# Cover Picture




**Philippe Brunet, Eric Demers, Thierry Maris, Gary D. Enright, and James D. Wuest***

**Permeable molecular crystals** can be specifically designed to let external agents enter, react, and produce single crystals of new substances with retention of the original crystalline architecture. Such topotactic processes can be made to cross-link molecular crystals covalently, thus capturing temporary supramolecular constructs as permanent crystalline macromolecular replicas. The Communication by J. D. Wuest et al on page 5303 ff. describes how suitable dithiols react with exposed allyl groups in such a manner.

# Contents

## Angewandte EarlyView

***The following articles are available online (in Wiley InterScience). You can find them at www.angewandte.org, under Full Text, Early View.***

*M. Lahav, T. Sehayek, A. Vaskevich, I. Rubinstein*:*
**Nanoparticle Nanotubes**
DOI: 10.1002/anie.200352216
Published online: October 23, 2003

*Z. Qin, C. M. Thomas, S. Lee, G. W. Coates*:*
**Cobalt-Based Complexes for the Copolymerization of Propylene Oxide and $CO_2$: Active and Selective Catalysts for Polycarbonate Synthesis**
DOI: 10.1002/anie.200352605
Published online: October 23, 2003

Articles judged by the referees or the editor as being either very important or very urgent are immediately edited, proof-read, and electronically published once the manuscript has arrived in the editorial office in final form. As long as there is no page number available these articles should be cited in the following manner:

Author(s) *Angew. Chem. Int. Ed.*, online publication date, DOI.

## Web Sites


http://www.sites.huji.ac.il/malaria/ **5266** — Malaria: A Parasite Goes Online — *Marcel Deponte, Katja Becker-Brandenburg*


## Books


Cellular Proteins and their Fatty Acids in Health and Disease **5267** — Asim K. Duttaroy, Friedrich Spener — *reviewed by Stefan Lorkowski*

Chemistry of Crop Protection **5267** — Günther Voss, Gerardo Ramos — *reviewed by Jörg Stetter*

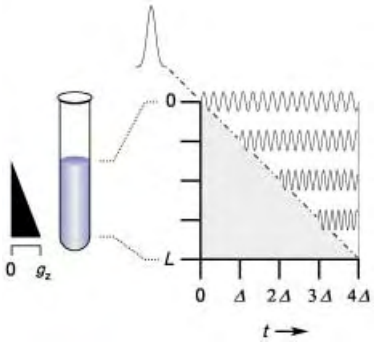

## Highlights

### *Imaging in NMR Spectroscopy*


T. Schulte-Herbrüggen* **5270 – 5272**

Imaging Techniques Boost NMR Spectroscopy: How To Remove Zero-Quantum Artifacts


**Slicewise excitation,** evolution, and detection are possible by using imaging techniques in NMR spectroscopy (see picture). Thus, spatial editing can be combined with spectral editing, for example, to remove zero-quantum artifacts from standard NOESY and TOCSY spectra, as recently described by Keeler and Thrippleton in this journal.



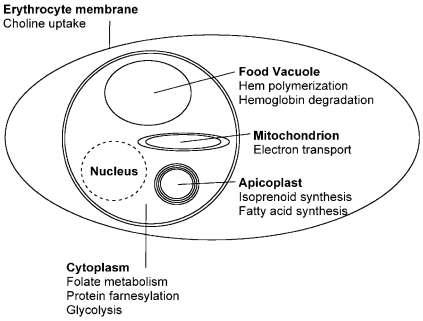

## Reviews

### *Medicinal Chemistry*


J. Wiesner,* R. Ortmann, H. Jomaa, M. Schlitzer* **5274 – 5293**

New Antimalarial Drugs

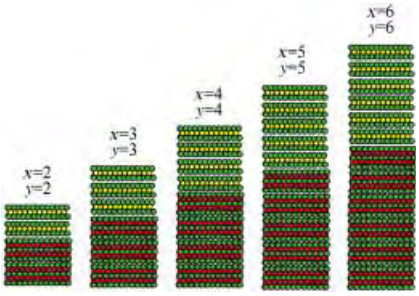

**Increasing resistance** of parasites to established therapeutics has resulted in malaria remaining one of the unsolved problems of modern medicine. Current research concentrates both on new compounds that act through established mechanisms and on new targets, such as the farnesyl transferase and the enzymes of the mevalonate-independent isoprenoid synthesis. (See picture: erythrocyte infected with *P. falciparum*.)






© 2003 Wiley-VCH Verlag GmbH & Co. KGaA, Weinheim

# Communications



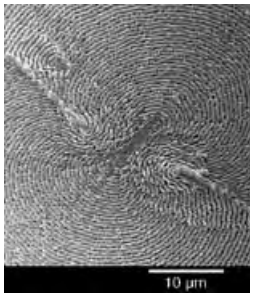

**Super Structures:** By thermally evaporating elemental layers onto substrates at ambient temperature, structural precursors are constructed with appropriate composition and modulation lengths to kinetically favor the formation of the desired superstructure. On annealing, these modulated elemental reactants form metastable $[(Bi_2Te_3)_x(TiTe_2)_y]$ superlattices (see picture).

## *Superlattices*

F. R. Harris, S. Standridge, C. Feik, D. C. Johnson* _____ **5296 – 5299**

Design and Synthesis of $[(Bi_2Te_3)_x(TiTe_2)_y]$ Superlattices

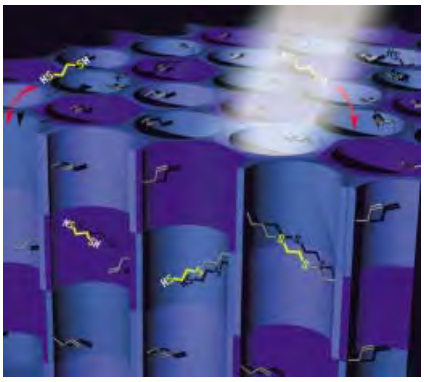
**$CaCO_3$ composites** with regular surface-relief structures have been synthesized (see picture). These sub-micrometer-scale structures are spontaneously formed on a thin matrix of a modified polysaccharide from aqueous solution containing an acidic polymer.




## *Patterned $CaCO_3$*

A. Sugawara, T. Ishii, T. Kato* _____ **5299 – 5303**

Self-Organized Calcium Carbonate with Regular Surface-Relief Structures



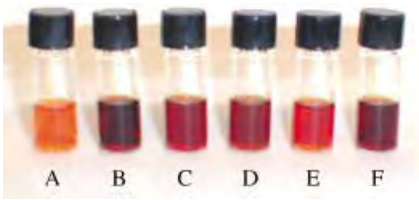
**Permeable molecular crystals** can be specifically designed to let external agents enter, react, and produce single crystals of new substances, with retention of the original crystalline architecture (see picture). Such topotactic processes can be made to cross-link molecular crystals covalently, thus capturing temporary supramolecular constructs as permanent crystalline macromolecular replicas.

## *Topotactic Reactions in Networks*

P. Brunet, E. Demers, T. Maris, G. D. Enright, J. D. Wuest* _____ **5303 – 5306**

Designing Permeable Molecular Crystals That React with External Agents To Give Crystalline Products

**Ion-induced assembly**: Supramolecular structures are obtained in solution by a new ion-induced assembly of conjugated Schiff-base macrocycles. A distinct color change accompanies the aggregation, as shown in the photo. Shown: Macrocycle (**A**); with $NaBPh_4$ (**B**); with $KBPh_4$ (**C**); with $RbBPh_4$ (**D**); with $CsBPh_4$ (**E**); and with $NH_4BPh_4$ (**F**) in $CH_2Cl_2$.




## *Conjugated Schiff-Base Macrocycles*

A. J. Gallant, M. J. MacLachlan* _____ **5307 – 5310**

Ion-Induced Tubular Assembly of Conjugated Schiff-Base Macrocycles

**For the USA and Canada:**
ANGEWANDTE CHEMIE International Edition (ISSN 1433-7851) is published weekly by Wiley-VCH PO Box 191161, D 69451 Weinheim, Germany. Air freight and mailing in the USA by Publications Expediting Inc. 200 Meacham Ave., Elmont, NY 11003. Periodicals postage paid at Jamaica NY 11431. US POSTMASTER: send address changes to *Angewandte Chemie*, Wiley-VCH, 111 River Street, Hoboken, NJ 07030. Annual institutional subscription price for institutions: Europe € 3430.00/3118.00. Outside Europe US$ 4499.00/4090.00 (valid for print and electronic/print or electronic delivery); for individuals who are personal members of a national chemical society, or whose institution already subscribes, or who are retired or self-employed consultants, print only. Europe € 248.00/Outside Europe US$ 378.00. Postage and handling charges included. All Wiley-VCH prices are exclusive VAT.

 © 2003 Wiley-VCH Verlag GmbH & Co. KGaA, Weinheim 

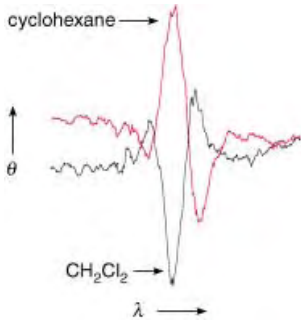
# Contents


## Solvent-Induced Chirality Switching

V. V. Borovkov,* G. A. Hembury, Y. Inoue* ——— **5310 – 5314**

The Origin of Solvent-Controlled Supramolecular Chirality Switching in a Bis(Zinc Porphyrin) System

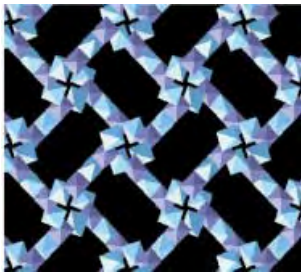
**Inducing chirality**: The supramolecular interaction of achiral bis(zinc porphyrin) with enantiopure amino acid derivatives in different solvents results in chirality induction. The sign and degree of the circular dichroims is controlled by the solvent polarity (see picture).




## Microporous Materials

N. Guillou,* C. Livage, M. Drillon, G. Férey ——— **5314 – 5317**

The Chirality, Porosity, and Ferromagnetism of a 3D Nickel Glutarate with Intersecting 20-Membered Ring Channels

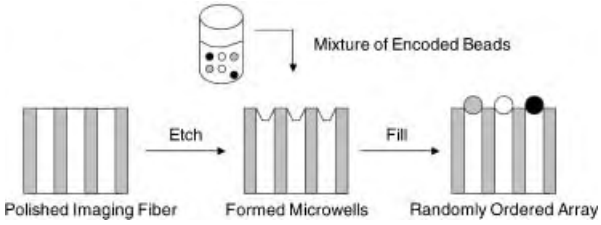


**A new dimension to nickel structures**: A three-dimensional nickel glutarate, $[Ni_{20}\{(C_5H_6O_4)_{20}(H_2O)_8\}]\cdot 40\,H_2O$, has been prepared under hydrothermal conditions. Its structure, solved from X-ray powder diffraction, is constructed from interconnected 20-rings, which form a remarkable open network of crossing channels (see picture). It is porous, and exhibits a ferromagnetic long-range ordering below 4 K.

## Biosensors

E. W. Adams, J. Ueberfeld, D. M. Ratner, B. R. O'Keefe, D. R. Walt,* P. H. Seeberger* ——— **5317 – 5320**

Encoded Fiber-Optic Microsphere Arrays for Probing Protein–Carbohydrate Interactions



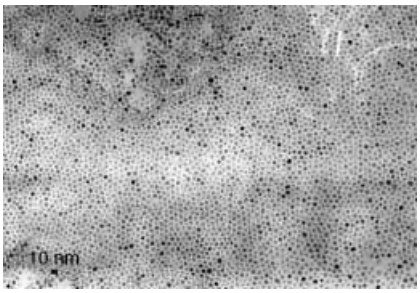

**Protein–carbohydrate interactions** can be evaluated by using randomly ordered fiber optic microsphere arrays bearing immobilized synthetic oligosaccharides (see scheme). Two systems are examined: the mannose-binding lectin concanavalin A, and cyanovirin N. The latter allows the simultaneous evaluation of five distinct structures against a carbohydrate-binding protein with unambiguous results.

## Zinc Oxide Nanoparticles

M. Monge, M. L. Kahn, A. Maisonnat, B. Chaudret* ——— **5321 – 5324**

Room-Temperature Organometallic Synthesis of Soluble and Crystalline ZnO Nanoparticles of Controlled Size and Shape

**Nanomaterials made easy**! The facile oxidation of $[Zn(c\text{-}C_6H_{11})_2]$ at room temperature in an organic solvent containing long-chain amine ligands leads to the formation of size- and shape-controlled crystalline ZnO nanoparticles (see picture). These particles, in the form of nanodisks and nanorods of low size dispersity in the 3–10 nm size range, are fully soluble in organic solvents (e.g., THF) and photoluminescent.





 © 2003 Wiley-VCH Verlag GmbH & Co. KGaA, Weinheim 



## Stabilizing the gp41 Trimer in HIV-1

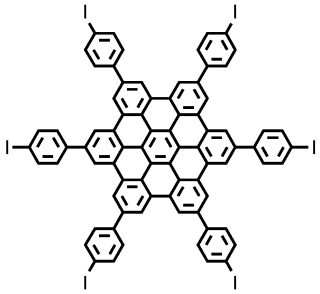
M. Gochin,* R. Kiplin Guy, M. A. Case ——— 5325 – 5328

A Metallopeptide Assembly of the HIV-1 gp41 Coiled Coil Is an Ideal Receptor in Fluorescence Detection of Ligand Binding

**A stable fragment** of the HIV-1 gp41 inner coiled coil has been designed. The addition of a transition-metal ion to bipyridylated gp41 peptides stabilizes the trimeric helical structure of the coiled coil through the formation of an octahedral tris-bipyridyl complex, and removes nonspecific aggregation of the hydrophobic peptide (see picture). The resulting structure recognizes peptides known to bind to the viral coiled coil and was used to develop a simple, useful and sensitive assay to rapidly detect binding of potential fusion-inhibiting drugs.

---

**An insoluble disclike building block** hexa(4-iodophenyl)-*peri*-hexabenzocoronene (see picture) was synthesized in an efficient way, and subsequent functionalization led to a series of soluble, star-type hexabenzocoronenes (HBCs), all showing remarkable self-assembly behavior: 1) highly ordered liquid-crystalline materials, 2) dendronized HBCs, and 3) triarylamine-substituted HBCs.

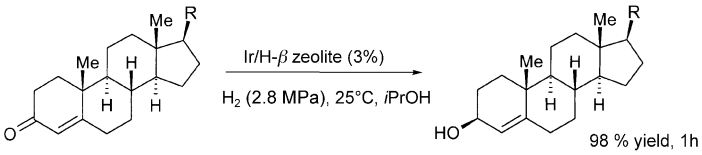


## Carbon-Rich Compounds

J. Wu, M. D. Watson, K. Müllen* ——— 5329 – 5333

The Versatile Synthesis and Self-Assembly of Star-Type Hexabenzocoronenes

---




## Chemoselective Hydrogenation

M. De bruyn, S. Coman, R. Bota, V. I. Parvulescu, D. E. De Vos, P. A. Jacobs* ——— 5333 – 5336

Chemoselective Reduction of Complex α,β-Unsaturated Ketones to Allylic Alcohols over Ir-Metal Particles on β Zeolites

**The combination of Ir**, which has a strong affinity for carbonyl groups, with an acid H-β zeolite as a support and promotor, provides an effective catalyst for the chemoselective hydrogenation of α,β-unsaturated aldehydes and ketones to the corresponding allylic alcohols. Steroidal enones are suitable substrates for this transformation (see scheme). R = CH(Me)$(CH_2)_3$CH$(Me)_2$.

---



## Imprinted Polymer Microspheres

J. Wang, P. A. G. Cormack,* D. C. Sherrington, E. Khoshdel ——— 5336 – 5338

Monodisperse, Molecularly Imprinted Polymer Microspheres Prepared by Precipitation Polymerization for Affinity Separation Applications

**Theophilline-imprinted** polymer microspheres were obtained in monodisperse form with diameters of about 5 μm (see picture) in a single synthetic step by precipitation polymerization. This robust material, which proved suitable for use in HPLC, can, in principle, also be applied in any application in which molecular recognition phenomena play a role.

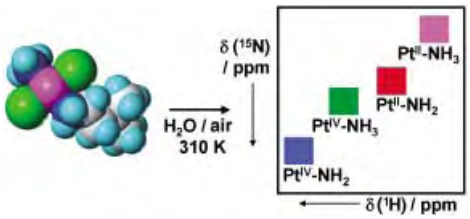
 © 2003 Wiley-VCH Verlag GmbH & Co. KGaA, Weinheim 

# Contents


## trans *Diamine Pt$^{II}$ Anticancer Complex*

A. M. Pizarro, V. P. Munk, C. Navarro-Ranninger, P. J. Sadler* _____ **5339 – 5342**

Hydrolysis Triggers Oxidation of a *trans* Diamine Platinum(II) Anticancer Complex

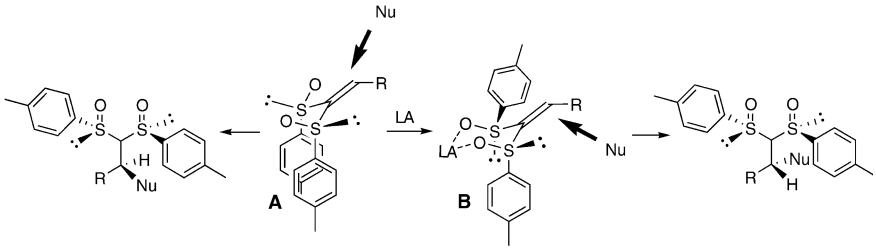



**$^{1}$H, $^{15}$N and $^{195}$Pt NMR** spectroscopy experiments show that the aqua adducts of a *trans* diamine platinum(II) anticancer complex unexpectedly undergo facile oxidation to platinum(IV) in aqueous solution in air (see picture).

## *Stereoselective Conjugate Addition*

F. Brebion, B. Delouvrié, F. Nájera, L. Fensterbank,* M. Malacria,* J. Vaissermann _____ **5342 – 5345**

Highly Diastereoselective Conjugate Addition to Alkylidene Bis(Sulfoxides): Asymmetric Synthesis of (+)-*erythro*-Roccellic Acid

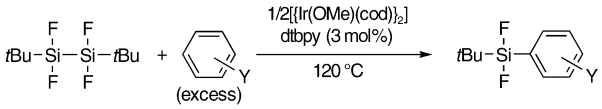



**Facial stereocontrol** is possible in Michael additions of nucleophiles (Nu) to alkylidene bis(sulfoxides), which proceed via nonchelated (**A**) or chelated (**B**) intermediates depending on the addition of an appropriate Lewis acid (LA). This intriguing reactivity could be applied to the first total synthesis of the succinate-based natural product, (+)-*erythro*-roccellic acid.

## *Ir-Catalyzed Silylation of Arenes*

T. Ishiyama,* K. Sato, Y. Nishio, N. Miyaura* _____ **5346 – 5348**

Direct Synthesis of Aryl Halosilanes through Iridium(I)-Catalyzed Aromatic C–H Silylation by Disilanes



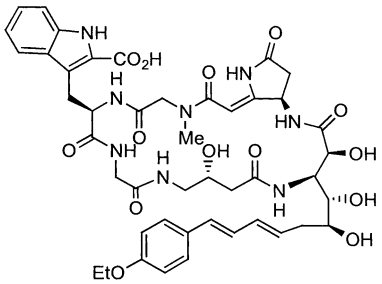

**Aromatic C–H silylation of arenes** by 1,2-di-*tert*-butyl-1,1,2,2-tetrafluorodisilane is efficiently catalyzed by iridium(I) complexes generated from [{Ir(OMe)(cod)}$_2$] (cod = cyclooctadiene) and 4,4′-di-*tert*-butyl-2,2′-bipyridine (dtbpy; see scheme) and provides the corresponding aryl fluorosilanes in excellent yields.

## *Hexapeptide Total Synthesis*

J. Zhu, D. Ma* _____ **5348 – 5351**

Total Synthesis of Microsclerodermin E

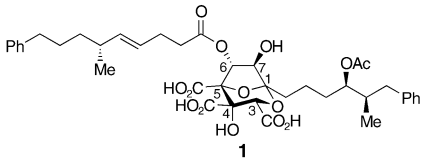
**Succumbing to total synthesis**: Microsclerodermin E, a 23-membered cyclic hexapeptide possessing antifungal activity, has been prepared for the first time. Key features in the synthesis include the construction of four unusual amino acid units, the assembly of the pyrrolidinone fragment with little racemization, and an effective macrocyclization.



microsclerodermin E


 © 2003 Wiley-VCH Verlag GmbH & Co. KGaA, Weinheim 

**Ketal isomers avoided**. The unique 2,8-dioxabicyclo[3.2.1]octane core of zaragozic acid C (**1**) was constructed in a Rh-catalyzed 1,3-dipolar cycloaddition of an alkyne to an ester carbonyl ylide. Another feature of this improved synthesis is the construction of the alkyl side chain at C1 by olefin cross-metathesis.

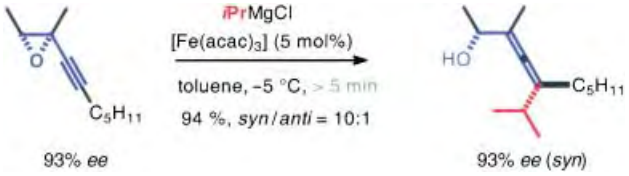



**1**

## Natural Products Total Synthesis

S. Nakamura, Y. Hirata, T. Kurosaki, M. Anada, O. Kataoka, S. Kitagaki, S. Hashimoto* ——— **5351 – 5355**

Total Synthesis of the Squalene Synthase Inhibitor Zaragozic Acid C by a Carbonyl Ylide Cycloaddition Strategy



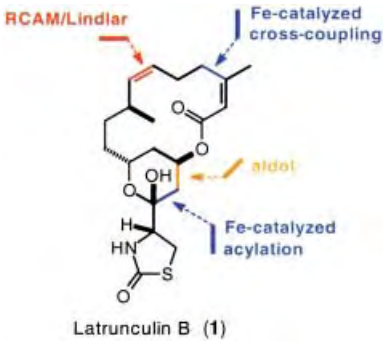

**Reliable chirality transfer** is one of the major advantages of a novel synthesis of 2,3-allenols from propargyl epoxides (see scheme) catalyzed by inexpensive and environmentally benign iron salts. The reactions proceed very rapidly in excellent yields and with moderate to good diastereoselectivity in favor of the *syn*-configured product.

## Iron-Catalyzed Allenol Formation

A. Fürstner,* M. Méndez ——— **5355 – 5357**

Iron-Catalyzed Cross-Coupling Reactions: Efficient Synthesis of 2,3-Allenol Derivatives

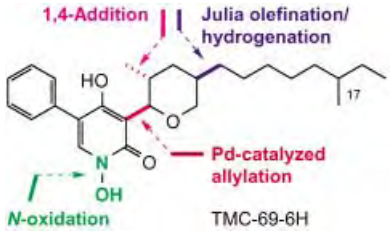
**The highly selective** actin-binding latrunculins (e.g. **1**) play a prominent role as probe molecules in chemical biology. A highly concise, productive, and inherently flexible approach to **1** illustrates the excellent profile and use of metal-catalyzed C–C bond formations.




## Natural Product Synthesis

A. Fürstner,* D. De Souza, L. Parra-Rapado, J. T. Jensen **5358 – 5360**

Catalysis-Based Total Synthesis of Latrunculin B




**The unexpected selectivity profile** of (17*R*)- and (17*S*)-TMC-69-6H (see formula) suggests that *N*-hydroxypyridone derivatives constitute a promising new lead structure in the search for selective phosphatase inhibitors. An unprecedented Pd-catalyzed C–C bond formation to a pyranone derivative was a key step in the synthesis of enantiopure (17*R*)- and (17*S*)-TMC-69-6H.

## Phosphatase Inhibitors

A. Fürstner,* F. Feyen, H. Prinz, H. Waldmann ——— **5361 – 5364**

Total Synthesis and Reassessment of the Phosphatase-Inhibitory Activity of the Antitumor Agent TMC-69-6H

Communications labeled with this symbol have been judged by two referees as being "very important papers".

The publication of Communications labeled with this symbol has been accelerated because of their topical or highly competitive nature.

 © 2003 Wiley-VCH Verlag GmbH & Co. KGaA, Weinheim 

# Contents


## Looking for outstanding employees?

**Do you need another expert for your excellent team?**
**...Chemists, PhD Students, Managers, Professors, Sales Representatives...**

Place an advert in the printed version and have it made available online for 1 month, free of charge!

***Angewandte Chemie International Edition***

**Advertising Sales Department: Marion Schulz**
**Phone: 0 62 01 - 60 65 65**
**Fax: 0 62 01 - 60 65 50**
**E-Mail: MSchulz@wiley-vch.de**


## Service


*Keywords* ——— 5366

*Authors* ——— 5367

*Preview* ——— 5369


# Corrigendum

In the Communication "Equilibrium and Kinetic Deuterium Isotope Effects on the Hetero-Diels–Alder Addition of Sulfur Dioxide" by P. Vogel, J. A. Sordo et al. (*Angew. Chem. Int. Ed* **2003**, *42*, 3924–3927), lines 7 and 11 as well as lines 8 and 12 of Table 2 (pg. 3926) have been swapped. The correct table is shown below:

***Table 2:*** Calculated kinetic deuterium isotope effect for concerted hetero-Diels–Alder additions.

| Reaction | | $T$ [°C] | | |
|---|---|---|---|---|
| | | −75 | −54 | +25 |
| **1**/**3** + 2 $SO_2$ → [**11**] → **4** + $SO_2$ | $k_H/k_D$[a] | 0.692 | 0.725 | 0.816[b] |
| | | (0.714) | (0.746) | (0.830)[c] |
| **1**/**3** + 2 $SO_2$ → [**12**] → **5** + $SO_2$ | $k'_H/k'_D$[d] | 0.776 | 0.801 | 0.869[b] |
| | | (0.734) | (0.763) | (0.841)[c] |
| Kinetic regioselectivity:[i] | Ratio | 1.12 | 1.10 | 1.06 |
| **15**/**16** + 2 $SO_2$ → [**11′**] → **4′** + $SO_2$ | $k_H/k_D$[e] | 0.707 | 0.741 | 0.829[b] |
| | | (0.721) | (0.754) | (0.842)[c] |
| | | 0.748 | 0.780 | 0.861[f] |
| | | (0.755) | (0.785) | (0.865)[g] |
| **15**/**16** + 2 $SO_2$ → [**12′**] → **5′** + $SO_2$ | $k'_H/k'_D$[h] | 0.693 | 0.729 | 0.824[b,j] |
| | | (0.673) | (0.709) | (0.806)[c,k] |
| | | 0.658 | 0.695 | 0.796[f] |
| | | (0.647) | (0.685) | (0.789)[g] |

[a] $k_H/k_D \triangleq k_1/2\,k_4$. [b] B3LYP/6-31G(d). [c] B3LYP/6-31G(d) for the reaction with only one equivalent of $SO_2$. [d] $k'_H/k'_D \triangleq k_1/2\,k_5$. [e] $k_H/k_D \triangleq$ butadiene + 2 $SO_2$ vs. 1,1-$D_2$-butadiene + 2 $SO_2$ giving a sultine analogous to **4**. [f] MP2/6-31G(d). [g] MP2/6-31G(d) for the reaction with only one equivalent of $SO_2$. [h] $k'_H/k'_D \triangleq$ butadiene + 2 $SO_2$ vs. 1,1-$D_2$-butadiene + 2 $SO_2$ giving sultine analogous to **5**. [i] $k'_H/k'_D$(**5**)/$k_H/k_D$(**4**); calculated (B3LYP/6-31G(d) including zero-point energy). [j] Energy barrier: 4.8 kcal mol$^{-1}$. [k] Energy barrier: 12.2 kcal mol$^{-1}$.

Imaging in NMR Spectroscopy

# Imaging Techniques Boost NMR Spectroscopy: How To Remove Zero-Quantum Artifacts

*Thomas Schulte-Herbrüggen**

**Keywords:**
imaging techniques · NMR spectroscopy

*Dedicated to Richard R. Ernst on the occasion of his 70th birthday*

> *"Fourier imaging ... can be considered as a typical 2D spectroscopy technique."*
> R. R. Ernst et al.[1]

## The Problem with Zero-Quantum Coherences

Magnetic resonance imaging[15] inherited its fundamental Fourier methods largely from NMR spectroscopy. In turn, spatial separation is just about to conquer spectroscopic domains by setting landmarks of progress. After allowing a multidimensional NMR experiment to be performed in a single scan,[2] imaging methods now solve the long-standing problem of purging NMR spectra of zero-quantum artifacts, as recently shown by Keeler and Thrippleton in this journal.[3]

Ironically, in the history of mathematics, the *zero* is widely recognized as one of the most helpful ingenious concepts introduced in antiquity, whereas *zero*-quantum coherences have all too often shown up as the devil's signature in a wide range of everyday NMR spectra. It is a safe bet that nearly every NMR spectroscopist has frowned over ugly dispersive trails and misleading *J* correlations, for example, in NOESY spectra. What a relief if a protein structure does not hinge on peaks interdispersed with (if not identical to) "ghost peaks"!

[*] Dr. T. Schulte-Herbrüggen
Institut für Organische Chemie und Biochemie II
Technische Universität München
Lichtenbergstrasse 4
85747 Garching (Germany)
Fax: (+49) 89-289-13210
E-mail: tosh@ch.tum.de

Why are zero-quantum coherences so difficult to eliminate? They simultaneously escape two of the most powerful purgative tools of NMR spectroscopy: phase cycling and pulsed-field gradients. They are both equally ineffective when it comes to separating zero quanta from $z$ polarization. It is therefore worth looking back in a bit more detail.

Only one year after the breakthroughs to pioneer 2D NMR spectroscopy,[4] Wokaun and Ernst showed in a seminal paper[5] that every component in a density operator (which represents the state of a spin ensemble) can be labeled with a phase factor $e^{-ip\varphi}$ according to its quantum order $p$ when subjected to a $z$ rotation or phase shift of angle $\varphi$. Moreover, they demonstrated how to exploit these phase labels to select the components of desired quantum order, while annihilating all others by way of phase cycling, that is, by Fourier analysis with respect to phase shifts of angle $\varphi$.[5] This method led to quantum filtering[6] and soon became routine.[1,7] Most prominently, it turned the crude look of early COSY spectra into the "well-groomed" appearance of double-quantum-filtered (DQF) COSY.[8] Without dispersive trails from the diagonal, they provide valuable connectivity and bond-angle information, which is complemented with NOESY-derived distance constraints to form the basis of structure elucidation by NMR spectroscopy.[9]

Why, then, does the same trick not purge NOESY-type spectra of zero-quantum artifacts? This reason lies in the fact that the NOE transfers polarization from one spin to the other ($I_{kz} \mapsto I_{lz}$), and $z$ polarization ($I_{kz}$) as well as longitudinal multispin order (e.g. $2I_{kz}I_{lz}$) both remain invariant under $z$ rotation. Hence they appear invariably with the phase label associated with $p = 0$—just as zero-quantum coherences do. Separation impossible!

Even worse, these three types of terms also remain largely unaffected by magnetic-field inhomogeneity.[5] The reason is similar: by applying pulsed-field gradients, terms of different quantum order receive different degrees of dephasing, again proportional to their quantum order.[10] This method, to which the group of Keeler has significantly contributed over the years,[11] quickly made it into the standard toolbox to select desired quantum orders in a single scan (mostly one each for the echo and anti-echo parts), whereas phase cycling usually requires the combination of more scans. However, since the phase labeling is similar in the two methods (phase cycling and gradients), both share largely the same blind spots—but not entirely so.

## The Solution of Keeler and Thrippleton

Keeler and Thrippleton[3] have now provided an elegant solution to the notorious conundrum of how to suppress zero-quantum coherences efficiently, while retaining polarizations or longitudinal multispin orders. Their experimental results are remarkably superior to any of the previous attempts at tackling the problem. This is made possible by state-of-the-art spectrometers that allow the combination of pulsed field gradients and selective pulses with adiabatic frequency sweeps, features which the pioneers could hardly have dreamt to be compatible with the

 © 2003 Wiley-VCH Verlag GmbH & Co. KGaA, Weinheim DOI: 10.1002/anie.200301689 

stability demands in high-resolution spectroscopy some day.

The basic trick derives from imaging and rests on spatial separation of different shift evolutions that sum to zero when averaged over the entire sample. The underlying refocusing module can readily be understood on a pictorial level in more detail. One needs to remember that a $z$ gradient makes the resonance frequency in each slice of the sample depend on the height ($z$ coordinate) within the NMR tube (Figure 1a). In other words, every layer has its unique Larmor frequency $\omega$. In the presence of such a $z$ gradient, a *selective* 180° pulse is swept during a time interval $\tau_f$ such that it will touch the resonance frequencies of different disks at different times, reaching from say $t=0$ for the top slice to $t=\tau_f$ for the bottom one. Thus, the chemical-shift evolution will be inverted (in the sense of Hahn's spin echo) first at the top ($t=0$), and at the bottom only from $t=\tau_f$ on (Figure 1b). In particular, this also holds for any evolution under a nonvanishing zero-quantum frequency $\Omega_{ZQ}=\Omega_k-\Omega_l$ of $I_k^- I_l^+$. If the spread of zero-quantum shift evolution between the slices is large enough, the average taken over the entire sample will be zero—even if another time interval (such as a mixing time) follows (Figure 1c).

This cancellation naturally results after a single scan and is robust to random processes such as diffusion between the slices as well as to convection driven by temperature gradients within the sample. However, in NOESY experiments the resonance-frequency bandwidth over the sample has to be much larger than the spectral width, otherwise the cross-peak buildup between two spins will be attenuated depending on their shift difference and thus hinder a quantitative interpretation. Yet, owing to its robustness and general applicability, for example, to isotropic TOCSY[12] and other experiments with mixing processes starting from $z$ magnetization, the method will surely find broad usage.

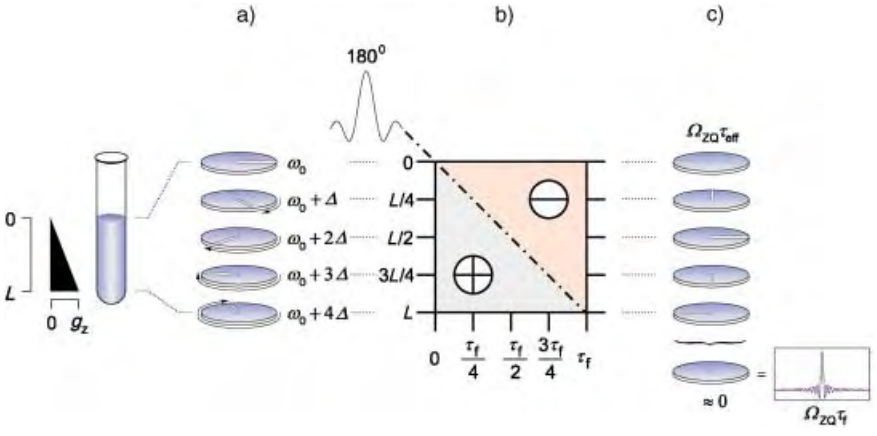



***Figure 1.*** Method to average out zero-quantum coherences while retaining polarization and longitudinal multispin order.[3] See text for details.

## *Multidimensional NMR Spectroscopy in One Shot*

Experimental robustness is certainly not the key point in a proposal for performing multidimensional NMR experiments in *single* scans—speed (short measuring time) is. Actually the paper by Frydman et al.[2] might well have served to inspire Keeler and Thrippleton. The principle of a one-scan 2D NMR experiment resides in parallel evolution of several $t_1$ increments, each in a spatially separated slice that also has to be detected distinctly. To fulfill these experimentally tricky demands, the authors exploit ideas of Fourier imaging.[13] However, in this case the phase labels of the slice position are not used for spatial resolution but are taken as $t_1$ evolutions (Figure 2). To this end, a selective excitation pulse (of flip angle 90°) has to be swept over discrete frequencies at discrete times in the presence of a position-encoding gradient. Thereby each slice is excited with a unique Larmor frequency and thus evolves with a unique $t_1$ increment. Only the subsequent mixing may proceed uniformly, whereas the detection process is slice-selective by making use of gradient echoes from echo-planar imaging,[14] a trick "borrowed" from medicinal NMR imaging. Confining each $t_1$ increment to a single spatially separated slice and thereby to a very small sample fraction requires high concentrations; this is feasible in the case of small molecules for which reduced resolution by diffusion and $t_1$ artifacts by convection are not detrimental. Therefore, particularly in routine analytical NMR spectroscopy, the new approach may well prove to be a valuable time saver, provided it can be reliably implemented and automated.

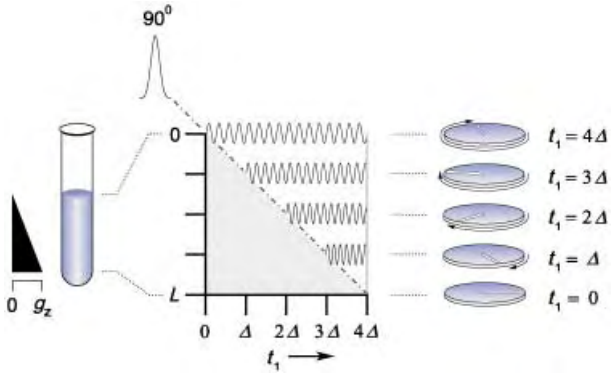


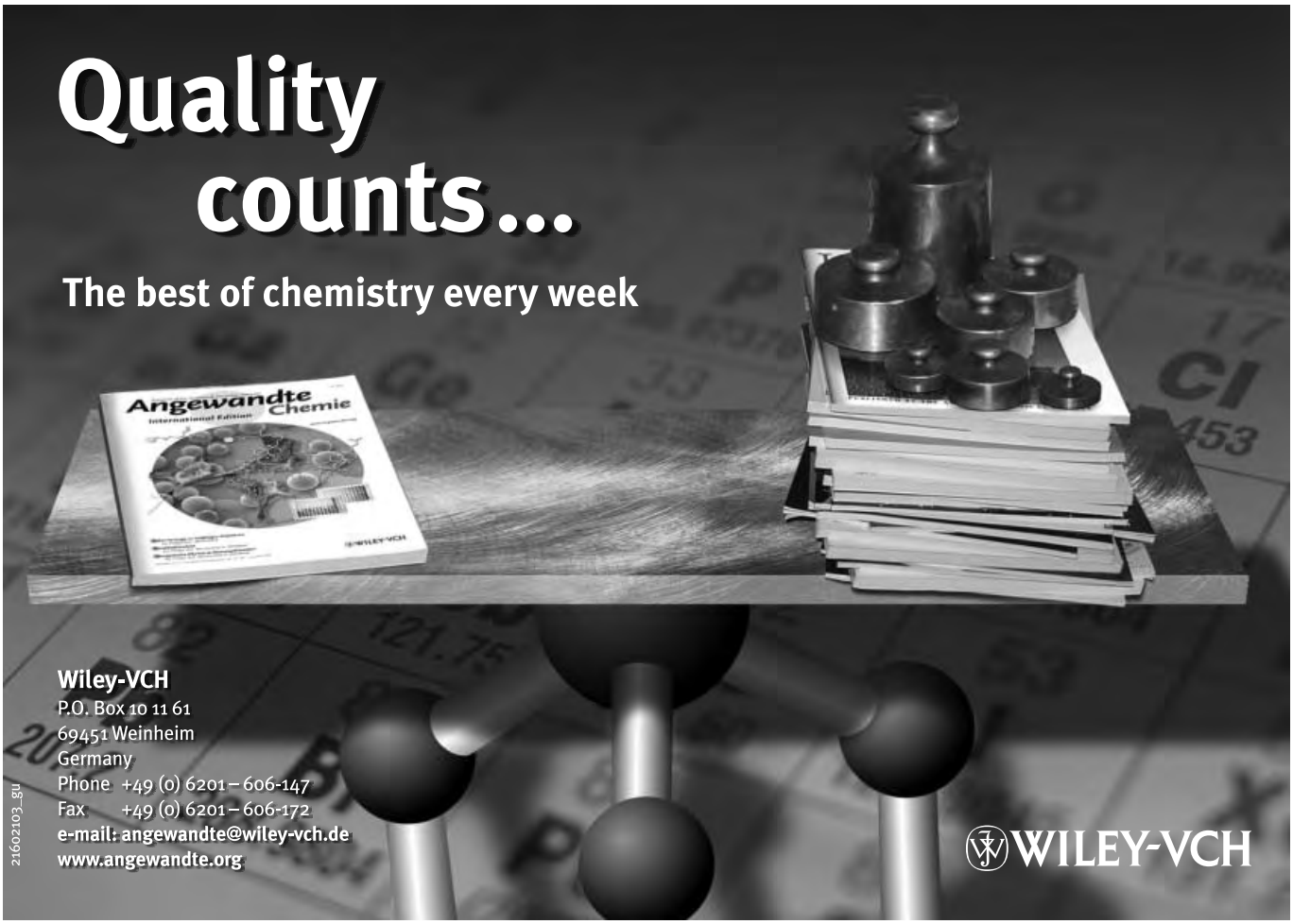

***Figure 2.*** Excitation scheme for a proposed singe-scan recording of a 2D spectrum.[2] The $z$ gradient ensures that every slice exhibits a distinct resonance frequency. A selective 90° pulse then excites every slice at a different time, so that the spins evolve slicewise in $t_1$. Only mixing can proceed uniformly. Echo-planar imaging[14] methods finally allow the signals from each disk to be separated upon detection.

In conclusion, imaging techniques allow the spectroscopist to separate the sample into spatially divided layers with different excitation, evolution, and detection. Depending on the transformation properties of the pertinent operator terms, spatial editing can thus be combined with spectral editing. Beyond purging or accelerating known techniques, this opens a perspective of creativity in designing novel experiments.

[1] R. R. Ernst, G. Bodenhausen, A. Wokaun, *Principles of Nuclear Magnetic Resonance in One and Two Dimensions*, Clarendon Press, Oxford, **1987**; see also Nobel Prize Lecture: R. R. Ernst, *An-*

 © 2003 Wiley-VCH Verlag GmbH & Co. KGaA, Weinheim 

*gew. Chem.* **1992**, *104*, 817 – 836; *Angew. Chem. Int. Ed.* **1992**, *31*, 805 – 823.
[2] L. Frydman, T. Scherf, A. Lupulescu, *Proc. Natl. Acad. Sci. USA* **2002**, *99*, 15858 – 15862.
[3] M. J. Thrippleton, J. Keeler, *Angew. Chem.* **2003**, *115*, 4068 – 4071; *Angew. Chem. Int. Ed.* **2003**, *42*, 3938 – 3941.
[4] W. Aue, E. Bartholdi, R. R. Ernst, *J. Chem. Phys.* **1976**, *64*, 2229 – 2246; "The Unpublished Baško Polje (1971) Lecture Notes": J. Jeener in *NMR and More* (Eds.: M. Goldman, A. Porneuf), Les Éditions de Physique, Les Ulis, **1994**, pp. 266 – 272.
[5] A. Wokaun, R. R. Ernst, *Chem. Phys. Lett.* **1977**, *52*, 407 – 412.
[6] G. Bodenhausen, H. Kogler, R. R. Ernst, *J. Magn. Reson.* **1984**, *58*, 370 – 388.
[7] H. Kessler, M. Gehrke, C. Griesinger, *Angew. Chem.* **1988**, *100*, 507 – 554; *Angew. Chem. Int. Ed. Engl.* **1988**, *27*, 490 – 536.
[8] U. Piantini, O. W. Sørensen, R. R. Ernst, *J. Am. Chem. Soc.* **1982**, *104*, 6800 – 6801.
[9] K. Wüthrich, *NMR of Proteins and Nucleic Acids*, Wiley, New York, **1988**; see also Nobel Prize Lecture: K. Wüthrich, *Angew. Chem.* **2003**, *115*, 3462 – 3484; *Angew. Chem. Int. Ed.* **2003**, *42*, 3340 – 3363.
[10] C. J. R. Counsell, M. H. Levitt, R. R. Ernst, *J. Magn. Reson.* **1985**, *64*, 470 – 478.
[11] G. Kontaxis, J. Stonehouse, R. D. Laue, J. Keeler, *J. Magn. Reson. Ser. A* **1994**, *111*, 70 – 76; A. L. Davis, J. Keeler, R. D. Laue, D. Moskau, *J. Magn. Reson.* **1992**, *98*, 207 – 216; see also: *Encyclopedia of Nuclear Magnetic Resonance* (Eds.: D. M. Grant, R. K. Harris), Wiley, Chichester, **1996**.
[12] S. J. Glaser, J. Quandt, *Adv. Magn. Reson.* **1996**, *19*, 59 – 252.
[13] A. Kumar, D. Welti, R. R. Ernst, *J. Magn. Reson.* **1975**, *18*, 69 – 83; W. A. Edelstein, J. M. S. Hutchinson, G. Johnson, T. Redpath, *Phys. Med. Biol.* **1980**, *25*, 751 – 756; P. T. Callaghan, *Principles of Nuclear Magnetic Resonance Microscopy*, Clarendon Press, Oxford, **1991**.
[14] P. Mansfield, *J. Phys. C* **1977**, *10*, L55 – L58; P. Mansfield, *Magn. Reson. Med.* **1984**, *1*, 370 – 386; see reference [15b] as well as: P. G. Morris, *NMR Imaging in Biology and Medicine*, Oxford University Press, Oxford, **1986**.
[15] During the revision of this Highlight, it was announced that Lauterbur and Mansfield had been awarded the Nobel Prize in Medicine for 2003. For more information on the techniques, see: a) P. C. Lauterbur, *Nature* **1973**, *242*, 190 – 191; b) P. Mansfield, P. G. Morris, *NMR Imaging in Biomedicine*, Academic Press, New York, **1982**; c) see also reference [14].

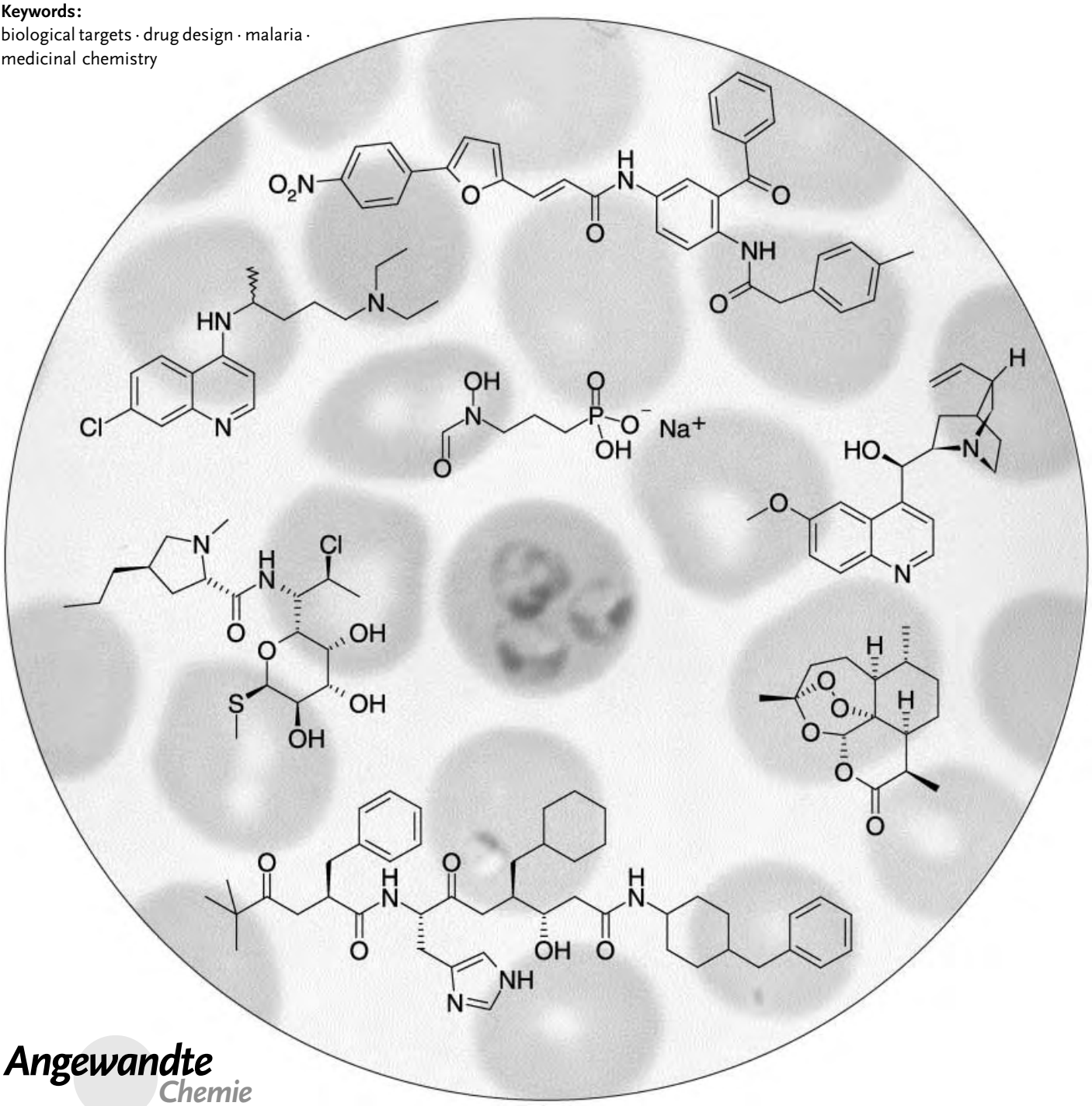


Medicinal Chemistry

# New Antimalarial Drugs**

*Jochen Wiesner,* Regina Ortmann, Hassan Jomaa, and Martin Schlitzer**

**Keywords:**
biological targets · drug design · malaria · medicinal chemistry





© 2003 Wiley-VCH Verlag GmbH & Co. KGaA, Weinheim
DOI: 10.1002/anie.200200569

*Approximately 40 % of the world population live in areas with the risk of malaria. Each year, 300–500 million people suffer from acute malaria, and 0.5–2.5 million die from the disease. Although malaria has been widely eradicated in many parts of the world, the global number of cases continues to rise. The most important reason for this alarming situation is the rapid spread of malaria parasites that are resistant to antimalarial drugs, especially chloroquine, which is by far the most frequently used. The development of new antimalarial drugs has been neglected since the 1970s owing to the end colonialism, changes in the areas of military engagement, and the restricted market potential. Only in recent years, in part supported by public funding programs, has interest in the development of antimalarial drugs been renewed. New data available from the recently sequenced genome of the malaria parasite* Plasmodium falciparum *and the application of methods of modern drug design promise to bring significant development in the fight against this disease.*

**From the Contents**


| | |
|---|---|
| 1. Introduction | 5275 |
| 2. Established Antimalarial Drugs | 5277 |
| 3. New Antimalarial Drugs in Clinical Use | 5280 |
| 4. Antimalarial Drugs in Clinical Development | 5280 |
| 5. Antimalarial Drugs in Preclinical Development | 5283 |
| 6. Summary and Overview | 5289 |
| 7. Abbreviations | 5290 |


## 1. Introduction

Malaria is caused by protozoal parasites of the genus *Plasmodium*. Four different *Plasmodium* species infect humans and cause distinct disease patterns: *P. falciparum* (malaria tropica), *P. vivax* (malaria tertiana), *P. malariae* (malaria tertiana), and *P. ovale* (malaria quartana). The latter two species are less common. The parasites are transmitted by mosquitoes of the genus *Anopheles*. After the bite of an infected mosquito, the parasites establish an initial asymptomatic infection of liver cells (Figure 1). After an average incubation period of one week, blood stages are released, which develop and multiply inside erythrocytes. A small proportion of the blood stages develop into sexual stages, the so-called gametocytes, which are able to infect a new mosquito when they are taken up with a meal of blood. The clinical symptoms of malaria are exclusively caused by the erythrocytic parasite stages. With the release of the parasites from infected erythrocytes, cell debris responsible for the characteristic fever spike pattern enters the blood stream. Most fatal malaria cases are caused by *P. falciparum*. This parasite produces specific proteins that are transported to and embedded in the cell membrane of the infected erythrocyte. As a consequence of this modification, the erythrocytes stick to the walls of pre-venous capillaries, which causes obstruction of the vessels. In cerebral malaria, an exceptionally dangerous complication of *P. falciparum* malaria, sequestration of infected erythrocytes in brain vessels is associated with loss of consciousness, and is lethal if not treated immediately. Parasites of the species *P. vivax* and *P. ovale* can persist for years as dormant stages in the liver (the so-called hypnozoites) and can cause clinical relapses at regular intervals.

Malaria was one of the best-studied diseases in Western medicine until the middle of the 20th century. Until that time, malaria was still endemic in parts of Europe and North America. The first attempts at a specific treatment of malaria date back to the early 18th century and made use of the bark of Cinchona trees (originally found in the high altitudes of South America), which had already been used in the treatment of fever since the beginning of the 17th century.[1] In 1820, quinine (**1**, Figure 2) was isolated as the active ingredient and successively replaced the crude bark for the treatment of malaria. Thus, malaria was among the first diseases to be treated with a pure chemical compound. In 1891, based on the observation that methylene blue (**2**, Figure 2) was selectively taken up by the parasites in microscopic specimens, Paul Ehrlich cured two malaria patients with the dye. This was the first time that a synthetic drug was ever used in humans.[2] Today it is known that methylene blue (**2**) inhibits glutathione reductase thereby disturbing the redox homoeostasis of the parasite.[3,4] By modifying the methylene blue structure, pamaquine (**3**, plasmoquine, Figure 2) was synthesized in 1925. This 8-amino quinoline was the first drug that was capable of preventing the relapses in *P. vivax* malaria.[5] In 1932, mepacrine (**4**, atebrine, quinacrine) was developed, which proved to be active against the blood stages of *P. falciparum*. Both drugs were used extensively in World War II, especially in the Southwest Pacific.

Chloroquine (**5**) had already been synthesized in 1934, but was not used until 1946 because it was considered to be too toxic. Since then, chloroquine (**5**) turned out to be the most

[*] Dr. J. Wiesner, Dr. H. Jomaa
Biochemisches Institut der Justus-Liebig-Universität
Friedrichstrasse 24, 35392 Giessen (Germany)
Fax: (+49) 641-9947529
E-mail: Jochen.Wiesner@biochemie.med.uni-giessen.de
Prof. Dr. M. Schlitzer, Dr. R. Ortmann
Department für Pharmazie – Zentrum für Pharmaforschung
Ludwig-Maximilians-Universität München
Butenandtstrasse 5–13, 81377 München (Germany)
Fax: (+49) 89-2180-79992
E-mail: Martin.Schlitzer@cup.uni-muenchen.de

[**] Protected trade names (trademarks) have not been indicated in this Review. The absence of such information in no way implies an unregistered or unprotected trade name.

 DOI: 10.1002/anie.200200569 © 2003 Wiley-VCH Verlag GmbH & Co. KGaA, Weinheim 

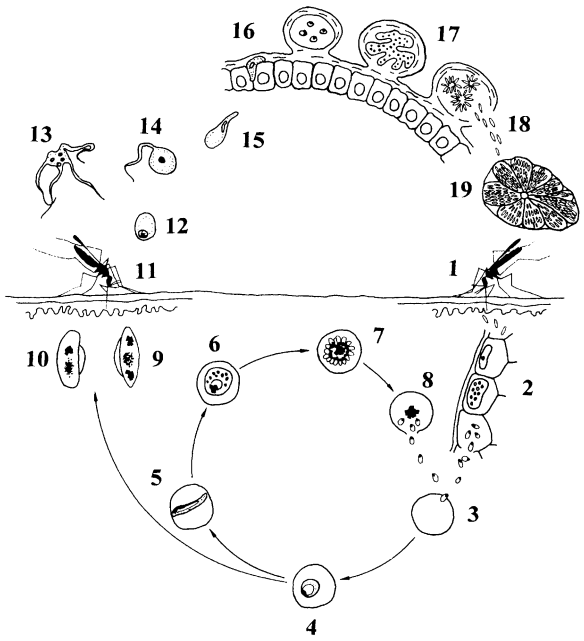



***Figure 1.*** Life cycle of the malaria parasite *P. falciparum*. With the bite of an infected female anopheles mosquito, the sporozoites are transferred into the human blood (1). The sporozoites invade the liver cells and start their asexual division (10000–30000-fold multiplication), resulting in the production of several thousands of merozoites (2). The merozoites are released from the liver cells to infect the erythrocytes in the blood stream (3). Within the erythrocytes, the asexual reproduction occurs in 48-hour cycles. The parasites develop through the stages of rings (4), trophozoites (5), and schizonts (6). In the segmenter stage (7), each schizont typically divides into 16 erythrocytic merozoites, which are released by lysis of the erythrocyte and immediately invade new erythrocytes (8). Induced by stress factors, a small proportion of blood stages undergo differentiation into female (9) and male (10) gametocytes, which enter the mosquito when it bites an infected individual (11). In the mosquito mid-gut, the female gametocytes develop into macrogametes (12), and the male gametocytes divide into four to eight flagellated microgametes (13). The male and female gametes fuse and form a zygote (14). This transforms into a motile ookinete (15), which penetrates the gut wall (16) and becomes the oocyst residing under the external membrane of the mosquito mid-gut (17). Asexual division inside the oocyst produces thousands of sporozoites, which are released when the oocyst ruptures (18) and migrate to the salivary glands (19).

effective and important antimalarial ever and became the drug of choice in several programs aimed at the global eradication of malaria. In an attempt at a widespread distribution of the drug as a prophylactic, chloroquine (**5**) was added to table salt in parts of South America, Africa, and Asia. Possibly as a result of the medicated salt program, the first cases of chloroquine resistance appeared at the end of the 1950s. Today, chloroquine-resistant strains of *P. falciparum* (and to some extent of *P. vivax*) are common in all endemic areas throughout the world. During World War II, British researchers developed proguanil (**6**, Figure 2), which in turn served as a lead compound for the development of pyrimethamine (**7**) in 1950. Faced with heavy losses as a result of chloroquine-resistant malaria during the Vietnam War, the development of new antimalarial drugs was encouraged by the American military and resulted in the development of mefloquine (**8**) and halofantrine (**9**).

A completely different group of drugs was derived from traditional Chinese medicine. The sweet wormwood *Artemisia annua* has been used in China for at least 2000 years, originally as a treatment for haemorrhoids, but since 1596 also for fever. In 1972, the sesquiterpene artemisinin (**10**, qinghaosu, Figure 2) was isolated as an active ingredient and was shown to have potent antimalarial activity.[6] At present, artemisinin derivatives are routinely administered for the treatment of malaria, in particular in Southeast Asia.

Since the 1920s routine screening for antimalarial drugs has been carried out on canaries infected with the avian malaria parasite *P. relictum*.[7] In 1935, *P. relictum* was completely replaced by *P. gallinaceum*, which infects day-old chicks. Since the discovery of the rodent parasite *P. berghei* in 1948, murine malaria models have been used increasingly and still represent the most important in vivo test systems for new antimalarial drugs.[8] Animal model studies against the *Plasmodium* species that infect humans can only be carried out in monkeys and, therefore, are of limited accessibility. The first in vitro culture of the human parasite *P. falciparum* was carried out in 1976 in a nutrient medium supplemented with human erythrocytes; this breakthrough provided the prerequisite methodology for the screening of large numbers of antimalarial test compounds.[9] Molecular biology methods can be applied in malaria research, although sometimes with difficulty as a consequence of the exceptionally high content of adenine and thymine base residues in the *P. falciparum* DNA. In particular, the recombinant expression of *P. falciparum* genes in *Escherichia coli* frequently causes problems. Nevertheless, the complete genome of *P. falciparum* has now been sequenced.[10] These data are expected to be extremely useful for the identification of new drug targets.

The high incidence of resistance against chloroquine (**5**) and the anti-folate combination pyrimethamine–sulfadoxine (**7**–**11**) (Figure 2) is the most important reason for the

*Prof. Dr. Martin Schlitzer studied pharmacy and chemistry at the Philipps-Universität Marburg, where he completed his doctorate in pharmaceutical chemistry in 1993. After postdoctoral studies with Prof. Carl R. Johnson in Detroit in 1993–1994, he completed his Habilitation in pharmaceutical chemistry at the Philipps-Universität Marburg. Since October 2001, he has been Professor of Pharmaceutical Chemistry at the Ludwig-Maximilians-Universität München.*

*Dr. Jochen Wiesner, born in 1971 in Bad Neustadt, Germany, studied biology at the University of Würzburg, where he received his doctorate in 1998 for his work in the group of Michael Lanzer on the interactions of the malaria parasite P. falciparum with the complement system and on the sodium–proton exchanger of P. falciparum as a potential drug target. Afterwards he worked at Jomaa Pharmaka GmbH in Giessen (Germany) on the development of fosmidomycin and other inhibitors of the mevalonate-independent isoprenoid biosynthesis pathway for the treatment of malaria. In 2002 he joined the research group of Hassan Jomaa at the University of Giessen.*

 © 2003 Wiley-VCH Verlag GmbH & Co. KGaA, Weinheim 

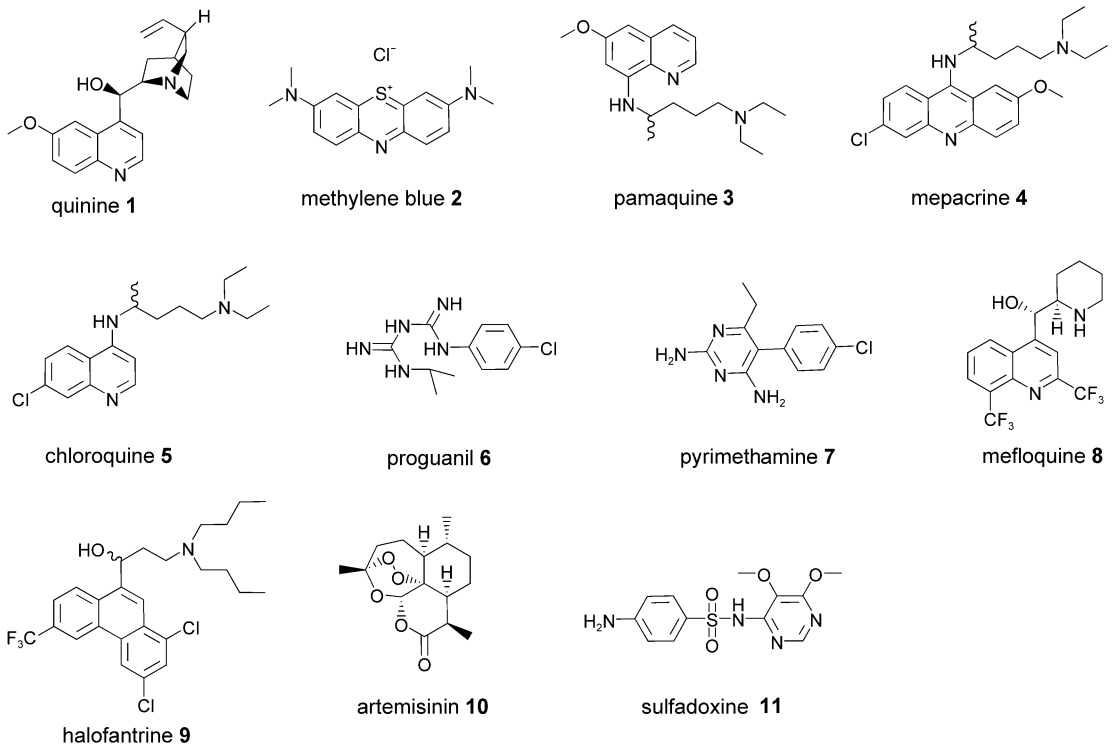



***Figure 2.*** Several antimalarial drugs of actual or historical importance.

increasing spread of malaria.[11] Existing alternative medications are virtually unaffordable in the countries affected most seriously. Additional factors that contribute to the deteriorating malaria situation are the collapse of control programs, resistance of the *Anopheles* mosquito against DDT (dichlorodiphenyltrichloroethane), the migration of refugee populations, as well as climatic and environmental changes.[12] Furthermore, industrial and military interest in the development of new antimalarial drugs declined in the mid 1970s. Despite various research activities, an effective vaccination against malaria will not become available in the near future. As a result, there is an urgent need for the rapid development of effective, safe, and affordable chemotherapeutics. Recently, increased funds have been provided by several public agencies to enable the development of new antimalarial compounds in spite of the poor economic interest.[12–14] The biological targets of these efforts are both cell functions (such as hem detoxification and folate metabolism) already exploited by established drugs, as well as novel biochemical pathways (such as fatty acid synthesis, protein farnesylation, and mevalonate-independent isoprenoid biosynthesis). Figure 3 gives an overview of old and new antimalarial targets and their intracellular localization.

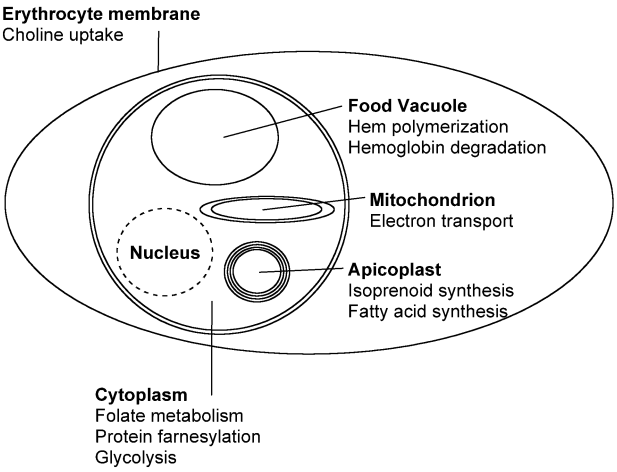



***Figure 3.*** Schematic presentation of an erythrocyte infected with *P. falciparum*, indicating the subcellular localization of different drug targets.

## 2. Established Antimalarial Drugs

### 2.1. 4-Amino Quinolines and Aryl Amino Alcohols

4-Amino Quinolines and aryl amino alcohols are structurally derived from quinine (**1**), the active ingredient of the Cinchona bark. Despite its relatively low efficacy and tolerability, quinine (**1**) still plays an important role in the treatment of multiresistant malaria. In particular, with respect to its high solubility, quinine (**1**) is used as an intravenous formulation in severe malaria when patients are unable to tolerate oral medication. Chloroquine (**5**, Figure 2), a synthetic 4-amino quinoline highly effective against sensitive parasites and generally well-tolerated, still represents the most frequently used antimalarial drug owing to its very low production costs. The use of the related amodiaquine (**12**,

 © 2003 Wiley-VCH Verlag GmbH & Co. KGaA, Weinheim 

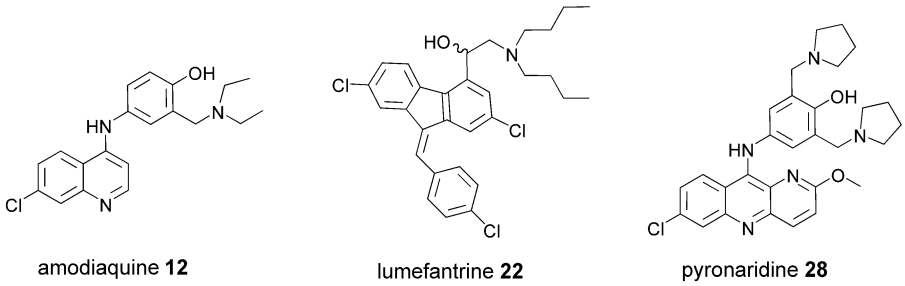



*Figure 4.* Aryl amino alcohol and 4-amino quinoline drugs.

Figure 4) has been limited since the mid 1980s after it was linked causally to the appearance of occasional agranulocytosis in travelers taking the drug prophylactically. But because it retains a high degree of efficacy against all but the most chloroquine-resistant parasites, there has been a recent increase in its use.[15] Mefloquine (**8**, Figure 2) and halofantrine (**9**) are aryl amino alcohols that are very similar to quinine. Mefloquine (**8**) is considered a standard therapeutic agent for chloroquine-resistant malaria; however, its use is limited by high costs and the appearance of neuropsychiatric side effects.[16] The administration of halofantrine (**9**), although highly effective, has strongly been restricted by its potential to induce heart arrhythmia.[17] In addition, there is cross-resistance with mefloquine (**8**).

It is generally accepted that the 4-amino quinolines interfere with the detoxification of free hem, which is generated during the degradation of hemoglobin.[18,19] Predominantly in the trophozoite and early schizont stages, hemoglobin is ingested with the cytoplasm of the host erythrocyte by a phagocytosis-like mechanism and transported into the central food vacuole (Figure 3). Inside the vacuole, hemoglobin is digested into small peptides, which are subsequently transported to the cytoplasm of the parasite. The hem moiety released during hemoglobin degradation is potentially toxic through an oxidative mechanism and, therefore, converted into insoluble crystals, the so-called hemozoin or malaria pigment, which can easily be recognized by light microscopy inside the food vacuole. Although it is now known that hemozoin is a crystal, this mechanism is commonly referred to as hem polymerization. As an additional mechanism, hem is degraded by reaction with hydrogen peroxide, which is generated by spontaneous oxidation of the released hem from an $Fe^{II}$ to an $Fe^{III}$ stage.[20] Some of the hem apparently diffuses into the cytoplasm of the parasite, where it may be destroyed by reduced glutathione.[21] There are quite convincing data that both the hem polymerization and the oxidative and glutathione-dependent hem degradation is inhibited by the 4-amino quinolines. Whether this is also the case for the aryl amino alcohols is less clear.[22] There is some evidence that mefloquine (**8**) and quinine (**9**) inhibit the uptake of hemoglobin from the host cell.[23]

### 2.2. Antifolates

Beside chloroquine (**5**), the antifolate combination sulfadoxine–pyrimethamine (fansidar, S/P; Figure 2) is the most common medication against malaria.[17] Pyrimethamine (**7**) inhibits dihydrofolate reductase, while the sulfonamide component sulfadoxine (**11**) inhibits dihydropteroate synthase, an additional enzyme of the folate metabolism. However, resistance develops rapidly when this combination is used excessively. Under a prophylactic regimen, occasional hypersensitivity to the sulfonamide component may give rise to a toxic epidermal necrolysis, known as Steve–Johnson Syndrome. For this reason, the approval of sulfadoxine–pyrimethamine has been retracted in several industrialized nations.

Another frequently used antimalarial drug is proguanil (**6**, Figure 5), which is transformed into cycloguanil (**13**), a further inhibitor of dihydrofolate reductase, by a cytochrome P450 dependent reaction. Proguanil (**6**) is well-tolerated, but has a low efficacy when used as a monotherapeutic. Thus, it is most commonly applied in combination with chloroquine (**5**).[16]

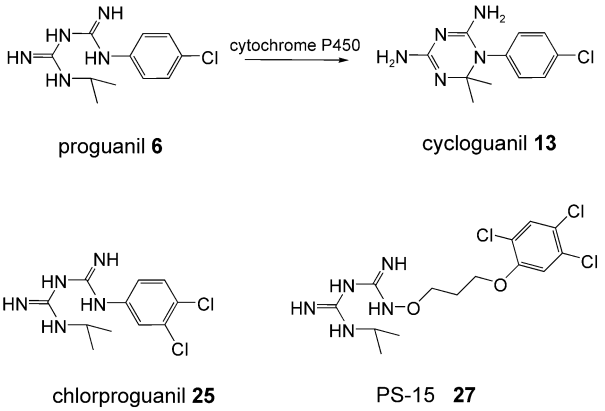



*Figure 5.* Antifolates: proguanil (**6**), chlorproguanil (**25**), and PS-15 (**27**) are transformed into the bioactive cyclic derivatives by a cytochrome P450-dependent reaction.

### 2.3. Artemisinin Derivatives

In addition to natural artemisinin (**10**) and dihydroartemisinin (**14**) the semisynthetic artemisinin derivatives artemether (**15**), arteether (**16**), and artesunate (**17**) have been increasingly used for about 20 years (Figure 6).[24b] These drugs are metabolized to dihydroartemisinin (**14**), the main bioactive compound. The artemisinins act faster than any other antimalarial drugs, with an approximate parasite- and fever-clearance time of 32 h, in contrast to 2–3 days needed with conventional antimalarial drugs to resolve the symptoms.[25] Moreover, the artemisinins are active against the sexual parasite stages (gametocytes), which are responsible for the infection of the *Anopheles* mosquito and for the transmission of the disease. As a consequence of the short

 © 2003 Wiley-VCH Verlag GmbH & Co. KGaA, Weinheim 

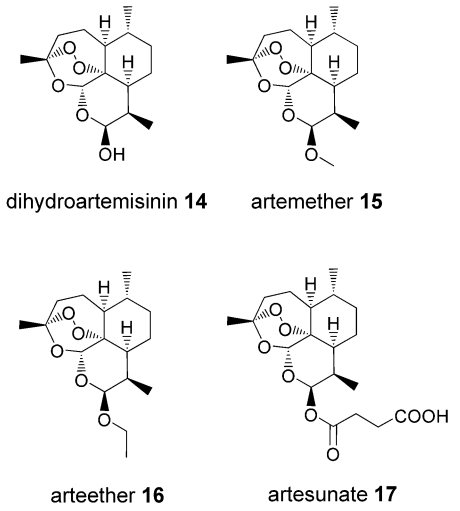



***Figure 6.*** Artemisinin derivatives in clinical use. Data on the stereochemistry of the acetal centers of **14** and **17** are contradictory in the literature.[24b]

plasma half-life of these drugs, a 5–7-day treatment is necessary to eliminate the parasites fully. To shorten the treatment duration and to prevent the development of resistance, the artemisinins are increasingly combined with other antimalarial drugs with longer half-lives. In some parts of Thailand, a combination of artesunate (**17**) with mefloquine (**8**) is recommended as standard therapy.[15] Also of increasing importance is the rectal application of artesunate (**17**) in small children with severe malaria, when an intravenous application of quinine is not possible for reasons of poor medical infrastructure.[26,27] Regardless of the neurotoxic and embryotoxic effects at higher doses in animal experiments, the application of artemisinins in humans seems to be very safe. With two million patients treated up to day, only two cases of severe adverse reactions owing to hypersensitivity were reported.[28–30]

The biological activity of the artemisinins evidently depends on the cleavage of the peroxide bond after contact with $Fe^{II}$ hem inside the food vacuole (Figure 3), thus generating free radicals that can alkylate the hem molecule.[31] By this mechanism, the detoxification of free hem may be inhibited, similar to the assumed process for the 4-amino quinolines (Figure 7).[32] Furthermore, alkylation of essential parasite proteins may contribute to the antimalarial activity.[33]

### *2.4. Antibiotics*

Various antibiotics that are known to be antibacterial agents also exhibit antimalarial activity. Their mode of action depends on the fact that malaria parasites, similar to other members of the phylum *Apicomplexa*, harbor an unusual plastidlike organelle, the so-called apicoplast (Figure 3).[34,35] In the course of the evolution, the apicoplast was acquired by endosymbiosis with a unicellular alga. The chloroplast of the alga has lost its photosynthetic activity and fulfils different metabolic functions, such as the synthesis of isoprenoids, fatty acids, and, potentially, hem (see Sections 4.4 and 5.4).[36] The apicoplast contains a residual genome that encodes tRNAs, rRNAs, RNA polymerases, and ribosomal proteins; for this reason the apicoplast genome is solely responsible for self-replication of this organelle. All enzymes involved in metabolic processes inside the apicoplast are encoded by the nuclear genome and are transported to the apicoplast, mediated by a specific amino-terminal-recognition sequence. The respective antibiotics act through inhibition of the prokaryote-like RNA (rifampicin (**18**); Figure 8) and protein synthesis (tetracyclines, macrolides, lincosamides) inside the apicoplast.[37] It is assumed that the tetracyclines also inhibit the mitochondrial protein synthesis of the parasites.[37] The metabolic functions of the apicoplast are not affected

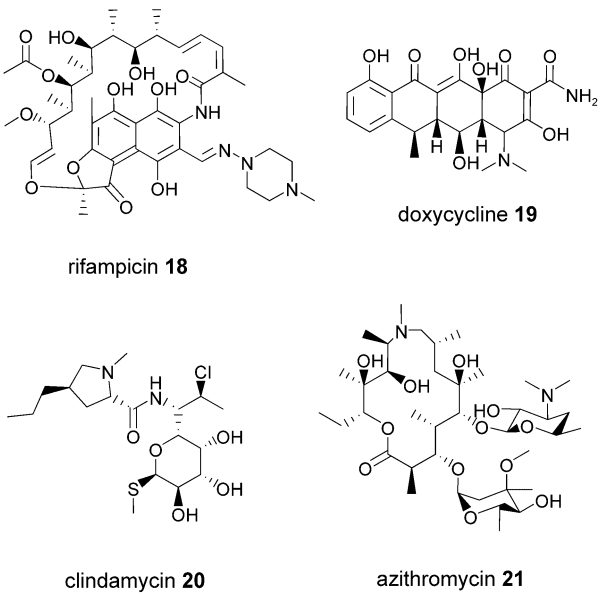



***Figure 8.*** Antibiotics used in the treatment of malaria.

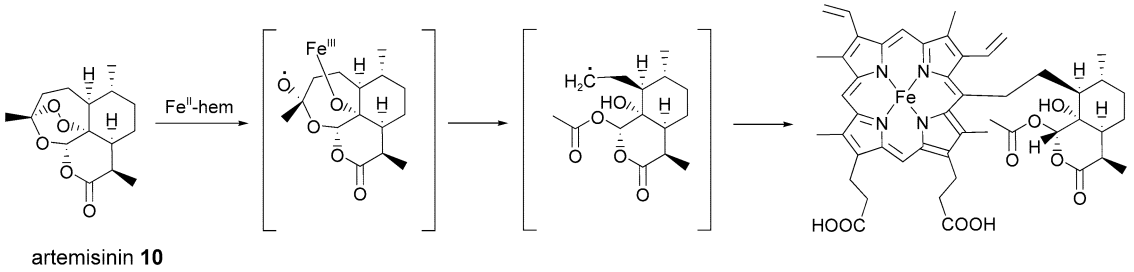



***Figure 7.*** Hypothetical mechanism for the radical alkylation of hem by artemisinin.

 © 2003 Wiley-VCH Verlag GmbH & Co. KGaA, Weinheim 

immediately after contact with these antibiotics, but self-replication of the organelle is then no longer possible. As a consequence, the parasites die with a characteristic delayed kinetic pattern in the second replication cycle after exposure to the drug. Thus, under clinical conditions, amelioration of symptoms is not observed earlier than 4 days after the beginning of the treatment with an antibiotic.[38] Because of their slow effect, antibiotics are only applied as prophylactics or in combination with other antimalarial drugs. In practice, doxycycline (**19**) is the most frequently used antibiotic in antimalarial therapy, either on its own as a prophylactic, or in combination (commonly with **1** or **17**) for treatment in cases of multiresistance.[16] Since **19** is contra-indicated in small children and pregnant women and is potentially responsible for photosensitizing reactions, clindamycin (**20**) provides an effective alternative.[39] It was also demonstrated that azithromycin (**21**) is an effective prophylactic against *P. vivax* malaria.[40]

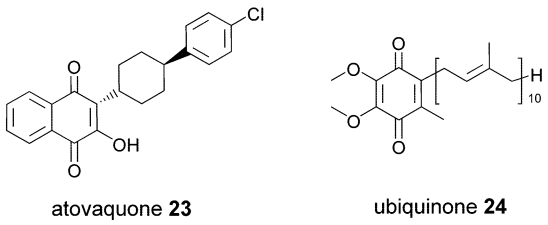
## 3. New Antimalarial Drugs in Clinical Use

### 3.1. Lumefantrine–Artemether

A fixed combination of lumefantrine (**22**, benflumethol; Figure 4) with artemether (**15**; Figure 6) for the treatment of uncomplicated *P. falciparum* malaria has recently been approved as riamet or co-artemether.[41] The structure of **22** includes an aryl amino alcohol similar to that of halofantrine (**9**). Compound **22** was already developed about 20 years ago by the Chinese military. There are no accessible clinical data on the efficacy of **22** as a monotherapeutic. Although less effective than **9**, lumefantrine (**22**) does not induce cardiotoxic side effects.[42] Also, no neurological side effects were observed with the combination (**15** and **22**), which may be expected as a result of the artemether component. A synergistic effect of the combination is potentially caused by interference of both components with hem detoxification inside the food vacuole.[43] The efficacy of lumefantrine–artemether seems to be somehow impaired by cross-resistance with mefloquine (**8**) and therefore the appropriate dosage is not yet clear in areas of complicated resistance.[44]

### 3.2. Atovaquone–Proguanil

Another drug recently approved for the treatment and prophylaxis of uncomplicated *P. falciparum* malaria is malarone, a fixed combination of atovaquone (**23**, Figure 9) with proguanil (**6**, Figure 5).[45,46] The hydroxynaphthoquinone **23** acts analogously to ubiquinone (**24**) by inhibiting the mitochondrial electron transport (Figure 3) through the cytochrome *c* reductase complex.[47] When atovaquone is used on its own, resistance emerges very rapidly owing to a mutation of the cytochrome *b* gene localized in the mitochondrial genome.[48] This problem was solved by combining **23** with **6**.[49] Unexpectedly, it is not cycloguanil (**13**) but rather proguanil (**6**) itself that is responsible for the striking synergistic effect of this combination, even though the intrinsic antimalarial activity of unmetabolized **6** is very low.[50] Almost nothing is known about the mechanism underlying this synergistic interaction. Some data suggest that proguanil (**6**) enhances the atovaquone-induced collapse of the mitochondrial membrane potential.[51] For the prophylactic application, the activity of atovaquone–proguanil against liver stages is particularly advantageous as the parasites are killed before an infection of erythrocytes can be established.[52] However, the long-term efficacy of atovaquone–proguanil seems to be limited, as there has been a report of treatment failure with a documented mutation of the cytochrome *b* gene.[53]



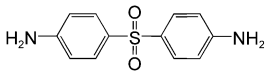

atovaquone **23** ubiquinone **24**

***Figure 9.*** Atovaquone (**23**) and the natural electron carrier ubiquinone (**24**).

## 4. Antimalarial Drugs in Clinical Development

### 4.1. Chlorproguanil–Dapsone

Lap-dap, a combination of chlorproguanil (**25**, Figure 5) with dapsone (**26**), is currently under development as a replacement for sulfadoxine–pyrimethamine.[54] Similar to proguanil (**6**), chlorproguanil (**25**) is transformed into the




dapsone **26**

dihydrofolate reductase inhibitor chlorcycloguanil. Dapsone (**26**), already used for treatment of leprosy since 1943, acts similarly to sulfadoxine (**11**, Figure 2) as an inhibitor of dihydropteroate synthase. Both compounds are inexpensive and relatively well-studied. A potential advantage of this combination is the short plasma half-life of both drugs. Thus, the parasites are exposed to subtherapeutic concentrations for a short time only, thereby deterring the emergence of resistance. As expected, it was shown in clinical studies that resistance to chlorproguanil–dapsone developed much slowly than resistance to sulfadoxine–pyrimethamine.[55,56] Clinical studies in Kenya have demonstrated that a 3-day regimen with chlorproguanil–dapsone is as effective as the sulfadoxine–pyrimethamine standard therapy with a single dose.[57,58] Additional studies in Tanzania and Malawi have shown that in most cases chlorproguanil–dapsone is effective against sulfadoxine–pyrimethamine-resistant parasite strains.[59,60] However, in a clinical study conducted in Thailand, the efficacy of chlorproguanil–dapsone was very low.[61] The reason was the common appearance of parasite strains with mutated dihy-

 © 2003 Wiley-VCH Verlag GmbH & Co. KGaA, Weinheim 

drofolate reductase, thus leading to chlorproguanil (**25**) resistance in Southeast Asia. In East Africa, such mutations are still rare.[62] In a phase III clinical study conducted in Nigeria, Kenya, Malawi, Tanzania, and Gabon, 2000 children were treated with chlorproguanil–dapsone. The study is finished, but the results have not yet been published.[54] In addition to the approval of chlorproguanil–dapsone in the near future, the development of a fixed combination of chlorproguanil (**25**), dapsone (**26**), and artesunate (**17**) is planned to lessen the chance of resistance development.[54] The proguanil derivative PS-15 (**27**, Figure 5) is also active against parasites that are resistant to established antifolates, but the drug is still in preclinical development.[63]

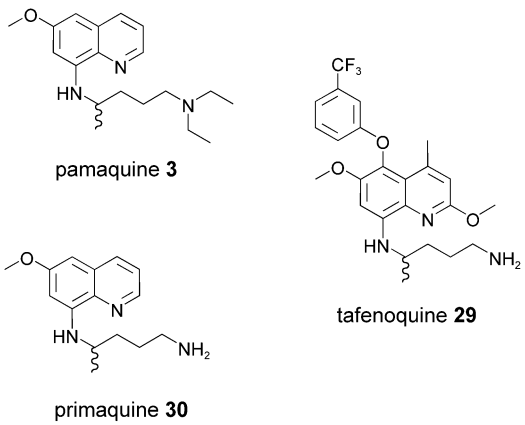



***Figure 10.*** 8-Amino quinoline drugs.

### *4.2. Pyronaridine*

The 9-anilinoacridine pyronaridine (**28**, Figure 4) is similar in structure to mepacrine (**4**), chloroquine (**5**), and amodiaquine (**12**). Pyronaridine (**28**) was developed in China and has been registered in that country since the 1980s. Outside China, none of the existing formulations are registered because of the failure to meet international regulatory standards.[64] Pyronaridine (**28**) is clearly the most active 4-amino quinoline derivative and is generally active against chloroquine-resistant parasites. Most likely, it acts through inhibition of hem polymerization, similarly to the other 4-amino quinolines. The efficacy of pyronaridine has been proven in clinical studies conducted in Cameroon and Thailand. In Cameroon, a 3-day regimen resulted in a 100% cure rate in adults and children.[65,66] In contrast, chloroquine (**5**) was used as a competitor drug and was only effective in 44% of the cases in adults and 40% in children. In Thailand, cure rates of 63% and 88% were observed after treatment for 3 and 5 days, respectively.[67] The different cure rates reported in Cameroon and Thailand may be partly explained by the fact that patients were observed for 28 days in Thailand but only 14 days in Cameroon.[68] Meanwhile, an improved capsule formulation of pyronaridine has been developed.[64] Recent work aims at the development of a combination of pyronaridine (**28**) with artesunate (**17**).[69] A synergistic effect of **28** with artemisinin (**10**) was demonstrated in vitro.[70]

### *4.3. Tafenoquine*

Tafenoquine (**29**) is an improved derivative of the 8-amino quinolines primaquine (**30**) and pamaquine (**3**, Figure 10). Primaquine (**30**) has already been used since the 1940s for the eradication of liver stages in course of *P. vivax* infections.[71] As a consequence of its activity against liver stages, **30** can also be used as a prophylactic. In addition, primaquine (**30**) prevents the maturation of fertile gametocytes. Against blood stages, however, **30** is inactive at pharmacologically achievable concentrations. Toxicological concerns have led to restrictions in the use of primaquine (**30**). Optimization of the structure of **30** led to tafenoquine (**29**), which is generally less toxic and has a longer plasma half-life of 2–3 weeks. Tafenoquine (**29**) is also active against erythrocytic stages; chloroquine- and multiresistant strains are significantly more susceptible than wild-types.[64] The mode of action of the 8-amino quinolines is largely unknown. The activity of **29** against blood stages possibly depends on the inhibition of hem polymerization by a mechanism similar to that assumed for the 4-amino quinolines. For the activity against liver stages and gametocytes, an alternative mechanism seems to be responsible. Potentially, mitochondrial processes are affected through the generation of toxic metabolites.[72]

The prophylactic activity of tafenoquine (**29**) was demonstrated in several clinical studies. Three out of four volunteers challenged with *P. falciparum* by being bitten by infected mosquitoes were protected by a single 600-mg dose.[73] In a field study conducted in Gabon, all 84 subjects who received 250 mg of **29** for 3 days were protected from malaria for the complete study time of 70 days.[74] In a similar study conducted in Kenya, a 3-day loading regimen followed by weekly administration of 200 mg of tafenoquine (**29**) for 13 weeks resulted in 86% protection (comparison with a placebo).[75] Also, elimination of hypnozoites from the liver for the radical cure of a *P. vivax* infection was demonstrated in a clinical setting. In this study, patients with acute *P. vivax* malaria were first treated with chloroquine (**5**) to eliminate all erythrocytic parasite stages. Only by subsequent treatment with tafenoquine (**29**), but not chloroquine (**5**), could relapse of the disease be prevented.[76] Clinical data on the treatment of acute malaria with tafenoquine (**29**) are not available. However, it was demonstrated in Aotus monkeys that tafenoquine (**29**) is effective against the blood stages of a chloroquine-resistant *P. vivax* strain.[77]

The major disadvantage of the 8-amino quinolines is the induction of hemolytic anemia in subjects with glucose 6-phosphate dehydrogenase (G6PD) deficiency as a potentially life-threatening adverse effect. The incidence of this genetic anomaly is particularly high in areas where malaria has been endemic, which suggests a certain selective advantage against the infection. The risk of hemolytic anemia with primaquine (**30**) in G6PD deficiency is well-established. Also, a hemolytic response was observed in two G6PD-deficient patients who accidentally received tafenoquine (**29**), one of whom required a blood transfusion.[72]

 © 2003 Wiley-VCH Verlag GmbH & Co. KGaA, Weinheim 

### 4.4. Fosmidomycin

Fosmidomycin (**31**, Figure 11) is an inhibitor of 1-deoxy-D-xylulose 5-phosphate (DOXP) reductoisomerase, a key enzyme in the recently described mevalonate-independent pathway of isoprenoid biosynthesis (also called DOXP pathway, MEP pathway, Rohmer pathway). The enzymes of this

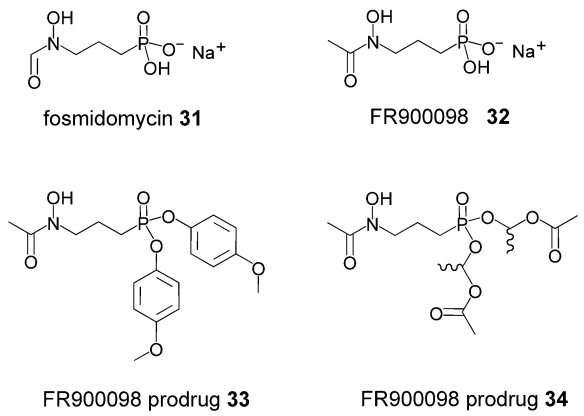



***Figure 11.*** Fosmidomycin (**31**) and some derivatives.

metabolic pathway are localized inside the apicoplast of the malaria parasite (Figure 3).[78] The mevalonate-independent isoprenoid synthesis pathway is also used by different bacteria and the plastids of algae and higher plants.[79] In animals and humans, isoprenoids are synthesized through the mevalonate pathway (Figure 12).

Fosmidomycin (**31**) was originally isolated as a natural antibiotic from *Streptomyces lavendulae* in the 1970s. After it

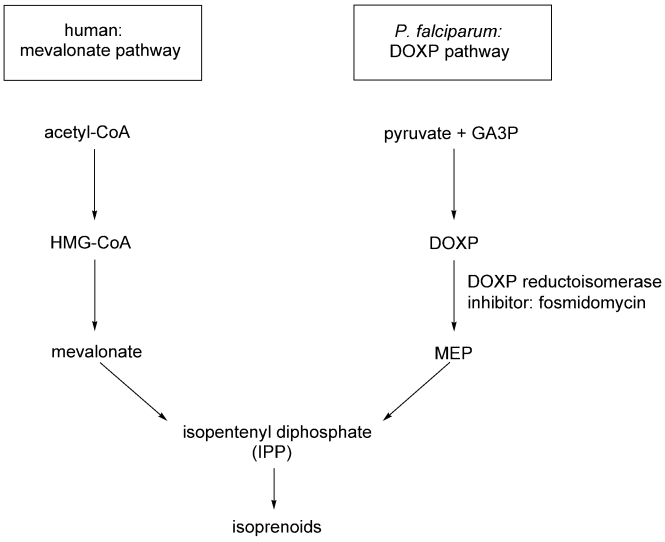



***Figure 12.*** Isoprenoid biosynthesis through the mevalonate and the DOXP pathway. In all organisms, isoprenoids are synthesized from $C_5$ units derived from isopentenyl diphosphate (IPP). In humans and other organisms that use the mevalonate pathway, IPP is synthesized from acetyl CoA. Alternatively, some organisms, including *P. falciparum*, synthesize IPP from pyruvate and glyceraldehyde 3-phosphate (GA3P) through the DOXP pathway.

was evaluated in an early phase II study for the management of bacterial infections, further development was abandoned.[80] The molecular target and the antimalarial activity of fosmidomycin (**31**) has only been known since 1998.[78,81–83] It was suggested that fosmidomycin (**31**) binds as a substrate analogue to the active site of the enzyme (Figure 13). Kinetic

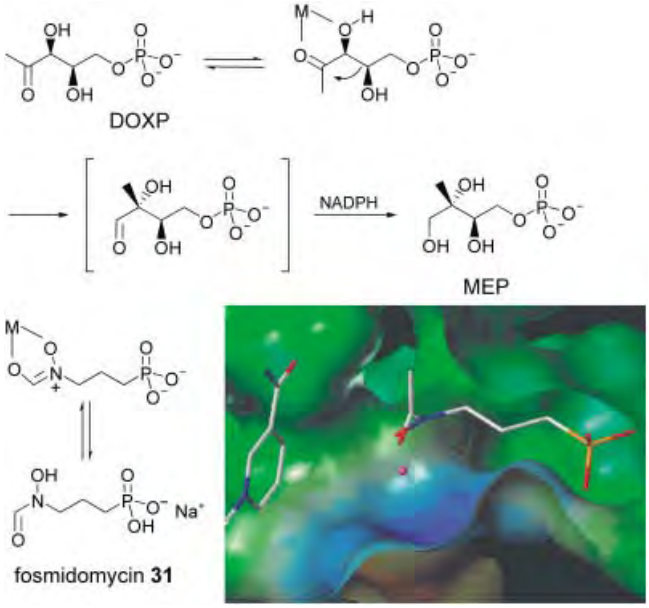



***Figure 13.*** Proposed mechanism for the reductoisomerase-catalyzed conversion of 1-deoxy-D-xylulose 5-phosphate (DOXP) into 2-C-methyl-D-erythritol-4-phosphate (MEP) and binding mode of the inhibitor fosmidomycin (**31**). The carbonyl and vicinal hydroxy group of the DOXP complex a metal ion (M; M = Mg or Mn) in the active site, before DOXP is transformed into MEP by an intramolecular rearrangement and concomitant reduction by NADPH. The result of the docking of FR900098 (**32**) into the crystal structure[86] of DOXP reductoisomerase is shown.[87] Hydrophilic (blue to green) and lipophilic (brown) properties of the active center are indicated on the Connolly surface. The metal ion (magenta) is chelated by the hydroxamate function of FR900098, whereas the phosphonate group occupies the phosphate-binding site. On the left, the pyridyl ring of NADPH is depicted.

analyses with *E. coli* DOXP reductoisomerase revealed that **31** initially binds with relatively low affinity to the active site, thereby inducing alterations in the enzyme conformation that result in a significantly higher affinity.[84] Thus **31** undergoes quasi-irreversible binding to the enzyme. Evidence for the highly flexible structure of the enzyme was also provided by the crystal structure of *E. coli* DOXP reductoisomerase.[85,86]

In a proof-of-concept study conducted in Gabon and Thailand, groups of ten patients infected with acute uncomplicated *P. falciparum* malaria were treated orally with 1200 mg of fosmidomycin (**31**) three times a day for 7 days.[88] The medication was generally well-tolerated, with the occasional appearance of mild gastrointestinal side effects such as loose stools and diarrhea, possibly related to the antibacterial activity of the drug. At both sites, the parasite- and fever-clearance times were approximately 2 days. Within 28 days of follow-up observations, parasites reappeared in two of the ten patients in Gabon and eight of the ten patients

 © 2003 Wiley-VCH Verlag GmbH & Co. KGaA, Weinheim 

in Thailand. This marked variation in the overall cure rate probably reflects the differences in immunity between a population from Central Africa where malaria is hyperendemic and a population from a hypoendemic area in Southeast Asia. In another study in Gabon, cure rates in excess of 80% on day 14 were observed after shortening the duration of the treatment to 4 days.[89]

Since the high recrudescence rate precludes the use of fosmidomycin (**31**) as a monotherapeutic agent, drug-interaction studies were performed to identify a potential combination partner. A synergistic interaction was observed with the combination of **31** and clindamycin (**20**, Figure 8).[90] A possible explanation is that clindamycin (**20**) inhibits the replication of the apicoplast, the organelle that harbors the enzymes of the mevalonate-independent isoprenoid biosynthesis pathway, including DOXP reductoisomerase. The first clinical studies with a fosmidomycin–clindamycin (**31**–**20**) combination are currently in progress in Gabon and Thailand. According to preliminary results, a significantly higher cure rate is observed after a shorter treatment duration, encouraging the development of a fixed fosmidomycin–clindamycin tablet formulation.[91]

The major advantages of fosmidomycin (**31**) are the remarkably low toxicity ($LD_{50}$ in rats (oral) $\approx 12\ g\,kg^{-1}$) and its activity against multiresistant parasite strains.[78] Limitations arise from the short plasma half-life ($\approx 2.5$ h) and the moderate resorption rate ($\approx 30\%$) as a consequence of the extremely hydrophilic properties (low lipophilicity) of the molecule.[80,92] The fosmidomycin derivative FR900098 (**32**) was approximately twice as active in vitro and in mice infected with *P. vinckei*.[78] Increased oral bioavailability resulted from the synthesis of prodrug derivatives of FR900098 in which the phosphonate moiety was masked as a biolabile aryl function (**33**) or with double esters (**34**, Figure 11).[93,94]

## 5. Antimalarial Drugs in Preclinical Development

### 5.1. New Hem-Polymerization Inhibitors

Notwithstanding the common appearance of chloroquine-resistant parasites nowadays, the development of resistance against 4-amino quinolines and related compounds is extremely rare. The emergence of chloroquine-resistant strains has possibly taken place only a few times, but led to a worldwide spread as a consequence of the excessive use of chloroquine (**5**).[95] The reason may be that hem polymerization, which is supposed to be inhibited by chloroquine (**5**), seems not to depend on any enzymes.[18] Therefore, resistance cannot develop by a simple mutation. Although the exact mechanism is still unclear, various data suggest that chloroquine resistance is linked to multiple factors, including changes in transport proteins.[59] In this context, there is still high interest in this class of compounds for the development of new antimalarial drugs.

The development of chloroquine derivatives with an altered side chain and of bisquinolines in which two quinoline cores are connected by various linkers is the focus of current work.[96–98]). Several of these compounds proved to be active against chloroquine-resistant parasites. The activity of 4-amino quinolines depends on the presence of a basic amino function: The basic drug is concentrated in the acidic food vacuole (Figure 3) in its membrane-impermeable protonated form, a mechanism commonly referred to as the weak base effect.[99] With the synthesis of the *N*-desbutyl derivative of halofantrine (**9**, Figure 2), already known as a metabolite of the drug, it was possible to eliminate the cardiotoxic side effects without changing the antimalarial activity.[100,101] Similarly, *N*-desbutyllumefantrine (*N*-desbutylbenflumetol) is fourfold more active in vitro than lumefantrine (**22**) itself.[102]

The dihydroacridinedione WR 243251 (**35**, Figure 14) is a derivative of floxacrine (**36**) that was developed from the lead compound mepacrine (**4**, Figure 2). The substance was highly active against a chloroquine-resistant *P. falciparum* strain in Aotus monkeys.[103] Moreover, **35** inhibited the development of *P. vivax* sporozoites in mosquitoes.[104] Inhibition of hem polymerization by **35** was demonstrated, but clearly does not represent the sole mechanism of activity.[105] Thus, similarly to atovaquone (**23**, Figure 9), **35** also inhibits the cellular respiration of the parasite, although its molecular target probably differs from that of **23**.[106] Possibly for this reason there is a moderate cross-resistance between **35** and **23**.

The indoloquinoline alkaloid cryptolepine was isolated from the West African climbing shrub *Cryptolepis sanguinolenta*, which is used in traditional medicine for the treatment of malaria and other diseases. A moderate antimalarial activity was demonstrated in vitro and in mice infected with *P. berghei*. The activity most probably depends on the inhibition of hem polymerization.[107] However, as a result of its DNA-intercalating properties, cryptolepine is cytotoxic.[108] Among different synthetic derivatives, 2,7-dibromocryptolepine (**37**, Figure 14) is the most active compound with approximately tenfold higher antimalarial activity, only slightly higher cytotoxicity against cancer cells, and lower toxicity in mice. The $ED_{90}$ in mice infected with *P. berghei* was $12.5\ mg\,kg^{-1}$ when administered intraperitoneally for 4 days.[107]

Aiming at the development of completely new inhibitors of hem polymerization, an in vitro microassay was established in which $^{14}C$-labeled hematin is incorporated into insoluble beta-hematin, which is chemically indistinguishable from hemozoin.[109] This assay was applied in the high-throughput screening of over 100000 compounds. As a result, the triarylmethanol Ro 06-9075 (**38**, Figure 14) and the benzophenone Ro 22-8014 (**39**, Figure 14) were identified. These compounds displayed oral antimalarial activity in mice infected with *P. berghei*, both with $ED_{90}$ values of about $100\ mg\,kg^{-1}$.

Also, substances such as compound **40**, which were originally developed as protease inhibitors, turned out to be potent inhibitors of hem polymerization.[110,111] In a series of related compounds, a clear correlation between in vitro antimalarial activity and inhibition of hem polymerization was demonstrated. The future potential of this class of compounds, however, may be questioned by the apparent cross-resistance with chloroquine (**5**). For instance, the $IC_{50}$ values measured with compound **40** were between 7 and

 © 2003 Wiley-VCH Verlag GmbH & Co. KGaA, Weinheim 

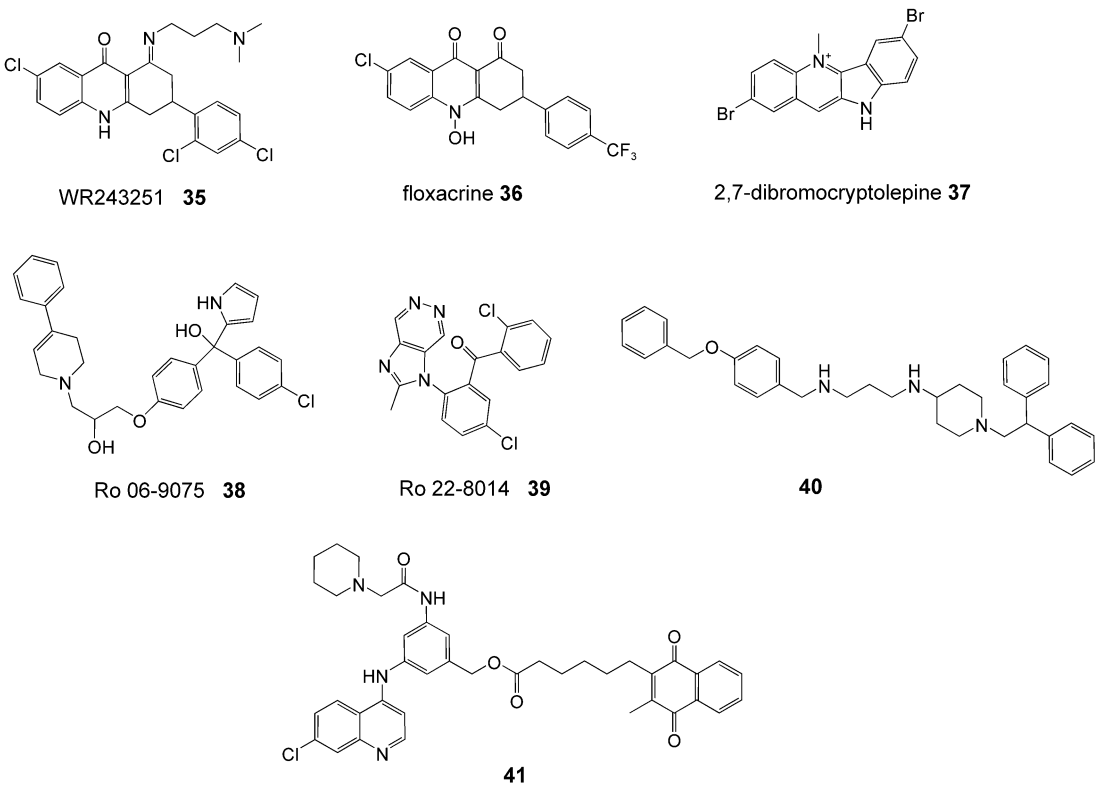



***Figure 14.*** New inhibitors of hem polymerization.

11 nM against a chloroquine-sensitive and 70 nM against a chloroquine-resistant *P. falciparum* strain.

A strategy to overcome resistance against 4-amino quinolines involved the synthesis of chimeric prodrugs that consist of a 4-amino quinoline with known antimalarial activity and a glutathione reductase inhibitor.[112] Both compounds were linked through a metabolically labile ester bond. The mutual prodrug **41** (Figure 14) exhibited in vitro activity against *P. falciparum* strains that were already resistant to the 4-amino quinoline component. In addition, the compound showed significant activity after oral administration (40 mg kg$^{-1}$) in mice infected with *P. berghei*.

As hem detoxification seems to depend on glutathione-mediated degradation and not only on hem polymerization, it was suggested that an increased intracellular content of reduced glutathione as consequence of increased glutathione reductase activity plays a crucial role in chloroquine resistance.[113] Thus, sensitivity to chloroquine (**5**) can be reconstituted by glutathione reductase inhibitors.[114] In addition, various glutathione reductase inhibitors possess antimalarial activity on their own.[4]

### 5.2. New Artemisinin Derivatives and Peroxides

With respect to their rapid onset of action, the artemisinin derivatives are superior to any other antimalarial drugs. Moreover, there have been no clinical reports on artemisinin resistance. Similarly, as discussed for the 4-amino quinolines, the reason for that may be that the mode of action does not depend on a specific enzyme target. As a major drawback, the currently available semisynthetic artemisinin derivatives are prone to hydrolysis, resulting in a short biological half-life and the generation of the potentially toxic dihydroartemisinin (**14**). Therefore, considerable effort has gone into the design of more-stable derivatives with improved bioavailability. With particular respect to intravenous treatment of severe malaria, artelinic acid (**42**, Figure 15), which is significantly more stable than artesunate (**17**) and is highly soluble in water, has been developed.[115] For other derivatives, such as compound **43**, water solubility was achieved by introduction of an amino side chain.[116] The *p*-trifluoromethylphenoxy derivative **44** proved to be superior to artesunate (**17**) after oral application in a malaria-infected mouse model.[117] Additional robust and orally active derivatives such as **45** (Figure 15) were obtained by non-acetal linkage of the side chain to the artemisinin core.[118] It was further rationalized that a piperazine ring in the side chain may lead to enrichment of the drug inside the food vacuole mediated by the weak base effect. Thus, in mice infected with *P. berghei*, **46** (Figure 15) was twice as active as artemether (**15**).[119] Also, artemisinin-derived trioxane dimers containing various linkers were synthesized.[120,121] The dimeric compound **47** exhibited an $IC_{50}$ value of 1.3 nM against the in vitro growth of *P. falciparum* (**10**: 9.7 nM).[120] Simplification of the artemisinin core led to synthetic 3-aryl trioxanes, for example, **48**.[122,123] Upon oral application in a murine model, **48** was twice as active as **10**.[123]

Based on the hypothesis that the mechanism of the artemisinins depends on the generation of free radicals by cleavage of the peroxide function, it can be assumed that

 © 2003 Wiley-VCH Verlag GmbH & Co. KGaA, Weinheim 

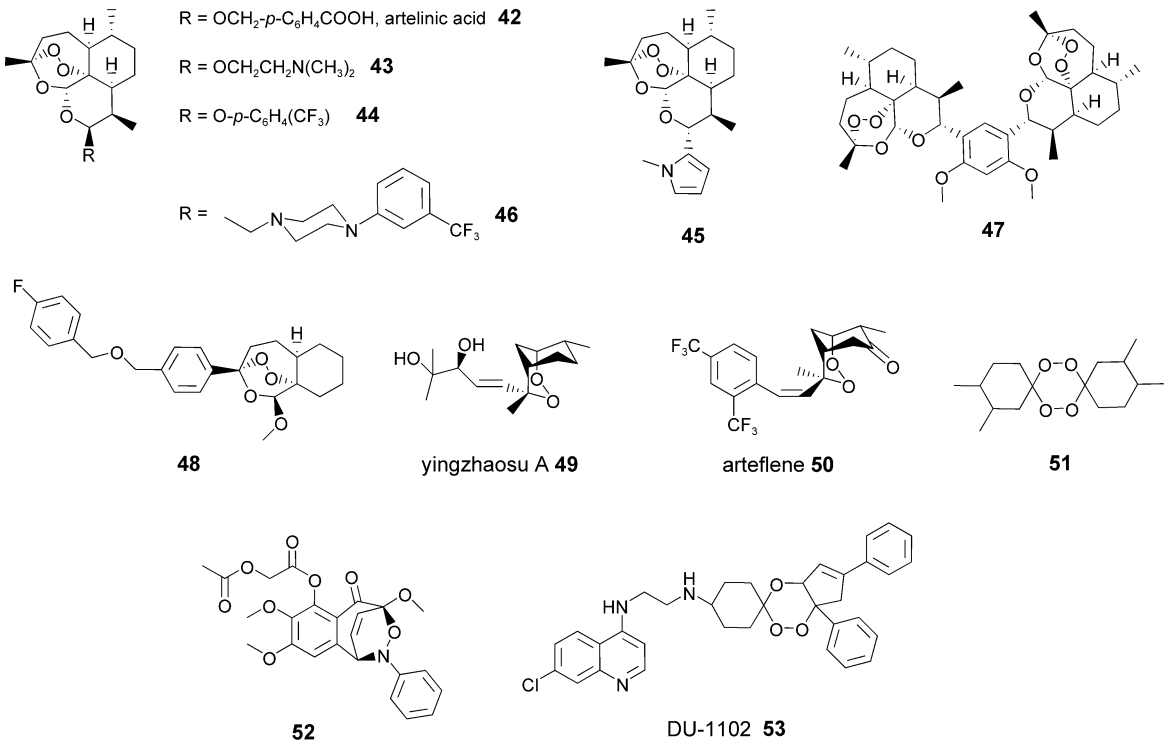



***Figure 15.*** New artemisinin derivatives and peroxides.

other endoperoxides not related to the artemisinin structure also exhibit antimalarial activity. Consequently, yingzhaosu A (**49**, Figure 15), which similarly to artemisinin was isolated from a traditional Chinese medicinal plant (*Artabotrys uncinatus*), and the synthetic derivative arteflene (**50**) are active against malaria.[124] After successful preclinical trials, arteflene (**50**) has already been tested on patients with uncomplicated malaria in Nigeria, Burkina Faso, Cameroon, and Gabon.[125–128] However, its moderate clinical efficacy and difficult synthesis prevented the further development of arteflene (**50**).[129]

More readily accessible are 1,2,4,5-tetraoxanes such as compound **51** (Figure 15), which differ significantly from artemisinin (**10**).[130] After oral application to mice infected with *P. berghei*, compound **51** was slightly more active than artemisinin (**10**), but less active than arteether (**16**). Furthermore, different oxazines were synthesized as potential antimalarial drugs. The standard dissociation energy of the N–O bond is similar to that of the O–O bond; the N–O bond is thus prone to undergo homolytic cleavage, resulting in the generation of radicals. As expected, some of these compounds exhibited significant in vitro activity against *P. falciparum*. By choosing a suitable substitution pattern, a relatively low cytotoxicity was achieved.[131] The growth of *P. falciparum* was inhibited by compound **52** with $IC_{50} = 3.2\ \mu M$ compared to mammalian cells (KB cells) with $IC_{50} = 128\ \mu M$.

The development of so-called trioxaquines aims at combining the pharmacological advantages of the artemisinin-like peroxides and the 4-amino quinolines. These compounds are covalent conjugates of a 4-amino quinoline entity with a trioxane motif. It is expected that the 4-amino quinoline moiety facilitates the transport to the food vacuole, where the trioxane is activated by free $Fe^{II}$–hem liberated during the digestion of hemoglobin. The most active trioxaquinone compound is DU-1102 (**53**, Figure 15), which is highly efficient against chloroquine-resistant *P. falciparum* strains.[132]

Possibly as a consequence of their quite unspecific mode of action, several of the peroxides mentioned exhibit additional pharmacological activities. Particularly antiproliferative and antitumor activity is often described, thus also attracting interest for the use of artemisinin-like compounds in anticancer therapy. However, such pleiotropic effects could imply a possible limitation for antimalarial therapy.

### 5.3. Protease Inhibitors

As mentioned before, the parasite digests most of the hemoglobin of the host cell during its intraerythrocytic growth. This hemoglobin degradation takes place in the food vacuole (Figure 3) and is catalyzed in a semiordered manner by a variety of proteases, which in part are well-characterized and available as recombinant proteins. The initial cleavage of hemoglobin is mediated by the aspartic proteases plasmepsin I, II, and IV.[133,134] Additional proteases such as the cysteine protease falcipain-2, the metalloprotease falcilysin, and an unusual histoaspartic protease (HAP) catalyze the further degradation into small peptides, which are finally transported into the cytoplasm of the parasite and cleaved into single amino acids.[135,136] The histoaspartic

 © 2003 Wiley-VCH Verlag GmbH & Co. KGaA, Weinheim 

protease is closely related to the plasmepsins, yet one of the two catalytic aspartate residues is replaced with histidine.

Protease inhibitors specific for the enzymes involved in hemoglobin degradation thus represent a further class of potential antimalarial drugs. Specific plasmepsin II inhibitors were obtained by modification of available inhibitors of cathepsin D, a lysosomal protease in mammalian cells.[137] Small-compound libraries were iteratively synthesized and led to the identification of **54** (Figure 16) with $IC_{50} = 4.3$ nM against plasmepsin II and 63 nM against cathepsin D. The high selectivity of such inhibitors for plasmepsin over cathepsin D is of particular importance, as cathepsin D is ubiquitous in mammals and, therefore, inhibition of this enzyme is expected to result in severe adverse effects. The low $IC_{50}$ values of plasmepsin II inhibitors such as compound **54** against the isolated enzyme translate only partially into their antiparasitic activity. The inhibition of the in vitro growth of *P. falciparum* was comparably weak with $IC_{50}$ values ranging from 1 to 2 μM.

The crystal structure of plasmepsin II, under consideration of a hypothetical induced-fit adaptation such as that known for the homologue renin, provided the base for the de novo design of inhibitors of the type **55** (Figure 16).[138] Compound **55** was virtually inactive against renin, but highly active against plasmepsin II ($IC_{50} = 2$ nM). The selectivity against cathepsin D and cathepsin E, however, was less pronounced ($IC_{50} = 7$ nM and 4 nM, respectively).

Some compounds such as Ro 42-1118 (**56**, Figure 16), originally described as plasmepsin II inhibitors,[139] exhibited a 16–80-fold higher potency against plasmepsin IV.[134] Different peptidyl fluoromethyl ketones and peptidyl vinyl sulfones were found to be highly potent falcipain-2 inhibitors. These inhibitors cause an accumulation of undegraded hemoglobin in the food vacuole, which is visible by light microscopy, and block parasite development.[140] The $IC_{50}$ values of **57** and **58** (Figure 16) against the growth of *P. falciparum* in vitro were 4 nM and 0.4 nM, respectively. The survival of mice infected with *P. vinckei* was significantly prolonged upon oral application of both compounds (100–200 mg kg$^{-1}$ twice daily). Theoretical limitations of these peptidic inhibitors are their susceptibility to hydrolysis by host proteases, their relatively low selectivity, and their irreversible mode of action, which leads to covalent modification of the target enzymes. Nevertheless, synthesis of such inhibitors with acceptable toxicity and pharmacokinetic profiles seems to be possible.[141]

Attempts to develop nonpeptide falcipain-2 inhibitors led to the identification of chalcones and phenothiazines with in vitro activity against *P. falciparum*. Compound **59** (Figure 16) is the chalcone with the highest reported in vitro activity ($IC_{50} = 230$ nM).[142] Inhibition of falcipain-2 by the phenothiazine **60** (Figure 16) has been demonstrated, although its antimalarial activity ($IC_{50} = 4$ nM in vitro) seems to be dominated by an unrelated mechanism similar to that of floxacrine (**36**).[143] It has been suggested that simultaneous inhibition of different classes of proteases that participate in the degradation of hem may result in potentiation of the antimalarial activity. In fact, a synergistic effect was observed by combining a peptidyl vinyl sulfone with pepstatin, a nonselective inhibitor of aspartic proteases.[144] The efficacy of this combination was also demonstrated in mice infected with *P. vinckei*.

### 5.4. Inhibitors of Fatty Acid Synthesis

Mammals, fungi, and some mycobacteria synthesize fatty acids with the aid of multifunctional proteins in which each reaction is catalyzed by a distinct region within a single polypeptide, the so-called type I fatty acid synthase (FAS-I).[145] In contrast, plant chloroplasts and most bacteria contain a type II system (FAS-II) in which each reaction is catalyzed by a discrete protein. The existence of a type II system has also been demonstrated in malaria parasites.[146] In this case, the individual enzymes are localized inside the apicoplast, similar to those involved in isoprenoid synthesis (Figure 3). The natural antibiotic thiolactomycin (**61**,

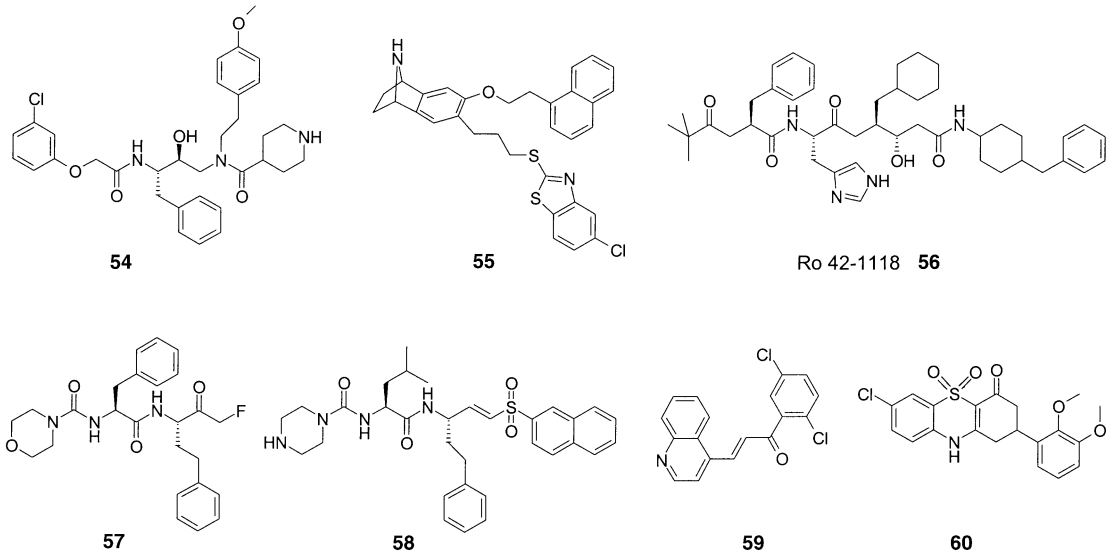



***Figure 16.*** Protease inhibitors.

 © 2003 Wiley-VCH Verlag GmbH & Co. KGaA, Weinheim 

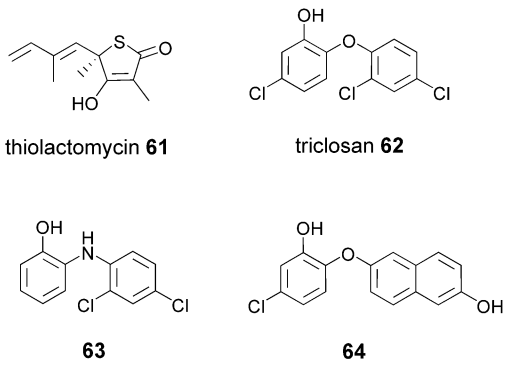



***Figure 17.*** Inhibitors of fatty acid synthesis.

Figure 17) inhibits the enzymes FabB, FabF, and FabH, which catalyze the different condensation steps of the type II fatty acid synthesis. Thiolactomycin (**61**) is active against the in vitro growth of *P. falciparum* ($IC_{50} = 50\ \mu M$).[146] Significantly more active against *P. falciparum* is triclosan (**62**, Figure 17), an inhibitor of the *trans*-2-enoyl-ACP reductase, FabI ($IC_{50} \approx 1\ \mu M$ in vitro. In addition, the efficacy of triclosan (**62**) was demonstrated in mice infected with *P. berghei*; the corresponding $ED_{50}$ and $ED_{90}$ values after subcutaneous injection were 3 and 30 $mg\,kg^{-1}$, respectively.[147] Triclosan (**62**) is active against a wide spectrum of bacteria and is used as a preservative in various household products, such as soaps and toothpastes, but is not suitable for oral treatment. Various triclosan derivates were tested for antimalarial activity. Compounds **63** and **64** were significantly active against the recombinant enzyme and the in vitro growth of *P. falciparum*, but were less active than triclosan (**62**).[148] The recombinant FabI protein of *P. falciparum* has been crystallized and its structure solved as a binary complex with the co-substrate NADH and as a ternary complex with $NAD^+$ and triclosan (**62**) or the derivatives **63** and **64**.[148]

### 5.5. Inhibitors of Choline Uptake

During the course of their intraerythrocytic development, the parasites have to synthesize considerable amounts of new biological membranes. In this process, phosphatidylcholine is used as the predominant membrane lipid. The synthesis of phosphatidylcholine in turn depends on the uptake of choline from the blood. Different choline analogues exhibit potent antimalarial activity. One can therefore assume that they inhibit choline uptake through a transporter localized in the membrane of the infected erythrocyte or the plasma membrane of the parasite (Figure 3). High activity was exhibited by quaternary ammonium salts with a long alkyl chain, such as E10 (**65**, Figure 18; in vitro $IC_{50} = 64$ nM).[149]

This activity was improved significantly by the synthesis of bisammonium salts that consist of two ammonium groups connected by a long alkyl spacer. G25 (**66**; in vitro $IC_{50} =$ 0.64 nM) is effective against *P. falciparum* in Aotus monkeys and *P. cynomolgi* (a species similar to *P. vivax*) in rhesus monkeys when administered by intramuscular injection.[150] Although its gastrointestinal resorption is very low, G25 (**66**) also proved to be effective against *P. falciparum* in monkeys after oral application in higher doses. Improved oral bioavailability was found by replacing the quaternary ammonium function with an aromatic amidine to form MS1 (**67**, Figure 18).[151] The bioavailability was further increased by

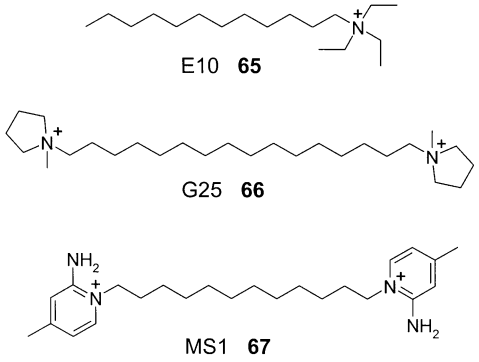



***Figure 18.*** Inhibitors of choline uptake.

synthesis of disulfide and thioester prodrugs, in which a thiazolium ring replaces the quaternary ammonium group after exposure to glutathione or an esterases or thioesterase, respectively (structural formulae and activity data have not been published).[151] The relatively high toxicity is probably due to an interaction with the cholinergic system and implies a possible limitation of this class of compounds. In this respect, the new prodrug derivatives should be tolerated significantly better than the quaternary ammonium compounds.[151]

### 5.6. Inhibitors of Farnesyl Transferase

Farnesyl transferase is a heterodimeric zinc protein that catalyzes the transfer of a farnesyl residue from farnesyl pyrophosphate to a cysteine side chain near the carboxy terminus of a number of proteins (Figure 19). In recent years, farnesyl transferase inhibitors were primarily developed as potential drugs for cancer therapy, as some proteins involved in intracellular signal transduction (the so-called small G proteins) are only active when anchored to the membrane by a farnesyl residue.[152–154] The majority of available farnesyl transferase inhibitors are peptide mimetics designed for the carboxy terminal CaaX-recognition sequence (C = cysteine; a = amino acid with aliphatic side chain; X = serine or methionine) of farnesylated proteins. The most recent development in this field involves thiol-free farnesyl transferase inhibitors in which the pharmacologically unfavorable thiol of former CaaX peptide mimetics has been replaced by alternative substructures.[155]

Protein farnesylation has been demonstrated in parasitic protozoa of the genera *Trypanosoma, Leishmania*, and *Plasmodium* (Figure 3).[156,157] Although sequences that code for both subunits of farnesyl transferase were identified in the *P. falciparum* genome, attempts to produce a recombinant protein by heterologous expression of these sequences have not yet been successful.[158] The in vitro growth of *P. falcipa-*

 © 2003 Wiley-VCH Verlag GmbH & Co. KGaA, Weinheim 

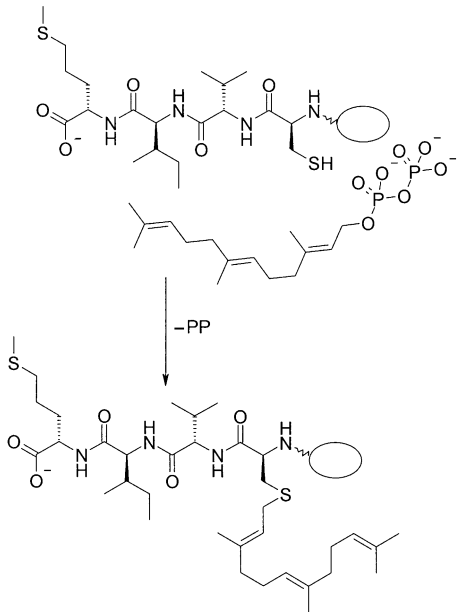


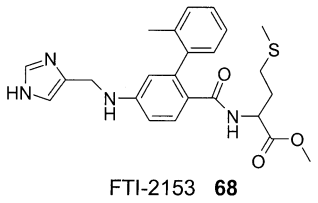

***Figure 19.*** The reaction catalyzed by farnesyl transferase. The substrate protein shown has the recognition sequence cysteine-valine-isoleucine-methionine. PP = pyrophosphate.

*rum* was inhibited by different farnesyl transferase inhibitors.[153,157] In a series of farnesyl transferase inhibitors developed by Sebti, Hamilton, and co-workers, the biphenyl derivative FTI-2153 (**68**, Figure 20) exhibited the highest in vitro antimalarial activity ($IC_{50} = 4.4\ \mu M$).[159] Highly active benzophenone-based farnesyl transferase inhibitors were developed by de novo design using the rat farnesyl transferase as a template.[160,161] Among this series, compound Schl-4116 (**69**, Figure 20) resulted in an in vitro $IC_{50}$ of 75 nM against *P. falciparum*.[162] Meanwhile, additional benzophenones with improved pharmacokinetic properties have been developed. With these compounds, mice infected with *P. vinckei* could be cured.[163]

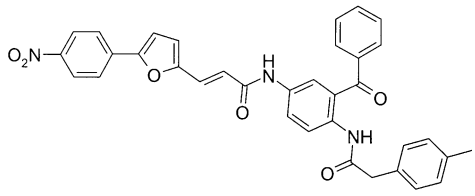
Despite high sequence homologies within the active sites of farnesyl transferases from different species, the development of specific inhibitors seems feasible. Thus, it was demonstrated that the antimalarial activity of a series of benzophenone derivatives did not necessarily correlate with the activity against yeast farnesyl transferase.[164]

### 5.7. Inhibitors of Glycolysis

A functional citric acid cycle is absent in malaria parasites, and therefore their energy metabolism depends mainly on anaerobic glycolysis



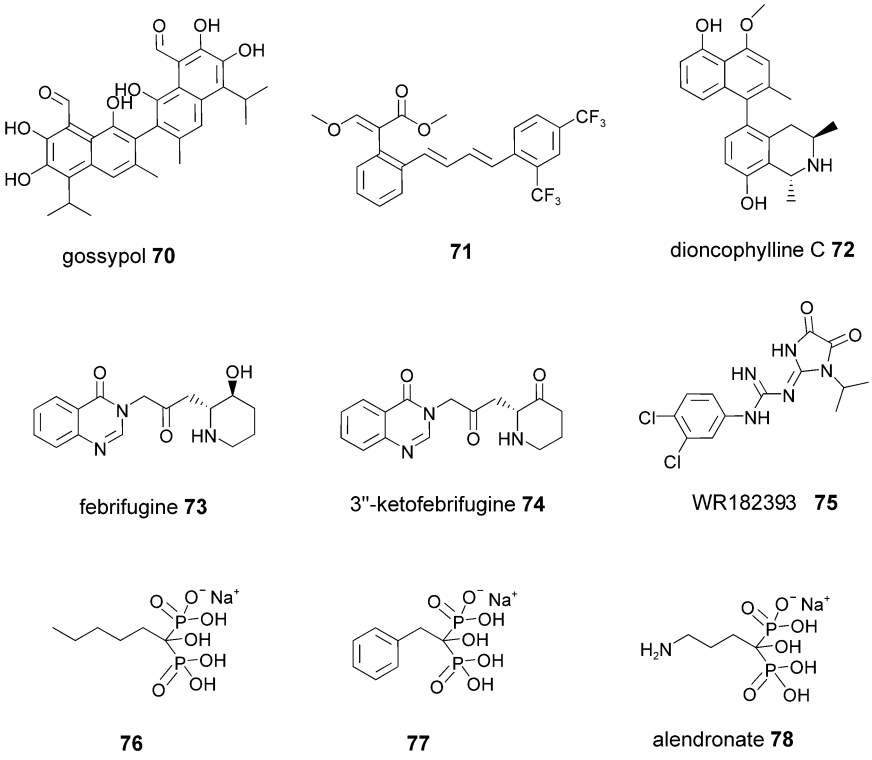
FTI-2153 **68**



Schl-4116 **69**

***Figure 20.*** Farnesyl transferase inhibitors.

(Figure 3).[165] $NAD^+$ needs to be regenerated by reduction of pyruvate to lactate. The lactate dehydrogenase of *P. falciparum* has been produced as a recombinant protein, and a high-resolution crystal structure is available. A combination of high-throughput screening and different structure-based design techniques is currently being used with the aim of identifying specific inhibitors that do not affect the human lactate dehydrogenase.[69] This may be feasible owing to significant structural differences between the mammalian and the parasite enzyme.[166] The disesquiterpene gossypol (**70**, Figure 21) isolated from cotton seeds inhibits *P. falciparum*



gossypol **70** | **71** | dioncophylline C **72**

febrifugine **73** | 3''-ketofebrifugine **74** | WR182393 **75**

**76** | **77** | alendronate **78**

***Figure 21.*** Further lead structures for new antimalarial drugs. A racemic mixture of 3''-ketofebrifugine (**74**) was used for in vivo experiments.

 © 2003 Wiley-VCH Verlag GmbH & Co. KGaA, Weinheim 

lactate dehydrogenase and displays moderate in vitro antimalarial activity ($IC_{50} = 15–29$ μM).[167] However, less-toxic derivatives are required for further development.

The crystal structures of two additional glycolytic enzymes of *P. falciparum* (fructose 1,6-bisphosphate aldolase and triosephosphate isomerase) have also been solved.[168,169] In both cases, structural differences between the parasite and the mammalian enzymes are evident, potentially providing a base for the design of specific inhibitors. Some sulfonated anionic dyes that inhibit the enzyme ($IC_{50} = 30.4$ (Congo Red) to 49.7 μM (Direct Red 23)) were identified by virtual screening based on the crystal structure of the *P. falciparum* triosephosphate isomerase.[170]

#### 5.8. Further New Lead Structures

β-Methoxyacrylates, which are used as agricultural fungicides, are known to act through a mechanism similar to that of atovaquone (**23**, Figure 9) by inhibition of the mitochondrial electron transfer at the cytochrome *c* reductase complex. Therefore, a series of β-methoxyacrylate derivatives was screened for antimalarial activity.[171] Compound **71** (Figure 21) was active in vitro against a chloroquine-sensitive and a chloroquine-resistant *P. falciparum* strain ($IC_{50} = 0.06$ and 0.13 nM, respectively). These are among the lowest $IC_{50}$ values ever recorded for an antimalarial drug. In mice infected with *P. berghei*, compound **71** was superior to chloroquine (**5**) by a factor of 5, but tenfold less active than atovaquone (**23**). As a potential limitation, rapid development of resistance is observed with these compounds.[15]

Tropical lianas of the families *Dioncophyllaceae* and *Ancistrocladaceae* have been widely applied in traditional medicine in several African and Asian countries for the treatment of malaria and other diseases. Naphthylisoquinoline alkaloids (dioncophyllines) with potent antimalarial activity have been isolated from these plants.[172] After oral administration of 50 mg kg$^{-1}$ of dioncophylline C (**72**, Figure 21), mice infected with *P. berghei* were cured completely. Febrifugine (**73**) is the active ingredient of the Chinese medicinal plant *Dichora febrifuga*. The antimalarial activity of febrifugine (**73**) has been demonstrated in vitro ($IC_{50} = 0.7$ nM) and in vivo. Its clinical use, however, is hampered by severe adverse effects. 3″-Ketofebrifugine (**74**), which is presumably a natural metabolite of febrifugine (**73**), was less toxic than febrifugine and slightly more active than chloroquine (**5**) in mice infected with *P. berghei* after intraperitoneal injection.[173] The mode of action of both the dioncophyllines and the febrifugines is unknown.

WR182393 (**75**, Figure 21) is formally a derivative of chlorproguanil (**25**) that cannot be cyclized into a dihydrofolate reductase inhibitor. Similar to the 8-amino quinolines primaquine (**30**) and pamaquine (**3**), **75** is only active against the hepatic parasite stages, but not against the blood stages.[174] Both the causal prophylactic activity and the prevention of relapses could be demonstrated in monkeys infected with *P. cynomolgi* after intramuscular injection of 31 mg kg$^{-1}$ of WR182393 for 3 days.[175]

Bisphosphonates such as those commonly used in the treatment and prophylaxis of osteoporosis may become important as a new class of antimalarial drugs. In a series of bisphosphonates with variable side chains, several compounds displayed activity against parasitic protozoa of the genera *Trypanosoma, Leishmania, Toxoplasma*, and *Plasmodium*.[176] Analysis of structure–activity relationships revealed that the absence of nitrogen in the side chain is clearly essential for antimalarial activity. The in vitro $IC_{50}$ values of **76** and **77** are 5.1 and 7.7 μM, respectively. In contrast, alendronate (**78**), the currently most frequently used bisphosphonate, was inactive against *P. falciparum* at the highest concentration tested (200 μM). It is assumed that the antiparasitic activity of the bisphosphonates is associated with inhibition of the farnesyl pyrophosphate synthase.

The reviews by Olliaro and Yuthavong,[177] Gutteridge,[178] Chauhan and Srivastava,[179] and Gelb and Hol[180] describe additional targets and lead structures.

## 6. Summary and Overview

The increasing spread of malaria together with the emergence of resistance against conventional antimalarial drugs has put enormous pressure on public health systems to introduce new treatments. Thus, drugs such as chlorproguanil (**25**), pyronaridine (**28**), and tafenoquine (**29**), which have been known for a relatively long time, have now been evaluated systematically in clinical trials. In parallel, several drug combinations with the artemisinin derivative artesunate (**17**) have been developed. Remarkably, the mechanisms of action of pyronaridine (**28**) and artesunate (**17**) are only partially understood, and that of tafenoquine (**29**) is virtually unknown. Fosmidomycin (**31**) is the only drug in clinical development that belongs to a new class of compounds and acts through a novel but well-understood mechanism. Also, in the field of preclinical research, well-established classes of compounds and molecular targets are still interesting, in particular 4-amino quinolines and other inhibitors of hem polymerization as well as artemisinin derivatives and other peroxides. With respect to the peroxides, there is a possible limitation owing to their less-specific mode of action pending as a result of the generation of free radicals.

Various inhibitors of proteases, choline uptake, and farnesyl transferase display promising activity in vitro and in animal models. However, as similar target molecules are present in humans, future development has to ensure a high degree of selectivity for the malarial enzymes. This is also the case for the development of inhibitors of glycolysis. The clinical application of a drug that has fully emerged by a rational design process cannot be foreseen in the near future. Nevertheless, the discovery of the type II fatty acid synthesis system and the mevalonate-independent isoprenoid biosynthesis pathway has demonstrated how fundamental research based on the *P. falciparum* genome sequence data can lead to the identification of new targets and to the rapid development of new drugs.

 © 2003 Wiley-VCH Verlag GmbH & Co. KGaA, Weinheim 

## 7. Abbreviations

$ED_{50}$ The dosage of a substance required to produce a defined therapeutic effect in 50% of the test animals.

$ED_{90}$ The dosage of a substance required to produce a defined therapeutic effect in 90% of the test animals.

$IC_{50}$ The concentration of a substance required to reduce a defined biological activity by 50%.

$LD_{50}$ The dosage of a substance that kills 50% of the test animals.

Received: December 27, 2002 [A569]


[1] S. R. Meshnick, M. J. Dobson in *Antimalarial Chemotherapy* (Ed.: P. J. Rosenthal), Humana Press, Totowa, NJ, **2001**, pp. 15–25.
[2] P. Guttmann, P. Ehrlich, *Berl. Klin. Wochenschr.* **1891**, *28*, 953–956.
[3] J. L. Vennerstrom, M. T. Makler, C. K. Angerhofer, J. A. Williams, *Antimicrob. Agents Chemother.* **1995**, *39*, 2671–2677.
[4] P. M. Farber, L. D. Arscott, C. H. Williams, Jr., K. Becker, R. H. Schirmer, *FEBS Lett.* **1998**, *422*, 311–314.
[5] D. Greenwood, *J. Antimicrob. Chemother.* **1995**, *36*, 857–872.
[6] D. L. Klayman, *Science* **1985**, *228*, 1049–1055.
[7] A. Bishop, *Parasitology* **1942**, *34*, 1–54.
[8] W. Peters, *Chemotherapy and Drug Resistance in Malaria*, Academic Press, New York, **1970**, pp. 64–136.
[9] W. Trager, J. B. Jensen, *Science* **1976**, *193*, 673–675.
[10] A. Bahl, B. Brunk, R. L. Coppel, J. Crabtree, S. J. Diskin, M. J. Fraunholz, G. R. Grant, D. Gupta, R. L. Huestis, J. C. Kissinger, P. Labo, L. Li, S. K. McWeeney, A. J. Milgram, D. S. Roos, J. Schug, C. J. Stoeckert, Jr., *Nucleic Acids Res.* **2002**, *30*, 87–90.
[11] P. B. Bloland, *Drug Resistance in Malaria*, World Health Organization, Geneva, **2001**, Report No. WHO/CDS/CSR/DRS/2001.4.
[12] B. Greenwood, T. Mutabingwa, *Nature* **2002**, *415*, 670–672.
[13] R. G. Ridley, *Lancet Infect. Dis.* **2002**, *2*, 54–59.
[14] W. E. Gutteridge, *Parassitologia* **1999**, *41*, 449–452.
[15] R. G. Ridley, *Nature* **2002**, *415*, 686–693.
[16] K. C. Kain, G. D. Shanks, J. S. Keystone, *Clin. Infect. Dis.* **2001**, *33*, 226–234.
[17] P. Newton, N. White, *Annu. Rev. Med.* **1999**, *50*, 179–192.
[18] C. P. Sanchez, M. Lanzer, *Curr. Opin. Infect. Dis.* **2000**, *13*, 653–658.
[19] H. Ginsburg, S. A. Ward, P. G. Bray, *Parasitol. Today* **1999**, *15*, 357–360.
[20] P. Loria, S. Miller, M. Foley, L. Tilley, *Biochem. J.* **1999**, *339*, 363–370.
[21] O. Famin, M. Krugliak, H. Ginsburg, *Biochem. Pharmacol.* **1999**, *58*, 59–68.
[22] M. Foley, L. Tilley, *Pharmacol. Ther.* **1998**, 79, 55–87.
[23] O. Famin, H. Ginsburg, *Biochem. Pharmacol.* **2002**, *63*, 393–398.
[24] a) G. A. Balint, *Pharmacol. Ther.* **2001**, *90*, 261–265; b) T. Klopp, C. Schroer, K. Bathe, M. Frieß, List of Pharmaceutical Substances, 13th ed., ABDATA Pharma-Daten-Service, Eschborn/Taunus, **2002**; *The Merck Index, An Encyclopedia of Chemicals, Drugs and Biologicals* (Eds.:M. J. O'Neil, A. Smith, P. E. Heckelman, J. R. Obenchain, J. A. R. Gallipeau, M. A. D'Arecca), 13th ed., Merck & Co. Inc., Whitehouse Station, NJ, **2001**; *Index Nominum, International Drug Directory* (Ed.: Schweizerischer Apothekerverein), Medpharm Scientific, Stuttgart, **2000**; X. D. Luo, H. J. C. Yeh, A. Brossi, J. L. Flippen-Anderson, R. Gilardi, *Helv. Chim. Acta* **1984**, *67*, 1515–1522; A. Brossi, B. Venugopalan, L. D. Gerpe, H. J. C. Yeh, J. L. Flippen-Anderson, P. Buchs, X. D. Luo, W. Milhous, W. Peters, *J. Med. Chem.* **1988**, *31*, 645–650; P. M. O'Neill, F. Scheinmann, A. V. Stachulski, J. L. Maggs, B. K. Park, *J. Med. Chem.* **2001**, *44*, 1467–1470; A. J. Lin, A. B. Zikry, D. E. Kyle, *J. Med. Chem.* **1997**, *40*, 1396–1400.
[25] R. N. Price, *Expert Opin. Invest. Drugs* **2000**, *9*, 1815–1827.
[26] D. A. Warrell, *Parassitologia* **1999**, *41*, 287–294.
[27] Artemether-Quinine Meta-analysis Study Group, *Trans. R. Soc. Trop. Med. Hyg.* **2001**, *95*, 637–650.
[28] I. R. Ribeiro, P. Olliaro, *Med. Trop.* **1998**, *58*, 50–53.
[29] R. McGready, T. Cho, N. K. Keo, K. L. Thwai, L. Villegas, S. Looareesuwan, N. J. White, F. Nosten, *Clin. Infect. Dis.* **2001**, *33*, 2009–2016.
[30] E. Leonardi, G. Gilvary, N. J. White, F. Nosten, *Trans. R. Soc. Trop. Med. Hyg.* **2001**, *95*, 182–183.
[31] P. L. Olliaro, R. K. Haynes, B. Meunier, Y. Yuthavong, *Trends Parasitol.* **2001**, *17*, 122–126.
[32] J. Cazelles, A. Robert, B. Meunier, *J. Org. Chem.* **2002**, *67*, 609–619.
[33] J. Bisutthibhan, X. Q. Pan, P. A. Hossler, D. J. Walker, C. A. Yowell, J. Carlton, J. B. Dame, S. R. Meshnick, *J. Biol. Chem.* **1998**, *273*, 16192–16198.
[34] M. E. Fichera, D. S. Roos, *Nature* **1997**, *390*, 407–409.
[35] S. Kohler, C. F. Delwiche, P. W. Denny, L. G. Tilney, P. Webster, R. J. Wilson, J. D. Palmer, D. S. Roos, *Science* **1997**, *275*, 1485–1489.
[36] R. J. Wilson, *J. Mol. Biol.* **2002**, *319*, 257–274.
[37] S. A. Ralph, M. C. D'Ombrain, G. I. McFadden, *Drug Resist. Updates.* **2001**, *4*, 145–151.
[38] S. Pukrittayakamee, R. Clemens, A. Chantra, A. Nontprasert, T. Luknam, S. Looareesuwan, N. J. White, *Trans. R. Soc. Trop. Med. Hyg.* **2001**, *95*, 524–528.
[39] B. Lell, P. G. Kremsner, *Antimicrob. Agents Chemother.* **2002**, *46*, 2315–2320.
[40] W. R. Taylor, T. L. Richie, D. J. Fryauff, H. Picarima, C. Ohrt, D. Tang, D. Braitman, G. S. Murphy, H. Widjaja, E. Tjitra, A. Ganjar, T. R. Jones, H. Basri, J. Berman, *Clin. Infect. Dis.* **1999**, *28*, 74–81.
[41] A. A. Omari, C. Preston, P. Garner, *Cochrane Database Syst. Rev.* **2002**, *3*, CD003125.
[42] M. van Agtmael, O. Bouchaud, D. Malvy, J. Delmont, M. Danis, S. Barette, C. Gras, J. Bernard, J. E. Touze, I. Gathmann, R. Mull, *Int. J. Antimicrob. Agents* **1999**, *12*, 159–169.
[43] M. Hassan Alin, A. Bjorkman, W. H. Wernsdorfer, *Am. J. Trop. Med. Hyg.* **1999**, *61*, 439–445.
[44] G. Lefevre, S. Looareesuwan, S. Treeprasertsuk, S. Krudsood, U. Silachamroon, I. Gathmann, R. Mull, R. Bakshi, *Am. J. Trop. Med. Hyg.* **2001**, *64*, 247–256.
[45] S. Looareesuwan, J. D. Chulay, C. J. Canfield, D. B. Hutchinson, *Am. J. Trop. Med. Hyg.* **1999**, *60*, 533–541.
[46] Atovaquone + Proguanil for Malaria Prophylaxis, *Drug Ther. Bull.* **2001**, *39*, 73–75.
[47] M. Fry, M. Pudney, *Biochem. Pharmacol.* **1992**, *43*, 1545–1553.
[48] I. K. Srivastava, J. M. Morrisey, E. Darrouzet, F. Daldal, A. B. Vaidya, *Mol. Microbiol.* **1999**, *33*, 704–711.
[49] C. J. Canfield, M. Pudney, W. E. Gutteridge, *Exp. Parasitol.* **1995**, *80*, 373–381.
[50] D. A. Fidock, T. Nomura, T. E. Wellems, *Mol. Pharmacol.* **1998**, *54*, 1140–1147.
[51] I. K. Srivastava, A. B. Vaidya, *Antimicrob. Agents Chemother.* **1999**, *43*, 1334–1339.
[52] J. D. Berman, R. Nielsen, J. D. Chulay, M. Dowler, K. C. Kain, K. E. Kester, J. Williams, A. C. Whelen, M. J. Shmuklarsky, *Trans. R. Soc. Trop. Med. Hyg.* **2001**, 95, 429–432.
[53] Q. L. Fivelman, G. A. Butcher, I. S. Adagu, D. C. Warhurst, G. Pasvol, *Malar. J.* **2002**, *1*, 1.


 © 2003 Wiley-VCH Verlag GmbH & Co. KGaA, Weinheim 

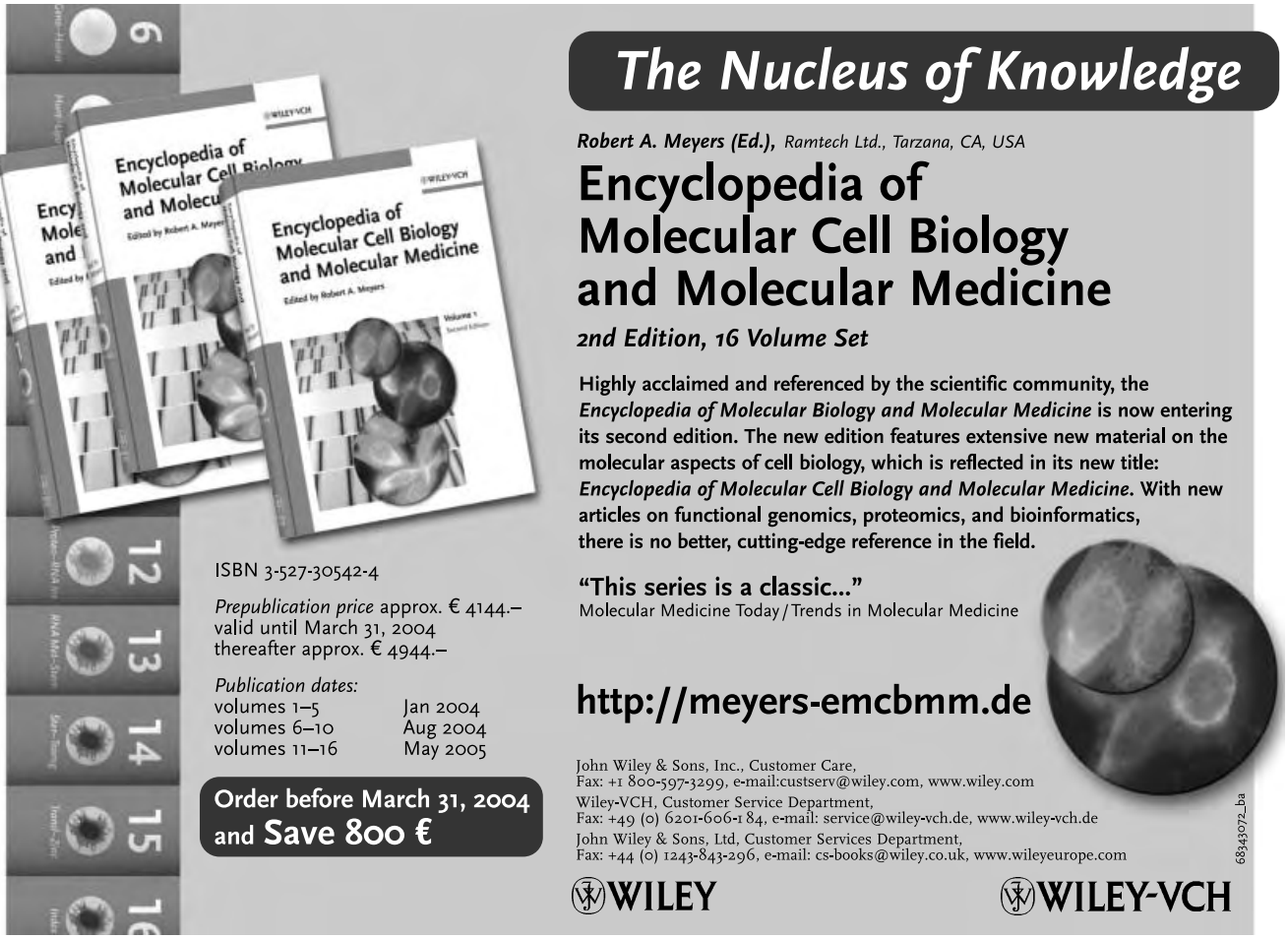
[54] P. Winstanley, *Trop. Med. Int. Health.* **2001**, *6*, 952 – 954.
[55] J. Curtis, M. T. Duraisingh, D. C. Warhurst, *J. Infect. Dis.* **1998**, *177*, 1429 – 1433.
[56] A. M. Nzila, E. Nduati, E. K. Mberu, C. Hopkins Sibley, S. A. Monks, P. A. Winstanley, W. M. Watkins, *J. Infect. Dis.* **2000**, *181*, 2023 – 2028.
[57] W. M. Watkins, A. D. Brandling-Bennett, C. G. Nevill, J. Y. Carter, D. A. Boriga, R. E. Howells, D. K. Koech, *Trans. R. Soc. Trop. Med. Hyg.* **1988**, *82*, 398 – 403.
[58] E. Amukoye, P. A. Winstanley, W. M. Watkins, R. W. Snow, J. Hatcher, M. Mosobo, E. Ngumbao, B. Lowe, M. Ton, G. Minyiri, K. Marsh, *Antimicrob. Agents Chemother.* **1997**, 41, 2261 – 2264.
[59] T. Mutabingwa, A. Nzila, E. Mberu, E. Nduati, P. Winstanley, E. Hills, W. Watkins, *Lancet* **2001**, *358*, 1218 – 1223.
[60] J. G. Kublin, F. K. Dzinjalamala, D. D. Kamwendo, E. M. Malkin, J. F. Cortese, L. M. Martino, R. A. Mukadam, S. J. Rogerson, A. G. Lescano, M. E. Molyneux, P. A. Winstanley, P. Chimpeni, T. E. Taylor, C. V. Plowe, *J. Infect. Dis.* **2002**. *185*, 380 – 388.
[61] P. Wilairatana, D. E. Kyle, S. Looareesuwan, K. Chinwongprom, S. Amradee, N. J. White, W. M. Watkins, *Ann. Trop. Med. Parasitol.* **1997**, *91*, 125 – 132.
[62] B. Khan, S. Omar, J. N. Kanyara, M. Warren-Perry, J. Nyalwidhe, D. S. Peterson, T. Wellems, S. Kaniaru, J. Gitonga, F. J. Mulaa, D. K. Koech, *Trans. R. Soc. Trop. Med. Hyg.* **1997**, *91*, 456 – 460.
[63] M. D. Edstein, S. Bahr, B. Kotecka, G. D. Shanks, K. H. Rieckmann, *Antimicrob. Agents Chemother.* **1997**, *41*, 2300 – 2301.
[64] P. L Olliaro, W. K. Milhous in *Antimalarial Chemotherapy* (Ed.: P. J. Rosenthal), Humana Press, Totowa, NJ, **2001**, pp. 219 – 232.
[65] P. Ringwald, J. Bickii, L. Basco, *Lancet* **1996**, *347*, 24 – 28.
[66] P. Ringwald, J. Bickii, L. K. Basco, *Clin. Infect. Dis.* **1998**, *26*, 946 – 953.
[67] S. Looareesuwan, D. E. Kyle, C. Viravan, S. Vanijanonta, P. Wilairatana, W. H. Wernsdorfer, *Am. J. Trop. Med. Hyg.* **1996**, *54*, 205 – 209.
[68] S. Looareesuwan, P. Olliaro, D. Kyle, W. Wernsdorfer, *Lancet* **1996**, *347*, 1189 – 1190.
[69] MMV—Medicines for Malaria Venture, Annual report **2000**.
[70] S. Gupta, M. M. Thapar, S. T. Mariga, W. H. Wernsdorfer, A. Bjorkman, *Exp. Parasitol.* **2002**, *100*, 28 – 35.
[71] G. D. Shanks, K. C. Kain, J. S. Keystone, *Clin. Infect. Dis.* **2001**, *33*, 381 – 385.
[72] R. P. Brueckner, C. Ohrt, J. K. Braid, W. Milhous in Antimalarial Chemotherapy (Ed.: P. J. Rosenthal), Humana Press, Totowa, NJ, **2001**, pp. 123–125.
[73] R. P. Brueckner, T. Coster, D. L. Wesche, M. Shmuklarsky, B. G. Schuster, *Antimicrob. Agents Chemother.* **1998**, *42*, 1293 – 1294.
[74] B. Lell, J. F. Faucher, M. A. Missinou, S. Borrmann, O. Dangelmaier, J. Horton, P. G. Kremsner, *Lancet* **2000**, *355*, 2041 – 2045.
[75] G. D. Shanks, A. J. Oloo, G. M. Aleman, C. Ohrt, F. W. Klotz, D. Braitman, J. Horton, R. P. Brueckner, *Clin. Infect. Dis.* **2001**, *33*, 1968 – 1974.
[76] D. S. Walsh, S. Looareesuwan, P. Wilairatana, D. G. Heppner, Jr., D. B. Tang, T. G. Brewer, W. Chokejindachai, P. Viriyavejakul, D. E. Kyle, W. K. Milhous, B. G. Schuster, J. Horton, D. J. Braitman, R. P. Brueckner, *J. Infect. Dis.* **1999**, *180*, 1282 – 1287.
[77] N. Obaldia III, R. N. Rossan, R. D. Cooper, D. E. Kyle, E. O. Nuzum, K. H. Rieckmann, G. D. Shanks, *Am. J. Trop. Med. Hyg.* **1997**, *56*, 508 – 510.
[78] H. Jomaa, J. Wiesner, S. Sanderbrand, B. Altincicek, C. Weidemeyer, M. Hintz, I. Turbachova, M. Eberl, J. Zeidler, H. K. Lichtenthaler, D. Soldati, E. Beck, *Science* **1999**, *285*, 1573 – 1576.
[79] M. Rohmer, *Nat. Prod. Rep.* **1999**, *16*, 565 – 574.
[80] H. P. Kuemmerle, T. Murakawa, H. Sakamoto, N. Sato, T. Konishi, F. De Santis, *Int. J. Clin. Pharmacol. Ther. Toxicol.* **1985**, *23*, 521 – 528.
[81] J. Zeidler, J. Schwender, C. Müller, J. Wiesner, C. Weidemeyer, E. Beck, H. Jomaa, H. K. Lichtenthaler, *Z. Naturforsch. C* **1998**, *53*, 980 – 986.
[82] T. Kuzuyama, T. Shizimu, S. Takahashi, H. Seto, *Tetrahedron Lett.* **1998**, *39*, 7913 – 7916.
[83] J. Wiesner, M. Hintz, B. Altincicek, S. Sanderbrand, C. Weidemeyer, E. Beck, H. Jomaa, *Exp. Parasitol.* **2000**, *96*, 182 – 186.
[84] A. T. Koppisch, D. T. Fox, B. S. Blagg, C. D. Poulter, *Biochemistry* **2002**, *41*, 236 – 243.
[85] K. Reuter, S. Sanderbrand, H. Jomaa, J. Wiesner, I. Steinbrecher, E. Beck, M. Hintz, G. Klebe, M. T. Stubbs, *J. Biol. Chem.* **2002**, *277*, 5378 – 5384.
[86] S. Yajima, T. Nonaka, T. Kuzuyama, H. Seto, K. Ohsawa, *J. Biochem. (Tokyo)* **2002**, *131*, 313 – 317.
[87] K. Silber, G. Klebe, unpublished results.
[88] B. Lell, R. Ruangweerayut, J. Wiesner, M. A. Missinou, A. Schindler, T. Baranek, M. Hintz, D. Hutchinson, H. Jomaa, P. G. Kremsner, *Antimicrob. Agents Chemother.* **2003**, *47*, 735 – 738.
[89] M. A. Missinou, S. Borrmann, A. Schindler, S. Issifou, A. Adegnika, P. B. Matsiegui, R. Binder, B. Lell, J. Wiesner, T. Baranek, H. Jomaa, P. G. Kremsner, *Lancet* **2002**, *360*, 1941 – 1942.
[90] J. Wiesner, D. Henschker, D. B. Hutchinson, E. Beck, H. Jomaa, *Antimicrob. Agents Chemother.* **2002**, *46*, 2889 – 2894.
[91] H. Jomaa, P. G. Kremsner, unpublished results.
[92] T. Tsuchiya, K. Ishibashi, M. Terakawa, M. Nishiyama, N. Itoh, H. Noguchi, *Eur. J. Drug Metab. Pharmacokinet.* **1982**, *7*, 59 – 64.
[93] A. Reichenberg, J. Wiesner, C. Weidemeyer, E. Dreiseidler, S. Sanderbrand, B. Altincicek, E. Beck, M. Schlitzer, H. Jomaa, *Bioorg. Med. Chem. Lett.* **2001**, *11*, 833 – 835.
[94] R. Ortmann, J. Wiesner, A. Reichenberg, D. Henschker, E. Beck, H. Jomaa, M. Schlitzer, *Bioorg. Med. Chem. Lett.*, **2003**, *13*, 2163 – 2166.
[95] T. E. Wellems, C. V. Plowe, *J. Infect. Dis.* **2001**, *184*, 770 – 776.
[96] S. Delarue, S. Girault, L. Maes, M. A. Debreu-Fontaine, M. Labaeid, P. Grellier, C. Sergheraert, *J. Med. Chem.* **2001**, *44*, 2827 – 2833.
[97] S. Girault, P. Grellier, A. Berecibar, L. Maes, P. Lemiere, E. Mouray, E. Davioud-Charvet, C. Sergheraert, *J. Med. Chem.* **2001**, *44*, 1658 – 1665.
[98] For a review, see: P. M. O'Neill, P. G. Bray, S. R. Hawley, S. A. Ward, B. K. Park, *Pharmacol. Ther.* **1998**, *77*, 29 – 58.
[99] H. Ginsburg, E. Nissani, M. Krugliak, *Biochem. Pharmacol.* **1989**, *38*, 2645 – 2654.
[100] L. K. Basco, G. Peytavin, F. Gimenez, B. Genissel, R. Farinotti, J. Le Bras, *Trop. Med. Parasitol.* **1994**, *45*, 45 – 46.
[101] D. L. Wesche, B. G. Schuster, W. X. Wang, R. L. Woosley, *Clin. Pharmacol. Ther.* **2000**, *67*, 521 – 529.
[102] H. Noedl, T. Allmendinger, S. Prajakwong, G. Wernsdorfer, W. H. Wernsdorfer, *Antimicrob. Agents Chemother.* **2001**, *45*, 2106 – 2109.
[103] J. Berman, L. Brown, R. Miller, S. L. Andersen, P. McGreevy, B. G. Schuster, W. Ellis, A. Ager, R. Rossan, *Antimicrob. Agents Chemother.* **1994**, *38*, 1753 – 1756.
[104] R. E. Coleman, N. Polsa, N. Eikarat, T. M. Kollars Jr., J. Sattabongkot, *Am. J. Trop. Med. Hyg.* **2001**, *65*, 214 – 218.
[105] A. Dorn, J. P. Scovill, W. Y. Ellis, H. Matile, R. G. Ridley, J. L. Vennerstrom, *Am. J. Trop. Med. Hyg.* **2001**, *65*, 19 – 20.

 © 2003 Wiley-VCH Verlag GmbH & Co. KGaA, Weinheim 

[106] E. Suswam, D. Kyle, N. Lang-Unnasch, *Exp. Parasitol.* **2001**, *98*, 180 – 187.
[107] C. W. Wright, J. Addae-Kyereme, A. G. Breen, J. E. Brown, M. F. Cox, S. L. Croft, Y. Gokcek, H. Kendrick, R. M. Phillips, P. L. Pollet, *J. Med. Chem.* **2001**, *44*, 3187 – 3194.
[108] J. N. Lisgarten, M. Coll, J. Portugal, C. W. Wright, J. Aymami, *Nat. Struct. Biol.* **2002**, *9*, 57 – 60.
[109] Y. Kurosawa, A. Dorn, M. Kitsuji-Shirane, H. Shimada, T. Satoh, H. Matile, W. Hofheinz, R. Masciadri, M. Kansy, R. G. Ridley, *Antimicrob. Agents Chemother.* **2000**, *44*, 2638 – 2644.
[110] K. M. Brinner, J. M. Kim, H. Habashita, I. Y. Gluzman, D. E. Goldberg, J. A. Ellman, *Bioorg. Med. Chem.* **2002**, *10*, 3649 – 3661.
[111] C. Y. H. Choi, E. L. Schneider, J. M. Kim, I. Y. Gluzman, D. E. Goldberg, J. A. Ellman, M. A. Marletta, *Chem. Biol.* **2002**, *9*, 881 – 889.
[112] E. Davioud-Charvet, S. Delarue, C. Biot, B. Schwobel, C. C. Boehme, A. Mussigbrodt, L. Maes, C. Sergheraert, P. Grellier, R. H. Schirmer, K. Becker, *J. Med. Chem.* **2001**, *44*, 4268 – 4276.
[113] H. Atamna, H. Ginsburg, *J. Biol. Chem.* **1995**, *270*, 24876 – 24883.
[114] H. Ginsburg, O. Famin, J. Zhang, M. Krugliak, *Biochem. Pharmacol.* **1998**, *56*, 1305 – 1313.
[115] Q. G. Li, J. O. Peggins, A. J. Lin, K. J. Masonic, K. M. Trotman, T. G. Brewer, *Trans. R. Soc. Trop. Med. Hyg.* **1998**, *92*, 332 – 340.
[116] Y. Li, Y. M. Zhu, H. J. Jiang, J. P. Pan, G. S. Wu, J. M. Wu, Y. L. Shi, J. D. Yang, B. A. Wu, *J. Med. Chem.* **2000**, *43*, 1635 – 1640.
[117] P. M. O'Neill, A. Miller, L. P. Bishop, S. Hindley, J. L. Maggs, S. A. Ward, S. M. Roberts, F. Scheinmann, A. V. Stachulski, G. H. Posner, B. K. Park, *J. Med. Chem.* **2001**, *44*, 58 – 68.
[118] G. H. Posner, M. H. Parker, J. Northrop, J. S. Elias, P. Ploypradith, S. Xie, T. A. Shapiro, *J. Med. Chem.* **1999**, *42*, 300 – 304.
[119] S. Hindley, S. A. Ward, R. C. Storr, N. L. Searle, P. G. Bray, B. K. Park, J. Davies, P. M. O'Neill, *J. Med. Chem.* **2002**, *45*, 1052 – 1063.
[120] G. H. Posner, P. Ploypradith, M. H. Parker, H. O'Dowd, S. H. Woo, J. Northrop, M. Krasavin, P. Dolan, T. W. Kensler, S. Xie, T. A. Shapiro, *J. Med. Chem.* **1999**, *42*, 4275 – 4280.
[121] G. H. Posner, J. Northrop, I. H. Paik, K. Borstnik, P. Dolan, T. W. Kensler, S. Xie, T. A. Shapiro, *Bioorg. Med. Chem.* **2002**, *10*, 227 – 232.
[122] G. H. Posner, H. B. Jeon, M. H. Parker, M. Krasavin, I. H. Paik, T. A. Shapiro, *J. Med. Chem.* **2001**, *44*, 3054 – 3058.
[123] G. H. Posner, J. N. Cumming, S. H. Woo, P. Ploypradith, S. Xie, T. A. Shapiro, *J. Med. Chem.* **1998**, *41*, 940 – 951.
[124] A. M. Szpilman, E. E. Korshin, R. Hoos, G. H. Posner, M. D. Bachi, *J. Org. Chem.* **2001**, *66*, 6531 – 6540.
[125] E. Weidekamm, E. Dumont, C. Jaquet, *Trop. Med. Parasitol.* **1994**, *45*, 278 – 283.
[126] L. A. Salako, R. Guiguemde, M. L. Mittelholzer, L. Haller, F. Sorenson, D. Sturchler, *Trop. Med. Parasitol.* **1994**, *45*, 284 – 287.
[127] R. Somo-Moyou, M. L. Mittelholzer, F. Sorenson, L. Haller, D. Sturchler, *Trop. Med. Parasitol.* **1994**, *45*, 288 – 291.
[128] P. D. Radloff, J. Philipps, M. Nkeyi, D. Sturchler, M. L. Mittelholzer, P. G. Kremsner, *Am. J. Trop. Med. Hyg.* **1996**, *55*, 259 – 262.
[129] G. H. Posner, M. Kravasin, M. McCutchen, P. Ploypradith, J. P. Maxwell, J. S. Elias, M. H. Parker in *Antimalarial Chemotherapy* (Ed.: P. J. Rosenthal), Humana Press, Totowa, NJ, **2001**, pp. 255 – 263.
[130] J. L. Vennerstrom, Y. Dong, S. L. Andersen, A. L. Ager, Jr., H. Fu, R. E. Miller, D. L. Wesche, D. E. Kyle, L. Gerena, S. M. Walters, J. K. Wood, G. Edwards, A. D. Holme, W. G. McLean, W. K. Milhous, *J. Med. Chem.* **2000**, *43*, 2753 – 2758.
[131] H. Ren, S. Grady, D. Gamenara, H. Heinzen, P. Moyna, S. L. Croft, H. Kendrick, V. Yardley, G. Moyna, *Bioorg. Med. Chem. Lett.* **2001**, *11*, 1851 – 1854.
[132] L. K. Basco, O. Dechy-Cabaret, M. Ndounga, F. S. Meche, A. Robert, B. Meunier, *Antimicrob. Agents Chemother.* **2001**, *45*, 1886 – 1888.
[133] G. H. Coombs, D. E. Goldberg, M. Klemba, C. Berry, J. Kay, J. C. Mottram, *Trends Parasitol.* **2001**, *17*, 532 – 537.
[134] D. M. Wyatt, C. Berry, *FEBS Lett.* **2002**, *513*, 159 – 162.
[135] K. K. Eggleson, K. L. Duffin, D. E. Goldberg, *J. Biol. Chem.* **1999**, *274*, 32411 – 32417.
[136] R. Banerjee, J. Liu, W. Beatty, L. Pelosof, M. Klemba, D. E. Goldberg, *Proc. Natl. Acad. Sci. USA* **2002**, *99*, 990 – 995.
[137] T. S. Haque, A. G. Skillman, C. E. Lee, H. Habashita, I. Y. Gluzman, T. J. Ewing, D. E. Goldberg, I. D. Kuntz, J. A. Ellman, *J. Med. Chem.* **1999**, *42*, 1428 – 1440.
[138] D. A. Carcache, S. R. Hörtner, A. Bertogg, C. Binkert, D. Bur, H. P. Märki, A. Dorn, F. Diederich, *ChemBioChem* **2002**, *3*, 1137 – 1141.
[139] R. P. Moon, L. Tyas, U. Certa, K. Rupp, D. Bur, C. Jaquet, H. Matile, H.-R. Loetscher, F. Grueninger-Leitch, J. Kay, B. M. Dunn, C. Berry, R. G. Ridley, *Eur. J. Biochem.* **1997**, *244*, 552 – 560.
[140] J. E. Olson, G. K. Lee, A. Semenov, P. J. Rosenthal, *Bioorg. Med. Chem.* **1999**, *7*, 633 – 638.
[141] J. H. McKerrow, *Int. J. Parasitol.* **1999**, *29*, 833 – 837.
[142] R. Li, G. L. Kenyon, F. E. Cohen, X. Chen, B. Gong, J. N. Dominguez, E. Davidson, G. Kurzban, R. E. Miller, E. O. Nuzum, P. J. Rosenthal, J. H. McKerrow, *J. Med. Chem.* **1995**, *38*, 5031 – 5037.
[143] J. N. Dominguez, S. Lopez, J. Charris, L. Iarruso, G. Lobo, A. Semenov, J. E. Olson, P. J. Rosenthal, *J. Med. Chem.* **1997**, *40*, 2726 – 2732.
[144] A. Semenov, J. E. Olson, P. J. Rosenthal, *Antimicrob. Agents Chemother.* **1998**, *42*, 2254 – 2258.
[145] R. J. Heath, S. W. White, C. O. Rock, *Appl. Microbiol. Biotechnol.* **2002**, *58*, 695 – 703.
[146] R. F. Waller, P. J. Keeling, R. G. Donald, B. Striepen, E. Handman, N. Lang-Unnasch, A. F. Cowman, G. S. Besra, D. S. Roos, G. I. McFadden, *Proc. Natl. Acad. Sci. USA* **1998**, *95*, 12352 – 12357.
[147] N. Surolia, A. Surolia, *Nat. Med.* **2001**, *7*, 167 – 173.
[148] R. Perozzo, M. Kuo, A. S. Sidhu, J. T. Valiyaveettil, R. Bittman, W. R. Jacobs, Jr., D. A. Fidock, J. C. Sacchettini, *J. Biol. Chem.* **2002**, *277*, 13106 – 13114.
[149] M. Calas, M. L. Ancelin, G. Cordina, P. Portefaix, G. Piquet, V. Vidal-Sailhan, H. Vial, *J. Med. Chem.* **2000**, *43*, 505 – 516.
[150] K. Wengelnik, V. Vidal, M. L. Ancelin, A. M. Cathiard, J. L. Morgat, C. H. Kocken, M. Calas, S. Herrera, A. W. Thomas, H. J. Vial, *Science* **2002**, *295*, 1311 – 1314.
[151] J. H. Vial, M. Calas in *Antimalarial Chemotherapy* (Ed.: P. J. Rosenthal), Humana Press, Totowa, NJ, **2001**, pp. 347 – 365.
[152] A. Wittinghofer, H. Waldmann, *Angew. Chem.* **2000**, *112*, 4360 – 4383; *Angew. Chem. Int. Ed.* **2000**, *39*, 4192 – 4214.
[153] J. Ohkanda, D. B. Knowles, M. A. Blaskovich, S. M. Sebti, A. D. Hamilton, *Curr. Top. Med. Chem.* **2002**, *2*, 303 – 323.
[154] P. Haluska, G. Dy, A. Adjei, *Eur. J. Cancer* **2002**, *38*, 1685.
[155] M. Schlitzer, *Curr. Pharm. Des.* **2002**, *8*, 1713 – 1721.
[156] F. S. Buckner, K. Yokoyama, L. Nguyen, A. Grewal, H. Erdjument-Bromage, P. Tempst, C. L. Strickland, L. Xiao, W. C. Van Voorhis, M. H. Gelb, *J. Biol. Chem.* **2000**, *275*, 21870 – 21876.
[157] D. Chakrabarti, T. Azam, C. DelVecchio, L. Qiu, Y. L. Park, C. M. Allen, *Mol. Biochem. Parasitol.* **1998**, *94*, 175 – 184.
[158] D. Chakrabarti, T. Da Silva, J. Barger, S. Paquette, H. Patel, S. Patterson, C. M. Allen, *J. Biol. Chem.* **2002**, *277*, 42066 – 42073.

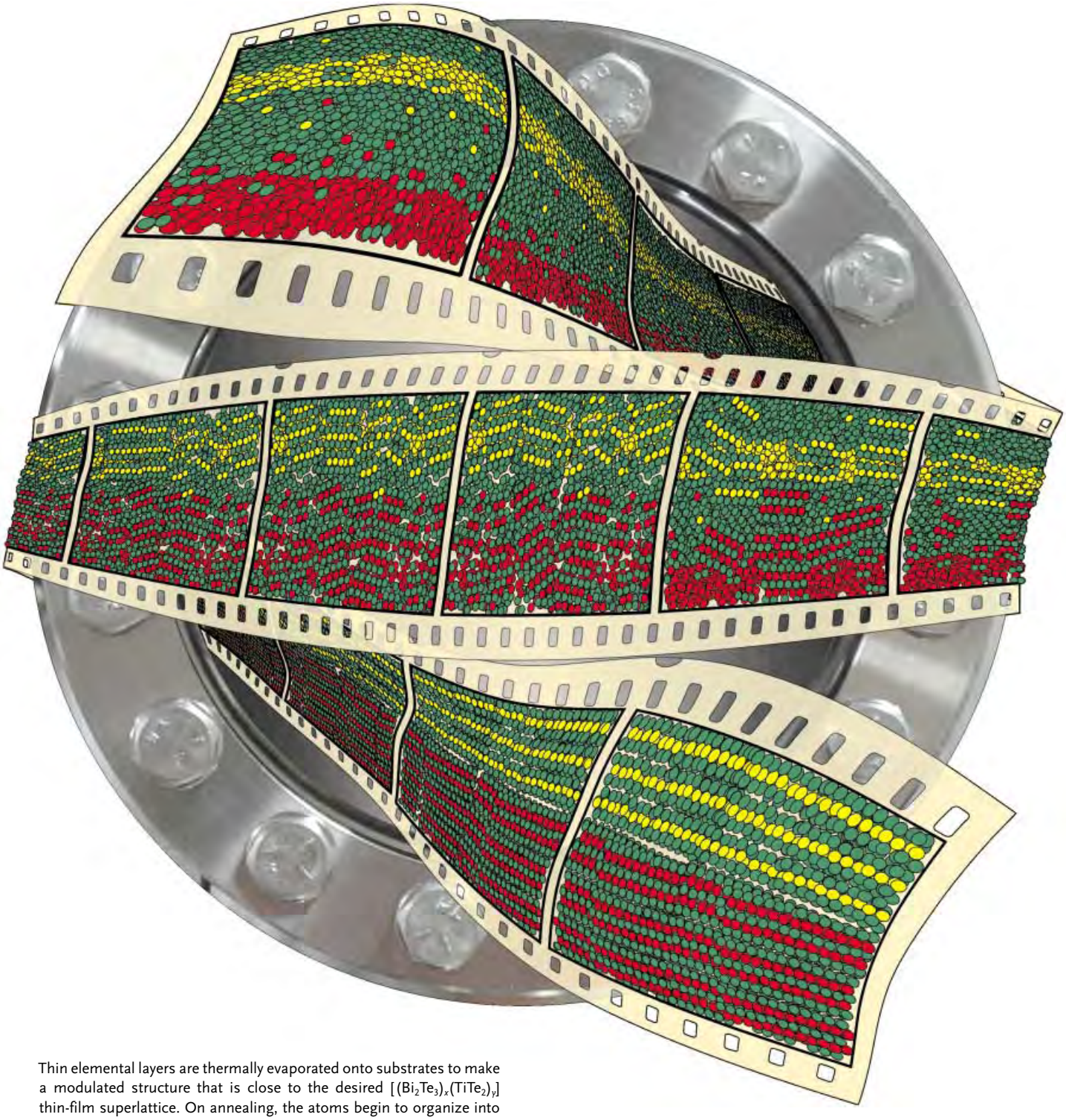
 © 2003 Wiley-VCH Verlag GmbH & Co. KGaA, Weinheim 

[159] J. Okhanda, J. W. Lockman, K. Yokoyama, M. H. Gelb, S. L. Croft, H. Kendrick, M. I. Harrell, J. E. Feagin, M. A. Blaskovich, S. M. Sebti, A. D. Hamilton, *Bioorg. Med. Chem. Lett.* **2001**, *11*, 761 – 764.
[160] A. Mitsch, M. Böhm, P. Wißner, I. Sattler, M. Schlitzer, *Bioorg. Med. Chem.* **2002**, *10*, 2657 – 2662.
[161] M. Böhm, A. Mitsch, P. Wißner, I. Sattler, M. Schlitzer, *J. Med. Chem.* **2001**, *44*, 3117 – 3124.
[162] J. Wiesner, A. Mitsch, P. Wißner, O. Krämer, H. Jomaa, M. Schlitzer, *Bioorg. Med. Chem. Lett.* **2002**, *12*, 2681 – 2683.
[163] M. Schlitzer, unpublished results.
[164] J. Wiesner, R. Ortmann, A. Mitsch, P. Wißner, I. Sattler, H. Jomaa, M. Schlitzer, *Pharmazie*, **2003**, *58*, 289 – 290
[165] I. W. Sherman, *Microbiol. Rev.* **1979**, *43*, 453 – 495.
[166] C. R. Dunn, M. J. Banfield, J. J. Barker, C. W. Higham, K. M. Moreton, D. Turgut-Balik, R. L. Brady, J. J. Holbrook, *Nat. Struct. Biol.* **1996**, *3*, 912 – 915.
[167] V. Razakantoanina, N. K. P. Phung, G. Jaureguiberry, *Parasitol. Res.* **2000**, *86*, 665 – 668.
[168] S. S. Velanker, S. S. Ray, R. S. Gokhale, S. Suma, H. Balaram, P. Balaram, M. R. Murthy, *Structure* **1997**, *5*, 751 – 761.
[169] H. Kim, U. Certa, H. Dobeli, P. Jakob, W. G. Hol, *Biochemistry* **1998**, *37*, 4388 – 4396.
[170] F. Joubert, A. W. Neitz, A. I. Louw, *Proteins Struct. Funct. Genet.* **2001**, *45*, 136 – 143.
[171] J. Alzeer, J. Chollet, I. Heinze-Krauss, C. Hubschwerlen, H. Matile, R. G. Ridley, *J. Med. Chem.* **2000**, *43*, 560 – 568.
[172] G. Francois, G. Timperman, W. Eling, L. A. Assi, J. Holenz, G. Bringmann, *Antimicrob. Agents Chemother.* **1997**, *41*, 2533 – 2539.
[173] H. Kikuchi, H. Tasaka, S. Hirai, Y. Takaya, Y. Iwabuchi, H. Ooi, S. Hatakeyama, H. S. Kim, Y. Wataya, Y. Oshima, *J. Med. Chem.* **2002**, *45*, 2563 – 2570.
[174] W. K. Milhous, *Med. Trop.* **2001**, *61*, 48 – 50.
[175] K. D. Corcoran, P. Hansukjariya, J. Sattabongkot, M. Ngampochjana, M. D. Edstein, C. D. Smith, G. D. Shanks, W. K. Milhous, *Am. J. Trop. Med. Hyg.* **1993**, *49*, 473 – 477.
[176] M. B. Martin, J. S. Grimley, J. C. Lewis, H. T. Heath III, B. N. Bailey, H. Kendrick, V. Yardley, A. Caldera, R. Lira, J. A. Urbina, S. N. Moreno, R. Docampo, S. L. Croft, E. Oldfield, *J. Med. Chem.* **2001**, *44*, 909 – 916.
[177] P. L. Olliaro, Y. Yuthavong, *Pharmacol. Ther.* **1999**, *81*, 91 – 110.
[178] W. E. Gutteridge, *Parassitologia* **1999**, *41*, 449 – 452.
[179] P. M. Chauhan, S. K. Srivastava, *Curr. Med. Chem.* **2001**, *8*, 1535 – 1542.
[180] M. H. Gelb, W. G. Hol, *Science* **2002**, *297*, 343 – 344.




 © 2003 Wiley-VCH Verlag GmbH & Co. KGaA, Weinheim 

# Communications



Thin elemental layers are thermally evaporated onto substrates to make a modulated structure that is close to the desired $[(Bi_2Te_3)_x(TiTe_2)_y]$ thin-film superlattice. On annealing, the atoms begin to organize into an oriented supperlattice. At temperatures around 280 °C, a well-defined superlattice forms. For more information see the following Communication by Johnson and co-workers.


**DOI: 10.1002/anie.200351724**
© 2003 Wiley-VCH Verlag GmbH & Co. KGaA, Weinheim

Superlattices

# Design and Synthesis of $[(Bi_2Te_3)_x(TiTe_2)_y]$ Superlattices**

*Fred R. Harris, Stacey Standridge, Carolyn Feik, and David C. Johnson**

The synthesis of new compounds has often been a necessary precursor to the discovery of new physical phenomena.[1] Unfortunately, predicting the structure and composition of undiscovered compounds with extended structures is quite difficult.[2] This is a result of many different possible coordination numbers and local environments for atoms in compounds. Most solid-state compounds are discovered serendipitously; however, solid-state chemists have recently begun searching for means to predict the structures of new compounds. For example, a prediction method proposed by Schön and Jansen utilizes energy calculations as a function of changes in the internal coordinates of atoms to find local energy minima.[3]

Another approach to predicting new compounds, used in the work presented here, is to combine the structural features of two or more known materials into a targeted new phase. We chose to target new materials consisting of interleaved layers of compounds containing van der Waals gaps (VWGs). We hypothesized that interleaving layers of already quasi 2D materials will result in products that are at local energy minima on the multidimensional energy surface. VWGs exist in many compounds, including layered transition-metal dichalcogenides (TMDC),[4] structural analogues of $Bi_2Te_3$,[5] and $MPX_3$ compounds (where M is a metal atom and X is a chalcogen),[6–8] to mention a few. Structural properties of the known VWG compounds support the hypothesis that the targeted structures are at local energy minima. For example, the existence of different stacking registries resulting in different polytypes suggests that there is only small free energy differences between them.[9–13] Additionally, interwoven TMDC films grown with molecular-beam epitaxy have been made with large lattice mismatches, thus implying that little strain energy is present between layers.[14] This reinforces the idea that there is little contribution to the stabilization energy of compounds from the weak, nondirectional VWG bonding between layers.

When considering which compounds to interleave to explore the effect of superstructure on physical properties, compounds that contain VWGs are also a logical choice. The bonding requirements of these compounds are satisfied within each layer, thus leaving interfaces between the layers with no dangling bonds. In addition, the weak bonding across the gaps reduces the effects of strain and eliminates the formation of dislocations that often result from lattice mismatch. The minimization of these defects between the layers in the targeted materials should result in the superstructure dominating the physical properties.

While dichalcogenide superlattices have been prepared (containing XMX layers)[15] and superlattices exhibiting the bismuth telluride structure have been prepared (containing XMXMX layers),[16] we believe this report of the synthesis of $[(Bi_2Te_3)_x(TiTe_2)_y]$ superlattices is the first preparation of a mixed superlattice (containing XMX–XMXMX layers), thus illustrating the general nature of the local energy arguments made above. This is an intriguing component pair in that $Bi_2Te_3$ is a narrow-bandgap semiconductor[17] while $TiTe_2$ is a semimetal.[18,19] An additional challenge in the $[(Bi_2Te_3)_x(TiTe_2)_y]$ superlattices is the immiscibility of the components. In the XMX–XMX and XMXMX–XMXMX superlattices made previously, the binary compounds formed solid solutions.[16,20–22]

The immiscibility of the components of the targeted superlattice presents a synthetic challenge that requires a low temperature synthesis approach.[23] We used a modulated elemental reactants (MER) synthesis technique to synthesize superlattice precursors. These films were prepared by thermally evaporating elements sequentially in an high vacuum chamber ($< 5 \times 10^{-7}$ torr) onto an ambient temperature substrate.[21] Bilayers of bismuth and tellurium, followed by bilayers of titanium and tellurium, were sequentially deposited to give the desired compositions of $Bi_2Te_3$ and $TiTe_2$ in the superlattice structure. The ratio of layer thicknesses was calibrated to yield the correct stoichiometry for each binary system. Samples were made by systematically changing the layer thickness of bismuth while holding the layer thickness of tellurium constant. Composition was determined by electron microprobe analysis (EPMA), and the ratio of layer thicknesses resulting in $Bi_2Te_3$ stoichiometry was selected for synthesis of the subsequent superlattice precursors. Similarly, titanium–tellurium binaries were synthesized and analyzed by EPMA to determine the thicknesses resulting in a $TiTe_2$ stoichiometry. Once the thickness ratios in the binaries were determined, samples with an approximate 1000 Å thickness were made by combining both binary systems into alternating layers. Absolute amounts of each binary multilayer were adjusted by analyzing X-ray reflectivity (XRR) for series of systematically changed superlattice precursors. These optimized precursors were then annealed to 280 °C for 20 minutes in a preheated box furnace under an inert $N_2$ atmosphere to kinetically trap the desired product.

Figure 1a shows X-ray diffraction (XRD) patterns collected with $Cu_{K\alpha}$ (1.54 Å) radiation which correspond to five isomeric superlattices with the formula $[(Bi_2Te_3)_x(TiTe_2)_x]$ synthesized by using the MER approach. Rietveld refinement of these superlattices shows that the structure within the layers and the VWG distance between $Bi_2Te_3$ sections is close to that of the distance found in bulk $Bi_2Te_3$ (2.6 $\pm$0.1 Å experimental; 2.60 Å reported in the literature,[24] and the same is true for the structure of and VWG distance between

[*] Prof. D. C. Johnson, F. R. Harris, S. Standridge, C. Feik
The University of Oregon
373 Klamath Hall, Eugene, OR 97403 (USA)
Fax: (+1) 541–346–0487
E-mail: davej@oregon.uoregon.edu

[**] This work was supported by the National Science Foundation (DGE 0114419, DMR 9813726, and DMR 0103409)

Supporting information for this article is available on the WWW under http://www.angewandte.org or from the author.

 © 2003 Wiley-VCH Verlag GmbH & Co. KGaA, Weinheim DOI: 10.1002/anie.200351724 

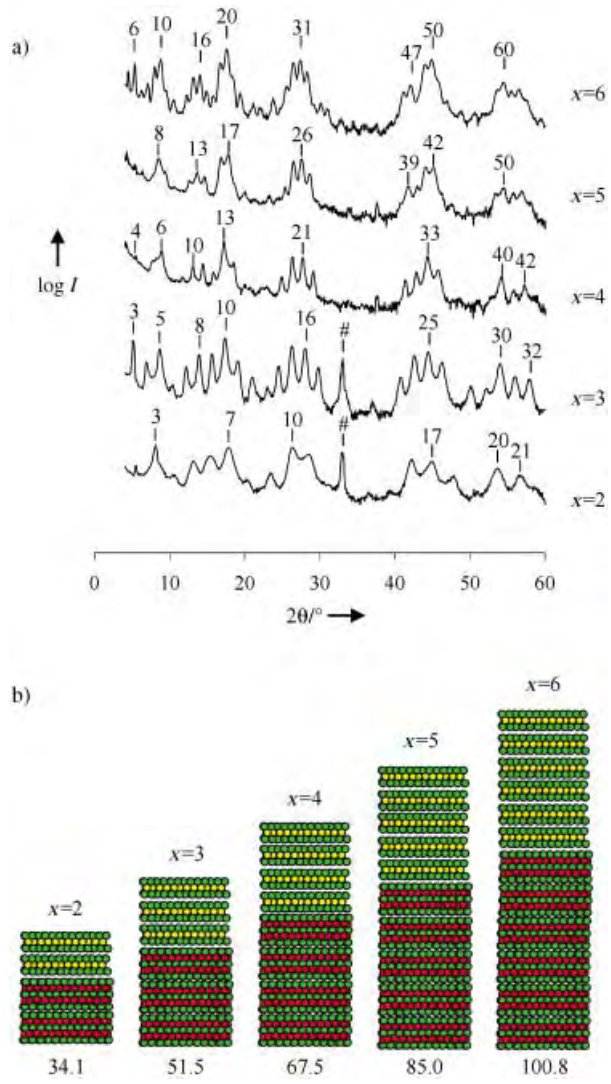



***Figure 1.*** a) X-ray diffraction of five isomeric superlattices with the formula $[(Bi_2Te_3)_x(TiTe_2)_x]$, $I$ = intensity. The # sign indicates peaks from the substrate. The numbers above the peaks are the $l$ component of the Miller indices of the superlattice. While all of the $l$ can be indexed, only some are listed owing to space restrictions. b) Idealized structures of each isomeric superlattice. The numbers listed underneath each structure indicates its $c$ lattice parameter.

$TiTe_2$ layers (3.2 ± 0.1 Å experimental; 3.08 Å reported in the literature)[25] The VWG distance between the $Bi_2Te_3$ and $TiTe_2$ layers is closer to that found in the pure $TiTe_2$ phase (3.2 ± 0.1 Å experimental).[26] This suggests that these isomeric structures along the $c$ axis look similar to the idealized structures shown in Figure 1b. Grazing incidence X-ray diffraction provides no evidence of alignment of the layers in the $a$ direction. Transmission electron microscopy shows that the films consist of small grains of the targeted superlattices (Figure 2).

The regular structure of the MER precursors provides a useful X-ray probe for studying the mechanism of product formation and optimizing annealing conditions. We chose to study the $[(Bi_2Te_3)_3(TiTe_2)_3]$ superlattice with a series of diffraction experiments designed to identify key structural

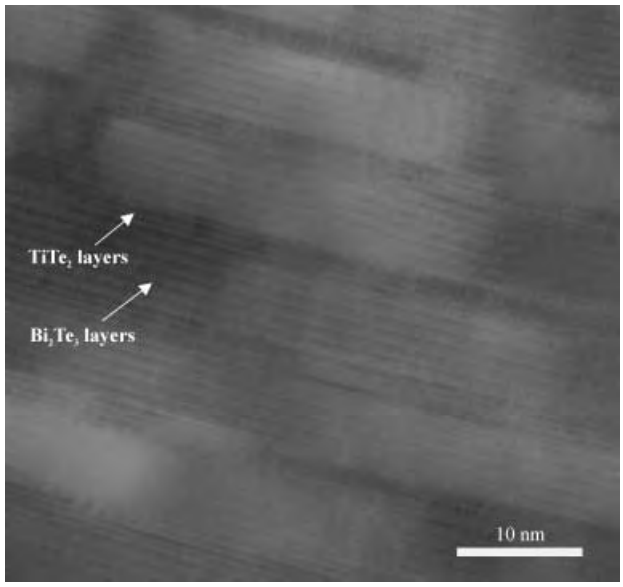



***Figure 2.*** TEM of $[(Bi_2Te_3)_6(TiTe_2)_3]$ superlattice. The different VWG spacings make the $Bi_2Te_3$ and $TiTe_2$ areas clearly visible.

changes and their associated annealing temperatures. Figure 3 contains a summary of a XRD study as a function of annealing temperature showing the increase in structural order perpendicular to the substrate. The 10.0 Å $Bi_2Te_3$ layer spacing produces diffraction maxima at $2\theta$ values of 8.8, 17.7, 26.7, and 45.3°, while the 6.5 Å $TiTe_2$ layer spacing results in diffraction maxima at $2\theta$ values of 13.6, 27.4, 41.6, and 56.6°. In the initially deposited sample, weak diffraction maxima are

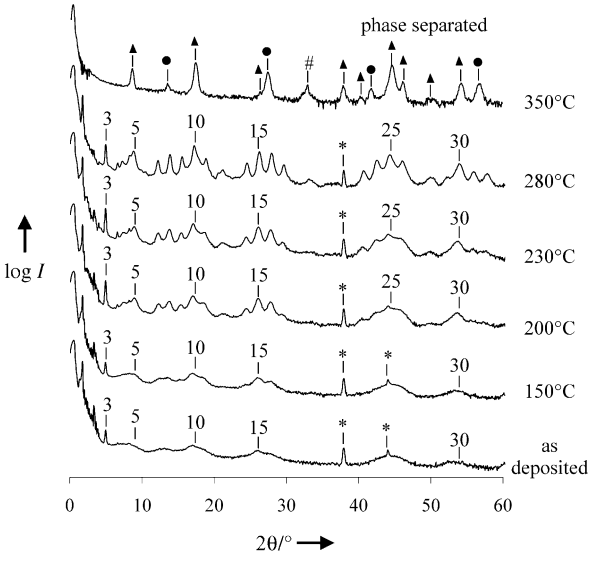



***Figure 3.*** X-ray diffraction study of a forming $[(Bi_2Te_3)_3(TiTe_2)_3]$ superlattice. (*) indicates diffraction from the sample holder. Numbers above the peaks indicate the $L$ component of the Miller Indices. Because of space restrictions, only a some of the peaks are labeled. In the phase separated material (▲) and (●) indicate peaks from $Bi_2Te_3$ and $TiTe_2$ respectiviely. (#) indicates substrate peaks.

 © 2003 Wiley-VCH Verlag GmbH & Co. KGaA, Weinheim 

observed at around 8 and 13°, thus indicating the presence of small crystallites of $Bi_2Te_3$ and $TiTe_2$ respectively. With annealing, these peaks grow in intensity and split. Higher-order Bragg peaks also grow and have the greatest intensity at the angles mentioned above. This reflects increased order and growth of crystallites perpendicular to the substrate containing layers similar to those found in the respective binary compounds. Only 00*l* diffraction lines are observed indicating the crystallographically aligned nature of the resulting superlattice. The superlattice disproportionates into a mixture of the binary compounds on annealing to 300 °C, thus reflecting the metastable nature of the superlattice structure.

Rocking curve scans were collected as a function of annealing to monitor the evolution of interfacial roughness in the multilayer (from the 001 reflection) and the changes in alignment of the crystallites that are forming from the 008 and 0010 reflections (related to the layer spacing of $TiTe_2$ and $Bi_2Te_3$ respectively). The 001 rocking curve shows little change in the diffuse scattering up to 240 °C. Above this temperature, the diffuse scattering becomes more intense, which suggests that the interfacial roughness of the multilayer is increasing.[27] The full width at half max (FWHM) of both the 008 and 0010 high angle rocking curves narrow steadily from 8 and 10° respectively at 160 °C to 3.2° at 280 °C reflecting a steady increase in the alignment of the crystallites as a function of annealing temperature. The crystallite size, determined from the FWHM of the XRD patterns collected at the same annealing temperatures, increases as well.

A possible mechanism for the formation of these superlattices consistent with this diffraction data is presented in Figure 4. The broad high angle maxima in the XRD scan of the as-deposited sample (Figure 3) suggest small crystallites of both $Bi_2Te_3$ and $TiTe_2$ are present as represented in Figure 4a. After annealing at 150 °C, the increased definition of the high angle 00*l* diffraction maxima (Figure 3) reflects the developing long range order in the *c* direction and rocking curve data shows a Gaussian distribution of orientation with a width of ~9° (Figure 4b). By 240 °C, TEM studies show that most of the material in the sample has crystallized while diffraction measurements show that the particle size and degree of orientation have significantly increased (Figure 4c). Continued Ostwald ripening increases alignment and decreases defects between 240 °C and 280 °C (Figure 4d). Annealing above 300 °C induces disproportionation into $Bi_2Te_3$ and $TiTe_2$ (Figure 4e). The diffraction data resulting from the modulated nature of the precursors track the evolution of the sample with temperature and time permitting the annealing conditions to be efficiently optimized.

The formation of these XMX–XMXMX superlattices suggests that there are a multitude of kinetic products that can potentially be made by interleaving VWG compounds. Properties are more likely to be dominated by the superlattice structure because of the lack of interfacial defects, such as dangling bonds, between the components. Fortunately VWG compounds have a host of intriguing properties including superconductivity, interesting magnetic properties, and charge density waves.[4,28–30] The understanding of how properties change with superlattice structure could ultimately lead to the tuning of the macroscopic properties of a material through the control of superlattice stoichiometry and unit cell size.[31,32]

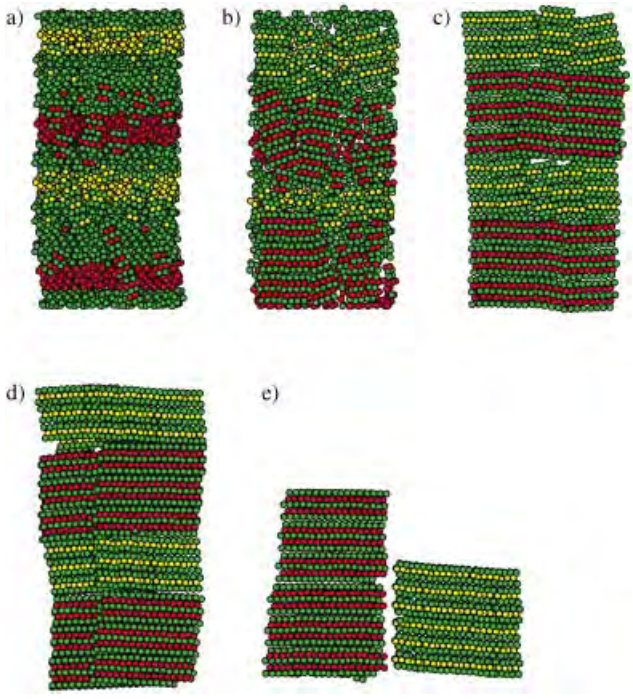



***Figure 4.*** Proposed mechanism of superlattice formation from MER. a) Shows the deposited precursor. Crystallites have begun to form. b) ~100 °C. Crystallites are growing larger and beginning to exhibit long range order. c) ~230 °C. Most of the material has crystalized. d) 240–300 °C Grains continue to grow by Ostwald ripening. e) >300 °C The superlattice dissociates into its constitutes.

Received: April 23, 2003
Revised: September 12, 2003 [Z51724]
Published Online: October 22, 2003

**Keywords:** crystal growth · layered compounds · nanostructures · superlattices · thin films

[1] F. J. DiSalvo, *Pure Appl. Chem.* **2000**, *72*, 1799.
[2] F. J. DiSalvo, *Science* **1990**, *247*, 649.
[3] J. C. Schön, M. Jansen, *Angew. Chem.* **1996**, *108*, 1358–1377; *Angew. Chem. Int. Ed. Engl.* **1996**, *35*, 1286–1304.
[4] R. H. Friend, A. D. Yoffe, *Adv. Phys.* **1987**, *36*, 1.
[5] A. F. Wells, *Structural Inorganic Chemistry. 5th Ed*, **1983**.
[6] M. Bernasconi, G. L. Marra, G. Benedek, L. Miglio, M. Jouanne, C. Julien, M. Scagliotti, M. Balkanski *Phys. Rev. B* **1988**, *38*, 12089.
[7] R. Brec, G. Ouvrard, J. Rouxel, *Mater. Res. Bull.* **1985**, *20*, 1257.
[8] G. Ouvrard, R. Brec, J. Rouxel, *Mater. Res. Bull.* **1985**, *20*, 1181.
[9] F. Hulliger, *Physics and Chemistry of Materials With Layered Structures, Vol. 5: Structural Chemistry of Layer-Type Phases*, **1976**.
[10] M. A. Wahab, G. C. Trigunayat, *Solid State Commun.* **1980**, *36*, 885.
[11] T. Shimada, Y. Furukawa, E. Arakawa, K. Takeshita, T. Matsushita, H. Yamamoto, A. Koma, *Solid State Commun.* **1994**, *89*, 583.
[12] T. Shimada, H. Nishikawa, A. Koma, Y. Furukawa, E. Arakawa, K. Takeshita, T. Matsushita, *Surf. Sci.* **1996**, *369*, 379.

 © 2003 Wiley-VCH Verlag GmbH & Co. KGaA, Weinheim 

[13] A. Meerschaut, C. Deudon, *Mater. Res. Bull.* **2001**, *36*, 1721.
[14] T. Ueno, H. Yamamoto, K. Saiki, A. Koma, *Appl. Surf. Sci.* **1997**, *113–114*, 33.
[15] M. Noh, Ph. D. thesis, University of Oregon (Eugene, OR), **1997**.
[16] R. Venkatasubramanian, E. Slivola, T. Colpitts, B. O′Quinn, *Nature* **2001**, *413*, 597.
[17] D. R. Lovett, *Semimetals and Narrow-Bandgap Semiconductors*, **1977**.
[18] D. K. G. De Boer, C. F. Van Bruggen, G. W. Bus, R. Coehoorn, C. Haas, G. A. Sawatzky, H. W. Myron, D. Norman, H. Padmore *Phys. Rev. B* **1984**, *29*, 6797.
[19] R. Claessen, R. O. Anderson, G. H. Gweon, J. W. Allen, W. P. Ellis, C. Janowitz, C. G. Olson, Z. X. Shen, V. Eyert, M. Skibowski, K. Friemelt, E. Bucher, S. Hüfner *Phys. Rev. B* **1996**, *54*, 2453.
[20] M. Noh, J. Thiel, D. C. Johnson, *Mater. Res. Soc. Symp. Proc.* **1995**, *382*, 71.
[21] M. Noh, C. D. Johnson, M. D. Hornbostel, J. Thiel, D. C. Johnson, *Chem. Mater.* **1996**, *8*, 1625.
[22] R. Venkatasubramanian, T. Colpitts, in *Thermoelectric Materials-New Directions and Approaches, Vol. 478* (Eds.: T. M. Tritt, M. G. Kanatzidis, J. Hylan B. Lyon, G. D. Mahan), Materials Research Society, San Francisco, California, **1997**, pp. 73.
[23] A. Stein, S. W. Keller, T. E. Mallouk, *Science* **1993**, *259*, 1558.
[24] M. Stordeur, *CRC Handb. Thermoelectr.* **1995**, 239.
[25] Y. Arnaud, M. Chevreton, *J. Solid State Chem.* **1981**, *39*, 230.
[26] The Rietveld analysis for $[(Bi_2Te_3)_x(TiTe_2)_x]$ ($x = 3, 4, 5, 6$) can be found in the Supporting Information.
[27] D. K. G. de Boer, A. J. G. Leenaers, *Phys. B* **1996**, *221*, 18.
[28] J. A. Wilson, F. J. Di Salvo, S. Mahajan, *Adv. Phys.* **1975**, *24*, 117.
[29] E. A. Marseglia, *Int. Rev. Phys. Chem.* **1983**, *3*, 177.
[30] W. Y. Liang, *NATO Adv. Study Inst. Ser. Ser. B* **1986**, *148*, 31.
[31] F. J. DiSalvo, in *Advancing Materials Research* (Eds.: P. A. Psaras, H. D. Langford), National Academy Press, Washington, D. C., **1987**, pp. 161.
[32] M. Cohen, in *Advancing Materials Research* (Eds.: P. A. Psaras, H. D. Langford), National Academy Press, Washington, D. C., **1987**, pp. 51.

 © 2003 Wiley-VCH Verlag GmbH & Co. KGaA, Weinheim 

*Patterned $CaCO_3$*

# Self-Organized Calcium Carbonate with Regular Surface-Relief Structures**

*Ayae Sugawara, Takeshi Ishii, and Takashi Kato**

Organisms produce complex nanostructures consisting of inorganic and organic components. These materials called biominerals form a variety of self-organized and hierarchical structures.[1,2] Calcium carbonate ($CaCO_3$) is one of the most abundant biominerals formed by organisms. $CaCO_3$-based biominerals such as nacre of mollusk shells and coccoliths have complex structures on submicrometer length scales. However, it is not easy to synthesize such elaborate structures in artificial systems. In biomineralization processes, organic matrices interacting with inorganic components play key roles in forming controlled structures. Synthetic approaches to a morphological control of $CaCO_3$ by using organic templates and/or additives led to the formation of a variety of shapes such as hollow spheres,[3] hollow porous spheres,[4] spherules with complex surface structures,[5] sponge-like structures,[6] thin films,[7–9] and helices.[9a] Micropatterning of $CaCO_3$ crystals was achieved by using template-directed systems.[10] Such bioinspired self-organization processes may result in the fabrication of highly functionalized and environmentally friendly materials.[2,11] Our strategy is to obtain $CaCO_3$-based functional composites with self-organized ordered structures by tuning the chemical structures of organic matrices.

Herein we report novel $CaCO_3$ composites with regular surface-relief structures, which have never been seen in natural biominerals nor synthetic materials based on $CaCO_3$. These self-organized $CaCO_3$ crystals with submicrometer-scale periodicity are formed from solution on the thin matrix of a hydrophobically modified polysaccharide in the presence of poly(acrylic acid) (PAA).

We previously reported that $CaCO_3$ thin films with smooth surfaces were formed by the cooperation of solid natural polysaccharides and acidic polymers.[7] We used chitin,

[*] Prof. Dr. T. Kato, A. Sugawara, T. Ishii
Department of Chemistry and Biotechnology
School of Engineering
The University of Tokyo
Hongo, Bunkyo-ku, Tokyo 113-8656 (Japan)
Fax: (+81) 3-5841-8661
E-mail: kato@chiral.t.u-tokyo.ac.jp

[**] This study was partially supported by Grant-in-aid for the 21st Century COE Program for Frontiers in Fundamental Chemistry (TK and AS) and Grant-in-aid for Exploratory Research (15655038) (TK) from the Ministry of Education, Culture, Sports, Science and Technology. Partial financial support of the Sasakawa Scientific Research Grant from the Japan Science Society (AS) is also acknowledged. We thank Prof. Dr. J. Sunamoto and Prof. Dr. K. Akiyoshi for valuable scientific discussions. We also thank Drs. H. Tsunakawa and C. Iwamoto for assistance in TEM observation.

Supporting information for this article is available on the WWW under http://www.angewandte.org or from the author.

 DOI: 10.1002/anie.200351541 © 2003 Wiley-VCH Verlag GmbH & Co. KGaA, Weinheim 

chitosan, and cellulose as thin film matrices. They are insoluble in water and provide solid surfaces for $CaCO_3$ crystallization. On the other hand, biominerals are often formed on soft surfaces such as lipid bilayers.[1a,b] We expected that the use of soft surfaces such as polymer gels is more effective for the morphological control of $CaCO_3$ because they can interact with inorganic components more easily. We have chosen cholesterol-bearing pullulans[12] as soft gel matrices for $CaCO_3$ crystallization (Figure 1). Pullulans are known to form hydrogels in water; these hydrogels form because of the association of the cholesteryl groups that function as physical cross-linking points.[12b,c] The formation of stable hydrogels was expected because of the high hydrophobicity of the cholesterol.

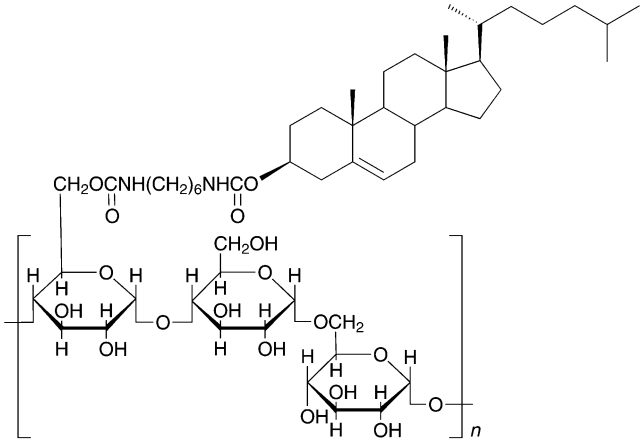



***Figure 1.*** Structure of cholesterol-bearing pullulans (CHPs).

Pullulans that have three and eight cholesteryl groups per 100 glucose units (CHP-3 and CHP-8) were synthesized. These CHPs were spin coated on glass substrates to give thin matrices for crystallization. They were then immersed in aqueous solutions of calcium chloride ($[Ca^{2+}] = 10$ mM) containing PAA. $CaCO_3$ crystallization was induced by the slow diffusion of ammonium carbonate vapor into calcium chloride solution for two days.[13]

Surprisingly, $CaCO_3$ films with periodic surface-relief structures developed on the CHP-3 matrix in the presence of PAA ($2.4 \times 10^{-3}$ wt%) at 20°C, as shown in the scanning electron microscopy (SEM) images (Figure 2a–e). The average distance between grooves is about 800 nm over the whole region of the patterned crystals and the height of the surface-relief structures is about 300 nm, as revealed by atomic force microscopy (AFM) (Figure 3). Since such relief structures function as diffraction gratings, the crystals appear to be iridescent (see Supporting Information).

The crystallization of $CaCO_3$ starts from multiple nucleation sites on the surface of the CHP-3 matrix. Figure 2a shows an area around a starting point of crystallization. In the initial stage of crystal growth, a bow-tie-shaped crystal is formed as shown in the inset of Figure 2a. The periodically patterned crystals then develop outwards on the CHP-3 matrix until they collide with each other (Figure 2b).

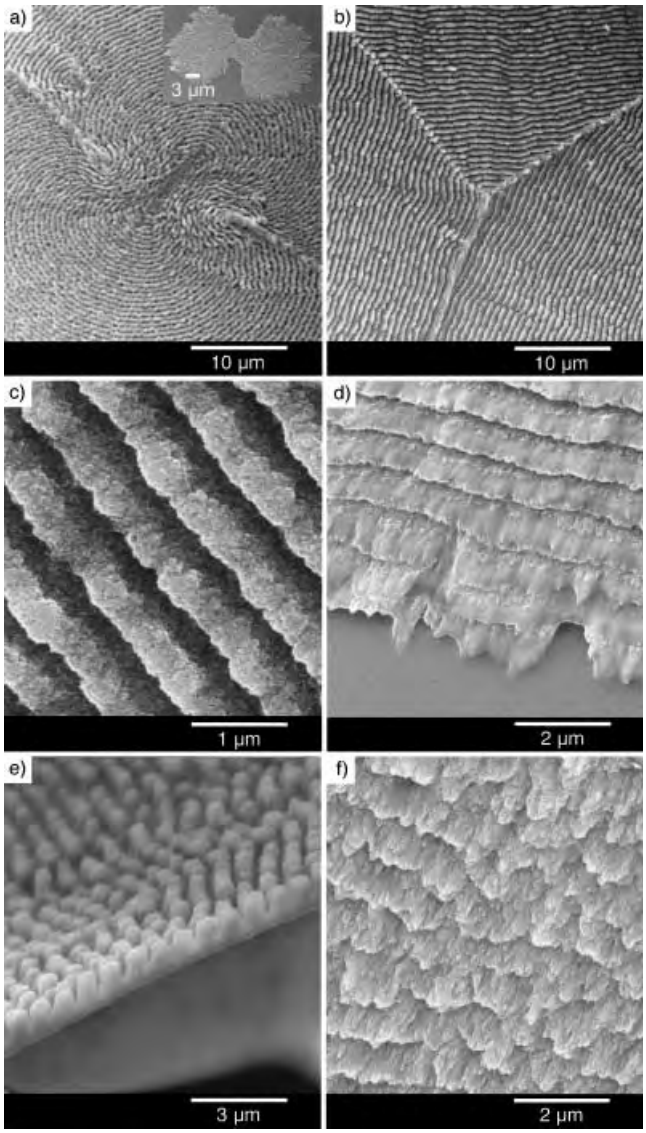



***Figure 2.*** SEM images of patterned $CaCO_3$ crystals grown on CHP-3 matrices, 20°C, 2 d, in the presence of PAA: a–e) $2.4 \times 10^{-3}$ wt% and f) $5.0 \times 10^{-3}$ wt%. a) An area around a starting point of crystallization (inset: $CaCO_3$ crystals obtained in the initial stage of crystal growth, 14 h); b) a boundary among patterned films; c) a magnified image; d) a front of patterned crystals; e) a cross-sectional image.

Figure 2c shows a magnified image of the patterned crystals. They are composed of calcite particles of about 30 nm in size.[14] At the front of the patterned crystals, we see needle-like crystals (Figure 2d), which are covered with nanoparticles composed of mature patterned structures. Electron diffraction analyses of the patterned crystals indicate that they are locally oriented polycrystalline calcite, although the overall crystallographic orientation is not unidirectional (see Supporting Information). A cross-sectional image of the fractured thin film crystals clearly demonstrates the formation of regular relief structure (Figure 2e), while the other side facing the CHP-3 matrix is smooth.

The regularity of the surface-relief structure of $CaCO_3$ is influenced by the concentration of PAA. The best concentration for the development of the regularly patterned crystals

 © 2003 Wiley-VCH Verlag GmbH & Co. KGaA, Weinheim 

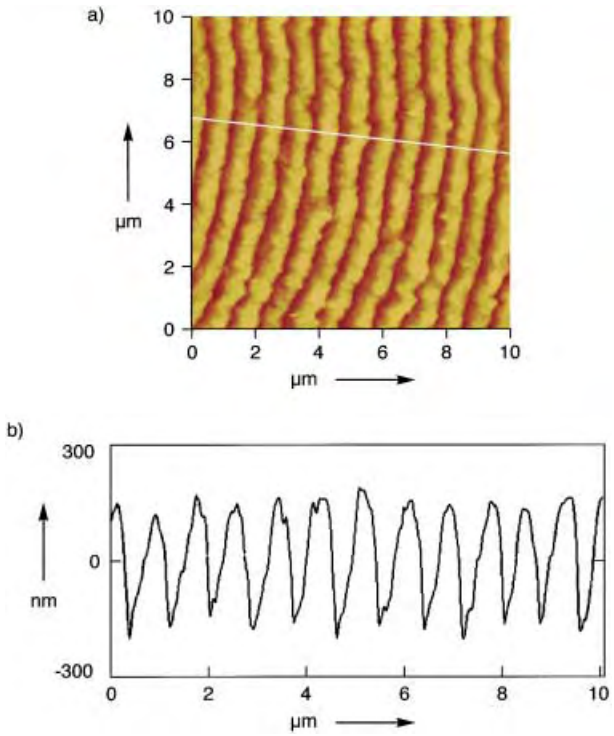



***Figure 3.*** AFM images of patterned $CaCO_3$ crystals developed on the CHP-3 matrix in the presence of PAA ($2.4\times10^{-3}$ wt%), 20°C, 2 d: a) top down view; b) cross-sectional image of the white line region depicted in (a).

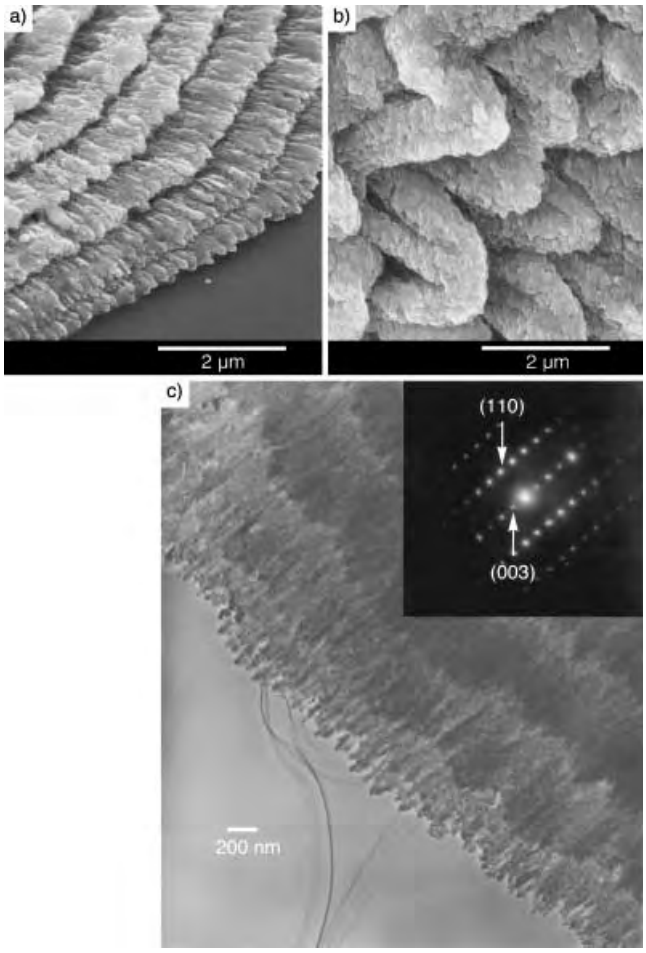



***Figure 4.*** Effects of crystallization temperature. a,b) SEM images of $CaCO_3$ crystals grown on the CHP-3 matrices in the presence of PAA ($2.4\times10^{-3}$ wt%): a) 10°C, 2 days; b) 50°C, 4 h. c) TEM image of the patterned $CaCO_3$ crystals grown on the CHP-3 matrix in the presence of PAA ($2.4\times10^{-3}$ wt%), 10°C, 2 days. The inset shows a selected-area diffraction pattern corresponds to the needlelike crystals. The crystals show the preferential orientation growth in length along the *c* axis of calcite.

is around $2.5\times10^{-3}$ wt%. Less-ordered structures are deposited when the concentration of PAA increases as shown in Figure 2f (PAA concentration: $5.0\times10^{-3}$ wt%). For higher concentrations (more than $6.0\times10^{-3}$ wt%), no crystals are obtained because of the inhibiting effect of PAA,[7b] whereas for lower concentrations of PAA (less than $1.0\times10^{-4}$ wt%), rhombohedral crystals of calcite and aggregated crystals of vaterite are formed on the matrix.

The crystallization temperature greatly affects the morphology of the patterned crystals. Figure 4a and b shows the surfaces of $CaCO_3$ films crystallized at 10 and 50°C, respectively. At 10°C, needlelike crystals of calcite that are preferentially oriented in the crystallographic *c* axis are grown (Figure 4c). However, the deposition of thin film crystals on the matrix is sporadic owing to the higher solubility of $CaCO_3$ at lower temperatures. At 50°C, random corrugations are formed on the surface of the calcite films (Figure 4b). The formation of this random structure may be attributed to the rapid crystallization at higher temperatures because of the increase of the sublimation rate of ammonium carbonate and the lower solubility of $CaCO_3$.[15]

The proper degree of substitution in the matrix is important for the periodic pattern formation. When more hydrophobically modified pullulan CHP-8 (containing eight cholesteryl moieties per 100 glucose units) is used as a matrix in place of CHP-3, $CaCO_3$ films with less regular surfaces are developed on the CHP-8 matrix in the presence of PAA at 20°C (see Supporting Information). Unmodified pullulan does not function as a thin film matrix because it is soluble in water. The presence of the unmodified pullulan in solution has no effect on crystallization; rhombohedral crystals of calcite and aggregated crystals of vaterite are formed in the presence of unmodified pullulan without PAA. In the presence of both unmodified pullulan and PAA ($2.4\times10^{-3}$ wt%), crystallization is inhibited.

It is difficult to fully understand the mechanism of the formation of the patterned crystals. We assume that the periodic pattern formation in the present study belongs to a self-organization process in the reaction-diffusion systems,[16,17] in which competition between precipitation and ion diffusion occurs. Such behavior is usually observed in gel media.[17] In the present material, the pullulan matrix is swollen with a calcium chloride solution to form the hydrogel as a result of the association of the cholesteryl group.[12b,c] When the CHP matrix is placed in a solution containing PAA, PAA may be adsorbed on the surface and incorporated into the matrix through the interaction between the CHP and PAA (see Supporting Information). The interaction of PAA

 © 2003 Wiley-VCH Verlag GmbH & Co. KGaA, Weinheim 

with calcium ions leads to a high local concentration of calcium ions in/on the matrix. When the calcium ions react with carbonate ions, the deposition of $CaCO_3$ occurs. These reactions induce a rapid decrease of ion concentration. The deposition is no longer sustained owing to the lack of ions because efficient ion transport to the reaction sites is prevented by the influence of the gel matrix. After some time, the high ion concentration recovers and the $CaCO_3$ is deposited once more. The cycling of these processes may result in the pattern generation.

The SEM image of the CHP matrix obtained after the dissolution of $CaCO_3$ grown on the matrix shows that the periodic pattern formation of $CaCO_3$ accompanies the deformation of the CHP matrix (see Supporting Information). One possible explanation on this behavior is that the transformation from amorphous to crystalline states that accompanies the matrix deformation occurs after patterned amorphous $CaCO_3$ is deposited (Figure 2d, and Supporting Information). Amorphous-to-crystalline transformation was often observed in the presence of acidic polymers.[8b,9b,18] Aizenberg and co-workers reported that micropatterned substrate-induced millimeter-sized single calcite crystals were a consequence of a relaxation of the tensile stress of the crystals on transforming from amorphous to crystalline states.[10d] This effect suggests the existence of a relationships between the formation of the crystals and tensile stress. In our system, the transformation the tensile stress of the crystals, which is increased by the transformation from amorphous to crystalline states, is relaxed, thus leading to the enhancement of the patterns formed in the amorphous states of $CaCO_3$.

In conclusion, we have succeeded in preparing periodically patterned calcium carbonate films for the first time. These self-organized $CaCO_3$ films with regular surface-relief structures are formed on the thin matrix of cholesterol-modified pullulan from an aqueous solution containing poly(acrylic acid). Such spontaneous pattern generation with remarkable regularity in the submicrometer length scale is unusual, even in other materials. The use of organic matrices in the fabrication of hybrid materials offers the potential to control structures in simple and mild synthetic conditions.

## Experimental Section

Cholesterol-bearing pullulans (CHPs) were synthesized according to literature procedures.[12a] Details can be found in the Supporting Information. CHP matrices were prepared by spin coating of their 2 wt% DMSO solution on glass substrates. They were annealed for 1 h at 180 °C to remove the solvent.

Purified water obtained from an Auto pure WT100 purification system (Yamato, relative resistivity: maximum $1.8\times10^7\,\Omega\,cm$) was employed for the crystallization of calcium carbonate. Poly(acrylic acid) ($\bar{M}_w = 2{,}000$) was added to calcium chloride aqueous solution ($[Ca^{2+}] = 10$ mM). The solution was transferred to vessels containing CHP matrices. The vessels were then placed in a closed desiccator together with a vial of ammonium carbonate.[13] An incubator (Fukushima) was used to maintain a constant crystallization temperature (10–50 °C). The pH value of the solution increased from 4.3 to 9.1 during the crystallization experiment.

SEM images were obtained using a Hitachi S-900S field-emission SEM operated at 5–10 kV. Samples were platinum coated by using a Hitachi E-1030 ion sputter. TEM images were taken with a JEOL JEM-4000FXII at 400 kV. AFM measurements were carried out by a Digital Instruments Nanoscope III system with standard Si tips. Fourier transform infrared spectra were recorded on a Jasco FT/IR-660Plus spectrometer using KBr pellet.

Received: April 1, 2003
Revised: August 12, 2003 [Z51541]

**Keywords:** biomineralization · crystal growth · materials science · self-organization

[1] a) S. Mann in *Biomineralization* (Eds: R. G. Compton, S. G. Davies, J. Evans), Oxford University Press, Oxford, **2001**; b) L. Addadi, S. Weiner, *Angew. Chem.* **1992**, *104*, 159–176; *Angew. Chem. Int. Ed. Engl.* **1992**, *31*, 153–169; c) S. V. Dorozhkin, M. Epple, *Angew. Chem.* **2002**, *114*, 3260–3277; *Angew. Chem. Int. Ed.* **2002**, *41*, 3130–3146.

[2] a) S. Mann, G. A. Ozin, *Nature* **1996**, *382*, 313–318; b) G. A. Ozin, *Acc. Chem. Res.* **1997**, *30*, 17–27.

[3] a) H. Cölfen, M. Antonietti, *Langmuir* **1998**, *14*, 582–589; b) L. Qi, J. Li, J. Ma, *Adv. Mater.* **2002**, *14*, 300–303.

[4] D. Walsh, S. Mann, *Nature* **1995**, *377*, 320–323.

[5] a) S.-H. Yu, H. Cölfen, J. Hartmann, M. Antonietti, *Adv. Funct. Mater.* **2002**, *12*, 541–545; b) J. Küther, R. Seshadri, W. Tremel, *Angew. Chem.* **1998**, *110*, 3196–3199; *Angew. Chem. Int. Ed.* **1998**, *37*, 3044–3047.

[6] a) D. Walsh, B. Lebeau, S. Mann, *Adv. Mater.* **1999**, *11*, 324–328; b) R. J. Park, F. C. Meldrum, *Adv. Mater.* **2002**, *14*, 1167–1169.

[7] a) T. Kato, *Adv. Mater.* **2000**, *12*, 1543–1546; b) T. Kato, T. Suzuki, T. Amamiya, T. Irie, M. Komiyama, H. Yui, *Supramol. Sci.* **1998**, *5*, 411–415; c) T. Kato, T. Suzuki, T. Irie, *Chem. Lett.* **2000**, 186–187; d) A. Sugawara, T. Kato, *Chem. Commun.* **2000**, 487–488; e) N. Hosoda, T. Kato, *Chem. Mater.* **2001**, *13*, 688–693.

[8] a) S. Zhang, K. E. Gonsalves, *Langmuir* **1998**, *14*, 6761–6766; b) G. Xu, N. Yao, I. A. Aksay, J. T. Groves, *J. Am. Chem. Soc.* **1998**, *120*, 11977–11985.

[9] a) L. A. Gower, D. A. Tirrell, *J. Cryst. Growth* **1998**, *191*, 153–160; b) L. B. Gower, D. J. Odom, *J. Cryst. Growth* **2000**, *210*, 719–734.

[10] a) J. Aizenberg, A. J. Black, G. M. Whitesides, *Nature* **1999**, *398*, 495–498; b) J. Aizenberg, A. J. Black, G. M. Whitesides, *J. Am. Chem. Soc.* **1999**, *121*, 4500–4509; c) J. Aizenberg, *J. Cryst. Growth* **2000**, *211*, 143–148; d) J. Aizenberg, D. A. Muller, J. L. Grazul, D. R. Hamann, *Science* **2003**, *299*, 1205–1208.

[11] a) E. Dujardin, S. Mann, *Adv. Mater.* **2002**, *14*, 775–788; b) T. Kato, A. Sugawara, N. Hosoda, *Adv. Mater.* **2002**, *14*, 869–877; c) S. I. Stupp, P. V. Braun, *Science* **1997**, *277*, 1242–1248; d) K. J. C. van Bommel, A. Friggeri, S. Shinkai, *Angew. Chem.* **2003**, *115*, 1010–1030; *Angew. Chem. Int. Ed.* **2003**, *42*, 980–999.

[12] a) K. Akiyoshi, S. Deguchi, N. Moriguchi, S. Yamaguchi, J. Sunamoto, *Macromolecules* **1993**, *26*, 3062–3068; b) K. Akiyoshi, S. Deguchi, H. Tajima, T. Nishikawa, J. Sunamoto, *Macromolecules* **1997**, *30*, 857–861; c) K. Kuroda, K. Fujimoto, J. Sunamoto, K. Akiyoshi, *Langmuir* **2002**, *18*, 3780–3786.

[13] G. Falini, S. Albeck, S. Weiner, L. Addadi, *Science* **1996**, *271*, 67–69.

[14] The Fourier transform infrared spectrum of the patterned crystals shows sharp bands at 875 and 714 $cm^{-1}$, which are characteristic of calcite. No other bands for aragonite, vaterite, and amorphous calcium carbonate are detected.

[15] The sublimation rates of ammonium carbonate in our experimental system at 10 °C, 20 °C, and 50 °C are about $6.3\times10^{-2}$ $mmol\,h^{-1}$, $7.1\times10^{-2}$ $mmol\,h^{-1}$, and $7.8\times10^{-1}$ $mmol\,h^{-1}$, respectively.

 © 2003 Wiley-VCH Verlag GmbH & Co. KGaA, Weinheim 

[16] a) G. M. Whitesides, B. Grzybowski, *Science* **2002**, *295*, 2418 – 2421; b) K. Iwamoto, S. Mitomo, M. Seno, *J. Colloid Interface Sci.* **1984**, *102*, 477 – 482; c) M. Tsapatsis, D. G. Vlachos, S. Kim, H. Ramanan, G. R. Gavalas, *J. Am. Chem. Soc.* **2000**, *122*, 12 864 – 12 865.
[17] a) H. K. Henisch in *Crystals in Gels and Liesegang Rings*, Cambridge University Press, Cambridge, **1988**; b) H.-J. Krug, H. Brandtstädter, *J. Phys. Chem. A* **1999**, *103*, 7811 – 7820.
[18] a) Y. Levi-Kalisman, S. Raz, S. Weiner, L. Addadi, I. Sagi, *Adv. Funct. Mater.* **2002**, *12*, 43 – 48; b) L. Addadi, S. Raz, S. Weiner, *Adv. Mater.* **2003**, *15*, 959 – 970.

 © 2003 Wiley-VCH Verlag GmbH & Co. KGaA, Weinheim 

*Topotactic Reactions in Networks*

# Designing Permeable Molecular Crystals That React with External Agents To Give Crystalline Products**

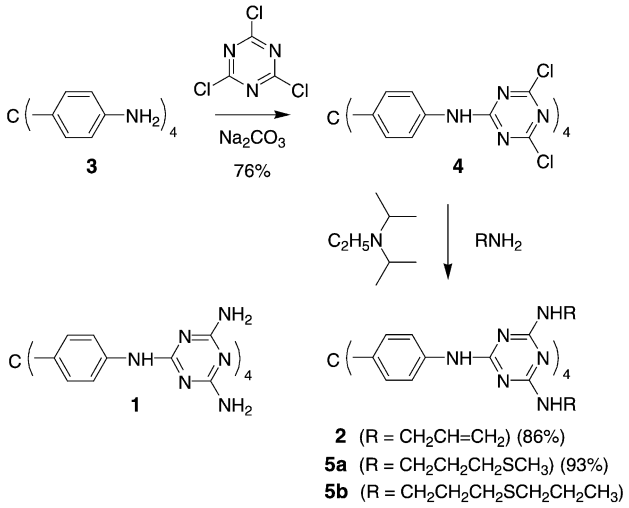
*Philippe Brunet, Eric Demers, Thierry Maris, Gary D. Enright, and James D. Wuest**

Topotactic reactions,[1] which convert single crystals of starting compounds directly into single crystals of products, are elegant and potentially useful processes that have fascinated solid-state chemists for many years. Unfortunately, such reactions are very rare. Mobility in solids is restricted, so known topotactic reactions in molecular crystals typically involve intramolecular processes or require that all necessary co-reactants be present within the solid, held in close proximity, and oriented properly.[2,3] These prerequisites can sometimes be satisfied by laborious crystal engineering, but new ways to devise topotactic reactions are needed. Here we describe a general strategy based on the use of permeable molecular crystals that are specifically designed to let external agents enter, react, and produce single crystals of new substances, with retention of the original crystalline architecture. Moreover, we show that such topotactic processes can be made to cross-link molecular crystals covalently, thereby capturing temporary supramolecular constructs as permanent crystalline macromolecular replicas.

Our strategy is related to the technique of isomorphous replacement in protein crystallography, a largely empirical process in which protein crystals are treated with agents that diffuse though water-filled channels in the crystal and bind at sites not normally determined in advance. We felt that single crystals of much smaller molecules might be made to react quantitatively with external agents at predetermined sites, thus providing a rational route to new substances in crystalline form. At present, such reactions are exceedingly rare, have been discovered by accident rather than by design, and involve only the smallest possible reactants.[3,4]

Suitable permeable molecular crystals can be made by an approach that has been called molecular tectonics.[5] This approach relies on the programmed association of special sticky molecules called tectons (derived from the Greek word for builder) that form directional interactions with neighbors according to well-established motifs. Such molecules do not typically crystallize in normal close-packed arrays; instead, they tend to form open networks filled with potentially mobile guests.[6] Tectonic networks held together by multiple hydrogen bonds are normally robust enough to allow the original guests to be exchanged or even partially removed without the loss of crystallinity, which renders their interiors accessible to various reagents.[7]

Initial experiments showed that in the porous hydrogen-bonded network formed by tecton **1** (Scheme 1), -$NH_2$ groups not used in intertectonic hydrogen bonding lie in guest-filled channels.[8] We reasoned that -NHR groups in substituted derivatives would be located similarly, thus making the substituents accessible to external agents. To test this hypothesis, we synthesized octaallyl derivative **2** by the route summarized in Scheme 1. X-ray diffraction established that tecton **2** crystallizes from dioxane in the tetragonal space




***Scheme 1.*** Tecton **1** and the synthesis of tectons **2** and **5a** in solution.

[*] Prof. J. D. Wuest, Dr. P. Brunet, E. Demers, Dr. T. Maris
Département de Chimie
Université de Montréal
Montréal, Québec H3C 3J7 (Canada)
Fax: (+1) 514-343-6281
E-mail: wuest@chimie.umontreal.ca
Dr. G. D. Enright
Steacie Institute for Molecular Sciences
National Research Council
Ottawa, Ontario K1A 0R6 (Canada)

[**] We thank Drs. James F. Britten and Michel Simard for preliminary crystallographic studies, Marjolaine Arseneault for her help in obtaining Raman spectra, and Prof. Denis Gravel for his expertise in photochemistry. We are grateful to the Natural Sciences and Engineering Research Council of Canada, the Ministère de l'Éducation du Québec, the Canada Research Chairs Program, and the Canada Foundation for Innovation for financial support. Cover picture illustration courtesy of Christian Gravel (Université de Montréal).

Supporting information for this article is available on the WWW under http://www.angewandte.org or from the author.

 DOI: 10.1002/anie.200352252 © 2003 Wiley-VCH Verlag GmbH & Co. KGaA, Weinheim 

group $I4_1/a$ to give the network represented by Figures 1 and 2. Each tecton forms a total of 16 hydrogen bonds with four neighbors, which results in a robust noninterpenetrated network with diamondoid connectivity.[9,10]

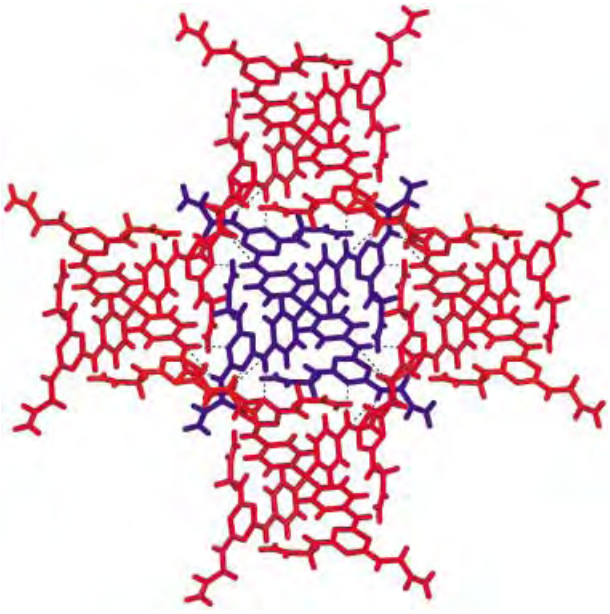


***Figure 1.*** View along the *c* axis of the crystal structure of tecton **2** showing a single tecton (blue) and the four neighbors (red) with which it forms hydrogen bonds (-----).

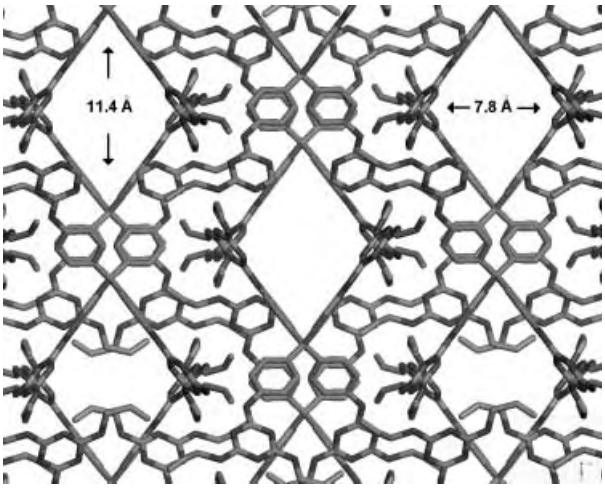



***Figure 2.*** View along the *b* axis of the crystal structure of tecton **2** showing the cross sections of helical channels. Hydrogen atoms and some allyl groups (upper channels) have been removed for clarity.

Dioxane occupies nearly 40% of the volume of the crystals,[11,12] which have the composition **2**·6 dioxane, as determined by X-ray crystallography and $^1$H NMR spectroscopy of dissolved samples. The guests fill interconnected helical channels that have a rhomboid cross section of approximately $7.8 \times 11.4$ Å$^2$ at the narrowest points (Figure 2). The channels themselves are represented by the surface shown in Figure 3.[13] In principle, guests diffusing inside the crystals can reach any point within the channels by multiple redundant pathways. As planned, the channels also include the allyl groups of tecton **2**.

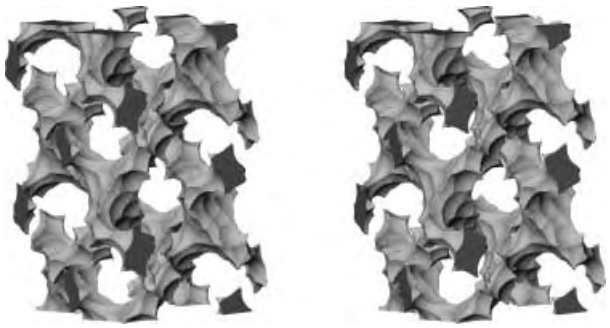


***Figure 3.*** Stereoscopic representation of the channels in the structure of tecton **2**.[13] The image shows a $1 \times 1 \times 2$ array of unit cells with the *c* axis vertical. The outsides of the channels appear in light gray, and dark gray is used to show where the channels are cut by the boundaries of the array. The surface is defined by the possible loci of the center of a sphere of diameter 3 Å as it rolls over the surface of the ordered tectonic network.

When single crystals of tecton **2**·6 dioxane of dimensions $0.5 \times 0.5 \times 0.5$ mm were treated with excess toluene at 25 °C for 24 h, they remained transparent and morphologically unchanged, continued to exhibit uniform extinction between crossed polarizers, and showed closely similar unit-cell parameters when studied by single-crystal X-ray diffraction. However, analysis of dissolved samples by $^1$H NMR spectroscopy established that the initial guest, dioxane, had been replaced completely by toluene. As a result, these crystals are well designed to allow a suitable reagent to enter by diffusion and react predictably with the exposed allyl groups without changing the architecture of the network, thereby yielding isostructural crystals of a new substance.

This possibility was tested by placing single crystals of tecton **2** in degassed toluene in a quartz vessel, then exposing them to $CH_3SH$ and irradiating them with a medium-pressure Hg lamp at 25 °C for 40 h. Under these conditions, photochemical solid-state addition of thiol to the allyl groups occurred to give thioether **5a**,[14,15] in which 70–85% of the allyl groups had reacted, as measured by $^1$H NMR spectroscopy of dissolved samples. Moreover, the process proved to be topotactic. The resulting crystals were morphologically unchanged, remained transparent, and continued to exhibit uniform extinction between crossed polarizers. X-ray diffraction confirmed that thioether **5a** had been formed isostructurally as single crystals belonging to the tetragonal space group $I4_1/a$, with unit-cell parameters similar ($\pm 9\%$) to those of precursor **2**.

A larger thiol ($CH_3CH_2CH_2SH$) also reacted topotactically in high yield with crystals of tecton **2** to give isostructural single crystals of thioether **5b** with similar ($\pm 2\%$) unit-cell parameters. In contrast, thiols that were too large to enter the channels in crystals of tecton **2** reacted negligibly under similar conditions, presumably because only the surfaces of

 © 2003 Wiley-VCH Verlag GmbH & Co. KGaA, Weinheim 

the crystals are accessible. For example, photochemical additions of 3,5-dimethylbenzenethiol and 2,4,6-trimethylbenzylthiol proceeded only to the extent of ≈3%. Such control experiments established that the observed solid-state photochemical additions to tecton **2** do not occur by a sequence of dissolution, reaction in solution, and subsequent recrystallization. The mass spectrum of thioether **5a** obtained topotactically showed the expected statistical distribution of molecules with reacted and unreacted allyl groups, which suggests that addition occurs relatively homogeneously throughout the crystal. A bimodal distribution, which would arise if addition occurred exclusively near the surface to leave an unreacted core, was not observed.

A sample of thioether **5a** prepared independently in solution by treating intermediate **4** (Scheme 1) with 3-methylthio-1-propanamine could be crystallized from $CH_3OH$/THF. In this case, the structure proved to be the same as the one obtained topotactically in the solid state. In other cases, however, we expect new polymorphs to be formed. Our strategy for devising topotactic reactions in porous crystals has two notable advantages: 1) It delivers single crystals of new compounds in polymorphic forms that are predetermined, based on the structure of the starting material, and 2) these polymorphs may be impossible to obtain by direct crystallization of the product, either because other polymorphs are favored or because crystallization does not occur at all.

A long-sought goal in supramolecular chemistry is covalent capture,[16] in which ordered structures formed reversibly by self-assembly are converted into analogues joined permanently by covalent bonds. Molecular tectonics allows predictable covalent capture to occur in the solid state by using permeable crystals with internally exposed reactive groups that can be cross-linked by external agents. This strategy extends conceptually related polymerizations, such as the cross-linking of porous protein crystals[17] and coordination complexes joined by metals,[18] to the realm of small molecular monomers and the production of single crystals of well-defined polymers.[19]

Single crystals of tecton **2**·6 dioxane were exposed to a series of liquid dithiols $HS(CH_2)_nSH$ and irradiated under standard conditions. The resulting materials proved to be insoluble in DMSO, hot aqueous HCl, and $CF_3COOH$, even after crushing to expose internal surfaces. This result indicates that extensive cross-linking had taken place. When $HSCH_2CH_2SH$ was used as the cross-linker, detailed studies of the resulting polymer by solid-state $^{13}C$ NMR spectroscopy and Raman spectroscopy confirmed the addition of the thiol to the allyl groups.[20] Remarkably, cross-linking of crystals of tecton **2** by both $HSCH_2CH_2SH$ and $HSCH_2CH_2CH_2SH$ occurred topotactically to give isostructural single crystals of the macromolecular products. Detailed single-crystal X-ray crystallographic analysis of the products confirmed directly that cross-linking had occurred and showed that each molecule of tecton **2** becomes joined not to its immediate hydrogen-bonded neighbors but to those somewhat farther away (Figure 4).

Despite close architectural similarity, the covalently cross-linked materials are vastly more stable than their hydrogen-bonded supramolecular precursor. In particular, variable-temperature X-ray powder diffraction established that the polymer derived from $HSCH_2CH_2SH$ loses its crystallinity only when it decomposes irreversibly above 200 °C, whereas the precursor loses crystallinity at 25 °C by spontaneous loss of included solvent. The topotactic cross-linking we observe in single crystals of tecton **2** has two unique characteristics: 1) Polymerization occurs in three dimensions to give a single crystalline macromolecular object, and 2) the composition of the product crystals is different from that of the starting crystals. In contrast, previously observed topotactic polymerizations have occurred in one direction to yield crystals with the same composition consisting of multiple copies of linear macromolecules.[2]

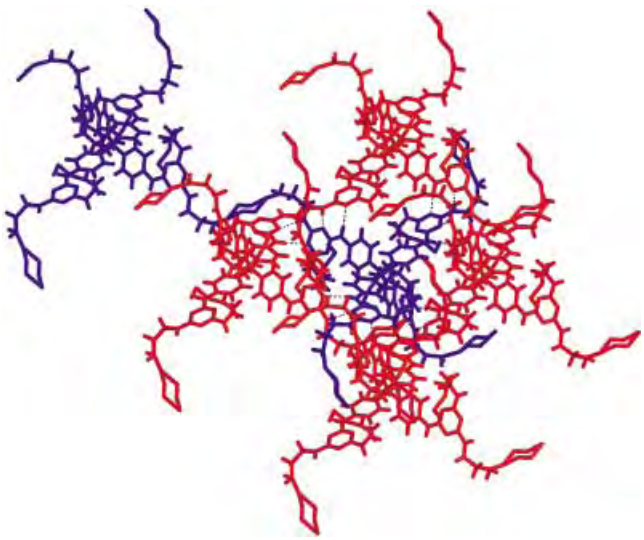


***Figure 4.*** Structure of the macromolecule obtained by cross-linking crystals of tecton **2** with $HSCH_2CH_2SH$, as viewed approximately along the *c* axis. The image shows a central unit derived from tecton **2** (blue), four neighboring units (red) joined by hydrogen bonds (-----), and one of the farther units (also in blue) to which the central unit has been linked covalently.

These observations demonstrate how molecular tectonics, by allowing the design of robust porous networks with reactive interiors, can give access to new molecular and macromolecular materials with predictably ordered structures that would be difficult or impossible to obtain by conventional methods.

## Experimental Section

X-ray structural analyses: Data were collected at 173 K using a Bruker SMART 1000 CCD diffractometer with $Mo_{K\alpha}$ radiation ($\lambda$ = 0.71070 Å). Intensities were integrated using SAINT[21] and corrected for absorption and other effects using SADABS.[22] Structures were solved and refined using the SHELX suite of programs.[23]

Crystal data for tecton **2**·6 dioxane: crystal size 0.15 × 0.20 × 0.30 mm, tetragonal, space group $I4_1/a$, $a = b = 23.0674(6)$, $c$ = 16.1892(6) Å, $V = 8614.4(4)$ Å$^3$, $Z = 4$. Least-squares refinement of 273 parameters based on 1759 reflections with $I > 2\sigma(I)$ (out of 2269 reflections) gave $R_1 = 0.0795$, w$R_2 = 0.230$, and GOF = 1.076.

 © 2003 Wiley-VCH Verlag GmbH & Co. KGaA, Weinheim 

Crystal data for thioether **5a** (as obtained from crystals of tecton **2**): crystal size $0.08 \times 0.15 \times 0.20$ mm, tetragonal, space group $I4_1/a$, $a = b = 20.988(2)$, $c = 16.816(3)$ Å, $V = 7407.6(16)$ Å$^3$, $Z = 4$. Least-squares refinement of 214 parameters based on 865 reflections with $I > 2\sigma(I)$ (out of 1976 reflections) gave $R_1 = 0.1210$, w$R_2 = 0.389$, and GOF = 1.306.

Crystal data for the product of cross-linking crystals of tecton **2** with $HSCH_2CH_2CH_2SH$: crystal size $0.15 \times 0.30 \times 0.30$ mm, tetragonal, space group $I4_1/a$, $a = b = 23.233(16)$, $c = 16.274(17)$ Å, $V = 8785(13)$ Å$^3$, $Z = 4$. Least-squares refinement of 182 parameters (with 192 restraints) based on 462 reflections with $I > 2\sigma(I)$ (out of 688 reflections) gave $R_1 = 0.1888$, w$R_2 = 0.461$, and GOF = 1.766.

Received: June 27, 2003 [Z52252]
Published Online: September 19, 2003

**Keywords:** crystal engineering · hydrogen bonding · porous networks · supramolecular chemistry · topotactic reactions

[1] J. M. Thomas, *Philos. Trans. R. Soc. London Ser. A* **1974**, *277*, 251.
[2] M. Morimoto, S. Kobatake, M. Irie, *Chem. Eur. J.* **2003**, *9*, 621; S. Takahashi, H. Miura, H. Kasai, S. Okada, H. Oikawa, H. Nakanishi, *J. Am. Chem. Soc.* **2002**, *124*, 10944; T. Hoang, J. W. Lauher, F. W. Fowler, *J. Am. Chem. Soc.* **2002**, *124*, 10656; T. Tanaka, A. Matsumoto, *J. Am. Chem. Soc.* **2002**, *124*, 9676; J. H. Kim, S. M. Hubig, S. V. Lindeman, J. K. Kochi, *J. Am. Chem. Soc.* **2001**, *123*, 87; K. Tanaka, E. Mochizuki, N. Yasui, Y. Kai, I. Miyahara, K. Hirotsu, F. Toda, *Tetrahedron* **2000**, *56*, 6853; K. Honda, F. Nakanishi, N. Feeder, *J. Am. Chem. Soc.* **1999**, *121*, 8246; Y. Ohashi, *Acta Crystallogr. Sect. A* **1998**, *54*, 842; H. Hosomi, Y. Ito, S. Ohba, *Acta Crystallogr. Sect. B* **1998**, *54*, 907; C. J. Keppert, D. Hesek, P. D. Beer, M. J. Rosseinsky, *Angew. Chem.* **1998**, *110*, 3335; *Angew. Chem. Int. Ed.* **1998**, *37*, 3158; J. D. Ranford, J. J. Vittal, D. Wu, *Angew. Chem.* **1998**, *110*, 1159; *Angew. Chem. Int. Ed.* **1998**, *37*, 1114; M. Leibovitch, G. Olovsson, J. R. Scheffer, J. Trotter, *J. Am. Chem. Soc.* **1997**, *119*, 1462; T. Suzuki, T. Fukushima, Y. Yamashita, T. Miyashi, *J. Am. Chem. Soc.* **1994**, *116*, 2793; A. Mori, N. Kato, H. Takeshita, Y. Kurahashi, M. Ito, *J. Chem. Soc. Chem. Commun.* **1994**, 869; V. Enkelmann, G. Wegner, K. Novak, K. B. Wagener, *J. Am. Chem. Soc.* **1993**, *115*, 10390; W.-N. Wang, W. Jones, *Tetrahedron* **1987**, *43*, 1273; B. Tieke, *J. Polym. Sci. Polym. Chem. Ed.* **1984**, *22*, 2895; E. J. Miller, T. B. Brill, A. L. Rheingold, W. C. Fultz, *J. Am. Chem. Soc.* **1983**, *105*, 7580; M. Hasegawa, *Chem. Rev.* **1983**, *83*, 507; H. Nakanishi, W. Jones, J. M. Thomas, M. B. Hursthouse, M. Motevalli, *J. Phys. Chem.* **1981**, *85*, 3636; R. Popovitz-Biro, H. C. Chang, C. P. Tang, N. R. Shochet, M. Lahav, L. Leiserowitz, *Pure Appl. Chem.* **1980**, *52*, 2693; K. Cheng, B. M. Foxman, *J. Am. Chem. Soc.* **1977**, *99*, 8102; G. M. J. Schmidt, *Pure Appl. Chem.* **1971**, *27*, 647.
[3] N. Tokitoh, Y. Arai, T. Sasamori, R. Okazaki, S. Nagase, H. Uekusa, Y. Ohashi, *J. Am. Chem. Soc.* **1998**, *120*, 433.
[4] For related reactions of guests with hosts in molecular inclusion complexes, see: R. Popovitz-Biro, H. C. Chang, C. P. Tang, N. R. Shochet, M. Lahav, L. Leiserowitz, *Pure Appl. Chem.* **1980**, *52*, 2693.
[5] S. Mann, *Nature* **1993**, *365*, 499; M. Simard, D. Su, J. D. Wuest, *J. Am. Chem. Soc.* **1991**, *113*, 4696.
[6] For recent references, see: J.-H. Fournier, T. Maris, J. D. Wuest, W. Guo, E. Galoppini, *J. Am. Chem. Soc.* **2003**, *125*, 1002.
[7] P. Brunet, M. Simard, J. D. Wuest, *J. Am. Chem. Soc.* **1997**, *119*, 2737; X. Wang, M. Simard, J. D. Wuest, *J. Am. Chem. Soc.* **1994**, *116*, 12119.
[8] S. Hetzel, T. Maris, M. Simard, J. D. Wuest, unpublished results.
[9] S. R. Batten, R. Robson, *Angew. Chem.* **1998**, *110*, 1558; *Angew. Chem. Int. Ed.* **1998**, *37*, 1460.
[10] M. J. Zaworotko, *Chem. Soc. Rev.* **1994**, *23*, 283.
[11] The percentage of volume accessible to guests was estimated by the PLATON program,[12] as described in detail in the Supporting Information.
[12] A. L. Spek, *PLATON, A Multipurpose Crystallographic Tool*, Utrecht University, Utrecht (The Netherlands), **2001**; P. van der Sluis, A. L. Spek, *Acta Crystallogr. Sect. A* **1990**, *46*, 194.
[13] Representations of channels were generated by the Cavities option in the ATOMS program (ATOMS, Version 5.1; Shape Software: 521 Hidden Valley Road, Kingsport, TN 37663; http:\www.shapesoftware.com). We are grateful to Eric Dowty of Shape Software for integrating this capacity into ATOMS at our suggestion.
[14] For a review of photochemical reactions in molecular crystals, see: V. Ramamurthy, K. Venkatesan, *Chem. Rev.* **1987**, *87*, 433.
[15] C. S. Marvel, R. R. Chambers, *J. Am. Chem. Soc.* **1948**, *70*, 993; W. E. Vaughan, F. F. Rust, *J. Org. Chem.* **1942**, *7*, 472.
[16] E. A. Archer, M. J. Krische, *J. Am. Chem. Soc.* **2002**, *124*, 5074.
[17] A. L. Margolin, M. A. Navia, *Angew. Chem.* **2001**, *113*, 2262; *Angew. Chem. Int. Ed.* **2001**, *40*, 2204.
[18] Z. Xu, S. Lee, Y.-H. Kiang, A. B. Mallik, N. Tsomaia, K. T. Mueller, *Adv. Mater.* **2001**, *13*, 637.
[19] For recent references to related polymerizations of guests in molecular inclusion complexes, see: K. Nakano, K. Sada, M. Miyata, *Polym. J.* **2001**, *33*, 172; K. Tajima, T. Aida, *Chem. Commun.* **2000**, 2399.
[20] Some allyl groups remain unreacted, and some molecules of $HSCH_2CH_2SH$ react only once, thus leaving free -SH groups; in addition, some unreacted $HSCH_2CH_2SH$ may remain trapped in the lattice. Spectroscopic and elemental analyses are consistent with the addition of approximately 6 equiv of $HSCH_2CH_2SH$ per tecton, rather than the 4 equiv required for ideal cross-linking.
[21] SAINT (Release 6.06), Integration Software for Single Crystal Data, Bruker AXS Inc., Madison, Wisconsin (USA), **1999**.
[22] G. M. Sheldrick, SADABS, Bruker Area Detector Absorption Corrections, Bruker AXS Inc., Madison, Wisconsin (USA), **1996**.
[23] G. M. Sheldrick, SHELXS-97, Program for the Solution of Crystal Structures and SHELXL-97, Program for the Refinement of Crystal Structures, University of Göttingen (Germany), **1997**.

 © 2003 Wiley-VCH Verlag GmbH & Co. KGaA, Weinheim 

*Conjugated Schiff-Base Macrocycles*

# Ion-Induced Tubular Assembly of Conjugated Schiff-Base Macrocycles**

*Amanda J. Gallant and Mark J. MacLachlan**

The supramolecular assembly of molecular precursors into well-defined architectures is a promising way to develop new materials and devices.[1,2] Supramolecular polymers are linear chains of molecules held together by noncovalent interactions, and they may have unusual properties in solution and in the solid-state.[3] Rigid molecular precursors (e.g., cyclic peptides[4] and hydrogen bonded rosettes[5]) can be assembled into nanotubes through hydrogen bonding or coordination chemistry.[6] Conjugated macrocycles, such as porphyrins and phthalocyanines, can also be assembled into polymers.[7,8] However, the coordination of metals to flexible macrocycles, such as crown ethers, does not usually lead to polymeric structures, though dimer formation is common.[9,10]

The assembly of rigid, shape-persistent macrocycles can lead to porous supramolecular architectures.[11] For example, in polar solvent, phenyleneacetylene macrocycles (e.g., **1**) self-associate through face-to-face π-π interactions to form tubular structures.[12–14] These assemblies can be useful models for the rational design of columnar liquid crystals and organic nanotubes. We are investigating new conjugated, shape-persistent macrocycles that may be used to build supramolecular architectures. In particular, macrocycles that are capable of both binding transition-metal atoms and assembling into tubes may form the basis of catalytic nanomaterials or ion-conducting channels. Herein we report the ion-induced assembly of new well-defined conjugated macrocycles to form supramolecular assemblies.

We identified organic macrocycles such as **2** as ideal candidates for supramolecular assembly (Figure 1).[15,16] These macrocycles contain three tetradentate $N_2O_2$ binding sites organized in an equilateral triangle, as well as a pocket in the center that is surrounded by six phenolic oxygen atoms resembling [18]crown-6. The binding of ions to these types of macrocycles has not yet been explored.

Macrocycle **2** is insoluble in most solvents and takes about two weeks to synthesize.[16] We therefore developed a general and convenient route to macrocycles that have peripheral alkoxy chains. The reaction of 3,6-diformylcatechol with 1,2-dihexyloxy-4,5-phenylenediamine afforded a red, crystalline product **3** in 70% yield (Scheme 1). The structure of the macrocycle was verified by mass spectrometry and by NMR spectroscopy. The $^1$H NMR spectrum of **3** shows the presence of single imine ($\delta = 8.54$ ppm) and OH resonances ($\delta =$ 13.23 ppm), which are consistent with the $D_{3h}$ symmetry of the macrocycle in solution. Unlike **2**, the macrocycles with peripheral alkoxy chains are soluble in a wide range of organic solvents such as chloroform and toluene.

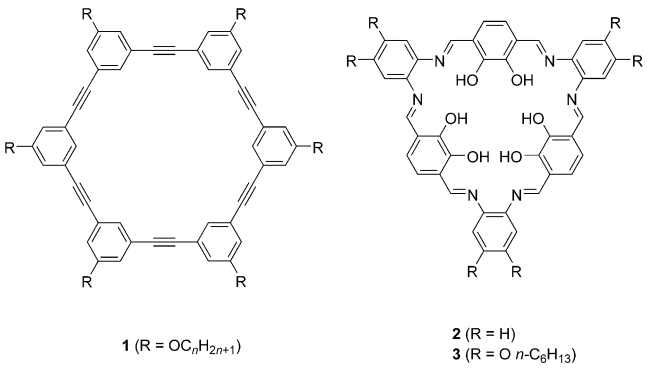
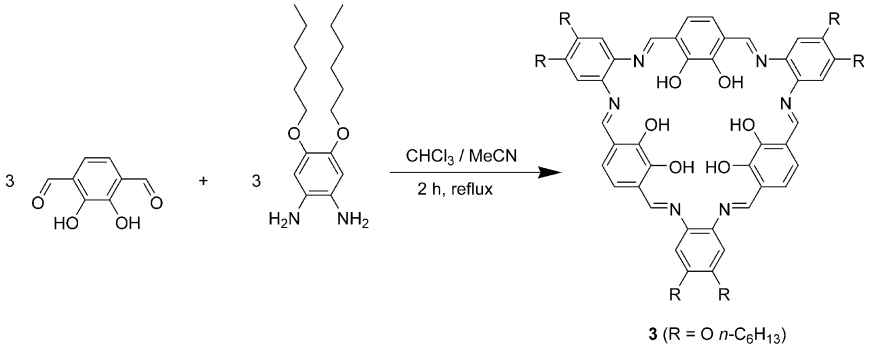



***Figure 1.*** Conjugated macrocycles **1**–**3**.




***Scheme 1.*** Synthesis of macrocycle **3**.

The electrospray mass spectrum (ESIMS) of macrocycle **3** shows the presence of not only the $[\mathbf{3}+H]^+$ ion, but also $[\mathbf{3}+Na]^+$ and $[\mathbf{3}_2+Na]^+$ species; the $Na^+$ ion is presumably a contaminant in the solvent or from the glass. When $NaBPh_4$ was added to a solution of **3**, the ESIMS (Figure 2) showed three sodium complexes—$[\mathbf{3}+Na]^+$, $[\mathbf{3}_2+Na]^+$, and $[\mathbf{3}_3+2Na]^{2+}$. As a mild ionization technique, ESIMS is known to give a meaningful picture of the species in solution.[17,18] Thus, it is most likely that these complex species are present in the solution before ionization. The observation of $[\mathbf{3}+H]^+$ but not any protonated aggregates also corroborates the formation of $Na^+$ bridged dimers and trimers.

The addition of alkali metal and ammonium salts ($MBPh_4$, $M^+ = Li^+$, $Na^+$, $K^+$, $Rb^+$, $Cs^+$, $NH_4^+$) to a solution of **3** in $CH_2Cl_2$ or $CHCl_3$ produced a change from orange to red-brown. Divalent metals (e.g., $Mg^{2+}$) caused precipitation of

[*] Prof. M. J. MacLachlan, A. J. Gallant
Department of Chemistry
University of British Columbia
2036 Main Mall, Vancouver, BC V6T 1Z1 (Canada)
Fax: (+1) 604-822-2847
E-mail: mmaclach@chem.ubc.ca

[**] We thank the University of British Columbia and the Natural Sciences and Engineering Research Council of Canada (NSERC) for funding this research. AJG thanks NSERC for a PGSA graduate fellowship award.

Supporting information for this article is available on the WWW under http://www.angewandte.org or from the author.

 DOI: 10.1002/anie.200352395 © 2003 Wiley-VCH Verlag GmbH & Co. KGaA, Weinheim 

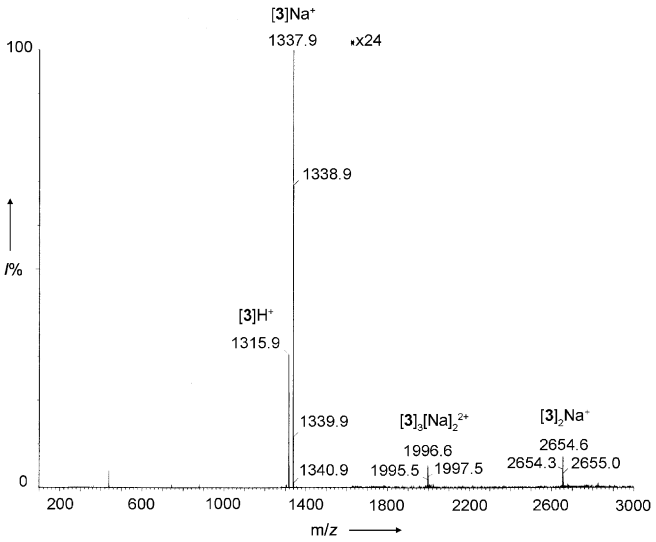



***Figure 2.*** ESIMS of **3** with $NaBPh_4$ ($CHCl_3$/MeOH), $I$ = relative intensity.

the macrocycle. The UV/Vis spectrum of **3** in $CHCl_3$ shows three large peaks centered near 310, 345, and 405 nm, as well as a weaker absorbance at 560 nm. To study the effect of small cations on the spectrum of **3**, a solution of **3** in about 95:5 $CHCl_3$:MeCN was prepared, and the salt in MeCN was added in aliquots.[19] All $MBPh_4$ ($M^+ = Na^+$, $K^+$, $Rb^+$, $Cs^+$, $NH_4^+$) produced similar changes to the visible spectrum of **3**. Figure 3 shows the effect of adding $NaBPh_4$ and $CsBPh_4$ to the macrocycle. Isosbestic points are seen at low salt concentrations (see insets in Figure 3), but are better defined in the case of $M^+ = Cs^+$. This can be rationalized as the conversion of the macrocycle to a cationic dimer, $[\mathbf{3}_2{+}Cs]^+$. In the case of $M = Na^+$, the macrocycle does not convert cleanly to a single product, even at low concentrations. As the ratio of salt to macrocycle is increased the isosbestic points disappear, which is consistent with the formation of trimers, tetramers, and higher aggregates.

The changes that occur in the electronic absorption spectrum of macrocycle **3** upon addition of small cations may arise from either electrostatic effects of coordinating the ions to the phenolic oxygen atoms or from an interaction between the π orbitals of the macrocycles as they are stacked. The lack of a single isosbestic point during the formation of the aggregates supports the latter conclusion, as the monomers, dimers, trimers, and larger aggregates appear to have different electronic spectra.

The interaction of macrocycle **3** with monovalent cations was also investigated by NMR spectroscopy. Figure 4a shows the $^1$H NMR spectrum of **3** with varying concentrations of $NaBPh_4$.[20,21] As the [$Na^+$]:[**3**] increases, there is a gradual upfield shift in the position of the peaks. Notably, the imine and aromatic peaks shift by as much as 1.5 ppm at the [$Na^+$]:[**3**] of about 1:1. This dramatic upfield shift is characteristic of π–π stacking whereby proton resonances are affected by the ring currents of adjacent macrocycles.[22] As two rings approach in proximity, the electron density surrounding an attached proton is increased, thus resulting in an upfield

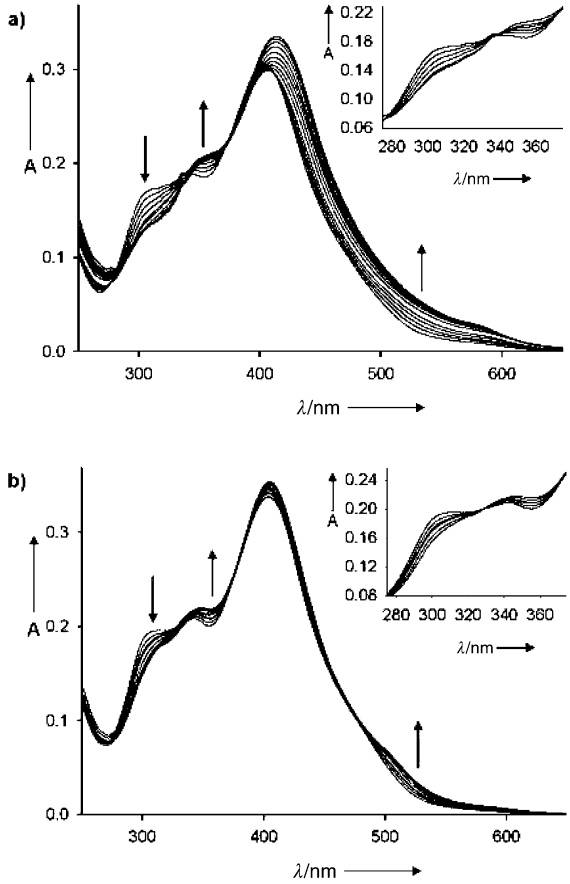



***Figure 3.*** UV/Vis spectra of **3** upon adding: a) $NaBPh_4$, and b) $CsBPh_4$. Each line represents an increase of about. 0.1 equivalents of $M^+$ to **3**. The spectra show a ratio of [$M^+$]:[**3**] up to about 1.5. Insets: Low concentration experiments (0 to 0.5 equivalents of $M^+$).

chemical shift.[23] The presence of a single product by $^1$H NMR spectroscopy, and the lack of any starting material after $NaBPh_4$ is added, indicates that the system is dynamic and that the macrocycles are freely interchanging between aggregates. Even at low concentrations of $Na^+$ ([$Na^+$]:[**3**] = 0.1:1), there is a single set of broad resonances that are consistent with this dynamic system.

The addition of $KBPh_4$ to **3** gives results similar to $NaBPh_4$, but $NH_4BPh_4$, $RbBPh_4$, and $CsBPh_4$ behave differently. Figure 4b shows the $^1$H NMR spectral changes that occur for the addition of $CsBPh_4$ to **3**. Above [$Cs^+$]:[**3**] equal to about 0.3:1, there are only broad peaks that are significantly shifted upfield from the pristine macrocycle **3**, but broadened because of dynamic exchange and/or a distribution of aggregate sizes similar to the case for $NaBPh_4$. At lower concentrations, however, signals from other species are observed to grow. At a concentration of [$Cs^+$]:[**3**] = 0.05:1, the macrocycle and a small amount of another species, **4**, are present. The intermediate **4** has an OH resonance at $\delta$ = 13.55 ppm, an imine resonance at $\delta$ = 8.0 ppm, and two aromatic resonances at $\delta$ = 6.2 ppm and 6.5 ppm. From the integration of the $^1$H NMR spectrum, the new species formed at low concentrations of $Cs^+$ has a formula of $[\mathbf{3}]_2Cs^+$, characteristic of a dimer. Moreover, the imine resonance at

 © 2003 Wiley-VCH Verlag GmbH & Co. KGaA, Weinheim 

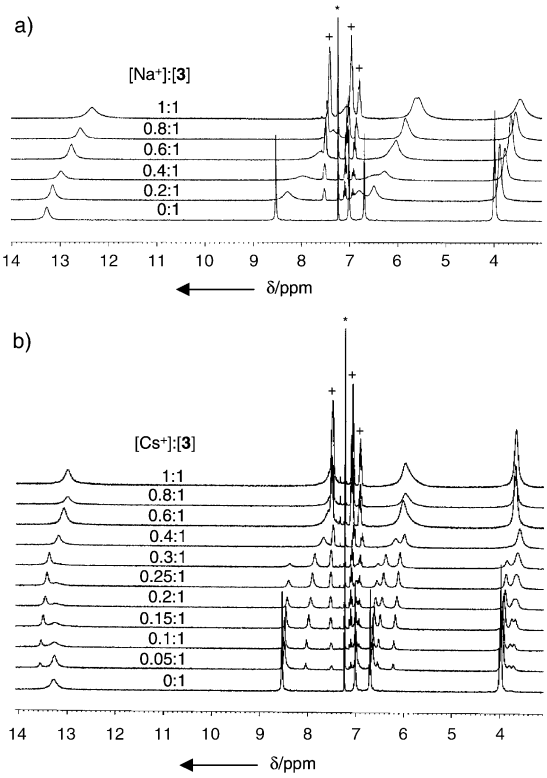



***Figure 4.*** Stacked $^1$H NMR spectra of macrocycle **3** with increasing amounts of a) $NaBPh_4$ and b) $CsBPh_4$. The ratio of $[M^+]$:[**3**] for each sample is shown. (∗ = $CHCl_3$; + = $BPh_4^-$).

$\delta = 8.0$ ppm is intermediate to that of the macrocycle ($\delta =$ 8.54 ppm) and the 1:1 $[Cs^+]$:[**3**] ($\delta = 7.5$ ppm) product. If the chemical shift of the 1:1 product corresponds to the macrocycle in a tubular assembly, the intermediate species **4** is most likely to be a dimeric sandwich complex. In this dimer, the aromatic protons would only experience the influence of the ring currents from a single neighbouring macrocycle, thus leading to half the change in chemical shift seen for a macrocycle in a tubular assembly.

In addition, the $OCH_2$ resonances of **4** are split into two multiplets. In a dimeric sandwich compound, these two protons are inequivalent (diastereotopic) as the mirror symmetry in the macrocycle is broken. Up to concentrations of $[Cs^+]$:[**3**] = 0.4:1, the free macrocycle is gradually replaced by species that result in broad peaks in the $^1$H NMR spectrum, which is characteristic of aggregates. The two resonances of the $OCH_2$ groups merge into a single broad resonance when the symmetry of the macrocycle is restored in a tubular structure. It appears that the dimer does not readily undergo exchange, but macrocycle exchange does occur once the aggregates have grown.

The change in chemical shift in the protons of **3** upon addition of a salt appears to depend on the size of the cation, with the imine peak shifted most dramatically for the smallest cation, $Na^+$ ($\Delta\delta = 1.48$ ppm), and least for the larger $Cs^+$ cation ($\Delta\delta = 0.98$ ppm). The imine peaks of **3** with the intermediate sized cations ($NH_4^+$, $K^+$, and $Rb^+$) are found between those of $Na^+$ and $Cs^+$, but are obscured by peaks assigned to $CHCl_3$ and $BPh_4^-$. In a tubular structure in which macrocycles are bridged by cations, the size of the cation should affect the chemical shifts as it changes the proximity of the neighbouring macrocycles and their relative shielding.[21]

The data obtained from ESIMS, UV/Vis and $^1$H NMR spectroscopies suggest that small cations induce the aggregation of macrocycles such as **3** to form tubular assemblies. At low $[M^+]$:[**3**] ratios, intermediate species (e.g., dimers) are observed while at higher concentrations dynamic stacked structures are formed. Postulated structures of the dimer **4** and the tubular assemblies are shown in Figure 5.

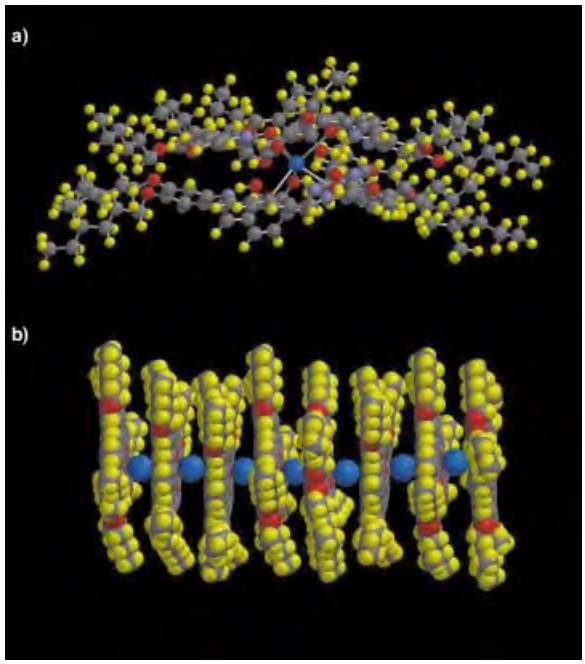
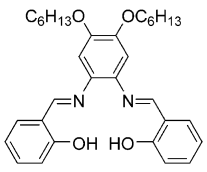



***Figure 5.*** Postulated structures of a) the dimeric intermediate **4** (minimized with molecular mechanics force field) and b) the ion-induced tubular assembly of macrocycle **3**.

We believe that in the tubular structure, the small cations are coordinated to the central phenolic oxygen atoms of macrocycle **3** rather than to the tetradentate $N_2O_2$ ligands. A control experiment in which salphen **5** was mixed with an excess of $NaBPh_4$ in $CDCl_3$ showed no change in color nor in its $^1$H NMR spectrum, thus indicating that **5** does not incorporate $NaBPh_4$ in $CDCl_3$. In addition, the final $[M^+]$:[**3**] ratio was nearly 1:1 for each cation; a larger ratio would be expected if the cations were coordinating to the $N_2O_2$ pockets of each macrocycle. Preliminary DFT calculations also indicate that a sodium ion has a strong affinity for binding to the phenolic oxygen atoms over the tetradentate $N_2O_2$ pockets offered by the macrocycle.




**5**

In summary, we report the first synthesis of soluble Schiff-base macrocycle, **3**, and show that upon addition of small cations, **3** changes color and aggregates to form ionic assemblies. Our results demonstrate that **3** can behave like a crown ether, in which the phenolic oxygen atoms inside the

 © 2003 Wiley-VCH Verlag GmbH & Co. KGaA, Weinheim 

macrocycle coordinate to small cations seated at the center of the macrocycle. These results provide a new avenue for self-assembled materials and small-cation sensors.

Received: July 16, 2003 [Z52395]

**Keywords:** alkali metals · macrocycles · Schiff bases · self-assembly · supramolecular chemistry

[1] A. P. Alivisatos, P. F. Barbara, A. W. Castleman, J. Chang, D. A. Dixon, M. L. Klein, G. L. McLendon, J. S. Miller, M. A. Ratner, P. J. Rossky, S. I. Stupp, M. E. Thompson, *Adv. Mater.* **1998**, *10*, 1297 – 1336.

[2] For recent interesting examples of self-assembled architectures, see: a) F. Würthner, S. Yao, U. Beginn, *Angew. Chem.* **2003**, *115*, 3368 – 3371; *Angew. Chem. Int. Ed.* **2003**, *42*, 3247 – 3250; b) E. R. Zubarev, M. U. Pralle, E. D. Sone, S. I. Stupp, *Adv. Mater.* **2002**, *14*, 198 – 203; c) Y.-H. Luo, H.-W. Liu, F. Xi, L. Li, X.-G. Jin, C. C. Han, C.-M. Chan, *J. Am. Chem. Soc.* **2003**, *125*, 6447 – 6451.

[3] L. Brunsveld, B. J. B. Folmer, E. W. Meijer, R. P. Sijbesma, *Chem. Rev.* **2001**, *101*, 4071 – 4098.

[4] a) W. S. Horne, C. D. Stout, M. R. Ghadiri, *J. Am. Chem. Soc.* **2003**, *125*, 9372 – 9376; b) J. Sanchez-Quesada, M. P. Isler, M. R. Ghadiri, *J. Am. Chem. Soc.* **2002**, *124*, 10004 – 10005.

[5] H. Fenniri, P. Mathivanan, K. L. Vidale, D. M. Sherman, K. Hallenga, K. V. Wood, J. G. Stowell, *J. Am. Chem. Soc.* **2001**, *123*, 3854 – 3855.

[6] For other examples of tube formation induced by ions, see: a) D. T. Bong, T. D. Clark, J. R. Granja, M. R. Ghadiri, *Angew. Chem.* **2001**, *113*, 1016 – 1041; *Angew. Chem. Int. Ed.* **2001**, *40*, 988 – 1011; b) V. Sidorov, F. W. Kotch, M. El-Kouedi, J. T. Davis, *Chem. Commun.* **2000**, 2369 – 2370.

[7] K. M. Kadish, K. M. Smith, R. Guilard, *The Porphyrin Handbook, Vol. 6.* Academic Press, San Diego, **2000**.

[8] Y. Kim, M. F. Mayer, S. C. Zimmerman, *Angew. Chem.* **2003**, *115*, 1153 – 1158; *Angew. Chem. Int. Ed.* **2003**, *42*, 1121 – 1126.

[9] J. W. Steed, *Coord. Chem. Rev.* **2001**, *215*, 171 – 221.

[10] a) V. Percec, G. Johansson, G. Ungar, J. Zhou, *J. Am. Chem. Soc.* **1996**, *118*, 9855 – 9866; b) R. J. M. Klein Gebbink, A. J. Sandee, F. G. A. Peters, S. J. van der Gaast, M. C. Feiters, R. J. M. Nolte, *J. Chem. Soc. Dalton Trans.* **2001**, 3056 – 3064; c) H. Engelkamp, R. J. M. Nolte, *J. Porphyrins Phthalocyanines* **2000**, *4*, 454 – 459; d) W.-S. Xia, R. H. Schmehl, C.-J. Li, J. T. Mague, C.-P. Luo, D. M. Guldi, *J. Phys. Chem. B* **2002**, *106*, 833 – 843.

[11] D. Zhao, J. S. Moore, *Chem. Commun.* **2003**, 807 – 818.

[12] a) S. Lahiri, J. L. Thompson, J. S. Moore, *J. Am. Chem. Soc.* **2000**, *122*, 11315 – 11319; b) A. S. Shetty, J. Zhang, J. S. Moore, *J. Am. Chem. Soc.* **1996**, *118*, 1019 – 1027; c) J. Zhang, J. S. Moore, *J. Am. Chem. Soc.* **1992**, *114*, 9701 – 9702.

[13] a) S. Höger, K. Bonrad, A. Mourran, U. Beginn, M. Möller, *J. Am. Chem. Soc.* **2001**, *123*, 5651 – 5659; b) S. Höger, J. Spickermann, D. L. Morrison, P. Dziezok, H. J. Rader, *Macromolecules* **1997**, *30*, 3110 – 3111.

[14] M. Pickholz, S. Stafström, *Chem. Phys.* **2001**, *270*, 245 – 251.

[15] W. T. S. Huck, F. C. J. M. van Veggel, D. N. Reinhoudt, *Recl. Trav. Chim. Pays-Bas* **1995**, *114*, 273 – 276.

[16] S. Akine, T. Taniguchi, T. Nabeshima, *Tetrahedron Lett.* **2001**, *42*, 8861 – 8864.

[17] F. Inokuchi, S. Shinkai, *J. Chem. Soc. Perkin Trans. 2* **1996**, 601 – 605.

[18] The mass spectrum was not obtained under conditions from which reliable quantification of the species could be made. See: E. Leize, A. Jaffrezic, A. Van Dorsselaer, *J. Mass Spectrom.* **1996**, *31*, 537 – 544.

[19] We tested the effect of adding MeOH and MeCN to the macrocycle in $CHCl_3$. The addition of MeOH to **3** led to continuous changes in the spectrum. MeOH may induce stacking of the macrocycles as the solvent polarity increases. MeCN caused small changes to the spectrum only below concentrations of about 1–2%. We believe that the MeCN is acting as a guest in the macrocycles as we see the chemical shift of MeCN in **3** at $\delta =$ 1.99 ppm in $CDCl_3$ (compare with $\delta = 2.10$ ppm in neat $CDCl_3$). As well, the crystalline compound contains MeCN that is difficult to remove under vacuum.

[20] Samples for the NMR experiments were prepared as follows: A solution of **3** (about $7.6 \times 10^{-3}$ M) in $CDCl_3$ was mixed for several minutes with a large excess of the tetraphenylborate salt of the cation ($M^+$). The resulting solution was filtered and aliquots were quantitatively transferred into NMR tubes. The salt solutions were then diluted with a standard solution of **3** in $CDCl_3$ so that the final volume and concentration of the macrocycle was approximately the same in each case. The original [$M^+$]:[**3**] ratio was determined by integration of the $^1$H NMR spectrum of the most concentrated solution, and was near 1:1 in each case (M = Na, K, Rb, Cs, $NH_4$,). It was not possible to get a larger ratio of [$M^+$]:[**3**].

[21] When a solution containing macrocycle **3** and $NaBF_4$ (in a ratio of about 1:1) was analyzed, it showed the same shifts in the NMR spectrum, thus eliminating the $BPh_4^-$ anion as the cause of the spectral shifts.

[22] D. Zhao, J. S. Moore, *J. Org. Chem.* **2002**, *67*, 3548 – 3554.

[23] C. Giessner-Prettre, B. Pullman, P. N. Borer, L.-S. Kan, P. O. P. Ts'o, *Biopolymers* **1976**, *15*, 2277 – 2286.

 © 2003 Wiley-VCH Verlag GmbH & Co. KGaA, Weinheim 

*Solvent-Induced Chirality Switching*

# The Origin of Solvent-Controlled Supramolecular Chirality Switching in a Bis(Zinc Porphyrin) System

*Victor V. Borovkov,* Guy A. Hembury, and Yoshihisa Inoue**

Chirogenic processes induced by means of supramolecular interactions have been one of the major focuses of research interest for chemists and material scientists in recent years due to their direct relation to many natural and artificial systems and potential applicability.[1] The understanding of chirality induction in supramolecular systems, including the detailed mechanisms and various driving forces, is of particular importance and allows rational control of these phenomena. Owing to the noncovalent nature of supramolecular interactions, the medium effect and solvent interactions with

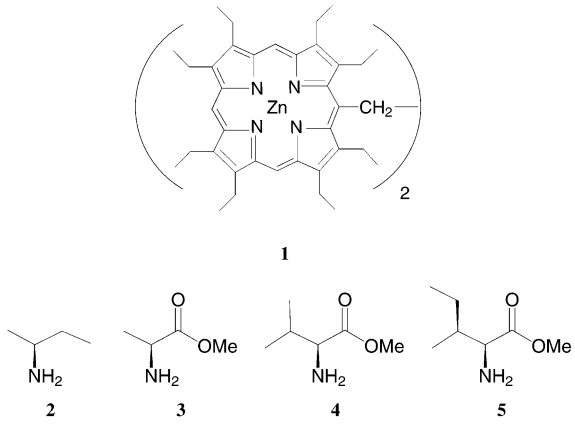
[*] Dr. V. V. Borovkov, Prof. Dr. Y. Inoue, Dr. G. A. Hembury
Entropy Control Project, ICORP, JST
4-6-3 Kamishinden, Toyonaka-shi, Osaka 560-0085 (Japan)
Fax: (+81) 6-6836-1636
E-mail: victrb@inoue.jst.go.jp
inoue@chem.eng.osaka-u.ac.jp

Supporting information for this article is available on the WWW under http://www.angewandte.org or from the author.

 © 2003 Wiley-VCH Verlag GmbH & Co. KGaA, Weinheim DOI: 10.1002/anie.200352493 

the molecular components of whole systems can play a key role in such association processes, thus influencing all aspects of the assembly, in particular the stereochemistry, and consequently the degree of induced chirality. Although a vast number of examples of the solvent effect on asymmetry transfer were reported,[1a,i–m,2] to our knowledge this important factor and its origin have not yet been well-investigated and rationalized, with consideration only going as far the observation of the results of these phenomena and the qualitative investigation into the influence of the bulk solvent properties. Herein, we describe a remarkable phenomenon that leads to the origin, and consequently a molecular-level understanding, of how the solvent may control and even switch the induced chirality in a supramolecular system that consists of an achiral host and a chiral guest.

To investigate the influence of the solvent on supramolecular chirality, a host–guest system on the basis of ethane-bridged bis(zinc porphyrin) host[3] (**1**) was chosen as the most suitable because the corresponding spectral changes upon the interaction of **1** with chiral guests (L) can be easily monitored.[4] Essentially, this host undergoes *syn*-to-*anti* conformational switching upon complexation with external ligands and unidirectional screw formation based on the stereochemistry of the chiral guests. To date the detailed mechanism, driving forces, and various external and internal controlling factors of this phenomenon have been thoroughly investigated and well-characterized. The choice of chiral guests was particularly important and dictated by a relatively small difference in the bulkiness between two of the largest substituents (excluding the binding amine) as it is the distinction between the competing steric interactions of these ligand substituents and the neighboring porphyrin that are responsible for the induced helical sense in **1**.[4] Another major factor is the considerable difference in the ability of the substituents of the ligand to interact with solvent molecules, which can be roughly represented by their polarity. Thus, with the aim of achieving a molecular-level understanding of the solvent effect, four enantiopure compounds **2**–**5** of *S* configuration were chosen as the corresponding chiral guests with comparably sized substituents as judged from the relatively modest amplitudes (*A*) of the induced circular dichroism (ICD)[5] observed with **1** in $CH_2Cl_2$.[4d,e] In addition, the amino acid derivatives **3**–**5** are expected to exhibit drastic distinctions in the polarity of their substituents, that is, between the carboxy ester *C*-terminus and the alkyl side chain, whilst **2** has only two nonpolar competing substituents (methyl and ethyl) and is an ideal "solvent-inert" reference compound.




As in the case of previously studied systems,[4] the UV/Vis spectra of **1**·$L_2$ in different solvents[6] show that the Soret (B) band is significantly bathochromically shifted (compared to initial **1**) and exhibits a well-resolved split into two major transitions arising from the through-space interactions of the corresponding pairs of porphyrin B electric dipoles of the two porphyrin rings in the *anti* conformation (see Figure 1 and Supporting Information), which is in full agreement with the exciton coupling theory of Kasha et al.[4j,7] The maxima positions and magnitude of their split (Davydov splitting) are essentially independent of the solvent. However, the relative ratio between the intensities of the high ($B_1$) and low($B_2$) energy components of the Soret band are noticeably affected by the solvent. Generally, in more polar solvents the intensity of $B_1$ transition is enhanced in comparison to that of the $B_2$ transition, whilst in nonpolar solvents the opposite tendency was observed.[8] This reflects the ability of polar and nonpolar solvents to form an overall solvation shell around the **1**·$L_2$ system, thus affecting the relative probability of light-absorption pathways to certain levels of the split $S_2$ excited states arising from the bisporphyrin coupling, whilst having little or no effect on its energy levels.

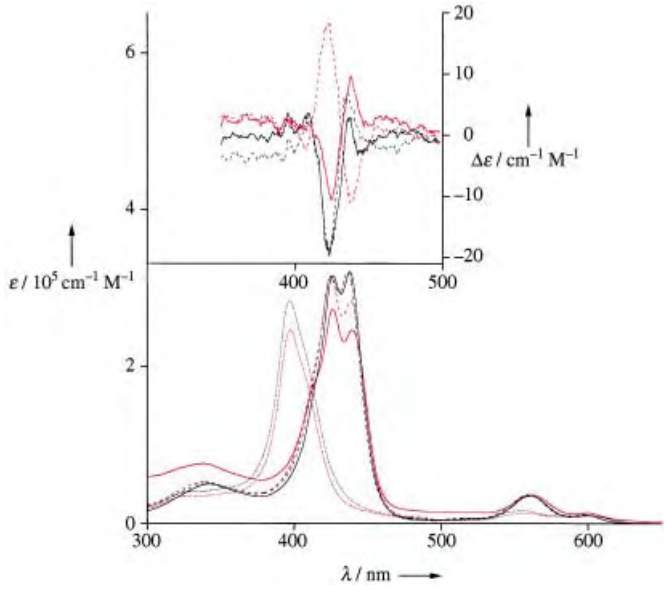



***Figure 1.*** UV/Vis and CD (inset) spectra of **1** without ligand (dotted lines) and in the presence of **2** (solid lines) and **3** (dashed lines) in $CH_2Cl_2$ (black lines) and in cyclohexane (red lines).

The CD spectra of **1**·$L_2$ in various solvents show similar features as reported previously for these systems in $CH_2Cl_2$,[4] including a bisignate CD signal comprising of two Cotton effects, the positions of which coincide very closely with the maxima of the split Soret band in UV/Vis spectra, thus indicating the same origin (see Figure 1, inset, and Supporting Information); these properties are also independent of the

 © 2003 Wiley-VCH Verlag GmbH & Co. KGaA, Weinheim 

solvent used. However, there was a dramatic difference in the spectral behavior between the amino acid-based systems $\mathbf{1}\cdot\mathbf{3}_2$–$\mathbf{1}\cdot\mathbf{5}_2$ that contain the polar ester group and the reference system $\mathbf{1}\cdot\mathbf{2}_2$ that contains only alkyl substituents. As can be seen, the intensity and sign of the CD couplets of $\mathbf{1}\cdot\mathbf{3}_2$–$\mathbf{1}\cdot\mathbf{5}_2$ are strongly affected by the surrounding medium, whilst $\mathbf{1}\cdot\mathbf{2}_2$ is largely unaffected by the solvent. Although in recent reports there were several examples of solvent-induced chirality switching, none of them give a rational or detailed insight at the molecular level into this remarkable and important phenomenon of solvent–solute interactions.[1i,2c,2e–2g] To highlight and understand the role of the solvent, the *A* values were plotted versus the dielectric constants ($\varepsilon_s$) of the solvents as a parameter of its polarity and thus its ability to interact with the ligands (Figure 2). As mentioned above, the *A* values of $\mathbf{1}\cdot\mathbf{2}_2$ are essentially independent of $\varepsilon_s$, whilst the chirality of $\mathbf{1}\cdot\mathbf{3}_2$–$\mathbf{1}\cdot\mathbf{5}_2$ correlates well with the solvent polarity, essentially, exhibiting positive ICD sign in polar media and negative ICD sign in nonpolar media.

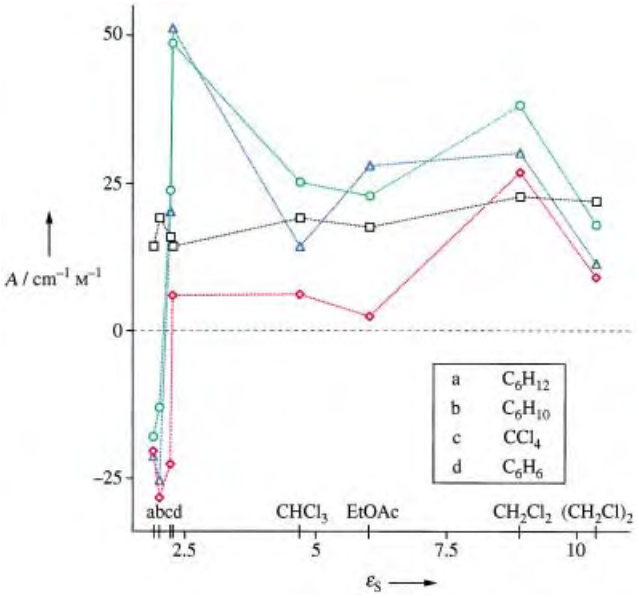



***Figure 2.*** The dependence of the ICD amplitudes of $\mathbf{1}\cdot L_2$, black L = **2**, red L = **3**, green L = **4**, and blue L = **5**, upon the dielectric constant of the solvent used.

In consideration of the main tendency of the experimentally observed solvent–ICD relationship, a general mechanism of the effect of the medium on supramolecular chirality induction at the molecular level of solvent–solute interactions can be schematically described (Figure 3).

In polar media the solvent molecules are able to interact electrostatically (through dipole–dipole, dipole–quadrupole interactions, etc.) with the ester group of the amino acid derivatives. Arising from such specific interactions with the solvent, a fairly well structurally organized solvent shell surrounding the polar substituent is formed. This is in sharp contrast to the nonpolar alkyl substituents that are unable to

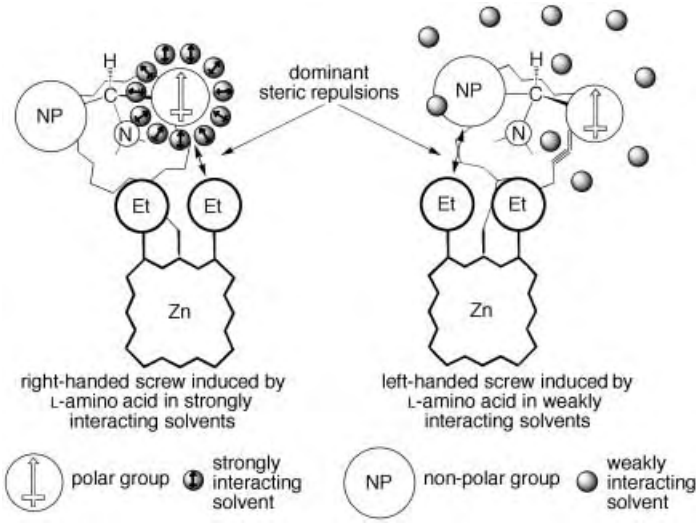



***Figure 3.*** Solvent effect on the mechanism of supramolecular chirality induction in $\mathbf{1}\cdot L_2$, in strongly and weakly interacting solvents (the ligand coordinated to the upper porphyrin has been omitted for clarity).

interact in such a manner, as they do not have such strong and defined permanent electrostatic distributions. As a result of the selective polar solvent–polar substituent interactions the relative "effective sizes" of the competing ligand substituents can be changed and even inverted. Thus, when both the *C*-terminus ester and the side-chain groups are comparable in size, or even if the nonpolar side-chain substituent is slightly larger than the polar *C*-terminus ester group (as in the present case), a "small" increase in the size of the polar group as a result of specific solvent–substituent interactions can cause a subsequent total equilibrium shift towards the formation of the right-handed screw structure in $\mathbf{1}\cdot L_2$ (when L has *S* configuration) (Figure 3). This helical orientation corresponds to positive-induced chirality, and is in accordance with the exciton chirality method[9] and also reported previously.[4] In contrast, in nonpolar solvents, because of the negligible solvent–solute electrostatic interactions there is no observable formation of any selective solvent–solute interaction around the polar group, and as a result, the dominant steric repulsion takes place between the larger side chain and ethyl group of the neighboring porphyrin ring. This interaction induces a corresponding equilibrium shift towards the formation of the left-handed screw structure in $\mathbf{1}\cdot L_2$, which corresponds to negative chirality. In the case of reference $\mathbf{1}\cdot\mathbf{2}_2$ it is obvious that both the methyl and ethyl nonpolar groups will interact to almost the same extent, thus preserving the right-handed screw owing to the larger size of ethyl substituent of **2** regardless of the medium used.

However, at first glance there is an apparent deviation of the proposed mechanism. This is the unexpected enhancement of the positive *A* values of $\mathbf{1}\cdot\mathbf{4}_2$ and $\mathbf{1}\cdot\mathbf{5}_2$ in benzene, whereas for the other solvents of corresponding low dielectric constant, small positive or highly negative *A* values are observed (Figure 2 and Supporting Information). This can occur either through the enhancement of the effective size of the ester group or reduction of the effective size of the alkyl side chain. Although benzene has a low $\varepsilon_s$ value, because of its

 © 2003 Wiley-VCH Verlag GmbH & Co. KGaA, Weinheim 

pronounced quadrupolar electrostatic distribution it is still able, in principle, to have significant electrostatic interaction with the polar ester group, which will consequently increase its effective size and thus result in the observed increase in positive chirality. Another possibility, although less probable, is a reduction in the effective size of the branched alkyl side-chain groups in **4** and **5** due to a conformational change that reduces their effective size as a result of CH-π interactions with benzene.[10]

To investigate the remarkable effect of high solvent sensitivity on supramolecular chirogenesis and particularly the chirality switching in a narrow polarity range,[11] the chirality induction processes in **1** were studied in mixed solvents. Thus, the CD and UV/Vis spectra of $\mathbf{1}\cdot\mathbf{3}_2$ were taken at different ratios by volume of $CH_2Cl_2$ (a strongly interacting solvent) to cyclohexane (a weakly interacting solvent) and the corresponding spectral data ($A$ values for CD and $B_1/B_2$ relative intensities ratio for UV/Vis) were plotted against the solvent content (Figure 4).

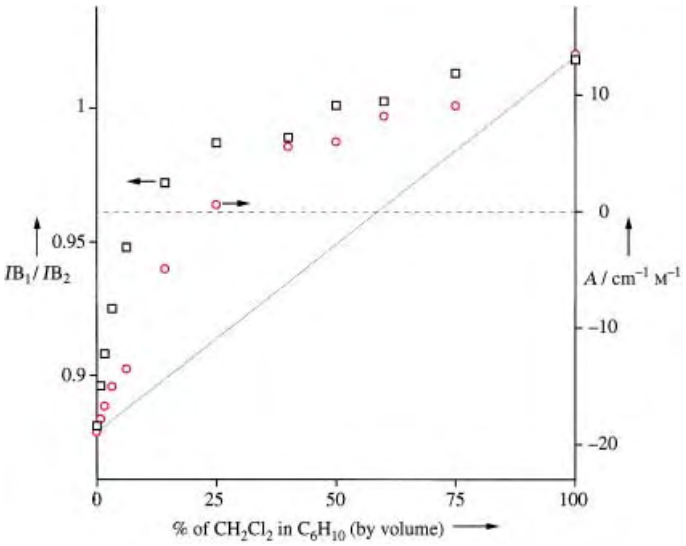



***Figure 4.*** Dependences of the ratio of the intensities of $B_1$ and $B_2$ transitions ($IB_1$ and $IB_2$) from UV/Vis data and ICD amplitude from CD data of $\mathbf{1}\cdot\mathbf{3}_2$ versus the percentage of $CH_2Cl_2$ in cyclohexane by volume.

The UV/Vis changes are associated with the overall solvation effect of the mixed solvents on the supramolecular system and essentially its chromophoric, that is, porphyrin, moiety. As expected from the above results, $CH_2Cl_2$ more strongly interacts with the zinc porphyrins that results in a considerable nonlinear increase in the probability of the $B_1$ transition on increasing $CH_2Cl_2$ content. In contrast, the CD dependence reflects specific solvent interactions with a certain part of the supramolecular system (particularly the polar group of L), thus resulting in a dramatic nonlinear dependence upon increasing the $CH_2Cl_2$ component. These significant deviations from linearity clearly indicate that the $CH_2Cl_2$ molecules much more strongly interact with the ester moiety than cyclohexane. Indeed, even at only 25% $CH_2Cl_2$ the sign of the chirality of the supramolecular system is switched from negative to positive as a result of the formation of a structurally organized solvent shell surrounding the polar substituent, which increases its effective size. Thus the behavior of the chiral supramolecular system is dictated not by the properties of the bulk solvent, but by the specific molecular solvent–solute interactions.

In summary, this work shows that through judicious control of the medium, the properties of supramolecular chirogenesis, including chirality switching phenomenon, may be controlled through specific solvent–solute interactions. Furthermore, as such interactions are common to all solution based supramolecular systems, and not just chiral ones, the realization and application of this approach to molecular control may have important implications for understanding the mechanisms and driving forces of numerous artificial and natural assemblies.

Received: July 28, 2003 [Z52493]

**Keywords:** chirality · circular dichroism · porphyrinoids · solvent effects · supramolecular chemistry

[1] a) T. S. Balaban, A. D. Bhise, M. Fischer, M. Linke-Schaetzel, C. Roussel, N. Vanthuyne, *Angew. Chem.* **2003**, *115*, 2190–2194; *Angew. Chem. Int. Ed.* **2003**, *42*, 2140–2144; b) V. V. Borovkov, T. Harada, G. A. Hembury, Y. Inoue, R. Kuroda, *Angew. Chem.* **2003**, *115*, 1788–1791; *Angew. Chem. Int. Ed.* **2003**, *42*, 1746–1749; c) M. Ishikawa, K. Maeda, E. Yashima, *J. Am. Chem. Soc.* **2002**, *124*, 7448–7458; d) T. Nabeshima, A. Hashiguchi, T. Saiki, S. Akine, *Angew. Chem.* **2002**, *114*, 499–502; *Angew. Chem. Int. Ed.* **2002**, *41*, 481–484; e) M. Ribó, J. Crusats, F. Sagués, J. Claret, R. Rubires, *Science* **2001**, *292*, 2063–2066; f) H. Nakashima, J. R. Koe, K. Torimitsu, M. Fujiki, *J. Am. Chem. Soc.* **2001**, *123*, 4847–4849; g) J. M. Fox, T. J. Katz, S. Van Elshocht, T. Verbiest, M. Kauranen, A. Persoons, T. Thongpanchang, T. Kraus, L. Brus, *J. Am. Chem. Soc.* **1999**, *121*, 3453–3459; h) R. Purrello, A. Raudino, L. M. Scolaro, A. Loisi, E. Bellacchio, R. Lauceri, *J. Phys. Chem. B* **2000**, *104*, 10900–10908; i) D. B. Steensgaard, H. Wackerbarth, P. Hildebrandt, A. R. Holzwarth, *J. Phys. Chem. B* **2000**, *104*, 10379–10386; j) D. Iarossi, A. Mucci, F. Parenti, L. Schenetti, R. Seeber, C. Zanardi, A. Forni, M. Tonelli, *Chem. Eur. J.* **2001**, *7*, 676–685; k) M. de Loos, J. van Esch, R. M. Kellogg, B. L. Feringa, *Angew. Chem.* **2001**, *113*, 633–636; *Angew. Chem. Int. Ed.* **2001**, *40*, 613–616; l) W. Steffen, B. Kohler, M. Altmann, U. Scherf, K. Stitzer, H.-C. zur Loye, U. H. F. Bunz, *Chem. Eur. J.* **2001**, *7*, 117–126; m) L. Brunsveld, E. W. Meijer, R. B. Prince, J. S. Moore, *J. Am. Chem. Soc.* **2001**, *123*, 7978–7984; n) J. H. Jung, H. Kobayashi, M. Masuda, T. Shimizu, S. Shinkai, *J. Am. Chem. Soc.* **2001**, *123*, 8785–8789; o) M. Wang, G. L. Silva, B. A. Armitage, *J. Am. Chem. Soc.* **2000**, *122*, 9977–9986; p) P. Wittung, P. Nielsen, O. Buchart, M. Egholm, B. Norden, *Nature* **1994**, *368*, 561–563.

[2] a) T. Aoki, T. Kaneko, N. Maruyama, A. Sumi, M. Takahashi, T. Sato, M. Teraguchi, *J. Am. Chem. Soc.* **2003**, *125*, 6346–6347; b) T. Kawasaki, M. Tokuhiro, N. Kimizuka, T. Kunitake, *J. Am. Chem. Soc.* **2002**, *124*, 11282–11283; c) H. Nakashima, M. Fujiki, J. R. Koe, M. Motonaga, *J. Am. Chem. Soc.* **2001**, *123*, 1963–1969; d) F. X. Redl, M. Lutz, J. Daub, *Chem. Eur. J.* **2001**, *7*, 5350–5358; e) T. Kurtan, N. Nesnas, Y.-Q. Li, X. Huang, K. Nakanishi, N. Berova, *J. Am. Chem. Soc.* **2001**, *123*, 5962–5973; f) K. Tomizaki, H. Nishino, T. Kato, A. Miike, N. Nishino, *Chem. Lett.* **2000**, 648–649; g) S. E. Boiadjiev, D. Lightner, *J. Am. Chem. Soc.* **2000**, *122*, 378–383; h) S. Yagi, T. Morinaga, T.

 © 2003 Wiley-VCH Verlag GmbH & Co. KGaA, Weinheim 

Nomura, T. Takagishi, T. Mizutani, S. Kitagawa, H. Ogoshi, *J. Org. Chem.* **2001**, *66*, 3848 – 3853; i) J. Recker, D. J. Tomcik, J. R. Parquette, *J. Am. Chem. Soc.* **2000**, *122*, 10298 – 10307; j) S. Saito, C. Nuckolls, J. Rebek, Jr., *J. Am. Chem. Soc.* **2000**, *122*, 9628 – 9630.

[3] a) V. V. Borovkov, J. M. Lintuluoto, Y. Inoue, *Helv. Chim. Acta* **1999**, *82*, 919 – 934.

[4] a) V. V. Borovkov, T. Harada, Y. Inoue, R. Kuroda, *Angew. Chem.* **2002**, *114*, 1436 – 1439; *Angew. Chem. Int. Ed.* **2002**, *41*, 1378 – 1381; b) V. V. Borovkov, J. M. Lintuluoto, M. Sugiura, Y. Inoue, R. Kuroda, *J. Am. Chem. Soc.* **2002**, *124*, 11282 – 11283; c) V. V. Borovkov, J. M. Lintuluoto, H. Sugeta, M. Fujiki, R. Arakawa, Y. Inoue, *J. Am. Chem. Soc.* **2002**, *124*, 2993 – 3006; d) V. V. Borovkov, J. M. Lintuluoto, Y. Inoue, *J. Am. Chem. Soc.* **2001**, *123*, 2979 – 2989; e) V. V. Borovkov, N. Yamamoto, J. M. Lintuluoto, T. Tanaka, Y. Inoue, *Chirality* **2001**, *13*, 329 – 335; f) V. V. Borovkov, J. M. Lintuluoto, Y. Inoue, *Org. Lett.* **2002**, *4*, 169 – 171; g) V. V. Borovkov, J. M. Lintuluoto, Y. Inoue, *Org. Lett.* **2000**, *2*, 1565 – 1568; h) V. V. Borovkov, J. M. Lintuluoto, M. Fujiki, Y. Inoue, *J. Am. Chem. Soc.* **2000**, *122*, 4403 – 4407; i) V. V. Borovkov, J. M. Lintuluoto, Y. Inoue, *J. Phys. Chem. A* **2000**, *104*, 9213 – 9219; j) V. V. Borovkov, J. M. Lintuluoto, Y. Inoue, *J. Phys. Chem. B* **1999**, *103*, 5151 – 5156.

[5] The term induced circular dichroism (ICD) was originally proposed by Prof. H. Falk for the phenomenon of asymmetry transfer from chiral solvents to achiral chromophores (for details, see H. Falk, W. Jungwirth, N. Müller, *Monatsh. Chem.* **1984**, *115*, 455 – 466).

[6] The choice of solvents (see Supporting Information) was limited to those that do not display any coordination to zinc porphyrins.

[7] M. Kasha, H. R. Rawls, M. A. El-Bayoumi, *Pure Appl. Chem.* **1965**, *11*, 371 – 392.

[8] $(CH_2Cl)_2$ is an exceptional case among the polar solvents studied with enhancement of the $B_2$ transition over $B_1$ transition, apparently because of its inability to form the corresponding solvation shell owing to steric hindrance.

[9] N. Harada, K. Nakanishi, *Circular Dichroic Spectroscopy. Exciton Coupling in Organic Stereochemistry*, University Science Books, Mill Valley, CA, **1983**.

[10] M. Nishio, M. Hirota, Y. Umezawa, *The CH/π Interaction: Evidence, Nature, and Consequence*, Wiley-VCH, New York, **1998**.

[11] In the case of **1**·(**3**)$_2$ the extremely narrow $\varepsilon_s$ gap of chirality switching is apparently because benzene also enhances a positive component of chirality induction for the same reasons as in the case of **1**·**4**$_2$ and **1**·**5**$_2$ but to a lesser extent.

 © 2003 Wiley-VCH Verlag GmbH & Co. KGaA, Weinheim 

Microporous Materials

# The Chirality, Porosity, and Ferromagnetism of a 3D Nickel Glutarate with Intersecting 20-Membered Ring Channels

*Nathalie Guillou,* Carine Livage, Marc Drillon, and Gérard Férey*

Hybrid edifices based on transition metals are currently one of the most productive areas of chemical research. Indeed, the ability of the organic moiety to diversify structural arrangements associated with the wide-ranging properties of transition metals (e.g. magnetic and optical properties, electronic conductivity and ferroelectricity) is very attractive as soon as the inorganic subnetwork is at least one-dimensional.[1] Whereas synthesis at room temperature leads only to coordination polymers, it is now well known that hydrothermal conditions considerably increase the dimensionality of the inorganic part and therefore the stability of the compounds.[2] In these conditions, divalent cations, such as Mn,[3] Fe,[4] Co,[5] Cu,[6] and Zn[7] generally lead to 1- and 2D inorganic subnetworks. The important feature is that the extent of the metal-oxide condensation seems to strongly depend on the electronic structure of the cation. For example, condensation becomes important with Mn species, which sometimes give pseudo 3D inorganic skeletons.[3b] With nickel, the inorganic condensation is even more diverse and first investigations on carboxylates showed that Ni could generate microporous materials with novel M-O-M connectivities in which polyhedra can share faces, edges, and/or corners.[8] Indeed, $[Ni_7(C_4H_4O_4)_6(OH)_2(H_2O)_2]\cdot 2H_2O$ presents a remarkable honeycomb nickel oxide network,[8a] while $[Ni_7(C_4H_4O_4)_4(OH)_6(H_2O)_3]\cdot 7H_2O$ or MIL-73 has a layered structure constructed from nickel oxide chains containing unprecedented hexanickel building blocks.[8e]

Herein we describe a ferromagnetic, porous, nickel glutarate which has a complex framework of helical octahedral chains and very large intersecting 20-membered ring tunnels.

The compound was synthesized by classical hydrothermal reaction. Its structure was solved by ab initio structure determination from laboratory data. A cubic solution ($a =$ 16.5812(7) Å; $V = 4558.8(6)$ Å$^3$) was consistent with the two chiral $P4_332$ and $P4_132$ space groups. Since it is impossible to

[*] Dr. N. Guillou, Dr. C. Livage, Prof. G. Férey
Institut Lavoisier, UMR CNRS 8637
Université de Versailles Saint-Quentin-en-Yvelines
45 avenue des Etats-Unis, 78035 Versailles Cedex (France)
Fax: (+33) 1-3925-4358
E-mail: guillou@chimie.uvsq.fr
Dr. M. Drillon
Institut de physique et de Chimie
des Matériaux de Strasbourg
23 rue du Loess, 67037 Strasbourg (France)

Supporting information for this article (selected analytical data and structural data) is available on the WWW under http://www.angewandte.org or from the author.

 © 2003 Wiley-VCH Verlag GmbH & Co. KGaA, Weinheim DOI: 10.1002/anie.200352520 

determine an absolute structure from powder diffraction, $P4_332$ was arbitrarily chosen to solve the structure. Nevertheless, because the starting materials are nonchiral, the final compound is probably a mixture of microcrystals of the two enantiomeric forms. At the final stage, the structural model contained 16 non-hydrogen atoms, and soft constraints were maintained for the organic molecules. The final Rietveld refinement (angular range 5–90° ($2\theta$); 416 reflections; 42 structural parameters; Figure 1) corresponds to satisfactory model indicators ($R_B = 0.033$ and $R_F = 0.030$) and profile factors ($R_P = 0.069$ and $R_{WP} = 0.095$).

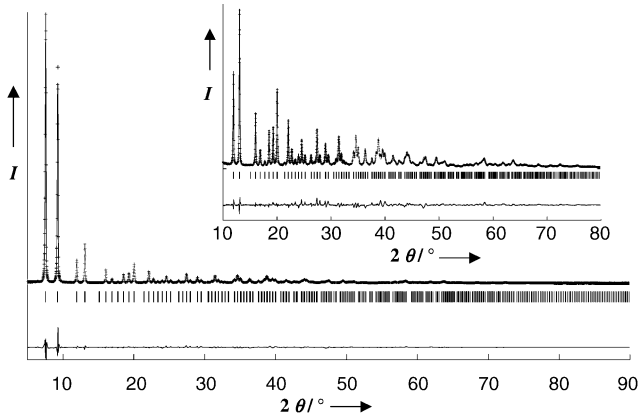



***Figure 1.*** Final Rietveld plot of MIL-77. Inset: an expansion at high angles.

Views of the structure (Figure 2) show that this new nickel glutarate, denoted MIL-77, presents an open 3D network of edge-sharing nickel octahedra. This complex framework is generated by two independent nickel atoms: Ni1 located on the threefold axis and Ni2 on the twofold one. The two independent nickel atoms have octahedral coordination with bond lengths ranging from 1.97(1) to 2.17(2) Å. Each Ni1 octahedron shares three edges with three Ni2 octahedra, each Ni2 octahedron shares two of its *trans* edges with two neighboring Ni1 octahedra. This complicated oxide network can be simply described from helixes running along the *a* axis, where Ni1 and Ni2 polyhedra alternate (Figure 2a). Each helix is connected to four out-of-phase parallel neighboring ones (above and below, and in front and behind), through a third Ni2 octahedron, which generates corrugated twenty-membered rings (Figure 2b). That also induces the formation of perpendicular helixes in this chiral structure. Topologically, a few analogies could be found with the (10–3)a network observed for nickel coordination polymers.[9] The oxide framework is decorated by two independent, deprotonated, glutarate anions (Figure 2b). One is located on the twofold axis and has two multidendate carboxylate groups which each coordinate to three nickel atoms, in an $\mu_2$ and a terminal fashion. This type of carboxylate connectivity is common and has been observed for numerous linear manganese, cobalt, and nickel dicarboxylates[3b,5a,5c,8a,8e] For the carboxylate groups of the second glutarate ion, one of the oxygen atoms coordinates through an $\mu_2$ manner and the other is non-coordinating. This type of carboxylate connectivity seems to be more specific to nickel compounds.[8a,f] In the case of dicarboxylates, it has been observed, to date, only for one of the carboxylate groups.[8a] Since this glutarate ion is located on a threefold axis, it is disordered with statistic occupancy of 2/3. To complete octahedral environment of the nickel centers, 1/3 of the Ni site filled by carboxylate oxygen atom is also occupied by a bridging water molecule. This situation corresponds to the chemical formula, $[Ni_{20}\{(C_5H_6O_4)_{20}(H_2O)_8\}]\cdot 40\,H_2O$.

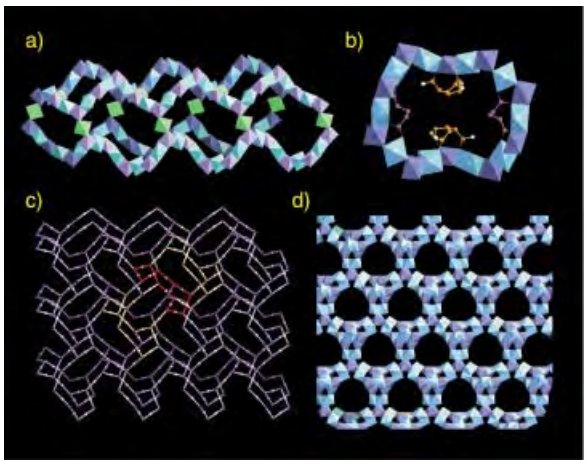



***Figure 2.*** a) View of four helixes with alternating Ni1 (mauve) and Ni2 (pale blue) connected by Ni2 octahedra (green), b) polyhedral view of a corrugated twenty-membered ring with the two independent glutarate ions; the orange one is disordered with statistic occupancy of 2/3, c) view of the nickel network showing interconnected rings, d) view of the nickel oxide tunnels down [111].

The twenty-membered rings intersect each other (Figure 2c) to generate crossing tunnels in the [111] direction (Figure 2d). The shortest opposite O···O distance in the corrugated ring is 9.1 Å and the longest one is 15.8 Å. The pores are partially obstructed by glutarate ions, mostly by the disordered one with a C–C distance of about 4 Å between central atoms of two glutarate molecules.

The thermal behavior of $[Ni_{20}\{(C_5H_6O_4)_{20}(H_2O)_8\}]\cdot 40\,H_2O$ was characterized by thermogravimetric analysis (TGA; flowing oxygen) and X-ray thermodiffraction (air). A gradual weight loss observed until 150 °C corresponds to the presence of the 40 occluded water molecules (found: 15.8 wt %, calcd: 15.5 wt %) without significant structural change. Then, the loss of the eight coordinated water molecules (found: 2.7 wt %, calcd: 3.1 wt %) occurs between 255 and 275 °C on the TGA curve and is combined to a crystallographic change observed at 240 °C. The anhydrous compound rehydrates very slowly (several days) under air at room temperature, even if no structural change is observed on thermodiffractometry from 250 °C to 50 °C. Its total rehydration can be obtained under water-saturated air in less than one day. This behavior may indicate sorption properties. Between 330 and 360 °C the structure collapses with the combustion of the organic moieties (found: 48.8 wt %, calcd: 49.2 wt %).

A sample activated at 200 °C under vacuum gives a typical Type-1 isotherm and a surface area of 346(10) $m^2g^{-1}$ which clearly indicates notable porosity for this compound. Curious-

 © 2003 Wiley-VCH Verlag GmbH & Co. KGaA, Weinheim 

ly, when the sample is activated under vacuum at 250 °C, the surface area decreases to 50(1) $m^2 g^{-1}$, which may indicate that important structural changes occur during the loss of the bridging water molecules. It is probably due to some motion of the organic molecules, which come to fill up the pores.

The magnetic properties of the compound, measured in a 3.5 Oe ac field, are displayed in Figure 3. Upon cooling from 9 to 4 K, $\chi T$ remains quite small, and then increases sharply at lower temperature, up to 1750 emu K $mol^{-1}$, followed by a moderate decay. The presence of an out-of-phase signal ($\chi''$)

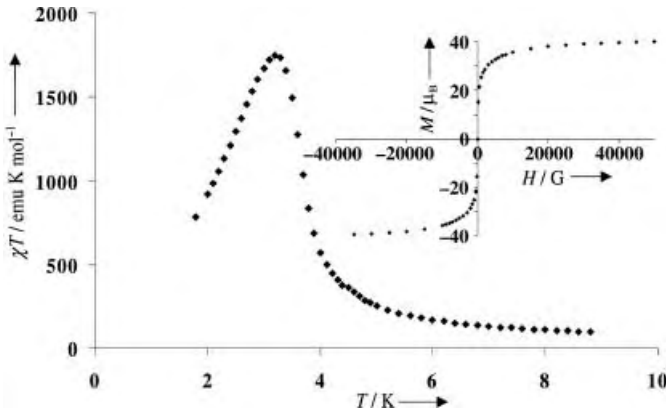



***Figure 3.*** Thermal dependence of the $\chi T$ product. The inset shows the magnetization versus the applied magnetic field at 2 K.

at the same temperature points to the stabilization of a magnetized state at low temperature. A plot of the field dependent magnetization at 2 K confirms these results (Figure 3). The saturation magnetization of 40 $\mu_B$ $mol^{-1}$ for $H = 60\,000$ G, demonstrates that this compound is a pure cooperative ferromagnet ($Ms = 40\ \mu_B$ expected for $g = 2$), without any spin frustration. Such a behavior is characteristic of ferromagnetic exchange interactions, which are expected for edge sharing nickel(II) octahedra (Ni1-O1-Ni2 99.9(4)° and Ni1-O3-Ni2 97.1(4)° with Ni1-Ni2 3.097(5) Å).[10] The low $T_c$ value is explained by the weakness of the ferromagnetic interaction for a bridge angle significantly larger than 90°.

In Summary, this nickel glutarate presents a chiral structure with very large crossing channels. For the first time, it has been possible to obtain a nickel carboxylate with a 3D network of pores, which is a pure ferromagnet at 4 K. Moreover, it becomes porous (346(10) $m^2 g^{-1}$) at 200 °C, after removing the water of hydration and can slowly reabsorb water molecules. A drastic decrease of the porosity, observed after activation of the sample at 250 °C, may correspond to a structural rearrangement. Some studies are in progress to explain this phenomenon. Once again, the originality of the structure illustrates the versatility of nickel-oxide networks and confirms the plasticity of nickel inorganic condensation under hydrothermal conditions.[5]

## Experimental Section

Reactions were carried out in a teflon container (23 mL) at 180 °C for two days under autogenous pressure. The reaction mixture contained $NiCl_2 \cdot 6H_2O$ (1.102 g), glutaric acid (0.916 g), KOH (0.518 g), and $H_2O$/ethanol (50/50 vol, 5 mL) in the molar ratio 1:1.5:2:60. After cooling (pH 5), the pale green powder was washed with distilled water. Elemental analysis (%): calcd: C 25.88, H 4.69, Ni 25.29; found: C 25.32, H 4.36, Ni 24.92.

The X-ray powder diffraction data were collected on a Siemens D5000 diffractometer by using $CuK_\alpha$ radiation ($\lambda = 1.5418$ Å). The powder diffraction pattern was scanned over an angular range 5–90°($2\theta$) with a step length of 0.02°($2\theta$). To improve the counting statistics at high angles, the pattern was divided in two $2\theta$ regions (1–35.98° and 36–90°), with times per step of 32 and 64 s, respectively. Pattern indexing was carried out with DICVOL91.[11] Structure solution was initialized with the EXPO package, integrating EXTRA, for extracting integrated intensities, and SIR97 for direct methods structure solution.[12] A list of 101 reflections was extracted in the angular range 7–70° ($2\theta$) and nickel atoms with their environments were found unambiguously from the E-map with the highest figure of merit. This partial structure was then used as fragment to complete the structural model. The corresponding atomic coordinates were used as starting model for Rietveld refinement, using FullProf integrated in WinPlotr.[13] Successive Fourier difference calculations were then performed with SHELXL to finalize the structural model.[14]

X-ray thermodiffractometry was performed under static air in an Anton Parr HTK16 high-temperature device of a Siemens D-5000 diffractometer ($\theta$–$\theta$ mode, $CoK_\alpha$ radiation) equipped with a M Braun linear position sensitive detector (PSD). The dehydration–rehydration processes have been studied at 10 °C intervals (40–250–50 °C) and decomposition at 20 °C intervals up to 600 °C; temperature ramp of 0.05 °C.$s^{-1}$; several hours at 250 and 50 °C. Thermogravimetric analysis was performed using a TA-Instruments TGA-2050 apparatus (oxygen flow 60 ml $min^{-1}$, 5 °C $min^{-1}$).

The BET surface area of samples activated under vacuum at 200 °C for 36 h and at 250 °C for 12 h was studied on a Micromeritics ASP200 porosimeter.

Magnetization measurements were performed on a Quantum Design Squid magnetometer (MPMS-5).

Received: July 30, 2003 [Z52520]
Published Online: October 20, 2003

**Keywords:** chirality · ferromagnetism · microporous materials · nickel · O ligands

[1] a) O. M. Yaghi, M. O'Keeffe, N. W. Ockwig, H. K. Chae, M. Eddaoudi, J. Kim, *Nature* **2003**, *423*, 705–714; b) G. Férey, *Chem. Mater.* **2001**, *13*, 3084–3098; c) S. Feng, R. Xu, *Acc. Chem. Res.* **2001**, *34*, 239–247; d) M. Eddaoudi, H. Li, O. M. Yaghi, *J. Am. Chem. Soc.* **2000**, *122*, 1391–1397.
[2] C. Livage, C. Egger, G. Férey, *Chem. Mater.* **2001**, *13*, 410–414.
[3] a) Y. Kim, E. Lee, D.-Y Jung, *Chem. Mater.* **2001**, *13*, 2684–2690; b) R. Vaidhyanathan, S. Natarajan, C. N. R. Rao, *J. Chem. Soc. Dalton Trans*, **2003**, 1459–1464; c) Y.-Q. Zheng, D. Sun, *J. Solid State Chem.* **2003**, *172*, 288–295.
[4] M. Sanselme, J. M. Grenèche, M. Riou-Cavellec, G. Férey, *Chem. Commun.* **2002**, 18, 2172–2173.
[5] a) C. Livage, C. Egger, G. Férey, *Chem. Mater.* **1999**, *11*, 1546–1550; b) Z.-L. Huang, M. Drillon, N. Masciocchi, A. Sironi, J.-T Zhao, P. Rabu, P. Panissod, *Chem. Mater.* **2000**, *12*, 2805–2812; c) L.-S. Long, X.-M. Chen, M.-L. Tong, Z.-G. Sun, Y.-P. Ren, R.-B. Huang, L.-S. Zheng, *J. Chem. Soc. Dalton trans.* **2001**, *19*, 2888–2890; d) M. Kurmoo, H. Kumagai, M. A. Green, B. W. Lovett, S. J. Blundell, A. Ardavan, J. Singleton, *J. Solid State Chem.* **2001**, *159*, 343–351.
[6] S. S.-Y. Chui, S. M.-F. Los, J. P. H. Charmant, A. G. Orpen, I. D. Williams, *Science* **1999**, *283*, 1148–1150.

 © 2003 Wiley-VCH Verlag GmbH & Co. KGaA, Weinheim 

[7] a) H. Li, M. Eddaoudi, M. O'Keeffe, O. M. Yaghi, *Nature* **1999**, *402*, 276 – 279; b) T. A. Bowden, H. L. Milton, A. M. Z. Slawin, P. Lightfoot, *J. Chem. Soc. Dalton trans.* **2003**, *5*, 936 – 939.
[8] a) P. M. Forster, A. K. Cheetham, *Angew. Chem.* **2002**, *114*, 475 – 477; *Angew. Chem. Int. Ed.* **2002**, *41*, 457 – 459; b) H. Kumagai, Y. Oka, M. M. Akita-Tanaka, K. Inoue, *Inorg. Chim. Acta* **2002**, *332*, 176 – 180; c) S. Konar, P. S. Mukherjee, E. Zangrando, F. Lloret, N. R. Chaudhuri, *Angew. Chem.* **2002**, *114*, 1631 – 1633; *Angew. Chem. Int. Ed.* **2002**, *41*, 1561 – 1563; d) N. Guillou, S. Pastre, C. Livage, G. Férey, *Chem. Commun.* **2002**, 2358 – 2359; e) N. Guillou, C. Livage, W. van Beek, M. Noguès, G. Férey, *Angew. Chem.* **2003**, *115*, 643 – 647; *Angew. Chem. Int. Ed.* **2003**, *42*, 457 – 459; f) P. M. Forster, Z. Yang, A. K. Cheetham, *Solid State Sci.* **2003**, *5*, 635 – 642.
[9] a) C. J. Kepert, M. J. Rosseinsky, *Chem. Commun.* **1998**, 31 – 32; b) C. J. Kepert, T. J. Prior, M. J. Rosseinsky, *J. Am. Chem. Soc.* **2000**, *122*, 5158 – 5168; c) T. J. Prior, M. J. Rosseinsky, *Inorg. Chem.* **2003**, *42*, 1564 – 1575.
[10] J. B. Goodenough *Magnetism and the Chemical Bond*, Wiley, New York, **1963**.
[11] A. Boultif, D. Louër, *J. Appl. Crystallogr.* **1991**, *24*, 987 – 993.
[12] a) A. Altomare, M. C. Burla, M. Camalli, B. Carozzini, G. L. Cascarano, C. Giacovazzo, A. Guagliardi, A. G. G. Moliterni, G. Polidori, R. Rizzi, *J. Appl. Crystallogr.* **1999**, *32*, 339 – 340; b) A. Altomare, M. C. Burla, G. Cascarano, C. Giacovazzo, A. Guagliardi, A. G. G. Moliterni, G. Polidori, *J. Appl. Crystallogr.* **1995**, *28*, 842 – 846; c) A. Altomare, M. C. Burla, M. Camalli, G. L. Cascarano, C. Giacovazzo, A. Guagliardi, A. G. G. Moliterni, G. Polidori, R. Spagna, *J. Appl. Crystallogr.* **1999**, *32*, 115 – 119.
[13] a) J. Rodriguez-Carvajal, *Collected Abstract of Powder Diffraction Meeting* (Toulouse) **1990**, p. 127; b) T. Roisnel, J. Rodriguez-Carvajal, *Mater. Sci. Forum* **2001** *378–381*, 118 – 123.
[14] G. M. Sheldrick, SHELXL-97, Program for the Solution of Crystal Structures, University of Göttingen, Göttingen (Germany), **1997**. CCDC 216165 contains the supplementary crystallographic data for this paper. These data can be obtained free of charge via www.ccdc.cam.ac.uk/conts/retrieving.html (or from the Cambridge Crystallographic Data Centre, 12 Union Road, Cambridge CB2 1EZ, UK; fax: (+44) 1223-336-033; or deposit@ccdc.cam.ac.uk).

 © 2003 Wiley-VCH Verlag GmbH & Co. KGaA, Weinheim 

Biosensors

# Encoded Fiber-Optic Microsphere Arrays for Probing Protein–Carbohydrate Interactions**

*Eddie W. Adams, Jörn Ueberfeld, Daniel M. Ratner, Barry R. O'Keefe, David R. Walt,* and Peter H. Seeberger**

Carbohydrate-binding proteins and their glycoconjugate ligands play significant roles in a number of critical biological processes. Immune response, viral membrane fusion, glycoprotein homeostasis, and signaling all involve carbohydrate-binding protein mediation at key steps.[1] A more detailed understanding of the exact nature of carbohydrate–protein interactions is expected to render them attractive therapeutic targets. To facilitate these biochemical investigations, glycobiologists require tools that will enable the simultaneous identification of carbohydrate-binding proteins and the oligosaccharide structures they bind.

Carbohydrate microarrays were introduced as a promising tool to aid in the discovery of oligosaccharide moieties necessary for carbohydrate-binding protein recognition.[2] Microarrays require small quantities of material, enable simultaneous screening of a defined set of structures against a host of potential binding partners, and, in some cases, are fully amenable to present high-throughput screening technologies, such as robotic printing and fluorescence scanning devices.

In the past year, several systems were described that present both natural and synthetically derived carbohydrate structures in array formats.[3] These systems differ in the mode of immobilization (covalent versus noncovalent), the surface upon which the immobilization was performed, and the

[*] Prof. Dr. P. H. Seeberger,[++] E. W. Adams,[+] D. M. Ratner
Department of Chemistry
Massachusetts Institute of Technology
Cambridge, MA 02139 (USA)
Fax: (+1) 617-253-2979
E-mail: seeberg@mit.edu

Prof. Dr. D. R. Walt, Dr. J. Ueberfeld[+]
The Max Tishler Laboratory for Organic Chemistry
Department of Chemistry
Tufts University
Medford, MA 02155 (USA)
E-mail: david.walt@tufts.edu

Dr. B. R. O'Keefe
Molecular Targets Development Program
NCI Center for Cancer Research
National Cancer Institute, NCI-Frederick
Frederick, MD 21702 (USA)

[+] These authors contributed equally to this work.

[++] Current address: Laboratory for Organic Chemistry. ETH Hönggerberg HCI F 315, Wolfgang Pauli Strasse 10,CH 8093 Zurich.

[**] This research was supported by a NDSEG Fellowship (for E.W.A.) and a NIH Biotechnology Training Grant (for D.M.R.). P.H.S. thanks GlaxoSmithKline (Scholar Award), the Alfred P. Sloan Foundation (Fellowship) and Merck for financial support. The Tufts effort was supported by a grant from NIH-NIDCR U01 DE14950-01.

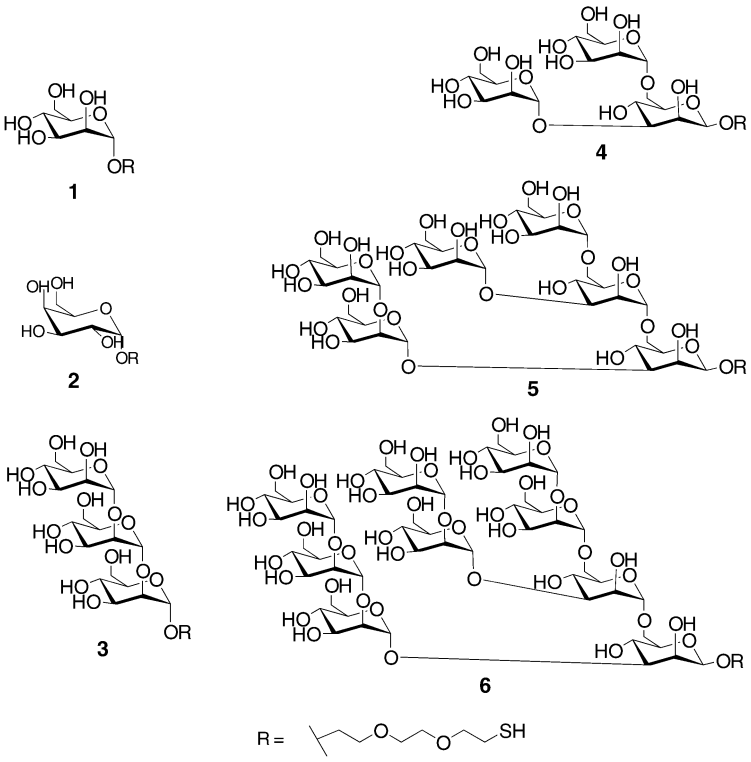
 DOI: 10.1002/anie.200351286 © 2003 Wiley-VCH Verlag GmbH & Co. KGaA, Weinheim 

means of detecting binding events (fluorescence and colorimetric detection). Herein we describe the use of fiber-optic microsphere arrays equipped with covalently immobilized synthetic oligosaccharides for the rapid analysis of protein–carbohydrate interactions.

Fiber-optic random microsphere arrays have been described in detail for DNA hybridization detection.[4] Here we use arrays with different populations of 4.5-μm microspheres of which each contains a unique carbohydrate structure covalently attached to its surface as well as an internally encoded spectral signature (an entrapped fluorescent dye with an emission maximum at 690 nm). The internal dye serves two purposes: it identifies the carbohydrate present on the surface of the bead surface and aids in determining the position of each type of microsphere in the array (Figure 1).

To demonstrate the utility of such arrays for studying protein–carbohydrate interactions, we examined two systems: the mannose-binding lectin concanavalin A (Con A), and cyanovirin N (CVN), a novel HIV-inactivating 11-kDa protein derived from the cyanobacterium *Nostoc ellipsosporum* with specificity for with a high mannose oligosaccharides.[5]

Mannose **1** and galactose **2** monosaccharides were prepared with a thiol-terminated ethylenedioxy linker at the anomeric center (Scheme 1).[6] Each monosaccharide was coupled to commercially available maleimide-activated bovine serum albumin (BSA). The neoglycoproteins were then attached to encoded microspheres by using a water-soluble carbodiimide. This conjugation strategy was used to achieve adequate spacing between the underlying polymer support and the carbohydrates. The resulting carbohydrate-functionalized microspheres were used to form a randomly ordered fiber-optic microsphere array. Con A binding was detected by incubating the fiber-optic array in a solution of Con A labeled with Alexa 488 at 50 μg mL$^{-1}$ for five minutes. Then, the lectin solution was removed, replaced with a fresh buffer solution and the fluorescence signal at the Alexa 488 wavelength (520 nm) was measured. Only those beads bearing **1** were bound by labeled Con A (Figure 2). The intrinsic nonspecific-binding levels of fiber-optic arrays in this assay were very low and the specificity of carbohydrate–protein interactions was clearly observed as no Con A was detected in the empty wells or associated with beads functionalized with **2**.




***Scheme 1.*** Carbohydrate structures used for the generation of randomly ordered microsphere arrays.

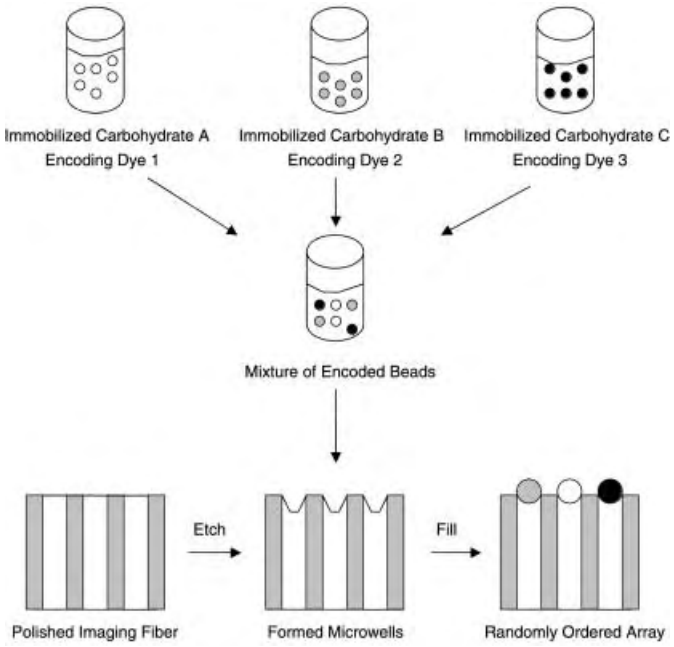



***Figure 1.*** Schematic representation of randomly ordered microsphere arrays.

To determine the concentrations of labeled Con A required to observe signals easily discriminated over background, the fiber-optic arrays were incubated with a dilution series of labeled Con A ranging from 0 to 400 μg mL$^{-1}$. Con A concentrations as low as 25 μg mL$^{-1}$ yielded fluorescence signals easily discernible over background (Figure 3). Even at very high lectin concentrations, no increase in fluorescence is observed associated with the beads presenting **2**.

After protein–carbohydrate interactions were detected with a simple lectin–monosaccharide system, five synthetic carbohydrates (**1**,**3**–**6**) were immobilized on microspheres carrying a unique internal code for each structure. Small aliquots of each of the five dispersions were mixed to form a random fiber-optic microsphere array and the array was probed with CVN.

CVN–oligosaccharide binding was assayed by incubating the array in a solution of BODIPY-labeled CVN at

 © 2003 Wiley-VCH Verlag GmbH & Co. KGaA, Weinheim 

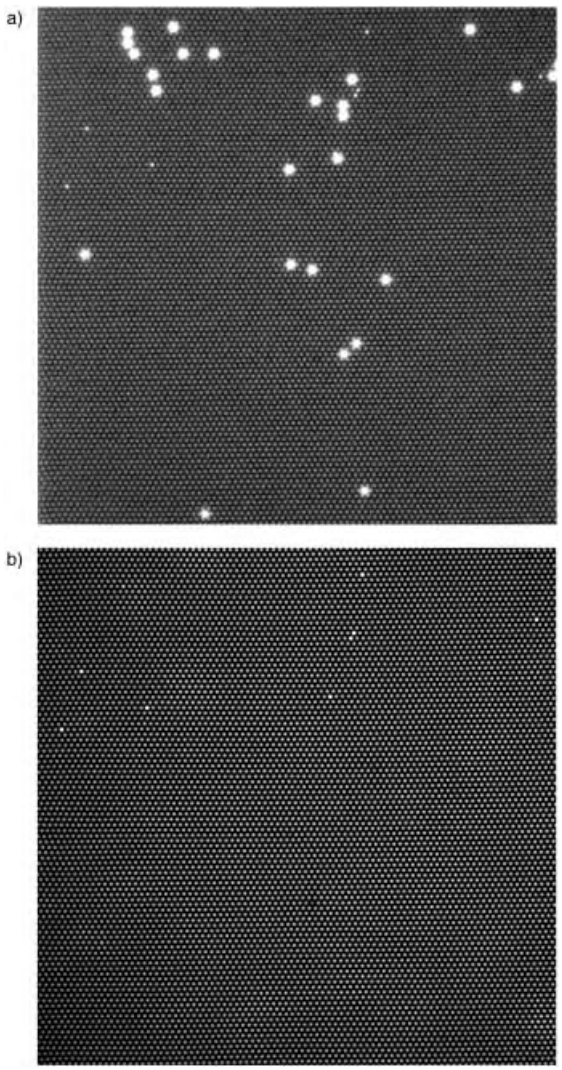



***Figure 2.*** Internally encoded microsphere array presenting immobilized **1** and **2**. a) Fluorescence at 690 nm prior to Con A incubation; b) fluorescence at 520 nm, post-Con A incubation.

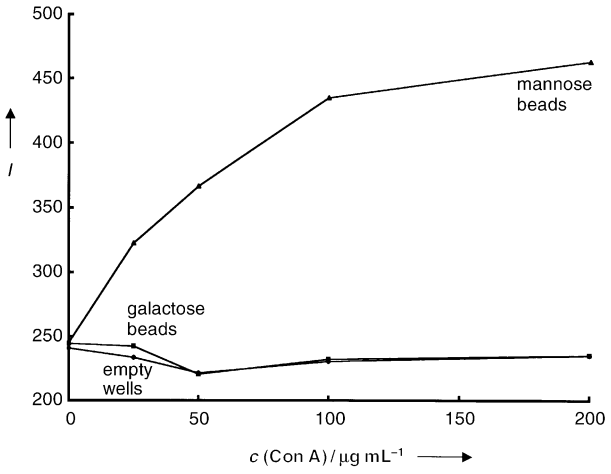



***Figure 3.*** Con A dilution series. Microsphere array containing **1** and **2** was probed with Con A labeled with Alexa 488 at various concentrations (plotted fluorescence intensities normalized to background fluorescence). $I$ = intensity of fluorescence (arbitrary units).

50 μg mL$^{-1}$ for five minutes before the CVN solution was removed and replaced with fresh buffer. Light at the BODIPY excitation wavelength (488 nm) was passed through the optical fiber bundle and the BODIPY emission was collected with a CCD camera. Three of the five structures (**3,5,6**) present were bound by CVN (Figures 4 and 5) in

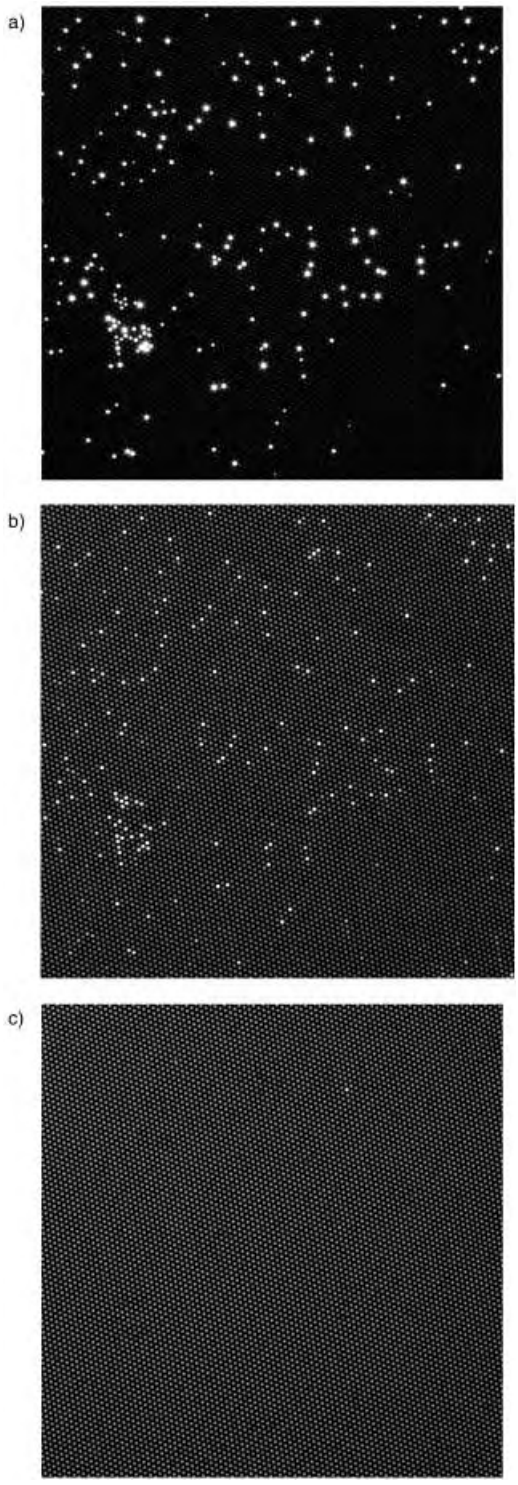



***Figure 4.*** Internally encoded microsphere array presenting **1** and **3**–**6** (see Scheme 1). a) Fluorescence at 690 nm prior to BODIPY-CVN incubation; b) fluorescence at 520 nm prior to CVN incubation; c) fluorescence at 520 nm post-CVN incubation.

 © 2003 Wiley-VCH Verlag GmbH & Co. KGaA, Weinheim 

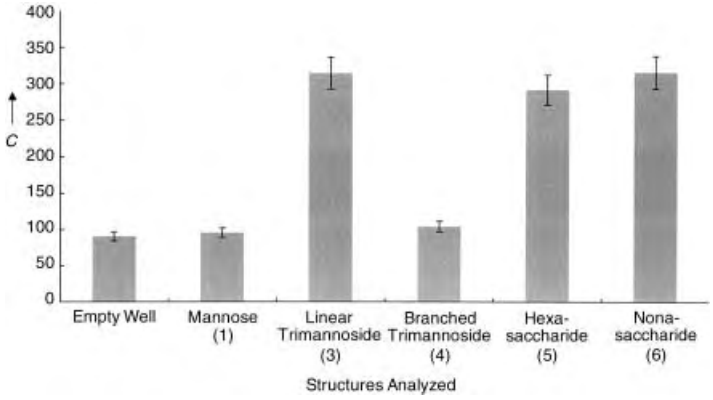



***Figure 5.*** Integrated fluorescence intensities from microsphere array. Fluorescence intensities were measured as detailed in the Experimental Section and normalized to background fluorescence. $C$ = fluorescence counts, 520 nm.

accordance with isothermal microcalorimetry studies.[7] Beads that were not bound by CVN did not show any fluorescence signals over background levels (Figure 5).

In summary, we have demonstrated that randomly ordered fiber-optic microsphere arrays bearing immobilized synthetic oligosaccharides can be used to evaluate protein–carbohydrate interactions. The system described herein allows for the simultaneous evaluation of five distinct structures against a carbohydrate-binding protein with unambiguous results. While this study makes use of synthetic structures, future efforts towards functionalizing small quantities of complex oligosaccharides from natural sources (e.g., glycoproteins) should readily extend the applicability of the described platform for the study of protein–carbohydrate interactions.

## Experimental Section

Carbohydrate synthesis: Thiol-terminated ethyleneglycol-derivatized saccharides were prepared as described previously.[6] In the syntheses, 2-[2-(2-benzylsulfanylethoxy)ethoxy]ethanol was substituted for pentenyl alcohol. This substitution affords an ethyleneglycol-modified thiol handle for covalent immobilization of the structures to a maleimide-modified surface or protein carrier.

Neoglycoprotein preparation: Maleimide-activated BSA and Tris(2-carboxyethyl)phosphane hydrochloride (TCEP) were purchased from Pierce Chemical. Compound **1** (50 μg, 152 nmol) was incubated with 1 equiv TCEP in 10 mM HEPES buffer (pH 7.5) at room temperature for 1 h with constant mixing. This solution was added to 100 μg maleimide-modified BSA in 100 μL of the same buffer. The solution was incubated overnight at room temperature with constant mixing. Without further purification the encoded microspheres were added to this neoglycoprotein solution. This coupling chemistry was used for all structures in this study.

Microsphere preparation: Internally encoded QuantumPlex microspheres (4.4 μm) were purchased from Bangs Laboratories. Stock beads (100 μL) were washed by centrifugation/re-dispersion (3× with 10 mM HEPES buffer, pH 7.5)and conjugated to neoglycoproteins with an excess of water-soluble carbodiimide. Beads were purified from excess neoglycoprotein by centrifugation/re-dispersion (3× in HEPES buffer). Microspheres were stored in 10 mM HEPES buffer with 0.1% Tween 20 at 4 °C until use.

Fiber-optic microsphere array formation: Equal amounts (10 μL) of bead suspensions were mixed and 1 μL of the mixture was added to the etched end of an imaging fiber (about 24000 microwells, well diameter 5 μm, Illumina, San Diego, USA). The mixture was left to dry before the excess beads were rinsed away with deionized water. About 30 beads of each type were present on the array.

Detection of protein–carbohydrate interactions: Images of the fiber-optic carbohydrate array were acquired with a custom-built epifluorescence microscope equipped with a xenon arc lamp and a CCD camera (Hamamatsu C4742-95-12-ER, Optical Analysis Corp., Nashua, NH). The system was controlled with IPLab software (Scananalytics, Fairfax, VA) which was also used for image processing. The positions of the microspheres were registered by exciting their internal encoding dye StarfireRed at 640 nm (emission maximum at 690 nm). The decoding of the different carbohydrate structures was achieved by analyzing the emission intensities at 690 nm. The array was incubated with the fluorescently labeled lectin at various concentrations for 5 min ($V$ = 200 μL). Then the lectin solutions were replaced with buffer and an image of the array was taken at the emission wavelength of the label (520 nm, exposure time 1 s). Fluorescence intensities in Figures 3 and 5 represent mean values of about 30 beads.

Received: February 26, 2003
Revised: July 28, 2003 [Z51286]

**Keywords:** biosensors · carbohydrates · proteins

[1] a) P. M. Rudd, T. Elliot, P. Cresswell, I. A. Wilson, R. A. Dwek, *Science* **2001**, *291*, 2370; b) D. C. Chan, P. S. Kim, *Cell* **1998**, *93*, 681; c) S. J. Lee, S. Evers, D. Roeder, A. F. Parlow, J. Risteli, L. Ristelli, Y. C. Lee, T. Feizi, H. Langen, M. Nussenzweig, *Science* **2002**, *295*, 1898; d) M. Demetriou, M. Granovksy, S. Quaggin, J. W. Dennis, *Nature* **2001**, *409*, 733.

[2] a) K. Love, P. H. Seeberger, *Angew. Chem.* **2002**, *114*, 3733; *Angew. Chem. Int. Ed.* **2002**, *41*, 3583; b) L. Kiessling, C. W. Cairo, *Nat. Biotechnol.* **2002**, *20*, 234; c) C. O. Mellet, J. M. Garcia Fernandez, *ChemBioChem* **2002**, *3*, 819.

[3] a) D. Wang, S. Liu, B. Trummer, C. Deng, A. Wang, *Nat. Biotechnol.* **2002**, *20*, 275; b) S. Fukui, T. Feizi, C. Galustian, A. Lawson, W. Chai, *Nat. Biotechnol.* **2002**, *20*, 1011; c) F. Fazio, M. C. Bryan, O. Blixt, J. C. Paulson, C. H. Wong, *J. Am. Chem. Soc.* **2002**, *124*, 14397; d) B. Houseman, M. Mrksich, *Chem. Biol.* **2002**, *9*, 443; e) S. Park, I. Shin, *Angew. Chem.* **2002**, *114*, 3312; *Angew. Chem. Int. Ed.* **2002**, *41*, 3180.

[4] a) F. J. Steemers, J. A. Ferguson, D. R. Walt, *Nat. Biotechnol.* **2000**, *18*, 91; b) J. A. Ferguson, F. J. Steemers, D. R. Walt, *Anal. Chem.* **2000**, *72*, 5618; c) D. R. Walt, *Acc. Chem. Res.* **1998**, *31*, 267.

[5] a) M. Boyd, K. Gustafson, J. McMahon, R. Shoemaker, B. O'Keefe, T. Mori, R. Gulakowski, L. Wu, M. Rivera, C. Laurencott, M. Currens, J. Cardellina, R. Buckheit, P. Nara, L. Pannell, R. Sowder, L. Henderson, *Antimicrob. Agents Chemother.* **1997**, *41*, 1521; b) A. J. Bolmstedt, B. R. O'Keefe, J. B. McMahon, M. R. Boyd, *Mol. Pharmacol.* **2001**, *59*, 949.

[6] D. M. Ratner, O. J. Plante, P. H. Seeberger, *Eur. J. Org. Chem.* **2002**, 826–833.

[7] S. Shenoy, L. Barrientos, D. Ratner, B. O'Keefe, P. H. Seeberger, A. Gronenborn, M. Boyd, *Chem. Biol.* **2002**, *9*, 1109.

 © 2003 Wiley-VCH Verlag GmbH & Co. KGaA, Weinheim 

*Zinc Oxide Nanoparticles*

# Room-Temperature Organometallic Synthesis of Soluble and Crystalline ZnO Nanoparticles of Controlled Size and Shape

*Miguel Monge, Myrtil L. Kahn, André Maisonnat, and Bruno Chaudret**

ZnO is a wide-band-gap semiconductor (3.37 eV) that displays interesting luminescent properties, which include the recent demonstration of ultraviolet lasing from nanowires.[1,2] These properties have stimulated the search for new synthetic methodologies for well-controlled ZnO nanostructures. Several reports on high-temperature physical[3,4] or chemical[5–9] ZnO syntheses have recently been published. The chemical methods appear to be of particular interest since they offer the potential of facile scale-up, and occur at moderate temperatures (100–200 °C). The synthesis is generally carried out in water or alcohols using zinc salts as starting materials in the presence of a base.[5–7] These methods are convenient and may lead to nanomaterials of controlled morphology. However, the synthesis makes use of ionic species, which may react with the growing oxide and modify the properties of the final material, whether chemical or physical. An alternative method using the organometallic complex $[Zn(C_2H_5)_2]$ (**1**) as a precursor was reported by Klabunde et al.[8] However, it involves the transformation of **1** into an alkoxide prior to hydrolysis and heat treatment. Complex **1** was also recently used for the synthesis of ZnO[9] following a "high-temperature organometallic method" derived from that originally reported by Bawendi et al.[10] in the presence of ligands, such as tri-*n*-octyl phosphane oxide (TOPO) and amines.

In separate studies, we have evidenced the interest of organometallic complexes for the preparation of metal nanoparticles of controlled size and shape.[11–15] This methodology was extended to the synthesis of metal oxide nanoparticles through a two-step approach : 1) the formation of metal nanoparticles through decomposition of the organometallic precursor, and 2) the oxidation of the as-formed nanoparticles.[16–18] This approach has allowed the preparation of $SnO_2$ and $In_2O_3$ particles for gas sensing[16,17] and was also used for the preparation of ZnO particles from the bisalkyl zinc precursor $[Zn(c\text{-}C_6H_{11})_2]$ (**2**).[18] However, we reasoned that most organometallic complexes are air-sensitive and decompose exothermically in air. A controlled oxidation of the precursor in solution could therefore lead in one step to oxidized nanomaterials (oxides or hydroxides), the shape and size of which could in principle be controlled by the ligands or surfactants present.

Herein we report the *room-temperature* synthesis of ZnO nanoparticles of controlled size and shape in solution. This route provides crystalline nanoparticles of regular disk or rod shapes depending on the characteristics of the solution, in terms of solvent, ligand, and concentration. The oxide particles are fully soluble in organic solvents giving rise to clear and luminescent solutions from which regular monolayers can be deposited.[19]

When a solution of the dicyclohexylzinc(II) compound **2** in THF[20] is left standing at room temperature in open air, the solvent slowly evaporates and leaves a white luminescent residue, which was characterized by XRD and TEM as being agglomerated nanoparticles of ZnO with a zincite structure that display no defined size or shape. If, however, ligands such as long chain amines are added under argon to a solution of **2** in THF, and the resulting mixture is treated as before, well-defined nano-objects are formed, the size and shape of which depend upon the reaction conditions. For example, the reaction can be carried out in THF using hexadecylamine (HDA) as a ligand. After a reaction time of 17 h and evaporation of the solvent (concentration of reagents: 0.042 mol $L^{-1}$; standard procedure[21]), homogeneous nanorods of approximately $8.1 \times 2.6$ nm are obtained, which can be redissolved in THF (Figure 1a). Several parameters were identified as important for controlling the size, shape, and homogeneity of the nanomaterials, namely the nature of the ligand, the relative concentration of the reagents, the solvent, the overall concentration of the reagents, the reaction time, the evaporation time, and the reaction/evaporation temperature. These parameters and their influence on the ZnO nano-objects produced are listed in Table 1 and, in some cases, illustrated in Figures 1 and 2.[21] All new materials were characterized by X-ray diffraction (XRD) and/or selected-area electron diffraction (SAED) and consistently display the same pattern. The XRD pattern corresponds to the hexagonal zincite phase, space group $P6_3mc$ (see Supporting Information; S1).

It is evident from Table 1 that the control of the size and morphology of the ZnO particles results from the nature of the solution (solvent, ligands, concentrations, and so on). We have previously shown, in particular by NMR spectroscopy, that the shape control of metal nanoparticles was related to ligand coordination.[13] A similar effect seemed however very surprising in the case of oxides and led us to undertake an NMR study. The addition of HDA to **2** in $[D_8]$THF leads to $^1H$ and $^{13}C\{^1H\}$ NMR spectra that suggest the coordination of the amine to **2** through nitrogen atoms. After oxidation, the $^{13}C\{^1H\}$ NMR spectra of the reaction mixture do not reveal the presence of any trace of **2** but show peaks attributed to HDA. The signals corresponding to the carbon atoms in the α, β, and γ positions relative to nitrogen at $\delta = 42.69$, 34.58, and 27.31 ppm, respectively, are very broad (see Figure 3). This phenomenon has been observed previously on ruthenium nanoparticles[13] and can be attributed to a fast exchange between free ligand molecules in solution and coordinated ligand molecules linked to ZnO through nitrogen atoms. This therefore demonstrates that throughout the process of

[*] Dr. B. Chaudret, Dr. M. Monge, Dr. M. L. Kahn, Dr. A. Maisonnat
Laboratoire de Chimie de Coordination du CNRS
205, route de Narbonne
31077 Toulouse Cédex 04 (France)
Fax: (+33) 5-6155-3003
E-mail: chaudret@lcc-toulouse.fr

Supporting information for this article is available on the WWW under http://www.angewandte.org or from the author.

 DOI: 10.1002/anie.200351949 © 2003 Wiley-VCH Verlag GmbH & Co. KGaA, Weinheim 

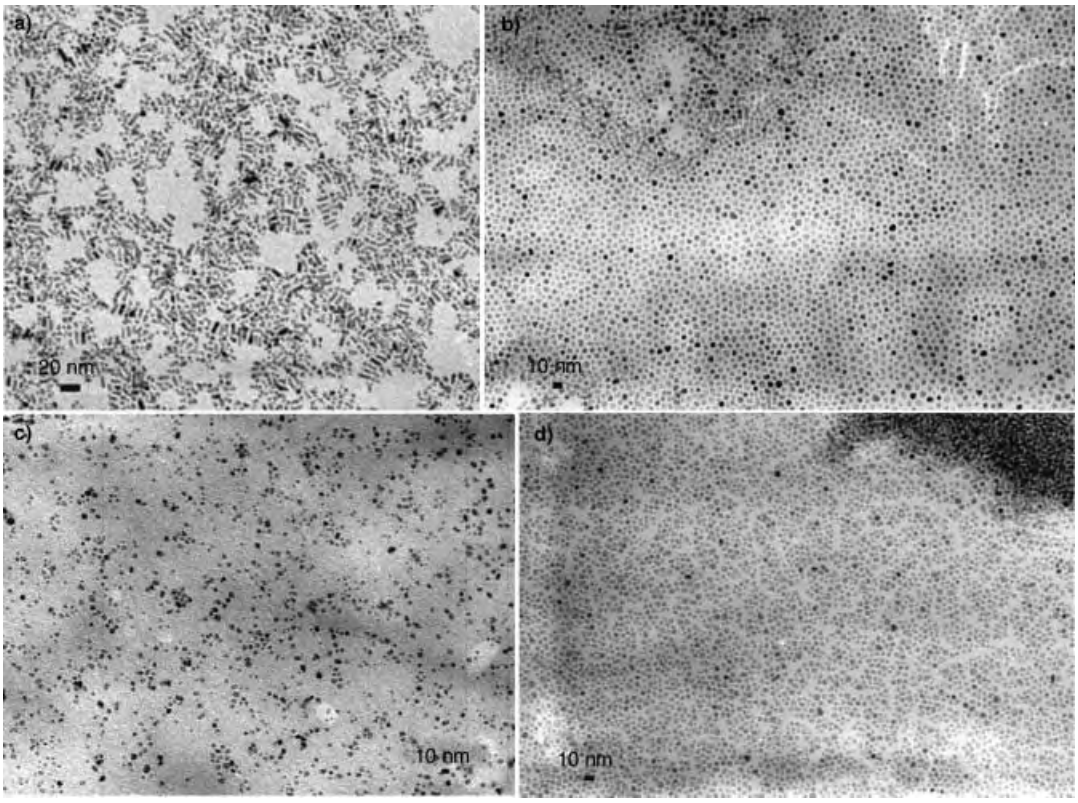



***Figure 1.*** TEM micrographs of ZnO nanoparticles. a) ZnO nanorods grown under standard conditions (see ref. [21]); b) ZnO nanodisks following a slow oxidation/evaporation process in THF (2 weeks); c) ZnO nanodisks using dodecylamine (DDA) instead of hexadecylamine (HDA) as the stabilizing ligand under standard conditions; d) ZnO nanodisks using octylamine (OA) instead of HDA under standard conditions.

***Table 1:*** Summary of the results obtained after oxidation of the $[Zn(c\text{-}C_6H_{11})_2]$ precursor under various reaction conditions.

| Ligand added | Solvent | Time | Overall concentration [M] | Temperature | Size [nm][b] | Morphology |
|---|---|---|---|---|---|---|
| – | THF | Standard[a] | 0.042 | RT | | Agglomerated nanoparticles |
| HDA | THF | Standard | 0.042 | RT | $8.1 \pm 3.3 \times 2.6 \pm 0.4$ | Nanorods |
| HDA | THF | Standard | 0.125 | RT | $11.4 \pm 5.7 \times 2.8 \pm 0.7$ | Nanorods |
| HDA | THF | 2 weeks | 0.042 | RT | $4.1 \pm 0.9$ | Nanodisks |
| HDA | THF | Standard | 0.042 | 45 °C | $4.8 \pm 0.3$ | Nanodisks |
| HDA | THF | Standard | 0.01 | RT | $< 3.0$ after 1 day<br>$4.3 \pm 0.5$ after 4 days | Nanodisks |
| HDA | THF | 5 min under Ar | 0.042 | RT | $5.8 \pm 1.3 \times 2.7 \pm 0.3$ | Nanorods |
| DDA | THF | Standard | 0.042 | RT | $3.0 \pm 0.5$ | Nanodisks |
| OA | THF | Standard | 0.042 | RT | $4.0 \pm 0.7$ | Nanodisks |
| HDA | Toluene | Standard | 0.042 | RT | $4.6 \pm 0.9$ | Nanodisks |
| HDA | Heptane | Standard | 0.042 | RT | $2.4 \pm 0.5$ | Nanodisks |
| HDA | – | Standard | – | RT | $10.7 \pm 1.2 \times 1.6 \pm 0.3$ | Nanorods |
| DDA | – | Standard | – | RT | $9.2 \pm 2.0 \times 3.7 \pm 1.8$ | Nanorods |
| OA | – | Standard | – | RT | $7.4 \pm 1.4 \times 2.8 \pm 0.6$ | Nanorods |
| 2 HDA | – | Standard | – | RT | ~5 | Not homogeneous |
| 2 DDA | – | Standard | – | RT | $17.1 \pm 3.4 \times 3.0 \pm 0.4$ | Nanorods |
| 2 OA | – | Standard | – | RT | $36.9 \pm 10.8 \times 2.8 \pm 0.3$ | Nanorods |

[a] Standard reaction time is 17 h under Ar and 1 or 2 days of oxidation/evaporation. [b] The values indicate the diameter of nanodisks or the length and width for nanorods; size dispersion is given after the mean size.

oxidation, the amine ligand remains coordinated to zinc and suggests that this coordination participates to the control of the growth of the particles.

The results reported in this communication highlight the possibility of synthesizing crystalline ZnO nanoparticles of controlled morphology at room temperature. If the length, width, or diameter of the particles are well characterized, TEM observations suggest that the particles are in fact plates or disks, which agrees with the layered structure of ZnO. The control of size and shape results from the characteristics of the solutions (presence of amine ligands; presence and nature of the solvent). Quite surprisingly, the zinc oxide nano-objects prepared in this way may change size and shape at room temperature in solution. For example, when carrying out the reaction with HDA, as described in the standard procedure, but with a

 © 2003 Wiley-VCH Verlag GmbH & Co. KGaA, Weinheim 

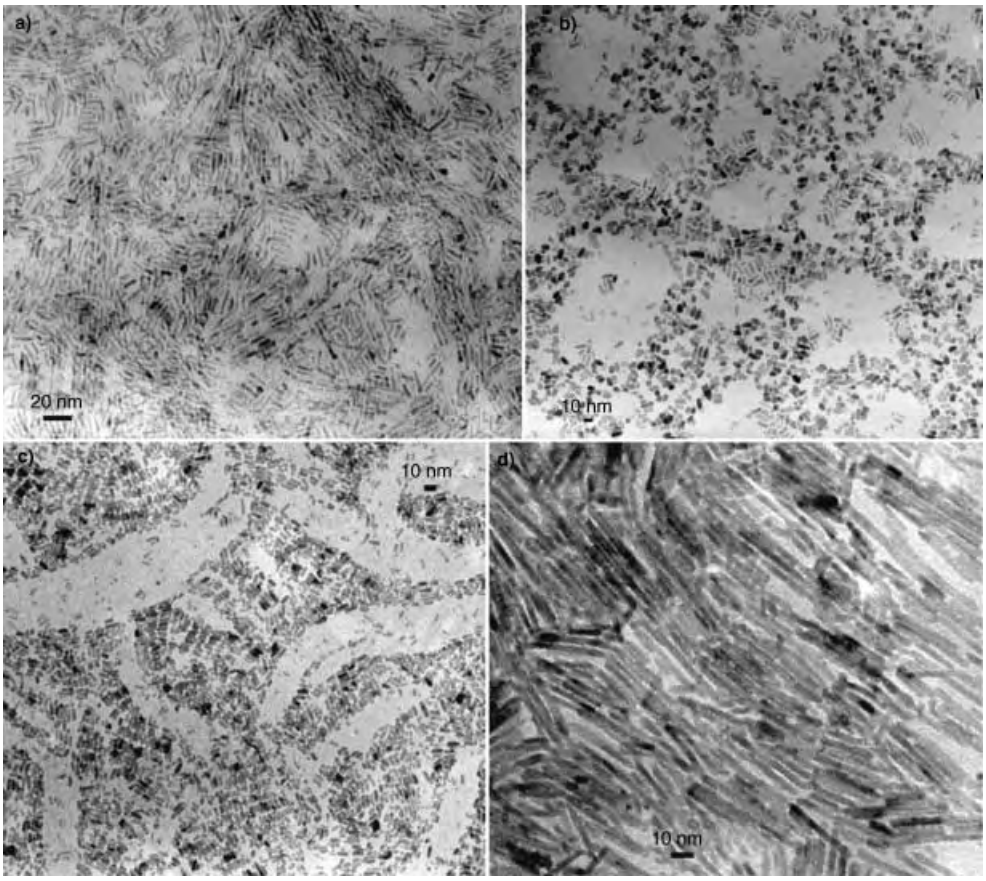



***Figure 2.*** TEM micrographs of various ZnO nanorods, which were prepared using 1 equiv HDA (a), DDA (b), or OA (c) ligands in the absence of solvent; d) long ZnO nanorods obtained in the presence of 2 equiv OA as ligand, in the absence of solvent.

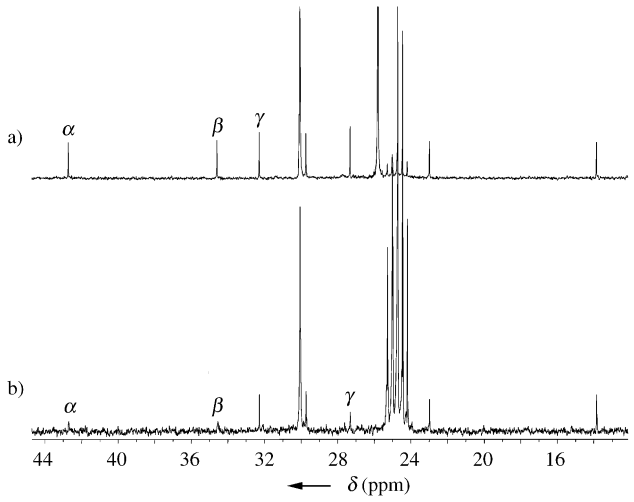



***Figure 3.*** $^{13}C\{^{1}H\}$ NMR spectra of a) the free HDA ligand; b) ZnO nanoparticles coated with HDA.

concentration of reagents of 0.01 mol $L^{-1}$, very small spherical particles are obtained after 24 h (less than 3 nm in diameter), which coalesce into nanodisks of approximately 4.3 nm diameter after 4 days, whereas nanorods form at higher HDA concentrations. This result is in agreement with the findings of Weller et al., where the shape of the ZnO nanoparticles formed were found to be very sensitive to the overall concentration of the precursors, and gave rise to rodlike ZnO particles by "oriented attachment" at high concentrations and quasi-spherical particles at low concentrations.[7] The anisotropic (nanorod) shape is observed either when the particles are synthesized in the presence of one equivalent of HDA in THF under otherwise standard conditions, or with one or two equivalents of amine in the absence of solvent. However, nanorods are not formed when the reaction mixture is heated or if the reaction is allowed to proceed very slowly, which strongly suggests that the rods are kinetic products and, as such, thermodynamically unstable, in contradiction with what has been found for cobalt nanorods.[15] This also suggests that the mesoscopic structure of the solution, present in the conditions described above, but absent when the solution is heated or diluted, may control the growth of the nanorods. The nature of the solvent and of the amine are also important since the growth of rods only occurs with the THF/HDA combination or in the presence of various amines but in the absence of solvent. This again suggests that the organization of the ligand in solution plays a decisive role for the shape control.

All ZnO nanoparticles described in this paper display, at room temperature, both in solution and in the solid state, two emission bands; one near 570 nm and the other near 365 nm,

 © 2003 Wiley-VCH Verlag GmbH & Co. KGaA, Weinheim 

in agreement with previous reports on ZnO particles.[3,22] It is interesting to note that the two emission bands are not quenched by the solvents and that they are intense enough to be directly observed by the human eye (See Supporting Information; S2 and S3).

In conclusion, we have described the unprecedented formation of crystalline zinc oxide nanoparticles in solution at room temperature. The exact mechanism of this astonishing reaction is difficult to assess. In principle, the decomposition in air of the organometallic precursor was expected to lead to an oxidized material. However, the absence of hydroxide formation is surprising and may result from the exothermicity of the oxidation reaction. Furthermore, the crystallinity, the coalescence phenomena, the changes of size and shape observed at room temperature in solution, and the formation of extended monolayers were not anticipated. This suggests that, like metal nanoparticles, oxide nanoparticles display a dynamic behavior in solution. This can be linked to the demonstration of ligand coordination throughout the synthesis process. It is moreover interesting that such semiconducting oxide nano-objects form clear and luminescent organic solutions. Finally, these nanoparticles can easily be deposited on various surfaces as monolayers or thick layers, and may thus be applied as photoluminescent probes or paints.

Received: May 22, 2003 [Z51949]

**Keywords:** colloids · luminescence · nanomaterials · oxides · zinc

[1] M. H. Huang, S. Mao, H. Feick, H. Yan, Y. Wu, H. Kind, E. Weber, R. Russo, P. Yang, *Science* **2001**, *292*, 1897.
[2] J. Johnson, H. Yan, R. Schaller, L. Haber, R. Saykally, P. Yang, *J. Phys. Chem. B* **2001**, *105*, 11387.
[3] P. Yang, H. Yan, S. Mao, R. Russo, J. Johnson, R. Saykally, N. Morris, J. Pham, R. He, H. Choi, *Adv. Funct. Mater.* **2002**, *12*, 323.
[4] W. I. Park, G. Yi, M. Kim, S. L. Pennycock, *Adv. Mater.* **2002**, *14*, 1841.
[5] L. Vayssieres, K. Keis, A. Hagfeldt, S. Lindquist, *Chem. Mater.* **2001**, *13*, 4395.
[6] L. Vayssieres, *Adv. Mater.* **2003**, *15*, 464.
[7] C. Pacholski, A. Kornowski, H. Weller, *Angew. Chem.* **2002**, *114*, 1234; *Angew. Chem. Int. Ed.* **2002**, *41*, 1188.
[8] C. L. Carnes, K. J. Klabunde, *Langmuir* **2000**, *16*, 3764.
[9] M. Shim, P. Guyot-Sionnest, *J. Am. Chem. Soc.* **2001**, *123*, 11651.
[10] C. B. Murray, D. J. Norris, M. G. Bawendi, *J. Am. Chem. Soc.* **1993**, *115*, 8706.
[11] K. Soulantica, A. Maisonnat, M.-C. Fromen, M.-J. Casanove, P. Lecante, B. Chaudret, *Angew. Chem.* **2001**, *113*, 462; *Angew. Chem. Int. Ed.* **2001**, *40*, 448.
[12] K. Soulantica, A. Maisonnat, F. Senocq, M.-C. Fromen, M.-J. Casanove, P. Lecante, B. Chaudret, *Angew. Chem.* **2001**, *113*, 3071; *Angew. Chem. Int. Ed.* **2001**, *40*, 2983.
[13] C. Pan, K. Pelzer, K. Philippot, B. Chaudret, *J. Am. Chem. Soc.* **2001**, *123*, 7584.
[14] N. Cordente, M. Respaud, F. Senocq, M.-J. Casanove, C. Amiens, B. Chaudret, *Nano Lett.* **2001**, *1*, 565.
[15] F. Dumestre, B. Chaudret, C. Amiens, M.-C. Fromen, M.-J. Casanove, P. Renaud, P. Zurcher, *Angew. Chem.* **2002**, *114*, 4462; *Angew. Chem. Int. Ed.* **2002**, *41*, 4286.
[16] C. Nayral, E. Viala, P. Fau, F. Senocq, J.-C. Jumas, A. Maisonnat, B. Chaudret, *Chem. Eur. J.* **2000**, *6*, 4082.
[17] K. Soulantica, L. Erades, M. Sauvan, F. Senocq, A. Maisonnat, B. Chaudret, *Adv. Funct. Mater.* **2003**, *13*, 553.
[18] F. Rataboul, C. Nayral, M.-J. Casanove, A. Maisonnat, B. Chaudret, *J. Organomet. Chem.* **2002**, *643–644*, 311.
[19] M. Monge, M. L. Kahn, A. Maisonnat, B. Chaudret, Fr 03-04285, **2003**.
[20] K. H. Thiele, S. Wilcke, M. Ehrhardt, *J. Organomet. Chem.* **1968**, *14*, 13.
[21] Standard experimental procedure: Both the precursor and the ligand are introduced in equal quantity under argon in a predried solvent (approximately 50 ppm of water is present, as measured by Karl-Fisher volumetric titration ; concentration of each reactant: 0.042 mol $L^{-1}$) and left to react at room temperature for a few hours. The solution is then exposed to ambient air and moisture, generally for one or two days, during which the solvent evaporates and the complex is oxidized and condenses into nanoparticles of zinc oxide (see Figure 1a). The nanoparticles can then be dissolved or suspended again in a solvent for further use. Interestingly, a similar reaction carried out in dry air leads to agglomerated nanoparticles of ZnO displaying no defined size or shape. Increasing the concentration of reagents in solution from 0.042 to 0.125 mol $L^{-1}$ leads to nano-objects of higher aspect ratio. Exchanging THF for toluene or heptane produces nanoparticles of isotropic morphology with mean diameters of 4.6 and 2.4 nm, respectively. A slow oxidation/evaporation process in THF (2 weeks) produces only nanodisks of very homogeneous size (4.1 nm; see Figure 1b). Reducing the reaction time under argon to 5 min, prior to oxidation leads to shorter nanorods $\approx 5.8 \times 2.7$ nm in size. Increasing the reaction temperature leads to isotropic disk-shaped nano-objects. Exchanging HDA for dodecylamine (DDA) or octylamine (OA) also leads to disks with mean diameters of 3.0 and 4.0 nm, respectively (Figure 1c and d). Finally, in the absence of solvent, mixing equimolar amounts of **1** and an amine (HDA, DDA, or OA) yields nanorods of $10.7 \times 1.6$, $9.2 \times 3.7$, and $7.4 \times 2.8$ nm, respectively. In this case, doubling the concentration of amine relative to zinc has little effect for HDA but produces nanorods of $17.1 \times 3.0$ nm or $36.9 \times 2.8$ nm in the case of DDA and OA, respectively (see Figure 2).
[22] A. van Dijken, E. A. Meulenkamp, D. Vanmaekelbergh, A. Meijerink, *J. Lumin.* **2000**, *90*, 123.

 © 2003 Wiley-VCH Verlag GmbH & Co. KGaA, Weinheim 

*Stabilizing the gp41 Trimer in HIV-1*

# A Metallopeptide Assembly of the HIV-1 gp41 Coiled Coil Is an Ideal Receptor in Fluorescence Detection of Ligand Binding**

*Miriam Gochin,* Rodney Kiplin Guy, and Martin A. Case*

The transmembrane subunit, gp41, of the envelope glycoprotein of HIV-1 plays a crucial role in the fusion of the virus to the target cell during infection.[1–3] During the conformational changes that accompany virus–cell binding, the coiled-coil domain of three HR1 helices of trimeric gp41 becomes exposed and vulnerable to attack by antiviral drugs that could prevent fusion and infection of cells.[4] To date, the only successful drug against fusion is the peptide T-20 (DP178), derived from the HR2 region of gp41.[5–8] T-20 binds tightly to the HR1 coiled coil, thus interfering with formation of the fusion-competent six-helix bundle structure of gp41, comprising three HR1 and three HR2 helices. There is considerable interest in the discovery and development of nonproteolytic alternatives to T-20, which is very expensive to produce and not orally bioavailable.

A key challenge to screening compound libraries for drugs that target the three stranded coiled coil of gp41 arises from the fact that it is unstable when excised from full-length gp41 and buried in intact gp41. Peptides from gp41 HR1 are hydrophobic and tend to aggregate in solution. Previous approaches for accessing the coiled coil domain have involved stabilizing it as part of a larger soluble protein construct. Prior work has included the addition of GCN4 trimeric helices which extend the coiled coil by several heptad repeats (IQN17),[9] the preparation of 5-helix, a gp41 protein lacking one HR2 domain,[10] and the use of mutant 6-helix protein in which the HR1–HR2 interaction is destabilized, thus allowing for transient exposure of the HR1 coiled coil.[11] We report herein on the design of a stable fragment of the HR1 coiled-coil domain that does not involve extra protein domains, and that can be used in a fluorescence assay for rapid screening of potential fusion inhibitors.

The basis of the design is depicted in Figure 1. A metal-ion-binding bidentate ligand, 2,2′-bipyridyl (bpy) is attached to the N-terminus of a 31 residue peptide that contains residues 565–584 of gp41. The region selected contains a prominent cavity within the grooves of the coiled coil.[12] Addition of a metal ion such as $Fe^{II}$ or $Ni^{II}$ should result in formation of a tris-bipyridyl metal complex, which stabilizes the coiled-coil structure, as has been shown previously for several designed peptides.[13–18]

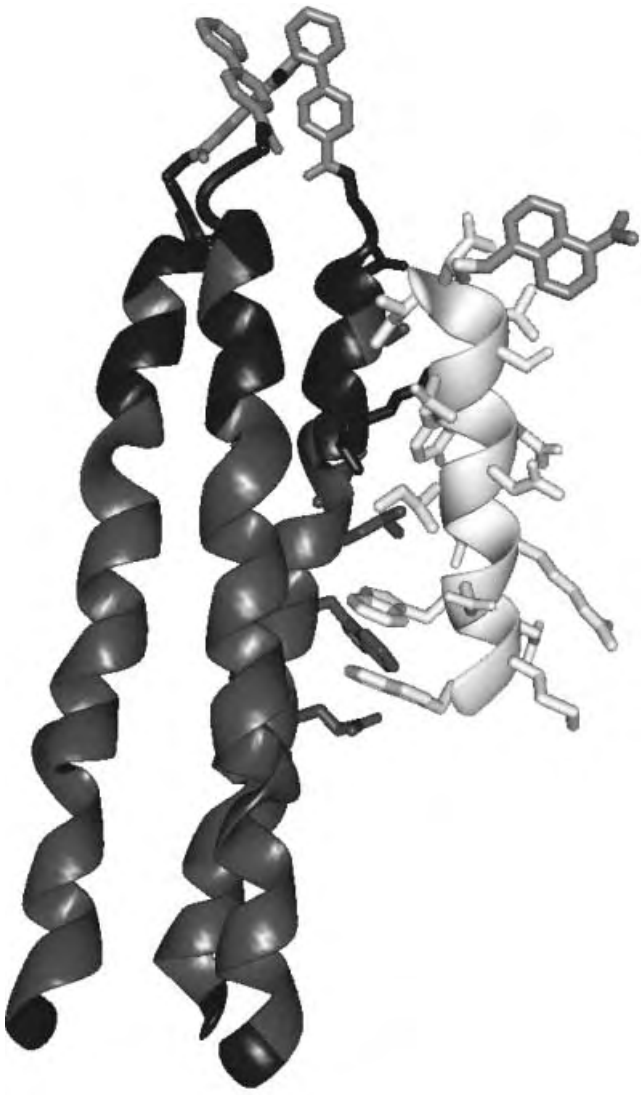


***Figure 1.*** Model of the expected Fe-env2.1—dansylated C-peptide interaction, derived by homology modeling from pdb2ez0. Residues of Fe–env2.1 corresponding to the native sequence of the gp41 coiled coil are shown in gray, and all other coiled coil residues in black. Iron(II) is shown in black, coordinated to the bipyridine groups in light gray. The C-peptide residues are off-white, with the dansyl group shown in light gray attached to the cysteine side chain in an arbitrary conformation. For clarity, side chains of coiled coil residues not in direct contact with the C-peptide are omitted. The distance between iron(II) and the dansyl group is estimated from the model to be about 15 Å.

[*] Prof. M. Gochin
Dept. Microbiology, University of the Pacific School of Dentistry, San Francisco, CA 94115 (USA)
and
Dept. Pharmaceutical Chemistry, University of California, San Francisco, CA 94143 (USA)
Fax (+1) 415-929-6564
E-mail: miriam@picasso.ucsf.edu, mgochin@uop.edu
R. Kiplin Guy
Dept. Pharmaceutical Chemistry
University of California
San Francisco, CA 94143 (USA)
M. A. Case
Department of Chemistry
University of Vermont
Burlington, VT 0540

[**] This work was supported by grants from the University-wide AIDS research project of the State of California (to M.G.), the American Foundation for AIDS Research (to M.G.), the National Science Foundation (to M.A.C.) and from the Sandler Research Foundation (to R.K.G).

 DOI: 10.1002/anie.200352006 © 2003 Wiley-VCH Verlag GmbH & Co. KGaA, Weinheim 

The $Fe^{II}$–bipyridyl complex is magenta, which corresponding to an absorbance maximum at 545 nm. This absorbance agrees well with the emission maximum of a dansyl fluorophore, which absorbs at 340 nm and emits at 542 nm (for the free probe). Thus, quenching of the dansyl fluorescence by fluorescent resonance energy transfer (FRET)[19] should occur if it is brought within 30 Å of the $Fe^{II}$–bipyridyl center. This is accomplished by using a C-peptide from the HR2 region of gp41, labeled with a dansyl fluorophore at a C-terminal cysteine (Figure 1). The C-peptide is expected to bind to the grooves of a properly folded coiled coil, thus inducing fluorescence quenching.

UV, Circular Dichroism, NMR and fluorescence spectroscopy have been used to characterize this system and demonstrate the effectiveness of the design. The peptide shown in Figure 1 has the sequence bpy–GQA **V**QA**L**EKL **L**QL**T**VWG **I**KQ**L**QAR **I**LA**V**EK-amide. It was prepared according to previously published procedures.[20] Residues native to gp41 are underlined, and positions a and d of the heptad repeat are highlighted in bold. In the first heptad repeat, the native gp41 sequence was substituted with a sequence designed to stabilize three-helix bundle formation.[21] The additional residues bpy–GQA at the N-terminal end were designed to fulfill structural requirements for metal–bpy ligation (unpublished results). This peptide is referred to as env2.1. Metal ion binding was readily observed in the UV spectrum with a red shift of the 291 nm $\pi$–$\pi^*$ band and a metal–ligand charge transfer band at 314 nm for $Ni^{II}$ and 545 nm for $Fe^{II}$ centers. The secondary structure was elucidated by measuring the mean residue ellipticity in the CD spectrum at 222 nm. A relatively high intrinsic helical content of 76 % was obtained for the apo-peptide and it increased to 87 % and 90 % upon addition of $Fe^{II}$ and $Ni^{II}$ ions, respectively.

The formation of discrete trimeric structure was assessed by NMR spectroscopy. Shown in Figure 2 are aromatic regions of the NMR spectra of env2.1 with and without $Ni^{II}$ ions. Line broadening of the Trp and bipyridyl resonances in the apo-peptide is indicative of nonspecific hydrophobic aggregation. In the presence of paramagnetic $Ni^{II}$ ions, which shift the aromatic bpy resonances far downfield,[18] the five Trp resonances sharpen significantly, thus demonstrating the alleviation of aggregation. NMR diffusion experiments conducted on $Ni^{II}$ ion-bound env2.1 confirmed the trimeric structure. The molecular weight estimated from diffusion lies within 12 % of the expected molecular weight of 11.08 kDa for the trimer. Thus the metal-bound form of this peptide should be able to present the binding surfaces of the hydrophobic coiled coil required for binding HR2 peptides or alternative drug candidates. This is a critical test for success of the design in creating a properly folded coiled coil.

The ability of the designed coiled coil to bind to known target peptides was examined by using CD and NMR spectroscopy. Target peptides included a 16-residue flanking peptide from the C-terminal heptad repeat of gp41 and a previously designed D-peptide, known as D10-p1–2K,[22] which binds to the hydrophobic pocket. The C-peptide has the sequence Ac-WMEWDRKIEEYTKKIC. It is altered from the native sequence Ac-WMEWDREINNYTSLIH according to a design suggested by Otaka et al.,[23] in which amino acids nonessential to the HR1–HR2 binding interaction are mutated to permit $i,i+3$ Lys-Glu salt bridges. These mutations are intended to stabilize the helical conformation and improve the solubility of the hydrophobic C-peptide. The C-terminal cysteine was introduced for dansyl-aziridine labeling.[25] The important binding interactions are hydrophobic contacts involving Trp 1, Trp 4 and Ile 8 in the hydrophobic pocket, as well as a salt bridge between Asp 5 and Lys 574 of the coiled coil.

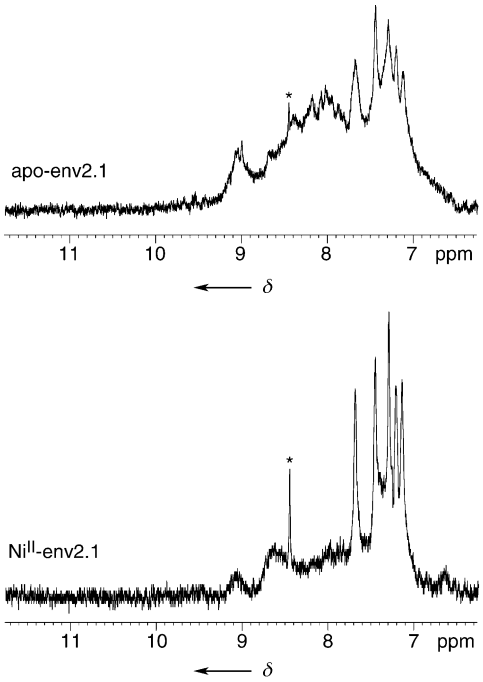



***Figure 2.*** Aromatic region of the $^1$H NMR spectra of 200 μM env2.1, free (top) and in the presence of 67 μM $NiCl_2$ (bottom). Spectra were taken at 500 MHz and 25 °C in 25 mM deuterated Tris/acetate buffer at pH 6. A spurious signal is indicated with an asterisk.

Figure 3 shows the results of CD experiments to test for binding between the 16 residue C-peptide and env2.1. The short C-peptide has no apparent helicity, despite the presence of three putative salt bridges. In the absence of a metal ion, the spectrum of an equimolar mixture of C-peptide and env2.1 is indistinguishable from the sum of the spectra of the two individual components, thus indicating that no interaction can be detected. This correlates with the result from NMR spectroscopy, in which aggregation of apo-env2.1 was observed. Aggregation is expected to interfere with formation of the correct helical fold or obscure the binding site. In the presence of $Fe^{II}$ ions, however, and in accordance with the NMR result, clear evidence of binding is obtained. The spectrum of the mixture of C-peptide and Fe-bound env2.1 differs from the sum of component spectra. There is a concomitant increase in the overall helicity of the system, presumably due to the increased helicity of the C-peptide upon binding.

The binding of the D-peptide D10-p1-2K to env2.1 was followed by NMR and compared to the results obtained with IQN17.[22] D10-p1-2K has the sequence

 © 2003 Wiley-VCH Verlag GmbH & Co. KGaA, Weinheim 

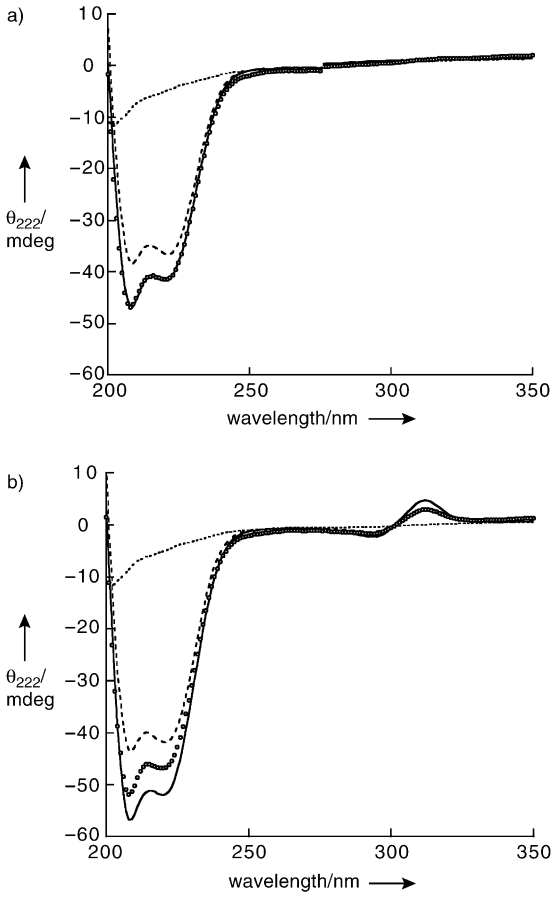



***Figure 3.*** CD spectra of env2.1 (-----) and C-peptide (••••) alone and combined in an equimolar ratio (——). Also shown is the sum of the env2.1 and C-peptide spectra (○).a) Results for apo-env2.1; b) results for $Fe^{II}$—bound env2.1.

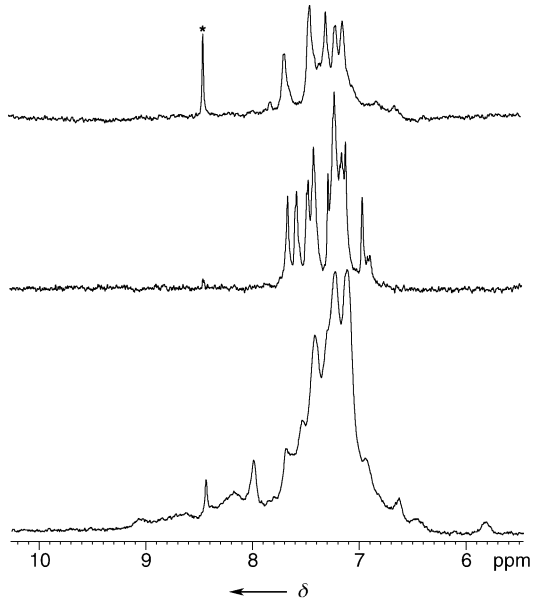



***Figure 4.*** 500 MHz aromatic $^1$H NMR spectra of: (top) 0.8 mM $Ni^{II}$-bound env2.1; (middle) 0.5 mM D10-p1–2 K; (bottom) a mixture of 0.8 mM $Ni^{II}$-bound env2.1 and 0.4 mM D10-p1–2 K. A spurious peak is indicated with an asterisk.

Ac-KKGACEARHREWAWLCAA-$NH_2$ with all D-amino acids. Binding between D10-p1-2K and env2.1 is characterized by line broadening and upfield shifting of Trp resonances (Figure 4), as was described previously with IQN17. The shifts were attributed to ring-current effects of the D-peptide on the resonances of Trp571 in the hydrophobic pocket. There is additional upfield shifting of a methyl group, possibly of Ile573 by the same mechanism (data not shown).

The ability of metal-bound env2.1 to recognize and bind the C- and D-peptides confirms the integrity of the construct. We then evaluated FRET as a means of detection of peptide binding. Figure 5a shows the observed fluorescence intensity of dansylated C-peptide as a function of $Fe^{II}$-env2.1 concentration. A 3.5-fold reduction in fluorescence intensity was observed as a result of peptide–coiled-coil binding. The curve was fit to a standard binding isotherm with a dissociation constant, $K_d$, of $0.40 \pm 0.09$ μM. It should be noted here that an alternative coiled-coil construct of the same length as env2.1 but with the native gp41 sequence in the first heptad repeat, binds the C-peptide with a similar $K_d$ ($0.65 \pm 0.20$ μM). This observation implies that the bulk of the binding affinity resides with the groups interacting in the hydrophobic pocket and not along the first heptad repeat of the coiled coil (Figure 1).

Figure 5b demonstrates a competitive inhibition assay with this system. Titration of unlabeled C-peptide was followed by measuring the fluorescence intensity in solutions containing 100 μM dansylated C-peptide and 5 μM $Fe^{II}$-env2.1. Recovery of the dansyl fluorescence at high C-peptide concentrations was observed, with an $IC_{50}$ value of $273 \pm 35$ μM. Most of the difference between $IC_{50}$ and $K_d$ can be accounted for by the effect of substrate concentration on $IC_{50}$

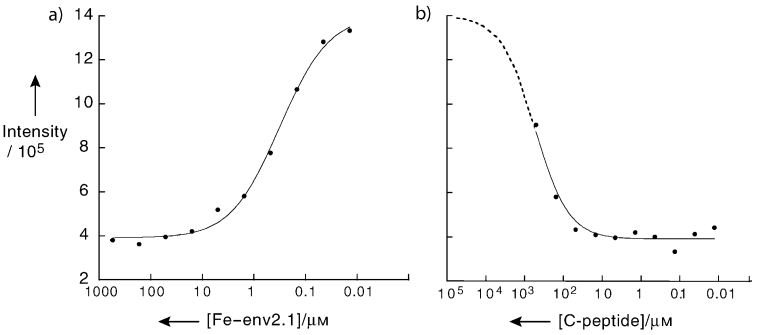



***Figure 5.*** a) Titration of $Fe^{II}$-env2.1 into wells of a 396-well plate containing a final concentration of 100 μM dansylated C-peptide in 25 mM Tris/acetate buffer, pH 6.6. $Fe^{II}$-env2.1 concentration is shown along the *x*-axis and fluorescence intensity above 400 nm following excitation at 340 nm is shown along the *y*-axis. The binding curve shown was fit to the binding isotherm $\Delta F = c_1(P_t - c_2\Delta F)/(K_d + P_t - c_2\Delta F)$ where $\Delta F$ is the reduction in fluorescence intensity compared to maximum, $P_t$ = [Fe–env2.1] and $c_1$,$c_2$ are constants. b) A competition experiment in which unlabeled C-peptide was titrated into wells of a 396-well plate containing a final concentration of 100 μM dansylated C-peptide and 5 μM Fe–env2.1. The data was fit to a competitive inhibition curve $\Delta F = \Delta F_0/(1 + L_t/IC_{50})$. $\Delta F_0$ is the maximum fluorescence change and $L_t$ = [C-peptide]. Part of the curve was inaccessible owing to limited solubility of the C-peptide.

 © 2003 Wiley-VCH Verlag GmbH & Co. KGaA, Weinheim 

in competitive inhibition kinetics.[24] In this experiment, the dansylated peptide concentration is 250 times the value of $K_d$. The additional factor of $\approx$2–3 in the observed ratio of $IC_{50}$ to $K_d$ may arise from a slightly different binding affinity of the dansylated peptide. $IC_{50}$ values are typically used to obtain the relative ranking of a series of ligands in a high-throughput assay. Translating $IC_{50}$ into $K_d$ must be approached cautiously, with accurate knowledge of substrate $K_d$ and component concentrations.

In summary, we have demonstrated that a peptide from the gp41 coiled coil region can be excised from the intact protein and stabilized by using metal ion–bipyridyl coordination at the peptide N-terminus. The resulting protein exhibits characteristics of the intact gp41 coiled coil, that is, it forms a trimeric unit in which the grooves along the coiled coil are accessible to binding by a small flanking peptide from the gp41 C-heptad repeat, as well as by a designed D-peptide known to bind to the coiled coil. Labeling the C-peptide with a fluorescent probe then enables direct determination of binding by using the phenomenon of FRET. Compounds which are able to bind to the coiled coil and displace the C-peptide can be measured with a competitive inhibition assay by following the increase in dansyl fluorescence intensity or lifetime with compound concentration. Naturally fluorescing organic compounds are not expected to interfere at the observed dansyl–peptide fluorescence maximum of 570 nm. Any residual fluorescence can be taken into account by using a negative control.

The molecules described here represent relatively short segments of the HR1 and HR2 regions of HIV-1 gp41. The design can be adapted to longer segments if desired, as well as to different regions of the gp41 coiled coil, and coiled coil domains in fusion proteins of other class 1 enveloped viruses. These include retroviruses, pneumoviruseses, orthomyxoviruses, paramyxoviruses and filoviruses, to which the particularly virulent Influenza, Ebola and Respiratory Syncytial Viruses belong, to name a few. In each case, the full-length fusion protein is unsuitable for biophysical binding studies, as the region of interest for drug targeting is masked by outer domains. This study suggests that the metallo-peptide design demonstrated here is a promising strategy for isolating the coiled coil domain and providing a built-in probe for high-throughput fluorescence screening of potential fusion inhibitors.

Received: May 30, 2003 [Z52006]

**Keywords:** FRET assay · metallopeptides · N ligands · NMR spectroscopy · viruses

[1] Y.-H. Chen, Y. Xiao, M. P. Dierich, *Immunobiology* **2000**, *201*, 308 – 316.
[2] M. P. D'Souza, J. S. Cairns, S. F. Plaeger, *JAMA J. Am. Med. Assoc.* **2000**, *284*, 215 – 222.
[3] R. W. Doms, J. P. Moore, *J. Cell Biol.* **2000**, *151*, F9-F13.
[4] D. M. Eckert, P. S. Kim, *Annu. Rev. Biochem.* **2001**, *70*, 777 – 810.
[5] C. T. Wild, T. Greenwell, T. Matthews, *AIDS Res. Hum. Retroviruses* **1993**, *9*, 1051 – 1053.
[6] C. T. Wild, D. C. Shugars, T. K, Greenwell, C. B. McDanal, T. J. Matthews, *Proc. Natl. Acad. Sci. USA* **1994**, *91*, 9770 – 9774.
[7] J. M. Kilby, S. Hopkins, T. M. Venetta, B. DiMassimo, G. A. Cloud, J. Y. Lee, L. Alldredge, E. Hunter, D. Lambert, D. Bolognesi, T. Matthews, M. R. Johnson, M. A. Nowak, G. M. Shaw, M. S. Saag, *Nat. Med.* **1998**, *4*, 1302 – 1307.
[8] C. D. Pilcher, J. J. Eron, Jr., L. Ngo, A. Dusek, P. Sista, J. Gleavy, D. Brooks, T. Venetta, E. DiMassimo, S. Hopkins, *Aids* **1999**, *13*, 2171 – 2173.
[9] W. Weissenhorn, L. J. Calder, A. Dessen, T. Laue, J. J. Skehel, D. C. Wiley, *Proc. Natl. Acad. Sci. USA* **1997**, *94*, 6065 – 6069.
[10] M. J. Root, M. S. Kay, P. S. Kim, *Science* **2001**, *291*, 884 – 888.
[11] C. A. Bewley, J. M. Louis, R. Ghirlando, G. M. Clore, *J. Biol. Chem.* **2002**, *277*, 14238 – 14245.
[12] D. C. Chan, C. T. Chutkowski, P. S. Kim, *Proc. Natl. Acad. Sci. USA* **1998**, *95*, 15613 – 15617.
[13] M. Lieberman, T. Sasaki, *J. Am. Chem. Soc.* **1991**, *113*, 1470 – 1471.
[14] M. R. Ghadiri, C. Soares, C. Choi, *J. Am. Chem. Soc.* **1992**, *114*, 825 – 831.
[15] M. Lieberman, M. Tabet, T. Sasaki, *J. Am. Chem. Soc.* **1994**, *116*, 5035 – 5044.
[16] M. W. Mutz, G. L. McLendon, J. F. Wishart, E. R. Gaillard, A. F. Corin, *Proc. Natl. Acad. Sci. USA* **1996**, *93*, 9521 – 9526.
[17] M. A. Case, M. R. Ghadiri, M. W. Mutz, G. L. McLendon, *Chirality* **1998**, *10*, 35 – 40.
[18] M. Gochin, V. Khorosheva, M. A. Case, *J. Am. Chem. Soc.* **2002**, *124*, 11018 – 11028.
[19] J. R. Lakowitz, *Principles of Fluorescence Spectroscopy*, Plenum, New York, **1986**.
[20] M. A. Case, G. L. McLendon, *J. Am. Chem. Soc.* **2000**, *122*, 8089 – 8090.
[21] N. L. Ogihara, M. S. Weiss, W. F. Degrado, D. Eisenberg, *Protein Sci.* **1997**, *6*, 80 – 88.
[22] D. M. Eckert, V. N. Malashkevich, L. H. Hong, P. A. Carr, P. S. Kim, *Cell* **1999**, *99*, 103 – 115.
[23] A. Otaka, M. Nakamura, D. Nameki, E. Kodama, S. Uchiyama, S. Nakamura, H. Nakano, H. Tamamura, Y. Kobayashi, M. Matsuoka, N. Fujii, *Angew. Chem.* **2002**, *114*, 3061 – 3064; *Angew. Chem. Int. Ed.* **2002**, *41*, 2938 – 2940.
[24] Y. Cheng, W. H. Prusoff, *Biochem. Pharmacol.* **1973**, *22*, 3099 – 3108.
[25] Probe and labeling procedures are from Molecular Probes, www.probes.com

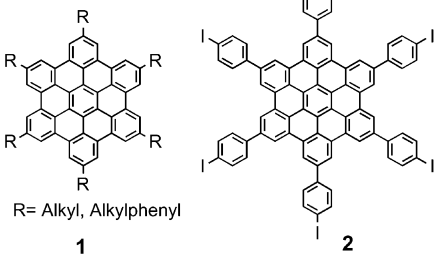
 © 2003 Wiley-VCH Verlag GmbH & Co. KGaA, Weinheim 

Carbon-Rich Compounds

# The Versatile Synthesis and Self-Assembly of Star-Type Hexabenzocoronenes**

*Jishan Wu, Mark D. Watson, and Klaus Müllen**

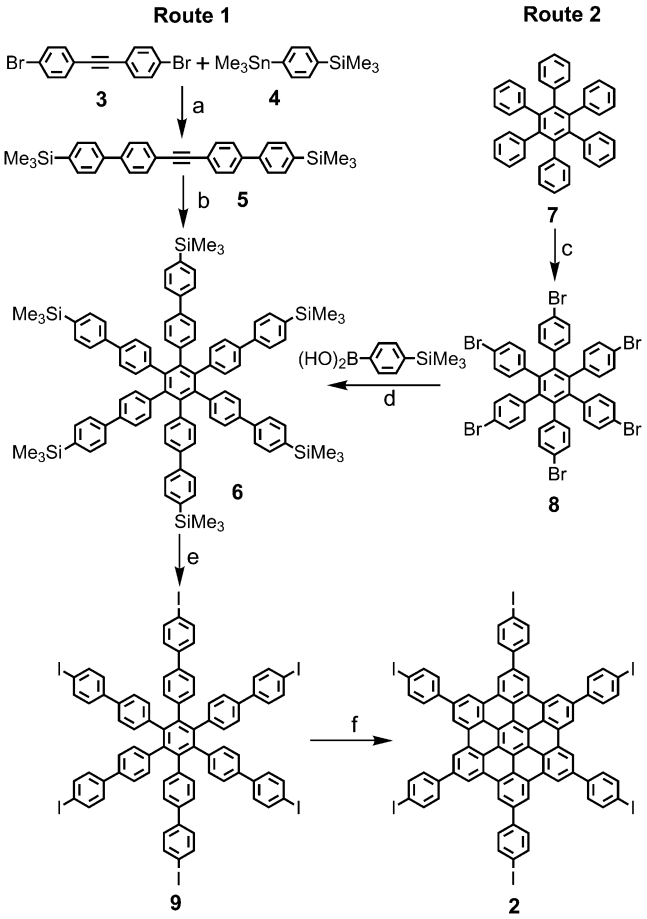
π-Stacking is a powerful motif for self-assembly that is ubiquitous in nature and utilized extensively by synthetic chemists to engineer complex supramolecular architectures—particularly in recent years, having been spurred on by the increasing technological promise of the π stacks as conducting pathways in organic-based electronics.[1] Hexa-*peri*-hexabenzocoronenes (HBCs) **1**[2] are larger than the widely studied triphenylenes,[3] porphyrins,[4] and phthalocyanines.[5] As a result, alkyl-substituted HBCs exhibit aggregation behavior in solution that persists to nanomolar concentrations, as well as bulk columnar mesophases with high order parameters, high charge-carrier mobilities, and exceptional thermal stability.[2] The bulk properties qualify them as active components in organic field-effect transistors (OFETs)[6] and as hole-conducting layers in photovoltaic devices or light-emitting diodes (LEDs).[7] Important targets include the understanding of the self-assembly of large disc molecules and improving device performance through 1) more specific assembly in solution, 2) further increasing the order in the columnar mesophases, and 3) modifying the electronic properties of the discs, in particular, for better hole stabilization.




1 2

Herein, we address these functions by varying pendant substituents; thus hexa(4-iodophenyl)-*peri*-hexabenzocoronene (**2**) acts as an HBC building block with versatile reactive sites, which can be converted into a range of useful functionalities. Such an atom economy is important when enriching the library of HBCs, since their synthetic modification has so far involved variation of the diphenylacetylene starting compounds.[2c]

The synthesis of the key building block **2** is outlined in Scheme 1. The precursor hexa(4-iodophenyl)hexaphenylbenzene (**9**) was prepared in 92% yield by reaction of excess iodine monochloride with hexa(4-trimethylsilylphenyl)hexaphenylbenzene (**6**), which was synthesized by two different routes. The first so-called convergent route (Route 1) involves a Stille coupling[8] and a cobalt-catalyzed cyclotrimerization.[2c] To avoid the toxic organotin chemistry, as well as to simplify the synthesis, an alternate divergent route (Route 2) requiring one sixfold bromination[9] and one sixfold Suzuki coupling reaction[10] was developed. Final cyclodehydrogenation of **9** with iron(III) chloride gave the desired compound **2** as a yellow powder in quantitative yield. Notably, this divergent route involves four sixfold transformations, all




***Scheme 1.*** Synthesis of compound **2**: a) $[Pd(PPh_3)_4]$, toluene, 125 °C, 75%; b) $[Co_2(CO)_8]$, dioxane, 125 °C, 92%; c) neat bromine, −20 °C → RT, 96%; d) $[Pd(PPh_3)_4]$, $K_2CO_3$(aq), 95 °C, 92%; e) ICl, chloroform, 92%; f) $FeCl_3$/nitromethane, $CH_2Cl_2/CS_2 = 2:1$.

[*] Prof. Dr. K. Müllen, J. Wu, Dr. M. D. Watson[+]
Max-Planck Institute for Polymer Research
Ackermannweg 10, 55128 Mainz (Germany)
Fax: (+49) 6131-379-350
E-mail: muellen@mpip-mainz.mpg.de

[+] Current address:
University of Kentucky
Department of Chemistry
Lexington, KY 40506-0055 (USA)

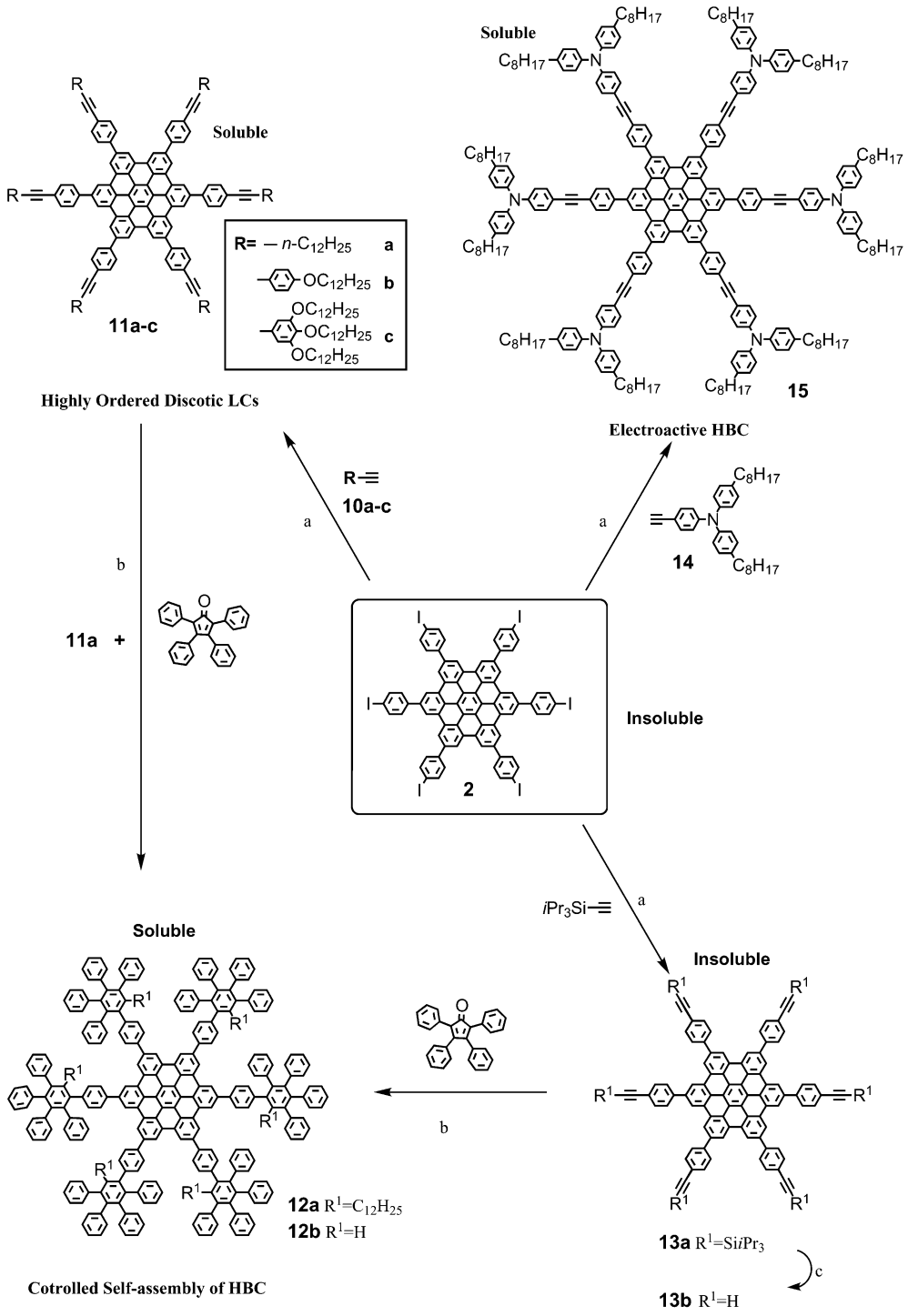
[**] This work was financially supported by the Zentrum für Multifunktionelle Werkstoffe und Miniaturisierte Funktionseinheiten (BMBF 03N6500), EU-TMR project SISITOMAS, the Deutsche Forschungsgemeinschaft (Schwerpunkt Feldeffekttransistoren), and the EU project DISCEL (G5RD-CT-2000-00321).

Supporting information for this article is available on the WWW under http://www.angewandte.org or from the author.

 DOI: 10.1002/anie.200352047 © 2003 Wiley-VCH Verlag GmbH & Co. KGaA, Weinheim 

in excellent to near quantitative yields and provides compound **2** on a gram scale.[11]

Despite the virtual insolubility of compound **2**, palladium-catalyzed Hagihara–Sonagashira coupling reactions[12] with solubilizing acetylene groups work smoothly, thus paving the way to versatile functionalization. Compared to *n*-alkyl substituents, 4-alkylphenyl groups provide the following advantages to HBCs: good solubility, longer range order in the columnar mesophase, and the highest reported room-temperature charge-carrier mobility for a discotic liquid-crystalline material.[2d,e] Thus a functionalizable core such as **2** is expected to provide a new series of highly ordered liquid-crystalline materials. As shown in Scheme 2, cross-coupling between **2** and soluble monoacetylenes **10a–c** gave a series of extended, star-type HBC derivatives **11a–c** in high yield. Their good solubility facilitates their full structural characterization, despite their size. The bulk thermotropic liquid-crystalline properties of **11a–c** were investigated by differ-




***Scheme 2.*** Versatile functionalization based on building block **2.** a) $[Pd(PPh_3)_4]$/CuI, piperidine, 50°C; b) $Ph_2O$, 250°C; c) tetrabutylammonium fluoride, THF, RT.

 © 2003 Wiley-VCH Verlag GmbH & Co. KGaA, Weinheim 

ential scanning calorimetry, polarized optical microscopy, and wide-angle X-ray diffraction (WAXD). As expected, highly ordered hexagonal columnar mesophases were observed at ambient temperature with compounds **11a**–**c**. Most interestingly, the 2D WAXD pattern of extruded fibers of **11b,c** revealed a helical stacking in the HBC column.[13] As a typical example, clear reflection peaks positioned in a first layer ($l=1$) above/below the equator corresponding to a repeating distance along the columns that is four times the π-π stacking distance of HBC disks are observed in the 2D X-ray pattern of **14b** (Figure 1). This pattern indicates the existence of super-

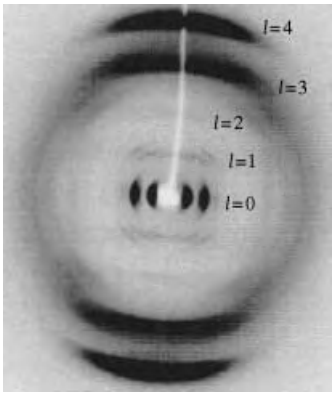



***Figure 1.*** 2D X-ray pattern of **11b** showing a typical helical column stacking. The sample was oriented by extrusion from a mini-extruder to give a fiber with a diameter of about 0.7 mm, then 2-D X-ray diffractograms were collected in transmission mode with the beam perpendicular to the fiber(fiber/column axes vertical).

lattice periodicity in the direction of stacks of discs. Further analysis discloses that every 5th disc along the column axis is positionally/rotationally correlated to form a helical superstructure. As a consequence, reflection peaks appear at $l=2$ and 3 in addition to the reflection peaks at $l=4$, which is correlated to the normal π-π stacking distance. This packing could arise from additional π-π interactions between, and space-filling requirements introduced by, the rigid-rod side groups in the star-type molecules. A helical arrangement has rarely been observed experimentally by X-ray diffraction for discs without chiral substituents,[14] and to the best of our knowledge, this is the first case from a disc with sixfold symmetry. For example, such a helical $D_{ho}$ mesophase was found in hexathioalkyltriphenylene and has exceptional one-dimensional charge-carrier mobilities.[14a]

Disc molecules and structurally related shape-persistent macrocycles are known to exhibit dynamic aggregation in solution.[15] This process is relevant for the formation of films from solution and also serves as a model for phase formation from the melt. Attaching bulky substituents is expected to inhibit or even completely suppress face-to-face aggregation of the HBC discoid core. As shown in Scheme 2, a sixfold Diels–Alder cycloaddition between **11a** and tetraphenylcyclopentadienone proceeds smoothly in refluxing diphenyl ether to provide HBC **12a**, which is substituted with oligophenylene dendrons. $^1$H NMR spectroscopic analysis reveals that molecule **12a** exhibits a unique monomer–dimer equilibrium in solution. The representative temperature-dependent $^1$H NMR spetra of **12a** in [$D_4$]tetrachloroethane are shown in Figure 2. Two independent species, one expected

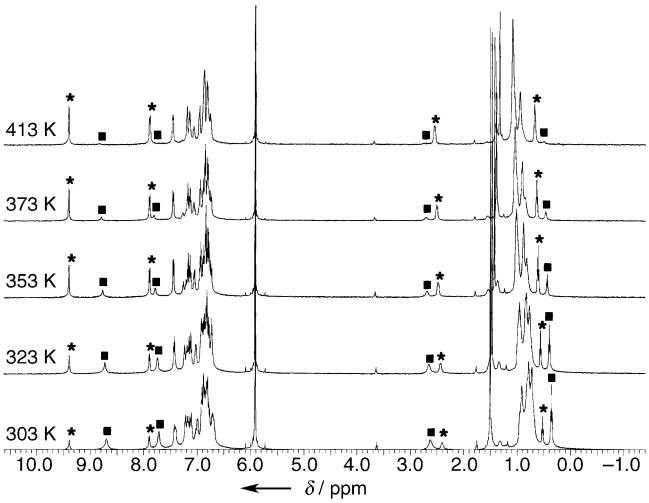


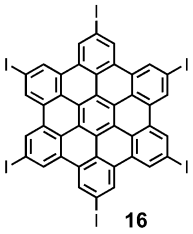

***Figure 2.*** Temperature-dependent $^1$H NMR (500 MHz) spectra of **12a** in [$D_4$]tetrachloroethane (3 mg mL$^{-1}$) which reveal two independent species, the ratio of which strongly depends on the temperature, concentration, and solvent. Resonances at about $\delta=8.7$ ppm and 9.4 ppm are assigned to HBC core protons in the dimer and monomer, respectively.

monomer (labeled by star) and another dimer (labeled by a square), were identified. The monomer/dimer ratio increases with increasing temperature or decreasing concentration. Furthermore, only dimer exists in a relatively poor solvent such as cyclohexane, while only monomer can be observed in carbon disulfide (an excellent solvent for large aromatic compounds). Clearly, the bulky dendrons suppress the formation of higher aggregates and allow only a dimer aggregate to exist in solution. The appearance of separate $^1$H NMR resonances, instead of averaged ones which shift with temperature/concentration/solvent, suggests that this self-assembly is slow on the NMR time scale. This could be ascribed to the bulky dendron structure as well as the steric hinderance produced by the dodecyl chains at the bay position. To further investigate the effect of the dodecyl group in **12a**, an analogous HBC molecule **12b**, in which the dodecyl groups are replaced by hydrogen atoms, was prepared (Scheme 2). Sixfold Hagihara–Sonogashira coupling between **2** and triisopropylacetylene gave the insoluble material **13a**, which was deprotected with tetrabutylammonium fluoride (TBAF) to provide insoluble material **13b**. Solid-state MALDI MS[11] of compounds **13a,b** indicated quantitative conversion even though both the starting materials and products are insoluble(!), further proving the high reactivity of the building block **2**. Diels–Alder cycloaddition between **13b** and tetraphenylcyclopentdienone proceeded smoothly to give the soluble **12b**. The $^1$H NMR spectra of **12b** in [$D_4$]tetrachloroethane reveal only one aggregated species,[16] which does not show concentration dependence, which thus most probably pointing toward a dimeric structure.

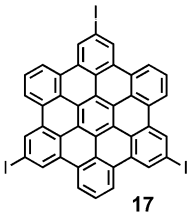
 © 2003 Wiley-VCH Verlag GmbH & Co. KGaA, Weinheim 

Triarylamines are commonly used as hole-transport materials in organic LEDs.[17] Sixfold triarylamine-substituted HBC **15** can be prepared by similar Hagihara–Sonogashira coupling reaction between compound **2** and *N,N′*-di(4-octylphenyl)-*N″*-(4-ethynylphenyl)amine (**14**) as shown in Scheme 2. It should be pointed out that the triarylamine-substituted hexaphenylbenzenes are usually excluded from the standard $FeCl_3$ oxidative cyclodehydrogenation conditions as a result of preferential formation of charge-localized radical cations.[18] The successful synthesis of the electroactive materials **15** suggests that more electroactive materials could be made from building block **2**. Besides the hole-transfer channel of the HBC column, the triarylamine moieties in molecule **15** are expected to form an additional hole-transport channel. By adapting the term "double-cable" used for conjugated polymers with tethered electronic functional units the columnar structures formed from **15** could be described as coaxial cables. Scientific interest in this molecule also includes the study, after formation of a radical cation, of the electronic coupling of the electroactive triarylamines through the rigid π system including the "superbenzene" HBC core.

A large number of useful peripheral substituents can now be attached to the HBC core as a last synthetic step, which leads to three new types of materials: 1) more highly ordered discotic columnar mesogens **11b,c** which exhibit unique helical superstructures, 2) peripherally dendronized large π systems **12a,b** which provide for programmed self-assembly in solution, and 3) a novel electroactive material **15** containing seven positionally defined hole-transport units of two different types. Work is under way to prepare new mesogenic versions with six peripheral electron acceptor/transport units that would lead to core–shell columns (coaxial cables) in which each individual column is a self-contained photovoltaic element. As an extension of the above synthetic concept, another two functionalizable HBC building blocks (**16** and **17**) have been prepared by shorter synthetic routes and



**16**



**17**

functionalized by palladium-catalyzed Hagihara–Sonogashira and Buchwald reactions.[19] The fact that substituents which may be incompatible with the normal synthetic build-up can be introduced to all three halo derivatives dramatically broadens the scope of HBC materials.

Received: June 4, 2003 [Z52047]

**Keywords:** cross-coupling · liquid crystals · polycycles · self-assembly · X-ray diffraction

[1] a) *Handbook of Liquid Crystals, Vol. 1* (Eds.: D. Demus, J. Goodby, G. W.Gray, H. W. Spiess, V. Vill), Wiley-VCH, Weinheim, **1998**; b) S. Chandrasekhar, *Liq. Cryst.* **1993**, *14*, 3–14; c) D. Adam, F. Closs, T. Frey, D. Funhoff, D. Haarer, H. Ringsdorf, P. Schuhmacher, K. Siemensmeyer, *Phys. Rev. Lett.* **1993**, *70*, 457–460.

[2] a) M. D. Watson, A. Fechtenkötter, K. Müllen, *Chem. Rev.* **2001**, *101*, 1267–1300; b) P. Herwig, C. Kayser, K. Müllen, H. W. Spiess, *Adv. Mater.* **1996**, *8*, 510–513; c) A. Stabel, P. Herwig, K. Mullen, *Angew. Chem.* **1995**, *107*, 335–339; *Angew. Chem. Int. Ed. Engl.* **1995**, *34*, 1609–1611; d) A. M. van de Craats, J. M. Warman, A. Fechenkötter, J. D. Brand, M. A. Harbison, K. Müllen, *Adv. Mater.* **1999**, *11*, 1469–1472; e) A. Fechtenkötter, K. Saalwächter, M. A. Harbison, K. Müllen, H. W. Spiess, *Angew. Chem.* **1999**, *111*, 3224–3228; *Angew. Chem. Int. Ed.* **1999**, *38*, 3039–3042.

[3] a) J. A. Rego, S. Kumar, H. Ringsdorf, *Chem. Mater.* **1996**, *8*, 1402–1409; b) D. Adam, P. Schuhmacher, J. Simmerer, L. Häussling, K Siemensmeyer, K. H. Etzbach, H. Ringsdorf, D. Haarer, *Nature* **1994**, *371*, 141–143; c) E. F. Gramsbergen, H. J. Hoving, W. H. de Jeu, K. Praefcke, B. Kohne, *Liq. Cryst.* **1986**, *1*, 397–400.

[4] a) B. A. Gregg, M. A. Fox, A. J. Bard, *J. Am. Chem. Soc.* **1989**, *111*, 3024–3029; b) M. Kimura, Y. Saito, K. Ohta, K. Hanabusa, H. Shirai, N. Kobayashi, *J. Am. Chem. Soc.* **2002**, *124*, 5274–5275.

[5] a) C. Piechoki, J. Simon, A. Skoulios, D. Guillon, P. Weber, *J. Am. Chem. Soc.* **1982**, *104*, 5245–5247; b) S. Chandrasekhar, *Mol. Cryst. Liq. Cryst.* **1981**, *63*, 171–180.

[6] a) A. Kraft, *ChemPhysChem* **2001**, *2*, 163–165; b) H. E. Katz, A. J. Lovinger, J. Johnson, C. Kloc, T. Siegrist, W. Li, Y.-Y. Lin, A. Dodabalapur, *Nature* **2000**, *404*, 478–481; c) A. M. van de Craats, N. Stutzmann, O. Bunk, M. M. Nielsen, M. D. Watson, K. Müllen, H. D. Chanzy, H. Sirringhaus, R. H. Friend, *Adv. Mater.* **2003**, *15*, 495–499.

[7] a) L. Schmidt-Mende, A. Fechtenkötter, K. Müllen, E. Moons, R. H. Friend, J. MacKenzie, *Science* **2001**, *293*, 1119–1122; b) C. W. Tang, *Appl. Phys. Lett.* **1986**, *48*, 183–185.

[8] T. N. Mitchell, *Synthesis* **1992**, 803–815.

[9] R. Rathore, C. L. Burns, M. I. Deselnicu, *Org. Lett.* **2001**, *3*, 2887–2890.

[10] N. Miyaura, A. Suzuki, *Chem. Rev.* **1995**, *95*, 2457–2483.

[11] The very poor solubility of **2** precludes standard $^1$H NMR and $^{13}$C NMR characterization, however, solid-state matrix-assisted laser-desorption/ionization mass spectroscopy (MALDI-MS) studies reveal a single species with an isotopic distribution in accord with that simulated for compound **2.** See Supporting Information and: L. Przybilla, J. D. Brand, K. Yoshimura, J. Räder, K. Müllen, *Anal. Chem.* **2000**, *72*, 4591–4597.

[12] S. Taskahashi, Y. Kuroyama, K. Sonogashira, N. Hagihara, *Synthesis* **1980**, 627–630.

[13] Details of the characterization of this unique helical $D_{ho}$ mesophase and nanoscale self-assembling properties of **11a–c** will be reported elsewhere; J. Wu, M. D. Watson, L. Zhang, Z. Wang, K. Müllen, unpublished results.

[14] a) D. Adam, P. Schuhmacher, J. Simmerer, L. Häussling, K. Siemensmeyer, K. H. Etzbach, H. Ringsdorf, D. Haarer, *Nature* **1994**, *371*, 141–143; b) F. Charra, J. Cousty, *Phys. Rev. Lett.* **1998**, *80*, 1682–1685; c) E. Fontes, P. A. Heiney, W. H. de Jeu, *Phys. Rev. Lett.* **1988**, *61*, 1202–1205.

[15] a) J.-S. Zhang, J. S. Moore, *J. Am. Chem. Soc.* **1992**, *114*, 9701–9702; b) A. S. Shetty, J.-S. Zhang, J. S. Moore, *J. Am. Chem. Soc.* **1996**, *118*, 1019–1027; c) Y. Tobe, N. Utsumi, K. Kawabata, A. Nagano, K. Adachi, S. Araki, M. Sonoda, K. Hirose, K. Naemura, *J. Am. Chem. Soc.* **2002**, *124*, 5350–5364.

 © 2003 Wiley-VCH Verlag GmbH & Co. KGaA, Weinheim 

[16] Only a single $^1$H NMR resonance (ca. $\delta = 8.7$ ppm) is observed above 8 ppm. A single crystal of **12b** has been obtained and hopefully will disclose the atom positions of this supramolecular dimer. A more detailed analysis of this unique self-assembly process will be presented in a separate publication.
[17] a) U. Mitschke, P. Bäuerle, *J. Mater. Chem.* **2000**, *10*, 1471 – 1507; b) S. J. Campbell, G. G. Malliaras, *Semicond. Polym.* **2000**, 411 – 461; c) M. D'Iorio, *Can. J. Phys.* **2000**, *78*, 231 – 241.
[18] a) C. Lambert, G. Nöll, *Angew. Chem.* **1998**, *110*, 2239 – 2242; *Angew. Chem. Int. Ed.* **1998**, *37*, 2107 – 2110; b) C. Lambert, G. Nöll, *Chem. Eur. J.* **2002**, *8*, 3467 – 3477.
[19] a) J. P. Wolfe, S. L. Buchwald, *J. Org. Chem.* **1997**, *62*, 6066 – 6068; b) M. H. Ali, S. L. Buchwald, *J. Org. Chem.* **2001**, *66*, 2560 – 2565.

 © 2003 Wiley-VCH Verlag GmbH & Co. KGaA, Weinheim 

*Chemoselective Hydrogenation*

# Chemoselective Reduction of Complex α,β-Unsaturated Ketones to Allylic Alcohols over Ir-Metal Particles on β Zeolites**

*Mario De bruyn, Simona Coman, Roxana Bota, Vasile I. Parvulescu, Dirk E. De Vos, and Pierre A. Jacobs**

Through chemoselective catalysis one aims to address only one of several similar functional groups in a molecule. The hydrogenation of an unsaturated carbonyl compound to an allylic alcohol in a chemoselective manner is a major challenge. Allylic alcohols have a wide range of applications, for example, as fragrances, or in the pharmaceutical industry.[1,2] The reduction of unsaturated aldehydes to primary allylic alcohols proceeds well on supported $Pt^0$ or $Ru^0$.[3,4] These metals may be modified by Lewis acids ($Sn^{n+}$, $Fe^{3+}$,...) or by specific supports, such as zeolites.[5] The chemoselective reduction of α,β-unsaturated ketones is much more difficult. Until recently, the most successful procedure was $CeCl_3$-assisted reduction with $NaBH_4$.[6] A homogeneous catalytic procedure has been proposed by Noyori and co-workers, which involves the use of a Ru–phosphane complex, a chiral diamine, and a base.[7] However, although the observed chemoselectivity is excellent, recuperation of the homogeneous catalyst is still a problem. Moreover, the selective activation of the C=O group of an unsaturated ketone on a simple, supported metal catalyst remains a formidable scientific challenge. Only two such reactions have been described: Ketoisophorone can be reduced by $Pd/Al_2O_3$ in $MeOH/CH_3COOH$ to the corresponding allylic alcohol,[8] and 4-phenyl-3-buten-2-one undergoes reduction to the unsaturated alcohol in the presence of $Au/Fe_2O_3$.[9] In both cases, the reaction has only been demonstrated for a single substrate. Thus, a catalyst with wider scope is required. One strategy toward the discovery of new, highly selective catalysts is to investigate the formation of metal particles on well-defined, porous supports.[10]

Herein we report that a new heterogeneous Ir catalyst facilitates the chemoselective reduction of a variety of unsaturated ketones and aldehydes to allylic alcohols. A strong-acid zeolite with a large external surface area, for example H-β, makes an optimal support. Iridium was selected because it is more oxophilic than other metals of the Pt group.[3] With a focus on specialty chemicals, seven unsaturated ketones and three unsaturated aldehydes were selectively transformed into allylic alcohols.

The standard catalyst was prepared by impregnation of a commercial H-β zeolite from PQ (surface area = 740 $m^2 g^{-1}$, average crystallite size = 0.2 μm, Si/Al = 12) with $Ir(acac)_3$ (acac = acetylacetone) as a solution in toluene. After calcination and reduction, the catalyst was tested on a series of α,β-unsaturated aldehydes. The desired allylic alcohols were obtained with high selectivity at high aldehyde conversion (Table 1). In the hydrogenation of citral, the isolated double bond was left intact, and a mixture of the allylic alcohols geraniol and nerol was obtained. When a Ru-containing catalyst was used under identical conditions, substantially lower chemoselectivity was observed in the hydrogenation of cinnamaldehyde (Table 1, entry 2). This demonstrates that Ir is essential for high selectivity in the reaction.

***Table 1:*** Hydrogenation of α,β-unsaturated aldehydes.[a]

| Entry | Catalyst | Substrate | *P* [MPa] | *t* [h] | Conv. [%] | Sel. [%] |
|---|---|---|---|---|---|---|
| 1 | Ir/H-β (2%) | cinnamaldehyde | 3 | 18 | 71 | 82 |
| 2 | Ru/H-β (2%) | cinnamaldehyde | 3 | 35 | 81 | 52 |
| 3 | Ir/H-β (2%) | α-$CH_3$-cinnamaldehyde | 3 | 3 | 72 | 89 |
| 4 | Ir/H-β (2%) | citral | 2.4 | 2.25 | >98 | 90 |

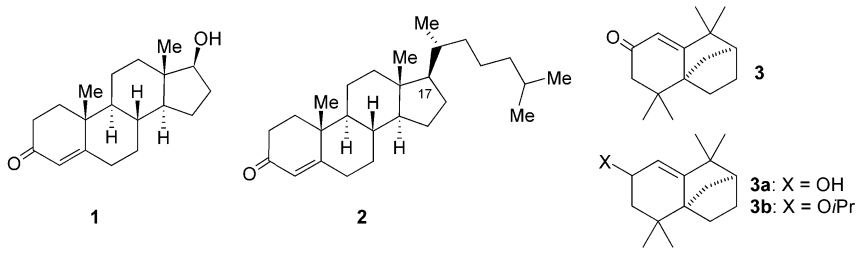
[a] Conditions: substrate (50 mg), isopropyl alcohol (6.5 g), catalyst (25 mg; calcined at 300°C and reduced at 450°C). Conv. = conversion, Sel. = selectivity.

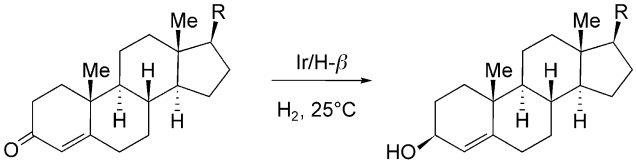
To extend the scope of the catalyst to α,β-unsaturated ketones, the reaction of the complex enone testosterone (**1**) was attempted (Scheme 1). We anticipated that the structural rigidity of this cyclic enone would lead to a decrease in the reactivity of the sterically hindered C=C double bond and an increase in the susceptibility of the carbonyl group to reduction, relative to enones in more flexible systems. The reaction was carried out with a 1% loading of Ir on H-β in

[*] Prof. P. A. Jacobs, M. De bruyn, Prof. D. E. De Vos
Centre for Surface Chemistry and Catalysis
Katholieke Universiteit Leuven
Kasteelpark Arenberg 23, 3001 Leuven (Belgium)
Fax: (+32) 16-32-1998
E-mail: pierre.jacobs@agr.kuleuven.ac.be
Dr. S. Coman, R. Bota, Prof. V. I. Parvulescu
Department of Chemical Technology and Catalysis
University of Bucharest
B-dul Regina Elisabeta 4–12, Bucharest 70346 (Romania)

[**] This research was supported by the Belgian Federal Government (IAP Program Supramolecular Catalysis) and by the Flemish Government (Bilateral Agreement Flanders–Romania). MDb is a fellow of IWT (Vlaanderen). PAJ is grateful for support in the frame of a concerted research action (GOA) of the Flemish Government.

 DOI: 10.1002/anie.200352275 © 2003 Wiley-VCH Verlag GmbH & Co. KGaA, Weinheim 




***Scheme 1.*** Ir/H-β-catalyzed hydrogenation of **1** and **2**.

conversion (Table 2, entries 8 and 10). The use of other solvents, such as methanol, invariably led to the formation of the saturated alcohol. In each of the above-mentioned cases, the allylic alcohol androst-4-ene-3β,17β-diol was formed with high diastereoselectivity (d.r. > 97:3).[11,12]

Next, the reaction of cholestenone (**2**, structurally related to **1**) was tested. As the large alkyl group at position 17 was found to affect the selectivity for allylic alcohol formation (Table 3, entries 1 and 2), slightly different conditions were required. With a Ir loading on H-β of 3%, the allylic alcohol was obtained within 1 h in 98% yield (Table 3, entry 3). As observed for testosterone, the formation of the 3-β-hydroxy-4-ene allylic alcohol was highly diastereoselective (d.r. > 97:3). In the reduction of the tricyclic compound (−)-isolongifolen-9-one (**3**) with Ir/H-β (1%) in *i*PrOH, the main product isolated was isolongifolen-9-yl isopropyl ether (**3b**; Table 3, entry 4). Such isolongifolenyl ethers are important fragrance compounds.[13] This two-step process mediated by a bifunctional metal/acid zeolite is more straightforward and more environmentally sound than alternative reduction–etherification procedures, in which, for example, NaH and 2-bromopropane are used. However, if desired, the etherification activity of the catalyst can be suppressed by supporting the $Ir^0$ on a Na-β zeolite (Table 3, entry 5). With this modified catalyst, complete chemoselectivity for the allylic alcohol is observed, even if the reaction is slow.

***Table 3:*** Hydrogenation of cholestenone (**2**) and isolongifolenone (**3**) with Ir on zeolite H-β.[a]

| Entry | Substrate | Catalyst | *P* [MPa] | *t* [h] | Conv. [%] | Selectivity [%] |
|---|---|---|---|---|---|---|
| 1 | **1** | Ir/H-β (2%) | 2.4 | 0.75 | 87 | 76 |
| 2 | **2** | Ir/H-β (2%) | 2.4 | 1 | 85 | 41 |
| 3 | **2** | Ir/H-β (3%) | 2.8 | 0.67 | 100 | > 98 |
| 4 | **3** | Ir/H-β (1%) | 6.0 | 47 | 59 | 21[b] (52)[c] |
| 5 | **3** | Ir/Na-β (1%) | 6.0 | 184.5 | 35 | 100[b] |

[a] Conditions: as in Table 2, but with cholestenone (66 mg) or isolongifolenone (40 mg) in *i*PrOH. [b] Racemic allylic alcohol. [c] Racemic isolongifolenyl ether.

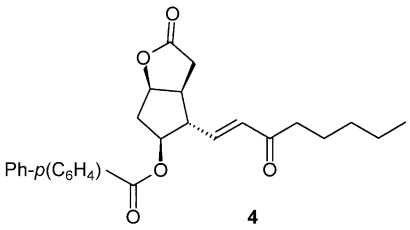
*i*PrOH, and the selectivities observed for the allylic alcohol were found to depend on the $H_2$ pressure used. Thus, the selectivity increased with increasing pressure to reach a maximum of 64% at ~2 MPa and ~60% conversion (Table 2, entries 1–5). With other zeolites, the selectivities observed were lower, for example, with H-USY (Si/Al = 5.75; Table 2, entry 7). When a H-Mordenite (Mor) with a Si/Al ratio of 11 was used, the selectivity remained relatively high (Table 2, entry 6). An increase in the Ir loading of H-β led to a dramatic decrease in reaction times and was also beneficial in terms of the selectivities observed, with 76% selectivity at 87% conversion (Table 2, entries 9–10). When isoamyl alcohol was used as the solvent, the selectivities could be further improved, for example, to 100% chemoselectivity at 30% enone

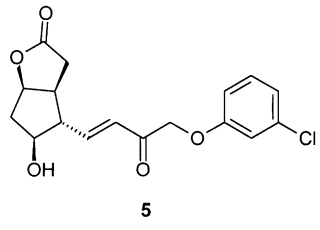
***Table 2:*** Hydrogenation of testosterone (**1**) over Ir/zeolite catalysts.[a]

| Entry | Catalyst | *P* [MPa] | Solvent | *t* [h] | Conv. [%] | Sel. [%] |
|---|---|---|---|---|---|---|
| 1 | Ir/H-β (1%) | 0.8 | *i*PrOH | 5 | 60 | 17 |
| 2 | Ir/H-β (1%) | 1.2 | *i*PrOH | 5 | 61 | 22 |
| 3 | Ir/H-β (1%) | 1.6 | *i*PrOH | 5 | 59 | 36 |
| 4 | Ir/H-β (1%) | 2.0 | *i*PrOH | 9 | 54 | 64 |
| 5 | Ir/H-β (1%) | 2.4 | *i*PrOH | 10 | 65 | 57 |
| 6 | Ir/H-Mor (1%) | 2.0 | *i*PrOH | 2 | 60 | 48 |
| 7 | Ir/H-USY (1%) | 2.0 | *i*PrOH | 25 | 67 | 32 |
| 8 | Ir/H-β (1%) | 2.0 | *i*AmOH | 9 | 30 | 100 |
| 9 | Ir/H-β (2%) | 2.0 | *i*PrOH | 0.75 | 87 | 76 |
| 10 | Ir/H-β (2%) | 2.0 | *i*AmOH | 1 | 75 | 86 |

[a] Conditions: testosterone (50 mg), solvent (6.5 g), catalyst (25 mg), 25°C. Catalysts were calcined at 300°C and reduced at 450°C. USY = ultra-stable Y zeolite, *i*Am = isoamyl.

Prostaglandins are important drugs and drug precursors. The Ir/H-β catalyst was used to reduce the two enone intermediates **4** and **5** in the prostaglandin synthesis,[2,14] which each contain a linear rather than a cyclic enone. In contrast with the reactions of the steroidal enones, the reduction of these prostaglandin intermediates was found to be more chemoselective when performed in MeOH, rather




 © 2003 Wiley-VCH Verlag GmbH & Co. KGaA, Weinheim 

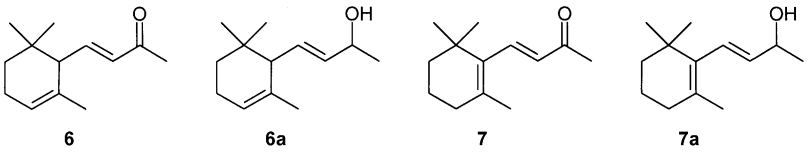
than in *i*PrOH (Table 4, entries 1 and 2). When **5** was used as the starting enone, the high selectivity of the reaction (80%) can be maintained up to very high conversion (95%), which implies that the corresponding unsaturated alcohol is a poor substrate for the Ir-catalyzed hydrogenation (Table 4, entry 3). Precalcination of the support at 700°C to convert part of the Brønsted acidity into Lewis acidity led to decreased chemoselectivity in the formation of the allylic alcohol, thus showing that the zeolite protons are important for the chemoselectivity of the catalyst (Table 4, entry 4). In contrast with the reactions of the steroids **1** and **2**, the reduction of the prostaglandin enones resulted in significant but low diastereoselectivities, typically about d.r 60:40.

***Table 4:*** Hydrogenation of prostaglandin intermediates **4** and **5** over Ir/H-β (1%).[a]

| Entry | Substrate | Solvent | *P* [MPa] | *t* [min] | Conv. [%] | Sel. [%] |
|---|---|---|---|---|---|---|
| 1 | **4** | *i*PrOH | 1.0 | 60 | 43 | 46 |
| 2 | **4** | MeOH | 1.0 | 120 | 59 | 71 |
| 3 | **5** | MeOH | 0.2 | 60 | 95 | 80 |
| 4[b] | **5** | MeOH | 0.2 | 15 | 50 | 55 |

[a] Conditions: **4** (18.6 mg) or **5** (14 mg), solvent (7 g), Ir/H-β (1%; 25 mg), 25°C. Catalyst was calcined at 300°C and reduced at 450°C. [b] H-β precalcined at 700°C prior to loading with Ir.

Finally, as representatives of smaller unsaturated ketones, α-ionone (**6**) and β-ionone (**7**) were subjected to the Ir/H-β-catalyzed reduction (Table 5). As anticipated based on the experiments with citral, hydrogenation of the isolated double bond in **6** is only a minor reaction, and 71% selectivity for the allylic alcohol is obtained at high conversion (Table 5, entries 1 and 3). Along with α-ionol (**6a**), some β-ionol (**7a**) is also formed, probably by isomerization to β-ionone, followed by reduction. With the Na zeolite, observed selectivities for the allylic alcohol were lower, thus providing further evidence that proton acidity is important for the chemoselectivity of the hydrogenation (Table 5, entry 2). Control experiments with α-ionol showed that further hydrogenation of α-ionol is very slow, which is consistent with the high chemoselectivity observed for the allylic alcohol. β-Ionone (**7**), in which the carbonyl group is conjugated to two double bonds, reacts much faster than α-ionone (**6**), and a selectivity of 65% for the allylic alcohol β-ionol was observed with Ir/H-β (2%) (Table 5, entry 8). Selectivities were lower or even much lower in the reactions of both **6** and **7** when commercial catalysts such as Ir/C, transition-metal-doped Ir/C (5%, Degussa), and Ir/$CaCO_3$ were used, as well as with Ir/$Al_2O_3$ and Ir/$TiO_2$ (Table 5, entries 4–7 and 9–13). These data unequivocally demonstrate the essential role of H-β as a selectivity-promoting support.




**6** **6a** **7** **7a**

***Table 5:*** Hydrogenation of **6** and **7** over Ir/H-β catalysts.[a]

| Entry | Substrate | Catalyst | *P* [MPa] | *t* [h] | Conv. [%] | Sel. [%][b] |
|---|---|---|---|---|---|---|
| 1 | **6** | Ir/H-β (2%) | 3.6 | 11 | 75 | 71 |
| 2 | **6** | Ir/Na-β (2%) | 3.6 | 5.8 | 69 | 45 |
| 3 | **6** | Ir/H-β (3%) | 2.8 | 22.2 | 92 | 70 |
| 4 | **6** | Ir/C (1%) | 4.4 | 19 | 97 | 50 |
| 5 | **6** | Ir/$CaCO_3$ (5%) | 2 | 2.3 | 75 | 15 |
| 6 | **6** | Ir/$Al_2O_3$ (1%) | 2.4 | 4 | 98 | 12 |
| 7[c] | **6** | Ir/$TiO_2$ (1%) | 4.4 | 48 | 90 | 47 |
| 8 | **7** | Ir/H-β (2%) | 3.6 | 1.5 | 84 | 65 |
| 9 | **7** | Ir/C (1%) | 4.4 | 2 | 73 | 7 |
| 10 | **7** | Ir/C (5%), doped | 3.6 | 18 | 94 | 10 |
| 11 | **7** | Ir/$CaCO_3$ (5%) | 2 | 0.8 | 70 | 2 |
| 12 | **7** | Ir/$Al_2O_3$ (1%) | 2.4 | 4 | 86 | 4 |
| 13 | **7** | Ir/$TiO_2$ (1%) | 4.4 | 23 | 77 | 14 |

[a] Conditions: substrate (70 mg), isopropanol (6.5 g), 25°C, catalyst (25 mg). Catalysts calcined at 300°C and reduced at 450°C (except in entries 4, 9, and 10). [b] Selectivity for ionols. [c] Catalyst: 50 mg, contains water (50%).

In addition, hydrogenation of the isolated double bond in **6** is only a minor reaction, and 71% selectivity for the allylic alcohol is obtained at high conversion (Table 5, entries 1 and 3). Along with α-ionol (**6a**), some β-ionol (**7a**) is also formed, probably by isomerization to β-ionone, followed by reduction. With the Na zeolite, observed selectivities for the allylic alcohol were lower, thus providing further evidence that proton acidity is important for the chemoselectivity of the hydrogenation (Table 5, entry 2). Control experiments with α-ionol showed that further hydrogenation of α-ionol is very slow, which is consistent with the high chemoselectivity observed for the allylic alcohol. β-Ionone (**7**), in which the carbonyl group is conjugated to two double bonds, reacts much faster than α-ionone (**6**), and a selectivity of 65% for the allylic alcohol β-ionol was observed with Ir/H-β (2%) (Table 5, entry 8). Selectivities were lower or even much lower in the reactions of both **6** and **7** when commercial catalysts such as Ir/C, transition-metal-doped Ir/C (5%, Degussa), and Ir/$CaCO_3$ were used, as well as with Ir/$Al_2O_3$ and Ir/$TiO_2$ (Table 5, entries 4–7 and 9–13). These data unequivocally demonstrate the essential role of H-β as a selectivity-promoting support.

Although the exact optimum conditions, for example, of pressure, solvent, and Ir content, vary from one substrate to another, it is very clear that the Ir/H-β (1–3 wt%) catalyst has unprecedented generality for the chemoselective reduction of unsaturated ketones and aldehydes. Combined CO-chemisorption/TEM/TPR studies have shown that at low Ir content (0.5–1 wt%), the Ir is finely distributed over the support, with hardly any TEM (transmittance electron microscopy)-detectable metal particles, and with Ir dispersions of up to 30%. The catalysts with a higher Ir content, which were more effective for many substrates, contain $Ir^0$ particles in the range of 2–10 nm, thus showing that extracrystalline $Ir^0$ particles play an important role. It should be stressed that the enones **1**–**7** are unable to enter the intracrystalline voids of zeolites with *BEA topology.[15] Based on TPR (temperature-programmed reduction, it appears that most of the Ir is in the metallic state. Reduction at high temperature is in any case required to obtain chemoselective catalysts.

In conclusion, by combining the carbonyl affinity of metallic iridium with the promotion effect of the H-β zeolite, which is a strong Brønsted acid, one can reduce a variety of α,β-unsaturated aldehydes and ketones to allylic alcohols effectively. Excellent conversions were paired with high selectivities. Thus, this Ir/H-β catalyst constitutes a breakthrough in selective reduction on heterogeneous catalysts, especially as many of the substrates used are highly relevant for fine-chemicals production.[14]

## *Experimental Section*

The catalyst was prepared by impregnation of zeolite H-β with $Ir(acac)_3$ as a solution in toluene (1.3 mM; 2 mL $g^{-1}$ zeolite). The catalyst was dried at 60°C for 2 h, after which it was calcined at 300°C for 4 h. The reduction of the unsaturated ketone or aldehyde in the presence of the catalyst (25 mg) was performed in the solvent indicated (6.5 g) under a stream of $H_2$ at 450°C for 6 h. Commercial catalysts were purchased from Alfa Aesar (Ir/C (1%), Ir/$CaCO_3$ (5%)) or were obtained as a generous gift from Degussa

 © 2003 Wiley-VCH Verlag GmbH & Co. KGaA, Weinheim 

(transition-metal-doped Ir/C (5%)). The reactions were performed at room temperature. Analysis of the reaction and products was performed by GC(MS), LC, and $^{1}H$ and $^{13}C$ NMR.

Received: July 2, 2003 [Z52275]

**Keywords:** allylic alcohols · heterogeneous catalysis · hydrogenation · iridium · zeolites

[1] K. Bauer, D. Garbe, H. Surburg, *Common Fragrance and Flavor Materials*, Wiley-VCH, Weinheim, **1997**.
[2] *Ullmann's Encyclopedia of Technical Chemistry*, 6th edition, electronic release, Wiley-VCH, **2000**.
[3] P. Gallezot in *Handbook of Heterogeneous Catalysis, Vol. 5* (Eds.: G. Ertl, H. Knözinger, J. Weitkamp), VCH, Weinheim, **1997**, pp. 2209–2221.
[4] P. Reyes, M. C. Aguirre, I. Melian-Cabrera, M. Lopez-Granados, J. L. G. Fierro, *J. Catal.* **2002**, *208*, 229.
[5] D. G. Blackmond, R. Oukaci, B. Blanc, P. Gallezot, *J. Catal.* **1991**, *131*, 401.
[6] J.-L. Luche, L. Rodriguez-Hahn, P. Crabbé, *J. Chem. Soc. Chem. Commun.* **1978**, 601.
[7] T. Ohkuma, H. Ikehira, T. Ikariya, R. Noyori, *Synlett* **1997**, 467.
[8] M. von Arx, T. Mallat, A. Baiker, *J. Mol. Catal. A* **1999**, *148*, 275.
[9] C. Milone, R. Ingoglia, M. L. Tropeano, G. Neri, S. Galvagno, *Chem. Commun.* **2003**, 868.
[10] A. Corma, A. Martinez, V. Martinez-Soria, *J. Catal.* **1997**, *169*, 480.
[11] R. C. Cambie, P. S. Rutledge, D. W. Scott, P. D. Woodgate, *Aust. J. Chem.* **1979**, *32*, 695.
[12] A. S. Campos Neves, M. L. Melo, M. J. Moreno, E. J. Tavares da Silva, J. A. R. Salvador, S. P. da Costa, R. M. Martins, *Tetrahedron* **1999**, *55*, 3255.
[13] W. Pickenhagen, D. Schatkowski, DE 10038544, **2002** [*Chem. Abstr.* **2002**, *136*, 134933].
[14] For the relevance of allylic alcohols derived from a) steroidal enones, see: S. Ring, G. Teichmüller, G. Weber, S. Schwarz, B. Erhart, B. Undeutsch, H. Raethe, P. Möllmann, C. Pfeiffer, H.-J. Palme, US 5831104, **1998** [*Chem. Abstr.* **1995**, *123*, 33509]; G. Humphrey, R. A. Miller, US 5696266, **1997** [*Chem. Abstr.* **1998**, *128*, 75585]; b) isolongifolenone, see reference [13]; c) prostaglandin precursors, see: M. Ohtani, T. Matsuura, Y. Hamada, I. Hamada, T. Sakata, K. Takahashi, M. Kishi, US 5585501, **1996** [*Chem. Abstr.* **1993**, *119*, 249777]; A. Gutman, G. Nisnevich, M. Etinger, I. Zaltzman, L. Yudovich, B. Pertsikov, WO PCT 01/55101, **2001** [*Chem. Abstr.* **2001**, *135*, 152659]; d) ionones, see: W. Kuhn, H. Surburg, US Appl. 2002/0082457, **2002** [*Chem. Abstr.* **2002**, *137*, 33431].
[15] http://www.iza-structure.org/

 © 2003 Wiley-VCH Verlag GmbH & Co. KGaA, Weinheim 

*Imprinted Polymer Microspheres*

# Monodisperse, Molecularly Imprinted Polymer Microspheres Prepared by Precipitation Polymerization for Affinity Separation Applications**

*Jinfang Wang, Peter A. G. Cormack,* David C. Sherrington, and Ezat Khoshdel*

Molecular imprinting is a versatile and facile method for preparing synthetic polymers with predetermined molecular recognition properties[1] (mimics of antibody binding) and hence is presently attracting widespread interest, especially as the technological potential of molecularly imprinted polymers (MIPs) in chromatographic separations,[2] biomimetic sensors,[3] solid-phase extraction (SPE)[4] and catalysis[5] has now been clearly established. To date, one of the simplest methods available for MIP production in the laboratory involves conventional free-radical solution polymerization, wherein a monolith of a highly cross-linked polymer forms upon copolymerization of functional monomer(s) with an excess of cross-linking agent in a porogenic solvent. When discrete, imprinted polymer particles of a particular size range are desired, which is often the case, particularly for HPLC and SPE applications, grinding and sieving of the monolith is necessary. Unfortunately, MIP particles of irregular size and shape are invariably obtained from grinding processes in low to moderate yields (typically less than 50%), and drawbacks associated with handling and application of such heterogeneous products are well documented. To streamline and optimize the production and performance of MIP particles, alternative synthetic strategies for obtaining discrete, imprinted, particulate products that obviate the need for grinding and sieving have been evolved; they include suspension,[6] dispersion[7] and seeded polymerization.[8] Whilst these methods have undoubted value, optimization of reliable experimental protocols can be lengthy, the general applicability is questionable in some cases, and residual emulsifier or stabilizer, which can remain absorbed on the surfaces of the particles, potentially compromises selective rebinding of molecules to the imprinted material.

As an alternative to the above approaches, precipitation polymerization has emerged as an attractive, simple, and seemingly general method for producing high-quality imprinted products as spherical particles. Precipitation poly-

[*] Dr. P. A. G. Cormack, J. Wang, Prof. D. C. Sherrington
Department of Pure and Applied Chemistry
University of Strathclyde
Thomas Graham Building
295 Cathedral Street, Glasgow, G1 1XL (UK)
Fax: (+44) 141-548-4246
E-mail: Peter.Cormack@strath.ac.uk
E. Khoshdel
Unilever Research, Port Sunlight
Quarry Road East, Bebington, Wirral, CH63 3JW (UK).

[**] This work was supported by Unilever Research.

 © 2003 Wiley-VCH Verlag GmbH & Co. KGaA, Weinheim DOI: 10.1002/anie.200352298 

merization is a surfactant-free method that involves polymerization of monomers in dilute solution (< 5 % w/v) in near-$\theta$ solvents.[9] Particle growth predominantly occurs by entropic precipitation of nanogel (seed) particles followed by continuous capture of oligomers from solution. Nearly monodisperse, spherical particles can be routinely prepared in good yields by this method, and it is possible to tune the size and porosity of the particles through control of the polymerization conditions. Application of precipitation polymerization to molecular imprinting has afforded high-quality, imprinted spherical particles with diameters typically less than 1 μm, which have been applied in analytical techniques such as competition assays[10] and capillary electrochromatography (CEC).[11]

To date, however, it has proved difficult to produce larger imprinted monodisperse microspheres by precipitation polymerization that are suitable for direct application in other important affinity-separation applications such as SPE and HPLC. Therefore, the main objective of the present work was to extend significantly the scope of application of imprinted polymers prepared by precipitation polymerization by the evolution of protocols for synthesizing micrometer-scale, spherical particulates. To realize this goal a clear understanding of the growth mechanism of the microspheres was necessary.[12] For example, in the preparation of larger particles, we found that matching the solubility parameter of the developing polymer network to that of the porogenic solvent(s) is particularly important, especially when simultaneous control of polymer morphology is also desirable. These criteria are usually met for copolymerization of divinylbenzene (DVB) in mixtures of acetonitrile and toluene (the solubility parameters for acetonitrile, toluene, and polydivinylbenzene are 24.6, 18.6, and ca. 17–18 $MPa^{0.5}$, respectively.[13,14]). Thus, when DVB is copolymerized under such conditions, phase separation is delayed and the polymer phase is solvated to a reasonable extent, so that products with well-developed, permanent pore structures and larger average diameters are obtained.[13] In addition, we have since also discovered, perhaps unsurprisingly, that the outcome of a precipitation polymerization is dependent on other factors, such as monomer concentrations and the method of agitation, albeit to a lesser extent. We will report upon these latter findings in full in a subsequent paper.

Under optimized polymerization conditions (see Experimental Section) relatively large microspheres of theophylline-imprinted polymer P1 and non-imprinted polymer P2 were obtained (Figure 1), which were easy to handle and of a size convenient for SPE and HPLC. The particle size distributions, measured by a Coulter Counter, were narrow; P1 and P2 had average particle diameters of 4.27 and 5.36 μm, respectively. Toluene was used as co-solvent in the polymerization of (predominantly) DVB 80; therefore, based on considerations of solubility parameters, P1 and P2 would be expected to be porous and to have high specific surface areas when prepared by precipitation polymerization.[9] This expectation was confirmed by nitrogen sorption porosimetry, which gave adsorption isotherms typical of porous polymer particles with a significant micropore population and BET specific surface areas of 550 and 660 $m^2 g^{-1}$ for P1 and P2,

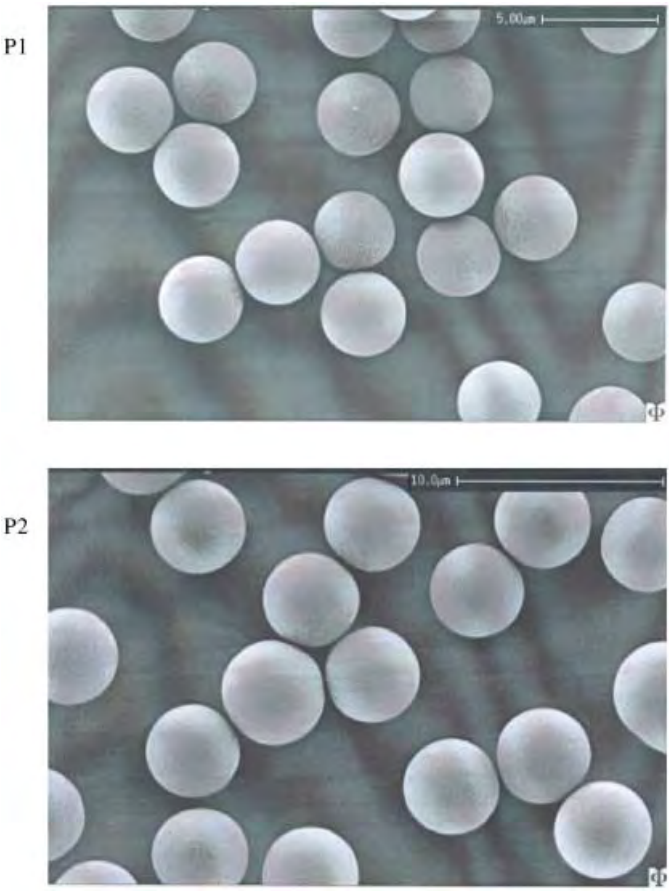



***Figure 1.*** Scanning electron micrographs of theophylline-imprinted (P1, bar = 5 μm) and non-imprinted (P2, bar = 10 μm) microspheres.

respectively. The similar morphologies of P1 and P2 in terms of average pore diameter (2.92 and 2.85 nm), pore volume (0.13 and 0.16 $cm^3 g^{-1}$), micropore volume (0.10 and 0.11 $cm^3 g^{-1}$), and micropore specific surface area (225 and 285 $m^2 g^{-1}$) demonstrated that the presence of template in the precipitation polymerization did not influence significantly the polymer morphology.

The molecular recognition properties of the microspheres were evaluated in HPLC mode after slurry packing of the microspheres, obtained directly after preparation, washing, and drying, into stainless steel HPLC columns (2.1 I.D. × 125 mm) by using an air-driven fluid pump operating at about 200 bar. Acetone was used as the void marker, and the capacity factors calculated according to standard chromatographic theory. The elution profiles under identical chromatographic conditions of theophylline with P1 and P2 as the stationary phase are shown in Figure 2. On the P1 column, theophylline was eluted with a capacity factor of 5.39 and, furthermore, showed the peak-tailing characteristic of an imprinted HPLC stationary phase. In contrast, and as expected, theophylline was relatively poorly retained on the non-imprinted control polymer P2 (capacity factor 2.43) with minimal tailing. The imprinting effect was confirmed by solid-phase extraction experiments under equilibrium rebinding conditions (data not shown), in which the rebinding capacity was found to be about 3 $\mu mol g^{-1}$.

 © 2003 Wiley-VCH Verlag GmbH & Co. KGaA, Weinheim 

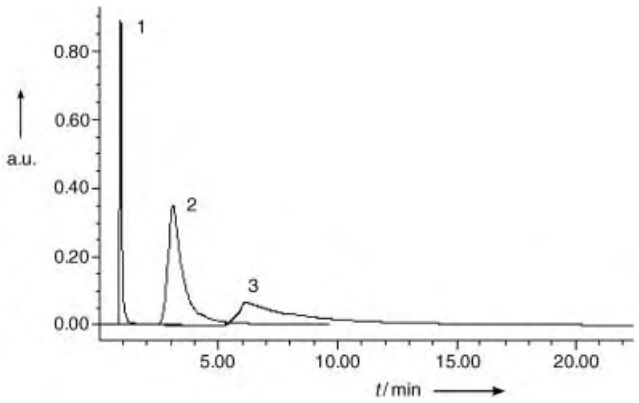



***Figure 2.*** Comparison of retention of theophylline on P1 (peak 3) and P2 (peak 2) and of acetone on P2 (peak 1). Mobile phase: acetonitrile; flow rate: 0.5 mL min$^{-1}$; detection: 270 nm. 2.5 μg of theophylline in 10 μL chloroform was injected. For acetone, the number of theoretical plates for P1 and P2 were calculated to be 5900 and 5300, respectively.

In summary, theophylline-imprinted and non-imprinted monodisperse, spherical, polymer particles of about 5 μm in diameter have been prepared in one step by precipitation polymerization in good yields and applied to HPLC and SPE separations. The advantages of the precipitation polymerization approach, as outlined herein, include the fact that it can quickly deliver, with minimal optimization, high-quality imprinted products in one step that are surfactant-free, and that it avoids the need for wasteful and time-consuming grinding procedures. In a subsequent paper we will report on how our method can be applied to different analytes, and describe how a variety of particulates can be produced by precipitation polymerization by varying the nature and amounts of functional monomers, cross-linkers, initiators, and porogenic solvents. Apart from the application of the imprinted microspheres to affinity separation described here, these materials can, in principle, be used wherever molecular recognition phenomena are of importance, and they thus have many other potential scientific applications.

## *Experimental Section*

Theophylline-imprinted polymer microspheres (P1) were prepared from divinylbenzene 80 (DVB 80) as cross-linker and methacrylic acid (MAA) as the functional monomer in a near-$\theta$[9] mixture of acetonitrile and toluene. In a typical synthesis, theophylline (1.5 mmol), MAA (6.0 mmol), DVB 80 (28.8 mmol) and free-radical initiator 2,2′-azobisisobutyronitrile (AIBN, 1.9 mmol) were dissolved in a mixture of acetonitrile and toluene (128 mL, 75/25 v/v) in a 250 mL round-bottomed flask. The solution was degassed in an ultrasonic bath for 5 min then sparged with oxygen-free nitrogen for 10 min while cooling on an ice bath. The flask was then attached to the rotor-arm of a Kugelrohr, submerged in a thermostatically controlled oil bath and rotated slowly (ca. 5–10 r.p.m.) to minimize turbulence. The temperature was increased from room temperature to 60 °C over 2 h and then maintained at 60 °C for a further 24 h. At the end of the reaction, the microspheres were separated from the reaction medium by vacuum filtration on a membrane filter, and were then washed successively with methanol/acetic acid (100 mL, 80/20 v/v) and methanol (100 mL) and dried in vacuo overnight at 40 °C. Non-imprinted, control microspheres (P2) were prepared under nominally identical conditions to P1 except that the theophylline template was omitted. By gravimetric analysis, the yields of P1 and P2 were found to be 62 and 55 %, respectively.

Received: July 3, 2003 [Z52298]

**Keywords:** imprinting · liquid chromatography · microporous solids · molecular recognition · polymerization

[1] K. Mosbach, O. Ramström, *Bio/Technology* **1996**, *14*, 163; b) G. Wulff, *Angew. Chem.* **1995**, *107*, 1958; *Angew. Chem. Int. Ed. Engl.* **1995**, *34*, 1812; c) K. J. Shea, *Trends Polym. Sci.* **1994**, *2*, 166; d) O. Brüggemann, K. Haupt, L. Ye, E. Yilmaz, K. Mosbach, *J. Chromatogr. A* **2000**, *889*, 15.

[2] a) M. Kempe, K. Mosbach, *J. Chromatogr. A* **1995**, *694*, 3; b) B. Sellergren, *J. Chromatogr. A* **2001**, *906*, 227; c) K. Haupt, *Analyst* **2001**, *126*,747.

[3] a) D. Kriz, O. Ramström, K. Mosbach, *Anal. Chem.* **1997**, *69*, 345A; b) S. A. Piletsky, Y. P. Parhometz, N. V. Lavryk, T. L. Panasyuk, A. V. Elskaya, *Sens. Actuators B* **1994**, *19*, 629; c) K. Haupt, K. Mosbach, *Chem. Rev.* **2000**, *100*, 2495.

[4] a) F. Lanza, B. Sellergren, *Chromatographia* **2001**, *53*, 599; b) D. Stevenson, *TrAC Trends Anal. Chem.* **1999**, *18*, 154; c) L. I. Andersson, *J. Chromatogr. B* **2000**, *739*, 163.

[5] G. Wulff, *Chem. Rev.* **2002**, *102*, 1.

[6] a) A. G. Mayes, K. Mosbach, *Anal. Chem.* **1996**, *68*, 3769; b) A. Flores, D. Cunliffe, M. J. Whitcombe, E. N. Vulfson, *J. Appl. Polym. Sci.* **2000**, *77*, 1841.

[7] B. Sellergren, *Anal. Chem.* **1994**, *66*, 1578.

[8] a) K. Hosoya, Y. Shirasu, K. Kimata, N. Tanaka, *Anal. Chem.* **1998**, *70*, 943; b) E. Yilmaz, O. Ramström, P. Moller, D. Sanchez, K. Mosbach, *J. Mater. Chem.* **2002**, *12*, 1577.

[9] a) K. Li, H. D. H. Stöver, *J. Appl. Polym. Sci.* **1993**, *31*, 3257; b) W. H. Li, H. D. H. Stöver, *J. Appl. Polym. Sci. Part A* **1998**, *36*, 1543; c) W. H. Li, K. Li, H. D. H. Stöver, *Macromolecules* **2000**, *33*, 4354.

[10] L. Ye, P. A. G. Cormack, K. Mosbach, *Anal. Commun.* **1999**, *36*, 35.

[11] T. de Boer, R. Mol, R. A. de Zeeuw, G. J. de Jong, D. C. Sherrington, P. A. G. Cormack, K. Ensing, *Electrophoresis* **2002**, *23*, 1296.

[12] J. S. Downey, R. S. Frank, W.-H. Li, H. D. H. Stöver, *Macromolecules* **1999**, *32*, 2838.

[13] D. C. Sherrington, *Chem. Commun.* **1998**, 2275.

[14] J. Brandrup, E. H. Immergut, *Polymer Handbook*, Wiley, New York, 3rd ed., **1989**, p. VII 519.

 © 2003 Wiley-VCH Verlag GmbH & Co. KGaA, Weinheim 

trans *Diamine Pt$^{II}$ Anticancer Complex*

# Hydrolysis Triggers Oxidation of a *trans* Diamine Platinum(II) Anticancer Complex**

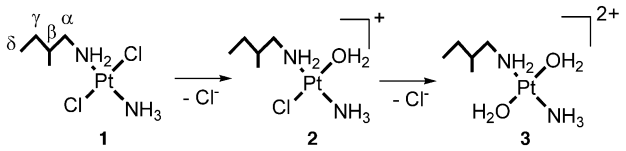
*Ana María Pizarro, Vivienne P. Munk, Carmen Navarro-Ranninger, and Peter J. Sadler**

The clinical success of cisplatin (*cis*-diamminedichloroplatinum(II)) as an anticancer drug has prompted the search for more effective platinum anticancer drugs that circumvent some of its limitations, for example, toxicity and resistance.[1–4] It was initially believed, because of the inactivity of transplatin (*trans*-diamminedichloroplatinum(II)), that all *trans*-platinum complexes are ineffective as antitumour agents.[5,6] Recently, several groups have reported that, with appropriate choice of amine, the cytotoxic activity of *trans*-diam(m)inedichloroplatinum(II) complexes can be comparable to, or even greater than, that of cisplatin.[7–11]

An understanding of the aqueous chemistry of diamine Pt$^{II}$ complexes is crucial for establishing their mechanism of action and hence for optimizing drug design. In particular, hydrolysis reactions of chloro Pt$^{II}$ complexes are thought to activate them prior to platination of the target site, DNA, since Pt–$OH_2$ bonds are more reactive than Pt–Cl bonds.[12] Although both the kinetics and thermodynamics of hydrolysis reactions of cisplatin and related *cis*-diaminodichloro Pt$^{II}$ complexes are well understood, surprisingly little is known about analogous reactions of *trans* complexes.[13–16]

Herein we report studies of the aqueous chemistry of *trans*-[$PtCl_2(NH_3)$(2-Me-butylamine)], **1**, a novel *trans*-platinum complex with cytotoxic activity comparable to that of cisplatin.[17] Unexpectedly, we have found that this complex undergoes facile redox reactions in aqueous solution. This shows that some *trans* complexes can exhibit novel chemistry that may be exploitable in further drug design, and could be relevant to the mechanism of biological activity.

We studied the hydrolysis pathway for **1**, Scheme 1, with ESIMS and $^1$H 1D and [$^1$H, $^{15}$N] 2D NMR spectroscopy.




***Scheme 1.*** Hydrolysis pathway for **1**.

Surprisingly, the $^1$H 1D NMR spectrum of [$^{15}NH_3$]**1** in water (Figure 1b) was complicated, in particular a range of $^1$H signals appeared in the $\delta = 5$–6.5 ppm region, which were not seen when NaCl was present to suppress hydrolysis (Figure 1a). Signals at about $\delta = 5$–6.5 ppm ($^1$H) were also observed in the 2D [$^1$H, $^{15}$N] spectrum of [$^{15}$N,$^{15}$N]**1** in water (see Supporting Information), with associated $^{15}$N shifts in the regions −55 to −45 ppm and −25 to −20 ppm.

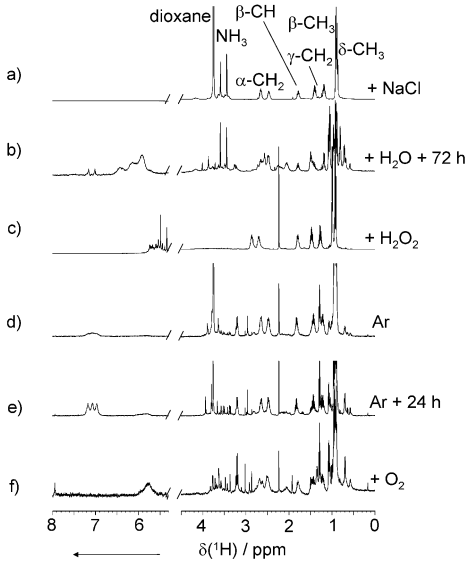



***Figure 1.*** $^1$H 1D NMR spectra of [$^{15}NH_3$]**1**. a) in 0.1 M NaCl in 90% $H_2O$/10% $D_2O$, 310 K; b) after reaction in the dark (72 h at 310 K) in 90% $H_2O$/10% $D_2O$, 310 K; c) complex [$^{15}$N,$^{15}$N]**1** treated with 25 equiv of $H_2O_2$; d) complex [$^{15}NH_3$]**1** after reaction with 0.95 equiv of $AgNO_3$ ($O_2$-free); e) sample from d) after it was allowed to stand for 24 h ($O_2$-free), and f) sample from e) after the sample had been purged with $O_2$(g) for 12 h. Signals assignable to Pt$^{IV}$ products (about 5.2–6.5 ppm) appear in spectra b), c) and f). The triplet at about $\delta = 7$ ppm arises from $NH_4^+$ ions ($^{14}$N, nuclear spin quantum number $I = 1$), and is observable at low pH values. This signal from $NH_4^+$ ions disappears after the sample has been purged with $O_2$(g), as $NH_3$ is volatile. Water resonances have been omitted for clarity.

To determine whether any of the product signals are assignable to aqua adducts, we investigated aqua complexes prepared by reaction of [$^{15}$N,$^{15}$N]**1** with 1.2 mol equivalents of $AgNO_3$ (with subsequent removal of AgCl(s)). Three $^1$H/$^{15}$N cross-peaks were observed in both the Pt$^{II}$–$^{15}NH_2$ and Pt$^{II}$–$^{15}NH_3$ regions of the spectrum (Figure 2a; $^1$H/$^{15}$N chemical shifts ($\delta$/ppm) 4.1 to 4.4/−47 to −44 and 3.5 to 3.8/−66 to −63, respectively). The $^1$H/$^{15}$N chemical shifts of these species (Table 1) are consistent with those expected for Pt$^{II}$ species with *trans*-nitrogen atoms,[18] and are assignable to the

[*] Prof. P. J. Sadler, Dr. V. P. Munk
School of Chemistry
The University of Edinburgh
King's Buildings, West Mains Road, Edinburgh EH9 3JJ (UK)
Fax: (+44) 131-650-6452
E-mail: p.j.sadler@ed.ac.uk
A. M. Pizarro, Prof. C. Navarro-Ranninger
Facultad de Ciencias
Departamento de Química Inorgánica
Universidad Autónoma de Madrid
Cantoblanco, 28049 Madrid (Spain)

[**] We thank the BBSRC, Spanish Ministry of Science and Technology, Spanish CICYT (Grants SAF00-0029 and SAF 03-01700) and Wellcome Trust (Edinburgh Protein Interaction Centre) for support, Dr. John Parkinson, Dr. Claudia Blindauer and Dr. Juraj Bella for their help and advice with NMR experiments, and colleagues in the EC COST D20 for support and stimulating discussions.

Supporting information for this article is available on the WWW under http://www.angewandte.org or from the author.

 DOI: 10.1002/anie.200352303 © 2003 Wiley-VCH Verlag GmbH & Co. KGaA, Weinheim 

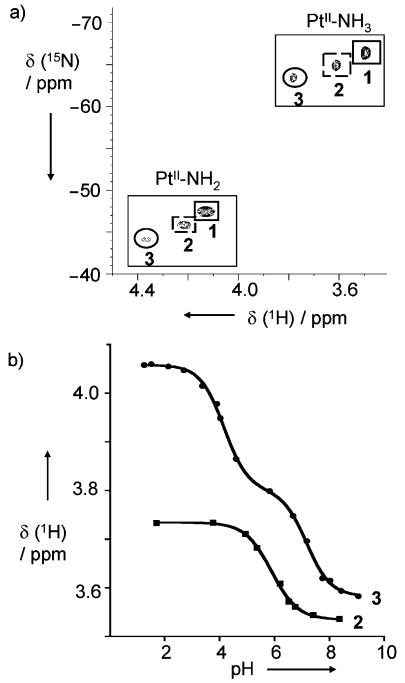



***Figure 2.*** a) [$^1$H, $^{15}$N] 2D NMR spectrum of the products formed after treatment of [$^{15}$N,$^{15}$N]**1** with $AgNO_3$ (molar ratio 1:1.2) in 0.1 M $NaClO_4$ in 90% $H_2O$/10% $D_2O$, 310 K, pH adjusted to 6.2. Assignments for the dichloro (**1**), monoaqua (**2**) and diaqua (**3**) complexes are shown. b) Variation in the Pt-$NH_3$ $^1$H NMR chemical shifts of peaks **2** and **3** in the 2D [$^1$H, $^{15}$N] NMR spectrum shown in a), assignable to the monoaqua/chloro and diaqua adducts of [$^{15}$N,$^{15}$N]**1** in 90% $H_2O$/10% $D_2O$, 310 K. The lines are computer-best fits with p$K_a$ values of 5.90 for **2** (monoaqua), and 4.16 and 7.17 for **3** (diaqua).

***Table 1:*** $^1$H and $^{15}$N NMR chemical shifts (ppm) for complexes **1, 2**, and **3** in 90% $H_2O$/10% $D_2O$ (pH 6.2, 310 K).

| Complex | $\delta$ $^1$H,$^{15}$N [ppm] | |
|---|---|---|
| | $Pt^{II}$-$NH_3$ | $Pt^{II}$-$NH_2$ |
| **1** | 3.49, −66.35 | 4.13, −47.38 |
| **2** | 3.61, −64.89 | 4.22, −45.85 |
| **3** | 3.78, −63.43 | 4.37, −44.08 |

dichloro complex, **1**, the monoaqua complex, **2**, and the diaqua complex, **3**. The assignments of signals for the aqua complexes were confirmed by their pH titration curves. Plots of the variation of the $^1$H NMR chemical shifts for the Pt–$NH_3$ signals versus pH were fitted to give p$K_a$ values of 5.90 for **2**, and of 4.16 and 7.17 for **3** (Figure 2b). These values are comparable with those reported for *trans*-$[PtCl(H_2O)(NH_3)_2]^+$ (p$K_a$ = 5.63) and *trans*-$[Pt(H_2O)_2(NH_3)_2]^{2+}$ (p$K_{a1}$ = 4.35, p$K_{a2}$ = 7.40), under similar conditions.[13]

The $^1$H/$^{15}$N cross-peaks assignable to monoaqua species were observed in the 2D HSQC spectrum for the hydrolysis products of [$^{15}$N,$^{15}$N]**1** formed after 24 h of reaction in 90% $H_2O$/10% $D_2O$ at 310 K (see Supporting Information). However, in this spectrum, no signals assignable to the diaqua species were observed. It might be expected that hydrolysis of one chloride ligand in a *trans*-$\{PtCl_2\}$ unit might occur at a faster rate than cisplatin on account of the higher *trans* effect of $Cl^-$ compared to $NH_3$, and that the second step to form *trans*-$\{Pt(H_2O)_2\}^{2+}$ would be very slow. This has indeed been reported to be the case.[14,16,19,20] In fact, it is very difficult to remove the second $Cl^-$ ligand from *trans*-$[PtCl(H_2O)(NH_3)_2]^+$ and requires extensive heating in the presence of $Ag^+$.[13,19]

Two additional sets of signals were also observed in all the 2D [$^1$H,$^{15}$N] HSQC spectra recorded for the hydrolysis of [$^{15}$N,$^{15}$N]**1** in water (see Supporting Information). Such signals also appeared when aqua adducts were generated by the reaction of [$^{15}$N,$^{15}$N]**1** with $AgNO_3$ (molar ratio 1:1.2, in 90% $H_2O$/10% $D_2O$, 310 K), Figure 3 (for the complete spectrum

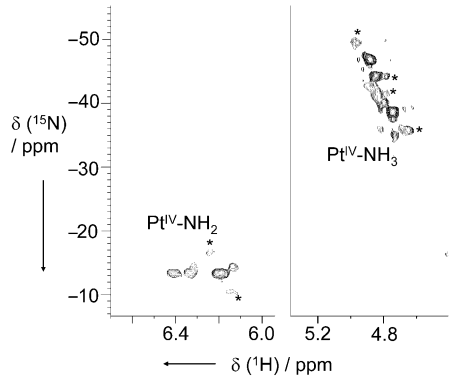



***Figure 3.*** [$^1$H, $^{15}$N] 2D NMR spectrum for the $Pt^{IV}$ reaction products formed after reaction of [$^{15}$N,$^{15}$N]**1** with $AgNO_3$ (molar ratio 1:1.2) in 0.1 M $NaClO_4$ in 90% $H_2O$/10% $D_2O$, 310 K. This spectrum was recorded during the pH titration at pH 1.5. Similar peaks were present at higher pH values, but the Pt–$NH_3$ signals overlap with the $H_2O$ signals. (* = $^{195}$Pt satellites).

see Supporting Information). It can be seen that at least three sets of signals, some with $^{195}$Pt satellites, appear in the regions with $^1$H/$^{15}$N chemical shifts ($\delta$/ppm) of 5.7 to 6.5/−20 to −10 ($Pt^{IV}$-$NH_2$) and 4.6 to 5.2/−50 to −35 ($Pt^{IV}$-$NH_3$). The shifts of these cross-peaks are similar to those that we observed for the reaction of [$^{15}$N,$^{15}$N]**1** with the strong oxidant $H_2O_2$, which gave rise to three new sets of Pt–$NH_2$ and Pt–$NH_3$ [$^1$H,$^{15}$N] NMR signals with chemical shifts ($\delta$/ppm) of about 5.6/−24 and 5.3/−40, respectively (see Supporting Information). These signals can be assigned to $^{15}NH_3$–$Pt^{IV}$-2-Me-($^{15}$N)butylamine complexes with additional Cl and OH ligands. Also, the $^1J(^{195}Pt–^{15}N)$ couplings (all about 260 Hz) are consistent with the presence of $Pt^{IV}$ centers.[21]

To investigate whether the presence of air influences the course of the hydrolysis reactions of **1**, aqua adducts were prepared by treating [$^{15}NH_3$]**1** with 0.95 mol equivalents of $AgNO_3$ under argon. In the absence of air, no $^1$H NMR signals were observed in the $\delta$ = 5.2–6.5 ppm region of the 1D $^1$H (Figure 1d). However, signals in this region appeared after the sample was purged with oxygen overnight (Figure 1f), which suggests that products from the hydrolysis of **1** in water react with oxygen.

Thus, the observed down-field shifts for both $^1$H and $^{15}$N NMR signals upon oxidation of [$^{15}$N,$^{15}$N]**1** with $H_2O_2$ are consistent with the formation of novel $Pt^{IV}$ complexes during the hydrolysis reactions of **1** in air, although they are not only

 © 2003 Wiley-VCH Verlag GmbH & Co. KGaA, Weinheim 

*trans* hydroxy adducts. We can find only one previous report of the spontaneous oxidation of aquated *trans*-diamine $Pt^{II}$ complexes.[13] Appleton et al. reported the detection of NMR peaks corresponding to $Pt^{IV}$ products from reactions of transplatin and silver salts after extensive heating, but did not investigate this reaction further. In the present study, $Pt^{IV}$ peaks appear directly during the hydrolysis of $[^{15}NH_3]$**1**, even in the absence of silver (see Figure 1b). In general, $Pt^{II}$ complexes with diam(m)ine and dihydroxo ligands are more easily oxidised than the dichloro analogues.[22]

Interestingly, $^1H$ NMR signals for $^{14}NH_4^+$ were observed for $[^{15}NH_3]$**1** in $H_2O$, under argon (triplet about $\delta = 7.1$ ppm; Figure 1d and 1e). The $NH_3$ ligand in the complex was labeled with $^{15}N$ (> 95%) in this experiment, and thus the only source of this $^{14}NH_4^+$ was the 2-Me-butylamine ligand (since $NO_3^-$ as a source seems unlikely). This suggests that during the hydrolysis reaction under these conditions the Pt–$NH_2$ bond of complex **1** is partially cleaved. The mechanism of this cleavage is unclear. Traces of a greyish-black precipitate were observed during the reaction, consistent with formation of $Pt^0$ (inductively coupled plasma atomic emission spectrometry (ICPAES) analysis after the solid was dissolved in $HNO_3$/HCl indicated the presence of Pt but not Ag atoms). Ammonia release, therefore, may involve oxidation of the amine.

The formation of $Pt^{IV}$ products was confirmed by $^{195}Pt$ NMR spectroscopy. Five sets of $^{195}Pt$ signals were observed in the $^{195}Pt$ NMR spectrum of **1** that had been treated with $AgNO_3$ (molar ratio **1**/$AgNO_3$ 1:1.2; 0.1 M $NaClO_4$, 90% $H_2O$/10% $D_2O$, 310 K), with shifts of −2178, −1867, −1471, −1157, and −50/−78 ppm (Figure 4). The signal at $\delta = -2178$ ppm (a) is assignable to the dichloro complex, **1**, and that at $\delta = -1867$ ppm (b) to the monoaqua complex, **2**. The signals at $\delta = -50$ and −78 ppm (e) are assignable to $Pt^{IV}$ species on the basis of their chemical shifts,[23,24] which confirms that the hydrolysis of **1** results in the formation of both $Pt^{II}$ and $Pt^{IV}$ products. The shift of peak (c), $\delta = -1471$ ppm, is consistent with either an hydroxy-bridged $Pt^{II}$ species or the diaqua complex, **3**, and that of signal (d), $\delta = -1157$ ppm, with an hydroxy-bridged $Pt^{II}$ dimer.[25,26]

ESIMS was used to identify further the products formed from reaction of complex **1** with $AgNO_3$ (0.95 mol equiv) in water. A large number of product signals was observed in the ESIMS spectrum (see Supporting Information), and each set of signals showed a cluster of ions with characteristic isotope splitting patterns for Pt, N and Cl atoms. Fragments observed at *m*/*z* 297, 331, and 349 are assignable to the mononuclear species $[PtC_5N_2H_{15}]^+$, $[PtC_5N_2O_2H_{17}]^+$, and $[PtC_5N_2OClH_{18}]^+$, respectively. With the aid of isotope modeling, the sets of peaks observed at *m*/*z* 667 and 982 can be assigned to the dinuclear species $[Pt_2C_{10}N_4O_2ClH_{35}]^+$ and trinuclear species $[Pt_3C_{15}N_6O_3ClH_{52}]^+$, respectively. This provides further evidence for the formation of di- and trinuclear $Pt^{II}$ hydroxy-bridged species in the hydrolysis reactions of **1**. Since hydroxy-bridged dimers and trimers of **1** appear to be readily formed in aqueous solution, further work on their isolation, DNA binding, and biological testing may be profitable. To our knowledge, no X-ray structures of hydroxy-bridged *trans* diamine complexes are available.

The findings of novel redox reactions of the complex **1** in aqueous solution may aid the design of *trans* diamine anticancer complexes, and the elucidation of structure–activity relationships. Hydrolysis of such *trans* complexes would be expected to be facile inside cells where the $Cl^-$ concentration is lower than outside cells. Oxidation of $Pt^{II}$ to $Pt^{IV}$ ions may be more prevalent in normal cells compared to cancer cells, since cells in solid tumours tend to be hypoxic. If oxidation to $Pt^{IV}$ inactivates the complex, this could provide a useful means of introducing selective toxicity, thus reducing side effects. It may be possible to vary the ease of oxidation by variation of the amine. It will be interesting to determine whether the oxidised products are stable even in the presence of the tripeptide glutathione, which is often present at millimolar concentrations in cells. Further work to investigate reaction pathways accessible to *trans* complexes which are not available to *cis* isomers is warranted.

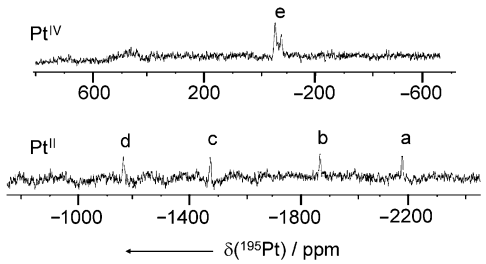



***Figure 4.*** $^{195}Pt$-{$^1H$} NMR spectrum of a solution containing **1** treated with 1.2 mol equivalents of $AgNO_3$ in 90% $H_2O$/10% $D_2O$ that contains 0.1 M $NaClO_4$ (310 K, about 75 mM). Signals assignable to $Pt^{II}$ complexes **1** and **2** ($\delta = -2178$ ppm (a) and $\delta = -1867$ ppm (b)) and $Pt^{IV}$ species (ca. −50 ppm (e)) are shown. The signal at $\delta = -1157$ ppm (d) may arise from dinuclear $Pt^{II}$ species, and peak **c** at $\delta = -1471$ ppm to an hydroxy-bridged $Pt^{II}$ complex or the diaqua complex **3**.

## *Experimental Section*

$K_2[PtCl_4]$ was provided on loan from Johnson Matthey plc. $^{15}NH_4Cl$, potassium phthalimide-$^{15}N$, 2-methylbutylamine and *S*-1-bromo-2-methylbutane were purchased from Aldrich. Cisplatin was synthesised by the Dhara method.[27]

The syntheses of *trans*-$[PtCl_2(NH_3)$(*rac*-2-Me-butylamine)], **1**, *trans*-$[PtCl_2(^{15}NH_3)$(*S*-2-Me-($^{15}$N)butylamine)], $[^{15}N,^{15}N]$**1**, and *trans*-$[PtCl_2(^{15}NH_3)$(*rac*-2-Me-butylamine)], $[^{15}NH_3]$**1**, were based on previously published procedures,[28,29] and are outlined in the Supporting Information. The monoaqua *trans*-$[PtCl(OH_2)(^{15}NH_3)$(*S*-2-Me-($^{15}$N)butylamine)]$NO_3$ complex, $[^{15}N,^{15}N]$**2**, was prepared in situ by addition of $AgNO_3$ (1.6 mg, 9.4 mmol) to a suspension of $[^{15}N,^{15}N]$**1** (3.7 mg, 9.9 mmol) in 90% $H_2O$/10% $D_2O$ (0.75 mL). The mixture was allowed to react for 24 h at ambient temperature in the dark, and then centrifuged to remove the white AgCl precipitate. $NaClO_4$ (9.2 mg, 75 mmol) was added to provide a constant ionic strength (0.1 M) for the pH titration. The same procedure was followed to give solutions containing the diaqua complex, *trans*-$[Pt(OH_2)_2(^{15}NH_3)$(*S*-2-Me-($^{15}$N)butylamine)]$(NO_3)_2$, $[^{15}N,^{15}N]$**3**, by using 1.2 mol equivalents of $AgNO_3$. In all experiments, it was determined by ICPAES that no residual silver remained in solution.

1D $^1H$, 1D $^{195}Pt$ and 2D [$^1H$, $^{15}N$] HSQC NMR spectra were recorded at 310 K in 5 mm (10 mm for $^{195}Pt$) NMR tubes on a Bruker DMX 500 MHz spectrometer ($^1H$ 500.13 MHz, $^{15}N$ 50.70 MHz, $^{195}Pt$ 53.76 MHz), with dioxane ($\delta(^1H)$ 3.76 ppm, internal), $^{15}NH_4Cl$ ($\delta(^{15}N)$ 0 ppm, external) and $K_2PtCl_4$ ($\delta(^{195}Pt)$ −1623 ppm, external)[30] as

 © 2003 Wiley-VCH Verlag GmbH & Co. KGaA, Weinheim 

standards. The pH values were determined at 298 K directly in the NMR tube, prior to and after NMR measurements, by using a Corning 145 pH meter equipped with a chloride-free microcombination electrode calibrated with Aldrich standard buffers (pH 4, 7 and 10). The pH was adjusted with dilute solutions of $HClO_4$ and NaOH. The pH titration curves were fitted to the Henderson–Hasselbalch equation by using the Kaleidagraph program (Synergy Software, Reading, PA, USA). ESIMS was performed on a Platform-II mass spectrometer (Micromass, Manchester, UK). ICPAES determination of platinum and silver concentrations were performed with a Thermo Jarrell Ash *IRIS* ICPAES, calibrated with 0–100 ppm standards.

Received: July 4, 2003 [Z52303]

**Keywords:** antitumor agents · hydrolysis · NMR spectroscopy · platinum

[1] T. W. Hambley, *Coord. Chem. Rev.* **1997**, *166*, 181.
[2] E. Wong, C. M. Giandomenico, *Chem. Rev.* **1999**, *99*, 2451.
[3] V. Brabec, *Prog. Nucleic Acid Res. Mol. Biol.* **2002**, *71*, 1.
[4] M. A. Fuertes, C. Alonso, J. M. Pérez, *Chem. Rev.* **2003**, *103*, 645.
[5] P. J. Stone, A. D. Kelman, F. M. Sinex, *J. Mol. Biol.* **1976**, *104*, 793.
[6] G. L. Cohen, J. A. Ledner, W. R. Bauer, H. M. Ushay, C. Caravana, S. J. Lippard, *J. Am. Chem. Soc.* **1980**, *102*, 2487.
[7] N. Farrell, L. R. Kelland, J. D. Roberts, M. van Beusichem, *Cancer Res.* **1992**, *52*, 5065.
[8] G. Natile, M. Coluccia, *Coord. Chem. Rev.* **2001**, *216–217*, 383.
[9] E. I. Montero, S. Díaz, A. M. González-Vadillo, J. M. Pérez, C. Alonso, C. Navarro-Ranninger, *J. Med. Chem.* **1999**, *42*, 4264.
[10] J. Kasparkova, O. Novakova, N. Farrell, V. Brabec, *Biochemistry* **2003**, *42*, 792.
[11] J. Kasparkova, V. Marini, Y. Najajreh, D. Gibson, V. Brabec, *Biochemistry* **2003**, *42*, 6321.
[12] R. B. Martin in *Cisplatin: Chemistry and Biochemistry of a leading anticancer drug* (Ed.: B. Lippert), Wiley-VCH, Zürich, **1999**, p. 183.
[13] T. G. Appleton, A. J. Bailey, K. J. Barnham, J. R. Hall, *Inorg. Chem.* **1992**, *31*, 3077.
[14] J. Arpalahti, R. Sillanpää, M. Mikola, *J. Chem. Soc. Dalton Trans.* **1994**, 1499.
[15] J. Arpalahti, *Met. Ions Biol. Syst.* **1996**, *32*, 379.
[16] B. I. Kankia, T. Funck, L. A. Marky, *J. Solution Chem.* **1999**, *28*, 1249.
[17] A. M. Pizarro, unpublished results.
[18] Y. Chen, Z. Guo, P. J. Sadler in *Cisplatin: Chemistry and Biochemistry of a Leading Anticancer Drug* (Ed.: B. Lippert), Wiley-VCH, Zürich, **1999**, p. 293.
[19] M. Mikola, J. Arpalahti, *Inorg. Chem.* **1994**, *33*, 4439.
[20] J. Arpalahti, E. Niskanen, R. Sillanpää, *Chem. Eur. J.* **1999**, *5*, 2306.
[21] R. Kuroda, S. Neidle, I. M. Ismail, P. J. Sadler, *Inorg. Chem.* **1983**, *22*, 3620.
[22] M. D. Hall, T. W. Hambley, *Coord. Chem. Rev.* **2002**, *232*, 49.
[23] P. S. Pregosin, *Coord. Chem. Rev.* **1982**, *44*, 247.
[24] K. Matsumoto, K. Sakai, *Adv. Inorg. Chem.* **2000**, *49*, 375.
[25] F. MacDonald, P. J. Sadler in *Biochemical Mechanisms of Platinum Antitumour Drugs* (Eds.: D. C. H. McBrien, T. F. Slater), IRL, Oxford, **1986**, p. 361.
[26] F. D. Rochon, C. Tessier, *Can. J. Chem.* **2002**, *80*, 379.
[27] S. C. Dhara, *J. Ind. Chem.* **1970**, *8*, 193.
[28] M. S. Gibson, R. W. Bradshaw, *Angew. Chem.* **1968**, *80*, 986; *Angew. Chem. Int. Ed. Engl.* **1968**, *7*, 919.
[29] G. B. Kauffman, D. O. Cowan, *Inorg. Synth.* **1960**, *6*, 211.
[30] D. P. Bancroft, C. A. Lepre, S. J. Lippard, *J. Am. Chem. Soc.* **1990**, *112*, 6860.

 © 2003 Wiley-VCH Verlag GmbH & Co. KGaA, Weinheim 

Stereoselective Conjugate Addition

# Highly Diastereoselective Conjugate Addition to Alkylidene Bis(Sulfoxides): Asymmetric Synthesis of (+)-*erythro*-Roccellic Acid**

*Franck Brebion, Bénédicte Delouvrié, Francisco Nájera, Louis Fensterbank,* Max Malacria,* and Jacqueline Vaissermann*

The conjugate addition of a nucleophile to an electron-deficient olefin is a key transformation for the synthesis of highly functionalized molecules.[1] Facial control relying on an appended chiral auxiliary as an electron-withdrawing moiety has been extensively studied,[2] and, despite recent advances in catalytic asymmetric processes,[3] this strategy still has important advantages such as predictability and generality. Whereas most methods for conjugate additions to olefins have dealt with chiral acrylic systems,[4] sulfoxides and congener auxiliaries have also been subject to versatile applications.[5] However, in the latter case, high diastereoselectivities have generally been reached when the acceptor is part of a ring, and/or an extra carbonyl moiety has been introduced so that additional steric constraints or chelation controls can operate.[6]

In this context alkylidene bis(sulfoxides) are appealing candidates[7] for asymmetric conjugate additions. Two types of these compounds have been developed: namely the 1,1-bis-*p*-tolyl derivatives[8] and the cyclic dithioacetal dioxides, which were studied more extensively by Aggarwal et al.[9] While these compounds have been utilized mainly as highly diastereoselective chiral ketene equivalents in cycloaddition[10] and epoxidation reactions,[11] their behavior as Michael acceptors has not been exploited.

Our approach has relied on (*S,S*)-bis-*p*-tolylsulfinyl acceptors **1** because of their direct availability from (−)-

[*] Dr. L. Fensterbank, Prof. Dr. M. Malacria, F. Brebion, B. Delouvrié, Dr. F. Nájera
Laboratoire de Chimie Organique
UMR 7611 CNRS, Case 229
Université Pierre et Marie Curie
4, place Jussieu, 75252 Paris Cedex 05 (France)
Fax: (+33) 1-4427-7360
E-mail: fensterb@ccr.jussieu.fr
malacria@ccr.jussieu.fr

Dr. J. Vaissermann
Laboratoire de Chimie Inorganique et Matériaux Moléculaires
UMR 7071 CNRS
Université Pierre et Marie Curie
4, place Jussieu, 75252 Paris Cedex 05 (France)

[**] We thank the Ministère de la Recherche for PhD grants to F.B. and B.D., and the CNRS for a Poste Rouge to F.N. as well as for their financial support. We also thank Carine Taboret for technical assistance, Patrick Herson (UPMC) for the X-ray analysis of **1c**, and Dr. Bernold Hasenknopf (UPMC) for helpful discussions. We are very grateful to Professor N. P. Argade (NCL Pune, India) for providing us with NMR spectra of *erythro*-roccellic acid.

Supporting information for this article is available on the WWW under http://www.angewandte.org or from the author.

 © 2003 Wiley-VCH Verlag GmbH & Co. KGaA, Weinheim DOI: 10.1002/anie.200352356 

menthol as a cheap chiral source.[8d] Moreover, structural examination of these substrates based on X-ray analysis of **1a** and **1c**[12] provided valuable information (see Figure 1 for the X-ray structure of **1a**). By introducing a dummy ligand (LP)

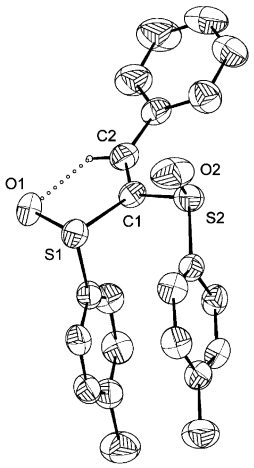
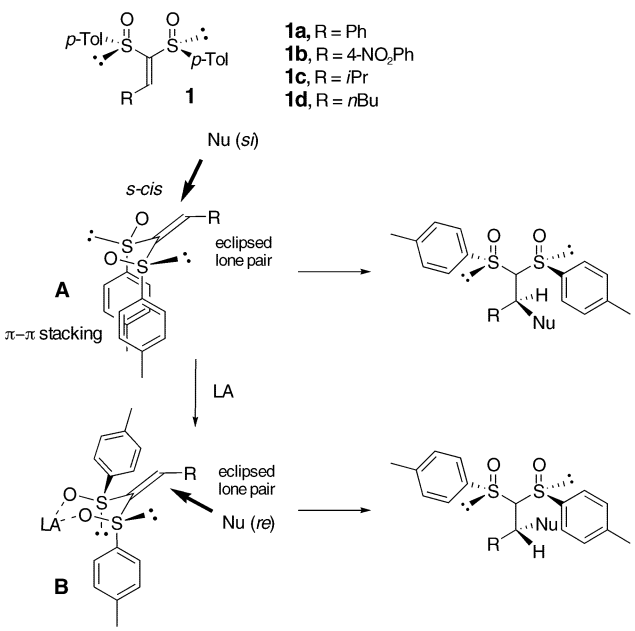



***Figure 1.*** X-ray structure of **1a**.



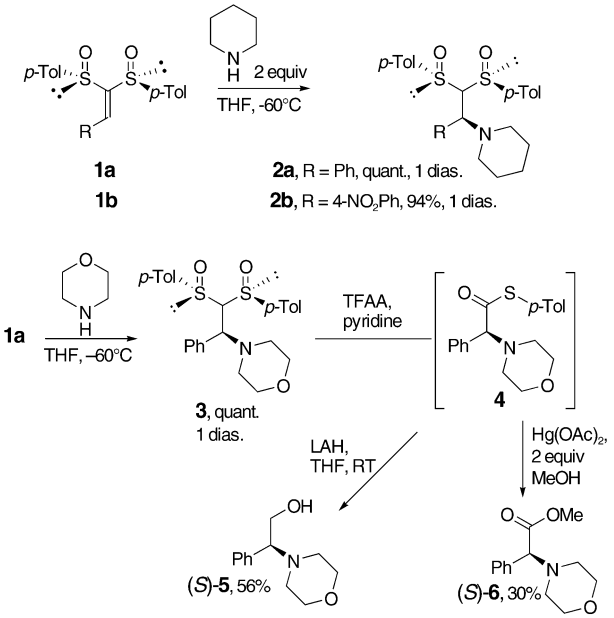

***Scheme 1.*** Dual mode of stereoselection.

in the structures of **1a** and **1c** in place of the lone pair, it was possible to deduce a dihedral angle C2-C1-S2-LP of 28° for **1a** and 14° for **1c**, which suggests that the lone pair of one sulfinyl group is quasi-eclipsing the *syn* R group on the alkene. Then, C2-C1-S1-O1 dihedral angles (4° for **1a** and 13° for **1c**) were even more consistent with an *s-cis* conformation of the other sulfinyl group. An additional intriguing feature of this *s-cis* arrangement is the interaction between the vinylic proton and the O1 atom ($d$(H–O1) = 2.28 Å for **1a** and **1c**). It is remarkable that these data corroborate the ab initio calculations by Tietze et. al on simpler vinylsulfoxides.[13] Finally, intramolecular π-stacking interactions between *p*-tolyl groups were established based on the following values[14] (distance between centroids: 3.53 Å for **1a**, 3.66 Å for **1c**, and ring normal–centroid vector angles of 25° for **1a**, and 27° for **1c**).

All these observations indicated to us that a dual mode (**A** or **B**) of diastereoselection was possible. If we assume that the conformations in solution are the same as those in the solid state, then the two interacting *p*-tolyl groups should lock the lower *re* face and promote the attack of the incoming nucleophile from the opposite *si* face (mode **A**, Scheme 1). In contrast, in presence of a proper Lewis acid (LA), a new organization of the reacting system based on chelation by the two sulfinyl groups should take place (mode **B**). This would favor attack from the *re* face, which minimizes steric interactions with the *p*-tolyl group present on the *si* face. Finally, a further attractive feature of this system is that the bis-sulfinyl moiety can serve as a masked carbonyl group,[15] which could be liberated after a Pummerer reaction.[8d]

To probe these points, we initially focused on the addition of amines to **1a** and **1b**. In contrast with the known reactivity of simple vinylsulfoxides,[16] this process provided amino adducts **2a** and **2b** more efficiently (quantitative yield at −60 °C) and in a completely diastereoselective manner following mode **A**. These amino adducts proved also to be versatile precursors of enantiopure amino esters and amino alcohols, as demonstrated by the transformation of **3** into (*S*)-**5** and (*S*)-**6**[17] via the Pummerer adduct **4** (Scheme 2).

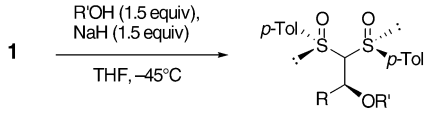
The addition of oxygenated nucleophiles required some optimization. Sodium alkoxides were the best nucleophiles and afforded adducts in high yields with total stereoselectivity following mode **A**, which sets an *S* absolute configuration at the α-alkoxy center.[18] It is worthy of note that products **10**




***Scheme 2.*** Diastereoselective addition of amines to compounds **1a** and **1b** and derivatizations. dias = diastereomer, LAH = lithium aluminum hydride, RT = room temperature, TFAA = trifluoroacetic anhydride.

 © 2003 Wiley-VCH Verlag GmbH & Co. KGaA, Weinheim 

and **11** are promising building blocks for the preparation of enantiopure diols and furan or pyran derivatives, respectively (Scheme 3, Table 1).



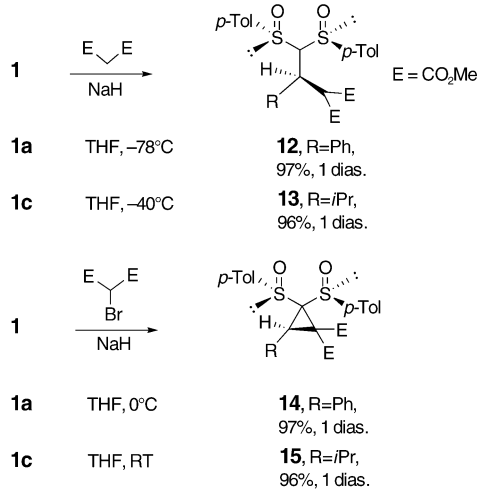

***Scheme 3.*** Diastereoselective addition of alkoxides.

***Table 1:*** Addition of sodium alkoxides to Michael acceptors **1**.

| Precursor | R′ | Prod. | Yield [%] | d.r., abs. conf.[a] |
|---|---|---|---|---|
| **1a** | Me | **7** | 90 | >98:2, *S* |
| **1c** | Me | **8** | 94 | >98:2, *S* |
| **1c** | Et | **9** | 93 | >98:2, *S* |
| **1c** | Bn | **10** | 84 | >98:2, *S* |
| **1c** | propargyl | **11** | 82 | >98:2, *S* |

[a] abs. conf.: absolute configuration of the α-alkoxy center.

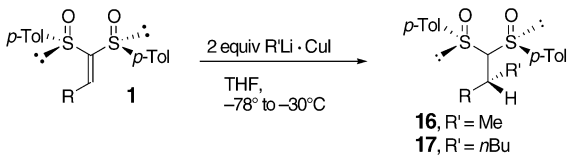
To further extend the scope of these Michael additions, we examined C–C bond formation with stabilized carbon nucleophiles such as sodium dimethylmalonate. High yields and complete stereoselectivity based on mode **A** were also observed (adducts **12**[19] and **13**, Scheme 4). More interest-




***Scheme 4.*** Diastereoselective C–C bond formation.

ingly, when the sodium anion of bromomalonate was used, the intriguing cyclopropane derivatives **14** and **15**, whose structure and absolute configuration were confirmed by X-ray analysis,[12] were also obtained in the same fashion.

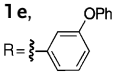
Because of the known complexation of copper salts with bis(sulfoxides) through sulfinyl oxygen atoms,[20] and previous results by Posner et al.,[21] we consider copper-based reagents to be good in Michael additions under chelation control (mode **B**, Scheme 5). Presumably also, formation of the initial Cu/olefin π-complex[22] with the double bond would be




***Scheme 5.*** Addition of copper reagents leads to a reversed diastereoselection.

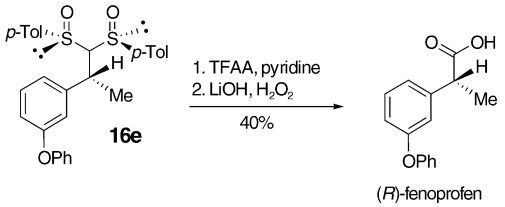
precluded on the *si* face because of the steric hindrance from the close *p*-tolyl group. Thus, addition reactions proceeded smoothly, affording products **16a, 16c–e**,and **17** in good yields and as single diastereomers with *R* absolute configuration at the newly alkylated center (Table 2).[23]

***Table 2:*** Addition of copper reagents to alkylidene acceptors **1**.

| Precursor | R′ | Prod. | Yield [%] | d.r., abs. conf.[a] |
|---|---|---|---|---|
| **1a** | Me | **16a** | 89 | >98:2, *R* |
| **1c** | Me | **16c** | 96 | >98:2, *R* |
| **1d** | Me | **16d** | 85 | >98:2, *R* |
| **1e**, R=  | Me | **16e** | 98 | >98:2, *R* |
| **1c** | *n*Bu | **17** | 77 | >98:2, *R* |

[a] abs. conf.: absolute configuration of the alkylated center.

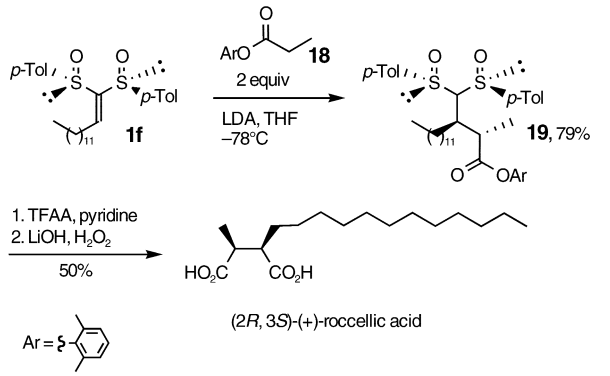
Derivatization of alkylidene **16e** through a Pummerer reaction and saponification provided the *R* enantiomer of fenoprofen (Scheme 6). *R* Enantiomers of profens have recently found applications in rheumatology,[24] and several members of this family should be readily available by this approach.




***Scheme 6.*** Application to the synthesis of (*R*)-fenoprofen.

Finally, exposure of alkylidene acceptor **1f** to the lithium enolate of Heathcock's ester[25] **18** afforded adduct **19** (79% yield) accompanied by minor diasteromers (10% yield; Scheme 7). The major diastereomer **19** was then engaged in a Pummerer reaction, followed by a double saponification to result in the first asymmetric synthesis of (+)-*erythro*-roccellic acid. Isolated from lichens,[26] and recently synthesized in a racemic form by Argade et al.,[27] roccellic acid exhibits a palette of biological activities such as plant growth promotion/inhibition and antituberculosis activity.[27] Remarkably, the succinate motif is found in a myriad of biologically relevant derivatives,[28] which this chemistry should render easily accessible.

 © 2003 Wiley-VCH Verlag GmbH & Co. KGaA, Weinheim 




***Scheme 7.*** Synthesis of (+)-*erythro*-roccellic acid.

In conclusion, we have shown that alkylidene bis(sulfoxide) derivatives are exceptional partners in high-yielding and totally diastereoselective Michael additions. The use of heteronucleophiles (amines and alkoxides) paves the way to enantiopure α-amino and α-hydroxy acids as well as β-amino alcohols and diols. C–C bond formation can also be achieved and the stereoselection conveniently controlled by means of chelation or lack of chelation by the choice of the counterion ($Li^+$, $Na^+$ vs. $Cu^+$). A new route to enantiopure succinate derivatives is also open, as demonstrated by the first asymmetric synthesis of (+)-*erythro*-roccelic acid, which relies on the highly diastereoselective addition of a lithium ester enolate to an appropriate, readily available bissulfinyl acceptor.

Received: July 11, 2003 [Z52356]

**Keywords:** allylic compounds · asymmetric synthesis · Michael addition · sulfoxides · total synthesis

[1] P. Perlmutter, *Conjugate Addition Reactions in Organic Synthesis*, Pergamon, Oxford, **1992**.
[2] H.-G. Schmalz in *Comprehensive Organic Synthesis, Vol. 4* (Ed.: M. F. Semmelhack), Pergamon, Oxford, **1991**, pp. 199–236.
[3] For reviews: a) M. P. Sibi, S. Manyem, *Tetrahedron* **2000**, *56*, 8033; b) N. Krause, A. Hoffmann-Roder, *Synthesis* **2001**, 171; c) A. Alexakis, C. Benhaim, *Eur. J. Org. Chem.* **2002**, 3221.
[4] B. E. Rossiter, N. M. Swingle, *Chem. Rev.* **1992**, *92*, 771.
[5] M. C. Carreño, *Chem. Rev.* **1995**, *95*, 1717.
[6] a) G. H. Posner, *Acc. Chem. Res.* **1987**, *20*, 72. For a radical version of this, see: b) N. Mase, Y. Watanabe, Y. Ueno, T. Toru, *J. Org. Chem.* **1997**, *62*, 7794; c) N. Mase, N. Watanabe, T. Toru, *J. Org. Chem.* **1998**, *63*, 3899.
[7] For an approach involving a phosphoryl sulfinyl alkylidene, see: W. H. Midura, M. Mikołajczyk, *Tetrahedron Lett.* **2002**, *43*, 3061.
[8] a) Y. Arai, S. Kuwayama, Y. Takeuchi, T. Koizumi, *Synth. Commun.* **1986**, *16*, 233; b) G. Solladié, F. Colobert, P. Ruiz, C. Hamdouchi, M. C. Carreño, J. L. García Ruano, *Tetrahedron Lett.* **1991**, *32*, 3695; c) J. C. Carretero, J. L. García Ruano, L. M. Martín Cabrejas, *Tetrahedron: Asymmetry* **1997**, *8*, 409; d) B. Delouvrié, F. Nájera, L. Fensterbank, M. Malacria, *J. Organomet. Chem.* **2002**, *643–644*, 130.
[9] For recent contributions of this group, see: a) V. K. Aggarwal, S. J. Roseblade, J. K. Barrell, R. Alexander, *Org. Lett.* **2002**, *4*, 1227; b) V. K. Aggarwal, R. M. Steele, Ritmaleni, J. K. Barrell, I. Grayson, *J. Org. Chem.* **2003**, *68*, 4087, and references therein.
[10] For a review, see: B. Delouvrié, L. Fensterbank, F. Nájera, M. Malacria, *Eur. J. Org. Chem.* **2002**, 3507.
[11] V. K. Aggarwal, J. K. Barrell, J. M. Worrall, R. Alexander, *J. Org. Chem.* **1998**, *63*, 7128.
[12] CCDC 213619–213621 contain the supplementary crystallographic data for this paper. These data can be obtained free of charge via www.ccdc.cam.ac.uk/conts/retrieving.html (or from the Cambridge Crystallographic Data Centre, 12 Union Road, Cambridge CB2 1EZ, UK; fax: (+44) 1223-336-033; or deposit@ccdc.cam.ac.uk).
[13] L. F. Tietze, A. Schuffenhauer, P. R. Schreiner, *J. Am. Chem. Soc.* **1998**, *120*, 7952.
[14] C. Janiak, *J. Chem. Soc. Perkin Trans. 1* **2000**, 3885.
[15] For the concept of chiral acyl anion, see : a) L. Colombo, C. Gennari, C. Scolastico, G. Guanti, E. Narisano, *J. Chem. Soc. Chem. Commun.* **1979**, 591; b) C. Gaul, K. Schärer, D. Seebach, *J. Org. Chem.* **2001**, *66*, 3059, and references therein.
[16] a) S. G. Pyne, P. Bloem, S. L. Chapman, C. E. Dixon, R. Griffith, *J. Org. Chem.* **1990**, *55*, 1086; b) D. J. Abbott, S. Colonna, J. M. Stirling, *J. Chem. Soc. Perkin Trans. 1* **1976**, 492.
[17] The *S* absolute configurations of **5** and **6** were determined by correlation: (*R*)-**5** was made independently from (*R*)-phenylglycinol, and LAH reduction of **6** afforded (*S*)-**5** with no loss of optical purity and with completely opposite optical activity, see the Supporting Information.
[18] The absolute configuration of **7** was determined by chemical correlation, see the Supporting Information.
[19] The absolute configuration of **12** was determined by chemical correlation with a compound described by G. Tsuchihashi, S. Mitamura, S. Inoue, K. Ogura, *Tetrahedron Lett.* **1973**, *14*, 323, see the Supporting Information.
[20] S. K. Madan, C. M. Hull, L. J. Herman, *Inorg. Chem.* **1968**, *7*, 491.
[21] a) G. H. Posner, T. P. Kogan, M. Hulce, *Tetrahedron Lett.* **1984**, *25*, 383; b) G. H. Posner, J. P. Mallamo, K. Miura, *J. Am. Chem. Soc.* **1981**, *103*, 2886.
[22] For the mechanism of copper-mediated addition reactions, see: S. Mori, E. Nakamura in *Modern Organocopper Chemistry* (Ed.: N. Krause), Wiley-VCH, Weinheim, **2002**.
[23] The *R* absolute configurations of **16a** and **16d** were determined by chemical derivatization. Pummerer reactions followed by reduction provided known enantiopure alcohols (see the Supporting Information).
[24] G. Geisslinger, S. Grösch, PCT Int. Appl. WO 02/24190A1, **2002**.
[25] C. H. Heathcock, M. C. Pirrung, S. H. Montgomery, J. Lampe, *Tetrahedron* **1981**, *37*, 4087.
[26] a) The Merck Index, 12th Edition, **1996**, article 8405; b) S. Huneck, J. Schmidt, A. Porzel, *Z. Naturforsch. B* **1994**, *49*, 561, and references therein.
[27] S. Mangaleswaran, N. P. Argade, *J. Chem. Soc. Perkin Trans. 1* **2001**, 1764.
[28] For an illustration of this, see: M. P. Sibi, H. Hasegawa, *Org. Lett.* **2002**, *4*, 3347.

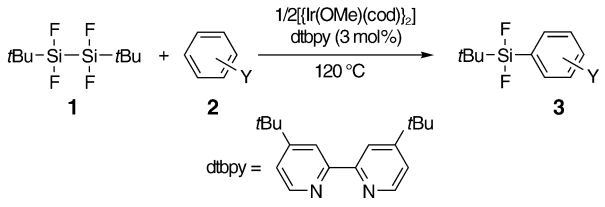
 © 2003 Wiley-VCH Verlag GmbH & Co. KGaA, Weinheim 

*Ir-Catalyzed Silylation of Arenes*

# Direct Synthesis of Aryl Halosilanes through Iridium(I)-Catalyzed Aromatic C–H Silylation by Disilanes**

*Tatsuo Ishiyama,* Kazuaki Sato, Yukihiro Nishio, and Norio Miyaura**

Aryl halosilanes and their hypervalent derivatives are versatile reagents for carbon–carbon[1–2] and carbon–heteroatom[3] bond formation in modern organic synthesis. Although they have been prepared by arylation of halosilanes with aryl magnesium or aryl lithium reagents,[4] and by Pd-catalyzed cross-coupling of halogenated disilanes with aryl electrophiles,[5] direct silylation of arenes through C–H bond activation would provide a more attractive route from the viewpoints of economy, efficiency, and environmental benignity. Indeed, aromatic C–H silylation by disilanes[6] or hydrosilanes[6a,7] catalyzed by a transition-metal complex has been developed by several research groups. However, the application of this protocol has been limited to the synthesis of aryl triorganosilanes. On the other hand, we recently found that $Ir^I$ complexes generated from 1/2[{IrCl(cod)}$_2$] (cod = 1,5-cyclooctadiene) or 1/2[{Ir(OMe)(cod)}$_2$] and 2,2′-bipyridine (bpy) or 4,4′-di-*tert*-butyl-2,2′-bipyridine (dtbpy) are excellent catalysts for aromatic C–H borylation by bis(pinacolato)diboron.[8] These results prompted us to extend the methodology to the aromatic C–H silylation of arenes (**2**) by 1,2-di-*tert*-butyl-1,1,2,2-tetrafluorodisilane (*t*BuF$_2$Si)$_2$ (**1**) in the presence of a 1/2[{Ir(OMe)(cod)}$_2$]-dtbpy catalyst. This process enables, for the first time, the direct synthesis of aryl halosilanes (**3**) through aromatic C–H bond activation (Scheme 1).




***Scheme 1.*** Aromatic C–H silylation.

[*] Prof. T. Ishiyama, Prof. N. Miyaura, K. Sato, Y. Nishio
Division of Molecular Chemistry
Graduate School of Engineering
Hokkaido University
Sapporo, 060-8628 (Japan)
Fax: (+81) 11-706-6562
E-mail: ishiyama@org-mc.eng.hokudai.ac.jp
miyaura@org-mc.eng.hokudai.ac.jp

[**] This work was partially supported by Grant-in-Aid for Scientific Research on Priority Areas (No. 14078101, "Reaction Control of Dynamic Complexes") from Ministry of Education, Culture, Sports, Science and Technology, Japan. T.I. thanks Itoh Science Foundation and The Akiyama Foundation for support of part of his work.

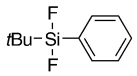
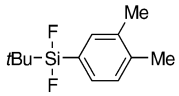
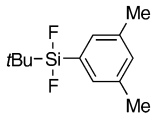
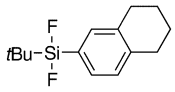
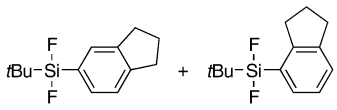
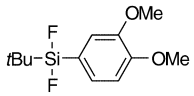
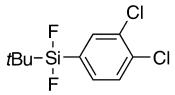
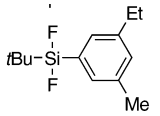
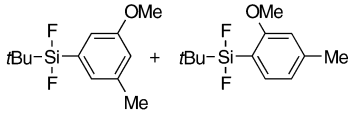
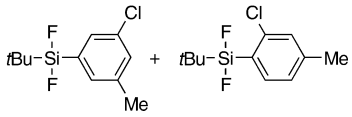
Our initial investigation focused on the effects of substituents on the disilanes on the reaction. The reactions were carried out at 80 °C for 16 h in a resealable Schlenk tube by using disilanes (1.0 mmol), benzene (60 mmol), [{Ir(OMe)(cod)}$_2$] (0.015 mmol), and dtbpy (0.03 mmol). Among the disilanes examined, **1** exhibited the highest reactivity to produce the corresponding phenylsilane in 28 % yield with 28 % conversion of **1**. The use of tetrafluorodisilanes is critical as (Me$_2$FSi)$_2$ gave the corresponding arylsilane in 9 % yield, and (*t*BuCl$_2$Si)$_2$ or (Me$_3$Si)$_2$ led to no reaction. The structures of alkyl substituents also had significant effects on silylation. For example, (*s*BuF$_2$Si)$_2$ and (*n*BuF$_2$Si)$_2$ formed no silylated product.

The reaction of *o*-xylene with **1** was carried out at 120 °C to optimize catalyst precursors and ligands. Of the precursors and ligands examined, the combination of 1/2[{Ir(OMe)(cod)}$_2$] and dtbpy was found to be the best catalyst to provide isomerically pure 4-silyl-1,2-dimethylbenzene in 99 % yield based on the molar amount of **1**. Although the substrate has weaker benzylic C–H bonds,[9] the reaction selectively occurred at the aromatic C–H bonds. The combination of dtbpy and either 1/2[{IrCl(cod)}$_2$] or [{Ir(cod)$_2$}BF$_4$] produced silylated products in 82 % and 78 % yield, respectively, but [Ni(acac)$_2$]–*n*BuLi (acac = acetylacetonato), 1/2[{RhCl(cod)}$_2$], 1/3[Ru$_3$(CO)$_{12}$], and [Pt(dba)$_2$] (dba = dibenzylideneacetone) with or without a dtbpy ligand formed no silylated product. Reactions with 1/2[{Ir(OMe)(cod)}$_2$] as a catalyst precursor were markedly affected by steric and electronic properties of bipyridine ligands. Bpy, 4,4′-di-Me-bpy, 5,5′-di-Me-bpy, and even 6,6′-di-Me-bpy displayed moderate reactivity (49–55 % yields), while 3,3′-di-Me-bpy showed little activity (8 % yield) owing to the importance of a parallel arrangement of two pyridine rings. Electronic effects of bpy derivatives were perplexing as electron-rich or -poor derivatives of bpy resulted in low yields, for example, 4,4′-di-Me$_2$N-bpy (1 %); 4,4′-di-MeO-bpy (34 %); 4,4′-di-Cl-bpy (2 %); and 4,4′-di-O$_2$N-bpy (0 %).

Reactions of **1** with representative arenes **2** catalyzed by the combination of 1/2[{Ir(OMe)(cod)}$_2$] and dtbpy at 120 °C are summarized in Table 1. Under optimized conditions, benzene produced phenylsilane in 97 % yield (entry 1). The orientation can be controlled by steric effects of substituents. Reactions occurred at C–H bonds located *meta* or *para* to a substituent in preference to those of *ortho* positions. Thus, *o*- and *m*-xylenes gave a single product (entries 2 and 3), but *p*-xylene resulted in no reaction because of steric hindrance. Bicyclic **2** such as tetralin and indan yielded silylated products (entries 4 and 5); indan gave a mixture of 5- and 4-silyl derivatives owing to only a small steric hindrance of the five-membered ring. Compounds **2** in which the rings were electron-rich or electron-poor participated in silylation reactions (entries 6 and 7). The reactions of 1,3-dialkylated **2** selectively occurred only at the common *meta* position; therefore, isomerically pure compounds of **3** were obtained even with two distinct substituents on **2** (entry 8), whereas analogous substrates of **2** that have less bulky substituents such as a MeO or Cl group produced a regioisomeric mixture of **3** (entries 9 and 10).

 © 2003 Wiley-VCH Verlag GmbH & Co. KGaA, Weinheim DOI: 10.1002/anie.200352399 

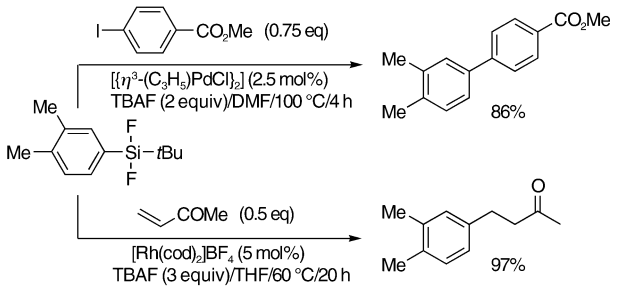
***Table 1:*** Synthesis of arylsilanes **3** (Scheme 1).[a]

| Entry | Arylsilane **3** | Yield [%][b] |
|---|---|---|
| 1 |  | 97 |
| 2 |  | 99 |
| 3 |  | 97 |
| 4 |  | 96 |
| 5 |  | 98 (82:18) |
| 6 |  | 73 |
| 7 |  | 46 |
| 8 |  | 75 |
| 9 |  | 79 (66:34) |
| 10 |  | 72 (87:13) |

[a] A mixture of $(t\mathrm{BuF_2Si})_2$ **1** (1.0 mmol), arene **2** (60 mmol), [{Ir(OMe)(cod)}$_2$] (0.015 mmol), and dtbpy (0.03 mmol) was stirred at 120 °C for 16 h. [b] GC yields based on **1**.

Although we have not investigated the reaction mechanism yet, the present C–H silylation may proceed through: (a) the generation of a (silyl)iridium intermediate (**4**) by the reaction of **1** with an iridium(I) complex; (b) oxidative addition of an aromatic C–H bond to **4** followed by reductive elimination of an arylsilane **3** or direct σ-bond metathesis between an Ir–Si bond of **4** and an aromatic H–C bond to form an iridium hydride complex (**5**); (c) oxidative addition of **1** to **5** followed by reductive elimination of a hydrosilane or direct σ-bond metathesis between **1** and **5** to regenerate a (silyl)iridium intermediate **4**. It is unclear at this moment whether the mechanism involves a mono(silyl)iridium(I) or a tris(silyl)iridium(III) intermediate, and why two of the silyl groups in **1** do not participate in the reaction.

Arylsilanes **3** thus obtained are useful reagents for carbon–carbon bond-formation reactions (Scheme 2). For example, **3** cross-coupled with aryl halides in the presence of a palladium catalyst and a fluoride-ion source in dimethylformamide (DMF) to produce the corresponding unsymmetrical biaryls in high yields.[1] Also, **3** participated in 1,4-addition to α,β-unsaturated ketones in the presence of a rhodium catalyst and a fluoride-ion source in THF to give β-arylketones in excellent yields.[2]




***Scheme 2.*** Synthetic utility of **3**.

In summary, iridium complexes composed of 1/2[{Ir(OMe)(cod)}$_2$] and 4,4′-di-*tert*-butyl-2,2′-bipyridine were found to be efficient catalysts for the aromatic C-H silylation by 1,2-di-*tert*-butyl-1,1,2,2-tetrafluorodisilane, thus enabling the first direct synthesis of arylhalosilanes from arenes in high yields. Further investigations to survey the scope and limitation of this C–H silylation, including that of monosubstituted arenes, heteroarenes, alkenes, and alkanes, as well as the application of this catalyst system to other types of C–H functionalization are in progress.

## *Experimental Section*

A representative procedure for **3**: A resealable Schlenk tube containing [{Ir(OMe)(cod)}$_2$][10] (0.015 mmol) and dtbpy (0.03 mmol) was flushed with nitrogen, then charged with *o*-xylene (60 mmol) and $(t\mathrm{BuF_2Si})_2$[11] **1** (1.0 mmol). The tube was sealed with a Teflon screwcap, and the mixture was stirred at 120 °C for 16 h. The product was isolated by Kugelrohr distillation to give an analytically pure sample: $^1$H NMR (400 MHz, $CDCl_3$, 25 °C, TMS): $\delta = 1.07$ (t, $J =$ 1.0 Hz, 9H), 2.29 (s, 3H), 2.30 (s, 3H), 7.21 (d, $J = 7.3$ Hz, 1H), 7.40 (d, $J = 9.8$ Hz, 1H), 7.42 ppm (s, 1H); $^{13}$C NMR (100 MHz, $CDCl_3$, 25 °C, TMS): $\delta = 17.87$ (t, $J = 15.3$ Hz), 19.67, 20.00, 24.83, 124.45 (t, $J = 16.5$ Hz), 129.55, 132.02, 135.41, 136.52, 140.68 ppm; HRMS calcd for $C_{12}H_{18}F_2Si$: 228.1145; found: 228.1140.

Received: July 16, 2003 [Z52399]

**Keywords:** arenes · C-H activation · homogeneous catalysis · iridium · silicon

[1] a) Y. Hatanaka, T. Hiyama, *Synlett* **1991**, 845; b) T. Hiyama in *Metal-Catalyzed Cross-Coupling Reactions* (Eds.: F. Diederich, P. J. Stang), Wiley-VCH, Weinheim, **1998**, p. 421; c) T. Hiyama, E. Shirakawa, *Top. Curr. Chem.* **2002**, *219*, 61; d) S. E. Denmark, R. F. Sweis, *Acc. Chem. Res.* **2002**, *35*, 835.

[2] a) S. Oi, M. Moro, Y. Inoue, *Organometallics* **2001**, *20*, 1036; b) T.-S. Huang, C.-J. Li, *Chem. Commun.* **2001**, 2348; c) K. Fagnou, M. Lautens, *Chem. Rev.* **2003**, *103*, 169.

[3] a) K. Tamao, N. Ishida, *J. Organomet. Chem.* **1984**, *269*, C37; b) G. R. Jones, Y. Landais, *Tetrahedron* **1996**, *52*, 7599; c) P. Y. S. Lam, S. Deudon, K. M. Averill, R. Li, M. Y. He, P. DeShong, C. G. Clark, *J. Am. Chem. Soc.* **2000**, *122*, 7600; d) P. Y. S. Lam, S.

 © 2003 Wiley-VCH Verlag GmbH & Co. KGaA, Weinheim 

Deudon, E. Hauptman, C. G. Clark, *Tetrahedron Lett.* **2001**, *42*, 2427.
[4] N. Auner in *Synthetic Methods of Organometallic and Inorganic Chemistry, Vol. 2* (Ed.: W. A. Herrmann), Thieme, New York, **1996**, p. 143.
[5] K. A. Horn, *Chem. Rev.* **1995**, *95*, 1317.
[6] a) T. Sakakura, Y. Tokunaga, T. Sodeyama, M. Tanaka, *Chem. Lett.* **1987**, 2375; b) M. Ishikawa, S. Okazaki, A. Naka, H. Sakamoto, *Organometallics* **1992**, *11*, 4135; c) M. Ishikawa, A. Naka, J. Ohshita, *Organometallics* **1993**, *12*, 4987; d) N. A. Williams, Y. Uchimaru, M. Tanaka, *J. Chem. Soc. Chem. Commun.* **1995**, 1129; e) A. Naka, K. K. Lee, K. Yoshizawa, T. Yamabe, M. Ishikawa, *Organometallics* **1999**, *18*, 4524.
[7] a) W. A. Gustavson, P. S. Epstein, M. D. Curtis, *Organometallics* **1982**, *1*, 884; b) Y. Uchimaru, A. M. M. El Sayed, M. Tanaka, *Organometallics* **1993**, *12*, 2065; c) K. Ezbiansky, P. I. Djurovich, M. LaForest, D. J. Sinning, R. Zayes, D. H. Berry, *Organometallics* **1998**, *17*, 1455; d) F. Kakiuchi, K. Igi, M. Matsumoto, N. Chatani, S. Murai, *Chem. Lett.* **2001**, 422; e) F. Kakiuchi, K. Igi, M. Matsumoto, T. Hayamizu, N. Chatani, S. Murai, *Chem. Lett.* **2002**, 396.
[8] a) T. Ishiyama, J. Takagi, K. Ishida, N. Miyaura, N. R. Anastasi, J. F. Hartwig, *J. Am. Chem. Soc.* **2002**, *124*, 390; b) J. Takagi, K. Sato, J. F. Hartwig, T. Ishiyama, N. Miyaura, *Tetrahedron Lett.* **2002**, *43*, 5649; c) T. Ishiyama, J. Takagi, J. F. Hartwig, N. Miyaura, *Angew. Chem.* **2002**, *114*, 3182; *Angew. Chem. Int. Ed.* **2002**, *41*, 3056.
[9] D. P. Curran in *Comprehensive Organic Synthesis, Vol. 4* (Ed.: B. M. Trost), Pergamon, Oxford, **1991**, p. 715.
[10] R. Uson, L. A. Oro, J. A. Cabeza, *Inorg. Synth.* **1985**, *23*, 126.
[11] B. Reiter, K. Hassler, *J. Organomet. Chem.* **1994**, *467*, 21.

 © 2003 Wiley-VCH Verlag GmbH & Co. KGaA, Weinheim 

Hexapeptide Total Synthesis

# Total Synthesis of Microsclerodermin E**

*Jidong Zhu and Dawei Ma**

Lithistid sponges are well-known among marine organisms for their ability to produce a diverse array of biologically active metabolites.[1] From several species of the lithistid sponge *Microscleroderma sp.* and *Theonella sp.*, Faulkner and co-workers have isolated a series of cyclic peptides named microsclerodermins A–I.[2] Structurally, each of them was shown to display several unique features, including a 23-membered cyclic hexapeptide core, featuring a very complex β-amino acid and three other unnatural amino acid residues. Preliminary studies have indicated that all these compounds possess intriguing antifungal activities and some of them show potent antitumor properties,[2,3] but further evaluation of their biological activities has been hampered by their relative scarcity. The biological activities and the structural complexity exhibited by the microsclerodermins have attracted much attention within the community of synthetic chemists. However, although some synthetic efforts towards these compounds have been reported,[4] no member of this family has been synthesized yet. Herein we wish to describe our total synthesis of microsclerodermin E. Notable elements of the synthesis are the concise assembly of its β-amino acid fragment, the assembly of the pyrrolidinone fragment with little racemization, and the effective macrocyclization at the Gly-GABOB site.

The retrosynthetic blueprint that guided this new campaign is defined in Figure 1. The macrocyclic core of the target molecule is disconnected into two fragments, the tetrapeptide

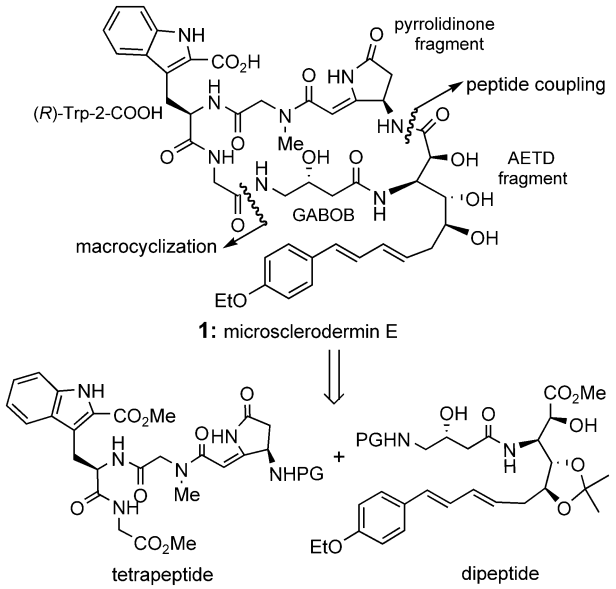



***Figure 1.*** Retrosynthetic analysis of microsclerodermin E. PG = protecting group.

portion and the dipeptide unit. Further disconnections of these two parts reveals that we need to employ Gly and *N*-MeGly as the starting materials and develop some efficient methods for assembling four unusual amino acid units, which include 3-amino-10-(*p*-ethoxyphenyl)-2,4,5-trihydroxydeca-7,9-dienoic acid (AETD), 4-amino-3-hydroxybutanoic acid (GABOB), (*R*)-Trp-2-carboxylic acid, and a pyrrolidinone fragment.

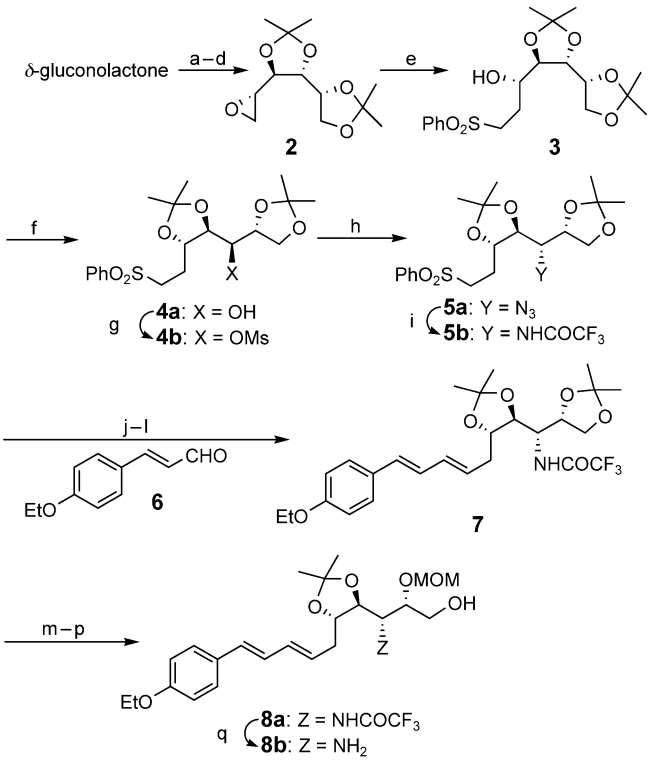
Our approach towards the AETD fragment is shown in Scheme 1 (see scheme legends for abbreviations). Treatment of lithiated methyl phenyl sulfone in THF at −78 °C with oxirane **2** (derived from δ-gluconolactone as shown) in the presence of $BF_3{\cdot}Et_2O$[5] afforded the desired γ-hydroxy

[*] Prof. Dr. D. Ma, J. Zhu
State Key Laboratory of Bioorganic and Natural Products Chemistry
Shanghai Institute of Organic Chemistry
Chinese Academy of Sciences
354 Fenglin Lu, Shanghai 200032 (China)
Fax: (+86) 21-6416-6128
E-mail: madw@pub.sioc.ac.cn

[**] The authors are grateful to the Chinese Academy of Sciences, the National Natural Science Foundation of China, and the Science and Technology Commission of the Municipality of Shanghai (grant 02 JC14032) for their financial support. We thank Professor T. Shioiri for his encouragement.

Supporting information for this article is available on the WWW under http://www.angewandte.org or from the author.

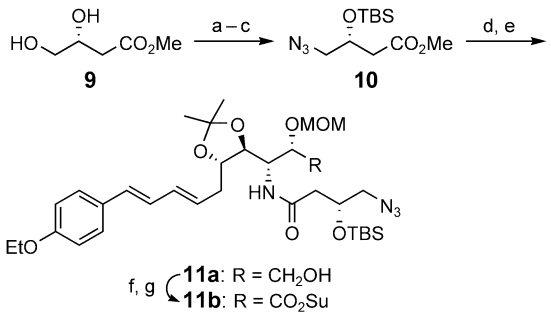
 © 2003 Wiley-VCH Verlag GmbH & Co. KGaA, Weinheim DOI: 10.1002/anie.200352423 




***Scheme 1.*** Reagents and conditions: a) 2,2-dimethoxypropane, acetone, TsOH, 80%; b) $NaBH_4$/MeOH, 100%; c) TsCl, Py, 85%; d) $K_2CO_3$, MeOH, 89%; e) $PhSO_2CH_2Li$, $BF_3{\cdot}Et_2O$, −78°C, 84%; f) 1N HCl, THF then 2,2-dimethoxypropane, acetone, TsOH, 67%; g) MsCl, DMAP, $Et_3N$, 97%; h) $NaN_3$, DMF, 120°C, 83%; i) Pd/C, $H_2$ then $(CF_3CO)_2O$, Py, 62%; j) *n*BuLi, THF, −78°C then **6**; k) PhCOCl, DMAP, $Et_3N$; l) Na(Hg), MeOH, 77% for 3 steps; m) PPTS, MeOH, 45°C, 87%; n) TBSCl, imidazole, 92%; o) MOMCl, $iPr_2NEt$, 100%; p) TBAF, THF, 100%; q) $NaBH_4$, EtOH, 100%. DMAP = 4-dimethylaminopyridine, DMF = dimethylformamide, MOM = methoxymethyl, Ms = methanesulfonyl, PPTS = pyridinium *p*-toluenesulfonate, Py = pyridine, TBAF = tetrabutylammonium fluoride, TBS = *tert*-butyldimethylsilyl, Ts = toluenesulfonyl.

sulfone **3**. Subsequent exposure of **3** to 1N HCl and regioselective reprotection of the resultant alcohol with 2,2-dimethoxypropane produced **4a** in 67% yield. This approach relied on the preferential formation of the acetonides with less steric hindrance. Mesylation of the hydroxy function of **4a**, followed by azidation of the resultant mesylate **4b** furnished azide **5a**, which was hydrogenated over Pd/C, and then treated with trifluoroacetic anhydride to provide amide **5b**. Julia reaction[6] of **5b** with α,β-unsaturated aldehyde **6** afforded the desired diene **7**, together with its *E*/*Z* isomer in a ratio of 5:1. After the terminal acetonide in **7** was selectively removed with the assistance of PPTS,[7] the two liberated hydroxy groups were protected selectively with TBSCl and MOMCl, and the TBS ether was then cleaved with TBAF to deliver amide **8a**. Removal of the $CF_3CO$ group in **8a** by reaction with $NaBH_4$[8] led to the free amine **8b**, which was required for the coupling with the GABOB unit.

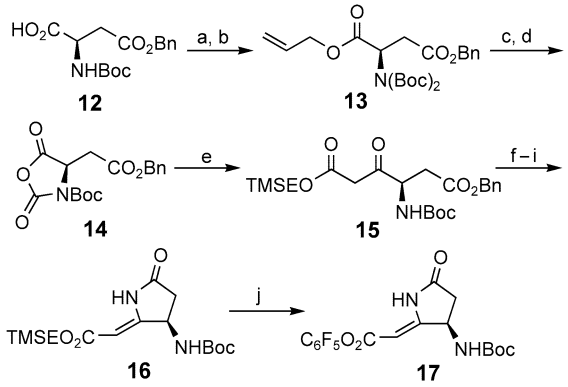
The GABOB unit **10** was constructed from methyl (*R*)-3,4-dihydroxybutanoate **9**[9] (Scheme 2). Selective tosylation[10] of the primary hydroxy group, followed by azidation of the resultant monotosylate afforded a hydroxy azide, which




***Scheme 2.*** Reagents and conditions: a) TsCl, Py, 60%; b) $NaN_3$, DMF, 80°C, 75%; c) TBSCl, imidazole, 100%; d) aq. NaOH, MeOH, then HOSu, EDCI, 100%; e) **8b**, EtOAc, reflux, 96%; f) Dess–Martin oxidation then $NaClO_2$, resorcinol, $NaH_2PO_4$, 74%; g) HOSu, EDCI, 85%. EDCI = 1-(3-dimethylaminopropyl)-3-ethylcarbodiimide hydrochloride, Su = succinimide.

was protected with TBSCl to give **10**. After **10** was hydrolyzed with NaOH, the resultant acid was converted into the corresponding activated ester,[11] which when coupled with the amine **8b**, to provide amide **11a** in 96% yield. The hydroxy group in **11a** was oxidated stepwise to the corresponding acid by reaction with the Dess–Martin reagent[12] and sodium chlorite, followed by esterification with HOSu and EDCI[13] to give dipeptide **11b** in 63% yield over three steps; this intermediate was ready for connection with the tetrapeptide part.

For the synthesis of the pyrrolidinone part, the starting D-aspartic acid derivative **12** was converted into the urethane *N*-carboxyanhydride **14** (Scheme 3),[14] and then treated with the lithium enolate of trimethylsilylethyl (TMSE) acetate to give β-keto ester **15**. This operation is essential for obtaining enantiopure **15** (>98% *ee* determined by HPLC) because attempts to use other activated esters prepared with *N,N*′-carbonyldiimidazole,[4c] *N*-hydroxysuccinimide, and pentafluorophenol led to partial or full racemization of **15**. After hydrogenolysis of the benzyl group over Pd/C, the resultant acid was converted into its mixed anhydride, which was

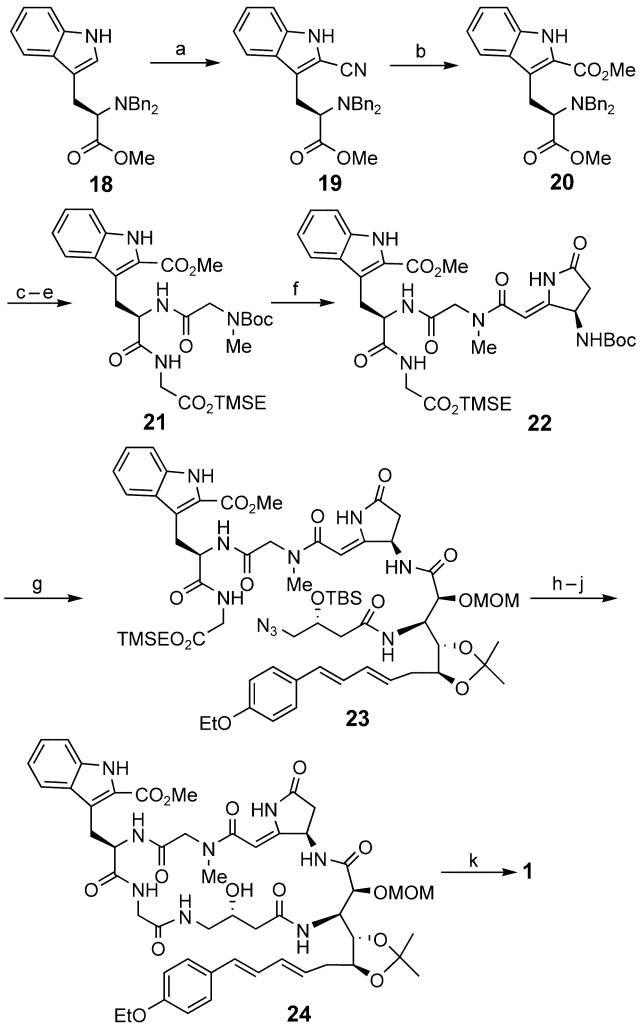



***Scheme 3.*** Reagents and conditions: a) Allyl bromide, $KHCO_3$, DMF, 97%; b) $(Boc)_2O$, DMAP, 100%; c) $[RhCl(PPh_3)_3]$, 90% EtOH, 81%; d) $SOCl_2$, Py, DMF, 90%; e) $LiCH_2CO_2TMSE$, THF, −78°C, 80%; f) Pd/C, $H_2$, 100%; g) *i*BuOCOCl, NMM; h) aq $NH_3$; i) MsCl, $Et_3N$, 81% for 3 steps; j) TBAF, TsOH then $C_6F_5OH$, EDCI, 73%. Boc = *tert*-butoxycarbonyl, NMM = *N*-methylmorpholine, TMSE = trimethylsilylethyl.

 © 2003 Wiley-VCH Verlag GmbH & Co. KGaA, Weinheim 

treated with aqueous ammonia to give a hydroxypyrrolidinone. Subjecting this intermediate to elimination through mesylation provided pyrrolidinone **16** in 81% overall yield. When the TMSE group was removed by treatment with TBAF, the liberated acid was found to be racemized due to the basic conditions directed by TBAF. The racemization could be hampered in the presence of TsOH,[15] although the best *R*/*S* ratio was 4:1. The free acid was converted to its PFP-activated ester[16] **17** by treatment with $C_6F_5OH$ and EDCI in 80% yield.

Construction of the (*R*)-Trp-2-carboxylic acid part commenced with introduction of a cyano group to the indole ring of **18**, which was derived from D-tryptophan according to Danishefsky's protocol[17] (Scheme 4). The cyano group of **19** was hydrolyzed to the acid function under alkali conditions and then esterified to afford the (*R*)-Trp-2-carboxylic acid derivative **20**.




***Scheme 4.*** Reagents and conditions: a) *t*BuOCl, $Et_3N$, −78 °C then TMSCN, $BF_3{\cdot}Et_2O$, 79%; b) aq KOH, MeOH then MeI, $KHCO_3$, DMF, 71%; c) $Pd(OH)_2$, $H_2$, MeOH, 70%; d) BocN(Me)$CH_2CO_2H$, EDCI, HOBt, DIEA, 96%; e) aq LiOH, MeOH then $NH_2CH_2CO_2TMSE$, EDCI, HOBt, DIEA, 88%; f) TFA then **17**, $NaHCO_3$, DMF, 45 °C; 81%; g) TFA then **11b**, $NaHCO_3$, MeCN, 80%; h) TBAF, THF; i) $Me_3P$, THF; j) DPPA, DMF, 40% for 3 steps; k) LiOH, MeOH, THF, then Amberlyst-15, MeOH, $H_2O$, 61%. DIEA = diisopropylethylamine, DPPA = diphenylphosphoryl azide, HOBt = 1-hydroxybenzotriazole, TFA = trifluoroacetic acid.

With the four unnatural amino acid fragments in hand, we set out on the next step—coupling these units to complete the synthesis of the macrocyclic core. The reaction was initially carried out on compound **20**. After catalytic removal of the benzyl groups over $Pd(OH)_2$, the free amine was coupled with Boc-*N*-MeGly-OH promoted by EDCI–HOBt[18] to provide a dipeptide (93%). Regioselective hydrolysis of the aliphatic carboxylic ester with LiOH, followed by coupling with H-Gly-OTMSE produced tripeptide **21**. The Boc group was removed by treatment with TFA, and without purification the free amine was coupled with the PFP-activated ester **17** to afford tetrapeptide **22** as a inseparable mixture (4:1), which resulted from the partial racemization of **17**. Removal of the Boc group in **22** followed by coupling with the dipeptide **11b** gave the linear precursor **23** in 80% yield. The TMSE group of **23** was removed with TBAF and TsOH to give the free carboxylic acid. Although attempts to reduce the azide group to the amine failed when **23** was treated with $Ph_3P$, $nBu_3P$, and $SnCl_2$,[19] less sterically hindered $Me_3P$[20] proved to be suitable for this transformation and furnished the reduced product in good yield.

The stage was now set for the crucial macrocyclization. To our delight, although EDCI–HOAt was not effective for this conversion, treatment of the above amino acid with DPPA[21] for 14 days afforded lactam **24** in 40% yield (three steps from **23**), together with its separable isomer (9% yield, resulting from the partial racemization during assembly of the pyrrolidinone fragment). Noteworthy is that much lower yields were observed when the reaction time was shortened to two to three days with either DPPA or HATU[22] as the coupling reagents. Removal of methyl ester was achieved by treatment with LiOH to give the free acid, and the next task was the removal of the MOM and acetonide group. This operation proved far from trivial, mainly because both the substrate and the product are unstable to strong acidic conditions. After some experimentation, we finally observed that the removal was accomplished with Amberlyst-15[23] to give **1**[24] in 61% yield (two steps). The analytical data of the synthetic compound were identical with those reported,[2b] thereby confirming the structure of microsclerodermin E proposed by Faulkner and co-workers.

In summary, we have developed a new, efficient strategy for the enantiospecific synthesis of microsclerodermins exemplified by the first total synthesis of microsclerodermin E (1% overall yield for 26 linear steps). The methods expressed here for the synthesizing AETD and the pyrrolidinone parts should be applicable for installation of the other polyhydroxy-β-amino acid residues and pyrrolidinone units in the microsclerodermins. We are currently extending these methods to the total synthesis of microsclerodermins A–D and their analogues for in-depth biological evaluation. Results will be reported in due course.

Received: July 21, 2003 [Z52423]

 © 2003 Wiley-VCH Verlag GmbH & Co. KGaA, Weinheim 

**Keywords:** amino acids · Julia reaction · macrocycles · peptides · total synthesis


[1] C. A. Bewley, D. J. Faulkner, *Angew. Chem.* **1998**, *110*, 2280; *Angew. Chem. Int. Ed.* **1998**, *37*, 2162.

[2] a) C. A. Bewley, C. Debitus, D. J. Faulkner, *J. Am. Chem. Soc.* **1994**, *116*, 7631; b) E. W. Schmidt, D. J. Faulkner, *Tetrahedron* **1998**, *54*, 3043; c) A. Qureshi, P. L. Colin, D. J. Faulkner, *Tetrahedron* **2000**, *56*, 3679.

[3] A. E. Wright, S. A. Pomponi, R. E. Longley, R. A. Isbrucker, US 6384187, **2002** [*Chem. Abstr.* **2002**, *136*, 319381]

[4] a) S. Sasaki, Y. Hamada, T. Shioiri, *Tetrahedron Lett.* **1997**, *38*, 3013; b) S. Sasaki, Y. Hamada, T. Shioiri, *Tetrahedron Lett.* **1999**, *40*, 3187; c) S. Sasaki, Y. Hamada, T. Shioiri, *Synlett* **1999**, *4*, 453.

[5] S. Marczak, J. Wicha, *Synth. Commun.* **1990**, *20*, 1511.

[6] S. L. Schreiber, H. V. Meyers, *J. Am. Chem. Soc.* **1988**, *110*, 5198.

[7] R. Van Rijsbergen, R. M. J. O. Anteunis, A. De Bruyn, *J. Carbohydr. Chem.* **1983**, *2*, 395.

[8] Z. H. Kudzin, P. Lyzwa, J. Luczak, G. Andrijewski, *Synthesis* **1997**, 44.

[9] S. Saito, T. Hasegawa, M. Inaba, R. Nishida, T. Fujii, S. Nomiz, T. Moriwake, *Chem. Lett.* **1984**, 1389.

[10] F. D. Bellamy, M. Bondoux, P. Dodey, *Tetrahedron Lett.* **1990**, *31*, 7323.

[11] E. Wunsch, E. Drees, *Chem. Ber.* **1966**, *99*, 110.

[12] D. B. Dess, J. C. Martin, *J. Org. Chem.* **1983**, *48*, 4155.

[13] J. C. Sheehan, P. A. Cruickshank, G. L. Boshart, *J. Org. Chem.* **1961**, *26*, 2525.

[14] M. Paris, J. Fehrentz, A. Heitz, A. Loffet, J. Martinez, *Tetrahedron Lett.* **1996**, *37*, 8489.

[15] J. P. Ferezou, M. Julia, Y. Li, L. W. Liu, A. Pancrazi, *Bull. Soc. Chim. Fr.* **1995**, *132*, 428.

[16] U. Schmidt, M. Kroner, H. Griesser, *Synthesis* **1989**, 832.

[17] J. M. Schkeryantz, J. G. Woo, P. Siliphaivanh, K. M. Depew, S. J. Danishefsky, *J. Am. Chem. Soc.* **1999**, *121*, 11969.

[18] W. König, R. Geiger, *Chem. Ber.* **1970**, *103*, 788.

[19] E. F. V. Scriven, K. Turnbull, *Chem. Rev.* **1988**, *88*, 297.

[20] B. M. Trost, S. R. Pulley, *Tetrahedron Lett.* **1995**, *36*, 8737.

[21] a) D. L. Boger, P. Yohannes, *Tetrahedron Lett.* **1989**, *30*, 5061; b) T. Sugiura, Y. Hamada, T. Shioiri, *Tetrahedron Lett.* **1987**, *28*, 2251; c) M. P. Forst, G. P. Concepcion, G. B. Caraan, C. M. Ireland, *J. Org. Chem.* **1992**, *57*, 6671.

[22] L. A. Carpino, A. El-Faham, C. A. Minor, F. Albericio, *J. Chem. Soc. Chem. Commun.* **1994**, 201.

[23] B. M. Trost, J. D. Chisholm, S. T. Wrobleski, M. Jung, *J. Am. Chem. Soc.* **2002**, *124*, 12420.

[24] $[\alpha]_D^{25} = -22.7$ ($c = 0.4$, 1:1 MeOH/0.1N $NH_4HCO_3$ (aq); lit.[2b]: $[\alpha]_D^{25} = -24$ ($c = 0.4$, 1:1 MeOH/0.1N $NH_4HCO_3$ (aq)); $^1$H NMR (300 MHz, [D$_7$]DMF with trace of TFA): $\delta = 11.58$ (s, 1H), 10.60 (s, 1H), 8.88 (d, $J = 4.8$ Hz, 1H), 8.62 (d, $J = 8.7$ Hz, 1H), 8.49 (t, $J = 6.2$ Hz, 1H), 7.72 (d, $J = 7.8$ Hz, 1H), 7.59 (br, 1H), 7.54 (d, $J = 8.1$ Hz, 1H), 7.40 (d, $J = 8.7$ Hz, 2H), 7.35 (m, 1H), 7.31 (t, $J = 7.8$ Hz, 1H), 7.16 (t, $J = 7.8$ Hz, 1H), 6.91 (d, $J = 8.7$ Hz, 2H), 6.73 (dd, $J = 15.9$, 10.8 Hz, 1H), 6.45 (d, $J = 15.9$ Hz, 1H), 6.24 (dd, $J = 15.0$, 10.8 Hz, 1H), 5.83 (m, 1H), 5.45 (s, 1H), 5.42 (m, 1H), 4.68 (s, 1H), 4.64 (d, $J = 15.9$ Hz, 1H), 4.33 (m, 1H), 4.27 (m, 1H), 4.05 (q, $J = 5.7$ Hz, 2H), 3.95 (br, 1H), 3.73 (m, 1H), 3.68 (m, 2H), 3.61 (m, 2H), 3.47 (d, $J = 15.9$ Hz, 1H), 3.45 (m, 2H), 3.07 (s, 3H), 2.91 (m, 2H), 2.59 (dd, $J = 18.9$, 4.8 Hz, 1H), 2.48 (d, $J = 13.5$ Hz, 1H), 2.39 (m, 2H), 2.21 (m, 1H), 1.35 ppm (t, $J = 5.7$ Hz, 3H); negative ESI-MS $m/z$ 929 $(M-H)^-$.


 © 2003 Wiley-VCH Verlag GmbH & Co. KGaA, Weinheim 

Natural Products Total Synthesis

# Total Synthesis of the Squalene Synthase Inhibitor Zaragozic Acid C by a Carbonyl Ylide Cycloaddition Strategy**

*Seiichi Nakamura, Yuuki Hirata, Takahiro Kurosaki, Masahiro Anada, Osamu Kataoka, Shinji Kitagaki, and Shunichi Hashimoto**

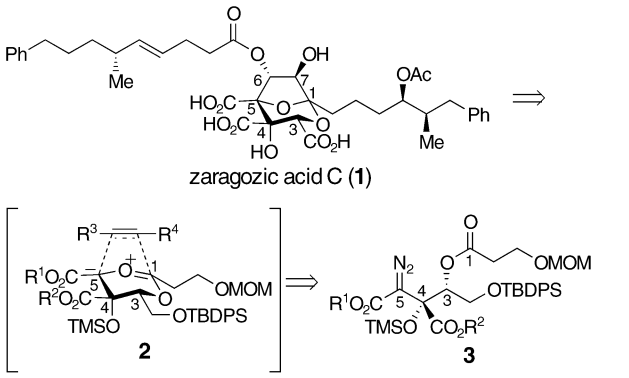
The zaragozic acids and squalestatins, a novel family of fungal metabolites isolated and characterized by researchers at Merck[1] and Glaxo,[2] respectively, in 1992, are the most potent inhibitors of squalene synthase known to date.[3] Some members of this family have also demonstrated the ability to inhibit Ras farnesyl transferase.[4] These molecules share a unique 4,6,7-trihydroxy-2,8-dioxabicyclo[3.2.1]octane-3,4,5-tricarboxylic acid core with six contiguous stereogenic centers and differ only with regard to the nature of the C1 alkyl and C6 O-acyl side chains. It is therefore not surprising that the zaragozic acids (squalestatins) have elicited considerable attention from synthetic chemists.[5] Apart from an enormous number of synthetic studies, eight total syntheses, including our own total synthesis of zaragozic acid C, have now been reported.[6–8] A strategic point in the synthesis of zaragozic acids lies in the construction of the fully or partially functionalized 2,8-dioxabicyclo[3.2.1]octane core structure. The majority of the reported synthetic strategies rely on the acid-catalyzed internal ketalization of a polyhydroxyketone or its equivalent under kinetically or thermodynamically controlled conditions. However, this key reaction often yields, apart from the target bicyclic ketal core, variable quantities of the isomeric 6,8-dioxabicyclo[3.2.1]octane ring. Departing from the ketalization-based approach, we now report a second-generation synthesis of zaragozic acid C capitalizing on the tandem carbonyl ylide formation/1,3-dipolar cycloaddition methodology extensively studied by the Padwa group.[9–11]

Our synthetic strategy based on the cycloaddition of a carbonyl ylide is outlined retrosynthetically in Scheme 1.[12–14] This approach would allow for the rapid assembly of the desired core system from α-diazo ester **3** and a suitable dipolarophile under the influence of a $Rh^{II}$ catalyst in a single step, wherein the problem of formation of the isomeric ketal can be avoided. We have previously demonstrated that

[*] Prof. Dr. S. Hashimoto, Dr. S. Nakamura, Y. Hirata, T. Kurosaki, Dr. M. Anada, Dr. O. Kataoka, Dr. S. Kitagaki
Graduate School of Pharmaceutical Sciences
Hokkaido University
Sapporo 060-0812 (Japan)
Fax: (+81) 11-706-3236
E-mail: hsmt@pharm.hokudai.ac.jp

[**] This research was supported in part by a Grant-in-Aid for Scientific Research on Priority Areas (A) "Exploitation of Multi-Element Cyclic Molecules" from the Ministry of Education, Culture, Sports, Science and Technology, Japan. We thank H. Matsumoto, A. Maeda, S. Oka, and M. Kiuchi of the Center for Instrumental Analysis, Hokkaido University, for technical assistance in MS and elemental analysis.

 DOI: 10.1002/anie.200352629 © 2003 Wiley-VCH Verlag GmbH & Co. KGaA, Weinheim 

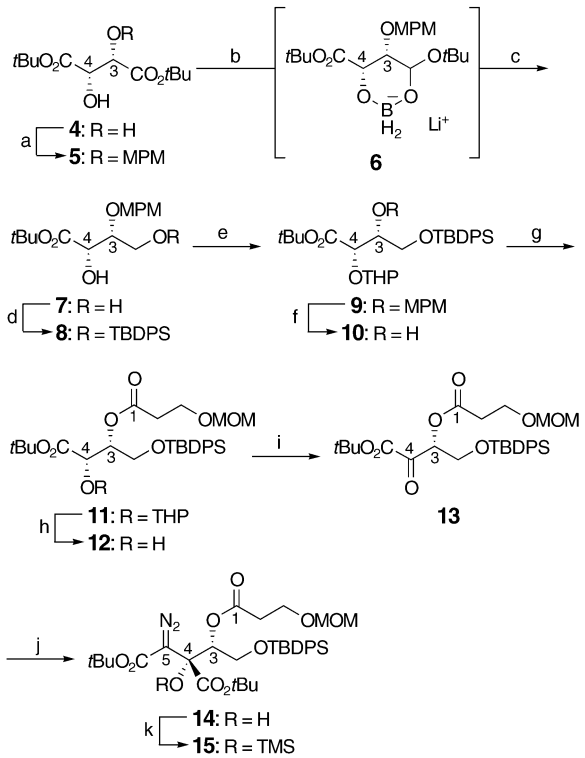



***Scheme 1.*** Retrosynthetic analysis of zaragozic acid C (**1**) based on the cycloaddition of a carbonyl ylide. MOM = methoxymethyl, TBDPS = *tert*-butyldiphenylsilyl, TMS = trimethylsilyl.

$Rh_2(OAc)_4$-mediated formation of the carbonyl ylide from α-diazo ester **3** ($R^1$ = Et, $R^2$ = Me) and subsequent 1,3-dipolar cycloaddition with (*E*)-3-hexene-2,5-dione as a dipolarophile proceeded with complete stereocontrol to give the desired core structure as a single isomer in 47% yield.[12] However, all of our efforts to convert the C6, C7 diacetyl groups into a diol unit by Baeyer–Villiger oxidation met with failure. Consequently, the judicious selection of dipolarophiles that could result in much higher yields as well as a completed synthesis was crucial to the success of our scenario.

Considering our previous finding that saponification and *tert*-butyl esterification at a later stage were problematic,[7d] we initiated the second-generation synthesis with protection of di-*tert*-butyl D-tartrate (**4**)[15] as its mono-MPM ether to give **5** in 92% yield (Scheme 2, see scheme legends for abbreviations). At this point, the synthetic plan called for the selective reduction of one of the *tert*-butyl esters in **5**.[16] After considerable experimentation, $LiBH_4$ proved to be the optimal choice for this purpose. Thus $LiBH_4$ reduction of **5** followed by aqueous workup afforded the aldehyde, which was reduced again with $LiBH_4$ to give 1,3-diol **7** in 72% yield along with 2% of the 1,2-diol. This highly beneficial result can be rationalized by assuming the predominant formation of a rigid, six-membered boronate intermediate **6** that is resistant to further reduction. Protective-group manipulations and subsequent oxidation proceeded uneventfully to give α-keto ester **13** in 63% yield, without any racemization over six steps from 1,3-diol **7**. Our effort was then directed toward the addition of metalated *tert*-butyl diazoacetate to **13** to set up the quaternary center at C4, which posed the serious problem of stereocontrol. After a number of unfruitful attempts, we were very pleased to find that the use of NaHMDS as a base in $CH_2Cl_2$/THF (20:1) at −93 °C led to acceptable diastereoselectivity (8:1), affording the desired α-diazo ester **14** in 65% yield after removal of its C4 epimer. It is noteworthy that the choice of $CH_2Cl_2$ as a cosolvent, which is not normally used in this type of reaction, was crucial to the high level of selectivity,[17] though the reason for this is not clear at present. The synthesis of the carbonyl ylide precursor **15** was then accomplished by TMS-protection of the C4 hydroxy group.

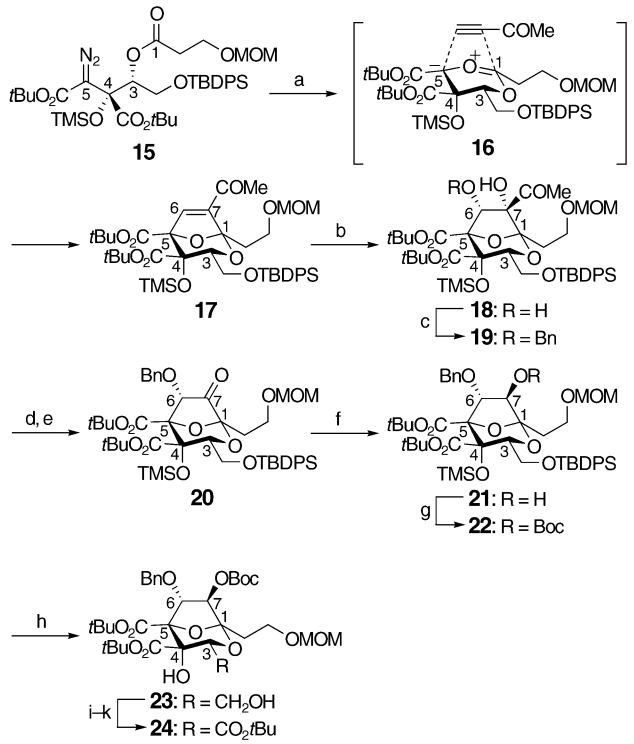
The stage was now set for the crucial tandem formation of the carbonyl ylide and 1,3-dipolar cycloaddition (Scheme 3).




***Scheme 2.*** Synthesis of α-diazo ester **15**. a) $Bu_2SnO$, toluene, reflux, 2 h, then CsF, MPMBr, DMF, 10 h, 92%; b) $LiBH_4$, THF, 4 h; c) $LiBH_4$, THF, −78 °C, 4 h, 74% (2 steps), 31:1 regioselectivity; d) TBDPSCl, imidazole, $CH_2Cl_2$, 0 °C, 30 min, 97%; e) DHP, PPTS, $CH_2Cl_2$, 5 h, 95%; f) DDQ, $CH_2Cl_2$, pH 7 buffer, 2 h, 96%; g) MOMO$(CH_2)_2CO_2H$, EDCI, DMAP, $CH_2Cl_2$, 3 h, 81%; h) TsOH, MeOH, 40 min, 91%; i) Dess–Martin periodinane, $CH_2Cl_2$, 2 h, 97%; j) $N_2CHCO_2tBu$, NaHMDS, $CH_2Cl_2$/THF (20:1), −93 °C, 5 min, 73%, 8:1 diastereoselectivity; k) HMDS, imidazole, THF, 48 h, 94%. DDQ = 2,3-dichloro-5,6-dicyano-1,4-benzoquinone, DHP = 3,4-dihydro-2*H*-pyran, DMAP = 4-(dimethylamino)pyridine, DMF = *N*,*N*-dimethylformamide, EDCI = 1-(3-dimethylaminopropyl)-3-ethylcarbodiimide hydrochloride, HMDS = 1,1,3,3-hexamethyldisilazane, MPM = 4-methoxybenzyl, PPTS = pyridinium *p*-toluenesulfonate, THP = tetrahydropyranyl, Ts = *p*-toluenesulfonyl.

With respect to the dipole reactivity of this type of ester-carbonyl ylide, we previously reported that the most dominant interaction of the frontier molecular orbitals (FMOs) is between the HOMO of the ester-carbonyl ylide and the LUMO of an electron-deficient dipolarophile.[12] The reaction was conducted by adding over one hour a solution of α-diazo ester **15** in benzene to a solution of $Rh_2(OAc)_4$ (5 mol%) and a dipolarophile candidate (3 equiv) in benzene heated at reflux. Apart from the dipolarophiles activated with two carbonyl groups described in the previous studies, we now found that a variety of α,β-ethylenic and α,β-acetylenic carbonyl compounds could be smoothly trapped by the ester-carbonyl ylide intermediate **16**. Furthermore, this reaction occurred exclusively from the β-face of the ylide so as to avoid the C4 pseudoaxial trimethylsilyloxy group on the opposite face. Of the various partners tested,[18] 3-butyn-2-one was chosen as the dipolarophile to most likely lead to the completed synthesis (vide infra); the desired cycloadduct **17** was obtained as a single diastereomer in 72% yield.[19] We

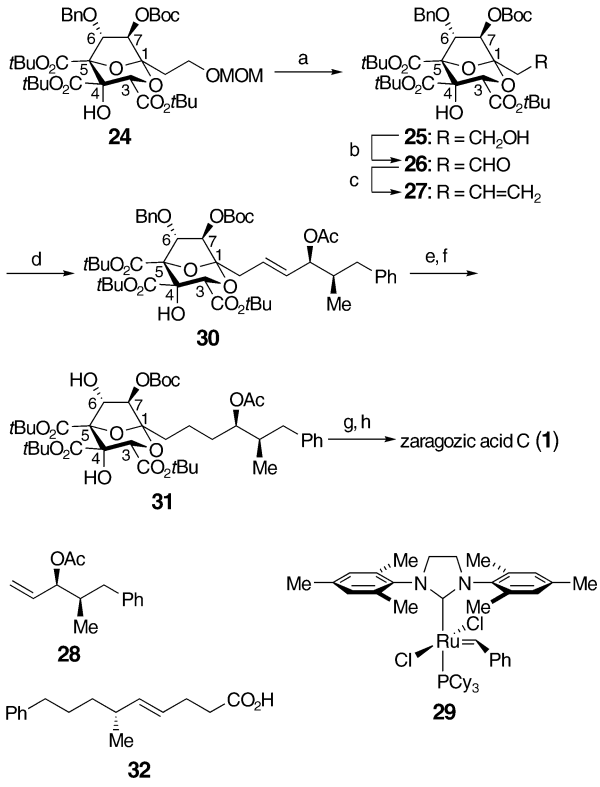
 © 2003 Wiley-VCH Verlag GmbH & Co. KGaA, Weinheim 




***Scheme 3.*** Construction of the fully functionalized bicyclic compound **24**. a) $Rh_2(OAc)_4$ (5 mol%), HC≡CCOMe (3 equiv), benzene, reflux, 1 h, 72%; b) $OsO_4$, NMO, aq acetone, 20 h, 88%; c) BnBr, $Ag_2O$, DMF, 48 h, 95%; d) DIBAL-H, toluene, −78°C, 30 min, quant.; e) $Pb(OAc)_4$, benzene, 30 min, 94%; f) DIBAL-H, $ZnCl_2$, $CH_2Cl_2$, −78°C, 0.5 h, 87%, 46:1 diastereoselectivity; g) $(Boc)_2O$, $Et_3N$, DMAP, $CH_2Cl_2$, 2 h, 96%; h) $Bu_4NF$, THF, 0°C, 30 min, 97%; i) Dess–Martin periodinane, $CH_2Cl_2$, 24 h; j) $NaClO_2$, $NaH_2PO_4$, 2-methyl-2-butene, aq *t*BuOH, 3 h; k) *i*PrN=C(O*t*Bu)NH*i*Pr, $CH_2Cl_2$, 24 h, 96% (3 steps). Bn = benzyl, Boc = *tert*-butoxycarbonyl, DIBAL-H = diisobutylaluminum hydride, NMO = 4-methylmorpholine *N*-oxide.

then proceeded to the installation of the C6, C7-*trans*-diol unit. Dihydroxylation of enone **17** with $OsO_4$ proceeded in accord with the facial bias of the C6–C7 double bond, affording diol **18** in 88% yield. Selective benzylation of the C6 hydroxy group furnished α-hydroxyketone **19**,[20] which was then converted into ketone **20** in 89% overall yield by DIBAL-H reduction and oxidative cleavage of the 1,2-diol with $Pb(OAc)_4$. In the next step, reduction of the C7 carbonyl group in **20**, we encountered serious difficulties in stereocontrol. After an exhaustive survey of reducing agents and solvents, it was found that this goal could best be achieved with DIBAL-H/$ZnCl_2$[21] in $CH_2Cl_2$ to give the desired alcohol **21** and its C7 epimer recyclable in 87% yield with excellent diastereoselectivity (46:1). It is noteworthy that the choice of the *O*-benzyl protecting group at C6 was crucial to the maximum efficiency of these transformations, particularly in terms of essentially perfect selectivities for its installation and C7 carbonyl reduction. Protection of the C7 hydroxy group with $(Boc)_2O$ and subsequent bisdesilylation with $Bu_4NF$ provided diol **23** in 93% yield, which, upon the three-step sequence without intervening purifications, gave tris(*tert*-butyl) ester **24** in 96% yield.

The remaining portion of the synthesis required elongation of the C1 alkyl side chain followed by installation of the C6 acyl side chain. Removal of the MOM ether in **24** with TMSCl/$Et_4NBr$[22] was followed by oxidation with Dess–Martin periodinane to give aldehyde **26** in 70% yield (Scheme 4).




***Scheme 4.*** Completion of the total synthesis of **1**. a) TMSCl, $Et_4NBr$, $CH_2Cl_2$, 20 h, 75%; b) Dess–Martin periodinane, $CH_2Cl_2$, 24 h, 93%; c) $Ph_3P^+CH_3Br^-$, *t*BuOK, toluene, 40°C, 30 min, 91%; d) **28** (1.2 equiv), **29** (5 mol%), benzene, 70°C, 8 h, 67%; e) $H_2$, 5% Pd/$BaSO_4$, EtOAc, 10 h; f) $H_2$, 20% $Pd(OH)_2$/C, EtOAc, 1 h, 87% (2 steps); g) **32**, DCC, DMAP, $CH_2Cl_2$, 48 h, 90%; h) TFA, $CH_2Cl_2$, 16 h, quant. Cy = cyclohexyl, DCC = dicyclohexylcarbodiimide, TFA = trifluoroacetic acid.

At this stage, we encountered a final key problem: how to install the full C1 side chain. Since initial attempts to adapt the Kocieński–Julia olefination[23] to this task met with failure, we were then attracted to the viability of the cross-metathesis of a terminal olefin.[24] Indeed, we were gratified to find that the cross-metathesis coupling between the terminal olefin **27** derived from **26** and allyl acetate **28**[25] (1.2 equiv) in benzene in the presence of 5 mol% of the second-generation Grubbs catalyst (**29**) at 70°C proceeded remarkably smoothly to give cross-product **30**[27] with exclusive *E* stereochemistry in 67% yield, along with recovered alkenes **27** (10%) and **28** (24%). As might be expected from the sterically hindered nature of the olefinic functionality adjacent to the core system, the dimer arising from self-metathesis of **27** was not detected. Hydrogenation of the C2′–C3′ double bond in **30** without concomitant reductive cleavage of the acetoxy group followed by hydrogenolysis of C6 benzyl ether furnished

 © 2003 Wiley-VCH Verlag GmbH & Co. KGaA, Weinheim 

tris(*tert*-butyl) ester **31** in 87% yield. Compound **31** was identical in all respects ($^1$H NMR, $^{13}$C NMR, IR, HRMS, $[\alpha]_D$) to the intermediate previously prepared by both the Carreira group[7b] and our group.[7d] Thus, acylation of the hydroxy group at C6 with (*R*)-9-phenyl-6-methyl-4-nonenoic acid (**32**) and global deprotection with TFA completed the total synthesis of zaragozic acid C (**1**).

In conclusion, we have accomplished a highly convergent and stereocontrolled total synthesis of zaragozic acid C in 30 steps (longest linear sequence) and 3.7% overall yield from di-*tert*-butyl D-tartrate (**4**). The synthesis illustrates the power of the carbonyl ylide cycloaddition methodology for rapidly assembling the unique 2,8-dioxabicyclo[3.2.1]octane core and the olefin cross-metathesis methodology to construct the C1 alkyl side chain. Importantly, the strategy is flexible with other types of ylides and potentially allows for the introduction of a variety of nonnatural heteroatomic substituents into the core structure. The synthesis of such analogues for biological and pharmacological investigations is currently underway.

Received: August 12, 2003 [Z52629]

**Keywords:** carbonyl ylides · cycloaddition · diazo compounds · metathesis · total synthesis

[1] K. E. Wilson, R. M. Burk, T. Biftu, R. G. Ball, K. Hoogsteen, *J. Org. Chem.* **1992**, *57*, 7151 – 7158.

[2] M. J. Dawson, J. E. Farthing, P. S. Marshall, R. F. Middleton, M. J. O'Neill, A. Shuttleworth, C. Stylli, R. M. Tait, P. M. Taylor, H. G. Wildman, A. D. Buss, D. Langley, M. V. Hayes, *J. Antibiot.* **1992**, *45*, 639 – 647.

[3] For a review, see: N. S. Watson, P. A. Procopiou, *Prog. Med. Chem.* **1996**, *33*, 331 – 378.

[4] J. B. Gibbs, D. L. Pompliano, S. D. Mosser, E. Rands, R. B. Lingham, S. B. Singh, E. M. Scolnick, N. E. Kohl, A. Oliff, *J. Biol. Chem.* **1993**, *268*, 7617 – 7620.

[5] For reviews, see: a) U. Koert, *Angew. Chem.* **1995**, *107*, 849 – 855; *Angew. Chem. Int. Ed. Engl.* **1995**, *34*, 773 – 778; b) A. Nadin, K. C. Nicolaou, *Angew. Chem.* **1996**, *108*, 1732 – 1766; *Angew. Chem. Int. Ed. Engl.* **1996**, *35*, 1622 – 1656; c) N. Jotterand, P. Vogel, *Curr. Org. Chem.* **2001**, *5*, 637 – 661; d) A. Armstrong, T. J. Blench, *Tetrahedron* **2002**, *58*, 9321 – 9349.

[6] Total synthesis of zaragozic acid A: a) K. C. Nicolaou, A. Nadin, J. E. Leresche, E. W. Yue, S. La Greca, *Angew. Chem.* **1994**, *106*, 2312 – 2313; *Angew. Chem. Int. Ed. Engl.* **1994**, *33*, 2190 – 2191; b) K. C. Nicolaou, E. W. Yue, S. La Greca, A. Nadin, Z. Yang, J. E. Leresche, T. Tsuri, Y. Naniwa, F. De Riccardis, *Chem. Eur. J.* **1995**, *1*, 467 – 494; c) S. Caron, D. Stoermer, A. K. Mapp, C. H. Heathcock, *J. Org. Chem.* **1996**, *61*, 9126 – 9134; d) K. Tomooka, M. Kikuchi, K. Igawa, M. Suzuki, P.-H. Keong, T. Nakai, *Angew. Chem.* **2000**, *112*, 4676 – 4679; *Angew. Chem. Int. Ed.* **2000**, *39*, 4502 – 4505.

[7] Total synthesis of zaragozic acid C: a) E. M. Carreira, J. Du Bois, *J. Am. Chem. Soc.* **1994**, *116*, 10825 – 10826; b) E. M. Carreira, J. Du Bois, *J. Am. Chem. Soc.* **1995**, *117*, 8106 – 8125; c) D. A. Evans, J. C. Barrow, J. L. Leighton, A. J. Robichaud, M. Sefkow, *J. Am. Chem. Soc.* **1994**, *116*, 12111 – 12112; d) H. Sato, S. Nakamura, N. Watanabe, S. Hashimoto, *Synlett* **1997**, 451 – 454; e) A. Armstrong, L. H. Jones, P. A. Barsanti, *Tetrahedron Lett.* **1998**, *39*, 3337 – 3340; f) A. Armstrong, P. A. Barsanti, L. H. Jones, G. Ahmed, *J. Org. Chem.* **2000**, *65*, 7020 – 7032.

[8] Total synthesis of 6,7-dideoxysqualestatin H5: a) S. F. Martin, S. Naito, *J. Org. Chem.* **1998**, *63*, 7592 – 7593; b) S. Naito, M. Escobar, P. R. Kym, S. Liras, S. F. Martin, *J. Org. Chem.* **2002**, *67*, 4200 – 4208.

[9] A. Padwa, G. E. Fryxell, L. Zhi, *J. Am. Chem. Soc.* **1990**, *112*, 3100 – 3109. For a copper-catalyzed reaction, see: T. Ibata, K. Jitsuhiro, *Bull. Chem. Soc. Jpn.* **1979**, *52*, 3582 – 3585.

[10] For reviews, see: a) A. Padwa, M. D. Weingarten, *Chem. Rev.* **1996**, *96*, 223 – 269; b) M. C. McMills, D. Wright in *Synthetic Applications of 1,3-Dipolar Cycloaddition Chemistry toward Heterocycles and Natural Products* (Eds.: A. Padwa, W. H. Pearson), Wiley, New York, **2002**, pp. 253 – 314; c) G. Mehta, S. Muthusamy, *Tetrahedron* **2002**, *58*, 9477 – 9504.

[11] For recent studies on the synthesis of bioactive molecules by a carbonyl ylide cycloaddition strategy, see: a) C. S. Straub, A. Padwa, *Org. Lett.* **1999**, *1*, 83 – 85; b) J. L. Wood, B. D. Thompson, N. Yusuff, D. A. Pflum, M. S. P. Matthäus, *J. Am. Chem. Soc.* **2001**, *123*, 2097 – 2098; c) F. Liu, D. J. Austin, *Org. Lett.* **2001**, *3*, 2273 – 2276; d) T. Graening, W. Friedrichsen, J. Lex, H.-G. Schmalz, *Angew. Chem.* **2002**, *114*, 1594 – 1597; *Angew. Chem. Int. Ed.* **2002**, *41*, 1524 – 1526.

[12] O. Kataoka, S. Kitagaki, N. Watanabe, J. Kobayashi, S. Nakamura, M. Shiro, S. Hashimoto, *Tetrahedron Lett.* **1998**, *39*, 2371 – 2374.

[13] For a carbonyl ylide cycloaddition approach to L-740,758, a product of the oxidative photodegradation of zaragozic acid A, see: H. Koyama, R. G. Ball, G. D. Berger, *Tetrahedron Lett.* **1994**, *35*, 9185 – 9188.

[14] For synthetic studies of zaragozic acids by a carbonyl ylide cycloaddition–rearrangement strategy, see: a) D. M. Hodgson, J. M. Bailey, T. Harrison, *Tetrahedron Lett.* **1996**, *37*, 4623 – 4626; b) D. M. Hodgson, C. Villalonga-Barber, *Tetrahedron Lett.* **2000**, *41*, 5597 – 5600; c) D. M. Hodgson, J. M. Bailey, C. Villalonga-Barber, M. G. B. Drew, T. Harrison, *J. Chem. Soc. Perkin Trans. 1* **2000**, 3432 – 3443.

[15] G. Uray, W. Lindner, *Tetrahedron* **1988**, *44*, 4357 – 4362.

[16] In this case it would be preferable to obtain the 1,2-diol; however, reduction of **5** under Saito conditions ($BH_3{\cdot}SMe_2$, $NaBH_4$, THF) did not work: S. Saito, T. Ishikawa, A. Kuroda, K. Koga, T. Moriwake, *Tetrahedron* **1992**, *48*, 4067 – 4086.

[17] Use of solvents other than $CH_2Cl_2$ led to a significant decline in diastereoselectivity: THF, 59%, 2.2:1; $Et_2O$, 64%, 3.2:1; toluene, 62%, 4.3:1.

[18] The following dipolarophiles gave the corresponding cycloadducts: methyl propiolate, 75%; methyl vinyl ketone, 59%; methyl acrylate, 68%; acrylonitrile, 62%.

[19] Product yields obtained with other $Rh^{II}$ complexes: $Rh_2(O\text{-}COC_7H_{15})_4$, 71%; $Rh_2(OCOPh)_4$, 66%; $Rh_2(OCOC_3F_7)_4$, 11%; $Rh_2(NHAc)_4$, 72%.

[20] The stereochemistry of **19** was verified by the diagnostic $^1$H NOE correlation (18%) between C3-H and C6-H.

[21] The combined use of DIBAL-H and $ZnCl_2$ in THF was reported to be effective for the diastereoselective reduction of β-ketosulfoxides: G. Solladié, G. Demailly, C. Greck, *Tetrahedron Lett.* **1985**, *26*, 435 – 438.

[22] S. Hanessian, D. Delorme, Y. Dufresne, *Tetrahedron Lett.* **1984**, *25*, 2515 – 2518.

[23] a) J. B. Baudin, G. Hareau, S. A. Julia, R. Lorne, O. Ruel, *Bull. Soc. Chim. Fr.* **1993**, *130*, 856 – 878; b) P. R. Blakemore, W. J. Cole, P. J. Kocieński, A. Morley, *Synlett* **1998**, 26 – 28.

[24] H. E. Blackwell, D. J. O'Leary, A. K. Chatterjee, R. A. Washenfelder, D. A. Bussmann, R. H. Grubbs, *J. Am. Chem. Soc.* **2000**, *122*, 58 – 71. For a review, see: S. J. Connon, S. Blechert, *Angew. Chem.* **2003**, *115*, 1944 – 1968; *Angew. Chem. Int. Ed.* **2003**, *42*, 1900 – 1923.

[25] Alkene **28** was prepared from (2*R*,3*R*)-2-(methanesulfonyl)oxy-3-methyl-4-phenyl-1-butanol[26] by the seven-step sequence:

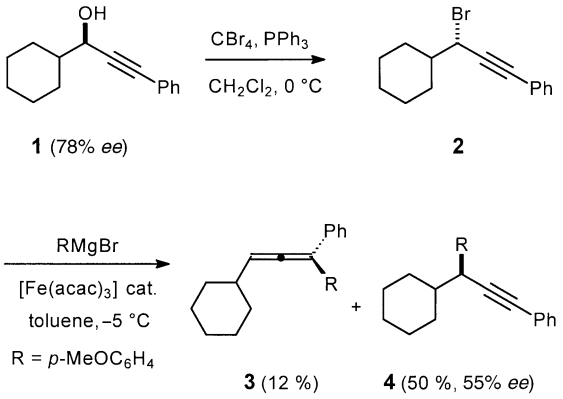
 © 2003 Wiley-VCH Verlag GmbH & Co. KGaA, Weinheim 

1) NaOMe, MeOH, then PhSH; 2) MPMBr, NaH, THF–DMF; 3) *m*CPBA, $CH_2Cl_2$, −25 °C; 4) TFAA, pyridine, $CH_2Cl_2$, 0 °C, then $NaHCO_3$, MeOH; 5) $Ph_3P{=}CH_2$, THF, 0 °C; 6) DDQ, aq $CH_2Cl_2$; 7) $Ac_2O$, pyridine, DMAP, $CH_2Cl_2$. *m*CPBA = 3-chloroperoxybenzoic acid, TFAA = trifluoroacetic anhydride.

[26] H. Sato, J. Kitaguchi, S. Nakamura, S. Hashimoto, *Chem. Pharm. Bull.* **1998**, *46*, 1816 – 1819.

[27] Since ruthenium byproducts act as poisons for the following hydrogenation, these impurities were removed by treatment with activated carbon: J. H. Cho, B. M. Kim, *Org. Lett.* **2003**, *5*, 531 – 533.

 © 2003 Wiley-VCH Verlag GmbH & Co. KGaA, Weinheim 




***Scheme 1.*** Preparation and iron-catalyzed reaction of a nonterminal propargyl bromide with a Grignard reagent.

*Iron-Catalyzed Allenol Formation*

# Iron-Catalyzed Cross-Coupling Reactions: Efficient Synthesis of 2,3-Allenol Derivatives**

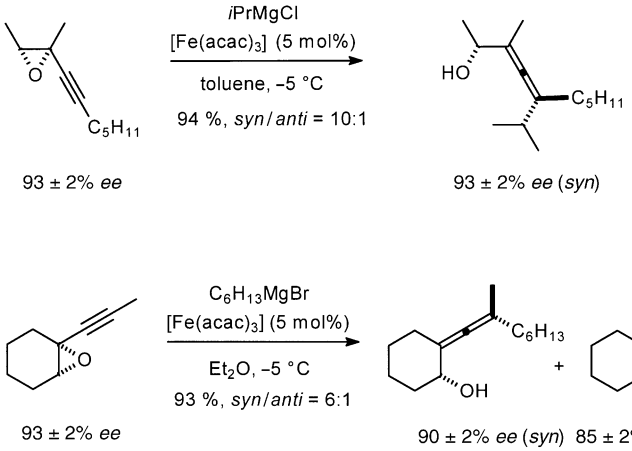
*Alois Fürstner* and María Méndez*

Allenes in general and 2,3-allenol derivatives in particular are versatile building blocks for advanced organic synthesis because of the reactivity inherent to their axially chiral backbones.[1] They are usually prepared by $S_N2'$-type reactions of propargylic substrates with organocopper reagents. Although this methodology has reached a high degree of sophistication and met with considerable success,[2] a literature survey shows that the stoichiometric regimen continues to prevail over the catalytic manifold in most applications.[1–3] Furthermore, strongly donating ligands to copper such as $PBu_3$ or $P(OMe)_3$ are required for efficient chirality transfer from the propargylic substrate to the incipient allene and/or to avoid the formation of reduction products derived from formal hydride delivery.[1f,4,5] Finally, a certain propensity of cuprates to racemize enantiomerically enriched allenes has been documented on several occasions.[6]

During our recent studies on iron-catalyzed cross-coupling reactions,[7] we became aware of an early, yet virtually inconsequential, report of Pasto et al. on the use of simple iron salts as precatalysts for the formation of allenes from propargylic halides and Grignard reagents.[8–10] In an attempt to apply this method, however, its limitations became immediately apparent (Scheme 1). Specifically, conversion of the scalemic propargyl alcohol **1** (78% *ee*)[11] into the corresponding bromide **2** followed by reaction with *p*-$MeOC_6H_4MgBr$ in the presence of $[Fe(acac)_3]$ catalyst furnished the desired allene **3** as the minor product only, together with compound **4** formed by direct $S_N2$-substitution. The *ee* of the latter was only 55%, thus showing that a considerable loss in enantiomeric purity accompanied this overall transformation.

Convinced of the preparative advantages of iron salts as user-friendly, inexpensive, and virtually nontoxic precatalysts,[7] however, various propargyl derivatives were screened in the search for better substrates. Gratifyingly, we found that propargyl epoxides perform exquisitely well. They are easily prepared in optically active form[12] and react with different Grignard reagents with exceptional efficiency in the presence of catalytic amounts of simple iron salts, preferentially the nonhygroscopic $[Fe(acac)_3]$. First and utmost, the central chirality of these substrates is transferred to the axial chirality of the resulting 2,3-allenols with high fidelity, as can be seen from the examples compiled in Scheme 2.

The reactions are virtually instantaneous, even at low temperatures ($\leqslant$5 min), the required catalyst loading is low (3–5 mol%),[13] no extra ligands are necessary, the yields are good to excellent, and the substrate scope is sufficiently broad. Importantly, propargyl epoxides with terminal or nonterminal alkyne units react with similar ease (Table 1). Moreover, the direct attack of the Grignard reagent at the epoxide ring[14] remains insignificant in all but the most activated cases (Table 1, entries 17 and 21).




***Scheme 2.*** Chirality transfer experiments.

[*] Prof. A. Fürstner, Dr. M. Méndez
Max-Planck-Institut für Kohlenforschung
45470 Mülheim an der Ruhr (Germany)
Fax: (+49) 208-306-2994
E-mail: fuerstner@mpi-muelheim.mpg.de

[**] Part 4. For Part 3, see reference [7b]. Generous financial support by the Deutsche Forschungsgemeinschaft (Leibniz program) and the Fonds der Chemischen Industrie is gratefully acknowledged. M.M. thanks the Alexander-von-Humboldt-Foundation for a fellowship.

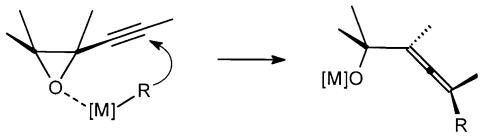
 DOI: 10.1002/anie.200352441 © 2003 Wiley-VCH Verlag GmbH & Co. KGaA, Weinheim 

***Table 1:*** Iron-catalyzed synthesis of 2,3-allenols from propargyl epoxides.[a]

| Entry | Substrate | $R^1$ | $R^2MgX$ | Major product | Solvent | *syn*/*anti* | Yield [%] |
|---|---|---|---|---|---|---|---|
| 1 | | H | $C_6H_{13}MgBr$ | | toluene | 78:22 | 72[b] |
| 2 | | H | PhMgBr | | toluene | 75:25 | 83 |
| 3 | | H | MeMgBr | | toluene | 55:45 | 71 |
| 4 | | Me | $C_6H_{13}MgBr$ | | $Et_2O$ | 86:14 | 93 |
| 5 | | Me | $C_6H_{13}MgBr$ | | $Et_2O$ | 78:22 | 75[c] |
| 6 | | Me | $C_6H_{13}MgBr$ | | $Et_2O$ | 50:50 | 54[d] |
| 7 | | Me | *i*PrMgCl | | $Et_2O$ | 84:16 | 79 |
| 8 | | Me | *i*PrMgCl | | toluene | 90:10 | 70 |
| 9 | | Me | PhMgBr | | $Et_2O$ | 66:34 | 98 |
| 10 | | Ph | MeMgBr | | $Et_2O$ | 65:35 | 69 |
| 11 | | $CH_2OH$ | $C_6H_{13}MgBr$ | | $Et_2O$ | 92:8 | 65[e] |
| 12 | | Me | $C_6H_{13}MgBr$ | | toluene | 80:20 | 73 |
| 13 | | Me | $C_6H_{13}MgBr$ | | toluene | 88:12 | 80 |
| 14 | | Me | *i*PrMgCl | | toluene | 84:16 | 79 |
| 15 | | Me | $C_6H_{13}MgBr$ | | toluene | 92:8 | 62 |
| 16 | | Me | $C_6H_{13}MgBr$ | | $Et_2O$ | 75:25 | 90 |
| 17 | | Me | *i*PrMgCl | | toluene | 86:14 | 75[f] |
| 18 | | Me | *i*PrMgCl | | $Et_2O$ | 60:40 | 89 |
| 19 | | $C_5H_{11}$ | *i*PrMgCl | | toluene | 91:9 | 94 |
| 20 | | $C_5H_{11}$ | *i*PrMgCl | | $Et_2O$ | 75:5 | 64 |
| 21 | | $C_5H_{11}$ | EtMgBr | | toluene | 82:18 | 55[g] |

[a] The reactions were carried out at $-5\,^{\circ}C$ in the presence of $[Fe(acac)_3]$ (3–5 mol%) precatalyst and Grignard reagent (1.3 equiv), unless stated otherwise. [b] Fe–salen precatalyst. [c] $-30\,^{\circ}C$. [d] $-60\,^{\circ}C$. [e] Grignard reagent (2.3 equiv). [f] A by-product (9%) was isolated that is formed by direct attack of the Grignard at the epoxide ring of the substrate. [g] In addition to the allenol, approximately 15% of by-products were formed from direct attack of the Grignard reagent at the epoxide ring of the substrate.

As can be seen from Table 1, the *syn*-configured 2,3-allenols are invariably formed as the major products.[15] Remarkably, this stereochemical outcome is *opposite* to that usually observed in reactions of propargyl epoxides with organocopper reagents,[4,6,16] which furnish the *anti*-configured allenols, except when carried out under "ligand-free" conditions in the presence of excess TMSCl.[4] Although the efficiency of the iron-catalyzed allenol formation is largely independent of the solvent used, the diastereoselectivity is higher in toluene than in $Et_2O$. This consistent trend (Table 1, entries 7/8, 15/16, 17/18, 19/20) is tentatively interpreted in terms of a "directed" delivery of the nucleophile to the alkyne,[17] which occurs only after the catalyst and/or the Grignard reagent has been coordinated to the oxygen atom of the substrate. Such a precoordination is likely more pronounced in a hydrocarbon solvent than in an ether medium (Scheme 3).




***Scheme 3.*** Proposed stereochemical rationale for the preferential formation of *syn*-configured 2,3-allenol derivatives by "directed" delivery of the nucleophile R.

The reasons, however, why the diastereoselectivity *decreases* upon lowering the reaction temperature are far less clear (Table 1, entries 4–6). Detailed mechanistic investigations will be necessary to shed light on this unusual behavior, which must include studies on the nature of the still elusive (and most likely highly reduced)[7] but exceptionally efficient iron catalyst formed in situ upon mixing of $[Fe(acac)_3]$ with an excess of an organomagnesium reagent. Investigations along these lines and further applications of iron-catalyzed cross-coupling reactions are currently underway and will be reported in due course.[18]

 © 2003 Wiley-VCH Verlag GmbH & Co. KGaA, Weinheim 

## Experimental Section

*i*PrMgCl (2 M in $Et_2O$, 0.42 mL, 0.83 mmol) was transferred by syringe into a solution of 1-prop-1-ynyl-9-oxa-bicyclo[6.1.0]nonane (105 mg, 0.64 mmol) and [Fe(acac)$_3$] (11 mg, 0.03 mmol) in toluene (14 mL) at −5 °C under Ar, causing an immediate color change from bright red to dark brown/black. After stirring for 5 min, the mixture was quenched with $NH_4Cl$ (5 mL) and diluted with $Et_2O$ (10 mL), the layers were separated, and the aqueous phase was extracted with $Et_2O$ (3 × 5 mL). The combined organic layers were dried over $MgSO_4$, and the residue was purified by flash chromatography (5:1 pentane/$Et_2O$) to provide 2-(2,3-dimethylbut-1-enylidene)-cyclooctanol as a colorless oil (100 mg, 75%, d.r. 86:14). IR (KBr): $\tilde{\nu}$ = 3402, 2931, 2858, 1943, 1115 cm$^{-1}$; $^1$H NMR (400 MHz, $CD_2Cl_2$): $\delta$ = 4.10 (dd, $J$ = 7.9, 3.7 Hz, 1H; *anti*), 4.07 (dd, $J$ = 8.8, 4.0 Hz, 1H; *syn*), 2.30–2.10 (m, 2H), 2.05 (m, 1H), 1.87 (m, 1H), 1.71 (s, 3H), 1.70–1.05 (m, 10H), 1.05 (d, $J$ = 1.9 Hz, 3H; *syn*), 1.04 (d, $J$ = 1.9 Hz, 3H; *syn*), 1.03 (d, $J$ = 1.9 Hz, 3H; *anti*), 1.01 ppm (d, $J$ = 1.9 Hz, 3H; *anti*); *syn* isomer: $^{13}$C NMR (100 MHz, $CD_2Cl_2$; DEPT) $\delta$ = 197.27 (C), 109.91 (C), 109.67 (C), 72.81 (CH), 33.36 ($CH_2$), 32.99 (CH), 29.66 ($CH_2$), 29.84 ($CH_2$), 26.50 ($CH_2$), 25.92 ($CH_2$), 23.24 ($CH_2$), 22.17 ($CH_3$), 22.04 ($CH_3$), 17.33 ppm ($CH_3$); *anti* isomer: $^{13}$C NMR (100 MHz, $CD_2Cl_2$; DEPT): $\delta$ = 196.67 (C), 110.58 (C), 110.04 (C), 71.97 (CH), 33.29 ($CH_2$), 33.08 (CH), 29.45 ($CH_2$), 29.18 ($CH_2$), 26.61 ($CH_2$), 26.04 ($CH_2$), 22.92 ($CH_2$), 22.04 ($CH_3$), 21.97 ($CH_3$), 17.37 ppm ($CH_3$); MS (EI, 70 eV): $m/z$ (%): 208 (10) [$M^+$], 193 (30), 165 (13), 137 (38), 110 (27), 95 (100); HMRS: calcd for $C_{14}H_{24}O$: 208.1828; found: 208.1827.

Received: July 22, 2003 [Z52441]

**Keywords:** alkynes · allenes · cross-coupling · epoxides · iron

[1] For selected reviews, see: a) J. A. Marshall, *Chem. Rev.* **2000**, *100*, 3163–3185; b) R. Zimmer, C. U. Dinesh, E. Nandanan, F. A. Khan, *Chem. Rev.* **2000**, *100*, 3067–3125; c) S. Ma, *Acc. Chem. Res.* **2003**, *36*, 701–712; d) A. S. K. Hashmi, *Angew. Chem.* **2000**, *112*, 3737–3740; *Angew. Chem. Int. Ed.* **2000**, *39*, 3590–3593; e) A. Hoffmann-Röder, N. Krause, *Angew. Chem.* **2002**, *114*, 3057–3059; *Angew. Chem. Int. Ed.* **2002**, *41*, 2933–2935; f) N. Krause, A. Hoffmann-Röder, J. Canisius, *Synthesis* **2002**, 1759–1774; g) H. F. Schuster, G. M. Coppola, *Allenes in Organic Synthesis*, Wiley, New York, **1984**, and references therein.

[2] For a review, see: N. Krause, A. Hoffmann-Röder, in *Modern Organocopper Chemistry* (Ed.: N. Krause), Wiley-VCH, Weinheim, **2002**, pp. 145–166, and references therein.

[3] For a recent exception, see: Z. Wan, S. G. Nelson, *J. Am. Chem. Soc.* **2000**, *122*, 10470–10471.

[4] For detailed studies on the effect of additives as well as for an in-depth mechanistic discussion, see the following for leading references: a) A. Alexakis, I. Marek, P. Mangeney, J. F. Normant, *J. Am. Chem. Soc.* **1990**, *112*, 8042–8047; b) A. Alexakis, I. Marek, P. Mangeney, J. F. Normant, *Tetrahedron* **1991**, *47*, 1677–1696.

[5] C. Sahlberg, A. Claesson, *J. Org. Chem.* **1984**, *49*, 4120–4122.

[6] a) C. J. Elsevier, P. Vermeer, *J. Org. Chem.* **1989**, *54*, 3726–3730; b) H. Westmijze, I. Nap, J. Meijer, H. Kleijn, P. Vermeer, *Recl. Trav. Chim. Pays-Bas* **1983**, *102*, 154–157; c) A. Claesson, L.-I. Olsson, *J. Chem. Soc. Chem. Commun.* **1979**, 524–525.

[7] a) A. Fürstner, A. Leitner, *Angew. Chem.* **2002**, *114*, 632–635; *Angew. Chem. Int. Ed.* **2002**, *41*, 609–612; b) A. Fürstner, A. Leitner, M. Méndez, H. Krause, *J. Am. Chem. Soc.* **2002**, *124*, 13856–13863; c) A. Fürstner, A. Leitner, *Angew. Chem.* **2003**, *115*, 320–323; *Angew. Chem. Int. Ed.* **2003**, *42*, 308–311.

[8] a) D. J. Pasto, G. F. Hennion, R. H. Shults, A. Waterhouse, S.-K. Chou, *J. Org. Chem.* **1976**, *41*, 3496; b) D. J. Pasto, S.-K. Chou, A. Waterhouse, R. H. Shults, G. F. Hennion, *J. Org. Chem.* **1978**, *43*, 1385–1388.

[9] A. S. K. Hashmi, G. Szeimies, *Chem. Ber.* **1994**, *127*, 1075–1089.

[10] For reports on the reaction of certain allylic substrates under iron catalysis, see: a) A. Yanagisawa, N. Nomura, H. Yamamoto, *Tetrahedron* **1994**, *50*, 6017–6028; b) A. Yanagisawa, N. Nomura, H. Yamamoto, *Synlett* **1991**, 513–514; c) M. Nakamura, K. Matsuo, T. Inoue, E. Nakamura, *Org. Lett.* **2003**, *5*, 1373–1375; d) M. Nakamura, A. Hirai, E. Nakamura, *J. Am. Chem. Soc.* **2000**, *122*, 978–979.

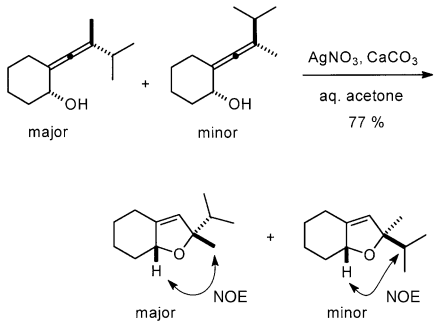
[11] D. E. Frantz, R. Fassler, E. M. Carreira, *J. Am. Chem. Soc.* **2000**, *122*, 1806–1807.

[12] The enantiomerically enriched substrates used in this study were prepared by enantioselective oxidation of the corresponding enynes; see: Z.-X. Wang, G.-A. Cao, Y. Shi, *J. Org. Chem.* **1999**, *64*, 7646–7650.

[13] Control experiments showed that the iron catalyst is essential; no productive allenol formation is observed in the absence of [Fe(acac)$_3$].

[14] Organocopper reagents show a certain tendency to undergo direct nucleophilic substitution of the epoxide, in particular if the reaction is carried out with only catalytic amounts of copper, see comments in reference [1f].

[15] The stereochemical assignment was corroborated by NOE measurements of the dihydrofuran derivatives formed from selected allenols upon treatment with $AgNO_3$.[16c] All other compounds were assigned by analogy. A representative example is shown below.




[16] a) P. Vermeer, J. Meijer, C. de Graaf, H. Schreurs, *Recl. Trav. Chim. Pays-Bas* **1974**, *93*, 46–47; b) A. C. Oehlschlager, E. Czyzewska, *Tetrahedron Lett.* **1983**, *24*, 5587–5590; c) J. A. Marshall, K. G. Pinney, *J. Org. Chem.* **1993**, *58*, 7180–7184; d) C. Spino, S. Fréchette, *Tetrahedron Lett.* **2000**, *41*, 8033–8036; e) C. R. Johnson, D. S. Dhanoa, *J. Org. Chem.* **1987**, *52*, 1885–1888; f) A. Doutheau, A. Saba, J. Gore, G. Quash, *Tetrahedron Lett.* **1982**, *23*, 2461–2464; g) P. R. Ortiz de Montellano, *J. Chem. Soc. Chem. Commun.* **1973**, 709–710; h) R. K. Dieter, L. E. Nice, *Tetrahedron Lett.* **1999**, *40*, 4293–4296; i) F. Bertozzi, P. Crotti, F. Macchia, M. Pineschi, A. Arnold, B. L. Feringa, *Tetrahedron Lett.* **1999**, *40*, 4893–4896.

[17] a) A similar rationale has been proposed for the formation of bromoallenes from propargyl alcohols and CuBr: N. Bernard, F. Chemea, J. F. Normant, *Tetrahedron Lett.* **1998**, *39*, 8837–8840; b) for a review, see: A. H. Hoveyda, D. A. Evans, G. C. Fu, *Chem. Rev.* **1993**, *93*, 1307–1370.

[18] For a recent application, see the following Communication in this issue: A. Fürstner, D. De Souza, L. Parra-Rapado, J. T. Jensen, *Angew. Chem.* **2003**, *115*, 5516–5518; *Angew. Chem. Int. Ed.* **2003**, *42*, 5358–5360.

 © 2003 Wiley-VCH Verlag GmbH & Co. KGaA, Weinheim 

Natural Product Synthesis

# Catalysis-Based Total Synthesis of Latrunculin B**

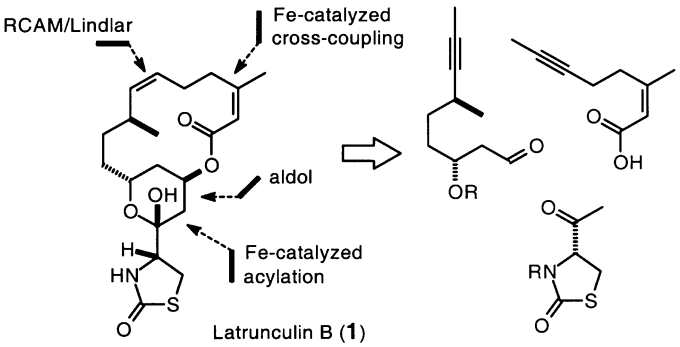
*Alois Fürstner,* Dominic De Souza, Liliana Parra-Rapado, and Jon T. Jensen*

Actin is one of the two major components of the cytoskeleton and not only determines the shape and mechanical properties of eukaryotic cells but is also responsible for cell motility processes as fundamental as cytokinesis or exo- and endocytosis. Our present knowledge about the many biological roles of actin derives to a large extent from a "chemical genetics" approach based on probe molecules able to dissect this highly sophisticated and inherently dynamic microfilament structure.[1] Among them, the latrunculins gained particular importance because of their striking selectivity and the surprisingly rapid onset of action.[2] They form 1:1 complexes with actin monomers that are incapable of polymerizing to the intact protein filament network.[3] Latrunculin B (**1**) and congeners were originally isolated as the ichthyotoxic principles of the Red Sea sponge *Latrunculia magnifica* and were also found later in taxonomically unrelated organisms from different marine habitats.[4,5]

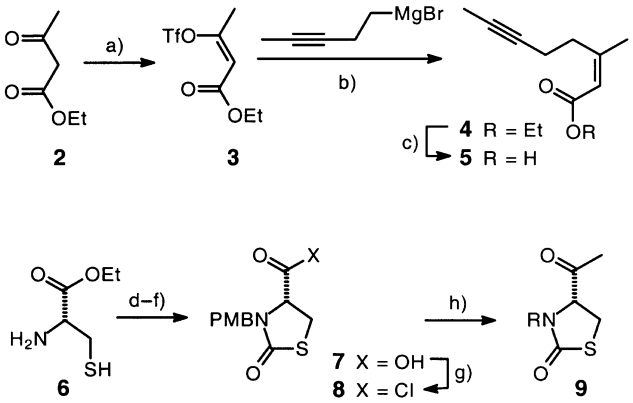
Despite the truly remarkable properties of the latrunculins and their widespread use as biochemical tools, the understanding of the structure–activity relationships (SAR) of these exquisite actin binders is fairly limited.[6] As a first step towards a synthesis-driven mapping of the structural elements essential for biological activity, a concise total synthesis of latrunculin B (**1**) was devised which is flexible enough to allow structural variations at a later stage. This flexibility was ensured by disconnecting **1** into three simple building blocks (Scheme 1) that are easy to modify and can be efficiently assembled through aldol chemistry, esterification, and formation of the macrocycle by the novel ring-closing alkyne metathesis (RCAM)/Lindlar reduction manifold.[7] Therefore, this new approach not only complements the previous total syntheses of **1** and its homologue latrunculin A based on macrolactonization,[8,9] but also illustrates the relevance of novel catalytic transformations recently developed in this laboratory.

The required acid component **5** was easily prepared from ethyl acetoacetate (**2**) via triflate **3** (Scheme 2). Reaction of the latter with the Grignard reagent derived from 1-bromo-3-pentyne in the presence of [Fe(acac)$_3$] as precatalyst afforded the desired product **4** in almost quantitative yield; the reaction proceeded stereoselectively and very rapidly under notably mild conditions. To the best of our knowledge, this is the first case of an iron-catalyzed cross-coupling reaction of an enol triflate. As such, it adds to the now rapidly growing number of examples in which cheap and benign iron salts serve as substitutes for established palladium or nickel catalysts in a variety of cross-coupling processes in general.[10,11]

In full accord with this notion, the synthesis of the cysteine-derived ketone **9** also takes advantage of iron catalysis (Scheme 2). Acid chloride **8** was prepared from **6** through standard reactions. Although **9** had previously been made by an uncatalyzed addition of MeMgBr to **8**,[8] we found the corresponding Fe-catalyzed process to be much more reliable and convenient; again, the rapid reaction rate is an additional bonus. The fact that attempted reactions of **8** with $Me_2CuLi$ led to complete decomposition of the starting material also bears witness to the superiority of the iron-catalyzed procedure.[12] Although acid chloride **8** is inherently prone to racemization, one recrystallization of the crude material sufficed to adjust the *ee* of ketone **9** to 99%.




***Scheme 1.*** Retrosynthetic analysis of latrunculin B.



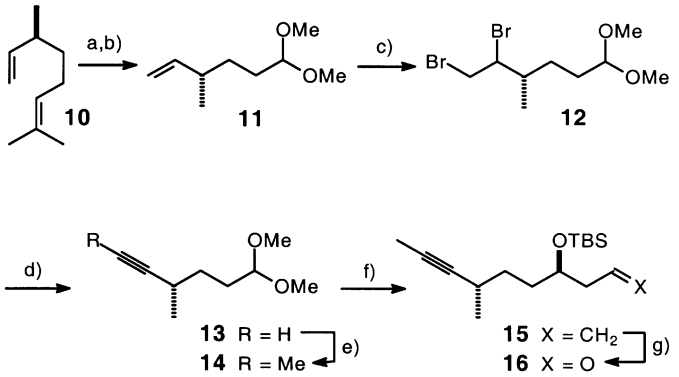

***Scheme 2.*** Synthesis of two building blocks by iron-catalyzed cross-coupling reactions: a) KHMDS, PhN(Tf)$_2$, THF, −78°C, 61%; b) [Fe(acac)$_3$] (10 mol%), THF, −30°C, 97%; c) aqueous NaOH, MeOH, 92%; d) CDI, THF, 71%; e) NaH, PMBBr, THF, 77%; f) aq. KOH, $Et_2O$, 98%; g) 1-chloro-2,*N*,*N*-trimethylprop-1-en-1-ylamine, THF, −18°C; h) [Fe(acac)$_3$] (1.5 mol%), MeMgBr, THF, −78°C→0°C, 80%. HMDS = hexamethyldisilazide, Tf = trifluoromethanesulfonyl, acac = acetylacetone, CDI = *N*,*N*′-carbonyldiimidazole, PMB = *p*-methoxybenzyl.

[*] Prof. A. Fürstner, Dr. D. De Souza, Dr. L. Parra-Rapado, Dipl.-Chem. J. T. Jensen
Max-Planck-Institut für Kohlenforschung
45470 Mülheim an der Ruhr (Germany)
Fax: (+49) 208-306-2994
E-mail: fuerstner@mpi-muelheim.mpg.de

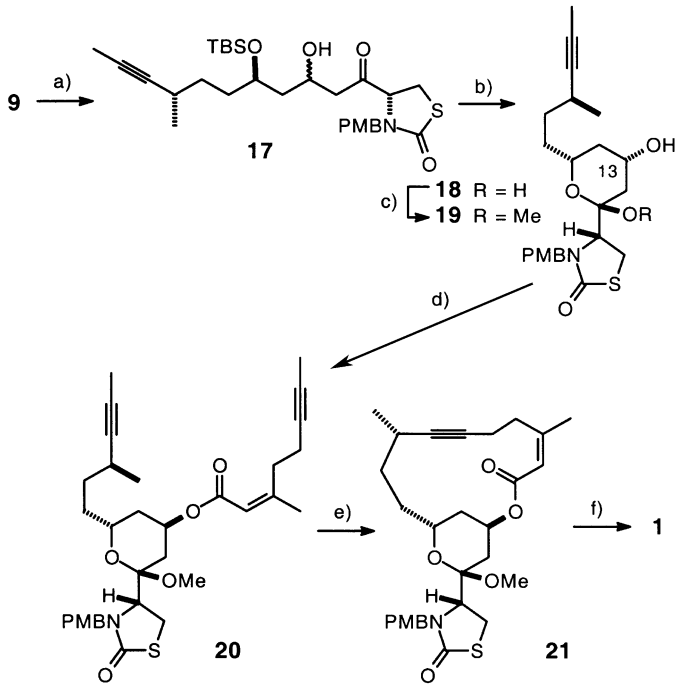
[**] Generous financial support by the DFG (Leibniz award to A.F.), the Swiss National Foundation (fellowship to L.P.-R.), the Fonds der Chemischen Industrie, the ACS (Cope Scholar Funds), and the Merck Research Council is gratefully acknowledged.

 © 2003 Wiley-VCH Verlag GmbH & Co. KGaA, Weinheim DOI: 10.1002/anie.200352413 

The third building block was derived from (+)-citronellene (**10**; 91% *ee*) by selective ozonolysis of the more highly substituted double bond and acetalization of the resulting aldehyde.[13] Bromination of **11** provided **12**, which was treated with LiHMDS to give **13** (Scheme 3). Alkyne **13** was




***Scheme 3.*** Synthesis of the third building block: a) $O_3$, $CH_2Cl_2$, −78 °C, then $Me_2S$; b) $HC(OMe)_3$, K10 montmorillonite, 75%; c) 4-dimethylaminopyridinium bromide perbromide, DMAP, $CH_2Cl_2$, 87%; d) LiHMDS, THF, 90%; e) BuLi, MeI, THF/DMPU, 95%; f) 1) aqueous HCl, THF; 2) (−)-$Ipc_2B$(allyl), −100 °C, $Et_2O$; (iii) TBSCl, imidazole, DMF, 78%; g) $O_3$, MeOH, Sudan red 7B, then $Me_2S$, 94%. DMAP = 4-dimethylaminopyridine, DMPU = 1,3-dimethyl-3,4,5,6-tetrahydro-2(1*H*)-pyrimidinone, Ipc = isopinocampheyl, TBS = *tert*-butyldimethylsilyl, DMF = *N*,*N*-dimethylformamide.




***Scheme 4.*** Completion of the total synthesis: a) $TiCl_4$, $iPr_2NEt$, $CH_2Cl_2$, −78 °C, 73%; b) aqueous HCl, THF; c) CSA, MeOH, 64% (over two steps); d) 1) $Tf_2O$, pyridine, $CH_2Cl_2$, −10 °C; 2) Na salt of **5**, 15[crown]-5, THF, 58%; e) [Mo{N(*t*Bu)(3,5-$Me_2C_6H_3$)}$_3$] (5 mol%), toluene, $CH_2Cl_2$, 80 °C, 70%; f) 1) $H_2$, Lindlar catalyst, $CH_2Cl_2$, quant.; 2) CAN, MeCN/$H_2O$, 78%. CSA = (+)-10-camphorsulfonic acid, CAN = ceric ammonium nitrate.

then methylated by reaction with BuLi and MeI. Deprotection of the acetal in **14**, allylation of the resulting aldehyde with (−)-$Ipc_2B$(allyl),[14] and subsequent protection of the alcohol with a TBS group furnished **15** in diastereomerically pure form (d.r. > 99.5:0.5). Selective ozonolysis of its alkene entity afforded the required product **16** for further elaboration.

Reaction of aldehyde **16** with the titanium enolate[15] derived from ketone **9** gave aldol **17** as a mixture (2:1) of diastereomers (Scheme 4). No attempt was made to improve this result as the stereochemical outcome was conveniently rectified at the next step by an equilibration process, which is well-precedented in the latrunculin series.[6a,8] Thus, acid-catalyzed cleavage of the TBS group in **17** delivered hemiacetal **18** (d.r. up to 7:1). Under these conditions, a transient oxonium ion is formed, which undergoes rapid loss of the axial OH group at C13; as 1,3-diaxial interactions are avoided during the re-addition of water to this intermediate, the formation of product **18** with an equatorially disposed OH function at that site is highly favored. Glycosylation with MeOH, conversion of product **19** into the corresponding triflate, and reaction with the sodium salt of acid **5** furnished diyne **20**, the substrate for the envisaged macrocyclization by RCAM.

This reaction proceeded exceptionally well in the presence of [Mo{N(*t*Bu)(3,5-$Me_2C_6H_3$)}$_3$] precatalyst, which was activated in situ with $CH_2Cl_2$ as recently described by our group.[16] Neither the dense array of functional groups nor the branching methyl substituent α to one of the alkyne units interfere with this catalytic system.[17] The chemoselective reaction of the triple bonds in the presence of a preexisting alkene is another noteworthy aspect of this transformation. The somewhat strained cycloalkyne **21** (Table 1) thus formed was subjected to a Lindlar reduction to ensure the stereoselective formation of the *Z*-alkene entity, followed by

***Table 1:*** Selected data for **21** and **1**.

**21:** $[\alpha]_D^{20} = +61.3°$ ($c = 0.75$, $CH_2Cl_2$); IR (ATR): $\tilde{\nu} = 2935, 1695, 1672, 1512, 1444, 1276, 1248, 1214, 1093, 1031\ cm^{-1}$; $^1H$ NMR (400 MHz, $CD_2Cl_2$): $\delta = 1.43$ (d, 3H, $J = 6.9$ Hz), 1.40–1.57 (m, 2H), 1.86 (d, 3H, $J = 1.3$ Hz), 1.75–1.90 (m, 4H), 2.08–2.40 (m, 5H), 2.49–2.53 (m, 1H), 3.14 (s, 3H), 3.17–3.32 (m, 4H), 3.79 (s, 3H), 3.83 (dd, 1H, $J = 3.3$ Hz, 9.0 Hz), 4.33 (d, 1H, $J = 14.4$ Hz), 4.91–4.99 (m, 1H), 5.00 (d, 1H, $J = 14.4$ Hz), 5.19–5.22 (m, 1H), 5.58 (d, 3H, $J = 1.3$ Hz), 6.87 (d, 2H, $J = 8.6$ Hz), 7.22 ppm (d, 2H, $J = 8.6$ Hz); $^{13}C$ NMR (100 MHz, $CD_2Cl_2$): $\delta = 19.05, 21.86, 24.99, 25.42, 26.33, 29.76, 31.09, 33.37, 33.92, 34.24, 47.36, 47.47, 55.28, 59.23, 65.66, 67.09, 80.96, 86.23, 101.98, 113.93, 118.73, 129.06, 130.00, 156.83, 159.22, 165.74, 172.59$ ppm; MS (ESI, 70 eV): *m*/*z* (%): 305 (100), 287 (20), 273 (13), 255 (26), 227 (15), 213 (23), 203 (15), 149 (11), 121 (91); HRMS: calcd for $C_{29}H_{37}NNaO_6S$ [*M*+Na$^+$]: 550.223930, found: 550.22450.

**1**: $[\alpha]_D^{20} = +122°$ ($c = 0.55$, $CHCl_3$); IR (ATR): $\tilde{\nu} = 3328, 2952, 1678, 1278, 1092, 1057\ cm^{-1}$; $^1H$ NMR (400 MHz, $CDCl_3$): $\delta = 0.95$ (d, 3H, $J = 6.3$ Hz), 1.07–2.39 (m, 11H), 1.90 (d, 3H, $J = 1.3$ Hz), 2.60–2.80 (m, 2H), 3.39 (dd, 1H, $J = 6.3$ Hz, 11.6 Hz), 3.47 (dd, 1H, $J = 8.8$ Hz, 11.6 Hz), 3.81–3.85 (m, 1H), 3.87 (s, 1H, OH), 4.24 (br t, 1H, $J = 10.6$ Hz), 5.05 (dt, 1H, $J = 1.5$ Hz, 11.2 Hz), 5.25 (dt, 1H, $J = 3.0$ Hz, 11.2 Hz), 5.43–5.46 (m, 1H), 5.68 (d, 1H, $J = 1.3$ Hz), 5.77 ppm (s, 1H, NH); $^{13}C$ NMR (100 MHz, $CDCl_3$): $\delta = 22.2, 24.0, 26.9, 28.7, 28.8, 30.9, 31.2, 31.4, 35.3, 35.8, 61.3, 62.5, 68.7, 97.8, 117.8, 127.4, 135.8, 154.5, 165.3, 174.7$ ppm.

 © 2003 Wiley-VCH Verlag GmbH & Co. KGaA, Weinheim 

concurrent cleavage of the *N*-PMB group and the methyl glycoside with CAN. Although this final deprotection was previously described as low-yielding,[8] we were pleased to find that it provided **1** (Table 1) in satisfactory yield (78%) simply upon prolongation of the reaction time.

In summary, a concise, productive, and inherently flexible route to latrunculin B (**1**) has been outlined based on Fe-catalyzed cross-coupling reactions[10–12] and alkyne metathesis[16,18] as the key steps. The longest linear sequence comprises 16 steps, which were performed in 14 operations, and provides an overall yield of approximately 6%. An extension of this approach to the synthesis of a focused library of latrunculin analogues is underway and will be reported in due course.

Received: July 18, 2003 [Z52413]

**Keywords:** alkynes · cross-coupling · macrocycles · metathesis · natural products

[1] a) J. R. Peterson, T. J. Mitchison, *Chem. Biol.* **2002**, *9*, 1275–1285; b) K.-S. Yeung, I. Paterson, *Angew. Chem.* **2002**, *114*, 4826–4847; *Angew. Chem. Int. Ed.* **2002**, *41*, 4632–4653.

[2] For leading references, see: a) I. Spector, N. R. Shochet, Y. Kashman, A. Groweiss, *Science* **1983**, *219*, 493–495; b) I. Spector, N. R. Shochet, D. Blasberger, Y. Kashman, *Cell Motil. Cytoskeleton* **1989**, *13*, 127–144; c) Molecular Motors and the Cytoskeleton, Part B: K. Ayscough, *Methods Enzymol.* **1998**, *298*, 18–25; d) K. R. Ayscough, J. Stryker, N. Pokala, M. Sanders, P. Crews, D. G. Drubin, *J. Cell Biol.* **1997**, *137*, 399–416.

[3] See i.a.: a) W. M. Morton, K. R. Ayscough, P. J. McLaughlin, *Nat. Cell Biol.* **2000**, *2*, 376–378; b) E. G. Yarmola, T. Somasundaram, T. A. Boring, I. Spector, M. R. Bubb, *J. Biol. Chem.* **2000**, *275*, 28120–28127.

[4] a) I. Neeman, L. Fishelson, Y. Kashman, *Mar. Biol.* **1975**, *30*, 293–296; b) Y. Kashman, A. Groweiss, U. Shmueli, *Tetrahedron Lett.* **1980**, *21*, 3629–3632; c) A. Groweiss, U. Shmueli, Y. Kashman, *J. Org. Chem.* **1983**, *48*, 3512–3516.

[5] a) R. K. Okuda, P. J. Scheuer, *Experientia* **1985**, *41*, 1355–1356; b) Y. Kakou, P. Crews, G. J. Bakus, *J. Nat. Prod.* **1987**, *50*, 482–484; c) C. W. Jefford, G. Bernardinelli, J. Tanaka, T. Higa, *Tetrahedron Lett.* **1996**, *37*, 159–162; d) N. K. Gulavita, S. P. Gunasekera, S. A. Pomponi, *J. Nat. Prod.* **1992**, *55*, 506–508; e) J. Tanaka, T. Higa, G. Bernardinelli, C. W. Jefford, *Chem. Lett.* **1996**, 255–256; f) D. Mebs, *J. Chem. Ecol.* **1985**, *11*, 713–716; g) T. R. Hoye, S.-E. N. Ayyad, B. M. Eklov, N. E. Hashish, W. T. Shier, K. A. El Sayed, M. T. Hamann, *J. Am. Chem. Soc.* **2002**, *124*, 7405–7410.

[6] This knowledge is entirely based on derivatizations of the natural product; see: a) D. Blasberger, S. Carmely, M. Cojocaru, I. Spector, N. R. Shochet, Y. Kashman, *Liebigs Ann. Chem.* **1989**, 1171–1188; b) I. Spector, N. R. Shochet, D. Blasberger, Y. Kashman, *J. Cell Biol.* **1986**, *103*, 1467.

[7] a) A. Fürstner, G. Seidel, *Angew. Chem.* **1998**, *110*, 1758–1760; *Angew. Chem. Int. Ed.* **1998**, *37*, 1734–1736; b) A. Fürstner, O. Guth, A. Rumbo, G. Seidel, *J. Am. Chem. Soc.* **1999**, *121*, 11108–11113.

[8] a) A. B. Smith, J. W. Leahy, I. Noda, S. W. Remiszewski, N. J. Liverton, R. Zibuck, *J. Am. Chem. Soc.* **1992**, *114*, 2995–3007; b) A. B. Smith, I. Noda, S. W. Remiszewski, N. J. Liverton, R. Zibuck, *J. Org. Chem.* **1990**, *55*, 3977–3979; c) R. Zibuck, N. J. Liverton, A. B. Smith, *J. Am. Chem. Soc.* **1986**, *108*, 2451–2453.

[9] a) J. D. White, M. Kawasaki, *J. Org. Chem.* **1992**, *57*, 5292–5300; b) J. D. White, M. Kawasaki, *J. Am. Chem. Soc.* **1990**, *112*, 4991–4993.

[10] a) A. Fürstner, A. Leitner, M. Méndez, H. Krause, *J. Am. Chem. Soc.* **2002**, *124*, 13856–13863; b) A. Fürstner, A. Leitner, *Angew. Chem.* **2002**, *114*, 632–635; *Angew. Chem. Int. Ed.* **2002**, *41*, 609–612; c) A. Fürstner, A. Leitner, *Angew. Chem.* **2003**, *115*, 320–323; *Angew. Chem. Int. Ed.* **2003**, *42*, 308–311.

[11] For Fe-catalyzed reactions of alkenyl halides, see: a) M. Tamura, J. K. Kochi, *J. Am. Chem. Soc.* **1971**, *93*, 1487–1489; b) S. M. Neumann, J. K. Kochi, *J. Org. Chem.* **1975**, *40*, 599–606; c) G. Cahiez, H. Avedissian, *Synthesis* **1998**, 1199–1205; d) G. A. Molander, B. J. Rahn, D. C. Shubert, S. E. Bonde, *Tetrahedron Lett.* **1983**, *24*, 5449–5452; e) A. Fürstner, H. Brunner, *Tetrahedron Lett.* **1996**, *37*, 7009–7012; f) B. Hölzer, R. W. Hoffmann, *Chem. Commun.* **2003**, 732–733.

[12] For iron-catalyzed syntheses of simple ketones, see: a) V. Fiandanese, G. Marchese, V. Martina, L. Ronzini, *Tetrahedron Lett.* **1984**, *25*, 4805–4808; b) C. Cardellicchio, V. Fiandanese, G. Marchese, L. Ronzini, *Tetrahedron Lett.* **1987**, *28*, 2053–2056.

[13] A. G. M. Barrett, R. A. E. Carr, S. V. Attwood, G. Richardson, N. D. A. Walshe, *J. Org. Chem.* **1986**, *51*, 4840–4856.

[14] U. S. Racherla, Y. Liao, H. C. Brown, *J. Org. Chem.* **1992**, *57*, 6614–6614.

[15] D. A. Evans, J. S. Clark, R. Metternich, V. J. Novack, G. S. Sheppard, *J. Am. Chem. Soc.* **1990**, *112*, 866–868.

[16] a) A. Fürstner, C. Mathes, C. W. Lehmann, *J. Am. Chem. Soc.* **1999**, *121*, 9453–9454; b) A. Fürstner, C. Mathes, C. W. Lehmann, *Chem. Eur. J.* **2001**, *7*, 5299–5317.

[17] This must be seen in light of the fact that steric hindrance close to a double bond can be a significant obstacle in conventional alkene metathesis; the same pertains to sulfur-containing compounds, which are usually highly problematic in alkene metathesis. For a Review, see: A. Fürstner, *Angew. Chem.* **2000**, *112*, 3140–3172; *Angew. Chem. Int. Ed.* **2000**, *39*, 3012–3043; see also: S. J. Connon, S. Blechert, *Angew. Chem.* **2003**, *115*, 1944–1968; *Angew. Chem. Int. Ed.* **2003**, *42*, 1900–1923.

[18] For previous applications of RCAM to total synthesis, see reference [16b] and the following: a) A. Fürstner, K. Grela, C. Mathes, C. W. Lehmann, *J. Am. Chem. Soc.* **2000**, *122*, 11799–11805; b) A. Fürstner, K. Radkowski, J. Grabowski, C. Wirtz, R. Mynott, *J. Org. Chem.* **2000**, *65*, 8758–8762; c) A. Fürstner, F. Stelzer, A. Rumbo, H. Krause, *Chem. Eur. J.* **2002**, *8*, 1856–1871; d) A. Fürstner, A.-S. Castanet, K. Radkowski, C. W. Lehmann, *J. Org. Chem.* **2003**, *68*, 1521–1528.

 © 2003 Wiley-VCH Verlag GmbH & Co. KGaA, Weinheim 

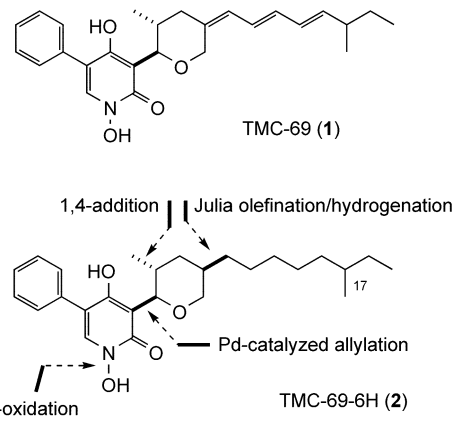
*Phosphatase Inhibitors*

# Total Synthesis and Reassessment of the Phosphatase-Inhibitory Activity of the Antitumor Agent TMC-69-6H**

*Alois Fürstner,* Fabian Feyen, Heino Prinz, and Herbert Waldmann*

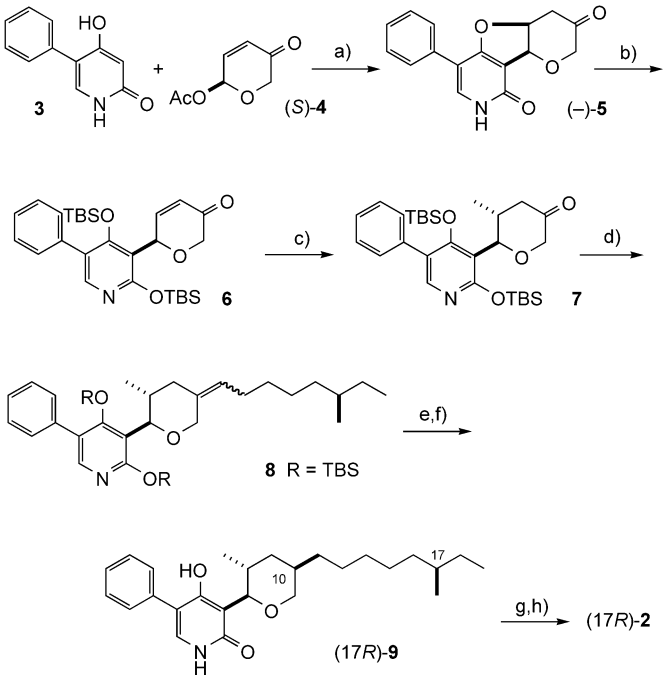
The family of the Cdc25 dual specific protein phosphatases is critically involved in cell-cycle control.[1] Their physiological substrates are cyclin-dependent kinases, which trigger key transitions in the process of eukaryotic cellular division. Therefore the homologous Cdc25 enzymes exert crucial regulatory functions at the crossroads between cellular proliferation, cell cycle arrest, and apoptosis. Their oncogenic properties together with the fact that Cdc25A and -B are overexpressed in many human tumors render these isoenzymes molecular targets of utmost interest in the quest for anticancer drugs.[1–3]

Despite this widely recognized fact, only a rather limited number of small molecules are presently known that might qualify as lead structures in the search for selective inhibitors of Cdc25 phosphatases.[3] One such compound is TMC-69 (**1**), a 2-pyridone derivative isolated from the culture broth of the fungus *Chrysosporium sp.* TC 1068 (Scheme 1).[4] According to the literature, this compound is distinguished by excellent activity ($IC_{50}$ values in the low micromolar range) and by a surprising selectivity for Cdc25A and -B over other phosphatases. Although pyridone **1** is inherently labile (it degrades within 2 weeks at 0 °C), hydrogenation of its triene moiety results in significantly improved stability and even further enhanced potency.[4] Importantly, TMC-69-6H (**2**) thus formed also exhibits a remarkable efficacy against P388 murine leukemia and B16 melanoma in nude mice.[4] Outlined below is the first total synthesis of the 17*R* and 17*S* isomers of **2** in enantiomerically pure form. The absolute stereochemistry at this remote stereogenic center in the natural product **1** and its derivative **2** has not yet been established.[4]




***Scheme 1.*** TMC-69 and TMC-69-6H. Retrosynthetic analysis for **2**.

The readily available pyranone **4**[5] served as a key building block en route to **2** (Scheme 2). Its enone moiety allowed the stereoselective installation of the methyl group by 1,4-addition, followed by attachment of the lateral chain by olefination of the remaining ketone. More importantly, however, the allylic leaving group in **4** opened several options for the introduction of the heteroaromatic ring. Rather than taking recourse to known oxo-carbenium cation chemistry,[6] we decided to rely on palladium-catalyzed C–C bond formations because they allow control of the stereochemical course of the envisaged allylation process more accurately (Scheme 2).




***Scheme 2.*** Synthesis of (17*R*)-**2**: [{(allyl)PdCl}$_2$] (0.5 %), **10** (1.5 %), $Et_3N$, DMF, 65 %, 96 % *ee*; b) TBSCl, $Et_3N$, 18 h, 78 %; c) $Me_2CuLi$, THF, −70 °C; d) LiHMDS, (*R*)-**15**, 69 % (over both steps); e) $H_2$, Pd/C, EtOH; f) TBAF, THF, 69 % (over two steps); g) $HN(SiMe_3)_2$, TMSCl cat., reflux; h) 1) [(pyridine)$MoO_5$(hmpa)], $CH_2Cl_2$; 2) saturated aqueous EDTA-Na, EtOAc, 61 % (over three steps). DMF = *N,N*-dimethylformamide, TBS = *tert*-butyldimethylsilyl, HMDS = hexamethyldisilazide, TBAF = tetrabutylammonium fluoride, TMS = trimethylsilyl, HMPA = hexamethylphosphortriamide, EDTA = ethylenediaminetetraacetate.

Surprisingly, though, palladium-catalyzed transformations of 6-hydroxy-6*H*-pyran-3-one derivatives are scarce and seem to be restricted to reactions with O nucleophiles.[7] To the best

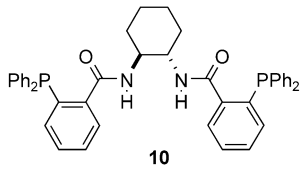
[*] Prof. A. Fürstner, Dipl.-Chem. F. Feyen
Max-Planck-Institut für Kohlenforschung
45470 Mülheim an der Ruhr (Germany)
Fax: (+49) 208-306-2994
E-mail: fuerstner@mpi-muelheim.mpg.de
Priv.-Doz. H. Prinz, Prof. H. Waldmann
Max-Planck-Institut für Molekulare Physiologie
44227 Dortmund (Germany)

[**] We thank Dr. J. Kohno, Tanabe Seiyaku Co. Ltd, Japan, for providing an authentic sample of TMC-69-6H for comparison. Financial support by the DFG (Leibniz award) and the Fonds der Chemischen Industrie is acknowledged with gratitude.

 DOI: 10.1002/anie.200352268 © 2003 Wiley-VCH Verlag GmbH & Co. KGaA, Weinheim 

of our knowledge, no Pd-catalyzed *C*-arylation of such a substrate with a phenol derivative has been described previously. Gratifyingly, however, (±)-**4** reacts smoothly and regioselectively at the enol site of 4-hydroxypyridone **3**[8] in the presence of $[Pd(PPh_3)_4]$ catalyst and $Et_3N$ in DMF to give the tricyclic product (±)-**5** in 89% yield. This novel palladium-catalyzed C–C bond formation is accompanied by a spontaneous 1,4-addition of the 4-OH group to the enone entity of the emerging product. Not only are we unaware of any precedence for this transformation, but this result must also be seen in the context of previous reports, which show that 2-pyridones tend to react with allylic substrates at their N atom in the presence of palladium catalysts.[9]

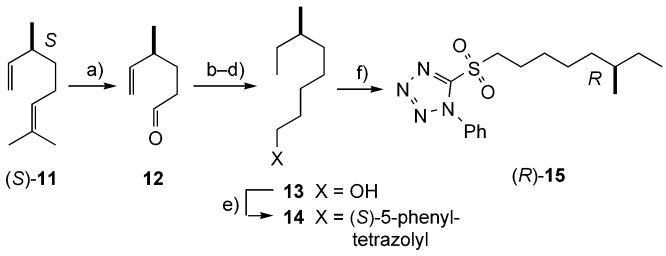
Attempts to perform this reaction enantioselectively with *rac*-**4** as the substrate and the chiral diphosphane **10**[10] as




**10**

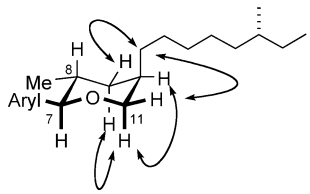
ligand to Pd were unrewarding (~30% *ee*). However, the use of **10** in combination with enantiomerically enriched (*S*)-**4** (81% *ee*), which is easily prepared on a multigram scale by a lipase-catalyzed dynamic resolution,[11] served our purpose very well, and delivered the tricyclic ketone (−)-**5** in good yield and with excellent enantiomeric purity (96% *ee*) (Scheme 2).

The cyclic ether moiety of **5** acts as a temporary protecting group for the enone which can be released by a retro-Michael reaction upon treatment with oxophilic reagents in the presence of a base.[12] Optimal results were obtained with TBSCl in combination with $Et_3N$. Exposure of the resulting disilyl ether derivative **6** to $Me_2CuLi$ afforded the somewhat labile *trans*-disubstituted ketone **7**, which was subjected to a Julia-Kocienski olefination reaction[13] with the lithiated sulfone (*R*)-**15** (prepared from (*S*)-citronellene **11** as shown in Scheme 3).[14] HPLC analyses of alkene **8** (*E*/*Z* 1:1) on chiral columns and comparison with the racemic series confirmed that no racemization had occurred during these




***Scheme 3.*** Reagents and conditions: a) $O_3$, $CH_2Cl_2$, −78 °C; then $Me_2S$, 98%; b) $(EtO)_2P(O)CH_2COOMe$, NaH, THF, −78 °C, 87%; c) DIBAL-H, $Et_2O$, 91%; d) $H_2$, Pd/C, 88%; e) 1-phenyl-1H-tetrazole-5-thiol, DEAD, $PPh_3$, THF, 68%; f) $(NH_4)_6Mo_7O_{24}\cdot 4H_2O$ (0.1 equiv), $H_2O_2$ (10 equiv), EtOH, 93%. DIBAL-H = diisobutylaluminum hydride, DEAD = diethyl azodicarboxylate.

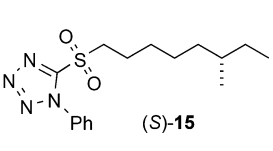
steps (97% *ee*). Subsequent hydrogenation of **8** over Pd/C followed by cleavage of the TBS groups furnished a separable mixture of the desired product **9** and its C10 epimer in 69% yield (over two steps). The axial orientation of the alkyl chain on the tetrahydropyran ring in **9** was evident from an analysis of the pertinent coupling constants and NOESY data (Scheme 4).[15]



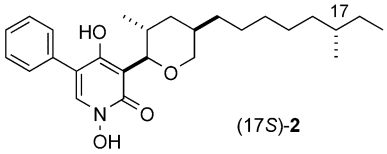

***Scheme 4.*** Schematic representation of compound **9** with characteristic NOESY data. Pertinent coupling constants: $^3J_{H7,H8} = 10.4$ Hz, $^3J_{H10,H11ax} = 2.5$ Hz, $^3J_{H10,H11eq} \leqslant 1$ Hz (TMC-69-6H numbering).

For the final *N*-oxidation to the desired hydroxamic acid derivative,[16] compound **9** was heated at reflux with hexamethyl disilazane and the resulting bis(silyl ether) was treated with the peroxo complex $[(pyridine)MoO_5(hmpa)]$.[17] Aqueous work-up with EDTA to sequester all metal cations then completed the first total synthesis of (17*R*)-TMC-69-6H ((17*R*)-**2**).

As mentioned above, no secured information concerning the absolute stereochemistry of the remote stereogenic center on the lateral chain of compound **2** derived from natural sources was available. Therefore the same sequence of reactions was repeated with ketone (−)-**5** and the antipodal sulfone (*S*)-**15** to give (17*S*)-**2** in similar overall yield. The




(*S*)-**15**




(17*S*)-**2**

diastereomeric compounds (17*R*)-**2** and (17*S*)-**2** thus obtained, however, are virtually indistinguishable by NMR spectroscopy and match the literature data reported for TMC-69-6H very well.[4] Even a direct comparison of their spectra recorded at 600 MHz with those of an authentic sample did not allow the rigorous assignment of the absolute stereochemistry of TMC-69-6H at that site.[18]

Since this excellent match leaves no doubt about the integrity of the synthetic materials, we were surprised to find that their phosphatase inhibitory activity *deviates significantly* from the reported profile both in terms of potency and selectivity. In contrast to what has been reported, the compounds prepared by total synthesis as well as an *authentic* sample of **2** all turned out to be only rather weak inhibitors of Cdc25A ($IC_{50} > 30$ μM) in our assay. Instead, they exhibit promising activities against the tyrosine protein phosphatase PTB1B, the dual specific phosphatase VHR, and the serine/

 © 2003 Wiley-VCH Verlag GmbH & Co. KGaA, Weinheim 

***Table 1:*** $IC_{50}$ values [μM] of authentic and synthetic TMC-69-6H and its immediate precursors against different phosphatases.[a]

| Compound | Cdc25A | PTP1B | VHR | PP1 |
|---|---|---|---|---|
| authentic **2** | ⩾50 | 3.2±1.6 | 7.0±3.5 | 6±3 |
| (17*R*)-**2** | 45±23 | 4±2.0 | 6±3 | 8.5±4.5 |
| (17*S*)-**2** | 32±16 | 3.5±1.7 | 5.5±3 | 8±4 |
| (17*S*)-**9** | ⩾50 | 11±5.5 | 9±5 | 30±5 |
| (17*S*)-**8b**[b] | ⩾50 | 23±11 | 11±5.5 | 32±16 |

[a] The enzymatic activity was determined by hydrolysis of *para*-nitrophenyl phosphate in standard buffers for PTP1B,[22a] VHR,[22b] and PP1.[22b] [b] The isomer with an *E* configuration between the $CH_2O$ group of the tetrahydropyran and C11 was tested.

threonine phosphatase PP1 (Table 1). PTP1B is a key negative regulator of insulin-receptor activity, and PTP1B-inhibitors are expected to enhance insulin sensitivity and act as effective therapeutics for the treatment of Type II diabetes, insulin resistance, and obesity. The vaccinia VH1-related phosphatase VHR is a physiological regulator of extracellular regulated kinases of the MAP (mitogen-activated protein) kinase family and influences signaling through the MAP kinase pathway. PP1 is a major eukaryotic phosphatase that regulates diverse cellular processes such as signal transduction, cell-cycle progression, protein synthesis, muscle contraction, carbohydrate metabolism, and transcription.

These phosphatases have been subject to intense research activities aimed at the development of inhibitors for biological studies and drug development.[19–22] Thus, PP1 inhibitors are expected to be potent anticancer drugs and have been used clinically for the treatment of cancers.[21] In particular, PTB1B is currently a major target of medicinal chemistry research in the pharmaceutical industry.[19]

Notably, TMC-69-6H incorporates a structural framework not present in any of the PTP1B and PP1 inhibitors developed so far. Thus, it provides a unique and unprecedented lead structure for the development of a new series of selective phosphatase inhibitors. Its proven activity in cellular assays (see above) renders such research activities particularly promising. Our preliminary results also seem to indicate that the presence of the *N*-OH group in the heterocycle, though not strictly required for phosphatase inhibition, enhances the potency of such compounds (compare, for instance, the $IC_{50}$ values determined for (17*S*)-**2** with the data for the corresponding amide (17*S*)-**9**).

Although we are unable to reconcile these findings with the literature reports concerning the physiological activity of TMC-69-6H,[4] the excellent reproducibility of our results, the internal control against authentic **2**, the consistency within the individual series, and the established validity of our Cdc25 assay[3b] leave no room for interpretation. These data also make clear that *N*-hydroxy-2-pyridone derivatives constitute a promising new class of selective phosphatase inhibitors and certainly deserve further studies to establish pertinent structure–activity relationships and assess their potency in more detail.[23,24] Synthesis-driven studies along these lines are underway and will be reported in due course.

Received: July 1, 2003 [Z52268]

**Keywords:** heterocycles · natural products · palladium · phosphatases · structure–activity relationships


[1] For reviews, see: a) K. Galaktinov, A. K. Lee, J. Eckstein, G. Draetta, J. Meckler, M. Loda, D. Beach, *Science* **1995**, *269*, 1575–1577; b) G. Draetta, J. Eckstein, *Biochim. Biophys. Acta* **1997**, *1332*, M53-M63; c) I. Nilsson, I. Hoffmann, *Prog. Cell Cycle Res.* **2000**, *4*, 107–114; d) Z.-Y. Zhang, *Curr. Opin. Chem. Biol.* **2001**, *5*, 416–423.

[2] Selected articles: a) M. G. Cangi, B. Cukor, P. Soung, S. Signoretti, G. Moreira, M. Ranashinge, B. Cady, M. Pagano, M. Loda, *J. Clin. Invest.* **2000**, *106*, 753–761; b) D. Dixon, T. Moyana, M. J. King, *Exp. Cell Res.* **1998**, *240*, 236–243; c) D. Gasparotto, R. Maestro, S. Piccinin, T. Vukosavljigevic, L. Barman, S. Sulfaro, M. Boiocchi, *Cancer Res.* **1997**, *57*, 2366–2368; d) W. Wu, Y. H. Fan, B. L. Kemp, G. Walsh, L. Mao, *Cancer Res.* **1998**, *58*, 4082–4085.

[3] a) For comprehensive literature coverage, see: M. A. Lyon, A. P. Ducruet, P. Wipf, J. S. Lazo, *Nat. Rev. Drug Discovery* **2002**, *1*, 961–976; b) for a representative study, see: D. Brohm, N. Philippe, S. Metzger, A. Bhargava, O. Müller, F. Lieb, H. Waldmann, *J. Am. Chem. Soc.* **2002**, *124*, 13171–13178.

[4] a) N. Hirano, J. Kohno, S. Tsunoda, M. Nishio, N. Kishi, T. Okuda, K. Kawano, S. Komatsubara, N. Nakanishi, *J. Antibiot.* **2001**, *54*, 421–427; b) J. Kohno, N. Hirano, K. Sugawara, M. Nishio, T. Hashiyama, N. Nakanishi, S. Komatsubara, *Tetrahedron* **2001**, *57*, 1731–1735; c) see also: K. Sugawara, J. Kohno, N. Nakanishi, T. Hashiyama, *Tennen Yuki Kagobutsu Toronkai Koen Yoshishu* **2000**, *42*, 661–666 [*Chem. Abstr.* **2001**, *134*, 340370].

[5] H. M. R. Hoffmann, H. Krumwiede, B. Mucha, H. Oehlerking, G. W. Prahst, *Tetrahedron* **1993**, *49*, 8999–9018.

[6] a) G. Grynkiewicz, A. Zamojski, *Z. Naturforsch. B* **1980**, *35*, 1024–1027; b) M. T. Reetz, H. Müller-Starke, *Liebigs Ann. Chem.* **1983**, 1726–1738.

[7] H. van der Deen, A. van Oeveren, R. M. Kellogg, B. L. Feringa, *Tetrahedron Lett.* **1999**, *40*, 1755–1758.

[8] a) B. B. Snider, Q. Lu, *J. Org. Chem.* **1996**, *61*, 2839–2844; b) J. Buck, J. P. Madeley, G. Pattenden, *J. Chem. Soc. Perkin Trans. 1* **1992**, 67–77.

[9] M. Moreno-Manas, R. Pleixats, M. Villarroya, *Tetrahedron* **1993**, *49*, 1457–1464.

[10] a) B. M. Trost, D. L. van Vranken, *Chem. Rev.* **1996**, *96*, 395–422; b) B. M. Trost, C. B. Lee, *J. Am. Chem. Soc.* **2001**, *123*, 3671–3686.

[11] M. van den Heuvel, A. D. Cuiper, H. van der Deen, R. M. Kellogg, B. L. Feringa, *Tetrahedron Lett.* **1997**, *38*, 1655–1658.

[12] a) M. J. Robins, C. Kaneko, M. Kaneko, *Can. J. Chem.* **1981**, *59*, 3356–3359; b) B. B. Snider, Q. Lu, *Tetrahedron Lett.* **1994**, *35*, 531–534.

[13] a) P. R. Blakemore, W. J. Cole, P. Kocienski, A. Morley, *Synlett* **1998**, 26–28; b) review: P. R. Blakemore, *J. Chem. Soc. Perkin Trans. 1* **2002**, 2563–2585; c) for a recent application, see: A. Fürstner, J. Mlynarski, M. Albert, *J. Am. Chem. Soc.* **2002**, *124*, 10274–10275.

[14] For the regioselective ozonolysis of citronellene and related olefinations of the resulting aldehyde, see: a) A. M. G. Barrett, R. Carr, S. V. Attwood, G. Richardson, N. D. A. Walshe, *J. Org. Chem.* **1986**, *51*, 4840–4856; b) M. G. Banwell, C. T. Bu, G. W. Simpson, *J. Chem. Soc. Perkin Trans. 1* **1998**, 791–800.

[15] The corresponding coupling constants of the minor product formed in the hydrogenation step are in full accord with an equatorial orientation of its alkyl side chain: $^3J_{H7,H8} = 10.0$ Hz, $^3J_{H10,H11ax} = 11.3$ Hz, $^3J_{H10,H11eq} = 2.6$ Hz.


 © 2003 Wiley-VCH Verlag GmbH & Co. KGaA, Weinheim 

[16] a) S. A. Matlin, P. G. Sammes, R. M. Upton, *J. Chem. Soc. Perkin Trans. 1* **1979**, 2481 – 2487; b) J. H. Rigby, M. Qabar, *J. Org. Chem.* **1989**, *54*, 5852 – 5853.

[17] a) E. Vedejs, S. Larsen, *Org. Synth.* **1986**, *64*, 127 – 137; b) H. Mimoun, I. S. de Roch, L. Sajus, *Bull. Soc. Chim. Fr.* **1969**, 1481 – 1492.

[18] Unfortunately, the optical rotations did also not allow us to make a final decision. The optical rotation reported for TMC-69-6H is $[\alpha]^{25} = +143.4$ ($c = 0.48$, MeOH);[4] the optical rotation of the authentic sample of **2** made available to us, however, was lower than this reported value. When corrected for the residual water in the sample, we record an $[\alpha]^{20}$ value of $\approx +99$ ($c = 0.18$, MeOH). The data of our analytically pure synthetic compounds are as follows: (17*R*)-**2**: $[\alpha]^{20} = +102.3$ ($c = 0.60$, MeOH); (17*S*)-**2**: $[\alpha]^{20} = +88.6$ ($c = 0.50$, MeOH).

[19] a) Z.-Y. Zhang, *Curr. Opin. Chem. Biol.* **2001**, *5*, 416 – 423; b) T. O. Johnson, J. Ermolieff, M. R. Jirousek, *Nat. Rev. Drug Discovery* **2002**, *1*, 696 – 709.

[20] a) J. L. Todd, K. G. Tanner, J. M. Denu, *J. Biol. Chem.* **1999**, *274*, 13271 – 13280; b) T. Usui, S. Kojima, S. Kidokoro, K. Ueda, U. Osada, M. Sodeoka, *Chem. Biol.* **2001**, *8*, 1209 – 1220.

[21] a) J. B. Aggen, A. C. Nairn, R. Chamberlin, *Chem. Biol.* **2000**, *7*, R13 – R23; b) A. McCluskey, J. A. Sakoff, *Mini-Rev. Med. Chem.* **2001**, *1*, 43 – 55.

[22] a) T. Hamaguchi, A. Masuda, T. Morino, H. Osada, *Chem. Biol.* **1997**, *4*, 279 – 286; b) A. Takai, G. Mieskes, *Biochem. J.* **1991**, *275*, 233 – 239; c) Vertebrate Phototransduction and the Visual Cycle Pt. A: X. Huang, M. R. Swingle, R. E. Honkanen, *Methods Enzymol.* **2000**, *315*, 579 – 593.

[23] While several other bioactive natural products that contain an *N*-hydroxy-2-pyridone motif are known in the literature, it appears that none have been checked for phosphatase inhibition; see: a) militarinone A: K. Schmidt, W. Günther, S. Stoyanova, B. Schubert, Z. Li, M. Hamburger, *Org. Lett.* **2002**, *4*, 197 – 199; b) militarinone D: K. Schmidt, U. Riese, Z. Li, M. Hamburger, *J. Nat. Prod.* **2003**, *66*, 378 – 383; c) tenellin: S. H. El Basyouni, D. Brewer, L. C. Vining, *Can. J. Bot.* **1968**, *46*, 441 – 448; d) bassianin: C.-K. Wat, A. G. McInnes, D. G. Smith, J. L. C. Wright, L. C. Vining, *Can. J. Chem.* **1977**, *55*, 4090 – 4098; e) fischerin: H. Fujimoto, M. Ikeda, K. Yamamoto, M. Yamazaki, *J. Nat. Prod.* **1993**, *56*, 1268 – 1275; f) pyridomacrolidin: S. Takahashi, N. Kakinuma, K. Uchida, R. Hashimoto, T. Yanagisawa, A. Nakagawa, *J. Antibiot.* **1998**, *51*, 596 – 598; g) leporin A: M. R. Tepaske, J. B. Gloer, D. T. Wicklow, P. F. Dowd, *Tetrahedron Lett.* **1991**, *32*, 5687 – 5690; h) fusaricide: K. D. McBrien, Q. Gao, S. Huang, S. E. Klohr, R. R. Wang, D. M. Pirnik, K. M. Neddermann, I. Bursuker, K. F. Kadow, J. E. Leet, *J. Nat. Prod.* **1996**, *59*, 1151 – 1153; i) pyridoxatin: Y. Teshima, K. Shin-ya, A. Shimazu, K. Furihata, H. S. Chul, K. Furihata, Y. Hayakawa, K. Nagai, H. Seto, *J. Antibiot.* **1991**, *44*, 685 – 687; j) BN-227: J. Itoh, S. Amano, Y. Ogawa, Y. Kodama, N. Ezaki, Y. Yamada, *J. Antibiot.* **1980**, *33*, 377 – 382. The same pertains to structurally related 2-pyridone alkaloids that are not oxidized at the nitrogen center; see: k) funiculosin: K. Ando, I. Matsuura, Y. Nawata, H. Endo, H. Sasaki, T. Okytomi, T. Saehi, G. Tamura, *J. Antibiot.* **1978**, *31*, 533 – 538; l) sambutoxin: J.-C. Kim, Y.-W. Lee, H. Tamura, T. Yoshizawa, *Tetrahedron Lett.* **1995**, *36*, 1047 – 1050; m) oxysporidinone: J. Breinholt, S. Ludvigsen, B. R. Rassing, C. N. Rosendahl, S. E. Nielsen, C. E. Olsen, *J. Nat. Prod.* **1997**, *60*, 33 – 35; n) harzianopyridone: J. M. Dickinson, J. R. Hanson, P. B. Hitchcock, N. Claydon, *J. Chem. Soc. Perkin Trans. 1* **1989**, 1885 – 1887.

[24] For a structurally different synthetic 2-pyridone derivative that bears an *N*-methylphosphonate moiety, which exhibits phosphatase-inhibiting properties, see: J.-M. Fu, A. L. Castelhano, *Bioorg. Med. Chem. Lett.* **1998**, *8*, 2813 – 2816.

 © 2003 Wiley-VCH Verlag GmbH & Co. KGaA, Weinheim 

# Cover Picture




**Ken Funabashi, Markus Jachmann, Motomu Kanai, and Masakatsu Shibasaki***

**The Senjyu Kannon statue** in the Koufukuji temple in Nara, Japan (see picture), has thousands of hands to manipulate thousands of things at once. A new catalyst, a 2,4-*cis*-hydroxyprolinol derivative, was developed for the enantioselective addition of dimethylzinc to α-ketoesters. The catalyst has three hands in a *cis*-stereochemical array, which activates both the ketoester substrate and the organozinc reagent simultaneously. M. Shibasaki et al. describe on page 5489 ff. the excellent enantioselectivities obtained from aromatic and heteroaromatic substrates.

# Contents

## Angewandte EarlyView

***The following articles are available online (in Wiley InterScience). You can find them at www.angewandte.org, under Full Text, Early View.***

*D. Stamou,* C. Duschl, E. Delamarche, H. Vogel*:*
**Self-Assembled Microarrays of Attoliter Molecular Vessels**
DOI: 10.1002/anie.200351866
Published online: November 5, 2003

*X. Gao, T. Friščić, L. R. MacGillivray*:*
**Supramolecular Construction of Molecular Ladders in the Solid State**
DOI: 10.1002/anie.200352713
Published online: November 5, 2003

*S. L. Tripp, R. E. Dunin-Borkowski, A. Wei*:*
**Flux Closure in Self-Assembled Cobalt Nanoparticle Rings**
DOI: 10.1002/anie.200352825
Published online: November 5, 2003

Articles judged by the referees or the editor as being either very important or very urgent are immediately edited, proof-read, and electronically published once the manuscript has arrived in the editorial office in final form. As long as there is no page number available these articles should be cited in the following manner:

Author(s) *Angew. Chem. Int. Ed.*, online publication date, DOI.

## Meeting Reviews


Nucleic Acids Chemistry and Biology ——— 5384 – 5385 — *J. Kurreck*


## Books


What Einstein Told his Cook ——— 5386 — Robert L. Wolke, Marlene Parrish — *reviewed by P. Weyerstahl*

De Artes Chemiae ——— 5386 — Lothar Beyer, Rainer Behrends — *reviewed by R. Zott, G. Boeck*

What's Cooking in Chemistry? ——— 5388 — Hubertus P. Bell, T. Feuerstein, C. E. Güntner, S. Hölsken, J. K. Lohmann — *reviewed by G. Märkl*

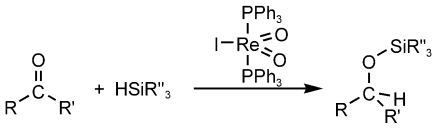

## Highlights

***Hydrosilylations***


W. R. Thiel* ——— 5390 – 5392

On the Way to a New Class of Catalysts—High-Valent Transition-Metal Complexes That Catalyze Reductions


**Surprise!** Owing to its rhenium(V) center, which bears two terminal oxo ligands, $[ReI(O)_2(PPh_3)_2]$ appears at first glance to be an oxygen-transfer reagent. The complex is, however, a novel catalyst for a reduction: the hydrosilylation of aldehydes and ketones (see scheme).




## Minireviews

***Cross-Coupling Reactions***


A. Zapf* ——— 5394 – 5399

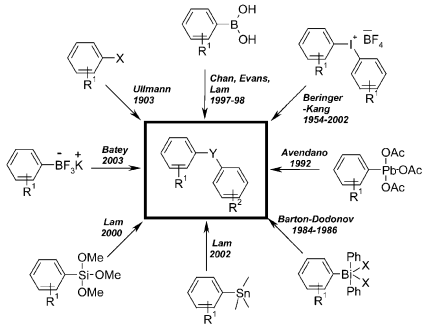
Novel Substrates for Palladium-Catalyzed Coupling Reactions of Arenes


**Alternative coupling partners**: Not only haloarenes, but also aryl carbonic acids and heteroaryl thioethers (see formulas) can take part in palladium-catalyzed coupling reactions. The substrate scope has thus become broader and the catalyst systems simpler. Furthermore, the reaction of carbonic acid derivatives allows the simple synthesis of ketones.




X = $OC(O)R^1$, OAryl, OH, $SR^1$
$R^1$ = Alkyl, Aryl

# Reviews




**The right conditions**: The development of new stoichiometric and catalytic variants of the copper-mediated arylation of heteroatoms (see figure) is of particular interest for the synthetic chemist. The authors give a thorough account of the state-of-the-art of the reaction and discuss the broad range of substrates and suitable choices of catalyst systems and reaction conditions.

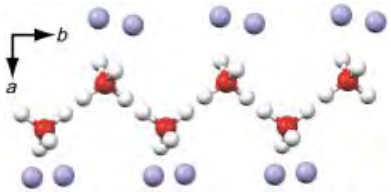
### *Ullmann Condensation*

S. V. Ley, A. W. Thomas* ___ **5400 – 5449**

Modern Synthetic Methods for Copper-Mediated C(aryl)–O, C(aryl)–N, and C(aryl)–S Bond Formation

# Communications

**Proton wires**: One-dimensional water chains play an important role in proton permeation through transmembrane proteins. The X-ray crystal structures as well as solid-state $^{2}H$ and $^{17}O$ NMR and calorimetry studies of two imidazole hydrates that stabilize infinite one-dimensional water chains are reported (see picture; N blue, O red, H white). The $^{2}H$ NMR spectroscopic studies

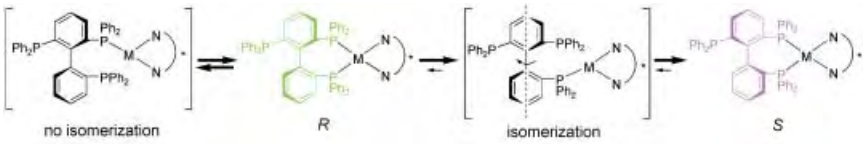



suggest that water molecules in both compounds undergo different reorientational dynamics.

### *One-Dimensional Water Chains*

L. E. Cheruzel, M. S. Pometun, M. R. Cecil, M. S. Mashuta, R. J. Wittebort, R. M. Buchanan* ___ **5452 – 5455**

Structures and Solid-State Dynamics of One-Dimensional Water Chains Stabilized by Imidazole Channels

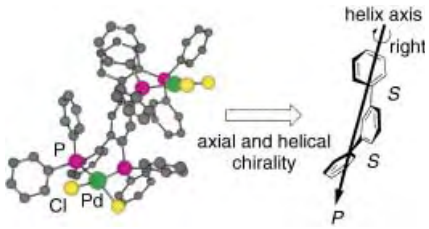



**Axial chirality is generated** upon complexation of the novel triphos ligand with a metal. In the presence of the diamine dm-dabn, isomerization to the enantiopure triphos–Ru complex was observed. The dm-dabn ligand of the Ru complex exchanges with dpen at room temperature without racemization. dm-dabn = 3,3′-dimethyl-2,2′-diamino-1,1′-binaphthyl, dpen = 1,2-diphenylethylenediamine.

### *Atropisomerism*

K. Aikawa, K. Mikami* ___ **5455 – 5458**

*Atropos* but Achiral Tris(phosphanyl)-biphenyl Ligands for Ru-Catalyzed Asymmetric Hydrogenation




**Both axial and helical chirality** are generated by complexation of the novel tetrakis(phosphanyl)terphenyl (tetraphos) ligand to a metal center (see picture). The *tropos* nature of the ligand was confirmed, and enantiopure Pd complexes controlled by diamines were applied as asymmetric Lewis acid catalysts in carbonyl–ene reactions.

### *Atropisomerism and Helicity*

K. Aikawa, K. Mikami* ___ **5458 – 5461**

Helical Chirality Control of Palladium Complexes That Bear a Tetrakis(phosphanyl)terphenyl Ligand: Application as Asymmetric Lewis Acid Catalysts

**For the USA and Canada:**
ANGEWANDTE CHEMIE International Edition (ISSN 1433-7851) is published weekly by Wiley-VCH PO Box 191161, D 69451 Weinheim, Germany. Air freight and mailing in the USA by Publications Expediting Inc. 200 Meacham Ave., Elmont, NY 11003. Periodicals postage paid at Jamaica NY 11431. US POSTMASTER: send address changes to *Angewandte Chemie*, Wiley-VCH, 111 River Street, Hoboken, NJ 07030. Annual institutional subscription price for institutions: Europe € 3430.00/3118.00. Outside Europe US$ 4499.00/4090.00 (valid for print and electronic/print or electronic delivery); for individuals who are personal members of a national chemical society, or whose institution already subscribes, or who are retired or self-employed consultants, print only. Europe € 248.00/Outside Europe US$ 378.00. Postage and handling charges included. All Wiley-VCH prices are exclusive VAT.

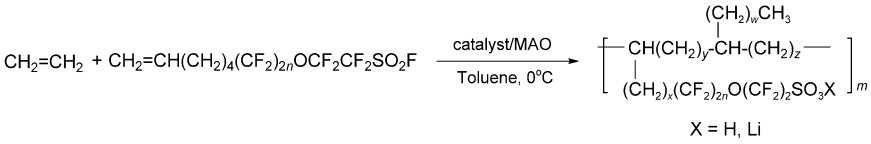
 © 2003 Wiley-VCH Verlag GmbH & Co. KGaA, Weinheim 

# Contents


## Super-Acid Catalysts

Z.-Y. Yang,* L. Wang,* N. Drysdale, M. Doyle, Q. Sun, S. K. Choi **5462 – 5464**

Benign by Molecular Design: Active Polymeric Super-Acid Catalysts and Highly Conductive Polymeric Lithium Electrolytes

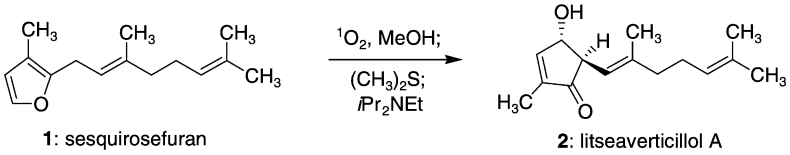



**Architectures of copolymers of ethylene** with α-olefinic fluorosulfonates are well controlled by tailoring palladium- or nickel-α-diimine catalysts and polymerization conditions (see scheme). These polymeric acids are shown to be "green" homogenous and heterogeneous super-acid catalysts for industrially important reactions. Their lithium salts exhibit excellent ionic conductivities as well as mechanical properties, and are attractive candidates for use in lithium batteries. (MAO = methylalumoxane)

## Natural Product Synthesis

G. Vassilikogiannakis,* M. Stratakis* **5465 – 5468**

Biomimetic Total Synthesis of Litseaverticillols A, C, D, F, and G: Singlet-Oxygen-Initiated Cascades



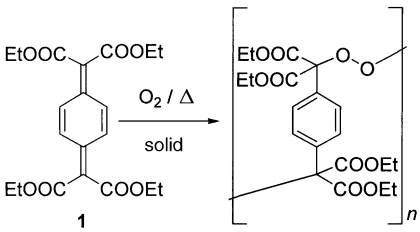

**Natural weapons against HIV,** litseaverticillols A (**2**) and C, have been synthesized from sesquirosefuran (**1**) by a rapid and efficient biomimetic total synthesis involving a chemo- and stereoselective singlet-oxygen-initiated tandem sequence (see scheme). Litseaverticillols D, F, and G were readily synthesized from litseaverticillol A through a regioselective $^1O_2$ ene reaction.

## Solid-State Reactions

S. Nomura, T. Itoh,* M. Ohtake, T. Uno, M. Kubo, A. Kajiwara, K. Sada, M. Miyata **5468 – 5472**

Polymerization by Insertion of Molecular Oxygen into Crystals of 7,7,8,8-Tetrakis-(ethoxycarbonyl)quinodimethane

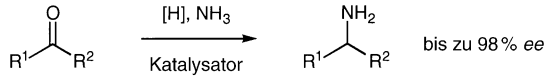
**Slipping through the lattice**: Molecular oxygen reacts with crystals of quinodimethane **1** to give highly crystalline alternating copolymers by means of a radical mechanism. An X-ray crystallographic study indicates that the unique arrangement of **1** in the crystal is crucial to the copolymerization.




## Asymmetric Reductive Amination

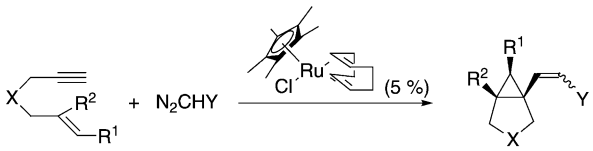
R. Kadyrov,* T. H. Riermeier **5472 – 5474**

Highly Enantioselective Hydrogen-Transfer Reductive Amination: Catalytic Asymmetric Synthesis of Primary Amines




**Ammonium formate is the hydrogen source** in the catalytic asymmetric reductive amination of ketones presented here (Leuckart–Wallach-type reaction). The reaction proceeds smoothly in methanol in the presence of Ir, Rh, and Ru catalysts. Primary amines were obtained as products in good yields with high enantioselectivities after hydrolytic workup when [((*R*)-tol-binap)$RuCl_2$] was used as the catalyst (see scheme). $R^1$, $R^2$ = alkyl, aryl.


 © 2003 Wiley-VCH Verlag GmbH & Co. KGaA, Weinheim 

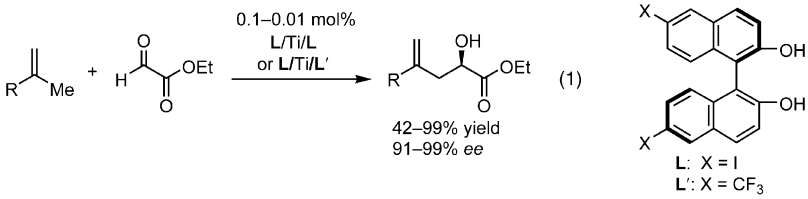



**[$C_p^*$RuCl(cod)]** ($C_p^* = C_5Me_5$, cod = cyclooctadiene) promotes the reaction of 1,6-enynes with an excess of diazoalkane in dioxane in one step to afford selectively 1-alkenyl bicyclo[3.1.0]hexane derivatives (see scheme, X = O, NTs; Y = $CO_2$Et; $R^1$ = H, Me; $R^2$ = H; Ts = *p*-toluenesulfonyl). This novel reaction involves the stereoselective formation of three C–C bonds and a cyclopropanation step.

## Enyne Cyclization

F. Monnier, D. Castillo, S. Dérien, L. Toupet, P. H. Dixneuf* — 5474 – 5477

Addition of Diazoalkanes to Enynes Promoted by a Ruthenium Catalyst: Simple Synthesis of Alkenyl Bicyclo[3.1.0]hexane Derivatives




**Simply mixing** the neat substrates and a small amount of the chiral catalyst (0.1–0.01 mol%) under nearly solvent-free conditions makes the enantioselective carbonyl-ene reaction of glyoxylate ester with a variety of olefins proceed smoothly to afford the corresponding α-hydroxy esters in high yields with excellent enantioselectivities [Eq. (1)].

## Catalytic Carbonyl-Ene Reaction

Y. Yuan, X. Zhang, K. Ding* — 5478 – 5480

Quasi Solvent-Free Enantioselective Carbonyl-Ene Reaction with Extremely Low Catalyst Loading



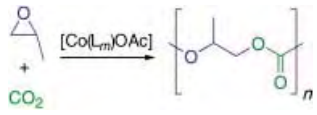

**Activity-based profiling** and reporter-group-tagged compounds were used to identify carboxylesterase-1 (CE-1) as a specific target of the natural product (−)-FR182877 (see scheme). Now that a target is known, specific modification of the lactone natural product may lead to even more effective inhibitors of CE-1.

## Chemical Biology

G. C. Adam, C. D. Vanderwal, E. J. Sorensen,* B. F. Cravatt* — 5480 – 5484

(−)-FR182877 Is a Potent and Selective Inhibitor of Carboxylesterase-1

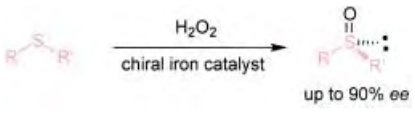
**$CO_2$ is an ideal feedstock** for chemical synthesis; unfortunately its thermodynamic stability is a barrier to widespread use. Active cobalt catalysts for the copolymerization of propylene oxide and $CO_2$ are reported (see scheme; L = *N*,*N*′-bis(3,5-di-*tert*-butylsalicylidene)-1,2-cyclohexanediamine), which have excellent regioselectivity for polycarbonate synthesis without concomitant production of cyclic carbonate by-products.




## Polycarbonate Synthesis

Z. Qin, C. M. Thomas, S. Lee, G. W. Coates* — 5484 – 5487

Cobalt-Based Complexes for the Copolymerization of Propylene Oxide and $CO_2$: Active and Selective Catalysts for Polycarbonate Synthesis




**An iron in the fire**: Iron-based catalysts promote the asymmetric oxidation of alkyl aryl sulfides to the corresponding sulfoxides with up to 90% *ee* (see scheme). Simple hydrogen peroxide (30% in water) serves as the terminal oxidant.

## Iron-Catalyzed Oxidations

J. Legros, C. Bolm* — 5487 – 5489

Iron-Catalyzed Asymmetric Sulfide Oxidation with Aqueous Hydrogen Peroxide

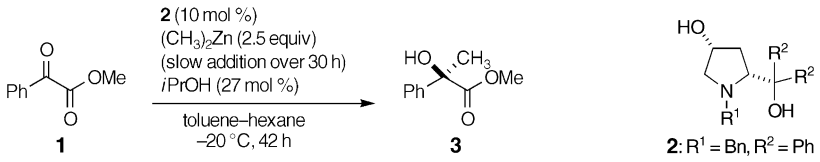
 © 2003 Wiley-VCH Verlag GmbH & Co. KGaA, Weinheim 

# Contents


## Asymmetric Alkylation of Ketones

K. Funabashi, M. Jachmann, M. Kanai, M. Shibasaki* ——— **5489 – 5492**

Multicenter Strategy for the Development of Catalytic Enantioselective Nucleophilic Alkylation of Ketones: $Me_2Zn$ Addition to α-Ketoesters

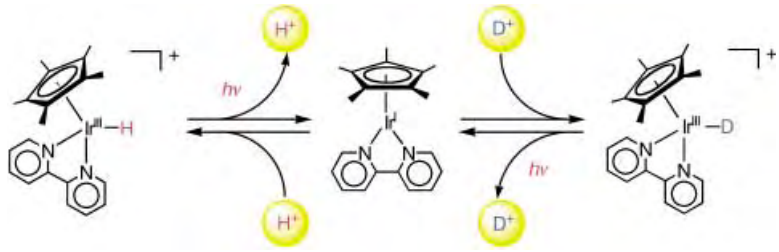



**An array of heteroatoms** is essential for the activity and enantioselectivity of the catalyst **2** in the addition of $Me_2Zn$ to α-ketoesters **1** (e.g. see equation). α-Hydroxyesters **3** were obtained with up to 96% *ee* in the presence of a catalytic amount of additive *i*PrOH, which serves to generate the catalytically active monomeric species (based on the observation of nonlinear effects).

## H/D Exchange in an Excited Hydride

T. Suenobu, D. M. Guldi,* S. Ogo, S. Fukuzumi* ——— **5492 – 5495**

Excited-State Deprotonation and H/D Exchange of an Iridium Hydride Complex



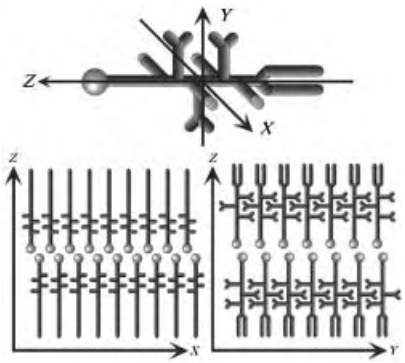

**Visible-light irradiation** of the hexafluorophosphate salt of $[Cp^*Ir^{III}(bpy)H]^+$ (**1**, $Cp^* = \eta^5\text{-}C_5Me_5$, bpy = 2,2′-bipyridine) results in excited-state deprotonation to form the conjugate base $[Cp^*Ir^{I}(bpy)]$. The H/D exchange reaction of **1** also occurs during photoirradiation of **1** in $[D_4]$methanol in the steady state (see picture).

## Elastic Films

N. Yamada,* T. Komatsu, H. Yoshinaga, K. Yoshizawa, S. Edo, M. Kunitake ——— **5496 – 5499**

Self-Supporting Elastic Film without Covalent Linkages as a Hierarchically Integrated β-Sheet Assembly

**Hierarchic self-assembly:** The formation of a self-supporting elastic film without the use of macromolecular materials is described. The film is prepared by using a peptide-containing amphiphile that has three or four consecutive leucinate residues. The amphiphile initially forms β-sheet structures, which stack in a fastenerlike fashion between the side chains of leucine within the different β-sheets (see picture).

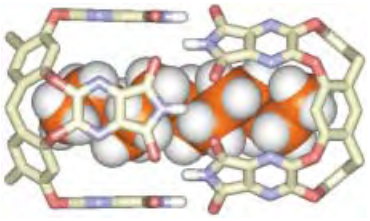



## Inclusion Complexes

A. Scarso, L. Trembleau, J. Rebek, Jr.* ——— **5499 – 5502**

Encapsulation Induces Helical Folding of Alkanes

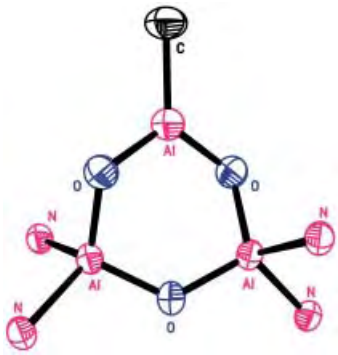
**Doing the twist**: Incorporation of long hydrocarbons during the self-assembly of a cylindrical capsule containing an elongated cavity lined with eight benzene rings and additional π surfaces induces helical conformations of the chains so that they are fully encapsulated within the cavity (see picture).





© 2003 Wiley-VCH Verlag GmbH & Co. KGaA, Weinheim

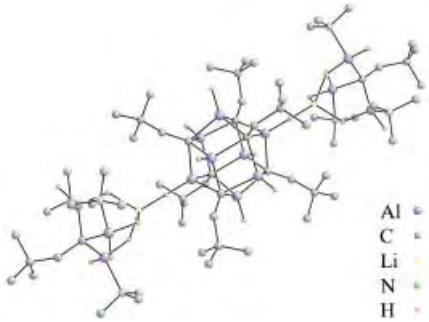
**Towards new polymerization-catalyst activators**: A new synthetic approach is described for the hitherto unknown $[\{LAl(OH)\}_2(\mu\text{-}O)]\cdot 0.5\,(C_7H_8)\cdot C_6H_{14}$ species (**1**; $L = HC[(CMe)(2,6\text{-}iPr_2C_6H_3N)]_2$). Further reaction of the Brönsted acidic OH groups of **1** with $Me_2AlH$ results in the formation of trimeric alumoxane containing a three coordinate Al center $[(LAl)_2(MeAl)(\mu\text{-}O)_3]\cdot 2\,C_7H_8$, the core of which is depicted. These compounds may have use as activators for olefin-polymerization catalysts.




## Terminal OH-Containing Alumoxane

G. Bai, H. W. Roesky,* J. Li, M. Noltemeyer, H.-G. Schmidt ——— **5502 – 5506**

Synthesis, Structural Characterization, and Reaction of the First Terminal Hydroxide-Containing Alumoxane with an $[\{Al(OH)\}_2(\mu\text{-}O)]$ Core

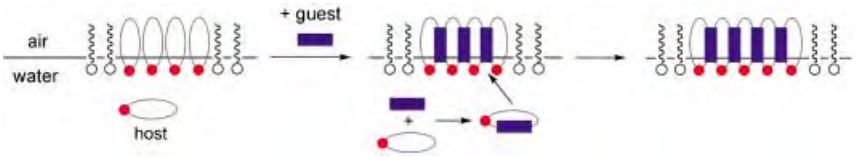



**The first carbaalanate** consists of a carbaalane dianion $[(AlH)_8(CCH_2tBu)_6]^{2-}$ that is coordinated through hydride bridges to two lithium ions on opposite sides of the cluster (see picture). Additionally, the lithium ions are each further coordinated to a neutral $[tBuCH_2C(AlH_2\cdot NMe_3)_3]$ unit. In this arrangement, the lithium ion prevents condensation of the $[tBuCH_2C(AlH_2\cdot NMe_3)_3]$ units.

## Cluster Compounds

A. Stasch, H. W. Roesky,* P. von R. Schleyer, J. Magull **5507 – 5509**

A Threefold $AlH_2$-Coordinated Carbon Atom as Part of the First Carbaalanate



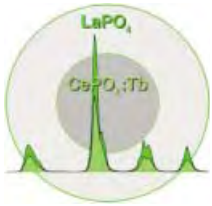

**Almost like the real thing**: Amphiphilic properties ensure that an artificial adrenaline receptor can be embedded in lipid monolayers just like the natural example. Here it forms large domains by self-assembly, which were investigated by Langmuir–Blodgett techniques. Embedded, the macrocyclic receptor is much more sensitive and selective than in solution. Monolayers containing receptor molecules can distinguish between adrenergic receptor substrates with similar structures.

## Artificial Adrenergic Receptors

O. Molt, T. Schrader* ——— **5509 – 5513**

Highly Sensitive Recognition of Substrates of Adrenergic Receptors at the Air/Water Interface

**Quantum leap**: Very high quantum yields, thought to be impossible for nanocrystalline phosphor materials, were achieved with $CePO_4$:Tb/$LaPO_4$ core–shell nanoparticles (see picture). Because the $LaPO_4$ shell reduces energy losses at the particle surface, transparent colloidal solutions of these 8-nm particles are highly photoluminescent.




## Core–Shell Particles

K. Kömpe, H. Borchert, J. Storz, A. Lobo, S. Adam, T. Möller, M. Haase* ——— **5513 – 5516**

Green-Emitting $CePO_4$:Tb/$LaPO_4$ Core–Shell Nanoparticles with 70% Photoluminescence Quantum Yield

 © 2003 Wiley-VCH Verlag GmbH & Co. KGaA, Weinheim 

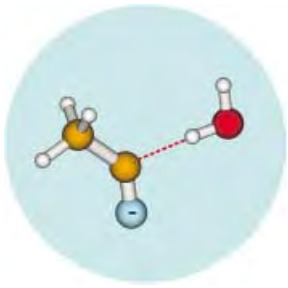
# Contents


**Reaction Mechanisms**

O. P. Balaj, I. Balteanu, B. S. Fox-Beyer, M. K. Beyer,* V. E. Bondybey* _____ **5516 – 5518**

Addition of a Hydrogen Atom to Acetonitrile by Hydrated Electrons in Nanodroplets


**Nanodroplets that contain hydrated electrons** provide information complementary to standard radiolysis techniques. Although the reaction of hydrated electrons with acetonitrile was observed in solution 25 years ago, its product has only now been identified in a gas-phase experiment as the hydrogen adduct. The picture shows a solvent-stabilized radical anion, which is suggested as a reactive intermediate.



VIP Communications labeled with this symbol have been judged by two referees as being "very important papers".

The publication of Communications labeled with this symbol has been accelerated because of their topical or highly competitive nature.


## Looking for outstanding employees?

**Do you need another expert for your excellent team?**
**... Chemists, PhD Students, Managers, Professors, Sales Representatives...**

Place an advert in the printed version and have it made available online for 1 month, free of charge!

***Angewandte Chemie International Edition***
**Advertising Sales Department: Marion Schulz**
**Phone: 0 62 01 - 60 65 65**
**Fax: 0 62 01 - 60 65 50**
**E-Mail: MSchulz@wiley-vch.de**

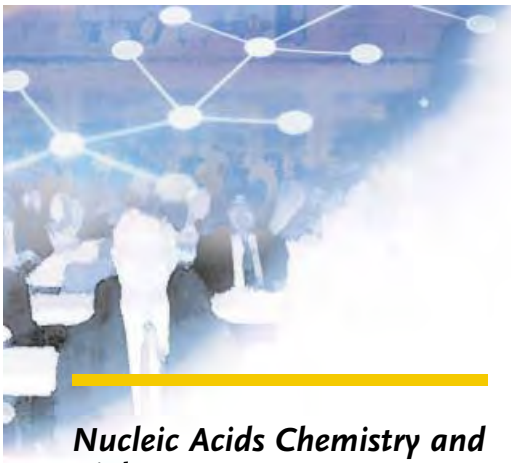

## Service


*Keywords* _____ *5522*

*Authors* _____ *5523*

*Angewandte's Sister Journals* _____ *5520 – 5521*

*Preview* _____ *5525*



# Nucleic Acids Chemistry and Biology**

Jens Kurreck*

In 2002 *Science* elected small RNAs as the Breakthrough of the Year. Therefore, it was not surprising that Thomas Tuschel, who recently moved from the Max-Planck-Institut für Biophysikalische Chemie in Göttingen (Germany) to The Rockefeller University in New York (USA), was chosen to give the opening lecture at the 5th Cambridge Symposium on Nucleic Acids Chemistry and Biology. He briefly referred to his landmark discovery in 2001 that short double-stranded RNA molecules (designated as small interfering RNAs or siRNAs) can be used for the sequence-specific silencing of gene expression through RNA interference in eukaryotic cells.[1] The focus of his talk was recent progress made in the micro-RNA (miRNA) field. Like siRNAs, these short RNAs are approximately 21 nucleotides long, but in contrast to siRNAs, miRNAs inhibit the synthesis of the target protein by binding to its homologous mRNA without degrading it. They are involved naturally in various regulatory processes within cells. Several hundred miRNAs have been identified in mammalians and *Drosophila melanogaster* to date, and researchers are currently trying to find further miRNAs and their targets.

The following speakers reported results on the use of siRNAs for target validation. François Natt (Basel, Switzerland) presented plans of the company Novartis to shut down the whole genome by RNA interference. In a large set of preliminary experiments with several thousand siRNAs, criteria for the design of efficient siRNAs were developed. The company now plans to synthesize 50000 siRNAs for target validation. During the discussions following the lectures about RNA interference in mammalian cells some warning statements were made with reference to a recent study in which the induction of an interferon response by siRNAs was described.[2]

Traditionally, nucleic acids chemistry has been an important topic of the Cambridge Symposia, which have taken place at irregular intervals since 1981. This year, too, numerous modified nucleotides were presented during the meeting. Several years ago, Jesper Wengel (Odense, Denmark) developed locked nucleic acids (LNAs) as a modification with various advantageous properties.[3] Meanwhile, his research group has been able to synthesize a variety of LNA analogues, for example, LNAs with a phosphorothioate backbone, α-L-LNAs, 2′-amino-LNAs, and *xylo*-configured nucleotides. Other speakers reported on the successful application of LNAs in antisense oligonucleotides, catalytically active deoxyribozymes, triplex-forming oligonucleotides (TOF), siRNAs, and aptamers.

Several talks dealt with recent progress made in the field of ribozymes. David Lilley (Dundee, UK) gave an impressive demonstration of how detailed structural information about molecules can be obtained by biochemical and biophysical methods even in the absence of a crystal structure. The VS ribozyme of *Neurospora* is the only known nucleolytic ribozyme for which there is no crystal structure. The global structure of this ribozyme was deduced from comparative gel electrophoresis, fluorescence resonance energy transfer (FRET) measurements, and mutational studies. In addition, the catalytic center was localized and a three-dimensional model of the ribozyme was constructed.[4] Sabine Müller (Bochum, Germany) presented a twin ribozyme that might become a new tool for RNA repair.[5] Two connected hairpin ribozymes are employed to cleave a fragment from a long RNA molecule. Since hairpin ribozymes do not only possess cleavage activity but also catalyze a ligation reaction, a repair oligonucleotide can subsequently be inserted into the processed RNA.

Without a doubt, Ronald Breaker's (New Haven, CT, USA) presentation on genetic control by metabolite-sensing riboswitches was one of the symposium's highlights.[6a] For many years Breaker has been developing artificial molecular switches for the allosteric control of ribozymes. For this, a ligand-binding aptamer is coupled to a ribozyme by an induction element. The addition of the ligand to an allosteric ribozyme induces a conformational change that activates the ribozyme and subsequently leads to the cleavage of a signal oligonucleotide. These allosteric ribozymes can be fixed to a solid surface, and the resulting chips can be used as biosensors for practical applications. Recently, Breaker and his co-workers discovered that nature had beaten them to the use of RNA biosensors. Generally, metabolic pathways are thought to be regulated by proteins that interact with metabolites and control gene expression by binding to the DNA. In some cases, however, the mRNA itself binds to the target molecule and thereby shuts down protein synthesis.[6b] For example, the purine metabolism in *Bacillus subtilis* is regulated by an RNA biosensor. The central riboswitch is located in the 5′ untranslated region of mRNAs that are involved in purine transport and biosynthesis. It is composed of two functional domains: an aptamer domain, which selectively binds the metabolite, and a control domain, which regulates gene expression by means of allosteric conformational changes after target-molecule binding. Figure 1 shows an example of the diverse mechanisms for gene control by riboswitches, which include the regulation of translation as well as control over transcription termination. Riboswitch classes known to date control 68 genes or 2% of the total genetic content of *B. subtilis*. Interestingly, riboswitches have not only been discovered in bacteria but appear to also occur in eukaryotic cells of plants and fungi.

Another highlight was the Nucleic Acids Award lecture given by Stephen J.

[*] J. Kurreck
Institut für Chemie (Biochemie)
Freie Universität Berlin (Germany)

[**] 5th Cambridge Symposium, Cambridge (UK), September 31 – October 3, 2003

 © 2003 Wiley-VCH Verlag GmbH & Co. KGaA, Weinheim DOI: 10.1002/anie.200320080 

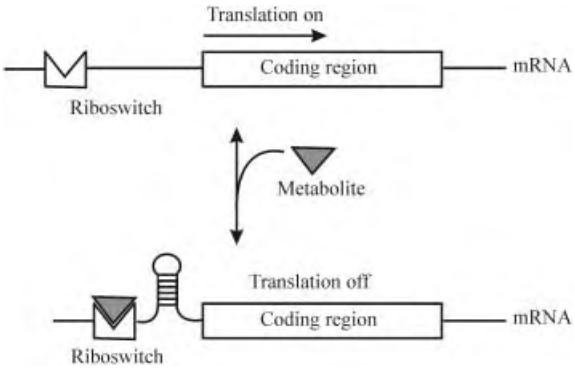



***Figure 1.*** Schematic representation of a riboswitch. In the absence of the target molecule the encoded protein is synthesized. Binding of the metabolite leads to a conformational change upon which translation is halted.

Benkovic (PA, USA). He talked about DNA replication by the T4 replisome. Eight proteins are directly involved in this process, and their assembly and interactions were analyzed in great detail by cross-linking experiments and single-molecule FRET measurements.

One session was dedicated to DNA arrays. Jörg Hoheisel (Heidelberg, Germany) gave an overview of methods for the generation and application of chips.[7] Currently, a DNA array is being developed to distinguish between various strains of the human papilloma virus. Most women are infected with the virus, and therefore it is important to identify dangerous strains that increase the probability of developing a cervix carcinoma. Another project deals with the diagnosis of single-nucleotide polymorphisms (SNPs), which will make a precise prognosis for cancer patients possible. The development of new dyes for the detection of DNA on the chips was also described in several lectures. Oliver Seitz (Berlin, Germany) and his co-workers generated fluorophors for homogeneous detection, for which the target and the probe are in solution.

Eric Wickstrom (Philadelphia, PA, USA) reported on recent results in noninvasive tumor diagnostics with radioactively labeled oligonucleotides. He uses PNAs that chelate a radionuclide, such as technetium, and bear a peptide that enables receptor-mediated endocytosis of the probe. These radionuclide-peptide-PNA-peptide chimeras are only taken up by invasive tumor cells that carry the IGF-1 receptor on their cell surface. In nude mice, tumor cells could be visualized specifically by the probe.

Hybridon, Inc. (Cambridge, MA, USA) develops immunomodulatory oligonucleotides as therapeutics for various diseases. Sundhir Agrawal presented results from the research of many years in this field. Oligonucleotides containing a CpG motif activate the vertebrate immune system by binding to toll-like receptors. They can be used as antiviral agents or as therapeutics for the treatment of cancer. In addition, CpG oligonucleotides are useful as adjuvants for vaccinations or for the treatment of asthma and allergies. Agrawal finished his talk with some critical remarks concerning the clinical trials of antisense oligonucleotides performed to date. These trials were very often disappointing and gave some questionable results. Agrawal pointed out that oligonucleotides with a CpG motif were used, and that immunostimulation might therefore have been observed rather than antisense effects. In this context, the disappointing news for researchers in the antisense field is that the only approved antisense drug, Vitravene, has recently been withdrawn from the European market. This decision, however, was not due to medical reasons but based on commercial motives, as the demand for Vitravene in Europe was less than 100 units per year.

These past disappointments increase the hope associated with new technologies in the field even further. The method of RNA interference might help to overcome efficiency problems of traditional antisense molecules. Furthermore, in recent years numerous modified nucleotides have been developed with desirable properties, such as nuclease resistance, high target affinity, and good cellular uptake. The Cambridge Symposium succeeds in bringing together chemists, molecular biologists, and physicians working in this field and initiating fruitful exchanges between various disciplines. In view of the dynamic nature of the field of nucleic acids, symposium participants expressed their hope that the organizers Mike Gait, Rick Cosstick, and Shankar Balasubramanian will soon find the time and energy to organize another symposium.

Meeting Reviews in *Angewandte Chemie* are meant to offer a view of the current state of a field rather than a comprehensive list of lectures. Authors are invited to describe what they feel were the most interesting contributions.

[1] a) M. S. Elbashir, J. Harborth, W. Lendeckel, A. Yalcin, K. Weber, T. Tuschl, *Nature* **2001**, *411*, 494–498; b) D. S. Conklin, *ChemBioChem* **2003**, *4*, 1033–1039.
[2] C. A. Sledz, M. Holko, M. J. de Veer, R. H. Silverman, B. R. G. Williams, *Nat. Cell Biol.* **2003**, *5*, 834–839.
[3] M. Petersen, J. Wengel, *Trends Biotechnol.* **2003**, *21*, 74–81.
[4] D. A. Lafontaine, D. G. Norman, D. M. J. Lilley, *EMBO J.* **2002**, *21*, 2461–2471.
[5] R. Welz, K. Bossmann, C. Klug, C. Schmidt, H.-J. Fritz, S. Müller, *Angew. Chem.* **2003**, *115*, 2526–2530; *Angew. Chem. Int. Ed.* **2003**, *42*, 2424–2427.
[6] a) W. C. Winkler, R. R. Breaker, *ChemBioChem* **2003**, *4*, 1024–1032; b) M. Mandal, B. Boese, J. E. Barrick, W. C. Winkler, R. R. Breaker, *Cell* **2003**, *113*, 77–586.
[7] M. C. Pirrung, *Angew. Chem.* **2002**, *114*, 1326–1341; *Angew. Chem. Int. Ed.* **2002**, *41*, 1276–1289.

 © 2003 Wiley-VCH Verlag GmbH & Co. KGaA, Weinheim 

Hydrosilylations

# On the Way to a New Class of Catalysts—High-Valent Transition-Metal Complexes That Catalyze Reductions

*Werner R. Thiel**

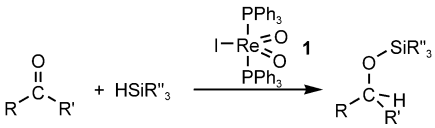
**Keywords:**
aldehydes · homogeneous catalysis · hydrosilylation · oxo ligands · rhenium

Over the last 40 years, homogeneous transition-metal catalysis has been developed into a versatile tool for fine and bulk chemical synthesis. If asked to classify the large number of different catalytically active species known to date, most chemists would consider the catalyzed transformation as a suitable criterion. If one proceeds in this way and at the same time initially neglects other important factors such as the influence of the ligand sphere, one can readily obtain a sketch of the periodic table, in which certain catalytic reactivities can be assigned to certain groups of elements.

The most active catalysts for reductions, such as hydrogenations, hydrosilylations, hydroformylations and others, contain electron-rich, late transition metals in low oxidation states. On the other hand, oxidations are mainly catalyzed by electron-poor species in high oxidation states. These statements are not only of relevance for homogeneous but also for heterogeneous catalysts; however, they raise a general question: has this simplified picture, which has without doubt didactic benefits, not contributed to us setting limits in the search for new catalytic reactions or new catalysts?

Following this argumentation, a review of catalyst research over the last 10–15 years reveals that genuine innovations were rather rare. Plenty of effort has been spent on the improvement of known structural motifs, which has proved vindicated and in many cases successful. The ruthenium-catalyzed metathesis ("Grubbs catalyst"),[1] the olefin polymerization catalyzed by late transition-metal complexes,[2] and the renaissance of N-heterocyclic carbene ligands for catalysis,[3] are among the few "really" new aspects that have been described. Depending on the individual interests, further examples can be added to this list.

It is therefore certainly of interest when an unexpected catalytic reaction is reported. In a publication and a patent, F. D. Toste and co-workers described the hydrosilylation of aldehydes and ketones catalyzed by the rhenium(v) complex $[ReI(O)_2(PPh_3)_2]$ (**1**) (Scheme 1).[4]




***Scheme 1.*** Rhenium-catalyzed hydrosilylation of aldehydes and ketones according to Toste et al.[4].

This is to our knowledge not only the first rhenium-catalyzed hydrosilylation, but also the first example for a hydrosilylation catalyst whose metal center is in the oxidation state +v and bears two terminal oxo ligands. The last two features in particular are remarkable.

Stable hydridorhenium complexes have been known for a long time.[5] Probably, the most famous compound of this type is the nonahydridorhenate(vii) $[ReH_9]^{2-}$, which is accessible from $[ReO_4]^-$ and sodium in EtOH.[6] In addition, a multitude of phosphane-stabilized hydridorhenium species has been synthesized by treating halogenorhenium–phosphane complexes with strong hydride-donating agents such as $Li[AlH_4]$, KH, $Na[BH_4]$, or $Li[BEt_3H]$.[7] However, silanes have not previously been used as the hydride source. Some of these hydridorhenium species have shown activity in the hydrogenation of C–C multiple bonds and/or in C–H activation.[8] In contrast, $[ReH_7(PPhiPr_2)_2]$ reacts with ethylene in the presence of various platinum catalysts to yield the hydrido–olefin complex $[ReH_3(C_2H_4)(PPhiPr_2)_2]$, which does not undergo hydrogenation of the olefin in the presence of 1 atm $H_2$ but gives the pentahydridorhenium complex $[ReH_5(C_2H_4)(PPhiPr_2)_2]$.[9]

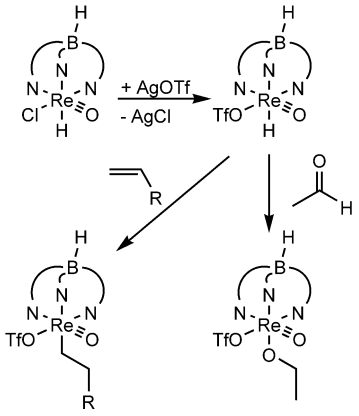
In their mechanistic interpretation of the catalytic cycle of the rhenium(v)-catalyzed hydrosilylation of aldehydes and ketones, Toste et al. proposed a hydrido-oxorhenium(v) intermediate. Such compounds have been known since 1989 and have been thoroughly investigated mainly by the groups of J. M. Mayer and A. Wojcicki. They are accessible by different synthetic routes: 1) decarboxylation of $[ReO(HCO_2)(R{-}C{\equiv}C{-}R)_2]$;[10] 2) spontaneous rearrangement (tautomerism) of the hydroxo complex $[Re(OH)(R{-}C{\equiv}C{-}R)_3]$, which can be obtained by deprotonation of the corresponding aqua complex, gives complexes of the type $[ReO(H)(R{-}C{\equiv}C{-}R)_2]$;[11] 3) treatment of [Tp*ReO(OMe)$_2$] (Tp* = hydridotris(3,5-dimethylpyrazol-1-yl)borate or [TpReO(OEt)Cl] (Tp = hydridotris(pyrazol-1-yl)borate) with $BH_3$·THF gives $[Tp^*ReO(H)_2]$ and [Tp*ReO(H)Cl], re-

[*] Prof. Dr. W. R. Thiel
Institut für Chemie
Technische Universität Chemnitz
Strasse der Nationen 62
09111 Chemnitz (Germany)
Fax: (+49) 371-5311833
E-mail:
werner.thiel@chemie.tu-chemnitz.de

 © 2003 Wiley-VCH Verlag GmbH & Co. KGaA, Weinheim DOI: 10.1002/anie.200301685 

spectively;[12] and 4) treatment of $[Re(H_2)H_4Cyttp]SbF_6$ to give fluorohydrido complexes of the type $[Re(F)(H)(O)Cyttp]SbF_6$ (Cyttp = PhP-$(CH_2CH_2CH_2PCy_2)_2$) by heating to reflux in a mixture of toluene and acetone[13].

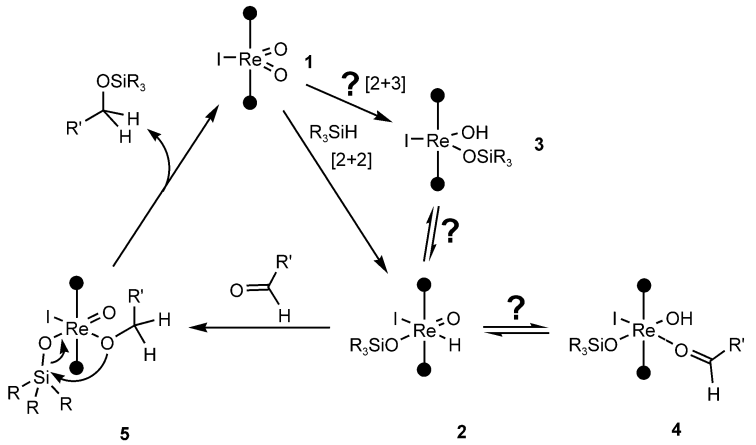
Here, only the synthesis of $[ReO(H)(R{-}C{\equiv}C{-}R)_2]$ (point 2) and the reactivity of the tris(3,5-dimethylpyrazol-1-yl)borate complex [Tp*ReO(H)Cl] (point 3) will be briefly mentioned: $[ReO(H)(R{-}C{\equiv}C{-}R)_2]$ is alternatively accessible by treatment of $[ReO(OEt)(R{-}C{\equiv}C{-}R)_2]$ with $Bu_3SnH$, a mild hydride-transfer agent. In contrast, the use of silanes such as $Et_3SiH$ or $Et_2SiH_2$ gives low yields.[10] [Tp*ReO(H)Cl] can be converted readily to the corresponding triflate complex [Tp*ReO(H)(OTf)] by treatment with AgOTf, which undergoes an insertion of acetaldehyde or a terminal olefin into the Re–H bond to yield [Tp*ReO(OEt)(OTf)] or $[Tp^*ReO(CH_2CH_2R)(OTf)]$, respectively (Scheme 2).[12]



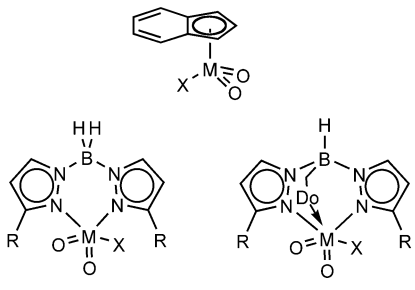

***Scheme 2.*** Insertion of alkenes and aldehydes into the Re–H bond of [Tp*ReO(H)(OTf)]. The hydridotris(3,5-dimethylpyrazol-1-yl)borate(Tp*) ligands are depicted in a simplified form for clarity.

These reactions correspond to the insertion of an aldehyde or ketone into the Re–H bond of the hydridorhenium(v) intermediate, obtained by Toste et al. in the addition of a silane to the rhenium complex **1**. In the reaction of **1** in the absence of a suitable substrate, a resonance signal occurs at $\delta = 6.60$ ppm in the $^1$H NMR spectrum, which was assigned to the hydridorhenium species **2** (Scheme 3). The position of this signal is consistent with the $^1$H NMR spectroscopic data of [Tp*ReO(H)Cl] ($\delta =$ 8.64 ppm) and $[ReO(H)(Et{-}C{\equiv}C{-}Et)_2]$ ($\delta = 6.05$ ppm). In constrast, the OH ligand of the tautomeric rhenium(III) hydroxo complex $[ReI(OH)(OSiR_3)(PPh_3)_2]$ (**3**) should give a proton resonance signal at higher field ($[Re(OH)(Et{-}C{\equiv}C{-}Et)_3]$: $\delta =$ 2.53 ppm). It still remains to be established whether the silane adds to one of the Re=O bonds by a [2+2] addition leading to the formation of a H-$Re^V$-OSi structure (**2**), or whether a HO-$Re^{III}$-OSi primary adduct (**3**) forms by a [2+3] addition to the O=Re=O moiety, which subsequently undergoes a rapid tautomerism. This question will probably be best answered with the aid of quantum-chemical calculations. A HO-$Re^{III}$-OSi intermediate may also play a role in the addition of the aldehyde or ketone, as it would open up a free coordination site for the docking of the substrate (**4**). The final elimination of the product is slow (**5**→**1**): the intermediate **5** could be detected by $^1$H NMR spectroscopy.

The results presented by Toste et al. will open up a discussion on whether compound **1** will remain a unique example for a high-valent transition-metal complex that catalyzes a reducing reaction. In my opinion, additional related systems will soon follow. If one considers the structural and electronic features of **1**, one can readily identify a series of alternative candidates. First, these compounds should have a coordination number of five or less, since it is increased to six by the addition of the Si–H unit (**1**→**2**). The metal center should be present in a high and stable oxidation state. A reduction by two units should be unachievable by mild reducing reagents such as silanes. The presence of at least one oxo ligand would be advantageous, since the addition of Si–H is favored by the formation of a stable Si–O bond. However, M=S and M=N groups may do the same job.[4b] Looking at the neighbors of rhenium in the periodic table, it appears that compounds of the type $[CpMoO_2X]$ (M = Mo, W; X = halogen) could be suitable candidates and may show analogous catalytic activity. The coordination number of six in these compounds could be lowered by the exchange of the cyclopentadienyl (Cp) ligand for an indenyl ligand (Scheme 4, top), which is known to undergo ring slippage ($\eta^5 \rightleftarrows \eta^3$) much easier than Cp. Alternatively, other bidentate ligands carrying one negative charge may be used. Scheme 4 (bottom)




***Scheme 3.*** Mechanism of the rhenium-catalyzed hydrosilylation of aldehydes. The reaction of **1** with $R_3SiH$ leads to **2**, presumably via **3** as the primary adduct. Comlpex **5** is formed by coordination of the aldehyde and insertion into the Re–H bond. The catalytic cycle is completed by elimination of the product and re-formation of **1**. ● = $PPh_3$.




***Scheme 4.*** Examples for oxo complexes with metal centers in high oxidation states, which can be considered as candidates for hydrosilylation catalysts. M = Mo, W; Do = optional donor function.

 © 2003 Wiley-VCH Verlag GmbH & Co. KGaA, Weinheim 

shows two complexes with bispyrazolyl ligands, which when necessary perhaps could be equipped with a third, labile donor site.

This is just a small and subjective collection, which may be completed by other complexes of Group 5, 8, or 9 elements in mid to high oxidation states, as well as by di- and polynuclear complexes. Variations in the ligand sphere of **1** should lead to further improvements in the catalytic performance of this type of compound. The exchange of the phosphane ligands for N-heterocyclic carbene ligands or the introduction of chiral (chelating) phosphane ligands for enantioselective hydrosilylation will certainly be investigated in the near future.


[1] a) S. T. Nguyen, R. H. Grubbs, J. W. Ziller, *J. Am. Chem. Soc.* **1993**, *115*, 9858 – 9859; b) G. C. Fu, S. T. Nguyen, R. H. Grubbs, *J. Am. Chem. Soc.* **1993**, *115*, 9856 – 9857; c) T. M. Trnka, R. H. Grubbs, *Acc. Chem. Res.* **2001**, *34*, 18 – 29.

[2] a) L. K. Johnson, S. Mecking, M. Brookhart, *J. Am. Chem. Soc.* **1996**, *118*, 267 – 268; b) L. K. Johnson, C. M. Killian, M. Brookhart, Maurice, *J. Am. Chem. Soc.* **1995**, *117*, 6414 – 6415; c) E. A. H. Griffiths, G. J. P. Britovsek, V. C. Gibson, I. R. Gould, *Chem. Commun.* **1999**, 1333 – 1334; d) G. J. P. Birtovsek, V. Gibson, B. S. Kimberley, P. J. Maddox, S. J. McTavish, G. A. Solan, A. J. P. White, D. J. Williams, *Chem. Commun.* **1998**, 849 – 850.

[3] W. A. Herrmann, *Angew. Chem.* **2002**, *114*, 1342 – 1363; *Angew. Chem. Int. Ed.* **2002**, *41*, 1290 – 1309.

[4] a) J. J. Kennedy-Smith, K. A. Nolin, H. P. Gunterman, F. D. Toste, *J. Am. Chem. Soc.* **2003**, *125*, 4056 – 4057; b) R. H. Grubbs, F. D. Toste (Cal. Inst. Tech., USA), US 2002-16178, **2002**.

[5] G. G. Hlatky, R. H. Crabtree, *Coord. Chem. Rev.* **1985**, *65*, 1 – 48.

[6] a) A. P. Ginsberg, C. R. Sprinkle, *Inorg. Chem.* **1969**, *8*, 2112 – 2114; b) J. G. Floss, A. V. Grosse, *J. Inorg. Nucl. Chem.* **1959**, *9*, 318 – 319.

[7] a) D. Guisto, *Inorg. Chim. Acta Rev.* **1972**, *6*, 91 – 110; b) J. Chart, R. S. Coffey, *Chem. Commun.* **1966**, 545 – 546; c) M. A. Green, J. C. Huffman, K. G. Caulton, *J. Am. Chem. Soc.* **1981**, *103*, 695 – 696; d) D. M. Lunder, M. A. Green, W. E. Streib, G. K. Caulton, *Inorg. Chem.* **1989**, *28*, 4527 – 4531; e) D. Alvarez, Jr., E. G. Lundquist, J. W. Ziller, W. J. Evans, K. G. Caulton, *J. Am. Chem. Soc.* **1989**, *111*, 8392 – 8398.

[8] a) D. G. DeWit, K. Folting, W. E. Streib, K. G. Caulton, *Organometallics* **1985**, *4*, 1149 – 1153; b) M. Dubeck, R. A. Schell, *Inorg. Chem.* **1964**, *3*, 1757 – 1760; c) D. Baudry, M. Ephritikhine, H. Felkin, *J. Chem. Soc. Chem. Commun.* **1982**, 606 – 607.

[9] N. J. Hazel, J. A. K. Howard, J. L. Spencer, *J. Chem. Soc. Chem. Commun.* **1984**, 1663 – 1664.

[10] E. Spaltenstein, T. K. G. Erikson, S. C. Critchlow, J. M. Mayer, M. James, *J. Am. Chem. Soc.* **1989**, *111*, 617 – 623.

[11] S. K. Tahmassebi, R. R. Conry, J. M. Mayer, *J. Am. Chem. Soc.* **1993**, *115*, 7553 – 7554.

[12] a) Y. Matano, S. N. Brown, T. O. Northcutt, J. M. Mayer, *Organometallics* **1998**, *17*, 2939 – 2941; b) Y. Matano, T. O. Northcutt, J. Brugman, B. K. Bennett, S. Lovell, J. M. Mayer, *Organometallics* **2000**, *19*, 2781 – 2790.

[13] a) D. E. Rende, Y. Kim, C. M. Beck, A. Wojcicki, *Inorg. Chim. Acta* **1995**, *240*, 435 – 439; b) Y. Kim, J. Gallucci, A. Wojcicki, *J. Am. Chem. Soc.* **1990**, *112*, 8600 – 8602.


 © 2003 Wiley-VCH Verlag GmbH & Co. KGaA, Weinheim 

Cross-Coupling Reactions

# Novel Substrates for Palladium-Catalyzed Coupling Reactions of Arenes

*Alexander Zapf**

**Keywords:**
carbonic acids · cross-coupling · homogeneous catalysis · ketones · palladium

*Dedicated to Professor Dr. Günther Oehme on the occasion of his 65th birthday*

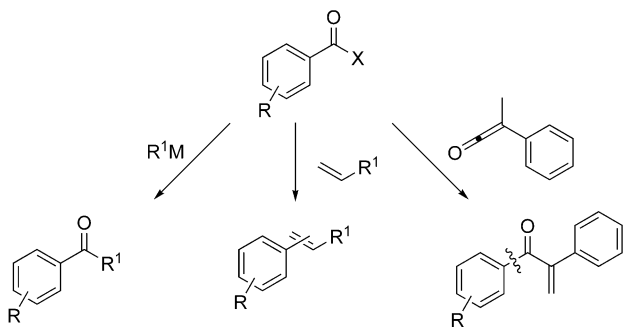
*Arenes and heteroarenes are ubiquitous substructures in biologically active agents and new materials. Thus, functionalization ("refinement") of simple arene precursors is still of major importance for preparative organic chemistry. During the last 20 years, especially transition-metal-catalyzed cross-coupling reactions of aryl halides and triflates have given arene chemistry new impetus. The first industrial applications were realized a few years ago. Quite recently, carbonic acid derivatives such as anhydrides and esters have added to the scope of substrates for these coupling reactions. Some recent developments in this area are presented in this Minireview.*

## 1. Introduction

Palladium-catalyzed coupling reactions allow a number of elegant derivatizations of aryl halides and similar aryl-X compounds.[1] Although these reactions have been known since the 1970s, there are currently only few examples of the industrial application of these reactions.[2] However, based on a considerable improvement of the catalyst systems since the mid 1990s, the prospects for this type of coupling chemistry in industry are much better today. Especially because of the high costs of palladium, the first applications were in the syntheses of relatively expensive drugs and fine chemicals.[2] A number of catalyst systems are now available that allow reactions of (in most cases) the most economical and readily available aryl halides, that is, the aryl chlorides, with high turnover numbers.[3] Other disadvantages have to be accepted to gain high catalytic activity and productivity: highly active catalysts are often based on costly and air-sensitive phosphane ligands. Furthermore, additives (e.g., cesium salts) are essential in many cases; these additives as well as the processing and disposal of their waste products come at a high price. Besides the development of new catalyst systems (e.g., catalysts that are based on N-heterocyclic carbenes[4] as ligands instead of phosphanes and that require simple or no additives), the search for novel substrates for the cross-coupling reactions has been the focus of much attention. The development of such substrates is covered in this Minireview. Functionalization reactions of arenes by C–H activation will not be discussed, as important progress in this area has already been summarized.[5]

## 2. Carbonic Acids, Anhydrides, and Esters

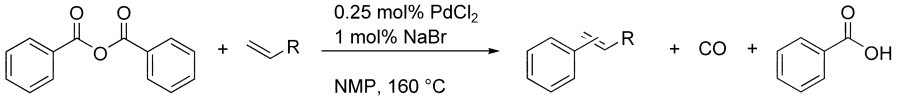
Carbonic acid chlorides are highly reactive species. It was shown in the 1970s for the first time that they also react with palladium(0) species and can therefore be employed in coupling reactions (Scheme 1).[6] The carbonyl group is either retained in the products (e.g. in cross-coupling reactions with organotin compounds as demonstrated by Stille and coworkers[7a]) or it is eliminated as carbon monoxide after



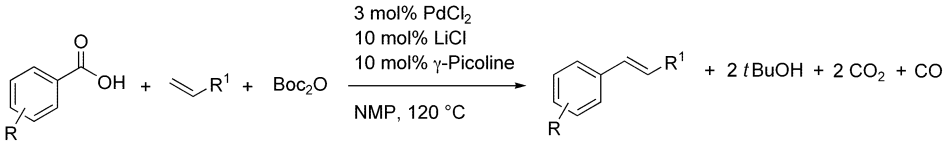

***Scheme 1.*** Palladium-catalyzed coupling reactions of aryl carbonic acid derivatives (for X = Cl, see references [6–8]). M = $SnR^2_3$, $BR^2_2$, ZnX, Cu, $AlR^1_2$, $PbR^1_3$, $SiR^1_3$.

[*] Dr. A. Zapf
Leibniz-Institut für Organische Katalyse
an der Universität Rostock e.V. (IfOK)
Buchbinderstrasse 5–6, 18055 Rostock (Germany)
Fax: (+49) 381-46693-24
E-mail: alexander.zapf@ifok.uni-rostock.de

 © 2003 Wiley-VCH Verlag GmbH & Co. KGaA, Weinheim DOI: 10.1002/anie.200301681 




(1)




(2)

oxidative addition of the acid chloride to $Pd^0$. The acyl–$Pd^{II}$ complex formed initially gives the corresponding aryl–$Pd^{II}$ complex, which undergoes aryl-X coupling reactions. Accordingly, Blaser and Spencer showed that olefins can be arylated with aryl carbonic acid chlorides in a Heck-type reaction (Blaser–Heck reaction).[7b]

It has also been known since the 1970s that nickel(0) can insert into the C–O bond of carbonic acid anhydrides[9] and esters.[10] Although the basis for new coupling reactions was laid early, it took about 20 years before it was demonstrated that palladium(0) also inserts into anhydride and ester groups[11] and that the resulting acyl complexes are suited for coupling reactions.[12] Stephan, de Vries et al. first described the use of aromatic carbonic acid anhydrides instead of aryl halides in the Heck reaction in 1998.[13] Under conditions similar to those for classical Heck reactions, arylated olefins were obtained in good yields in most cases [Eq. (1); NMP = *N*-methyl-2-pyrrolidone].

This protocol has some advantages over the Heck reaction of aryl halides: no large amounts of waste salts are generated, stoichiometric amounts of base to neutralize the liberated acid are unnecessary, and the addition of phosphane ligands for activation or at least stabilization of the palladium catalyst is not required (in fact, they are even detrimental!). The role of the phosphane ligands is played by sodium bromide, which must be added in catalytic amounts; evidently, bromine–palladium complexes are involved in the reaction. Carbon monoxide, which is released by the coupling reaction, is harmless on a laboratory scale and can easily be burned to carbon dioxide in industrial processes. The carbonic acid that is generated concomitantly can be reconverted into its anhydride, so that the overall reaction produces comparatively little waste.



*Alexander Zapf was born in Coburg, Germany, in 1970 and studied chemistry at the Technische Universität München. He completed his PhD in 1998 in the group of M. Beller on the topic of palladium-catalyzed cross-coupling reactions of aryl chlorides. He then joined the Leibniz-Institut für Organische Katalyse an der Universität Rostock e.V. (IfOK), where he is in charge of the "Aryl-X Activation" group. He was a fellow of the Studienstiftung des deutschen Volkes and the Max-Buchner-Forschungsstiftung.*

Investigations into the oxidative addition of benzoic acid to $Pd^0$–phosphane complexes have shown that the resulting acyl–$Pd^{II}$ complexes are comparatively stable and have barely any tendency to undergo CO elimination.[14] Under conditions of decarbonylative Heck reaction (phosphane-free, but halide-containing reaction mixture),[13,15–18] however, CO is eliminated quickly—the formation of vinyl ketones resulting from the insertion of the olefin into the acyl–Pd instead of into the aryl–Pd bond has never been observed.

In the following years, several variants of this first palladium-catalyzed coupling of carbonic acid anhydrides were described. Ionic liquids can be used instead of NMP as solvent, although a decrease in catalytic activity and productivity is observed.[15] Shmidt and Smirnov observed that the use of lithium chloride instead of sodium bromide increases catalyst activity and productivity, as chloride accelerates CO elimination from the oxidative addition product more than bromide does.[16]

A significant drawback of the olefination reaction with anhydrides compared to the classical Heck reaction is that few substituted aryl carbonic acid anhydrides are commercially available. Gooßen et al. reported a significant improvement of this method: They found conditions that allow the coupling of free aryl and heteroaryl carbonic acids.[17] In the presence of $Boc_2O$, the free acids are converted in situ into the corresponding mixed anhydrides, which can be coupled with olefins [Eq. (2)].

Besides carbon monoxide and carbon dioxide, only *tert*-butanol is formed as waste product. Again, the addition of lithium chloride is required to enhance CO elimination and ligands must be added to stabilize the catalyst. Whereas phosphanes reduce the activity of the system significantly, amines (especially γ-picoline) lead to active and comparatively productive catalysts. Besides extension of the substrate scope, activation of carbonic acids in situ has the advantage that all the applied acid equivalents are available for coupling, that is, half does not function as a leaving group, which would then either have to be discarded or reconverted into its anhydride.

The same result, although in a different way, was obtained by Myers and co-workers, who described the coupling of free aryl carbonic acids with styrene or α,β-unsaturated carbonyl compounds.[19] Under their conditions, $Pd^0$ is not inserted into an activated C–O bond, but $CO_2$ is eliminated from a $Pd^{II}$–carboxylate complex to give an aryl–$Pd^{II}$ complex, which is required for the coupling reaction. After olefin insertion, β-

 © 2003 Wiley-VCH Verlag GmbH & Co. KGaA, Weinheim 

hydride elimination and reductive elimination, a $Pd^0$ species results which must be reoxidized to $Pd^{II}$ for the next catalytic cycle with stoichiometric amounts of an oxidant (e.g., silver carbonate). A further drawback of this interesting protocol is the high catalyst concentration required (20 mol%).

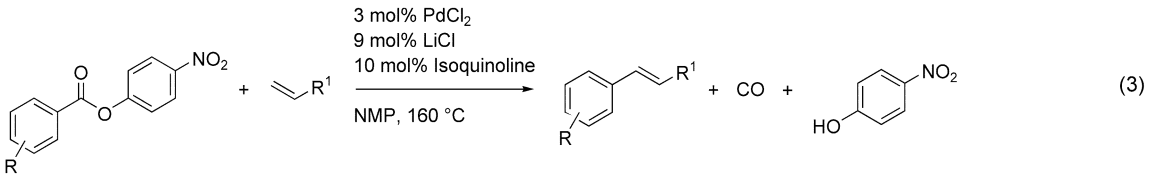
Activation of C–O bonds of carbonic acids for oxidative addition to $Pd^0$ can be realized not only by the formation of anhydrides but also by esterification [Eq. (3)]. If electron-deficient phenols are employed as the alcohol-derived portion of the esters (*p*-nitrophenol and pentafluorophenol are suited best), the coupling reaction with olefins occurs under conditions similar to those for mixed anhydrides formed in situ (see [Eq. (2)]).[18] The liberated phenol can be acylated again, so that only carbon monoxide is released as stoichiometric side product.

Activated carbonic acids can be used not only in Heck-type reactions, but also in coupling reactions with other types of nucleophiles. In contrast to olefination reactions under CO elimination, the carbonyl group is retained in the products. The palladium-catalyzed coupling of trifluoroacetic anhydride with aryl tri-*n*-butylstannane to yield trifluoromethyl ketones was already described in 1995.[20] However, this Stille-type reaction was developed further. On the other hand the Suzuki-analogous coupling with aryl or alkyl boronic acids was elaborated to a widely applicable method by the groups of Gooßen and Yamamoto. The first coupling reactions with aryl boronic acids led to the syntheses of trifluoromethyl ketones.[21] Phenyl trifluoroacetate was treated with various aryl boronic acids in the presence of palladium(II) acetate and tri-*n*-butylphosphane under comparatively mild conditions [Eq. (4)].

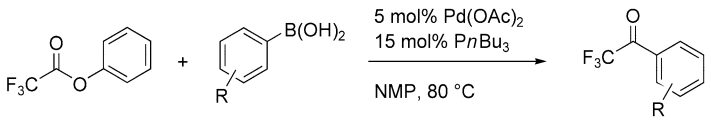
For the coupling of more-electron-rich, nonfluorinated carbonic acids, activation by esterification with simple alcohols is not sufficient. In this case, more-reactive anhydrides have to be applied. Accordingly, substituted benzoic anhydrides react smoothly with aryl boronic acids to give the corresponding unsymmetrical diaryl ketones.[22,23] $[Pd(PPh_3)_4]$ is a good catalyst in refluxing THF or dioxane at 80 °C,[23] but, depending on the steric and electronic properties of the anhydrides, other phosphanes such as tris(*p*-methoxyphenyl)-phosphane or tricyclohexylphosphane lead to improved results.[22] Aliphatic carbonic anhydrides (e.g., acetic anhydride) can also be coupled smoothly, but sterically congested substrates such as pivalic anhydride hardly react. Mixed anhydrides of pivalic acid and different aryl carbonic acids therefore react with $Pd^0$ to give aryl carbonyl–$Pd^{II}$–pivaloate complexes selectively, so that activation of free benzoic acids in situ with pivalic anhydride is possible [Eq. (5)].[22,24] Under these conditions, the addition of a small amount of water was found to enhance the reaction rate strongly.

The use of pivalic anhydride for carbonic acid activation sometimes makes the isolation of the coupling products more difficult, because 2 equivalents of pivalic acid are formed in the reaction. An activating agent that leaves just readily separable residues would thus be of some advantage. Di-(*N*-succinimidyl) carbonate[25a] as well as dimethyl dicarbonate[24,25b,26] fulfill this requirement. The former coupling reagent is successful in the presence of electron-rich trialkyl phosphanes and a base such as sodium carbonate. By activating the acid, carbon dioxide and *N*-hydroxysuccinimide are generated and can be removed simply by washing with water. Coupling reactions with dimethyl dicarbonate are best performed in the presence of tris(*p*-methoxyphenyl)phosphane and small amounts of water at 20–50 °C.[25b] In the absence of water, reaction temperatures of 80 °C are required to ensure efficient coupling.[24,26] Besides carbon dioxide, methanol is formed as a by-product, but does not disrupt the workup of the reaction.

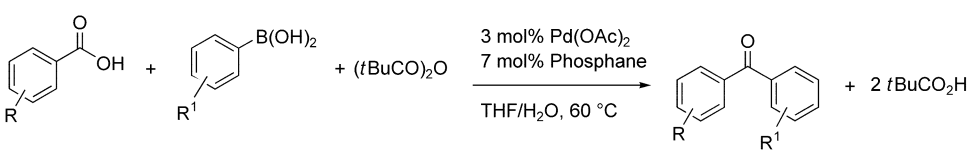
Benzoic acid can also be coupled with phenylacetylene under similar reaction conditions to yield the corresponding alkynyl ketone.[24,26] So far, only this single example of a Sonogashira-type reaction has been described, but more should follow.




(3)




(4)




(5)

 © 2003 Wiley-VCH Verlag GmbH & Co. KGaA, Weinheim 

### 3. Sulfonium Salts, Thiol Esters, and Thioethers

A new type of coupling reagent for palladium-catalyzed reactions was developed by Liebeskind and co-workers towards the end of the 1990s:[27] They employ various organosulfur compounds, and thiols or thioethers act as leaving groups. As sulfur in low oxidation states generally coordinates well to palladium and thus blocks free coordination sites, the corresponding sulfur compounds must be trapped or their complexation ability restricted to enable palladium-catalyzed coupling reactions. Initially this was accomplished by using sulfonium salts. For instance, *S*-aryl and *S*-heteroaryl tetramethylenesulfonium hexafluorophosphates were coupled with aryl or heteroaryl boronic acids under mild conditions [Eq. (6), 40 °C in ethanol or THF/water].[28] [Pd(dppf)$Cl_2$] was used as catalyst and potassium carbonate monohydrate as base. Tetrahydrothiophene, which is released during the coupling reaction, does not poison the palladium catalyst, in contrast to thiols.

Further investigations have shown that the leaving group does not have to be preformed within the substrate. Thiol esters of 4-iodobutylthiol can also be coupled with aryl boronic acids to yield diaryl ketones. It is assumed that cyclization of the iodoalkyl thiolate does not occur before insertion of the Pd catalyst into the carbonyl C–S bond to form an acyl–Pd$^{II}$–thiolate complex.[29] In this way, the thiolate is removed from the catalyst and allows the aryl group of the boronic acid to be transferred to the palladium center.

For coupling reactions with organozinc reagents, alkyl thiol esters do not require any masking. Zinc(II) compounds simultaneously act as trapping agents for thiolates because of their high thiophilicity. Thus, ethanethiol esters of substituted benzoic acids (as well as of aliphatic carbonic acids), for instance, can be coupled with ethylzinc iodide to give the corresponding propiophenone derivatives [Eq. (7)].[30] As the reactions proceed even at room temperature, functional groups such as aldehydes and esters remain unchanged. Methylthioheterocycles can also be alkylated in this way.[31]

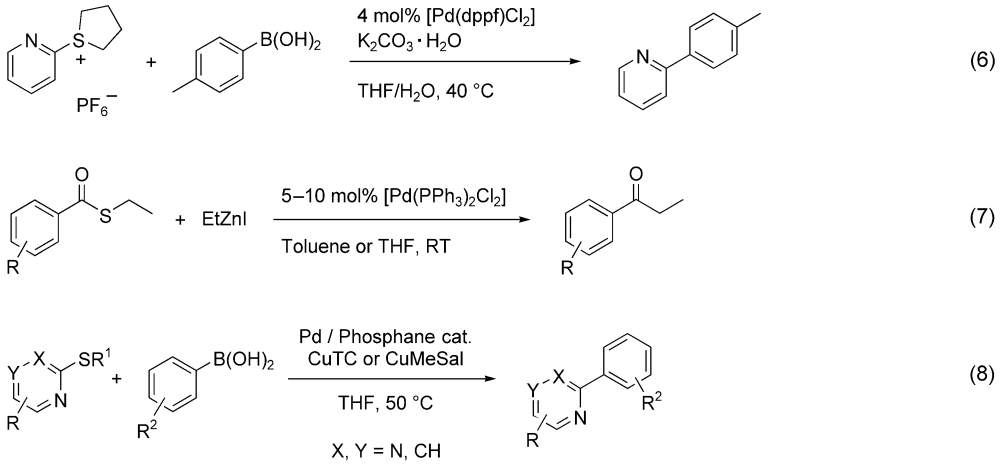
For the coupling reactions of aryl boronic acids with thiol esters or heteroaryl thioethers, a new method was found that avoids blocking of the Pd catalyst: The leaving thiolate is removed from the catalyst by complexation to copper(I).[32] However, an excess amount of a suitable copper salt has to be added, which makes the reaction less attractive from both an economical and ecological point of view. On the other hand, the substrate scope tolerated by this "external" masking is much larger than that of the "internal" masking through alkylation of the leaving group. Accordingly, simple thiol esters of aryl carbonic acids can be coupled with aryl boronic acids in good yields in the presence of 1.6 equivalents of copper(I) thiophene-2-carboxylate (CuTC).[33] Alkylthio-substituted heterocycles can be arylated with the same catalyst system[34a] or by utilizing copper(I) 3-methylsalicylate (CuMeSal)[34b] [Eq. (8)]. However, this reaction is thus far limited to various π-electron-deficient heterocycles such as pyridines, pyrazines, and benzothiazoles.

The analogous coupling of heteroaryl thioethers with aryl or vinyl stannanes was described very recently.[35] Again, only π-electron-deficient heterocycles can be converted in this reaction. Nevertheless, some progress has been reported: A stoichiometric amount of a simple cocatalyst, copper(I) bromide, can be used in this Stille-type coupling instead of the copper complexes.[35b]

### 4. Summary and Outlook

The introduction of aryl carbonic acid derivatives for palladium-catalyzed coupling reactions has significantly broadened the substrate scope of these reactions. These new substrates are interesting alternatives to aryl halides under conditions that lead to the elimination of carbon monoxide. If the carbonyl group is preserved in the product, this new method for the synthesis of ketones is even superior to the carbonylation cross-coupling sequence with haloarenes or the coupling of highly reactive acid chlorides. However, the accessibility of substituted aryl carbonic acids will be the limiting factor in most cases.

In terms of atom economy, the novel coupling reactions do not have significant general advantages over the old ones. Stoichiometric amounts of base are often consumed in coupling reactions with aryl halides. However, the halide released in the coupling reaction can be reused for the synthesis of haloarenes after oxidation (bromide, iodide) or it




 © 2003 Wiley-VCH Verlag GmbH & Co. KGaA, Weinheim 

can be disposed economically (chloride). The coupling of carbonic acids does produce relatively small amounts of waste, but the synthesis of the carbonic acids themselves often generates stoichiometric amounts of salts as by-products.

The "old" reactions have at least one important advantage: They have reached the stage at which the catalyst productivities are suitable for many industrial applications. In most cases, the new reactions still have to be improved significantly towards this goal. The coupling reactions of thio-substituted (hetero)arenes is of great interest for researchers, especially as a method to avoid deactivation of the catalyst, but are most likely to remain laboratory methods for the derivatization of special substrates. The functionalization of aryl fluorides, one of the last great challenges in the area of coupling reactions with haloarenes, is also more of academic interest. First such successful reactions were described recently.[36]

The opinion that "arene chemistry is dead" has been quite common at universities during the last decades. The work on transition-metal-catalyzed coupling reactions shows, however, that this field of research is alive and well and still holds much potential.

Received: July 11, 2003 [M1681]

[1] a) *Transition Metals for Organic Synthesis* (Eds.: M. Beller, C. Bolm), Wiley-VCH, Weinheim, **1998**; b) *Metal-catalyzed Cross-coupling Reactions* (Eds.: F. Diederich, P. J. Stang), Wiley-VCH, Weinheim, **1998**.

[2] a) A. Zapf, M. Beller, *Top. Catal.* **2002**, *19*, 101 – 109; b) M. Beller, A. Zapf in *Handbook of Organopalladium Chemistry for Organic Synthesis, Vol. 1* (Ed.: E.-i. Negishi), Wiley, New York, **2002**, pp. 1209 – 1222; c) J. G. de Vries, *Can. J. Chem.* **2001**, *79*, 1086 – 1092.

[3] a) L. Botella, C. Nájera, *Angew. Chem.* **2002**, *114*, 187 – 189; *Angew. Chem. Int. Ed.* **2002**, *41*, 179 – 181; b) N. Kataoka, Q. Shelby, J. P. Stambuli, J. F. Hartwig, *J. Org. Chem.* **2002**, *67*, 5553 – 5566; c) A. Zapf, A. Ehrentraut, M. Beller, *Angew. Chem.* **2000**, *112*, 4315 – 4317; *Angew. Chem. Int. Ed.* **2000**, *39*, 4153 – 4155; d) R. B. Bedford, S. M. Draper, P. N. Scully, S. L. Welch, *New J. Chem.* **2000**, *24*, 745 – 747; e) J. P. Wolfe, S. L. Buchwald, *Angew. Chem.* **1999**, *111*, 2570 – 2573; *Angew. Chem. Int. Ed.* **1999**, *38*, 2413 – 2416; f) M. Beller, H. Fischer, W. A. Herrmann, K. Öfele, C. Broßmer, *Angew. Chem.* **1995**, *107*, 1992 – 1993; *Angew. Chem. Int. Ed. Engl.* **1995**, *34*, 1848 – 1849.

[4] W. A. Herrmann, *Angew. Chem.* **2002**, *114*, 1342 – 1363; *Angew. Chem. Int. Ed.* **2002**, *41*, 1290 – 1309.

[5] G. Dyker, *Angew. Chem.* **1999**, *111*, 1808 – 1822; *Angew. Chem. Int. Ed.* **1999**, *38*, 1699 – 1712.

[6] Review: R. K. Dieter, *Tetrahedron* **1999**, *55*, 4177 – 4236.

[7] a) J. W. Labadie, D. Tueting, J. K. Stille, *J. Org. Chem.* **1983**, *48*, 4634 – 4642; b) H.-U. Blaser, A. Spencer, *J. Organomet. Chem.* **1982**, *233*, 267 – 274.

[8] T.-a. Mitsudo, M. Kadokura, Y. Watanabe, *J. Org. Chem.* **1987**, *52*, 3186 – 3192.

[9] a) B. M. Trost, F. Chen, *Tetrahedron Lett.* **1971**, 2603 – 2607; b) H.-F. Klein, H. H. Karsch, *Chem. Ber.* **1976**, *109*, 2515 – 2523; c) E. Uhlig, G. Fehske, B. Nestler, *Z. Anorg. Allg. Chem.* **1980**, *465*, 141 – 146; d) S. Komiya, A. Yamamoto, T. Yamamoto, *Chem. Lett.* **1981**, 193 – 196; e) K. Sano, T. Yamamoto, A. Yamamoto, *Chem. Lett.* **1983**, 115 – 118.

[10] a) J. Ishizu, T. Yamamoto, A. Yamamoto, *Chem. Lett.* **1976**, 1091 – 1094; b) T. Yamamoto, J. Ishizu, T. Kohara, S. Komiya, A. Yamamoto, *J. Am. Chem. Soc.* **1980**, *102*, 3758 – 3764.

[11] a) K. Nagayama, F. Kawataka, M. Sakamoto, I. Shimizu, A. Yamamoto, *Chem. Lett.* **1995**, 367 – 368; b) K. Nagayama, I. Shimizu, A. Yamamoto, *Bull. Chem. Soc. Jpn.* **1999**, *72*, 799 – 803.

[12] The coupling of pyridylzinc halides with benzoic anhydride in the presence of $[Pd(PPh_3)_4]$ to yield phenyl pyridyl ketones could be the first published coupling reaction of an anhydride. However, the authors did not compare the results with a Pd-free system, and the yields were $< 40\,\%$: T. Sakamoto, Y. Kondo, N. Murata, H. Yamanaka, *Tetrahedron* **1993**, *49*, 9713 – 9720.

[13] a) M. S. Stephan, A. J. J. M. Teunissen, G. K. M. Verzijl, J. G. de Vries, *Angew. Chem.* **1998**, *110*, 688 – 690; *Angew. Chem. Int. Ed.* **1998**, *37*, 662 – 664; b) "*Catalysis of Organic Reactions*": M. S. Stephan, J. G. de Vries, *Chem. Ind.* **2001**, *82*, 379 – 390.

[14] a) A. Jutand, S. Négri, J. G. de Vries, *Eur. J. Inorg. Chem.* **2002**, 1711 – 1717; b) V. V. Grushin, H. Alper, *J. Am. Chem. Soc.* **1995**, *117*, 4305 – 4315.

[15] A. J. Carmichael, M. J. Earle, J. D. Holbrey, P. B. McCormac, K. R. Seddon, *Org. Lett.* **1999**, *1*, 997 – 1000.

[16] a) A. F. Shmidt, V. V. Smirnov, *Kinet. Catal.* **2000**, *41*, 743 – 744; b) A. F. Shmidt, V. V. Smirnov, *Kinet. Catal.* **2002**, *43*, 195 – 198.

[17] L. J. Gooßen, J. Paetzold, L. Winkel, *Synlett* **2002**, 1721 – 1723.

[18] L. J. Gooßen, J. Paetzold, *Angew. Chem.* **2002**, *114*, 1285 – 1289; *Angew. Chem. Int. Ed.* **2002**, *41*, 1237 – 1241.

[19] A. G. Myers, D. Tanaka, M. R. Mannion, *J. Am. Chem. Soc.* **2002**, *124*, 11250 – 11251.

[20] J. W. Guiles, *Synlett* **1995**, 165 – 166.

[21] R. Kakino, S. Shimizu, A. Yamamoto, *Bull. Chem. Soc. Jpn.* **2001**, *74*, 371 – 376.

[22] a) L. J. Gooßen, K. Gosh, *Angew. Chem.* **2001**, *113*, 3566 – 3568; *Angew. Chem. Int. Ed.* **2001**, *40*, 3458 – 3460; b) L. J. Gooßen, K. Gosh, *Eur. J. Org. Chem.* **2002**, 3254 – 3267.

[23] R. Kakino, S. Yasumi, I. Shimizu, A. Yamamoto, *Bull. Chem. Soc. Jpn.* **2002**, *75*, 137 – 148.

[24] R. Kakino, H. Narahashi, I. Shimizu, A. Yamamoto, *Bull. Chem. Soc. Jpn.* **2002**, *75*, 1333 – 1345.

[25] a) L. J. Gooßen, K. Gosh, *Chem. Commun.* **2001**, 2084 – 2085; b) L. J. Gooßen, L. Winkel, A. Döhring, K. Gosh, J. Paetzold, *Synlett* **2002**, 1237 – 1240.

[26] R. Kakino, H. Narahashi, I. Shimizu, A. Yamamoto, *Chem. Lett.* **2001**, 1242 – 1243.

[27] The coupling of allyl sulfides with Ni or Pd catalysts has already been known for some time: H. Okamura, J. Takei, *Tetrahedron Lett.* **1979**, 3425 – 3428.

[28] J. Srogl, G. D. Allred, L. S. Liebeskind, *J. Am. Chem. Soc.* **1997**, *119*, 12376 – 12377. *S*-Benzylsulfonium salts are more reactive than the corresponding aryl derivatives and can also be coupled with organotin or -zinc reagents; see: S. Zhang, D. Marshall, L. S. Liebeskind, *J. Org. Chem.* **1999**, *64*, 2796 – 2804.

[29] C. Savarin, J. Srogl, L. S. Liebeskind, *Org. Lett.* **2000**, *2*, 3229 – 3231.

[30] H. Tokuyama, S. Yokoshima, T. Yamashita, T. Fukuyama, *Tetrahedron Lett.* **1998**, *39*, 3189 – 3192.

[31] M. E. Angiolelli, A. L. Casalnuovo, T. P. Selby, *Synlett* **2000**, 905 – 907.

[32] A "simple" coupling of aryl thiol esters with aryl boronic acids has only been described as a side reaction in the Suzuki coupling of acyl thiophenyl bromides: B. Zeysing, C. Gosch, A. Terfort, *Org. Lett.* **2000**, *2*, 1843 – 1845.

[33] L. S. Liebeskind, J. Srogl, *J. Am. Chem. Soc.* **2000**, *122*, 11260 – 11261. In the same way alkynyl thioethers can be coupled to aryl acetylenes (C. Savarin, J. Srogl, L. S. Liebeskind, *Org. Lett.* **2001**, *3*, 91 – 93) as well as methylthiopseudoureas to aryl amidines

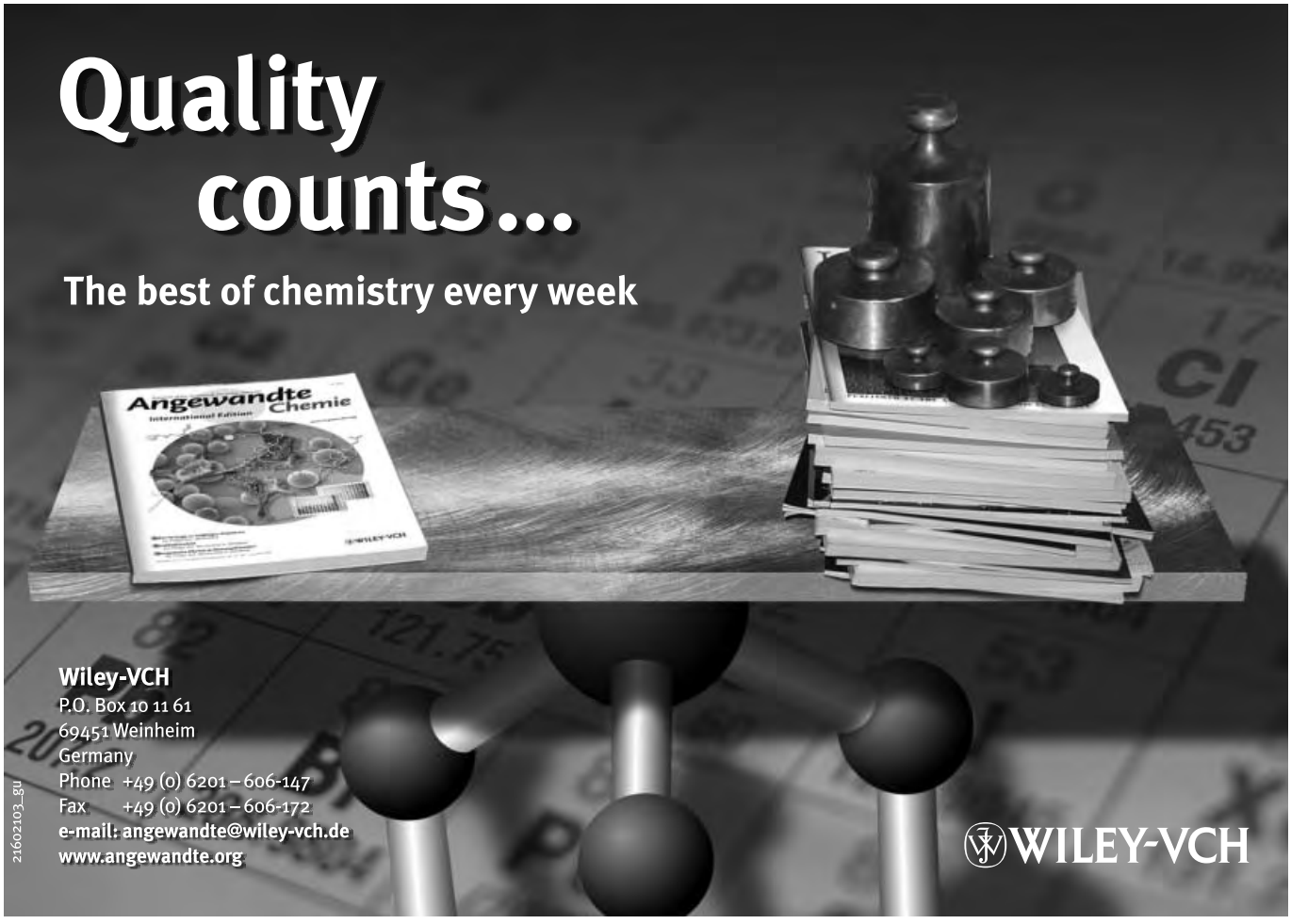
 © 2003 Wiley-VCH Verlag GmbH & Co. KGaA, Weinheim 

(C. L. Kusturin, L. S. Liebeskind, W. L. Neumann, *Org. Lett.* **2002**, *4*, 983 – 985).

[34] a) L. S. Liebeskind, J. Srogl, *Org. Lett.* **2002**, *4*, 979 – 981; b) F.-A. Alphonse, F. Suzenet, A. Keromnes, B. Lebret, G. Guillaumet, *Synlett* **2002**, 447 – 450.

[35] a) M. Egi, L. S. Liebeskind, *Org. Lett.* **2003**, *5*, 801 – 802; b) F.-A. Alphonse, F. Suzenet, A. Keromnes, B. Lebret, G. Guillaumet, *Org. Lett.* **2003**, *5*, 803 – 805.

[36] For the Ni-catalyzed Kumada reaction of aryl fluorides, see: V. P. W. Böhm, C. W. K. Gstöttmayr, T. Weskamp, W. A. Herrmann, *Angew. Chem.* **2001**, *113*, 3500 – 3503; *Angew. Chem. Int. Ed.* **2001**, *40*, 3387 – 3389; for the Kumada reaction of alkyl fluorides, see: J. Terao, A. Ikumi, H. Kuniyasu, N. Kambe, *J. Am. Chem. Soc.* **2003**, *125*, 5646 – 5647; for the Pd-catalyzed coupling of *o*-nitrofluorobenzenes, in which Pd presumably inserts into the C–F bond through an $S_NAr$ mechanism, see: Y. M. Kim, S. Yu, *J. Am. Chem. Soc.* **2003**, *125*, 1696 – 1697.



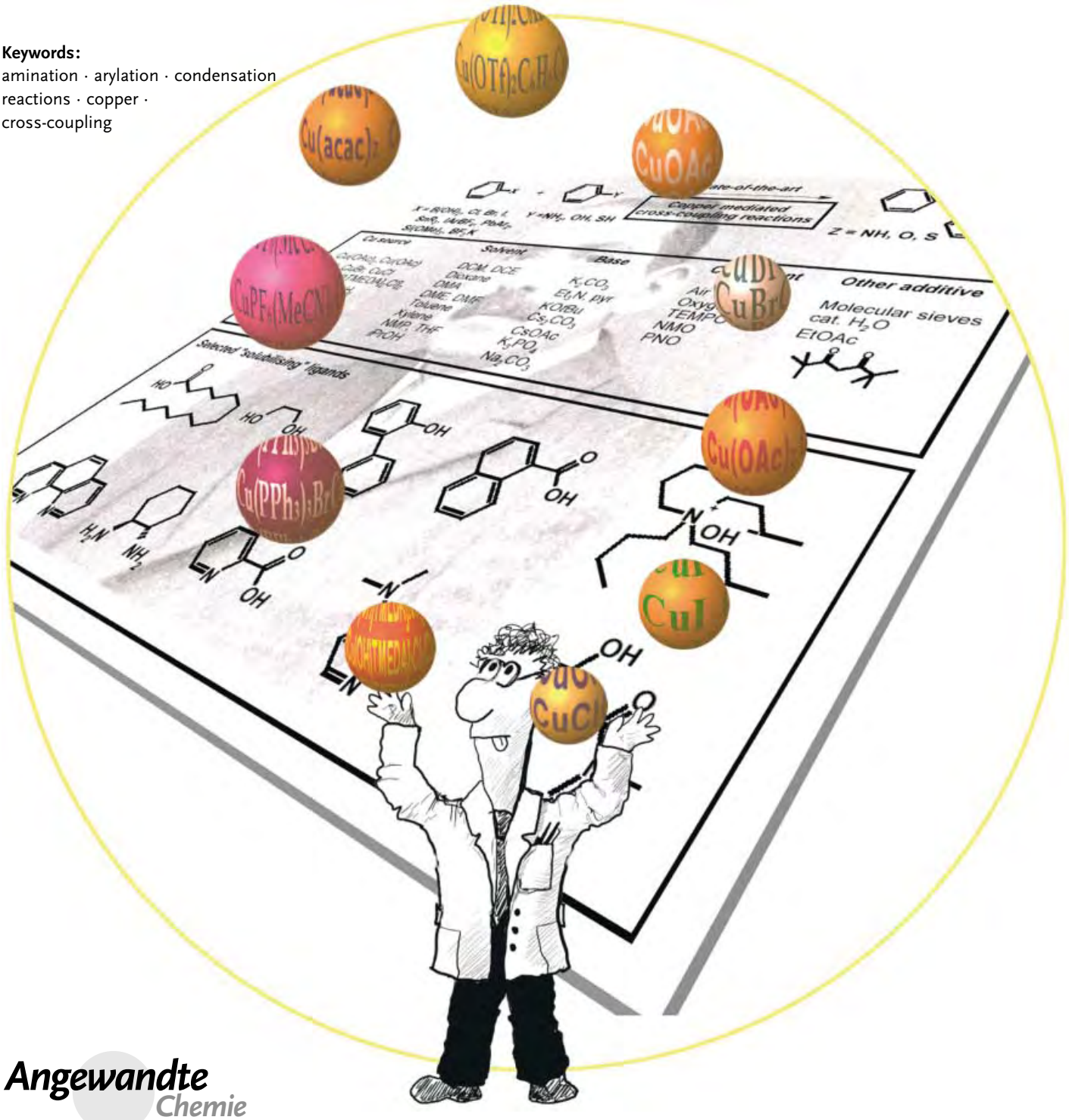

 © 2003 Wiley-VCH Verlag GmbH & Co. KGaA, Weinheim 

Ullmann Condensation

# Modern Synthetic Methods for Copper-Mediated C(aryl)–O, C(aryl)–N, and C(aryl)–S Bond Formation

*Steven V. Ley and Andrew W. Thomas**

**Keywords:**
amination · arylation · condensation reactions · copper · cross-coupling




 © 2003 Wiley-VCH Verlag GmbH & Co. KGaA, Weinheim DOI: 10.1002/anie.200300594 

*The copper-mediated C(aryl)–N, C(aryl)–O, and C(aryl)–S bond formation is an important transformation and has been developed to include a wide range of substrates. This Review highlights the recent developments in the copper-mediated (both stoichiometric and catalytic) reactions of aryl boronic acids, aryl halides, iodonium salts, siloxanes, stannanes, plumbanes, bismuthates, and trifluoroborate salts as aryl donors. In particular, the recent introduction of boronic acids as reaction partners in both* O- *and* N*-arylation has been a significant discovery and will occupy centre-stage in this review. Clear improvements can be obtained by the correct choice of copper source, base, ligands, and other additives. Mechanistic investigations should provide insight into the catalytically active species, which would aid in the development of milder, more-efficient methods.*

## 1. Introduction: The Legacy of the Past[1]

There is high demand for new methods to facilitate the synthesis of diaryl ethers, alkylaryl ethers, diaryl amines, alkylaryl amines, diaryl thioethers, and alkylaryl thioethers owing to their importance as structural motifs in a wide range of molecules with numerous and important applications. The classical copper-mediated Ullmann reaction (Figure 1) has



***Figure 1.*** Fritz Ullmann, 1875–1939. Reproduced courtesy of the Library and Information Centre, Royal Society of Chemistry, from *Helv. Chim. Acta* **1939**, *23*, 94–100.

underpinned the research community when functionalities of these sorts are required. However, the harsh reaction conditions (high temperatures, strong bases, stoichiometric amounts of copper or copper salts, long reaction times) needed to effect these transformations, usually only in moderate yields, led to severe limitations in the general use of this reaction, especially on a large scale. Notable advances in the use of ultrasound[2] and use of alternative bases[3] required for the transformation have been reported, however these have not resulted in widespread popularity or use. Furthermore, activation of the aryl halide with a nitro group[4] or a triazene[5] has proven to be a valid method for diaryl ether synthesis with "copper phenoxides". However, removal of the

### From the Contents

1. Introduction: The Legacy of the Past[1] 5401

2. Boronic Acids as the Aryl Donor: A Long-Standing Problem Has Been Solved[13] 5404

3. Aryl Halides as the Aryl donor: C(aryl)–N Bond Formation 5418

4. Aryl Halides as the Aryl Donor: C(aryl)–O Bond Formation 5431

5. Aryl Halides as the Aryl Donor: C(aryl)–S Bond Formation 5434

6. Aryl Siloxanes as the Aryl Donor: C(aryl)–Heteroatom Bond Formation 5436

7. Aryl Stannanes as the Aryl Donor: C(aryl)–Heteroatom Bond Formation 5437

8. Iodonium Salts as the Aryl Donor: C(aryl)–Heteroatom Bond Formation 5438

9. Aryl Lead(IV) Triacetates as the Aryl Donor: C(aryl)–Heteroatom Bond Formation 5439

10. Pentavalent Organobismuth Reagents as the Aryl Donor: C(aryl)–Heteroatom Bond Formation 5439

11. Pentavalent Organotrifluoroborate Reagents as the Aryl Donor: C(aryl)–N Bond Formation 5441

12. Mechanistic Considerations for the Copper-Mediated Heteroatom-Arylation Reaction 5442

13. Summary and Outlook 5445

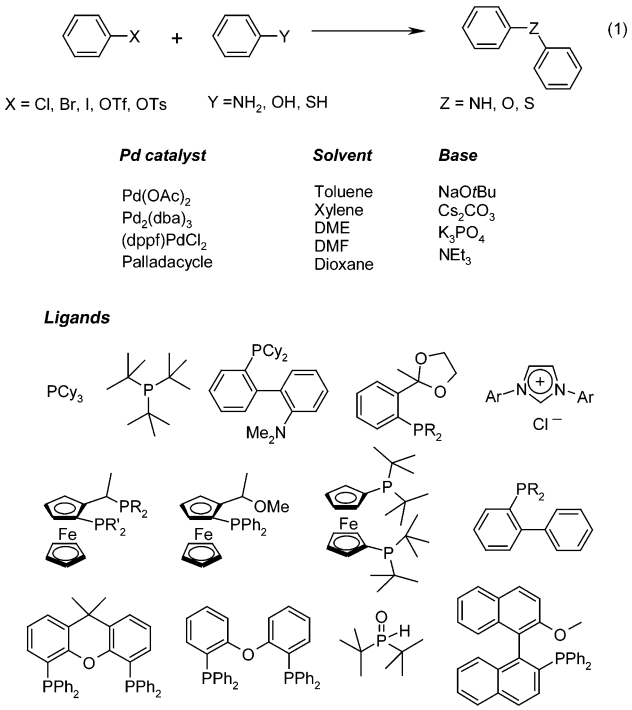
[*] Dr. A. W. Thomas
F. Hoffmann-La Roche AG
Pharmaceutical Research, Discovery Chemistry
4070 Basel (Switzerland)
Fax: (+41) 61-688-8714
E-mail: andrew.thomas@roche.com

Prof. Dr. S. V. Ley
Department of Chemistry, University of Cambridge
Lensfield Road, Cambridge CB2 1EW (England)

 DOI: 10.1002/anie.200300594 © 2003 Wiley-VCH Verlag GmbH & Co. KGaA, Weinheim 

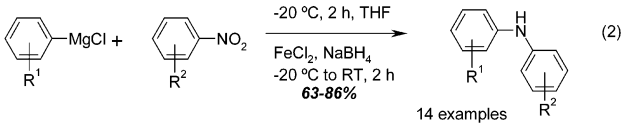
activating group by additional reaction steps renders these methods less efficient.

Current direct routes to form diaryl ethers, alkylaryl ethers, diaryl amines, alkylaryl amines, diaryl thioethers, and alkylaryl thioethers are, not surprisingly, mainly based on palladium-catalyzed reactions [Eq. (1)]. An extensive toolbox




of reaction variables allows the synthetic chemist to prepare a vast array of desired products in an efficient and practical manner, and a recent survey of palladium-mediated arylations using soft, non-organometallic nucleophiles has been compiled.[6]

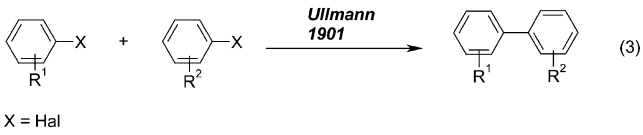
An interesting, novel, practical method for the synthesis of polyfunctionalized diaryl amines from the reaction of nitroarenes and functionalized aryl magnesium reagents (formed through Mg–halogen exchange from the corresponding aryl iodides or bromides with *i*PrMgCl) and has been developed by Knochel and Sapountzis [Eq. (2)].[7] Owing, in




part, to the recent emergence of this method, these reaction conditions are currently underdeveloped but do show great promise as a complementary route to prepare a range of diaryl amines, and interesting improvements are anticipated.

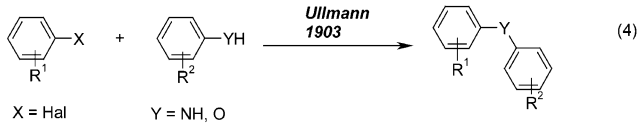
### 1.1. The Copper-Mediated Arylation Reaction Revisited: Reaction Nomenclature

Ullmann Reaction (synthesis of biaryl compounds): The formation of a C–C bond between two aryl units, which originate from two aryl halides, mediated by a copper species, although the transformation can be performed with various transition metals [Eq. (3)]. This transformation has recently




been reviewed in detail.[8] In this Review we associate Ullmann's name mainly with the synthesis of diaryl ethers and diaryl amines.

Ullmann Condensation Reaction (synthesis of diaryl ethers, diaryl amines, or diaryl thioethers): The formation of a C(aryl)–O, a C(aryl)–N, or a C(aryl)–S bond by the reaction of an aryl halide with a phenol, an aniline, or a thiophenol, respectively, mediated (originally catalytic) by a copper species [Eq. (4)].




Goldberg-Modified Ullmann Condensation Reaction: The copper-mediated (originally catalytic) formation of a C(aryl)–N bond after the reaction between an amide and an aryl halide [Eq. (5)].

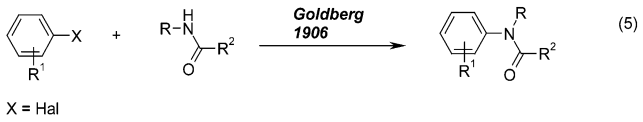


*Andrew Thomas earned his PhD under the guidance of Dr. R. Alan Aitken at the University of St. Andrews as a St. Leonard's College Fellow. He then spent two years as a postdoctoral student with Professor Steve V. Ley at the University of Cambridge as a Glaxo-Wellcome Research Fellow. In 1991 he moved to "Discovery Chemistry", F. Hoffmann-La Roche AG in Basel, Switzerland, and is currently a group leader and senior scientist in the central nervous system therapy area.*



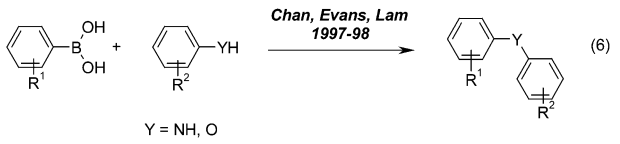
*Steven V. Ley was appointed to the faculty at Imperial College in 1975 and made Head of Department in 1989. In 1992 he was appointed Professor of Organic Chemistry at the University of Cambridge and Fellow of Trinity College. He is Immediate Past President of the RSC and was made a CBE in January 2002. Steve's research involves the discovery and development of new synthetic methods and their application to biologically active systems. His group has reported the synthesis of over 90 target compounds in nearly 500 papers. In recognition of his work, he has been awarded 14 major prizes, most recently the Ernest Guenther Award.*

 © 2003 Wiley-VCH Verlag GmbH & Co. KGaA, Weinheim 



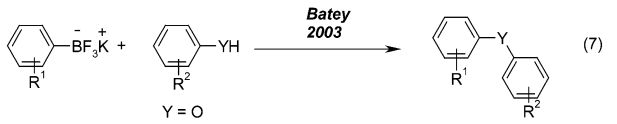

(5)

Chan–Evans–Lam-Modified Ullmann Condensation Reaction: The formation of a C(aryl)–O, a C(aryl)–N, or a C(aryl)–S bond by the reaction of an aryl boronic acid with a phenol, an aniline (or other N nucleophile), or thiophenol, respectively, mediated by a copper species [Eq. (6)].



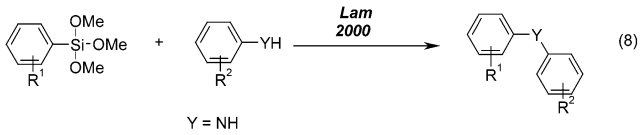

(6)

Batey-Modified Ullmann Condensation Reaction: The formation of a C(aryl)–O bond by the reaction of a phenol with a potassium aryltrifluoroborate mediated by a copper species [Eq. (7)].



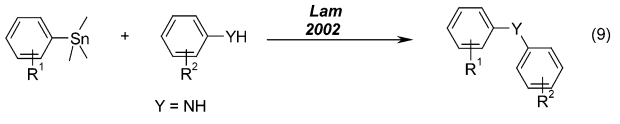

(7)

Lam-Modified Ullmann Condensation Reaction: The formation of a C(aryl)–O, a C(aryl)–N, or a C(aryl)–S bond by the reaction of an aryl siloxane with a phenol, an aniline (or other N nucleophile), or a thiophenol, respectively, mediated by a copper species [Eq. (8)].




(8)

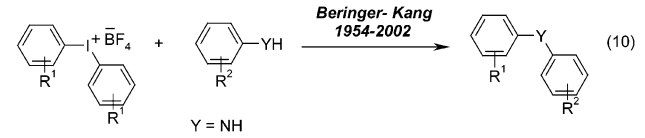
Lam Stannane-Modified Ullmann Condensation Reaction: The formation of a C(aryl)–O, a C(aryl)–N, or a C(aryl)–S bond by the reaction of an aryl stannane with a phenol, an aniline (or other N nucleophile), or a thiophenol, respectively, mediated by a copper species [Eq. (9)].



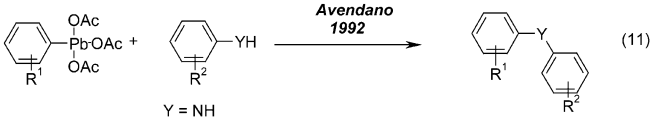

(9)

Beringer–Kang-Modified Ullmann Condensation Reaction: The formation of a C(aryl)–O, a C(aryl)–N, or a C(aryl)–S bond by the reaction of an aryl iodonium salt with a phenol, an aniline (or other N nucleophile), or a thiophenol, respectively, mediated by a copper species [Eq. (10)].

Avendano-Modified Ullmann Condensation Reaction: The formation of a C(aryl)–O, a C(aryl)–N, or a C(aryl)–S bond by the reaction of an aryl lead reagent with a phenol, an aniline (or other N nucleophile), or a thiophenol, respectively, mediated by a copper species [Eq. (11)].

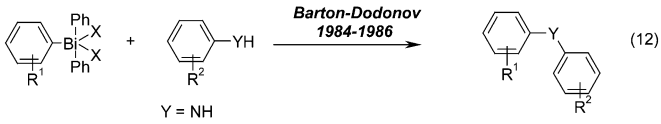



(10)




(11)

Barton-Modified Ullmann Condensation Reaction: The formation of a C(aryl)–O, a C(aryl)–N, or a C(aryl)–S bond by the reaction of an aryl bismuth reagent with a phenol, an aniline (or other N nucleophile), or a thiophenol, respectively, mediated by a copper species [Eq. (12)].




(12)

Cross-Coupling Reactions: The reaction of organometallic reagents with organic electrophiles in the presence of group 8–10 metal catalysts, notably Ni and Pd complexes. This reaction is currently a popular method for a wide range of C–C, C–H, C–N, C–O, C–S, C–P, or C–M bond-forming processes.

Throughout the remainder of this Review we use the same terminology as Sir Derek Barton did in examining advances in the "arylation reaction".[9] Arylation in this context means replacement of an H atom on an heteroatom by an aryl group.

### 1.2. Following in the Footsteps of Success: Palladium-Mediated Strategies

Buchwald and co-workers[10] and Hartwig and co-workers[11] have endeavored to develop "user-friendly" palladium-mediated methods for C(aryl)–O and C(aryl)–N bond formation. This has been a very successful research program, as evidenced by the enormous popularity of these reactions, which has led to a fascinating number of potentially biologically active molecules that incorporate these structural motifs. Indeed, the vast amount of published material available describing a wide range of Pd-catalyzed methods, ligands, solvents, temperatures, and substrates has led to a toolbox of tunable reaction conditions whose scope should allow access to most target molecules that incorporate an aryl amine motif.

These research groups, and others, are continually providing important new advances and insight through iterative development of new catalytic methods, routinely using mechanistic investigations in the design cycle. Fu and co-

 © 2003 Wiley-VCH Verlag GmbH & Co. KGaA, Weinheim 

workers have also contributed significantly and have recently summarized the state of the art of palladium-catalyzed coupling reactions of aryl chlorides.[12]

### 1.3. Organization of this Review

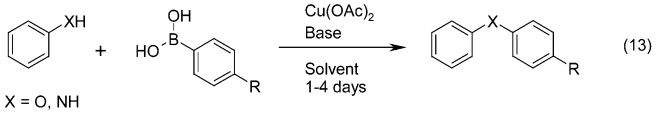
Each section of this Review presents the most recent developments in the formation of C(aryl)–N, C(aryl)–O, and C(aryl)–S bonds. Each section describes a class of aryl donor and is further subclassified by the nature of the two reaction partners, and then further elaborated in the development of the transformation, whether stoichiometric or catalytic in nature. In each section, a survey of the reaction scope is also shown schematically: these "visual tables" can be used as a quick reference guide to search for first-attempt reaction conditions for a planned transformation.

For clarity, in cases in which more than one aryl moiety is present in the product (attached to the same type of heteroatom used in the transformation), the unit that originates from the electrophile is colored in red.

The comprehensive Sections 2 and 3 (boronic acids and aryl halides as aryl donors, respectively) are concluded by drawing specific attention to the state of the art as well as briefly outlining current deficiencies.

## 2. Boronic Acids as the Aryl Donor: "A Long-Standing Problem Has Been Solved"[13]

Independent reports by the groups of Chan,[14] Evans,[15] and Lam[16] in 1998 revolutionized the copper-mediated heteroatom arylation reaction for the formation of C(aryl)–O and C(aryl)–N bonds [Eq. (13)]. In these key contributions, the groups successfully and simply devised new milder methods for the construction of these bonds. This Review describes the discovery and development of the transformation into a practical and reliable method, which can be used either stoichiometrically or catalytically and overcomes some of the deficiencies associated with the classical Ullmann and Goldberg arylation protocols.




(13)

### 2.1. Starting Off: Why Boronic Acids? Why Cupric Acetate?

Chan's previous experiences using triarylbismuth[17] and the quest to introduce new aryl-transfer reagents as the electrophilic reaction partner in heteroatom–aryl bond construction using cupric acetate as a promoter led his group at DuPont to try a new combination of reagents. By replacing the palladium with a copper species (copper acetate) and the use of a boronic acid and a heteroatom donor, they discovered that these new conditions were ideal to effect an Ullmann condensation. At this point, there was little deliberation on the mechanistic rationale for these precise reaction conditions, although the outcome is of considerable importance.

Chan and co-workers[18] first described a collection of *N*- and *O*-arylation transformations under novel reaction conditions as early as in June 1997, but only part of the work was disclosed at this meeting. However in the first publication[14] it was already demonstrated that this method with a boronic acid as the aryl donor was applicable to a wide range of nucleophilic reaction partners, including phenols (C(aryl)–O bonds) and amines, anilines, amides, imides, ureas, carbamates, and sulfonamides (C(aryl)–N bonds). The method quickly attracted interest and Evans and co-workers[15] were quick to exploit the process in an expedient formal synthesis of throxine; they also suggested a speculative mechanism analogous to that proposed by Barton for the amine arylation reaction. In the final of the back-to-back series of papers, Lam, Chan, and co-workers[16] also reported that aromatic heterocycles (imidazoles, pyrazoles, triazoles, tetrazoles, benzimidazoles, and indazoles) participate efficiently in this reaction mediated by copper acetate and using aryl boronic acids as the aryl donor.

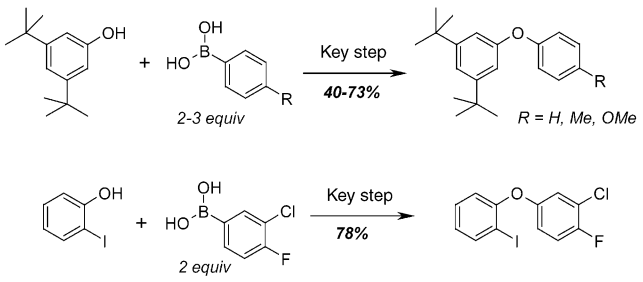
The stage was now set, and the remainder of this section is focused on the development of these preliminary reaction conditions to effect these transformations, charting its emergence from a stoichiometric to a catalytic method. The scope of the reaction was expanded by incorporating different substrates, solvents, reaction temperatures, reaction times, as well as by the introduction of new "nontailored" ligands. These developments led to a potentially powerful new and general methodology for *O*- and *N*-arylation reactions. Efficient *S*-arylation involved overcoming challenges associated with thiol oxidations during the reaction process, and the successful work of Guy and co-workers and Liebeskind and co-workers is discussed in detail (Section 2.4).

### 2.2. Copper-Mediated C(aryl)–O Bond Formation

#### 2.2.1. The Original Discovery: Stoichiometric $Cu^{II}$ Methods

The simultaneous papers by the groups of Chan and Evans are important, as they set the standard for attracting the interest of the synthetic community: Both showed in detail the remarkable simplicity of the new reaction conditions. A mixture of the phenol (1 equiv), aryl boronic acid (2–3 equiv), anhydrous $Cu(OAc)_2$ (1–2 equiv), and $Et_3N$ (2–3 equiv) in dichloromethane were stirred at room temperature for 1–2 days and then the product was isolated in good yield after chromatography (Scheme 1). These reaction conditions have therefore greatly improved the standard classic reaction protocols for the formation of diaryl ethers. Although Chan and co-workers described only four examples of the unoptimized synthesis of trisubstituted unsymmetrical diaryl ethers using only two phenolic substrates, they both underwent efficient cross-coupling with electronic-rich, electron-deficient, and *ortho*-substituted boronic acids. In these first examples, only $Et_3N$ was used as the tertiary base along with either 1 or 2 equivalents of cupric acetate.

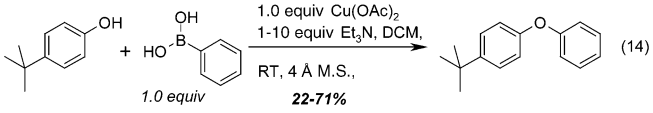
 © 2003 Wiley-VCH Verlag GmbH & Co. KGaA, Weinheim 




***Scheme 1.*** Key step: $Cu(OAc)_2$ (1–2 equiv), $Et_3N$, $CH_2Cl_2$, room temperature.

### 2.2.2. *Molecular Sieves as Water Scavengers*

Evans and co-workers, on the other hand, who used the method to great effect for the synthesis of diaryl ether functionalities present in multifunctionalized macrocycles, further evaluated the scope and limitations of the new stoichiometric copper-mediated procedure (Table 1, [Eq. (14)]).




(14)

***Table 1:*** Reaction conditions for the *O*-arylation of phenols with aryl boronic acids [Eq. (14)].

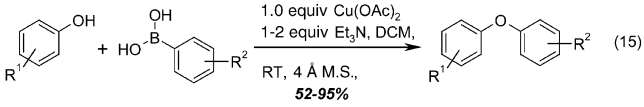
| Atmosphere | $Et_3N$ [equiv] | $Cu(OAc)_2$ [equiv] | Yield [%] |
|---|---|---|---|
| Ar | 1 | 1 | 22 |
| Ar | 10 | 1 | 34 |
| air | 1 | 1 | 41 |
| air | 10 | 1 | 71 |
| $O_2$ | 5 | 1 | 71 |

They confirmed that the reaction conditions outlined above worked well in most cases. In fact they realized that $Cu(OAc)_2$ was an optimal $Cu^{II}$ source and that the use of other copper salts, for example, $Cu(OPiv)_2$, $Cu(NO_3)_2$, $Cu(acac)_2$, and $Cu(OCOCF_3)_2$, gave inferior results and did not lead to the products of an arylation reaction. Neither did the use of $CuSO_4$, $CuCl_2$, or $Cu(ClO_4)_2$, and the use of $Cu(OTf)_2$ resulted in significant C–C bond formation. To allow the synthesis of more products with higher molecular complexity, milder conditions were sought. The reaction was monitored by GC–MS; it was shown that during the reaction, significant amounts of phenol and diphenyl ether were produced which may be due to the formation of water during the reaction. This water could be formed from the boronic acid, which forms the trimeric triaryl boroxine that may then participate in the reaction. Indeed this was found to be the case in independent experiments when using 0.33 equivalents of the boroxines. Investigations into the need for inert gas during the reaction also led to the observation that ambient atmospheric air or even oxygen offered a better reaction outcome, leading to more than double the yields observed under an argon atmosphere. Moreover, the addition of excess base to the reaction medium did not impede the reaction and may infer that this component plays a dual role as a base and as a participating ligand with a possible organocopper species in the reaction.

These observations then developed into a new *general* reaction procedure**:** A heterogeneous mixture of the phenol (1 equiv), aryl boronic acid (1–3 equiv), $Cu(OAc)_2$ (1–2 equiv), powdered molecular sieves (4 Å, amount not indicated) and $Et_3N$ (5 equiv) in dichloromethane was stirred at room temperature for 18 h exposed to the atmosphere; the product was then isolated in good yield after chromatography. The use of molecular sieves resulted in a significant enhancement in the product yield. Notably, excess amounts of the aryl donor were still necessary (1–3 equiv) for higher-yielding reactions. Presumably the minimum amount of molecular sieves to be added should correspond to at least the amount of water that can be produced by the hydrolysis of the boronic acid during the reaction.

### 2.2.3. *Substrate Scope*

It was shown that all types of structurally and electronically diverse boronic acids and phenols, even *ortho*-substituted phenols, which had caused problems with previous procedures, underwent smooth reaction to afford products in near quantitative yields (Table 2, [Eq. (15)]).




(15)

***Table 2:*** Substrate scope examined for the *O*-arylation of phenols with aryl boronic acids [Eq. (15)].

| $R^1$ | $R^2$ | $Et_3N$ [equiv] | Yield [%] |
|---|---|---|---|
| *p*-*t*Bu | H | 1.5 | 95 |
| *p*-*t*Bu | *p*-Me | 2.0 | 87 |
| *p*-*t*Bu | *p*-F | 2.0 | 42 |
| *p*-*t*Bu | *p*-OMe | 2.0 | 85 |
| *p*-*t*Bu | *m*-OMe | 1.0 | 68 |
| *p*-*t*Bu | *m*-$NO_2$ | 2.0 | 68 |
| *o*-Cl | H | 2.0 | 95 |
| *o*-Cl | *p*-Me | 1.0 | 70 |
| *o*-Cl | *p*-F | 2.0 | 61 |
| *o*-OMe | H | 1.0 | 92 |
| *o*-OMe | *p*-Me | 1.0 | 95 |
| *o*-OMe | *p*-F | 1.0 | 97 |
| *o*-OMe | *p*-OMe | 2.0 | 82 |
| *o*-OMe | *o*-Me | 1.0 | 52 |

### 2.2.4. *Applications: L-Thyroxine, (S, S)-Isodityrosine, Teicoplanin Aglycon, MMP Inhibitors*

The diaryl ether motif is abundant in a number of naturally occurring compounds, including important medicinal compounds such as vancomycin[19] and chloropeptins[20] as well as molecules of potential clinical use such as RA-I–IV,[21]

 © 2003 Wiley-VCH Verlag GmbH & Co. KGaA, Weinheim 

OF4949-I–IV,[22] piperazinomycin,[23] and K-13 (Figure 2).[24] However, the synthesis of this class of molecules currently relies on classical Ullmann condensation reactions between aryl halides and phenols.[25] This problem was addressed by Evans and co-workers, who further expanded the scope of these transformations whilst investigating the coupling of functionalized phenolic tyrosine derivatives **1**–**3** (Scheme 2, Table 3). In these reactions pyridine (2.0 equiv) was used as the base (in place of $Et_3N$) to afford the desired diaryl ethers **4**–**6**, respectively, in good to excellent yields with no apparent

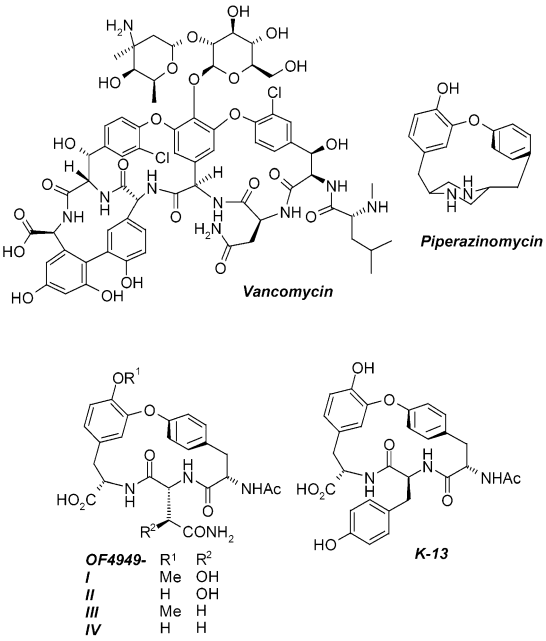
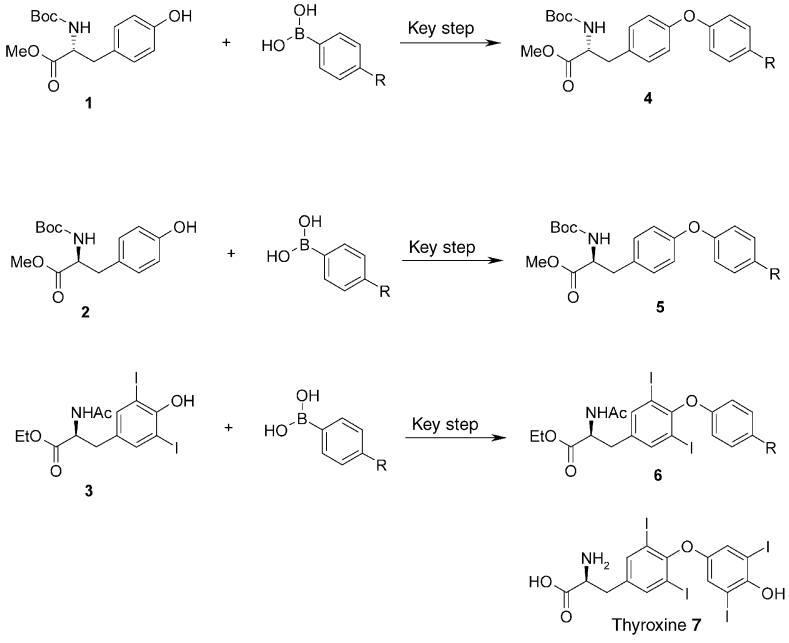



***Figure 2.*** Selected examples of biologically active macrocyclic diaryl ethers.




***Scheme 2.*** Key step: $Cu(OAc)_2$ (1 equiv) pyr and $Et_3N$, 4 Å molecular sieves, $CH_2Cl_2$, room temperature, time not specified.

***Table 3:*** Synthesis of diaryl ethers **4**–**6** in the $Cu(OAc)_2$-mediated arylation of phenols with aryl boronic acids (Scheme 2).

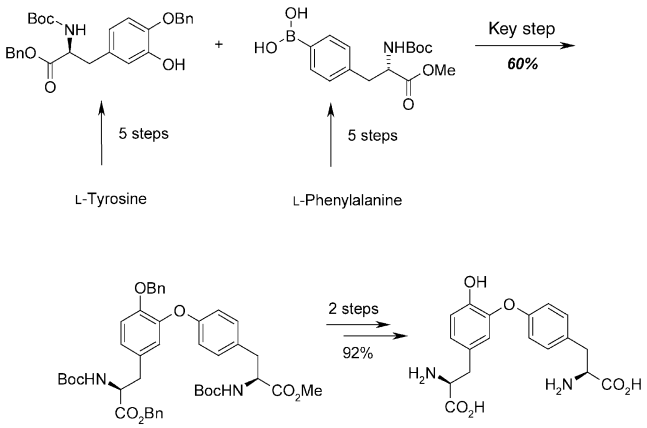
| R | Compound | Yield [%] |
|---|---|---|
| H | **4a** | 95 |
| *p*-Me | **4b** | 98 |
| *p*-F | **4c** | 97 |
| *p*-OMe | **4d** | 96 |
| *m*-OMe | **4e** | 97 |
| *m*-$NO_2$ | **4f** | 98 |
| *o*-Me | **4g** | 98 |
| *o*-OMe | **4h** | 37 |
| Cl | **4i** | 7 |
| *p*-Me | **5a** | 81 |
| *p*-OMe | **5b** | 76 |
| Me | **6a** | 81 |
| TBDMS | **6b** | 84 |

change in the integrity of the racemization-prone stereogenic centers. The only problems were found with *ortho*-methoxy and -chloro substituents on the boronic acid, and although no details were given, it is implied that some reactions in this series were more sluggish and needed a second equivalent of the boronic acid. It was shown that *ortho*-alkyl substitution was well-tolerated (Table 3, **4g**). In the synthesis of thyroxine (**7**), the impact of steric hindrance on the course of the reaction was crucial as two iodine atoms are present in the phenolic substrate *ortho* to the OH group. In the event a slight, but important, variation was required in the general reaction procedure in which a mixture of $Et_3N$/pyr (1:1, 5 equiv) was used to obtain the desired intermediate **6a** in 81% yield which was previously used by Hems and co-workers.[26] Furthermore, the silylated phenol **6b** was also prepared in 84% yield to demonstrate the generality of this method in the efficient synthesis of functionalized unsymmetrical diaryl ethers.

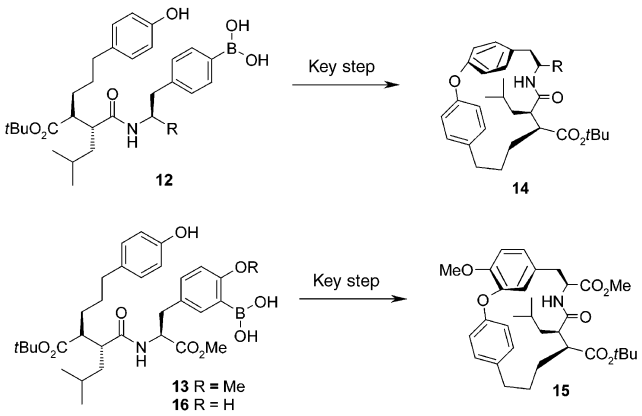
In these syntheses, the boronic acid was chosen as the aryl donor, and tyrosine derivatives were used as the phenolic partner. Jung and Lazarova,[27] however, demonstrated that the role of reaction partners can be reversed in a new efficient convergent total synthesis of (*S,S*)-isodityrosine starting from the two aromatic α-amino acids L-tyrosine and L-phenylalanine (Scheme 3).

Evans and co-workers planned the total synthesis of the teicoplanin agylcon **8** based on the coupling reaction of the aryl boronic acid **9** and the phenol **10** (Scheme 4).[28] In the key transformation, the desired diaryl ether **11** was formed in 80% yield with no detection of epimerization at any of the three stereogenic centers under the previously optimized conditions using molecular oxygen as co-oxidant. An elegant collection of organic transformations, including two atropdiastereoselective nucleophilic aromatic substitution reactions (between a phenol and an aryl fluoride), led to completion of the synthesis of **8**.

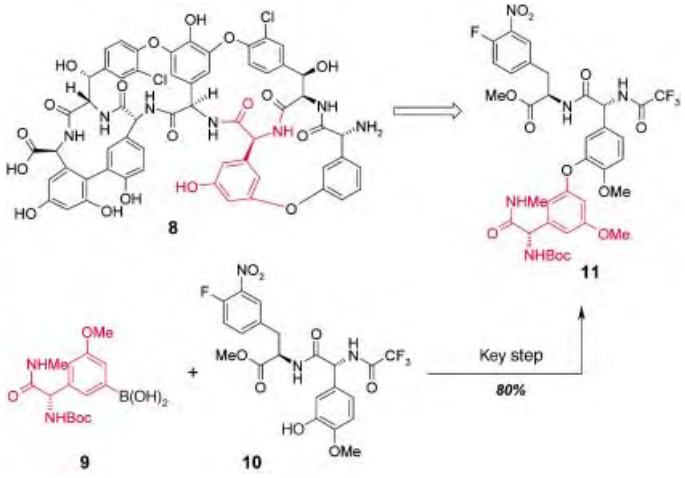
 © 2003 Wiley-VCH Verlag GmbH & Co. KGaA, Weinheim 




***Scheme 3.*** Key step: $Cu(OAc)_2$ (1 equiv), pyr, 4 Å molecular sieves, $CH_2Cl_2$, room temperature, 18 h.




***Scheme 5.*** Key step: dilute conditions, $Cu(OAc)_2$ (amount not specified), $Et_3N$, $CH_2Cl_2$, room temperature, 48 h (note: no molecular sieves/no air or $O_2$).



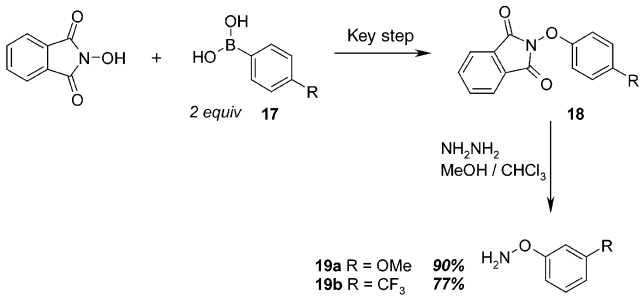

***Scheme 4.*** Key step: $Cu(OAc)_2$, $O_2$, pyr, 4 Å molecular sieves, $CH_2Cl_2$, room temperature, time not specified.

### 2.2.5. *Intramolecular Coupling*

Decicco, Song, and Evans have extended the generality of this transformation to intramolecular *O*-arylation in their novel synthesis of a small series of inhibitors of the metalloproteinases collagenase 1 and gelatinases A and B (Scheme 5).[29] The key step relied on the development of a novel intramolecular macrocyclization in which a diaryl ether was formed by the reaction of the boronic acid function and the phenol group in precursors **12** and **13**; a pinacol boronate was not a suitable substrate. Stoichiometric amounts of $Cu(OAc)_2$ and $Et_3N$ as base under dilute conditions (1 μM in $CH_2Cl_2$) afforded the desired products **14** and **15**, respectively, in good yields. One exception was the macrocyclization of the bisphenol boronic acid **16**, which only proceeded in a disappointing 5% yield. The resulting scaffolds were elaborated further to the target hydroxamic acids under standard reaction conditions to provide active ($K_i = 91$–$5000$ nM) matrix metalloproteinase (MMP) inhibitors.

### 2.2.6. **N-*Hydroxyimides as the Nucleophilic Reaction Partner***

Synthetic routes to *N*-aryl hydroxylamines are rare.[30] In response to this, Sharpless, Kelly and Petrassi recently extended the wide range of oxygen-centered nucleophiles that can participate in the copper-mediated arylation reaction; they investigated the coupling of *N*-hydroxyimides with a variety of boronic acids **17** under slightly modified conditions, with molecular sieves and ambient air in 1,2-dichloroethane (Scheme 6, Table 4).[31] It was shown that in the presence of base, preferably pyridine (1 equiv), all copper sources ($Cu(OAc)_2$, $Cu(OTf)_2$, CuCl, and $CuBr{\cdot}SMe_2$) resulted in the desired coupling products **18** in up to 98% yield. In fact, there was no direct correlation between the effectiveness of a specific salt or its oxidation state except that Cu, Cu(OAc), $CuCl_2$,and $Cu(OCOCF_3)_2$ were not suitable in effecting the transformation. The use of $Et_3N$ resulted in lower yields (13–37%), and neither DMAP, DABCO, or $Cs_2CO_3$ were effective bases in the reactions. In line with earlier reports, electronically and structurally diverse substituents on the boronic acid are tolerated, and the only recorded exceptions were *ortho*-fluorine and *para*-boronic acid precursors (which can undergo oligomerization). Two examples of **18** were converted into the correspoding *O*-arylhydroxylamine **19** in good yields after hydrazinolysis in methanol (Scheme 6). The main limitations




***Scheme 6.*** Key step: Cu salt (1 equiv), pyr, 4 Å molecular sieves, $C_2H_4Cl_2$, room temperature, 24–48 h.

 © 2003 Wiley-VCH Verlag GmbH & Co. KGaA, Weinheim 

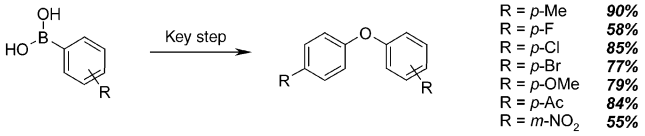
*Table 4:* $Cu(OAc)_2$-mediated arylation of aryl boronic acids with *N*-hydroxyphthalimide (Scheme 6).

| Compound | R | Yield [%] |
|---|---|---|
| **18a** | H | 90 |
| **18b** | *p*-Br | 73 |
| **18c** | *p*-I | 57 |
| **18d** | *p*-OMe | 37 |
| **18e** | *p*-CH=$CH_2$ | 87 |
| **18f** | *p*-$CO_2$Me | 64 |
| **18g** | *p*-CHO | 52 |
| **18h** | *p*-CN | 66 |
| **18i** | *p*-$CF_3$ | 65 |
| **18j** | *p*-$B(OH)_2$ | 0 |
| **18k** | *m*-*i*Pr | 68 |
| **18l** | *m*-F | 65 |
| **18m** | *m*-OMe | 57 |
| **18n** | *m*-$CF_3$ | 87 |
| **18o** | *o*-OMe | 60 |
| **18p** | *o*-F | 0 |
| **18q** | *m*,*m*,-di-F | 72 |

of the method are the requirement for 2 equivalents of the boronic acid and the incompatability of an *ortho*-heteroatom substituent or a second boronic acid functionality in the substrate.

#### 2.2.7. One-Pot Preparation of Symmetrical Diaryl Ethers[32]

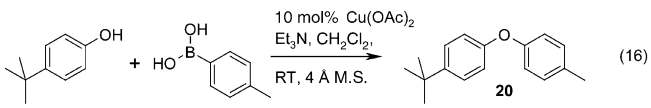
A recent extension of this coupling process involves the reaction of a phenol formed in situ (regioselective reaction of a boronic acid (1.0 equiv) with hydrogen peroxide (0.25 equiv)) followed by further reaction with the adduct boronic acid (2.0 equiv) in the presence of $Cu(OAc)_2$ (0.5 equiv) and $Et_3N$ (3.0 equiv) in $CH_2Cl_2$. As Evans and co-workers found previously, the addition of molecular sieves to sequester the water formed during triarylboroxine formation was beneficial in terms of yield (Scheme 7). The reaction worked particularly well with electron-rich boronic acids (up to 90% yield), although satisfactory yields (> 55%) were obtained with electron-deficient boronic acids. No *ortho*-substituted boronic acids were reported.




*Scheme 7.* Symmetrical diaryl ether synthesis. Key step: $Cu(OAc)_2$ (0.5 equiv), $H_2O_2$, $Et_3N$, 4 Å molecular sieves, $CH_2Cl_2$, room temperature, overnight.

#### 2.2.8. Catalytic Cu Methods: The Original Discovery

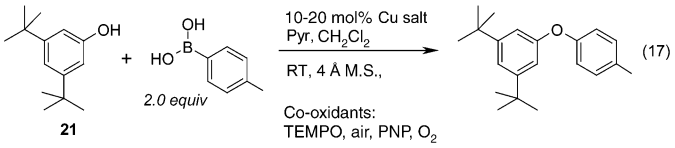
The potential for a catalytic variant was recognized early on in the synthesis of **20**. The use of less than stoichiometric amounts of $Cu(OAc)_2$ (10 mol%) in $CH_2Cl_2$, in the presence of $Et_3N$ (5 equiv) under argon or oxygen, gave rise to product, albeit in low yield [Eq. (16)].[15] Unfortunately, no studies



(16)

profiting from this early observation followed until some time later.

Lam et al, however, improved on the catalytic version by employing a co-oxidant in the cross-coupling of the phenol **21** with *p*-tolylboronic acid [Eq. (17)].[33] Although the best

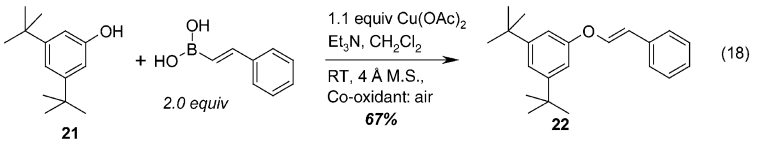


(17)

yields (79%) were obtained with oxygen as oxidant, it was possible to use TEMPO (1.1 equiv)/air, pyridinium *N*-oxide (1.1 equiv)/air, or $[\{Cu(\mu\text{-}OH)(tmeda)\}_2]Cl_2$/oxygen in the presence of $Cu(OAc)_2$ (20 mol%) as the $Cu^{II}$ source. These reactions were best performed in refluxing $CH_2Cl_2$ using pyridine as base.

#### 2.2.9. Styrylboronic Acids

As can be seen in the following sections, a variety of structurally diverse boronic acids function well in these transformations. In an interesting extension to the method, Lam et al. showed that a vinyl boronic acid could function well in the coupling reaction [Eq. (18)].[33] Although a



(18)

catalytic system was not successful, the electron-rich phenol **21** provided **22** in good yield when using $Cu(OAc)_2$ (stoichiometric) and $Et_3N$ (2 equiv) as base under air as oxidant at room temperature. Dichloromethane was the optimal solvent of choice; DMF could also be used, but increasing the temperature to 50 °C led to inferior results.

### 2.3. Copper-Mediated C(aryl)–N Bond Formation

#### 2.3.1. The Original Discovery: Stoichiometric $Cu^{II}$ Methods

The simultaneously published original papers by Chan and co-workers and Lam and co-workers had a significant impact on establishing the substrate scope and preoptimal reaction conditions in the cross-coupling of aryl boronic acids and nitrogen nucleophiles.[14,16]

 © 2003 Wiley-VCH Verlag GmbH & Co. KGaA, Weinheim 

### 2.3.2. *Substrate Scope*

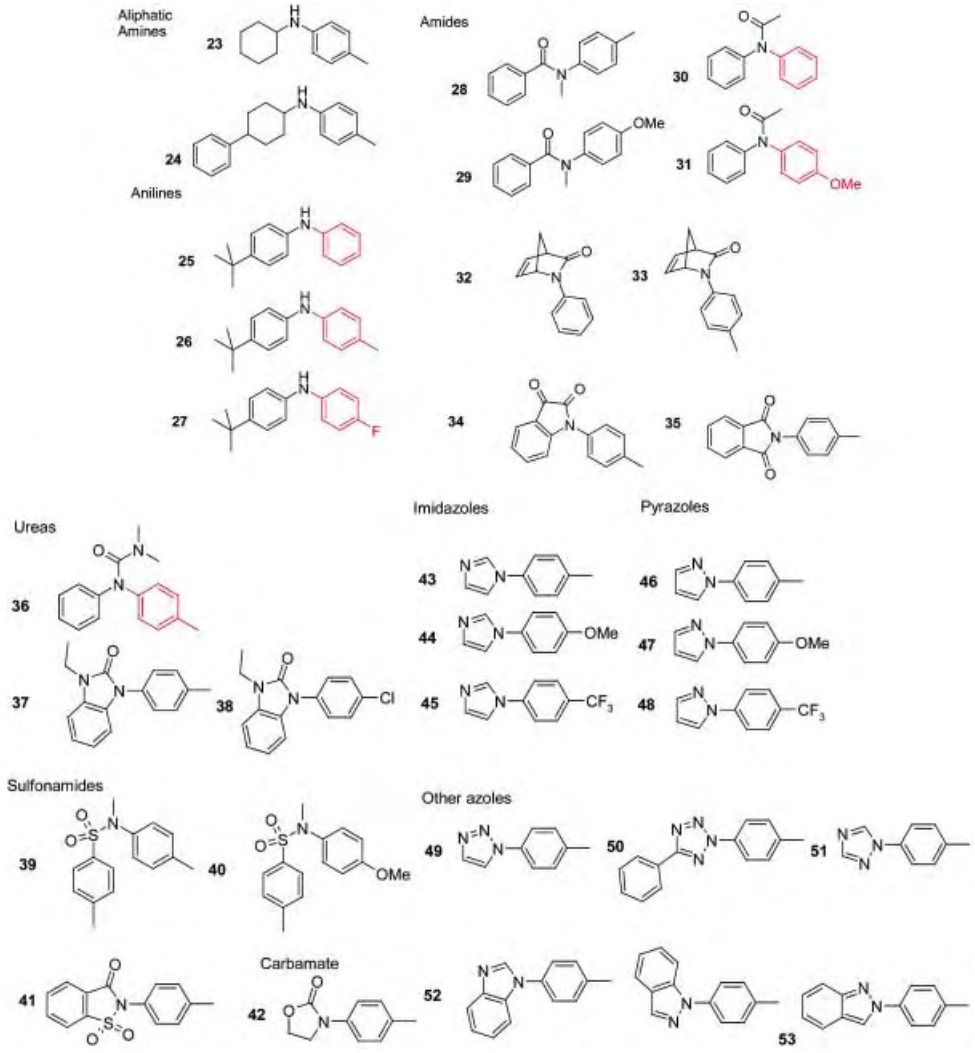
In the first[14] of the two communications, an impressive range of nucleophiles were successful, and suitable substrates for the reaction, which included amines, anilines, amides, imides, ureas, carbamates, sulfonamides, and aromatic heterocycles (imidazoles, pyrazoles, triazoles, tetrazoles, benzimidazoles, and indazoles) were reported. Table 5 and (Scheme 8) show the range of products **23**–**53** prepared by using a slightly modified form of the general reaction procedure. However, no true substrate trend emerged in these reactions, in contrast to the analogous process when bismuthates were employed as the aryl donor.

### 2.3.3. *Which Base Is Best?*

Much of the early base screening was carried out on the reaction with *p*-tolylboronic acid as aryl donor. For this limited substrate, it would appear that $Et_3N$ was the best choice. In all the reactions investigated with N nucleophiles, the use of $Et_3N$ as a base resulted in yields superior to those obtained with pyridine. However, for the preparation of

***Table 5:*** $Cu(OAc)_2$-mediated arylation of aryl boronic acids with N nucleophiles (Scheme 8).

| Compound | Base | *t* [h] | Yield [%] | Compound | Base | *t* [h] | Yield [%] |
|---|---|---|---|---|---|---|---|
| **23** | $Et_3N$ | 45 | 56 | **37** | $Et_3N$ | 66 | 96 |
| **23** | Pyr | 45 | 63 | **37** | Pyr | 66 | 52 |
| **24** | $Et_3N$ | 48 | 50 | **38** | $Et_3N$ | 66 | 37 |
| **24** | Pyr | 48 | 74 | **39** | $Et_3N$ | 65 | 72 |
| **25** | $Et_3N$ | 48 | 58 | **39** | Pyr | 65 | 23 |
| **26** | $Et_3N$ | 24 | 90 | **40** | $Et_3N$ | 48 | 67 |
| **27** | $Et_3N$ | 18 | 93 | **41** | $Et_3N$ | 53 | 23 |
| **28** | $Et_3N$ | 66 | 17 | **41** | Pyr | 53 | 92 |
| **28** | Pyr | 67 | 4 | **42** | $Et_3N$ | 50 | 60 |
| **29** | $Et_3N$ | 48 | 5 | **43** | Pyr | 48 | 72 |
| **30** | $Et_3N$ | 48 | 59 | **44** | Pyr | 48 | 62 |
| **30** | Pyr | 48 | 4 | **45** | Pyr | 48 | 71 |
| **31** | $Et_3N$ | 48 | 41 | **46** | Pyr | 48 | 76 |
| **32** | $Et_3N$ | 64 | 12 | **47** | Pyr | 48 | 64 |
| **33** | $Et_3N$ | 40 | 77 | **48** | Pyr | 48 | 45 |
| **34** | $Et_3N$ | 65 | 53 | **49** | Pyr | 48 | 11 |
| **34** | Pyr | 65 | 72 | **50** | Pyr | 48 | 26 |
| **35** | $Et_3N$ | 35 | 92 | **51** | Pyr | 48 | 6 |
| **35** | Pyr | 35 | 83 | **52** | Pyr | 48 | 67 |
| **36** | $Et_3N$ | 47 | 45 | **53** (4.5:1) | Pyr | 48 | 88 |
| **36** | Pyr | 47 | 7 | | | | |




***Scheme 8.*** Initial array of *N*-arylated products formed. Key step: $Cu(OAc)_2$ (1–2 equiv), $Et_3N$ or pyr (see Table 5), $CH_2Cl_2$, room temperature, 18–66 h.


© 2003 Wiley-VCH Verlag GmbH & Co. KGaA, Weinheim

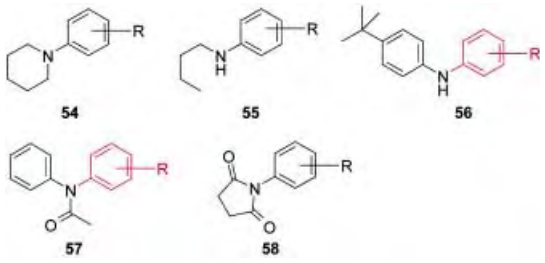
compounds **43–53** from the range of heteroarenes examined as nucleophiles, it appears that pyridine was the base of choice as no examples were recorded with the supposedly equally efficient $Et_3N$. For the tetrazole **50** NMO and DBU were studied as alternative bases, but were found to be less effective. It was also shown that in the slower reactions (with less-nucleophilic amines), substantial amounts of the phenol and symmetrical diaryl ethers were formed, even in the presence of molecular sieves.

### 2.3.4. Which Solvent Is Best?

An empirical order has been established for the solvent in terms of reaction yield:

$$CH_2Cl_2 \gg 1,4\text{-dioxane} = NMP = THF = DMF \gg > EtOAc = \text{toluene} = DMSO \gg \gg MeOH$$

Cundy and Forsyth presented several additional examples **54–58** and confirmed the capricious nature of the reaction: No substrate trend was observed in terms of the basicity of the amine and the sigma-donating effect of the aryl boronic acids (Scheme 9, Table 6).[34] In fact, on the basis of these findings




***Scheme 9.*** Key step: $Cu(OAc)_2$ (1 equiv), $Et_3N$, $CH_2Cl_2$, room temperature, 48–72 h.

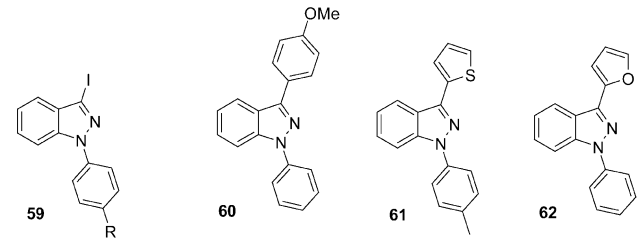
***Table 6:*** $Cu(OAc)_2$-mediated arylation of aryl boronic acids with N nucleophiles.

| Compound | Yield [%] | | | | | | |
|---|---|---|---|---|---|---|---|
| | *p*-$NMe_2$ | *p*-OMe | *o*-OMe | *p*-Me | H | *m*-$CF_3$ | *m*-$NO_2$ |
| **54** | – | 82 | 14 | 58 | – | – | 11 |
| **55** | – | 39 | 17 | 43 | 6 | 21 | n.d.[a] |
| **56** | n.d. | n.d. | – | 56 | 42 | 10 | < 10 |
| **57** | 11 | n.d. | – | 12 | – | 53 | 18 |
| **58** | – | – | – | 69 | 72 | 65 | 36 |

[a] Not determined.

and those of Chan and Lam, it could be concluded that the general reaction conditions had to be adapted for each substrate type in the *N*-arylation reaction. This is possibly best achieved by using a "Design of Experiment" (DoE) protocol.[35]

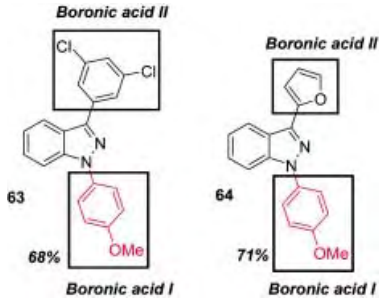
Rault and co-workers developed a regioselective copper-mediated *N*-arylation of 3-iodoindazole (Scheme 10) with four different boronic acids to form compounds of type **59–62** in good yields in only 1–2 h.[36] These results show a




***Scheme 10.*** Key step: $Cu(OAc)_2$ (1.5 equiv), $Et_3N$, $CH_2Cl_2$, room temperature, 1–2 h.

remarkable rate enhancements for this particular substrate (3-iodoindazole) relative to that observed by the groups of Chan and Lam, who reported that indazoles were only *N*-arylated to completion after 48 h when using pyridine as base.[16]

The efficient preparation of the 1,3-diaryl indazoles **63** and **64** from the 3-iodoindazole can be carried out in a one-pot process that combines two processes mediated by different catalysts (Scheme 11): The first process led to a surprisingly rapid *N*-arylation mediated by $Cu(OAc)_2$ (1 equiv), aryl boronic acid (1 equiv), $Et_3N$ (3 equiv). A subsequent Suzuki reaction in the *same* reaction pot upon the simultaneous addition of $[Pd(PPh_3)_4]$ (5 mol%), $NaHCO_3$ (3 equiv) in DME, and the second boronic acid (1 equiv) gave the desired product. This is the first report of this sequence of reactions being performed in one pot with two catalysts efficiently functioning independently of one another. This strategy has enormous potential for the design and preparation of combinatorial libraries of compounds in which both N– and C–aryl moieties are fundamental features.

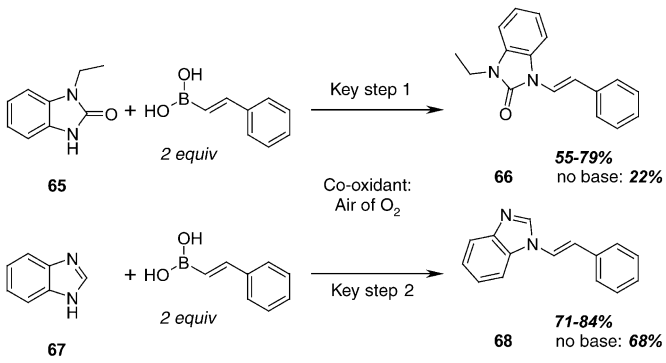



***Scheme 11.*** Reagents and conditions: Boronic acid I (1 equiv), $Cu(OAc)_2$ (1 equiv), $[Pd(PPh_3)_4]$ (0.05 equiv), $Et_3N$, $NaHCO_3$, DME, room temperature, 1 h; then boronic acid II (1 equiv), 80°C, 3 h.

### 2.3.5. Not Only Aryl Boronic Acids React

In an interesting extension of the substrate scope of the reaction, it was shown that the aryl boronic acid reaction partner could be extended with a vinyl group. In the reaction

 © 2003 Wiley-VCH Verlag GmbH & Co. KGaA, Weinheim 



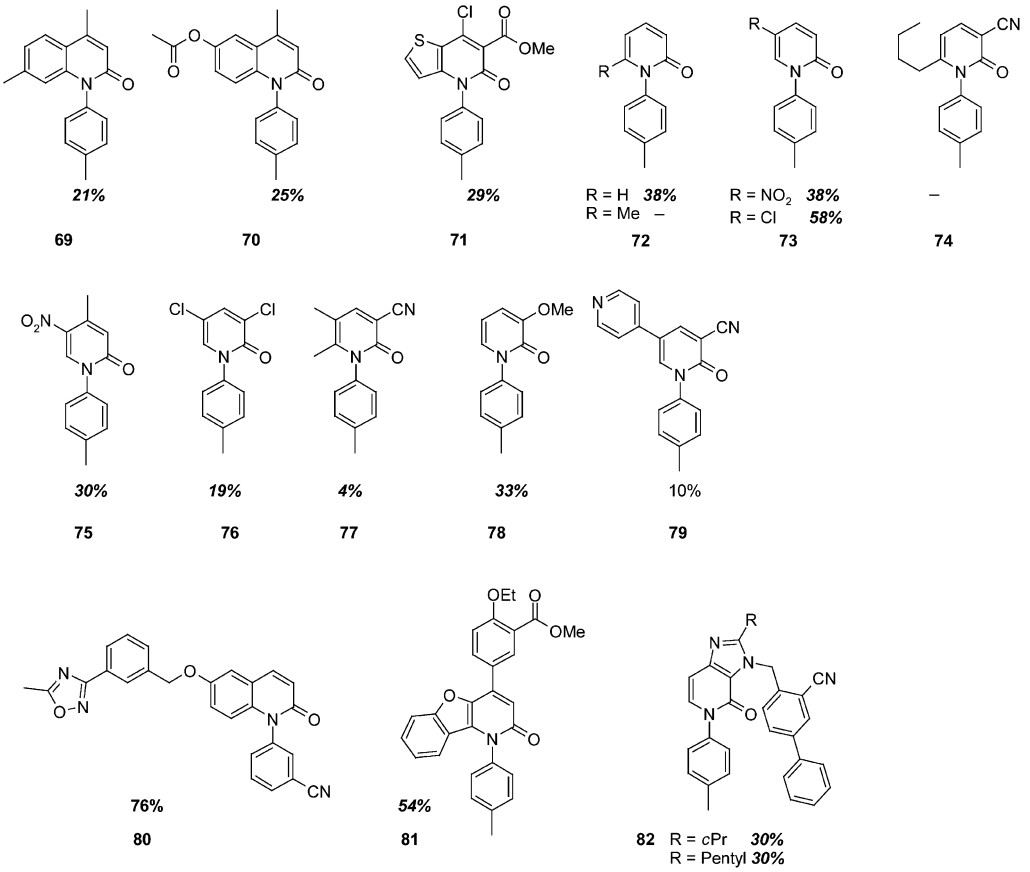

***Scheme 12.*** Key step: 1) $Cu(OAc)_2$ (1.1 equiv), $Et_3N$, 4 Å molecular sieves, $CH_2Cl_2$, room temperature or 50 °C, 4 days; 2) $Cu(OAc)_2$ (1 equiv), pyr, 4 Å molecular sieves, $CH_2Cl_2$, room temperature, 4 days.

of the benzimidazolones and benzimidazoles, the best yields of the desired coupling products were obtained in the presence of stoichiometric amounts of $Cu(OAc)_2$ exposed to air (Scheme 12).[33] Interestingly, $Et_3N$ was the base of choice for the substrate **65**, whereas pyridine was preferred in the cross-coupling of benzimidazole **67**. Both reactions proceeded best at room temperature, although in the case of **65** the yield was comparable at 50 °C. No explanation or comparison of bases were reported.

### 2.3.6. *Applications: Medicinal Chemistry and Solid-Phase Organic Synthesis*

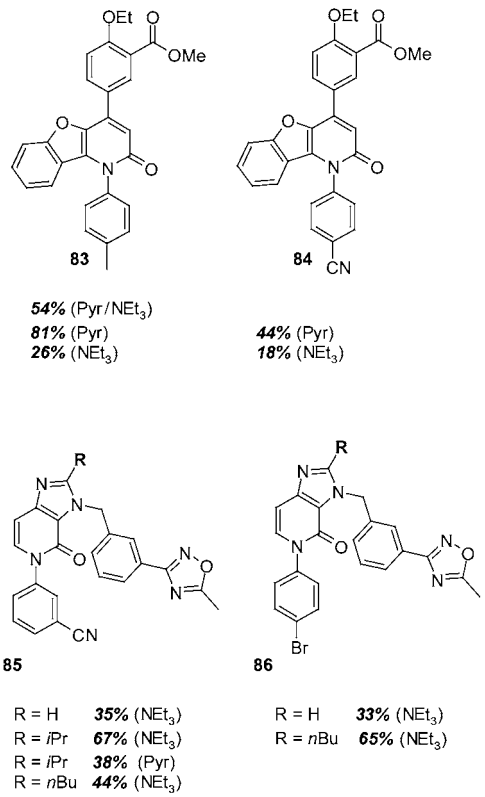
Researchers at Merck showed that 2-pyridones were useful N nucleophiles in the arylation reaction with aryl boronic acids in a program dedicated towards the discovery of novel and potent Factor Xa inhibitors (Scheme 13).[37] Notably, in this transformation it was possible to selectively form the *N*-aryl product **69** with none of the corresponding *O*-arylated product being observed. Under different conditions (KO*t*Bu, DMF), a mixture of *N*-/*O*-arylated products (2:1) was observed. Interestingly, partly perhaps because there was no precedent for which base to use, Mederski et al. employed both $Et_3N$ *and* pyridine in the reaction. No examples are given in which only one base was used. Scheme 13 shows the diverse range of substrates examined and products **69**–**82** formed. Again, there appears to be no general trend with respect to the impact of the electronic nature of the N nucleophiles; electron-poor and -rich systems behave similarly. However, in all cases, no trace of the aromatic *O*-arylated product was observed.

The acceptable to good yields of **83**–**86** were encouraging, as these were key molecular units in the quest for new Factor Xa inhibitors (Scheme 14). Further investigation showed that pyridine alone as base in these reactions offered the best yields for the benzo[3,2-*b*]pyridone moieties, but




***Scheme 13.*** Key step: $Cu(OAc)_2$ (2 equiv), $Et_3N$ *and* pyr, 4 Å molecular sieves, $CH_2Cl_2$, room temperature, 48 h.

 © 2003 Wiley-VCH Verlag GmbH & Co. KGaA, Weinheim 



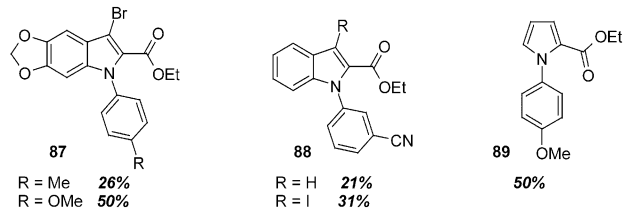

***Scheme 14.*** Key step: $Cu(OAc)_2$ (2 equiv), $Et_3N$ *and/or* pyr, 4 Å molecular sieves, $CH_2Cl_2$, room temperature, 48 h.

$Et_3N$ proved to be the base of choice for the fused imidazolepyridone unit.

Moreover, Mederski et al. showed that indoles and pyrroles activated with an *ortho* carboxylate functional group were suitable N nucleophiles and they developed a general procedure for the formation of the products **87**–**89**, using pyridine as base (Scheme 15).

Potential MMP inhibitors that incorporate electron-deficient pyrrole scaffolds were constructed by using the stoichiometric $Cu(OAc)_2$ method described above by researchers at Pfizer.[38] In general these molecular motifs appear to be excellent substrates for *N*-arylation reactions, and in nearly all cases high yields of the products **90**–**95** were obtained (Scheme 16). However, the reaction times ranged from 2–13 days, but generally were in the 2-day range (Scheme 16). Heteroaryl boronic acids do not function well in this reaction: 3-pyridyl-, 2-thienyl-, and 2-furanylboronic acids all failed to give any of the desired product. This method was used to prepare a pivotal intermediate **95** for the synthesis of the MMP inhibitor AG3433, which is currently in preclinical trials.

The 3-pyrroleglyoxalates **96**, which lack the activating 2-acyl functionality, are not good substrates, whereas the 2-acetylpyrroles **97** react very well (Scheme 17). In each case, longer reaction times than those for the 2-formyl-3-glyoxalates

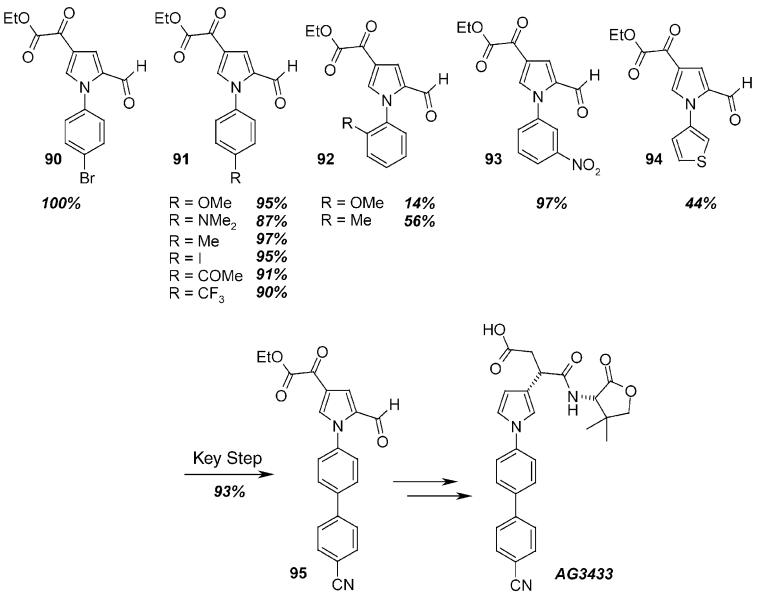



***Scheme 15.*** Key step: $Cu(OAc)_2$ (2 equiv), pyr, 4 Å molecular sieves, $CH_2Cl_2$, room temperature, 48 h.

were required for complete conversion of reactants. This effect may be due to a possible chelating effect of the pyrrole N atom, the Cu complex, and the oxygen atom of the 2-carbonyl unit.

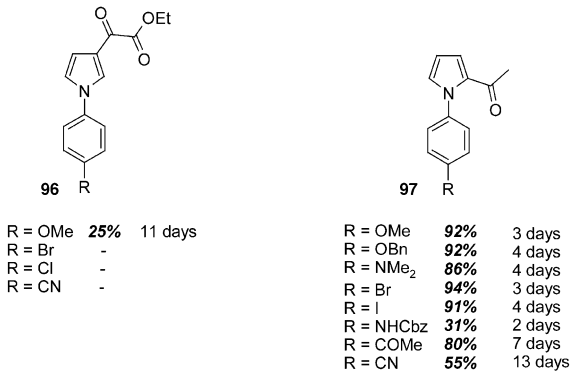
Amino acids and aminoesters are useful substrates for the Ullmann condensation reaction (see Section 3) with or without the use of solubilizing agents. Lam et al showed that the standard substrate *p*-tolylboronic acid couples smoothly with a range of 15 α-aminoesters (lipophilic examples and hence more soluble in the reaction medium) to form the *N*-arylated products in generally acceptable yields (Scheme 18).[39] Although the reactions required 1–2 days for complete conversion into product and the standard use of 2.0 equivalents of the boronic acid and stoichiometric amounts of copper acetate for optimum yields, the reactions were performed at room temperature. This represents a much milder alternative to the use of aryl halides as the electrophilic reaction partner. Furthermore, the reaction products were formed with almost complete retention of configuration for both enantiomers (94–99 % *ee*), which will ensure that this new method will continue to be an important method for the preparation of molecules of this type.

A rapid and direct synthesis of 9-aryl purines, which display diverse biological activities,[40] was sought, as standard

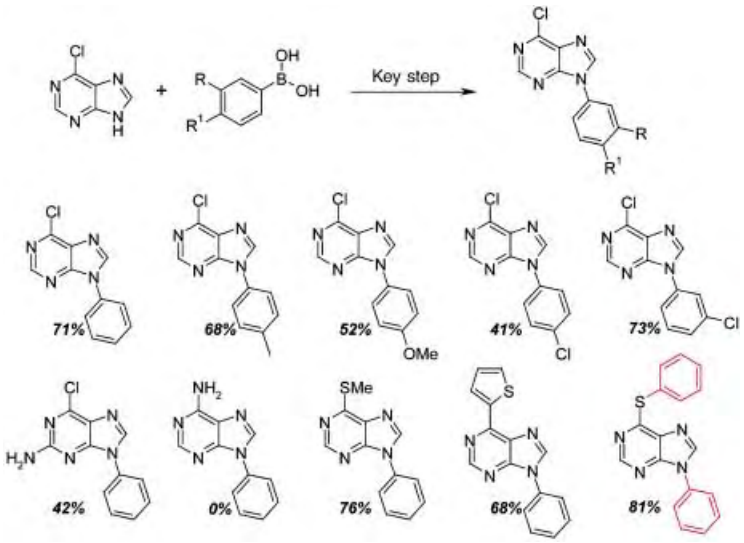



***Scheme 16.*** Key step: $Cu(OAc)_2$ (1.5 equiv), pyr, air, $CH_2Cl_2$, room temperature, 3 days.

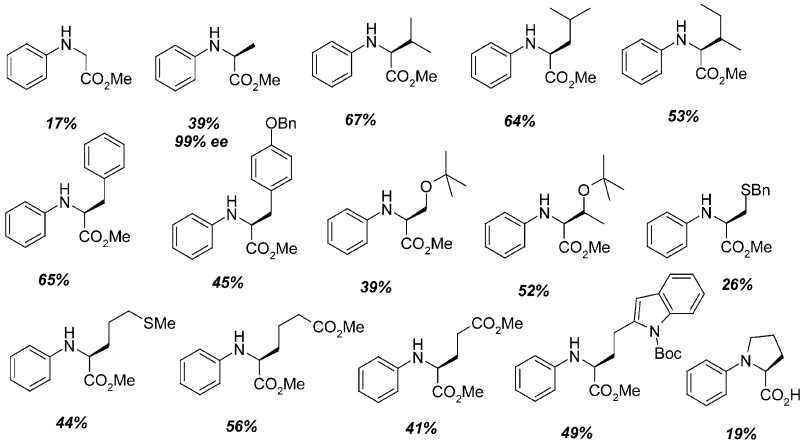
 © 2003 Wiley-VCH Verlag GmbH & Co. KGaA, Weinheim 




***Scheme 17.*** Key step: $Cu(OAc)_2$ (1.5 equiv), pyr, air, $CH_2Cl_2$, room temperature, 2–11 days.




***Scheme 19.*** Key step: Boronic acid (3 equiv), $Cu(OAc)_2$ (1.0 equiv), phen (2 equiv), $CH_2Cl_2$, 4 Å molecular sieves, air, room temperature, 4 days.



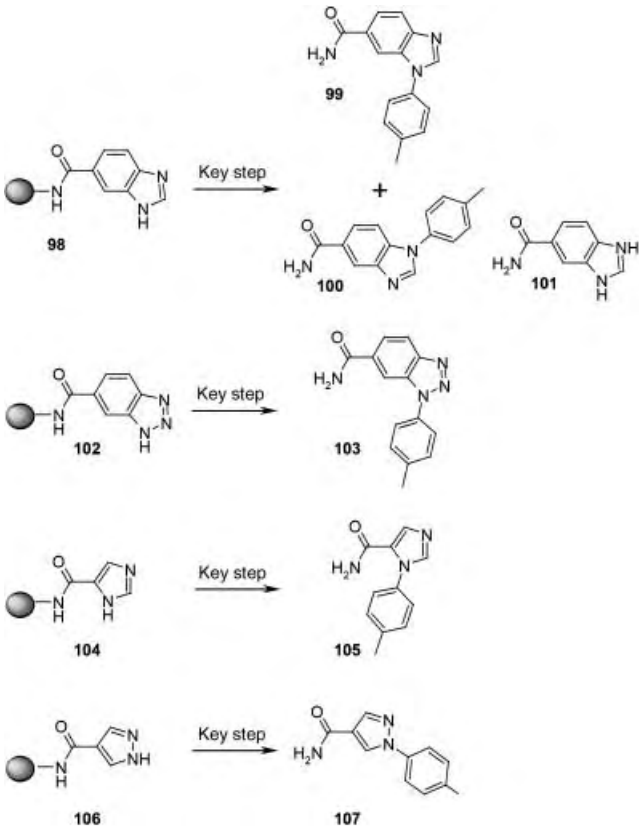

***Scheme 18.*** Key step: Boronic acid (2 equiv), $Cu(OAc)_2$ (1.1 equiv), $Et_3N$ (2 equiv), $CH_2Cl_2$, 4 Å molecular sieves, room temperature, 1–2 days.

routes to molecules of this type involve cyclization strategies with the aryl unit already in place.[41] These strategies are not suitable for rapid exploration of structure–activity relationships (SAR). To meet these demands, Gunderson and Bakkestuen recently showed that purines react regio- and chemoselectively at N9, thus allowing the first direct access to the desired compounds in average to good yields (Scheme 19).[42] The use of 1,10-phenanthroline as a stoichiometric (see Section 3 for catalytic variant) ligand for the copper center proved optimal over the standard choices of $Et_3N$, pyridine and 2,2′-bipyridine, TMEDA and *N,N′*-diarylethanediimines, which had already shown promise in coupling reactions with aryl iodides (see Section 3).

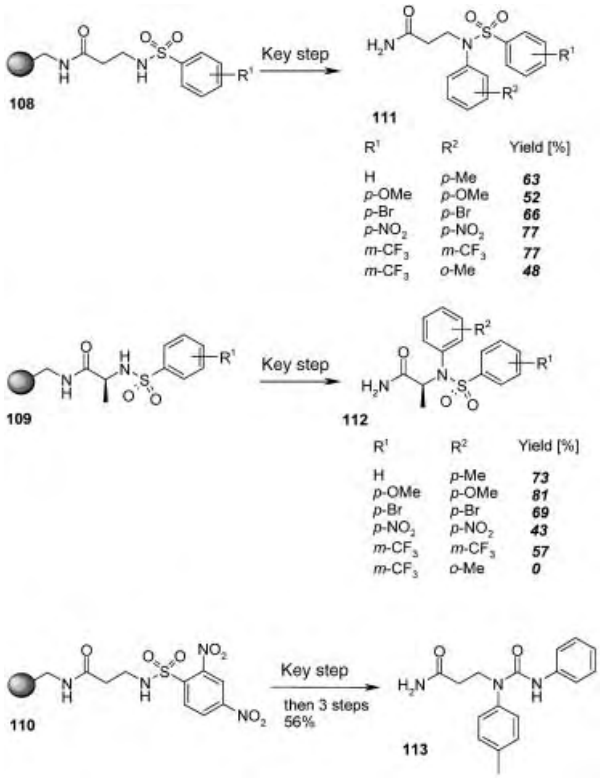
The impact of solid-phase organic chemistry in academic and medicinal chemistry communities has been significant.[43] Combs et al. reported efficient examples of the solid-supported aryl and heteroaryl C–N cross-coupling reactions mediated by microwave irradiation: *p*-tolylboronic acid reacted with a range of solid-supported benzimidazoles, imidazoles, pyrazoles, and benzotriazoles (Scheme 20).[44] In preliminary experiments with the supported benzimidazole **98** and the *p*-tolylboronic acid, it was shown that the arylation reaction could not be driven to completion under standard conditions. However, with the aid of microwave irradiation from a domestic microwave oven, five heating, reagent addition, and agitation cycles allowed the reactions to proceed to completion (no benzimidazole (**101**) was observed after cleavage from the resin) and afforded the regioisomeric products **99** and **100** (56% yield, 96% pure). After establishing the route, a range of aryl and heteroaryl acids **102, 104**, and **106** were then attached to the PEG-supported amine to form an amide linker (apparently, polystyrene can also be employed as the support), and in each case the desired products **103, 105**, and **107** were obtained in good overall yields (56–64%) and acceptable purities (73–96%) after washing away excess reagents, cleavage with TFA, and purification by silica-gel chromatography. Notably, no *N*- or *O*-arylation of the amide linker was observed. The reaction could be performed in 96-well microtiter plates and thus lends itself well to the synthesis of libraries.

Combs and Rafalski also showed that solid-supported sulfonamides **108–110** can be used as the N nucleophile in copper-mediated *N*-arylation reactions (Scheme 21).[45] Optimization of the general protocol revealed that $Et_3N$ as base, THF as solvent, and the use of molecular sieves was optimal (DIPEA, pyridine, and dichloromethane were explored as alternatives). As a result, a small array of products of type **111** and **112** were formed in good yields, even at room temperature. Importantly, no racemization was observed in compounds of type **112**. The study was extended to include Fukuyama's sulfonamide strategy involving *N*-arylation of

 © 2003 Wiley-VCH Verlag GmbH & Co. KGaA, Weinheim 



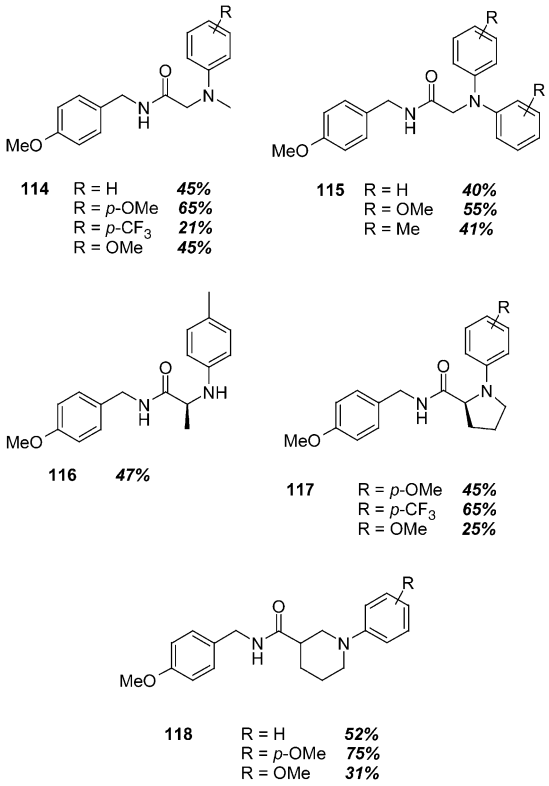

***Scheme 20.*** Key step: Boronic acid (3 equiv), $Cu(OAc)_2$ (5 equiv), pyr/NMP, 80 °C, > 2 days; then optimized to: boronic acid (3 equiv), $Cu(OAc)_2$ (5 equiv), pyr/NMP, 4 Å molecular sieves, microwave heating (3 × 10 s 1000 W, 5 applications of reagents).




***Scheme 21.*** Key step: Boronic acid (4 equiv), $Cu(OAc)_2$ (2 equiv), $Et_3N$, THF, 4 Å molecular sieves, repeat twice.

*o,p*-dinitroarylsulfonamides. In the event, copper(II)-mediated *N*-arylation followed by cleavage with *t*-butylamine to afford the amine and subsequent reaction with phenylisocyanate afforded **113** in 56% overall yield. Supported carbamates, amides, and ureas were also investigated as nucleophiles, but all failed to react under these reaction protocols.

The substrate scope of the solid-phase *N*-arylation reaction was also extended to include aliphatic secondary amines in a CNS-directed medicinal chemistry program at DuPont (Scheme 22).[46] The conditions previously optimized[41] for




***Scheme 22.*** Key step: Boronic acid (4 equiv), $Cu(OAc)_2$ (2 equiv), $Et_3N$, 4 Å molecular sieves, THF, repeat twice.

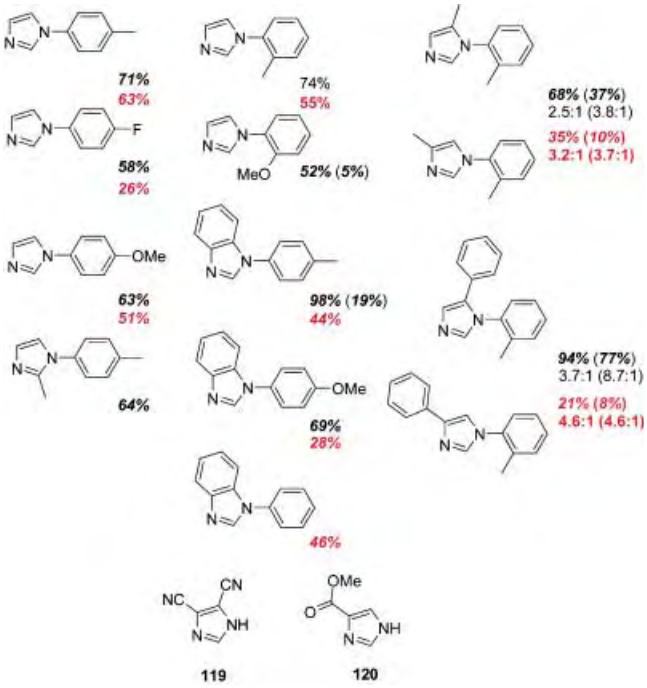
the *N*-arylation of supported sulfonamides (use of *powdered* molecular sieves) proved to be best for this class of substrate. The range of products **114**–**118** prepared demonstrates the scope and utility of the reaction; yields are representative of the *N*-arylation/cleavage/purification sequence. Notably, the primary amine **115** derived from glycine was bisarylated, and only traces of the monoarylated products were evident. However, in the case of α substitution (e.g. an alanine derivative) selective mono-*N*-arylation was predominant (e.g. to form **116**).

### 2.3.7. *Catalytic $Cu^{II}$ methods*

In perhaps the most important development since the copper-mediated *N*-arylation of boronic acids, Collman and Zhong reported the catalytic version of this reaction.[47]

 © 2003 Wiley-VCH Verlag GmbH & Co. KGaA, Weinheim 

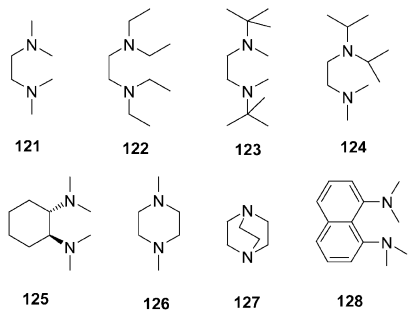
Imidazole was used as a standard N nucleophile with phenylboronic acid as the aryl donor. It was also shown that $Cu^{II}$ alternatives in the form of [Cu(OH)Cl·tmeda] (formed in situ by the reaction of oxygen and the commercially available dimer $[\{Cu(OH)\cdot tmeda\}_2]Cl_2$) were potent catalysts. Several reaction parameters were optimized (amount of catalyst, aryl boronic acid, imidazole, solvent, time, atmosphere, molecular sieves), which resulted in an optimized general reaction procedure in which a mixture of aryl boronic acid (2 equiv), imidazole (1 equiv), $[\{Cu(OH)\cdot tmeda\}_2]Cl_2$ (10 mol%) in dichloromethane are stirred at room temperature overnight under oxygen. Scheme 23 shows the electronic and structural diversity in the boronic acids selected for this study. In all cases, reaction conditions were found that led to good to excellent yields (52–98%). Although benzimidazoles were also suitable substrates, the imidazoles **119**–**120** did not take part in the reaction.




***Scheme 23.*** Key step: Boronic acid (2 equiv), $[\{Cu(OH)\cdot tmeda\}_2]Cl_2$ (10 mol%), $O_2$, $CH_2Cl_2$, room temperature, overnight. Yields in red for reactions in water.

Environmentally friendly reaction procedures are fashionable, especially when performed in water.[48] Collman et al. studied exactly the above reaction with the same substrates and catalyst species, and reported the first examples of *N*-arylation of imidazoles in water.[49] The yields for the same products are shown in *red* in Scheme 23. This reaction system differs from the general reaction procedure only in the replacement of dichloromethane with water (2.5× dilution). Notably, the addition of phase-transfer catalysts offered no substantial benefit in terms of yield or reaction time. It was also shown that a neutral pH value for the reaction was optimal, as in both slightly acidic or basic media, the reaction yields were lower. The increased potential for water to intercept the putative reaction intermediates led to slightly lower yields for these transformations, but nevertheless in useful preparative amounts (26–63%).

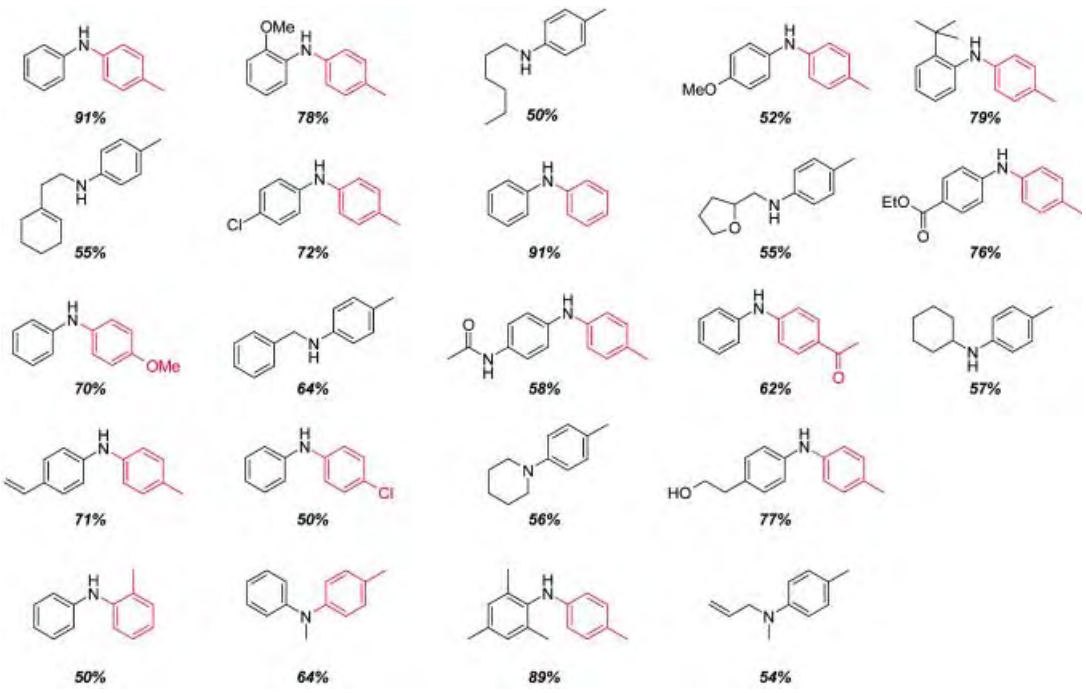
Although perhaps the most efficient system for the arylation of imidazoles was discovered, Collman et al. attempted to make the route even better by closely investigating other copper catalysts and ligands.[50] The use of a commercially available μ-hydroxo $Cu^{II}$ complex with the bidentate tmeda ligand was investigated first. This was followed by studies with other bidentate nitrogen ligands and counterions. In this report, a bidentate ligand **121**–**128** (Scheme 24) and a $Cu^{I}$ salt (CuCl, CuBr, CuI, or CuOTf) in the presence of oxygen and water, were used to generates a $Cu^{II}$ species that efficiently catalyzes the cross-coupling of imidazoles (and benzimidazoles) with aryl boronic acids. Although all ligands led to acceptable yields (19–68%), the most efficient ligand was tmeda (**121**).




***Scheme 24.*** Key step: Boronic acid (2 equiv), $[\{Cu(OH)\cdot(\mathbf{121}–\mathbf{128})\}_2]Cl_2$ (10 mol%), $O_2$, $CH_2Cl_2$, room temperature, overnight.

Building on these studies, further improvements to the catalytic variation of the boronic acid cross-coupling have been reported. Buchwald and Antilla, for example, developed a general reaction involving the use of catalytic $Cu(OAc)_2$ and myristic acid ($n$-$C_{13}H_{27}COOH$) as an additive along with stoichiometric amounts of 2,6-lutidine as base at room temperature. Substituted anilines as well as primary and secondary aliphatic amines reacted with a series of aryl boronic acids (Scheme 25).[51] Mainly *p*-tolylboronic acid was used in the optimization of the reaction, and in early observations it was shown by screening copper salts that $Cu(OAc)_2$, CuOAc, and $Cu^{II}$ isobutyrate all efficiently catalyzed the reaction between aniline and phenylboronic acid, allowing conversions up to 55%. Vigorous stirring of the reaction mixture (which presumably allowed better oxygen uptake and hence an increased oxidative efficiency of a reduced copper intermediate in the reaction), allowed the complete cross-coupling of aniline derivatives when the reaction was performed in reaction flasks with large volumes (100 mL) relative to the amount of solvent (2 mL). It was discovered that the addition of a small amount of myristic acid enhanced the speed of the reactions, perhaps by rendering the copper species more soluble in the reaction medium.[52] Scheme 25 shows the range of products formed under these

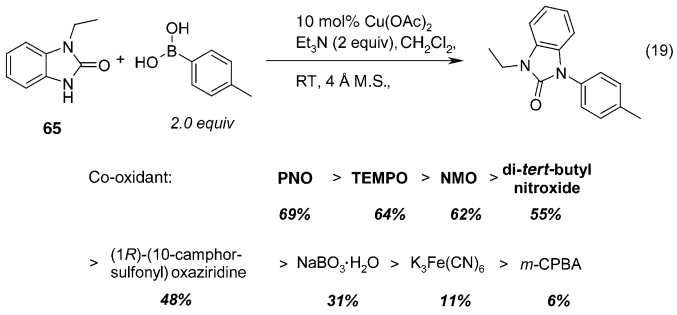
 © 2003 Wiley-VCH Verlag GmbH & Co. KGaA, Weinheim 




***Scheme 25.*** Key step: Boronic acid (1.5 equiv), $Cu(OAc)_2$ (5–20 mol%), myristic acid (10–40 mol%), air, 2,6-lutidine, toluene, room temperature, vigorous stirring, 24 h.

new conditions, demonstrating the versatility of this procedure. The reaction tolerates a wide range of electronically and structurally diverse substrates with other functionalities already incorporated in the products (e.g. alkene, ester, alcohol, acetamides), which did not interfere with the desired reaction pathway. In the reaction with primary amines, no bisarylated products were observed.

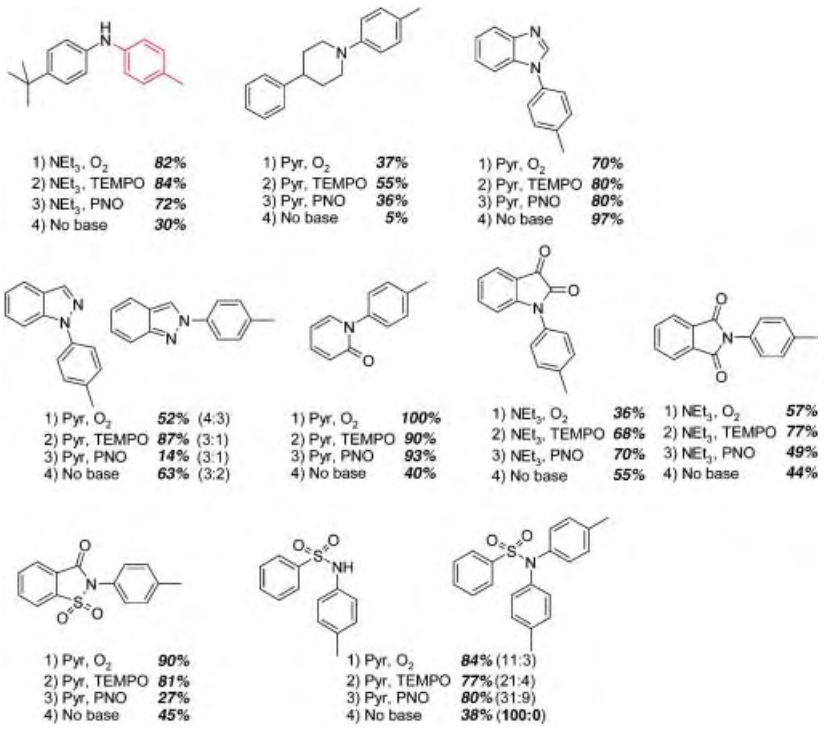
Lam et al. also reported an important alternative to this catalytic cross-coupling of aryl boronic acids and amines in the presence of $Cu(OAc)_2$ (10 mol%) and a co-oxidant additive (other than oxygen).[33] The best systems explored involved $Cu(OAc)_2$ and a combination of pyridine *N*-oxide (PNO) (1.1 equiv) and air, TEMPO (1.1 equiv) and air, or just oxygen. Most substrates reacted well, although no single catalytic system worked for *all* the substrates examined. The original study also screened NMO (62%), di-*tert*-butylnitroxide (55%), (1*R*)-(10-camphorsulfonyl)oxaziridine (48%), $NaBO_3{\cdot}H_2O$ (31%), $K_3Fe(CN)_6$ (11%), and *m*CPBA (6%) as co-oxidants in the *p*-tolylation of the benzimidazolone [Eq. (19)].



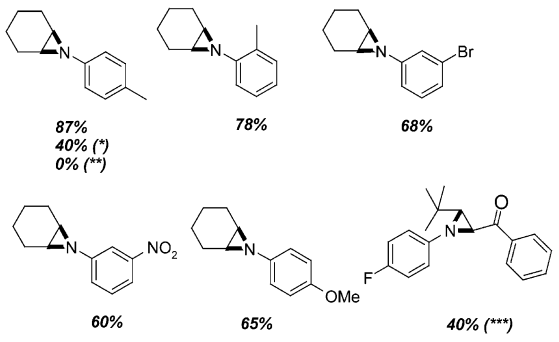

These investigations led to the following general reaction procedure: aryl boronic acid (2.0 equiv), the amine (1.0 equiv), $Cu(OAc)_2$ (0.1–0.2 equiv), PNO (1.1 equiv) or TEMPO (1.1 equiv), and $Et_3N$ (2.0 equiv) or pyridine (2.0 equiv) and *powdered* molecular sieves were stirred under air at room temperature for 4 days. The range of substrates that work well in this transformation includes, benzimidazolones, isatins, phthalimides, piperidines, indazoles, anilines, pyridones, sulfonamides, saccharin, and benzimidazoles (Scheme 26). Although no general catalytic copper system works equally well for *all* substrates examined, choosing the best of the four systems leads to yields in the range 55–100%. The average yields for each of the four procedures in the presence of $Cu(OAc)_2$ (10 mol%) were: 1) 67% ($O_2$), 2) 75% (TEMPO/air), 3) 59% (PNO/air), and 4) 42%. A modified Collman catalytic system in the presence of $[\{Cu(OH){\cdot}tmeda\}_2]Cl_2$ (10 mol%)/oxygen was a less-efficient system, although it was best for benzimidazole derivatives.

Classic routes to *N*-arylated aziridines have not involved transition-metal-catalyzed *N*-arylation.[53] However, Yudin and co-workers recently showed that *N*-arylation is possible under the modifications of the Buchwald method. Both palladium- and copper-catalyzed routes were successful with a range of boronic acids (Scheme 27).[54]

 © 2003 Wiley-VCH Verlag GmbH & Co. KGaA, Weinheim 




***Scheme 26.*** Key step: 1) Boronic acid (2 equiv), $Cu(OAc)_2$ (10 mol%), $O_2$, 4 Å molecular sieves, $CH_2Cl_2$, room temperature, 4 days; 2) boronic acid (2 equiv), $Cu(OAc)_2$ (10 mol%), TEMPO (1.1 equiv) and air, 4 Å molecular sieves, $CH_2Cl_2$, room temperature, 4 days; 3) boronic acid (2 equiv), $Cu(OAc)_2$ (10 mol%), PNO (1.1 equiv) and air, 4 Å molecular sieves, $CH_2Cl_2$, room temperature, 4 days; 4) boronic acid (2 equiv), $Cu(OAc)_2$ (10 mol%), $[\{Cu(OH)\cdot tmeda\}_2]Cl_2$, $O_2$, 4 Å molecular sieves, dichloromethane, room temperature, 4 days.




***Scheme 27.*** Key step: Boronic acid (1.5 equiv), $Cu(OAc)_2$ (10 mol%), 2,6-lutidine (1 equiv), myristic acid (20 mol%), toluene, room temperature, 24 h; (*) with camphanic acid; (**) with 2-phenylbutyric acid; (***) at 50 °C, time not stated.

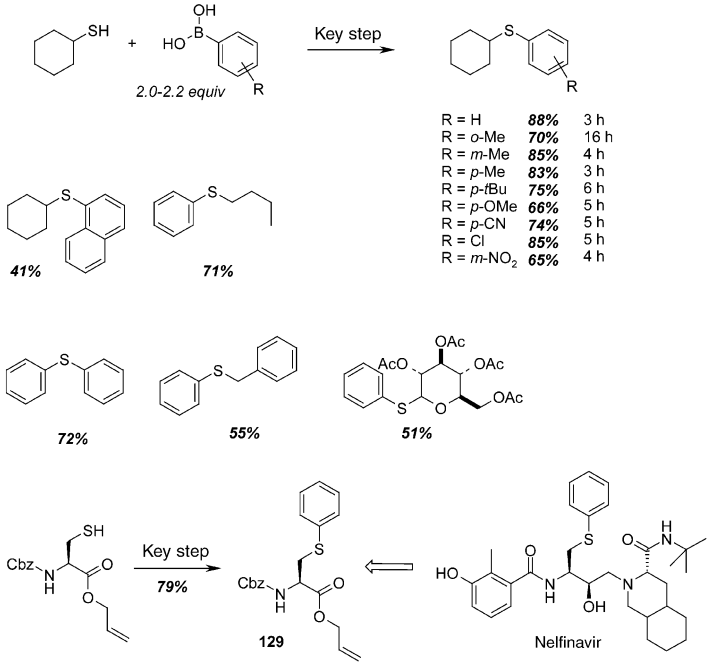
### 2.4. Copper-Mediated C(aryl)–S Bond Formation

#### 2.4.1. The Original Stoichiometric $Cu^{II}$ Methods and Their Substrate Scope

The need for better synthetic access to **129** led Guy and co-workers to explore a copper-mediated *S*-arylation of thiols (cysteine derivative) with phenylboronic acids in a formal synthesis of nelfinavir.[55] In a model study with cyclohexanethiol and *p*-tolylboronic acid, it was shown that under the conditions developed by the groups of Lam and Chan for *N*- and *O*-arylation reactions, the reactions were too slow for *S*-arylation because of significant disulfide formation as a result of competitive oxidation. However, it was shown that the reaction of a wide range of thiolate substrates with electronically and structurally diverse boronic acids proceeded well when heated to 155 °C in DMF to afford the desired cross-coupled products in good yields (Scheme 28). No racemization was observed during the synthesis of cysteine phenylsulfides. Unfortunately, tertiary thiols, thiolacetic acids, and α-methoxycarbonylthiolates did not react under these conditions.

#### 2.4.2. The Original Catalytic $Cu^{I}$ Method

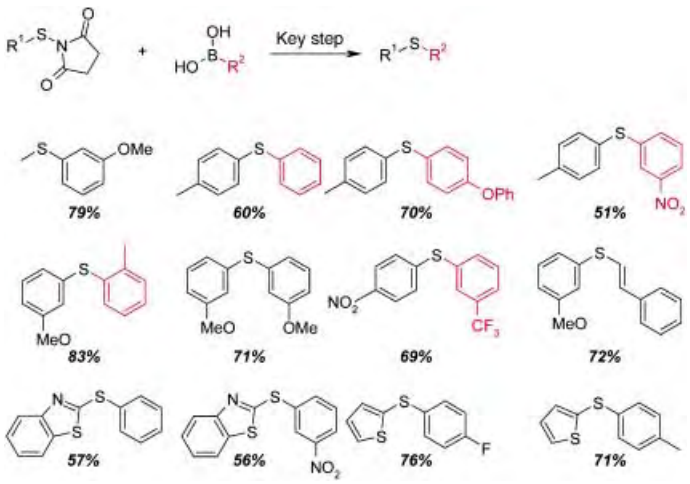
Improvements to this method were clearly needed and Liebeskind et al. reported a novel, interesting, mild, copper(I)-mediated strategy for the synthesis of thioethers in the absence of base. They proposed that the mechanism for alkylaryl sulfide formation does not parallel that of the *O* and *N* counterparts (see Section 11), but instead it is more likely that a $Cu^{I}$-mediated transformation takes place owing to the facile oxidation of thiols to disulfides by $Cu^{II}$.[56] This postulate was supported by the preparation of diphenylsulfide (74%) from the reaction between phenylboronic acid and $Cu^{I}$–3-methylsalicylate [CuMeSal]




***Scheme 28.*** Key step: Boronic acid (2 equiv), $Cu(OAc)_2$ (1.5 equiv), pyr, 4 Å molecular sieves (75 wt%), DMF, reflux, argon, 2–16 h.


© 2003 Wiley-VCH Verlag GmbH & Co. KGaA, Weinheim

in DMA at 100 °C for 18 h. This result was particularly significant since it showed for the first time that *S*-arylation was possible under *non-basic* conditions. In fact the use of base (TBAF, $K_2CO_3$, NaOH, $Et_3N$, or pyridine) in the reaction actually impedes its progress. Accepting the empirical assumption that $Cu^I$ is required in stoichiometric amounts (50 % is converted into the catalytically inactive $Cu^I$ thiolate) led the investigators to develop a reaction protocol in which *N*-thioimides serve as the electrophilic sulfide source. In the reaction, a range of boronic acids (1.4 equiv) smoothly reacted with *N*-thioimides (1.0 equiv) in the presence of [CuMeSal] (20–30 mol %) in THF at 45–50 °C to afford the desired cross-coupled products in moderate to good yields of 51–79 % (Scheme 29). It was noted that disulfides can be used




***Scheme 29.*** Key step: Boronic acid (1.4 equiv), CuMeSal (20–30 mol %), THF, 45–50 °C, 4–5 h. R = *p*-tolyl, *m*-methoxyphenyl, 2-benzothiazolyl, 2-thienyl.

efficiently in the reaction, although stoichiometric amounts of $Cu^I$ are necessary. Alternative copper(I) carboxylates (CuOAc and CuTC; TC = [$Cu^I$–thiophene-2-carboxylate]) were effective in promoting the *S*-arylation, however CuCN, $Cu_2O$, and CuCl were not.

### 2.5. Reaction with Aryl Boronic Acids: Summary

When forming C(aryl)–O, C(aryl)–N, and C(aryl)–S bonds, the use of aryl boronic acids as the aryl donor is very much dependent on the oxidation state of the Cu catalyst. $Cu^{II}$ salts are most commonly used, although it is not known for sure that $Cu^{II}$ is the form of the active catalytic species during these processes. In nearly all reports with O, N, and S nucleophiles, $Cu(OAc)_2$ has proved to be the best source of $Cu^{II}$ for the Chan, Evans, and Lam modifications of the Ullmann condensation reaction. The reactions are carried out with either $Et_3N$ or pyridine as base in dichloromethane, and stirred vigorously to help with the uptake of oxygen. As the solubility of oxygen decreases at higher temperatures, the reactions are generally carried out at room temperature. These conditions seem to be critical to the success of the reaction with an impressive range of substrates. However, these reactions are generally slow (18 h–13 days to proceed to completion). As an exception, iodoindazoles react much quicker.

Although the reaction conditions in these powerful new methods are significant improvements over classical Ullmann condensation conditions, there is still room for improvement. The enhanced rates of reaction in the microwave-mediated process has only been shown for some solid-supported reactions of N nucleophiles. A parallel study with O and S nucleophiles has not yet been reported. In all cases, the use of excess aryl boronic acid is also a major limitation of the method. The reasons for this are discussed later (see Section 12). In general, the presence of molecular sieves results in better yields.

Catalytic variants of this transformation are possible and closely parallel the stoichiometric $Cu^{II}$ route. These reactions rely on an efficient reoxidation of the active catalytic species involved in the reaction processes with molecular oxygen or other co-oxidants such as TEMPO. Again the reaction times are in excess of 24 h and rely on the use of excess aryl boronic acid. Additives such as myristic acid, which may aid solubilization of the $Cu^{II}$ species, offer distinct advantages when used in combination with 2,6-lutidine and air or dioxygen. Collman et al. used [Cu(OH)Cl·tmeda] and related systems, which led to a considerable understanding of the catalytic process when employing $Cu^I$ salts and a range of bidentate nitrogen-ligand systems. This has allowed environmentally benign variations of the reactions in water with air as reoxidant.

The reaction of sulfides with aryl boronic acids needed much more optimization as disulfide formation was a predominant reaction outcome with $Cu(OAc)_2$ under the standard conditions developed for O and N nucleophiles. Increasing reaction temperature to 155 °C, excluding air from the reaction, and use of DMF as solvent allowed the successful formation of C(aryl)–S bonds. The significant discovery by Liebeskind and co-workers, who used $Cu^I$ (from [CuMeSal], CuOAc or CuTC) as the active catalytic species, showed that it was possible to form the desired *S*-arylated products from the reaction between excess aryl boronic acid and *N*-thioimides (as the *S* electrophile) under *nonbasic* conditions.

These reactions were used successfully in a range of studies into the substrate scope, in natural product directed synthesis, as well as in medicinal chemistry directed programs, and it is anticipated that the use of these methods will continue to escalate.

## 3. Aryl Halides as the Aryl donor: C(aryl)–N Bond Formation

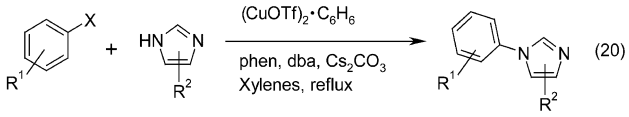
The first *ipso* substitution of an aryl halide by a nucleophile was first reported in 1901 by Ullmann. It was shown that "Cu" can oxidatively insert into and thus polarize a carbon–halogen bond effectively. The polarized bond then undergoes further attack (either inter- or intramolecular) by a nucleophilic species, as was demonstrated in the early cases with phenoxides and aryl amines. Possible mechanisms of this Ullmann condensation reaction have already been reviewed.[57]

 © 2003 Wiley-VCH Verlag GmbH & Co. KGaA, Weinheim 

### 3.1. The Original Discovery: Catalytic Cu Methods and Substrate Scope

The groups of Buchwald and Hartwig pioneered a renaissance in the C(aryl)–heteroatom bond construction with their seminal contributions using palladium salts and "tailored ligands and bases" to cope with a broad range of heteroatom-containing substrates.

Since this time, Buchwald and co-workers have continued to make further important contributions to the introduction of a general Ullmann-type synthesis of diaryl amines [Eq. (20)].[58] Perhaps the first modern variant was

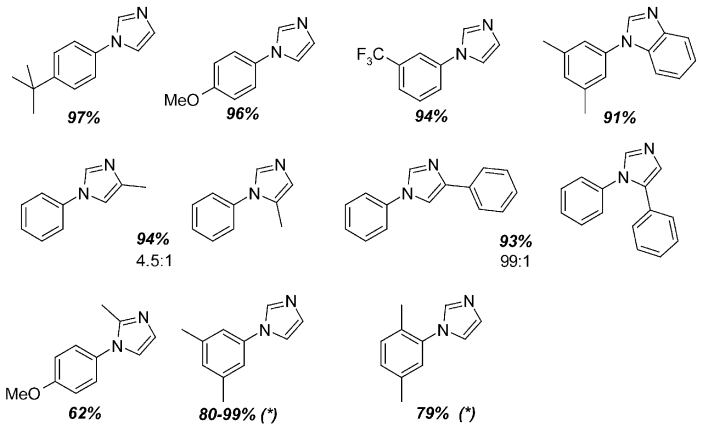



(20)

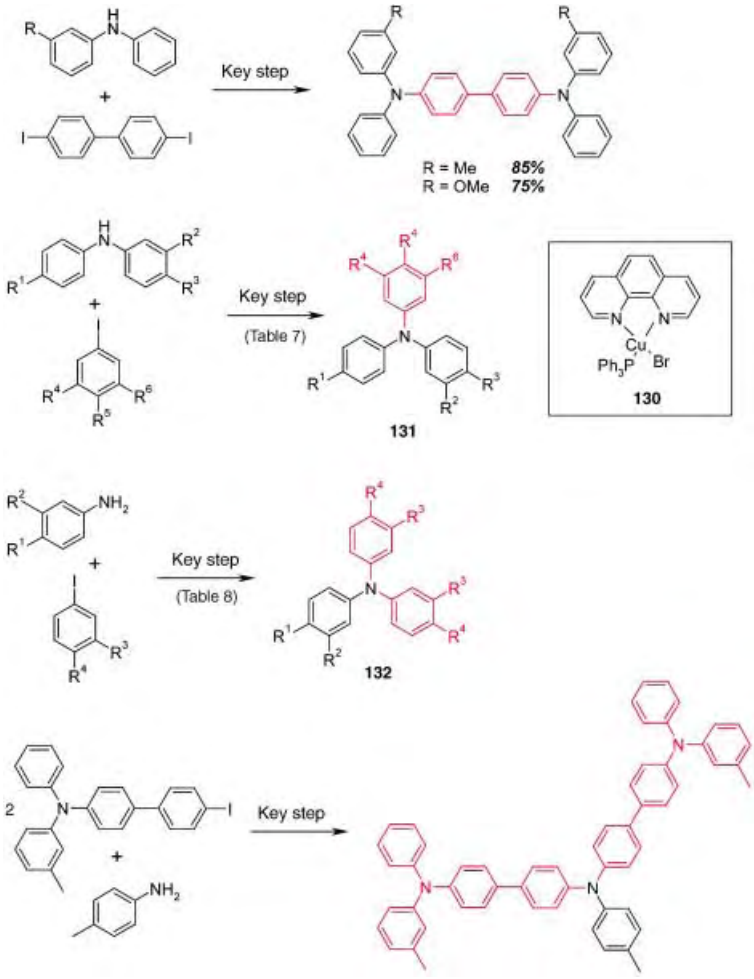
the report that $(CuOTf)_2$ can efficiently catalyze the reaction between imidazoles and aryl halides which revitalized this area of research, as reflected by the increasing number of reports in the scientific literature.

Although the reaction conditions used were certainly not yet general (100–125 °C in xylenes), it was clear that a new strategy for investigating improved catalytic systems had commenced. The use of catalytic amounts of $(CuOTf)_2{\cdot}C_6H_6$ and the addition of stoichiometric amounts of 1,10-phenanthroline, *trans,trans*-dibenzylidineacetone, and $Cs_2CO_3$ (as base) were critical to the effectiveness and reproducibility of the imidazole arylation. Both electron-rich and electron-deficient aryl iodides and bromides reacted well, offering the desired products in near-quantitative yields (Scheme 30).

Goodbrand and Hu also used a similar system to prepare "hole-conducting" triaryl amines in the presence of [Cu(phen)($PPh_3$)Br] (**130**) as an accelerating ligand (Scheme 31).[59] In this case, lower temperatures were




***Scheme 30.*** Key step: Aryl iodide (2 equiv), imidazole (3 equiv), $(CuOTf)_2{\cdot}C_6H_6$ (10 mol%), phen (2 equiv), dba (10 mol%), $Cs_2CO_3$, xylenes, 110–125 °C, 24–48 h; (*) from aryl bromide.




***Scheme 31.*** Key step: Aryl iodide (1 equiv), diaryl amine (1 equiv), CuCl (4 mol%), phenanthroline (4 mol%), KOH, toluene, 125 °C, 4–5 h.

***Table 7:*** Ligand-accelerated catalysis of the Ullmann condensation with CuCl and phenanthroline.

| Compound | $R^1$ | $R^2$ | $R^3$ | $R^4$ | $R^5$ | $R^6$ | Yield [%] |
|---|---|---|---|---|---|---|---|
| **131a** | H | H | H | Me | H | Me | 85 |
| **131b** | H | OMe | H | H | Me | H | 61 |
| **131c** | Ph | Me | Me | OMe | H | H | 80 |
| **131d** | Ph | Me | Me | H | Ph | H | 78 |
| **131e** | Ph | Me | Me | Me | Me | H | 80 |
| **131f** | Ph | Me | Me | H | H | H | 80 |
| **131g** | H | Me | H | H | *p*-$BrC_6H_4$ | H | 80 |

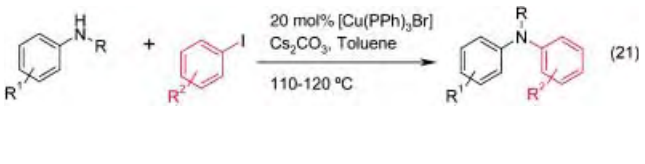
***Table 8:*** Ligand-accelerated catalysis of the Ullmann condensation with CuCl and phenanthroline.

| Compound | $R^1$ | $R^2$ | $R^3$ | $R^4$ | Yield [%] |
|---|---|---|---|---|---|
| **132a** | H | H | H | Me | 73 |
| **132b** | Br | H | H | Me | 85 |
| **132c** | Br | H | Me | Me | 83 |
| **132d** | Me | Me | Me | Me | 70 |
| **132e** | Ph | H | Me | Me | 83 |
| **132f** | Br | H | H | Br | 73 |

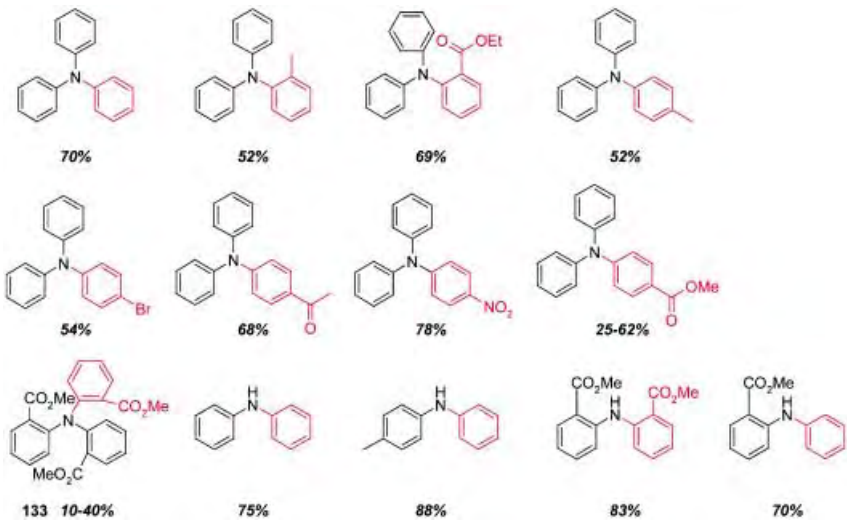

© 2003 Wiley-VCH Verlag GmbH & Co. KGaA, Weinheim

required when using catalytic CuCl and KOH as base. Some examples of the products formed are shown in Tables 7 and 8.

Venkataraman and co-workers also showed that a *soluble* copper(I) species can be used as a catalyst in the construction of C(aryl)–N bonds [Eq. (21)].[60] $[Cu(PPh_3)_3Br]$ is air-stable,

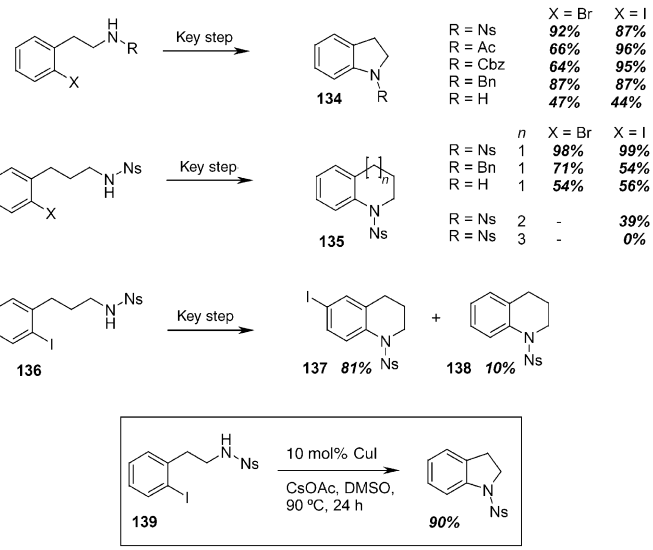



readily prepared from $CuBr_2$ and $PPh_3$ in methanol, and is soluble in a wide range of solvents, including THF, $CH_2Cl_2$, MeCN, $CHCl_3$, NMP, DMF, DMSO, toluene, and benzene. It is, however, insoluble in methanol, ethanol, and diethyl ether. A general reaction procedure followed, which included heating a mixture of the aryl iodide with the $[Cu(PPh_3)_3Br]$ catalyst (20 mol%) and $Cs_2CO_3$ at 120 °C for 24–36 h. In general, the desired diaryl amines were obtained in good yields (Scheme 32). Importantly, the diaryl amines can be formed only if the amine, catalyst, and $Cs_2CO_3$ are preheated together at 110 °C for 5 min prior to the addition of the aryl iodide. Of note was the successful preparation of **133**, which with an *ortho* ester functionality had eluded synthesis by modern palladium-catalyzed methods.




***Scheme 32.*** Key step: Aryl iodide (1 equiv), diphenylamine (1 equiv), $[Cu(PPh_3)_3Br]$ (20 mol%), $Cs_2CO_3$ (1.5 equiv), toluene, 110–175 °C, 24 h.

Fukuyama and co-workers used a novel combination of CuI (2.0 equiv) and CsOAc in an efficient intramolecular cyclization route to dihydroindoles **134** and tetrahydroquinolines **135**; reactions were usually complete after 1–24 h at temperatures ranging from room temperature to 90 °C (Scheme 33).[61] This remarkably mild method signifies a breakthrough in the Ullmann condensation reactions at room temperature, although it should be noted that the reaction

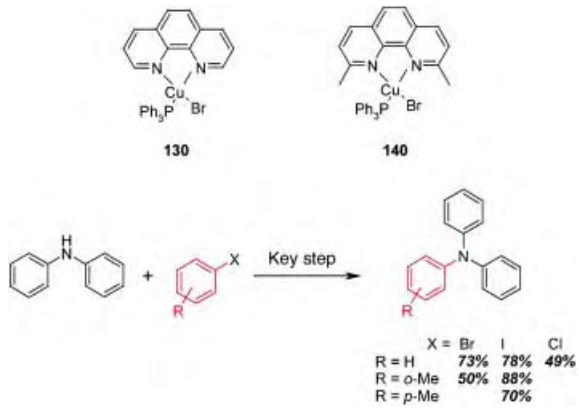



***Scheme 33.*** Key step: CuI (2 equiv), CsOAc, DMSO, RT→90 °C, 1–24 h.

required 2 equivalents of CuI and that the intermolecular variant failed. The scope of the reaction was established using both *o*-bromo- and *o*-iodophenethylamines and a small range of amino-protecting groups (Ac, Ns, Cbz, Bn). The intramolecular reaction was also successful with six- and seven-membered fused ring systems, but failed in the case of the eight-membered system. Remarkably, for substrate **136**, the desired product **137** was only accompanied by 10% of the deiodinated compound **138**—a distinct advantage over palladium-mediated methods. A catalytic system also provided product, although for the same substrate **139** the reaction times needed to be extended from 1 to 24 h.

Venkataraman used diaryl amines substrates to exploit the use of the air-stable and soluble $Cu^I$ catalysts **130** and **140**.[62] The synthesis and characterization of these chemically well-defined, stable, and soluble copper(I) complexes was inspired by the fact *soluble* cuprous ions are proposed as the active catalytic species in Ullmann condensation reactions. In the first examples it was shown that the catalyst **140** is soluble in a wide range of solvents, including $CH_2Cl_2$, $CHCl_3$, toluene (warm), benzene, NMP, DMF and DMSO. However, it is insoluble in diethyl ether and hexane. The catalyst **140** was shown to be twice as fast as **130** in mediating *N*-arylations, and its use was demonstrated in the preparation of the triaryl amines shown (Scheme 34). Thus far, *N*-arylation of primary amines in the presence of **140** has not been reported.

The synthesis of triaryl amines (from aryl iodides and aryl amines) in a *one-pot* reaction was reported to proceed under

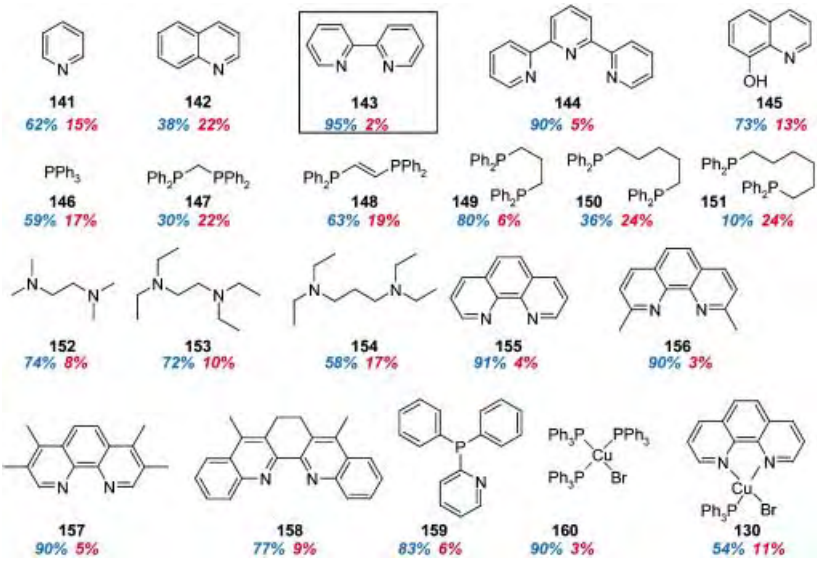



***Scheme 34.*** Key step: [Cu(neocup)(PPh)$_3$Br] (**140**) (10 mol%), KO*t*Bu, toluene, 110°C, 6–36 h.

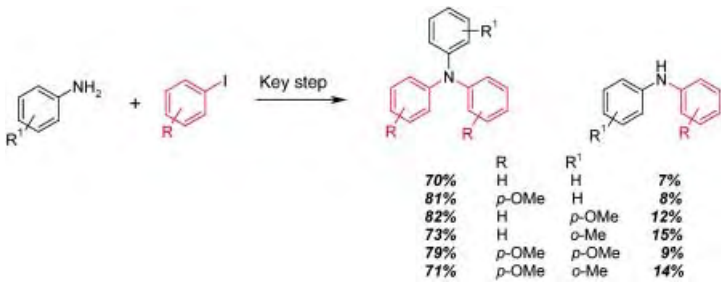
ligand-free Cu-catalyzed conditions in the presence of potassium *tert*-butoxide (Scheme 35).[63] The first system involved the reaction of an aryl amine, aryl halide (3 equiv), and CuI (5 mol% gave moderate turnover numbers of 30–40) in the presence of KO*t*Bu (3 equiv) in toluene at 135°C for 14 h which provided the desired triaryl amines in yields of 28–82%. Other bases (such as NaO*t*Bu, NaOMe, DBU, $Cs_2CO_3$, KOH, and $NaHCO_3$) were less effective. Best results were obtained with electron-rich aryl amines and aryl iodides; the *o*- or *p*-nitroaniline did not afford any triaryl amine.

A systematic study was undertaken on the mono- and bidentate chelating ligands **141**–**160** (Scheme 36). Their ability to form an active copper catalyst species with CuI and to form triphenylamine in the reaction of iodobenzene with aniline was investigated. Contrary to the results of Venkataram and co-workers,[62] it was shown that the $PPh_3$ ligand only accelerated the reaction when the $PPh_3$/Cu ratio was $>2:1$. Quinolines and pyridines were shown to be less efficient ligands. The most efficient chelating bisphosphanes was dppf; however, the diamino chelating ligands gave consistently better yields. 2,2′-Bipyridine (**143**) gave the highest yield and selectivity in favor of the triaryl amine. The yields of triphenylamine and diphenylamine are given in blue and red, respectively, for the representative ligand set (Scheme 36). Further investigation of a single-step transformation showed that the CuI/2,2′-bipyridine-catalyzed amination reaction with electron-rich aryl amines and aryl iodides proceeded with 100% conversion in excellent yields in only 3.5 h at 115°C.

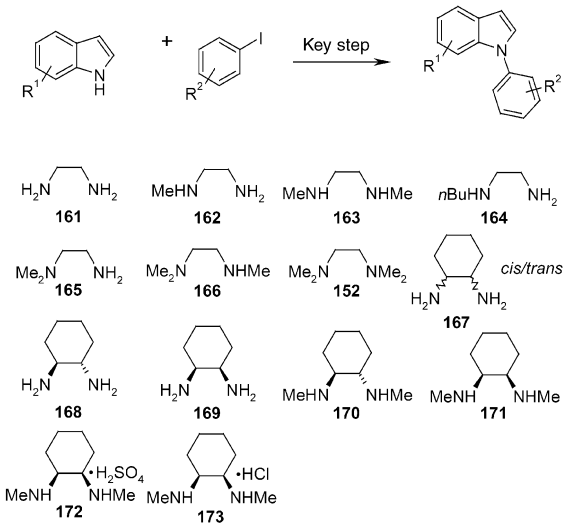
Buchwald and co-workers showed that the known copper-chelating diamine ligands **152** and **161**–**173** are efficient catalysts in the *N*-arylation of a range of substituted indoles (Scheme 37).[64] The desired products were obtained in yields up to 99% under the usual conditions (CuI (1–5 mol%), ligand (**161**–**173, 152**) (10–20 mol%), $K_3PO_4$ base, and preferably toluene as solvent at 110°C for 24 h). From these initial studies, **168** and **170** were shown to be the best ligands (Scheme 38). In studies with **170**, CuI and $Cu^0$ (bronze) were shown to be the most efficient copper sources. Copper(II)




***Scheme 36.*** Key step: Aryl halide (3 equiv), aryl amine (1 equiv), CuI (5 mol%), KO*t*Bu, toluene, 135°C, 14 h.

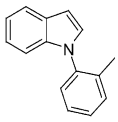



***Scheme 35.*** Key step: Aryl halide (3 equiv), aryl amine (1 equiv), CuI (5 mol%), KO*t*Bu, toluene, 135°C, 14 h.




***Scheme 37.*** Key step: Aryl iodide (1 equiv), indole (1 equiv), CuI (5 mol%), $K_3PO_4$, ligand **152** or **161**–**173**, toluene, 135°C, 14 h.


© 2003 Wiley-VCH Verlag GmbH & Co. KGaA, Weinheim



| Ligand | Yield [%] 4 h | 24 h | Ligand | Yield [%] 4 h | 24 h |
|---|---|---|---|---|---|
| **163** | 52 | 99 | **168** | 66 | 93 |
| **161** | 22 | 96 | **169** | 59 | 88 |
| **162** | 52 | 90 | **170** | 52 | 98 |
| **164** | 52 | 90 | **171** | 39 | 90 |
| **165** | 5 | 43 | **172** | 55 | 94 |
| **166** | 8 | 71 | **173** | 19 | 85 |
| **152** | <1 | 2 | **167** | 41 | 80 |

***Scheme 38.*** Key step: Aryl bromide (1.2 equiv), indole (1 equiv), CuI (5 mol%), $K_3PO_4$, ligand **152** or **161**–**173** (20 mol%), toluene, 110°C, 4–24 h.

sources such as $Cu(OAc)_2$, $CuCl_2$, and $Cu(OMe)_2$ were less efficient, but still suitable. In each case, arylation of the ligand was observed as a side reaction (up to 10%).

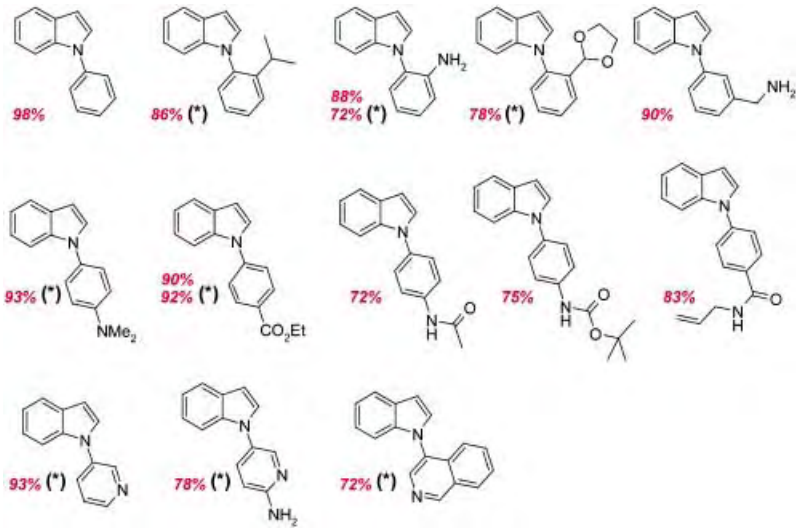
The generality of this transformation was shown with a wide range of functionally substituted indoles (Scheme 39) and aryl halides (Scheme 40) in the presence of ligands **168** (yields in blue) or **170** (yields in red). No reaction occurred with benzoic acids, phenols, or when both reaction partners were substituted at C2.

A variety of diol ligands, **174**–**185**, were assessed in the CuI-catalyzed amination of aryl iodides (Scheme 41).[65] The most efficient system involved a combination of CuI (5 mol%), ethylene glycol (**174**) (2 equiv), and $K_3PO_4$ base in 2-propanol at 80°C; the desired products were obtained in consistently high yields, without the need to protect the reaction from air or moisture.

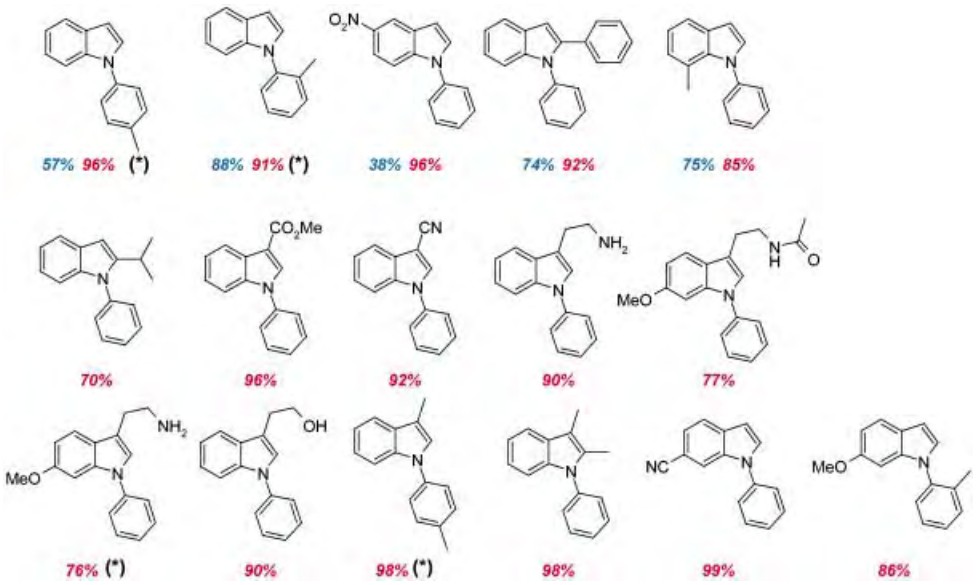
Alternative copper sources (CuBr, CuCl, and CuOAc) were possible, and $Cs_2CO_3$ could be used as base; however, larger amounts of the *O*-arylated ethylene glycol were formed. 2-Propanol was the best choice of solvent, butanol gave acceptable results, but toluene, dioxane, and DMF were much less effective.

Products from the reactions of benzylamine with a variety of substituted aryl iodides are shown in Scheme 42. A range of amines (primary and secondary aliphatic, as well as bi- and tri-functionalized) were also shown to be suitable substrates and all reacted selectively under these new conditions (Scheme 43). Interestingly, neither amides nor anilines are efficient substrates in these reactions.

Aryl bromides were also useful substrates. The products shown in Scheme 44 were formed in initial investigations with the phenol ligands **186a,b**. Driven by the goal to develop even better conditions for the *N*-arylation of primary alkyl amines under which only a stoichiometric amount of the aryl donor is used, Buchwald and co-workers examined a further range of anionic O-donor ligands (Scheme 45).[66] They concluded that



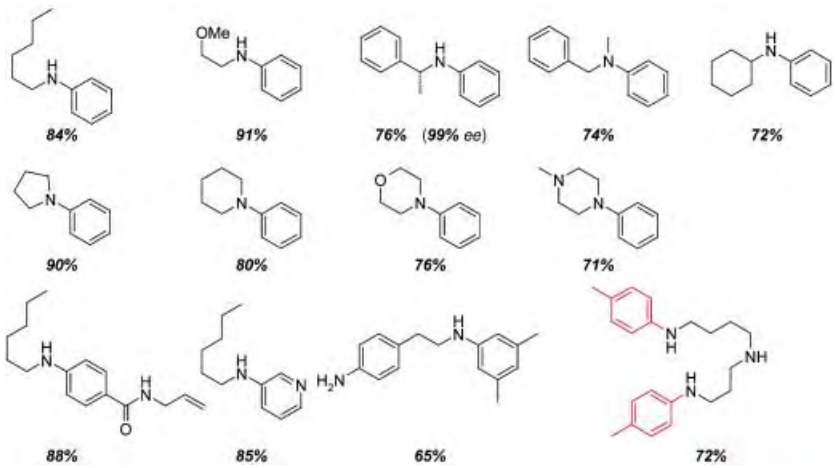

***Scheme 40.*** Key step: Aryl iodide (1 equiv), indole (1.2 equiv), CuI (5 mol%), $K_3PO_4$, ligand **170** (20 mol%), toluene, 110°C, 24 h; (*) from aryl bromide.



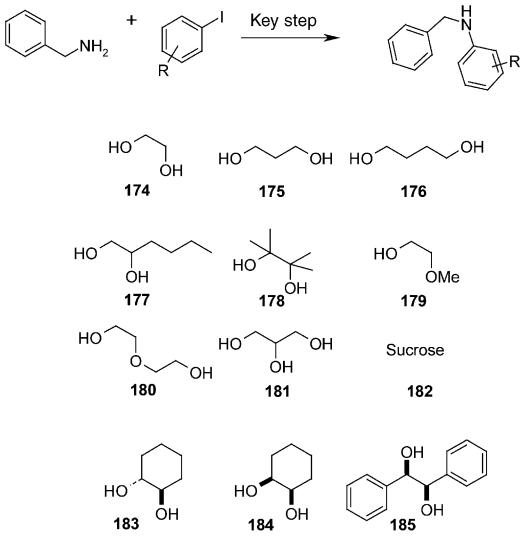

***Scheme 39.*** Key step: Aryl iodide (1 equiv), indole (1.2 equiv), CuI (5 mol%), $K_3PO_4$, ligand **170** (20 mol%), toluene, 110°C, 24 h; (*) from aryl bromide.

 © 2003 Wiley-VCH Verlag GmbH & Co. KGaA, Weinheim 

the commercially available *N,N*-diethylsalicylamide (**187**) provided the best results in terms of yield and conversion. A range of products accessible through this method are shown in Scheme 46, including a variety of *ortho*-substituted and heteroaryl substrates, which normally pose significant challenges owing to their poor reactivity. A limitation of this new method is that secondary amines have provided poor results so far. Both $K_3PO_4$ and $K_2CO_3$ were found to be effective bases. However, the amine bases DBU or DABCO were inefficient. DMF was shown to be a better solvent than toluene, DME, dioxane, and $Et_3N$, although the reaction can also be run under solvent-free conditions. In this case, although the reaction mixture maintains its appearance as a solid throughout the reaction, a range of products were formed in good yields (shown in red in Scheme 46).

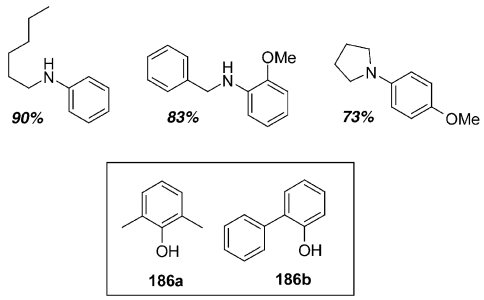



***Scheme 43.*** Key step: Aryl iodide (1 equiv), amine (1.2 equiv), CuI (5 mol%), $K_3PO_4$, ethylene glycol (**174**) (200 mol%), *i*PrOH, 80°C, 12–40 h.

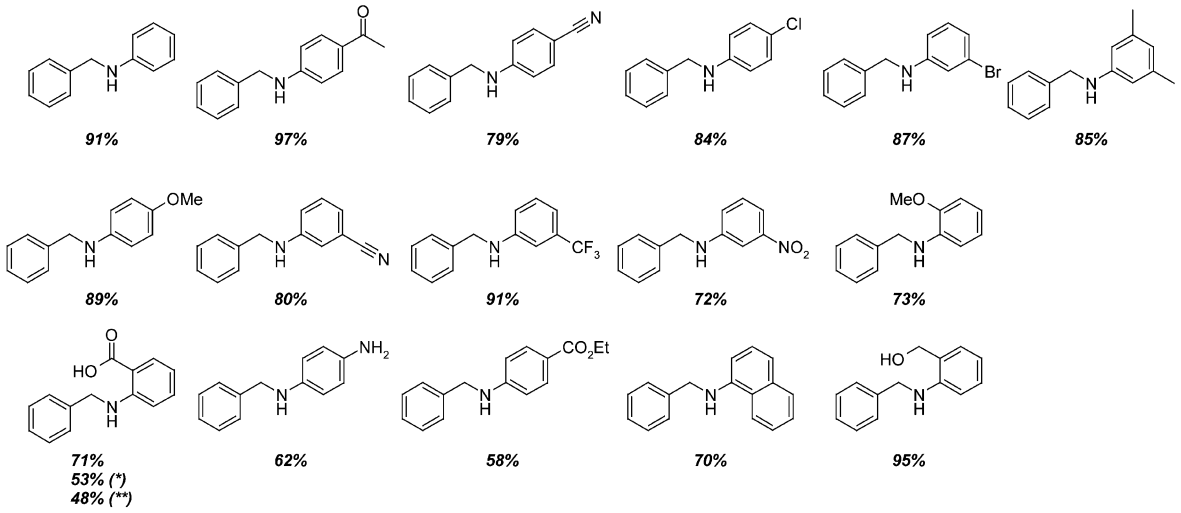



***Scheme 41.*** Key step: Aryl iodide (1 equiv), benzylamine (1.2 equiv), CuI (10 mol%), $K_3PO_4$, ligand **174**–**185** (10–20 mol%), *i*PrOH, 80°C, 18 h.

An intramolecular CuOAc-catalyzed amination of *o*-bromo- and *o*-chlorophenethylamines, in which the *N*-atoms are not protected, provided direct access to dihydroindoles and tetrahydroquinolines (Scheme 47, cf. Scheme 33). Aryl

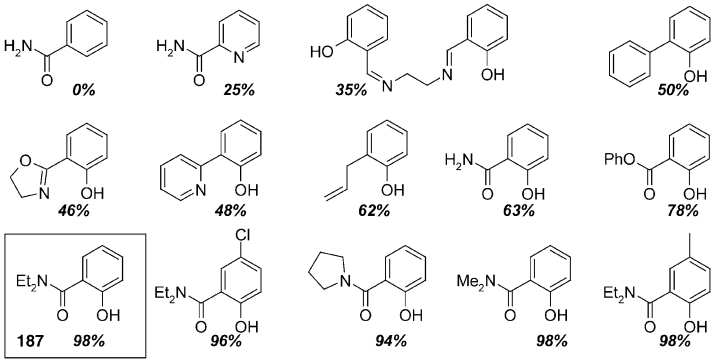



***Scheme 44.*** Key step: Aryl bromide (1 equiv), amine (1.2 equiv), CuI (5 mol%), $K_3PO_4$, **186a** or **186b** (20 mol%), *n*Hex$NH_2$, toluene, 100°C, 5–72 h.

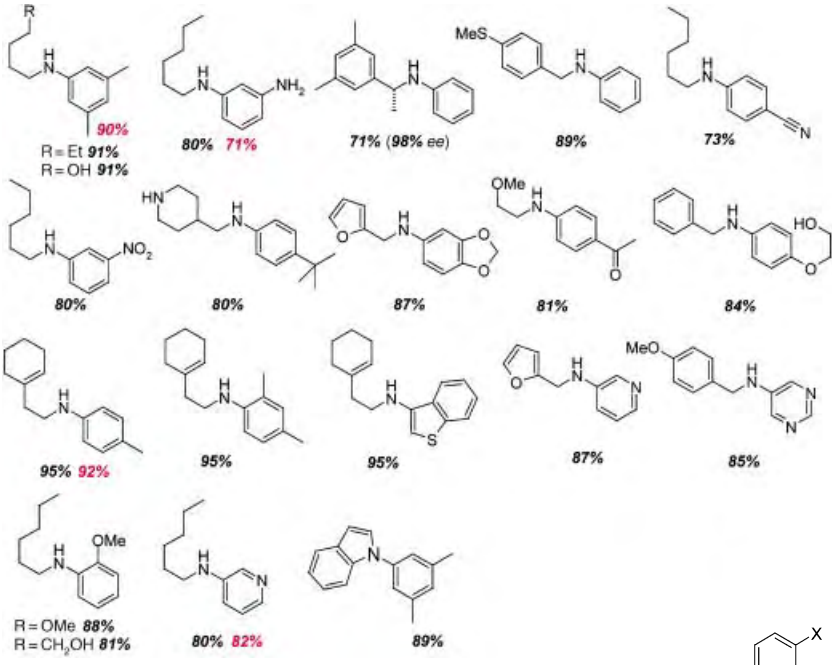



***Scheme 42.*** Key step: Aryl iodide (1 equiv), benzylamine (1.2 equiv), CuI (5 mol%), $K_3PO_4$, ethylene glycol (**174**) (200 mol%), *i*PrOH, 80°C, 5–72 h; (*) from aryl bromide; (**) from aryl chloride.


© 2003 Wiley-VCH Verlag GmbH & Co. KGaA, Weinheim



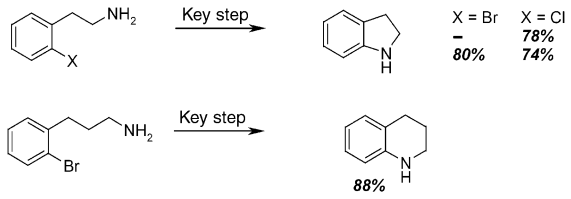

***Scheme 45.*** Range of ligands used in the reaction between 5-bromo-*m*-xylene and *n*HexNH$_2$.




***Scheme 46.*** Key step: Aryl iodide (1 equiv), Amine (1.5 equiv), CuI (5 mol%), $K_3PO_4$, **177** (20 mol%), DMF, 90°C, 18–22 h; yields in red solvent-free, 100°C, 18–22 h.

bromides were the best substrates, but aryl chlorides also reacted even though longer reaction times were required. When CuI was used as catalyst the yield was much lower, which implies that the solubilizing effect of the preformed CuOAc is responsible for this pronounced effect.

Under conditions similar to those in Scheme 41 (CuI (2.5 mol%), $K_3PO_4$ (2 equiv), $HO(CH_2)_2OH$ (1 equiv) in *i*PrOH at 75°C), the selective *N*-arylation of amino alcohols (1.2 equiv) with aryl iodides proceeded in good yields (Scheme 48).[67] A general reaction procedure was developed in which the amino alcohol is the limiting reagent and reacts with the aryl iodide in the presence of CuI (2.5 mol%) and NaOH (2 equiv) in DMSO/$H_2O$ (2:1) or *i*PrOH at 90°C. It was also possible to use

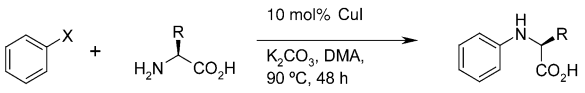



***Scheme 47.*** Key step: CuOAc (5 mol%), $K_3PO_4$ (200 mol%), **177** (20 mol%), DMF, 35–100°C, 12–48 h.

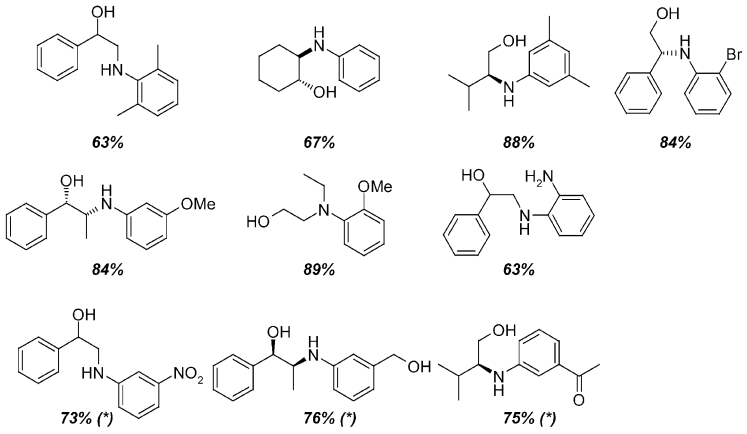
the aryl iodide as the limiting reagent, hence sparing the more valuable chiral material. $K_3PO_4$ can be used as the base instead of NaOH. In both systems, the reaction times were in the 16-h range and only the *N*-arylated product was formed. These protocols offer complementary approaches to epoxide aminolysis, and offer new strategies in planning stereoselective routes to enantiopure arylated β-amino alcohols.

A general *N*-arylation coupling reaction of α-amino acids with aryl halides has also been reported [Eq. (22)].[68]

The accelerating affect induced by α-amino acids has allowed Ullmann-type condensations to be carried out at temperatures significantly lower than those under classic experimental conditions. A systematic study of a variety of amino acids (Schemes 49–51) as well as different aryl halides and copper ion sources allowed the formation of a wide range of products.

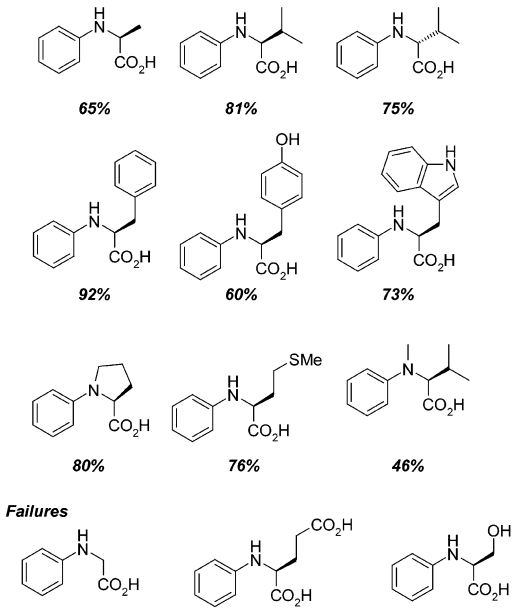



(22)

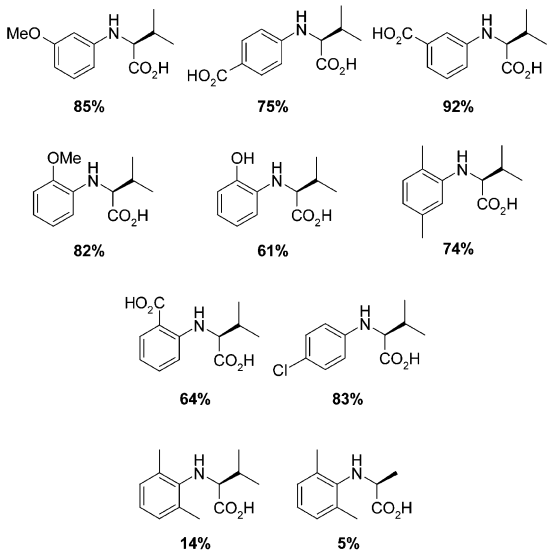



***Scheme 48.*** Key step: Aryl iodide (1.2 equiv), amino alcohol (1 equiv), CuI (2.5 mol%), NaOH, DMSO/$H_2O$ (2:1) or *i*PrOH, 90°C, 15–17 h; (*) aryl iodide (1.2 equiv), amino alcohol (1 equiv), CuI (2.5 mol%), $K_3PO_4$, ethylene glycol (**174**) (100 mol%), *i*PrOH, 75°C, 16 h.

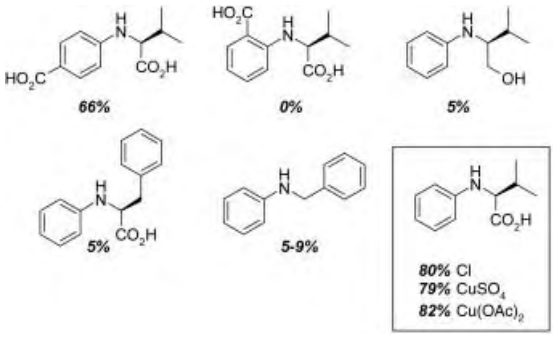
 © 2003 Wiley-VCH Verlag GmbH & Co. KGaA, Weinheim 




***Scheme 49.*** Key step: Aryl halide (1 equiv), amino acid (1 equiv), CuI (10 mol%), $K_2CO_3$ (150 mol%), DMA, 90°C, 48 h.



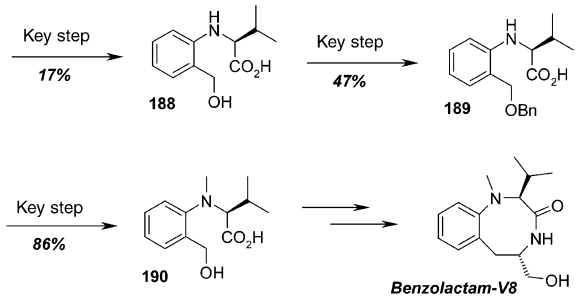

***Scheme 50.*** Key step: Aryl halide (1 equiv), amino acid (1 equiv), CuI (10 mol%), $K_2CO_3$ (150 mol%), DMA, 90–110°C, 48 h.




***Scheme 51.*** Key step: Aryl halide (1 equiv), amino acid (1 equiv), CuI (10 mol%), $K_2CO_3$ (150 mol%), DMA, 75°C, 24–48 h.

### *3.1.1. Application to the Total Synthesis of Molecules of Potential Pharmaceutical Interest*

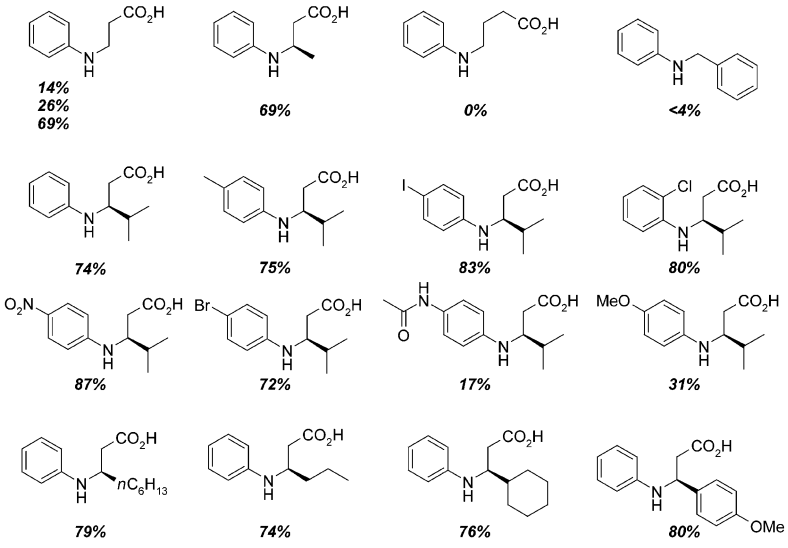
The above-mentioned conditions (see Schemes 49–51) were applied in three copper-mediated strategies in which *o*-iodobenzoic acid derivatives were used as aryl donors in coupling reactions with L-valine to afford the key intermediates **188–190**. Further elaboration with standard reactions allowed an efficient total synthesis of benzolactam-V8 (Scheme 52).




***Scheme 52.*** Key step: Aryl halide (1 equiv), amino acid (1 equiv), CuI (10 mol%), $K_2CO_3$ (150 mol%), DMA, 90°C, 48 h.

A survey of amino acids revealed that β-amino esters were also useful substrates for the CuI-catalyzed coupling reaction with a variety of aryl halides. Higher yields were obtained with aryl iodides after shorter reaction times at lower temperatures than with aryl bromides; aryl chlorides did not react. During the reaction, the ethyl esters were efficiently cleaved in situ to reveal the desired acidic products (Scheme 53).

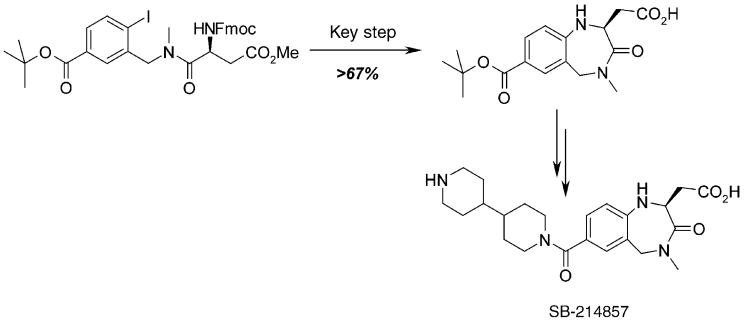
An intramolecular version of this transformation evolved and was used in a facile synthesis of SB-214857. A β-amino




***Scheme 53.*** Key step: Aryl halide (1 equiv), amino acid (1 equiv), CuI (10 mol%), DMF (250 mol%), $H_2O$ (cat.), 90–110°C, 48 h.


© 2003 Wiley-VCH Verlag GmbH & Co. KGaA, Weinheim

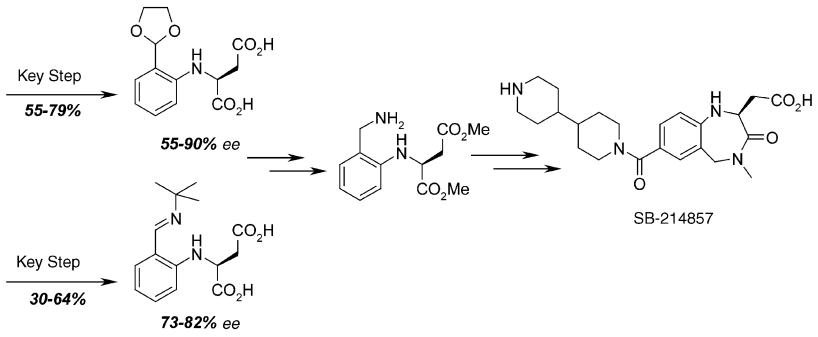
acid was used to accelerate the CuI-catalyzed key intramolecular *N*-arylation reaction, which proceeded in >67% yield (Scheme 54).[69a] No racemization was observed, in contrast to the original aryl fluoride displacement reaction in which 5% racemization was detected.



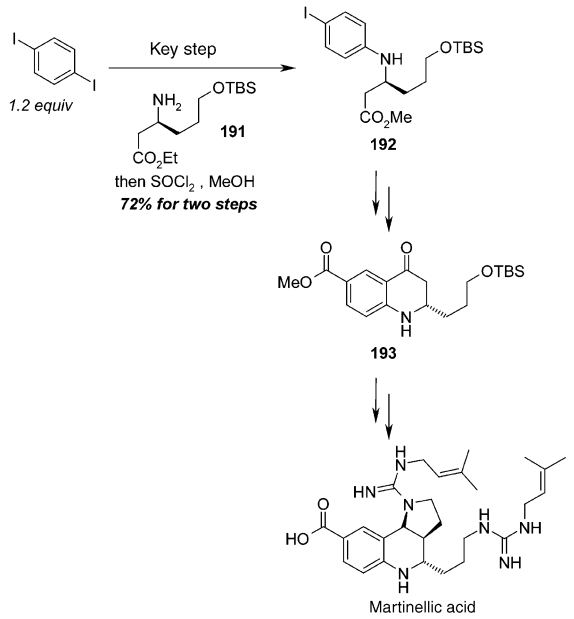

***Scheme 54.*** Key step: CuI (10 mol%), DMF (250 mol%), $H_2O$ (cat.), 90°C, 48 h.

In parallel, Hayes and co-workers examined a similar synthetic strategy to allow efficient access to SB-214857.[69b] The work described above established that there was a tendency for the amino acids with α-hydrophilic substituents to react poorly under the conditions used. It was proposed that the poor reaction outcome may be in part due to the low solubility of this substrate in the reaction medium, and therefore a method was sought to solubilize the substrates. Upon the addition of tetrabutylammonium hydroxide, aspartic acid (which failed to react under the conditions described above, Scheme 49) pleasingly provided access to the desired products, albeit in modest yield, in the presence of CuI in either MeCN, DMF, or DMA (Scheme 55). To improve on these early promising results, a range of copper catalysts were screened. It was shown that the catalytic efficiency was mainly influenced by the oxidation state of copper ($Cu^0 > Cu^I > Cu^{II}$). However, the best system was an unusual combination of Raney copper (19 mol%) mixed with $Cu_2O$ (1 mol%), which was used to prepare lotrifiban SB-214857 (Scheme 55). Notably, the enantiomeric purity tends to decrease with increasing reaction time.

Ma et al. also demonstrated that 1,4-diiodobenzene is a good electrophile in the arylation reaction with the β-amino



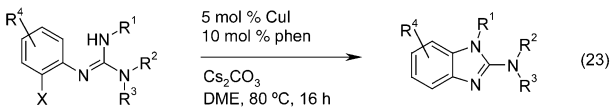

***Scheme 55.*** Key step: Aryl bromide (1 equiv), aspartic acid (1 equiv), Raney copper (19 mol%), $Cu_2O$ (1 mol%), tetrabutylammonium hydroxide (40% aq., 200 mol%), MeCN, reflux, 18 h.




***Scheme 56.*** Key step: CuI (10 mol%), $K_2CO_3$ (300 mol%), DMF, $H_2O$ (cat.), 100°C, 48 h.

ester **191**. No diamination was observed. Although the reaction times were long (2 days), the product was obtained in good yield (>72%) on a >10-g scale. The product **192** was used as a key intermediate en route to **193**, which was then converted into the natural product martinellic acid (Scheme 56).[70]

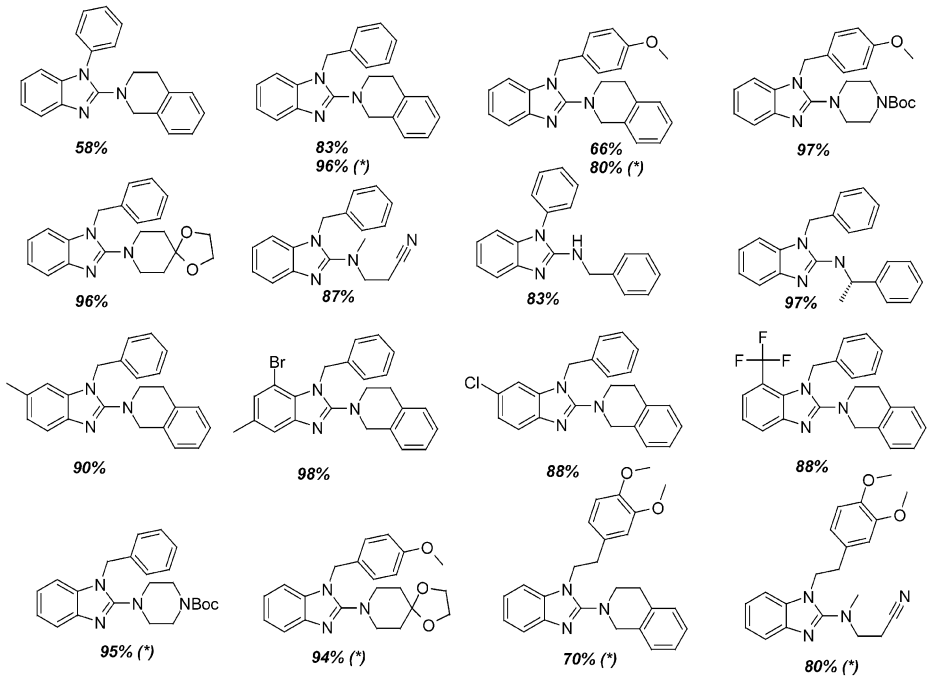
An efficient intramolecular aryl guanidinylation reaction allows access to a number of 2-aminobenzimidazoles [Eq. (23)].[71]




(23)

A direct comparison of a CuI/phenanthroline catalytic system with a palladium-mediated reaction protocol showed that the optimized copper-catalyzed system was superior in terms of yield and selectivity, and a wide range of products were formed in good to excellent yields (Scheme 57). Another comparison between copper- and palladium-catalyzed systems was reported by Buchwald and co-workers, who described a facile route to 6-aminoimidazo[1,2-*a*]pyridines from an aryl iodide substrate (Scheme 58).[72] Again, a copper-catalyzed (Scheme 38, CuI (5–15 mol%), **174**, $K_3PO_4$)[65] proved to be of significant synthetic use, although in some cases the reaction temperature had to be optimized (85–112°C). Scheme 58 shows a range of products obtained in the copper- and palladium-mediated syntheses (yields shown in black and red, respectively).

 © 2003 Wiley-VCH Verlag GmbH & Co. KGaA, Weinheim 

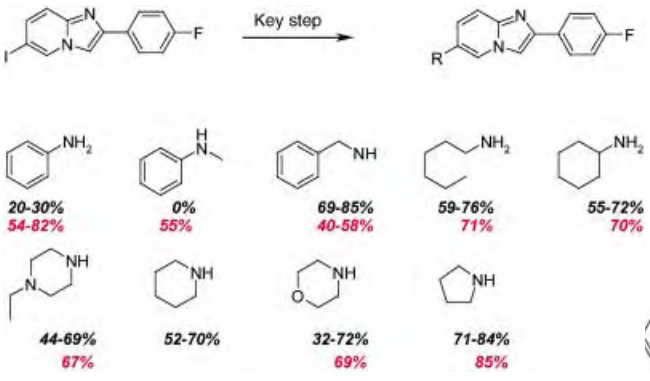



***Scheme 57.*** Key step: CuI (5 mol%), $Cs_2CO_3$ (2 equiv), phenanthroline (10 mol%), DME, 80°C, 16 h; (*) from aryl iodide.

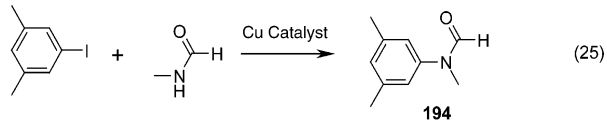
ligands was also performed. When *n*-hexylamine was used as solvent, the product was obtained in near-quantitative yield. This study also revealed that the inexpensive racemic *trans*-1,2-cyclohexanediamine (**168**) in the presence of a base ($K_3PO_4$, $K_2CO_3$, $Cs_2CO_3$, or NaO*t*Bu) in combination with CuI comprised a general and efficient protocol for the *N*-arylation of a variety of amides with aryl and heteroaryl iodides and bromides.

#### 3.2.1. *Choice of Copper Source*

For the formation of **194**, a range of readily available copper sources were screened, which revealed that $Cu^0$ (bronze), CuCl, CuSCN, $Cu_2O$, $CuCl_2$, $CuSO_4 \cdot 5H_2O$, $Cu(OAc)_2$, and $Cu(acac)_2$ were suitable alternatives to CuI [Eq. (25)]. Although in the following investigations only CuI was examined in detail,




***Scheme 58.*** Key step: N nucleophile (1.1 equiv), CuI (5–15 mol%), $HOCH_2CH_2OH$ (200 mol%), $K_3PO_4$, *i*PrOH, 85–112°C, 20–48 h.



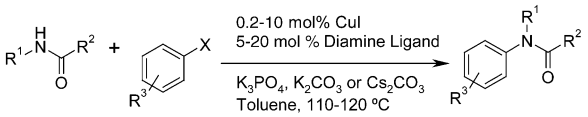

(25)

it can be assumed that for most of the transformations these other reagents can be used as alternatives.

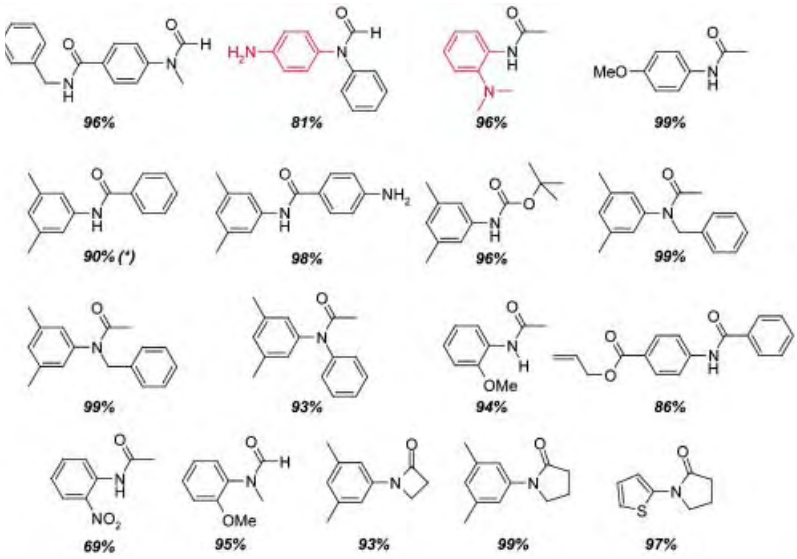
### 3.2. N-*Arylation of Amides: Improvements in the Goldberg-Modified Ullmann Condensation Reaction*

Buchwald and co-workers have made major contributions to the copper-catalyzed amidation of aryl halides [Eq. (24), Schemes 59–63].[73–75]

These studies confirmed that bidentate chelating ligands such as **168** and **170** have an accelerating effect on these transformations. A systematic screening of

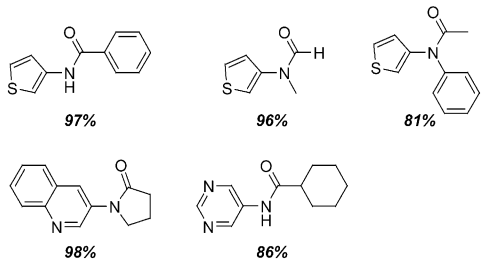



(24)

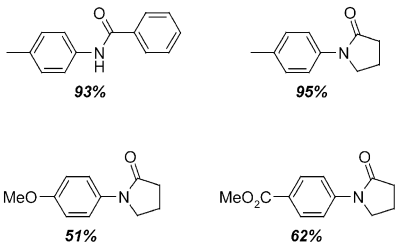



***Scheme 59.*** Key step: Aryl iodide (1 equiv), amide (1 equiv), CuI (10 mol%), **168** (10 mol%), $K_3PO_4$, dioxane, 90–110°C, 23 h. (*) Aryl iodide (1 equiv), amide (1 equiv), CuI (10 mol%), **168** (5 mol%), $Cs_2CO_3$ (2 equiv), dioxane, room temperature, 46 h.


© 2003 Wiley-VCH Verlag GmbH & Co. KGaA, Weinheim



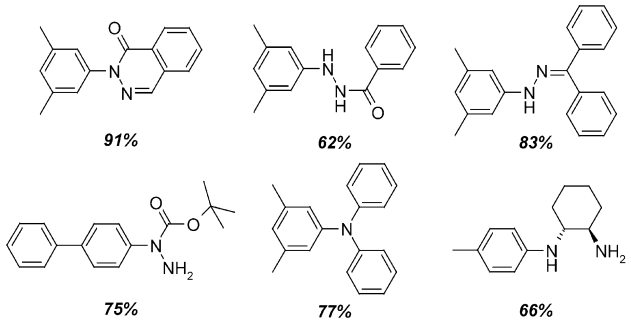

***Scheme 60.*** Key step: Aryl bromide (1 equiv), amide (1 equiv), CuI (1–10 mol%), **168** (10 mol%), $K_3PO_4$, dioxane, 110°C, 15–24 h.




***Scheme 62.*** Key step: Aryl chloride (1 equiv), amide (1 equiv), CuI (5 mol%), **170** (11 mol%), $K_3PO_4$, dioxane, 110–130°C, 23 h.

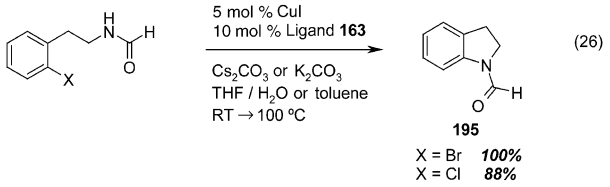
An interesting relationship between the $pK_{HA}$ values of the amide and the base was observed: for enhanced yields, the $pK_{HA}$ value of the base should be lower than that of the amide substrate. Further studies on the effect of chelating and nonchelating ligands on the stability constant for the catalytically active copper–amine species are clearly needed since working guidelines for the use and design of these catalytic systems are required.

Aryl chlorides were also used as electrophilic arylation partners, although ligand **170** was the best choice (Scheme 62). A variety of other *N* nucleophiles efficiently reacted with aryl iodides and in each case only one isomer was formed (Scheme 63).



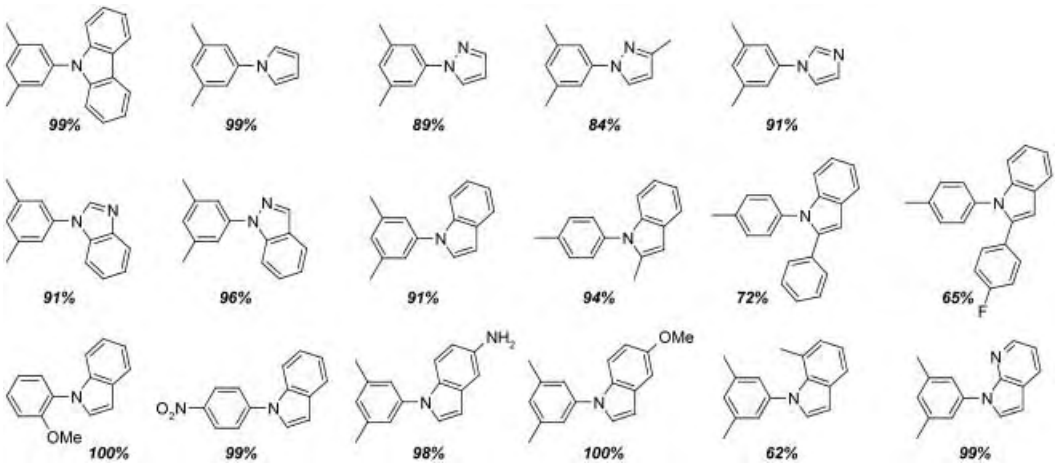

***Scheme 63.*** Key step: Aryl iodide (1 equiv), Aza-nucleophile (1 equiv), CuI (1–20 mol%), **168** or **170** (10 mol%), $K_2CO_3$, $K_3PO_4$, $Cs_2CO_3$ or NaO*t*Bu, dioxane, 110°C, 24 h.

The room-temperature intramolecular aryl amidation reaction with an aryl chloride or bromide was also developed which afforded **195** in yields of 88 and 100%, respectively [Eq. (26)]. This striking result parallels the outcome from palladium-mediated strategies in which the intramolecular amidation reaction is more facile. In the absence of the ligand, no reaction occurs.



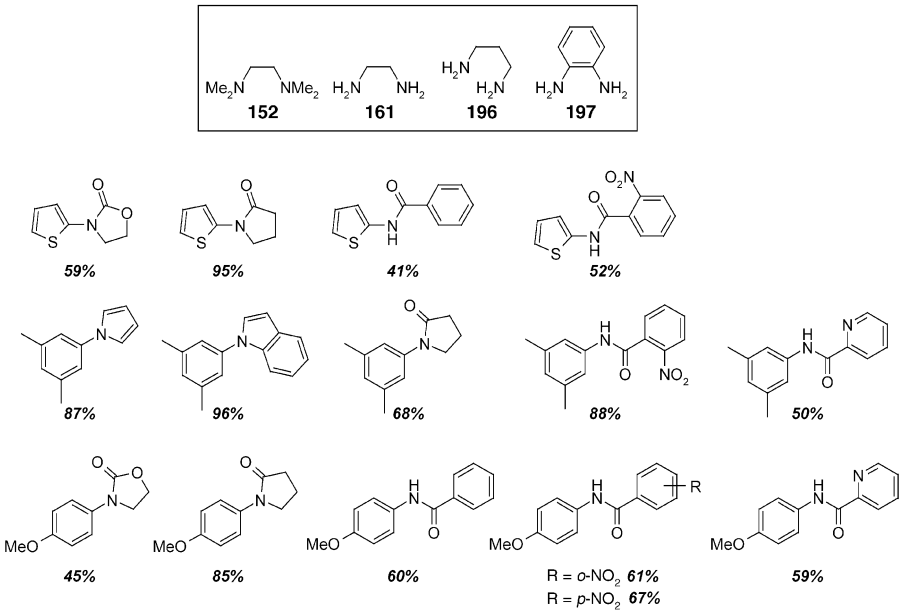

(26)

Kang et al. demonstrated that the cross-coupling of primary and secondary amides as well as carbamates with heteroaryl halides was most efficient in the presence of CuI/**161** (10 mol%) and $K_3PO_4$ base (Scheme 64).[75] These studies also showed that a range of other diamines were suitable ligands (e.g. **152, 196, 197**) in combination with the correct base to affect the amidation of iodothiophene, 3,5,-dimethyliodobenzene, and *p*-methoxyiodobenzene in 45–96% yields.




***Scheme 61.*** Key step: Aryl iodide (1 equiv), azole (1.2 equiv), CuI (10 mol%), 168 (10 mol%), $K_3PO_4$, dioxane, 110°C, 24 h.

 © 2003 Wiley-VCH Verlag GmbH & Co. KGaA, Weinheim 




***Scheme 64.*** Key step: Aryl iodide (1 equiv), amide (1.2 equiv), CuI (10 mol%), **161** (10 mol%), $K_3PO_4$, dioxane, 110°C, 24 h.

Padwa and co-workers also recently exploited these routes in a ligand-free arylation of thiopheno and furano halides to prepare a range of 2- and 3-amido-substituted thiophenes and furans after their reactions with a variety of amides and carbamates (Scheme 65). Thiazole was also examined and afforded the desired product in 58% yield.[76]

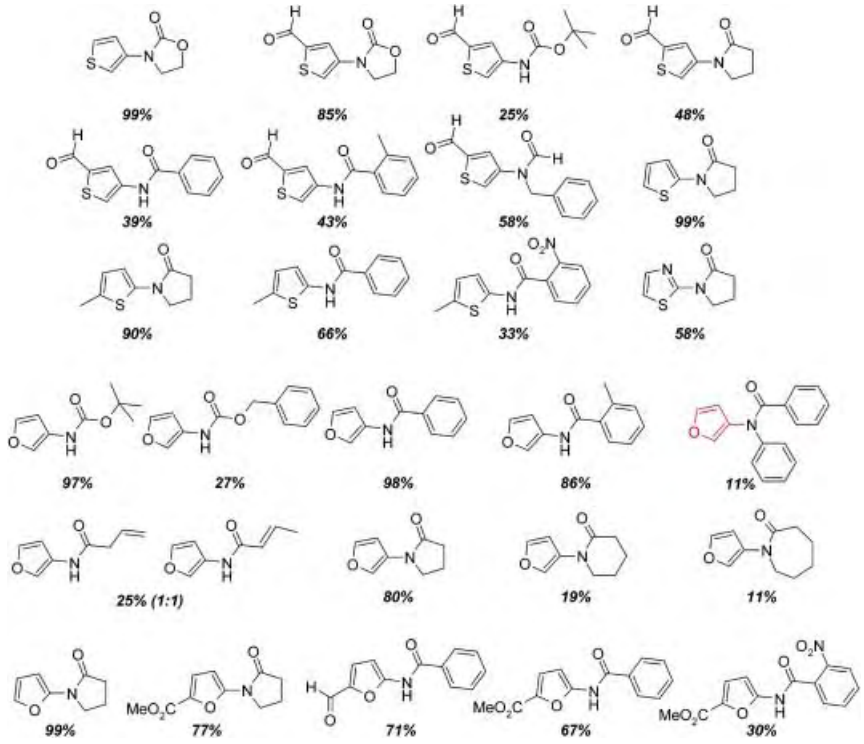
### 3.2.2. *Enhancing Reaction Rates by Microwave Irradiation*

Lange et al used the amidation of aryl bromides in a key strategic step in the efficient syntheses of *N*-aryl piperazinones, piperazinediones, and 3,4-dihydroquinolinones (Scheme 66).[77] In each case, the substrates were combined with CuI (10 mol%) and $K_2CO_3$ base in NMP and exposed to microwave irradiation to afford the desired products very rapidly (20–40 min) in good yields.

### 3.2.3. N-*Aminoamides as Substrates*

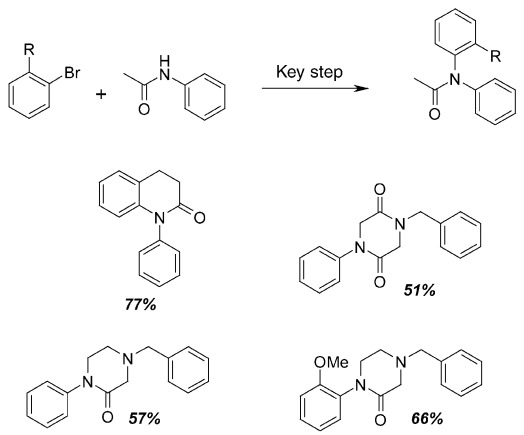
Acyl hydrazides are also suitable substrates under slightly modified conditions with CuI and $Cs_2CO_3$ in combination with phenanthroline (Schemes 67 and 68).[78] Consistently high yields were obtained with long reaction times (24 h), although the temperatures were reduced to 80°C [Eq. (27)]. In these series of examples, a remarkably wide range of functional groups (enolizable ketones, primary and phenolic OH, aniline $NH_2$, ester, and cyano) was tolerated.

The transformation described above was found to be completely regioselective, and the *N*-Boc hydrazine reacted

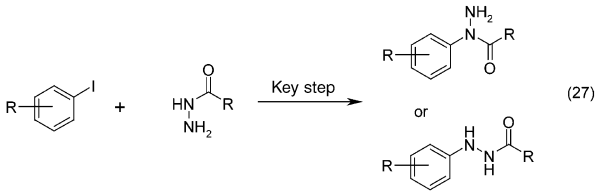



***Scheme 65.*** Key step: Thiophene halide or furan halide (1 equiv), amide (1.2 equiv), (10 mol% CuI), $K_2CO_3$ (430 mol%), dioxane, 110°C, 24 h.

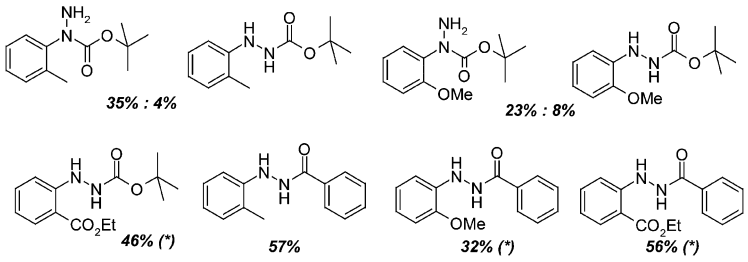
 © 2003 Wiley-VCH Verlag GmbH & Co. KGaA, Weinheim 




***Scheme 66.*** Key step: Aryl bromide (1.5 equiv), Amide (1 equiv), CuI (10 mol%), $K_2CO_3$ (100 mol%), NMP, microwave irradiation (250 W), 190 °C, 20–40 min.

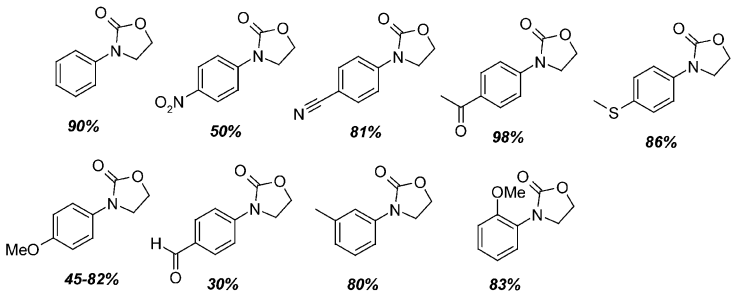



exclusively with *meta*- and *para*-substituted aryl iodides (Scheme 67). When using *ortho*-substituted aryl iodides as the electrophile, a poorer regioselectivity was observed. In the absence of ligand, there was a complete loss of regioselectivity. The use of benzoic hydrazide afforded regioselectively the *N*′-arylated products regioselectively in moderate to good yields (Scheme 68).

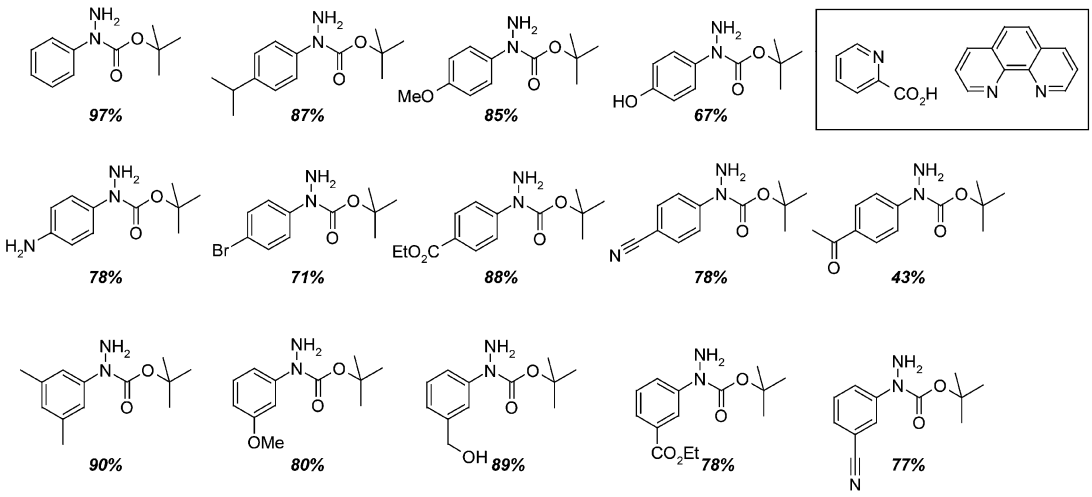



***Scheme 68.*** Key step: Aryl iodide (1 equiv), hydrazide (1.2 equiv), CuI (1–5 mol%), **130** (10–20 mol%), $Cs_2CO_3$ (1.4 equiv), DMF, 80 °C, 21 h; (*) with picolinic acid.

Oxazolidinones are excellent substrates in the *N*-arylation reaction and allow access to a range of substituted *N*-aryl oxazolidinones after some optimization of the conditions previously reported by Buchwald and co-workers (Scheme 69; recrystallized CuI (3 mol%), freshly distilled (±)-**168** (10 mol%), $K_2CO_3$ (200 mol%)).[79] Substituted oxazolidinones also reacted well, and Trehan and co-workers also used this method in an efficient synthesis of racemic linezolid and toloxatone (Scheme 70).

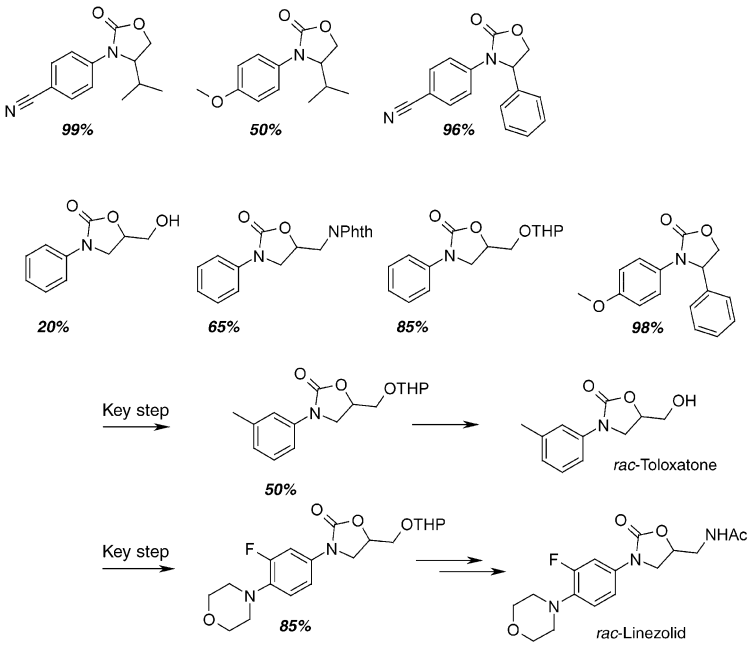



***Scheme 69.*** Key step: Aryl bromide (1 equiv), CuI (3 mol%), **168** (10 mol%), $K_2CO_3$ (2 equiv), dioxane, 110 °C, 15 h.




***Scheme 67.*** Key step: Aryl iodide (1 equiv), hydrazide (1.2 equiv), CuI (1–5 mol%), phenanthroline (10–20 mol%), $Cs_2CO_3$ (1.4 equiv), DMF, 80 °C, 21 h. In box: applied ligands.

 © 2003 Wiley-VCH Verlag GmbH & Co. KGaA, Weinheim 

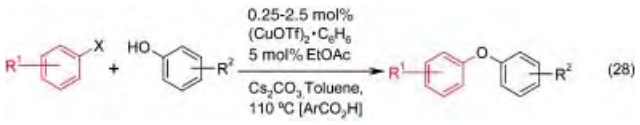



***Scheme 70.*** Key step: Aryl bromide (1 equiv), CuI (3–5 mol%), **168** (10 mol%), $K_2CO_3$ (2 equiv), dioxane, 110°C, 15 h.

## 4. Aryl Halides as the Aryl Donor: C(aryl)–O Bond Formation

### 4.1. The Original Discovery: Catalytic Cu Methods and Substrate Scope

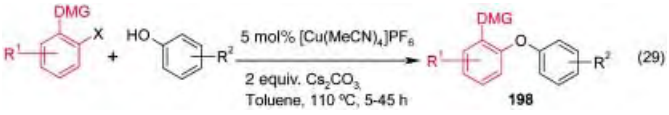
The introduction of cesium carbonate as a base by Buchwald and co-workers for the Ullmann arylation reaction has led to much better procedures for the synthesis of diaryl ethers from a variety of phenols and aryl bromides or iodides [Eq. (28)].[80] Reaction times were in the range of 12–26 h, and ethyl acetate was necessary as a catalytic additive in the reactions.



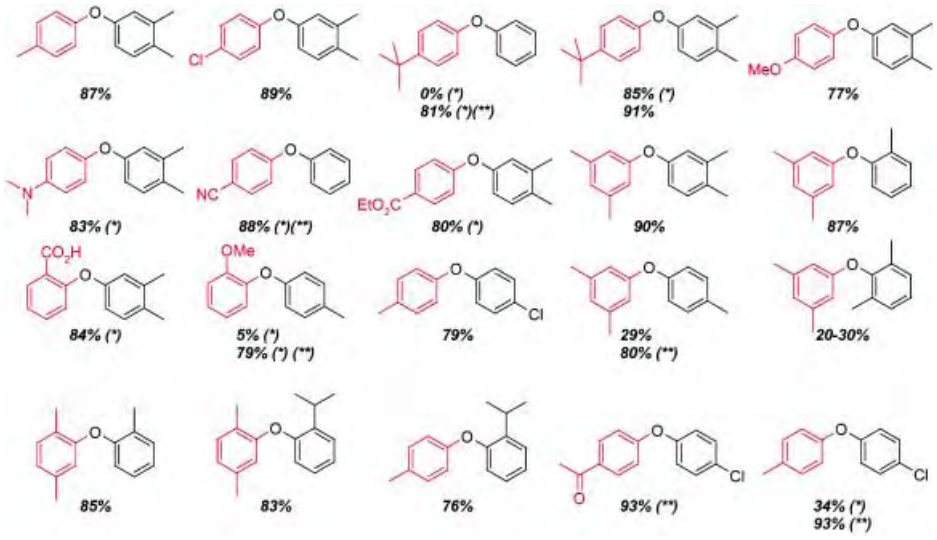

A variety of copper sources, namely $(CuOTf)_2{\cdot}C_6H_6$, CuCl, CuBr, CuI, $CuBr_2$, and $CuSO_4$, displayed similar efficiencies (Scheme 63). Interestingly, less reactive phenols required an equimolar amount of 1-napthoic acid (presumably to solubilize the copper–phenoxide complex or the cesium phenoxide), and molecular sieves greatly facilitated the transformation, presumably by enhancing the reactivity of the system. Under these new conditions, the Ullmann condensation between unactivated aryl halides and less reactive or hindered phenols was now possible (Scheme 71).

The 2-hydroxy-2′-methoxydiphenyl ether framework present in verbenachalcone was assembled through the copper-catalyzed coupling of the 2-benzyloxybromobenzene derivative with a 2-methoxyphenol (Scheme 72). An alternative disconnection using a 2-bromoanisole derivative as the electrophile failed.[81]

Snieckus and co-workers elegantly used a directed *ortho* and remote metalation concept to prepare a series of 1,2,3-contiguous aromatic substitution patterns for compounds of type **198** [Eq. (29)].[82]

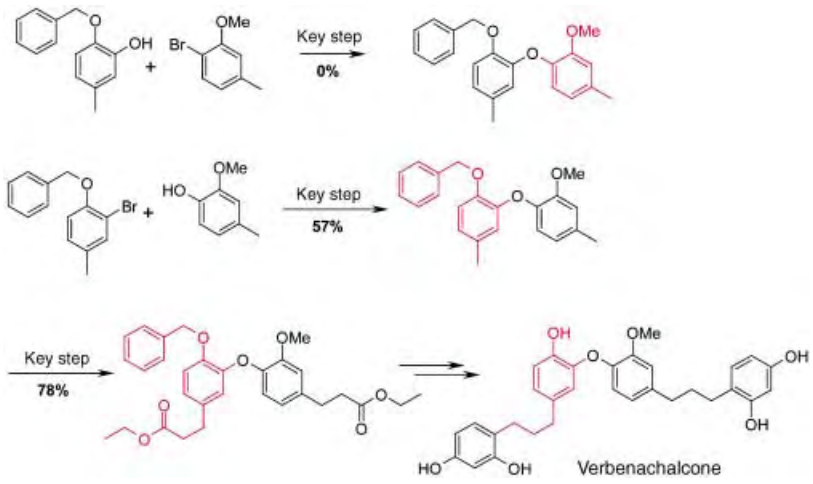



The methodology employed the catalytic (5 mol%) use of $[CuPF_6(MeCN)_4]$ instead of the air-sensitive $(CuOTf)_2{\cdot}C_6H_6$




***Scheme 71.*** Key step: Aryl iodide (1 equiv), phenol (1.4–2 equiv), $(CuOTf)_2{\cdot}C_6H_6$ (2.5 mol%), $Cs_2CO_3$ (1.4 equiv), EtOAc (5 mol%), toluene, 110°C, 12–26 h; (*) from aryl bromide; (**) with 1-naphthoic acid (1 equiv) and 5 Å molecular sieves.

 © 2003 Wiley-VCH Verlag GmbH & Co. KGaA, Weinheim 

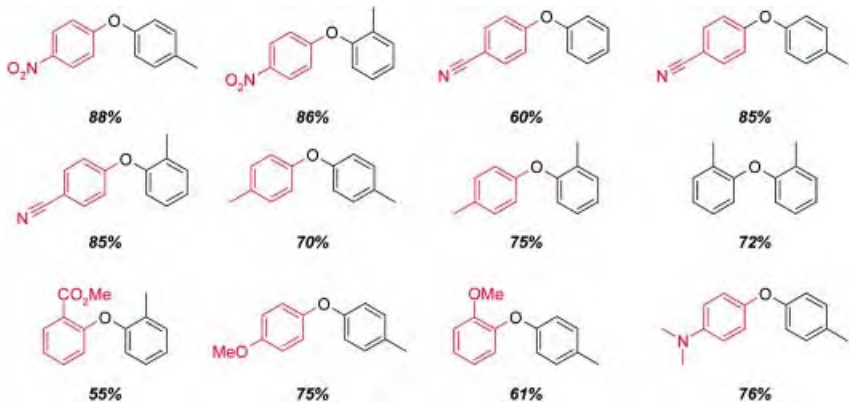



***Scheme 72.*** Key step: Aryl bromide (1.1 equiv), $(CuOTf)_2$·PhMe (2.5 mol%), $Cs_2CO_3$ (1.1 equiv), Pyr, 110°C, 24 h.

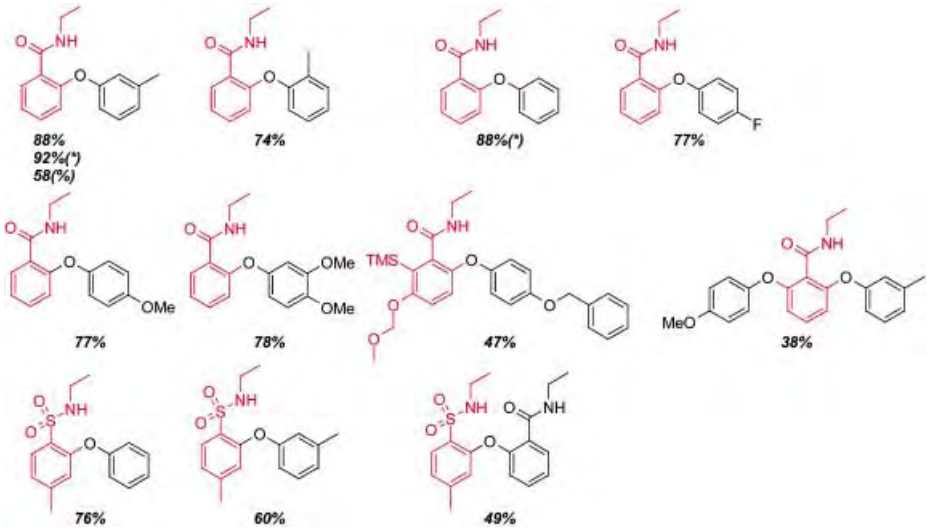
along with $Cs_2CO_3$ in boiling toluene or xylenes. This protocol allowed the preparation of a range of products (Scheme 73) from aryl iodides, bromides, and even secondary chloro benzamides, which are reported to be poor substrates for the Ullmann condensation. Thiophenols and benzylamines were also found to be suitable substrates.

$[Cu(PPh_3)_3Br]$ is an easy-to-prepare air-stable copper(I) catalyst and was found to be a suitable catalyst for the synthesis of diaryl ethers from electron-rich aryl bromides and electron-rich phenols in the presence of $Cs_2CO_3$ in NMP (Scheme 74).[83] With 5 mol% catalyst, long reactions times were required (up to 48 h) to provide the products in good to excellent yields. However, the reaction times could be decreased to 24 h by increasing the catalyst concentrations to 20 mol% or even to stoichiometric amounts. Efficient stirring of the reaction mixture was obligatory, and the reactions did not proceed when using $K_2CO_3$, KO*t*Bu, or DMAP, or when using toluene as solvent.

The choice of protecting group for the aniline in the synthesis of *p*-aminomethoxy derivatives was crucial for the Ullmann reaction of 2-fluoro-4-iodoaniline.[84] Unprotected aniline, methylacetamide, methylcarbamate, phthalate, or benzophenone imine all failed to provide any trace of




***Scheme 74.*** Key step: Aryl halide (1 equiv), phenol (1 equiv), $[Cu(PPh_3)_3Br]$ (20 mol%), $Cs_2CO_3$, NMP, 100°C, 17–24 h.

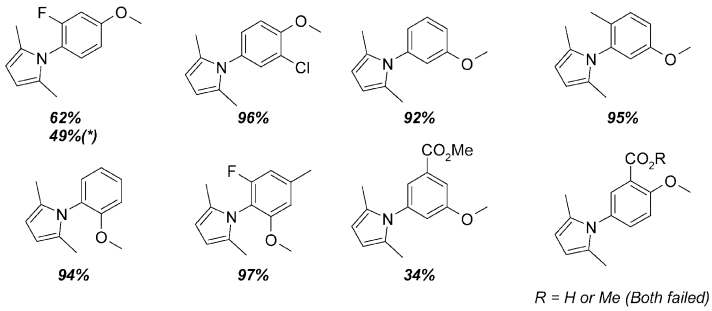



***Scheme 73.*** Key step: Aryl halide (1 equiv), phenol (1.2–1.5 equiv), $[Cu(MeCN)_4]PF_6$ (5 mol%), $Cs_2CO_3$, toluene or xylene, reflux, 5–45 h.

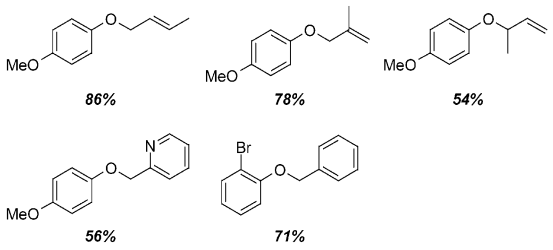
the desired products. However, protection with a 2,5-dimethylpyrrole unit followed by methoxylation with NaOMe/MeOH in the presence of CuI or CuCl (15 mol%) as catalyst gave the desired products in good yields (Scheme 75).

Buchwald and co-workers also demonstrated that alkoxide bases can be replaced during the coupling of aryl iodides with aliphatic alcohols by using neat alcohol in the presence of catalytic amounts of CuI and phenanthroline with cesium carbonate as base (Scheme 76).[85] The range of products shown in Scheme 77 demonstrates the use of alcohol as solvent; with more valuable alcohols, 2 equivalents were used in the presence of toluene as solvent.

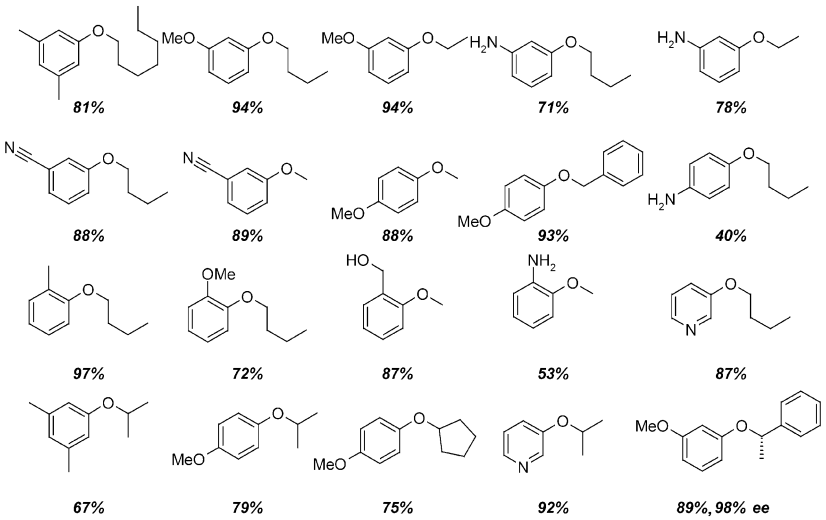
 © 2003 Wiley-VCH Verlag GmbH & Co. KGaA, Weinheim 




***Scheme 75.*** Key step: Aryl iodide, CuCl (15 mol%), NaOMe (3 equiv), MeOH/DMF (3:1), 80°C, 4 h; (*) from aryl bromide.




***Scheme 77.*** Key step: Aryl iodide (1 equiv), alcohol (2 equiv), CuI (10 mol%), phenanthroline (20 mol%), $Cs_2CO_3$ (1.4–2 equiv), toluene, 110°C, 22–38 h.

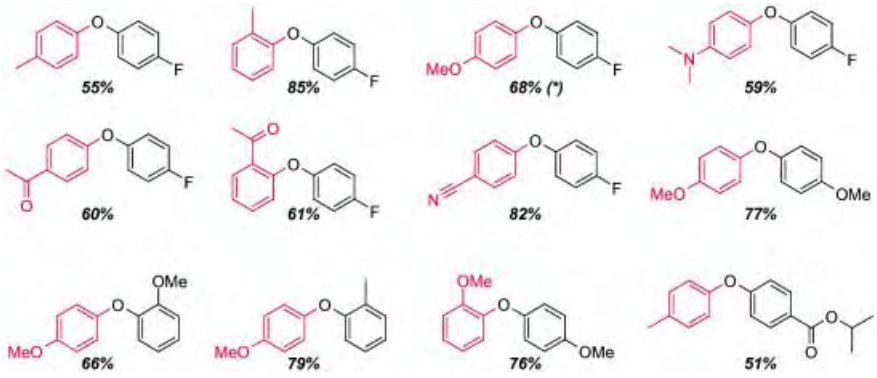



***Scheme 76.*** Key step: Aryl iodide (1 equiv) in alcohol, CuI (10 mol%), **155** (20 mol%), $Cs_2CO_3$ (1.4–2.0 equiv), 110°C, 18–24 h.

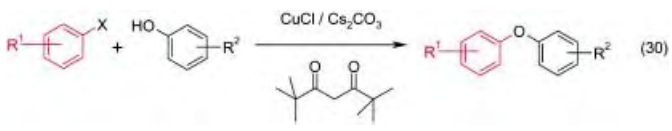
### 4.2. Enhancing Reaction Rates by Additives

In another recent development in the synthesis of diaryl ethers by an Ullmann condensation reaction, it was found that rate enhancements (10–15-fold) could be obtained by using 2,2,6,6-tetramethylheptane-3,5-dione (TMHD) as an additive along with CuCl as catalyst and $Cs_2CO_3$ as base [Eq. (30)].[86]

The reason behind the accelerating effect of this ligand is still unclear, but interestingly this ligand works best with $Cs_2CO_3$, and no accelerating effect was observed with other bases. The optimum amount of TMHD was found to be 25 mol%. 8-Hydroxyquinoline, 2-aminopyridine, and 1,10-phenenthroline **155** were possible alternative ligands. In addition, the use of acetylacetone offered only small rate enhancements. It was proposed that the diketone (TMHD) exists mainly as the diketo tautomer under the reaction conditions and forms a co-complex with the copper(I)–phenolate species which equilibrates rapidly and hence accelerates the rate-determining step. A range of products formed under these conditions are shown in Scheme 78.



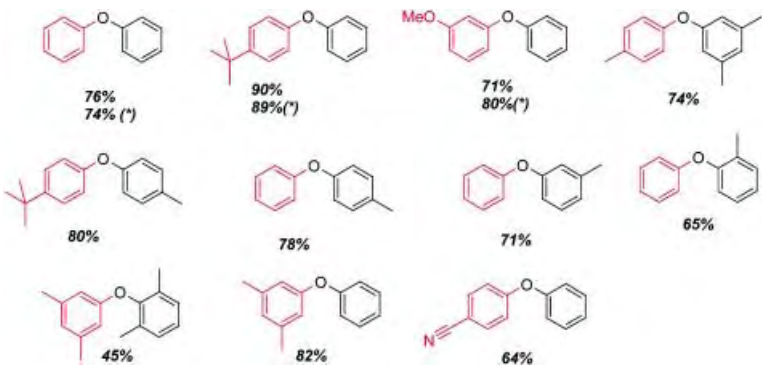

***Scheme 78.*** Key step: Aryl bromide (1 equiv), phenol (2 equiv), CuCl (50 mol%), TMHD (10 mol%), NMP, 120°C, 4 h; (*) from aryl iodide.




### 4.3. Enhancing Reaction Rates by Microwave Irradiation

An operationally simplistic protocol using microwave irradiation and based on the conventional thermally induced protocol developed by Buchwald and co-workers was used by He and Wu for the reaction of aryl bromides and iodides with a range of phenols (Scheme 79).[87] The reaction appears to be general with respect to the electronic nature of both reaction partners, although so far only CuI has been examined as the copper catalyst. Aryl chlorides do not need to react under these conditions; even after 14 h at 195°C under microwave irradiation, mainly starting materials were recovered unchanged.

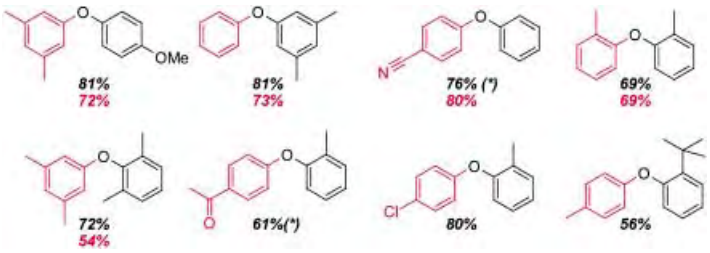
 © 2003 Wiley-VCH Verlag GmbH & Co. KGaA, Weinheim 




***Scheme 79.*** Key step: Aryl bromide (1 equiv), phenol (2 equiv), CuI (10 mol%), $Cs_2CO_3$ (2 equiv), NMP, microwave heating, 195 °C, 2 h; (*) from aryl bromide.

### 4.4. Enhancing Reaction Rates with Phosphazene Bases

Palomo et al. have developed an efficient method for the coupling of aryl halides with phenols in the presence of $P_4$-*t*Bu base in combination with $Cu^I$ salts in dioxane or toluene.[3] CuBr proved to be the best $Cu^I$ source, but CuCl, CuI, and $(CuOTf)_2{\cdot}C_6H_6$ were also possible. A catalytic version with CuBr (20 mol%) was also established (Scheme 80, yields given in red) but no reaction was observed when $Cu^{II}$ salts were used.




***Scheme 80.*** Key step: Aryl iodide (1 equiv), phenol (2 equiv), CuBr (200 mol%), $P_4$-*t*Bu (2 equiv), toluene or dioxane, reflux, 16–20 h; (*) from aryl bromide.

## 5. Aryl Halides as the Aryl Donor: C(aryl)–S Bond Formation

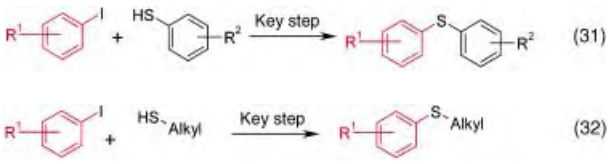
### 5.1. Phosphazene Bases and $Cu^I$ Catalysis

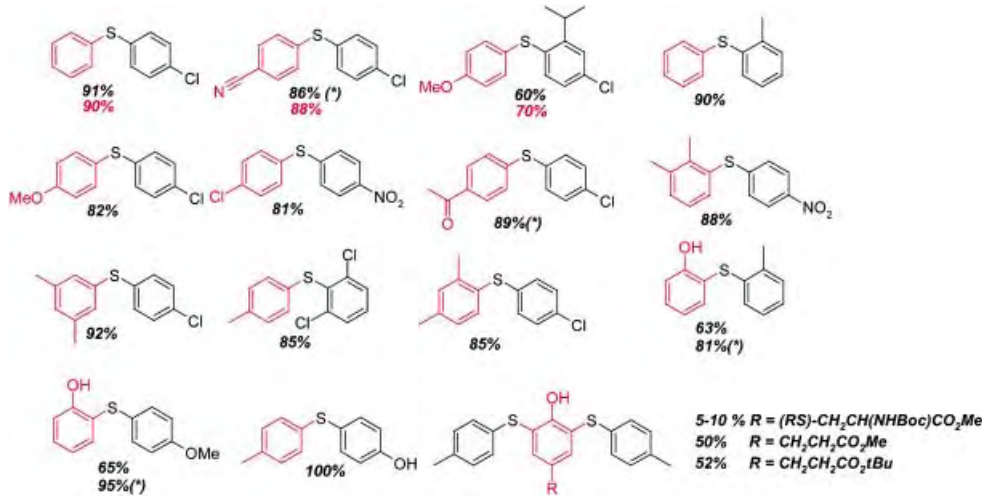
Palomo et al. also used the $P_2$-Et base (the $P_4$-*t*Bu base was ineffective) in combination with catalytic amounts of CuBr (20 mol%) to prepare a range of diaryl sulfides in good yields (Scheme 81).[88] Chemoselectivity was observed with dihalo aryl-donor substrates; aryl chlorides do not react at all. As thiophenol is much more reactive than phenol, selective reaction of the sulfur atom was observed in the catalytic version of the reaction. Higher yields were obtained when CuBr was used in stoichiometric amounts. Notably, DBU was an efficient alternative to the phosphazene base, although longer reaction times were required (yields given in red).

### 5.2. Catalytic $Cu^I$ Methods and Substrate Scope

Transition-metal-mediated C(aryl)–sulfur bond formation is a much less studied transformation.[89] A variety of diaryl sulfides and arylalkyl sulfides have been prepared under the new conditions in the presence of CuI (10 mol%), neocuproine (10 mol%), and NaO*t*Bu base in toluene [Eq. (31) and Eq. (32)].[90]

Under other conditions, especially when $Cs_2CO_3$ was used as base, significant amounts of the disulfides were formed. It was also shown that [Cu(neocuproine)($PPh_3$)Br] (**140**)




***Scheme 81.*** Key step: Aryl iodide (1 equiv), thiophenol (2 equiv), CuBr (20 mol%), $P_2$-Et (2 equiv), toluene, reflux, 4–6 h; (*) from aryl bromide.

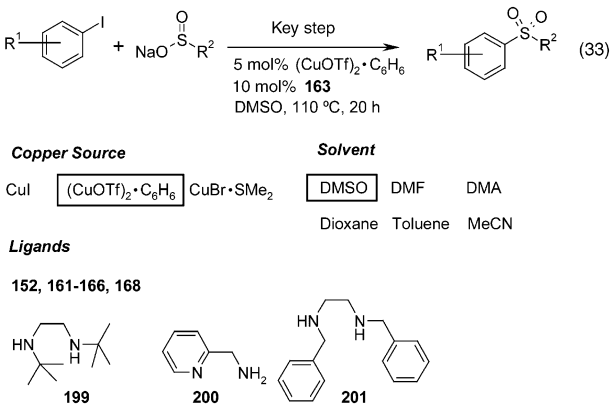
 © 2003 Wiley-VCH Verlag GmbH & Co. KGaA, Weinheim 

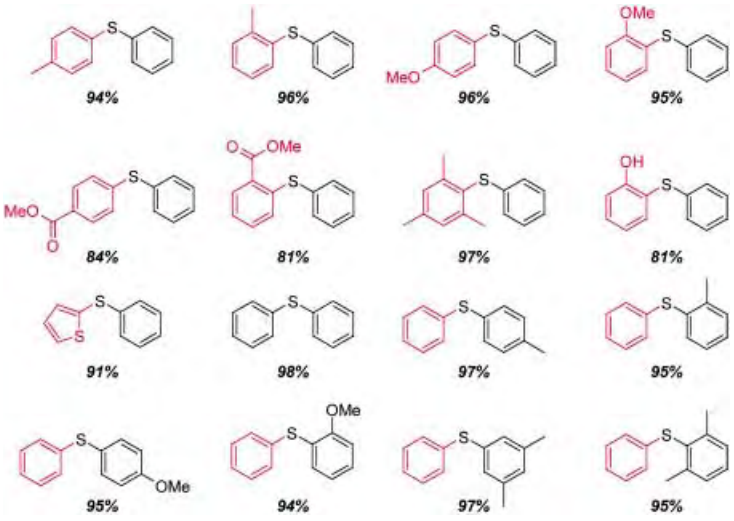
afforded the desired products in yields up to 50%, but was much less efficient overall than CuI/neocuproine/NaO*t*Bu (Scheme 82). $K_3PO_4$ was also a suitable base for the reaction; $Et_3N$ and $K_2CO_3$ were not. Alkyl thiolates were also useful nucleophiles in this process (Scheme 83).

Buchwald and co-workers introduced an alternative method for the same transformation which is reported to be experimentally simple, highly general, and displays an exceptional level of functional-group tolerance.[91] The system relies on an optimized copper(I)-catalyzed coupling of aryl iodides with aromatic and alkane thiols in the presence of CuI (5 mol%), $K_2CO_3$ (2 equiv), and **174** (2 equiv) in 2-propanol at 80°C under argon. Schemes 84–86 show the formidable range of products that can be formed in high yields under these relatively mild conditions.

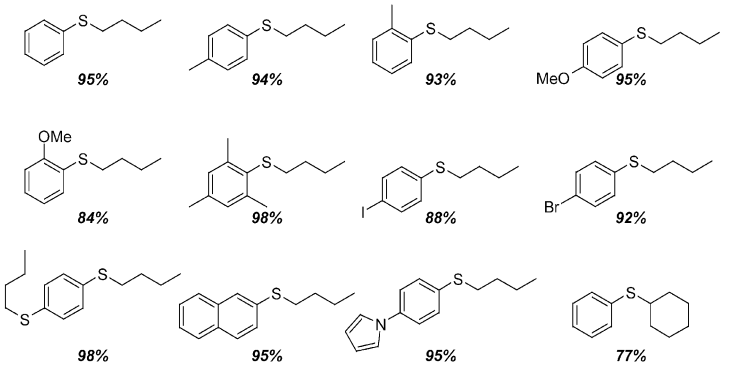
Baskin and Wang have reported a new reaction sequence for the preparation of a range of methylaryl and diaryl sulfones from aryl iodides and the corresponding sulfinic acid salts after screening a range of conditions [Eq. (33)].[92a]

This method tolerates a wide range of functional groups (Scheme 87). The utility of this methodology will rely heavily on efficient access to sulfinic acid salts.[92b] The scope of the reaction is further limited by the fact that aryl bromides do not react.




***Scheme 82.*** Key step: CuI (10 mol%), **156** (10 mol%), NaO*t*Bu, toluene, 110°C, 18–22 h.



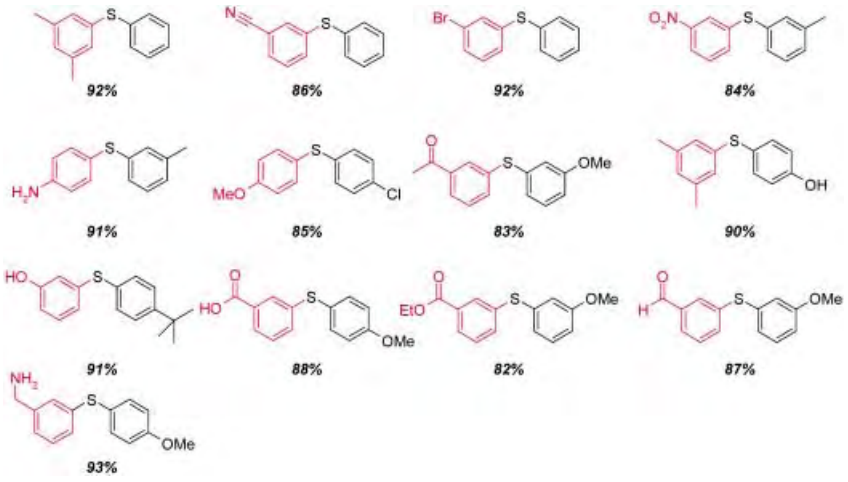

***Scheme 83.*** Key step: CuI (10 mol%), **156** (10 mol%), NaO*t*Bu, toluene, 110°C, 18–20 h.

### *5.3. Aryl Halides as Aryl Donors: Summary*

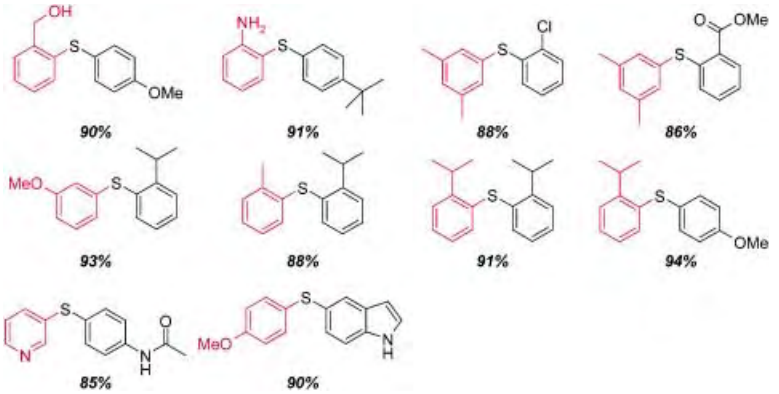
When forming C(aryl)–O, C(aryl)–N, and C(aryl)–S bonds with aryl halides as the aryl donor, the oxidation state of the Cu in the precatalyst plays a decisive role. In general, $Cu^I$ gives the best results, and nearly all recent improvements on the classic Ullmann method have examined the catalytic variation in the presence of $Cu^I$ salts. The first copper-catalyzed method ($(CuOTf)_2/Cs_2CO_3$/phenanthroline) led to numerous studies of different ligand/catalyst/base combinations in the quest for the "holy grail" of room-temperature Ullmann condensation reactions, which so far have not been developed. Thus far it appears that catalytic CuI together with phenanthroline is optimal for a range of substrates, especially when KO*t*Bu is used as base, although reaction temperatures are usually still in excess of 120°C. The discovery of ethylene glycol and *N,N*-diethylsalicylamide as copper ligands is particularly important in C(aryl)–N bond formation. Fewer studies have been carried out on new ligand systems for the related C(aryl)–O and C(aryl)–S bond formation. Important contributions include the use of phosphazene bases to effect both C(aryl)–O and C(aryl)–S bond formation. Microwave irradiation has been shown to enhance the reaction rates of C(aryl)–O bond formation. TMHD as an additive can significantly enhance reaction rates by up to 15-fold. Both concepts need to be further investigated. These reaction processes have been used successfully in several studies into substrate scope, natural product synthesis, as well as in medicinal chemistry.

In general, the current state-of-the-art in modern variants of the classic Ullmann condensation has not reached the goal of being able to perform these intermolecular transformations at temperatures less than 80–100°C, apart from one isolated example by

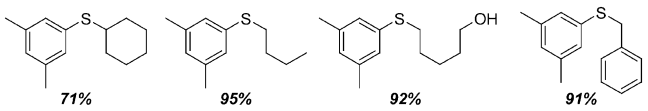

© 2003 Wiley-VCH Verlag GmbH & Co. KGaA, Weinheim



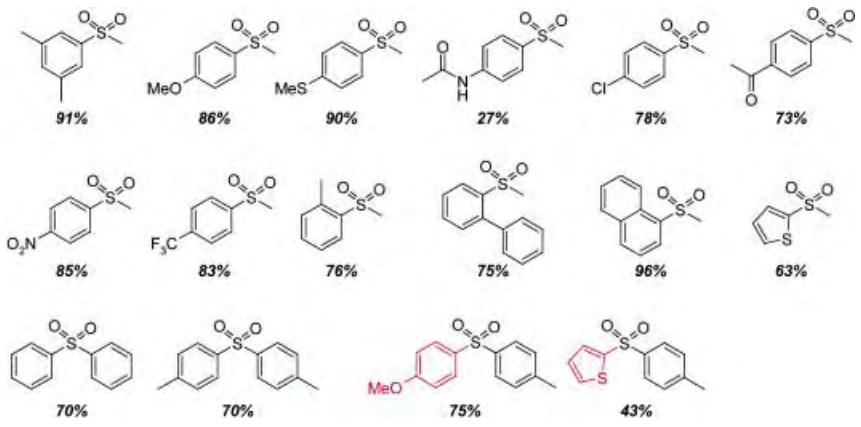

***Scheme 84.*** Key step: Aryl iodide (1 equiv), ArSH (1 equiv), CuI (5 mol%), $HOCH_2CH_2OH$ (**174**) (200 mol%), $K_2CO_3$, *i*PrOH, 80°C, 18–22 h.




***Scheme 85.*** Key step: Aryl iodide (1 equiv), ArSH (1 equiv), CuI (5 mol%), $HOCH_2CH_2OH$ (**174**) (200 mol%), $K_2CO_3$, *i*PrOH, 80°C, 18–22 h.




***Scheme 86.*** Key step: Aryl iodide (1 equiv), ArSH (1 equiv), CuI (5 mol%), $HOCH_2CH_2OH$ (**174**) (200 mol%), $K_2CO_3$, *i*PrOH, 80°C, 18–22 h.



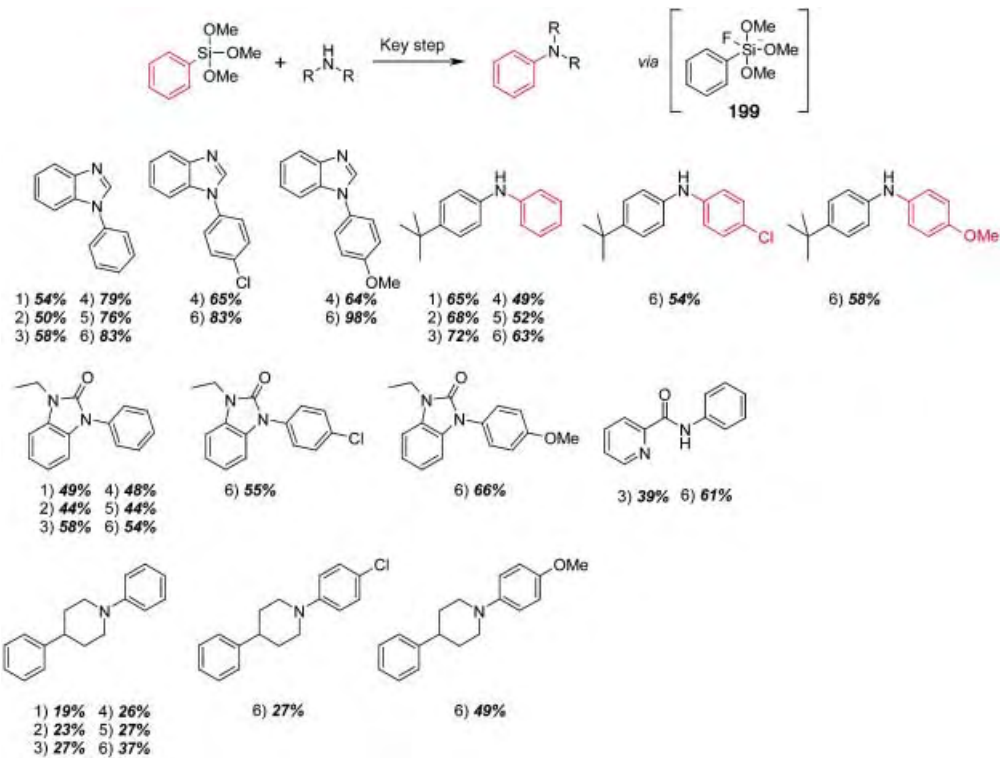

***Scheme 87.*** Key step: Aryl iodide (1 equiv), sodium sulfinate (1.2 equiv), $(CuOTf)_2{\cdot}C_6H_6$ (5 mol%), air, DMSO, 110°C, 20 h.

Buchwald and co-workers for the Goldberg-modified Ullmann condensation reaction.[73] Strikingly, however, Fukuyama and co-workers have shown that intramolecular C(aryl)–N bond formation at room temperature was successful when using 2 equivalents of Cu salt.[61] The key to this mild method relies on the use of CuI and CsOAc, which presumably form CuOAc in situ. The fact that this catalytic system is much less efficient in intermolecular reactions reflects the accelerating effect described by Ma and co-workers on the intermolecular amination of α-and β-amino acids with aryl halides. Buchwald and co-workers recently showed that CuOAc can be used catalytically in a similar intramolecular reaction with *N,N*-diethylsalicylamide as ligand, although the reaction needs higher temperatures for aryl bromides (35–40°C) and aryl chlorides (50–100°C). The range of aryl donors used in the modern Ullmann condensation reaction encompasses aryl iodides, bromides, and chlorides but so far no investigations with pseudohalides (ArOTf, ArONf, etc) have been reported.

## 6. Aryl Siloxanes as the Aryl Donor: C(aryl)–Heteroatom Bond Formation

The hypervalent siloxane species **199**, which is generated in situ, is an excellent reagent for the one-pot arylation of a suitable N nucleophile in the presence of cupric acetate at room temperature exposed to that atmosphere. This was the first room-temperature *N*-arylation of an aryl iodide in the *absence* of a strong base. The rate of reactions were found to be one order of magnitude quicker than the corresponding reactions with the boronic acids, and no further base, ligand, or molecular sieves were necessary (Scheme 88).[93–94] A one-pot version of the C–N cross-coupling of aryl iodides with a range of amines was also possible. Essentially, the reaction proceeded well with most N nucleophiles, except for piperidine derivatives, and gave yields in excess of 50%. A catalytic version was possible when using 10 mol% of $[\{Cu(OH){\cdot}tmeda\}_2]Cl_2$, and was used for the efficient (69%) phenylation of benzimidazole with phenyltrimethoxysiloxane albeit at 50°C.

 © 2003 Wiley-VCH Verlag GmbH & Co. KGaA, Weinheim 

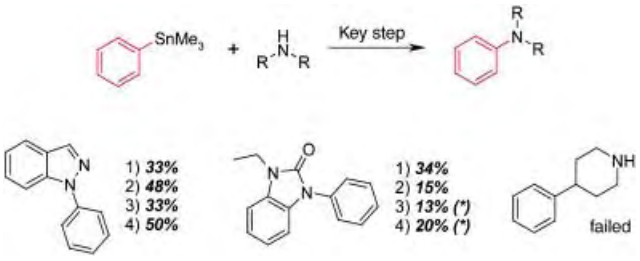



***Scheme 88.*** Key step: 1) $Cu(OAc)_2$ (1.1 equiv), TBAF (2 equiv), pyr (2 equiv), $CH_2Cl_2$, air, room temperature; 2) with $Et_3N$; 3) no base; 4) in DMF; 5) with $Et_3N$ in DMF; 6) no base in DMF.

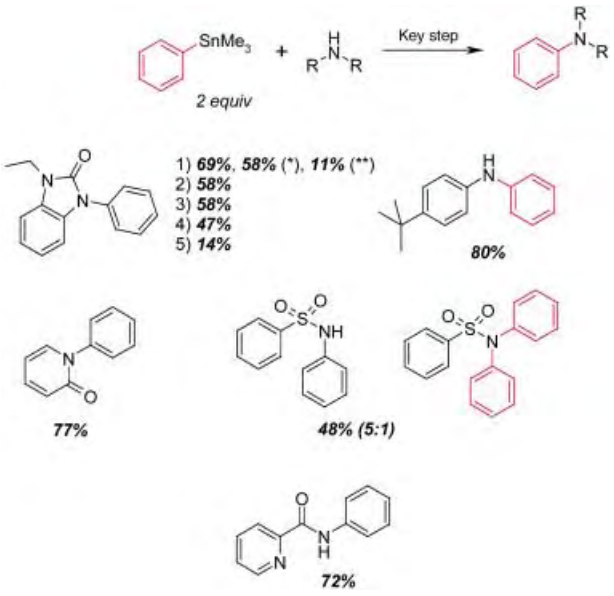
## 7. Aryl Stannanes as the Aryl Donor: C(aryl)–Heteroatom Bond Formation

In the search for alternative arylating reagents, Lam et al. also demonstrated the use of commercially available aryl stannanes as electrophiles in the copper(II) acetate mediated *N*-arylation (Scheme 89).[95] However, the yields are modest and in some cases the reaction completely fails. In most cases, even after prolonged heating, homocoupling was a major side reaction. Changing the copper source to CuCl resulted in a similar outcome, but, remarkably, the reaction could be effected at room temperature.

An improvement to these modest results soon followed, and it was found that the addition of TBAF to the reaction mixture resulted in enhanced yields in the reaction of benzimidazolones with the fluorophilic phenylstannane. As is the case with the siloxanes, it can be postulated that the addition of fluoride anion can lead to the formation of the hypervalent stannane anion, which accelerates the transmetalation step. Other fluoride sources such as CsF and TASF were also suitable, but pyridinium fluoride was not. A range of products accessible under these conditions are shown in Scheme 90.




***Scheme 89.*** Key step: 1) $Cu(OAc)_2$ (1.5 equiv), pyr (2 equiv), dioxane, 80 °C, 2 days; 2) $Cu(OAc)_2$ (1.5 equiv), $Et_3N$ (2.0 equiv), dioxane, 80 °C, 2 days; 3) CuCl (5 equiv), pyr (2 equiv), dioxane, room temperature, 2 days; 4) CuCl (5 equiv), pyr (2 equiv), dioxane, room temperature, 2 days; (*) at 80 °C.

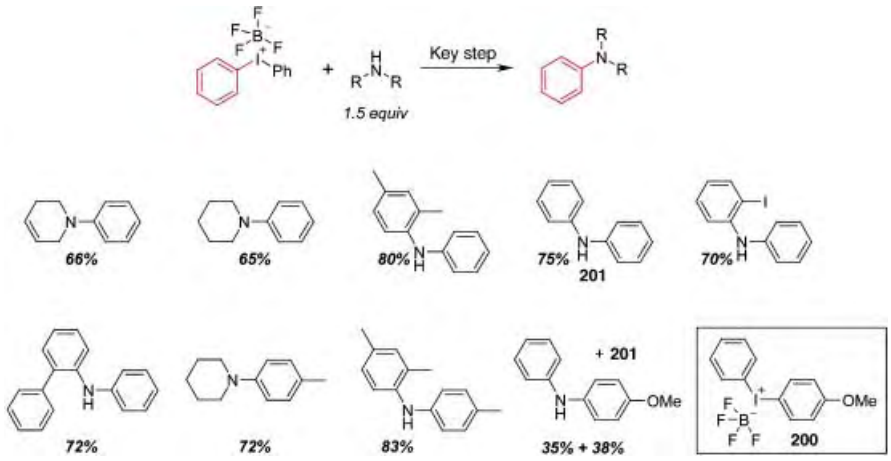



***Scheme 90.*** Key step: 1) $Cu(OAc)_2$ (1.1 equiv), TBAF (2 equiv), $CH_2Cl_2$, room temperature, 2 days; 2) with TBAF and $Et_3N$; 3) CsF; 4) TASF; 5) with $Et_3N$; (*) in DMF; (**) in 1,4-dioxane.

 © 2003 Wiley-VCH Verlag GmbH & Co. KGaA, Weinheim 

### 8. Iodonium Salts as the Aryl Donor: C(aryl)–Heteroatom Bond Formation

The copper-catalyzed or noncatalytic *N*-arylation of aryl iodonium salts has been known for some time.[96] However, a new milder method employing CuI (10 mol%) and $Na_2CO_3$ (2 equiv) in $CH_2Cl_2$ at room temperature allows the *N*-arylation of a number of piperidines and anilines (Scheme 91).[97] In general, the yields of the reactions are good (65–83%), and the reaction times are short (< 6 h). $Na_2CO_3$ is a better base than $K_2CO_3$ and $Cs_2CO_3$, and alkoxides bases such as NaOMe and NaO*t*Bu are ineffective. CuBr and $CuCl_2$ were less effective than CuI. Interestingly, when the unsymmetrical iodonium salt **200** was used, the two aryl groups competitively participated in the transfer of the aryl unit in a 1:1 ratio to give a mixture of **201** and the expected product. This is in line with the observations of Barton and co-workers with unsymmetrical aryl bismuth reagents.

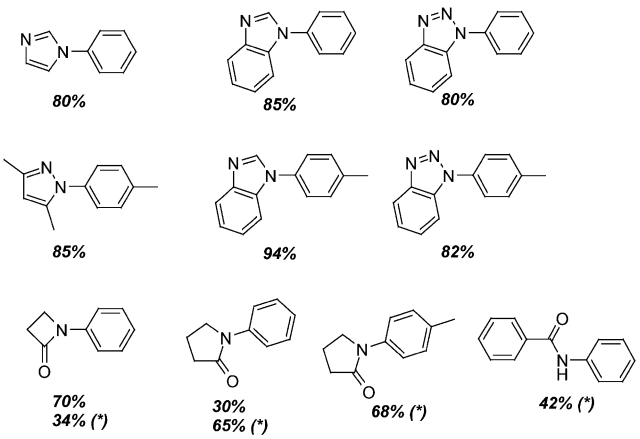



***Scheme 91.*** Key step: CuI (10 mol%), $Na_2CO_3$ (2 equiv), $CH_2Cl_2$, room temperature, 6 h.

The procedure was extended to a range of azole derivatives, including imidazole, benzimidazole, benzotriazoles, and a pyrazole. $Cu(acac)_2$ was the preferred catalyst, but the reactions only proceeded to completion at 50 °C (Scheme 92). Furthermore, cyclic secondary amides and benzamide were efficient substrates and provided the desired products under the same reaction protocol, although in these cases CuI was a better catalytic copper ion source.

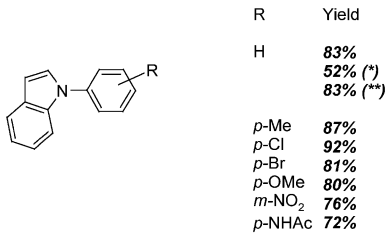
Zhou and Chen later extended the scope of the nucleophiles to indoles. Their catalytic system involved CuI (10 mol%) and $K_2CO_3$ (3 equiv) in DMF, although much higher temperatures (140–150 °C) were required to afford the desired products in good yields after 6–7 h (Scheme 93).[98]

Tetrazoles (in the form of sodium salts) are also suitable nucleophilic reaction partners in the *N*-arylation of diaryl iodonium salts (Scheme 94).[99] It was observed that in the presence of [$Cu^{II}$–phenylcyclopropyl carboxylate], the desired coupling product **202** was formed in 35% yield after 18 h at 80 °C; **203** was not observed. The use of a $Pd^0$ catalyst reduced the reaction times to 6 h. However, mixtures of




***Scheme 92.*** Key step: $Cu(acac)_2$ (5 mol%), $K_2CO_3$ (2 equiv), toluene, 50 °C, 6 h; (*) with CuI (10 mol%).

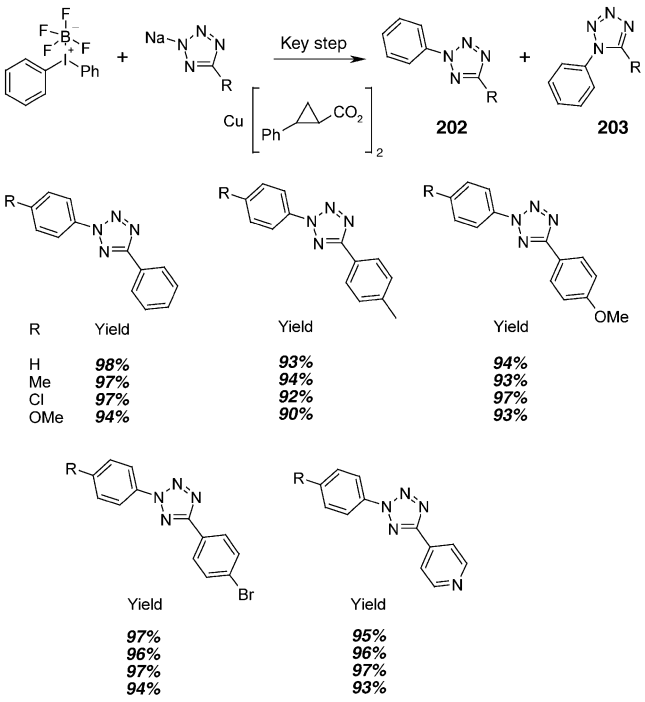
isomers were formed. It was shown that the positive synergistic effects of the two catalysts ($Cu^{II}$ enhances selectivity and $Pd^0$ leads to better yields) could be combined: When the sodium salt of 5-phenyltetrazole was treated with $Ar_2I^+BF_4^-$ at reflux in *t*BuOH for 8 h in the presence of both $Cu^{II}$ and $[Pd(dba)_2]$, all products were formed in near-quantitative yields as only one isomer. Scheme 94 shows that a range of electron-donating or electron-withdrawing substituents on both the aryl tetrazoles and iodonium moiety are tolerated. Aryl iodides and bromides were examined as suitable electrophiles, but all conditions examined proved to be ineffective.




***Scheme 93.*** Key step: CuI (10 mol%), $K_2CO_3$ (3 equiv), DMF, 140–150 °C, 6–7 h; (*) with $Cu(OAc)_2$; (**) with $Cu(acac)_2$.

However, the nucleophile species could be changed, and the use of the stannylated tetrazole **204** with either diaryl iodonium salt **205** or **206** resulted in selective arylation in yields of 72 and 75%, respectively, for the 2,5-disubstituted tetrazoles in the presence of $Cu(OAc)_2$ (1.1 equiv) in $CH_2Cl_2$ at room temperature for 8 h. Products successfully formed under these conditions are shown in Scheme 95.[100] Aryl halides, aryl bismuth reagents, and aryl boronic acids were not suitable aryl donors.

 © 2003 Wiley-VCH Verlag GmbH & Co. KGaA, Weinheim 



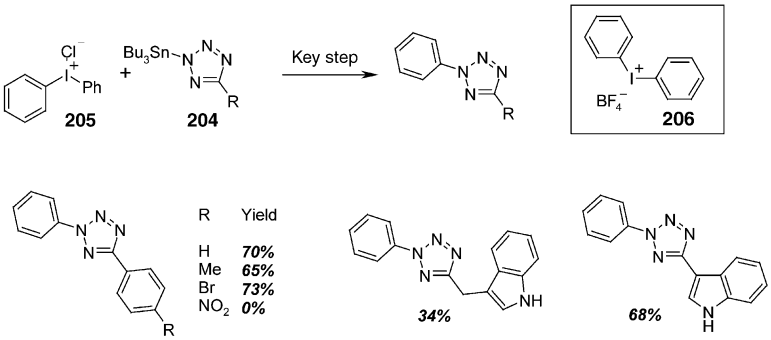

***Scheme 94.*** Key step: [Cu$^{II}$–phenylcyclopropyl carboxylate] (5 mol%), *rac*-binap/[Pd(dba)$_2$] (5 mol%), *t*BuOH, 80°C, 8 h.

## 9. Aryl Lead(IV) Triacetates as the Aryl Donor: C(aryl)–Heteroatom Bond Formation

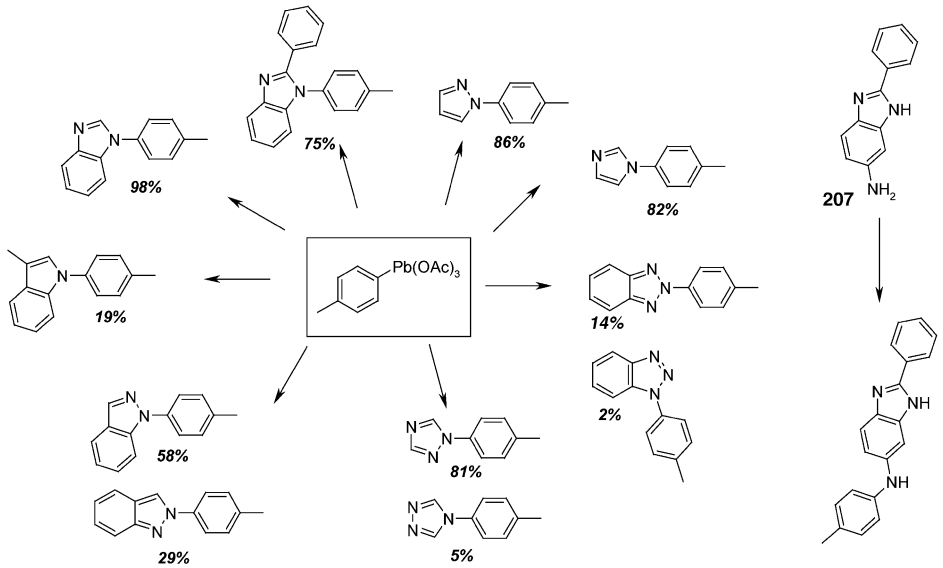
Barton and co-workers previously reported that indoles and carbazoles failed to react under their standard procedure for the arylation of aromatic amines.[104] However, Avendano and co-workers showed that imidazoles, pyrazoles, indazoles, and benzimidazoles were all suitable substrates for *N*-arylation with *p*-tolyllead triacetate (1.1–1.5 equiv) as the aryl donor with the copper catalyst [Cu(OAc)$_2$] in stoichiometric amounts (Scheme 96).[101–102] 1,2,4-Triazole was a poor substrate, but it was shown that the sodium salt reacted much better under the same conditions to afford only one regioisomer in high yield. In a chemoselectivity study, it was shown that the aminobenzimidazole **207** reacted solely at the N atom of the aniline group, although the product was only isolated in 50% yield.

## 10. Pentavalent Organobismuth Reagents as the Aryl Donor: C(aryl)–Heteroatom Bond Formation

David and Thieffry first showed that triphenylbismuth diacetate was capable of donating a phenyl moiety in the monoarylation of glycols.[103] The original conditions proved to be extremely capricious (solvent specific, need for thermal and photochemical activation, long induction times). Barton and co-workers as well as Dodonov and Gushchin independently reported that the aryl transfer from triarylbismuth diacetates to alcohols proceeded much more smoothly (room temperature, 15 min, various solvents) in the presence of




***Scheme 95.*** Key step: Cu(OAc)$_2$ (1.2 equiv), $CH_2Cl_2$, room temperature, 8 h.



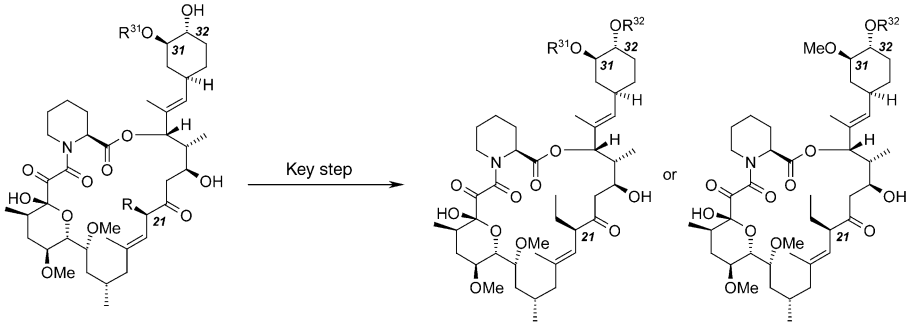

***Scheme 96.*** Key step: Cu(OAc)$_2$ (1.2 equiv), $CH_2Cl_2$, 4–48 h.


© 2003 Wiley-VCH Verlag GmbH & Co. KGaA, Weinheim

catalytic amounts of copper acetate.[104] Over the last 20 years, the arylation of heteroatoms with aryl bismuthates has become standard and was recently reviewed by Finet et al.[105] As a result, we only discuss the most recent advances in synthesis and application to natural products.

### 10.1. C(aryl)–O Bond Formation

The natural product ascomycin and its derivative L-683,742 were arylated by researchers at Merck when searching for novel immunosuppresive macrolides similar to FK-506 (Scheme 97).[106] The key arylation reaction worked best under the conditions shown to selectively transfer one aryl group to the secondary alcohol group at C32, albeit in modest yields. In the case of L-683,742, a 1:1 mixture of mono- and diarylated product was formed. Enhanced levels of activity were observed with the simple phenyl ethers and led the team to perform the aryl-transfer reaction with functionalized bismuth derivatives (Table 9).

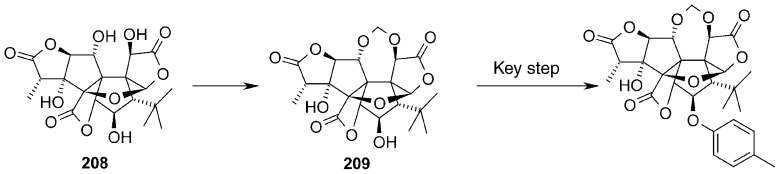



*Scheme 97.* Key step: $Cu(OAc)_2$ (amount not stated), $BiAr_3(OAc)_2$, peracetic acid (1–1.2 equiv), AcOH, $THF/CH_2Cl_2$, room temperature.

*Table 9:* Preparation of derivatives of FK-506 and ascomycin-related macrolides (Scheme 97).

| $R^{32}$ | Yield [%] |
|---|---|
| phenyl | 42 |
| 2-naphthyl | 18 |
| 5-indolyl | 10 |
| *N*-methyl-5-indolyl | 50 |
| 3,5-di-$(CF_3)C_6H_3$ | 46 |
| *p*-$CF_3C_6H_4$ | 51 |
| *m*-$MeC_6H_4$ | 42 |
| *p*-$MeC_6H_4$ | 42 |
| *p*-$MeSC_6H_4$ | 14 |
| *m*-$MeOC_6H_4$ | 62 |
| *p*-$MeOC_6H_4$ | 18 |
| *p*-$Me_2NC_6H_4$ | 17 |
| *m*-$OHC_6H_4$ | 34 |
| *p*-$OHC_6H_4$ | 65 |

Finet and co-workers attempted the selective arylation of the ginkgolide tetrahydroxy compound **208**. Under the standard conditions, only a complex mixture of products was formed. However, protection of the hydroxy groups at C1 and C10 with a methylenedioxy bridge to afford the diol **209** allowed the introduction of the *p*-tolyl moiety at the relatively less-hindered hydroxy functional group at C7, albeit in only 21% yield (Scheme 98).[107]

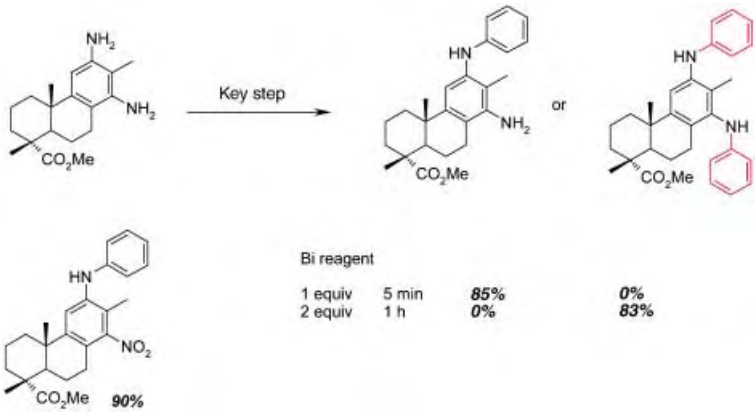



*Scheme 98.* Key step: $Cu(OAc)_2$ (cat.), $Bi(p\text{-Me-Ar})_3(OAc)_2$, DMAP, $CH_2Cl_2$, room temperature.

### 10.2. C(aryl)–N Bond Formation

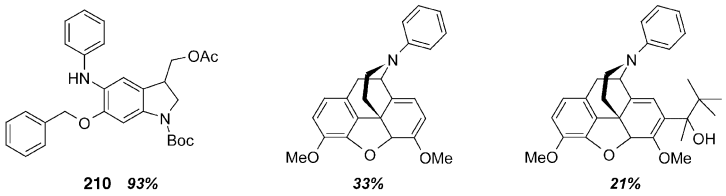
Selective monoarylation of dehydroabietate derivatives was possible at room temperature in only 5 minutes when using $Cu(Piv)_2$ in catalytic amounts with triphenylbismuth diacetate as the aryl donor (Scheme 99).[108] The di-*N*-arylated product was exclusively formed in good yield in the presence of 2 equivalents of the aryl donor.

In the quest for novel cytotoxic compounds based on the aminoindoline scaffold,[109] an aniline was selectively monoarylated in high yield to give **210**. It was also shown that morphine alkaloids could be efficiently arylated at the N atom (Scheme 100).[110]



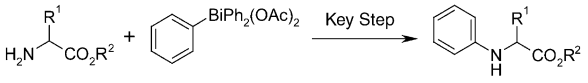

*Scheme 99.* Key step: $Cu(OPiv)_2$ (cat.), $BiPh_3(OAc)_2$, $CH_2Cl_2$, room temperature.

 © 2003 Wiley-VCH Verlag GmbH & Co. KGaA, Weinheim 



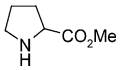
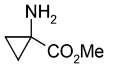

210 93% 33% 21%

***Scheme 100.*** Key step: $Cu(OAc)_2$ (cat.), $Ph_3Bi(OAc)_2$, $CH_2Cl_2$, room temperature




***Scheme 101.*** Key step: Cu (cat.), $Ph_3Bi(OAc)_2$, $CH_2Cl_2$, room temperature

***Table 10:*** *N*-arylation of amino acid derivatives with triarylbismuth diacetates as aryl donors (Scheme 101)

| $R^2$ | $R^1$ | Yield [%] |
|---|---|---|
| H | Et | 81 |
| $PhCH_2$ | $PhCH_2$ | 80 |
| $PhCH_2O_2CCH_2$ | $PhCH_2$ | 50 |
| $PhCH_2O_2CCH_2$ | $PhCH_2$ | 58 |
| 3-Indolylmethyl | Me | 66 |
| (*S*)-*i*Pr | Me | 85–92 |
| (*S*)-*i*Bu | Me | 86 |
| (*R*)-Ph | Me | 92 |
|  | | 61 |
|  | | 94 |

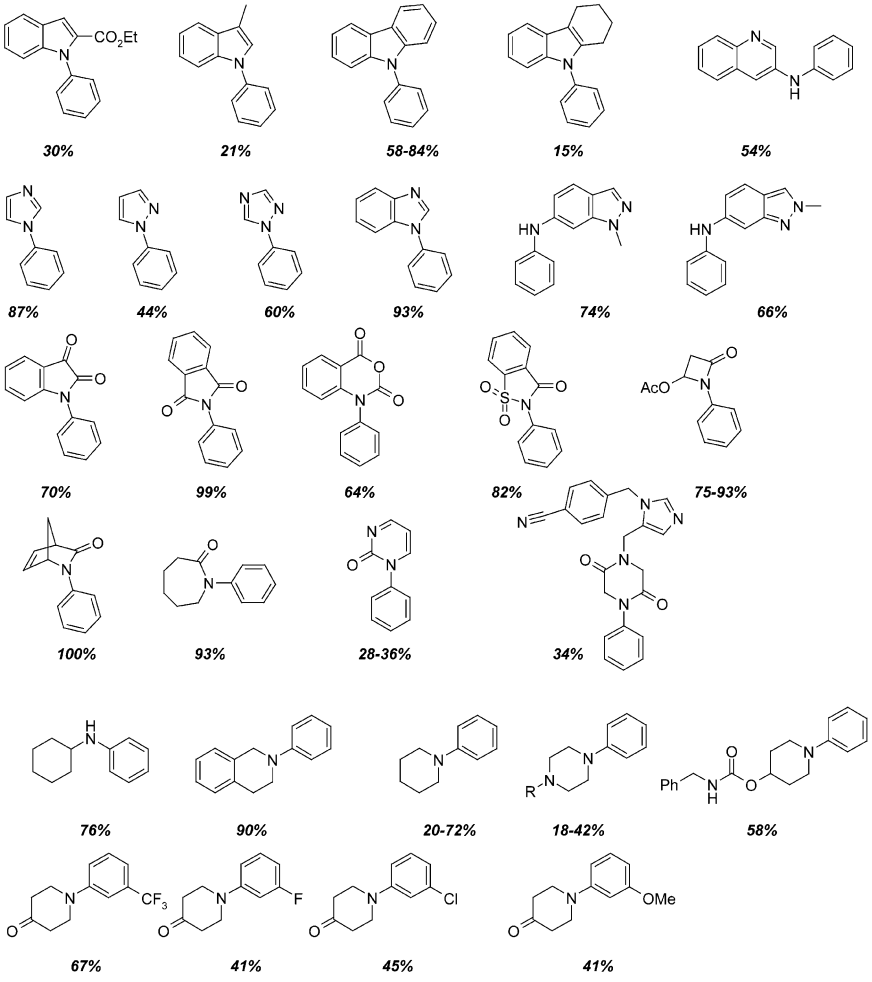
Barton and co-workers had already shown that α-amino acids were not useful aryl acceptors from triaryl bismuth diacetate, but their corresponding esters were indeed efficient substrates (Scheme 101, Table 10).[111] Recently, it was found that the addition of $Et_3N$ has a dramatic effect and increases the yield to 94% for the cyclopropylamino acid derivative.[112]

As can be seen from Table 10, the monoarylation product was formed predominant in all cases when using 1 equivalent of the bismuth reagent. However, if the diarylated product was desired, then 1.5–2 equivalents were needed. The arylation reaction proceeded well for glycine or valine (14 days reaction time). However, for phenylalanine, even after extended reaction times, the diarylated product could not be formed in yields greater than 8%. Notably, no racemization was detected, thus offering a significant advantage over the corresponding palladium-mediated transformation in which full racemization of the products was reported.[113]

A range of heterocyclic (Scheme 102) and nonheterocyclic (Scheme 103) products were formed under these standard conditions.[17,114–128] These substrates were, in general, the first true exploration of the substrate scope of copper-catalyzed heteroatom-arylation reactions, as can be witnessed in the similarity between the schemes in earlier sections.

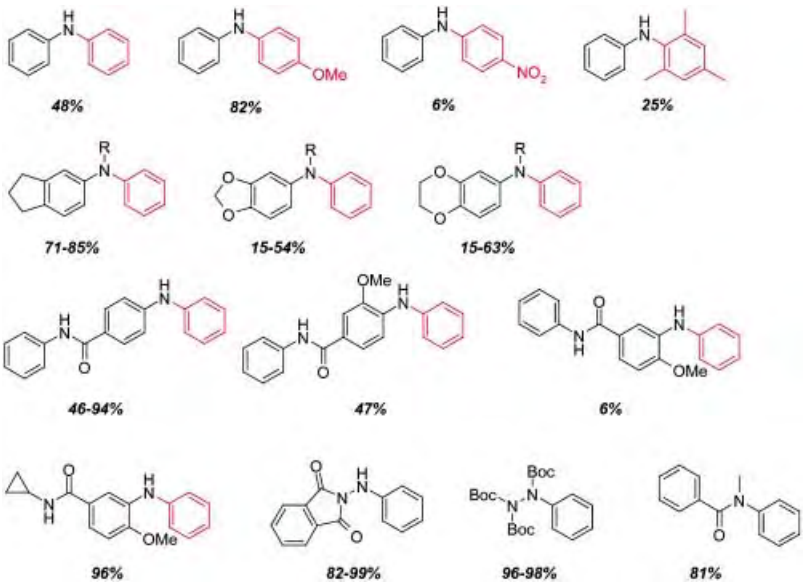
## 11. Pentavalent Organotrifluoroborate Reagents as the Aryl Donor: C(aryl)–N Bond Formation

Batey and Quach have developed a novel protocol for the $Cu^{II}$-mediated etherification of alcohols (1 equiv) under essentially neutral conditions in the presence of air- and moisture-stable potassium alkenyl and aryl trifluoroborate salts (2 equiv) at room temperature.[129] The optimized reaction procedure involves catalytic amounts of $Cu(OAc)_2$




***Scheme 102.*** Key step: $Cu(OAc)_2$, $Ar_3Bi$, $Et_3N$ or pyr, $CH_2Cl_2$, room temperature.

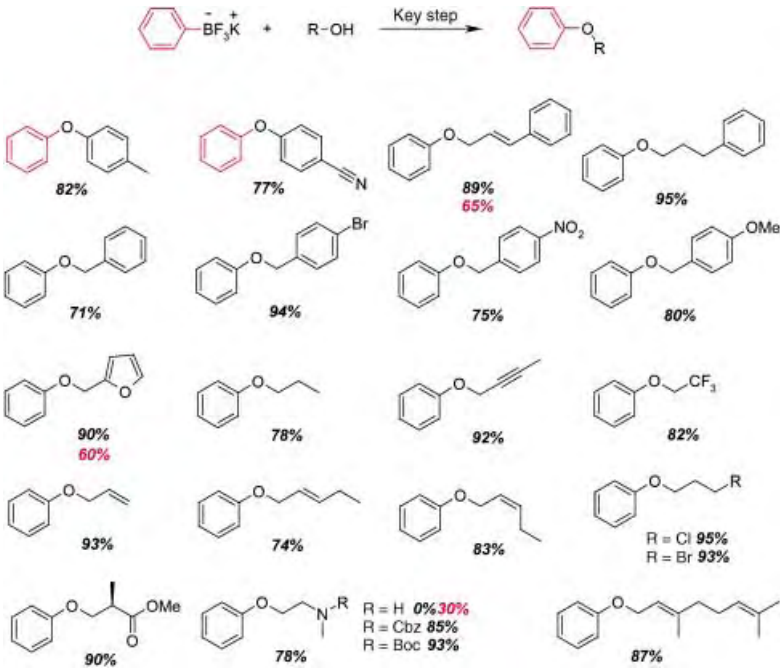

© 2003 Wiley-VCH Verlag GmbH & Co. KGaA, Weinheim



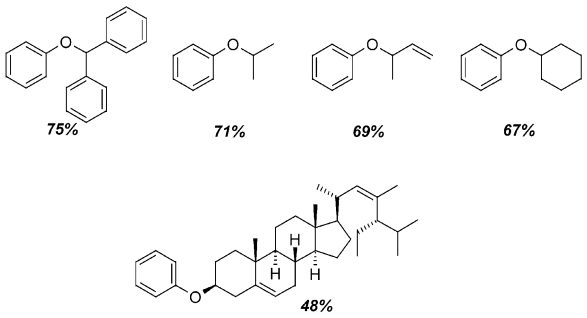

***Scheme 103.*** Key step: $Cu(OAc)_2$, $Ph_3Bi$, $Et_3N$ or pyr, $CH_2Cl_2$, room temperature.

(10 mol%) with DMAP (20 mol%) as a ligand in the presence of oxygen and molecular sieves. A variety of aliphatic primary and secondary alcohols as well as phenols are suitable reaction partners, thus displaying a broad functional-group tolerance (Schemes 104 and 105). A comparison between the efficiency of these reagents with that of the aryl boronic acids (yields given in red) revealed that the organotrifluoroborate salts give higher yields. However, although standard methods to prepare these salts are known,[130] increased commercial availability is required for this method to attract more widespread use.

A range of secondary alcohols also participate in the reaction, although tertiary alcohols do not react under the previously optimized conditions (Scheme 105). Moreover, the nature of the electrophilic reaction partner is important, and the electron-rich 4-methoxyphenyltrifluoroborate gave the best results, whereas the electron-deficient 4-acetylphenyltrifluoroborate did not afford any product when treated with 2-furfuryl alcohol (Scheme 106). Alkenyl trifluoroborate salts were also found to be effective reaction partners, but alkyl trifluoroborate derivatives did not react, presumably as a result of the low efficiency of transmetalation with Cu salts.




***Scheme 104.*** Key step: Potassium aryl trifluoroborate (2 equiv), alcohol (1 equiv), $Cu(OAc)_2 \cdot H_2O$ (10 mol%), DMAP (20 mol%), $O_2$, 4 Å molecular sieves, $CH_2Cl_2$, room temperature, 24 h.

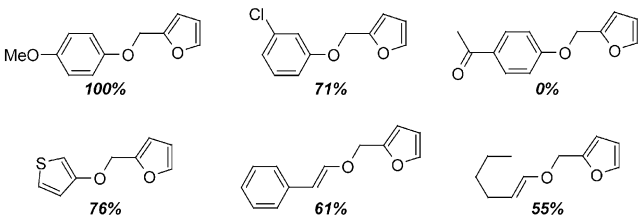



***Scheme 105.*** Key step: Potassium aryl trifluoroborate (2 equiv), alcohol (1.0 equiv), $Cu(OAc)_2H_2O$ (10 mol%), DMAP (20 mol%), $O_2$, 4 Å molecular sieves, $CH_2Cl_2$, room temperature, 24 h.

## 12. Mechanistic Considerations for the Copper-Mediated Heteroatom-Arylation Reaction

The mechanism of the Ullmann arylation of alcohols has not been well-established.[131] As most studies devoted to the use of this reaction are synthetically driven, only themes and proposals for the mechanistic rationale have been discussed, some which are relatively speculative in nature. In general, much still has to be done for all types of metal-mediated C–heteroatom bond formation, including all Group 8–10 metals. Hartwig already commented that "In general, catalytic organometallic chemistry that forms carbon–heteroatom bonds is less developed than that forming C–C bonds and is less well understood".[11a]

As can be seen from the many examples in this Review, copper sources are diverse, but, in general, the most universal starting copper source is a $Cu^{I}$ or $Cu^{II}$ species. It seems most likely that $Cu^{II}$ is not the catalytic species in the reaction. Furthermore, it has been ascertained that radical mechanisms are ruled out as the reactions are not inhibited when radical scavenger additives (such as 1,1-diphenylethylene) are included. For copper-mediated C(aryl)–heteroatom bond formation, the original investigations and proposals by




***Scheme 106.*** Key step: Potassium aryltrifluoroborate (2 equiv), alcohol (1.0 equiv), $Cu(OAc)_2H_2O$ (10 mol%), DMAP (20 mol%), $O_2$, 4 Å molecular sieves, $CH_2Cl_2$, room temperature, 24 h.

Lockhardt[132] and by Barton et al.[133] dealing with the intermediacy of hypervalent copper(III) species during the reactions of diaryl iodonium salts and pentavalent bismuth reagents are the most prevailing mechanistic suggestions.

Aryl donors can be as follows:

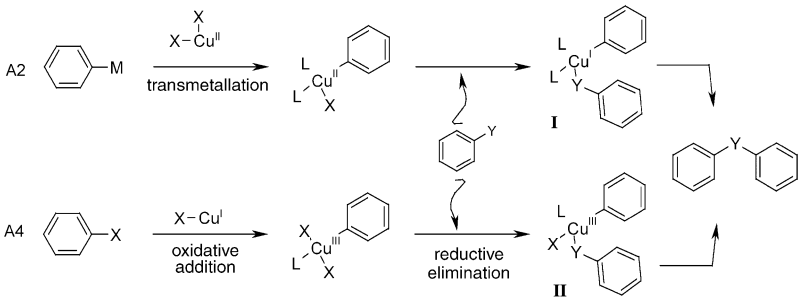
A1 = Hypervalent reagents ($Sb^{5+}$, $Pb^{4+}$, $I^{3+}$)
A2 = Low-valent organometallic reagents ($Bi^{3+}$, $B^{4+}$, $Si^{4+}$, $Sn^{4+}$), stoichiometric in copper
A3 = Low-valent organometallic reagents with a co-oxidant, catalytic in copper
A4 = Aryl halides (I, Br, Cl), no examples of F, or pseudohalides OTf, ONf, etc.

A1: The mechanism involved in the transfer of an aryl moiety to X (X = heteroatom) has been rationalized with the following steps (Scheme 107):

1) $Cu^{II}$ reduced to $Cu^{I}$ by a nucleophile.
2) $Cu^{I}$ species **I** forms **II**, another $Cu^{I}$ species, by ligand exchange.
3) Oxidative addition to the $Cu^{I}$ species **II** forms a $Cu^{III}$ species.
4) The latter undergoes reductive elimination of the product, and the active catalytic species **I** is regenerated.

A2: Evans speculated that the paths of A2 and A4 intersect at the plausible aryl copper phenoxide intermediates, which are both capable of forming the observed diaryl ether products by reductive elimination (Scheme 108). The unresolved issue is whether the oxidation state of the intermediate is $Cu^{I}$ or $Cu^{III}$ or indeed an equilibrium (or disproportionation) controlled by the reduction potential of the Cu couple. It was later shown that the presence of an oxidizing atmosphere (air, oxygen, or co-oxidant) improves the process of the arylation reaction and lends some substantial supporting evidence that perhaps **I** can be oxidized to **II** prior to the reductive elimination.

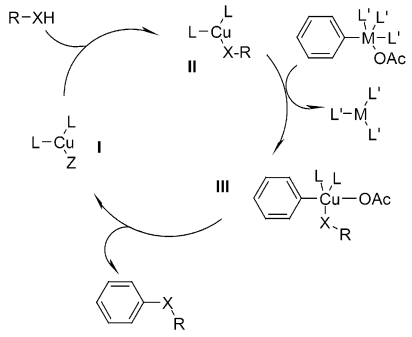
1) Transmetalation of boronic acid and copper catalyst.
2) N nucleophile coordinates to $Cu^{II}$: reduction potential of the $Cu^{III}/Cu^{II}$ couple decreases
3) Oxygen oxidizes $Cu^{II}$ to $Cu^{III}$ (putative) ready for reductive elimination.
4) Product eliminated and $Cu^{I}$ species ready to regenerate catalytic species.



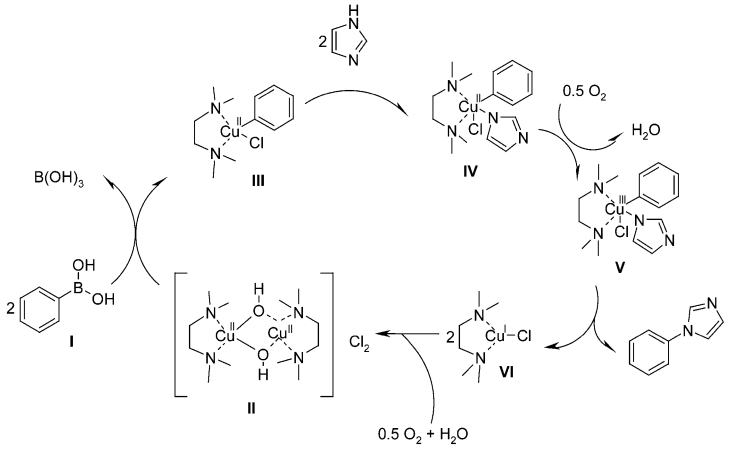

***Scheme 108.*** Plausible mechanism for the copper-catalyzed arylation with class A2 and A4 reagents. M = $B(OH)_2$, $BiAr_2(OAc)_2$, or $SnBu_3$; X = Cl, Br, I; Y = NH, O.

A3: Building on this proposal, Collman and Zhong[47] have proposed the follow catalytic cycle for the coupling of imidazole with aryl boronic acids (Scheme 109). Although, as yet, no experimental evidence exists for any of the putative steps, the hypothesis can be supported.[134] The individual steps may include:

1) Transmetalation of the aryl boronic acid **I** with the catalyst **II**, generating the $Cu^{II}$ species **III**.
2) Coordination of the imidazole nucleophile to give **IV**.
3) Oxidation of **IV** to **V** in the presence of oxygen or air.
4) Reductive elimination of the desired product and oxidation to regenerate the active bis-μ-hydroxo $Cu^{II}$ catalytic species **II** via **VI**.



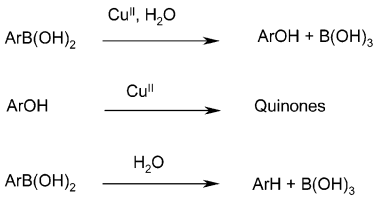

***Scheme 107.*** Catalytic cycle for the copper-catalyzed arylation with polyvalent reagents. Y = NH,O; L, Z = exchangeable ligands; M = polyvalent center.




***Scheme 109.*** Catalytic cycle for the arylation of imidazole with phenylboronic acid and $[\{Cu(\mu\text{-}OH)(tmeda)\}_2]Cl_2$ as catalyst.


© 2003 Wiley-VCH Verlag GmbH & Co. KGaA, Weinheim

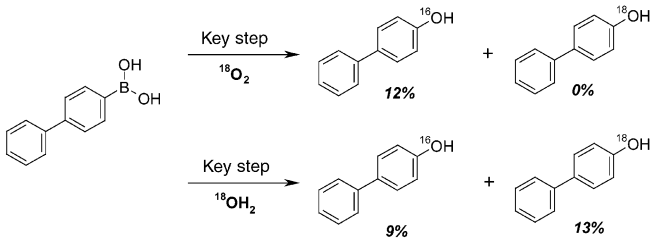
During these processes (catalytic or stoichiometric), possible side reactions do occur and are shown in Scheme 110). These explain why the use of $>1$ equivalent



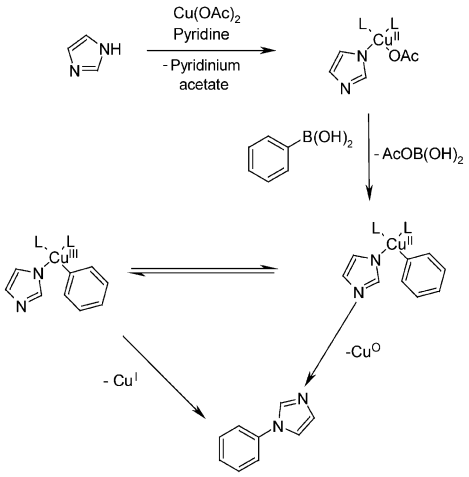

***Scheme 110.*** Possible side reactions in the arylation of imidazole with aryl boronic acids.

of the boronic acid is necessary. Furthermore, during the oxidation of $Cu^{II}$ to $Cu^{III}$, hydrogen peroxide is produced, which can decrease the yields of the reaction as a result of a reaction with the aryl boronic acid. This may also explain why $>1$ equivalent of the aryl boronic acid results in enhanced yields.[135] Moreover, the aryl boronic acid can form triaryl boroxines[136] and in doing so forms water, which can be removed from the reaction by molecular sieves. Evans and co-workers postulated that phenolic products are formed as a result of the competitive arylation of water formed during the reaction process. Lam and co-workers conducted oxygen isotope incorporation studies to validate Evans's hypotheses.[39] The use of $^{18}O_2$ demonstrated that the phenols are not formed from atmospheric oxygen, which suggests that the phenol is formed from water produced during the reaction. Indeed, when $H_2{}^{18}O$ was used, the isotope label was incorporated into the biphenylphenol product, as shown (Scheme 111). An alternative proposal follows the sequence: a) coordination and deprotonation; b) transmetalation; c) oxidation or disproportionation; and d) reductive elimination (Scheme 112).

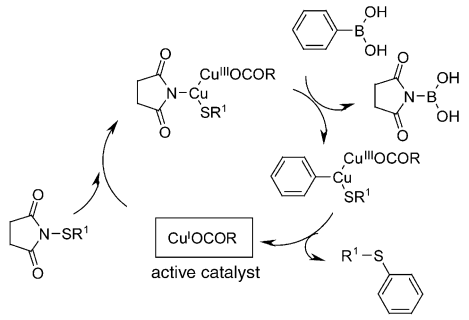
Liebeskind et al. have reported a novel, interesting, mild, non-base copper(I)-mediated strategy for the synthesis of thioethers. They proposed that the mechanism for alkylaryl sulfide formation does not parallel that of the O and N (see Section 11) counterparts but instead, it is more likely that a $Cu^{I}$-mediated transformation takes place (due to the facile oxidation of thiols to disulfides by $Cu^{II}$).[56] This postulate was supported by the preparation of diphenylsulfide (74%) from the reaction between phenylboronic acid and $Cu^{I}$–3-methylsalicylate (CuMeSal) in DMA at 100°C for 18 h (Section 2.4.2). A possible mechanism for the copper-catalyzed coupling of boronic acids and *N*-thioimides proceeds through a reversible oxidative addition of the *N*-thioimide to $Cu^{I}$ followed by transmetalation from boron to copper. Regeneration of the active catalytic $Cu^{I}$ species is viable through carbon–sulfur bond reductive elimination to afford the observed thioether product. Again, the postulated mechanism proceeds through $Cu^{I}$ and $Cu^{III}$ intermediates (Scheme 113).




***Scheme 111.*** Oxygen-isotope-incorporation studies: Under the conditions for the Ullmann reaction, $^{18}O$ from $H_2{}^{18}O$ is incorporated into phenol derivatives.




***Scheme 112.*** Alternative mechanism for the copper-catalyzed arylation of imidazole with aryl boronic acids.

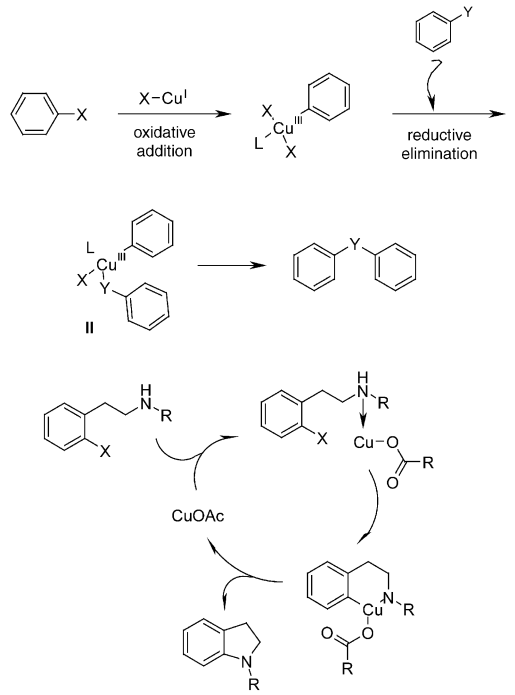



***Scheme 113.*** Plausible catalytic cycle for the copper-catalyzed arylation of *N*-thioimides with boronic acids.

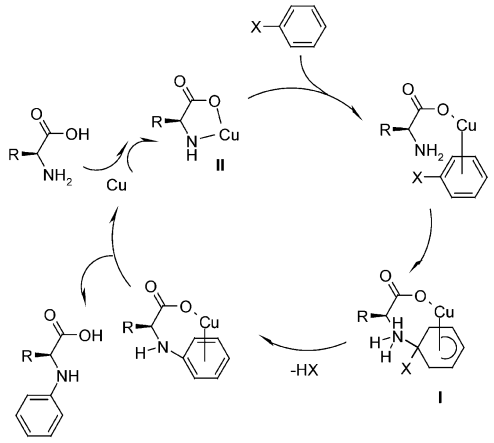
A4: The Ullmann reaction may proceed as shown in Scheme 114, and an intramolecular variant is also given. A possible reaction mechanism was proposed which proceeds via the air-sensitive CuOAc. This was not cross-checked by adding the commercially available material as a control. Interestingly, another advantage over the palladium-mediated reaction was noted in which a *meta*-iodo substrate did indeed produce the desired product and not only a product formed from the oxidative addition of copper to the aryl iodide.[61]

The nature of the carboxylate ligand has a significant accelerating effect on the heteroatom arylation reaction. Ma and co-workers proposed a catalytic cycle (Scheme 115) based on some underlying principles. A mechanistic rational

 © 2003 Wiley-VCH Verlag GmbH & Co. KGaA, Weinheim 




***Scheme 114.*** Plausible mechanism for the copper-catalyzed Ullmann reaction with aryl halides as aryl donors. Reductive elimination releases the coupling product. X = Cl, Br, I; Y = NH, O.




***Scheme 115.*** Catalytic cycle for the copper-catalyzed *N*-arylation of amino acids.

discussing the accelerating effects of α-, β-, and γ-amino acids has been proposed. α-Amino acids can chelate copper ions through the amine and acid functionalities, and since the π complex mechanism is a common proposal for the mechanism of the Ullmann condensation, the intermediate **I** is proposed to form as follows:

1) Formation of the amino acid–Cu$^{I}$ salt **II**.
2) π Complex formation with an aryl halide.
3) Intramolecular $S_NAr$ reaction to form **I** as a transition-state intermediate.
4) Elimination of HX (base-mediated) to form the π complex copper salt of the desired *N*-arylated product.

A similar mechanism has been proposed for β-amino acids.

## *13. Summary and Outlook*

The copper-mediated C(aryl)–O, C(aryl)–N, and C(aryl)–S bond formation is a powerful reaction used routinely for the preparation of a wide variety of compounds ranging from simple to complex molecular targets. Leading contributions have clearly been the use of aryl boronic acids as the aryl donor, which react efficiently in the presence of Cu$^{II}$ sources such as $Cu(OAc)_2$ at room temperature to form products of the Ullmann condensation reaction. When using aryl halides as the aryl donor, major progress has been made in the presence of Cu$^{I}$ sources, in particular CuOAc in combination with chelating and/or solubilizing ligands in approaching the ultimate goal of a room-temperature Ullmann condensation reaction. So far, this goal has only been reached in the intramolecular transformation.

In general it is apparent from a synthetic perspective that the recent discoveries described in this Review have had a considerable impact in organic synthesis. This is represented by the increasing amount of publications in the areas encompassing a) substrate design, b) optimization of reaction conditions, bases, additives, time, solvent, c) nature of the copper species involved, and d) introduction of new ligands, paralleling to a small extent the progress made in the corresponding palladium-mediated arylation reactions. However, in the Pd-mediated field, today's state-of-the-art has been the incorporation of iterative design cycles in the use and developmental design of new ligands to offer the synthetic chemists a bountiful toolbox of opportunities for the synthesis of a wide range of targets. To continue the initial rapid progress of the copper-mediated arylation, still relatively in its infancy, it is imperative to apply many of the principles precedented in the palladium-mediated work. Despite many important contributions and significant progress, many challenges remain. To meet these, many more mechanistic studies have to be performed to shed more light on the copper species involved during the reactions, including identifying the substrate/ligand/catalyst intermediates.

However, with few exceptions, most of the work carried out thus far reports yields after chromatographic purification and in some case yields judged by GC are presented. For this process to be used more widely in industry, it is prudent to encourage the reporting of ICP analyses of the copper residues within final products to give an adequate indication of product purity. In particular, for a major impact on industry, higher turnover numbers of the catalytic cycles must be established and new and effective supported ligand/catalyst combinations are necessary. Clearly, the low cost price [Pd = \$1000 per ounce; Cu = \$0.1 per ounce] of copper relative to palladium offers a distinct financial advantage on an industrial scale.

Many substrates fail to react under some of the reaction conditions, and the choice of reaction conditions is still open to trial and error attempts. Improvement in both scope and the mildness of the reaction conditions are necessary for all of the methods described above. Owing to the increased amount of research work being conducted in this field, major steps to solve these challenges should emerge in the near future. The continued development and discovery of new and efficient

 © 2003 Wiley-VCH Verlag GmbH & Co. KGaA, Weinheim 

aryl-transfer reagents[137] is also essential to keep pace with competing methods[138] to prepare the usual products from C(aryl)–O, C(aryl)–N, and C(aryl)–S bond formation.

## Addendum

Further improvements, novel applications, and new classes of Ullmann condensation reactions are continually appearing in the literature. The latest developments are described below.

Snapper, Hoveyda, and co-workers used a $Cu(OAc)_2$-mediated formation of a macrocyclic diaryl ether as a key step in the stereoselective total synthesis of the anti-HIV agent chloropeptin I.[139] The reaction was carried out under dilute conditions with 10 equivalents of $Et_3N$. Methanol (10 equiv) was used as an additive to increase the solubility of the copper salt and in situ formation of the dimethylboronate. Takeya and co-workers investigated the use of a variety of bases and copper ligands in a similar diaryl ether formation, as a significant amount of protodeborylated products was formed. In the synthesis of two cycloisodityrosines, the use of DMAP allowed respectable yields (35–56%) of the desired products (free from epimerization), with less than 6% of the side product formed under dilute reaction conditions.[140]

Sagar et al. reported the synthesis of symmetrical diaryl ethers through the arylation of phenols generated in situ from boronic acids.[141] Their method is complementary to that of Petasis and co-workers.[32] The products were all formed in high yields using water (rather than $H_2O_2$ previously used) as a key additive (10–12 equiv) with $Cu(OAc)_2$ and $Et_3N$.

Kabalka and Guchhait have reported the room temperature synthesis of diprotected monosubstituted hydrazine derivatives by the reaction of *t*-butyl carbazates and aryl boronic acids in the presence of CuCl with pyridine as base and air as co-oxidant.[142]

The introduction of deanol (2-(*N,N*-dimethylamino)ethanol) as a solvent for the amination of aryl halides by Twieg and co-workers is significant. A wide range of substrates, copper salts, additive contents, and reaction temperatures were studied.[143]

Ma et al. elegantly used *N*-methylglycine and L-proline as accelerating ligands in the formation of aryl amines. The reaction temperatures used (40–90 °C) are some of the lowest reported to date to effect the Ullmann condensation of aryl halides.[144] Under these conditions and with *N,N*-dimethylglycine·HCl salt (instead of *N*-methylglycine or L-proline), a range of diaryl ethers were prepared at only 90 °C from aryl bromides or iodides and substituted phenols.[145]

Wu et al. used microwave radiation to effect the amination of a number or azole substrates with (*S*)-1-(3-bromophenyl)-ethylamine as the electrophile in the presence of CuI (10 mol%) with $K_2CO_3$ in NMP as solvent.[146] Under the same conditions, Wu and He effected the *N* arylation of a number of sulfonamides with aryl bromides and iodides,[147] as well as *S* arylation of a thiophenols with aryl bromides and iodides.[148]

Buchwald and co-workers compared the regioselective arylation of difunctionalized nucleophiles with copper and palladium catalysts, which lead to complementary products:[149] Aniline derivatives with carbamoyl, indolyl, or aliphatic amino functions are arylated at the nitrogen atom of the aniline function in the presence of palladium catalysts. When copper catalysts are used, mainly the other functional group is arylated. Although outside the scope of this Review, the reaction conditions developed initially by Buchwald and co-workers for the arylation of amides has proven to be general for the amidation of vinyl halides, providing rapid access to a wide range of enamides in good yields.[150] Miyashita and co-workers recently reported the total synthesis of scytophcin C in which a crucial terminal amidation of a vinyl iodide was used at an advanced stage.[151] Under the Buchwald-modified Goldberg amidation conditions, the desired coupling product was formed in 85% yield.

Pellon Comdom and Docampo Palacious have shown that water can be used as the solvent in the copper- and ultrasound-mediated preparation of 2-carboxy-substituted diphenyl ethers.[152]]

Heaney and co-workers have illustrated the desymmetrization of resorcinol with 3-benyloxyiodobenzene as a substrate with a range of alcohol donors under previously developed conditions (CuI, 1,10-phenanthroline, $Cs_2CO_3$).[154]

Again, although outside the scope of this Review, the reaction conditions developed initially by Lam and co-workers for the arylation of NH and OH substrates with aryl boronic acids has proven to be general, and the use of vinyl boronic acids provided rapid access to a wide range of products in good yields. Both stoichiometric and catalytic reactions (with or without co-oxidants) were developed for $Cu(OAc)_2$- and base-mediated *O* and *N* vinylation. The range of products formed were then elaborated as protecting groups or as substrates for ring-closing metathesis or for Simmons–Smith cyclopropanations.[154]

This Review has dealt with *O, N*, and *S* arylations, but other C(aryl)–heteroatom bond formations are possible. Recently, the introduction of copper-mediated methods for the formation of C(aryl)–Se bonds was demonstrated by Gujadhur and Venkataraman, who effected the $Cu^I$-mediated cross-coupling of aryl iodides with phenylselenol.[155] The best reaction conditions involved the use of CuI (10 mol%), neocuproine, and NaO*t*Bu (or $K_2CO_3$) as base in toluene at 100 °C. Recently, Taniguchi and Onami showed that unsymmetrical diaryl selenides can be formed from aryl iodides and diphenyl selenides in the presence of $Cu_2O$ and Mg under neutral conditions.[156] Beletskaya et al. used a complimentary approach with $Bu_3SnSeAr$ and aryl bromides to prepare unsymmetrical diaryl selenides.[157] Buchwald and co-workers[158] and Venkataraman and Van Allen[159] reported improved conditions for copper-catalyzed C–P bond formations from aryl and vinyl iodides.

## Abbreviations

| | |
|---|---|
| Ac | acetyl |
| acac | acetylacetone |
| Bn | benzyl |

 © 2003 Wiley-VCH Verlag GmbH & Co. KGaA, Weinheim 

| | |
|---|---|
| Boc | *tert*-butoxycarbonyl |
| cat. | catalytic |
| Cbz | benzyloxycarbonyl |
| CNS | Central Nervous System |
| DABCO | 1,4-diazabicyclo[2.2.2]octane |
| dba | dibenzylidene acetone |
| DBU | 1,8-diazabicyclo[5.4.0]undec-7-ene |
| DIPEA | *N,N*-diisopropylethylamine |
| DMA | dimethylacetamide |
| DME | 1,2,-dimethoxyethane |
| DMAP | 4-dimethylaminopyridine |
| DMF | *N,N*-dimethylformamide |
| DMSO | dimethyl sulfoxide |
| Fmoc | 9-fluorenylmethyl |
| ICP | inductively coupled plasma |
| *m*CPBA | *m*-chloroperoxybenzoic acid |
| NMO | 4-methylmorpholine-*N*-oxide |
| NMP | *N*-methylpyrolidinone |
| Ns | 2-nitrobenzenesulfonamide |
| PEG | poly(ethylene glycol) |
| phen | phenanthroline |
| Piv | pivaloyl |
| pyr | pyridine |
| $P_2$-Et | 1-ethyl-2,2,4,4,4-pentakis(dimethylamino)-2$\Lambda^5$-catenadi(phosphazene) |
| $P_4$-*t*Bu | 1-*tert*-butyl-2,2,4,4,4-pentakis(dimethylamino)-2$\Lambda^5$-catenadi(phosphazene) |
| TBAF | tetra-*n*-butylammonium fluoride |
| TBDMS | *tert*-butyldimethylsilyl |
| TEMPO | tetramethylpiperidinyloxy |
| TFA | trifluoroacetic acid |
| tmeda | tetramethylethylenediamine |
| TMHD | 2,2,6,6-tetramethylheptane-3,5-dione |

*AWT thanks Prof. Erick Carreira, Dr. Geo Adam, Dr. Alex Alanine, and Prof. Jochen Böhm for support during the preparation of this manuscript. The constant encouragement, stimulating scientific discussions, and proofreading of the manuscript by Dr. Matthias Nettekoven, Dr. Mark Rogers-Evans, and Dr. Thomas Woltering are highly appreciated. Matthias is also thanked for his valuable input whilst preparing the German translation. Dr. Simona Ceccarelli is thanked for the excellent frontispiece, which gracefully encapsulates the message of this Review. Finally, heartfelt thanks are extended to Anke Kurt, Axel Maier, Debi Studer, Eva Krafft, Christophe Rochais, and Pierre-Emmanuel Broutin for their excellent contributions to our medicinal chemistry research programs in our quest to discover new and improved treatments for diseases of the CNS.*

Received: March 19, 2003 [A594]

[1] a) F. Ullmann, *Ber. Dtsch. Chem. Ges.* **1903**, *36*, 2389 – 2391; b) F. Ullmann, *Ber. Dtsch. Chem. Ges.* **1904**, *37*, 853 – 857; c) I. Goldberg, *Ber. Dtsch. Chem. Ges.* **1906**, *39*, 1691 – 1696.
[2] J.-P. Hanoun, J.-P. Galy, A. Tanaglia, *Synth. Commun.* **1995**, *25*, 2443 – 2448.
[3] C. Palomo, M. Oiarbide, R. Lopez, E. Gomez-Bengoa, *Chem. Commun.* **1998**, 2091 – 2092.
[4] a) T. Eicher, M. Walter, *Synthesis* **1991**, 469 – 473; b) T. Eicher, S. Fey, W. Puhl, E. Buechel, A. Speicher, *Eur. J. Org. Chem.* **1998**, 877 – 888.
[5] K. C. Nicolaou, C. N. C. Boddy, H. Li, A. E. Koumbis, R. Hughes, S. Natarjan, N. F. Jain, J. M. Ramanjulu, S. Brase, M. E. Solomon, *Chem. Eur. J.* **1999**, *5*, 2602 – 2621.
[6] D. Prim, J. M. Campagne, D. Joseph, B. Andrioletti, *Tetrahedron* **2002**, *58*, 2041 – 2075.
[7] I. Sapountzis, P. Knochel, *J. Am. Chem. Soc.* **2002**, *124*, 9390 – 9391.
[8] J. Hassan, M. Sevingnon, C. Gozzi, E. Shulz, M. Lemaire, *Chem. Rev.* **2002**, *102*, 1359 – 1469.
[9] a) D. H. R. Barton, J. P. Finet, *Pure Appl. Chem.* **1987**, *59*, 937 – 946; b) R. A. Abramovitch, D. H. R. Barton, J. P. Finet, *Tetrahedron* **1988**, *44*, 3039 – 3071.
[10] a) A. R. Muci, S. L. Buchwald, *Top. Curr. Chem.* **2002**, *219*, 131 – 209; b) J. P. Wolfe, S. Wagaw, J. F. Marcoux, S. L. Buchwald, *Acc. Chem. Res.* **1998**, *31*, 805 – 818; c) B. Y. Yang, S. L. Buchwald, *J. Organomet. Chem.* **1999**, *576*, 125 – 146.
[11] a) J. F. Hartwig, *Angew. Chem.* **1998**, *37*, 2154 – 2177; *Angew. Chem. Int. Ed.* **1998**, *37*, 2046 – 2067; b) J. F. Hartwig in *Handbook of Organopalladium Chemistry for Organic Synthesis, Vol. 1*, (Eds.: E.-i. Negishi, A de Meijere), John Wiley & Sons, New York, S. 1051–1096; c) J. F. Hartwig, *Pure Appl. Chem.* **1999**, *71*, 1417 – 1423; d) J. F. Hartwig, *Acc. Chem. Res.* **1998**, *31*, 852 860; e) J. F. Hartwig, *Synlett* **1997**, 329 – 340; f) D. Baranano, G. Mann, J. F. Hartwig, *Curr. Org. Chem.* **1997**, *1*, 287 – 305.
[12] A. F. Littke, G. C. Fu, *Angew. Chem.* **2002**, *114*, 4350 – 4386; *Angew. Chem. Int. Ed.* **2002**, *41*, 4177 – 4211.
[13] F. Theil, *Angew. Chem.* **1999**, *111*, 2493 – 2495; *Angew. Chem. Int. Ed.* **1999**, *38*, 2345 – 2347.
[14] D. M. T. Chan, K. L. Monaco, R.-P. Wang, M. P. Winters, *Tetrahedron Lett.* **1998**, *39*, 2933 – 2936.
[15] D. A. Evans, J. L. Katz, T. R. West, *Tetrahedron Lett.* **1998**, *39*, 2937 – 2940.
[16] P. Y. S. Lam, C. G. Clark, S. Saubern, J. Adams, M. P. Winters, D. M. T. Chan, A. Combs, *Tetrahedron Lett.* **1998**, *39*, 2941 – 2944.
[17] D. M. T. Chan, *Tetrahedron Lett.* **1996**, *37*, 9013 – 9016.
[18] D. M. T. Chan, Abstract M92, 35th National Organic Symposium, TX, USA, **1997**.
[19] D. L. Boger, Y. Nomoto, B. R. Teegarten, *J. Org. Chem.* **1993**, *58*, 1425 – 1433.
[20] S. B. Singh, H. Jayasuiriya, G. M. Salituro, D. L. Zink, A. Shafiee, B. Heimbuch, K. C. Silverman, R. B. Lingham, O. Genilloud, A. Teran, D. Vilella, P. Felock, D. Hazuda, *J. Nat. Prod.* **2001**, *64*, 874 – 882.
[21] H. Itokawa, K. Takeya, N. Mori, T. Sonobe, S. Mihashi, T. Hamanaka, *Chem. Pharm. Bull.* **1983**, *31*, 1424 – 1427.
[22] a) S. Nishiyama, Y. Suzuki, S. Yamamura *Tetrahedron Lett.* **1988**, *29*, 559 – 562; b) U. Schmidt, D. Weller, A. Holder, A. Lieberknecht, *Tetrahedron Lett.* **1988**, *29*, 3227 – 3230.
[23] M. E. Jung, J. C. Rohloff, *J. Org. Chem.* **1985**, *50*, 4909 – 4912.
[24] D. L. Boger, D. Yohannes, *J. Org. Chem.* **1989**, *54*, 2498 – 2502.
[25] A. V. R. Rao, M. K. Gurjar, K. L. Reddy, A. S. Rao, *Chem. Rev.* **1995**, *95*, 2135 – 2167.
[26] J. R. Chalmers, G. T. Dickson, J. Elks, B. A. Hems, *J. Chem. Soc.* **1949**, 3424.
[27] M. E. Jung, T. I. Lazarova, *J. Org. Chem.* **1999**, *64*, 2976 – 2977.
[28] D. A. Evans, J. L. Katz, G. S. Peterson, T. Hintermann, *J. Am. Chem. Soc.* **2001**, *123*, 12411 – 12413.
[29] C. P. Decicco, Y. Song, D. A. Evans, *Org. Lett.* **2001**, *3*, 1029 – 1032.
[30] I. C. Choong, J. A. Ellman, *J. Org. Chem.* **1999**, *64*, 6528 – 6529.
[31] H. M. Petrassi, K. B. Sharpless, J. W. Kelly, *Org. Lett.* **2001**, *3*, 139 – 142.

 © 2003 Wiley-VCH Verlag GmbH & Co. KGaA, Weinheim 

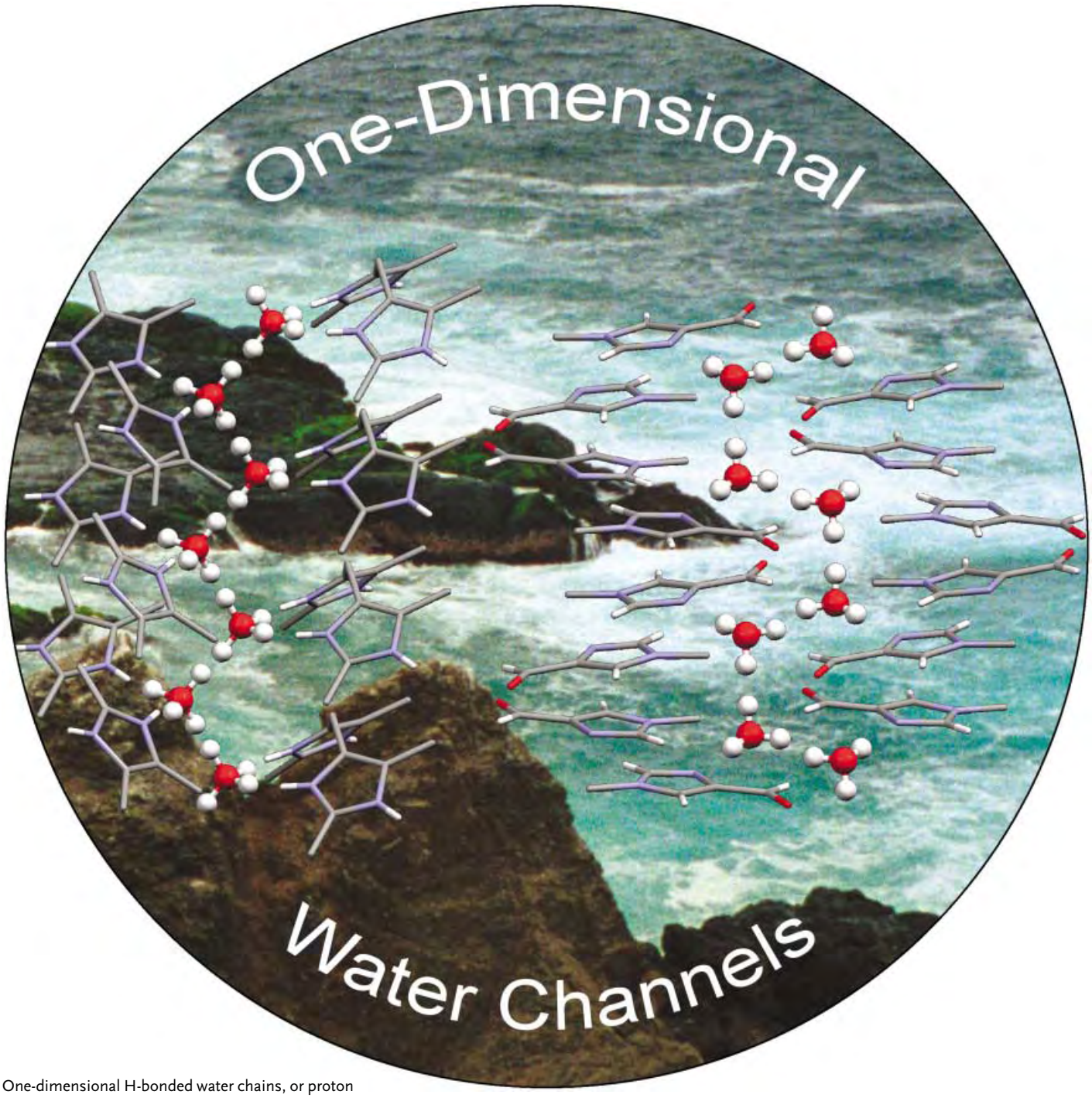
[32] J. Simon, S. Salzbrunn, G. K. S. Prakash, N. A. Petasis, G. A. Olah, *J. Org. Chem.* **2001**, *66*, 633 – 634.
[33] P. Y. S. Lam, G. Vincent, C. G. Clark, S. Deudon, P. K. Jadhav, *Tetrahedron Lett.* **2001**, *42*, 3415 – 3418.
[34] D. J. Cundy, S. A. Forsyth, *Tetrahedron Lett.* **1998**, *39*, 7979 – 7982.
[35] C. Jamieson, M. S. Congreave, D. F. Emiabata-Smith, S. V. Ley, J. J. Scicinski, *Org. Process Res. Dev.* **2002**, *6*, 823 – 827.
[36] V. Collot, P. R. Bovy, S. Rault, *Tetrahedron Lett.* **2000**, *41*, 9053 – 9057.
[37] W. W. K. R. Mederski, M. Lefort, M. Germann, D. Kux, *Tetrahedron* **1999**, *55*, 12757 – 12770.
[38] S. Yu, J. Saenz, J. K. Srirangam, *J. Org. Chem.* **2002**, *67*, 1699 – 1702.
[39] P. Y. S. Lam, D. Bonne, G. Vincent, C. G. Clark, A. P. Combs, *Tetrahedron Lett.* **2003**, *44*, 1691 – 1694.
[40] R. D. Thompson, S. Secunda, J. W. Daly, R. A. Olsson, *J. Med. Chem.* **1991**, *34*, 2877 – 2882.
[41] S. M. Greenberg, L. O. Ross, R. K. Robins, *J. Org. Chem.* **1959**, *24*, 1314 – 1317.
[42] A. K. Bakkestuen, L.-L. Gundersen, *Tetrahedron Lett.* **2003**, *44*, 3359 – 3362.
[43] a) R. E. Dolle, *J. Comb. Chem.* **2002**, *4*, 369 – 418; b) R. E. Dolle, *J. Comb. Chem*, **2003**, *5*, ASAP.
[44] A. P. Combs, S. Saubern, M. Rafalski, P. Y. S. Lam, *Tetrahedron Lett.* **1999**, *40*, 1623 – 1626.
[45] A. P. Combs, M. Rafalski, *J. Comb. Chem.* **2000**, *2*, 29 – 32.
[46] A. P. Combs, S. Tadesse, M. Rafalski, T. S. Haque, P. Y. S. Lam, *J. Comb. Chem.* **2002**, *4*, 179 – 182.
[47] J. P. Collman, M. Zhong, *Org. Lett.* **2000**, *2*, 1233 – 1236.
[48] *Organic Synthesis in Water* (Ed.: P. A. Grieco), Blackie Academic & Professional, London, **1998**.
[49] J. P. Collman, M. Zhong, L. Zeng, S. Costanzo, *J. Org. Chem.* **2001**, *66*, 1528 – 1531.
[50] J. P. Collman, M. Zhong, C. Zhang, S. Costanzo, *J. Org. Chem.* **2001**, *66*, 7892 – 7897.
[51] J. C. Antilla, S. L. Buchwald, *Org. Lett.* **2001**, *3*, 2077 – 2079.
[52] H. Weingarten, *J. Am. Chem. Soc.* **1964**, *86*, 3624 – 3626.
[53] a) A. Padwa, A. D. Woodhouse in *Comprehensive Heterocyclic Chemistry* (Ed.: A. R. Katrizky, C. W. Rees), Pergamon, Oxford, UK, **1984**; b) D. Tanner, *Angew. Chem.* **1994**, *96*, 625 – 646; *Angew. Chem. Int. Ed. Engl.* **1994**, *33*, 599 – 619; c) V. K. Aggarwal, R. A. Stenson, R. V. H. Jones, R. Fieldhouse, J. Blacker, *Tetrahedron Lett.* **2001**, *42*, 1587 – 1590; d) P. Magdolen, M. Meciarova, S. Toma, *Tetrahedron* **2001**, *57*, 4781 – 4787.
[54] M. Sasaki, S. Dalili, A. K. Yudin, *J. Org. Chem.* **2003**, *68*, 2045 – 2047.
[55] P. S. Herradura, K. A. Pendola, R. K. Guy, *Org. Lett.* **2000**, *2*, 2019 – 2022.
[56] C. Savarin, J. Srogl, L. S. Liebeskind, *Org. Lett.* **2002**, *4*, 4309 – 4312.
[57] J. Lindley, *Tetrahedron* **1984**, *40*, 1433 – 1456.
[58] A. Kiyomori, J.-F. Marcoux, S. L. Buchwald, *Tetrahedron Lett.* **1999**, *40*, 2657 – 2660.
[59] H. B. Goodbrand, N.-X. Hu, *J. Org. Chem.* **1999**, *64*, 670 – 674.
[60] R. Gujadhur, D. Venkataraman, J. T. Kintigh, *Tetrahedron Lett.* **2001**, *42*, 4791 – 4793.
[61] K. Yamada, T. Kubo, H. Tokuyama, T. Fukuyama, *Synlett* **2002**, 231 – 234.
[62] R. K. Gujadhur, C. G. Bates, D. Venkataraman, *Org. Lett.* **2001**, *3*, 4315 – 4317.
[63] A. A. Kelkar, N. M. Patil, R. V. Chaudhari, *Tetrahedron Lett.* **2002**, *43*, 7143 – 7146.
[64] J. C. Antila, A. Klapars, S. L. Buchwald, *J. Am. Chem. Soc.* **2002**, *124*, 11684 – 11688.
[65] F. Y. Kwong, A. Klapars, S. L. Buchwald, *Org. Lett.* **2002**, *4*, 581 – 584.
[66] F. Y. Kwong, S. L. Buchwald, *Org. Lett.* **2003**, *5*, 793 – 796.
[67] G. E. Job, S. L. Buchwald, *Org. Lett.* **2002**, *4*, 3703 – 3706.
[68] D. Ma, Y. Zhang, J. Yao, S. Wu, F. Tao, *J. Am. Chem. Soc.* **1998**, *120*, 12459 – 12467.
[69] a) D. Ma, C. Xia, *Org. Lett.* **2001**, *3*, 2583 – 2586; b) J.-B. Clement, J. F. Hayes, H. M. Sheldrake, P. W. Sheldrake, A. S. Wells, *Synlett* **2001**, 1423 – 1427.
[70] D. Ma, C. Xia, J. Jiang, J. Zhang, W. Tang, *J. Org. Chem.* **2003**, *68*, 442 – 451.
[71] G. Evindar, R. A. Batey, *Org. Lett.* **2003**, *5*, 133 – 136.
[72] C. Enguehard, H. Allouchi, A. Gueiffier, S. L. Buchwald, *J. Org. Chem.* **2003**, *68*, 4367 – 4370.
[73] A. Klapars, J. C. Antila, X. Huang, S. L. Buchwald, *J. Am. Chem. Soc.* **2001**, *123*, 7727 – 7729.
[74] A. Klapars, X. Huang, S. L. Buchwald, *J. Am. Chem. Soc.* **2002**, *124*, 7421 – 7428.
[75] S.-K. Kang, D.-H. Kim, J.-N. Pak, *Synlett* **2002**, 427 – 430.
[76] a) K. R. Crawford, A. Padwa, *Tetrahedron Lett.* **2002**, *43*, 7365 – 7368; b) A. Padwa, K. R. Crawford, P. Rashatasakhon, M. Rose, *J. Org. Chem.* **2003**, *68*, 2609 – 2617 .
[77] J. H. M. Lange, L. J. F. Hofmeyer, F. A. S. Hout, S. J. M. Osnabrug, P. C. Verveer, C. G. Kruse, R. W. Feenstra, *Tetrahedron Lett.* **2002**, *43*, 1101 – 1104.
[78] M. Wolter, A. Klapars, S. L. Buchwald, *Org. Lett.* **2001**, *3*, 3803 – 3805.
[79] B. Mallesham, B. M. Rajesh, P. Rajmohan-Reddy, D. Srinivas, S. Trehan, *Org. Lett.* **2003**, *5*, 963 – 965.
[80] J. F. Marcoux, S. Doyle, S. L. Buchwald, *J. Am. Chem. Soc.* **1997**, *119*, 10539 – 10540.
[81] X. Xing, D. Padmanaban, L.-A. Yeh, G. D. Cuny, *Tetrahedron* **2002**, *58*, 7903 – 7910.
[82] A. V. Kalinin, J. F. Bower, P. Reibel, V. Snieckus, *J. Org. Chem.* **1999**, *64*, 2986 – 2987.
[83] K. Gujadhur, D. Venkataraman, *Synth. Commun.* **2001**, *31*, 2865 – 2879.
[84] J. A. Ragan, T. W. Makowski, M. J. Castaldi, P. D. Hill, *Synthesis* **1998**, 1599 – 1603.
[85] M. Wolter, G. Nordmann, G. E. Job, S. L. Buchwald, *Org. Lett.* **2002**, *4*, 973 – 976.
[86] E. Buck, Z. J. Song, D. Tschaen, P. G. Dormer, R. P. Volante, P. J. Reider, *Org. Lett.* **2002**, *4*, 1623 – 1626.
[87] H. He, Y.-J. Wu, *Tetrahedron Lett.* **2003**, *43*, 3445 – 3446.
[88] C. Palomo, M. Oiabide, R. Lopez, E. Gomez-Bengoa, *Tetrahedron Lett.* **2000**, *41*, 1283 – 1286.
[89] T. Kondo, T. Mitsudo, *Chem. Rev.* **2000**, *100*, 3205 – 3220.
[90] C. G. Bates, R. K. Gujadhur, D. Venkataraman, *Org. Lett.* **2002**, *4*, 2803 – 2806.
[91] F. Y. Kwong, S. L. Buchwald, *Org. Lett.* **2002**, *4*, 3517 – 3520.
[92] a) J. M. Baskin, Z. Wang, *Org. Lett.* **2002**, *4*, 4423 – 4425; b) J. M. Baskin, Z. Wang, *Tetrahedron Lett.* **2002**, *43*, 8479 – 8483.
[93] P. Y. S. Lam, S. Deudon, K. M. Averill, R. Li, M. Y. He, P. DeShong, C. G. Clark, *J. Am. Chem. Soc.* **2000**, *122*, 7600 – 7601.
[94] P. Y. S. Lam, C. G. Clark, S. Saubern, J. Adams, K. M. Averill, D. M. T. Chan, A. Combs, *Synlett* **2000**, 674 – 676.
[95] P. Y. S. Lam, G. Vincent, D. Bonne, C. G. Clark, *Tetrahedron Lett.* **2002**, *43*, 3091 – 3094.
[96] a) F. M. Beringer, A. Brierley, M. Drexler, E. M. Gindler, C. C. Lumpkin, *J. Am. Chem. Soc.* **1953**, *75*, 2708 – 2712; b) R. A. Scherer, H. R. Beatty, *J. Org. Chem.* **1980**, *45*, 2127 – 2131.
[97] S.-K. Kang, S.-H. Lee, D. Lee, *Synlett* **2000**, 1022 – 1024.
[98] T. Zhou, Z.-C. Chen, *Synth. Commun.* **2002**, *32*, 903 – 907.
[99] I. P. Beletskaya, D. V. Davydov, M. S. Gorovoy, *Tetrahedron Lett.* **2002**, *43*, 6221 – 6223.


 © 2003 Wiley-VCH Verlag GmbH & Co. KGaA, Weinheim 

[100] D. V. Davydov, I. P. Beleskaya, B. S. Semenov, Y. I. Smushkevich, *Tetrahedron Lett.* **2002**, *43*, 6217 – 6219.
[101] P. Lopez-Alvarado, C. Avendano, J. C. Mendendez, *Tetrahedron Lett.* **1992**, *33*, 659 – 662.
[102] P. Lopez-Alvarado, C. Avendano, J. C. Mendendez, *J. Org. Chem.* **1995**, *60*, 5678 – 5682.
[103] a) S. David, A. Thieffry, *Tetrahedron Lett.* **1981**, *22*, 5063 – 5066; b) S. David, A. Thieffry, *J. Org. Chem.* **1983**, *48*, 441 – 447.
[104] a) D. H. R. Barton, J.-P. Finet, *Pure Appl. Chem.* **1987**, *59*, 937 – 946; b) R. A. Abramovitch, D. H. R. Barton, J.-P. Finet, *Tetrahedron* **1988**, *44*, 3039 – 3071; c) V. A. Dodonov, A. V. Gushchin, *Russ. Chem. Bull.* **1993**, *12*, 2043 – 2047.
[105] J.-P. Finet, A. Y. Federov, S. Combes, G. Boyer, *Curr. Org. Chem.* **2002**, *6*, 597 – 626.
[106] a) P. J. Sinclair, F. Wong, M. Wyvratt, M. J. Staruch, F. Dumont, *Bioorg. Med. Chem. Lett.* **1995**, *5*, 1035 – 1038; b) P. J. Sinclair, F. Wong, M. J. Staruch, G. Wiederrecht, W. H. Parsons, F. Dumont, M. Wyvratt, *Bioorg. Med. Chem. Lett.* **1996**, *6*, 2193 – 2196; c) K. M. J. Brands, U.-H. Dolling, R. B. Jobson, G. Marchesini, R. A. Reamer, J. M. Williams, *J. Org. Chem.* **1998**, *63*, 6721 – 6726.
[107] S. Pietri, T. Liebgott, J.-P. Finet, M. Culcasi, L. Billottet, C. Bernard-Henriet, *Drug Dev. Res.* **2001**, *54*, 191 – 201.
[108] M. A. Esteves, M. Narander, M. J. Marcelo-Curto, B. Gigante, *J. Nat. Prod.* **2001**, *64*, 761 – 766.
[109] Y. Fukuda, H. Furata, Y. Kusama, H. Ebisu, Y. Oomori, S. Terashima, *Heterocycles* **1998**, *49*, 53 – 58.
[110] S. K. Moiseev, I. V. Bakhanova, H. Schmidhammer, V. N. Kalinin, *Russ. Chem. Bull.* **1999**, *48*, 589 – 592.
[111] a) D. H. R. Barton, J.-P. Finet, J. Khamsi, *Tetrahedron Lett.* **1989**, *30*, 937 – 940; b) J. C. Anderson, M. Harding, *Chem. Commun.* **1998**, 393 – 394; c) J. C. Anderson, R. Cubbon, M. Harding, D. S. James, *Tetrahedron: Asymmetry* **1998**, *9*, 3461 – 3490.
[112] C. Balsamini, A. Bedini, G. Spadoni, G. Tarzia, A. Tontini, W. Balduini, M. Cimino, *Farmaco* **1998**, *53*, 181 – 188.
[113] G. A. Doherty, T. Kamenecka, E. McCauley, G. Van Riper, R. A. Mumford, S. Tong, W. K. Hagmann, *Bioorg. Med. Chem. Lett.* **2002**, *12*, 729 – 731.
[114] T. Arnauld, D. H. R. Barton, E. Doris, *Tetrahedron* **1997**, *53*, 4137 – 4144.
[115] S. Combes, J.-P. Finet, *Tetrahedron* **1998**, *54*, 4313 – 4318.
[116] a) S. Morel, F. Chatel, G. Boyer, J.-P. Galy, *J. Chem. Res. Miniprint* **1998**, 4 – 5; b) S. Morel, F. Chatel, G. Boyer, J.-P. Galy, *J. Chem. Res. Miniprint* **1998**, 761 – 766; c) S. Morel, F. Chatel, G. Boyer, J.-P. Galy, *J. Chem. Res. Miniprint* **1998**, 4 – 5; d) S. Morel, F. Chatel, G. Boyer, J.-P. Galy, *Heterocycles* **2000**, *53*, 2535 – 2552; e) S. Morel, F. Chatel, G. Boyer, J.-P. Galy, *Arkivoc* **2000**, *1*, 563 – 575; f) G. Boyer, J.-P. Galy, J. Barbe, *Heterocycles* **1995**, *41*, 487 – 496.
[117] D. H. R. Barton, J.-P. Finet, J. Khamsi, *Tetrahedron Lett.* **1988**, *29*, 1115 – 1118.
[118] A. Federov, J.-P. Finet, *Tetrahedron Lett.* **1999**, *40*, 2747 – 2748.
[119] a) P. Fan, S. Y. Ablordeppey, *J. Heterocycl. Chem.* **1997**, *34*, 1789 – 1794; b) S. Y. Ablordeppey, P. Fan, A. M. Clark, A. Nimrod, *Bioorg. Med. Chem.* **1999**, *7*, 343 – 349.
[120] A. Banfi, M. Bartoletti, E. Bellora, M. Bignotti, M. Turconi, *Synthesis* **1994**, 775 – 776.
[121] R. Naito, M. Takeuchi, K. Morihira, M. Hayakawa, K. Ikeda, T. Shibanuma, Y. Isomura, *Chem. Pharm. Bull.* **1998**, *46*, 1274 – 1285.
[122] E. Vassileva, M. Shopova, C. Fugier, E. Henry-Basch, *Synth. Commun.* **1997**, *27*, 1669 – 1675.
[123] I. W. J. Still, R. Natividad-Preyra, F. D. Toste, *Can. J. Chem.* **1999**, *77*, 113 – 121.
[124] Y. Aoki, Y. Saito, T. Sakamoto, Y. Kikuguwa, *Synth. Commun.* **2000**, *30*, 131 – 140.
[125] a) O. Loog, U. Maeorg, U. Ragnarsson, *Synthesis* **2000**, 1591 – 1597; b) O. Tsubrik, U. Maeorg, U. Ragnarsson, *Tetrahedron Lett.* **2002**, *43*, 6213 – 6215.
[126] J.-P. Meigh, M. Alvarez, J. A. Joule, *J. Chem. Soc. Perkin Trans. 1* **2001**, 2012 – 2121.
[127] C. J. Dinsmore, J. M. Bergman, D. D. Wei, C. B. Zartman, J. P. Davide, I. B. Greenberg, D. Liu, T. J. O'Neill, J. B. Gibbs, K. S. Koblan, N. E. Kohl, R. B. Lobell, I.-W. Chen, D. A. McLoughlin. T. V. Olah, S. L. Graham, G. D. Hartman, T. M. Williams, *Bioorg. Med. Chem. Lett.* **2001**, *11*, 537 – 540.
[128] R. J. Sorensen, *J. Org. Chem.* **2000**, *65*, 7747 – 7749.
[129] T. D. Quach, R. A. Batey, *Org. Lett.* **2003**, *5*, 1381 – 1384.
[130] E. Vedejs, S. C. Fields, M. R. Scheimpf, *J. Am. Chem. Soc.* **1993**, *115*, 11612 – 11613.
[131] a) V. V. Litvak, S. M. Shein, *Zh. Org. Khim.* **1975**, *11*, 92 – 94; b) A. Paine, *J. Am. Chem. Soc.* **1987**, *109*, 1496 – 1497.
[132] T. P. Lockhardt, *J. Am. Chem. Soc.* **1983**, *105*, 1940 – 1946.
[133] D. H. R. Barton, J.-P. Finet, J. Khamsi, *Tetrahedron Lett.* **1987**, *28*, 887 – 890.
[134] a) A. S. Hay, *J. Org. Chem.* **1962**, *27*, 3320 – 3321; b) S. G. Bratsch, *J. Phys. Chem. Ref. Data* **1989**, *18*, 1 – 21.
[135] M. F. Lappert, *Chem. Rev.* **1956**, *56*, 959 – 1064.
[136] L. Santucci, C. Triboulet, *J. Chem. Soc. Chem. Commun.* **1969**, 392 – 396.
[137] For the first report on the successful use of cyclic borate esters for copper(II)-promoted *O*- and *N*-arylation, see: D. M. T. Chan, K. L. Monaco, R. Li, D. Bonne, C. G. Clark, P. Y. S. Lam, *Tetrahedron Lett.* **2003**, *44*, 3863 – 3865.
[138] For a catalyst-free method for the Ullmann condensation, see: F. Li, Q. Wang, Z. Ding, F. Tao, *Org. Lett.* **2003**, *5*, 2169 – 2171.
[139] H. Deng, J.-K. Jung, T. Liu, K. W. Kuntz, M. L. Snapper, A. H. Hoveyda, *J. Am. Chem. Soc.* **2003**, *125*, 9032 – 9034.
[140] Y. Hitotsuanagi, H. Ishikawa, S. Naito, K. Takeya, *Tetrahedron Lett.* **2003**, *44*, 5901 – 5903.
[141] A. D. Sagar, R. H. Tale, R. N. Adude, *Tetrahedron Lett.* **2003**, *44*, 7061 – 7063.
[142] G. W. Kabalka, S. K. Guchhait, *Org. Lett.* **2003**, *5*, im Druck.
[143] Z. Lu, R. Tweig, S. D. Huang, *Tetrahedron Lett.* **2003**, *44*, 6289 – 6292.
[144] D. Ma, Q. Cai, H. Zhang, *Org. Lett.* **2003**, *5*, 2453 – 2455.
[145] D. Ma, Q. Cai, *Org. Lett.* **2003**, *5*, 3799 – 3802.
[146] Y.-J. Wu, H. He, A. L'Heureux, *Tetrahedron Lett.* **2003**, *44*, 4217 – 4218.
[147] H. He, Y.-J. Wu, *Tetrahedron Lett.* **2003**, *44*, 3385 – 3386.
[148] Y.-J. Wu, H. He, *Synlett* **2003**, 1789 – 1790.
[149] X. Huang, K. W. Anderson, D. Zim, L. Jiang, A. Klapars, S. L. Buchwald, *J. Am. Chem. Soc.* **2003**, *125*, 6653 – 6655.
[150] L. Jiang, G. E. Job, A. Klapars, S. L. Buchwald, *Org. Lett.* **2003**, *5*, 3667 – 3669.
[151] R. Nakamura, K. Tanino, M. Miyashita, *Org. Lett.* **2003**, *5*, 3579 – 3582.
[152] R. F. Pellon Comdom, M. L. Docampo Palacios, *Synth. Commun.* **2003**, *33*, 921 – 926.
[153] J. Y. Boxhall, P. C. B. Page, Y. Chan, C. M. Hayman, H. Heaney, M. J. McGrath, *Synlett* **2003**, 997 – 1001.
[154] P. Y. S. Lam, G. Vincent, D. Bonne, C. G. Clark, *Tetrahedron Lett.* **2003**, *44*, 4927 – 4931.
[155] R. K. Gujadhur, D. Venkataraman, *Tetrahedron Lett.* **2003**, *44*, 81 – 84.
[156] N. Taniguchi, T. Onami, *Synlett* **2003**, 829 – 832.
[157] I. R. Beletskaya, A. S. Sigeev, A. S. Peregudov, P. V. Petrovskii, *Tetrahedron Lett.* **2003**, *44*, 7039 – 7041.
[158] D. Gelman, L. Jiang, S. L. Buchwald, *Org. Lett.* **2003**, *5*, 2315 – 2318.
[159] D. Van Allen, D. Venkataraman, *J. Org. Chem.* **2003**, *68*, 4590 – 4593.

 © 2003 Wiley-VCH Verlag GmbH & Co. KGaA, Weinheim 

# Communications




One-dimensional H-bonded water chains, or proton wires, are of interest because of their involvement in proton permeation through transmembrane proteins such as cytochrome oxidase. Buchanan and co-workers describe in their Communication on the following pages their attempt to stabilize 1D water chains and evaluate the proton dynamics by using biologically relevant imidazole compounds.


**DOI: 10.1002/anie.200352157**
© 2003 Wiley-VCH Verlag GmbH & Co. KGaA, Weinheim

One-Dimensional Water Chains

# Structures and Solid-State Dynamics of One-Dimensional Water Chains Stabilized by Imidazole Channels**

*Lionel E. Cheruzel, Maxim S. Pometun, Matthew R. Cecil, Mark S. Mashuta, Richard J. Wittebort, and Robert M. Buchanan**

One-dimensional (1D) water chain structures constitute a potentially important form of water that is poorly understood.[1] Many fundamental biological processes[2–9] appear to depend on the unique properties of water chains. For example, water chains may assist in proton translocation through membranes by functioning as "proton wires".[10a] Such behavior is illustrated by the membrane protein gramicidin A (gA)[2] in which protons are envisioned[10b] to either hop along a single-file chain of water molecules according to the Grotthuss relay mechanism,[11] or migrate as $H_9O_4^+$[12] or $H_5O_2^+$[13] ionic water clusters.[14] In addition, water chains appear to be important to the proton pathways in the cytochrome b6f complex of plant chloroplast thylakoid membrane and mitochondrial ATPase,[3] and carbonic anhydrase II,[4] as well as in redox proteins such as cyctochrome oxidase,[5] bacteriorhodopsin,[6] and the photosynthetic reaction center of *Rhodobacter sphaeroides*.[7] Water chains are also found in membrane aquapores, which are important to the function of the nicotinic receptor M2$\delta_5$[8] as well as the influenza A M2 virus.[9]

Curiously, little is known of the structural constraints required in stabilizing 1D water chains. Unlike bulk water or ice,[15] 1D water chains appear to be stabilized by strong H-bonding between neighboring water molecules along the chain as well as H-bonding between water molecules and donor–acceptor groups associated with channels.[2,8–9] Recently, we have discovered that certain imidazole compounds stabilize infinite 1D water chains relevant to the biological structures mentioned above. Herein we describe the crystal structures of the hydrated compounds and preliminary data from solid-state $^2$H NMR studies and calorimetric analyses that establish the possibility of reorientation dynamics of the water-chain nanostructures.

The crystal structures of hydrates of 1-methylimidazole-4-carboxaldehyde (**1**)[16] and 4,4′-methylene-bis(2,5-dimethylimidazole) (**2**)[17] are shown in Figure 1, along with their respective packing representations in Figure 2, which also display the arrangement of imidazole N atoms in both compounds in relation to their infinite 1D water chains. The water channels in **1** are generated by weak π interactions between imidazole molecules in alternating layers along the crystallographic *c* axis. The closest intermolecular interactions between layers are 3.282 Å (C1′–C3), 3.297 Å (C1′–N1) and 3.323 Å (C3–N1′), and individual channels are linked together by weak interactions (C3···O1″ 3.273 Å) between neighboring imidazole molecules (see Supporting Information). The approximate dimension of the water channels in compound **1** is $6.62 \times 3.44$ Å$^2$.

The water molecules in **1** are trigonally distorted and form strong hydrogen bonds with symmetry related molecules in the chain as well as with imidazole nitrogen atoms directed towards the channel. Each water molecule has a full-occupancy H-atom (H1o) that is strongly hydrogen bonded to N2 (N2···O2 2.8424(16) Å). The other H-atoms (H2ao and H2bo) are positionally disordered and were treated as half-occupancy atoms during refinement. Both H2ao and H2bo are hydrogen bonded (see Supporting Information) to symmetry related waters, and the O2···O2′ ($-x+1,-y,-z+1$) and O2···O2″ ($-x+1$, $y$,$-z+3/2$) separations are 2.763(2) and 2.783(2) Å, respectively, thus indicating the presence of strong H-bonding between water molecules in the chain. Overall, the shape of the water chain resembles the "arm chair" motif proposed by Nagle and Morowitz[20] for 1D proton wires.

Compound **2** has a different packing arrangement of imidazole molecules (Figure 2) that results in water channels oriented along the crystallographic *b* axis. The imidazole (N–H) and water hydrogen atoms where located and refined as half-occupancy atoms. Both water molecules associated with the asymmetric unit were found to be tetrahedrally disordered. The first water molecule containing O1 forms strong hydrogen bonds (see also Supporting Information) with imidazole N1 (O1···N1 2.828(2) Å) and N3 (O1···N3 2.854(2) Å) atoms, while the second water molecule, containing O2, is hydrogen bonded to N2′ ($x+1/2$, $y+1/2$, $z$) (O2···N2′ 2.827(2) Å) and N4″ (x, $-y+1$, $z-1/2$) (O2···N4″ 2.786(2) Å) associated with different imidazole molecules on opposite sides of the water channel. In addition, both water molecules are strongly hydrogen bonded to each other (O1···O2 2.778(2) Å) and form a "zig-zag" motif, which is the second probable proton wire structure proposed by Nagle and Morowitz.[20] The water channel formed by the stacking of **2** has an approximate rectangular shape ($\approx 4.80 \times 3.02$ Å$^2$) and a smaller pore size compared to **1** (Supporting Information). The apparent smaller pore diameter of **2** appears better suited for stabilizing the zig-zag arrangement of water molecules over the arm-chair motif.[21]

Curiously, there have been no comprehensive studies of water dynamics in systems containing infinite water-chain

[*] Prof. Dr. R. M. Buchanan, L. E. Cheruzel, M. S. Pometun, M. R. Cecil, Dr. M. S. Mashuta, Prof. Dr. R. J. Wittebort
Department of Chemistry
University of Louisville
2320 S. Brook Street, Louisville, KY 40292 (USA)
Fax: (+1) 502-852-8149
E-mail: bob.buchanan@louisville.edu

[**] We gratefully acknowledge the support of the University of Louisville and the National Science Fundation (Grant No. CHE-0328406) (R.M.B. and RJW), the Kentucky Science and Engineering Foundation (Grant No. KSEF-275-RDE-003) (R.M.B.), the National Institutes of Health (Grant No. AR41751-07) (R.J.W.), and the Kentucky Research Challenge Trust Fund for the upgrade of our X-ray facilities. Special thanks to Dr. George R. Pack and Dr. Craig A. Grapperhaus for helpful discussions, and Dr. Usha M. Gundusharma (Kimberly-Clark) and Rodica McCoy for their assistance with the TGA and DSC measurements.

Supporting information for this article is available on the WWW under http://www.angewandte.org or from the author.

 © 2003 Wiley-VCH Verlag GmbH & Co. KGaA, Weinheim DOI: 10.1002/anie.200352157 

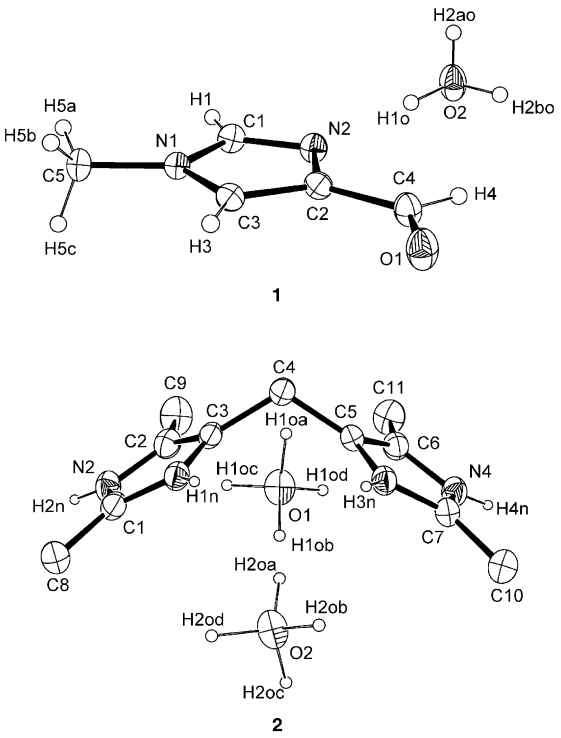



***Figure 1.*** ORTEP[18] views of the molecular structures of compounds **1** ($C_5H_6N_2O{\cdot}H_2O$) and **2** ($C_{11}H_{16}N_4{\cdot}2\,H_2O$). Thermal ellipsoids are drawn at 40% probability level. The hydrates in both structures are disordered and form strong N–H···O and O–H···O hydrogen bonds. In compound **2**, the methyl and methylene H atoms are omitted for clarity.

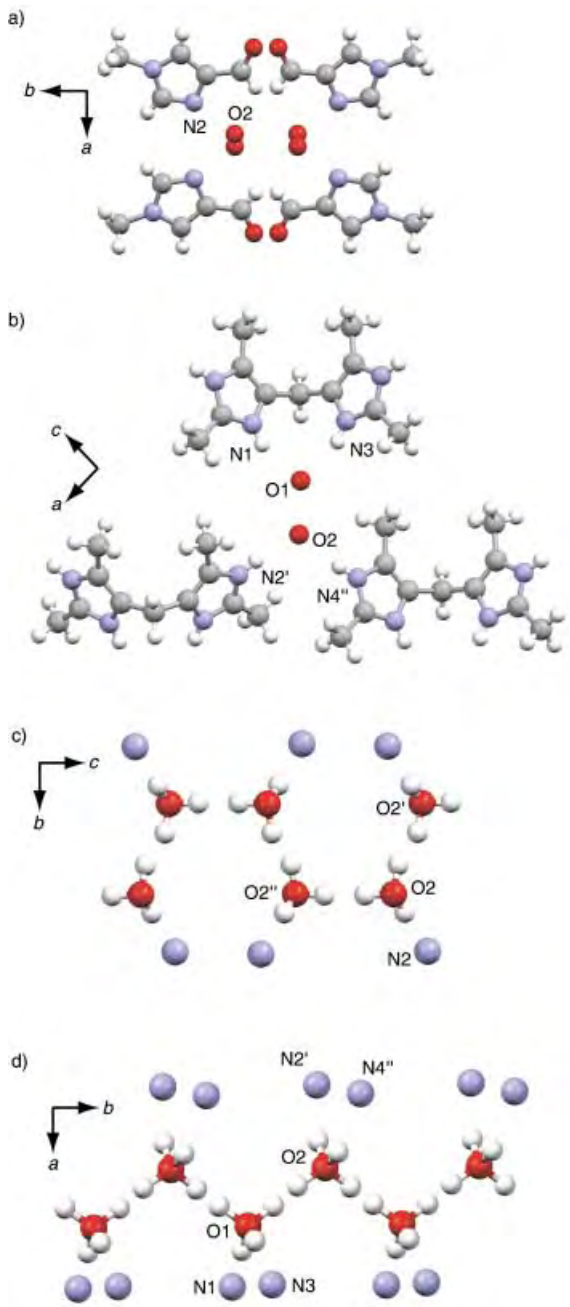



***Figure 2.*** Packing representations[19] viewed down the water channel of compound **1** and **2** are shown in frames a) and b), respectively. In both representations water H atoms have been omitted for clarity. In addition, hydrogen-bonding representations illustrating the nanostructure of the water chains of **1** and **2** are shown in frames c) and d), respectively, with each channel oriented along the horizontal axis of the figure. Imidazole nitrogen atoms involved in hydrogen bonding are included in frames c) and d). Imidazole N–H atoms are omitted in frame d) for clarity. For more detailed packing representations of **1** and **2**, see the Supporting Information.

structures. This fact may be due in part to the limited number of well-characterized continuous water chain structures involving small molecules.[22–25] To determine if **1** and **2** serve as models of biological proton wires, we have studied the dynamics of the water chains by using solid state $^2H$ and $^{17}O$ NMR spectroscopy and examined the calorimetric behavior of the compounds by thermogravimetric analysis (TGA) and differential scanning calorimetry (DSC).

In the context of proton transfer along an H-bonded chain of water molecules, dynamical disorder plays a central role. In particular, the proton positions between adjacent waters in the structures **1** and **2** are refined in the X-ray structure at half-occupancy and we probed the dynamics of this disorder by using $^2H$ and $^{17}O$ solid-state NMR. Water dynamics affect $^2H$ and $^{17}O$ spectra if O–H bonds reorient, thereby modulating the NMR spectrum in a manner completely analogous to chemical exchange. In both experiments, orientation dependent NMR frequencies arise from quadrupole coupling and the breadth of the powder spectrum defines the characteristic timescales for intermediate and fast exchange.[26] For $^2H$ ($S = 1$), this is the first-order quadrupole coupling with $\chi_{zz} \approx 170$ kHz. While for $^{17}O$, in which the observed central transition of the $S = 5/2$ spin is effected only in second order, the spectrum breadth is $\approx 50$ kHz at a field of 11.7 T for a typical hydrate water with $\chi_{zz} \approx 6$ MHz. For both experiments, we use an echo sequence to detect the broad powder spectra. Consequently, when intermediate exchange is present signals are substantially attenuated making their detection difficult. Reorientation of O–H bonds in both **1** and **2** occurs not only if waters reorient but also if a proton is transferred because, in contrast to the ice structure, the half-occupied O–H bonds for adjacent waters in **1** and **2** are not antiparallel. $^2H$ spectra are shown in Figure 3 and clearly

 © 2003 Wiley-VCH Verlag GmbH & Co. KGaA, Weinheim 

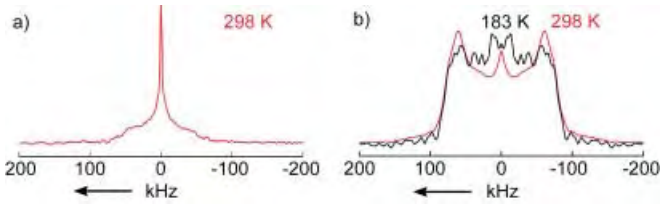



***Figure 3.*** $^2$H NMR powder spectra of a) compound **1** and b) compound **2**.

display different water dynamics in **1** and **2.** The room-temperature spectrum of **2** is dominated by features for stationary deuterons, supported on a lower time-scale by the $^{17}$O spectrum of **2** (see Supporting Information). In contrast, the spectrum of **1** has a different shape with substantially reduced breadth and intensity indicative of intermediate exchange dynamics. Similar spectra were observed for ice where they could be uniquely attributed to molecular rotation.[26]

Interestingly, on lowering the temperature of **2** to 183 K, the corresponding spectrum (obtained with long recycle delay to avoid spectral distortion from saturation) shows the appearance of a narrow central feature indicative of a dynamic water. This suggests that one of the two water molecules in **2** is dynamically disordered and not seen in the $^2$H spectrum at 298 K owing to intermediate exchange. Upon lowering the temperature, water motion slows and approaches slow exchange resulting in increased signal intensity. Over the range of temperature studied, the amine deuteron signals are saturated and not observed because of long $T_1$ values ($>60$ s). Similar proton dynamics are observed for other small molecule proton wire models, which include discontinuous water chain structures[27] and hydrated tripeptide crystals.[28] In the latter system, for example, Pometun et al.[28] have demonstrated the presence of dynamic deuterium exchange consistent with the Grotthuss mechanism.[10,11]

Crystalline samples of **1** and **2** also were examined by TGA and DSC under open conditions (see Supporting Information). TGA analyses show weight losses of 14.2 and 15.2 % for **1** and **2**, respectively. These results are consistent with the loss of one (**1**) and two (**2**) water molecules per imidazole molecule, which is in good agreement with the X-ray crystal structures. DSC for **1** shows a single sharp endotherm centered at 37 °C with a molar enthalpy of 16 kJ, which corresponds to 16 kJ per water molecule and 5 kJ per H-bond. The DSC measurements for compound **2** show the dehydration endotherm has two peaks indicating that the water molecules are in different environments, which is consistent with the X-ray crystal structure and differences in the $^2$H exchange dynamics observed for the two water molecules. The total molar enthalpy was 44 kJ per water molecule and corresponds to 11 kJ per H-bond. Results similar to **2** have been reported previously for hydrated tripeptides[28] and theophylline monohydrate[29] and are in good agreement with the strength of a hydrogen bond.[30]

In conclusion, the X-ray crystal structures, solid state $^2$H reorientation dynamics and calorimetry measurements suggest that compound **1** and **2** are potential models of biologically relevant proton wires. Future studies on these and related 1D water chain structures will include proton conductivity measurements, more detailed examination of deuterium exchange and hydrate reorientation dynamics in crystalline and powdered samples, as well as molecular modeling.

## *Experimental Section*

Compound **1** was prepared by using a procedure reported previously and a $^1$H NMR spectrum of **1** in $CDCl_3$ was in good agreement with previously reported results.[16] The off-white powder was crystallized by dissolving the compound (40 mg, 0.31 mmol) in 9:1 MeOH:$H_2O$ (0.5 mL) layered with diethyl ether and cooled to 270 K. Colorless block crystals were isolated from the crystallization solution prior to the X-ray diffraction analysis.

Compound **2** was prepared by using a procedure reported elsewhere[17] and isolated in approximately 60 % yield. The white powder was crystallized by dissolving **2** (0.2 g, 0.83 mmol) in 9:1 MeOH:$H_2O$ (1 mL) followed by slow evaporation of the crystallization solution. Colorless block crystals were isolated from the crystallization solution prior to the X-ray diffraction analysis. Characterization: ESIMS: 205.28 $[M+H]^+$; $^1$H NMR (500 MHz, $CD_3OD$, 25 °C): $\delta = 3.65$ (s, 2H, -$CH_2$-), 2.15 (s, 3H, -$CH_3$), 2.05 ppm (s, 3H, -$CH_3$).

Crystallographic Studies: Single crystals of **1** and **2** were mounted on a 0.05 mm CryoLoop with Paratone oil for collection of X-ray data using omega scans on a Bruker SMART APEX CCD diffractometer. The following programs were used during data collection and refinement: SMART (V 5.625 to acquire frame data),[31a] SAINT (V 6.22 to determine final unit cell parameters and integrate frame data)[31b] and structures were solved by direct methods with SHELXS-90[31c] and refined by least square methods on $F^2$ with SHELXL-97[31d] incorporated into the SHELXTL (V 6.12)[31e] suite of programs.

Crystal structure analysis of $C_5H_6N_2O{\cdot}H_2O$ (**1**): $0.32\times0.25\times0.14$ mm, monoclinic, space group $C2/c$, $a = 20.149(4)$ Å, $b = 8.5299(17)$ Å, $c = 7.3447(15)$ Å, $\beta = 96.41(3)°$, $V = 1254.5(4)$ Å$^3$, $\rho_{calcd} = 1.357$ Mg m$^{-3}$, $Z = 8$, $\mu = 0.106$ mm$^{-1}$, $2\theta_{max} = 4.08$ to 56.52, $Mo_{K\alpha}$ radiation ($\lambda = 0.71073$ Å), $T = 100$ K, F(000) 544, total reflections = 5325, independent reflections = 1466 ($R_{int} = 0.023$), observed data = 1350 ($I > 2\sigma(I)$), adsorption correction: SADABS (V 2.02),[31f] transmission factors max: 0.99, min: 0.90. All non-hydrogen atoms were refined anisotropically. Hydrogen atoms of the water molecule are disordered. One full occupancy hydrogen atom (H1o) and two half-occupancy hydrogen atoms (H2ao and H2bo) were located by difference maps and refined isotropically in a trigonal arrangement about O2. Imidazole and carbonyl hydrogen atoms also were located by difference maps and refined isotropically. Methyl hydrogen atoms were placed in their geometrically generated positions and refined as a riding model. The final anisotropic full matrix least-squares refinement on $F^2$ for 102 variables converged at $R1 = 0.043$ and $wR2 = 0.107$ with a GOF of 1.04, 0.33 e Å$^{-3}$, residual based on $I > 2\sigma(I)$.

Crystal structure analysis of $C_{11}H_{16}N_4{\cdot}2H_2O$ (**2**): $0.36\times0.28\times0.25$ mm, monoclinic, space group $Cc$, $a = 17.9264(19)$ Å, $b = 4.5526(5)$ Å, $c = 17.8364(19)$ Å, $\beta = 105.623(2)°$, $V = 1401.9(3)$ Å$^3$, $\rho_{calcd} = 1.139$ Mg m$^{-3}$, $Z = 4$, $\mu = 0.081$ mm$^{-1}$, $2\theta_{max} = 4.72$ to 56.38, $Mo_{K\alpha}$ radiation ($\lambda = 0.71073$ Å), $T = 296$ K, $F(000)$ 520, total reflections = 5680, independent reflections = 2963 ($R_{int} = 0.0224$), observed data = 2597 ($I > 2\sigma(I)$), adsorption correction: SADABS,[31f] transmission factors max: 0.98, min: 0.97. All non-hydrogen atoms were refined anisotropically. Hydrogen atoms on the water molecules and the imidazole NH atoms are disordered and were located by difference electron density maps. Both sets of hydrogen atoms were refined isotropically as half-occupancy atoms and constrained by using the DFIX command in SHELXTL. Methyl and methylene

 © 2003 Wiley-VCH Verlag GmbH & Co. KGaA, Weinheim 

hydrogen atoms were placed in their geometrically generated positions and refined as a riding model. The final anisotropic full matrix least-squares refinement on $F^2$ for 184 variables converged at $R1 = 0.045$ and $wR2 = 0.096$ with a GOF of 1.02, 0.17 e Å$^{-3}$, residual based on $I > 2\sigma(I)$.

CCDC-212688 (**1**) and -212689 (**2**) contain the supplementary crystallographic data for this paper. These data can be obtained free of charge via www.ccdc.cam.ac.uk/conts/retrieving.html (or from the Cambridge Crystallographic Data Centre, 12 Union Road, Cambridge CB2 1EZ, UK; fax: (+44) 1223-336-033; or deposit@ccdc.cam.ac.uk).

Supporting Information available: Views showing important intermolecular contacts in **1** and illustrations of the water channels in **1** and **2**, $^{17}$O NMR spectrum of **2**, TGA and DSC data for compound **1** and **2**, and H-bonding distances and angles for both compounds.

Received: June 17, 2003
Revised: August 25, 2003 [Z52157]
Published Online: October 6, 2003

**Keywords:** calorimetry · NMR spectroscopy · proton transport · solid-state structures

[1] G. Hummer, J. C. Rasaiah, J. P. Noworyta, *Nature* **2001**, *414*, 188 – 190.
[2] S. Cukierman, *Biophys. J.* **2000**, *78*, 1825 – 1834.
[3] J. K. Lanyi, *Biochim. Biophys. Acta* **2000**, *1460*, 1 – 3.
[4] K. M. Jude, S. K. Wright, C. Tu, D. N. Silverman, R. E. Viola, D. W. Christianson, *Biochemistry* **2002**, *41*, 2485 – 2491.
[5] D. Zaslavsky, R. B. Gennis, *Biochim. Biophys. Acta* **2000**, *1458*, 164 – 179.
[6] M. Wilkstrom, *Curr. Opin. Struct. Biol.* **1998**, *8*, 480 – 488.
[7] H. Kandori, *Biochim. Biophys. Acta* **2000**, *1460*, 177 – 191.
[8] R. J. Law, L. R. Forrest, K. M. Ranatunga, P. LaRocca, D. P. Tieleman, M. S. Sansom, *Proteins Struct. Funct. Genet.* **2000**, *39*, 47 – 55.
[9] Q. Zhong, T. Husslein, P. B. Moore, D. M. Newns, P. Pattnaik, M. L. Klein, *FEBS Lett.* **1998**, *434*, 265 – 271.
[10] a) D. P. Tieleman, P. C. Biggin, G. R. Smith, M. S. P. Sansom, *Q. Rev. Biophys.* **2001**, *34*, 473 – 561; b) R. Pomès, B. Roux, *Biophys. J.* **2002**, *82*, 2304 – 2316, and references therein.
[11] a) C. J. T. de Grotthuss, *Ann. Chim.* **1806**, *58*, 54 – 74; b) N. Agmon, *Chem. Phys. Lett.* **1995**, *244*, 456 – 462.
[12] M. Eigen, *Angew. Chem.*, **1963**, 75, 489 – 508; *Angew. Chem. Int. Ed. Engl.* **1964**, *3*, 1 – 19.
[13] G. Zundel, H. Metzger, *Z. Phys. Chem.* **1968**, *58*, 225 – 245.
[14] R. Ludwig, *Angew. Chem.*, **2003**, *115*, 268 – 271; *Angew. Chem. Int. Ed.* **2003**, *42*, 258 – 260.
[15] a) H. E. Stanley, *Introduction to Phase Transitions and Critical Phenomena 2*, Oxford University Press, New York, **1971**; b) L. J. Barbour, G. W. Orr, J. L. Atwood, *Nature* **1998**, *393*, 671 – 673; c) L. J. Barbour, G. W. Orr, J. L. Atwood, *Chem. Commun.* **2000**, 859 – 860; d) K. Liu, J. D. Cruzan, R. J. Saykally, *Science* **1996**, *271*, 929 – 933.
[16] S. Chen, J. F. Richardson, R. M. Buchanan, *Inorg. Chem.* **1994**, *33*, 2376 – 2382.
[17] Shikoku Chemicals Corps, Jpn. Kokai Tokkyo Koho, JP 59,190,972, **1984**. [*Chem. Abstr.* **1985**, *102*, 149268a].
[18] ORTEP-3 for Windows,:L. J. Farrugia, *J. Appl. Crystallogr.* **1997**, *30*, 565.
[19] Mercury (the "Program"), copyright work belonging to the Cambridge Crystallographic Data Center ("CCDC"), can be found under http://www.iucr.ac.uk.
[20] J. F. Nagle, H. J. Morowitz, *Proc. Natl. Acad. Sci. USA* **1978**, *75*, 298 – 302.
[21] K. Koga, G. T. Gao, X. C. Zeng, *Nature* **2001**, *412*, 802 – 805.
[22] a) D. J. Sutor, *Acta Crystallogr.* **1958**, *11*, 83 – 87; D. J. Sutor, *Acta Crystallogr.* **1958**, *11*, 453 – 458; b) C. Q. Sun, D. L. Zhou, D. J. W. Grant, V. G. Young, Jr., *Acta Crystallogr. Sect. E* **2002**, *58*, o368-o370.
[23] a) K. Stahl, A. Kvick, S. Ghose, *Zeolites* **1989**, *9*, 303 – 311; b) Y. Lee, T. Vogt, J. A. Hriljac, J. B. Parise, J. C. Hason, S. J. Kim, *Nature* **2002**, *420*, 485 – 489; c) Y. Lee, T. Vogt, J. A. Hriljac, J. B. Parise, G. Artioli, *J. Am. Chem. Soc.* **2002**, *124*, 5466 – 5475; d) E. Fois, A. Gamba, G. Tabacchi, S. Quartieri, G. Vezzalini, *Phys. Chem. Chem. Phys.* **2001**, *3*, 4158 – 4163.
[24] S. A. Kim, H. Küppers, *Z. Kristallogr.* **1994**, *209*, 789 – 793.
[25] D. Cheng, M. A. Khan, R. P. Houser, *Inorg. Chem.* **2001**, *40*, 6858 – 6859.
[26] R. J. Wittebort, M. G. Usha, D. J. Ruben, D. E. Wemmer, A. Pines, *J. Am. Chem. Soc.* **1988**, *110*, 5668 – 5671.
[27] H. Terao, T. Sugawara, Y. Kita, N. Sato, E. Kaho, S. Takeda, *J. Am. Chem. Soc.* **2001**, *123*, 10468 – 10474.
[28] M. S. Pometun, U. M. Gundsusharma, J. F. Richardson, R. J. Wittebort, *J. Am. Chem. Soc.* **2002**, *124*, 2345 – 2351.
[29] E. Suihko, J. Ketolainen, A. Poso, M. Ahlgren, J. Gynther, P. Paronen, *Int. J. Pharm.* **1997**, *158*, 47 – 55.
[30] S. Schneider, *Reviews in Computational Chemistry, Vol. II*, VCH, New York, **1991**.
[31] a) SMART, V.5.625, Bruker Advanced X-ray Solutions, Inc., Madison, WI, **2001**; b) SAINT, V. 6.22, Bruker Advanced X-ray Solutions, Inc., Madison, WI, **2001**; c) SHELXS-90: G. M. Sheldrick, *Acta Crystallogr. Sect. A* **1990**, *46*, 467; d) G. M. Sheldrick, SHELXL-97, Program for the Refinement of Crystal Structures, University of Göttingen, Göttingen (Germany), **1997**; e) SHELXTL 6.12, Program Library for Structure Solution and Molecular graphics, Bruker Advanced X-ray Solutions, Madison, WI, **2001**; f) G. M. Sheldrick, SADABS, V. 2.02, Area Detector Absorption Correction, University of Göttingen, Göttingen, Germany, **1997**.

 © 2003 Wiley-VCH Verlag GmbH & Co. KGaA, Weinheim 

*Atropisomerism*

# *Atropos* but Achiral Tris(phosphanyl)biphenyl Ligands for Ru-Catalyzed Asymmetric Hydrogenation**

*Kohsuke Aikawa and Koichi Mikami**

In modern synthetic and pharmaceutical chemistry, the advance of asymmetric catalysts is of central importance.[1] The design of chiral ligands is the key to attaining high asymmetric induction and to increasing catalytic activity from an achiral precatalyst ("ligand-accelerated catalysis").[2] How-

[*] Prof. Dr. K. Mikami, K. Aikawa
Department of Applied Chemistry
Graduate School of Science and Engineering
Tokyo Institute of Technology
Ookayama, Meguro-ku, Tokyo 152-8552 (Japan)
Fax: (+81) 3-5734-2776
E-mail: kmikami@o.cc.titech.ac.jp

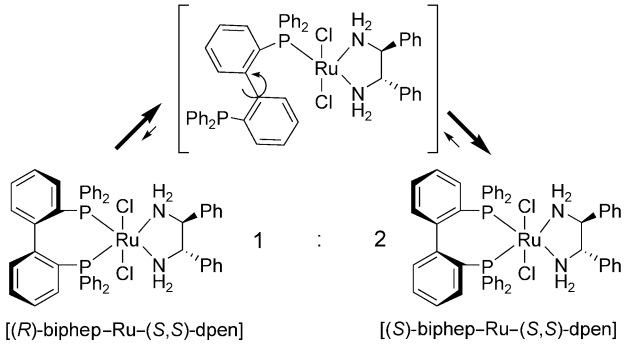
[**] K. Aikawa is grateful to the Japan Society for the Promotion of Science for Young Scientists for a research fellowship.

 DOI: 10.1002/anie.200352277 © 2003 Wiley-VCH Verlag GmbH & Co. KGaA, Weinheim 

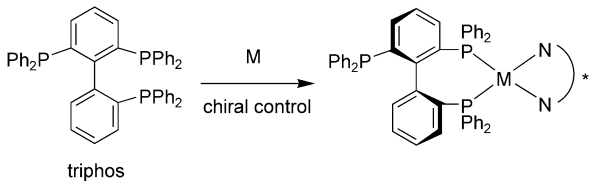
ever, to obtain enantiopure forms of atropisomeric (from Greek *atropos*; *a* = not, *tropos* = turn) ligands,[3] asymmetric synthesis or resolution is requisite. In contrast, we reported a new strategy for asymmetric catalysis with chirally flexible (*tropos*) 2,2′-bis(diphenylphosphanyl)biphenyl (biphep) ligands.[3,4] The chirality of the biphep–Ru complex can be controlled through isomerization by (*S,S*)-1,2-diphenylethylenediamine ((*S,S*)-dpen) as a chiral controller. As a result, a 2:1 mixture of *S,S,S* and *R,S,S* diastereomers was formed at room temperature (Scheme 1).[4c,5] The isomerization of the [biphep–Ru–dpen] complex could take place through disconnection of a Ru–P bond followed by the rotation of the biphenyl rings, and then recoordination of the Ru–P bond (Scheme 1).[4c,6]

Herein we report a novel strategy that employs *atropos* but achiral triphos (2,6,2′-tris(diphenylphosphanyl)biphenyl) ligands for Ru catalysts through chiral control by chiral diamines (Scheme 2). The three *ortho* substituents of the biphenyl compound prevent rotation about the single bond,[7] but axial chirality is created upon complexation with a metal.

A racemic and *atropos* binap–Ru complex gives a 1:1 mixture of two diastereomers when combined



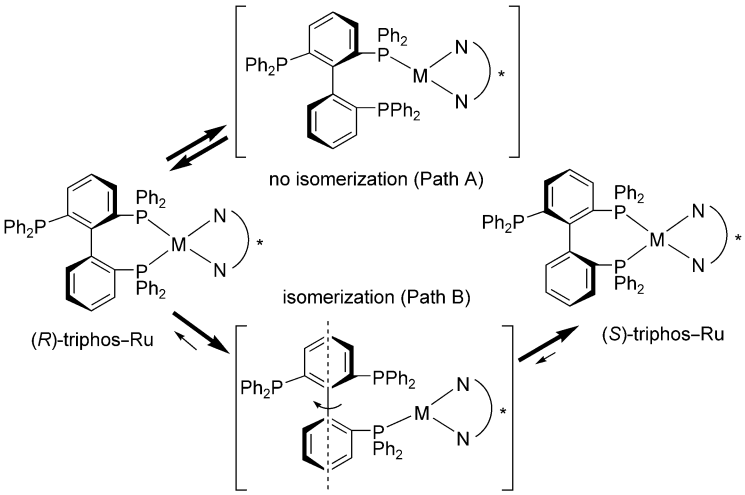

***Scheme 1.*** Isomerization of the *tropos* biphep–Ru complex at room temperature.




***Scheme 2.*** Chiral control of the *atropos* triphos–M complex.

with an equimolar amount of an enantiopure diamine controller. However, if biphep is used as a ligand instead of binap, the diastereomer ratio can be increased up to 2:1, even at room temperature, by virtue of the *tropos* nature.[4c]

In spite of the *atropos* nature, the diastereomer ratio of the triphos–Ru complex can, in principle, be increased by a chiral controller (Scheme 3). However, the isomerization process is different from that of the biphep–Ru complex. At low temperatures, the monophosphane part might dissociate easily, but should re-form the identical enantiomer upon recomplexation with the metal (Scheme 3, Path A). At higher



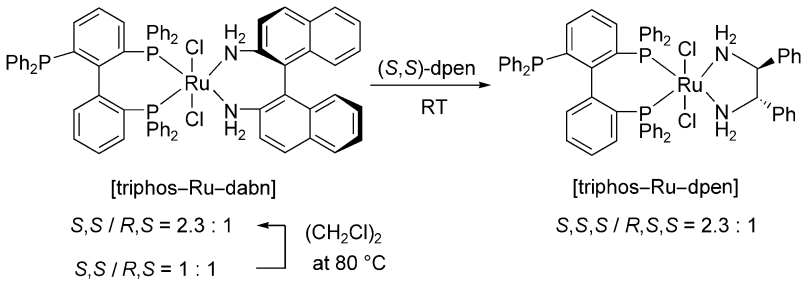

***Scheme 3.*** Mechanism of isomerization of the triphos–Ru complex.

temperatures, the bisphosphane portion can dissociate to give the opposite enantiomer (Scheme 3, Path B).

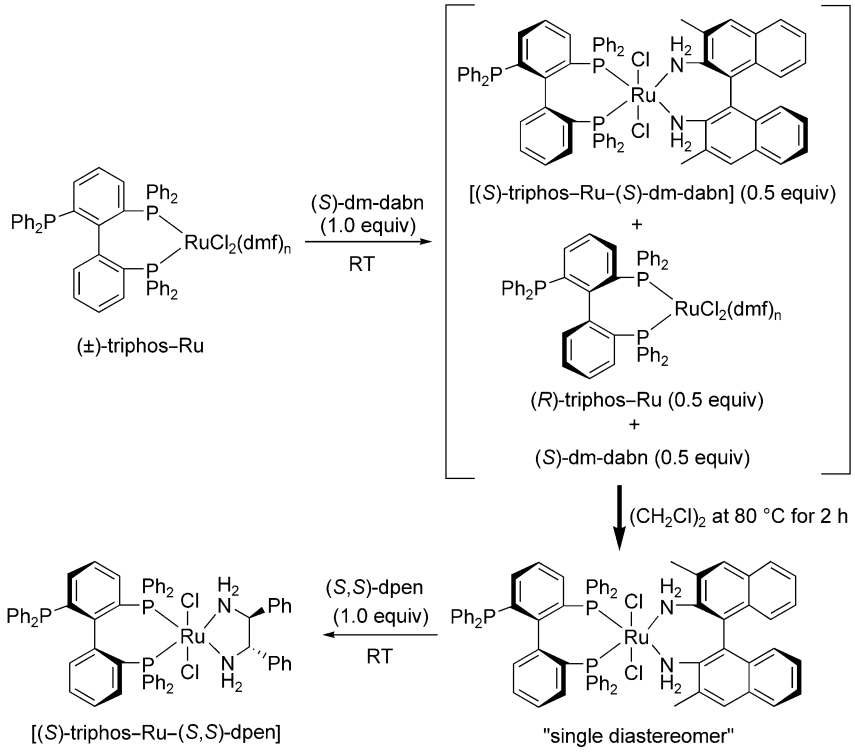
First, the complexation of the triphos–Ru complex and enantiopure (*S,S*)-dpen was examined to give a mixture of diastereomers in a kinetic (1:1) ratio (see below).[8] Next, isomerization was attempted to convert the diastereomeric mixture of [(*S*)-triphos–Ru–(*S,S*)-dpen] and [(*R*)-triphos–Ru–(*S,S*)-dpen] (1:1) into a single diastereomer. Unfortunately, no change was observed in the diastereomeric ratio at room temperature or even at 80 °C. Similarly, the 1:1 diastereomeric mixture of [triphos–Ru–dabn] (dabn = 2,2′-diamino-1,1′-binaphthyl) did not isomerize at room temperature.[9] However, the isomerization did proceed at 80 °C over 2 hours to the favorable [(*S*)-triphos–Ru–(*S*)-dabn] (*S,S*/*R,S* 2.3:1) (Scheme 4). Upon addition of an equimolar amount of (*S,S*)-dpen to the diastereomer mixture, the aliphatic diamine dpen exchanged with the aromatic diamine dabn without racemization at room temperature (Scheme 4). In sharp contrast to [biphep–Ru–dpen], which readily isomerizes, the triphos ligand of [triphos–Ru–dpen] retained its configuration under the same conditions. Additionally, heating at 80 °C for 24 h did not change the 2.3:1 diastereomeric ratio (see above).

The use of 3,3′-dimethyl-2,2′-diamino-1,1′-binaphthyl (dm-dabn), which can readily discriminate between enantiomers owing to its sterically demanding methyl substituents,[4b,10] resulted in isomerization to give the diastereopure triphos–Ru complex (Scheme 5). The combination of racemic (±)-triphos–Ru and an equimolar amount of (*S*)-dm-dabn gave the single diastereomer by isomerization of the (*R*)-triphos–Ru complex in dichloroethane at 80 °C.[11] Significantly, an equimolar amount of (*S,S*)-dpen did exchange with dm-dabn upon addition to the enantiopure complex, to give enantiopure [(*S*)-triphos–Ru–(*S,S*)-dpen] without racemiza-

 © 2003 Wiley-VCH Verlag GmbH & Co. KGaA, Weinheim 

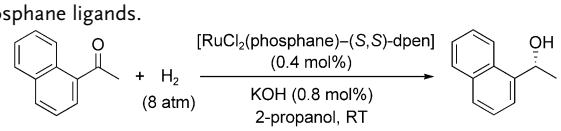



***Scheme 4.*** Isomerization and chiral stability of the triphos–Ru–diamine complexes.




***Scheme 5.*** Resolution and subsequent isomerization by (*S*)-dm-dabn, and *atropos* nature of the triphos–Ru complex.

***Table 1:*** Enantioselective hydrogenation by Ru catalysts with different phosphane ligands.




| Entry | Phosphane | *S,S,S*/*R,S,S*[a] | *t* [h] | *ee* [%] | Yield [%] |
|---|---|---|---|---|---|
| 1 | (±)-binap | 1:1 | 4 | 71 | >99 |
| 2 | biphep | 1:1 | 4 | 54 | >99 |
| 3[b] | biphep | 2:1 | 4 | 69 | >99 |
| 4 | triphos | 1:1 | 6 | 66 | >99 |
| 5 | triphos | 100:0 | 6 | 85 | >99 |

[a] The *S,S,S*/*R,S,S* ratio was determined by $^1$H and $^{31}$P NMR spectroscopic analysis. [b] [biphep–Ru–(*S,S*)-dpen] in 2-propanol was prestirred at room temperature for 3 h.

tion of the triphos–Ru moiety at room temperature (Scheme 5).

The enantiopure [triphos–Ru–dpen] was used in the enantioselective hydrogenation of a simple ketone in the presence of KOH (Table 1).[12] The enantioselectivity observed with [(±)-binap–Ru–(*S,S*)-dpen][13] was higher than that found with chirally flexible [biphep–Ru–(*S,S*)-dpen], even after isomerization (Table 1, entries 1–3).[14] The [triphos–Ru–(*S,S*)-dpen] complex (d.r. 1:1) also resulted in lower enantioselectivity (Table 1, entry 4). However, the enantioselectivity exhibited by enantiopure [(*S*)-triphos–Ru–(*S,S*)-dpen] was much higher than that by [(±)-binap–Ru–(*S,S*)-dpen] under the same conditions (Table 1, entries 1 and 5).

In summary, we have demonstrated that the axial chirality of a Ru complex with an *atropos* but achiral triphos ligand can be controlled perfectly and retained at room temperature, in contrast to the *tropos* biphep–Ru complex. The enantiopure [triphos–Ru–dm-dabn] complex underwent exchange with dpen without racemization of the triphos–Ru moiety at room temperature, and the enantiopure [triphos–Ru–dpen] complex led to higher enantioselectivity than that attained with (±)-binap–Ru and biphep–Ru complexes in the asymmetric hydrogenation of a ketone.

## Experimental Section

[(*S*)-triphos–Ru–(*S*)-dm-dabn]: Degassed *N,N*-dimethylformamide (3.5 mL) was added to a mixture of [{$RuCl_2$(benzene)}$_2$] (25.0 mg, 0.05 mmol) and triphos (70.7 mg, 0.10 mmol) under an argon atmosphere in a Schlenk tube. After stirring for 3 h at 100 °C, the clear reddish-brown solution was concentrated at 50 °C under reduced pressure. Degassed dichloroethane (5.0 mL) was added to the mixture of the triphos–Ru complex and (*S*)-dm-dabn (31.2 mg, 0.10 mmol) under an argon atmosphere in a Schlenk tube. The solution was stirred for 2 h at 80 °C and then concentrated under reduced pressure to give [(*S*)-triphos–Ru–(*S*)-dm-dabn] quantitatively. $^1$H NMR (300 MHz, $CDCl_3$): $\delta = 1.82$ (s, 3H), 1.85 (s, 3H), 3.94–3.99 (m, 2H; $NH_2$), 4.69 (d, $J = 6.6$ Hz, 1H; $NH_2$), 4.74 (d, $J = 6.6$ Hz, 1H; $NH_2$), 5.45–5.47 (m, 1H), 6.19 (t, $J = 5.7$ Hz, 1H), 6.77–8.18 ppm (m, 45H); $^{31}$P NMR (162 MHz, $CDCl_3$): $\delta = -11.3$ (d, $J_{P\text{-}P} = 6.2$ Hz, 1P), 44.6 (d, $J_{P\text{-}P} = 39.7$ Hz, 1P), 47.7 ppm (dd, $J_{P\text{-}P} = 6.2$, 39.7 Hz, 1P).

Asymmetric hydrogenation: An autoclave (100 mL) was charged with solid [(*S*)-triphos–Ru–(*S*)-dm-dabn] (14.3 mg, 0.012 mmol) and (*S*)-dpen (2.5 mg, 0.012 mmol). After replacing the air in the

 © 2003 Wiley-VCH Verlag GmbH & Co. KGaA, Weinheim 

autoclave with argon, degassed $CH_2Cl_2$ (2.0 mL) was added. The solution was stirred for 24 h at room temperature, and then concentrated under reduced pressure. The autoclave was again charged with an argon atmosphere, and 2-propanol (3.3 mL) and KOH/2-propanol (0.5 M; 48 μL, 0.024 mmol) was added under a stream of argon. The mixture was stirred for 30 min at room temperature. 1′-Acetonaphthone (0.46 mL, 3.0 mmol) was added under a stream of argon, and hydrogen was then introduced at a pressure of 8 atm. The reaction mixture was vigorously stirred for 6 h at room temperature. After concentration under reduced pressure, the residue was filtered through a short column of silica gel. The yield and *ee* values were determined by chiral GC analysis. The product was isolated by column chromatography on silica gel (hexane/EtOAc 3:1) in 99% yield; GC (column: CP-Cyclodextrin-β-2,3,6-M-19, i.d. 0.25 mm × 25 m, CHROMPACK; carrier gas: nitrogen 75 kPa; column temperature: 160 °C; injection and detection temperature: 190 °C; split ratio: 100:1): $t_R$ (*S* isomer) = 31.6 min, $t_R$ (*R* isomer) = 32.5 min.

Received: July 3, 2003 [Z52277]

**Keywords:** atropisomerism · chirality · hydrogenation · phosphane ligands · ruthenium

[1] a) E. N. Jacobsen, A. Pfaltz, H. Yamamoto, *Comprehensive Asymmetric Catalysis, Vol. 1–3*, Springer, Berlin, **1999**; b) *Transition Metals for Organic Synthesis*, (Ed.: M. Beller, C. Bolm), VCH, Weinheim, **1998**; c) R. Noyori, *Asymmetric Catalysis in Organic Synthesis*, Wiley, New York, **1994**; d) H. Brunner, W. Zettlmeier, *Handbook of Enantioselective Catalysis*, VCH, Weinheim, **1993**; e) *Catalytic Asymmetric Synthesis, Vol. I and II* (Ed.: I. Ojima), VCH, New York, **1993**, **2000**; f) H. B. Kagan, *Comprehensive Organic Chemistry, Vol. 8*, Pergamon, Oxford, **1992**; g) *Asymmetric Catalysis* (Ed.: B. Bosnich), Martinus Nijhoff Publishers, Dordrecht, **1986**.

[2] D. J. Berrisford, C. Bolm, K. B. Sharpless, *Angew. Chem.* **1995**, *107*, 1159 – 1171; *Angew. Chem. Int. Ed. Engl.* **1995**, *34*, 1059 – 1070.

[3] K. Mikami, K. Aikawa, Y. Yusa, J. J. Jodry, M. Yamanaka, *Synlett* **2002**, *10*, 1561 – 1578.

[4] a) K. Mikami, T. Korenaga, M. Terada, T. Ohkuma, T. Pham, R. Noyori, *Angew. Chem.* **1999**, *111*, 517 – 519; *Angew. Chem. Int. Ed.* **1999**, *38*, 495 – 497; b) K. Mikami, K. Aikawa, T. Korenaga, *Org. Lett.* **2001**, *3*, 243 – 245; c) T. Korenaga, K. Aikawa, M. Terada, S. Kawauchi, K. Mikami, *Adv. Synth. Catal.* **2001**, *343*, 284 – 288; For similar work on the biphep ligand, see: d) M. D. Tudor, J. J. Becker, P. S. White, M. R. Gagne, *Organometallics* **2000**, *19*, 4376 – 4484; e) J. J. Becker, P. S. White, M. R. Gagne, *J. Am. Chem. Soc.* **2001**, *123*, 9478 – 9479.

[5] The diastereomeric ratios were determined by $^1$H NMR analysis at 25 °C in $(CD_3)_2CDOD/CDCl_3$ (2:1).

[6] M. Yamanaka, K. Mikami, *Organometallics* **2002**, *21*, 5847 – 5851.

[7] a) E. L. Eliel, S. H. Wilen, *Stereochemistry of Organic Compounds*, Wiley, New York, **1994**, chap. 14–15; b) "Moleculare Asymmetrie": R. Kuhn in *Stereochemie* (Ed.: H. Freudenberg), Franz Deutike, Leipzig, **1933**, pp. 803 – 824; c) "Recent Advances in Atropisomerism": M. Oki, *Top. Stereochem.* **1983**, *14*, 1 – 81.

[8] [(±)-triphos–Ru–(*S,S*)-dpen]: $^{31}$P NMR (162 MHz, $CDCl_3$): *R,S,S*: $\delta = -11.1$ (d, $J_{P\text{-}P} = 6.2$ Hz, 1P), 46.7 (d, $J_{P\text{-}P} = 36.6$ Hz, 1P), 48.0 ppm (dd, $J_{P\text{-}P} = 6.2$, 36.6 Hz, 1P); *S,S,S*: $\delta = -10.8$ (d, $J_{P\text{-}P} = 5.3$ Hz, 1P), 46.2 (d, $J_{P\text{-}P} = 36.6$ Hz, 1P), 47.4 ppm (dd, $J_{P\text{-}P} = 5.3$, 36.6 Hz, 1P).

[9] [(±)-triphos–Ru–(*S*)-dabn]: $^{31}$P NMR (162 MHz, $CDCl_3$): *R,S*: $\delta = -12.5$ (d, $J_{P\text{-}P} = 5.3$ Hz, 1P), 50.9 (d, $J_{P\text{-}P} = 45.0$ Hz, 1P), 53.5 ppm (dd, $J_{P\text{-}P} = 5.3$, 45.0 Hz, 1P); *S,S*: $\delta = -11.5$ (d, $J_{P\text{-}P} = 5.3$ Hz, 1P), 50.3 (d, $J_{P\text{-}P} = 42.8$ Hz, 1P), 52.1 ppm (dd, $J_{P\text{-}P} = 5.3$, 42.8 Hz, 1P).

[10] a) K. Mikami, T. Korenaga, T. Ohkuma, R. Noyori, *Angew. Chem.* **2000**, *112*, 3854 – 3857; *Angew. Chem. Int. Ed.* **2000**, *39*, 3707 – 3710; b) K. Mikami, Y. Yusa, T. Korenaga, *Org. Lett.* **2002**, *4*, 1643 – 1645.

[11] [(*S*)-triphos–Ru–(*S*)-dm-dabn]: $^{31}$P NMR (162 MHz, $CDCl_3$): $\delta = -11.3$ (d, $J_{P\text{-}P} = 6.2$ Hz, 1P), 44.6 (d, $J_{P\text{-}P} = 39.7$ Hz, 1P), 47.7 ppm (dd, $J_{P\text{-}P} = 6.2$, 39.7 Hz, 1P).

[12] Hydrogenation with enantiopure [binap–Ru–dpen]: a) for an excellent review, see: R. Noyori, T. Ohkuma, *Angew. Chem.* **2001**, *113*, 40 – 75; *Angew. Chem. Int. Ed.* **2001**, *40*, 40 – 73; see also: b) T. Ohkuma, H. Ooka, S. Hashiguchi, T. Ikariya, R. Noyori, *J. Am. Chem. Soc.* **1995**, *117*, 2675 – 2676; c) T. Ohkuma, H. Ooka, T. Ikariya, R. Noyori, *J. Am. Chem. Soc.* **1995**, *117*, 10417 – 10418.

[13] Examples of asymmetric hydrogenation: a) [(±)-tol-binap–Ru–(*S,S*)-dpen]: T. Ohkuma, H. Doucet, T. Pham, K. Mikami, T. Korenaga, M. Terada, R. Noyori, *J. Am. Chem. Soc.* **1998**, *120*, 1086 – 1087; b) [(±)-dm(xyl)-binap–Ru–(*S,S*)-dpen]: K. Mikami, T. Korenaga, Y. Matsumoto, M. Ueki, M. Terada, S. Matsukawa, *Pure. Appl. Chem.* **2001**, *73*, 255 – 259.

[14] We have already reported that a Ru complex with a 3,3′-dimethyl-substituted biphep ligand (dm-biphep) can be controlled to a 3:1 diastereomeric ratio by enantiopure dpen. In asymmetric hydrogenation, the complex gave a higher enantioselectivity than the racemic dm-binap–Ru complex.[4a]

 © 2003 Wiley-VCH Verlag GmbH & Co. KGaA, Weinheim 

*Atropisomerism and Helicity*

# Helical Chirality Control of Palladium Complexes That Bear a Tetrakis(phosphanyl)terphenyl Ligand: Application as Asymmetric Lewis Acid Catalysts**

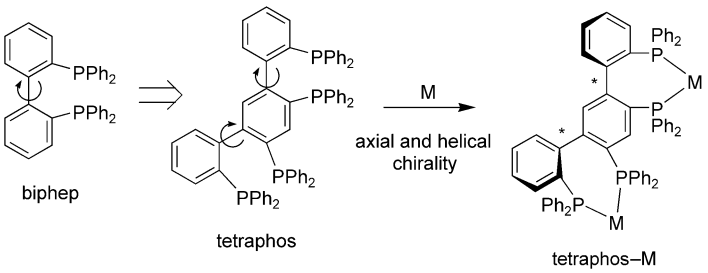
*Kohsuke Aikawa and Koichi Mikami**

Helical structures (e.g. classical helicenes[1]) have attracted much attention for quite some time. The helical chirality stems from the nonplanar structure and, therefore, we designed the novel 2,4′,6′,2″-tetrakis(diphenylphosphanyl)-[1,1′;3′,1″]terphenyl (tetraphos) ligand model, which exhibits nonplanar helicity when complexed to metal centers (Scheme 1).

[*] Prof. Dr. K. Mikami, K. Aikawa
Department of Applied Chemistry
Graduate School of Science and Engineering
Tokyo Institute of Technology
Ookayama, Meguro-ku, Tokyo 152-8552 (Japan)
Fax: (+81) 3-5734-2776
E-mail: kmikami@o.cc.titech.ac.jp

[**] We are grateful to Dr. Kenji Yoza and Mr. Kazuyoshi Kitajima in the Nippon Bruker Co. for X-ray crystallographic analysis. K. Aikawa is grateful to the Japan Society for the Promotion of Science for Young Scientists for a research fellowship.

 © 2003 Wiley-VCH Verlag GmbH & Co. KGaA, Weinheim DOI: 10.1002/anie.200352300 




***Scheme 1.*** *Tropos* nature of the tetraphos–M complex.

Many chiral phosphane ligands have been reported to induce high enantioselectivity in catalytic asymmetric reactions,[2] and much attention has been devoted to their syntheses. However, the synthesis and resolution of these chiral P ligands are difficult because of racemization at higher temperature.[3] We have reported the chirally flexible (*tropos*, meaning turn in Greek) biphep ligand, which has a biphenyl backbone[4] whose axial chirality can be controlled by chiral controllers without resolution. Herein we report a further advanced strategy that employs the *tropos* nature of the designed tetraphos ligand to generate helicity upon complexation with a metal and its application as an asymmetric Lewis acid catalyst.

The tetraphos–Pd complex was quantitatively obtained from the tetraphos ligand and 2 equivalents of $[PdCl_2(cod)]$ (cod = cycloocta-1,5-diene) in $CH_2Cl_2$. Recrystallization from $CH_2Cl_2$/MeOH gave single crystals, which allowed the 3D structure of this complex to be clarified by X-ray crystallographic analysis (Figure 1a).[5] The complex has two biphep–Pd units in which the phenyl groups adopt either axial or equatorial orientations (Figure 1b). The biphep portions of the tetraphos–Pd complex are quite similar not only to the biphep–Pd complex but also to many binap–metal complexes.[4d,6] In Figure 1, the axial chirality is *S,S* and the helical chirality is *P* (plus), that is, clockwise around the helix axis. The *meso* diastereomer complex, which would have *S,R* axial chirality, was not obtained, apparently as a consequence of the sterically demanding diphenylphosphane groups. Once the axial chirality (*S* or *R*) is determined in one biphenyl unit, the axial and helical chirality in the other unit is inevitably fixed as *S,P* or *R,M*, respectively.

3,3′-Dimethyl-2,2′-diamino-1,1′-binaphthyl (dm-dabn) with sterically demanding methyl substituents in the 3,3′-positions of 2,2′-diamino-1,1′-binaphthyl (dabn)[4b,7] was used for the enantiomeric resolution and isomerization of the tetraphos–Pd complex (±)-**1** complex (Scheme 2). Complex (±)-**1** was treated with 2 equivalents of (*S*)-dm-dabn to give the single diastereomer (*P,S,S*)-**2**, along with remaining (*M,R,R*)-**1** and (*S*)-dm-dabn. Importantly, no isomerization of the remaining (*M,R,R*)-**1** to (*P,S,S*)-**1** was observed to complex with (*S*)-dm-dabn at room temperature for more than 120 h. After heating at 80 °C for 12 h, however, only (*P,S,S*)-**2** was obtained through isomerization of (*M,R,R*)-**1**.[8]

Under the same conditions, the combination of biphep–Pd complex (±)-**3** and 1 equivalent of (*S*)-dm-dabn gave the single diastereomer (*S*)-**4** through isomerization of (*R*)-**3** at

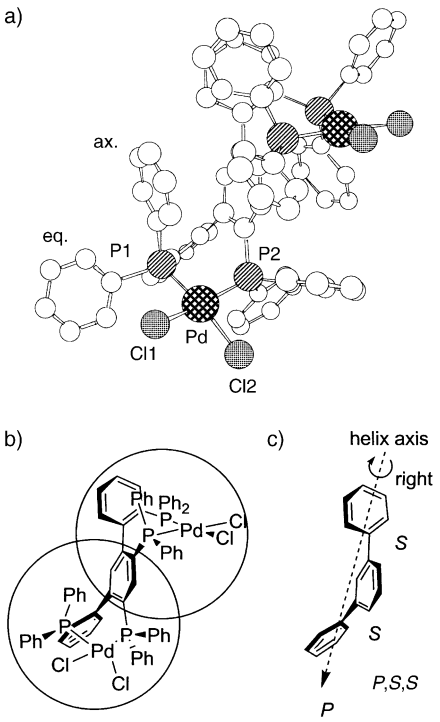



***Figure 1.*** a) X-ray crystal structure of the tetraphos–Pd complex. Selected bond lengths [Å]: Pd-P1 2.241(2), Pd-P2 2.261(2), Pd-Cl1 2.369(3), Pd-Cl2 2.347(2), selected bond angles [°]: P1-Pd-P2 93.67(3), Cl1-Pd-Cl2 91.42(4). b) tetraphos–Pd complex with two biphep units c) Helical chirality of the tetraphos–Pd complex.

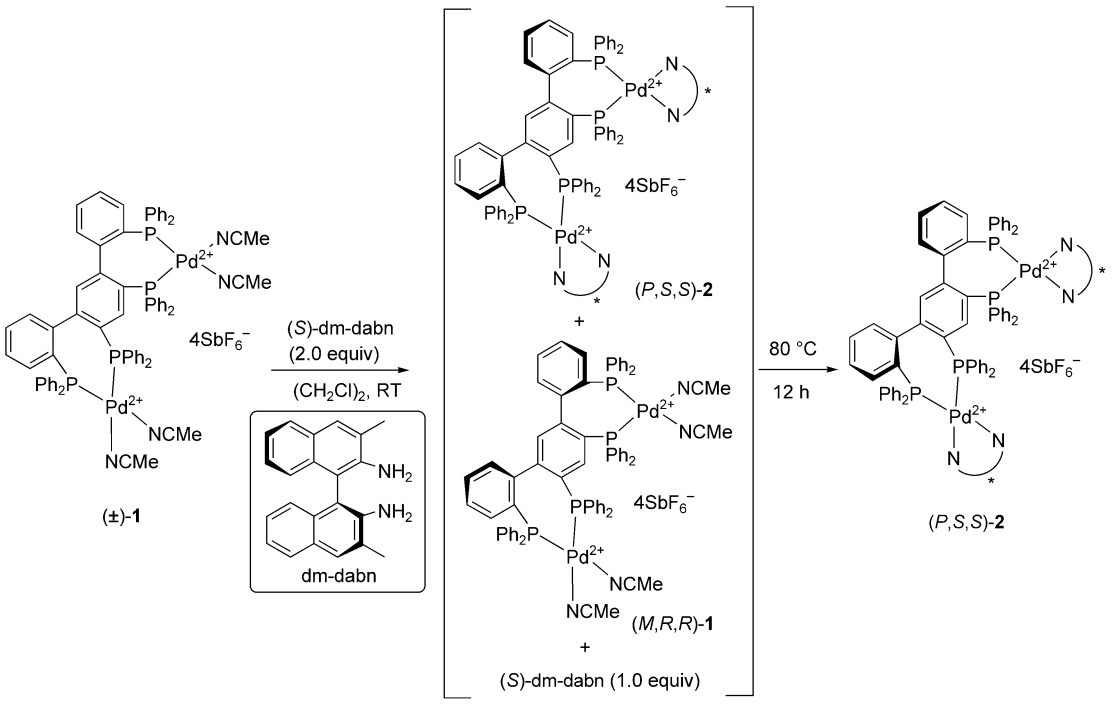
80 °C within a shorter period of time (Scheme 3).[4d] It was therefore clear that tetraphos–Pd complex **1** changes its conformation much less readily than biphep–Pd complex **3**.

Next, complexation of (±)-**1** and 2 equivalents of (*S*)-dabn also gave a diastereomeric mixture in a nonselective manner ((*P,S,S*)-**5**/(*M,R,R*)-**5** = 1:1) (Scheme 4).[9] However, the diastereomeric mixture was converted into the single diastereomer, even at room temperature for 120 h (or 80 °C for 2 h). While the configuration of **1** was retained at room temperature as shown in Scheme 2, the dabn complex **5** isomerized under the same conditions. Therefore, the flexibility of tetraphos–Pd complex **1** can be increased by association of the chiral controller dabn.

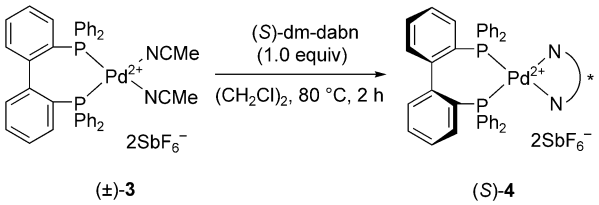
In the combination of biphep–Pd complex (±)-**3** and 1 equivalent of (*S*)-dabn, isomerization of (*R*)-**6** took place at 80 °C for 8 h to give the single *S* diastereomer, but not at room temperature (Scheme 5).[4e] It can therefore be seen that tetraphos–Pd complex **1** is more rigid than biphep–Pd complex **3** by itself, but more flexible with a chiral diamine controller.

These enantiopure tetraphos–Pd complexes obtained through isomerization by diamines were employed as asymmetric catalysts for carbon–carbon bond-forming reactions. As a probe reaction, the carbonyl-ene reaction of methylenecyclohexane (**7**) and ethyl glyoxylate (**8**) was examined (Table 1).[2a,10] Enantiopure [(*S*)-binap–Pd–(*S*)-dabn] resulted in moderate enantioselectivity and yield (Table 1, entry 1). The [biphep–Pd–dabn] complex led to a decrease in enantio-

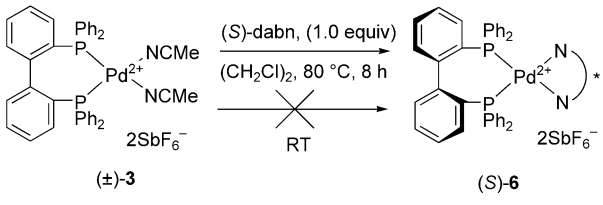
 © 2003 Wiley-VCH Verlag GmbH & Co. KGaA, Weinheim 




***Scheme 2.*** Chirally stable tetraphos–Pd complex at room temperature and its isomerization to the diastereopure form at 80 °C.



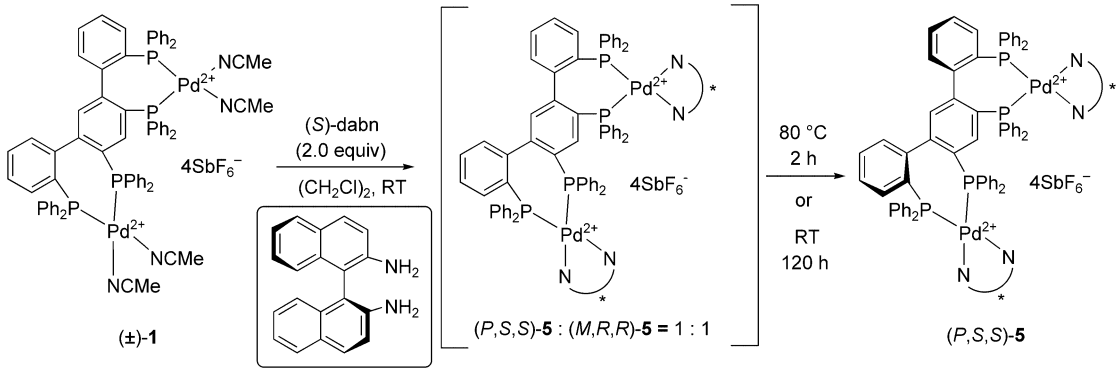

***Scheme 3.*** Isomerization of the biphep–Pd complex by (*S*)-dm-dabn.




***Scheme 5.*** Isomerization of the biphep–Pd complex by (*S*)-dabn.

selectivity (Table 1, entry 2). However, a higher yield and enantioselectivity was observed with [tetraphos–Pd–dabn] ((*P,S,S*)-**5**) than with [biphep–Pd–dabn] ((*S*)-**6**) and [(*S*)-binap–Pd–(*S*)-dabn] (Table 1, entry 3). These results unambiguously prove the efficiency of *tropos* but sterically demanding and hence relatively rigid helical tetraphos ligands. The complex (*P,S,S*)-**2**, which bears dm-dabn, gave a slightly lower enantioselectivity (Table 1, entry 4).

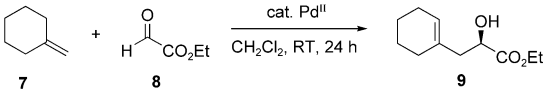
In summary, we have succeeded in control over not only axial but also helical chirality of Pd complexes that bear the *tropos* tetraphos ligand. Significantly, the flexibility of the tetraphos–Pd complex can be increased by association of the chiral controller dabn. The tetraphos–Pd complexes, through isomerization into single enantiomers, lead to a higher enantioselectivity and yield, as integrated asymmetric catalysts for the carbon–carbon bond-forming reaction.




***Scheme 4.*** Isomerization of the [tetraphos–Pd–dabn] complex in diastereopure form at room temperature.

 © 2003 Wiley-VCH Verlag GmbH & Co. KGaA, Weinheim 

***Table 1:*** Asymmetric carbonyl-ene reaction by Pd catalysts with chirally flexible phosphane ligands.




7 8 9

| Entry | $Pd^{II}$ catalyst[a] | [mol%] | *ee* [%][b] | Yield [%][c] |
|---|---|---|---|---|
| 1 | [(*S*)-binap–Pd–(*S*)-dabn] | 5.0 | 78 | 80 |
| 2 | [(*S*)-biphep–Pd–(*S*)-dabn] | 5.0 | 69 | 78 |
| 3 | [(*P,S,S*)-tetraphos–Pd–(*S*)-dabn] | 2.5 | 81 | 86 |
| 4 | [(*P,S,S*)-tetraphos–Pd–(*S*)-dm-dabn] | 2.5 | 76 | 85 |

[a] All reactions were examined through isomerization by enantiopure diamines except for (*S*)-binap. [b] Enantiopurity was determined by chiral GC analysis on a CP-Cyclodextrin-β-2,3,6-M-19 column. [c] Yield of isolated product.

## *Experimental Section*

Dichloroethane (2.0 mL) was added to a mixture of (±)-**1** (22.9 mg, 0.01 mmol) and (*S*)-dabn (6.0 mg, 0.021 mmol) in a 10-mL Schlenk tube under an argon atmosphere, and the reaction mixture was stirred at 80 °C for 2 h. After concentration under reduced pressure, the flask was replenished with argon, and dichloromethane (2.0 mL), ethyl glyoxylate (**8**) (30.6 mg, 0.6 mmol), and methylenecyclohexane (**7**) (48 μL, 0.4 mmol) was added sequentially to the solution. The reaction mixture was stirred at room temperature for 24 h, directly loaded onto a silica-gel column, and eluted with hexane/EtOAc (3:1) to afford (*R*)-**9** in 86% yield as a colorless oil. The enantiomeric excess was determined by chiral GC analysis; GC (column: CP-Cyclodextrin-β-2,3,6-M-19, i.d. 0.25 mm × 25 m, CHROMPACK; carrier gas: nitrogen, 75 kPa; column temperature: 130 °C; injection and detection temperature: 160 °C; split ratio: 100:1), $t_R$ (*R* isomer): 31.3 min, $t_R$ (*S* isomer): 32.4 min; $^1$H NMR (300 MHz, $CDCl_3$): $\delta =$ 1.26 (t, $J = 6.9$ Hz, 3H), 1.48–1.63 (m, 4H), 1.93–1.99 (m, 4H), 2.24 (dd, $J = 7.8$, 14.1 Hz, 1H), 2.40 (dd, $J = 4.5$, 14.1 Hz, 1H), 2.60 (d, $J =$ 6.3 Hz, 1H), 4.19 (q, $J = 6.9$ Hz, 2H), 5.50 ppm (m, 1H); $^{13}$C NMR (75 MHz, $CDCl_3$): $\delta = 14.4$, 22.4, 23.0, 25.5, 28.7, 43.5, 61.8, 69.6, 126.0, 133.7, 175.9 ppm.

Received: July 3, 2003 [Z52300]

**Keywords:** chirality · ene reaction · helical structures · isomerization · palladium

[1] a) H. Hopf, *Classics in Hydrocarbon Chemistry*, Wiley-VCH, Weinheim, **2000**; b) C. Schmuck, *Angew. Chem.* **2003**, *115*, 2552 – 2556; *Angew. Chem. Int. Ed.* **2003**, *42*, 2448 – 2452; c) A. Urbano, *Angew. Chem.* **2003**, *115*, 4116 – 4119; *Angew. Chem. Int. Ed.* **2003**, *42*, 3986 – 3989.

[2] a) E. N. Jacobsen, A. Pfaltz, H. Yamamoto, *Comprehensive Asymmetric Catalysis, Vol. 1–3*, Springer, Berlin, **1999**; b) *Transition Metals for Organic Synthesis* (Ed.: M. Beller, C. Bolm), VCH, Weinheim, **1998**; c) R. Noyori, *Asymmetric Catalysis in Organic Synthesis*, Wiley, New York, **1994**; d) H. Brunner, W. Zettlmeier, *Handbook of Enantioselective Catalysis*, VCH, Weinheim, **1993**; e) *Catalytic Asymmetric Synthesis, Vol. I and II* (Ed.: I. Ojima), VCH, New York, **1993**, **2000**.

[3] R. Noyori, H. Takaya, *Acc. Chem. Res.* **1990**, *23*, 345 – 350.

[4] a) K. Mikami, T. Korenaga, M. Terada, T. Ohkuma, T. Pham, R. Noyori, *Angew. Chem.* **1999**, *111*, 517 – 519; *Angew. Chem. Int. Ed.* **1999**, *38*, 495 – 497; b) K. Mikami, K. Aikawa, T. Korenaga, *Org. Lett.* **2001**, *3*, 243 – 245; c) T. Korenaga, K. Aikawa, M. Terada, S. Kawauchi, K. Mikami, *Adv. Synth. Catal.* **2001**, *343*, 284 – 288; d) K. Mikami, K. Aikawa, Y. Yusa, M. Hatano, *Org. Lett.* **2002**, *4*, 91 – 94; e) K. Mikami, K. Aikawa, Y. Yusa, *Org. Lett.* **2002**, *4*, 95 – 97; f) K. Mikami, K. Aikawa, Y. Yusa, J. J. Jodry, M. Yamanaka, *Synlett* **2002**, *10*, 1561 – 1578; for similar work on the biphep ligand, see: g) M. D. Tudor, J. J. Becker, P. S. White, M. R. Gagne, *Organometallics* **2000**, *19*, 4376 – 4484; h) J. J. Becker, P. S. White, M. R. Gagne, *J. Am. Chem. Soc.* **2001**, *123*, 9478 – 9479.

[5] X-ray crystallographic analysis was performed with a Bruker SMART 1000 diffractometer (graphite monochromator, $Mo_{K\alpha}$ radiation, $\lambda = 0.71073$ Å) at 299 K. Crystal data for $[Pd_2Cl_4(tetraphos)]\cdot 2\,MeOH$ ($C_{66}H_{58}O_2P_4Cl_4Pd_2$): monoclinic, *C*2/*C*, $a =$ 18.796(19) Å, $b = 12.631(13)$ Å, $c = 27.10(3)$ Å, $\alpha = 90°$, $\beta =$ 105.748(18)°, $\gamma = 90°$, $V = 4249.9(3)$ Å$^3$, $Z = 4$, $\rho_{calcd} =$ 1.486 g cm$^{-3}$, crystal dimensions $0.37 \times 0.11 \times 0.05$ mm$^3$, range for data collection $2\theta max = 54.96°$, reflections collected 18277, independent reflections 6783 ($R_{int} = 0.0382$). The structures were solved by direct methods (SHELXL-97); the final cycle of full-matrix least-squares on $F^2$ was based on 6783 observed reflections ($I > 2\sigma(I)$) and 390 variable parameters, and converged to $R = 0.038$, $Rw = 0.080$, and goodness of fit = 1.001. CCDC-213825 contains the supplementary crystallographic data for this paper. These data can be obtained free of charge via www.ccdc.cam.ac.uk/conts/retrieving.html (or from the Cambridge Crystallographic Data Centre, 12, Union Road, Cambridge CB21EZ, UK; fax: (+44) 1223-336-033; or deposit@ccdc.cam.ac.uk). $^1$H NMR (300 MHz, $CD_2Cl_2$): $\delta = 6.24$–6.28 (m, 3H), 6.77 (dd, $J = 8.1$, 11.7 Hz, 2H), 6.92 (t, $J = 8.1$ Hz, 2H), 7.13–7.18 (m, 2H), 7.23–7.62 (m, 35H), 7.77–7.83 (m, 2H), 7.89 ppm (dd, $J = 7.5$, 12.6 Hz, 4H); $^{31}$P NMR (162 MHz, $CD_2Cl_2$): $\delta = 25.0$ (s, 2P), 27.8 ppm (s, 2P).

[6] a) M. Ogasawara, K. Yoshida, T. Hayashi, *Organometallics* **2000**, *19*, 1567 – 1571; b) F. Ozawa, A. Kubo, Y. Matsumoto, T. Hayashi, *Organometallics* **1993**, *12*, 4188 – 4196.

[7] a) K. Mikami, T. Korenaga, T. Ohkuma, R. Noyori, *Angew. Chem.* **2000**, *112*, 3854 – 3857; *Angew. Chem. Int. Ed.* **2000**, *39*, 3707 – 3710; b) K. Mikami, Y. Yusa, T. Korenaga, *Org. Lett.* **2002**, *4*, 1643 – 1645.

[8] (±)-**1**: $^{31}$P NMR (162 MHz, $CD_2Cl_2$): $\delta = 25.9$ (s, 2P), 29.3 ppm (s, 2P). (*P,S,S*)-**2**: $^{31}$P NMR (162 MHz, $CD_2Cl_2$): $\delta = 22.0$ (d, $J_{P\text{-}P} = 25.9$ Hz, 2P), 25.7 ppm (d, $J_{P\text{-}P} = 25.9$ Hz, 2P).

[9] (*P,S,S*)-**5**: $^{31}$P NMR (162 MHz, $CD_2Cl_2$): $\delta = 24.8$ (d, $J_{P\text{-}P} =$ 19.9 Hz, 2P), 26.3 ppm (d, $J_{P\text{-}P} = 19.9$ Hz, 2P). (*M,R,R*)-**5**: $^{31}$P NMR (162 MHz, $CD_2Cl_2$): $\delta = 22.7$ (d, $J_{P\text{-}P} = 19.1$ Hz, 2P), 28.2 ppm (d, $J_{P\text{-}P} = 19.1$ Hz, 2P).

[10] For a general review of enantioselective ene reactions, see: a) K. Mikami, M. Shimizu, *Chem. Rev.* **1992**, *92*, 1021 – 1050; b) L. C. Dias, *Curr. Org. Chem.* **2000**, *4*, 305 – 342; for an excellent recent example, see: c) D. A. Evans, S. W. Tregay, C. S. Burgey, N. A. Paras, T. Vojkovsky, *J. Am. Chem. Soc.* **2000**, *122*, 7936 – 7943.

 © 2003 Wiley-VCH Verlag GmbH & Co. KGaA, Weinheim 

Super-Acid Catalysts

# Benign by Molecular Design: Active Polymeric Super-Acid Catalysts and Highly Conductive Polymeric Lithium Electrolytes**

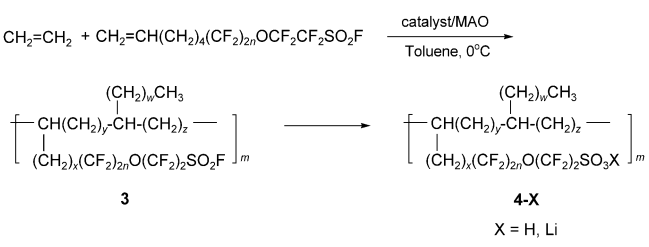
*Zhen-Yu Yang,* Lin Wang,* N. Drysdale, Marc Doyle, Qun Sun, and Susan K. Choi*

The development of polymeric strong acids as benign catalysts, and their lithium salts as electrolytes for lithium batteries, to replace very hazardous, corrosive, difficult-to-recover materials such as HF, $H_2SO_4$, and $LiPF_6$, has received growing attention for environmental reasons. Although perfluorinated sulfonic acid ionomers such as the Nafion resins are superior to polystyrene-based sulfonic acids such as Dowex and Amberlite in terms of acidity, they have a high equivalent weight (low-acid capacity), a high cost, and relatively low catalytic activity in nonpolar media.[1] The lithium-salt form of the Nafion membrane does not absorb enough quantities of organic solvents as is necessary for high ion conductivity. The polymeric lithium salts can offer significant advantages over conventional electrolytes, which includes fast cation transport, anion exclusion, and the absence of added thermally and hydrolytically unstable lithium salts such as $LiPF_6$ in addition to their environmental benefits.[2–3] We anticipate the catalytic activity, the ionic conductivity, and ease of process of these materials could be improved by proper architectural design of their microstructure, molecular topology, and chemical composition. The synthesis of polymers with new structures generally requires exotically designed monomers, which direct new architectures of the polymers.[4] It is highly desirable to directly polymerize existing commodity monomers to give controllable architectures that can exhibit unique properties.[5–8] Herein we report active polymeric acid catalysts and highly conductive polymeric lithium electrolytes by carefully designing molecular architectures by using metal catalyzed copolymerization of ethylene with an α-olefin that contains fluorosulfonyl fluorides.

The activities of polymeric acid catalysts are generally determined by the acid strength, surface area, or accessibility of the catalysts.[9] Homogeneous catalysts usually exhibit high activity, whereas heterogeneous catalysts also could exhibit excellent properties if they have high a surface area or swell in the reaction media.[10] The ability of polymeric lithium electrolytes to swell in selected organic solvents is particularly important for high ionic conductivity. Lithium electrolytes suitable for commercial applications also require that the electrolytes have sufficient mechanical integrity to fabricate a functional multilayered laminate that does not dissolve in battery solvents in addition to having good electrochemical stability and low cost.[3,11] To meet these diverse criteria, it is critical to synthesize polymeric materials with new architectures from low-cost monomers. Branched structures may be desirable as they could lower the crystallinity, increase the ability of the polymer to swell in organic solvents, and improve the processing of the system while maintaining excellent mechanical properties. A practical method for introducing the branched structure is to use a catalyst that can chain walk to control the position of monomer insertion during propagation, thus avoiding the use of costly monomers. The catalysts used for ethylene polymerization that chain walk are late transition metal complexes such as those recently discovered by Brookhart, Johnson, and co-workers.[12–14] Unlike Ziegler-Natta and metallocene catalysts that are readily poisoned by most functional olefins because of their high oxophilicity, the late-transition-metal catalysts such as nickel and palladium complexes not only catalyze the homo- or copolymerization of ethylene with functionalized olefins such as acrylates but are also able control the polymer topology when the right catalysts and the polymerization conditions are chosen.

We copolymerized ethylene and α-olefins that contain fluorinated sulfonyl fluoride by using α-diimine-palladium and nickel catalysts. For the palladium catalyst, the polymerization reactions were conducted under one atmosphere of ethylene in methylene chloride at room temperature. For Ni catalysts, the polymerization reactions were conducted with a cocatalyst, methylalumoxane (MAO), under one atmosphere of ethylene in toluene at 0 °C (Scheme 1).

During polymerization, the Pd catalyst does extensive chain walking to generate highly branched polymers, whereas the nickel catalysts undergo moderate chain walking to afford moderately branched polymers as determined by $^{13}C$ NMR




***Scheme 1.*** Synthesis of the copolymers **3**, which can be transformed into superacids and their Li derivatives, **4**.

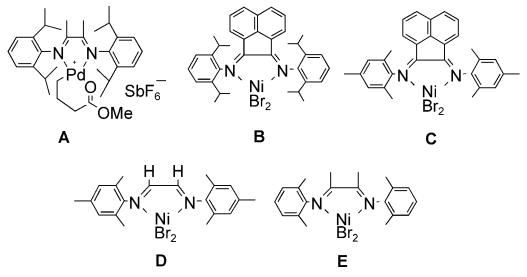
[*] Dr. Z.-Y. Yang, Dr. L. Wang, Dr. N. Drysdale
DuPont Central Research and Development
Experimental Station
Wilmington, DE 19880-0328 (USA)
E-mail: zhenyu.yang-1@usa.dupont.com
lin.wang@usa.dupont.com
Dr. M. Doyle
DuPont Electronic Technologies
14 T.W. Alexander Drive
Research Triangle Park, NC 27709-3999 (USA)
Dr. Q. Sun, Dr. S. K. Choi
DuPont T&I
Experimental Station
Wilmington, DE 19880 (USA)

[**] Publication No.: 8400. The authors thank W. Hyde, A. Woolard, R. E. Smith, Jr., C. Naples, and M. Barker for technical assistance, Dr. E. F. McCord for $^{13}C$ NMR analysis, Dr. M. Subramanian for helpful discussions, and Professor S. Zhu at Shanghai Institute of Organic Chemistry for precursors of the monomers.

Supporting information for this article is available on the WWW under http://www.angewandte.org or from the author.

 © 2003 Wiley-VCH Verlag GmbH & Co. KGaA, Weinheim DOI: 10.1002/anie.200351725 

analysis. The Pd catalyst **A** produced high molecular weight oil copolymers with glass transition temperatures ($T_g$s) below




**A** **B** **C** **D** **E**

$CH_2{=}CH(CH_2)_4(CF_2)_2OCF_2CF_2SO_2F$, **1**

$CH_2{=}CH(CH_2)_4(CF_2)_4OCF_2CF_2SO_2F$, **2**

−55 °C (Table 1, entries 1–3); Ni catalysts gave semi-crystalline copolymers with melting points ($T_m$s) ranging from 94 °C to 126 °C (Table 1, entries 4–10). These semi-crystalline polymers can be thermally fabricated into strong and tough thin films or other shaped articles. The precise polymer structures can be controlled by tailoring the α-diimine backbone and the *ortho* substituents on the phenyl rings of the catalysts and the polymerization conditions. The less bulky catalysts, **C, D, E**, gave less branched and more crystalline copolymers under similar conditions (Table 1, entries 6 to 10). In addition, the comonomer content increased in the polymer as the concentration of the comonomer increased in the polymerization mixture (Table 1, entries 8 to 10). When catalyst **E** was used, under the same conditions, 0.51 M of **1** in the precharged mixture gave polymer containing 2.6 mol % of **1**. When the concentration of **1** was increased to 1.20 M and 3.60 M, polymers containing 3.7 mol % of **1** and 10.8 mol % of **1**, respectively, were obtained. More interestingly, the number of methyl groups in the polymers decreased as the mole % of **1** increased, and the melting points of the polymers were similar. Under low-pressure conditions, highly branched copolymers with more incorporated comonomer **2** were obtained because of the increase in the rate of chain walking relative to that of ethylene insertion.[6]

***Table 1:*** High value copolymers of ethylene with $CH_2{=}CH(CH_2)_4(CF_2)_nO(CF_2)_2SO_2F$.

| Entry | Catalyst | Monomer (M) | Comonomer in **3** (mol %) | No. of Me per 1000 $CH_2$ | $T_g$ or $T_m$ [°C] | $\bar{M}_w \times 10^{-4}$ (PDI) |
|---|---|---|---|---|---|---|
| **1** | **A** | **2** (0.40) | **2** (8.5) | 89 | $T_g$ −57 | 7.89 (1.5) |
| **2** | **A** | **1** (1.20) | **1** (6.7) | 89 | $T_g$ −69 | 9.0 (1.7) |
| **3** | **A** | **1** (0.42) | **1** (2.9) | 113 | $T_g$ −66 | 9.05 (2.1) |
| **4** | **B** | **2** (0.67) | **2** (3.9) | 77 | $T_m$ 102 | 33 (2.3) |
| **5** | **B** | **1** (1.18) | **1** (4.4) | 49 | $T_m$ 94 | 18.6 (2.6) |
| **6** | **C** | **1** (1.18) | **1** (6.9) | 6 | $T_m$ 126 | 6.66 (2.7) |
| **7** | **D** | **1** (1.18) | **1** (5.3) | 4 | $T_m$ 126 | 2.55 (3.0) |
| **8** | **E** | **1** (0.51) | **1** (2.6) | 20 | $T_m$ 118 | 17.3 (4.8) |
| **9** | **E** | **1** (1.20) | **1** (3.7) | 11 | $T_m$ 124 | 25.1 (5.1) |
| **10** | **E** | **1** (3.60) | **1** (10.8) | 8 | $T_m$ 127 | 24.6 (5.6) |

These copolymers were readily hydrolyzed with KOH or LiOH in aqueous MeOH to give polymeric fluorosulfonates, which underwent ion exchange with concentrated HCl to give various polymeric acids. Because of the strong electron-withdrawing effect of the fluorinated group, these polyethylene based copolymeric acids **4**-*x* showed super acid properties (*x* refers to the entry numbers in Table 1, thus indicating how the acids were obtained). The highly branched polymeric sulfonic acids **4**-1 and **4**-2 (Table 1, entries 1 and 2) are elastic materials and soluble in polar solvents such as THF. Thus, these materials can be used as homogeneous polymeric super-acid catalysts in certain polar solvents. While polymeric super acids **4**-4–10 (from entries 4–10) are usually not soluble in organic solvent, they can be swelled and used as heterogeneous super acid catalysts. Although homogenous catalysts exhibit excellent activity for some acid-catalyzed reactions, heterogeneous catalysts offer advantages in the isolation step as simple filtration can remove the catalysts from the reaction mixture and the recovered catalyst can be reused. We have demonstrated that these catalysts exhibit excellent catalytic activities in several types of industrially important reactions.[15,16] Table 2 tabulates the polymerization of THF with acetic anhydride with the new polyethylene/sulfonic acid catalysts to generate diacetate-capped polyethers. The polymerization of THF occurs readily with a catalyst that contains a low mole percent of **1**. Thus with catalyst **4**-3, which only contains 2.9 mole % of comonomer **1**, the polymerization occurs rapidly to give a conversion of 45 % after 2 h. With catalyst **4**-2, 50 % conversion was observed within 2 hrs. More importantly, the catalyst **4**-2 also catalyzed the copolymerization of THF and 3-methyl THF, which is usually difficult to achieve with other acid catalysis. Although the new catalysts contain much less sulfonic acid comonomer than the standard Nafion resin, which contains 16 mol % of fluorosulfonic acid comonomer, the new catalysts are more active than the Nafion resin. This is probably because the new catalysts swell more or are soluble in the THF solutions. After one hour at a loading of 0.57 g the new polyethylene/sulfonic acid catalyst gave a conversion of 39 % compared to 6.8 % for Nafion (Table 2, entries 2, 3, 6, and 7).

***Table 2:*** Polymerization of THF with acetic anhydride.

| Entry | THF [g] | $Ac_2O$ [g] | Catalyst | Quantity[a] [g] | Time [h] | Conv. [%] | $\bar{M}_w \times 10^{-4}$[b] (PDI) |
|---|---|---|---|---|---|---|---|
| **1** | 10.00 | 0.53 | **4**-3 | 0.66 | 20 | 74.4 | 2.2 (1.80) |
| **2** | 10.10 | 0.65 | **4**-3 | 0.57 | 1 | 39.2 | 2.6 (1.48) |
| **3** | 10.10 | 0.56 | **4**-3 | 0.37 | 2 | 45.1 | 4.2 (1.65) |
| **4** | 10.08 | 0.50 | **4**-2 | 0.43 | 2 | 50.0 | 5.2 (1.57) |
| **5** | 10.15[c] | 0.50 | **4**-2 | 0.35 | 18 | 56.2 | 3.5 (1.76) |
| **6** | 10.10 | 0.56 | Nafion NR50 | 0.57 | 1 | 6.8 | 1.6 (2.64) |
| **7** | 10.10 | 0.62 | Nafion NR50 | 0.37 | 2 | 12.7 | 2.9 (2.14) |

[a] Quantity of catalyst present. [b] $\bar{M}_w$ is the weight average molecular mass. [c] 3-Me-THF copolymerization, approximately 30 mole % in initial THF solution. From $^1$H NMR spectroscopy the resulting polymer contains ca. 14 mole % 3-Me-THF.

 © 2003 Wiley-VCH Verlag GmbH & Co. KGaA, Weinheim 

After the quantity of catalyst was decreased to 0.37 g and the polymerization time increased to two hours, Nafion gave a conversion of 13% and the catalyst **4**-3 gave a conversion of 45%. Isolation was easy and the polymer was readily separated from catalyst by the addition of a mixture of ether, THF and water to the reaction mixture. More importantly, the new catalysts gave polymers of designed molecular weight with narrow polydispersity (PDI less than 2), whereas polymers made with Nafion catalysts have broad bimodal molecular weight distributions.

We also tested catalytic activity of **4**-6 in acylation of substituted-benzenes with acyl chloride and isomerization of olefins. We found that the new catalyst is not soluble but it is more active than Nafion and other acid catalysts. For example, in the benzoylation of *m*-xylene at 140°C, the reaction rate with 0.25 g of **4**-6 was 380 mM $g^{-1}$ of catalyst $h^{-1}$, whereas the rate with 1.0 g of Nafion and 1.0 g of SAC-13A (Nafion/silica composite) was 108 and 68 mM $g^{-1}$ of catalyst $h^{-1}$, respectively. Upon isomerization of 1-dodecene at 75°C, the rate with **4**-6 was 45 times faster than that with Nafion, four times faster than that with Amberlst-15 and more than 88 times faster than with 70% $H_3PO_4/SiO_2$.

After they have been converted into lithium form, the strong and tough thin films of copolymers made with Ni catalysts have almost the same melting point as the nonionic copolymers and are thermally stable up to 350°C. Our preliminary results have demonstrated that branching in ionomers remarkably affects the uptake of solvent and lithium ion conductivity. The films swell in selected organic solvents such as propylene carbonate (PC) but still have excellent mechanical properties. The more branched the polymers are, the more solvent they absorb although contents of comonomer **1** (or equivalent weight) also have a pronounced effect (Table 3). The relatively high-branching ionomer of entry 2 exhibited the same conductivity as the ionomer of entry 3, which had 50% more of the comonomer **1**, but less branching. More interestingly, the film **4** containing 6.8 mol% of **1** with 20 methyl groups per 1000 $CH_2$ units was 3.7 fold more conductive than the film of Table 3, entry 5, which contained 10.8 mol% **1** but only eight methyl groups per 1000 $CH_2$ units, although they absorbed similar amounts of PC. These examples have indicated that moderate branching in the ionomers significantly improved ionic conductivity and overall properties. Ionomers with highly branched structures made from the Pd catalyst resulted in poor mechanical properties, while ionomers with little alkyl branches exhibited poor conductivity and low uptake of solvents.

***Table 3:*** Lithium ion conductivity and PC uptake of ionomer films.

| Entry | Content of **1** [mol%] in **4** | $CH_3$ per 1000 $CH_2$ | $T_m$ [°C] | PC uptake [%] | Conductivity [mS $cm^{-1}$] |
|---|---|---|---|---|---|
| **1** | 3.7 | 11 | 124 | 56 | 0.233 |
| **2** | 4.4 | 49 | 93 | 70 | 0.369 |
| **3** | 6.9 | 6 | 120 | 84 | 0.341 |
| **4** | 8.0 | 20 | 118 | 84 | 0.702 |
| **5** | 10.8 | 8 | 125 | 87 | 0.189 |

The molecular architecture design of copolymers of ethylene described here provides new opportunities for green solid super-acid catalysts and polymeric lithium-ion-conducting electrolytes. In principle, various polymeric molecular structures can be synthesized by tailoring the polymerization catalysts and the polymerization conditions with commodity monomers, which offers a promising approach for making new materials at low cost. We have demonstrated that the materials with new structures exhibit desirable properties to meet specific applications. The polymeric acid catalysts from copolymers of ethylene showed enhanced catalytic activity for industrially important reactions and their lithium ionomers not only have excellent conductivity but can also be processed more easily, have better mechanical properties, and are inexpensive.

Received: April 23, 2003
Revised: August 8, 2003 [Z51725]

**Keywords:** copolymerization · electrolytes · homogeneous catalysis · lithium batteries · superacidic systems

[1] a) M. A. Harmer, Q. Sun, *Appl. Catal. A* **2001**, *221*, 45, and references therein; b) G. A. Olah, S. I. Pradeep, G. K. S. Prakash, *Synthesis* **1986**, 513.
[2] M. E. Doyle, M. G. Lewittes, M. A. Roelofs, S. A. Perusich, *J. Phys. Chem. B* **2001**, *105*, 9387.
[3] a) J. M. Tarascon, M. Armand, *Nature* **2001**, *414*, 359; b) G. S. MacGlashan, Y. G. Andreev, P. Bruce, *Nature* **1998**, *398*, 792; c) F. Croce, G. B. Appetecchi, L. Persi, B. Scrosati, *Nature* **1998**, *394*, 456.
[4] a) O. W. Webster, *Science* **1991**, *251*, 887; b) K. Ishizu, K. Tsubaki, A. Mori, S. Uchida, *Prog. Polym. Sci.* **2003**, *28*, 27.
[5] a) Z. Guan, P. M. Cotts, E. F. McCord, S. J. Mclain, *Science* **1999**, *283*, 2059; b) Z. Guan, *J. Am. Chem. Soc.* **2002**, *124*, 5616.
[6] C. W. Bielawski, D. Benitez, R. H. Grubbs, *Science* **2002**, *297*, 2041.
[7] J. M. Frechet, M. Henmi, I. Gitsov, S. Aoshima, M. R Leduc, R. B. Grubbs, *Science* **1995**, *269*, 1080.
[8] A. W. Bosman, R. Vestberg, A. Heumann, J. M. Frechet, C. J. Hawker, *J. Am. Chem. Soc.* **2003**, *125*, 715.
[9] a) K. Ishihara, A. Hasegawa, H. Yamamoto, *Angew. Chem.* **2001**, *113*, 4201; *Angew. Chem. Int. Ed.* **2001**, *40*, 4077; b) K. Ishihara, A. Hasegawa, H. Yamamoto, *Synlett* **2002**, 1296.
[10] D. J. Cole-Hamilton, *Science* **2003**, *299*, 1702.
[11] a) A. Feiring, S. K. Choi, M. E. Doyle, E. R. Wonchoba, *Macromolecules* **2000**, *33*, 9262; b) A. U. Schnurer, N. R. Holcomb, G. L. Gard, D. G. Castner, D. W. Grainger, *Chem. Mater.* **1996**, *8*, 1475.
[12] a) L. K. Johnson, C. M. Killian, M. Brookhart, *J. Am. Chem. Soc.* **1995**, *117*, 6414; b) S, Mecking, L. K. Johnson, L. Wang, M. Brookhart, *J. Am. Chem. Soc.* **1998**, *120*, 888; c) D. P. Gates, S. A. Svejda, E. Onate, C. M. Killian, L. K. Johnson, P. S. White, M. Brookhart, *Macromolecules* **2000**, *33*, 2320; d) P. Preishuber-Pflugl, M. Brookhart, *Macromolecules* **2002**, *35*, 6074.
[13] S. D. Ittel, L. K. Johnson, M. Brookhart, *Chem. Rev.* **2000**, *100*, 1169, and references therein.
[14] T. R. Younkin, E. F. Connor, J. I. Henderson, S. K. Friedrich, R. H. Grubbs, D. A. Bansleben, *Science* **2000**, *287*, 460.
[15] F. E. Bailey, J. V. Koleske, *Ullmann's Encyclopedia of Industrial Chemistry, Vol. 28*, 6th ed., VCH, Weinheim, **2003**, p. 497.
[16] M. Schneider, K. Zimmermann, F. Aquino, W. Bonrath, *Appl. Catal. A* **2001**, *220*, 51.

 © 2003 Wiley-VCH Verlag GmbH & Co. KGaA, Weinheim 

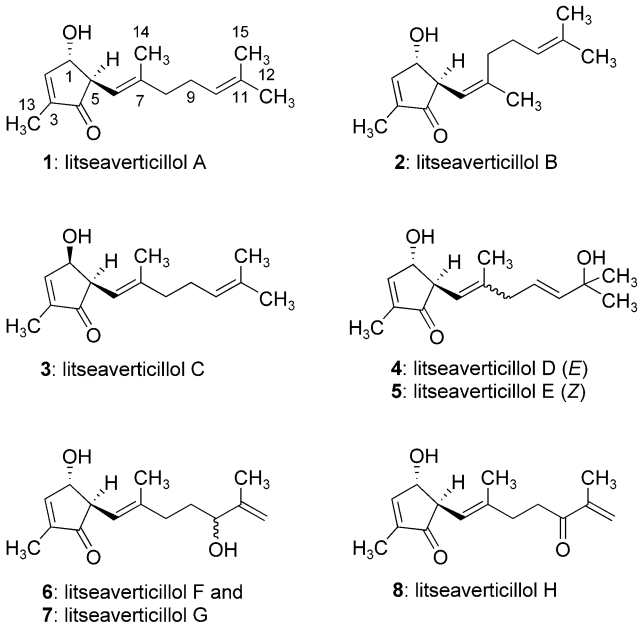
*Natural Product Synthesis*

# Biomimetic Total Synthesis of Litseaverticillols A, C, D, F, and G: Singlet-Oxygen-Initiated Cascades**

*Georgios Vassilikogiannakis* and Manolis Stratakis**

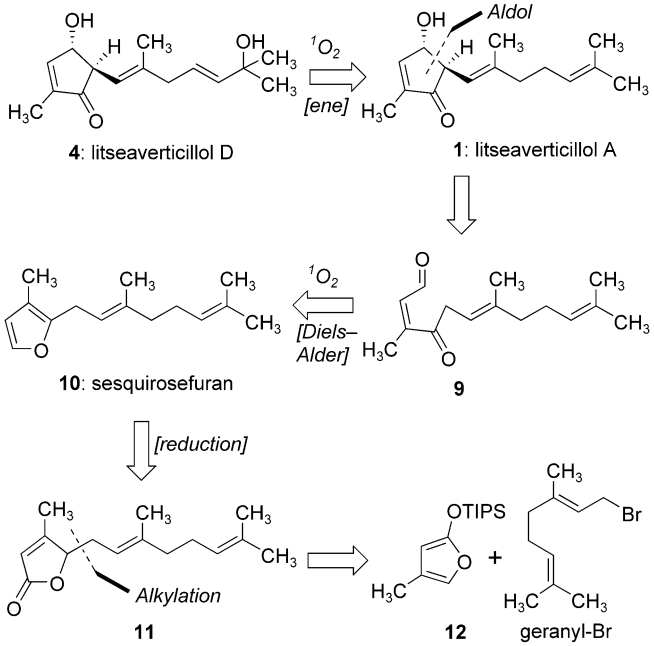
*Dedicated to Professor Christopher S. Foote*

The litseaverticillols (A–H, **1**–**8**, Scheme 1) are a recently isolated novel class of bioactive natural products. They were identified as the result of bioassay-guided fractionation of chloroform extracts from the leaves and twigs of a perennial shrub, *Litsea verticillata* Hance, found in Cuc Phuong National Park, Vietnam.[1] The eight new sesquiterpenes (**1**–**8**) were fully characterized because of their potent anti-HIV activity. More advanced biological studies revealed that compounds **1**–**8** inhibit HIV-1 replication in HOG.R5 cells (a reporter cell line)[2] with $IC_{50}$ values (the concentration required for 50% inhibition) ranging from 2 to 15 μg mL$^{-1}$ (8–85 μM). Furthermore, this viral inhibition was shown to be selective; HOG.R5 cell growth was only significantly affected at concentrations two- to threefold higher than the $IC_{50}$ values. The demonstrated anti-HIV activity in the absence of any apparent toxicity to host cells shows these molecules to have an impressive selectivity and makes them attractive candidates for further study. Of equal interest is the puzzle of how the racemic litseaverticillols (**1**–**8**) are derived in the natural environment. Racemic mixtures are highly atypical of natural products, whose syntheses are usually templated by homochiral enzymes. Herein, we provide a potential answer to this dichotomy in the form of a proposed biomimetic synthesis that delivers litseaverticillols A (**1**) and C (**3**) as the products of a one-pot, five-operation cascade sequence beginning with an achiral precursor and initiated by a cycloaddition reaction involving singlet oxygen ($^1O_2$).[3] Further support for the biogenetic hypothesis is garnered from the subsequent elaboration of litseaverticillol A through singlet-oxygen-mediated transformations to afford three additional family members.




***Scheme 1.*** Structures of litseaverticillols A–H.

Careful examination of these structurally related sesquiterpenes revealed that litseaverticillols D–H (**4**–**8**) could arise from direct oxidation of the first-generation litseaverticillols A–C (**1**–**3**). For example, litseaverticillols D, F, and G are the three possible products that can be derived from an ene reaction with $^1O_2$[4] at the side-chain double bond most distal to the cyclopentenone ring in litseaverticillol A (Scheme 2). In a similar manner, litseaverticillol B could be expected to be the precursor to litseaverticillol E, while litseaverticillol H may represent the oxidation product of both litseaverticillols F and G. This proposed biogenetic origin of the litseaverticillols D–H is in full accord with the high natural abundance of the three components necessary for the photochemical formation of highly reactive singlet oxygen, which are: a) molecular dioxygen (ca. 20% in atmospheric air),




***Scheme 2.*** Retrosynthetic analysis and strategy.

[*] Prof. Dr. G. Vassilikogiannakis, Prof. Dr. M. Stratakis
Department of Chemistry
University of Crete
71409 Iraklion, Crete (Greece)
Fax: (+30) 2810-393-601
E-mail: vasil@chemistry.uoc.gr
stratakis@chemistry.uoc.gr

[**] We thank Dr. T. Montagnon for her valuable discussions and comments. This work was financially supported by the Greek Ministry of Education (Β' ΕπΕΑΕΚ Graduate Program).

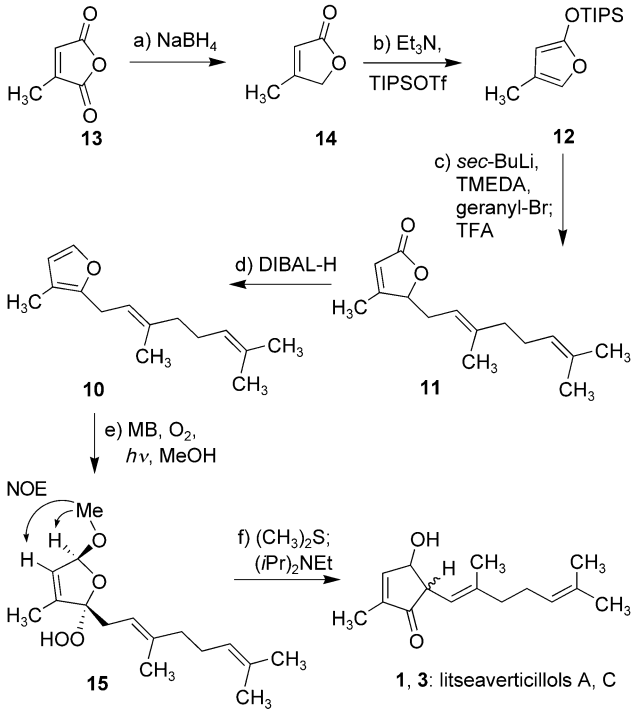
Supporting information for this article is available on the WWW under http://www.angewandte.org or from the author.

 DOI: 10.1002/anie.200352180 © 2003 Wiley-VCH Verlag GmbH & Co. KGaA, Weinheim 

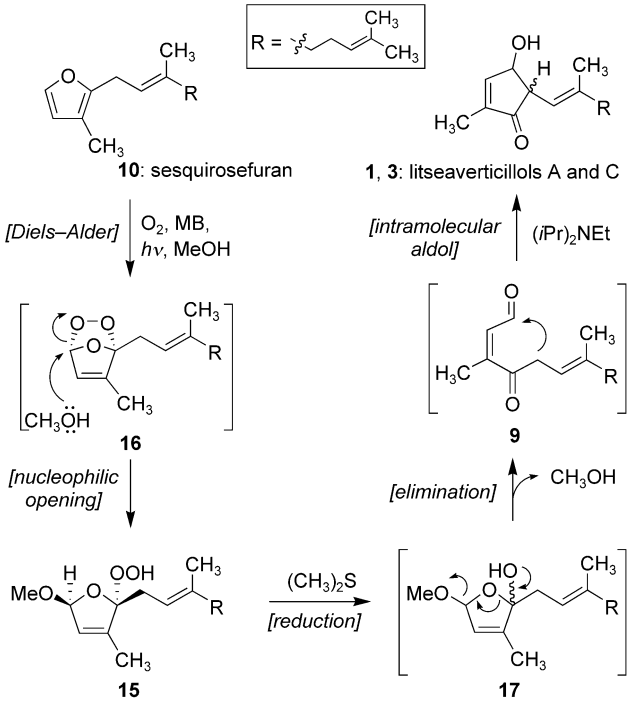
b) photosensitizers such as tannins and chlorophylls, and c) visible light.

We envisioned that the first generation listeaverticillols A–C might be derived from keto aldehyde **9** (an achiral precursor) through an intramolecular aldol reaction in a scenario that is proposed to mimic the natural nonenzymatic biogenesis and is consistent with the fact that compounds **1**–**8** were isolated as racemates (see above and Scheme 2). In turn, we anticipated that ketoaldehyde **9** could arise from the naturally occurring sesquirosefuran (**10**)[5] through a chemoselective $^1O_2$ oxidation of its furan moiety.[6] Finally, sesquirosefuran (**10**) might be synthesized by alkylation of the known furan **12**.[7]

The clear strategy that emerged from our retrosynthetic analysis enabled us to embark on the synthetic phase of the investigation. Furan derivative **12** was easily prepared by using a known two-step procedure[7,8] that begins with commercially available and inexpensive citraconic anhydride (**13**; Scheme 3). *Ortho*-metalation of **12** with *sec*-butyllithium followed by alkylation of the resultant anion with geranyl bromide and in situ acidic hydrolysis of the triisopropylsilyl ether moiety afforded lactone **11**. When DIBAL-H (1.7 equiv) was employed[9] as the reducing agent for lactone **11**, accompanied by an acidic work-up (10% HCl), sesquirosefuran **10** could be obtained in 85% yield (Scheme 3). This efficient transformation (**11**→**10**) prompted us to turn our attention towards accomplishing the direct oxidation of sesquirosefuran (**10**) to obtain keto aldehyde **9**. A serious obstacle to this process was expected to be the concomitant, if not faster, oxidation of the double bonds present in the appended side chain of **10**. Indeed, application of literature protocols for the direct oxidation of furans to *cis*-1,4-enediones, which involve treatment with magnesium monoperoxyphtalate[10] and $Br_2$/MeOH/dilute $H_2SO_4$,[11] led to rapid epoxidation and bromination, respectively, of the side-chain double bonds of **10**. These failures led us to examine the application of the pioneering work of Foote and Schenck[12] for the photosensitized oxygenation ($^1O_2$) of alkyl-substituted furans. The conditions used in this approach are also closer to the original biomimetic proposal. The photoinduced oxidation of the furan moiety of sesquirosefuran (**10**; 30 s irradiation with visible light of a methanolic solution bubbled through with $O_2$ and containing $10^{-4}$ M methylene blue as photosensitizer) led to the quantitative and exclusive formation of adduct **15**. The structure of hydroperoxide **15** was confirmed by NOE experiments (Scheme 3) and was found to be the opposite regioisomer to that proposed for the photooxidation of 2-methylfuran and menthofuran in MeOH.[12] Hydroperoxide **15** was treated with 5.0 equivalents $(CH_3)_2S$ in $CDCl_3$ and the reaction monitored by $^1H$ NMR spectroscopy. Complete reduction of **15** to a mixture of diastereomeric hemiacetals (**17**, Scheme 4) was observed after 2 h stirring at room temperature. At the same time, a substantial amount of the keto aldehyde **9** was observed. Futhermore, prolonged stirring of this solution (3 h more) at room temperature afforded keto aldehyde **9** in high yield (90%), accompanied




***Scheme 3.*** Biomimetic total synthesis of litseaverticillols A and C. Reagents and conditions: a) Ref. [8]; b) $Et_3N$ (1.4 equiv), TIPSOTf (1.2 equiv), $CH_2Cl_2$, 0→25 °C, 6 h, 81%; c) TMEDA (1.8 equiv), *sec*-BuLi (1.8 equiv), THF, 0 °C, 2 h, geranyl-Br (2.0 equiv), 0 °C, 3 h; then TFA (5.0 equiv), 25 °C, 1 h, 63%; d) DIBAL-H (1.7 equiv), THF, −78→−5 °C, 3 h, 85%; e) MB ($10^{-4}$ M), $O_2$ (bubbling), MeOH, *hν*, 0 °C, 30 sec, 97%; f) $(CH_3)_2S$ (5.0 equiv), $CHCl_3$, 25 °C, 5 h; then $(iPr)_2NEt$ (1.0 equiv), 25 °C, 4 h, 55% **1**/**3** (19:1). TIPSOTf = triisopropylsilyl trifluoromethanesulfonate; TMEDA = *N,N,N′,N′*-tetramethylethylenediamine; THF, tetrahydrofuran; TFA = trifluoroacetic acid; DIBAL-H = diisobutylaluminium hydride; MB = methylene blue.




***Scheme 4.*** Mechanistic rationale for the tandem tranformation of sesquirosefuran to litseaverticillols A and C.

 © 2003 Wiley-VCH Verlag GmbH & Co. KGaA, Weinheim 

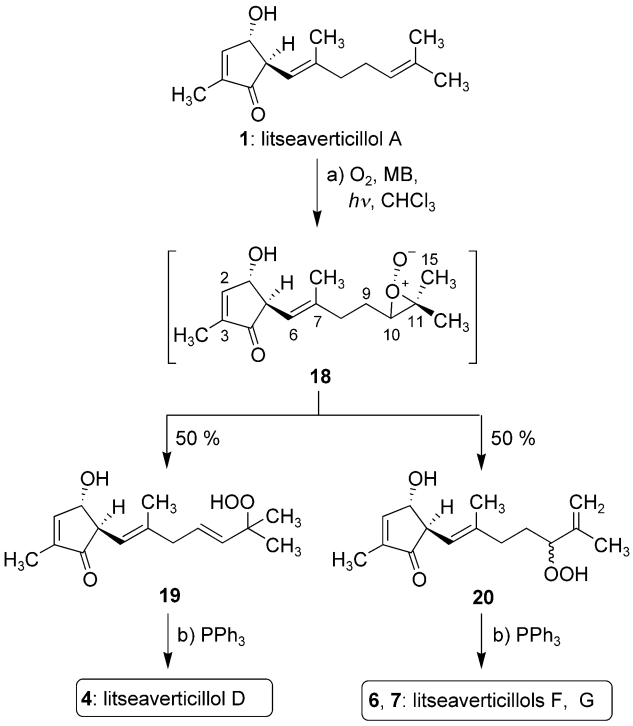
by just 10% unidentified byproducts. In situ treatment of the solution of keto aldehyde **9** with $(i\text{Pr})_2\text{NEt}$ (1.0 equiv), 4 h stirring, and subsequent chromatographic purification gave a 19:1 mixture of litseaverticillols A (**1**) and C (**3**) in 53% overall yield from sesquirosefuran **10**.

Keto aldehyde **9** is a labile compound and decomposed completely upon standing for two days. However, premature addition of Hünig's base before the complete disappearance of hemiacetals **17** (7:3 mixture of **17**/**9**) suppressed the elimination of MeOH and led to a 7:3 mixture of **17**/**1**. This ratio remained unchanged even after three days at room temperature. Only replacement of the solvent (MeOH) with $CH_2Cl_2$ or $CHCl_3$ prior to the addition of $(CH_3)_2S$ was necessary for the entire one-pot, five-operation sequence (**10**→**1** and **3**).

A detailed mechanistic rationale for this tandem sequence transforming sesquirosefuran (**10**) to litseaverticillols A (**1**) and C (**3**) is given in Scheme 4. The first step involves the [4+2] cycloaddition of singlet oxygen to the furan moiety[13] of **10** and is followed by regio- and diastereoselective[14] nucleophilic opening of endoperoxide **16** by MeOH. Reduction of the resulting hydroperoxide **15** to the fleeting anomeric hemiacetals **17** leads to the achiral keto aldehyde **9**, after elimination of MeOH. The final step is a base-induced intramolecular aldol reaction of the labile keto aldehyde **9** to form a 19:1 thermodynamic mixture of litseaverticillols A (**1**) and C (**3**).

With the synthesis of litseaverticillol A (**1**) secured, the stage was set for the application of a second type of singlet-oxygen reaction. Visible light irradiation of a solution of **1** in $CDCl_3$ ($10^{-4}$ M methylene blue) bubbled through with $O_2$ for 2 min at 0°C afforded an equimolar mixture ($^1$H NMR analysis) of tertiary hydroperoxide **19** and diastereomeric secondary hydroperoxides **20** (Scheme 5). In situ reduction of this mixture with $PPh_3$ instantaneously produced the corresponding naturally occurring diols litseaverticillol D (**4**) and litseaverticillols F (**6**), and G (**7**), which were separated by flash chromatography. Like synthetic litseaverticillols A (**1**) and C (**3**), the litseaverticillols D (**4**), F, and G (**6** and **7**) derived from the above procedure were shown to be identical to the natural substances[1] by IR, $^1$H NMR, $^{13}$C NMR, and HRMS analyses. Only trace amounts of a more polar mixture of triols resulting from oxidation of both side-chain double bonds were isolated under the reaction conditions used (2 min irradiation at 0°C). The regioselective oxidation of one of the three trisubstituted double bonds of **1** occurs for a combination of electronic and steric reasons:[15] the C10=C11 double bond is more accessible to the electrophilic $^1O_2$ than C6=C7, and the C2=C3 bond is electron deficient. The equimolar formation of the tertiary and secondary allylic hydroperoxides (**19** and **20**) is consistent with the formation of intermediate perepoxide **18**[16] (Scheme 5), in which the negatively charged oxygen atom is directed towards the more-substituted side of the previously present double bond (*cis* effect).[17] Allylic hydrogen abstraction from C9 and C15 of perepoxide **18** results in balanced formation of the ene reaction products, allylic hydroperoxides **19** and **20**.

In conclusion, we have developed a fast and reliable synthesis for the laboratory preparation of this new and biologically promising class of natural products by using a sequence of reactions proposed to be biomimetic. This initially convergent route provides the first generation of litseaverticillols A (**1**) and C (**3**) in four steps with an overall yield of 29% (starting from known furan **12**), and then diverges at this late stage to allow the preparation of the second-generation litseaverticillols D (**4**), F (**6**), and G (**7**). The developed technology should be easy to adapt for the synthesis of litseaverticillols B (**2**) and E (**5**) by replacing geranyl-Br with neryl-Br in the alkylation step (Scheme 3). This route will be utilized for the synthesis of selected analogues for further chemical biology studies.[18] For example, based on our proposed biomimetic synthesis, we believe that the $\Delta^{6,7}$ *Z*-geometrical isomers of litseaverticillols F and G (**6** and **7**) exist in nature, despite the fact that they have not yet been isolated. It is important to test the anti-HIV activity of these analogues since it has been shown that a change in configuration at $\Delta^{6,7}$ from *E* to *Z* generates a two- to threefold enhancement in activity when comparing **1** and **4** with **2** and **5**, respectively.[1] Perhaps, most significantly, these studies add considerably to the scope of syntheses employing different modes of singlet-oxygen reactions as a means to mimic nature in the construction of natural products.




***Scheme 5.*** Biomimetic transformation of litseaverticillol A into litseaverticillols D, F, and G through a regioselective singlet-oxygen-ene reaction. Reagents and conditions: a) MB ($10^{-4}$ M), $O_2$ (bubbling), $CHCl_3$, *hν*, 0°C, 2 min; b) $PPh_3$ (2.0 equiv), $CHCl_3$, 25°C, 5 min, 35% **4** plus 35% **6** and **7** over 2 steps.

Received: June 23, 2003 [Z52180]

**Keywords:** biomimetic synthesis · ene reaction · natural products · singlet oxygen · total synthesis

 © 2003 Wiley-VCH Verlag GmbH & Co. KGaA, Weinheim 

[1] a) H.-J. Zhang, G. T. Tan, V. D. Hoang, N. V. Hung, N. M. Cuong, D. D. Soejarto, J. M. Pezzuto, H. H. S. Fong, *Tetrahedron* **2003**, *59*, 141 – 148; for the isolation of litseaverticillol A, see: b) H.-J. Zhang, G. T. Tan, V. D. Hoang, N. V. Hung, N. M. Cuong, D. D. Soejarto, H. H. S. Fong, J. M. Pezzuto, *Tetrahedron Lett.* **2001**, *42*, 8587 – 8591.

[2] V. D. Hoang, G. T. Tan, H.-J. Zhang, P. A. Tamez, N. V. Hung, N. M. Cuong, D. D. Soejarto, H. H. S. Fong, J. M. Pezzuto, *Phytochemistry* **2002**, *59*, 325 – 329.

[3] For a review of cascade sequences employed in synthesis, as well as a discussion of examples of biomimetic variants that give racemic natural products from achiral precursors, see: K. C. Nicolaou, T. Montagnon, S. A. Snyder, *Chem. Commun.* **2003**, 551 – 564.

[4] a) H. H. Wasserman, R. W. Murray, *Singlet Oxygen*, Academic Press, New York, **1979**, pp. 287 – 427; for recent reviews, see: b) M. Stratakis, M. Orfanopoulos, *Tetrahedron* **2000**, *56*, 1595 – 1615; c) E. L. Clennan, *Tetrahedron* **2000**, *56*, 9151 – 9179.

[5] N. Hayashi, H. Komae, S. Eguchi, M. Nakayama, S. Hayashi, T. Sakao, *Chem. Ind.* **1972**, 572.

[6] For other singlet-oxygen oxidations of furans in natural products synthesis, see: a) J. A. Marshall, G. S. Bartley, E. M. Wallace, *J. Org. Chem.* **1996**, *61*, 5729 – 5735; b) M. R. Kernan, D. J. Faulkner, *J. Org. Chem.* **1988**, *53*, 2773 – 2776; c) G. C. M. Lee, E. T. Syage, D. A. Harcourt, J. M. Holmes, M. E. Garst, *J. Org. Chem.* **1991**, *56*, 7007 – 7014; d) R. Shiraki, A. Sumino, K. Tadano, S. Ogawa, *J. Org. Chem.* **1996**, *61*, 2845 – 2852.

[7] S. F. Martin, K. J. Barr, D. W. Smith, S. K. Bur, *J. Am. Chem. Soc.* **1999**, *121*, 6990 – 6997.

[8] a) M. M. Kayser, L. Breau, S. Eliev, P. Morand, H. S. Ip, *Can. J. Chem.* **1986**, *64*, 104 – 109; b) A. W. Johnson, G. Gowda, A. Hassanali, S. Knox, Z. Monaco, Z. Razavi, G. Rosebery, *J. Chem. Soc. Perkin Trans. 1* **1981**, 1734; c) F. V. D. Ohe, R. Brückner, *New J. Chem.* **2000**, *24*, 659 – 669.

[9] a) H. Minato, T. Nagasaki, *J. Chem. Soc. C* **1966**, 377; b) C. W. Jefford, A. W. Sledeski, J.-C. Rossier, J. Boukouvalas, *Tetrahedron Lett.* **1990**, *31*, 5741 – 5744.

[10] C. Domínguez, A. G. Csáky, J. Plumet, *Tetrahedron Lett.* **1990**, *31*, 7669 – 7670.

[11] a) S. Al-Busafi, J. R. Doncaster, M. G. B. Drew, A. C. Regan, R. C. Whitehead, *J. Chem. Soc. Perkin Trans. 1* **2002**, 476 – 484; b) J. A. Hirsch, A. J. Szur, *J. Heterocycl. Chem.* **1972**, *9*, 523.

[12] C. S. Foote, M. T. Wuesthoff, S. Wexler, I. G. Burstain, R. Denny, G. O. Schenck, K. H. Schulte-Elte, *Tetrahedron* **1967**, *23*, 2583 – 2599.

[13] For a mechanistic work, see: E. L. Clennan, M. E. Mehrsheikh-Mohammadi, *J. Am. Chem. Soc.* **1984**, *106*, 7112 – 7118.

[14] K. Gollnick, A. Griesbeck, *Angew. Chem.* **1983**, *95*, 751; *Angew. Chem. Int. Ed. Engl.* **1983**, *22*, 726 – 727.

[15] For a review about the regioselectivity and stereoselectivity of the singlet-oxygen-ene reaction, see: M. Prein, W. Adam, *Angew. Chem.* **1996**, *108*, 519 – 538; *Angew. Chem. Int. Ed. Engl.* **1996**, *35*, 477 – 494.

[16] L. M. Stephenson, M. J. Grdina, M. Orfanopoulos, *Acc. Chem. Res.* **1980**, *13*, 419 – 425.

[17] M. Stratakis, R. Nencka, C. Rabalakos, W. Adam, O. Krebs, *J. Org. Chem.* **2002**, *67*, 8758 – 8763.

[18] W. C. Greene, M. B. Peterlin, *Nat. Med.* **2002**, *8*, 673 – 680.


 © 2003 Wiley-VCH Verlag GmbH & Co. KGaA, Weinheim 

Solid-State Reactions

# Polymerization by Insertion of Molecular Oxygen into Crystals of 7,7,8,8-Tetrakis(ethoxycarbonyl)quinodimethane

*Shinji Nomura, Takahito Itoh,* Masaki Ohtake, Takahiro Uno, Masataka Kubo, Atsushi Kajiwara, Kazuki Sada, and Mikiji Miyata*

Polymerizations in crystals lead to polymers with highly controlled structures because of the structural restraints of the crystal lattice, and thus, they are promising methods for controlling polymer structures. However, it is still difficult to predict and control the polymerization properties of compounds in the crystal, because the arrangements of the monomers play a significant role. In particular, the monomers that undergo topochemical polymerizations, such as derivatives of 2,5-distyrylpyrazines[1] and diacetylenes,[2] triacetylenes,[3] dienes,[4] and quinodimethanes,[5] are known to have strict requirements for the monomer arrangements in the crystal. Therefore, the investigation of the crystal structures of monomers related to those that undergo solid-state polymerizations should enable us to control the reactivities of the monomers and provide us with models for the reaction pathway of the polymerization reactions.

Molecular oxygen is a well-known oxidizing agent in organic chemistry,[6] and in polymer chemistry it acts as an inhibitor and a retarder of radical polymerizations. Sometimes it can be incorporated as a comonomer to afford copolymers.[7] Until now, solution polymerizations of vinyl monomers[8] such as styrene, methyl methacrylate, vinylnaphthalene, α-methylstyrene, and unsubstituted quinodimethane[9] with oxygen afforded random copolymers. More recently, it was reported that solid-state polymerizations of dibenzofulvene[10] and alkyl sorbate[11] under air and oxygen produce a random copolymer and an alternating copolymer, respectively. However, this work did not report crystal

[*] Prof. Dr. T. Itoh, S. Nomura, M. Ohtake, Dr. T. Uno, Dr. M. Kubo
Department of Chemistry for Materials
Faculty of Engineering
Mie University
1515 Kamihama-cho, Tsu-shi, Mie 514-8507 (Japan)
Fax: (+81) 59-231-9410
E-mail: itoh@chem.mie-u.ac.jp

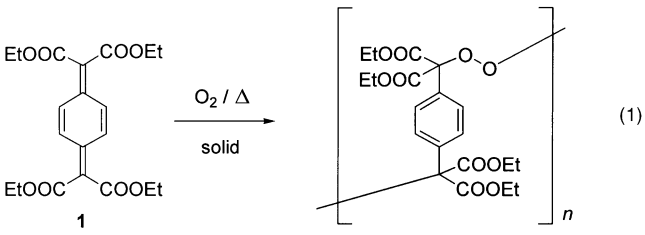
Dr. A. Kajiwara
Department of Materials Science
Nara University of Education
Takabatake-cho, Nara 630-8528 (Japan)

Dr. K. Sada
Department of Chemistry and Biochemistry
Graduate School of Engineering
Kyushu University
6-10-1 Hakozaki, Higashi-ku, Fukuoka 812-8581 (Japan)

Prof. Dr. M. Miyata
Department of Material and Life Science
Graduate School of Engineering
Osaka University and Handai FRC
2-1 Yamadaoka, Suita, Osaka 565-0871 (Japan)

 © 2003 Wiley-VCH Verlag GmbH & Co. KGaA, Weinheim DOI: 10.1002/anie.200352355 

structures of the monomers suitable for copolymerization with molecular oxygen. In this communication we describe how 7,7,8,8-tetrakis(ethoxycarbonyl)quinodimethane (**1**) copolymerizes with molecular oxygen in the solid state to give a highly crystalline alternating copolymer [Eq. (1)]. An X-ray crystallographic study shows that the unique arrangement of **1** in the crystal is conducive to copolymerization with molecular oxygen.




(1)

Monomer **1** was prepared according to the method reported previously.[5] Knoevenagel condensation of 1,4-cyclohexanedione with diethyl malonate using titanium tetrachloride and pyridine as a dehydrating system[12] afforded 1,4-[bis(ethoxycarbonyl)methylene]cyclohexane (**2**) (43% yield). Oxidation of **2** with activated manganese dioxide in benzene heated at reflux gave **1** (34% yield), which was recrystallized from hexane to afford yellow needles. Crystals of **1** were polymerized under air or in vacuo by irradiation with a high-pressure Hg lamp at room temperature, or by heating in the dark. When crystals of **1** were exposed to UV light at 34 °C in air for 25 h, or heated at 60 °C in air for 24 h, polymers formed as white needlelike solids in 16% and quantitative yields, respectively (entries 1 and 4 in Table 1). In contrast, **1** did not polymerize in vacuo with irradiation or heating, or under air but in the dark and not heated, and **1** was recovered quantitatively (entries 2, 3, and 5 in Table 1). Therefore, polymer formation upon irradiation with UV light is due to photoinitiation, not to thermal initiation. These results strongly suggest the participation of oxygen in the polymerizations. To clarify role of oxygen, thermal polymerizations of **1** in the solid state at 60 °C were performed in the presence of oxygen and in the presence of nitrogen (entries 6 and 7 in Table 1). Monomer **1** polymerized only in the presence of oxygen to give a polymer in quantitative yield as a white needlelike solid. This indicates that oxygen truly participates in both thermal polymerizations and photopolymerizations in the solid state.

***Table 1:*** Thermal polymerizations and photopolymerizations of **1** in the solid state, and thermal polymerization of **1** in benzene.

| Entry | Amount of **1** [mg] | Light source | Atm. | $T$ [°C] | $t$ [h] | Conv. [%] | $M_n \times 10^3$[b] |
|---|---|---|---|---|---|---|---|
| 1 | 20.4 | Hg lamp | air | 34 | 25 | 16 | 1.5 |
| 2 | 21.0 | Hg lamp | vacuo | 34 | 25 | 0 | |
| 3 | 11.1 | dark | air | 35 | 24 | 0 | |
| 4 | 10.5 | dark | air | 60 | 24 | 100 | 18 |
| 5 | 10.1 | dark | vacuo | 60 | 24 | 0 | |
| 6 | 10.9 | dark | $N_2$ | 60 | 15 | 0 | |
| 7 | 11.4 | dark | $O_2$ | 60 | 15 | 100 | 18 |
| 8[a] | 370 | dark | vacuo | 60 | 50 | 72 | 2.5 |

[a] Solution-phase polymerization in benzene (1 mL) initiated by AIBN (5.1 mg). [b] Determined by GPC measurement with THF as the eluent and standard polystyrene as the reference.

The white needlelike solids obtained by the thermal polymerization of **1** in the solid state at 60 °C (entry 4 in Table 1) were characterized by $^1$H and $^{13}$C NMR and IR spectroscopy, GPC, elemental analysis, and powder X-ray diffraction. The data were also compared with those of the polymer obtained from the solution polymerization initiated by α,α′-azobisisobutyronitrile (AIBN; entry 8 in Table 1). Number-average molecular weights ($M_n$) of the products obtained by the solid-state polymerization and by the solution polymerization were 18000 and 2500, respectively. The solid-state polymerization produced higher-molecular-weight polymer than the solution polymerization. A characteristic absorption band at 1540 cm$^{-1}$ assigned to the exocyclic conjugated C=C bond of **1** was absent in the IR spectra of both polymers, signals arising from the C=C bond of the ring were observed at 1486, 1445, and 1369 cm$^{-1}$, and a signal arising from the out-of-plane deformation of the *para*-disubstituted benzene was observed at 852 cm$^{-1}$. The changes in the IR spectrum observed in the solid-state polymerization of **1** lend support to the proposition that this reaction follows the conventional mode observed for substituted quinodimethane molecules: the polymerization takes place at the disubstituted exomethylene carbon atoms with formation of the corresponding stable aromatic structure.[13]

The $^1$H NMR peak at $\delta = 7.53$ ppm assigned to the phenylene protons of the polymer obtained by the thermal solid-state polymerization was observed at a lower field than the corresponding one ($\delta = 6.70$ ppm) of the polymer obtained by the solution polymerization. In the $^{13}$C NMR spectrum the peak at $\delta = 89.4$ ppm assigned to the quaternary carbon atom in the solid-state polymerization polymer was observed 19 ppm further downfield than the corresponding signal ($\delta = 70.0$ ppm) in the solution-phase polymerization polymer (Figure 1).

These deshieldings observed in the NMR spectra indicate the presence of electron-withdrawing groups such as oxygen atoms next to the units of **1** in the polymer. The elemental analysis of the polymer obtained from the solid-state polymerization (H 5.62, C 56.42) is not in good agreement with the found data for the homopolymer of **1** obtained from the solution polymerization (H 6.10, C 60.89), but is in good agreement with the figures calculated for the alternating copolymer of **1** with oxygen (H 5.70, C 56.60).

The thermogravimetric analysis (TGA) measurements showed that the solution-phase polymerization polymer begins to decompose at 217 °C, but the solid-state polymerization polymer shows a two-stage decomposition and begins to decompose already at 111 °C. The weight loss from 111 to 150 °C amounts to 17%, which corresponds approximately to the loss of an ethoxycarbonyl group from each unit of **1**. Upon heating the polymer obtained in the solid-state polymerization at 150 °C for 15 min, 1,4-bis(ethoxalyl)benzene (18% yield) was isolated. These results indicate that the polymer has thermally degradable bonds, which are reasonably assumed to be peroxide groups. It is concluded from the

 © 2003 Wiley-VCH Verlag GmbH & Co. KGaA, Weinheim 

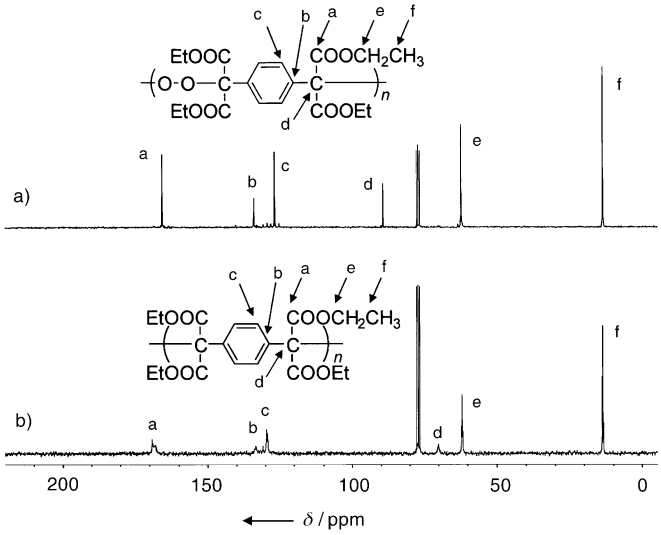



***Figure 1.*** $^{13}C$ NMR spectra (in $CDCl_3$) of the polymers of **1** obtained from a) the solid-state polymerization under air and b) the solution-phase polymerization.

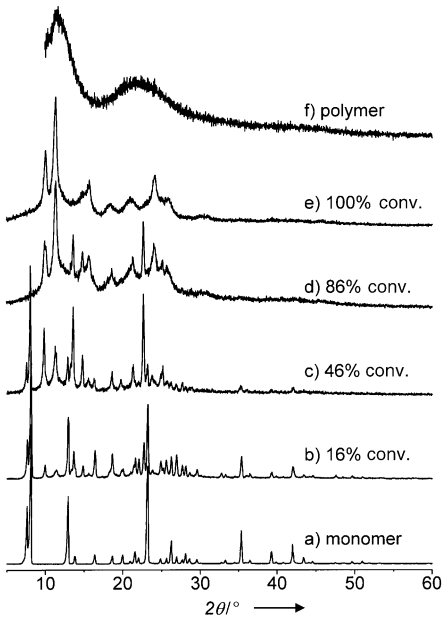



***Figure 2.*** Powder X-ray diffraction patterns for a) monomer **1**, aliquots from the solid-state polymerization at b) 16% conversion, c) 46% conversion, d) 86% conversion, and e) 100% conversion, and f) reprecipitated polymer.

analysis results that the polymer produced in the solid-state polymerization under air and oxygen is a completely alternating copolymer of **1** with oxygen molecules. This is the first example for the alternating copolymerization of quinodimethanes with molecular oxygen in the solid state.

Thermal polymerization of **1** in the solid state under air was investigated by ESR spectroscopy. When crystals of **1** were heated in air at 62 °C, the ESR spectrum showed a broad triplet at a *g*-value of 2.0030 with a coupling constant of 5.0 G due to the two equivalent *ortho* hydrogens ($H^a$) of the phenylene group, which strongly supports the bis(ethoxycarbonyl)benzyl structure of the propagating radical. Thus, this indicates that polymerization reaction takes place at the disubstituted exomethylene carbon atoms and proceeds through a radical mechanism, and that the propagating species is a bis(ethoxycarbonyl)benzyl radical. The radical concentration in the polymerization reaction, $6.9 \times 10^{-5}$ mol kg$^{-1}$ in 1 h, was evaluated by using 4-hydroxy-2,2,6,6-tetramethyl-1-piperidinyloxy as a standard, and was kept as high as $2.3 \times 10^{-5}$ mol kg$^{-1}$ in 24 h after even 100% conversion. This indicates that a long-lived radical is formed in this solid-state polymerization because of immobility of the polymer chain produced.

The powder X-ray diffraction (XRD) patterns of monomer **1**, reaction mixtures at conversions of 16%, 46%, and 86%, the polymer of **1** obtained at complete conversion by thermal polymerization in the solid state under air, and the polymer of **1** reprecipitated from chloroform–hexane are shown in Figure 2. The relatively sharp diffraction patterns of the reaction mixtures at conversions of 46% and 86%, and even at 100% conversion indicate that the monomer **1** maintains crystallinity during and after completion of the polymerization. However, there are no significant peaks in the powder XRD patterns of the reprecipitated polymer, which implies that it is amorphous (Figure 2 f). This indicates that the thermal polymerization of **1** in the solid state proceeds under the influence of the crystal lattice to form an alternating copolymer with a highly ordered structure.

To clarify the steric requirement of the polymerization, we investigated the crystal structure of **1** by X-ray crystallography.[15] In the crystal structure of **1**, the molecules form a one-dimension column by the stacking of the quinodimethane rings along the crystallographic *c* axis (Figure 3). The stacking axes are nearly perpendicular to the plane of the quinodimethane ring, and the stacked molecules are rotated successively by 60°. The face-to-face distance between units of **1** in

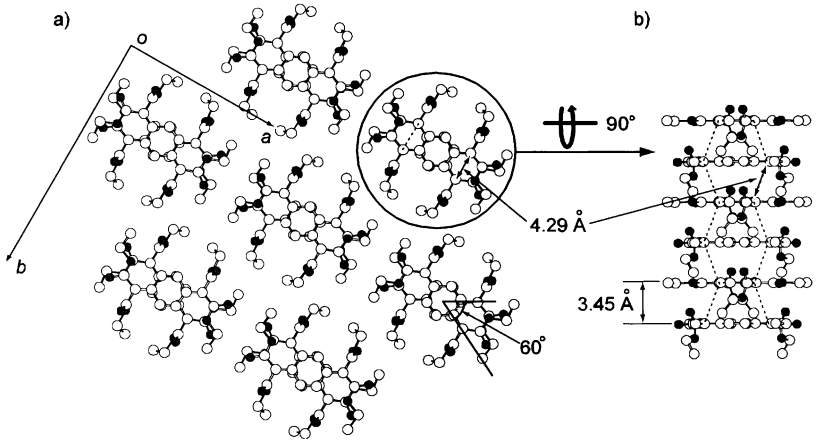



***Figure 3.*** Crystal structure of **1** a) viewed down the crystallographic *c* axis and b) viewed down the crystallographic *b* axis. Hydrogen atoms are omitted for clarity. Open and filled circles represent carbon and oxygen atoms, respectively.

 © 2003 Wiley-VCH Verlag GmbH & Co. KGaA, Weinheim 

the stacked column is 3.45 Å, which corresponds to the π–π stacking distance of the aromatic rings.[14] The distance between the reacting exomethylene carbon atoms in the column is 4.29 Å. This packing of molecules of **1** in the crystal is quite different from that found for the methyl analogue, which undergoes topochemical polymerization.[5] Therefore, monomer **1** does not undergo homopolymerization in the solid state by thermal and photoinitiation due to the different packing mode in the crystals.

Instead, **1** copolymerizes with molecular oxygen. Molecular oxygen normally exists as a triplet (i.e. a diradical) in its ground state with a bond length of 1.21 Å, which is much shorter than the distance between the reacting exomethylene carbon atoms (4.29 Å) and also the face-to-face distance between the quinodimethane rings (3.45 Å). A dioxygen unit may act as a hinge to bind neighboring quinodimethane molecules at their exomethylene carbon atoms. These distances are just suitable for the insertion of oxygen into the polymer chains to yield copolymers. The reaction mechanism (polyaddition or chain reaction) is not clear at present and more experimental data are needed.

In conclusion, we described the first example of the solid-state alternating copolymerization of **1** with oxygen molecules, which leads to highly crystalline needlelike white solids by means of a radical mechanism. No thermal or photo solid-state polymerizations of **1** in vacuo were observed, which was explained by the lack of structural prerequisites for topochemical polymerization. In crystals of **1** the crystal packing is suitable for insertion of oxygen diradicals between the bis(ethoxycarbonyl)benzyl radicals. Detailed studies on the application of this peroxide polymer, the reaction mechanism of the polymerization, and the crystal structures and polymerization reactivities of other substituted quinodimethanes are now in progress.

## Experimental Section

**2**: Compound **2** was synthesized from 1,4-cyclohexanedione and diethyl malonate by the same procedure reported previously[5]: white needles by recrystallization from hexane (43% yield); m.p. 59–60°C; IR (KBr): $\nu = 2940$ (CH), 1688 (C=O), 1610 (C=C), 1232 and 1050 $cm^{-1}$ (C–O); UV/Vis ($CH_3CN$): 215 ($\varepsilon = 1.75 \times 10^4$) nm; $^1H$ NMR (270 MHz, $CDCl_3$, TMS): $\delta = 4.26$ (q, $J = 7.26$ Hz, 8H, $CH_2$), 2.76 (s, 8H, $CH_2$), 1.29 ppm (t, $J = 7.26$ Hz, 12H, $CH_3$); $^{13}C$ NMR (67.7 MHz, $CDCl_3$, TMS): $\delta = 165.2$ (C=O), 157.7 (>C<), 123.5 (>C<), 61.1 ($CH_2$), 29.4 ($CH_2$), 14.1 ppm ($CH_3$); elemental analysis calcd for $C_{20}H_{28}O_8$: H 7.12, C 60.59, O 32.29; found: H 7.03, C 59.85, O 33.12.

**1**: A solution of compound **2** (678 mg, 1.71 mmol) in benzene (50 mL) was added in one portion to activated manganese dioxide (5.42 g) and molecular sieves 4 Å (2.84 g) in benzene (350 mL) at reflux. After the reaction mixture had been stirred for 15 min at reflux, the activated manganese dioxide and molecular sieves were removed by filtration and the solvent was removed by evaporation under reduced pressure. The crude yellow solids were purified by column chromatography ($SiO_2$, chloroform) followed by recrystallization from hexane to give **1** as yellow needles (225 mg, 34%): m.p. 72–73°C; IR (KBr): $\nu = 2938$ (CH), 1690 (C=O), 1639 (C=C), 1542 (C=C), 1209, and 1044 $cm^{-1}$ (C–O); UV/Vis ($CH_3CN$): 360 ($\varepsilon = 5.75 \times 10^4$) nm; $^1H$ NMR (270 MHz, $CDCl_3$, TMS): $\delta = 7.45$ (s, 4H, CH), 4.32 (q, $J = 7.26$ Hz, 8H, $CH_2$), 1.33 ppm (t, $J = 7.26$ Hz, 12H, $CH_3$); $^{13}C$ NMR (67.7 MHz, $CDCl_3$, TMS): $\delta = 164.7$ (C=O), 138.8 (>C<), 130.0 (CH), 126.1 (>C<), 61.7 ($CH_2$), 14.0 ppm ($CH_3$); elemental analysis calcd for $C_{20}H_{24}O_8$: H 6.16, C 61.22, O 32.62; found: H 6.15, C 60.77, O 33.08.

Polymerization: A given amount of **1** (see Table 1) was put in a Pyrex ampoule, which was sealed either without degassing (in air) or with degassing under reduced pressure (in vacuo). Thermal polymerizations were carried out by setting the ampoule in an oil bath at 35 or 60°C for a given time. The conversion was determined by removing an aliquot from the reaction system after a certain reaction time, dissolving it in $CDCl_3$, and recording the $^1H$ NMR spectrum. The conversion was calculated from the ratio of the peak area at $\delta =$ 7.45 ppm due to quinonoid structure of **1** to that at $\delta = 7.53$ ppm due to the phenylene group of polymer. Photopolymerizations were carried out at 34°C under UV irradiation by using a high-pressure mercury lamp (Fuji Glass Work Type HB-400, 400 W) at a distance of 12 cm. Conversion was determined by the same procedure as that described above.

Received: July 11, 2003 [Z52355]

**Keywords:** oxygen · polymerization · quinodimethanes · solid-state reactions · structure elucidation

[1] a) M. Hasegawa, *Chem. Rev.* **1983**, *83*, 507–518; b) M. Hasegawa, *Adv. Phys. Org. Chem.* **1995**, *30*, 117–171.

[2] a) G. Z. Wegner, *Z. Naturforsch. B* **1969**, *24*, 824–832; b) G. Wegner, *Pure Appl. Chem.* **1977**, *49*, 443–454; c) V. Enkelmann, *Adv. Polym. Sci.* **1984**, *63*, 91–131; d) T. Ogawa, *Prog. Polym. Sci.* **1995**, *20*, 943–985.

[3] a) J. Kiji, J. Kaiser, J. G. Wegner, R. C. Schulz, *Polymer* **1973**, *14*, 433–439; b) V. Enkelmann, *Chem. Mater.* **1994**, *6*, 1337–1340; c) J. Xiao, M. Yang, J. W. Lauher, F. W. Fowler, *Angew. Chem.* **2000**, *112*, 2216–2219; *Angew. Chem. Int. Ed.* **2000**, *39*, 2132–2135; d) T. Hoang, J. W. Lauher, F. W. Fowler, *J. Am. Chem. Soc.* **2002**, *124*, 10656–10657.

[4] a) A. Matsumoto, T. Matsumura, S. Aoki, *Macromolecules* **1996**, *29*, 423–432; b) A. Matsumoto, K. Yokoi, S. Aoki, K. Tashiro, T. Kamae, M. Kobayashi, *Macromolecules* **1998**, *31*, 2129–2136; c) A. Matsumoto, K. Katayama, T. Odani, K. Oka, K. Tashiro, S. Saragami, S. Nakamoto, *Macromolecules* **2000**, *33*, 7786–7792; d) A. Matsumoto, K. Sada, K. Hashiro, M. Miyata, T. Tubouchi, T. Tanaka, T. Odani, S. Nagahara, T. Tanaka, K. Inoue, S. Saragai, S. Nakamoto, *Angew. Chem.* **2002**, *114*, 2612–2615; *Angew. Chem. Int. Ed.* **2002**, *41*, 2502–2505; e) A. Matsumoto, T. Tashiro, T. Tsubouchi, K. Tashiro, S. Saragai, S. Nakamoto, *J. Am. Chem. Soc.* **2002**, *124*, 8891–8902.

[5] T. Itoh, S. Nomura, T. Uno, M. Kubo, K. Sada, M. Miyata, *Angew. Chem.* **2002**, *114*, 4482–4485; *Angew. Chem. Int. Ed.* **2002**, *41*, 4306–4309.

[6] H. O. House, *Modern Synthetic Reactions*, W. A. Benjamin, California, **1972**, pp. 337–352.

[7] a) G. Odian, *Principles of Polymerization*, Wiley, New York, **1991**, pp. 259–266; b) V. A. Bhanu, K. Kishore, *Chem. Rev.* **1991**, *91*, 99–116.

[8] a) R. E. Cais, F. A. Bovey, *Macromolecules* **1977**, *10*, 169–178; b) T. Mukundan, K. Kishore, *Macromolecules* **1987**, *20*, 2382–2385; c) T. Mukundan, K. Kishore, *Macromolecules* **1989**, *22*, 4430–4433; d) J. Jayaseharan, K. Kishore, *Macromolecules* **1997**, *30*, 3959–3964.

[9] L. A. Errede, S. L. Hopwood, Jr., *J. Am Chem. Soc.* **1957**, *20*, 6507–6510.

[10] T. Nakano, O. Nakagawa, T. Yade, Y. Okamoto, *Macromolecules* **2003**, *36*, 1433–1435.

[11] a) A. Matsumoto, Y. Ishizu, K. Yokoi, *Macromol. Chem. Phys.* **1998**, *199*, 2511–2516; b) A. Matsumoto, H. Higashi, *Macromolecules* **2000**, *33*, 1651–1655.

 © 2003 Wiley-VCH Verlag GmbH & Co. KGaA, Weinheim 

[12] W. Lehnert, *Tetrahedron* **1973**, *29*, 635 – 638.
[13] T. Itoh, *Prog. Polym. Sci.* **2001**, *26*, 1019 – 1059.
[14] a) T, Dahl, *Acta Chem. Scand. Ser. A* **1988**, *42*, 1 – 7; b) J. H. Williams, J. K. Cockcroft, J. K. Fitch, *Angew. Chem.* **1992**, *104*, 1666 – 1669; *Angew. Chem. Int. Ed. Engl.* **1992**, *31*, 1655 – 1657; c) G. W. Coates, A. R. Dunn, L. M. Henling, J. W. Ziller, E. B. Lobkovsky, R. H. Grubbs, *J. Am. Chem. Soc.* **1998**, *120*, 3641 – 3649.
[15] Crystal structure data for **1** (single crystal from isopropyl ether): $C_{10}H_{12}O_4$, $M_r = 196.20$, crystal dimensions $0.15 \times 0.30 \times 0.10$ mm, orthorhombic, space group *Iba*2 (no. 45), $a = 13.483(2)$, $b = 21.392(3)$, $c = 6.8956(9)$ Å, $\alpha = 90°$, $\beta = 90°$, $\gamma = 90°$, $V = 1988.9(5)$ Å$^3$, $Z = 8$, $\rho_{calcd} = 1.310$ g cm$^{-3}$, $2\theta_{max} = 136.3°$, Rigaku RAXIS-RAPID Imaging Plate diffractometer ($Cu_{K\alpha}$, $\lambda = 1.54178$ Å, graphite monochromator), $\omega$ scans, $T = 296$ K, 860 measured reflections, all 832 independent reflections used in the refinement, Lorenz and polarization factors were applied, $\mu = 8.56$ cm$^{-1}$. Structure solution and refinement: direct methods (SIR92), full-matrix least-squares refinement of $F^2$, 127 parameters, all non-hydrogen atoms were refined anisotropically, and hydrogen atoms were located in ideal positions without further refinement, $R_1 = 0.072$, $R = 0.291$, $Rw = 0.156$, GOF = 1.56, $\Delta\rho_{max} = 0.45$ e Å$^{-3}$, $\Delta\rho_{min} = -0.61$ e Å$^{-3}$. CCDC-214888 (**1**) contains the supplementary crystallographic data for this paper. These data can be obtained free of charge via www.ccdc.cam.ac.uk/conts/retrieving.html (or from the Cambridge Crystallographic Data Centre, 12, Union Road, Cambridge CB2 1EZ, UK; fax: (+44) 1223-336-033; or deposit@ccdc.cam.ac.uk).

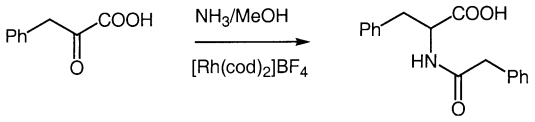
 © 2003 Wiley-VCH Verlag GmbH & Co. KGaA, Weinheim 

Asymmetric Reductive Amination

# Highly Enantioselective Hydrogen-Transfer Reductive Amination: Catalytic Asymmetric Synthesis of Primary Amines**

*Renat Kadyrov* and Thomas H. Riermeier*

Optically active amines are attracting increasing interest in the food, agrochemical, and pharmaceutical industries as building blocks for novel compounds and as templates for asymmetric synthesis. One of the most common methods for preparing amines is the reductive amination of carbonyl compounds.[1] We have successfully explored the rhodium-catalyzed asymmetric reductive amination with hydrogen as the reducing agent.[2] Recently, we developed a highly active and enantioselective catalytic system for the reductive amination of α-keto acids.[3] In the course of our studies we observed that the reaction of phenylpyruvic acid in methanolic ammonia at 60 °C in the presence of a Rh catalyst smoothly furnished *N*-(phenylacetyl)phenylalaninamide [Eq. (1)]. The formation of this product from phenylpyruvic acid and ammonium sulfate proceeds in the absence of a catalyst at a higher temperature (105 °C).[4]




(1)

This observation prompted us to investigate a reductive amination mediated by chiral catalysts under hydrogen-transfer conditions. The reduction of carbonyl compounds to amines with formic acid or formamide is known as the Leuckart–Wallach reaction.[5] Few studies on the use of catalysts in this reaction have been reported in the literature.[6] As part of our ongoing research into the asymmetric hydrogen-transfer reductive amination,[7] we report herein our results from the screening of a variety of catalyst types and describe an effective catalytic system for the production of simple amines with high enantioselectivity.

Two conventional hydrogen sources, isopropyl alcohol and formic acid,[8] were considered. In the reductive amination of acetophenone with ammonia in isopropyl alcohol only $[Rh(C_5Me_5)Cl_2]_2$ demonstrated acceptable activity. In the presence of this catalyst, 1-phenylethylamine (**1**) and 1-phenylethanol (**2**) were produced in 12 h at 70 °C in yields of 30 % and 1 %, respectively. Figure 1 shows the yields determined by GC of **1** and **2** and the enantiomeric excess of **1** in the reaction of acetophenone with ammonium formate for the different Rh, Ir, and Ru complexes that were tested as catalysts. The use of Rh and Ir complexes resulted in poor enantioselectivities under all conditions investigated. Therefore, we concentrated on Ru systems with ammonium formate as the hydrogen donor (Leuckart–Wallach-type reductive amination).

As can be seen in Figure 1, the best enantioselectivities were observed with Ru catalysts with a binap or a tol-binap ligand. The degree of asymmetric induction by both catalysts was evaluated for a number of aryl ketones. The reactions were quenched after 24 h, and the crude reaction mixtures were analyzed directly by HPLC for the *ee* values of the products. The results indicate that the Ru–tol-binap complex gives higher enantioselectivities than the Ru–binap complex (Table 1). As a result of the very broad peaks observed with our fast method of HPLC analysis, we were unable to detect another enantiomer in the reactions represented in entries 2, 3, and 5 of Table 1.

Optimization of the reaction conditions by screening additives was performed with acetophenone in the presence of [((*R*)-tol-binap)$RuCl_2$] (Table 2). Acids were found to accelerate the reaction but to lower the asymmetric induction. The addition of ammonia led to enhancement of the enantioselectivity but a decrease in the reactivity. However, aqueous ammonia was found to increase the yield of the alcohol. The best enantioselectivities were generally observed when 5 to 10 equivalents of $HCOONH_4$ in $NH_3$/methanol (15–25 %) and temperatures between 60 and 85 °C were used.

[*] Dr. R. Kadyrov, Dr. T. H. Riermeier
Degussa AG, Projekthaus Katalyse
Industriepark Höchst, G 830, 65926 Frankfurt/Main (Germany)
Fax: (+49) 69-305-27338
E-mail: renat.kadyrov@degussa.com

[**] We thank Prof. A. Börner, Prof. K.-H. Drauz, Dr. J. Almena, Dr. A. Monsees, and Dr. V. I. Tararov for stimulating and helpful discussions.

 © 2003 Wiley-VCH Verlag GmbH & Co. KGaA, Weinheim DOI: 10.1002/anie.200352503 

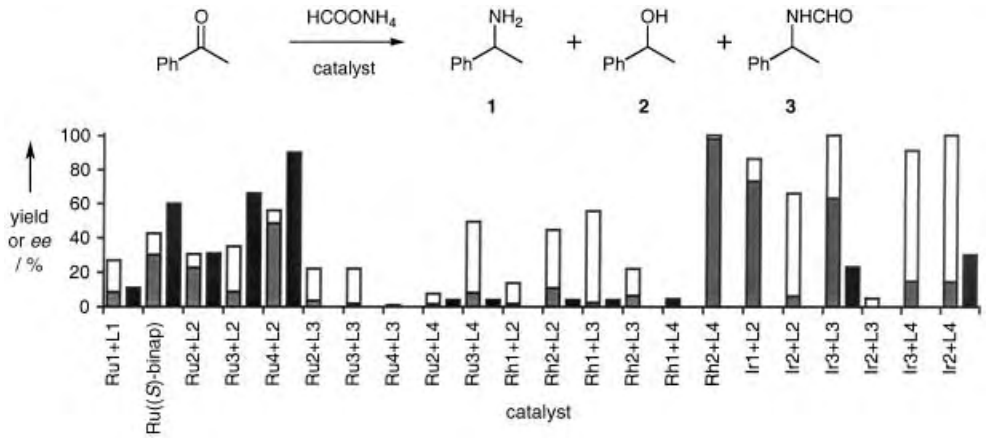



***Figure 1.*** The yields of **1** (shadowed bars) and **2** (white bars), as determined by GC analysis, and the enantiomeric excess of **1** (black bars) after 24 h in the reductive amination of acetophenone (0.5 mmol) with ammonium formate in ammonia solution (15–25%, 1 mL) in methanol at 70°C in the presence of the catalyst indicated (0.5 μmol): Ru1 = $[Ru(DMSO)_4Cl_2]$; Ru2 = $[Ru(cymene)_4Cl_2]_2/2$; Ru3 = $[Ru(PPh_3)_3Cl_2]$; Ru4 = $[Ru(C_4H_7)_2$-(cod)]; Rh1 = $[Rh(cod)_2]OTf$; Rh2 = $[Rh(C_5Me_5)Cl_2]_2/2$; Ir1 = $[Ir(cod)Cl]_2/2$; Ir2 = $[Ir(C_5Me_5)Cl_2]_2/2$; Ir3 = $[Ir(C_8H_{14})_2Cl]_2/2$; L1 = (1*R*,2*R*)-1,2-diaminocyclohexane-*N*,*N*′-bis(2′-diphenylphosphanylbenzoyl); L2 = (*R*)-2,2′-bis(di-*p*-tolylphosphanyl)-1,1′-binaphthyl; L3 = (2*R*,3*R*)-2,3-bis(diphenylphosphanyl)bicyclo[2.2.1]hept-5-ene; L4 = (1*R*,2*R*)-1,2-diphenyl-1,2-ethylenediamine. DMSO = dimethyl sulfoxide; cod = cyclooctadiene; Tf = trifluoromethanesulfonate.

***Table 1:*** Enantioselectivities in the Leuckart–Wallach-type reductive amination of ketones.[a]

| Entry | Ketone | *ee* [%][b] | |
|---|---|---|---|
| | | Catalyst A[c] | Catalyst B[d] |
| 1 | acetophenone | 83 (*S*) | 91 (*R*) |
| 2 | 4′-methylacetophenone | 10 (*R*) | >95 (*R*) |
| 3 | 4′-methoxyacetophenone | 6 (*R*) | >95 (*R*) |
| 4 | 4′-bromoacetophenone | 60 (*S*) | 84 (*R*) |
| 5 | 2-acetylnaphthalene | 90 (*S*) | >95 (*R*) |

[a] Ketone (0.5 mmol), ammonium formate (1 mmol), catalyst (5 μmol), $NH_3$/MeOH (15–20%, 1 mL), 24 h, 70°C. [b] The *ee* values were determined by HPLC analysis. [c] [((*S*)-binap)$RuCl_2$]. [d] [((*R*)-tol-binap)-$RuCl_2$].

***Table 2:*** Effect of additives in the enantioselective Leuckart–Wallach-type reductive amination of acetophenone with [((*R*)-tol-binap)$RuCl_2$] as the catalyst.[a]

| Entry | Additive | Yield [%] | | | *ee* of **1** [%] |
|---|---|---|---|---|---|
| | | **1** | **2** | **3** | |
| 1 | – | 37.3 | 2.9 | 48.0 | 85 |
| 2 | $NH_3$[b] | 15.0 | 2.0 | 17.2 | 90 |
| 3 | $NH_4OH/H_20$[c] | 13.6 | 14.4 | 3.4 | 92 |
| 4 | TsOH[d] | 57.5 | 13.1 | 20.8 | 69 |
| 5 | HCl[d] | 78.9 | 10.8 | 10.3 | 60 |
| 6 | $HBF_4$[d] | 69.7 | 13.7 | 12.1 | 20 |

[a] Acetophenone (0.5 mmol), ammonium formate (2.5 mmol), [((*R*)-tol-binap)$RuCl_2$] (10 μmol), MeOH (1 mL), 10 h, 60°C. The product ratio was determined by GC analysis. [b] $NH_3$/MeOH (20%); [c] Aqueous ammonia (25%, 0.5 mL). [d] Additive: 0.5 mmol.

A series of ketones were examined under the optimized conditions (Table 3). The desired products were formed as the free amines and in their *N*-formylated form. The *N*-formyl derivatives are the main products in the Leuckart–Wallach reductive amination of aromatic ketones.[5b] The amines were obtained in good yields with moderate to high enantioselectivities (86–98% *ee*) after hydrolysis when aromatic ketones were used as substrates. The best asymmetric induction was observed in the reaction of 4′-nitroacetophenone at 60°C (98% *ee*).

In the reaction of 2-octanone under the standard conditions, full consumption of the starting material occurred within 24 h, but only a

***Table 3:*** Enantioselective Leuckart–Wallach-type reductive amination of ketones with [((*R*)-tol-binap)-$RuCl_2$] as the catalyst.[a]

| Entry | Substrate | *t* [h] | Ketone [%] | Amine [%] | Formyl amine [%] | Alcohol [%] | Yield[d] [%] | ee[e] [%] |
|---|---|---|---|---|---|---|---|---|
| 1 | acetophenone | 20 | 5 | 75 | 19 | 1 | 92 | 95 |
| 2 | propiophenone | 21 | 0 | 22 | 78 | 0 | 89 | 95 |
| 3 | 3′-methylacetophenone | 24 | 23 | 38 | 39 | 0 | 74 | 89 |
| 4 | 4′-methylacetophenone | 21 | 0 | 8 | 91 | 0 | 93 | 93 |
| 5 | 4′-methoxyacetophenone | 24 | 3 | 64 | 32 | 1 | 83 | 95 |
| 6 | 4′-chloroacetophenone | 24 | 0 | 6 | 94 | 0 | 93 | 92 |
| 7 | 4′-bromoacetophenone | 48 | 0 | 10 | 90 | 0 | 56 | 91 |
| 8 | 4′-nitroacetophenone | 48 | 0 | 45 | 55 | 0 | 92 | 95[f] |
| 9 | 1-acetylnaphthalene | 30 | 14 | 11 | 69 | 6 | 69 | 86 |
| 10 | 2-acetylnaphthalene | 30 | 0 | 18 | 82 | 0 | 91 | 95 |
| 11 | 2-octanone[b] | 17 | 0 | 36 | 64 | 0 | 44 | 24 (*S*) |
| 12 | 2-methylcyclohexanone[b,c] | 20 | 0 | (33:22) | (32:13) | 0 | 63 (64:36) | 17:64[g] |

[a] For the reaction conditions, see Experimental Section: substrate (5 mmol), ammonium formate (50 mmol), [((*R*)-tol-binap)$RuCl_2$] (1 mol%), 85°C, $NH_3$/MeOH (15–20%, 20 mL). The product ratio was determined by GC analysis. [b] In MeOH (20 mL), without ammonia. [c] *Cis/trans* ratios are given in brackets. [d] Yield of the isolated amine after hydrolysis. [e] Products have the *R* configuration, with the exception of the last two entries. [f] When the reaction was carried out at 60°C, 98% *ee* was observed. [g] *Cis* isomer: 17% *ee*, *trans* isomer: 64% *ee*.

 © 2003 Wiley-VCH Verlag GmbH & Co. KGaA, Weinheim 

trace amount of 2-octylamine was detected. However, a 44% yield of the desired product was isolated with 24% *ee* in the absence of ammonia as additive (Table 3, entry 11). The reductive amination of 2-methylcyclohexanone proceeded well under both sets of conditions. Although the *cis*/*trans* stereoselectivity was not affected by the inclusion of ammonia as an additive, inferior enantioselectivities were observed. Thus, the *cis* isomer was obtained in 9% *ee* and the *trans* isomer in 43% *ee* under the standard reaction conditions, whereas in the absence of ammonia 17% *ee* was observed for the *cis* isomer and 64% *ee* for the *trans* isomer (Table 3, entry 12). Interestingly, a nearly identical *cis*/*trans* ratio of 3:2 was reported for the corresponding Leuckart–Wallach reaction.[9]

In summary, we have developed a new and efficient method for the synthesis of primary amines from ketones in an asymmetric catalytic manner. This method displays a high level of asymmetric induction for aromatic ketones. Ammonia is a crucial parameter in the catalytic system described, in terms of the enantioselectivities observed.

## Experimental Section

[((*R*)-tol-binap)$RuCl_2(DMF)_x$][10] (50 mg, ca. 50 μmol; DMF = dimethylformamide), the ketone (5 mmol), and ammonium formate (3.16 g, 50 mmol) were placed in a 35-mL Ace pressure tube (Aldrich) under argon. Freshly condensed ammonia in dry methanol (20–25%, 20 mL) was added, then the tubes were sealed under argon and stirred at 85 °C for the time indicated. Following evaporation of the volatile components, the residue was dissolved in ethanol (10 mL), and hydrochloric acid (6N, 5 mL) was added. The mixture was then heated at reflux for 1 h to hydrolyze the formyl derivatives, then cooled, diluted with water (10 mL), and extracted with ether to remove any unreacted ketone. The aqueous layer was made alkaline by the addition of ammonia solution (25%, 4 mL), then extracted with dichloromethane (3 × 5 mL). The combined organic extracts were dried over $Na_2SO_4$ and concentrated to afford the crude amine, which was shown to be pure by $^1H$ NMR spectroscopy. The optical purity was determined by GC analysis of the corresponding acetamide on a chiral phase (Chrompack, CP Chirasil-DEX CB), as reported previously.[11]

Received: July 29, 2003 [Z52503]

**Keywords:** amination · amines · asymmetric catalysis · ketones · ruthenium

[1] a) S. Gomez, J. A. Peters, T. Maschmeyer, *Adv. Synth. Catal.* **2002**, *344*, 1037–1057; b) V. A. Tarasevich, N. G. Kozlov, *Russ. Chem. Rev.* **1999**, *68*, 55–72; c) P. N. Rylander, *Hydrogenation Methods*, Academic Press, New York, **1985**, pp. 82–93; d) W. S. Emerson, *Org. React.* **1948**, *4*, 174–255.

[2] V. I. Tararov, R. Kadyrov, T. H. Riermeier, A. Börner, *Chem. Commun.* **2000**, 1867–1868.

[3] R. Kadyrov, T. H. Riermeier, U. Dingerdissen, V. I. Tararov, A. Börner, *J. Org. Chem.* **2003**, *68*, 4067–4070.

[4] H. Yanagawa, Y. Makino, K. Sato, M. Nishizawa, F. Egami, *Origins Life* **1984**, *14*, 163–169.

[5] a) S. Ram, R. E. Ehrenkaufer, *Synthesis* **1988**, 91–95; b) M. L. Moore, *Org. React.* **1949**, *5*, 301–330.

[6] a) M. Kitamura, D. Lee, S. Hayashi, S. Tanaka, M. Yoshimura, *J. Org. Chem.* **2002**, *67*, 8685–8687; b) B. A.Hay (Pfizer Inc.), US 4851548, **1989** [*Chem. Abstr.* **1990**, *112*, 76922]; c) N. Kost, *Nauchn. Dokl. Vyssh. Shk. Khim. Khim. Tekhnol.* **1958**, 125–129 [*Chem. Abstr.* **1959**, *53*, 3112i]; d) N. Kost, I. I. Grandberg, *Zh. Obshch. Khim.* **1955**, *25*, 1432–1437 [*Chem. Abstr.* **1956**, *50*, 4800i]; e) R. Stroh (Farbenfabriken Bayer), DE 861844, **1953** [*Chem. Zentralbl.* **1953**, *5926*]; f) J. F. Bunnett, J. L. Marks, *J. Am. Chem. Soc.* **1949**, *71*, 1587–1589.

[7] A. Börner, U. Dingerdissen, R. Kadyrov, T. H. Riermeier, V. I. Tararov (Degussa AG), DE 10138140, **2001** [*Chem. Abstr.* **2003**, *138*, 189782].

[8] a) R. A. W. Johnstone, A. H. Wilby, I. D. Entwisle, *Chem. Rev.* **1985**, *85*, 129–170; b) H. W. Gibson, *Chem. Rev.* **1969**, *69*, 673–692.

[9] D. S. Noyce, F. W. Bachelor, *J. Am. Chem. Soc.* **1952**, *74*, 4577–4579.

[10] M. Kitamura, M. Tokunaga, T. Ohkuma, R. Noyori, *Org. Synth.* **1993**, *71*, 1–13.

[11] a) E. Fernandez, K. Maeda, M. W. Hooper, J. M. Brown, *Chem. Eur. J.* **2000**, *6*, 1840–1846; b) E. Fernandez, M. W. Hooper, F. I. Knight, J. M. Brown, *Chem. Commun.* **1997**, 173–174.

 © 2003 Wiley-VCH Verlag GmbH & Co. KGaA, Weinheim 

*Enyne Cyclization*

# Addition of Diazoalkanes to Enynes Promoted by a Ruthenium Catalyst: Simple Synthesis of Alkenyl Bicyclo[3.1.0]hexane Derivatives**

*Florian Monnier, Dante Castillo, Sylvie Dérien, Loïc Toupet, and Pierre H. Dixneuf**

Molecular catalysts are currently playing a key role in innovative synthetic methods.[1] They promote the synthesis of complex, useful molecules, through highly simplified pathways that involve the combination of simple substrates and the formation of several consecutive bonds with high selectivity.[2,3] The activation of these molecules under mild

[*] Prof. P. H. Dixneuf, F. Monnier, D. Castillo, Dr. S. Dérien
Institut de Chimie de Rennes, UMR 6509
CNRS-Université de Rennes
Organométalliques et Catalyse
Campus de Beaulieu, 35042, Rennes (France)
Fax: (+33) 2-2323-6939
E-mail: pierre.dixneuf@univ-rennes1.fr
Dr. L. Toupet
Groupe Matière Condensée et Matériaux, UMR 6626
CNRS-Université de Rennes
Campus de Beaulieu, 35042, Rennes (France)

[**] This work was supported by the CNRS and the Ministère de la recherche. The authors are grateful to the latter for a PhD grant to FM and, for additional support, to the European Union through the Cost Program D17, and the Region Bretagne, through a PRIR program (169AOC), and to Institut Universitaire de France for membership (PHD).

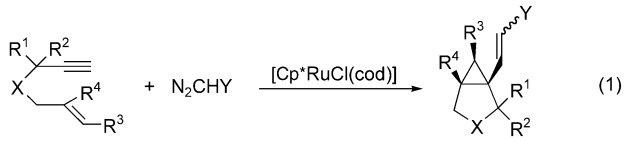
Supporting information for this article is available on the WWW under http://www.angewandte.org or from the author.

 © 2003 Wiley-VCH Verlag GmbH & Co. KGaA, Weinheim DOI: 10.1002/anie.200352477 

conditions are also opening the way to transform stoichiometric reactions into catalytic ones such as the Pauson–Khand[4] or Nicholas[5] reactions. Enynes have recently been at the center of general, useful catalytic transformations. In the presence of alkene metathesis catalysts, they lead to a variety of functional alkenyl cycloalkenes with the 1,3-diene moiety.[6] The research groups of Trost, Murai, and Fürstner have shown that enynes constitute the basis of straightforward routes to bicyclo[3.1.0]hexane[7,8] or bicyclo[4.1.0]heptane[9] derivatives in the presence of $Pd^{II}$ centers,[8] $[RuCl_2L_n]$[7] or $[PtCl_2]$[9–11] catalysts. One aspect that these transformations have in common is the initial electrophilic activation of the triple bond, which favors its coupling with the double bond and leads to either bicyclic alkylidene–metal[7,8] or stabilized by cationic carbenoid resonance [9] intermediates.

Recently, the ruthenium catalyzed double addition of diazoalkanes to alkynes, has offered a direct route to 1,3-dienes.[12] The attempt to apply this reaction to enynes has actually led to the discovery of a new catalytic reaction that contrasts with the above electrophilically initiated transformations of enynes.[7–9]

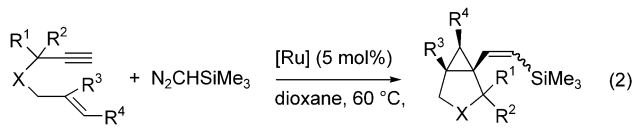
Herein we report the novel one-step reaction of enynes with diazoalkanes, catalyzed by [(Cp*RuCl(cod)] ([Rh]; Cp* = $C_5Me_5$, cod = cyclooctadiene). The reaction involves the selective formation of three C–C bonds including a cyclopropanation step and directly leads to 1-alkenyl bicyclo[3.1.0]hexane derivatives [Eq. (1)]. This highly stereoselective reaction has potential in synthesis as alkenylcyclopropanes easily give access to 5-membered cycles.[13]



(1)

The reaction of enyne **1a** with an excess of trimethylsilyldiazomethane in dioxane in the presence of 5 mol% of [Cp*RuCl(cod)] under inert atmosphere does not lead to the expected diazoalkane carbene double addition to the C≡C bond,[12] but selectively affords the bicyclic 1-alkenyl bicyclo[3.1.0]hexane product **2a** in 70% yield after 24 h at 60 °C and with complete conversion of **1a** [Eq. (2)]. Under the same conditions the enyne **1b** led to **2b,** which was isolated in 85% yield ($Z/E = 3:1$).[14] For the C=C bond disubstituted ether **1c**, the reaction was slower and **2c** was isolated in only 40% yield as a mixture of diastereoisomers (9:1). All compounds **2** formed as a mixture of $Z > E$ isomers but the cyclopropanation is highly stereoselective.

The enynes that contain nitrogen are more reactive. The reaction of **3a** with $N_2CHSiMe_3$ after 1 h at 60 °C led to **4a** in 95% yield ($Z/E = 4:1$) [Eq. (2)] (Ts = *p*-toluenesulfonyl). It is noteworthy that in this case substitutions at the C=C bond in enynes **3b** and **3c** do not affect either reaction time or yield, and the formation of the bicyclo[3.1.0]hexane derivatives **4b** (80%) and **4c** (85%) is observed. In the case of enyne **3b**, the diastereoisomers **4b** (d.r. = 3:1) are formed and had only a *Z* configuration of the C=C bond.



(2)

X = O, 20-48 h

**1a** $R^1$ = Me, $R^2$ = Ph, $R^3$ = $R^4$ = H — **2a** (70%) *Z/E* 10:1

**1b** $R^1$, $R^2$ =-$(CH_2)_5$-, $R^3$ = $R^4$ = H — **2b** (85%) *Z/E* 3:1

**1c** $R^1$, $R^2$ =-$(CH_2)_5$-, $R^3$ = H, $R^4$ = Ph — **2c** (40%) *Z/E* <1:20 (d.r. = 9:1)

X = NTs, 1-2 h

**3a** $R^1$ = $R^2$ = $R^3$ = $R^4$ = H — **4a** (95%) *Z/E* 4:1

**3b** $R^1$ = $R^2$ = $R^3$ = H, $R^4$ = $CH_3$, (E/Z = 85:15) — **4b** (80%) *Z/E* >20:1 (d.r. = 3:1)

**3c** $R^1$ = $R^2$ = $R^4$ = H, $R^3$ = $CH_3$ — **4c** (85%) *Z/E* 9:1

The major diastereoisomer of **4b** was purified by chromatography over silica gel. Crystals of this diastereoisomer that were suitable for X-ray crystal-structure analysis were obtained in a mixture of pentane and diethyl ether (Figure 1.)[15] The structure reveals the relative spacial substituent positions on the cyclopropane moiety: both *Z* trimethylsilylvinyl and methyl groups are *cis* and this observation is confirmed by NMR experiments (hmqc, hmbc, NOESY) for the derivatives **2** and **4**.

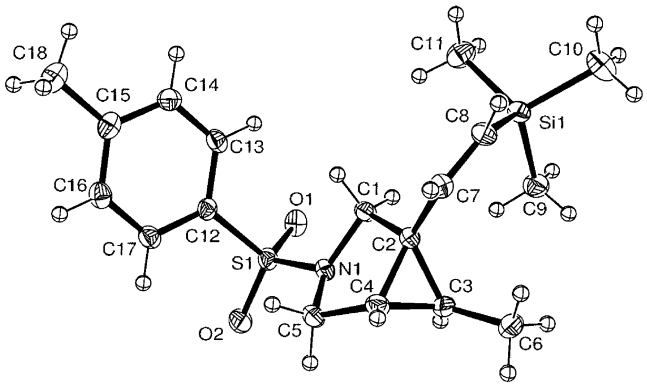
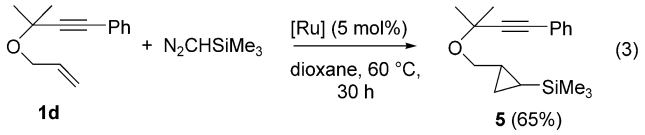



***Figure 1.*** ORTEP drawing of the molecular structure of the major diastereoisomer of **4b**. Thermal ellipsoids are set at the 50% probability level.

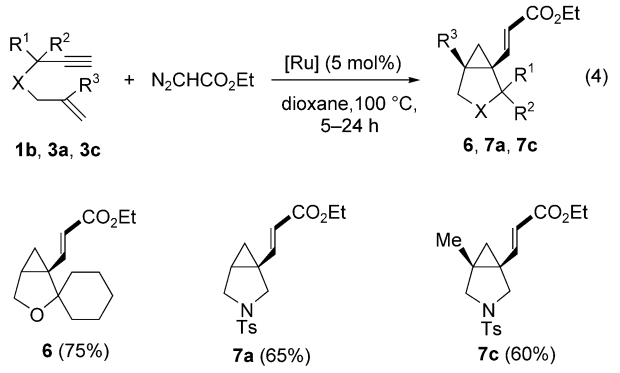
The above catalytic reaction seems general, as it is not inhibited by different substitutions on the C=C bond of the starting enynes. The only observed limitation is related to the disubstituted triple bond of the starting enyne **1d**. In that case, the reaction affords the compound **5**, which results from classical cyclopropanation of the double bond. This result suggests that an enyne with sterically hindered C≡C bond inhibits the coordination of the catalyst to the advantage of the C=C bond [Eq. (3)].

Ethyl diazoacetate and phenyldiazomethane are less reactive than trimethylsilyldiazomethane and require more energetic conditions. Thus, the reaction of **1b, 3a** and **3c** to afford derivatives **6, 7a**, and **7c,** respectively, in yields of 60–

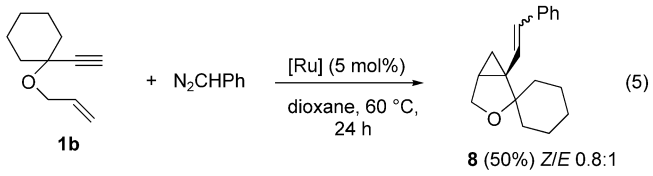
 © 2003 Wiley-VCH Verlag GmbH & Co. KGaA, Weinheim 




75% requires three equivalents of $N_2CHCO_2Et$ in dioxane at 100°C for 5–24 h [Eq. (4)]. Under these conditions the reaction affords exclusively the *E* isomer.



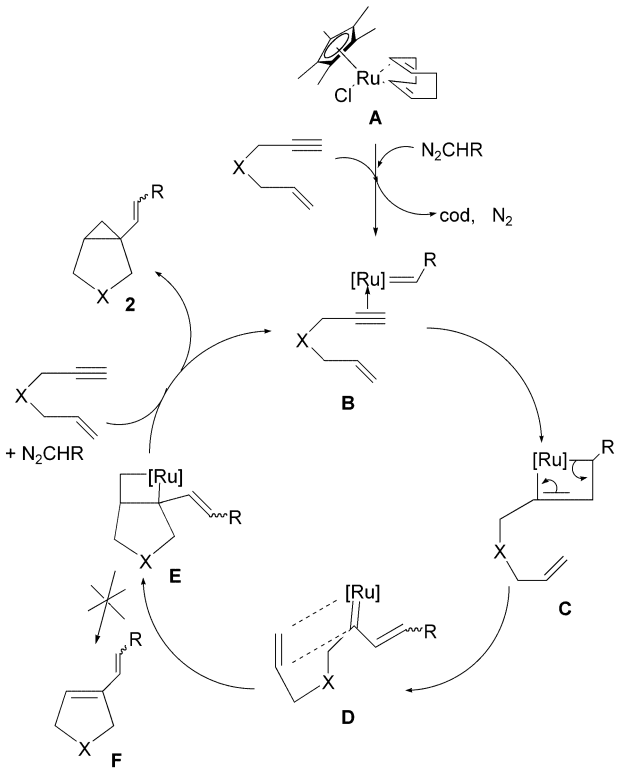

The reaction of **1b** with an excess of $N_2CHPh$ at 60°C in dioxane and after 24 h led to **8** isolated in 50% yield. This relatively low yield is related to the parallel formation of stilbene by decomposition of the phenyldiazomethane [Eq. (5)].




These results show that the catalyst [Cp*RuCl(cod)] selectively transforms 1,6-enynes into 1-alkenyl bicyclo[3.1.0]hexanes and the stereochemistry of the alkene group depends on the nature of the diazoalkane and thus reaction conditions. For the enynes **1a, 1b, 3a** with $N_2CHSiMe_3$ the isomer *Z* is the major product formed at 60°C and $N_2CHCO_2Et$ preferentially leads to the *E* isomer at 100°C.

It is noteworthy that the stoichoimetric reaction of enynes with metal–carbene complexes, $[(OC)_5M{=}C(OR)R^1]$ derivatives of chromium[16] and molybdenum,[17] have been shown to lead to the synthesis of alkenyl bicyclo[3.1.0]hexane derivatives.[18] Thus the above reaction appears to be the first catalytic version of the Hoye–Harvey reaction.[16,17]

The mechanism of the reaction can be explained according to Scheme 1. The initial step is expected to involve the formation of a Ru=CHR moiety from the diazoalkane and its coupling with the alkyne to form **C**, as postulated for the first step of the catalytic double diazoalkane addition to alkyne by




***Scheme 1.*** Catalytic cycle.

the same catalyst,[12] or as shown for the first step of stoichiometric addition of metal carbenes to enyne.[19] This is also supported by the reaction inhibition of disubstituted hindered enyne C≡C bond (**1d** to **5**, [Eq. (3)]). The formation of intermediates **D** and **E** corresponds to alkene and enyne metathesis key steps. The novelty of this catalytic reaction is related to the last step: a promoted reductive elimination from **E** to give **2**, rather than the classical formation of the enyne metathesis product the alkenylcycloalkene **F**. On interaction of ruthenium–carbene moiety with an alkene, this reductive elimination step is favoured[20] probably because of the steric hindrance of the $C_5Me_5$–Ru group, as we showed that [Cp*RuCl(cod)] also catalyzed the same reaction but afforded derivatives of **2** in lower yield.

In the reaction reported here, the diazoalkane carbene, which is known to involve a variety of functional groups, is not involved in the cyclopropane ring but in the pendent chain. Thus, this new reaction leading to alkenyl cyclopropane derivatives has a broad spectrum of applications in synthesis.

## Experimental Section

General procedure for the catalytic synthesis of **2,4–8**: [Cp*RuCl(cod)] (0.0625 mmol, 5 mol%) was added to a solution of enyne (1.25 mmol, 1 equiv) and diazoalkane (2–4 equiv) in 1 mL of degassed dioxane at 60–100°C under an inert atmosphere. The reaction mixture was stirred for between 1 h to 48 h according to the natures of the enyne and diazoalkane. The solvent was then removed under vacuum, and the products were isolated by column chromatography on silica gel to give bicyclic products (1-alkenyl bicyclo[3.1.0]hexane). The yields are based on the enyne. All compounds were fully characterized by spectroscopic methods (see Supporting Informa-

 © 2003 Wiley-VCH Verlag GmbH & Co. KGaA, Weinheim 

tion). Selected data for **7c**: $^1$H NMR (200.131 MHz, $CDCl_3$): $\delta = 0.89$ (d, 1H, $J = 5.3$ Hz, $CH_2$); 1.16 (s, 3H, Me); 1.26 (t, 3H, $J = 7.1$ Hz, $CH_3$) ; 1.29 (d, 1H, $J = 5.3$ Hz, $CH_2$); 2.44 (s, 3H, Me); 2.80 (d, 1H, $J = 9.1$ Hz, $CH_2N$); 3.10 (d, 1H, $J = 9.0$ Hz, $CH_2N$); 3.60 (d, 2H, $J = 9.1$ Hz, $CH_2N$); 4.16 (q, 2H, $J = 7.1$ Hz, $OCH_2$); 5.68 (d, 1H, $J = 15.8$ Hz, = CH); 6.66 (d, 1H, $J = 15.8$ Hz, = CH); 7.34 (d, 2H, $J = 8.0$ Hz, Ph); 7.68 ppm (d, 2H, $J = 8.0$ Hz, Ph). $^{13}$C NMR (50.329 MHz, $CDCl_3$): $\delta = 166.5$, 147.3, 144.2, 133.3, 130.2, 128.1, 120.1, 60.8, 55.1, 51.7, 33.4, 33.3, 23.2, 22.0, 15.8, 14.7. HRMS: *m/z* calcd for ($C_{18}H_{23}NO_4S$) [$M^+$] 349.1347, found 349.1348; FTIR (KBr): $\tilde{\nu} = 2928$, 1707, 1637, 1598 cm$^{-1}$. Elemental analysis calcd (%) for $C_{18}H_{23}NO_4S$: C 61.87, H 6.63; found: C 61.87, H 6.71.

Received: July 25, 2003 [Z52477]

**Keywords:** cyclization · diazo compounds · enynes · heterocycles · ruthenium

[1] a) S. J. Connon, S. Blechert, *Angew. Chem.* **2003**, *115*, 1944; *Angew. Chem. Int. Ed.* **2003**, *42*, 1900; b) B. M. Trost, F. D. Toste, A. B. Pinkerton, *Chem. Rev.* **2001**, *101*, 2067; c) B. Cornils, W. A. Herrmann, *Applied homogeneous catalysis with organometallic compounds*, Wiley-VCH, Weinheim **2002**; d) A. Fürstner, *Topics in Organometallic Chemistry, Vol. 1*, Springer, Heidelberg, **1998**; e) T. Naota, H. Takaya, S. Murahashi, *Chem. Rev.* **1998**, *98*, 2599.

[2] a) B. M. Trost, *Acc. Chem. Res.* **2002**, *35*, 695; b) C. Bruneau, P. H. Dixneuf, *Acc. Chem. Res.* **1999**, *32*, 311; c) C. Bruneau, P. H. Dixneuf, *Chem. Commun.* **1997**, 507.

[3] N. Chatani, A. Kamitani, S. Murai, *J. Org. Chem.* **2002**, *67*, 7014.

[4] a) T. Morimoto, N. Chatani, Y. Fukumoto, S. Murai, *J. Org. Chem.* **1997**, *62*, 3762; b) T. Kondo, N. Suzuki, T. Okada, T. Mitsudo, *J. Am. Chem. Soc.* **1997**, *119*, 6187.

[5] a) K. M. Nicholas, *Acc. Chem. Res.*, **1987**, *20*, 207; b) Y. Nishibayashi, M. Yoshikawa, Y. Inada, M. Hidai, S. Uemura, *J. Am. Chem. Soc.* **2002**, *124*, 11846.

[6] a) S. Imhof, S. Blechert, *Synlett*, **2003**, 609; b) A. Kinoshita, M. Mori, *Synlett*, **1994**, 1020; c) M. Mori, *Topics in Organometallic Chemistry, Vol. 1*, Springer, Heidelberg, **1998**, 133.

[7] a) N. Chatani, T. Morimoto, T. Muto, S. Murai, J . *Am. Chem. Soc.* **1994**, *116*, 6049; b) N. Chatani, K. Kataoka, S. Murai, N. Furukawa, Y. Seki, *J. Am. Chem. Soc.* **1998**, *120*, 9104.

[8] a) B. M. Trost, M. K. Trost, *J. Am. Chem. Soc.* **1991**, *113*, 1850; b) B. M. Trost, A. S. K. Hashmi, *Angew. Chem.* **1993**, *105*, 1130; *Angew. Chem. Int. Ed. Engl.* **1993**, *32*, 1085; c) B. M. Trost, A. S. K. Hashmi, R. G. Ball, *Adv. Synth. Catal.*, **2001**, *343*, 490; d) B. M. Trost, A. S. K. Hashmi, *J. Am. Chem. Soc.* **1994**, *116*, 2183.

[9] A. Fürstner, F. Stelzer, H. Szillat, *J. Am. Chem. Soc.* **2001**, *123*, 11863.

[10] M. Mendez, M. Paz Munoz, C. Nevado, D. J. Cardenas, A. M. Echavarren, *J. Am. Chem. Soc.* **2001**, *123*, 10511.

[11] E. Mainetti, V. Mouriès, L. Fensterbank, M. Malacria, J. Marco-Contelles, *Angew. Chem.* **2002**, *114*, 2236; *Angew. Chem. Int. Ed.* **2002**, *41*, 2132.

[12] J. Le Paih, S. Dérien, I. Özdemir, P. H. Dixneuf, *J. Am. Chem. Soc.* **2000**, *122*, 7400.

[13] a) A. de Meijere, S. I. Kozhushkov, *Chem. Rev.* **2000**, *100*, 93; b) H.-U. Reissig, R. Zimmer, *Chem. Rev.* **2003**, *103*, 1151; c) J. E. Baldwin, *Chem. Rev.* **2003**, *103*, 1197.

[14] The double-bond stereochemistry of all products obtained with trimethylsilyldiazomethane was based on larger coupling constants between the two vinyl protons for the *trans* (18–19 Hz) with respect to the *cis* (14–15 Hz) isomer and was confirmed by X-ray structure of **4b**.

[15] Crystal structure analysis: $SSiNC_{18}H_{27}O_2$, $M_r = 349.56$, monoclinic, $P2_1/a$, $a = 13.5714(2)$, $b = 7.3787(1)$, $c = 19.5966(4)$ Å, $\beta = 104.157(1)°$, $V = 1902.8(1)$ Å$^{-3}$, $Z = 4$, $D_x = 1.220$ Mg.m$^{-3}$, l(MoKα) = 0.71073 Å, $\mu = 2.42$ cm$^{-1}$, F(000) = 752, $T = 120$ K. The sample ($0.25 \times 0.12 \times 0.12$ mm) is studied on a NONIUS Kappa CCD with graphite monochromatized $Mo_{K\alpha}$ radiation. The cell parameters are obtained with Denzo and Scalepack (Otwinowski & Minor , 1997) with ten frames (psi rotation: 1° per frame). The data collection (Nonius, 1999) ($2\theta_{max} = 54°$, 230 frames through 1.8° omega rotation and 20 s per frame, range HKL: H 0.17, K 0.9, L −25.24) gives 27966 reflections. The data reduction with Denzo and Scalepack (Otwinowski and Minor, 1997) leads to 4323 independent reflections from which 3489 with $I > 2.0\sigma(I)$. The structure was solved with SIR-97 (Altomare et al., 1998) which reveals the non hydrogen atoms of the molecule. After anisotropic refinement, many hydrogen atoms may be found with a Fourier Difference. The whole structure was refined with SHELXL97: G. M. Sheldrick, SHELXS-97, Program for the Solution of Crystal Structures, University of Göttingen, Göttingen (Germany), **1997** by the full-matrix least-square techniques (use of F square magnitude; *x, y, z*, $\beta_{ij}$ for Si, S, O, C, and N atoms, *x, y, z* in riding mode for H atoms ; 208 variables and 3489 observations with $I > 2.0\sigma(I)$; calcd $w = 1/[\sigma^2(Fo^2) + (0.098P)^2 + 1.48P]$ in which $P = (Fo^2 + 2Fc^2)/3$ with the resulting $R = 0.050$, $R_w = 0.142$ and $S_w = 1.020$, $\Delta\rho < 0.54$ eÅ$^{-3}$. CCDC 215613 (**4b**) contains the supplementary crystallographic data for this paper. These data can be obtained free of charge via www.ccdc.cam.ac.uk/conts/retrieving.html (or from the Cambridge Crystallographic Data Centre, 12 Union Road, Cambridge CB21EZ, UK; fax: (+44) 1223-336-033; or deposit@ccdc.cam.ac.uk).

[16] a) P. F. Korkowski, T. R. Hoye, D. B. Rydberg, *J. Am. Chem. Soc.* **1988**, *110*, 2676; b) T. R. Hoye, G. M. Rehberg, *J. Am. Chem. Soc.* **1990**, *112*, 2841; c) T. R. Hoye, T. J. Katz, G. X.-Q. Yang, *Tetrahedron Lett.* **1991**, *32*, 5895.

[17] D. F. Harvey, M. F. Brown, *Tetrahedron Lett.* **1991**, *32*, 5253.

[18] More recently such a stoichiometric reaction was observed with [$RuCl_2$(=CHPh)($PCy_3$)(heterocyclic carbene)] and enyne as a side reaction of the catalytic enyne metathesis. In that case the reductive elimination step in the absence of a source of carbene does not allow the regeneration of the ruthenium carbene catalyst. See: T. Kitamura, Y. Sato, M. Mori, *Chem. Commun.* **2001**, 1258.

[19] a) T. J. Katz, T. M. Sivavec, *J. Am. Chem. Soc.* **1985**, *107*, 737; b) T. M. Sivavec, T. J. Katz, M. Y. Chiang, G. X.-Q. Yang, *Organometallics* **1989**, *8*, 1620.

[20] Y. Yamamoto, H. Kitahara, R. Ogawa, H. Kawaguchi, K. Tatsumi, K. Itoh, *J. Am. Chem. Soc.* **2000**, *122*, 4310.

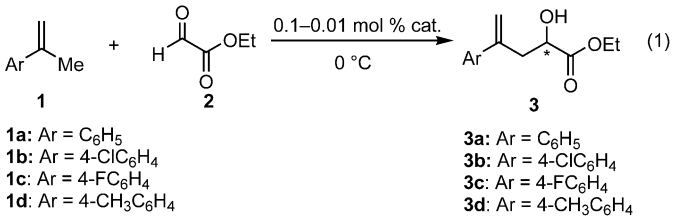
 © 2003 Wiley-VCH Verlag GmbH & Co. KGaA, Weinheim 

*Catalytic Carbonyl-Ene Reaction*

# Quasi Solvent-Free Enantioselective Carbonyl-Ene Reaction with Extremely Low Catalyst Loading**

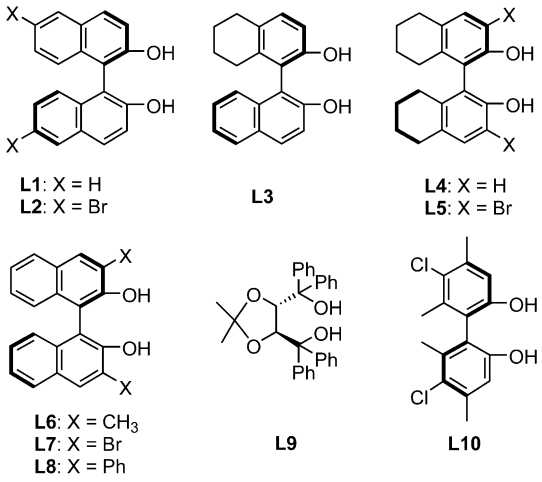
*Yu Yuan, Xue Zhang, and Kuiling Ding**

Asymmetric catalysis of organic reactions to provide enantiomerically enriched products is of central importance to modern synthetic and pharmaceutical chemistry.[1] The development of chiral catalysts for the enantioselective carbon–carbon bond-forming reactions is a fundamental topic in asymmetric catalysis.[1] However, many currently accessible methods are impractical, for example, in terms of efficiency and environmental considerations.[2] Therefore the development of truly efficient and practical synthesis has been one of the greatest challenges for synthetic chemists. As part of our continuing effort in this area,[3] we report in this communication the first quasi solvent-free enantioselective carbonyl-ene reaction. The reaction of ethyl glyoxylate with a variety of olefins could be carried out with 0.1–0.01 mol % of catalysts to give α-hydroxy esters in good to excellent yields and up to 99 % *ee* [Eq. (1)].




For practical synthesis, solvent-free processes are ideal in terms of volumetric productivities and environmental safety.[4] Although most catalytic asymmetric processes are highly sensitive to the polarity of solvent and the concentration of substrates, a solvent-free procedure might be suitable for an asymmetric reaction with a concerted mechanism[3] because its transition state is less influenced by the polarity of the solvents. The thermal pericyclic ene reaction represents a typical concerted pathway involving six electrons with a suprafacial orbital interaction,[5] and its asymmetric version has been achieved with various chiral Lewis acids including Al, Ti, Ni, Pt, Pd, Yb, and Cu complexes.[6,7] The catalyst loadings employed in most cases were in the range from 1 to 10 mol %. In our experiments we employed binolate-Ti, which was prepared in situ by the reaction of (*R*)-binol (2,2′-dihydroxy-1,1′-biphenyl) and titanium isopropoxide (2:1 molar ratio in dichloromethane/toluene). Under nearly solvent-free conditions (the solvent volume from the catalyst was about 13 % of the whole system) and with a catalyst loading of 0.1 mol %, α-methylstyrene (**1a**) reacted with ethyl glyoxylate (**2**) [Eq. (1)] efficiently at room temperature to give α-hydroxy ester (*R*)-**3a** in quantitative yields and good enantioselectivity (90 % *ee*). The practical advantages of this strategy—the easy preparation of the catalyst, the nearly solvent-free conditions, the high yield and enantiopurity of the product, and the extremely low catalyst loading—make this protocol attractive for the preparation of enantiomerically enriched α-hydroxy esters of biological and synthetic importance.

Tuning the sterics and electronics of the diol ligands in their metal complexes is essential to achieving highly efficient catalysts for asymmetric reactions, and the combinatorial-chemistry approach may be a powerful strategy for this purpose.[8] We searched for more efficient catalysts for the reaction of **1a** with **2** by high-throughput screening of a catalyst library generated from the parallel combination of any two of the ligands shown in Scheme 1 with titanium isopropoxide. We found that both the electronic effect and the steric bulk of the substituents of these binol derivatives have significant impact on the catalytic activity and enantioselectivity of the binol-Ti catalysts (see the Supporting Information). The serious steric hindrance of the substituents (e.g. $CH_3$, Ph, Br) at the 3,3′-positions of binol proved to be disadvantageous for the reaction. The partially reduced binaphthyl ligands **L3** and **L4** were inferior to the parent ligand **L1**. The modification of diol ligand at the 6,6′-positions of binol with Br (**L2**) is quite effective for enhancing both the reactivity and the enantioselectivity of the reaction.




***Scheme 1.*** Chiral ligands employed for asymmetric induction.

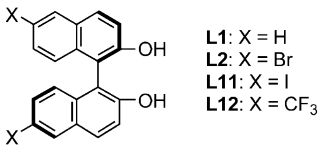
[*] Prof. Dr. K. Ding, Dr. Y. Yuan, X. Zhang
State Key Laboratory of Organometallic Chemistry
Shanghai Institute of Organic Chemistry
Chinese Academy of Sciences
354 Fenglin Road, Shanghai 200032 (P.R. China)
Fax: (+86) 21-6416-6128
E-mail: kding@mail.sioc.ac.cn

[**] Financial support from the NSFC, the CAS, the Major Basic Research Development Program of China (grant no. G2000077506), and the Ministry of Science and Technology of Shanghai Municipality is gratefully acknowledged.

Supporting information for this article is available on the WWW under http://www.angewandte.org or from the author.

 © 2003 Wiley-VCH Verlag GmbH & Co. KGaA, Weinheim DOI: 10.1002/anie.200352535 

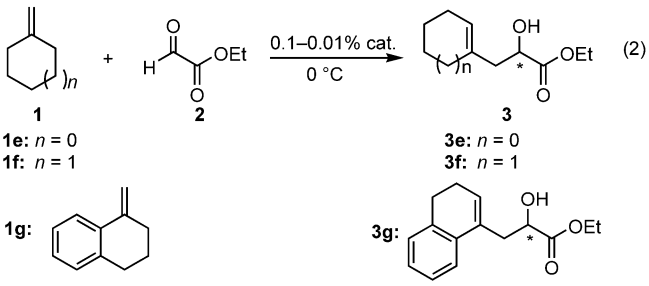
All these results demonstrated that enhancing the Lewis acidity of the titanium complexes might be a key point for achieving high efficiency and enantioselectivity in the carbonyl-ene reaction. Therefore, we decided to set up a second-generation library of chiral binol ligands with various electron-withdrawing groups (X = Br, I, $CF_3$) at the 6,6′-positions (Scheme 2). As we expected, the catalyst library




***Scheme 2.*** Second-generation chiral binol ligands employed for asymmetric induction.

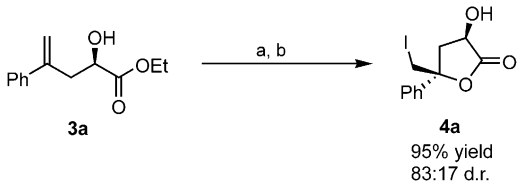
generated by either homocombination or heterocombination of these chiral ligands with titanium isopropoxide showed excellent enantioselectivity (> 94.9 % *ee*) (see the Supporting Information) under nearly solvent-free conditions even though the catalyst loading was reduced to 0.01 mol %. (The solvent volume of the catalyst system was only ca. 1.3 % of the whole system in these cases!) The catalysts formed by homocombination of **L11** or heterocombination of **L11** and **L12** with titanium isopropoxide were found to be superior to other catalysts, affording α-hydroxy ester **3a** in 97.1 % yield and 97.7 % *ee*.

The reactions promoted by the optimized catalysts (**L11**/Ti/**L11** and **L11**/Ti/L**12**) were then carried out on a gram scale with catalyst loadings of 0.1–0.01 mol % at 0 °C. We found that both **L11**/Ti/**L11** and **L11**/Ti/**L12** are highly efficient catalysts for the reactions of a variety of 2-arylpropenes (**1a–d**), including derivatives with electron-withdrawing or electron-donating substituents (Table 1). The olefin substrates could be also extended to cyclic systems (**1e,f**). The reactions of ethyl glyoxylate with methylenecyclopentane (**1e**) and methylenecyclohexane (**1f**) proceeded with excellent enantioselectivities [Eq. (2)]. Incidentally, product **3e** is a key intermediate in the synthesis of the collagenase-selective inhibitor Trocade.[9] In the case of benzocyclic olefin substrate **1g**, the corresponding α-hydroxy ester **3g** could be obtained in 94–97 % yields with 92.6–96.3 % *ee*.




(2)

To demonstrate the preparative utility of this methodology, we conducted the reaction of ethyl glyoxylate with α-methylstyrene at 0 °C on a 0.1-mole scale employing 0.05 mol % **L11**/Ti/**L12**; the desired adduct **3a** was generated in > 99 % yield and 95 % *ee*. To the best of our knowledge, this is the lowest catalyst loading for a Lewis acid catalyzed asymmetric carbonyl-ene reaction.[6h] The resulting product **3a** could be converted stereoselectively into functionalized γ-butyrolactone **4a** by iodolactionization in excellent yield with the (*R,S*) isomer as the major product (Scheme 3).[10] This is a powerful approach for the synthesis of biologically important products.




***Scheme 3.*** Preparation of γ-butyrolactone **4a**. Conditions: a) 20 % aq KOH, $CH_3OH$, 40 °C, 4 h; b) $I_2$, $NaHCO_3$, $CH_3CN$, room temperature, 16 h.

***Table 1:*** Enantioselective ene reactions between ethyl glyoxylate and representative olefins under nearly solvent-free conditions.

| Olefin | Product[a] | Cat. (mol %) | *t* [h] | Yield[b] [%] | *ee* [%][c] |
|---|---|---|---|---|---|
| **1a** | (*R*)-**3a** | **L11**/Ti/**L11** (0.1) | 48 | 98 | 98.2 |
| **1a** | (*R*)-**3a** | **L11**/Ti/**L12** (0.1) | 48 | 85 | 97.6 |
| **1a** | (*R*)-**3a** | **L11**/Ti/**L11** (0.01) | 72 | 76 | 97.2 |
| **1a** | (*R*)-**3a** | **L11**/Ti/**L12** (0.01) | 72 | 49 | 97.9 |
| **1b** | (−)-**3b**[d] | **L11**/Ti/**L11** (0.1) | 48 | 89 | 99.4 |
| **1b** | (−)-**3b**[d] | **L11**/Ti/**L12** (0.1) | 36 | 96 | 98.2 |
| **1c** | (+)-**3c**[d] | **L11**/Ti/**L11** (0.1) | 48 | 83 | 98.4 |
| **1c** | (+)-**3c**[d] | **L11**/Ti/**L12** (0.1) | 48 | 96 | 98.4 |
| **1d** | (−)-**3d**[d] | **L11**/Ti/**L11** (0.1) | 36 | 92 | 97.1 |
| **1d** | (−)-**3d**[d] | **L11**/Ti/**L12** (0.1) | 36 | > 99 | 97.0 |
| **1f** | (*R*)-**3e** | **L11**/Ti/**L11** (0.1) | 24 | > 99 | 91.6 |
| **1f** | (*R*)-**3f** | **L11**/Ti/**L12** (0.01) | 42 | 42 | 91.8 |
| **1g** | (*R*)-**3g** | **L11**/Ti/**L11** (0.1) | 48 | 97 | 92.2 |
| **1g** | (*R*)-**3g** | **L11**/Ti/**L12** (0.1) | 48 | 94 | 96.3 |

[a] Absolute configurations were assigned by comparing the optical rotations with literature values. [b] Yields of isolated products. [c] Enantiomeric excesses were determined by GC (Cyclodex B column) or HPLC (Chiral OJ column). [d] Absolute configuration was not determined.

In conclusion, we have first demonstrated that the enantioselective carbonyl-ene reaction of glyoxylate ester with a variety of olefins can be carried out under nearly solvent-free conditions with the catalysis of 6,6′-$I_2$- or 6,6′-$(CF_3)_2$-binol-Ti at very low catalyst loadings (up to 0.01 mol %), affording the corresponding α-hydroxy esters in high yields and excellent enantioselectivities. The transformation of product **3a** into a new type of functionalized γ-butyrolactone **4a** was also achieved by stereoselective iodolactonization in excellent yield.

## *Experimental Section*

General procedure for the quasi solvent-free enantioselective carbonyl ene reaction of ethyl glyoxylate with α-methylstyrene. To a solution of **L11** (27 mg, 0.05 mmol) and **L12** (21 mg, 0.05 mmol) in

 © 2003 Wiley-VCH Verlag GmbH & Co. KGaA, Weinheim 

toluene (1 mL) was added 0.5 M $Ti(OiPr)_4$ in $CH_2Cl_2$ (100 μL, 0.05 mmol), and the mixture was stirred for 2 h at room temperature. The mixture was cooled to 0 °C, and then α-methylstyrene (**1a**) (12.5 mL, 0.1 mol) and ethyl glyoxylate (**2**) (15 mL, 0.2 mol) were added. After stirring for 48 h at 0 °C, the reaction mixture was directly submitted to flash column separation on silica gel with EtOAc/hexane (1:4) as eluent to give (*R*)-**3a** (22 g, >99% yield with 95% *ee*). The enantiomeric excess of the product was determined by HPLC on a Chiralcel OJ column; eluent: hexane/2-propanol (97:3); flow rate: 0.7 mL $min^{-1}$; UV detection at $\lambda = 254$ nm; $t_R$((*S*)-**3a**) = 23.3 min (minor), $t_R$((*R*)-**3a**) = 30.7 min (major).

Received: August 1, 2003 [Z52535]

**Keywords:** asymmetric catalysis · carbonyl-ene reaction · ligand effects · titanium

[1] For comprehensive reviews on asymmetric catalysis, see: a) R. Noyori, *Asymmetric Catalysis in Organic Synthesis*, Wiley-Interscience, New York, **1994**; b) *Catalysis Asymmetric Synthesis*, 2nd ed. (Ed.: I. Ojima), Wiley-VCH, New York, **2000**; c) *Advances in Catalytic Processes: Asymmetric Chemical Transformations, Vol. 1* (Ed.: M. Doyle), JAI, Greenwich, **1995**; d) *Comprehensive Asymmetric Catalysis, Vol. I–III* (Eds.: E. N. Jacobsen, A. Pfaltz, H. Yamamoto), Springer, Berlin, **1999**; e) *Lewis Acids in Organic Synthesis* (Ed.: H. Yamamoto), Wiley-VCH, New York, **2001**.

[2] R. Noyori, *Adv. Synth. Catal.* **2001**, *343*, 1.

[3] J. Long, J. Hu, X. Shen, B. Ji, K. Ding, *J. Am. Chem. Soc.* **2002**, *124*, 10–11.

[4] For examples of solvent-free asymmetric catalysis, see: a) M. Tokunaga, J. F. Larrow, F. Kakiuchi, E. N. Jacobsen, *Science* **1997**, *277*, 936; b) N. K. Anand, E. M. Carreira, *J. Am. Chem. Soc.* **2001**, *123*, 9687; c) S. J. Dolman, E. S. Sattely, A. H. Hoveyda, R. R. Schrock, *J. Am. Chem. Soc.* **2001**, *123*, 6991; d) T. Shibata, N. Toshida, K. Takagi, *J. Org. Chem.* **2002**, *67*, 7446; e) T. Perrard, J.-C. Plaquevent, J.-R. Desmurs, D. Hebrault, *Org. Lett.* **2000**, *2*, 2959; see also ref. [3].

[5] For a mechanistic study of the ene reaction, see: a) G. D. Paderes, W. L. Jorgensen, *J. Org. Chem.* **1992**, *57*, 1904; b) E. J. Corey, D. Barnes-Seeman, T. W. Lee, S. N. Goodman, *Tetrahedron Lett.* **1997**, *38*, 6513.

[6] For examples, see: a) K. Maruoka, Y. Hoshino, T. Shirasaka, H. Yamamoto, *Tetrahedron Lett.* **1988**, *29*, 3967; b) A. Graven, M. Johannsen, K. A. Jorgensen, *Chem. Commun.* **1996**, 2373; c) K. Mikami, M. Terada, T. Nakai, *J. Am. Chem. Soc.* **1989**, *111*, 1940; d) K. Mikami, M. Terada, T. Nakai, *J. Am. Chem. Soc.* **1990**, *112*, 3949; f) C. Qian, T. Huang, *Tetrahedron Lett.* **1997**, *38*, 6721; g) M. Johannsen, K. A. Jorgensen, *J. Org. Chem.* **1995**, *60*, 5757; h) D. A. Evans, C. S. Burgey, N. A. Paras, T. Vojkovsky, S. W. Tregay, *J. Am. Chem. Soc.* **1998**, *120*, 5824, where the reaction was carried at −78 °C in $CH_2Cl_2$ (0.65 M) with 0.2 mol% of Box-Cu catalyst to afford the corresponding α-hydroxy esters in 86% yield and 97% *ee*; Pt, Pd, Ni catalysts, see: i) J. J. Becker, P. S. White, M. R. Gagne, *J. Am. Chem. Soc.* **2001**, *123*, 9478; j) K. Mikami, K. Aikawa, *Org. Lett.* **2002**, *4*, 99; k) J. Hao, M. Hatano, K. Mikami, *Org. Lett.* **2000**, *2*, 4059; for reviews on enantioselective carbonyl-ene reaction, see: l) K. Mikami, M. Shimizu, *Chem. Rev.* **1992**, *92*, 1021; n) K. Mikami, M. Terada in *Comprehensive Asymmetric Catalysis, Vol. III* (Eds.: E. N. Jacobsen, A. Pfaltz, H. Yamamoto), Springer, Berlin, **1999**, chap. 32; o) L. C. Dias, *Curr. Org. Chem.* **2000**, *4*, 305.

[7] For asymmetric activation of the binol-Ti catalyst in the ene reaction, see: a) K. Mikami, S. Matsukawa, *Nature* **1997**, *385*, 613; b) K. Mikami, S. Matsukawa, T. Volk, M. Terada, *Angew. Chem.* **1997**, *109*, 2936; *Angew. Chem. Int. Ed. Engl.* **1997**, *36*, 2768; c) S. Pandiaraju, G. Chen, A. Lough, A. K. Yudin, *J. Am. Chem. Soc.* **2001**, *123*, 3850.

[8] For comprehensive reviews on combinatorial catalysts, see: a) K. D. Shimizu, M. L. Snapper, A. H. Hoveyda, *Chem. Eur. J.* **1998**, *4*, 1885; b) M. B. Francis, T. F. Jamison, E. N. Jacobsen, *Curr. Opin. Chem. Biol.* **1998**, *2*, 422; c) B. Jandeleit, D. J. Schaefer, T. S. Powers, H. W. Turner, W. H. Weinberg, *Angew. Chem.* **1999**, *111*, 2648; *Angew. Chem. Int. Ed.* **1999**, *38*, 2494; d) M. T. Reetz, K.-E. Jaeger, *Chem. Eur. J.* **2000**, *6*, 407; e) M. T. Reetz, *Angew. Chem.* **2001**, *113*, 292; *Angew. Chem. Int. Ed.* **2001**, *40*, 284; f) M. T. Reetz, *Angew. Chem.* **2002**, *114*, 1391; *Angew. Chem. Int. Ed.* **2002**, *41*, 1335; g) M. Tsukamoto, H. B. Kagan, *Adv. Synth. Catal.* **2002**, *344*, 453; h) C. Gennari, U. Pilarulli, *Chem. Rev.* **2003**, *103*, 3071.

[9] P. Brown, H. Hilpert (F. Hoffmann-La Roche AG), EP Appl96110814.9, **1996**.

[10] The absolute configuration of **4a** was determined by X-ray diffraction analysis, see the Supporting Information. CCDC-216977 contains the supplementary crystallographic data for this paper. These data can be obtained free of charge via www.ccdc.cam.ac.uk/conts/retrieving.html (or from the Cambridge Crystallographic Data Centre, 12, Union Road, Cambridge CB21EZ, UK; fax: (+44) 1223-336-033; or deposit@ccdc.cam.ac.uk).

 © 2003 Wiley-VCH Verlag GmbH & Co. KGaA, Weinheim 

Chemical Biology

# (−)-FR182877 Is a Potent and Selective Inhibitor of Carboxylesterase-1**

*Gregory C. Adam, Christopher D. Vanderwal, Erik J. Sorensen,* and Benjamin F. Cravatt**

Natural products constitute a rich source of structurally diverse compounds that display exceptional biochemical and cellular activities. Although many natural products bind reversibly to their protein targets to alter protein–protein interactions[1] and/or catalytic activity,[2–4] others produce their biological effects through the covalent modification of specific proteins and/or protein families. Members of this latter class of natural products are typically endowed with electrophilic functionalities that react with nucleophilic residues in structured sites of proteins, such as the active

[*] Prof. E. J. Sorensen, Prof. B. F. Cravatt, G. C. Adam,[+]
C. D. Vanderwal[+]
The Skaggs Institute for Chemical Biology and
The Departments of Chemistry and Cell Biology
The Scripps Research Institute
10550 North Torrey Pines Road, La Jolla, CA 92037 (USA)
Fax: (+1) 858-784-8023
E-mail: ejs@princeton.edu
cravatt@scripps.edu

[+] These authors contributed equally to this work.

[**] This research was supported by the NIH (CA87660 and CA085526) and the Skaggs Institute for Chemical Biology.

Supporting information for this article is available on the WWW under http://www.angewandte.org or from the author.

 © 2003 Wiley-VCH Verlag GmbH & Co. KGaA, Weinheim DOI: 10.1002/anie.200352576 

sites of enzymes. Key examples of protein-reactive natural products include fumagillin,[5] lipstatin,[6] microcystin,[7] and wortmannin,[8] which label the active sites of methionine aminopeptidases (MetAPs), pancreatic lipases, serine/threonine phosphatases, and lipid kinases, respectively.

Within the domain of natural products bearing electrophilic functional groups, the structure of FR182877 (**1**) is particularly provocative in that it displays two potential sites for protein reactivity: a strained bridgehead olefin and a lactone carbonyl group.[9–11] The unprecedented architecture of **1** (Scheme 1) has attracted the attention of several groups in organic synthesis.[12–19] Additionally, preliminary biological studies of **1** have revealed that this molecule displays several interesting activities, including promotion of microtubule polymerization,[9] induction of cell-cycle arrest in human cancer cell lines,[9] and antitumor effects in mouse models.[10] Nonetheless, whether **1** produces its pharmacological effects through binding and/or modifying specific proteins in the proteome remains unknown. The recent establishment of efficient routes for the synthesis of **1** and derivatives thereof[14–16] has provided an opportunity to investigate the biological activity of this natural product. Toward this end, we report here the synthesis of a series of biotin/fluorophore-conjugated forms of both the natural (−) and unnatural (+) enantiomers of FR182877 and their application to mouse-tissue proteomes to identify specific sites of protein reactivity.

Reporter-group-tagged versions of (−)-**1** were synthesized in a two-stage sequence in which the natural product was first treated with 10-azidodecanoyl chloride (**2**) to create **3** (Scheme 1).[20] Reaction of **3** with an alkyne-derivatized rhodamine or rhodamine–biotin bifunctional agent in the presence of a copper(I) catalyst[21] provided **4** and **6**, respectively. The analogous tagged variant **5** of the unnatural enantiomer (+)-FR182877 was also synthesized in this manner.

The tagged derivative **4** was incubated at 0.1 μM for 1 h with a mouse-heart proteome (2 mg protein $mL^{-1}$) and found by SDS-PAGE analysis to specifically label a diffuse 70-kDa protein (Figure 1a, lane 2). Heat denaturation of the proteome prior to treatment with **4** completely blocked labeling of the 70-kDa target (Figure 1a, lane 1), suggesting that this

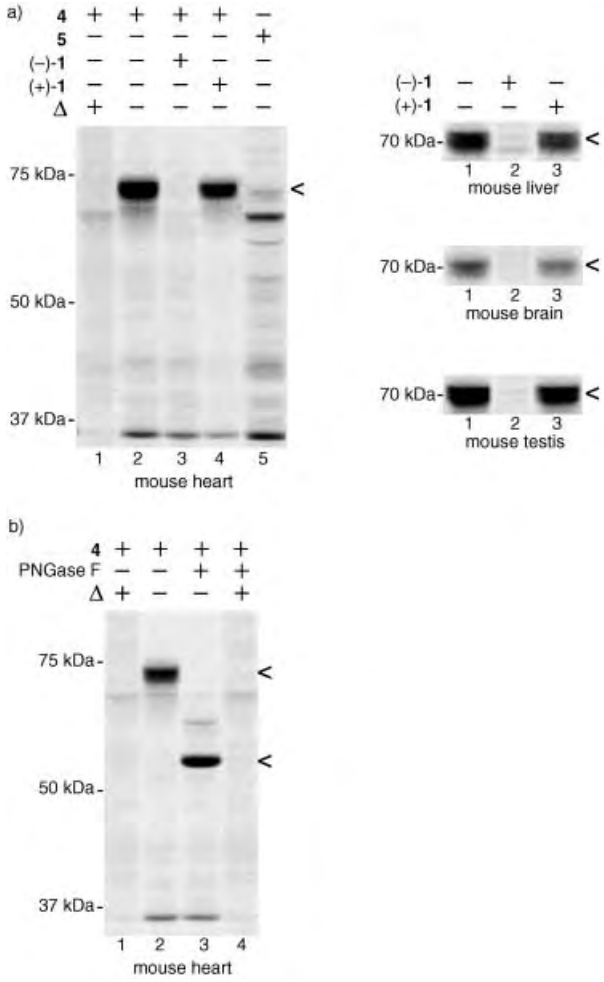
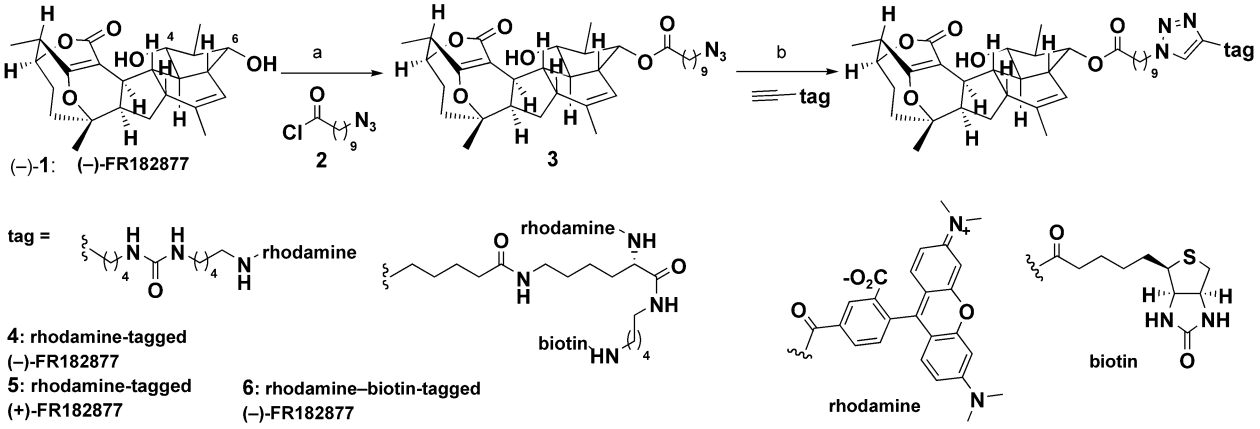



***Figure 1.*** Profiling mouse-tissue proteomes with rhodamine/(−)-FR182877 (**4**). a) Left panel: **4** but not **5** labeled a diffuse 70-kDa protein in mouse-heart proteome (lanes 2 and 5, respectively) (reaction conditions: 0.1 μM **4** or **5**, 2 mg $mL^{-1}$ protein, 50 mM Tris, pH 8.0, 60 min). This protein labeling event was heat sensitive (lane 1) and blocked by pretreatment with 10 μM unlabeled (−)-**1** (lane 3). Right panel: The 70-kDa **4**-labeled protein was found in many tissues. b) Treatment of the **4**-labeled mouse-heart proteome with PNGaseF reduced the size of the 70-kDa target to 55 kDa, indicating that this protein is glycosylated.




***Scheme 1.*** Synthesis of reporter-tagged versions of (−)-**1**. a) **2** (4 equiv), 2,4,6-collidine (10 equiv), $CH_2Cl_2$, 77%; b) alkyne-tag (rhodamine or rhodamine–biotin) (0.5 equiv), cat. $CuSO_4$, cat. sodium ascorbate, $t$BuOH/$H_2O$, ca. 50%.

 © 2003 Wiley-VCH Verlag GmbH & Co. KGaA, Weinheim 

event occurs in a structured binding site in the protein. Interestingly, the 70-kDa protein was not labeled by **5** (Figure 1a, lane 5), indicating that it is a specific target of the natural enantiomer. Consistent with this premise, labeling of this protein was completely blocked by preincubation with 10 μM untagged (−)-**1**, but was unaffected by (+)-**1** (Figure 1a, lanes 3 and 4, respectively). A few additional protein targets of **4** were also detected, but the labeling of these proteins was also observed with **5** and was not competed by untagged forms of either enantiomer (e.g., 35-kDa band, lanes 2–6, Figure 1a). Treatment of the mouse-heart proteome with higher concentrations of **4** (5–20 μM) did not uncover additional protein targets that were selectively labeled by this natural product (data not shown). Collectively, these initial data suggest that (−)-**1** specifically labels a single protein in the mouse-heart proteome.

The 70-kDa target of (−)-**1** was detected in several other mouse tissues, including brain, liver, and testis (Figure 1b). The target was glycosylated as determined by its conversion to a 55-kDa band following treatment with the glycosidase PNGaseF (Figure 1c). To identify this protein, a version of (−)-**1** coupled to both rhodamine and biotin was employed (derivative **6**, Scheme 1) This type of "trifunctional" probe permits the affinity isolation of labeled proteins by avidin chromatography and direct visualization of affinity-purified proteins by in-gel fluorescence scanning.[22] The avidin-purified 70-kDa protein was excised from an SDS-PAGE gel, digested with trypsin, and identified by mass spectrometry (MS) analysis as carboxylesterase-1 (CE-1) (for MS data, see Supporting Information).

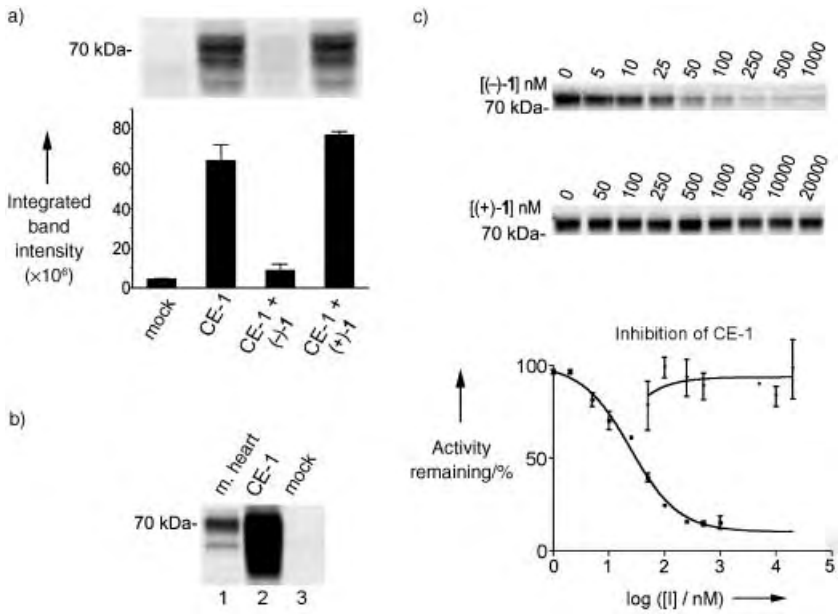



***Figure 2.*** Evidence that (−)-**1** is an active site-directed inhibitor of mouse CE-1. a) Derivative **4** labels recombinant CE-1 expressed by transient transfection in COS-7 (lane 2) and this labeling event was blocked by pretreatment with 10 μM unlabeled (−)-**1** (lane 3), but not (+)-**1** (lane 4). Mock-transfected COS-7 cells did not contain CE-1 (lane 1). Proteomes shown represent soluble extracts from homogenized COS-7 cells; the conditioned media of CE-1-transfected COS-7 cells also contained this enzyme (data not shown). b) Native and recombinantly expressed CE-1 (lanes 1 and 2, respectively) were labeled by the serine hydrolase-directed activity-based probe, FP-rhodamine[28] (0.1 μM, 10 min). c) Upper panel: Inhibition of FP-rhodamine labeling of CE-1 by increasing concentrations of unlabeled (−)- and (+)-**1** [preincubated with heart proteomes for 10 min prior to addition of FP-rhodamine (0.1 μM, 10 min)]. Lower panel: Plotting of these competitive profiling data determined an $IC_{50}$ value of 34 nM (28–41 nM, 95% confidence limits) for (−)-**1** inhibition of CE-1. No inhibition of CE-1 by (+)-**1** was detected at concentrations up to 20 μM.

CE-1 is a secreted serine hydrolase implicated in lipid metabolism and detoxification of xenobiotics.[23–25] To confirm that CE-1 is the target of modification by (−)-**1**, the cDNA for the enzyme was subcloned into the vector pcDNA3.1 and expressed in COS-7 cells by transient transfection following previously described procedures.[26] CE-1-transfected COS extracts, but not mock-transfected cell extracts (transfected with empty vector), were found to possess a diffuse 70-kDa protein that was labeled by derivative **4** (Figure 2a). Importantly, the labeling of recombinant CE-1 by **4** was blocked by pretreatment with untagged (−)-**1**, but not (+)-**1** (Figure 2a), verifying that this enzyme is a specific target of the natural enantiomer.

To determine whether (−)-**1** acted as an inhibitor of CE-1, an assay for the activity of this enzyme was needed. Although CE-1 has been hypothesized to participate in the metabolism of lipids in vivo,[23–25] its natural substrates remain unknown. Thus, few assays to measure CE-1 activity have been developed, other than those that employ a nonspecific substrate such as *p*-nitrophenyl acetate,[27] which are complicated to perform in cell/tissue extracts because of the presence of contaminating esterases. Considering that CE-1 is a member of the serine hydrolase superfamily, the activity of this enzyme should be measurable in whole proteomes by using a rhodamine-tagged fluorophosphonate probe (FP-rhodamine).[28] Previous studies have shown that FP-rhodamine serves as a general activity-based profiling tool for serine hydrolases[29] and can been used to evaluate the potency and selectivity of inhibitors that target this enzyme class directly in complex proteomes.[30,31]

FP-rhodamine was found to label both native and recombinantly expressed CE-1 (Figure 2b). The effect of (−)-**1** on FP-labeling of CE-1 was tested by preincubating mouse-heart extracts with the natural product over a concentration range of 0.001–1 μM for 10 min, followed by addition of FP-rhodamine (0.1 μM) (Figure 2c). From these data, an $IC_{50}$ value of 34 nM (28–41 nM, 95% confidence limits) was calculated for the inhibition of CE-1 by (−)-**1**. In contrast, (+)-**1** failed to inhibit the FP-labeling of CE-1, even at the highest concentration tested (20 μM). Notably, (−)-**1** completely blocked the FP-labeling of CE-1 at a concentration (1 μM) that was at least 20-fold lower than that required to

 © 2003 Wiley-VCH Verlag GmbH & Co. KGaA, Weinheim 

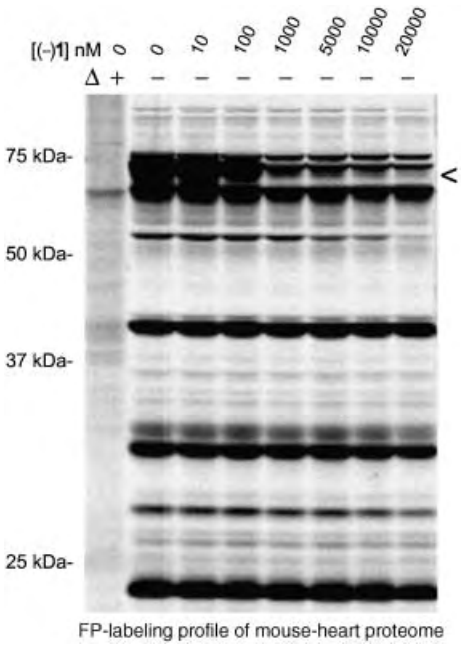



***Figure 3.*** Evidence that (−)-**1** is a selective inhibitor of mouse CE-1. Preincubation of the mouse-heart proteome with increasing concentrations of (−)-**1** (0.01–20 μM) prior to treatment with FP-rhodamine (0.1 μM) identified CE-1 as a selective target of this natural product. FP-labeling of CE-1 was completely blocked by 1 μM (−)-**1** (for a lighter exposure of this profile, see upper panel in Figure 2c), while additional serine hydrolase targets of (−)-**1** were not detected until 20 μM of this natural product was added to the proteome [at this concentration, one additional serine hydrolase target of (−)-**1** was detected (60 kDa protein)].

reduce the FP-labeling of other heart hydrolases (Figure 3). Collectively, these inhibitor profiling data indicate that (−)-**1** is a potent and selective inhibitor of CE-1.

In summary, we have synthesized a series of rhodamine–biotin-tagged forms of (−)- and (+)-**1** and applied these reagents to identify the mouse enzyme carboxylesterase-1 (CE-1) as a specific target of this natural product. Considering that the association of (−)-**1** with CE-1 was stable to protein denaturation, this interaction appears to be covalent in nature. Activity-based profiling experiments with the serine hydrolase directed probe FP-rhodamine determined that (−)-**1** acts as a highly potent ($IC_{50} = 34$ nM) and selective inhibitor of CE-1. Notably, the inhibition of CE-1 by (−)-**1** occurs at much lower concentrations than the reported effects of this natural product on tubulin polymerization (~100 μM[9]). These findings raise the intriguing possibility that at least some of the pharmacological activities of (−)-**1** in vivo may be due to CE-1 inhibition. For example, the antitumor effects of (−)-**1** would not be inconsistent with CE-1 inhibition, as carboxylesterases are expressed in a variety of cancers.[32,33] However, establishing a direct link between the biochemical properties of (−)-**1** and its pharmacological activities in vivo will require more detailed investigations. In this regard, it is important to emphasize that (−)-**1** may also possess non-covalent protein targets that would have eluded detection by the methodologies employed in this study.

As mentioned previously, the complex and rigid molecular architecture of FR182877 (**1**) is distinguished by two electrophilic groups, a strained bridgehead olefin and a lactone carbonyl group. One or both of these functional groups may represent sites for protein modification. Although it remains unclear which, if either, of these moieties is responsible for covalent binding to CE-1, instances of lactone natural products serving as inhibitors of serine hydrolases are known. For example, lipstatin is a covalent inactivator of the pancreatic lipases,[6] and, in its tetrahydro form (Orlistat), it is in clinical use for the treatment of obesity.[34] Considering further that many synthetic serine hydrolase inhibitors suffer from poor target selectivity within this large enzyme class,[31,35] the apparent specificity that FR182877 and lipstatin display for their respective targets is provocative and suggests that lactone natural products, or natural product-like compounds, may be a fertile source for novel hydrolase inhibitors. Toward this end, the creation of diverse compounds based on the structure of FR182877,[36] coupled with an activity-based proteomic screen,[31] may provide a general strategy to discover potent and selective inhibitors of many members of the serine hydrolase superfamily.

Received: August 6, 2003 [Z52576]

**Keywords:** activity-based profiling · hydrolases · inhibitors · natural products · proteomics

[1] S. L. Schreiber, *Science* **1991**, *251*, 283–287.
[2] N. Gray, L. Detivaud, C. Doerig, L. Meijer, *Curr. Med. Chem.* **1999**, *6*, 859–875.
[3] J. F. Dawson, C. F. Holmes, *Front. Biosci.* **1999**, *4*, D646–658.
[4] C. M. Grozinger, S. L. Schreiber, *Chem. Biol.* **2002**, *9*, 3–16.
[5] S. Liu, J. Widom, C. W. Kemp, C. M. Crews, J. Clardy, *Science* **1998**, *282*, 1324–1327.
[6] P. Hadvary, W. Sidler, W. Meister, W. Vetter, H. Wolfer, *J. Biol. Chem.* **1991**, *266*, 2021–2027.
[7] M. Runnegar, N. Berndt, S.-M. Kong, E. Y. C. Lee, L. Zhang, *Biochem. Biophys. Res. Commun.* **1995**, *216*, 162–169.
[8] M. P. Wymann, G. Bulgarelli-Leva, M. J. Zvelebil, L. Pirola, B. Vanhaesebroeck, M. D. Waterfield, G. Panayotou, *Mol. Cell. Biol.* **1996**, *16*, 1722–1733.
[9] B. Sato, H. Muramatsu, M. Miyauchi, Y. Hori, S. Takase, M. Hino, S. Hashimoto, H. Terano, *J. Antibiot.* **2000**, *53*, 123–130.
[10] B. Sato, M. Nakajima, Y. Hori, M. Hino, S. Hashimoto, H. Terano, *J. Antibiot.* **2000**, *53*, 204–206.
[11] S. Yoshimura, B. Sato, T. Kinoshita, S. Takase, H. Terano, *J. Antibiot.* **2000**, *53*, 615–622.
[12] C. D. Vanderwal, D. A. Vosburg, S. Weiler, E. J. Sorensen, *Org. Lett.* **1999**, *1*, 645–648.
[13] C. D. Vanderwal, D. A. Vosburg, E. J. Sorensen, *Org. Lett.* **2001**, *3*, 4307–4310.
[14] D. A. Vosburg, C. D. Vanderwal, E. J. Sorensen, *J. Am. Chem. Soc.* **2002**, *124*, 4552–4553.
[15] C. D. Vanderwal, D. A. Vosburg, S. Weiler, E. J. Sorensen, *J. Am. Chem. Soc.* **2003**, *125*, 5393–5407.
[16] D. A. Evans, J. T. Starr, *Angew. Chem.* **2002**, *114*, 1865–1868; *Angew. Chem. Int. Ed.* **2002**, *41*, 1787–1790.
[17] A. Armstrong, F. W. Goldberg, D. A. Sandham, *Tetrahedron Lett.* **2001**, *42*, 4585–4587.
[18] P. A. Clarke, R. L. Davie, S. Peace, *Tetrahedron Lett.* **2002**, *43*, 2753–2756.

 © 2003 Wiley-VCH Verlag GmbH & Co. KGaA, Weinheim 

[19] T. Suzuki, M. Nakada, *Tetrahedron Lett.* **2002**, *43*, 3263 – 3267.
[20] The conditions originally reported by Yamamoto for the selective acylation of primary alcohols in the presence of secondary alcohols were utilized to effectively discriminate between the C6 and the more sterically encumbered C4 hydroxy groups. K. Ishihara, H. Kurihara, H. Yamamoto, *J. Org. Chem.* **1993**, *58*, 3791 – 3793.
[21] V. V. Rostovtsev, L. G. Green, V. V. Fokin, K. B. Sharpless, *Angew. Chem.* **2002**, *114*, 2708 – 2711; *Angew. Chem. Int. Ed.* **2002**, *41*, 2596 – 2599. Due to the sensitivity of FR182877 toward nucleophiles, other methods for derivatization of the natural product were complicated by side reactions.
[22] G. C. Adam, E. J. Sorensen, B. F. Cravatt, *Mol. Cell. Proteomics* **2002**, *1*, 828 – 835.
[23] B. Yan, D. Yang, P. Bullock, A. Parkinson, *J. Biol. Chem.* **1995**, *270*, 19128 – 19134.
[24] S. Krishnasamy, A. L. Teng, R. Dhand, R. M. Schultz, N. J. Gross, *Am. J. Physiol.* **1998**, *275*, L969 – 975.
[25] M. R. Redinbo, S. Bencharit, P. M. Potter, *Biochem. Soc. Trans.* **2003**, *31*, 620 – 624.
[26] G. C. Adam, E. J. Sorensen, B. F. Cravatt, *Nat. Biotechnol.* **2002**, *20*, 805 – 809.
[27] E. W. Morgan, B. Yan, D. Petersen, D. Greenway, A. Parkinson, *Arch. Biochem. Biophys.* **1994**, *315*, 513 – 526.
[28] M. P. Patricelli, D. K. Giang, L. M. Stamp, J. J. Burbaum, *Proteomics* **2001**, *1*, 1067 – 1071.
[29] N. Jessani, Y. Liu, M. Humphrey, B. F. Cravatt, *Proc. Natl. Acad. Sci. USA* **2002**, *99*, 10335 – 10340.
[30] D. Kidd, Y. Liu, B. F. Cravatt, *Biochemistry* **2001**, *40*, 4005 – 4015.
[31] D. Leung, C. Hardouin, D. L. Boger, B. F. Cravatt, *Nat. Biotechnol.* **2003**, *21*, 687 – 691.
[32] G. Xu, W. Zhang, M. K. Ma, H. L. McLeod, *Clin. Cancer Res.* **2002**, *8*, 2605 – 2611.
[33] S. O. Lim, S. J. Park, W. Kim, S. G. Park, H. J. Kim, Y. I. Kim, T. S. Sohn, J. H. Noh, G. Jung, *Biochem. Biophys. Res. Commun.* **2002**, *291*, 1031 – 1037.
[34] A. Ballinger, S. R. Peikin, *Eur. J. Pharmacol.* **2002**, *440*, 109 – 117.
[35] D. Leung, G. Abbenante, D. P. Fairlie, *J. Med. Chem.* **2000**, *43*, 305 – 341.
[36] A recently described route for the enantioselective synthesis of multigram quantities of FR182877[15] should make feasible the creation of structurally diverse compounds based on the scaffold of this natural product. E. J. Sorensen, *Bioorg. Med. Chem.* **2003**, *11*, 3225 – 3228.

 © 2003 Wiley-VCH Verlag GmbH & Co. KGaA, Weinheim 

Polycarbonate Synthesis

# Cobalt-Based Complexes for the Copolymerization of Propylene Oxide and $CO_2$: Active and Selective Catalysts for Polycarbonate Synthesis**

*Zengquan Qin, Christophe M. Thomas, Stephen Lee, and Geoffrey W. Coates**

$CO_2$ is an ideal feedstock for chemical synthesis as it is safe and abundant.[1] However its thermodynamic stability hinders its utility as a starting material in synthetic reactions. A topic of current interest is the development of catalysts that can exploit $CO_2$ by combining it with highly reactive reagents, thus resulting in thermodynamically and kinetically viable reactions. Perhaps the most promising reaction of this type is the alternating copolymerization of $CO_2$ with epoxides to aliphatic polycarbonates,[2] which was first reported by Inoue et al. in the late 1960's.[3] More recently, highly active discrete complexes have been discovered that offer significant advantages over traditional heterogeneous catalysts. Although noteworthy successes were realized for the copolymerization of $CO_2$ with alicyclic epoxides (such as cyclohexene oxide),[4–12] catalysts that exhibit high activities with aliphatic epoxides (such as propylene oxide, PO),[13–16] without the concomitant production of cyclic carbonates, have not been reported. Herein we report the use of cobalt-based catalysts that exhibit excellent activity and selectivity for the synthesis of poly(propylene carbonate) (PPC).

The generalized mechanism of $CO_2$/epoxide copolymerization involves two steps: 1) epoxide ring opening by a metal carbonate, followed by 2) $CO_2$ insertion into a metal alkoxide (Scheme 1). When aliphatic epoxides such as propylene oxide are used, a common side-product is the cyclic carbonate, likely formed by a back-biting reaction from the propagating alkoxide.[14] In fact, the most active PPC catalysts reported to date produce 10–30% of the unwanted cyclic propylene carbonate byproduct under optimized conditions.[14,16]

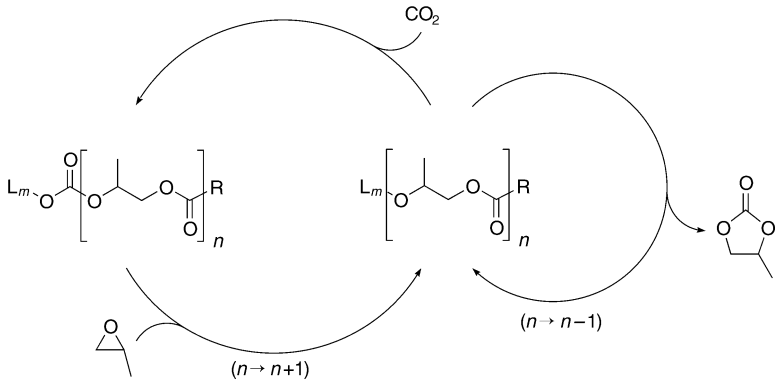
In our search for new polymerization catalysts, we focused our efforts on ligand/metal combinations known to effect both of the productive steps of polycarbonate formation. Although cobalt catalysts have essentially no precedent in $CO_2$/epoxide polymerization,[17] recent reports documented the utility of discrete cobalt complexes in each of the vital

[*] Prof. Dr. G. W. Coates, Dr. Z. Qin, Dr. C. M. Thomas, Prof. Dr. S. Lee
Department of Chemistry and Chemical Biology
Baker Laboratory, Cornell University
Ithaca, NY 14853-1301 (USA)
Fax: (+1) 607-255-4137
E-mail: gc39@cornell.edu

[**] G.W.C. gratefully acknowledges a Packard Foundation Fellowship in Science and Engineering and an Arnold and Mabel Beckman Foundation Young Investigator Award, as well as funding from the NSF (CHE-0243605) and the Cornell Center for Materials Research, supported through the NSF MRSEC program (DMR-0079992).

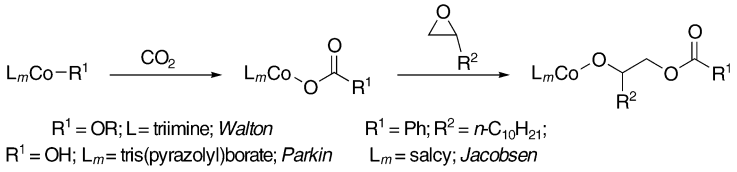
Supporting information for this article is available on the WWW under http://www.angewandte.org or from the author.

 © 2003 Wiley-VCH Verlag GmbH & Co. KGaA, Weinheim DOI: 10.1002/anie.200352605 




***Scheme 1.*** Mechanism of $CO_2$/epoxide copolymerization by using discrete metal alkoxides (R = OR′) and carboxylates (R = alkyl, aryl).

steps of the copolymerization (Scheme 2).[18] Jacobsen and coworkers have recently shown that (salcy)$Co^{III}$ carboxylates (salcy = *N,N′*-bis(3,5-di-*tert*-butylsalicylidene)-1,2-cyclohexanediamine) can efficiently ring-open epoxides,[19,20] whereas Co hydroxides[21,22] and alkoxides[23,24] have been documented




***Scheme 2.*** Recent examples of reactions of cobalt complexes that suggest the potential utility of [$L_m$CoOR] complexes for epoxide/$CO_2$ copolymerization.

to form carbonates in the presence of $CO_2$. Furthermore, to suppress unwanted cyclic carbonate formation, we proposed that catalysts incapable of lactone polymerization might exhibit improved selectivities because of the mechanistic similarity between lactone enchainment and cyclic carbonate extrusion (Scheme 1). Interestingly, efficient cobalt complexes have not been reported for lactone polymerization, thus suggesting possible selectivity for polycarbonate formation.[25] We focused our initial efforts on $Co^{III}$(salcy) complexes given their spectacular performance in the hydrolytic kinetic resolution of aliphatic epoxides,[19,20] as well as the documented performance of their chromium counterparts for the synthesis of cyclic-[26] and polycarbonates.[12,15,16]

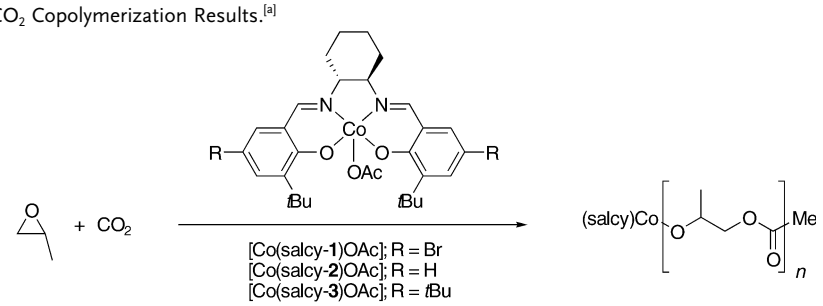
We initially investigated the use of various [Co(salcy)OAc] complexes for the polymerization of propylene oxide with $CO_2$ at low pressures, but found them to be inactive. Given the known reactivity of Co(salcy) carboxylates with epoxides,[19,20] we reasoned the problematic sequence in the reaction pathway was $CO_2$ insertion. Upon exploring reactions at higher pressures of $CO_2$, we discovered [Co(salcy)OAc] complexes were highly active and selective catalysts. Shown in Table 1 are the complexes used as well as their polymerization data. Catalysts [Zn(BDI)OAc][14] (BDI = β-diiminate) and [Cr(salph)Cl]/DMAP[16] (salph = bis(3,5-di-*tert*–butylsalicylidine)-1,2-phenylenediamine dianion; DMAP = dimethylaminopyridine) are included for comparison (entry 14, [Zn(BDI)OAc] and entry 15, [Cr(salph)Cl]/DMAP. All of the cobalt catalysts are enantiomerically pure (*R,R*-stereochemistry), thus enabling the stereoselectivity of epoxide enchainment to be measured (see below). The complex [Co(salcy–**1**)OAc] was used to study the effect of the reaction conditions on polymer formation. Entry 1 shows the $CO_2$ pressure and reaction temperature for optimal catalyst activity. [Co(salcy–**1**)OAc] requires high pressure (800 psi) for the most favorable activity, which is approximately half of that of the benchmark Zn and Cr catalysts. However, a notable advantage of [Co(salcy–**1**)OAc] is a much higher selectivity for polymer formation; the cyclic by-product propylene carbonate is not formed in measurable quantities. The resultant polycarbonates are highly alternated with 95% carbonate linkages. Molecular weight distributions of the polycarbonates produced by [Co(salcy)OAc] complexes are generally narrow, consistent with a controlled polymerization, however values of $\bar{M}_n$ ($\bar{M}_n$ is the number-average molar mass) are about half those expected, [14] which we tentatively attribute to chain transfer to water or acetic acid molecules that were coordinated to the catalyst during synthesis.[19] Entry 2 shows the profound effect of lowering the $CO_2$ pressure; at 600 psi, the reaction rate is quartered and at lower pressures the catalyst is essentially inactive. Entries 3–6 show the strong influence of reaction temperature. Catalyst activity decreases at temperatures above and below 25 °C; ether linkages are notably present in higher content (10%) at 40 °C. Entry 7 shows that propylene oxide conversion is acceptable (77%) at higher catalyst loadings, while entry 8 shows that high-molecular-weight polymer can be formed at low catalyst loadings.

[Co(salcy–**2**)OAc] shows minor difference in catalytic properties versus [Co(salcy–**1**)OAc] (entries 9, 10), although [Co(salcy–**3**)OAc] with the sterically bulky *para tert*-butyl group shows notable differences (entries 11–13). Although the activities of [Co(salcy–**3**)OAc] are slightly lower than [Co(salcy–**1**)OAc], the polymers produced are almost perfectly alternating polycarbonates. As with the other [Co(salcy)OAc] complexes, cyclic propylene carbonate is not formed. Regarding the regioselectivity of propylene oxide enchainment,[27] [Co(salcy–**3**)OAc] is highly selective with 80% head-to-tail linkages. In contrast, the catalysts [Co(salcy–**1**)OAc], [Co(salcy–**2**)OAc], and [Zn(BDI)OAc][14] have typical regioselectivities of 70, 75, and 60%, respectively. Polymerization of (*S*)-propylene oxide with enantiomerically-pure [Co(salcy–**3**)OAc] (entry 13), yields an isotactic (*S*) polymer with an unprecedented head-to-tail content of 93% was obtained. [Co(salcy–**3**)OAc] preferentially consumes (*S*)-propylene oxide over (*R*)-propylene oxide with a $k_{rel}$ of 2.8 (entry 12); given the same absolute configuration and similar $k_{rel}$ observed by Jacobsen in the ring-opening of aliphatic epoxides with benzoic acid,[19] we propose a related mechanism occurs in the polymerization to give the active alkoxide regiochemistry as shown in Table 1.

In summary, we report the first discrete cobalt complexes for the copolymerization of $CO_2$ and epoxides. In contrast to

 © 2003 Wiley-VCH Verlag GmbH & Co. KGaA, Weinheim 

***Table 1:*** Propylene Oxide/$CO_2$ Copolymerization Results.[a]




| Entry | Catalyst | Epoxide | [PO]:[Cat] | Pressure [psi] | Temp [°C] | Time [h] | TOF[b] [$h^{-1}$] | Selectivity (% PPC)[c] | Carbonate Linkages [%][c] | $\bar{M}_n$[d] [g $mol^{-1}$] | PDI ($\bar{M}_w/\bar{M}_n$) |
|---|---|---|---|---|---|---|---|---|---|---|---|
| 1 | [Co(salcy–**1**)OAc] | *rac*-PO | 500 | 800 | 25 | 3 | 81 | >99 | 95 | 15300 | 1.22 |
| 2 | [Co(salcy–**1**)OAc] | *rac*-PO | 500 | 600 | 25 | 3 | 19 | >99 | 94 | 3100 | 2.60 |
| 3 | [Co(salcy–**1**)OAc] | *rac*-PO | 500 | 800 | 40 | 3 | 17 | >99 | 90 | 5600 | 1.21 |
| 4 | [Co(salcy–**1**)OAc] | *rac*-PO | 500 | 800 | 30 | 3 | 69 | >99 | 94 | 12200 | 1.26 |
| 5 | [Co(salcy–**1**)OAc] | *rac*-PO | 500 | 800 | 20 | 3 | 42 | >99 | 95 | 8000 | 1.44 |
| 6 | [Co(salcy–**1**)OAc] | *rac*-PO | 500 | 800 | 15 | 3 | 31 | >99 | 95 | 7600 | 1.51 |
| 7 | [Co(salcy–**1**)OAc] | *rac*-PO | 200 | 800 | 25 | 3 | 51 | >99 | 95 | 8200 | 1.25 |
| 8 | [Co(salcy–**1**)OAc] | *rac*-PO | 2000 | 800 | 25 | 8 | 38 | >99 | 95 | 21700 | 1.41 |
| 9 | [Co(salcy–**2**)OAc] | *rac*-PO | 200 | 800 | 25 | 3 | 51 | >99 | 96 | 6600 | 1.21 |
| 10 | [Co(salcy–**2**)OAc] | *rac*-PO | 500 | 800 | 25 | 3 | 66 | >99 | 96 | 9000 | 1.31 |
| 11 | [Co(salcy–**3**)OAc] | *rac*-PO | 200 | 800 | 25 | 3 | 42 | >99 | 99 | 5700 | 1.28 |
| 12 | [Co(salcy–**3**)OAc] | *rac*-PO | 500 | 800 | 25 | 3 | 59 | >99 | 99 | 8100 | 1.57 |
| 13 | [Co(salcy–**3**)OAc] | *(S)*-PO | 500 | 800 | 25 | 3 | 71 | >99 | 99 | 6900 | 1.58 |
| 14[e] | [Zn(BDI)OAc] | *rac*-PO | 2000 | 300 | 25 | 2 | 184 | 87 | 99 | 35900 | 1.11 |
| 15[f] | [Cr(salph)Cl] | *rac*-PO | 1500 | 490 | 75 | 4 | 160 | 71 | 98 | 16700 | 1.38 |

[a] All of the polymerizations were carried out in 3.5 mL of neat propylene oxide (PO). [b] Turnover frequency of PO to PPC. [c] Determined by using $^1$H NMR spectroscopy. [d] Determined by gel permeation chromatography in tetrahydrofuran at 40°C, calibrated with polystyrene standards. [e] Reference [14]. [f] Reference [16].

the chromium catalysts, [Co(salcy)OAc] complexes do not require heterocyclic additives for optimal catalytic activity. Although [Co(salcy)OAc] catalysts are only half as active as highly active Cr and Zn catalysts, they have notable advantages such as high selectivity to polymer as well as excellent regioselectivity. In addition, [Co(salcy)OAc] catalysts are remarkably robust, thus allowing the use of unpurified monomers and bench-top reaction setup. Our future efforts are directed toward the study of the reaction mechanism, as well as development of catalysts that exhibit higher stereoselectivities for epoxide ring-opening.

Received: August 8, 2003 [Z52605]
Published Online: October 20, 2003

**Keywords:** carbon dioxide · cobalt · green chemistry · homogeneous catalysis · ligand effects · polymerization

[1] H. Arakawa, M. Aresta, J. N. Armor, M. A. Barteau, E. J. Beckman, A. T. Bell, J. E. Bercaw, C. Creutz, E. Dinjus, D. A. Dixon, K. Domen, D. L. DuBois, J. Eckert, E. Fujita, D. H. Gibson, W. A. Goddard, D. W. Goodman, J. Keller, G. J. Kubas, H. H. Kung, J. E. Lyons, L. E. Manzer, T. J. Marks, K. Morokuma, K. M. Nicholas, R. Periana, L. Que, J. Rostrup-Nielson, W. M. H. Sachtler, L. D. Schmidt, A. Sen, G. A. Somorjai, P. C. Stair, B. R. Stults, W. Tumas, *Chem. Rev.* **2001**, *101*, 953–996.

[2] For reviews on epoxide/$CO_2$ copolymerizations, see: a) D. J. Darensbourg, M. W. Holtcamp, *Coord. Chem. Rev.* **1996**, 153, 155–174; b) M. S. Super, E. Beckman, *Trends Polym. Sci.* **1997**, 5, 236–240; c) A. Rokicki, W. Kuran, *J. Macromol. Sci. Rev. Macromol. Chem. Phys.* **1981**, 21, 135–186.

[3] S. Inoue, H. Koinuma, T. Tsuruta, *J. Polym. Sci. Part B* **1969**, *7*, 287–292.

[4] D. J. Darensbourg, M. W. Holtcamp, *Macromolecules* **1995**, *28*, 7577–7579.

[5] M. S. Super, E. Berluche, C. Costello, E. J. Beckman, *Macromolecules* **1997**, *30*, 368–372.

[6] D. J. Darensbourg, S. A. Niezgoda, J. D. Draper, J. H. Reibenspies, *J. Am. Chem. Soc.* **1998**, *120*, 4690–4698.

[7] M. Cheng, E. B. Lobkovsky, G. W. Coates, *J. Am. Chem. Soc.* **1998**, *120*, 11018–11019.

[8] D. J. Darensbourg, J. R. Wildeson, J. C. Yarbrough, J. H. Reibenspies, *J. Am. Chem. Soc.* **2000**, *122*, 12487–12496.

[9] S. Mang, A. I. Cooper, M. E. Colclough, N. Chauhan, A. B. Holmes, *Macromolecules* **2000**, *33*, 303–308.

[10] M. Cheng, D. R. Moore, J. J. Reczek, B. M. Chamberlain, E. B. Lobkovsky, G. W. Coates, *J. Am. Chem. Soc.* **2001**, *123*, 8738–8749.

[11] D. R. Moore, M. Cheng, E. B. Lobkovsky, G. W. Coates, *Angew. Chem.* **2002**, *114*, 2711–2714; *Angew. Chem. Int. Ed.* **2002**, *41*, 2599–2602.

[12] D. J. Darensbourg, J. C. Yarbrough, *J. Am. Chem. Soc.* **2002**, *124*, 6335–6342.

[13] M. Ree, J. Y. Bae, J. H. Jung, T. J. Shin, *J. Polym. Sci. Part A* **1999**, *37*, 1863–1876.

[14] S. D. Allen, D. R. Moore, E. B. Lobkovsky, G. W. Coates, *J. Am. Chem. Soc.* **2002**, *124*, 14284–14285.

[15] D. J. Darensbourg, J. C. Yarbrough, C. Ortiz, C. C. Fang, *J. Am. Chem. Soc.* **2003**, *125*, 7586–7591.

 © 2003 Wiley-VCH Verlag GmbH & Co. KGaA, Weinheim 

[16] R. Eberhardt, M. Allmendinger, B. Rieger, *Macromol. Rapid Commun.* **2003**, *24*, 194 – 196.
[17] $Co(OAc)_2$ has been shown to exhibit extremely low activity ($TOF = 1.4\ d^{-1}$) for the copolymerization of propylene oxide and $CO_2$: K. Soga, K. Uenishi, S. Ikeda, *J. Poly. Sci. Poly. Chem. Ed.* **1979**, *17*, 415 – 423.
[18] For the synthesis of propylene carbonate from propylene oxide and $CO_2$ using [$Co^{II}$(salen)]/DMAP as a catalyst, see: Y.-M. Shen, W.-L. Duan, M. Shi, *J. Org. Chem.* **2003**, *68*, 1559 – 1562. $CoCl_2/PPh_3$ also produces propylene carbonate, although with much lower activity: M. Ratzenhoefer, H. Kisch, *Angew. Chem.* **1980**, *92*, 303; *Angew. Chem. Int. Ed. Engl.* **1980**, *19*, 317 – 318.
[19] M. Tokunaga, J. F. Larrow, F. Kakiuchi, E. N. Jacobsen, *Science* **1997**, *277*, 936 – 938.
[20] E. N. Jacobsen, F. Kakiuchi, R. G. Konsler, J. F. Larrow, M. Tokunaga, *Tetrahedron Lett.* **1997**, *38*, 773 – 776.
[21] A. Werner, *Ber. Dtsch. Chem. Ges. A* **1907**, *40*, 4098 – 4145.
[22] C. Bergquist, T. Fillebeen, M. M. Morlok, G. Parkin, *J. Am. Chem. Soc.* **2003**, *125*, 6189 – 6199.
[23] T. Funaioli, P. Biagini, P. F. Zanazzi, G. Fachinetti, *Gazz. Chim. Ital.* **1991**, *121*, 321 – 324.
[24] S. J. Archibald, S. P. Foxon, J. D. Freeman, J. E. Hobson, R. N. Perutz, P. H. Walton, *J. Chem. Soc. Dalton Trans.* **2002**, 2797 – 2799.
[25] B. J. O'Keefe, M. A. Hillmyer, W. B. Tolman, *J. Chem. Soc. Dalton Trans.* **2001**, 2215 – 2224.
[26] R. L. Paddock, S. T. Nguyen, *J. Am. Chem. Soc.* **2001**, *123*, 11498 – 11499.
[27] M. H. Chisholm, D. Navarro-Llobet, Z. Zhou, *Macromolecules* **2002**, *35*, 6494 – 6504.

 © 2003 Wiley-VCH Verlag GmbH & Co. KGaA, Weinheim 

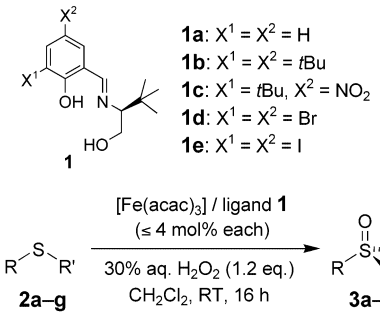
*Iron-Catalyzed Oxidations*

# Iron-Catalyzed Asymmetric Sulfide Oxidation with Aqueous Hydrogen Peroxide**

*Julien Legros and Carsten Bolm**

*Dedicated to Dr. Jean-Pierre Bégué on the occasion of his 65th birthday*

Research concerning new catalytic asymmetric reactions is often focused on the efficiency of the chemical transformation itself (i.e. yield and enantioselectivity) and less so on the practicability of the process and on environmental as well as economic issues. In the development of practical syntheses, however, the latter points become more dominant and aspects such as the simplicity of the process and the availability and toxicity of the reactants play a very significant role.[1] With respect to metal-catalyzed asymmetric oxidation reactions, this means that the choice of metal and terminal oxidant is of primary concern.[2] Along these lines, we now report an iron-catalyzed asymmetric sulfide oxidation, which provides optically active sulfoxides with up to 90% *ee*.[3] The catalysis proceeds under very simple reaction conditions (room temperature in a capped flask) and utilizes a readily available chiral iron complex ($\leqslant$4 mol%) as well as inexpensive and safe 30% aqueous hydrogen peroxide (Scheme 1).[4]




***Scheme 1.*** Iron-catalyzed asymmetric oxidation of sulfides to sulfoxides.

Enantioselective oxidation of sulfides with titanium, manganese, and vanadium complexes has been widely studied.[5,6] Conversely, iron is relatively underrepresented in this field, and the few systems developed so far fail in terms of efficiency and practicability.[5] Most involve structurally complex iron porphyrins and iodosylbenzene[7a–d] or alkyl hydroperoxides[7e] as terminal oxidant, and the enantioselectivities are only moderate (<55% *ee*).[8] The iron complex $[Fe_2O(pb)_4(H_2O)_2](ClO_4)_4$ (pb = (−)-4,5-pinene-2,2′-bipyridine) as a catalyst for sulfide oxidations with $H_2O_2$ was reported by Fontecave and co-workers but, unfortunately, the enantioselectivity remained rather low (max. 40% *ee*).[9]

We have now found that sulfides can rapidly be oxidized to give chiral sulfoxides (max. 90% *ee*) by using an iron catalyst formed in situ from $[Fe(acac)_3]$ and a Schiff base of type **1** (Scheme 1).[10] The process is synthetically interesting for the following reasons: 1) The oxidation can be performed without particular precautions as the presence of water and air does not affect the outcome. 2) Aqueous hydrogen peroxide (30%, 1.2 equiv) is the most efficient oxidizing agent.[11] 3) Iron is abundant and relatively nontoxic in comparison to other transition metals, and $[Fe(acac)_3]$ is commercially available and inexpensive. 4) Ligands of type **1** are easily prepared from the corresponding aminoalcohol and salicylaldehyde derivatives. Already the first screening with simple ligands revealed that products with high enantioselectivities could be obtained (Table 1). Further ligand adjustments for specific target structures appear to be possible.

The influence of the structure of the ligand on the enantioselectivity of the reaction was studied in the oxidation

[*] Prof. Dr. C. Bolm, Dr. J. Legros
Institut für Organische Chemie
Rheinisch-Westfälische Technische Hochschule Aachen
Professor-Pirlet-Strasse 1, 52056 Aachen (Germany)
Fax: (+49) 241-809-2391
E-mail: carsten.bolm@oc.rwth-aachen.de

[**] We are grateful to the Fonds der Chemischen Industrie and to the Deutsche Forschungsgemeinschaft (DFG) within the SFB 380 "Asymmetric Synthesis by Chemical and Biological Methods" for financial support. We thank the Alexander von Humboldt Foundation for a postdoctoral fellowship (J.L.).

 DOI: 10.1002/anie.200352635 © 2003 Wiley-VCH Verlag GmbH & Co. KGaA, Weinheim 

***Table 1:*** Catalytic enantioselective oxidation of sulfides with $H_2O_2$ and a chiral iron complex.[a]

| Entry | Ligand | Sulfide **2** | Sulfoxide | Yield [%][b] | *ee* [%][c] | Config.[d] |
|---|---|---|---|---|---|---|
| 1 | **1a** | Ph-S-Me (**2a**) | **3a** | 27 | 26 | (*S*)-(−) |
| 2 | **1b** | Ph-S-Me (**2a**) | **3a** | 15 | 13 | (*S*)-(−) |
| 3 | **1c** | Ph-S-Me (**2a**) | **3a** | 27 | 23 | (*S*)-(−) |
| 4 | **1d** | Ph-S-Me (**2a**) | **3a** | 30 | 55 | (*S*)-(−) |
| 5 | **1e** | Ph-S-Me (**2a**) | **3a** | 36 | 59 | (*S*)-(−) |
| 6[e] | **1e** | Ph-S-Me (**2a**) | **3a** | 40 | 51 | (*S*)-(−) |
| 7 | **1e** | Ph-S-Et (**2b**) | **3b** | 30 | 44 | (*S*)-(−) |
| 8 | **1e** | Ph-S-Bn (**2c**) | **3c** | 40 | 27 | (*S*)-(−) |
| 9 | **1e** | *p*-ClPh-S-Me (**2d**) | **3d** | 32 | 65 | (*S*)-(−) |
| 10 | **1e** | *p*-BrPh-S-Me (**2e**) | **3e** | 41 | 78 | (*S*)-(−) |
| 11 | **1e** | *p*-$NO_2$Ph-S-Me (**2f**) | **3f** | 21 | 90 | (*S*)-(−) |
| 12 | **1e** | 2-Naphthyl-S-Me (**2g**) | **3g** | 44 | 70 | (−) |

[a] Reaction conditions: $[Fe(acac)_3]$ (0.02 mmol), ligand (0.04 mmol), sulfide (1 mmol), aqueous $H_2O_2$ (30%; 1.2 mmol), $CH_2Cl_2$. [b] Yield of isolated product. [c] The enantiomer ratios were determined by HPLC on a chiral stationary phase. [d] The absolute configurations were assigned by comparing optical rotations and HPLC elution orders with known literature data. [e] Urea–$H_2O_2$ adduct (UHP, 1.2 mmol) was used instead of aqueous $H_2O_2$.

of thioanisole (**2a**) (Table 1, entries 1–5). The highest enantioselectivities were obtained with ligands derived from (*S*)-*tert*-leucinol. In contrast to large substituents such as *tert*-butyl (less than 23% *ee* for ligands **1b** and **1c**) on the aryl moiety, halogen atoms such as Br or I (ligands **1d** and **1e**[10d]) increase the enantioselectivity significantly (55 and 59% *ee*, respectively; Table 1, entries 4 and 5).

The chiral iron/$H_2O_2$ system affords products with particularly high *ee* values in the oxidation of aryl methyl sulfides (59–90% *ee*). Under the conditions described, no sulfones are formed, which indicates that the enantioselectivities are a direct result of the asymmetric sulfide oxidation and not of a kinetic resolution by overoxidation of the resulting sulfoxide.[12] A limitation of the reported catalysis stems from the fact that under the reaction conditions optimized to achieve high enantioselectivities, significant amounts of the substrates remain and the yields do not exceed 44%. All attempts to reach higher sulfide conversions (by increasing the catalyst loading and/or the amount of oxidant,[12] slow addition of the oxidant, or performing the reaction under homogeneous conditions[13]) afforded sulfoxides with lower *ee* values.

The results described herein, albeit not as good as those already reported with chiral complexes of other metals,[5] constitute the basis for a promising new approach and a major step in the ascent of iron-catalyzed asymmetric oxidation in general, and sulfoxidation in particular. Investigations are currently underway to improve the efficiency of the catalysts and to determine which iron species is responsible for the observed enantioselectivity.

## Experimental Section

$[Fe(acac)_3]$ (7.1 mg, 0.02 mmol) and ligand **1** (0.04 mmol) were dissolved in dichloromethane (1 mL) in a 10-mL flask, and the clear red solution was stirred until it turned brown (15 min). A solution of the sulfide (1 mmol) in dichloromethane (1 mL) was then added, followed by the dropwise addition of aqueous $H_2O_2$ (30%; 1.2 mmol). The flask was then capped and the reaction mixture was slowly stirred at room temperature (approximately 150 rpm). After 16 h, the aqueous layer was separated, and the organic layer was dried over $MgSO_4$, filtered, and the solvent removed in vacuo. The product was then purified by flash chromatography on silica gel (pentane/diethyl ether 1:1, then ethyl acetate). The enantiomeric excesses were determined by HPLC on chiral stationary phases (Gynkotek apparatus; UV detector UVD 170S (254 nm); 20°C; flow rate 0.5 mL $min^{-1}$ unless indicated otherwise). Retention times [min]: (*R*)-**3a** 26.6, (*S*)-**3a** 31.7 (Chiralcel OD, heptane/*i*PrOH 9:1); (*R*)-**3b** 20.5, (*S*)-**3b** 25.7 (Chiralcel OD, heptane/*i*PrOH 9:1); (*R*)-**3c** 31.3, (*S*)-**3c** 38.7 (Chiralcel OD, heptane/*i*PrOH 9:1); (*S*)-**3d** 23.2, (*R*)-**3d** 34.3 (Chiralcel OD, heptane/*i*PrOH 9:1); (*S*)-**3e** 26.1, (*R*)-**3e** 35.0 (Chiralcel OB-H, heptane/*i*PrOH 8:2, flow rate 0.4 mL $min^{-1}$); (*R*)-**3f** 44.2, (*S*)-**3f** 49.7 (Chiralcel OJ, heptane/*i*PrOH 7:3); (+)-**3g** 38.9, (−)-**3g** 43.5 (Chiralcel OD, heptane/*i*PrOH 9:1; optical rotation measured in $CHCl_3$).

Received: August 12, 2003 [Z52635]

**Keywords:** asymmetric catalysis · iron · oxidation · peroxides · sulfoxides

[1] a) R. A. Sheldon, *Chem. Tech.* **1994**, *24*, 38–47; b) see also: C. Bolm, O. Beckmann, O. A. G. Dabard, *Angew. Chem.* **1999**, *111*, 957–959; *Angew. Chem. Int. Ed.* **1999**, *38*, 907–909.

[2] For a recent comparative assessment of asymmetric oxidations, see: C. Bonini, G. Righi, *Tetrahedron* **2002**, *58*, 4981–5021.

[3] Efficient asymmetric sulfide oxidations are required in various processes towards pharmaceutically relevant molecules. One of the most important is the synthesis of the chiral sulfoxide, omeprazole, which is one of the most sold drugs in the world (sales in 2002: US$6.6 billion). For a summary of recent developments and data, see: A. M. Rouhi, *Chem. Eng. News* **2003**, *81*(19), 56–61.

[4] For overviews on the use of $H_2O_2$ in oxidation reactions, see: a) *Catalytic Oxidations with Hydrogen Peroxide as Oxidant* (Ed.: G. Strukul), Kluwer Academic, Dordrecht, **1992**; b) C. W. Jones, *Applications of Hydrogen Peroxide and Derivatives*, Royal Society of Chemistry, Cambridge, **1999**; c) B. S. Lane, K. Burgess, *Chem. Rev.* **2003**, *103*, 2457–2473.

[5] a) H. B. Kagan, T. Luukas in *Transition Metals for Organic Synthesis* (Eds.: M. Beller, C. Bolm), Wiley-VCH, Weinheim, **1998**, pp. 361–373; b) H. B. Kagan in *Catalytic Asymmetric Synthesis*, 2nd ed. (Ed.: I. Ojima), Wiley-VCH, New York, **2000**, pp. 327–356; c) C. Bolm, K. Muñiz, J. Hildebrand in *Comprehensive Asymmetric Catalysis* (Eds.: E. N. Jacobsen, A. Pfaltz, H. Yamamoto), Springer, Berlin, **1999**, pp. 697–713.

[6] Recently, niobium and tungsten complexes have also been involved in asymmetric sulfoxidation reactions: a) Nb: T. Miyazaki, T. Katsuki, *Synlett* **2003**, 1046–1048; b) W: V. V. Takur, A. Sudalai, *Tetrahedron: Asymmetry* **2003**, *14*, 407–410.

[7] a) J. T. Groves, P. Viski, *J. Org. Chem.* **1990**, *55*, 3628–3634; b) Y. Naruta, F. Tani, K. Maruyama, *J. Chem. Soc. Chem. Commun.* **1990**, 1378–1380; c) Y. Naruta, F. Tani, K. Maruyama, *Tetrahe-*

 © 2003 Wiley-VCH Verlag GmbH & Co. KGaA, Weinheim 

*dron: Asymmetry* **1991**, *2*, 533 – 542; d) L.-C. Chiang, K. Konishi, T. Aida, S. Inoue, *J. Chem. Soc. Chem. Commun.* **1992**, 254 – 256; e) Q. L. Zhou, K. C. Chen, Z. H. Zhu, *J. Mol. Catal.* **1992**, *72*, 59 – 65.

[8] For an exception, see references [7b,c]. In these cases, Naruta et al. reported that the oxidation of methyl pentafluorophenyl sulfide gave a product with 73% *ee*.

[9] a) C. Duboc-Toia, S. Ménage, C. Lambeaux, M. Fontecave, *Tetrahedron Lett.* **1997**, *38*, 3727 – 3730; b) Y. Mekmouche, H. Hummel, R. Y. N. Ho, L. Que, V. Schünemann, F. Thomas, A. X. Trautwein, C. Lebrun, K. Gorgy, J.-C. Leprêtre, M.-N. Collomb, A. Deronzier, M. Fontecave, S. Ménage, *Chem. Eur. J.* **2002**, *8*, 1196 – 1204.

[10] Such ligands have also been used in vanadium-catalyzed asymmetric sulfide oxidations; see: a) C. Bolm, F. Bienewald, *Angew. Chem.* **1995**, *107*, 2883 – 2885; *Angew. Chem. Int. Ed. Engl.* **1995**, *34*, 2640 – 2642; b) C. Bolm, G. Schlingloff, F. Bienewald, *J. Mol. Catal. A* **1997**, *117*, 347 – 350; c) C. Bolm, F. Bienewald, *Synlett* **1998**, 1327 – 1328; d) B. Pelotier, M. S. Anson, I. B. Campbell, S. J. F. Macdonald, G. Priem, R. F. W. Jackson, *Synlett* **2002**, 1055 – 1060; e) S. A. Blum, R. G. Bergman, J. A. Ellman, *J. Org. Chem.* **2003**, *68*, 150 – 155; f) D. J. Weix, J. A. Ellman, *Org. Lett.* **2003**, *5*, 1317 – 1320; g) for a review, see: C. Bolm, *Coord. Chem. Rev.* **2003**, *237*, 245 – 256, and references therein.

[11] Urea–$H_2O_2$ adduct (UHP) also gives satisfactory results.

[12] After a reaction time of 16 h, a potassium iodide test revealed that no more oxidant was present in the reaction medium. In the presence of a large excess of $H_2O_2$, complete conversion of sulfide into racemic sulfoxide and sulfone was observed. In independent experiments, it was demonstrated that the sulfoxide to sulfone oxidation proceeded in a non-enantioselective manner.

[13] Attempts to substitute dichloromethane with other solvents such as acetonitrile, acetone, toluene, or *tert*-butyl methyl ether were unsuccessful.

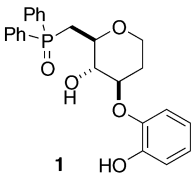
 © 2003 Wiley-VCH Verlag GmbH & Co. KGaA, Weinheim 

Asymmetric Alkylation of Ketones

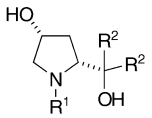
# Multicenter Strategy for the Development of Catalytic Enantioselective Nucleophilic Alkylation of Ketones: $Me_2Zn$ Addition to α-Ketoesters**

*Ken Funabashi, Markus Jachmann, Motomu Kanai, and Masakatsu Shibasaki**

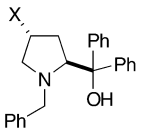
The catalytic construction of stereogenic tetrasubstituted carbon centers through the addition of carbon nucleophiles to ketones or ketoimines is very challenging, partly because of the lower reactivity of these substrates relative to aldehydes and aldoimines.[1] This task requires strong activation of the substrate and/or the nucleophile by an asymmetric catalyst. We developed Lewis acid–Lewis base two-center asymmetric catalysts (titanium and lanthanide complexes of **1**) that promote the cyanosilylation of ketones and ketoimines with broad substrate generality.[2] The fundamental concept for the catalyst design was that the Lewis acid metal and the Lewis base (the phosphane oxide) activate both the substrate and the nucleophile (TMSCN) simultaneously at defined positions in the transition state. A logical extension of this concept is to target the diorganozinc addition to ketones,[3] because both Lewis acid activation of the substrate and Lewis base activation of the reagent are required to promote the reaction.[4] We report herein our initial investigations toward this goal: the catalytic enantioselective addition of $Me_2Zn$ to α-ketoesters. Our newly designed catalyst **2**, which



**1**



**2**: $R^1$ = Bn, $R^2$ = Ph
**3**: $R^1$ = Bn, $R^2$ = Me
**4**: $R^1$ = Bn, $R^2$ = *p*–$ClC_6H_4$
**5**: $R^1$ = Bn, $R^2$ = *p*–$MeOC_6H_4$
**6**: $R^1$ = allyl, $R^2$ = Ph
**7**: $R^1$ = β–naphthyl, $R^2$ = Ph
**8**: $R^1$ = 9–anthracenyl, $R^2$ = Ph



**9**: X = H
**10**: X = OH

[*] Prof. Dr. M. Shibasaki, K. Funabashi, Dr. M. Jachmann, Dr. M. Kanai
Graduate School of Pharmaceutical Sciences
The University of Tokyo
Hongo, Bunkyo-Ku, Tokyo 113-0033 (Japan)
Fax: (+81) 3-5684-5206
E-mail: mshibasa@mol.f.u-tokyo.ac.jp
Dr. M. Kanai
PRESTO, Japan Science and Technology Corporation
Graduate School of Pharmaceutical Sciences
The University of Tokyo
Hongo, Bunkyo-Ku, Tokyo 113-0033 (Japan)

[**] Financial support was provided by RFTF of the Japan Society for the Promotion of Science (JSPS) and PRESTO of the Japan Science and Technology Corporation (JST). K.F. thanks JSPS Research Fellowships for Young Scientists. M.J. is an Alexander von Humboldt Foundation–JSPS fellow.

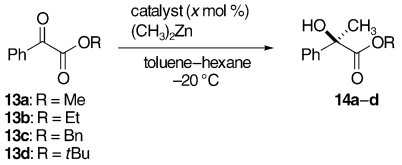
Supporting information for this article is available on the WWW under http://www.angewandte.org or from the author.

 DOI: 10.1002/anie.200351650 © 2003 Wiley-VCH Verlag GmbH & Co. KGaA, Weinheim 

contains arranged multicenters (alcohols and an amine), produced the corresponding products with up to 96% *ee* from aromatic and acetylenic α-ketoesters. This type of catalytic enantioselective reaction was recently reported by DiMauro and Kozlowski; however the enantioselectivity and substrate generality were not necessarily high (up to 78% *ee*).[5] The products are useful chiral building blocks for the synthesis of pharmaceutical agents and natural products.[6]

Because **1** did not produce satisfactory catalyst activity and enantioselectivity in the reaction of $Me_2Zn$ with ethyl benzoylformate (**13b**; see Table 1), we developed a new catalyst system. Based on the transition-state model initially proposed by Noyori and co-workers (Figure 1, **11**),[7] we expected that the presence of an additional Lewis base coordinating to $Me_2Zn$ would more strongly activate the nucleophile (Figure 1, **12**). Moreover, we planned to use a zinc alkoxide as the additional Lewis base, because anionic Lewis bases have a greater electron-donating ability than neutral Lewis bases such as amines or phosphane oxides. The combination of these two factors should allow the reaction to proceed through a dual activation pathway with the strongly activated nucleophilic $Me_2Zn$, and both high catalyst activity and enantioselectivity should be observed. Based on these considerations, we designed new enantioselective catalysts **2**–**8**. These catalysts could be readily synthesized in two steps from commercially available 2,4-*cis*-4-hydroxy-D-proline methyl ester.[8] Catalyst **9**, which lacks the 4-hydroxy group,[9] and the 2,4-*trans* catalyst **10**[10] were also prepared as control catalysts.

***Table 1:*** Optimization of the reaction conditions.[a]




| Entry | 13/14 | Catalyst | *x* [mol%] | *t* [h][b] | Yield [%][c] | *ee* [%][d] |
|---|---|---|---|---|---|---|
| 1 | **b** | **2** | 20 | 24 | 72 | 82 |
| 2 | **b** | **9** | 20 | 24 | 45 | 0 |
| 3 | **b** | **10** | 20 | 24 | 28 | 7[e] |
| 4 | **b** | **2** | 10 | 36 | 63 | 53 |
| 5 | **b** | **2** | 10 | 30+12 | 69 | 83 |
| 6 | **b** | **3** | 10 | 30+12 | 89 | 4 |
| 7 | **b** | **4** | 10 | 30+12 | 85 | 80 |
| 8 | **b** | **5** | 10 | 30+12 | 89 | 77 |
| 9 | **b** | **6** | 10 | 30+12 | 78 | 33 |
| 10 | **b** | **7** | 10 | 30+12 | 55 | 56 |
| 11 | **b** | **8** | 10 | 30+12 | 89 | 33 |
| 12 | **a** | **2** | 10 | 30+12 | 85 | 81 |
| 13 | **c** | **2** | 10 | 30+12 | 74 | 40 |
| 14 | **d** | **2** | 10 | 30+12 | 17 | n.d.[f] |

[a] $Me_2Zn$: 1.8 equiv (entries 1–4) or 2.5 equiv (entries 5–14). [b] In entries 1–4, $Me_2Zn$ was added in one portion, whereas in entries 5–14, $Me_2Zn$ was added slowly over 30 h, and the reaction was continued for 12 h. [c] Yield of isolated product. [d] Determined by chiral HPLC analysis. [e] The opposite enantiomer was the major isomer. [f] Not determined.

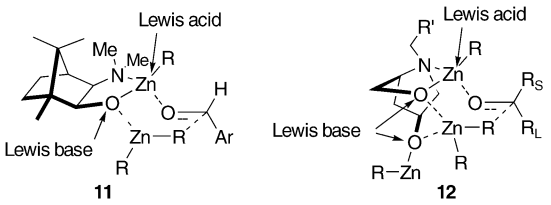



***Figure 1.*** Fundamental concepts of catalyst design.

The function of catalysts **2**, **9**, and **10** (20 mol%) was first investigated for the reaction of $Me_2Zn$ and **13b** in toluene at −20 °C for 24 h. As shown in Table 1, 2,4-*cis* catalyst **2** gave product **14b** in 72% yield with 82% *ee* (entry 1). Catalysts **9** and **10**, however, gave the product in only moderate yield with very low enantioselectivity (Table 1, entries 2 and 3). It can therefore be concluded that the 2,4-*cis* configuration of the diols is essential for high yield and enantioselectivity. Based on molecular-modeling studies, these two oxygen atoms must be in close proximity so that the two alkoxides can chelate $Me_2Zn$, which acts as a nucleophile. The sharp contrast between the catalytic activity and enantioselectivity of **2** and **9** or **10** might be due to the ability of the zinc alkoxides to chelate the nucleophile.[11]

Next, we investigated a decrease in the catalyst loading. When the amount of **2** was decreased to 10 mol%, the enantioselectivity was significantly decreased to 53% *ee* (Table 1, entry 4). This might be due partly to the competitive catalyst-independent background reaction. Thus, we tried slow addition (30 h) of $Me_2Zn$. The product was obtained with 83% *ee* (Table 1, entry 5), which was comparable to the results obtained with 20 mol% of the catalyst. Under these optimized reaction conditions, the catalyst structure was further modified. When the diaryl alcohol was changed into a dimethyl alcohol (catalyst **3**), a significant loss of enantioselectivity occurred (Table 1, entry 6). The electron-withdrawing or -donating group on the aryl group, however, did not have a significant effect (Table 1, entries 7 and 8). Finally, catalyst **2**, which contains a benzyl substituent on the nitrogen atom, produced the best enantioselectivity, and catalysts that bear smaller (*N*-allyl; Table 1, entry 9) and larger (*N*-β-naphthyl and *N*-9-anthracenyl; Table 1, entries 10 and 11) substituents gave lower enantioselectivity. The yield of the product was dependent on the bulkiness of the ester moiety of the substrate (Table 1, entries 12–14), and the best results were obtained with the small methyl ester **13a** as the substrate (Table 1, entry 12).

To improve the enantioselectivity further, several additives were screened.[12] Although neither coordinating additives such as $Ph_3P(O)$, $Et_3N$, $Ph_3P$, or LiBr, nor Brönsted acids such as trifluoromethanesulfonic acid or trifluoroacetic acid produced positive effects, the addition of protic additives such as MeOH, EtOH, *i*PrOH, or *t*BuOH improved both the yield and enantioselectivity (Figure 2). Although the tendency was slightly different depending on the alcohol, the chemical yield increased up to 96% (in the presence of 27 mol% EtOH) and the enantioselectivity up to 95% *ee* (in the presence of 18 mol% EtOH). The best results in terms of yield and enantioselectivity were obtained in the presence of 27 mol%

 © 2003 Wiley-VCH Verlag GmbH & Co. KGaA, Weinheim 

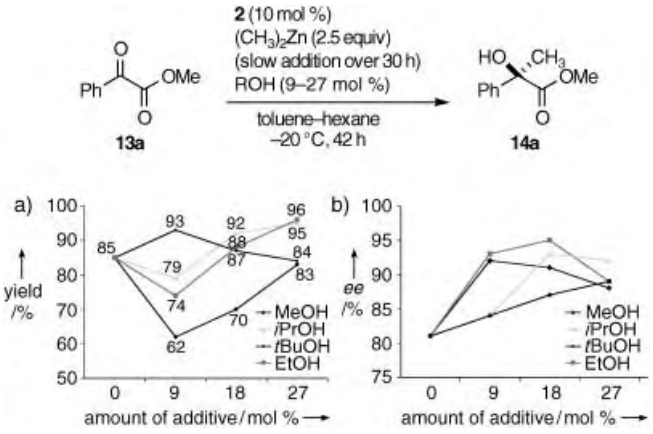



***Figure 2.*** Effect of additive alcohol on yield and enantioselectivity. a) Relationship between yield and amount of additive. b) Relationship between *ee* and amount of additive.

*i*PrOH, and product **14a** was obtained in 95% yield with 92% *ee*.

Substrate generality was then investigated under the optimized reaction conditions. High *ee* values were obtained with aromatic and heteroaromatic ketones (Table 2, entries 1–7). Although the enantioselectivity was moderate, the present reaction could also be applied to acetylenic ketoester **13j** (Table 2, entry 8). The product is a versatile precursor for functionalized or α,α-dialkyl-substituted hydroxy esters. Ketoester **13k** that is constrained to the *s-cis* form of the ketone and amide carbonyls gave 76% *ee* (Table 2, entry 9). Thus, this is the first example of a catalytic enantioselective addition of $Me_2Zn$ to α-ketoesters that affords products with high enantioselectivity.[13,14]

Although a detailed mechanistic discussion is difficult at present owing to the lack of information on the structure of the catalyst, we obtained important information regarding the role of the additive, based on the differences in the nonlinear effects[15] in the absence or presence of *i*PrOH (Figure 3).

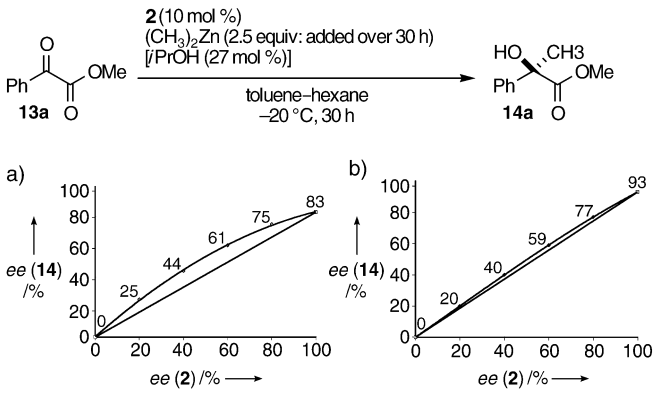
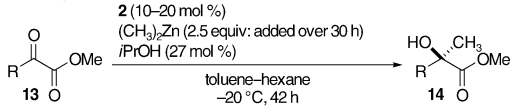



***Figure 3.*** Nonlinear effects a) in the absence of and b) in the presence of *i*PrOH.

Positive nonlinear effects were observed in the absence of *i*PrOH, however the nonlinearity almost disappeared in the presence of 27 mol% *i*PrOH. These results suggest that the additive *i*PrOH (thus, zinc isopropoxide in the reaction mixture) changes the catalyst structure into a monomeric form by mixed aggregate formation, which might be the actual catalytic species that results in the high enantioselectivity and reactivity.

In summary, we developed a new enantioselective catalyst for the addition of $Me_2Zn$ to α-ketoesters. The *cis* arrangement of the two hydroxy groups on the pyrrolidine ring is essential for high catalyst activity and enantioselectivity. Addition of a catalytic amount of *i*PrOH improved the yield and enantioselectivity. The nonlinear effects suggest that the additive forms a monomeric catalyst species. The information obtained in the present study will be useful for the development of an enantioselective catalyst of diorganozinc addition to simple ketones. Studies toward this end and to clarify the reaction mechanism are underway.

***Table 2:*** Catalytic enantioselective addition of $Me_2Zn$ to α-ketoesters.[a]




| Entry | **13** | **2** [mol%] | Yield [%][b] | *ee* [%][c] |
|---|---|---|---|---|
| 1 | R = Ph (**13a**) | 10 | 95 | 92[d] |
| 2[f] | R = Ph (**13a**) | 10 | 70 (91) | 85[d] |
| 3 | R = *p*-Br-$C_6H_4$ (**13e**) | 10 | 89 | 85 |
| 4 | R = *p*-MeO-$C_6H_4$ (**13f**) | 10 | 42 | 92 |
| 5 |  (**13g**) | 10 | 77 | 80 |
| 6 |  (**13h**) | 10 | 91 | 96 |
| 7 |  (**13i**) | 20 | 89 | 72 |
| 8 | Ph—≡– (**13j**) | 10 | 75 | 59[d] |
| 9 |  (**13k**) | 20 | 82 | 76[e] |

[a] For experimental procedure, see reference [13]. [b] Yield of isolated product. [c] Determined by chiral HPLC analysis. [d] The absolute configuration was determined to be *R*. [e] The absolute configuration was determined to be *S*. [f] Reaction carried out on a 1.6-g scale. Conversion yield is in parenthesis. Recovery of chiral ligand **2**: 98%.

Received: April 14, 2003 [Z51650]
Published Online: August 1, 2003

**Keywords:** alkylation · asymmetric catalysis · homogeneous catalysis · ketoesters · nonlinear effects

[1] a) E. J. Corey, A. Guzman-Perez, *Angew. Chem.* **1998**, *110*, 402–415; *Angew. Chem. Int. Ed.* **1998**, *37*, 388–401; b) J. Christoffers, A. Mann, *Angew. Chem.* **2001**, *113*, 4725–4732; *Angew. Chem. Int. Ed.* **2001**, *40*, 4591–4597.

 © 2003 Wiley-VCH Verlag GmbH & Co. KGaA, Weinheim 

[2] For a review, see: M. Shibasaki, M. Kanai, K. Funabashi, *Chem. Commun.* **2002**, 1989 – 2183.
[3] For the catalytic enantioselective addition of diorganozinc reagents to simple ketones, see: a) P. I. Dosa, G. C. Fu, *J. Am. Chem. Soc.* **1998**, *120*, 445 – 446; b) D. J. Ramón, M. Yus, *Tetrahedron* **1998**, *54*, 5651 – 5666; c) M. Yus, D. J. Ramón, O. Prieto, *Tetrahedron: Asymmetry* **2002**, *13*, 2291 – 2293; d) C. Garcia, L. K. LaRochelle, P. J. Walsh, *J. Am. Chem. Soc.* **2002**, *124*, 10970 – 10971.
[4] a) R. Noyori, M. Kitamura, *Angew. Chem.* **1991**, *103*, 34 – 55; *Angew. Chem. Int. Ed. Engl.* **1991**, *30*, 49 – 69; b) R. Noyori, *Asymmetric Catalysis in Organic Synthesis*, Wiley, New York, **1994**; c) K. Soai, T, Shibata in *Comprehensive Asymmetric Catalysis, Vol. 2* (Eds.: E. N. Jacobsen, A. Pfaltz, H. Yamamoto), Springer, Berlin, **1999**, pp. 911 – 922; d) C. Bolm, K. Muñiz, *Chem. Soc. Rev.* **1999**, *28*, 51 – 59; e) L. Pu, H.-B. Yu, *Chem. Rev.* **2001**, *101*, 757 – 824.
[5] For a bifunctional asymmetric catalyst that promotes alkylation selectively with $Et_2Zn$, see: a) E. F. DiMauro, M. C. Kozlowski, *J. Am. Chem. Soc.* **2002**, *124*, 12668 – 12669; b) E. F. DiMauro, M. C. Kozlowski, *Org. Lett.* **2002**, *4*, 3781 – 3784; for highly enantioselective alkynylation of α-ketoesters, see: B. Jiang, Z. Chen, X. Tang, *Org. Lett.* **2002**, *4*, 3451 – 3453; however, this method cannot be applied to the synthesis of methyl-substituted chiral tertiary alcohols (low yield).
[6] Many biologically active compounds contain methyl-substituted chiral tertiary alcohols.
[7] M. Kitamura, S. Okada, S. Suga, R. Noyori, *J. Am. Chem. Soc.* **1989**, *111*, 4028 – 4036.
[8] For details, see Supporting Information.
[9] For enantioselective addition of dialkylzinc to aldehydes with prolinol-derived catalysts, see: K. Soai, A. Ookawa, T. Kaba, K. Ogawa, *J. Am. Chem. Soc.* **1987**, *109*, 7111 – 7115.
[10] For enantioselective addition of $Et_2Zn$ to aldehydes with 2,4-*trans* hydroxyproline-derived catalysts, see: a) G. Liu, J. A. Ellmann, *J. Org. Chem.* **1995**, *60*, 7712 – 7713; b) S. J. Bae, S.-W. Kim, T. Hyeon, B. M. Kim, *Chem. Commun.* **2000**, 31 – 32. The secondary alcohol groups (C4) were protected as ethers in these cases.
[11] No useful information was obtained from $^1H$ and $^{13}C$ NMR spectroscopic measurements of the [Zn–**2**] complex. Studies to determine the catalyst structure by X-ray crystallography are underway.
[12] For a review on the additive effect on catalytic enantioselective reactions, see: E. M. Vogl, H. Gröger, M. Shibasaki, *Angew. Chem.* **1999**, *111*, 1672 – 1680; *Angew. Chem. Int. Ed.* **1999**, *38*, 1570 – 1577.
[13] General procedure: $Me_2Zn$ (1.0 M in hexane, 18 μL, 0.018 mmol) was added to a solution of the catalyst **2** (7.2 mg, 0.020 mmol) in toluene (0.45 mL), and the mixture was stirred for 30 min at room temperature. *i*PrOH (4.13 μL) in toluene (0.050 mL) was then added and the mixture was stirred for 30 min. The mixture was cooled to −20 °C and the α-ketoester (0.20 mmol) was added, followed by the dropwise addition of $Me_2Zn$ (1.0 M in hexane, 482 μL, 0.482 mmol) over 30 h by using a syringe pump. The reaction vessel has to be strictly sealed so as not to lose the volatile $Me_2Zn$. After all the $Me_2Zn$ was added, the reaction was stirred for 12 h and then quenched with aqueous citric acid (10%). Extraction with EtOAc and purification by column chromatography ($SiO_2$, EtOAc/hexane, 1:8→1:4) provided the product.
[14] Further scope and limitations: A vinyl-substituted ketoester [R = (*E*)-PhCH=CH] gave the product in 92% yield with 15% *ee*. An alkyl-substituted ketoester ($R = PhCH_2CH_2$) gave a complex mixture of products. The reaction of $Et_2Zn$ and **13a** did not give any products, and **13a** was recovered.

 © 2003 Wiley-VCH Verlag GmbH & Co. KGaA, Weinheim 

H/D Exchange in an Excited Hydride

# Excited-State Deprotonation and H/D Exchange of an Iridium Hydride Complex**

*Tomoyoshi Suenobu, Dirk M. Guldi,* Seiji Ogo, and Shunichi Fukuzumi**

*Dedicated to Professor Fritz Wasgestian on the occasion of his 70th birthday*

Excited-state proton transfer from hydroxyarenes has been known for long time[1] and studied extensively.[2–8] Simple thermodynamic considerations, for both the ground and excited states of any proton-containing molecule and its conjugate base, indicate that the excited state is a much stronger acid than the corresponding ground state.[2–4] Extremely strong acids can be produced by photoexciting hydroxyaromatic compounds that carry electron withdrawing groups—commonly referred to as "super" photoacids.[1,5] A widely accepted rationalization for the enhanced acidity in the excited state infers an intramolecular charge transfer (ICT)—in the excited state of the acid from the hydroxyl oxygen to the aromatic ring.[1–4] In addition to hydroxyarene-type photoacids, so-called photoacid generators (PAG) exhibit promising activities.[9] The performance of such PAGs is, however, limited to exposure of UV light ($\lambda <$ 400 nm). A photoacid that operates under visible light illumination is desired when visible light lasers such as He–Cd, YAG, and Ar ion lasers are necessary as a high-power and stable light source for microlithographic and holographic applications.[10]

In contrast to organic photoacids, metal hydride complexes, which also contain removable protons, have never been shown to act as photoacids. In particular, the hydride in metal hydride complexes is believed to be electronegative and, in turn, difficult to remove in the form of protons.

[*] Prof. Dr. S. Fukuzumi, Dr. T. Suenobu, Dr. S. Ogo
Department of Material and Life Science
Graduate School of Engineering, Osaka University
CREST, Japan Science and Technology Corporation
2-1 Yamada-oka Suita Osaka 565-0871 (Japan)
Fax: (+81) 6-6879-7370
E-mail: fukuzumi@chem.eng.osaka-u.ac.jp
Prof. Dr. D. M. Guldi
Radiation Laboratory
University of Notre Dame
Notre Dame, Indiana 46556 (USA)
Fax: (+1) 574-631-8068
E-mail: guldi.1@nd.edu

[**] This work was partially supported by Grants-in-Aid for Scientific Research on Priority Area (Nos. 13555247 and 14045249) from the Ministry of Education, Culture, Sports, Science and Technology, Japan, and the offices of Basic Energy Sciences of the US Department of Energy (contribution no. NDRL-4481 from the Notre Dame radiation laboratory. The authors thank the reviewers for their useful comments and suggestions.

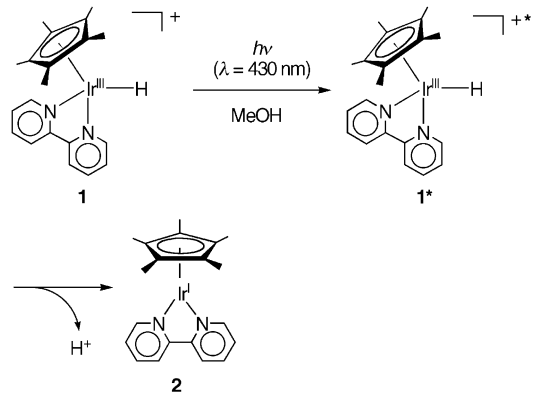
Supporting information for this article is available on the WWW under http://www.angewandte.org or from the author.

 © 2003 Wiley-VCH Verlag GmbH & Co. KGaA, Weinheim DOI: 10.1002/anie.200352061 

However, the release of protons occurs in some metal hydride complexes as indicated by the H/D exchange reactions in water.[11]

We wish to report herein the first example of: 1) excited state deprotonation in a hexafluorophosphate salt of an iridium hydride complex (**1**)[12,13] which absorbs visible light ($\lambda_{max} = 430$ nm); and 2) the H/D exchange reaction in the excited state.

No spectral changes of the absorption features are noted when a methanol solution of **1** was photoirradiated in the steady state with visible light ($\lambda > 400$ nm) at room temperature. Transient absorption bands at $\lambda_{max} = 490$, 530(sh), 620, 670, and 730 nm are, on the other hand, observed upon nanosecond laser pulse excitation ($\lambda = 430$ nm) as shown in Figure 1 a. These newly formed absorption bands are assigned




***Scheme 1.*** Photoinduced deprotonation of **1** to form **2**.

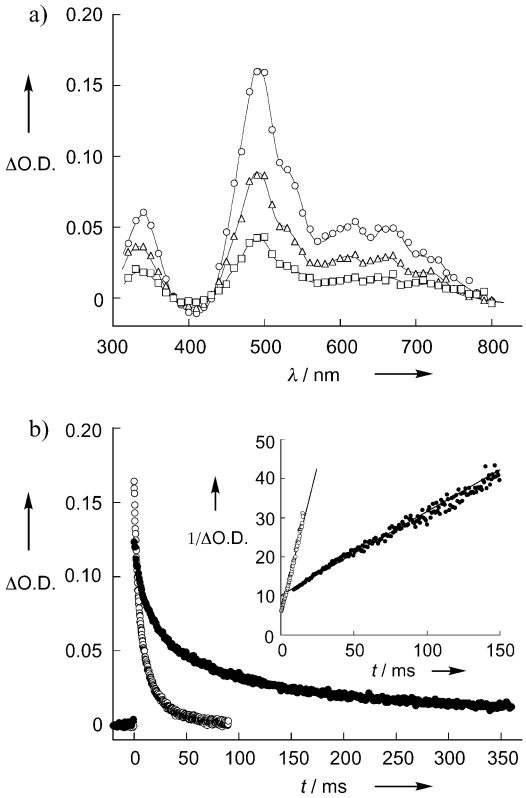



***Figure 1.*** a) Transient absorption spectra observed in photoinduced deprotonation of **1** ($2.4 \times 10^{-4}$ M) at 10 μs (○), 4 ms (△), and 12 ms (□) after laser excitation ($\lambda = 430$ nm, 10 mJ/pulse) in deaerated $CH_3OH$; b) time-course of the absorbance change at $\lambda = 490$ nm in deaerated $CH_3OH$ (○) and $CH_3OD$ (●). Inset: second-order plots.

to the reactive intermediate iridium(I) complex (**2**).[14] This indicates that deprotonation of **1** occurs in the excited state and that the iridium hydride complex **1** acts as an efficient photoacid. Scheme 1 summarizes the photoactivity of **1**.

The decay of the transient absorption band (Figure 1 b), which arises from the instability of **2**, obeys second-order kinetics (see inset of Figure 1 b). Thus, the following mechanism evolves: after the initial deprotonation of excited state of **1** (**1***), which generates **2** and a proton; protonation of **2** occurs in $CH_3OH$ and regenerates the ground state **1**. This mechanism was further confirmed by the change of deprotonation kinetics from second-order to psuedo-first-order in the presence of large excess trifluoroacetic acid ($CF_3COOH$). The pseudo-first-order rate constant linearly increases with increasing [$CF_3COOH$] (see Supporting Information).

When we replaced $CH_3OH$ with [$D_1$]methanol ($CH_3OD$), the decay rate of **2** became significantly slower (Figure 1 b). A large kinetic deuterium isotope effect ($k_H/k_D = 8.2$) is derived from the slopes of the second-order plots.[15]

The formation of **1*** and the subsequent deprotonation process were successfully observed by picosecond laser flash photolysis as shown in Figure 2. Upon laser excitation ($\lambda =$ 355 nm) of **1** in deaerated $CH_3OH$, a new absorption band with a maximum at 500 nm increase steadily up to 100 ps. This absorption band is assignable to the ICT excited state of **1** and the underlying growth dynamics corresponds to the intersystem crossing (ISC) to form the lowest triplet excited state of **1**. In this lowest triplet excited state of **1**, the 2,2′-bipyridine (bpy) ligand is reduced to its radical anion, exhibiting the characteristic visible absorption band at 500–600 nm.[16] Moreover, the absorption maximum at 500 nm is consistent with that observed for metal-to-ligand charge transfer

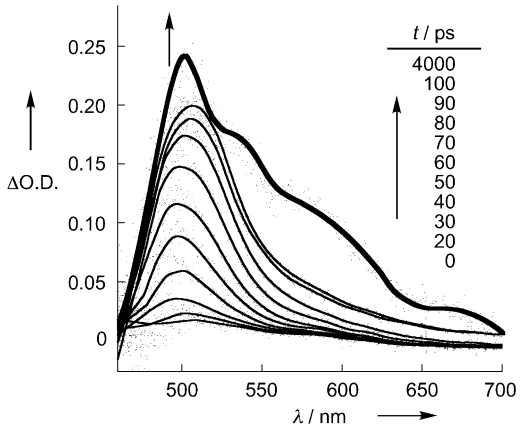



***Figure 2.*** Transient absorption spectra observed upon formation of the ICT excited state of **1** ($1.5 \times 10^{-4}$ M; thin lines) and the following deprotonation of **1** (thick line) after laser excitation ($\lambda = 355$ nm, 1.5 mJ/pulse) in deaerated $CH_3OH$.

 © 2003 Wiley-VCH Verlag GmbH & Co. KGaA, Weinheim 

(MLCT) excited state of other $Ir^{III}$-bpy complexes (490–500 nm) containing *ortho*-metalating ligands 2-phenylpyridine or benzo[*h*]quinoline.[17] The rise of the ICT band at 500 nm obeys to first-order kinetics (see Supporting Information). The first-order rate constant ($1.4\times10^{10}\ s^{-1}$) is consistent with that determined for the ISC of the excited state of an $Ir^{III}$ complex bearing a 1,10-phenanthroline ligand ($3–4\times10^{10}\ s^{-1}$).[18,19] With the completion of the fast ISC process, the slower deprotonation process sets in, as shown in Figure 2. Here, the characteristic absorption band that relates to **2** increases with first-order kinetics (see Supporting Information). From the first-order plot the deprotonation rate constant for **1** is determined as $k_H = 8.1\times10^8\ s^{-1}$.[20]

Although no deprotonation of **1** is observed when a $CH_3OH$ solution of **1** is photoirradiated in the steady state (see above), the H/D exchange of **1** clearly occurs during photoirradiation in $CD_3OD$. For example, when a $CD_3OD$ solution of **1** is photoirradiated in the steady state, the $^1H$ NMR signal at $\delta = -10.7$ ppm due to the hydride proton of **1** disappears gradually as the photoirradiation progresses (see Figure 3a). The addition of $H_2O$ [$H_2O/CD_3OD$ (1:4 v/v)] to the photoirradiated solution results in no change in the $^1H$ NMR signal (Figure 3b). However, the photoirradiation of the sample in the presence of $H_2O$ results in the

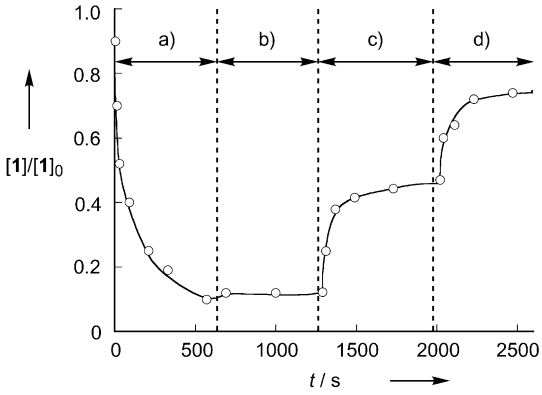
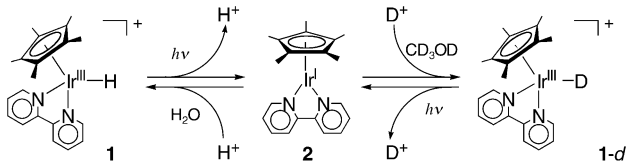



***Figure 3.*** Plot of $[\mathbf{1}]/[\mathbf{1}]_0$ versus time in the photoinduced H/D exchange reaction of **1** ($8.2\times10^{-3}$ M) at 298 K; a) during irradiation of monochromatized visible light at $\lambda = 430$ nm in deaerated $CD_3OD$; b) in the dark in the presence of $H_2O$ [$H_2O/CD_3OD$ (1:4 v/v)], and during irradiation with monochromatized visible light at $\lambda = 430$ nm in deaerated c) $H_2O/CD_3OD$ (1:4 v/v) and d) $H_2O/CD_3OD$ (1:2 v/v).

reappearance of the hydride proton of **1** (Figure 3c).[21] A further addition of $H_2O$ [$H_2O/CD_3OD$ (1:2 v/v)] followed by photoirradiation of the sample results in an increase in the hydride proton signal up to 80% of **1** (Figure 3d).[22] This observation indicates that the H/D exchange occurs efficiently during the photoirradiation of **1** in $CD_3OD$ in the steady state as shown in Scheme 2.

The deprotonation of the excited state of **1** may be understood by comparing the case of photoacid formation of hydoxyarenes, in which the enhanced acidity in the excited state is ascribed to an ICT from the hydroxyl oxygen to the aromatic ring. Figure 4 shows the HOMO and LUMO orbitals of **1**, obtained by DFT calculations.[23] The HOMO




***Scheme 2.*** The H/D exchange reaction between **1** and [$D_1$]-**1** under steady-state photoirradiation.

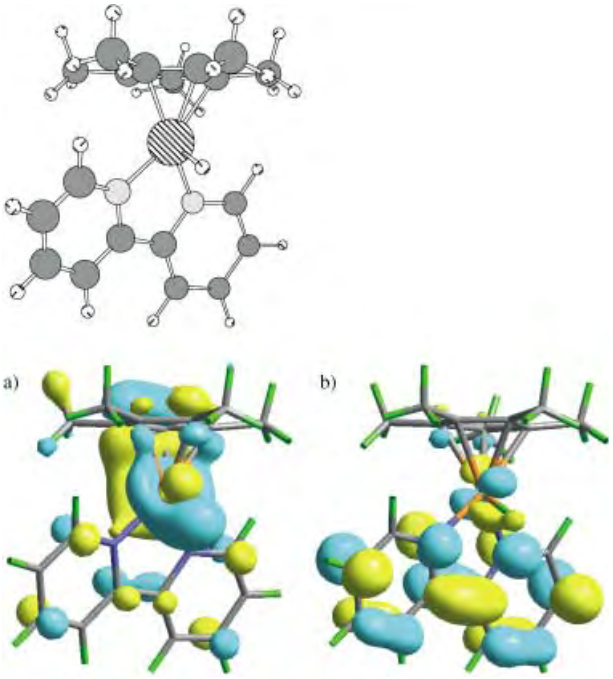



***Figure 4.*** a) The HOMO and b) LUMO orbitals of **1** calculated based on a density functional theory using ADF 2003.01 program.[23]

orbital is highly localized on the metal center, whereas the LUMO orbital is mainly localized on the ligand moiety. Thus, the MLCT excitation reduces the basicity of the iridium metal center, thus facilitating the release of a proton from **1**. The lifetime of the excited state of the conjugate base **2** is too short to be detected in the transient absorption spectra in Figure 2. On the other hand, the oxygen-centered hydroxyarenes have fluorescent conjugate bases with nonbonding molecular orbitals and excited states with charge distribution at distant sites from the oxygen atom. This reduces the basicity of the conjugate base. The latter scenario is equivalent to Weller's "intramolecular charge transfer" rationalization of the enhanced acidity in photoexcited hydroxyarenes.[2] The iridium hydride complex **1** also has a conjugate base **2** in which the MLCT transition reduces the basicity of the iridium metal center, thus facilitating the release of protons from the excited state of **1**.[24,25]

In summary, the present study documents a detailed investigation regarding 1) photoinduced deprotonation and 2) H/D exchange processes in a metal hydride complex **1**. We believe that **1** represents a new class of unique candidates that exhibit promising features as visible light-sensitive PAG.

 © 2003 Wiley-VCH Verlag GmbH & Co. KGaA, Weinheim 

## Experimental Section

The iridium hydride complex, **1**, was synthesized according to the literature procedure.[12] The methanol solution of deuterium-exchanged complex **1** ([$D_1$]-**1**) for picosecond laser flash photolysis experiments is obtained by the photoirradiation of **1** in the steady-state for 20 min by continuous exposure to light from a Xe-lamp (150 W, $\lambda > 390$ nm) in deaerated [$D_1$]methanol ($CH_3OD$).

Laser flash photolysis: For nanosecond laser flash photolysis experiments, the deaerated methanol solution of **1** was excited by a Panther OPO pumped by Nd:YAG laser (Continuum, SLII-10, 4–6 ns fwhm) at $\lambda = 430$ nm with the power of 10 mJ per pulse. The photochemical reactions were monitored by continuous exposure to a Xe-lamp (150 W) as a probe light and a photomultiplier tube (Hamamatsu 2949) as a detector. Picosecond laser flash photolysis experiments were carried out with 355 nm laser pulses from a mode-locked, Q-switched Quantel YG-501 DP Nd:YAG laser system (pulse width ~18 ps, 1–3 mJ/pulse).[26] The white continuum picosecond probe pulse was generated by passing the fundamental output through a $D_2O/H_2O$ solution.

Theoretical calculation: Electrons in orbitals up to and including 1s (C,N) and 4f but excluding 5s and 5p (Ir) were treated in accordance with the frozen-core approximation. Calculations for **1** and **2** were spin-restricted. Geometry optimizations were performed by using the local density approximation (LDA) with double-ζ quality Slater type basis sets (type II) for C, H, and N atoms and triple-ζ (type IV) for Ir atom. Nonlocal and relativistic corrections to the LDA were effected employing the B-LYP nonlocal exchange and correlation functionals and the ZORA scalar relativistic correction for each atom.[23]

Received: June 5, 2003
Revised: August 11, 5206 [Z52061]

**Keywords:** hydrides · iridium · isotope effects · kinetics · photochemistry

[1] L. M. Tolbert, K. M. Solntsev, *Acc. Chem. Res.* **2002**, *35*, 19.
[2] a) T. Förster, *Z. Elektrochem.* **1950**, *54*, 531; b) A. Weller, *Z. Elektrochem.* **1952**, *56*, 662; c) A. Weller, *Prog. React. Kinet.* **1961**, *1*, 187.
[3] a) H. Shizuka, *Acc. Chem. Res.* **1985**, *18*, 141; b) L. M. Tolbert, *Acc. Chem. Res.* **1986**, *19*, 268; c) E. M. Kosower, D. Huppert, *Annu. Rev. Phys. Chem.* **1986**, *37*, 127; d) P. Wan, G. Zhang, *Res. Chem. Intermed.* **1993**, *19*, 119.
[4] a) P. Wan, D. Shukla, *Chem. Rev.* **1993**, *93*, 571; b) S. G. Schulman in *Modern Fluorescence Spectroscopy* (Ed.: E. L. Wehry), Plenum, New York, **1976**, pp. 239–275; c) N. Mataga, T. Kubota, *Molecular Interactions and Electronic Spectra*, Marcel Dekker, New York, **1970**.
[5] a) L. M. Tolbert, J. E. Haubrich, *J. Am. Chem. Soc.* **1990**, *112*, 8163; b) L. M. Tolbert, J. E. Haubrich, *J. Am. Chem. Soc.* **1994**, *116*, 10593; c) K. M. Solntsev, D. Huppert, L. M. Tolbert, N. Agmon, *J. Am. Chem. Soc.* **1998**, *120*, 7981; d) K. M. Solntsev, L. M. Tolbert, B. Cohen, D. Huppert, Y. Hayashi, Y. Feldman, *J. Am. Chem. Soc.* **2002**, *124*, 9046.
[6] a) M. Lukeman, P. Wan, *J. Am. Chem. Soc.* **2002**, *124*, 9458; b) P.-T. Chou, J.-H. Liao, C.-Y. Wei, C.-Y. Yang, W.-S. Yu, Y.-H. Chou, *J. Am. Chem. Soc.* **2000**, *122*, 986; c) M. Fischer, P. Wan, *J. Am. Chem. Soc.* **1999**, *121*, 4555.
[7] a) N. Agmon, W. Rettig, C. Groth, *J. Am. Chem. Soc.* **2002**, *124*, 1089; b) I. V. Gopich, K. M. Solntsev, N. Agmon, *J. Chem. Phys.* **1999**, *110*, 2164.
[8] a) P. Dutta, A. Halder, S. Mukherjee, P. Sen, S. Sen, K. Bhattacharyya, *Langmuir* **2002**, *18*, 7867; b) K. Bhattacharyya, B. Bagchi, *J. Phys. Chem. A* **2000**, *104*, 10603.
[9] a) S. P. Pappas, *J. Imaging Technol.* **1985**, *11*, 146; b) D. A. Doshi, N. K. Huesing, M. Lu, H. Fan, Y. Lu, K. Simmons-Potter, B. G. Potter, Jr., A. J. Hurd, C. J. Brinker, *Science* **2000**, *290*, 107.
[10] a) B. J. Scott, G. Wirnsberger, M. D. McGehee, B. F. Chmelka, G. D. Stucky, *Adv. Mater.* **2001**, *13*, 1231; b) T. J. Trout, J. J. Schmieg, W. J. Gambogi, A. M. Weber, *Adv. Mater.* **1998**, *10*, 1219.
[11] S. Ogo, H. Nakai, Y. Watanabe, *J. Am. Chem. Soc.* **2002**, *124*, 597.
[12] a) S. Ogo, N. Makihara, Y. Watanabe, *Organometallics* **1999**, *18*, 5470; b) S. Ogo, N. Makihara, Y. Kaneko, Y. Watanabe, *Organometallics* **2001**, *20*, 4903; c) T. Abura, S. Ogo, Y. Watanabe, S. Fukuzumi, *J. Am. Chem. Soc.* **2003**, *125*, 4149.
[13] R. Ziessel, *J. Am. Chem. Soc.* **1993**, *115*, 118.
[14] M. Ladwig, W. Kaim, *J. Organomet. Chem.* **1992**, *439*, 79.
[15] The observed kinetic deuterium isotope effect may originate from the difference in the rate of proton transfer from protonated $CH_3OH$ as compared with deuteron transfer from deuterated $CH_3OD$.
[16] a) C. Creutz, *Comments Inorg. Chem.* **1982**, *1*, 293; b) T. Shida in *Electronic Absoption Spectra of Radical Ions*, Elsevier, Amsterdam, **1988**, p. 197.
[17] K. Ichimura, T. Kobayashi, K. A. King, R. J. Watts, *J. Phys. Chem.* **1987**, *91*, 6104.
[18] Y. Ohashi, T. Kobayashi, *J. Phys. Chem.* **1979**, *83*, 551.
[19] The ISC process is further confirmed by the observation of no kinetic deuterium isotope effect on the ISC rate for **1*** in comparison with that for [$D_1$]-**1***.
[20] The kinetic deuterium isotope effect ($k_H/k_D$) on the rate of deprotonation of **1*** is significantly smaller than that observed in the protonation process of **2**.
[21] The reappearance of the hydride proton signal by the addition of $H_2O$ (part c, Figure 3) clearly indicates the formation of the Ir-D complex, although we have not confirmed its formation by $^2H$ NMR.
[22] Addition of $H_2O$ obviously accelerates the rate of H/D exchange. It takes more than 600 seconds for reaching H/D exchange equilibrium of **1** (Figure 3a), however, less than 300 seconds in the presence of $H_2O$ (Figure 3c and d).
[23] G. te Velde, F. M. Bickelhaupt, E. J. Baerends, C. Fonseca-Guerra, S. J. A. Van Gisbergen, J. G. Snijders, T. Ziegler, *J. Comput. Chem.* **2001**, *22*, 931.
[24] The DFT calculations of **2** indicate that the HOMO orbital is more metal-centered (24%) than the LUMO orbital (21%). However, this is not a genuine MLCT example and there exists considerable orbital mixing between the metal and ligand orbitals.[14]
[25] Alternatively photoinduced opening of a coordination site followed by binding of methanol may result in intramolecular H/D exchange. Such intramolecular H/D exchange in an Ir-H complex has previously been reported, see: R. Koelliker, D. Milstein, *J. Am. Chem. Soc.* **1991**, *113*, 8524.
[26] C. Luo, D. M. Guldi, H. Imahori, K. Tamaki, Y. Sakata, *J. Am. Chem. Soc.* **2000**, *122*, 6535.

 © 2003 Wiley-VCH Verlag GmbH & Co. KGaA, Weinheim 

Elastic Films

# Self-Supporting Elastic Film without Covalent Linkages as a Hierarchically Integrated β-Sheet Assembly**

*Norihiro Yamada,* Tsukasa Komatsu, Hirotsugu Yoshinaga, Kayo Yoshizawa, Susumu Edo, and Masashi Kunitake*

In general, an amphiphilic molecule that can form an aggregate in a certain medium, especially an aqueous bilayer aggregate, forms a self-supporting film when the solution is cast onto an appropriate substrate then air dried.[1] The orderly molecular alignment within the cast film is useful for forming an ultrathin layer or coating with few defects. However, the supramolecular cast film has neither mechanical strength nor elasticity. Our aim in the present study is to improve the mechanical strength of the cast film, and to form an elastic supramolecular film that has the elastic properties of a macromolecular film. The prominent advantages of macromolecular films, namely, strength and elasticity, are ascribed to the covalent linkage that constitutes a sequence of the lowest unit molecule, the monomer. Therefore, an alternative interaction is needed to replace the covalent linkage to obtain an elastic supramolecular film. By using multiple H bonding as an alternative, Meijer and co-workers have demonstrated a supramolecular polymer.[2] The monomer of the supramolecular polymer has two sets of H-bonding blocks, for example, pyrimidon, at both edges of the molecule, which links the other molecules by multiple H bonding. The bora-type monomers yield a highly viscous, resinlike liquid. A similar substance has also been reported by Rebek, Jr. and coworkers.[3] Furthermore, the research group of Hutchison demonstrated that the self-assembled monolayer of a glycylglycine-containing amphiphile was stabilized by 3D networks of H bonding.[4] On the other hand, multiple H bonding has been observed as a β-sheet structure in the cast films of the tripeptide-containing amphiphiles.[5] These amphiphiles produce a self-supporting transparent film, but they are extremely brittle. This result means that another interaction that immobilizes the β-sheets will be needed for improving the mechanical strength of the supramolecular film. Thus, we attempted to use the side chains of the peptide part. Because the side chains of the adjacent amino-acid residues locate in opposite directions across the β-sheet plane,[6] the side chains could interlock with counterparts of the other β-sheet planes. This specific interdigitated structure should fasten the β-sheet planes when the peptide part contains at least three consecutive leucine residues as illustrated in Figure 1, which is similar to a zipper or a fastener. To reduce the confusion with the leucine zipper peptides, we prefer to call the aforementioned structure "leucine fastener". The leucine fastener will not be formed if a β-sheet structure is absent. Emphasis is placed on this hierarchy. However, until now, such hierarchic integration has not yet been realized. We demonstrate herein the hierarchic integration of supramolecular monomers, and aim to form a self-supporting elastic film without covalent linkage between the monomers.

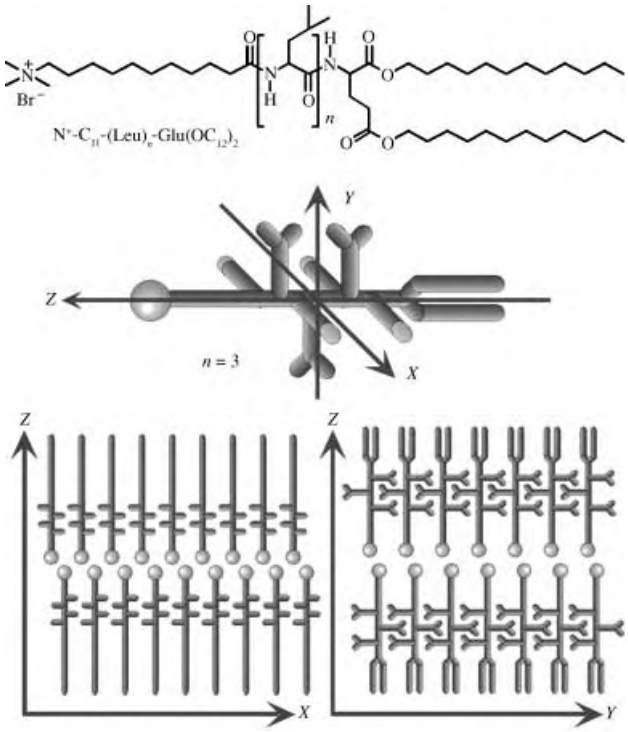



***Figure 1.*** Schematic illustration of two-dimensional immobilization of trileucine-containing amphiphile. Parallel β-sheet form in the *X*–*Z* plane, and leucine fastener form in the *Y*–*Z* plane.

The supramolecular monomers used in the study are leucine-containing amphiphiles ($N^+C_{11}(Leu)_nGlu(OC_{12})_2$; $n =$ 2, 3, 4). These amphiphiles dissolve in solvents with a low dielectric constant, namely, $CCl_4$, benzene, toluene, and cyclohexane, and form a gel at concentrations greater than 1 mM. In organic solvents with a higher dielectric constant, for example $CHCl_3$, the amphiphiles produce a clear solution. These results are consistent with our previous results with the other tripeptide or tetrapeptide-containing amphiphiles.[5,7]

We prepared the air-dried cast film from a $CCl_4$ gel and an isotropic $CHCl_3$ solution; the solutions were cast onto silicon-coated paper then air dried. The silicon-coated paper is available as cooking paper, which is helpful for the formation

[*] Prof. Dr. N. Yamada, T. Komatsu, H. Yoshinaga, K. Yoshizawa
Faculty of Education
Chiba University
Yayoi-cho, Inage-ku, Chiba 263-8522 (Japan)
Fax: (+81) 43-290-2519
E-mail: yamadan@faculty.chiba-u.jp
S. Edo, Prof. Dr. M. Kunitake
Faculty of Engineering, Kumamoto University
Kurokami, Kumamoto 860–8555 (Japan)

[**] This work was supported in part by a Grant-in-Aid for Scientific Research on Priority Areas (A), "Dynamic Control of Strongly Correlated Soft Materials" (No. 413/14045208), and a Grant-in-Aid for Scientific Research (No. 14550831) from the Ministry of Education, Science, Sports, Culture, and Technology, Japan.

 © 2003 Wiley-VCH Verlag GmbH & Co. KGaA, Weinheim DOI: 10.1002/anie.200352185 

of a self-supporting film. The cast film was easily peeled off from the substrate by using tweezers. Although all of the leucine-containing amphiphiles formed a self-supporting transparent cast film, a flexible film was obtained from a $CHCl_3$ solution of the trileucine- or tetraleucine-containing amphiphile. The cast film of the tetraleucine-containing amphiphile formed from the $CHCl_3$ solution was extraordinary. This cast film, which was brittle immediately after peeling off from the silicon-coated paper, became flexible when the film was warmed to about 70 °C. The reason for this phenomenon is discussed below. The other films were brittle despite the thermal treatment. The characteristics of the $N^+C_{11}(Leu)_nGlu(OC_{12})_2$ cast films are summarized in Table 1.

***Table 1:*** Characteristics of the Cast Films of $N^+C_{11}$ $(Leu)_nGlu(OC_{12})_2$.

| $N^+C_{11}(Leu)_nGlu(OC_{12})_2$ | $CHCl_3$ solution | $CCl_4$ gel |
|---|---|---|
| $n=2$ | brittle | brittle |
| $n=3$ | nonbrittle | brittle |
| $n=4$ | nonbrittle[a] | brittle |

[a] This cast film was brittle immediately after peeling from the silicon-coated paper, but turned flexible when the film was warmed to ca. 70 °C.

Figure 2 depicts an example of the flexible cast film of $N^+C_{11}(Leu)_3Glu(OC_{12})_2$ formed from a $CHCl_3$ solution (10 mM). We can bend (Figure 2A) and fold (Figure 2B) the film without fragmentation. However, the film is not tensible and tears under strain. Although the tensile strength was inferior to a macromolecular film, importance is placed on the flexibility of the cast film.

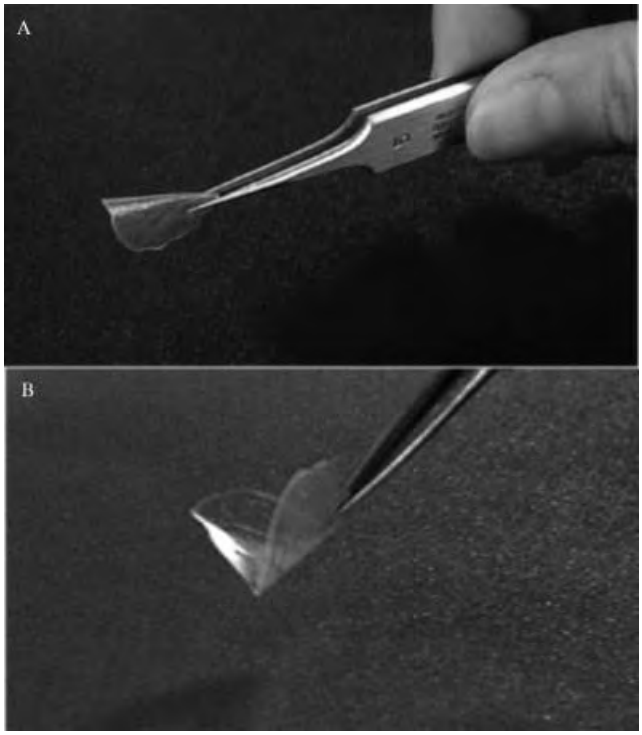



***Figure 2.*** Flexible cast film formed from a $CHCl_3$ solution. We can bend (A) or fold (B) the cast film without fragmentation.

The interpeptide H bonding is not the cause for the elasticity as all of the cast films contain a β-sheet structure regardless of the elasticity. The secondary structure of the peptide-containing amphiphiles are easily diagnosed by Fourier transform infrared (FTIR) spectroscopy.[5] As shown in Figure 3, all of the cast films, except for the film formed on a

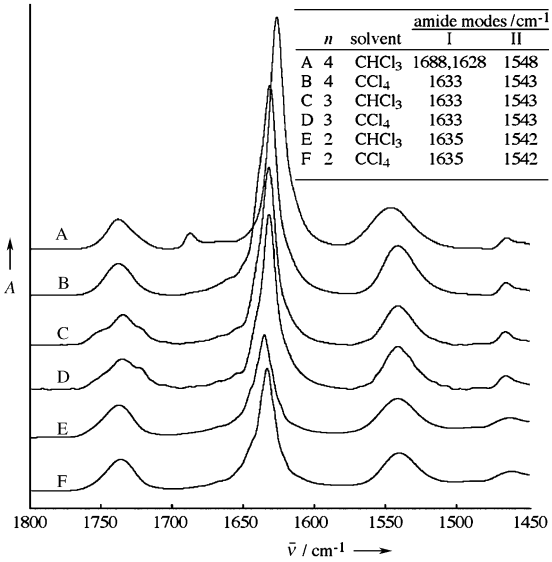



***Figure 3.*** FTIR spectra of $N^+C_{11}Leu_nGlu(OC_{12})_2$ cast films. A $CHCl_3$ or $CCl_4$ solution (2 mM) was spread onto a $CaF_2$ window then air dried. All of the spectra were measured at 25 ± 0.5 °C. Spectrum A ($n=4$, cast film from $CHCl_3$ solution) indicates formation of an antiparallel β-sheet structure, whereas the others (B–F) indicate formation of a parallel β-sheet structure. Details of the measurement and the diagnostics of the secondary structure in the peptide region have been reported elsewhere.[5]

$CaF_2$ window from the $CHCl_3$ solution of $N^+C_{11}(Leu)_4Glu(OC_{12})_2$, gave the same FTIR spectra, which was attributed to a parallel β-sheet structure. Strong and narrow amide I bands at 1630 $cm^{-1}$ indicate the presence of a well-developed parallel β-sheet structure within every cast film, whereas the amide I bands accompanying a small peak at 1690 $cm^{-1}$ meant that the cast film formed from the $CHCl_3$ solution of $N^+C_{11}(Leu)_4Glu(OC_{12})_2$ adopted an antiparallel β-sheet structure. Therefore, either the brittle or nonbrittle property should depend on another factor. The leucine fastener is thus most plausible factor, because the other peptide-containing amphiphiles without leucine residues formed only a fragile film. For example, pentapeptide-containing amphiphiles ($N^+C_{11}(Phe)_4Glu(OC_{12})_2$,[7] $N^+C_{11}(Ala)_4Glu(OC_{12})_2$[8]), tetrapeptide-containing amphiphiles ($N^+C_{11}(Phe)_3Glu(OC_{12})_2$,[7] $N^+C_{11}(Gly)_3Glu(OC_{12})_2$[8]), and the other tripeptide-containing amphiphiles previously reported,[5] which did not contain any leucinate residue, formed a self-supporting cast film, but never formed a flexible cast film. On the other hand, the leucine fastener needs at least three consecutive leucinate residues, because dileucine-containing amphiphiles could not form the specific interdigitated structure shown in Figure 1.

 © 2003 Wiley-VCH Verlag GmbH & Co. KGaA, Weinheim 

The next question is why did the $CCl_4$ gels of $N^+C_{11}(Leu)_n$-$Glu(OC_{12})_2$ ($n=3$ and 4) not produce an elastic film? The answer was obtained from the observation of the surface morphology by using a differential interference contrast microscope (DIM) and an atomic force microscope (AFM). Figure 4 and Figure 5 show the DIM and AFM images,

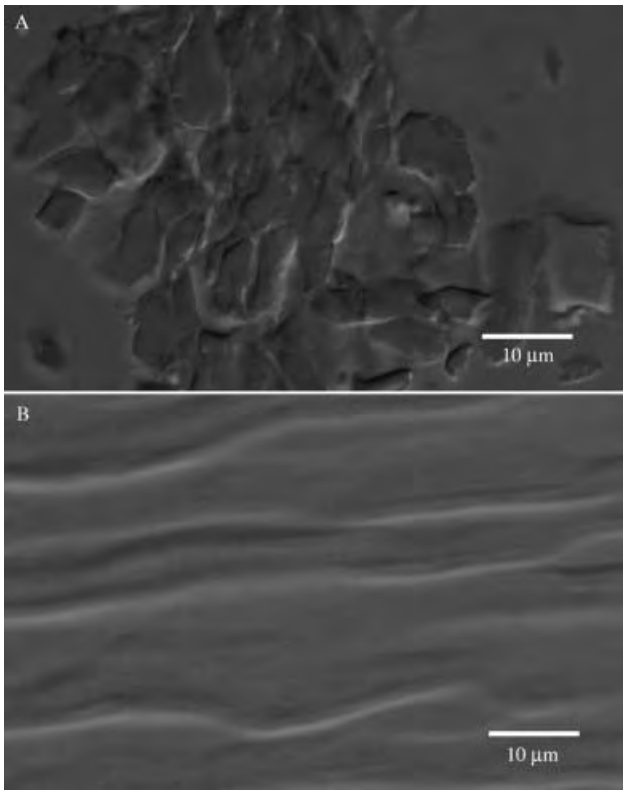



***Figure 4.*** DIM pictures of the surface morphology. The cast films on slide-glass were prepared from a $CCl_4$ (A) or a $CHCl_3$ (B) solution of $N^+C_{11}Leu_3Glu(OC_{12})_2$.

respectively, of the cast films of $N^+C_{11}(Leu)_3Glu(OC_{12})_2$. The surface morphology of the cast film prepared from the $CCl_4$ gel looked like a pile of platelets (Figure 4A). These platelets should be the aggregate formed in an original $CCl_4$ solution. On the other hand, the surface morphology of the cast film prepared from the $CHCl_3$ solution was a continuous sheet (Figure 4B). These images were consistent with the AFM images (Figure 5). A part of the platelet observed in Figure 4A is depicted in Figure 5A. This platelet should be an adsorbed monolayer or a tilted bilayer membrane, because the thickness of the platelet is about 3 nm, which corresponds to the expanded length of the $N^+C_{11}(Leu)_3Glu(OC_{12})_2$ molecule (about 4 nm). An important point is the discontinuity of the surface structure. The discontinuity should make the cast film fragile. On the other hand, the continuous sheet of the cast film from a $CHCl_3$ solution has a flat surface structure at the atomic level, although many clefts were observed. This flat surface morphology of the cast film formed from an isotropic $CHCl_3$ solution should reflect the flat surface of freshly cleaved mica. The clefts are very interesting,

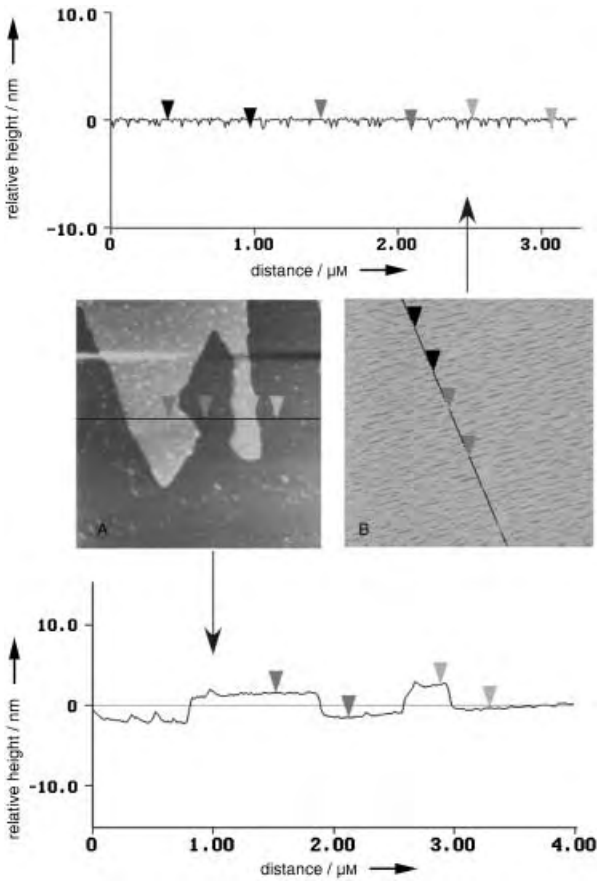



***Figure 5.*** AFM images of the surface morphology and cross-section profiles. The cast films on freshly cleaved mica prepared from 10 mM of $CCl_4$ (A) or $CHCl_3$ (B) solution of $N^+C_{11}Leu_3Glu(OC_{12})_2$.

because their formation should be related to the continuous sheet formation process. Figure 6A shows the AFM image of the surface of the mica, on which a thinner $CHCl_3$ solution of $N^+C_{11}(Leu)_3Glu(OC_{12})_2$ ($10^{-4}$ M) was spread then air dried. We consider that the rodlike objects are the single or doubled β-sheet as shown in Figure 6B. The fragmented β-sheet assemblages are closely packed when a solution with a higher concentration ($10^{-3}$ M) was cast. In this process, clefts have been left behind, especially at both edges of the β-sheet (Figure 6C). Therefore, the H bonding could form along the direction of the clefts, and the leucine fastener is formed along the perpendicular direction to the β-sheet plane. The H bonding and the leucine fastener achieve a two-dimensional immobilization of $N^+C_{11}(Leu)_3Glu(OC_{12})_2$, which should be the reason for the elasticity of the cast film formed from the $CHCl_3$ solution.

At the present stage, there remains one question: why did the thermal treatment produce flexibility in the cast film of $N^+C_{11}(Leu)_4Glu(OC_{12})_2$ formed from the $CHCl_3$ solution? In general, an increase in H bonding tends to result in solidity rather than fluidity. As solidity results in the lose of elasticity, thermal treatment could transform the solid film into a fluid film. Therefore, the cast film of $N^+C_{11}(Leu)_4Glu(OC_{12})_2$ formed from $CHCl_3$ should be fluid at the alkyl chains by thermal treatment. Such a partial fluid state should be related

 © 2003 Wiley-VCH Verlag GmbH & Co. KGaA, Weinheim 

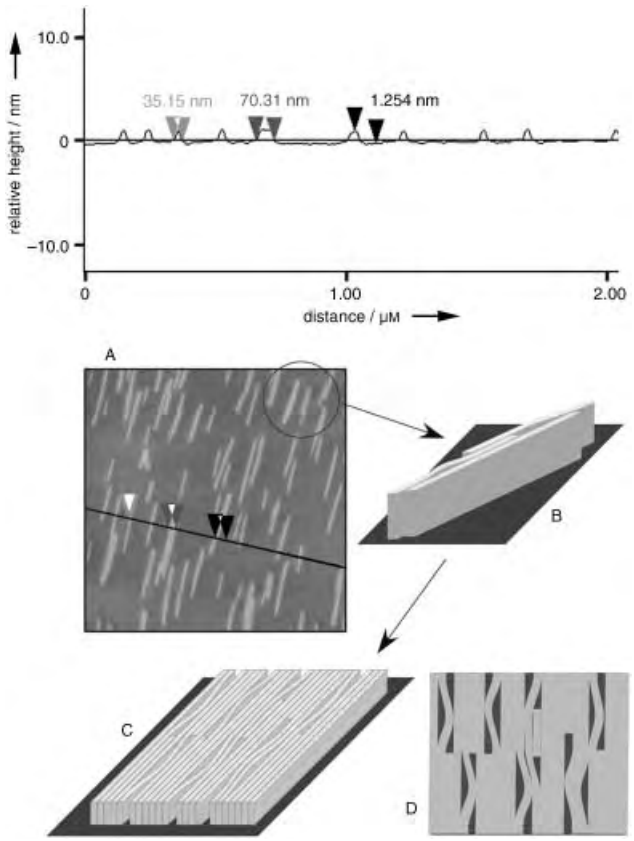



***Figure 6.*** Plausible mechanism for the formation of a flat surface at the atomic level. The cast film formed from a thinner solution yields rodlike objects (A), which should be a single or stacked β-sheet (B). The cluster should accumulate when a thick solution was spread (C). Overhead scanning of (C) should give the image like (D), which bears a resemblance to Figure 5(B).

to a plastic crystal phase. We are now investigating such details of the thermal treatment.

In conclusion, we have demonstrated the first example of a self-supporting, elastic supramolecular film. The supramolecular monomer, tri- or tetraleucine-containing amphiphile self-assembles and forms a β-sheet. The β-sheets stack upon each other, which was immobilized by interlocking at the side chains of the leucinate residues. This hierarchic integration is characteristic of an elastic supramolecular film. Furthermore, the elastic film should not be a solid, but forms a metastable state, because crystallization definitely reduces film elasticity. To maintain the elasticity, some functional group that prevents the film from crystallizing will be needed.

Received: June 25, 2003 [Z52185]

**Keywords:** amphiphiles · hydrogen bonds · self-assembly · supramolecular chemistry · thin films

[1] T. Kunitake, *Angew. Chem.* **1992**, *104*, 692–710; *Angew. Chem. Int. Ed. Engl.* **1992**, *31*, 709–726.
[2] L. Brunsveld, B. J. B. Folmer, E. W. Meijer, R. P. Sijbesma, *Chem. Rev.* **2001**, *101*, 4071–4097.
[3] R. K. Castellano, R. Clark, S. L. Craig, C. Nuckolls, J. Rebek, Jr., *Proc. Natl. Acad. Sci. USA* **2000**, *97*, 12418–12421.
[4] R. S. Clegg, S. M. Reed, J. Hutchison, *J. Am. Chem. Soc.* **1998**, *120*, 2486–2487.
[5] N. Yamada, K. Ariga, M. Naito, K. Matsubara E. Koyama, *J. Am. Chem. Soc.* **1998**, *120*, 12192–12199.
[6] J. Bandekar, *Biochim. Biophys. Acta* **1992**, *1120*, 123–143.
[7] N. Yamada, T. Imai, E. Koyama, *Langmuir* **2001**, *17*, 961–963.
[8] N. Yamada, unpublished results.

 © 2003 Wiley-VCH Verlag GmbH & Co. KGaA, Weinheim 

*Inclusion Complexes*

# Encapsulation Induces Helical Folding of Alkanes**

*Alessandro Scarso, Laurent Trembleau, and Julius Rebek, Jr.**

Helical structures occur frequently in proteins and nucleic acids but are not encountered as conformations of naturally occurring hydrocarbons. In the gel state of membranes, for example, the long alkyl chain components of membranes adopt strain-free extended conformations. Folding to more compact forms reduces the hydrophobic surface but generates strain in the form of *gauche* interactions. We recently observed that the alkane chains of two common surfactants in aqueous solution are bound within an open-ended synthetic receptor by assuming helical coil conformations.[1] The formation of the complex buries the hydrophobic surfaces of both the surfactant and receptor. Here we show that complete encapsulation of long-chain, normal alkanes ($C_{12}$–$C_{14}$) in organic media also results in folding to helical structures. Molecular recognition occurs between the $\pi$ lining of the rigid receptor and the C-H surface of the flexible alkane: the coiled alkane better complements the size, shape, and chemical surface of the receptor, even at the cost of $> 6$ kcal mol$^{-1}$ in *gauche* strain. Shorter alkanes are encapsulated in more extended conformations.

The synthetic receptor $\mathbf{1}_2$ (Figure 1) offers an elongated cavity, lined with eight benzene rings and additional $\pi$ surfaces. The calculated size of its cavity depends on the software

[*] Prof. J. Rebek, Jr., A. Scarso,[+] L. Trembleau[+]
The Skaggs Institute for Chemical Biology and
Department of Chemistry
The Scripps Research Institute
10550 North Torrey Pines Road, La Jolla, CA (USA)
Fax: (+1) 858-784-2876
E-mail: jrebek@scripps.edu

[+] These authors contributed equally to this work.

[**] We thank E. Bosa for valuable advice on NMR experiments. We are grateful to the Skaggs Institute for Research, the NASA Astrobiology Institute, and the National Institutes of Health (GM 50174) for financial support. L.T. and A.S. are Skaggs Postdoctoral Fellows.

Supporting information for this article is available on the WWW under http://www.angewandte.org or from the author.

 DOI: 10.1002/anie.200352235 © 2003 Wiley-VCH Verlag GmbH & Co. KGaA, Weinheim 

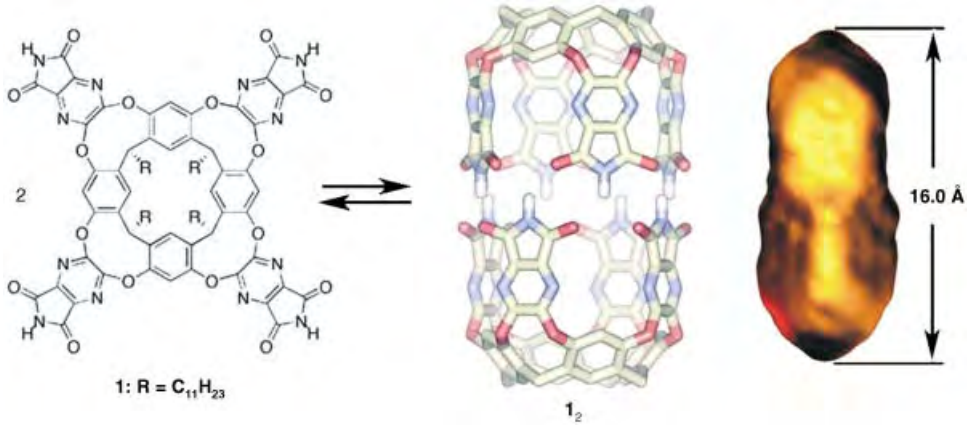
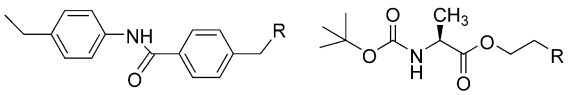



***Figure 1.*** a) Schematic drawing of the synthetic receptor; b) the energy-minimized dimer; and c) the size and shape of its cavity.

used, for example, the Swiss PDB viewer gives a volume of 425 Å$^3$ and a length of approximately 16 Å, but the tapered ends can accommodate only the smallest of atoms. The capsule is a host to guests that fill about half of its volume. The binding of rigid guest structures is strictly limited by length: the anilide **2a** (Scheme 1) with a methyl group is encapsulated, but the slightly longer ethyl compound **2b** is not. Flexible guests are also accepted if they can assume complementary lengths.[2,3] The Boc-Ala-ethyl ester **3a** (Boc = *tert*-butoxycarbonyl) is a good guest, while its homologues, even up to the pentyl ester **3b**, are bound to some extent.[4] The longer esters must adopt nonlinear conformations to be accommodated. The capsules are held together through a cyclic seam of bifurcated hydrogen bonds (Figure 1) and guest exchange involves the rupture of the seam as well as a conformational change of the receptor. Activation barriers for the in/out exchange process in [$D_{12}$]mesitylene are in the range of about 20 kcal mol$^{-1}$ for large guests,[5] and this process is slow on the NMR time scale: separate signals are seen in the spectra for the free and bound guest.




***Scheme 1.*** Examples of common guests for $\mathbf{1}_2$.

Only undefined aggregates of the host with broad NMR signals are observed in distilled [$D_{12}$]mesitylene. The maximum number of hydrogen bonds per subunit are present only in the dimeric capsular form, but mesitylene cannot fit inside. Without an appropriate guest, the inner surfaces remain unsolvated and a vacuum would exist in the capsule since; this provides the driving force for the assembled complexes.

We examined the encapsulation of straight-chain alkanes $C_{10}$ to $C_{15}$. At first glance, the hydrocarbons are ill fits as they are too narrow to complement the cavity of the capsule. A summary of the relevant properties of the guests, including their dimensions, surface areas, and volumes in both the extended and entirely helical conformations are given in Table 1. Even tightly coiled, alkane $C_{15}$ is seen to exceed the capsule's length, but alkane $C_{10}$ can fit in a fully extended conformation. The hydrocarbons $C_{10}$ to $C_{14}$ were found by experiment to be encapsulated in $\mathbf{1}_2$, but $C_{15}$ was not. The NMR spectra (Figure 2) showed separate signals for each encapsulated methylene and methyl group; the latter appeared at −4 ppm. This chemical shift ($\Delta\delta \sim 5$ ppm) is associated with a methyl group positioned at the very end of the cavity; the magnetic environment changes gradually as the guest moves toward the center of the capsule, where $\Delta\delta$ changes of approximately 1 ppm is typically observed.[6]

***Table 1:*** Dimensions of the hydrocarbons.

| Alkane[a] | Length [Å] | Surface area [Å$^2$] | Volume [Å$^3$] | PC[b] [%] | $K_{rel.}$[c] |
|---|---|---|---|---|---|
| $C_{10}H_{22}$ extended | 15.0 | 196 | 167 | 39 | 1.00 |
| $C_{12}H_{26}$ extended | 17.5 | 230 | 200 | 47 | 1.35 |
| $C_{12}H_{26}$ coiled | 13.6 | 207 | 206 | 48 | |
| $C_{14}H_{30}$ extended | 20.0 | 264 | 235 | – | 0.80 |
| $C_{14}H_{30}$ coiled | 15.5 | 235 | 240 | 56 | |
| $C_{14}H_{28}$ coiled | 16.0 | 239 | 239 | 56 | 0.32 |
| $C_{15}H_{32}$ coiled | 16.3 | 251 | 258 | – | |

[a] $C_{10}H_{22}$: *n*-decane; $C_{12}H_{26}$: *n*-dodecane; $C_{14}H_{30}$: *n*-tetradecane; $C_{14}H_{28}$: *trans*-7-tetradecene; $C_{15}H_{32}$: *n*-pentadecane. [b] Packing coefficients of alkanes in capsule $\mathbf{1}_2$ were calculated using Grasp[13] (1.5 Å probe) after energy minimization of the structures. [c] Relative association constants $K_{rel}$ were determined by NMR spectroscopy at 300 K by direct competition experiments.

Since no more than 10 carbon atoms can be accommodated in a fully extended conformation, folding must occur during the encapsulation of the longer alkanes. The conformation of the longest alkane guest ($C_{14}$) was determined through nuclear Overhauser enhancement (NOE) experiments. Cross-peaks between the hydrogen atoms on C1 and C4, and C1 and C5 were observed, and in accord with *gauche* interactions at the carbon atoms at the ends of the chain (Figure 3). The hydrogen atoms on C2 showed cross-peaks

 © 2003 Wiley-VCH Verlag GmbH & Co. KGaA, Weinheim 

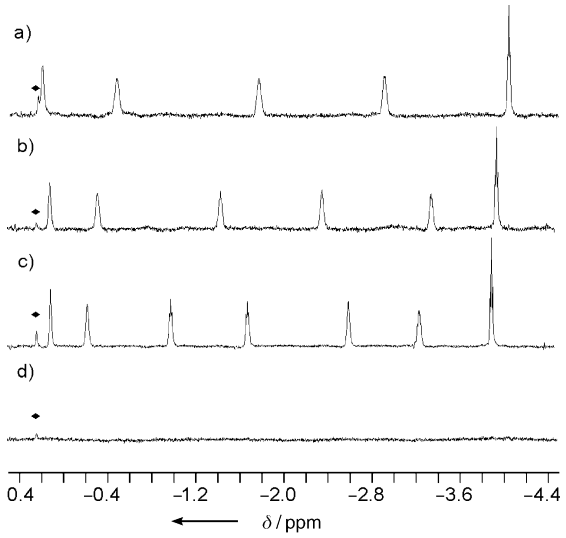



***Figure 2.*** $^1$H NMR spectra at 600 MHz in [$D_{12}$]mesitylene at 300 K of $\mathbf{1}_2$ (2 mM) with a) *n*-$C_{10}H_{22}$ (100 mM); b) *n*-$C_{12}H_{26}$ (100 mM); c) *n*-$C_{14}H_{30}$ (100 mM); d) *n*-$C_{15}H_{32}$ (100 mM). ◆indicates an impurity from the deuterated solvent.

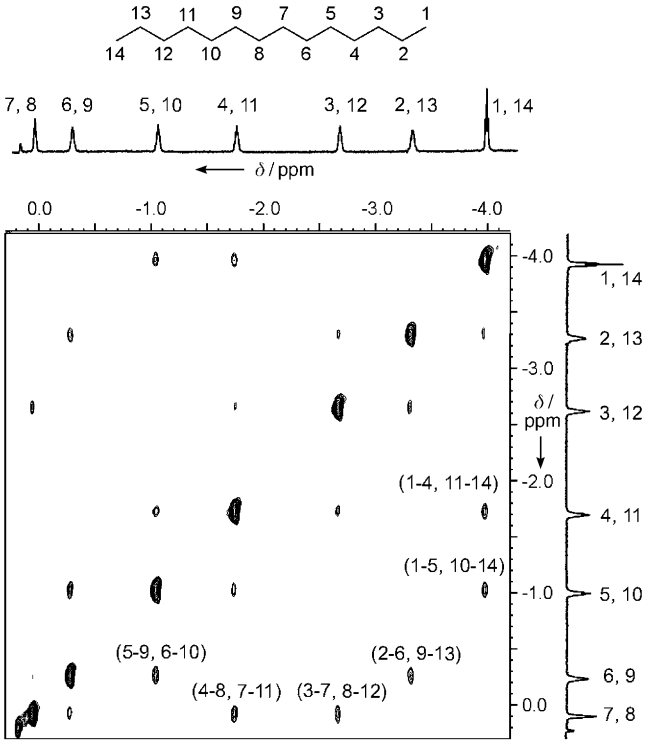



***Figure 3.*** Upfield portion of the 2D NOESY spectrum of the encapsulation complex of $\mathbf{1}_2$ [2 mM] with *n*-$C_{14}H_{30}$ [100 mM] (600 MHz; 300 K in [$D_{12}$]mesitylene; mixing time of 300 ms).

with C6 and those on C3 with C7—in general, C*i* interacted with C*i*+4 (*i* = 2 to 6)—thus indicating a tightly coiled helical structure. At least five *gauche* interactions exist at both ends of the $C_{14}$ alkane chain, each at an energy cost of 0.5–0.6 kcal mol$^{-1}$ in the liquid phase.[7,8] Direct competition experiments gave the relative binding affinities reported in Table 1 and revealed that the rate of equilibration in mesitylene is very slow at 300 K: more than 20 days was required to reach equilibrium in some cases. Dodecane ($C_{12}H_{26}$) was bound the strongest and reflects the balance of forces involved in encapsulation: as the chain length increases so do the unfavorable *gauche* interactions, but better packing coefficients and more favorable CH/π interactions[9,10] result between the guest and host (Figure 4). Accordingly, the

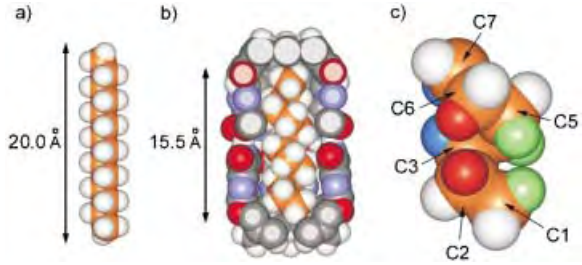



***Figure 4.*** Energy-minimized structures of $C_{14}H_{30}$@$\mathbf{1}_2$ complex:[12] a) extended conformation of tetradecane ($C_{14}H_{30}$); b) space-filling model and cross-section of the cavity showing C-H/π contacts; c) the origins of the intramolecular NOE interactions between hydrogen atoms at C1 and C4/C5, Ci and C*i*+4 (*i* = 2 to 6).

binding affinity of the $C_{14}$ alkane for the capsule is reduced by only a factor of 0.6. Liberation of the mesitylene solvent in contact with the alkanes outside the capsule undoubtedly provides an entropic benefit to offset the limitations of the guest inside the organized walls of the capsule. Size complementarity also exists: the volume of the cavity is about 425 Å$^3$ while that of the helical alkane is approximately 240 Å$^3$. The packing coefficient for the $C_{14}$ alkane within this space is 56%, which is near the ideal value for the liquid state.[11]

The signals in the $^1$H NMR spectrum corresponding to the methylene groups of alkane $C_{10}$ are shifted downfield in accord with positions nearer the center of the capsule (Figure 2a,c) and its NOE patterns correspond to those of a fully extended conformation (see Supplementary Information). Both conformations were present with alkane $C_{12}$ as a guest: the ends showed the characteristics of a coil and the central segment those of an extended conformation.

Finally, there are the motions of the alkanes while inside the capsule. The resting state of encapsulated alkane $C_{14}$ is helical, but the system is dynamic. Helices are, of course, chiral and the hydrogen atoms on C2 (and C3, etc) are then diastereotopic. Yet in the $^1$H NMR spectrum C2 appears as a fairly sharp hextet pattern, as would be expected of rapid rotation about the C2–C3 bond. A frozen helical conformation would generate signals of higher multiplicity than those actually observed (Figure 2c). Consequently, the enantiomeric helical forms must interconvert rapidly (racemize) on the NMR time scale while within the capsule. The eclipsed transition states for rotation about each *gauche* bond contribute only a barrier of about 2.7 kcal mol$^{-1}$, and rapid racemization seems energetically quite reasonable. There is not enough room in the capsule for this interconversion to take place through a fully extended conformation, but

 © 2003 Wiley-VCH Verlag GmbH & Co. KGaA, Weinheim 

crankshaft motions of a few carbon atoms up and down the chain are a likely mechanism for the interconversion, and some evidence of this is provided by the olefin *trans*-7-tetradecene. This alkene has its central four carbon atoms fixed in an extended conformation and is encapsulated almost as well as the $C_{14}$ alkane: direct competition experiments with the $C_{14}$ alkene and alkane showed the alkane is favored by only a factor of 2.5. In other words, the energetic cost of an extended conformation for four carbon atoms of the $C_{14}$ alkane is less than 0.5 kcal mol$^{-1}$.

Received: June 26, 2003 [Z52235]

**Keywords:** helical structures · host–guest systems · hydrocarbons · pi interactions · supramolecular chemistry

[1] L. Trembleau, J. Rebek, Jr., *Science* **2003**, 301, 1219 – 1220.
[2] T. Heinz, D. M. Rudkevich, J. Rebek, Jr., *Angew. Chem.* **1999**, *111*, 1206 – 1209; *Angew. Chem. Int. Ed.* **1999**, *38*, 1136 – 1139.
[3] T. Heinz, D. M. Rudkevich, J. Rebek, Jr., *Nature* **1998**, *394*, 764 – 766.
[4] O. Hayashida, L. Sebo, J. Rebek, Jr., *J. Org. Chem.* **2002**, *67*, 8291 – 8298.
[5] S. L. Craig, S. Lin, J. Chen, J. Rebek, Jr., *J. Am. Chem. Soc.* **2002**, *124*, 8780 – 8781.
[6] A. Shivanyuk, J. Rebek, Jr., *Angew. Chem.* **2003**, *115*, 708 – 710; *Angew. Chem. Int. Ed.* **2003**, *42*, 684 – 686.
[7] E. Eliel, S. H. Wilen, *Stereochemistry of organic compounds*, Wiley, New York, **1994**.
[8] Molecular modeling calculations performed with the program Maestro (MM3 force field) gave an energy gap of 0.83 kcal mol$^{-1}$ between *anti* and *gauche* conformations of hexane in the gas phase.
[9] a) M. Nishio, M. Hirota, Y. Umezawa, *The CH/π interaction*, Wiley, New York, **1998**; b) W. Blokzijl, J. B. F. N. Engberts, *Angew. Chem.* **1993**, *105*, 1610 – 1648; *Angew. Chem. Int. Ed. Engl.* **1993**, *32*, 1545.
[10] E. A. Meyer, R. K. Castellano, F. Diederich, *Angew. Chem.* **2003**, *115*, 1244 – 1287; *Angew. Chem. Int. Ed.* **2003**, *42*, 1210 – 1250.
[11] S. Mecozzi, J. Rebek, Jr., *Chem. Eur. J.* **1998**, *4*, 1016 – 1022.
[12] F. Mohamadi, N. G. J. Richards, W. C. Guida, R. Liskamp, M. Lipton, C. Caufield, G. Chang, T. Hendrickson, W. C. Still, *J. Comput. Chem.* **1990**, *11*, 440.
[13] A. Nicholls, K. Sharp, B. Honig, *Proteins* **1991**, *11*, 281.

 © 2003 Wiley-VCH Verlag GmbH & Co. KGaA, Weinheim 

Terminal OH-Containing Alumoxane

# Synthesis, Structural Characterization, and Reaction of the First Terminal Hydroxide-Containing Alumoxane with an [{Al(OH)}$_2$(μ-O)] Core**

*Guangcai Bai, Herbert W. Roesky,* Jiyang Li, Mathias Noltemeyer, and Hans-Georg Schmidt*

*Dedicated to Professor Alan H. Cowley on the occasion of his 70th birthday*

Considerable attention has been focused on the investigations of their structure and mode of catalytic activity of alumoxanes since the discovery of methylalumoxane (MAO) as a highly active cocatalyst in ethylene and propylene polymerization by group 4 metallocenes in 1980.[1] The role of MAO seems clear,[2] but the molecular structure of the active alumoxane species remains an open question. In the course of numerous investigations of the controlled hydrolysis of aluminum compounds, some alumoxanes have been isolated and structurally characterized by introducing bulky alkyl or aryl groups in place of methyl groups,[3] but none of them perform as well as MAO in the metallocene mediated olefin polymerization. Although three coordinate aluminum sites are present in the compounds in which oligomerization is sterically hindered by bulky ligands,[4] alumoxanes containing terminal hydroxide are very rare.

Recently we demonstrated that the liquid ammonia/toluene two phase system is highly effective for the hydrolysis and ammonolysis of transition metal compounds. The organozirconium oxide and hydroxide clusters [{($EtMe_4C_5$)Zr}$_6$-(μ$_6$-O)(μ$_3$-O)$_8$]·($C_7H_8$),[5] [(Cp*Zr)$_6$(μ$_4$-O)(μ-O)$_4$(μ-OH)$_8$]·2($C_7H_8$),[6] and related systems[7] were prepared by the hydrolysis and ammonolysis of metal chlorides in a liquid ammonia/toluene two-phase system at low temperatures. More recently, the first hydrolysis by a main-group metal halide in a two phase system led to an unprecedented congener of boronic acid LAl(OH)$_2$ (**1**; L = HC[(CMe)(2,6-*i*Pr$_2$$C_6H_3$N)]$_2$).[8] Herein we report on the synthesis of the first dinuclear alumoxane that contains a terminal hydroxide and a six-membered alumoxane with a three coordinate Al center and two coordinate O atoms.

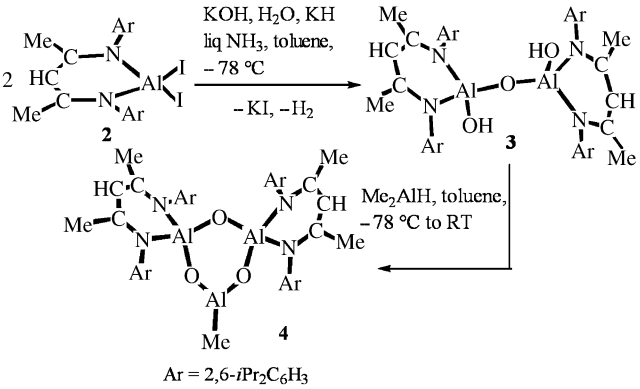
The reaction of LAlI$_2$ (**2**) with KOH that contained 10–15% $H_2O$ (1.0:0.71 molar ratio of pure KOH) and KH (1.0:1.4 molar ratio) in liquid ammonia and toluene at −78 °C results in the complete removal of iodide and the formation of

[*] Prof. Dr. H. W. Roesky, Dr. G. Bai, Dr. J. Li, Dr. M. Noltemeyer, H.-G. Schmidt
Institut für Anorganische Chemie
Universität Göttingen
Tammannstrasse 4, 37077 Göttingen (Germany)
Fax: (+49) 551-39-3373
E-mail: hroesky@gwdg.de

[**] This work was supported by the Deutsche Forschungsgemeinschaft and the Fonds der Chemischen Industrie.

 © 2003 Wiley-VCH Verlag GmbH & Co. KGaA, Weinheim DOI: 10.1002/anie.200352163 

β-diketiminatoalumoxane [{LAl(OH)}$_2$(μ-O)]·0.5($C_7H_8$)·$C_6H_{14}$ (**3**; Scheme 1). A proposed mechanism for the formation of **3** is similar to that of **1**.[8] In this reaction dihydroaluminum **1** is obtained as an intermediate in the first




***Scheme 1.*** Synthesis of **3** and **4**.

steps. Meanwhile, we assume that the amidohydroaluminum {LAl(OH)($NH_2$)} intermediate is formed because of the excess of the starting material **2**. After intermolecular ammonia elimination, the two intermediates are converted to **3**. However, no {LAl(OH)($NH_2$)} was found after the reaction was complete. Moreover, it is well documented that ammonolysis of aluminum triiodide yields potassium aluminate $KAl(NH_2)_4$ in the presence of K or $K(NH_2)$ in liquid ammonia.[9] We suppose that the excess of **2** and the intermediate [LAl(OH)($NH_2$)] react with $KNH_2$ (resulting from the reaction of KH and $NH_3$), thus leading to insoluble or noncrystalline products under the above condition. Furthermore, increase of the molar ratio of **2**:(KOH+$H_2O$), such as 1.0 to 1.5, led to the mixture of products **1** and **3**. Therefore, we assume that the liquid ammonia/toluene two phase system and the excess of **2** and KH in this reaction are essential for the formation of **3**, and the bulky L ligand on aluminum is stabilizing the terminal hydroxide-containing alumoxane. Further reaction of **3** with $Me_2AlH$ (1.0:1.0 molar ratio) in toluene results in the formation of trimeric alumoxane [$(LAl)_2$(MeAl)(μ-O)$_3$]·2$C_7H_8$ (**4**; Scheme 1). The steric hindrance of the L ligands attached to two Al atoms leads to the coordinatively unsaturated third Al atom in **4**.

Compounds **3** and **4** are colorless crystalline solids with melting points of 265 and 152 °C, respectively. No decomposition or polymerization was observed when **3** or **4** were kept in the toluene solution or as solids in a glove box. The most intense peak in the EI mass spectrum of **3** appears at *m*/*z* 905 [$M^+$–0.5$C_7H_8$–$C_6H_{14}$–$H_2O$–Me], and the signal at 938 (42%) is assigned to the [$M^+$–0.5$C_7H_8$–$C_6H_{14}$] fragment. Compound **4** exhibits the fragments [$M^+$–2$C_7H_8$], [$M^+$–2$C_7H_8$–Me] and [$L^+$–Me] at 979 (56), 964 (48) and 403 (100), respectively. In the IR spectrum of **3**, a sharp band (3716 $cm^{-1}$) for the stretching frequency of the free hydroxide is observed.

The molecular structures of **3** and **4**[10] are shown in Figure 1 and Figure 2, respectively. Compounds **3** and **4** crystallize in the monoclinic space groups *P*2(1)/*n* and *C*2/*c*,

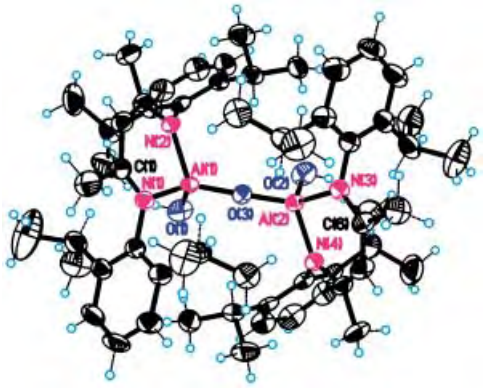


***Figure 1.*** The crystal structure of **3**. The toluene and hexane molecules are omitted for clarity. Selected bond lengths [Å] and angles [°]: Al(1)-O(1) 1.738(3), Al(1)-O(3) 1.698(3), Al(2)-O(2) 1.741(3), Al(2)-O(3) 1.694(3), Al(1)-N(1) 1.912(3), Al(1)-N(2) 1.928(3), Al(2)-N(3) 1.911(3), Al(2)-N(4) 1.919(3); O(1)-Al(1)-O(3) 112.33(14), O(1)-Al(1)-N(1) 111.76(15), O(1)-Al(1)-N(2) 106.84(13), N(1)-Al(1)-N(2) 95.64(13), Al(1)-O(3)-Al(2) 143.84(16).

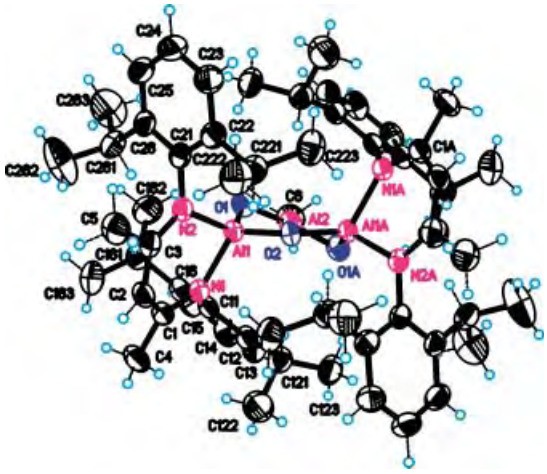


***Figure 2.*** The crystal structure of **4**. The two toluene molecules are omitted for clarity. Selected bond lengths [Å] and angles [°]: Al(1)-O(1) 1.726(2), Al(1)-O(2) 1.7122(16), Al(2)-O(1) 1.708(2), Al(1)-N(1) 1.930(3), Al(1)-N(2) 1.909(2); O(1)-Al(1)-O(2) 108.28(11), O(1)-Al(1)-N(1) 101.23(11), O(1)-Al(1)-N(2) 125.16(11), N(1)-Al(1)-N(2) 95.26(11), Al(1)-O(1)-Al(2) 117.69(13), Al(1)-O(2)-Al(1A) 125.73(18), O(1)-Al(2)-O(1A) 115.53(16).

respectively. Compound **3** contains a bent AlOAl species without a center of symmetry. Each of the Al atoms exhibits a highly distorted tetrahedral geometry with two nitrogen atoms of the ligand L, an OH group and one (μ-O) unit. The two ligands L adopt an approximately staggered *anti* conformation (the angles between the N(1)Al(1)N(2) and N(3)Al(2)N(4) planes are 87.70°), and the bulky *ortho* substituents (2,6-*i*$Pr_2C_6H_3$) of the ligands L are arranged *trans* to each other at the same side of the two Al centers, which minimizes the steric repulsion between the two ligands. The OH groups are bent out of the Al(1)O(3)Al(2) plane (31.26° and 30.71°) towards the opposite side where the 2,6-*i*$Pr_2C_6H_3$ substituents are oriented. The Al-(μ-O) bond lengths (1.698(3) and 1.694(3) Å) are comparable, and the

 © 2003 Wiley-VCH Verlag GmbH & Co. KGaA, Weinheim 

Al-(μ-O)-Al angle (143.84(16)°) is significantly smaller than those found in compounds [{[$(Me_3Si)_2HC]_2Al$}$_2$(μ-O)] (1.6877(4) Å; 180°),[11] [{($t$Bu)$_2$Al[NH(Me)$CH_2CH_2$N-$Me_2$]}$_2$](μ-O) (1.690(7) Å; 173.0(4)°),[12] and [{HC[(CMe)(N-Me)]$_2$AlCl}$_2$(μ-O)] (1.6770(6) Å; 180°).[13] The Al–OH bond lengths (1.738(3) and 1.741(3) Å) of **3** are significantly longer than those in **1** (1.6947(15) and 1.7107(16) Å),[8] but considerably shorter than those of the Al–(μ-OH) and Al–($\mu_3$-OH) bonds exhibited by compounds [$(Ph_2Si)_2O_3]_4Al_4$(μ-OH)$_4$ (1.787(3) to 1.814(3) Å, average 1.800 Å),[14] [{$Mes_2$Al(μ-OH)}$_2$]·2THF (1.822 Å; Mes = mesityl),[3e] and [$Al_5$($t$Bu)$_5$($\mu_3$-O)$_2$($\mu_3$-OH)$_2$(μ-OH)$_2$(μ-$O_2$CPh)$_2$] (Al–($\mu_3$-OH), 1.914(5) to 2.086(4) Å; Al–(μ-OH), 1.820(3) to 1.828(3) Å).[15] The Al–N bond lengths (1.912(3) and 1.928(3) Å) are longer than those observed in **1** (1.8881(17) and 1.8903(16) Å) and [{HC[(CMe)(NMe)]$_2$AlCl}$_2$(μ-O)] (1.8611(16) and 1.8617(16) Å).[13]

The structure of **4** contains two four coordinate Al and one three coordinate Al linked by μ-oxo bridges to form a highly distorted six-membered $(AlO)_3$ ring. The coordination sphere of Al(1), Al(1A) or Al(2) is completed by two nitrogen atoms of L or one Me group, respectively. The Al(2)–(μ-O) bond lengths (1.708(2) Å) are slightly shorter than those of Al(1)–(μ-O) and Al(1A)-(μ-O) (1.7122(16) and 1.726(2) Å) in **4**, but longer than those in **3** and other dimeric compounds containing an {$Al_2$(μ-O)} unit. Furthermore, the Al–(μ-O) bond lengths of **3** are considerable shorter than those of the Al–(μ-OH) bonds found in the six-membered ring compound [($t$Bu)$_2$Al(μ-OH)]$_3$ (1.846(3) to 1.851(2) Å) and in a complex containing three coordinate Al centers [($t$Bu)$_2$Al{μ-OAl($t$Bu)$_2$}]$_2$ (1.750(3) to 1.871(4) Å).[4a]

It has been demonstrated that compounds with linear centrosymmetric {$Al_2$(μ-O)} building units have significant Al-(μ-O) double bond character.[16] Compound **3** contains a bent {$Al_2$(μ-O)} unit but short Al-(μ-O) bonds, which should increase the steric interaction between the bulky L groups on adjacent aluminum atoms. The calculated molecular electrostatic potential (MESP) isosurface of **3** is presented in Figure 3.[17] The negative potential regions (−20 kcal mol$^{-1}$) of the lone pairs arrange outside of the one bridged and two terminal oxygen atoms, which interact with the π electrons of the two aryl rings. Because of this interaction the π electron density in the MESP map of the two aromatic rings becomes stronger. The bending of the Al-O-Al bond (143.86°) leads to an effective overlap of the lone pairs of the oxygen atoms with the π electrons of the two aromatic rings. The argument that the lone pair electron density of the bridged oxygen atom is partially transferred to the aromatic rings is supported by the partial double bond character of the Al-(μ-O) bonds.

Because of the Lewis acidic $Al^{3+}$ centers, the OH groups of **3** are expected to function as Brönsted acids. The solid state IR spectrum (Nujol) of **3** exhibits a sharp band (3716 cm$^{-1}$) for the OH groups, which is similar to that found for the free OH groups of compound **1** (3727 cm$^{-1}$). Therefore, **3** contains free and strong Brönsted acidic OH groups.[18] Furthermore, these protons of the OH groups are expected to resonate at very low field in the $^1$H NMR spectrum. However, no resonance was observed at low field in the $^1$H NMR spectrum of **3**. It can be clearly seen that the protons of the two OH groups are surrounded by the two aromatic rings because of the high π electron density of the aromatic rings in **3** (Figure 3). As a result the aromatic rings give rise to unusual shielding, which causes the two OH protons to resonate at high field ($\delta = -0.30$ ppm).

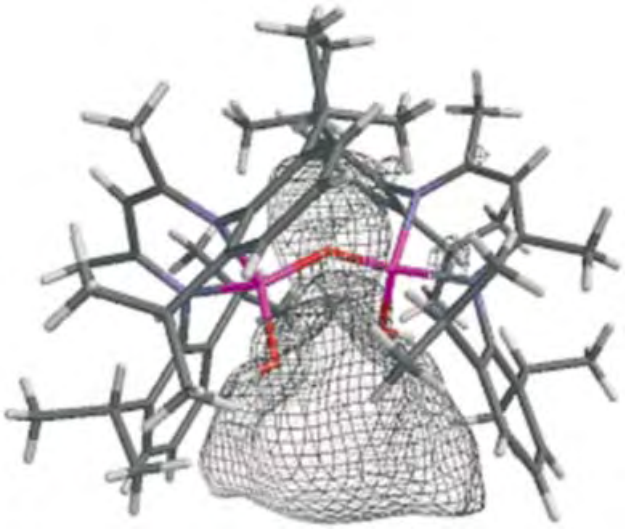


***Figure 3.*** The calculated molecular potential isosurfaces (−20 kcal mol$^{-1}$) for **3** (area: 150.67 Å$^2$, volume: 95.19 Å$^3$) at the HF/STO-3G level, showing the interaction of the lone pairs on the oxygen atoms and the π electrons of the aromatic rings.

It has been traditionally proposed that alumoxanes containing three coordinate Al centers are strong Lewis acids and vital for the catalytic activity. Although **4** contains a three coordinate Al center, no catalytic activity was observed when **4** was used as a cocatalyst for the dimethylzirconocene polymerization of ethylene in toluene solution at room temperature. This result is in agreement with that obtained by Barron and co-workers, although they used no methyl-containing aluminum three coordinate species.[19]

Herein, we present the hydrolysis of an aluminum compound that involves a liquid $NH_3$/toluene two phase system and yields the hitherto unknown [{LAl(OH)}$_2$(μ-O)] species. The partial transfer of the lone pair electron density of the three O atoms of **3** results in the formal double bond character of the Al–(μ-O) bonds and in a stronger electron density of the two aromatic rings with the consequence that the two Brönsted acidic OH protons resonate at very high field in the $^1$H NMR spectrum. Because of the presence of the Brönsted acidic OH groups, **3** should react with organometallic compounds, which provides possibilities in the field of design and synthesis of low molecular weight organoaluminum-containing compounds, such as **4**, and newer and unusual applications in the catalysis of olefins. Such an investigation is currently underway in our laboratories.

## Experimental Section

Synthesis of **3**: Ammonia (40 mL) was condensed onto a suspension of **2** (1.50 g, 2.15 mmol), KOH (KOH > 85%, $H_2O$ 10–15%; 0.10 g, 1.52 mmol KOH (85%), 0.83 mmol $H_2O$ (15%)) and KH (0.12 g, 3.00 mmol) in toluene (80 mL) at −78 °C while the reaction mixture

 © 2003 Wiley-VCH Verlag GmbH & Co. KGaA, Weinheim 

was stirred. The mixture was stirred continuously for an additional 1 h at this temperature. The excess ammonia was then allowed to evaporate from the reaction mixture over a period of 4 h. During this time the mixture was warmed slowly to room temperature. After filtration and subsequent concentration (to 5 mL) in vacuo, hexane (5 mL) was added to the filtrate. The resulting colorless solution was kept at −20 °C for two days to give colorless crystals of **3** (0.56 g). Yield 67 % (according to O containing reactants). Mp: 265 °C; IR (Nujol): $\tilde{\nu}$ = 3716, 1549, 1534, 1439, 1401, 1383, 1317, 1226, 1176, 1099, 1023, 975, 935, 873, 798, 760 $cm^{-1}$; $^1H$ NMR (200 MHz, $C_6D_6$; the sample isolated from toluene was used, in which one molecule of aluminum dimer contains one molecule of toluene): $\delta$ = 7.24–7.00 (m, *Ph*Me and *Ar*), 4.87 (s, 2H, γ-C*H*), 3.73 (sept, $^3J_{HH}$ = 6.8 Hz, 2H, C*H*$Me_2$), 3.57 (sept, $^3J_{HH}$ = 6.9 Hz, 2H, C*H*$Me_2$), 3.24 (sept, $^3J_{HH}$ = 6.8 Hz, 2H, C*H*$Me_2$), 3.12 (sept, $^3J_{HH}$ = 6.6 Hz, 2H, C*H*$Me_2$), 2.10 (s, 3H, Ph*Me*), 1.55 (d, $^3J_{HH}$ = 7.5 Hz, 6H, CH*Me*$_2$), 1.50 (s, C*Me*), 1.48 (d, $^3J_{HH}$ = 6.7 Hz, CH*Me*$_2$), 1.45 (s, C*Me*) (18H), 1.35 (d, $^3J_{HH}$ = 6.9 Hz, 12H, CH*Me*$_2$), 1.14, 1.13 (dd, $^3J_{HH}$ = 6.9 Hz, 12H, CH*Me*$_2$), 0.82 (d, $^3J_{HH}$ = 6.6 Hz, 6H, CH*Me*$_2$), 0.73 (d, $^3J_{HH}$ = 6.7 Hz, 6H, CH*Me*$_2$), −0.30 ppm (s, 2H, O*H*); EI-MS: *m*/*z* (%): 938 (42) [$M^+$−0.5 $C_7H_8$−$C_6H_{14}$], 920 (19) [$M^+$−0.5 $C_7H_8$−$C_6H_{14}$−$H_2O$], 905 (100) [$M^+$−0.5 $C_7H_8$−$C_6H_{14}$−$H_2O$−Me]; elemental analysis calcd (%) for $C_{67.5}H_{102}Al_2N_4O_3$ (1071.5): C 75.7, H 9.6, N 5.2; found: C 75.1, H 9.4, N 5.2.

Synthesis of **4**: $Me_2AlH$ (20 % in heptane, 0.29 g, 1.0 mmol) was added to the solution of **3** (1.07 g, 1.0 mmol) in toluene (60 mL) at −78 °C while the reaction mixture was stirred. The mixture was warmed slowly to room temperature and stirred continuously overnight at this temperature. After filtration and subsequent concentration (to 5 mL) in vacuo, the resulting colorless solution was kept at −20 °C for two weeks to give colorless crystals of **4** (0.61 g). After concentration of the filtrate to 3 mL, the solution was kept at −20 °C for three days and an additional crop of **4** (0.12 g) was formed. Yield 0.73 g (63 %). Mp: 152 °C; IR (Nujol): $\tilde{\nu}$ = 1550, 1533, 1466, 1382, 1318, 1252, 1178, 1024, 936, 904, 884, 798, 760, 729 $cm^{-1}$; $^1H$ NMR (300 MHz, $C_6D_6$): $\delta$ = 7.31–6.99 (m, *Ph*Me and *Ar*), 4.87 (s, 2H, γ-C*H*), 4.15 (sept, $^3J_{HH}$ = 6.7 Hz, 2H, C*H*$Me_2$), 3.33 (sept, $^3J_{HH}$ = 6.8 Hz, 2H, C*H*$Me_2$), 3.11, 3.06 (dsept, $^3J_{HH}$ = 6.8 and 6.7 Hz, 4H, C*H*$Me_2$), 2.10 (s, 6H, Ph*Me*), 1.58 (d, $^3J_{HH}$ = 6.5 Hz, 6H, CH*Me*$_2$), 1.48 (s, 6H, C*Me*), 1.46 (s, 6H, C*Me*), 1.42, 1.38 (dd, $^3J_{HH}$ = 6.8 and 6.9 Hz, 18H, CH*Me*$_2$), 1.12, 1.09 (dd, $^3J_{HH}$ = 7.0 and 7.1 Hz, 12H, CH*Me*$_2$), 0.87 (d, $^3J_{HH}$ = 6.7 Hz, 6H, CH*Me*$_2$), 0.72 (d, $^3J_{HH}$ = 6.7 Hz, 6H, CH*Me*$_2$), −1.48 ppm (s, 3H, *Me*); EI-MS: *m*/*z* (%): 979 (56) [$M^+$−2 $C_7H_8$], 964 (48) [$M^+$−2 $C_7H_8$−Me], 403 (100) [L−Me]; elemental analysis calcd. for $C_{73}H_{101}Al_3N_4O_3$ (1163.5): C 75.3, H 8.7, N 4.8; found: C 74.5, H 8.7, N 4.8.

Received: June 18, 2003 [Z52163]

**Keywords:** aluminum · ammonia · biphasic system · hydrolysis · hydroxide

[1] a) H. Sinn, W. Kaminsky, H.-J. Vollmer, R. Woldt, *Angew. Chem.* **1980**, *92*, 396 – 402; *Angew. Chem. Int. Ed. Engl.* **1980**, *19*, 390 – 392; b) E. Y.-X. Chen, T. J. Marks, *Chem. Rev.* **2000**, *100*, 1391 – 1434; c) H. W. Roesky, M. G. Walawalkar, R. Murugavel, *Acc. Chem. Res.* **2001**, *34*, 201 – 211.

[2] a) H. Sinn, W. Kaminsky, *Adv. Organomet. Chem.* **1980**, *18*, 99 – 149; b) W. Kaminsky, R. Steiger, *Polyhedron* **1988**, *7*, 2375 – 2381; c) L. Resconi, F. Piemontesi. G. Franciscono, L. Abis, T. Fiorani, *J. Am. Chem. Soc.* **1992**, *114*, 1025 – 1032; d) C. Sishta, R. M. Hathorn, T. J. Marks, *J. Am. Chem. Soc.* **1992**, *114*, 1112 – 1114.

[3] a) T. L. Feng, P. L. Gurian, M. D. Healy, A. R. Barron, *Inorg. Chem.* **1990**, *29*, 408 – 411; b) C. J. Harlan, M. R. Mason, A. R. Barron, *Organometallics* **1994**, *13*, 2957 – 2969; c) R. J. Wehmschulte, W. J. Grigsby, B. Schiemenz, R. A. Bartlett, P. P. Power, *Inorg. Chem.* **1996**, *35*, 6694 – 6702; d) J. Storre, A. Klemp, H. W. Roesky, H.-G. Schmidt, M. Noltemeyer, R. Fleischer, D. Stalke, *J. Am. Chem. Soc.* **1996**, *118*, 1380 – 1386; e) J. Storre, C. Schnitter, H. W. Roesky, H.-G. Schmidt, M. Noltemeyer, R. Fleischer, D. Stalke, *J. Am. Chem. Soc.* **1997**, *119*, 7505 – 7513; f) Y. Koide, A. R. Barron, *Organometallics* **1995**, *14*, 4026 – 4029; g) M. Veith, M. Jarczyk, V. Huch, *Angew. Chem.* **1998**, *110*, 109 – 112; *Angew. Chem. Int. Ed.* **1998**, *37*, 105 – 108; h) W. Schmitt, E. Baissa, A. Mandel, C. E. Anson, A. K. Powell, *Angew. Chem.* **2001**, *113*, 3689 – 3693; *Angew. Chem. Int. Ed.* **2001**, *40*, 3577 – 3581.

[4] a) M. R. Mason, J. M. Smith, S. G. Bott, A. R. Barron, *J. Am. Chem. Soc.* **1993**, *115*, 4971 – 4984; b) M. D. Healy, A. R. Barron, *Angew. Chem.* **1992**, *104*, 939 – 941; *Angew. Chem. Int. Ed. Engl.* **1992**, *31*, 921 – 922.

[5] G. Bai, H. W. Roesky, P. Lobinger, M. Noltemeyer, H.-G. Schmidt, *Angew. Chem.* **2001**, *113*, 2214 – 2217; *Angew. Chem. Int. Ed.* **2001**, *40*, 2156 – 2159.

[6] G. Bai, H. W. Roesky, J. Li, T. Labahn, F. Cimpoesu, J. Magull, *Organometallics* **2003**, *22*, 3034 – 3038.

[7] a) G. Bai, H. W. Roesky, P. Müller, *Bull. Pol. Acad. Sci. Chem.* **2002**, *50*, 1 – 10; b) G. Bai, H. W. Roesky, M. Noltemeyer, H. Hao, H.-G. Schmidt, *Organometallics* **2000**, *19*, 2823 – 2825; c) G. Bai, P. Müller, H. W. Roesky, I. Usón, *Organometallics* **2000**, *19*, 4675 – 4677; d) G. Bai, H. W. Roesky, H.-G. Schmidt, M. Noltemeyer, *Organometallics* **2001**, *20*, 2962 – 2965.

[8] G. Bai, Y. Peng, H. W. Roesky, J. Li, H.-G. Schmidt, M. Noltemeyer, *Angew. Chem.* **2003**, *115*, 1164 – 1167; *Angew. Chem. Int. Ed.* **2003**, *42*, 1132 – 1135.

[9] a) W. L. Taylor, E. Griswold, J. Kleinberg, *J. Am. Chem. Soc.* **1955**, *77*, 294 – 298; b) G. W. Watt, J. L. Hall, G. R. Choppin, *J. Phys. Chem.* **1953**, *57*, 567 – 570.

[10] a) Crystal data for **3**: Single crystals of **3** suitable for X-ray structural analysis were obtained from a solution of toluene and hexane by maintaining the reaction mixture at −20 °C for one week. $C_{67.5}H_{102}Al_2N_4O_3$, $M_r$ = 1071.49, monoclinic, space group *P*2(1)/*n*, *a* = 13.731(3) Å, *b* = 21.352(4) Å, *c* = 22.877(5) Å, β = 103.58(3)°, *V* = 6520.0(1) Å$^3$, *Z* = 4, $\rho_{calcd}$ = 1.092 Mg m$^{-3}$, *F*(000) = 2340, λ = 0.71073 Å, *T* = 203(2) K, μ($Mo_{K\alpha}$) = 0.090 mm$^{-1}$. Of the 16982 measured reflections, 8498 were independent ($R_{int}$ = 0.0844). The final refinement converged at *R*1 = 0.0657 for $I > 2\sigma(I)$, *wR*2 = 0.1908 for all data. The final difference Fourier synthesis gave a min./max. residual electron density −0.425/+0.347 e Å$^{-3}$; b) Crystal data for **4**: Single crystals of **4** suitable for X-ray structural analysis were obtained from a solution of toluene by maintaining the reaction mixture at −20 °C for two weeks. $C_{73}H_{101}Al_3N_4O_3$, $M_r$ = 1163.52, monoclinic, space group *C*2/*c*, *a* = 19.515(3) Å, *b* = 14.738(2) Å, *c* = 24.414(5) Å, β = 102.974(10)°, *V* = 6842.6(19) Å$^3$, *Z* = 4, $\rho_{calcd}$ = 1.129 Mg m$^{-3}$, *F*(000) = 2520, λ = 0.71073 Å, *T* = 200(2) K, μ($Mo_{K\alpha}$) = 0.103 mm$^{-1}$. Of the 5788 measured reflections, 5670 were independent ($R_{int}$ = 0.0982). The final refinement converged at *R*1 = 0.0672 for $I > 2\sigma(I)$, *wR*2 = 0.2049 for all data. The final difference Fourier synthesis gave a min./max. residual electron density −0.457/+0.669 e Å$^{-3}$; c) Data for the structures **3** and **4** were collected on a Stoe-Siemens-AED2 four-circle diffractometer. Intensity measurements were performed on a rapidly cooled crystal with the dimensions 0.8 × 0.6 × 0.5 mm$^3$ in the range $7.04 \le 2\theta \le 45.02°$ and 1.0 × 0.5 × 0.4 mm$^3$ in the range $7.00 \le 2\theta \le 49.90°$ for **3** and **4**, respectively. The structures were solved by direct methods (SHELXS-97)[20] and refined with all data by full-matrix least-squares on $F^2$. The hydrogen atoms of C–H bonds were placed in idealized positions. CCDC 212660 and 212661 (**3** and **4**) contain the supplementary crystallographic data for this paper. These data can be obtained free of charge via www.ccdc.cam.ac.uk/conts/retrieving.html (or from the Cam-

 © 2003 Wiley-VCH Verlag GmbH & Co. KGaA, Weinheim 

bridge Crystallographic Data Centre, 12, Union Road, Cambridge CB21EZ, UK; fax: (+44) 1223-336-033; or deposit@ccdc.cam.ac.uk).
[11] W. Uhl, M. Koch, W. Hiller, M. Heckel, *Angew. Chem.* **1995**, *107*, 1122 – 1124; *Angew. Chem. Int. Ed. Engl.* **1995**, *34*, 117 – 119.
[12] C. N. McMahon, A. R. Barron, *J. Chem. Soc. Dalton Trans.* **1998**, 3703 – 3704.
[13] N. Kuhn, S. Fuchs, E. Niquet, M. Richter, M. Steimann, *Z. Anorg. Allg. Chem.* **2002**, *628*, 717 – 718.
[14] M. Veith, M. Jarczyk, V. Huch, *Angew. Chem.* **1997**, *109*, 140 – 142; *Angew. Chem. Int. Ed. Engl.* **1997**, *36*, 117 – 119.
[15] Y. Koide, A. R. Barron, *Organometallics* **1995**, *14*, 4026 – 4029.
[16] a) Y. Kushi, Q. Fernando, *J. Am. Chem. Soc.* **1970**, *92*, 91 – 96; b) K. J. Wynne, *Inorg. Chem.* **1985**, *24*, 1339 – 1343; d) Y. Kushi, Q. Fernando, *Chem. Commun.* **1969**, 555 – 556.
[17] a) The RHF (Restricted Hartree-Fock) calculations with STO-3G basis set were performed with the Spartan '02 program: W. J. Hehre, R. F. Stewart, J. A. Pople, *J. Chem. Phys.* **1969**, *51*, 2657 – 2664; b) All calculations are based on the experimental structure of **3**.
[18] The stretching mode of the O–H group is a qualitative indicator for the acidity of the proton: G. Sastre, D. W. Lewis, *J. Chem. Soc. Faraday Trans.* **1998**, *94*, 3049 – 3058.
[19] a) C. J. Harlan, S. G. Bott, A. R. Barron, *J. Am. Chem. Soc.* **1995**, *117*, 6465 – 6474; b) A. R. Barron, *Macromol. Symp.* **1995**, *97*, 15 – 26.
[20] G. M. Sheldrick, SHELXL-97, *Program for Crystal Structure Refinement*, Universität Göttingen, **1997**.

 © 2003 Wiley-VCH Verlag GmbH & Co. KGaA, Weinheim 

Cluster Compounds

# A Threefold $AlH_2$-Coordinated Carbon Atom as Part of the First Carbaalanate**

*Andreas Stasch, Herbert W. Roesky,* Paul von Ragué Schleyer, and Jörg Magull*

*Dedicated to Professor F. Albert Cotton*

Carbaalanes[1] were first prepared by Wilke and Schneider[2] and unambiguously characterized by Uhl and Breher in 1999.[3] The corresponding dianions of this class of compounds, the carbaalanates, have not been reported so far, although they are widely known in boron chemistry. Some of the boron congeners are among the weakest coordinating anions and stabilize reactive cationic species, which could only be isolated because of the unique properties of these anions.[4]

By the reaction of a terminal alkyne with 3 equivalents of $AlH_3{\cdot}NMe_3$ in boiling toluene we obtained the carbaalane $[(AlH)_6(AlNMe_3)_2(CCH_2R)_6]$ (R = Ph, $CH_2SiMe_3$) in good yields.[5] However, the reaction of *t*BuC≡CH with $AlH_3{\cdot}NMe_3$ under the same conditions resulted in traces of $[(AlH)_6(AlNMe_3)_2(CCH_2tBu)_6]$, which could not be characterized unambiguously. As a result of the low boiling point of *t*BuC≡CH (37–38 °C), the compound evaporates from the mixture before any reaction takes place. Therefore, we decided to treat solid *t*BuC≡CLi, prepared from *t*BuC≡CH and *n*BuLi in hexane, with equivalent amounts of $AlH_3{\cdot}NMe_3$ and $ClAlH_2{\cdot}NMe_3$ [Eq. (1)]. The latter species was prepared in situ by the addition of 1 equivalent of chlorotrimethylsilane to 3 equivalents of $AlH_3{\cdot}NMe_3$. When the reagents were combined (at 0 °C or room temperature), an exothermic reaction occurred. The suspension was stirred at room temperature, heated at reflux for 45 min, and filtered while hot. Colorless crystals were obtained from the reaction mixture at room temperature and at 4 °C.

$$8\ tBuC{\equiv}CLi + 6\ ClAlH_2\cdot NMe_3 + 8\ AlH_3\cdot NMe_3 \xrightarrow[-\,6\ LiCl\ -\,8\ NMe_3]{\text{toluene},\ \Delta} [\{tBuCH_2C(AlH_2\cdot NMe_3)_3Li\}_2\{(AlH)_8(CCH_2tBu)_6\}] \quad (1)$$

**1**

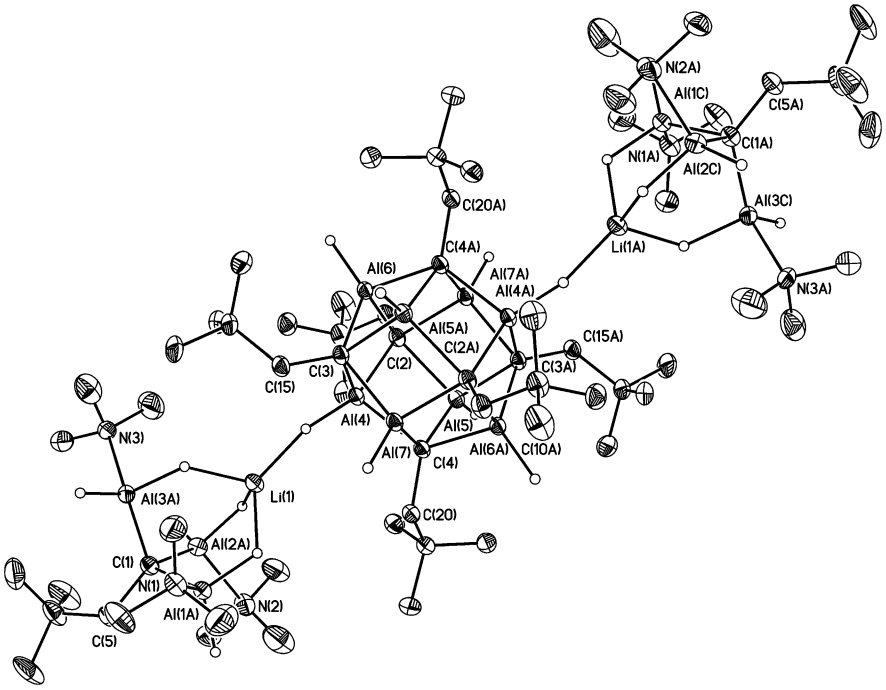



***Figure 1.*** Molecular structure of **1**. Only hydrogen atoms on aluminum atoms are shown. Selected bond lengths [pm] and angles [°]: Al(1A)-C(1) 201.9(4), Al(2A)-C(1) 196.1(4), Al(3A)-C(1) 193.5(4), Al(1B)-C(1) 191.0(4), Al(2B)-C(1) 204.2(4), Al(3B)-C(1) 196.5(4), Al(1A)-N(1) 206.1(3), Al(2A)-N(2) 206.7(3), Al(3A)-N(3) 213.2(4), Al(1B)-N(2) 216.8(4), Al(2B)-N(3) 221.2(5), Al(3B)-N(1) 217.4(4), Al(4)-C(2) 202.7(3), Al(5)-C(2) 210.3(3), Al(4)-Al(7) 257.0(1), Al(5)-Al(6)#1 262.5(1); Al(2A)-C(1)-Al(1A) 103.76(16), C(1)-Al(1A)-N(1) 117.68(14), Al(7)#1-Al(5)-Al(4) 87.65(4), Al(5)#1-Al(7)-Al(6)#1 93.10(4).

The X-ray single-crystal structural analysis[6] revealed a composition of $[\{tBuCH_2C(AlH_2{\cdot}NMe_3)_3Li\}_2\{(AlH)_8(CCH_2tBu)_6\}]{\cdot}2\,C_7H_8$ (**1**·2 $C_7H_8$; Figure 1). The central part of the molecule is a carbaalanate cluster $[(AlH)_8(CCH_2tBu)_6]^{2-}$, which is isoelectronic with the previously characterized $[(AlX)_6(AlNMe_3)_2(CCH_2R)_6]$ (X = H, Cl) carbaalane system and therefore implies the same aromatic stabilization.[5] Two lithium cations are each coordinated through hydride bridges to the neutral $[tBuCH_2C(AlH_2{\cdot}NMe_3)_3]$ moiety in which three $AlH_2{\cdot}NMe_3$ groups are bound covalently to one carbon atom. The three Al atoms are disordered with two different positions (~68% for Al(A) and ~32% for Al(B)) for each Al atom (Figure 2). In the neutral $[tBuCH_2C(AlH_2{\cdot}NMe_3)_3]$ moiety, the Al–C bond lengths range from 193.5(4) to

[*] Prof. Dr. H. W. Roesky, Dipl.-Chem. A. Stasch, Prof. Dr. J. Magull
Institut für Anorganische Chemie, Georg-August-Universität
Tammannstrasse 4, 37077 Göttingen (Germany)
Fax: (+49) 551-393-373
E-mail: hroesky@gwdg.de
Prof. Dr. P. von R. Schleyer
Computational Chemistry Annex, The University of Georgia
Athens, GA 30602-2525 (USA)
and
Institut für Organische Chemie 1, Universität Erlangen-Nürnberg
Henkestrasse 42, 91054 Erlangen (Germany)

[**] This work was supported by the Deutsche Forschungsgemeinschaft, the Fonds der Chemischen Industrie, and the Göttinger Akademie der Wissenschaften.

Supporting information for this article is available on the WWW under http://www.angewandte.org or from the author.

 DOI: 10.1002/anie.200352502 © 2003 Wiley-VCH Verlag GmbH & Co. KGaA, Weinheim 

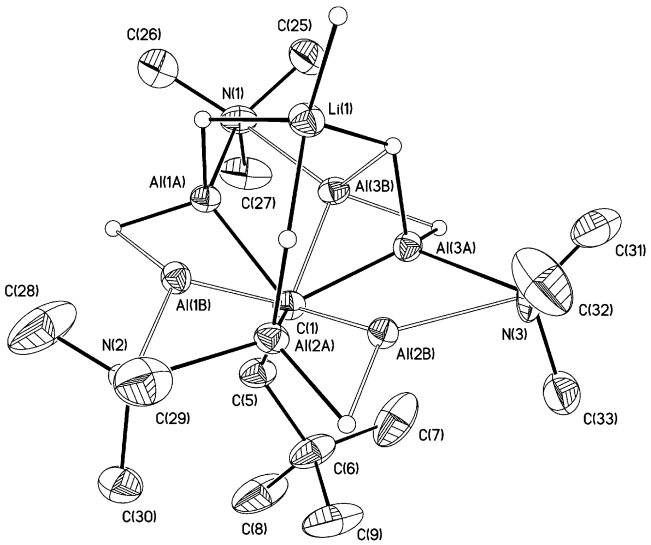



***Figure 2.*** View of the disordered [$t$BuCH$_2$C(AlH$_2$·NMe$_3$)$_3$LiH] unit of **1**. Hydrogen atoms between Al(B) and Li(1) were not found. Shorter contacts were observed between the hydrogen atom and Al(3A), Li(1), and Al(3B).

201.9(4) pm for the Al(A) atoms and from 191.0(4) to 204.2(4) pm for the Al(B) atoms. The Al–N bond lengths show a large variation, ranging from 206.1(3) pm for Al(1A)–N(1) to 221.2(5) pm for Al(2B)–N(3). The Al–C and Al–Al bond lengths in the cluster anion are in the expected region when compared with those of previously reported systems.[5]

Compound **1** is poorly soluble in toluene or benzene and therefore NMR spectroscopic analysis was difficult and poor-quality spectra were obtained. However, the $^1$H NMR data does not contradict the crystallographically determined composition. EIMS analysis did not provide any molecular ion or significant fragments. Furthermore the fragments obtained by ESIMS (dilute solution in toluene) could not be assigned. The IR spectrum shows several absorptions for the Al–H bonds in the region 1768–1650 cm$^{-1}$. When the reaction mixture or the isolated solid is exposed to traces of air, it adopts a violet to lavender-blue color, which persists when the oxidized solution is stored at low temperatures (room temperature: hours, $-25\,^\circ$C: days). An EPR spectrum of an air-oxidized, dilute, violet solution of **1** at room temperature does not show any resonances. The violet color is not exclusively seen in this sample. We observed this phenomenon in general in some (but not all) reaction mixtures that contained AlH$_3$·NMe$_3$ and $t$BuC≡C groups. The synthesis of **1** is reproducible, and the crystal structure was determined twice from the products obtained in the same way from two different reaction mixtures.

DFT calculations at the B3LYP6-311+G** level for the simplified model, [H$_3$CC(AlH$_2$·NH$_3$)$_3$Li]$^+$ (an optimized $C_3$ symmetry minimum), reproduced the structural findings and showed that the Li$^+$ interacts strongly with the three endo Al–H bonds. As a consequence, these Al–H bond lengths increase (from 160.2 to 165.1 pm), whereas the terminal Al–H bonds become shorter (163.3 to 159.8 pm). The Li$^+$ ion (natural charge +0.90) fits well in the "pocket", where it interacts electrostatically with the three Al-H groups. The natural charges on these three hydrides increase from −0.36 to −0.45 upon coordination with Li$^+$. The resulting very large Li$^+$ binding energy to the free [H$_3$CC(AlH$_2$·NH$_3$)$_3$] species (77.5 kcal mol$^{-1}$, calculated with the zero-point energy correction) stabilizes the complex considerably. In the crystal, the Li$^+$ interacts at its fourth coordination site with an additional Al-H hydrogen atom of the dianion moiety.

As described above, the reaction of a terminal alkyne RC≡CH (R = Ph, CH$_2$SiMe$_3$) with 3 equivalents of AlH$_3$·NMe$_3$ under similar conditions (solvent, temperature, and time) as those used for **1** resulted in a condensed cluster [(AlH)$_6$(AlNMe$_3$)$_2$(CCH$_2$R)$_6$] with aromatic stabilization.[5] No reactive intermediates such as RCH$_2$C(AlH$_2$·NMe$_3$)$_3$ were detected in the reaction mixture.

Based on the calculations and chemical behavior of carbaalanes, we concluded that the coordination to the lithium cation stabilizes the [$t$BuCH$_2$C(AlH$_2$·NMe$_3$)$_3$] moiety and prevents condensation to a cluster compound. The $t$BuCH$_2$C(BCl$_2$)$_3$ analogue is known in boron chemistry.[7] Compounds of this type are synthesized by hydroboration of $t$BuC≡CBCl$_2$ with HBCl$_2$ (formed in situ) and are further converted into a *closo*-C$_2$B$_3$-carborane cluster. Very recently, a compound with a [(Me$_2$Al)$_2$(μ-CH)(AlCl$_2$Me$_2$)$_2$]$^-$ anion in which the central CH unit is surrounded by four aluminum atoms was synthesized by a C–H activation reaction.[8] In compound **1**, the [$t$BuCH$_2$C(AlH$_2$·NMe$_3$)$_3$] moiety acts as a chelating ligand to the lithium atom. Clearly, the organolithium starting material is also essential for the formation of the carbaalanate and the formation of the cluster dianion via aluminate intermediates.

In summary, we have prepared and structurally characterized the first carbaalanate [(AlH)$_8$(CCH$_2$$t$Bu)$_6$]$^{2-}$ and isolated it as a dilithium salt. This unit stabilizes the neutral molecule [$t$BuCH$_2$C(AlH$_2$·NMe$_3$)$_3$] by coordination of the hydride H atoms to the lithium cation. Although the aromatic carbaalanes are not stable under protic conditions, as is the case with many carboranes, we proved its stability through calculations and through its reaction behavior.[5] Therefore the isoelectronic carbaalanates are a promising new class of compounds for trapping reactive species.

## Experimental Section

All manipulations were performed under a dry and oxygen-free atmosphere (N$_2$ or Ar) using Schlenk-line and glovebox techniques.

**1**: Me$_3$SiCl (1.56 mL, 1.34 g, 12.4 mmol, 0.95 equiv) was added dropwise to a solution of AlH$_3$·NMe$_3$ (51.5 mL of a 0.80 M solution in toluene, 41.2 mmol, 3.15 equiv) at room temperature and stirred for 20 min. The resulting solution was cooled by using an ice bath and transferred immediately to solid $t$BuC≡CLi (1.15 g, 13.1 mmol, 1.0 equiv). An exothermic reaction occurred. The suspension was stirred for 20 min, heated at reflux for 45 min and then filtered while hot. The solution was stored overnight to give colorless crystals of **1**·2C$_7$H$_8$. After filtration, the solution was stored for some weeks at 4 °C to provide additional single crystals of **1**·2C$_7$H$_8$. Yield: 1.63 g (62 %). M.p. > 180 °C (decomp. to a gray solid); the NMR spectra are of poor quality as a result of the poor solubility of **1** and therefore interpretation of the spectra is questionable: $^1$H NMR (500 MHz, C$_6$D$_6$, 298 K): $\delta$ = 5.3, 3.9 (s, very broad, 20H; Al-H), 2.52 and 2.40–2.30 (m, 16+4H; CH$_2$), 1.93 (s, 54H; NMe$_3$), 1.49, 1.46, 1.44 ppm

 © 2003 Wiley-VCH Verlag GmbH & Co. KGaA, Weinheim 

(several singlets, 54 + 18 H; *t*Bu); NMR recordings in $C_7D_8$ at variable temperatures gave similar results with shifted resonances; $^7$Li NMR (116.6 MHz, $C_6D_6$, 298 K): $\delta = 0.36$ (s) and a weaker resonance at $-0.4$ ppm; $^{13}$C NMR (123.8 MHz, $C_6D_6$, 298 K): $\delta = 54.4$ (broad), 51.1, 49.9, 49.4, 47.5 ($NCH_3$), 35.9, 35.8, 35.6, 30.9, 30.7, 30.5, 30.2 ppm; IR (Nujol, KBr plates): $\tilde{\nu} = 1768, 1746, 1680, 1650, 1262, 1099, 1032, 1008, 890, 800, 755, 722, 640$ cm$^{-1}$; elemental analysis calcd for $C_{80}H_{178}Al_{14}Li_2N_6$ (%): C 59.46, H 11.10, N 5.20; found: C 59.02, H 11.30, N 5.31.

Details of the calculations are given in the Supporting Information.

Received: July 29, 2003 [Z52502]

**Keywords:** alanes · aluminum · carbaalanes · cluster compounds · hydrides

[1] W. Uhl, F. Breher, *Eur. J. Inorg. Chem.* **2000**, 1–11.
[2] G. Wilke, W. Schneider, *Bull. Soc. Chim. Fr.* **1963**, 1462–1467.
[3] W. Uhl, F. Breher, *Angew. Chem.* **1999**, *111*, 1578–1580; *Angew. Chem. Int. Ed.* **1999**, *38*, 1477–1479.
[4] For some examples, see: a) K.-C. Kim, C. A. Reed, D. W. Elliot, L. J. Mueller, F. Tham, L. Lin, J. B. Lambert, *Science*, **2002**, *297*, 825–827; b) C. A. Reed, K.-C. Kim, R. D. Bolskar, L. J. Mueller, *Science* **2000**, *289*, 101–104; c) C. A. Reed, *Acc. Chem. Res.* **1998**, *31*, 133–139.
[5] A. Stasch, M. Ferbinteanu, J. Prust, W. Zheng, F. Cimpoesu, H. W. Roesky, J. Magull, H.-G. Schmidt, M. Noltemeyer, *J. Am. Chem. Soc.* **2002**, *124*, 5441–5448.
[6] **1**·2 $C_7H_8$: $C_{80}H_{178}Al_{14}Li_2N_6$; Stoe IPDS II diffractometer with $Mo_{K\alpha}$-radiation ($\lambda = 71.073$ pm); crystal dimensions: $0.30 \times 0.20 \times 0.20$ mm$^3$; monoclinic; *C*2/*c*; $a = 2075.32(5)$ pm, $b = 1973.34(8)$ pm, $c = 2698.09(7)$ pm, $\alpha = 90°$, $\beta = 105.926(2)°$, $\gamma = 90°$; $V = 10.625.4(6)$ nm$^3$; $Z = 4$; $\rho_{calcd} = 1.01$ Mg m$^{-3}$; absorption coefficient: 0.164 mm$^{-1}$; $\theta$: 1.45–23.50°; index ranges: $-23 \leqslant h \leqslant 23$, $-22 \leqslant k \leqslant 22$, $-30 \leqslant l \leqslant 30$; reflections collected/unique: 65409/7809; $R_{int} = 0.0443$; observed reflections ($I > 2\sigma(I)$): 6940; completeness to $\theta$: 99.4%; data/restraints/parameter: 7809/0/521; goodness-of-fit on $F^2$: 1.007; final $R$ indices ($I > 2\sigma(I)$): $R_1 = 0.0658$, $wR_2 = 0.1616$; $R$ indices (all data): $R_1 = 0.0728$, $wR_2 = 0.1673$; residual electron density (largest maximum and minimum): 897 and $-682$ e nm$^{-3}$. The structure was solved by direct methods and was refined with SHELX-97 with full-matrix least-squares methods on $F^2$ (G. M. Sheldrick, programs for crystal-structure refinement; Universität Göttingen, Göttingen (Germany), **1997**). The hydrogen atoms of the Al–H groups were found and refined free. Others were calculated at their positions. CCDC-216081 contains the supplementary crystallographic data for this paper. These data can be obtained free of charge via www.ccdc.cam.ac.uk/conts/retrieving.html (or from the Cambridge Crystallographic Data Centre, 12, Union Road, Cambridge CB2 1EZ, UK; fax: (+44) 1223-336-033; or deposit@ccdc.cam.ac.uk).
[7] M. J. Bayer, H. Pritzkow, W. Siebert, *Eur. J. Inorg. Chem.* **2002**, 1293–1300.
[8] P. Wei, D. W. Stephan, *Organometallics* **2003**, *22*, 1992–1994.

 © 2003 Wiley-VCH Verlag GmbH & Co. KGaA, Weinheim 

*Artificial Adrenergic Receptors*

# Highly Sensitive Recognition of Substrates of Adrenergic Receptors at the Air/Water Interface**

*Oliver Molt and Thomas Schrader**

One of the major classes of receptors in the human body are the G-protein-coupled receptors (GPCRs).[1] Their signals arise from a special binding site incorporated in the phospholipid bilayer: seven membrane-spanning helices create a binding pocket for the incoming hormones that has a largely unpolar environment.[2] One of the major subclasses is the family of adrenergic receptors. Amino alcohols of varying length and polarity are distinguished and lead to different transduction processes. In light of the enormous biological and pharmaceutical importance of this recognition site[3] the question arises whether it is possible to imitate this microenvironment in a lipid layer and use it for highly efficient and selective recognition.[4]

Recent developments in the field of artificial catecholamine receptor molecules include bipyridinium/gold nanoparticle arrays,[5] phenyl boronates,[6] and pyrazole-containing cryptands.[7] Bioorganic alternatives have also been presented featuring RNA aptamers[8] and copper-containing redox enzymes.[9] In keeping with the natural image,[10] we have recently designed a new type of synthetic adrenaline receptor with the following features: 1) a xylylene bisphosphonate unit serves as an established amino alcohol binder,[11] with enough flexibility for an induced fit; 2) the core unit is linked to rigid building blocks, assuring a high level of preorganization.[12] Thus, stiff aromatic tolan side walls[13] create a deep hydrophobic cleft, which is flanked by inwards-oriented amide NH groups that can form hydrogen bonds with the hydroxy groups of catechol derivatives. Monte Carlo simulations of this host molecule in its complex with noradrenaline indicate that there is enough room at the bottom part of the receptor for accomodating the amino alcohol, and all minimum-energy conformations find the guest inside the cavity. Subsequent molecular dynamics calculations suggest a high mobility of host and guest within the complex—an entropically most favorable situation.[14]

A modular retrosynthesis leads to three building blocks: a bisphosphonate-modified *p*-xylylene dibromide, a tolandicarboxylic acid, and *m*-xylylene diamine. These can be prepared by a very direct synthetic route. Arbuzov reaction and

[*] Prof. T. Schrader, Dr. O. Molt
Fachbereich Chemie
Universität Marburg
Hans-Meerwein-Strasse, 35032 Marburg (Germany)
Fax: (+49) 6421-28-25544
E-mail: schradet@mailer.uni-marburg.de

[**] We gratefully acknowledge support by the Deutsche Forschungsgemeinschaft (DFG SCHR 604/1-3).

Supporting information for this article is available on the WWW under http://www.angewandte.org or from the author.

 DOI: 10.1002/anie.200352186 © 2003 Wiley-VCH Verlag GmbH & Co. KGaA, Weinheim 

subsequent NBS bromination give bisphosphonate **6**, while two successive Sonogashira couplings furnish the mono-*tert*-butyl ester component **3** of the tolan spacer.[15] After the ester function is converted into first the carboxylic acid and then the acid chloride, this unit is connected to *m*-xylylene diamine to give compound **4** after cleavage of the ester. Subsequent macrocyclization with bisphosphonate **6** via the cesium carboxylate relied on the intramolecular directing effect of cesium ions.[16] Final mild monodealkylation of the phosphonates with LiBr completes the high-yielding synthesis of the new receptor molecule.[17] Host **1** is well soluble in polar solvents such as DMSO, methanol, and water.

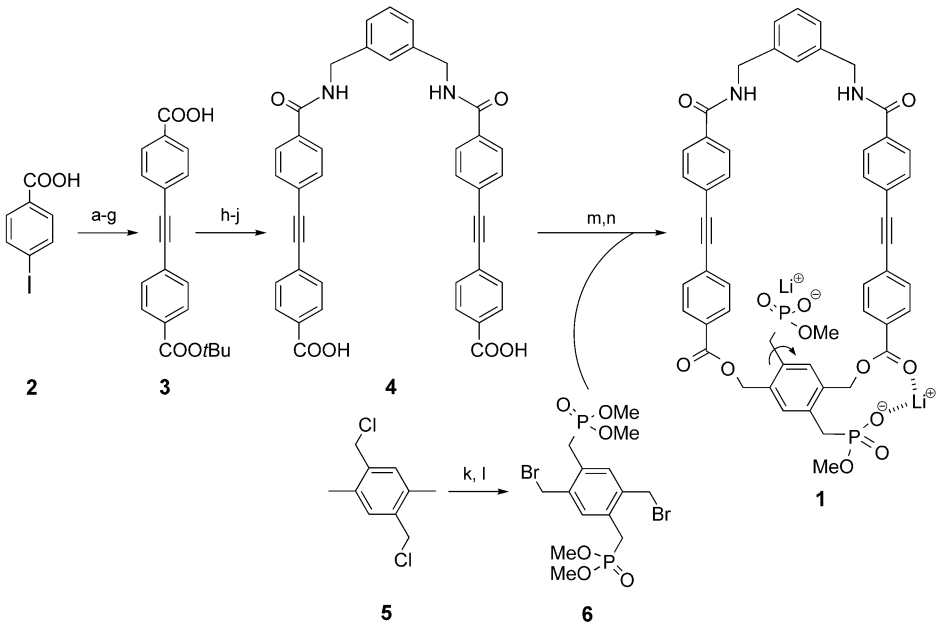
The $^1$H NMR spectrum of the **1** displays remarkably broad signals for the P-$CH_2$ and the O-$CH_2$ methylene groups. Variable-temperature experiments in methanol reveal a clean and large splitting for the diastereotopic protons at −45 °C. This is explained by a ten-membered chelate ring in which the lithium cation bridges the phosphonate and the ester carbonyl oxygen atoms of the neighboring carboxylate group (Scheme 1). The phosphonate arm is thus directed inwards ready to receive the amino alcohol guest.[18] No sharp NMR signals were observed for **1** in $D_2O$. In a dilution titration experiment large shifts were found for the unpolar aromatic parts of **1**, and a self-association constant in the order of $10^2$–$10^3\,M^{-1}$ was determined.[19] Considering the structural similarity of **1** to amphiphilic phospholipids, an incorporation of the new host into lipid monolayers seemed feasible in imitation of the natural adrenergic receptor.

For a quantitative evaluation of the new receptor's binding profile we performed NMR titrations in methanol and calculated the association constants by standard non-linear regression methods.[20] The assumed 1:1 stoichiometry was confirmed by a representative Job plot.[21] In most cases all signals of the guest shifted and produced similar binding constants. However, the results of a systematic variation of the amino alcohol were disappointing: from small ethanolamine to propranolol the $K_a$ values ranged only between 700 and $1600\,M^{-1}$ (Table 1). Only amino acids with an additional α substituent were bound less effectively by one order of magnitude. Considering the relatively small NMR shifts for the aromatic protons of the host and guest, we must conclude that in polar solution the macrocyclic host **1** probably does not

***Table 1:*** $A_0$ and $\Delta A_0$ values for stearic acid monolayers with embedded receptor **1** over different subphases.

| Monolayer[a] | Aqueous subphase | $A_0$[b] [Å$^2$ molecule$^{-1}$] | $\Delta A_0$[c] [Å$^2$ molecule$^{-1}$] |
|---|---|---|---|
| S | – | 21.2 | – |
| S+**1** | – | 21.6 | 0 |
| S+**1** | phenethylamine | 21.9 | 0.3 |
| S+**1** | (*R*/*S*)-isoproterenol | 21.9 | 0.3 |
| S+**1** | ethanolamine | 22.0 | 0.4 |
| S+**1** | L-tyrosine methyl ester | 22.0 | 0.4 |
| S+**1** | dopamine | 22.2 | 0.6 |
| S+**1** | (*R*/*S*)-adrenaline | 22.7 | 1.1 |
| S+**1** | (*R*/*S*)-noradrenaline | 25.6 | 4.0 |
| S+**1** | (*R*/*S*)-atenolol | 27.3 | 5.7 |
| S+**1** | (*R*)-propranolol | 17.3 | −4.3 |

[a] S = stearic acid. [b] $A_0$ = apparent total area of molecule of stearic acid in the liquid-condensed phase. [c] Net influence of the guest: $\Delta A_0$ = $A_0$ (monolayer with **1** over subphase with guest) − $A_0$ monolayer with **1** over water).




***Scheme 1.*** Synthesis of macrocycle **1**. a) $SOCl_2$, MeOH, 0 °C (92 %); b) 2-methyl-but-3-yn-2-ol, $[Pd(PPh_3)_2Cl_2]$, CuI, $PPh_3$, $NEt_3$, pyridine, Δ (98 %); c) NaOH, 1-butanol, Δ (99 %); d) $SOCl_2$, cat. DMF, $CHCl_3$, 0 °C (99 %); e) phenol, $NEt_3$, THF (45 %); f) 4-iodobenzoic acid *tert*-butyl ester, $[PdCl_2(PPh_3)_2]$, CuI, $PPh_3$, $NEt_3$, 80 °C (93 %); g) 1. $Na_2CO_3$, $H_2O_2$, dioxane, $H_2O$, Δ; 2. $KHSO_4$ (86 %); h) $(COCl)_2$, cat. DMF, $CH_2Cl_2$ (99 %); i) *m*-xylylenediamine, $NEt_3$, $CH_2Cl_2$ (89 %); j) TFA, $CH_2Cl_2$ (99 %); k) $P(OMe)_3$, Δ (99 %); l) NBS, AIBN, $CCl_4$, Δ (64 %); m) **6**, $Cs_2CO_3$, DMF, high dilution (28 %); n) LiBr, $CH_3CN$, Δ (81 %). AIBN = azoisobutyronitrile, DMF = dimethylformamide, NBS = *N*-bromosuccinimide, TFA = trifluoroacetic acid.

 © 2003 Wiley-VCH Verlag GmbH & Co. KGaA, Weinheim 

embrace adrenaline-type guests but merely lets them dock onto its hydrophobic region with their catechol moiety. Other spectroscopic methods indicate the same: a clean ESI mass spectrum was obtained from methanol showing peaks for host and 1:1 complex exclusively (Figure 1), but no change of the receptor's extinction maxima could be detected in a UV/Vis experiment in the same solvent.

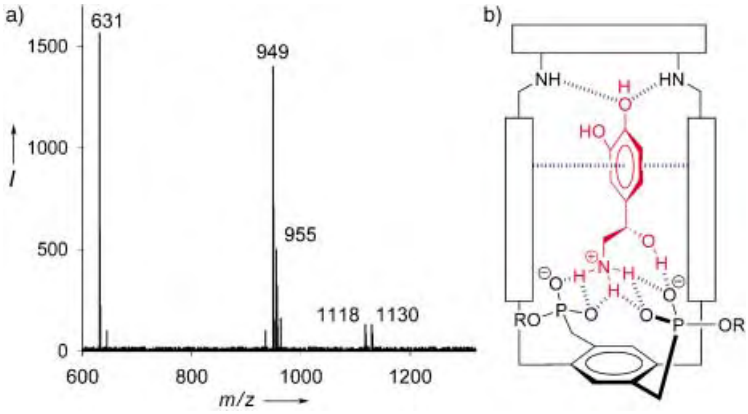



***Figure 1.*** a) ESI mass spectrum (negative-ion detection) of a solution of receptor **1** and noradrenaline hydrochloride (NA) in methanol. Host: $m/z = 631$ [**4**−H$^+$]$^-$, 949 [**1**−Li$^+$+H$^+$]$^-$, 955 [**1**−Li$^+$]$^-$; 1:1 complex: $m/z = 1118$ [**1**−2 Li$^+$+NA-Cl$^-$]$^-$, 1130 [**1**−2 H$^+$+NA-Cl$^-$]$^-$. b) Schematic drawing of the planned binding mode, featuring inclusion inside the rigid cavity of **1**, accompanied by an induced fit of the bisphosphonates.

The situation changed profoundly when we embedded the new amphiphilic receptor molecule in a monomolecular layer of stearic acid at the air/water interface.[22] A marked increase in the pressure–area ($\pi$–$A$) diagram of the Langmuir film balance always indicated the incorporation of additional material into the monolayer.[23] This was accompanied by the development of new stable, large patches in the Brewster angle microscope (BAM) images (Figure 2), which we attribute to the formation of domains within the monolayer consisting mainly of self-aggregated receptor molecules.[24] Recent bioanalytical results show that even the natural adrenergic receptors form dimeric structures.[25]

Subsequent subinjection of noradrenaline into the subphase led to a drastic increase in the $\pi$–$A$ isotherm, but the patches in the BAM picture remained (Figure 2). These effects were reproducible and strongly dependent on the nature of the guest dissolved in the aqueous subphase. Since the host molecules present their amino alcohol binding site towards the water phase, the guest molecules are bound by their bisphosphonate moieties and drawn into the monolayer. Now a new binding mode becomes operative which distinguishes between minute structural variations with high sensitivity. Figure 3 shows the $\pi$–$A$ diagrams for noradrenaline, adrenaline, and isoproterenol, which differ only in the size of their *N*-alkyl substituent (Scheme 2). Comparison of these curves to those of β-blockers propranolol and atenolol reveals the exquisite selectivity of the new binding mode: although the only structural difference between both antihypertensives consists of the replacement of an α-naphthyl moiety by a phenylacetamide, the receptor–ligand interaction produces in one case the strongest of all positive substrate shifts, in the other case even a drastically negative $\pi$–$A$ shift.

The affinity of the embedded receptor molecules within the monolayer for their guests is so high that noradrenaline can be detected even at micromolar concentrations.[26] A rough estimation of the binding constants at the air/water interface leads to $K_a$ values that must clearly surpass $10^5\,\text{M}^{-1}$; thus **1** might be used in new adrenaline-sensing devices. All the other catecholamines did not show any appreciable shifts in the $\pi$–$A$ diagram at concentrations between $10^{-5}$ and $10^{-6}$ M. Their association constants must therefore be at least one order of magnitude lower than that of noradrenaline. A complete list of changes in the $\pi$–$A$

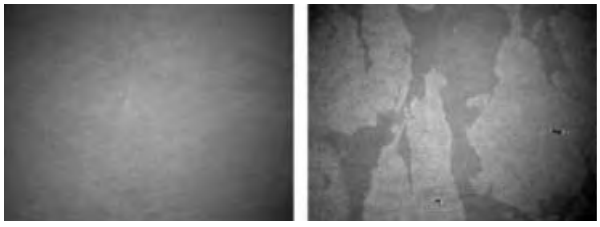


***Figure 2.*** BAM images (4.8×6.4 mm$^2$) of a stearic acid monolayer (left) and a monolayer with embedded receptor **1** (dark gray areas, right) in the condensed liquid phase.

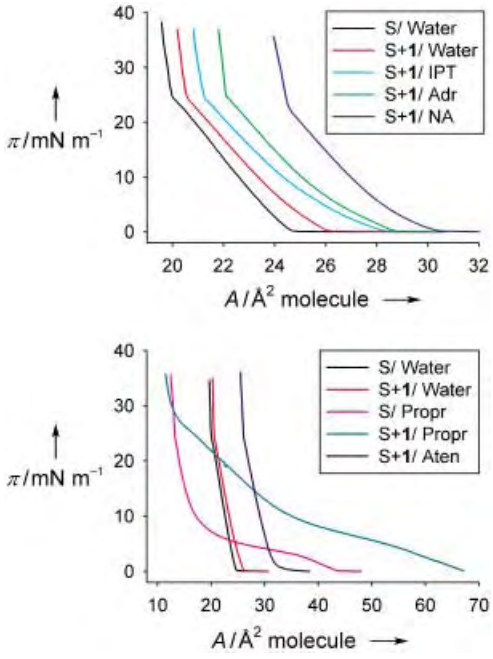
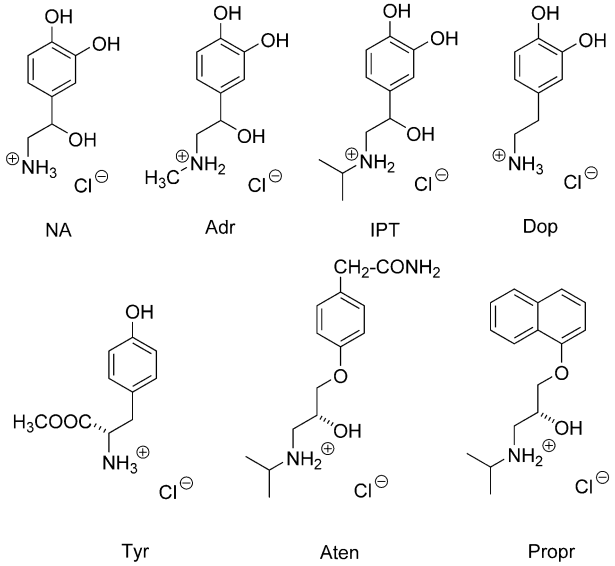



***Figure 3.*** Pressure–area ($\pi$–$A$) isotherms of stearic acid (S) and receptor **1** in a monolayer over water: with a) isoproterenol (IPT), adrenaline (Adr), and noradrenaline (NA); and b) propranolol (Propr) and atenolol (Aten.).

 © 2003 Wiley-VCH Verlag GmbH & Co. KGaA, Weinheim 




***Scheme 2.*** Guest molecules with structures similar to that of adrenaline. NA = noradrenaline, Adr = adrenaline, IPT = isoproterenol, Dop = dopamine, Tyr = tyrosine methyl ester, Aten = atenolol, Propr = propranolol. (The hydrochloride salts employed in the experiments are shown.)

diagrams induced by a range of guest molecules is summarized in Table 1.

With Langmuir–Blodgett (LB) techniques it was possible to immobilize 160 ($2 \times 80$) layers of the receptor-containing stearic acid monolayer on quartz slides. These immobilized multilayers were observed directly with UV/Vis spectroscopy, which revealed a drastic blue shift of the receptor's extinction maximum.[27] The multilayers were subsequently washed off the glass carrier with methanol, which leads to a complete reversal of the blue shift and restores the UV/Vis spectrum of the free receptor molecule (Figure 4). Since solvatochromic effects with the lipid layer would result in a red shift,[28] this effect must be attributed to the self-aggregation of the receptor molecule within the monolayer, as already indicated in the BAM picture. If noradrenaline was present in the subphase, the LB deposition on quartz led to a markedly decreased blue shift, which was shown to be dependent on the analyte concentration and could again be completely reverted on washing with methanol. This effect sheds light on the binding mechanism inside the monolayer. We propose that the red shift originates from the insertion of the electron-rich catechol ring into the ensemble of stacked electron-poor aromatic rings of the surrounding receptor molecules.[29] We could detect this bathochromic shift down to a noradrenaline concentration in the subphase of $5 \times 10^{-5}$ M, indicating again a similar lowest limit for the dissociation constant of the complex as judged from the Langmuir $\pi$–$A$ diagrams (Figure 3).

From all the experimental data we infer the following tentative mechanism of noradrenaline binding by the monolayer. When guest molecules are subinjected into the aqueous phase, they are bound by solvated receptor molecules close to the monolayer. The host molecules' negative charges become neutralized in part and their lipophilicity increases. This in turn leads to reincorporation of the whole complex into the monolayer (Figure 5). However, the catechol moiety is not inserted into a single host's cavity, but rather into the ensemble of host molecules in receptor domains within the stearic acid monolayer. The new microenvironment leads to high selectivity for minute structural changes in the analytes.

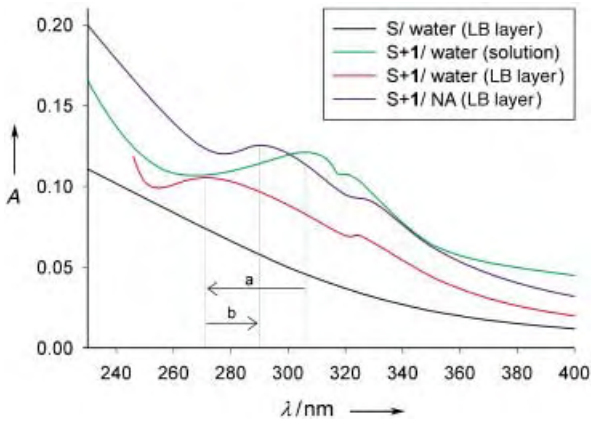



***Figure 4.*** UV/Vis spectra of LB layers of stearic acid (alone, with embedded **1**, and with attached guest) on quartz slides and in methanol solution.

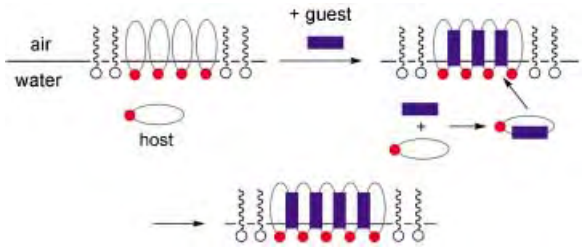



***Figure 5.*** Schematic representation of the proposed binding mode within the monolayer.

We conclude that the incorporation of an artificial receptor molecule for substrates of the adrenergic receptor into a monolayer leads to a dramatic increase in both the recognition efficiency and selectivity for a whole range of substrates. Thus, noradrenaline can be detected quantitatively at micromolar concentrations. The basis for this enormous progress is the altered microenvironment created in the monolayer.[30] Not only is the dielectric constant lowered dramatically compared to that of the free aqueous phase,[27] but the receptor molecules also self-aggregate into assemblies that are highly sensitive towards the structural features of amino alcohol guests. In the future we intend to incorporate the new macrocyclic receptor molecules into vesicles made from lipids and diacetylenes for colorimetric detection of adrenaline derivatives.[31]

Received: June 23, 2003 [Z52186]

**Keywords:** adrenergic receptors · β-blockers · interfaces · Langmuir–Blodgett films · molecular recognition · monolayers

 © 2003 Wiley-VCH Verlag GmbH & Co. KGaA, Weinheim 

[1] a) T. P. Iismaa, T. J. Biden, J. Shine, *G Protein-Coupled Receptors*, Springer, Heidelberg, **1995**; b) *Special Issue: G-Protein-Coupled Receptors, ChemBioChem* **2002**, *3*, 913 – 1034.

[2] a) D. A. Doyle, J. Morais Cabral, R. A. Pfuetzner, A. Kuo, J. M. Gulbis, S. L. Cohen, B. T. Chait, R. MacKinnon, *Science* **1998**, *280*, 69; b) K. Palczewski, T. Kumasaka, T. Hori, C. A. Behnke, H. Motoshima, B. A. Fox, I. Le Trong, D. C. Teller, T. Okada, R. O. Stenkamp, M. Yamamoto, M. Miyano, *Science* **2000**, *289*, 739; c) R. E. Stenkamp, S. Filipek, C. A. G. G. Driessen, D. C. Teller, K. Palczewski, *Biochim. Biophys. Acta* **2002**, *1565*, 168.

[3] Approximatively 50% of all commercially available drugs interact with GPCRs: a) D. T. Chalmers, D. P. Behan, *Nat. Rev. Drug Discovery* **2002**, *1*, 599; b) T. Klabunde, G. Hessler, *ChemBioChem* **2002**, *3*, 928.

[4] H. Brockman, *Curr. Opin. Struct. Biol.* **1999**, *9*, 438.

[5] M. Lahav, A. N. Shipway, I. Willner, *J. Chem. Soc. Perkin Trans. 2* **1999**, 1925.

[6] a) S. M. Strawbridge, S. J. Green, J. H. R. Tucker, *Chem. Commun.* **2000**, 2393; b) S. M. Strawbridge, S. J. Green, J. H. R. Tucker, *Phys. Chem. Chem. Phys.* **2000**, *2*, 2393.

[7] L. Lamarque, P. Navarro, C. Miranda, V. J. Arán, C. Ochoa, F. Escarti, E. García-España, J. Latorre, S. V. Luis, J. F. Miravet, *J. Am. Chem. Soc.* **2001**, *123*, 10560.

[8] C. Mannironi, A. Di Nardo, P. Fruscoloni, G. P. Tocchini-Valentini, *Biochemistry* **1997**, *36*, 9726.

[9] a) D. R. Shankaran, M.-S. Won, Y.-B. Shim, *Anal. Sci.* **2001**, *17*, 9; b) M. Del Pilar Taboada Sotomayor, A. A. Tanaka, L. T. Kubota, *Anal. Chim. Acta* **2002**, *455*, 215.

[10] a) S. Trumpp-Kallmeyer, J. Hoflack, A. Bruinfels, M. Hibert, *J. Med. Chem.* **1992**, *35*, 3448; b) K. Wieland, H. M. Zuurmond, C. Krasel, A. P. Ijzerman, M. J. Lohse, *Proc. Natl. Acad. Sci. USA* **1996**, *93*, 9276.

[11] a) T. Schrader, *Angew. Chem.* **1996**, *108*, 2816; *Angew. Chem. Int. Ed. Engl.* **1996**, *35*, 2649; b) T. Schrader, *J. Org. Chem.* **1998**, *63*, 264; c) T. Schrader, M. Herm, *Chem. Eur. J.* **2000**, *6*, 47.

[12] The last generation of advanced biomimetic adrenaline hosts suffered from multiple benzylic connections with their high torsional entropy: a) T. Schrader, M. Herm, O. Molt, *Angew. Chem.* **2001**, *113*, 3244; *Angew. Chem. Int. Ed.* **2001**, *40*, 3148; b) T. Schrader, M. Herm, O. Molt, *Chem. Eur. J.* **2002**, *8*, 1485.

[13] a) T. Kawase, Y. Seirai, H. R. Darabi, M. Oda, Y. Sarakai, K. Tashiro, *Angew. Chem.* **2003**, *115*, 1659; *Angew. Chem. Int. Ed.* **2003**, *42*, 1621; b) M. M. Haley, J. J. Pak, S. C. Brand, *Top. Curr. Chem.* **1999**, *201*, 82.

[14] Monte Carlo simulations: MacroModel 7.0, Schrödinger Inc. 2000, Force field Amber*, water, 3000 steps; subsequent molecular dynamics simulations: 300 K, 10 ps.

[15] S. Takahashi, Y. Kuroyama, K. Sonogashira, N. Hagihara, *Synthesis* **1980**, 627.

[16] A. Ostrowicki, E. Koepp, F. Vögtle, *Top. Curr. Chem.* **1992**, *161*, 37.

[17] a) R. Karaman, A. Goldblum, E. Breuer, H. Leader, *J. Chem. Soc. Perkin Trans. 1* **1989**, 765; b) E. Breuer, M. Safadi, M. Chorev, D. Gibson, *J. Org. Chem.* **1990**, *55*, 6147.

[18] Protonation of the lithium salt leads to sharp NMR signals in methanol and a complete loss of the splitting of the diastereotopic methylene protons.

[19] Dilution titration to determine self-association constants: C. S. Wilcox, *Frontiers in Supramolecular Chemistry and Photochemistry* (Eds.: H.-J. Schneider, H. Dürr), VCH, Weinheim, **1991**.

[20] L. Fielding, *Tetrahedron* **2000**, *56*, 6151.

[21] M. T. Blanda, J. H. Horner, M. Newcomb, *J. Org. Chem.* **1989**, *54*, 4626.

[22] For experimental details see Supporting Information.

[23] a) M. Higuchi, T. Koga, K. Taguchi, T. Kinoshita, *Langmuir* **2002**, *18*, 813; b) D. Y. Sasaki, T. A. Waggoner, J. A. Last, T. M. Alam, *Langmuir* **2002**, *18*, 3714; c) J. Lahiri, G. D. Fate, S. B. Ungashe, J. T. Groves, *J. Am. Chem. Soc.* **1996**, *118*, 2347.

[24] J. Meunier, *Colloids Surf. A* **2000**, *171*, 33.

[25] a) C. Lavoie, J.-F. Mercier, A. Salahpour, D. Umapathy, A. Breit, L.-R. Villeneuve, W.-Z. Zhu, R.-P. Xiao, E. G. Lakatta, M. Bouvier, T. E. Hebert, *J. Biol. Chem.* **2002**, *277*, 35402; b) J. Xu, M. Paquet, A. G. Lau, J. D. Wood, C. A. Ross, R. A. Hall, *J. Biol. Chem.* **2001**, *276*, 41310.

[26] Other sensors for adrenaline derivatives reach comparable detection limits of $\sim 10^{-6}$ M.[5–9]

[27] K. Ariga, T. Kunitake, *Acc. Chem. Res.* **1998**, *31*, 371.

[28] Solvatochromic red shifts with unpolar solvents originate from the stabilization of their more polarizable LUMO: C. Reichardt, *Solvents and Solvent Effects in Organic Chemistry*, Wiley-VCH, Weinheim, **2003**, pp. 340 – 341.

[29] A CT band does not develop, as judged from the colorless monolayer. However, a sandwich arrangement would be conceivable for the guest's catechol ring within the host aggregates.

[30] A simple lipid-modified bisphosphonate embedded in the stearic acid monolayer did not produce any changes in the $\pi$–$A$ diagram even at high guest concentrations in the aqueous subphase.

[31] S. Kolusheva, T. Shahal, R. Jelinek, *J. Am. Chem. Soc.* **2000**, *122*, 776.


 © 2003 Wiley-VCH Verlag GmbH & Co. KGaA, Weinheim 

*Core–Shell Particles*

# Green-Emitting $CePO_4$:Tb/$LaPO_4$ Core–Shell Nanoparticles with 70 % Photoluminescence Quantum Yield**

*Karsten Kömpe, Holger Borchert, Jörg Storz, Arun Lobo, Sorin Adam, Thomas Möller, and Markus Haase**

Luminescent nanocrystals may serve as active components in light-emitting devices,[1a] low-threshold lasers,[1b] optical amplifiers,[1c] and as markers for biomolecules,[1d] provided that their photoluminescence quantum yield is high. In recent years, strategies have been developed to significantly increase the quantum yield of nanoparticles by suppressing energy-loss processes at the particle surface. In the case of semiconducting nanoparticles, this is possibly by growing a crystalline shell of a suitable large-bandgap material around each nanocrystal.[2] Examples of such core–shell systems are CdSe/CdS,[2a] CdSe/ZnS,[2b] InAs/CdSe, InAs/ZnS,[2c] and InP/ZnS[2d] nano-

[*] Dr. M. Haase, Dr. K. Kömpe, H. Borchert, J. Storz
Institute of Physical Chemistry, University of Hamburg
Bundesstrasse 45, 20146 Hamburg (Germany)
Fax: (+49) 40-42838-3452
E-mail: haase@chemie.uni-hamburg.de
Dr. A. Lobo, S. Adam, Dr. T. Möller
HASYLAB/DESY
Nottkestrasse 85, 22603 Hamburg (Germany)

[**] We thank A. Kornowski and S. Bartholdi-Nawrath for TEM investigations and Dr. Lühmann at Malvern Instruments GmbH for dynamic light-scattering measurements. This work was supported in part by the BMBF.

 DOI: 10.1002/anie.200351943 © 2003 Wiley-VCH Verlag GmbH & Co. KGaA, Weinheim 

crystals. All these systems are based on two materials with similar lattice constants to avoid the formation of defects at the core–shell interface.

Another class of redispersible luminescent nanoparticles is formed by lanthanide(III)-doped large-bandgap materials with compositions similar to those of solid-state laser materials or of bulk phosphors used in lighting and display applications.[3] Unlike most molecular lanthanide complex compounds, the nanocrystals provide a rigid crystal environment for the dopant ions, resulting in a higher photoluminescence quantum yield of the latter. However, the quantum yield of doped nanoparticles is usually lower than that of the corresponding bulk material as a result of energy-transfer processes to the surface through adjacent dopant ions or because the luminescence of surface dopant ions is quenched.[3e,f,i] These processes could be suppressed if one were able to grow a shell of an undoped material around each doped nanoparticle, that is, a shell made up of a material through which energy cannot be transferred. Herein we report the successful synthesis of redispersible $CePO_4$:Tb/$LaPO_4$ core–shell particles, which to our knowledge is the first realization of the core–shell principle for a nanocrystalline phosphor material.

Figure 1 displays luminescence spectra of dilute colloidal solutions of $CePO_4$:Tb particles and $CePO_4$:Tb/$LaPO_4$ core–shell particles, which have identical optical densities at the

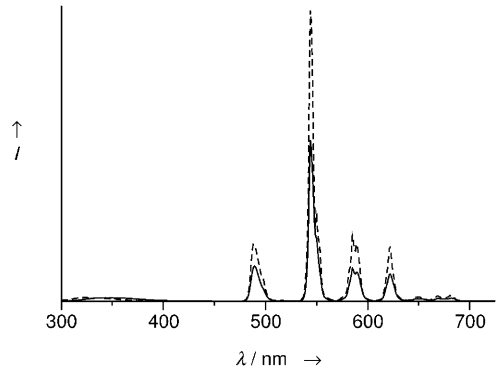



***Figure 1.*** Fluorescence spectra of colloidal solutions of $CePO_4$:Tb nanoparticles (solid line) and of $CePO_4$:Tb/$LaPO_4$ core–shell particles (dashed line).

excitation wavelength ($\lambda_{exc.} = 277$ nm). The spectra consist mainly of four groups of signals, which correspond to the f–f transitions of the $Tb^{3+}$ ions, and a weak band in the UV region as a result of the d–f transitions of $Ce^{3+}$.[3f,g] The photoluminescence quantum yield of the $CePO_4$:Tb core particles in Figure 1 is 43% for the terbium emission (53% if the Ce emission is taken into account) and depends on the surface treatment of the particles and the solvent as described earlier.[3f] Growth of the $LaPO_4$ shell around these core particles increases the quantum yield of the terbium emission to 70% and the total quantum yield to 80%. These values are obtained reproducibly and are not far from the quantum yield of the bulk material, which is 86% for the terbium emission and 93% for the total emission.[4]

TEM images of $CePO_4$:Tb nanoparticles before (upper part) and after (lower part) growth of the $LaPO_4$-shell are shown in Figure 2. The mean particle diameter increases from 4–6 nm for the almost spherical $CePO_4$:Tb core-particles to 8–10 nm for the slightly elongated $CePO_4$:Tb/$LaPO_4$ core–shell

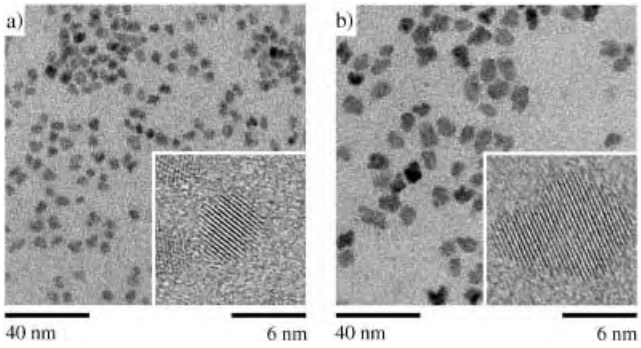



***Figure 2.*** TEM micrographs of a) $CePO_4$:Tb nanoparticles and b) $CePO_4$:Tb/$LaPO_4$ core–shell particles. Insets: High-resolution images of nanoparticles.

particles. High-resolution images (insets) exhibit lattice fringes for most particles and show that each particle consists of a single crystalline domain. As the lattice constants of monazite-type $CePO_4$ and $LaPO_4$ are virtually identical, the core and the shell of these particles cannot be distinguished in the TEM images. These observations are in accord with the powder X-ray diffraction (XRD) data of both samples (Figure 3). The Debye–Scherrer approximation was used to calculate mean particle sizes of $\approx 5$ and $\approx 8$ nm for the core and the core–shell particles, respectively. However, the widths of the reflections of the elongated $CePO_4$:Tb/$LaPO_4$ core–shell particles show some anisotropy, which is most pronounced for the 200 reflection. The width of this peak corresponds to a particle size of approximately 11 nm, which indicates that the elongated shape of the nanoparticles is caused by preferential growth along the *a* axis of the unit cell. The $CePO_4$:Tb core nanoparticles as well as the $CePO_4$:Tb/$LaPO_4$ core–shell particles display almost identical XRD

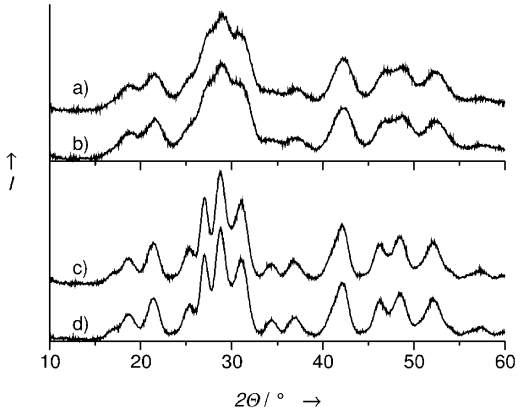



***Figure 3.*** Top: XRD patterns of $CePO_4$:Tb core particles after a) 2 h and b) 16 h of heating at 200 °C. Bottom: XRD patterns of $CePO_4$:Tb/$LaPO_4$ core–shell particles after c) 2 h and d) 16 h of heating at 200 °C.

 © 2003 Wiley-VCH Verlag GmbH & Co. KGaA, Weinheim 

patterns after 2 h and after 16 h of growth at 200 °C. This result indicates that the reactants initially present in solution are consumed within 2 h and that the resulting particles do not grow further by Ostwald ripening, that is, by exchange of material among the particles. The absence of Ostwald ripening is a considerable advantage in the synthesis of core–shell particles, as dissolution of the smaller particles during Ostwald ripening leads finally to an intermixing of the core and the shell materials.

In fact, X-ray photoelectron spectroscopy (XPS) measurements performed with varying excitation energy provides further evidence that a shell was grown on the core particles and that no intermixing of lanthanum and cerium phosphate took place (Figure 4). If a photoelectron is generated by an X-ray photon in the core of a core–shell nanoparticle, the probability of its escape through the shell scales and its detection depends on its kinetic energy.[5] If a synchrotron is used as the X-ray source, the kinetic energy of the photoelectrons can be adjusted by choosing a suitable X-ray photon energy ($h\nu$) according to $E_{kin} = h\nu - E_{bind}$ ($E_{bind}$ is the electron-binding energy in the solid). The average shell thickness can then be extracted from the dependence of the experimental XPS peak intensities on the X-ray photon energy.[5] The simulation shows that the intensities of the XPS signals (data points in Figure 4) cannot be explained by the formation of a mixed phosphate (La,Ce,Tb)$PO_4$ (dashed line in Figure 4). If, on the other hand, a $CePO_4$:Tb core particle with a diameter of 5 nm is assumed (see TEM images in Figure 2) a good fit to the measured data is obtained for a $LaPO_4$ shell thickness of $1.13 \pm 0.05$ nm. This value is in reasonable agreement with the expected value of 1.5 nm, the difference presumably being due to the slight elongation of the particles and local variations of the shell thickness which could not be taken into account.

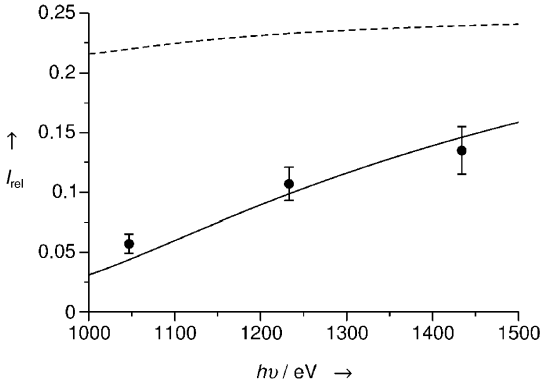



***Figure 4.*** XPS data for the $CePO_4$:Tb/$LaPO_4$ core–shell particles: experimental intensity ratio of the Ce and La 3d peaks versus X-ray photon energy (dots with error bars). Expected pattern for a mixed phosphate of composition $La_3Ce_{0.75}Tb_{0.25}(PO_4)_4$ (dashed line) and for core–shell particles with a 5-nm $CePO_4$:Tb core and 1.13-nm-thick $LaPO_4$ shell (solid line).

Finally, we determined the particle-size distribution of the core and the core–shell particles in a colloidal solution in methanol (1 wt %) by dynamic light-scattering measurements

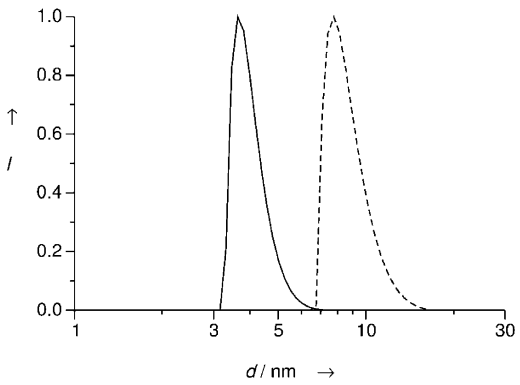



***Figure 5.*** Semilogarithmic plot of the number-averaged particle size distribution curves of $CePO_4$:Tb nanoparticles (solid line) and $CePO_4$:Tb/$LaPO_4$ core–shell particles (broken line) in a colloidal solution (1 wt %), determined by dynamic light scattering.

(Figure 5). From the full width at half maximum of the distribution curves, particle sizes of $\approx$3.5–4.5 nm and of about $\approx$7–10 nm are derived for the $CePO_4$:Tb core nanoparticles and $CePO_4$:Tb/$LaPO_4$ core–shell particles, respectively. These values are similar to those derived from the TEM images, which indicates that the 1-wt % colloidal solutions consist mainly of well-separated particles.

In summary, we succeeded in preparing $CePO_4$:Tb/$LaPO_4$ core–shell particles with a total quantum yield of 80 %. Until recently, quantum yields this close to the value of the bulk material were believed to be impossible for a nanocrystalline phosphor material, because phosphors prepared by conventional solid-state methods display lower quantum yields already when their grain size is smaller than about 0.5 μm. The quantum yield of these nanoparticles can probably be increased further by optimizing the thickness of the shell and by employing metal salts of very high purity.

## Experimental Section

The $CePO_4$:Tb core nanoparticles were prepared as described previously by using hydrated metal chlorides with a purity of 99.9 %:[6] $CeCl_3 \cdot 7H_2O$ (2.66 g, 7.5 mmol) and $TbCl_3 \cdot 6H_2O$ (0.93 g, 2.5 mmol) were dissolved in methanol (10 mL). The clear solution was mixed with tributylphosphate (10.98 mL, 40 mmol), and the methanol was removed on a rotary evaporator. Diphenyl ether (30 mL) was added, and the released water content was removed under vacuum at 50–80 °C. Subsequently, trihexylamine (10.15 mL, 30 mmol) and a solution of dry phosphoric acid in dihexyl ether (2 M; 7.0 mL) were added, and the mixture was heated to 200 °C under dry nitrogen. After 2 h, one third of the solution was removed, cooled to 50 °C, diluted with methanol (200 mL), and purified by diafiltration (5000-Dalton filter, Millipore; Diafiltration cell (Berghof); solvent: methanol). The nanoparticles were isolated as a white powder (0.8 g) by removing the methanol on a rotary evaporator.

After an additional 14 h of heating at 200 °C, one half of the remaining reaction solution was removed and treated in the same way. Colloidal solutions of the resulting white powder (yield: 0.8 g) were used for the measurements on $CePO_4$:Tb core nanoparticles.

Synthesis of core–shell nanoparticles: Phosphoric acid in dihexyl ether (2 M; 12.7 mmol) was added to the transparent solution remaining in the reaction vessel (i.e., one third of the initial content) at 20 °C. The mixture was stirred vigorously and heated to 200 °C. A solution of $LaCl_3 \cdot 7H_2O$ (3.89 g, 10 mmol) in methanol was mixed

 © 2003 Wiley-VCH Verlag GmbH & Co. KGaA, Weinheim 

with tributylphosphate (10.98 mL, 40 mmol), the methanol was removed by distillation, and the residue was taken up in diphenyl ether (30 mL). After the water had been removed by vacuum distillation as described above, the solution was mixed with trihexylamine (10.15 mL, 30 mmol) and added to the reaction mixture through a dropping funnel within 2 h. After an additional 2 h of heating at 200 °C, half of the solution was removed, purified by diafiltration, and the nanoparticles were isolated as described above (white powder, 1.0 g yield). The remaining solution was treated in the same way after 14 h of further heating at 200 °C (white powder; 1.4 g yield) and used as core–shell particles.

Dilute colloidal solutions were obtained by redispersing the nanoparticles in methanol and were transparent. Transparent methanolic solutions of higher concentration were obtained by the addition of a few drops of a solution of tetra-*n*-butylammonium hydroxide in methanol (25 wt %).

Powder XRD measurements were performed on a Philips X'pert system, TEM investigations on a Philips CM 300 UT transmission electron microscope, and dynamic light-scattering measurements on a Malvern HPPS system. The absorption and luminescence spectra were recorded in cuvettes (1 cm path length; Hellma, QS-series) on a Cary 500 Scan UV/vis spectrometer (Varian) and on a Fluorolog-03 spectrometer (Jobin-Yvon), respectively.

Photoluminescence quantum yields of colloidal solutions were measured by comparing their integrated emission to the emission of a solution of Rhodamin 6G (Lambda Physik, laser grade; solution in spectroscopic grade absolute ethanol; quantum yield 95 %[7]), which has the same optical density of 0.1 at the excitation wavelength (277 nm). A dilution series of the dye showed that the quantum yield at this concentration was 3 % lower than in more dilute solutions. A comparison of the absorption and luminescence excitation spectrum between 250 and 550 nm gave no indication for a notable dependence of the quantum yield on the excitation wavelength.

Received: May 21, 2003 [Z51943]

**Keywords:** colloids · fluorescence · lanthanides · luminescence · nanostructures

[1] a) V. L. Colvin, M. C. Schlamp, A. P. Alivisatos, *Nature* **1994**, *370*, 354; N. Tessler, V. Medvedev, M. Kazes, S. H. Kan, U. Banin, *Science* **2002**, *295*, 1506; B. O. Dabousi, M. G. Bawendi, O. Onitsuka, M. F. Rubner, *Appl. Phys. Lett.* **1995**, *66*, 1316; b) V. I. Klimov, A. A. Mikhailovsky, S. Xu, J. A. Hollingsworth, C. A. Leatherdale, H. J. Eisler, M. G. Bawendi, *Science* **2000**, *290*, 314; c) M. T. Harrison, S. V. Kershaw, M. G. Burt, A. L. Rogach, A. Kornowski, A. Eychmüller, H. Weller, *Pure Appl. Chem.* **2000**, *72*, 314; d) B. Dubertret, P. Skourides, D. J. Norris, V. Noireaux, A. H. Brivanlou, A. Libchaber, *Science* **2002**, *298*, 1759; M. P. Bruchez, M. Moronne, P. Gin, S. Weiss, A. P. Alivisatos, *Science* **1998**, *281*, 2013.

[2] a) X. Peng, M. C. Schlamp, A. V. Kadavanich, A. P. Alivisatos, *J. Am. Chem. Soc.* **1997**, *119*, 7019; b) B. O. Dabousi, J. Rodriguez-Viejo, F. V. Mikulec, J. R. Heine, H. Mattoussi, R. Ober, K. F. Jensen, M. Bawendi, *J. Phys. Chem. B* **1997**, *101*, 9463; D. V. Talapin, A. L. Rogach, A. Kornowski, M. Haase, H. Weller, *Nano Lett.* **2001**, *1*, 207; c) Y. W. Cao, U. Banin, *J. Am. Chem. Soc.* **2000**, *122*, 9692; d) S. Haubold, M. Haase, A. Kornowski, H. Weller, *ChemPhysChem* **2001**, *5*, 331.

[3] a) M. Yin, W. Zhang, S. Xia, J.-C. Krupa, *J. Lumin.* **1996**, *68*, 335; b) B. Tissue, *Chem. Mater.* **1998**, *10*, 2837; K. Riwotzki, M. Haase, *J. Phys. Chem. B* **1998**, *102*, 10129; c) Y. L. Soo, S. W. Huang, Z. H. Ming, Y. H. Kao, G. C. Smith, E. Goldburt, R. Hodel, B. Kulkarni, J. V. D. Veliadis, R. N. Bhargava, *J. Appl. Phys.* **1998**, *83*, 5404; d) H. Meyssamy, K. Riwotzki, A. Kornowski, S. Naused, M. Haase, *Adv. Mater.* **1999**, *11*, 840; e) A. Huignard, Th. Gacoin, J.-P. Boilot, *Chem. Mater.* **2000**, *12*, 1090; f) H. Meyssamy, K. Riwotzki, A. Kornowski, S. Naused, M. Haase, *J. Phys. Chem. B* **2000**, *104*, 2824; g) K. Riwotzki, H. Meyssamy, H. Schnablegger, A. Kornowski, M. Haase, *Angew. Chem.* **2001**, *113*, 574; *Angew. Chem. Int. Ed.* **2001**, *40*, 573; h) Z. Wie, L. Sun, C. Liao, C. Yan, Sh. Huang, *Appl. Phys. Lett.* **2002**, *80*, 1447; i) G. A. Hebbink, J. W. Stouwdam, D. N. Reinhoudt, F. J. M. van Veggel, *Adv. Mater.* **2002**, *14*, 1147.

[4] B. M. J. Smets, *Mater. Chem. Phys.* **1987**, *16*, 283.

[5] H. Borchert, S. Haubold, M. Haase, H. Weller, C. McGinley, M. Riedler, T. Möller, *Nano Lett.* **2002**, *2*, 151.

[6] O. Lehmann, H. Meyssamy, K. Kömpe, H. Schnablegger, M. Haase, *J. Phys. Chem. B* **2003**, *107*, 7449.

[7] R. F. Kubin, A. N. Fletcher, *J. Lumin.* **1982**, *27*, 455.

 © 2003 Wiley-VCH Verlag GmbH & Co. KGaA, Weinheim 

*Reaction Mechanisms*

# Addition of a Hydrogen Atom to Acetonitrile by Hydrated Electrons in Nanodroplets**

*O. Petru Balaj, Iulia Balteanu, Brigitte S. Fox-Beyer, Martin K. Beyer,* and Vladimir E. Bondybey**

Solvated electrons are the most fundamental model systems used to study electron-transfer reactions and they play an important role in radiation chemistry and biology as well as in organic and inorganic synthesis.[1] The hydrated electron ($e_{aq}^-$) as well as other transient species in aqueous solutions, such as the hydrogen atom (·H), the hydroxyl radical (·OH), and the oxide radical anion ($\cdot O^-$), have been studied in radiation chemistry, especially with the aid of the pulsed radiolysis technique.[2] However, interpretation of the results is complicated by the fact that even for the radiolysis of pure water, 33 distinct reactions occur,[2] which convert the primary species not only into new radicals, but also into each other. To study the reactivity of the hydrated electron ($e_{aq}^-$) the experiments are carried out in buffer solutions at pH 12 to prevent the formation of hydrogen atoms by the recombination of protons with the hydrated electrons.[3] An alternative way to eliminate such problems is to solvate the electron in a nanodroplet. Hydrated electrons ($(H_2O)_n^-$) in the gas phase were first observed by Haberland and co-workers, and their

[*] Dr. M. K. Beyer, Prof. Dr. V. E. Bondybey, O. P. Balaj, I. Balteanu, Dr. B. S. Fox-Beyer
Institut für Physikalische und Theoretische Chemie
Technische Universität München
Lichtenbergstrasse 4, 85 747 Garching (Germany)
Fax: (+49) 89-289-13416
E-mail: beyer@ch.tum.de
bondybey@ch.tum.de

[**] Financial support by the Deutsche Forschungsgemeinschaft, the Fonds der Chemischen Industrie, and the European Union through the Research Training Network Reactive Intermediates is gratefully acknowledged.

 © 2003 Wiley-VCH Verlag GmbH & Co. KGaA, Weinheim DOI: 10.1002/anie.200351953 

spectroscopic properties[4] and decay kinetics[5] were studied extensively. Studies into the reactivity of $(H_2O)_n^-$ involved mainly electron-scavenging reactions.[6] Recently, it was demonstrated that nanodroplets that consist of as few as 10–50 water molecules are sufficiently large to exhibit solution-phase behavior,[7] and a number of well-known bulk-solution reactions were shown to have their counterparts in the nanodroplet.[7a] In the work presented herein, we investigated the reactions of acetonitrile with hydrated electrons ($(H_2O)_n^-$, $n = 25$–$60$) in a Fourier transform ion cyclotron resonance (FTICR) mass spectrometer. More than 25 years ago, this reaction was observed by ESR spectroscopy in solution, but the product was not identified.[3]

The progress of the reaction was monitored at different intervals, as shown in the mass spectra in Figure 1. As a constant pressure of the acetonitrile reactant is present in the

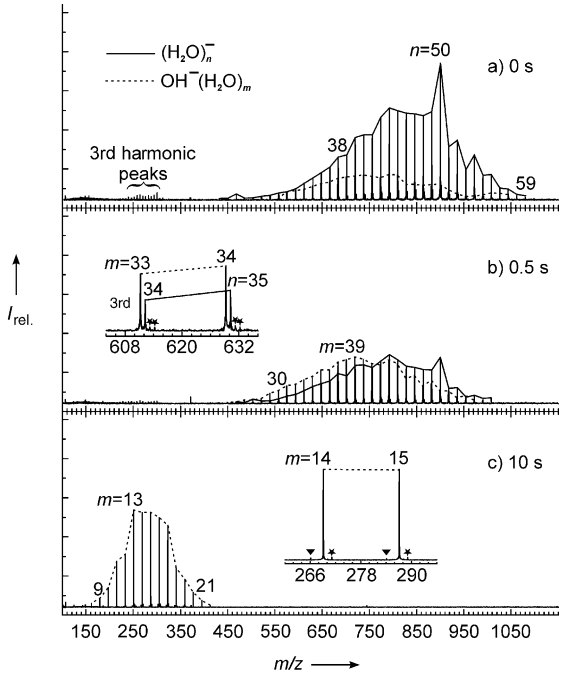



***Figure 1.*** Mass spectra of the reaction of $(H_2O)_n^-$ with acetonitrile after a) 0 s, b) 0.5 s, and c) 10 s. Already at 0 s, one can clearly see (shifted lower by one AMU) the presence of the reaction products, $OH^-(H_2O)_m$. After 0.5 s, about 50% of the ions have reacted, and after 10 s all the initial $(H_2O)_n^-$ has been completely converted into products. The peaks marked with ⋆ are due to the natural abundance of $^{18}O$ in the water molecules. The peaks marked with ▼ result from $O_2^-(H_2O)_p$ impurities after long reaction delays.

instrument during the entire experiment, the reaction already takes place during the accumulation of the $(H_2O)_n^-$ nanodroplets in the ICR cell, so that products are already clearly observable at the nominal time $t = 0$. The product peaks are shifted by one unit to lower masses with respect to the reactant that contains the solvated electron, indicating that a hydrogen atom has been lost from the cluster. The distribution of the products is broad and, except for a slight shift towards smaller values of $n$, similar to that of the reactant clusters, which suggests that the reaction rate is not strongly size-dependent. The overall reaction can be described by Equation (1).

$$(H_2O)_n^- + CH_3CN \rightarrow OH^-(H_2O)_{n-m-1} + m\,H_2O + C_2H_4N, \quad m = 1,2 \tag{1}$$

Clearly, one of the water molecules in the nanodroplet loses a hydrogen atom, and a hydrated hydroxide anion is formed. In addition, the shift in the distribution of the product towards a smaller number of ligands suggests that the overall reaction is sufficiently exothermic to evaporate one or several water molecules. After 0.5 s, almost exactly half of the ions have reacted, and after 10 s, virtually all the $(H_2O)_n^-$ is converted into $OH^-(H_2O)_n$. Although the $CH_3CN$ clearly is an essential participant of the reaction, no clusters that contained acetonitrile were detected in the first reaction step.

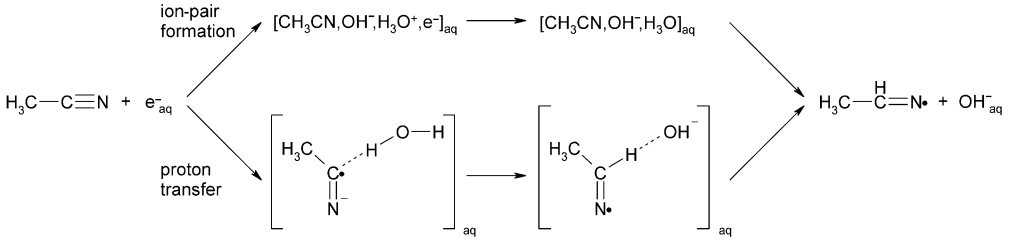
The reaction is accompanied by collisional and blackbody-radiation-induced cluster fragmentation, which causes the nanodroplets to undergo sequential loss of single water molecules.[7a] After even longer reaction times, when the number of water molecules drops to below about $n = 15$, the uptake of one acetonitrile molecule in the strongly basic $OH^-(H_2O)_n$ clusters becomes feasible, resulting in $OH^-(H_2O)_nCH_3CN$ species. The final product of their further fragmentation is an $OH^-(H_2O)_2CH_3CN$ complex, which appears stable under the conditions of our experiment.

Although mass spectrometric analysis unambiguously reveals the loss of a hydrogen atom, it cannot identify the neutral species formed in the reaction and does not show if it is lost as a free atom, if it recombined with the acetonitrile molecule, or if other fragments (e.g. CN or HCN) have been formed. However, the observed reaction must be both thermochemically allowed and mechanistically feasible. The potential energy surface of $CH_3CN + H$ was recently studied by Wang et al. at the G3 level of theory, and the results were in excellent agreement with available experimental data.[8] Among the eleven different possibilities investigated by these authors, the product of hydrogen addition at the carbon atom, $CH_3CHN$, is clearly the thermochemically most favorable and at the same time the product most likely to be produced from a mechanistic point of view, as it poses the smallest barrier for hydrogen addition.

As shown in Scheme 1, the observations can be rationalized by two mechanisms, which differ in the initially activated species. Recent calculations suggest that structures that contain the $H_3O^+$–$OH^-$ ion pair are stable minima on the potential energy surface of $(H_2O)_n^-$ with $n = 11$ and $n = 14$.[9] Even though these structures are not the lowest-energy species, the formation of such ion pairs in the collision complex could be promoted by the large dipole moment of $CH_3CN$ (3.924 D). Once formed, the $H_3O^+$ might recombine with the electron, and the resulting H atom is added to acetonitrile, as previously observed in radiolysis studies.[10]

The second, equally speculative mechanism, involves a solvent-stabilized covalent radical anion as the reactive intermediate. It is well-established for $CO_2^-$ [11] and the uracil anion[12] that solvation with a single water molecule leads to a greatly increased electron affinity and, at least in the case of $CO_2^-$, a significant change in geometry and

 © 2003 Wiley-VCH Verlag GmbH & Co. KGaA, Weinheim 




***Scheme 1.*** Proposed mechanisms for the formation of $OH^-(H_2O)_m$. In the first mechanism, the large dipole moment of acetonitrile induces $H_3O^+$–$OH^-$ ion-pair formation in the collision complex, followed by a hydronium ion–electron recombination. The resulting H atom is added to acetonitrile. The second mechanism involves a solvent-stabilized covalent radical anion as an intermediate. A proton can be transferred from a water molecule, the $CH_3CHN$ evaporates, and $OH^-(H_2O)_m$ remains.

electronic structure. Whereas $CH_3CN^-$ is a dipole-bound anion in the gas phase,[13] it was recently shown that excess electrons in condensed acetonitrile lead to reactive species,[14] and quantum-chemical calculations (polarizable continuum model) yield a C-C-N angle of 125.4°.[14c] It is quite conceivable that hydration may have a similar effect and that $CH_3CN^-$ is transformed into a covalent radical anion. When formed in the collision of $CH_3CN$ with $(H_2O)_n^-$, this radical anion may be able to extract a proton from the nanodroplet, and a neutral $CH_3CHN$ entity evaporates, leaving behind an $OH^-(H_2O)_n$ cluster.

Our studies indicate that reactivity studies of organic molecules in nanodroplets that contain hydrated electrons can yield information that is not available by pulsed radiolysis studies of bulk solutions. In the cluster study, the product compositions can be clearly identified by mass spectrometry. In the present case, it was shown that the hydrated electron induces the transfer of an H atom from water to acetonitrile. The formation of a solvent-stabilized radical anion as a reactive intermediate is suggested to be a possible first step in the organic chemistry of the hydrated electron.

## Experimental Section

The experiments were performed on a modified Bruker/Spectrospin CMS47X mass spectrometer equipped with an Apex III data station and an external homebuilt laser vaporization source.[15] Hydrated electrons ($(H_2O)_n^-$, $n = 25$–$60$) were produced by laser vaporization of a solid zinc target with the 5-ns pulse of a frequency-doubled Nd:YAG laser (Continuum Surelite II, 10 Hz, 5 mJ pulse energy), followed by supersonic expansion of the hot plasma entrained in a 50-μs helium pulse, which was seeded with traces of water. The $(H_2O)_n^-$ ions formed were transferred by a series of electrostatic lenses through four stages of differential pumping, decelerated, and stored in the ICR cell. The reactant acetonitrile (Aldrich, 99.93 + %) was degassed by three freeze–pump–thaw cycles and then admitted into the ultrahigh-vacuum region of the ICR cell through a leak valve. The base pressure was thus raised from $2 \times 10^{-10}$ to $9.6 \times 10^{-9}$ mbar, which, based on the average dipole orientation theory,[16] translates into a collision rate of $0.55\ s^{-1}$. The true collision rate is, however, probably larger owing to the finite size of the nanodroplets.

Received: May 22, 2003 [Z51953]

**Keywords:** gas-phase reactions · hydrated electrons · hydrogen transfer · nanodroplets · radical ions

[1] a) R. A. Marcus, *Rev. Mod. Phys.* **1993**, *65*, 599; b) M. Anbar, *Adv. Phys. Org. Chem.* **1969**, *7*, 115; c) U. Schindewolf, *Angew. Chem.* **1968**, *80*, 165; *Angew. Chem. Int. Ed. Engl.* **1968**, *7*, 190; d) P. A. Anderson, D. Barr, P. P. Edwards, *Angew. Chem.* **1991**, *30*, 1511; *Angew. Chem. Int. Ed. Engl.* **1991**, *30*, 1501.
[2] For a review, see: G. V. Buxton, C. L. Greenstock, W. P. Helman, A. B. Ross, *J. Phys. Chem. Ref. Data* **1988**, *17*, 513.
[3] N. C. Verma, R. W. Fessenden, *J. Chem. Phys.* **1976**, *65*, 2139.
[4] a) J. V. Coe, G. H. Lee, S. T. Arnold, H. W. Sarkas, K. H. Bowen, C. Ludewigt, H. Haberland, D. R. Worsnop, *J. Chem. Phys.* **1990**, *92*, 3980; b) P. Ayotte, M. A. Johnson, *J. Chem. Phys.* **1997**, *106*, 811.
[5] M. K. Beyer, B. S. Fox, B. M. Reinhard, V. E. Bondybey, *J. Chem. Phys.* **2001**, *115*, 9288, and references therein.
[6] a) L. A. Posey, M. J. DeLuca, P. J. Campagnola, M. A. Johnson, *J. Phys. Chem.* **1989**, *93*, 1178; b) S. T. Arnold, R. A. Morris, A. A. Viggiano, M. A. Johnson, *J. Phys. Chem.* **1996**, *100*, 2900.
[7] a) V. E. Bondybey, M. K. Beyer, *Int. Rev. Phys. Chem.* **2002**, *21*, 277, and references therein; b) B. S. Fox, O. P. Balaj, I. Balteanu, M. K. Beyer, V. E. Bondybey, *Chem. Eur. J.* **2002**, *8*, 5534.
[8] B. S. Wang, H. Hou, Y. S. Gu, *J. Phys. Chem. A* **2001**, *105*, 156.
[9] A. L. Sobolewski, W. Domcke, *Phys. Chem. Chem. Phys.* **2003**, *5*, 1130.
[10] a) I. Draganić, Z. Draganić, L. Petković, A. Nikolić, *J. Am. Chem. Soc.* **1973**, *95*, 7193; b) P. Neta, R. W. Fessenden, R. H. Schuler, *J. Phys. Chem.* **1971**, *75*, 1654.
[11] T. Tsukuda, M. Saeki, R. Kimura, T. Nagata, *J. Chem. Phys.* **1999**, *110*, 7846; M. Saeki, T. Tsukuda, S. Iwata, T. Nagata, *J. Chem. Phys.* **1999**, *111*, 6333.
[12] J. H. Hendricks, S. A. Lyapustina, H. L. de Clercq, K. H. Bowen, *J. Chem. Phys.* **1998**, *108*, 8.
[13] a) C. G. Bailey, C. E. H. Dessent, M. A. Johnson, *J. Chem. Phys.* **1996**, *104*, 6976; b) M. Gutowski, K. D. Jordan, P. Skurski, *J. Phys. Chem. A* **1998**, *102*, 2624.
[14] a) I. A. Shkrob, M. C. Sauer, Jr., *J. Phys. Chem. A* **2002**, *106*, 9120; b) I. A. Shkrob, K. Takeda, F. Williams, *J. Phys. Chem. A* **2002**, *106*, 9132; c) C.-G. Xia, J. Peon, B. Kohler, *J. Chem. Phys.* **2002**, *117*, 8855.
[15] C. Berg, T. Schindler, G. Niedner-Schatteburg, V. E. Bondybey, *J. Chem. Phys.* **1995**, *102*, 4870.
[16] L. Bass, T. Su, W. J. Chesnavich, M. T. Bowers, *Chem. Phys. Lett.* **1975**, *34*, 119.

 © 2003 Wiley-VCH Verlag GmbH & Co. KGaA, Weinheim 

# Cover Picture




**Dimitrios Stamou,* Claus Duschl, Emmanuel Delamarche, and Horst Vogel***

**Parallel, fast, and effortless** self-assembly of nanosized components results in their organization of into functional objects. In their Communication on page 5580 ff., Stamou, Vogel, et al. describe how receptor–ligand recognition allows the assembly of single attoliter molecular vessels in a two-dimensional array format, thus allowing the rapid detection, identification, and manipulation of biologically active compounds in a parallel manner.

# Contents

## Angewandte EarlyView

***The following articles are available online (in Wiley InterScience). You can find them at www.angewandte.org, under Full Text, Early View.***

*N. Gommermann, C. Koradin, K. Polborn, P. Knochel*:*
**A New Enantioselective, Copper(I)-Catalyzed Three-Component Reaction for the Preparation of Propargylamines**
DOI: 10.1002/anie.200352578
Published online: November 11, 2003

*J. M. C. A. Kerckhoffs, F. W. B. van Leeuwen, A. L. Spek, H. Kooijman, D. N. Reinhoudt,* M. Crego-Calama*:*
**Regulatory Strategies in the Complexation and Release of a Noncovalent Guest Trimer by a Self-Assembled Molecular Cage**
DOI: 10.1002/anie.200352733
Published online: November 11, 2003

*S. Quideau,* M. Jourdes, C. Saucier, Y. Glories, P. Pardon, C. Baudry:*
**DNA Topoisomerase Inhibitor Acutissimin A and Other Flavano-Ellagitannins in Red Wine**
DOI: 10.1002/anie.200352089
Published online: November 11, 2003

Articles judged by the referees or the editor as being either very important or very urgent are immediately edited, proof-read, and electronically published once the manuscript has arrived in the editorial office in final form. As long as there is no page number available these articles should be cited in the following manner:

Author(s) *Angew. Chem. Int. Ed.*, online publication date, DOI.

## Obituary


Virgil Boekelheide (1919–2003) — **5540** — From Alkaloids to Superphane — *Henning Hopf*


## Books


Biophysical Chemistry—Membranes and Proteins — **5541** — Richard H. Templer, Robin Leatherbarrow — *reviewed by W. Binder*

Cell Membrane — **5541** — Yoshihito Yawata — *reviewed by C. Steinem*

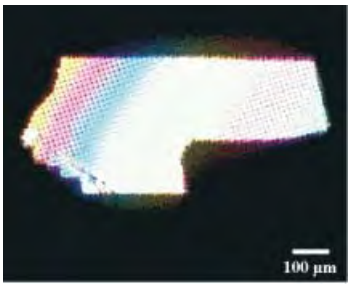

## Highlights

*Crystal Engineering*


D. Braga* — **5544–5546**

From Amorphous to Crystalline by Design: Bio-Inspired Fabrication of Large Micropatterned Single Crystals


**Clear as crystal?** There are still many questions to be answered before we can truly understand the mysteries of crystallization. However, there has been some remarkable progress towards finding some of these answers; for example, the use of ordered, functionalized templates to prepare oriented single crystals (see the polarized-light image of a single micropatterned calcite crystal)

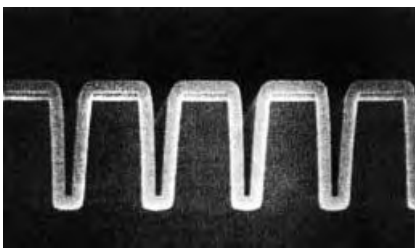



## Minireviews

*Electronic Materials*


M. Leskelä,* M. Ritala — **5548–5554**

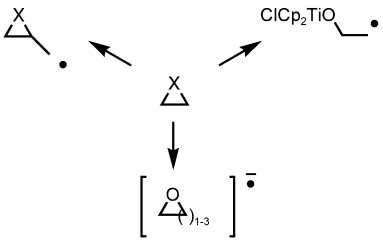
Atomic Layer Deposition Chemistry: Recent Developments and Future Challenges

**One step at a time**: Atomic layer deposition (ALD) is a most promising technique for the design of future integrated circuits. The self-limiting mechanism of ALD lends itself to the preparation of pure high-permittivity oxides for gate dielectrics and memory capacitors, and transition-metal nitride and metal films for interconnects (the picture shows a 300-nm layer of $Al_2O_3$ deposited onto a patterned Si substrate).

# Reviews

**Unusual radicals** efficiently prepared by the ring opening of heterocycles have enormous potential in organic synthesis. Three different types of valuable radical intermediates can be generated from strained heterocycles by properly choosing the reaction conditions (see scheme; X = O, NR). Applications in the synthesis of complex molecules amply demonstrate the usefulness of the methods.

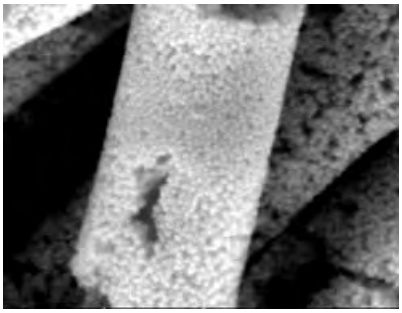



***Radicals from Ring Opening***

A. Gansäuer,* T. Lauterbach, S. Narayan ——— **5556 – 5573**

Strained Heterocycles in Radical Chemistry

# Communications

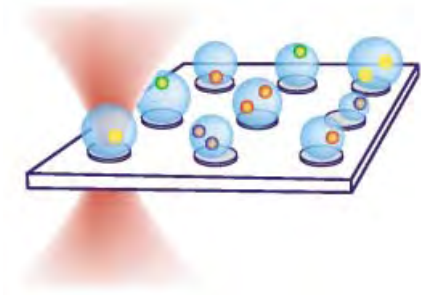


**Electrically conducting nanoparticle nanotubes** (NPNTs) with a high surface area are obtained by a novel procedure. The assembly of gold nanoparticles on the pore walls of surface-modified nanoporous alumina membrane templates under flow conditions is accompanied by spontaneous room-temperature coalescence of the bound nanoparticles, which results, after membrane dissolution, in self-sustained NPNTs that preserve the nanoparticle morphology (see picture).

***Nanostructures***

M. Lahav, T. Sehayek, A. Vaskevich, I. Rubinstein* ——— **5576 – 5579**

Nanoparticle Nanotubes



**High-density microarrays** of attoliter volume elements can be created (see figure) within minutes in a parallel and effortless manner by using self-assembly of nanometer-size components based on biological recognition. These ultrasmall volumes allow localization of single molecules, screening for (bio)chemical properties, and assessing the performance of confined chemical reactions.

***Vesicular Microarrays***

D. Stamou,* C. Duschl, E. Delamarche, H. Vogel* ——— **5580 – 5583**

Self-Assembled Microarrays of Attoliter Molecular Vessels

**For the USA and Canada:**
ANGEWANDTE CHEMIE International Edition (ISSN 1433-7851) is published weekly by Wiley-VCH PO Box 191161, D 69451 Weinheim, Germany. Air freight and mailing in the USA by Publications Expediting Inc. 200 Meacham Ave., Elmont, NY 11003. Periodicals postage paid at Jamaica NY 11431. US POSTMASTER: send address changes to *Angewandte Chemie*, Wiley-VCH, 111 River Street, Hoboken, NJ 07030. Annual institutional subscription price for institutions: Europe € 3430.00/3118.00. Outside Europe US$ 4499.00/4090.00 (valid for print and electronic/print or electronic delivery); for individuals who are personal members of a national chemical society, or whose institution already subscribes, or who are retired or self-employed consultants, print only. Europe € 248.00/Outside Europe US$ 378.00. Postage and handling charges included. All Wiley-VCH prices are exclusive VAT.

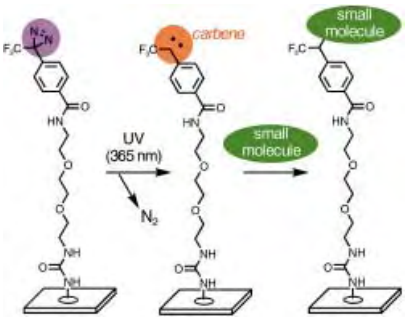
 © 2003 Wiley-VCH Verlag GmbH & Co. KGaA, Weinheim 

# Contents


## Microarrays

N. Kanoh, S. Kumashiro, S. Simizu, Y. Kondoh, S. Hatakeyama, H. Tashiro, H. Osada* _____ **5584 – 5587**

Immobilization of Natural Products on Glass Slides by Using a Photoaffinity Reaction and the Detection of Protein–Small-Molecule Interactions



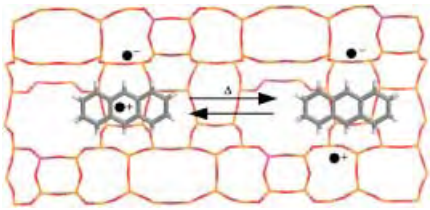

**Library on a glass slide:** A variety of small molecules, including complex natural products, are introduced to glass slides using a photoaffinity reaction (see picture). The small molecules retain the inherent ability to interact with the relevant binding proteins. Importantly, this immobilization procedure does not require a specific functional group, and can be applied for use with a diverse small-molecule library.

## Zeolites

H. Vezin, A. Moissette,* C. Brémard _____ **5587 – 5591**

Temperature-Dependent Interconversion of an Anthracene Radical Cation/Electron Moiety to an Electron–Hole Pair in the Pores of Al-ZSM-5 Zeolites

**Trappings of success**: The reversible interconversion between an anthracene radical cation and its ejected electron, and an electron–hole pair in the acidic zeolite Al-ZSM-5 was thermally induced. The void space of the porous material facilitates anthracene ionization at room temperature and the electron–hole formation under gentle heating.



●$^-$ = trapped electron
●+ = electron-deficient site in the radical cation or hole

## Magnetic Effects in Nanomaterials

S. L. Tripp, R. E. Dunin-Borkowski, A. Wei* _____ **5591 – 5593**

Flux Closure in Self-Assembled Cobalt Nanoparticle Rings



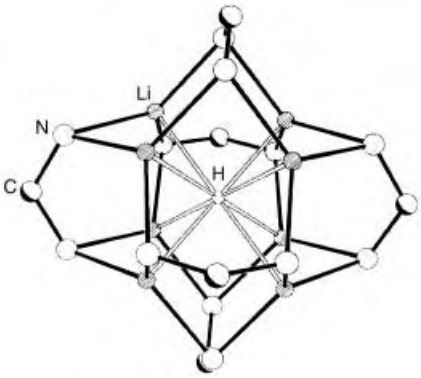

**Closing the circle**: Chiral magnetic domains are observed when ferromagnetic Co nanoparticles self-assemble into bracelet-like rings (see picture). The magnetic dipoles of the particles collectively contribute toward flux closure, a bistable state with potential utility for nonvolatile data storage.

## Main-Group Clusters

S. R. Boss, M. P. Coles,* R. Haigh, P. B. Hitchcock, R. Snaith, A. E. H. Wheatley* _____ **5593 – 5596**

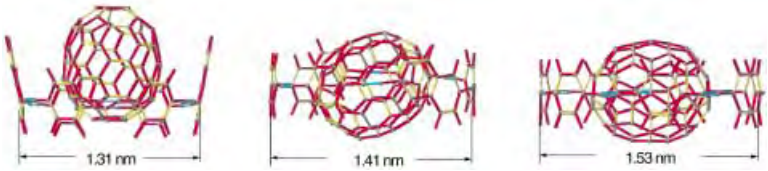
Ligand and Metal Effects on the Formation of Main-Group Polyhedral Clusters

**The reaction of $AlMe_3$ or $ZnMe_2$ with hppH** (hppH = 1,3,4,6,7,8-hexahydro-2*H*-pyrimido[1,2-*a*]pyrimidine) and then with *t*BuLi affords $[Li_8(H)_m(hpp)_6]^{n+}[X]^-_n$, $X = [ZntBu_3]$, $m = n = 1$ (the cation core of which is shown); $X = [Li(Me_2AltBu_2)_2]$, $m = 0$, $n = 2$, as the major product in each case. These data reveal that non-aromatic heterocycle hppH and $ZnMe_2$ can be employed to generate novel hydride-encapsulation main-group-metal clusters, and that related polylithium architectures can also incorporate a central void.





 © 2003 Wiley-VCH Verlag GmbH & Co. KGaA, Weinheim 




**Tuning up**: Carbon nanorings are structurally tuned to optimize their complexation with fullerenes ($C_{60}$ and $C_{70}$; see picture). The affinity of carbon nanorings with fullerenes correlates with the width of the contact area. As the intense fluorescence emission of the cyclic-paraphenyleneacetylene host is quenched by the complexation of a fullerene, this effect can be used as a basis of a fullerene sensor.

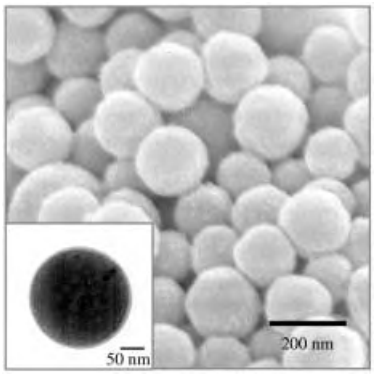
***Supramolecular Dynamics***

T. Kawase,* K. Tanaka, Y. Seirai, N. Shiono, M. Oda* ——— **5597 – 5600**

Complexation of Carbon Nanorings with Fullerenes: Supramolecular Dynamics and Structural Tuning for a Fullerene Sensor

---

**A variety of polymer shells** with controlled and uniform thickness are easily formed on the surfaces of silica and titania colloids by vapor deposition polymerization (VDP; see picture of silica–PMMA core–shell nanoparticles). Carbon capsules derived from polydivinylbenzene shells can be used in applications such as the encapsulation of pyrene molecules, which is a photochromic dye. These results demonstrate the usefulness of VDP as a simple method to fabricate various capsule materials as well as core–shell nanoparticles.



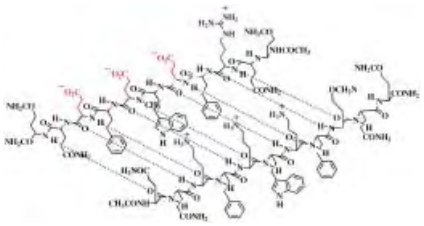

***Core–Shell Nanostructures***

J. Jang,* B. Lim ——— **5600 – 5603**

Facile Fabrication of Inorganic-Polymer Core–Shell Nanostructures by a One-Step Vapor Deposition Polymerization

---

**Fibrillar networks** built up from polyelectrolyte β-sheet complexes (see picture) are formed by spontaneous self-assembly when solutions of appropriately designed cationic and anionic oligopeptides are mixed. At the macroscopic level the resulting solutions are nematic hydrogels, which are quite robust to variations in pH or peptide concentration.



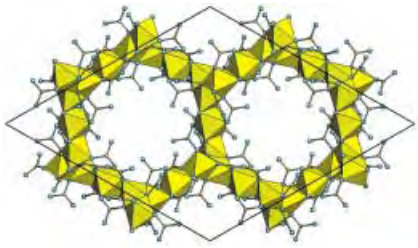
***Peptide Polyelectrolyte Complexes***

A. Aggeli, M. Bell, N. Boden,* L. M. Carrick, A. E. Strong — **5603 – 5606**

Self-Assembling Peptide Polyelectrolyte β-Sheet Complexes Form Nematic Hydrogels

---

**A framework of $AlO_6$ octahedra** is present in the microporous aluminoborate $HAl_3B_6O_{12}(OH)_4$ (PKU-1; see picture), which was synthesized from $AlCl_3$ in a boric acid flux. The octahedra share two or three edges with neighboring octahedra to form a framework with 18-ring tunnels along [001] and 10-ring tunnels along {100}. The borate groups share vertices with the octahedra, compensating the negative charge of the octahedral framework and almost completely blocking the 10-ring channels.



***Octahedron-Based Molecular Sieves***

J. Ju, J. Lin,* G. Li, T. Yang, H. Li, F. Liao, C.-K. Loong, L. You ——— **5607 – 5610**

Aluminoborate-Based Molecular Sieves with 18-Octahedral-Atom Tunnels

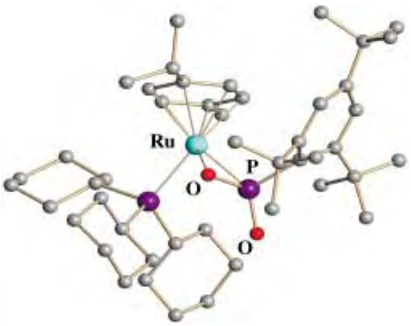
 © 2003 Wiley-VCH Verlag GmbH & Co. KGaA, Weinheim 

# Contents


## Phosphorus Coordination Chemistry

R. Menye-Biyogo, F. Delpech,* A. Castel, H. Gornitzka, P. Rivière* — **5610 – 5612**

Ruthenium-Stabilized Low-Coordinate Phosphorus Atoms: Structural Evidence for Monomeric Metaphosphonate

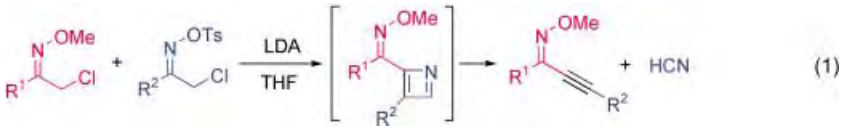



**Monomeric metaphosphonate** is generated and stabilized within the coordination sphere of a ruthenium atom. The π system of a PO moiety coordinates to the transition metal center and this allows thermodynamic stabilization to give the first structural evidence for monomeric dioxophosphorane.

## Synthetic Methods

T. Tsuritani, K. Yagi, H. Shinokubo,* K. Oshima* — **5613 – 5615**

Base-Induced Condensation of α-Chloro Oxime Derivatives Furnishes Alkynes

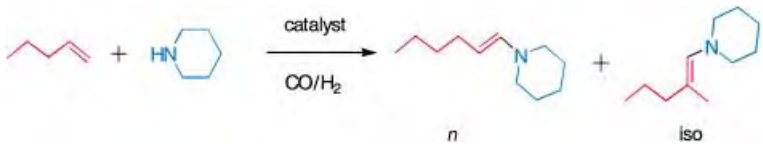



**A one-carbon unit is lost** in the condensation of α-chloro oxime ethers induced by lithium diisopropylamide [Eq. (1)]. This reaction, which provides alkynyl oxime ethers in good yields, is proposed to proceed via a 2-(iminomethyl)azacyclobutadiene intermediate.

## Synthesis of Enamines

M. Ahmed, A. M. Seayad, R. Jackstell, M. Beller* — **5615 – 5619**

Highly Selective Synthesis of Enamines from Olefins



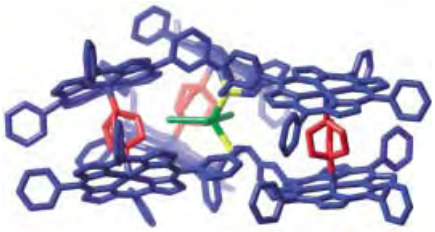

**Astonishing chemoselectivity** is observed in the rhodium-catalyzed formation of enamines from olefins, CO, $H_2$, and amines (see scheme). This new reaction can be used with a broad range of substrates and is high-yielding and highly selective (*n*/iso = 99:1 in most cases).

## Supramolecular Catalysts

V. F. Slagt, P. W. N. M. van Leeuwen, J. N. H. Reek* — **5619 – 5623**

Multicomponent Porphyrin Assemblies as Functional Bidentate Phosphite Ligands for Regioselective Rhodium-Catalyzed Hydroformylation

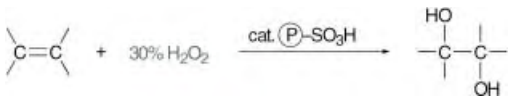
**Selectivity from a rigid sandwich-type complex**: A supramolecular approach was used to prepare chelating ligands that give high selectivity for the linear aldehyde in the rhodium-catalyzed hydroformylation of 1-octene. The multicomponent assembly consists of two tris(zinc(II) porphyrin)-phosphite ligands (blue) and three ditopic templates (red) with the rhodium complex (green) in the middle of the structure.



## Green Chemistry

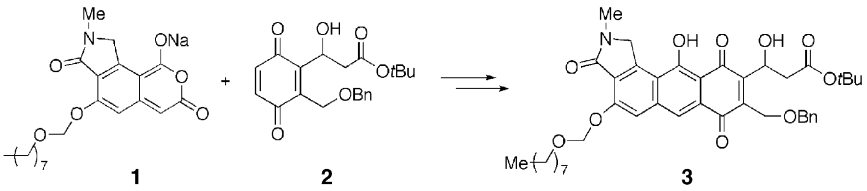
Y. Usui, K. Sato,* M. Tanaka — **5623 – 5625**

Catalytic Dihydroxylation of Olefins with Hydrogen Peroxide: An Organic-Solvent- and Metal-Free System




**Green and convenient**: Olefins are oxidized to 1,2-diols in high yield with 30% $H_2O_2$ in the presence of resin-supported sulfonic acid (see scheme) under metal-free conditions without any organic solvent. The catalyst can be recycled easily and is effective for at least 10 cycles.


 © 2003 Wiley-VCH Verlag GmbH & Co. KGaA, Weinheim 

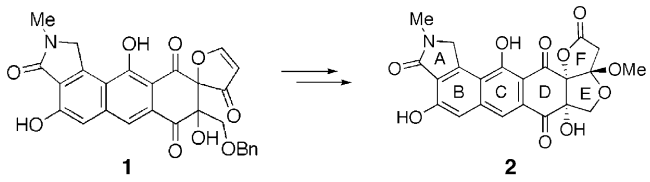



**The rapid assembly** of the ABCD tetracyclic ring system of lactonamycin involved the strong-base-induced regioselective Diels–Alder reaction of **1** and **2** to form advanced precursor **3**. Regiochemical control results from the suitably positioned hydroxy group, and thus only the desired isomer of **3** is obtained.

**Natural Product Synthesis**

C. D. Cox, T. Siu,
S. J. Danishefsky* ——— **5625 – 5629**

Studies Directed toward the Total Synthesis of Lactonamycin: Control of the Sense of Cycloaddition of a Quinone through Directed Intramolecular Catalysis

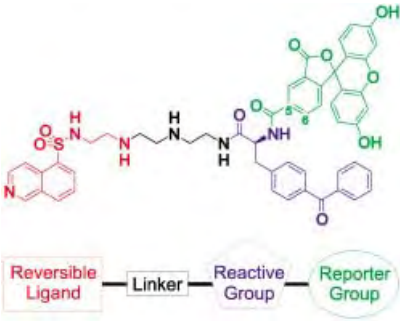



**A revised strategy** was required for the installation of the remaining polyoxygenated E and F rings of lactonamycinone (**2**). Key features in the successful route include dihydroxylation of a ketoquinone, the use of a furanone as a lactone surrogate (see **1**), and an acid-induced ketalization reaction to install the angular methoxy substituent.

**Natural Product Synthesis**

T. Siu, C. D. Cox,
S. J. Danishefsky* ——— **5629 – 5634**

Total Synthesis of Lactonamycinone

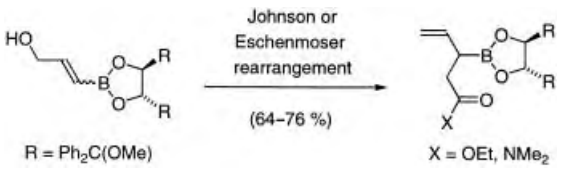



**Kinases** can be tagged with an engineered chemical probe that comprises a reversibly binding protein ligand, a photoreactive group (4-benzoylphenylalanine), and a fluorescent reporter group (carboxyfluorescein). This principle, which does not require irreversible inhibitors, allows affinity-based detection of protein families in functional proteomics.

**Functional Proteomics**

M. C. Hagenstein, J. H. Mussgnug, K. Lotte, R. Plessow, A. Brockhinke, O. Kruse,* N. Sewald* ——— **5635 – 5638**

Affinity-Based Tagging of Protein Families with Reversible Inhibitors: A Concept for Functional Proteomics




**Enantiomerically pure reagents** for allyl additions were prepared by [3,3] sigmatropic rearrangements (see scheme) followed by a separation of the diastereoisomers. The highly stable allylboronic esters with a stereogenic center $\alpha$ to a boron atom were used to synthesize *Z*-configured homoallylic alcohols with an enantiomeric excess $>94\%$.

**Allylation Reagents**

J. Pietruszka,* N. Schöne ——— **5638 – 5641**

[3,3] Sigmatropic Rearrangement of Boron-Containing Allyl Alcohols: Synthesis of Allyl Addition Reagents

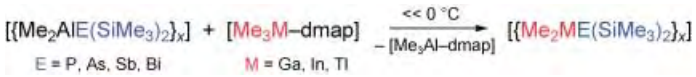
 © 2003 Wiley-VCH Verlag GmbH & Co. KGaA, Weinheim 

# Contents


**Group 13/15 Heterocycles**

F. Thomas, S. Schulz,* H. Mansikkamäki, M. Nieger ——— **5641 – 5644**

A Versatile Metathesis Reaction for the Formation of Labile Bonds between Group 13 and Group 15 Atoms




**The heterocycles $[\{Me_2AlE(SiMe_3)_2\}_x]$** (E = P–Bi) are powerful metathesis reagents in the presence of 4-dimethylaminopyridine (dmap), thus allowing the synthesis of previously unknown Group 13/15 compounds. Reactions with $[Me_3M{-}dmap]$ (M = In, Tl) proceed with $E(SiMe_3)_2$ transfer to form the corresponding heterocycles $[\{Me_2InBi(SiMe_3)_2\}_3]$ and $[\{Me_2TlE(SiMe_3)_2\}_2]$ (E = P, As), which were characterized by NMR and MS analysis, and by single-crystal X-ray diffraction.


VIP Communications labeled with this symbol have been judged by two referees as being "very important papers".

The publication of Communications labeled with this symbol has been accelerated because of their topical or highly competitive nature.


# Sources

## Product and Company Directory

You can start the entry for your company in "Sources" in any issue of *Angewandte Chemie*.

If you would like more information, please do not hesitate to contact us.

**Wiley-VCH Verlag – Advertising Department**
Tel.: 0 62 01 - 60 65 65
Fax: 0 62 01 - 60 65 50
E-Mail: MSchulz@wiley-vch.de


## Service


*Keywords* ——— *5648*

*Authors* ——— *5649*

*Angewandte's Sister Journals* ——— *5646 – 5647*

*Sources* ——— *A67*

*Preview* ——— *5651*

## Virgil Boekelheide (1919–2003): From Alkaloids to Superphane

Virgil Boekelheide, Professor of Organic Chemistry in the Department of Chemistry at the University of Oregon, died in Eugene, Oregon (USA) on September 24 at the age of 84.

Boekelheide was descended from a family of German immigrants, who had emigrated in the 19th century from Emsland to the present South Dakota (USA). He spent his childhood and student years in the Midwest and completed his PhD in 1943 under the supervision of C. F. Koelsch at the University of Minnesota. He was an instructor at the University of Illinois from 1943 to 1946, and from there moved as professor to the University of Rochester. From 1960 until 1984 he worked at the University of Oregon, where he played a leading role in the development of this institution and contributed to the establishment of its scientific reputation. Until the beginning of the 1960s, alkaloid chemistry remained at the center of Boekelheide's research. However, his interests shifted more and more toward aromatic chemistry, especially after his move to the West Coast. Again and again he had come across new and unusual aromatic and related π systems—tropones, cyclooctatetraenes, cyclazines—in his natural product work.



By the middle of the 1960s his reorientation was complete, and Boekelheide reported new aromatic compounds he had made with substituents inside the π-electron cloud.[1] Aromatic chemistry experienced unprecedented progress during that period, almost 100 years after Kekulé had reported his structure of benzene. New valence isomers of benzene were prepared, the Hückel theory had been generally accepted by organic chemists, and new synthetic methods were developed, particularly in the field of nonbenzenoid aromatic systems (for example, by Sondheimer for higher annulenes and by Nozoe and Hafner for tropones and azulenes). Crucial to these developments was that NMR spectroscopy now provided a method for recording "aromaticity" experimentally. However, an impasse existed at first in the area of medium-sized rings: The synthesis of [10]- and [14]annulenes and their derivatives caused difficulties. The breakthrough was made by E. Vogel in the case of [10]- and by Boekelheide in the case of [14]annulenes, through an elegant and highly effective trick. They eliminated the steric interactions between transannular hydrogen atoms inside the ring of these systems, which were the root of the synthetic problems, by replacing these atoms with a methano bridge and an ethano bridge, respectively, to make a 15,16-dihydropyrene system in the latter case.[2]

Bridged aromatic compounds are now known as cyclophanes. The π stacking of planar aromatic systems had been an obvious step to Boekelheide from the start. He used this approach in the synthesis of his new π systems through the valence isomerization of [2.2]*meta*-cyclophanedienes, a (photochromic) process that enjoys popularity in the development of new photoswitchable systems to this day. From this point Boekelheide's research developed in two directions. While he studied the chemical, electronic, structural, and theoretical properties of dihydropyrenes in the broadest sense, often in cooperation with other research groups, he also started to solve one of the big problems in phane chemistry—the synthesis of "superphane", a compound in which the two benzene rings are clamped together by a total of six ethano bridges. This target molecule was not only aesthetically attractive, on account of its high symmetry, but was interesting above all in terms of how closely two π systems, in this case two benzene rings on top of one another, could be pushed together, and what the consequences of forcing them together would be. Whereas the distance between the layers in graphite is 3.4 Å, the distance is only 3.1 Å between the decks of [2.2]*para*-cyclophane. How far apart would the aromatic rings be in superphane? Superphane was prepared through an extremely elegant iterative synthesis, which made use of the Diels–Alder addition of *o*-xylylene intermediates. With an interdeck distance of 2.6 Å, this compound still holds the record for π-stacked aromatic systems.[3]

Boekelheide, who for many years was on the editorial boards of the *Journal of the American Chemical Society*, the *Journal of Organic Chemistry*, *Organic Reactions*, and *Organic Syntheses*, received many awards and honors for his scientific achievements. He was invited to give innumerable plenary lectures, received distinctions from the chemical societies of many countries, and was made a member of the National Academy of Science of the USA. Particularly during his two periods in Germany as a Senior Alexander von Humboldt Fellow he was able to build up and strengthen contacts with German colleagues and friends. During his first stay in Karlsruhe from 1974 to 1975 I came to know him as a modest and friendly person with a great sense of humor, always ready to share not only his ideas, but also his vast experimental know-how. Our own work in the field of cyclophanes would not have developed so rapidly without his help. He was convinced that good relations between countries could only be developed through personal contact between people and made his research group a meeting place for countless undergraduate and PhD students, postdoctoral researchers, and colleagues from all over the world, whom he encouraged and assisted long after they had left Eugene. As he got older his generosity shifted increasingly toward the arts and music. Having always been fond of classical music, he became one of the main patrons of the music and theater scene in Oregon. Boekelheide will be always remembered by his friends around the world as an outstanding experimental chemist and philanthropist.

*Henning Hopf*
TU Braunschweig

[1] V. Boekelheide, J. B. Phillips, *Proc. Natl. Acad. Sci. USA* **1964**, *51*, 550.
[2] V. Boekelheide, J. B. Phillips, *J. Am. Chem. Soc.* **1967**, *89*, 1695–1704.
[3] Y. Sekine, M. Brown, V. Boekelheide, *J. Am. Chem. Soc.* **1979**, *101*, 3126–3127.

 © 2003 Wiley-VCH Verlag GmbH & Co. KGaA, Weinheim 

Crystal Engineering

# From Amorphous to Crystalline by Design: Bio-Inspired Fabrication of Large Micropatterned Single Crystals**

*Dario Braga**

**Keywords:**
amorphous materials · calcium carbonate · crystal engineering · crystal growth · micropatterning

Crystals have always fascinated mankind[1] and yet crystallization, the process by which crystals are formed, remains to a large extent a mystery that remains to be unravelled.[2] No recipe exists to predict the shape, size, or system of crystals that may form from a solution of a new compound, nor whether the crystals will be thermodynamically stable or metastable, whether they will undergo phase changes with temperature or pressure, or whether they will include solvent molecules upon crystallization. In most cases, we are unable to predict whether crystallization will yield a powder, single crystals, or an amorphous material, or indeed all of these at the same time.

All materials can be solid, but not every solid obeys Bragg's law. Indeed, many of the most interesting materials are disordered or amorphous and their characterization and evaluation is particularly challenging.[3] This seems to contrast with the belief of many people (including the author of this article) in the possibility of engineering crystals at the molecular level.[4] There is no doubt that crystal design can be performed by choosing building blocks and/or crystallization conditions, but in order for a crystal to have any practical utilization it must have a controllable size and a shape, and often orientation, that is adequate to the desired function. Crystalline materials are finding important applications in optics, microelectronics, biomedical implants, gas sensors, traps, reservoirs, separation technologies, and catalysis. Engineering implies transferability and reproducibility at an extreme level of precision; even the smallest fragment, visible only under a microscope, requires recognition and the self-arrangement of billions of molecules or ions.

Nature knows how to build extremely specialized materials, which are constructed, indeed *engineered*, to exert specific biological functions, which may require the crystals to adopt specific shapes, crystallographic orientations,[5] or to possess specific dimensions. In bones or mollusc shells, for example, the material is polycrystalline, while in sea urchin spines and plates the whole skeletal element is one large crystal. It is fascinating to realize that the odd shapes of many biominerals correspond to perfect single crystals (see Figure 1). Can we learn from nature how to build "tailor-made" crystals? This paper highlights a success story: The controlled generation of microdecorated single crystals using a bio-inspired approach.

It is now well established that nature often uses amorphous material as a reservoir for crystalline material. For example biogenic single crystals of calcium carbonate (in its three forms, calcite, aragonite, and vaterite) are often produced by the conversion of amorphous calcium carbonate (ACC).[6] An amorphous form of calcium carbonate hydrate can be obtained in vitro from highly saturated solutions.[7] This phase is metastable and rapidly transforms into crystalline calcium carbonate (as calcite, vaterite, or aragonite) unless stabilized with the aid of additives.[8] In biological environments, ACC is stabilized by macromolecules containing hydroxyamino acids, glycine, glutamate, phosphate, or polysaccharide groups.[3b,9]

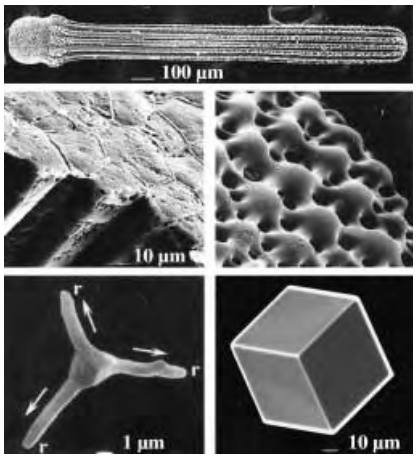



***Figure 1.*** Scanning electron micrographs of biogenic and synthetic calcite crystals. Top: sea urchin spine (single crystal of calcite); center left: mollusc shell (crystalline/organic composite); center right: brittle star lens array (single crystal of calcite); bottom left: sea urchin larval spicule (amorphous-to-crystalline transition); bottom right: a laboratory grown calcite crystal.

If the paradigm of the crystalline state is the ordered distribution of molecules and ions through the space of the crystal, an amorphous material is a solid that does not possess periodicity. An amorphous solid appears isotropic under polarized light and does not diffract X-rays in the same way as crystals do. Because of this lack of structural information, the full characterization of an amorphous phase is very difficult. In the case of ACC, however,

[*] Prof. D. Braga
Department of Chemistry
The University of Bologna
Via F. Selmi 2, 40126 Bologna (Italy)
Fax: (+39) 051-209-9456
E-mail: dbraga@ciam.unibo.it

[**] I am grateful to Prof. L. Addadi and F. Grepioni for comments. Original drawings and images used herein were kindly provided by Dr. Aizenberg.

 © 2003 Wiley-VCH Verlag GmbH & Co. KGaA, Weinheim DOI: 10.1002/anie.200301677 

based on EXAFS experiments (EXAFS provides information on the local short-range order around selected atoms) it has been shown that biogenic amorphous ACC is not one single structural phase, but a family of at least three different forms. These forms possess roughly the same composition as that of monohydrocalcite and differ mainly in the number of calcium atoms in the first, second, and third coordination shell.[10]

The differences between the various amorphous phases appear to be under genetic control and depend on the organism producing the phase. Any step towards the understanding of the factors controlling ACC biogenesis and its subsequent crystallization into a functional structure would be fundamental for the deliberate engineering of biomimetic function-oriented crystalline materials.

Whitesides, Aizenberg, and coworkers have shown that control over crystallization can be obtained by using ordered, functionalized templates. For instance, when self-assembled monolayers (SAMs) of ω-terminated alkanethiols supported on gold or silver[11a] are used as crystallization templates, calcite nucleation in various crystallographic orientations can be controlled.[11b] Much higher control was achieved when SAMs were combined with micropatterning. Using this approach, it has been possible to generate high-resolution patterns and multicrystalline arrays of microcrystals of calcium carbonate with controlled sizes, crystallographic orientation, and density of nucleation by varying the SAM, solution concentration, and/or the features of the deposition surface.[12]

Aizenberg et al.[13] have combined SAMs, micropatterning, and the controlled transformation of transient ACC to prepare large, micropatterned, oriented calcite single crystals that originate from a single nucleation site (the imprinted SAM).[13]

In Aizenberg's crystallization strategy, the micropattern design is obtained by photolithography and serves to generate the microstructure of the metastable ACC; this microstructure will be retained in the single-crystal structure once the amorphous-to-crystalline transition starts at the imprinted SAM nanoregion. Formation of ACC will be controlled via functionalization of the substrate with methyl, phosphate, and hydroxy groups while the amorphous-to-crystal transformation will be controlled by incorporating just one nucleation site specific for calcite on the patterned substrate beneath the ACC film. Figure 2 helps to understand how the experiment has been conducted:

a) First a template structure with posts spaced regularly on the surface of a glass slide was prepared by utilizing a photoresist technique.
b) The glass substrate was then coated with a transparent 5–10 nm thick layer of gold (or silver).
c) The tip of an AFM microscope was used to deposit a nanoregion of a self-assembled monolayer (SAM) of $HS(CH_2)_nA$ (A = OH, COOH, $SO_3H$) onto the metal surface, which was required to induce the calcite nucleation.
d) The metal surface around the SAM was then covered with a mixture of alkanethiols of different lengths terminated in phosphate, methyl, and hydroxy groups to create a disordered organic surface that could inhibit calcite nucleation and favor formation of ACC.
e) The functionalized substrate was covered with a thin film of gas-permeable polydimethylsiloxane (PDMS).
f) ACC deposition was attained by placing the assembly in a 1 M $CaCl_2$ solution in a desiccator containing $(NH_4)_2CO_3$ powder whereby, by means of diffusion of $CO_2$ through the PDMS film, metastable ACC was formed among the regularly spaced posts.

Nucleation of crystalline calcite from the metastable ACC started at the imprinted SAM region after approximately 30 min. The calcite crystal growth took place in between the micro-patterned posts and resulted in the formation of a large (up to 1 mm) micropatterned single crystal of calcite (Figure 3).[13] The pore size in the micropatterned crystals was larger than in the ACC mesh probably because the microchannels around the posts were used to discharge the excess water contained in the ACC. It was noted that defects in the micropattern were responsible for stopping crystal growth in certain directions and determined the final macroscopic shape of the crystal.

An important discovery presented in the paper is that the presence of micropatterns plays multiple roles during crystal growth (over and above shape determination). This includes "sump action" for the release of water (and possibly other impurities) during the amorphous-to-crystal transition and the relaxation of stress; as a result, large defect-free single crystals can be grown.

Nature knows very well how to make crystals. Aizenberg and her coworkers have learned three general biomineralization principles, which can

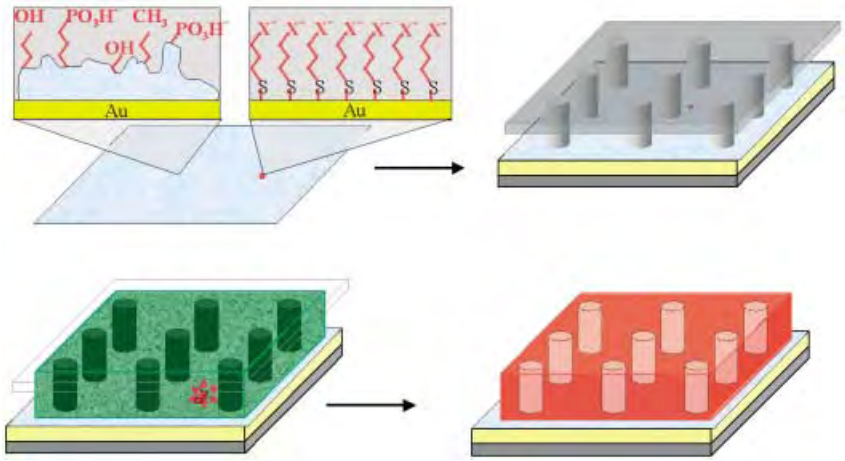



***Figure 2.*** Experimental set up for the crystallization strategy of Aizenberg et al.[13] Top left: a SAM nucleation site is implanted on the gold (or silver) surface with an AFM tip, while the surroundings are covered with ACC-stabilizing organic molecules; top right: coating with porous inert polymer; bottom left: deposition of ACC. Nucleation of a calcite single crystal starts at the SAM; bottom right: growth of the micropatterned calcite single crystal.

 © 2003 Wiley-VCH Verlag GmbH & Co. KGaA, Weinheim 

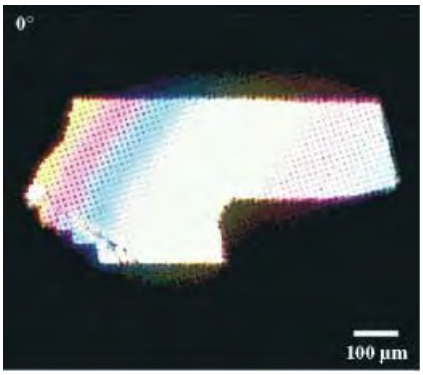



***Figure 3.*** Polarized-light image of the micropatterned single crystal of calcite.

be exploited in planning their crystal design experiment. First of all, they knew that biocrystals usually grow inside organic frameworks that confine mineral deposition within predetermined spatial patterns.[14] Furthermore they have exploited the knowledge that the formation of biogenic calcite single crystals often arises from the transformation of a transient amorphous ACC phase, which is stabilized by phosphate, hydroxy, and methyl-functionalized molecules (as discussed above). The crystallographic orientation of the crystal growth in living organisms is achieved through oriented nucleation at well-defined chemically modified intracellular sites, hence artificial crystal formation can be controlled at the molecular level by organized assemblies of selected organic molecules.

The successful fabrication of macrocrystals with controlled crystallographic orientation and micropatterns relies upon the engineering of a template with essential chemical and structural features. By using appropriate surface patterning agents it is possible to control not only the formation of a transient amorphous ACC phase with an extended lifetime, but also to decorate the ACC phase in a manner that will be remembered by the single crystals subsequently constructed. This can be obtained by placing a nucleation site where appropriate on the amorphous substrate.

While the formation of a large single crystal from an amorphous phase can be expected to lead to unbearable mechanical stress because of the density differences and release of impurities, a three-dimensional array of self-assembling biological macromolecules and/or cells serving as structural templates will provide stress relaxation and impurity discharge, thus giving rise to the formation of large microporous single crystals. It is noteworthy that the diameter of the channels in the fabricated synthetic crystal ($< 10\ \mu m$) is comparable with the mesh observed in biologically formed single calcite crystals. This raises the interesting possibility that the mechanistic implications proposed in this study are directly relevant to the formation of analogous structures in the biological world.

In summary, the work describes a new, bio-inspired crystal design strategy that take advantage of controlled amorphous-to-crystalline transitions using specially engineered, organically modified, three-dimensional templates with integrated nucleation sites. This new concept, which was demonstrated through the crystallization of calcium carbonate, made it possible to directly fabricate millimetre-sized single crystals with an arbitrary sub-10-micrometer pattern and controlled crystallographic orientation. The mechanism underlying this process may provide a new, general, bottom-up approach to the engineering of oriented, micropatterned crystalline materials and, ultimately, may help to explain how organisms evolved their sophisticated, nanopatterned mineralized structures. The prospective applications of bio-inspired crystal design are limited only by … the imagination of the researcher!


[1] G. R. Desiraju, *Nature* **2003**, *423*, 485.
[2] P. Ball, *Nature* **1996**, *381*, 648.
[3] a) L. Addadi, M. Geva, *CrystEngComm* **2003**, *5*, 140; b) J. Aizenberg, G. Lambert, S. Weiner, L. Addadi, *J. Am. Chem. Soc.* **2002**, *124*, 32.
[4] a) D. Braga, G. R. Desiraju, J. Miller, A. G. Orpen, S. S. Price, *CrystEngComm* **2002**, *4*, 500; b) D. Braga, *Chem. Commun.* **2003** (Advance Article, DOI:10.1039/b306269b).
[5] a) S. Mann, *New Sci.* **1990**, 42; b) S. Mann, *Biomineralization. Principles and Concepts in Bioinorganic Materials Chemistry*, Oxford University Press, Oxford, **2001**; c) H. Cölfen, S. Mann, *Angew. Chem.* **2003**, *115*, 2452; *Angew. Chem. Int. Ed.* **2003**, *42*, 2350.
[6] a) E. Beniash, J. Aizenberg, L. Addadi, S. Weiner, *Proc. R. Soc. London Ser. B* **1997**, *264*, 461; b) L. Addadi, S. Raz, S. Weiner, *Adv. Mater.* **2003**, *15*, 959.
[7] J. Johnston, H. E. Merwin, E. D. Williamson, *Am. J. Sci.* **1916**, *41*, 473.
[8] a) S. Raz, S. Weiner, L. Addadi, *Adv. Mater.* **2000**, *12*, 38; b) E. Loste, F. C. Meldrum, *Chem. Commun.* **2001**, 901.
[9] J. Aizenberg, G. Lambert, L. Addadi, S. Weiner, *Adv. Mater.* **1996**, *8*, 222.
[10] a) Y. Levi-Kalisman, S. Raz, S. Weiner, L. Addadi, I. Sagi, *J. Chem. Soc. Dalton Trans.* **2000**, 3977; b) Y. Levi-Kalisma, S. Raz, S. Weiner, L. Addadi, I. Sagi, *Adv. Funct. Mater.* **2002**, *12*, 43.
[11] a) A. Kumar, N. L. Abbott, E. Kim, H. A. Biebuyck, G. M. Whitesides, *Acc. Chem. Res.* **1995**, *28*, 219; b) J. Aizenberg, A. J. Black, G. M. Whitesides, *J. Am. Chem. Soc.* **1999**, *121*, 4500.
[12] J. Aizenberg, A. J. Black, G. M. Whitesides, *Nature* **1999**, *398*, 495; b) J. Aizenberg, *J. Chem. Soc. Dalton Trans.* **2000**, 3963.
[13] J. Aizenberg, D. A. Muller, J. L. Grazul, D. R. Hamann, *Science* **2003**, *299*, 1205.
[14] H. A. Lowenstam, S. Weiner, *On Biomineralization* Oxford University Press, Oxford, **1989**.


 © 2003 Wiley-VCH Verlag GmbH & Co. KGaA, Weinheim 

Electronic Materials

# Atomic Layer Deposition Chemistry: Recent Developments and Future Challenges**

*Markku Leskelä* and Mikko Ritala*

**Keywords:**
atomic layer deposition · microelectronics · nitrides · oxides · thin films

*New materials, namely high-k (high-permittivity) dielectrics to replace $SiO_2$, Cu to replace Al, and barrier materials for Cu, are revolutionizing modern integrated circuits. These materials must be deposited as very thin films on structured surfaces. The self-limiting growth mechanism characteristic to atomic layer deposition (ALD) facilitates the control of film thickness at the atomic level and allows deposition on large and complex surfaces. These features make ALD a very promising technique for future integrated circuits. Recent ALD research has mainly focused on materials required in microelectronics. Chemistry, in particular the selection of suitable precursor combinations, is the key issue in ALD; many interesting results have been obtained by smart chemistry. ALD is also likely to find applications in other areas, such as magnetic recording heads, optics, demanding protective coatings, and micro-electromechanical systems, provided that cost-effective processes can be found for the materials required.*

## 1. Introduction

Atomic layer deposition (ALD) has recently received much interest as a potential deposition method for advanced thin-film structures. However, ALD had already been developed and introduced worldwide with the name Atomic Layer Epitaxy (ALE) in the late 1970s.[1] The motivation for the development of ALD was the need for a deposition method for thin-film electroluminescent (TFEL) flat-panel displays. For such an application, high-quality dielectric and luminescent films are required on large-area substrates.[2] ALD is still used today in the industrial production of TFEL displays.[3] In the mid-1980s the applicability of ALD to epitaxial compound semiconductors was demonstrated, and great efforts were made in the preparation of III–V compounds in the late 1980s.[4] Due to the unfavorable chemistry between group III alkyl compounds and group V hydrides, no real benefits were achieved with ALD, compared to metal–organic vapor phase epitaxy (MOVPE) or molecular beam epitaxy (MBE). The renaissance of ALD began in the mid-1990s, with the interest focused on silicon-based microelectronics. Shrinking device dimensions and increasing aspect ratios in integrated circuits (IC) require the introduction of new materials and thin-film deposition techniques. ALD is considered as one deposition method with the greatest potential for producing very thin, conformal films with control of the thickness and composition of the films possible at the atomic level.

In the following the principles and characteristic features of the ALD method are presented. The comprehensive review made by the authors[5] covers the ALD literature to summer 2000. This minireview focuses mostly on more recent literature. Since the major part of the ALD research at the moment is focused on thin films needed in microelectronics, the recent achievements are mostly connected to this area.

## 2. The Principle of ALD

ALD is a special modification of chemical vapor deposition (CVD) with the distinct feature that film growth takes place in a cyclic manner. Normally one growth cycle consists

[*] Prof. M. Leskelä, Prof. M. Ritala
Department of Chemistry
University of Helsinki
P.O. Box 55, 00014 Helsinki (Finland)
Fax: (+357) 9-191-50198
E-mail: markku.leskela@helsinki.fi

[**] Throughout this Minireview, nomenclature common to the area of semiconductor materials science is employed. For example, group III elements are those of group 13 of the periodic table and group V elements are those of group 15. Hence, GaAs is an example of a III–V material.


© 2003 Wiley-VCH Verlag GmbH & Co. KGaA, Weinheim
DOI: 10.1002/anie.200301652

of four steps (Figure 1): 1) Exposure of the first precursor, 2) purge of the reaction chamber, 3) exposure of the second precursor, and 4) a further purge of the reaction chamber.[5] The growth cycles are repeated as many times as required for the desired film thickness. Depending on the process and the reactor being used, one cycle can take time from 0.5 s to a few seconds, and may deposit between 0.1 and 3 Å of film material. The cycle time depends particularly on the aggressiveness of the film-formation reaction. In ALD, in contrast to CVD, reactions with as negative a value of $\Delta G$ as possible are desired.[5] The film thickness obtained per cycle may depend on the size of the precursor molecule, because steric hindrance between large precursors limits the number of molecules capable to adsorb on the surface. With small molecules and elements as precursors, a full monolayer growth per cycle is possible. In addition, the number of adsorption sites at the surface also affects the amount of molecules adsorbed.

Ideally each exposure and purge step in ALD is complete. The precursor molecules chemisorb or react with the surface groups saturatively, and after the formation of the chemisorbed layer no further adsorption takes place. Under these saturative reaction conditions the film growth is self-limiting; that is, the amount of film material deposited in each reaction cycle is constant. The self-limiting growth mechanism brings several advantages to ALD: 1) Film thickness depends only on the number of reaction cycles, which makes the thickness control accurate and simple; 2) unlike CVD, there is less need of reactant flux homogeneity, which gives large area (large batch and easy scale-up) capability, excellent conformality (Figure 2) and reproducibility, and simplifies the use of solid precursors. Separate dosing of the precursors prevents gas-phase reactions, which allows the use of highly reactive precursors and gives enough time for each reaction step to reach completion. This results in pure films being deposited at relatively low temperatures. The ALD processing window is often wide, which makes the process insensitive to small changes in temperature and precursor flows, and allows the processing of different materials to multilayer structures in a continuous process (Figure 3).[6]

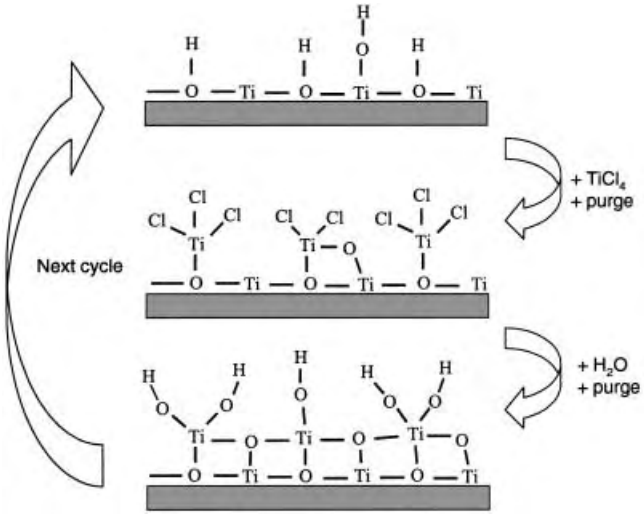



***Figure 1.*** An ALD deposition cycle showing schematically the deposition of $TiO_2$ films from $TiCl_4$ and $H_2O$.

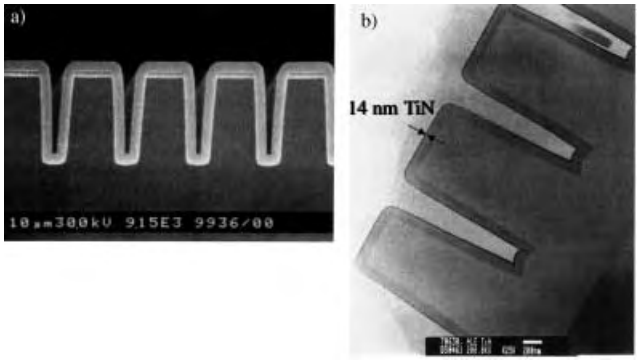



***Figure 2.*** Cross-sectional SEM images for a 300-nm $Al_2O_3$ film (a) and a 14-nm TiN film (b) deposited on a patterned silicon substrate.

## 3. Precursors

ALD precursors may be gases, volatile liquids, or solids. The vapor pressure must be high enough for effective mass transportation; all solid, and some liquid precursors need to be heated. Thanks to the self-limiting growth, demands for the evaporation rates to remain constant are more relaxed



*Markku Leskela received a PhD in inorganic chemistry in 1980 (Helsinki University of Technology). He worked as both Associate Professor (University of Oulu, 1980–86) and as Professor (University of Turku, 1986–90) before taking his present position as Professor of inorganic chemistry at the University of Helsinki. His research includes thin-film growth by various chemical methods for micro- and optoelectronics, ranging from precursor synthesis to applications. He also has an interest in coordination compound catalysts for olefin polymerization and oxidation. He has published over 370 papers and holds several patents.*



*Mikko Ritala received a PhD in inorganic chemistry in 1994 (University of Helsinki), and from 1995–2003 he worked as a postdoctoral researcher, then as an academic research fellow at the same institution. He is currently Professor of inorganic materials chemistry at the University of Helsinki. His research is in the area of thin-film growth by atomic layer deposition and electrodeposition for microelectronics and other applications. Real-time reaction mechanism studies form an important part of his research. He has published 150 papers and holds several patents.*


© 2003 Wiley-VCH Verlag GmbH & Co. KGaA, Weinheim

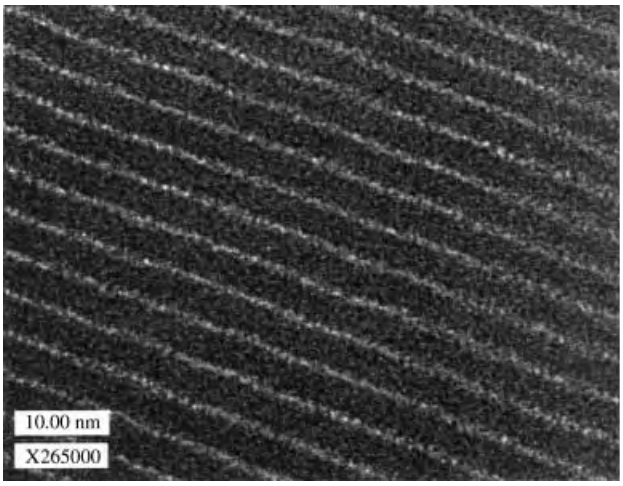



***Figure 3.*** Cross-sectional TEM image of a $Zr_xSi_yO_z$–$Zr_xTi_yO_z$ nanolaminate.

than in CVD, thus making it easier to use solid precursors. The challenging task of pulsing precursors evaporated at high temperatures is solved by inert-gas valving.[5,7] The precursors must be thermally stable at the growth temperature. Decomposition would destroy the self-limiting growth mechanism and the related advantages. In some applications, such as protective coatings, slightly thermally unstable precursors can be acceptable if their decomposition is slow (compared to the pulsing sequence times), and makes only a small contribution to the overall growth. The precursors must adsorb or react with the surface sites, such as hydroxyl groups on oxide surfaces (Figure 1). The type of adsorption, molecular or dissociative, and reaction mechanisms have recently been extensively studied in situ with quartz-crystal microbalance and mass spectrometric measurements. Different mechanisms have been found for different precursors.[5]

Typical metal precursors used in ALD are halides, especially chlorides, alkyl compounds, and alkoxides. Organometallic compounds, such as cyclopentadienyl complexes and alkyl and silyl amides have gained more attention recently.[6] The nonmetal precursors used are: water, hydrogen peroxide, and ozone for oxygen; hydrides for chalcogens; ammonia, hydrazine, and amines for nitrogen; hydrides for group V elements.[5]

## 4. ALD in Microelectronics

In microelectronics, ALD is studied as a potential technique to deposit high-k (high permittivity) gate oxides, high-k memory capacitor dielectrics, ferroelectrics, and metals and nitrides for electrodes and interconnects. In high-k gate oxides, where the control of ultrathin films is essential, ALD is only likely to come in to wider use at the 45-nm technology.[8] In metallizations, conformal films are required; currently it is expected that ALD will be used in mainstream production at the 65-nm node. In dynamic random access memories (DRAMs), the conformality requirements are even higher and ALD is the only method that can be used when feature sizes become smaller than 100 nm.[8]

### 4.1. Gate Oxides

Deposition of the high-k oxides $Al_2O_3$, $ZrO_2$, and $HfO_2$ has been the most widely examined area of ALD during the past few years. The motivation for this work comes from the detrimentally high tunneling currents through the currently used $SiO_2$ metal–oxide semiconductor field-effect transistor (MOSFET) gate dielectric, when it is downscaled to a thickness of about 1.0 nm and below for device generations in the near future.[9] When a high-k oxide is used, the gate dielectric can be made physically thicker for the required capacitance density, thus lowering the tunneling current. A convenient measure for the capacitance density is the equivalent oxide thickness ($EOT = d_{high\text{-}k}\,k_{SiO2}/k_{high\text{-}k} = 3.9(d_{high\text{-}k})/k_{high\text{-}k}$), and for future devices with high-k-based dielectrics this should be 1.0 nm or less. However, silicon is easily oxidized from its surface and a thin interface layer of $SiO_2$ or a mixture of $SiO_2$ and the high-k oxide is easily formed, which adds to the overall EOT. On the other hand, the Si–$SiO_2$ interface is commonly recognized as the best semiconductor–insulator interface. Therefore, to achieve an EOT of less than 1.0 nm with good electrical characteristics, a very thin, one-to-two monolayer thick interfacial $SiO_2$ layer should preferably be left between the silicon and the high-k oxide. Controlling such a thin $SiO_2$ layer is very challenging (Figure 4).

ALD high-k gate oxide research has mainly focused on three basic systems: $Al(CH_3)_3/H_2O$, $ZrCl_4/H_2O$, and $HfCl_4/H_2O$. These systems have all yielded good results in an EOT range of 1–2 nm,[9] but scaling the EOT down further is difficult and requires careful attention to the pretreatment of the silicon surface. Despite many efforts, better processes than those mentioned above have not been found. The lowest EOT should be achievable by using native-oxide free, hydrogen-terminated silicon as the starting surface. However,

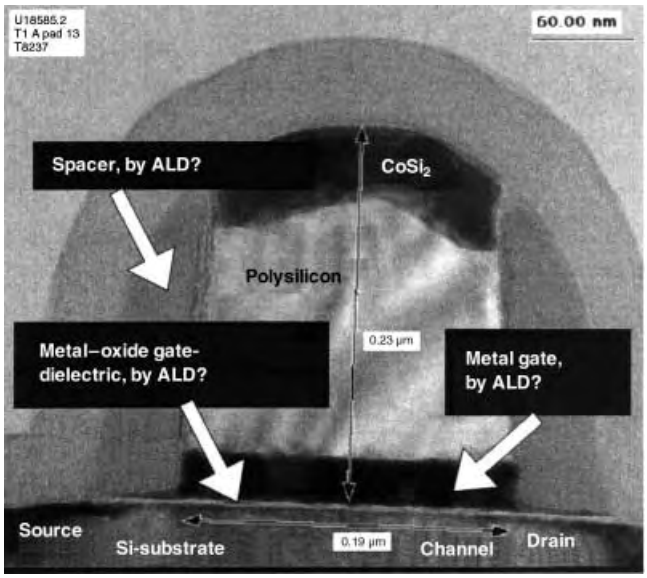



***Figure 4.*** A cross-sectional TEM image of a MOSFET (channel length = 0.19 µm) showing three application areas where ALD films could be used. See text for details.

 © 2003 Wiley-VCH Verlag GmbH & Co. KGaA, Weinheim 

nucleation on this surface, particularly for $ZrO_2$ and $HfO_2$, is poor and results in inhomogeneous microstructure, thereby preventing their direct application on hydrogen-terminated surfaces.[10] More work is needed to tailor the interface to an optimum level. Alternative chemistry developed for the ALD of oxides involves the use of metal alkoxides as oxygen sources, which react with other metal compounds, most often chlorides.[11,12] Because oxygen atoms are bound to the metal centers in the alkoxides, they oxidize silicon less strongly than water, which results in a sharp interface. Unfortunately, these processes leave a somewhat higher content of chloride residue ($\approx$1 atom %), as compared with the conventional metal chloride–water processes.

Progress in the application of high-k gate oxides has been somewhat slower than what was assumed a few years ago. The problem is the high-k materials themselves rather than the ALD processing.[8] Direct contact with silicon often degrades electron and hole mobility in the MOSFET channel region and the interaction with the polysilicon top electrode may create charges which shift the threshold voltage.

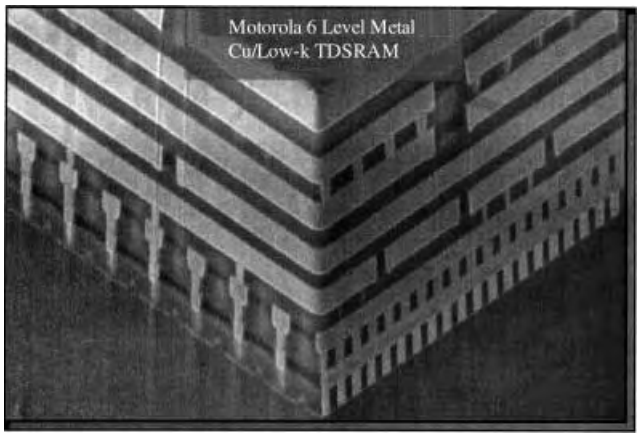



***Figure 5.*** Focused ion beam (FIB) cross section through a six-layer Cu/low-k dielectric interconnect metallization. Here ALD could be used for depositing thin metal or metal nitride barrier layers (not resolved in the image) encapsulating the copper wires (bright features) as well as depositing seed layers for Cu electroplating.

### *4.2. DRAM Capacitors*

The development of DRAM capacitor dielectrics has been similar to that of gate dielectrics: $SiO_2$ has dominated thus far, but is likely to be phased out in the near future. The DRAM capacitors will be three dimensional, thus requiring good conformality, but permittivity values above 200 will still be required, and thus the candidate materials are different from those explored for MOSFET gate dielectrics. The most extensively studied candidate has been (Ba,Sr)$TiO_3$. Due to the high conformal requirements of DRAM applications, ALD is a very promising method, although ternary and quaternary compounds are very challenging for chemical thin-film deposition techniques. Totally new ALD chemistry has been developed for $SrTiO_3$ and $BaTiO_3$ using strontium and barium cyclopentadienyl compounds, [Ti(O*i*Pr)$_4$], and water as precursors.[13] A permittivity of 180 was measured for $SrTiO_3$ and 165 for $BaTiO_3$ when films thicker than 200 nm were post-deposition annealed, but when the film thickness was decreased to 50 nm, the permittivity decreased to only 100.

### *4.3. Transition-Metal Nitrides*

Transition-metal nitrides, such as TiN and TaN find potential use both as metallization barriers and as gate metals. Metallization barriers are needed on one hand to avoid Cu diffusion into the surrounding insulators and the silicon substrate and, on the other hand, to prevent Cu contamination by elements diffusing from the insulators (Figure 5). Metal gates (Figure 4), in turn, will be needed to eliminate the EOT-increasing effect of the depletion layer capacitance in the presently used polysilicon gate electrodes. The most studied ALD nitride process has been that where TiN is deposited from $TiCl_4$ and $NH_3$. Films with low resistivity ($<200\ \mu\Omega$ cm) and excellent conformality are obtained with this process at 400 °C (Figure 2b).[14] The process is not ideal, however, because of the modest reactivity of ammonia, the halide residue content, the modest deposition rate and, most importantly, the fact that the HCl formed as a byproduct in the process causes pitting of copper.[14] Many alternative titanium precursors have been studied but an ideal solution for the TiN process has not yet been found. Simultaneously, ALD chemistry has been developed for TaN and $WN_x$ materials, which are more demanding to prepare than TiN since they require stronger reduction. In the deposition of TaN a three-precursor process ($TaCl_5$/Zn/$NH_3$) using Zn as a reducing agent has given the best results.[15] The use of zinc, however, is not accepted in microelectronics applications, and therefore alternative reducing agents, such as trimethylaluminum,[16] dimethylhydrazine,[17] and *tert*-butylamine[18] have been studied with varying success. Plasma enhancement offers new possibilities for the ALD of TaN and other transition-metal nitrides. TaN has been deposited using *tert*-butylimidotris(diethylamido)tantalum, [$(Et_2N)_3Ta$=N*t*Bu], and hydrogen radicals as precursors.[19] The process takes place at low temperature (260 °C), has a good growth rate (0.8 Å/cycle), but needs long hydrogen plasma exposure times (30 s). Another plasma-enhanced ALD process for TaN uses $TaCl_5$ together with hydrogen and nitrogen plasma.[20] The N/Ta ratio was controlled from 0.3 to 1.4 by varying the nitrogen partial pressure, which indicated that the process was not completely self-limited. However, the films had a low resistivity of 350 $\mu\Omega$ cm. WN is an alternative barrier material, which has been deposited from $WF_6$ and $NH_3$ with a rate of 0.42 Å/cycle at 350 °C.[14] In a high-vacuum chamber and with longer exposure times, the same process resulted in a much higher deposition rate of 2.55 Å/cycle.[21] Some copper pitting was observed also in this process, however.[14] Recently, a new process utilizing $WF_6$, $NH_3$, and $B(C_2H_5)_3$ was reported for depositing $WC_xN_y$ (atomic composition: W 57 %, C 30 %, N 13 %).[22] A resistivity of 600–900 $\mu\Omega$ cm was measured for 7-nm films of this material. Unlike TiN and $WN_x$, $WC_xN_y$ barriers deposited by ALD do not show Cu pitting voids in dual-damascene (Figure 6) copper metallization nor passiva-

 © 2003 Wiley-VCH Verlag GmbH & Co. KGaA, Weinheim 

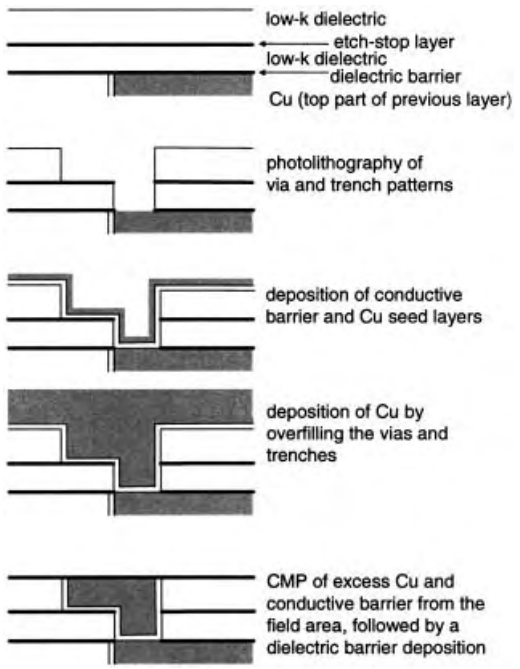



***Figure 6.*** Dual-damascene process flow for the fabrication of copper interconnects. This approach was developed because the dry etching of copper is difficult because of a lack of suitable volatile copper compounds. In the damascene process, copper patterning into wires and via plugs is realized by dry etching appropriate trench and via patterns into the dielectric film, then filling these with copper, and finally removing the excess copper by chemical mechanical polishing (CMP).

tion blistering, and is the best ALD barrier material reported so far.

### 4.4. Metal Films

An interest in metal ALD has several motivations: 1) Cu interconnects and W plugs, or at least Cu seed layers for Cu electrodeposition and W seeds for W CVD, 2) Ti and Ta for Cu interconnect barriers, 3) noble metals for ferroelectric random access memory (FRAM) and DRAM capacitor electrodes, and 4) high- and low-workfunction metals for dual-gate MOSFETs. Metals have been quite problematic for ALD techniques; most trials to employ metal CVD chemistry in ALD have been unsuccessful. The reasons for these difficulties are thought to be related to a lack of an appropriate mechanism by which metal precursors can adsorb on metal surfaces that do not contain reactive sites, such as hydroxyl groups in the oxide processes, and the low reactivity of the common reducing agent $H_2$. George et al.[23] demonstrated that tungsten may be deposited from $WF_6$ and $Si_2H_6$. Based on detailed mechanistic studies, the overall reaction was suggested to be that which is displayed in Equation (1).

$$WF_6 + Si_2H_6 \rightarrow W + 2\,SiHF_3 + 2\,H_2 \quad (1)$$

Amorphous films, free of silicon and fluorine, could be deposited at a rate of 2.5 Å/cycle. The noble metals Ru and Pt have been deposited from the organometallic precursors $[Ru(C_5H_5)_2]$ and $[CH_3C_5H_4Pt(CH_3)_3]$ and oxygen.[24] A key feature of the growth mechanism is that oxygen atoms remain adsorbed on the Ru and Pt surfaces after the oxygen pulse and the following purge sequence. When the organometallic compounds are exposed on the surface, the oxygen atoms oxidize part of the hydrocarbon ligands to carbon oxides and water. The remaining ligands and hydrocarbon fragments are oxidized during the next oxygen pulse, which also reforms the adsorbed oxygen-atom layer. The films were pure and had resistivities of 10–20 μΩ cm. It is quite apparent that this kind of ALD chemistry is applicable to all noble metals capable of catalyzing the dissociation of molecular oxygen.

The use of radicals has introduced many new possibilities for metal ALD, as compared with just thermally activated processes. Titanium and tantalum, for example, are such electropositive elements that their deposition without additional activation is apparently impossible at reasonable temperatures. But by using highly reactive hydrogen radicals generated in a remote plasma discharge these metals have been deposited from the corresponding chlorides.[25] Reasonable deposition rates, resistivities, and step coverages have been reported for these metal films, and the barrier performance in separating copper and silicon was better than that of sputtered tantalum with a similar thickness. Even aluminum has been deposited at low temperatures with a good growth rate (1.5 Å/cycle) by a hydrogen-plasma-enhanced ALD process using trimethylaluminum as an aluminum precursor.[26] Nickel films have been deposited indirectly by first making the oxide and reducing that with hydrogen[27] or hydrogen radicals.[28]

Despite some initial reports[29] on copper ALD this metal has remained quite problematic. Recently, it was shown that copper seed layers may be formed indirectly by first depositing a copper oxide film using $[Cu(thd)_2]/O_3$ (thd = 2,2,6,6-tetramethyl-3,5-heptanedionate) as precursors and then reducing CuO to metallic copper with alcohols, aldehydes, or carboxylic acids.[30] It has also been shown that copper may be deposited from $[Cu(acac)_2]$ (acac = acetylacetonate) using hydrogen radicals from an upstream microwave plasma discharge.[31] The films deposited on glass were quite rough, however, and had resistivities of 14 μΩ cm when 30-nm thick.

## 5. Recent Discoveries

The increasing interest in ALD over the last few years has resulted in some interesting new innovations. The results show clearly that the key issue in ALD is proper chemistry. With smart thermal-activated chemistry, it has been possible to develop new processes and new film materials grown by ALD. A good example of this development is the discovery of Gordon et al., who deposited $SiO_2$ with a small amount of $Al_2O_3$ at an exceptionally high growth rate (12 nm/cycle) from tris(*tert*-butoxy)silanol activated by trimethylaluminum.[32] A low growth temperature (250 °C) was employed and yielded materials with complete conformality in trenches with an aspect ratio of 70:1. The proposed mechanism relies on a polymerization reaction where silanol molecules insert into Al–O bonds. The chains that are formed may then crosslink

 © 2003 Wiley-VCH Verlag GmbH & Co. KGaA, Weinheim 

via the decomposition of *tert*-butyl groups and the elimination of isobutene and *tert*-butanol. Though this deposition rate is too high for gate dielectric applications, the process may find applications for ALD-grown $SiO_2$ in spacers (Figure 4) and trench insulators between transistors, multilayer optical filters, planar waveguides, protective layers, and microelectromechanical system (MEMS) devices.

The deposition of tungsten films from tungsten hexafluoride and disilane is another example of the new smart chemistry.[23] Non-noble metals are difficult to prepare in thermally activated processes, but it is possible with a suitable combination of precursors. The new chemistry introduced for high-k gate oxides that utilizes metal alkoxides as oxygen sources is also showing the importance of chemistry in ALD processes.[11]

The use of a third component in an ALD cycle of binary compounds opens up many possibilities. The use of bases to catalyze the reaction $SiCl_4 + 2H_2O \rightarrow SiO_2 + 4HCl$, and reductive pulses in the preparation of nitride films represent some existing examples.[15,33] The third component may introduce a new element into the film, as is in the serendipitous case of $WC_xN_y$, where improved barrier properties and process integration were obtained.

Ternary and quaternary compounds needed for the preparation of ferroelectric oxides are apparently the greatest challenge for ALD. There are two major issues: Ferroelectric oxides contain several cations whose stoichiometry must be accurately controlled. Second, for some of these elemental cations, such as lead, bismuth, and also to some extent strontium, there is no good ALD binary oxide process available. One solution for controlling the cation stoichiometry is to employ bimetallic complexes where the cations are present in the same ratio as in the desired film. $SrTa_2O_6$ has been deposited from such a precursor ($[SrTa_2(OEt)_{10}(dmae)_2]$; dmae = *N,N*-dimethylaminoethoxide) using either water[34] or oxygen plasma[35] as the other precursor. Currently, the addition of bismuth to this film is being studied with an aim to obtain the ferroelectric $SrBi_2Ta_2O_9$. A large amount of work is still required for controlled ALD processes for ferroelectrics.

Radical enhancement has opened new possibilities for developing ALD processes for materials which have remained outside the capabilities of thermally activated chemistry. Illustrative examples of this are the successful depositions of titanium, tantalum, and aluminum metals. Besides materials completely new to ALD, radical enhancement will also offer alternative, apparently lower temperature routes for those materials which have so far been deposited by traditional ALD processes. Radical enhancement is also likely to assist in keeping precursor chemistry relatively simple, however, one obvious drawback of the radical enhanced processes is the need for a more complicated reactor design.

High-surface-area substrates have been a subject of ALD studies because of their importance in heterogeneous catalysis, and because they offer plenty of materials for detailed chemical characterization.[36] Some good results have been obtained from depositions on porous silicon, for example.[37] Slow precursor transportation makes the processes very slow, but as there are no other viable alternatives, ALD is and will remain an important method for deposition on porous materials and holes.

Selective ALD is a very attractive concept but also very challenging. With self-assembled monolayers (SAMs) as passivation agents, $ZrO_2$ was recently deposited selectively for $Cu/ZrO_2/Si$ capacitors.[38] The patterning of spin-coated octadecyl tetrachlorosilane (OTS) was achieved by microcontact printing.

## 6. The Limitations of ALD

The major limitation of ALD is its slowness; usually only a fraction of a monolayer is deposited in one cycle. Typically deposition rates are 100–300 $nm\,h^{-1}$. Therefore it is not very practical to grow micrometer-thick films by ALD. The slow growth rate can be compensated by processing large batches of substrates in one process, as is done in TFEL production. In microelectronics, however, single-wafer processing is preferred. Fortunately the films needed for future-generation ICs are very thin and thus the slowness of ALD is not such an important issue.

Although the selection of film materials grown by ALD is wide,[5] many technologically important materials (Si, Ge, $Si_3N_4$, several multicomponent oxides, certain metals) cannot currently be deposited by ALD in a cost-effective way. Only a small number of groups have been studying new ALD precursors and processes and this has limited the development of the technique.

ALD is a chemical technique and thus there is always a risk of residues being left from the precursors. The impurity content of the films depends on the completeness of the reactions. In typical oxide processes where metal halides or alkyl compounds are used together with water as precursors, impurities found in the films are at the 0.1–1 atom% level. The carrier gas is also an important source of impurities, as has been exemplified, for example, with oxygen-sensitive AlN films. In physical vapor deposition (PVD) methods the environment is much cleaner due to the high vacuum used and the lack of precursor compounds with unwanted elements.

Because of their unique impurity background, ALD-grown materials may have different properties than those made by PVD, for example. This has been seen in transition-metal nitride films, where small variations in composition markedly affects the electrical properties.[8] Also microstructure and morphology of ALD films may differ from PVD films. Therefore the ALD materials have to be characterized thoroughly before use. Post-deposition treatments, particularly high-temperature annealing under varied atmospheres, form an important part of this research as they may have both beneficial and adverse effects on purity and microstructure.

## 7. Future Aspects

Despite the achievements made over recent years, many challenges still remain for the future development of ALD in

 © 2003 Wiley-VCH Verlag GmbH & Co. KGaA, Weinheim 

microelectronics applications. Basic research on precursor chemistry and film deposition will remain important, especially when expanding the application of ALD to new materials and devices, for example, to ferroelectric oxides for nonvolatile memories. Integration of the ALD processes and materials to the overall process flow forms another important area of the research, and this should be properly addressed during the early stages of the process development.

The intense research into using ALD in microelectronics has brought the technique wider publicity. As the general awareness of ALD has increased, an interest in its usage in other potential application areas has also increased. Such areas include insulator layers in magnetic write–read heads, MEMS, and a number of demanding applications in optics and protective coatings. It is evident that in the future, research into ALD will expand further.

*Dr. David Gilmer (Motorola, Austin) is thanked for Figures 4 and 5. Funding from the Academy of Finland and the Finnish Technology Development Agency Tekes is gratefully acknowledged.*

Received: April 1, 2003 [M1652]

[1] T. Suntola, J. Antson, U.S. Patent 4,058,430, **1977**.
[2] M. Leskelä, W.-M. Li, M. Ritala, *Semicond. Semimetals* **1999**, *64*, 413 – 487.
[3] http://www.planar.com.
[4] *Atomic Layer Epitaxy* (Eds.: T. Suntola, M. Simpson) Blackie, Glasgow, **1990**, p. 182.
[5] M. Ritala, M. Leskelä in *Handbook of Thin Film Materials, Vol. 1* (Ed.: H. S. Nalwa), Academic Press, San Diego, **2001**, pp. 103 – 156.
[6] M. Leskelä, M. Ritala, *J. Phys. IV* **1999**, *9*(8), 837 – 852; M. Leskelä, M. Ritala, *Thin Solid Films* **2002**, *409*, 138 – 146.
[7] T. Suntola, *Mater. Sci. Rep.* **1989**, *4*, 261 – 312.
[8] A. Hand, *Semicond. Int.* **2003**, *26*(May), 46 – 51.
[9] G. D. Wilk, R. M. Wallace, J. M. Anthony, *J. Appl. Phys.* **2001**, *89*, 5243 – 5275.
[10] E. P. Gusev, E. Cartier, D. A. Buchanan, M. Gribelyuk, M. Copel, H. Okorn-Schmidt, C. D'Emic, *Microelectron. Eng.* **2001**, *59*, 341 – 349; M. Copel, M. Gribelyuk, E. Gusev, *Appl. Phys. Lett.* **2000**, *76*, 436 – 438.
[11] M. Ritala, K. Kukli, A. Rahtu, P. I. Räisänen, M. Leskelä, T. Sajavaara, J. Keinonen, *Science* **2000**, *288*, 319 – 321.
[12] A. Rahtu, M. Ritala, *Langmuir* **2002**, *18*, 10046 – 10048.
[13] M. Vehkamäki, T. Hatanpää, T. Hänninen, M. Ritala, M. Leskelä, *Electrochem. Solid-State Lett.* **1999**, *2*, 504 – 506; M. Vehkamäki, T. Hänninen, M. Ritala, M. Leskelä, T. Sajavaara, E. Rauhala, J. Keinonen, *Chem. Vap. Deposition* **2001**, *7*, 75 – 80.
[14] K.-E. Elers, V. Saanila, P. J. Soininen, W.-M. Li, J. T. Kostamo, S. Haukka, J. Juhanoja, W. A. Besling, *Chem. Vap. Deposition* **2002**, *8*, 149 – 153.
[15] M. Ritala, P. Kalsi, D. Riihelä, K. Kukli, M. Leskelä, J. Jokinen, *Chem. Mater.* **1999**, *11*, 1712 – 1718.
[16] P. Alén, M. Juppo, M. Ritala, T. Sajavaara, J. Keinonen, M. Leskelä, *J. Electrochem. Soc.* **2001**, *148*, G566 – G571; M. Juppo, P. Alén, M. Ritala, M. Leskelä, *Chem. Vap. Deposition* **2001**, *7*, 211 – 217.
[17] M. Juppo, M. Ritala, M. Leskelä, *J. Electrochem. Soc.* **2000**, *147*, 3377 – 3381.
[18] M. Juppo, P. Alén, M. Ritala, T. Sajavaara, J. Keinonen, M. Leskelä, *Electrochem. Solid-State Lett.* **2002**, *5*, C4 – C6; P. Alén, M. Juppo, M. Ritala, T. Sajavaara, J. Keinonen, M. Leskelä, *J. Mater. Res.* **2002**, *17*, 107 – 114.
[19] J.-S. Park, H.-S. Park, S.-W. Kang, *J. Electrochem. Soc.* **2002**, *149*, C28 – C30.
[20] H. Kim, A. J. Kellock, S. M. Rossnagel, *J. Appl. Phys.* **2002**, *92*, 7080 – 7085.
[21] J. W. Klaus, S. J. Ferro, S. M. George, *J. Electrochem. Soc.* **2000**, *147*, 1175 – 1181.
[22] S. Smith, W.-M. Li, K.-E. Elers, K. Pfeiffer, *Microelectron. Eng.* **2002**, *64*, 247 – 253.
[23] J. W. Klaus, S. J. Ferro, S. M. George, *Thin Solid Films* **2000**, *360*, 145 – 153.
[24] T. Aaltonen, P. Alén, M. Ritala, M. Leskelä, *Chem. Vap. Deposition* **2003**, *9*, 45 – 49; T. Aaltonen, P. Alén, M. Ritala, M. Leskelä, *Chem. Mater.* **2003**, *15*, 1924 – 1928.
[25] S. M. Rossnagel, A. Sherman, F. Turner, *J. Vac. Sci. Technol. B* **2000**, *18*, 2016 – 2020; H. Kim, C. Cabral, Jr., C. Lavoie, S. M. Rossnagel, *J. Vac. Sci. Technol. B* **2002**, *20*, 1321 – 1326.
[26] J. Lee, S.-W. Kang, *Electrochem. Solid-State Lett.* **2002**, *5*, C91 – C93.
[27] M. Utriainen, M. Kröger-Laukkanen, L.-S. Johansson, L. Niinistö, *Appl. Surf. Sci.* **2000**, *157*, 151 – 158.
[28] J. Chae, H.-S. Park, S. Kang, *Electrochem. Solid-State Lett.* **2002**, *5*, C64 – C66.
[29] P. Mårtensson, J.-O. Carlsson, *J. Electrochem. Soc.* **1998**, *145*, 2926 – 2931.
[30] J. Kostamo, V. Saanila, M. Tuominen, S. Haukka, K.-E. Elers, M. Soininen, W.-M. Li, M. Leinikka, S. Kaipio, H. Huotari, *AVS Topical Conference on Atomic Layer Deposition—ALD2002*, (August 2002, Seoul), Abstracts p. 21.
[31] A. Niskanen, M. Ritala, M. Leskelä, unpublished results.
[32] D. Hausmann, J. Becker, S. Wang, R. G. Gordon, *Science* **2002**, *298*, 402 – 406.
[33] J. W. Klaus, O. Sneh, S. M. George, *Science* **1997**, *278*, 1934 – 1936.
[34] M. Vehkamäki, M. Ritala, M. Leskelä, A. C. Jones, H. O. Davies, E. Rauhala, T. Sajavaara, J. Keinonen, *J. Electrochem. Soc.*, submitted.
[35] W.-J. Lee, I.-K. You, S.-O. Ryu, B.-G. Yu, K.-I. Cho, S.-G. Yoon, C.-S. Lee, *Jpn. J. Appl. Phys. Part 1* **2001**, *40*, 6941 – 6944.
[36] S. Haukka, E.-L. Lakomaa, T. Suntola, *Stud. Surf. Sci. Catal.* **1998**, *120*, 715 – 750.
[37] C. Ducso, N. Q. Khanh, Z. Hovarth, I. Barsony, M. Utriainen, S. Lehto, M. Nieminen, L. Niinistö, *J. Electrochem. Soc.* **1996**, *143*, 683 – 687.
[38] D. Jeong, J. Park, N. Park, H.-J. Yang, J.-G. Lee, H. Shin, M.-M. Sung, J. Kim, *AVS 4th International Conference on Microelectronics and Interfaces* (March 2003, Santa Clara) Abstracts p. 225.

 © 2003 Wiley-VCH Verlag GmbH & Co. KGaA, Weinheim 

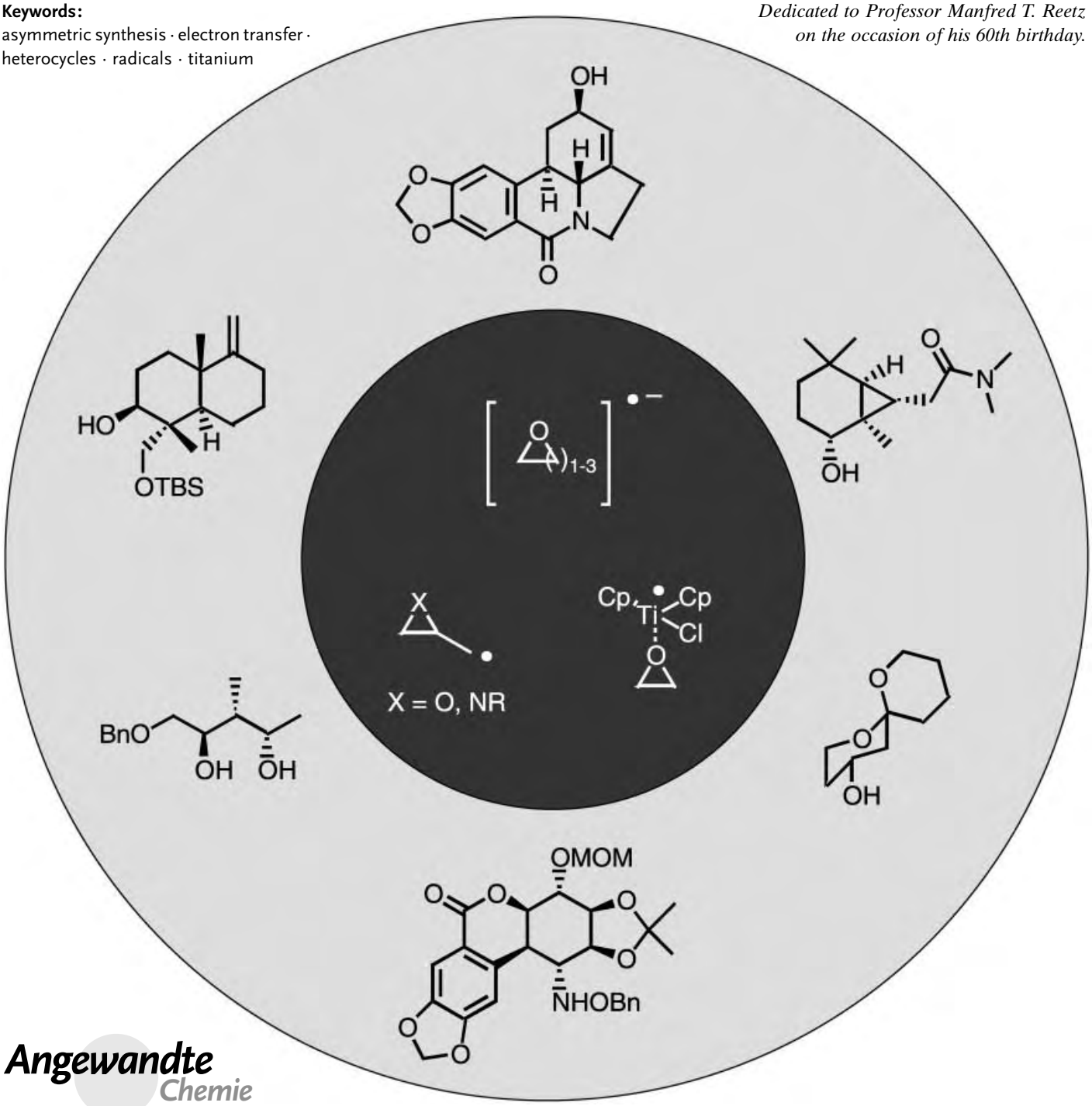
Radicals from Ring Opening

# Strained Heterocycles in Radical Chemistry

*Andreas Gansäuer,* Thorsten Lauterbach, and Sanjay Narayan*

**Keywords:**
asymmetric synthesis · electron transfer · heterocycles · radicals · titanium

*Dedicated to Professor Manfred T. Reetz on the occasion of his 60th birthday.*





© 2003 Wiley-VCH Verlag GmbH & Co. KGaA, Weinheim
DOI: 10.1002/anie.200300583

*Over the last few decades the use of radicals in synthesis has witnessed an explosive growth through introduction of efficient chain and electron-transfer reactions. Strained heterocycles, in particular, have emerged as a highly versatile and readily available class of radical precursors. The generation of carbinyl radicals of heterocycles has resulted in many elegant applications of heteroatom-centered radicals, such as β fragmentations, cyclizations, and intramolecular hydrogen atom abstractions. Direct electron transfer to strained heterocycles has been realized through the use of arene radical anions. The method combines the virtues of radical and organometallic chemistry to yield useful functionalized organolithium compounds. Epoxides have been opened with high regioselectivity by titanocene(III) reagents in either stoichiometric or catalytic quantities to yield β-titanoxy radicals. This development has resulted in many new applications in natural product synthesis.*

**From the Contents**

1. Introduction 5557

2. Epoxide, Oxetane, and Aziridine Opening through Generation of Carbinyl Radicals 5557

3. Reductive Cleavage of Heterocycles by Electron Transfer from Arene Radical Anions 5562

4. Epoxide Opening by Single Electron Transfer from Metal Complexes 5564

5. Summary and Outlook 5570

## 1. Introduction

Over the last few decades radical chemistry has developed into a central part of organic chemistry.[1] The evolution of efficient chain reactions and their applications constituted the single most important reason for this development.[1]

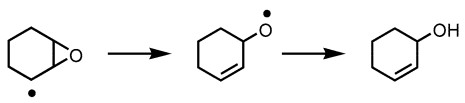
Strained heterocycles that can be opened through radical chemistry are especially valuable and readily available radical precursors. It is possible to generate three important classes of intermediates in this manner: heteroatom-centered radicals, carbon-centered radicals, and radical anions. The purpose of this Review is to highlight the evolution of this active field of research.[2]

## 2. Epoxide, Oxetane, and Aziridine Opening through Generation of Carbinyl Radicals

### 2.1. Epoxide Opening

#### 2.1.1. Early Examples

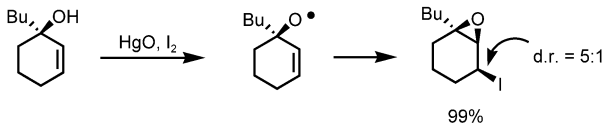
The first opening of a heterocycle through free-radical chemistry was reported in 1963. Epoxycarbinyl radicals, which were generated through hydrogen-atom abstraction from epoxides, were found to undergo C–O bond cleavage to give an allyloxy radical (Scheme 1).[3] The analogy to the opening of the cyclopropylcarbinyl radical was immediately recognized.[2c]




***Scheme 1.*** The first epoxycarbinyl radical opening by Sabatino and Gritter.[3]

#### 2.1.2. Kinetics and Mechanism of Epoxide Opening

As in the case of the cyclopropylcarbinyl radical, ring opening was demonstrated to be reversible. Both radicals could be intercepted with high selectivity, as in epoxide opening. The electrophilic allyloxy radicals could be efficiently reduced by $Bu_3SnH$.[4,5] Iodo epoxides could be obtained from the exposure of allyl alcohols to electrophilic radical traps such as mercury oxide and iodine (Scheme 2)[6] or to diacetoxyiodobenzene and iodine.[7]



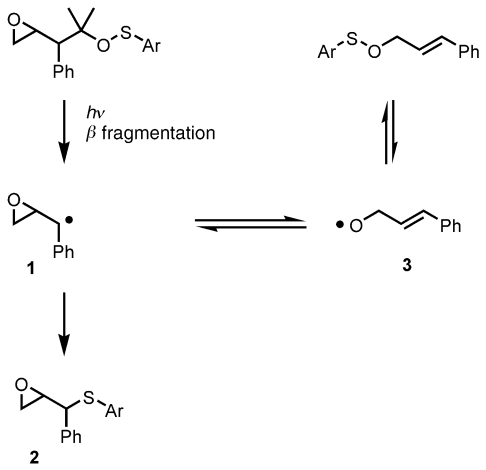

***Scheme 2.*** The first trapping of epoxycarbinyl radicals by Sugimone and Wang.[6]

More recent experiments and calculations confirmed the reversibility of epoxide opening (Scheme 3).[8] Compound **2** was exclusively obtained after extended periods of time from radical **1** by epoxycarbinyl radical trapping; radical **3** was demonstrated to be an intermediate. Radical **1** was calculated to be about 20 kJ mol$^{-1}$ more stable than **3** because of conjugation with the arene.

Early lower limits for the rate constants of ring opening of the oxiranylcarbinyl radical were established to be $4 \times 10^8$ s$^{-1}$

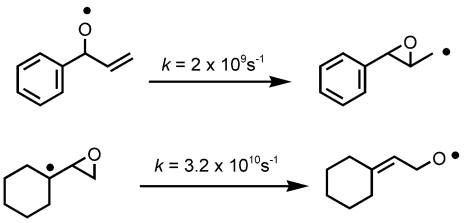
[*] Prof. Dr. A. Gansäuer, T. Lauterbach, Dr. S. Narayan
Kekulé-Institut für Organische Chemie und Biochemie
Universität Bonn
Gerhard Domagk Strasse 1, 53127 Bonn (Germany)
Fax: (+49) 228-73-4760
E-mail: andreas.gansaeuer@uni-bonn.de.


DOI: 10.1002/anie.200300583
© 2003 Wiley-VCH Verlag GmbH & Co. KGaA, Weinheim




***Scheme 3.*** Reversible trapping of epoxycarbinyl radicals by Amaudrut and Wiest.[8] Ar = *p*-$NO_2C_6H_4$.

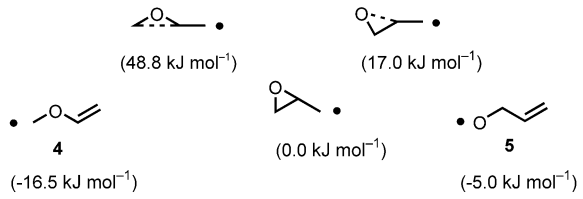
by EPR spectroscopy and $10^{10}\ s^{-1}$[9] by competition experiments between epoxide and cyclopropane opening.[10] The first spectroscopic evidence for epoxycarbinyl radicals was reported from spin-trapping methods with EPR spectroscopy.[11] Direct measurements of the rate constants (Scheme 4) confirmed the above limits.[12,13]




***Scheme 4.*** Kinetic data for epoxycarbinyl radical opening.

These kinetic studies have established a full quantitative picture of the ring opening of the epoxycarbinyl radical, and have established it as one of the fastest radical reactions known.[14]

Indispensable information about the intermediates has been obtained from ab initio molecular calculations.[15,16] It was found that ring opening is exothermic for cleavage of both C–O or C–C bonds (Scheme 5). Radical **4** is predicted to be more stable than **5** by about 11 kJ mol$^{-1}$. The transition




***Scheme 5.*** Computational analysis of ring opening by Radom and co-workers.[16]

structure **7** arising from C–O bond cleavage is, however, lower in energy by about 30 kJ mol$^{-1}$ than **6** arising from C–C bond cleavage. Thus, C–O bond cleavage is favored kinetically, as observed experimentally.

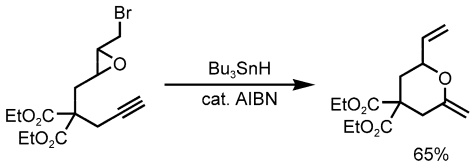
### 2.1.3. *Synthetic Applications of Epoxide Opening*

Epoxide opening has attracted considerable synthetic interest because of the allyloxy radicals generated,[17] which display unique reactivity profiles, for example, in cyclizations, hydrogen atom abstractions, group-transfer reactions, and β fragmentations. Many valuable precursors for epoxycarbinyl radicals are available, for example, "Sharpless epoxides",[18] vinyl epoxides, and keto epoxides, and this has certainly contributed to the popularity of the overall transformation.

#### 2.1.3.1. *Epoxide Opening through C–O Bond Cleavage*

##### 2.1.3.1.1. *Radical Generation through Chain Reactions*

The first attempts to use alkoxyl radicals in reactions other than their simple reduction[3,4] involved 5-*exo* and 6-*exo* cyclizations to yield tetrahydrofurans and tetrahydropyrans (Scheme 6).[19] More elaborate tandem sequences have led to numerous applications. The first example described the




***Scheme 6.*** Synthesis of enol ethers by Murphy and co-workers.[19]



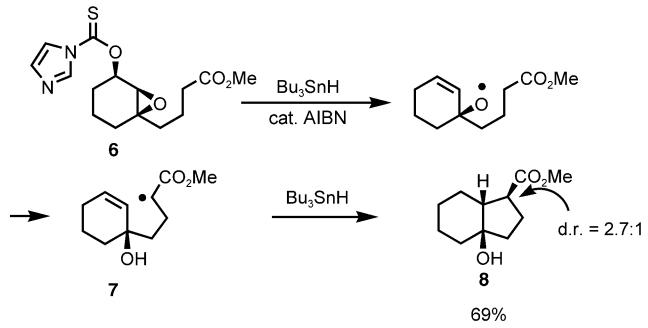
*Andreas Gansäuer was born in Paris, France. After studying chemistry at the Universities of Bonn and Oxford he obtained his PhD in 1994 in the group of Prof. M. Reetz at the MPI für Kohlenforschung Mülheim/Ruhr. After a postdoctoral position in the group of Prof. B. M. Trost at Stanford University, he completed his Habilitation with Prof. Brückner in Göttingen. Since 2000 he has been a professor of organic chemistry at the University of Bonn.*



*Thorsten Lauterbach was born in Aurich, Ostfriesland, and studied chemistry at the Universities of Göttingen and Barcelona. He is currently a PhD student in the group of Prof. A. Gansäuer.*

 © 2003 Wiley-VCH Verlag GmbH & Co. KGaA, Weinheim 

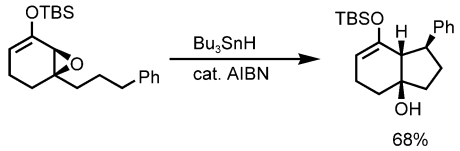
reactions of **6** and similar systems (Scheme 7).[20] Formation of an alkoxyl radical was followed by a 1,5-hydrogen abstraction to give radical **7**. The bicyclic hydroxy ester **8** was obtained




***Scheme 7.*** Sequence of ring opening, hydrogen atom abstraction, and cyclization by Rawal et al.[20]

after cyclization and reduction. Compounds such as **8** constitute important intermediates for the synthesis of cardiotonic steroids.

The preparative usefulness of this tandem sequence has been increased even further by the introduction of enol acetates,[21a] silylenol ethers,[21b] and ketones[21c] as radical precursors (Scheme 8). Iodides could also be formed as the final products under atom-transfer conditions.[22]



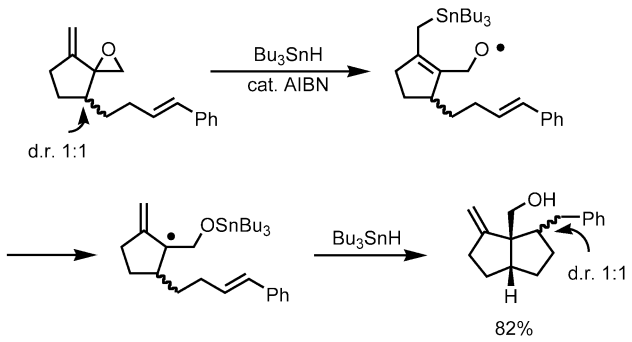

***Scheme 8.*** Synthesis of bicyclic enol ethers by Kim and Koh.[21b] TBS = *tert*-butyldimethylsilyl.

Tributylstannyl radicals have been added to vinyl epoxides to generate epoxycarbinyl radicals.[23] A shift of the tributyltin group resulted in an allyl radical that could be used in cyclizations or intermolecular additions (Scheme 9). Shifts of silyl groups were also reported.[24]

The addition of sulfur-centered radicals to vinyl epoxides has been used in model studies for DNA cleavage.[25]

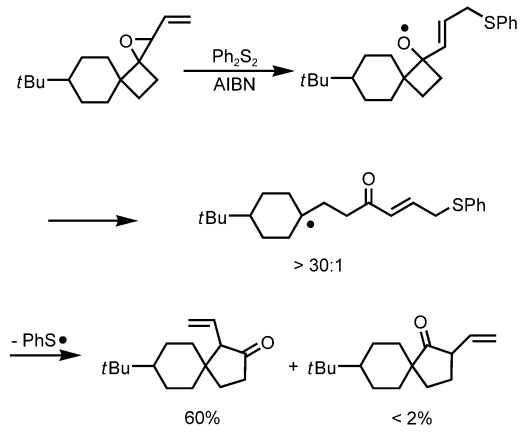


*Sanjay Narayan was born in Varanasi, India, studied chemistry at Mumbai University, and obtained his PhD under the supervision of Dr. V. K. Jain. After a post-doctoral position in Stockholm with Prof. K. J. Szábo, he joined Prof. Gansäuer's group in 2001.*



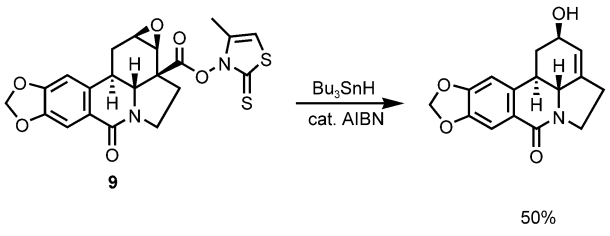

***Scheme 9.*** Tandem sequence of epoxide opening featuring a [1,5]-shift of the $Bu_3Sn$ group by Kim et al.[23]

The β-scission reaction that generates carbonyl groups and alkyl radicals has also found widespread use.[17] One example is the ring-enlargement reactions shown in Scheme 10.[26]




***Scheme 10.*** β-Fragmentation sequence for the synthesis of spiro ketones by Kim and Lee.[26a]

Epoxycarbinyl radicals have also been applied to natural product synthesis, the critical test for novel methodology. The opening of the epoxide ring of **9** via the formation of a carboxy radical, decarboxylation, and opening of the epoxycarbinyl radical yielded an important intermediate in the synthesis of (+)-deoxylycorine (Scheme 11).[27] A key intermediate for prostaglandin B1 compounds was obtained by a tandem cyclopropylcarbinyl and epoxycarbinyl radical rearrangement.[28a,b]

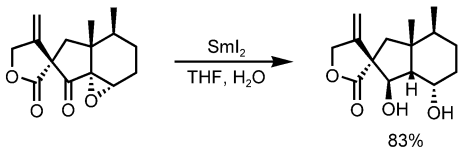



***Scheme 11.*** Key step in the synthesis of deoxylycorine.

 © 2003 Wiley-VCH Verlag GmbH & Co. KGaA, Weinheim 

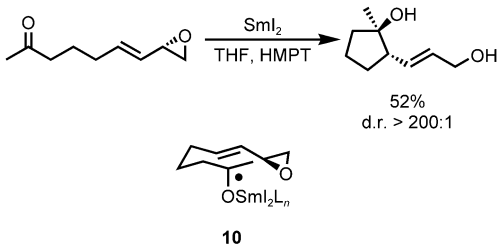
*2.1.3.1.2. Radical Generation by Electron Transfer*

The usefulness of the opening of epoxycarbinyl radicals has been further expanded by preparing radicals through reduction of suitable precursors in the presence of $SmI_2$. α,β-Epoxy ketones proved to be especially valuable in this respect because of the generation of ketyl radicals next to an epoxide ring.[29] The easy access of the epoxides from α,β-unsaturated ketones has resulted in this method finding widespread application in synthesis. The ketones can be reduced further for the construction of cyclic compounds or 1,3-diols (Scheme 12). The reaction also worked well for α,β-epoxyamides.[29d]



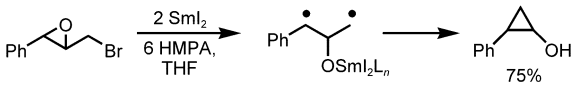

***Scheme 12.*** Ring opening and reduction of an epoxyketone with $SmI_2$.

Epoxycarbinyl radicals were also generated by intramolecular addition of ketyl radicals to vinyl epoxides (Scheme 13).[30] The observed selectivities supported radical




***Scheme 13.*** Addition of ketyl radicals to vinyl epoxides by Molander and Shakaya.[30]

pathways in which **10** was a transition structure. The mechanistic analysis for the intermolecular variations of this transformation[31] was less clear cut and it is therefore not clear whether allyl anions are involved in the reaction pathway.[32] Cyclopropanols could be synthesized from α-bromo epoxides with $SmI_2$ (Scheme 14).[33]

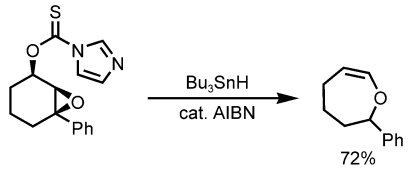



***Scheme 14.*** Synthesis of cyclopropanols by Kim and co-workers.[33]

*2.1.3.2.* ***Epoxide Opening through C–C Bond Cleavage***

The first examples of C–C bond cleavage were realized by introduction of radical-stabilizing groups, for example, phenyl or vinyl.[34] The first application in the synthesis of more complex molecules involved the synthesis of tetrahydrofurans[35] in a sequence similar to the transformations of vinylcyclopropanes.[36]

Ring expansions leading to enol ethers as precursors for oxepane and oxocane derivatives[37] (Scheme 15) and for the synthesis of chromenes were also realized.[38] The opening of



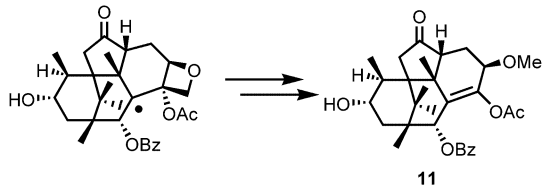

***Scheme 15.*** Synthesis of cyclic enol ethers by Marples and co-workers.[37]

naphthyl-substituted epoxides in $SmI_2$-initiated ring-opening reactions took place partially through a radical reaction. However, the interference of anionic pathways could not be fully suppressed.[39]

***2.2. Oxetane and β-Lactone Opening***

The opening of oxetanes and β-lactones through formation of their carbinyl radicals is less common than the opening of epoxides. Once generated, the carbinyl radicals showed similar behavior as epoxycarbinyl radicals. Fragmentation occurs readily to give homoallyloxy radicals. The rate constant for the opening of the 3-methyl-3-oxetanylcarbinyl radical was determined as 890 $s^{-1}$. The corresponding methyl-substituted cyclobutylcarbinyl radical reacted about three times faster ($2.5 \times 10^3$ $s^{-1}$).[9]

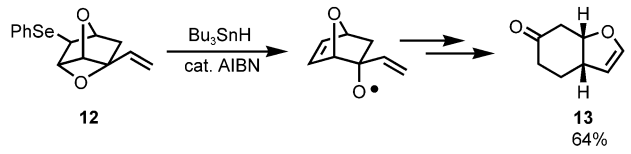
In a study aimed at the preparation of deoxytaxol compounds a radical formed through a number of skeletal rearrangements from taxol opened to give **11** (Scheme 16).[40]




***Scheme 16.*** Opening of a oxetanylcarbinyl radical by Farina and co-workers.[40] Bz = benzoyl.

A vinyloxetane was opened in a tributylstannyl group transfer reaction.[41] Oxetanonylcarbinyl radicals, obtained from β-lactones, were opened to prepare allyl and cyclohexadienyl radicals.[42] Ring opening was very fast ($10^6$–$10^7$ $s^{-1}$). Very recently a radical alternative to the anionic oxy-Cope rearrangement was reported; the key step in the synthesis of **13** was the opening of the strained oxetane **12** (Scheme 17).[43]

 © 2003 Wiley-VCH Verlag GmbH & Co. KGaA, Weinheim 



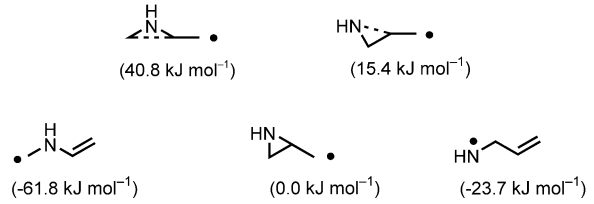

***Scheme 17.*** Radical alternative to the oxy-Cope rearrangement by Renaud and co-workers.[43]

### 2.3. Opening of Aziridines

The opening of aziridinylcarbinyl radicals occupies a prominent position among the useful methods for the generation of aminyl radicals,[44] which display a rich chemistry.

#### 2.3.1. Mechanism of Aziridine Opening

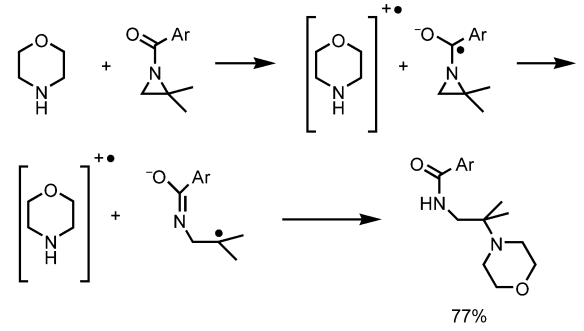
The energy barrier for the cleavage of the C–C bond in aziridine is high (40.8 kJ mol$^{-1}$), while a much lower value has been reported for cleavage of the C–N bond (15.4 kJ mol$^{-1}$). Thus, ring opening by cleavage of the C–N bond is kinetically preferred even though the product is distinctly less stable (−61.8 kJ mol$^{-1}$ versus −23.7 kJ mol$^{-1}$; Scheme 18).[16]




***Scheme 18.*** Computational analysis of the opening of an aziridinylcarbinyl radical by Radom and co-workers.[16]

#### 2.3.2. Synthetic Applications

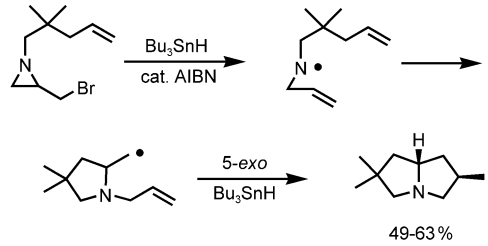
The first ring opening was reported with *N*-acylated aziridines.[45] The pivotal ketyl radicals were formed by electron transfer from easily oxidized nucleophiles, for example, amines, or from metals. The higher substituted alkyl radicals were formed (Scheme 19).




***Scheme 19.*** The first opening of an aziridinylcarbinyl radical by Stamm et al.[45] Ar = *p*-$NO_2C_6H_4$

The exclusive mode of ring opening of aziridinylcarbinyl radicals prepared under free-radical conditions involved C–N bond cleavage and resulted in the formation of aminyl radicals.[46] After activation by complexation with magnesium bromide,[44] cyclization of the radicals led to pyrrolidines. An efficient method for C–C bond cleavage has until now unfortunately remained elusive.[47,48]

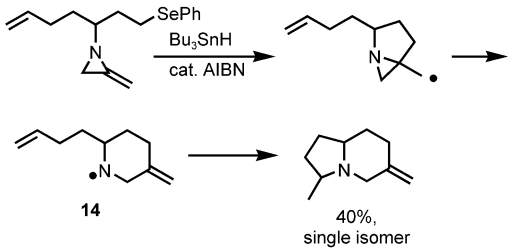
Readily available 2-(bromomethyl)aziridine derivatives were also used for ring opening[49] and pyrrolizidines were synthesized by tandem cyclizations (Scheme 20). 2-Acylazir-




***Scheme 20.*** Tandem sequence for the preparation of pyrrolizidines by De Kimpe et al.[49]

idines were opened in the presence of $SmI_2$ via formation of aziridinylketyl radicals. The reaction yielded β-amino ketones, esters, and amides with a variety of protecting groups.[50]

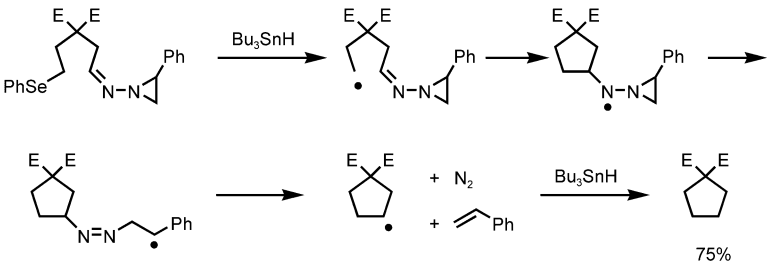
A [3+2] annulation sequence that used the initial opening of an aziridinylcarbinyl radical for the synthesis of pyrrolidine derivatives was described recently.[51] 2-Methyleneaziridines were introduced as functional groups for the generation of aziridinylcarbinyl radicals.[52] Ring opening resulted in the formation of cyclic aminyl radical **14** which could be reduced or subjected to another cyclization reaction (Scheme 21).




***Scheme 21.*** Tandem sequence for the synthesis of octahydroindolizines by Prévost and Shipman.[52]

A very elegant and useful application of aziridine opening has been developed with *N*-(1-aziridinyl)imine.[53] After radical addition and ring opening, a fragmentation resulted in the cleavage of styrene and nitrogen. The resulting cyclic radical could be further used in tandem reactions (Scheme 22). The method was also unique because formally *5-endo* cyclization products were obtained; a number of structurally complex molecules, for example, modhephene,[53d] zizaene,[53f] and deoxypancratistatins,[53h] were prepared from aziridinylimines.

 © 2003 Wiley-VCH Verlag GmbH & Co. KGaA, Weinheim 




***Scheme 22.*** Aziridinylimines as precursors for aziridine opening by Kim et al.[53] E = COOR.

The opening of carbinyl and heterocarbinyl radicals of epoxides, oxetanes, β-lactones, and aziridines has led to numerous useful synthetic applications that could be initiated from virtually any radical precursor.

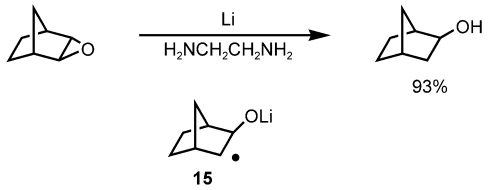
## 3. Reductive Cleavage of Heterocycles by Electron Transfer from Arene Radical Anions

The opening of heterocyclic radical anions combines the virtues of organometallic chemistry with radical chemistry.

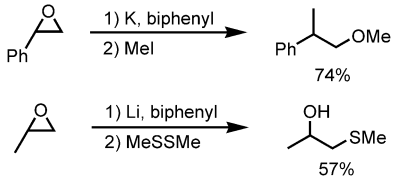
### 3.1. Epoxide Opening

#### 3.1.1. Early Examples and Mechanism

The first reductive opening of epoxides through electron transfer was achieved under Birch conditions[54] through formation of the lithiated radical anion **15** (Scheme 23). The




***Scheme 23.*** Reduction of norbornene oxide under Birch conditions.



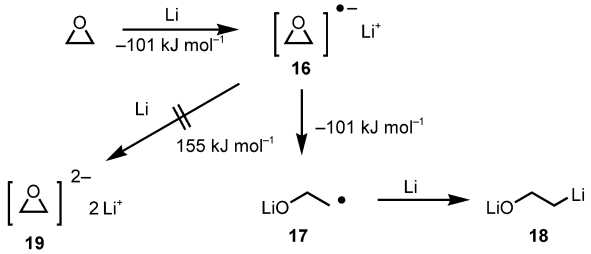

***Scheme 24.*** Epoxide opening with arene radical anions by Bartmann.[56]

preparatively interesting β-lithioalkoxides, which could also be obtained by different routes,[55] could not be trapped by electrophiles other than protons because of the acidic medium.

The first direct electron transfer to epoxides under nonprotic conditions was realized by employing radical anions of aromatic compounds.[56] It was found that alkyl-substituted epoxides were opened to give the less-substituted organolithium compounds (Scheme 24). The regioselectivity was reversed with ester- or phenyl-substituted epoxides, and enolates or benzylic organometallic compounds could be prepared and trapped.

The intermediate β-lithioalkoxides were thermally labile, and the reactions usually had to be conducted at −90 °C. Thus, only very reactive electrophiles, for example, $H_2O$, $D_2O$, $CO_2$, MeI, and disulfides, could be employed for quenching.

Houk, Cohen, and Dorigo have carried out a comprehensive theoretical study of oxirane opening (Scheme 25).[57] The most important result was the identification of the lithiated radical anion **16** as the decisive




***Scheme 25.*** Analysis of epoxide opening through electron transfer by Dorigo, Houk, and Cohen.[57]

intermediate. Opening of this intermediate was exothermic (about −100 kJ mol$^{-1}$) and produced radical **17**, which was subsequently reduced to **18**. Dianion **19** was not formed. The calculations also suggested that **20** was favored over **21** by about 10 kJ mol$^{-1}$, thus confirming the experimental results (Scheme 26). The reason for this preference was attributed to




***Scheme 26.*** Calculated stabilities of the regioisomeric products of epoxide opening.

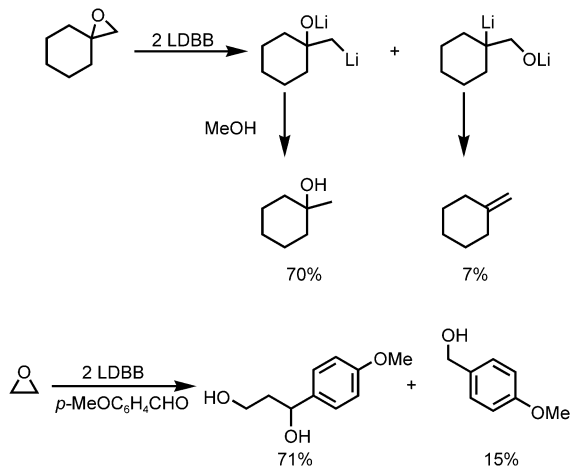
the higher stability of a tertiary alkoxide compared to a primary alkoxide[58] which outweighed the opposite trend for radical stabilization. Epoxide opening was irreversible.[59]

#### 3.1.2. Synthetic Applications

The scope and limitations of reductive epoxide cleavage were subsequently investigated more thoroughly.[60] The regioselectivity of the ring opening was usually high but not necessarily complete. Hydride transfer was observed as a minor competing pathway (Scheme 27).

Stable organolithium compounds were only obtained from 1,2-disubstituted epoxides if an elimination reaction was impossible. This was the case only rarely, for example, for

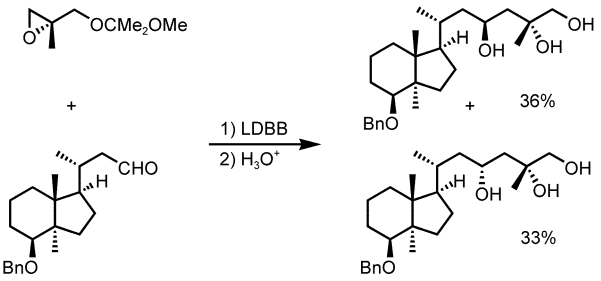
 © 2003 Wiley-VCH Verlag GmbH & Co. KGaA, Weinheim 




***Scheme 27.*** Scope and limitation of reductive epoxide opening. LDBB = lithium 4,4′-di-*tert*-butylbiphenylidene.

cyclohexene oxide at low temperature. Vinyl oxiranes were opened to give allyllithium compounds through electron transfer to the olefin. Stereoselective additions to aldehydes were only possible after transmetalation with cerium or titanium.

Enantiomerically pure epoxides constituted excellent starting materials for electron transfer. One example is the formal synthesis of calcitriollactone (Scheme 28).[61] Unfortunately, the diastereoselectivity for the key reaction was low. A study of the use of enantiomerically pure epoxides as substrates in the synthesis of 1,3-diols was later disclosed,[62] but the problem of low selectivity could not be resolved. Structural modification of sugars[63] and steroids[64] as well as openings of α,β-epoxy ketones[65] were also reported.

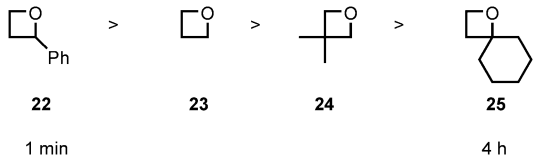



***Scheme 28.*** Synthesis of modified steroids through reductive epoxide opening. Bn = benzyl.

The nature of the reductant was found to be dependant on the amount of lithium employed.[66] Dianions that were more potent reductants than the radical anions were formed with two or more equivalents of lithium.

### *3.2. Oxetane and Tetrahydrofuran Opening*

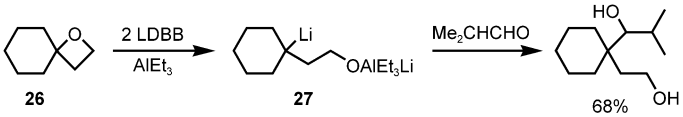
Rings that were larger than epoxides turned out to be harder to reduce because of the reduced ring strain. Nevertheless, it was demonstrated that oxetanes could be cleaved by arene radical anions at 0 °C to yield γ-lithioalkoxides.[67] The ease of ring opening depended on the substitution pattern of the oxetane (Scheme 29).




***Scheme 29.*** The rate of oxetane opening depends on the substitution pattern.

Oxetanes **23, 24**, and **25** yielded the less-substituted organolithium compounds, when possible, after exposure to the reductant for up to 4 h. Presumably, the same mechanism[57] as in epoxide opening was operating. Substrate **22** displayed two distinctly different features: Reduction occurred much quicker and the opposite regioselectivity was observed. The reaction of **22** must be considered as a simple reductive cleavage of a benzyl ether through initial reduction of the arene[68] and not an electron-transfer reaction of the heterocycle.

Complexation with the Lewis acid $AlMe_3$ resulted in exclusive formation of **27** from **26**, and thus in a reversal of regioselectivity (Scheme 30).[69] This observation was rationalized by elongation of the C–O bond involving the higher substituted carbon atom upon complexation. The resulting lowering in energy of the LUMO enabled electron transfer to occur at −70 °C!



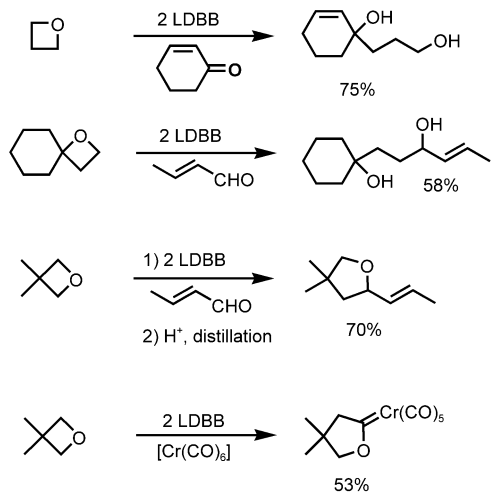

***Scheme 30.*** Reversal of regioselectivity of oxetane opening through complexation.

A number of highly useful applications of oxirane opening have been described (Scheme 31).[69] The thermally stable organolithium reagents that possessed no β-elimination pathway for decomposition could even react with less reactive electrophiles such as $Cr(CO)_6$.[70]

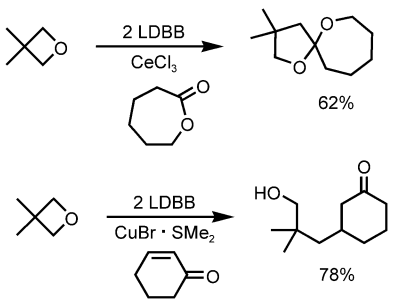
Transmetalation reactions, for example, with $CeCl_3$ or copper salts, were also feasible.[71] In this manner conjugate addition reactions were carried out and spiroketals and oxaspirolactones were prepared (Scheme 32). Many enantiomerically pure compounds of interest for the preparation of biologically active compounds could also be synthesized, although usually with low selectivities.[72]

Activation of tetrahydrofuran derivatives, which are usually inert to towards electron transfer, could be achieved by complexation with the Lewis acid $BF_3{\cdot}Et_2O$. This approach enabled the preparation of synthetically valuable organolithium compounds (Scheme 33).[73,74] The more highly substituted organometallic compounds were usually formed with

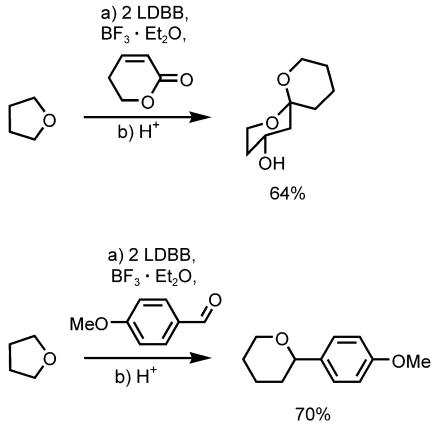
 © 2003 Wiley-VCH Verlag GmbH & Co. KGaA, Weinheim 




***Scheme 31.*** Synthetic applications of reductive oxetane opening.




***Scheme 32.*** Transmetalation reactions after oxetane opening.




***Scheme 33.*** Reductive opening of tetrahydrofuran rings.

excellent selectivity (94:6 to > 99:1).[73] As in the case of the oxetanes, phenyl substitution led to the benzyllithium species exclusively.[74,75] So far, it has been impossible to reductively cleave tetrahydropyrans.[66]

The series of oxygen heterocycles discussed has demonstrated that a reduction in ring strain dramatically reduced the ease of reduction. Mild conditions could only be achieved through Lewis acid activation.

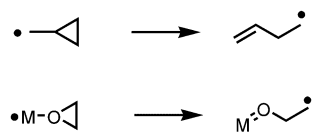
### 3.3. Opening of Nitrogen and Sulfur Heterocycles

In comparison to oxygen heterocycles, nitrogen and sulfur heterocycles are less strained because C–N and C–S bonds are longer and less polarized than C–O bonds. Thus, their σ* orbitals will be higher in energy and hence less readily available for electron-transfer reactions. The reductive cleavage of the C–N bond is therefore expected to occur less readily. This has indeed been observed, and only phenyl-substituted heterocycles were found to be useful precursors. Since electron transfer occurred to the phenyl substituent and not to the heterocycle in these reactions the resulting transformations[76–78] will not be discussed here.

## 4. Epoxide Opening by Single Electron Transfer from Metal Complexes

### 4.1. Introductory Remarks

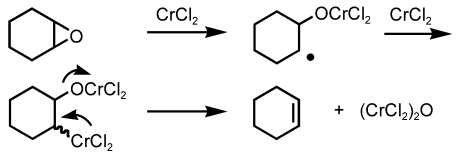
A different and promising approach to radical generation involves Lewis acid activation of and electron transfer to the heterocycle by a metal complex that can potentially act as a catalyst. The general idea of this concept was first outlined for epoxides by Nugent and RajanBabu in 1988[79] (Scheme 34), although the transformation had been realized before.




***Scheme 34.*** Synthesis of β-metaloxy radicals from epoxides by the strategy of Nugent and RajanBabu.[79]

### 4.2. Epoxide Deoxygenation

The first attempts reported in the area of metal complex mediated epoxide opening were only concerned with the deoxygenation of epoxides. β-Metaloxy radicals were proposed as crucial intermediates for the first time in the deoxygenation of styrene and cyclohexene oxide with chromium(II) compounds (Scheme 35).[80] However, this study did

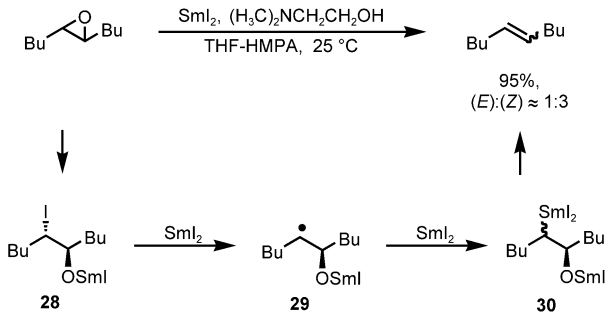



***Scheme 35.*** First use of β-metaloxy radicals in deoxygenation reactions by Kochi et al.[80]

not address any issues of stereoselectivity and was only of limited use for synthetic applications.

An example in which $SmI_2$[81] was used under optimized conditions[82,83] is shown in Scheme 36. The reactions most

 © 2003 Wiley-VCH Verlag GmbH & Co. KGaA, Weinheim 



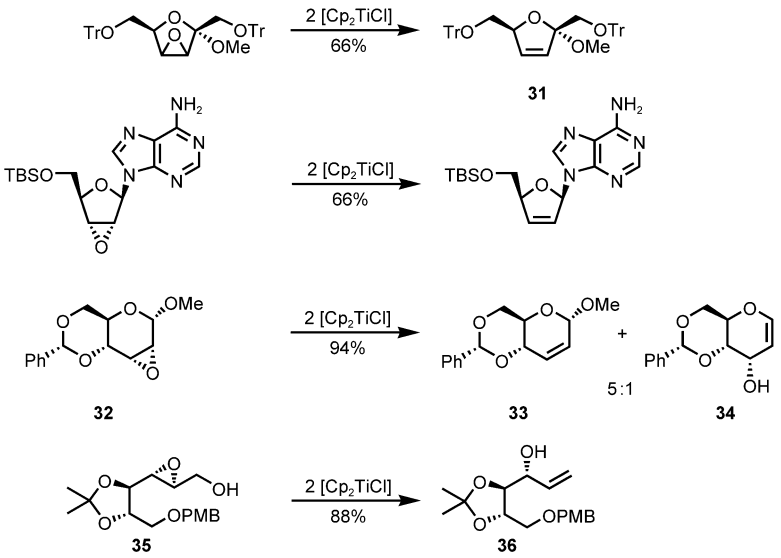

***Scheme 36.*** Epoxide deoxygenation with $SmI_2$.

likely proceeded through the samarium complex of iodohydrin **28**, formed through a metal-mediated $S_N2$ process. The crucial intermediate, the β-samariumoxy radical **29**, was subsequently formed by the reduction of the C–I bond and not by direct opening of the epoxide through electron transfer. The low stereoselectivity of the deoxygenation was explained by the presence of the configurationally labile radical and/or its unselective reduction to **30** and ensuing elimination.

Transformations proceeding by two-electron processes, for example, oxidative insertions or $S_N2$-type reactions with metals, often display excellent stereoselectivity, but will not be discussed here.[84] In the design of suitable reagents for epoxide opening through electron transfer it is essential to exclude the possibility of any competing epoxide opening by $S_N1$ or $S_N2$ reactions. This goal was achieved by using non-nucleophilic ligands and by modulating the Lewis acidity of the metal center by choosing σ- and/or π-donor ligands.

Low-valent titanocene chlorides were found to constitute a highly chemoselective and mild class of electron-transfer reagents for the deoxygenation of epoxides. Titanocene(III) reagents, formed in the presence of strong reductants, did not necessarily lead to stepwise electron transfer and will not be discussed further.[85,86] Nugent and RajanBabu described that 5-decenes were observed in an *E* to *Z* ratio of 3–4:1 from either *cis*- or *trans*-5-decene oxide by using $[Cp_2TiCl]$, which had been isolated and purified prior to use.[79c,d] Therefore, it seems clear that a common, long-lived β-titanoxy radical intermediate was formed from both epoxides. The formation of the mixture of olefins was observed after further reduction and elimination.

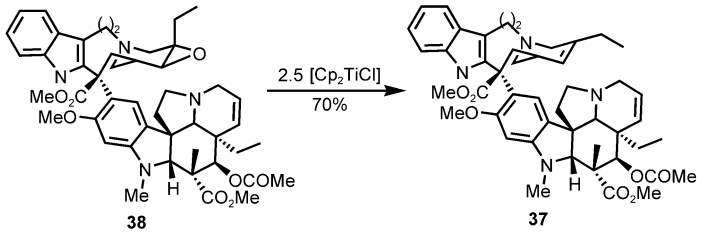
The deoxygenation of epoxides was applied in useful transformations of highly functionalized substrates (Scheme 37). The preparation of **31**,[79d] which is highly unstable towards elimination even in the presence of traces of acids, in 66% yield was remarkable; other routes failed.[87] A 5:1 mixture of the regioisomeric olefins **33** and **34** was isolated in an excellent combined yield of 94% in the case of the glucose derivative **32**. However, the reaction was neither selective in terms of epoxide opening nor in terms of the final elimination.[79d] A very useful deoxygenation uses enantiomerically pure primary allylic alcohols, for example, **35**, to give enantiomerically pure secondary allylic alcohols, for example, **36**.[88] This approach circumvented kinetic resolution




***Scheme 37.*** Synthetic applications of titanocene-mediated epoxide deoxygenation. PMB = *p*-$MeOC_6H_4CH_2$, Tr = triphenylmethyl.

of secondary allylic alcohols by the method of Sharpless and co-workers, which gives a maximum yield of 50%.[89]

Anhydrovinblastine (**37**), an important intermediate for the anticancer drug navelbine, was prepared from leurosine (**38**), an abundant alkaloid from the Madagaskan periwinkle *Catharantus roseus*, in 70% yield by deoxgenation with $[Cp_2TiCl]$ (Scheme 38).[90] Stereospecific deoxygenations in the cryptophycin family of natural products from *Nostocaceae* were also reported.[91]




***Scheme 38.*** Synthesis of anhydrovinblastine by Doris and co-workers.[90]

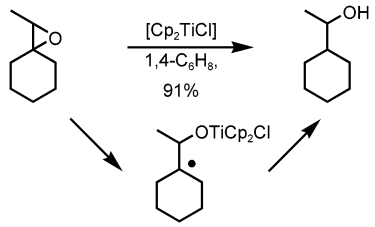
### *4.3. Reductive Epoxide Opening to Alcohols*

#### *4.3.1. Introductory Remarks*

Reactions of β-titanoxy radicals other than the deoxygenation of epoxide-derived radicals will be discussed first by considering reductions with hydrogen atom donors. In this manner the underlying reactivity profiles and the reaction mechanism can be presented.

Titanocene(III) chloride[79c,d] constitutes the best reagent reported so far for carrying out this reductive epoxide opening. The β-titanoxy radicals were reduced efficiently by hydrogen atom donors, for example, 1,4-cyclohexadiene or *tert*-butylthiol. The highly regioselective opening of unsymmetrical epoxides (Scheme 39) to give the less-substituted alcohols is particularly important. Up to 33% deoxygenation and a lower regioselectivity (90:10) in favor of the primary

 © 2003 Wiley-VCH Verlag GmbH & Co. KGaA, Weinheim 



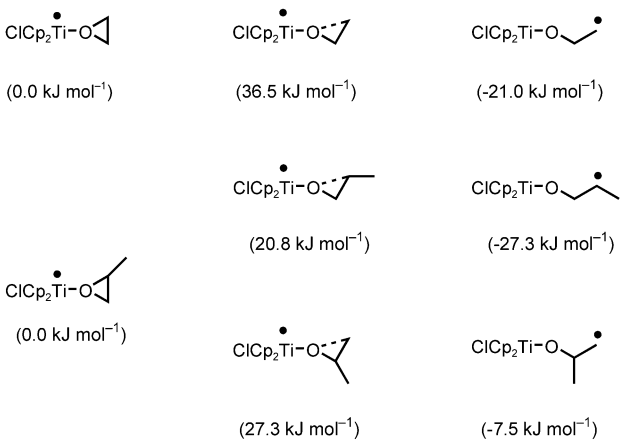

***Scheme 39.*** Mechanism of $[Cp_2TiCl]$-mediated reductive epoxide opening.

alcohol were observed in the case of monosubstituted epoxides.[79d] Thus, the method is complementary to the typical opening of epoxides with hydrides[92] by an $S_N2$ mechanism or the opening of epoxides with arene radical anions.

#### 4.3.2. *Structure of the Titanocene Reagent and Mechanism*

Daasbjerg, Skrydstrup, and co-workers recently disclosed an electrochemical study on the structure of titanocene(III) reagents in solution.[93] It was established that the reduction of $[Cp_2TiCl_2]$ with either Mn or Zn led to the same redox-active intermediate. Most likely, this active species was $[Cp_2TiCl]$, which was in equilibrium with its dimer.[94]

The transition structures and intermediates of the reaction were studied by DFT methods (Scheme 40).[95] All the

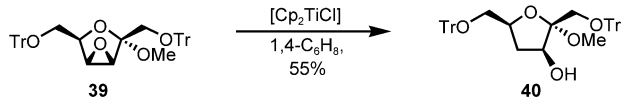



***Scheme 40.*** Computational analysis of $[Cp_2TiCl]$-mediated epoxide opening by Grimme et al.[95]

epoxide openings were exothermic and, in agreement with the experimental results, the higher substituted radicals were formed preferentially. According to the Hammond postulate,[96] the transition structures are early and thus the spin density is mostly located on the titanium center. The regioselectivity of epoxide opening was correctly predicted as 9:1 for the case of propene oxide.

#### 4.3.3. *Synthetic Applications*

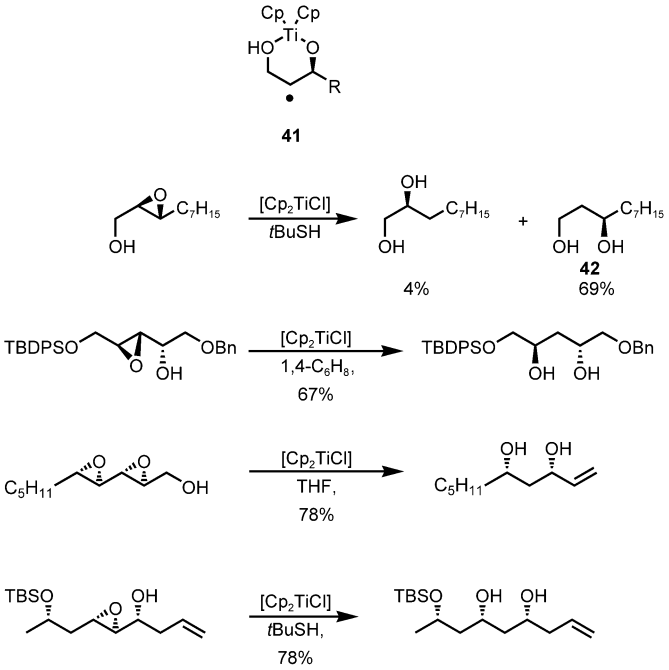
High regioselectivity of ring opening was not confined to unsymmetrical substitution patterns of the epoxide. In many cases excellent results could be observed with 1,2-disubstituted epoxides for electronic reasons,[97] for example, exclusive formation of **40** from **39**, (Scheme 41).[79d] 2,3-Epoxy




**39** **40**

***Scheme 41.*** Regioselective opening of 1,2-disubstituted epoxides by RajanBabu and Nugent.[79d]

alcohols[18] are especially valuable substrates in this respect. Chelated radicals, such as **41**, have been proposed as key intermediates in the preparation of 1,3-diols (Scheme 42).

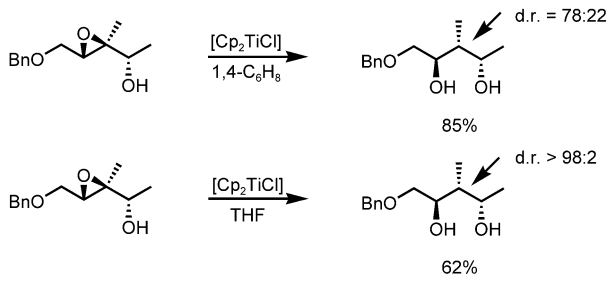



***Scheme 42.*** Synthesis of 1,3-diols from Sharpless epoxides with $[Cp_2TiCl]$. TBPDS = *tert*-butyldiphenylsilyl.

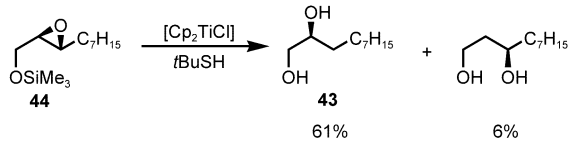
Nugent and RajanBabu were the first to reduce these radicals when they prepared 1,3-diols, for example, **42**[79d] in excellent regioselectivity (94:6). More elaborate 1,3-diols could also be obtained.[98–100] Various 2-methyl-1,3-diol frameworks were also synthesized (Scheme 43).[101] Better selectivities were observed with THF as the hydrogen donor.[102]

Ring opening of 3-heptyl-2-hydroxymethyloxirane generated 1,3-diol **42**. The opposite regioisomer **43**, was obtained when the free hydroxy group was converted into the trimethylsilyl ether **44** (Scheme 44).[79d] Both methods compared very well with the established nucleophilic conditions for regioselective epoxide opening performed using hydride reagents.[103] α,β-Epoxy ketones could be opened with $[Cp_2TiCl]$ in good to excellent yields.[104] $[Cp_2TiCl]$ even performed better than $SmI_2$ in some cases.[29]

 © 2003 Wiley-VCH Verlag GmbH & Co. KGaA, Weinheim 



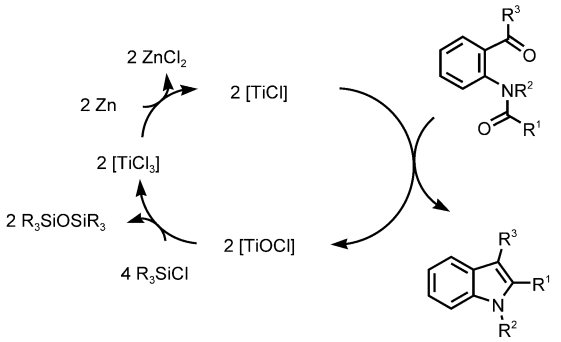

***Scheme 43.*** Stereoselective access to stereotriads by titanocene-mediated epoxide opening by Chakraborty and Das.[101]




***Scheme 44.*** [$Cp_2TiCl$]-mediated synthesis of 1,2-diols from Sharpless epoxides.

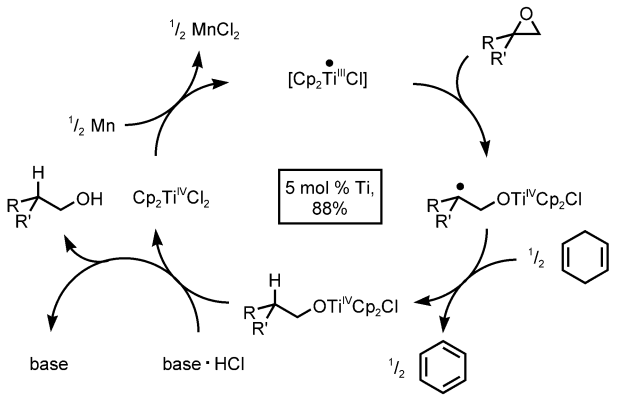
### 4.3.4. *Titanocene-Catalyzed Reductive Epoxide Opening*

No attempt has so far been made to use ligands other than simple cyclopentadienyl in the stoichiometric applications of titanocene complexes. The use of more complex titanocenes[105] in catalytic reactions is very promising for obtaining reagent-controlled radical reactions.[106,2a] The solution of the conceptually similar problem of achieving catalytic turnover[107] in McMurry couplings,[108] Nozaki–Hiyama reactions,[109] and pinacol couplings[110] were reported by Fürstner et al. and by Hirao et al. by in situ silylation of titanium, vanadium, and chromium oxides and alkoxides with $Me_3SiCl$ (Scheme 45). This concept was later also extended to other applications.[111–113]




***Scheme 45.*** Titanium-catalyzed McMurry reaction by Fürstner.[108]

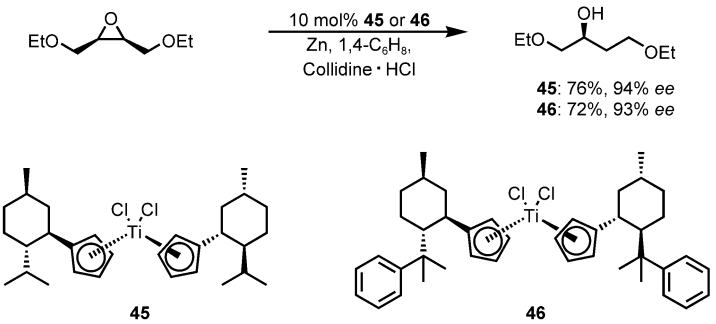
In the case of the epoxide openings, $Me_3SiCl$ was not an appropriate reagent for the cleavage of a Ti–O bond because of the high Lewis acidity of the silicon atom that led to undesired epoxide opening. Substituted pyridine hydrochlorides[114,115] emerged as excellent mediators for catalysis. Collidine and lutidine hydrochloride performed best in the presence of manganese dust as a stoichiometric reductant. Collidine hydrochloride was preferred because it is distinctly less hygroscopic than lutidine hydrochloride. The resulting catalytic cycle, which preserves all the attractive features of the stoichiometric reaction, is shown in Scheme 46.




***Scheme 46.*** Titanocene-catalyzed reductive epoxide opening. R = $CH_2CH_2Ph$, R′ = Me, base = 1.5 equiv 2,4,6-collidine.

The opening of epoxy ketones, which leads to sensitive β-hydroxy ketones, could also be carried out with catalytic amounts of [$Cp_2TiCl$].[104] The catalytic conditions proved valuable in the opening of *meso*-epoxides through electron transfer from enantiomerically pure titanocene derivatives through preferential cleavage of one of the C–O bonds of the titanocene(III) bound epoxide.[116]

Inspection of the extensive literature on titanocene and zirconocene derivatives[105] suggested that complexes derived from menthol[117] and phenylmenthol[118] would be suitable catalysts for asymmetric epoxide opening (Scheme 47).




***Scheme 47.*** Titanocene-catalyzed enantioselective epoxide opening.

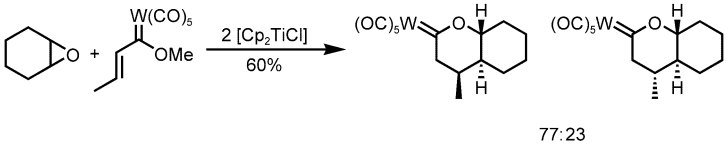
Surprisingly, complex **45** with a menthol substituent was as efficient as the phenylmenthol derivative **46**, even though phenylmenthol is usually a much better reagent in asymmetric synthesis than menthol.[119] The structure of both complexes were demonstrated to be essentially the same in solution and in the solid state.[120] The reaction described was conceptually different from epoxide openings proceeding by an $S_N2$ mechanism.[121]

 © 2003 Wiley-VCH Verlag GmbH & Co. KGaA, Weinheim 

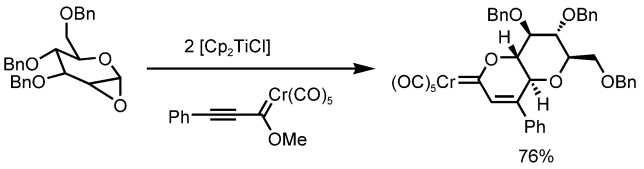
### 4.4. Intermolecular Addition Reactions to Activated Alkenes

β-Titanoxy radicals are generated under exceptionally mild reaction conditions and can act as highly reactive intermediates in intermolecular C–C bond-forming reactions.[79b,d] The resulting products, δ-hydroxy esters or δ-lactones constitute valuable synthetic intermediates. Similar transformations cannot be achieved with organometallic reagents, for example, cuprates, because of competing β-elimination pathways.

Epoxide-derived radicals added efficiently to α,β-unsaturated carbene complexes as reactive radical acceptors (Scheme 48) under these conditions.[122] Extensions of this concept by using sugar-derived carbenes as radical acceptors and by adding radicals derived from glycal epoxides to unsaturated carbenes were also investigated.[123] The products obtained (Scheme 49) should be of interest for the synthesis of biologically active substances. The same system was later employed to organic acceptors and the same selectivities as above were found.[124]

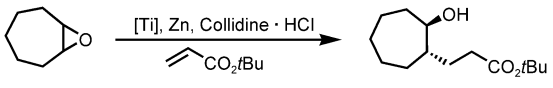



***Scheme 48.*** Synthesis of functionalized tungsten carbenes by Merlic et al.[122]




***Scheme 49.*** The first use of glycal epoxides as radical precursors by Dötz and Gomess da Silva.[123]

The catalytic conditions were well-suited for the preparation of δ-hydroxy esters, lactones, and δ-hydroxynitriles.[115c] Alkyl-substituted titanocenes are efficient catalysts for the often highly diastereoselective addition of radicals to α,β-unsaturated carbonyl compounds (Scheme 50).[116c] The preferential formation of the *trans* isomers was explained by Giese's *anti* rule through the shielding of the bulky ligands.[125]



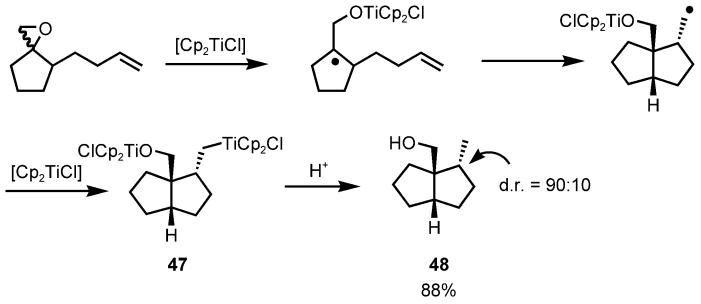

***Scheme 50.*** Titanocene-catalyzed reagent-controlled addition of epoxides to acrylates.

### 4.5. Titanocene-Mediated and -Catalyzed Cyclizations

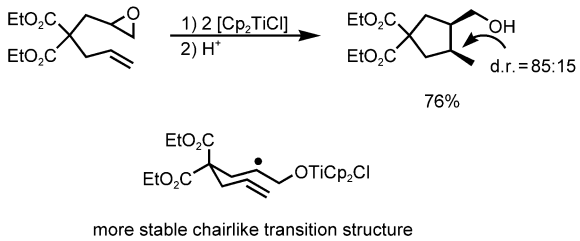
Cyclization reactions,[126] especially 5-*exo* cyclizations,[127] have been of outstanding importance to radical chemistry. The titanocene-mediated cyclization of suitably unsaturated epoxides offers a number of attractive features for these reactions.

The mechanism of the formation of a bicyclo[3.3.0] system is outlined in Scheme 51.[79a,d] The generation of organotitanium compounds, such as **47**, as intermediates in the formation of **48** was demonstrated by trapping with $D_2SO_4$ or $I_2$.[79a,d] The relative configurations of the major products were in accordance with the rules outlined by Beckwith and Houk.[128] Scheme 52 shows a reaction that proceeded through a more-stable chairlike transition structure.

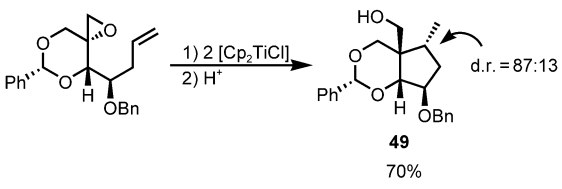
The cyclization was especially powerful in the generation of radicals from highly functionalized epoxides, for example, in the synthesis of **49** (Scheme 53), to yield products with functional groups that were typically not tolerated under polar conditions. The cyclization conditions have since been applied in numerous synthetic endeavors. A stereospecific cyclization–elimination sequence that allowed a highly selective synthesis of preparatively useful




***Scheme 51.*** Titanocene-mediated cyclization of unsaturated epoxides.



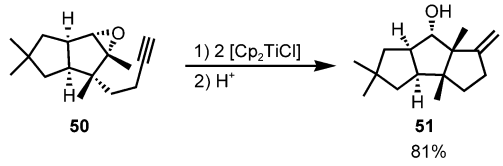

***Scheme 52.*** Control of diastereoselectivity in titanocene-mediated cyclizations.




***Scheme 53.*** Synthesis of highly functionalized carbocycles from carbohydrates by RajanBabu.[79d]

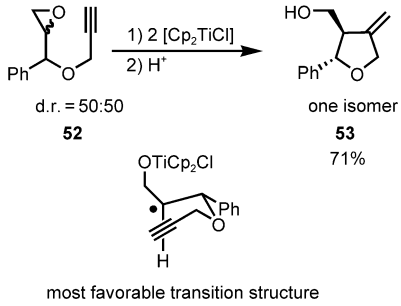
 © 2003 Wiley-VCH Verlag GmbH & Co. KGaA, Weinheim 

*exo*-cyclopentylidene compounds was amongst the first examples.[129] The cyclization of epoxy alkyne **50** to yield homoallylic alcohol **51** was employed in the synthesis of (±)-ceratopicanol (Scheme 54).[130] The vinyl radicals generated could not be controlled under free-radical conditions.




***Scheme 54.*** 5-*exo* cyclization on the way to ceratopicanol by Clive et al.[130]

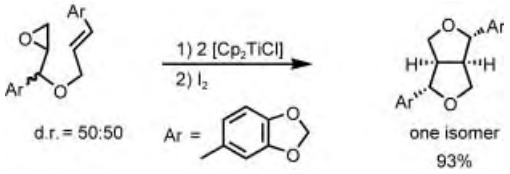
The titanocene-mediated 5-*exo* cyclization was used extensively in the synthesis of tetrahydrofuran derivatives that were further transformed into numerous natural products (Scheme 55).[131] This synthetically highly attractive method




***Scheme 55.*** Diastereoconvergent synthesis of substituted tetrahydrofuran derivatives by Roy and co-workers.[131]

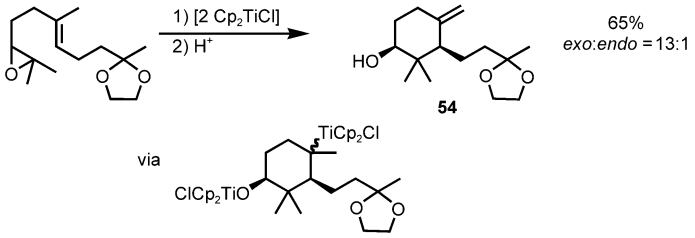
used the configurational lability of radicals to convert the 1:1 diastereomeric mixture of substrates **52** into **53** as a single isomer in a diastereoconvergent reaction.[131b] The *trans* arrangement of the $CH_2O(TiCp_2Cl)$ group and the phenyl moiety seems to have been enforced by avoidance of steric interactions between the alkyne and the bulky $CH_2O$-($TiCp_2Cl$) group.

Furanolignans, for example, (±)-sesamin, could be obtained by trapping the organotitanium intermediate formed after cyclization with iodine and a subsequent $S_N2$ reaction to close the second ring (Scheme 56). More recently, the titanocene-based protocol was extended to the formation




***Scheme 56.*** Stereoconvergent synthesis of sesamin by Roy and coworkers.[131]

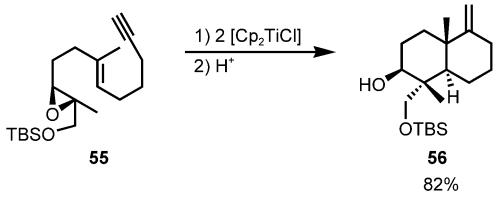
of larger rings through 6-*exo*, 6-*endo*, and 7-*endo* cyclizations. In this way the synthesis of cyclic terpenoids based on the radical opening of acyclic epoxypolyenes[132a] and of achilleol A[132b] was developed. As shown in Scheme 57, the




***Scheme 57.*** Synthesis of achilleol using a 6-*endo* approach by Barrero et al.[132]

cyclization of the epoxide-derived radical was terminated by a β-hydride elimination to give olefin **54**. This pathway is reminiscent of the hydrozirconation reaction with the Schwartz reagent.[133]

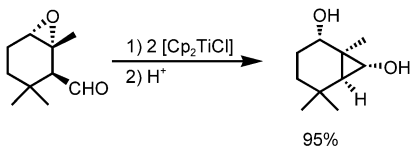
The use of a 6-*endo*-6-*exo* tandem sequence for the synthesis of (±)-smenospondiol from **55** (Scheme 58) and A- and C-ring synthons of paclitaxel was described recently.[134] The key to obtaining a high yield of the desired product **56** in this remarkable process was found to be the use of a mixture of benzene and THF (5:1) at reflux.




***Scheme 58.*** Tandem approach to smenospondiol by Takahashi and coworkers.[134]

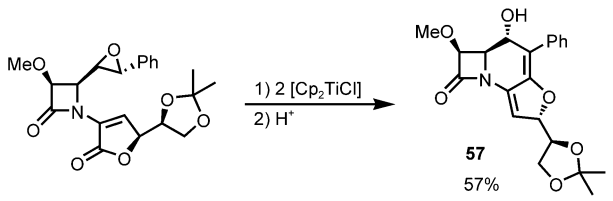
Other less-common but interesting titanocene-mediated radical cyclizations have begun to emerge recently. A unique example of a 3-*exo* cyclization with aldehydes as radical traps for the synthesis of cyclopropanols has been reported (Scheme 59).[135] Cyclobutanols and cyclopentanols could also be obtained efficiently. All the reaction products are difficult to synthesize by other methods. The reduction of highly electrophilic alkoxyl radicals by titanocene derivatives has been proposed as the driving force of the reaction.

Surprisingly, β-titanoxy radicals could even add to the carbonyl group of butenolides (Scheme 60).[136a] The method




***Scheme 59.*** 3-*exo* cyclizations with aldehydes by Fernández-Mateos et al.[135]

 © 2003 Wiley-VCH Verlag GmbH & Co. KGaA, Weinheim 

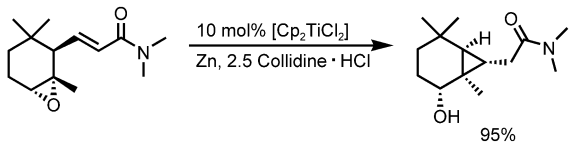



***Scheme 60.*** Synthesis of functionalized β-lactams by Grande and coworkers.[136a]

is of great interest for the synthesis of β-lactam antibiotics such as **57** that are not available by other routes, as yet. Other examples of the synthesis of functionalized β-lactams were concerned with cyclizations of α,β-unsaturated carbonyl compounds[136b] and aldehydes.[136c]

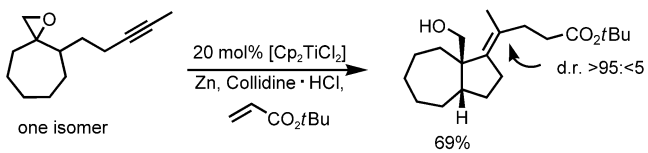
A titanocene-catalyzed *5-exo* cyclization of unsaturated epoxides was developed as a first step towards the goal of practical reagent-controlled cyclizations.[115a,c] The key step of the mechanism was the protonation of Ti–O and Ti–C bonds by collidine hydrochloride. This catalytic reaction allowed the synthesis of useful heterocyclic products.[137]

Transformations other than 5-*exo* cyclizations could also be realized efficiently.[138] The preparation of cyclopropanols could be performed catalytically if collidine was added to the reaction mixture to buffer the acidity of the system. The alkoxyl radicals generated through radical addition were most likely reduced by THF through hydrogen atom abstraction in a reaction supported by polar effects.[139] Cyclopropane derivatives with many different substitution patterns were formed in excellent yields by the efficient catalysis of 3-*exo* cyclizations (Scheme 61).




***Scheme 61.*** Titanocene-catalyzed 3-*exo* cyclizations.

A very attractive characteristic of radical chemistry is the generation of a novel radical after cyclization or any other radical translocation.[140] This feature allows for ensuing C–C bond-forming events. The resulting tandem reactions[141,142] can be extremely useful for the construction of complex molecules. The conditions used for the titanocene-catalyzed reactions also allowed the realization of tandem reactions.[143] An example with a vinyl radical as a crucial intermediate is shown in Scheme 62. The use of alkynes in the cyclization




***Scheme 62.*** Titanocene-catalyzed tandem radical reactions.

resulted in a rapid assembly of polycyclic compounds with exocyclic double bonds that are of substantial importance for the synthesis of modified steroids.

## 5. Summary and Outlook

The use of strained heterocycles, especially epoxides and aziridines, as readily available radical precursors has led to many mechanistically and synthetically pertinent investigations and applications over the last few decades. Three complementary modes of ring opening allow the generation of the pivotal radical intermediates, usually with very high selectivity. The reactions of heteroatom-centered radicals (hydrogen atom abstractions, cyclizations, and fragmentations) and β-titanoxy radicals arising from reductive epoxide opening are of special relevance.

A thorough understanding of the kinetic and theoretical intricacies of the reaction mechanisms has meant that the reactions are highly predictable, which is essential for applications in the synthesis of complex targets. We expect that in the future the reactions described here will be applied more frequently in large-scale applications and in the synthesis of complex molecules and natural products.

*We are indebted to the Deutsche Forschungsgemeinschaft (Gerhard-Hess-Programm) and the Fonds der Chemischen Industrie (Dozentenstipendium to A.G.) for financial support.*

Received: February 11, 2003 [A583]

[1] a) B. Giese, *Radicals in Organic Synthesis: Formation of Carbon–Carbon Bonds*, Pergamon, Oxford, **1986**; b) W. B. Motherwell, D. Crich, *Free Radical Chain Reactions in Organic Synthesis*, Academic Press, London, **1991**; c) J. Fossey, D. Lefort, J. Sorba, *Free Radicals in Organic Chemistry*, Wiley, New York, **1995**; d) D. P. Curran, N. A. Porter, B. Giese, *Stereochemistry of Radical Reactions*, VCH, Weinheim, **1996**; e) T. Linker, M. Schmittel, *Radikale und Radikalionen in der Organischen Synthese*, Wiley-VCH, Weinheim, **1998**; f) *Radicals in Organic Synthesis, Vol. 1–2* (Eds.: P. Renaud, M. P. Sibi), Wiley-VCH, Weinheim, **2001**.

[2] For recent reviews on isolated aspects, see a) A. Gansäuer, H. Bluhm, *Chem. Rev.* **2000**, *100*, 2771; b) J. J. Lie, *Tetrahedron* **2001**, *57*, 1; c) A. Gansäuer in *Radicals in Organic Synthesis, Vol. 2* (Eds.: P. Renaud, M. P. Sibi), Wiley-VCH, Weinheim, **2001**, p. 207.

[3] E. C. Sabatino, R. J. Gritter, *J. Org. Chem.* **1963**, *28*, 3437.

[4] D. H. R. Barton, R. S. H. Motherwell, W. B. Motherwell, *J. Chem. Soc. Perkin Trans. 1* **1981**, 2363.

[5] a) J. C. Scaiano, *J. Am. Chem. Soc.* **1980**, *102*, 5399; b) A. L. J. Beckwith, B. P. Hay, *J. Am. Chem. Soc.* **1988**, *110*, 4415.

[6] H. Suginome, J. B. Wang, *J. Chem. Soc. Chem. Commun.* **1990**, 1629.

[7] P. Galatsis, S. D. Millan, *Tetrahedron Lett.* **1991**, *32*, 7493.

[8] J. Amaudrut, O. Wiest, *Org. Lett.* **2000**, *2*, 1251.

[9] D. Laurie, D. C. Nonhebel, C. J. Suckling, J. C. Walton, *Tetrahedron* **1993**, *49*, 5869.

[10] K. W. Krosley, G. J. Gleicher, *J. Phys. Org. Chem.* **1993**, *6*, 228.

[11] a) L. Grossi, S. Strazzari, *Chem. Commun.* **1997**, 917; b) L. Grossi, S. Strazzari, B. C. Gilbert, A. C. Whitwood, *J. Org. Chem.* **1998**, *63*, 8366.

 © 2003 Wiley-VCH Verlag GmbH & Co. KGaA, Weinheim 

[12] F. E. Ziegler, A. K. Petersen, *J. Org. Chem.* **1995**, *60*, 2666.
[13] V. Krishnamurthy, V. H. Rawal, *J. Org. Chem.* **1997**, *62*, 1572.
[14] M. Newcomb in *Radicals in Organic Synthesis, Vol. 1*, (Eds.: P. Renaud, M. P. Sibi), Wiley-VCH, Weinheim, **2001**, p. 317.
[15] D. J. Pasto, *J. Org. Chem.* **1996**, *61*, 252.
[16] D. M. Smith, A. Nicolaides, B. T. Golding, L. Radom, *J. Am. Chem. Soc.* **1998**, *120*, 10223.
[17] Recent reviews: a) J. Hartung in *Radicals in Organic Synthesis, Vol. 2* (Eds.: P. Renaud, M. P. Sibi), Wiley-VCH, Weinheim, **2001**, p. 417; b) J. Hartung, T. Gottwald, K. Spehar, *Synthesis* **2002**, 1469.
[18] For a recent review, see T. Katsuki in *Comprehensive Asymmetric Catalysis, Vol. 2* (Eds.: E. N. Jacobsen, A. Pfaltz, H. Yamamoto), Springer, Berlin, **1999**, p. 621.
[19] a) A. Johns, J. A. Murphy, *Tetrahedron Lett.* **1988**, *29*, 837; b) R. C. Gash, F. MacCorquodale, J. C. Walton, *Tetrahedron* **1989**, *45*, 5531; c) A. Johns, J. A. Murphy, M. S. Sherburn, *Tetrahedron* **1989**, *45*, 7835.
[20] V. H. Rawal, R. C. Newton, V. Krishnamurthy, *J. Org. Chem.* **1990**, *55*, 5181.
[21] a) V. H. Rawal, V. Krishnamurthy, *Tetrahedron Lett.* **1992**, *33*, 3439; b) S. Kim, J. S. Koh, *Tetrahedron Lett.* **1992**, *33*, 7391; c) V. H. Rawal, V. Krishnamurthy, A. Fabre, *Tetrahedron Lett.* **1993**, *34*, 2899.
[22] V. H. Rawal, S. Iwasa, *Tetrahedron Lett.* **1992**, *33*, 4867.
[23] a) S. Kim, S. Lee, J. S. Koh, *J. Am. Chem. Soc.* **1991**, *113*, 5106; b) S. Kim, S. K. Koh, *J. Chem. Soc. Chem. Commun.* **1992**, 1377.
[24] J. Robertson, J. N. Burrows, *Tetrahedron Lett.* **1994**, *35*, 3777.
[25] a) A. P. Breen, J. A. Murphy, *J. Chem. Soc. Chem. Commun.* **1993**, 191; b) A. P. Breen, J. A. Murphy, *J. Chem. Soc. Chem. Commun.* **1993**, 193.
[26] a) S. Kim, S. Lee, *Tetrahedron Lett.* **1991**, *32*, 6575; b) P. Galatsis, S. D. Millan, T. Faber, *J. Org. Chem.* **1993**, *58*, 1215; c) V. H. Rawal, H. M. Zhong, *Tetrahedron Lett.* **1993**, *34*, 5197; d) M. Afzal, J. C. Walton, *J. Chem. Soc. Perkin Trans. 2* **1999**, 937.
[27] a) A. G. Schultz, M. A. Holoboski, M. S. Smyth, *J. Am. Chem. Soc.* **1993**, *115*, 7904; b) A. G. Schultz, M. A. Holoboski, M. S. Smyth, *J. Am. Chem. Soc.* **1996**, *118*, 6210.
[28] a) F. E. Ziegler, A. K. Petersen, *Tetrahedron Lett.* **1996**, *37*, 809; b) F. E. Ziegler, A. K. Petersen, *J. Org. Chem.* **1994**, *59*, 2707.
[29] a) G. A. Molander, G. Hahn, *J. Org. Chem.* **1986**, *51*, 2596; b) M. Kito, T. Sakai, N. Haruta, H, Shirahama, F. Matsuda, *Synlett* **1996**, 1057; c) E. Hasegawa, K. Ishiyama, F. Fujita, T. Kato, T. Abe, *J. Org. Chem.* **1997**, *62*, 2396; d) B. H. Lee, M. F. Clothier, *J. Org. Chem.* **1997**, *62*, 1795; e) G. A. Molander, C. del Pozo Losada, *J. Org. Chem.* **1997**, *62*, 1935; f) L. A. Paquette, H. L. Wang, Z. Su, *Synthesis* **1998**, 1123; g) G. A. Molander, C. del Pozo Losada, *Tetrahedron* **1998**, *54*, 5819; h) O. Hamelin, Y. Wang, J.-P. Deprés, A. E. Greene, *Angew. Chem.* **2000**, *112*, 4484; *Angew. Chem. Int. Ed.* **2000**, *39*, 4314.
[30] G. A. Molander, S. R. Shakaya, *J. Org. Chem.* **1996**, *61*, 5885.
[31] a) J. M. Aurrecoechea, E. Iztueta, *Tetrahedron Lett.* **1995**, *36*, 7129; b) J. M. Aurrecoechea, M. Solay, *Tetrahedron Lett.* **1995**, *36*, 2501.
[32] G. A. Molander, B. E. La Belle, G. Hahn, *J. Org. Chem.* **1986**, *51*, 5259.
[33] H. S. Park, S. H. Chung, Y. H. Kim, *Synlett* **1998**, 1073.
[34] E. L. Stogryn, M. H. Gianni, *Tetrahedron Lett.* **1970**, 3025.
[35] K. S. Feldman, T. E. Fisher, *Tetrahedron* **1989**, *45*, 2969.
[36] a) K. Miura, K. Fugami, K. Oshima, K. Utimoto, *Tetrahedron Lett.* **1988**, *29*, 5135; b) K. S. Feldman, A. L. Romanelli, R. E. Ruckle, Jr., R. F. Miller, *J. Am. Chem. Soc.* **1988**, *110*, 3300.
[37] D. A. Corser, B. A. Marples, R. K. Dart, *Synlett* **1992**, 987.
[38] J. A. Murphy, C. W. Patterson, *Tetrahedron Lett.* **1993**, *34*, 867.
[39] E. Hasegawa, M. Takahashi, T. Horaguchi, *Tetrahedron Lett.* **1995**, *36*, 5215.
[40] a) S.-H. Chen, S. Huang, J. Kant, C. Fairchild, J. Wei, V. Farina, *J. Org. Chem.* **1993**, *58*, 5028; b) S.-H. Chen, S. Huang, Q. Gao, J. Golik, V. Farina, *J. Org. Chem.* **1994**, *59*, 1475.
[41] S. Kim, K. M. Lim, *J. Chem. Soc. Chem. Commun.* **1993**, 1152.
[42] a) D. Crich, X.-S. Mo, *J. Org. Chem.* **1997**, *62*, 8624; b) D. Crich, X.-S. Mo, *J. Am. Chem. Soc.* **1998**, *120*, 8298.
[43] R. Chuard, A. Giraud, P. Renaud, *Angew. Chem.* **2002**, *114*, 4499; *Angew. Chem. Int. Ed.* **2002**, *41*, 4323.
[44] For a recent review, see L. Stella in *Radicals in Organic Synthesis, Vol. 2* (Eds.: P. Renaud, M. P. Sibi), Wiley-VCH, Weinheim, **2001**, p. 407.
[45] a) H. Stamm, P. Assithianakis, B. Buchholz, R. Weiss, *Tetrahedron Lett.* **1982**, *23*, 5021; b) H. Stamm, P. Assithianakis, R. Weiss, G. Bentz, B. Buchholz, *J. Chem. Soc. Chem. Commun.* **1984**, 753; c) D. Archier-Jay, N. Besbes, A. Laurent, H. Stamm, R. Tardivel, *Tetrahedron Lett.* **1989**, *30*, 2271; d) J. Werry, H. Stamm, P.-Y. Lin, R. Falkenstein, S. Gries, H. Irngartinger, *Tetrahedron* **1989**, *45*, 5015.
[46] a) J. M. Dickinson, J. A. Murphy, *J. Chem. Soc. Chem. Commun.* **1990**, 434; b) J. M. Dickinson, J. A. Murphy, *Tetrahedron* **1992**, *48*, 1317.
[47] A. L. Schwan, M. D. Refvik, *Tetrahedron Lett.* **1993**, *34*, 4901.
[48] B. A. Marples, R. C. Toon, *Tetrahedron Lett.* **1999**, *40*, 4873.
[49] a) N. De Kimpe, D. De Smaele, P. Bogaert, *Synlett* **1994**, 287; b) N. De Kimpe, R. Julie, D. De Smaele, *J. Chem. Soc. Chem. Commun.* **1994**, 1221; c) D. De Smaele, P. Bogaert, N. De Kimpe, *Tetrahedron Lett.* **1998**, *39*, 9797; d) K. A. Tehrani, T. NguyenVan, M. Karikomi, M. Rottiers, N. De Kimpe, *Tetrahedron* **2002**, *58*, 7145.
[50] G. A. Molander, P. J. Stengel, *Tetrahedron* **1997**, *53*, 8887.
[51] O. Kitagawa, Y. Yamada, H. Fujiwara, T. Taguchi, *Angew. Chem.* **2001**, *113*, 3983; *Angew. Chem. Int. Ed.* **2001**, *40*, 3865.
[52] N. Prévost, M. Shipman, *Org. Lett.* **2001**, *3*, 2383; b) N. Prévost, M. Shipman, *Tetrahedron* **2002**, *58*, 7165.
[53] a) S. Kim, I. S. Kee, S. Lee, *J. Am. Chem. Soc.* **1991**, *113*, 9882; b) S. Kim, I. S. Kee, *Tetrahedron Lett.* **1993**, *34*, 4213; c) S. Kim, J. H. Cheong, K. S. Yoon, *Tetrahedron Lett.* **1995**, *36*, 6069; d) H. Y. Lee, S. Kim, *Chem. Commun.* **1996**, 1539; e) H. Y. Kang, W. S. Hong, S. H. Lee, K. I. Choi, H. Y. Koh, *Synlett* **1997**, 33; f) S. Kim, J. H. Cheong, *Synlett* **1997**, 947; g) H. Y. Lee, S. Lee, D. Kim, B. K. Kim, J. S. Bahn, S. Kim, *Tetrahedron Lett.* **1998**, *39*, 7713; h) G. E. Keck, T. T. Wager, S. F. McHardy, *J. Org. Chem.* **1998**, *63*, 9164; i) D. A. Ellis, D. J. Hart, L. Zhao, *Tetrahedron Lett.* **2000**, *41*, 9357.
[54] a) A. J. Birch, *J. Proc. R. Soc. N. S. W.* **1949**, *83*, 245; b) A. S. Hallsworth, H. B. Henbest, *J. Chem. Soc.* **1957**, 4604; c) H. C. Brown, S. Ikegami, J. H. Kawakami, *J. Org. Chem.* **1970**, *35*, 3243; d) R. A. Benkesser, A. Rappa, L. A. Wolsieffer, *J. Org. Chem.* **1986**, *51*, 3391.
[55] a) J. Barluenga, F. J. Fañanás, J. Villamaña, M. Yus, *J. Chem. Soc. Perkin Trans. 1* **1984**, 2685; b) J. Barluenga, J. Flórez, M. Yus, *J. Chem. Soc. Chem. Commun.* **1982**, 1153; c) J. Barluenga, J. L. Fernández-Simón, J. M. Concellón, M. Yus, *J. Chem. Soc. Chem. Commun.* **1987**, 915; d) J. Barluenga, J. L. Fernández-Simón, J. M. Concellón, M. Yus, *J. Chem. Soc. Perkin Trans. 1* **1988**, 3339.
[56] E. Bartmann, *Angew. Chem.* **1986**, *98*, 629; *Angew. Chem. Int. Ed. Engl.* **1986**, *25*, 653.
[57] A. E. Dorigo, K. N. Houk, T. Cohen, *J. Am. Chem. Soc.* **1989**, *111*, 8976.
[58] J. D. Cox, G. Pilcher, *Thermochemistry of Organic and Organometallic Compounds*, Academic Press, London, **1970**.
[59] J. I. Seeman, *Chem. Rev.* **1983**, *83*, 83.
[60] T. Cohen, I.-H. Jeong, B. Mudryk, M. Bhupathy, M. M. A. Awad, *J. Org. Chem.* **1990**, *55*, 1528.
[61] R. E. Conrow, *Tetrahedron Lett.* **1993**, *34*, 5533.

 © 2003 Wiley-VCH Verlag GmbH & Co. KGaA, Weinheim 

[62] a) A. Bachki, F. Foubeto, M. Yus, *Tetrahedron: Asymmetry* **1995**, *6*, 1907; b) A. Bachki, F. Foubeto, M. Yus, *Tetrahedron: Asymmetry* **1996**, *7*, 2997.

[63] a) T. Soler, A. Bachki L. R. Falvello, M. Yus, *Tetrahedron: Asymmetry* **1998**, *9*, 3939; b) T. Soler, A. Bachki, L. R. Falvello, F. Foubelo, M. Yus, *Tetrahedron: Asymmetry* **2000**, *11*, 493.

[64] M. Yus, T. Soler, F. Foubelo, *Tetrahedron: Asymmetry* **2001**, *12*, 801.

[65] R. Jankoska, G. L. Mhehe, H.-J. Liu, *Chem. Commun.* **1999**, 1581.

[66] a) M. Yus, R. P. Herrera, A. Guijarro, *Tetrahedron Lett.* **2001**, *42*, 3455; b) M. Yus, R. P. Herrera, A. Guijarro, *Chem. Eur. J.* **2002**, *8*, 2574.

[67] B. Mudryk, T. Cohen, *J. Org. Chem.* **1989**, *54*, 5657.

[68] I. D. Entwistle, W. W. Wood in *Comprehensive Organic Synthesis, Vol. 8* (Eds.: B. M. Trost, I. Fleming), Pergamon, Oxford, **1991**, p. 402.

[69] B. Mudryk, T. Cohen, *J. Org. Chem.* **1991**, *56*, 5760.

[70] E. Licandro, S. Maiorana, A. Papagni, A. Zanotti-Gerosa, *J. Chem. Soc. Chem. Commun.* **1992**, 1623.

[71] B. Mudryk, C. A. Shook, T. Cohen, *J. Am. Chem. Soc.* **1990**, *112*, 6389.

[72] A. Bachki, L. R. Falvello, F. Foubelo, M. Yus, *Tetrahedron: Asymmetry* **1997**, *8*, 2633.

[73] B. Mudryk, T. Cohen, *J. Am. Chem. Soc.* **1991**, *113*, 1866.

[74] D. J. Ramón, M. Yus, *Tetrahedron* **1992**, *48*, 3585.

[75] a) U. Azzena, S. Demartis, M. G. Fiori, G. Melloni, L. Pisano, *Tetrahedron Lett.* **1995**, *36*, 8123; b) U. Azzena, S. Demartis, G. Melloni, *J. Org. Chem.* **1996**, *61*, 4913.

[76] a) J. Almena, F. Foubelo, M. Yus, *Tetrahedron Lett.* **1993**, *34*, 1649; b) J. Almena, F. Foubelo, M. Yus, *J. Org. Chem.* **1994**, *59*, 3210.

[77] J. Almena, F. Foubelo, M. Yus, *Tetrahedron* **1994**, *50*, 5775.

[78] a) J. Almena, F. Foubelo, M. Yus, *Tetrahedron* **1997**, *53*, 5563; b) M. Yus, F. Foubelo, *Tetrahedron Lett.* **2001**, *42*, 2469.

[79] a) W. A. Nugent, T. V. RajanBabu, *J. Am. Chem. Soc.* **1988**, *110*, 8561; b) T. V. RajanBabu, W. A. Nugent, *J. Am. Chem. Soc.* **1989**, *111*, 4525; c) T. V. RajanBabu, W. A. Nugent, M. S. Beattie, *J. Am. Chem. Soc.* **1990**, *112*, 6408; d) T. V. RajanBabu, W. A. Nugent, *J. Am. Chem. Soc.* **1994**, *116*, 986.

[80] J. K. Kochi, D. M. Singleton, L. J. Andrews, *Tetrahedron* **1968**, *24*, 3503.

[81] For some reviews on $SmI_2$, see a) H. B. Kagan, J.-L. Namy, *Tetrahedron* **1986**, *42*, 6573; b) H. B. Kagan, *New J. Chem.* **1990**, *14*, 453; c) J. A. Soderquist, *Aldrichimica Acta* **1991**, *24*, 15; d) G. A. Molander, *Chem. Rev.* **1992**, *92*, 29; e) G. A. Molander, C. R. Harris, *Chem. Rev.* **1996**, *96*, 307; f) T. Skrydstrup, *Angew. Chem.* **1997**, *109*, 355; *Angew. Chem. Int. Ed. Engl.* **1997**, *36*, 345; g) A. Krief, A.-M. Laval, *Chem. Rev.* **1999**, *99*, 745.

[82] P. Girard, J.-L. Namy, H. B. Kagan, *J. Am. Chem. Soc.* **1980**, *102*, 2693.

[83] M. Matsukawa, T. Tabuchi, J. Inanaga, M. Yamaguchi, *Chem. Lett.* **1987**, 2101.

[84] For some examples, see a) K. B. Sharpless, M. A. Umbreit, M. T. Nieh, T. C. Flood, *J. Am. Chem. Soc.* **1972**, *94*, 6538; b) H. Su, L. Walder, Z.-d. Zhang, R. Scheffold, *Helv. Chim. Acta* **1988**, *71*, 1073; c) P. Bonhote, R. Scheffold, *Helv. Chim. Acta* **1991**, *74*, 1425.

[85] R. Schobert, *Angew. Chem.* **1988**, *100*, 869; *Angew. Chem. Int. Ed. Engl.* **1988**, *27*, 855.

[86] M. Berry, S. G. Davies, M. L. H. Green, *J. Chem. Soc. Chem. Commun.* **1978**, 99.

[87] O. R. Martin, R. J. Rafka, W. A. Szarek, *Carbohydr. Res.* **1989**, *185*, 77.

[88] J. S. Yadav, T. Shekharam, V. R. Gadgil, *J. Chem. Soc. Chem. Commun.* **1990**, 843.

[89] V. S. Martin, S. S. Woodward, T. Katsuki, Y. Yamada, M. Ikeda, K. B. Sharpless, *J. Am. Chem. Soc.* **1981**, *103*, 6237; for a review, see R. A. Johnson, K. B. Sharpless in *Catalytic Asymmetric Synthesis*, 2nd ed. (Ed.: I. Ojima), Wiley-VCH, Weinheim, **2000**, p. 231.

[90] a) C. Hardouin, E. Doris, B. Rousseau, C. Mioskowski, *Org. Lett.* **2002**, *4*, 1151; b) C. Hardouin, E. Doris, B. Rousseau, C. Mioskowski, *J. Org. Chem.* **2002**, *67*, 6571.

[91] T. Golakoti, J. Ogino, C. E. Heltzel, T. L. Husebo, C. M. Jensen, L. K. Larsen, G. M. L. Petterson, R. E. Moore, S. L. Mooberry, T. H. Corbett, F. A. Valeriote, *J. Am. Chem. Soc.* **1995**, *117*, 12030.

[92] For a review, see S. Murai, T. Murai, S. Kato in *Comprehensive Organic Synthesis, Vol. 8* (Eds.: B. M. Trost, I. Fleming), Pergamon, Oxford, **1991**, p. 871.

[93] R. J. Enemærke, G. H. Hjøllund, K. Daasbjerg, T. Skrydstrup, *C. R. Acad. Sci. Ser. IIc* **2001**, *4*, 435.

[94] Y. Handa, J. Inanaga, *Tetrahedron Lett.* **1987**, *28*, 5717.

[95] S. Grimme, M. Gerenkamp, C. Mück-Lichtenfeld, A. Gansäuer, unpublished results.

[96] G. S. Hammond, *J. Am. Chem. Soc.* **1955**, *77*, 334.

[97] A. G. Myers, R. Glatthar, M. Hammond, P. M. Harrington, E. Y. Kuo, J. Liang, S. E. Schaus, Y. Wu, J.-N. Xiang, *J. Am. Chem. Soc.* **2002**, *124*, 5380.

[98] S. Weigand, R. Brückner, *Synlett* **1997**, 225.

[99] J. S. Yadav, D. Srinivas, *Chem. Lett.* **1997**, 905.

[100] K. B. Jørgensen, T. Suenaga, T. Nakata, *Tetrahedron Lett.* **1999**, *40*, 8855.

[101] T. K. Chakraborty, S. Dutta, *J. Chem. Soc. Perkin Trans. 1* **1997**, 1257.

[102] T. K. Chakraborty, S. Das, *Tetrahedron Lett.* **2002**, *43*, 2313.

[103] J. M. Finan, Y. Kishi, *Tetrahedron Lett.* **1982**, *23*, 2719.

[104] C. Hardouin, F. Chevallier, B. Rousseau, E. Doris, *J. Org. Chem.* **2001**, *66*, 1046.

[105] a) R. L. Halterman, *Chem. Rev.* **1992**, *92*, 965; b) R. L. Halterman in *Metallocenes, Vol. 1* (Eds.: A. Togni, R. L. Halterman), Wiley-VCH, Weinheim, **1998**, p. 455.

[106] For recent reviews, see a) P. Renaud, M. Gerster, *Angew. Chem.* **1998**, *110*, 2704; *Angew. Chem. Int. Ed.* **1998**, *37*, 2562; b) B. P. Roberts, *Chem. Soc. Rev.* **1999**, *28*, 35; c) M. P. Sibi, N. A. Porter, *Acc. Chem. Res.* **1999**, *32*, 163; d) M. P. Sibi in *Radicals in Organic Synthesis, Vol. 1* (Eds.: P. Renaud, M. P. Sibi), Wiley-VCH, Weinheim, **2001**, p. 461.

[107] a) A. Fürstner, *Pure Appl. Chem.* **1998**, *70*, 1071; b) A. Fürstner, *Chem. Eur. J.* **1998**, *4*, 567.

[108] A. Fürstner, A. Hupperts, *J. Am. Chem. Soc.* **1995**, *117*, 4468.

[109] a) A. Fürstner, N. Shi, *J. Am. Chem. Soc.* **1996**, *118*, 2533; b) A. Fürstner, N. Shi, *J. Am. Chem. Soc.* **1996**, *118*, 12349.

[110] a) T. Hirao, T. Hasegawa, Y. Muguruma, I. Ikeda, *J. Org. Chem.* **1996**, *61*, 366; b) T. Hirao, *Synlett* **1999**, 175.

[111] a) R. Nomura, T. Matsuno, T. Endo, *J. Am. Chem. Soc.* **1996**, *118*, 11666; b) E. J. Corey, G. Z. Zheng, *Tetrahedron Lett.* **1997**, *38*, 2045.

[112] a) A. Gansäuer, *Chem. Commun.* **1997**, 457; b) A. Gansäuer, *Synlett* **1997**, 363; c) A. Gansäuer, M. Moschioni, D. Bauer, *Eur. J. Org. Chem.* **1998**, 1923.

[113] a) M. Bandini, P. G. Cozzi, P. Melchiorre, A. Umani-Ronchi, *Angew. Chem.* **1999**, *111*, 3558; *Angew. Chem. Int. Ed.* **1999**, *38*, 3357; b) M. Bandini, P. G. Cozzi, A. Umani-Ronchi, *Angew. Chem.* **2000**, *112*, 2417; *Angew. Chem. Int. Ed.* **2000**, *39*, 2327.

[114] a) A. Gansäuer, *Synlett* **1998**, 810; b) A. Gansäuer, S. Narayan, *Adv. Synth. Catal.* **2002**, *344*, 465.

[115] a) A. Gansäuer, M. Pierobon, H. Bluhm, *Angew. Chem.* **1998**, *110*, 107; *Angew. Chem. Int. Ed.* **1998**, *37*, 101; b) A. Gansäuer, H. Bluhm, *Chem. Commun.* **1998**, 2143; c) A. Gansäuer, H. Bluhm, M. Pierobon, *J. Am. Chem. Soc.* **1998**, *120*, 12849; for the realization of this concept in pinacol couplings, see d) A.

Gansäuer, D. Bauer, *J. Org. Chem.* **1998**, *63*, 2070; e) A. Gansäuer, D. Bauer, *Eur. J. Org. Chem.* **1998**, 2673; for reviews, see f) A. Gansäuer, *Synlett* **1998**, 801; g) A. Gansäuer, S. Narayan, *Adv. Synth. Catal.* **2002**, *344*, 465.

[116] a) A. Gansäuer, T. Lauterbach, H. Bluhm, M. Noltemeyer, *Angew. Chem.* **1999**, *111*, 3113; *Angew. Chem. Int. Ed.* **1999**, *38*, 2909; b) A. Gansäuer, H. Bluhm, T. Lauterbach, *Adv. Synth. Catal.* **2001**, *343*, 785; c) A. Gansäuer, H. Bluhm, B. Rinker, S. Narayan, M. Schick, T. Lauterbach, M. Pierobon, *Chem. Eur. J.* **2003**, *9*, 531.

[117] E. Cesarotti, H. B. Kagan, R. Goddard, C. Krüger, *J. Organomet. Chem.* **1978**, *162*, 297.

[118] R. L. Halterman, K. P. C. Vollhardt, *Organometallics* **1988**, *7*, 883.

[119] J. K. Whitesell, *Chem. Rev.* **1992**, *92*, 953.

[120] A. Gansäuer, H. Bluhm, M. Pierobon, M. Keller, *Organometallics* **2001**, *20*, 914.

[121] For a recent review, see E. N. Jacobsen, *Acc. Chem. Res.* **2000**, *33*, 421.

[122] a) C. A. Merlic, D. Xu, *J. Am. Chem. Soc.* **1991**, *113*, 9855; b) C. A. Merlic, D. Xu, M. C. Nguyen, V. Truong, *Tetrahedron Lett.* **1993**, *34*, 227.

[123] K. H. Dötz, E. Gomes da Silva, *Tetrahedron* **2000**, *56*, 8291.

[124] J. D. Parrish, R. D. Little, *Org. Lett.* **2002**, *4*, 1439.

[125] B. Giese, *Angew. Chem.* **1989**, *101*, 993; *Angew. Chem. Int. Ed. Engl.* **1989**, *28*, 969.

[126] B. Giese, B. Kopping, T. Göbel, J. Dickhaut, G. Thoma, K. J. Kulicke, F. Trach in *Organic Reactions* (Ed.: L. A. Paquette), Wiley, New York, **1996**, p. 301.

[127] J. E. Baldwin, *J. Chem. Soc. Chem. Commun.* **1976**, 734.

[128] a) A. L. J. Beckwith, *Tetrahedron* **1981**, *37*, 3073; b) D. P. Curran, D. M. Rakiewicz, *Tetrahedron* **1985**, *41*, 3943; c) D. C. Spellmeyer, K. N. Houk, *J. Org. Chem.* **1987**, *52*, 959; d) T. V. RajanBabu, *Acc. Chem. Res.* **1991**, *24*, 139.

[129] T. B. Lowinger, L. Weiler, *Can. J. Chem.* **1990**, *68*, 1636.

[130] a) D. L. J. Clive, S. R. Magnusson, *Tetrahedron Lett.* **1995**, *36*, 15; b) D. L. J. Clive, S. R. Magnusson, H. W. Manning, D. L. Mayhew, *J. Org. Chem.* **1996**, *61*, 2095.

[131] a) G. Maiti, S. C. Roy, *J. Chem. Soc. Perkin Trans. 1* **1996**, 403; b) P. K. Mandel, G. Maiti, S. C. Roy, *J. Org. Chem.* **1998**, *63*, 2829; c) P. K. Mandal, S. C. Roy, *Tetrahedron* **1999**, *55*, 11395; d) K. K. Rana, C. Guin, S. C. Roy, *Tetrahedron Lett.* **2000**, *41*, 9337; e) K. K. Rana, C. Guin, S. C. Roy, *Synlett* **2001**, 1249; f) S. C. Roy, K. K. Rana, C. Guin, *J. Org. Chem.* **2002**, *67*, 3242.

[132] a) A. F. Barrero, J. M. Cuerva, M. M. Herrador, M. V. Valdivia, *J. Org. Chem.* **2001**, *66*, 4074; b) A. F. Barrero, J. M. Cuerva, E. J. Alvarez-Manzaneda, J. E. Oltra, R. Chahboun, *Tetrahedron Lett.* **2002**, *43*, 2793.

[133] J. Schwartz, J. A. Labinger, *Angew. Chem.* **1976**, *88*, 402; *Angew. Chem. Int. Ed. Engl.* **1976**, *15*, 333.

[134] a) Y. Haruo, T. Hasegawa, H. Tanaka, T. Takahashi, *Synlett* **2001**, 1935; b) K. Nakai, M. Kamoshita, T. Doi, H. Yamada, T. Takahashi, *Tetrahedron Lett.* **2001**, *42*, 7855.

[135] A. Fernández-Mateos, E. Martín de la Nava, G. P. Coca, A. R. Silvo, R. R. González, *Org. Lett.* **1999**, *1*, 607.

[136] a) G. Ruano, M. Grande, J. Anaya, *J. Org. Chem.* **2002**, *67*, 8243; b) J. Anaya, A. Fernández-Mateos, M. Grande, J. Martiáñez, G. Ruano, M. R. Rubio-González, *Tetrahedron* **2003**, *59*, 241; c) G. Ruano, J. Martiáñez, M. Grande, J. Anaya, J. Org. Chem. *2003*, **68**, 2024.

[137] a) A. Gansäuer, M. Pierobon, *Synlett* **2000**, 1357; b) A. Gansäuer, M. Pierobon, H. Bluhm, *Synthesis* **2001**, 2500.

[138] A. Gansäuer, T. Lauterbach, unpublished results.

[139] a) C. Walling, *Free Radical Reactions in Solution*, Wiley, New York, **1957**; b) V. Paul, B. P. Roberts, C. R. Willis, *J. Chem. Soc. Perkin Trans. 2* **1989**, 1953.

[140] J. Robertson, J. Pillai, R. K. Lush, *Chem. Soc. Rev.* **2001**, *30*, 94.

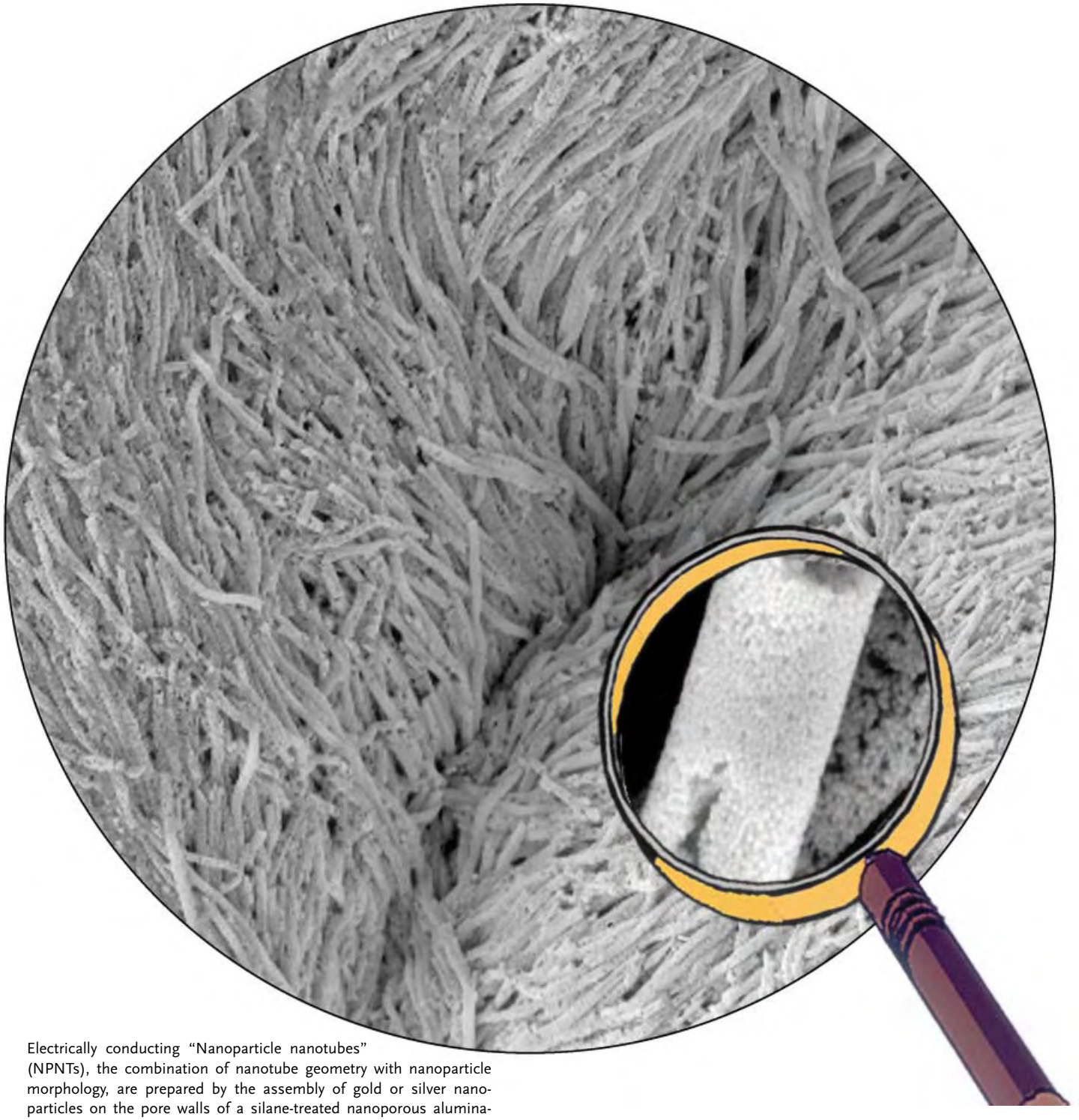
[141] a) L. F. Tietze, U. Beifuß, *Angew. Chem.* **1993**, *105*, 137; *Angew. Chem. Int. Ed. Engl.* **1993**, *32*, 131; b) L. F. Tietze, *Chem. Rev.* **1996**, *96*, 115; c) M. Malacria, *Chem. Rev.* **1996**, *96*, 289.

[142] See, for example, a) G. Stork, P. M. Sher, *J. Am. Chem. Soc.* **1983**, *105*, 6765; b) G. Stork, P. M. Sher, *J. Am. Chem. Soc.* **1986**, *108*, 303; c) G. Stork, *Bull. Chem. Soc. Jpn.* **1988**, *61*, 149.

[143] A. Gansäuer, M. Pierobon, H. Bluhm, *Angew. Chem.* **2002**, *114*, 3341; *Angew. Chem. Int. Ed.* **2002**, *41*, 3206.

 © 2003 Wiley-VCH Verlag GmbH & Co. KGaA, Weinheim 

# Communications



Electrically conducting "Nanoparticle nanotubes" (NPNTs), the combination of nanotube geometry with nanoparticle morphology, are prepared by the assembly of gold or silver nanoparticles on the pore walls of a silane-treated nanoporous alumina-membrane template. Self-sustained NPNTs can be obtained by dissolving the template. For more information, see the Communication by Rubinstein and co-workers on the following pages.


**DOI: 10.1002/anie.200352216**
© 2003 Wiley-VCH Verlag GmbH & Co. KGaA, Weinheim

Nanostructures

# Nanoparticle Nanotubes**

*Michal Lahav, Tali Sehayek, Alexander Vaskevich, and Israel Rubinstein**

In recent years there has been considerable interest in the synthesis of structured materials and control of their shape and geometry on different length scales, from molecular to macroscopic.[1,2] Special attention has been given to materials structured on the nanometer scale, representing a step down in size from present technology. Two prominent components of such systems are nanoparticles[3,4] and nanotubes.[5,6]

Nanoparticles, which are particularly attractive building blocks for nanomaterial architectures,[7] can be prepared from a variety of materials including metals,[8] semiconductors, and polymers.[4] Their dimensions, typically several to hundred nm, provide unique flexibility in the synthesis of composite nanomaterials. Examples include controlled aggregation in solution,[9] as well as binding to templates such as macromolecules,[10] and to solid substrates of planar[3,11] or curved[12] geometries. By using such methods a variety of self-sustained structures, including hollow spheres,[13] rods,[14] and chainlike multiparticle assemblies,[15] have been obtained. Binding of (sub)monolayer amounts of Au colloids to the pore walls of nanoporous alumina membranes was reported.[16,17]

Nanotubes of various kinds have been prepared in the last decade, starting from the discovery of carbon nanotubes by Iijima.[18] Recently other types of nanotubes have been produced, including metallic (e.g., Au), [19] other inorganic (e.g., $TiO_2$, $HfS_2$, $V_7O_{16}$, CdSe, $MoS_2$),[5,20–22] and polymeric (e.g., polyaniline, polyacrylonitrile) nanotubes.[23] These are synthesized by several methods,[5] including, for example, hydrothermal synthesis, surfactant-assisted synthesis, and decomposition in $H_2$ or electron radiation.

A common method for producing nanotubes is template synthesis in nanoporous membranes.[24,25] Template synthesis of nanotubes is achieved by using different strategies[26] such as electrochemical deposition, electroless deposition, polymerization, sol–gel deposition, or chemical vapour deposition (CVD) in the nanoporous templates.

Herein we present a novel synthetic procedure leading to a new kind of porous, high-surface-area "nanoparticle nanotube" (NPNT). The NPNTs are prepared by assembly of gold (or silver) nanoparticles on the pore walls of a silane-treated nanoporous alumina membrane template, accompanied by spontaneous room-temperature coalescence of the bound nanoparticles. Under well-defined conditions this process results in a solid tubular structure spanning the entire pore length. Self-sustained NPNTs, which preserve the nanoparticle morphology, are obtained by template dissolution.

Alumina membranes (about 220 nm average pore diameter) were pretreated with 3-aminopropyl trimethoxysilane (APMS) according to a reported procedure.[27] The silyl groups react with the hydroxyl groups on the alumina surface, thus leaving the amine groups available for binding Au nanoparticles. Au colloid solution ($14 \pm 2$ nm diameter, citrate stabilized, prepared according to a literature procedure,[28] but with five times the original concentrations of the starting materials) was then passed through the modified membrane pores by vacuum suction (Figure 1). Au nanoparticles interact with the amine groups of the APMS and

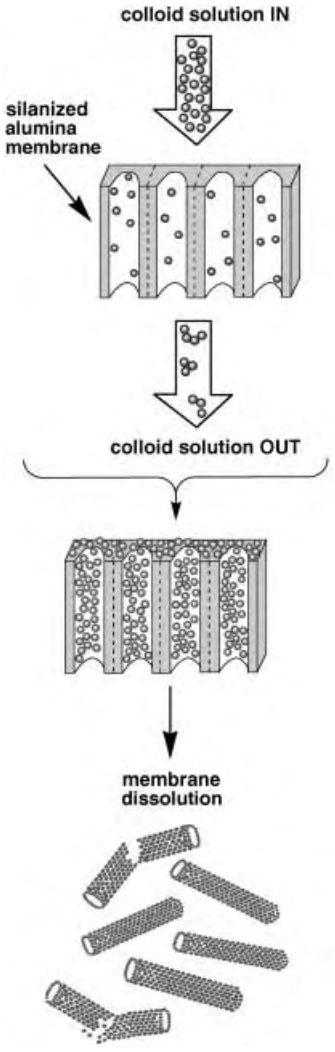



***Figure 1.*** Schematic diagram showing the preparation of metal NPNTs. A nanoparticle solution is passed through a silanized alumina membrane, followed by membrane dissolution (dimensions are not to scale).

[*] Prof. I. Rubinstein, Dr. M. Lahav, T. Sehayek, Dr. A. Vaskevich
Department of Materials and Interfaces
Weizmann Institute of Science
Rehovot 76100 (Israel)
Fax: (+972) 8-934-4137
E-mail: israel.rubinstein@weizmann.ac.il

[**] We thank Dr. R. Popovitz-Biro for assisting with the TEM imaging. Support from the Minerva Foundation, Munich, and the Faivovich Foundation (Weizmann Institute), is gratefully acknowledged. A.V. acknowledges support from the Kamea Program, Israel Ministry of Absorption.

Supporting information for this article is available on the WWW under http://www.angewandte.org or from the author.

 © 2003 Wiley-VCH Verlag GmbH & Co. KGaA, Weinheim DOI: 10.1002/anie.200352216 

become immobilized on the pore walls, similar to the process observed on flat surfaces.[3,11] The Au nanoparticle arrangement in the membrane pores is visualized by cross-section environmental scanning electron microscope (ESEM) imaging of the membrane following colloid binding, as shown in Figure 2a. The nanoparticles are seen as bright spots on the pore walls. Note that no nanoparticle immobilization is observed when the same process is carried out with membranes that have not been silanized.

In marked contrast with Au nanoparticle binding to amino-terminated flat surfaces in stagnant solutions,[3,11] immobilization on the pore walls under the present conditions is not restricted to the first layer of nanoparticles. Continued flow of the colloid solution through the pores promotes additional nanoparticle binding and formation of a multilayer structure. The immobilization is assumed to involve aggregation of surface-confined Au nanoparticles accompanied by spontaneous coalescence (possibly during membrane drying) to yield continuous, solid NPNTs. Although the NPNT formation mechanism is not yet fully understood, partial stripping of the citrate stabilizing shell on the Au nanoparticles may be the primary step in the immobilization, rearrangement and coalescence.[13,15,29]

Dissolution of the colloid-treated (and dried) alumina membrane in 1.0 M NaOH followed by removal of the solution led to the release of solid, self-sustained Au NPNTs. Figure 2b–d and Figure 3 show ESEM and transmission electron microscope (TEM) images, respectively, of the free-standing nanotubes, presented at different magnifications. The nanotubes are composed of a continuous, multilayered nanoparticle array. Some nanotubes are partly bent as a result of the dissolution and drying (Figure 2b, c), which indicates limited mechanical strength. Defects are frequently seen along the nanotubes, but the geometrical shape is preserved. Electron diffraction (not shown) produced a pattern characteristic of an assembly of randomly-oriented Au crystallites.

The process of NPNT formation can be observed by passing an increasing volume (5–18 mL) of Au nanoparticle solution through the surface-modified alumina membrane. Figure 4a–c presents ESEM images taken at different stages

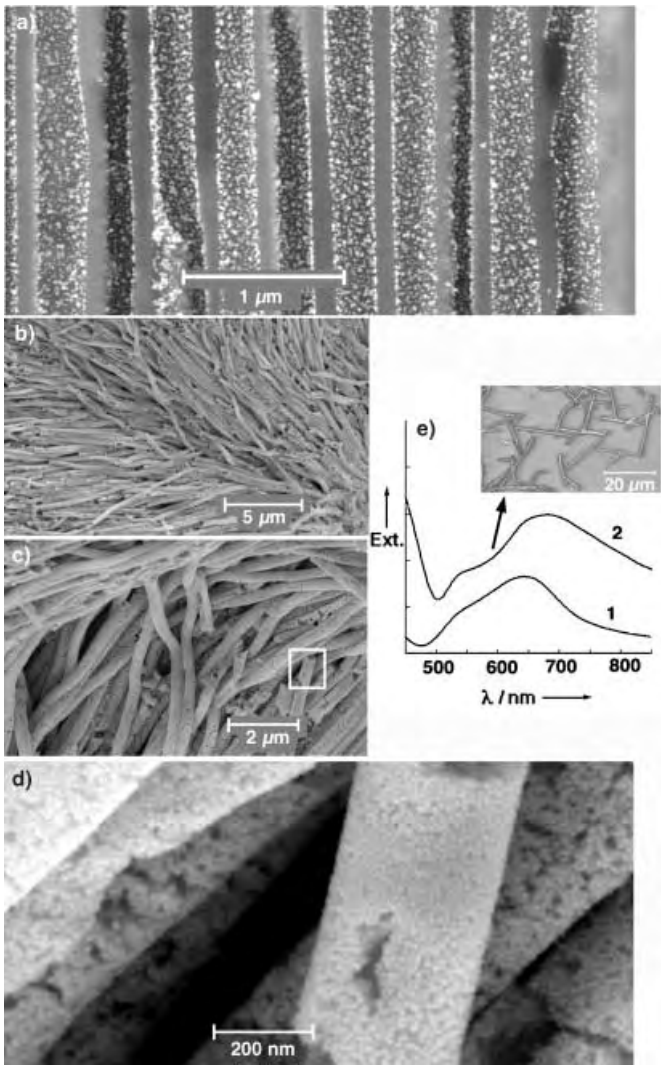



***Figure 2.*** a) ESEM image showing the cross-section of a silanized nanoporous alumina membrane after passing a Au nanoparticle solution and drying. b–d) ESEM images of Au NPNTs obtained after alumina membrane dissolution in 1.0 M NaOH, shown at different magnifications. d) A magnified image of the area marked in (c), showing the arrangement of individual nanoparticles. e) Transmission UV/Vis spectrum (extinction versus wavelength) of Au NPNTs in solution (1) and on a glass slide (2). Inset: ESEM image of the sample used for obtaining spectrum (2).

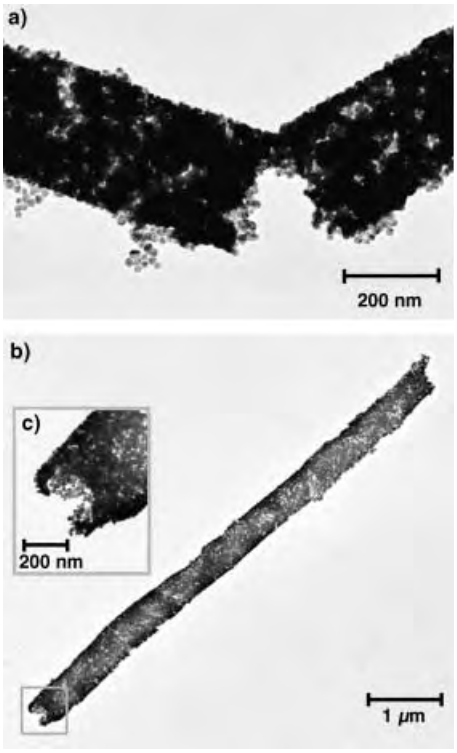



***Figure 3.*** a) and b): TEM images of NPNTs obtained after alumina membrane dissolution in 1.0 M NaOH, shown at different magnifications. c) A magnified image of the area marked in (b), showing the tubular structure.

 © 2003 Wiley-VCH Verlag GmbH & Co. KGaA, Weinheim 

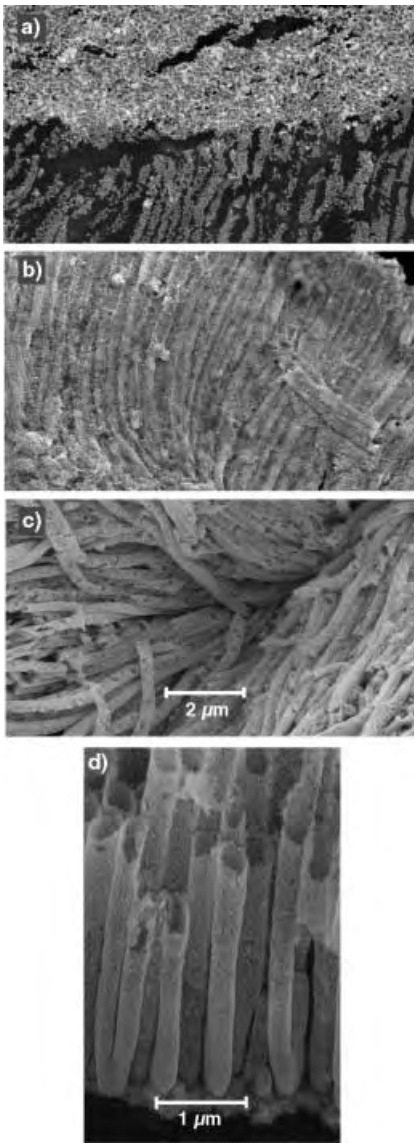



***Figure 4.*** NPNT development and modification. (a–c) ESEM images showing the progress of Au NPNT formation after passing a) 5 mL, b) 9 mL, c) 18 mL of Au nanoparticle solution, followed by drying and membrane dissolution. d) ESEM image of Au NPNTs after Cu electrodeposition and membrane dissolution.

of NPNT formation, obtained after membrane dissolution. At the initial stage (5 mL) most of the nanoparticles appeared as random aggregates (Figure 4a, top), with sporadic appearance of elongated structures that survived membrane dissolution (Figure 4a, bottom). When more nanoparticles (9 mL) were passed through the membrane, a rather fragile nanotube arrangement resulted (Figure 4b), whereas when the maximal amount in these experiments was used (18 mL), fully developed, mechanically stable, multilayered NPNTs were produced (Figure 4c).

In contrast with the system reported by Steinhart et al.[30] in which annealing was necessary to convert Pd nanoparticles formed on membrane walls to nanotubes, the opposite effect was observed with the spontaneously formed Au NPNTs. Hence, membranes with fully grown NPNTs were annealed (220 °C, 17 h) followed by membrane dissolution. ESEM imaging (not shown) revealed severely damaged nanotube fractions, which arise from local conversion of nanoparticle aggregates into large, separated lumps.

Transmission UV/Vis spectroscopy of the NPNTs was carried out both in solution (Figure 2e, line 1) and with a sample dried on a glass slide (Figure 2e, line 2). The weak extinction band at about 530 nm is attributed to a small amount of free nanoparticles. The more intense band, attributed to the NPNTs, appears at longer wavelengths, characteristic of nanoparticle aggregates. The latter is shifted more to the red in the dry sample (about 675 nm) versus the wet sample (about 645 nm) and this shift is due to the different media, different orientations of the nanotubes in the solution and on the slide, and possibly a structural change (additional aggregation) upon nanotube drying. The dry sample was also imaged by ESEM (Figure 2e, inset) to confirm the presence of Au NPNTs on the glass slide.

The NPNTs are electrically conductive and show perfect ohmic behavior with no hysteresis. A resistance of about 0.3 ohm·cm$^2$ was measured across the nanoparticle-modified membrane (see Experimental Section); the apparent specific resistivity, $\rho \approx 6$ ohm·cm, was calculated by using the overall NPNT wall thickness and ignoring the interconnected nanoparticulate structure. The NPNT electrical conductivity can be used to modify their chemical, structural, and mechanical properties by using electrodeposition. In the present case a small amount of copper was electrodeposited on the NPNTs following Au colloid immobilization and prior to membrane dissolution.[31] The presence of Cu along the tubes was confirmed by energy dispersive spectroscopy (EDS) measurements (see Supporting Information). Figure 4d shows ESEM side view of the hybrid NPNTs after membrane dissolution. A well-ordered assembly of continuous, rigid, hollow, Cu-covered nanotubes is observed. The Cu-modified NPNTs are considerably more robust than the pristine Au NPNTs, as evident in the cross-sectional images (compare Figure 2a, with Supporting Information). Careful inspection suggests that most of the defects are "repaired" by the deposited Cu, while the basic nanoparticulate structure is maintained.

The procedure for producing Au NPNTs can be adopted with other metals, by replacing the Au colloid solution with, for example, a solution of citrate-stabilized Ag nanoparticles. This results in self-sustained Ag NPNTs (see Supporting Information).

In conclusion, a novel procedure is presented, providing metal "nanoparticle nanotubes" (NPNTs) that combine nanotube geometry with nanoparticle morphology and properties (e.g., high surface-to-volume ratio; surface plasmon optical absorption). The process involves passing a metal (Au, Ag) colloid solution in the pores of a surface-modified nanoporous alumina membrane, followed by spontaneous room-temperature coalescence of the surface-confined nanoparticles to yield solid, multilayered nanotubes. These nanotubes can be obtained as free-standing NPNTs by dissolution of the membrane template. The mechanism of NPNT formation is not yet fully understood and is currently being studied. The new process opens the way to the synthesis of novel kinds of nanomaterials that have a tube geometry, high

 © 2003 Wiley-VCH Verlag GmbH & Co. KGaA, Weinheim 

surface area, mechanical stability, electrical conductivity, and distinct optical properties. The synthesis of various new types of NPNTs, for example, other metal NPNTs, as well as more complicated structures such as bimetallic NPNTs, is being investigated.

Modification of the NPNT properties can be achieved by exploiting their electrical conductivity for electrochemical deposition on the nanotube surface, as exemplified here with Cu coating. This, as well as possible chemical (electroless) deposition, enables formation of composite NPNT systems that have modified mechanical, electrical and optical properties, as well as diverse surface chemistries. These unique properties of NPNTs may be particularly useful in catalysis and electrocatalysis,[32] as well as in sensing, microfluidic, chemistry-on-a-chip, binding of biological molecules, and future device applications.

## Experimental Section

NPNT synthesis: Au NPNTs were prepared as follows: 18 mL (unless otherwise specified) of Au nanoparticle solution were passed by vacuum suction through the silanized alumina membrane (Whatman, Anodisc 0.2 μm) by using the following procedure: (1) 10 mL of the red nanoparticle solution was passed through the membrane (note: the first 5–6 mL coming out of the membrane are colorless, the remaining amount comes out colored). (2) The membrane was sonicated for 4 min. (3) A few mL of triply distilled water were passed through the membrane. (4) An additional 8 mL of Au nanoparticle solution was passed through the membrane. (5) Distilled water was passed through the membrane (an indication that the nanotubes are not blocked). The membranes were then dried under a stream of nitrogen. To obtain self-sustained NPNTs the alumina membrane was dissolved in 1.0 M NaOH over 2.5 h then washed with triply distilled water.

Samples for UV/Vis spectroscopy: A NPNT solution was prepared by dissolving the colloid-treated alumina membrane in 1.0 M NaOH, followed by removal of the solution and redispersion of the NPNTs in water. The dry sample was prepared by applying a drop of the NPNT solution on a cleaned microscope cover slide followed by evaporation of the solution.

NPNT conductivity: A gold contact layer (100 nm thick) was evaporated on both faces of the Au nanoparticle-modified membrane, avoiding the membrane edges. The membrane resistivity was then measured using a cyclic voltage scan. An apparent specific resistivity ($\rho$) of the NPNTs was estimated by using the following values: a measured resistance of 0.3 ohm·cm$^2$ across the membrane; a membrane pore density of $10^9$ cm$^{-2}$; a pore diameter of 220 nm; a membrane thickness of 60 μm; a NPNT wall thickness (estimated from ESEM images, ignoring the nanoparticluate morphology) of 40 nm. A control experiment with a similar membrane that was not exposed to a Au nanoparticle solution showed infinite resistance.

Cu electrodeposition: The membrane was mounted in a special holder, leaving the "outlet" side (bottom side of the membrane in Figure 1, middle) in contact with a $Cu^{2+}$ solution (0.3 M $CuSO_4$ + 0.1 M $H_2SO_4$).[31] Electrical connection (cathode) was established by contacting the "inlet" side of the alumina membrane, covered with bound Au nanoparticles (Figure 1). A standard electrochemical cell was used with a $K_2SO_4$-saturated $Hg/Hg_2SO_4$ (MSE) reference electrode and a Pt counter electrode. Electrodeposition was carried out at −0.8 V (versus MSE) for 60 s.

Received: June 24, 2003
Revised: September 10, 2003 [Z52216]
Published Online: October 23, 2003

**Keywords:** gold · membranes · nanoparticles · nanotubes · silver · template synthesis

[1] D. L. Feldheim, C. D. Keating, *Chem. Soc. Rev.* **1998**, *27*, 1–12.
[2] S. I. Stupp, V. LeBonheur, K. Walker, L. S. Li, K. E. Huggins, M. Keser, A. Amstutz, *Science* **1997**, *276*, 384–389.
[3] R. G. Freeman, K. C. Grabar, K. J. Allison, R. M. Bright, J. A. Davis, A. P. Guthrie, M. B. Hommer, M. A. Jackson, P. C. Smith, D. G. Walter, M. J. Natan, *Science* **1995**, *267*, 1629–1632.
[4] A. N. Shipway, E. Katz, I. Willner, *Chemphyschem* **2000**, *1*, 18–52.
[5] C. N. R. Rao, M. Nath, *J. Chem. Soc. Dalton Trans.* **2003**, *1*, 1–25.
[6] R. Tenne, A. K. Zettl, *Top. Appl. Phys.* **2001**, *80*, 81–112.
[7] P. C. Hidber, W. Helbig, E. Kim, G. M. Whitesides, *Langmuir* **1996**, *12*, 1375–1380.
[8] D. L. Feldheim, C. A. Foss in " *Metal Nanoparticles*", Marcel Dekker, New York-Basel **2002**, p. 338.
[9] C. A. Mirkin, R. L. Letsinger, R. C. Mucic, J. J. Storhoff, *Nature* **1996**, *382*, 607–609.
[10] R. Djalali, Y. Chen, H. Matsui, *J. Am. Chem. Soc.* **2002**, *124*, 13660–13661.
[11] A. Doron, E. Katz, I. Willner, *Langmuir* **1995**, *11*, 1313–1317.
[12] A. Dokoutchaev, J. T. James, S. C. Koene, S. Pathak, G. K. S. Prakash, M. E. Thompson, *Chem. Mater.* **1999**, *11*, 2389–2399.
[13] S. Chah, J. H. Fendler, J. Yi, *J. Colloid Interface Sci.* **2002**, *250*, 142–148.
[14] J. T. Hu, T. W. Odom, C. M. Lieber, *Acc. Chem. Res.* **1999**, *32*, 435–445.
[15] Z. Y. Tang, N. A. Kotov, M. Giersig, *Science* **2002**, *297*, 237–240.
[16] T. Hanaoka, H. P. Kormann, M. Kroll, T. Sawitowski, G. Schmid, *Eur. J. Inorg. Chem.* **1998**, 807–812.
[17] S. M. Marinakos, L. C. Brousseau, A. Jones, D. L. Feldheim, *Chem. Mater.* **1998**, *10*, 1214–1219.
[18] S. Iijima, *Nature* **1991**, *354*, 56.
[19] M. Wirtz, M. Parker, Y. Kobayashi, C. R. Martin, *Chem. Eur. J.* **2002**, *8*, 3573–3578.
[20] T. Kasuga, M. Hiramatsu, A. Hoson, T. Sekino, K. Niihara, *Langmuir* **1998**, *14*, 3160–3163.
[21] M. Worle, F. Krumeich, F. Bieri, H. J. Muhr, R. Nesper, *Z. Anorg. Allg. Chem.* **2002**, *628*, 2778–2784.
[22] R. Tenne, *Colloids Surf., A,* **2002**, *208*, 83–92.
[23] L. Feng, S. H. Li, H. J. Li, J. Zhai, Y. L. Song, L. Jiang, D. B. Zhu, *Angew. Chem.* **2002**, *114*, 1269–1271; *Angew. Chem. Int. Ed.* **2002**, *41*, 1221–1223.
[24] C. R. Martin in *Electroanalytical Chemistry, Vol. 21* (Eds.: A. J. Bard, I. Rubinstein), Marcel Dekker, New York **1999**, pp. 1–74.
[25] C. John, C. R. Martin, *J. Mater. Chem.* **1997**, *7*, 1075–1087.
[26] R. A. Caruso, J. H. Schattka, A. Greiner, *Adv. Mater.* **2001**, *13*, 1577–1579.
[27] C. A. Goss, D. H. Charych, M. Majda, *Anal. Chem.* **1991**, *63*, 85–88.
[28] J. Turkevich, P. C. Stevenson, J. Hiller, *Discuss. Faraday Soc.* **1951**, *11*.
[29] N. A. Alcantar, C. Park, J. M. Pan, J. N. Israelachvili, *Acta Mater.* **2003**, *51*, 31–47.
[30] M. Steinhart, Z. Jia, A. K. Schaper, R. B. Wehrspohn, U. Gösele, J. H. Wendroff, *Adv. Mater.* **2003**, *15*, 706–709.
[31] T. Sehayek, A. Vaskevich, I. Rubinstein, *J. Am. Chem. Soc.* **2003**, *125*, 4718–4719.
[32] A. Cho, *Science* **2003**, *299*, 1684–1685.

 © 2003 Wiley-VCH Verlag GmbH & Co. KGaA, Weinheim 

Vesicular Microarrays

# Self-Assembled Microarrays of Attoliter Molecular Vessels**

*Dimitrios Stamou,* Claus Duschl, Emmanuel Delamarche, and Horst Vogel**

Spatial compartmentalization is a prerequisite for the creation of living matter.[1] Without the existence of clearly defined borders,[2] differentiation and diversity at the cellular level would not be possible. Most scientific disciplines that deal with dissolved molecules are concerned with the same problem of subdividing solutions into miniaturized autonomous units, either to increase the functional complexity of a system,[3] reduce reagent consumption,[4] monitor fast chemical kinetics,[5] or even to study single molecules.[6] We describe a method that allows the parallel isolation of attoliter ($1\ aL = 10^{-18}\ L$) volumes of experimental solutions and their self-assembly into ordered arrays on surfaces with 100-nm precision. By using lipid-bilayer vesicles[1] as molecular shuttles,[7] we transported and localized molecules encapsulated in their aqueous interior or embedded in the lipid matrix. The site-selective immobilization of intact single vesicles (SVs) was mediated by patterns of receptor molecules defined by microcontact printing (μCP)[8] on glass. One-step directed self-assembly (SA)[9] produced arrays of around $10^6$ volume elements per $mm^2$ within minutes. As shown below, this approach can create random arrays of vesicles of varied content that may serve as libraries of miniaturized experimental systems.

The strategy employed to realize arrays of surface-immobilized SVs is illustrated in Figure 1. Similar concepts have been recently applied to the immobilization of colloids[10] or vesicles[11] in regular patterns. We defined regions on the substrate that specifically bind vesicles and are surrounded by areas that prevent nonspecific attachment.

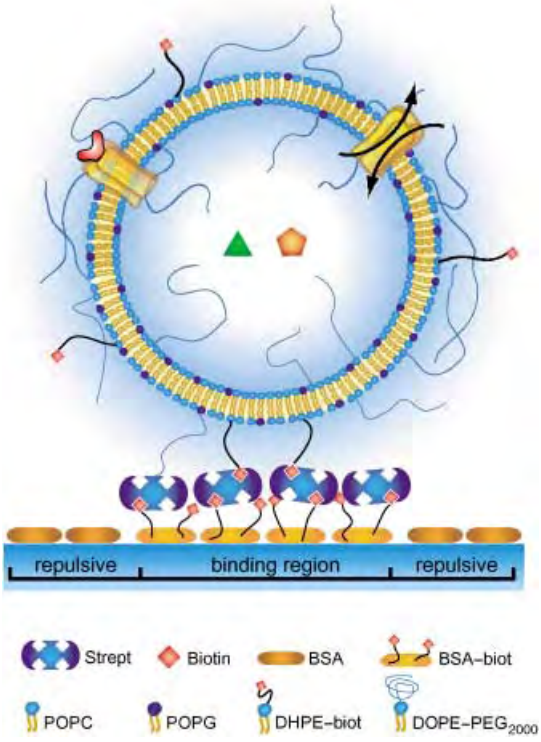



***Figure 1.*** Strategy to self-assemble SVs on a surface with spatial control. First, biotinylated bovine serum albumin (BSA–biot) is fixed on the surface in a defined pattern by means of μCP. The nonprinted regions are passivated by adsorbtion of BSA from solution. Streptavidin (Strept) is then bound to the printed BSA–biot. Biotinylated lipids mediate the specific immobilization of vesicles. The vesicles carry charged and poly(ethylene glycol) (PEG)-derivatized lipids to prevent nonspecific interactions with the surface: 1-palmitoyl-2-oleoyl-*sn*-glycero-3-phosphocholine, POPC; 1-palmitoyl-2-oleoyl-*sn*-glycero-3-phospho-rac-(1-glycerol), POPG; *n*-((6-(biotinoyl)amino)hexanoyl)-1,2-dihexadecanoyl-*sn*-glycero-3-phosphoethanolamine, DHPE–biotin; 1,2-dioleoyl-*sn*-glycero-3-phosphoethanolamine-*n*-[methoxy (polyethylene glycol)-2000], DOPE–$PEG_{2000}$. The colored triangle and pentagon represent different water-soluble molecules confined in the vesicle interior.

Specific binding is mediated through the receptor–ligand pair, streptavidin–biotin.[12] Vesicles with exposed biotin ligands on their surface lock exclusively onto the parts of the substrate where the active complementary receptor was immobilized.[13] In this manner, the positioning of vesicles and their content becomes a diffusion-limited SA process guided by the patterned surface functionalization.

The properties of the vesicles can be tailored for optimum interaction with the surface by selecting an appropriate lipid composition for their bilayer. We adjusted the lipid composition to introduce two long-range repulsive forces that prevent nonspecific interactions between the vesicles and the surface. Electrostatic repulsion was controlled by setting the ratio of charged to uncharged lipids. The presence of 10% charged lipids (POPG) also increases the bending energy[14] of the lipid membrane, which prevents vesicles from deforming and fusing upon immobilization. To establish a second barrier against intimate contact between surface and vesicles, we used lipids modified with a hydrophilic polymeric chain (PEG).[15] The PEG molecules induce a force that is entropic

[*] Dr. D. Stamou, Prof. Dr. H. Vogel, Dr. C. Duschl[+]
Institut de Sciences Biomoléculaires
Ecole Polytechnique Fédérale de Lausanne, EPFL-CHB
1015 Lausanne (Switzerland)
Fax: (+41) 21-693-6190
E-mail: dimitrios.stamou@epfl.ch
horst.vogel@epfl.ch
Dr. E. Delamarche
IBM Research
Zurich Research Laboratory
8803 Rüschlikon (Switzerland)
[+] Present address: Fraunhofer Institute
Biomedical Technology (AMBT)
Invalidenstrasse 42, 10115 Berlin (Germany)

[**] We thank A. Brecht and C. Bieri for critically reading the manuscript, and A. Bietsch and B. Michel for the high-resolution μCP stamps. This work was in part funded by the TOP NANO 21 program and the IHP/Networks Programme of the European Community (Project HPRN-CT-2000-00159).

Supporting information for this article is available on the WWW under http://www.angewandte.org or from the author.

 © 2003 Wiley-VCH Verlag GmbH & Co. KGaA, Weinheim DOI: 10.1002/anie.200351866 

in nature and independent of the immobilization conditions (pH, ionic strength) that affect electrostatic-based repulsion. To maintain the membrane in a fluid state and avoid leakage, POPC was chosen as the main lipid constituent, which ensured an ordered-to-fluid phase transition far below room temperature. A balance of contributions from the three most important interactions, that is, the receptor–ligand binding, the electrostatic repulsion, and the entropic repulsion, was crucial to achieving selective deposition of intact vesicles.

We chose the dimensions of the vesicles and the resolution of the patterning method to be complementary to the probe volume of fluorescence-based detection techniques. Most of the vesicles used in this work were prepared by extrusion, with an average diameter of 100 nm.[16] The surface onto which the vesicles are immobilized was structured by μCP, a versatile technique for patterning surfaces with a variety of biomolecules[17] with a resolution of less than 100 nm.[18] In this patterning step, we directly defined both the geometry and the resolution of the subsequent vesicle assembly.

One strategy to immobilize small numbers of vesicles onto predefined areas of a surface is to reduce the number of vesicles available for binding per printed area. This reduction is readily accomplished in the SA step by reducing the vesicle concentration. The fluorescence image in Figure 2a shows vesicles with an average diameter of 100 nm immobilized on an array composed of 2-μm-wide dots separated by 8 μm. The vesicles are localized within $\pm 1$ μm of the center of the printed areas. Vesicles did not bind to surfaces preincubated with biotin (results not shown), which emphasizes the specificity of this immobilization procedure and indicates the successful suppression of nonspecific interactions by this approach. The occupation of potential binding regions was on the order of 80%. The mean number of vesicles per dot is estimated to be 1.3 (all resolved features were assumed to be SVs because their solution density was too low). To verify that vesicles neither leaked nor fused with the surface upon immobilization, we loaded them with the water-soluble dye carboxyfluorescein. Figure 2b shows the simultaneously recorded fluorescence emmision originating from the membrane and from the interior of the vesicles and the co-localization of the two signals. CF was retained for periods of several days, which proves that the immobilized vesicles had an ability to confine molecules that is comparable to that of vesicles in suspension. As long as equiosmolar solutions were used, immobilized vesicles were stable against washes/buffer exchange. The absence of nonspecific deposition of vesicles together with the precise localization of the immobilized vesicles create the contrast that is key for proceeding to the immobilization of single vesicles.

Extension of the technique from statistical placement of small numbers of vesicles on predefined areas to SV positioning required reduction of the pattern size to the dimensions of the vesicles.[10] We functionalized glass by using high-resolution μCP stamps that had various features with sizes as small as 60 nm.[18] The simultaneous presence of different patterns on the surface allowed us to screen in one step for the geometries and sizes that were appropriate for immobilization of a single vesicle on a printed feature. The highest occupation of printed sites by SVs (80%) was obtained for

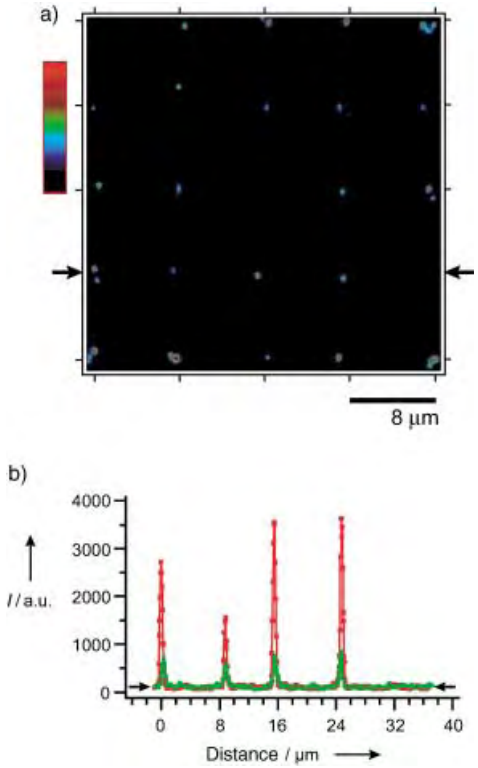



***Figure 2.*** Confocal fluorescence microscopy characterization of groups of vesicles arrayed on a glass surface (LSM 510, Zeiss). Binding sites were 2 μm in diameter and situated on an 8-μm quadratic lattice. Vesicles were labeled with 1% rhodamine–lipid in the bilayer and loaded with d-sorbitol (200 mM) and carboxyfluorescein (CF; 100 μM, approximately 30 CF molecules per 100-nm vesicle). a) Fluorescence from the lipid bilayer indicates the position of the vesicles. b) Line trace from the image in (a) showing the rhodamine signal (red) and the simultaneously acquired fluorescence signal of CF (green). The vesicles are positioned site-specifically on the surface and remain intact, as indicated by their retention of CF.

'linelets' with dimensions of $100 \times 400$ nm$^2$ spaced 800 nm apart (Figure 3a). Vacancies (for example, first row, positions 2 and 5 in Figure 3a) are due to patterning defects (incomplete stamping) and size-related binding constraints (for example, number of receptors available). Decreasing the size of the patterns lowered the occupation percentage, whereas increasing it resulted in multiple occupation (results not shown). Vesicles are localized on the linelets to within $\pm 50$ nm in the vertical and $\pm 200$ nm in the horizontal direction. The vesicles are kept at an average separation of 800 nm, which is twice their resolution-limited diameter. The different intensities observed probably originate from differences in size and, therefore, different numbers of fluorophores per vesicle. Incubation times to self-assemble vesicles onto printed sites were 5–10 min for vesicle concentrations of 3 nM.

In addition we incubated the linelet patterns with a mixture of two vesicle populations, each tagged with a different fluorophore (Figure 3b). The occupation of one site by multiple vesicles would result in the co-localization of the two fluorescence signals. No co-localization was observed, which proves that each occupied site of the pattern contains only one vesicle. The size of the arrays we fabricated was $0.4 \times$

 © 2003 Wiley-VCH Verlag GmbH & Co. KGaA, Weinheim 

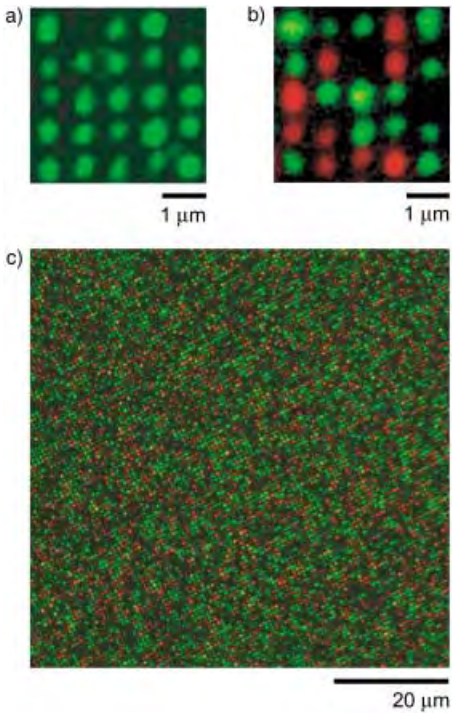



***Figure 3.*** High-density arrays of SVs immobilized on 100×400-nm$^2$ binding sites, separated by 800 nm. The confocal fluorescence images show a) an array of one type of vesicles labeled with oregon488–lipid, and b) the same patterns incubated with a mixture of two differently labeled vesicle populations (red: rhodamine; green: oregon488). Overlay of the two signals shows no co-localization of fluorescence, which proves that only one vesicle is immobilized per binding site. c) Directed SA permits the construction of complex high-density SV arrays over large areas.

0.4 mm$^2$ and this size can be extended into the centimeter range. The fluorescence image in Figure 3c shows a small part of a mixed array with an SV density of about $10^6$ mm$^{-2}$. All SVs in the image are placed in an ordered fashion on the surface, which renders their localization simple. The positioning of different SVs on the array is random, but various encoding schemes (such as oligonucleotide tagging) can be employed to ascertain the identity of each SV, even in the case of complex mixtures.[19]

To assess the stability of the controlled environment of molecules confined inside immobilized vesicles, we investigated the permeability of the lipid bilayer. Low passive influx/efflux of ions into/out of vesicles is a prerequisite for keeping the pH value or ionic composition of an SV stable and the function of a protein or the reactivity of solutes inside an SV reliable. The experiments whose results are reported in Figure 4 take advantage of the pH sensitivity of CF to monitor the pH value inside SVs 0.5–1 μm in diameter, immobilized on 10-μm-wide stripes. The vesicles were prepared with a pH value of around 5.5 and were immobilized in a buffer of pH 7.4. After immobilization, the pH value of the vesicles shifted to about 6.2, where it remained stable because of the established diffusion potential (Figure 4, Experiment A). The SVs proved capable of maintaining pH gradients of more than one unit over the course of several hours as a result of the low counterion exchange rate.

In a subsequent step, we addressed the interior of these tightly sealed containers and initiated a simple chemical reaction. We triggered the deprotonation of CF inside the SVs by treatment with an ion-channel-forming peptide (gramicidin A). Gramicidin forms cation-selective channels in lipid membranes. Upon incorporation into a bilayer, the channels allow $Na^+$ ions to diffuse down their concentration gradient, in this case into the vesicle. The sodium influx induces a pH increase (proton efflux) so as to maintain electroneutrality. In Experiment B shown in Figure 4, we monitored individual vesicles over time and recorded how the fluorophores trapped in their interior responded to the gramicidin stimulus. As a result of the high single-channel conductance of gramicidin

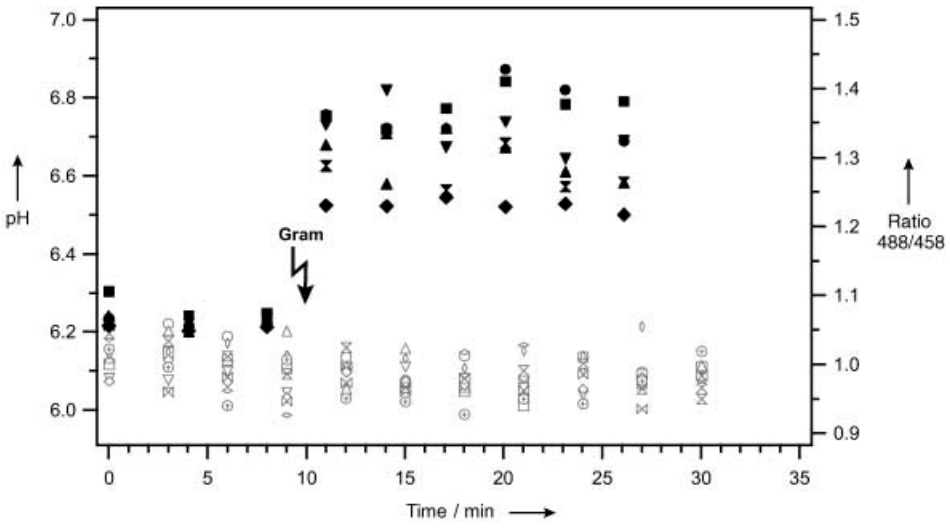



***Figure 4.*** The internal pH value of SVs monitored over time. Vesicles were loaded with CF (100 μM). The pH value was inferred from the excitation ratio 488/458 nm of the dye, at an emission bandwidth of 505–550 nm (see the Supporting Information). Experiment A (open symbols) monitored the stable pH value of SVs after their immobilization. In Experiment B (solid black symbols), we triggered a chemical reaction (deprotonation of CF) in the interior of the SVs in a second sample by the addition of gramicidin (Gram; 10 nM). In both experiments, we selected vesicles 0.5–1 μm in diameter to ensure a sufficient number of fluorophores were present. For clarity, the results of Experiment A are shifted vertically by −0.1.

 © 2003 Wiley-VCH Verlag GmbH & Co. KGaA, Weinheim 

(~40 pS), equilibrium was reached milliseconds after the first channel opened,[20] much faster than the time resolution of the results shown in Figure 4 (see also the Supporting Information). Ion channels with smaller conductivities (for example, the 5-$HT_{3A}$ receptor[21]) would need seconds or minutes to establish equilibrium and would therefore potentially allow real-time monitoring of channel activity.[22] This experiment illustrates how the selective permeability properties of membrane-associated transporters or channels can be employed to perform chemistry inside individually addressed nanocontainers.

Hierarchical SA is an emerging approach to the fabrication of functional nanometer-scale architectures.[9] In this work, we combined SA principles and receptor–ligand interactions first to define attoliter autonomous experimental volumes, and then to order them on a surface. Incorporation of multifunctional recognition elements, such as oligonucleotides, would further increase the complexity of the assembled structures.[23] The lipid-bilayer vesicles we used as molecular vessels are arrayed at high densities (every 800 nm, $\sim 10^6\ mm^{-2}$). Nevertheless, each one maintains its cargo dissolved in a protective environment[24] of defined chemical composition (pH, ionic strength, etc.) and at the same time localizes its position with 100-nm precision. Such ultrasmall-volume libraries allow simultaneous screening[6] of (bio)-chemical properties, molecular function, or confined chemical reactions over millions of samples, while consuming total reagent volumes of a few picoliters. A natural extension of this work is the use of vesicles produced directly from cells to form arrays.[25] To array native vesicles individually, the employment of a more versatile surface modification[26] might be crucial since their properties are not so easily controlled as those of synthetic vesicles. Native vesicles are of primary importance as they can carry receptor proteins expressed in cell membranes and/or signal transduction machinery from the cytosol. In array format, such vesicles may thus be used to screen binding of pharmaceutical compounds (drug candidates) or the functional responses induced by such binding.

## Experimental Section

Vesicle production: A dried lipid film was rehydrated overnight in d-sorbitol (200 mM). A vesicle cloud was then harvested (ca. 1 $mg\,mL^{-1}$), freeze-thawed, and extruded through 100-nm filter pores (typical vesicle diameters were $100 \pm 40$ nm). The vesicles used for the experiments in Figure 4 were passed once through a 1-μm pore-size filter after harvesting to create a sharp upper cut-off in their size distribution. Before incubation with the microarray surface, vesicles were diluted (1:10) in the immobilization buffer (80 mM NaCl and 10 mM $NaHPO_4$ at pH 7.4). All experiments presented herein used vesicles composed of POPC (88%), POPG (10%), DHPE–biot (2%), and DOPE–$PEG_{2000}$ (0.3%). We used two fluorescently labeled lipids: *n*-(6- tetramethylrhodaminethiocarbamoyl)-1,2- dihexadecanoyl-*sn*-glycero-3- phosphoethanolamine and Oregon green 488–1,2-dihexadecanoyl-*sn*-glycero-3-phosphoethanolamine.

Patterned surface functionalization: Poly(dimethylsiloxane) stamps for μCP were inked with BSA–biot ($0.1\ mg\,mL^{-1}$). After washing the stamps with phosphate-buffered saline and removing residual buffer under an $N_2$ stream, we printed BSA–biot onto a clean glass substrate, which was subsequently passivated with BSA ($0.5\ mg\,mL^{-1}$). The patterned substrate was then functionalized by incubation with streptavidin ($0.025\ mg\,mL^{-1}$) for 10 min. The final streptavidin surface density was approximately 10% of a complete monolayer.

Received: May 12, 2003 [Z51866]
Published Online: November 5, 2003

**Keywords:** liposomes · microarrays · nanostructures · self-assembly · vesicles

[1] R. Lipowsky, E. Sackmann, *Structure and Dynamics of Membranes. From Cells to Vesicles*, Elsevier Science, Amsterdam, **1995**.
[2] R. B. Gennis, *Biomembranes. Molecular Structure and Function*, 1st ed., Springer, New York, NY, **1989**.
[3] A. Bernard, B. Michel, E. Delamarche, *Anal. Chem.* **2001**, *73*, 8.
[4] A. v. d. Berg, W. Olthouis, P. Bergveld, *Micro Total Analysis Systems 2000*, Kluwer Academic, Dordrecht, **2000**.
[5] K. Jensen, *Nature* **1998**, *393*, 735.
[6] M. J. Levene, J. Korlach, S. W. Turner, M. Foquet, H. G. Craighead, W. W. Webb, *Science* **2003**, *299*, 682.
[7] D. T. Chiu, C. F. Wilson, F. Ryttsen, A. Stromberg, C. Farre, A. Karlsson, S. Nordholm, A. Gaggar, B. P. Modi, A. Moscho, R. A. Garzalopez, O. Orwar, R. N. Zare, *Science* **1999**, *283*, 1892.
[8] B. Michel, A. Bernard, A. Bietsch, E. Delamarche, M. Geissler, D. Juncker, H. Kind, J. P. Renault, H. Rothuizen, H. Schmid, P. Schmidt-Winkel, R. Stutz, H. Wolf, *IBM J. Res. Dev.* **2001**, *45*, 697; Y. Xia, G. M. Whitesides, *Angew. Chem.* **1998**, *110*, 568; *Angew. Chem. Int. Ed.* **1998**, *37*, 551.
[9] G. M. Whitesides, B. Grzybowski, *Science* **2002**, *295*, 2418.
[10] Y. D. Yin, Y. Lu, B. Gates, Y. N. Xia, *J. Am. Chem. Soc.* **2001**, *123*, 8718.
[11] S. Svedhem, I. Pfeiffer, C. Larsson, C. Wingren, C. Borrebaeck, F. Hook, *ChemBioChem* **2003**, *4*, 339; R. Michel, I. Reviakine, D. Sutherland, C. Fokas, G. Csucs, G. Danuser, N. D. Spencer, M. Textor, *Langmuir* **2002**, *18*, 8580.
[12] S. A. Walker, M. T. Kennedy, J. A. Zasadzinski, *Nature* **1997**, *387*, 61.
[13] A. Albersdorfer, T. Feder, E. Sackmann, *Biophys. J.* **1997**, *73*, 245.
[14] R. Lipowsky, *Nature* **1991**, *349*, 475.
[15] D. Kroger, F. Hucho, H. Vogel, *Anal. Chem.* **1999**, *71*, 3157.
[16] B. J. Frisken, C. Asman, P. J. Patty, *Langmuir* **2000**, *16*, 928.
[17] C. Bieri, O. P. Ernst, S. Heyse, K. P. Hofmann, H. Vogel, *Nat. Biotechnol.* **1999**, *17*, 1105.
[18] J. P. Renault, A. Bernard, A. Bietsch, B. Michel, H. R. Bosshard, E. Delamarche, M. Kreiter, B. Hecht, U. P. Wild, *J. Phys. Chem. B* **2003**, *107*, 703.
[19] D. R. Walt, *Science* **2000**, *287*, 451.
[20] C. M. Biegel, J. M. Gould, *Biochemistry* **1981**, *20*, 3474.
[21] S. P. Kelley, J. I. Dunlop, E. F. Kirkness, J. J. Lambert, J. A. Peters, *Nature* **2003**, *424*, 321.
[22] M. Tschodrich-Rotter, U. Kubitscheck, G. Ugochukwu, J. T. Buckley, R. Peters, *Biophys. J.* **1996**, *70*, 723.
[23] L. M. Demers, D. S. Ginger, S. J. Park, Z. Li, S. W. Chung, C. A. Mirkin, *Science* **2002**, *296*, 1836.
[24] E. Rhoades, E. Gussakovsky, G. Haran, *Proc. Natl. Acad. Sci. USA* **2003**, *100*, 3197.
[25] D. T. Chiu, S. J. Lillard, R. H. Scheller, R. N. Zare, S. E. Rodriguez-Cruz, E. R. Williams, O. Orwar, M. Sandberg, J. A. Lundqvist, *Science* **1998**, *279*, 1190.
[26] R. Michel, J. W. Lussi, G. Csucs, I. Reviakine, G. Danuser, B. Ketterer, J. A. Hubbell, M. Textor, N. D. Spencer, *Langmuir* **2002**, *18*, 3281.

 © 2003 Wiley-VCH Verlag GmbH & Co. KGaA, Weinheim 

Microarrays

# Immobilization of Natural Products on Glass Slides by Using a Photoaffinity Reaction and the Detection of Protein–Small-Molecule Interactions**

*Naoki Kanoh, Saori Kumashiro, Siro Simizu, Yasumitsu Kondoh, Satoru Hatakeyama, Hideo Tashiro, and Hiroyuki Osada**

Small molecules, especially from natural resources, are an important source of bioprobes which are useful in the study of protein function and cell signaling networks.[1] The identification of target proteins for small molecules which modulate particular biological process has not only provided new insights in biology,[2] but has also provided chemists and pharmacologists with the opportunity to create new synthetic molecules which efficiently regulate specific protein–protein interactions and biological processes.[3] Using a split-pool strategy, for chemical library synthesis, and biochemical technology, high-throughput processes for creating and identifying synthetic ligands for any protein have recently been developed.[4] Printing small molecules and carbohydrates as microarrays on glass slides or on other solid surfaces has been reported as one of the most frequently used approaches to date.[4a–d,5] A key aspect of such approaches is the immobilization of small molecules on solid surfaces; recently, mild and selective coupling reactions have been developed which include a Michael addition,[4a,5c] the addition of alcohol to silyl chloride,[4b] 1,3-dipolar cycloaddition,[5b] and a Diels–Alder reaction.[5d] Very recently, Schreiber and co-workers developed diazobenzilidene-functionalized glass slides and used these slides for the covalent capture of phenols as well as of other compounds containing functional groups of comparable acidity.[4g]

However, there remain some drawbacks to using these selective coupling approaches. Small molecules have to possess certain functional groups to be attached to solid surfaces. Combinatorial chemical libraries prepared by solid-phase synthesis inherently have such functional groups, but small-molecule libraries derived from natural resources contain a variety of structures and functional groups which are not always compatible with the selective coupling process. Even though the small molecules could be introduced onto the solid surfaces, a certain area of the small molecule faces towards the solid surface, and therefore some of the immobilized compounds will not come into contact with the relevant binding proteins. As it is difficult to predict the binding domain of small molecules that interact with unknown proteins, this poses a major drawback to such studies, especially when the goal is to discover new target proteins for small molecules by using microarray technology. To overcome these drawbacks, we describe herein a "non-selective" universal coupling method that enables the introduction of a variety of small molecules to glass slides by using a photoaffinity reaction. The small molecules introduced onto the glass slide by this method have the inherent ability to interact with their binding proteins.

Photoaffinity labeling has been used for investigating ligand–receptor interactions and analyzing binding sites within receptor molecules.[6] Photoreactive groups introduced to ligands are promoted upon UV irradiation to highly reactive species, which in turn bind irreversibly to the receptor at the interaction site. These species, in many cases aryl nitrenes and carbenes, are so reactive that they can insert into a heteroatom–hydrogen and even into a carbon–hydrogen bond. Recently, photoinduced cross-linking reactions using an aryl nitrene[7a] and an aryl carbene[7b] have been reported to anchor proteins on the solid supports. We expected that these photoinduced reactions could be used to immobilize not only proteins but also various types of small molecules on glass slides. Our strategy is summarized in Figure 1. Small-molecule solutions are first printed on glass slides, which are coated by a photoreactive group. The slides are then dried to remove the solvent used in the printing

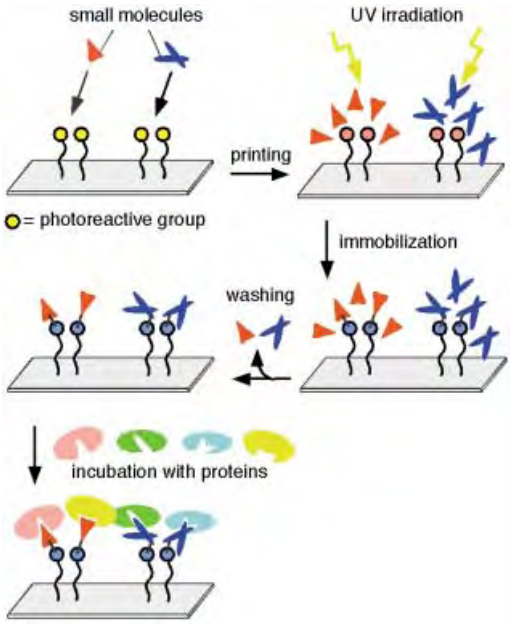



***Figure 1.*** Immobilization of small molecules using a photoaffinity reaction.

[*] Dr. H. Osada, Dr. N. Kanoh, S. Kumashiro, Dr. S. Simizu
Antibiotics Laboratory
Discovery Research Institute
RIKEN (The Institute of Physical and Chemical Research)
2-1 Hirosawa, Wako, Saitama 351-0198 (Japan)
Fax: (+81) 48-462-4669
E-mail: osadah@riken.jp
Dr. Y. Kondoh, S. Hatakeyama, Dr. H. Tashiro
Advanced Engineering Center
RIKEN (The Institute of Physical and Chemical Research)
2-1 Hirosawa, Wako, Saitama 351–0198 (Japan)

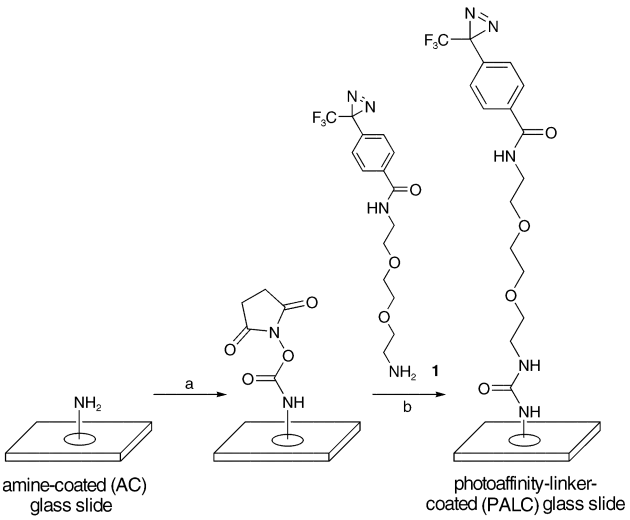
[**] We are especially grateful to Fujisawa Pharmaceuticals (Osaka, Japan) for the generous gift of FK506, and to Y. Ichikawa and R. Nakagawa (Bioarchitect Research Group, RIKEN) for DNA sequencing.

Supporting information for this article is available on the WWW under http://www.angewandte.org or from the author.

 © 2003 Wiley-VCH Verlag GmbH & Co. KGaA, Weinheim DOI: 10.1002/anie.200352164 

process. Irradiation of the resulting slides activates the photoreactive group on the slides, generating highly reactive species that can insert into or add to proximate small molecules. The immobilized small molecules remain on the glass slides after washing, and the washed slides can be used to detect the interactions between proteins and small molecules by incubating the slides with labeled proteins. Immobilization should occur in a functional-group-independent manner; using this method, some, but not all, of the immobilized small molecules are expected to retain binding affinity towards all of the possible binding proteins. As discussed above, this is important when discovering new target proteins for each small molecule.

To test this concept, we prepared photoaffinity linker **1** from *N-tert*-butoxycarbonyl-2,2′-ethylenedioxybis(ethylamine)[8] and 4-[3-(trifluoromethyl)-3*H*-diazirin-3-yl]benzoic acid,[9] and introduced it onto amine-coated (AC) glass slides (Scheme 1). A variety of photoaffinity reagents was screened,




***Scheme 1.*** The introduction of a photoaffinity linker on an amine-coated glass slide. Reagents and conditions: a) immersed in a solution of *N,N*-disuccinimidyl carbonate (1.0 M) and diisopropylethylamine (1.0 M) in DMF, RT, overnight, then washed, b) immersed in a solution of **1** (100 mM) and diisopropylethylamine (500 mM) in DMF, RT, overnight, then washed.

and the 4-[3-(trifluoromethyl)-3*H*-diazirin-3-yl]benzoyl group was found to be most suitable for our purposes. The AC slides were first treated with *N,N*-disuccinimidyl carbonate to yield mixed carbonate on the slides. The resultant succinimidyl slides were then treated with **1** to give photoaffinity linker-coated (PALC) glass slides.

Rhodamine B (RhoB) and biotin solutions in DMSO were printed in quadruplicate at various concentrations (100, 10, 1, 0.1, and 0.01 mM) on both PALC and AC surfaces (Figure 2a), and the slides were dried in vacuo to remove DMSO. After the printed surface of a slide was irradiated at 365 nm for 30 min, it was washed successively with organic solvents and water. The slide was then probed with streptavidin–Alexa$_{633}$ conjugate in reaction buffer (see Supporting Information), washed with TBST buffer, and scanned for

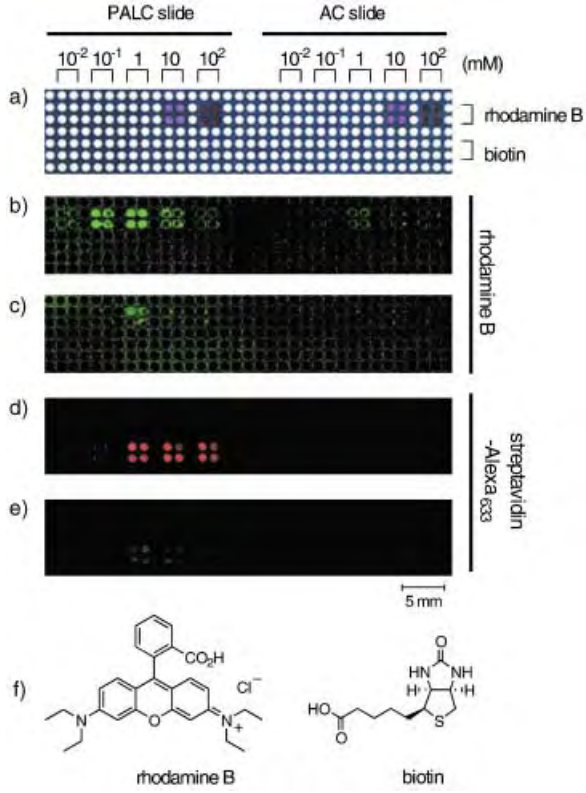



***Figure 2.*** Immobilized small molecules on PALC and AC slides and the detection of the biotin–streptavidin interaction. a) Image of PALC and AC slides on which rhodamine B and biotin solution were printed in quadruplicate. The concentration of printed solution decreases 10-fold with each interval from the right to the left, as indicated. b)–e) Fluorescent images: After the slides were irradiated at 365 nm (irradiation time: 30 min for b and d, 7 min for c and e), they were washed successively with organic solvents and water. The resultant slides were incubated with streptavidin–Alexa$_{633}$ conjugate (3.7 μg mL$^{-1}$), washed, and scanned for rhodamine (b and c) and Alexa$_{633}$ fluorescence (d and e). f) Structure of rhodamine B and biotin.

RhoB and Alexa$_{633}$ fluorescence by using a DNA scope IV fluorescence slide scanner (Biomedical Photometrics Inc., Waterloo, ON, Canada). The results are shown in Figure 2b and 2d. Strong RhoB and Alexa$_{633}$ fluorescence was observed only on the PALC slides. Note that the spots where 100 and 10 mM RhoB were printed showed weak fluorescence signals relative to 1 and 0.1 mM areas. When 100 and 10 mM solutions of RhoB were printed on the slides, the printed areas were deep red owing to the high concentration of RhoB (Figure 2a). Therefore, it is probable that UV light did not pass through the RhoB layer, and the photoaffinity reaction did not occur efficiently in these areas. The fluorescence intensity of RhoB and Alexa$_{633}$ depended on the irradiation time (30 min for Figure 2b and d; 7 min for Figure 2c and e). Furthermore, when the compounds were washed off without irradiation, no RhoB and Alexa$_{633}$ fluorescence was observed after the probe with streptavidin–Alexa$_{633}$ conjugate (data not shown). These results strongly suggest that RhoB and biotin were immobilized by a photoaffinity reaction.

We applied this approach for immobilizing a variety of natural products on the PALC slides to observe specific

 © 2003 Wiley-VCH Verlag GmbH & Co. KGaA, Weinheim 

interactions between small molecules and proteins (Figure 3). Digoxin is a cardiac steroidal glycoside that is recognized by mouse monoclonal antibody DI-22 (Sigma). A DI-22 clone is also known to show cross-reactivity with digoxigenin (strong) and digitoxin (< 5 %), and almost no cross-reactivity has been observed with progesterone and hydrocortisone (< 0.1 %).[10] The immunosuppressive agent FK506 and rapamycin are known to bind their target protein FKBP12.[2c,11] Also, immunosuppressant cyclic peptide cyclosporin A is recognized by its monoclonal antibody CSZ.22 (HyTest). These molecules were immobilized on a PALC slide, and the resultant slide was probed with a solution of labeled proteins and scanned. All the immobilized molecules were successfully recognized in a specific manner by their protein targets. This is the first example in which complex natural products have been immobilized on a solid surface as arrays in a uniform process.

Because the spots that contained steroids exhibited a similar fluorescent signal (Figure 3c), we prepared a "steroid array" to determine whether or not other steroids could interact with the DI-22 clone on the slide (Figure 4). Five

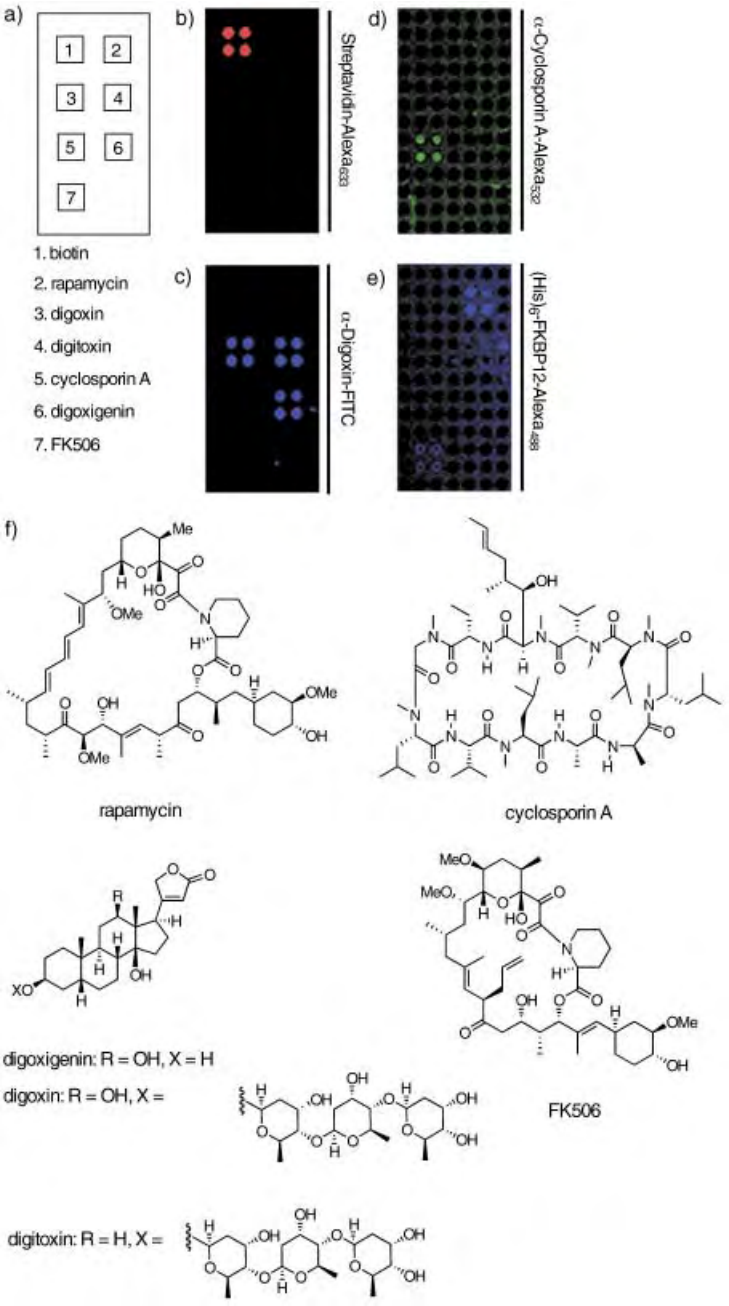



***Figure 3.*** The detection of specific interactions between small molecules and proteins. a) Each slide was printed with 10 mM solutions of small molecules according to the pattern illustrated. b)–e) Fluorescent images: b) probed with streptavidin–$Alexa_{633}$ conjugate (5 μg mL$^{-1}$), c) probed with anti-digoxin DI-22-FITC conjugate (150 μg mL$^{-1}$), d) probed with anti-cyclosporin A CSZ.22–$Alexa_{532}$ conjugate (10 μg mL$^{-1}$) and $(His)_6$-FKBP12–$Alexa_{488}$ conjugate (10 μg mL$^{-1}$), and then scanned for $Alexa_{532}$; e) probed with anti-cyclosporin A CSZ.22–$Alexa_{532}$ conjugate (10 μg mL$^{-1}$) and $(His)_6$-FKBP12–$Alexa_{488}$ conjugate (10 μg mL$^{-1}$), and then scanned for $Alexa_{488}$. f) Structures of the test compounds.

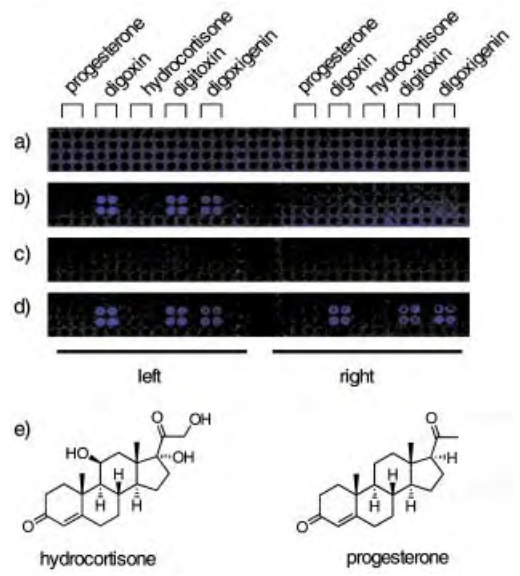



***Figure 4.*** Steroid arrays: 10 mM solutions of five different steroids were printed on a PALC slide. a) Background, b) fluorescent image after the probe with anti-digoxin DI-22-FITC conjugate (150 μg mL$^{-1}$) in the presence (right) or absence (left) of digoxin (10 μM), c) fluorescent image of the slide stripped with stripping buffer (see text), d) fluorescent image of the slide reprobed with anti-digoxin DI-22-FITC conjugate (150 μg mL$^{-1}$), e) structures of hydrocortisone and progesterone; digoxin, digitoxin, and digoxigenin are depicted in Figure 3 f.

steroidal compounds were immobilized on the slide and probed with DI-22-FITC conjugate. As expected, spots containing progesterone and hydrocortisone had no FITC fluorescence, demonstrating that DI-22 did not interact with these compounds (Figure 4b, left). In the presence of digoxin (10 μM), no fluorescence was observed, showing that fluorescence on the slides is the result of specific interactions between steroids and antibody (Figure 4b, right). According to these observations, it appears that this type of natural products array could be useful for testing the antigen specificity of an antibody. In addition, it should be noted that the captured antibody was stripped by stripping buffer (62.5 mM Tris·HCl, pH 6.8, 100 mM β-mercaptoethanol, 2 % SDS) at 50 °C for 1 h (Figure 4c), and the stripped slide was then available for reuse (Figure 4d).

In summary, we prepared PALC slides and, using a photoaffinity reaction, we immobilized structurally distinct

 © 2003 Wiley-VCH Verlag GmbH & Co. KGaA, Weinheim 

small molecules on these slides. The immobilized molecules were shown to retain specific binding activity towards their binding proteins. Importantly, this immobilization procedure does not require a specific functional group, and can be applied for use with a diverse small-molecule library.

Received: June 18, 2003 [Z52164]

**Keywords:** high-throughput screening · immobilization · natural products · photochemistry · protein–ligand interactions

[1] *Bioprobes: Biochemical Tools for Investigating Cell Function* (Ed.: H. Osada), Springer, Tokyo, **1999**.

[2] a) K. Miyake, S. Horinouchi, M. Yoshida, N. Chiba, K. Mori, N. Nogawa, N. Morikawa, T. Beppu, *J. Bacteriol.* **1989**, *171*, 4298; b) J. J. Siekierka, S. H. Y. Hung, M. Poe, C. S. Lin, N. H. Sigal, *Nature* **1989**, *341*, 755; c) M. W. Harding, A. Galat, D. E. Uehling, S. L. Schreiber, *Nature* **1989**, *341*, 758; d) L. Whitesell, E. G. Mimnaugh, B. De Costa, C. E. Myers, L. M. Neckers, *Proc. Natl. Acad. Sci. USA* **1994**, *91*, 8324.

[3] a) F. F. Zheng, S. D. Kuduk, G. Chiosis, P. N. Munster, L. Sepp-Lorenzino, S. J. Danishefsky, N. Rosen, *Cancer Res.* **2000**, *60*, 2090; b) G. R. Crabtree, S. L. Schreiber, *Trends Biochem. Sci.* **1996**, *21*, 418.

[4] a) G. MacBeath, A. N. Koehler, S. L. Schreiber, *J. Am. Chem. Soc.* **1999**, *121*, 7967; b) P. J. Hergenrother, K. M. Depew, S. L. Schreiber, *J. Am. Chem. Soc.* **2000**, *122*, 7849; c) G. MacBeath, S. L. Schreiber, *Science* **2000**, *289*, 1760; d) F. G. Kuruvilla, A. F. Shamji, S. M. Sternson, P. J. Hergenrother, S. L. Schreiber, *Nature* **2002**, *416*, 653; e) H. E. Blackwell, L. Pérez, R. A. Stavenger, J. A. Tallarico, E. C. Eatough, M. A. Foley, S. L. Schreiber, *Chem. Biol.* **2001**, *8*, 1167; f) P. A. Clemons, A. N. Koehler, B. K. Wagner, T. G. Sprigings, D. R. Spring, R. W. King, S. L. Schreiber, *Chem. Biol.* **2001**, *8*, 1183; g) D. Barnes-Seeman, S. B. Park, A. N. Koehler, S. L. Schreiber, *Angew. Chem.* **2003**, *115*, 2474; *Angew. Chem. Int. Ed.* **2003**, *42*, 2376; h) N. Winssinger, J. L. Harris, B. J. Backes, P. G. Schultz, *Angew. Chem.* **2001**, *113*, 3254; *Angew. Chem. Int. Ed.* **2001**, *40*, 3152; i) N. Winssinger, S. Ficarro, P. G. Schultz, J. L. Harris, *Proc. Natl. Acad. Sci. USA* **2002**, *99*, 11139.

[5] a) D. Wang, S. Liu, B. J. Trummer, C. Deng, A. Wang, *Nat. Biotechnol.* **2002**, *20*, 275; b) F. Fazio, M. C. Bryan, O. Blixt, J. C. Paulson, C.-H. Wong, *J. Am. Chem. Soc.* **2002**, *124*, 14397; c) S. Park, I. Shin, *Angew. Chem.* **2002**, *114*, 3312; *Angew. Chem. Int. Ed.* **2002**, *41*, 3180; d) B. T. Houseman, M. Mrksich, *Chem. Biol.* **2002**, *9*, 443; e) K. R. Love, P. H. Seeberger, *Angew. Chem.* **2002**, *114*, 3733; *Angew. Chem. Int. Ed.* **2002**, *41*, 3583.

[6] F. Kotzyba-Hibert, I. Kapfer, M. Goeldner, *Angew. Chem.* **1995**, *107*, 1391; *Angew. Chem. Int. Ed. Engl.* **1995**, *34*, 1296, and references therein.

[7] a) J. C. Miller, H. Zhou, J. Kwekei, R. Cavallo, J. Burke, E. D. Butler, B. S. Teh, B. B. Haab, *Proteomics* **2003**, *3*, 56; b) I. Caelen, H. Gao, H. Sigrist, *Langmuir* **2002**, *18*, 2463.

[8] P. D. Beer, J. Cadman, J. M. Lloris, R. Martínez-Máñez, J. Soto, T. Pardo, M. D. Marcos, *J. Chem. Soc. Dalton Trans.* **2000**, 1805.

[9] Y. Hatanaka, H. Nakayama, Y. Kanaoka, *Heterocycles* **1993**, *35*, 997. This material is commercially available from Bachem AG (Bubendolf, Switzerland).

[10] This information was obtained from the Sigma product information sheet.

[11] B. E. Bierer, P. S. Mattila, R. F. Standaert, L. A. Herzenberg, S. J. Burakoff, G. Crabtree, S. L. Schreiber, *Proc. Natl. Acad. Sci. USA* **1990**, *87*, 9231.

 © 2003 Wiley-VCH Verlag GmbH & Co. KGaA, Weinheim 

*Zeolites*

# Temperature-Dependent Interconversion of an Anthracene Radical Cation/Electron Moiety to an Electron–Hole Pair in the Pores of Al-ZSM-5 Zeolites**

*Hervé Vezin, Alain Moissette,* and Claude Brémard*

One of the most intriguing properties of acidic zeolites is their ability to generate organic radical cations spontaneously upon mere sorption of organic molecules.[1] The rigid framework of silicoaluminate porous materials with specific molecular-sieve properties can stabilize radical cations over several months at room temperature. It appears that the presence of heteroatoms such as aluminum in the siliceous framework and a proton as the counterion is a requirement for the efficient stabilization of radical cations. In addition, the tight fit of the radical cation in the pore is also considered to be an important factor for the stabilization of short-lived radical cations.

The characterization of many occluded radical cations is well documented. In contrast, direct evidence of the fate of the ejected electron is rare.[1–3] Typically, the ejected electrons are suggested to be highly delocalized in the zeolite framework. The zeolite framework is also known to contain electron-donor sites capable of transferring electrons to strong acceptors. The nature and structure of the centers responsible for the electron-donating or electron-accepting ability of zeolites is still the subject of controversy and debate.[1,4,5] Understanding the fate of ejected or abstracted electrons may lead to better control in producing high-yielding ionizations. These features have obvious implications in the area of the acid catalysis of hydrocarbons based on zeolites.[1,4,5]

Previously, we have characterized electron–hole pairs stabilized in acidic $H_n$ZSM-5 zeolites loaded with biphenyl.[3] The sorption of biphenyl resulted in spontaneous ionization to give the radical cation and the electron. However, the

[*] Dr. A. Moissette, Dr. C. Brémard
Laboratoire de Spectrochimie Infrarouge et Raman
UMR-CNRS 8516
Centre d'Etudes et de Recherches Lasers et Applications
FR-CNRS 2416, Bât. C5
Université des Sciences et Technologies de Lille
59655 Villeneuve d'Ascq cedex (France)
Fax: (+33) 3-2043-6755
E-mail: alain.moissette@univ-lille1.fr
Dr. H. Vezin
Laboratoire de Chimie Organique et Macromoléculaire
UMR-CNRS 8009, Bât. C4
Université des Sciences et Technologies de Lille
59655 Villeneuve d'Ascq cedex (France)

[**] The authors are very grateful to Dr. J. Patarin for providing ultrapure zeolites. The Centre d'Etudes et de Recherches Lasers et Applications (CERLA) is supported by the Ministère chargé de la recherche, the région Nord/Pas de Calais, and the Fonds Européen de Développement Economique des Régions.

Supporting information for this article is available on the WWW under http://www.angewandte.org or from the author.

 DOI: 10.1002/anie.200352269 © 2003 Wiley-VCH Verlag GmbH & Co. KGaA, Weinheim 

system evolved too rapidly to an electron–hole pair to be characterized by pulsed electron paramagnetic resonance (EPR) techniques. In addition, the ionization occurred after activation of zeolites under $O_2$ at high temperature, and the yield was found to be low.[3] Recently, we have reported the results of investigations by UV/Vis absorption and Raman scattering of the sorption of anthracene (Anth) and parent molecules in $H_n$ZSM-5 dehydrated at moderate temperature.[6] Spontaneous Anth ionization occurs in high yield, and the occluded radical cation $Anth^{+\bullet}$ is found to be stable over several months at room temperature.

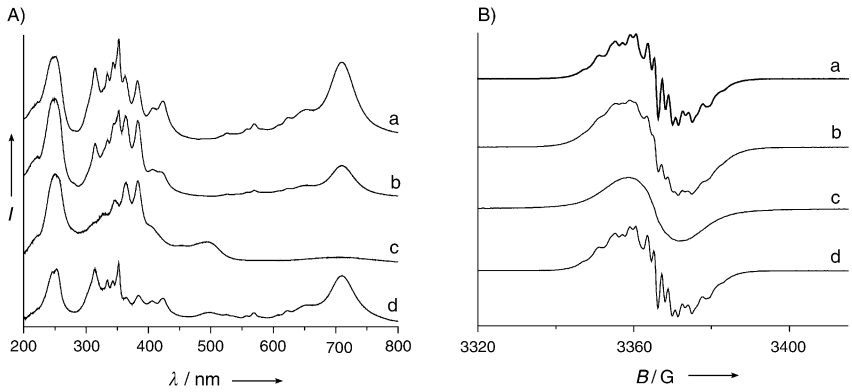



***Figure 1.*** A) Diffuse reflectance UV/Vis spectra for Anth occluded in $H_3$ZSM-5 at a) room temperature, b) 400 K, c) 473 K, and d) 24 h after cooling to room temperature. Loading: one molecule of Anth per unit cell. B) CW X-band EPR spectra for Anth occluded in $H_3$ZSM-5 at the same temperatures as in A).

Here, we report the results of EPR and UV/Vis absorption studies of the temperature-dependent reversible conversion of the $Anth^{+\bullet}$/electron moiety to electron–hole pairs in the pores of $H_3$ZSM-5 zeolite. The emphasis of this paper is set on the characterization of the $Anth^{+\bullet}$/electron moiety and electron–hole pair occluded in the pores of $H_3$ZSM-5 zeolites by pulsed EPR techniques.

The evacuation of template molecules from the framework of the as-synthesized ZSM-5 zeolite was performed at 773 K under $O_2$. Subsequent rehydration at room temperature and dehydration at 673 K under Ar provide the porous $H_3$ZSM-5 material. The comparison of all the physicochemical measurements—powder XRD, $^{29}$Si and $^{27}$Al MAS-NMR, EPR, Raman, UV/Vis, IR absorption, and chemical analyses—with previous works provides clear evidence of a pure ZSM-5 phase with unit cells of the chemical composition $H_3(AlO_2)_3(SiO_2)_{93}$. In particular, no evidence was found for either extraframework aluminum species or iron(III) impurities.[7,8,9] The framework topology of $H_3$ZSM-5 is composed of a three-dimensional network of straight and sinusoidal channels. The entrance of the channels is controlled by ten-membered rings of oxygen atoms with dimensions reported as $0.54 \times 0.56$ nm$^2$ for the straight channels and $0.51 \times 0.55$ nm$^2$ for the zigzag ones.[10] The straight channels are sufficiently wide to allow Anth molecules to pass through the openings and to diffuse into the void space.[6]

Bare $H_3$ZSM-5 zeolite as microcrystals several μm in size was exposed in the dark, under argon, and at room temperature to a weighted amount of dry Anth ($C_{14}H_{10}$). The Anth loading corresponds to one Anth molecule per unit cell of zeolite ($Anth/H_3(AlO_2)_3(SiO_2)_{93}$). The sorption was monitored by diffuse-reflectance UV/Vis absorption (DRUVv), Raman scattering, and continuous-wave (CW)-EPR spectroscopies. The sorption and equilibration were found to be complete after three months at room temperature. The Raman and UV/Vis spectra were found to be typical for $Anth^{+\bullet}$ as the major occluded organic species (spectrum a, Figure 1 A). Nevertheless, no evidence of the ejected electron was obtained with these techniques.[6]

In the CW-EPR spectra recorded after equilibrium at room temperature (spectrum a, Figure 1 B) sharp signals are superimposed over a broad signal of 10 G. No half-field ($g \sim 4$) signal was detected. The double integration of the EPR signal in the $g = 2$ region indicates that the ionization is nearly complete after three months and that it generates spin density corresponding to two unpaired electrons per unit cell. The reference standard sample was obtained by loading 2,2,5,5-tetramethyl-3-pyrrolin-1-yloxy nitroxide radical in ZSM-5 zeolite. The excitation of the complex CW-EPR signal obtained after complete ionization with a two-pulse echo sequence yields a two-spin-process phenomenon. Effectively, in combination with the echo generation, a strong free-induction-decay (FID) process is observed due to the presence of a homogeneous spin packet. These two jointly observed phenomena result from the presence in the sample of two nonequivalent chemical magnetic species.

We performed spin-lattice $T_1$ measurements using FID inversion recovery with 16-step phase cycling to suppress the echo process and echo inversion recovery and found very long $T_1$ times for both processes with threefold higher values for the echo process (Figure 2 A). The $T_1$ values recorded at room temperature were found to be 100 μs and 310 μs for FID and echo processes, respectively. Such behavior gives us the possibility to identify the paramagnetic species responsible for the two distinct spin-magnetic processes.

We recorded two-dimensional spectra for $T_1$ versus the field sweep for the FID signal and observed along the field direction the typical CW $Anth^{+\bullet}$ spectrum with numerous lines due to the proton hyperfine coupling (Figure 2). The spectrum in Figure 2 A is indicative of the formation of $Anth^{+\bullet}$ in accurate agreement with DRUVv and Raman spectroscopy.[6] This spectrum consists of at least twenty split components. Comparison of these $^1$H hyperfine splittings with those of a pure $Anth^{+\bullet}$ isotropic spectrum recorded in solution indicates some $^1$H hyperfine splittings have disappeared due to anisotropic broadening effects. This feature has also previously been observed for $Anth^{+\bullet}$ generated on a silica–alumina catalyst surface and during oxidation by polyoxometalate.[11,12]

Similar experiments with echo detection only yield the observation of the echo shape along the field direction. The

 © 2003 Wiley-VCH Verlag GmbH & Co. KGaA, Weinheim 

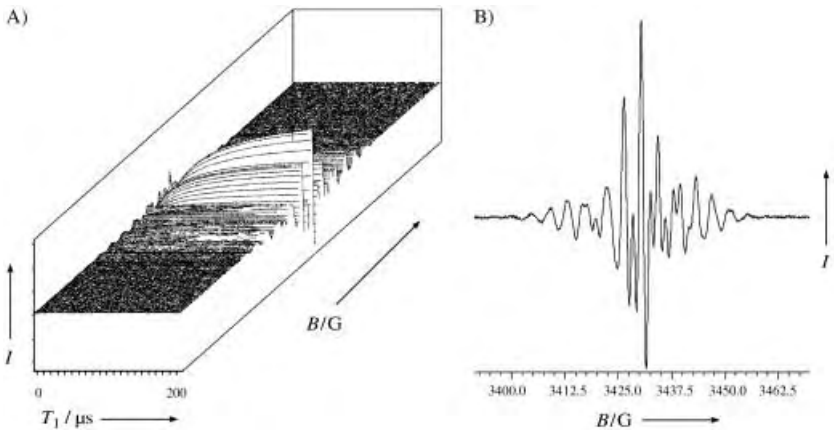



***Figure 2.*** A) 2D spin-lattice relaxation time $T_1$ versus field-sweep measurements recorded at room temperature for Anth occluded in $H_3$ZSM-5 relevant to radical cation/electron moiety. The FID inversion recovery with 16-step phase cycling to suppress echo processes was used. B) Projection slice spectrum of pure Anth$^{+\cdot}$ as observed along the field direction.

echo signal is relevant to the electron trapped in the zeolite framework but needs supplementary pulsed EPR experiments.

The differences in $T_1$ values allow us to characterize separately Anth$^{+\cdot}$ and the trapped electron by spin-echo correlation spectroscopy (SECSY). We performed at room temperature and 4.2 K the analysis of the structure of these two species by using SECSY for the FID (Figure 3 A) and echo SECSY for the echo signal (Figure 3 B). The SECSY spectra give the usual EPR spectrum along the $f_2$-axis and the nuclear frequencies along the $f_1$-axis, respectively. This method provides the distribution of nuclear modulation frequency included in inhomogeneous EPR spectrum. In addition, the characterization of the echo signal was completed by hyperfine sublevel correlation spectroscopy (HYSCORE) experiments (not shown). It has been shown that these HYSCORE experiments offer excellent resolution of the hyperfine splittings.

Firstly, we recorded a 2D SECSY spectrum of the FID process (Figure 3 A), and we observe along the diagonal the signature of the proton–electron coupling of Anth$^{+\cdot}$ that was observed on the projection along the CW domain in Figure 2 B. Moreover we can observe that the diagonal signal measured at the resonance is not completely symmetric and that on both negative and positive quadrants some cross-peaks appear and occur from Heisenberg spin-exchange mechanisms. This result confirms that an equilibrium should exist between the radical cation and trapped electron.

Secondly, due to the strong FID process, a 16-step phase cycling SECSY sequence was used to suppress completely the anti-echo FID process. The 2D echo SECSY contour plot shows in both positive and negative $f_1$ quadrants the double-quantum peak ($2\tilde{\nu}(^{13}C) = 7.4$ MHz) of $^{13}C$ nuclear modulation ($\tilde{\nu}(^{13}C) = 3.7$ MHz) centered at 0 MHz in the $f_2$ domain (Figure 3 B). This is consistent with an unpaired isolated electron coupled with carbon. An additional proton pattern centered at the carbon nuclear frequency is observed with $\nu(^1H) = 14.5$ MHz and combination lines at $2\nu(^1H) = 29$ MHz. Such changes were also observed in the HYSCORE spectrum (not shown) where the $^1H$ anisotropic constant measured is 9.8 MHz and a weak carbon coupling is observed in the (+,+) $f_2$ domain with an anisotropic constant of 2.1 MHz and a positive sign for the hyperfine splitting constant. Moreover, no signal features arising from zeolite interactions through $^{29}Si$ or $^{27}Al$ were evident in the HYSCORE spectrum. In HYSCORE and SECSY spectra the same patterns are observed at room temperature and at 4.2 K. Due to its quadrupolar moment, the $^{27}Al$ nucleus can be observed only at 4.2 K. Consequently, the HYSCORE pattern observed at 3.7 MHz at room temperature and at 4.2 K must be attributed to $^{13}C$ modulation and not to the $^{27}Al$ nucleus, for which the nuclear modulation frequency is 3.8 MHz. Such results seem to indicate that the electron is trapped in close proximity to the occluded Anth$^{+\cdot}$ radical cation. It should be noted that the trapped electron is stabilized in the zeolite framework with no visible coupling to $^{27}Al$ or $^{29}Si$ nuclei and is probably in close proximity to oxygen.

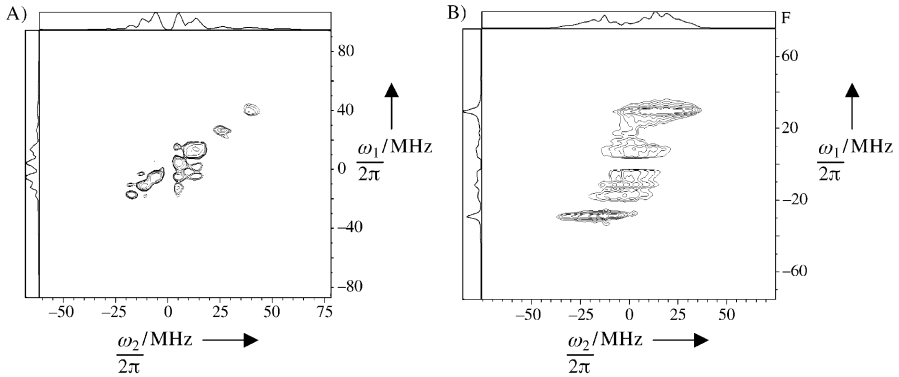



***Figure 3.*** SECSY spectra of Anth occluded in $H_3$ZSM-5 zeolite relevant to the radical cation/electron moiety. A) Two-pulse FID SECSY spectrum of the radical cation. B) Two-pulse echo SECSY spectrum of the trapped electron. The spectra were recorded at 4.2 K at the maximum of the CW EPR signal. The two-pulse SECSY spectrum was recorded with pulse lengths of 12 ns for $\pi/2$ pulses, and a 16-step phase cycling ($\pi/2-t_1-\pi/2-t_1-t_2-$echo) was applied.

When we heated the sample that had equilibrated at room temperature over three months, the hyperfine structure of the CW spectra disappeared and only a featureless signal was obtained after one hour at 473 K. Double integration of the signals, (spectrum c, Figure 1 B) indicates a spin density close to two unpaired electrons per unit cell. The hyperfine splittings reappeared when the sample was cooled to room temperature after an equili-

 © 2003 Wiley-VCH Verlag GmbH & Co. KGaA, Weinheim 

bration period of several hours (spectrum d, Figure 1B). An identical phenomenon was observed by DRUVv spectrometry, (Figure 1A). The intense absorption bands around 300 and 700 nm characteristic of $Anth^{+\cdot}$ disappeared gradually upon heating. This development was complete at 473 K. The resulting spectral maxima (383, 364, 347 nm) were found to be analogous to those exhibited by occluded Anth in the ground state (384, 364, 347 nm) except for a weak and broad-band absorption around 500 nm (spectrum c, Figure 1A). Both the broad EPR signal and the absorption at 500 nm were straightforwardly attributed to occluded electron–hole pairs with respect to Anth occluded in ground state.

The remanence of the electron–hole pair at room temperature for one hour before the reverse electron-transfer permitted us to perform pulsed EPR investigations. The two-pulse echo experiment recorded for the the so-called electron–hole pair shows the complete disappearance of the FID process in accordance with the disappearance of $Anth^{+\cdot}$. Moreover, $T_1$ echo measurements yield the same value as that measured for the ejected electron of the $Anth^{+\cdot}$/electron moiety, demonstrating identical relaxation times for the ejected electron and for unpaired electrons involved in the electron–hole pair.

Both the 2D echo SECSY contour plot and the HYSCORE pattern of electron–hole pair were found to be analogous to those recorded for the $Anth^{+\cdot}$/electron moiety. In particular, the 3.7-MHz pattern observed in the HYSCORE spectrum is assigned to $^{13}C$ nuclei in a straightforward fashion. Such results seem to indicate that the electrons of the electron–hole pairs are in the vicinity of the occluded Anth in ground state. Unfortunately, no evidence was found for coupling between the electrons and the $^{27}Al$ or $^{29}Si$ nuclei of the zeolite framework. The electrons of the electron–hole pairs are probably stabilized in the zeolite framework in close proximity to oxygen nuclei. In contrast, coupling between electrons and $^{29}Si$ and $^{27}Al$ nuclei was observed previously for the electron–hole pairs stabilized by sorption of biphenyl in $H_3ZSM\text{-}5$.[3] In addition, no half-field signal was detected in the CW spectrum. Thus, there is no evidence for a spin-coupling interaction between the two paramagnetic centers of the electron–hole pair stabilized in the $H_3ZSM\text{-}5$ zeolite loaded with Anth. It should be noted that weak ferromagnetic coupling was previously detected in the electron–hole pair stabilized by biphenyl.[3]

The exposure of solid Anth to the bare zeolite $H_3ZSM\text{-}5$ ($H_3(AlO_2)_3(SiO_2)_{93}$) results in the uptake of Anth molecules at the openings of the pores and diffusion into the straight channels of the zeolite framework. Because of the relatively low ionization potential of Anth in the gas phase (7.44 eV), the electrostatic field in the void space of $H_3ZSM\text{-}5$ suffices to completely ionize Anth, and it is found trapped exclusively as the radical cation [Eq. (1)].

$$Anth + H_3ZSM\text{-}5 \rightarrow Anth^{+\cdot}/H_3ZSM\text{-}5^{-\cdot} \quad (1)$$

The ejected electron was found to be in close proximity to $Anth^{+\cdot}$, and the $Anth^{+\cdot}$/electron moiety was found occluded in the straight channel (Figure 4). However, we found no evidence for the interaction of unpaired electrons with the zeolite nuclei. The $Anth^{+\cdot}/H_3ZSM\text{-}5^{-\cdot}$ moiety exhibits temperature-dependent behavior in agreement with the observation of temperature-dependent electron transfer from the $H_3ZSM\text{-}5$ framework to the $Anth^{+\cdot}$ radical cation through Equation (2).

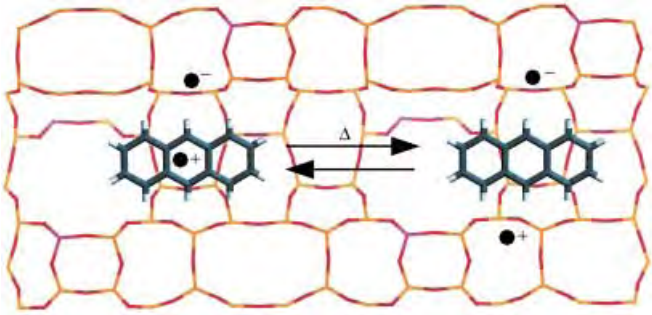



***Figure 4.*** Schematic structures of the $Anth^{+\cdot}$/electron moiety and the electron–hole pair in the straight channel of $H_3ZSM\text{-}5$ zeolite. Yellow, red, and pink sticks represent the Si, O, and Al atoms of zeolite, respectively. Dark gray and white cylinders represent the C and H atoms of anthracene. ● − = trapped electron, ● + = electron-deficient sites in $Anth^{+\cdot}$ and in hole.

$$Anth^{+\cdot}/H_3ZSM\text{-}5^{-\cdot} \overset{\Delta}{\rightleftarrows} Anth/H_3ZSM\text{-}5^{+\cdot -\cdot} \quad (2)$$

The conversion appears to be gradual and fully reversible. In contrast to the behavior of biphenyl in the same zeolite, the spontaneous ionization of Anth and subsequent formation of the electron–hole pair were found to be nearly total. However, no interaction of the unpaired electrons with the zeolite framework was detected. The electron–hole pair appears to be stabilized in high yield in the straight channel of $H_3ZSM\text{-}5$ by anthracene in the ground state in close proximity.

The ability of some porous materials to generate and stabilize electron–hole pairs appears to be the conjunction of intrinsic and complementary properties of both the host and the guest. The process is initiated by the sorption of electron-donor molecules, the shape and size of which are suitable for penetrating the void space of the zeolite.[6] The electrostatic field imposed by the incorporation of $Al^{III}$ and $H^+$ as the counterion leads to complete ionization. The charge recombination is hampered by the restricted mobility of the sorbed radical cation and efficient electron trapping. The electron capture from the framework by the radical cation rather than direct charge recombination is the most intriguing feature under the confinement of the void space. The long life of the electron–hole pair stabilized by anthracene occluded in $H_3ZSM\text{-}5$ zeolite is attributed to both efficient electron and hole trapping.

Received: July 1, 2003 [Z52269]

**Keywords:** anthracene · electron transfer · EPR spectroscopy · UV/Vis spectroscopy · zeolites

 © 2003 Wiley-VCH Verlag GmbH & Co. KGaA, Weinheim 

[1] H. Garcia, H. D. Roth, *Chem. Rev.* **2002**, *102*, 3947 – 4007.
[2] R. I. Samoilova, A. A. Shubin, M. K. Bowman, J. Hüttermann, S. A. Dikanov, *Chem. Phys. Lett.* **2000**, *316*, 404 – 410.
[3] A. Moissette, H. Vezin, I. Gener, J. Patarin, C. Brémard, *Angew. Chem.* **2002**, *114*, 1289 – 1292; *Angew. Chem. Int. Ed.* **2002**, *41*, 1241 – 1244.
[4] I. Kirisci, H. Förster, G. Tasi, J. B. Nagy, *Chem. Rev.* **1999**, *99*, 2085 – 2114.
[5] M. Hunger, J. Weitkamp, *Angew. Chem.* **2001**, *113*, 3040 – 3059; *Angew. Chem. Int. Ed.* **2001**, *40*, 2954 – 2971.
[6] A. Moissette, S. Marquis, I. Gener, C. Brémard, *Phys. Chem. Chem. Phys.* **2002**, *4*, 5690 – 5696.
[7] G. Catana, D. Baetens, T. Mommaerts, R. A. Schoonheydt, B. M. Weckhuysen, *J. Phys. Chem. B* **2001**, *105*, 4904 – 4911.
[8] B. Staudte, A. Gutsze, W. Böhlmann, H. Pfeifer, B. Pichewitz, *Microporous Mesoporous Mater.* **2000**, *40*, 1 – 7.
[9] D. Goldfarb, K. G. Strohmaier, D. E. W. Vaughan, H. Thomann, O. G. Poluektov, J. Schmidt, *J. Am. Chem. Soc.* **1996**, *118*, 4665 – 4671.
[10] H. Van Koningsveld, J. C. Jansen, H. Van Bekkum, *Zeolites* **1990**, *10*, 235 – 242.
[11] G. M. Muha, *J. Phys. Chem.* **1967**, *71*, 640 – 649.
[12] A. M. Khenkin, L. Weiner, Y. Wang, R. Neumann, *J. Am. Chem. Soc.* **2001**, *123*, 8531 – 8542.

 © 2003 Wiley-VCH Verlag GmbH & Co. KGaA, Weinheim 

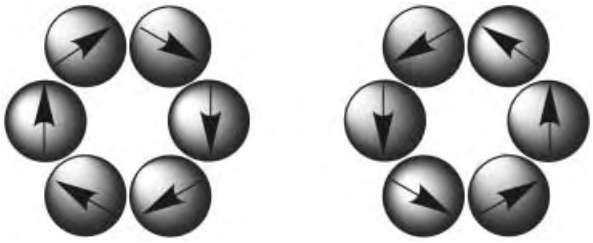


*Figure 1.* Flux-closure domains produced by cyclic ensembles of magnetic dipoles, in clockwise and counterclockwise configurations.

*Magnetic Effects in Nanomaterials*

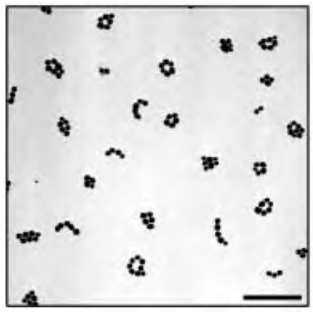
# Flux Closure in Self-Assembled Cobalt Nanoparticle Rings**

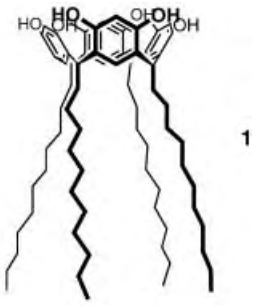
*Steven L. Tripp, Rafal E. Dunin-Borkowski, and Alexander Wei**

The drive toward ultradense information storage has stimulated considerable interest in magnetic nanostructures, particularly those with bistable domains and minimal crosstalk between elements.[1] Magnetic rings are appealing candidates for such applications because their magnetostatic fields can be entrained into chiral domains commonly referred to as flux-closure (FC) states (see Figure 1). Here magnetic dipoles are aligned into a closed circuit and produce a net moment of zero, which minimizes both the magnetic energy and the field outside of the ring. Bistable FC states have been used extensively in early data-storage applications involving ferrite cores, which served as bits in electronically addressable magnetic memory devices.[2] More recently, magnetic rings have been proposed as elements in novel device architectures for magnetoresistive random-access memory (MRAM), with subsequent studies directed at the FC states of Co microrings fabricated by lithography.[3–5] However, these structures are far from the physical size limit of flux closure, which ultimately depends on the magnetic remanence of the host material.

In this Communication, we demonstrate that single-walled Co nanoparticle rings can support stable FC states at room temperature, using off-axis electron holography to visualize magnetic flux with nanometer spatial resolution.[6] These bracelet-like rings are created by dipole-directed self-assembly, with dimensions well below the limits of conventional lithography: A ring of six 27-nm Co particles (the average size used in this study) is less than 100 nm in diameter.[7,8] Self-assembled nanorings also have intriguing possibilities for integration with nanopatterned surfaces, with application toward spin-polarized electronic devices.[3]

Co nanoparticles encapsulated in a 3–4 nm CoO shell ($27 \pm 4$ nm, $10^{12}$–$10^{13}$ particles $mL^{-1}$) were dispersed in toluene with varying amounts of *C*-undecylcalix[4]resorcinarene (**1**) as a surfactant (1–100 μM) as previously described, then deposited onto carbon-coated copper grids and dried in air using a standardized procedure.[7] These dispersion conditions produce a variety of self-assembled nanostructures as imaged by transmission electron microscopy (TEM) including five- and six-particle rings, short chains, and close-packed aggregates containing three or more particles (see Figure 2). A statistical analysis suggests that the relative yield of dipole-






1

*Figure 2.* TEM image (Philips EM-400, 80 kV) showing nanoparticle rings and chains formed by dipole-directed self-assembly. Co nanoparticles ($27 \pm 4$ nm, $10^{12}$ particles $mL^{-1}$) were dispersed in toluene with resorcinarene **1** ($10^{-6}$ M), then deposited as a thin wetting layer onto a carbon-coated Cu grid and dried in air. Scale bar = 250 nm.

[*] Prof. A. Wei, Dr. S. L. Tripp
Department of Chemistry, Purdue University
West Lafayette, IN 47907 (USA)
Fax: (+1) 765-494-0239
E-mail: alexwei@purdue.edu
Dr. R. E. Dunin-Borkowski
Department of Materials Science
University of Cambridge, Pembroke Street
Cambridge CB2 3QZ (UK)

[**] A.W. and S.L.T. gratefully acknowledge support from the National Science Foundation (0243496-CHE), the Department of Defense, and the Birck Nanotechnology Center at Purdue University. R.E.D.B. thanks the Royal Society for financial support.

 DOI: 10.1002/anie.200352825 © 2003 Wiley-VCH Verlag GmbH & Co. KGaA, Weinheim 

directed aggregates (rings and chains) is optimal at an initial concentration of $10^{12}$ particles $mL^{-1}$ and surfactant concentrations of 10 μM or more (see Figure 3). The latter parameter is important for increasing the viscosity of the residual wetting

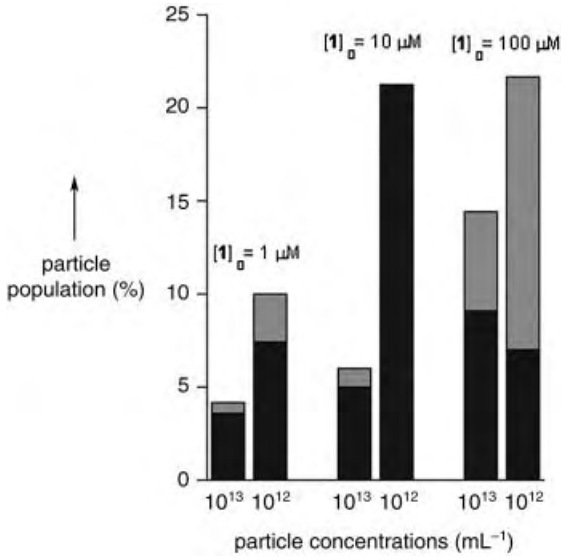



***Figure 3.*** Distribution of Co nanoparticles observed in dipole-directed assemblies, as a function of initial particle and surfactant concentrations. Particle populations in self-assembled rings and chains are plotted as dark and light grey areas, respectively. Particle counts were taken over areas of at least 8 $\mu m^2$.

layer, which stabilizes the rings against van der Waals "collapse" during the drying stage.[7] However, higher levels of **1** correlate with a greater percentage of nanoparticles in open chains, which indicates that ring formation is most favored at intermediate surfactant concentrations. The self-assembled rings and chains captured in the TEM images do not necessarily represent an equilibrium distribution: While these nanostructures are likely to equilibrate in solution at zero field, additional shear forces during surface adsorption and drying may affect the final distribution of immobilized species.

Remanent magnetic FC states in individual nanoparticle rings were recorded at room temperature under zero-field conditions by electron holography (see Figure 4). Continuous magnetic flux lines revealed the in-plane induction to be confined within each ring ensemble, despite irregularities in particle shape and deviations from radial symmetry in the self-assembled nanostructures. Magnetic force microscopy did not indicate any out-of-plane magnetization, which signified the absence of magnetic vortex cores such as those observed in planar magnetic disks.[9–11] These observations are consistent with a magnetostatic description of FC states in cyclic ensembles of single-domain particles.[12]

Electron holography records additional phase information which reveals the handedness of the magnetic domains within the Co nanoparticle rings (see Figure 4, bottom row). A statistical sampling of FC states indicates an approximately 50:50 (racemic) mixture of clockwise and counterclockwise ground-state configurations, to which the rings relaxed after

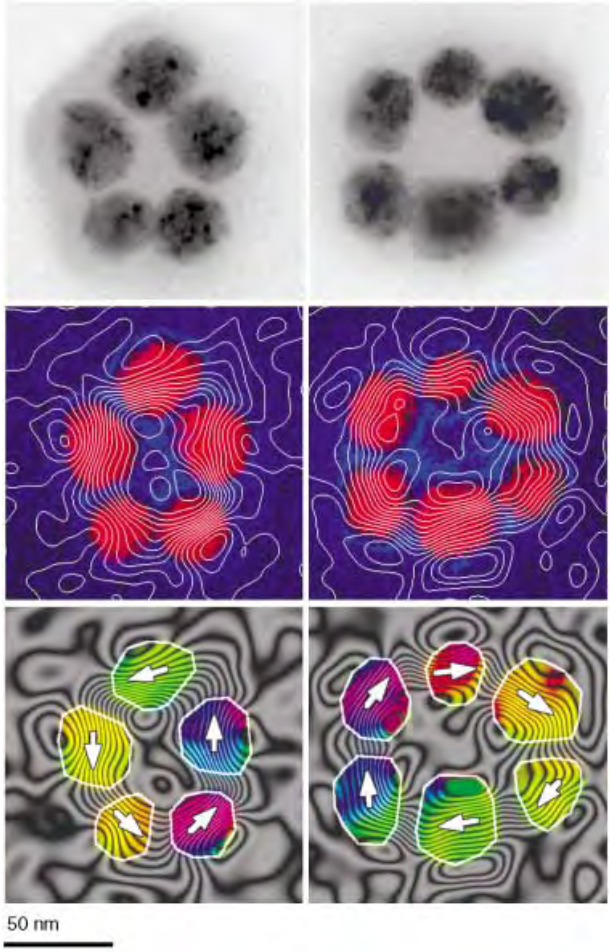



***Figure 4.*** TEM and electron holography images of self-assembled Co nanoparticle rings, taken with a Philips CM-300 equipped with a Lorentz lens (300 kV). Samples were briefly subjected to plasma cleaning prior to TEM analysis. Top: bright-field images of nanoparticle rings; middle: magnetic FC states imaged in zero-field conditions using off-axis electron holography and displayed in the form of contours, superimposed on elemental maps obtained by energy-filtered TEM analysis (red = Co, blue = C). The magnetic flux enclosed between adjacent contours is $h/128e$; bottom: direction of the magnetic flux indicated using arrows and colors (red = right, yellow = down, green = left, blue = up). The magnetic contribution to the measured holographic phase shift was separated from the mean inner potential contribution by taking the difference between phase images recorded with the sample turned over in the electron microscope.

exposure to a 2 T out-of-plane magnetic field. The chiral FC states are stable at room temperature and persist in low magnetic fields. This coercivity implies cooperativity in magnetic coupling, and suggests that FC states may be achieved at room temperature using even smaller nanoparticles.[13] This is in stark contrast to vortex states in thin magnetic disks of similar material, which are stable only for diameters of 100 nm or more.[14]

The Co nanoparticle rings presented here offer at least two unique opportunities for studying magnetism on the nanoscale. First, the FC states comprise discrete single domains, whose magnetization behaviors and reversals can be modeled precisely by micromagnetic simulations.[12]

 © 2003 Wiley-VCH Verlag GmbH & Co. KGaA, Weinheim 

Second, the chirality of the FC states can be switched by out-of-plane or circularly polarized magnetic fields generated by electrical currents, as demonstrated recently with a submicron magnetic cylinder.[15] Explorations in this direction would require integrating magnetic nanorings with electrically conductive nanowires. Self-assembly may prove to be pivotal in the construction of such hybrid nanomaterials.

Received: September 9, 2003 [Z52825]
Published Online: November 3, 2003

**Keywords:** chirality · cobalt · magnetic properties · nanostructures · self-assembly

[1] R. E. Dunin-Borkowski, M. R. McCartney, B. Kardynal, D. J. Smith, M. R. Scheinfein, *Appl. Phys. Lett.* **1999**, *75*, 2641 – 2643.
[2] L. A. Russell, R. M. Whalen, H. O. Leilich, *IEEE Trans. Magn.* **1968**, *4*, 134 – 145.
[3] J.-G. Zhu, Y. Zheng, G. A. Prinz, *J. Appl. Phys.* **2000**, *87*, 6668 – 6673.
[4] J. Rothman, M. Kläui, L. Lopez-Diaz, C. A. F. Vaz, A. Bleloch, J. A. C. Bland, Z. Cui, R. Speaks, *Phys. Rev. Lett.* **2001**, *86*, 1098 – 1101.
[5] S. P. Li, D. Peyrade, M. Natali, A. Lebib, Y. Chen, U. Ebels, L. D. Buda, K. Ounadjela, *Phys. Rev. Lett.* **2001**, *86*, 1102 – 1105.
[6] R. E. Dunin-Borkowski, M. R. McCartney, B. Kardynal, S. S. P. Parkin, M. R. Scheinfein, D. J. Smith, *J. Microsc.* **2000**, *200*, 187 – 205.
[7] S. L. Tripp, S. V. Pusztay, A. E. Ribbe, A. Wei, *J. Am. Chem. Soc.* **2002**, *124*, 7914 – 7915.
[8] For magnetic rings assembled from $Fe_3O_4$ nanoparticles, see: A. P. Philipse, D. Maas, *Langmuir* **2002**, *18*, 9977 – 9984.
[9] T. Shinjo, T. Okuno, R. Hassdorf, K. Shigeto, T. Ono, *Science* **2000**, *289*, 930 – 932.
[10] J. Raabe, R. Pulwey, R. Sattler, T. Schweinböck, J. Zweck, D. Weiss, *J. Appl. Phys.* **2000**, *88*, 4437 – 4439.
[11] A. Wachowiak, J. Wiebe, M. Bode, O. Pietzsch, M. Morgenstern, R. Wiesendanger, *Science* **2002**, *298*, 577 – 580.
[12] P. Jund, S. G. Kim, D. Tománek, J. Hetherington, *Phys. Rev. Lett.* **1995**, *74*, 3049 – 3052.
[13] Although the critical field strengths for magnetization reversal remain to be determined, we have observed the FC states of 6- and 7-membered rings to be reproducibly switched by an out-of-plane field of 1600 Oe.
[14] R. P. Cowburn, D. K. Koltsov, A. O. Adeyeye, M. E. Welland, D. M. Tricker, *Phys. Rev. Lett.* **1999**, *83*, 1042 – 1045.
[15] K. Bussmann, G. A. Prinz, R. Bass, J.-G. Zhu, *Appl. Phys. Lett.* **2001**, *78*, 2029 – 2030.

 © 2003 Wiley-VCH Verlag GmbH & Co. KGaA, Weinheim 

Main-Group Clusters

# Ligand and Metal Effects on the Formation of Main-Group Polyhedral Clusters**

*Sally R. Boss, Martyn P. Coles,* Robert Haigh, Peter B. Hitchcock, Ronald Snaith[+], and Andrew E. H. Wheatley**

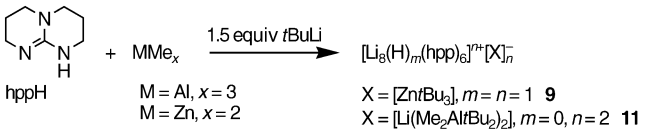
Anion-containing metal clusters in general and interstitial hydrides in particular have a range of uses. The ability of main-group hydrides to store and deliver reactive hydride ions means that they have long been utilised synthetically as reducing agents.[1] They do, however, also have the ability to act as convenient sources of hydrogen and, as such, have potential applications in the hydrogen economy.[2] In the context of such species, we previously reported that the sequential treatment of *N*-2-pridylaniline with one equivalent $AlMe_3$ yields dimethylaluminium(*N*-2-pyridylanilide) (**1**), which then reacts with excess *t*BuLi to give species that X-ray crystallographic analysis suggests to be the cluster complexes $[Li_8(H)\{N(2\text{-}C_5H_4N)Ph\}_6]^+[Li(Me_2Al\mathit{t}Bu_2)_2]^-$ (**2**), and $Li_7(H)\{N(2\text{-}C_5H_4N)Ph\}_6$ (**3**).[3] Such compounds, postulated to incorporate interstitial hydride, are extremely rare with the convoluted hydride/*t*-butoxide superaggregate $[Li_{33}H_{17}(O\mathit{t}Bu)_{16}]$[4] and heterobimetallic $[Li\{(\mathit{t}BuCH_2O)_5Al_3H_5\}]\cdot OEt_2$[5] and $[\{NaMg[N(\mathit{i}Pr)_2](\mu\text{-}H)\cdot PhMe\}_2]$[6] being the only clusters of main-group metals suggested to incorporate hydride in what is otherwise a field dominated by transition-metal species.[7] Recently, a succession of complexes related to **2** and **3** have been characterized in the solid state. However, $[Li_8(H)\{N(2\text{-}C_5H_4N)(C_6H_4\text{-}4\text{-}Me)\}_6]^+[Li(Me_2Al\mathit{t}Bu_2)_2]^-$ (**4**), $[Li_8(H)\{N(2\text{-}C_5H_4N)(C_6H_4\text{-}2\text{-}Me)\}_6]^+[Me(Al\mathit{t}Bu_3)_2]^-$ (**5**), $[Li_8(H)\{N(2\text{-}C_5H_4N)Ph\}_6]^+[Li(Et_2Al\mathit{t}Bu_2)_2]^-$ (**6**, obtained by using $AlEt_3$), and $[Li_8(H)\{N(2\text{-}C_5H_4N)(\mathit{c}\text{-}C_6H_{11})\}_6]^+[Li(Me_2Al\mathit{t}Bu_2)_2]^-$ (**7**) have also yielded only circumstantial evidence for the existence and identity of the interstitial hydride ion.[8] It is only very recently that categorical evidence has been obtained in this respect, with the solution of a single crystal neutron diffraction structure of **2**.[8] To date, attempts to significantly alter the composition of such hydride-yielding systems have met with little success; the employment of, for example, *N,N′*-diphenylbenzamidine gives the hydride-free superlithiate $[Li_4\{PhNC(Ph)NPh\}_3]^+[Li(Me_2AlMe\mathit{t}Bu)_2]^-$

[*] Dr. M. P. Coles, Dr. P. B. Hitchcock
The Chemical Laboratories
University of Sussex
Brighton, BN1 9QJ (UK)
Fax: (+44) 1273-677-196
E-mail: m.p.coles@sussex.ac.uk
Dr. A. E. H. Wheatley, S. R. Boss, Dr. R. Haigh
Department of Chemistry
University of Cambridge
Lensfield Road, Cambridge, CB2 1EW (UK)
Fax: (+44) 1223-336-362
E-mail: aehw2@cam.ac.uk
[+] Deceased.

[**] This work was supported by the U.K. EPSRC (S.R.B., R.H.).

 DOI: 10.1002/anie.200351921 © 2003 Wiley-VCH Verlag GmbH & Co. KGaA, Weinheim 

(**8**).[9] In seeking to probe the generality of cage–cluster formation and hydride entrapment, two variations on the methodology that yields **2** and **3** (and also **4**–**7**) have been deployed; 1) *N*-2-pridylaniline has been replaced by a non-aromatic guanidine ligand, and 2) while the use of MeLi and HMDSLi (HMDS = hexamethyldisilazide) has circumstantially established the importance of β-hydrogen-containing *t*BuLi in hydride encapsulation chemistry[10] the Group 13 organometallic substrate is now replaced by a Group 12 analogue. We report herein that a hydride-entrapment cluster can be generated by using bicyclic 1,3,4,6,7,8-hexahydro-2*H*-pyrimido[1,2-*a*]pyrimidine (hppH) in tandem with $ZnMe_2$ and *t*BuLi. Remarkably, the use of $AlMe_3$ in such a system leads to the formation of a hydride-free polyhedral cluster of the type known to encapsulate an anion in **2** (see Scheme 1).




***Scheme 1.*** Synthesis of complexes **9** and **11**.

Sequential reaction of $ZnMe_2$ with hppH and 1.5 equivalents of *t*BuLi in toluene gives an oil from which crystals deposit (see Experimental Section). Consistent with $^1$H NMR spectroscopy (which indicates the presence of hpp and *t*Bu in a 2:1 ratio), X-ray crystallography reveals this product to be ion-separated $[Li_8(H)(hpp)_6]^+[Zn tBu_3]^-$ (**9**, see Figure 1). For this formula there also exists half a lattice toluene molecule and, of the two crystallographically independent separated ion pairs that exist in the unit cell, one representative example will be discussed in detail.[11] The tris(*t*-butyl)zincate anion in **9** contains a metal center that deviates only nominally from trigonal planar coordination (sum of angles at the Zn atom = 359.4°, mean Zn–C = 2.065 Å). The cationic component of **9** incorporates an almost exactly cubic array of closely packed alkali-metal centers (Li···Li range 2.473(14)–2.527(14) Å); each metal face is symmetrically straddled by a {hpp}$^-$ ion (mean ∠C(NLi$_2$)$_2$ 118.3°). The Fourier difference map reveals observable interstitial electron density that can only be satisfactorily refined as hydride. Such an assignment is consistent not only with the $[Li_8(hpp)_6]^{2+}$:$[Zn tBu_3]^-$ stoichiometry observed both crystallographically and by NMR spectroscopy but also with the recent fundamental demonstration of the existence of molecular interstitial hydrides of this type.[8] However, in contrast to previously reported structures the regularity of the alkali-metal cluster in **9** suggests a $\mu^8$-coordination sphere for the trapped anion (see also **2**, which has an octahedrally coordinated hydride by virtue of the displacement of two $Li^+$ centers away from the cluster core). The observation of a distorted alkali-metal array in **2** correlates with the ligand asymmetry therein. Charge delocalization over all three N centers is suggested in each {hpp}$^-$ ligand (mean sum of angles at N3/N6/N9 = 359.5°; Figure 1b). It is reasonable that the ligand symmetry demonstrated by the {hpp}$^-$ ligand is responsible for the more regular and thus higher coordination state of the interstitial

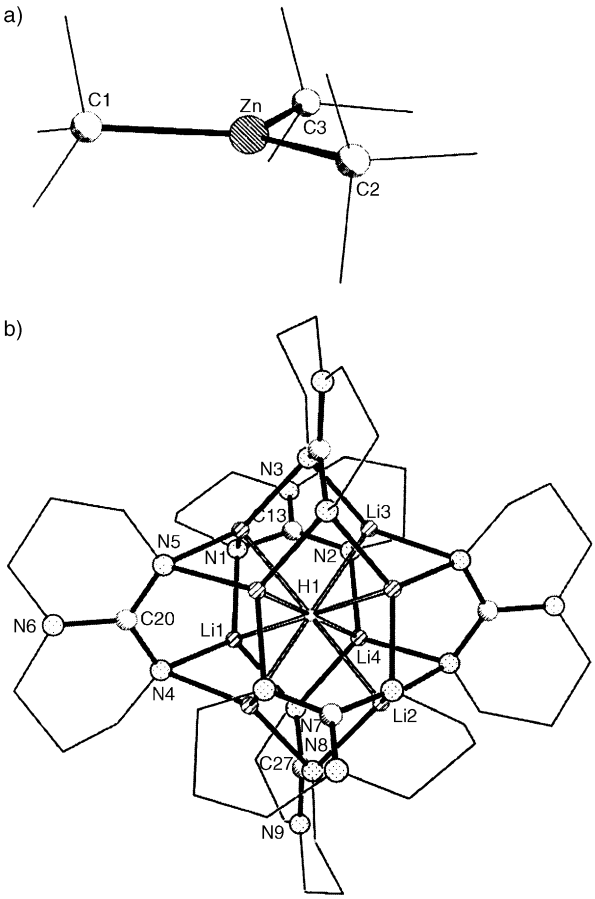



***Figure 1.*** a) Anionic part of **9**. Selected bond lengths [Å] and angles [°]: Zn-C1 2.080(7), Zn-C2 2.059(7), Zn-C3 2.057(8), C1-Zn-C2 118.1(2), C1-Zn-C3 120.7(3), C2-Zn-C3 120.6(3). b) Cationic part of **9**: Li1-H1 2.21(1), Li2-H1 2.17(1), Li3-H1 2.16(1), Li4-H1 2.10(1), Li1-N1 2.019(11), Li1-N4 2.014(11), Li1-N7 2.029(10), Li2-N1A 2.026(11), Li2-N5A 1.984(11), Li2-N8 1.999(11), Li3-N2 2.007(11), Li3-N4A 2.000(11), Li3-N8A 2.030(10), Li4-N2 1.974(11), Li4-N5A 2.031(11), Li4-N7 2.001(11), C13-N1 1.349(8), C13-N2 1.316(8), C13-N3 1.396(8), C20-N4 1.353(7), C20-N5 1.329(7), C20-N6 1.386(7), C27-N7 1.340(7), C27-N8 1.332(7), C27-N9 1.377(7), N1-C13-N2 119.1(5), N4-C20-N5 118.9(5), N7-C27-N8 117.6(5), Li1-N1-Li2A 76.8(4), Li3-N2-Li4 77.4(4), Li1-N4-Li3A 78.0(4), Li2A-N5-Li4A 76.0(4), Li1-N7-Li4 76.2(4), Li2-N8-Li3A 76.5(4).

anion. Consistent with this enhanced coordination, the mean Li–H bond length in **9** (2.16 Å; Li1–H1 2.21(1), Li2–H1 2.17(1), Li3–H1 2.16(1), Li4–H1 2.10(1) Å) is longer than those in both **2** (2.015 Å) and **3** (2.06 Å) and of that in octahedral $(LiH)_\infty$ (2.04 Å).[12] All Li–H bond lengths in **9** are significantly shorter than the nonbonding Li···H distance in **2** (2.828(9) Å) or the extended metal-hydride distance of 2.49(3) Å in **3**. Nevertheless, in the structure of **9**, Li1 (and its symmetry equivalent) are nominally extruded (see **2**) such that they are incorporated both in the most extended Li–H bonds (2.21(1) Å) and in the longest cube–edge distances (mean Li1···Li2A/3A/4 2.509 Å). All metal–hpp bond lengths in **9** are normal for Li–N interactions (range 1.984(11)–2.030(10) Å, mean 2.010 Å).[13]

The reaction of hppH with $AlMe_3$ is known to afford the dimethylaluminium(guanidinate) Al(hpp)Me$_2$ (**10**)[14] the

 © 2003 Wiley-VCH Verlag GmbH & Co. KGaA, Weinheim 

treatment of which with 1.5 equivalents of *t*BuLi gives a single isolable product (**11**). However, $^1$H NMR spectroscopy reveals that this species does not contain hpp, *t*Bu, and AlMe units in the ratio 3:1:1 (expected for a hydride-encapsulating analogue of **2**) but in the ratio 3:2:2 (see Experimental Section). Rather than pointing to the formation of a **2**-type interstitial hydride, these data suggest the existence of two aluminium-containing anions for each $[Li_8(hpp)_6]^{2+}$ cluster ion and obviates the need for interstitial hydride to achieve electrical neutrality. Accordingly, and in contrast to the data for **2, 3**, and **9** (in all of which the Fourier difference map revealed residual electron density attributable to the trapped anion)[3,8] an X-ray crystallographic study of **11** reveals the existence of an interstitial void and thus the formulation of ion-separated $[Li_8(hpp)_6]^{2+}[\{[Li(Me_2AltBu_2)_2]^-\}_2]$ (see Figure 2).[15] The two observed lithium bis(aluminate) anionic components are precisely analogous to that reported for **2**[3] and closely related to that noted recently in **8**.[9] The single countercation incorporates an array of alkali metal centers that is almost perfectly cubic and each face of which is straddled by an $\{hpp\}^-$ ion. This polyhedral regularity contrasts with that seen in the structure of **2**[3] and suggests a relationship with the cationic component of **9**. However, any similarity proves to be superficial, with the intermetal cube edges in **11** being significantly longer those in **9** (namely Li···Li in **9**: 2.473(14)–2.527(14) Å; in **11** 2.751(7)–2.795(7) Å) and are comparable only to those in **2** that involve the extruded alkali-metal centers. Hence, in spite of the similar bite angles of *N*-2-pyridylanilide and $\{hpp\}^-$ (mean $C(NLi_2)_2$ in **2**: 115.5°; in **11**: 117.3°) it is clear that the cluster cation of **11** incorporates a somewhat enlarged alkali-metal cage. To compensate, the Li–N distances in **11** (mean Li–N 1.987 Å, range 1.964(5)–2.013(5) Å) are shorter than those reported for either **2** (mean 2.048 Å, range 1.966(8)–2.130(8) Å) or **9** (mean 2.010 Å, range 1.984(11)–2.030(10) Å). Such geometry is consistent with the absence of bonding interactions involving an interstitial anion. Rather, the positions of the $Li^+$ ions in **11** are borne of intermetal electrostatic repulsion and the action of $\{hpp\}^-$ ligands only.

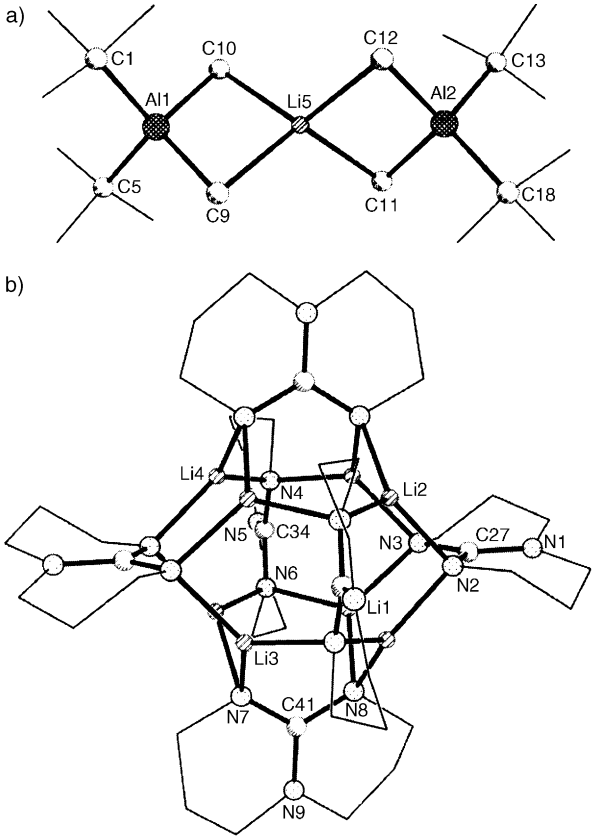



***Figure 2.*** a) Anionic part of **9**. Selected bond lengths [Å] and angles [°]: Li5-C9 2.260(7), Li5-C10 2.271(7), Li5-C11 2.270(8), Li5-C12 2.279(7), Al1-C9 2.035(3), Al1-C10 2.050(3), Al2-C11 2.046(4), Al2-C12 2.047(4), C9-Li5-C10 95.7(3), C11-Li5-C12 95.6(3), Li5-C9-Al1 76.97(19), Li5-C10-Al1 76.43(19), Li5-C11-Al2 76.9(2), Li5-C12-Al2 76.7(2), C9-Al1-C10 110.67(16), C11-Al2-C12 110.82(17). b) Cationic part of **9**: Li1-N3 1.987(5), Li1-N6 2.004(5), Li1-N8 1.973(5), Li2-N2 1.989(5), Li2-N6A 1.969(5), Li2-N7A 2.013(5), Li3-N3A 1.981(5), Li3-N4A 1.998(5), Li3-N7 1.964(5), Li4-N2A 1.981(5), Li4-N4 1.993(5), Li4-N8A 1.993(5), C27-N1 1.365(3), C27-N2 1.346(4), C27-N3 1.349(4), C34-N4 1.353(3), C34-N5 1.359(4), C34-N6 1.340(4), C41-N7 1.348(3), C41-N8 1.348(3), C41-N9 1.360(3), N2-C27-N3 117.6(2), N4-C34-N6 117.4(2), N7-C41-N8 117.0(2), Li1-N3-Li3A 89.4(2), Li2-N2-Li4A 89.5(2), Li1-N6-Li2A 88.0(2), Li3A-N4-Li4 88.2(2), Li1-N8-Li4A 89.4(2), Li2A-N7-Li3 87.5(2).

The observation that $ZnMe_2$ is capable of yielding a hydride-encapsulation complex of the type $[Li_8(H)R_6]^+[X]^-$ is noteworthy and suggests some generality to the organometallic components that evolve such a cluster cation. Moreover, employment of the guanidine substrate hppH yields results that contrast with recent attempts to generate analogues of **2** by using *N,N′*-diphenylbenzamidine,[9] and they suggest that the employment of less sterically demanding amidines should further extend this area of hydride-capture chemistry. The view that the presence of a pyridyl moiety (see **2** and **3**) is not necessary for hydride encapsulation to proceed (see **9**) is borne of the non-aromatic nature of hppH. Evidently, the (known) reductive addition of LiH to pyridines[16] does not represent a required intermediate step in hydride capture of the type noted here. Moreover, previously published data that strongly suggest *t*BuLi to be the lithium hydride source in the preparation of complexes such as **2** point to the role of *t*BuLi differing in the two syntheses reported here.[10,17] That this dichotomy gives a structural congener of **9** that incorporates not a hydride but a core void introduces the possibility of a truly polyhedral structural chemistry for alkali metals.

## *Experimental Section*

Synthesis of **9**: A solution of $ZnMe_2$[18] (2.0 M in toluene; 0.5 mL, 1.0 mmol) was added to hppH (0.139 g, 1.0 mmol) in toluene (8 mL) at room temperature under $N_2$ and this solution was stirred until the effervescence subsided. A solution of *t*BuLi (0.88 mL, 1.7 M in pentane, 1.5 mmol) was added at −78 °C and this mixture was allowed to reach ambient temperature. The addition of toluene (6 mL) gave a suspension that was heated to reflux and filtered. The resulting oil was stored at room temperature whereupon a solution formed over a period of hours and crystals of **9** deposited over two days. Yield 35 % (based on *t*BuLi), m.p. 314–316 °C. Elemental analysis calcd (%) for $C_{54}H_{100}Li_8N_{18}Zn{\cdot}0.5\,C_7H_8$: C 59.10, H 8.97, N 21.58 %; found, C 58.94, H 8.68, N 21.55 %. $^1$H NMR spectroscopy (400 MHz, $[^2H_6]$DMSO): $\delta = 7.24$–$7.11$ (m, 2.5 H; Ph), 3.04 (t,

 © 2003 Wiley-VCH Verlag GmbH & Co. KGaA, Weinheim 

$^3J$(H,H) = 5.4 Hz, 24H; $NCH_2$), 2.92 (t, $^3J$(H,H) = 6.2 Hz, 24H; $NCH_2$), 2.29 (s, 1.5H; Me), 1.62 (quint, $^3J$(H,H) = 5.8 Hz, 24H; $CH_2$), 0.85–0.84 ppm (m, 27H, *t*Bu). $^{13}$C NMR spectroscopy (100 MHz, [$^2H_6$]DMSO): $\delta$ = 159.8 ($CN_3$), 137.2 (*i*Ph), 129.3, 128.6 (*o*-, *m*-Ph), 125.8 (*p*-Ph), 49.1, 44.5 ($NCH_2$), 25.5 ($CH_2$), 24.9 ppm (ZnC*Me*).

Synthesis of **11**: A solution of $AlMe_3$ (2.0 M in hexane; 0.5 mL, 1.0 mmol) was added to hppH (0.139 g, 1.0 mmol) in toluene (5 mL) at room temperature under $N_2$. The resultant yellow solution was stirred until the reaction ceased. A solution of *t*BuLi (1.7 M in pentane; 0.88 mL, 1.5 mmol) was added at −78 °C and the mixture allowed to reach room temperature giving a suspension. Toluene (2.5 mL) was added to the mixture, which was then filtered and stored at room temperature for one day to give crystals of **11**. Yield 57% (based on *t*BuLi), m.p. 218–220 °C. Elemental analysis calcd (%) for $C_{41}H_{84}Al_2Li_5N_9$: C 62.19, H 10.69, N 15.92%; found, C 62.18, H 10.54, N 15.43%. $^1$H NMR spectroscopy (400 MHz, [$^2H_6$]DMSO): $\delta$ = 7.24–7.11 (m, 0.5H; Ph), 2.99 (t, $^3J$(H,H) = 5.8 Hz, 24H; $NCH_2$), 2.96 (t, $^3J$(H,H) = 5.8 Hz, 24H; $NCH_2$), 2.27 (s, 0.3H; Me), 1.70 (quint, $^3J$(H,H) = 5.8 Hz, 24H; $CH_2$), 0.75–0.69 (m, 36H; *t*Bu), −1.40 ppm (sext, $^2J$(H,Al) = 6.0 Hz, 12H; Me). $^{13}$C NMR spectroscopy (125 MHz, [$^2H_6$]DMSO): $\delta$ = 150.2 ($CN_3$), 137.4 (*i*-Ph), 129.0, 128.3 (*o*-, *m*-Ph), 125.4 (*p*-Ph), 47.5, 41.1 ($NCH_2$), 32.9–32.0 (AlC*Me*), 23.0 ($CH_2$), 21.1 (Ph*Me*), −7.9 ppm (AlMe, $^1J$(C,Al) = 71.0 Hz).

Received: May 19, 2003
Revised: September 4, 2003 [Z51921]

**Keywords:** aluminium · cluster compounds · hydrides · lithium · zinc

[1] *Comprehensive Organic Synthesis, Vol. 8* (Ed.: B. M. Trost), Elsevier Science, Oxford, **1991**.
[2] a) G. Sandrock, *J. Alloys Compd.* **1999**, *293–295*, 877–888; b) K. J. Gross, G. J. Thomas, C. M. Jensen, *J. Alloys Compd.* **2002**, *330–332*, 683–690.
[3] W. Clegg, R. P. Davies, S. T. Liddle, D. J. Linton, P. R. Raithby, R. Snaith, A. E. H. Wheatley, *Angew. Chem.* **1999**, *111*, 3568–3570; *Angew. Chem. Int. Ed.* **1999**, *38*, 3367–3370.
[4] D. Hoffmann, T. Kottke, R. J. Lagow, R. D. Thomas, *Angew. Chem.* **1998**, *110*, 1630–1633; *Angew. Chem. Int. Ed.* **1998**, *37*, 1537–1539.
[5] H. Nöth, A. Schlegel, J. Knizek, H. Schwenk, *Angew. Chem.* **1997**, *109*, 2754–2758; *Angew. Chem. Int. Ed. Engl.* **1997**, *36*, 2640–2643.
[6] D. J. Gallagher, K. W. Henderson, A. R. Kennedy, C. T. O'Hara, R. E. Mulvey, R. B. Rowlings, *Chem. Commun.* **2002**, 376–377.
[7] a) V. G. Albano, G. Ciamician, G. Ciani, S. Martinengo, A. Sironi, *J. Chem. Soc. Dalton Trans.* **1979**, 978–982; b) C. R. Eady, P. F. Jackson, B. F. G. Johnson, J. Lewis, M. C. Malatesta, M. McPartlin, *J. Chem. Soc. Dalton Trans.* **1980**, 383–392; c) P. F. Jackson, B. F. G. Johnson, J. Lewis, P. R. Raithby, M. McPartlin, W. J. H. Nelson, K. D. Rouse, J. Allibon, S. A. Mason, *J. Chem. Soc. Chem. Commun.* **1980**, 295–297; d) C. E. Housecroft, A. L. Rheingold, X. Song, *Inorg. Chem.* **1992**, *31*, 4023–4025.
[8] A. E. H. Wheatley, unpublished results.
[9] R. P. Davies, D. J. Linton, P. Schooler, R. Snaith, A. E. H. Wheatley, *Eur. J. Inorg. Chem.* **2001**, 619–622.
[10] D. R. Armstrong, R. P. Davies, D. J. Linton, P. Schooler, R. Snaith, A. E. H. Wheatley, *J. Chem. Soc. Dalton Trans.* **2001**, 2838–2843.
[11] Crystal data for **9**: $C_{54}H_{100}Li_8N_{18}Zn{\cdot}0.5\,C_7H_8$, $M_r$ = 1168.48, monoclinic, space group $P2(1)/n$, $a$ = 16.4567(7), $b$ = 18.6532(8), $c$ = 22.6602(9) Å, $\beta$ = 105.527(2)°, $V$ = 6702.1(5) Å$^3$, $Z$ = 4, $\rho_{calcd}$ = 1.158 g cm$^{-3}$, $Mo_{K\alpha}$ radiation, $\lambda$ = 0.71073 Å, $\mu$ = 0.415 mm$^{-1}$, $T$ = 173(2) K. 27354 data (8151 unique, $R_{int}$ = 0.1003, $\theta$ < 21.99°) were collected on a Nonius Kappa CCD diffractometer. The structure was solved by direct methods and refined by full-matrix least-squares on $F^2$ values of all data (G. M. Sheldrick, SHELX-97, Program for Crystal Structure Refinement, University of Göttingen, **1997**) to give $wR2 = \{\Sigma[w(F_o^2-F_c^2)^2]/\Sigma[w(F_o^2)^2]\}^{1/2}$ = 0.2025, conventional $R$ = 0.0770 on $F$ values of 5139 reflections with $F^2 > 2\sigma(F^2)$, $S$ = 1.025, 763 parameters. Residual electron density extrema ±0.509 e Å$^{-3}$. Crystallographic data (excluding structure factors) for **9** and **11** have been deposited with the Cambridge Crystallographic Data Centre as supplementary publications CCDC-209673 and CCDC-209674 contain the supplementary crystallographic data for this paper. These data can be obtained free of charge via www.ccdc.cam.ac.uk/conts/retrieving.html (or from the Cambridge Crystallographic Data Centre, 12 Union Road, Cambridge CB2 1EZ, UK; fax: (+44) 1223-336-033; or deposit@ccdc.cam.ac.uk).
[12] K. M. Mackay in *Comprehensive Inorganic Chemistry, Vol. 1* (Eds.: J. C. Bailar, H. J. Emeléus, R. Nyholm, A. F. Trotman-Dickenson), Pergamon, Oxford, **1973**, p. 30.
[13] K. Gregory, P. von R. Schleyer, R. Snaith, *Adv. Inorg. Chem.* **1991**, *37*, 47–142.
[14] S. L. Aeilts, M. P. Coles, D. C. Swenson, R. F. Jordan, V. G. Young, Jr., *Organometallics* **1998**, *17*, 3265–3270.
[15] Crystal data for **11**: $C_{41}H_{84}Al_2Li_5N_9$, $M_r$ = 791.83, monoclinic, space group $P2(1)/n$, $a$ = 14.349(3), $b$ = 20.752(4), $c$ = 18.272(4) Å, $\beta$ = 107.79(3)°, $V$ = 5180.7(19) Å$^3$, $Z$ = 4, $\rho_{calcd}$ = 1.015 g cm$^{-3}$, $Mo_{K\alpha}$, $\lambda$ = 0.71069 Å, $\mu$ = 0.090 mm$^{-1}$, $T$ = 180(2) K. 25541 data (9051 unique, $R_{int}$ = 0.0405, $\theta$ < 25.03°) were collected on a Nonius Kappa CCD diffractometer. The structure was solved by direct methods and refined by full-matrix least-squares on $F^2$ values of all data (G. M. Sheldrick, SHELX-97, Program for Crystal Structure Refinement, University of Göttingen, **1997**) to give $wR2 = \{\Sigma[w(F_o^2-F_c^2)^2]/\Sigma[w(F_o^2)^2]\}^{1/2}$ = 0.2209, conventional $R$ = 0.0649 on $F$ values of 6397 reflections with $F^2 > 2\sigma(F^2)$, $S$ = 1.090, 526 parameters. Residual electron density extrema ±0.518 e Å$^{-3}$.
[16] W. Clegg, L. Dunbar, L. Horsburgh, R. E. Mulvey, *Angew. Chem.*, **1996**, *108*, 815–816; *Angew. Chem. Int. Ed. Engl.* **1996**, *35*, 753–755.
[17] D. R. Armstrong, R. P. Davies, W. Clegg, S. T. Liddle, D. J. Linton, P. Schooler, R. Snaith, A. E. H. Wheatley, *Phosphorus Sulfur Silicon Relat. Elem.* **2001**, 168, 93–98.
[18] A. L. Galyer, G. Wilkinson, *Inorg. Synth.* **1979**, *19*, 253–257.

 © 2003 Wiley-VCH Verlag GmbH & Co. KGaA, Weinheim 

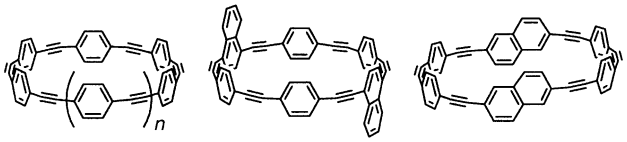
*Supramolecular Dynamics*

# Complexation of Carbon Nanorings with Fullerenes: Supramolecular Dynamics and Structural Tuning for a Fullerene Sensor**

*Takeshi Kawase,* Kenji Tanaka, Yohko Seirai, Nami Shiono, and Masaji Oda**

Recently we have found that a carbon nanoring **1**, cyclic [6]paraphenyleneacetylene ([6]CPPA), which has a smooth belt-shaped structure with a 1.31 nm diameter, forms stable inclusion complexes with fullerenes ($C_{60}$ and a methano[60]-fullerene derivative) in solution as well as in the solid state.[1] Although the host molecule is composed of only carbon and hydrogen atoms, the association constants are quite high ($>10^4$).[2] From these results, together with crystallographic analysis, we concluded that the novel noncovalent interaction, namely concave–convex π–π interaction, plays an important role in the complexation.[3] The same interaction should also be important in the formation and properties of multiwalled carbon nanotubes,[4] Bucky onions[5] and "fullerene Peapods".[6] On the other hand, the molecular structure also reveals that the cavity size of **1** is slightly smaller than that of $C_{60}$. These findings promoted us to investigate the structural tuning of carbon nanorings for optimizing complexation with fullerenes ($C_{60}$ and $C_{70}$).

We previously prepared "carbon nanorings" **1**–**4** ([6]–[9]CPPAs).[7] According to theoretical calculation (AM1 method),[8] the diameters of **2**, **3**, **4** are 1.53, 1.74, and



**1**; $n=1$, **2**; $n=2$
**3**; $n=3$, **4**; $n=4**

**5**

**6**

1.96 nm, respectively. We have designed new carbon nanorings **5** and **6**, isomers of **2**, which have 1,4- or 2,6-naphthylene units at diametrically opposed positions in place of 1,4-phenylene units of **1**. In contrast with **1**–**4**, rotational isomers are possible for **5** and **6**. While the cavity size of **5** is equal to that of **1**, the cavity sizes of **6** (1.41 nm for *syn*-**6** and 1.39 nm for *anti*-**6**) are between those of **1** (or **5**) and **2**. When the van der Waals distance between carbon atoms with $sp^2$ hybridized orbitals are taken into account (0.34 nm), the cavity of **6** is slightly larger than the $C_{60}$ molecule but is just right to accommodate a $C_{70}$ molecule. However, the cavity of **2** is slightly too large even for a $C_{70}$ molecule (Figure 1c). Herein

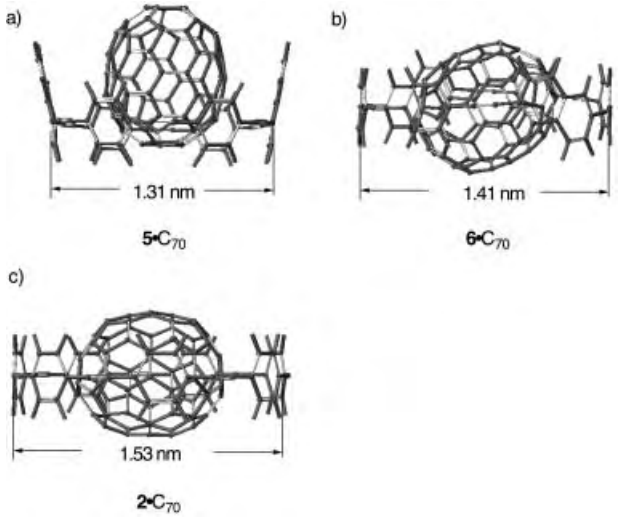



***Figure 1.*** The optimized structures of **5**·$C_{70}$, **6**·$C_{70}$, and **2**·$C_{70}$ by AM1 calculation.

we report on the formation of unusually stable complexes of new carbon nanorings with fullerenes and their novel supramolecular dynamics based on NMR spectroscopic analysis. Moreover, we have found that these carbon nanorings can act as efficient fluorescence sensors for fullerenes, and that the host **6** is the best sensor known to date.

Syntheses of **5** and **6** (see Table 1) were carried out as shown in Scheme 1. These compounds are susceptible to acid and oxygen, but stable enough to be stored in dilute solution

***Table 1:*** Selected data for **5** and **6**

**5**:Yellow fine crystals, mp 120 °C (decomp); MS (FAB): $m/z=700$ ($M^+$);IR-Raman (KBr): $\tilde{\nu}=2189.86$ (C≡C, s), 2168.43 (C≡C, s), 1593.55 $cm^{-1}$ (C=C, s); $^1H$ NMR (270 MHz, $CDCl_3$): $\delta=7.36$ (AA′BB′, $J_{AB}=8.6$ Hz, 8H), 7.41 (AA′BB′, $J_{AB}=8.6$ Hz, 8H), 7.56 (s, 4H), 7,58 (*m*-naphthyl, 4H), 8.31 ppm (*m*-naphthyl, 4H); $^{13}C$ NMR (67.8 MHz, $CDCl_3$): $\delta=96.97$, 97.58, 100.55, 122.37, 123.83, 124.09, 126.47, 127.23, 129.35, 130.93, 130.97, 133.07 ppm; UV (cyclohexane): $\lambda$max [nm](log $\varepsilon$) = 354(5.14); Fluorescence (cyclohexane): $\lambda$max [nm] = 418, 448; quantum yields $\Phi=0.24$;

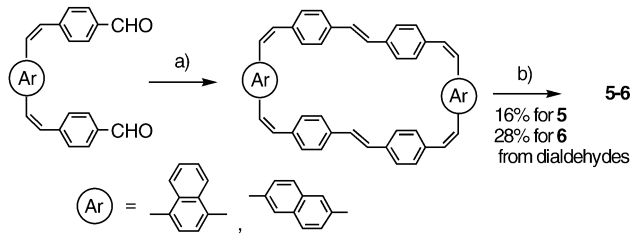
**6**: Yellow fine crystals, mp >97 °C (decomp); MS (FAB): $m/z=700$ [$M^+$]; IR-Raman (KBr): $\tilde{\nu}=2199.12$ (C≡C, m), 2184.19 (C≡C, s), 2160.56 (C≡C, w), 1592.27 $cm^{-1}$ (C=C, s); $^1H$ NMR (270 MHz, $CDCl_3$): $\delta=7.34$ (AA′BB′, $J_{AB}=8,6$ Hz, 8H), 7.38 (AA′BB′, $J_{AB}=8.6$ Hz, 8H), 7.44 (dd, $J=1.3$, 8.6 Hz, 4H), 7.67 (d, $J=8.6$ Hz, 4H), 7.83 ppm (d, $J=1.3$ Hz, 4H); $^{13}C$ NMR (100 MHz, $CDCl_3$): $\delta=96.88$, 97.10, 97.50, 121.75, 123.86, 124.02, 127.79, 128.82, 130.53, 130.91, 130.96, 132.89 ppm; UV (cyclohexane): $\lambda$max [nm](log $\varepsilon$) = 338(5.2) s, 358(5.4), 405(4.5); Fluorescence (cyclohexane): $\lambda$max [nm] = 472; quantum yields $\Phi=0.20$.

[*] T. Kawase, M. Oda, K. Tanaka, Y. Seirai, N. Shiono
Department of Chemistry
Graduate School of Science
Osaka University
Toyonaka, Osaka 560-0043 (Japan)
Fax: (+81) 6-6850-5387
E-mail: tkawase@chem.sci.osaka-u.ac.jp
moda@chem.sci.osaka-u.ac.jp

[**] This work was supported by a Grant-in-Aid for Scientific Research (No.14654112 and 14340197) from the Ministry of Education, Culture, Sports, Science and Technology (Japan).

Supporting information for this article is available on the WWW under http://www.angewandte.org or from the author.

 DOI: 10.1002/anie.200352033 © 2003 Wiley-VCH Verlag GmbH & Co. KGaA, Weinheim 




***Scheme 1.*** Synthesis of **5** and **6**: a) $TiCl_4$-Zn(CuI), 1,2-dimethoxyethane/toluene (1:1), room temperature, 12 h, then reflux 6 h; b) $Br_2$, $CHCl_3$, RT, 6 h, then *t*BuOK, ether, room temperature, 12 h.

at 0 °C over a month. The NMR spectra of **5** and **6** at 30 °C reveal $D_2$ symmetry of the molecules, and the signals are almost unchanged even at −90 °C (in $CD_2Cl_2$) except for some slight broadening. The results clearly indicate that each aromatic ring rotates faster than the NMR time scale in the measurable temperature range.

The stability of fullerene complexes is generally evaluated in terms of the association constant ($K_a$) determined by absorption spectra.[9,10] The titration experiment of **1**·$C_{70}$ determined the $K_a$ value to be $(1.8 \pm 0.2) \times 10^4$ dm$^3$mol$^{-1}$, which is slightly larger than that of **1**·$C_{60}$, $(1.6 \pm 0.3) \times 10^4$ dm$^3$mol$^{-1}$. The rather small differences in the values of $K_a$, however, indicate that the symmetry mismatching between **1** (*D6h*) and $C_{70}$ (*D5h*) is not an important factor for complexation. On the other hand, we have found that the $K_a$ values for the complexes of **5** and **6** with fullerenes in benzene are too large ($> 5 \times 10^4$) to be determined precisely.[10] The $K_a$ value of **6**·$C_{60}$ and **6**·$C_{70}$, in fact, can be roughly estimated to be about $1 \times 10^5$ and $1 \times 10^6$ dm$^3$mol$^{-1}$, which would indicate that the host forms extremely stable complexes for a hydrocarbon.

In a previous paper,[1c] we described that variable-temperature NMR spectra of **1**·$C_{60}$ in $CD_2Cl_2$ provide the Gibbs energies of activation ($\Delta G^{\neq}$) for the dissociation of the complex, and indicate the high mobility of the guest molecule in the cavity. Similarly, the $^1$H NMR spectra of the complexes, **1**·$C_{70}$, **5**·$C_{60}$, **5**·$C_{70}$, and **6**·$C_{70}$, in $CD_2Cl_2$ at −100 °C revealed that the dissociation rates of these complexes also are slower than the NMR time scale. The variable-temperature NMR experiments thus afforded the $\Delta G^{\neq}$ values of these complexes (Table 2), and further important information about their supramolecular dynamics.[11]

***Table 2:*** Coalescence temperatures (*Tc*) and $\Delta G^{\neq}$ values of the complexes.

| complex | $T_c$[a] | $\Delta G^{\neq}$ ($CD_2Cl_2$)[b] |
|---|---|---|
| **1**·$C_{60}$ | $-80 \pm 5$ | $9.9 \pm 0.2$ |
| **1**·$C_{70}$ | $-60 \pm 5$ | $9.6 \pm 0.2$ |
| **5**·$C_{60}$ | $-50 \pm 5$ | $10.8 \pm 0.3$ |
| **5**·$C_{70}$ | $-60 \pm 5$ | $10.1 \pm 0.2$ |
| **6**·$C_{60}$ | $< -100$ | $< 9$ |
| **6**·$C_{70}$ | $-30 \pm 10$ | $11.9 \pm 0.8$ |
| **2**·$C_{60}$ | $< -100$ | $< 9$ |
| **2**·$C_{70}$ | $< -100$ | $< 9$ |

[a] °C. [b] kcal mol$^{-1}$.

Whereas the signal of **1**·$C_{60}$ complex appears as a singlet at −100 °C, the $^1$H NMR spectrum of complex **1**·$C_{70}$ (1:1) has two singlets (7.484 and 6.929 ppm) of equal intensity at −90 °C (Figure 2). The $\Delta G^{\neq}$ value is estimated to be $(9.6 \pm 0.2)$ kcal mol$^{-1}$ ($T_c = -60 \pm 5$ °C) in $CD_2Cl_2$. The two signals

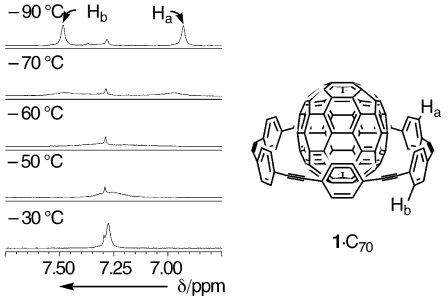



***Figure 2.*** $^1$H NMR spectra of a 1:1 mixture of **1** and $C_{70}$.

show the presence of two sets of non-equivalent aromatic protons because the center of $C_{70}$ is not aligned with the center of **1** (Figure 2). Thus, these results indicate that the activation energy of the passage of the $C_{70}$ through the cavity of **1** is at least as high as the value of dissociation, which is in contrast to the case of complex **1**·$C_{60}$. In addition, the appearance of the signals as singlets again suggests fast rotation of $C_{70}$ probably around the long axis. In the structure of **1**·$C_{70}$, which has lower symmetry than that of **1**·$C_{60}$, the inner and outer aromatic protons should receive a different anisotropic effect from $C_{70}$. The large barrier as well as the relatively large anisotropic effect would be attributable to the high π-electron density of the relatively flat midsection of $C_{70}$.[12]

The spectra of **5**·$C_{60}$ and **5**·$C_{70}$ (Figure 3 a and b) show that these complexes exist in a mixture of *syn*- and *anti*-isomers at low temperatures, where the *syn*-isomers would be predominant probably because they have a wider contact area than the *anti*-isomers. The appearance of some aromatic signals of **5**·$C_{70}$ at a relatively high magnetic field provides evidence for the assignment, because, according to the calculated molecular structure (Figure 1 b), the corresponding protons should receive the anisotropic effect of the midsection of $C_{70}$. In agreement with considerably high $K_a$ value, the $\Delta G^{\neq}$ for dissociation of **6**·$C_{70}$ ($11.9 \pm 0.8$ kcal mol$^{-1}$) is the highest. However, the NMR spectra at low temperatures appear to be relatively simple (Figure 3 c), thus indicating the high mobility of the guest in the cavity. Unlike these complexes, the variable-temperature NMR spectra of **6**·$C_{60}$, **2**·$C_{60}$ and **2**·$C_{70}$ indicate that the $\Delta G^{\neq}$ values are immeasurably low ($< 9$ kcal mol$^{-1}$). The activation energies thus correlate with the van der Waals contact between the host and guest. In one of our previous papers,[1c] we pointed out the importance of the electrostatic attractive force between the concave and convex surfaces in addition to the dispersion force, because the high affinity between a carbon nanoring **1** and $C_{60}$ can be hardly explained in terms of dispersion forces alone.[1c,3,13] The formation of the extremely stable complexes such as **6**·$C_{70}$

 © 2003 Wiley-VCH Verlag GmbH & Co. KGaA, Weinheim 

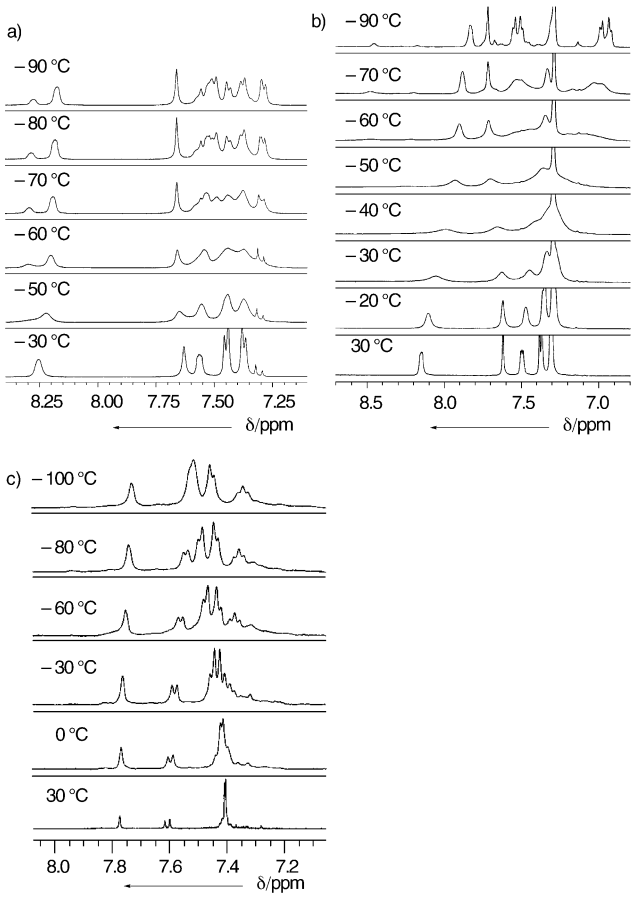



***Figure 3.*** Temperature-variable NMR spectra of an equimolar solution of a) **5** and $C_{60}$, b) **5** and $C_{70}$, and c) **6** and $C_{70}$.

provides additional evidence for our conclusion, and also has the novel feature of a curved conjugated systems.

Furthermore, we have found that the presence of a fullerene quenches the intense fluorescence emission of CPPAs very effectively. We have monitored the titration experiments by means of fluorescence spectra to determine the Stern–Völmer constant ($K_{SV}$).[9] Although the $K_{SV}$ values are not direct measures of the complexation because of the quenching mechanisms, they are informative in estimating the relative stability of these complexes.[14–16] Table 3 lists the $K_{SV}$ values of the complexes. The order of the values are $\mathbf{5} \geq \mathbf{6} > \mathbf{1} > \mathbf{2} > \mathbf{3}$ for the $C_{60}$ complexes, and $\mathbf{6} > \mathbf{5} > \mathbf{2} > \mathbf{1} > \mathbf{3}$ for the $C_{70}$ complexes, respectively. The ratio of the $K_{SV}$ values for $\mathbf{6}\cdot C_{70}/\mathbf{6}\cdot C_{60}$ is roughly consistent with the ratio of the $K_a$ values for $\mathbf{6}\cdot C_{70}/\mathbf{6}\cdot C_{60}$ ($K_a$ $\mathbf{6}\cdot C_{70}/\mathbf{6}\cdot C_{60} \approx 10$). It is noteworthy that **6** can act as the best fluorescence sensor for fullerenes among all the known hosts.[14]

Moreover, the significantly larger $K_a$ and $K_{SV}$ values of $\mathbf{6}\cdot C_{70}$ than that of $\mathbf{6}\cdot C_{60}$ suggests that the complexation of **6** with $C_{70}$ is highly selective; in fact, upon competitive complexation of **6** through solid-to-liquid extraction from a fullerite ($C_{60}$:$C_{70}$ = about 1:1) in $CD_2Cl_2$, the NMR spectrum of the extract was almost identical to that of $\mathbf{6}\cdot C_{70}$, thus indicating the considerably high selectivity (>10:1) for $C_{70}$ against $C_{60}$.[17] A similar experiment with the host **1** shows a relatively low and inverse selectivity (1:4). These findings will also open the way to create tailor-made hosts for the separation of higher fullerenes and carbon nanotubes.

***Table 3:*** Diameters ($\Phi$)[a] of the cavity of hosts and $K_{SV}$ values[b] of the complexes.

| | **1** | **5** | **6** | **2** | **3** |
|---|---|---|---|---|---|
| $\Phi$ | 1.31 | 1.31 | 1.41 | 1.53 | 1.74 |
| $K_{SV}$ $C_{60}$ | $7.0\times10^4$ | $2.7\times10^5$ | $2.6\times10^5$ | $5.6\times10^4$ | $<10^4$ |
| $K_{SV}$ $C_{70}$ | $1.4\times10^5$ | $2.6\times10^5$ | $4.3\times10^6$ | $2.1\times10^5$ | $<10^4$ |
| $K_{C70}/K_{C60}$ | 2.0 | 1.0 | 16.5 | 3.7 | |

[a] nm, evaluated by AM1 calculations. [b] $dm^3\,mol^{-1}$, in $C_6H_6$.

Received: June 3, 2003
Revised: September 1, 2003 [Z52033]

**Keywords:** cycloalkynes · fullerenes · inclusion compound · luminescence · noncovalent interactions

[1] a) T. Kawase, H. R. Darabi, M. Oda, *Angew. Chem.* **1996**, *108*, 2803–2805; *Angew. Chem. Int. Ed. Engl.* **1996**, *35*, 2664–2667; b) T. Kawase, Y. Seirai, H. R. Darabi, M. Oda, Y. Sarakai, K. Tashiro, *Angew. Chem.* **2003**, *115*, 1659–1662; *Angew. Chem. Int. Ed.* **2003**, *42*, 1621–1624; c) T. Kawase, K. Tanaka, N. Fujiwara, H. R. Darabi, M. Oda, *Angew. Chem.* **2003**, *115*, 1662–1666; *Angew. Chem. Int. Ed.* **2003**, *42*, 1624–1628.

[2] Recent articles related to belt-shaped conjugated systems: M. Ohkita, K. Ando, T. Tsuji, *Chem. Commun.* **2001**, 2570–2571; E. Nakamura, K. Tahara, Y. Matsuo, M. Sawamura, *J. Am. Chem. Soc.* **2003**, *125*, 2834–2835; R. Herges, M. Deichmann, T. Wakita, Y. Okamoto, *Angew. Chem.* **2003**, *115*, 1202–1204; *Angew. Chem. Int. Ed.* **2003**, *42*, 1170–1172; N. Treitel, M. Deichmann, T. Sternfeld, T. Sheradsky, R. Herges, M. Rabinovitz, *Angew. Chem.* **2003**, *115*, 1204–1206; *Angew. Chem. Int. Ed.* **2003**, *42*, 1172–1176.

[3] Recent reviews related to supramolecular chemistry of curved conjugated systems: a) L. T. Scott, H. E. Bronstein, D. V. Preda, R. B. M. Ansems, M. S. Bratcher, S. Hagen, *Pure Appl. Chem.* **1999**, *71*, 209–219; b) F. Diederich, M. Gomez-Lopez, *Chem. Soc. Rev.* **1999**, *28*, 263–277; c) M. J. Hardie, C. L. Raston, *Chem. Commun.* **1999**, 1153–1163; d) G. J. Bodwell, T. Satou, *Angew. Chem.* **2002**, *114*, 4175–4178; *Angew. Chem. Int. Ed.* **2002**, *41*, 4003–4006.

[4] S. Iijima, *Nature* **1991**, *354*, 56–58; B. W. Smith, M. Monthioux, D. E. Luzzi, *Nature* **1998** *396*, 323–325.

[5] H. W. Kroto, K. G. Mckay, *Nature* **1988**, *331*, 328–331; S. Iijima, *J. Cryst. Growth* **1989**, *50*, 675–683; D. Ugarte, *Nature* **1992**, *359*, 707–709.

[6] B. W. Smith, M. Monthioux, D. E. Luzzi, *Nature* **1998**, *396*, 323; J. Sloan, A. I. Kirkland, J. L. Hutchison, M. L. H. Green, *Chem. Commun.* **2002**, 1319–1332.

[7] T. Kawase, N. Ueda, K. Tanaka, Y. Seirai, M. Oda, *Tetrahedron Lett.* **2001**, *42*, 5509–5511.

[8] J. J. P. Stewart, *J. Comput. Chem.* **1989**, *10*, 209–220.

[9] J.-M. Lehn, J. L. Atwood, J. E. D. Davies, D. D. MacNicol in *Supramolecular Chemistry, Vol. 8*, Pergamon Press, Oxford, **1996**.

[10] K. Hirose, *J. Inclusion Phenom. Macrocyclic Chem.* **2001**, *39*, 193–209.

[11] K. Tashiro, Y. Hirabayashi, T. Aida, K. Saigo, K. Fujiwara, K. Komatsu, S. Sakamoto, K. Yamaguchi, *J. Am. Chem. Soc.* **2002**, *124*, 12086–12087.

 © 2003 Wiley-VCH Verlag GmbH & Co. KGaA, Weinheim 

[12] C. Thilgen, A. Herrmann, F. Diederich, *Angew. Chem.* **1997**, *109*, 2362 – 2374; *Angew. Chem. Int. Ed. Engl.* **1997**, *36*, 2268 – 2280; M. S. Meier, G.-W. Wang, R. C. Haddon, C. P. Brock, M. A. Lloyd, J. P. Selegue, *J. Am. Chem. Soc.* **1998**, *120*, 2337 – 2342; Y.-B. Wong, Z. Lin, *J. Am. Chem. Soc.* **2003**, *125*, 6072 – 6073.

[13] Recent reviews related to interactions with arenes: F. Cozzi, J. S. Siegel, *Pure Appl. Chem.* **1995**, *67*, 683 – 689; M. Nishio, M. Hirota, Y. Umezawa, *The CH/π Interaction. Evidence, Nature and Consequences*, Wiley-VCH, New York, **1998**; A. Hunter, K. R. Lawson, J. Perkins, C. J. Urch, *J. Chem. Soc. Perkin Trans. 2* **2001**, 651 – 666; D. Zhao, J. S. Moore, *Chem. Commun.* **2003**, 807 – 818; E. A. Meyer, R. K. Castellano, F. Diederich, *Angew. Chem.* **2003**, *115*, 1244 – 1287; *Angew. Chem. Int. Ed.* **2003**, *42*, 1210 – 1250.

[14] a) T. Haino, Y. Yamanaka, H. Araki, Y. Fukazawa, *Chem. Commun.* **2002**, 402 – 403; b) D. I. Schuster, J. Rosenthal, S. MacMahon, P. D. Jarowski, C. A. Alabi, D. M. Guldi, *Chem. Commun.* **2002**, 2538 – 2539; c) S. R. Wilson, S. MacMahon, F. T. Tat, P. D. Jarowski, D. I. Schuster, *Chem. Commun.* **2003**, 226 – 227.

[15] Quenching of the fluorescence takes place by an intermolecular energy-transfer process from the excited states of CPPAs to fullerenes. The Stern–Völmer plots show straight lines, which suggest the quenching mechanism through 1:1 complexes involve several mechanisms (Figure 4). Further investigation of the energy-transfer mechanisms of the systems will be reported in due course.

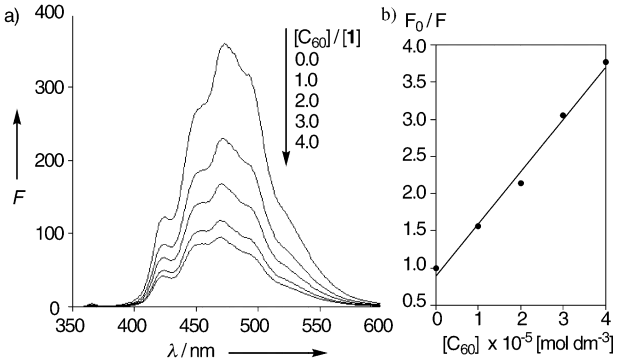



***Figure 4.*** a) Emission spectral change of **1** in the presence of $C_{60}$ in benzene. $\lambda_{excitation} = 363$ nm, $[\mathbf{1}] = 1.0 \times 10^{-5}$ mol dm$^{-3}$ constant. $[C_{60}] = [\mathbf{1}] \times 0 \sim 4.0$ mol dm$^{-3}$. b) Stern–Völmer plot.

[16] For recent reviews related to photochemistry of fullerenes and their derivatives see: H. Imahori, Y. Sakata, *Adv. Mater.* **1997**, *9*, 537; D. M. Guldi, *Chem. Commun.* **2000**, 321 – 327; D. M. Guldi, P. V. Kamat in *Fullerenes: Chemistry, Physics and Technology* (Eds.: K. M. Kadish, R. S. Ruoff), Wiley, New York, **2000**.

[17] For recent articles related to selective complexation with fullerenes see: T. Haino, M. Yanase, Y. Fukazawa, *Angew. Chem.* **1998**, *110*, 1044 – 1046; *Angew. Chem. Int. Ed.* **1998**, *37*, 997 – 998; H. Matsubara, S. Ogura, K. Asano, K. Yamamoto, *Chem. Lett.* **1999**, 431 – 432; F. C. Tucci, D. M. Rudkevich, J. Rebek, Jr., *J. Org. Chem.* **1999**, *64*, 4555 – 4559; N. Komatsu, *Tetrahedron Lett.* **2001**, *42*, 1733 – 1736; J.-Y. Zheng, K. Tashiro, Y. Hirabayashi, K. Kinbara, K. Saigo, T. Aida, S. Sakamoto, K. Yamaguchi, *Angew. Chem.* **2001**, *113*, 1909 – 1913; *Angew. Chem. Int. Ed.* **2001**, *40*, 1858 – 1860; N. Komatsu, *Org. Biomol. Chem.* **2003**, *1*, 204 – 209.

 © 2003 Wiley-VCH Verlag GmbH & Co. KGaA, Weinheim 

*Core–Shell Nanostructures*

# Facile Fabrication of Inorganic-Polymer Core–Shell Nanostructures by a One-Step Vapor Deposition Polymerization**

*Jyongsik Jang* and Byungkwon Lim*

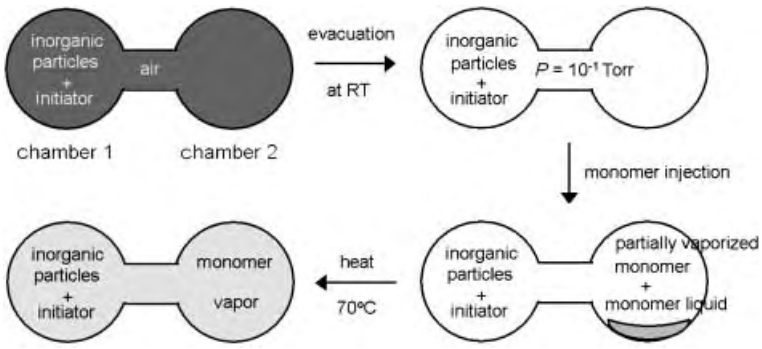
The enhanced stability and tunable surface properties derived from the selective polymer coating of inorganic colloids have expedited the development of a variety of methods to fabricate inorganic-polymer core–shell nanostructures.[1] To date, the preparation of polymer-coated inorganic nanoparticles has largely depended upon the solution-based approaches, which include emulsion or dispersion polymerization[2] and adsorption of polymers onto the inorganic particles.[3] However, these methods have often been limited by the large particle–particle aggregations, the formation of the isolated polymer particles from the inorganic colloids, or the requirement for the complicated multistep procedure. Therefore, it is desirable to develop a simple and reliable method to fabricate inorganic colloid-polymer nanoparticles with the well-defined core–shell morphology. Vapor deposition techniques can provide the creation of a smoother and more uniform polymer layer by the consecutive polymerization of vaporized monomer under a vacuum onto the desired surface. While vapor deposition polymerization (VDP) has been performed on the metal and semiconductor with macroscopically flat surfaces by radiation-induced polymerization,[4] considerably less attention has been paid to the coating of inorganic colloids with polymers. Herein we report a facile route for the fabrication of various inorganic colloid-vinyl polymer core-shell nanostructures by one-step VDP. Having demonstrated the feasibility of the above approach, we were prompted to apply it to encapsulate silica and titania nanoparticles with poly(methyl methacrylate) (PMMA) and polydivinylbenzene (PDVB).

Spherical silica colloids of two different sizes (200 and 25 nm) and irregularly shaped titania nanoparticles were used as the cores and pretreated with a silane coupling agent to improve the chemical affinity of the inorganic particle surfaces towards organic monomers. The surface-modified inorganic colloids were encapsulated with two vinyl polymers; PMMA as an optically transparent material, and PDVB as a carbon precursor. The overall synthetic procedure is represented in Scheme 1. The reactor containing the inorganic nanoparticles and a solid initiator was evacuated at room temperature until the pressure inside reached about $10^{-1}$ Torr,

[*] Prof. Dr. J. Jang, B. Lim
Hyperstructured Organic Materials Research Center and
School of Chemical Engineering
Seoul National University
Shinlimdong 56-1, Seoul 151-742 (Korea)
Fax: (+82) 2-888-1604
E-mail: jsjang@plaza.snu.ac.kr

[**] This work was supported by the Brain-Korea 21 Program of the Korea Ministry of Education and by Hyperstructured Organic Materials Research Center in Seoul National University.

 © 2003 Wiley-VCH Verlag GmbH & Co. KGaA, Weinheim DOI: 10.1002/anie.200352113 




***Scheme 1.*** Illustration of the VDP for the encapsulation of the inorganic nanoparticles.

which put the system under a static vacuum. Then, liquid monomer was introduced into the reactor by injection. The monomers were partially vaporized as soon as they were injected inside the reactor at room temperature and completely vaporized by heating the reactor at 70 °C. Polymerization was initiated by thermal decomposition of a radical initiator and the inorganic particles were stirred with a magnetic to prevent the formation of particle–particle aggregations.

In the case of 200 nm sized silica colloid-PMMA nanocomposites, FTIR spectrum indicated PMMA C–H stretching bands at 2957 $cm^{-1}$ and 3000 $cm^{-1}$ and a carbonyl stretching band at 1737 $cm^{-1}$ as well as the characteristic peaks of silica at 3400, 1630, 1100, 956, and 474 $cm^{-1}$. The C=C stretching band at 1620 $cm^{-1}$ from the MMA monomer disappeared after polymerization. An X-ray photoelectron spectroscopy (XPS) study showed the C 1s peak at 284 eV and O 1s peak at 533 eV with a shoulder at 531 eV. The XPS spectrum of the pure silica particles showed the O 1s peak of the symmetrical shape near at 533 eV with no shoulder peak. Therefore, XPS confirmed the presence of carbon and oxygen atoms originating from PMMA. Thermogravimetric analysis (TGA) showed that PMMA decomposed completely below 500 °C. These results demonstrate the successful polymerization of methyl methacrylate (MMA) and also the availability of a radical initiator for the initiation of the VDP.[5]

A scanning electron microscopy (SEM) image shows 200 nm spherical silica particles (Figure 1 a). PMMA-coated silica nanoparticles obtained with an MMA/silica weight ratio of 0.25 are shown in Figure 1 b. These nanoparticles have a morphology similar to silica particles, thus indicating uniform PMMA layers on the silica particle surfaces. In transmission electron microscopy (TEM) images, the PMMA-coated silica particles have a uniform and remarkably thin PMMA layer (shell thickness 8 nm) on their outer surface (Figure 1 c and 1 d). In addition, we did not observe the polymer particle that had not encapsulated the inorganic particle in TEM investigation. The formation of the highly uniform PMMA layer and the absence of polymer particles might result from the nature of the VDP and the high specific surface area of inorganic nanoparticles to be encapsulated. The inorganic nanoparticles provide the considerably large surfaces even with a small number of particles compared to semiconductor or metallic flat surfaces, on which the most of monomers can adsorb from the vapor phase. Under these conditions, polymerization of the monomers proceeds exclusively by growing polymer radicals confined in the adsorbed layers and is not significantly affected by polymerization in the gas phase.[6] The growth of the polymer layer in the particle surfaces leads to the formation of the highly uniform polymer shell.

The degree of polymerization depended on the reaction time, the initiators, and the reaction temperature. In the control of the thickness of the polymer, we selected the loading amount of the monomer as a control parameter and fixed other reaction parameters to simplify the reaction system such as the reaction time of 24 h and the reaction temperature of 70 °C. The shell thickness could be tuned by varying the MMA/silica weight ratio. As the MMA/silica weight ratio increased, the polymer shell thickness increased gradually. The PMMA shell thickness of about 25 nm was obtained with an MMA/silica weight ratio of 0.75 (Figure 1 e) and increased up to about 39 nm at the weight ratio of 1.5 (Figure 1 f). VDP provided a uniform PMMA shell regardless of the increment in shell thickness.

The VDP method was also applied to encapsulate colloidal silica less than 50 nm. It was found that the aggregation of particles during the polymerization often occurred with higher quantities of monomer, without stirring the inorganic particles, especially in the coating of nano-

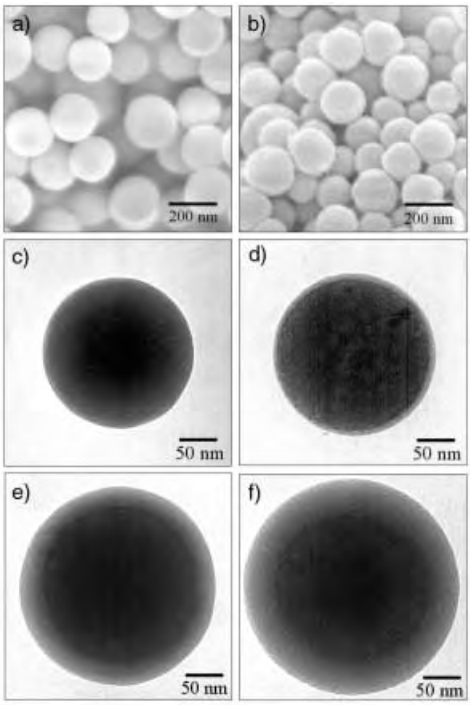



***Figure 1.*** SEM images of a) 200 nm silica particles as synthesized and b) silica particles coated with PMMA. TEM images of c) 200 nm silica particle and d–f) silica–PMMA core–shell nanoparticles with the various shell thickness (MMA/silica weight ratio of 0.25 in d), 0.75 in e), and 1.5 in f).

 © 2003 Wiley-VCH Verlag GmbH & Co. KGaA, Weinheim 

particles less than 50 nm compared to that of relatively large nanoparticles of 200 nm in diameter. However, the particle–particle aggregations were remarkably reduced by stirring the nanoparticles during polymerization and by using the appropriate choice of synthetic conditions. Stirring of the particles decreases the contact time between the neighboring particles so that it effectively prevents the formation of the polymer layer connecting the inorganic particles. Figure 2a and b

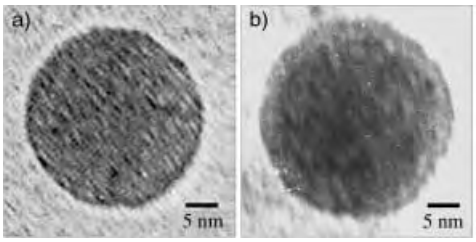



***Figure 2.*** TEM images of a) 25 nm silica particle and b) PMMA-coated silica particle with the shell thickness of about 2.5 nm.

represent the highly magnified TEM images of 25 nm silica colloids before and after the deposition of PMMA with an MMA/silica weight ratio of 0.75 at 70 °C. Figure 2b shows the outer shell of the particle brighter than the dark inner core, which confirms the silica–PMMA core–shell nanostructure. The shell thickness of PMMA was about 2.5 nm. Our results show that the core–shell morphology can be obtained with the silica particles as small as 25 nm.

Titania is well-known for its use in optical and photocatalytic applications. In our experiment, titania nanoparticles of irregular shapes were encapsulated with a PMMA shell to improve their stability and dispersibility for a variety of applications. The representative TEM micrograph of titania–PMMA nanoparticles (MMA/titania weight ratio of 1.5; Figure 3) proved that 200 nm titania nanoparticles were

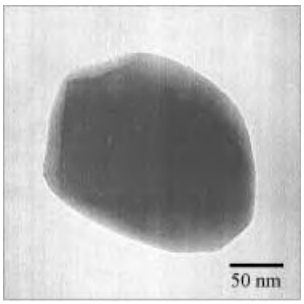



***Figure 3.*** TEM image of titania–PMMA core–shell nanoparticle. The titania nanoparticle was completely encapsulated with the PMMA layer.

successfully coated with a PMMA shell, and the shell had the same morphology as that of the titania nanoparticles. The shell thickness ranged from 10 to 20 nm. This result suggests that VDP is also available for the encapsulation of the irregularly shaped inorganic particles as well as spherical silica particles.

PDVB is a typical crosslinked polymer and can be used as a carbon precursor. Figure 4a presents the TEM image of the silica–carbon core-shell nanoparticle with a shell thickness of about 15 nm, which was prepared by the carbonization of the

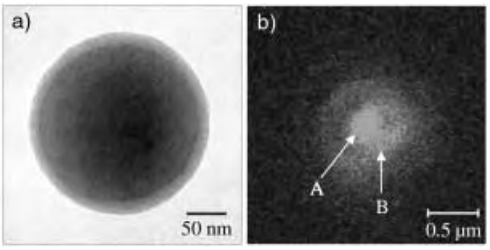



***Figure 4.*** a) TEM image of silica-carbon core-shell nanoparticle and b) CLSM fluorescence image of pyrene-encapsulated hollow carbon nanoparticle. Green emission results from pyrene. The emission in region A originates from pyrene inside the carbon capsule and that in region B from pyrene adsorbed on the outer surface of carbon capsule.

silica–PDVB core-shell nanoparticle. Carbon nanocapsules were obtained by HF etching of the silica core. TGA of the carbon capsules confirmed that the residual amount of sample was less than 5 wt % under an oxygen flow and confirmed the successful removal of the silica. This fact also implies that the wall of carbon capsule is porous and permeable towards small molecules.[7] The carbon capsule was used as a host container for the encapsulation of pyrene, a photochromic dye material. The confocal-laser scanning microscope (CLSM) image of pyrene-embedded carbon capsule dispersed in water showed a green emission resulting from the pyrene molecules (Figure 4b). It is noticeable that the pyrene emission could be divided into two, that is, one originating from pyrene molecules inside the carbon capsule (labeled A in Figure 4b), and the other with a donut shape originating from pyrene molecules adsorbed on the outer surface of the carbon capsule (labeled B in Figure 4b). The diameter of the emission from the region A was about 200 nm, which was in good agreement with the size of the capsule core. When the CLSM observation was performed in benzene instead of water, the pyrene emission was no longer concentrated in the carbon capsule, but displayed from the entire benzene media. This is because hydrophobic pyrene tends to locate at the hydrophobic interior of the carbon capsule in water, but the encapsulated pyrene is released from the carbon capsule in hydrophobic benzene. This result indicates the potential of the carbon capsule as the container for storage and release of organic guest molecules in a different environment.

In summary we have demonstrated the VDP methodology as a new strategy to fabricate various inorganic colloid–vinyl polymer core–shell nanostructures. This conceptually new and simple process has allowed the formation of highly uniform PMMA shells on silica and titania nanoparticle surfaces. The shell thickness could be controlled from about 2.5 to 40 nm by changing the monomer/inorganic particle weight ratio. In addition, carbon capsules derived from the silica–PDVB nanoparticles realized the encapsulation and selective release property of pyrene in a different environment and can be applied as a novel nanohybrid material in

 © 2003 Wiley-VCH Verlag GmbH & Co. KGaA, Weinheim 

optical and electronic devices. This novel approach might be expanded to allow the preparation of the various core–shell structures, which include metallic, inorganic, and polymeric materials.

## Experimental Section

Uniform silica spheres of about 200 nm were synthesized according to the method of Stöber et al.[8] Ludox TM-40 solution (Aldrich) was used as a source of 25 nm silica nanoparticle. Titanium dioxide (Junsei Chemical) was chosen as 200 nm titania nanoparticles. Silica and titania nanoparticles (2 g) were treated with chlorodimethylvinylsilane (CDVS, 0.2 mL) in a mixture solution of ethanol (75 mL) and water (15 mL) overnight, and then dried at 50 °C. A reactor was designed for VDP by connecting two modified round bottom flasks as reaction chambers. The total volume of the reactor was about 200 mL. 0.3 g of CDVS-treated inorganic particle and 0.01 g of a radical initiator was added to the one chamber of the reactor. 2,2′-azobis-[2-(2-imidazolin-2-yl)-propane] dihydrochloride or 2,2′-azobisisobutyronitrile (AIBN) was used as a radical initiator. The reactor was evacuated to about $10^{-1}$ torr at room temperature, and then the vacuum valve was closed to obtain the system in a static vacuum. Liquid monomer was introduced into the other chamber of the reactor by injection (0.075–0.6 mL). The monomer was completely vaporized by heating at 70 °C. The vapor deposition polymerization proceeded with magnetic stirring of the inorganic particles in an atmosphere of the monomer vapor for 24 h. After the polymerization, the residual monomer vapor was removed from the reactor by venting and the final product of inorganic-polymer core-shell nanoparticle was obtained.

The silica–PDVB core–shell nanoparticles were carbonized under $N_2$ gas flow. The sample was heated up to 900 °C at a heating rate of 3 °C $min^{-1}$, held at that temperature for 5 h, and then cooled to room temperature. Carbon capsule was prepared by removal of the silica core with HF solution. To obtain pyrene-embedded carbon nanocapsule, pyrene (1 mg) in THF (1 mL) was introduced into the mixture of carbon nanocapsule (2 mg) in water (10 mL), and then vigorously stirred for 30 min. TEM and SEM images were taken by a JEOL 2010 high-resolution microscope and a JEOL 6700F field emission scanning electron microscope, respectively. Fluorescence image of pyrene–carbon nanoparticle was obtained by using a Carl Zeiss LSM510 confocal laser scanning microscope. XPS spectra were recorded using Kratos Model AXIS-HS system. An $Al_{K\alpha}$ X-ray source was operated at a power of 100 W (10 mA and 10 kV). Infrared spectra were recorded on a Bomem MB 100 Fourier Transform Infrared (FTIR) Spectrometer with a transmission technique.

Received: June 11, 2003
Revised: September 3, 2003 [Z52113]

**Keywords:** colloids · nanostructures · polymers · silicon · titanium

[1] F. Caruso, *Adv. Mater.* **2001**, *13*, 11 – 22.
[2] a) L. Quaroni, G. Chumanov, *J. Am. Chem. Soc.* **1999**, *121*, 10642 – 10643; b) C. Barthet, A. J. Hickey, D. B. Cairns, S. P. Armes, *Adv. Mater.* **1999**, *11*, 408 – 410; c) S. Reculusa, C. Poncet-Legrand, S. Ravaine, S. Mingotaud, E. Duguet, E. Bourgeat-Lami, *Chem. Mater.* **2002**, *14*, 2354 – 2359; d) J. Luna-Xavier, A. Guyot, E. Bourgeat-Lami, *J. Colloid Interface Sci.* **2002**, *250*, 82 – 92.
[3] a) F. Caruso, R. A. Caruso, H. Möhwald, *Science* **1998**, *282*, 1111 – 1114; b) E. Donath, G. B. Sukhorukov, F. Caruso, S. A. Davis, H. Möhwald, *Angew. Chem.* **1998**, *110*, 2324 – 2327; *Angew. Chem. Int. Ed.* **1998**, *37*, 2202 – 2205.
[4] a) M. A. Bruk, S. A. Pavlov, A. D. Abkin, *Radiat. Phys. Chem.* **1981**, 17, 113 – 117; b) M. A. Bruk, K. K. Chuiko, A. D. Abkin, S. V. Kirpikov, *Polym. Sci. U.S.S.R.* **1982**, 24, 696 – 703; c) M. A. Bruk, S. V. Kirpikov, *Polym. Sci. U.S.S.R.* **1988**, 30, 130 – 136; d) J. Bai, C. M. Snively, W. N. Deglass, J. Lauterbach, *Macromolecules* **2001**, *34*, 1214 – 1220; e) J. Bai, C. M. Snively, W. N. Deglass, J. Lauterbach, *Adv. Mater.* **2002**, *14*, 1546 – 1549.
[5] a) J. Jang, B. Lim, J. Lee, T. Hyeon, *Chem. Commun.* **2001**, 1, 83 – 84; b) K. Moller, T. Bein, R. X. Fischer, *Chem. Mater.* **1998**, *10*, 1841 – 1852.
[6] M. A. Bruk, S. V. Kiroikov, *Colloid J.* **1995**, 57, 160 – 165.
[7] J. Jang, B. Lim, *Adv. Mater.* **2002**, *14*, 1390 – 1393.
[8] W. Stöber, A. Fink, E. Bohn, *J. Colloid Interface Sci.* **1968**, *26*, 62 – 69.

 © 2003 Wiley-VCH Verlag GmbH & Co. KGaA, Weinheim 

*Peptide Polyelectrolyte Complexes*

# Self-Assembling Peptide Polyelectrolyte β-Sheet Complexes Form Nematic Hydrogels**

*Amalia Aggeli, Mark Bell, Neville Boden,* Lisa M. Carrick, and Andrew E. Strong*

An emergent activity is exploration of the prospect for exploiting proteinlike self-assembly as a route to novel soft solidlike materials, with the objective of being able to incorporate proteinlike responsivity into their nanostructure.[1–5] Our approach has been to exploit the intrinsic one-dimensional self-assembling propensity of peptides to form cross-β-structures.[2–4] A hierarchy of structures: helical tapes (single-molecule thick), twisted ribbons (double tapes), fibrils (twisted stacks of ribbons), and fibers (entwined fibrils) are formed successively with increasing concentration in water.[2,3] The fibrils are semirigid and can form nematic fluids at concentrations of about 0.001 v/v, whilst fiber formation occurs at higher concentrations and gives rise to networks comprised of fibrils linked at fiberlike junctions that create nematic hydrogels.[3] This behavior has been shown to stem from the chirality of the peptide molecule, which in turn originates from the intrinsic chirality of the constituent amino acids (L in the case of naturally occurring ones). Another ubiquitous property of peptides is their ability to become electrostatically charged in response to changes in pH values.

[*] Prof. Dr. N. Boden, Dr. A. Aggeli, Dr. M. Bell, Dr. L. M. Carrick, Dr. A. E. Strong
Centre for Self-Organising Molecular Systems
Department of Chemistry
University of Leeds, Leeds LS2 9JT (UK)
Fax: (+44) 113-343-6452
E-mail: n.boden@chem.leeds.ac.uk

[**] The work was supported by the UK Engineering and Physical Sciences Research Council and the Royal Society (University research fellowship to A.A.).

Supporting information for this article is available on the WWW under http://www.angewandte.org or from the author.

 DOI: 10.1002/anie.200352207 © 2003 Wiley-VCH Verlag GmbH & Co. KGaA, Weinheim 

Here we demonstrate how the Coulombic attraction between oppositely charged monomeric peptides, in appropriate pH windows, leads to the spontaneous self-assembly of fibrillar networks and associated nematic hydrogels simply by mixing the component solutions. This behavior may be likened to the polyelectrolyte complexes (PECs) formed on mixing oppositely charged polyelectrolytes.[6]

To illustrate this principle, we make use of two peptides A and C, whose phase behavior[4] in 6.3 mM aqueous solutions is depicted as a function of pH in Figure 1 a. (In previous work,[4] A and C were termed $P_{11}$-4 and $P_{11}$-5, respectively.) Both peptides are in their monomeric states in the pH window $7.2 < pH > 7.4$. The three Glu ($-CH_2CH_2COOH$) residues at positions 5, 7, and 9 in A are in their deprotonated states which gives the peptide a net two units of negative charge (Figure 1 b). The resultant Coulombic repulsion keeps the peptides apart and suppresses self-assembly. Similarly, for peptide C, the three Orn ($-CH_2CH_2CH_2NH_2$) residues in positions 3, 5, and 7 are positively charged and give the peptide three units of net positive charge (Figure 1 b).

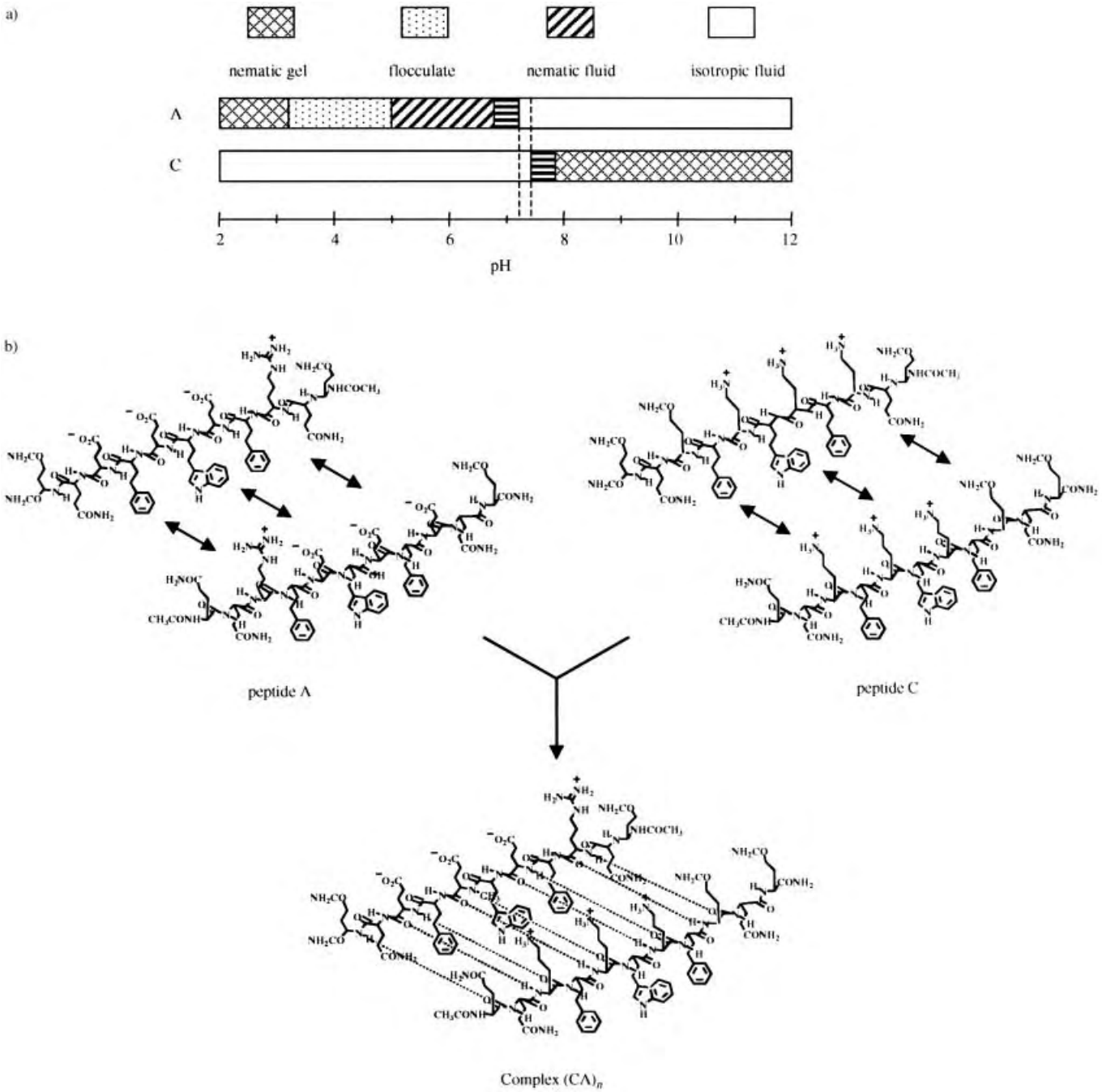



***Figure 1.*** a) Phase behavior of 6.3 mM aqueous solutions of peptides A and C as a function of pH. The nematic-to-isotropic biphasic region of A extends from pH 6.8 to 7.2 and for C from 7.4 to 7.8, which defines the pH interval 7.2 to 7.4 for the mixing of A and C. The horizontal lines spanning the biphasic intervals denote pH values of co-existing nematic and isotropic phases. b) Molecular structures of A, C, and the complex CA showing the electrostatic charge distributions at pH 7.3.

 © 2003 Wiley-VCH Verlag GmbH & Co. KGaA, Weinheim 

When equal quantities of these two solutions at pH 7.3 were mixed a self-supporting, turbid gel was obtained instantaneously. The gel is birefringent when viewed between crossed polarizers, and the optical micrograph (Figure 2a) is characteristic of a nematic gel.[7] The FTIR (Figure 3a) and

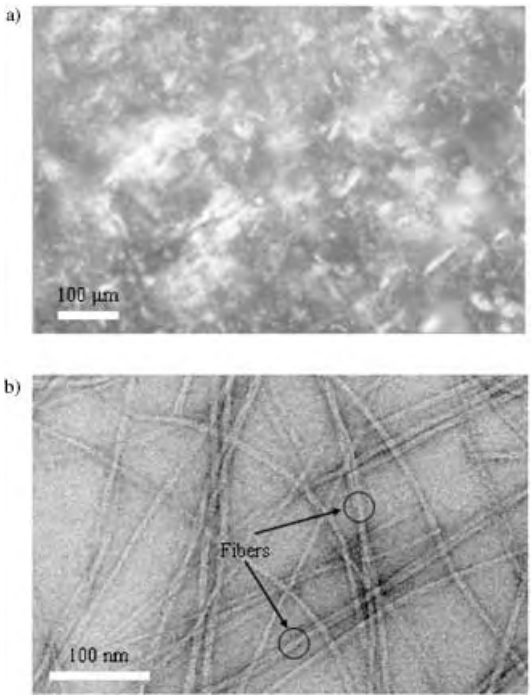



***Figure 2.*** a) Polarizing optical micrograph of the gel ($c = 6.3$ mM) formed after mixing aqueous solutions of monomeric peptides A and C at pH 7.3 showing a typical nematic gel texture.[7] b) Transmission electron micrograph showing mainly fibrils and a few fibers (having twice the diameter of the fibrils) in the nematic gel ($c = 6.3$ mM).

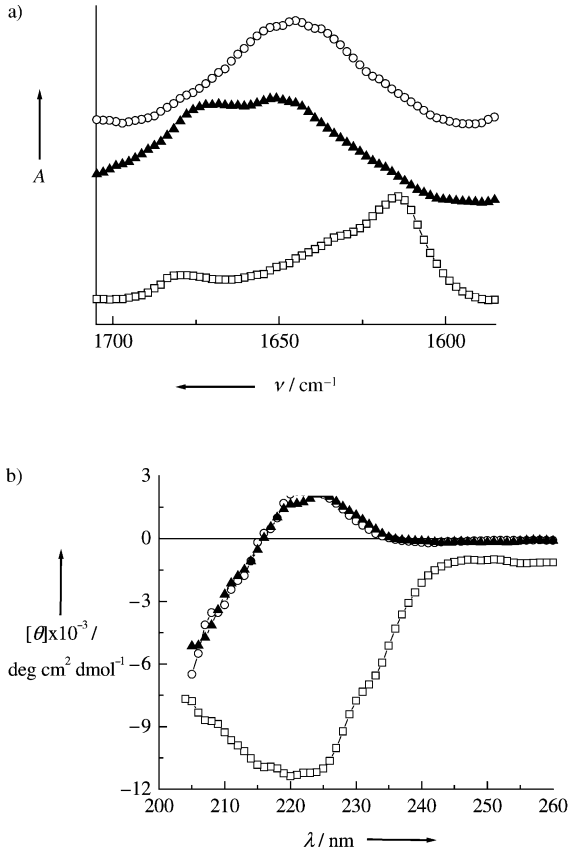



***Figure 3.*** a) FTIR spectra showing amide I′ bands centered at 1645 $cm^{-1}$, a signature of the initial random coil state of peptide A (○) and peptide C (▲) in 6.3 mM aqueous solutions at pH 7.3 prior to mixing, and the β-sheet conformation of the polyelectrolyte complex after mixing (□). b) Far-UV CD spectra showing the initial random coil states of peptide A (○) and peptide C (▲) in aqueous solutions ($c = 3.1$ mM) prior to mixing, and the β-sheet complex formed after mixing (□).

CD (Figure 3b) spectra of both A (○) and C (▲) prior to mixing are indicative of monomeric (random coil) peptide.[4] After mixing, the spectra (□) are characteristic of an antiparallel cross-β-sheet structure within fibrils.[8] The $^1$H NMR spectra also reveal distinctive changes. The high-resolution spectra obtained from monomeric solutions of A or C (Figure 4a and b) are indicative of peptide molecules undergoing fast, random, reorientational motion. In contrast, a solidlike, structureless, broad-banded spectrum (Figure 4c) is obtained from the nematic gel state of A ($c = 3.13$ mM, pH 2), which is indicative of peptide molecules locked into a relatively static fibrillar network. On mixing equal volumes of the solutions of A and C, as used to obtain the spectra in Figure 4a and b, respectively, the spectrum in Figure 4d was obtained, which is indicative of the formation of a gel with a small excess (5%) of monomeric C arising from the slight inequality of the molar ratios of A and C in the mixture. Addition of a greater excess of C led to the spectrum in Figure 4e (ca. 66% monomeric C). In contrast, the corresponding addition of an excess of A led to the spectrum in Figure 4f (ca. 66% monomeric A). These spectroscopic results are consistent with the fibrils being a 1:1 complex of A and C which we anticipate must be arranged alternately in an antiparallel cross-β-structure within the tapelike fibrillar substructure (Figure 1b).

The bulk viscosity and $^1$H NMR experiments reveal that the peptide PECs and their nematic hydrogels appear to be stable over a wider pH interval (ca. 1–12) than the access window (ca. 7.2–7.4). The peptide PEC was converted into a gel of C and a monomeric solution of the anionic peptide A over a period of days at pH values higher than about 12 (see Supporting Information). The stability of the peptide PEC to pH appears to arise from the effects of the electrostatic attractive forces between neighboring $Glu^-$ and $Orn^+$ residues in the complex (Figure 1b). This would shift the effective p$K$ values of the Glu and Orn units to lower and higher values, respectively, than those of the free amino acids (Glu 4.1, Orn 10.8). Typically, the gels were stable up to approximately 90 °C.

The fibrillar structure of the CA complex (Figure 2b) is similar to those of pure A and pure C: all have cross-sections of $8 \times 4$ nm and are comprised of four ribbons (eight tapes; see Supporting Information). This observation might appear surprising in view of the different cross-β-strand forces between peptides in the tapelike substructure of the CA

 © 2003 Wiley-VCH Verlag GmbH & Co. KGaA, Weinheim 

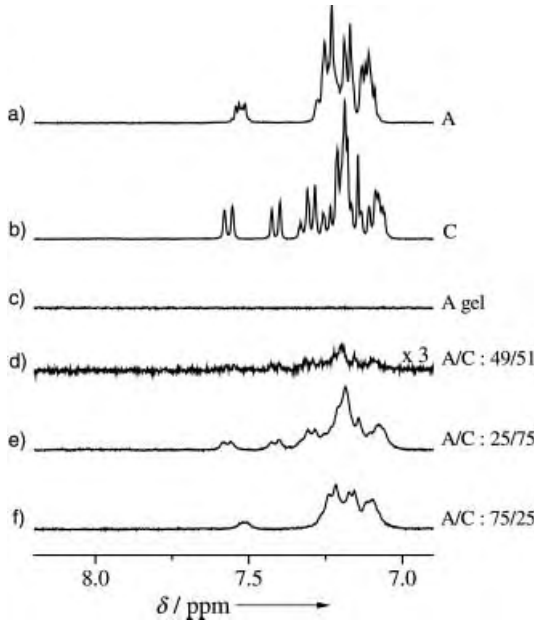



***Figure 4.*** $^1$H NMR (300 MHz) spectra of the aromatic side chains of residues 4, 6, and 8 in a) a solution of monomeric A at $c = 3.13$ mM, pH 7.46, b) a solution of monomeric C at $c = 3.28$ mM, pH 7.1, c) the nematic gel state of A at $c = 3.13$ mM, pH 2, d) the nematic gel state obtained by mixing equal volumes of solutions (a) and (b), e) as in (d) but with a 3:1 excess of peptide C, and f) as in (d) but with a 3:1 excess of peptide A (pH values are uncorrected meter readings).

complex as compared with the corresponding ones in those of pure A or C. This is because fibril structure is goverened primarily by the intrinsic twist of the ribbons and their mutual attraction.[3] Nevertheless, we might expect the apparently stronger mutual attraction between neighboring A and C peptides in the tapelike structure of the complex to be reflected in a significantly lower value of the onset concentration $c^*_{tape}$ for self-assembly of tapes of CA compared to those of pure A and C.[3] From CD measurements we estimate $c^*_{tape} \approx (2 \pm 1)$ mM) for the CA complex, a value significantly greater than for either A ($c^*_{tape} \sim 20$ μM at pH 2) or C ($c^*_{tape} \sim 400$ μM at pH 10) at pH values appropriate for the formation of a gel (see Supporting Information). This paradoxical behavior would appear to have its origin in a high kinetic barrier, which leads to supersaturation of the solution beyond $c^*_{tape}$. To test this hypothesis a 6.3 mM gel at pH 7.5 was carefully diluted down to 0.05 mM. CD measurements revealed a transition in the peptide conformation from β-sheet to random coil at about 100 μM, which is a more realistic value for $c^*_{tape}$.

The stability of β-sheet fibrillar networks toward flocculation has previously[4] been linked to the electrical double layer forces resulting from the presence of a net positive or negative charge on each peptide monomer. One unit of net positive charge per CA pair of peptides appears to be sufficient in the case of the peptide polyelectrolyte complex CA. This charge comes from the single net positive charge located on the $Arg^+$ residue of A. We can expect this minimum net charge requirement to be raised with increasing ionic strength of the solution.

In conclusion, it has been demonstrated that polyelectrolyte β-sheet complexes (PECs) are formed on mixing aqueous solutions of cationic and anionic peptides and this results in the spontaneous self-assembly of fibrillar networks and the production of nematic hydrogels. These complexes have a 1:1 stoichiometry and their networks are quite robust to variations in pH values or peptide concentration. They may be likened to the PECs formed on mixing oppositely charged polymeric polyelectrolytes,[6] except that their supramolecular structures are quite different. In the case of peptide complexes, the fibrils have more definitive molecular and mesoscopic structures which makes it easier to specify the requisite molecular design. The two peptides C and A must have a propensity to form antiparallel β-sheets, appropriate complementarity in the disposition of their charged amino acid side chains, and at least one additional charged amino acid per peptide pair to stabilize the peptide PEC fibrillar network against flocculation. The presence of salt will attenuate the electrostatic forces and this must be accounted for in the peptide design. Potential applications envisaged for these biocompatible, biodegradable nematic hydrogels are, for example, encapsulation, immobilization, and separation of cells, proteins, antibodies, or enzymes.

Received: June 23, 2003 [Z52207]

**Keywords:** β-sheets · gels · peptides · phase transitions · self-assembly

[1] A. Aggeli, N. Boden, S. Zhang, *Self-Assembling Peptide Systems in Biology, Medicine and Engineering*, Kluwer Academic Publishers, Dordrecht, **2001**.
[2] A. Aggeli, M. Bell, N. Boden, J. N. Keen, P. F. Knowles, T. C. B. McLeish, M. Pitkeathly, S. E. Radford, *Nature* **1997**, *386*, 259–262.
[3] A. Aggeli, I. A. Nyrkova, M. Bell, R. Harding, L. Carrick, T. C. B. McLeish, A. Semenov, N. Boden, *Proc. Natl. Acad. Sci. USA* **2001**, *98*, 11 857–11 862.
[4] A. Aggeli, M. Bell, L. M. Carrick, C. W. G. Fishwick, R. Harding, P. J. Mawer, S. E. Radford, A. E. Strong, N. Boden, *J. Am. Chem. Soc.* **2003**, *125*, 9619–9628.
[5] a) D. Bong, T. D. Clark, J. R. Granja, M. R. Ghadiri, *Angew. Chem.* **2001**, *113*, 1016–1041; *Angew. Chem. Int. Ed.* **2001**, *40*, 988–1011; b) S. Zhang, T. Holmes, C. Lockshin, A. Rich, *Proc. Natl. Acad. Sci. USA* **1993**, *90*, 3334–3338; c) H. A. Lashuel, S. R. LaBrenz, L. Woo, L. C. Serpell, J. W. Kelly, *J. Am. Chem. Soc.* **2000**, *122*, 5262–5277.
[6] E. Tsuchida, K. Abe, *Adv. Polym. Sci.* **1982**, 45, 1–119.
[7] M. G. Dobb, D. J. Johnson, B. P. Saville, *J. Polym. Sci.* **1977**, *15*, 2201–2211.
[8] a) S. Krimm, J. Bandekar, *Adv. Protein Chem.* **1986**, *38*, 181–364; b) A. Muga, H. H. Mantsch, W. K. Surewicz, *Biochemistry* **1991**, *30*, 2629–2635.

 © 2003 Wiley-VCH Verlag GmbH & Co. KGaA, Weinheim 

*Octahedron-Based Molecular Sieves*

# Aluminoborate-Based Molecular Sieves with 18-Octahedral-Atom Tunnels**

*Jing Ju, Jianhua Lin,* Guobao Li, Tao Yang, Hongmei Li, Fuhui Liao, Chun-K. Loong, and Liping You*

Microporous frameworks composed of tetrahedra, particularly zeolites, have been extensively studied. These materials are of technological importance as shape-selective catalysts and ion-exchange materials and are widely used in various industrial and technological processes.[1] On the other hand, although a number of microporous materials consisting of mixed octahedra/tetrahedra were established in recent years,[2] microporous frameworks based purely on octahedra are rare. The todorokite family of manganese oxides,[3] including pyrolusite, todorokite, hollandite, and romanechite, is a well-known example among the pure-octahedron frameworks. In these materials, the octahedra share edges to form cubic close-packed rock salt (111) layers, which are interconnected by sharing corners at 90° angles (rutile-like connection), forming one-dimensional tunnels with different pore sizes. The large square tunnels and mixed manganese valences endow these materials with potential applications as redox catalysts, batteries, and chemical sensors.[4] Here we report the novel aluminoborate PKU-1, in which $AlO_6$ octahedra share edges to form a three-dimensional porous framework consisting of 18- and 10-ring windows. The search for new zeolite-like aluminoborates was carried out several years ago, and several aluminoborates and aluminum boron oxide chlorides were identified under hydrothermal conditions, but their stuctures remain unknown.[5]

[*] Prof. Dr. J. Lin, Dr. J. Ju, Dr. G. Li, T. Yang, H. Li, F. Liao
College of Chemistry and Molecular Engineering
Peking University
Beijing 100871 (P. R. China)
Fax: (+86) 10-6275-1708
E-mail: jhlin@chem.pku.edu.cn
Dr. C.-K. Loong
Intense Pulsed Neutron Source Division
Argonne National Laboratory
Argonne, IL 60439 (USA)
L. You
Electron Microscopy Laboratory
College of Physics
Peking University
Beijing 100871 (P. R. China)

[**] We thank Profs. Xuanwen Li, Youchang Xie, and Xiyao Yang at PKU for stimulating discussions and Prof. Feng Deng at Wuhan Institute of Physics and Mathematics for his support with MAS NMR analysis. This work was supported by the Natural Science Foundation of China and by the State Key Basic Research Program of China. Work performed at Argonne National Laboratory was supported by the U.S. DOE, Basic Energy Sciences, under contracts No. W-31-109-ENG-38.

Supporting information for this article is available on the WWW under http://www.angewandte.org or from the author.

Aluminoborate PKU-1 was synthesized by reaction of $AlCl_3 \cdot 6H_2O$ with an excess of $H_3BO_3$ at 240 °C in an autoclave (yield: 95% in Al), whereby the boric acid was used as both reaction medium and reactant. The product consists of needle-shaped polycrystallites. X-ray diffraction identified a trigonal structure ($R\bar{3}$) with lattice parameters $a = 22.0381(2)$ and $c = 7.0261(1)$ Å at room temperature. Analysis of boron and aluminum by inductively coupled plasma emission spectroscopy (ICP-ES) gave a B/Al ratio of about 2. The $^{27}$Al MAS-NMR, $^{11}$B MAS-NMR, and IR data indicated that the Al and B atoms are exclusively in octahedral and triangular coordination, respectively. The detailed structure of PKU-1 was established by analysis of the XRD data with an ab initio method and subsequently by Rietveld refinements with the GSAS program,[6,7] which allowed all non-hydrogen atoms in the compound to be located.[8] The refined structural parameters are listed in the Supporting Information. The presence of protons in the structure was established by consideration of charge balance, as well as thermogravimetric analysis (TGA), IR spectroscopy, and valence calculation.

Figure 1 shows the structure of PKU-1 projected along the *c* axis. The structure can be considered as a framework of octahedra that is enveloped by triangular borate groups. The

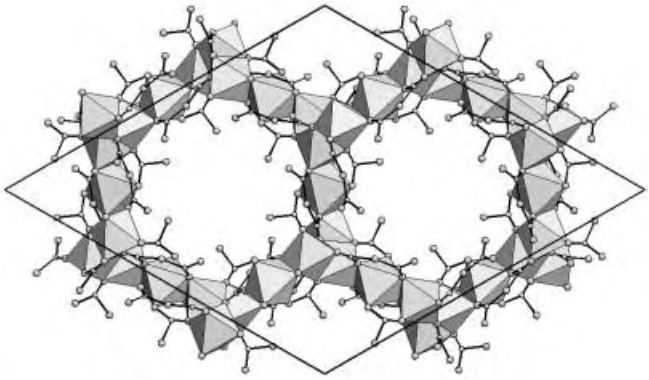


***Figure 1.*** Projection of the PKU-1 structure along the *c* axis; $AlO_6$ octahedra are shown as polyhedra, and oxygen and boron atoms as dark and light spheres, respectively; water molecules in the channels are omitted for clarity.

aluminum atoms are all octahedrally coordinated, and the octahedra share edges to form a framework with three-dimensional porosity. The structure contains two crystallographically independent types of Al atoms [Al1-(18*f*) and Al2-(9*d*)]. The Al1 octahedra share three edges with two Al1 and one Al2 octahedra and act as "nodes" in the framework. The Al2 atoms, on the other hand, share two opposite edges with Al1 octahedra, leaving two opposite corners as terminal oxygen atoms. An alternative description of the framework is that the Al1 octahedra form one-dimensional edge-sharing chains along the *c* axis (threefold helix with an approximate Al1-Al1-Al1 angle of 120°). The Al2 octahedra share two opposite edges with the Al1 chains to form a three-dimensional porous framework. Thus Al2 octahedra act as "girders" in the framework. Figure 2 displays a perspective view of the

 DOI: 10.1002/anie.200352263 © 2003 Wiley-VCH Verlag GmbH & Co. KGaA, Weinheim 

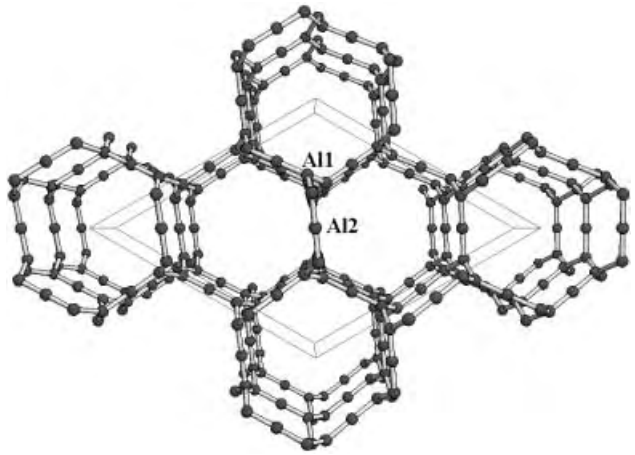



***Figure 2.*** Perspective view of the framework of octahedra in PKU-1 showing the large, parallel hexagonal channels (18-ring) along [001] and the smaller rectangular channels (10-ring) along {100}.

framework of PKU-1, which clearly shows the connectivity of octahedra in the structure. The cavity of the framework is three-dimensional and contains 18-ring hexagonal channels along the [001] direction and 10-ring rectangular channels along each of the {100} directions. The structural model of PKU-1 was also supported by high-resolution TEM data (Figure 3). The HREM image (central inset), simulated by using the structural parameters of PKU-1, agrees reasonably well with the observed pattern. In addition, electron diffraction (insert left) also confirms the trigonal cell of the structure.

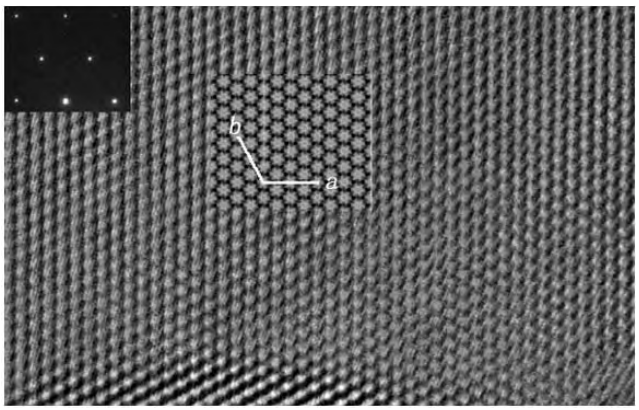



***Figure 3.*** HREM image of PKU-1 in the basal plane; the electron diffraction pattern (top, left inset) shows a typical trigonal symmetry. The inset at the center is a simulated HREM image based on the structural parameters of PKU-1. The basal axes *a* and *b* are shown in the figure, and the length of the axis bars is about 44 Å.

The framework of edge-sharing Al octahedra in PKU-1 is highly negatively charged ($[Al_3O_{10}]^{11-}$). This is a common feature of three-dimensional porous frameworks of octahedra and may also be the reason that these frameworks are rare. To stabilize the octahedral framework, other positively charged species are needed. As shown in Figure 1, all of the oxygen atoms of the octahedral framework are further shared by surrounding borate groups [i.e., $BO_2(OH)$ and $B_2O_4(OH)$] that compensate most of the negative charges ($[Al_3B_6O_{12}(OH)_4]^-$). The remaining negative charge could be compensated by countercations in the channels. In this case, it is likely that protons act as the countercations. The IR spectrum of a sample after calcination at 200 °C under vacuum clearly shows three distinct OH vibrations at 3180, 3440, and 3650 $cm^{-1}$ for the hydroxy groups (see Supporting Information). The overall composition of PKU-1 can be expressed as $HAl_3B_6O_{12}(OH)_4$.

The borate groups partially block the channels of the framework and thus reduce the porosity of the structure. Figure 4 shows the structures of the 18- and 10-rings. The $B_2O_4(OH)$ groups are located within the 10-ring rectangular

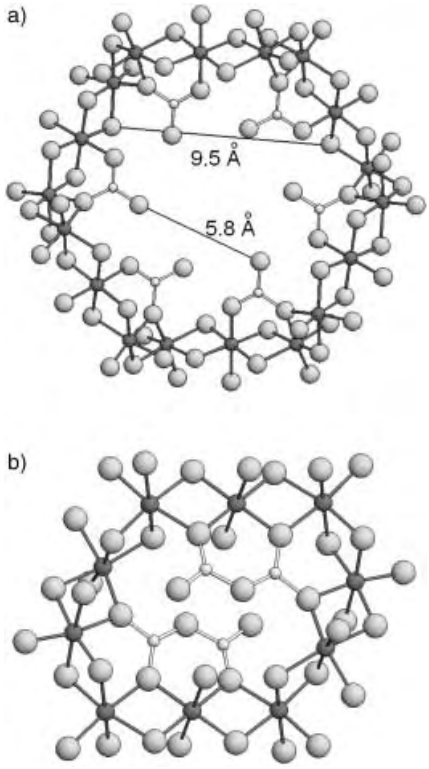



***Figure 4.*** a) 18- and b) 10-ring windows in PKU-1; the borate groups in the channel are also shown. The distances of 5.8 and 9.5 Å shown in the 18-ring are between crystallographically equivalent terminal oxygen atoms and oxygen atoms of the octahedra, which result in diameters of 6.7 and 11.0 Å, respectively, for the channel.

windows and almost completely block the channels along the {100} directions. The $BO_2(OH)$ groups are located within the 18-ring windows and narrow the channels along the [001] direction. The O–O distances of about 5.8 Å between the terminal oxygen atoms on borate groups and about 9.5 Å between those on the Al octahedra correspond to columns 6.7 Å and 11.0 Å in diameter, respectively. The nitrogen adsorption isotherm of a PKU-1 sample degassed at 200 °C under vacuum was characteristic of a microporous material, with a maximum uptake of about 71.4 $cm^3$ of nitrogen per gram of sample.

 © 2003 Wiley-VCH Verlag GmbH & Co. KGaA, Weinheim 

***Table 1:*** Reaction and lattice parameters for PKU-1.[a]

| Compound | Synthesis conditions Reactants | | $T$ [°C] | $t$ [d] | Lattice parameter $a$ [Å] | $c$ [Å] |
|---|---|---|---|---|---|---|
| $HAl_3B_6O_{12}(OH)_4$ | 5 mmol $AlCl_3{\cdot}6H_2O$ | 100 mmol $H_3BO_3$ | 240 | 4 | 22.0381(2) | 7.0261(1) |
| $HGa_3B_6O_{12}(OH)_4$ | 5 mmol $Ga_2O_3$ | 200 mmol $H_3BO_3$ | 220 | 10 | 22.6212(9) | 7.2441(8) |
| $HAl_{2.4}Fe_{0.6}B_6O_{12}(OH)_4$ | 4 mmol $AlCl_3{\cdot}6H_2O$<br>1 mmol $Fe(NO_3)_3{\cdot}6H_2O$ | 100 mmol $H_3BO_3$ | 220 | 14 | 22.2130(5) | 7.1024(3) |
| $HAl_{2.5}Cr_{0.5}B_6O_{12}(OH)_4$ | 4 mmol $AlCl_3{\cdot}6H_2O$<br>1 mmol $Cr(NO_3)_3{\cdot}6H_2O$ | 100 mmol $H_3BO_3$ | 220 | 14 | 22.2041(9) | 7.0716(1) |

[a] The lattice constants were determined by refinement with EXTRA.

The structure refinement also indicated that the as-synthesized sample contains a considerable number of partially ordered water molecules in the 18-octahedron channels. These water molecules are mobile and can be removed completely without affecting the integrity of the framework structure. Structure refinement carried out on a PKU-1 sample calcined at 200 °C showed that the residual electron density in the channels was completely removed (see Supporting Information). Furthermore, TGA shows two-stage weight loss. The weight loss below 200 °C (ca. 8.1 wt %) originates from removal of water, and that between 300 and 600 °C (ca. 10.1 wt %) is related to dehydration of the borate hydroxy groups. Above 600 °C the framework eventually collapses.

The microporous materials known so far are mostly based on corner-sharing tetrahedra, and octahedron-based molecular sieves are rare. One reason for this might be the high negative charge of the three-dimensional porous frameworks of octahedra for common $M^{III}$ and $M^{IV}$ cations. Two different approaches may reduce the negative charge: sharing the octahedral edges more extensively throughout the framework or compensating with other positively charged species. The OMS (octahedral molecular sieves) family of manganese oxides[4] exemplifies extensive sharing of octahedral edges, in this case to form rock salt (111) layers. The oxygen atoms in this family all exhibit threefold coordination by $Mn^{4+}$ and $Mn^{2+}$. PKU-1 is a representative in which the negative charge is compensated by borate groups. In the structure of PKU-1, most of the oxygen atoms on the framework of octahedra of PKU-1 are also threefold coordinated by Al and B (except for the opposite vertices on the Al2-octahedron, which are two-coordinate). Such a mode of compensation allows the formation of a three-dimensional framework of octahedra containing tunnels.

It is noteworthy that this octahedron-based molecular sieve was synthesized in boric acid flux without using any organic template. Although the reaction mechanism is not yet understood, the formation of the microporous structure implies the assembly of borate groups and water molecules, perhaps mediated by hydrogen bonding during the reaction. In fact, in addition to PKU-1, many new polyborates, including rare-earth polyborates and transition-metal polyborates, were obtained.[9] Moreover, some other metal ions can also be accommodated at the octahedral sites in the PKU-1 structure. Galloborate ($HGa_3B_6O_{12}(OH)_4$) also crystallizes in the PKU-1 structure under the same reaction conditions. The lattice constants are significantly larger than those of the aluminum analogue, as shown in Table 1. We also applied similar reaction conditions to the transition metal salts and found that most transition metals do not themselves form PKU-1 structures, but can partially replace Al to form solid solutions such as $HAl_{2.4}Fe_{0.6}B_6O_{12}(OH)_4$ and $HAl_{2.5}Cr_{0.5}B_6O_{12}(OH)_4$. As shown in Table 1, substitution by transition-metal ions modifies the lattice parameters and the porosity of the frameworks. In terms of potential applications, the octahedral molecular sieves containing d-block elements are considerably more interesting because they may provide a means of tailoring not only chemical and physical properties such as catalysis, ion exchange, and molecular sieving, but also electronic properties.

## *Experimental Section*

PKU-1 was synthesized by direct reaction of aluminum salts with boric acid in a flux of boric acid in a closed autoclave. In a typical reaction $AlCl_3{\cdot}6H_2O$ (5 mmol) and $H_3BO_3$ (100 mmol) were charged to a 50 $cm^3$ Teflon autoclave, and the mixture was heated at 240 °C for four days. After cooling to room temperature, the solid (containing PKU-1 and residual $H_3BO_3$) was washed with hot water (50 °C) until the residual boric acid was completely removed. The yield was about 95 % in Al. Other aluminum sources, such as $Al_2O_3$ and $Al(NO_3)_3$, also yielded the same product. Ga-PKU-1 and transition-metal-substituted PKU-1 (AlCr-PKU-1 and AlFe-PKU-1) were synthesized from gallium oxide and the transition-metal nitrates by a similar method at 220 °C for 10–14 days. Table 1 summarizes the reaction conditions for these compounds. The degree of substitution by transition-metal cations was analyzed by the ICP method.

Received: June 30, 2003 [Z52263]

**Keywords:** aluminoborates · aluminum · boron · microporous materials · zeolite analogues

[1] M. E. Davis, *Nature* **2002**, *417*, 813.
[2] a) M. W. Anderson, O. Terasaki, T. Ohsuna, A. Philippou, S. P. Mackay, A. Ferrreira, J. Rocha, S. Lidin, *Nature* **1994**, *367*, 347; b) R. C. Haushalter, K. G. Strohmaier, F. W. Lai, *Science* **1989**, *246*, 1289; c) S. M. Kuznicki, V. A. Bell, S. Nair, H. W. Hillhouse, R. M. Jacubinas, C. M. Braunbarth, B. H. Toby, M. Tsapatsis, *Nature* **2001**, *412*, 720; d) C. H. Lin, S. L. Wang, K. H. Lii, *J. Am. Chem. Soc.* **2001**, *123*, 4649; e) N. Guillou, Q. Gao, P. M. Forster, J. Chang, M. Noguès, S. Park, G. Férey, A. K. Cheetham, *Angew. Chem.* **2001**, *113*, 2913; *Angew. Chem. Int. Ed.* **2001**, *40*, 2831; f) S. Ekambaram, S. C. Sevov, *Angew. Chem.* **1999**, *111*, 384; *Angew. Chem. Int. Ed.* **1999**, *38*, 372.

 © 2003 Wiley-VCH Verlag GmbH & Co. KGaA, Weinheim 

[3] a) F. V. Chukhrov, A. I. Gorshkov, A. V. Sivtsov, V. V. berezovskaya, *Nature* **1979**, *278*, 631; b) S. Turner, P. R. Buseck, *Science* **1981**, *212*, 1024; c) R. G. Burns, V. M. Burns, H. W. Stockman, *Am. Mineral.* **1983**, *68*, 972.

[4] a) Y. F. Shen, R. P. Zerger, R. N. DeGuzman, S. L. Suib, L. McCurdy, D. I. Potter, C. L. O'Young, *Science* **1993**, *260*, 511; b) X. Chen, Y. Shen, S. L. Suib, C. L. O'Young, *Chem. Mater.* **2002**, *14*, 940; c) Y.-C. Son, V. D. Makwana, A. R. Howell, S. L. Suib, *Angew. Chem.* **2001**, *113*, 4410; *Angew. Chem. Int. Ed.* **2001**, *40*, 4280.

[5] a) J. Wang, S. Feng, R. Xu, *J. Chem. Soc. Chem. Commun.* **1989**, 265; b) J. Yu, R. Xu, Y. Xu, Y. Yue, *J. Solid State Chem.* **1996**, *122*, 200; c) J. Yu, R. Xu, J. Chen, Y. Yue, *J. Mater. Chem.* **1996**, *6*, 465.

[6] a) C. Dong, *Appl. Crystallogr.* **1999**, *32*, 838; b) A. Altomare, M. C. Burla, G. Cascarano, G. Giacovazzo, A. Guagliardi, A. G. G. Moliterni, G. Polidori, *J. Appl. Crystallogr.* **1995**, *28*, 842.

[7] A. C. Larson, R. B. von Dreele, Report LAUR 86-748, Los Alamos National Laboratory, Los Alamos, NM, **1985**.

[8] Powder XRD data of PKU-1 were collected at room temperature on a Bruker D8 diffractometer in the Bragg–Brentano geometry with a curved germanium primary monochromator ($Cu_{K\alpha1}$, $\lambda = 1.5406$ Å). Tube voltage and current were 50 kV and 40 mA. Step-scan size and time: 0.02° ($2\theta$) and 30 s. The patterns were indexed to trigonal unit cells, $a = 22.0392(2)$ and $c = 7.02643(8)$ Å by using TREOR90-PowderX,[6] and the analysis of the observed systematic absences narrowed the possible space groups to $R\bar{3}$, $R3$, $R32$, $R3m$, and $R\bar{3}m$. PKU-1 does not show nonlinear optical behavior, so the space group was restricted to $R\bar{3}$ or $R\bar{3}m$. The crystal structure was established by using EXPO with space group $R\bar{3}$ and was further developed by difference Fourier analysis during the Rietveld refinement.[6,7] All non-hydrogen atoms in the structure were refined with geometric constraints of triangular borate groups. The first reflection peak at about 8.0° was not used in the structure refinement. The number of contributing reflections was 421 with 29 structure and profile variables in the final refinement. The residual factors of the refinement were $R_{wp} = 0.069$ and $R_p = 0.049$. The Rietveld refinement was also carried out for a PKU-1 sample calcined at 200 °C. The structure parameters are almost the same as those of the as-synthesized sample (with $R_{wp} = 0.048$ and $R_p = 0.036$), but the disappearance of all of the electron density in the channels indicated complete removal of the mobile water from the channels. Crystallographic data, atomic parameters, and selected bond lengths and angles are given in the Supporting Information. Further details on the crystal structure investigations may be obtained from the Fachinformationszentrum Karlsruhe, 76344 Eggenstein-Leopoldshafen, Germany (fax: (+49) 7247-808-666; e-mail: crysdata@fiz-karlsruhe.de), on quoting the depository number CSD-413233.

[9] a) L. Y. Li, P. C. Lu, Y. Y. Wang, X. L. Jin, G. B. Li, Y. X. Wang, L. P. You, J. H. Lin, *Chem. Mater.* **2002**, *14*, 4963; b) L. Y. Li, X. L. Jin, G. B. Li, Y. X. Wang, F. H. Liao, G. Q. Yao, J. H. Lin, *Chem. Mater.* **2003**, *15*, 2253; c) P. C. Lu, Y. X. Wang, L. P. You, J. H. Lin, *Chem. Commun.* **2001**, 1178.

 © 2003 Wiley-VCH Verlag GmbH & Co. KGaA, Weinheim 

Phosphorus Coordination Chemistry

# Ruthenium-Stabilized Low-Coordinate Phosphorus Atoms: Structural Evidence for Monomeric Metaphosphonate**

*Richard Menye-Biyogo, Fabien Delpech,* Annie Castel, Heinz Gornitzka, and Pierre Rivière**

The metaphosphate anion has attracted steady interest since 1955[1] in connection with wide applications in phosphorylation reactions.[2] It has relevance in biochemistry in particular with respect to ATP hydrolysis.[3] However, despite considerable efforts, monomeric metaphosphates and other dioxophosphoranes are only known as transient species in solution and their existence can be inferred from trapping experiments.[2–4] Their high reactivity arises from the powerful electrophilic character at the phosphorus center. Several approaches have been tested to stabilize these highly reactive species. Kinetic stabilization by steric protection[5] proved to be ineffective for dioxophosphorane and led to products that resulted from the insertion of the $PO_2$ moiety in a neighboring group.[6] The electrophilicity and the tendency to expand the valence shell were exploited for their stabilization as Lewis salts. This strategy allowed only spectroscopic characterization by $^{31}P$ NMR in a few cases.[7] Thus, the chemistry of dioxophosphorane suffers from a paucity of information and new approaches to stabilize and enable deeper investigation are highly desirable. This work describes the first isolation and full characterization, including X-ray structural analysis, of stabilized metaphosphonate.

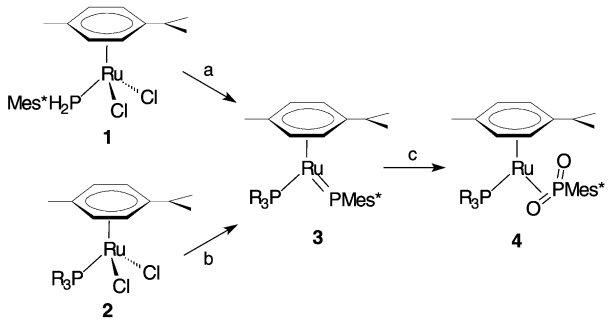
We have developed a novel and successful route to ruthenium-stabilized monomeric metaphosphonate by oxidation of a nucleophilic terminal phosphinidene complex of ruthenium. As recently described by Lammerstma and coworkers, the terminal phosphinidene ruthenium complexes $[(\eta^6\text{-}p\text{-cymene})Ru(PR_3)(PMes^*)]$ (**3a**: R = Cy, **3b**: R = Ph[8]) are formed as dark green solids by the reaction of the primary phosphane complex $[(\eta^6\text{-}p\text{-cymene})RuCl_2(PH_2Mes^*)]$(**1**; *p*-cymene = 4-methyl-*iso*-propylbenzene; Mes* = 2,4,6-tri-*tert*-butylphenyl) with two equivalents of 1,8-diazabicyclo[5-4-0]undec-7-ene (DBU) in the presence of $PR_3$ as a stabilizing ligand (R = Ph, Cy).[8] Alternatively, treatment of $[(\eta^6\text{-}p\text{-cymene})RuCl_2(PR_3)]$ (**2a**: R = Cy, **2b**: R = Ph) and $PH_2Mes^*$ with DBU affords **3** in high yields (Scheme 1).

[*] Dr. F. Delpech, P. Rivière, R. Menye-Biyogo, Dr. A. Castel, Dr. H. Gornitzka
Laboratoire d'Hétérochimie Fondamentale et Appliquée, UMR 5069
Université Paul Sabatier
118, Route de Narbonne, 31062 Toulouse Cédex 04 (France)
Fax: (+33) 5–6155–8204
E-mail: delpech@chimie.ups-tlse.fr
riviere@chimie.ups-tlse.fr

[**] This work was supported by the Ministère de la Jeunesse, de L'Education Nationale et de la Recherche and by the CNRS. R.M.B. is grateful to the Gabonese government for a fellowship.

Supporting information for this article is available on the WWW under http://www.angewandte.org or from the author.

 © 2003 Wiley-VCH Verlag GmbH & Co. KGaA, Weinheim DOI: 10.1002/anie.200352306 




***Scheme 1.*** Synthesis of the complexes **3, 4**: a) $PR_3$, DBU, $C_7H_8$; b) $PH_2Mes^*$, DBU, $C_7H_8$; c) $O_2$, $Et_2O$.

The $^{31}P$ NMR spectra show a high-field resonance ($\delta =$ 811 ppm for **3a** and $\delta = 835$ ppm for **3b**) in the typical region for terminal phosphinidene complexes[8,9] as well as a signal which corresponds to the $PR_3$ ligand.[10] X-ray diffraction study ascertains the structure of **3a**, which compares well with those of [($\eta^6$-*p*-cymene)($PPh_3$)Os(PMes*)] and [($\eta^6$-benzene)($PPh_3$)Ru(PMes*)].[8] The nucleophilic behavior of the phosphinidene ligand in these complexes arises from a substantial back-donation from the metal. Thus, complexes **3** offer an attractive opportunity to stabilize strong electrophilic phosphorus species such as dioxophosphorane.

Using similar oxidation route to that reported to generate metaphosphonate from related $\sigma^2$-$\lambda^3$ phosphorus in diphosphene,[11] we obtained the first monomeric stabilized-dioxophosphorane. Indeed, upon oxidation with $O_2$, the dark green solution of **3** turned instantly yellow and yielded [($\eta^6$-*p*-cymene)($PR_3$)Ru($\eta^2$-OPOMes*)] (**4a**: R = Cy, **4b**: R = Ph) in high yields (Scheme 1). Interestingly, **4** are mildly air-sensitive and the high electrophilicity of dioxophosphorane is thoroughly quenched since no reaction occurs in the presence of any of the typical trapping agents ($CH_3OH$, $PhNH_2$). The formulation of **4** was confirmed by spectroscopic studies. Conversion of **3** into **4** was followed by IR spectroscopy and the spectra (nujol) show appearance of two strong and characteristic absorptions (at 1168 $cm^{-1}$ and 907 $cm^{-1}$; 1153 $cm^{-1}$ and 925 $cm^{-1}$ for **4a** and **4b** respectively) assigned to asymmetric and symmetric OPO stretches. Although these bands cannot be considered as pure modes (coupling with Ru–P and Ru–O must be present), they are clearly shifted to low frequencies by comparison to the band observed in $RPO_2$ (1448 $cm^{-1}$ and 1143 $cm^{-1}$)[12] and indicate a significant weakening of the P=O bond consistent with ligation to ruthenium. Analogous behavior has been reported in the well-documented coordination chemistry of the somewhat related $CO_2$ ligand.[13] $^{31}P$ NMR resonances are in the expected region for four-coordinate phosphorus atoms ($\delta =$ 40.8 ppm for $PO_2Mes^*$ and $\delta = 27.1$ ppm for $PCy_3$ in **4a** and $\delta = 38.5$ ppm for $PO_2Mes^*$ and $\delta = 25.7$ ppm for $PPh_3$ in **4b**). $^1H$ NMR spectroscopic data provide additional structural information. $^1H$ NMR spectra show for the aryl protons of the *p*-cymene ligand three resonances in a 2:1:1 ratio, which are significantly shifted upfield relative to those of **1**–**3**. Such a behavior had been previously observed for half-sandwich complexes exposed to magnetic anisotropy cone of phenyl substituent (known as "β-phenyl effect").[14] Consistently, the proximity between *p*-cymene and Mes* moieties results in restricted rotation about the P–C(Mes*) bond as evidenced by the presence of two Mes* aryl signals in addition to two *o*-Me resonances. No change is observed in the NMR spectra over the temperature range of 20 °C to 100 °C. The molecular geometry of **4a** was determined by X-ray crystallographic analysis (Figure 1).[15]

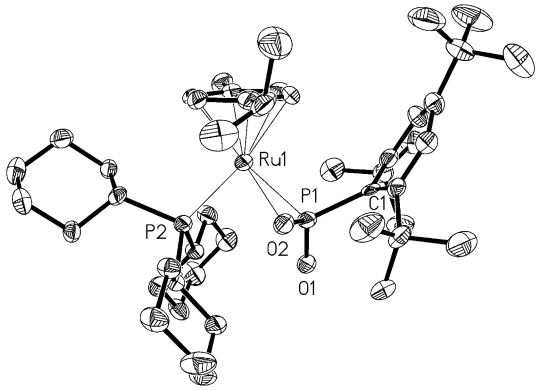



***Figure 1.*** Molecular structure of **4a** (50% thermal ellipsoids; hydrogen atoms and noncoordinated ether molecules are omitted for clarity). Selected bond lengths (Å) and angles (°): Ru1-O2 2.130(4), Ru1-P1 2.2963(17), Ru1-P2 2.3830(17), P1-O1 1.491(5), P1-O2 1.569(4), P1-Ru1-P2 89.91(6), P2-Ru1-O2 87.09(11), O1-P1-O2 120.1(2), O1-P1-C1 115.2(3), O2-P1-C1 104.2(3).

The environment around the ruthenium center can be considered as a two-legged piano stool with a P=O bond occupying one of the coordination sites. Complex **4a** features a side-on $\eta^2$-coordinated metaphosphonate, which is unprecedented (Figure 1). The metal-coordinated P(1)–O(2) bond (1.569(4) Å) is longer than the P(1)=O(1) double bond (1.491(5) Å) which is similar to that found in phosphinidene oxide complexes.[16] However, P(1)–O(2) bond is still shorter than a single P–O bond ($\approx$1.63 Å) and indicates significant residual double-bond character. The lengthening of the P=O bond and the planarity of the *p*-cymene ligand (deviations out the plane from 0.001 to 0.005 Å) in **4** are strong signs of substantial Ru (dπ) to P=O (π*) back-donation.[17,18] This bonding mode induces pyramidalization at the P atom with a sum of bond angles of 339° and loss of the planarity for metaphosphonate as observed upon coordination of olefin[19] or of related bis(imino)- and amino(imino) thiophosphorane[20] toward a transition metal. Interestingly, the acute P(2)-Ru-A angle (A is the projection of the metal Ru on the P(1)–O(2) bond, O(2)–A = 0.551 Å) of 88.02 ° does not vary significantly than P-M-P (M = Ru, Os) angle in related terminal phosphinidene complexes,[8] despite the increased steric congestion between the Mes* group and *p*-cymene ligand. This unexpected arrangement has its origin in orbital factors. Ab initio calculations performed on monomeric dioxophosphorane have shown that OPO moiety may be described as a four-electron, three-center π system, in which HOMO is mainly localized at the oxygen positions while the LUMO corresponds to P = O (π*) antibonding orbitals.[21] Examination of the bonding situation for the metaphosphonate ligand in **4** by using the Dewar–Chatt–Duncanson model

 © 2003 Wiley-VCH Verlag GmbH & Co. KGaA, Weinheim 

(by analogy with olefin complexes) provides pertinent information. Both donation and back-donation involving the metaphosphonate ligand implicate orbitals that are perpendicular to the plane of the free dioxophosphorane and impose such a face-on orientation for the Mes* group.

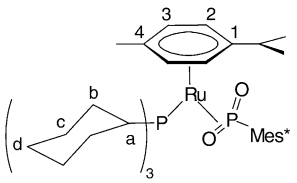
In conclusion, the accessibility of monomeric metaphosphonate relies on its complexation to electron-rich species which reduce electrophilicity. Complexes **4**, in which dioxophosphorane Mes*$PO_2$ has been generated and stabilized within the coordination sphere of a transition metal, represent the first direct observation of fully characterized monomeric metaphosphonate.

## Experimental Section

**3a**: DBU (0.29 mL; 1.97 mmol) was added to a red slurry of [($\eta^6$-*p*-cymene)($PCy_3$)$RuCl_2$] (0.602 g; 1.03 mmol) and Mes*$PH_2$ (0.274 g; 0.98 mmol) in toluene (10 mL). The mixture was stirred for 1 h at room temperature to afford a dark green solution. The toluene was removed in vacuo and the dark green solid then extracted with pentane (10 mL) and filtered to remove DBU·HCl. Removal of the pentane to a minimal volume and cooling to −25 °C gave 0.780 g of a crystalline solid in 80 % yield.[10]

**4a**: A cold (0 °C) ether solution of **3a** (0.166 g; 0.21 mmol) was bubbled with oxygen for 1 min. Removal of the ether to a minimal volume and cooling to −25 °C gave 0.150 g of a yellow crystalline solid in 87 % yield. m.p.: 176 °C.

Atom labeling used in the NMR assignments of **4a** is given below.




$^{31}$P NMR (81 MHz, $C_6D_6$): $\delta = 27.1$ (d, $^2J$(P,P) = 45.8 Hz, $PCy_3$), 40.8 ppm (d, $^2J$(P,P) = 45.8 Hz, $PO_2$Mes*). $^1$H NMR (200 MHz, $C_6D_6$): $\delta = 1.05$ (d, $^3J$(H,H) = 6.8 Hz, 3H, CH($CH_3$)$_2$ *p*-cymene), 1.20 (d, $^3J$(H,H) = 6.6 Hz, 3H, CH($CH_3$)$_2$ *p*-cymene), 1.29 (m, 12H, $C_cH_2$), 1.41 (s, 9H, *p*-C($CH_3$)$_3$), 1.56 (m, 6H, $C_dH_2$), 1.81 (s, 3H, $CH_3$ *p*-cymene), 1.88 (s, 9H, *o*-C($CH_3$)$_3$), 1.91 (m, 12H, $C_bH_2$), 2.14 (s, 9H, *o*-C($CH_3$)$_3$), 2.53 (m, 4H, $C_aH$ and $CH(CH_3)_2$ *p*-cymene), 2.95 (s, 1H, $C_2H$ *p*-cymene), 4.17 (s, 1H, $C_3H$ *p*-cymene), 5.40 (s, 2H, $C_2H$ and $C_3H$ *p*-cymene), 7.43 (s, 1H, *m*-Mes*), 7.55 ppm (s, 1H, *m*-Mes*). $^{13}$C{$^1$H} NMR (50 MHz, $C_6D_6$): $\delta = 19.1$ (s, $CH_3$ *p*-cymene), 20.5 (s, CH($CH_3$)$_2$ *p*-cymene), 25.3 (s, CH($CH_3$)$_2$ *p*-cymene), 27.3 (s, $C_d$), 28.4 (d, $^3J$(C,P) = 10.2 Hz, $C_c$), 30.6 (d, $^2J$(C,P) = 33.3 Hz, $C_b$), 31.1 (s, CH($CH_3$)$_2$ *p*-cymene), 31.6 (s, *p*-C($CH_3$)$_3$), 33.7 (s, *o*-C($CH_3$)$_3$), 33.8 (s, *o*-C($CH_3$)$_3$), 34.9 (s, *p*-C($CH_3$)$_3$), 37.3 (d, $^3J$(C,P) = 8.3 Hz, $C_a$), 39.8 (d, $^3J$(C,P) = 2.8 Hz, *o*-C($CH_3$)$_3$), 40.7 (d, $^3J$(C,P) = 2.8 Hz, *o*-C($CH_3$)$_3$), 73.7 (s, $C_4$ *p*-cymene), 75.2 (d, $^2J$(C,P) = 11.1 Hz, $C_2$ *p*-cymene), 84.6 (d, $^2J$(C,P) = 9.2 Hz, $C_2$ *p*-cymene), 86.3 (s, $C_3$ *p*-cymene), 93.9 (s, $C_3$ *p*-cymene), 99.4 (s, $C_1$ *p*-cymene), 119.1 (d, $^3J$(C,P) = 12.9 Hz, *m*-Mes*), 121.7 (d, $^3J$(C,P) = 10.2 Hz, *m*-Mes*), 137.9 (d, $^1J$(C,P) = 65.7 Hz, *ipso*-Mes*), 147.7 (d, $^4J$(C,P) = 3.7 Hz, *p*-Mes*), 153.6 (s, *o*-Mes*), 153.9 ppm (s, *o*-Mes*); IR (nujol): 1168, 907 $cm^{-1}$ (asym and sym OPO); elemental analysis (%) calcd. for **4a**·2$Et_2O$ $C_{54}H_{96}O_4P_2Ru$: C 66.70, H 9.95; found: C 66.33, H 9.46.

The derivatives **3b** and **4b** were prepared by an analogous method.[10]

Received: July 4, 2003 [Z52306]

**Keywords:** coordination modes · P ligands · phosphanes · pi interactions · ruthenium

[1] a) W. W. Butcher, F. H. Westheimer, *J. Am. Chem. Soc.* **1955**, *77*, 2420; b) D. W. C. Barnard, C. A. Bunton, D. R. Llewellyn, K. G. Oldham, L. B. Silver, C. A. Vernon, *Chem. Ind. (London, U.K.)* **1955**, 760.

[2] a) L. D. Quin, *Coord. Chem. Rev.* **1994**, *137*, 525; b) I. Lukes, M. Borbaruah, L. D. Quin, *J. Am. Chem. Soc.* **1994**, *116*, 1737.

[3] a) F. H. Westheimer, *Chem. Rev.* **1981**, *81*, 313; b) F. H. Westheimer, *Science* **1987**, *235*, 1173; c) A. C. Hengge, W. A. Edens, H. Elsing, *J. Am. Chem. Soc.* **1994**, *116*, 5045; d) J. Y. Choe, C. V. Iancu, H. J. Fromm, B. B. Honzatko, *J. Biol. Chem.* **2003**, *278*, 16015.

[4] M. Meisel in *Multiple Bonds and Low Coordination in Phosphorus Chemistry* (Eds.: M. Regitz, O. J. Scherer), Thieme, Stuttgart, **1990**, pp. 415 – 442.

[5] M. Larbig, M. Nieger, V. von der Gönna, A. V. Ruban, E. Niecke, *Angew. Chem.* **1995**, *107*, 505; *Angew. Chem. Int. Ed. Engl.* **1995**, *34*, 460.

[6] a) S. Bracher, J. I. G. Cadogan, I. Gosney, S. Yaslak, *J. Chem. Soc. Chem. Commun.* **1983**, 857; b) J. I. G. Cadogan, A. H. Cowley, I. Gosney, M. Pakulski, S. Yaslak, *J. Chem. Soc. Chem. Commun.* **1983**, 1408.

[7] H. Teichmann, *Phosphorus Sulfur Silicon Relat. Elem.* **1993**, *76*, 95.

[8] A. T. Termaten, T. Nijbacker, M. Schakel, M. Lutz, A. L. Spek, K. Lammertsma, *Chem. Eur. J.* **2003**, *9*, 2200.

[9] F. Mathey, *Angew. Chem.* **2003**, *115*, 1616; *Angew. Chem. Int. Ed.* **2003**, *42*, 1578.

[10] For synthesis, spectroscopic data, and elemental analysis see Supporting Information.

[11] B. Kramer, E. Niecke, M. Nieger, R. W. Yaslak, *Chem. Commun.* **1996**, 513.

[12] R. Ahlrichs, C. Ehrhardt, M. Lakenbrink, S. Schunck, H. Schnöckel, *J. Am. Chem. Soc.* **1986**, *108*, 3596.

[13] D. H. Gibson, *Chem. Rev.* **1996**, *96*, 2063.

[14] H. Brunner, T. Zwack, M. Zabel, W. Beck, A. Böhm, *Organometallics* **2003**, *22*, 1741.

[15] CCDC 213806 contains the supplementary crystallographic data for this paper. These data can be obtained free of charge via www.ccdc.cam.ac.uk/conts/retrieving.html (or from the Cambridge Crystallographic Data Centre, 12 Union Road, Cambridge CB2 1EZ, UK; fax: (+44) 1223-336-033; or deposit@ccdc.cam.ac.uk). Information about crystal data and structure measurements and refinements are summarized in the Supporting Information.

[16] a) E. Niecke, M. Engelmann, H. Zorn, B. Krebs, G. Henkel, *Angew. Chem.* **1980**, *92*, 737; *Angew. Chem. Int. Ed. Engl.* **1980**, *19*, 710; b) P. B. Hitchcock, J. A. Johnson, M. A. N. D. A. Lemos, M. F. Meidine, J. F. Nixon, A. J. L. Pombeiro, *J. Chem. Soc. Chem. Commun.* **1992**, 645; c) I. V. Kourkine, D. S. Glueck, *Inorg. Chem.* **1997**, *36*, 5164.

[17] P. Rosa, L. Ricard, F. Mathey, P. Le Floch, *Organometallics* **1999**, *18*, 3348.

[18] L. J. Radonovich, F. J. Koch, T. A. Albright, *Inorg. Chem.* **1980**, *19*, 3373.

[19] C. Elschenbroich, A. Salzer, *Organometallics*, VCH, Weinheim, **1992**, pp. 252 – 266.

[20] a) O. J. Scherer, H. Jurgmann, C. Krüger, G. Wolmershäuser, *Chem. Ber.* **1984**, *117*, 2382; b) O. J. Scherer, R. Walter, P. Bell, *Chem. Ber.* **1987**, *120*, 1885.

[21] W. W. Schoeller, T. Bush, *Chem. Ber.* **1992**, *125*, 1319.

 © 2003 Wiley-VCH Verlag GmbH & Co. KGaA, Weinheim 

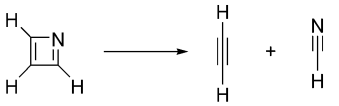
*Synthetic Methods*

# Base-Induced Condensation of α-Chloro Oxime Derivatives Furnishes Alkynes**

*Takayuki Tsuritani, Kazunari Yagi, Hiroshi Shinokubo,* and Koichiro Oshima**

The carbon–carbon triple bond is a fundamental structural unit in natural and unnatural organic molecules. Alkynes also serve as important synthetic intermediates in a number of organic transformations, and their chemistry has recently received particular attention with respect to new materials. The alkynyl linkage is often a key building block in highly conjugated molecules used in light-emitting devices and molecular wires.[1]

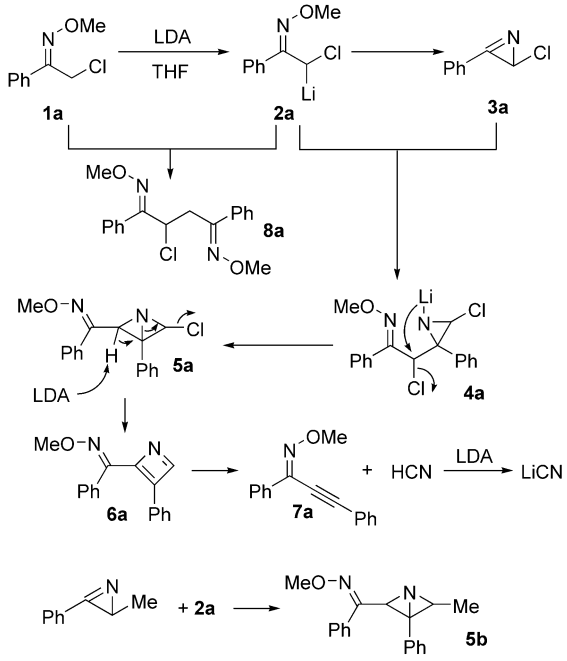
Azacyclobutadiene (azete) is a highly reactive and unstable molecule, the physical properties of which have been investigated experimentally and theoretically.[2] Although the reaction of an isolable azacyclobutadiene kinetically stabilized by bulky substituents has been reported,[2d–f] the utility of such compounds in organic synthesis has remained largely unexplored. In particular, azacyclobutadiene is known to undergo [2+2] cycloreversion to provide acetylene and hydrogen cyanide (Scheme 1).[2b,h] However, no



***Scheme 1.*** Fragmentation of azacyclobutadiene.

applications of azacyclobutadienes for the preparation of alkynes have been reported. Here we wish to describe a base-induced novel condensation reaction of α-chloro oxime derivatives to furnish alkynyl oximes via an azacyclobutadiene intermediate.

The reaction of α-chloroacetophenone *O*-methyloxime (**1a**) with 1.1 equiv of lithium diisopropylamide (LDA) afforded 1,3-diphenylpropyn-1-one *O*-methyloxime (**7a**) and 2-chloro-1,4-diphenyl-1,4-butanedione bis(*O*-methyloxime) (**8a**) in yields of 7% and 38%, respectively.[3] The formation of **7a** is rationalized by assuming the fragmentation of an intermediate 1-aza-2-chlorobicyclo[1.1.0]butane **5a** (Scheme 2).[4] Deprotonation of **1a** affords the lithio oxime ether **2a**, which then undergoes Neber-type cyclization to



***Scheme 2.*** Plausible reaction pathway.

provide the highly reactive azirine **3a**.[5,6] The reaction of **3a** with **2a** affords **4a**, which yields 1-aza-2-chlorobicyclo[1.1.0]-butane **5a**. The formation of **5a** is likely because **5b** was isolated in the case of the reaction of **2a** with 2-methyl-3-phenyl-2*H*-azirine. Removal of an α-proton of **5a** with LDA leads to the highly unstable azacyclobutadiene **6a** by ring expansion and elimination of chloride ion. The [2+2] cycloreversion of **6a** yields the alkynyl oxime ether **7a** accompanied by HCN, which is then deprotonated by lithium amide. Consequently, 2.0 equiv of lithium amide are necessary for the reaction. With this in mind, we treated **1a** with 2.2 equiv of lithium diisopropylamide at −78 °C and allowed the reaction mixture to warm to room temperature. We obtained **7a** in 76% yield without the formation of **8a** (entry 1 in Table 1).[7]

We examined the conversion of various α-chloro oxime ethers into alkynyl oxime ethers under the same conditions (Table 1). Oxime ether **1b** provided the corresponding alkynyl oxime ether **7b** in 81% yield, whereas **1c** furnished **7c** in poor yield along with other unidentified products. The low yield was ascribed to the lower stability of the corresponding lithio oxime ether **2**. However, the addition of 0.5 equiv of magnesium bromide increased the yield of **7c** up to 70% yield. A noteworthy observation is the fact that the reaction in the presence of $MgBr_2$ proceeded even at −78 °C, suggesting that magnesium bromide acts as a Lewis acid and accelerates the conversion of **2** into **3**.

In order to verify the reaction mechanism, an additional experiment was performed. When the reaction mixture

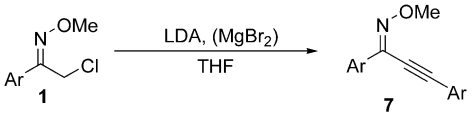
[*] Dr. H. Shinokubo, Prof. Dr. K. Oshima, T. Tsuritani, K. Yagi
Department of Material Chemistry
Graduate School of Engineering
Kyoto University
Kyoto-Daigaku Katsura, Nishikyo-ku, Kyoto 615-8510 (Japan)
Fax: (+81) 75-753-2438
E-mail: shino@fm1.kuic.kyoto-u.ac.jp
oshima@fm1.kuic.kyoto-u.ac.jp

[**] This work was supported by a Grant-in-Aid for Scientific Research on Priority Area No. 412: Exploitation of Multi-Element Cyclic Molecules) and by a COE research grant from the Ministry of Education, Culture, Sports, Science, and Technology, Japan. H.S. thanks Tokuyama Science Foundation for financial support.

Supporting information for this article is available on the WWW under http://www.angewandte.org or from the author.

 DOI: 10.1002/anie.200352317 © 2003 Wiley-VCH Verlag GmbH & Co. KGaA, Weinheim 

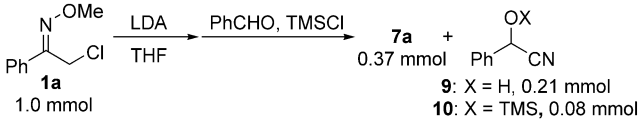
***Table 1:*** Self-condensation of α-chloro oxime ethers.




| Entry | Starting cmpd. | Ar | Cond.[a] | Prod. | Yield [%] | Sel. [*Z*/*E*] |
|---|---|---|---|---|---|---|
| 1 | **1a** | Ph | A | **7a** | 76 | >95/5 |
| 2 | **1b** | 4-MeO-$C_6H_4$ | A | **7b** | 81 | >95/5 |
| 3 | **1c** | 4-Cl-$C_6H_4$ | A | **7c** | 19 | >95/5 |
| 4 | **1c** | 4-Cl-$C_6H_4$ | B | **7c** | 70 | 95/5 |
| 5 | **1d** | 4-Br-$C_6H_4$ | B | **7d** | 65 | 94/6 |
| 6 | **1e** | 2-naphthyl | C | **7e** | 67 | >95/5 |

[a] Conditions: A: LDA (2.2 equiv), −78 °C to room temperature; B: LDA (2.5 equiv), $MgBr_2$ (0.5 equiv), −78 °C, 3 h; C: same conditions as B, but −78 °C to room temperature.

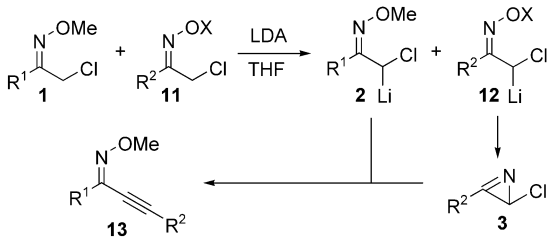
derived from **1a** in the absence of $MgBr_2$ was treated with benzaldehyde and TMSCl, mandelonitrile (**9**) and its silylated product **10** were obtained along with **7a** (Scheme 3). This supports the generation of HCN from the fragmentation of **6a**.




***Scheme 3.*** Trapping of HCN with an aldehyde. TMS = trimethylsilyl.

Next, we attempted to perform a cross-condensation reaction. The reaction of **2** with 2-halo-2*H*-azirine **3** would furnish alkynyl oxime ethers. Although the synthesis of azirines has been extensively explored, there are very few reports on the synthesis of haloazirine **3**.[8] The reaction of chlorine azide with chloroalkenes followed by elimination of hydrogen chlorides yields the corresponding chlorovinylazides, which can be converted into chloroazirines. However, not only is this complicated synthetic route inconvenient but also haloazirines are unstable (e.g., 2-chloro-3-ethyl-2-methyl-2*H*-azirine rearranges into 2-chloro-2-ethyl-3-methyl-2*H*-azirine).[8c] We therefore turned our attention towards a preparation of haloazirines in situ (Scheme 4).

Deprotonation of **1** and **11**, which possesses a good leaving group on the nitrogen atom,



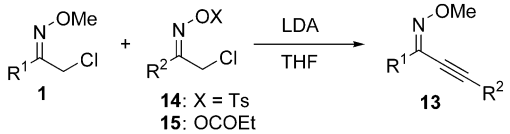

***Scheme 4.*** Cross-condensation of oxime derivatives.

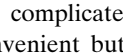
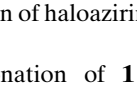
affords **2** and **12**, respectively. If the cyclization of **12** proceeds much faster than that of **2**, haloazirine **3** is selectively generated and then reacts with **2** to furnish alkynyl oxime ether **13**. With this working hypothesis, we examined the reaction of various imines derived from α-chloroacetophenone.

After screening a series of leaving groups, we found that oxime *p*-toluenesulfonate (X = Ts, **14**) and ethoxycarbonate (X = EtOCO, **15**) are both good partners with oxime methyl ether **1** in this cross-condensation.[9] It is noteworthy that the cross-condensation reaction proceeded even at −78 °C, whereas homocondensation did not occur without magnesium bromide at −78 °C. Furthermore, no homocondensation product was obtained in any reaction.

With the cross-condensation protocol in hand, we synthesized a variety of alkynyl oxime ethers (Table 2). Several observations are worth noting: 1) Alkyl-substituted α-chloro oxime ethers **1h–j**, which have α-protons on both sides, afforded the corresponding products in moderate to good yields (entries 9–12). 2) The use of **14j** with $R^2$ = Me afforded none of the desired product. 3) The initial stereochemistry of

***Table 2:*** Cross-condensation of α-chloro oxime derivatives.




| Entry | **1**, $R^1$ | **14** or **15**, $R^2$[a] | Prod. | Yield [%] | Sel. [*Z*/*E*] |
|---|---|---|---|---|---|
| 1 | **1a**, Ph | **14c**, 4-Cl-$C_6H_4$ | **13ac** | 73 | 94/6 |
| 2 | **1a**, Ph | **15l**, *i*Pr | **13al** | 63 | >95/5 |
| 3 | **1a**, Ph | **14j**, Me (*Z*/*E* = 88/12) | – | – | – |
| 4 | **1b**, 4-MeO-$C_6H_4$ | **14a**, Ph | **13ba** | 68 | >95/5 |
| 5 | **1c**, 4-Cl-$C_6H_4$ | **14a**, Ph | **13ca** | 65 | >95/5 |
| 6 | **1c**, 4-Cl-$C_6H_4$ | **15a**, Ph | **13ca** | 63 | >95/5 |
| 7 | **1f**,  | **15a**, Ph | **13fa** | 54 | 84/16 |
| 8[b] | **1g**, *t*Bu | **14a**, Ph | **13ga** | 63 | 62/38 |
| 9 | **1h**, *c*-$C_5H_9$ | **14a**, Ph | **13ha** | 73 | >95/5 |
| 10 | **1i**, *n*-$C_8H_{17}$ | **14a**, Ph | **13ia** | 69 | >95/5 |
| 11 | **1i**, *n*-$C_8H_{17}$ | **15l**, *i*Pr (*Z*/*E* = 57/43) | **13il** | 74 | >95/5 |
| 12 | **1j**, Me | **14a**, Ph | **13ja** | 57 | >95/5 |
| 13 | **1k**,  | **15a**, Ph | **13ka** | 40 | ca. 1/4 |

[a] Configuration of **14** and **15** is *Z*/*E* = >95/5 except for entries 3 and 11. [b] Reaction temperature −78 °C to room temperature.

 © 2003 Wiley-VCH Verlag GmbH & Co. KGaA, Weinheim 

the oxime carbonates does not have a significant effect on the reaction (entries 2 and 11).[10]

In conclusion, we have achieved a facile synthesis of alkynyl oxime ethers from α-chloro oxime derivatives with lithium diisopropylamide. This reaction probably involves azacyclobutadienes as a key intermediate. Further efforts to verify the reaction mechanism and develop applications of this highly reactive heterocycle are currently under way in our laboratory.

Received: July 7, 2003 [Z52317]

**Keywords:** alkynes · nitrogen heterocycles · oximes · small ring systems

[1] *Modern Acetylene Chemistry* (Eds.: P. J. Stang, F. Diederich), VCH, Weinheim, **1995**.

[2] a) N. de Kimpe in *Comprehensive Heterocyclic Chemistry II, Vol. 1A* (Eds.: A. R. Katritzky, C. W. Rees, E. F. V. Scriven), Pergamon, Oxford, **1996**, p. 507; b) M. N. Glukhovtsev, S. Laiter, *J. Phys. Chem.* **1996**, *100*, 1569; c) F. Neumann, K. Jug, *J. Org. Chem.* **1994**, *59*, 6442; d) U.-J. Vogelbacher, M. Regitz, R. Mynott, *Angew. Chem.* **1986**, *98*, 835; *Angew. Chem. Int. Ed. Engl.* **1986**, *25*, 842; e) M. Ledermann, M. Regitz, K. Angermund P. Binger, C. Krüger, R. Mynott, R. Gleiter, I. Hyla-Kryspin, *Angew. Chem.* **1988**, *100*, 1615; *Angew. Chem. Int. Ed. Engl.* **1988**, *27*, 1559; f) U. Hess, U.-J. Vogelbacher, G. Michels, M. Regitz, *Tetrahedron* **1989**, *45*, 3115; g) R. K. Mishra, B. K. Mishra, *Chem. Phys. Lett.* **1988**, *151*, 44; h) G. Maier, U. Schäfer, *Liebigs Ann. Chem.* **1980**, 798; i) W. W. Schoeller, T. Busch, *Angew. Chem.* **1993**, *105*, 635; *Angew. Chem. Int. Ed. Engl.* **1993**, *32*, 617.

[3] We assume **8a** resulted from $S_N2$-type displacement of **1a** by **2a**.

[4] For review on 1-azabicyclo[1.1.0]butane, see: R. Bartnik, A. P. Marchand, *Synlett* **1997**, 1029. No studies of this type of 1-azabicyclo[1.1.0]butane with a halo substituent at C2 have been reported to our knowledge.

[5] P. W. Neber, A. Friedolsheim, *Justus Liebigs Ann. Chem.* **1926**, *449*, 109.

[6] For mechanistic study of the Neber reaction, see: a) H. O. House, W. F. Berkowitz, *J. Org. Chem.* **1963**, *28*, 2271; b) T. Ooi, M. Takahashi, K. Doda, K. Maruoka, *J. Am. Chem. Soc.* **2002**, *124*, 7640.

[7] Similar results were obtained when lithium tetramethylpiperidide was used instead of lithium diisopropylamide. The reaction with lithium hexamethyldisilazide yielded 1,4-diphenyl-2-butene-1,4-dione bis(*O*-methyloxime) as a single product.

[8] a) F. Palacios, A. M. Ochoa de Retana, E. Martines de Marigorra, J. M. de los Santos, *Eur. J. Org. Chem.* **2001**, 2401; b) T. M. V. D. Pinho e Melo, C. S. J. Lopes, A. L. Cardoso, A. M. d'A. Rocha Gonsalves, *Tetrahedron* **2001**, *57*, 6203; c) J. Ciabattoni, M. Cabell, Jr., *J. Am. Chem. Soc.* **1971**, *93*, 1482.

[9] The corresponding oxime methanesulfonate and benzoate provided **13ca** in yields of 38% and 51%, respectively.

[10] According to the report by House and Berkowitz,[6a] the initial stereochemistry of oxime sulfonates is irrelevant in the Neber reaction. However, Maruoka's group has recently reported that the stereochemistry has some effects. They suggested that the generation of azirines from oxime sulfonates with a base favors *anti* displacement.[6b]

 © 2003 Wiley-VCH Verlag GmbH & Co. KGaA, Weinheim 

*Synthesis of Enamines*

# Highly Selective Synthesis of Enamines from Olefins**

*Moballigh Ahmed, Abdul Majeed Seayad, Ralf Jackstell, and Matthias Beller**

*Dedicated to Professor Manfred T. Reetz on the occasion of his 60th birthday*

A major challenge for synthetic chemists constitutes the development of cleaner (green) and practical catalytic technologies for organic synthesis. In this respect, we have been interested for some years in the development of novel methods for the synthesis of nitrogen-containing compounds, for example, amines,[1] enamines,[2] and imines.[3] Members of this class of compounds are useful as dyes, fine chemicals, and biologically active substances for pharmaceuticals. An ideal chemical synthesis of amines and their derivatives should make use of easily available raw materials and produce a minimum of waste.[4] On the one hand, atom economy[5] or atom efficiency[6] of the reaction should be as high as possible, on the other hand, a minimum amount of reaction steps should be performed to avoid tedious workup procedures and to save solvents and energy. These latter points are especially important for large-scale synthesis. Hence, the use of multicomponent coupling reactions[7] or domino reactions[8] is highly desirable compared to classic multistep procedures.

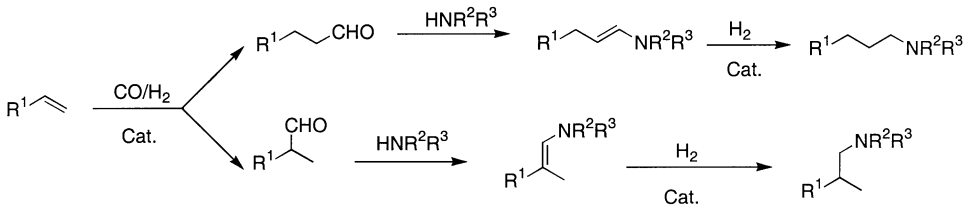
An environmentally benign synthesis of amines constitutes the so-called hydroaminomethylation[9] of olefins. This catalytic domino reaction starting from readily available olefins and consists of an initial hydroformylation step, to give aldehydes, and a subsequent reductive amination (Scheme 1).

Since the discovery of this reaction by Reppe and Vetter at BASF,[10] the hydroaminomethylation reaction has been considered mainly in industry.[11] Notable advances in the last decade have been especially reported by Eilbracht and coworkers, who developed elegant domino variants of hydroaminomethylation reactions.[12] More recently, we presented a rhodium catalyst based on the xantphos ligand (**3**; Scheme 2),[13] which allowed for the first general, efficient, and highly regioselective (typically *n*/iso > 98:2) hydroaminomethylation of simple as well as of functionalized

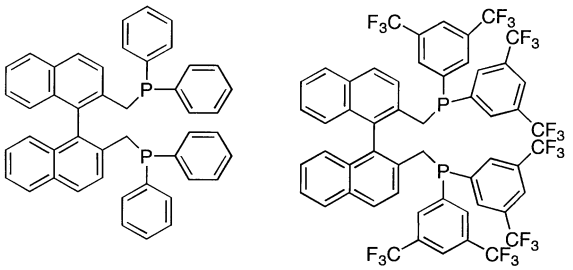
[*] Prof. Dr. M. Beller, M. Ahmed, A. M. Seayad, R. Jackstell
Leibniz-Institut für Organische Katalyse
Universität Rostock e.V. (IfOK)
Buchbinderstraße 5–6, 18055 Rostock (Germany)
Fax: (+49) 381-46693-23
E-mail: matthias.beller@ifok.uni-rostock.de

[**] The authors thank Dr. Holger Klein (IfOK) for help with the preparation of the ligand iphos and for his work on the high-pressure infrastructure, Susann Buchholz for GC analyses, and Hannelore Baudisch for GC–MS experiments. Financial support from the BMBF (Bundesministerium für Bildung und Forschung), the Ministry of Education, Science, and Cultural Affairs of Mecklenburg-Vorpommern and the Fonds der Chemischen Industrie (FCI) is gratefully acknowledged.

 DOI: 10.1002/anie.200352320 © 2003 Wiley-VCH Verlag GmbH & Co. KGaA, Weinheim 

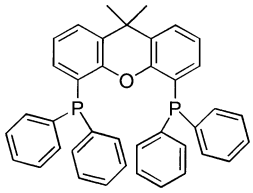


***Scheme 1.*** Hydroaminomethylation of alkenes.



**1** naphos

**2** iphos



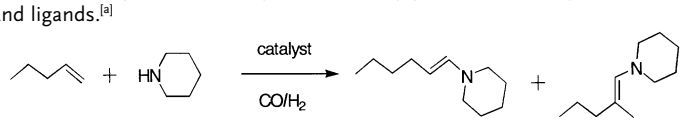
**3** xantphos

***Scheme 2.*** Ligands used in the hydroaminomethylenation of 1-pentene with piperidine (Table 1).

α-olefins.[14] During our studies on the improvement of tailor-made catalyst systems for hydroaminomethylations,[15] we noted that the reaction steps of the sequence (1. hydroformylation, 2. imine/enamine formation, 3. hydrogenation) are influenced by the ligand in different ways. Among the ligands tested in the model reaction of 1-pentene with piperidine, 2,2′-bis(diphenylphosphanylmethyl)-1,1′-binaphthyl (naphos (**1**); Scheme 2)[16] and its derivatives provided relatively large amounts of the corresponding enamine (*N*-1-hexenylpiperidine). After studying the literature, we were surprised to find that there was no general protocol for the direct and highly selective synthesis of enamines from olefins.[17] Clearly, such a domino reaction has advantages over the stepwise procedure of hydroformylation and amination, but also over other catalytic syntheses of enamines.[18] Furthermore, this transformation is interesting because it allows the synthesis of unsaturated products in the presence of hydrogen. Therefore, we investigated this new hydroaminomethylenation reaction in more detail. In general the reaction was carried out in the presence of $[Rh(CO)_2(acac)]$ (0.1 mol%), ligand (0.2 mol%), and a 1:1 mixture of synthesis gas. Ligands such as triphenylphosphane and bidentate phosphanes such as naphos, xantphos, or their derivatives were used.

Examination of different solvents, temperatures, time, pressure, and concentration of starting materials in the presence of naphos led to highly selective reaction under remarkably mild conditions (Table 1, entries 1–9). At 65 °C and under 10 bar pressure of synthesis gas ($CO/H_2 = 1:1$), good conversion (90%) and excellent chemoselectivity (>97%) as well as regioselectivity (>99:1) are observed. The high chemoselectivity is noteworthy because of the relatively easy hydrogenation of the produced enamines. We thought that the ligand controls this unusual selectivity to a

***Table 1:*** Hydroaminomethylenation of 1-pentene with piperidine in the presence of different Rh complexes and ligands.[a]



*n* iso

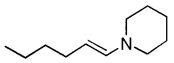
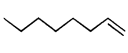
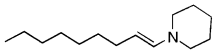
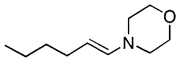
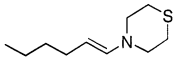
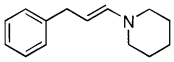
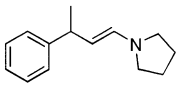
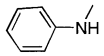
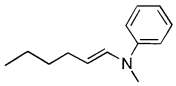
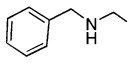
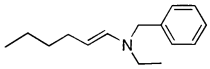
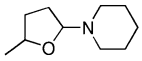
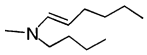
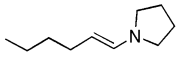
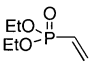
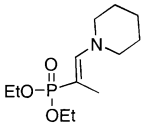
| Entry | Ligand | *T* [°C] | $CO/H_2$ [bar] | Conv. [%] | Yield [%] *n*-enamine | Selectivity [%][b] *n*-enamine | iso enamine | *n* amine | aldol product | *n*/iso |
|---|---|---|---|---|---|---|---|---|---|---|
| 1 | **1** | 65 | 20 | 69 | 50 | 72 | 8 | 5 | 11 | 90:10 |
| 2 | **1** | 85 | 20 | 85 | 76 | 89 | 1 | 1 | 3 | 99:1 |
| 3 | **1** | 100 | 20 | 83 | 75 | 90 | 1 | 2 | 3 | 99:1 |
| 4 | **1** | 120 | 20 | 80 | 70 | 87 | 5 | – | 4 | 95:5 |
| 5 | **1** | 75 | 10 | 95 | 85 | 89[c] | – | – | 1 | >99:1 |
| 6 | **1** | 65 | 40 | 42 | 41 | 98 | – | – | – | >99:1 |
| **7**[d] | **1** | **65** | **10** | **90** | **87** | **97** | **–** | **–** | **–** | **>99:1** |
| 8[e] | **1** | 65 | 20 | 92 | 44 | 48 | 29 | 23 | – | 62:38 |
| 9[f] | **1** | 65 | 20 | 99 | 15 | 15 | 1 | 76[g] | 2 | 94:6 |
| 10[i,j] | **1** | 125 | 40 | 100 | – | – | – | 89 | – | 94:6 |
| 11 | – | 65 | 10 | 57 | – | – | – | 35[h] | 18 | – |
| 12 | $PPh_3$ | 65 | 10 | 76 | 37 | 49 | 20 | 13 | 17 | 71:29 |
| 13 | **2** | 65 | 10 | 79 | 61 | 77 | – | – | 23 | 99:1 |
| 14 | **3** | 65 | 10 | 39 | 39 | 39 | – | – | – | 99:1 |
| 15[i,j] | **3** | 125 | 40 | 100 | – | – | – | 97 | – | 98:2 |

[a] Reaction conditions: 1-pentene (15 mmol), piperidine (15 mmol), $[Rh(CO)_2(acac)]$ (0.1 mol%), ligand (0.2 mol%), toluene (30 mL), 12 h. [b] Selectivities were determined by GC analysis with bis(methoxyethyl) ether as an internal standard. [c] Linear aldehyde (5%), iso-aldehyde (4%). [d] 16 h. [e] THF (30 mL). [f] MeOH (30 mL). [g] Iso-amine (6%). [h] Iso-amine (48%). [i] Alkene (10 mmol), amine (10 mmol), methanol (15 mL), (toluene) 15 mL, CO (7 bar), $H_2$ (33 bar), 125 °C, 5 h. [j] $[Rh(cod)_2]BF_4$. cod = cycloocta-1,5-diene.

 © 2003 Wiley-VCH Verlag GmbH & Co. KGaA, Weinheim 

large extent. Indeed, as shown in Table 1 (entries 7, 11–14), both the chemoselectivity and the regioselectivity (*n*/iso)[19] of the reaction are controlled by the added ligand. Whereas in the absence of any phosphane ligand essentially no enamine and a nearly 1:1 mixture of linear and iso-amine is formed, the use of the "standard ligand" triphenylphosphane leads to lower conversion (76%), chemoselectivity (69%), and regioselectivity (*n*/iso = 71:29). Furthermore, it is shown that rhodium catalysts based on xantphos or iphos (**3**)[20] also gave significantly lower conversion and selectivities. Apart from the ligand, the solvent appeared to be important for preventing hydrogenation of the enamine. In this case, aromatic solvents, which are known to coordinate to the rhodium center and thus slow down hydrogenation reactions,[21] seem to be especially suitable. Interestingly, at higher temperature (125 °C) and slightly higher pressure (40 bar), high selectivity to the corresponding amine is observed (Table 1, entries 10 and 15).[14]

***Table 2:*** General synthesis of enamines.[a]

| Entry | Alkene | Amine | Major product | Conv. [%] | Selec. [%][b] | *n*/iso |
|---|---|---|---|---|---|---|
| 1 |  |  |  | 100 | 97 | 99:1 |
| 2 |  |  |  | 95 | 95 | 99:1 |
| 3 |  |  |  | 90 | >99 | 99:1 |
| 4[c] |  |  |  | 80 | >99 | 99:1 |
| 5[d] |  |  |  | 100 | 90 | 73:27 |
| 6[d] |  |  |  | 75 | >99 | 99:1 |
| 7 |  |  |  | 40 | >99 | 99:1 |
| 8 |  |  |  | 98 | 85[d] | 89:11 |
| 9 |  |  |  | 100 | 98 | 99:1 |
| 10 |  |  |  | 98 | >98 | 99:1 |
| 11 |  |  |  | 100 | >98 | 99:1 |
| 12[e] |  |  |  | 95 | 86 | 99:1 |

[a] Reaction conditions: substrate (1:1, 15 mmol), [$Rh(CO)_2(acac)$] (0.1 mol%), naphos (0.2 mol%), toluene (30 mL), $P_{CO/H_2}$ (1:1, 10 bar), 65 °C, 16 h. [b] Selectivities were determined by GC analysis with bis(methoxyethyl) ether as an internal standard. [c] Thiomorpholine (30 mmol). [d] 20 h. [e] THF (30 mL).

Evidently, the new procedure for enamine synthesis is only of significant importance to synthetic organic chemists if different aliphatic and aromatic olefins with various functional groups as well as various amines can be applied with success. Therefore, we were interested in the scope and limitations of our new reaction (Table 2).

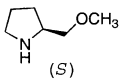
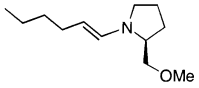
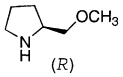
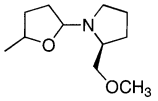
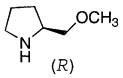
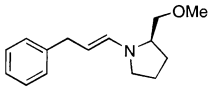
We were pleased to find that not only lower but also higher aliphatic as well as aromatic olefins react well with piperidine to give the linear products with good to excellent selectivity (Table 2, entries 1–8). *N*-Methylaniline, *N*-ethylbenzylamine, and other aliphatic secondary amines (morpholine, thiomorpholine, pyrrolidine, *N*-methyl-*N*-butylamine) react well to give the corresponding enamine in high yield and selectivity. Notably, an unprotected allylic alcohol is efficiently converted into the corresponding N,O acetal, which is the cyclization product of the 4-hydroxyenamine, with high *n*/iso ratio (99:1) (Table 2, entry 9). In most cases, the reaction proceeds with an extremely high degree of chemo- (typically >95%) and regioselectivity (>99:1) towards the linear enamines. In case of aliphatic olefins, only the *E* enamine is detected. This is of special importance because the separation of mixtures of the branched and the linear enamine products is often very tedious owing to similar physical properties of both compounds. Hence, regioselectivities >98% are an important factor for the application of the method. Among the different reactions studied, the hydroaminomethylenation of α-methylstyrene with pyrrolidine and of 1-pentene with *N*-methylaniline needed longer reaction time and/or higher reaction temperature for complete conversion.

Notably, chiral secondary amines such as 2-methoxymethylpyrrolidine also produce the chiral aliphatic enamines in excellent yields and selectivities (chemoselectivity >98%; *n*/iso >98:2; Table 3, entry 1). In the case of styrene, the regioselectivity is somewhat lower. It is evident that these chiral enamines are useful building blocks for asymmetric synthesis.[22]

In conclusion, we have shown the first direct synthesis of enamines from olefins. Remarkably, excellent selectivities are observed under mild reaction conditions. Aliphatic olefins give the corresponding linear products in general with regioselectivities of 99:1, which allows easy isolation of the product. Key to the success of the reaction is the use of a catalyst system consisting of a neutral rhodium precursor together with naphos as ligand. The reported catalyst system is tolerant to a variety of potentially reactive functional groups, making the procedure valuable for the synthesis of interesting organic building blocks, including chiral enamines.

 © 2003 Wiley-VCH Verlag GmbH & Co. KGaA, Weinheim 

***Table 3:*** Synthesis of various enamines using chiral amines.[a]

| Entry | Alkene | Amine | Major product | Conv. [%] | Selec. [%][b] | *n*/iso |
|---|---|---|---|---|---|---|
| 1 |  |  (*S*) |  | 100 | 98 | 98:2 |
| 2 |  |  (*R*) |  | 100 | 98 | 99:1 |
| 3[c] |  |  (*R*) |  | 90 | 82[d] | 63:37 |

[a] Reaction conditions: substrate (1:1, 10 mmol), $[Rh(CO)_2(acac)]$ (0.1 mol%), naphos (0.2 mol%), toluene (30 mL), $P_{CO/H_2}$ (1:1, 10 bar), 65 °C, 16 h. [b] Selectivities were determined by GC analysis with bis(methoxyethyl) ether as an internal standard. [c] 20 h. [d] Major side product is amine (15%, 80:20).

Clearly, this new synthesis of enamines is atom-economic and environmentally friendly (i.e., water is the only by-product), and the starting materials are both inexpensive and readily available.

## *Experimental Section*

$^1$H and $^{13}$C NMR spectra were recorded on a Bruker ARX 400 spectrometer ($^1$H: 400.1, $^{13}$C: 100.6 MHz). Chemical shifts ($\delta$) are given in ppm relative to residual solvent as internal standard. Gas chromatographic analyses were performed on a Hewlett Packard HP 5890 chromatograph with flame-ionization detector and an HP5 column (cross-linked 5% PH ME siloxane). Mass spectra (GC–MS) experiments were conducted on an Agilent-6890. The products were isolated from the reaction mixture by evaporation of the solvent and/or further purified by vacuum distillation wherever necessary. All yields reported in Tables 1–3 refer to GC yields using bis(methoxyethyl) ether as an internal standard. All yields of isolated compounds (which vary by 5–10% from those determined by GC) were estimated to be >95% pure as determined by GC and NMR. All new compounds were further characterized by HRMS. Linear/branched ratios were determined by GC analysis of the crude reaction mixtures. Compounds known in the literature were characterized by comparing their $^1$H NMR, $^{13}$C NMR, and GC–MS data with the previously reported data. The purity of known compounds was confirmed by GC.

General procedure: All hydroaminomethylenation experiments were carried out in a Parr stainless-steel autoclave (100 mL). In a typical experiment, the autoclave was charged with $[Rh(CO)_2(acac)]$ (0.1 mol%), naphos (0.2 mol%), olefin (15.0 mmol), amine (15.0 mmol), and toluene (30 mL) under argon. The autoclave was pressurized with CO (5 bar) and hydrogen (5 bar), and the reaction was carried out at 65 °C for 16 h. The autoclave was then cooled to room temperature and depressurized. The reaction mixture was transferred to a Schlenk flask under an argon atmosphere, dried over $MgSO_4$, and analyzed by GC with bis(methoxyethyl) ether as internal standard.

*N*-1-Hexenylpiperidine: Yield: 99% (GC); $^1$H NMR (400 MHz, $CDCl_3$): $\delta = 5.79$ (d, $J = 14$ Hz, 1H), 4.36 (quint, $J = 14$ Hz, $J = 7$ Hz, 1H), 2.78–2.69 (m, 4H), 1.95–1.90 (m, 2H), 1.58-1.46 (br m, 4H), 1.29–1.26 (m, 6H), 0.86 ppm (t, $J = 7$ Hz, 3H); $^{13}$C NMR (100 MHz, $CDCl_3$): $\delta = 140.1$, 101.4, 50.1, 33.5, 30.2, 25.4, 24.3, 22.0, 13.9 ppm; MS (EI, 70 eV): *m*/*z* (%): 167 [$M^+$], 152, 138, 124, 110, 96, 80, 68, 55, 41, 27; HRMS: calcd for $C_{11}H_{21}N$ [$M^+$]: 167.16795; found: 167.16740.

2-Methyl-5-piperidinyltetrahydrofuran: Yield: 99% (GC); $^1$H NMR (400 MHz, $CDCl_3$): $\delta = 4.54$ and 4.51 (t, $J = 6.4$ Hz and dd, $J = 6.4$ Hz, 4.0 Hz, 1H of the two isomers), 3.98–3.90 and 3.81–3.73 (m, 1H of the two isomers), 2.71–2.40 (br m, 4H), 1.98–1.78 (m, 4H), 1.53–1.36 (m, 6H), 1.16 and 1.11 ppm (d, $J = 6.0$ Hz and d, $J = 6.0$ Hz, 3H of the two isomers); $^{13}$C NMR (100 MHz, $CDCl_3$): $\delta = 95.9$, 95.7, 74.3, 73.4, 48.3, 47.8, 32.9, 32.1, 28.2, 25.5, 24.0, 20.7, 19.8 ppm; MS (EI, 70 eV): *m*/*z* (%): 169 [$M^+$], 154, 140, 125, 114, 98, 84, 69, 55, 41, 29; HRMS: calcd for $C_{10}H_{19}NO$ [$M^+$]: 169.14443; found: 169.1466.

*N*-(1-Hexenyl)-2-methoxymethylpyrrolidine: Yield: 98% (GC); $^1$H NMR (400 MHz, $CDCl_3$): $\delta = 6.21$ (d, $J = 14$ Hz, 1H), 4.16 (quint, $J = 14$ Hz, $J = 7$ Hz, 1H), 3.36 (d, $J = 3$ Hz, 2H), 3.34 (s, 3H), 3.22–3.17 (m, 1H), 2.82 (t, $J = 8.12$ Hz, 2H), 1.98–1.93 (m, 2H), 1.89–1.79 (m, 2H), 1.73–1.69 (m, 2H), 1.31–1.27 (m, 4H), 0.87 ppm (t, $J = 7$ Hz, 3H); $^{13}$C NMR (100 MHz, $CDCl_3$): $\delta = 135.4$, 99.0, 75.7, 60.2, 59.0, 49.0, 33.9, 30.3, 28.4, 23.5, 22.1, 14.0 ppm; MS (EI, 70 eV): *m*/*z* (%):197 [$M^+$], 182, 166, 152, 122, 108, 94, 81, 70, 54, 41, 27; HRMS: calcd for $C_{12}H_{23}NO$ [$M^+$]: 197.15984. found: 197.16231.

Received: July 7, 2003 [Z52320]

**Keywords:** amines · enamines · homogeneous catalysis · rhodium · synthetic methods

[1] M. Beller, C. Breindl, T. H. Riermeier, M. Eichberger, H. Trauthwein, *Angew. Chem.* **1998**, *110*, 3571–3573; *Angew. Chem. Int. Ed.* **1998**, *37*, 3389–3391.
[2] M. Beller, M. Eichberger, H. Trauthwein, *Angew. Chem.* **1997**, *109*, 2306–2308; *Angew. Chem. Int. Ed. Engl.* **1997**, *36*, 2225–2227.
[3] a) A. Tillack, I. Garcia Castro, C. G. Hartung, M. Beller, *Angew. Chem.* **2002**, *114*, 2646–2648; *Angew. Chem. Int. Ed.* **2002**, *41*, 2541–2543; b) C. G. Hartung, H. Trauthwein, A. Tillack, M. Beller, *J. Org. Chem.* **2001**, *66*, 6339–6343.
[4] For reviews, see: a) T. E. Müller, M. Beller, *Chem. Rev.* **1998**, *98*, 675–703; b) Y. Yamamoto, U. Radhakrishnan, *Chem. Soc. Rev.* **1999**, *28*, 199–207; c) M. Nobis, B. Driessen-Hölscher, *Angew. Chem.* **2001**, *113*, 4105–4108; *Angew. Chem. Int. Ed.* **2001**, *40*, 3983–3986; d) M. Beller, C. Breindl, M. Eichberger, C. G. Hartung, J. Seayad, O. R. Thiel, A. Tillack, H. Trauthwein, *Synlett* **2002**, *10*, 1579–1594; e) J. Seayad, A. Tillack, C. G. Hartung, M. Beller, *Adv. Synth. Catal.* **2002**, *344*, 795–813.
[5] a) B. M. Trost, *Science* **1991**, *254*, 1471–1477; b) B. M. Trost, *Angew. Chem.* **1995**, *107*, 285–307; *Angew. Chem. Int. Ed. Engl.* **1995**, *34*, 259–281.
[6] R. A. Sheldon, *Pure Appl. Chem.* **2000**, *72*, 1233–1246.
[7] a) H. Bienaymé, C. Hulme, G. Oddon, P. Schmitt, *Chem. Eur. J.* **2000**, *6*, 3321–3329; b) G. H. Posner, *Chem. Rev.* **1986**, *86*, 831–844; c) R. W. Armstrong, A. P. Combs, P. A. Tempest, S. D. Brown, T. A. Keating, *Acc. Chem. Res.* **1996**, *29*, 123–131.
[8] a) L. F. Tietze, F. Haunert in *Stimulating Concepts in Chemistry* (Eds.: M. Shibasaki, J. F. Stoddart, F. Vögtle), Wiley-VCH, Weinheim, **2000**, pp. 39–64; b) L. F. Tietze, *Chem. Rev.* **1996**, *96*, 115–136; c) L. F. Tietze, A. Modi, *Med. Res. Rev.* **2000**, *20*, 304–322.
[9] For a review, see: P. Eilbracht, L. Bärfacker, C. Buss, C. Hollmann, B. E. Kitsos-Rzychon, C. L. Kranemann, T. Rische, R. Roggenbuck, A. Schmidt, *Chem. Rev.* **1999**, *99*, 3329–3365.
[10] W. Reppe, H. Vetter, *Justus Liebigs Ann. Chem.* **1953**, *582*, 133–163.

 © 2003 Wiley-VCH Verlag GmbH & Co. KGaA, Weinheim 

[11] a) B. Zimmermann, J. Herwig, M. Beller, *Angew. Chem.* **1999**, *111*, 2515 – 2518; *Angew. Chem. Int. Ed.* **1999**, *38*, 2372 – 2375; b) A. F. M. Iqbal, *Chem. Acta* **1971**, *54*, 1440; b) F. Jachimowicz, J. W. Raksis, *J. Org. Chem.* **1982**, *47*, 445 – 447; c) E. MacEntire, J. F. Knifton (Texaco Inc.), EP-B 241093, **1987** [*Chem. Abstr.* **1989**, *110*, 134785 h]; d) J. J. Brunet, D. Neibecker, F. Agbossou, R. S. J. Srivastav, *J. Mol. Catal.* **1994**, *87*, 223 – 230; e) E. Drent, A. J. M. Breed (Shell Int. Res.M.), EP-B 457386, **1992** [*Chem. Abstr.* **1992**, *116*, 83212 h]; f) S. Törös, I. Gemes-Pesci, B. Heil, S. Maho, Z. Tubar, *J. Chem. Soc. Chem. Commun.* **1992**, 585 – 589; g) T. Baig, P. Kalck, *J. Chem. Soc. Chem. Commun.* **1992**, 1373 – 1374; h) T. Baig, J. Molinier, P. Kalck, *J. Organomet. Chem.*. **1993**, *455*, 219 – 224; i) M. D. Jones, *J. Organomet. Chem.* **1989**, *366*, 403 – 408; j) G. Diekhaus, D. Kampmann, C. Kniep, T. Müller, J. Walter, J. Weber (Hoechst AG), DE-B 4334809, **1993** [*Chem. Abstr.* **1995**, *122*, 314160 g]; k) H. Schaffrath, W. Keim, *J. Mol. Catal. A* **1999**, *140*, 107 – 113.

[12] a) T. Rische, L. Bärfacker, P. Eilbracht, *Eur. J. Org. Chem.* **1999**, *3*, 653 – 660; b) T. Rische, B. Kitsos-Rzychon, P. Eilbracht, *Tetrahedron* **1998**, *54*, 2723 – 2742; c) C. L. Kranemann, P. Eilbracht, *Synthesis* **1998**, *1*, 71; d) T. Rische, P. Eilbracht, *Synthesis* **1997**, *11*, 1331 – 1337; e) B. Breit, *Tetrahedron Lett.* **1998**, *39*, 5163 – 5166.

[13] For a review, see: a) P. C. J. Kamer, P. W. N. M. van Leeuwen, J. N. H. Reek, *Acc. Chem. Res.* **2001**, *34*, 895 – 904; b) M. Kranenburg, Y. E. M. van der Bugt, P. C. J. Kamer, P. W. N. M. van Leeuwen, *Organometallics* **1995**, *14*, 3081 – 3083; c) L. A. van der Veen, P. C. J. Kamer, P. W. N. M. van Leeuwen, *Angew. Chem.* **1999**, *111*, 349 – 351; *Angew. Chem. Int. Ed.* **1999**, *38*, 336 – 338; d) L. A. van der Veen, P. C. J. Kamer, P. W. N. M. van Leeuwen, *Organometallics* **1999**, *18*, 4765 – 4777; e) L. A. van - der Veen, P. H. Keeven, G. C. Schoemaker, J. N. H. Reek, P. C. J. Kamer, P. W. N. M. van Leeuwen, M. Lutz, A. L. Spek, *Organometallics* **2000**, *19*, 872 – 883; f) J. M. Fox, X. H. Huang, A. Chieffi, S. L. Buchwald, *J. Am. Chem. Soc.* **2000**, *122*, 1360 – 1370; g) P. W. N. M. van Leeuwen, A. J. Sandee, J. N. H. Reek, P. C. J. Kamer, *J. Mol. Catal. A* **2002**, *182*, 107 – 123; h) C. R. Landis, J. Uddin, *J. Chem. Soc. Dalton Trans.* **2002**, 729 – 742; i) C. Botteghi, M. Marchetti, S. Paganelli, S. Scognamillo, *J. Mol. Catal. A* **2002**, *179*, 79 – 86; j) W. Goertz, P. C. J. Kamer, P. W. N. M. van Leeuwen, D. Vogt, *Chem. Eur. J.* **2001**, *7*, 1614 – 1618.

[14] M. Ahmed, A. M. Seayad, R. Jackstell, M. Beller, *J. Am. Chem. Soc.* **2003**, *125*, 10311–10318.

[15] a) A. Seayad, M. Ahmed, H. Klein, R. Jackstell, T. Gross, M. Beller, *Science* **2002**, *297*, 1676 – 1678; b) for a commentary on this work, see: J. F. Hartwig, *Science* **2002**, *297*, 1653 – 1654.

[16] a) T. J. Devon, G. W. Philips, T. A. Puckette, J. L. Satvinoha, J. J. Vanderbilt, (Eastman Kodak), WO 87/07600, **1987**; b) M. Beller, J. G. E. Krauter, *J. Mol. Catal. A* **1999**, *143*, 31 – 39; c) W. A. Herrmann, R. Schmid, C. W. Kohlpaintner, T. Priermeier, *Organometallics* **1995**, *14*, 1961 – 1968; d) H. B. Bahrmann, K. Bergrath, H.-J. Kleiner, P. Lapper, C. Naumann, D. Peters, D. Regnat, *J. Organomet. Chem.* **1996**, *520*, 97 – 100; e) F. A. Rampf, M. Spiegler, W. A. Herrmann, *J. Organomet. Chem.* **1999**, *582*, 204 – 210; f) R. W. Eckl, T. Priermeier, W. A. Herrmann, *J. Organomet. Chem.* **1997**, *532*, 243 – 249; g) M. Beller, B. Cornils, C. D. Frohning, C. W. Kohlpaintner, *J. Mol. Catal. A* **1995**, *104*, 17 – 85; h) S. Okucu, A. Karacar, M. Freytag, P. G. Jones, R. Schmutzler, *Z. Anorg. Allg. Chem.* **2002**, *628*, 1339 – 1345; f) A. C. Da Silva, K. C. B. De Oliveira, E. V. Gusevskaya, E. N. Dos Santos, *J. Mol. Catal. A* **2002**, *179*, 133 – 141.

[17] a) Y.-S. Lin, B. E. Ali, H. Alper, *J. Am. Chem. Soc.* **2001**, *123*, 7719 – 7720; b) C. A. Busaca, Y. Dong, *J. Org. Chem.* **1997**, *62*, 6464 – 6465.

[18] a) X. Zhang, A. Fried, S. Knapp, A. S. Goldman, *Chem. Commun.* **2003**, 2060 – 2061; b) M. C. Willis, G. N. Brace, *Tetrahedron Lett.* **2002**, *43*, 9085 – 9088; c) N. Fujiwara, Y. Yamamoto, *Tetrahedron Lett.* **1998**, *39*, 4729 – 4732; d) P. W. Hickmott, *Tetrahedron* **1982**, *38*, 1975 – 2050; e) P. W. Hickmott, *Tetrahedron* **1982**, *38*, 3363 – 3446.

[19] The *n*/iso ratios were determined by GC analysis of the crude reaction mixture.

[20] H. Klein, R. Jackstell, K.-D. Wiese, C. Borgmann, M. Beller, *Angew. Chem.* **2001**, *113*, 3505 – 3508; *Angew. Chem. Int. Ed.* **2001**, *40*, 3408 – 3411.

[21] D. Heller, H.-J. Drexler, A. Spannenberg, B. Heller, J. S. You, W. Baumann, *Angew. Chem.* **2002**, *114*, 814 – 817; *Angew. Chem. Int. Ed.* **2002**, *41*, 777 – 780.

[22] a) C. Agami, L. Dechoux, C. Menard, S. Hebbe, *J. Org. Chem.* **2002**, *67*, 7573 – 7576; b) B. Jiang, F. Zhang, W. Xiong, *Tetrahedron*, **2002**, *58*, 261 – 264; c) V. I. Tararov, R. Kadyrow, T. H. Riermeier, J. Holz, A. Börner, *Tetrahedron Lett.* **2000**, *41*, 2351 – 2355; d) M. Nour, K. Tan, C. Cave, D. Villeneuve, D. Desmale, J. D'Angelo, C. Riche, *Tetrahedron: Asymmetry* **2000**, *11*, 995 – 1002; e) E. Caballero, P. Puela, M. Sanchez, M. Medarde, L. M. del Prado, A. San Feliciano, *Tetrahedron: Asymmetry* **1995**, *6*, 1985 – 1994; f) R. C. F. Jones, I. Turner, K. J. Howard, *Tetrahedron Lett.* **1993**, *34*, 6329 – 6332; g) W. S. Saari, T. E. Fischer, *Synthesis* **1990**, 6, 453 – 454; h) W. Keim, A. Koehnes, T. Roethel, D. Enders, *J. Organomet. Chem.* **1990**, *382*, 295 – 301.

 © 2003 Wiley-VCH Verlag GmbH & Co. KGaA, Weinheim 

*Supramolecular Catalysts*

# Multicomponent Porphyrin Assemblies as Functional Bidentate Phosphite Ligands for Regioselective Rhodium-Catalyzed Hydroformylation**

*Vincent F. Slagt, Piet W. N. M. van Leeuwen, and Joost N. H. Reek**

Noncovalent synthesis of well-defined molecular structures of nanometer dimensions has proven to be an attractive alternative to covalent synthesis.[1] Several examples of large and complex multicomponent assemblies have been reported,[2] and the number of medium-sized structures based on hydrogen bonds as well as metal–ligand interactions is enormous.[1,3] The current challenge in this field comprises the translation of these esthetically appealing structures into functional materials.[4] Catalysis has been one of the longstanding proposed applications of supramolecular chemistry,[5] and one of the more recent strategies involves the encapsulation[6] of substrates within self-assembled host molecules to invoke new

[*] Dr. J. N. H. Reek, V. F. Slagt, P. W. N. M. van Leeuwen
Institute of Molecular Chemistry
University of Amsterdam
Nieuwe Achtergracht 166, 1018 WV Amsterdam (The Netherlands)
Fax: (+31)-20-525-6422
E-mail: reek@science.uva.nl

[**] The NRSCC is kindly acknowledged for financial support.

Supporting information for this article is available on the WWW under http://www.angewandte.org or from the author.

 DOI: 10.1002/anie.200352525 © 2003 Wiley-VCH Verlag GmbH & Co. KGaA, Weinheim 

reaction pathways.[7] So far, however, only a few examples exist that describe the modification of transition-metal catalysts by supramolecular encapsulation.[8] Here we report on a multicomponent porphyrin-based assembly that serves as a bidentate ligand in a sandwich-type rhodium complex. The bidentate ligand system held together by three bridging ditopically coordinated template molecules shows a high selectivity for the linear aldehyde in the rhodium-catalyzed hydroformylation of 1-octene.

The tris(zinc(II) porphyrin)phosphite ligand **1** was prepared by the reaction of phosphorus trichloride with three equivalents of 5-(3-hydroxyphenyl)-10,15,20-tris(phenyl)-zinc(II) porphyrin (see the Supporting Information). The monomeric phosphite ligand **1** contains three zinc(II) porphyrin moieties that can be used as anchoring points for the formation of multicomponent assemblies. The phosphorus donor atom of **1** does not coordinate to the zinc(II) porphyrins[8a] and is therefore accessible for selective transition-metal coordination to form the catalytically active complex. We used 1,4-diazabicyclo[2.2.2]octane (dabco, **a**) as a ditopic template ligand, since it has been shown previously to form strong, well-defined 1:2 complexes with zinc(II) porphyrins,[9] and we applied quinuclidine (**b**) as a monotopic reference template.

UV/Vis spectroscopic titrations in toluene were performed to study the binding of ditopic template **a** to ligand **1** (Scheme 1). The titration curve representing the binding of **a** to **1** shows two distinct inflection points, indicating that there are two different binding sites (see the Supporting Information). These binding modes likely consist of a ditopically bound species **I** corresponding to the inflection point at **a**/**1** = 1, and monotopically bound dabco **II**,[10] as was also found for other flexible trimeric porphyrin systems.[9a] The binding constants obtained from curve fitting[11] ($K_{\mathbf{I}} = 1.1 \times 10^7\,\text{M}^{-1}$ and $K_{\mathbf{II}} = 5.5 \times 10^5\,\text{M}^{-1}$) are in line with the expected values for these two different binding modes. As expected, the curve for the titration of complex [Rh(acac)(**1**)$_2$][12] with **a** shows one inflection point only, indicating that all dabco molecules are bound in a similar ditopic fashion (see the Supporting Information). The stoichiometry of the supramolecular complex formed (**a**/[Rh(acac)(**1**)$_2$] = 3/1) is in line with the proposed structure **2**. The titration curve could be fitted with the equation for a complex with a 3:1 stoichiometry assuming identical binding sites, with an average binding constant calculated of $1.9 \times 10^7\,\text{M}^{-1}$, which is typical for ditopic complexation.[9] Interestingly, the ditopic binding is stronger in the complex [Rh(acac)(**1**)$_2$] than in the free ligand **1**, showing that the ditopic binding between two ligands of the complex is preferred over ditopic binding within the ligand of the complex.

To investigate the coordination properties of these new multicomponent ligand assemblies, their rhodium carbonyl hydride complexes were studied with high-pressure NMR spectroscopy at various **a**/**1** ratios (Figure 1). The NMR experiments in [D$_8$]-toluene under 20 bars of H$_2$/CO show

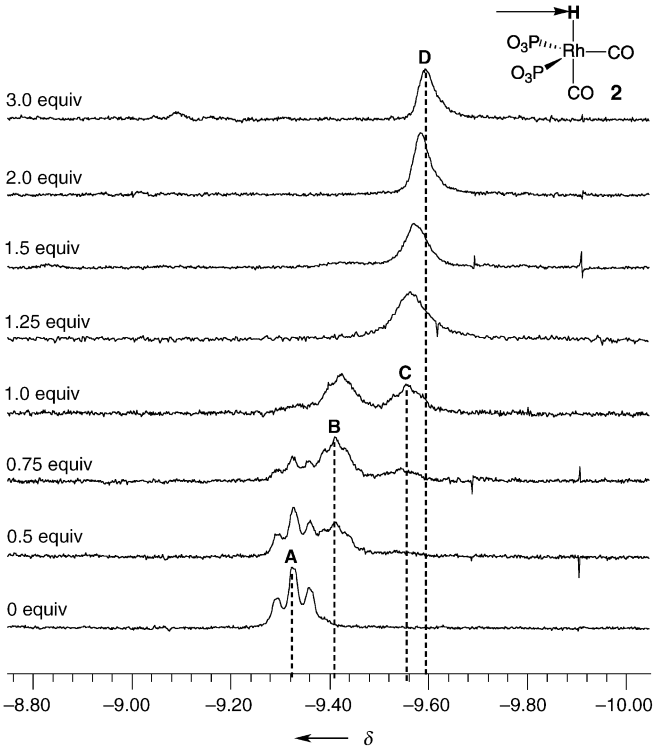
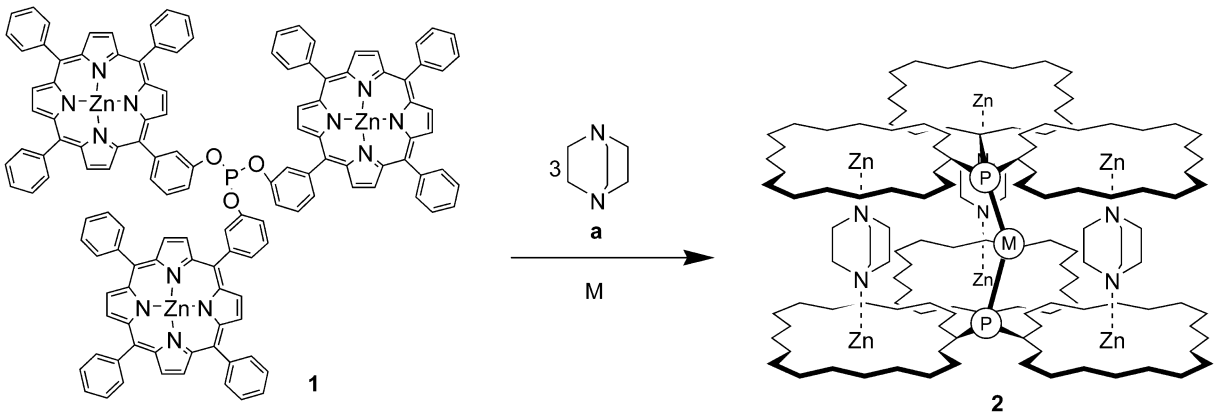



***Figure 1.*** $^1$H NMR spectra (hydride region) of rhodium catalyst assemblies of tris(zinc(II) porphyrin)phosphite **1** and various amounts of dabco **a** under high pressure.




***Scheme 1.*** Representation of the formation of a multicomponent assembly from ligand **1**, template **a** (= dabco), and a transition-metal catalyst M. P = monodentate phosphorus ligand.

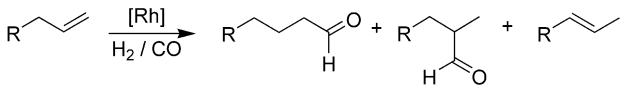
 © 2003 Wiley-VCH Verlag GmbH & Co. KGaA, Weinheim 

that monomeric tris(zinc(II) porphyrin)phosphite **1** in the presence of a rhodium precursor forms the hydridorhodium(biscarbonyl)diphosphite complex; $^{31}P\{^1H\}$ NMR spectroscopy shows the formation a doublet ($\delta = 148.0$ ppm, $J_{Rh\text{-}P} = 232$ Hz), and a rhodium hydride signal **A** ($\delta = -9.3$ ppm, $J_{H\text{-}P} = 9$ Hz) appears as a triplet in the $^1H$ NMR spectrum.[13]

The gradual addition of dabco **a** (**a**/**1** = 0–0.75) to this complex resulted in a decrease of intensity of **A** and the formation of a new rhodium complex with hydride signal **B** ($\delta = -9.4$ ppm). This shows that under these conditions two catalyst systems are in slow exchange on the NMR timescale (300 MHz, 298 K), which suggests the ditopic complexation of dabco. This is substantiated by the chemical shift of the bound dabco at −4.9 ppm.[9] The addition of more dabco (**a**/**1** = 1–1.5) resulted in the rise of a new distinct rhodium hydride signal **C** ($\delta = -9.54$ ppm) that is in slow exchange with **B**. At the **a**/**1** ratio of 1.5, **C** is the only hydride signal present and is therefore likely that of the proposed structure **2**. In this highly symmetrical complex the phosphites are fixed in space by the complexation of three ditopic templates. Increasing the concentration to an excess of dabco resulted in a gradual small upfield shift of hydride signal **C**, finally giving hydride signal **D** ($\delta = -9.6$ ppm, **a**/**1** = 3). This shows that complex **2** is in fast exchange on the NMR timescale with another assembly in which some of the dabco templates are monotopically bound to the zinc(II) porphyrin, indicating that assembly **2** is not stable in the presence of excess dabco.

The rhodium catalysts based on the assemblies consisting of phosphite **1** and either ditopic dabco **a** or monotopic quinuclidine **b** were studied in the rhodium-catalyzed hydroformylation of 1-octene[14] (Scheme 2, Table 1). The monomeric tris(zinc(II) porphyrin)phosphite **1** yields a rhodium catalyst with an activity and regioselectivity that is typical of rhodium bisphosphite complexes (turnover frequency (TOF) = $2.0 \times 10^3$ and ratio of linear to branched aldehyde products (*l*/*b*) = 2.5).[14] In the presence of three equivalents of monotopic ligand **b**, **1** is transformed into the bulkier system **1**(**b**)$_3$, which is even more active in the rhodium-catalyzed hydroformylation. In addition, the selectivity decreased (TOF = $3.4 \times 10^3$ and *l*/*b* = 1.9) and the amount of 2-octene formed increased. Likely, the more bulky ligand assembly **1**(**b**)$_3$ leads to monophosphite rhodium complexes, which explains the increase in activity and decreases in selectivity.[15] Interestingly, the rhodium catalyst based on assembly **2**, [Rh(CO)$_2$H(**1**$_2$**a**$_3$)], shows a high selectivity (*l*/*b* = 15.1) and a lower activity, which is characteristic for bidentate chelating ligand systems.[14] This shows that the multicomponent ligand assembly based on noncovalent interactions acts as a chelating bisphosphite![16] Surprisingly, lowering the temperature to 30 °C resulted in an even more selective catalyst, and the *l*/*b* ratio increased to 22.8,[17] suggesting that the assembled supramolecular catalyst system **2** is more stable at lower temperatures; this is explained by the stronger binding of the nitrogen donor atoms of the template to the zinc(II) porphyrin moieties.[18]

To obtain more information on the performance of the various catalyst assemblies we studied the rhodium-catalyzed hydroformylation of 1-octene at 40 °C using various **a**/**1** ratios; the results are displayed in Figure 2. The catalyst shows a gradual decrease in activity at increasing **a**/**1** ratios (Figure 2a). Bidentate chelating phosphorus ligands typically show lower activity in the rhodium-catalyzed hydroformylation, and the decrease thus confirms the assembly of a bidentate chelating ligand system in situ. Interestingly, the




***Scheme 2.*** Rhodium-catalyzed hydroformylation of alkenes.

***Table 1:*** Hydroformylation of 1-octene with rhodium catalysts based on tris(zinc(II) porphyrin)phosphite assemblies with various template ligands.[a]

| Ligand[b] | Template[b] | *T* [°C] | TOF[c] | *l*/*b*[d] | 2-Octene[e] [%] |
|---|---|---|---|---|---|
| **1** | – | 80 | $2.0 \times 10^3$ | 2.5 | 10.6 |
| **1** | **b** | 80 | $3.4 \times 10^3$ | 1.9 | 16.1 |
| **1** | **a** | 80 | $1.1 \times 10^3$ | 15.1 | 11.9 |
| **1** | **a** | 30 | 25 | 22.8 | 10.3 |

[a] [Rh(acac)(CO)$_2$] = 0.084 mmol L$^{-1}$ in toluene, pressure = 20 bar (CO/H$_2$ = 1/1), 1-octene/rhodium = 5160. [b] [**1**] = 2.1 mmol L$^{-1}$, [**b**] = 6.3 mmol L$^{-1}$, [**a**] = 3.1 mmol L$^{-1}$. [c] TOF = average turnover frequency = (mol aldehyde) (mol Rh)$^{-1}$ h$^{-1}$. The reaction was stopped after 1 h (80 °C) or 17 h (30 °C). [d] *l*/*b* = ratio of linear to branched oxidation product. [e] Amount of isomerization based on converted 1-octene.

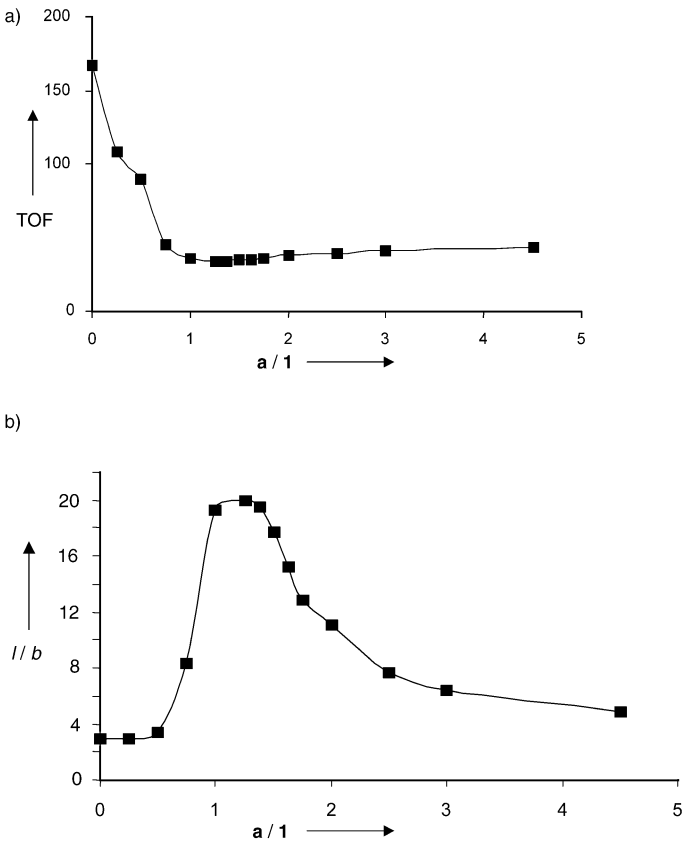



***Figure 2.*** The activity (a, TOF) and selectivity (b, *l*/*b* ratio) of the rhodium complexes based on the assemblies formed from tris(zinc(II) porphyrin)phosphite **1** and various amounts of dabco **a** in the rhodium-catalyzed hydroformylation of 1-octene.

 © 2003 Wiley-VCH Verlag GmbH & Co. KGaA, Weinheim 

activity remains the same upon the addition of more than 0.8 equiv of **a** to **1** (even up to 4.5 equiv), indicating that in this region the catalysis is dominated by self-assembled chelating ligands. The decrease in activity observed in the presence of small amounts of **a** confirms that dabco is ditopically bound between two porphyrins of different ligands.

The selectivity of the reaction is very sensitive to the **a**/**1** ratio, and only around **a**/**1** = 1.5 does the catalyst assembly give high selectivity for the linear aldehyde (Figure 2b). Apparently, the sandwich-type complex must have three bridging dabco molecules to be highly selective. The selectivity is likely associated with the rigidity of the assembly formed. If there is a shortage of dabco, the sandwich assembly has only one or two bridging dabco units, and in the presence of excess dabco the binding of a fourth dabco will compete with the third ditopically bound dabco molecule. In both situations this leads to less rigid chelate assemblies and lower selectivities.

In conclusion, a new supramolecular approach is presented for the preparation of self-organized transition-metal catalyst systems. The multicomponent assembly of two (zinc(II) porphyrin)phosphite ligands **1** and three ditopic dabco ligands into the sandwich-type structure **2** leads to a supramolecular chelating bidentate ligand. This chelate effect was responsible for the high selectivity for the linear aldehyde in the rhodium-catalyzed hydroformylation of 1-octene. The selectivity is very sensitive to the **a**/**1** ratio used, and we showed that three bridging dabco ligands are required for high selectivity. This novel supramolecular approach for the preparation of chelating ligands has proven to be successful, and the regioselectivity and activity in the hydroformylation observed for the catalyst assembly ranks it among the best systems at present.[19]

## Experimental Section

For the synthesis of tris(5-(phenyl-2-yl)-10,15,20-tris(phenyl)zinc(II) porphyrin)phosphite **1** and further experimental details, see the Supporting Information.

Received: July 31, 2003 [Z52525]

**Keywords:** homogenous catalysis · hydroformylation · porphyrinoids · self-assembly · supramolecular chemistry

[1] L. J. Prins, D. N. Reinhoudt, P. Timmerman, *Angew. Chem.* **2001**, *113*, 2446; *Angew. Chem. Int. Ed.* **2001**, *40*, 2382.

[2] a) B. Olenyuk, J. A. Whiteford, A. Fechtenkötter, P. J. Stang, *Nature* **1999**, *398*, 796; b) M. Fujita, N. Fujita, K. Ogura, K. Yamaguchi, *Nature* **1999**, *400*, 52; c) L. J. Prins, J. Huskens, F. de Jong, P. Timmerman, D. N. Reinhoudt, *Nature* **1999**, *398*, 498; d) N. Takeda, K. Umemoto, K. Yamaguchi, M. Fujita, *Nature* **1999**, *398*, 794; e) K. A. Jolliffe, P. Timmerman, D. N. Reinhoudt, *Angew. Chem.* **1999**, *111*, 983; *Angew. Chem. Int. Ed.* **1999**, *38*, 933; f) L. R. MacGillivray, J. L. Atwood, *Nature* **1997**, *389*, 469; g) L. J. Prins, F. de Jong, P. Timmerman, D. N. Reinhoudt, *Nature* **2000**, *408*, 181.

[3] a) J.-M. Lehn in *Supramolecular Chemistry: Concepts and Perspectives*, VCH, Weinheim, **1995**; b) M. Ortega Lorenzo, C. J. Baddeley, C. Muryn, R. Raval, *Nature* **2000**, *404*, 376; c) J. L. Atwood, L. J. Barbour, M. J. Hardie, C. L. Raston, *Coord. Chem. Rev.* **2001**, *222*, 3; d) G. F. Swiegers, T. J. Malefetse, *Chem. Rev.* **2000**, *100*, 3483; e) M. Albrecht, *Chem. Rev.* **2001**, *101*, 3457; f) S. Leininger, B. Olenyuk, P. J. Stang, *Chem. Rev.* **2000**, *100*, 853; g) B. J. Holliday, C. A. Mirkin, *Angew. Chem.* **2001**, *113*, 2076; *Angew. Chem. Int. Ed.* **2001**, *40*, 2022.

[4] a) D. N. Reinhoudt, M. Crego-Calama, *Science*, **2002**, *295*, 2403; b) O. Ikkala, G. ten Brinke, *Science*, **2002**, *295*, 2407; c) G. R. Desiraju, *Nature*, **2001**, *412*, 397; c) R. F. Service, *Science* **2001** *293*, 782.

[5] For reviews see: a) J. K. M. Sanders, *Chem. Eur. J.* **1998**, *4*, 1378; b) P. D. Beer, P. A. Gale, *Angew. Chem.* **2001**, *113*, 502; *Angew. Chem. Int. Ed.* **2001**, *40*, 486; c) M. C. Feiters, in *Compr. Supramol. Chem., Vol. 10*, Elsevier, Oxford **1996**, 267; d) R. Breslow, S. D. Dong, *Chem. Rev.* **1998**, *98*, 1997; e) K. Takahashi, *Chem. Rev.* **1998**, *98*, 2013; f) W. B. Motherwell, M. J. Bingham, Y. Six, *Tetrahedron*, **2001**, *57*, 4663; g) M. T. Reetz, *Top Catal.* **1997**, *4*, 187; h) Y. Murakami, J.-I Kikuchi, Y. Hisaeda, O. Hayashida, *Chem. Rev.* **1996**, *96*, 721.

[6] a) R. Wyler, J. de Mendoza, J. Rebek Jr., *Angew. Chem.* **1993**, *105*, 1820; *Angew. Chem. Int. Ed. Engl.* **1993**, *32*, 1699; b) M. Morgan, J. Rebek Jr., *Chem. Rev.* **1997**, *97*, 1647–1668; c) J. Rebek Jr., *Chem. Soc. Rev.* **1996**, *25*, 255–264; d) J. Rebek Jr., *Chem. Commun.* **2000**, 637–643; e) F. Hof, S. L. Craig, C. Nuckolls, J. Rebek Jr. , *Angew. Chem.* **2002**, *114*, 1556; *Angew. Chem. Int. Ed.* **2002**, *41*, 1488; f) A. Jasat, J. C. Sherman, *Chem. Rev.* **1999**, *99*, 931; g) L. R. MacGillivray, J. L. Atwood, *Angew. Chem.* **1999**, *111*, 1080; *Angew. Chem. Int. Ed.* **1999**, *38*, 1018; h) C. J. Jones, *Chem. Soc. Rev.* **1998**, *27*, 289.

[7] a) J. Kang, J. Rebek Jr., *Nature*, **1997**, *385*, 50; b) J. Kang, G. Hilmersson, J. Santamaria, J. Rebek Jr., *J. Am. Chem. Soc.* **1998**, *120*, 3650; c) J. Kang, J. Santamaria, G. Hilmersson, J. Rebek Jr., *J. Am. Chem. Soc.* **1998**, *120*, 7389; d) M. Yoshizawa, T. Kusukawa, M. Fujita, S. Sakamoto, K. Yamaguchi, *J. Am. Chem. Soc.* **2001**, *123*, 10454; e) M. Yoshizawa, Y. Takeyama, T. Okano, M. Fujita, *J. Am. Chem. Soc.* **2003**, *125*, 3243; f) M. Yoshizawa, Y. Takeyama, T. Kusukawa, M. Fujita, *Angew. Chem.* **2002**, *114*, 1403; *Angew. Chem. Int. Ed.*, **2002**, *41*, 1347; g) R. Warmuth, J. L. Kerdelhue, S. S. Carrera, K. J. Langenwalter, N. Brown, *Angew. Chem.* **2002**, *114*, 102; *Angew. Chem. Int. Ed.*, **2002**, *41*, 96.

[8] a) V. F. Slagt, J. N. H. Reek, P. C. J. Kamer, P. W. N. M. van-Leeuwen, *Angew. Chem.* **2001**, *113*, 4401; *Angew. Chem. Int. Ed.* **2001**, *40*, 4271; b) G. A. Morris, S. T. Nguyen, J. T. Hupp, *J. Mol. Catal. A: Chem.* **2001**, *174*, 15; c) M. L. Merlau, M. Del. Pilar Meija, S. T. Nguyen, J. T. Hupp, *Angew. Chem.* **2001**, *113*, 4369; *Angew. Chem. Int. Ed.* **2001**, *40*, 4239.

[9] a) N. Bampos, V. Marvaud, J. K. M. Sanders, *Chem. Eur. J.* **1998**, *4*, 335; b) C. C. Mak, N. Bampos, J. K. M. Sanders, *Angew. Chem.* **1998**, *110*, 3169; *Angew. Chem. Int. Ed.* **1998**, *37*, 3020; c) C. C. Mak, N. Bampos, S. L. Darling, M. Montalti, L. Prodi, J. K. M. Sanders, *J. Org. Chem.* **2001**, *66*, 4476; d) C. A. Hunter, M. N. Meah, J. K. M. Sanders, *J. Am. Chem. Soc.* **1990**, *112*, 5773; e) C. A. Hunter, M. N. Meah, J. K. M. Sanders, *J. Am. Chem. Soc.* **1990**, *112*, 5780.

[10] At these concentrations the formation of larger assemblies is unlikely, and indeed the spectroscopic data did not indicate formation of such species.

[11] We have analyzed the titration curves with a fitting program developed by Hunter et al.: A. P. Bisson, C. A. Hunter, J. Carlos, K. Young, *Chem. Eur. J.* **1998**, *4*, 845.

[12] This complex was prepared *in situ* by mixing $[Rh(acac)(CO)_2]$ with (zinc(II) porphyrin)phosphite **1** in a 1:2 ratio.

[13] These signals are similar to those found for other phosphite rhodium complexes: a) G. J. H. Buisman, E. Vos, P. C. J. Kamer, P. W. N. M. van Leeuwen, *J. Chem. Soc. Dalton Trans.* **1995**, 409;

 © 2003 Wiley-VCH Verlag GmbH & Co. KGaA, Weinheim 

b) A. van Rooy, P. C. J. Kamer, P. W. N. M. van Leeuwen, *Organometallics* **1996**, *15*, 835.
[14] P. W. N. M. van Leeuwen, C. Claver, in *Rhodium-catalyzed Hydroformylation*, Kluwer, Dordrecht, **2000**.
[15] A. van Rooy, P. C. J. Kamer, P. W. N. M. van Leeuwen, *Organometallics* **1996**, *15*, 835.
[16] During the preparation of this manuscript a chelating bisphosphane based on hydrogen bonds yielding highly selective hydroformylation catalysts was reported: B. Breit, W. Seiche, *J. Am. Chem. Soc.* **2003**, *125*, 6608.
[17] Usually the *l*/*b* ratio decreases at lower temperatures: a) R. Lazzaroni, R. Settambolo, G. Uccello-Barretta, A. Caiazzo, *Organometallics* **1996**, *15*, 4657; b) C. Botteghi, L. Cazzolato, M. Marchetti, S. Paganelli, *J. Org. Chem.* **1995**, *60*, 6612.
[18] G. Szintay, A. Horvath, *Inorg. Chim. Acta* **2000**, *310*, 175.
[19] S. C. van der Slot, J. Duran, J. Luten, P. C. J. Kamer, P. W. N. M. van Leeuwen, *Organometallics* **2002**, *21*, 3873.

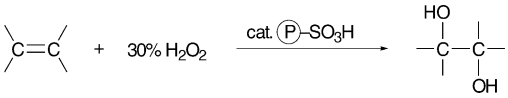
 © 2003 Wiley-VCH Verlag GmbH & Co. KGaA, Weinheim 

*Green Chemistry*

# Catalytic Dihydroxylation of Olefins with Hydrogen Peroxide: An Organic-Solvent- and Metal-Free System**

*Yoko Usui, Kazuhiko Sato,* and Masato Tanaka*

1,2-Diols are widely used as intermediates in the perfume and fragrance industry, for the manufacture of cosmetics, for the synthesis of commercial products such as photographic materials and lubricants, and in drugs and foods.[1] Dihydroxylation of olefins is a straightforward method for the synthesis of 1,2-diols, and various oxidants are now used for this purpose both in the laboratory and in industry.[2] The *syn* dihydroxylation of olefins is most commonly performed in the presence of metal oxides, including $KMnO_4$[3] and $OsO_4$,[4] and *t*-$C_4H_9OOH$ with a catalytic amount of $OsO_4$.[5] The *anti* dihydroxylation can be achieved with $CH_3CO_3H$[6] and *m*-$ClC_6H_4CO_3H$[7] in water. However, the atom efficiency of these oxidants is low, and they form equimolar amounts of the deoxygenated compounds as waste.[8,9] Hydrogen peroxide is an ideal oxidant, because the atom efficiency is excellent and water is theoretically the sole by-product. However, $H_2O_2$ can be a clean oxidant only if it is used in a controlled manner without organic solvents and other toxic compounds.[10] In this context, we developed various oxidation reactions with aqueous $H_2O_2$ under organic-solvent-free conditions.[11,12] Although mixtures of aqueous $H_2O_2$ and $CH_3CO_2H$ or $HCO_2H$ have been known as an effective reagents for the dihydroxylation of olefins,[13] neutralization of the acid solvent with a strong alkali is necessary for isolation of the product. The dihydroxylation of olefins with $H_2O_2$ catalyzed by transition metal complexes has also been reported.[14] However, the selectivity for 1,2-diols in these catalytic reactions is moderate, with formation of epoxides as by-products or overoxidation involving C–C bond cleavage. Furthermore, all these methods require chlorohydrocarbons or other organic solvents. The use of zeolites as catalysts has allowed dihydroxylation without organic solvents,[15] but the selectivity for 1,2-diols was lower than 59% as a result of the formation of epoxides, alcohols, ketones, and/or ethers along with the desired 1,2-diols. We report herein a procedure for the synthesis of 1,2-diols by the dihydroxylation of olefins with aqueous 30% $H_2O_2$ catalyzed by resin-supported sulfonic acid [Eq. (1)]. The present method satisfies the following conditions: 1) organic-solvent- and metal-free system; 2) high yield and selectivity for 1,2-diols; 3) the catalyst is easily recycled; and 4) simple and safe manipulation.




(1)

The dihydroxylation of cyclohexene with 30% $H_2O_2$ in the presence of nafion NR50[16] beads (0.04 equiv, 0.8 mmol $g^{-1}$ of $SO_3H$ group) at 70 °C for 20 h produced *trans*-1,2-cyclohexanediol in 98% yield. The catalyst was recycled very easily. After the first dihydroxylation, the catalyst was filtrated and washed with water, then reused for the second reaction. Ten cycles of dihydroxylation of cyclohexene could be catalyzed by the recycled resin-supported sulfonic acid without a decrease in the catalytic activity. The yield of each reaction was over 94% (Table 1).

Some examples of the dihydroxylation of a range of substrates with 30% $H_2O_2$ are given in Table 2. The reactivity of internal olefins is higher than that of terminal olefins (Table 2, entry 1 vs. entries 2 and 3). The dihydroxylation of (*E*)- and (*Z*)-2-hexene proceeded stereospecifically to give

***Table 1:*** Dihydroxylation of cyclohexene with 30% $H_2O_2$ in the presence of recycled resin-supported sulfonic acid as catalyst.[a]

| Run | Yield [%][b] | Run | Yield [%][b] |
|---|---|---|---|
| 1 | 98 | 6 | 94 |
| 2 | 96 | 7 | 94 |
| 3 | 96 | 8 | 96 |
| 4 | 97 | 9 | 95 |
| 5 | 96 | 10 | 96 |

[a] Reaction conditions: cyclohexene (10 mmol)/30% $H_2O_2$/nafion NR50 (25:50:1), 70 °C, 20 h. [b] Yield of isolated *trans*-1,2-cyclohexanediol.

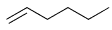
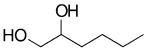
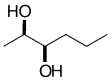
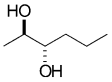
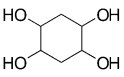
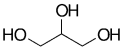
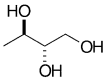
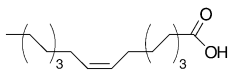
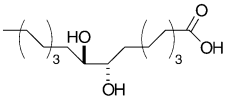
[*] Dr. K. Sato, Dr. Y. Usui, Prof. Dr. M. Tanaka[+]
Research Institute for Green Technology
National Institute of Advanced Industrial Science and Technology (AIST)
Tsukuba Central 5, Tsukuba, Ibaraki, 305-8565 (Japan)
Fax: (+81) 29-861-4852
E-mail: k.sato@aist.go.jp

[+] Present address:
Chemical Resources Laboratory
Tokyo Institute of Technology
4259 Nagatsuda, Midori-ku, Yokohama 226-8503 (Japan)

[**] This work was supported in part by the New Energy and Industrial Technology Development Organization (NEDO)–Research Institute of Innovative Technology for the Earth (RITE) and the Japan Science and Technology Corporation (JST)–Core Research for Evolutional Science and Technology (CREST) program.

 DOI: 10.1002/anie.200352568 © 2003 Wiley-VCH Verlag GmbH & Co. KGaA, Weinheim 

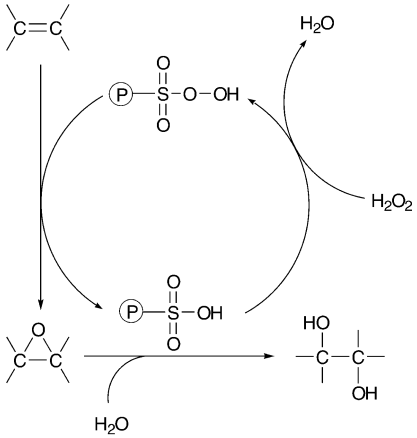
***Table 2:*** Dihydroxylation of olefins with 30% $H_2O_2$ in the presence of resin-supported sulfonic acid catalyst.[a]

| Entry | Olefin | Product | Yield [%][b] |
|---|---|---|---|
| 1[c] |  |  | 40[d] |
| 2[c] |  |  | 67 |
| 3[c] |  |  | 85 |
| 4 |  |  | 83[d] |
| 5 |  |  | 86 |
| 6 |  |  | 98 |
| 7[c] | | | 95 |
| 8[e] | | | 83 |
| 9 |  |  | 92[d] |
| 10 |  |  | 100 |
| 11 |  |  | 93 |
| 12[f] |  |  | 80 |

[a] Unless otherwise stated, the reactions were run with olefin (10 mmol), 30% $H_2O_2$, and nafion NR50 (25:50:1) at 70°C for 20 h. [b] Yield of isolated product. [c] Olefin/30% $H_2O_2$/nafion SAC-13 (25:50:1). [d] Determined by GC analysis. Based on olefin charged. [e] Olefin/30% $H_2O_2$/amberlyst 15 (25:50:1). [f] Olefin/30% $H_2O_2$/nafion SAC-13 (8:32:1), 90°C.

the corresponding *anti*- and *syn*-2,3-hexanediols, respectively (Table 2, entries 2 and 3). Functionalized olefins were also easily oxidized to produce the corresponding 1,2-diols without affecting alcohol and carboxylic acid groups present in the substrate (Table 2, entries 10–12). Nafion SAC-13 (powder, supported on silica) showed almost the same catalytic activity as nafion NR50 (Table 2, entries 6 and 7). The ion-exchange resin, amberlyst 15[17] (polystyrene-supported sulfonic acid) also proved to be a good catalyst for dihydroxylation, producing *trans*-1,2-cyclohexanediol from cyclohexene in 83% yield (Table 2, entry 8). Interestingly, the catalytic activity of resin-supported sulfonic acids is much higher than that of homogeneous acid catalysts. For example, the yields of *anti*-2,3-hexanediol from the dihydroxylation of (*E*)-2-hexene were 85% when using nafion SAC-13, 36% when using $CF_3SO_3H$, 19% when using $H_2SO_4$, 11% when using $C_6H_5SO_3H$, and 0% when using $CH_3CO_2H$. Resin-supported carboxylic acid (amberlite IRC76[17]) did not work as a catalyst.

This dihydroxylation of olefins proceeds through two steps (Scheme 1): 1) epoxidation of the olefin by $H_2O_2$ and 2) hydration of the epoxide to form 1,2-diol. The rate-determining step seems to be the epoxidation of olefins as epoxides could not be detected in the reaction mixtures. Indeed, under these reaction conditions, cyclohexene oxide produced *trans*-1,2-cyclohexanediol quantitatively within 10 min. The initial epoxidation is probably carried out by resin-supported peroxysulfonic acid formed in situ.[18,19] Competitive experiments showed the following relative reactivity: 1-hexene/(*Z*)-2-hexene/(*E*)-2-hexene/2-methyl-2-pentene = 1:24:46:153. These values are similar to the epoxidation ratio of these olefins with peroxycarboxylic acid (1:22:20:230).[20]




***Scheme 1.*** Proposed catalytic cycle for the dihydroxylation reaction.

In summary, we have developed a clean and safe method for the dihydroxylation of alkenes under organic-solvent- and metal-free conditions. The resin-supported sulfonic acid catalyst is easily recycled.

## *Experimental Section*

Typical procedure: A 50-mL round-bottomed flask equipped with a magnetic stirring bar and reflux condenser was charged with nafion NR50 (501 mg) and aqueous $H_2O_2$ (30%; 2.23 g, 20 mmol). The mixture was stirred at room temperature for 10 min, after which cyclohexene (821 mg, 10 mmol) was added. The triphasic mixture was heated at 70°C with vigorous stirring for 20 h and then cooled to room temperature. After the nafion NR50 was removed by filtration, $MnO_2$ (ca. 10 mg) was added to the solution. The absence of $H_2O_2$ was examined by testing with starch–iodide paper. After filtration of $MnO_2$, the water was removed by evaporation to provide *trans*-1,2-cyclohexanediol[21] was obtained as a white powder (1.14 g, 98% yield). M.p. 101–102°C. $^1$H NMR (500 MHz, $D_2O$): $\delta = 1.38$ (br s, 2H), 1.80 (br s, 2H), 2.06 (br s, 1H), 3.50 ppm (br s, 1H); $^{13}$C NMR (125 MHz, $D_2O$): $\delta = 76.0$, 33.6, 24.4 ppm. The nafion NR50 used above was washed with water (5 × 5 mL), and the same dihydroxylation reaction was carried out under the same conditions to give *trans*-1,2-cyclohexanediol (1.12 g, 96% yield).

Received: August 5, 2003 [Z52568]

 © 2003 Wiley-VCH Verlag GmbH & Co. KGaA, Weinheim 

**Keywords:** alkenes · dihydroxylation · green chemistry · hydrogen peroxide · oxidation


[1] a) *Kirk-Othmer Encyclopedia of Chemical Technology, Vol. 12*, 4th ed. (Eds.: J. I. Kroscwitz, M. Howe-Grant), Wiley, New York, **1991**; b) K. Kulkaand, J. W. Dittrick, *Cosmet. Perfum.* **1975**, *90*, 90 – 95.

[2] a) M. Hudlicky, *Oxidations in Organic Chemistry*, American Chemical Society, Washington, DC, **1990**, pp. 174 – 184 (ACS Monograph Ser. 186); b) A. H. Haines in *Comprehensive Organic Synthesis, Vol. 7.*, 1st ed. (Eds.: B. M. Trost, I. Fleming), Pergamon, Oxford, **1991**, pp. 437 – 438; c) J. March, *Advanced Organic Chemistry*, 4th ed., Wiley, New York, **1992**, pp. 822 – 825.

[3] a) G. Wagner, *Ber. Dtsch. Chem. Ges.* **1888**, *21*, 1230 – 1240; b) G. Wagner, *Ber. Dtsch. Chem. Ges.* **1888**, *21*, 3347 – 3355; c) G. Wagner, *Ber. Dtsch. Chem. Ges.* **1890**, *23*, 2307 – 2319; d) A. J. Fatiadi, *Synthesis* **1989**, 85 – 127.

[4] a) R. Criegee, *Justus Liebigs Ann. Chem.* **1936**, *522*, 75 – 97; b) R. Criegee, B. Marchand, H. Wannowius, *Justus Liebigs Ann. Chem.* **1942**, *550*, 99 – 133; c) M. Schröder, *Chem. Rev.* **1980**, *80*, 187 – 213.

[5] K. Akashi, R. E. Palermo, K. B. Sharpless, *J. Org. Chem.* **1978**, *43*, 2063 – 2066.

[6] D. Swern, *Chem. Rev.* **1949**, *49*, 1 – 68.

[7] F. Fringuelli, R. Germani, F. Pizzo, G. Savelli, *Synth. Commun.* **1989**, *19*, 1939 – 1943.

[8] B. M. Trost, *Angew. Chem.* **1995**, *107*, 285 – 307; *Angew. Chem. Int. Ed. Engl.* **1995**, *34*, 259 – 281.

[9] R. A. Sheldon, *Chem. Ind.* **1997**, 12 – 15.

[10] a) J. O. Metzger, *Angew. Chem.* **1998**, *110*, 3145 – 3148; *Angew. Chem. Int. Ed.* **1998**, *37*, 2975 – 2978; b) P. T. Anastas, J. C. Warner, *Green Chemistry, Theory and Practice*, Oxford University Press, New York, **1998**.

[11] a) K. Sato, M. Aoki, M. Ogawa, T. Hashimoto, R. Noyori, *J. Org. Chem.* **1996**, *61*, 8310 – 8311; b) K. Sato, M. Aoki, J. Takagi, R. Noyori, *J. Am. Chem. Soc.* **1997**, *119*, 12386 – 12387; c) K. Sato, M. Aoki, M. Ogawa, T. Hashimoto, D. Penyella, R. Noyori, *Bull. Chem. Soc. Jpn.* **1997**, *70*, 905 – 915; d) K. Sato, M. Aoki, R. Noyori, *Science* **1998**, *281*, 1646 – 1647; e) K. Sato, J. Takagi, M. Aoki, R. Noyori, *Tetrahedron Lett.* **1998**, *39*, 7549 – 7552; f) K. Sato, M. Aoki, J. Takagi, K. Zimmermann, R. Noyori, *Bull. Chem. Soc. Jpn.* **1999**, *72*, 2287 – 2306; g) K. Sato, M. Hyodo, J. Takagi, M. Aoki, R. Noyori, *Tetrahedron Lett.* **2000**, *41*, 1439 – 1442; h) K. Sato, M. Hyodo, M. Aoki, X.-Q. Zheng, R. Noyori, *Tetrahedron* **2001**, *57*, 2469 – 2476; i) Y. Usui, K. Sato, *Green Chem.* **2003**, *5*, 373 – 375.

[12] R. Noyori, M. Aoki, K. Sato, *Chem. Commun.* **2003**, 1977 – 1986.

[13] For dihydroxylation with aqueous $H_2O_2$ in acetic acid, see: a) T. P. Hilditch, *J. Chem. Soc.* **1926**, 1828 – 1836; in formic acid, see: b) D. Swern, G. N. Billen, T. W. Findley, J. T. Scanlan, *J. Am. Chem. Soc.* **1945**, *67*, 1786 – 1789; c) A. Roebuck, H. Adkins in *Org. Synth. Coll. Vol., Vol. 3* (Ed.: E. C. Horning), Wiley, New York, **1962**, pp. 217 – 219.

[14] For $H_2WO_4$-catalyzed dihydroxylation with $H_2O_2$, see: a) M. Mugdan, D. P. Young, *J. Chem. Soc.* **1949**, 2988 – 3000; b) G. B. Payne, C. W. Smith, *J. Org. Chem.* **1957**, *22*, 1682 – 1685; c) V. Singh, P. T. Deota, *Synth. Commun.* **1988**, *18*, 617 – 624; d) T. Oguchi, T. Ura, Y. Ishii, M. Ogawa, *Chem. Lett.* **1989**, 857 – 860; for the use of a heteropoly acid catalyst, see: e) M. Schwegler, M. Floor, H. van Bekkum, *Tetrahedron Lett.* **1988**, *29*, 823 – 826; f) C. Venturello, M. Gambaro, *Synthesis* **1989**, 295 – 297; for the use of $CH_3ReO_3$ as catalyst, see: g) W. A. Herrmann, R. W. Fischer, D. W. Marz, *Angew. Chem.* **1991**, *103*, 1706 – 1708; *Angew. Chem. Int. Ed. Engl.* **1991**, *30*, 1638 – 1641.

[15] For dihydroxylation with $H_2O_2$ in the presence of $(NH_4)_{10}W_{12}O_{41}$/hydrotalcite catalyst, see: a) T. Tatsumi, K. Yamamoto, H. Tajima, H. Tominaga, *Chem. Lett.* **1992**, 815 – 818; For the use of Ti-beta zeolites as catalyst, see: b) A. Corma, M. A. Camblor, P. Esteve, A. Martínez, J. Pérez-Pariente, *J. Catal.* **1994**, *145*, 151 – 158; for the use of Ti-MCM zeolites as catalysts, see: c) A. Corma, M. T. Navarro, J. Pérez-Pariente, *J. Chem. Soc. Chem. Commun.* **1994**, 147 – 148; d) T. Tatsumi, K. A. Koyano, N. Igarashi, *Chem. Commun.* **1998**, 325 – 326; for the use of Nb-MCM-41 zeolites as catalyst, see: e) J. Xin, J. Suo, X. Zhang, Z. Zhang, *New J. Chem.* **2000**, *24*, 569 – 570.

[16] Nafion resins were first synthesized at DuPont; see: a) D. C. England, US Patent, 2852554, **1958** [*Chem. Abstr.* **1959**, *53*, 2253]; b) D. J. Conolly, W. F. Gresham, US Patent 3282875, **1966**; for a review on the use of nafion for organic syntheses, see: c) G. A. Olah, P. S. Iyer, G. K. Surya Prakash, *Synthesis* **1986**, 513 – 531.

[17] Amberlyst and amberlite products are ion-exchange resins produced by the ORGANO Corporation.

[18] S. Vayssié, H. Elias, *Liebigs Ann.* **1997**, 2567 – 2572.

[19] One of the referees for this Communication suggested the possibility that $H_2O_2$ is activated by the resin-supported sulfonic acid through hydrogen-bond formation; for example, see: a) M. C. A. van Vliet, I. W. C. E. Arends, R. A. Sheldon, *Synlett* **2001**, 248 – 250; b) J. Wahlen, D. E. De Vos, P. A. Jacobs, *Org. Lett.* **2003**, *5*, 1777 – 1780.

[20] a) D. Swern, *Org. React.* **1953**, *7*, 378 – 433; b) J. Rebek, Jr., L. Marshall, R. Wolak, *J. Org. Chem.* **1986**, *51*, 1649 – 1653.

[21] W. D. Emmons, A. S. Pagano, J. P. Freeman, *J. Am. Chem. Soc.* **1954**, *76*, 3472 – 3474.


 © 2003 Wiley-VCH Verlag GmbH & Co. KGaA, Weinheim 

*Natural Product Synthesis*

# Studies Directed toward the Total Synthesis of Lactonamycin: Control of the Sense of Cycloaddition of a Quinone through Directed Intramolecular Catalysis**

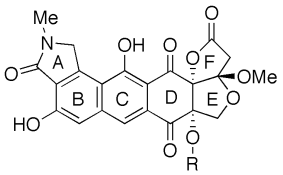
*Christopher D. Cox, Tony Siu, and Samuel J. Danishefsky**

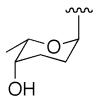
As part of a screening program for the discovery of new antibiotics, Matsumoto et al. isolated lactonamycin (**1**) from a culture broth of *Streptomyces rishirienisi* MJ773–88K4.[1] Its

[*] Prof. S. J. Danishefsky, Dr. C. D. Cox, T. Siu
Department of Chemistry, Columbia University
Havemeyer Hall, New York, NY 10021 (USA)
E-mail: s-danishefsky@ski.mskcc.org
Prof. S. J. Danishefsky
Laboratory for Bioorganic Chemistry
Sloan-Kettering Institute for Cancer Research
1275 York Ave., New York, N.Y. 10021 (USA)
Fax: (+1) 212-772-8691

[**] This work was supported by the National Institutes of Health (Grant number: HL25848). A Postdoctoral Fellowship is gratefully acknowledged by C.D.C. (NIH, Grant Number F32-CA84758). The authors thank Yashuiro Itagaki for high-resolution mass spectral analyses.

 **DOI: 10.1002/anie.200352591** © 2003 Wiley-VCH Verlag GmbH & Co. KGaA, Weinheim 



**1** R = 

**2** R = H

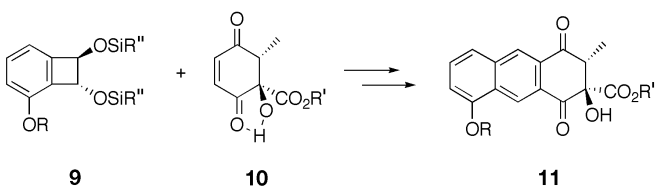
structure and absolute configuration were assigned through spectroscopic and X-ray crystallographic measurements in conjunction with degradation protocols. Biological evaluation of lactonamycin revealed it to have antimicrobial activity against Gram-positive bacteria, including methicillin- and vancomycin-resistant strains ($IC_{50} = 0.20$–$1.56\ mg\,mL^{-1}$). In addition to its antimicrobial activities, lactonamycin is cytotoxic against various tumor cell lines ($IC_{50} = 0.06$–$3.3\ mg\,mL^{-1}$).

The novel, highly functionalized hexacyclic aglycone domain of lactonamycin, lactonamycinone (**2**), inherently poses some significant issues at the planning level of a chemical synthesis. Furthermore, the feasibility of glycosylation of a tertiary α-hydroxyketone acceptor site with an appropriate L-rhodinose donor species under high anomeric stereoselectivity could hardly be taken for granted. These concerns notwithstanding, the challenges confronting any attempt to construct lactonamycin in a laboratory setting and its promising profile of antibiotic action drew us into a total synthesis venture. We report herein an important milestone in that effort, that is, the first total synthesis of the aglycone, lactonamycinone (**2**).[2] We expand upon the concept of intramolecular directed catalysis, which enabled the highly concise assembly of the key tetracyclic intermediate **35** (see Scheme 7), and we discuss how we overcame the many difficulties associated with the synthesis of this intermediate and its conversion into lactonamycinone.[3]

Our strategy hinged on the condensation of a homophthalic anhydride (see generalized structure **3**) with a quinone **4** in a process that is initiated by an anionically mediated "cycloaddition" reaction (Scheme 1). We use the term cycloaddition in an empirical rather than mechanistic sense, thereby sidestepping difficultly resolvable issues related to the concerted nature of the reaction. Cycloadduct **5** would be expected to undergo transformation into **6** upon the loss of carbon dioxide. Although this type of overall reaction is, in itself, well-known as a Tamura–Diels–Alder reaction,[4] in this case it was to be applied to the unsymmetrical quinone **4**. Even if unlikely initial cycloaddition at the more hindered of the quinone double bonds is neglected, in principle, two regioisomeric products **6** and **8**, arising from primary cycloadducts **5** and **7**, respectively, could be produced.

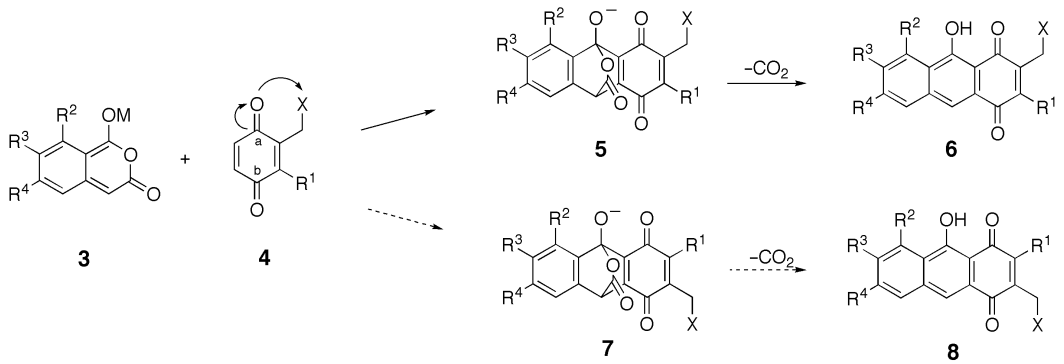
In Scheme 1, a general format for solving this type of problem is suggested by building an internal activating group into the quinone **4**. In the case at hand, we imply that the formal ketone group (a) can be rendered more active than its counterpart (b) by means of the biasing element X.[5a–c] Whether through hydrogen bonding or metal-ion bridging (see below), the consequences of this intramolecular directed catalysis would be to favor the eventual formation of **6** over **8**.

Indeed, in our recently described total synthesis of rishirilide B, we demonstrated this type of locally biased catalysis (Scheme 2, **9** + **10**→**11**).[6] In the total synthesis of lactonamycin, we hoped to extend the local biasing strategy to quinones rather than to a cyclohexene-1,4-dione **10**. Since quinones are particularly reactive substrates, the applicability of the findings in the case of rishirilide was open to question. Moreover, we would be seeking to extend the generalized idea of regiocontrol by intramolecular catalysis from a clear cycloaddition case (**9** + **10**) conducted under neutral conditions to a less-well-defined, anion-mediated setting (**3** + **4**).



**9** **10** **11**

***Scheme 2.*** Application of locally biased catalysis in the total synthesis of rishirilide B.

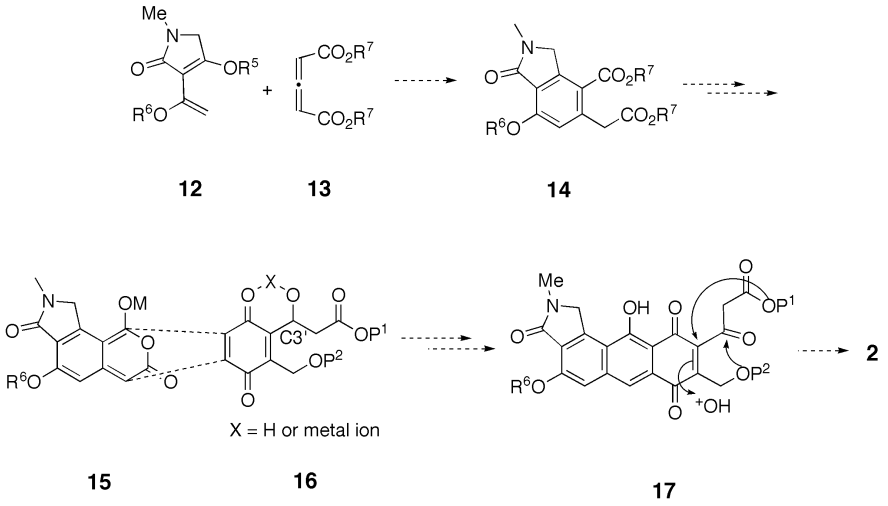


**3** **4** **5** **6** **7** **8**

***Scheme 1.*** Tamura–Diels–Alder reaction with an unsymmetrical quinone.

 © 2003 Wiley-VCH Verlag GmbH & Co. KGaA, Weinheim 

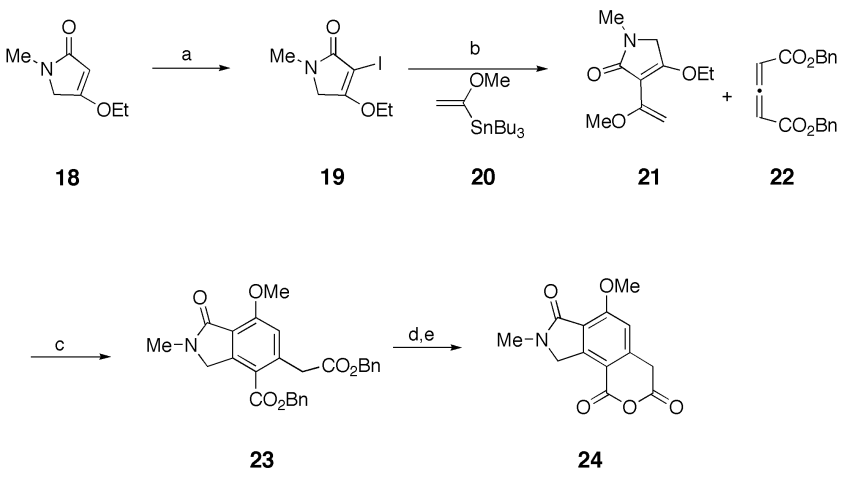
Viewed from the perspective of lactonamycinone, we envisioned the cycloaddition of **15** and **16** (Scheme 3). The orienting function would be the strategically placed hydroxy group at C3′, which would differentiate the two ketone-like centers of quinone **16**. We hoped to reach the homophthalic anhydride **15** by a Diels–Alder reaction of **12** and **13**. In this way, we would ultimately have connected the diverse functionalities of the ABCD ensemble through *two* defining cycloaddition reactions (see product **17**). Some of the necessary connections to proceed from **17** to lactonamycinone (**2**) are suggested in Scheme 3.




**12** **13** **14** **15** **16** **17**

***Scheme 3.*** Proposed synthesis of lactonamycinone

Implementation of the ideas outlined above commenced with tetramic acid derivative **18**[7] (Scheme 4). Iodination[8] of this compound gave rise to **19**, which served as a substrate for a Stille reaction with **20**,[9] thereby giving rise to diene **21** in 42% yield (two steps). For our allene component, we took recourse to the 1,3-dicarbobenzyloxyallene (**22**).[10] In the event, cycloaddition of **21** and **22** was possible and gave **23**, albeit in 15–25% yield. Hydrogenolysis of the two benzyl esters gave rise to a diacid. However, dehydration with trimethylsilylethoxyacetylene[11] only produced trace amounts of the desired homophthalic anhydride **24**, presumably as a result of solubility issues. It is possible that the difficulties in the cycloaddition reaction of **21** and **22** reflect the usual complexities associated with Diels–Alder reactions of 1,1-disubstituted dienes, in which the required 2,3-*s-cis* coplanar conformer may be of high energy. In the case at hand, the situation is perhaps further aggravated by the presence of substituents at C2 and C3 in **21**. Given the difficulties of the Diels–Alder reaction and anhydride formation, we also explored an alternative route, which, though somewhat less concise, lends itself to larger-scale development.



**18** **19** **20** **21** **22** **23** **24**

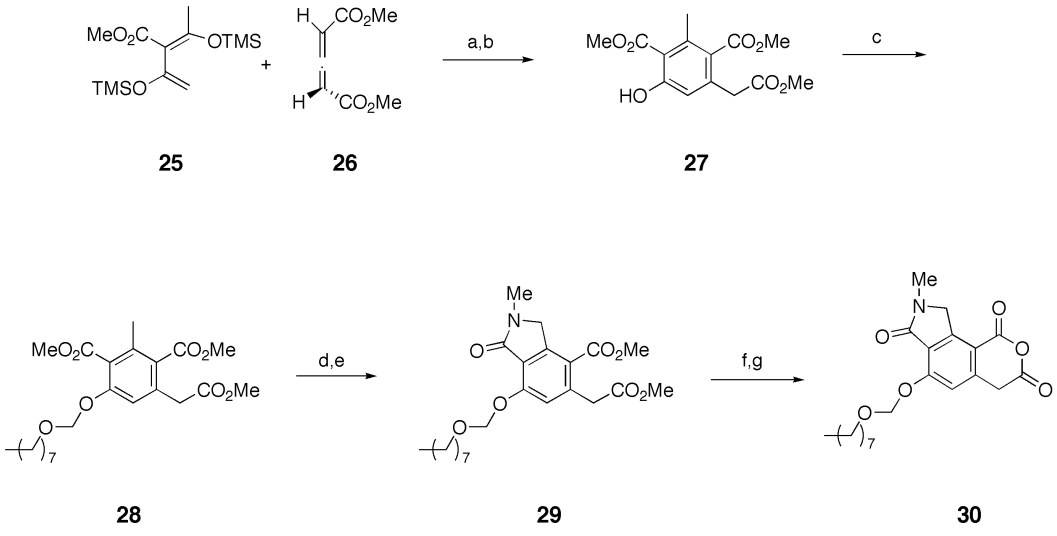
***Scheme 4.*** Reagents and conditions. a) $I_2$, PIFA, pyridine, 51%; b) **20**, $[PdCl_2(PPh_3)_2]$, PhMe, reflux, 83%; c) **22**, neat, 200°C, 15–25%; d) $H_2$, Pd/C, 50%; e) trimethylsilylethoxyacetylene, $CH_3CN/CH_2Cl_2$, trace amounts of product. PIFA = bis(trifluoroacetoxy)iodobenzene.

The second path started with the known bis(silyl enol ether) **25**.[12] Cycloaddition of **25** with the 1,3-dicarbomethoxyallene (**26**)[10] gave rise to **27** in 75% yield (Scheme 5). To overcome issues of solubility later in the synthesis, the phenolic function of **27** was protected as an unconventional octyloxymethyl ether[13] derivative **28**. The aryl methyl group of **28** was brominated with *N*-bromosuccinimide and benzoyl peroxide under irradiation from a UV lamp. Revisiting a type of chemistry that we had studied in 1969, we treated the resulting compound with methylamine, which gave rise primarily to lactam **29**[14] (30% yield based on recovered starting material) along with the isomeric isoindolinone (3.5:1). Hydrolysis of the ester linkages gave rise to a diacid, which was dehydrated to produce the protected pyrrolo homophthalic anhydride **30** (Scheme 5).

The building of a suitable quinone system started with the known **31**[15] (Scheme 6). Protection of the primary alcohol as a benzyl ether followed by deprotection of the dithiane[16] afforded **32** in 74% yield. The smooth chain extension of the benzaldehyde derivative by the Rathke methodology[17] gave rise to **33** in excellent yield. Oxidative demethylation of this substrate afforded quinone **34** in 96% yield. It was this compound that would serve as the coupling partner with the previously described homophthalic anhydride **30**.

With the appropriately functionalized quinone **34** and homophthalic anhydride **30** in hand, the crucial Tamura–Diels–Alder reaction was examined. In the event, treatment of **30** with 2 equivalents of NaH at −78°C, followed by the addition of 2 equivalents of quinone **34** and warming to 0°C, led to a rapid cycloaddition reaction followed by extrusion of

 © 2003 Wiley-VCH Verlag GmbH & Co. KGaA, Weinheim 

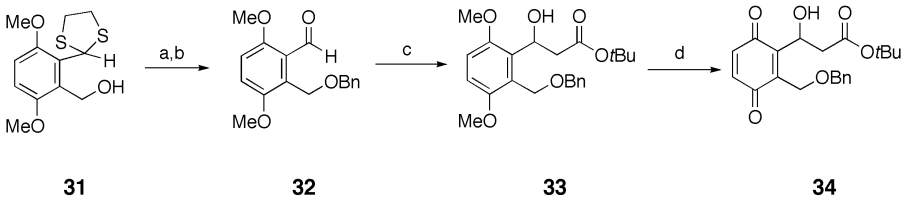



***Scheme 5.*** Reagents and conditions. a) **25, 26**, neat, 105 °C; b) $NH_4F$, MeOH, 75 %; c) $CH_3(CH_2)_7OCH_2Cl$, DIPEA, DMF, 95 %; d) NBS, benzoyl peroxide (cat.), UV, benzene; e) $K_2CO_3$, $NH_2Me$, MeOH/$CH_3CN$ (1:2), 30 % yield based on recovered starting material, 3.5:1; f) KOH, MeOH, 98 %; g) trimethysilylethoxyacetylene, $CH_3CN/CH_2Cl_2$, quantitative. DIPEA = *N,N*-diisopropylethylamine; DMF = *N,N*-dimethylformamide.

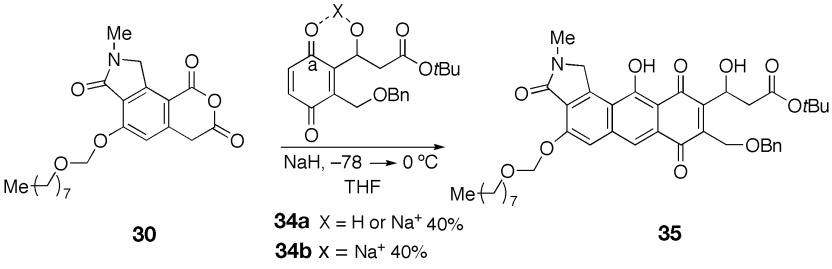
carbon dioxide to provide quinone **35** in 40 % yield (Scheme 7). As we had hoped, only a single regioisomer was formed, as determined by NMR spectroscopic analysis at 500 MHz. The structure of the product was first inferred from precedent and later confirmed by X-ray crystallography to correspond to that depicted in **35**. Notably, 2 equivalents of quinone were needed for optimum yield—presumably the extra equivalent is required to oxidize the resulting hexacyclic intermediate to quinone **35**. Efforts to use 1 equivalent of quinone and an external source of oxidant gave lower yields.

Although we had indeed predicted the preferred formation of **35** under mediation by a strategically placed activating group, it was appropriate to test this rationale in a closely related setting, thereby enabling further understanding of the issues involved. Accordingly, the hydroxy group of **34** was protected as its *tert*-butyldimethylsilyl ether **36**. The latter compound reacted smoothly under the same Tamura–Diels–Alder reaction conditions employed for **35** (Scheme 8). However, in this case a 1:1 mixture of **37** and **38** was produced. Certainly, this experiment is fully in keeping with the governing paradigm sketched out in Scheme 1 (see structure **4**).

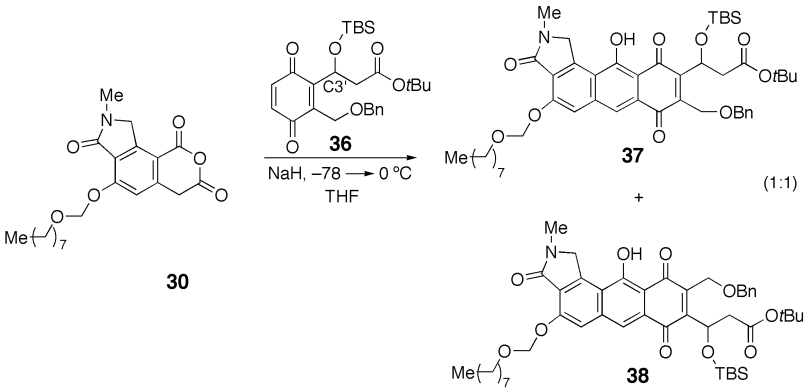
In presenting this model for directed activation we were appropriately vague as to the precise nature of the activating




***Scheme 6.*** Reagents and conditions. a) NaH, BnBr, TBAI, THF, 86 %; b) PIFA, $CH_3CN/H_2O$ (1:1), 86 %; c) LDA, *t*BuOAc, −78 °C, THF, 99 %; d) CAN, 0 °C, $CH_3CN/H_2O$ (9:1), 96 %. TBAI = tetrabutylammonium iodide; LDA = lithium diisopropylamide; CAN = ceric ammonium nitrate.




***Scheme 7.*** Regioselective Tamura–Diels–Alder reaction.




***Scheme 8.*** Disruption of the locally biased catalysis.

 © 2003 Wiley-VCH Verlag GmbH & Co. KGaA, Weinheim 

effect. One possibility would be that of a local intramolecular hydrogen bond. Alternatively, carbonyl a (**34a**) could be differentially activated by a chelation effect (sodium in the case of our application of the Tamura reaction). Clearly, a metal chelate effect might, in principle, have been possible even if the oxygen atom of the side chain were protected as the TBS ether. Since TBS ethers projecting from carbons α or β to a carbonyl function tend to be poor donors to support metal-mediated chelates,[18] the 1:1 ratio of products resulting from the reaction of **30** and **36** is not surprising.

Finally, we probed the possibility of exerting control through an alkoxide-based metal bridge. Toward this end, compound **34** was pretreated with NaH. Treatment of **34b**, thus produced, with **30** under the same conditions used above again led to **35** as the only isolated regioisomer (Scheme 7). Hence, metal-induced positionally directed selective activation is clearly possible with a hydroxy-based anchor (see **34b**). It remains to be shown whether a hydrogen-bonded counterpart can intervene under these basic conditions.

In summary, we have shown how the otherwise complicated ABCD domain of lactonamycin can be assembled with high regiocontrol through two cycloaddition reactions from readily synthesized components. This enabling strategy was crafted around the notion of gaining regiochemical control through mediation of a suitably positioned hydroxy group. The concept was reduced to practice but does not extend to the corresponding TBS ether of the hydroxy group. In the following Communication in this issue, we describe the completion of the total synthesis of lactonamycinone utilizing the key ideas and intermediates illustrated herein.

Received: August 7, 2003 [Z52591]

**Keywords:** antibiotics · Diels–Alder reaction · natural products · quinones · total synthesis

[1] a) N. Matsumoto, T. Tsuchida, M. Maruyama, R. Sawa, N. Kinoshita, Y. Homma, Y. Takahashi, H. Iinuma, H. Naganawa, *J. Antibiot.* **1996**, *49*, 953 – 954; b) N. Matsumoto, T. Tsuchida, M. Maruyama, N. Kinoshita, Y. Homma, H. Iinuma, T. Sawa, M.; T. Hamada, T. Takeuchi, N. Heida, T. Yoshioka, *J. Antibiot.* **1999**, *52*, 269 – 275; c) N. Matsumoto, T. Tsuchida, H. Nakamura, R. Sawa, Y. Takahashi, H. Naganawa, H. Iinuma, T. Sawa, T. Takeuchi, M. Shiro, *J. Antibiot.* **1999**, *52*, 276 – 280.

[2] For synthetic and model studies toward the synthesis of lactonamycin, see: a) C. Cox, S. J. Danishefsky, *Org. Lett.* **2000**, *2*, 3493 – 3496; b) C. Cox, S. J. Danishefsky, *Org. Lett.* **2001**, *3*, 2899 – 2902; c) J. P. Deville, V. Behar, *Org. Lett.* **2002**, *4*, 1403 – 1405d) T. R. Kelly, D. Xu, G. Martinez, H. Wang, *Org. Lett.* **2002**, *4*, 1527 – 1529.

[3] T. Siu, C. D. Cox, S. J. Danishefsky, *Angew. Chem.* **2003**, *115*, 5787 – 5792; *Angew. Chem. Int. Ed.* **2003**, *42*, 5629 – 5634.

[4] Y. Tamura, F. Fukata, M. Sasho, T. Tsugoshi, Y. Kita, *J. Org. Chem.* **1985**, *50*, 2273 – 2277, and references therein.

[5] For a related use of this concept in a Diels–Alder reaction, see: a) H. Fujioka, H. Yamamoto, H. Annoura, H. Maeda, Y. Kita, *Chem. Pharm. Bull.* **1992**, *40*, 32 – 35; for a related use of this concept in juglone and naphthazarin systems, see: b) V. H. Powell, A. J. Birch, *Tetrahedron Lett.* **1970**, *11*, 3467 – 3469; c) T. R. Kelly, J. W. Gillard, R. N. Goerner, Jr. J. M. Lyding, *J. Am. Chem. Soc.* **1977**, *99*, 5513 – 5514.

[6] J. G. Allen, S. J. Danishefsky, *J. Am. Chem. Soc.* **2001**, *123*, 351 – 352.

[7] H. W. Pinnick, K. S. Kochhar, *J. Org. Chem.* **1989**, *54*, 3222 – 3224.

[8] R. Benhida, P. Blanchard, T. L. Fourrey, *Tetrahedron Lett.* **1998**, *39*, 6849 – 6852.

[9] J. A. Soderquist, J.-H. Hsu, *Organometallics* **1982**, *1*, 830 – 833.

[10] M. Node, T. Fujiwara, S. Ichihashi, K. Nishide, *Tetrahedron* **1986**, *42*, 6645 – 6656.

[11] P. Müller, N. Pautex, *Helv. Chim. Acta* **1991**, *74*, 55 – 64.

[12] P. Allevi, M. Anastasia, S. Bingham, P. Ciuffreda, A. Fiecchi, G. Cighetti, A. Scala, J. Tyman, *J. Chem. Soc. Perkin Trans. 1* **1998**, 575 – 582.

[13] A. Warshawsky, A. Deshe, *J. Polym. Sci. Part. A* **1985**, *23*, 1839.

[14] S. J. Danishefsky, T. A. Bryson, J. Puthenpurayil, *J. Org. Chem.* **1975**, *40*, 1846 – 1848.

[15] G. A. Kraus, L. Chen, R. A. Jacobson, *Synth. Commun.* **1993**, *23*, 2041 – 2049.

[16] G. Stork, K. Zhao, *Tetrahedron Lett.* **1989**, *30*, 287 – 290.

[17] M. J. Rathke, D. F. Sullivan, *J. Am. Chem. Soc.* **1973**, *95*, 3050 – 3051.

[18] G. E. Keck, S. Castellino, *Tetrahedron Lett.* **1987**, *28*, 281 – 284.

 © 2003 Wiley-VCH Verlag GmbH & Co. KGaA, Weinheim 

*Natural Product Synthesis*

# Total Synthesis of Lactonamycinone**

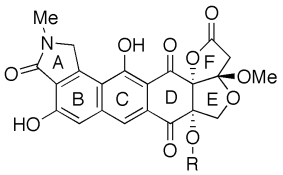
*Tony Siu, Christopher D. Cox, and Samuel J. Danishefsky**

In the previous Communication in this issue, we described an approach to the total synthesis of lactonamycinone (**2**), the aglycone of the antibiotic of lactonamycin (**1**). This effort culminated in a highly concise assembly of the tetracyclic intermediate **3** (see Scheme 1),[1] containing the core functionality, which, in principle, could be exploited in a total synthesis of **2**. As described herein, the first total synthesis of lactonamycinone (**2**) has now been completed. To reach our

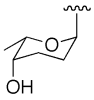
[*] Prof. S. J. Danishefsky, T. Siu, Dr. C. D. Cox
Department of Chemistry, Columbia University
Havemeyer Hall, New York, NY 10021 (USA)
E-mail: s-danishefsky@ski.mskcc.org
Prof. S. J. Danishefsky
Laboratory for Bioorganic Chemistry
Sloan-Kettering Institute for Cancer Research
1275 York Ave., New York, NY 10021 (USA)
Fax: (+1) 212-772-8691

[**] This work was supported by the National Institutes of Health (Grant number: HL25848). A Postdoctoral Fellowship is gratefully acknowledged by C.C. (NIH, Grant Number F32-CA84758). The authors thank Dr. Tekeuchi of The Institute of Microbial Chemistry for kindly providing the $^1$H NMR spectra of **33** and lactonamycin, Yashuiro Itagaki for high-resolution mass spectral analyses, and Professor Ged Parkin and Dr. David Churchill for crystallographic analysis of compound **8**.

 DOI: 10.1002/anie.200352592 © 2003 Wiley-VCH Verlag GmbH & Co. KGaA, Weinheim 



**1** R =

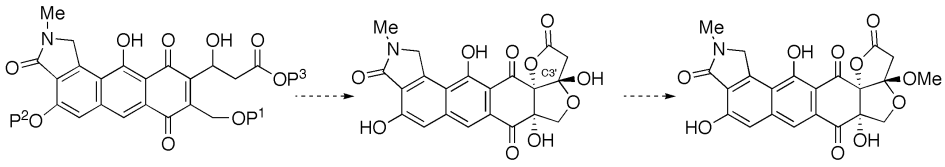


**2** R = H

goal, it became necessary to devise a new end-game sequence to overcome a virtually complete breakdown of the chemistry that was workable in several model settings.[2] The new route highlights some important principles, which are likely to prove valuable in any future synthesis of lactonamycinone.

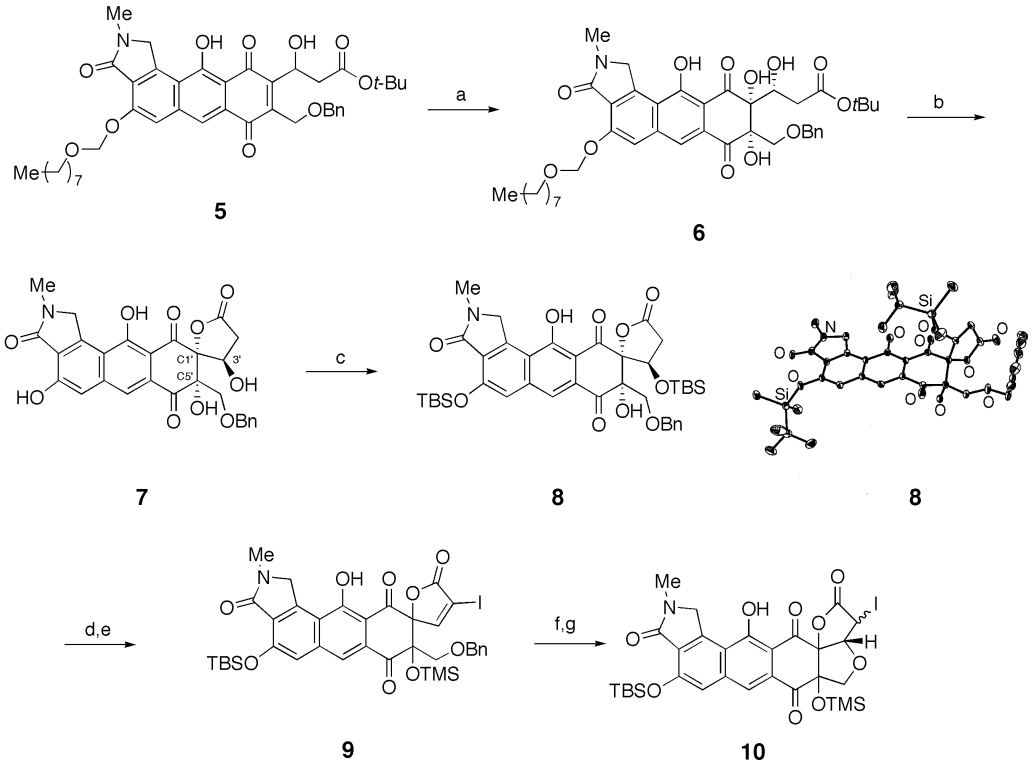
Our original strategy for constructing the E and F rings is summarized in Scheme 1 (**3**→**4**→**2**). Although the protecting groups in the ABC domain are not specified, the concept suggests progression of **3** to hemiacetal **4**. The introduction of the methyl ether at C3′ (in **2**) might involve methanolysis of a system such as **4** through oxonium formation at C3′.

The effort began with a novel and highly diastereoselective dihydroxylation of the quinone moiety of **5** with osmium tetroxide and pyridine. This reaction led to the clean formation (90% yield) of compound **6**, which incorporates the required *cis* relationship of the hydroxy groups at C1′ and C5′ (Scheme 2). The stereochemical sense of this dihydroxylation reaction follows well from Kishi's model, in which $OsO_4$ approaches the olefin in its lowest-energy conformer (based on minimization of the 1,3-allylic strain) from the face opposite to the hydroxy group.[3] Notably, had the C3′ alcohol been homochiral and of the required absolute configuration, the diol at C1′ and C5′ would have been installed with enantiotopic control. Treatment of **6** with TFA brought about concurrent cleavage of the octyloxymethyl acetal and of the *tert*-butyl ester linkages as well as cyclization to afford lactone **7** in 97% yield. A variety of conditions were screened to



**3** **4** **2**

***Scheme 1.*** Proposed construction of the E and F rings.



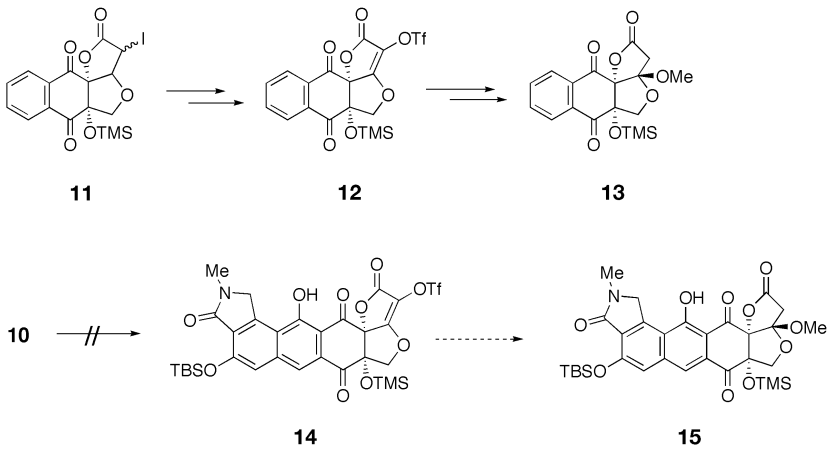
**5** **6** **7** **8** **8** **9** **10**

***Scheme 2.*** Reagents and conditions. a) 1) $OsO_4$, pyridine, THF; 2) $NaHSO_3$, 90%; b) TFA, $CH_2Cl_2$, $H_2O$, 97%; c) TBSOTf, 2,6-lutidine, 73%. d) LDA, TMSCl, NIS, THF, −78°C, 61%; e) $Cs_2CO_3$, THF, 83%; f) $BBr_3$, $CH_2Cl_2$, −78°C; g) $Al_2O_3$, $CHCl_3$, 65% (two steps). TFA = trifluoroacetic acid; TBS = *tert*-butyldimethylsilyl; Tf = trifluoromethanesulfonyl; LDA = lithium diisopropylamide; TMS = trimethylsilyl; NIS = *N*-iodosuccinimide.

 © 2003 Wiley-VCH Verlag GmbH & Co. KGaA, Weinheim 

oxidize the alcohol at C3′ to the ketolactone. As was the case in our earlier model studies,[2] all attempts were unsuccessful, The inability to execute this seemingly simple operation forced recourse to new methods to install the angular methoxy function. The "C3′" alcohol was converted into its *tert*-butyldimethylsilyl ether derivative with concomitant silylation of one of the phenolic hydroxy groups to give **8**. X-ray crystallographic analysis confirmed this structure and, accordingly, the structures of the precursors throughout the project.[4]

α-Iodination of lactone **8** was achieved through initial formation of an intermediate silyl ketene acetal (not isolated), which was treated with NIS (Scheme 2). Elimination of the β-siloxy group with $Cs_2CO_3$ furnished vinyl iodide **9** in 51% yield (over two steps). Deprotection of the benzyl ether followed by stirring with weakly acidic alumina yielded tetrahydrofuran **10** in 65% yield (over two steps). The complete hexacyclic ring system of lactonamycin was now in place as a mixture of iodo diastereomers. Interestingly, no intramolecular Michael addition occurs without the activation of the double bond by the iodide substituent.



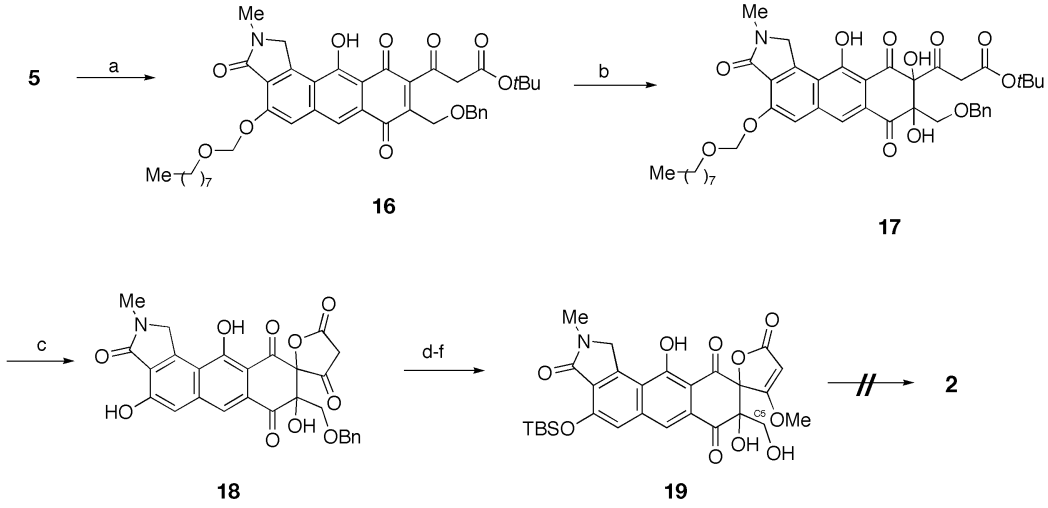

***Scheme 3.*** Failure to adapt model studies **11**→**12**→**13** to **10**→**14**→**15**.

The total synthesis project now appeared to be almost complete. In our model studies, compound **11** had been converted into **13** through methanolysis of the strained double bond of vinyl triflate **12** (Scheme 3).[2] However, various attempts to adapt this chemistry to the case of **10** were unsuccessful. Without presently describing all these initiatives in detail, the overriding difficulty was our inability, in the hexacyclic series, to generate a junction olefin (as in **14**).

Given that the oxidation of the alcohol at C3′ was apparently not feasible at the stage of lactone **7**, it became difficult to install the angular methoxy functional group. It was decided to try to oxidize quinone **5** to the unstable ketoquinone **16** (Scheme 4). Accordingly, the oxidation was conducted with Dess–Martin periodinane[5] at the stage of **5** to afford **16** in 96% yield. Dihydroxylation was now difficult, reflecting electronic depletion of the quinone by the proximal acyl group. However, the transformation was accomplished by using osmium tetroxide coordinated to TMEDA.[6] Reductive cleavage of the osmate ester afforded **17** in 77% yield.

Treatment of **17** with TFA did indeed give rise to ketolactone **18** (along with variable amounts of the decarboxylated product of **18**). Unfortunately, we were unable to cleave the benzyl ether of the labile ketolactone **18**, which was required to trigger the proposed hemiacetal formation. It was found that **18** could be converted into its methyl enol ether **19** (22% over two steps).[7,8] With the added robustness of the vinylogous carbonate ensemble, came the ability to cleave the benzyl ether (see **19**). Unfortunately, all attempts at intramolecular conjugate addition, which would have delivered **2**, failed. Essentially, the vinylogous carbonate double bond in **19** had resisted Michael addition by the now liberated hydroxy group at C5. In fact, methyl tetronate is apparently rather inert to 1,4-additions under acidic conditions.[9]

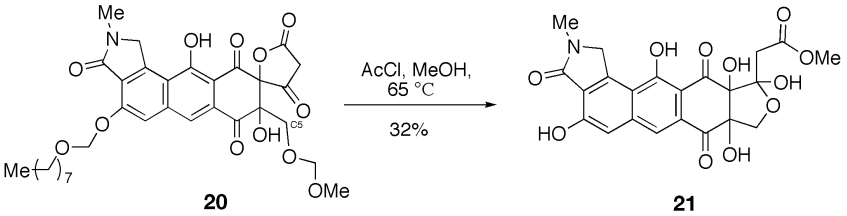
Given the nonreactivity of methyl enol ether **19**, we revisited the ketolactone concept (see **4**). The main stumbling




***Scheme 4.*** Reagents and conditions. a) Dess–Martin periodinane, $CH_2Cl_2$, 96%; b) 1) $OsO_4$, TMEDA, $CH_2Cl_2$, 2) HCl (1 N), $NaHSO_3$, THF, 77%; c) TFA/$CH_2Cl_2$, 20–55%; d) TBSOTf, 2,6-lutidine, −78 °C, $CH_2Cl_2$; e) $TMSCHN_2$, DIPEA, MeCN/$CH_2Cl_2$, 22% (two steps); f) $BBr_3$, $CH_2Cl_2$, −78 °C, 95%. TMEDA = *N*,*N*,*N*′,*N*′-tetramethylethylenediamine; DIPEA = *N*,*N*-diisopropylethylamine.

 © 2003 Wiley-VCH Verlag GmbH & Co. KGaA, Weinheim 

block in obtaining the ketolactone with a free hydroxy group at C5 had been our inability to remove the benzyl ether with the ketolactone moiety in place. As we were unable to deprotect the alcohol from its benzyl ether, it would be necessary to have the latent hydroxy group at C5 protected in an acid-labile form (**20**). Accordingly, in this connection, following protocols very similar to those described above and previously,[1] compound **20**, which contains the acid-labile MOM group on the C5 alcohol, was synthesized. Treatment of this compound with acid did indeed result in liberation of the primary alcohol by cleavage of its protecting group. However, instead of prompting cyclization to lactonamycinone (**2**), the principal product of treatment of **20** with acid in methanol was **21** (Scheme 5). Thus, the hemiacetal cyclization step that we sought had occurred, but was accompanied by opening of the lactone ring. We

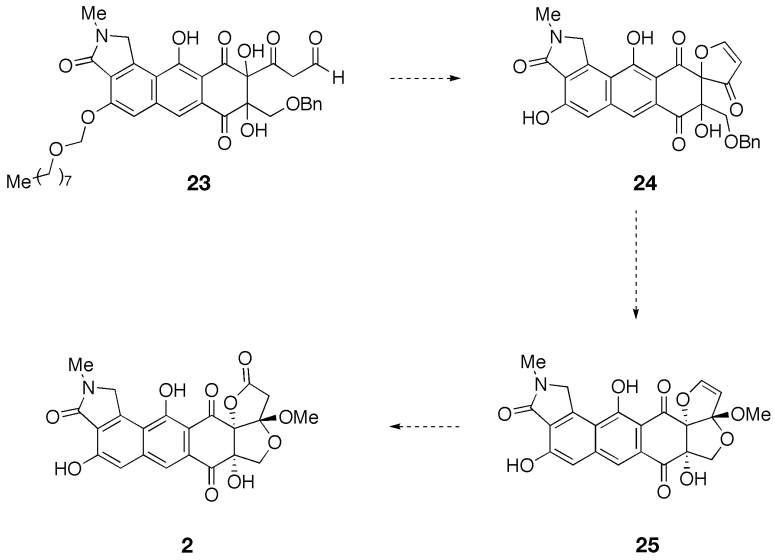



***Scheme 5.*** Failed attempt at lactonamycinone.

cannot speak rigorously as to the timing of these events, but preliminary experiments suggest that lactone degradation precedes hemiacetal formation.

At this point, a new approach was needed to overcome the limitations encountered in the previous routes. In compound **10**, the hexacyclic ring system had been reached; however, all efforts to introduce the angular methoxy were unsuccessful. Methyl enol ether **19** contains the required methoxy functional group and the correct oxidation state at C3′, but the cyclization of the E ring did not occur, apparently due to the stable nature of the vinylogous system. Ketolactone **20** contains the functionality to cyclize the E ring with the addition of the angular methoxy group, but the lactone moiety is vulnerable to the harshly acidic conditions of the cyclization reaction.

The key departure in our new approach was the presentation of the F ring as a vinylogous butenolide **24** (Scheme 6). Given the instability of ketolactone **20**, it was hoped that the stable, structurally simpler vinylogous butenolide could function as a more durable surrogate. Moreover, since decarboxylation was a serious problem in reaching the lactone, the vinylogous butenolide would prove to be more amenable to a straightforward construction of the F ring. The hope was that methanol-induced cyclization would lead to **25**. Conversion of **25** into **2** should be straightforward, even though the oxidation state would require adjustment.




***Scheme 6.*** Proposed new strategy to form the E and F rings.

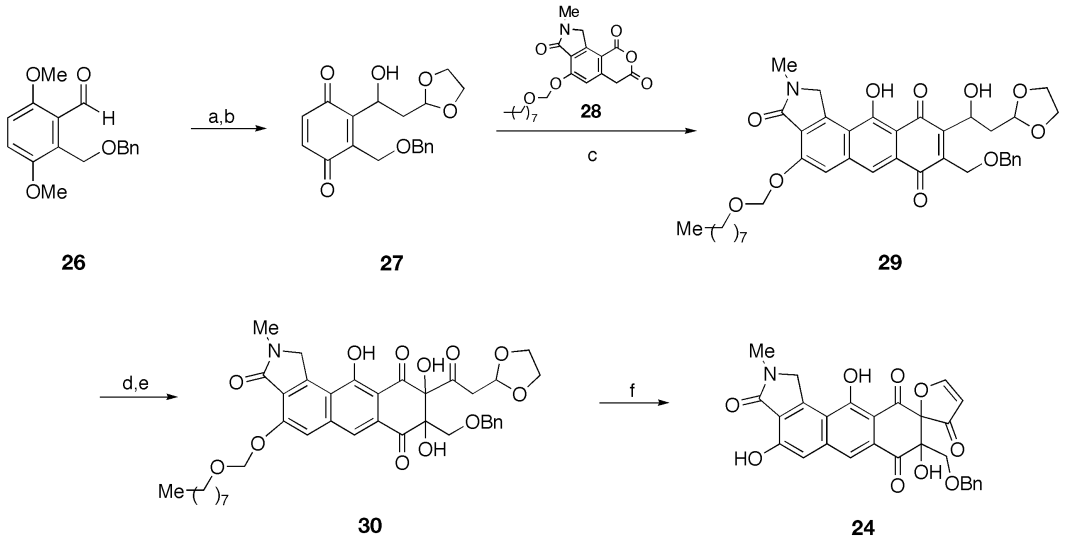
Our campaign commenced with the addition of (1,3-dioxolan-2-ylmethyl)magnesium bromide[10] to aldehyde **26**[1] followed by oxidation to produce quinone **27** in 55% yield over two steps (Scheme 7). As described earlier, the strategic alcohol function at the future C3′ in **27** directed the Tamura reaction with the previously described homophthalic anhydride **28**,[1] thereby affording **29** in 42% yield. Subsequent oxidation followed by dihydroxylation afforded **30** (89%, two steps). With diol **30** in hand, treatment with aqueous HCl (3N) led to deprotection of the octyloxymethyl ether with concomitant intramolecular attack of the tertiary alcohol at the proximal acetal to afford butenolide **24** in 82% yield.

Deprotection of the benzyloxy ether produced the pivotal intermediate **31** (Scheme 8). Gratifyingly, when this compound was heated at reflux with HCl/dioxane/methanol, acetal **32** was obtained in 51% yield (over two steps, based on recovered starting material). Hydrolysis of **32** gave rise to an anomeric mixture of lactols in quantitative yield, with the C3′ methoxy group intact.

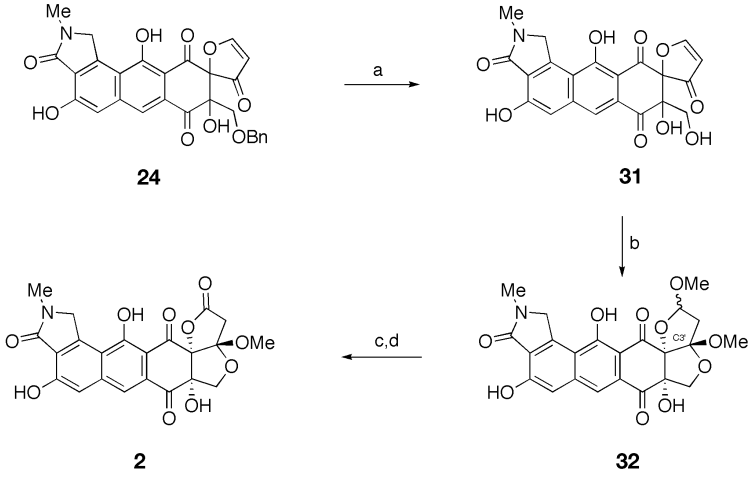
During the planning stages of the new strategy, the task of oxidizing a lactol to a lactone seemed straightforward. Unfortunately, what had initially been anticipated to be an uneventful oxidation turned out to be anything but routine. After a systematic survey of many oxidants, it was discovered that only TEMPO[11]-mediated oxidation was able to complete the transformation to lactonamycinone (**2**) (58% yield). The $^{1}H$ and $^{13}C$ NMR spectra of the synthetic aglycone of lactonamycin were similar to those of the natural product, lactonamycin, which bears the carbohydrate attachment.[12] Conclusive comparison data came from the identical NMR spectra of synthetic peracetylated lactonamycinone **33** and naturally derived peracetylated lactonamycinone, kindly provided by Tekeuchi and co-workers.

In the total synthesis of lactonamycinone, it was found that there was considerable kinetic resistance to fashioning a

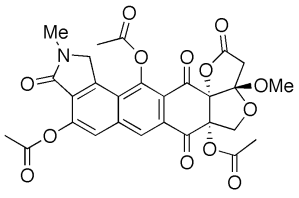
 © 2003 Wiley-VCH Verlag GmbH & Co. KGaA, Weinheim 




***Scheme 7.*** Reagents and conditions. a) (1,3-dioxolan-2-ylmethyl)-magnesium bromide, LiBr, THF, reflux, 69%; b) CAN, 0°C, $CH_3CN/H_2O$ (1:1), 80%; c) NaH, **28**,[1] THF, 42%; d) Dess–Martin periodinane, $CH_2Cl_2$, quantitative; e) 1) $OsO_4$, TMEDA, $CH_2Cl_2$, 2) HCl (1 N), $NaHSO_3$, THF, 89%; f) HCl (3 N), acetone/THF, reflux, 82% (based on recovered starting material).




***Scheme 8.*** Reagents and conditions. a) $BBr_3$, $CH_2Cl_2$, −78°C, b) HCl (4.0 N), dioxane/MeOH, 65°C, 51% (two steps, based on recovered starting material); c) HCl (1 N)/THF, quantitative yield; d) TEMPO, $PhI(OAc)_2$, $CH_2Cl_2$, 58%.
TEMPO = 2,2,6,6 tetramethyl-1-piperidinyloxy free radical.




full hexacyclic system by closure of the tetrahydrofuran E ring at C3′ in a reversible reaction. A dihydrofuranone was used to overcome this problem. This allowed us to craft a setting for closure, by which concurrent methanolysis at C3′ caps the reaction in the "forward" sense (see formation of compound **32**). Clearly, there is much still to be learnt about the origins of the resistance to formation of this hexacyclic array at the ring F lactone level of oxidation.

It is tempting to conjecture that, with such understanding, could come valuable insight into the role of this novel ring system in the biological function of the antibiotic itself. Although some yield issues must be overcome,[1] and a scheme for an enantiocontrolled synthesis implemented, the conciseness of the present synthesis will be of great advantage in dealing with these problems.

As we address these challenges, we also plan to generalize the concept of using proximal intramolecular catalytic devices to differentiate closely balanced functional groups.[1] The ability to distinguish between cognate functions in a multifunctional setting is surely one of the continuing challenges of organic synthesis.

Received: August 7, 2003 [Z52592]

**Keywords:** antibiotics · Diels–Alder reaction · natural products · quinones · total synthesis

[1] C. D. Cox, T. Siu, S. J. Danishefsky, *Angew. Chem.* **2003**, *115*, 5783–5787; *Angew. Chem. Int. Ed.* **2003**, *42*, 5625–5629.
[2] a) C. Cox, S. J. Danishefsky, *Org. Lett.* **2000**, *2*, 3493–3496; b) C. Cox, S. J. Danishefsky, *Org. Lett.* **2001**, *3*, 2899–2902.
[3] a) J. K. Cha, W. J. Christ, Y. Kishi, *Tetrahedron Lett.* **1983**, *24*, 3943; b) W. J. Christ, J. K. Cha, Y. Kishi, *Tetrahedron Lett.* **1983**, *24*, 3947c) J. K. Cha, W. J. Christ, Y. Kishi, *Tetrahedron* **1984**, *40*, 2247.
[4] CCDC-216742 (**8**) contains the supplementary crystallographic data for this paper. These data can be obtained free of charge via www.ccdc.cam.ac.uk/conts/retrieving.html (or from the Cam-

 © 2003 Wiley-VCH Verlag GmbH & Co. KGaA, Weinheim 

bridge Crystallographic Data Centre, 12, Union Road, Cambridge CB21EZ, UK; fax: (+44) 1223-336-033; or deposit@ccdc.cam.ac.uk).
[5] D. B. Dess, J. C. Martin, *J. Am. Chem. Soc.* **1991**, *113*, 7277–7287.
[6] E. J. Corey, S. Sarshar, M. D. Azimioara, R. C. Newbold, M. C. Noe, *J. Am. Chem. Soc.* **1996**, *118*, 7851.
[7] T. Aoyama, S. Terasawa, K. Sudo, T. Shioiri, *Chem. Pharm. Bull.* **1984**, *32*, 3759.
[8] Intermediate **19** was assigned as the methyl tetronate as opposed to the ketene acetal by comparison with related systems in the literature: W. R. Roush, B. B. Brown, *J. Org. Chem.* **1993**, *58*, 2162, and references therein.
[9] A. Bertucco, J. Brennan, M. Fachini, S. Kliage, P. J. Murphy, F. Pasutto, R. Signorini, H. L. Williams, *Tetrahedron* **1994**, *50*, 8237.
[10] M. Schmeichel, H. Redlich, *Synthesis* **1996**, *8*, 1002–1006.
[11] A. De Mico, R. Margarita, L. Parlanti, A. Vescovi, G. Piancatelli, *J. Org. Chem.* **1997**, *62*, 6974.
[12] The spectra of lactonamycin and its aglycone are quite similar, except for the protons from the glycoside and one of the protons at C5, whose signal differs by 0.2 ppm presumably due to the perturbation of the glycoside.

 © 2003 Wiley-VCH Verlag GmbH & Co. KGaA, Weinheim 

Functional Proteomics

# Affinity-Based Tagging of Protein Families with Reversible Inhibitors: A Concept for Functional Proteomics**

*Miriam C. Hagenstein, Jan H. Mussgnug, Kirsten Lotte, Regina Plessow, Andreas Brockhinke, Olaf Kruse,* and Norbert Sewald**

*Dedicated to Professor Hans-Dieter Jakubke on the occasion of his 70th birthday*

Proteomics, one of the most powerful techniques of the postgenomic era, relies on the two-dimensional separation of proteins.[1] However, as more than 10000 different proteins are usually expressed by a cell at the same time, resolution often remains incomplete. Sensitive detection and quantification represent further problems, because conventional staining methods are nonselective and sometimes difficult to reproduce. Detection methods with fluorescent dyes are highly sensitive, but quantification is problematic, because the dye is covalently linked to the proteins in an unselective manner prior to the separation step. Uniform labeling is not possible, and extensive labeling may lead to fluorescence quenching and solubility problems.[2] Consequently, selective labeling with reporter groups (e.g. fluorescent labels, radioactive tags, or biotin) on a mechanistic basis is desirable.

Selective labeling is possible when the reporter groups are conjugated to irreversible enzyme inhibitors and, hence, form covalent links to enzymes in the course of the enzyme reaction. Activity-based profiling has proven to be amenable for serine proteases with fluorophosphonates[3] and cysteine proteases with epoxides[4] as the irreversible inhibitors (Figure 1a). This intriguing concept suffers from the fact that irreversible enzyme inhibitors are required, which severely limits its applicability as irreversibly binding ligands are not known for many classes of proteins. As separation of protein mixtures by 2D-PAGE (2D polyacrylamide gel electrophoresis) usually involves denaturing conditions, the vast majority of protein families can only be addressed by substantial modification of this approach.

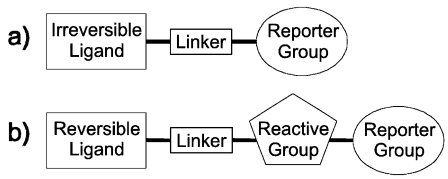



***Figure 1.*** Mechanism-based tagging of proteins with a) irreversible and b) reversible inhibitors.

We have rendered this strategy generally applicable for protein profiling in proteomics. As a covalent bond between the proteins and the reporter group is necessary to prevent dissociation under the conditions of 2D electrophoresis, an additional chemical step is required. Only a few chemical reactions are appropriate for this kind of protein modification; among them are photoreactions, which are well-known in biochemistry and widely used for photoaffinity labeling.[5] An engineered chemical probe was designed on this basis, comprising a (semi-)specific, reversibly binding protein ligand (inhibitor) linked to a reporter group and a reactive group (photoaffinity label) (Figure 1b). This concept is suited for many different classes of proteins and may facilitate the discovery of new members of a protein family. Any method capable of decreasing the amount of data and detecting mechanistically related proteins in 1D- or 2D-PAGE will be helpful for the retrieval of hitherto unknown proteins and for the future development of proteome research. To prove the principle of our concept, the class of isoquinolinesulfonamides of the H series (H-8, H-9, etc.)[6] was envisaged as the first model inhibitors.

Isoquinolinesulfonamides competitively inhibit a broad range of kinases, including protein kinases, by occupying the ATP-binding sites. Kinases play a major role in many regulatory mechanisms of living cells. Phosphorylation/dephosphorylation reactions trigger important metabolic or pathologic pathways and participate in internal and external adaptation mechanisms. Recent advances in protein kinase research rely on systematic analyses of completely sequenced genomes, but the correlation between genome and proteome remains difficult.

Our initial experiments are directed towards the detection of plant kinases. Despite the progress in understanding detailed functions of plant protein kinases, it is still very difficult to assign the vast amount of recently identified kinase genes by systematic genomics. Serine/threonine kinases can be divided into more than twelve groups based on the sequence relationships and are of special interest in plants. In particular, chloroplasts are reported to contain several serine/threonine kinases that are functionally involved in adaptation mechanisms as biological responses to changes in environmental conditions (e.g. light).[7–9] The sensitivity of protein

[*] Prof. Dr. N. Sewald, Dipl.-Chem. M. C. Hagenstein
Department of Chemistry, Organic and Bioorganic Chemistry
University of Bielefeld
Universitätsstrasse 25, 33615 Bielefeld (Germany)
Fax: (+49) 521-106-8094
E-mail: norbert.sewald@uni-bielefeld.de
Dr. O. Kruse, Dipl.-Biol. J. H. Mussgnug
Department of Biology, Molecular Cell Physiology
University of Bielefeld
Universitätsstrasse 25, 33615 Bielefeld (Germany)
Fax: (+49) 521-106-6410
E-mail: olaf.kruse@uni-bielefeld.de
Dipl.-Chem. K. Lotte, Dipl.-Chem. R. Plessow, Dr. A. Brockhinke
Department of Chemistry, Physical Chemistry
University of Bielefeld
Universitätsstrasse 25, 33615 Bielefeld (Germany)

[**] This project was supported by the University of Bielefeld and the Fonds der Chemischen Industrie. The authors thank Professor Dr. J. Mattay for providing access to photochemical equipment, Dr. K. Niehaus and N. Kuepper for MALDI TOF MS analysis, Dr. M. Letzel for ESIMS analysis, and Dr. K. Stembera for helpful discussions regarding SPR analysis.

Supporting information for this article is available on the WWW under http://www.angewandte.org or from the author.

 DOI: 10.1002/anie.200352084 © 2003 Wiley-VCH Verlag GmbH & Co. KGaA, Weinheim 

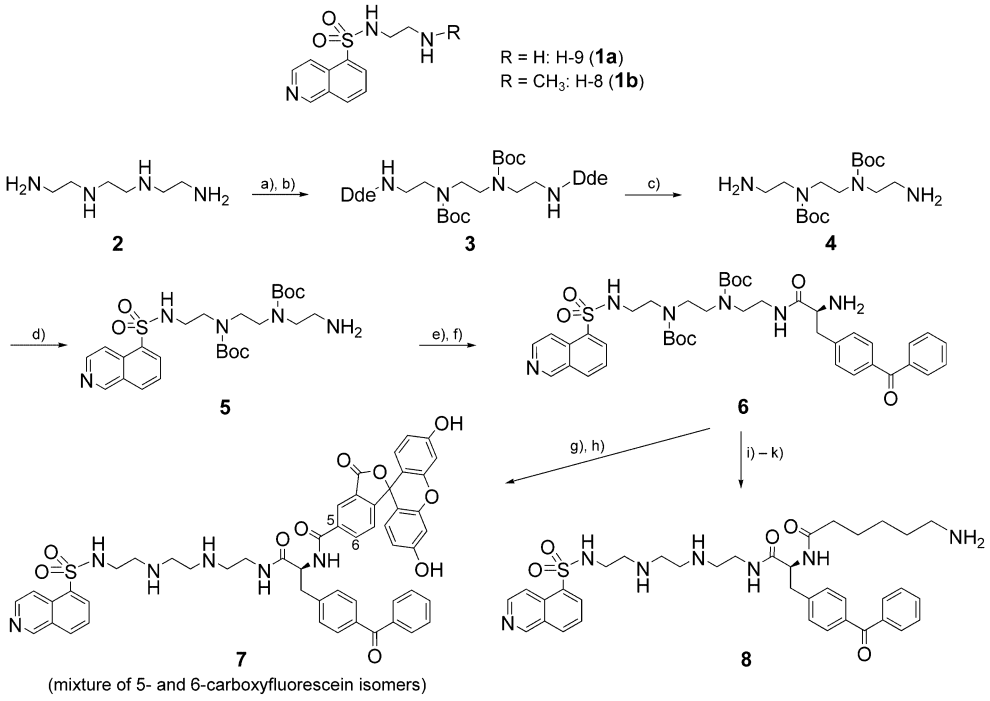
phosphorylation of the light-harvesting proteins (LHC) and photosystem II proteins to inhibitors of kinase C and cAMP-dependent kinases has been described.[10,11] The isoquinolinesulfonamide-type inhibitor H-9 (**1a**)[12] inhibits the phosphorylation of LHCII proteins at concentrations of about 50–100 μM, presumably by interacting with the ATP-binding site of membrane-associated threonine kinases. No unambiguous proof of a kinase in *Chlamydomonas reinhardtii* thylakoid membranes existed before a kinase that is assumed to be involved in LHC phosphorylation was identified only recently by a genome-based approach.[13]

The conjugate **7**, which consists of H-9 with a polar linker, a photoreactive group, and a fluorophore, was designed as an engineered chemical probe to identify kinases after covalent tagging and protein separation by SDS-PAGE (SDS = sodium dodecyl sulfate). The linker attachment was chosen on the basis of the crystal structure of a protein kinase–inhibitor complex (with H-8, **1b**) in such a way that inhibitor binding would only be minimally affected by the conjugation.[14] 4-Benzoylphenylalanine was selected as the photoreactive group, because it can be activated reversibly by excitation–relaxation cycles, and the triplet state exclusively inserts into C–H bonds within a 3.1-Å distance of the oxygen atom of the carbonyl group. It is stable in common protic solvents and leads to efficient single-site modification.[5]

The synthesis of **7** starts with protection of the primary amino groups in **2** with Dde (Scheme 1). Protection of the secondary amino functions with a Boc group gives the orthogonally protected linker **3**. Hydrazinolysis of the Dde groups yields **4**, which reacts with 5-isoquinolinesulfonyl chloride to give **5**. The isoquinolinesulfonamide **5** is then coupled to Fmoc-protected L-4-benzoylphenylalanine (Fmoc-Bpa-OH). The free amine **6** is obtained by cleavage of the Fmoc group and then coupled to the isomeric mixture of 5- and 6-carboxyfluorescein. Any other dye or any other reporter group can be used. In the final step, the Boc groups are removed to yield the target molecule **7**.

The kinase-binding ability of modified H-9 **7** was proved by surface plasmon resonance experiments (Figure 2). The conjugate **8**, an immobilizable analogue of **7** (Scheme 1), was synthesized by coupling **6** to Fmoc-6-aminohexanoic acid, followed by complete deprotection.

It was proven that protein kinase A (PKA) and creatine kinase[15] bind in a concentration-dependent manner (Figure 2a). Binding could be reduced or even totally eliminated by preincubation of the corresponding protein with a series of soluble ligands such as H-9 (**1a**; Figure 2b), **7**, and **8**.[15] These experiments clearly prove that conjugation of H-9 (**1a**) with Bpa and reporter groups does not significantly affect binding to the model kinases. The $K_D$ value for the interaction of PKA with immobilized **8**[16] was calculated to be $(2\pm3)\times10^{-7}$ M, which is similar to the $K_D$ value reported for **1a** and PKA ($1.9\times10^{-6}$ M).[12] Moreover, unspecific binding of a series of non-kinase proteins (hemoglobin, ovalbumin, bovine serum




***Scheme 1.*** Synthesis of the chemical probe **7**, which comprises the kinase inhibitor moiety H-9 (**1a**), the photoreactive group 4-benzoylphenylalanine, and the fluorescent reporter group 5-/6-carboxyfluorescein. Conjugate **8** is a derivative of **7** that can be immobilized to surfaces, for example, on a surface plasmon resonance sensor chip. Reagents and Conditions: a) 2-acetyldimedone, DMF, 74%; b) $Boc_2O$, $CH_2Cl_2$, 89%; c) $N_2H_4\cdot H_2O$, $CH_2Cl_2$, 45%; d) 5-isoquinolinesulfonyl chloride·HCl, $NEt_3$, $CHCl_3$, 63%; e) EDC·HCl, NMM, Fmoc-Bpa-OH, $HOBt\cdot H_2O$, $CH_2Cl_2$, 68%; f) 4-(aminomethyl)piperidine, $CH_2Cl_2$, 85%; g) EDC·HCl, NMM, 5-/6-carboxyfluorescein (isomeric mixture), $HOBt\cdot H_2O$, $CH_2Cl_2$/DMF (1:1), 45%; h) TFA (30% in $CH_2Cl_2$), 99%; i) EDC·HCl, NMM, Fmoc-6-aminohexanoic acid, $HOBt\cdot H_2O$, $CH_2Cl_2$, 52%; j) 4-(aminomethyl)piperidine, $CH_2Cl_2$, 92%; k) TFA (30% in $CH_2Cl_2$), 98%. Dde = 2-(4,4-dimethyl-2,6-dioxocyclohexylidene)ethyl; DMF = *N*,*N*-dimethylformamide, Boc = *tert*-butoxycarbonyl, EDC = 1-ethyl-3-(3-dimethylaminopropyl)carbodiimide, NMM = *N*-methylmorpholine, Fmoc = 9-fluorenylmethyloxycarbonyl, HOBt = 1-hydroxy-1*H*-benzotriazole.

 © 2003 Wiley-VCH Verlag GmbH & Co. KGaA, Weinheim 

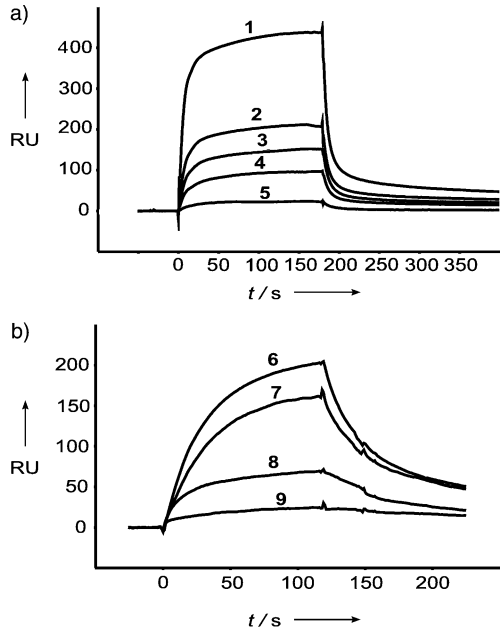



***Figure 2.*** Surface plasmon resonance sensorgrams: a) concentration-dependent binding of cAMP-dependent protein kinase A (PKA) to immobilized **8**: 1) 120 nM, 2) 60 nM, 3) 30 nM, 4) 15 nM, 5) 7.5 nM; $K_D = (2 \pm 3) \times 10^{-7}$ M. b) Competition with H-9 (**1a**): 6) 24 nM PKA, 7) 24 nM PKA+19 nM H-9, 8) 24 nM PKA+184 nM H-9, 9) 24 nM PKA+1.85 μM H-9. RU = Response Unit.

albumin, and α-glucosidase) to immobilized **8** was shown to be negligible.

Excitation–emission spectroscopy (EES) was used to study the effects of potential radiation-free fluorescence resonance energy transfer (FRET) in **7**, particularly between the benzophenone triplet state and the neighboring fluorescein.[15,17] We found the fluorescence quantum yield to be very low for both **1a** and 4-benzoylphenylalanine ($\Phi_{Fl} \approx 10^{-4}$).

By comparing normalized emission spectra of **7** and of the analogous compound without a photoreactive group, no significant FRET could be found at $\lambda_{exc} = 350$ nm ($\Phi_{FRET} \leqslant 10^{-2}$). Energy transfer between H-9 and fluorescein was found to be negligible in all cases ($\Phi_{FRET} \leqslant 10^{-4}$). Therefore, quenching and chemical reactions are the dominant channels of loss after photoactivation at this wavelength.

In the next step, purified proteins were used for tagging experiments with **7**. Four commercially available kinases were compared to prove the specificity of the photoaffinity labeling with the photoreactive and fluorescent inhibitor **7**. Three kinases (Figure 3, lanes 1, 2, and 4) were fluorescently tagged by photoaffinity labeling with **7** to a high extent, whereas the fourth (Figure 3, lane 3), although present in a higher concentration, exhibited a very low binding tendency for **7**. The specificity of photoaffinity labeling of a particular kinase is highlighted by the fact that in the case of the hexokinase and the cAMP-dependent protein kinase A assays, only the catalytic unit is tagged, whereas the regulatory unit remains unlabeled.

To prove the feasibility of our concept for the affinity-based identification of putative kinases, creatine kinase was treated with SDS prior to incubation and photoreaction with **7**

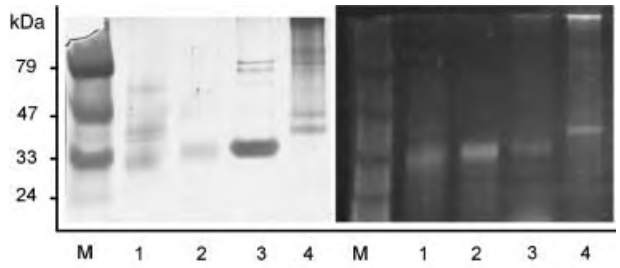



***Figure 3.*** Specific photoaffinity labeling of different kinases with the H-9 derivative **7**. Left: silver stain; right: fluorescence image. M: prestained protein marker; Lane 1: hexokinase; lane 2: creatine kinase; lane 3: 3PGA phosphokinase; lane 4: cAMP-dependent protein kinase A.

(Figure 4A, lanes 2 and 4). The drastic decrease in fluorescence of this preincubated preparation (Figure 4A, lane 4) relative to the reference sample (Figure 4A, lane 3) clearly demonstrates that photoaffinity labeling with **7** occurs specifically, as the SDS-denatured protein was not tagged.

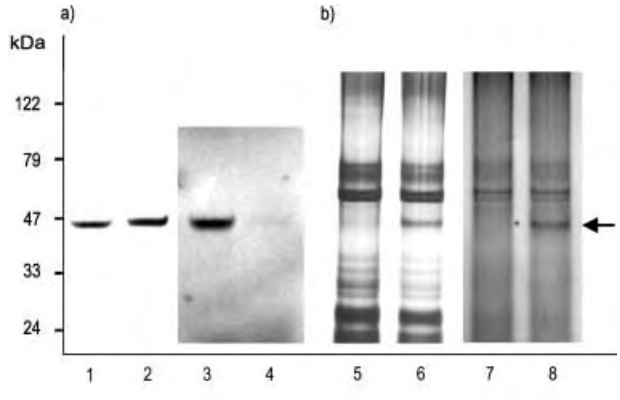



***Figure 4.*** Selective kinase tagging by photoaffinity labeling with derivative **7**. a) Comparison of photoaffinity labeling efficiency of native creatine kinase with labeling of denatured creatine kinase. Lane 1: silver stain, native creatine kinase; Lane 2: silver stain, denatured creatine kinase; Lane 3: fluorescence image, native creatine kinase; Lane 4: fluorescence image, denatured creatine kinase. b) Retrieval of added creatine kinase from thylakoid membrane preparations after photoaffinity labeling. Lane 5: silver stain; Lane 6: silver stain, with additional 150 ng creatine kinase; Lane 7: fluorescence image; Lane 8: fluorescence image, with additional 150 ng creatine kinase (see arrow).

In a second approach creatine kinase was added to isolated thylakoid proteins prior to labeling with **7**. The results demonstrate that the H-9 derivative **7** targeted several thylakoid membrane proteins predominantly in a molecular mass range between 40 and 80 kDa (Figure 4B, lane 7). The creatine kinase that was added to the thylakoid membrane preparation could be found again (Figure 4B, lane 8). The subsequent identification of the labeled protein band at 45 kDa by MALDI TOF MS fingerprint analysis[15] as the supplemented creatine kinase clearly demonstrates the functionality of the tagging system in combination with mass

 © 2003 Wiley-VCH Verlag GmbH & Co. KGaA, Weinheim 

spectrometry.[18] The identification and characterization of the other labeled proteins is currently underway.

Notably, the selectivity of the labeling process with **7** is also shown by the fact that the LHC proteins (Figure 4B, proteins with molar masses $< 33$ kDa) are not labeled. To exclude the possibility that other photochemical processes (e.g. photooxidation) prevail over the desired CH insertion of the benzophenone triplet, photoaffinity control experiments with a conjugate that lacks the inhibitor moiety (linker-Bpa-carboxyfluorescein) and with carboxyfluorescein alone were carried out.[15]

In summary, the engineered chemical probe **7**, which comprises the reversibly binding protein ligand H-9, a fluorescent reporter group, and a photoreactive group, allows affinity-based tagging of kinases. Selective detection of kinases in functional proteomics is now possible. The concept is generally applicable to affinity-based tagging of proteins and will be exploited in the first instance for plastidial plant serine/threonine kinases by using new techniques[18] for thylakoid protein separation by 2D gel electrophoresis followed by isolation and further identification. The presence of basic groups in **7** may change the pI value of the protein after the tagging step. This could lead to a decoupling of tagged and untagged proteins in the isoelectric focusing domain of 2D gel electrophoresis. Further experiments to improve this shortcoming are currently in progress. However, the concept may, in its current state, be applied to the discovery of new kinases.

Received: June 10, 2003
Revised: September 15, 2003 [Z52084]

**Keywords:** fluorescent probes · inhibitors · kinases · photoaffinity labeling · proteomics

[1] F. Lottspeich, *Angew. Chem.* **1999**, *111*, 2630 – 2647; *Angew. Chem. Int. Ed.* **1999**, *38*, 2476 – 2492.
[2] *Proteome Research: Two-Dimensional Gel Electrophoresis and Identification Methods* (Ed.: T. Rabilloud), Springer, Heidelberg, **2000**.
[3] Y. Liu, M. P. Patricelli, B. F. Cravatt, *Proc. Natl. Acad. Sci. USA* **1999**, *96*, 14694 – 14699.
[4] D. Greenbaum, K. F. Medzihradszky, A. Burlingame, M. Bogyo, *Chem. Biol.* **2000**, *7*, 569 – 581.
[5] G. Dormán, G. N. Prestwich, *Trends Biotechnol.* **2000**, *18*, 64 – 77.
[6] N. Ono-Saito, I. Niki, H. Hidaka, *Pharmacol. Ther.* **1999**, *82*, 123 – 131.
[7] A. Gal, H. Zer, I. Ohad, *Physiol. Plant.* **1997**, *100*, 869 – 885.
[8] J. F. Allen, *Biochim. Biophys. Acta* **1992**, *1098*, 275 – 335.
[9] O. Kruse, *Naturwissenschaften* **2001**, *88*, 284 – 292.
[10] Z. Ishak, I. R. White, P. A. Millner, *Biochem. Soc. Trans.* **1992**, *20*, 8S.
[11] J. Farchaus, R. A. Dilley, W. A. Cramer, *Biochim. Biophys. Acta* **1985**, *809*, 17 – 26.
[12] H. Hidaka, M. Inagaki, S. Kawamoto, Y. Sasaki, *Biochemistry* **1984**, *23*, 5036 – 5041.
[13] N. Depège, S. Bellfiore, J.-D. Rochaix, *Science* **2003**, *299*, 1572 – 1575.
[14] R. A. Engh, A. Girod, V. Kinzel, R. Huber, D. Bossemeyer, *J. Biol. Chem.* **1996**, *271*, 26157 – 26164.
[15] See Supporting Information.
[16] Compound **8** was immobilized on a BIAcore CM5 sensor chip by activation of surface-bound carboxy groups with EDC/NHS. It can be assumed that amide bond formation proceeds predominantly through the primary amino group.
[17] A. Brockhinke, R. Plessow, P. Dittrich, K. Kohse-Höinghaus, *Appl. Phys. B* **2000**, *71*, 755 – 763.
[18] M. Hippler, J. Klein, A. Fink, T. Allinger, P. Hoerth, *Plant J.* **2001**, *28*, 595 – 606.

 © 2003 Wiley-VCH Verlag GmbH & Co. KGaA, Weinheim 

*Allylation Reagents*

# [3,3] Sigmatropic Rearrangement of Boron-Containing Allyl Alcohols: Synthesis of Allyl Addition Reagents**

*Jörg Pietruszka* and Niklas Schöne*

Over the past decades a major effort has been directed toward the selective formation of homoallylic alcohols by the addition of allylmetal compounds to aldehydes and ketones. Allylboron reagents have proved to be especially versatile: a closed, chairlike transition structure with the boron atom coordinated to the carbonyl oxygen atom is responsible for the highly selective transformations.[1] While auxiliary-controlled reactions are well established, the use of reagents with a stereogenic center in the position α to the boronic ester moiety (structure **1**; Figure 1) is reported less often.[2] Hoffmann et al. have developed a family of derivatives and

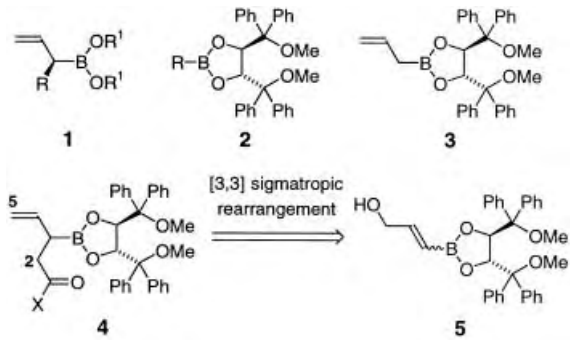



***Figure 1.*** Retrosynthesis of allylboronic esters **4**. X = OEt, $NMe_2$.

[*] Priv.-Doz. Dr. J. Pietruszka, N. Schöne
Institut für Organische Chemie
Universität Stuttgart
Pfaffenwaldring 55, 70569 Stuttgart (Germany)
Fax: (+49) 711-685-4269
E-mail: joerg.pietruszka@po.uni-stuttgart.de

[**] The authors thank the Deutsche Forschungsgemeinschaft, the Fonds der Chemischen Industrie, the Otto-Röhm-Gedächtnisstiftung, and Novartis AG for their generous support. We are grateful to Dr. Wolfgang Frey for performing the X-ray structure analysis.

Supporting information for this article is available on the WWW under http://www.angewandte.org or from the author.

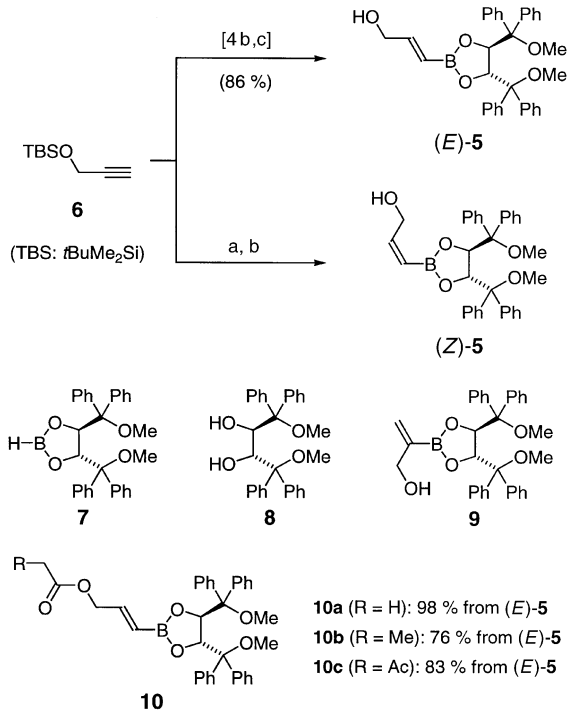
 © 2003 Wiley-VCH Verlag GmbH & Co. KGaA, Weinheim DOI: 10.1002/anie.200352210 

have demonstrated their versatility in the synthesis of complex (polypropionate-derived) natural products.[3] It was shown that a high degree of enantioselectivity can be observed, but a drawback is the problem of preparing α-chiral 2-allylboronic esters in an enantiomerically pure form. The fact that boronic esters **2**—derived from an "inverse-TADDOL"—show remarkable stability towards a variety of reaction conditions, and in addition allow the chromatographic separations of diastereoisomers,[4] started our investigation to synthesize a new type of reagent. Furthermore, since preliminary results with allylboronic ester **3** showed that the auxiliary has only a minor influence on the stereoselection,[5] it was envisaged that the allyl addition should almost exclusively be controlled by an additional stereogenic center in the α-position.

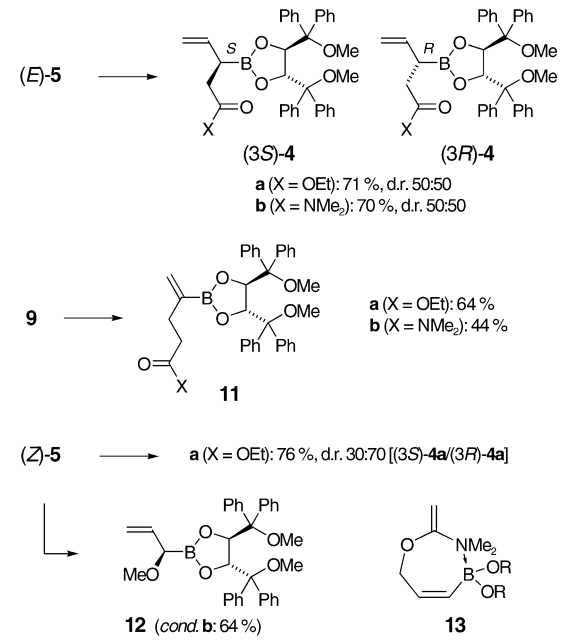
In connection with an ongoing problem in a natural product synthesis, we were especially interested in developing a method to synthesize enantiomerically pure reagents of the general type **4** (Figure 1). A simple retrosynthetic analysis of this γ,δ-unsaturated carbonyl compound revealed a possible [3,3] sigmatropic rearrangement for the conversion,[6] another key reaction in organic synthesis that has already been used for the corresponding Si or Sn derivatives.[7] However, an application to boron chemistry was not known. It is important to note that the *E*/*Z* selectivity of the reaction with boronic esters depends on the substituent in the α-position and the steric bulk of the ester, thus enabling the stereochemical course of the reaction to be directed.[8] Furthermore, our approach should easily allow the introduction of additional substituents in the 2- or 5-position of reagent **4** by altering either the reagent for the rearrangement or using a modified allyl alcohol **5**.

The starting materials are readily available from silyl-protected propargyl alcohol **6** (Scheme 1): Direct hydroboration with 1,3,2-dioxaborolane **7**—derived from the $BH_3{\cdot}SMe_2$ complex and diol **8**—yielded the allyl alcohol (*E*)-**5** after deprotection. Regioisomer **9** was also isolated as a minor by-product.[4] For the initial step in the improved synthesis of the olefin (*Z*)-**5**[4d] we followed the procedure reported by Miyaura and co-workers;[9] the consecutive transesterification with diol **8** and deprotection furnished the allyl alcohol (*Z*)-**5**. Transformation to the esters **10**—starting materials for the envisaged Claisen–Ireland or Carroll rearrangement—proceeded smoothly under standard conditions.

Initial attempts to perform rearrangements under basic conditions (as required for Claisen–Ireland or Carroll reactions) failed, no matter which variation was used. Reactions under acidic conditions were more successful: The best results were obtained by using the standard procedure under the harsh conditions of the Johnson rearrangement.[10] The allyl alcohol (*E*)-**5** reacted with triethyl orthoacetate at 135 °C in the presence of catalytic amounts of propionic acid to yield the γ,δ-unsaturated esters **4a** in 71 % yield as a 1:1 mixture of readily separable diastereoisomers (Scheme 2). Similar results were obtained with the alternative starting materials (*Z*)-**5** and **9**. Ester **11a** was isolated in 64 % yield (from **9**). The transformation of (*Z*)-**5** gave the same products as the olefin (*E*)-**5**, however, quite unexpectedly an increase of selectivity was observed [(3*S*)-**4a**:(3*R*)-**4a** 30:70, 76 % yield].




***Scheme 1.*** Synthesis of starting materials for the [3,3] sigmatropic rearrangements: a) 1. Catecholborane, cat. $[Rh(cod)Cl]_2$, $(iPr)_3P$, $Et_3N$, cyclohexane, RT; 2. **8**, RT (63 %); b) HCl, EtOH (62 %). Cod = cyclo-octa-1,5-diene.



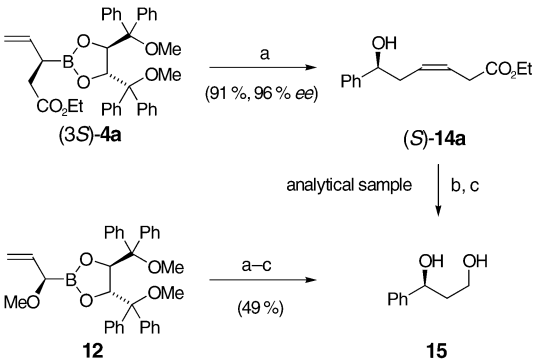

***Scheme 2.*** [3,3] Sigmatropic rearrangement of boron-containing allyl alcohols. Conditions: "**a**": $MeC(OEt)_3$, 135 °C, cat. $EtCO_2H$; "**b**": $Me(OMe)_2NMe_2$, toluene, 80 °C.

Eschenmoser rearrangements[7a,11] gave similar results: At 80 °C allyl alcohol (*E*)-**5** reacted with the orthoamide to furnish the diastereoisomeric amides **4b** (70 % yield of a 1:1 mixture, separated by medium-pressure liquid chromatogra-

 © 2003 Wiley-VCH Verlag GmbH & Co. KGaA, Weinheim 

phy (MPLC)), while compound **9** gave product **11b** in moderate yield (44%). No formation of products **4b** was detected when olefin (*Z*)-**5** was exposed to the same reaction conditions. Instead, the only compound isolated was the homoenolate equivalent **12** as a single, configurationally stable diastereoisomer. One possible explanation for this could be that an intramolecular occurred complexation through the amino group (for example, intermediate **13**) which prevented the rearrangement, but also favored the substitution by the released methanol. A similar intramolecular activation was previously observed when attempting a cyclopropanation of the olefin (*Z*)-**5**.[4d]

The absolute configuration of the new reagents was assigned after the allyl addition of pure diastereoisomer (3*S*)-**4a** (configuration determined after this sequence) to benzaldehyde (Scheme 3). Homoallyl alcohol (*S*)-**14a** was obtained




***Scheme 3.*** Assignment of absolute configuration: a) PhCHO, toluene, −100→RT; b) 1. $CH_2Cl_2$, $O_3$, −78 °C; 2. $Me_2S$, RT; c) $LiAlH_4$, THF, 0 °C. **15**: $[\alpha]_D^{20} = -70$ (*c* = 0.1 in $CHCl_3$) [ref.[13]: −70.5 (c = 1.0 in $CHCl_3$)].

in 91% yield; the enantiomeric excess was determined (ca. 96% *ee*) by the Mosher method.[12] It is important to note that the *Z*-configured olefin was formed exclusively and no traces of the diastereoisomer could be detected in the crude product. This also has important implications for the preferred transition state of the addition (see below). An analytical sample was further converted into diol **15**, and the configuration determined by comparing the optical rotation with the literature data.[13] The same sequence was used to ascertain both the configuration and diastereomeric purity of **12**.

The stereochemical assignment of the allyl addition product (*S*)-**14a** enabled the configurations of all products **4** to be deduced: In full agreement with the work of Hoffmann et al.,[8] the outcome of the reaction between benzaldehyde and (*S*)-**14a** can be explained by a favored chairlike transition state (Figure 2, left). The phenyl group would—as expected—preferentially take up an equatorial position, whereas bulky boronic ester moieties would favor the substituent α to the boron atom to be in an axial position. Indeed, this reasoning was later indirectly confirmed by an X-ray structure analysis of the second diastereoisomer (3*R*)-**4a** (Figure 2, right).[14] The configuration of amide **4b** were assigned by comparison of the NMR data as well as by an X-ray structure analysis of (3*S*)-**4b**.

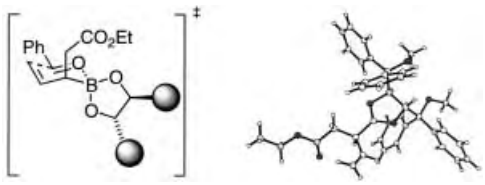



***Figure 2.*** Left: Favored transition state for the allyl addition of (3*S*)-**4a** to benzaldehyde; right: X-ray structure analysis of (3*R*)-**4a**.

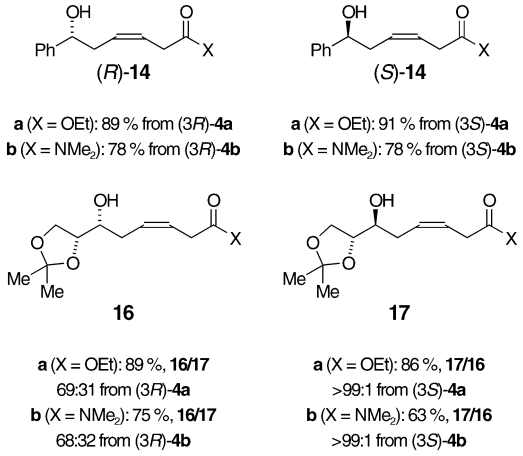



***Figure 3.*** Allyl addition products—influence of a stereogenic center in the aldehyde moiety.

In our initial studies, we applied *all* new reagents **4** to some simple allyl additions (Figure 3). It was generally shown that the reactions with benzaldehyde could be performed in good yield (78–91%) and enantiomeric excess (> 94% *ee* as determined as the Mosher ester). An attempt at a kinetic resolution by introducing a 1:1 mixture of diastereoisomers (3*S*)- and (3*R*)-**4a** (2 equiv reagent used for 1 equiv of benzaldehyde) failed: Homoallylalcohol **14** was obtained as a racemic mixture and the ratio of the recovered allylboronic esters (3*S*)- and (3*R*)-**4a** did not change. We could not observe a reagent-controlled addition when introducing aldehydes with an additional stereogenic center, for example, 2,3-*O*-isopropylidene-D-glyceraldehyde, instead a mismatched (with (*3R*)-**4** to *syn*-product **16**) and a matched (with (3*S*)-**4** to *anti*-product **17**) interaction occurred.[15] Nevertheless, the *anti* alcohols **17a**/**b** were obtained in high yield and in no case was a second diastereoisomer detected.

In conclusion, we have synthesized a new type of allyl addition reagent. For the first time, Johnson and Eschenmoser rearrangements were used to obtain enantiomerically pure allylboronic esters. The synthesis of homoenolate equivalent **12** as a single diastereoisomer in good yield from (*Z*)-**5** was an especially pleasant surprise. We unequivocally assigned the absolute configuration of all reagents by means of chemical correlation or X-ray structure analysis, and successfully performed allyl additions.

Received: June 24, 2003
Revised: September 15, 2003 [Z52210]

 © 2003 Wiley-VCH Verlag GmbH & Co. KGaA, Weinheim 

**Keywords:** allyl additions · boronic esters · rearrangements · sigmatropic reactions · stereoselectivity

[1] a) D. Hoppe in *Stereoselective Synthesis, Vol. E21*, 3rd ed (Eds.: G. Helmchen, R. W. Hoffmann, J. Mulzer, E. Schaumann), Thieme, Stuttgart, **1996**, pp. 1357 – 1409; b) W. R. Roush, in *Stereoselective Synthesis, Vol. E21*, 3rd ed (Eds.: G. Helmchen, R. W. Hoffmann, J. Mulzer, E. Schaumann), Thieme, Stuttgart, **1996**, pp. 1410 – 1486; c) S. E. Denmark, N. G. Almstead, in *Modern Carbonyl Chemistry* (Ed.: J. Otera), Wiley-VCH, Weinheim, **2000**, pp. 299 – 401; d) S. R. Chemler, W. R. Roush, in *Modern Carbonyl Chemistry* (Ed.: J. Otera), Wiley-VCH, Weinheim, **2000**, pp. 403 – 490; e) Y. Yamamoto, N. Asao, *Chem. Rev.* **1993**, *93*, 2207 – 2293.

[2] For recent publications, see a) E. M. Flamme, W. R. Roush, *J. Am. Chem. Soc.* **2002**, *124*, 13644 – 13645; b) A. Schlapbach, R. W. Hoffmann, *Eur. J. Org. Chem.* **2001**, 323 – 328; c) J. Mortier, M. Vaultier, B. Plunian, L. Toupet, *Heterocycles* **1999**, *50*, 703 – 711; d) J.-Y. Lallemand, Y. Six, L. Ricard, *Eur. J. Org. Chem.* **2002**, 503 – 513.

[3] Review: a) R. W. Hoffmann, *Pure Appl. Chem.* **1988**, *60*, 123 – 130; synthesis by Matteson homologation (D. S. Matteson, *Tetrahedron* **1998**, *54*, 10555 – 10607): b) R. W. Hoffmann, K. Ditrich, G. Köster, R. Stürmer, *Chem. Ber.* **1989**, *122*, 1783 – 1789; c) R. Stürmer, R. W. Hoffmann, *Synlett* **1990**, 759 – 761; synthesis by allylic rearrangement with $SOCl_2$: d) R. W. Hoffmann, S. Dresely, *Angew. Chem.* **1986**, *98*, 186 – 187; *Angew. Chem. Int. Ed. Engl.* **1986**, *25*, 189; e) R. W. Hoffmann, S. Dresely, *Chem. Ber.* **1989**, *122*, 903 – 909; synthesis by Diels–Alder reactions: f) M. Vaultier, F. Truchet, B. Carboni, R. W. Hoffmann, I. Denne, *Tetrahedron Lett.* **1987**, *28*, 4169 – 4172.

[4] a) J. E. A. Luithle, J. Pietruszka, *Liebigs Ann.* **1997**, 2297 – 2302; b) J. E. A. Luithle, J. Pietruszka, *J. Org. Chem.* **1999**, *64*, 8287 – 8297; c) J. E. A. Luithle, J. Pietruszka, *J. Org. Chem.* **2000**, *65*, 9194 – 9200; d) J. E. A. Luithle, J. Pietruszka, *Eur. J. Org. Chem.* **2000**, 2557 – 2562.

[5] With benzaldehyde and **3**: 30% *ee* (T. Wilhelm, J. Pietruszka, Universität Stuttgart).

[6] Recent review: U. Nubbemeyer, *Synthesis* **2003**, 961 – 1008, and references therein.

[7] Si derivatives: a) P. R. Jenkins, R. Gut, H. Wetter, A. Eschenmoser, *Helv. Chim. Acta* **1979**, *62*, 1922 – 1931; b) G. Procter, A. T. Russel, P. J. Murphy, T. S. Tan, A. N. Mather, *Tetrahedron* **1988**, *44*, 3953 – 3973; c) J. S. Panek, R. Beresis, F. Xu, M. Yang, *J. Org. Chem.* **1991**, *56*, 7341 – 7344; d) R. T. Beresis, J. S. Solomon, M. G. Yang, N. F. Jain, J. S. Panek, *Org. Synth.* **1998**, *75*, 78 – 88, and references therein; Sn derivatives: e) K. Ritter, *Tetrahedron Lett.* **1990**, *31*, 869 – 872; f) J. C. Anderson, C. A. Roberts, *Tetrahedron Lett.* **1998**, *39*, 159 – 162; g) U. Kazmaier, D. Schauß, S. Raddatz, M. Pohlmann, *Chem. Eur. J.* **2001**, *7*, 456 – 464.

[8] R. W. Hoffmann, U. Weidmann, *J. Organomet. Chem.* **1980**, *195*, 137 – 146.

[9] T. Ohmura, Y. Yamamoto, N. Miyaura, *J. Am. Chem. Soc.* **2000**, *122*, 4990 – 4991.

[10] W. S. Johnson, L. Werthemann, W. R. Bartlett, T. J. Brockson, T.-T. Li, D. J. Faulkner, M. R. Petersen, *J. Am. Chem. Soc.* **1970**, *92*, 741 – 743.

[11] a) H. Meerwein, W. Florian, N. Schön, G. Stopp, *Justus Liebigs Ann. Chem.* **1960**, *641*, 1 – 39; b) A. E. Wick, D. Felix, K. Steen, A. Eschenmoser, *Helv. Chim. Acta* **1964**, *47*, 2425 – 2429.

[12] J. A. Dale, D. L. Dull, H. S. Mosher, *J. Org. Chem.* **1969**, *34*, 2543 – 2549.

[13] N. W. Boaz, *J. Org. Chem.* **1992**, *57*, 4289 – 4292.

[14] CCDC-212769 [(3*R*)-**4a**] contains the supplementary crystallographic data for this paper. These data can be obtained free of charge via www.ccdc.cam.ac.uk/conts/retrieving.html (or from the Cambridge Crystallographic Data Centre, 12 Union Road, Cambridge CB2 1EZ, UK; fax: (+44) 1223-336-033; or deposit@ccdc.cam.ac.uk).

[15] For other investigations on matched/mismatched interactions of allyl additions to 2,3-*O*-isopropylidene-D-glyceraldehyde with boron reagents see, for example, a) I. Chataigner, J. Lebreton, F. Zammattio, J. Villiéras, *Tetrahedron Lett.* **1997**, *38*, 3719 – 3722; b) W. R. Roush, L. K. Hoong, M. A. J. Palmer, J. C. Park, *J. Org. Chem.* **1990**, *55*, 4109 – 4117; c) W. R. Roush, L. K. Hoong, M. A. J. Palmer, J. A. Straub, A. D. Palkowitz, *J. Org. Chem.* **1990**, *55*, 4117 – 4126; d) R. W. Hoffmann, B. Landmann, *Chem. Ber.* **1986**, *119*, 2013 – 2024; and references therein.

 © 2003 Wiley-VCH Verlag GmbH & Co. KGaA, Weinheim 

Group 13/15 Heterocycles

# A Versatile Metathesis Reaction for the Formation of Labile Bonds between Group 13 and Group 15 Atoms**

*Florian Thomas, Stephan Schulz,* Heidi Mansikkamäki, and Martin Nieger*

*Dedicated to Professor Peter Jutzi on the occasion of his 65th birthday*

Although Group 13/Group 15 compounds have been intensely studied for some decades, no generally applicable synthetic pathway for the formation of M–E bonds (M = Al–Tl; E = N–Bi) is known to date. Dihydrogen- and salt-elimination reactions as well as metathesis reactions with organolithium reagents are well-established methods for the formation of $M–NR_2$ and $M–PR_2$ bonds, but they are generally ineffective for the synthesis of compounds containing the heaviest Group 13/15 elements (M = In, Tl; E = Sb, Bi). To date, dehydrosilylation reactions represent the most versatile reaction pathway for the generation of this type of compound.[1] The activation energy is low, thus allowing the reaction to be performed at low temperature. Additionally, the tendency of silyl-substituted compounds of the type

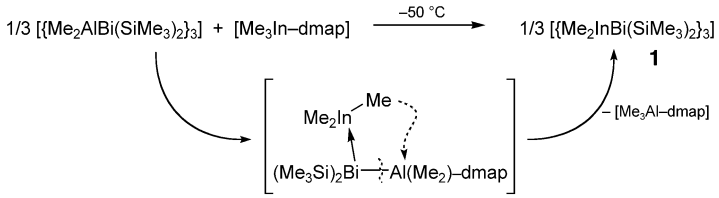
[*] Priv.-Doz. Dr. S. Schulz, Dipl.-Chem. F. Thomas, Dr. M. Nieger
Institut für Anorganische Chemie
Universität Bonn
Gerhard-Domagk-Strasse 1, 53121 Bonn (Germany)
Fax: (+49) 228-73-5327
E-mail: sschulz@uni-bonn.de
MSc H. Mansikkamäki
Department of Chemistry
University of Jyväskylä (Finland)

[**] S. Schulz gratefully acknowledges financial support by the Deutschen Forschungsgemeinschaft (DFG), the Fonds der Chemischen Industrie (FCI), the Bundesministerium für Bildung, Wissenschaft, Forschung und Technologie (BMBF), and Prof. E. Niecke, Universität Bonn. F. Thomas thanks the FCI, and H. Mansikkamäki, of the Academy of Finland for fellowship awards.

 DOI: 10.1002/anie.200352332 © 2003 Wiley-VCH Verlag GmbH & Co. KGaA, Weinheim 

$R_2ESiMe_3$ to undergo redox reactions is rather low compared to that of organolithium compounds, $R_2ELi$. Unfortunately, this reaction pathway cannot be used for the synthesis of In–E and Tl–E compounds because of the instability of the required dialkylindium hydrides $R_2InH$ and dialkylthallium hydrides $R_2TlH$.[2] Consequently, we became interested in an alternative route to Group 13/15 compounds, in particular those compounds that contain the heaviest elements of both groups. Herein, we report a new metathesis reaction, which is used for the synthesis of the previously unknown heterocycles of the type $[\{Me_2ME(SiMe_3)_2\}_x]$.

$[\{Me_2AlBi(SiMe_3)_2\}_3]$[3] reacts with the Lewis acid–base adduct $[Me_3In{-}dmap]$[4] (dmap = 4-dimethylaminopyridine) at −50 °C with the formation of $[Me_3Al{-}dmap]$ and $[Me_2InBi(SiMe_3)_2]_3$ (**1**). We believe this reaction to proceed through the cleavage of the Al–Bi heterocycle by the reaction with the strong Lewis base dmap. The subsequent coordination of $InMe_3$ results in the formation of $[dmap{-}Al(Me_2)Bi(SiMe_3)_2{-}InMe_3]$,[5] which undergoes fragmentation with Al–Bi and In–Me bond breakage to give **1** and $[Me_3Al{-}dmap]$ (Scheme 1).




***Scheme 1.*** Synthesis of the six-membered In–Bi heterocycle **1**.

Compound **1** is heat labile and sensitive towards oxygen and water. Whereas isolated **1** can be stored in the dark at −30 °C for several weeks, it decomposes in solution at temperatures above −30 °C within minutes with the formation of $Bi_2(SiMe_3)_4$, $InMe_3$, and elemental In and Bi. Consequently, NMR spectra ($^1H$, $^{13}C$) were recorded at −40 °C in [D$_8$]toluene. Both spectra show only two resonances arising from the $InMe_2$ and $SiMe_3$ groups, as observed for the corresponding AlBi[3] and GaBi heterocycles.[6] The mass spectrum of **1** only shows decomposition fragments, thus indicating the lability of **1**. Single crystals of **1** were obtained from a toluene solution at −60 °C (Figure 1). Compound **1** crystallizes in the monoclinic space group $P2_1/n$ (No. 14)[7] and is isostructural to $[\{Me_2AlBi(SiMe_3)_2\}_3]$[3] and $[\{Me_2GaBi(SiMe_3)_2\}_3]$.[6] The central structural feature of this first organometallic In–Bi compound[8] is the nonplanar six-membered $In_3Bi_3$ ring. Both the In and the Bi atoms adopt distorted tetrahedral environments, in which the average endocyclic Bi-In-Bi bond angle (101.1°) is significantly smaller than the average In-Bi-In bond angle (127.1°). The In–Bi bond lengths range from 2.903(1) to 2.935(1) Å (av 2.915 Å), which is about 0.15 Å longer than the corresponding M–Bi bond lengths in $[\{Me_2AlBi(SiMe_3)_2\}_3]$ (av 2.774 Å)[3] and $[\{Me_2GaBi(SiMe_3)_2\}_3]$ (av 2.762 Å).[6] However, this increase in bond length is less pronounced than was expected because of the increase of the covalent radii of the In atom (1.44 Å) compared to Al (1.25 Å) and Ga (1.26 Å) atoms.[9]

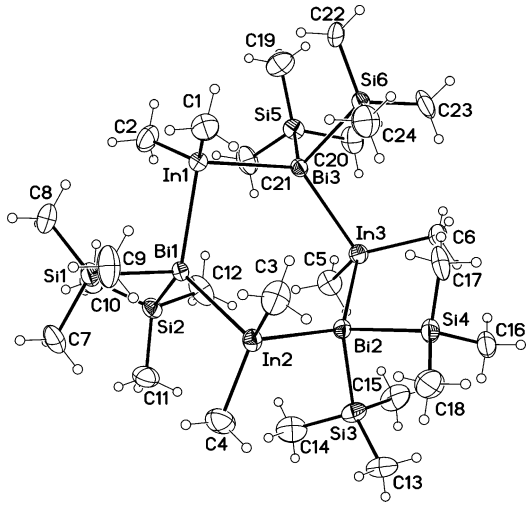
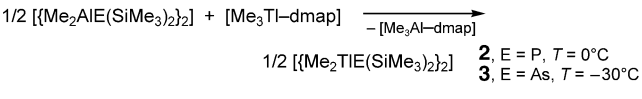



***Figure 1.*** Solid-state structure of **1**. Selected bond lengths [Å] and angles [°]: Bi1-In1 2.907(1), Bi1-In2 2.903(1), Bi2-In2 2.914(1), Bi2-In3 2.911(1), Bi3-In1 2.935(1), Bi3-In3 2.920(1), Bi1-Si1 2.628(2), Bi1-Si2 2.622(2), In1-C1 2.182(7), In1-C2 2.165(8), Bi2-Si3 2.637(2), Bi2-Si4 2.635, In2-C3 2.162(8), In2-C4 2.171(8), Bi3-Si5 2.639(2), Bi3-Si6 2.642(2), In3-C5 2.180(8), In3-C6 2.195(8); In1-Bi1-In2 123.0(1), In2-Bi2-In3 129.1(1), In1-Bi3-In3 129.2(1), Bi1-In1-Bi3 99.7(1), Bi1-In2-Bi2 99.4(1), Bi2-In3-Bi3 104.2(1), C1-In1-C2 126.9(3), Si1-Bi1-Si2 102.3(1), C3-In2-C4 125.6(3), Si3-Bi2-Si4 100.1(1), C5-In3-C6 116.6(3), Si5-Bi3-Si6 101.6(1).

Detailed studies on the reactivity of $[\{Me_2AlE(SiMe_3)_2\}_x]$ (E = P, As, Sb, Bi) towards $[Me_3M{-}dmap]$ (M = Ga, In) clearly demonstrated that the described reaction pathway is generally applicable for the formation of heterocycles of the type $[\{Me_2ME(SiMe_3)_2\}_x]$ (M = Ga, In; E = P, As, Sb, Bi).[10] The presence of the Lewis base dmap was found to be essential, as the reactivity of $[\{Me_2AlE(SiMe_3)_2\}_x]$ is significantly increased owing to the initial formation of Lewis base stabilized, monomeric $[R_2E{-}AlR_2(dmap)]$. This is also known for organolithium reagents, whose reactivity increases in the presence of donor solvents (disaggregation and formation of RLi(donor)).[11] Comparable results have been reported by Driess et al. on the reactivity of $[(iBu)_2AlPH_2]_3$, which was found to be a mild $PH_2$-transfer reagent in coordinating solvents such as THF.[12]

In an attempt to explore the synthetic potential of this new metathesis reaction, we focused our interest on the synthesis of TlE heterocycles $[\{R_2TlER'_2\}_x]$. To date, heterocycles of this type are completely unknown owing to the high oxidation potential and the low thermal resistance of $Tl^{III}$ compounds and because dialkylthallium hydrides $R_2TlH$ are not available. Our initial studies on the reactions of $[\{Me_2AlE(SiMe_3)_2\}_2]$ (E = P, As)[13] with $[Me_3Tl{-}dmap]$[4] resulted in the formation of the corresponding four-membered TlE heterocycles $[\{Me_2TlP(SiMe_3)_2\}_2]$ **2** and $[\{Me_2TlAs(SiMe_3)_2\}_2]$ **3** in good yields (Scheme 2).




***Scheme 2.*** Synthesis of the four-membered Tl–E heterocycles **2** (E = P) and **3** (E = As).

 © 2003 Wiley-VCH Verlag GmbH & Co. KGaA, Weinheim 

The presence of a triplet in the $^{31}P$ NMR spectrum of **2** with a $^{1}J_{Tl,P}$ coupling constant of 2462 Hz proves the formation of a Tl–P heterocycle.[14] The $^{1}H$ and $^{13}C$ NMR spectra of **2** and **3** each show a doublet arising from the $TlMe_2$ groups (**2**: $^{2}J_{Tl\text{-}H} = 317$ Hz, $^{1}J_{Tl\text{-}C} = 2391$ Hz; **3**: $^{2}J_{Tl\text{-}H} = 313$ Hz, $^{1}J_{Tl\text{-}C} = 2304$ Hz), whereas the $SiMe_3$ groups only show a singlet. The mass spectra of **2** and **3** do not show the molecular ion peaks. The mass spectrum of **2** shows the presence of two fragments at *m/z* 557 $[(Me_3Si)_2PTlP(SiMe_3)_2]^+$ and *m/z* 395 $[MeTlP(SiMe_3)_2]^+$) that contain a Tl–P bond, whereas the mass spectrum of **3** only shows decomposition fragments.

Crystals of **2** and **3** suitable for single-crystal X-ray diffraction analyses were obtained from solutions in toluene at −30 °C (**2**) and −60 °C (**3**) (Figure 2). Compounds **2** and **3**

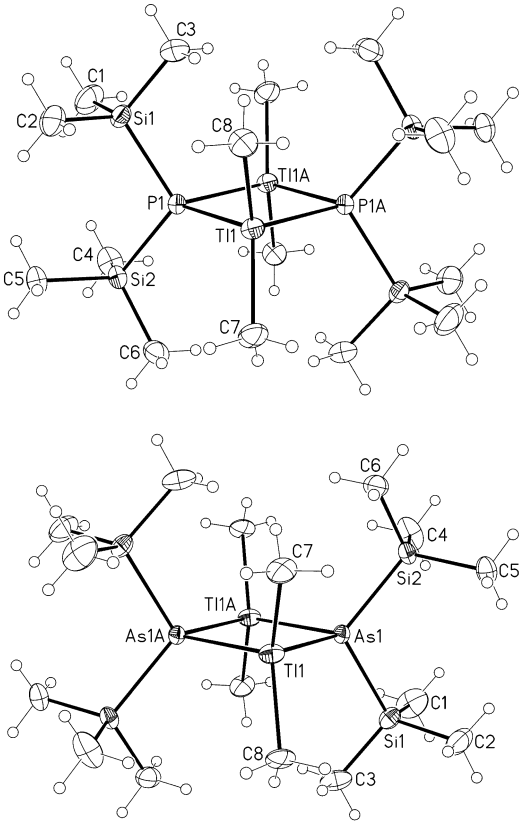



***Figure 2.*** Solid-state structures of **2** (above) and **3** (below): Selected bond lengths [Å] and angles [°]. **2**: Tl1-P1 2.695(2), Tl1-P1A 2.688(2), P1-Si1 2.246(2), P1-Si2 2.245(2), Tl1-C7 2.198(5), Tl1-C8 2.210(5); Tl1-P1-Tl1A 95.5(1), P1-Tl1-P1A 84.5(1), C7-Tl1-C8 122.3(2), Si1-P1-Si2 109.0(1). **3**: Tl1-As1 2.781(1), Tl1-As1A 2.743(1), As1-Si1 2.334(2), As1-Si2 2.338(2), Tl1-C7 2.192(6), Tl1-C8 2.202(6); Tl1-As1-Tl1A 96.7(1), As1-Tl1-As1A 83.3(1), C7-Tl1-C8 124.6(3), Si1-As1-Si2 108.5(1).

are isostructural and crystallize in the triclinic space group $P\bar{1}$ (No. 2).[15] The central structural units of **2** and **3** are the four-membered planar $Tl_2E_2$ rings. The Tl- and P- or As-atoms each adopt distorted tetrahedral environments. To date, only two Lewis acid–base adducts containing a $Tl^{III}$ center with a Tl–P bond have been structurally characterized. The Tl–P σ-bond in **2** (2.688(1), 2.695(1) Å) is significantly shorter than the dative Tl–P bond observed in the intramolecularly stabilized adduct $[Tl\{o\text{-}(Ph_2PCH_2)C_6H_4\}_3]$ (2.795 Å) as well as in $[(Me_3SiCH_2)_3Tl{-}P(SiMe_3)_3]$ (2.992 Å).[16] Compound **3** is the first organometallic compound that contains a Tl–As bond. Consequently, the Tl–As bond lengths (2.743(1), 2.781(1) Å) can only be compared with the Tl–As bond lengths in Zintl anions such as $[TaAs_4Tl_2]^{5-}$ (2.74–2.88 Å).[17] The average Tl–C bond lengths (**2**: 2.204 Å, **3**: 2.197 Å) are almost the same as those in $[Me_3Tl{-}dmap]$ (2.180 Å).[4] The endocyclic E-Tl-E bond angles are smaller than the Tl-E-Tl bond angles, as is generally observed for four-membered heterocycles of the type $[\{Me_2ME(SiMe_3)_2\}_2]$.[18] However, the differences within the thallium heterocycles **2** (P-Tl-P = 84.5(1)° versus Tl-P-Tl = 95.5(1)°) and **3** (As-Tl-As = 83.1(1)° versus Tl-As-Tl = 96.7(1)°), are significantly more pronounced than in analogous heterocycles containing the lighter elements of Group 13.

The synthesis of the heat-labile heterocycles **1**–**3** provides evidence for the preparative potential of this new synthetic pathway and extends the methods available for the formation of Group 13/Group 15 atom bonds. The driving force of the described reaction is the formation of the stable Lewis acid–base adduct $[Me_3Al{-}dmap]$. Because of the excellent reactivity of the starting Al/Group 15 atom heterocycles of the type $[\{Me_2AlE(SiMe_3)_2\}_x]$ and the mild reaction conditions (low temperature), this metathesis reaction has a promising potential for the formation of compounds containing yet unknown bonds between Group 15 atoms and atoms of other elements.

## *Experimental Section*

**1**: A suspension of $[\{Me_2AlBi(SiMe_3)_2\}_3]$ (0.41 g, 0.33 mmol) in toluene (10 mL) at −50 °C was combined with $[Me_3In{-}dmap]$ (0.28 g, 1.0 mmol) dissolved in toluene (5 mL). The resulting brownish suspension was allowed to warm to −30 °C over 30 min. Thereafter, the suspension was quickly warmed until a clear solution was formed, which was then stored at −60 °C. Colorless crystals of **1** were obtained after 24 h. Yield: 0.15 g, 0.10 mmol, 30 %. M.p. 68–73 °C (decomp). $^{1}H$ NMR (300 MHz, $[D_8]$toluene, −40 °C): $\delta = 0.62$ (s, 6H; $InMe_2$), 0.70 ppm (s, 18H; $SiMe_3$). $^{13}C\{^{1}H\}$ NMR (75 MHz, $[D_8]$toluene, −40 °C): $\delta = -1.1$ ($InMe_2$), 6.8 ppm ($SiMe_3$). MS (EI, 12 eV, 50 °C) *m/z* (%) = 428 (13) $[Bi(SiMe_3)_3]^+$, 282 (13) $[BiSiMe_3]^+$, 145 (65) $[InMe_2]^+$, 131 (100) $[Si_2Me_5]^+$, 73 (39) $[SiMe_3]^+$.

**2**: A suspension of $[\{Me_2AlP(SiMe_3)_2\}_2]$ (0.23 g 0.5 mmol) in toluene (10 mL) at 0 °C was combined with $[Me_3Tl{-}dmap]$ (0.37 g, 1.0 mmol) dissolved in toluene (5 mL). The resulting clear solution was stirred for an additional 30 min and stored at −30 °C. Colorless crystals of **2** were obtained after 24 h. Yield: 0.33 g, 0.28 mmol, 56 %. M.p. 107–111 °C (decomp). $^{1}H$ NMR (300 MHz, $C_6D_6$, 30 °C): $\delta = 0.35$ (s, 18H; $SiMe_3$), 1.00 ppm (d, $^{2}J_{Tl\text{-}H} = 317$ Hz, 6H; $TlMe_2$). $^{13}C\{^{1}H\}$ NMR (75 MHz, $C_6D_6$, 30 °C): $\delta = 5.0$ (s; $SiMe_3$), 12.8 ppm (d, $^{1}J_{Tl\text{-}C} = 2391$ Hz; $TlMe_2$). $^{31}P\{^{1}H\}$ NMR (120 MHz, $C_6D_6$, 30 °C): $\delta = -234$ ppm (t, $^{1}J_{Tl\text{-}P} = 2462$ Hz). MS (EI, 12 eV, 75 °C) *m/z* (%) = 557 (5) $[(Me_3Si)_2PTlP(SiMe_3)_2]^+$, 416 (26) $[P_4(SiMe_3)_4]^+$, 401 (100) $[P_4(SiMe_3)_3(SiMe_2)]^+$, 395 (20) $[MeTlP(SiMe_3)_2]^+$, 328 (12) $[P_4(SiMe_3)_2(SiMe_2)]^+$, 313 (24) $[P_4(SiMe_3)(SiMe_2)_2]^+$, 203 (7) $Tl^+$, 178 (36) $[HP(SiMe_3)_2]^+$, 163 (5) $[P(SiMe_3)(SiMe_2)]^+$, 73 (25) $[SiMe_3]^+$.

**3**: A suspension of $[\{Me_2AlAs(SiMe_3)_2\}_2]$ (0.28 g, 0.5 mmol) in toluene (10 mL) at −30 °C was combined with $[Me_3Tl{-}dmap]$ (0.37 g, 1.0 mmol) dissolved in toluene (5 mL). The resulting slightly brown suspension was stirred for 30 min, then warmed quickly until a clear solution was formed, and finally stored at −60 °C. Colorless crystals of **3** were obtained after 24 h. Yield: 0.29 g, 0.32 mmol, 64 %. M.p. 118–

 © 2003 Wiley-VCH Verlag GmbH & Co. KGaA, Weinheim 

121 °C (decomp, darkening above 70 °C). $^1$H NMR (300 MHz, [D$_8$]toluene, −10 °C): $\delta = 0.32$ (s, 18 H; $SiMe_3$), 0.97 ppm (d, $^2J_{Tl\text{-}H} =$ 313 Hz, 6 H; $TlMe_2$). $^{13}C\{^1H\}$ NMR (75 MHz, [D$_8$]toluene, −10 °C): $\delta = 4.3$ (s; $SiMe_3$), 12.4 ppm (d, $^1J_{Tl\text{-}C} = 2304$ Hz; $TlMe_2$). MS (EI, 12 eV, 150 °C) $m/z$ (%) = 442 (76) $[As_2(SiMe_3)_4]^+$, 354 (11) $[As_2(SiMe_3)_2(SiMe_2)]^+$, 339 (11) $[As_2(SiMe_3)(SiMe_2)_2]^+$, 294 (30) $[(As(SiMe_3)_3]^+$, 266 (61) $[As_2(SiMe_2)_2]^+$, 233 (24) $[TlMe_2]^+$, 203 (9) $Tl^+$, 131 (15) $[Si_2Me_5]^+$, 73 (100) $[SiMe_3]^+$.

Received: July 8, 2003 [Z52332]

**Keywords:** Group 13 elements · Group 15 elements · heterocycles · main group element · metathesis

[1] See the following and references in: S. Schulz, *Struct. Bonding (Berlin)* **2002**, *103*, 117.
[2] Several indium hydrides have been synthesized within the last decade, whereas to the best of our knowledge molecular thallium hydrides are unknown to date. S. Aldridge, A. J. Downs, *Chem. Rev.* **2001**, *101*, 3305.
[3] S. Schulz, M. Nieger, *Angew. Chem.* **1999**, *111*, 1020; *Angew. Chem. Int. Ed.* **1999**, *38*, 967.
[4] F. Thomas, T. Bauer, S. Schulz, M. Nieger, *Z. Anorg. Allg. Chem.* **2003**, *629*, 2018.
[5] Detailed studies on the reaction of base-stabilized compounds of the type [dmap−Al(Me$_2$)E(SiMe$_3$)$_2$] (E = P, Sb) with MMe$_3$ (M = Al, Ga, In) demonstrate the initial formation of the corresponding adducts [dmap−Al(Me$_2$)E(SiMe$_3$)$_2$−MR$_3$], which consequently undergo Al−E bond breakage and M−E bond formation reactions. F. Thomas, S. Schulz, M. Nieger, *Organometallics* **2003**, *22*, 3471.
[6] F. Thomas, S. Schulz, M. Nieger, *Organometallics* **2002**, *21*, 2793.
[7] Single-crystal X-ray diffraction: Nonius Kappa CCD diffractometer ($Mo_{K\alpha}$ radiation, $\lambda = 0.71073$ Å; $T = 123(2)$ K). The structures were solved by direct methods (SHELXS-97, G. M. Sheldrick, *Acta Crystallogr. Sect. A* **1990**, *46*, 467) and refined by full-matrix least-squares on $F^2$ (G. M. Sheldrick, SHELXL-97, Program for Crystal Structure Refinement, Universität Göttingen, Göttingen (Germany), **1997**). All non-hydrogen atoms were refined anisotropically and hydrogen atoms by a riding model. Empirical absorption corrections were applied. **1**: $C_{24}H_{72}Bi_3In_3Si_6$, $M_r = 1500.76$, colorless crystal, 0.45 × 0.40 × 0.35 mm; monoclinic, space group $P2(1)/n$ (No. 14); $a =$ 9.6601(2), $b = 20.9419(4)$, $c = 24.8825(5)$ Å, $\beta = 96.354(1)°$, $V =$ 5002.83(17) Å$^3$; $Z = 4$; $\mu = 12.031$ mm$^{-1}$; $\rho_{calcd} = 1.993$ g cm$^{-3}$; 41 988 reflections ($2\theta_{max} = 50°$), 8812 unique ($R_{int} = 0.070$), 325 parameters; largest max./min. in the final difference Fourier synthesis: 1.068 e Å$^{-3}$/−1.366 e Å$^{-3}$; max./min. transmission 0.1084/0.0751; $R_1 = 0.035$ ($I > 2\sigma(I)$), $wR_2 = 0.065$.
[8] In addition to the binary intermetallic phases In$_x$Bi$_y$ only some Zintl anions are known with In−Bi bond lengths ranging from 2.83–3.15 Å. a) R. Kubiak, *Z. Anorg. Allg. Chem.* **1977**, *431*, 261; b) L. Xu, S. C. Sevov, *Inorg. Chem.* **2000**, *39*, 5383; c) S. Bobev, S. C. Sevov, *J. Solid State Chem.* **2002**, *163*, 436.
[9] A. F. Holleman, E. Wiberg, *Lehrbuch der Anorganischen Chemie*, 101th ed., W. de Gruyter, Berlin, **1995**, p. 1838.
[10] The formation of the heterocycles was unequivocally proven by NMR spectroscopy.
[11] [{Me$_2$AlBi(SiMe$_3$)$_2$}$_3$] fails to react with InMe$_3$ at the required low-temperature conditions (−50 °C). Only upon the addition of an equimolar amount of dmap is a fast and complete reaction achieved.
[12] In THF, solvent-stabilized monomeric units [(*i*Bu)$_2$Al(thf)PH$_2$] are formed. M. Driess, C. Monse, *Z. Anorg. Allg. Chem.* **2000**, *626*, 1091.
[13] a) E. Hey-Hawkins, M. F. Lappert, J. L. Atwood, S. G. Bott, *J. Chem. Soc. Dalton Trans.* **1991**, 939; b) R. L. Wells, A. T. McPhail, T. M. Speer, *Eur. J. Solid State Inorg. Chem.* **1992**, *29*, 63.
[14] Despite the presence of two NMR-active Tl isotopes, only a single coupling is observed in the NMR spectra.
[15] **2**: $C_{16}H_{48}P_2Si_4Tl_2$, $M_r = 823.58$, colorless crystal 0.40 × 0.30 × 0.20 mm; triclinic, space group $P\bar{1}$ (No. 2); $a = 9.2585(2)$, $b =$ 9.5727(2), $c = 9.6569(3)$ Å, $\alpha = 77.581(1)$, $\beta = 81.497(1)$, $\gamma =$ 64.991(2)°, $V = 755.92(3)$ Å$^3$; $Z = 1$; $\mu = 10.910$ mm$^{-1}$; $\rho_{calcd} =$ 1.809 g cm$^{-3}$; 10 498 reflections ($2\theta_{max} = 55°$), 3378 unique ($R_{int} = 0.049$), 109 parameters; largest max./min. in the final difference Fourier synthesis: 1.709 e Å$^{-3}$/−2.514 e Å$^{-3}$; max./min. transmission 0.1589/0.0846; $R_1 = 0.029$ ($I > 2\sigma(I)$), $wR_2 =$ 0.072. **3**: $C_{16}H_{48}As_2Si_4Tl_2$, $M_r = 911.48$, colorless crystal 0.40 × 0.35 × 0.30 mm; triclinic, space group $P\bar{1}$ (No. 2); $a = 9.2985(4)$, $b = 9.4604(3)$, $c = 9.7580(4)$ Å, $\alpha = 78.332(2)$, $\beta = 82.125(2)$, $\gamma =$ 66.191(2)°, $V = 767.64(5)$ Å$^3$; $Z = 1$; $\mu = 12.779$ mm$^{-1}$; $\rho_{calcd} =$ 1.972 g cm$^{-3}$; 6618 reflections ($2\theta_{max} = 55°$), 3321 unique ($R_{int} =$ 0.055), 109 parameters; largest max./min. in the final difference Fourier synthesis: 2.177 e Å$^{-3}$/−3.042 e Å$^{-3}$; max./min. transmission 0.1311/0.0639; $R_1 = 0.038$ ($I > 2\sigma(I)$), $wR_2 = 0.093$. CCDC-213920 (**1**), CCDC-213921 (**2**), and CCDC-213922 (**3**) contain the supplementary crystallographic data for this paper. These data can be obtained free of charge via www.ccdc.cam.ac.uk/conts/retrieving.html (or from the Cambridge Crystallographic Data Centre, 12 Union Road, Cambridge CB2 1EZ, UK; fax: (+44) 1223-336-033; or deposit@ccdc.cam.ac.uk).
[16] a) G. Müller, J. Lachmann, *Z. Naturforsch. B* **1993**, *48*, 1544; b) R. A. Baldwin, R. L. Wells, P. S. White, *Main Group Chem.* **1997**, *2*, 67.
[17] D. Huang, J. D. Corbett, *Inorg. Chem.* **1998**, *37*, 4006.
[18] F. Thomas, S. Schulz, M. Nieger, *Z. Anorg. Allg. Chem.* **2002**, *628*, 235.

 © 2003 Wiley-VCH Verlag GmbH & Co. KGaA, Weinheim 

# Cover Picture




**Jessica M. C. A. Kerckhoffs, Fijs W. B. van Leeuwen, Anthony L. Spek, Huub Kooijman, Mercedes Crego-Calama,* and David N. Reinhoudt***

***An artificial enzyme or virus?*** The cover picture shows the single crystals and X-ray crystal structure of a hydrogen-bonded trimeric guest complexed by a self-assembled molecular container. Not only is the structure topologically very similar to that of viruses and enzymes, the receptor also exhibits primitive regulatory strategies of the type featured by these natural systems. For further details, see the Communication by D. N. Reinhoudt, M. Crego-Calama, and co-workers on page 5717 ff.

# Angewandte EarlyView

***The following articles are already available online (in Wiley InterScience). You can find them at www.angewandte.org, under Full Text, Early View.***

*R. Hoffmann,* D. J. Tantillo*:*
**Breaking Down Barriers: The Liaison Between Sigmatropic Shifts, Electrocyclic Reactions, and Three-Center Cations**
DOI: 10.1002/anie.200352853
Published online: November 19, 2003

*F. W. Lichtenthaler,* K. Nakamura, J. Klotz:*
**(−)-Daucic Acid: Revision of Configuration, Synthesis, and Biosynthetic Implications**
DOI: 10.1002/anie.200352718
Published online: November 18, 2003

Articles judged by the referees or the editor as being either very important or very urgent are immediately edited, proof-read, and electronically published once the manuscript has arrived in the editorial office in final form. As long as there is no page number available these articles should be cited in the following manner:

Author(s) *Angew. Chem. Int. Ed.*, online publication date, DOI.

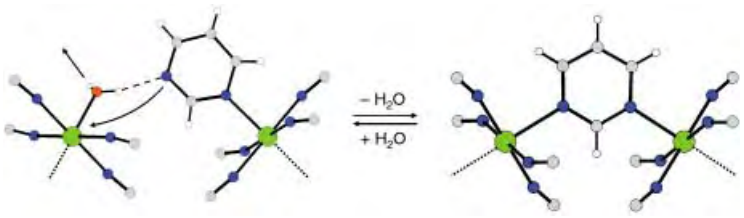
## Web Sites

http://www.brenda.uni-koeln.de — **5666** BRENDA: Everything You Always Wanted To Know about Enzymes — *C. Weise*

## Books

Handbook of Molecular Physics and Quantum Chemistry — **5667** Stephen Wilson, Peter F. Bernath, Roy McWeeny — *reviewed by C. van Wüllen*

## Highlights

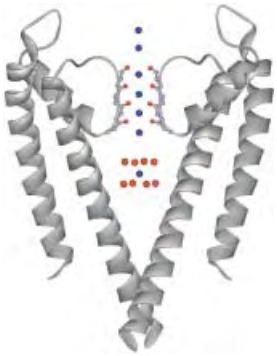



**A reversible ligand-substition reaction** in the crystal provides a possibility to switch spin-crossover materials (see picture). The merger of spin-crossover with the nanoporosity of metal–organic frameworks allows a dramatic variation of the cooperative interactions between the spin transition centers by sorption/desorption of guest molecules.

***Functional Materials***

T. Glaser* — **5668 – 5670**

Switching of a Spin-Crossover-Material Incorporated in Metal–Organic Frameworks by a Reversible Ligand-Substitution Reaction in the Crystalline State



**Crystallized and elucidated**: Our understanding of the basic functions of ion channels—the selective guidance of ions through cell membranes and the control of this process by "gates"—is derived to a large extent from the contributions of Roderick MacKinnon, who was awarded a Nobel Prize this year for his work. The picture shows the X-ray crystal structure of the prokaryotic potassium channel KcsA (blue: $K^+$ ions, red: carbonyl groups of the peptide backbone and water molecules).

***Ion Channels***

D. Trauner* — **5671 – 5675**

Potassium Channels: Symmetric, Selective, and Sensitive

 © 2003 Wiley-VCH Verlag GmbH & Co. KGaA, Weinheim 

# Contents

## Minireviews


**Conservation Techniques**

H. Langhals,* D. Bathelt — **5676 – 5681**

The Restoration of the Largest Archaeological Discovery—a Chemical Problem: Conservation of the Polychromy of the Chinese Terracotta Army in Lintong





**The monomer of choice** for the preservation of the lacquer base of the Chinese terracotta warriors through polymerization is hydroxyethyl methacrylate (**1**). The treated artifacts (such as the shown cuirass) remain unchanged for years.

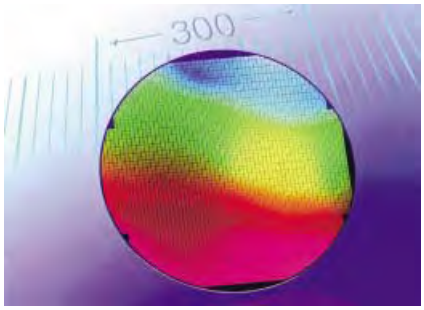
## Reviews


**Single-Crystal Growth of Silicon**

J. Evers,* P. Klüfers, R. Staudigl,* P. Stallhofer — **5684 – 5698**

Czochralski's Creative Mistake: A Milestone on the Way to the Gigabit Era


**Purely by accident**: Silicon chips for the microelectronic industry are continually being developed to improve performance. We now live in the era of the 300-mm Si wafer (see picture), with which the manufacture of one-gigabit chips began in 2001. The high-purity Si single crystals used to make such wafers are prepared by a method devised by Jan Czochralski, which, as has only now been revealed, he discovered through a failed experiment.

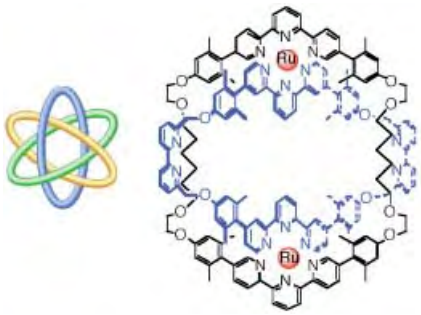



## Communications


**Macrocycles**

J. C. Loren, M. Yoshizawa, R. F. Haldimann, A. Linden, J. S. Siegel* — **5702 – 5705**

Synthetic Approaches to a Molecular Borromean Link: Two-Ring Threading with Polypyridine Templates

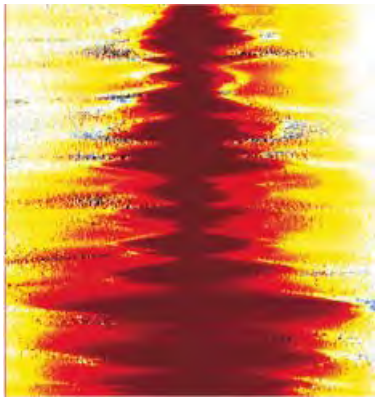




**"One ring to bind them"**: The Borromean link, which consists of three rings connected such that no two are concatenated, is a challenging synthetic target. The synthesis of an orthogonal two-ring system that could be a precursor for such a link was prepared from a polypyridine template (see picture).


**For the USA and Canada:**
ANGEWANDTE CHEMIE International Edition (ISSN 1433-7851) is published weekly by Wiley-VCH PO Box 191161, D 69451 Weinheim, Germany. Air freight and mailing in the USA by Publications Expediting Inc. 200 Meacham Ave., Elmont, NY 11003. Periodicals postage paid at Jamaica NY 11431. US POSTMASTER: send address changes to *Angewandte Chemie*, Wiley-VCH, 111 River Street, Hoboken, NJ 07030. Annual institutional subscription price for institutions: Europe € 3430.00/3118.00. Outside Europe US$ 4499.00/4090.00 (valid for print and electronic/print or electronic delivery); for individuals who are personal members of a national chemical society, or whose institution already subscribes, or who are retired or self-employed consultants, print only. Europe € 248.00/Outside Europe US$ 378.00. Postage and handling charges included. All Wiley-VCH prices are exclusive VAT.




© 2003 Wiley-VCH Verlag GmbH & Co. KGaA, Weinheim

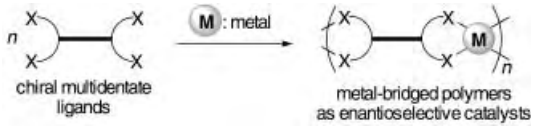


**What's in the middle matters little!** Differential conductance measurements made on single-molecule rotaxanes and their precursor dumbbells in transistors with platinum electrodes reflect the molecule–electrode contacts rather than the middle section of the molecules (see diagram; the color reflects the conductance, with dark corresponding to zero current). Interface states dominate electron transport. Molecular signatures are masked and even constitutional asymmetry in the molecule is difficult to detect.

***Molecular Electronics***

H. Yu, Y. Luo, K. Beverly, J. F. Stoddart, H.-R. Tseng, J. R. Heath* — **5706 – 5711**

The Molecule–Electrode Interface in Single-Molecule Transistors

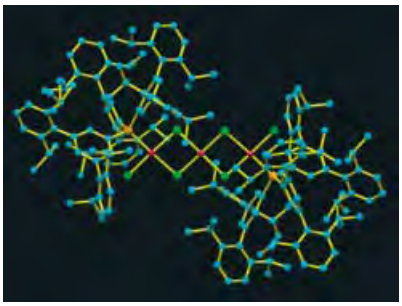



**Immobile without support**: The first synthesis of chiral Al-bridged and Ti-bridged polymers by a metal-mediated self-assembly of (*R*,*R*)-6,6′-bi(binol) (binol = 1,1′-bi-2-naphthol), which bears two pairs of phenolic hydroxy groups at the opposite sides in the molecule, is described (see scheme, X = OH or O). The polymers are found to promote asymmetric Michael reaction and carbonyl–ene reaction with high enantioselectivity and can be reused.

***Multicomponent Asymmetric Catalysis***

S. Takizawa, H. Somei, D. Jayaprakash, H. Sasai* — **5711 – 5714**

Metal-Bridged Polymers as Insoluble Multicomponent Asymmetric Catalysts with High Enantiocontrol: An Approach for the Immobilization of Catalysts without Using any Support

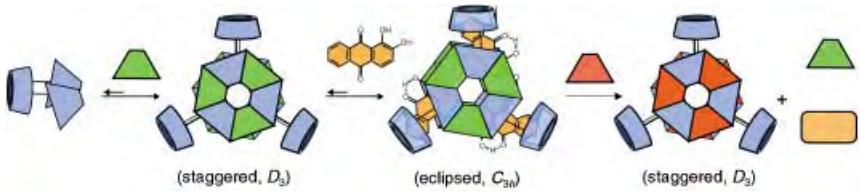


**A trinuclear palladium(II) chloride phosphane complex**, $[(PdCl_2)_3(PAr_3)_2]$, is obtained in the reaction of a bowl-shaped triarylphosphane with a deep cavity with $PdCl_2$ even when an excess amount of the phosphane is employed. X-ray crystallography established the structure of the complex: a trimer of $PdCl_2$ is terminated by two phosphane ligands (see picture).

***Coordination Chemistry***

Y. Ohzu, K. Goto,* T. Kawashima* — **5714 – 5717**

A Bowl-Shaped Triarylphosphane with a Large Cone Angle: Synthesis and Crystallographic Analysis of a $[(PdX_2)_3(PR_3)_2]$-Type Complex




**Primitive similarities** with regulatory strategies of natural systems have been mimicked by a synthetic self-assembled receptor. The complexation of a hydrogen-bonded trimer inside a hydrogen-bonded molecular cage triggers similar large conformational changes to the ones occurring in enzymes upon complexation of a specific substrate. Controlled release is also achieved (see scheme).

***Host–Guest Systems***

J. M. C. A. Kerckhoffs, F. W. B. van Leeuwen, A. L. Spek, H. Kooijman, M. Crego-Calama,* D. N. Reinhoudt* — **5717 – 5722**

Regulatory Strategies in the Complexation and Release of a Noncovalent Guest Trimer by a Self-Assembled Molecular Cage

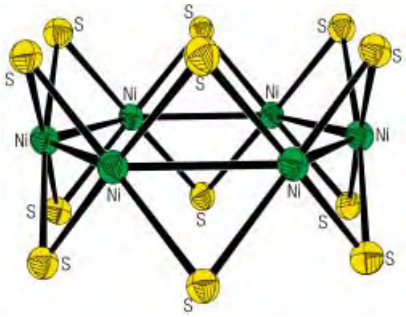
 © 2003 Wiley-VCH Verlag GmbH & Co. KGaA, Weinheim 

# Contents


## Crown Complexes

F.-F. Jian,* K. Jiao, Y. Li, P.-S. Zhao, L.-D. Lu ——— **5722 – 5724**

$[Ni_6(SCH_2CH_2OH)_{12}]$: A Double Crown [12]Metallacrown-6 Nickel(II) Cluster




**Crowning Glory**: Twelve $\mu_2$-sulfur donors are located above and below an $Ni_6$ ring to form a double crown cluster (see picture). This [12]metallacrown-6 nickel(II) cluster was synthesized by spontaneous self-assembly from 2-sulfanylethanol, carbon bisulfide, NaOH, and $NiSO_4$. The hydroxy groups of 2-sulfanylethanol form strong intermolecular hydrogen-bonding interactions, and thus help in sustaining the metallacrown complex.

## Metal–Alkene Complexes

I. Krossing,* A. Reisinger ——— **5725 – 5728**

A Stable Salt of the Tris(ethene)silver Cation: Structure and Characterization of $[Ag(\eta^2\text{-}C_2H_4)_3]^+[Al\{OC(CF_3)_3\}_4]^-$

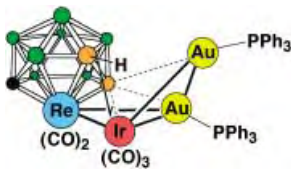


**More than 50 years** after the proposal of the Dewar–Chatt–Duncanson model for the binding of olefins to transition-metal atoms, the first structurally characterized example of a silver–$C_2H_4$ complex ($[Ag(\eta^2\text{-}C_2H_4)_3]^+$, see picture) was obtained with the help of the very weakly coordinating $[Al\{OC(CF_3)_3\}_4]^-$ ion. By contrast, earlier gas-phase investigations only suggested the existence of $[Ag(\eta^2\text{-}C_2H_4)_x]^+$ ions ($x = 1$ and 2).

## Carborane Clusters

S. Du, J. A. Kautz, T. D. McGrath, F. G. A. Stone* ——— **5728 – 5730**

Heterometallic Cluster Assembly on a Rhenium–Monocarborane Substrate

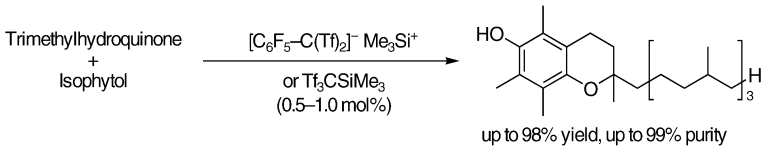



**Building butterflies**: A carborane-supported $\{ReIrAu_2\}$ butterfly has been assembled by stepwise addition of iridium and then gold to a rhenium-monocarborane complex (see picture green = BH, orange = B, black = CPh). The method of preparation has considerable potential for the synthesis of other new heteropolymetallic species.

## Super Lewis Acid Catalyst

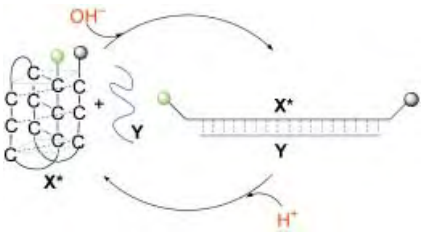
A. Hasegawa, K. Ishihara,* H. Yamamoto* ——— **5731 – 5733**

Trimethylsilyl Pentafluorophenylbis(trifluoromethanesulfonyl)methide as a Super Lewis Acid Catalyst for the Condensation of Trimethylhydroquinone with Isophytol




**Acid and vitamin E**: Trimethylsilyl super Lewis acids, such as $[C_6F_5\text{–}C(Tf)_2]^-Me_3Si^+$ and $Tf_3CSiMe_3$, are extremely active and highly effective catalysts for the regioselective condensation of trimethylhydroquinone with isophthyol to afford (±)-α-tocopherol (vitamin E; see scheme, Tf = $CF_3SO_2$).


 © 2003 Wiley-VCH Verlag GmbH & Co. KGaA, Weinheim 

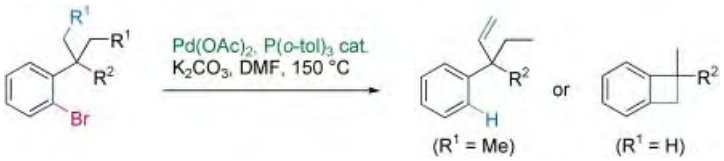



**Making DNA blink**: A molecular machine based on the DNA *i*-motif structure is driven by changing pH (see picture). At pH 5, oligonucleotide X* folds into the *i*-motif (closed state), and complementary strand Y adopts a random-coil structure. At pH 8, X* unfolds and forms an extended duplex with Y. This reversible process can be monitored by means of a rhodamine green label (green circle), whose fluorescence is quenched by a dabcyl moiety (gray circle) in the closed but not in the open state.

## Molecular Devices

D. Liu,
S. Balasubramanian* ——— **5734 – 5736**

A Proton-Fuelled DNA Nanomachine



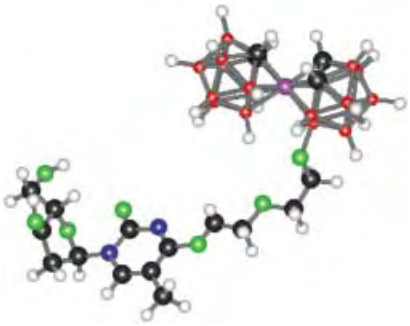

**Palladacyclic intermediates** effectively lower the high energy barrier to cleavage of a C($sp^3$)—H bond. C—H activation of benzylic *gem*-dialkyl groups of bromo- and iodobenzenes produces olefins and cyclobutabenzenes, respectively, without homocoupling (see scheme).

## Organometallic Chemistry

O. Baudoin,* A. Herrbach,
F. Guéritte ——— **5736 – 5740**

The Palladium-Catalyzed C–H Activation of Benzylic *gem*-Dialkyl Groups

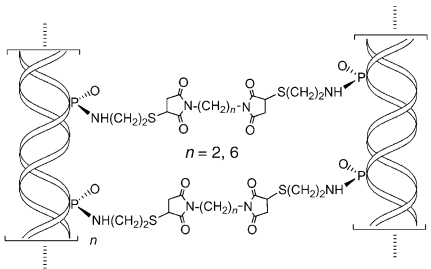
**Nucleoside–metallacarborane conjugates** (for example, $T^{BEMC}$; see picture with low toxicity were synthesized and coupled as a redox label to DNA oligonucleotide. The labeled oligonucleotide acted as a primer for Taq polymerase.



## Biometallic Materials

A. B. Olejniczak, J. Plešek, O. Kříž,
Z. J. Lesnikowski* ——— **5740 – 5743**

A Nucleoside Conjugate Containing a Metallacarborane Group and Its Incorporation into a DNA Oligonucleotide




**Micrometer-scale rodlike** DNA architectures can be synthesized by one-step molecular assembly using cross-linked oligonucleotides with bismaleimide linkers and subsequent DNA ligation (see scheme). Atomic force microscopy studies have shown that the flexibility of the DNA structures in the parallel double-helix structure is reduced.

## DNA Structures

M. Endo, T. Majima* ——— **5744 – 5747**

Parallel, Double-Helix DNA Nanostructures Using Interstrand Cross-Linked Oligonucleotides with Bismaleimide Linkers

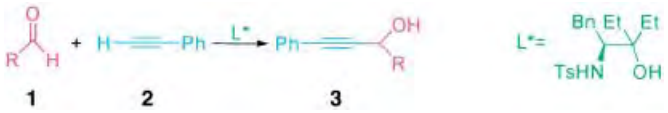
 © 2003 Wiley-VCH Verlag GmbH & Co. KGaA, Weinheim 

# Contents


## Asymmetric Additions

Z. Xu, R. Wang,* J. Xu, C.-s. Da, W.-j. Yan, C. Chen ——— 5747 – 5749

Highly Enantioselective Addition of Phenylacetylene to Aldehydes Catalyzed by a β-Sulfonamide Alcohol–Titanium Complex

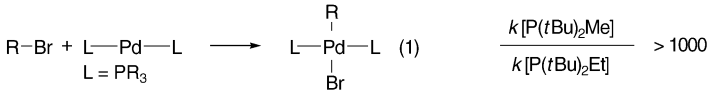



**Three simple steps** were required to prepare the β-sulfonamide alcohol ligand (L*) from L-phenylalanine. Its titanium complex efficiently catalyzes the asymmetric addition of phenylacetylene (**2**) to aromatic aldehydes **1** to form enantiomerically pure propargyl alcohols **3**. Ts = *p*-toluenesulfonyl, R = substituted phenyl or naphthyl group.

## Reaction Mechanisms

I. D. Hills, M. R. Netherton, G. C. Fu* ——— 5749 – 5752

Toward an Improved Understanding of the Unusual Reactivity of $Pd^0$/Trialkylphosphane Catalysts in Cross-Couplings of Alkyl Electrophiles: Quantifying the Factors That Determine the Rate of Oxidative Addition



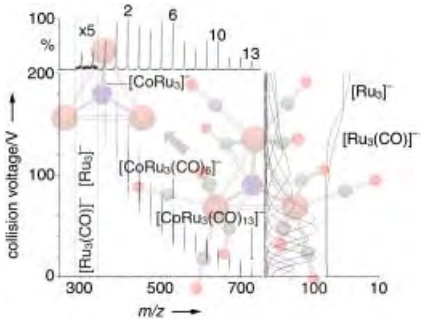

**What a difference a ligand makes!** The reactivity of $Pd^0$/trialkylphosphane complexes is of great interest because of their unusual effectiveness as cross-coupling catalysts for alkyl electrophiles [Eq. (1)]. This study sheds light on various aspects of the critical oxidative-addition step of the catalytic cycle.

## Cluster Compounds

C. P. G. Butcher, A. Dinca, P. J. Dyson, B. F. G. Johnson, P. R. R. Langridge-Smith, J. S. McIndoe* ——— 5752 – 5755

A Strategy for Generating Naked-Metal Clusters for Gas-Phase Reactivity Studies by FTICR–MS

**Facile generation of naked-metal** particles by stripping the ligands from transition-metal–carbonyl clusters for gas-phase studies by FTICR–MS is achieved by using ESI combined with collision induced dissociation (see picture).

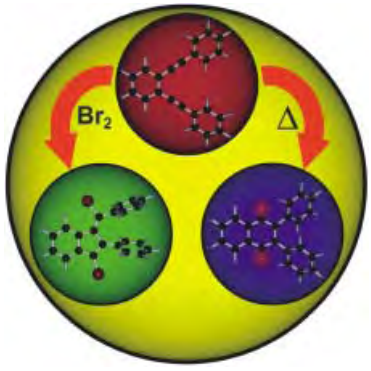



## Polycyclic Aromatic Hydrocarbons

P. R. Schreiner,* M. Prall, V. Lutz ——— 5757 – 5760

Fulvenes from Enediynes: Regioselective Electrophilic Domino and Tandem Cyclizations of Enynes and Oligoynes

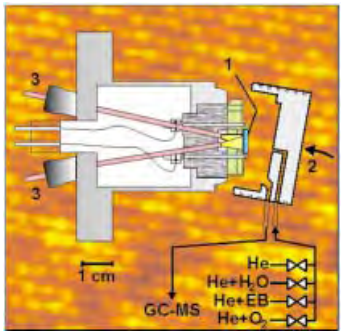
**Complementary products**: the electrophilic cyclizations of *ortho*-benzooligoynes upon bromination give benzopentafulvenes with orthogonal, peripheral phenyl groups. In contrast, the thermal cyclizations of the same starting materials give naphthalene derivatives. This strategy was used for the synthesis of anellated benzopentafulvenes in domino reactions.





 © 2003 Wiley-VCH Verlag GmbH & Co. KGaA, Weinheim 

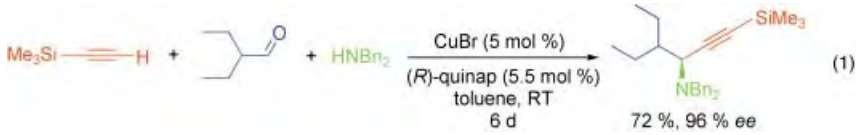
**Rates ten times faster** for the conversion of ethylbenzene (EB) into styrene are possible over unpromoted hematite catalysts if reduction to magnetite and coking is prevented by adding traces of oxygen. This finding results from measurements made with the stagnation-point microflow reactor shown (1: model catalyst, 2: cap, 3: diode laser).




## Heterogeneous Catalysis

O. Shekhah, W. Ranke,* A. Schüle, G. Kolios, R. Schlögl ——— **5760 – 5763**

Styrene Synthesis: High Conversion over Unpromoted Iron Oxide Catalysts under Practical Working Conditions

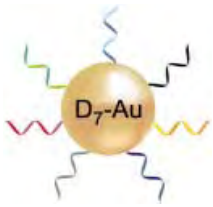



**The one-pot reaction** of alkynes, aldehydes, and secondary amines in the presence of CuBr/quinap as the catalytic system provides various enantiomerically enriched propargylamines in good yields (up to 99%) and good selectivities (up to 96% *ee*) [Eq. (1)].

## C–H Activation

N. Gommermann, C. Koradin, K. Polborn, P. Knochel* ——— **5763 – 5766**

Enantioselective, Copper(I)-Catalyzed Three-Component Reaction for the Preparation of Propargylamines




**Highly-functionalized reagents** can be produced from gold nanoparticles containing up to seven different DNA oligonucleotide sequences (see picture). The individual oligomers are orthogonally addressable and reveal an efficient reactivity that is comparable to that of the analogous monofunctional conjugates.

## Nanotechnology

C. M. Niemeyer,* B. Ceyhan, P. Hazarika ——— **5766 – 5770**

Oligofunctional DNA–Gold Nanoparticle Conjugates

VIP Communications labeled with this symbol have been judged by two referees as being "very important papers".

The publication of Communications labeled with this symbol has been accelerated because of their topical or highly competitive nature.

**Sources**

***Product and Company Directory***

You can start the entry for your company in "Sources" in any issue of *Angewandte Chemie*.

If you would like more information, please do not hesitate to contact us.

**Wiley-VCH Verlag – Advertising Department**
Tel.: 0 62 01 - 60 65 65
Fax: 0 62 01 - 60 65 50
E-Mail: MSchulz@wiley-vch.de

## Service

***Keywords*** ——— ***5772***

***Authors*** ——— ***5773***

***Preview*** ——— ***5775***

 © 2003 Wiley-VCH Verlag GmbH & Co. KGaA, Weinheim 

Functional Materials

# Switching of a Spin-Crossover-Material Incorporated in Metal–Organic Frameworks by a Reversible Ligand-Substitution Reaction in the Crystalline State**

*Thorsten Glaser**

**Keywords:**
bistability · cooperative effects · host–guest systems · magnetic properties · spin-crossover

The synthesis of new magnetic materials from molecular organic, organometallic, or coordination-chemistry building blocks is a fast-growing area of research with a high potential for applications in molecular electronics.[1] The scientific motivation to rationally construct nanoscale materials from chemically well-defined substructures merges ideally in this area with anticipated future technologies.

The molecular storage of information is one of the essential challenges in molecular electronics. Devices for such purposes must incorporate compounds that exhibit the phenomenon of bistability,[2] which may be defined as the ability of a compound to exist in two stabile (or metastabile) electronic states under the control of an external stimulus. For use in memory devices, the bistability of the compound has to be connected with a measurable change of the properties (e.g., magnetic or optical) of the two states. Two examples of bistability are provided in the field of molecular magnetism: single-molecule magnets and spin-crossover materials.

Single-molecule magnets are polynuclear transition metal complexes with a high spin ground state, which have an energy barrier for relaxation of the magnetic moment due to a strong magnetic anisotropy respectively zero-field splitting.[3] Thus, in the first step the magnetic moments may be aligned by an external magnetic field and this state might be frozen in the second step at a temperature below the so-called blocking temperature. This step results in the magnetization of the sample even in the absence of an external magnetic field. The direction of the magnetization can occur in two ways. Therefore, single-molecule magnets have been regarded as the ultimate dense-storage media in computer technology and as the heart of a quantum computer.[4] Unfortunately, the blocking temperatures are still too low for single-molecule magnets to attract technological interest. However, a lot of effort in research is currently aimed at increasing the blocking temperatures.

Spin-crossover materials are the second class of compounds that exhibit bistability. Transition-metal complexes with a $d^4$–$d^7$ electron configuration may possess a transition between a low-spin (LS) and a high-spin (HS) configuration which is initiated photochemically, or by changes in pressure or temperature.[5] This spin-crossover is accompanied by a change in the magnetic susceptibilities, the electronic absorption spectra, the vibrational spectra, and the metal–ligand distances, thus opening many possibilities for the detection of such a transition. In many cases, there is such a strong modification of the absorption bands that the naked eye can follow the color change due to the spin-crossover. Applications of such materials for displays have already been successfully tested.[6] Although the underlying principle for a spin transition is of a purely molecular nature, intermolecular interactions are essential for the occurrence of hysteresis effects in the spin transition. In these cases, the transition temperature depends on the history of the sample: the critical temperature of the LS→HS transition when increasing the temperature ($T_c^{\uparrow}$) is higher than the critical temperature when decreasing the temperature ($T_c^{\downarrow}$), thus giving rise to a bistability in the temperature range between $T_c^{\downarrow}$ and $T_c^{\uparrow}$. This property, which is particularly interesting for potential applications, occurs only if cooperative interactions between the individual transition-metal complexes exist. Therefore, a lot of effort deals with the transition from molecular solids to higher-dimensional aggregates.[7]

It is known that the critical temperatures in spin-crossover materials can be tuned by rational design from low temperatures even to temperatures above room temperature. In this respect, the polymeric system based on tris-μ-triazol $Fe^{II}$ has been optimized in such a way that room temperature falls in the middle of the hystereses loop ($T_c^{\downarrow} = 288$ K, $T_c^{\uparrow} = 304$ K).[8] Consequently, this compound can exists at room temperature with a white (HS, starting from temperatures above room temperature) or a red color (LS, starting from temperatures below room temperature).

[*] Dr. T. Glaser
Institut für Anorganische und Analytische Chemie
Westfälische Wilhelms-Universität Münster
Wilhelm-Klemm-Strasse 8
48149 Münster (Germany)
Fax: (+49) 251-833-3108
E-mail: tglaser@uni-muenster.de

[**] I am grateful to Professor Dr. F. E. Hahn for his generous and continuous support of my work as well as to the Fonds der Chemischen Industrie, the Deutsche Forschungsgemeinschaft, the Bundesministerium für Bildung und Forschung, and the Dr. Otto Röhm Gedächtnisstiftung.

 © 2003 Wiley-VCH Verlag GmbH & Co. KGaA, Weinheim DOI: 10.1002/anie.200301693 

This kind of externally inducible transitions, which can be measured by a color change, a variation of the magnetic susceptibility, and other physical properties, make spin-crossover compounds ideal materials for information storage. Recent developments in this field have aimed at the incorporation of spin-crossover materials in metal–organic frameworks. Such frameworks exhibit a number of interesting properties that can be varied and switched by sorption/desorption processes.[9] The combination of spin-crossover compounds and metal–organic frameworks represents a fascinating approach for the generation of new materials with multiple functionalities.

In this respect, Kepert and co-workers reported the first successful integration of spin-crossover materials in metal–organic frameworks.[10] The nanoporous network $[Fe_2(azpy)_4(NCS)_4]$ (azpy = *trans*-4,4′-azopyridine) incorporates reversibly guest molecules such as EtOH, MeOH, or *n*PrOH. While in the absence of the guests the host exhibits no spin-crossover, the inclusion of alcohol molecules induce a spin-crossover that originates from one of the two different kinds of iron centers. The sorbed guest molecules do not only induce a distortion of the networks but also form hydrogen bonds with the coordinated thiocyanate ligands of one kind of iron centers, which may explain the variation of the electronic properties.

Real and co-workers reported recently on a multifunctional material exhibiting, on the one hand, all properties of a spin-crossover material including hysteresis and, on the other hand, a reversible dehydration/rehydration crystal reaction whereby the critical spin-transition temperatures vary dramatically.[11] The compounds $[Fe(pmd)(OH_2)\{M(CN)_2\}_2]\cdot H_2O$ **1**-M (pmd = pyrimidine M = Ag: **1**-Ag, M = Au: **1**-Au) each contain two different types of iron centers, Fe1 und Fe2. Both types of iron centers are coordinated by four nitrogen-bound $CN^-$ ligands. The coordination sphere around Fe1 is saturated by two monodentate pyrimidine ligands *trans* to each other whereas the coordination sphere around Fe2 is saturated by two water molecules. The iron centers are connected by $[M(CN)_2]^-$ units leading to three-dimensional networks. The crystal structure contains three identical networks that interpenetrate each other and are only weakly connected with one another.

Both compounds show spin-crossover behavior with hysteresis (**1**-Ag: $T_c^{\downarrow} = 215$ K, $T_c^{\uparrow} = 223$ K; **1**-Au: $T_c^{\downarrow} = 163$ K, $T_c^{\uparrow} = 171$ K) accompanied by a color change from yellow (HS) to deep-red (LS). These spin-crossover properties alone make **1**-Ag and **1**-Au interesting materials, but the nanoporous nature of the metal–organic frameworks adds a remarkable new attribute: on warming or on reducing the pressure, the uncoordinated and the coordinated water molecules are removed completely (**2**-Ag and **2**-Au). Although the single crystals crack during this dehydration process, the crystal structure of **2**-Au was ingeniously determined based on X-ray powder diffraction data![12] The two water molecules that were coordinated to the Fe2 center are lost, which leads to an unfavorable four coordination of the Fe2 center. However, the pyrimidine ligand with monodentate coordination to the Fe1 center is located geometrically in such a favorable position that the noncoordinated nitrogen atoms of two independent pyrimidine molecules occupy the vacant coordination sites on Fe2. The pyrimidine ligand now bridges an Fe1 center and an Fe2 center (Figure 1), which were part of two independent networks in **1**-Au. Thus, the crystal reaction joins the three independent networks to one three-dimensional network in **2**-Au. This solid-state reaction is completely reversible because exposing a dehydrated phase to an atmosphere of water induces the back reaction to the hydrated phase.

These changes in the three-dimensional arrangement, and thus of the cooperative interactions between the metal centers, result in extensive variations of the spin-crossover behavior. While **2**-Au exhibit no spin-crossover, **2**-Ag shows a spin-crossover with hysteresis at lower temperatures as compared to **1**-Ag ($T_c^{\downarrow} = 124$ K, $T_c^{\uparrow} = 141$ K; Figure 2). Changes in spin-crossover by dehydration/hydration were reported before.[13] The reversible crystal reaction elucidated by Real and co-workers provides a new way to switch spin-crossover materials. Further optimized systems with hysteresis cycles around room temperature have potential applications as display and memory devices, or even moisture sensors with magnetic detection.

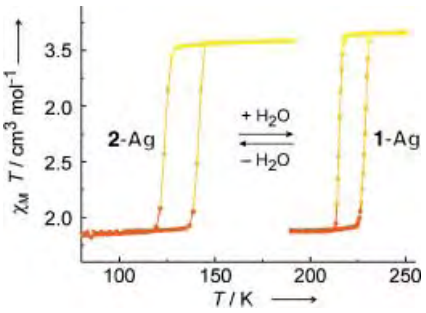



***Figure 2.*** Effect of the crystal reaction on the hysteresis of the magnetic properties of **1**-Ag and **2**-Ag.

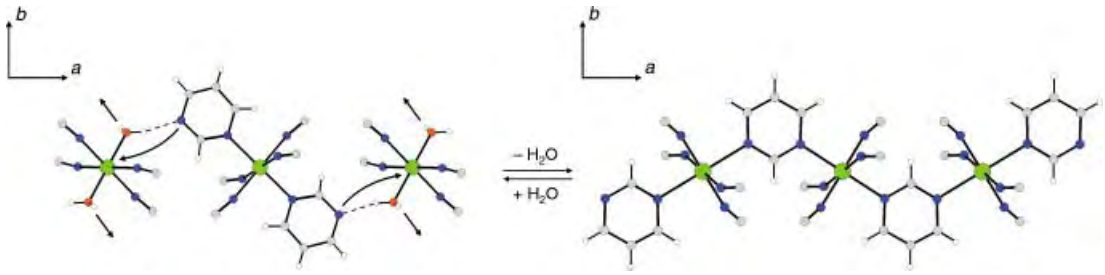



***Figure 1.*** Reversible ligand-substitution reaction in the crystal: the unbound nitrogen atoms in **1**-Au (left) substitute the coordinated water molecules, which then leave the crystal. In **2**-Au (right) the pyrimidine ligands bridge two iron atoms.

 © 2003 Wiley-VCH Verlag GmbH & Co. KGaA, Weinheim 

[1] *Magnetism: Molecules to Materials*, *Vol. I–IV* (Eds.: J. S. Miller, M. Drillon), Wiley-VCH, Weinheim, **2001–2003**.
[2] a) J. S. Miller, *Angew. Chem.* **2003**, *115*, 27 – 29; *Angew. Chem. Int. Ed.* **2003**, *42*, 27 – 29; b) O. Kahn, J. P. Launay, *Chemtronics* **1988**, *3*, 140 – 151.
[3] R. Sessoli, D. Gatteschi, *Angew. Chem.* **2003**, *115*, 278 – 309; *Angew. Chem. Int. Ed.* **2003**, *42*, 268 – 297.
[4] M. N. Leuenberger, D. Loss, *Nature* **2001**, *410*, 789 – 793.
[5] a) P. Gütlich, A. Hauser, H. Spiering, *Angew. Chem.* **1994**, *106*, 2109 – 2141; *Angew. Chem. Int. Ed. Engl.* **1994**, *33*, 2024 – 2054; b) P. Gütlich, H. Spiering, A. Hauser in *Inorganic Electronic Structure and Spectroscopy*, *Vol II* (Eds.: E. I. Solomon, A. B. P. Lever), Wiley-Interscience, New York, **1999**, pp. 575 – 622; c) H. Toftlund, *Coord. Chem. Rev.* **1989**, *94*, 67 – 108.
[6] O. Kahn, J. Kröber, C. Jay, *Adv. Mater.* **1992**, *4*, 718 – 728.
[7] a) O. Kahn, C. J. Martinez, *Science* **1998**, *279*, 44 – 48; b) J. A. Real, E. Andrés, M. C. Munoz, M. Julve, T. Granier, A. Bousseksou, F. Varret, *Science* **1995**, *268*, 265 – 267.
[8] J. Kröber, E. Codjovi, O. Kahn, F. Grolière, C. Jay, *J. Am. Chem. Soc.* **1993**, *115*, 9810 – 9811.
[9] a) B. Chen, M. Eddaoudi, S. T. Hyde, M. O'Keeffe, O. M. Yaghi, *Science* **2001**, *291*, 1021 – 1023; b) P. J. Langley, J. Hulliger, *Chem. Soc. Rev.* **1999**, *28*, 279 – 291; M. Eddaoudi, D. B. Moler, H. Li, B. Chen, T. M. Reeke, M. O'Keeffe, A. M. Yaghi, *Acc. Chem. Res.* **2001**, *34*, 319 – 330.
[10] G. J. Halder, C. J. Kepert, B. Moubaraki, K. S. Murray, J. D. Cashion, *Science* **2002**, *298*, 1762 – 1765.
[11] V. Niel, A. L. Thompson, M. C. Munoz, A. Galet, A. E. Goeta, J. A. Real, *Angew. Chem.* **2003**, *115*, 3890 – 3893; *Angew. Chem. Int. Ed.* **2003**, *42*, 3760 – 3763.
[12] The following review provides a current overview on the structure determination by X-ray powder diffraction: K. D. M. Harris, M. Tremayne, B. M. Kariuki, *Angew. Chem.* **2001**, *113*, 1675 – 1700; *Angew. Chem. Int. Ed.* **2001**, *40*, 1626 – 1651.
[13] a) W. Vreugdenhil, J. H. Van Diemen, A. G. De Graaff, J. G. Haasnoot, J. Reedijk, A. M. van der Kraan, O. Kahn, J. Zarembowitch, *Polyhedron* **1990**, *9*, 2971 – 2979; b) E. Codjovi, L. Sommier, O. Kahn, C. Jay, *New J. Chem.* **1996**, *20*, 503 – 505; c) Y. Garcia, P. J. van Koningsbruggen, E. Codjovi, R. Lapouyade, L. Rabardel, *J. Mater. Chem.* **1997**, *7*, 857 – 858; d) O. Roubeau, J. G. Haasnoot, E. Codjovi, F. Varret, J. Reedijk, *Chem. Mater.* **2002**, *14*, 2559 – 2566.

 © 2003 Wiley-VCH Verlag GmbH & Co. KGaA, Weinheim 

Ion Channels

# Potassium Channels: Symmetric, Selective, and Sensitive

*Dirk Trauner**

**Keywords:**
ion channels · membranes · neurobiology · protein structures · structure elucidation

Potassium channels occur in virtually all eukaryotic and prokaryotic cells. Their ability to guide potassium ions across biological membranes and thereby control the membrane potential underpins elementary cellular functions, such as excitability, proliferation, secretion, and volume regulation. In higher organisms potassium channels fulfill many important physiological roles, ranging from the propagation of action potentials to the complex functions of central nervous systems. Potassium channels are associated with every heartbeat, sensation, and thought. Their significance can not be overestimated.[1]

Some very poisonous animals have recognized the importance of potassium channels as well.[2] The venoms produced by the green mamba, the tarantula, and the death stalker scorpion, to name just a few, contain small peptides that block potassium channels and prevent them from functioning properly. Blocking potassium channels is a clever strategy when prey or foes have to be killed or immobilized as quickly as possible. The toxins are fast acting—no cell membranes have to be crossed—and they paralyze vital components of the nervous system reliably. In neurobiology potassium-channel toxins are important tools with which to probe the structure and function of channels. These investigations gave the first clues about the extracellular surface of potassium channels and provided insight into their structural conservation.[3]

The extent to which the basic structure of potassium channels is conserved is indeed remarkable. For instance, KvAP, a voltage-gated potassium channel found in an archaebacterium that lives at 96 °C at the bottom of the Sea of Japan, is very similar to eukaryotic Kv channels, which control the transmembrane potential of T-lymphocytes and neurons.[4] In fact, certain toxins produced by the Chilean rose tarantula to block Kv channels (and inflict painful bites on Chilean rose workers) also block KvAP! Presumably, potassium channels evolved long before they assumed the main function they have today in the nervous system. The remarkable structural conservation of potassium channels and their participation in a wide range of physiological processes is a nice example of how evolution manages great leaps forward: by "hijacking" existing functional elements, modifying them, combining them, and applying them to new tasks.

Potassium channels, like most ion channels, have two basic functional properties: the ability 1) to pass ions along their electrochemical gradient selectively (for example, potassium ions in the presence of sodium ions) and 2) to control this process with "gates". Depending on the type of channel, the main gate can open and close in response to changes in membrane potential ("voltage gating") or upon binding to small messenger molecules, other proteins, or even other ions ("ligand gating"). Some potassium channels possess additional "inactivation gates", which close slowly following the opening of the ligand or voltage gate.

Since the end of the 1990s, Roderick MacKinnon and co-workers (The Rockefeller University, New York) have shed light on most of these functional properties by analyzing a series of progressively more complex and more informative X-ray crystal structures, and have thus essentially elucidated how potassium channels work. These seminal studies were recently rewarded with the Nobel Prize in Chemistry—only five years after the first crystal structure appeared in the literature!

The Nobel Prize in Chemistry 2003, awarded for "discoveries concerning channels in cell membranes", was shared equally between MacKinnon and Peter Agre (Johns Hopkins University, Baltimore, USA). Agre identified the long-sought-after water channels in 1988. Water channels, also known as aquaporins, pass water molecules across lipid membranes while maintaining the pH gradient—not a simple task when one considers that protons can be transferred along water networks by "proton hopping". Aquaporins have little in common with potassium channels in terms of structure or function, but are of equal physiological importance.

The first X-ray crystal structure to emerge from the MacKinnon laboratory was of the relatively simple bacterial potassium channel KcsA, with a resolution of 3.2 Å (Figure 1).[5] Its disclosure made a big splash, as at that time nobody had thought the crystallization and structural elucidation of ion channels possible. KcsA contains only two transmembrane helices per subunit (Figure 1b), in contrast to more complex eukaryotic potassium channels, which have been traditionally assigned six. As shown in Figure 1a, four subunits form the central pore, which consists of a narrow region known as the selectivity filter and a water-filled wider inner cavity. This tetrameric quaternary struc-

[*] Prof. Dr. D. Trauner
Center for New Directions in Organic Synthesis
Department of Chemistry
University of California, Berkeley
Berkeley, CA 94720 (USA)
Fax: (+1) 510-643-9480
E-mail: trauner@cchem.berkeley.edu


DOI: 10.1002/anie.200301724
© 2003 Wiley-VCH Verlag GmbH & Co. KGaA, Weinheim

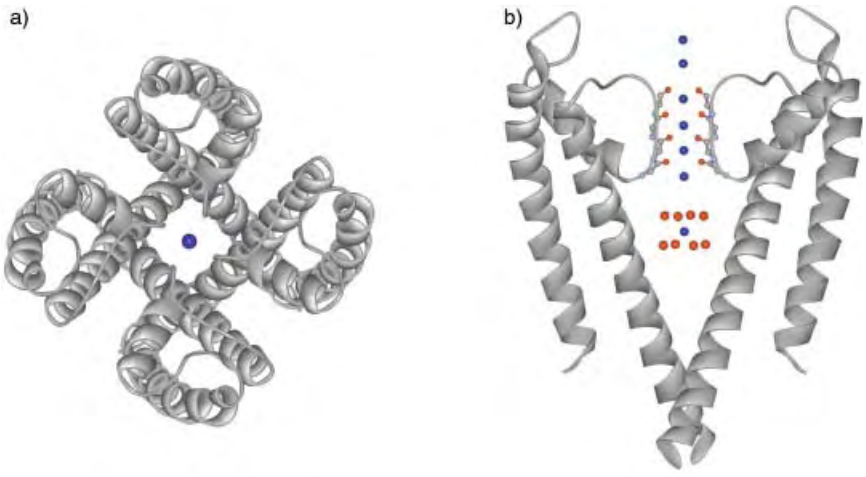



***Figure 1.*** The X-ray crystal structure of KcsA: a) view from the extracellular side; b) side view; only two of the four subunits are shown; blue: potassium ions, red: carbonyl groups of the selectivity filter and water molecules.

ture is a general feature of potassium channels. The selectivity filter is lined with the carbonyl groups of the peptide backbone, the amino acid residues of which are given by the highly conserved TXXTXGYG signature sequence. In the tetrameric structure the orientation of these carbonyl groups can be likened to a stack of crown ethers. They stabilize the potassium ion as it sheds its hydration sphere and passes through the pore. Presumably this process is energetically more favorable for the potassium ion than for the smaller sodium ion, which explains the greater-than-10000-fold selectivity for the former. However, coordination by the carbonyl groups is weak enough that the potassium ion passes through the channel essentially at the diffusion limit.

A second, higher-resolution structure of KcsA (2.0 Å) resolved some of the remaining questions and doubts and provided further insight into how the potassium ions pass through the selectivity filter.[6] Furthermore, it gave clues as to how the ions are stabilized in the middle of the membrane. The new electron-density map even showed a potassium ion residing in the central cavity of the channel, complete with its inner hydration sphere, an array of eight water molecules in a square antiprismatic orientation around the ion (Figure 1b). A remarkable feature of these studies was the cocrystallization of antibodies with the channel protein to stabilize the crystal lattice. This strategy has also been used in subsequent structure determinations.

With the next X-ray crystal structure disclosed by the MacKinnon research group, they were able to explain the basic gating mechanism of potassium channels.[7] The MthK channel, identified in the genome of *Methanobacterium thermoautotrophicum*, was expressed in the presence of $Ca^{2+}$ ions and was crystallized in its open form. The X-ray crystal structure was solved at a resolution of 3.3 Å (Figure 2). MthK is a ligand-gated channel that opens and closes in response to intracellular changes in $Ca^{2+}$ concentration. The intracellular calcium-sensitive domain is connected to the C-terminal end of the transmembrane domain, which forms the actual channel. In the tetrameric state these intracellular domains interact to form a "gating ring", which opens up like the shutter of a camera when calcium ions bind to it.

From the X-ray crystal structure and concomitant sequence-alignment studies, MacKinnon and co-workers identified a highly conserved glycine residue situated in the middle of the S6 helix, the transmembrane helix closest to the pore. According to MacKinnon's gating model, this residue acts like a hinge. Upon gating, the lower section of the inner helix appears to bend backwards at the glycine hinge, away from the central axis of the channel, creating an opening on the intracellular side of the channel. In the closed state, the four S6 helices of the subunits form a tight bundle, which has been likened to an "inverted tepee". Thus, the structure of KcsA (Figure 1) represents the closed state.

In MthK the shutterlike expansion of the gating ring is mechanically coupled to the bending movement of the four inner helices. Unfortunately, the amino acid residues linking the gating ring with the transmembrane domain of the channel are disordered in the crystal structure. Some of the details of the gating mechanism have therefore not been fully clarified. However, the gating mechanism proposed for MthK appears to be general for potassium channels, including voltage-gated channels (see below). Flexible domains of a channel can be allosterically coupled to the bending of the lower part of the S6 helix and can thus effect the opening or closing of the gate.

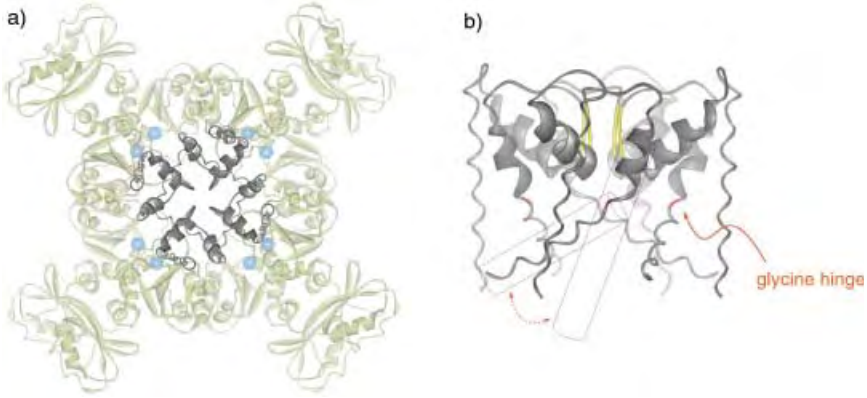



***Figure 2.*** The X-ray crystal structure of MthK: a) view from the extracellular side (gray: transmembrane domain, gray–green: gating ring, blue: calcium ions); b) side view of the transmembrane domain in which the bending of the S6 helix is indicated (red: glycine hinge).

 © 2003 Wiley-VCH Verlag GmbH & Co. KGaA, Weinheim 

MacKinnon and co-workers recently disclosed the structure of a complete voltage-gated channel.[8] According to hydrophobicity plots, voltage-gated channels contain six helical transmembrane segments per subunit (S1–S6), as opposed to their simpler congeners KcsA and MthK, which have just two. The fourth segment, S4, typically contains an array of four to seven positively charged amino acids, most often arginine residues, which had long been thought to act as the "voltage sensor". Remarkably, charged lysine residues are rarely found in the voltage-sensor region. As the membrane is depolarized, that is, as the extracellular side becomes more negative, the positively charged voltage sensor physically moves across the cell membrane, a movement that is mechanically coupled with the opening of the gate.

After many attempts with more common voltage-gated channels, which were ill fated as a result of the inherent flexibility of these proteins, a change in strategy brought about a breakthrough, when a channel from an unusual organism was chosen. The voltage-gated channel KvAP was identified by sequence comparison in the genome of *Aeropyrum pernix*, a thermophilic archaebacterium found near deep-sea hot springs (black smokers). Genetic and electrophysiological studies showed that KvAP behaves essentially as a voltage-gated channel and is very similar to the previously mentioned eukaryotic Kv channels. The idea was that a channel that operates at 96 °C in its native environment would be less flexible at or below room temperature and thus should be easier to crystallize. To further stabilize the channel and provide hydrophilic contacts for the crystal lattice, antibodies were raised against the channel and crystallized in the complex with the channel protein.

The X-ray crystal structure of KvAP, solved at a resolution of 3.2 Å, provided some surprises (Figure 3). Although the transmembrane helices closest to the pore, S5 and S6, showed the now canonical fold and closely resembled the open MthK structure, the remaining four "transmembrane" segments were not oriented as anticipated, that is, perpendicular to the (imaginary) membrane. In fact, S3 and S4 were not even situated in a region corresponding to the membrane, and S1 and S2 were oriented almost parallel to the plane of the membrane. The question now was how, with this structure, which clearly did not represent a physiologically relevant conformation of the channel in the membrane, voltage gating could be explained.

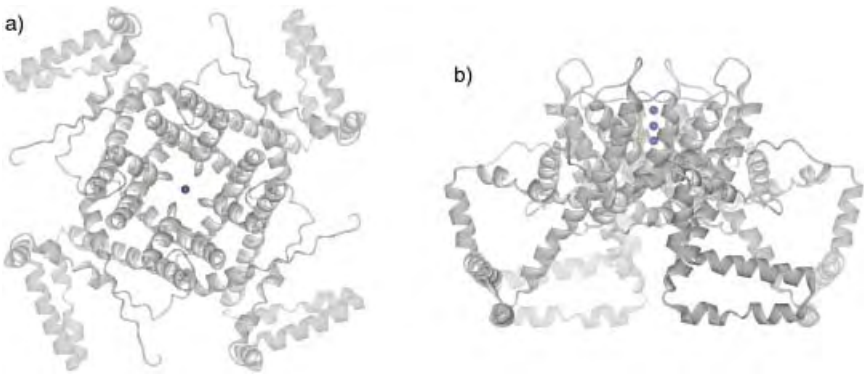



***Figure 3.*** The X-ray crystal structure of KvAP: a) view from the extracellular side; b) side view.

Further supported by an independent crystal structure of the S1–S4 segment and by a series of sophisticated biochemical experiments, MacKinnon proposed a refined model for voltage gating (Figure 4). According to his model, S4 and parts of S3 form a "voltage paddle", which is not embedded in the protein core but resides at the periphery of the channel in contact with the membrane. Upon depolarization, the four voltage paddles on the tetrameric channel cross the membrane to display their edges on the extracellular side. The delocalized positive charges on the arginine residues could render this movement through the lipophilic membrane energetically feasible. As mentioned previously, this membrane crossing is mechanically coupled with the bending of S6 and opening of the gate.

This interpretation has stirred up some controversy. Indirect evidence accumulated over many years had led to a "standard model" for the voltage sensor. According to this model, the positively charged residues of S4 are embedded in the core of the protein, thus avoiding direct contact with the membrane lipids, and move up and down in response to changes in the membrane potential. This movement would essentially occur perpendicular to the membrane. It will be interesting to see whether the new voltage-paddle model can be reconciled with the results of previous biophysical experiments, which were carried out with different voltage-gated channels.[9]

Although the essential structural and functional features of potassium channels have been mapped out, many questions remain: How is the S1–S6 domain folded in the open and closed states of a voltage-gated channel? How does the voltage sensor move across the membrane? What are the energetic details of this process? How exactly is this movement coupled to the opening and closing of the gate? How do inactivation gates work? What role does the

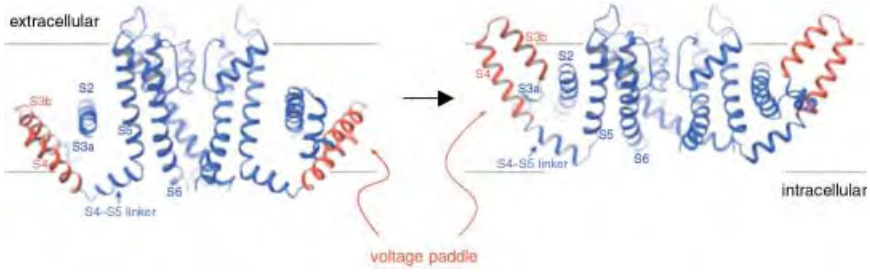



***Figure 4.*** MacKinnon's model for voltage-gating: Upon depolarization the voltage paddle moves towards the extracellular side of the membrane; reproduction from reference [8b].

 © 2003 Wiley-VCH Verlag GmbH & Co. KGaA, Weinheim 

β subunit associated with some potassium channels play?

Perhaps all these questions will be answered through the elucidation of the three-dimensional structure of the Shaker channel. Shaker is the archetypical potassium channel and the model for voltage-gated channels of the Kv class in the human genome. Its name is derived from a *Drosophila melanogaster* phenotype whose legs shake "under the influence" of ether. Shaker was the first potassium channel to be cloned, an achievement that opened the door for all the structural elucidations described above.[10] Shaker is a voltage-gated channel with characteristics similar to those of KvAP. It undergoes inactivation upon prolonged opening. Despite continuing attempts, the X-ray crystal structure of Shaker or a mammalian Kv channel has not yet been solved. Nevertheless, if the elements from the crystal structures disclosed so far are combined, a functional model of a complete voltage-gated potassium channel emerges.

The work of MacKinnon and coworkers has provided most of the key components of this model (Figure 5). The selectivity filter of Shaker and related Kv channels contains the characteristic TXXTXGYG signature sequence and presumably closely resembles the corresponding regions found in the four potassium-channel structures elucidated to date.[3–8,11] The gate is formed by the lower portion of S6, which bends at the glycine hinge upon opening. The voltage sensor possibly consists of a voltage paddle, whose movements are mechanically coupled to the gate. At the N-terminal end of S1, the polypeptide chain continues with a connector whose three-dimensional structure remains as yet unknown. The connector links S1 with the tetramerization domain (T1 domain), a region that was once believed to be essential for the self-assembly of potassium channels. Finally, at the N teminus of the T1 domain (and of the entire channel) resides a flexible loop and a well-defined short sequence of amino acids, which have been collectively dubbed the "ball and chain". These domains are responsible for the fast inactivation of the open channel. According to the ball-and-chain mechanism of inactivation, initially proposed by Armstrong, the N-terminal peptide sequence threads into the open pore from the intracellular side, presumably through openings between the four connectors, and literally plugs the channel.[1]

In the case of certain mammalian channels, a fourfold symmetric β subunit has been shown to bind to the T1 domain. To complete the detailed model of a voltage-gated potassium channel, the structures of an isolated β subunit and of a β-subunit–T1-domain assembly have also been solved by X-ray crystallographic analysis.[12] Surprisingly, the β subunit was found to contain a binding pocket for $NADPH/H^+$, the functional significance of which remains unclear. It is quite tempting to speculate about the existence of a direct link between the redox state of a cell and its transmembrane potential.

The detailed crystal structures of potassium channels disclosed by MacKinnon and co-workers will certainly benefit the design and development of drugs against ion-channel diseases (channelopathies). Indeed, potassium channels are involved in numerous diseases, such as episodic ataxia, epilepsy, cardiac arrhythmia, and diabetes. Furthermore, the voltage-gated potassium channel Kv1.3 plays a crucial role in the activation of human T-lymphocytes. Molecules that selectively block this channel depolarize the lymphocytes and prevent their proliferation. The resulting immunosuppressive effect could be useful for organ transplantations or help treat autoimmune disorders.

With their fourfold symmetry, their relatively uncomplicated protein folding pattern, and their fascinating functional properties, potassium channels appeal to chemists and biologists alike. They are an excellent example of the self-assembly of supramolecular species with highly complex functions from much simpler components. MacKinnon's work will have an impact beyond neurobiology and medicine on diverse fields, such as supramolecular chemistry, molecular recognition,[13] nanotechnology, and materials science. Voltage-gated potassium channels are in essence field-effect transistors on a nanometer scale, that is, devices that change their conductance in response to fluctuations in an electromagnetic field. Compared with other nanoscale "molecular machines", such as ATP synthases, transporters, or ion pumps, their structure and function are now relatively well understood, thus provoking scientists to use them as a starting point for further elaboration.

More than fifty years after Hodgkin and Huxley (Nobel Prize 1963) postulated their existence and twenty-five

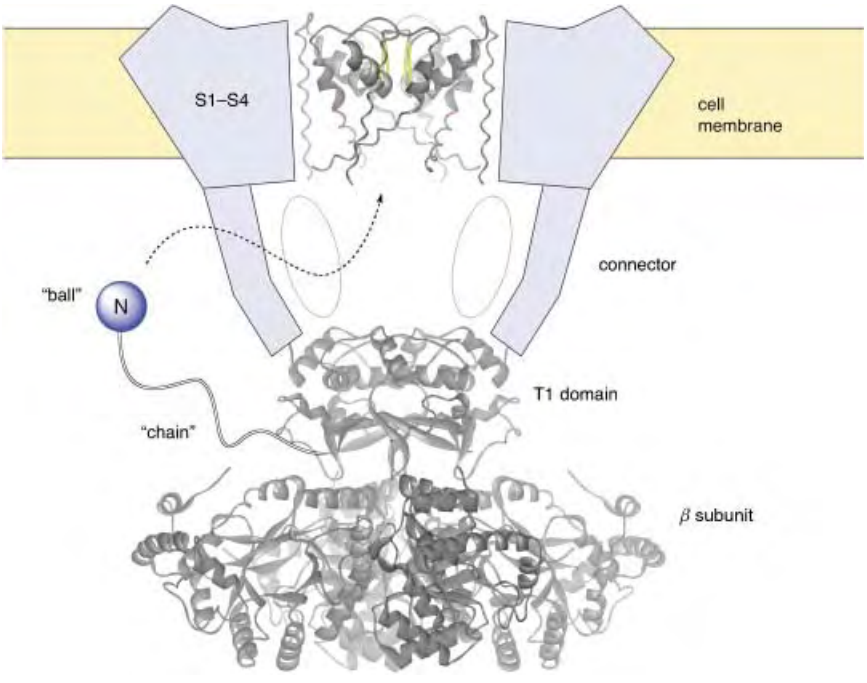



***Figure 5.*** Composite model of a voltage-gated potassium channel.

 © 2003 Wiley-VCH Verlag GmbH & Co. KGaA, Weinheim 

years after Neher and Sakmann (Nobel Prize 1991) provided the necessary techniques to study them on a "single molecule" level, detailed structures of potassium channels have been disclosed—and again this research has been rewarded with a Nobel Prize. Many of the lessons learned from studying potassium channels will be applicable to related transmembrane proteins, such as sodium or calcium channels, and perhaps even to ion channels in general. With an improved understanding of the structure and function of ion channels, neurobiology is bound to mature into a "true" molecular science. Chances are that structures of other key elements of neurobiology, in particular G-protein-coupled receptors and ion pumps, will soon follow, and push back even further what promises to be one of the most exciting scientific frontiers of the 21st century.


[1] a) B. Hille, *Ion Channels of Excitable Membranes*, 3rd ed., Sinauer, Sunderland, **2001**; b) F. M. Ashcroft, *Ion Channels and Disease*, Academic, San Diego, **2000**; c) C. A. Hübner, T. J. Jentsch, *Hum. Mol. Genet.* **2002**, *11*, 2435; d) G. Yellen, *Nature* **2002**, *419*, 35.

[2] M. L. Garcia, Y. D. Gao, O. B. McManus, G. J. Kaczorowski, *Toxicon* **2001**, *39*, 739.

[3] R. MacKinnon, S. L. Cohen, A. Kuo, A. Lee, B. T. Chait, *Science* **1998**, *280*, 106.

[4] Y. X. Jiang, V. Ruta, J. Y. Chen, A. Lee, R. MacKinnon, *Nature* **2003**, *423*, 42.

[5] D. A. Doyle, J. M. Cabral, R. A. Pfuetzner, A. L. Kuo, J. M. Gulbis, S. L. Cohen, B. T. Chait, R. MacKinnon, *Science* **1998**, *280*, 69.

[6] Y. F. Zhou, J. H. Morais-Cabral, A. Kaufman, R. MacKinnon, *Nature* **2001**, *414*, 43.

[7] a) Y. X. Jiang, A. Lee, J. Y. Chen, M. Cadene, B. T. Chait, R. MacKinnon, *Nature* **2002**, *417*, 515; b) Y. X. Jiang, A. Lee, J. Y. Chen, M. Cadene, B. T. Chait, R. MacKinnon, *Nature* **2002**, *417*, 523.

[8] a) Y. X. Jiang, A. Lee, J. Y. Chen, V. Ruta, M. Cadene, B. T. Chait, R. MacKinnon, *Nature* **2003**, *423*, 33; b) Y. X. Jiang, V. Ruta, J. Y. Chen, A. Lee, R. MacKinnon, *Nature* **2003**, *423*, 42.

[9] a) B. E. Cohen, M. Grabe, L. Y. Jan, *Neuron* **2003**, *39*, 395; b) C. Miller, *Nat. Struct. Biol.* **2003**, *10*, 422.

[10] D. M. Papazian, T. L. Schwarz, B. L. Tempel, Y. N. Jan, L. Y. Jan, *Science* **1987**, *237*, 749.

[11] A. L. Kuo, J. M. Gulbis, J. F. Antcliff, T. Rahman, E. D. Lowe, J. Zimmer, J. Cuthbertson, F. M. Ashcroft, T. Ezaki, D. A. Doyle, *Science* **2003**, *300*, 1922.

[12] J. M. Gulbis, M. Zhou, S. Mann, R. MacKinnon, *Science* **2000**, *289*, 123.

[13] S. N. Gradl, J. P. Felix, E. Y. Isacoff, M. L. Garcia, D. Trauner, *J. Am. Chem. Soc.* **2003**, *125*, 12668.


 © 2003 Wiley-VCH Verlag GmbH & Co. KGaA, Weinheim 

Conservation Techniques

# The Restoration of the Largest Archaeological Discovery—a Chemical Problem: Conservation of the Polychromy of the Chinese Terracotta Army in Lintong

*Heinz Langhals* and Daniela Bathelt*

**Keywords:**
archaeology · hydroxyethyl methacrylate · lacquer · polymerization · terracotta army

*The conservation of the polychromy of the terracotta army of the first Chinese emperor Qin Shihuangdi represents a special problem because of the deterioration of the ground layer consisting of organic material. This was triggered due to it having spent more than 2200 years in water-saturated soil. The consolidation of the polychromy was achieved through polymerisation of a specially adapted combination of monomers.*

## 1. Introduction

The first Chinese emperor, Qin Shihuangdi, is known as the founder of united China. He subjugated all other kingdoms in China in 221 B.C. and put an end to the dynasty of the Warring States (Table 1). He started an era of large-scale construction and reforms. Not only are there a number of important buildings dating from this era, such as the Great Wall of China, but the unified Chinese script also brought about appreciable progress.

***Table 1:*** Selected Chinese Dynasties.

| | |
|---|---|
| 5000 B.C. | Beginnings of the bronze period |
| 1045–771 B.C. | Western Zhou Dynasty |
| 770–256 B.C. | Eastern Zhou Dynasty |
| 445–221 B.C. | Warring States Dynasty |
| 221–206 B.C. | Qin Dynasty |
| **210 B.C.** | **Death of the Emperor Qin Shihuangdi** |
| 206 B.C.–9 A.D. | Western Han Dynasty |
| 9–24 | Xin Dynasty |
| 25–220 | Eastern Han Dynasty |
| 220–280 | Three Kingdoms Dynasty |
| 304–439 | Sixteen Kingdoms Dynasty |
| 386–589 | Northern and Southern Dynasties |
| 581–618 | Sui Dynasty |
| 618–907 | Tang Dynasty |

[*] Prof. Dr. H. Langhals, Dipl.-Chem. D. Bathelt
Department Chemie, Universität München
Butenandtstrasse 13, 81377 München (Germany)
Fax: (+49) 89-2180-77640
E-mail: langhals@lrz.uni-muenchen.de

There is a fantastic description of the mausoleum of the emperor (Sima Qian, 91 B.C.[1]), in which the whole world is said to be represented. This description is the only written source of the mausoleum from this time and should be at least partially verified by archaeological discoveries: Terracotta fragments were found during the construction of wells in Lintong, approximately 30 km east of the provincial capital Xi'an ("western peace"), in 1974. This important archaeological discovery consisted of the terracotta army as part of the mausoleum of the first Chinese emperor Qin Shihuangdi (see Figure 1).



***Figure 1.*** Part of the terracotta army of the Chinese emperor Qin Shihuangdi in pit 1.

It is clear in the meantime that the archaeological field covers an area of at least $4 \times 4.5\ km^2$. The field comprises more than 100 single pits and is probably the largest archaeological find worldwide. To date, more than 1500 life-sized terracotta warriors have been excavated and restored.

 © 2003 Wiley-VCH Verlag GmbH & Co. KGaA, Weinheim DOI: 10.1002/anie.200301633 

Many statues of animals such as life-sized horses were found, and 7000 to 8000 individual statues are estimated in the already opened pits. Moreover, complete war-chariots with terracotta horses were excavated.

However, soon after the first excavations it became clear that this was not only an extraordinary archaeological find, but also a special conservation and restoration challenge, because the terracotta warriors and animals were initially polychrome.[2] They lose their coloration irreversibly soon after excavation. Since the excavation, the terracotta warriors such as in Figure 1 are in a similar unfinished state as they were prior to being polychromed. The consolidation of the polychromy proved to be extraordinarily difficult, because none of the methods and materials commonly used in conservation could be applied successfully. Thus, it became clear that novel methods for the consolidation of the polychromy had to be developed.

The restoration was complicated by the special fate of the terracotta warriors. Soon after the death of the emperor Qin Shihuangdi, a rebellion broke out and the statues were damaged and their weapons looted. Also, the underground wooden structures that housed the warriors were set on fire. Residues of charcoal can be found in the pits even today (Figure 2a). The wooden ceiling of the shafts collapsed and the warriors were buried by the loamy soil. The terracotta warriors remained in the water-saturated layer of soil, which at times could reach a thickness of 200 meters, for more than 2000 years. All organic materials, especially the polychromy of the figures, were damaged by the previous fire and the long-lasting effect of water.

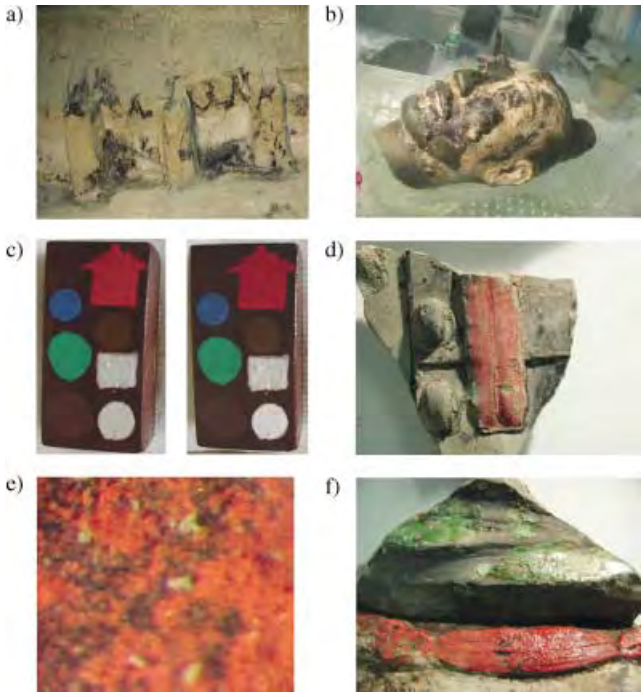



***Figure 2.*** Excavations in Lintong. a) Traces of the big fire in the walls of pit 2. b) Head of a terracotta warrior with partially consolidated polychromy. Treatment with polyethylene glycol (PEG) in a climatized chamber. c) Modern pigments on terracotta: left: before irradiation with an electron beam; right: after irradiation with an electron beam (50 kGy). Pigments on the sample: left column from top to bottom: azurite, malachite, hematite; right column from top to bottom: cinnabar, ochre, coquina (aragonite), white lead pigment. d) Fragment from the cuirass of a warrior (fragment nr. 007/2000) consolidated by electron-beam curing. e) Microscopic view of the red pigment layer. f) Consolidated terracotta fragment with glossy spots (fragment 005/2000).

## 2. Layer Structure of the Polychromy

An investigation showed that the polychromy was made up of a layer structure consisting of a base followed by a pigment layer.[3] The base, which consists essentially of qi-lacquer (east Asian lacquer) probably with additives such as rice starch, was generally applied in two layers. Things were made especially difficult by the fact that no documentation was found on the production of the terracotta warriors and no clues were found in the pits themselves. No binding media was present in the pigment layer. The two-layered base of qi-lacquer has altered during its time in the stratified soil, which leads to cleavage, curling, and flaking followed by the loss of the top paint layer and the qi-lacquer base when the relative humidity sinks below 84%. Conventional methods for conservation can not stop this process, and therefore new methods are required.

## 3. Properties and Processing of Qi-Lacquer

Qi-lacquer[4] is formulated from the sap of the lacquer tree (*Rhus vernificera* Stokes, new nomenclature: *Toxicodendron*



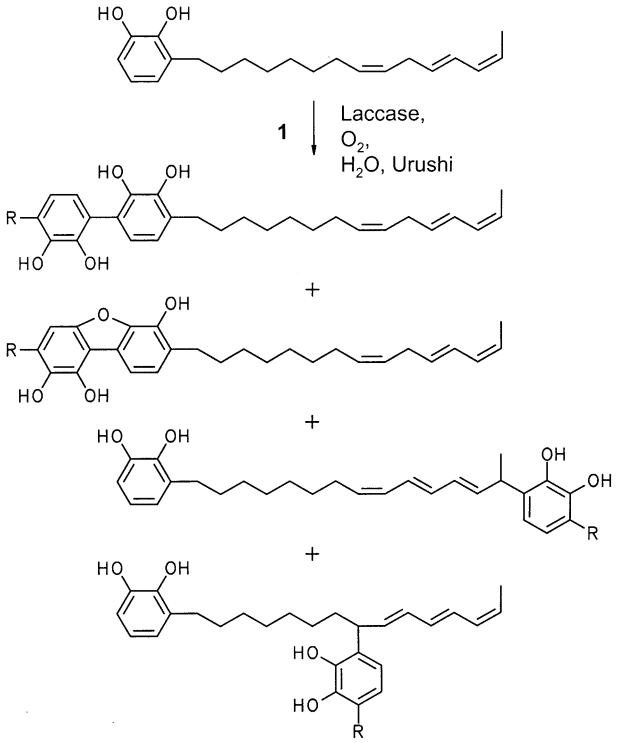
*Heinz Langhals was born in Altena (Germany) in 1948. In 1967 he began his chemistry studies at the University of Münster. In 1974 he obtained his PhD in Freiburg (with Prof. C. Rüchardt). After postdoctoral studies in Paris (Organic Chemistry, Prof. M. Julia) and in Zürich (Physical Chemistry, Prof. H. Fischer), he was appointed C3 Professor at the Universität München in 1984. His research interests lie in the fields of organic and macromolecular chemistry. In 2002, he was a visiting researcher at the Bingmayong Museum in China.*



*Daniela Bathelt was born in 1974 in Neuendettelsau (Germany) and studied chemistry at the Universities of Erlangen-Nürnberg and Oslo. She completed her Diploma studies in Erlangen under the supervision of Prof. R. Saalfrank. Since 2001 she has been working on her PhD thesis with Prof. H. Langhals, and is involved in the BMBF-sponsored "China Project" at the Bavarian State Department of Historical Monuments with Prof. R. Snethlage. Her research is focused on the conservation of aged qi-lacquer.*

 © 2003 Wiley-VCH Verlag GmbH & Co. KGaA, Weinheim 

*vernicifluum (Stokes) F. A. Barkley*) and is still used today. The lacquer is first conditioned by stirring and warming. The crude lacquer sap contains urushiol (**1**) and analogous components with a smaller number of double-bonds in the side chain.[*] The content of urushiol should be more than 45% (preferably 70%) to obtain a smooth layer of lacquer. Hardening in air is induced by the copper-containing enzyme laccase (content 1% in the crude sap). Polymerization of urushiol proceeds through electron-transfer reactions with participation of both the aromatic structure and the side chains (Scheme 1, compare also reference [5]). The formation




***Scheme 1.*** Chemical reactions in the consolidation of qi-lacquer. Urushi[24] means crude lacquer, whose content of **1** amounts to 58%.

of a smooth layer of lacquer is influenced by carbohydrate components,[6] which give structure to the polymer. No nitrogen is detected in the hardened lacquer (detection limit $\leqslant 0.01$% by elemental analysis) as residues from laccase.[7] A constant high humidity of 75–85% and a temperature of 25–30°C are important for the formation of a high-quality lacquer layer. The strong allergenic effect[8] of **1** must be considered for all work with fresh qi-lacquer; urushiol has similar chemical properties to that of poison ivy. Fortunately, the hardened lacquer does not induce any allergic reactions.

[*] The name urushiol usually refers to a mixture of pyrocatechols with a side chain of 15 or 17 carbon atoms which contains up to three double bonds. The configuration at the double bonds and the exact composition depends on the source of the natural product mixture (W. P. Armstrong, W. L. Epstein, *HerbalGram* **1995**, *34*, 36–42; this journal is published by the American Botanical Council and the Herb Research Foundation).

The hardened lacquer is brownish black, nontransparent, absolutely insoluble, and can only swell slightly with water and even less with organic solvents. The lacquer resembles phenol formaldehyde resins in many respects. However, it is more sensitive, for example, against UV radiation. The insolubility and nontransparency of the lacquer is a handicap both for the investigation and the conservation of the lacquer because polymers cannot penetrate the layer.

## 4. Consolidation of the Polychromy of the Terracotta Statues

The fine porous structure of the water-saturated lacquer is the fundamental problem in the restoration of the polychromy. Polymers for conservation are too big to penetrate the layer, so that established materials for consolidation failed. Transportation of the consolidant through fissures is not sufficient because the lacquer layer still curls and falls off. One option is the partial replacement of water by a high-boiling-point, non-evaporating material. This way, a complete desiccation can be prevented.

The detachment and cleavage of the polychromy can be prevented or at least delayed by a slow exchange of the water in the terracotta by polyethylene glycol with a low molecular weight (PEG 200 or PEG 400; Figure 2b).[9] The latter is very hygroscopic, so that desiccation is prevented. The wet surfaces attract dust and remain mechanically sensitive, and therefore the handling of artifacts is problematic.

A more stable consolidation of the lacquer layer was possible by the application of a water-soluble organic monomer. The latter was diffused into the water-saturated terracotta fragments by poultices.[10] Hydrophilic organic monomers are especially suited for this purpose because they can penetrate the aged layer of lacquer and partially replace the water in its porous structure. Consecutive anionic or cationic polymerization methods are problematic because of the high water content, and therefore radical polymerization is preferred. The application of thermal radical initiators is less appropriate in this special case because the diffusion of monomers is a slow process so that hardening at the surface of the terracotta is difficult to control. Even hardening with UV radiation is not possible because qi-lacquer is nontransparent. Thus, a hardening is only possible at the surface and not at the important connection between lacquer and terracotta.

Hardening with penetrating ionizing radiation is therefore a solution to this problem. However, X- and $\gamma$ rays are not really suitable as they easily penetrate the layer of lacquer but are more likely to be absorbed by the terracotta. Electron radiation ($\beta$-rays)[11,12] is optimal because it penetrates the layer of lacquer without any problem and is then stopped efficiently by the terracotta.[13] Thus, polymerization is more strongly induced within the barrier layer important for the adhesion and proceeds from there towards the surface.[14] Finally, the polymerization reaction stops at the border with the surrounding air, where oxygen acts as a radical trap. This is of special interest for conservation and restoration because it prevents the formation of a glossy surface. Such an artificial

 © 2003 Wiley-VCH Verlag GmbH & Co. KGaA, Weinheim 

surface gloss would very much detract from the natural appearance of the terracotta warriors.

Electron rays are favorably obtained by an electron accelerator (Figure 3). Nuclear processes are excluded if the voltage of acceleration does not exceed 1 MV. Thus, the



***Figure 3.*** Electron accelerator near Lintong.

radiation vanishes as soon as the accelerating voltage is switched off. During irradiation, a large amount of X-rays are emitted as bremstrahlung from decelerated electrons. This must be appropriately shielded. This secondary radiation is also of interest for the preservation of the lacquer because it causes complete sterilization of the sample. A slow deterioration of the lacquer by microorganisms and mould is thus efficiently prevented. An accelerating voltage of 1 MV proved to be optimal.

The polychromy contains pigments such as cinnabar or malachite in addition to the qi-lacquer base layer (Table 2, compare also reference [15]). These are also not only exposed to the radiation, but can also stop it efficiently because they

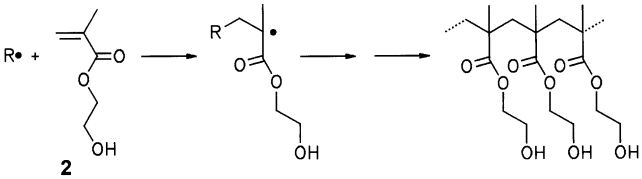
***Table 2:*** Pigments of the terracotta army.

| Pigment | Formula | CAS-Nr. | Chinese name |
|---|---|---|---|
| orpiment | $As_2S_3$ | 1303-33-9 | 雌黄 |
| azurite | $Cu_3(CO_3)_2(OH)_2$ | 1319-45-5 | 石青、佛青 |
| bone white | $Ca_5(PO_4)_3OH$ | 12167-74-7 | 磷灰石、骨白 |
| cerussite | $PbCO_3$ | 598-63-0 | 白铅矿 |
| China ink | C | 7440-44-0 | 炭黑 |
| cinnabar | HgS | 1344-48-5 | 朱砂 |
| hematite | $Fe_2O_3$ | 1309-37-1 | 赤铁矿 |
| Han blue | $BaCuSi_4O_{10}$ | | 汉蓝 |
| Han purple | $BaCuSi_2O_6$ | 169122-88-7 | 汉紫 |
| kaolinite | $Al_2O_3{\cdot}SiO_2{\cdot}2\,H_2O$ | 1332-58-7 | 高岭土 |
| malachite | $Cu_2CO_3(OH)_2$ | 12069-91-1 | 石绿 |
| massicot | PbO | 1317-36-8 | 铅黄 |
| ochre, yellow and red | $Fe_2O_3$ | 1309-37-1 | 黄色和红色的赭石 |
| red lead | $Pb_3O_4$ | 1314-41-6 | 铅丹 |
| white lead pigment | $2\,Pb(CO_3)_2{\cdot}Pb(OH)_2$ | 1319-46-6 | 铅白、胡粉 |

contain heavy elements. These pigments proved to be inert to electron radiation, even when an appreciably higher dose was applied than is necessary for hardening (Figure 2c). Even an extreme dose (400 kGy) does not affect the colors. Thus, hardening by electron radiation does not have negative consequences on the color of the pigments.

## *5. Requirements of the Monomer for the Consolidation of the Polychromy*

The monomeric consolidant must fulfill a number of requirements. For example, it should be water-soluble to penetrate the water-saturated surface of the terracotta and it should contain polar groups to bind firmly to the polar surface of the terracotta. To guarantee the long-term stability of the consolidation, a high persistence of the polymer is an important prerequisite. We applied hydroxyethyl methacrylate (HEMA (**2**) and the cross-linker PEG-DMA 330 (see below); Scheme 2) as a monomer because it forms a highly stable polymer and is water-soluble, so that it can be applied directly to the water-saturated terracotta to fill the pores. Polyethylene glycol may be applied for the partial replacement of water even before this hardening.




***Scheme 2.*** Formation of free radicals in the electron-beam-induced polymerization of HEMA.

Several processes can initiate the polymerization of HEMA. The relative tendencies for the formation of free radicals *G*, which indicates the number of radicals formed per 100 eV of absorbed radiation, is a suitable measure (Table 3 and Equation 1).[16] In Equation (1), *c* is the concentration of

$$c = \rho\, G\, D\, N_{\mathrm{L}}^{-1} \qquad (1)$$

reaction products in $\mathrm{mol\,L^{-1}}$, $\rho$ is the density of the target in $\mathrm{kg\,L^{-1}}$, *D* is the absorbed dose in Gy, and $N_L$ is the Loschmidt constant. The reaction of the electron beam with water is clearly a process with low efficiency.[17] The reaction of the monomer is appreciably more efficient. The polymerization reaction proceeds more quickly in the presence of a cross-linker such as polyethylene glycol dimethacryl ester (PEG-DMA 330).[18] The reaction of the electron beam with the polymeric material is possible, but with appreciably lower yields.[19] Thus polymerization is favored over depolymerization, so that overall polymeric material is formed. The poorly efficient reaction of the polymeric material with the electron beam is also of interest because, in principle, it offers the possibility of refreshing aged polymeric material.[20] The

 © 2003 Wiley-VCH Verlag GmbH & Co. KGaA, Weinheim 

already long lifetime of the polymer can be thus multiplied, so that an extraordinarily long-lasting conservation is guaranteed. The permeability of water vapor through polymeric HEMA is a further advantage because it enables exchange of humidity. This prevents accumulation of humidity or water vapor below the consolidation layer, which could cause the formation of bubbles and subsequent detachment.

***Table 3:*** *G* values for some compounds.

| Target | *G* |
|---|---|
| water | 0.45 |
| alkanes | 4 |
| methylacrylate | 15 |
| methyl methacrylate | 11.5 |
| polymethyl methacrylate[a] | 1.1 |

[a] Chain fission.

The polychromy of the excavated terracotta fragments can be consolidated piece by piece with electron-beam curing. The conserved fragments can then be combined, and the statues reconstructed. The success of electron-beam curing was verified by laser video holography.[21] A complete insensitivity towards alteration of the humidity was found for single fragments. For others, some curling of the broken perimeters of the lacquer base occurred, and in extreme cases, cracks and even craquelure caused by humidity fluctuations occurred. However, even in these cases the lacquer remained firmly fixed to the base so that no detachment took place.[22] A consolidated terracotta fragment from the cuirass of a warrior is shown in Figure 2 d. The impression of color was in no way disturbed by the consolidation, and no gloss occurred at the surface. A microscopic view of the red polychromy is shown in Figure 2 e. One can see the agglomerates of cinnabar and the brownish background of the qi-lacquer in areas where the paint layer has been lost. The average diameter of single particles is 4–5 μm, often even smaller. There have been a few single particles of 20 μm in size. One can observe agglomerates of these particles with a microscope.

The electron-beam curing has had a successful debut as the consolidated polychromy has remained unchanged for several years. Many technical details are still to be optimized. For example, glossy spots (Figure 2 f) occurred in a few cases over three years as a consequence of a consecutive reaction of excess HEMA owing to the hot, humid Lintong summers. The consolidating of strongly curved areas of fragments is a further problem and requires the development of special types of radiation techniques. Electron-beam curing delivers the most stable conservation of the polychromy of the excavated fragments. Many details are still to be solved; however, the results thus far make this a worthwhile task.

## 6. Outlook

Electron-beam curing with the use of HEMA promises to become the method of choice for a durable conservation of the polychromy of the terracotta army. This has recently been given a special significance and timeliness, since in the framework of new excavations (end of 2002) sites were discovered that exceed even those known to date (see daily press, for example, K. Strittmatter, *Süddeutsche Zeitung* 59/2, No. 8 of January 11, 2003, p. 12).[23] To preserve an archaeological treasure of such a magnitude requires the development of conservation methods that on the one hand give lasting results and on the other can be applied routinely.

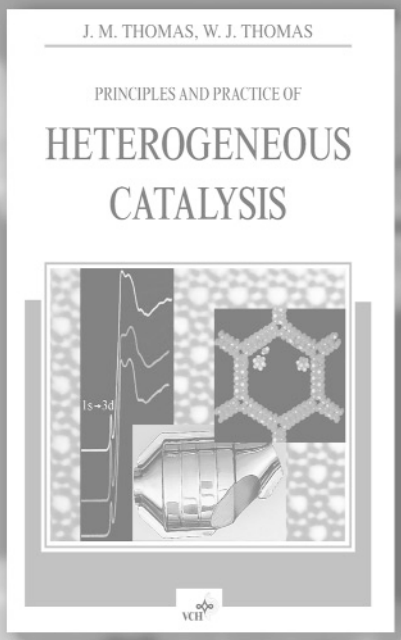
*We especially thank Professor Dr. R. Snethlage, Prof. Dr. C. Herm (Schule für Bildende Künste, Dresden), Mr. H. Dorschner and Mr. G. Neubert (IPF, Dresden), Mrs. C. Blänsdorf, Mrs. M. Weichert, and Mrs. C. Thieme (presently at the Munich University of Technology) of the Bavarian State Department of Historical Monuments, Mr. Zhou Tie, Mr. Zhang Zhijun, and Mr. Rong Bo of the Museum of the Terracotta Army of Qin Shihuang in Lintong (Bingmayong-Museum), and Mr. Xing Dong Jian of the Xi'an Radiation Research Center and many other co-workers of these three institutes. We also thank Dr. I. Rogner for his pioneering work in the field of electron-beam curing. We thank the BMBF for financial support of this project.*

Received: February 3, 2003 [M1633]

[1] Sima Qian, *Report of the Historian (Shiji)*, Beijing, **91 B.C.**; translation: H.-Y. Yang, G. Yang, *Selections from Records of the Historian*, Commercial Press, Hong Kong, **1974**, chap. 6, p. 256.
[2] "On the Polychromy of the Terracotta Army": C. Thieme, E. Emmerling in *The Terracotta Army of the First Chinese Emperor Qin Shihuang (Arbeitshefte des Bayerischen Landesamtes für Denkmalpflege, Vol. 83)*, Karl Lipp, München, **2001**, p. 335 – 370 (ISBN 3-87490-711-2).
[3] "Analysis of Painting Materials of the Polychrome Terracotta Army of the First Emperor Qin Shi Huang": C. Herm, C. Thieme, E. Emmerling, W. Yong Qi, Z. Tie, Z. Zhijun in *The Ceramics Cultural Heritage (Techna—Monographs in Materials and Society, Vol. 2)* (Ed.: P. Vincenzini), Gruppo Editoriale Faenza Editrice, Faenza, **1995**, p. 675 – 684.
[4] J. Mills, R. White, *Organic Chemistry of Museum Objects*, 1st ed., Butterworth–Heinemann, London, **1987**, p. 104.
[5] S. Kobayashi, H. Uyama, R. Ikeda, *Chem. Eur. J.* **2001**, *7*, 4755 – 4760.
[6] L. Zhang, X. Qiu, J. Xu, Y. Du, B. Qian, J. F. Kennedy, *Carbohydr. Polym.* **1992**, *19*, 161 – 166 [*Chem. Abstr.* **1993**, *117*, 214558w].
[7] H. Langhals, U. Ring, unpublished results.
[8] G. Dupuis, *Br. J. Dermatol.* **1979**, *101*, 617 – 624.
[9] Restored by K. Blänsdorf, **2002**.
[10] I. Rogner, PhD Thesis, Universität München, **2000**.
[11] I. Rogner, H. Langhals, *ARC-Nucléat, Grenoble* **1999**, 294 – 298.
[12] I. Rogner, H. Langhals, *J. Macromol. Sci. Part A* **1999**, *36*, 461 – 469 (*Notes part*).
[13] "Consolidation and Preservation of the Polychrome Qi-Lacquer Layers of the Terracotta Army of Qin Shihuang by Treatment with Methacrylic Monomers and Electron-Beam Curing": I. Rogner, H. Langhals, Z. Tie, Z. Zhijun, R. Bo, C. Blänsdorf, C. Herm in *The Terracotta Army of the First Chinese Emperor Qin Shihuang (Arbeitshefte des Bayerischen Landesamtes für Denkmalpflege, Vol. 83)*, Karl Lipp, München, **2001**, p. 594 – 617, ISBN 3-87490-711-2.
[14] I. Rogner, H. Langhals, Ger. Offen. DE 19859549.2, **1998**; [*Chem. Abstr.* **2000**, *133*, 75374y].

 © 2003 Wiley-VCH Verlag GmbH & Co. KGaA, Weinheim 

[15] H. Berke, *Angew. Chem.* **2002**, *114*, 2595 – 2600; *Angew. Chem. Int. Ed.* **2002**, *41*, 2483 – 2487.
[16] *Ullmann's Encyclopedia of Industrial Chemistry*, 6th ed., Wiley-VCH, **1999**, *Electronic Release, Radiation Chemistry*, Table 1.
[17] *Ullmann's Encyclopedia of Industrial Chemistry*, 6th ed., Wiley-VCH, **1999**, *Electronic Release, Hydrogen, 4.4.1 Thermolytic and Radiolytic Processes.*
[18] D. Bathelt, H. Langhals, unpublished results.
[19] J. Pacansky, R. J. Waltman, *J. Radiat. Curing* **1988**, *10*, 12 – 25.
[20] D. C. McHerron, G. L. Wilkes, *Polymer* **1993**, *34*, 915 – 924.
[21] R. Jones, C. Wykes, *Holographic and Speckle Interferometry*, Cambridge University Press, Cambridge, **1983**.
[22] G. Gülker, A. El Jarad, A. Kraft, Universität Oldenburg, and I. Rogner, H. Langhals, Universität München, unpublished results.
[23] Mr. Rong Bo of the Museum of the Terracotta Army of Qin Shihuang in Lintong, personal communication.
[24] For an overview, see: Y. Du in *Urushi—Proceedings of the 1985 Urushi Study Group* (Eds. N. S. Brommelle, P. Smith), Getty Conservation Institute, Los Angeles, **1998**, pp. 189 – 197 (ISBN 0-89236-096-8).




Register now for the free
**WILEY-VCH Newsletter!**
http://www.wiley-vch.de/home/pas

**Principles and Practice of**
**Heterogeneous Catalysis**

***J. M. THOMAS**, The Master's Lodge, Peterhouse, Cambridge, UK;*
***W. J. THOMAS**, University of Bath, UK*

*3-527-29239-X 1996 XIX, 669 pp*
*375 figures 25 tables. SC.*
*€ 55.00*/£32.50*

Catalysis occupies a pivotal position in the physical and biological sciences. As well as being the mainstay of the chemical industry, it is the means of effecting many laboratory syntheses and the root cause of all enzymatic processes.

This book is an eminently readable introduction to the fundamental principles of heterogeneous catalysis. Written by world-renowned experts, it explains the vocabulary, grammar and literature of catalysis from the laboratory-oriented model study through to the operating plant.

Didactically skillful and using many lucidly designed figures, the authors present an insightful exposition of all important concepts, new developments and techniques in this rapidly advancing field.

* *The €-prices refer to Germany only!*

73901111_vi

*Wiley-VCH · P. O. Box 10 11 611 · 69451 Weinheim, Germany*
*Fax: +49 (0) 62 01-60 61 84 · service@wiley-vch.de · www.wiley-vch.de*

WILEY-VCH

 © 2003 Wiley-VCH Verlag GmbH & Co. KGaA, Weinheim 

Single-Crystal Growth of Silicon

# Czochralski's Creative Mistake: A Milestone on the Way to the Gigabit Era

*Jürgen Evers,* Peter Klüfers, Rudolf Staudigl,* and Peter Stallhofer*

*Dedicated to Professor Heinrich Nöth on the occasion of his 75th birthday*

**Keywords:**
crystal growth · Czochralski, Jan · defect engineering · microelectronics · silicon




 © 2003 Wiley-VCH Verlag GmbH & Co. KGaA, Weinheim DOI: 10.1002/anie.200300587 

*Much of the rapid change in industry, science, and society is brought about by the meteoric development of the microelectronics industry. Daily life is affected by this development; one has only to think of mobile telephones and the chips on modern credit cards. The raw material for microelectronics is the single crystal of silicon, with very high purity and almost perfect crystal structure. About 95% of the world's current production of silicon single crystals is achieved using the process that Jan Czochralski discovered in 1916. Today, single crystals of silicon can be grown that are up to 2 m long, 300 mm in diameter, and weigh up to 265 kg. The use of magnetic fields has led to significant advances in crystal-drawing technology. Intensive research and development reveals that in addition to the technology, which provides crystals of ever-increasing diameter, defect engineering, and the control of the numerous temperature-dependent reactions of crystal defects, are of paramount importance.*

**From the Contents**


| | |
|---|---|
| 1. Introduction | 5685 |
| 2. Jan Czochralski (1885–1953) | 5686 |
| 3. Czochralski's Creative Mistake: Single Crystals of Tin Drawn from the Melt | 5688 |
| 4. Preparation of Silicon Single Crystals with a Diameter of 300 mm | 5689 |
| 5. Summary and Outlook | 5697 |


> *"...spreading understanding for technological issues... If we could only have travel diaries for the technical countryside that could be measured against Goethe's Italian Journey or Bismarck's Reflections and Reminiscences, the public could look at technical things with Goethe's open eyes, free them from the cold usefulness of purpose, and recognize their wonderful laws and the beauty of their existence."*
> Wichard von Moellendorf[80]

## 1. Introduction

Single-crystal rods of silicon with large diameters and few defects are fundamental raw materials of the microelectronics industry that have assumed a key position in information and communication technology. The production of microelectronic components based upon silicon is a field of high technology that is under particular pressure for rapid innovation. According to the findings of G. E. Moore,[1] the capacity of electronic components (microchips) doubles in just two years with a concomitant halving in their price. Maintenance of this rapid technological advance is only possible because the line width of the incorporated electronic components is constantly reduced and consequently more functions can be accommodated on a single chip. Furthermore, with the increasing diameter of single-crystalline silicon wafers, more chips can be accommodated on a wafer and produced at the same time. It has only recently been possible to overcome this considerable cost degression per microchip through enormous technological advances. The progression from wafers of 150 mm to 200 mm diameter was achieved in 1990,[2] while the development of 300 mm wafers became possible in 1995. Since then, worldwide production of the most highly integrated chips have been produced on wafers with a diameter of 300 mm,[3] and before long the first one gigabit chips, with enough storage capacity to contain a 25-volume encyclopedia, will be available.

About 95% of the world's production of silicon single crystals[4] is manufactured by the method devised by the Pole Jan Czochralski. His method for drawing single crystals from a crucible, discovered in 1916 and described in 1918,[5] has dramatically changed daily life. Whether we communicate with a mobile telephone, pay with a chip-containing credit card in the supermarket, activate the anti-theft device in a car, or, as may soon be possible, are recognized as an individual by biometric systems, it is clear that without microchips made from single crystals of silicon, nothing would work!

In spite of this it is not an easy task to uncover anything about the life of Jan Czochralski, or the circumstances that surround his discovery. In the reading room of the Bavarian State Library in Munich it was a slow process to find out anything about the man himself. It is true that there are many references to the Czochralski method for drawing single crystals: in the Encyclopedia Britannica, the Encyclopedia Americana; in English, French, Russian, Italian, and German. However, the recent editions of reference books, sometimes comprising 20 volumes, possess no entry on Jan Czochralski himself. And in Poland? In the Wielka Encyclopedia Powszechna (12 volumes, 1962–1969), there is also no entry for Jan Czochralski. Although there is a 17-line text entry in the supplementary volume published in 1970, a search for a photograph proved unsuccessful.[6]

The first biographical data on Jan Czochralski and the quite unusual circumstances surrounding the discovery of

[*] Prof. Dr. J. Evers, Prof. Dr. P. Klüfers
Department Chemie
Ludwig-Maximilians-Universität München
Lehrbereich Anorganische Chemie
Butenandtstrasse 5–13, 81377 München (Germany)
Fax: (+49) 89-2180-77950
E-mail: eve@cup.uni-muenchen.de
Dr. R. Staudigl, Dr. P. Stallhofer
Wacker-Chemie GmbH
Hanns-Seidel-Platz 4, 81737 München (Germany)
Fax: (+49) 89-6279-1466
E-mail: Rudolf.Staudigl@wacker.com

 DOI: 10.1002/anie.200300587 © 2003 Wiley-VCH Verlag GmbH & Co. KGaA, Weinheim 

crystal drawing were published in 1987 by P. E. Tomaszewski of the Polish Academy of Science (Wrocław) in a poorly circulated Polish-language journal.[7] Further biographical data followed two years later from J. Żmija in a report of another Polish journal,[8] and again from P. E. Tomaszewski in 1998, 2002, and 2003.[9–11]

## 2. Jan Czochralski (1885–1953)

Jan Czochralski (Figure 1) was born in Kcynia in what is now Poland on October 23, 1885 as the eighth child of an artisan family. Kcynia lies a little north of the communication link between Berlin and Warsaw, almost exactly 300 km from both cities. The region of Bydgoszcz, which contained Kcynia, was annexed by Prussia in the three Polish partitions (1772–1795), and assimilated into the German Reich in 1871. It was only after the Treaty of Versailles that Czochralski's homeland again became Polish in 1919. Therefore, Jan Czochralski had a German upbringing. He had already become interested in chemistry while at school, but he left senior school (Teacher's Seminary in Kycnia) without graduating. At first he was only able work on chemistry in a perfumery in Krotoszyn near his home town. This soon became too restrictive for him, and in 1904 he moved to Berlin. In an apothecary in Altglienicke owned by a pharmacist with a doctorate in chemistry he improved his knowledge of chemistry. Under expert guidance he carried out analyses of metals, ores, oils, and fats, and was found to be diligent, talented, and accurate. In 1906 he worked for a short time in the analytical laboratory of the Kunheim chemical company in Niederschöneweide near Berlin-Köpenick, and in 1907 he moved to the Allgemeine Elektricitäts-Gesellschaft (AEG), firstly in the laboratory of the Oberspree cable works in Oberschöneweide, and then in other laboratories.[7]



***Figure 1.*** Jan Czochralski, circa 1907, in Berlin.[9] (Photograph by kind permission of Dr. P. E. Tomaszewski)

In addition to his professional activities, from 1905 Czochralski attended lectures in chemistry at the technical high school in Berlin-Charlottenburg (now the Technical University of Berlin), where in 1910 he was awarded the title "Diplom-Ingenieur" for chemistry.[7] In the same year he married the Dutch pianist M. Haase.[8] He had considerable interest in music and literature, wrote poetry, and purportedly attended lectures on art and literature at Berlin University.[7,9]

From 1911 to 1914 Czochralski was assistant to Wichard von Moellendorf (Figure 2),[12] chief technologist[13] and assistant director of AEG,[14] in their metals laboratory. Von Moellendorf was an influential personality. He worked in fields stretching across science, economics, and politics; he was later undersecretary in the German Economics Ministry, was appointed Professor of National Economy, then director of the state-run Materialprüfungsamt in Berlin-Dahlem, the current Bundesanstalt für Materialforschung und -prüfung (BAM), and of the Kaiser-Wilhelm-Institut für Metallforschung. He was a member of the supervisory boards of S. Fischer Verlag, the IG Farbenindustrie, and the Metallbank und Metallurgische Gesellschaft AG (since 1928: Metall-Gesellschaft AG). From 1912 to 1916 he published a number of cultural criticisms in which he warned of the consequences of a profit-orientated economy and presented his ideas of an economic order committed to public welfare.




*Jürgen Evers, born in 1941 (Dortmund), received his doctorate in 1974 with A. Weiss (LMU München) on the preparation of highly purified alkaline earths and their silicides. After postdoctoral research at ETH Zürich (1975) he gained his Habilitation in 1982 at the LMU (high-pressure investigations of silicides). He received a Heisenberg Stipendium (1985) and was appointed supernumerary professor in 1994. His research includes the study of Zintl phases at high pressure. Moreover, he is one of a rare breed who can draw a silicon single crystal by hand, albeit with 1970s technology that gives crystals of 12-mm diameter rather than 300 mm!*



*Rudolf Staudigl, born in 1954 (Neufahrn, Germany), received his doctorate with H. Nöth on the reaction mechanisms of boron compounds. In 1981 he joined W. N. Lipscomb (Harvard) where he worked on quantum-chemical calculations of enzyme–substrate interactions. In 1983 he moved to Wacker-Siltronic, the silicon-producing subsidiary of Wacker-Chemie GmbH, where he worked on optical fibers and GaAs crystal growth. He was president of the American subsidiary responsible for the production of high-purity silicon chips (1990–1993) and is now a company manager of Wacker-Chemie.*


 © 2003 Wiley-VCH Verlag GmbH & Co. KGaA, Weinheim 

At AEG von Moellendorff took considerable interest in metallurgic investigations on copper and aluminum, important for electrotechnology, in which he recognized the problems of "purity and minor impurities".[15] AEG was an innovative company that promoted research and development, and rapidly converted new scientific knowledge into technology.[12] With this research von Moellendorff awakened in his assistant Czochralski, who had until then worked essentially on analytical chemistry, an interest in metallurgy and crystallography. In 1913 a joint publication appeared on "technological conclusions from the crystallography of metals".[16] Amongst other things, the authors showed for the first time that it was possible "by stripping from coarsely crystalline castings… to obtain individual crystals of up to the size of a finger."[17]



***Figure 2.*** The metals scientist, economic theorist, and politician Wichard von Moellendorff.[15] (Photograph by kind permission of the Bundesanstalt für Materialforschung und -prüfung).

While still a student von Moellendorff was introduced to the Rathenau family of industrialists. Since 1887 Emil Rathenau had been director general of AEG, and his son Walther (Figure 3), with a doctorate in physics, had been a member of the board of directors since 1903. After his diploma examination in 1906, von Moellendorff was employed in the AEG Oberspree cable factory. He built up a metals laboratory[14] that contained "a mechanical, a chemical, and a microscopic station" for "centralized control and research work",[16] and he soon became chief technologist. Von Moellendorff was impressed by Walther Rathenau,[14] and a friendly relationship soon developed between the two, such that Rathenau had "great hope" in von Moellendorff.[14] In 1914 along with Rathenau, von Moellendorff encouraged the formation of the department for military raw materials[12] which was incorporated into the Ministry of War.



***Figure 3.*** The scientist, industrialist, and politician Walter Rathenau, seen here as a student (circa 1890).[20] The ink well shown to the left of Rathenau has a shape consistent with that period.[21] (Photograph by kind permission of S. Fischer Verlag).

From 1914 to 1915, Rathenau was director of this new authority,[19] and he appointed von Moellendorff as one of its first co-workers.[14] With von Moellendorff's move into the "government sphere"[14] Czochralski's assistantship came to an end in 1914, and he was able to begin his own research in the metals laboratory, which he was later to lead.

From 1917 everything progressed well for Czochralski. First he moved from AEG to join the Metallbank und Metallurgische Gesellschaft AG in Frankfurt am Main, where in 1918 von Moellendorff was economic advisor[14] and, from 1919, a member of the supervisory board.[12] There, as head of the metals laboratory, Czochralski combined excellent research with economic awareness. With a number of scientific colleagues he founded the German Society for Metals Science in 1919, of which he was president from 1925 until his appointment as professor at the chemical faculty of the Technical University in Warsaw in 1929. After a short period he founded a department for metallurgy and metals science at the university. He even acquired his own research institute, a very rapid ascent for an artisan's son who failed to graduate from high school. His successful work in industry and science in his country of birth brought him high recognition in his homeland. But the Second World War brought about Jan Czochralski's downfall.

The German invasion of Poland in 1939 and the effects of the war eventually led to the complete cessation of his research in Warsaw. At the request of his co-workers he founded a workshop in the institute that produced replacement parts for both the German and Polish self-administration in occupied Warsaw. For those living under duress, that not only brought a means of existence, but also, since official documentation was issued, protection from the random incursions of occupying forces. Czochralski actively supported the Polish underground army and helped many of those in need in the Warsaw ghetto, but after the war the senate of the Technical University of Warsaw accused him of collaboration with the Germans, and in 1945 excluded him from the university.[7,9]

Embittered, he returned to his home town of Kcynia, and using his acquired knowledge of pharmacy and perfumery

 © 2003 Wiley-VCH Verlag GmbH & Co. KGaA, Weinheim 

founded BION, a small company for cosmetics and household chemicals in 1946. He died in Poznañ on April 22, 1953 at the age of 68 and was buried in Kcynia.[7,9] The tragedy of his ever-active life was publicized in 2001 by the fact that in the list of unclaimed Swiss bank accounts with assets deposited before or during the Second World War, there is an entry for a "Czochralski, Jan [Poland]".[22]. However, Swiss banks give detailed information only to persons with a valid claim.

The bond between Walther Rathenau, Wichard von Moellendorff, and Jan Czochralski is typified by the manner their lives were thwarted by the tragic circumstances of the age: Rathenau, appointed German Foreign Minister in 1922, was shot by two young radical right-wing officers in June of the same year.[19] Von Moellendorf killed himself four years after the seizure of power by the National Socialist Party and the suicide of his Jewish second wife.[12]

Jan Czochralski's first publication, in 1913 with Wichard von Moellendorff at AEG, dealt with technological aspects of the crystallography of metals.[17] His final publication appeared in 1940 in the Swiss Archive for Applied Science and Technology and dealt with the results of some basic research on aluminum.[23] At that time the first European aluminum facility in Neuhausen am Rheinfall (Switzerland), in which Walther Rathenau once worked as technical appointee, was only 50 years old. In 27 years Czochralski published 101 metallurgic publications,[7] of which 70 are referenced in Chemical Abstracts. These include a text book (Modern Metal Science in Theory and Practice), which was published by Julius Springer in 1924 and which was later translated into several languages.[24]

After his exclusion from the Warsaw Technical University, Jan Czochralski sank into obscurity under the communist regime. He found greater recognition only after his death. Seventy years after the discovery of crystal drawing, the 10th European Crystallographic Meeting in Wrocław (1986) was dedicated to his memory.[7] Today, Jan Czochralski is recognized as one of the most highly regarded Polish natural scientists (a list of 14 outstanding natural scientists born in Poland was published by the Polish Physical Society[25]). Jan Czochralski stands alongside Maria Skłodowska-Curie, Walther Nernst, Otto Stern, and Albert Michelson. On the occasion of the 50th anniversary of Czochralski's death the Polish Society for Crystal Growth held an international symposium in Toruñ and Kcynia at the end of April 2003.[26]

## 3. Czochralski's Creative Mistake: Single Crystals of Tin Drawn from the Melt

The famous discovery, the effects of which can be felt today, was made by Czochralski at AEG in Berlin.[5] He submitted a paper to Zeitschrift für Physikalische Chemie in August 1916, which appeared in the February issue of 1917, but was only classified for the first time in Volume 92 in 1918. He had also communicated his results briefly to the Zeitschrift des Vereines Deutscher Ingenieure in April 1917.[27] In retrospect, it is surprising to note that Czochralski made this fundamental discovery through a creative mistake!

According to the research of P. E Tomaszewski,[7,9–11] Czochralski was working on the rate of crystallization of metals and one evening had terminated an unsuccessful experiment with a tin melt. He carefully placed the full, hot crucible on the edge of the desk to cool. He then began to enter notes into the laboratory notebook. The necessary utensils of the time (pen and ink well) were on the desk. Then, as Czochralski confirmed nine years later, a "remarkable coincidence" took place.[18] He was totally fixated on the notes, and deep in thought he dipped his pen not into the ink well, but into the crucible with molten tin.[7,9–11] Alarmed, he quickly lifted his arm and noted that a long, thin thread was hanging onto the pen. It was, through etching with acid, to be the first single crystal drawn out of a crucible by the Czochralski method! A single crystal of tin had separated from the liquid tin due to the capillary-like constriction of the tip of the steel pen on its removal. This thin single crystal acted as a seed to which further tin atoms from the melt attached themselves to the single crystal.

Figure 4 illustrates the apparatus of 1916, unpretentious by modern standards, with which Jan Czochralski made his discovery reproducible "with ease" as he himself later put it.[24] With this apparatus he prepared single crystals of tin, lead, and zinc. The length of the single crystals of tin drawn in the first Czochralski apparatus was about 15 cm with a diameter of about 1 mm and a mass of about 1 g.

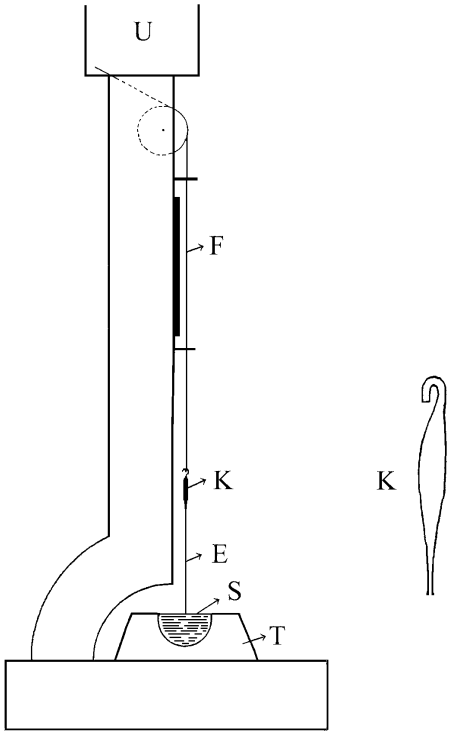



***Figure 4.*** Czochralski's crystal drawing apparatus of 1916.[5] The clockwork motor (U) draws the single crystal (E) out of the melt (S) which sits in the crucible (T). The seed crystal resides in a capillary (K), which is attached to a thread (F). The capillary (K) is shown on the right-hand side of the apparatus, magnified six times. From a diagram by J. Czochralski.[5]

 © 2003 Wiley-VCH Verlag GmbH & Co. KGaA, Weinheim 

## 4. Preparation of Silicon Single Crystals with a Diameter of 300 mm

### 4.1. A Backward Glance

As previously stated, about 95% of the world's production of silicon single crystals is manufactured by the Czochralski (CZ) procedure.[4] It is interesting to note how rapidly the diameter of silicon single crystals has increased over the last three decades. At the beginning of the 1970s one of the authors (J.E.) had prepared crystals of 12 mm diameter on a hand-operated drawing apparatus (Siemens VZA 3) at the Inorganic Chemistry Institute of the Ludwig Maximillian University in Munich. At that time, industrial technology was already at 50 mm. In 1980 this had reached 100 mm, then 200 mm by 1995, and by 2002 the technology was at a diameter of 300 mm. Wacker-Chemie GmbH (Burghausen, Germany) supplies 300-mm diameter wafers (the only supplier of such wafers outside of Japan) on which the chips are produced at Infineon Technology AG (Dresden, Germany).[28] The Shin-Etsu group and the company Sumco are involved in manufacture of wafers in Japan.

### 4.2. Industrial Growth of Silicon Single Crystals with a Diameter of 300 mm

Figure 5 displays a cooled silicon single crystal with a diameter of 300 mm, about 2 m in length, and weighing approximately 265 kg that was produced by the CZ method. At the top of the single crystal is situated the thin seed which at the start of drawing is dipped into a crucible containing molten silicon and then, as with Jan Czochralski in 1916, pulled out again, but in this case very slowly.

Figure 6 schematically illustrates a CZ drawing plant in which such silicon single crystals of 300-mm diameter are produced.[29] The total height is about 15 m, hence the upper part of the drawing mechanism is shown in a somewhat truncated form.

The silica crucible (4) from which the single crystal (3) is drawn from the melt (1) on a seed (2) at about 1420 °C is supported by a graphite crucible (5) because silica softens at these temperatures. The $SiO_2$ crucible and the Si single crystal may be rotated and each is adjustable upwards or downwards. External magnetic coils (7) can be attached at the furnace chamber so that the single crystal may also be drawn from the melt under the influence of a magnetic field. The furnace chamber may be sealed under high vacuum, but during the growth period it is filled with argon as protective gas. The growth process may be monitored and controlled directly with an optical sensor (13).

Six steps in the CZ growth of a silicon single crystal are illustrated in Figure 7. After evacuating to $10^{-3}$ mbar, polycrystalline pieces of highest-purity silicon are heated to a temperature just above the melting point of silicon (1414 °C) under a pressure of 10–200 mbar of high-purity argon (Figure 7a).[30,31] When thermal equilibrium has been reached in the melt (Figure 7b) the thin Si seed crystal (3–5 mm in diameter) with the desired crystallographic orientation (in almost all cases [100]) is dipped into the melt (Figure 7c). Slight cooling induces crystallization at the Si seed as a thin neck ("necking"; Figure 7d). With a rapid rate of crystalliza-



*Figure 5.* A single crystal of silicon, 300 mm in diameter, 2 m long, and weighing 265 kg, drawn using the CZ process. (Photograph: Wacker-Chemie).

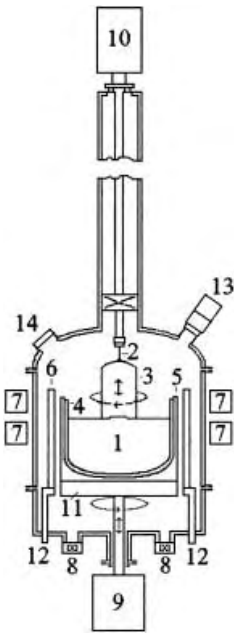



*Figure 6.* Diagram of a CZ drawing plant for 300-mm diameter silicon single crystals. The total height of the drawing plant is about 15 m, therefore the upper section of the installation is somewhat truncated (diagram after B. Altenkrüger and M. Gier).[29] 1 melt, 2 seed, 3 single crystal, 4 silica crucible, 5 graphite crucible, 6 heating elements, 7 magnetic coils, 8 argon outlet, 9 rotating equipment for the crucible, 10 drawing and rotating equipment for the crystal, 11 crucible mounting, 12 current supply for the heating elements, 13 optical sensor, 14 viewing glass.

 © 2003 Wiley-VCH Verlag GmbH & Co. KGaA, Weinheim 

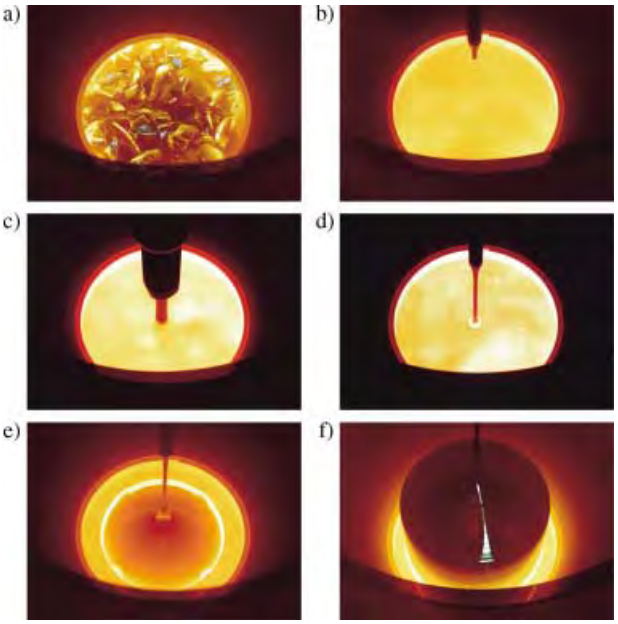



***Figure 7.*** Six steps in the CZ growth of a silicon single crystal: a) Evacuation and heating of the polycrystalline silicon ("pumping"); b) setting the temperature of the Si melt just above 1414 °C ("melting"); c) dipping the thin Si seed crystal into the homogeneous Si melt ("dipping"); d) initiating crystallization at the neck of the thin Si seed ("necking"); e) adjustment of the shoulder of the desired single crystal diameter ("shoulder"; four positions which portray the fourfold drawing axis [100] are visible at the hot, light marginal zone of the single crystal); f) growing phase of the single crystal with constant diameter ("body"). (Photographs: Wacker-Chemie)

tion, drawing is then carried out at a rate of a few millimeters per minute. Because of the high growth rate, one-dimensional crystal defects (dislocations) can no longer spread because their diffusion-controlled growth in the [100] direction no longer keeps pace. They grow laterally and end up at the surface of the thin necks. (The migration of dislocations will be discussed in more detail in Section 4.6.). In this way dislocation-free silicon ("DF-Si") is formed after a few centimeters of growth.[32] By further reduction in temperature the diameter is increased. Finally, at the desired diameter, the growth in thickness is slowed down and the crystal is "bent over" ("shoulder"; Figure 7e). Four points are visible at the hot, bright marginal zone of the single crystal which form an image of the fourfold drawing axis [100]. The main process, namely, the drawing of the Si crystal from the melt with constant diameter, then begins. For the 300-mm single crystal shown in Figure 5, a total time of 3–4.5 days is needed for a crystal length of 2 m. The drawing rate in the cylindrical part is 0.4–1.2 mm min$^{-1}$, depending on the desired crystal properties and the intended use. The process parameters must be continuously adjusted during drawing because the mass of the Si melt of 300 kg at the start falls to 35 kg towards the end of the process. B. Altekrüger and M. Gier have detailed the technology of CZ drawing of 300-mm silicon single crystals.[29]

The transition from the 200-mm to the 300-mm technology was a considerable technological advance.[33] Above all, with this increase in diameter, the amount of polycrystalline silicon had to be increased from 110 kg to about 300 kg, which necessitated an enlargement of the diameter of the silica crucible from 60 to 80 cm. The tripling of the silicon charge for crystal growth also required reconstruction of the drawing apparatus. To maintain the previous demands for axial accuracy of the drawing plant and to exclude any oscillation during crystal growth, the drawing plant was equipped with three-column, rather than single-column hydraulics.[34] Figure 8 shows the CZ crystal-drawing apparatus EKZ 3000/400 of CGS-Crystal Growth Systems GmbH (Hanau, Germany) for crucible diameters of up to 102 cm and a maximum Si melt of 600 kg.[35]

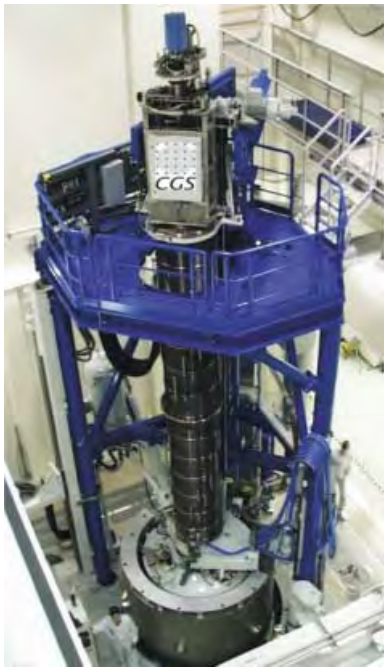



***Figure 8.*** CZ crystal drawing apparatus for crucible diameters of up to 102 cm and a maximum of 600 kg silicon melt.[35] (Photograph with kind permission of Crystal Growing Systems GmbH).

### *4.3. Technical Problems*

Two serious problems occurred during the growth of 300-mm single crystals from crucibles with up to 300 kg silicon melt. First, as a result of the long processing time, the high load demanded an extremely clean and bubble-free silica crucible. In addition, the heat balance and thus the temperature distribution in the Si melt had to be precisely controlled because turbulent flows occurred in the total melt volume. These factors greatly impaired single-crystal drawing and made it difficult to achieve a homogeneous temperature distribution in the crystal during cooling because of the large crystal diameters and masses.

The maximum drawing rates are reduced in comparison to the 200-mm crystals, since latent heat ($1.8 \times 10^6$ J kg$^{-1}$)[36] is released during crystallization (enthalpy of crystallization, $\Delta H = -50.21$ kJ mol$^{-1}$).[37] This heat at the crystallization interface of silicon single crystals of 300-mm diameter is, with respect to surface area, 2.25 times greater than for those

 © 2003 Wiley-VCH Verlag GmbH & Co. KGaA, Weinheim 

of 200-mm diameter. This heat, which arises in the center of the crucible, must be dispersed. In addition, the temperature of the melt at the crystal/melt boundary must be cooler so that the crystal grows truly. Moreover, the axial temperature gradient across the crystal is changed.[33]

The reduced drawing rate for 300-mm single crystals and the increased weight leads to a doubling of the time in which the crucible material ($SiO_2$) is in contact with the Si melt. This can cause corrosion phenomena, and in extreme cases, to the release of $SiO_2$ particles into the Si melt, which can lead to dislocations in the Si crystal. However, the reaction of silica with liquid silicon[38] leads to desired doping of the melt with oxygen [Eq. (1)].

$$SiO_2 + Si \rightarrow 2\,SiO \qquad (1)$$

Oxygen is transported in part by convection and diffusion to the free melt-gas surface where it evaporates as SiO and is blown off with high-purity argon and pumped away. Some of the oxygen dissolved in the melt is transported to the melt–crystal phase boundary and incorporated into the crystal lattice, which leads to oxygen doping of the crystal and wafer. An oxygen doping $N_O$ of $4\times10^{17}$ to $\approx7\times10^{17}$ O atoms per $cm^3$ (hereafter given as $N_O$ [$cm^{-3}$]) is desired depending upon the application and process methodology used during chip manufacture. In the case of silicon, which has a density of 2.329 $g\,cm^{-3}$ and a molar mass of 28.08553 $g\,mol^{-1}$,[37] an $N_O$ value of $5\times10^{17}$ $cm^{-3}$[38] corresponds to $5\times10^{22}$ Si atoms per $cm^3$ (or 0.001 at%), and to 10 ppma O (ppma = atoms per million). To be able to maintain such oxygen doping it is necessary that 99% of the oxygen that is carried into the Si melt through crucible corrosion diffuses to the free melt–gas interface and is removed as SiO. Only the residue of about 1% of the oxygen may be incorporated into the single crystal,[38,39] but this amount must be maintained very accurately.

### 4.4. The Magnetic Czochralski Procedure (MCZ)

The high demands placed upon oxygen control in the large melt volumes, crucible surfaces, and the changed ratio of free-melt surface to crystal diameter could no longer be totally fulfilled by conventional CZ growth. In addition, for certain process conditions there were problems in governing precise temperature control over three times the melt volume, relative to that used to prepare 200-mm technology. The temperature stability required for good single-crystal quality cannot always be guaranteed with mechanical rotation alone (e.g., 5 rotations $min^{-1}$ for the crucible in one direction and 15 rotations $min^{-1}$ in the opposite direction for the single crystal); at high melt volumes convection is unstable, which corresponds to turbulent flow.

A turbulent flow in the melt can be suppressed more effectively through electromagnetic forces[40] than with mechanically produced forces, or can be actively driven using dynamic magnetic fields; this process is known as the magnetic CZ procedure (MCZ). Unlike crystalline silicon at room temperature, liquid silicon is a good conductor of electricity. According to the fundamental electrodynamic laws,[41] Lorentz forces are exerted by a static magnetic field (a "cusp" or horizontal magnetic field) on moving charges that are perpendicular to the magnetic-field vector and the rate vector, in the sense of a right-handed helix. The Lorentz forces in the Si melt are greatest when an orthogonal arrangement of both vectors exists.

Three possible arrangements of the magnetic coils in the MCZ procedure are shown in Figure 9, and are the state of the art for static fields: The magnetic field can be produced

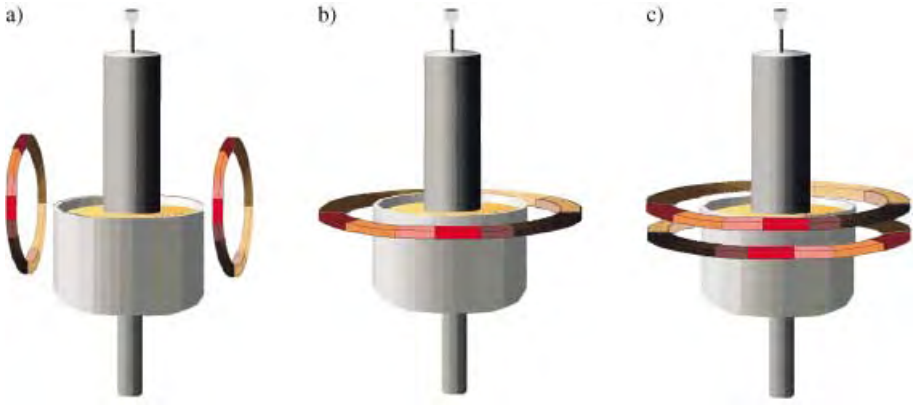



***Figure 9.*** Arrangement of the magnetic coils for the magnetic CZ process with static fields: a) Horizontal, b) axial, c) cusp magnetic fields. To produce the cusp magnetic field the currents must flow in opposite directions in the two coils.

transversally through two horizontal toroids (HMCZ; Figure 9a). The magnetic field lines run perpendicular to the drawing direction of the crystal. In the second variant (Figure 9b) the toroid is arranged vertically and produces an axial magnetic field, while in the third arrangement (Figure 9c) two coaxial toroids, in which the electric currents flow in opposite directions, are arranged symmetrically about the melt–crystal interface to produce a cusp magnetic field (the word "cusp" is derived from the Latin *cuspis* = point, lance.[42] The points in the tracery of a gothic church window are known as "cusps".[43,44]) The opposed toroids produce the cusp magnetic field, which leads to zero magnetic-field strength at the center of the melt–crystal interface. However, the magnetic-field strength increases rapidly in all other directions.

Systematic investigations in MCZ plants have shown that oxygen transport through convection is reduced and thus lower oxygen concentrations can be regulated using cusp magnetic fields.[39] In addition, turbulent fluctuations are suppressed.[45] Fields of up to 3000 G can be produced at the rim of the crucible with superconducting magnets that produce cusp-geometry fields, in which the field at the

 © 2003 Wiley-VCH Verlag GmbH & Co. KGaA, Weinheim 

growth boundary is practically zero.[46] Horizontal fields also make these high fields possible at the crystal.

A new technology (developed by Wacker) is the dynamic magnetic field ("traveling magnetic field", or the combination of a cusp field with alternating current fields), which actively imposes the desired convection pattern and thus allows far more possibilities for influencing the melt than passive, static fields can offer. The convection pattern can be set according to the direction of the traveling magnetic fields. This can be advantageous with respect to stabilization of growth and oxygen control, since convection affects both heat and oxygen transport. In addition, significantly less power and space are required for dynamic fields, which offers advantages in respect of the demands for lower production costs. Figure 10 illustrates a MCZ arrangement in which dynamic fields are employed.

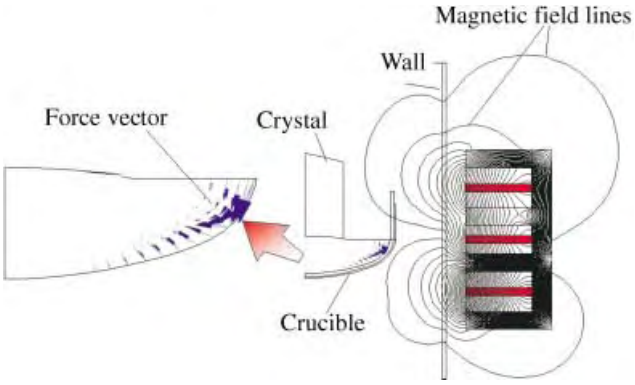



***Figure 10.*** Dynamic fields (traveling magnetic fields) in the magnetic CZ process. On the right the arrangement of the coils and the resulting magnetic field lines are illustrated schematically. On the left the resulting forces on the melt are shown. By changing the direction of the traveling field the direction of force, and thus the flow of the melt, can be reversed.

The active driving of the melt using traveling magnetic fields is based on the same principle that applies in linear motors, for example, in transport through magnetic levitation, such as with the Transrapid train. When the magnetic field is at a maximum, the alternating field induces a current at a certain point that interacts with the traveling magnetic field and thus drives the melt.

### *4.5. Mathematical Modeling of Crystal Drawing*

Recently it has become possible to mathematically simulate oxygen diffusion and temperature distribution in a silicon melt in the silica crucible of a MCZ plant with cusp magnetic fields.[39] Figure 11 shows schematically the model for calculating[39] the number of oxygen atoms $N_O$ at three positions: in the Si melt at point M and in the Si single crystal at points S and Z, which is viewed both from the side (Figure 11, top) and from above (Figure 11, bottom).

The coils producing the cusp magnetic fields (1 and 2) are aligned parallel to the melt–crystal interface (Figure 11, top;

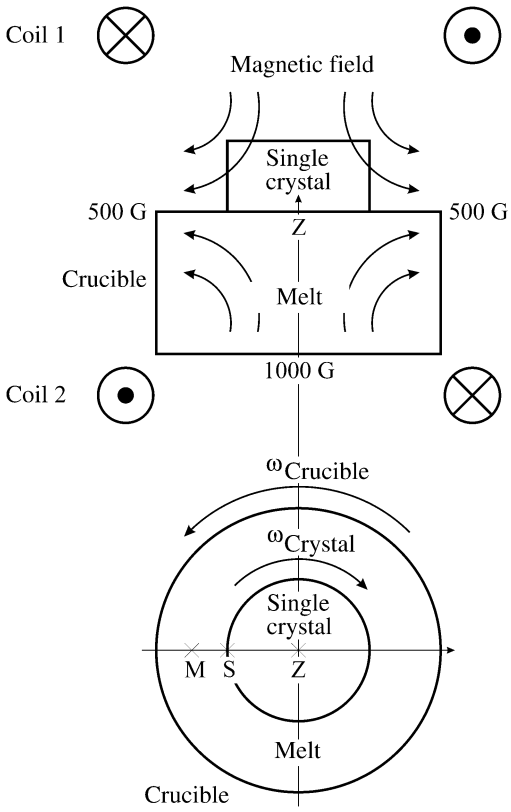



***Figure 11.*** Model for the calculation of the oxygen concentration in the silicon melt and in the silicon single crystal of a MCZ arrangement with a static cusp magnetic field. Top: side view, bottom: plan view.[39,47]

the symbols ⊗ and ⊙ represent the opposite directions of the current within the two coils that produce the cusp magnetic field). The path of the field lines of the cusp magnets is also shown. At the base of the silica crucible the magnetic field has a strength of 1000 G, while at the upper rim both sides of the crucible it is 500 G. The center (point Z) of the melt–crystal interface is magnetic-field free. Owing to the considerable computational expenditure of the model, the single crystal is calculated to be only 37.5 mm in diameter (i.e., 1/8 of the real diameter). Correspondingly, the crucible, with a diameter of 75 mm, is considerably smaller than that which is used in 300-mm technology. The crucible and crystal are rotated in opposing directions. In the plan view (Figure 11, bottom) two further points for oxygen calculation are shown: point M is located between the crucible rim and the crystal surface, and point S is at the crystal surface. The magnetic field is entered into the calculation as the dimensionless Hartmann number $Ha$,[47,48] which in magnetohydrodynamics describes the flow field of an electrically conducting liquid in a magnetic field.

Figure 12 shows the concentration of oxygen atoms $N_O$ as a function of time $t$ in the melt at points M, S, and Z.[39,47] On the left side of the chart, the cusp magnetic field ($Ha = 161$) is switched on, and on the right side it is switched off ($Ha = 0$). Between $t = 400$ and $t = 600$ s, $N_O \approx 1.3 \times 10^{18}$ cm$^{-3}$ at point M (Figure 12). During this time period, the plot for point M shows sharp periodic signals, which clearly demonstrates that the cusp magnetic field suppresses turbulent aperiodic

 © 2003 Wiley-VCH Verlag GmbH & Co. KGaA, Weinheim 

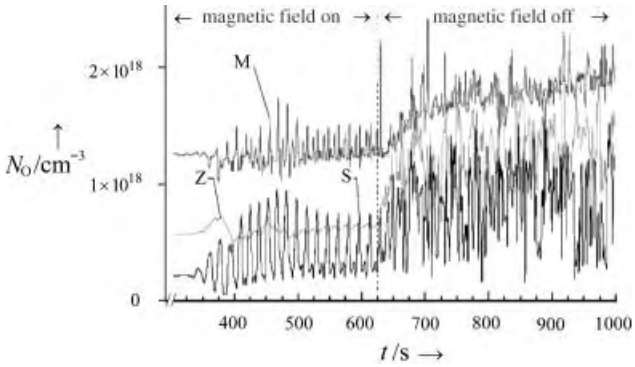



***Figure 12.*** Number of oxygen atoms $N_O$ [cm$^{-3}$] as a function of time $t$ with and without static cusp magnetic field in the melt (M), on the crystal surface (S), and in the center of the melt–crystal interface (Z). Data from Ref. [39]; see text for more details and Ref. [47].

fluctuations.[45] The periodic oscillations are caused by convective instabilities[49] when dominant vertical temperature gradients occur in rotating liquids.[50] With the cusp magnetic field switched off ($Ha = 0$), the oscillations lose their periodicity in the model described. If a weak cusp magnetic field is applied, as observed at point Z (Figure 11, top), the periodic signals at that point are correspondingly weak (Figure 12).

Switching off the magnetic field at $t = 625$ s results in an increase in $N_O$ to $1.8\times10^{18}$ cm$^{-3}$ at point M. Thus, more oxygen atoms are carried into the melt at M. At the same time intense aperiodic fluctuations in the oxygen concentration occur. With the cusp magnetic field switched on, the $N_O$ values are about $0.3\times10^{18}$ for S, $0.6\times10^{18}$ for Z, and $1.3\times10^{18}$ cm$^{-3}$ for M. Switching off the magnetic field also causes an increase in oxygen concentration at points Z and S. With the cusp magnetic field applied, the value of $N_O$ at Z ($\approx0.6\times10^{18}$ cm$^{-3}$) and S ($\approx0.3\times10^{18}$ cm$^{-3}$) is only one third and one sixth, respectively, of that at point M when no magnetic field is applied ($\approx1.8\times10^{18}$ cm$^{-3}$). Switching on the cusp magnetic field thus brings about a purifying effect with regard to the concentration of oxygen impurities in CZ silicon.

A cusp magnetic field also has a favorable effect on temperature distribution in the Si melt and at the boundary zone of a CZ-grown Si single crystal.[45] For calculations of these effects, a model with a smaller silica crucible (107 mm high with a diameter of 360 mm) and crystal diameter (104 mm) was required. The cusp magnetic field was set at a maximum of 400 G. The whole melt and the lower part of the single crystal were broken down into a matrix of 450000 control volumes to calculate the temperature distribution. Figure 13 illustrates the measured and calculated normalized temperature distribution (isothermal lines) in the melt of a MCZ plant with the cusp magnetic field switched off (Figure 13a) and switched on (Figure 13b).[45,51]

The left side of Figure 13a shows the temperature measured in the crucible of a 20-kg CZ silicon melt without magnetic field, and the right side shows the equivalent calculated temperature. Figure 13b shows the same information with an applied cusp magnetic field of 400 G. The maximum temperature difference measured ($\Delta T_{max}$) is 36 °C with no applied field, and 42 °C with the cusp magnetic field switched on.[45] By this method, direct temperatures may again be calculated from the normalized isothermal lines at a known silicon melt temperature, which allows greater insight into the temperature distribution within the crystal.[51]

The agreement between experiment and simulation is very good: The difference between measured and calculated temperature is no more than 4 °C without field, and 6 °C with the magnetic field switched on.[45] Figure 13b shows that a considerable dampening of convective heat transport and a greater temperature difference between crystal and crucible rim is achieved with the magnetic field switched on. This is exemplified by comparison of, for example, the experimental

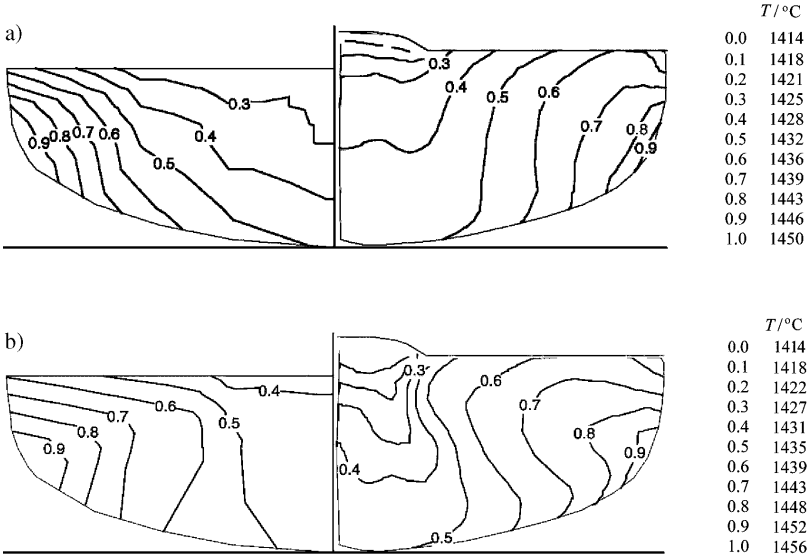



***Figure 13.*** Normalized temperature distribution of a 20-kg silicon CZ melt; [45] left: measured, right: calculated for a) without field, and b) with a cusp magnetic field of 400 G. See text and Ref. [51] for details.

isotherms 0.6 on the left-hand side of Figure 13a and b: The isotherms run almost perpendicularly; there is less heat exchange through convection in a radial direction since the cusp field inhibits melt movement in a radial direction at the crucible rim (that is, perpendicular to the magnetic field lines).

Mathematical modeling of crystal-growth processes is also a useful tool for simulating changes in furnace construction and thus the optimization of cooling rates and defect kinetics. Corrosion of the silica crucible by the Si melt at different process parameters may also be estimated in this way. Costs are reduced dramatically if expensive experimental investigations can be simulated by a click of a mouse. Thus computer programs, for example, CrysVUN++[52] or FEMAG-CZ,[53] are of considerable economic significance when it comes to increasing the diameters of silicon single crystals beyond 300 mm.

 © 2003 Wiley-VCH Verlag GmbH & Co. KGaA, Weinheim 

### 4.6. Defects in Silicon Single Crystals

A manufactured crystal of silicon with a diameter of 300 mm is very different from the fictional ideal crystal with a three-dimensionally extended translational periodic structure; a multitude of deviations from the perfect crystal arise. These defects can be produced by silicon itself, or by impurities. Since these defects are mobile at elevated temperatures they react with each other in many ways during the cooling phase of the large single crystal, which takes several days. In addition to the desired reactions, undesired processes can take place whose consequential products can produce fatal defects in the active switching region of the microchip and cause considerable economic damage. The defects that arise are divided into point, line, surface, and volume defects depending upon their dimensionality.[54]

Point defects occur if atoms are missing or placed at irregular sites. In real single crystals a series of such defects can occur, and can be due to silicon itself, or to foreign atoms. In the first case the point defects are said to be intrinsic, and in the second case, extrinsic. An intrinsic point defect can be either a vacancy ($V_{Si}$) at a normal Si site, or a matrix atom at an interstitial site between regular Si sites. An extrinsic point defect is produced by an atom of another element substituting a silicon atom at a normal lattice site, or by occupying an interstitial site. The controlled introduction of foreign atoms into regular sites by doping silicon (e.g., n-type doping with P or p-type doping with B at doping levels of between $10^{17}$ and $10^{20}$ atoms $cm^{-3}$) is what makes the multifarious functionality of microchips possible.

The number of intrinsic point defects in silicon depends upon the temperature and the growth conditions of the CZ growth. At between 700 and 1200 °C there may be $10^{15}$ to $10^{17}$ $cm^{-3}$ vacancies in CZ Si single crystals.[55] Occupation of the interstitial sites occurs somewhat less extensively. It is interesting to note that just one type of intrinsic point defect predominates within certain regions of CZ Si single crystals. Voronkov has shown that the occurrence of these point defects is dependent upon the relationship between the growth rate $v$ and the axial temperature gradient $G$ at the melt–crystal interface (the $v/G$ rule).[56] Above a critical value $(v/G)_{crit} \approx 0.13\ mm^2\,K^{-1}\,min^{-1}$,[31,57] intrinsic point defects will only survive as vacancies; below this value, they only occur at interstitial sites. For $(v/G) > 0.13\ mm^2\,K^{-1}\,min^{-1}$, the majority of vacancies are initially formed on drawing from the melt, whilst "interstitial atoms" are present to a lesser extent. Recombination of the deficient number of interstitial atoms with vacancies leads eventually to their complete disappearance. For $(v/G) < 0.13\ mm^2\,K^{-1}\,min^{-1}$, this mechanism is reversed. Most of the CZ Si single crystals produced industrially are manufactured under conditions in which Si vacancies are formed.[58]

During cooling the Si vacancies can coalesce to form agglomerates (voids, D defects).[59] The agglomeration of point defects during cooling can increase the dimensionality of the defects. In this way, one-dimensional line defects (dislocations) are formed. These are also formed during crystallization when mismatched crystal domains occur in the crystal due to mechanical strain, high temperature gradients, or plastic deformation. Dislocations compensate such mismatches and can then extend across large regions of a single crystal. This can mean that half of a 300-mm diameter single crystal of about 2 m in length (Figure 5) is ruined[33] if dislocations subsequently spread into an originally displacement-free region with lengths that correspond approximately to the crystal diameter. Considerable economic damage is then accrued, since the growth of a large single crystal is a high-cost process that lasts several days. However, with the correct process control and the use of high-quality silica crucibles, such dislocations do not occur as the rapid crystallization of a thin, orientated Si seed leads to a neck being formed ("necking"; Figure 7d) so that further dislocations in the [100] direction can no longer occur. Through this process, a large single crystal of dislocation-free silicon ("DF-Si") is obtained on drawing from the melt.[32]

On cooling the defects in the Si single crystal are subjected to strong dynamic forces, which must be controlled experimentally to ensure successful growth. Disklike accumulations of vacancies and additional Si atoms at interstitial sites can coalesce to form "dislocation loops" with enclosed stacking defects, which can involve either a deficiency or an excess of silicon atoms. In a two-dimensional representation lines are formed, however, in the real three-dimensional crystal, rings or loops with a radius of 10–15 lattice constants can form.[60] When the drawn CZ Si single crystal is cooled, dislocations can also "climb" up the lattice through interactions with point defects, as shown in Figure 14, where dislocations are marked by the dislocation symbol $\perp$, which symbolizes the start of the insertion of additional sites.

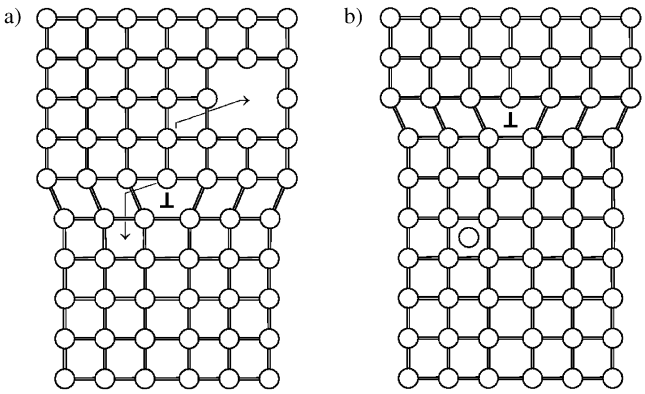



***Figure 14.*** Schematic representation of the positive climbing of a dislocation in a two-dimensional lattice: a) the two arrows show the migration of the two neighboring atoms necessary for the climbing of the dislocation. b) After climbing an "interstitial site" is produced (emission) and an empty site is occupied (absorption). Explanation in text.

Of the two atoms labeled with arrows in Figure 14a, the lower becomes an interstitial atom (emission; Figure 14b), whereas the upper occupies a vacancy (absorption). In this way the step displacement climbs two horizontal rows vertically (positive climbing).[60] Negative climbing would occur during the emission of a vacancy and the absorption of an interstitial site.[60]

 © 2003 Wiley-VCH Verlag GmbH & Co. KGaA, Weinheim 

Intrinsic defects are able not only to react with other intrinsic defects, but also with extrinsic defects, that is, with foreign atoms which are present in low concentration within the single crystal. Oxygen is the most important impurity atom, and is thus the focus of numerous research projects. In spite of this a number of properties remain unexplained to this day and are thus still the subject of discussion.[55,61] Through their production in $SiO_2$ crucibles, industrially prepared CZ Si single crystals contain on the order of 10 ppma oxygen atoms, which corresponds to $N_O = 5 \times 10^{17}$ cm$^{-3}$. The interstitial oxygen atoms ($O_i$) present in solid solution are electronically neutral and occupy sites between two silicon atoms.[55,61]. For decades it was firmly believed that the Si-$O_i$-Si arrangement in CZ silicon was angular (bond angle = 160°),[55,61] that is, similar to α-quartz (144°).[62] The Si–$O_i$ bond length in CZ silicon at 1.60 Å should be almost as long as that in α-quartz (1.61 Å).[62] More recently, a linear Si-$O_i$-Si arrangement with a Si–$O_i$ bond length of 1.61 Å has also been discussed.[63] This Si-$O_i$-Si configuration would arise when the energy threshold between the six possible angular configurations in the [111] direction and the linear version is only a few meV,[63] so that the $O_i$ atoms are able to move through the Si–Si matrix and are delocalized to a small degree.[64]

Figure 15 displays the silicon-rich part of the Si–O phase diagram.[65] Above 1414 °C (the melting point of silicon[30,31]) the $O_i$ atoms are found in liquid solution ($L_1$, monophasic) up

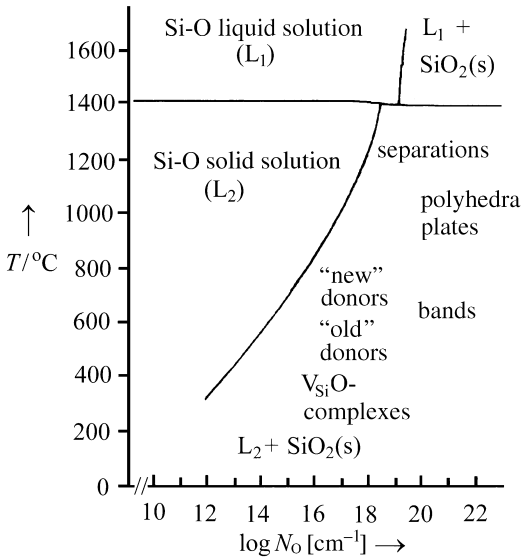



***Figure 15.*** Silicon-rich section of the Si–O phase diagram. Data after Ref. [65].

to $N_O \approx 10^{19}$ cm$^{-3}$. An increase in $N_O$ by a factor of 10 leads to segregation of solid $SiO_2$ in the melt ($L_1$ + $SiO_2$(s), biphasic). On cooling to just below 1414 °C the solid Si–O solution is stable only to $N_O = 2 \times 10^{18}$ cm$^{-3}$ (Figure 15), which corresponds to 0.004 at % oxygen (40 ppma). With falling temperature the oxygen solubility in solid silicon falls further: at 1100 °C $N_O$ is only $3 \times 10^{17}$ cm$^{-3}$ (0.0006 at %; 6 ppma), and at 1000 °C it is merely $1 \times 10^{17}$ cm$^{-3}$ (0.0002 at %; 2 ppma). A CZ Si single crystal which at its melting point contains homogeneously dissolved oxygen at a concentration of about 10 ppma is supersaturated with oxygen on cooling to 1000 °C. According to the solubility curve only a fraction (≈ 2 ppma) remains homogeneously dissolved in the silicon (homogeneously solid Si–O phase, $L_2$), whilst the main fraction (≈ 8 ppma) separates as a solid $SiO_x$ phase in the heterogeneous mixture $L_2$ + $SiO_2$(s). The separation of solid $SiO_x$ phases continues with further cooling. A number of $SiO_x$ phases for an oxygen concentration of about $N_O = 10^{20}$ cm$^{-3}$ are shown in the phase diagram (Figure 15; for example, separations, polyhedra, plates, bands, thermal donors, vacancy–oxygen complexes ($V_{Si}O$ complexes). This complicated behavior is indicative of the ability of silicon and oxygen to form modified Si–O bonds, the structural variety of which is also shown in $SiO_2$ modifications.

On further cooling between 1400 and 700 °C, the CZ Si single crystal may exhibit smaller separations of amorphous $SiO_2$ at dislocation rings. These separations may coalesce to give somewhat larger agglomerates due to the lowering of interfacial energy through Ostwald ripening.[66] The agglomerates produce new dislocations in order to reduce mechanical stress arising from the local volume increase during $SiO_2$ separation. According to thermal studies, and as is characterized by the diffusion kinetics highlighted in Figure 15, the separations can also form polyhedra, plates, or bands. At higher temperatures (above 950 °C) polyhedra of minimal surface energy are formed. The preferred polyhedron is the octahedron because for silicon the surface energy is here lower than for a sphere.[67] At moderate temperatures (950–650 °C) plates can separate by reaction with dislocations, and needles can form at low temperatures (650–400 °C).[67]

An oxygen concentration of about $N_O = 10^{20}$ cm$^{-3}$ (Figure 15) is sufficient to allow imagery of the $SiO_x$ separations obtained between 700 and 1400 °C with transmission electron microscopy (TEM), but these defects are electronically inactive. In contrast, by tempering the single crystals at lower temperatures(350–550 °C)[67] and by using a lower oxygen concentration ($N_O \approx 10^{18}$ cm$^{-3}$) defects are obtained that are electrically active; these defects are known as thermal donors (TDs).[67] TDs are detectable through electrical resistance, infrared absorption, electron paramagnetic resonance (EPR), and electron–nucleus double resonance (ENDOR) spectroscopy, but are not observed in TEM because of their small size and the low oxygen concentration.[67]

TDs were initially divided into two groups with the poorly characteristic definitions "old" and "new" (Figure 15). In thermal donors electrons occupy states near the conduction band. There are, therefore, more appropriate names that characterize the electrical properties of the "old" thermal donors: single thermal donors are known as "shallow thermal donors" (STDs) and double thermal donors are called "thermal double donors" (TDDs).[68] The STDs are located in the electronic band structure of silicon at 0.035 eV,[69] an ionization energy close to that of n-type P-doped silicon (0.044 eV),[70] and lying near to the minimum of the con-

 © 2003 Wiley-VCH Verlag GmbH & Co. KGaA, Weinheim 

duction band (hence, a shallow donor), whereas double donors with ionization energies of 0.053–0.155 eV.[68] are more distant. The TDDs are thought to consist of $O_{ni}$ clusters with $n = 2$–13 oxygen atoms inserted between the silicon atoms in either chain or ring-shaped configurations.[61,68,71] The slow formation of the first thermal donors $O_{ni}$ ($n = 2$), to which further $O_i$ atoms attach themselves, is the rate-determining step in the formation of higher members of the $O_{ni}$ series.[61,71] Seventeen different TDDs are thought to occur.[68] Since thermal donors affect the conductivity of the CZ Si wafers they are of considerable significance in microprocessor technology.

Optimization of the technical processes that lead to oxygen aggregation in CZ Si single crystals will remain dependent upon empirical knowledge, so long as attempts to understand the complete atomic mechanism remain unsuccessful. Thus oxygen atoms triply coordinated with silicon atoms, and formally positively charged ions are responsible for the electrical activity of the thermal donors.[68] Density functional theory calculations on simple defects in CZ silicon have proved to be very helpful in estimating energies for the migration, restructuring, and dissociation of oxygen defects (e.g., $O_{ni}$ with $n = 3$–6) along a reaction coordinate.[72] Figure 16 illustrates some concepts for five simple oxygen defects:[68,73] Figure 16a shows the interstitial oxygen atom $O_i$ in the angular configuration,[73] Figure 16b displays the interstitial oxygen dimer $O_{2i}$ in the staggered configuration,[73]

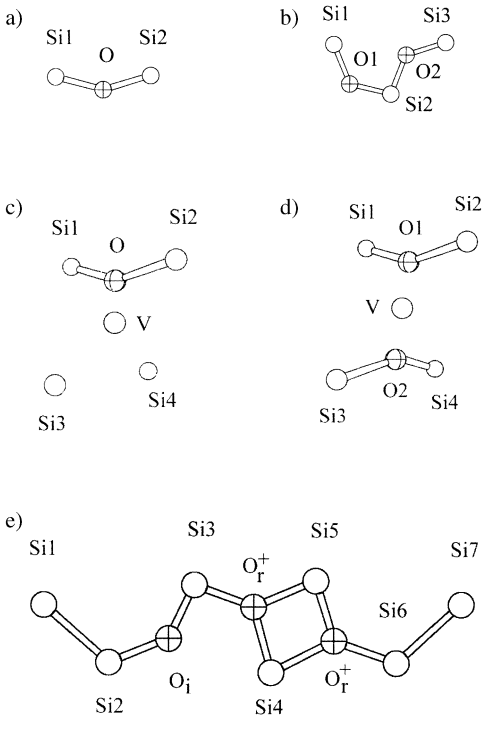



***Figure 16.*** The arrangement of five possible oxygen defects in CZ silicon single crystals, as obtained by density functional theory (using the LDA approximation).[68,73] a) An interstitial oxygen atom $O_i$ in the angular configuration, b) an interstitial oxygen dimer $O_{2i}$ in the staggered configuration, c) a 1:1 vacancy–oxygen defect $V_{Si}O$, d) a 1:2 vacancy–oxygen defect $V_{Si}O_2$, e) thermal double donor $O_i$-$O_{2r}^{2+}$.

Figure 16c and d show the 1:1 and 1:2 vacancy–oxygen defects $V_{Si}O$ and $V_{Si}O_2$,[73] and Figure 16e describes the TDD $O_i$-$O_{2r}^{2+}$.[68] The Si-O-Si bond angles of approximately 140–160° and the Si–O bond lengths of approximately 1.62–1.65 Å are assigned as the $O_i$, $O_{2i}$, $V_{Si}O$ and $V_{Si}O_2$ defects (Figure 16a–d).[73] Thus the interactions lie in the range that has also been found experimentally for α-quartz.[62] The doubly bound $O_i$ atom in the TDD $O_i$-$O_{2r}^{2+}$[68] (Figure 16e) is also coordinated in a manner similar to that in α-quartz, whereas for the two triply bonded, formally positively charged $O_r^+$ ring atoms, pyramidal or planar configurations are possible. Molecular-dynamics calculations on oxygen atoms triply coordinated with silicon predict Si–O bond lengths of 1.81 Å(2×) and 1.90 Å[74] and angles in the region of 120°.[75]

Electrically inactive oxygen agglomerates (with oxygen concentrations higher than those of the thermal donors; Figure 15) are in part advantageous because they render harmless the rapidly diffusing transition-metal impurities such as Fe, Cu, and Ni, which can interfere many microchip applications at concentrations as low as $10^{11}$ atoms cm$^{-3}$.[76] For silicon with $5 \times 10^{22}$ Si atoms per cm$^3$, this corresponds to an Fe content of $2 \times 10^{-10}$ at%, or 2 ppta (1 ppt $= 10^{-3}$ ppb $= 10^{-6}$ ppm). The transition-metal impurities reduce the lifetime of the minority carriers through the recombination of corresponding electron hole pairs. Therefore it is advantageous to capture them along with oxygen agglomerates in an "internal gettering" (IG) process.[77]

In thin silicon wafers a two-hour tempering process at 1100 °C precedes the IG process in a three-stage cycle. Through this procedure the internal oxygen concentration is greatly reduced since oxygen atoms diffuse out to the surface of the wafer, forming a low-defect surface or denuded zone (DZ).[78] Finally the wafer is cooled to 600 °C for 4 h so that a large number of microdefect nuclei are formed at which $SiO_x$ separations are established through heating for 12 h at 1100 °C. This process is of considerable importance in the manufacture of microprocessors, as two objectives are achieved, namely, the preparation of a low-defect surface zone and a region inside the wafer in which the damaging transition-metal impurities Fe, Cu, and Ni are captured by IG.

It is evident that very careful thermal processing of the CZ Si single crystal drawn from the melt, and of the wafer that is then produced, is necessary to control the numerous defect reactions (defect engineering) that are possible.[79] Crystal drawing and defect engineering represent two equally strong but mutually dependent pillars which underpin 300-mm silicon technology. With an increasing diameter of the silicon single crystal and, in addition, ever diminishing cross-link structures in microchips, it is necessary continually to improve the construction of the crystals.[33] These improvements will become more difficult because CZ Si single crystals with increasing diameters must be produced with a respectively lower drawing rate, and for economic reasons greater crucible batch weights will have to be used. The residence time of the Si melt in the $SiO_2$ crucible is then correspondingly increased. This demands continually better crucible qualities and more rigorous process control. Consequently the oxygen contamination of future CZ Si single crystals with large diameters will become problematic, and with it the defect engineering.

 © 2003 Wiley-VCH Verlag GmbH & Co. KGaA, Weinheim 

## 5. Summary and Outlook

In the CZ process large silicon single crystals are drawn and processed into wafers, the new generation of which (since December 2001) have a diameter of 300 mm. Production strategies estimate[2] that in 2009 the diameter will have increased to 450 mm, and in 2015 (99 years after Czochralski's discovery[5]) perhaps as large as 675 mm. With these predicted leaps in innovation, the wafer area will double in size in each instance. It would appear that along with the findings of G. E. Moore[1] (namely, doubling the capacity of the electronic components within just two years with a concomitant halving in price), a further criterion is included, that is, further perfecting of the single crystal!

Today, however, 170 one-gigabit microchips can be produced from a 300-mm wafer, compared to only 70 64-megabit chips per 200-mm wafer. The enormous value of these developments must continue to be backed up by considerable industrial investment, developments which, let us not forget, originated from Jan Czochralski's creative mistake!

*The authors extend their thanks to Dr. P. E. Tomaszewski (Polish Academy of Sciences) for the photographs of J. Czochralski and for his critical review of Sections 2 and 3, D. Schreiber (S. Fischer Verlag) for the photograph of W. Rathenau, Dr. C. Maywald-Pitellos (Gutenberg Museum, Mainz) for authentication of the photograph of W. Rathenau, Dr. J. Lexow (Bundesanstalt für Materialforschung und -prüfung) for the photograph of von Moellendorff, Dr. B. Altekrüger (Crystal Growing Systems GmbH) for the photographs of the EKZ 3000/400 crystal drawing plant and for information on the publication of 300-mm silicon single-crystal technology, Dr. M. Kämper for his stimulating assistance, and last, but not least, R. Singer-Schülmers for her untiring dedication to this manuscript.*

Received: February 18, 2003 [A587]

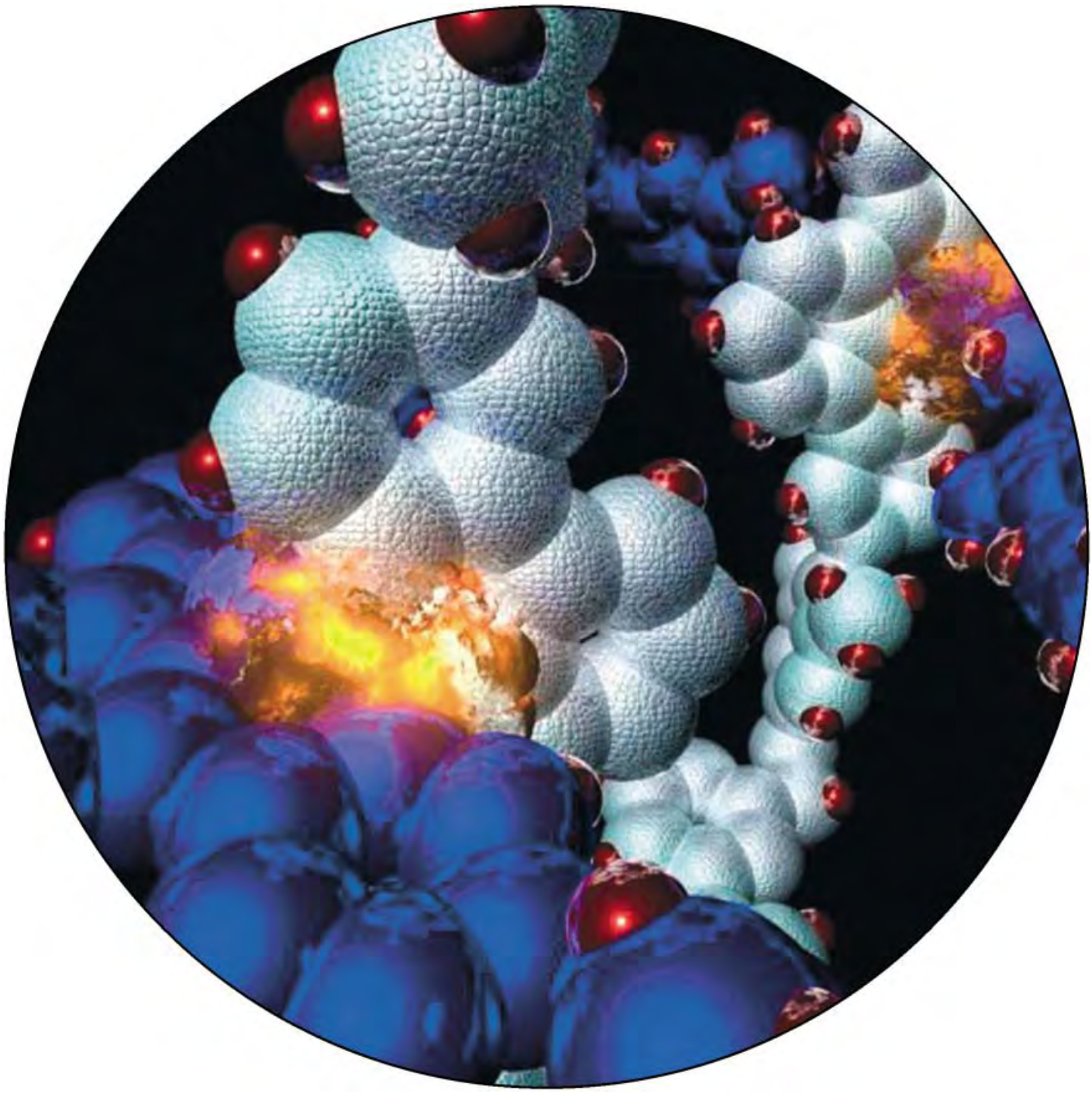
[1] Moore's Law: G. E. Moore, *Electronics* **1965**, *38*, 114 – 117.
[2] A. P. Mozer, *Mater. Sci. Eng. B* **2000**, *73*, 36 – 41.
[3] Infineon Technologies AG (München), press release (December 12, 2001), *Pioneering 300.* http://www.pioneering300.com/pioneering300/de/
[4] W. Zulehner, *Mater. Sci. Eng. B* **2000**, *73*, 7 – 15.
[5] J. Czochralski, *Z. Phys. Chem. (München)* **1918**, *92*, 219 – 221.
[6] *Wielka Encyklopedia Powszechna PWN*, supplement, Państwowe Wydawnictwo Naukowe, Warszawa, **1970**, p. 99.
[7] P. E. Tomaszewski, *Wiad. Chem.* **1987**, *41*, 597 – 634.
[8] J. Żmija, *Zesz. Nauk. – Politech. Łodz. Fiz.* **1989**, *10*, 7 – 22 (Conf. Cryst. Growth Liq. Cryst. 1986).
[9] P. E. Tomaszewski, *American Association for Crystal Growth*, *Vol. 27*(2), newsletter, **1998**, p. 12–18. http://www.ptwk.org.pl/art2.htmDr. P. E. Tomaszewski, Institute of Low Temperature and Structure Research, Polish Academy of Sciences, P. Nr. 1410, 50 – 950 Wrocław 2, Poland.
[10] P. E. Tomaszewski, *J. Cryst. Growth* **2002**, *236*, 1 – 4.
[11] P. Tomaszewski, *Jan Czochralski i jego metoda – Jan Czochralski and his Method*, Instytut Niskich Temperatur i Badań Stukturalnych PAN (Institute of Low Temperature and Structure Research), Polish Academy of Sciences, Wrocław, Poland.
[12] Biography: *Wichard von Moellendorff*, 1881 – 1937; Deutsches Historisches Museum (Berlin); *Lebendiges Virtuelles Museum Online(LeMo)*. http://www.dhm.de/lemo/html/biografien/MoellendorffWichard/
[13] W. von Moellendorff, *Elektrotech. Maschinenbau* **1913**, *31*, 242 – 244. Lecture: "Über das Kabelwerk Oberspree", February 4, **1913**, Vienna.
[14] K. Braun, *Konservatismus und Gemeinwirtschaft. Eine Studie über Wichard von Moellendorff*, Walter Braun, Duisburg, **1978.**
[15] W. Ruske, G. W. Becker, H. Czichos, *125 Jahre Forschung und Entwicklung, Prüfung, Analyse, Zulassung, Beratung und Information in Chemie- und Materialtechnik*, Bundesanstalt für Materialforschung und -prüfung (BAM), Berlin, Wirtschaftsverlag NW, Verlag für neue Wissenschaft GmbH, Bremerhaven, **1996**, p. 133
[16] W. von Moellendorff, *Giesserei-Ztg.* **1914**, *11*, 506 – 509 and 521–525.
[17] W. von Moellendorff, J. Czochralski, *Z. Ver. Dtsch. Ing.* **1913**, *57*, 931 – 935 and 1014–1020.
[18] J. Czochralski, *Z. Metallkd.* **1925**, *17*, 1 – 11.
[19] Biography: *Walther Rathenau*, *1867–1922*; Deutsches Historisches Museum (Berlin); *Lebendiges Virtuelles Museum Online (LeMo)*. http://www.dhm.de/lemo/html/biografien/RathenauWalther/
[20] "*Walther Rathenau. Sein Leben und sein Werk*": H. Kessler, *Gesammelte Schriften in drei Bänden*, *Vol. 3* (Eds.: C. Blasberg, G. Schuster), Fischer Taschenbuch, Frankfurt am Main, **1988.**
[21] According to information from the ink-well specialist, Dr. C. Maywald-Pitellos (Gutenberg Museum, Mainz), it is an ink well with "a drop-shaped glass body… with a metal ring. Probably a cover, not seen in the photograph, belongs to the ink well. Ink wells with this shape could be obtained from department stores up until the Second World War."
[22] *Claims Resolution Tribunal*, Zürich, CRT-II, **2001** Published List of Accounts.
http://www.crt-ii.org/_lists/publication_list1_C.phtm
[23] J. Czochralski, *Schweiz. Arch. Angew. Wiss. Tech.* **1940**, 167 – 176.
[24] J. Czochralski, *Moderne Metallkunde in Theorie und Praxis*, Springer, Berlin, **1924.**
[25] Polish Physical Society, ul. Hoża 69, 00 – 681, Warsaw, Poland. http://ptf.fuw.edu.pl/ptftabp.htm
[26] Polish Society for Crystal Growth, Institute of Technology of Electronic Materials, ul. Wólczyńska 133, 01 – 919 Warszawa, Poland. http://www.ptwk.org.pl/cz-symposium03/index/htmL
[27] J. Czochralski, *Z. Ver. Dtsch. Ing.* **1917**, *16*, 345 – 351.
[28] Business, Concentrates, *Chem. Eng. News* **2002**, *80*(42), 19.
[29] B. Altekrüger, M. Gier, *Vak. Forsch. Prax.* **1999**, 31 – 36.
[30] According to Ref. [31], the precise melting point of silicon is very difficult to measure because thermoelements based on metals of the platinum group age readily in the region of 1400 °C and can thus indicate temperatures up to 3 °C too low. In addition the chemically aggressive silicon melt dissolves most impurities, with a concomitant drop in melting point. Since 1958, 20 melting points have been published: 1408, 1410, 1412(7×), 1414(8×), and 1416(3×) °C. That gives a mean value of 1413.1 °C with a standard deviation of the mean of ±0.31 °C. A temperature of 1414.0 ± 0.9 °C is recommended as the melting point for silicon; this value is slightly higher than the mean value and should have a statistical reliability of 90 %.
[31] "Properties of Crystalline Silicon": *Electronic Materials Information Service: EMIS Datareviews Series*, *Vol. 20* (Ed.: Robert Hull), INSPEC, The Institution of Electrical Engineers, London, **1999**.
[32] W. Dash, *J. Appl. Phys.* **1959**, *30*, 459 – 474.
[33] "Festkörperprobleme": A. P. Mozer, *Adv. Solid State Phys.* **1998**, 37, 1 – 14.

 © 2003 Wiley-VCH Verlag GmbH & Co. KGaA, Weinheim 

[34] E. Tomzig, W. von Ammon, E. Dornberger, U. Lambert, W. Zulehner, *Microelectron. Eng.* **1999**, *45*, 113 – 125.
[35] Crystal-drawing plant EKZ 3000/400 of CGS-Crystal Growing Systems GmbH, Hanau; crucible diameter: 1.02 m, charge weight: 600 kg, crystal movement: 4 m, furnace chamber diameter: 1.7 m, total height: 14.74 m.
[36] T. Zhang, G.-X. Wang, H. Zhang, F. Ladeinde, V. Prassad, *J. Cryst. Growth* **1999**, *198*/199, 141 – 146.
[37] "Elemente, anorganische Verbindungen und Materialien, Minerale": *D'Ans-Lax*, *Taschenbuch für Chemiker und Physiker*, Vol. III, 4th revised edition (Ed.: R. Blachnik), Springer, Berlin, **1998**, p. 193.
[38] G. Müller, A. Mühe, R. Backofen, E. Tomzig, W. von Ammon, *Microelectron. Eng.* **1999**, *45*, 135 – 147.
[39] Y. C. Won, K. Kakimoto, H. Ozoe, *J. Cryst. Growth* **2001**, *233*, 622 – 630.
[40] R. W. Series, D. T. J. Hurle, *J. Cryst. Growth* **1991**, *113*, 305 – 328.
[41] W. H. Westphal, *Physik: Ein Lehrbuch*, Springer, Berlin, **1959**, p. 370.
[42] M. Petschenig, *Der kleine Stowassser*, Lateinisch-Deutsches Schulwörterbuch, G. Freytag, München, **1963**, p. 150.
[43] *The New Encyclopaedia Britannica*, *Vol. 3*, *Micropaedia*, Encyclopaedia Britannica, Chicago, **1997**, p. 810.
[44] *Langenscheidts Fachwörterbuch Technik und angewandte Wissenschaften*, English-German (Ed.: P. A. Schmitt), Langenscheidt, Berlin, **2002**, p. 466.
[45] D. Vizman, J. Friedrich, G. Müller, *J. Cryst. Growth* **2001**, *230*, 73 – 80.
[46] H. Yamagishi, M. Kuramoto, Y. Shiraishi, N. Machida, K. Takano, N. Takase, T. Iida, J. Matsubara, H. Minami, M. Imai, K. Takada, *Microelectron. Eng.* **1999**, *45*, 101 – 111.
[47] Data according to Ref. [39]: coil separation: 750 mm; distance from the coils to the melt surface: 230 mm; crucible diameter: 75 mm; crucible height: 37.5 mm; crystal diameter: 37.5 mm; $\omega_{crystal} = -3$ revolutions per minute ($r\,min^{-1}$), $\omega_{crucible} = 10\,r\,min^{-1}$; The Hartmann number *Ha* is dimensionsless. It is defined as $Ha = B\,h\,(\sigma\mu^{-1})^{1/2}$, with $B$ is the magnetic field strength, $H$ is the height, $\sigma$ is the electrical conductivity, and $\mu$ is the viscosity.[48] According to a private communication from H. Ozoe the calculations are first carried out with a dimensionless mathematical model in order to obtain results independent of specific parameters. Therefore in the original figure (Figure 2 in Ref. [39]) the oxygen concentration (atoms per $cm^3$) is shown on the ordinate and the dimensionless time on the abscissa. Multiplication of this time by the factor $t_0 = 0.0123$ s (Table 1 in Ref. [39]), which is appropriate for the above model, gives $t$ [s] for the abscissa of Figure 12.
[48] *dtv-Lexikon der Physik*, *Vol. 4 Glu-Kel* (Ed.: H. Franke), Deutscher Taschenbuch Verlag, München, **1970**, p. 81.
[49] "Modelling of Transport Phenomena in Crystal Growth": K. Kakimoto, *Developments in Heat Transfer*, *Vol. 6* (Ed.: J. S. Szmyd), WIT Press, Southampton, **2000**, p. 181 – 200.
[50] A. Seidl, G. McCord, G. Müller, H.-J. Leister, *J. Cryst. Growth* **1994**, *137*, 326 – 334.
[51] The isothermal lines[45] $(T-T_m)(T_{max}-T_m)^{-1}$ of Figure 12 were converted into temperatures $T$ in ?C for $T_m = 1414$ °C (melting point of Si[30,31]) and $\Delta T_{max} = 36$ °C and 42 °C,[45] respectively, and are inserted on the right of the figure.
[52] M. Kurz, A. Pusztai, G. Müller, *J. Cryst. Growth* **1999**, *198/199*, 101 – 106.
[53] N. Van den Bogaert, F. Dupret, *J. Cryst. Growth* **1997**, *171*, 65 – 76 und 77–93.
[54] W. Kleber, *Einführung in die Kristallographie*, extended and revised by H. J. Bautsch, J. Bohm, I. Kleber, 15th Edition, VEB Verlag Technik, Berlin, **1983**, p. 164.
[55] S. Pizzini, *Solid State Phenom.* **2002**, *85*–86, 1 – 66.
[56] V. V. Voronkov, *J. Cryst. Growth* **1982**, *59*, 625 – 643.
[57] W. von Ammon, E. Dornberger, H. Oelkrug, H. Weidner, *J. Cryst. Growth* **1995**, *151*, 273 – 277.
[58] R. Falster, V. V. Voronkov, *Mater. Sci. Eng. B* **2000**, *73*, 87 – 94.
[59] V. V. Voronkov, R. Falster, *J. Cryst. Growth* **1999**, *204*, 462 – 474.
[60] J. Bohm, *Realstruktur von Kristallen*, E. Schweizerbart'sche Verlagsbuchhandlung (Nägele and Obermiller), Stuttgart, **1995**, p. 126 and 162.
[61] R. C. Newman, *J. Phys. Condens. Matter* **2000**, *12*, R335 – R365.
[62] A. F. Wells, *Structural Inorganic Chemistry*, Clarendon Press, Oxford, **1984**, p. 1006.
[63] J. Coutinho, R. Jones, P. R. Briddon, S. Öberg, *Phys. Rev. B* **2000**, *62*, 10824 – 10840.
[64] E. Artacho, F. Ynduráin, B. Pajot, R. R. Ramírez, C. P. Herrero, L. I. Khiruenko, K. M. Ito, E. E. Haller, *Phys. Rev. B* **1997**, *56*, 3820 – 3833.
[65] J. C. Mikkelsen, *Mater. Res. Soc. Symp. Proc.*, **1986**, *59*, 3 – 5 and 19–30.
[66] W. Ostwald, *Z. Phys. Chem. (München)* **1900**, *34*, 495 – 503.
[67] A. Borghesi, B. Pivac, A. Sassella, A. Stella, *Appl. Phys. Rev.* **1995**, *77*, 4169 – 4244.
[68] M. Pesola, Y. J. Lee, J. von Boehm, M. Kaukonen, R. M. Nieminen, *Phys. Rev. Lett.* **2000**, *84*, 5343 – 5346.
[69] J. A. Griffin, H. Navarro, J. Weber, L. Genzel, J. T. Borenstein, J. W. Corbett, L. C. Snyder, *J. Phys. C* **1986**, *19*, L579 – L584.
[70] G. Busch, H. Schade, *Vorlesungen über Festkörperphysik*, Birkhäuser, Basel, **1973**, p. 299.
[71] R. C. Newman, *Mater. Sci. Eng. B* **1996**, *36*, 1 – 12.
[72] Y. J. Lee, J. von Boehm, M. Pesola, R. M. Nieminen, *Phys. Rev. B* **2002**, *65*, 085205-1–085205-12.
[73] M. Pesola, J. von Boehm, T. Mattila, R. M. Nieminen, *Phys. Rev. B* **1999**, *60*, 11449 – 11463.
[74] A. Pasquarello, *Appl. Surf. Sci.* **2000**, *166*, 451 – 454.
[75] A. Pasquarello, M. S. Hybertsen, R. Car, *Nature* **1998**, *396*, 58 – 60.
[76] M. L. Polignano, F. Cazzaniga, A. Sabbadini, F. Zanderigo, F. Priolo, *Mater. Sci. Semicond. Process.* **1998**, *1*, 119 – 130.
[77] F. Shimura, *Solid State Phenom.* **1991**, *19*–20, 1 – 12.
[78] K. Nagasawa, Y. Matsushita, S. Kishino, *Appl. Phys. Lett.* **1980**, *37*, 622 – 624.
[79] T. Sinno, E. Dornberger, W. von Ammon, R. A. Brown, F. Dupret, *Mater. Sci. Eng. R* **2000**, *28*, 149 – 198.
[80] Wichard von Moellendorff, executive engineer at the Allgemeinen Elektricitäts-Gesellschaft (AEG), "On the Oberspree Cable Factory, with cinematographic presentation"; lecture given at 7 p.m. on February 4, 1913, in Vienna.[13]

 © 2003 Wiley-VCH Verlag GmbH & Co. KGaA, Weinheim 

# Communications



The Borromean link of three rings connected such that no two are concatenated is an exceptionally challenging target and any synthetic approach must address both representative and methodological aspects of the problem. Methodological advances toward an orthogonal two-ring target are detailed by J. S. Siegel et al. on the following pages.


**DOI: 10.1002/anie.200352562**
© 2003 Wiley-VCH Verlag GmbH & Co. KGaA, Weinheim

Macrocycles

# Synthetic Approaches to a Molecular Borromean Link: Two-Ring Threading with Polypyridine Templates**

*Jon C. Loren, Michito Yoshizawa, Richard F. Haldimann, Anthony Linden, and Jay S. Siegel**

The molecular Borromean link is one of the most challenging synthetic targets generated from molecular graphs[1] of complex topology.[2,3] Its structural complexity stems from the interweaving of three macrocycles such that no two of the macrocycles are concatenated nor covalently connected, yet collectively they form an integral molecular unit. The origins of this link in human culture go back to antiquity[4] and the novelty of its form has been richly discussed.[5] The design of molecular targets and retrosyntheses from topological graphs often correlate with a specific representation (often printed in two dimensions).[6,7] Three principal representations of the Borromean link that inspire targets for molecular design and synthesis are the Venn rings, chain rings, and orthogonal rings (Figure 1).[8] The Venn rings highlight threefold symmetry and embellish upon the triskelion[9] or related trefoil knot[10] precursor. The chain rings betray a rack[11] or grid[12] substructure from which functionalized end groups close the macrocycles. The orthogonal rings beseech a single-step template-driven synthesis[13] but readily succumb to a ring-by-ring retrosynthesis. From this humble strategy, we begin.

To illustrate a specific strategy, we look to an orthogonal-ring representation using metal coordination as the template method, built up by a kinetically selective reaction sequence (Figure 2). Two key structural intermediates along this synthetic route are the assembly of a principal base macrocycle with *endo*- or *exo*-oriented metal-binding sites and the completion of a threaded two-ring structure, in which the two rings are orthogonal and at least one of the two rings possesses a second set of metal-binding sites, compatible with the threading and knitting together of the third ring.

Macrocycles, abstracted as form **e** (cf. Figure 2), have substantial precedence in the literature;[14] however, the relatively simple conceptual extension to a bismacrocycle of form **c** (cf. Figure 2) represents a curious threaded-ring structure of which there are few examples.[15,16] Our

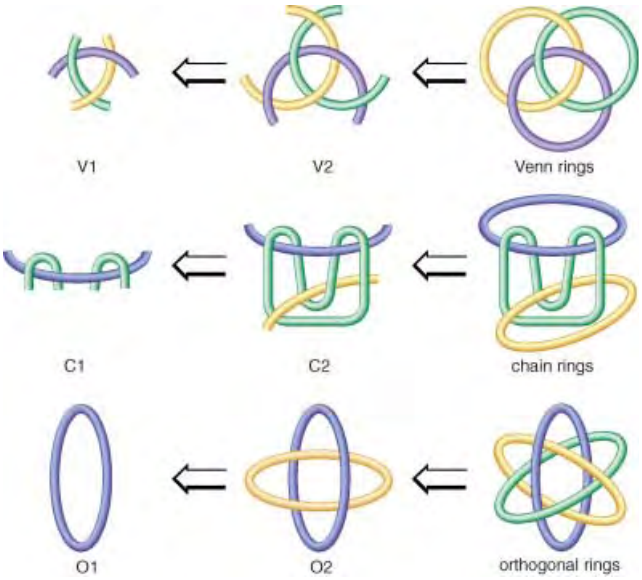



***Figure 1.*** Three retrosynthetic representations of the Borromean link (Venn rings, chain rings, orthogonal rings).

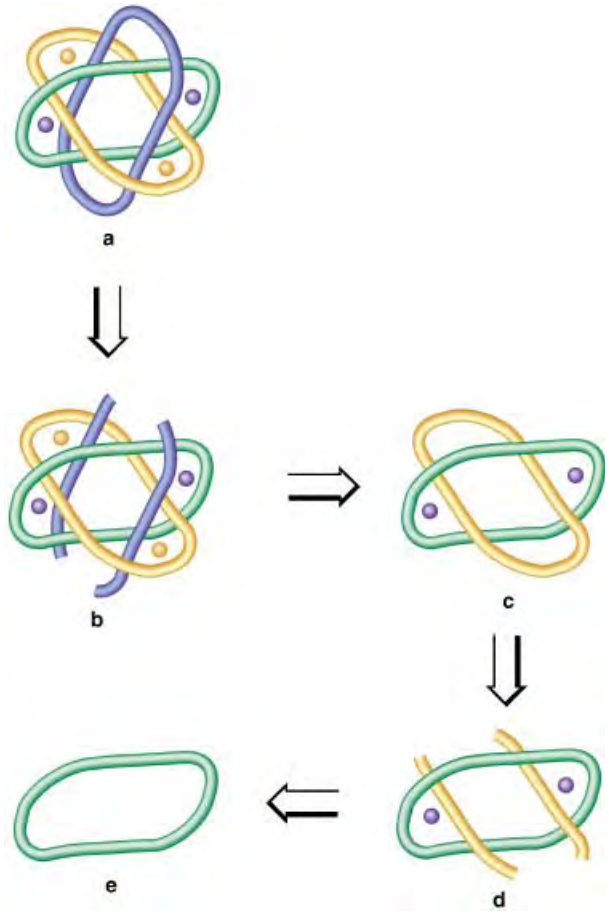



***Figure 2.*** Retrosynthesis of a Borromean link from the orthogonal-ring representation.

[*] Prof. J. S. Siegel, Dr. A. Linden
Organic Chemistry Institute, University of Zürich
Winterthurerstrasse 190, 8057 Zürich (Switzerland)
Fax (+41) 1-635-6888
E-mail: jss@oci.unizh.ch

J. C. Loren, M. Yoshizawa, Dr. R. F. Haldimann
Department of Chemistry, University of California-San Diego
La Jolla, California 92093-0358 (USA)
Fax: (+1) 858-822-0386

[**] This work was supported by the US National Science Foundation (CHE-0213323) and the Swiss National Fond. Gail Bamber prepared the graphical art in Figure 1. Kim Baldridge and Steve Cutchin rendered Figure 3. Bruno Bürgi assisted with the crystal structure determination.

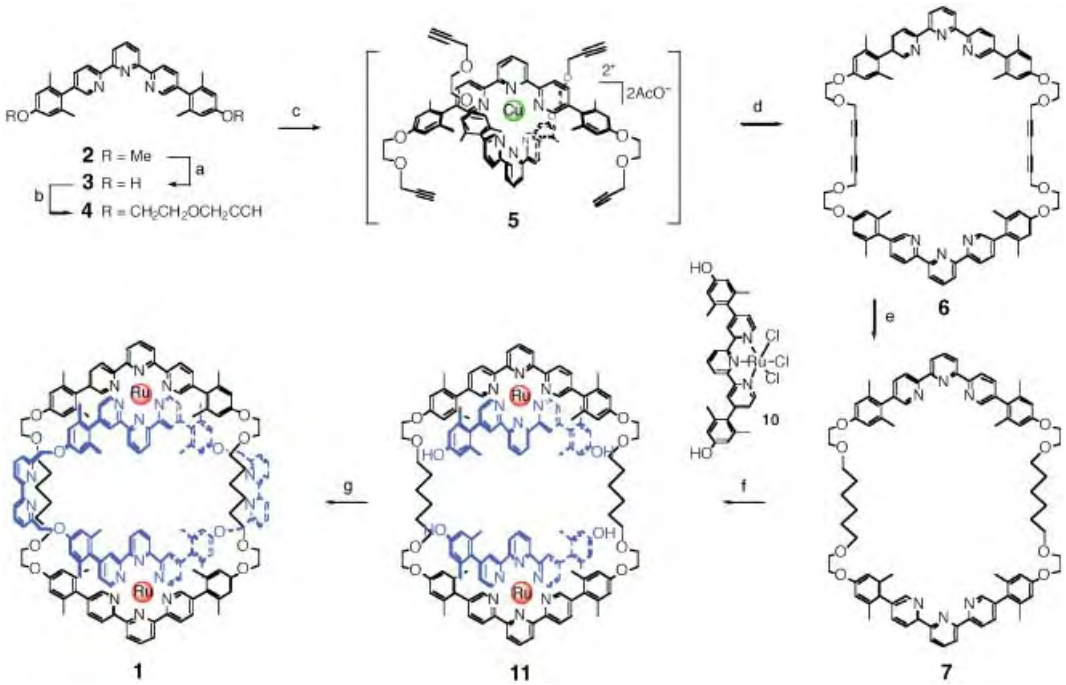
Supporting information for this article is available on the WWW under http://www.angewandte.org or from the author.

 © 2003 Wiley-VCH Verlag GmbH & Co. KGaA, Weinheim DOI: 10.1002/anie.200352562 

strategy focuses on those macrocycles with polypyridine units,[15,17] which would suit a metal-template-based retrosynthesis.

The macrocycle **6** can be synthesized in a multistep procedure from the previously reported terpyridine **2**[18] (Scheme 1). Elaboration of **2** into a related terpyridine **4** with alkyne-terminated side chains, proceeds by standard demethylation and realkylation methods. Terpyridine **4** forms an intermediate homoleptic copper(II) complex[19] with four dangling arms, terminating in alkynes. These arms are too short for the ends to form a [2]catanane, as seen in related work,[20] but are optimal to form the so-called "figure-eight" complex.[21] The combined one-pot operation of forming **5** from **4** and copper ions followed by addition of excess copper ion, under modified Eglinton conditions in ethanol without pyridine, leads directly to the 66-membered macrocycle **6** in over 90% yield. Hydrogenation of the diynes in **6** affords macrocycle **7**, which bears two *endo*-oriented terpyridines and saturated bridging arms. Preformation of the ruthenium complex **10** by standard methods[22] provides the reagent necessary to complex two 4,4″-diarylterpyridyl–Ru units (LRu) to macrocycle **7**, thus forming **11**. These LRu units serve as *exo*-oriented precursors of ring 2 threaded within ring 1. The ends of the 4,4″-aryl units are juxtaposed with each other and macrocyclization to form the threaded two-ring architecture **1** is effected by Williamson ether synthesis with the known biselectrophile 6,6′-bisbromomethyl-2,2′-bipyridine.[23] The bridging bipyridine units represent the *endo*-oriented portions of a tetrahedral or trigonal bipyramidal metal-binding site through which the third ring would ultimately be threaded, oriented, and cyclized.

Crystals of **1** were grown from acetone/diethyl ether as the $PF_6$ salt, and the crystal structure was elucidated in space group $P\bar{1}$ with molecules residing on $C_i$ special positions (Figure 3).[24] The two rings are clearly threaded within one another in an orthogonal orientation. The largest dimension of the complex is roughly 29 Å from the hydrogen atoms in the saturated arm of ring 1 to their symmetry-related partners. The Ru–Ru span is 16.4 Å; on the outer ring (ring 1) the span from the *para*-hydrogen atom of the central ring of the terpyridine to its symmetry partner is approximately 27 Å. The dimensions of ring 2 are slightly smaller, with a long diagonal of 26.1 Å measured between manisyl aryl hydrogen atoms. The conformation of ring 1 is not planar and bows into a chair form. The two *endo*-oriented terpyridines of ring 1 sit in parallel planes, offset by about 5 Å. One might anticipate considerable uncertainty about the exact conformation of the saturated arms and this is supported by residual disorder, which required a two-conformation model for these arms in the crystal structure analysis. The conformation of ring 2 is also readily likened to a macrocyclic chair. The *exo*-oriented terpyridines sit in planes parallel to one another but shifted by roughly 6.5 Å. The bridging bipyridines, adopt the expected *anti* conformation in the absence of a metal. The idealized symmetry of ring 2 would be $C_{2h}$, with the twofold axis bisecting each of the 2,2′ bonds of each bipyridine, and the horizontal mirror plane bisecting the *exo*-oriented terpyridines. The structure shows that there is ample space for the arms of the third ring to be threaded inside of ring 2 and outside of ring 1. The dimensions of this third ring will again need to be over 20 Å to span even the smallest region of ring 1.




***Scheme 1.*** Reaction conditions: a) molten py·HCl, 185 °C, 4 h, 97%; b) $Cs_2CO_3$, $TsOCH_2CH_2OCH_2CCH$ (2.2 equiv), DMF, 80 °C, 10 h, 69%; c) $Cu(OAc)_2{\cdot}H_2O$ (0.5 equiv), ethanol, room temperature, 1 h; d) 1) $Cu(OAc)_2{\cdot}H_2O$ (10.0 equiv), ethanol, high dilution, reflux, 72 h; 2) KCN (aq), $CH_2Cl_2$, 91%; e) $H_2$ 80 psi, Pd/C (10%), ethanol/$CH_2Cl_2$ (1:1), 6 h, 91%; f) **10** (2.0 equiv), $CH_2Cl_2$/EtOH/ethylene glycol (2:2:1), reflux, 12 h, 65%; g) 6,6′-bisbromomethyl-2,2′-bipyridine (2.0 equiv), $Cs_2CO_3$, acetonitrile, reflux, 72 h, 49%.

 © 2003 Wiley-VCH Verlag GmbH & Co. KGaA, Weinheim 

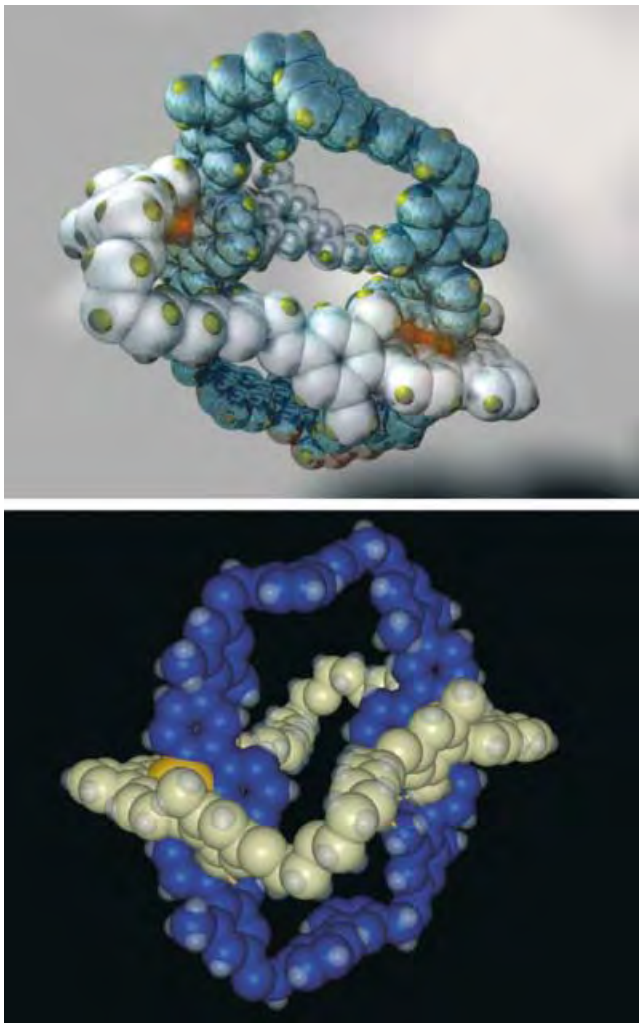
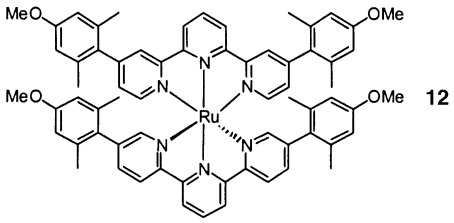


***Figure 3.*** Space-filling model of the crystal structure of **1**: colored to emphasize connectivity; aspect to show chair form of ring 1 (bottom)

The photophysical and electrochemical properties of **1**, relative to its parent mono ruthenium heteroleptic complex **12**, indicate that the ruthenium centers behave independently of one another (Table 1). Excitation near 312 nm results in




**12**

what appears to be a ligand-centered emission at 407 and 419 nm for **1** and **12**, respectively. These values coincide with the emission wavelength range of the free ligands.[18] Excitation at 480 nm results in no detectable emission for either. Cyclic voltametry (CV) shows only quasi-reversible behavior, and electrodeposition occurs on the electrodes after multiple scans for both **1** and **12**.

***Table 1:*** UV/Vis, fluorescence, and electrochemical reduction potentials for **1** and **12**.

| | UV/Vis[a] | | Fluorescence ($\lambda$)[a] | | |
|---|---|---|---|---|---|
| | $\lambda_{abs}$ | $\log \varepsilon$ | Excitation | Emission | $E_{1/2}$ [V][b] |
| **1** | 201 | 5.6 | 312 | 407 | 0.99 |
| | 273 | 5.0 | | | |
| | 312 | 5.1 | | | |
| | 480 | 4.4 | | | |
| **12** | 202 | 5.0 | 313 | 419 | 0.95 |
| | 271 | 4.8 | | | |
| | 313 | 5.9 | | | |
| | 480 | 4.1 | | | |

[a] In acetonitrile. [b] 0.1 M tetrabutylammonium hexafluorophosphate in acetonitrile vs $Ag/AgNO_3$ in acetonitrile.

The synthesis of the two-ring intermediate en route to a Borromean link in the orthogonal-ring representation marks a milestone. The challenge of this target lead to a highly efficient strategy for the synthesis of macrocycle **7**, which in turn made 100 mg quantities of **1** readily accessible. The elucidation of the structure of **1** provides evidence that the molecule adopts a structure close to the idealized scheme and, more importantly, gives insight into the stereochemistry and structural dimensions necessary to assemble the last ring of the Borromean link. Beyond the mere technical details, these studies illustrate an important aspect of the pursuit of chemistry: the human conception of molecular structure.[31]

Received: August 4, 2003 [Z52562]
Published Online: November 20, 2003

**Keywords:** macrocycles · nitrogen heterocycles · ruthenium · supramolecular chemistry · template synthesis

[1] D. M. Walba, *Tetrahedron* **1985**, *41*, 3161.
[2] For a review of the field of chemical topology, see: a) J. P. Sauvage, C. Dietrich-Buchecker, *Molecular Catenanes, Rotaxanes and Knots: A Journey Through the World of Molecular Topology*, Wiley-VCH, Weinheim, **1999**, p. 368; b) G. Schill, *Catenanes, Rotaxanes, and Knots, Vol. 22*, Academic, New York, **1971**, p. 192 (Organic Chemistry, A Series of Monographs); c) J. M. Lehn, *Supramolecular Chemistry: Concepts and Perspectives*, VCH, Weinheim, **1995**, p. 262.
[3] For pioneering work in the field, see: a) E. Wasserman, *J. Am. Chem. Soc.* **1960**, *82*, 4433–4434; b) G. Schill, A. Lüttringhaus, *Angew. Chem.* **1964**, *76*, 567; *Angew. Chem. Int. Ed. Engl.* **1964**, *3*, 546; c) A. Lüttringhaus, F. Cramer, H. Prinzbach, F. M. Henglein, *Justus Liebigs Ann. Chem.* **1958**, *613*, 158; d) A. Lüttringhaus, F. Cramer, H. Prinzbach, *Angew. Chem.* **1957**, *69*, 137.
[4] P. R. Cromwell, E. Beltrami, M. Rampichini, *Mathematical Intelligencer* **1998**, *20*, 53–62; see also: http://www.liv.ac.uk/~spmr02/rings/.
[5] C. Liang, K. Mislow, *J. Math. Chem.* **1994**, *16*, 27–35.
[6] In contrast, the one existing molecular effigy of a Borromean link comes from the creative use of molecular biological methods for connecting DNA analogous to the well-known Holiday-junction construction. This form, albeit topologically equivalent to the Borromean link, is not visually equivalent to a simple Borromean-link representation. This lack of direct visual correlation between the actual structure and the ideal represen-

 © 2003 Wiley-VCH Verlag GmbH & Co. KGaA, Weinheim 

tation is also characteristic of Whiteside's novel micromachined model of a Borromean link.

[7] a) N. C. Seeman, *Angew. Chem.* **1998**, *110*, 3408 – 3428; *Angew. Chem. Int. Ed.* **1998**, *37*, 3220 – 3238; b) C. Mao, W. Sun, N. C. Seeman, *Nature* **1997**, *386*, 137 – 138; c) H. Wu, S. Brittain, J. Anderson, B. Grzybowski, S. Whitesides, G. M. Whitesides, *J. Am. Chem. Soc.* **2000**, *122*, 12691 – 12699.

[8] These representations exemplify but do not limit the number of ways this topology can be visually appreciated or structurally realized; however it is through the connections between these representations and the designed molecular targets that we enrich our conceptualization of molecular structure and envision retrosyntheses. For an example of how this has been interpreted in crystal engineering, see: L. Carlucci, G. Ciani, D. M. Proserpio, *Cryst. Eng. Comm.* **2003**, *5*, 269 – 279.

[9] C. R. Woods, M. Benaglia, S. Toyota, K. Hardcastle, J. S. Siegel, *Angew. Chem.* **2001**, *113*, 771 – 773; *Angew. Chem. Int. Ed.* **2001**, *40*, 749 – 751.

[10] a) O. Safarowsky, M. Nieger, R. Fröhlich, F. Vögtle, *Angew. Chem.* **2000**, *112*, 1699 – 1701; *Angew. Chem. Int. Ed.* **2000**, *39*, 1616 – 1618; b) G. Rapenne, C. Dietrich-Buchecker, J.-P. Sauvage, *J. Am. Chem. Soc.* **1999**, *121*, 994 – 1001; c) G. Schill, R. Henschel, J. Boeckmann, *Justus Liebigs Ann. Chem.* **1974**, 709 – 733; d) H. Adams, E. Ashworth, G. A. Breault, C. A. Hunter, P. C. Mayers, *Nature* **2001**, *411*, 763.

[11] M. Benaglia, F. Ponzini, C. R. Woods, J. S. Siegel, *Org. Lett.* **2001**, *3*, 967 – 969.

[12] a) G. S. Hanan, D. Volkmer, U. S. Schubert, J. M. Lehn, G. Baum, D. Fenske, *Angew. Chem.* **1997**, *109*, 1929 – 1931; *Angew. Chem. Int. Ed. Engl.* **1997**, *36*, 1842 – 1844; b) S. Toyota, C. R. Woods, M. Benaglia, R. Haldimann, K. Warnmark, K. Hardcastle, J. S. Siegel, *Angew. Chem.* **2001**, *113*, 773 – 776; *Angew. Chem. Int. Ed.* **2001**, *40*, 751 – 754.

[13] For a review on template-directed approaches, see: a) Breault, C. A. Hunter, P. C. Mayers, *Tetrahedron* **1999**, *55*, 5265 – 5293; b) S. Anderson, H. L. Anderson, J. K. M. Sanders, *Acc. Chem. Res.* **1993**, *26*, 469 – 475; c) T. J. Hubin, D. H. Busch, *Coord. Chem. Rev.* **2000**, *200*, 5 – 52; d) F. Diederich, P. J. Stang, *Templated Organic Synthesis*, Wiley-VCH, Weinheim, **2000**, p. 410.

[14] a) D. Parker in *Macrocycle Synthesis: A Practical Approach* (Ed.: C. J. Moody, L. M. Harwood), Oxford University, Oxford, **1996**; b) E. C. Constable, *Coordination Chemistry of Macrocyclic Compounds*, Oxford University, Oxford, **1999**.

[15] M. Schmittel, A. Ganz, D. Fenske, *Org. Lett.* **2002**, *4*, 2289 – 2292.

[16] S.-H. Chiu, A. R. Pease, J. F. Stoddart, A. J. P. White, D. J. Williams, *Angew. Chem.* **2002**, *114*, 280 – 284; *Angew. Chem. Int. Ed.* **2002**, *41*, 270 – 274.

[17] a) M. Schmittel, A. Ganz, *Synlett* **1997**, 710 – 712; b) U. Lehmann, A. D. Schlüter, *Eur. J. Org. Chem.*, **2000**, 3483 – 3487; c) O. Henze, D. Lentz, A. D. Schlüter, *Chem. Eur. J.* **2000**, *6*, 2362 – 2367; d) G. R. Newkome, H.-W. Lee, *J. Am. Chem. Soc.* **1983**, *105*, 5956 – 5957; e) T. W. Bell, F. Albert, *J. Am. Chem. Soc.* **1986**, *108*, 8109 – 8111.

[18] J. C. Loren, J. S. Siegel, *Angew. Chem.* **2001**, *113*, 776 – 779; *Angew. Chem. Int. Ed.* **2001**, *40*, 754 – 757.

[19] U. S. Schubert, C. Eschbaumer, P. Andres, H. Hofmeier, C. H. Weidl, E. Herdtweck, E. Dulkeith, A. Morteani, N. E. Hecker, J. Feldmann, *Synth. Met.* **2001**, *121*, 1249 – 1252.

[20] a) By optimizing the arm length, the mixture of catenane and "figure-eight" products can be controlled (J. Loren, P. Gantzel, J. S. Siegel, unpublished results); b) the length and flexibility of the arms has been noted as a crucial factor in a related RCM-based synthesis of catenanes; see: a) M. Weck, B. Mohr, J. P. Sauvage, R. H. Grubbs, *J. Org. Chem.* **1999**, *64*, 5463 – 5471; b) B. Mohr, M. Weck, J. P. Sauvage, R. H. Grubbs, *Angew. Chem.* **1997**, *109*, 1365 – 1367; *Angew. Chem. Int. Ed. Engl.* **1997**, *36*, 1308 – 1310.

[21] a) N. Belfrekh, C. Dietrich-Buckecker, J.-P. Sauvage, *Inorg. Chem.* **2000**, *39*, 5169 – 5172; b) A. G. Fallis, M. A. Heuft, *Angew. Chem.* **2002**, *114*, 4702 – 4705; *Angew. Chem. Int. Ed.* **2002**, *41*, 4520 – 4523.

[22] P. B. Sullivan, J. M. Calvert, T. J. Meyer, *Inorg. Chem.* **1980**, *19*, 1404 – 1407.

[23] U. S. Schubert, J. L. Kersten, A. E. Pemp, C. D. Eisenbach, G. R. Newkome, *Eur. J. Org. Chem.* **1998**, 2573 – 2581.

[24] Crystal-structure analysis of **1**: crystals from acetone/$Et_2O$; $C_{204}H_{232}F_{24}N_{16}O_{24}P_4Ru_2$, $M_r = 4074.0$; triclinic, space group $P\bar{1}$, $a = 14.8913(6)$, $b = 15.6077(7)$, $c = 24.010(1)$ Å, $\alpha = 98.044(2)$, $\beta = 90.089(2)$, $\gamma = 90.936(2)°$, $V = 5524.6(4)$ Å$^3$, $Z = 1$, $\rho = 1.224$ g cm$^{-3}$, $T = -113$ °C, crystal dimensions: $0.20 \times 0.25 \times 0.30$ mm, Nonius Kappa CCD area detector diffractometer, graphite-monochromated $Mo_{K\alpha}$ radiation, $\lambda = 0.71073$ Å, $\mu = 0.249$ mm$^{-1}$, $2\theta_{max} = 55°$, 62117 total reflections, 18576 symmetry-independent reflections, $R_{int} = 0.072$, 11249 reflections with $I > 2\sigma(I)$. Data reduction performed with HKL Denzo and Scalepack;[25] absorption correction applied.[26] The structure was solved by using the Patterson and Fourier expansion routines of DIRDIF94.[27] The SQUEEZE routine[28] of the program PLATON[29] was employed to omit the contribution to the reflection data from the highly disordered solvent molecules, estimated to be six acetone molecules per asymmetric unit. This significantly improved the refinement results. The six $CH_2$ groups of the hexamethylene chain and one $PF_6^-$ anion are disordered and two conformations were modelled for each. The structure was refined on $F^2$ by full-matrix least-squares methods using SHELXL97.[30] The H atoms were placed in geometrically calculated positions and were allowed to ride on their parent atom. The refinement of 1136 parameters using 18576 reflections and 739 restraints gave $R(F)$ ($I > 2\sigma(I)$ data) = 0.103, $Rw(F^2)$ (all data) = 0.306, goodness of fit on $F^2 = 1.040$, $\Delta\rho_{max} = 2.27$ e Å$^{-3}$. CCDC-216666 contains the supplementary crystallographic data for this paper. These data can be obtained free of charge via www.ccdc.cam.ac.uk/conts/retrieving.html (or from the Cambridge Crystallographic Data Centre, 12, Union Road, Cambridge CB2 1EZ, UK; fax: (+44) 1223-336-033; or deposit@ccdc.cam.ac.uk).

[25] Z. Otwinowski, W. Minor, *Methods Enzymol.* **1997**, *276*, 307 – 326.

[26] R. H. Blessing, *Acta Crystallogr. Sect. A* **1995**, *51*, 33.

[27] P. T. Beurskens, G. Admiraal, G. Beurskens, W. P. Bosman, R. de Gelder, R. Israel, J. M. M. Smits, DIRDIF94: The DIRDIF program system, Technical Report of the Crystallography Laboratory, University of Nijmegen, The Netherlands, **1994**.

[28] P. van der Sluis, A. L. Spek, *Acta Crystallogr. Sect. A* **1990**, *46*, 194 – 201.

[29] A. L. Spek, PLATON, Program for the Analysis of Molecular Geometry, University of Utrecht, The Netherlands, **2003**.

[30] G. M. Sheldrick, SHELXL97, Program for the Refinement of Crystal Structures, University of Göttingen, Germany, **1997**.

[31] Note added in Proof: An example of a related topological structure can be found in: O. V. Dolomanov, A. J. Blake, N. R. Champness, M. Schröder, C. Wilson, *Chem. Commun.* **2003**, 682 – 683.

 © 2003 Wiley-VCH Verlag GmbH & Co. KGaA, Weinheim 

Molecular Electronics

# The Molecule–Electrode Interface in Single-Molecule Transistors**

*Hongbin Yu, Yi Luo, Kristen Beverly, J. Fraser Stoddart, Hsian-Rong Tseng, and James R. Heath**

A fundamental goal of molecular electronics[1] is to design useful transport signatures into solid-state devices through control[2] over the molecular components. In principle, theory and experiment should unite to provide a "chemical intuition" that guides 1) the direction of molecular design and synthesis and 2) the choice of the device materials and architectures that are employed in molecular electronics. To date, however, the field has advanced largely through the development of phenomenological—rather than quantitative—models of molecular devices. For example, traditional models for correlating properties, such as intermolecular charge transfer with molecular structure (electron-transfer theory) are designed for the solution phase.[3] Similarly, such structure–property relationships can be tested by using a variety of sophisticated spectroscopic techniques, such as optical measurements and multidimensional NMR spectroscopy, which have been designed to work in solution on statistical numbers of molecules.

Consider the case of a single molecule bridging two electrodes. Any theory of such a system must consider the molecule and the electrode as a single nonseparable entity.[4] The objectives of the theory would be 1) to predict the alignment of the Fermi levels of the electrodes with the molecular orbital energies in the molecule, 2) to forecast the voltage-dependent electron conductance across the molecule–electrode interfaces of the device junction, and 3) to provide fundamental insight that can be fed back into molecular and device design for optimization of properties. Ideal experiments should be able to provide a robust test of such predictions. This theory does not exist yet, and, until recently, there were very few experiments that could be used to guide or test such a theory. The situation is now changing, as increasingly reliable measurements of molecular electronic devices have been carried out in many laboratories.[5]

[*] Prof. J. R. Heath, Dr. H. Yu, Dr. Y. Luo, K. Beverly
Caltech Chemistry, MC 127-72
1200 East California Boulevard, Pasadena, CA 91125 (USA)
Fax: (+1) 310-206-4038
E-mail: heath@caltech.edu
Prof. J. F. Stoddart, Dr. H.-R. Tseng
The California NanoSystems Institute and
Department of Chemistry and Biochemistry
University of California, Los Angeles
405 Hilgard Avenue, Los Angeles, CA 90095-1569 (USA)

[**] We thank Professor Hongkun Park and Wenjie Liang for helpful discussions, and the Department of Energy (DOE) and the Defense Advanced Research Projects Agency (DARPA), including the MARCO Center, for funding.

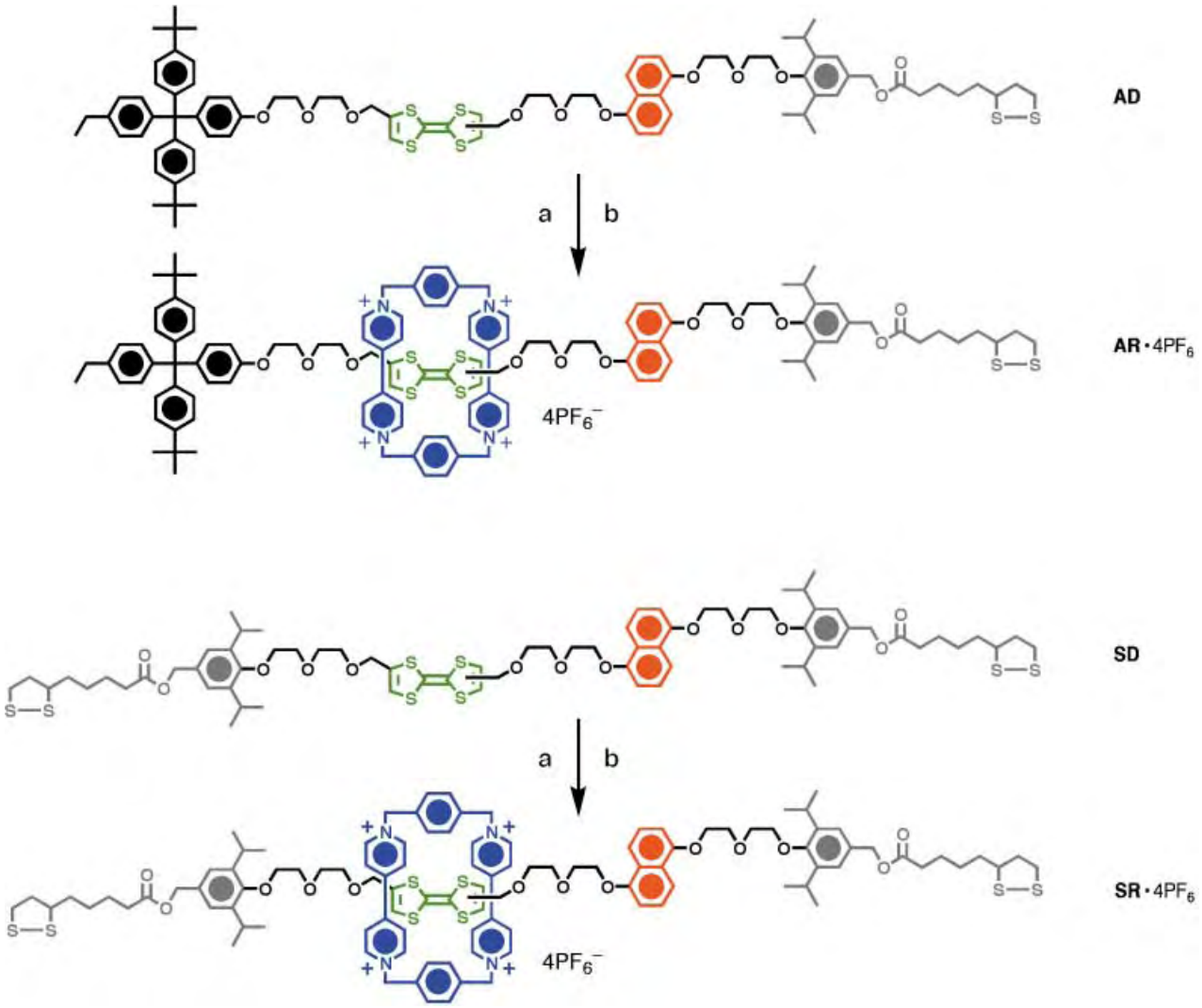
Supporting information for this article is available on the WWW under http://www.angewandte.org or from the author.

In particular, single-molecule devices are emerging as a powerful high-resolution spectroscopic tool for molecular electronics. Early experiments utilized[6] two-terminal break junctions in which one or a few molecules were suspended across a mechanically adjusted electrode gap. More recent experiments have employed[7–9] an electrical break junction, together with a gate electrode, to form a three-terminal device (3TD). The gate can be utilized to correlate the molecular energy levels with the Fermi energies of the electrodes, and thus somewhat normalize out the device-to-device fluctuations that are observed in the two-electrode measurements.

Herein we utilize single-molecule 3TDs with a Pt break-junction source and drain electrodes to investigate four molecules—namely, the bistable [2]rotaxane $\mathbf{AR}^{4+}$ and $\mathbf{SR}^{4+}$ and the corresponding dumbbell-shaped compounds **AD** and **SD**, from which the mechanically, redox-switchable rotaxanes were obtained (Scheme 1) by a template-directed protocol[10] that clips a tetracationic ring around the tetrathiafulvalene (TTF) units in the dumbbell-shaped compounds. Our goal was to address the nature of the molecule–electrode contact. We had previously found that similar amphiphilic, bistable [2]rotaxanes[11] and bistable [2]catenanes[12]—rendered amphiphilic with dimiristoylphosphatidic acid (DMPA) counterions—could be utilized[13,14] as solid-state, bistable switches in devices in which a Langmuir–Blodgett (LB) monolayer is sandwiched between a Si bottom electrode—passivated with the native oxide—and a Ti/Al top electrode. In the case of bistable [2]catenanes that were specially designed to interact noncovalently with the side walls of single-walled carbon nanotubes (SWNTs), we have also found[15] that usable switching devices could be fabricated using a semiconducting SWNT bottom electrode. Various control molecules, including the dumbbell precursors of the bistable [2]rotaxanes and nondegenerate [2]catenanes, were also explored, and none of these controls yielded a switch. Thus, we attributed the bistable character of working solid-state devices as arising from hysteretical mechanical motions in these redox-switchable interlocked molecules.[11,12] Conversely, we have never observed switching signatures attributable to a molecular bistability when we have utilized a metal (Au or Pt) bottom electrode.[16] One possible reason for the difference between Group IV (Si or C) electrode materials and transition metal electrodes is that the increased ionic character of the organic/metal interface leads to Schottky-like barriers to charge-flow, and that those barriers dominate the device characteristics. We report here that the device characteristics of 3TDs containing bistable [2]rotaxanes and Pt electrodes are extremely sensitive to the chemical nature of the molecule–-electrode contact, but are much less sensitive to the details of the molecular structure away from those contacts. This result has strong implications for the design of molecular electronic devices.

While the bistable [2]rotaxane $\mathbf{AR}^{4+}$ can form "chemical" bonds between the terminal, incipient five-membered disulfide ring and a Pt electrode, the tetraarylmethane stopper at the other end of $\mathbf{AR}^{4+}$ will, at most, become physisorbed onto platinum, thus the molecule–electrode contacts are asymmetric. In the case of the bistable [2]rotaxane $\mathbf{SR}^{4+}$, both ends

 © 2003 Wiley-VCH Verlag GmbH & Co. KGaA, Weinheim DOI: 10.1002/anie.200352352 




***Scheme 1.*** Template-directed synthesis of **AR**·4 $PF_6$ from **AD**, and **SR**·4 $PF_6$ from **SD** in 77 and 34% yields, respectively. Reagents and conditions: a) α,α′-[1,4-phenylenebis(methylene)]bis(4,4′-bipyridium) bis(hexafluorophosphate), 1,4-bis(bromomethyl)benzene, DMF, RT, 10 days; b) chromatography on $SiO_2$ with $Me_2CO/NH_4PF_6$, followed by addition of $H_2O$ to the eluent.

of the molecule are terminated by five-membered disulfide rings and so the molecule–electrode contacts are symmetric. It should be noted, however, that both molecules are asymmetric in their middle regions away from the contacts.

The devices used to conduct the single-molecule experiments are shown in Figure 1. A degeneratively doped ($n^+$)poly-Si substrate served as the gate electrode on top of which was grown a 30-nm thick $SiO_2$ film.[17] Each experimental run utilized 14 Pt junctions (thickness ca. 7 nm; width ca. 160 nm; length ca. 500 nm). These junctions were patterned by electron-beam lithography into a poly(methyl methacrylate) (PMMA) resist on top of the $SiO_2$ layer, and then developed by electron beam evaporation of Pt from a metal target. The patterns were cleaned with $Me_2CO$ and an $O_2$ plasma, and then a drop of a dilute solution (ca. $10^{-6}$ M to $10^{-7}$ M) of the molecules of interest in $CH_2Cl_2$ was placed onto the device. These devices were dried under flowing $N_2$. The individual junctions were then wire-bonded, mounted into a chip carrier, and then loaded into the cold-finger of a He cryostat, which was cooled to 1.7 K. The junctions were broken by applying a voltage to the wire, as has been described by other research groups.[8,9] After forming the break junction, current–voltage ($I$–$V$) curves were measured across the source and drain electrodes as a function of varying gate voltage ($V_G$). Since the object was to prepare junctions containing just one molecule, most junctions were simply open circuits, which implies that no molecule was bridging the gap. For the device prepared with $\mathbf{AR}^{4+}$, 5 out of 40 broken junctions exhibited a gating response while, for $\mathbf{SR}^{4+}$ 7 out of 25 broken junctions exhibited a gating response. This higher yield for $\mathbf{SR}^{4+}$—which is chemisorbed to both the source and drain sides of the junction—was observed, even though the solution of $\mathbf{SR}^{4+}$ was a factor of four more dilute than for $\mathbf{AR}^{4+}$. Several break junctions were investigated by electron microscopy after completing the $I$–$V$ measurements, and the gap was observed to be about 4 nm. Although this distance is hard to quantify, the result is consistent with a nonmeasurable tunneling current between the two electrodes in the absence

 © 2003 Wiley-VCH Verlag GmbH & Co. KGaA, Weinheim 

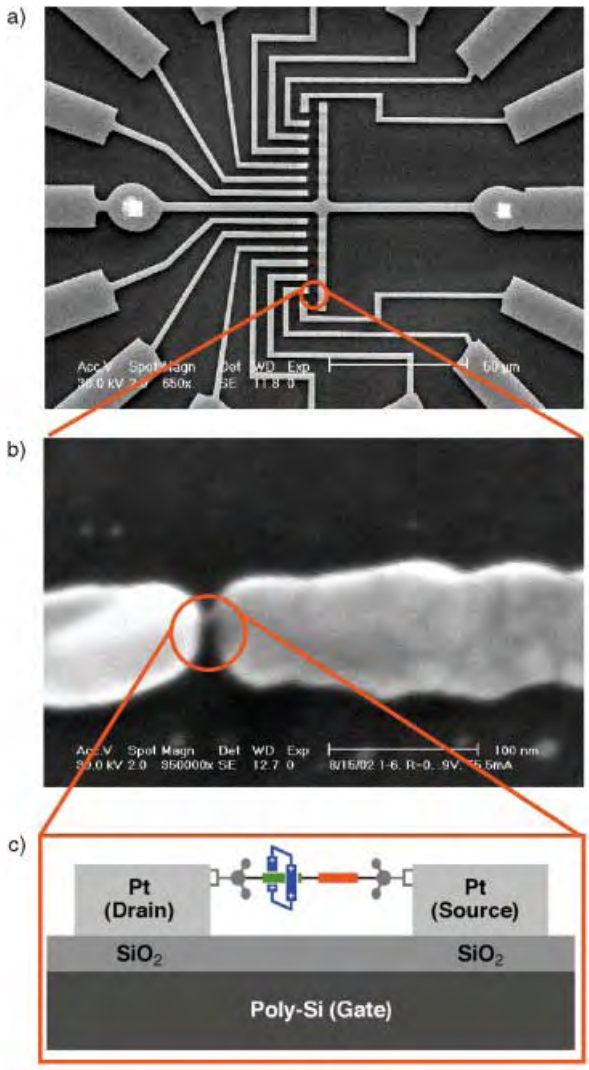



***Figure 1.*** a) Scanning electron microscope (SEM) pictures of single-molecule devices fabricated on a Si substrate. A 30-nm thick low-temperature thermal oxide of Si was grown on top of a degenerately doped Si substrate. The center metal electrode, where the break junction is made of 7-nm thick Pt, followed by 100-nm thick gold wires and pads for wire bonding. b) The SEM image after the break junction is made. The separation between the two metal electrodes is around 4 nm. c) A section through a single-molecule transistor.

of a molecule. Tunneling current can be used to estimate the width of gaps in the 1–2-nm range.[7]

Figure 2a,b display data from break junctions formed in the presence of $\mathbf{AR}^{4+}$ and $\mathbf{SR}^{4+}$. Here, the x-axis is the applied source-drain voltage ($V_{SD}$), and the $y$-axis is $V_G$.[18] The color represents the conductance ($dI/dV$) of the junction, which is typically $\geq 0$ for all $V_{SD}$ values. The darkest areas in the center of the plots indicate the regions of no current. The edges of these dark regions correspond to the current steps in the $I$–$V$ graph near the threshold voltage. This behavior is that of a single-electron transistor—that is, a device containing a small island (the molecule) connected to electrodes by tunnel barriers at either end and with gate-voltage-tunable electronic states.[19] At low $V_{SD}$ values, the electron energy is not high enough to tunnel to the island and, therefore, current is blocked (Coulomb blockade).[14] When voltage passes beyond the threshold, the electron gains sufficient energy and can tunnel to an electronic state on the molecule.

Although amphiphilic, bistable [2]rotaxanes that are structurally similar to $\mathbf{AR}^{4+}$ and $\mathbf{SR}^{4+}$ have been shown to work as solid-state switches in two-terminal tunnel junctions, such switching behavior is thermally activated.[14] The data displayed in Figure 2 was collected at 1.7 K, and so we expect that all activated processes will be quenched. With this type of measurement, it is never completely clear whether each device contains just one molecule, although each individual triangular-shaped resonance undoubtedly originates from a single molecule because of the extreme unlikelihood of having any two molecules coupled in the same way to the source, drain, and gate electrodes. In each plot, a region where the conductance gap narrows has been chosen (indicated by the red arrows). In Figure 2c,d, the current–voltage response that correlates with the $V_G$ values is presented, indicated by the arrows located at the sides of Figure 2a,b, respectively.

Two significant results are illustrated in Figure 2. First, the conductance spectrum for $\mathbf{AR}^{4+}$ is quite asymmetric, while the corresponding spectrum for $\mathbf{SR}^{4+}$ is symmetric. This result was found for all of the devices measured. We may clearly ascribe it to the asymmetric/symmetric nature of the molecule–electrode chemical interactions. Both molecules are asymmetric structures, although only $\mathbf{SR}^{4+}$ can have similar bonding at both the source and drain electrodes. Second, the junction resistance, measured at the point where the conductance gap narrows, is approximately a factor of $10^2$ lower for $\mathbf{SR}^{4+}$ than for $\mathbf{AR}^{4+}$. Again, this result was observed in every device that was measured, and implies that this reduced junction resistance is attributable to the additional "chemical" bonding interaction possible for $\mathbf{SR}^{4+}$. A third observation (Figure 3) was that, for junctions prepared using the dumbbell-shaped compounds **AD** and **SD**, the first two observations remained valid, namely, the conductance spectra (Figure 3a,b) for **AD** and **SD** are asymmetric and symmetric, respectively. In Figure 3c,d, the current–voltage response that correlates with a $V_G$-tuned closing of the conductance gap are presented, indicated by the arrows located at the sides of Figure 3a,b, respectively. In other words, while changing the chemical nature of the molecule–electrode contacts has a profound effect on the conductance characteristics of the junction, changing the nature of the molecule away from those contacts had only a minor effect. A last relevant observation (not shown) involves the temperature-dependent stability of these devices. For devices containing $\mathbf{AR}^{4+}$, the current decreased to below our detection limit of about $10^{-12}$ A when the temperature was raised to about 20 K. This result indicates that the molecule moved so that it was no longer bridging the source and drain electrodes. For $\mathbf{SR}^{4+}$, conductance plots such as that presented in Figure 2b could still be recorded when the temperature was raised to above 100 K, albeit with thermally broadened line widths, but also with increased current magnitudes. This observation is consistent with the fact that $\mathbf{AR}^{4+}$ is chemisorbed to just one electrode and is loosely anchored (physisorbed) onto the other, while $\mathbf{SR}^{4+}$ is chemisorbed to both electrodes.

 © 2003 Wiley-VCH Verlag GmbH & Co. KGaA, Weinheim 

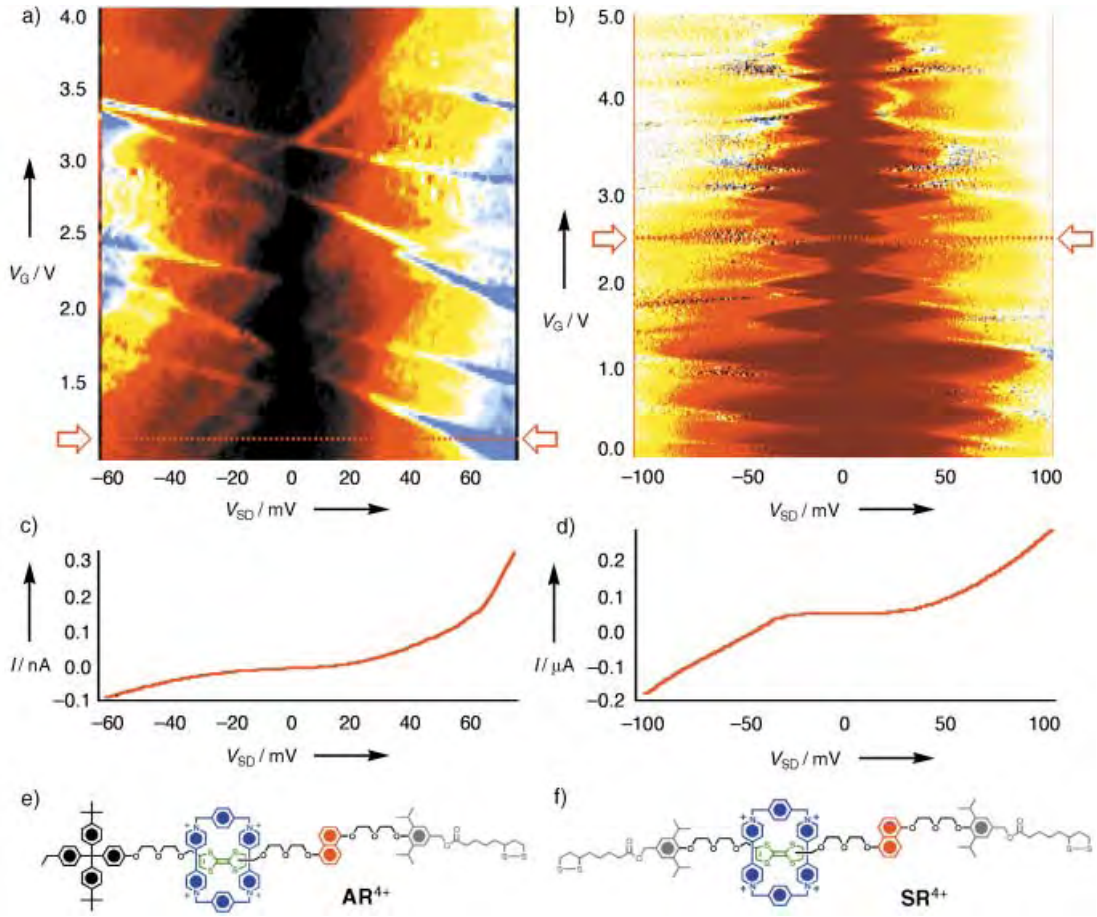



***Figure 2.*** Differential conductance (d*I*/d*V*) plots (a and b) and current–voltage (*I*–*V*) curves (c and d) for rotaxane $\mathbf{AR}^{4+}$ and $\mathbf{SR}^{4+}$ (e and f). The *I*–*V* curves shown in (c) and (d) were taken at the gate voltages ($V_G$) indicated by the red arrows in (a) and (b), respectively.

The conclusion from all of these results taken together is that it is very easy to identify the molecular components involved in the molecule–electrode contacts in a system consisting of Pt electrodes and a molecule containing a large number of low-lying molecular orbitals. However, those same interface states also dominate the transport characteristics. The molecular orbitals that are not involved in the electrode contacts are effectively masked. Even something as simple as molecular asymmetry is difficult to detect.

These results, coupled with other results[13–15] using Si and SWNT electrodes, outline a significant chemical challenge for molecular electronics. If the goal of achieving interesting device signatures that are molecular in origin is achieved, then the implication is that such devices might be scalable to the dimensions of just a few molecules. However, at such small dimensions, the choice of conductors is limited. SWNTs are both "good molecular electronics electrodes" and good conductors, but, in spite of recent progress, sorting SWNTs by electrical character is still a significant challenge, and organizing SWNTs into well-defined circuit architectures is also nontrivial.[20,21] Ultra-high density circuits[22] of metal and semiconductor nanowires can be patterned with wire diameters of only a few nanometers, but at wire diameters below a few nanometers, only the metal wires are expected to be good conductors. Thus, the challenge is to design *chemically* a molecule–metal electrode interface that does not mask the electronic structure of the molecule. Yaliraki et al.[4a] have calculated that simply varying the electrode-binding atom on the organic molecule from O to S to Se for an Au electrode has a strong impact on the resulting transport characteristics through the molecular junction. Similarly, the exploration of other metals and metal alloys as electrode materials is likely to be fruitful. Theoretical guidance in such an exploration would be extremely helpful.

Received: July 10, 2003 [Z52352]

**Keywords:** break junctions · differential conductance · molecular devices · molecule electrode contact · rotaxanes

[1] A. Aviram, M. A. Ratner, *Chem. Phys. Lett.* **1974**, *29*, 277–283.
[2] J. R. Heath, M. A. Ratner, *Phys. Today* **2003**, *56*, 43–49.
[3] J. Jortner, M. Bixon, A. A. Voityuk, N. Rösch, *J. Phys. Chem. A* **2002**, *106*, 7599–7606.
[4] a) S. N. Yaliraki, M. Kemp, M. A. Ratner, *J. Am. Chem. Soc.* **1999**, *121*, 3428–3434; b) K. W. Hipps, *Science* **2001**, *294*, 536–537; c) X. D. Cui, A. Primak, X. Zarate, J. Tomfohr, O. F. Sankey, A. L. Moore, T. A. Moore, D. Gust, G. Harris, S. M. Lindsay, *Science* **2001**, *294*, 571–574.

 © 2003 Wiley-VCH Verlag GmbH & Co. KGaA, Weinheim 

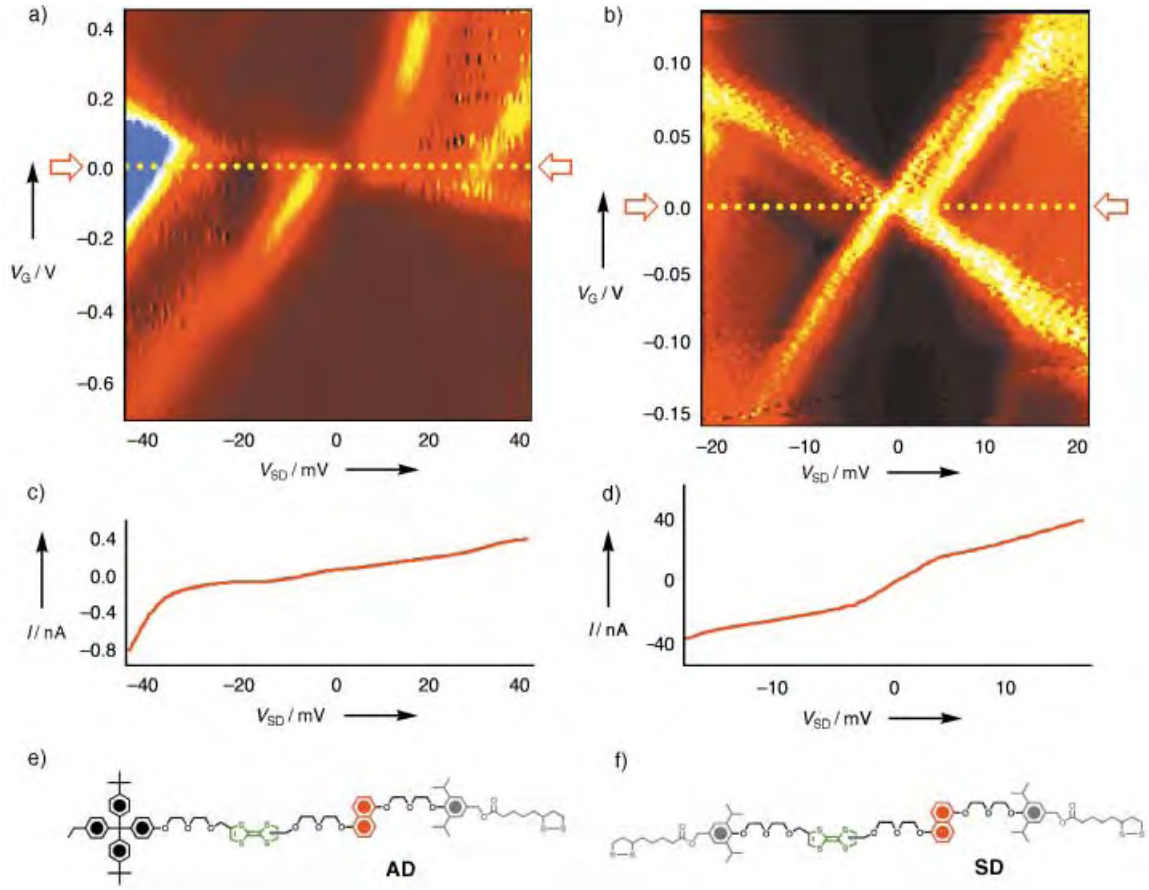



***Figure 3.*** Differential conductance (d*I*/d*V*) plots (a and b) and current–voltage (*I*–*V*) curves (c and d) for the dumbbell-shaped compounds **AD** and **SD** (e and f). Note that, in concert with the data for the [2]rotaxanes, the chemical nature of the molecule–electrode contacts dominate both the magnitude of the current and the symmetry of the conductance plots. These high-resolution scans reveal the type of excited-state structure that is observed in simpler molecules. While the fine structure is relatively symmetric about $V_{SD} = 0$, the current magnitude is not. The conductance plots are normalized such that the value of $V_C$, for which the conductance gap closes, is set to 0.


[5] a) D. Goldhaber-Gordon, M. S. Montemerlo, J. C. Love, G. J. Opiteck, *Proc. IEEE.* **1997**, *85*, 521–540; b) C. Joachim, J. K. Gimzewski, A. Aviram, *Nature* **2000**, *408*, 541–548; c) R. L. Carroll, C. B. Gorman, *Angew. Chem.* **2002**, *114*, 4556–4579; *Angew. Chem. Int. Ed.* **2002**, *41*, 4378–4400; d) M. Mayor, H. B. Weber, R. Waser in *Nanoelectronics and Information Technology. Advanced Electronic Materials and Novel Devices* (Ed.: R. Waser), Wiley-VCH, Weinheim, **2003**, pp. 501–525.

[6] M. A. Reed, C. Zhou, C. T. Muller, T. P. Burgin, J. M. Tour, *Science* **1997**, *278*, 252–254.

[7] H. Park, J. Park, A. K. L. Lim, E. H. Anderson, A. P. Alivisatos, P. L. McEuen, *Nature* **2000**, *407*, 57–60.

[8] J. Park, A. N. Pasupathy, J. I. Goldsmith, C. Chang, Y. Yaish, J. R. Petta, M. Rinkoski, J. P. Sethna, H. D. Abruña, P. L. McEuen, D. C. Ralph, *Nature* **2002**, *417*, 722–725.

[9] W. Liang, M. P. Shores, M. Bockrath, J. R. Long, H. Park, *Nature* **2002**, *417*, 725–729.

[10] J. F. Stoddart, H.-R. Tseng, *Proc. Natl. Acad. Sci. USA* **2002**, *99*, 4797–4800.

[11] a) J. O. Jeppesen, J. Perkins, J. Becher, J. F. Stoddart, *Org. Lett.* **2000**, *2*, 3547–3550; b) H.-R Tseng, S. A. Vignon, J. F. Stoddart, *Angew. Chem.* **2003**, *115*, 1529–1533; *Angew. Chem. Int. Ed.* **2003**, *42*, 1491–1495; c) J. O. Jeppesen, K. A. Nielsen, J. Perkins, S. A. Vignon, A. Di Fabio, R. Ballardini, M. T. Gandolfi, M. Venturi, V. Balzani, J. Becher, J. F. Stoddart, *Chem. Eur. J.* **2003**, *9*, 2982–3007.

[12] V. Balzani, A. Credi, G. Mattersteig, O. A. Matthews, F. M. Raymo, J. F. Stoddart, M. Venturi, A. J. P. White, D. J. Williams, *J. Org. Chem.* **2000**, *65*, 1924–1936.

[13] C. P. Collier, G. Mattersteig, E. W. Wong, Y. Luo, K. Beverly, J. Sampaio, F. M. Raymo, J. F. Stoddart, J. R. Heath, *Science* **2000**, *289*, 1172–1175.

[14] Y. Luo, C. P. Collier, J. O. Jeppesen, K. A. Nielsen, E. DeIonno, G. Ho, J. Perkins, H.-R. Tseng, T. Yamamoto, J. F. Stoddart, J. R. Heath, *ChemPhysChem* **2002**, *3*, 519–525.

[15] M. Diehl, D. W. Steuerman, H.-R. Tseng, S. A. Vignon, A. Star, P. C. Celestre, J. F. Stoddart, J. R. Heath, *ChemPhysChem* **2003**, *4*, in press.

[16] Other researchers have described bistability in junctions sandwiching a molecular monolayer between a metal bottom electrode and a Ti/Al top electrode. This bistability, however, is not dependent upon the details of the molecular material, and exhibits a very different electrical signature of the switching. For example, it is not thermally activated; see a) Y. Chen, D. A. A. Ohlberg, X. Li, D. R. Stewart, R. S. Williams, J. O. Jeppesen, K. A. Nielsen, J. F. Stoddart, D. L. Olynick, E. Anderson, *Appl. Phys. Lett.* **2003**, *82*, 1610–1612; b) Y. Chen, G.-Y. Jung, D. A. A. Ohlberg, X. Li, D. R. Stewart, J. O. Jeppesen, K. A. Nielsen, J. F. Stoddart, R. S. Williams, *Nanotechnology* **2003**, *14*, 462–468.

[17] The 30-nm thick $SiO_2$ gate insulator was grown at 450 °C using low-pressure chemical vapor deposition. Leakage currents between the gate and the source or drain electrodes were less than $10^{-12}$ A for gate voltages up to 35 V.


 © 2003 Wiley-VCH Verlag GmbH & Co. KGaA, Weinheim 

[18] We note that the gate coupling to the molecules is strong in our devices. From the slope of the differential conductance plot, we can estimate that a change of about 300 mV in the gate-voltage translates into a change of about 100 mV in the source-drain bias. This coupling strength is significantly greater than any previously reported, and allows us to access a larger range of the molecular electronic energy levels by varying the gate bias. This increased coupling strength is probably attributable to the use of Pt break junctions, which allows for the fabrication of much thinner electrodes.
[19] H. Grabert, M. H. Devoret, *Single Charge Tunneling*, Plenum, New York, **1992**.
[20] D. Chattopadhyay, I. Galeska, F. Papadimitrakopoulos, *J. Am. Chem. Soc.* **2003**, *125*, 3370 – 3375.
[21] R. Krupke, F. Hennrich, H. v. Löhneysen, M. M. Kappes, *Science*, **2003**, *301*, 344 – 347.
[22] N. Melosh, A. Boukai, F. Diana, B. Geradot, A. Badolato, P. Petroff, J. R. Heath, *Science* **2003**, *300*, 112 – 114.

 © 2003 Wiley-VCH Verlag GmbH & Co. KGaA, Weinheim 

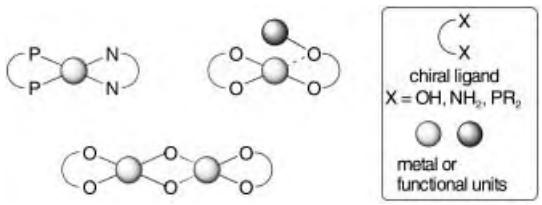



***Figure 1.*** Schematic representation of multicomponent asymmetric catalysts.

tional units onto a sterically irregular polymer backbone, resulted in less effective catalysts. Multidentate ligands with attached sites for metals at the opposite sides in the molecular skeleton readily form insoluble metal-bridged polymers (Figure 2). If chiral metal-bridged regions on the generated

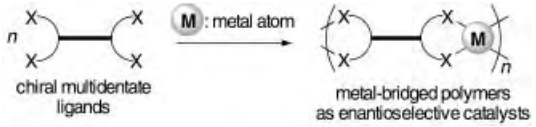



***Figure 2.*** A concept of metal-bridged polymers as enantioselective catalysts.

polymer function as asymmetric catalysts, a simple and efficient approach for the immobilization of multicomponent asymmetric catalysts without the need for a polymer support would be realized. While metal–organic coordination networks, including metal-bridged polymers, have been utilized for catalytic asymmetric reactions, the enantioselectivity of the products obtained has been very low.[4]

Herein, the synthesis of insoluble multicomponent asymmetric catalysts by the self-assembly of multidentate ligands containing binol (binol = 1,1′-bi-2-naphthol)[5] with metal ions such as $Al^{3+}$ or $Ti^{4+}$ is described. To obtain the metal-bridged polymers, (*R*,*R*)-6,6′-bis(binol) derivatives (**2a**–**c**) and (*R*,*R*)-6,6′-bi(binol) (**2d**) were synthesized[6] by linking the binol units at 6-position (Figure 3).[7]

We have reported the ready preparation of Al–Li–bis(binaphthoxide) complex (ALB) as a multicomponent asymmetric catalyst by the reaction of $LiAlH_4$ with two molar equivalents of binol (Figure 4).[2b] ALB was revealed to have

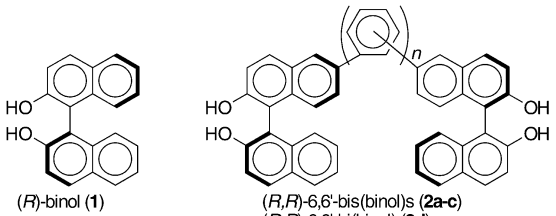



***Figure 3.*** (*R*,*R*)-6,6′-bis(binol) derivatives (**2a**–**c**) and (*R*,*R*)-6,6′-bi(binol) (**2d**).

*Multicomponent Asymmetric Catalysis*

# Metal-Bridged Polymers as Insoluble Multicomponent Asymmetric Catalysts with High Enantiocontrol: An Approach for the Immobilization of Catalysts without Using any Support**

*Shinobu Takizawa, Hidenori Somei, Doss Jayaprakash, and Hiroaki Sasai**

Immobilization, as a methodology to effectively recover and reuse asymmetric catalysts, has attracted the interest of many research groups resulting in a large number of catalysts being subjected to investigation.[1] Multicomponent asymmetric catalysts,[2,3] composed of plural ligands, metals, and functional moieties, have proved to be challenging systems in this regard (Figure 1). Multicomponent asymmetric catalysts function like enzymes in facilitating a wide range of regio- and stereoselective reactions that make use of the synergistic cooperation between the active sites; it is important to maintain the structural motif during immobilization if high reactivities are to be realized. The conventional approach, which involves the random introduction of ligand and func-

[*] Prof. Dr. H. Sasai, Dr. S. Takizawa, Dr. H. Somei, Dr. D. Jayaprakash
The Institute of Scientific and Industrial Research (ISIR)
Osaka University
Mihogaoka, Ibaraki, Osaka 567-0047 (Japan)
Fax: (+81) 6-6879-8469
E-mail: sasai@sanken.osaka-u.ac.jp

[**] This work was supported by a Grant-in-Aid for Scientific Research from the Ministry of Education, Culture, Sports, Science and Technology, Japan. We thank the technical staff in the Materials Analysis Center of ISIR, Osaka University.

Supporting information for this article is available on the WWW under http://www.angewandte.org or from the author.

 DOI: 10.1002/anie.200352354 © 2003 Wiley-VCH Verlag GmbH & Co. KGaA, Weinheim 

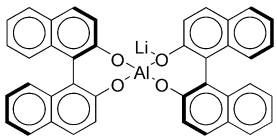
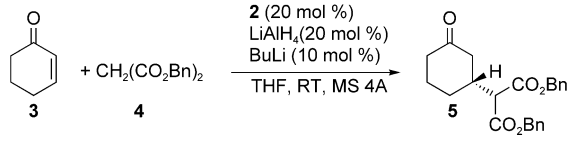



***Figure 4.*** Al-Li-bis(binaphthoxide) complex (ALB).

high enantioselectivity in the asymmetric Michael reaction (e.g., 2-cyclohexenone (**3**) with dibenzyl malonate (**4**)). The catalyst activity of ALB can be increased by the addition of about one equivalent of a basic reagent such as BuLi to form ALB II catalyst while maintaining high enantiocontrol.[2c] Ligands **2a–d** were examined in the first attempt at creating a chiral metal-bridged polymer that could function as ALB II-type catalyst in the enantioselective Michael reaction of **3** with **4**. The addition of $LiAlH_4$ (1 equivalent) to a homogeneous solution of **2** (1 equivalent) in THF at 0 °C spontaneously gave a white precipitate. After the reaction mixture was stirred for 0.5 h, BuLi (0.5 equivalents) was added to the obtained white solid. ALB II (20 mol %) was used as the heterogeneous catalyst in the enantioselective Michael reaction. The results with ligands **2a–d** are summarized in Table 1.

***Table 1:*** Enantioselective Michael reaction catalyzed by Al-bridged polymer.




**3** **4** **5**

| Entry | **2a–d** | *t* [h] | Yield [%][a] | *ee* [%][b] |
|---|---|---|---|---|
| 1 | **2a** | 48 | 94 | 6 |
| 2 | **2b** | 48 | 69 | 17 |
| 3 | **2c** | 48 | 89 | 88 |
| 4 | **2d** | 48 | 86 | 96 |
| 5 | ALB[c] | 72 | 88 | 99 |
| 6 | ALB II[c] | 12 | Quant | 97 |

[a] Isolated yield. [b] Determined by HPLC (Daicel Chiralpak AS). [c] 10 mol % of catalyst was used. See reference [2c].

Heterogeneous catalysts derived from **2a** and **2b** afforded the Michael adduct **5** with *ee* values of 6 % and 17 %, respectively (entries 1 and 2). The low *ee* values are attributable to the bent shape of the ligands that facilitate the formation of unsuitable aggregates.[2d] In contrast, heterogeneous catalysts derived from **2c** and **2d**, in which each pair of the phenolic hydroxy groups is situated at the opposite sides in the multidentate ligands, gave the Michael adduct **5** with high enantioselectivity. As we have previously reported that polystyrene-supported ALB derived from randomly introduced binol derivatives on polystyrene resin afforded **5** with no enatiomeric excess,[8] there is obviously an advantage in the present method that uses a metal-bridged polymer for immobilizing ALB. The ability of the insoluble polymer to act as an asymmetric catalyst was confirmed by the following experiments: The heterogeneous catalyst derived from **2d** and $LiAlH_4$ was allowed to settle and the clear supernatant solution removed with a syringe under argon. The supernatant solution exhibited no catalyst activity in the Michael reaction, whereas the precipitate afforded **5** with *ee* value of 91 %. In addition two reactions were carried out with **3** and **4** under optimized conditions. One reaction was quenched after 8 h during which **5** was obtained in 22 % yield with an *ee* value of 94 %. The supernatant solution of the other reaction was separated from the heterogeneous catalyst and stirred further for 40 h. This reaction afforded **5** in 19 % yield with an *ee* value of 90 %. In addition ligand **2d** was not observed in the supernatant solution. These results confirm the absence of catalyst activity in the solution phase. The heterogeneous catalyst as Al-bridged polymer, derived from **2d** and $LiAlH_4$, was characterized by elemental analysis and by a comparison of its IR spectrum with that of the ALB complex. Characteristic absorptions for Al-bridged polymer are similar to ALB complex.[9]

Having been encouraged by the success with Al-bridged polymer as an insoluble asymmetric catalyst, we examined the reuse of the catalyst in asymmetric Michael reaction (Table 2). The reuse experiments were performed by removal of the clear supernatant solution containing the product with a syringe under argon followed by the addition of substrates. The metal-bridged polymer maintained its activity even after being reused three times, albeit with a slight decrease in enantioselectivity (yield: 74 %, *ee* value of 85 %).

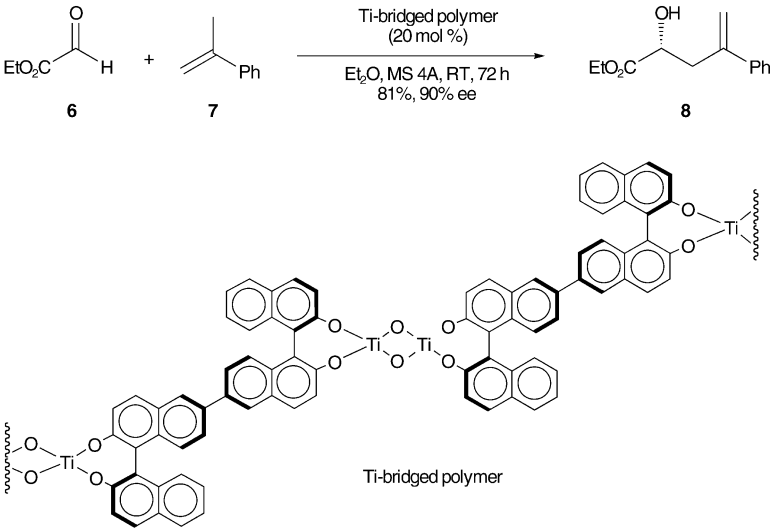
***Table 2:*** Reuse of Al-bridged polymer in enantioselective Michael reaction of **3** with **4**.[a]

| Cycle | *t* [h] | Yield [%][b] | *ee* [%][c] |
|---|---|---|---|
| 1 | 72 | 88 | 96 |
| 2 | 98 | 86 | 87 |
| 3 | 98 | 74 | 85 |
| 4 | 98 | 60 | 77 |
| 5 | 98 | 59 | 77 |

[a] Al-bridged polymer generated from **2d** (1 mol equiv), $LiAlH_4$ (1 mol equiv) and BuLi (0.5 mol equiv) in the presence of MS 4A was used. [b] Isolated yield. [c] Determined by HPLC (Daicel Chiralpak AS).

The generality of the concept of chiral metal-bridged polymer catalysis was also demonstrated through asymmetric carbonyl–ene reaction by using a Ti–binol complex.[2i] A solution of $Ti(O\text{-}iPr)_4$ (2 equivalents) in toluene and $H_2O$ (four molar equivalents) were added to a solution of **2d** in $CH_2Cl_2$. The solution was stirred at room temperature for 24 h to afford the precipitate. After removal of the solvents at 80 °C under reduced pressure, the residue was dried in vacuo at 80 °C for 19 h. The resulting red solid was characterized by elemental analysis and by comparison of its IR spectrum with hitherto known titanium complex,[2i] and found to be a titanium-bridged polymer. The characteristic absorptions for titanium-bridged polymer are similar to the parent titanium complex.[10] As shown in Scheme 1, the titanium-bridged polymer catalyzed the reaction of aldehyde **6** and olefin **7** to give the product **8** in 81 % yield with an *ee* value of 90 %. In contrast to the Al-bridged polymer, Ti-bridged polymer could be recovered in air. After being reused four times the Ti-

 © 2003 Wiley-VCH Verlag GmbH & Co. KGaA, Weinheim 




***Scheme 1.*** Asymmetric carbonyl–ene reaction catalyzed by Ti-bridged polymer.

***Table 3:*** Reuse of Ti-bridged polymer in enantioselective carbonyl–ene reaction of **6** with **7**.

| Cycle | *t* [h] | Yield [%][a] | *ee* [%][b] |
|---|---|---|---|
| 1 | 98 | 88 | 88 |
| 2 | 98 | 72 | 92 |
| 3 | 98 | 71 | 89 |
| 4 | 147 | 88 | 88 |
| 5 | 147 | 66 | 88 |

[a] Yield of isolated product. [b] Determined by HPLC (Daicel Chiralpak AS).

bridged polymer exhibited consistent catalytic selectivity affording **8** with an *ee* value of 88% (Table 3).

The results presented herein is the first example of a chiral metal-bridged polymer, formed by a metal-mediated self-assembly of chiral multidentate ligands, that functions as an asymmetric catalyst with high enantioselectivity. This novel method offers the possibility of immobilization of multicomponent asymmetric catalysts without using any support.[8,11] The design of other types of chiral multidentate ligands is currently being pursued.

Received: July 11, 2003
Revised: August 18, 2003 [Z52354]

**Keywords:** asymmetric catalysis · heterogeneous catalysis · immobilization · self-assembly · synthetic methods

[1] For recent reviews, see: a) N. E. Leadbeater, M. Marco, *Chem. Rev.* **2002**, *102*, 3217; b) C. A. McNamara, M. J. Dixon, M. Bradley, *Chem. Rev.* **2002**, *102*, 3275; c) T. J. Dickerson, N. N. Reed, K. D. Janda, *Chem. Rev.* **2002**, *102*, 3325; d) D. E. Bergbreiter, *Chem. Rev.* **2002**, *102*, 3345; e) R. van Heerbeek, P. C. J. Kamer, P. W. N. M. van Leeuwen, J. N. H. Reek, *Chem. Rev.* **2002**, *102*, 3717.

[2] Representative examples of multicomponent asymmetric catalysts: a) S. Kobayashi, H. Ishitani, *J. Am. Chem. Soc.* **1994**, *116*, 4083; b) T. Arai, H. Sasai, K. Aoe, K. Okamura, T. Date, M. Shibasaki, *Angew. Chem.* **1996**, *108*, 103; *Angew. Chem. Int. Ed. Engl.* **1996**, *35*, 104; c) T. Arai, Y. M. A. Yamada, N. Yamamoto, H. Sasai, M. Shibasaki, *Chem. Eur. J.* **1996**, *2*, 1368; d) T. Arai, H. Sasai, K. Yamaguchi, M. Shibasaki, *J. Am. Chem. Soc.* **1998**, *120*, 441; e) K. Mikami, T. Korenaga, M. Terada, T. Ohkuma, T. Pham, R. Noyori, *Angew. Chem.* **1999**, *111*, 517; *Angew. Chem. Int. Ed.* **1999**, *38*, 495; f) H. Ishitani, M. Ueno, S. Kobayashi, *J. Am. Chem. Soc.* **2000**, *122*, 8180; g) H. Furuno, T. Hanamoto, Y. Sugimoto, J. Inanaga, *Org. Lett.* **2000**, *2*, 49; h) H. Du, K. Ding, *Org. Lett.* **2003**, *5*, 1091; i) D. Kitamoto, H. Imma, T. Nakai, *Tetrahedron Lett.* **1995**, *36*, 1861. See also reference [3].

[3] For recent reviews, see: a) M. Shibasaki, H. Sasai, T. Arai, *Angew. Chem.* **1997**, *109*, 1290; Angew. *Chem. Int. Ed. Engl.* **1997**, *36*, 1236; b) G. J. Rowlands, *Tetrahedron* **2001**, *57*, 1865; c) M. Shibasaki, N. Yoshikawa, *Chem. Rev.* **2002**, *102*, 2187.

[4] a) C. J. Kepert, T. J. Prior, M. J. Rosseinsky, *J. Am. Chem. Soc.* **2000**, *122*, 5158; b) J. S. Seo, D. Whang, H. Lee, S. I. Jun, J. Oh, Y. J. Jeon, K. Kim, *Nature* **2000**, *404*, 982; c) O. R. Evans, H. L. Ngo, W. Lin, *J. Am. Chem. Soc.* **2001**, *123*, 10395.

[5] For the design and synthesis of the new metal-bridged polymer, binol was chosen to be modified as chiral multidentate ligands because binol as a ligand is used in various chiral metal catalysts. a) C. Roshini, L. Franzini, A. Raffaelli, P. Salvadori, *Synthesis* **1992**, 503; b) R. Noyori, I. Tomino, Y. Tanimoto, *J. Am. Chem. Soc.* **1979**, *101*, 3129; c) H. Yamamoto, A. Yanagisawa, K. Ishihara, S. Saito, *Pure Appl. Chem.* **1998**, *70*, 1507; d) C. Qian, C. Zhu, T. Huang, *J. Chem. Soc. Perkin Trans. 1* **1998**, 2131; e) H. Sasai, T. Arai, S. Watanabe, M. Shibasaki, *Catal. Today* **2000**, *62*, 17; f) L. Pu, *Chem. Rev.* **1998**, *98*, 2405; g) S. Kobayashi, H. Ishitani, *Chem. Rev.* **1999**, *99*, 1069; h) J. Inanaga, H. Furuno, T. Hayano, *Chem. Rev.* **2002**, *102*, 2211; i) H. C. Aspinall, *Chem. Rev.* **2002**, *102*, 1807.

[6] Starting from known (*R*)-6-Br-2,2′-bis(methoxymethyloxy)-1,1′-binaphthalene, novel chiral multidentate ligands **2a-c** were prepared in four steps by using the Suzuki–Miyaura coupling reaction as the key step (See the Supporting Information). The ligand **2d** was also prepared in four steps by using the Suzuki–Miyaura coupling reaction and was identical in all the respects with spectra reported by Lin and co-workers. (See Supporting Information). L. Ma, P. S. White, W. Lin, *J. Org. Chem.* **2002**, *67*, 7577.

[7] Shibasaki and co-workers reported an efficient enantioselective reaction by linking binol at C3. Y. S. Kim, S. Matsunaga, J. Das, A. Sekine, T. Ohshima, M. Shibasaki, *J. Am. Chem. Soc.* **2000**, *122*, 6506.

[8] T. Arai, T. Sekiguti, Y. Iizuka, S. Takizawa, S. Sakamoto, K. Yamaguchi, H. Sasai, *Tetrahedron: Asymmetry* **2002**, *13*, 2083.

[9] Al-bridged polymer (generated from ligand **2d** with $LiAlH_4$ in the ratio of 1:1): Elemental analysis calcd (%) for polymeric $C_{52}H_{46}AlLiO_7$ (containing three molecules of THF per active site): C 76.46, H 5.68; found: C 76.26, H 5.75. IR: ALB complex 2871, 1591, 1502, 1463, 1425, 1340, 1126, 1049, 953, 860, 816, 746 $cm^{-1}$, Al-bridged polymer 2862, 1587, 1499, 1458, 1423, 1339, 1126, 1045, 949, 862, 820, 746 $cm^{-1}$.

[10] Ti-bridged polymer: Elemental analysis calcd (%) for polymeric $C_{47}H_{30}O_6Ti_2$ (containing one molecule of toluene per active site): C 71.78, H 3.84; found: C 71.96, H 4.15. IR: Ti-binol complex 1585, 1499, 1458, 1333, 1234, 1113, 1078, 974, 935, 814, 746 $cm^{-1}$,

 © 2003 Wiley-VCH Verlag GmbH & Co. KGaA, Weinheim 

Ti-bridged polymer 1583, 1499, 1454, 1427, 1333, 1236, 1074, 976, 941, 820, 727 $cm^{-1}$.

[11] Recent progress in immobilized multicomponent asymmetric catalysts: a) T. Arai, Q.-S. Hu, X.-F. Zheng, L. Pu, H. Sasai, *Org. Lett.* **2000**, *2*, 4261; b) D. Jayaprakash, H. Sasai, *Tetrahedron: Asymmetry* **2001**, *12*, 2589; c) T. Arai, T. Sekiguti, K. Otsuki, S. Takizawa, H. Sasai, *Angew. Chem.* **2003**, *115*, 2194; *Angew. Chem. In. Ed.* **2003**, *42*, 2144; d) T. Sekiguti, Y. Iizuka, S. Takizawa, D. Jayaprakash, T. Arai, H. Sasai, *Org. Lett.* **2003**, *5*, 2647; e) S. Matsunaga, T. Ohshima, M. Shibasaki, *Tetrahedron Lett.* **2000**, *41*, 8473; f) T. Ohkuma, H. Takeno, Y. Honda, R. Noyori, *Adv. Synth. Catal.* **2001**, *343*, 369; g) H.-B. Yu, Q.-S. Hu, L. Pu, *J. Am. Chem. Soc.* **2000**, *122*, 6500; h) G. Sundararajan, N. Prabagaran, *Org. Lett.* **2001**, *3*, 389; i) A. Fujii, M. Sodeoka, *Tetrahedron Lett.* **1999**, *40*, 8011; j) Y. M. A. Yamada, M. Ichinohe, H. Takahashi, S. Ikegami, *Tetrahedron Lett.* **2002**, *43*, 3431.

 © 2003 Wiley-VCH Verlag GmbH & Co. KGaA, Weinheim 

*Palladium Chloride Trimer Complex*

# A Bowl-Shaped Triarylphosphane with a Large Cone Angle: Synthesis and Crystallographic Analysis of a $[(PdX_2)_3(PR_3)_2]$-Type Complex**

*Yoshiko Ohzu, Kei Goto,* and Takayuki Kawashima**

There has been a growing interest in the molecular design of bulky phosphane ligands,[1] which can facilitate the formation of catalytically active low-coordinate species by their steric properties. The tertiary phosphane complexes of divalent palladium are well recognized as important species because of their effectiveness in organic synthesis and as homogeneous catalysts.[2] Generally, the reactions of tertiary phosphanes with palladium(II) halides produce the 2:1 complexes $[PdX_2(PR_3)_2]$ (X = halide), which may or may not be converted to the 2:2 complexes $[(PdX_2)_2(PR_3)_2]$ upon heating.[3] Although bulky phosphane ligands tend to favor the direct formation of 2:2 complexes,[3] there has been no report of a phosphane ligand bulky enough to form the 2:3 trinuclear complex $[(PdX_2)_3(PR_3)_2]$. Most of the bulky phosphane ligands thus far reported have the substituents in the vicinity of the phosphorus center, which often results in facile intramolecular cyclometallation. For example, trimesitylphosphane ($P(Mes)_3$) reacts with palladium(II) chloride under a wide range of reaction conditions to produce only the cyclometallated dinuclear complex.[4] Although such cyclometallation reactions have attracted much attention in view of the catalytic utility of the resulting metallacycles,[5] they are undesirable when one intends to synthesize a metal complex with the phosphane ligands intact. It is usually difficult, however, to increase the steric bulk of the phosphane ligands without an increase in the steric congestion around the phosphorus center.

In the course of our study on bowl-shaped molecules,[6] we previously designed the triarylmethane,[7a] triarylsilane,[7b] and triarylgermane[7c] derivatives **1**–**3**, in which the radially extended *m*-terphenyl units form a large cavity. It is expected that replacement of the central atom of these molecules by a phosphorus atom will produce very bulky phosphane ligands without severe steric congestion in the vicinity of the phosphorus center. Recently, Tatsumi and co-workers[8] and our group[9] independently reported the synthesis of triarylphosphane TRMP.[10] TRMP was applied to the highly efficient rhodium-catalyzed hydrosilylation of ketones by Tsuji et al.[11] In this communication, we report the synthesis and structure of the first example of the $[(PdX_2)_3(PR_3)_2]$-type trinuclear complex by taking advantage of a novel bowl-shaped phosphane TRIP,[10] in which the methyl groups of TRMP are replaced by isopropyl groups (Figure 1).

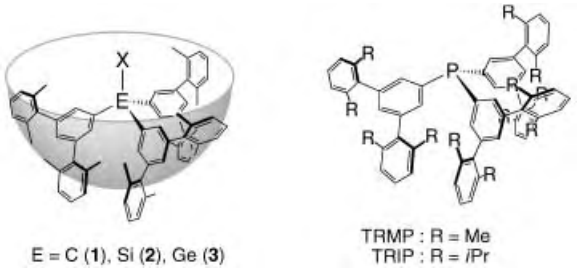
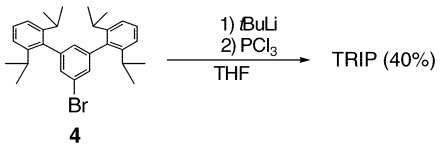



***Figure 1.*** Bowl-shaped molecules that bear *m*-terphenyl units.

TRIP was prepared by lithiation of the corresponding *m*-terphenyl bromide **4**[6e] followed by treatment with $PCl_3$ (Scheme 1). The $^{31}P$ NMR spectra ($CDCl_3$) of TRIP showed a signal at $\delta = -6.60$ ppm, which is almost the same as the chemical shifts of TRMP ($\delta = -7.16$ ppm) and triphenylphosphane ($\delta = -6.0$ ppm).[12] X-ray crystallographic analysis established the structure of TRIP (Figure 2),[13] in which the central phosphorus atom is embedded in a bowl-shaped cavity. The space-filling models of the crystal structures of TRMP[9b] and TRIP are shown in Figure 3. Both phosphanes have a diameter of about 16 Å, but the cavity of TRIP is




**4**

***Scheme 1.*** Synthesis of TRIP.

[*] Dr. K. Goto, Prof. Dr. T. Kawashima, Y. Ohzu
Department of Chemistry
Graduate School of Science
The University of Tokyo
7–3–1 Hongo, Bunkyo-ku, Tokyo 113–0033 (Japan)
Fax: (+81) 3-5800-6899
E-mail: goto@chem.s.u-tokyo.ac.jp
takayuki@chem.s.u-tokyo.ac.jp

[**] This work was partly supported by Grants-in-Aid for The 21 st Century COE Program for Frontiers in Fundamental Chemistry (T.K.) and for Scientific Research (Nos. 14703066 (K.G.) and 15105001 (T.K.)) from the Ministry of Education, Culture, Sports, Science and Technology, Japan. We also thank Tosoh Finechem Corporation for the generous gifts of alkyllithiums.

 © 2003 Wiley-VCH Verlag GmbH & Co. KGaA, Weinheim DOI: 10.1002/anie.200352616 

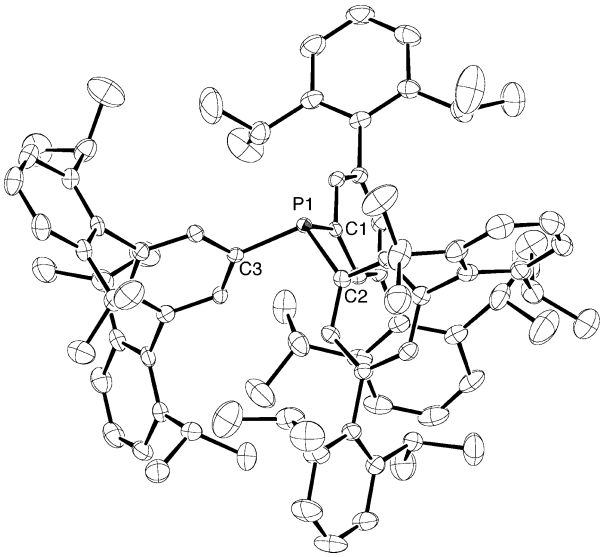
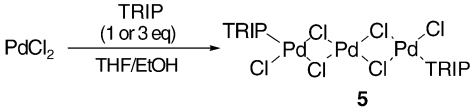



***Figure 2.*** X-ray crystal structure of TRIP (ORTEP drawing, 50% probability). Selected bond lengths [Å] and angles [°]: P1-C1, 1.829(3); P1-C2, 1.830(3); P1-C3, 1.836(3); C1-P1-C2, 101.52(13); C2-P1-C3, 103.48(13); C1-P1-C3, 104.52(13).

deeper than that of TRMP (3.3 Å for TRIP versus 2.1 Å for TRMP). The cone angle of TRIP is estimated to be 206°, which is much larger than those of TRMP (174°),[9b] tri-*t*-butylphosphane (182°)[12] and triphenylphosphane (145°).[12] On the other hand, the averaged C-P-C bond angle of TRIP is 103°, which is almost the same as those of TRMP (102°)[9b] and $PPh_3$ (103°),[12] in contrast to other bulky phosphanes such as $P(Mes)_3$ (110°).[14] These results indicate that in phosphane TRIP, which bears a dendritic framework, the molecular size is enlarged in comparison with $PPh_3$ without increasing steric repulsion among the three aryl groups.

The reactions of tertiary phosphanes with divalent palladium chloro salts usually produce the mononuclear complex $[PdCl_2(PR_3)_2]$ or dinuclear complex $[(PdCl_2)_2(PR_3)_2]$, depending on the relative amount of the phosphane ligand. Tatsumi et al. reported that, even in the case of TRMP, the reactions with $PdCl_2$ in the ratio of 1:2 and 1:1 (Pd/ligand) yielded the corresponding mononuclear complex, $[PdCl_2(TRMP)_2]$, and the dinuclear complex, $[(PdCl_2)_2(TRMP)_2]$, respectively.[8a] In contrast, the treatment of $PdCl_2$ with an equimolar amount of TRIP in refluxing ethanol/THF produced the trinuclear palladium(II) chloride complex, $[(PdCl_2)_3(TRIP)_2]$ (**5**), as a single product (Scheme 2). In the $^{31}P$ NMR spectrum ($CDCl_3$), **5** showed a signal at $\delta = 34.77$ ppm. The structure of **5** was established by X-ray crystallographic analysis (Figure 4).[13]

The X-ray crystal structure (Figure 4) shows that **5** contains three Pd atoms linked by bridging chloride ligands




**5**

***Scheme 2.*** Reaction of $PdCl_2$ with TRIP.

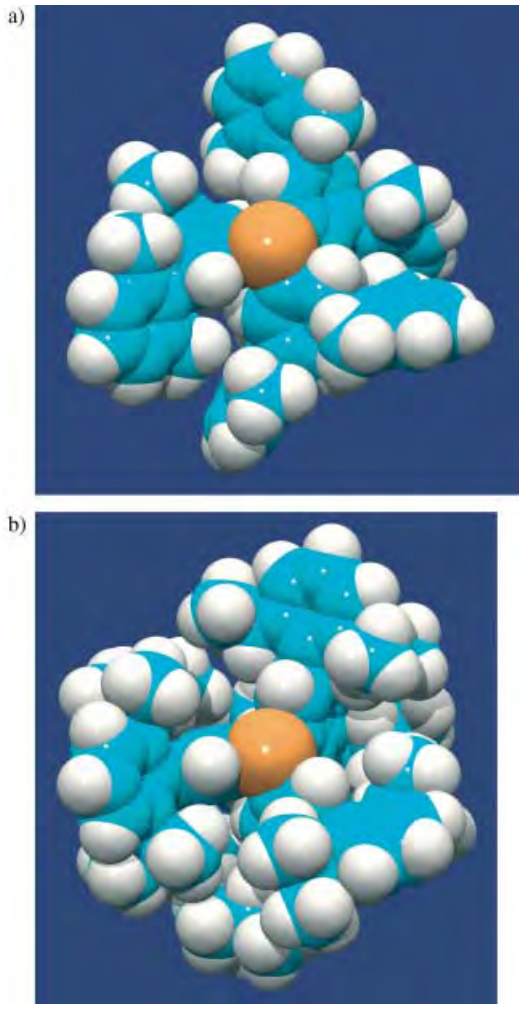



***Figure 3.*** Space-filling models of the crystal structures of a) TRMP and b) TRIP.

with the Pd2 atom residing at a crystallographic inversion center. It is known that $PdCl_2$ has a polymeric structure in the solid state,[15] and the structure of **5** can be regarded as a trimer of $PdCl_2$ cut out from the polymeric chain by two phosphane ligands. The formation of a $PdCl_2$ trimer terminated by organic ligands at each end has been postulated in some references, but based only on indirect evidence.[16] This is the first example of a structurally characterized $PdCl_2$ trimer complex. The bond length of Pd1–Cl3 is substantially longer than that of Pd1–Cl1, indicating the stronger *trans* influence of the phosphane ligand compared with that of the chloride. Similar asymmetry in the Pd–Cl bond lengths was reported for many dinuclear palladium chloride phosphane complexes, such as $[PdCl_2(PPh_3)_2]$.[17] On the other hand, there is no significant difference between the Pd2–Cl1 and Pd2–Cl3 bond lengths, both of which are close to the Pd–($\mu$-Cl) bond lengths in the central $PdCl_4$ unit of the chloride-bridged trinuclear $Pd^{II}$ complex, $[Pd_3Cl_4(\mu^3\text{-2-methylallyl})_2]$ (2.30–2.31 Å).[18] It was found that **5** is solvated by ten molecules of $CHCl_3$ (omitted for clarity in Figure 4), all of which are located outside the cavity of the TRIP ligand.

 © 2003 Wiley-VCH Verlag GmbH & Co. KGaA, Weinheim 

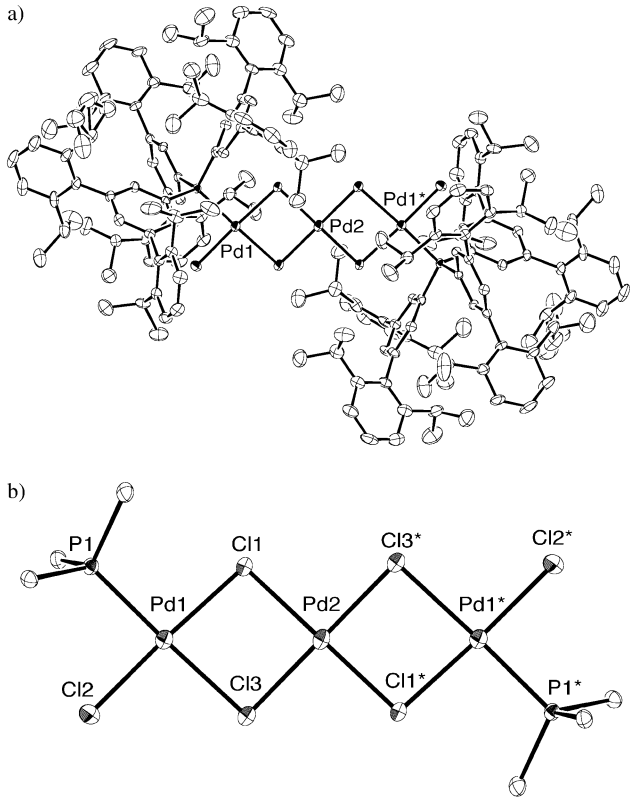



***Figure 4.*** X-ray crystal structure of a) whole structure and b) partial structure of **5** (ORTEP drawing, 50% probability). Selected bond lengths [Å] and angles [°]: Pd1-Cl1, 2.3389(14); Pd1-Cl2, 2.2782(14); Pd1-Cl3, 2.4214(15); Pd1-P1, 2.2249(14); Pd2-Cl1, 2.2901(14); Pd2-Cl3, 2.3054(14); P1-Pd1-Cl3, 176.26(5); Cl1-Pd1-Cl2, 176.48(5).

It is noteworthy that the reaction of $PdCl_2$ with an excess of TRIP (three equivalents) also produced only trinuclear complex **5**; no dinuclear or mononuclear complexes were detected (Scheme 2). This is in sharp contrast with the reactions of tertiary phosphanes thus far reported, including TRMP, which produced $[PdCl_2(PR_3)_2]$-type complexes. The present results suggest that only one molecule of TRIP can coordinate to one palladium atom because the phosphorus center of TRIP is embedded in the bowl-shaped cavity, which is deeper than that of TRMP. On the other hand, the $^1$H NMR spectrum of **5** in $CDCl_3$ at room temperature showed the signals for only one kind of isopropyl group; two non-equivalent methyl signals and one methyne signal were observed similar to *m*-terphenyl bromide **4**, thus indicating that there is a space around the phosphorus center large enough to ensure the rapid rotation of the P–C bonds. This space is largely due to the absence of any substituent in the ortho positions of phosphorus, which also contributes to the suppression of intramolecular metallation. Such an inert and large cavity in the ligand TRIP is considered to have enabled the formation of the $[(PdX_2)_3(PR_3)_2]$-type complex.

## Experimental Section

Synthesis of TRIP: *tert*Butyllithium (2.36 M hexane solution, 6.14 mmol) was added to a solution of 5′-bromo-2,2″,6,6″-tetraisopropyl-1,1′:3′,1″-terphenyl (**4**)[6e] (1.42 g, 2.97 mmol) in THF (25 mL) at −70 °C under Ar. The mixture was stirred at −70 °C for 25 min. $PCl_3$ (84 μL, 0.963 mmol) was added to this solution and the mixture was stirred at −70 °C for 2.5 h and at room temperature for 2 h. After removal of the solvent, the residue was treated with degassed $H_2O$, and extracted with degassed $CHCl_3$ under Ar. The extracts were dried over anhydrous $MgSO_4$. After removal of the solvent under reduced pressure, the residue was washed thoroughly with degassed ethanol to give TRIP as colorless crystals (0.475 g, 40%). M.p. 345 °C; $^1$H NMR (500 MHz, $CDCl_3$) $\delta = 0.77$ (d, $J_{HH} = 6.8$ Hz, 36H), 0.95 (d, $J_{HH} = 6.8$ Hz, 36H), 2.52 (sept, $J_{HH} = 6.8$ Hz, 12H), 6.97 (s, 3H), 7.10 (d, $J_{HH} = 7.8$ Hz, 12H), 7.26 (t, $J_{HH} = 7.8$ Hz, 6H), 7.50 ppm (dd, $J_{PH} = 8.7$ Hz, $J_{HH} = 1.6$ Hz, 6H); $^{31}$P NMR (109 MHz, $CDCl_3$) $\delta = -6.60$ ppm; $^{13}$C{$^1$H} NMR (126 MHz, $CDCl_3$) $\delta = 23.60$ (s), 23.99 (s), 30.38 (s), 122.41 (s), 127.91 (s), 131.58 (s), 133.45 (d, $J_{PC} = 23.2$ Hz), 135.60 (d, $J_{PC} = 13.7$ Hz), 138.77 (s), 140.61 (d, $J_{PC} = 8.6$ Hz), 146.61 ppm (s). Elemental analysis calcd (%) for $C_{90}H_{113}OP$: C 87.05, H 9.17; found: C 86.89, H 9.27. Atmospheric-pressure chemical ionization (APCI)-MS *m*/*z* 1224 $[M+H]^+$.

Synthesis of **5**: A solution of TRIP (134.9 mg, 0.110 mmol) in THF (30 mL) was added to a solution of $PdCl_2$ (29.8 mg, 0.168 mmol) in ethanol (10 mL). The mixture was heated at reflux for 3 h under Ar. After removal of the solvent, the residue was treated with $CHCl_3$ and filtered. After evaporation of the solvent, the residue was washed with hexane and recrystallized from $CHCl_3$/hexane to give **5** as yellow crystals (80.3 mg, 49%). M.p. 380 °C (decomp); $^1$H NMR (500 MHz, $CDCl_3$) $\delta = 0.69$ (d, $J_{HH} = 6.8$ Hz, 72H), 0.89 (d, $J_{HH} = 6.8$ Hz, 72H), 2.53 (sept, $J_{HH} = 6.8$ Hz, 24H), 7.07 (d, $J_{HH} = 7.8$ Hz, 24H), 7.10 (s, 6H), 7.29 (t, $J_{HH} = 7.8$ Hz, 12H), 7.76 ppm (d, $J_{PH} = 9.3$ Hz, 12H); $^{31}$P NMR (109 MHz, $CDCl_3$) $\delta = 34.77$ ppm; $^{13}$C{$^1$H} NMR (126 MHz, $CDCl_3$) $\delta = 23.64$ (s), 24.02 (s), 30.31(s), 122.65 (s), 126.72 (d, $J_{PC} = 57$ Hz), 128.10 (s), 133.72 (brs), 134.15 (s), 137.78 (s), 140.77 (m: virtual coupling), 146.80 ppm (s). Elemental analysis calcd (%) for $C_{180}H_{222}Cl_6P_2Pd_3$: C 72.56, H 7.51; found: C 72.27, H 7.79.

Received: August 11, 2003 [Z52616]

**Keywords:** bowl-shaped molecules · palladium · phosphane ligands · steric hindrance · structure elucidation

[1] For recent examples, see: a) S. Sasaki, K. Sutoh, F. Murakami, M. Yoshifuji, *J. Am. Chem. Soc.* **2002**, *124*, 14830; b) T. Hamada, A. Chieffi, J. Åhman, S. L. Buchwald, *J. Am. Chem. Soc.* **2002**, *124*, 1261; c) J. P. Stambuli, S. R. Stauffer, K. H. Shaughnessy, J. F. Hartwig, *J. Am. Chem. Soc.* **2001**, *123*, 2677; d) V. F. Slagt, J. N. H. Reek, P. C. J. Kamer, P. W. N. M. van Leeuwen, *Angew. Chem.* **2001**, *113*, 4401; *Angew. Chem. Int. Ed.* **2001**, *40*, 4271; e) M. Naiki, S. Shirakawa, K. Kon-i, Y. Kondo, K. Maruoka, *Tetrahedron Lett.* **2001**, *42*, 5467; f) B. S. Balaji, Y. Obora, D. Ohara, S. Koide, Y. Tsuji, *Organometallics* **2001**, *20*, 5342.

[2] *Handbook of Organopalladium Chemistry for Organic Synthesis* (Ed.: E. Negishi), Wiley-Interscience, New York, **2002**.

[3] A. T. Hutton, C. P. Morley in *Comprehensive Coordination Chemistry, Vol. 5* (Ed.: G. Wilkinson), Pergamon, Oxford, **1987**, p. 1157.

[4] a) S. A. Dias, E. C. Alyea, *Transition Met. Chem.* **1979**, *4*, 205; b) E. C. Alyea, J. Malito, *J. Organomet. Chem.* **1988**, *340*, 119; c) E. C. Alyea, G. Ferguson, J. Malito, B. L. Ruhl, *Organometallics* **1989**, *8*, 1188.

[5] a) W. A. Herrmann, C. Brossmer, K. Öfele, C.-P. Reisinger, T. Priermeier, M. Beller, H. Fischer, *Angew. Chem.* **1995**, *107*, 1989; *Angew. Chem. Int. Ed. Engl.* **1995**, *34*, 1844; b) W. A. Herrmann, C. Brossmer, C.-P. Reisinger, T. H. Riermeier, K. Öfele, M. Beller, *Chem. Eur. J.* **1997**, *3*, 1357.

[6] For examples, see: a) K. Goto, N. Tokitoh, R. Okazaki, *Angew. Chem.* **1995**, *107*, 1202; *Angew. Chem. Int. Ed. Engl.* **1995**, *34*,

 © 2003 Wiley-VCH Verlag GmbH & Co. KGaA, Weinheim 

1124; b) K. Goto, M. Holler, R. Okazaki, *J. Am. Chem. Soc.* **1997**, *119*, 1460; c) T. Saiki, K. Goto, R. Okazaki, *Angew. Chem.* **1997**, *109*, 2320; *Angew. Chem. Int. Ed. Engl.* **1997**, *36*, 2223; d) K. Goto, R. Okazaki, *Liebigs Ann./Recl.* **1997**, 2393; e) K. Goto, G. Yamamoto, B. Tan, R. Okazaki, *Tetrahedron Lett.* **2001**, *42*, 4875; f) K. Goto, Y. Hino, Y. Takahashi, T. Kawashima, G. Yamamoto, N. Takagi, S. Nagase, *Chem. Lett.* **2001**, 1204.

[7] a) K. Goto, Y. Hino, T. Kawashima, M. Kaminaga, E. Yano, G. Yamamoto, N. Takagi, S. Nagase, *Tetrahedron Lett.* **2000**, *41*, 8479; b) K. Goto, T. Okumura, T. Kawashima, *Chem. Lett.* **2001**, 1258; c) K. Goto, I. Shimo, T. Kawashima, *Bull. Chem. Soc. Jpn.*, in press.

[8] a) T. Kasai, T. Matsumoto, K. Tatsumi, *79th Spring Annual Meeting of the Chemical Society of Japan* (Tokyo, Japan) March 2001, Abstr. No. 1PA104; b) T. Matsumoto, T. Kasai, K. Tatsumi, *Chem. Lett.* **2002**, 346.

[9] a) K. Goto, Y. Ohzu, H. Sato, T. Kawashima, *15th International Conference on Phosphorus Chemistry* (Sendai, Japan), July 2001, Abstr. No. PB072; b) K. Goto, Y. Ohzu, H. Sato, T. Kawashima, *Phosphorus Sulfur Silicon Relat. Elem.* **2002**, *177*, 2179.

[10] TRMP and TRIP denote *tri*s(2,2″,6,6″-tetra*m*ethyl[1,1′:3′,1″-terphenyl]-5′-yl)*p*hosphane and *tri*s(2,2″,6,6″-tetra*i*sopropyl[1,1′:3′,1″-terphenyl]-5′-yl)*p*hosphane, respectively.

[11] O. Niyomura, M. Tokunaga, Y. Obora, T. Iwasawa, Y. Tsuji, *Angew. Chem.* **2003**, *115*, 1325; *Angew. Chem. Int. Ed.* **2003**, *42*, 1287.

[12] C. A. Tolman, *Chem. Rev.* **1977**, *77*, 313.

[13] Crystallographic data for TRIP·2CHCl$_3$: $C_{92}H_{113}Cl_6P$, $M_r$ = 1462.49, triclinic, space group $P\bar{1}$, $a$ = 14.855(5), $b$ = 14.885(4), $c$ = 21.813(7) Å, $\alpha$ = 76.152(12), $\beta$ = 84.394(13), $\gamma$ = 67.948(10)°, $V$ = 4340(2) Å$^3$, $Z$ = 2, $\rho_{calcd}$ = 1.119 g cm$^{-3}$, $T$ = 120 K, $\mu(Mo_{K\alpha})$ = 0.258 mm$^{-1}$, 28146 measured reflections, 14872 independent, 971 parameters, $R1$ = 0.0816 ($I > 2\sigma(I)$), $wR2$ = 0.1865 (all data). Crystallographic data for **5**·10CHCl$_3$: $C_{95}H_{116}Cl_{18}PPd_{1.5}$, $M_r$ = 2086.55, triclinic, space group $P\bar{1}$, $a$ = 15.920(6), $b$ = 17.486(7), $c$ = 20.339(8) Å, $\alpha$ = 82.825(16)°, $\beta$ = 71.934(14)°, $\gamma$ = 74.785(14)°, $V$ = 5189(4) Å$^3$, $Z$ = 2, $\rho_{calcd}$ = 1.336 g cm$^{-3}$, $T$ = 120 K, $\mu(Mo_{K\alpha})$ = 0.783 mm$^{-1}$, 33449 measured reflections, 17768 independent, 1075 parameters, $R1$ = 0.0676 ($I > 2\sigma(I)$), $wR2$ = 0.1779 (all data). The intensity data were collected on a Rigaku/MSC Mercury CCD diffractometer with graphite-monochromated MoK$_\alpha$ radiation ($\lambda$ = 0.71069 Å). The structures were solved by the direct method and refined by full-matrix least squares on $F^2$ using SHELXL 97 (G. M. Sheldrick, University of Göttingen, 1997). The non-hydrogen atoms were refined anisotropically. The hydrogen atoms were idealized by using the riding models. CCDC-216987 (TRIP) and CCDC-216988 (**5**) contain the supplementary crystallographic data for this paper. These data can be obtained free of charge via www.ccdc.cam.ac.uk/conts/retrieving.html (or from the Cambridge Crystallographic Data Centre, 12 Union Road, Cambridge CB21EZ, UK; fax: (+44) 1223-336-033; or deposit@ccdc.cam.ac.uk).

[14] J. F. Blount, C. A. Maryanoff, K. Mislow, *Tetrahedron Lett.* **1975**, *16*, 913.

[15] P. M. Maitlis, P. Espinet, M. J. H. Russell in *Comprehensive Organometallic Chemistry, Vol. 6* (Ed.: G. Wilkinson), Pergamon, Oxford, **1982**, p. 233.

[16] a) R. Hüttel, H. J. Neugebauer, *Tetrahedron Lett.* **1964**, *5*, 3541; b) P. M. Maitlis, D. Pollock, M. L. Games, W. J. Pryde, *Can. J. Chem.* **1965**, *43*, 470; c) K. Tani, M. Yabuta, S. Nakamura, T. Yamagata, *J. Chem. Soc. Dalton Trans.* **1993**, 2781.

[17] J. Vicente, M. C. Lagunas, E. Bieuel, Cambridge Structural Database, refcode ROQZAY, **1997**.

[18] P. M. Bailey, E. A. Kelley, P. M. Maitlis, *J. Organomet. Chem.* **1978**, *144*, C52.

 © 2003 Wiley-VCH Verlag GmbH & Co. KGaA, Weinheim 

*Host–Guest Systems*

# Regulatory Strategies in the Complexation and Release of a Noncovalent Guest Trimer by a Self-Assembled Molecular Cage**

*Jessica M. C. A. Kerckhoffs, Fijs W. B. van Leeuwen, Anthony L. Spek, Huub Kooijman, Mercedes Crego-Calama,* and David N. Reinhoudt**

Self-assembly,[1] nowadays recognized as one of the most promising techniques for building nanoscale structures,[2] is nature's favorite way of building objects, probably because it is the most economic and reliable strategy. Life is made possible by highly complex functional structures built with great perfection by self-assembly, which allows for errors to be minimized and/or spontaneously corrected.[3] The same supramolecular principles have made it possible to assemble synthetic building blocks into predictable assemblies.[4] However, the organizational complexity and control found in biological structures for the creation of recognition sites is still far beyond the ability of chemists. Building complex synthetic structures with specific function through self-assembly remains a challenge.[5] One of the more intriguing aspects of biological and chemical self-assembly is the capture and organization of guest molecules in self-assembled cages and capsules.[6] The entrapment of guest molecules in synthetic self-assembled systems is mainly achieved by steric constraints in rigid preorganized building blocks. Bulky solvents that cannot occupy the cavities are used for efficient encapsulation of guests. There are few examples where the self-organization of the enclosure occurs through noncovalent interactions.[7] Furthermore, supramolecular systems with higher hierarchy of assembly in both the host and guest obtained through the use of the same type of noncovalent interactions were until now unknown.

Here we report a dynamic self-assembled system where the reversibility of the association allows changes in the constitution by all of the most characteristic processes of supramolecular chemistry, namely, internal rearrangement,

[*] Dr. M. Crego-Calama, Prof. D. N. Reinhoudt,
Dr. J. M. C. A. Kerckhoffs, F. W. B. van Leeuwen
Laboratory of Supramolecular Chemistry and Technology
MESA+ Research Institute, University of Twente
P.O. Box 217, 7500 AE Enschede (The Netherlands)
Fax: (+31) 534-894-645
E-mail: m.crego-calama@ct.utwente.nl
d.n.reinhoudt@ct.utwente.nl
Prof. A. L. Spek, Dr. H. Kooijman
Department of Crystal and Structural Chemistry
Bijvoet Center for Biomolecular Research, Utrecht University
Padualaan 8, 3584 CH Utrecht (The Netherlands)

[**] This work has been financially supported in part by the Technology Foundation of the Netherlands (J.M.C.A.K.) and the Council for Chemical Sciences of the Netherlands Organization for Scientific Research (CW-NOW to A.L.S.). The research of M.C.-C. has been made possible by a fellowship from the Royal Netherlands Academy of Arts and Sciences.

 DOI: 10.1002/anie.200352733 © 2003 Wiley-VCH Verlag GmbH & Co. KGaA, Weinheim 

incorporation, exchange, and extrusion of components.[8] More specifically, we describe here the template-assisted assembly of a hydrogen-bonded trimer inside a molecular cage that itself is also assembled through the formation of hydrogen bonds.[9] Remarkably, this self-assembled receptor shows some primitive similarities with regulatory strategies of natural systems such as enzymes and viruses.[3b] The self-assembled receptor has the ability to adapt its geometry to that of the guest trimer by undergoing large conformational changes. Furthermore, the receptor has the capacity to release the encapsulated material when it receives a specific external molecular signal.

Recently, we have exploited the circular network (rosette)[10] of complementary hydrogen bonds formed between melamine and barbituric (BAR) or 1,3,5-triazine-2,4,6-triol (cyanuric acid, CYA) for the noncovalent synthesis of self-assembled nanometer-sized molecular boxes, $\mathbf{1}_3\cdot(\mathrm{DEB})_6$ (DEB = diethylbarbituric acid) or $\mathbf{1}_3\cdot(\mathrm{BuCYA})_6$ (BuCYA = butylcyanuric acid), respectively.[11] The assemblies are formed spontaneously through the formation of 36 cooperative hydrogen bonds by mixing calix[4]arene dimelamines **1** with either two equivalents of barbiturates or cyanurates in apolar solvents such as chloroform, toluene, or benzene. These thermodynamically highly stable molecular boxes consist of two flat rosette motifs connected through three calix[4]arene moieties (Figure 1).

During the course of our studies on these self-assembled nanostructures as potential mimics for antibodies[12] we identified a complex $\mathbf{1a}_3\cdot(\mathrm{DEB})_6\cdot\mathbf{2}_3$ in which the hydrogen-bonded molecular box $\mathbf{1a}_3\cdot(\mathrm{DEB})_6$ encapsulates the also hydrogen-bonded alazarine trimer $\mathbf{2}_3$, both in organic solvents and in the solid state. Besides the formation of the complex, we were able to elucidate, by a combination of X-ray and $^1$H NMR studies, the conformational changes experienced by the molecular box $\mathbf{1a}_3\cdot(\mathrm{DEB})_6$ upon encapsulation and release of $\mathbf{2}_3$.

Crystallization of assembly $\mathbf{1a}_3\cdot(\mathrm{DEB})_6\cdot\mathbf{2}_3$ by diffusion of hexane into a solution of the complex in dichloromethane gave cubic red/orange crystals (0.25–1 mm).[13] The X-ray crystallographic analysis (Figure 2) revealed that the space between the two rosette layers is filled by a layer of three coplanar alazarine molecules that are interlocked by an array of hydrogen bonds, with the OH groups in the alazarine (**2**) pointing outwards from the threefold rotation axis of the complex. The O···O distance (between the carbonyl group of one guest molecule and the hydroxy group of the adjacent guest molecule) in the hydrogen-bonded network forming the $\mathbf{2}_3$ trimer is 2.7 Å, which is within the distance for the formation of a hydrogen bond. Furthermore, the crystal structure reveals that the two melamine units of one calix[4]arene molecule are in an eclipsed orientation, thus inferring that the complex $\mathbf{1a}_3\cdot(\mathrm{DEB})_6\cdot\mathbf{2}_3$ has $C_{3h}$ symmetry (Figure 1b). In this way the electron-deficient aromatic ring of **2** is stacked in between the two relatively electron poor aromatic rings of the melamine unit, thus maximizing the π–π interactions.[14] The eclipsed orientation adopted by the

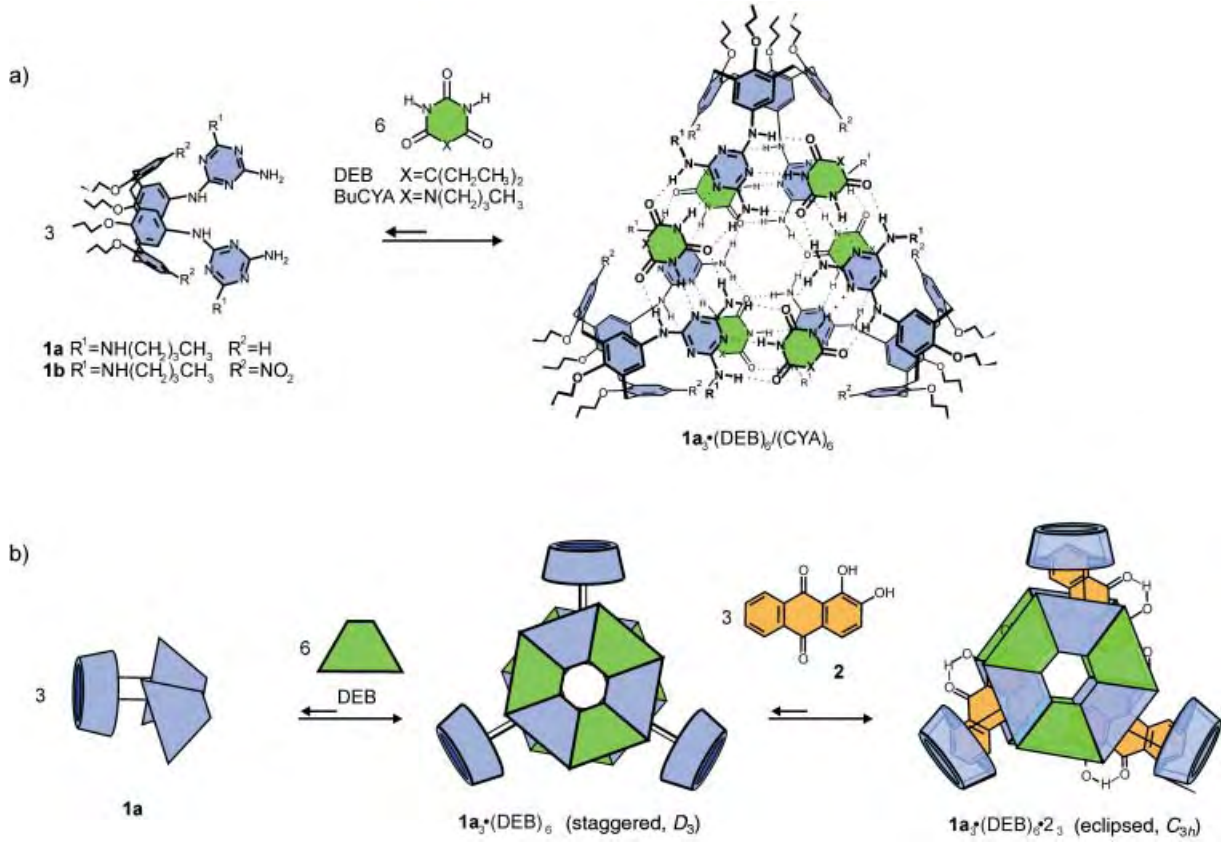



***Figure 1.*** a) Self-assembly of $\mathbf{1}_3\cdot(\mathrm{DEB})_6/\mathrm{CYA}_6$). b) Schematic representation of the formation of $\mathbf{1a}_3\cdot(\mathrm{DEB})_6$ and $\mathbf{1a}_3\cdot(\mathrm{DEB})_6\cdot\mathbf{2}_3$ showing the rearrangement of the double rosette $\mathbf{1a}_3\cdot(\mathrm{DEB})_6$ from a staggered to an eclipsed conformation after encapsulation of $\mathbf{2}_3$.

 © 2003 Wiley-VCH Verlag GmbH & Co. KGaA, Weinheim 

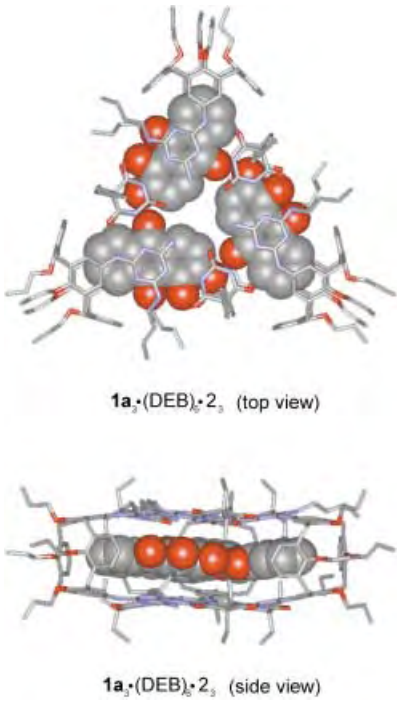



***Figure 2.*** Top and side view of the crystal structure of the complex $\mathbf{1a}_3\cdot(\mathrm{DEB})_6\cdot\mathbf{2}_3$ (a space-filling model representation for the trimer $\mathbf{2}_3$ and a stick model for the molecular box, $\mathbf{1a}_3\cdot(\mathrm{DEB})_6$). Only the main component of the disordered butyl and propyl groups are shown. Hydrogen atoms are not shown for clarity.

melamine units in the solid state is surprising because, as demonstrated by X-ray and $^1$H NMR spectroscopy,[11] empty assemblies of type $\mathbf{1}_3\cdot(\mathrm{DEB})_6$ are formed exclusively as the staggered isomer with a $D_3$ symmetry.

Other important structural information can be extracted by comparing the crystal structure of the complex $\mathbf{1a}_3\cdot(\mathrm{DEB})_6\cdot\mathbf{2}_3$ with that of the empty double rosette $\mathbf{1b}_3\cdot(\mathrm{DEB})_6$.[11b] In the empty assembly $\mathbf{1b}_3\cdot(\mathrm{DEB})_6$, the two rosette layers are practically stacked on top of each other with an intermolecular separation of 3.5 Å at the edges and 3.2 Å in the center, while the crystal structure of $\mathbf{1a}_3\cdot(\mathrm{DEB})_6\cdot\mathbf{2}_3$ reveals that the intermolecular separation between the two rosette layers increases to 6.7 Å at the edges and to 6.4–6.9 Å at the center upon encapsulation of $\mathbf{2}_3$ (Figure 3). This very efficient structural regulation is possible because of the impressive structural flexibility of the calix[4]arene platform.

These structural changes suggest that the two rosette floors in the self-assembled nanostructure $\mathbf{1a}_3\cdot(\mathrm{DEB})_6$ undergo some sort of allosteric regulation upon encapsulation of the guest. In the resulting structure the two rosette floors, as defined by the barbiturates, move apart 3.0–3.5 Å and turn 60° (from staggered to eclipsed) in the formation of the $\mathbf{1a}_3\cdot(\mathrm{DEB})_6\cdot\mathbf{2}_3$ complex. This ability to transmit conformational changes between spatially distinct sites within this "super"-structure is possible because of the inherent dynamic character of the self-assembled structures.

Such regulatory strategies occur widely in nature.[3b] For example, the catalytic trimers in aspartate transcarbamoylase

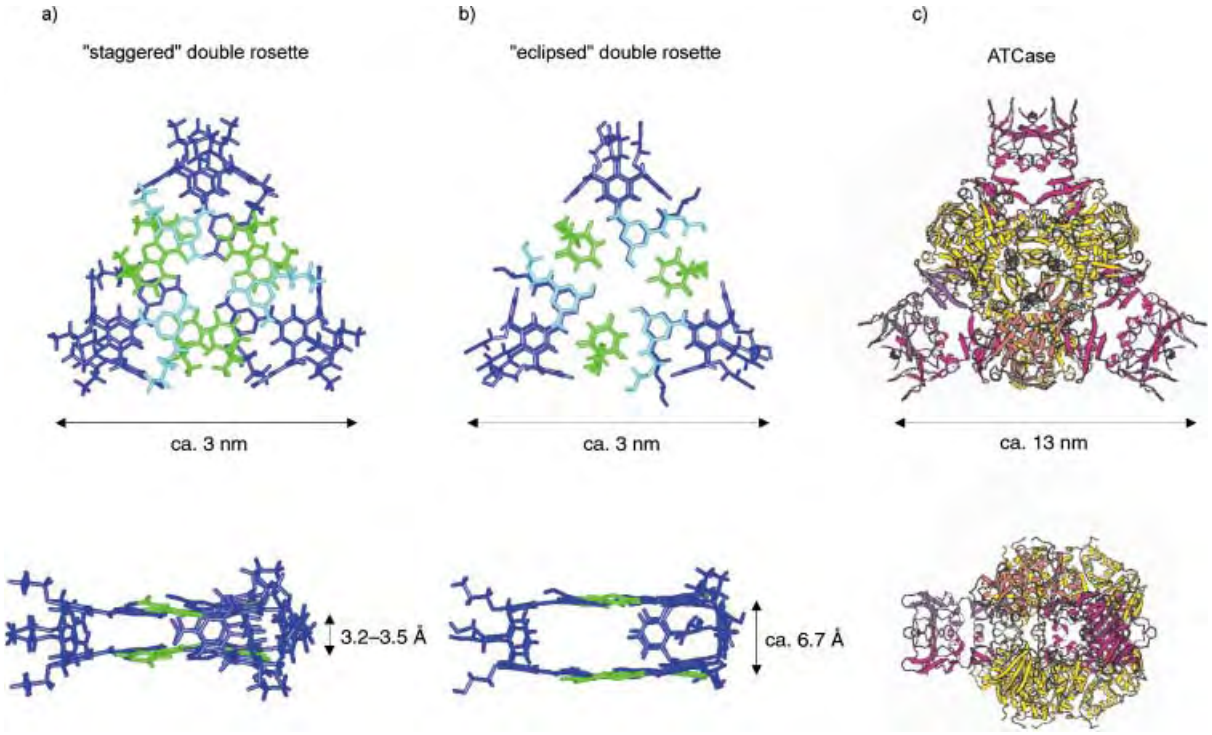



***Figure 3.*** a) X-ray crystal structure of double rosette $\mathbf{1b}_3\cdot(\mathrm{DEB})_6$ ($D_3$ symmetry) showing the staggered conformation of the melamine rings. The two melamine rings of each calixarene has been colored differently (dark and light blue) to highlight the staggered orientation). The top view (top) shows the width of the rosette (ca. 3 nm) and the side view (bottom) shows the height of the internal cavity of the structure (ca. 3.2–3.5 Å); b) X-ray crystal structure of complex $\mathbf{1a}_3\cdot(\mathrm{DEB})_6\cdot\mathbf{2}_3$ ($C_{3h}$ symmetry) showing the eclipsed conformation of the melamine rings (the encapsulated $\mathbf{2}_3$ in the top and side view as well as the ethyl and butyl side chains of the rosettes in the side view are not shown). The top view (top) shows the width of the rosette (ca. 3 nm) and the side view (bottom) shows the height of the internal cavity of the box (ca. 6.4–6.9 Å); c) three-dimensional structure of the natural ATCase enzyme. (Figure 3c is repinted with permission from Ref. [3b].)

 © 2003 Wiley-VCH Verlag GmbH & Co. KGaA, Weinheim 

(ATCase) are moved apart 12 Å and turned by 10° after binding of *N*-(phosphonacetyl)-L-aspartate and also adopt a more eclipsed position.[15] Remarkably, a reduction in symmetry from $D_3$ to $C_3$ is also observed in the enzymatic recognition and formation of the complex (Figure 3).[16]

In addition, the $^1$H NMR studies shows that the structure of complex $\mathbf{1a}_3\cdot(\mathrm{DEB})_6\cdot\mathbf{2}_3$ in $CDCl_3$ is in full accord with the structure found in the solid state. Furthermore, the solution studies confirm the structural changes proposed from the X-ray analysis. We observed that addition of three equivalents of alizarin **2** to the self-assembled host $\mathbf{1a}_3\cdot(\mathrm{DEB})_6$, which has $D_3$ symmetry,[17] resulted in the quantitative self-assembly of a single and highly symmetrical complex in $CDCl_3$ (Figure 4). Integration of the signals in the $^1$H NMR spectrum clearly showed a 3:1 complexation of **2** to $\mathbf{1a}_3\cdot(\mathrm{DEB})_6$. The presence of only two signals for the barbiturate NH protons confirm the formation of a "super" complex with an eclipsed orientation of the two melamine rings of the calix[4]arene moieties and thus the $C_{3h}$ symmetry (four signals are expected for the staggered complex, $C_3$ symmetry). This symmetry implies a change in the spatial disposition of the melamine rings of each calix[4]arene from staggered in the empty assembly to an eclipsed orientation upon complexation of alazarin (Figure 1), as found in the solid state. The titration of $\mathbf{1a}_3\cdot(\mathrm{DEB})_6$ with 0–3 equivalents of **2** was monitored by $^1$H NMR spectroscopy. The $^1$H NMR spectrum for a $\mathbf{2}$:$\mathbf{1a}_3\cdot(\mathrm{DEB})_6$ ratio of less than 3:1 showed the signals corresponding to the $\mathbf{1a}_3\cdot(\mathrm{DEB})_6\cdot\mathbf{2}_3$ complex as well as the signal for the free $\mathbf{1a}_3\cdot(\mathrm{DEB})_6$ assembly, thus indicating that slow exchange occurs between the free and complexed assemblies on the NMR timescale. The kinetic stability of the assembly is remarkable; when the sample was heated to 60 °C the $^1$H NMR spectrum still showed the two independent assemblies. Furthermore, separate signals corresponding to free **2** and $\mathbf{1a}_3\cdot(\mathrm{DEB})_6\cdot\mathbf{2}_3$ could be seen at a $\mathbf{2}$:$\mathbf{1a}_3\cdot(\mathrm{DEB})_6$ ratio of 4:1. Significant signals for the intermediates $\mathbf{1a}_3\cdot(\mathrm{DEB})_6\cdot\mathbf{2}_n$ ($n = 1, 2$) were not observed, which indicates that the complexation is strongly cooperative.

2D $^1$H NMR spectroscopic analysis of complex $\mathbf{1a}_3\cdot(\mathrm{DEB})_6\cdot\mathbf{2}_3$ (1 mM, $CDCl_3$, 298 K) allowed the assignment of the signals in the $^1$H NMR spectrum. The large shifts observed for the alizarin protons ($\Delta\delta > 3$ ppm) confirmed the encapsulation of the guest molecules in solution. The aromatic protons $H_r$, $H_s$, and $H_t$ of **2** (ring A, see Figure 4) shifted 3.28–3.88 ppm upfield, thus demonstrating that ring A is partially included in the calix[4]arene cone. The observed shift arises from the anisotropy provided by the numerous aromatic rings that line the interior of the cage.[18] Many other protons also show very large shifts upon complexation of **2**. For example, the $NH_{DEB}$ protons $H_a$ and $H_b$ in the complex $\mathbf{1a}_3\cdot(\mathrm{DEB})_6\cdot\mathbf{2}_3$ are shifted upfield 0.58 ppm and 0.30 ppm, repectively relative to those of the free host $\mathbf{1a}_3\cdot(\mathrm{DEB})_6$. Interestingly, the alizarin hydroxy $OH_n$ shifts from 6.24 ppm in free **2** to 9.87 ppm ($\Delta\delta = 3.63$ ppm) in the complex, which suggests that the $OH_n$ group is involved in the formation of a hydrogen bond, probably with the carbonyl functionality of an adjacent **2** molecule. The other hydroxy group $OH_m$ which is involved in the formation of a intramolecular hydrogen bond before complexation hardly shifted ($\Delta\delta =$ −0.02 ppm).[19] Therefore, $^1$H NMR spectroscopy confirms that the hydrogen-bonded scaffold $\mathbf{1a}_3\cdot(\mathrm{DEB})_6$ encapsulates the hydrogen-bonded trimer of alizarin ($\mathbf{2}_3$) in between the two rosette layers in a highly organized manner in solution. The structure of the complex $\mathbf{1a}_3\cdot(\mathrm{DEB})_6\cdot\mathbf{2}_3$ in solution matches exactly that of the X-ray crystal structure, thus confirming the change from the $D_3$ symmetry of the "empty cage" to the $C_{3h}$ symmetry of the "filled cage". In addition, it is important to highlight that the self-assembled template

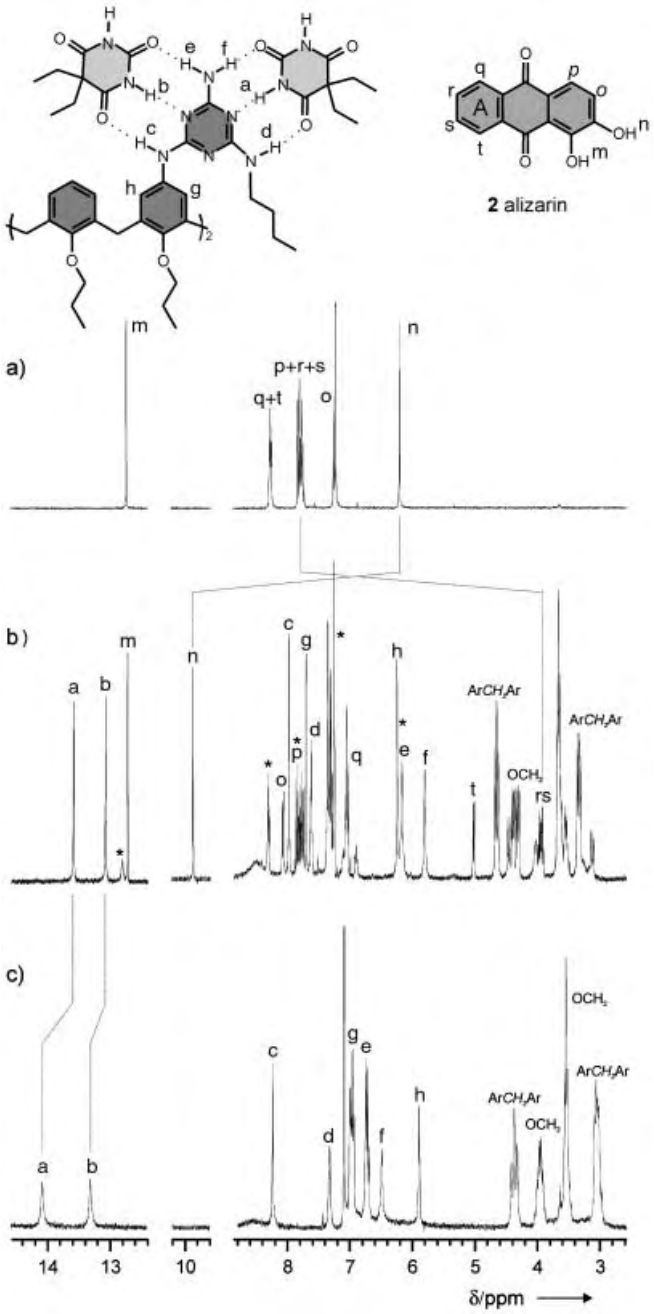



***Figure 4.*** Part of the $^1$H NMR spectra (400 MHz, in $CDCl_3$ at 298 K relative to residual $CHCl_3$) of a) guest molecule **2**; b) complex $\mathbf{1a}_3\cdot(\mathrm{DEB})_6\cdot\mathbf{2}_3$; c) assembly $\mathbf{1a}_3\cdot(\mathrm{DEB})_6$. Signals marked with ⋆ belong to **2**. The molecular structure of alazarin and part of the double rosette with the corresponding proton assignments are shown.

 © 2003 Wiley-VCH Verlag GmbH & Co. KGaA, Weinheim 

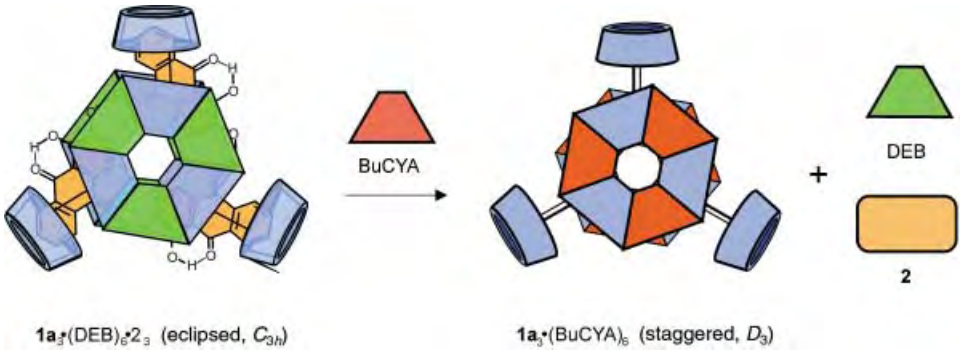



***Figure 5.*** Schematic representation of the release of the encapsulated dye trimer $\mathbf{2}_3$ and the "rearrangement" of the eclipsed to staggered conformation after substitution of the DEB for BuCYA.

$\mathbf{1a}_3{\cdot}(\mathrm{DEB})_6$ allows formation of the $\mathbf{2}_3$ trimer, which is not otherwise observed in solution.

Whereas the common characteristic of all the biological self-assembly systems is the high level of organization of the encapsulated material, specific viruses present another interesting feature, that is, the release of their encapsulated self-assembled genetic material after binding to the wall of a host cell. Also, full control over guest release is of fundamental importance for the development of encapsulation-based applications with synthetic systems.[20] The controlled release of the guest in hydrogen-bonded capsules is achieved by pH changes or by the addition of a competitive solvent or molecule, which in all cases results in the breaking of the capsule.[21]

We have achieved the release of the encapsulated material from our hydrogen-bonded cage $\mathbf{1a}_3{\cdot}(\mathrm{DEB})_6{\cdot}\mathbf{2}_3$ by a specific external molecular recognition stimulus that retains the basic structural topology of the assembly.

Our strategy was based on our previous work where we have shown that barbiturate building blocks (DEB) in assemblies of type $\mathbf{1}_3{\cdot}(\mathrm{DEB})_6$ can be substituted by cyanurate derivatives (CYA) to form assemblies $\mathbf{1}_3{\cdot}(\mathrm{CYA})_6$.[22] The barbiturate–cyanurate exchange occurs because cyanurates form much stronger hydrogen bonds with melamines than barbiturates.[23]

The controlled addition of butyl cyanurate to the complex $\mathbf{1a}_3{\cdot}(\mathrm{DEB})_6{\cdot}\mathbf{2}_3$ releases the encapsulated molecules. This results in an empty self-assembled molecular cage $\mathbf{1a}_3{\cdot}(\mathrm{BuCYA})_6$ and free guest (Figure 5). The release is achieved because assembly $\mathbf{1a}_3{\cdot}(\mathrm{BuCYA})_6$ is not able to template the encapsulation of $\mathbf{2}_3$ because of the different geometry of the cyanurates compared to that of the barbiturates.[24]

The release of the encapsulated guest has been studied by $^1$H NMR spectroscopy. The addition of 2.1 equivalents of BuCYA to the $C_{3h}$-symmetric complex $\mathbf{1a}_3{\cdot}(\mathrm{DEB})_6{\cdot}\mathbf{2}_3$ showed that all the signals of $\mathbf{1a}_3{\cdot}(\mathrm{DEB})_6{\cdot}\mathbf{2}_3$ had disappeared from the $^1$H NMR spectrum and that only signals corresponding to assembly $\mathbf{1a}_3{\cdot}(\mathrm{BuCYA})_6$, free **2**, and free DEB were present. NMR spectroscopic analysis also revealed a structrural rearrangement of the melamine calix[4]arene derivative from a staggered to an eclipsed conformation of the melamines.[25] This reorganization results in the empty assembly $\mathbf{1a}_3{\cdot}(\mathrm{BuCYA})_6$ formed after the release of $\mathbf{2}_3$ having $D_3$ symmetry.

Thus, we have now achieved a high control over the self-organization process. The work presented here compiles in a single system many separated supramolecular strategies that chemists have used over the last three decades to master the molecular self-assembly process. We have designed building blocks that not only show a strong affinity for each other and form a predictable self-assembled molecular cage with self-assembled encapsulated material, but which display topological and regulatory strategies similar to those found in nature that allow functions such as templating and guest release.

Received: August 28, 2003 [Z52733]
Published Online: November 11, 2003

**Keywords:** enzyme mimics · host–guest systems · hydrogen bonds · receptors · self-assembly

[1] Special Issue "Supramolecular Chemistry and Self-Assembly": *Science* **2002**, *295*, 2400 – 2421.
[2] a) N. C. Seeman, A. M. Belcher, *Proc. Natl. Acad. Sci. USA* **2002**, *99*, 6451 – 6455; b) Special Issue "Nanostructures": E. A. Chandross, R. D. Miller, *Chem. Rev.* **1999**, *99*, 1644 – 1990.
[3] a) J. S. Lindsey, *New J. Chem.* **1991**, *15*, 153 – 180; b) L. Stryer, *Biochemistry*, 4th ed, Freeman and Company, New York, **1995**.
[4] M. Lyndsey, D. Philp, *Chem. Soc. Rev.* **2001**, *30*, 287 – 302.
[5] R. Fiammengo, M. Crego-Calama, D. N. Reinhoudt, *Curr. Opin. Chem. Biol.* **2001**, *5*, 660 – 673.
[6] a) M. M. Conn, J. Rebek, Jr., *Chem. Rev.* **1997**, *97*, 1647 – 1668; b) F. Hof, S. L. Craig, C. Nuckolls, J. Rebek, Jr., *Angew. Chem.* **2002**, *114*, 1556 – 1578; *Angew. Chem. Int. Ed.* **2002**, *41*, 1488 – 1508, and references therein; c) C. A. Schalley, *Angew. Chem.* **2002**, *114*, 1583 – 1586; *Angew. Chem. Int. Ed.* **2002**, *41*, 1513 – 1515, and references therein.
[7] a) J. Kang, J. Rebek, Jr., *Nature* **1996**, *382*, 239 – 241; b) T. Heinz, D. M. Rudkevich, J. Rebek, Jr., *Nature* **1998**, *394*, 764 – 766; c) T. Kusukawa, M. Fujita, *J. Am. Chem. Soc.* **2002**, *124*, 13576 – 13582; d) M. Ziegler, J. L. Brumaghim, K. N. Raymond, *Angew. Chem.* **2000**, *112*, 4285 – 4287; *Angew. Chem. Int. Ed.* **2000**, *39*, 4119 – 4121.
[8] J.-M. Lehn, *Science* **2002**, *295*, 2400 – 2403.
[9] L. J. Prins, D. N. Reinhoudt, P. Timmerman, *Angew. Chem.* **2001**, *113*, 2446 – 2492; *Angew. Chem. Int. Ed.* **2001**, *40*, 2382 – 2426.
[10] C. T. Seto, G. M. Whitesides, *J. Am. Chem. Soc.* **1993**, *115*, 905 – 916.
[11] a) P. Timmerman, R. H. Vreekamp, R. Hulst, W. Verboom, D. N. Reinhoudt, K. Rissanen, K. A. Udachin, J. Ripmeester, *Chem. Eur. J.* **1997**, *3*, 1823 – 1832; b) R. H. Vreekamp, J. P. M. Van

 © 2003 Wiley-VCH Verlag GmbH & Co. KGaA, Weinheim 

Duynhoven, M. Hubert, W. Verboom, D. N. Reinhoudt, *Angew. Chem.* **1996**, *108*, 1306 – 1309; *Angew. Chem. Int. Ed. Engl.* **1996**, *35*, 1215 – 1218.

[12] P. Timmerman, D. N. Reinhoudt, *Adv. Mater.* **1999**, *11*, 71 – 74.

[13] A crystal of $\mathbf{1a}_3{\cdot}(\mathrm{DEB})_6{\cdot}\mathbf{2}_3$ with dimensions $0.25 \times 0.25 \times 0.25$ mm was placed on a Lindemann glass capillary and placed in the cold nitrogen stream ($T = 150$ K) of a Nonius KappaCCD diffractometer ($\lambda_{\mathrm{MoK}\alpha} = 0.71073$ Å). Crystal data: cubic, $Pa\bar{3}$ (no. 205), $a = 41.043(6)$ Å, $V = 69138(18)$ Å$^3$, $Z = 8$, no absorption correction was applied. The structure was solved by direct methods (SHELXS97). 35 % of the unit cell is filled with disordered solvent molecules, which were incorporated in the model with the PLATON/SQUEEZE procedure. A total of 5360 electrons was found in the disordered solvent region. Some butyl and propyl moieties, which bordered the disordered solvent region, displayed disorder, which could be described with a two-site model. 186112 reflections were measured, $\theta_{\max} = 21.05°$, of which 12481 were unique, and 1009 parameters refined. Final $wR2 = 0.2551$, $R1 = 0.0899$ $S = 1.053$, min./max. residual density $= -0.30/0.43$ e Å$^{-3}$. CCDC-218142 contains the supplementary crystallographic data for this paper. These data can be obtained free of charge via www.ccdc.cam.ac.uk/conts/retrieving.html (or from the Cambridge Crystallographic Data Centre, 12 Union Road, Cambridge CB2 1EZ, UK; fax: (+44) 1223-336-033; or deposit@ccdc.cam.ac.uk).

[14] Other interactions such as van der Waals, attractive electrostatic, and interactions between hydrogen-bonding arrays and aromatic or heteroaromatic rings may play a role. a) E. A. Meyer, R. K. Castellano, F. Diederich, *Angew. Chem.* **2003**, *115*, 1244 – 1287; *Angew. Chem. Int. Ed.* **2003**, *42*, 1210 – 1250; b) C. A. Hunter, J. K. M. Sanders, *J. Am. Chem. Soc.* **1990**, *112*, 5525 – 5534c) C. A. Hunter, *Chem. Soc. Rev.* **1994**, *23*, 101 – 109.

[15] K. L. Krause, K. W. Volz, W. N. Lipscomb, *Proc. Natl. Acad. Sci. USA* **1985**, *82*, 1643 – 1647.

[16] A $C_3$ symmetry would also be obtained for our complex if the building blocks were chiral.

[17] L. J. Prins, J. Huskens, F. De Jong, P. Timmerman, D. N. Reinhoudt, *Nature* **1999**, *398*, 498 – 502.

[18] S. Saito, C. Nuckolls, J. Rebek, Jr., *J. Am. Chem. Soc.* **2000**, *122*, 9628 – 9630.

[19] NOE connectivities between $OH_n$ and $H_q$ of the same molecule **2** and between $OH_n$ and $H_o$ of the neighboring molecule **2** can be seen in the 2D NMR sprectrum. The last connectivity is only possible if the OH groups in the trimer $\mathbf{2}_3$ are pointing outwards (for assignment of the protons see Figure 2).

[20] a) K. Park, *Controlled Drug Delivery: Challenges and Strategies*, American Chemical Society, Washington DC, **1997**; b) T. Douglas, M. Young, *Nature* **1998**, *393*, 152 – 155; c) N. K. Mal, M. Fujiwara, Y. Tanaka, *Nature* **2003**, *421*, 350 – 353.

[21] a) S. K. Körner, F. C. Tucci, D. M. Rudkevich, T. Heinz, J. Rebek, Jr., *Chem. Eur. J.* **2000**, *6*, 187 – 195; b) B. C. Hamann, K. D. Shimizu, J. Rebek, Jr., *Angew. Chem.* **1996**, *108*, 1425 – 1427; *Angew. Chem. Int. Ed. Engl.* **1996**, *35*, 1326 – 1329; c) N. Branda, R. M. Grotzfeld, C. Valdés, J. Rebek, Jr., *J. Am. Chem. Soc.* **1995**, *117*, 85 – 88.

[22] L. J. Prins, F. De Jong, P. Timmerman, D. N. Reinhoudt, *Nature* **2000**, *408*, 181 – 184.

[23] A. G. Bielejewska, C. E. Marjo, L. J. Prins, P. Timmerman, F. De Jong, D. N. Reinhoudt, *J. Am. Chem. Soc.* **2001**, *123*, 7518 – 7533.

[24] Somehow the structure of DEB, with its tetrahedral $sp^3$ carbon atom, allows a better fit for the **2** trimer than CYA with its flatter $sp^3$ nitrogen atom.

[25] L. J. Prins, K. A. Jolliffe, R. Hulst, P. Timmerman, D. N. Reinhoudt, *J. Am. Chem. Soc.* **2000**, *122*, 3617 – 3627.

 © 2003 Wiley-VCH Verlag GmbH & Co. KGaA, Weinheim 

Crown Complexes

# $[Ni_6(SCH_2CH_2OH)_{12}]$: A Double Crown [12]Metallacrown-6 Nickel(II) Cluster**

*Fang-Fang Jian,* Kui Jiao, Yan Li, Pu-Su Zhao, and Lu-De Lu*

Metallacrowns represent a new class of multinuclear clusters that are analogous to crown ethers in both structure and function.[1,2] One may substitute heteroatoms, such as transition metals and nitrogen atoms, for the methylene carbon atoms of the parent ether complexes to form metallacrowns. There has been considerable interest in metallacrown chemistry owing to potential applications in chemically modified electrodes, anion-selective separation agents, liquid-crystal precursors, and magnetic materials.[3]

Generally, the metallacrowns can be synthesized using either multidentate ligands that bridge two metal ions[4] or bridging chalcogen ligands, such as NaSR,[5] NaSeR,[6] and OR anions.[7] We wanted to synthesize the bidentate ligand $[NaS_2COCH_2CH_2SCS_2Na]$ from 2-sulfanylethanol $[HSCH_2CH_2OH]$ by reaction with carbon bisulfide in aqueous NaOH solution, and then treat this ligand with aqueous nickel sulfate to produce the polymer $[NiS_2COCH_2CH_2SCS_2Ni]_n$. However, we unexpectedly obtained $[Ni_6(SCH_2CH_2OH)_{12}]$ (**1**), a novel [12]metallacrown-6 nickel cluster as shown by single-crystal X-ray diffraction. We repeated the experiment and were able to form this product in high yield. Herein we report the spontaneous self-assembly and crystal structure of compound **1** as well as investigations on its UV/Vis spectrum and thermal stability.

The crystal lattice of compound **1**[8] is made up of a centrosymmetric $[Ni_6(SCH_2CH_2OH)_{12}]$ molecule (Figure 1). Each Ni atom is surrounded by four S atoms of the $\mu_2$-$SCH_2CH_2OH$ ligands in a distorted square-planar fashion. As a result, the edge-sharing $NiS_4$ planes connect to form a ring. The six nickel atoms approximately form a hexagon, with Ni–Ni separations in the range of 2.9010(15)–2.9378(17) Å, vertex angles of 119.08(5)–121.38(5)°, and an average deviation of $\pm 0.001$ Å from the best least-squares $Ni_6$ plane. The diameter of the ring, defined as the average distance between two opposing nickel atoms, is 5.84 Å. Two $\mu_2$-S bridges

[*] Prof. Dr. F.-F. Jian, Prof. Dr. K. Jiao, Y. Li
New Materials & Function Coordination Chemistry Laboratory
Qingdao University of Science and Technology
Qingdao, 266042 (P.R. China)
Fax: (+86) 532-4023-606
E-mail: ffj2003@163169.net
Dr. P.-S. Zhao, Prof. Dr. L.-D. Lu
Materials Chemistry Laboratory
Nanjing University of Science and Technology
Nanjing, 210094 (P.R. China)

[**] This work was supported by the Natural Science Foundation of Shandong province (no. Y2002B06).

Supporting information for this article (views of the crystal structure) is available on the WWW under http://www.angewandte.org or from the author.

 © 2003 Wiley-VCH Verlag GmbH & Co. KGaA, Weinheim DOI: 10.1002/anie.200351896 

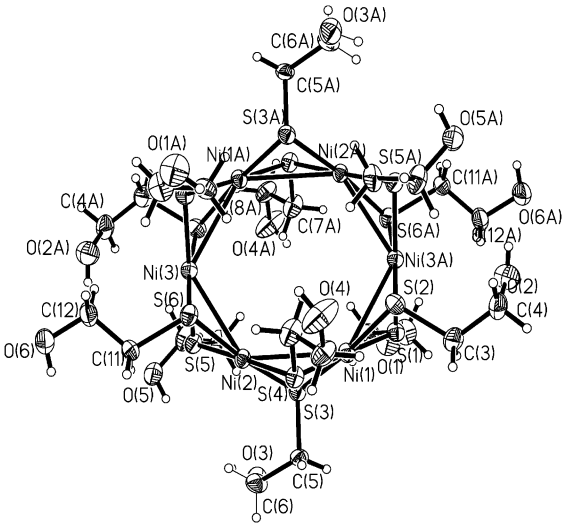



***Figure 1.*** Molecular structure of $[Ni_6(SCH_2CH_2OH)_{12}]$ (**1**). Thermal ellipsoids are shown at the 50% probability level. Selected bond lengths [Å] and angles [°]: Ni(1)-S(3) 2.194(2), Ni(1)-S(1) 2.197(2), Ni(1)-S(4) 2.200(2), Ni(1)-S(2) 2.208(2), Ni(1)-Ni(2) 2.934(2), Ni(1)-Ni(3)#1 2.9378(17), Ni(2)-S(5) 2.183(2), Ni(2)-S(4) 2.198(2), Ni(2)-S(3) 2.204(2), Ni(2)-S(6) 2.214(2), Ni(2)-Ni(3) 2.9010(15), Ni(3)-S(1)#1 2.192(2), Ni(3)-S(5) 2.204(2), Ni(3)-S(2)#1 2.205(2), Ni(3)-S(6) 2.213(2); S(3)-Ni(1)-S(1)97.21(8), S(3)-Ni(1)-S(4)82.28(8), S(1)-Ni(1)-S(4)178.64(9), S(3)-Ni(1)-S(2)173.95(9), S(1)-Ni(1)-S(2)81.86(8), S(4)-Ni(1)-S(2)98.78(8), Ni(2)-Ni(1)-Ni(3)#1 121.38(5), S(5)-Ni(2)-S(4) 178.55(9), S(5)-Ni(2)-S(3) 97.69(8), S(4)-Ni(2)-S(3) 82.11(8), S(5)-Ni(2)-S(6) 82.25(8), S(4)-Ni(2)-S(6) 98.11(8), S(3)-Ni(2)-S(6) 173.29(8), Ni(3)-Ni(2)-Ni(1) 119.53(5), S(1)#1- Ni(3)-S(5) 179.39(8), S(1)#1-Ni(3)-S(2)#1 82.05(8), S(5)-Ni(3)-S(2)#1 98.51(8), S(1)#1-Ni(3)-S(6) 97.60(8), S(5)-Ni(3)-S(6) 81.82(8),S(2)#1-Ni(3)-S(6) 174.20(9), Ni(2)-Ni(3)- Ni(1)#1 119.08(5). Symmetry transformations used to generate equivalent atoms: #1: $-x+1,-y+2,-z+1$; #2: $-x,-y+2,-z+1$.

originating from two 2-sulfanylethanol ligands connect adjacent nickel atoms. One of the $\mu_2$-S atoms is above and the other is below the $Ni_6$ plane. As a consequence, the six nickel(II) atoms nearly show virtual $C_6$ symmetry, and the twelve $\mu_2$-S atoms form double crowns, one above and the other below the nickel ring (Figure 2). This type of complex

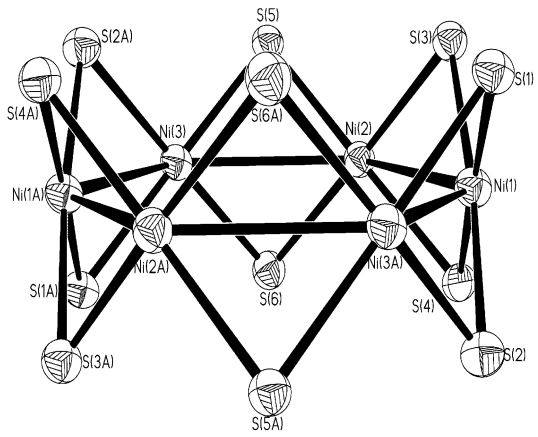



***Figure 2.*** The double crowns in **1** made up of a $Ni_6$ ring and twelve $\mu_2$-S atoms.

with a $Ni_6$ ring and a double-crown structure is to our knowledge the first of its kind.

Owing to geometrical restrictions introduced by the bridging sulfur atoms, the $NiS_4$ units are not strictly planar, with S-Ni-S bond angles ranging from 81.82 to 98.78°. The Ni–S bond lengths are 2.183–2.213 Å, and thus slightly longer than that found in another nickel(II) complex with square-planar coordination (2.172(2) Å).[9] Within the $Ni_6$ ring, the average Ni–Ni separations of 2.9276 Å are significantly longer than the Ni–Ni separations between nearest neighbors in cubic close-packed nickel (2.492 Å) and hexagonal close-packed nickel (2.492 Å).[10] They are also longer than the mean Ni–Ni separations in nickel metal (2.49 Å),[11] but are comparable to the Ni–Ni bond lengths in other nickel clusters such as $[Ni_6Se_4Cp'_5]$ (2.502–3.194 Å) and $[Ni_{15}Se_{10}(CO)_3Cp'_8]$ (2.523–2.948 Å; $Cp' =$ methylcyclopentadienyl).[12] In addition, the triangle plane laminas (NiSNi) of the double crown are not perpendicular to the $Ni_6$ ring. The plane comprising Ni(2), S(5), and Ni(3) makes a dihedral angle of 58.65° with the plane formed by Ni(2), S(6), and Ni(3). These two planes form dihedral angles of 57.60° and 63.74° with the $Ni_6$ ring plane, respectively.

The salient feature in the crystal packing of compound **1** is that the hydroxy groups of 2-sulfanylethanol form strong intermolecular hydrogen bonding interactions with each other, with donor–acceptor separations of 2.6458–2.8811 Å. This situation results in the formation of a one-dimensional chain structure (Figure 3), in which hydrogen bonding plays a

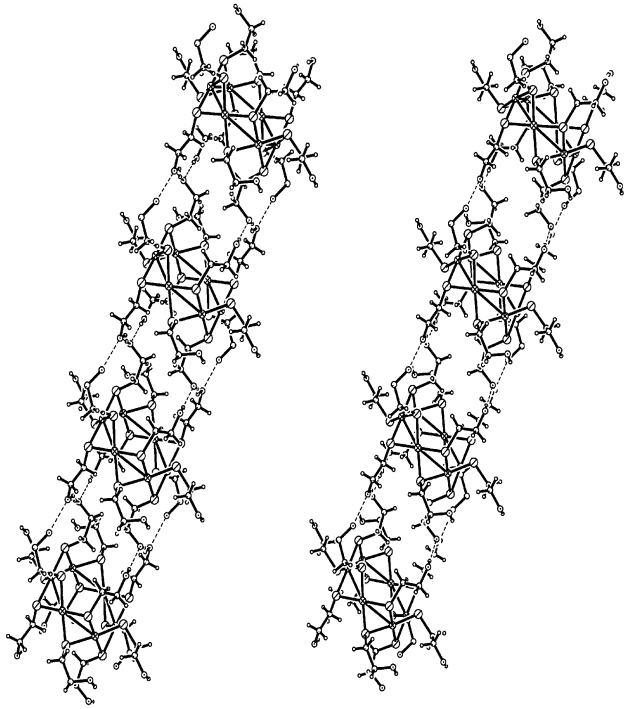


***Figure 3.*** Crystal packing of **1** as viewed down the *a* axis, showing the one-dimensional chain formed by hydrogen-bonding interactions. Selected hydrogen-bond lengths [Å] and angles [°]: O(1)-H···O(5) $[x,1+y,z]$ 2.8811, 161.24; O(2)-H···O(3) $[-1+x,y,z]$ 2.6802, 175.41; O(3)-H···O(4) $[x,-1+y,z]$ 2.6458, 142.85; O(4)-H···O(5) $[x,1+y,z]$ 2.7033, 146.76; O(5)-H···O(4) $[x,-1+y,z]$ 2.7033, 172.64; O(6)-H···O(2) $[-x,1-y,-z]$ 2.6933, 160.59.

 © 2003 Wiley-VCH Verlag GmbH & Co. KGaA, Weinheim 

significant part in sustaining the assembly of the metallacrown complex.

The solid-state UV/Vis spectrum of **1** shows there is a low-energy absorption band at $\lambda = 782$ nm. This band can be attributed to an electronic transition based on principal d orbital contribution for nickel ions because of the direct metal–metal bonding system.

Thermogravimetric (TG) analysis and differential scanning calorimetry (DSC) analysis show that the thermal decomposition of compound **1** includes four transitions (Figure 4). There are three peaks corresponding to endothermic processes—that is, weak heat-absorbing processes at 146.6, 174.2, and 217.0 °C—and a broad peak for an exothermal process at about 300 °C. Decomposition occurs at 146.6 °C. On the basis of weight changes in the TG curve, the first process of weight loss corresponds to the loss of hydroxy groups from the 2-sulfanylethanol ligands (146.6–174.2 °C; found 8.04, calcd 7.98 %) with a weak endothermic event; the second process of the weight loss is attributed to the cleavage of C–S bonds (174.2–217.0 °C; found 40.81, calcd 42.26 %). Finally, $Ni_6S_{12}$ decomposes gradually (217.0–1000 °C) with the broad peak for this exothermal is at about 300 °C, the residue may be Ni atom (found 71.69, calcd 72.43 %).

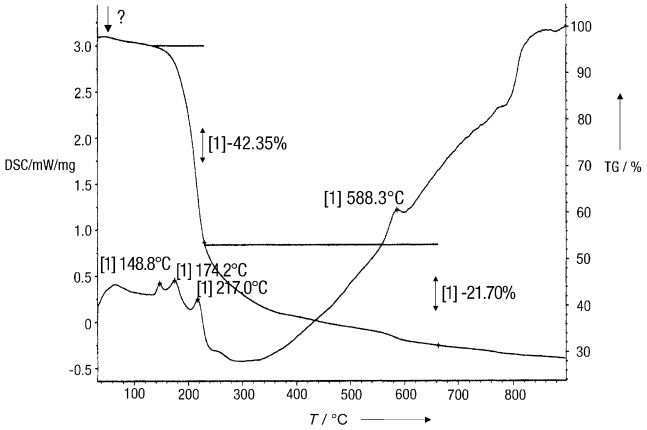



***Figure 4.*** The TG and DSC curves obtained for compound **1**.

Noteworthy is that we could not obtain the novel nickel cluster if 2-sulfanylethanol was allowed to react with aqueous NaOH solution and nickel sulfate directly, without adding carbon bisulfide. Further studies on this reaction, including the use of other metals, are in progress.

## *Experimental Section*

**1**: Warm aqueous NaOH solution (1.1 mL, 50 wt %) was added in a dropwise manner to $HOCH_2CH_2SH$ (1.00 g, 13.0 mmol) and carbon bisulfide (1.00 g 13.0 mmol) in acetonitrile (10 mL) with stirring, and the mixture was allowed to reflux for 1.5 h at 30 °C. The solution turned light yellow and then formed an orange-red viscous matter that dissolved in water easily. Then an excess of aqueous $NiSO_4$ solution (1.5 g, 8.0 ml) was added, upon which brown gelatinous precipitates formed. The brown precipitate was isolated by filtration, washed with water, and dried overnight in air. Yield 2.5 g, 92.3 % based on $HOCH_2CH_2SH$; elemental analysis: found C 21.08, H 2.38 %; the identity of this substance is not yet clear. The brown solid was ground into dust, and then recrystallized from EtOH; thus, large, dark green crystals suitable for X-ray diffraction experiments were obtained. These crystals were all collected and dried (Yield 0.4 g, 16 %. Elemental analysis calcd (%) for $C_{24}H_{60}Ni_6O_{12}S_{12}$: C 22.56, H 4.73; found: C 22.23, H 4.38.

Received: May 14, 2003
Revised: July 24, 2003 [Z51896]

**Keywords:** cluster compounds · crown compounds · nickel · S ligands

[1] V. L. Pecoraro, A. J. Stemmler, B. R. Gibeny, J. J. Bodwin, H. Wang, J. W. Kampf, A. Barwinski, *Prog. Inorg. Chem.* **1997**, *45*, 83–177.
[2] M. S. Lah, V. L. Pecoraro, *J. Am. Chem. Soc.* **1989**, *111*, 7258.
[3] a) M. S. Lah, M. L. Kirk. W. Hatfield, V. L. Pecoraro, *J. Chem. Soc. Chem. Commun.* **1989**, 1606; b) M. S. Lah, V. L. Pecoraro, *Comments Inorg. Chem.* **1990**, *11*, 59.
[4] a) S. X. Liu, S. Lin, B. Z. Lin, C. C. Lin, J. Q. Huang, *Angew. Chem.* **2001**, *113*, 1118; *Angew. Chem. Int. Ed.* **2001**, *40*, 1084; b) B. Kwak, H. Rhee, S. Park, M. S. Lah, *Inorg. Chem.* **1998**, *37*, 3599.
[5] a) T. Krüger, B. Krebs, G. Henkel, *Angew. Chem.* **1989**, *101*, 54; *Angew. Chem. Int. Ed. Engl.* **1989**, *28*, 61; b) G. Henkel, M. Kriege, K. Matsumoto, *J. Chem. Soc. Chem. Commun.* **1988**, 657.
[6] D. Fenske, A. Fischer, *Angew. Chem.* **1995**, *107*, 340; *Angew. Chem. Int. Ed. Engl.* **1995**, *34*, 307.
[7] A. Caneschi, A. Cornia, S. J. Lippard, *Angew. Chem.* **1995**, *107*, 511; *Angew. Chem. Int. Ed. Engl.* **1995**, *34*, 467.
[8] Crystal data for compound **1** ($C_{24}H_{60}Ni_6O_{12}S_{12}$): $M_r = 1277.7$, $0.3 \times 0.5 \times 0.5$ mm, $Mo_{K\alpha}$ radiation, $\lambda = 0.71073$ Å, triclinic space group, $P\bar{1}$, $a = 10.500(2)$, $b = 11.110(2)$, $c = 11.390(2)$ Å, $\alpha = 108.30(3)$, $\beta = 103.30(3)$, $\gamma = 100.90(3)°$, $Z = 1$, $V = 1177.5(4)$ Å$^3$, $T = 293(2)$ K, $\rho_{calcd} = 1.802$ Mg m$^{-3}$, $F(000) = 660$, $\mu = 2.930$ mm$^{-1}$. Of 4392 reflections collected [$(2\theta)_{max} = 49.94°$], 4144 were unique ($R_{int} = 0.0723$) and 2867 with $I > 2\sigma(I)$ were used for structure solution and refinement on $F^2$ by full-matrix least-squares techniques (SHELXL-97); $R1 = 0.0380$, $wR2 = 0.1328$, GOF ($F^2$) = 1.073; max./min. residual electron density = 0.978/−0.948 e Å$^{-3}$. CCDC-221211 contains the supplementary crystallographic data for this paper. These data can be obtained free of charge via www.ccdc.cam.ac.uk/conts/retrieving.html (or from the Cambridge Crystallographic Data Centre, 12 Union Road, Cambridge CB2 1EZ, UK; fax: (+44) 1223-336-033; or deposit@ccdc.cam.ac.uk).
[9] M. B. Ferrari, S. Capacchi, F. Bisceglie, G. Pelosi, P. Tarasconi, *Inorg. Chim. Acta* **2001**, *312*, 81.
[10] H. Donohue, *The Structures of the Elements*, Wiley, New York, **1974**, p. 213.
[11] A. I. Baranov, L. Kloo, A. V. Olenev, B. A. Popovkin, A. I. Romanenko, A. V. Shevelkov, *J. Am. Chem. Soc.* **2001**, *123*, 12375.
[12] D. Fenske, A. Hollnagel, *Angew. Chem.* **1989**, *101*, 1412; *Angew. Chem. Int. Ed. Engl.* **1989**, *28*, 1390.

 © 2003 Wiley-VCH Verlag GmbH & Co. KGaA, Weinheim 

# Apology

In the Communication "[$Ni_6(SCH_2CH_2OH)_{12}$]: A Double Crown [12]Metallacrown-6 Nickel(II) Cluster" by **F.–F. Jian**, **K. Jiao**, **Y. Li**, **P.–S. Zhao**, **L.–D. Lu** (*Angew. Chem. Int. Ed*. **2003**, *42*, 5722) the crystal structure of the main compound has already been reported: "Nickel and Palladium Complexes of 1-Hydroxyethane-2-thiol and Analogues. Part 1. Crystal Structure of Cyclohexakis[bis-(μ-1-hydroxyethane-2-thiolato)-nickel(II)]" R. O. Gould, M. M. Harding, *J. Chem. Soc.* (A) **1970**, 875–881. The authors also missed several important references to related species, these include: "A New Type of Cyclic Transition Metal Complex, $[Ni(SC_2H_5)_2]_6$" P. Woodward, L. F. Dahl, E. W. Abel, B. C. Crosse, *J. Am. Chem. Soc.* **1965**, *87*, 5251–5253; "The Structure of a Toroidal, Neutral, Homoleptic Ni(II) Complex with a Chelate Dithiolate Ligand, $[Ni_6(SCH_2CH_2CH_2S)_6]$" J. Sletten, J. A. Kovacs, *Acta Chem. Scand.* **1994**, *48*, 929–932; "Cyclo-$[Ni(\mu_2\text{-}SPh)_2]_9$ and Cyclo-$[Ni(\mu_2\text{-}SPh)_2]_{11}$: New Oligomeric Types of Toroidal Nickel(II) Thiolates Containing Geometrically Unprecedented 9- and 11-Membered Ring Systems" S. A. Ivanov, M. A. Kozee, W. Alex Merrill, S. Agarwal, L. F. Dahl "*J. Chem. Soc. Dalton Trans.* **2002**, 4105–4115. The authors apologize for these oversights.

 © 2004 Wiley-VCH Verlag GmbH & Co. KGaA, Weinheim 

*Metal–Alkene Complexes*

# A Stable Salt of the Tris(ethene)silver Cation: Structure and Characterization of $[Ag(\eta^2\text{-}C_2H_4)_3]^+[Al\{OC(CF_3)_3\}_4]^-$**

*Ingo Krossing* and Andreas Reisinger*

Since the discovery of Zeise's salt $K[PtCl_3(C_2H_4)]$ in 1827[1] the investigation of simple ethene–metal complexes is an area of continuing interest in all fields of chemistry, fueled by the interest in transformations of the coordinated $C_2H_4$ molecule. Several ethene–metal coordination modes including $\mu,\eta^2{:}\eta^2$ are known,[2] and ethene–silver complexes with no or very little back-bonding served to formulate the Dewar–Chatt–Duncanson model for the binding of olefins to transition-metal atoms.[3] However, there is still much controversy about the nature of the bonding in $[Ag(\eta^2\text{-}C_2H_4)_x]^+$ ions ($x = 1$–$3$) with proposals ranging from mainly electrostatic[4] to mainly covalent[5] and mixtures thereof.[6,7] Several weak addition compounds $[Ag(C_2H_4)_x]^+[Y]^-$ ($x = 1$–$3$; e.g., $Y = BF_4$) were prepared by applying $C_2H_4$ pressure on solid Ag[Y] salts. They were characterized by complexation constants, NMR, and vibrational spectroscopy.[8] In addition, the experimental silver complexation enthalpies for the binding of one ($-142\ kJ\,mol^{-1}$) and two ($-136\ kJ\,mol^{-1}$) equivalents of $C_2H_4$ in the gas phase were determined by FT-ICR mass spectrometry;[9] $Ag^+$ complexes with three ethene molecules are unknown in the gas phase and were only once reported in a recent computational study.[7] However, although silver–ethene complexes are textbook compounds, no solid-state structure of a $[Ag(C_2H_4)_x]^+$ moiety ($x > 0$) has been determined. This is possibly due to the instability of the compounds already prepared. The complexation of one gaseous $C_2H_4$ molecule to a silver salt at 298 K diminishes the Gibbs energy of the $Ag{-}C_2H_4$ bond compared to its bond-dissociation enthalpy by $65\ kJ\,mol^{-1}$, owing to the loss of entropy. In contrast, a huge quantity of silver complexes with less volatile and/or chelating (di-)olefins is known, some of which contain a silver atom coordinated by three or four C=C double bonds (see for example $2\,Ag[ClO_4]\cdot 3\,C_6H_{10}$[10] or $Ag[SO_3CF_3]\cdot C_{24}H_{32}$[11]). These olefins are solids or liquids and, therefore, the entropic contribution to dissociation (and thus decomposition) is much smaller than that for the lightest parent $C_2H_4$ olefin.

Recently we prepared the silver salt of the very weakly coordinating $[Al\{OC(CF_3)_3\}_4]^-$ ($[A]^-$) ion [12,13] and reported its use in stabilizing silver complexes of very weak Lewis bases such as $S_8$,[14] $P_4$,[15] and $P_4S_3$,[16] as well as reactive cations such as $CI_3^+$,[17] $P_3I_6^+$, and $P_5X_2^+$ ($X = Br$, I).[18] Large weakly coordinating anions (WCAs[19]) such as $[A]^-$ stabilize weakly bound Lewis acid–base adducts through their ability to produce "pseudo-gas-phase conditions"[14] in condensed phases, which were used herein to prepare and characterize a stable $[A]^-$ salt of the $[Ag(\eta^2\text{-}C_2H_4)_3]^+$ ion, a weakly bound isoelectronic cation analogue of the neutral tris(ethene)-nickel,[20] -palladium, and -platinum molecules.[21]

When three equivalents of $C_2H_4$ were added to Ag[A] in $CH_2Cl_2$, cooling of the concentrated clear colorless solution to $+7\,°C$ resulted in the precipitation of an almost quantitative amount of large colorless blocks of a compound that was identified by NMR, IR, and X-ray studies as $[Ag(\eta^2\text{-}C_2H_4)_3]^+[A]^-$ [Eq. (1)].[22]

$$Ag[A] + 3\,C_2H_4 \xrightarrow[+7\,°C]{CH_2Cl_2} Ag(\eta^2\text{-}C_2H_4)_3^+[A]^- \qquad [A]^- = [Al(OC(CF_3)_3)_4]^- \tag{1}$$

It is noteworthy that the affinity of the dissolved Ag[A] silver ion towards the $C_2H_4$ molecule is so high that a stoichiometric amount of ethene is sufficient to prepare the $[Ag(\eta^2\text{-}C_2H_4)_3]^+[A]^-$. The latter salt is stable in a closed nitrogen-filled container at room temperature and may be handled quickly in the atmosphere of a glove box. Compared to free $C_2H_4$, the $^1H$ and $^{13}C$ NMR spectra of a $CD_2Cl_2$ solution of $[Ag(\eta^2\text{-}C_2H_4)_3]^+[A]^-$ showed a downfield shift of $\Delta(\delta^1H) = +0.49$ ppm and an upfield shift of $\Delta(\delta^{13}C) = -6.9$ ppm, which is in good agreement with the DFT-calculated[23–28] NMR shifts of $[Ag(\eta^2\text{-}C_2H_4)_3]^+$ and free $C_2H_4$ ($\Delta(\delta^1H) = +0.3$ ppm; $\Delta(\delta^{13}C) = -7.3$ ppm; Table 1).

***Table 1:*** Comparison of experimental and DFT-calculated properties of $[Ag(\eta^2\text{-}C_2H_4)_3]^+$ and free $C_2H_4$.

| | $[Ag(\eta^2\text{-}C_2H_4)_3]^+$ | | $C_2H_4$ | |
|---|---|---|---|---|
| Property | expt | calcd | expt | calcd |
| $\delta^1H$ [ppm] | 5.77 | 5.3[a] | 5.28 | 5.0[a] |
| $\delta^{13}C$ [ppm] | 116.4 | 114.4[a] | 123.3 | 121.7[a] |
| $d$(C=C) [Å] | 1.307[b] | 1.364[c] | 1.313[b] | 1.333[c] |
| $d$(Ag–C) [Å] | 2.396 | 2.388[c] | – | – |
| $\nu$(C=C) [$cm^{-1}$] | 1581 (vw; e′) | 1610 (vw; $a_1'$) | 1623 | 1656[a] |
| | 1575 (3 km $mol^{-1}$, e′)[a] | 1577 (0 km $mol^{-1}$, $a_1'$)[a] | | |

[a] BP86/SV(P). [b] In the solid state, corrected for libration. [c] BP86/TZVPP. vw = very weak.

This agreement suggests that the planar spoke-wheel structure of solid $[Ag(\eta^2\text{-}C_2H_4)_3]^+[A]^-$ may be retained in solution (see below).

In the solid state[29] $[Ag(\eta^2\text{-}C_2H_4)_3]^+[A]^-$ forms an ionic lattice with the almost planar $[Ag(\eta^2\text{-}C_2H_4)_3]^+$ ions in a spoke-wheel arrangement (Figure 1). Short C=C bond lengths of 1.30(1) to 1.309(9) Å (av 1.304 Å) were found in the $[Ag(\eta^2\text{-}C_2H_4)_3]^+$ ion. An additional correction for libration elongates the C=C bonds by 0.003 to 0.005 Å[30] (av 1.307 Å). These C=C bond lengths compare well to those in solid ethane (1.313 Å, corrected for libration).[31] In conclusion it may be

[*] Priv.-Doz. Dr. I. Krossing, Dipl.-Chem. A. Reisinger
Universität Karlsruhe, Institut für Anorganische Chemie
Engesserstrasse Geb. 30.45, 76128 Karlsruhe (Germany)
Fax: (+49) 721-608-4854
E-mail: krossing@chemie.uni-karlsruhe.de

[**] This work was supported by the Deutsche Forschungsgemeinschaft and the Fonds der Chemischen Industrie. We thank Prof. H. Schnöckel and Dr. H.-J. Himmel for valuable discussions.

 DOI: 10.1002/anie.200352080 © 2003 Wiley-VCH Verlag GmbH & Co. KGaA, Weinheim 

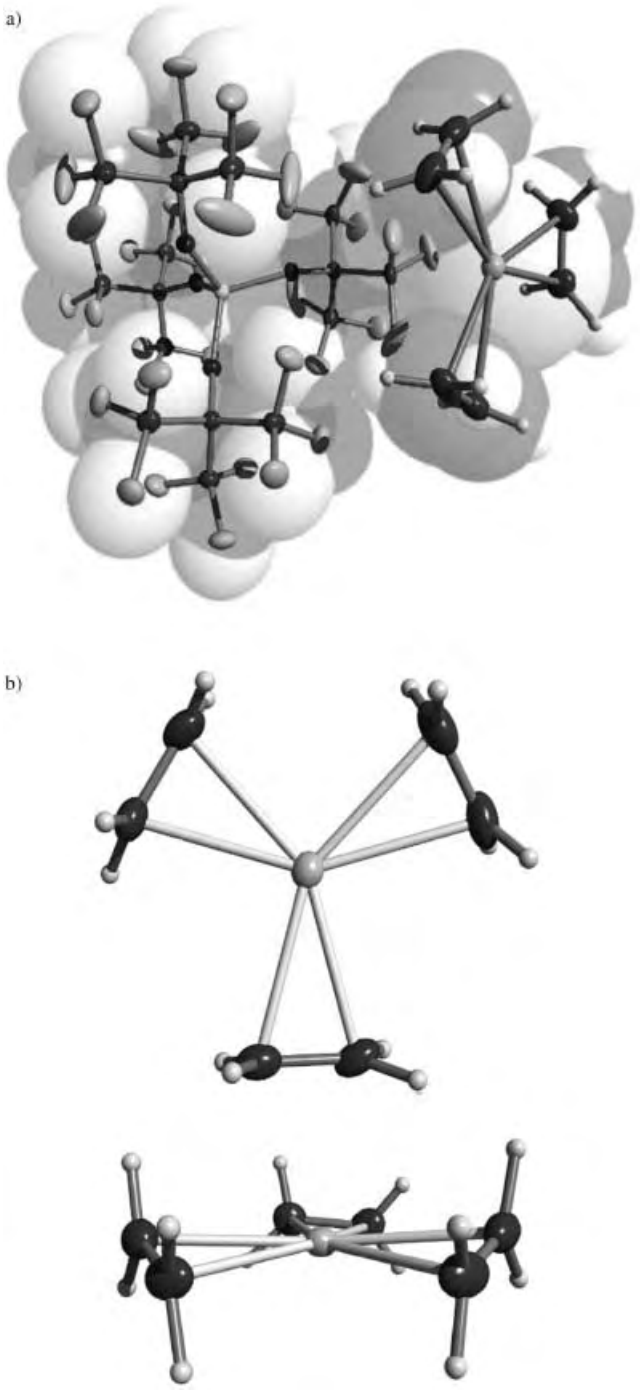



***Figure 1.*** a) Section of the solid-state structure of $[Ag(\eta^2\text{-}C_2H_4)_3]^+[A]^-$. Superposition of a space-filling (faint in gray scale) and a 25% probability ellipsoid model; b) two additional views of the cation. The positions of the hydrogen atoms were found in the difference Fourier map.

stated that the C=C bond in $C_2H_4$ is unaffected upon coordination in the $[Ag(\eta^2\text{-}C_2H_4)_3]^+$. This stands in sharp contrast to the solid-state structure of the isoelectronic $[Pt(\eta^2\text{-}C_2H_4)_3]$ molecule, in which the average C=C bond length is elongated to 1.402(7) Å.[21d] The Ag–C separations range from 2.385(5) to 2.410(5) Å (av 2.396 Å) and are ≈0.22 Å longer than those in $[Pt(\eta^2\text{-}C_2H_4)_3]$.[21d] However $d$(Ag–C) is in good agreement with other Ag–C bonds in silver complexes, for example, in $[Ag(toluene)_2\{Al(OR)_4\}]$ (2.363(5)–2.647(6) Å; R = C(H)$(CF_3)_2$).[12a] The overall structure of the $[Ag(\eta^2\text{-}C_2H_4)_3]^+$ ion approaches $D_{3h}$ symmetry, but the three individual $AgC_2$ planes deviate from the mean plane defined by the silver atom and all carbon atoms by 11.7 to 17.5°. This distortion is attributed to packing effects, which are underlined by 10 weak H···F contacts between the cation and the anion that range from 2.56 to 2.93 Å (av 2.79 Å; sum of van der Waals radii: 2.90 Å). In contrast, no contacts between fluorine and carbon atoms were observed, while the silver atom forms two weak contacts to fluorine atoms at 3.07 and 3.19 Å (sum of van der Waals radii: 3.20 Å). By employing the bond valence method of Brown,[32] the nature of the two Ag···F contacts correspond to a partial charge of +0.14 v.u. residing on the silver atom. The remainder (+0.86 v.u.) is distributed over the hydrogen atoms only, since no close contacts between carbon and fluorine atoms were observed. The latter assignment of positive partial charges to hydrogen but no (or even negative) charge to the carbon atoms is in agreement with the trends concluded from $^1H$ and $^{13}C$ NMR spectroscopy of $[Ag(\eta^2\text{-}C_2H_4)_3]^+[A]^-$ (Table 1).

The infrared spectra of $[Ag(\eta^2\text{-}C_2H_4)_3]^+[A]^-$ contain the bands of the isolated nondistorted $[A]^-$ ion as well as some less intense bands assigned to the almost $D_{3h}$-symmetric $[Ag(\eta^2\text{-}C_2H_4)_3]^+$ ion. The C=C stretches are expected to be intense in the Raman spectrum, however, all attempts to obtain such a spectrum of $[Ag(\eta^2\text{-}C_2H_4)_3]^+[A]^-$ failed and led to immediate decomposition of several independently prepared samples. Nevertheless, two very weak C=C stretches at 1581 and 1610 $cm^{-1}$ assigned to the e′- and $a_1$′-modes were observed in the IR spectrum and fit with the DFT-calculated[23,33] frequencies (Table 1). The weighted average[34] of those two bands is 1591 $cm^{-1}$ and $\Delta\nu$ with respect to free ethene (1623 $cm^{-1}$) is −32 $cm^{-1}$. This is in line with earlier reports on $[Ag(C_2H_4)_2]^+$ ($\Delta\nu = -37$)[8] and $[Ag(C_2H_4)]^+$ ($\Delta\nu = -44$).[8] As expected, $\Delta\nu$ decreases with an increasing number of coordinated $C_2H_4$ molecules, which is indicative of weaker interactions.[35] It should be noted that although the observed average C=C frequency fits very well with the trend of other $[Ag(C_2H_4)_x]^+$ cations ($x = 1, 2$), the DFT-calculated frequencies as well as the calculated C=C bond distance indicate a greater weakening of the C=C bond in $[Ag(\eta^2\text{-}C_2H_4)_3]^+$ than expected from the experimental data (compare $\Delta\nu$ and $d$(C=C) in Table 2).

To understand the formation of a planar, almost $D_{3h}$-symmetric $[Ag(\eta^2\text{-}C_2H_4)_3]^+$ ion and relate its structure and bonding to the (known) isoelectronic $[Pd(\eta^2\text{-}C_2H_4)_3]$ molecule, as well as the hypothetic $[Na(\eta^2\text{-}C_2H_4)_3]^+$ ion, additional DFT[23] and ab initio[23,36] calculations were performed on spoke-wheel $D_{3h}$ molecules, as well as trigonal-prismatic barrel-like $[M(\eta^2\text{-}C_2H_4)_3]$ (M = $Ag^+$, Pd, and $Na^+$) with all $C_2H_4$ molecules perpendicular to the mean central plane (Table 2). From Table 2 it is evident that the planar form of $[M(\eta^2\text{-}C_2H_4)_3]$ is highly favored for M = Pd (by 186.5 kJ $mol^{-1}$), with M = $Ag^+$ (44.4 kJ $mol^{-1}$) being intermediate, while for M = $Na^+$ both the planar and prismatic arrangements are isoenergetic within 1.5 kJ $mol^{-1}$. The sodium structure contains the longest M–C separations and the structural/vibrational parameters of the coordinated $C_2H_4$

 © 2003 Wiley-VCH Verlag GmbH & Co. KGaA, Weinheim 

***Table 2:*** Experimental and calculated properties of $[M(\eta^2\text{-}C_2H_4)_3]$ (M = $Ag^+$, Pd, $Na^+$). $\Delta E$ represents the energy difference between the planar spoke-wheel and the prismatic barrel structure and $\Delta\tilde{\nu}$ is the difference between the C=C stretching frequency of free ethene and $[M(\eta^2\text{-}C_2H_4)_3]$.

| Property (Level or expt) | $Pd(C_2H_4)_3$ | $[Ag(C_2H_4)_3]^+$ | $[Na(C_2H_4)_3]^+$ | $C_2H_{4\,free}$ |
|---|---|---|---|---|
| $\Delta E$ [kJ mol$^{-1}$] (MP2/TZVPP) | 186.5 | 44.4 | 1.5 | – |
| $d$(M–C) [Å] (BP86/TZVPP) | 2.216 | 2.388 | 2.852 | – |
| $d$(C=C) [Å] (BP86/TZVPP) | 1.389 | 1.364 | 1.340 | 1.333 |
| $d$(C=C) [Å] (expt) | – | 1.307[a] | – | 1.313[a] |
| $\nu$ (C=C) [cm$^{-1}$] (BP/SV(P)) | 1522[b] | 1576[b] | 1631 | 1656 |
| $\nu$ (C=C) [cm$^{-1}$] (expt) | 1522[b] | 1591[b] | – | 1623 |
| $\Delta\nu$ [cm$^{-1}$] (computed/expt) | 134/101 | 80/32 | 24/– | – |

[a] In the solid state, corrected for libration. [b] weighted average of the e′ and $a_1$′ modes.[33]

molecule are least affected upon coordination to M. Therefore the Na–C bonding in $Na(\eta^2\text{-}C_2H_4)_3^+$ is best described as being of electrostatic nature. In contrast, $Ag^+$ and Pd have an accessible $4d^{10}$ shell. The large energetic differences $\Delta E$ of the planar versus the prismatic form, as well as the short M–C separation, suggest that d-orbital bonding contributions are most important for the Pd complex but are, to a lesser extent, also important for the Ag complex.[37] A full analysis of the nature of this bonding is in progress.[35]

The synthesis and full characterization of a stable $[Ag(\eta^2\text{-}C_2H_4)_3]^+[A]^-$ salt gives the first structural information on the $[Ag(C_2H_4)_x]^+$ textbook ions ($x > 0$). It is rather remarkable that a tris(ethene)silver cation can be stabilized in condensed phases considering the fact that in the gas phase this was hitherto impossible.[9] This is certainly due to the low binding energy of the third $C_2H_4$ molecule of $\Delta G_{298} = -55$ kJ mol$^{-1}$ in the gas phase (MP2/TZVPP).[23] According to an estimation of the lattice potential enthalpies in a suitable Born–Fajans–Haber cycle, solid $[Ag(\eta^2\text{-}C_2H_4)_3]^+[A]^-$ is stable against the loss of one gaseous $C_2H_4$ molecule by only 17 kJ mol$^{-1}$.[38] Therefore we consider the preparation of $[Ag(\eta^2\text{-}C_2H_4)_3]^+[A]^-$ as a further proof for the validity of the concept of pseudo-gas-phase conditions[14] in condensed phases.

## *Experimental Section*

All manipulations were performed using grease-free Schlenk or dry-box techniques and a dinitrogen or argon atmosphere. $CH_2Cl_2$ was rigorously dried by multiple additions of 20-g quantities of $P_2O_5$, followed by distillation and degassing prior to use. Solvents were added by condensation techniques. Stoichiometric quantities of ethene were added by condensation techniques from flasks with a known volume and pressure of ethene. Ag[A] was prepared as previously described.[12a]

Received: June 6, 2003
Revised: July 21, 2003 [Z52080]

**Keywords:** alkenes · cations · density functional calculations · silver

[1] Crystal structure: M. Black, R. H. B. Mais, P. G. Owston, *Acta. Crystallogr. Sect. B* **1969**, *25*, 1753.
[2] a) F. A. Cotton, P. A. Kibala, *Polyhedron* **1987**, *6*, 645; b) F. A. Cotton, E. V. Dikarev, M. A. Petrukhina, R. E. Taylor, *J. Am. Chem. Soc.* **2001**, *123*, 5831.
[3] a) M. J. S. Dewar, *Bull. Soc. Chim. Fr.* **1951**, *79*, 18; b) J. Chatt, L. A. Duncanson, *J. Chem. Soc.* **1953**, 2939.
[4] a) M. Sodupe, C. W. Bauschlicher, *J. Phys. Chem.* **1991**, *95*, 8640; b) J. Miralles-Sabater, M. Merchan, I. Nebot-Gil, P. M. Viruela-Martin, *J. Phys. Chem.* **1996**, *100*, 4853.
[5] a) G. Frenking, N. Froehlich, *Chem. Rev.* **2000**, *100*, 717; b) R. H. Hertwig, W. Koch, D. Schröder, H. Schwarz, J. Hrušák, P. Schwerdtfeger, *J. Phys. Chem.* **1996**, *100*, 12253.
[6] a) T. Ziegler, A. Rauk, *Inorg. Chem.* **1979**, *18*, 1558; b) D. V. Deubel, *J. Am. Chem. Soc.* **2002**, *124*, 12312; c) J. C. Ma, D. A. Dougherty, *Chem. Rev.* **1997**, *97*, 1303; d) G. W. Gokel, S. L. De Wall, E. S. Meadows, *Eur. J. Org. Chem.* **2000**, 2967.
[7] J. Kaneti, L. de Smet, R. Boom, H. Zuilhof, E. Sudhölter *J. Phys. Chem. A* **2002**, *106*, 11197.
[8] a) H. W. Quinn, J. S. McIntyre, *Can. J. Chem.* **1965**, *43*, 2896; b) D. B. Powell, J. G. V. Scott, N. Sheppard, *Spectrochim. Acta Part A* **1972**, *28*, 327; c) H. W. Quinn, D. N. Glew, *Can. J. Chem.* **1962**, *40*, 1103.
[9] a) B. C. Guo, A. W. Castleman, Jr., *Chem. Phys. Lett.* **1991**, *181*, 16; b) D. Schröder, R. Wesendrup, R. H. Hertwig, T. K. Dargel, H. Grauel, W. Koch, B. R. Bender, H. Schwarz, *Organometallics* **2000**, *19*, 2608.
[10] I. W. Bassi, G. Fagherazzi, *J. Organomet. Chem.* **1968**, *13*, 535.
[11] J. McMurry, G. J. Haley, J. R. Matz, J. C. Clardy, J. Mitchell, *J. Am. Chem. Soc.* **1986**, *108*, 515.
[12] a) I. Krossing, *Chem. Eur. J.* **2001**, *7*, 490; b) I. Krossing, H. Brands, R. Feuerhake, S. König, *J. Fluorine Chem.* **2001**, *112*, 83; c) M. Gonsior, I. Krossing, N. Mitzel, *Z. Anorg. Allg. Chem.* **2002**, *628*, 1821.
[13] S. M. Ivanova, B. G. Nolan, Y. Kobayashi, S. M. Miller, O. P. Anderson, S. H. Strauss, *Chem. Eur. J.* **2001**, *7*, 503.
[14] T. S. Cameron, A. Decken, I. Dionne, M. Fang, I. Krossing, J. Passmore, *Chem. Eur. J.* **2002**, *8*, 3386.
[15] a) I. Krossing, *J. Am. Chem. Soc.* **2001**, *123*, 4603; b) I. Krossing, L. van Wüllen, *Chem. Eur. J.* **2002**, *8*, 700.
[16] A. Adolf, M. Gonsior, I. Krossing, *J. Am. Chem. Soc.* **2002**, *124*, 7111
[17] A. Bihlmeier, I. Krossing, I. Raabe, N. Trapp, *Angew. Chem.* **2003**, *115*, 1569; *Angew. Chem. Int. Ed.* **2003**, *42*, 1531.
[18] a) I. Krossing, *J. Chem. Soc. Dalton Trans.* **2002**, 500; b) I. Krossing, I. Raabe, *Angew. Chem.* **2001**, *113*, 4544; *Angew. Chem. Int. Ed.* **2001**, *40*, 4406; c) M. Gonsior, I. Krossing, L. Müller, I. Raabe, M. Jansen, L. van Wüllen, *Chem. Eur. J.* **2002**, *8*, 4475; d) I. Krossing, I. Raabe, *Angew. Chem.* **2004**, *116*; *Angew. Chem. Int. Ed.* **2004**, *43*, in press.
[19] For recent reviews see: a) C. Reed, *Acc. Chem. Res.* **1998**, *31*, 133; b) S. H. Strauss, *Chem. Rev.* **1993**, *93*, 927; c) E. Y.-X. Chen, T. J. Marks, *Chem. Rev.* **2000**, *100*, 1391.
[20] a) K. Fischer, K. Jonas, G. Wilke, *Angew. Chem.* **1973**, *85*, 620; *Angew. Chem. Int. Ed. Engl.* **1973**, *12*, 565; b) J. Mink, M. Gal, P. L. Goggin, J. L. Spencer, *J. Mol. Struct.* **1986**, *142*, 467.
[21] a) M. Green, J. A. K. Howard, J. L. Spencer, F. G. A. Stone, *J. Chem. Soc. Chem. Commun.* **1975**, 449; b) M. Green, J. A. K. Howard, J. L. Spencer, F. G. A. Stone, *J. Chem. Soc. Dalton Trans.* **1977**, 271; c) P. Csaszar, P. L. Goggin, J. Mink, J. L. Spencer, *J. Organomet. Chem.* **1989**, *379*, 337; d) J. A. K. Howard, J. L. Spencer, S. A. Mason, *Proc. R. Soc. London Ser. A* **1983**, *386*, 145.

 © 2003 Wiley-VCH Verlag GmbH & Co. KGaA, Weinheim 

[22] Synthesis of $[Ag(C_2H_4)_3]^+[Al(OC(CF_3)_3)_4]^-$: $Ag^+[Al(OC(CF_3)_3)_4]^-$ (1.045 g, 0.901 mmol) was weighed into a two-bulb frit plate vessel with a glass stem that was closed with two J. Young valves. The salt was dissolved in $CH_2Cl_2$ ($\approx$40 mL), cooled to 77 K, and the flask was evacuated. Next, ethene (76 mg, 2.70 mmol) was condensed onto the mixture. The vessel was allowed to reach ambient temperature where a small quantity of a gray precipitate was observed in the clear solution, which was then filtered. The filtrate was very slowly cooled to +7 °C and within about 12 h a large quantity of colorless blocks of $[Ag(C_2H_4)_3]^+[Al(OC(CF_3)_3)_4]^-$ had formed (0.892 g, 80 %). $^1$H NMR (250 MHz, $CD_2Cl_2$, 300 K): $\delta = 5.77$ ppm (s); $^{13}$C[$^1$H] NMR (63 MHz, $CD_2Cl_2$, 300 K): $\delta = 116.4$ (s, $C_2H_4$); 121.5 ppm (q, $CF_3$, $^1J_{CF} = 292.5$ Hz); $^{19}$F NMR (235 MHz, $CD_2Cl_2$, 300 K): $\delta = -75.38$ (s); $^{27}$Al NMR (78 MHz, $CD_2Cl_2$, 300 K): $\delta = 36.0$ ppm (s). IR (CsI plates, Nujol): $\tilde{\nu} = 206$ (mw), 285 (mw), 315 (m), 330 (w), 368 (mw), 379 (mw), 444 (ms), 536 (ms), 560 (m), 571 (w), 727 (s), 756 (mw), 833 (ms), 966 (vs), 999 (m), 1065 (mw), 1224 (vs), 1243 (vs), 1274 (vs), 1299 (s), 1354 cm$^{-1}$ (ms); IR (CsI plates, perfluoropolyalkylether): $\tilde{\nu} =$ 1581 (vw), 1612 (vw), 3007(vw), 3114 cm$^{-1}$ (vw).

[23] All quantum chemical calculations were carried out with the TUBOMOLE program of R. Ahlrichs.[24] The geometries of all species $[M(C_2H_4)_3]$ (M = Pd, $Ag^+$, $Na^+$) were fully optimized in $D_{3h}$ symmetry in the spoke-wheel as well as the trigonal-prismatic barrel structure by DFT calculations using the BP86/SV(P) or BP86/TZVPP basis sets,[25–27] as well as the (RI-)MP2/TZVPP levels.[36] The nature of the obtained minima was verified by the calculation of vibrational frequencies[33] at the BP86/SV(P) level and, unless otherwise stated, all species are true minima. The 28 core electrons of Ag were replaced by a scalar relativistic effective core potential,[28] however, the entire $4d^{10}$ shell was explicitly treated in the MO calculations.

[24] a) R. Ahlrichs, M. Bär, M. Häser, H. Horn, C. Kölmel, *Chem. Phys. Lett.* **1989**, *162*, 165; b) M. von Arnim, R. Ahlrichs, *J. Chem. Phys.* **1999**, *111*, 9183.

[25] K. Eichkorn, O. Treutler, H. Oehm, M. Häser, R. Ahlrichs, *Chem. Phys. Lett.* **1995**, *242*, 652.

[26] a) A. D. Becke, *Phys. Rev. A* **1988**, *38*, 3098; b) J. P. Perdew, *Phys. Rev. B* **1986**, *33*, 8822.

[27] K. Eichkorn, F. Weigend, O. Treutler, R. Ahlrichs, *Theor. Chem. Acc.* **1997**, *97*, 119.

[28] D. Andrae, U. Haeussermann, M. Dolg, H. Stoll, H. Preuss, *Theor. Chim. Acta* **1990**, *77*, 123.

[29] Crystal-structure determination of $[Ag(C_2H_4)_3]^+[Al(OC(CF_3)_3)_4]^-$: IPDS (Stoe), graphite-monochromated $Mo_{K\alpha}$ radiation, $T = 150(2)$ K, 5000 reflections, Lorentz, polarization, and numerical absorption corrections, $\mu = 0.807$ cm$^{-1}$, direct methods with SHELXS-97, refinement against $F^2$ with SHELXL-97; $P2_1/c$, $Z = 4$, $a = 11.2881(3)$, $b = 14.984(3)$, $c = 19.092(4)$ Å, $\beta = 103.47(3)°$; $V = 3469.4(12)$ Å$^3$, $\rho_{calcd} = 2.148$ g cm$^{-1}$, $2\theta_{max} = 50°$, reflections: 10365 collected, 6102 unique ($R_{int} = 0.0469$), 5586 observed (2σ), 654 parameter, $R_1 = 0.0548$, $wR_2$ (all data) = 0.1470, GOF = 1.019. CCDC-211689 contains the supplementary crystallographic data for this paper. These data can be obtained free of charge via www.ccdc.cam.ac.uk/conts/retrieving.html (or from the Cambridge Crystallographic Data Centre, 12, Union Road, Cambridge CB21EZ, UK; fax: (+44) 1223-336-033; or deposit@ccdc.cam.ac.uk).

[30] Librational correction done with XP (SHELXTL suite of programs, LIBR keyword) based on the method of V. Schomaker, K. N. Trueblood, *Acta Crystallogr. Sect. B* **1968**, *24*, 63.

[31] G. H. van Nes, A. Vos, *Acta. Crystalogr. B* **1979**, *35*, 2593.

[32] The contacts s (in valency units v.u.) have been defined as $s = (R/R_0)^{-N}$, where R is the observed distance, $R_0$ is the covalent bond distance (bond order = 1) of the bond in question and $N$ is an empirically derived constant. For $Ag^I\cdots F$ contacts $N = -6.5$ and $R_0 = 1.95$ Å. see: I. D. Brown in *Structure and Bonding in Crystals*, *Vol. 2* (Eds.: M. O'Keefe, A. Navrotsky), Academic Press, London, **1981**, p. 1.

[33] P. Deglmann, F. Furche, R. Ahlrichs, *Chem. Phys. Lett.* **2002**, *362*, 511.

[34] Weighted average: the e′ mode is degenerate and counts double, that is, 1591 cm$^{-1}$ = (2 × 1581 + 1610)/3.

[35] Full details and assignments of the vibrational spectrum as well as a full analysis of the bonding in $[Ag(\eta^2\text{-}C_2H_4)_3]^+$ and related species will appear in an upcoming full paper; A. Reisinger, I. Krossing, unpublished results.

[36] a) F. Weigend, M. Häser, *Theor. Chem. Acc.* **1997**, *97*, 331; b) F. Weigend, M. Häser, H. Patzelt, R. Ahlrichs, *Chem. Phys. Lett.* **1998**, *294*, 143.

[37] An analysis of the related Ag–($\eta^2$-C=C) bonding in $Ag^+$[2,2,2]cyclophane prismands is found in: P. Saarenketo, R. Suontamo, T. Jödicke, K. Rissanen, *Organometallics* **2000**, *19*, 2346.

[38] A. Reisinger, Diplomarbeit, Universität Karlsruhe **2003**.


 © 2003 Wiley-VCH Verlag GmbH & Co. KGaA, Weinheim 

*Carborane Clusters*

# Heterometallic Cluster Assembly on a Rhenium–Monocarborane Substrate**

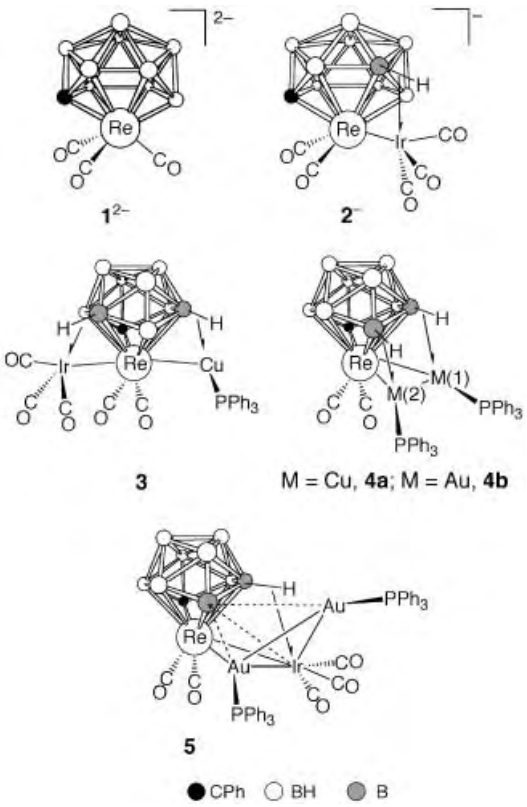
*Shaowu Du, Jason A. Kautz, Thomas D. McGrath, and F. Gordon A. Stone**

The carborane ions [*nido*-7,8-$C_2B_9H_{11}$]$^{2-}$ and [*nido*-7-$CB_{10}H_{11}$]$^{3-}$ may be compared with the ubiquitous cyclopentadienide ion [$C_5H_5$]$^-$, in that all three act as pentahapto, six-π-electron donor ligands to transition-metal centers.[1] However, compared to the relative wealth of information available on metal complexes of anionic dicarbon *nido*-carboranes, the corresponding complexes of monocarbon carboranes have scarcely been studied.[1] One aspect of particular interest derives from the monocarborane anions having a higher negative charge than their dicarbon analogues. Consequently their metal complexes also carry a higher negative charge, a property resulting in reactivity towards various electrophiles, which leads to functionalization at the carborane cage.[2] Moreover, cationic metal–ligand fragments react to give bimetallic species.[3,4] We have recently expanded our studies to non-icosahedral metal–monocarborane complexes with the rhenacarborane ion **1**$^{2-}$ (Scheme 1).[5] Herein we demonstrate that **1**$^{2-}$ may be used as

[*] Prof. F. G. A. Stone, Dr. S. Du, Dr. J. A. Kautz, Dr. T. D. McGrath
Department of Chemistry and Biochemistry
Baylor University
Waco, TX 76798–7348 (USA)
Fax: (+1) 254-710-2403
E-mail: gordon stone@baylor.edu

[**] We thank the Robert A. Welch Foundation for support (Grant AA-1201).

 © 2003 Wiley-VCH Verlag GmbH & Co. KGaA, Weinheim DOI: 10.1002/anie.200352310 




***Scheme 1.*** Structures of the species $\mathbf{1}^{2-}$, $\mathbf{2}^{-}$, and **3**–**5**.[7]

a scaffold for the stepwise assembly of heteropolymetallic clusters.

When $[N(PPh_3)_2][NEt_4]$-**1**[5] is treated in $CH_2Cl_2$ with $[IrCl(CO)_2(NH_2C_6H_4Me\text{-}1,4)]$[6] and $Tl[PF_6]$, the ionic rhenium–iridium complex $\mathbf{2}^{-}$ is formed. Its structure is reasonably inferred from its NMR spectra and from the known structures of compounds **3**–**5** (Scheme 1). Noting that $\mathbf{2}^{-}$ retains a single negative charge, it was of interest to establish whether a further, but different, cationic metal fragment could be added to the cage system. Accordingly, $\mathbf{2}^{-}$ was treated in $CH_2Cl_2$ with $[CuCl(PPh_3)]_4$[8] or $[AuCl(PPh_3)]$[9] in the presence of $Tl[PF_6]$, each reaction unexpectedly giving rise to two products.

In the copper system the anticipated product, a trimetallic Ir-Re-Cu species **3** was indeed observed and its structure was confirmed by a preliminary X-ray diffraction study. However, the major product was a rhenium–dicopper species **4a**, also characterized structurally. The metal atom arrangement in **3** resembles that of the Cu-Re-Cu compound formed by direct reaction of $\mathbf{1}^{2-}$ with $[CuCl(PPh_3)]_4/Tl[PF_6]$.[5] However, the latter trimetallic complex has a Cu-Re-Cu angle of 93.89(2)° (Cu–Re 2.7563(8), 2.7866(7) Å), whilst the Ir-Re-Cu angle in **3** is 164.27(4)° (Ir–Re 2.8860(12), Re–Cu 2.666(3) Å). These "V-shaped" trimetallic units contrast with **4a**, where there is an $\{ReCu_2\}$ triangle (Re–Cu(1) 2.6838(9), Re–Cu(2) 2.6117(9), Cu(1)–Cu(2) 2.9093(15) Å; Cu(1)-Cu(2)-Re 57.87(3), Cu(1)-Re-Cu(2) 66.64(3), Re-Cu(1)-Cu(2) 55.50(3)°). However, solution $^{11}B\{^1H\}$ and $^{31}P\{^1H\}$ NMR spectral data for **4a** are consistent with a time-averaged symmetric structure, suggesting that the exopolyhedral $\{Cu(PPh_3)\}$ fragments are fluxional over the carborane surface.[4] Such a process might involve migration of the entire $\{Cu_2(PPh_3)_2\}$ unit, or else a breaking of the Cu–Cu connectivity to give an intermediate with a V-shaped trimetal unit akin to **3**.

The reaction of $\mathbf{2}^{-}$ with the source of $\{Au(PPh_3)\}^{+}$ also gives two products, namely complexes **4b** and **5** (Scheme 1). No Ir-Re-Au analogue of compound **3** was observed, but the major product **4b** is the rhenium-digold analogue of **4a** described above. Single crystals of **4b** were not available for an X-ray diffraction study but its structure is, nevertheless, reasonably assumed to be similar to that of **4a**: the $\{Au(PPh_3)\}_2$ derivative of $\mathbf{1}^{2-}$ is known to be isostructural with its dicopper analogue.[5] Although complex **5** is isolated in lesser amounts from this reaction its structure (Figure 1), confirmed by X-ray diffraction methods,[10] is of interest.

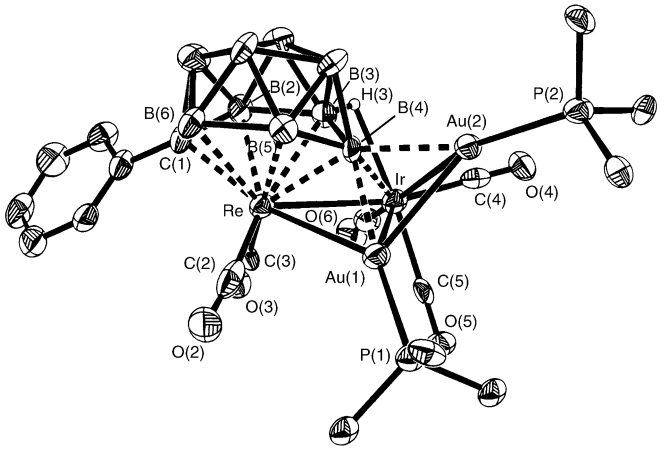



***Figure 1.*** Molecular structure of **5** (thermal ellipsoids set at 40% probability). For clarity, only *ipso* C atoms of $PPh_3$ ligands are shown and all H atoms are omitted except that in the B-H→Ir bridge. Selected interatomic distances [Å] and angles [°] are: Re-C(1) 2.165(13), Re-B(2) 2.434(18), Re-B(3) 2.346(16), Re-B(4) 2.236(15), Re-B(5) 2.362(16), Re-B(6) 2.385(17), Re-Au(1) 2.9126(8), Re-Ir 2.9540(9), B(3)···Ir 2.337(17), B(3)-H(3) 1.05(13), Ir-H(3) 2.21(13), B(4)-Au(1) 2.262(17), B(4)-Au(2) 2.270(14), B(4)-Ir 2.328(18), Ir-Au(1) 2.9765(8), Ir-Au(2) 2.8738(8), Au(1)-Au(2) 2.7723(8); Au(1)-Re-Ir 60.97(2), Au(2)-Ir-Re 96.53(2), Au(2)-Ir-Au(1) 56.54(2), Re-Ir-Au(1) 58.83(2), Au(2)-Au(1)-Re 99.79(2), Au(2)-Au(1)-Ir 59.86(2), Re-Au(1)-Ir 60.20(2), Au(1)-Au(2)-Ir 63.60(2).

In **5**, the $\{Ir(CO)_3\}$ and $\{Au(PPh_3)\}$ moieties are bonded to the rhenium center and to each other. The Au–Ir vector is bridged by a second $\{Au(PPh_3)\}$ fragment, so that overall an $\{ReIrAu_2\}$ "butterfly" has been assembled upon the starting rhenacarborane template. The iridium center is supported by an additional B–H→Ir interaction and the terminal hydrogen atom has been lost from one boron vertex. Note that this naked boron vertex B(4) is in contact with all four metal centers, in an arrangement reminiscent of $\{M_4B\}$ transition-metal boride clusters.[11] However, the $^{11}B$ NMR chemical shift of B(4) ($\delta = 37.9$ ppm) is substantially upfield of those of genuine borides.

Mechanistically, the mode of formation of **5** remains unclear. However, it seems likely that an Ir-Re-Au species akin to **3** might be its precursor. Moreover, it is conceivable

 © 2003 Wiley-VCH Verlag GmbH & Co. KGaA, Weinheim 

that ejection of an iridium fragment from **5** and H capture from the medium would be sufficient to formally convert **5** into **4b**. Conversely, it is equally possible that a gold fragment simply displaces iridium from an Ir-Re-Au intermediate to give **4b** directly. Similar considerations would apply to the copper system.

Compound **5** represents a novel class of hybrid multiple cluster in which an {ReIrAu$_2$} butterfly has been constructed on a rhenacarborane substrate. Although carborane-supported heterometallic clusters have been reported,[12] we are not aware of three different metals being introduced in such a stepwise fashion, nor of any example of such intimate contact between the metal cluster and metallacarborane subunits. The ions **1**$^{2-}$ and **2**$^{-}$ appear to offer considerable potential for the synthesis of other new heteropolymetallic species. Complexes **2**$^{-}$, **3** and **4** are interesting in their own right and the details of their structures, and those of the many other species that are accessible by a similar synthetic methodology, will undoubtedly reveal yet further architectural novelty.

## Experimental Section

[N(PPh$_3$)$_2$]-**2**:[13] Treatment (16 h) of [N(PPh$_3$)$_2$][NEt$_4$]-**1** in $CH_2Cl_2$ with [IrCl(CO)$_2$(NH$_2$C$_6$H$_4$Me-1,4)] and Tl[PF$_6$] (1 equiv each), followed by filtration, evaporation, and column chromatography of the residue, gave yellow [N(PPh$_3$)$_2$]-**2** (63%). Elemental analysis calcd (%) for $C_{48}H_{44}B_9IrNO_5P_2Re$: C 46.0, H 3.5, N 1.1; found: C 45.8, H 3.6, N 1.2; IR ($CH_2Cl_2$): $\tilde{\nu}_{max}$ = 2048 s, 2011 s, 1985 s, 1915 br s cm$^{-1}$ (CO); $^1$H NMR (360.1 MHz, $CD_2Cl_2$, 298 K): $\delta$ = ca. −7.9 ppm (vbr, B-H→Ir); $^{13}$C{$^1$H} NMR (90.6 MHz, $CD_2Cl_2$, 298 K): $\delta$ = 197.7 (Ir-CO), 173.1 (br, Re-CO), 56.8 ppm (br, cage C); $^{11}$B{$^1$H} NMR (115.5 MHz, $CD_2Cl_2$, 298 K; unit integral except where indicated): $\delta$ = 23.1, 16.1, 4.2, −6.2 (br, B-H→Ir), −16.4, −18.6, −22.8, −24.0, −35.8 ppm.

**3** and **4a**:[13] Reaction (16 h) of [N(PPh$_3$)$_2$]-**2** with [CuCl(PPh$_3$)]$_4$ and Tl[PF$_6$] (equimolar ratio Re:Cu:Tl) in $CH_2Cl_2$ and workup as above gave, successively, pale yellow **3** (12%) and yellow **4a** (41% based on Re). For **3**: elemental analysis calcd (%) for $C_{30}H_{29}B_9CuIrO_5PRe{\cdot}C_5H_{12}$: C 37.8, H 3.7; found: C 37.4, H 3.5; IR ($CH_2Cl_2$): $\tilde{\nu}_{max}$ = 2067 s, 2035 s, 2019 s, 1944 br s cm$^{-1}$ (CO); $^1$H NMR ($CD_2Cl_2$, 298 K): $\delta$ = −6.73 (br q, $^1J$(B,H) ≈ 100 Hz, B-H→Ir), −9.18 ppm (br q, $^1J$(B,H) ≈ 110 Hz, B-H→Cu); $^{13}$C{$^1$H} NMR ($CD_2Cl_2$, 298 K): $\delta$ = 192.9, 192.5, 189.4 (Ir-CO), 176.4, 168.0 (Re-CO), 47.8 ppm (br, cage C); $^{11}$B{$^1$H} NMR ($CD_2Cl_2$, 298 K): $\delta$ = 38.4 (br), 6.9, 2.9, −9.4 (br), −13.9, −16.8 (br), −22.5, −23.7, −32.0 ppm; $^{31}$P{$^1$H} NMR (145.8 MHz, $CD_2Cl_2$, 298 K): $\delta$ = 9.2 ppm (br). For **4a**: elemental analysis calcd (%) for $C_{45}H_{44}B_9Cu_2O_2P_2Re{\cdot}0.5\,CH_2Cl_2$: C 48.3, H 4.0; found: C 48.2, H 4.1; IR ($CH_2Cl_2$): $\tilde{\nu}_{max}$ = 2023 s, 1974 s cm$^{-1}$ (CO); $^{13}$C{$^1$H} NMR ($CD_2Cl_2$, 298 K): $\delta$ = 172.3 (Re-CO), 63.5 ppm (br, cage C); $^{11}$B{$^1$H} NMR ($CD_2Cl_2$, 298 K): $\delta$ = 7.6, ca. 6.3 (vbr), −7.1, −10.4 (br, 2B), −28.8 (2B), −31.3 ppm (2B); $^{31}$P{$^1$H} NMR ($CD_2Cl_2$, 298 K): $\delta$ = 9.2 ppm (br).

**4b** and **5**[13] Similarly, [N(PPh$_3$)$_2$]-**2**, [AuCl(PPh$_3$)] and Tl[PF$_6$] in $CH_2Cl_2$ gave orange **5** (16% based on Re, not optimized) and then yellow **4b** (39% based on Re). For **4b**: elemental analysis calcd (%) for $C_{45}H_{44}Au_2B_9O_2P_2Re{\cdot}0.5\,CH_2Cl_2$: C 39.1, H 3.2; found: C 39.1, H 3.2; IR ($CH_2Cl_2$): $\tilde{\nu}_{max}$ = 2044 s, 2000 s cm$^{-1}$ (CO); $^{13}$C{$^1$H} NMR ($CD_2Cl_2$, 298 K): $\delta$ = 172.8 (Re-CO), 54.2 ppm (br, cage C); $^{11}$B{$^1$H} NMR ($CD_2Cl_2$, 298 K): $\delta$ = 11.1, 9.2 (br), 0.5, −5.2 (br, 2B), −27.6 ppm (4B); $^{31}$P{$^1$H} NMR ($CD_2Cl_2$, 298 K): $\delta$ = 44.7 ppm. For **5**: elemental analysis calcd (%) for $C_{48}H_{43}Au_2B_9IrO_5P_2Re$: C 35.3, H 2.7; found: C 35.1, H 2.7; IR ($CH_2Cl_2$): $\tilde{\nu}_{max}$ = 2051 s, 2009 vs, 1929 s, 1915 br s cm$^{-1}$ (CO); $^1$H NMR ($CD_2Cl_2$, 298 K): $\delta$ ≈ −8.9 ppm (vbr, B-H→Ir); $^{13}$C{$^1$H} NMR ($CD_2Cl_2$, 298 K): $\delta$ = 198.0, 194.8, 192.6 (br, Ir-CO), 175.4, 171.0 (Re-CO), 56.1 ppm (br, cage C); $^{11}$B{$^1$H} NMR ($CD_2Cl_2$, 298 K): $\delta$ = 37.9 (B(4)), 18.3, 8.6 (br), −5.6 (vbr), −10.2 (br), −18.8 (br), −21.2 (2B), −33.6 ppm; $^{31}$P{$^1$H} NMR ($CD_2Cl_2$, 298 K): $\delta$ = 58.7 (br), 51.1 ppm (br).

Received: July 4, 2003 [Z52310]

**Keywords:** carboranes · cluster compounds · gold · heterometallic compounds · rhenium

[1] R. N. Grimes in *Comprehensive Organometallic Chemistry II, Vol. 1* (Eds.: E. W. Abel, F. G. A. Stone, G. Wilkinson), Pergamon, Oxford, **1995**, pp. 373–430, and references therein.
[2] For example: A. Franken, S. Du, P. A. Jelliss, J. A. Kautz, F. G. A. Stone, *Organometallics* **2001**, *20*, 1597; S. Du, A. Franken, P. A. Jelliss, J. A. Kautz, F. G. A. Stone, P.-Y. Yu. , *J. Chem. Soc. Dalton Trans.* **2001**, 1846; S. Du, J. A. Kautz, T. D. McGrath, F. G. A. Stone, *J. Chem. Soc. Dalton Trans.* **2001**, 2791.
[3] For example: S. A. Batten, J. C. Jeffrey, P. L. Jones, D. F. Mullica, M. D. Rudd, E. L. Sappenfield, F. G. A. Stone, A. Wolf, *Inorg. Chem.* **1997**, *36*, 2570; I. Blandford, J. C. Jeffery, P. A. Jelliss, F. G. A. Stone, *Organometallics* **1998**, *17*, 1402.
[4] D. D. Ellis, A. Franken, P. A. Jelliss, J. A. Kautz, F. G. A. Stone, P.-Y. Yu, *J. Chem. Soc. Dalton Trans.* **2000**, 2509.
[5] S. Du, J. A. Kautz, T. D. McGrath, F. G. A. Stone, *Organometallics* **2003**, *22*, 2842.
[6] U. Klabunde, *Inorg. Synth.* **1974**, *15*, 82.
[7] Metal–metal interactions are shown simply as a single line, which indicates a connectivity but not any particular electron distribution.[5] A more detailed discussion will be presented elsewhere, along with full synthetic details and the crystallographic analyses of **3** and **4a**.
[8] F. H. Jardine, J. Rule, G. A. Vohra, *J. Chem. Soc. A* **1970**, 238.
[9] M. I. Bruce, B. K. Nicholson, O. Bin Shawkataly, *Inorg. Synth.* **1989**, *26*, 325.
[10] Single crystals were grown by slow diffusion of 40–60 petroleum ether into a dichloromethane solution of **5** at −30°C. Enraf-Nonius CAD-4 diffractometer, graphite monochromated $Mo_{K\alpha}$ X-ray radiation ($\lambda$ = 0.71073 Å), 293(2) K, Lorentz and polarization corrections, numerical absorption correction based on measurement of crystal faces ($T_{max}$ = 0.087, $T_{min}$ = 0.033), solution by direct methods, refinement by full-matrix least-squares methods using all $F^2$ data. Crystal data for **5**·2$CH_2Cl_2$: $C_{50}H_{47}Au_2B_9Cl_4IrO_5P_2Re$, $M_r$ = 1801.24, crystal size 0.246 × 0.262 × 0.344 mm, monoclinic, $P2_1/n$, $a$ = 18.467(3), $b$ = 17.1872(14), $c$ = 19.797(2) Å, $\beta$ = 115.338(9)°, $V$ = 5679.0(12) Å$^3$, $Z$ = 4, $\rho_{calcd}$ = 2.107 g cm$^{-3}$, $F(000)$ = 3360, $\mu$ = 9.900 mm$^{-1}$. 10363 data collected ($\theta_{max}$ = 25.0°), 10030 unique ($R_{int}$ = 0.0401) and 6952 observed reflections [$F_o > 4\sigma(F_o)$], final $R_1$ = 0.0534 and $wR_2$ = 0.1104 (observed), $R_1$ = 0.0931 and $wR_2$ = 0.1257 (all data), max. and min. residual electron density: 1.661 (near Ir), −1.256 e Å$^{-3}$. CCDC 213812 contains the supplementary crystallographic data for this paper. These data can be obtained free of charge via www.ccdc.cam.ac.uk/conts/retrieving.html (or from the Cambridge Crystallographic Data Centre, 12 Union Road, Cambridge CB2 1EZ, UK; fax: (+44) 1223-336-033; or deposit@ccdc.cam.ac.uk).
[11] For example: C. E. Housecroft, *Coord. Chem. Rev.* **1995**, *143*, 297.
[12] For example: J. A. K. Howard, J. C. Jeffery, P. A. Jelliss, T. Sommerfeld, F. G. A. Stone, *J. Chem. Soc. Chem. Commun.* **1991**, 1664.
[13] Only selected NMR data are given. Signals for B-H→M are not observed in the $^1$H NMR spectra of compounds **4**.[4,5]

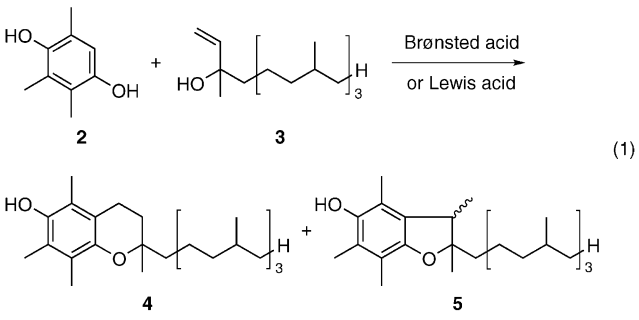
 © 2003 Wiley-VCH Verlag GmbH & Co. KGaA, Weinheim 

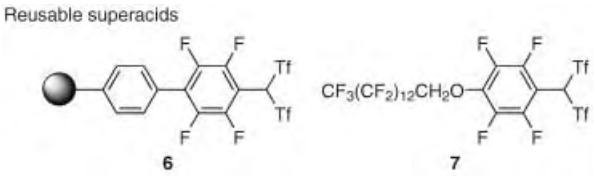
*Super Lewis Acid Catalyst*

# Trimethylsilyl Pentafluorophenylbis(trifluoromethanesulfonyl)methide as a Super Lewis Acid Catalyst for the Condensation of Trimethylhydroquinone with Isophytol**

*Aiko Hasegawa, Kazuaki Ishihara,* and Hisashi Yamamoto**

Recently, Ghosez and co-workers demonstrated that a surprising reversal of relative acidity on going from Brønsted acids to trimethylsilyl derivatives thereof could result from the difference in size between the trifluoromethanesulfonate anion ($TfO^-$) and the trifluoromethanesulfonimide anion ($Tf_2N^-$).[1] The order of Brønsted acidity is HOTf ($pK_a = -0.96$ in HOAc (Ac = acetyl)[2,3]) > $HNTf_2$ ($pK_a = 0.67$ in HOAc [2,3]),[4] whereas the order of Lewis acidity is $Me_3SiNTf_2 > Me_3SiOTf$. $Me_3SiNTf_2$ is a highly efficient Lewis acid catalyst for various carbon–carbon bond-forming reactions.[1,5] Our interest in a genuine silyl cation, such as $Me_3SiNTf_2$, prompted us to study the physical properties and catalytic efficiency of a new silicon super Lewis acid, namely, trimethylsilyl pentafluorophenylbis(trifluoromethanesulfonyl)methide $Me_3Si[C_6F_5CTf_2]$ (**1**), since the $pK_a$ value of $C_6F_5CHTf_2$ ($pK_a = 1.5$ in HOAc[2]) is higher than that of $HNTf_2$.[6] Herein we report that **1**, which is a stronger Lewis acid than $Me_3SiNTf_2$, is an extremely active and highly effective catalyst for the regioselective condensation of trimethylhydroquinone (**2**) with isophytol (**3**) to afford (±)-α-tocopherol (**4**, vitamin E) [Eq. (1)].[7] The use of **1** limited the yield of byproducts (two diastereomers of dihydrobenzofuran **5**) to less than 2%. In addition, we demonstrate that the reusable super Brønsted acids polystyrene-bound 2,3,5,6-tetrafluorophenylbis(trifluoromethanesulfonyl)methane (**6**)[6a,b] and 4-(1*H*,1*H*-perfluorotetradecanoxy)-2,3,5,6-tetrafluorophenylbis(trifluoromethanesulfonyl)methane (**7**),[6c] and their trimethylsilyl derivatives are also effective for the regioselective synthesis of **4**.




The new silicon superacid **1** was prepared by the protodesilylation of allyltrimethylsilane (2 equiv) with $C_6F_5CHTf_2$ (1 equiv)[8] in the absence of solvent, analogous to $Me_3SiNTf_2$.[1] The reaction was fast at room temperature and yielded **1** in essentially quantitative yield (0 °C to RT, 1 h). This compound could be isolated as a white solid by distillation (8 Pa, 120 °C).

Following the report of Ghosez and co-workers,[1] we used the NMR method of Childs et al.[9] to assess the Lewis acidity of **1**. This involves measuring the variation of the chemical shift of the proton in the 3-position of an α,β-unsaturated carbonyl compound on complexation with a Lewis acid. A prerequisite for this study is knowledge of the stoichiometry of the complex. Therefore, we monitored the change in the $^1H$ NMR spectrum of a solution of crotonaldehyde in $CDCl_3$ on successive addition of small amounts of **1**. This spectrometric titration showed a homogeneous variation in chemical shift for all of the protons up to a saturation level of slightly above 1 equivalent of **1**. Hence, the complex has 1:1 stoichiometry.

The effects of Lewis and Brønsted acids on the chemical shift of $H^3$ of crotonaldehyde are summarized in Table 1. The largest value of $\Delta\delta(H^3)$ for **1** shows that it is very effective in complexing crotonaldehyde. In contrast, $C_6F_5CHTf_2$ has a small value of $\Delta\delta(H^3)$. Thus, **1** is clearly a much stronger Lewis acid than $Me_3SiNTf_2$ and $Me_3SiOTf$. This is consistent with predictions based on the $^{29}Si$ chemical shifts of the three silicon Lewis acids. Therefore, the order of Lewis acidity is **1** > $Me_3SiNTf_2 > Me_3SiOTf$. However, the order of Brønsted acidity is $HOTf > HNTf_2 > C_6F_5CHTf_2$, as judged on the basis not only of $pK_a$ values but also $\Delta\delta(H^3)$ values. This reversal of the acidity sequence on going from a Brønsted acid to a trimethylsilyl derivative can be easily understood by means of the hypothesis of Ghosez and co-workers.[1]

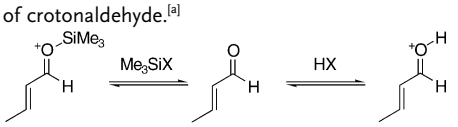
The difference in Lewis acidity between **1** and $Me_3SiOTf$ was dramatically illustrated by their effect on the rate of cycloaddition of methyl acrylate with 1-phenyl-3-(trimethylsilyloxy)buta-1,3-diene in the presence of 2,6-di-*tert*-butyl-4-

[*] Prof. Dr. K. Ishihara, A. Hasegawa
Graduate School of Engineering
Nagoya University
Furo-cho, Chikusa, Nagoya 464-8603 (Japan)
Fax: (+81) 52-789-3222
E-mail: ishihara@cc.nagoya-u.ac.jp
Prof. Dr. H. Yamamoto
Department of Chemistry
The University of Chicago
5735 South Ellis Avenue, Chicago, IL 60637 (USA)
Fax: (+1) 773-702-5059
E-mail: yamamoto@uchicago.edu

[**] This work was supported by SORST, Japan Science and Technology Agency (JST), the 21st Century COE Program "Nature-Guided Materials Processing" of the Ministry of Education, Culture, Sports, Science and Technology, the Izumi Science and Technology Foundation, the Mazda Foundation's Research Grant, and the Noguchi Fluorous Project of the Noguchi Institute.

 DOI: 10.1002/anie.200352382 © 2003 Wiley-VCH Verlag GmbH & Co. KGaA, Weinheim 

***Table 1:*** Effect of Lewis and Brønsted acids on the chemical shifts of the $H^3$ proton of crotonaldehyde.[a]




| HX | $\Delta\delta(H^3)$[b] | $Me_3SiX$ [$\delta(^{29}Si)$][d] | $\Delta\delta(H^3)$[b] |
|---|---|---|---|
| $C_6F_5CHTf_2$ | 0.086 | **1** (58.5) | 1.99 |
| $HNTf_2$ | 0.76 (0.46[c]) | $Me_3SiNTf_2$ (55.9)[e] | 1.74 (1.74[c]) |
| HOTf | 1.27 (1.28[c]) | $Me_3SiOTf$ (43.5)[f] | 0.003 (ca. 0[c]) |

[a] NMR samples were prepared by mixing crotonaldehyde (0.4 mmol) and HX or $Me_3SiX$ (0.6 mmol) in $CDCl_3$ (0.6 mL) at RT. [b] $^1H$ NMR shift differences of crotonaldehyde owing to its coordination to acids were downfield shifts in all cases. [c] Data from ref. [1]. [d] $^{29}Si$ chemical shift of $Me_3SiX$ in $CDCl_3$ in the absence of crotonaldehyde. [e] Ref. [15]. [f] Ref. [16].

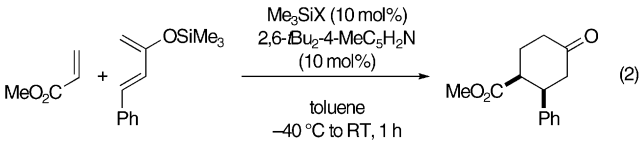
***Table 2:*** Condensation of **2** with **3** catalyzed by silicon Lewis or Brønsted acids.[a]

**2** + **3** $\xrightarrow[\text{heptane, azeotropic reflux}]{\text{HX or } Me_3SiX\ (10\,mol\%)}$ **4**

| HX | **4** | | $Me_3SiX$ | **4** | |
|---|---|---|---|---|---|
| | Yield [%][b] | Purity [%][c] | Yield [%][b] | Purity [%][c] | |
| $C_6F_5CHTf_2$ | 95 | 90.0 | **1**[e] | 97 | 99.2 |
| $HNTf_2$ | 95 | 90.8 | $Me_3SiNTf_2$[f] | 94 | 92.5 |
| HOTf[d] | 92[d] | 89[d] | $Me_3SiOTf$ | > 79 | 85.9 |

[a] A solution of **3** (3.1 mmol) in heptane (1.0 mL) was added by syringe drive (1.3 mL $h^{-1}$) to a solution of a catalyst (10 mol%) and **2** (3.0 mmol) in heptane (1.5 mL) under azeotropic reflux with removal of water (bath temperature 115 °C). The reaction mixture was then stirred for an additional 2 h under the same conditions. [b] Yield of product isolated by column chromatography on silica gel. [c] Determined by GLC analysis of the isolated products. [d] Data from ref. [7c]. [e] 2,6-Di-*tert*-butylpyridine (5 mol%) was added. [f] 2,6-Di-*tert*-butylpyridine (10 mol%) was added.

methylpyridine[10] [Eq. (2)]. According to Ghosez and coworkers, $Me_3SiOTf$ is unable to catalyze this Diels–Alder reaction, whereas $Me_3SiNTf_2$ acts as an excellent Lewis acid




(2)

**1**, $Me_3SiCTf_3$, or $Me_3SiNTf_2$[1]: 85~90% yield; $Me_3SiOTf$: 0% yield[1]

catalyst.[1] Both **1** and $Me_3SiCTf_3$ are highly active catalysts. $Me_3SiCTf_3$ was prepared from $HCTf_3$ and allyltrimethylsilane in situ, but could not be isolated by distillation since it was too unstable. Although $HCTf_3$ and $Me_3SiCTf_3$ are also very attractive superacids, since their counteranion is much larger than the $OTf^-$ and $NTf_2^-$ ions,[11] we could not assess their acidities because of their low solubility in HOAc and $CDCl_3$.[4]

Vitamin E is the most important fat-soluble antioxidant in biological systems.[12] The most economically valuable form of vitamin E is synthetic (all-*rac*)-α-tocopherol (**4**) an equimolar mixture of all eight stereoisomers, mainly applied as its acetate derivative.[12,13] The world market for vitamin E is about 25000 t/a and is constantly growing.[14] Most industrial syntheses of **4** are based on the reaction of **2** with **3** in the presence of Brønsted or Lewis acids [Eq. (1)].

From the perspective of green and sustainable chemistry, most of these methods suffer from three major disadvantages: low catalytic activities, formation of byproduct **5**, and/or the difficulty of reusing catalysts. In particular, it is important to develop a highly regioselective condensation to give **4** in high purity, because it is difficult to separate **5** from the desired product **4**. To overcome these disadvantages, based on our earlier experimental results,[7] we examined several superacids as catalysts for the condensation of **2** with **3** under azeotropic reflux with removal of water in heptane. Representative results are shown in Table 2. All the reactions were carried out in the presence of 10 mol% of catalyst under a nitrogen atmosphere and in the dark to prevent loss of yield of **4** by oxidation of **2**. Silicon Lewis acids were used for condensation in the presence of 2,6-di-*tert*-butylpyridine instead of 2,6-di-*tert*-butyl-4-methylpyridine, because the former is a weaker Lewis base.[10] As expected, the use of **1** afforded **4** in high yield, as did $Me_3SiNTf_2$. Similar catalytic activity was observed with the corresponding Brønsted acids. It is noteworthy that **4** was obtained in 99.2% purity only in the condensation catalyzed by **1**. In contrast, the purity of **4** was about 90% in other cases.

To optimize the reaction conditions, catalysts and additives were investigated in more detail (Table 3). In the presence of 2,6-di-*tert*-butylpyridine, decreasing the amount

***Table 3:*** Effects of additives on the condensation of **2** with **3** catalyzed by silicon Lewis or Brønsted acids.[a]

**2** + **3** $\xrightarrow[\text{heptane, azeotropic reflux}]{Me_3SiX\ +\ \text{additive}}$ **4**

| $Me_3SiX$ or HX (mol%) | Additive (mol%) | **4** Yield [%] | **4** Purity[b] [%] |
|---|---|---|---|
| **1** (1) | 2,6-$tBu_2C_5H_3N$ (1) | 58 | 98.3 |
| **1** (0.5) | $CH_2{=}CMeCH_2SiMe_3$ (2) | 89 | 98.1 |
| **1** (0.5) | none | 81 | 98.0 |
| $HCTf_3$ (0.5) | $CH_2{=}CMeCH_2SiMe_3$ (2.5) | 98 | 98.7 |
| $HCTf_3$ (0.5) | none | 93 | 98.2 |

[a] Unless otherwise noted, the reaction (6 mmol scale) was carried out by the same procedure as in Table 2. [b] Determined by GLC analysis of the isolated products.

of **1** to less than 10 mol% dramatically lowered the yield of **4**, but its purity remained above 98%. However, the condensation proceeded smoothly with 0.5 mol% of **1** in the presence of 2 mol% of methallyltrimethylsilane instead of a hindered base, and gave **4** in 89% yield and 98.1% purity. Methallyltrimethylsilane was added to transform residual $C_6F_5CHTf_2$ into **1**. Surprisingly, the use of a combination of $HCTf_3$ and methallyltrimethylsilane was slightly superior to **1**.

Finally, we examined reusable superacids **6** (1.01 mmol $Tf_2CHC_6F_4$ units per gram of polystyrene resin) and **7** for the condensation of **2** with **3** (Table 4). Both superacids were effective for the condensation, and their regioselectivities were slightly improved by adding methallyltrimethylsilane. Solid catalyst **6** was easily recovered in quantitative yield by filtration after the reaction, and there was no decrease in yield

 © 2003 Wiley-VCH Verlag GmbH & Co. KGaA, Weinheim 

***Table 4:*** Condensation of **2** with **3** catalyzed by reusable super Brønsted or Lewis acids.[a]

$$\mathbf{2} + \mathbf{3} \xrightarrow[\text{heptane, azeotropic reflux}]{\text{HX (5 mol\%) } CH_2{=}CMeCH_2SiMe_3} \mathbf{4}$$

| Entry | HX | Methallyl-trimethyl-silane [mol%] | **4** Yield [%] | **4** Purity [%][b] | Recovery [%] of HX |
|---|---|---|---|---|---|
| 1[c] | **6** | 25 | 81 | 97.6 | >95 |
| 2 (1st run) | **6** | 0 | 82 | 96.5 | >95 |
| 3 (2nd run)[d] | **6** | 0 | 83 | 96.0 | >95 |
| 4 | **7** | 25 | 86 | 98.2 | 77 |

[a] Unless otherwise noted, the reaction (3 mmol scale) was carried out by the same procedure as in Table 2. [b] Determined by GLC analysis of the isolated products. [c] The mixture of HX and methallyltrimethylsilane was stirred at 40°C for 1 h to prepare $Me_3SiX$ in situ before adding heptane, **2**, and **3**. [d] The reaction was carried out with **6** recovered from the first run (entry 2).

in consecutive reaction cycles with recovered catalyst **6** (entries 2 and 3). Fluorous catalyst **7** prompted the condensation and subsequent acetylation to give the acetate of **4** and was recovered in 77% yield by extraction with perfluoromethylcyclohexane. The polymer-bound catalyst **6** gave higher regioselectivity in the condensation than $C_6F_5CHTf_2$, probably because the polymeric anion is much bulkier than $C_6F_5C^-Tf_2$.

In conclusion, trimethylsilyl super Lewis acids are superior to the corresponding super Brønsted acids with respect to both catalytic activity and regioselectivity in the condensation of **2** with **3**. In particular, bulkier anions in superacids greatly contributed to improved regioselectivity: hindered anions such as $C_6F_5C^-Tf_2$ and $^-CTf_3$ were more effective than $^-NTf_2$ and $^-OTf$. Furthermore, high catalytic activities, high regioselectivity, and recycling of catalysts by using reusable superacids, such as **6** and **7**, were achieved.

Received: July 15, 2003 [Z52382]

**Keywords:** green chemistry · Lewis acids · silicon · superacidic systems · vitamins

[1] a) B. Mathieu, L. de Fays, L. Ghosez, *Tetrahedron Lett.* **2000**, *41*, 9561; b) B. Mathieu, L. Ghosez, *Tetrahedron* **2002**, *58*, 8219.

[2] The $pK_a$ values in glacial acetic acid were measured by $^1H$ NMR spectroscopy: B. M. Rode, A. Engelbrecht, J. Schantl, *Z. Phys. Chem. (Leipzig)* **1973**, *253*, 17.

[3] The $pK_a$ values of $HNTf_2$ and HOTf in glacial acetic acid are 7.8 and 4.2, respectively: J. Foropoulos, D. D. DesMarteau, *Inorg. Chem.* **1984**, *23*, 3720.

[4] The order of gas-phase acidity is $HCTf_3$ ($\Delta G_{acid} = 289.0$ kcal mol$^{-1}$) > $HNTf_2$ ($\Delta G_{acid} = 291.8$ kcal mol$^{-1}$) > TfOH ($\Delta G_{acid} = 299.5$ kcal mol$^{-1}$) > $PhCHTf_2$ ($\Delta G_{acid} = 301.3$ kcal mol$^{-1}$): I. A. Koppel, R. W. Taft, F. Aniva, S.-Z. Zhu, L.-Q. Hu, K.-S. Sung, D. D. DesMarteau, L. M. Yagupolskii, Y. L. Yagupolskii, V. M. Vlasov, R. Notario, P.-C. Maria, *J. Am. Chem. Soc.* **1994**, *116*, 3047.

[5] a) B. Mathieu, L. Ghosez, *Tetrahedron Lett.* **1997**, *38*, 5497; b) A. Ishii, O. Kotera, T. Saeki, K. Mikami, *Synlett* **1997**, *10*, 1145; c) N. Kuhnert, J. Peverley, J. Robertson, *Tetrahedron Lett.* **1998**, *39*, 3215; d) K. Ishihara, Y. Hiraiwa, H. Yamamoto, *Synlett* **2001**, *12*, 1851; e) K. Ishihara, Y. Hiraiwa, H. Yamamoto, *Chem. Commun.* **2002**, 1564.

[6] a) K. Ishihara, A. Hasegawa, H. Yamamoto, *Angew. Chem.* **2001**, *113*, 4201; *Angew. Chem. Int. Ed.* **2001**, *40*, 4077; b) K. Ishihara, A. Hasegawa, H. Yamamoto, *Synlett* **2002**, 1296; c) K. Ishihara, A. Hasegawa, H. Yamamoto, *Synlett* **2002**, 1299.

[7] a) M. Matsui, N. Karibe, K. Hayashi, H. Yamamoto, *Bull. Chem. Soc. Jpn.* **1995**, *68*, 3569; b) M. Matsui, H. Yamamoto, *Bull. Chem. Soc. Jpn.* **1996**, *69*, 137; c) K. Ishihara, M. Kubota, H. Yamamoto, *Synlett* **1996**, 1045; d) W. Bonrath, A. Haas, E. Hoppmann, T. Netscher, H. Pauling, F. Schager, A. Wildermann, *Adv. Synth. Catal.* **2002**, *344*, 37.

[8] $C_6F_5CHTf_2$ is commercially available from Tokyo Kasei Kogyo Co., Ltd.

[9] R. F. Childs, D. L. Mulholland, A. Nixon, *Can. J. Chem.* **1982**, *60*, 801.

[10] A strongly hindered base, namely, 2,6-di-*tert*-butyl-4-methylpyridine, was added to neutralize traces of HX, which might contaminate the reaction mixture, without deactivating $Me_3SiX$, since degradation of the reactants was promoted by residual HX. However, 2,6-di-*tert*-butyl-4-methylpyridine somewhat suppressed the catalytic activity of $Me_3SiX$. For the use of 2,6-di-*tert*-butyl-4-methylpyridine, see a) T. K. Hollis, B. Bosnich, *J. Am. Chem. Soc.* **1995**, *117*, 4570; b) Ref. [1].

[11] a) L. Turowaky, K. Seppelt, *Inorg. Chem.* **1988**, *27*, 2135; b) F. J. Waller, A. G. M. Barrett, D. C. Braddock, D. Ramprasad, R. M. McKinnell, A. J. P. White, D. J. Williams, R. Ducrsy, *J. Org. Chem.* **1999**, *64*, 2910; c) J. Nishikido, F. Yamamoto, H. Nakajima, Y. Mikami, Y. Matsumoto, K. Mikami, *Synlett* **1999**, 1990; d) A. G. M. Barrett, D. C. Braddock, R. Ducray, R. M. McKinnell, F. J. Waller, *Synlett* **2000**, 57; e) K. Ishihara, Y. Hiraiwa, H. Yamamoto, *Synlett* **2000**, 80.

[12] O. Isler, G. Brubacher, S. Ghisla, B. Kräulter in *Vitamine II*, Theime, Stuttgart, **1988**, pp. 126–151.

[13] K.-U. Baldenius, L. von dem Bussche-Hünnefeld, E. Hilgemann, P. Hoppe, R. Stürmer in *Ullmann's Encyclopedia of Industrial Chemistry, Vol. A27*, VCH, Weinheim, **1996**, pp. 478–488.

[14] *Chemical Market Reporter*, November 10, **1997**, p. 5.

[15] A. Vij, Y. Y. Zheng, R. L. Kirchmeier, J. M. Shreeve, *Inorg. Chem.* **1994**, *33*, 3281.

[16] H. C. Marsmann, H. G. Hon, *Z. Naturforsch. B* **1972**, *27*, 1448.

 © 2003 Wiley-VCH Verlag GmbH & Co. KGaA, Weinheim 

Molecular Devices

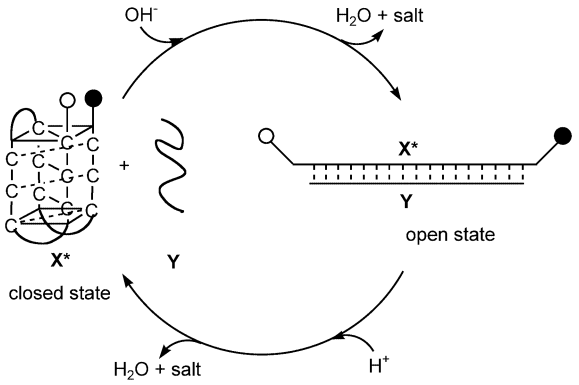
# A Proton-Fuelled DNA Nanomachine**

*Dongsheng Liu and Shankar Balasubramanian**

The molecular-recognition properties of DNA are sufficiently well understood to enable the self-assembly of defined structures and devices on the nanometer scale.[1,2] DNA machines based on a competing hybridization mechanism have been reported.[2] These nanomachines are fuelled by complementary oligonucleotides and accumulate double-stranded DNA waste products that poison the system. Herein we report a novel molecular machine driven by a distinct mechanism that is fast and relatively clean. It is based on a four-stranded DNA structure, called the *i*-motif, that can be formed from sequences containing stretches of cytosine (C) residues.[3–7] In this structure protonated C forms a noncanonical base pair with an unprotonated C (i.e., a $C{:}C^+$ base pair), and these base pairs interdigitate to form a quadruple helix that is stable under slightly acidic conditions.[3–7] A pH titration of the formation of the *i*-motif folded structure shows a sharp transition around pH 6.5;[4,5] thus, the design of a DNA nanomachine driven by pH changes is enabled.

As illustrated in Figure 1, our system comprises a 21mer single-stranded oligonucleotide X containing four stretches of CCC. The second component is a 17 mer DNA strand Y, whose sequence is complementary to X with the exception of two bases. The two mismatches are necessary to stop strand Y folding into a G-quadruplex, a four-stranded structure that results from stacked tetrads of hydrogen-bonded guanine residues,[8] and to moderate the melting point of the double helix formed (see Supporting Information). At acidic pH (pH 5.0) strand X folds into the closed *i*-motif structure.[3,4,7] In this closed state, complementary strand Y adopts a floppy random-coil conformation. When the pH value is raised to 8.0, strand X unfolds and is captured by hybridization to Y with formation of an extended duplex structure (the open state). Interconversion of the closed and open states of the machine is thus mediated by alternating addition of $H^+$ and $OH^-$.

To visualize the open and closed states of this machine, a doubly labeled version of X (i.e., X*) was synthesized with a rhodamine green fluorophore at the 5′ end and a dabcyl quencher at the 3′ end. When the 5′ and 3′ ends of strand X* are nearby, the fluorescence of rhodamine green is quenched by dabcyl, whereas rhodamine green fluorescence is strong when it is held away from the dabcyl moiety.[7,9] Rhodamine green was chosen since its fluorescence yield is insensitive to pH value in the range pH 4.0–9.0;[10] therefore, the fluorescence of this system depends only on whether the machine is open or closed.[2,7] Fluorescence quenching was also exploited as an internal indicator for titrating the required amount of $H^+$ or $OH^-$ to switch between the open and closed states. In the fully extended, open state (pH 8.0), when rhodamine green is excited at 504 nm strong emission is observed at 534 nm; when closed by lowering the pH to 5.0, the fluorescence emission is reduced to 16% (Figure 2a).




X: 5′ CCCTAACCCTAACCCTAACCC 3′
X* 5′ Rhodamine Green-CCCTAACCCTAACCCTAACCC-Dabcyl 3′
Y: 3′ GATTGTGATTGTGATTG 5′

***Figure 1.*** Oligonucleotide sequences and working cycle of the pH-driven DNA machine. The underlined DNA bases indicate the mismatched nucleotide positions in the duplex. The open circle represents rhodamine green dye, and the filled circle the dabcyl group.

The structures associated with the open and closed states were further confirmed by circular dichroism (CD) spectroscopy. At pH 5.0 the closed state (X/Y 1/1) has a CD spectrum which shows the distinct characteristics of the *i*-motif structure, with a strong positive band near 285 nm, a smaller negative band near 260 nm, and a crossover around 270 nm[11] (Figure 2b and Supporting Information). By studying the temperature dependence at 287 nm, the melting point of the closed structure was determined to be 60 °C. Examination of the open state at pH 8.0 by CD spectroscopy shows distinct characteristics of a *B*-form duplex DNA structure with a positive band near 275 nm, a negative band near 240 nm, and a crossover at 258 nm[11] In particular, the crossover at 258 nm rules out a random-coil structure (Supporting Information). By studying the variation of the UV absorbance at 260 nm with temperature, the melting temperature for the transition from the duplex (open state) to the random-coil structure was found to be 32 °C.

Thermodynamic data were obtained for the open and closed states by analysis of the respective melting curves with an established method[12] (see Supporting Information). The $\Delta G$ value for the formation of the *i*-motif structure is $-19.15\ \text{kcal mol}^{-1}$ (pH 5.0, 20 °C), while $\Delta G$ for duplex

[*] Dr. S. Balasubramanian, Dr. D. Liu
University Chemical Laboratory
University of Cambridge
Lensfield Road, Cambridge CB21EW (UK)
Fax: (+44) 1223-336913
E-mail: sb10031@cam.ac.uk

[**] We thank Drs. Paul Barker, Yamuna Krishnan-Ghosh, and Liming Ying for helpful discussions. Dr. Dongsheng Liu is supported by The Interdisciplinary Research Collaboration (IRC) in Nanotechnology.

Supporting information for this article is available on the WWW under http://www.angewandte.org or from the author.

 © 2003 Wiley-VCH Verlag GmbH & Co. KGaA, Weinheim DOI: 10.1002/anie.200352402 

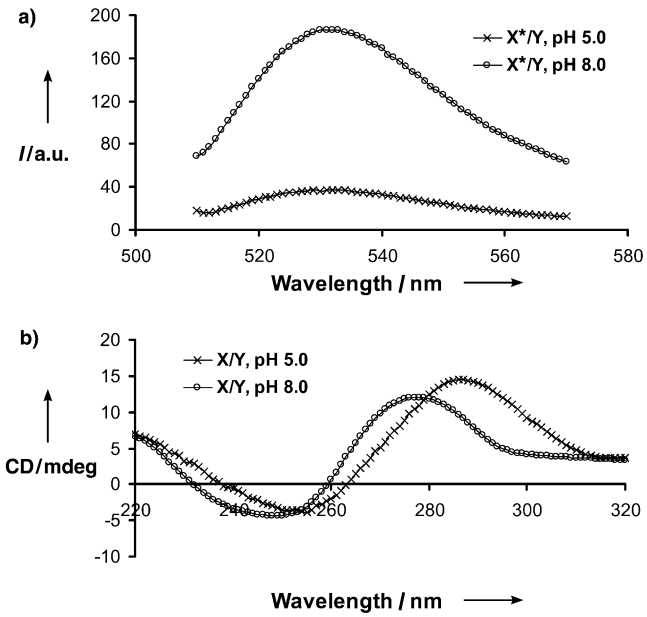



***Figure 2.*** Characterization of the open and closed structures by CD spectroscopy (for X/Y) and fluorescence spectroscopy (for X*/Y). a) Fluorescence emission spectra of the open and closed states at 20 °C with excitation at 504 nm. 1 μM X*/Y in 50 mM MES/50 mM NaCl buffer at the pH value indicated. b) CD spectra of the open and closed states at 20 °C. 1 μM X/Y in 50 mM MES/50 mM NaCl buffer at the pH value indicated.

formation by X/Y is $-8.03\,\mathrm{kcal\,mol^{-1}}$ (pH 8.0, 20 °C). Given that the stability of the X/Y duplex will decrease when the pH value is reduced from 8.0 to 5.0, the magnitude of the change in $\Delta G$ (i.e., $\Delta\Delta G$) associated with the transition from open to closed state must have a lower limit of $-11.12\,\mathrm{kcal\,mol^{-1}}$. In the closed state of the machine the 5′ and 3′ ends of X are held 0.8 nm apart according to an X-ray crystal structure of the *i*-motif.[6] In the open state X/Y forms a 17-nucleotide duplex in which the ends are held 5.8 nm apart.[13] Thus, in a complete cycle the machine undergoes a linear movement of about 5 nm. Therefore, we estimate the closing force of this system to be 15.5 pN, while the opening (or extending) force is 11.2 pN.

Multiple cycling of the machine (X*/Y 1/1) can be demonstrated by alternating addition of HCl and NaOH. Figure 3a shows the cyclical changes in fluorescence emission that result from controlled opening and closing of the system. Over 30 cycles the decrease in the amplitude of the system is negligible ($206 \pm 7$ a.u. throughout). The same output was observed by monitoring cyclical changes in the CD signal at 287 nm that result from driving the machine with pH changes (data not shown). Evidently, the accumulating "waste products" ($H_2O$ and NaCl) do not interfere with the molecular mechanism of this machine. The response time of the system can be gauged by analysis of a single opening or closing event. For a strand stoichiometry of X*/Y = 1/1 at 20 °C, the opening (Figure 3b) and closing (Figure 3c) processes are both completed in about 5 s.

Our system is based on just two strands of DNA, one of which reversibly undergoes a precise structural change driven by a pH change. The linear motion generated by this machine is associated with extending and shrinking forces in the range of 10–16 pN. The magnitudes of these forces are at the upper end of the range of forces generated by natural single-

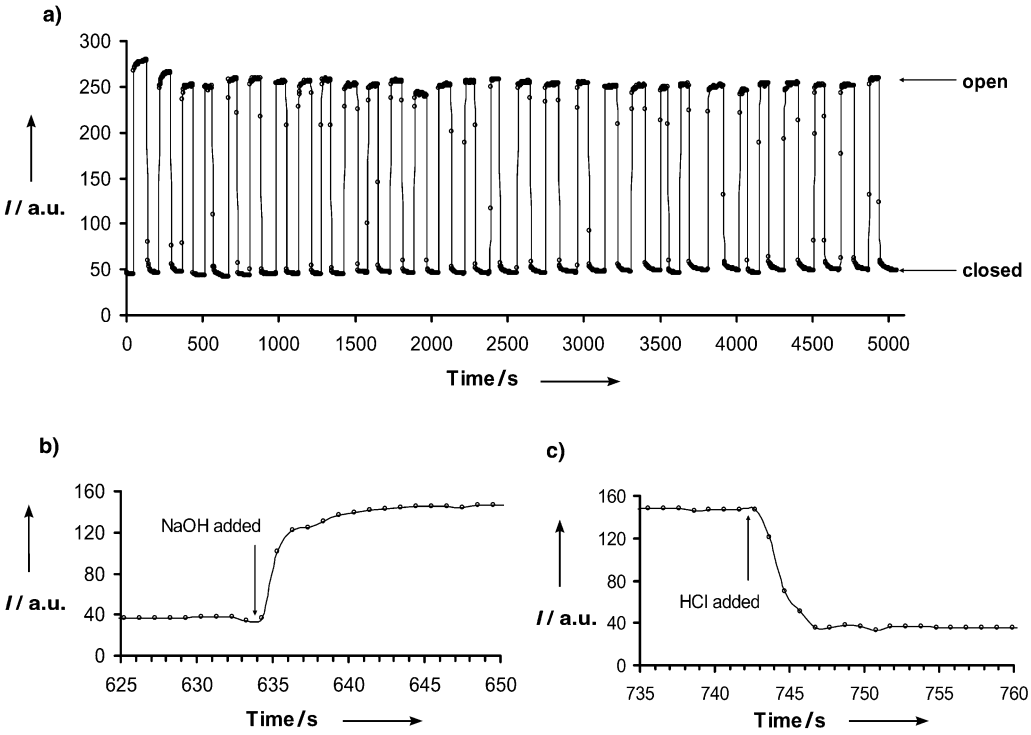



***Figure 3.*** Cycling of the machine (X*/Y), as observed by fluorescence spectroscopy. Excitation at 503 nm and emission monitored at 534 nm at a sampling interval of 0.3 s. a) Cycling of the machine (X*/Y, 1.5 μM). b) Opening of the machine (X*/Y, 1 μM). c) Closing of the machine (X*/Y, 1 μM).

 © 2003 Wiley-VCH Verlag GmbH & Co. KGaA, Weinheim 

molecule protein motors, such as kinesin[14] and myosin,[15] and also compare favorably with those of other artificial DNA machines.[2] Furthermore, since the machine exerts comparable opening and closing forces, it could be used to do work in both strokes of a working cycle. The switching mechanism has the advantage of being fast compared to DNA machines that employ competitive hybridization mechanisms. As the waste products are nontoxic, one can envisage many working cycles without apparent loss in efficiency. The modular design of this system could be employed to generate a wider range of motion that spans multiples of 5 nm by connecting *i*-motif-forming DNA sequences in tandem. By chemically tethering the ends to components such as proteins, nucleic acids, or other, synthetic molecules, adapted X/Y systems could reversibly and controllably bring two selected entities together in space, and the resulting interaction could be explored. One could also readily immobilize the X or the Y strand using DNA recognition or established covalent chemistry for integration into more complex devices. This system provides new possibilities for exploiting pH-driven motion in nanoscale structures.

## Experimental Section

Oligonucleotides X and Y were purchased from Qiagen (salt-free, resuspended in $H_2O$ prior to use). Oligonucleotide X* was purchased from Sigma Genosys.

All CD spectra were recorder on a JASCO-810 spectropolarimeter equipped with a programmable temperature-control unit. All UV spectroscopic studies were conducted on a Varian CARY 1E UV/Vis spectrophotometer. Fluorescence spectroscopy was carried out on a Varian fluorescence spectrometer.

Cycling of the system (X*/Y) visualized by fluorescence spectroscopy: X* and Y were dissolved in a buffer solution (400 μL) containing 2-morpholinoethanesulfonic acid (MES, 50 mM) and NaCl (50 mM) to give a final concentration of 1.5 μM X*/Y in a quartz fluorescence cuvette. The pH value of the buffer was cycled between 5.0 and 8.0 by alternatively adding 16 μL of 1M HCl and 1.5 μM X*/Y (to maintain a constant concentration of X* and Y), or 16 μL of 1M NaOH and 1.5 μM X*/Y to 400 μL of buffer solution at 20 °C. Under these conditions the ionic strength would gradually increase to a maximum of 1M NaCl. A lower buffer concentration may allow switching with smaller additions of NaOH/HCl and hence lead to reduced accumulation of NaCl.

Received: July 17, 2003 [Z52402]

**Keywords:** DNA · molecular devices · nanostructures · nanotechnology

[1] a) N. C. Seeman, *Nature* **2003**, *421*, 427 – 431; b) C. M. Niemeyer, M. Adler, *Angew. Chem.* **2002**, *114*, 3933 – 3937; *Angew. Chem. Int. Ed.* **2002**, *41*, 3779 – 3783; c) N. C. Seeman, *Trends Biotechnol.* **1999**, *11*, 437 – 443; d) Y. Benenson, R. Adar, T. Paz-Elizur, Z. Livneh, E. Shapiro, *Proc. Natl. Acad. Sci. USA* **2003**, *100*, 2191 – 2196; e) V. Balzani, A. Credi, M. Venturi, *Molecular Devices and Machines*, VCH, Weinheim, **2003**.

[2] a) B. Yurke, A. J. Turberfield, A. P. Mills, Jr., F. C. Simmel, J. L. Neumann, *Nature* **2000**, *406*, 605 – 608; b) H. Yan, X. Zhang, Z. Shen, N. C. Seeman, *Nature* **2002**, *415*, 62 – 65; c) J. J. Li, W. Tan, *Nano Lett.* **2002**, *2*, 315 – 318; d) P. Alberti, J. L. Mergny, *Proc. Natl. Acad. Sci. USA* **2003**, *100*,1569 – 1573.

[3] a) K. Gehring, J. L. Leroy, M. Gueron, *Nature* **1993**, *363*, 561 – 565; b) J. L. Leroy, M. Gueron, J. L. Mergny, C. Helene, *Nucleic Acids Res.* **1994**, *22*, 1600 – 1606; c) M. Gueron, J.-L. Leroy, *Curr. Opin. Struct. Biol.* **2000**, *10*, 326 – 331; d) D. E. Gilbert, J. Feigon, *Curr. Opin. Struct. Biol.* **1999**, *9*, 305 – 314.

[4] J. L. Leroy, K. Gehring, A. Kettani, M. Gueron, *Biochemistry* **1993**, *32*, 6019 – 6031.

[5] S. Ahmed, A. Kintanar, E. Henderson, *Nat. Struct. Biol.* **1994**, *1*, 83 – 88.

[6] C. Kang, I. Berger, C. Lockshin, R. Ratliff, R. Moyzis, A. Rich, *Proc. Natl. Acad. Sci. USA* **1994**, *91*, 11636 – 11640.

[7] J. L. Mergny, *Biochemistry* **1999**, *38*, 1573 – 1581.

[8] T. Simonsson, *Biol. Chem.* **2001**, *382*, 621 – 628.

[9] S. Tyagi, F. R. Kramer, *Nat. Biotechnol.* **1996**, *14*, 303 – 308.

[10] R. P. Haugland, *Handbook of Fluorescent Probes and Research Products*, 9th ed., Molecular Probes, Eugene, **2003**, p. 53.

[11] N. Berova, K. Nakanishi, R. W. Woody, *Circular Dichroism: Principles and Application*, 2nd ed., Wiley, New York, **2000**, pp. 707 – 727.

[12] L. A. Marky, K. J. Breslauer, *Biopolymers* **1987**, *26*,1601 – 1620.

[13] a) J. D. Watson, F. H. C. Crick, *Nature* **1953**, *171*, 737 – 738; b) S. B. Smith, L. Finzi, C. Bustamante, *Science* **1992**, *258*, 1122 – 1126; c) G. S. Manning, *Biopolymers* **1981**, *20*, 1751 – 1755.

[14] a) K. Svoboda, C. F. Schmidt, B. J. Schnapp, S. M. Block, *Nature* **1993**, *365*, 721 – 727; b) S. C. Kuo, M. P. Sheetz, *Science* **1993**, *260*, 232 – 234.

[15] J. T. Finer, R. M. Simmons, J. A. Spudich, *Nature* **1994**, *368*, 113 – 119.

 © 2003 Wiley-VCH Verlag GmbH & Co. KGaA, Weinheim 

*Organometallic Chemistry*

# The Palladium-Catalyzed C–H Activation of Benzylic *gem*-Dialkyl Groups

*Olivier Baudoin,* Audrey Herrbach, and Françoise Guéritte*

The activation of C($sp^3$)–H bonds is one of the current challenges in chemistry that is expected to have a major impact on both industrial and academic research. In the past years, it was shown that C–H bond activations in alkanes can be performed by low- and high-valent transition-metal complexes and in stoichiometric and catalytic processes, giving rise to synthetically useful and structurally diverse functionalized hydrocarbons.[1]

The high energy barrier of C–H bond cleavage is lowered when it is preceded by cyclometalation, which is initiated by precoordination of the metal complex to a carbon or heteroatom in the molecule. This precoordination directs

[*] Dr. O. Baudoin, Dr. A. Herrbach, Dr. F. Guéritte
Institut de Chimie des Substances Naturelles, CNRS
Avenue de la Terrasse, 91198 Gif-sur-Yvette (France)
Fax: (+33) 1-6907-7247
E-mail: baudoin@icsn.cnrs-gif.fr

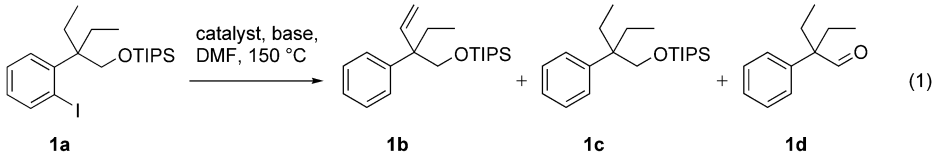
Supporting information for this article is available on the WWW under http://www.angewandte.org or from the author.

 © 2003 Wiley-VCH Verlag GmbH & Co. KGaA, Weinheim DOI: 10.1002/anie.200352461 

the metal center to the vicinity of the C–H bond to be broken. Among transition metals, it was shown that palladium(0) is particularly suitable for this process since the precoordination step can arise from the oxidative insertion into a carbon–halogen bond, such as that occurring in cross-coupling reactions. Indeed, a number of intramolecular arylations that proceed by catalytic C–H activation of arenes have been described.[2] Much less data is available regarding catalytic activation of a $C(sp^3)$–H bond through cyclometalation. In particular, it was shown that benzylic or α-benzylic C–H bonds can be cleaved through cyclometalation from $Pd^{II}$ intermediates, giving rise to homo- or cross-coupling products.[3–6] In this report, we describe our own findings regarding the catalytic C–H activation of benzylic *gem*-dialkyl groups, which occurs by formation of five- and six-membered palladacycles, and gives rise to benzocylobutadienes and olefins, respectively, without formation of homo- or cross-coupling products.

During the course of our studies directed to the synthesis of bridged biaryls with antimitotic properties, we found that a mixture of olefin **1b**, the protodeiodinated compound **1c**, and aldehyde **1d** was obtained in different ratios when phenyl iodide **1a** was heated at 150 °C in DMF in the presence of a palladium catalyst and a base [Eq. (1), Table 1]. Initially, cesium carbonate was used as base, and different palladium catalysts were tested (entries 1–7). Thus, in the presence of a phosphane-free catalyst, olefin **1b** was the major product, accompanied by starting material **1a** and by-product **1c** (entry 1). When a phosphane ligand was added, the starting iodide was completely converted into the mixture of **1b** (major product) and **1c** (entries 2–7). Among the ligands tested, tri-*o*-tolylphosphane gave the highest yield of **1b** (entry 6). From these results, it seems that a bulky triarylmonophosphane gives better results than other types of phosphanes in this reaction. Among triarylmonophosphanes with large cone angles—$PPh_3$ (145°), P(*o*-tol)$_3$ (194°), and P(mesityl)$_3$ (212°) (entries 3, 6, and 7)[7]— P(*o*-tol)$_3$ seems to have the optimal bulkiness for this reaction. Interestingly aldehyde **1d** was formed in substantial amounts when $PPh_3$ and dppp were employed as ligands (entries 3 and 5). In most other cases **1d**, which probably arises from desilylation and dehydrogenation of the resulting primary alcohol, was formed in negligible quantities. The influence of the base was then assessed (entries 8–11). Among the bases tested, $K_2CO_3$ (entry 8) and $K_3PO_4$ (entry 9) gave the highest yields of **1b** and the highest **1b**:**1c** ratio. Besides, high-boiling solvents other than DMF (e.g. dimethyl sulfoxide, xylenes) gave lower yields of **1b** (data not shown). In DMF, the reaction did not proceed at temperatures below 140–150 °C. Repeating the reaction under the optimal conditions (entries 8–9) with 5 mol % palladium acetate and 10 mol % phosphane gave the same results as with 10 mol % palladium. However, lower yields were obtained when less than 5 mol % palladium was employed (data not shown).

Using the optimal conditions, i.e. $Pd(OAc)_2$/P(*o*-tol)$_3$ as the catalyst and $K_2CO_3$ as the base, we evalulated the scope of this new dehydrogenation reaction with a number of different substrates (Table 2).[8] These were obtained in few steps from commercially available iodo- or bromobenzenes according to procedures described in our previous reports.[9] First, the influence of the benzylic R substituent and of the halogen X was studied (entries 1–8). As shown with iodides **1a, 2a, 3a**, and **4a**, substrates with relatively large R groups gave higher yields of olefin than those with smaller groups. Remarkably, phenyl bromides **5a** and **6a** gave olefins **1b** and **4b**, respectively, in high yield and with no protodehalogenated by-products (entries 5 and 6), in contrast to the reactions of the corresponding iodides **1a** and **4a**. The same temperature (150 °C) was required for the reactions of bromides and iodides. In contrast, the chloro ethyl ester (R = $CO_2Et$, X = Cl) was not reactive under these conditions. The fact that the reaction of bromides is more efficient than that of iodides may be related to the high reactivity of the latter at this temperature and consequently their higher propensity to undergo protodehalogenation. Nitrile **7a** gave olefin **7b** as the sole product in 65 % yield, indicating again that substrates with smaller R groups give lower yields. The methoxymethyl(MOM)-protected tertiary alcohol **8a** gave only 11 % yield of olefin **8b**. In this case, the use of protecting groups other than MOM (Me, Ac, TES) did not prove more satisfactory. These data indicate that the reaction is quite dependent on the nature of the benzylic R substituent, with poor reactivity when an oxygen atom is directly attached to the quaternary carbon atom, perhaps




(1)

**1a** **1b** **1c** **1d**

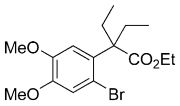
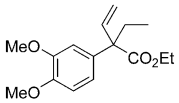
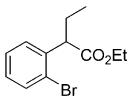
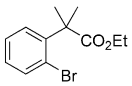
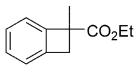
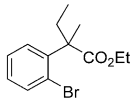
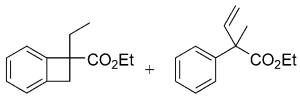
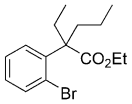
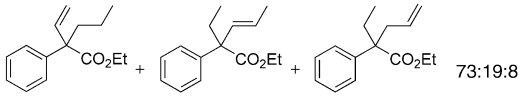
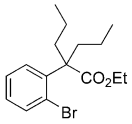
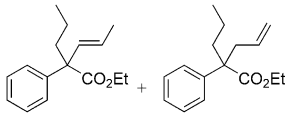
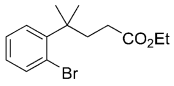
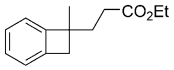
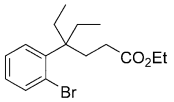
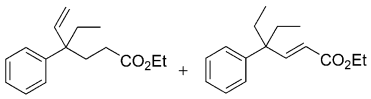
***Table 1:*** Optimization of the reaction conditions.[a]

| Entry | Catalyst[a] | Base | **1a** [%][b] | **1b** [%][b] | **1c** [%][b] | **1d** [%] |
|---|---|---|---|---|---|---|
| 1 | $Pd(OAc)_2$ | $Cs_2CO_3$ | 19 | 55 | 6 | < 5 |
| 2 | $[PdCl_2(dppf)]$ | $Cs_2CO_3$ | 0 | 57 | 18 | < 5 |
| 3 | $Pd(OAc)_2/PPh_3$ | $Cs_2CO_3$ | 0 | 39 | 7 | 28[c] |
| 4 | $Pd(OAc)_2$/P(*t*Bu)$_3$ | $Cs_2CO_3$ | 0 | 58 | 6 | < 5 |
| 5 | $Pd(OAc)_2$/dppp | $Cs_2CO_3$ | 0 | 32 | 10 | 28[c] |
| 6 | $Pd(OAc)_2$/P(*o*-tol)$_3$ | $Cs_2CO_3$ | 0 | 82 | 8 | < 5 |
| 7 | $Pd(OAc)_2$/P(mesityl)$_3$ | $Cs_2CO_3$ | 0 | 75 | 6 | < 5 |
| 8 | $Pd(OAc)_2$/P(*o*-tol)$_3$ | $K_2CO_3$ | 0 | 82 | 4 | < 5 |
| 9 | $Pd(OAc)_2$/P(*o*-tol)$_3$ | $K_3PO_4$ | 0 | 83 | 5 | < 5 |
| 10 | $Pd(OAc)_2$/P(*o*-tol)$_3$ | DBU | 47 | 42 | nd | < 5 |
| 11 | $Pd(OAc)_2$/P(*o*-tol)$_3$ | KOAc | 56 | 32 | nd | < 5 |

[a] Reaction conditions: 10 mol % palladium, 20 mol % phosphane (when used), 2 equiv base, DMF (0.1 mmol **1a** $L^{-1}$), 150 °C, 30 min. Abbreviations: dppf = 1,1′-bis(diphenylphosphanyl)ferrocene, dppp = 1,3-bis(diphenylphosphanyl)propane, TIPS = triisopropylsilyl. [b] Yields after flash chromatography; **1a**:**1b**:**1c** ratio was determined by GC and $^1$H NMR analysis. [c] Yield of isolated product.

 © 2003 Wiley-VCH Verlag GmbH & Co. KGaA, Weinheim 

***Table 2:*** Dehydrogenation of phenyl iodides and bromides.[a]

| Entry | Phenyl halide | Products[b] | Yield [%][c] |
|---|---|---|---|
| 1 | **1a**: R = $CH_2OTIPS$, X = I | **1b** | 82 (4) |
| 2 | **2a**: R = $CH_2OTES$, X = I | **2b** | 12 (2) |
| 3 | **3a**: R = $CO_2Me$, X = I | **3b** | 47 (8) |
| 4 | **4a**: R = $CO_2Et$, X = I | **4b** | 62 (6) |
| 5 | **5a**: R = $CH_2OTIPS$, X = Br | **1b** | 83 (0) |
| 6 | **6a**: R = $CO_2Et$, X = Br | **4b** | 83 (0) |
| 7 | **7a**: R = CN, X = Br | **7b** | 65 (0) |
| 8 | **8a**: R = OMOM, X = Br | **8b** | 11 (7) |
| 9 |  **9a** |  **9b** | 93 |
| 10 |  **10a** | – | 0 |
| 11 |  **11a** |  **11b** | 60[d] |
| 12 |  **12a** |  **12b** **12c** 95:5 | 71 |
| 13 |  **13a** |  **13b** **13c** **13d** 73:19:8 | 75 |
| 14 |  **14a** |  **14b** **14c** 81:19 | 74 |
| 15 |  **15a** |  **15b** | 78 |
| 16 |  **16a** |  **16b** **16c** 86:14 | 80 |

[a] Reaction conditions: 10 mol% $Pd(OAc)_2$, 20 mol% P(*o*-tol)$_3$, 2 equiv $K_2CO_3$, DMF, 150 °C, 30 min.[8] Abbreviation: TES = triethylsilyl. [b] The ratio of regioisomers was determined by GC analysis. [c] After flash chromatography; yields in brackets refer to the protodehalogenated by-product (see **1c**, Table 1). [d] Reaction time: 90 min.

due to electronic effects. By contrast, as shown with bromide **9a**, it seems that substituted benzenes can be employed successfully, though more examples are still needed.

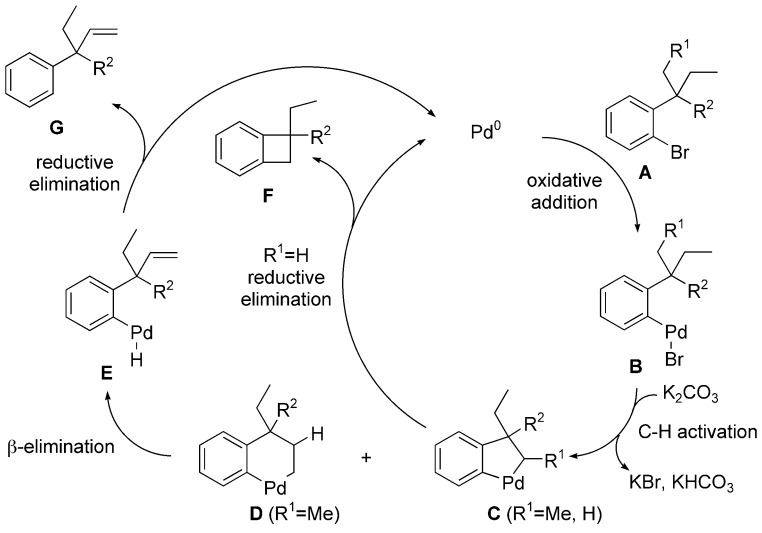
Next, the influence of different benzylic alkyl groups was evaluated (entries 10–16) starting from bromophenyl ethyl esters **10a**–**16a**. When only one ethyl group was present, no reaction occurred (entry 10). With a *gem*-dimethyl group, substrate **11a** (entry 11) is obviously unable to undergo double-bond formation. The benzocyclobutene **11b** was formed exclusively in 60% yield, and a longer time (90 min) was necessary for the reaction to reach completion. A related example of benzocyclobutene formation, concomitant with homocoupling, was described by Dyker.[3d] The controlled formation of **11b** (without homocoupling) may provide convenient access to functionalized benzocyclobutenes, which are traditionally difficult to synthesize and which, in particular, are useful substrates for Diels–Alder reactions and intermediates in the synthesis of natural products.[10] Starting

 © 2003 Wiley-VCH Verlag GmbH & Co. KGaA, Weinheim 

from dissymmetric methyl ethyl bromide **12a**, a 95:5 mixture of the two possible products **12b** and **12c** was obtained in 71% yield, showing that the formation of the cyclobutarene is much preferred over the olefin. When the ethyl propyl bromide **13a** was employed, a 73:19:8 mixture of regioisomeric olefins **13b, 13c**, and **13d** was obtained in 75% yield, showing that the dehydrogenation of the less substituted alkyl group is predominant. With the symmetrical dipropyl bromide **14a**, a 81:19 mixture of regioisomers **14b** and **14c** was obtained in 74% yield, and **14b** has exclusively the *E* geometry (like **13c**). Thus, as shown with **13a** and **14a**, it seems that the dehydrogenation of the *n*-propyl group occurs such as to give the thermodynamically more stable product with the more substituted double bond.

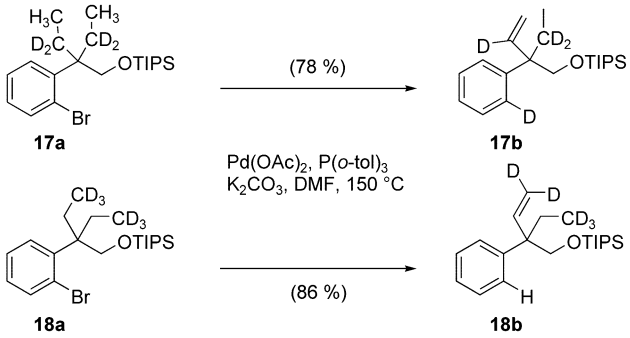
Finally, the two-carbon homologated compounds **15a** and **16a** were reacted in order to determine whether the conjugated double bond was formed preferentially as a consequence of thermodynamic factors. In the case of *gem*-dimethyl bromide **15a**, the benzocyclobutene **15b** was formed exclusively in 78% yield. Similarly, with *gem*-diethyl bromide **16a**, both olefins **16b** and **16c** were formed (80% yield), but in a 86:14 ratio in favor of the nonconjugated product **16b**. These data suggest again that steric factors prevail in this reaction.

A plausible mechanism for the formation of olefins (when alkyl groups have at least two carbons) or benzocyclobutenes (when at least one alkyl group is a methyl) is shown in Scheme 1. The oxidative addition of $Pd^0$ to phenyl bromide **A** gives rise to intermediate **B**, which would undergo C–H activation of one of the alkyl C–H bonds to give either the five-membered palladacycle **C** or the six-membered palladacycle **D**. If a methyl group is present ($R^1 = H$), intermediate **C** is formed and gives directly benzocyclobutene **F** by reductive elimination. If alkyl groups having at least two carbons are present ($R^1$ = Me, Et), both five- and six-membered palladacycles can explain the formation of olefin **G** by β-elimination followed by reductive elimination from the palladium hydride intermediate **E**.[11]




***Scheme 1.*** Mechanistic proposal for the formation of olefins and benzocyclobutenes.

In order to determine whether palladacycle **C** or **D** is involved in the formation of olefin **G**, the dehydrogenation was conducted with deuterated bromides **17a** and **18a** (Scheme 2). The corresponding olefins **17b** and **18b**, having




***Scheme 2.*** Deuterium-labeling experiments.

a deuterium atom and an hydrogen atom, respectively, in the place of the bromine, were obtained in good yield.[12] These experiments show that the deuterium or hydrogen atom incorporated on the benzene ring originated from the carbon α to the quaternary benzylic position and lends support for the six-membered palladacycle intermediate **D** in Scheme 1. The observation of terminal olefins **13d** and **14c** in the dehydrogenation of propyl-containing substrates (Table 2) also argues in favor of intermediate **D** (with β-elimination from the terminal position).[11] Thus, it appears that benzocyclobutenes **F** and olefins **G** are formed initially through C–H activation at the α- and β-benzylic position, respectively, (**B** → **C** or **D**). When the competition between the two routes leading to **F** and **G** is allowed (Table 2, entries 12, 15), the route leading to cyclobutarene **F** is preferred, perhaps because of steric factors or because in this case no β-elimination step is involved.

In conclusion, we have reported a novel palladium-catalyzed C–H activation of *gem*-dialkyl groups on bromo- and iodobenzenes to give olefins or benzocyclobutenes. This process is simple, efficient, and regioselective and utilizes common reagents. The reaction products are valuable molecules containing a quaternary stereocenter as well as a new chemical function (olefin, cyclobutene) potentially useful for further reactions. A full description of the synthesis and physical data of reaction substrates and products as well as further development of the methodology will be reported in due course.

Received: July 24, 2003 [Z52461]

**Keywords:** alkenes · C–H activation · catalysis · dehydrogenation · palladium

[1] For reviews, see: a) A. E. Shilov, G. B. Shul'pin, *Chem. Rev.* **1997**, *97*, 2879–2932; b) G. Dyker, *Angew. Chem.* **1999**, *111*, 1808–1822; *Angew. Chem. Int. Ed.* **1999**, *38*, 1698–1712; c) Y. Guari, S.

 © 2003 Wiley-VCH Verlag GmbH & Co. KGaA, Weinheim 

Sabo-Etienne, B. Chaudret, *Eur. J. Inorg. Chem.* **1999**, 1047 – 1055; d) J. A. Labinger, J. E. Bercaw, *Nature* **2002**, *417*, 507 – 514.
[2] a) J. Hassa, M. Sévignon, C. Gozzi, E. Schultz, M. Lemaire, *Chem. Rev.* **2002**, *102*, 1359 – 1470; b) A. M. Echavarren, B. Gómez-Lor, J. J. González, O. de Frutos, *Synlett* **2003**, 585 – 597.
[3] a) G. Dyker, *Angew. Chem.* **1992**, *104*, 1079 – 1081; *Angew. Chem. Int. Ed. Engl.* **1992**, *31*, 1023 – 1025; b) G. Dyker, *J. Org. Chem.* **1993**, *58*, 6426 – 6428; c) G. Dyker, *Chem. Ber.* **1994**, *127*, 739 – 742; d) G. Dyker, *Angew. Chem.* **1994**, *106*, 117 – 119; *Angew. Chem. Int. Ed. Engl.* **1994**, *33*, 103 – 105.
[4] M. Catellani, E. Motti, S. Ghelli, *Chem. Commun.* **2000**, 2003 – 2004.
[5] a) J. L. Portscheller, H. C. Malinakova, *Org. Lett.* **2002**, *4*, 3679 – 3681; b) J. L. Portscheller, S. E. Lilley, H. C. Malinakova, *Organometallics* **2003**, *22*, 2961 – 2971.
[6] a) B. D. Dangel, K. Godula, S. W. Youn, B. Sezen, D. Sames, *J. Am. Chem. Soc.* **2002**, *124*, 11 856 – 11 857; b) B. Sezen, R. Franz, D. Sames, *J. Am. Chem. Soc.* **2002**, *124*, 13 372 – 13 373.
[7] C. A. Tolman, *Chem. Rev.* **1977**, *77*, 313 – 348.
[8] Representative procedure: A dry resealable Schlenk tube containing a magnetic rod was charged with bromide **6a** (145 mg, 0.48 mmol), palladium acetate (11 mg, 0.048 mmol), tri-*o*-tolylphosphane (30 mg, 0.097 mmol), and potassium carbonate (134 mg, 0.97 mmol). The Schlenk tube was evacuated and backfilled with argon twice, then capped with a rubber septum. Dry *N,N*-dimethylformamide (3 mL) was injected under argon, then the septum was replaced by a screwcap and the mixture was stirred at 150 °C (preheated oil bath) for 30 min. After cooling, the mixture was diluted with diethyl ether and filtered through celite. The organic solution was washed with water, dried over magnesium sulfate, and concentrated to dryness. The residue was purified by flash chromatography (silica gel, heptanes) to afford olefin **4b** as an oil (88 mg, 83 %); $^1$H NMR ($CDCl_3$, 300 MHz): $\delta = 0.86$ (t, $J = 7.3$ Hz, 3H), 1.22 (t, $J = 7.2$ Hz, 3H), 2.18 (m, 2H), 4.18 (q, $J = 7.2$ Hz, 2H), 5.03 (d, $J = 17.7$ Hz, 1H), 5.31 (d, $J = 11.1$ Hz, 1H), 6.38 (dd, $J = 17.7$, 10.8 Hz, 1H), 7.27 ppm (m, 5H); $^{13}$C NMR ($CDCl_3$, 62.9 MHz): $\delta = 9.2$, 14.0, 29.3, 57.9, 60.8, 115.9, 126.6, 127.3, 128.1, 139.6, 142.0, 174.3 ppm; IR (film) $\tilde{\nu} = 2975$, 1729 cm$^{-1}$; HRMS (ESI) calcd for $C_{14}H_{18}NaO_2$ [$(M+Na)^+$]: 241.1204, found: 241.1212.
[9] a) C. Pascal, J. Dubois, D. Guénard, F. Guéritte, *J. Org. Chem.* **1998**, *63*, 6414 – 6420; b) C. Pascal, J. Dubois, D. Guénard, L. Tchertanov, S. Thoret, F. Guéritte, *Tetrahedron* **1998**, *54*, 14 737 – 14 756.
[10] a) G. Mehta, S. Kotha, *Tetrahedron* **2001**, *57*, 625 – 659; b) A. K. Sadana, R. K. Saini, W. E. Billups, *Chem. Rev.* **2003**, *103*, 1539 – 1602.
[11] In the case of propyl groups ($R^1 = Et$), it could be possible that the terminal methyl C–H bond is activated selectively to form a seven-membered palladacycle giving the terminal olefin, and that isomerization of the double bond occurs afterwards to give the mixture of olefins.
[12] Selected physical data: **17b**: $^1$H NMR (300 MHz, $CDCl_3$): $\delta =$ 0.78 (s, 3H), 0.99 (m, 21H), 3.86 (d, $J = 9.9$ Hz, 1H), 3.96 (d, $J =$ 9.3 Hz, 1H), 5.02 (m, 1H), 5.21 (m, 1H), 7.15–7.33 ppm (m, 4H); $^{13}$C NMR (62.9 MHz, $CDCl_3$): $\delta = 8.5$, 12.0, 18.0, 26.5, 50.1, 68.7, 113.8, 125.9 (*C*H-Ar), 127.3 (*C*D-Ar), 127.7 (*C*H-Ar), 127.8 (*C*H-Ar), 128.0 (*C*H-Ar), 143.3, 144.2 ppm (*C*q-Ar); HRMS (EI) calcd for $C_{18}H_{25}D_4OSi$ [$(M-i\mathrm{Pr})^+$]: 293.2239; found: 293.2242. **18b**: $^1$H NMR (250 MHz, $CDCl_3$): $\delta = 0.98$ (m, 21H), 1.91 (m, 2H), 3.86 (d, $J = 8.8$ Hz, 1H), 3.95 (d, $J = 9.2$ Hz, 1H), 6.01 (m, 1H), 7.14–7.35 ppm (m, 5H); $^{13}$C NMR (75.5 MHz, $CDCl_3$): $\delta = 8.5$, 11.9, 17.9, 26.8, 50.1, 68.6, 113.9, 125.8 (*C*H-Ar), 127.7 (*C*H-Ar), 127.9 (*C*H-Ar), 143.2, 144.1 ppm (*C*q-Ar); HRMS (EI) calcd for $C_{18}H_{24}D_5OSi$ [$(M-i\mathrm{Pr})^+$]: 294.2302; found: 294.2312.

 © 2003 Wiley-VCH Verlag GmbH & Co. KGaA, Weinheim 

Biometallic Materials

# A Nucleoside Conjugate Containing a Metallacarborane Group and Its Incorporation into a DNA Oligonucleotide**

*Agnieszka B. Olejniczak, Jaromir Plešek, Otomar Křiž, and Zbigniew J. Lesnikowski**

Nucleosides, nucleotides, and oligonucleotides site-specifically modified with metal complexes are of interest for analytical applications (hybridization probes, electrochemical sensors)[1,2] and therapeutic uses (anticancer agents and radiopharmaceuticals),[3,4] as novel materials for the assembly of nanostructures,[5,6] for structural and mechanistic studies (DNA-mediated electron and energy transfer),[7] and for the construction of artificial chemical nucleases.[8,9]

Metal-containing nucleosides, the precursors of the corresponding metal-derivatized nucleic acids, have been predominantly constructed by the synthesis of nucleoside–chelator conjugates followed by metal complexation (chelator-type metallanucleosides).[10] Another kind of metal-containing nucleoside is obtained by coupling the nucleoside moiety with a metallocene such as ferrocene (the $\pi$ complex type of metallanucleoside).[11,12] Herein we describe a new type of metal-bearing nucleoside obtained by conjugation of the nucleoside with a metallacarborane moiety.

Metallacarboranes are a vast family of metallocene-type complexes consisting of at least one carborane cage ligand and one or more metal atoms. Carborane (borane) clusters are versatile and efficient ligands for metals like Al, Au, Co, Cr, Cu, Fe, Ir, Mn, Ni, Pt, and many others,[13,14] and potentially allow incorporation of an array of metals with different properties into a nucleic acid or its components. For

[*] Prof. Z. J. Lesnikowski
Center for Microbiology and Virology
Laboratory of Molecular Virology and Biological Chemistry
Polish Academy of Sciences
106 Lodowa St., 93-232 Lodz (Poland)
Fax: (+48) 42-677-1249
E-mail: zlesnik@cmiwpan.lodz.pl

Dr. A. B. Olejniczak
Center for Microbiology and Virology
Polish Academy of Sciences
106 Lodowa St., Lodz 93-232 (Poland)

Prof. J. Plešek, Dr. O. Křiž
Institute of Inorganic Chemistry
Academy of Sciences of the Czech Republic
250-68 Rez (Czech Republic)

[**] This work was supported by the Polish Committee for Scientific Research (KBN; Grant no. PBZ-KBN 059/T09/08). The authors thank Dr. Clara Viñas for her assistance in the cyclic voltametry measurements, Dr. Edyta Paradowska and Mrs. Slawomira Studzinska for the cytotoxicity assay, and Mrs Marzena Przepiorkiewicz for the polymerase chain reaction experiments. A.B.O thanks the Polish Academy of Sciences and Spanish Academy of Sciences for the award of a travel grant.

Supporting information for this article is available on the WWW under http://www.angewandte.org or from the author.

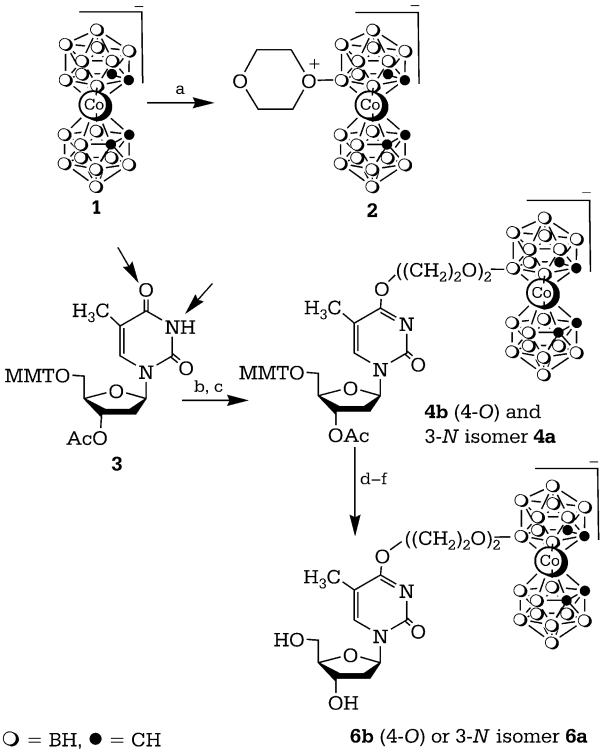
 © 2003 Wiley-VCH Verlag GmbH & Co. KGaA, Weinheim DOI: 10.1002/anie.200352505 

example, depending upon the radioisotope of the metal component of the metallacarborane cluster, the metal-containing nucleosides and oligonucleotides produced could potentially be used for different types of radiotherapy of tumors, such as alpha, beta, and Auger therapy.[4,15–17] In addition, the nucleoside–metallacarborane conjugates described herein contain twice as many boron atoms as nucleosides with a standard carborane modification, and up to twenty times more than nucleosides modified with boronic acid. Therefore, nucleoside–metallacarborane conjugates are potentially useful as boron carriers for boron neutron capture therapy (BNCT) of cancers.[18,19]

Conjugation of the metallacarborane complex with a nucleoside unit was achieved by application of the nucleophilic reaction of a base-activated nucleoside with the dioxane group of the 8-dioxane-[(1,2-dicarba-*closo*-undecaborane)-3,3′-cobalt(−1)(1′,2′-dicarba-*closo*-undecaborane)] zwitterion {**2**; [3,3′-Co(8-$C_4H_8O_2$-1,2-$C_2B_9H_{10}$)(1′,2′-$C_2B_9H_{11}$)]}. The ring-opening of a tetrahydropyran or dioxane group attached to a [bis(1,2-dicarbollido)-3-cobalt(−1)]ate ion through attack by simple nucleophiles such as fluoride, chloride, or hydroxide anions,[20] phenolates and phosphorus-containing nucleophiles,[21] potassium phtalimide, diethyl acetamidomalonate, and cyanide ions,[22] or potassium pyrrolyl, indolyl, and carbazolyl compounds[23] has been described before.

Herein, we describe for the first time dioxane ring-opening of a dioxane–metallacarborane zwitterion by a biomolecule. We propose a novel type of metal-containing nucleoside with a metallacarborane modification, describe the incorporation of such a nucleoside into a DNA oligonucleotide, and present the results of studies on some of the physicochemical and biological properties of the modified products.

Nucleosides containing a metallacarborane complex were obtained by the synthetic procedure shown in Scheme 1. First, the [3,3′-Co(8-$C_4H_8O_2$-1,2-$C_2B_9H_{10}$)(1′,2′-$C_2B_9H_{11}$)] zwitterion (**2**; 8-dioxane-COSAN) was obtained by treatment of [Cs{3-Co-(1,2-$C_2B_9H_{11}$)$_2$}] (see **1**) with dioxane in the presence of dimethyl sulfate and sulfuric acid.[24] Alkylation of the thymine base in 5′-*O*-monomethoxytrityl-3′-*O*-acetylthymidine (**3**)[25] with metallacarborane derivative **2** was performed by activation of the 4-*O* (and competitively, the 3-*N*) atom in protected nucleoside **3** by treatment with sodium hydride.[26] The fully protected products of 3-*N* and 4-*O* alkylation, **4a** and **4b**, respectively, were separated by chromatography on silica gel. The 3-*N* or 4-*O* location of the bisethyleneoxy-8-[(1,2-dicarba-*closo*-undecaborane)-3,3′-cobalt(−1)(1′,2′-dicarba-*closo*-undecaborane)] moiety (BEMC) was determined by comparison of the UV spectra recorded for compounds **4a** and **4b** with those of 4-*O*- and 3-*N*-methylthymidine. The assignment is based on the characteristic bathochromic shift of the maximum in the spectra of the 4-*O*-alkylated derivatives.[27,28] The deacetylation of the 3′-OH group in **4b** (4-*O*)[29] yielded 5′-*O*-monomethoxytrityl-4-*O*-bisethyleneoxy-8-{(1,2-dicarba-*closo*-undecaborane)-3,3′-cobalt(−1)(1′,2′-dicarba-*closo*-undecaborane)]}thymidine (**5**), which was used in the synthesis of a metallacarborane-containing phosphoramidite monomer **7** and oligonucleotide **8**. Detritylation of the 5′-OH functional group in **5** under acidic conditions[30] gave the fully



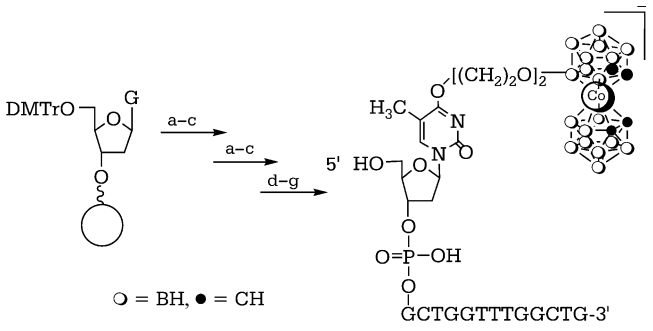

***Scheme 1.*** Synthesis of 5′-*O*-monomethoxytrityl-3′-*O*-acetyl-3-*N*-(bisethyleneoxy-8-COSAN)thymidine (**4a**), 5′-*O*-monomethoxytrityl-3′-*O*-acetyl-4-*O*-(bisethyleneoxy-8-COSAN)thymidine (**4b**), and 4-*O*-(bisethyleneoxy-8-COSAN)thymidine (**6b**). a) Dioxane/$Me_2SO_4$, $H_2SO_4$; b) NaH/toluene; c) **2**/toluene; d) separation of **3**-*N* and **4**-*O* isomers; e) 80% $CH_3COOH$; f) aq $NH_3$. MMT = monomethoxytrityl.

deprotected metallacarborane–nucleoside conjugate 4-*O*-bisethyleneoxy-8-{(1,2-dicarba-*closo*-undecaborane)-3,3′-cobalt(−1)(1′,2′-dicarba-*closo*-undecaborane)]}thymidine (**6b**). The isomer **6a**, which has BEMC attached to *N*-3, was prepared from **4a** in an analogous manner.

Phosphitylation of **5** was performed according to the standard procedure[31,32] and led to modified monomer 5′-*O*-monomethoxytrityl-4-*O*-diethyleneoxy-8-{(1,2-dicarba-*closo*-undecaborane)-3,3′-cobalt(−1)(1′,2′-dicarba-*closo*-undecaborane)]}-3′-*O*-(*N,N*-diisopropyl-β-cyanoethyl)phosphoramidite (**7**). Synthesis of metallacarborane-modified oligonucleotide **8** [5′-d($^{BEMC}$TGCTGGTTTGGCTG)-3′] was performed by using a β-cyanoethyl cycle on an automated DNA synthesizer[33] (Scheme 2). After completion of the synthesis of the unmodified part of the oligonucleotide, the metallacarborane-modified nucleoside was attached to the 5′-end of the oligomer chain manually by using monomer **7**.[34] In the oxidation step, *t*BuOOH was applied instead of $J_2$, which is routinely used as the oxidizing agent.[35,36] The capping step was omitted in the manual cycle. Complete deprotection of the nucleic acid bases was achieved by treatment with concentrated ammonia solution for 2 h at 50 °C.

The products were characterized by TLC, reverse-phase (RP) HPLC, UV and $^1$H NMR spectroscopies, MS, and $^{11}$B- and $^{31}$P NMR spectroscopy where applicable. The purity of oligonucleotide **8** was checked by polyacrylamide gel electrophoresis and RP-HPLC; the molecular weight was confirmed

 © 2003 Wiley-VCH Verlag GmbH & Co. KGaA, Weinheim 




**8**

***Scheme 2.*** Synthesis of a tetradecanucleotide [5′-d($^{BEMC}$TGCTGGTTTGGCTG)-3′] (**8**) containing the modified base 4-*O*-(bisethyleneoxy-8-COSAN)thymidine ($^{BEMC}$T). a) Detritilation: 3% dichloroacetic acid in $CH_2Cl_2$; b) coupling: unmodified monomers; c) oxidation: 0.1 M $I_2$ in THF/pyridine/$H_2O$ (13:6:1); capping: 1 M $(CH_3CO)_2O$ in THF/pyridine (1:8) and 0.5 M 4-dimethylaminopyridine in THF; d) coupling: modified monomer **7**; e) oxidation: 0.5 M *t*BuOOH in dodecane; d) cleavage from the support: 30% aq $NH_3$, 1 h, RT; f) base deprotection: 30% aq $NH_3$, 2 h, 50 °C. THF, tetrahydrofuran; DMTr, dimethoxytrityl.

by mass spectrometry. Experimental procedures and analytical data for compounds **5**–**8** are available in the Supporting Information.

Selected physicochemical and biochemical properties of conjugates **6a** and **6b** and metallacarborane-containing oligonucleotide **8** were studied. To check the applicability of the metallacarborane group as a redox label for nucleosides, the electrochemical properties of conjugate **6b** and its counterpart with the metallacarborane complex attached to *N*-3, **6a**, were studied by cyclic voltammetry. A three-electrode cell with acetonitrile as the solvent, 0.1 M $[NBu_4]ClO_4$ as the supporting electrolyte, and platinum as the working electrode was used.[37–39] The *E* values representing the average of the forward and return peak potentials were: **6b** (4-*O*): $E° = -964$ mV; 3-*N* isomer **6a**: $E° = -1007$ mV. Under the same conditions, 3,3′-Co(8-[bis-$(C_2H_4O)$]OH]-1,2-$C_2B_9H_{10}$)(1′,2′-$C_2B_9H_{11}$) and thymidine (taken as standards), had E° values of −964 and 0 mV, respectively (cyclic voltammetry plots are available in the Supporting Information). These observations illustrate the potential usefulness of metallacarborane complexes as redox labels for nucleosides.

To test the susceptibility of the oligonucleotide labeled with the metallacarborane cage to elongation by the polymerase chain reaction (PCR), the oligonucleotide 5′-d($^{BEMC}$TGCTGGTTTGGCTG)-3′ (**8**) was used as one of two primers in PCR amplification of a fragment of human cytomegalovirus (HCMV) DNA, strain AD 169. The other primer was unmodified nucleotide P12 (5′-AAACGGCG-CAGCCACATAAGG-3′). Part of gene US14 and gene US13 were amplified to yield a 812-bp product, as expected. This result proves the susceptibility of the oligonucleotide with the metallacarborane modification at its 5′ end to amplification by Taq DNA polymerase.

In addition, studies were carried out on the cytotoxicity of compound **6a** and its 4-*O* isomer **6b** in two cell lines, Vero and A549, by using the 3-(4,5-dimethylthiazol-2-yl)-2,5-diphenyltetrazolium bromide (MTT) method.[40] The toxicity of nucleoside **6a**, measured as the 50% inhibitory concentration ($IC_{50}$) value, was found to be 94 μM and 82 μM in the Vero and A549 cell lines, respectively; for the 4-*O* isomer **6b**, toxicity was detected at concentrations higher than 100 μM for both cell lines. The toxicities of nucleoside conjugates **6a** and **6b** to Vero cells are lower than that of 5-carboranyl-2′-deoxyuridine, whose $IC_{50}$ value is 17 μM,[41,42] but more than an order of magnitude higher than the toxicity of L-4-(dihydroxyboryl)phenylalanine in the TIG-1–20 cell line ($IC_{50} = 2.2 \times 10^3$ μM).[43] These findings show that both nucleoside–metallacarborane conjugates **6a** and **6b** are low enough in toxicity to be considered as a potential new type of boron carrier for BNCT.

In summary, we have described a new class of metal-containing nucleosides and shown their application in the synthesis of oligonucleotide–metal conjugates, as well as the ability of a metallacarborane-modified oligonucleotide to serve as a primer for Taq DNA polymerase in PCR amplification of HCMV DNA. The applicability of metallacarboranes as redox labels for nucleosides was also demonstrated. In addition, the nucleoside–metallacarborane conjugates were found to have low toxicity, which could lead to their application as a new type of boron-rich carrier for BNCT of tumors.

## Experimental Section

Synthesis of key intermediates 5′-*O*-monomethoxytrityl-3′-*O*-acetyl-3-*N*-{bisethyleneoxy-8-[(1,2-dicarba-closo-undecaborane)-3,3′-cobalt-(−1)(1′,2′-dicarba-closo-undecaborane)]}thymidine (**4a**) and 5′-*O*-monomethoxytrityl-3′-*O*-acetyl-4-*O*-{bisethyleneoxy-8-[(1,2-dicarba-closo-undecaborane)-3,3′-cobalt(−1)(1′,2′-dicarba-closo-undecaborane)]}thymidine (**4b**): The procedure was performed under a positive pressure of argon. 5′-*O*-Monomethoxytrityl-3′-*O*-acetylthymidyne (**3**; 0.9 g, 1.6 mmol) and 8-dioxane-COSAN (**2**; 1.4 g, 3.3 mmol) were mixed together then dried over $P_2O_5$ under high vacuum for 24 h. NaH (60% suspension in mineral oil, 80 mg, 3.3 mmol) was added, followed by anhydrous toluene (18 mL). The reaction mixture was stirred at 70 °C in an oil bath. After 8 h, excess NaH was removed by centrifugation and the supernatant added dropwise to hexane (135 mL). The resultant precipitate was separated by centrifugation and the sediment was dried under vacuum to yield crude **4** (2.4 g) as a mixture of 3-*N* and 4-*O* isomers (**4a** and **4b**, respectively). Crude **4** was purified by silica gel column chromatography (70 g silica gel, 230–400 mesh) with 12% $CH_3OH$ in $CHCl_3$ containing 1% $Et_3N$ as the eluting solvent system. Yield: **4a**, 221 mg; **4b**, 450 mg. **4a**: TLC ($CH_3CN/CHCl_3$, 1:2): $R_f = 0.14$; UV/Vis ($CH_3CN$): $\lambda_{min} = 227.46$, 249.18, 287.30 nm, $\lambda_{max} = 234.43$, 261.89, 313.93 nm; $^1$H NMR (500 MHz, $[D_3]CHCl_3$, 25 °C, tetramethylsilane (TMS)): $\delta = 1.8$–3.5 (br m, 21 H; BH-COSAN), 1.58 (s, 3 H; $CH_3CO$), 1.71 (s, 3 H; $CH_3$–5), 2.54 (m, 2 H; H-2′), 2.95–3.08 (m, 4 H; 4 × CH-COSAN), 3.28–3.41 (br s, 4 H; 2 × $OCH_2$), 3.43 (s, 3 H; $CH_3O$), 3.46–3.52 (q, 2 H; H-5′,5″), 3.92 (br s, 2 H; $OCH_2$), 3,96 (s, 1 H; H-4′), 4.48–4.59 (m, 2 H; $OCH_2$), 5.36 (s, 1 H; H-3′), 6.31 (s, 1 H; H-1′), 6.87 (d, 2 H; α-arom. in $CH_3OPh$), 7.28–7.60 (m, 12 H; H arom. in MMTr), 8.11 (s, 1 H; H-6) ppm; $^{13}$C NMR (125 MHz, $[D_3]CHCl_3$, 25 °C, TMS): $\delta = 13.62$ ($CH_3$-5), 20.99 ($CH_3$ in $CH_3CO$), 39.76 (C-2′), 48.10, 51.94 (C-COSAN), 55.72 ($CH_3O$), 64.61 (C-5′), 68.73, 73.48 ($OCH_2$), 75.67 (C-3′), 86.41 (C-4′), 87.46 (C-1′), 88.74 (C-methylidene in MMTr), 114.65,

 © 2003 Wiley-VCH Verlag GmbH & Co. KGaA, Weinheim 

129.23, 131.40, 144.85, 145.06 (MMTr), 135.92 (C-6), 156.91 (C-2), 160.24 ($\delta$-C in $CH_3OPh$), 170.30 (CO in $CH_3CO$), 176.38 (C-4) ppm; $^{11}$B NMR (160 MHz, $[D_3]CHCl_3$, 25 °C, $BF_3/(C_2H_5)_2O$): $\delta = 25.4$ (s, 1B), 20.0 to −35.0 ppm (br s, max. at 8.0, −5.3 and −16.7, 17B) ppm; FAB-MS (negative, nitrobenzylalcohol): $m/z$: 966.9 [$M-1$]. **4b**: TLC ($CH_3CN/CHCl_3$, 1:2): $R_f = 0.41$; UV/Vis ($CH_3CN$): $\lambda_{min} = 252.87$ nm, $\lambda_{max} = 283.91$, 311.84 nm; $^1$H NMR (500 MHz, $[D_3]CHCl_3$, 25 °C, TMS): $\delta = 1.50$–4.00 (br m, 21H; BH-COSAN), 1.48 (s, 3H; $CH_3$–5), 1.62 (s, 3H; $CH_3CO$), 2.55 (m, 2H; H-2′), 2.77–3.07 (m, 4H; 4 × CH-COSAN), 3.21 (br s, 4H; 2 × $OCH_2$), 3.37 (s, 3H; $CH_3O$), 3.45–3.51 (q, $J(5', 5'') = 9.04$ Hz, 2H; H-5′,5″), 3.88 (br s, 2H; $OCH_2$), 4.08 (s, 1H; H-4′), 4.37–4.43 (m, 2H; $OCH_2$), 5.43 (s, 1H; H-3′), 6.64 (s, 1H; H-1′), 6.82 (d, 2H; α-H arom. in $CH_3OPh$), 7.06–7.52 (m, 12H; H arom. in MMTr), 8.20 ppm (s, 1H; H-6) ppm; $^{13}$C NMR (125 MHz, $[D_3]CHCl_3$, 25 °C, TMS): $\delta = 12.33$ ($CH_3$-5), 21.09 ($CH_3$-acetyl), 40.22 (C-2′), 48.12, 51.85, 51.95 (C-COSAN), 55.60 ($CH_3O$), 64.43 (C-5′), 68.27, 71.68, 73.26 ($OCH_2$), 75.53 (C-3′), 85.97 (C-4′), 87.75 (C-1′), 88.56 (C-methylidene in MMTr), 114.55, 129.14, 129.23, 129.55, 131.41, 142.33, 144.94, 145.09 (MMTr), 135.95 (C-6), 158.93 (C-2), 160.21 (C-4 in 4-$CH_3OPh$), 170.58 (C-4), 172.52 ($CH_3$-acetyl) ppm; $^{11}$B NMR (160 MHz, $[D_3]CHCl_3$, 25 °C, $BF_3/(C_2H_5)_2O$): 25.6 (s, 1B), 20.0 to −30.0 (br s, max at 9.0, −5.1 and −15.8, 17B) ppm; FAB-MS (negative, nitrobenzylalcohol): $m/z$: 966,7 [$M-1$].

Received: July 29, 2003 [Z52505]

**Keywords:** DNA · metallacarboranes · molecular probes · nucleosides · redox chemistry

[1] T. Ihara, M. Nakayama, M. Murata, K. Nakano, M. Maeda, *Chem. Commun.* **1997**, 1609 – 1610.
[2] *Probing of Nucleic Acids by Metal Ion Complexes of Small Molecules, Vol. 33* (Eds.: A. Siegel, H. Siegel), Marcel Dekker, New York, **1996**, pp. 1 – 678.
[3] C. K. Younes, R. Boisgard, B. Tavitian, *Curr. Pharm. Des.* **2002**, *8*, 1451 – 1466.
[4] A. I. Kassis, S. J. Adelstein, G. Mariani, *Q. J. Nucl. Med.* **1996**, *40*, 301 – 319.
[5] J. J. Storhoff, C. A. Mirkin, *Chem. Rev.* **1999**, *99*, 1849 – 1862.
[6] N. C. Seeman, *Synlett* **2000**, 1536 – 1548.
[7] B. Giese, *Curr. Opin. Chem. Biol.* **2002**, *6*, 612 – 618.
[8] D. M. Perrin, A. Mazumder, D. S. Sigman, *Progr. Nucl. Acid Res. Mol. Biol.* **1996**, *52*, 123 – 151.
[9] J. A. Cowan, *Curr. Opin. Chem. Biol.* **2001**, *5*, 634 – 642.
[10] R. Haner, J. Hall, *Antisense Nucleic Acid Drug Dev.* **1997**, *7*, 423 – 430.
[11] C. J. Yu, H. Yowanto, Y. Wan, T. J. Meade, Y. Chong, M. Strong, L. H. Donilon, J. F. Kayyem, M. Gozim, G. F. Blackburn, *J. Am. Chem. Soc.* **2000**, *122*, 6767 – 6768.
[12] M. Nakayama, T. Ihara, K. Nakano, M. Maeda, *Talanta* **2002**, *56*, 857 – 866.
[13] A. K. Saxena, N. S. Hosmane, *Chem. Rev.* **1993**, *93*, 1081 – 1124.
[14] R. N. Grimes, *Coord. Chem. Rev.* **2000**, *200*, 773 – 811.
[15] R. N. Hanson, *Curr. Pharm. Des.* **2000**, *6*, 1457 – 1468.
[16] M. T. Ercan, M. Caglar, *Curr. Pharm. Des.* **2000**, *6*, 1085 – 1121.
[17] R. Schibili, P. A. Schubiger, *Eur. J. Nucl. Med. Mol. Imaging* **2002**, *29*, 1529 – 1542.
[18] Z. J. Lesnikowski, J. Shi, R. F. Schinazi, *J. Organomet. Chem.* **1999**, *581*, 156 – 169, and references cited therein.
[19] J. F. Valliant, K. J. Guenther, A. S. King, P. Morel, P. Schaffer, O. O. Sogbein, K. A. Stephenson, *Coord. Chem. Rev.* **2002**, *232*, 173 – 230.
[20] T. Peymann, K. Kück, D. Gabel, *Inorg. Chem.* **1997**, *36*, 5138 – 5139.
[21] J. Plesek, B. Grüner, J. Baca, P. Selucky, J. Rais, N. V. Šistkova, B. Casensky, *Proc. 6th Int. Inform. Exch. Meet. (Madrid, 2000)*, NEA OECD Publications, Paris Cedex 16, France, **2001**, paper N43, p. 659.
[22] I. B. Sivaev, Z. A. Starikova, S. Sjöberg, V. I. Bregadze, *J. Organomet. Chem.* **2002**, *649*, 1 – 8.
[23] J. Llop, C. Masalles, C. Viñas, F. Teixidor, R. Sillanpää, R. Kivekäs, *J. Chem. Soc. Dalton Trans.* **2003**, 556 – 561.
[24] J. Plesek, S. Hermanek, A. Franken, I. Cisarova, C. Nachtigal, *Collect. Czech. Chem. Commun.* **1997**, *62*, 47 – 56.
[25] H. Schaller, G. Weiman, B. Lerch, H. G. Khorana, *J. Am. Chem. Soc.* **1963**, *85*, 3821 – 3827.
[26] A. Shabarova, A. Bogdanov, *Advanced Organic Chemistry of Nucleic Acids*, Wiley-VCH, Weinheim, **1994**, pp. 413 – 414.
[27] P. D. Lawley, D. J. Orr, S. A. Shah, P. B. Farmer, M. Jarman, *J. Biochem.* **1973**, *135*, 193 – 201.
[28] K. Takenuki, H. Itoh, A. Matsuda, T. Ueda, *Chem. Pharm. Bull.* **1990**, *38*, 2947 – 2952.
[29] J. P. H. Verheyden, J. G. Moffat in *Synthetic Procedure in Nucleic Acid Chemistry* (Eds.: W. W. Zorbach, R. S. Tipson), Wiley-Interscience, New York, **1968**, pp. 383 – 387.
[30] H. Weber, H. G. Khorana, *J. Mol. Biol.* **1972**, *72*, 219.
[31] T. Atkinson, M. Smith in *Oligonucleotide Synthesis: A Practical Approach* (Ed.: M. Gait), **1984**, IRL, Oxford, pp. 35 – 81.
[32] S. L. Beaucage in *Methods in Molecular Biology, Vol. 20, Protocols for Oligonucleotides and Analogs. Synthesis and Properties* (Ed.: S. Agrawal), Humana, Totowa, **1993**, pp. 33 – 61.
[33] *Oligo 1000 DNA Synthesizer Operating Instructions*, Beckman Instruments Inc., Fullerton, CA, **1992**.
[34] A. B. Olejniczak, M. Koziołkiewicz, Z. J. Leśnikowski, *Antisense Nucleic Acid Drug Dev.* **2002**, *12*, 79 – 94.
[35] Y. Hayakawa, M. Uchiyama, R. Noyori, *Tetrahedron Lett.* **1986**, *27*, 4191 – 4194.
[36] Y. Hayakawa, S. Wakabayashi, H. Kato, R. Noyori, *J. Am. Chem. Soc.* **1990**, *112*, 1691 – 1696.
[37] M. F. Hawthorne, D. C. Young, T. D. Andrews, D. V. Howe, R. L. Pilling, A. D. Pitts, M. Reintjes, L. F. Warren, P. A. Wegner, *J. Am. Chem. Soc.* **1968**, *90*, 879 – 895.
[38] C. Viñas, J. Pedrajas, J. Bertran, F. Teixidor, R. Kivekäs, R. Sillanapää, *Inorg. Chem.* **1997**, *36*, 2482 – 2486.
[39] W. G. Geiger Jr. , *Metal Interactions with Boron Clusters* (Ed.: R. N. Grimes), **1982**, Plenum, New York, pp. 239 – 267.
[40] T. Mosmann, *J. Immunol. Methods* **1983**, *65*, 55 – 63.
[41] Y. Yamamoto, T. Seko, H. Nakamura, H. Niemoto, H. Hojo, N. Mukai, Y. Hashimoto, *J. Chem. Soc. Chem. Commun.* **1992**, 157 – 158.
[42] R. F. Schinazi, N. M. Goudgaon, G. Fulcrand, Y. El Kattan, Z. J. Lesnikowski, J. Moravek, D. C. Liotta, *Intl. J. Radiat. Oncol. Biol. Phys.* **1994**, 28, 1113 – 1120.
[43] H. Nemoto, J. Cai, N. Asao, S. Iwamoto, Y. Yamamoto, *J. Med. Chem.* **1995**, *38*, 1673 – 1678.

 © 2003 Wiley-VCH Verlag GmbH & Co. KGaA, Weinheim 

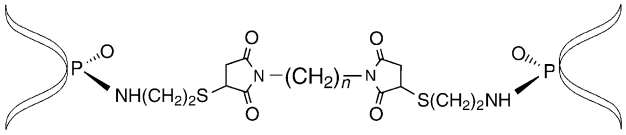
DNA Structures

# Parallel, Double-Helix DNA Nanostructures Using Interstrand Cross-Linked Oligonucleotides with Bismaleimide Linkers**

*Masayuki Endo and Tetsuro Majima**

The creation of functional nanometer-scale wires and arrays has attracted increasing interest in the field of material sciences and molecular electronics.[1] For this purpose, molecular scaffolds, including polymers and supramolecules, with well-defined architectures are required for placing and arranging the desired functional molecules.[1] Nucleic acids provide a good scaffold for the following reasons: 1) The structure of DNA is well-defined and considered to be a periodic double-helical polymer; 2) association of DNA strands can be controlled by programming the sequence of DNA; 3) DNA molecules are easily modified chemically and biochemically for introduction of various functional molecules and nanoparticles;[2] and 4) DNA can be manipulated with modifying enzymes such as DNA ligase, kinase, polymerase, and restriction enzymes. Although DNA is an ideal scaffold, the flexibility of a long DNA chain makes the construction of desirable rigid structures difficult. Seeman and co-workers have built micrometer-scale DNA architectures by arranging previously prepared rigid DNA components.[3] The preparation and creation of wires and arrays would be much easier if such rigid DNA structures could be prepared simply by the addition of a chemical connector to the DNA strands.

Here we describe the design, synthesis, and properties of novel cross-linked oligonucleotides (XL-DNA) for the construction of a micrometer-scale rodlike DNA structure. Cross-linked oligonucleotides were designed to connect two double-helix DNA strands using a tether from a diastereochemically pure phosphoramidate (Scheme 1). Interstrand DNA cross-linking has been investigated in previous studies in which modification of a specific nucleic acid base was employed.[4] Our design is advantageous for connecting two duplex strands with less structural stress because the phosphate groups are located in the outer positions of the double-helical DNA. We employed a bifunctional cross-linker, alkyl bismaleimide, which can form a covalent bond with a thiol residue of a DNA strand under mild conditions. In addition, the distance between two DNA strands can be controlled using two different lengths of bismaleimide linkers.




$C_2$-bismaleimide linker: $n = 2$
$C_6$-bismaleimide linker: $n = 6$

***Scheme 1.*** Interstrand cross-linked DNA having bismaleimidoethane ($C_2$) and bismaleimidohexane ($C_6$) linkers.

The diastereochemically pure oligonucleotides were prepared according to a literature method.[5] We used two DNA sequences, 5′-CGGCTpACTCC-3′ (**1XL**) and 5′-GTGCTpAGCGG-3′ (**2XL**; p denotes a phosphoramidate linkage where a cross-linker is introduced). Analysis by reversed-phase HPLC revealed two diastereomers, **A** (faster eluting) and **B** (slower eluting; see Supporting Information). The DNA was cross-linked according to Scheme 2. Oligonucleotides having a cystamine linker were treated with dithiothreitol (DTT) to reduce the disulfide linker. Thiol-tethered DNA (SH-DNA) was treated with excess 1,2-bismaleimidoethane ($C_2$) or 1,6-bismaleimidohexane ($C_6$) to produce a monocapped bismaleimide–DNA conjugate. This DNA conjugate and the SH-DNA were incubated in a 1:1 mol ratio, and the resulting XL-DNA was purified by HPLC. The extent of cross-linking was examined by 20% denaturing polyacrylamide gel electrophoresis (PAGE, Figure 1). All the cross-linked oligonucleotides migrated to a similar degree as a 20 mer single strand; no original 10 mer strand was observed, thus indicating that these oligonucleotides were cross-linked. The cross-linked oligonucleotides having a $C_6$ linker migrated slower than those with a $C_2$ linker.

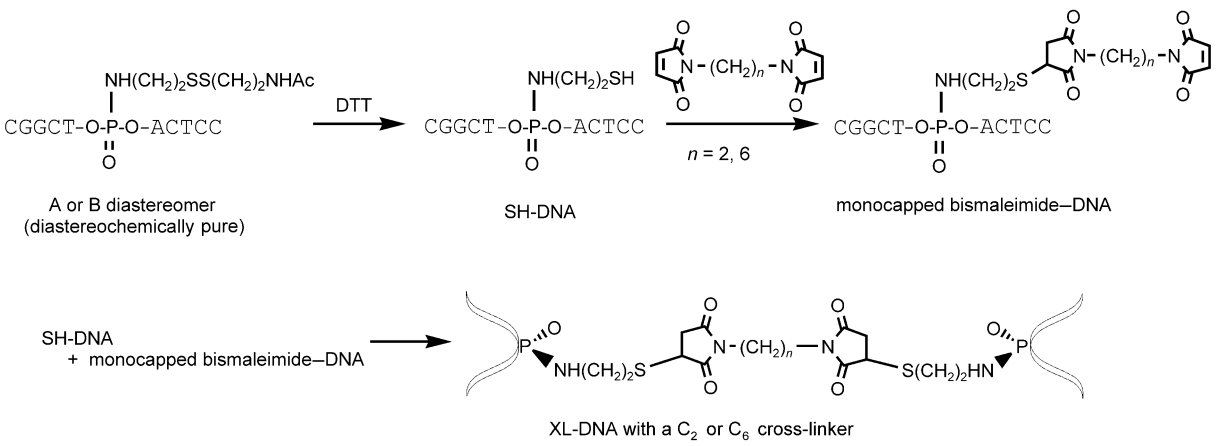
The stabilities of the DNA assemblies with one cross-linked oligonucleotide (Scheme 3a) were examined by measurement of the melting temperature ($T_m$) (Table 1). All the DNA assemblies containing one XL-DNA helix were destabilized relative to that of unmodified DNA, which indicates that the stabilities of the DNA assemblies are reduced by electrostatic repulsion of the two proximal double helixes connected by a cross-linker. However, the assemblies with one XL-DNA helix still form thermally stable complexes. We employed two different cross-linked oligonucleotides (**1XL, 2XL**) and one complementary strand (**1c, 2c**) for assembling two double-helix strands in a parallel orientation (Scheme 3b). The $T_m$ values show that these parallel DNA assemblies are largely stabilized relative to those with a single XL-DNA helix, which indicates that the two cross-linked oligonucleotides cooperatively function to stabilize the DNA assemblies. The length of the bismaleimide linkers affected the stabilities of the DNA assemblies, and the cross-linked oligonucleotides with a $C_2$ linker formed more-stable assemblies than those with a $C_6$ linker. The stereochemical effects of the phosphoramidates were also observed,[5] and the assemblies containing the **B** diastereomers were thermally more stable than those with the **A** diastereomers.

[*] Dr. T. Majima, Dr. M. Endo
Institute of Scientific and Industrial Research
Osaka University
8–1 Mihogaoka, Ibaraki, Osaka 567-0047 (Japan)
Fax: (+81) 6-6879-8499
E-mail: majima@sanken.osaka-u.ac.jp

[**] This work has been partly supported by a Grant-in-Aid for Scientific Research on Priority Area (417), 21st Century COE Research, and others from the Ministry of Education, Culture, Sports, Science, and Technology (MEXT) of the Japanese Government.

Supporting information for this article is available on the WWW under http://www.angewandte.org or from the author.

 © 2003 Wiley-VCH Verlag GmbH & Co. KGaA, Weinheim DOI: 10.1002/anie.200352546 




***Scheme 2.*** Synthetic scheme for a diastereochemically pure cross-linked oligonucleotide having a $C_2$ and $C_6$ bismaleimide cross-linker.

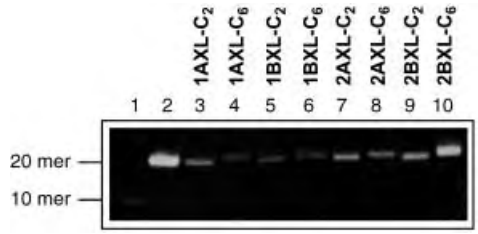
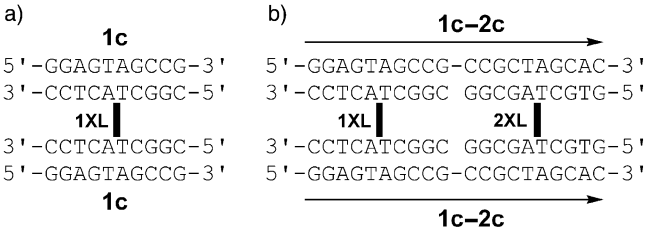



***Figure 1.*** Polyacrylamide gel electrophoresis (PAGE) of cross-linked oligonucleotides having a $C_2$- and $C_6$-bismaleimide linker. **A** and **B** denote the diastereomers. **XL** represents XL-DNA.



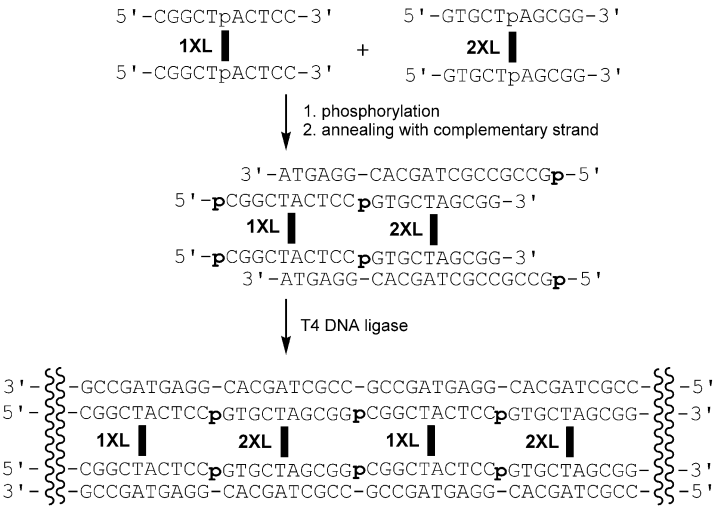

***Scheme 3.*** DNA assemblies with cross-linked oligonucleotides and complementary strands for the $T_m$ measurements. The bold bars represent cross-linkers. The arrows indicate the orientations of the double helixes.

***Table 1:*** Melting temperatures ($T_m$) of the DNA assemblies with **1XL** and 10 mer complementary strand **1c**, and those with two cross-linked oligonucleotides **1XL, 2XL**, and 20 mer complementary strand **1c-2c**.[a]

| XL-DNA | $T_m$ [°C] | $\Delta T_m$ [°C] |
|---|---|---|
| **1AXL-$C_2$** | 44.1 | −6.2 |
| **1AXL-$C_6$** | 42.0 | −8.3 |
| **1BXL-$C_2$** | 44.7 | −5.6 |
| **1BXL-$C_6$** | 42.6 | −7.7 |
| **1** (native) | 50.3 | – |
| **1AXL-$C_2$ + 2AXL-$C_2$** | 55.2 | +2.2 |
| **1AXL-$C_6$ + 2AXL-$C_6$** | 53.6 | +0.6 |
| **1BXL-$C_2$ + 2BXL-$C_2$** | 58.3 | +5.3 |
| **1BXL-$C_6$ + 2BXL-$C_6$** | 56.5 | +3.5 |
| **1 + 2** (native) | 53.0 | – |

[a] The measurement conditions are described in the Experimental Section.

Micrometer-scale parallel duplex DNA constructs (300 base pairs, 0.1 μm) were prepared by molecular assembly (first step) and DNA ligation (second step) from these cross-linked oligonucleotides. The two phosphorylated cross-linked oligonucleotides **1XL** and **2XL** were annealed with a phosphorylated complementary strand to form a DNA assembly (Scheme 4). The assembly was then treated with




***Scheme 4.*** Schematic representation of the procedure for the construction of the DNA nanostructures with cross-linked oligonucleotides by self-assembly of the DNA and subsequent DNA ligation. The bold bars represent cross-linkers.

T4 DNA ligase to enable extension and formation of the tandem double-helix constructs. The DNA assemblies containing cross-linked oligonucleotides were extended in the presence of T4 DNA ligase, as shown by agarose gel electrophoresis (Figure 2). Interestingly, differences in the distribution of the ligated products were observed. The products with the cross-linked oligonucleotides having a $C_2$ linker contained 200–400 base pairs (lanes 4 and 8) and those with **1BXL-$C_6$** and **2BXL-$C_6$** contained 200–800 base pairs (lane 10). On the other hand, the reactions with **1AXL-$C_6$** and **2AXL-$C_6$** showed broad distributions of products with

 © 2003 Wiley-VCH Verlag GmbH & Co. KGaA, Weinheim 

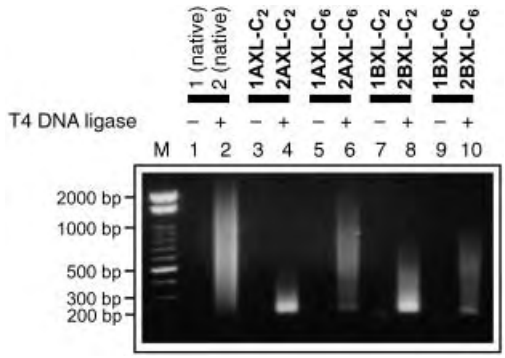



***Figure 2.*** Agarose gel electrophoresis of DNA ligation products containing cross-linked oligonucleotides having a $C_2$-and $C_6$-bismaleimide linker. The cross-linked oligonucleotides used for the ligation reaction, with (+) and without (−) addition of T4 DNA ligase, are indicated above the lane number.

200 to over 2000 base pairs after ligation, a result similar to that found with the unmodified DNA (lanes 2 and 6). These results indicate that the $C_2$ linker is not long enough for efficient ligation because of some steric hindrance between the XL-DNA and T4 DNA ligase.[6] Clearly, the length of the cross-linker is the determinant for the ligation efficiency. In the cases of the $C_6$ linker, the cross-linked oligonucleotides of the **A** diastereomers do not seem to inhibit the ligation reaction relative to those of the **B** diastereomers.

The structures of the ligated products containing **1AXL-$C_6$** and **2AXL-$C_6$** were analyzed by atomic force microscopy (AFM; Figure 3).[7] The products can be observed at low concentrations as straight structures up to 0.6 μm in length (Figure 3a). This observation is consistent with the results obtained by gel electrophoresis. On the other hand, the ligated products seem rather flexible at a high concentration, but they are not aggregated (Figure 3b). Only aggregated products were detected by AFM analysis in the case of the ligated products generated from the other cross-linked oligonucleotides. The long DNA double strand can usually be observed as a flexible chain by AFM,[7] but the parallel double helixes in these cross-linked oligonucleotides suppress the mobility of the flexible DNA structures and form rigid structures.

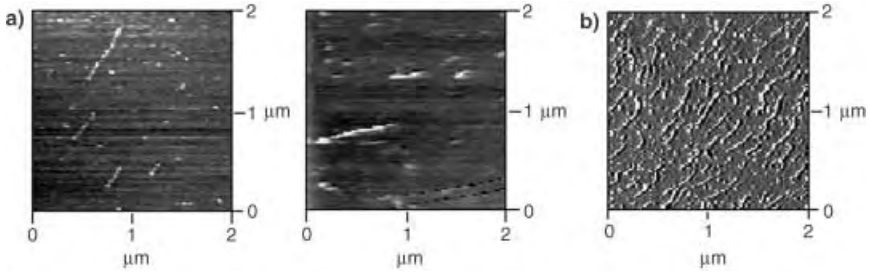



***Figure 3.*** AFM images of the ligated products containing **1AXL-$C_6$** and **2AXL-$C_6$**. The samples containing low (a) and high (b) concentrations of DNA were adsorbed onto a mica plate.

In conclusion, we have designed and synthesized cross-linked oligonucleotides to form potentially rigid DNA assemblies. We have demonstrated the construction of a micrometer-scale rodlike DNA architecture, which can be achieved by a one-step molecular assembly using these cross-linked oligonucleotides and subsequent DNA ligation. The DNA assemblies can be extended into two-dimensional structures simply by changing the direction of the connection. These DNA structures can act as a scaffold for functionalized wires and arrays through modification of the DNA strands with reactive and small molecules followed by introduction of nanoparticles and biomolecules such as proteins and enzymes.[2b,c]

## *Experimental Section*

Preparation of cross-linked oligonucleotides: A disulfide tether was introduced through a phosphoramidate linkage in the center of a 10 mer single-strand DNA according to a previously reported method.[5] Two diastereomers were separated by reversed-phase HPLC (see Supporting Information).

The purified diastereochemically pure oligonucleotides (10 nmol) were treated with DTT (10 mM) in tris(hydroxymethyl)aminomethane hydrochloride (Tris-HCl; pH 8.0, 50 mM) at 50 °C for 30 min, and thiol-tethered DNA (SH-DNA) was purified by reversed-phase HPLC (HPLC conditions are described in the Supporting Information). SH-DNA (5 nmol) was treated with 1,2-bismaleimidoethane ($C_2$, 1 μmol) or 1,6-bismaleimidohexane ($C_6$) in a 10% DMF/water solution at 50 °C for 2 h, and the monocapped bismaleimide–DNA conjugate was purified by HPLC. This DNA conjugate and the SH-DNA were then reacted in a 1:1 mol ratio at 37 °C overnight. After treatment with DTT (10 mM) at 37 °C for 2 h to remove any trace of an unwanted disulfide XL-DNA,[8] the bismaleimide XL-DNA was purified by HPLC. All the reaction steps were quantitative. The cross-linking was confirmed by 20% denatured PAGE analysis and the gel was visualized by staining with ethidium bromide.

Melting temperature measurements: Thermal denaturation profiles were obtained on a JASCO V-530 UV/VIS spectrophotometer equipped with a JASCO ETC-505T temperature controller. A solution containing XL-DNA (0.5 μM), complementary DNA (1.0 μM), Tris-HCl (pH 7.6; 10 mM), and 1.0 M NaCl was heated at 80 °C, then gradually cooled down to 10 °C. Measurements were carried out by heating from 10 to 80 °C at a rate of 1.0 °C $min^{-1}$, and monitored at 260 nm. The first derivative calculated from a melting profile was used to determine the $T_m$ value. Complementary strands used here are **1c**: 5′-GGAG-TAGCCG-3′ (10 mer) and **1c**–**2c**: 5′-GGAG-TAGCCGCCGCTAGCAC-3′ (20 mer).

Enzymatic reactions: Phosphorylation of XL-DNA was carried out at 37 °C for 2 h in a solution (30 μL) containing XL-DNA (0.5 nmol), Tris-HCl (pH 7.5, 50 mM), $MgCl_2$ (5 mM), DTT (1 mM), ATP (1 mM), and T4 polynucleotide kinase (10 units). After the reaction, the solutions were heated at 65 °C for 20 min to inactivate the kinase. The ligation of a DNA assembly was carried out in a solution (20 μL) containing phosphorylated cross-linked oligonucleotides (0.2 nmol each), phosphorylated complementary DNA (0.4 nmol), Tris-HCl (pH 7.5; 50 mM), 0.1 M NaCl, $MgCl_2$ (10 mM), DTT (10 mM), ATP (1 mM), bovine serum albumin (BSA, 0.5 μg), and T4 DNA ligase (4 units). Mixtures (10 μL) were loaded onto a 1% agarose gel in a 1 × tris-borate-edta (tris = tris(hydroxymethyl)aminomethane, edta = ethylenediaminetetraacetate) buffer. The ligated products were visualized by staining with ethidium bromide.

AFM: The ligated DNA samples (0.5 pmol or 10 pmol) were placed on a freshly cleaved mica plate pretreated with a 0.01%

 © 2003 Wiley-VCH Verlag GmbH & Co. KGaA, Weinheim 

aminopropyltriethoxysilane/95% ethanol/water solution.[7b] After incubating the plate at RT for 5 min, it was rinsed with MilliQ water twice and dried under reduced pressure. The samples were observed by SP400-AFM (Seiko Instruments, Inc., Tokyo, Japan) with a silicon nitrite cantilever (SN-AF01, Olympus Optical Co., Ltd., Tokyo, Japan), and the collected data were processed on a Spise132 software (Seiko Instruments, Inc.).

Received: August 1, 2003 [Z52546]

**Keywords:** DNA structures · DNA · molecular assembly · nanostructures · supramolecular chemistry

[1] a) J. M. Tour, *Chem. Rev.* **1996**, *96*, 537–553; b) P. F. H. Schwab, M. D. Levin, J. Michl, *Chem. Rev.* **1999**, *99*, 1863–1933; c) R. E. Martin, F. Diederich, *Angew. Chem.* **1999**, *111*, 1440–1469; *Angew. Chem. Int. Ed.* **1999**, *38*, 1350–1377; d) J. M. Tour, *Acc. Chem. Res.* **2000**, *33*, 791–804; e) U. H. F. Bunz, *Chem. Rev.* **2000**, *100*, 1605–1644; f) L. Brunsveld, B. J. B. Folmer, E. W. Meijer, R. P. Sijbesma, *Chem. Rev.* **2001**, *101*, 4071–4097; g) V. Hensel, A. Godt, R. Popovitz-Biro, H. Cohen, T. R. Jensen, K. Kjaer, I. Weissbuch, E. Lifshitz, M. Lahav, *Chem. Eur. J.* **2002**, *8*, 1413–1423; h) S. Westenhoff, N. A. Kotov, *J. Am. Chem. Soc.* **2002**, *124*, 2448–2449.

[2] a) J. Goodchild, *Bioconjugate Chem.* **1990**, *1*, 165–187; b) C. A. Mirkin, *Inorg. Chem.* **2000**, *39*, 2258–2272; c) C. M. Niemeyer, *Angew. Chem.* **2001**, *113*, 4254–4287; *Angew. Chem. Int. Ed.* **2001**, *40*, 4128–4158.

[3] a) E. Winfree, F. Liu, L. A. Wenzler, N. C. Seemen, *Nature* **1998**, *394*, 539–544; b) C. Mao, W. Sun, N. C. Seeman, *J. Am. Chem. Soc.* **1999**, *121*, 5437–5443; c) R. Sha, F. Liu, D. P. Millar, N. C. Seemen, *Chem. Biol.* **2000**, *7*, 743–751; d) R. Sha, F. Liu, N. C. Seeman, *Biochemistry* **2002**, *41*, 5950–5955.

[4] a) G. D. Glick, S. E. Osborne, D. S. Knitt, J. P. Marino, Jr., *J. Am. Chem. Soc.* **1992**, *114*, 5447–5448; b) A. E. Ferentz, T. A. Keating, G. L. Verdine, *J. Am. Chem. Soc.* **1993**, *115*, 9006–9014; c) H. Wang, E. R. P. Zuiderweg, G. D. Glick, *J. Am. Chem. Soc.* **1995**, *117*, 2981–2991; d) R. J. Cain, E. R. Zuiderweg, G. D. Glick, *Nucleic Acids Res.* **1995**, *23*, 2153–2160; e) D. A. Erlanson, J. N. M. Glover, G. L. Verdine, *J. Am. Chem. Soc.* **1997**, *119*, 6927–6928; f) C. R. Allerson, S. L. Chen, G. L. Verdine, *J. Am. Chem. Soc.* **1997**, *119*, 7423–7433; g) E. J. Maglott, G. D. Glick, *Nucleic Acids Res.* **1998**, *26*, 1301–1308; h) E. A. Harwood, S. T. Sigurdsson, N. B. F. Edfeldt, B. R. Reid, P. B. Hopkins, *J. Am. Chem. Soc.* **1999**, *121*, 5081–5082; i) D. M. Noll, A. M. Noronha, P. S. Miller, *J. Am. Chem. Soc.* **2001**, *123*, 3405–3411.

[5] a) J. A. Fidanza, L. W. McLaughlin, *J. Org. Chem.* **1992**, *57*, 2340–2346; b) M. Endo, M. Komiyama, *J. Org. Chem.* **1996**, *61*, 1994–2000.

[6] H. S. Subramanya, A. J. Doherty, S. R. Ashford, D. B. Wigley, *Cell* **1996**, *17*, 607–615.

[7] a) L. S. Shlyakhtenko, V. N. Potaman, R. R. Sinden, A. A. Gall, Y. L. Lyubchenko, *Nucleic Acids Res.* **2000**, *28*, 3472–3477; b) K. Umemura, M. Ishikawa, R. Kuroda, *Anal. Biochem.* **2001**, *290*, 232–237.

[8] A disulfide linkage of an interstrand cross-linked oligonucleotide was completely cleaved at 37 °C after 30 min in a solution containing Tris-HCl (pH 8.0; 50 mM) and DTT (10 mM).

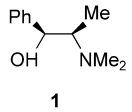
 © 2003 Wiley-VCH Verlag GmbH & Co. KGaA, Weinheim 

Asymmetric Additions

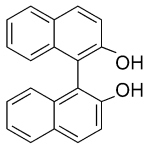
# Highly Enantioselective Addition of Phenylacetylene to Aldehydes Catalyzed by a β-Sulfonamide Alcohol–Titanium Complex**

*Zhaoqing Xu, Rui Wang,* Jiangke Xu, Chao-shan Da, Wen-jin Yan, and Chao Chen*

The enantioselective formation of C–C bonds is an area of intense research.[1,2] The asymmetric addition of alkynyl reagents to aldehydes is very useful for the synthesis of chiral secondary propargyl alcohols, which are important building blocks for many chiral organic compounds.[3] Several studies into the alkynylation of aldehydes with amino alcohol ligands have led to methods that give moderate to good yields and enantioselectivities.[4] Carreira and co-workers reported the addition of terminal acetylenes to aliphatic aldehydes in the presence of stoichiometric or catalytic amounts of amino alcohol **1** to give the desired products in high yields and enantioselectivities. However, this method was not suitable for the addition reaction to aromatic aldehydes because of significant competition from the Cannizzaro reaction.[5]




**1**




**2**

Recently, Chan and co-workers reported that binol (**2**) can catalyze the addition of alkynyl zinc reagents to aromatic aldehydes with high *ee* values. However, the reaction also requires 1 equivalent of a sulfonamide ligand and must be run at 0 °C for 1–2 days.[6] Pu and co-workers reported that a

[*] Prof. R. Wang
Department of Biochemistry and Molecular Biology
School of Life Science, Lanzhou University
and
State Key Laboratory for Oxo Synthesis and Selective Oxidation
Lanzhou Institute of Chemical Physics
Chinese Academy of Sciences
Lanzhou 730000 (China)
Fax: (+86) 931-891-2561
E-mail: wangrui@lzu.edu.cn
Dr. Z. Xu, J. Xu, C.-s. Da, W.-j. Yan, C. Chen
Department of Biochemistry and Molecular Biology
School of Life Science, Lanzhou University
Lanzhou 730000 (China)

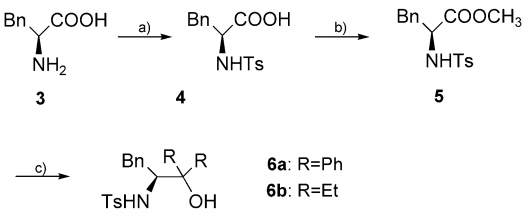
[**] This work was supported by the National Natural Science Foundation of China, the Ministry of Science and Technology of China, the Teaching and Research Award Program for Outstanding Young Teachers, the Specialized Research Fund for the Doctoral Program in Higher Education Institutions, and the Key Research Program of Science and Technology of the Ministry of Education of China.

 DOI: 10.1002/anie.200352572 © 2003 Wiley-VCH Verlag GmbH & Co. KGaA, Weinheim 

binol–Ti complex can also catalyze this reaction, but this method requires a separate step for the preparation of the alkynyl zinc reagent at high temperatures for 5 h.[7] Thus there is a growing need to find an inexpensive and novel catalyst for the asymmetric addition of terminal acetylenes to aromatic aldehydes; the reaction should be fast, occur in a single step under mild and convenient conditions, and should also lead to has *ee* values.

The N-H group of sulfonamides is acidic owing to the highly electron-withdrawing nature of the sulfonyl group. Therefore, unlike traditional metal amides (M-$NR_2$), the sulfonamide nitrogen atom is a poor electron donor and sulfonamide–Ti complexes are Lewis acids.[8] Aminoalcohols derived from natural amino acids are among the best and most economical ligands available.[9] We therefore decided to prepare a few β-sulfonamide alcohols **6** (Scheme 1). As a result of the acidic N-H and O-H groups, a titanium complex is readily formed when combined with Ti(O*i*Pr)$_4$ under basic conditions.[10] These complexes behave similarly to binol–Ti complexes, and we therefore applied them in the enantioselective addition of phenylacetylene to aldehydes.

Three simple steps were required to prepare **6a** and **6b** from L-phenylalanine in overall yields of 67% and 62%, respectively (Scheme 1). The two ligands were initially tested

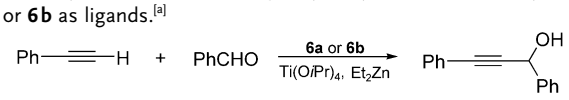



***Scheme 1.*** Preparation of sulfonamide from L-phenylalanine. a) NaOH (2 equiv), $H_2O$, TsCl (1 equiv), $Et_2O$, room temperature, 24 h; b) $SOCl_2$ (1.2 equiv), MeOH, −30°C, 30 min; then reflux, 2 h; c) RMgBr (5 equiv), THF, room temperature, 24 h. Ts = *p*-toluenesulfonyl.

in the asymmetric addition of phenylacetylene to benzaldehyde in the presence of diethylzinc (Table 1). Interestingly, **6a**, which has the bulkier, less-flexible phenyl substituents at the hydroxy-bearing carbon atom, resulted in a lower enantioselectivity (Table 1, entry 1) than **6b**, which has the more-flexible ethyl substituents (Table 1, entry 2). We varied the amount of Ti(O*i*Pr)$_4$ and found that the best *ee* are obtained when the **6b**/Ti(O*i*Pr)$_4$ ratio is 1:3 (Table 1, entries 2–6). We also found that this reaction was strongly influenced by the solvent: Low enantioselectivities were found in $CH_2Cl_2$ and THF (Table 1, entries 7 and 8). When the amount of ligand increased from 10% to 15 and 20%, the *ee* values improved slightly (Table 1, entries 9 and 10). No significant changes in *ee* values were observed when the temperature of the reaction was decreased from room temperature to 0°C (Table 1, entry 11).

Under these optimized reaction conditions, ligand **6b** was employed to induce the enantioselective addition of phenylacetylene to a number of aromatic aldehydes,[11] all of which gave rise to products with high enantioselectivity (up to 98% *ee*; Table 2).

***Table 1:*** Asymmetric addition of phenylacetylene to benzaldehyde with **6a** or **6b** as ligands.[a]




| Entry | Ligand | [mol%] | Ligand/Ti(O*i*Pr)$_4$[b] | Solvent | *T* | *ee* [%][c] |
|---|---|---|---|---|---|---|
| 1 | **6a** | 10 | 1:3 | toluene | RT | 10 |
| 2 | **6b** | 10 | 1:3 | toluene | RT | 90 |
| 3 | **6b** | 10 | 1:1 | toluene | RT | 11 |
| 4 | **6b** | 10 | 1:2 | toluene | RT | 88 |
| 5 | **6b** | 10 | 1:4 | toluene | RT | 85 |
| 6 | **6b** | 10 | 1:5 | toluene | RT | 78 |
| 7 | **6b** | 10 | 1:3 | $CH_2Cl_2$ | RT | 4 |
| 8 | **6b** | 10 | 1:3 | THF | RT | 6 |
| 9 | **6b** | 15 | 1:3 | toluene | RT | 93 |
| 10 | **6b** | 20 | 1:3 | toluene | RT | 95 |
| 11 | **6b** | 20 | 1:3 | toluene | 0°C | 95 |

[a] Phenylacetylene/$Et_2Zn$/benzaldehyde = 3:3:1. [b] Ti(O*i*Pr)$_4$ was freshly distilled. [c] The enantiomeric excess was determined by HPLC analysis of the corresponding products on a Chiralcel OJ-H column.

***Table 2:*** Asymmetric addition phenylacetylene to aromatic aldehydes promoted by ligand **6b**.[a]

| Entry | Aldehyde | *t* [h] | Yield [%] | *ee* [%][b] |
|---|---|---|---|---|
| 1 | benzaldehyde | 12 | 92 | 95 |
| 2 | 3-tolualdehyde | 12 | 89 | 92 |
| 3 | 4-tolualdehyde | 12 | 90 | 93 |
| 4 | 3-anisaldehyde | 12 | 88 | 90 |
| 5 | 4-anisaldehyde | 14 | 91 | 92 |
| 6 | 4-chlorobenzaldehyde | 12 | 80 | 98 |
| 7 | 4-fluorohenzaldehyde | 12 | 87 | 93 |
| 8 | α-naphthaldehyde | 18 | 70 | 90 |
| 9 | β-naphthaldehyde | 18 | 71 | 95 |

[a] $Et_2Zn$/phenylacetylene/aldehyde/Ti(O*i*Pr)$_4$/**6b** = 3:3:1:0.6:0.2. All the reactions were processed under argon and at room temperature. Ti(O*i*Pr)$_4$ was fresh distilled before use. [d] The *ee* values were determined by chiral HPLC on a Chiracel OJ-H column.

In conclusion, we successfully prepared two β-sulfonamide alcohol ligands from natural L-phenylalanine in three steps in good yields. Ligand **6b** exhibits excellent catalytic activity in the enantioselective addition of phenylacetylene to aromatic aldehydes under very mild conditions.

## *Experimental Section*

All manipulations were carried out under an argon atmosphere in dried and degassed solvent. β-Sulfonamide alcohols **6a** and **6b** were synthesized according to literature procedures.[12]

(*S*)-**6a**. White needles (67% yield); m.p. 122–123°C; $[\alpha]_D^{20} = +105$ ($c = 0.121$ in $CHCl_3$); IR (KBr): $\tilde{\nu} = 3528, 3303, 3066, 3028, 2926, 1660, 1598, 1493, 1448, 1324, 1153, 1087, 968, 908, 811, 740, 700\ cm^{-1}$; $^1H$ NMR (200 MHz, $CDCl_3$, TMS): $\delta = 2.37$ (s, 3H; $CH_3$), 2.53 ( s, 1H; OH), 2.86 (dd, $^3J$(H-H) = 6.0, $^2J$(H-H) = 14.2 Hz, 1H; Ph$CH_AH_B$), 3.27 (dd, $^3J$(H-H) = 3.6 Hz, $^2J$(H-H) = 14.2 Hz, 1H; Ph$CH_AH_B$), 4.69 (m, 1H; CHN), 4.86 (d, $^3J$(H-H) = 8.2 Hz, 1H; NH), 6.96–7.52 ppm (m, 19H; 4 × Ph-H); MS (ESI): *m*/*z*: 456 $[M-H]^-$.

(*S*)-**6b**. White needles (62% yield); m.p. 95–96°C; $[\alpha]_D^{20} = -39$ ($c = 0.102$ in $CHCl_3$); IR(KBr): $\tilde{\nu} = 3512, 3287, 3066, 3028, 2969, 2882, 1648, 1599, 1457, 1321, 1152, 1086, 960, 908, 812, 736, 698\ cm^{-1}$; $^1H$ NMR (200 MHz, $CDCl_3$, TMS): $\delta = 0.84$–$0.95$ (m, 6H; $CH_3$), 1.43–1.75 (m, 4H; $CH_2Me$), 2.01 (s, 1H; OH), 2.37 (s, 3H; $PhCH_3$), 2.48

 © 2003 Wiley-VCH Verlag GmbH & Co. KGaA, Weinheim 

(dd, $^3J$(H-H) = 9.2 Hz, $^2J$(H-H) = 14.2 Hz, 1H; PhC$H_A$H$_B$), 2.94 (dd, $^3J$(H-H) = 6.2 Hz, $^2J$(H-H) = 14.2 Hz, 1H; PhCH$_A$$H_B$), 4.65 (m, 1H; CHN), 4.75 (s, 1H; NH), 6.93–7.40 ppm (m, 9H; 2 × Ph-H); MS (ESI): *m/z*: 360 $[M-H]^-$.

General addition procedure: Under argon, the ligand **6b** (18 mg, 0.05 mmol) and Ti(O*i*Pr)$_4$ (41.2 μL, 0.15 mmol) were mixed in dry toluene at room temperature. A solution of $Et_2Zn$ (1.0 M in toluene, 0.75 mL) was then added. After the mixture was stirred at the room temperature for 2 h, phenylacetylene (82.4 μL, 0.75 mmol) was added and the stirring continued for 1 h. The orange solution was cooled to 0 °C and treated with aldehyde (0.25 mmol). The resulting mixture was allowed to warm to room temperature and stirred for 12–18 h. After the reaction was complete (monitoring with TLC), it was cooled to 0 °C and quenched with aqueous HCl (5%). The mixture was extracted with diethyl ether. The organic layer was washed with brine, dried over $Na_2SO_4$, and concentrated under vacuum. The residue was purified by flash column chromatography (silica gel, 12.5% EtOAc in hexane) to give the product.

Received: August 5, 2003 [Z52572]

**Keywords:** addition · aldehydes · alkynes · asymmetric catalysis · sulfonamides

[1] For a review, see: L. Pu, H. B. Yu, *Chem. Rev.* **2001**, *101*, 757.
[2] For selected recent examples from our group, see: a) X. W. Yang, J. H. Shen, C. S. Da, H. S. Wang, W. Su, R. Wang, A. S. C. Chan, *J. Org. Chem.* **2000**, *65*, 295; b) X. W. Yang, W. Su, D. X. Liu, H. S. Wang, J. H. Shen, C. S. Da, R. Wang, A. S. C. Chan, *Tetrahedron* **2000**, *56*, 3511; c) X. W. Yang, J. H. Shen, C. S. Da, H. S. Wang, W. Su, D. X. Liu, R. Wang, M. C. K. Choi, A. S. C. Chan, *Tetrahedron Lett.* **2001**, *42*, 6573; d) D. X. Liu, L. C. Zhang, Q. Wang, C. S. Da, Z. Q. Xin, R. Wang, M. C. K. Choi, A. S. C. Chan, *Org. Lett.* **2001**, *3*, 2733.
[3] a) S. Niwa, K. Soai, *J. Chem. Soc. Perkin Trans. 1* **1990**, 937; b) M. Ishizaki, O. Hoshino, *Tetrahedron: Asymmetry* **1994**, *5*, 1901; c) Z. Li, V. Vpadhyay, A. Z. DeCamp, L. DiMichele, P. Reider, *Synthesis* **1999**, 1453.
[4] a) J. A. Marsh, X. J. Wang, *J. Org. Chem.* **1992**, *57*, 1242; b) A. G. Meyers, B. Zhang, *J. Am. Chem. Soc.* **1996**, *118*, 4492; c) M. E. Fox, C. Li, J. P. Marino, Jr, L. E. Overman, *J. Am. Chem. Soc.* **1999**, *121*, 5467.
[5] a) D. E. Frantz, R. Fassler, E. M. Carreira, *J. Am. Chem. Soc.* **2000**, *122*, 1806; b) N. K. Anand, E. M. Carreire, *J. Am. Chem. Soc.* **2001**, *123*, 9687.
[6] X. S. Li, G. Lu, W. H. Kwok, A. S. C. Chan, *J. Am. Chem. Soc.* **2002**, *124*, 12636.
[7] a) G. Gao, D. Moore, R. G. Xie, L. Pu, *Org. Lett.* **2002**, *4*, 4143; b) M. H. Xu, L. Pu, *Org. Lett.* **2002**, *4*, 4555.
[8] S. Pritchett, P. Gantzel, P. J. Walsh, *Organometallics* **1997**, *16*, 5130.
[9] For some selected examples of aminoalcohols derived from natural amino acids, see: a) K. Soai, A. Ookawa, T. Kaba, K. Ogawa, *J. Am. Chem. Soc.* **1987**, *109*, 7111; b) P. Delair, C. Einhorn, J. Einhorn, J. L. Luche, *J. Org. Chem.* **1994**, *59*, 4680; c) C. Wolf, C. J. Francis, P. A. Hawes, M. Shah, *Tetrahedron: Asymmetry* **2002**, *13*,1733.
[10] S. Pritchett, D. H. Woodmansee, P. Gantzel, P. J. Walsh, *J. Am. Chem. Soc.* **1998**, *120*, 6423.
[11] Under the same conditions, we also used **6b** in the addition of phenylacetylene to two aliphatic aldehydes: isobutylaldehyde and cyclohexanecarboxaldehyde. The enantioselectivities were determined by chiral HPLC on a Chiracel OD column and were found to be 81 and 70% *ee*, respectively.
[12] J. S. You, M. Y. Shao, H. M. Gau, *Tetrahedron: Asymmetry* **2001**, *12*, 2971.

 © 2003 Wiley-VCH Verlag GmbH & Co. KGaA, Weinheim 

Reaction Mechanisms

# Toward an Improved Understanding of the Unusual Reactivity of $Pd^0$/Trialkylphosphane Catalysts in Cross-Couplings of Alkyl Electrophiles: Quantifying the Factors That Determine the Rate of Oxidative Addition**

*Ivory D. Hills, Matthew R. Netherton, and Gregory C. Fu**

Palladium- and nickel-catalyzed cross-couplings are widely used tools in synthetic chemistry.[1] No doubt, such processes would be even more broadly employed if they were not largely restricted to reactions of *aryl* and *vinyl* halides and sulfonates. Recognizing the significance of this limitation, several groups have recently turned their attention to the development of methods for cross-coupling *alkyl* halides and sulfonates.[2–7] Among the palladium catalysts that have been described to date, the majority are based on sterically demanding trialkylphosphanes ($PCy_3$ or $P(t\text{Bu})_2\text{Me}$).[8]

The catalytic cycle for most cross-coupling reactions presumably includes a sequence of oxidative addition, transmetalation, and reductive elimination (Figure 1). With regard to the challenge of coupling alkyl electrophiles, the difficulty

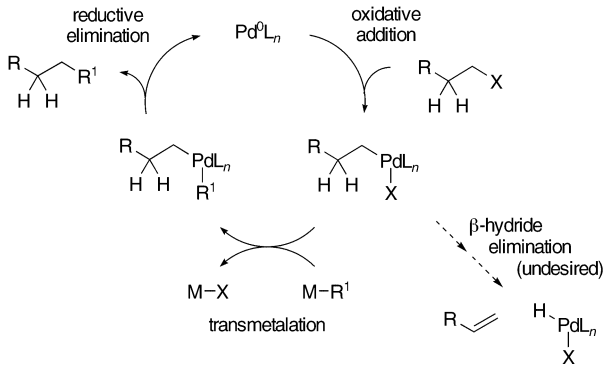



***Figure 1.*** Generalized mechanism for a palladium-catalyzed cross-coupling reaction.

[*] Prof. Dr. G. C. Fu, I. D. Hills, Dr. M. R. Netherton
Department of Chemistry
Massachusetts Institute of Technology
Cambridge, MA 02139 (USA)
Fax: (+1) 617-324-3611
E-mail: gcf@mit.edu

[**] Support has been provided by the National Institutes of Health (National Institute of General Medical Sciences, R01-GM62871 to G.C.F. and R01-GM57034 supplement to I.D.H.), the American Chemical Society (Organic Division Fellowship to I.D.H., sponsored by Abbott Laboratories), the Natural Sciences and Engineering Research Council of Canada (Postdoctoral Fellowship to M.R.N.), Merck, and Novartis. Funding for the MIT Department of Chemistry Instrumentation Facility has been furnished in part by NSF CHE-9808061 and NSF DBI-9729592. We thank Johnson Matthey for supplying palladium compounds.

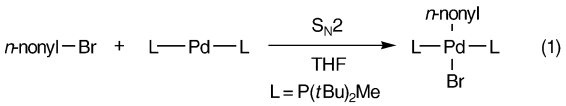
Supporting information for this article is available on the WWW under http://www.angewandte.org or from the author.

 DOI: 10.1002/anie.200352858 © 2003 Wiley-VCH Verlag GmbH & Co. KGaA, Weinheim 

has generally been attributed to relatively slow oxidative addition and to facile β-hydride elimination (Figure 1). To complement our methods-development studies of Pd/trialkylphosphane catalysts for coupling alkyl electrophiles, we have recently initiated mechanistic work on these systems. As part of this new program, in this communication we describe a wide-ranging investigation of the initial step of the catalytic cycle, oxidative addition of an alkyl electrophile to a Pd/trialkylphosphane complex.

In an earlier study, we discovered that $PdL_2$ ($L = PCy_3$ or $P(tBu)_2Me$) can react with an alkyl electrophile (R–X) to generate an oxidative-addition adduct that, in the absence of a cross-coupling partner, can be isolated and even crystallographically characterized.[9] The relative stability of $PdL_2RX$ toward β-hydride elimination was a pleasant surprise for us. Recognizing that there are no systematic, quantitative investigations of oxidative addition of alkyl electrophiles to palladium(0),[10] we decided to remedy this deficiency.

Through kinetics studies, we have determined that, for the oxidative addition of *n*-nonyl bromide to $Pd(P(tBu)_2Me)_2$ [Eq. (1)],[11] the activation parameters are: $\Delta G^{\ddagger} = 20.8$ kcal mol$^{-1}$ at 20 °C; $\Delta H^{\ddagger} = 2.4$ kcal mol$^{-1}$; $\Delta S^{\ddagger} = -63$ eu. The large



(1)

negative $\Delta S^{\ddagger}$ is consistent with the associative $S_N2$-type pathway suggested by our earlier stereochemical investigations.[12]

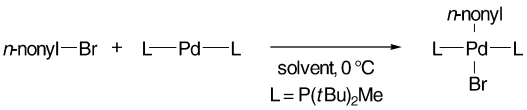
The addition of $P(tBu)_2Me$ (e.g., 2 or 4 equiv) to the reaction illustrated in Equation (1) does not affect the rate, suggesting that the alkyl bromide oxidatively adds to $PdL_2$, not PdL or $PdL_3$.[13] In contrast, in the case of cross-couplings of aryl bromides that are catalyzed by $Pd/P(tBu)_3$, the available data indicate that a palladium–monophosphane adduct undergoes oxidative addition.[14]

We have examined the relationship between solvent polarity and the rate of oxidative addition. As illustrated in Table 1, we have determined that an increase in polarity[15] leads to a decrease in the activation energy, consistent with the expectation for an $S_N2$-type nucleophilic attack of $PdL_2$ on R–X.[16]

We have also investigated the impact of the leaving group X on the rate of oxidative addition of alkyl electrophiles R–X to $Pd(P(tBu)_2Me)_2$ (Table 2). We have established that an alkyl iodide rapidly oxidatively adds to $Pd(P(tBu)_2Me)_2$ even at −60 °C (entry 1), whereas the corresponding bromide requires a temperature of 0 °C to achieve a comparable rate (entry 2). Upon heating to 60 °C, an alkyl chloride (entry 3), but not a fluoride (entry 4), reacts with $Pd(P(tBu)_2Me)_2$. Finally, we have determined that an alkyl tosylate (entry 5) is intermediate between a bromide and a chloride in reactivity. The relative propensity of alkyl electrophiles to oxidatively add to $Pd(P(tBu)_2Me)_2$ (Table 2) is consistent with an $S_N2$ pathway for oxidative addition.[17]

Unfortunately, no catalyst, including $Pd(P(tBu)_2Me)_2$, has yet been reported to be effective for cross-couplings of unactivated secondary alkyl electrophiles. Naturally, we were interested in whether this shortcoming may be attributable to a reluctance of these compounds to undergo oxidative addition. We therefore examined the relationship between the rate of oxidative addition to $Pd(P(tBu)_2Me)_2$ and the steric demand of the electrophile.

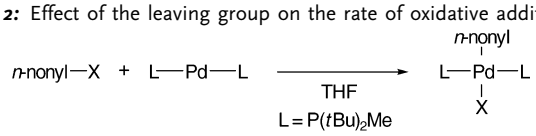
***Table 1:*** Correlation between solvent polarity and the activation barrier for oxidative addition.[a]




| Entry | Solvent | Polarity | $\Delta G^{\ddagger}$ [kcal mol$^{-1}$] |
|---|---|---|---|
| 1 | hexane | 0.68 | > 23.0[b] |
| 2 | toluene | 1.66 | 20.0 |
| 3 | THF | 2.08 | 19.5 |
| 4 | *tert*-amyl alcohol | 2.46[c] | 18.1 |
| 5 | NMP[d] | 2.62 | 18.0 |
| 6 | DMF[e] | 2.80 | 17.8 |

[a] All data are the average of two runs. [b] No reaction at 0–60 °C. $\Delta G^{\ddagger}$ was calculated for 60 °C. [c] Value for *tert*-butanol. [d] NMP = *N*-methylpyrrolidinone. [d] DMF = dimethylformamide.

***Table 2:*** Effect of the leaving group on the rate of oxidative addition.[a]




| Entry | X | $t_{1/2}$ |
|---|---|---|
| 1 | I | 2.2 h at −60 °C |
| 2 | Br | 2.3 h at 0 °C |
| 3 | Cl | 2.0 d at 60 °C |
| 4 | F | < 2% reaction after 43 h at 60 °C |
| 5 | OTs[b] | 10.4 h at 40 °C |

[a] All data are the average of two runs. [b] Ts = toluenesulfonyl.

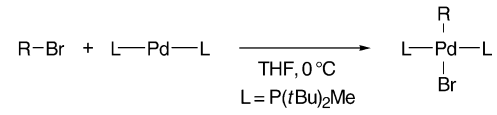
As illustrated in Table 3, the bulk of the electrophile has a large impact on the reaction rate. Branching in the γ-position leads to a roughly fivefold decrease in reactivity relative to an unbranched substrate (entry 2 vs. entry 1), and branching in the β-position attenuates the reactivity by a factor of ~20 (entry 3 vs. entry 1). Consistent with the failure of $Pd(P(tBu)_2Me)_2$ to catalyze cross-couplings of secondary alkyl electrophiles, no oxidative addition occurs if the branch is in the α-position (entry 4).

For couplings of primary alkyl electrophiles catalyzed by $Pd/PR_3$, in earlier work we observed a remarkable dependence of the efficiency of the reaction on the structure of the phosphane.[3d,e] We have now determined that cross-coupling efficiency correlates with the propensity of $PdL_2$ to undergo oxidative addition (Table 4). Thus, adducts of $P(tBu)_2Me$ or $PCy_3$ readily add *n*-nonyl bromide (Table 4, entries 1 and 2), in keeping with their effectiveness in a range of coupling processes. In contrast, complexes of $P(tBu)_2Et$ or $P(tBu)_3$ are relatively unreactive toward oxidative addition (entries 3 and 4), as well as ineffective at cross-coupling alkyl electrophiles.

The divergent reactivity of $PdL_2$ complexes of $P(tBu)_2Me$ (cone angle: 161°) and $P(tBu)_2Et$ (cone angle: 165°),[18] which

 © 2003 Wiley-VCH Verlag GmbH & Co. KGaA, Weinheim 

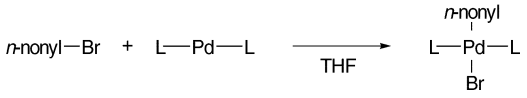
***Table 3:*** Correlation between the steric demand of the electrophile and the activation barrier for oxidative addition.[a]




| Entry | R–Br | $k_{rel}$ | $\Delta G^{\neq}$ [kcal mol$^{-1}$] |
|---|---|---|---|
| 1 | *n*-pentyl–Br | 1.0 | 19.5 |
| 2 | Me, Me, Br | 0.19 | 20.3 |
| 3 | Me, Me, Me, Br | 0.054 | 21.0 |
| 4 | Me, Me, Me, Br | < 0.0001 | > 24.0[b] |

[a] All data are the average of two runs. [b] Extrapolated from a reaction run at 60 °C.

***Table 4:*** Effect of the phosphane on the activation barrier for oxidative addition.[a]




| Entry | L | $\Delta G^{\neq}$ [kcal mol$^{-1}$][b] |
|---|---|---|
| 1 | $P(tBu)_2Me$ | 19.5 (0 °C) |
| 2 | $PCy_3$ | 20.0 (0 °C) |
| 3 | $P(tBu)_2Et$ | 25.4 (60 °C) |
| 4 | $P(tBu)_3$ | > 28.4 (60 °C) |

[a] All data are the average of two runs. [b] The temperature at which $\Delta G^{\neq}$ was measured is noted in parentheses.

at first glance appear to be nearly isosteric, is particularly striking (Table 4, entries 1 and 3; $k_{rel} > 10^3$). However, computation of the energy of the various conformers of palladium–phosphane adducts leads to a reasonable explanation for this initially surprising difference. Through B3LYP/LanL2DZ DFT calculations, we have determined that conformer **1**, in which Me and Pd are eclipsed, is ~3.5 kcal mol$^{-1}$ lower in energy than conformer **2**, in which Me and Pd are *anti*, due to the presence of additional *syn*-pentane-like interactions in **2** (Figure 2a).[19] Figure 2b shows that, in the illustrated conformation of $Pd(P(tBu)_2Et)_2$ (**3**), approach of an electrophile to Pd would be impeded significantly by the Me groups. In contrast, higher energy conformation **4** presents a steric environment around Pd that resembles that of $Pd(P(tBu)_2Me)_2$.[20] We believe that this analysis provides an adequate rationalization for the difference in reactivity between $Pd(P(tBu)_2Et)_2$ and $Pd(P(tBu)_2Me)_2$.

In conclusion, we have described the first systematic investigation of the oxidative addition of alkyl electrophiles to $Pd^0$, specifically, adducts of trialkylphosphanes. The reactivity of these complexes is of high current interest due to their unusual effectiveness as cross-coupling catalysts for alkyl electrophiles. We have determined that the species that undergoes oxidative addition is $PdL_2$ and that the activation parameters for this $S_N2$ process are: $\Delta G^{\neq} = 20.8$ kcal mol$^{-1}$ at 20 °C; $\Delta H^{\neq} = 2.4$ kcal mol$^{-1}$; $\Delta S^{\neq} = -63$ eu. In addition, we

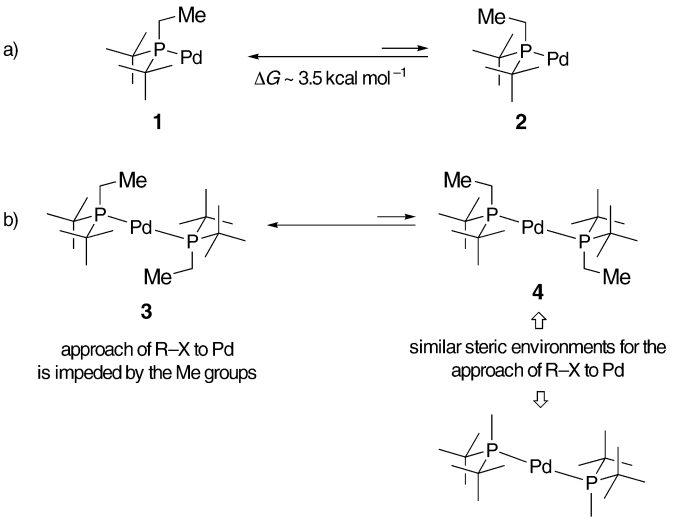



***Figure 2.*** A rationale for the divergent reactivity of $Pd(P(tBu)_2Me)_2$ and $Pd(P(tBu)_2Et)_2$.

have quantified the impact of the following parameters on the rate of oxidative addition of R–X to $PdL_2$: the solvent, the leaving group (X = I, Br, Cl, F, OTs), and the steric demand of the electrophile (R) and the ligand (L). Furthermore, based on DFT calculations, we have provided a rationale for the remarkable difference in reactivity between $Pd(P(tBu)_2Me)_2$ and $Pd(P(tBu)_2Et)_2$. Additional mechanistic studies of these intriguing cross-coupling catalysts are underway.

Received: September 12, 2003 [Z52858]

**Keywords:** cross-coupling · homogeneous catalysis · palladium · phosphane ligands · reaction mechanisms

[1] For reviews of metal-catalyzed cross-coupling reactions, see: a) *Metal-Catalyzed Cross-coupling Reactions* (Eds.: F. Diederich, P. J. Stang), Wiley-VCH, New York, **1998**; b) "Cross-Coupling Reactions: A Practical Guide": *Top. Curr. Chem.* **2002**, *219* (Ed.: N. Miyaura); c) *Handbook of Organopalladium Chemistry for Organic Synthesis* (Ed.: E.-i. Negishi), Wiley Interscience, New York, **2002**.

[2] For an overview of the difficulty of achieving coupling reactions of $C(sp^3)$–X electrophiles, see: D. J. Cárdenas, *Angew. Chem.* **1999**, *111*, 3201–3203; *Angew. Chem. Int. Ed.* **1999**, *38*, 3018–3020; D. J. Cárdenas, *Angew. Chem.* **2003**, *115*, 398–401; *Angew. Chem. Int. Ed.* **2003**, *42*, 384–387. See also: T.-Y. Luh, M.-k. Leung, K.-T. Wong, *Chem. Rev.* **2000**, *100*, 3187–3204.

[3] Suzuki reaction: a) T. Ishiyama, S. Abe, N. Miyaura, A. Suzuki, *Chem. Lett.* **1992**, 691–694; b) M. R. Netherton, C. Dai, K. Neuschütz, G. C. Fu, *J. Am. Chem. Soc.* **2001**, *123*, 10099–10100; c) J. H. Kirchhoff, C. Dai, G. C. Fu, *Angew. Chem.* **2002**, *114*, 2025–2027; *Angew. Chem. Int. Ed.* **2002**, *41*, 1945–1947; d) M. R. Netherton, G. C. Fu, *Angew. Chem.* **2002**, *114*, 4066–4068; *Angew. Chem. Int. Ed.* **2002**, *41*, 3910–3912; e) J. H. Kirchhoff, M. R. Netherton, I. D. Hills, G. C. Fu, *J. Am. Chem. Soc.* **2002**, *124*, 13662–13663.

[4] Negishi reaction: a) A. Devasagayaraj, T. Stüdemann, P. Knochel, *Angew. Chem.* **1995**, *107*, 2952–2954; *Angew. Chem. Int. Ed. Engl.* **1995**, *34*, 2723–2725; b) R. Giovannini, T. Stüdemann, G. Dussin, P. Knochel, *Angew. Chem.* **1998**, *110*, 2512–2515;

 © 2003 Wiley-VCH Verlag GmbH & Co. KGaA, Weinheim 

*Angew. Chem. Int. Ed.* **1998**, *37*, 2387 – 2390; c) R. Giovannini, P. Knochel, *J. Am. Chem. Soc.* **1998**, *120*, 11186 – 11187; d) R. Giovannini, T. Stüdemann, A. Devasagayaraj, G. Dussin, P. Knochel, *J. Org. Chem.* **1999**, *64*, 3544 – 3553; e) M. Piber, A. E. Jensen, M. Rottländer, P. Knochel, *Org. Lett.* **1999**, *1*, 1323 – 1326; f) A. E. Jensen, P. Knochel, *J. Org. Chem.* **2002**, *67*, 79 – 85; g) J. Zhou, G. C. Fu, *J. Am. Chem. Soc.* **2003**, *125*, 12527 – 12530.

[5] Kumada reaction: a) J. Terao, H. Watanabe, A. Ikumi, H. Kuniyasu, N. Kambe, *J. Am. Chem. Soc.* **2002**, *124*, 4222 – 4223; b) A. C. Frisch, N. Shaikh, A. Zapf, M. Beller, *Angew. Chem.* **2002**, *114*, 4218 – 4221; *Angew. Chem. Int. Ed.* **2002**, *41*, 4056 – 4059; c) J. Terao, A. Ikumi, H. Kuniyasu, N. Kambe, *J. Am. Chem. Soc.* **2003**, *125*, 5646 – 5647.

[6] Stille reaction: a) K. Menzel, G. C. Fu, *J. Am. Chem. Soc.* **2003**, *125*, 3718 – 3719; b) H. Tang, K. Menzel, G. C. Fu, *Angew. Chem.* **2003**, *115*, 5233 – 5236; *Angew. Chem. Int. Ed.* **2003**, *42*, 5079 – 5082.

[7] Hiyama reaction: J.-Y. Lee, G. C. Fu, *J. Am. Chem. Soc.* **2003**, *125*, 5616 – 5617.

[8] For exceptions, see refs. [3a] and [6b].

[9] a) Ref. [3e]; b) I. D. Hills, M. R. Netherton, unpublished results.

[10] For an excellent review of oxidative addition, including the chemistry of $Pd^0$, see: J. K. Stille in *The Chemistry of the Metal–Carbon Bond* (Ed.: S. Patai), Wiley, New York, **1985**, chap. 9. See also: M. Huser, M.-T. Youinou, J. A. Osborn, *Angew. Chem.* **1989**, *101*, 1427 – 1430; *Angew. Chem. Int. Ed. Engl.* **1989**, *28*, 1386 – 1388.

[11] We chose to focus on complexes of $P(t\mathrm{Bu})_2\mathrm{Me}$ because it generally furnishes the most active catalyst.

[12] a) Ref. [3d]; b) I. D. Hills, M. R. Netherton, unpublished results.

[13] When $Pd(P(t\mathrm{Bu})_2\mathrm{Me})_2$ is dissolved in THF, the only phosphorus-containing species that is present according to $^{31}$P NMR spectroscopy is the $PdL_2$ adduct (e.g., no $PdL_1$), and there is no change in the spectrum in the presence of excess $P(t\mathrm{Bu})_2\mathrm{Me}$ (e.g., no $PdL_3$).

[14] a) A. F. Littke, G. C. Fu, *Angew. Chem.* **1998**, *110*, 3586 – 3587; *Angew. Chem. Int. Ed.* **1998**, *37*, 3387 – 3388; A. F. Littke, C. Dai, G. C. Fu, *J. Am. Chem. Soc.* **2000**, *122*, 4020 – 4028; b) J. P. Stambuli, R. Kuwano, J. F. Hartwig, *Angew. Chem.* **2002**, *114*, 4940 – 4942; *Angew. Chem. Int. Ed.* **2002**, *41*, 4746 – 4748, and references therein; M. Prashad, X. Y. Mak, Y. Liu, O. Repic, *J. Org. Chem.* **2003**, *68*, 1163 – 1164. See also: E. Galardon, S. Ramdeehul, J. M. Brown, A. Cowley, K. K. Hii, A. Jutand, *Angew. Chem.* **2002**, *114*, 1838 – 1841; *Angew. Chem. Int. Ed.* **2002**, *41*, 1760 – 1763.

[15] The values for solvent polarity are according to the S′ scale. For an overview, see: J. Zou, Q. Yu, Z. Shang, *J. Chem. Soc. Perkin Trans. 2* **2001**, 1439 – 1443.

[16] In our methods-development studies, we have consistently found nonpolar solvents such as hexane and toluene to be unsuitable for cross-coupling reactions of alkyl electrophiles.

[17] Consistent with the possibility that oxidative addition is the turnover-limiting step of the catalytic cycle, the same order of reactivity (Br > OTs > Cl) is observed for Suzuki reactions catalyzed by $Pd/PR_3$.[3b–d]

[18] These values were calculated by the method of Tolman: C. A. Tolman, *Chem. Rev.* **1977**, *77*, 313 – 348.

[19] Notes: a) The only other energy minimum that was located is the conformation in which Me and Pd are *gauche*. This lies ~0.6 kcal mol$^{-1}$ higher in energy than the eclipsed conformation. b) These calculations are, of course, imperfect, since they do not account for effects such as solvation.

[20] The $PdL_2$ structures in Figure 2b are not the direct result of calculations—they are derived from computed structures **1** and **2**.

 © 2003 Wiley-VCH Verlag GmbH & Co. KGaA, Weinheim 

Cluster Compounds

# A Strategy for Generating Naked-Metal Clusters for Gas-Phase Reactivity Studies by FTICR–MS**

*Colin P. G. Butcher, Adriana Dinca, Paul J. Dyson, Brian F. G. Johnson, Patrick R. R. Langridge-Smith, and J. Scott McIndoe**

Cluster reactivity in the gas phase has been probed extensively with clusters generated by using a variety of custom-built sources. These include pulsed-laser vaporisation, continuous-operation ovens, fast-atom and secondary-ion sputtering, dc discharge, and pulsed-arc cluster-ion sources.[1] All generate an assortment of clusters of different nuclearities, and $MS^n$ techniques make selection of a particular sized cluster relatively straightforward. Both homo- and heteronuclear clusters are known.[2] All of these techniques employ a similar strategy to cluster synthesis; that is, the target is vaporised, the gas-phase metal atoms condensed, and the resulting clusters examined by mass spectrometry. We report herein an entirely different approach for the production of bare-metal gas-phase clusters, in which presynthesised transition-metal–carbonyl-cluster anions are delivered into the gas phase by a standard electrospray ionisation (ESI) source and stripped free of ligands by using collision-induced dissociation (CID) at the skimmer cone. The benefits of this approach are high yields of a specific cluster, no requirement for a special source, easy access to heteronuclear clusters and/or those with interstitial atoms, and a vast library of known clusters to draw from.

Because mixed-metal–carbonyl clusters are currently extensively used as precursors for metal nanoparticle catalysts (the clusters are absorbed inside mesoporous silica and calcined to remove the ligands),[3] examination of their gas-phase reactivity may provide insight into their action as

[*] Dr. J. S. McIndoe
Department of Chemistry, University of Victoria
P.O. Box 3065, Victoria, BC V8W 3V6 (Canada)
Fax: (+1) 250-721-7147
E-mail: mcindoe@uvic.ca.

C. P. G. Butcher, Prof. B. F. G. Johnson
Department of Chemistry, University of Cambridge
Lensfield Road, Cambridge CB2 1EW (UK)

Dr. A. Dinca, Dr. P. R. R. Langridge-Smith
Department of Chemistry, The University of Edinburgh
West Mains Road, Edinburgh, EH9 3JJ (UK)

Prof. P. J. Dyson
Institut de chimie moléculaire et biologique
Ecole Polytechnique Fédérale de Lausanne
EPFL-BCH, 1015 Lausanne (Switzerland)

[**] Thanks to the EPSRC, ICI and Newton Trust for funding (CPGB), Aventis Pharma (Dagenham (UK)) for the donation of the FTICR-MS, and Dr. Don Daley (Argenta Discovery Ltd., Harlow (UK)) for his support.

Supporting information for this article is available on the WWW under http://www.angewandte.org or from the author.

 © 2003 Wiley-VCH Verlag GmbH & Co. KGaA, Weinheim DOI: 10.1002/anie.200352859 

catalysts in the solid state and represent a means of high throughput screening of potential catalysts for activity. Clusters used as catalysts are usually bimetallic, with well defined nuclearities and metal ratios (e.g. $[Pd_6Ru_6]$, $[Ru_{12}Cu_4C_2]$, $[Ru_5PtC]$, $[Ru_{10}Pt_2C_2]$)[4] and often have interstitial atoms that confer extra structural stability. Generating such naked nanoparticles in the gas phase in useable yield presents what would appear to be an insurmountable challenge for conventional cluster sources, but is essentially trivial by using our approach. Most cluster syntheses form a number of products, and this is an advantage with a mass-spectrometric approach. The reaction mixture may be analysed directly, and separation, ligand stripping, and reactivity studies may be carried out on the various clusters in the gas phase. We have previously demonstrated the efficiency of the stripping process for a wide range of anionic clusters, with nuclearities up to 20 metal atoms and with up to 40 carbonyl ligands.[5] Neutral clusters may also be readily chemically derivatized and stripped in the same manner.[6] A report of a related strategy concerns stripping the cluster $[Pt_4(PF_3)_8]$ by electron ionisation to provide the clusters $[Pt_n]^+$ $(n = 1–4)$,[7] but this approach relies on the precursor cluster being able to be transferred into the gas phase from the solid by heating under vacuum, thus the size and type of cluster that can be studied is limited (in particular, the anionic clusters of interest as catalyst precursors).

The high efficiency of the ligand-stripping process is illustrated in Figure 1, the energy dependent ESIMS/MS[8] of $[CoRu_3(CO)_{13}]^-$.[9] Carbonyl ligands are removed from the core as free CO by collision-induced dissociation (CID) of the cluster ions with an inert target gas (e.g. Ar). The energy of the ion–molecule collisions is represented by the collision voltage, which may be smoothly increased from 0 to 200 V (other instruments alter different parameters to achieve CID, but the principle remains the same). The cross-peak in the bottom right-hand corner of the contour map represents the intact parent ion; the remainder are fragment ions. In addition to the carbonyl loss ions $[CoRu_3(CO)_n]^-$ $(n = 0–12)$, all present in high intensity, at the highest collision voltages the metal core itself may be fragmented, and the ions $[Ru_3]^-$, $[CoRu_2]^-$, $[Ru_2]^-$ and $[Ru]^-$ generated (see Supporting Information).

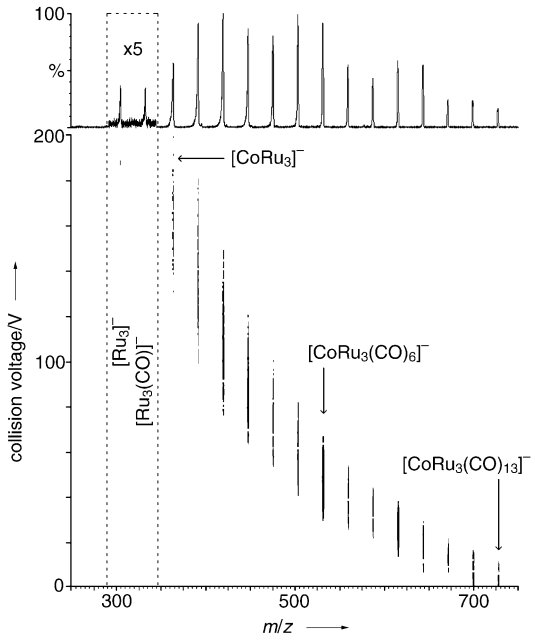



***Figure 1.*** EDESIMS/MS of $[CoRu_3(CO)_{13}]^-$. The highlighted area has been enhanced in intensity (×5).

Any of the fragment ions may be selected for reaction with neutral molecules using an FTICR mass spectrometer.[10] The reactivity of clusters in the gas phase has been investigated by many groups, often with the intention of developing gas-phase models for heterogenous catalysis.[11] We have taken a similar approach and, as a preliminary study, have investigated the reactivity of the naked cluster $[CoRu_3]^-$ with $CH_4$ and $H_2$.

The $[CoRu_3]^-$ cluster reacts with methane after activation by SORI (sustained off-resonance irradiation). In Figure 2 are shown the spectra collected by reaction of $[CoRu_3]^-$ with $10^{-7}$ Torr of $CH_4$ after SORI for 0, 1, 5 and 15 seconds. The primary process is dehydrogenation of methane molecules by the naked anionic metal cluster to produce carbide species [Eq. (1)].

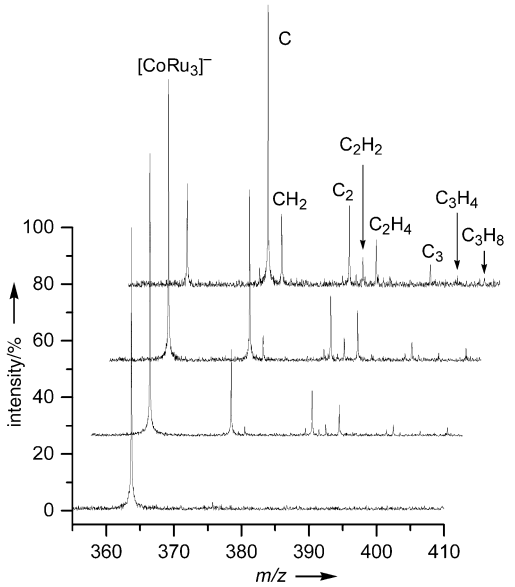



***Figure 2.*** FTICRMS$^n$ of $[CoRu_3]^-$ + $CH_4$ after SORI activation for 0 s (bottom), 1 s, 5 s, and 15 s (top).

$$[CoRu_3]^- + n\,CH_4 \rightarrow [CoRu_3C_n]^- + 2n\,H_2 \quad (n = 1-3) \qquad (1)$$

Additionally, the partially hydrogenated species $[CoRu_3CH_2]^-$, $[CoRu_3C_2H_2]^-$ and $[CoRu_3C_2H_4]^-$, $[CoRu_3C_3H_4]^-$ and $[CoRu_3C_3H_8]^-$ are observed. Long periods of activation do not lead preferentially to higher carbide species, nor to a significant change in the ratio of carbide species to the hydrogenated species. Rather, the main effect is enhancement of the C and $CH_2$ species at the expense of the

 © 2003 Wiley-VCH Verlag GmbH & Co. KGaA, Weinheim 

bare-metal core. Formation of the higher hydrocarbon species necessarily proceeds sequentially [e.g. Eq. (2), (3)].

$$[CoRu_3C]^- + CH_4 \rightarrow [CoRu_3C_2H_2]^- + H_2 \quad (2)$$

$$\text{or} \rightarrow [CoRu_3C_2H_4]^- \quad (3)$$

Similar reaction of the above products with methane will yield $[CoRu_3C_3H_4]^-$ and $[CoRu_3C_3H_8]^-$. However, there is a limit to this process, as the intensity of the $C_2$ and $C_3$ species do not increase upon prolonged activation. Further reaction of these species may lead to hydrocarbon elimination [e.g. Eq. (4)].

$$[CoRu_3C_2H_2]^- + CH_4 \rightarrow [CoRu_3C]^- + C_2H_6 \quad (4)$$

These reactions are consistent with the observation that for the monocarbide species signal intensity increases significantly, mostly at the expense of the naked-metal core. Higher levels of C/H addition could be obtained by the selection of the $[CoRu_3C]^-$ core followed by further reaction with $CH_4$ (without additional activation), thus allowing observation of $[CoRu_3C + nCH_4]^-$ ($n = 1, 2, 3$; see Supporting Information). We plan experiments with larger clusters to determine whether the extent of reactivity can be increased further.

The oligomerization of hydrocarbons on a metal surface is important, especially for the Fischer–Tropsch synthesis of hydrocarbons from CO and $H_2$.[12] Many features of the synthesis indicate that the mechanism is complicated and leads to a range and distribution of products, the appearance of different functional groups and variations with catalysts and conditions.[13] Experimental information on the various elementary reactions that make up the Fischer–Tropsch synthesis is important to overall understanding, and we consider that our strategy will provide fundamental data on certain steps in this process.

To extend the analogy to the Fischer–Tropsch synthesis, pulsed-in hydrogen gas was used to hydrogenate the mixture of clusters prepared from the reactions with methane. Figure 3 shows the results of this process, and the preferential hydrogenation of the carbides suggests that it is the carbon atom rather than the metal atoms that preferentially react with hydrogen. However, the presence of $[CoRu_3H_2]^-$, $[CoRu_3CH_4]^-$, and $[CoRu_3C_2H_6]^-$ indicate that at least some of the hydrogen is adsorbed on the metal atoms, consistent with mechanisms in which $M_n$–H and $M_n$–$C_xH_y$ species coexist on the metal surface.

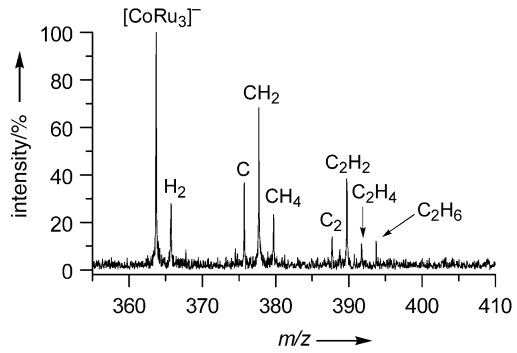



***Figure 3.*** FTICRMS$^n$ of $[CoRu_3]^- + CH_4$ after SORI activation for 5 s, followed by pulsed-in hydrogen gas.

In summary, transition-metal carbonyl clusters are a potentially rich source of naked (or partially ligated) clusters for gas-phase reactivity studies. Advantages of this approach include the direct analogy that can be drawn with supported nanocatalysts prepared from identical precursors, the potential of using the technique as a means of rapidly screening new clusters for catalytic activity,[14] and the fact that a conventional electrospray source can be used for the preparation of naked clusters. Work is underway to evaluate other clusters and their reactions with various gases, including CO, $H_2$, $C_xH_y$, $O_2$, and NO.

## *Experimental Section*

EDESI mass spectra were collected on a Micromass Quattro LC triple-quadrupole instrument, and reactivity studies were carried out by using a Bruker Daltonics 3 T APEX II FTICR mass spectrometer. See supporting information for further details.

Received: September 12, 2003 [Z52859]

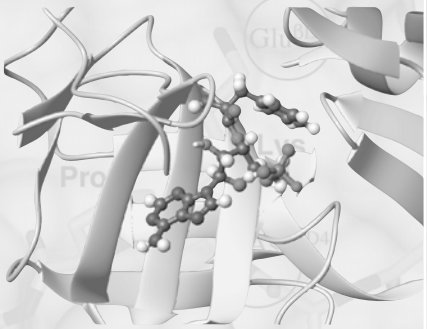
**Keywords:** cluster compounds · gas-phase reactions · mass spectrometry · surface chemistry

[1] K. M. Ervin, *Int. Rev. Phys. Chem.* **2001**, *20*, 127, and references therein.
[2] a) J. A. Barrow, D. J. Sordelet, M. F. Besser, C. J. Jenks, P. A. Thiel, E. F. Rexer, S. J. Riley, *J. Phys. Chem. A* **2002**, *106*, 9204; b) W. Bouwen, P. Thoen, F. Vanhoutte, S. Bouckaert, F. Despa, H. Weidele, R. E. Silverans, P. Lievans, *Rev. Sci. Instrum.* **2000**, *71*, 54; c) M. Heinebrodt, N. Malinowski, F. Tast, W. Branz, I. M. L. Billas, T. P. Martin, *J. Chem. Phys.* **1999**, *110*, 9915.
[3] a) S. Hermans, R. Raja, J. M. Thomas, B. F. G. Johnson, G. Sankar, D. Gleeson, *Angew. Chem.* **2003**, *115*, 1251; *Angew. Chem. Int. Ed.* **2001**, *40*, 1211; b) R. Raja, T. Khimyak, J. M. Thomas, S. Hermans, B. F. G. Johnson, *Angew. Chem.* **2001**, *113*, 4774; *Angew. Chem. Int. Ed.* **2001**, *40*, 4638.
[4] J. M. Thomas, R. Raja, B. F. G. Johnson, T. J. O'Connell, G. Sankar, T. Khimyak, *Chem. Commun.* **2003**, 1126.
[5] C. P. G. Butcher, P. J. Dyson, B. F. G. Johnson, T. Khimyak, J. S. McIndoe, *Chem. Eur. J.* **2003**, *9*, 944.
[6] a) P. J. Dyson, N. Feeder, B. F. G. Johnson, J. S. McIndoe, P. R. R. Langridge-Smith, *J. Chem. Soc. Dalton Trans.* **2000**, 1813; b) W. Henderson, J. S. McIndoe, B. K. Nicholson, P. J. Dyson *J. Chem. Soc. Dalton Trans.* **1998**, 519.
[7] G. S. Jackson, F. M. White, C. L. Hammill, R. J. Clark, A. G. Marshall, *J. Am. Chem. Soc.* **1997**, *119*, 7567.
[8] a) P. J. Dyson, B. F. G. Johnson, J. S. McIndoe, P. R. R. Langridge-Smith, *Rapid Commun. Mass Spectrom.* **2000**, *14*, 311; b) P. J. Dyson, A. K. Hearley, B. F. G. Johnson, J. S. McIndoe, P. R. R. Langridge-Smith, C. Whyte, *Rapid Commun. Mass Spectrom.* **2001**, *15*, 895; c) C. P. G. Butcher, P. J. Dyson, B. F. G. Johnson, P. R. R. Langridge-Smith, J. S. McIndoe, *Rapid Commun. Mass Spectrom.* **2002**, *16*, 1595.
[9] $[N(PPh_3)_2][CoRu_3(CO)_{13}]$ was prepared according to a reported procedure: G. L. Geoffroy, J. R. Fox, E. Burkhardt, H. C. Foley, A. D. Harley, R. Rosen, *Inorg. Synth.* **1982**, *21*, 57.
[10] K. J. Fisher, *Prog. Inorg. Chem.* **2001**, *50*, 343.

 © 2003 Wiley-VCH Verlag GmbH & Co. KGaA, Weinheim 

[11] a) K. Koszinowski, D. Schröder, H. Schwarz *J. Phys. Chem. A* **2003**, *107*, 4999; b) P. B. Armentrout, *Annu. Rev. Phys. Chem.* **2001**, *52*, 423; c) P. A. Hintz, K. M. Ervin, *J. Chem. Phys.* **1995**, *103*, 7897; d) G. M. Koretsky, K. P. Kerns, G. C. Nieman, M. B. Knickelbein, S. J. Riley, *J. Phys. Chem. A* **1999**, *103*, 1997; e) M. Andersson, A. Rosen, *J. Chem. Phys.* **2002**, *117*, 7051; f) W. T. Wallace, R. L. Whetten, *J. Am. Chem. Soc.* **2002**, *124*, 7499; g) K. Koszinowski, D. Schröder, H. Schwarz, *J. Am. Chem. Soc.* **2003**, *125*, 3676; h) D. Schröder, M. Engeser, M. Brönstrup, C. Daniel, J. Spandl, H. Hartl, *Int. J. Mass Spectrom.* **2003**, *228*, 743.
[12] M. J. Overett, R. O. Hill, J. R. Moss, *Coord. Chem. Rev.* **2000**, *206*, 581.
[13] C. K. Rofer-DePoorter, *Chem. Rev.* **1981**, *81*, 447.
[14] P. Chen, *Angew. Chem.* **2003**, *115*, 2938; *Angew. Chem. Int. Ed.* **2003**, *42*, 2832.

This book is definitely a must for all who want to read, or to read again, where we stand in our chemical comprehension of the fascinating relationship between chemical structure and biological processes, how we got here, and what the future might hold.



*Contributors:*
Peter B. Dervan, Jack D. Dunitz, Albert Eschenmoser, Christian Griesinger, Jean-Marie Lehn, Thomas F. Prisner, Gerhard Quinkert, Peter G. Schultz, Helmut Schwarz, Dieter Seebach, Ernst-Ludwig Winnacker, Ahmed Zewail

47423025_ba

# Essays in Contemporary Chemistry

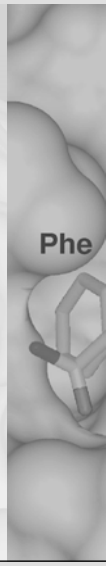
Gerhard Quinkert / M. Volkan Kisakürek (Eds.)

## From Molecular Structure towards Biology

2001. 471 pages with 230 figures (116 in color).
Hardcover. € 149.00/ sFr 220.00/ £ 80.00
ISBN 3-906390-28-4
*The €-Price is valid only for Germany.

In this volume internationally renowned chemists recount their roles in the progress of structural chemistry research toward elucidation of biological processes. Beginning with a historical perspective on the development of X-ray crystallography, the reader is regaled with first-hand accounts of research milestones.

Additionally there is a prologue by *Albert Eschenmoser*, for whom this collection was conceived, and an epilogue that contains facsimiles of notes from his landmark lecture 'Synthesis of Co-Enzyme $B_{12}$: A Vehicle for Teaching Organic Synthesis'.



Wiley-VCH, Customer Service Department, P.O. Box 10 11 61 , D-69451 Weinheim, Germany, Fax +49 (0) 6201 606-184, e-mail: service@wiley-vch.de, www.wiley-vch.de

John Wiley & Sons, Ltd., Customer Services Department, 1 Oldlands Way, Bognor Regis, West Sussex, PO22 9SA England, Fax: +44 (0) 1243-843-296, www.wileyeurope.com

VCH WILEY-VCH

 © 2003 Wiley-VCH Verlag GmbH & Co. KGaA, Weinheim 

*Polycyclic Aromatic Hydrocarbons*

# Fulvenes from Enediynes: Regioselective Electrophilic Domino and Tandem Cyclizations of Enynes and Oligoynes**

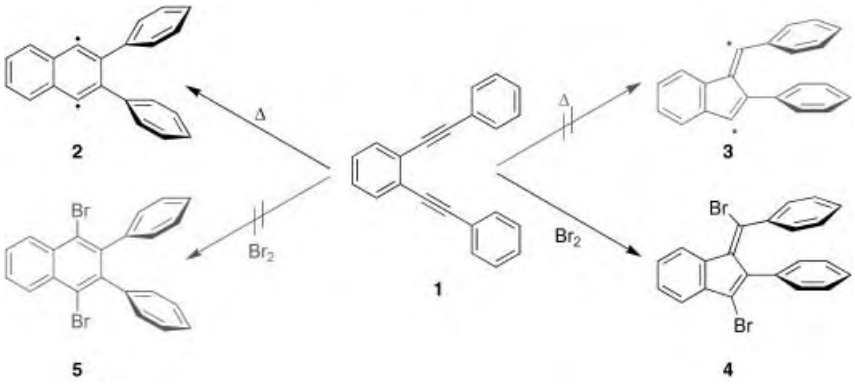
*Peter R. Schreiner,* Matthias Prall, and Volker Lutz*

The anellation of fulvenoid five- and aromatic six-membered rings in fullerenes is responsible for the curvature in these and many nonplanar polyaromatic hydrocarbons (PAHs).[1] Hence, the rational design of closed nanotubes or fullerenes[2] must include strategies for building five-membered rings, ideally from easily accessible starting materials that would also allow (by means of different reaction conditions) the formation of six-membered rings.

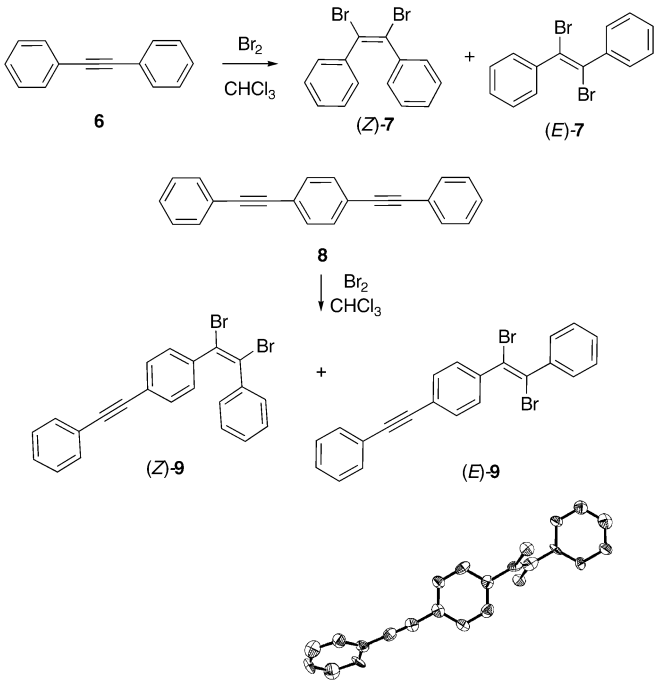
We recently became aware of such a possibility in our studies on alternatives to the $C^1$–$C^6$ cyclization of enediyne derivatives such as *o*-bis(phenylethynyl)benzene (**1**, Bergman reaction[3] to short-lived biradical **2**) that can, in principle, also lead to benzopentafulvenes ($C^1$–$C^5$ cyclization to biradical **3**; Scheme 1).[4] While the thermal cyclization yielding **3** is unlikely because of the high barrier for cyclization (ca. 40 kcal mol$^{-1}$ at UBS-B3LYP6-31G*), pentafulvenes do form when starting materials such as **1** react with electrophiles (e.g., bromine, to give **4** but not **5**),[5–7] carbanions,[6] and radicals.[8] Hence, the thermal and reagent-controlled reactions of **1** and its derivatives are nicely complementary and lend themselves to the production of novel carbon-rich architectures by means of well-established acetylene chemistry.[9]

The incorporation of halogens in compounds such as **4** may be useful in the context of rational fullerene syntheses.[2,10] Although the mechanisms of these reactions appear to be straightforward, it is startling that not even the electrophilic addition of bromine to diphenylacetylene (**6**, Scheme 2) is entirely understood.[11] The present communication sheds light on these as well as related reactions, which provide benzopentafulvenes by regioselective, electrophilic cyclizations.[6,7,12]

Surprisingly, the reported spectroscopic data for the isomeric dibromostilbenes **7** are incomplete. One source provides a $^1$H NMR spectrum for (*E*)-**7**, and the assigned configuration is corroborated by an X-ray crystal structure.[13] Another source reports the $^{13}$C NMR signals for (*E*)-**7**,[14] which, however, match ours for (*Z*)-**7**. NMR coupling constants are equally inconclusive. To resolve this issue by means of an analogy we brominated **8**[15] under identical conditions to those that gave **7** (0.4 M $Br_2$ in $CHCl_3$). The resulting mixture of (*E*)-**9** and (*Z*)-**9** (60:40) had the same proportions as the mixture of (*E*)-**7** and (*Z*)-**7** formed in the bromination of **6**. Fractional crystallization gave crystals of (*E*)-**9** (Scheme 2); its $^{13}$C NMR signals at $\delta = 118.48$ and




***Scheme 1.*** The thermal reaction of **1** proceeds by Bergman cyclization to form a six-membered ring, whereas the bromination yields the benzopentafulvene derivative **4**.




***Scheme 2.*** Addition of bromine to phenylalkynes **6** and **8** gives *E*/*Z* mixtures of products **7** and **9**, respectively. The X-ray crystal structure of (*E*)-**9** is also shown.

[*] Prof. Dr. P. R. Schreiner, Dr. M. Prall, V. Lutz
Institut für Organische Chemie
Justus-Liebig-Universität
Heinrich-Buff-Ring 58, 35392 Giessen (Germany)
Fax: (+49) 641-99-34309
E-mail: prs@org.chemie.uni-giessen.de

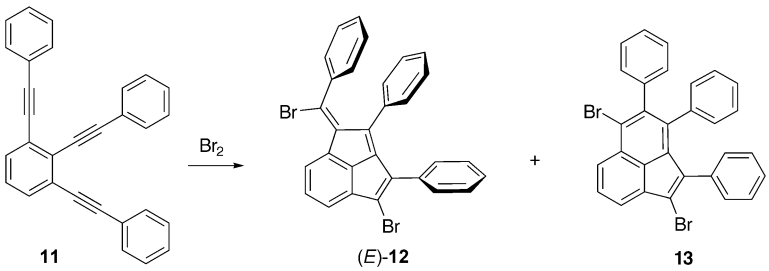
[**] This work was supported by the Deutsche Forschungsgemeinschaft, the Fonds der Chemischen Industrie, and the National Science Foundation (CHE-0209857). We thank Prof. M. Schmittel for valuable comments.

Supporting information for this article is available on the WWW under http://www.angewandte.org or from the author.

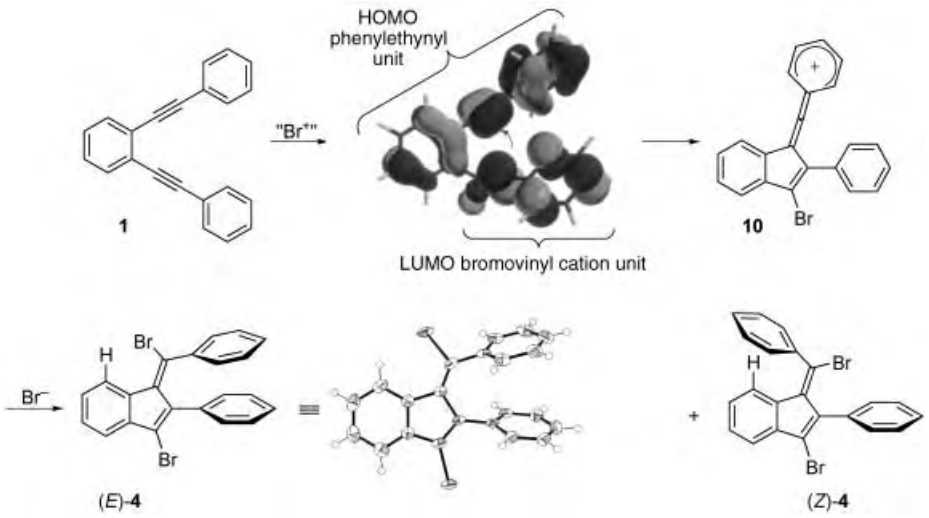
 DOI: 10.1002/anie.200351195 © 2003 Wiley-VCH Verlag GmbH & Co. KGaA, Weinheim 

117.34 ppm are closer to those for (*E*)-**7** than for (*Z*)-**7**. Hence, the $^{13}C$ NMR signal assignment in ref. [14] is likely to be incorrect. The lack of selectivity of the bromine addition supports the notion of an open cationic intermediate.[14]

The electrophilic cyclization of **1** to give **4** (Scheme 3) can be rationalized by the formation of the stabilized cation **10**.[6] The cyclization to give an aromatic six-membered ring would yield a highly unfavorable naphthyl cation. The isomers of **4** can be separated by recrystallization, and




***Scheme 4.*** Electrophilic domino cyclization of **11** to give (*E*)-**12** and **13** ((*E*)-**12**/**13** = 4:1, NMR).




***Scheme 3.*** Electrophilic domino cyclization of **1** to give (*E*)-**4** and (*Z*)-**4** (5:1). The X-ray crystal structure of (*E*)-**4** is also shown. The LUMO of the bromovinyl unit and the HOMO of the phenylethynyl unit are shown to demonstrate the orbital-controlled preference of the fulvene cyclization.

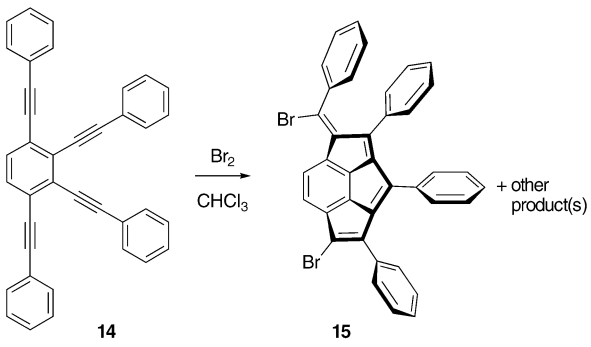
the crystal structure of the major product (*E*)-**4** (> 80 %) supports the structural assignment. The peripheral phenyl groups are oriented coplanar with a separation of about 3.8 Å and are perpendicular to the fully conjugated benzopentafulvene moiety. These results and the calculations for (*E*)-**4** in the gas phase (B3LYP6-31G*)[16] concur.

The approach of the LUMO of the bromovinyl moiety and the HOMO of the phenylethynyl moiety shows that the endergonic cyclization is initially orbital-controlled. This is evident from the reduced distance between the orbital lobes responsible for the C–C bond formation. In contrast to earlier work, we note that the bromovinyl cation is a true minimum (at B3LYP6-31G*) with a classic, nonbridging structure.[14]

As one of the resonance structures of **10** is a vinyl cation,[17] we envisaged that an adjacent third phenylethynyl moiety (as in **11**, Scheme 4) could be attacked in a domino reaction[5] to give a product with a second fulvene ring. The reaction of **11** with bromine yields not only the major product (*E*)-**12** but also the acenaphthalene derivative **13** (Scheme 4; (*E*)-**12**/**13** = 4:1, NMR). The separation of these two products is not easy. The major product (*E*)-**12** readily isomerizes to (*Z*)-**12** during column chromatography and even in $CDCl_3$ (due to traces of HCl). In the computed structure of (*E*)-**12** the phenyl groups are also coplanar; the distance between the second and third phenyl group (3.1 Å) is significantly shorter than that between the first and the second, and is comparable to that in [3.3]paracyclophanes (3.2 Å).[18] This synthesis of **12** allows convenient access to cyclopent[*cd*]indenes, which can be exploited as redox-active PAHs.[19]

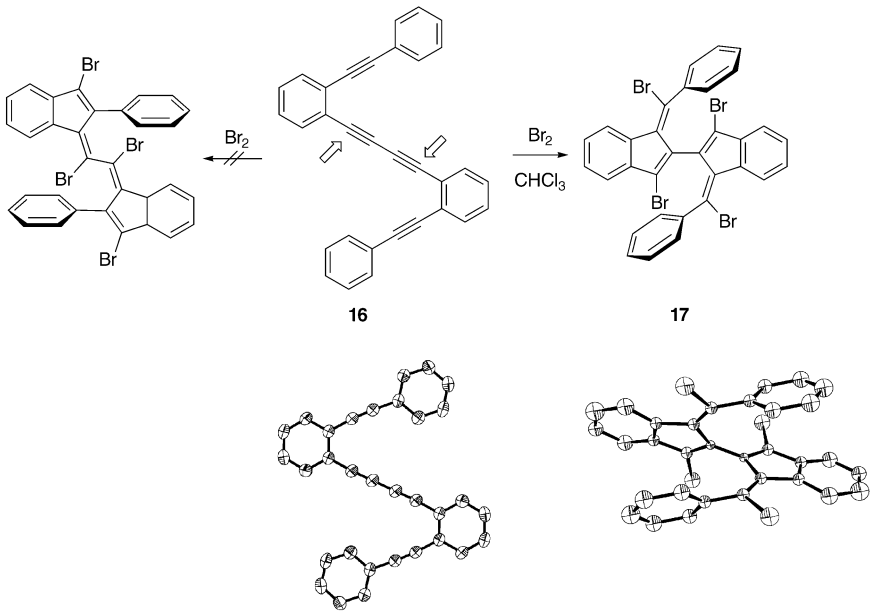
This strategy can be extended for the electrophilic domino cyclization of more highly substituted phenylethynylbenzene derivatives to produce carbon-rich fulvenoid materials. Indeed, the cyclization of **14** gives the half-bowl compound **15** (based on the NMR spectrum of the product mixture; Scheme 5). At least one other compound is present, which is likely the next higher analogue of **13**. Owing to their similarity and insolubility, the products cannot be separated. We are currently preparing *p*-alkyl-substituted phenylethynyl derivatives, which should display less self-association and better solubility. When these problems typical for PAHs are solved, the electrophilic "zipper" cyclization should be an interesting alternative for the synthesis of anellated benzopentafulvenes.

As a test of the pronounced regioselectivity of the cyclization, we brominated the tetrayne **16** (Scheme 6). The selective formation of the previously unknown bisfulvene **17** can be explained only by the attack of "$Br^+$" at the more electron-rich diyne unit (arrows in Scheme 6). The cyclizations to give the two pentafulvene units occur in a tandem




***Scheme 5.*** Electrophilic domino cyclization of **14** leads to the half-bowl compound **15**.

 © 2003 Wiley-VCH Verlag GmbH & Co. KGaA, Weinheim 




***Scheme 6.*** Electrophilic tandem cyclization of tetrayne **16** upon bromination to give bisfulvene **17**. The X-ray crystal structures of **16** and **17** are depicted.

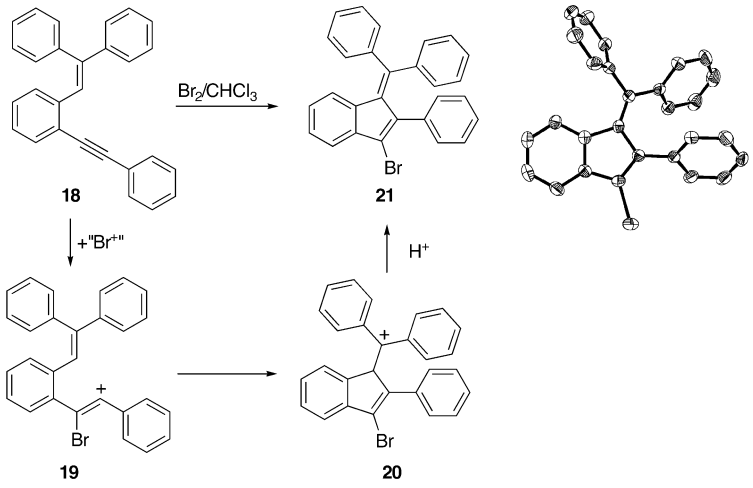
fashion, and the domino cyclization to give naphthyl derivatives does not compete. Note that in the crystal structure of **17** the two benzopentafulvene moieties are not in conjugation (twist angle at the central butadiene moiety = 88°).

Finally, the question of differences in the reactivity of double and triple bonds in electrophilic reactions[11,20] was also addressed through the bromination of the novel eneyne **18** (Scheme 7). Remarkably, the addition of the $Br^+$ ion is followed by the expected regioselective fulvene cyclization and then by formal loss of a proton. Hence, this reaction is an example for a rare electrophilic vinylic substitution.[21] The alternative mechanism—an addition/elimination—is unlikely because the $Br^-$ ion is a weak base. The observed mode of the reaction is explained by the occurrence of the stabilized cation **20**. The subsequent loss of a proton with formation of an extended conjugated system is preferred over bromide capture. However, maximizing conjugation alone does not explain the formation of product **21**, which displays significant twisting around the exocyclic double bond (dihedral angle: 22°, computed: 23°). The computed structure also indicates that the phenyl groups are not aligned for perfect conjugation; in other words, this is not a packing effect.

The electrophilic cyclizations of aromatic systems having adjacent alkyne moieties to give benzopentafulvene derivatives complement their thermal reactions, which give aromatic six-membered rings. This strategy can be used to introduce curved structure elements into carbon-rich compounds that are synthesized by, for example, by the vaporization of graphite. After electrophilic aromatic halogenation and alkynylation, the resulting *ortho*-oligoynes can then be cyclized to give anellated benzopentafulvenes. This approach is not limited to bromine (or other halogens) as the electrophile; acid-catalyzed cyclizations of enediynes are also known, which after air oxidation give five-membered derivatives.[22] As all of the fulvene cyclization products contain bromine as a heteroatom, further functionalization is straightforward and should make this approach broadly applicable to the rational synthesis of a large variety of PAHs.

## Experimental Section

Details of the preparation and characterization of **4**, **9**, **12**, **16**–**18**, and **21** can be found in the Supporting Information.




***Scheme 7.*** Vinylic electrophilic substitution at eneyne **18** provides the fulvene derivative **21**. The X-ray crystal structure of **21** is also shown.

Received: February 17, 2003
Revised: August 20, 2003 [Z51195]

**Keywords:** alkynes · bromine · cyclization · polycycles · tandem reactions

[1] M. Zander, *Polycyclische Aromaten. Kohlenwasserstoffe und Fullerene*, Teubner, Stuttgart, **1995**.
[2] L. T. Scott, M. M. Boorum, B. J. McMahon, S. Hagen, J. Mack, J. Blank, H. Wegner, A. de Meijere, *Science* **2002**, *295*, 1500.
[3] R. R. Jones, R. G. Bergman, *J. Am. Chem. Soc.* **1972**, *94*, 660.
[4] M. Prall, A. Wittkopp, P. R. Schreiner, *J. Phys. Chem. A* **2001**, *105*, 9265.
[5] B. J. Whitlock, H. W. Whitlock, *J. Org. Chem.* **1972**, *37*, 3559.
[6] H. W. Whitlock, P. E. Sandvick, L. E. Overman, P. B. Reichardt, *J. Org. Chem.* **1969**, *34*, 879.

 © 2003 Wiley-VCH Verlag GmbH & Co. KGaA, Weinheim 

[7] H. W. Whitlock, P. E. Sandvick, *J. Am. Chem. Soc.* **1966**, *88*, 4525.
[8] B. König, W. Pitsch, M. Klein, R. Wasold, M. Prall, P. R. Schreiner, *J. Org. Chem.* **2001**, *66*, 1742.
[9] P. J. Stang, F. Diederich, *Modern Acetylene Chemistry*, VCH, Weinheim, **1996**.
[10] M. M. Boorum, Y. V. Vasil'ev, T. Drewello, L. T. Scott, *Science* **2001**, *294*, 828.
[11] G. Melloni, G. Modena, U. Tonellato, *Acc. Chem. Res.* **1981**, *14*, 227.
[12] a) J. Blum, W. Baidossi, Y. Badrieh, R. E. Hoffman, *J. Org. Chem.* **1995**, *60*, 4738; b) Q. Zhou, P. J. Carroll, T. M. Swager, *J. Org. Chem.* **1994**, *59*, 1294.
[13] J. H. Espenson, Z. Zhu, T. H. Zauche, *J. Org. Chem.* **1999**, *64*, 1191.
[14] R. Bianchini, C. Chiappe, G. Lo Moro, D. Lenoir, P. Lemmen, N. Goldberg, *Chem. Eur. J.* **1999**, *5*, 1570.
[15] H.-F. Chow, C.-W. Wan, K.-H. Low, Y.-Y. Yeung, *J. Org. Chem.* **2001**, *66*, 1910.
[16] Gaussian 98 (Revision A.11), M. J. Frisch, G. W. Trucks, H. B. Schlegel, G. E. Scuseria, M. A. Robb, J. R. Cheeseman, V. G. Zakrzewski, J. A. Montgomery, R. E. Stratmann, J. C. Burant, S. Dapprich, J. M. Millam, A. D. Daniels, K. N. Kudin, M. C. Strain, O. Farkas, J. Tomasi, V. Barone, M. Cossi, R. Cammi, B. Mennucci, C. Pomelli, C. Adamo, S. Clifford, J. Ochterski, G. A. Petersson, P. Y. Ayala, Q. Cui, K. Morokuma, D. K. Malick, A. D. Rabuck, K. Raghavachari, J. B. Foresman, J. Cioslowski, J. V. Ortiz, B. B. Stefanov, G. Liu, A. Liashenko, P. Piskorz, I. Komaromi, R. Gomperts, R. L. Martin, D. J. Fox, T. Keith, M. A. Al-Laham, C. Y. Peng, A. Nanayakkara, C. Gonzalez, M. Challacombe, P. M. W. Gill, B. G. Johnson, W. Chen, M. W. Wong, J. L. Andres, M. Head-Gordon, E. S. Replogle, J. A. Pople, Gaussian, Inc., Pittsburgh, PA, **1998**.
[17] P. J. Stang, Z. Rappoport, M. Hanack, L. R. Subramanian, *Vinyl Cations*, Academic Press, New York, **1979**.
[18] P. K. Gantzel, K. N. Trueblood, *Acta Crystallogr.* **1965**, *18*, 958; P. G. Jones, H. Hopf, Z. Pechlivanidis, R. Boese, *Z. Kristallogr.* **1994**, *209*, 673.
[19] P. Eilbracht, K. Hafner, *Angew. Chem.* **1971**, *83*, 802; *Angew. Chem. Int. Ed. Engl.* **1971**, *10*, 751.
[20] G. H. Schmid in *The Chemistry of the Carbon–Carbon Triple Bond* (Ed.: S. Patai), Wiley-Interscience, Chichester, England, **1978**.
[21] M. Hojo, R. Masuda, Y. Kamitori, E. Okada, *J. Org. Chem.* **1991**, *56*, 1975; Z. Rappoport, I. Schnabel, *J. Chem. Soc. Perkin Trans. 2* **1972**, 146.
[22] M. Schmittel, S. Kiau, *Liebigs Ann.* **1997**, 1391.

 © 2003 Wiley-VCH Verlag GmbH & Co. KGaA, Weinheim 

Heterogeneous Catalysis

# Styrene Synthesis: High Conversion over Unpromoted Iron Oxide Catalysts under Practical Working Conditions**

*Osama Shekhah, Wolfgang Ranke,* Achim Schüle, Grigorios Kolios, and Robert Schlögl*

The standard catalyst for the dehydrogenation of ethylbenzene (EB) to give styrene (St) consists of potassium-promoted iron oxides,[1–5] but unpromoted iron oxides are active as well.[5–7] In order to understand the actual role of the iron oxide, we have resumed studies on unpromoted hematite, $\alpha$-$Fe_2O_3$. In an attempt to bridge the gap between real and ideal systems we compare experiments on powder pellets in a fixed-bed reactor under technical conditions with model catalysis studies. In the latter we prepare and characterize single-crystalline samples in ultrahigh vacuum (UHV) and measure the conversions for reactions with these samples under realistic conditions in an in-situ microflow reactor.

Figure 1 shows the time dependence of the rate of St production over pressed pellets of hematite powder in a small fixed-bed reactor under the conditions of the technical reaction and compares them with a measurement where

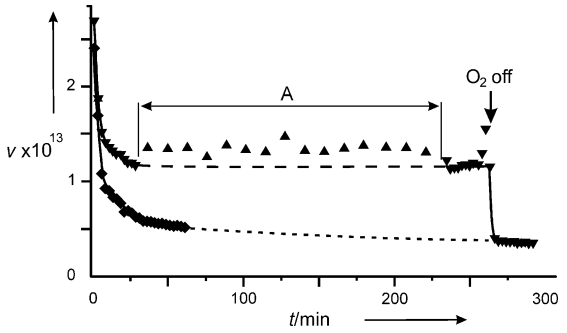



***Figure 1.*** Time dependence of the rate of styrene production ($\nu$ in molecules per s and $cm^2$ BET surface) for the dehydrogenation of ethylbenzene (EB) over pressed pellets of $Fe_2O_3$ powder in a fixed-bed reactor. Reaction temperature 895 K, atmospheric pressure. ◆: $EB/H_2O \approx 1:6$, ▲: $EB/H_2O/O_2 \approx 1:6:0.4$. Around point A the GC measurement was switched from fast FID analysis to the combined FID-TCD method. This caused a shift in the baseline. For details see the Experimental Section.

[*] Dr. W. Ranke, O. Shekhah, Prof. Dr. R. Schlögl
Abteilung Anorganische Chemie
Fritz-Haber-Institut der Max-Planck-Gesellschaft
Faradayweg 4–6, 14195 Berlin (Germany)
Fax: (+49) 30-8413-4401
E-mail: ranke@fhi-berlin.mpg.de

A. Schüle, Dr. G. Kolios
Institut für Chemische Verfahrenstechnik
Universität Stuttgart
Böblinger Strasse 72, 70199 Stuttgart (Germany)

[**] Supported by the Deutsche Forschungsgemeinschaft (RA376/2-2 and KO2049/2-2).

 © 2003 Wiley-VCH Verlag GmbH & Co. KGaA, Weinheim DOI: 10.1002/anie.200352135 

traces of oxygen were added to the feed. In both cases the reaction rate drops initially, but in the presence of oxygen the rate is stabilized at a value about three times higher than without. Possible reasons could be a stabilization of the hematite phase or burning of coke or both. Interruption of the oxygen feed leads to a quick drop in rate to the level of the experiment without oxygen. X-ray diffraction (XRD) analysis of the spent catalyst shows that it is completely reduced to magnetite, confirming previous observations.[2,4,8]

In order to identify the active phases and to understand the role of oxygen and the deactivation processes, we performed studies using well-characterized $\alpha$-$Fe_2O_3(0001)$ (hematite) and $Fe_3O_4(111)$ (magnetite) model catalysts. They were prepared in ultrahigh vacuum (UHV) in the form of single-crystalline epitaxial films on Pt(111) substrates.[9] The surface composition was characterized by Auger electron spectroscopy (AES), and the oxide phase was characterized by low-energy electron diffraction (LEED). The catalysts were transferred under vacuum into a stagnation-point microflow reactor[10] with a void volume of only 4 $cm^3$, where the reaction was performed under atmospheric pressure with variable feed composition. The catalytic activity was monitored in the flow-through mode by gas chromatography from the moment of admission. The model catalysts were then transferred back to the UHV chamber for postreaction characterization by AES. If carbonaceous deposits formed, they were removed in a number of temperature-programmed oxidation (TPO) runs before the oxide surface was analyzed by LEED.

In order to study the role of water and oxygen in the reactant mixture, experiments with different feed composition were conducted: with EB alone in the carrier gas (He), with EB and water as in the technical process, and with EB, water, and oxygen. Figure 2 shows the time dependence of the rate of styrene production over the model catalysts for the three different feed compositions. For the dehydrogenation of EB in the presence of water (Figure 2b) the rate drops within about 70 min from a high initial to a low final value. It should be stressed, however, that the final rate is not zero. Postreaction surface analysis by AES at point E (see Table 1) shows that the surface is covered by carbonaceous deposits. After carbon removal the LEED pattern shows, as expected,[1,4,8] that the hematite is reduced to magnetite.

A very similar decrease occurs when no water but only EB is present in the feed (Figure 2a). The final rate is about the same, although the surface now is totally covered by carbon (no Auger signals for Fe or O; Table 1). Carbon removal requires many TPO cycles, and the oxide turns out to be reduced, in part even to metallic $Fe^0$. We conclude that the catalytically active phase in this final regime is carbon. Carbon deposits are always present under steady-state reaction conditions without oxygen,[4] especially on unpromoted catalysts.[6] It is therefore likely that coke was the catalytically active phase in all previous studies performed on unpromoted catalysts. That certain forms of carbon are catalytically active was only known for oxidative dehydrogenation up to this point.[11] The turnover frequency (TOF) calculated from the rate in the final state in Figure 2a,b is approximately 1.4 molecules per s and site.[12]

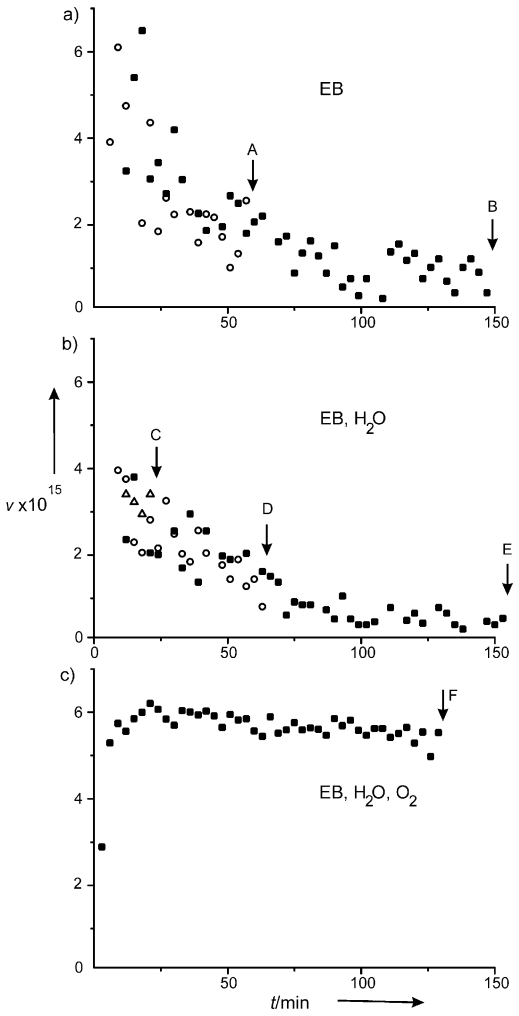



***Figure 2.*** Time dependence of the rate of styrene production ($\nu$ in molecules per s and $cm^2$) for the dehydrogenation of ethylbenzene (EB) in the microflow reactor for different reactant compositions: a) only EB in He, b) EB/$H_2O$ (molar ratio 1:10) in He, c) EB/$H_2O$/$O_2$ (molar ratio 1:10:0.55) in He. At points A–F the reaction was stopped and Auger measurements were performed. Each time, the measurement was started again with a freshly prepared film (different symbols △, ○, and ■). The corresponding Auger intensity ratios are given in Table 1.

Table 1 summarizes the results of the surface characterization of the model catalysts at different stages of the conversion experiments. When the reaction is interrupted in the high-conversion regime (point C in Figure 2b), analysis of the catalyst surface shows that only a small amount of carbon (C/Fe Auger peak height ratio ca. 1) has been deposited. The O/Fe ratio has decreased only slightly, and, accordingly, LEED after only one TPO cycle shows the pattern of hematite. Increased spot widths indicate increased disorder. In an intermediate regime (point D in Figure 2b) the carbon deposits have increased. LEED analysis after two TPO cycles exhibits a superposition of the patterns of hematite and magnetite, suggesting partial reduction close to the surface.[13] The appearance of separated and ordered domains of both phases is certainly a result of the heating during TPO experiments. When we started the measurements with a clean magnetite sample ($Fe_3O_4(111)$) under the same con-

 © 2003 Wiley-VCH Verlag GmbH & Co. KGaA, Weinheim 

***Table 1:*** LEED patterns and intensity ratios for the main Auger peaks of oxygen, iron, and carbon after different treatments.

| Treatment | LEED pattern | Phase (from LEED) | Intensity ratios (AES) C/Fe | O/Fe | Label in Figure 2 |
|---|---|---|---|---|---|
| $Fe_2O_3$ before reaction |  | $Fe_2O_3$ | 0 | 3.5[a] | – |
| Reaction with EB | no pattern | | 5.3 | 2.0 | A |
| | | | [b] | – | B |
| Reaction with EB + $H_2O$ |  | $Fe_2O_3$[c] | 1.1 | 3.2 | C |
| | | | 3.6 | 4.0 | D |
| | | | 3.4 | 3.8 | E |
| Reaction with EB + $H_2O$ + $O_2$ |  | $Fe_2O_3$, disordered[d] | 0.8 | 3.4 | F |

[a] If O/Fe = 3.5 corresponds to $Fe_2O_3$, then O/Fe = 3.1 would correspond to $Fe_3O_4$. [b] Only C is observed in the spectrum. [c] After three TPO cycles. [d] After one TPO cycle.

ditions as in Figure 2b, the initial rate was the same as at point D. After about 60 min it dropped to the same final value as that for hematite and was covered by coke. We can thus attribute the high initial rate to hematite as the active phase. The intermediate rate at point D may be due to reduction to magnetite or to reduction and partial coking, while the final rate is characteristic for coke.

When traces of oxygen are added to the reaction mixture, a high conversion rate is stabilized (Figure 2c). Surface analysis at point F reveals only little carbon on weakly ordered $Fe_2O_3$ (Table 1), which proves that oxygen prevents reduction of hematite and oxidizes coke deposits. When the oxygen content in the feed exceeds that of EB, total oxidation effects start to dominate. The initial high-rate regime in Figure 2a,b is thus maintained as long as the near-surface region consists of hematite. Without oxygen, the hematite is reduced to magnetite by the hydrogen formed in the dehydrogenation reaction.

We have shown that the initial rate of St production over unpromoted hematite is high. Deactivation occurs within roughly one hour, and previously only this final state with the lowest rate had been observed. The initial rate is almost an order of magnitude higher and thus similar to that of potassium-promoted catalysts.[2,3] Deactivation occurs by reduction of the hematite catalyst to magnetite and by coke deposition. Water prevents further reduction of magnetite and reduces carbon accumulation by coal gasification. The deactivation can be suppressed largely by adding even low concentrations of oxygen; this prevents the reduction of hematite to magnetite and oxidizes carbon deposits. The absolute rates (per $cm^{-2}$) obtained for the flat model catalysts are about two orders of magnitude higher than for the porous powder pellets. The model studies using surface-science methods have thus shown that the performance of the technical process for styrene synthesis is not limited by elementary surface processes but by mass and energy transport. An essential improvement of the overall performance is thus not to be expected by varying the catalyst but by optimizing the process engineering.

## *Experimental Section*

Real catalysis: Cylindrical pellets (diameter 7.1 mm, length 8.8 mm, BET area 2.8 $m^2 g^{-1}$) were pressed from hematite powder. Sixteen pellets were put into a small fixed-bed reactor (bed diameter 20 mm, height 35 mm) installed in a tube furnace. The reaction was conducted at 895 K and under atmospheric pressure. The feed consisted of 26 mL $h^{-1}$ of liquid water and 30 mL $h^{-1}$ of liquid EB, both evaporated and mixed. For the experiments with oxygen, 37.2 mL $h^{-1}$ of $O_2$ was added. The product gas mixture was analyzed by gas chromatography. Two methods were implemented: A fast analysis mode with a runtime of 2.5 min using a FID (flame ionization detector) for detecting the aromatics and a detailed mode with a runtime of 13 min using the FID and a TCD (thermal conductivity detector) for detecting gas compounds as well.

Model catalysis: The main ultrahigh-vacuum chamber (base pressure $10^{-10}$ mbar) was equipped with facilities for sample preparation and cleaning, standard LEED optics, and a cylindrical mirror analyzer for AES. Films of $Fe_3O_4$(111) 100–200-Å thick were prepared by iron deposition at room temperature on a clean Pt(111) substrate with an area of 0.5 $cm^2$,[9] followed by oxidation at 950 K in $5 \times 10^{-7}$ mbar of oxygen. These films were transformed into $\alpha$-$Fe_2O_3$(0001) by treatment with oxygen at pressures above $10^{-1}$ mbar and temperatures around 1050 K. Order and cleanliness were monitored by LEED and AES. The samples were transferred under vacuum into a preparation cell where high-pressure oxidation treatment and the reaction experiments were performed in a stationary-flow reactor.[10] The samples were heated by radiation from two fiber-coupled diode laser stacks (total power max. 100 W). After the sample was transferred into the reactor cell, the reactor cap was closed and the cell preheated to 470 K under vacuum. The reactor chamber was then vented with nitrogen and the sample heated to the reaction temperature (870 K). During this period, a He flow of 20 mL $min^{-1}$ at 1 bar passing through a water saturator at 303 K ($p_{H_2O}$ = 42 mbar), together with a flow of 0.5 mL $min^{-1}$ of $O_2$ was introduced into the reactor. When the reaction temperature stabilized, the $O_2$ flow was stopped and a flow of 5 mL $min^{-1}$ of He passing through an ethylbenzene saturator at 303 K ($p_{EB}$ = 17 mbar) was added to the He + $H_2O$ flow, resulting in an EB/$H_2O$ molar ratio of ~1:10. For the experiments with water and oxygen, a flow of 0.24 mL $min^{-1}$ of 20% $O_2$ in He was added. For the experiments without water and oxygen, 20 mL of He alone was introduced to keep the total flow constant. From the product gas mixture, aliquots of 250 µL were injected every 3 min into the column of a gas chromatograph and analyzed with an ion trap mass spectrometer (GCMS). Temperature-programmed oxidation (TPO) was performed after the sample had been transferred back to the main chamber by heating at a rate of 5 K $s^{-1}$ to 1000 K in $10^{-6}$ mbar oxygen, which is sufficient to remove carbon without reoxidation of the substrate.

Received: June 13, 2003 [Z52135]

 © 2003 Wiley-VCH Verlag GmbH & Co. KGaA, Weinheim 

**Keywords:** dehydrogenation · ethylbenzene · heterogeneous catalysis · iron oxide · styrene

[1] K. Kochloefl in *Handbook of heterogeneous catalysis*, *Vol. 5* (Eds.: G. Ertl, H. Knözinger, J. Weitkamp), Wiley, Weinheim, **1997**, p. 2151.
[2] E. H. Lee, *Catal. Rev.* **1973**, *8*, 285.
[3] T. Hirano, *Appl. Catal.* **1986**, 26, 65.
[4] G. M. Meima, P. G. Menon, *Appl. Catal. A* **2001**, *212*, 239.
[5] M. Muhler, J. Schütze, M. Wesemann, T. Rayment, A. Dent, R. Schlögl, G. Ertl, *J. Catal.* **1990**, *126*, 339.
[6] K. Coulter, D. W. Goodman, R. G. Moore, *Catal. Lett.* **1995**, *31*, 1.
[7] W. P. Addiego, C. A. Estrada , D. W. Goodman, M. P. Rosynek, *J. Catal.* **1994**, *146*, 407.
[8] W. Weiss, D. Zscherpel, R. Schlögl, *Catal. Lett.* **1998**, *52*, 215.
[9] W. Weiss, W. Ranke, *Prog. Surf. Sci.* **2002**, *70*, 1.
[10] C. Kuhrs, M. Swoboda, W. Weiss, *Top. Catal.* **2001**, *15*, 13.
[11] a) G. Mestl, N. I. Maksimova, N. Keller, V. V. Roddatis, R. Schlögl, *Angew. Chem.* **2001**, *113*, 2122 – 2125; *Angew. Chem. Int. Ed.* **2001**, *40*, 2066; b) N. Keller, N. I. Maksimova, V. V. Roddatis, M. Schur, G. Mestl, Y. V. Butenko, V. L. Kuznetsov, R. Schlögl, *Angew. Chem.* **2002**, *114*, 1966 – 1966; *Angew. Chem. Int. Ed.* **2002**, *41*, 1885 – 1888.
[12] The TOF was calculated assuming that the density of $Fe_2O_3(0001)$ surface units ($4.6 \times 10^{14}\,cm^{-2}$) is the same as the site density. In experiments under temperature and pressure conditions similar to ours, Coulter et al.[6] give a TOF of $5 \times 10^{-3}$ styrene molecules per s and site for reactions on an oxidized polycrystalline slice of iron. They comment that this is a lower limit because of the assumption of a high density of active sites.
[13] For $Fe_2O_3$ reduction, the following stoichiometric reaction may be suggested: $C_8H_{10} + 3\,Fe_2O_3 \rightarrow C_8H_8 + 2\,Fe_3O_4 + H_2O$. Here, the oxygen liberated by reduction is consumed by the hydrogen formed in the dehydrogenation of ethylbenzene. Our model catalyst films are 100–200 Å thick. Assuming reduction of the whole film to $Fe_3O_4$ during the initial high-conversion regime in Figures 2 a, b, we can estimate the amount of liberated oxygen. It turns out that the styrene production is about a factor of 700 higher than explainable by the above stoichiometric reaction. The factor 700 is a lower limit since oxygen may also be consumed in the oxidation of coke. We can conclude that the dehydrogenation reaction of ethylbenzene to styrene over clean $Fe_2O_3$ is essentially catalytic. The stoichiometric reaction may be a side reaction.

 © 2003 Wiley-VCH Verlag GmbH & Co. KGaA, Weinheim 

C–H Activation

# Enantioselective, Copper(I)-Catalyzed Three-Component Reaction for the Preparation of Propargylamines**

*Nina Gommermann, Christopher Koradin, Kurt Polborn, and Paul Knochel**

The catalytic enantioselective formation of new C–C bonds is an important class of reactions.[1] Especially attractive are multicomponent reactions which allow the formation of several bonds including new C–C bonds in a one-pot procedure.[2] For achieving optimum atom economy[3] and avoiding the production of stoichiometric amounts of metal salts as by-products, we[4] and others[5] have examined the use of an alkyne as the precursor for the nucleophilic reaction component. Alkynes of type **1** can be deprotonated catalytically in situ by means of cesium salts and reacted subsequently with aldehydes and ketones, leading to propargyl alcohols.[6] Recently, we have shown that various enamines react with terminal alkynes in the presence of copper(I) salts and quinap (**2**),[7] providing propargylamines in up to 90% *ee*.[4]

In order to avoid the generation of sensitive enamines and to extend the scope of this propargylamine synthesis to nonenolizable aldehydes (i.e. aldehydes from which enamines cannot be prepared), we have examined a new three-component reaction[8] between an alkyne **1**, an aldehyde **3**, and a secondary amine **4**. We have found that propargylamines of type **5** are formed in toluene at room temperature in the presence of CuBr (5 mol%), (*R*)-quinap ((*R*)-**2**) (5.5 mol%), and molecular sieves 4 Å in excellent yields (up to 99%) and good enantioselectivities (up to 96% *ee*; Scheme 1 and Table 1).

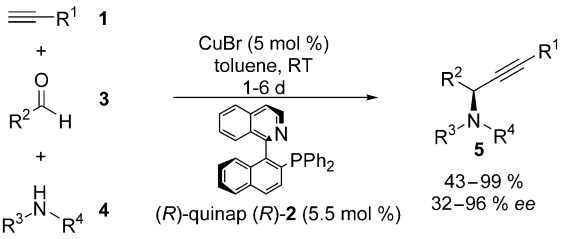
The reaction is usually complete within 12 to 48 h for the racemic reaction without ligand and within one to six days for the enantioselective reaction with high yields in most cases. The alkyne can bear either an aryl substituent ($R^1 = Ph$) or an alkyl substituent ($R^1 = Bu$; entries 1 and 2 in Table 1). The resulting propargylamines **5a** and **5b** were obtained in 98 and 85% yield and 86 and 82% *ee*, respectively. Branched aliphatic aldehydes like isobutyraldehyde lead to the expected propargylamines **5c** and **5d** in 60 and 99% yield and 84 and 83% *ee*, respectively (entries 3 and 4). The use of

[*] Prof. Dr. P. Knochel, Dipl.-Chem. N. Gommermann, Dr. C. Koradin, Dr. K. Polborn
Department Chemie
Ludwig-Maximilians-Universität München
Butenandtstrasse 5–13, Haus F, 81377 München (Germany)
Fax: (+49) 89-2180-77680
E-mail: paul.knochel@cup.uni-muenchen.de

[**] We thank Chemetall GmbH (Frankfurt), Degussa (Frankfurt), and BASF AG (Ludwigshafen) for generous gifts of chemicals. N.G. thanks the DFG for a fellowship in the context of SPP 1118 "Sekundäre Wechselwirkungen als Steuerungsprinzip zur gerichteten Funktionalisierung reaktionsträger Substrate".

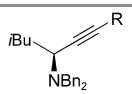
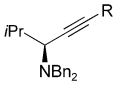
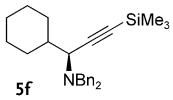
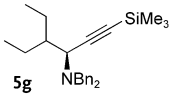
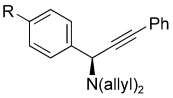
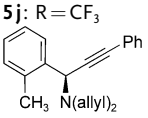
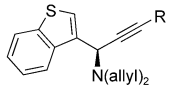
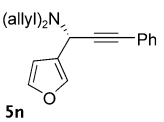
Supporting information for this article is available on the WWW under http://www.angewandte.org or from the author.

 DOI: 10.1002/anie.200352578 © 2003 Wiley-VCH Verlag GmbH & Co. KGaA, Weinheim 




***Scheme 1.*** Enantioselective three-component reaction for the synthesis of proparylamines. RT = room temperature.

***Table 1:*** Enantioselective, copper(I)-catalyzed three-component synthesis of propargylamines **5**.

| Entry | $R^1$ | $R^2$ | $R^3$ | **5** | Yield [%][a] | Sel. [% *ee*][b] |
|---|---|---|---|---|---|---|
| | | | |  | | |
| 1 | Ph | *i*Bu | Bn | **5a**: R = Ph | 98 | 86 |
| 2 | *n*Bu | *i*Bu | Bn | **5b**: R = *n*Bu | 85 | 82 |
| | | | |  | | |
| 3 | Ph | *i*Pr | Bn | **5c**: R = Ph | 60 | 84 |
| 4 | *p*-$BrC_6H_4$ | *i*Pr | Bn | **5d**: R = *p*-$BrC_6H_4$ | 99 | 83 |
| 5 | $SiMe_3$ | *i*Pr | Bn | **5e**: R = $SiMe_3$ | 87 | 92[c] |
| 6 | $SiMe_3$ | *c*-Hex | Bn |  **5f** | 99 | 92[c] |
| 7 | $SiMe_3$ | 1-ethylpropyl | Bn |  **5g** | 72 | 96[c] |
| | | | |  | | |
| 8 | Ph | Ph | allyl | **5h**: R = H | 91 | 70 |
| 9 | Ph | *p*-MeO-$C_6H_4$ | allyl | **5i**: R = OMe | 76 | 60 |
| 10 | Ph | *p*-$CF_3$-$C_6H_4$ | allyl | **5j**: R = $CF_3$ | 43 | 63 |
| 11 | Ph | *o*-$CH_3$-$C_6H_4$ | allyl |  **5k** | 84 | 32 |
| | |  | |  | | |
| 12 | Ph | | allyl | **5l**: R = Ph | 80 | 78 |
| 13 | *c*-Hex | | allyl | **5m**: R = *c*-Hex | 61 | 74 |
| 14 | Ph |  | allyl |  **5n** | 55 | 64[d] |

[a] Yield of analytically pure product. [b] Enantiomeric excess determined by HPLC with a Chiracel OD-H column (*n*-heptane:*i*PrOH). [c] The *ee* value was determined after desilylation. [d] The *ee* value was determined after deprotection to give the monodeallylated derivative.

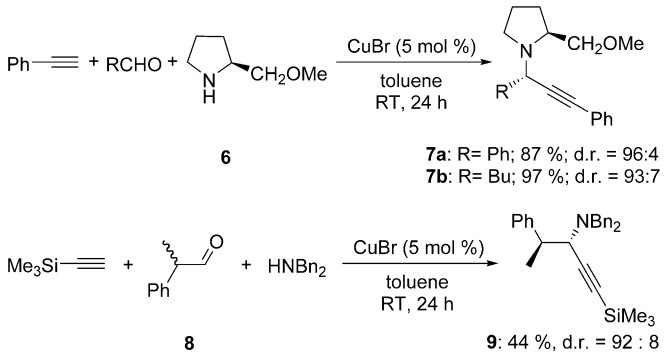
trimethylsilylacetylene leads to a further increase of enantioselectivity with these branched aldehydes, affording the propargylamines **5e–g** in 72–99% yield and 92–96% *ee*. Aromatic aldehydes can also be used. The presence of either an electron-donating or an electron-withdrawing substituent in *para* position has only a moderate influence on the enantioselectivity of the reaction (entries 8–10). However, the yield of the product **5j** (R = $CF_3$) is strongly reduced (43%) compared to that of **5i** (R = OMe; 76%) due to a dramatic decrease in reactivity. Steric effects are more important and the presence of an *ortho* substituent in the aldehyde (2-methylbenzaldehyde) leads to a dramatic decrease of the selectivity (**5k**: 84%, 32% *ee*; cf. entries 8 and 11). Heterocyclic aldehydes like 3-formylbenzothiophene and 3-furfural are also compatible and allow the preparation of the corresponding propargylic products **5l** and **5n** in yields of 80% (78% *ee*) and 55% (64% e*e*), respectively.

Remarkably, this reaction is highly diastereoselective if a chiral amine or aldehyde is used. Thus, the reaction of the prolinol derivative **6** with aromatic or aliphatic aldehydes and phenylacetylene produces the desired propargylamines **7a** and **7b** in yields of 87 and 97% and good diastereoselectivities of 96:4 and 93:7, respectively.[9] By using the racemic aldehyde **8**, the corresponding propargylamine **9** can also be obtained in good diastereoselectivity (92:8) (Scheme 2). The relative configuration of **9** has been determined by X-ray structure analysis.[10]

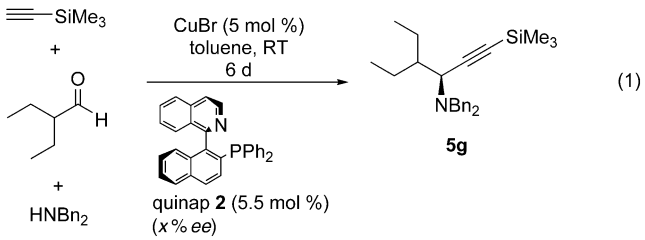
Preliminary mechanistic investigations [Eq. (1)] show that the enantioselective reaction displays a strong positive nonlinear effect (Figure 1). This suggests that a dimeric Cu/quinap complex is the catalytically active species and is in good agreement with the previously reported crystal structure of the $[CuBr\{(R)\text{-quinap}\}]_2$ complex.[11] The heterochiral complex $[Cu_2Br_2\{(R)/(S)\text{-quinap}\}]$ seems to react at a much slower rate than the corresponding homochiral complex $[Cu_2Br_2\{(R)/(R)\text{-quinap}\}]$. This explains the strong positive amplification. Thus, a ligand having an enantiomeric excess of 10% leads to the formation of the propargylamine **5g** in 68% *ee*. A lower conversion rate and product yield is observed when the ligand has lower *ee*.

A tentative reaction mechanism is described in Scheme 3. The dimeric[11] chiral copper complex **10** complexes the alkyne **1,** leading to the side-on complex **11**. The complexation of **11** with the intermediate aminal **12** (obtained by the reaction of the amine **4** with the aldehyde **3**) provides the complex **13**. Deprotonation of the

 © 2003 Wiley-VCH Verlag GmbH & Co. KGaA, Weinheim 




***Scheme 2.*** Diastereoselective three-component reactions.



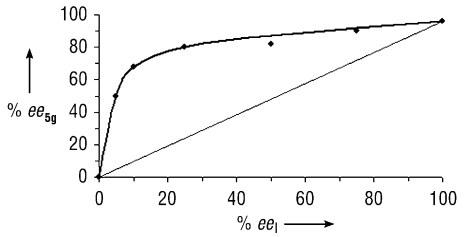
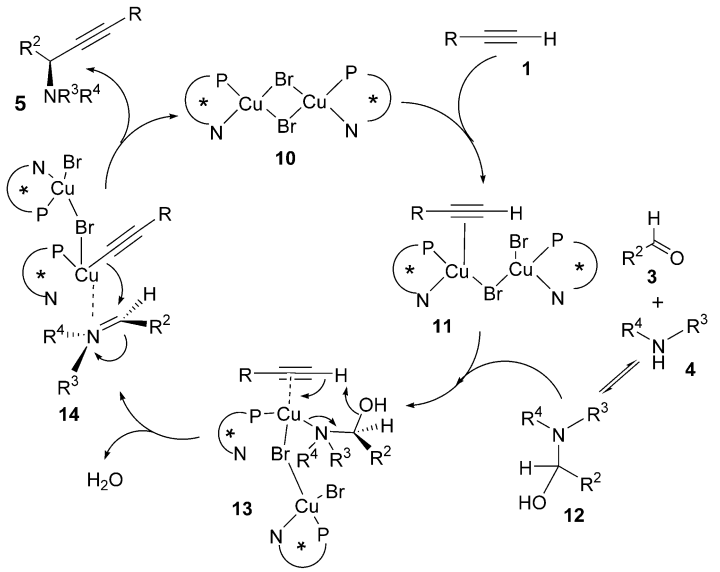




***Figure 1.*** Nonlinear effects in the three-component reaction leading to **5g** [Eq. (1)]. $\%ee_l$: enatiomeric excess of the ligand, $\%ee_{5g}$: enantiomeric excess of the product.




***Scheme 3.*** Tentative mechanism of the three-component reaction.

coordinated alkyne and the elimination of $H_2O$ gives complex **14**, an end-on copper acetylide with a coordinated iminium ion. The addition of the acetylide to the iminium salt in the coordination sphere of the chiral copper(I) complex leads to the chiral propargylamine **5** and regenerates the catalyst **10**.

In summary, we have shown that a wide range of chiral propargylamines can be prepared in a one-pot three-component reaction in good yield and good enantioselectivity. Further applications in natural-product synthesis and mechanistic studies of this reaction are currently underway in our laboratories.

## *Experimental Section*

(−)-**5a**: A dry and argon-flushed 10-mL flask equipped with a magnetic stirrer and a septum was charged with copper(I) bromide (3.6 mg, 0.0250 mmol) and (*R*)-quinap (12.1 mg, 0.0275 mmol). Anhydrous toluene (2 mL) was added, the mixture was stirred at room temperature for 30 min. Molecular sieves (4 Å, 0.3 g) and *n*-decane (30 mg, as internal standard) were added, followed by phenylacteylene (51 mg, 0.5 mmol), 3-methylbutanal (43 mg, 0.5 mmol), and dibenzylamine (99 mg, 0.5 mmol). The reaction mixture was stirred for 70 h at room temperature. The molecular sieves were removed by filtration and washed with diethyl ether. The crude product was concentrated in vacuo and purified by chromatography on silica gel (pentane:diethyl ether = 98:2) yielding the propargylamine ((−)-**5a**) as a colorless oil (180 mg, 98 %, 86 % *ee*).

Received: August 6, 2003 [Z52578]
Published Online: November 11, 2003

**Keywords:** alkynes · asymmetric catalysis · C–H activation · multicomponent reactions · propargylamines

[1] a) R. Noyori, *Asymmetric Catalysis in Organic Synthesis*, Wiley, Weinheim, **1994**; b) G. Helmchen, R. W. Hoffmann, J. Mulzer, E. Schaumann, *Houben-Weyl: Stereoselective Synthesis*, Thieme, Stuttgart **1996**; c) E. N. Jacobsen, A. Pfaltz, H. Yamamoto, *Comprehensive Asymmetric Catalysis*, Springer, Berlin **1999**; d) R. A. Aitken, S. N. Kilényi, *Asymmetric Synthesis*, Blackie A&P, London, **1992**.

[2] For recently described three-component reactions, see: a) S. Kamijo, Y. Yamamoto, *J. Am. Chem. Soc.* **2002**, *124*, 11940; S. Kamijo, T. Jin, Y. Yamamoto, *J. Am. Chem. Soc.* **2001**, *123*, 9453; b) F. Bertozzi, M. Gustafsson, R. Olsson, *Org. Lett.* **2002**, *4*, 4333; c) G. W. Kabalka, Z. Wu, Y. Ju, *Org. Lett.* **2002**, *4*, 3415; d) T.-P. Loh, S.-L. Chen, *Org. Lett.* **2002**, *4*, 3647; e) A. Dömling, I. Ugi, *Angew. Chem.* **2000**, *112*, 3300; *Angew. Chem. Int. Ed.* **2000**, *39*, 3168; f) B. List, P. Pojarliev, W. T. Biller, H. J. Martin, *J. Am. Chem. Soc.* **2002**, *124*, 827; g) U. Bora, A. Saikia, R. C. Boruah, *Org. Lett.* **2003**, *5*, 435; h) R. Dhawan, R. D. Dghaym, B. A. Arndtsen, *J. Am. Chem. Soc.* **2003**, *125*, 1474; i) C. Cao, Y. Shi, A. L. Odom, *J. Am. Chem. Soc.* **2003**, *125*, 2880; j) S. J. Patel, T. F. Jamison, *Angew. Chem.* **2003**, *115*, 1402, *Angew. Chem. Int. Ed.* **2003**, *42*, 1364; k) J. R. Porter, J. F. Traverse, A. H. Hoveyda, M. L. Snapper, *J. Am. Chem. Soc.* **2001**, *123*, 10409.

[3] a) B. M. Trost, *Angew. Chem.* **1995**, *107*, 285; *Angew. Chem. Int. Ed. Engl.* **1995**, *34*, 259; b) B. M. Trost, *Science* **1991**, *254*, 1471.

[4] a) C. Koradin, K. Polborn, P. Knochel, *Angew. Chem.* **2002**, *114*, 2651; *Angew. Chem. Int. Ed.* **2002**, *41*, 2535;

 © 2003 Wiley-VCH Verlag GmbH & Co. KGaA, Weinheim 

b) C. Koradin, N. Gommermann, K. Polborn, P. Knochel, *Chem. Eur. J.* **2003**, *9*, 2797.

[5] a) C. M. Wei, C. J. Li, *J. Am. Chem. Soc.* **2002**, *124*, 5638; b) N. K. Anand, E. M. Carreira, *J. Am. Chem. Soc.* **2001**, *123*, 9687; c) E. El-Sayed, N. K. Anand, E. M. Carreira, *Org. Lett.* **2001**, *3*, 3017; d) D. E. Frantz, R. Faessler, C. S. Tomooka, E. M. Carreira, *Acc. Chem. Res.* **2000**, *33*, 373; e) D. E. Frantz, R. Faessler, E. M. Carreira, *J. Am. Chem. Soc.* **2000**, *122*, 1806; f) K. C. Brannock, R. D. Burpitt, J. G. Thweatt, *J. Org. Chem.* **1963**, *28*, 1462; g) J. J. McNally, M. A. Youngman, S. L. Dax, *Tetrahedron Lett.* **1998**, *39*, 967; M. A. Youngman, S. L. Dax, *Tetrahedron Lett.* **1997**, *38*, 6347.

[6] a) D. Tzalis, P. Knochel, *Angew. Chem.* **1999**, *111*, 1547; *Angew. Chem. Int. Ed.* **1999**, *38*, 1463; b) D. Tzalis, C. Koradin, P. Knochel, *Tetrahedron Lett.* **1999**, *40*, 6193.

[7] a) J. M. Valk, G. A. Whitlock, T. P. Layzell, J. M. Brown, *Tetrahedron: Asymmetry* **1995**, *6*, 2593; b) E. Fernandez, K. Maeda, M. W. Hooper, J. M. Brown, *Chem. Eur. J.* **2000**, *6*, 1840.

[8] a) During the preparation of the manuscript, an analogous racemic, gold-catalyzed reaction was reported: C. Wei, C.-J. Li, *J. Am. Chem. Soc.* **2003**, *125*, 9584; b) for an analogous racemic, iridium-catalyzed reaction see: S. Sakaguchi, T. Kubo, Y. Ishii, *Angew. Chem.* **2001**, *113*, 2602; *Angew. Chem. Int. Ed.* **2001**, *40*, 2534; c) for solid-phase three-component reactions leading to racemic propargylamines, see: J. J. McNally, M. A. Youngman, S. L. Dax, *Tetrahedron Lett.* **1998**, *39*, 967; A. B. Dyatkin, R. A. Rivero, *Tetrahedron Lett.* **1998**, *39*, 3647; d) for a microwave-enhanced heterogeneous three-component reaction, see: G. W. Kabalka, L. Wang, R. M. Pagni, *Synlett* **2001**, 676.

[9] The absolute configuration was determined by comparison to a known compound (see the Supporting Information).

[10] The crystal structure is shown in the Supporting Information. CCDC 216200 contains the supplementary crystallographic data for this paper. These data can be obtained free of charge via www.ccdc.cam.ac.uk/conts/retrieving.html (or from the Cambridge Crystallographic Data Centre, 12, Union Road, Cambridge CB21EZ, UK; fax: (+44) 1223-336-033; or deposit@ccdc.cam.ac.uk).

[11] An X-ray analysis of quinap–CuBr shows that the complex is dimeric (see ref. [4]).

 © 2003 Wiley-VCH Verlag GmbH & Co. KGaA, Weinheim 

Nanotechnology

# Oligofunctional DNA–Gold Nanoparticle Conjugates**

*Christof M. Niemeyer,* Bülent Ceyhan, and Pompi Hazarika*

*Dedicated to Professor Manfred T. Reetz on the occasion of his 60th birthday*

Hybrid conjugates comprised of inorganic nanoparticles and biomolecules, such as proteins and nucleic acids, are currently attracting much attention for their use as building blocks in the self-assembly of nanometer-sized functional devices.[1] Because of their tremendous molecular-recognition capabilities, DNA molecules play an important role in this approach. For instance, DNA oligomers have been used to functionalize gold nanoparticles, thus enabling the bottom-up fabrication of nanostructured materials[2] as well as highly sensitive assays for detecting nucleic acids[3] and proteins.[4] These studies, however, have been carried out exclusively using DNA–nanoparticle conjugates containing just a single recognition site, that is, a single oligonucleotide sequence.[5] Thus, the conjugates can be considered as monofunctional with respect to their recognition capabilities for complementary nucleic acids. Herein we report on the preparation and characterization of oligofunctional gold nanoparticle conjugates containing different DNA sequences (**$D_n$-Au** in Scheme 1). The index *n* in **$D_n$-Au** denotes the number of different sequences attached to the nanoparticle, ranging from one (monofunctional) up to seven (heptafunctional). The oligofunctional particles are extremely versatile, such that they are capable of hybridizing to more than one complementary target. The **$D_n$-Au** nanoparticles reveal almost unaltered hybridization capabilities as compared to monofuctional conjugates. Moreover, due to the extraordinary specificity of Watson–Crick base pairing, the various oligonucleotides can be individually and selectively addressed as members of an orthogonal coupling system present on the surface of the particle. For example, individual sequences can be unambiguously employed for coupling with DNA-functionalized surfaces and the connection with DNA-tagged molecular and colloidal building blocks.

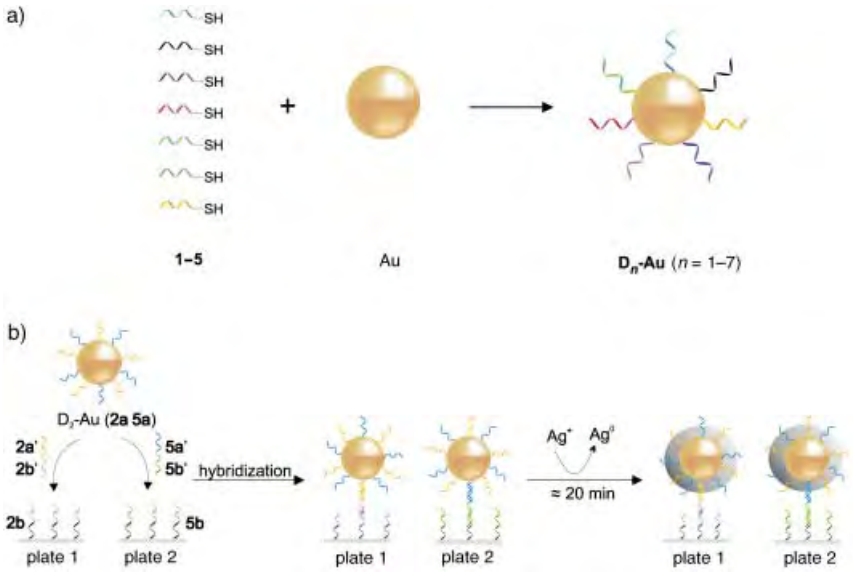
To prepare the oligofunctional DNA–nanoparticle conjugates **$D_n$-Au**, the method of Mirkin and co-workers[6] was

[*] Prof. Dr. C. M. Niemeyer, Dipl.-Chem. B. Ceyhan, P. Hazarika
Universität Dortmund, Fachbereich Chemie
Biologisch-Chemische Mikrostrukturtechnik
Otto-Hahn Strasse 6, 44227 Dortmund (Germany)
Fax: (+49) 231-755-7082
E-mail: cmn@chemie.uni-dortmund.de

[**] This work was supported by Deutsche Forschungsgemeinschaft (DFG) in Schwerpunktprogramm 1072. We wish to thank Martina Reibner for her help with the AAS measurements.

Supporting information for this article is available on the WWW under http://www.angewandte.org or from the author.

 © 2003 Wiley-VCH Verlag GmbH & Co. KGaA, Weinheim DOI: 10.1002/anie.200352744 




***Scheme 1.*** a) Schematic drawing of the preparation of oligofunctional DNA–gold nanoparticle conjugates $D_n$-Au, illustrating the heptafunctional conjugate $D_7$-Au containing sequences **1a**, **1b**, **2a**, **2b**, **3a**, **4a**, and **5a**; b) Schematic drawing of the DNA-directed immobilization of bifunctional DNA–gold nanoparticles $D_2$-Au containing the oligonucleotide sequences **2a** and **5a** with a subsequent silver development step.

employed, using citrate-stabilized gold nanoparticles and oligonucleotides **1**–**5** containing thiol groups at their 3′ or 5′-termini, respectively (Table 1). To initially study the feasibility of our concept, bifunctional $D_2$-Au conjugates were prepared from an equimolar mixture of two thiolated oligonucleotides, for instance, **2a** and **5a**. The absolute amounts of the two DNA oligomers in the resulting $D_2$-Au conjugates were experimentally determined by the method of Demers et al.,[7] and the results indicated that, in fact, about half of the 260 oligomers were either **2a** or **5a** (Figure S1a; Supporting Information). The hybridization capabilities of this **$D_2$-Au(2a5a)** conjugate were measured in a solid-phase hybridization assay (Scheme 1b). To this end, biotinylated capture oligomers **2b** and **5b** were immobilized in streptavidin-coated microplates, and saturated with complementary linker oligonucleotides (**2a′b′** and **5a′b′**, respectively) providing a 5′ dangling end sequence complementary to the gold-particle-bound oligonucleotides. Subsequent to hybridization of **$D_2$-Au(2a5a)**, immobilized particles were subjected to a silver development, which led to the formation of a silver precipitate that was quantified photometrically by absorbance measurements at 490 nm.[4,8] The signal intensity was equal to that of the analogous monoconjugate, containing only **2a** or **5a**. (Figure S1b; Supporting Information). Further investigations with other bifunctional conjugates, namely **$D_2$-Au(2a1a)**, **$D_2$-Au(2a3a)**, and **$D_2$-Au(2a4a)** led to identical results, which indicated that $D_2$-Au conjugates show unaltered hybridization efficiency, compared to the monoconjugate **$D_1$-Au**, and that neither surface coverage nor hybridization capabilities are affected by variations of the second sequence present on the surface of the nanoparticle (Figure S1; Supporting Information).

***Table 1:*** Oligonucleotide sequences used in this study.

| Compound | Sequence |
|---|---|
| **1a** | 5′-TCT CAA CTG GTA-SH-3′ |
| **1b** | 5′-SH-CGC ATT CAG GAT-3′ |
| **2a** | 5′-AAG ACC ATC CTG-SH-3′ |
| **2b** | 5′-SH-GGT GAA GAG ATC-3′ |
| **3a** | 5′-GAA GAC TGG GAA T-SH-3′ |
| **4a** | 5′-GCA CTT GAG AGC-SH-3′ |
| **5a** | 5′-TTC GGA TCC CGG-SH-3′ |
| **1a′1b′** | 5′-TAC GAG TTG AGA ATC CTG AAT GCG-3′ |
| **2a′2b′** | 5′-CAG GAT GGT CTT GAT CTC TTC ACC-3′ |
| **5a′5b′** | 5′-CCG GGA TCC GAA TTC AAG CTT CGA-3′ |
| **1a′2b′** | 5′-TAC GAG TTG AGA GAT CTC TTC ACC-3′ |
| **3a′2b′** | 5′-ATT CCC AGT CTT CGA TCT CTT CAC C-3′ |
| **4a′2b′** | 5′-GCT CTC AAG TGC GAT CTC TTC ACC-3′ |
| **5a′2b′** | 5′-CCG GGA TCC GAA GAT CTC TTC ACC-3′ |
| **2a′1b′** | 5′-CAG GAT GGT CTT ATC CTG AAT GCG-3′ |

To further elucidate the influence of the surface coverage on the hybridization capabilities of bifunctional conjugates, **$D_2$-Au(2a5a)** conjugates were prepared by coating gold particles with mixtures of oligomers **2a** and **5a** using systematic variations of the relative amounts of the two oligomers ranging between 100% to 0%. The absolute numbers of the two DNA oligomers determined experimentally for the various **$D_2$-Au(2a5a)** conjugates indicated that the surface coverage correlated with the ratio of the thiolated oligomers present in the coating solution (Figure S2; Supporting Information). The hybridization capabilities of the various **$D_2$-Au(2a5a)** conjugates were investigated by solid-phase hybridization. As shown in Figure 1a, rather than the gradual decrease in hybridization efficiency that one might have expected from a gradual decrease of oligomer binding sites, maximum signal intensities were observed at fairly low surface coverages of less than 20%. With a typical surface coverage of $27 \pm 4$ pmol cm$^{-2}$, this correlates with the presence of only about 60 complementary oligomer molecules in the presence of $\approx$230 noncomplementary oligonucleotides. These somewhat unexpected hybridization characteristics are explained by the fact that, due to electrostatic repulsion, only 10% of the particle-bound oligomers can hybridize.[7] It is less important for binding if 90% of the oligomers possess a different sequence.

It can also be seen in Figure 1a that the maximum signal intensities varied for the two sequences **2a** and **5a**. These differences in hybridization efficiency, that is, the amount of material which is immobilized by nucleic acid hybridization in a certain time period, do not correlate with the thermodynamic stability of the respective DNA duplexes. The differences can be attributed to sequence-specific variations in the formation of intra- and intermolecular oligomer structures,

 © 2003 Wiley-VCH Verlag GmbH & Co. KGaA, Weinheim 

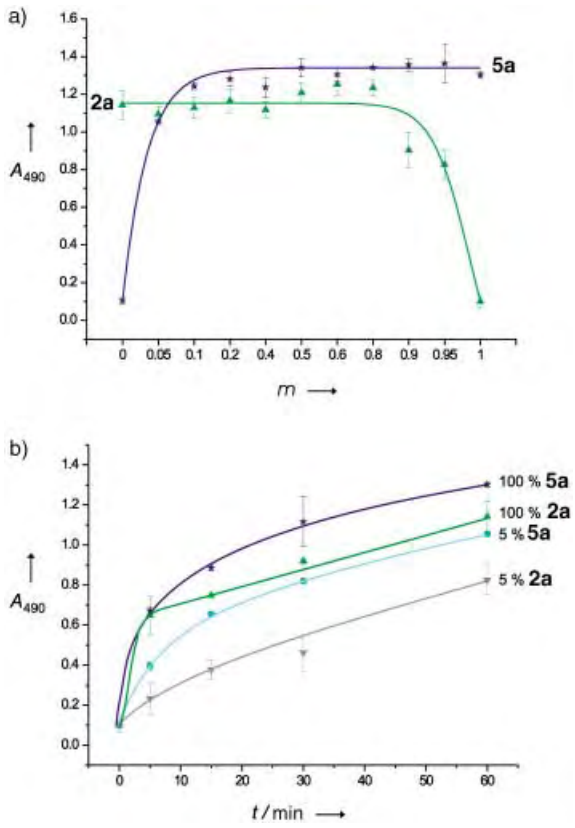



***Figure 1.*** Solid-phase hybridization of bifunctional **$D_2$-Au(2a5a)** conjugates containing varying amounts of the two oligonucleotides **2a** and **5a**, respectively. The hybridization capabilities were monitored in a microplate assay using the two complementary capture systems, that is, biotinylated **2b** with linker **2a′b′** (for **2a**) and biotinylated **5b** with linker **5a′b′** (for **5a**), respectively. Note that the signal intensities were obtained by absorbance measurements at 490 nm subsequent to silver enhancement. a) Signal intensities depending on the relative surface coverage *m* of **2a** and **5a**. The values $m = 0$ and $m = 1$ represent monofunctional conjugates **$D_1$-Au** containing **2a** and **5a**, respectively. The values $m = 0.95$–$0.05$ represent bifuctional conjugates **$D_2$-Au** with varying amounts of **2a** and **5a**. The signals were obtained after a hybridization time of 60 min. Note that the hybridization efficiency of **$D_2$-Au** changes only at a low surface coverage of less than 20%; b) time-dependent hybridization curves of monofunctional **$D_1$-Au** and bifunctional **$D_2$-Au** conjugates, the latter of which contain a low surface coverage (5%) of the hybridizing oligomer. Note that the slope of the curves is significantly steeper for the monofunctional **$D_1$-Au** conjugates.

which influences the hybridization kinetics and stability of the respective double helices.[9]

Time-dependent hybridization measurements were carried out to compare monofunctional **$D_1$-Au** with bifunctional **$D_2$-Au** conjugates that contained a low surface coverage (5%) of the hybridizing oligomer. As shown in Figure 1b, the decrease in surface coverage leads to a decreased slope compared to the respective monofunctional nanoparticles, which suggests that hybridization kinetics are significantly slowed down when low concentrations of the hybridizing oligomer are present at the surface of the nanoparticle. Additional measurements with analogous bifunctional **$D_2$-Au** conjugates containing mixed 12-mer and 24-mer coding sequences led to comparable results, which confirms that only low surface coverage is required for efficient hybridization of the particles (Figure S3; Supporting Information).

To demonstrate the functionality of the two individual binding sites within the bifunctional conjugates, **$D_2$-Au(1a2a)** and **$D_2$-Au(3a5a)** were used for the assembly of surface-bound particle layers by solid-phase hybridization (Figure 2). Sequence **1a** of **$D_2$-Au(1a2a)** was used for generating a surface-bound layer of particles and sequence **2a** was used for interconnecting a second layer comprised of monofunctional **$D_1$-Au(2b)**. In the next step the sequence **3a** of **$D_2$-Au(3a5a)** was utilized for generating a third layer of particles, and sequence **5a** of **$D_2$-Au(3a5a)** was used as an interconnect to a fourth layer of **$D_1$-Au(5b)**. Each conjugate was immobilized through hybridization via individual linkers, with sequences that only allowed a single type of conjugate interconnection to occur. As shown in Figure 2, UV/Vis measurements revealed that each layer immobilization leads to a linear increase in absorbance at 526 nm. Control experiments, in which the layers were formed either with or without non-complementary linkers, showed no such increase in absorbance at 526 nm (Figure S4; Supporting Information). These results confirm the unbiased specificity of DNA-base-pairing in bifunctional DNA–Au nanoparticle conjugates. It should be noted that the employment of oligofunctional conjugates, for example **$D_2$-Au**, generally allows for enhanced variability in the rational construction of multilayered assemblies in which direct binding of one layer to any of the underlying layers can be easily prevented by the choice of appropriate oligomer combinations. This exceeds the complexity that can be obtained with monofunctional conjugates, usually employed for the assembly of nanoparticle layers.[8,10]

The interesting hybridization characteristics of the bifunctional **$D_2$-Au** conjugates prompted us to investigate whether higher functionalization of nanoparticles can be realized by using appropriate stoichiometric mixtures containing three or more thiolated oligonucleotides during conjugate formation. We prepared oligofunctional **$D_n$-Au** conjugates ($n = 1$–$7$) using combinations of oligomers **1a**–**5a** (Figure 3). In the case of pentafunctional conjugates (**$D_5$-Au**), an average of 63 oligomers of each type were experimentally determined, which corresponds to about 20% of $317 \pm 20$ oligomers present per particle (Figure S5; Supporting Information). The solid-phase hybridization assay of the various oligofunctional **$D_n$-Au** conjugates indicated that all of the sequences are functional (Figure 3). Even in the case of the heptafunctional conjugate **$D_7$-Au**, just two of the sequences (out of seven) were significantly affected by the presence of the other oligomers. While five sequences revealed hybridization efficiencies of more than 85% of the analogous monofunctional conjugates, the hybridization efficiencies of oligomers **1b** and **4a** dropped to about 40% in the heptafunctional conjugate **$D_7$-Au**. It is likely that the decrease in hybridization capabilities is due to sequence-specific features of these individual oligomers. Systematic optimization of the sequence design will help to overcome the non-optimal binding properties of individual sequences attached to nanoparticles.

In conclusion, a new concept for the preparation of highly functionalized, versatile DNA–gold nanoparticles has been demonstrated where modification with up to seven different

 © 2003 Wiley-VCH Verlag GmbH & Co. KGaA, Weinheim 

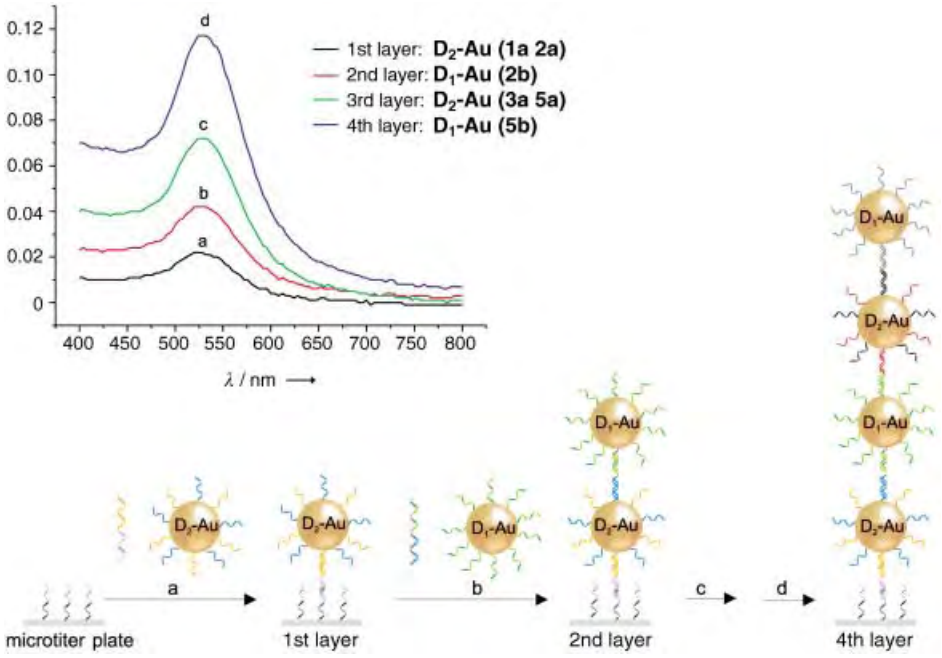



***Figure 2.*** Generation of surface-bound layers of particles by DNA hybridization using mono- and bifunctional DNA–gold nanoparticle conjugates in a microplate; Spectra: absorbance measurements of layer assembly. First, a surface-bound particle layer was generated by subsequent hybridization of linker **1a′1b′** and conjugate **$D_2$-Au(1a2a)** to the biotinylated capture oligonucleotide (sequence **1b** (a)). Further hybridization steps were linker **2a′2b′** and **$D_1$-Au(2b)** (b), linker **2b′3a′** and **$D_2$-Au(3a5a)** (c), and linker **5a′5b′** and **$D_1$-Au(5b)** (d). The formation of particle layers was recorded photometrically over a range of 400–800 nm in a microplate reader.

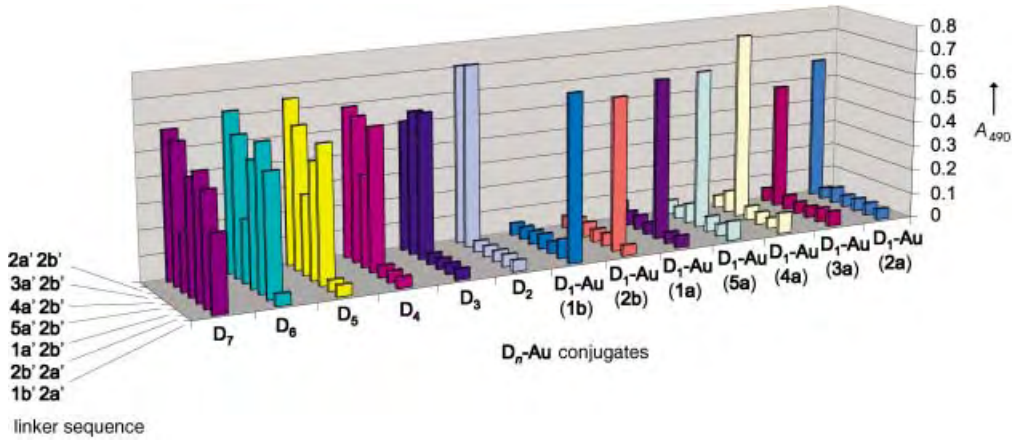



***Figure 3.*** Solid-phase hybridization of various oligofunctional **$D_n$-Au** conjugates ($n = 1$–7). The following conjugates were studied: **$D_1$-Au(1a)**, **$D_1$-Au(1b)**, **$D_1$-Au(2a)**, **$D_1$-Au(2b)**, **$D_1$-Au(3a)**, **$D_1$-Au(4a)**, **$D_1$-Au(5a)**, **$D_2$-Au(2a3a)**, **$D_3$-Au(2a3a4a)**, **$D_4$-Au(2a3a4a5a)**, **$D_5$-Au(1a2a3a4a5a)**, **$D_6$-Au(1a2a2b3a4a5a)**, and **$D_7$-Au(1a1b2a2b3a4a5a)**.

oligomers leads to the formation of a complex orthogonal coupling system, in which individual oligomers can be selectively addressed by highly specific nucleic acid base pairing. Individual sequences can be specifically functionalized with DNA-tagged molecular and colloidal components, thus enabling the bottom-up assembly of complex biomolecular functionalized nanoparticles. The approach reported here is not only simple, robust, and efficient, but also should open up new applications of DNA- and protein-modified nanoparticles. For example, oligofunctional DNA nanoparticles may be applied in materials science for fabricating surface-bound heterostructures comprised of various types of metal and semiconductor nanoparticles,[11] and also in life sciences for generating functional biomolecular hybrid probes for the detection of proteins and nucleic acids.[4] Moreover, this concept is fully compatible with the DNA-directed assembly of nanostructured protein conjugates, currently investigated for the fabrication of oligovalent receptor devices, multienzymes, artifical antennas, and other biomolecular devices.[12]

 © 2003 Wiley-VCH Verlag GmbH & Co. KGaA, Weinheim 

## Experimental Section

The preparation of DNA–gold nanoparticle conjugates was carried out as described by Mirkin and co-workers[6] using citrate-stabilized gold nanoparticles of $23.6 \pm 5.3$ nm diameter (ICN) and thiol-modified DNA oligomers (Thermo Hybaid). For determination of surface coverages, 5′-fluorescein, 3′-thiol-labeled oligonucleotides were used for preparing the DNA–nanoparticle conjugates. In a typical reaction, bifunctional DNA–Au nanoparticle conjugates were prepared by adding a mixture containing the desired ratio of two different oligonucleotides to an aqueous nanoparticle solution. The final oligonucleotide concentration was 4 μM. Oligofunctional DNA–Au nanoparticle conjugates were prepared in the same way by using appropriate mixtures of oligonucleotides.

Solid-phase hybridization experiments were carried out using streptavidin-coated microplates functionalized with biotinylated capture oligonucleotides[9] containing a $dT_{12}$ spacer between the biotin group and the coding sequence (for sequences, see Table 1). The immobilized capture oligomers (e.g., 5′-biotin-$dT_{12}$-**2b**) were saturated by 30 min incubation of 50 μL linker oligomers (e.g., **2a′b′**, 200 nM in a Tris-buffer containing 300 mM NaCl). Finally, 0.04 nM of DNA-modified gold nanoparticles containing a DNA sequence complementary to the linker sequence (e.g., **$D_1$-Au(2a)**) were added to the wells and incubated for 1 h to bind to the immobilized linker oligomer. Subsequent to hybridization, a silver-amplification step was carried out using silver-enhancer-kits (Sigma Aldrich or ICN). Quantification of immobilized particles was conducted photometrically by absorbance measurements at 490 nm.

For layer experiments (Figure 2), 0.6 nM of DNA-modified gold nanoparticles in the Tris-buffer solution were used for particle immobilization. After each particle hybridization, the conjugates immobilized were saturated with 200 nM of the appropriate linkers (see legend to Figure 2). Each particle layer was measured spectrophotometrically over a range of 400–800 nm using a Synergy-HT microtiterplate reader.

Received: August 29, 2003 [Z52744]

**Keywords:** analytical methods · DNA · nanostructures · nucleic acids · supramolecular chemistry

[1] C. M. Niemeyer, *Angew. Chem.* **2001**, *113*, 4254 – 4287; *Angew. Chem. Int. Ed.* **2001**, *40*, 4128 – 4158.
[2] J. J. Storhoff, C. A. Mirkin, *Chem. Rev.* **1999**, *99*, 1849 – 1862.
[3] R. A. Reynolds, C. A. Mirkin, R. L. Letsinger, *J. Am. Chem. Soc.* **2000**, *122*, 3795 – 3796.
[4] C. M. Niemeyer, B. Ceyhan, *Angew. Chem.* **2001**, *113*, 3798 – 3801; *Angew. Chem. Int. Ed.* **2001**, *40*, 3685 – 3688.
[5] Noncoding oligomers, such as $dT_{12}$, have previously been used to change the surface density of the coding oligomers. For example, see: a) S. R. Nicewarner Pena, S. Raina, G. P. Goodrich, N. V. Fedoroff, C. D. Keating, *J. Am. Chem. Soc.* **2002**, *124*, 7314 – 7323; b) R. Jin, G. Wu, Z. Li, C. A. Mirkin, G. C. Schatz, *J. Am. Chem. Soc.* **2003**, *125*, 1643 – 1654.
[6] J. J. Storhoff, R. Elghanian, R. C. Mucic, C. A. Mirkin, R. L. Letsinger, *J. Am. Chem. Soc.* **1998**, *120*, 1959 – 1964.
[7] L. M. Demers, C. A. Mirkin, R. C. Mucic, R. A. Reynolds, R. L. Letsinger, R. Elghanian, G. Viswanadham, *Anal. Chem.* **2000**, *72*, 5535 – 5541.
[8] T. A. Taton, C. A. Mirkin, R. L. Letsinger, *Science* **2000**, *289*, 1757 – 1760.
[9] Kinetic data of DNA hybridization are rare, and it is impossible to a priori predict hybridization efficiency from mere sequence data. For a discussion, see: C. M. Niemeyer, W. Bürger, R. M. J. Hoedemakers, *Bioconjugate Chem.* **1998**, *9*, 168 – 175, and references therein.
[10] Examples: a) T. A. Taton, R. C. Mucic, C. A. Mirkin, R. L. Letsinger, *J. Am. Chem. Soc.* **2000**, *122*, 6305 – 6306; b) F. Patolsky, K. T. Ranjit, A. Lichtenstein, I. Willner, *Chem. Commun.* **2000**, 1025 – 1026; c) I. Willner, F. Patolsky, J. Wasserman, *Angew. Chem.* **2001**, *113*, 1913 – 1916; *Angew. Chem. Int. Ed.* **2001**, *40*, 1861 – 1864; d) S. J. Park, T. A. Taton, C. A. Mirkin, *Science* **2002**, *295*, 1503 – 1506; e) A. Csaki, R. Möller, W. Straube, J. M. Köhler, W. Fritzsche, *Nucleic Acids Res.* **2001**, *29*, E81 – 81; f) R. Möller, A. Csaki, J. M. Köhler, W. Fritzsche, *Langmuir* **2001**, *17*, 5426 – 5430; g) C. M. Niemeyer, B. Ceyhan, S. Gao, L. F. Chi, S. Peschel, U. Simon, *Colloid Polym. Sci.* **2001**, *279*, 68 – 72; h) S. Peschel, B. Ceyhan, C. M. Niemeyer, S. Gao, L. F. Chi, U. Simon, *Mater. Sci. Eng. C* **2002**, *19*, 47 – 50; i) D. Gerion, W. J. Parak, S. C. Williamson, D. Zanchet, C. M. Micheel, A. P. Alivisatos, *J. Am. Chem. Soc.* **2002**, *124*, 7070 – 7074.
[11] Bifunctional nanoparticles have been employed as building blocks for the self-assembly of cross-linked particle layers: C. M. Niemeyer, B. Ceyhan, M. Noyong, U. Simon, *Biochem. Biophys. Res. Commun.* **2003**, *311*, in press.
[12] Examples: a) C. M. Niemeyer, T. Sano, C. L. Smith, C. R. Cantor, *Nucleic Acids Res.* **1994**, *22*, 5530 – 5539; b) C. M. Niemeyer, W. Bürger, J. Peplies, *Angew. Chem.* **1998**, *110*, 2391 – 2395; *Angew. Chem. Int. Ed.* **1998**, *37*, 2265 – 2268; c) C. M. Niemeyer, J. Koehler, C. Wuerdemann, *ChemBioChem* **2002**, *3*, 242 – 245; d) for a recent review, see: C. M. Niemeyer, *Trends Biotechnol.* **2002**, *20*, 395 – 401.

 © 2003 Wiley-VCH Verlag GmbH & Co. KGaA, Weinheim 

# Cover Picture




**Roald Hoffmann* and Dean J. Tantillo***

**Orbital-symmetry control** was initially explored almost 40 years ago. However, new principles can still be discovered: There is a striking congruence in the geometries of the transition states (not reactants and products) of electrocyclic reactions and sigmatropic shifts related by a proton. A link between these reactions and three-center hydride transfers in a cation is forged, and the idea of a transition-state proton affinity is reintroduced by R. Hoffmann and D. J. Tantillo in their Communication on page 5877 ff.

# Contents

## Angewandte EarlyView

***The following articles are available online (in Wiley InterScience). You can find them at www.angewandte.org, under Full Text, Early View.***


*A. Albinati, P. Leoni,* L. Marchetti, S. Rizzato:*
**Assembling Metal Clusters with Covalent Linkers: Synthesis and Structure of a Quasi-Planar $Pt_{18}$ Dendrimer Containing Five Clusters Connected by σ-Alkynyl Spacers**
DOI: 10.1002/anie.200352954
Published online: November 24, 2003

*N. Schiefenhövel, H.-J. Himmel, M. Binnewies*:*
**Plasmachemistry: $N_2(SiCl_3)_4$—A Tetrakissilylhydrazine as an Unexpected Product of the Reaction between $N_2$ and $SiCl_4$**
DOI: 10.1002/anie.200352575
Published online: November 24, 2003


Articles judged by the referees or the editor as being either very important or very urgent are immediately edited, proof-read, and electronically published once the manuscript has arrived in the editorial office in final form. As long as there is no page number available these articles should be cited in the following manner:

Author(s) *Angew. Chem. Int. Ed.*, online publication date, DOI.

## News


R. Noyori, A. Müller, and W. A. Herrmann honored ——— **5790**


## Books


Magnetic Materials ——— **5791** Nicola Spaldin *reviewed by S. Decurtins*

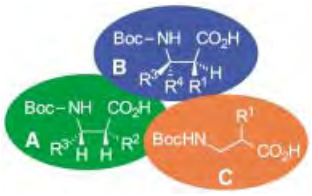
Textures of Liquid Crystals ——— **5791** Ingo Dierking *reviewed by M. Hird*


## Highlights

### *Amino Acid Synthesis*


N. Sewald* ——— **5794 – 5795**

Synthetic Routes towards Enantiomerically Pure β-Amino Acids

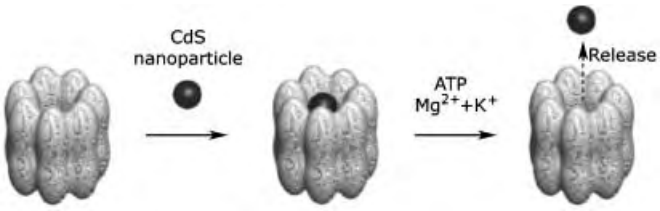




**Unusual representatives** of the synthetically attractive β-amino acids can be accessed by two novel synthetic routes. The synthesis of $\beta^{2,3}$- and $\beta^{2,3,3}$-amino acids (**A** and **B**, respectively) involves a diastereoselective 1,3-dipolar cycloaddition, whereas $\beta^2$-amino acids **C** are obtained by enantioselective $Cu^I$-catalyzed conjugate addition of dialkyl zinc compounds to nitroalkenes.

### *Nanotechnology*


C. M. Niemeyer* ——— **5796 – 5800**

Functional Hybrid Devices of Proteins and Inorganic Nanoparticles

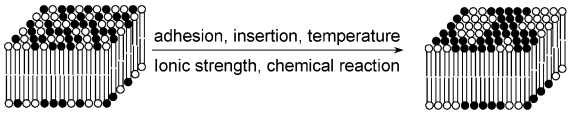




**The combination of inorganic nanoparticles** with biological functionality, such as the ATP-triggered release of CdS nanoparticles from inclusion complexes with chaperonins (see schematic illustration), opens up innovative approaches to novel hybrid devices applicable in biomedical sensing and the fabrication of advanced functional materials.



© 2003 Wiley-VCH Verlag GmbH & Co. KGaA, Weinheim

# Reviews




**Barriers with function**: Domains and rafts play an important role in the amazing behavior of lipid membranes. The phase separation of mixed lipid membranes (see scheme) generates a new hierarchy of membrane organization within lipid and polymer vesicles. The biological impact of this structuring as well as the chemical background is described.

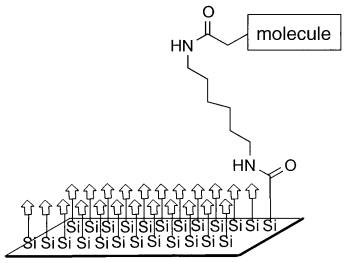
## Lipid membranes

W. H. Binder,* V. Barragan, F. M. Menger ——— **5802 – 5827**

Domains and Rafts in Lipid Membranes

# Communications

**Chemoselective coupling**: The Staudinger ligation between azide-functionalized small molecules and a phosphane-modified glass surface offers a new immobilization strategy for the preparation of drug arrays through the formation of a thermodynamically stable amide (see scheme).



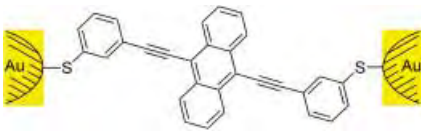

small-molecule array

## Microarrays

M. Köhn, R. Wacker, C. Peters, H. Schröder, L. Soulère, R. Breinbauer,* C. M. Niemeyer,* H. Waldmann* ——— **5830 – 5834**

Staudinger Ligation: A New Immobilization Strategy for the Preparation of Small-Molecule Arrays

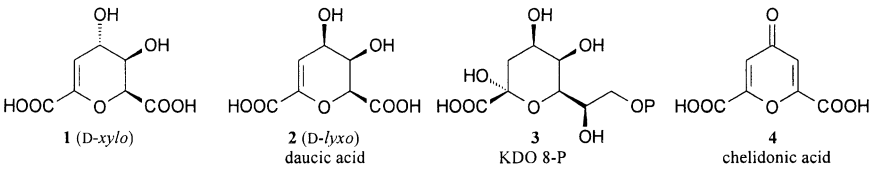
**The electronic resistance** of an electrode-molecule-electrode device strongly depends on the relative position of the anchor group in the molecular structure. The molecular rod, immobilized through two sulfur groups in the *meta* position on a pair of electrodes (see picture), displays a considerably increased resistance compared to the rod with the sulfur groups in the *para* position.




## Electron Transport Mechanism

M. Mayor,* H. B. Weber,* J. Reichert, M. Elbing, C. von Hänisch, D. Beckmann, M. Fischer ——— **5834 – 5838**

Electric Current through a Molecular Rod—Relevance of the Position of the Anchor Groups




The synthesis of dihydropyrans with the D-*xylo* (**1**), D-*ribo*, L-*arabino*, and D-*lyxo* (**2**) configuration by one-carbon-atom homologation of D-mannose or D-galactose, terminal oxidation, and directed β elimination revealed (−)-daucic acid isolated from carrots to be **2**, rather than **1** as previously thought. The identical configuration of **2** and KDO 8-P (**3**) and available biosynthetic information about chelidonic acid (**4**) suggest a KDO 8-P based pathway for the generation of **2** and **4** in plants.

## Plant Acids

F. W. Lichtenthaler,* K. Nakamura, J. Klotz ——— **5838 – 5843**

(−)-Daucic Acid: Revision of Configuration, Synthesis, and Biosynthetic Implications

**For the USA and Canada:**
ANGEWANDTE CHEMIE International Edition (ISSN 1433-7851) is published weekly by Wiley-VCH PO Box 191161, D 69451 Weinheim, Germany. Air freight and mailing in the USA by Publications Expediting Inc. 200 Meacham Ave., Elmont, NY 11003. Periodicals postage paid at Jamaica NY 11431. US POSTMASTER: send address changes to *Angewandte Chemie*, Wiley-VCH, 111 River Street, Hoboken, NJ 07030. Annual institutional subscription price for institutions: Europe € 3430.00/3118.00. Outside Europe US$ 4499.00/4090.00 (valid for print and electronic/print or electronic delivery); for individuals who are personal members of a national chemical society, or whose institution already subscribes, or who are retired or self-employed consultants, print only. Europe € 248.00/Outside Europe US$ 378.00. Postage and handling charges included. All Wiley-VCH prices are exclusive VAT.

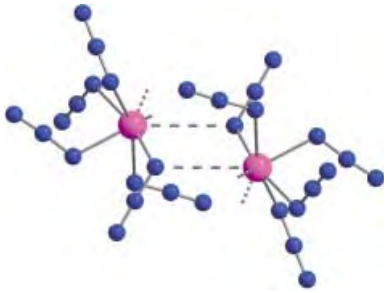
 © 2003 Wiley-VCH Verlag GmbH & Co. KGaA, Weinheim 

# Contents


## Azide Complexes (1)

T. M. Klapötke,* B. Krumm, P. Mayer, I. Schwab ——— **5843 – 5846**

Binary Tellurium(IV) Azides: $Te(N_3)_4$ and $[Te(N_3)_5]^-$

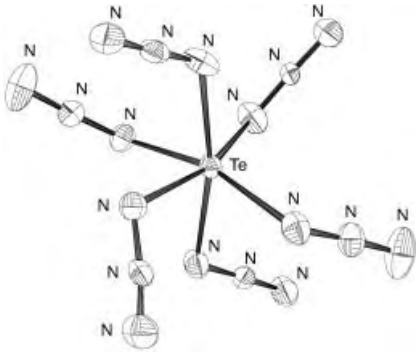


**Very sensitive materials**: Tellurium tetraazide, $Te(N_3)_4$, was prepared directly from $TeF_4$ and $Me_3SiN_3$ as an extremely sensitive solid; azidation of a pentafluorotellurate(IV) anion gave the pentaazidotellurate(IV) anion. The crystal structure of the pyridinium salt $[pyH][Te(N_3)_5]$ consists of $[Te(N_3)_5]^-$ units, considerably distorted from ideal square-pyramidal symmetry, that are linked through Te···N interactions (see picture).

## Azide Complexes (2)

R. Haiges, J. A. Boatz, A. Vij, M. Gerken, S. Schneider, T. Schroer, K. O. Christe* ——— **5847 – 5851**

Polyazide Chemistry: Preparation and Characterization of $Te(N_3)_4$ and $[P(C_6H_5)_4]_2[Te(N_3)_6]$ and Evidence for $[N(CH_3)_4][Te(N_3)_5]$

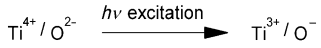



**Highly explosive** $Te(N_3)_4$ was prepared by the fluoride-ion-catalyzed reaction of $TeF_6$ and $Me_3SiN_3$, and converted to the more stable $[P(C_6H_5)_4]_2[Te(N_3)_6]$ salt by reaction with $[P(C_6H_5)_4]N_3$. The sterically active free valence-electron pair at the Te center strongly distorts the structure of the $[Te(N_3)_6]^{2-}$ ion from the predicted ideal $S_6$ symmetry (see picture). Evidence for the formation of the $[Te(N_3)_5]^-$ ion is also presented.

## Surface UV/Vis Spectroscopy

V. A. de la Peña O'Shea, M. Capel-Sanchez, G. Blanco-Brieva, J. M. Campos-Martin, J. L. G. Fierro* ——— **5851 – 5854**

The Usefulness of Time-Dependent Density Functional Theory to Describe the Electronic Spectra of Ti-Containing Catalysts

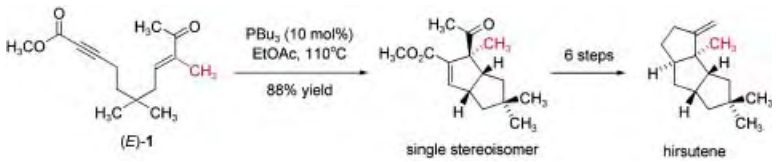



**A good correlation** between the experimental UV/Vis spectra of titanium-containing catalysts and the photophysical properties calculated using time-dependent density functional theory (TD-DFT) has been found for a ligand to metal charge transfer (LMCT) from an oxygen atom to a $Ti^{IV}$ ion (see scheme). This finding makes the TD-DFT methodology an excellent tool to generate and interpret the electronic spectra of isolated atoms on the surface of heteroatom-containing inorganic substrates.

## Natural Product Synthesis

J.-C. Wang, M. J. Krische* ——— **5855 – 5857**

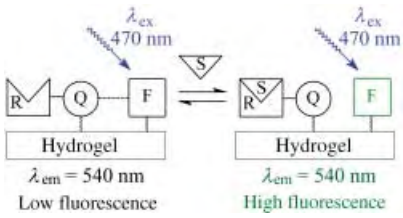
Intramolecular Organocatalytic [3+2] Dipolar Cycloaddition: Stereospecific Cycloaddition and the Total Synthesis of (±)-Hirsutene




**A testing ground for cyclopentannulation strategies**: the triquinane natural product hirsutene is obtained through the intramolecular organocatalytic [3+2] cycloaddition of the 1,7-enyne (*E*)-**1** . The cycloaddition is stereospecific: reaction of the corresponding *Z* isomer provides the epimeric diquinane.


 © 2003 Wiley-VCH Verlag GmbH & Co. KGaA, Weinheim 

**Sweetness and light**: A fluorescent thin-film hydrogel that contains a covalently bound boronic-acid-functional quencher (Q) and a fluorescent dye (F; see Figure) continuously senses glucose under physiological conditions through binding of the sugar (S) to a labeled receptor (R).




## Carbohydrate Sensors

J. T. Suri, D. B. Cordes, F. E. Cappuccio, R. A. Wessling, B. Singaram* ——— **5857 – 5859**

Continuous Glucose Sensing with a Fluorescent Thin-Film Hydrogel




**From three simple starting materials**, the diastereoselective synthesis of pentasubstituted cyclopentanols or tetrasubstituted cyclohexane-1,4-diols can be controlled by the appropriate choice of lithium enolate (see scheme). The overall one-pot transformation leads to the formation of up to five new C–C bonds and up to four contiguous stereogenic centers.

## Carbene Complexes

J. Barluenga,* I. Pérez-Sánchez, E. Rubio, J. Flórez ——— **5860 – 5863**

Three/Four/Five-Component Diastereoselective Cyclization of Fischer Carbene Complexes, Lithium Enolates, and Allylmagnesium Bromide

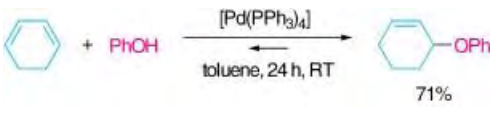
**The importance of the thiadiazole ring**: While electrostatic interactions between the thiadiazole rings is responsible for the 2D close packing in the solid-state structure of tetrakis(thiadiazole)porphyrazine ($TTDPzH_2$, see X-ray crystal structure), the formation of a coordination bond between the ring and the cobalt ion results in the cobalt derivative TTDPzCo having a chain structure.



## Solid-State Structures

M. Fujimori, Y. Suzuki, H. Yoshikawa, K. Awaga* ——— **5863 – 5865**

Packing Motifs in Porphyrazine Macrocycles Carrying Peripherally Annulated Thiadiazole Rings: Crystal Growths of Metal-Free and Cobalt Tetrakis(1,2,5-thiadiazole)porphyrazines




**Mildly acidic** O–H groups undergo transition-metal-catalyzed reversible addition across the C=C bonds of cyclic and acyclic dienes. For example, the simple complex $[Pd(PPh_3)_4]$ (1 mol%) effectively catalyzes both the forward addition of phenol across dienes and the reverse elimination of phenol from allylic ethers (see scheme).

## Addition reactions

M. Utsunomiya, M. Kawatsura, J. F. Hartwig* ——— **5865 – 5868**

Palladium-Catalyzed Equilibrium Addition of Acidic OH Groups across Dienes

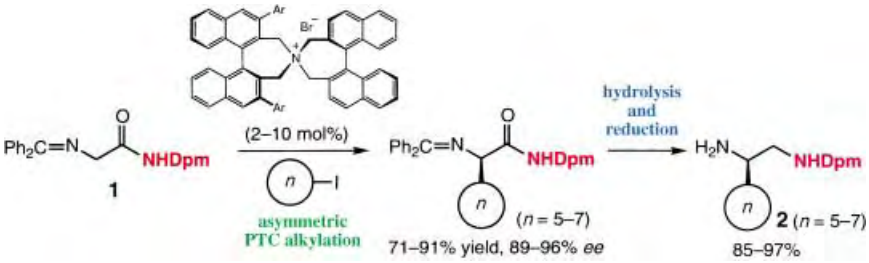
 © 2003 Wiley-VCH Verlag GmbH & Co. KGaA, Weinheim 

# Contents


## Asymmetric Catalysis

T. Ooi, D. Sakai, M. Takeuchi, E. Tayama, K. Maruoka* ——— **5868 – 5870**

Practical Asymmetric Synthesis of Vicinal Diamines through the Catalytic Highly Enantioselective Alkylation of Glycine Amide Derivatives

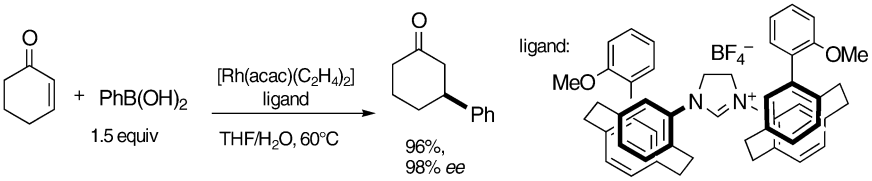



**Phase-transfer catalysis** (PTC) by a designer chiral quaternary ammonium bromide facilitated the direct, highly enantioselective introduction of a wide variety of substituents including cycloalkyl side chains at the α position of the prochiral glycine amide derivative **1**. A general, practical procedure for the asymmetric synthesis of structurally diverse monosubstituted vicinal diamines of type **2** is presented. Dpm = diphenylmethyl.

## Rh-Catalyzed 1,4-Additions

Y. Ma, C. Song, C. Ma, Z. Sun, Q. Chai, M. B. Andrus* ——— **5871 – 5874**

Asymmetric Addition of Aryl Boron Reagents to Enones with Rhodium Dicyclophane Imidazolium Carbene Catalysis

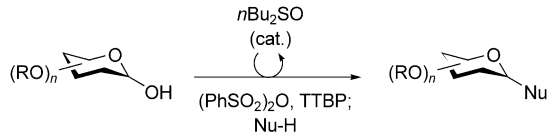



**Chiral N-heterocyclic carbene ligands** based on [2.2]paracyclophanes form complexes with rhodium. These catalysts can be used in the high-yielding and enantioselective asymmetric conjugate addition of arylboron compounds to cyclic and acyclic enones (see scheme).

## Covalent Catalysis

T. A. Boebel, D. Y. Gin* ——— **5874 – 5877**

Sulfoxide Covalent Catalysis: Application to Glycosidic Bond Formation



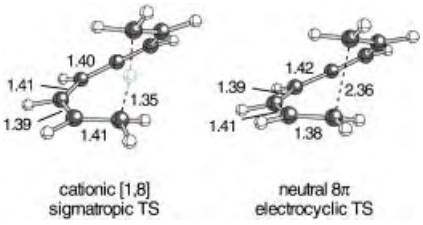

**A versatile glycosylation reaction** is used to establish the process of sulfoxide covalent catalysis. Hemiacetals are activated by benzenesulfonic anhydride and a dialkyl sulfoxide catalyst, $nBu_2SO$, for coupling with various nucleophiles (Nu; see scheme, TTBP = 2,4,6-tri-*tert*-butylpyridine). The sulfoxide catalyst functions uniquely in three capacities, first as an O nucleophile, then as a $S^+$ electrophile, and finally as a leaving group to fulfill turnover.

## Hydrogen Shifts

R. Hoffmann,* D. J. Tantillo* ——— **5877 – 5882**

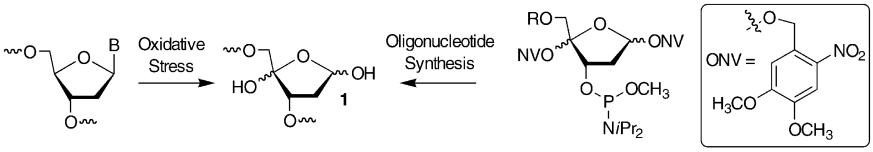
Breaking Down Barriers: The Liaison Between Sigmatropic Shifts, Electrocyclic Reactions, and Three-Center Cations

**Almost indistinguishable** transition-state (TS) geometries, which differ only by the presence or absence of a simple proton, were found for electrocyclic and sigmatropic rearrangements with the same electron count (see picture).





 © 2003 Wiley-VCH Verlag GmbH & Co. KGaA, Weinheim 

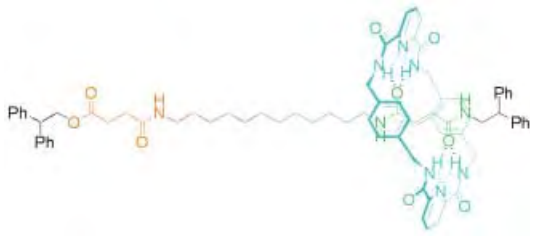



**Selective introduction of damage**: The C4′-position of DNA serves as the site of attack for a number of DNA damaging agents, including bleomycin. The C4′-abasic site is a major product found in damaged DNA following abstraction of the hydrogen atom from this position. The first general method for the synthesis of oligonucleotides **1** containing the C4′-abasic site at defined positions is described (see scheme). This method should facilitate physicochemical, biochemical, and biological studies on this commonly formed DNA lesion.

## Synthesis of Oligonucleotides

J. Kim, J. M. Gil, M. M. Greenberg* ——— **5882 – 5885**

Synthesis and Characterization of Oligonucleotides Containing the C4′-Oxidized Abasic Site Produced by Bleomycin and Other DNA Damaging Agents

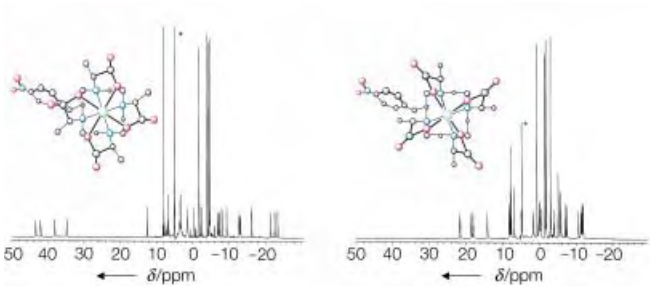



**Two's company but three's allowed!** An entropy-driven tristable molecular shuttle has been developed, where shuttling between two of three stations is brought about through a photochemical isomerization, but a further stable co-conformation is unexpectedly observed simply upon changing the temperature (the picture shows the molecular shuttle in one of the three possible co-conformations).

## Molecular Shuttles

G. Bottari, F. Dehez, D. A. Leigh,* P. J. Nash, E. M. Pérez, J. K. Y. Wong, F. Zerbetto* ——— **5886 – 5889**

Entropy-Driven Translational Isomerism: A Tristable Molecular Shuttle




**Controlling water exchange**: Square antiprism (SAP; left) and twisted square antiprism (TSAP; right) coordination isomers of $Ln^{III}$DOTA-type complexes (DOTA = 1,4,7,10-tetraazacyclododecane-1,4,7,10-tetraacetic acid) may be isolated by choosing substituents on the ring and arms with identical chirality for the TSAP isomer, or with opposite chirality for the SAP isomer. The water exchange rates of the complexes differ by an order of magnitude.

## Coordination Isomers

M. Woods, Z. Kovacs, S. Zhang, A. D. Sherry* ——— **5889 – 5892**

Towards the Rational Design of Magnetic Resonance Imaging Contrast Agents: Isolation of the Two Coordination Isomers of Lanthanide DOTA-Type Complexes

 © 2003 Wiley-VCH Verlag GmbH & Co. KGaA, Weinheim 

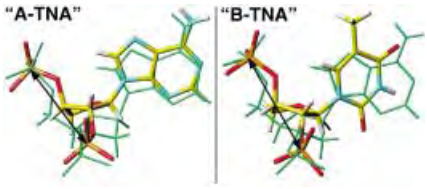
# Contents


## Nucleic Acids

P. S. Pallan, C. J. Wilds, Z. Wawrzak, R. Krishnamurthy, A. Eschenmoser, M. Egli* _____ **5893 – 5895**

Why Does TNA Cross-Pair More Strongly with RNA Than with DNA? An Answer From X-ray Analysis

**The TNA twist**: L-α-threofuranosyl (3′→2′) nucleic acid (TNA) residues adopt a C4′-*exo* pucker when incorporated into an A- (left) or a B-form DNA duplex (right). The resulting intranucleotide P···P distance in TNA is very similar to that in RNA (represented by a C3′-*endo* puckered adenosine residue; green). The structural data explain earlier observations that TNA hydridizes more stably with RNA than



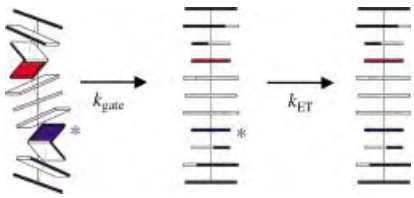

with DNA and that RNA constitutes the better template for ligating TNA fragments.

## Electron Transfer

M. A. O'Neill, H.-C. Becker, C. Wan, J. K. Barton,* A. H. Zewail* **5896 – 5900**

Ultrafast Dynamics in DNA-Mediated Electron Transfer: Base Gating and the Role of Temperature

**The ultrafast dynamics** of electron transfer (ET) between bases in DNA have been determined to elucidate the critical role of base-pair gating on the timescale of the electron transport and the temperature dependence of the rates. ET occurs only through DNA duplexes that adopt a specific, well-coupled alignment of bases (ET-active; see picture). Descriptions of




ET dynamics must include fluctuations of DNA bases.


Communications labeled with this symbol have been judged by two referees as being "very important papers".

The publication of Communications labeled with this symbol has been accelerated because of their topical or highly competitive nature.


**Looking for outstanding employees?**

**Do you need another expert for your excellent team?**
**... Chemists, PhD Students, Managers, Professors, Sales Representatives...**

Place an advert in the printed version and have it made available online for 1 month, free of charge!

***Angewandte Chemie International Edition***
**Advertising Sales Department: Marion Schulz**
**Phone: 0 62 01 - 60 65 65**
**Fax: 0 62 01 - 60 65 50**
**E-Mail: MSchulz@wiley-vch.de**


## Service

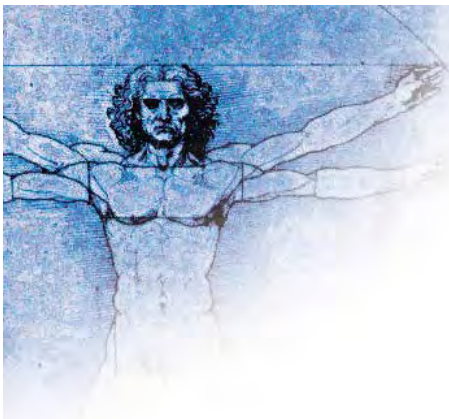

*Keywords* _____ *5904*

*Authors* _____ *5905*

*Angewandte's Sister Journals* _____ *5902 – 5903*

*Vacancies* _____ *5787*

*Preview* _____ *5907*



## R. Noyori Takes up RIKEN Presidency

As of October 1, Ryoji Noyori has taken over as president of RIKEN, the national research institute of Japan. He is now head of an institution with around 3000 employees, 1800 visiting scientists per year, and 1000 students, at seven locations in Japan and three centers in the UK and the USA. RIKEN (Rikagaku Kenkyusho, meaning school for science and research center) was founded in 1917 as a private foundation and has been run since 1958 as a public institution. Since October 2003 it has been an independent administrative institution under the auspices of the Japanese government.



R. Noyori

Noyori acquired bachelor's and master's degrees from Kobe University (Japan) and completed his PhD there in 1967, under the supervision of H. Nozaki, on the first example of organometallic asymmetric catalysis. He was then appointed associate professor at Nagoya University, and only later, in 1969, had the opportunity to carry out postdoctoral research with E. J. Corey (Harvard). Back in Nagoya he was promoted to professor in 1972 and to this day has remained faithful to this institution. His work on asymmetric hydrogenation earned him the Nobel Prize in 2001,[1] together with W. S. Knowles and K. B. Sharpless. Noyori is a member of the International Advisory Board of *Angewandte Chemie* and chairman of the Editorial Board of *Advanced Synthesis & Catalysis*. In 2002 he was president of the Chemical Society of Japan, which celebrated its 125th birthday this year.

## Distinctions to A. Müller

Achim Müller (Universität Bielefeld, Germany), whose large metal clusters always cause a sensation (see the cover of issue 19/2002),[2a] has received two further honors: The Russian Academy of Sciences (Moscow) has awarded him an honorary doctorate, and The University of Kentucky in Lexington (USA) has invited him as the Lyle Dawson Lecturer on the topic "From Protein-Sized Clusters to Super-Supramolecular Chemistry".



A. Müller

Müller completed his PhD in 1965 in Göttingen (Germany) under the guidance of O. Glemser and complete his habilitation there. In 1971 he moved to the Universität Dortmund as professor; he has been at the Universität Bielefeld since 1977. His research encompasses synthetic, spectroscopic, and theoretical aspects of transition-metal inorganic-supramolecular and bioinorganic chemistry. His most recent Communication in *Angewandte Chemie* deals with nanochemistry at its best: the fixing of cations in well-defined positions in tunable artificial cell channels.[2b] In addition to numerous other honors he holds several honorary doctorates.

## W. A. Herrmann Awarded Honorary Doctorate

Wolfgang A. Herrmann has been awarded an honorary doctorate by the University of Rennes (France). Professor of Inorganic Chemistry at the Technische Universität München (TUM, Germany), Herrmann has been recognized for his work in the field of metal complexes and their application in catalysis. His research is mainly focused on metal carbenes,[3a] metal oxides, and lanthanoid organic and bimetallic compounds with multiple bonds. Through this work he has also contributed to numerous industrial processes. He recently reported "New Catalyst Systems for the Catalytic Conversion of Methane into Methanol" in *Angewandte Chemie*.[3b]



W. A. Herrmann

Herrmann studied in Munich (under the Nobel Laureate E. O. Fischer), completed his PhD and his habilitation in Regensburg (under the guidance of H. Brunner), and spent a postdoctoral period in the research group of P. S. Skell in Pennsylvania (USA). He became professor in 1979 at the Universität Regensburg (Germany), took up an appointment in Frankfurt am Main in 1982, and in 1985 moved on to the TUM, where he has been president since 1995. He already holds honorary doctorates from several universities. He is a recipient of the Bundesverdienstkreuz (Federal Cross of Merit) and is an officer of the French Legion of Honor. Herrmann is a member of the Editorial Board of *Angewandte Chemie* and co-editor of several handbooks. From July 5 to 9, 2004 he will chair the 14th International Symposium on Homogeneous Catalysis in Munich.


[1] R. Noyori, *Angew. Chem.* **2002**, *114*, 2108; *Angew. Chem. Int. Ed.* **2002**, *41*, 2008.

[2] A. Müller, E. Krickemeyer, H. Bögge, M. Schmidtmann, S. Roy, A. Berkle, *Angew. Chem.* **2002**, *114*, 3756; *Angew. Chem. Int. Ed.* **2002**, *41*, 2805; A. Müller, S. K. Das, S. Talismanov, S. Roy, E. Beckmann, H. Bögge, M. Schmidtmann, A. Merca, A. Berkle, L. Allouche, Y. Zhou, L. Zhang, *Angew. Chem.* **2003**, *115*, 5193; *Angew. Chem. Int. Ed.* **2003**, *42*, 5039

[3] a) W. A. Herrmann, *Angew. Chem.* **2002**, *114*, 1342; *Angew. Chem. Int. Ed.* **2002**, *41*, 1290; b) M. Muehlhofer, T. Strassner, W. A. Herrmann, *Angew. Chem.* **2002**, *114*, 1817; *Angew. Chem. Int. Ed.* **2002**, *41*, 1745.


 © 2003 Wiley-VCH Verlag GmbH & Co. KGaA, Weinheim 

Amino Acid Synthesis

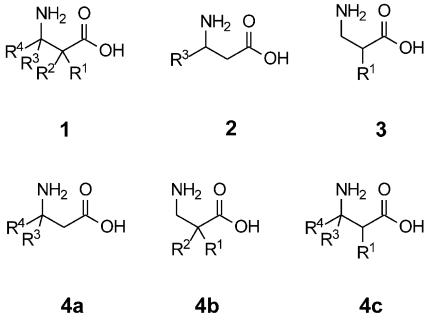
# Synthetic Routes towards Enantiomerically Pure β-Amino Acids

*Norbert Sewald**

**Keywords:**
amino acids · cycloaddition · diastereoselectivity · enantioselectivity · Michael addition

Enantiomerically pure β-amino acids emerged as an interesting and rewarding synthetic target during the past decade, not only because of the fact that the corresponding oligomers, the β-peptides, display a high tendency towards the formation of stable secondary structures (turns, sheets, and helices).[1] The hydrogen-bond pattern and the conformation of β-peptides strongly depend on the substituents and the stereochemistry at $C^{\alpha}$ and $C^{\beta}$, respectively.

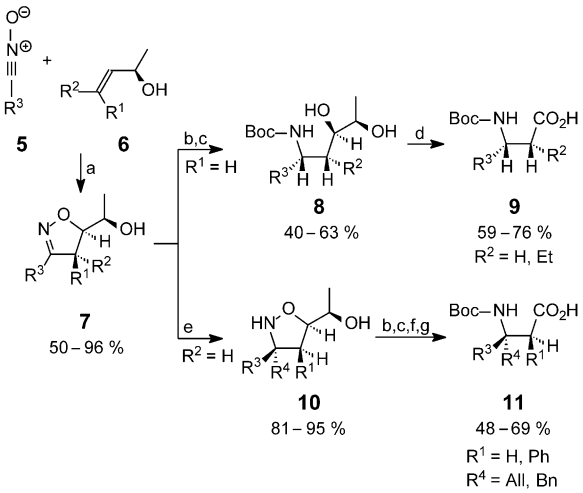
β-Amino acids **1** differ structurally from their α-amino acid correlates, because the amino group is shifted away from the carboxy group by one atom in the skeleton.[2] They do not occur in nature as frequently as α-amino acids, but especially representatives of the class of $\beta^3$-amino acids **2** may be found in free form or as components of naturally occurring biologically active peptides. In contrast, natural products that contain $\beta^2$-amino acids **3** occur more rarely. β-Amino acids often exhibit interesting pharmacological properties and are increasingly finding applications in medicinal chemistry, as peptides that contain β-amino acids display increased metabolic stability.[3]




Stereoselective syntheses of β-amino acids have been the subject of a series of recent review articles.[4–6] Efficient stereoselective synthesis protocols, especially for $\beta^{3,3}$-amino acids **4a** ($R^3 \neq R^4$), $\beta^{2,2}$-amino acids **4b** ($R^1 \neq R^2$),[5] and $\beta^{2,3,3}$-amino acids **4c** still represent a challenge for the synthetic chemist, as a quaternary stereogenic center has to be formed. Furthermore, efficient procedures for the preparation of $\beta^2$-amino acids **3** are also of general interest.[7]

Mapp and co-workers presented a diastereoselective route to $\beta^3$-, $\beta^{3,3}$-, and $\beta^{2,3,3}$-amino acids **2**, **4a**, and **4c**, respectively,[8] which relies on the application of the $Mg^{2+}$-mediated diastereoselective 1,3-dipolar cycloaddition of nitrile oxides **5** to allylic alcohols **6** as originally described by Kanemasa et al.[9] and Bode et al (Scheme 1).[10]

Following the generation of nitrile oxides **5** in situ from the corresponding oximes, 1,3-dipolar cycloaddition with the magnesium allyl alcoholates occurs regio- and diastereoselectively to yield the 2-isoxazolines **7.** The C=N and N–O bonds of these compounds are simultaneously reduced and cleaved, respectively, by hydride donors (Scheme 1). After introduction of an appropriate amino-protecting group (e.g. Boc), the 1,2-diol **8** is subsequently cleaved by oxidation to provide, depending on the allyl alcohol **6** employed, a $\beta^3$-amino acid **9** ($R^2 = H$, $R^3 \neq H$) or a $\beta^{2,3}$-amino acid **9** ($R^2 = Et$, $R^3 = \neq H$) in three steps. Alternatively, instead of a reduction, an additional carbon substituent $R^4$ may be introduced by the addition of a Grignard compound to yield the isoxazolidine **10.** In these cases, the N–O bond requires subsequent reductive cleavage. While the free hydroxy group directs the diastereofacial *syn* selectivity of the hydride transfer reaction, the addition of a carbon nucleophile occurs—for steric reasons—selectively from the



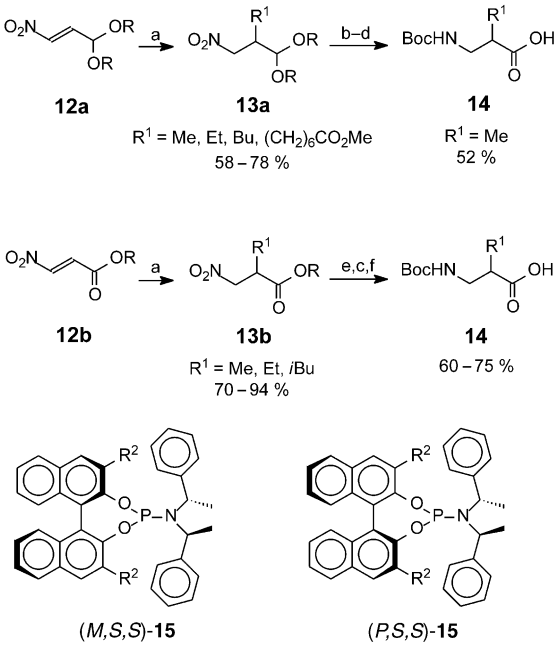

***Scheme 1.*** Synthesis of β-amino acids by 1,3-dipolar cycloaddition.[8] a) EtMgBr, *i*PrOH, d.r. 7:1 to >20:1; b) $LiAlH_4$; c) $Boc_2O$; d) $NaIO_4$, $RuCl_3$; e) $R^4MgCl$, $BF_3{\cdot}OEt_2$; f) $NaIO_4$; g) $NaClO_2$, 2-methyl-2-butene. Boc = *tert*-butoxycarbonyl, All = allyl, Bn = benzyl.

[*] Prof. Dr. N. Sewald
Organische und Bioorganische Chemie,
Universität Bielefeld
PO Box 100131, 33501 Bielefeld (Germany)
Fax: (+49) 521-106-8094
E-mail: norbert.sewald@uni-bielefeld.de

 © 2003 Wiley-VCH Verlag GmbH & Co. KGaA, Weinheim DOI: 10.1002/anie.200301692 

complementary face. As the authors investigated only one example of the addition of $R^4MgCl$ in which a substituent is located at C4 of isoxazoline **7** ($R^1 = Ph$, $R^2 = H$), no proof is yet provided that all other diastereomers of a certain $\beta^{2,3,3}$-amino acid **11** are formed with comparable stereoselectivity.

Protection of the amino group is again followed by oxidative cleavage of the glycol to provide either $\beta^{3,3}$-amino acids **11** (type **4a**) or $\beta^{2,3,3}$-amino acids **11** (type **4c**). Substituents at C2 and the sense of chirality at this carbon atom are carried over from the enantiomerically pure allyl alcohol, which is easily accessible in both enantiomeric forms. The substituents at C3 of the isoxazoline and, consequently, of the β-amino acid either originate from the nitrile oxide **5** or the carbon nucleophile $R^4M$. In principle, a broad variety of differently substituted $\beta^{2,3,3}$-amino acids **11** (type **4c**) should be accessible in both stereochemical series with good stereoselectivity and acceptable to good yields. However, Mapp and co-workers described only one single derivative of this type, and a racemic allyl alcohol was used in this synthesis. Moreover, the sterically demanding compounds ($R^1 \neq H$, $R^2 \neq H$) are only obtained in moderate yields.




***Scheme 2.*** Synthesis of $\beta^2$-amino acids by enantioselective $Cu^I$-catalyzed conjugate addition of dialkyl zinc compounds to nitroalkenes.[12,14–16] a) $R^1_2Zn$, $Cu^I$, **15a** for **12a**, **15a,b** for **12b**, < 98% *ee*, < 94% yield; b) Raney nickel, $H_2$; c) $Boc_2O$, $NEt_3$; d) $H_5IO_6$, $CrO_3$; e) $NH_4^+$ $HCO_2^-$, Pd/C; f) LiOH.

Enantiomerically pure $\beta^2$-amino acids **2** were recently obtained by asymmetric $Cu^I$-catalyzed addition of diorganozinc compounds to nitroalkenes. Organozinc compounds have found broad application in asymmetric synthesis and catalysis, as they tolerate a broad range of functional groups and, hence, allow the introduction of sensitive functionalities (e.g. esters, nitriles).[11]

The $Cu^I$-catalyzed enantioselective addition of diethylzinc to 3-nitroacrolein dimethylacetal (**12a**) proceeds with excellent enantioselectivity and yield (Scheme 2).[12,13] Especially enantiomerically pure phosphoramidites of type **15** (**a**: $R^2 = H$; **b**: $R^2 = CH_3$) based on BINOL and *N*,*N*′-bis(1-phenylethyl)-amine provide good results. They act as ligands for $Cu^I$ and as mediators of the stereochemical information. Suitably functionalized nitroalkenes already contain the substituent pattern required for $\beta^2$-amino acids **3**. The nitro group is easily reduced to give an amino group (Scheme 2). Feringa and co-workers took up this concept and developed it further, for example, with respect to the substituents on the side chain.[14] Besides Boc-protected $\beta^2$-amino acids, $\beta^2$-aminoaldehydes and the corresponding aminoalcohols are also accessible. In contrast to results by Feringa and co-workers,[14] the reactivity and the Michael acceptor capability of the nitroalkene moiety allows 3-nitroacrylates **12b** to be employed directly for the regioselective and stereoselective synthesis of $\beta^2$-amino acids, as independently shown by our group[15] and Eilitz et al.[16] Again, enantioselective $Cu^I$/phosphoramidite catalysis in the 1,4-addition of diorganozinc compounds is followed by hydrogenation of the nitro group, Boc protection of the amino group, and hydrolysis of the ester (Scheme 2).


[1] R. P. Cheng, S. H. Gellman, W. F. DeGrado, *Chem. Rev.* **2001**, *101*, 3219–3232.

[2] Besides the IUPAC nomenclature, the trivial names of the α-amino acids are frequently used in a modified form for β-amino acids. The expression β-homoamino acid means that formally an additional methylene group is inserted between the carboxy group and the carbon atom that bears the amino group. The CIP nomenclature sometimes changes in contrast to the D,L nomenclature when comparing stereochemically equivalent α- and β-amino acids. To distinguish between position isomers, Seebach et al. suggested that the side-chain attachment be classified by a superscripted digit following the greek letter β.

[3] J. V. Schreiber, J. Frackenpohl, F. Moser, T. Fleischmann, H.-P. E. Kohler, D. Seebach, *ChemBioChem* **2002**, *3*, 424–432.

[4] *Enantioselective Synthesis of* β*-Amino Acids* (Ed.: E. Juaristi), Wiley-VCH, New York, **1997**.

[5] S. Abele, D. Seebach, *Eur. J. Org. Chem.* **2000**, 1–15.

[6] M. Liu, M. P. Sibi, *Tetrahedron* **2002**, *58*, 7991–8035.

[7] D. Seebach, L. Schaeffer, F. Gessie, P. Bindschädler, C. Jäger, D. Josien, S. Kopp, G. Lelais, Y. R. Mahajan, P. Micuch, R. Sebesta, B. W. Schweizer, *Helv. Chim. Acta* **2003**, *86*, 1852–1861.

[8] A. R. Minter, A. A. Fuller, A. K. Mapp, *J. Am. Chem. Soc.* **2003**, *125*, 6846–6847.

[9] S. Kanemasa, M. Nishiuchi, A. Kamimure, K. Hori, *J. Am. Chem. Soc.* **1994**, *116*, 2324–2339.

[10] J. W. Bode, N. Fraefel, D. Muri, E. M. Carreira, *Angew. Chem.* **2001**, *113*, 2128–2131; *Angew. Chem. Int. Ed.* **2001**, *40*, 2082–2084.

[11] P. Knochel, R. D. Singer, *Chem. Rev.* **1993**, *93*, 2117–2188.

[12] N. Sewald, V. Wendisch, *Tetrahedron: Asymmetry* **1998**, *9*, 1341–1344.

[13] A. Alexakis, C. Benhaim, *Org. Lett.* **2000**, *2*, 2579–2581.

[14] A. Duursma, A. J. Minnaard, B. L. Feringa, *J. Am. Chem. Soc.* **2003**, *125*, 3700–3701.

[15] A. Rimkus, N. Sewald, *Org. Lett.* **2003**, *5*, 79–80.

[16] U. Eilitz, F. Leßmann, O. Seidelmann, V. Wendisch, *Tetrahedron: Asymmetry* **2003**, *14*, 189–191.


 © 2003 Wiley-VCH Verlag GmbH & Co. KGaA, Weinheim 

Nanotechnology

# Functional Hybrid Devices of Proteins and Inorganic Nanoparticles**

*Christof M. Niemeyer**

**Keywords:**
chaperonins · enzymes · nanostructures · proteins · supramolecular chemistry

*Dedicated to Professor Manfred T. Reetz on the occasion of his 60th birthday*

Currently there is great interest in the rational self-assembled fabrication of hybrid materials from inorganic nanoparticles and biomolecules.[1] These approaches are motivated by the broad range of applications of such hybrids which range from life sciences to materials and nanosciences. The motivation is based on the unique properties of the two classes of building blocks. Inorganic nanoparticles possess strongly size-dependent optical, electrical, magnetic, and electrochemical properties, while biomolecules, such as proteins and nucleic acids, reveal perfect binding properties and biochemical functionality that has been optimized over billions of years of evolution. Nucleic acids have preferentially been used in the early stages of the research on the functionalization of nanoparticles to provide highly specific binding sites since they are more readily available by synthetic chemical means and are more convenient to handle than proteins.[2] Proteins have also been employed to extend the binding capabilities of inorganic nanoparticles.[3] However, in addition to simply utilizing their binding properties, a particular challenge is to combine the intrinsic functionality of many proteins, for example, optic, catalytic, mechanic, or switching capabilities, with the special properties of nanoparticles.[4,5]

To this end, initial studies concerned the optical interaction between cadmium chalcogenide semiconductor nanoparticles (CdS, CdSe, CdTe), often refered to as quantum dots (QDs), and proteins chemisorbed to their surface.[6,7] QDs have a broad excitation and size-tunable photoluminescence spectra with narrow emission bandwidths that span the visible spectrum, which allows simultaneous excitation of several particle sizes at a single wavelength. QDs are also being developed as luminescent probes in biological labeling studies since they reveal exceptional photochemical stability and relatively high quantum yields,.[3f–l] Mamedova et al. showed that the cross-linking of the 67 kDa protein bovine serum albumin (BSA) and cysteine-capped 2-nm-sized CdTe QDs using glutaric dialdehyde led to conjugates, which preferentially contained one molecule of the cigar-shaped ellipsoidal BSA (ca. $6 \times 6 \times 10$ nm) per QD.[6] Circular dichroism spectroscopy indicated that the tertiary structure of the protein remained largely intact after the conjugation. The conjugates revealed effective interaction between the excited states of the biological and inorganic parts as a consequence of the spatial closeness of BSA and the nanoparticle. The luminescence of two aromatic tryptophan residues of BSA, which normally emits at 340 nm, was quenched completely, while the emission peak of the CdTe QDs increased twofold in amplitude and about threefold in area. This enhancement in luminescence was attributed to the concentration of adsorbed energy collected by the nanoparticle from the protein units through resonance energy transfer—analogous to the classical Förster resonance energy transfer (FRET).[6]

In a related study by Willard et al. (Figure 1a), approximately 3-nm CdSe-ZnS core-shell particles were coated by chemisorption with biotinylated BSA (bBSA) containing about twenty thiol groups, which had been previously incorporated using 2-iminothiolane.[7] Conjugates were formed which contained two bBSA molecules per nanoparticle. The biotin groups of bBSA allowed for the specific coupling of tetramethylrhodamine-labeled streptavidin (TMR-STV), and thus, the formation of a FRET system. The addition of various amounts of the TMR-STV, in fact, induced a quenching of the nanoparticle's emission while the emission of the TMR increased. It was observed that the fraction of emission quenched through FRET depended on the relative amounts of TMR-STV added to the bBSA-coated QDs. Only 11% of the quenching arose from FRET with one molar equivalent of TMR-STV while this value increased up to 54% with five molar equivalents. A further increase in the TMR-STV concentration again decreased the fraction of FRET. Alternative energy-transfer mechanisms which account for additional quenching include self-quenching as a result of nanoparticle aggregation as well as nanoparticle-to-TMR electron transfer.[7]

These initial studies indicate that specific binding events of proteins can be observed by utilizing the unique optical properties of inorganic nanoparticles. They also suggest that such hybrid conjugates might be used in the design of homogeneous assays for antibody–antigen binding, nucleic acid hybridiza-

[*] Prof. Dr. C. M. Niemeyer
Universität Dortmund
Fachbereich Chemie
Biologisch-Chemische Mikrostrukturtechnik
Otto-Hahn Strasse 6
44227 Dortmund (Germany)
Fax: (+49) 231-755-7082
E-mail: cmn@chemie.uni-dortmund.de

[**] I wish to thank P. Alhorn for her help in preparing the figures.

 © 2003 Wiley-VCH Verlag GmbH & Co. KGaA, Weinheim DOI: 10.1002/anie.200301703 

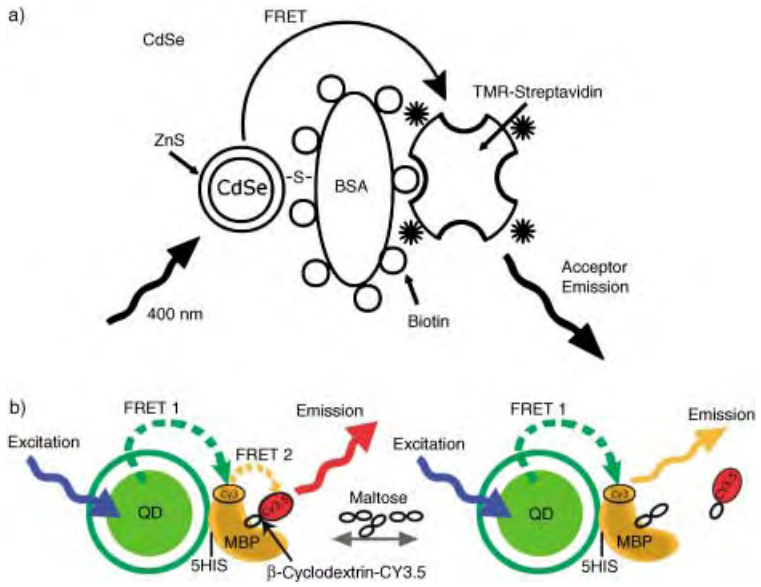



***Figure 1.*** Optical communication between biomolecular and semiconductor nanoparticles. a) Schematic drawing of a FRET system assembled by chemisorption of thiol-modified biotinylated bovine serum albumin (BSA) to CdSe quantum dots (QD) and subsequent coupling of tetramethylrhodamine-labeled streptavidin (TMR-STV).[7] b) Maltose nanosensor assembled from CdSe-ZnS QDs (emitting at 530 nm) coated with a recombinant maltose-binding protein (MBP) containing a pentahistidine segment (5His) and a single Cy3 fluorophore. The maltose binding site is occupied by the β-cyclodextrin–Cy3.5 conjugate, which is replaced upon competition with free maltose.[8]

tion, or enzyme–substrate interaction.[7] This has recently been conducted by Medintz et al., who reported on the design, formation, and testing of QD–protein assemblies that function as a specific chemical sensor for saccharides.[8] CdSe-ZnS core-shell QDs of approximately 3-nm diameter, stabilized by dihydrolipoic acid ligands, were coated with a recombinant variant of maltose-binding protein (MBP) containing a pentahistidine segment at its C-terminus and a single Cy3 fluorophore covalently attached to a distinct cysteine residue (Figure 1b). The binding sites of the about 10 MBP molecules per QD were occupied by β-cyclodextrin–Cy3.5 (β-CD–Cy3.5) conjugates. Within these defined assemblies, the protein-bound Cy3 served as a "FRET relay station", that is, a bridging acceptor/donor for the energy transfer from the QD to the maltose-displacable β-CD–Cy3.5. Added maltose readily competes with and displaces the β-CD–Cy3.5 leading to an increase in the Cy3 emission, thus allowing the detection of about 0.1 μM maltose.

In an alternative nanosensor assembly, the binding sites of the MBPs were occupied by β-CD–QSY9 conjugates. QSY9 is a nonfluorescent dye which efficiently quenched the QD emission. Maltose and other sugars containing an α-1,4-glucosidic linkage replaced the quencher–CD complex, thereby increasing the QDs photoluminescence. This nanosensor configuration showed similar sensitivity as the double-FRET system depicted in Figure 1b. FRET efficiencies of the β-CD–QSY9 and the β-CD–Cy3.5 assemblies were estimated to be about 75% and 20%, respectively. In the latter assembly, the Cy3.5 received the energy of the QDs either directly (ca. 6%) or relayed through the 10 MBP-bound Cy3 dyes (ca. 14%). This study represents not only an innovative approach to transducing sugar binding into an optical signal, it also sheds more light on energy-transfer mechanisms occuring within QD–protein conjugates. While earlier studies could not rule out whether energy transfer was mainly a result of FRET or other processes, such as electron transfer or surface activation,[7] the recent study clearly confirmed FRET to be the dominant process.[8] Moreover, the recent study also highlights some aspects of our incomplete understanding of molecular-scale energetics and the chemical behavior of optically active assemblies bound to QD surfaces.[8]

Nanoparticles often coagulate in aqueous media and so lose their size-dependent properties. Shape-persistent three-dimensional stabilizers that enfold nanoparticles are thus required which do not interfere with the particle's optical properties and their accessibility to external stimuli. Ishii et al. recently reported on the biomolecular enfolding of CdS nanoparticles by chaperonin proteins which allow for a triggered release of the encapsulated guest.[9] The chaperonin proteins GroEL and *T.th* encapsulate denatured proteins inside a cylindrical cavity; after refolding, the encapsulated proteins are released by the action of ATP which induces a conformational change of the chaperonin's cavity. The *Escherichia coli* protein GroEL consists of two supramolecular rings, each comprised of seven subunits of 60 kDa, which are stacked to form a double-decker architecture (Figure 2), thereby forming a cyclindrical cavity with a diameter of 4.5 nm and a wall thickness of 4.6 nm. Chaperonin *T.th* originates from thermophilic bacterium *Thermus thermophilus* HB8, and consists of a GroEL-like tetradecamer which is capped with a protein assembly [cpn10] of 70 kDa. The cavity size and wall thickness of *T.th*–cpn complexes are comparable to those of GroEL.

For complexation, a solution of 2–4-nm-sized CdS particles in dimethylformamide was mixed with an aqueous solution of the chaperonin proteins in Tris-HCl buffer. The formation of an inclusion complex was verified by CD spectroscopy, analytical size-exclusion chromatography, and transmission electron microscopy (TEM). The TEM images clearly revealed a dark central region within the *T.th*–cpn–CdS nanoparticle complex which corresponds to the presence of a CdS particle within the protein cavity. Statistical analysis showed that about 75% of the *T.th*–cpn complexes had a dark central cavity, while no CdS nanoparticles were observed at the exterior of the protein surface.

The characteristic photoluminescence of the CdS particles within the chaperonin–CdS nanoparticle complex

 © 2003 Wiley-VCH Verlag GmbH & Co. KGaA, Weinheim 

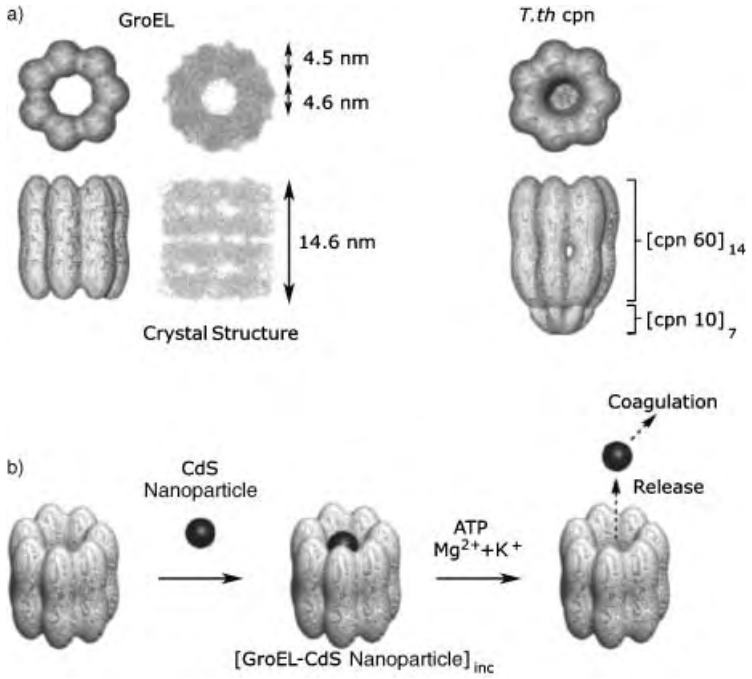



***Figure 2.*** Chaperonin proteins as ATP-responsive barrels for inclusion of semiconductor nanoparticles. a) Top and side views of GroEL and *T.th*–cpn. b) Formation of GroEL–CdS nanoparticle complexes by inclusion of CdS nanoparticles into the cyclindrical cavity of GroEL, and its ATP-triggered guest release. Reproduced with permission from Ref. [9].

lasted for an ununsually long period of time (for example, more than 400 days in the case of GroEL complexes), while in the absence of GroEL the photoluminescence dissappeared within two hours. It was also established by repeated heating–cooling cycles that the thermal stability of the QDs was dramatically increased by the chaperonin proteins: at elevated temperatures, for example, 70 °C, the photoluminescence of the *T.th*–cpn–CdS inclusion complex was quenched, but the original intensity was recovered upon cooling down to 4 °C. The luminescence recovery was possible as long as the heating did not exceed the temperature of protein denaturation, that is, about 80 °C for *T.th*–cpn complexes. Similarly, the GroEL–CdS complex showed thermoresponsive photoluminescence activity, but became irreversible upon heating for 20 min at 60 °C, which is just below the thermal denaturation temperature of intact GroEL. In contrast, a solution of the CdS nanoparticles in DMF also revealed a temperature-dependent photoluminescence profile, but it became irreversible at only 30 °C, with formation of a colloidal precipitate of CdS.

The CdS nanoparticles within the chaperonin proteins were electronically insulated by the approximately 4.5-nm-thick protein wall around them. This was demonstrated by fluorescence titration with methyl viologen ($MV^{2+}$), an electron acceptor which is known to quench the photoexited singlet state of CdS QDs. The Stern–Vollmer constant of the GroEL–CdS complex was more than 15 times smaller than for isolated CdS particles in DMF, which indicates that the thickness of the protein envelope was sufficient to shield the particles from electron transfer.

The encapsulation of semiconductor nanoparticles by protein components[10] as well as the changes in the optical and physicochemical properties of the nanoparticles as a result of (bio)organic enwrapping, and thus, shielding from the aqueous solvent, have previously been described.[11] However, the chaperonin ligand system offers a unique option, namely, a triggered release of the encapsulated nanoparticle. Treatment of the GroEL–CdS nanoparticle inclusion complex with ATP in the presence of $Mg^{2+}$ and $K^+$ resulted in the immediate release of inorganic species within seconds as a consequence of the large conformational change in protein conformation. This led to the formation of colloidal substances and the immediate quenching of fluorescence, and did not occur when either ATP or $Mg^{2+}$ was missing or when ADP was used instead of ATP. This report is a clear demonstration of how highly specific biological mechanisms can be integrated into materials science, and will surely stimulate many new approaches to conceptually new bioresponsive devices.

Another fascinating example of coupling biomolecular functionality with inorganic nanoparticles was recently reported by Willner and co-workers.[12] They nanowired redox enzymes with gold nanoparticles to enhance the routing of electrons from the enzymes to electrodes. Previous approaches using redox-relay groups or the immobilization of enzymes in redox-active polymers had led to the establishment of electrical communication between the biocatalyst and electrodes, however, the electron-transfer rate constants in such assemblies were always far lower than those between the enzymes and their natural electron acceptor (most often $O_2$).[13] An "electrical nanoplug" was obtained by synthesizing a conjugate from 1.4-nm-sized Au nanoparticles containing a single *N*-hydroxysuccinimide group and N6-(2-aminoethyl)-FAD (FAD = flavin adenin dinucleotide) to yield an FAD-functionalized gold nanoparticle (Figure 3). FAD is the cofactor of the redox enzyme glucose oxidase (GOx). The Au–FAD conjugate was then used in the reconstitution of apo-GOx, thereby bringing the metallic nanoparticle in proximity to the enzyme's redox center. The kinetics of reconstitution was probed by following the increase in the fluorescence of FAD upon reconstitution which presumably originated from the spatial separation of the FAD from the nanoparticle by incorporation in the hydrophobic microenvironment of the protein.

Two alternative routes for the attachment of the bioinorganic hybrid enzyme with a macroscopic electrode were studied (Figure 3). In one case Au nanoparticle-reconstituted GOx was adsorbed onto a dithiol monolayer associated with a gold electrode (route a in Figure 3). In the second case the Au

 © 2003 Wiley-VCH Verlag GmbH & Co. KGaA, Weinheim 

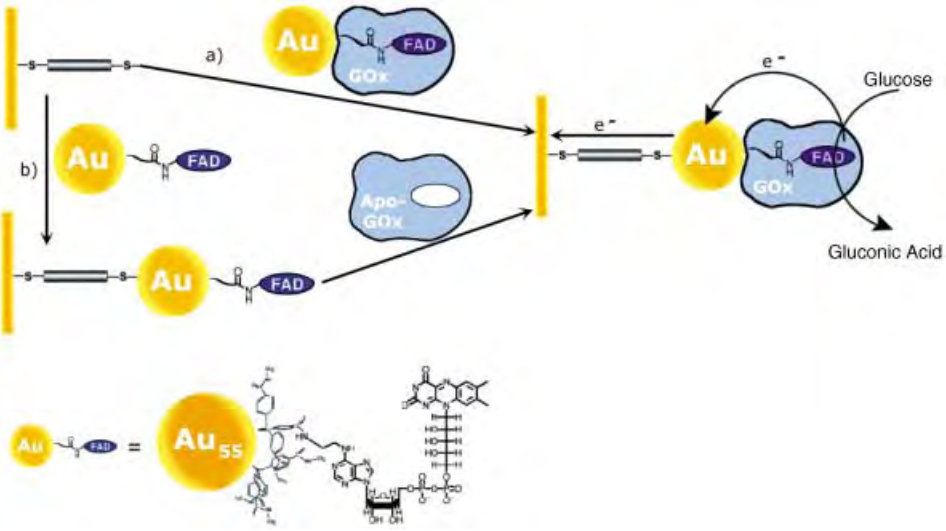



***Figure 3.*** "Plugging into enzymes": Assembly of an Au nanoparticle–glucose oxidase (GOx) conjugate at macroscopic Au electrodes by two alternative routes: a) adsorption of Au nanoparticle-reconstituted GOx to a dithiol monolayer associated with a gold electrode; b) adsorption of Au nanoparticle–FAD conjugates on the dithiol-modified gold electrode, followed by reconstitution of apo-GOx on the functionalized nanoparticles. The bridge between the macroscopic electrode and the gold nanoparticle is achieved by dithiol spacer units. Adapted from Ref. [12].

nanoparticle-FAD conjugates were adsorbed onto a dithiol-modified gold electrode, followed by reconstitution of apo-GOx on the functionalized nanoparticles (route b in Figure 3). Both methods yielded almost identical surface coverages of reconstituted GOx of $1 \times 10^{12}$ mol cm$^{-2}$, which corresponds to approximately 60 % of a random, densely packed GOx monolayer on the electrode surface. Investigation of the catalytic properties of the assembly by cyclic voltammetry revealed that the oxidation of glucose occured with an unexpectedly high unimolecular electron-transfer rate constant of $5 \times 10^3$ s$^{-1}$. This value is seven times higher than the electron-transfer rate constant of native GOx with $O_2$ and, thus, the results suggest that the incorporation of gold nanoparticles into the enzyme greatly increases its maximum turnover rate. Further experiments showed that the biocatalytic assembly is unperturbed by $O_2$ or the presence of an oxidizable interfering species, such as ascorbic acid. It was also shown that the length and structure of the bridging dithiol spacer units between the electrode and the nanoparticle influence the electron transfer between the FAD and the electrode. This process is reflected in the overall bioelectrocatalytic oxidation of glucose.

The reports highlighted here are very illustrative examples of how biological systems can be tuned by nanostructured inorganic components and how the properties of inorganic particles can be extended by biomolecular mechanisms. The present studies,[8,9,12] in particular, add new facets to nanobiotechnology, and will clearly stimulate plenty of new exciting developments in this young field of research.


[1] C. M. Niemeyer, *Angew. Chem.* **2001**, *113*, 4254 – 4287; *Angew. Chem. Int. Ed.* **2001**, *40*, 4128 – 4158.

[2] C. A. Mirkin, *Inorg. Chem.* **2000**, *39*, 2258 – 2272.

[3] For examples of gold nanoparticles, see a) C. M. Niemeyer, W. Bürger, J. Peplies, *Angew. Chem.* **1998**, *110*, 2391 – 2395; *Angew. Chem. Int. Ed.* **1998**, *37*, 2265 – 2268; b) S. Connolly, D. Fitzmaurice, *Adv. Mater.* **1999**, *11*, 1202 – 1205; c) M. Li, K. W. K. Wong, S. Mann, *Chem. Mater.* **1999**, *11*, 23 – 26; d) C. M. Niemeyer, B. Ceyhan, *Angew. Chem.* **2001**, *113*, 3798 – 3801; *Angew. Chem. Int. Ed.* **2001**, *40*, 3685 – 3688; e) histochemical applications: J. Kreuter in *Microcapsules and Nanoparticles in Medicine and Pharmacy* (Ed.: M. Donbrow), CRC, Boca Raton, **1992**; for examples of semiconductor nanoparticles, see f) M. Bruchez, Jr., M. Moronne, P. Gin, S. Weiss, A. P. Alivisatos, *Science* **1998**, *281*, 2013 – 2015; g) W. C. W. Chan, S. M. Nie, *Science* **1998**, *281*, 2016 – 2018; h) H. Mattoussi, J. M. Mauro, E. R. Goldmann, G. P. Anderson, V. C. Sundar, F. V. Miculec, M. G. Bawendi, *J. Am. Chem. Soc.* **2000**, *122*, 12142 – 12150; i) X. Wu, H. Liu, J. Liu, K. N. Haley, J. A. Treadway, J. P. Larson, N. Ge, F. Peale, M. P. Bruchez, *Nat. Biotechnol.* **2003**, *21*, 41 – 46; k) J. K. Jaiswal, H. Mattoussi, J. M. Mauro, S. M. Simon, *Nat. Biotechnol.* **2003**, *21*, 47 – 51; l) M. Han, X. Gao, J. Z. Su, S. M. Nie, *Nat. Biotechnol.* **2001**, *19*, 631 – 635.

[4] Examples of enyzme–nanoparticle conjugates: a) proteases: A. Gole, C. Dash, C. Soman, S. R. Sainkair, M. Rao, M. Sastry, *Bioconjugate Chem.* **2001**, *12*, 684 – 690; N. O. Fischer, C. M. McIntosh, J. M. Simard, V. M. Rotello, *Proc. Natl. Acad. Sci. USA* **2002**, *99*, 5018 – 5023; b) cytochrom C: C. D. Keating, K. M. Kovaleski, M. J. Natan, *J. Phys. Chem. B* **1998**, *102*, 9414 – 9425; C. D. Keating, K. M. Kovaleski, M. J. Natan, *J. Phys. Chem. B* **1998**, *102*, 9404 – 9413, and references therein; c) electrode-immobilized adsorbates of nanoparticles and enzymes: J. G. Stonehuerner, J. Zhoa, J. P. O'Daly, A. L. Crumbliss, R. W. Henkens, *Biosens. Bioelectron.* **1992**, *7*, 421 – 428; A. L. Crumbliss, S. C. Perine, J. G. Stonehuerner, K. R. Tubergen, J. Zhao, J. P. O'Daly, *Biotechnol. Bioeng.* **1992**, *40*, 483 – 490; J. Zhao, J. P. O'Daly, R. W. Henkens, J. G. Stonehuerner, A. L. Crumbliss, *Biosens. Bioelectron.* **1996**, *11*, 493 – 502; F. Patolsky, T. Gabriel, I. Willner, *J. Electroanal. Chem.* **1999**, *479*, 69 – 73; V. Pardo-Yissar, E. Katz, J. Wasserman, I. Willner, *J. Am. Chem. Soc.* **2003**, *125*, 622 – 623.

[5] Recently, the enzymatic manipulation of DNA-functionalized gold nanoparticles has been studied: S. R. Nicewarner Pena, S. Raina, G. P. Goodrich, N. V.


 © 2003 Wiley-VCH Verlag GmbH & Co. KGaA, Weinheim 

Fedoroff, C. D. Keating, *J. Am. Chem. Soc.* **2002**, *124*, 7314 – 7323; C. S. Yun, G. A. Khitrov, D. E. Vergona, N. O. Reich, G. F. Strouse, *J. Am. Chem. Soc.* **2002**, *124*, 7644 – 7645; A. G. Kanaras, Z. Wang, A. D. Bates, R. Cosstick, M. Brust, *Angew. Chem.* **2003**, *115*, 201 – 204; *Angew. Chem. Int. Ed.* **2003**, *42*, 191 – 194.

[6] N. N. Mamedova, N. A. Kotov, A. L. Rogach, J. Studer, *Nano Lett.* **2001**, *1*, 281 – 286.

[7] D. M. Willard, L. L. Carillo, J. Jung, A. Van Orden, *Nano Lett.* **2001**, *1*, 469 – 474.

[8] I. L. Medintz, A. R. Clapp, H. Mattoussi, E. R. Goldman, B. Fisher, J. M. Mauro, *Nat. Mater.* **2003**, *2*, 630 – 638.

[9] D. Ishii, K. Kinbara, Y. Ishida, N. Ishii, M. Okochi, M. Yohda, T. Aida, *Nature* **2003**, *423*, 628 – 632.

[10] For the growth of inorganic nanoparticles in apo-ferritin, see a) F. C. Meldrum, V. J. Wade, D. L. Nimmo, B. R. Heywood, S. Mann, *Nature* **1991**, *349*, 684 – 687; b) F. C. Meldrum, B. R. Heywood, S. Mann, *Science* **1992**, *257*, 522 – 523; c) K. K. W. Wong, T. Douglas, S. Gider, D. D. Awschalom, S. Mann, *Chem. Mater.* **1998**, *10*, 279 – 285; growth of iron oxide in Lumazin synthase capsid: d) W. Shenton, S. Mann, H. Cölfen, A. Bacher, M. Fischer, *Angew. Chem.* **2001**, *113*, 456 – 459; *Angew. Chem. Int. Ed.* **2001**, *40*, 442 – 444; for virus capsid proteins as hosts for particle growth, see e) T. Douglas, M. Young, *Nature* **1998**, *393*, 152 – 155; f) Q. Wang, T. Lin, L. Tang, J. E. Johnson, M. G. Finn, *Angew. Chem.* **2002**, *114*, 477 – 480; *Angew. Chem. Int. Ed.* **2002**, *41*, 459 – 462; g) W. Shenton, T. Douglas, M. Young, G. Stubbs, S. Mann, *Adv. Mater.* **1999**, *11*, 253 – 256 for chaperonins as templates for the organization of metal and semiconductor nanoparticles, see h) R. A. McMillan, C. D. Paavola, J. Howard, S. L. Chan, N. J. Zaluzec, J. D. Trent, *Nat. Mater.* **2002**, *1*, 247 – 252, see also Ref. [1], and references therein.

[11] For example, trioctylphosphane oxide (TOPO) stabilized semiconductor quantum dots can be protected by adsorption of a layer of an amphiphilic polymer (octylamine modified polyacrylic acid) and the two organic components are covalently cross-linked. The resulting particles are stable against coagulation in aqueous solutions, and reveal luminescence intensity similar as in organic solvents (Ref. [3i], see also www.qdots.-com).

[12] Y. Xiao, F. Patolsky, E. Katz, J. F. Hainfeld, I. Willner, *Science* **2003**, *299*, 1877 – 1881.

[13] I. Willner, E. Katz, *Angew. Chem.* **2000**, *112*, 1230 – 1269; *Angew. Chem. Int. Ed.* **2000**, *39*, 1180 – 1218.

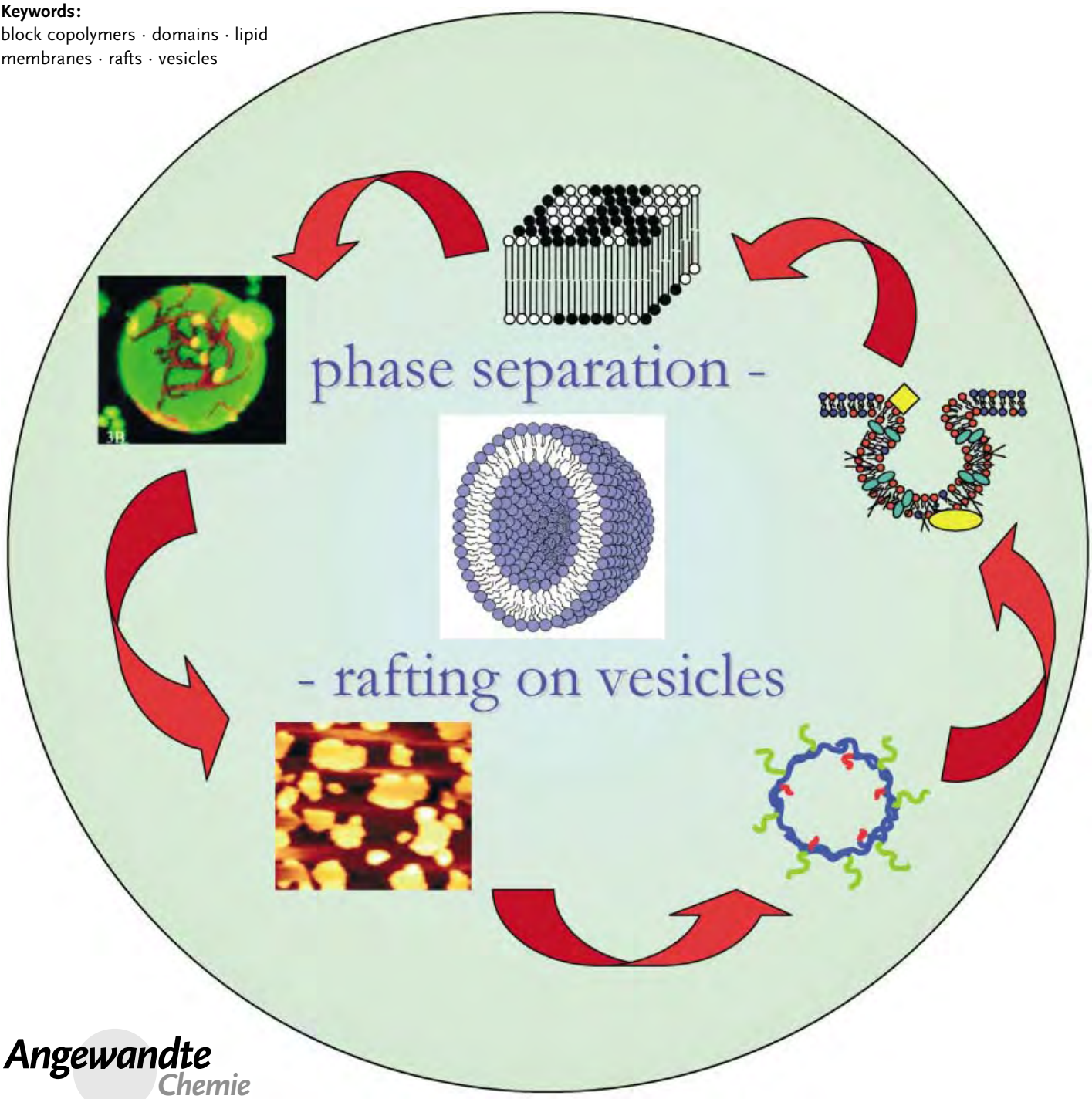
 © 2003 Wiley-VCH Verlag GmbH & Co. KGaA, Weinheim 

Lipid membranes

# Domains and Rafts in Lipid Membranes

*Wolfgang H. Binder,* Veronique Barragan, and Fredric M. Menger*

**Keywords:**
block copolymers · domains · lipid membranes · rafts · vesicles





© 2003 Wiley-VCH Verlag GmbH & Co. KGaA, Weinheim
DOI: 10.1002/anie.200300586

*"It takes a membrane to make sense out of disorder in biology. You have to be able to catch energy and hold it, storing precisely the needed amount and releasing it in measured shares". So wrote Lewis Thomas in* The Lives of Cells. *Domains and rafts are shown in the present Review to play an important role in this amazing behavior of lipid membranes. Topics touched upon include the experimental detection of domains, their composition, domain induction, properties of rafts (a special form of domain), and the relationship of rafts to human diseases. Lipids, polymers, and proteins can contribute to this type of micro- and nanostructuring within membranes, thus imposing a new structural hierarchy on top of the classical bilayer membrane. The purpose of this Review is to develop an appreciation for the multiple organizational levels in self-assembling systems.*

### From the Contents


| | |
|---|---|
| 1. Introduction | 5803 |
| 2. Experimental Grounds of Domain and Raft Research | 5804 |
| 3. Phase Separation and Domain Formation in Model Lipid Bilayers | 5807 |
| 4. Rafts | 5814 |
| 5. Polymer-Induced Phase Separation | 5817 |
| 6. Biological Impacts of Phase Separation | 5822 |
| 7. Outlook | 5825 |


## 1. Introduction

Lipid assemblies are, in one sense, more complex than other biological constituents, such as polynucleotides, proteins, and polysaccharides, whose units are covalently connected and cannot undergo rapid sequence rearrangements. In contrast, lipids self-assemble noncovalently, and in so doing create membranes within which the lipid molecules can relocate themselves in a variety of ways. To visualize the complexity of lipid motions, one need only know that biomembranes are composed of lipid bilayers (Figure 1) in which polar groups lie on the outer membrane surfaces, while the hydrophobic chains extend inwardly adjacent to each other. A lipid molecule can drift within one of the two membrane layers of a bilayer, may "flip-flop" from one layer to the other, or might even depart from the bilayer altogether, depending upon the lipid structure and conditions. A host of molecular motions within a given lipid molecule are also coupled with these events. As shall be shown in the following sections, membrane properties are to a large degree determined by the motional freedom of its component lipids.

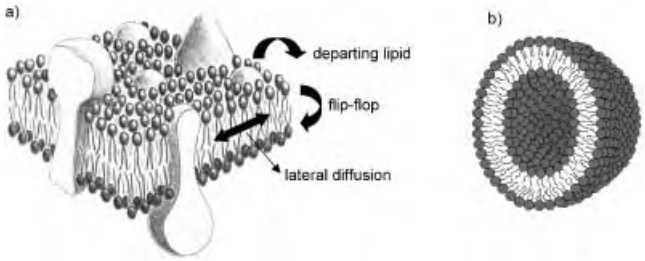



***Figure 1.*** a) Lipid bilayer membrane. b) Schematic drawing of (half) a vesicle.

If a membrane is composed of two or more lipids (as most biomembranes are), then the possibility exists that one of the lipid components will segregate into a domain. Certain domains (rafts) are rich in cholesterol and sphingolipids, and have been implicated recently in signal transduction and membrane trafficking pathways.[1] Domains and rafts are the subject of this Review, with emphasis on chemical aspects.

Vesicles (also called liposomes) are closed, hollow spheres with shells composed of a bilayer membrane (Figure 1). Several methods of preparing vesicles exist,[2] but for our purposes it suffices to say that lipids have a natural propensity to self-assemble into vesicles. Physical agitation, for example, as caused by sonication or by filtration through a porous membrane, can facilitate the process. The appropriate choice of starting lipid or lipid mixture can fine-tune the membrane with regard to properties such as temperature stability, stiffness, electrical charge, surface roughness, and overall vesicle size. Thus, the following vesicle types are commonly described in the literature (unilamellar signifies a single bilayer shell): small unilamellar vesicles (SUVs) with diameters of 30–100 nm, large unilamellar vesicles (LUVs) with diameters of 100–200 nm, and giant vesicles (GUVs) ranging from 1 to 100 μ and visible by light microscopy. Vesicles allow the easy and fairly realistic mimicking of biomembranes, and

[*] Prof. Dr. W. H. Binder
Institute of Applied Synthetic Chemistry
Division of Macromolecular Chemistry
Vienna University of Technology
Getreidemarkt 9/163/MC, 1060 Wien (Austria)
Fax: (+43) 1-58801-16299
E-mail: wbinder@mail.zserv.tuwien.ac.at
Dr. V. Barragan
University of Montpellier, ENSCM
Laboratoire de Chimie Biomoléculaire
8, rue de L'Ecole Normale
34296 Montpellier cedex 05 (France)
Prof. Dr. F. M. Menger
Chemistry Department
Emory University
1515-Pierce Drive, 30322 Atlanta, GA (USA)

 DOI: 10.1002/anie.200300586 © 2003 Wiley-VCH Verlag GmbH & Co. KGaA, Weinheim 

thus have been important tools in research on domains and rafts.

As already mentioned, biomembranes are usually composed of lipid mixtures. The main components include phospholipids, glycerolipids, sphingolipids, cholesterol, and a large number of minor components such as lysolipids, glycolipids, and cerebrosides. Together with membrane-bound proteins, which can occupy up to 70% of the membrane surface, the biomembrane is an enormously complex entity. Each kind of cell and each membrane type has its own lipid composition (that is, percentage ratio of each particular lipid).[3] Lipid compositions can also change as a cell grows and develops.[4] Lipid compositions might even, to some degree, depend upon diet.[5] In comparison, the combination of four nucleotides or even twenty amino acids is trivial, especially because their covalent sequences are more-or-less stable and uniform throughout a cell.

It was once assumed that the rather weak intermolecular forces between lipid molecules would promote a statistical distribution of lipids in a membrane. As already mentioned, clustering into domains or rafts is now believed to occur and to dictate in part the properties of the biomembrane. Figure 2

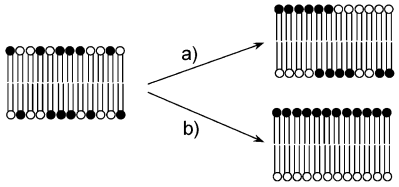



***Figure 2.*** Mixed lipid bilayer with two main types of phase separation of two double-chain lipids: a) lateral phase separation, b) vertical phase separation.

illustrates the consequences of mixing and demixing effects within a bilayer membrane composed of two different lipids. There are at least two types of demixing: a) lipids within one layer can congregate (lateral phase segregation), thereby creating domains and rafts, and b) the opposite layers of a bilayer membrane may assume different compositions (vertical phase segregation). Both processes occur in natural (cells) and synthetic systems (vesicles).

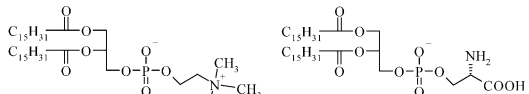
If more than two lipids are involved, the mechanism of domain/raft formation can become even more complex as a result of the multiple interactions involved. In any event, formation of a domain/raft resembles a phase-segregation process that is triggered by such external stimuli as a change in temperature, ionic strength, or lateral pressure. Integration of a macromolecule into a bilayer can also promote a rearrangement of the lipid molecules which corresponds to formation of a domain/raft.

## 2. Experimental Grounds of Domain and Raft Research

In this section we cover diverse experimental approaches that have been used to detect and characterize domain formation. We begin with four older studies that still remain instructive after more than two decades. More recent experiments with domain/raft systems are then considered.

In 1975 Jacobson and Papahadjopoulos[6] created a domain (referred to by them as a molecular segregation or phase separation) by adding $Ca^{2+}$ ions to a mixed-lipid membrane. To understand their experiment, something needs to be known about the so-called "gel to liquid-crystalline phase transition" (henceforth referred to here as the solid to fluid transition). Thus, a bilayer undergoes a highly cooperative order-to-disorder transition as one exceeds the transition temperature $T_m$. The bilayer expands laterally and decreases in thickness in a melting-type transformation when the linear *all-trans* chains present below the $T_m$ value undergo rotation and assume diverse *gauche* conformations above the $T_m$ value. Differential scanning calorimetry (DSC) is a popular way of determining $T_m$ values. In this method a membrane suspension is simply heated up in a calorimeter and the temperature determined at which an endothermic peak appears.

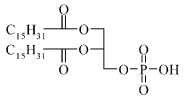
The lipid dipalmitoylphosphatidylcholine (**1**, DPPC) has a sharp transition temperature of 42 °C. When 34% of this lipid is mixed with 66% beef-brain phosphatidylserine (**2**, PS) the



DPPC **1**



DPPS **2**



DPPA **3**



*Wolfgang Binder completed his PhD in carbohydrate chemistry at the University of Vienna (Austria) with Prof. W. Schmid in 1995. After carrying out postdoctoral research with Prof. F. M. Menger on combinatorial polymer chemistry, he worked with Prof. J. Mulzer (University of Vienna) on total organic synthesis. Since 1997 he has been an assistant professor at the Vienna University of Technology (TU-Wien). His research interests include nanostructured polymers, membranes, and polymer networks.*



*Veronique Barragan received her PhD from the University of Montpellier after which she carried out postdoctoral research with Prof. F. M. Menger. She returned to Montpellier where she is now on the faculty of the chemistry department (Laboratoire de Chimie Biomoleculaire of Prof. Montero). Her research interests concern biomedical aspects of carbohydrate chemistry, liposomes, and membrane chemistry.*

 © 2003 Wiley-VCH Verlag GmbH & Co. KGaA, Weinheim 

DSC trace shows a broad peak between 5 and 28 °C. In the presence of 10 mM $Ca^{2+}$ ions, however, two peaks are formed which are centered at 29 and 42 °C. This result indicates that "pure" DPPC domains, with a $T_m$ value of 42 °C, has phase-separated as a result of the binding of $Ca^{2+}$ ions to the PS carboxylate groups.

In 1978 Hartmann and Galla[7] investigated polylysine-induced molecular organization of a lipid in bilayer membranes. Spin labels, fluorescence methods, and electron microscopy were used to prove that association between the membrane and the polypeptide causes an anionic lipid to assemble into patches. The experimental design will now be discussed.

Pyrene (**4**) forms 1:1 complexes (excimers) consisting of a monomer in the ground state and a first excited singlet state. The monomer fluorescence and excimer emissions are well separated. When a fluid state is converted into the solid state (by lowering the temperature below the $T_m$ value, for example), pyrene probe molecules tend to take up residence in whatever fluid membrane happens to coexist with the solid membrane. It is as if the solid membrane "squeezes" out the pyrene, which is consequently concentrated within the remaining fluid membrane. An increased excimer-to-monomer fluorescence ratio is thereby observed.



pyrene **4**

A vesicle membrane can be made from dipalmitoyl phosphatidic acid (**3**, DPPA; an anionic lipid with a $T_m$ value of 50 °C) plus 3 mol % pyrene **4**. In an experiment polylysine (a polycation) was then added at 60 °C, a temperature at which the lipid is fluid. The polylysine binds to the anionic vesicle through electrostatic interactions which causes the anionic lipid at the binding site to gather into a solid aggregate (Figure 3). Evidence for the formation of such a domain comes from an enhanced excimer-to-monomer emission upon addition of polylysine, a result which is consistent with pyrene being concentrated in the fluid lipid outside of polylysine-triggered solid domains.

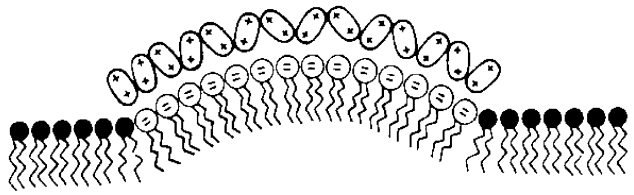
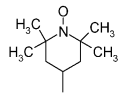


***Figure 3.*** Domain formation triggered by electrostatic interaction between polylysine and anionic phospholipids. Reprinted from Ref. [7] with permission from Elsevier Science.



*Fredric M. Menger is professor of chemistry at Emory University. When he reflects upon his most long-lasting contribution to science, he unhesitatingly thinks of his collaborations with students such as Wolfgang and Veronique who, themselves professors now, continue the chain.*

Shimshick and McConnell investigated lateral phase separation in phospholipid membranes by EPR spectroscopy in the early 1970s.[8] The method was based on the partitioning of 2,2,6,6-tetramethylpiperidine *N*-oxide (TEMPO, **5**) between the fluid membrane interior and the external water. As the temperature is reduced, the fluid bilayer transforms into a solid bilayer, and the TEMPO is ejected into the aqueous phase. Since the probe has different paramagnetic resonance spectral characteristics in the fluid membrane than in water, the probe concentrations in the two environments could be assessed. If, for example, a membrane loses 50 % of its probe to the water, then one can deduce that 50 % of the membrane has been converted into the solid state. Discontinuities in phase diagrams (that is, plots of the phase state at various temperatures and lipid ratios) are taken as evidence for the spontaneous formation of domains.



TEMPO **5**

A binary mixture of phosphatidylcholines with saturated chains differing by only two carbon atoms in length tend to result in ideal mixing. Thus, there is only a single homogeneous solid phase when DMPC (dimyristoylphosphatidylcholine; two $C_{14}$ chains) and DPPC (two $C_{16}$ chains) are mixed. The bilayer is fluid at 30 °C and 0–25 mol % of DPPC, according to ESR data; both solid and liquid phases coexist at 25–60 mol % DPPC, and the bilayer is solid but (as mentioned) uniform in structure at above 60 mol % DPPC. Heterogeneous solid phases are possible when the chain lengths of the two phospholipids differ by more than two carbon atoms, or when the lipid head groups differ (as with phosphatidylcholine and phosphatidylethanolamine). Lipid molecules can migrate within a bilayer to form single-lipid solid-state clusters provided that sufficient time is allowed to reach equilibrium conditions within the solid phase. The formation of these simple domains in fluid bilayers is known, but is less common.

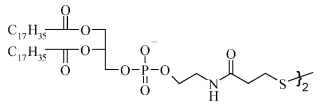
In 1979 Wilkinson and Nagle[9] used a dilatometric method to detect immiscibility (domains) in binary mixtures of DMPC and D-$C_{20}$PC (having two $C_{14}$ and $C_{20}$ chains, respectively). Multilamellar vesicles were prepared by mixing the two lipids in chloroform, removing the solvent, and exposing the resulting film to water. Alternatively, the lipid mixture was suspended in water, sonicated to near transparency above the $T_m$ value, stripped of water, and resuspended in water. Dilatometric scans were obtained on solutions of 10–15 mg $mL^{-1}$ mixtures and the abrupt increase in the specific volume was determined as the temperature was elevated above the $T_m$ value.

DMPC and D-$C_{20}$PC have $T_m$ values of about 24 and 63 °C, respectively. A phase diagram, based on dilatometric data, gave a constant solid-to-fluid transition of 24 °C for vesicles composed of 1 to 90 mol % D-$C_{20}$PC admixed with DMPC. The D-$C_{20}$PC segregates from the DMPC and, as a consequence, has no affect on the normal DMPC transition temperature (24 °C).

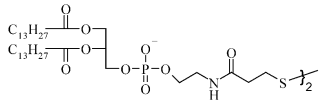
 © 2003 Wiley-VCH Verlag GmbH & Co. KGaA, Weinheim 

NAP-22, a protein isolated from rat brain, is derivatized with hydrophobic myristoyl chains. The protein binds only to vesicles containing cholesterol in vitro. A recent study by Epand et al.[10] concerned whether NAP-22, with its cholesterol binding specificity, can induce the formation of cholesterol-rich domains in membranes. In situ atomic force microscopy was one of the techniques used in this study. In the experiments a film of dioleoylphosphatidylcholine (DOPC) with 40 mol % cholesterol was hydrated and then sonicated to form small vesicles (1 mg mL$^{-1}$). This suspension was injected into an AFM fluid cell, previously fitted with a piece of freshly cleaved mica, on which the spontaneous formation of bilayers was observed. After the cell was flushed with buffer, an AFM reference image was acquired on the protein-free sample. An NAP-22 solution was then added to the cell, and the sample was imaged again. The surface morphology of the supported bilayer changed markedly upon addition of NAP-22: the bilayer was molecularly smooth prior to exposure to the protein, while a rough "protein blanket" approximately 1 nm thick was formed in the presence of NAP-22. Since this thickness is much less than the diameter of NAP-22 (ca. 3.7 nm) it is clear that the NAP-22 is only partially embedded within the lipid bilayer. Closer inspection of the protein blanket by AFM showed that it was composed of protein-rich regions that are spatially segregated and elevated in height. Circular dichroism and DSC experiments suggest that these NAP-22-induced domains contain particularly high levels of cholesterol.

The thiolate-disulfide interchange method of Regen and co-workers[11] can be considered as a unique experimental approach. It utilizes lipids connected as dimers by an S–S linkage. If two different lipid homodimers ($R^1$–S–S–$R^1$ (**6**) and $R^2$–S–S–$R^2$ (**7**)) are mixed in equal amounts, then an equilibrium [Eq. (1)] will be established in the presence of a catalyst. In the absence of a preference for the formation of homodimers, one would expect a statistical ratio of the hetero- and homodimers to be 2:1:1.



disulfide-lipid **6**



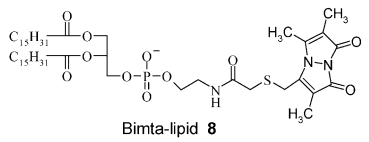
disulfide-lipid **7**

$$R^1\text{–S–S–}R^1 + R^2\text{–S–S–}R^2 \rightleftharpoons R^1\text{–S–S–}R^2 \quad (1)$$

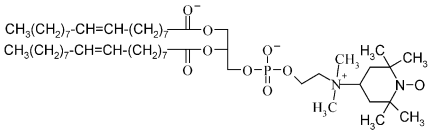
The two phospholipid homodimers **6** and **7** (one with a $C_{18}$ chain, and the other with a $C_{14}$ chain) were mixed and equilibrated within large unilamellar vesicles. HPLC analysis showed that the heterodimer-to-homodimer ratio was 1.55:1 when the vesicles initially contained only the two homodimers. This result signifies that there is a nonstatistical distribution of lipid dimers, that is, a preference for the formation of the homodimer. The effect has been termed "nearest neighbor recognition" although an *intramolecular* preference of $R^1$ for $R^1$ and/or $R^2$ for $R^2$ might also play a role. (Curiously, when the two homodimers were admixed in the bilayer with 50 mol % DPPC, a statistical ratio of 2:1:1 was attained.) A preference ratio such as 1.55:1 is not easy to explain in terms of the actual domain size and composition.

We now describe experiments with cell membranes that can indeed provide information on lipid composition in membrane domains. Non-ionic detergents at low temperatures are commonly used to solubilize membrane components of animal cells, however, it was discovered that a fraction of the membrane lipids of mammalian cells are resistant to such solubilization. Electrospray ionization mass spectrometry (ESI-MS) investigations showed that the fractions were found to be enriched in cholesterol.[12] These lipid rafts exist as liquid-ordered domains ($l_o$) that lie side-by-side with liquid-disordered ($l_d$) regions within the membrane bilayer ($l_o$ and $l_d$ are both fluid, but of differing fluidity). The identity of the various membrane components comprising the $l_o$ and $l_d$ domains has been inferred largely from chemical analysis of the insoluble and soluble fractions, respectively, after treating the biomembrane with detergent.

Silvius and co-workers used fluorescent-quenching methods to secure information on lipid distribution within rafts.[13] In simplified terms, the experiment involved vesicle bilayers with several components (the first two of which are found in most biological rafts): a) sphingolipid/phospholipid, b) a constant 33 mol % cholesterol, c) small amounts of a fluorescent phospholipid (for example, **8**), and d) a spin-labeled phosphatidylcholine (for example, **9**) that served as a fluorescent quencher. Quenching curves for the fluorescent probes were obtained by measuring the decrease in fluorescence as the percentage of spin-labeled phosphatidylcholine (relative to the total unlabeled sphingolipid and phospholipid) was increased from 0 to 100 %.



Bimta-lipid **8**



TEMPO-lipid **9**

Two sets of behavior were observed: quenching curves consistent with the lipid components forming a single phase over the full range of bilayer compositions, and quenching curves consistent with a $l_o/l_d$ phase separation. The analysis proved, for example, that a fluorescent phospholipid possessing two saturated $C_{20}$ chains partitions readily into the $l_o$-phase domain, while a fluorescent phospholipid possessing two saturated $C_{14}$ chains is only modestly successful in entering the rafts. If the fluorescent lipid chains have two

 © 2003 Wiley-VCH Verlag GmbH & Co. KGaA, Weinheim 

*cis*-double bonds within them, the lipid fails to partition at all into the $l_o$ phase.

One final example of the experimental methods used in domain/raft investigations entails the spreading of lipid films one molecule thick onto a water surface using a Langmuir surface balance (Figure 4).[14a] The device confines a monolayer film within a rectangular area bound on one side by a movable barrier and on the opposite side by a float attached to a torsion wire arrangement. When the moveable barrier is adjusted to compress the film (that is, to decrease its area) the surface pressure, measured directly by the float assembly, is increased. A decrease in area (caused by an increase in pressure) may have the effect of forcing molecules lying flat on the water into vertical (or partially vertical) positions where they require less room. Therefore, the capability is available of manipulating the orientation of molecules and of determining their orientation by comparing the area per molecule in the film with the actual molecular area.

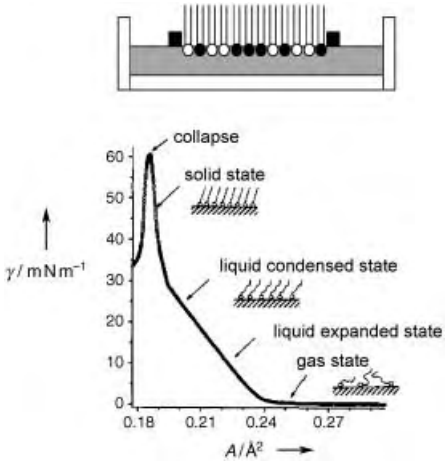



***Figure 4.*** The behavior of lipids on a Langmuir trough and their different phases. Reprinted from Ref. [14a] with permission from Elsevier Science.

What does this have to do with bilayers? In a compressed lipid film the head groups reside in the water while the tails project more-or-less vertically. It can be seen that this closely resembles half a bilayer. Thus, the information acquired on molecular packing in a lipid monolayer can be reasonably extrapolated to bilayer systems. An experiment by Janshoff and co-workers[14b] illustrates the point clearly. A monolayer was prepared with DPPC/DPPS (4:1) containing 1 mol% of a fluorescently labeled phosphatidylcholine. When the subphase underneath the film was pure water, and no pressure from the moveable barrier was applied to the film, one could see circular black domains (looking somewhat like leopard skin) under a fluorescent microscope which accounted for roughly 19% of the film area. The black spots grew continuously as the film pressure was increased to 4 mN m$^{-1}$. The domains were interpreted as DPPS-rich areas that had squeezed out the fluorescent phosphatidylcholine. Films at air/water interfaces have an advantage over vesicle systems in that phase changes in the former can be easily induced by the application of pressure.

## 3. Phase Separation and Domain Formation in Model Lipid Bilayers

Lateral (within a layer) and vertical (between layers) phase separation may occur either spontaneously or as a result of external stimuli. These processes may be coupled to each other or occur separately. As depicted in Figure 5, a variety of external stimuli can lead to phase separation and subsequent modification of the membrane structure. In principle, two different types of interactions can be involved: forces between the head groups and forces between the lipid chains. For example, a change in the external pH value which alters the head-group charge or hydration can decrease the attractive forces among two lipid head groups, thereby causing a phase segregation. As we have seen, charged ions such as $Ca^{2+}$ can also lead to clustering through metal complexation, and adsorption of ionic polymers can enhance the packing density of lipids attracted electrostatically to the polymer.

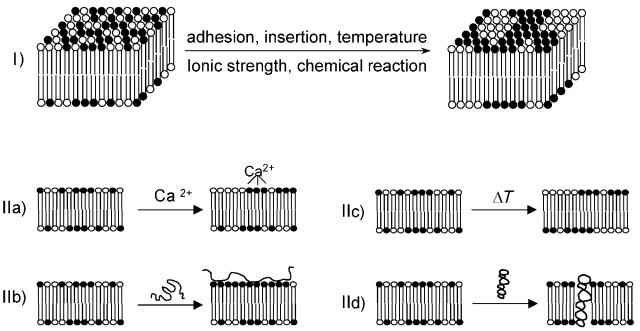



***Figure 5.*** The different modes of phase separation in lipid bilayer membranes: I) Phase separation of two lipids in a lateral manner; II) various external effects leading to different modes of phase separation: a) lateral phase separation in the outer layer induced by ion complexation, b) vertical phase separation induced by the adsorption of polymers, c) lateral phase separation in both layers induced by temperature, and d) lateral phase separation around an incorporated macromolecule.

Forces acting primarily on the hydrophobic interior of the lipid bilayer can induce phase separation in a similar manner. For example, a temperature change can lead to the phase separation of two lipids with different melting temperatures ($T_m$). Molecules penetrating the lipid bilayer can induce the formation of domains by surrounding themselves with a nonstatistical population of lipids. Domains can vary greatly in size, from a few molecules to substantial stretches of lipid. The point at which domain formation can be considered as an outright phase separation is largely a matter of semantics.

### 3.1. Lipid Components

The structure of the main components in living and artificial cellular membranes are depicted in Figure 6.[15] In principle there are three main classes of lipids: a) diacylglycerol-derived lipids, b) sphingosine-derived lipids, and c) sterol lipids (cholesterol). The dimensions of the head

 © 2003 Wiley-VCH Verlag GmbH & Co. KGaA, Weinheim 

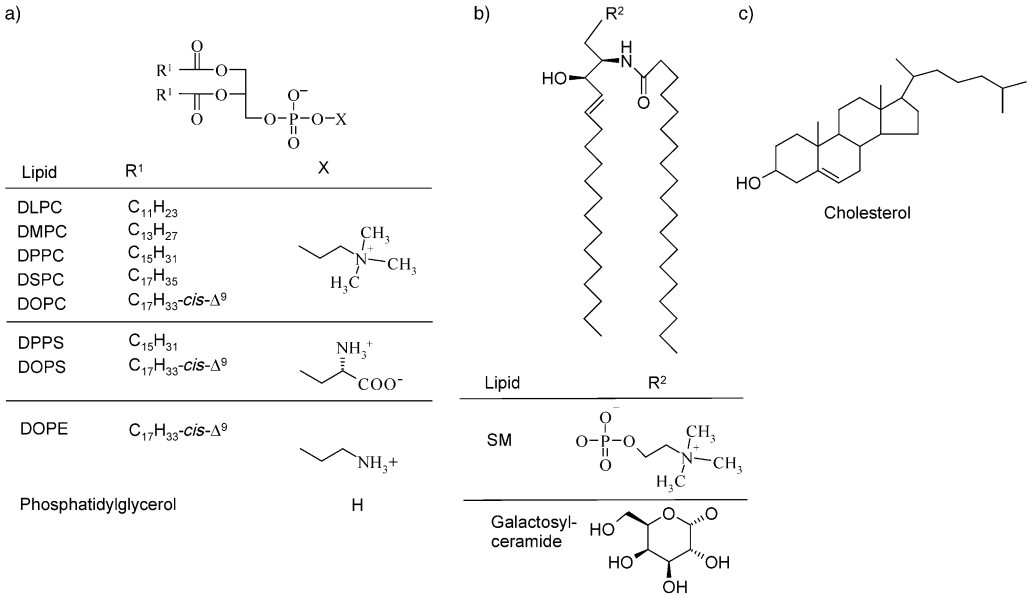



***Figure 6.*** Structure of membrane lipids: a) diacylgycolipids, b) sphingolipids, and c) sterol lipids (cholesterol).

groups and tails, as well as charge interactions between the head groups are important factors for dictating the ordering properties within the bilayer.

Block copolymers are also capable of forming thin membranes,[16] but this is controlled by a different combination of forces. Whereas lipid bilayers assemble mainly as a result of the hydrophobic association between the alkyl chains, membranes of block copolymers assemble as a result of both solvent–polymer and polymer–polymer interactions. Thus, polymeric membranes have additional ordering forces which may be present even in nonaqueous solvents. Most notably, the immiscibility of polymer chains residing in different regions of a block copolymer may serve as a driving force for their ordering into vesicular membranes. Vesicles derived from block copolymers ("polymersomes", see Section 5) exhibit a stronger and stiffer membrane structure than do membranes composed of lipid bilayers.

Diacylglycerol-derived lipids include phosphatidylcholines (PCs), phosphatidylethanolamines (PEs), as well as diacylglycerols (DAGs) and the corresponding glycolipids in which a carbohydrate residue is attached to the head group through a glycosidic bond. All of these lipids, with the exception of PEs, spontaneously assemble into planar bilayer membranes as a result of their cylindrical shape (that is, the head group and sum of the two chains have roughly the same cross-sectional area). The head-group surface area varies between 40 to 60 $Å^2$ depending on the phase state of the lipid. Thus, the areas are smaller in the solid (gel) state where all the alkyl chains are ordered in a crystalline hexagonal lattice and adopt an *all-trans* conformation. A head-group expansion of about 5–10 $Å^2$ is observed upon melting above the main transition temperature, and leads to the fluid (liquid-crystalline) phase in which one or more of the C–C bonds twist into a *gauche* conformation. The temperature of this transition varies with the length and degree of saturation of the acyl chains. Thus, lower transition temperatures are associated with shorter chains and a higher degree of unsaturation (compare, for example, DMPC ($T_m = 24\,°C$) to DPPC ($T_m = 42\,°C$) and DOPC ($T_m = -22\,°C$; Figure 6). Lateral diffusion rates, however, do not seem to be greatly affected by the nature of the alkyl chains. As might be expected, the thickness of the lipid bilayer depends on the chain length of the alkyl moieties (the longer the chain, the thicker the bilayer membrane). If the two chains of a lipid are unequal in length, bilayer formation may involve chain interdigitation to best fill the space.

Sphingolipids are derived from the sphingosine base, which possesses an unsaturated chain. The sphingosine backbone, a rather stiff and planar entity, is linked to an acyl chain through an amide bond to yield sphingolipids. Structural variations similar to those found in glycerolipids are possible and include the phosphorylcholine head group (sphingomyelins) typical of sphingomyelin (SM; see Figure 6) derived from bovine brain. Acyl chains of varying length can be attached to the sphingosine to give highly asymmetric sphingolipids. Cerebrosides, which are the main constituents of neuronal cells, are generated when carbohydrates are attached to a sphingosine. Although the effective dimensions within the lipid bilayer are comparable to the glycerophospholipids (head-group areas between 45 and 57 $Å^2$),[17] the hydrophobic chain length can be much longer (for example, the lignoceroylsphingosines have 24 carbon atoms) The melting temperatures of the sphingolipid chains are usually higher than those of the corresponding glycerolipids and may exceed 60 °C.[17b]

Sterol lipids (mainly cholesterol)[15] are unique among the various lipids because of their annelated structures, which imply they have highly condensed hydrophobic areas. The only hydrophilic part, the 3-hydroxy moiety, is much smaller than in the sphingo- or glycerolipids. The length of cholesterol, about 17.5 Å, is also shorter than the tail length of most nonsteroidal lipids.[15b] Cholesterol tends to increase mem-

 © 2003 Wiley-VCH Verlag GmbH & Co. KGaA, Weinheim 

brane stiffness while increasing the lateral mobility of other membrane components.

The miscibility of two (or more) lipids within a lipid bilayer membrane is graphically represented by simple phase diagrams.[18] Figure 7a shows an example of two lipids A and

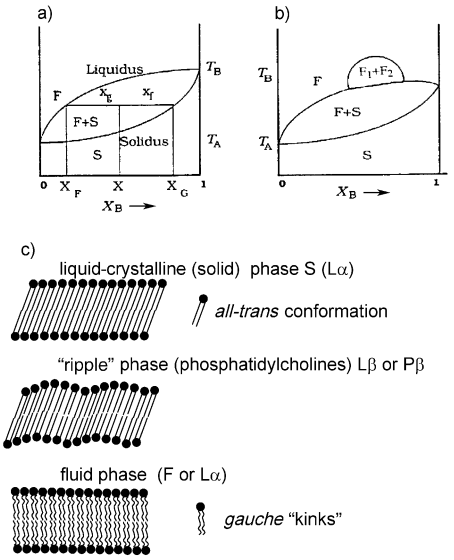



***Figure 7.*** Phase behavior of lipid mixtures (lipid A and lipid B): a) full miscibility of lipids in the liquid state and b) partial immiscibility of lipids in the fluid state. Reprinted from Ref. [18] with permission from Academic Press.

B which are homogeneously miscible in both the solid and fluid states. In the following discussion we assume that lipid A has a lower transition temperature ($T_A$) than does lipid B ($T_B$), and that the fluid phase and the solid phase coexist between the pure melting temperatures of both lipids (namely, between $T_A$ and $T_B$). Thus, starting with a 1:1 lipid mixture in the solid phase ($x_B = 0.5$), the fluid phase is enriched by the lower melting lipid (lipid A), while the solid phase is enriched with the higher melting lipid B. Similar to ice, the solid domains (enriched in lipid B) will float across the fluid parts (enriched in lipid A). This is perhaps the simplest mode of domain formation within lipid bilayer membranes. Complete lipid miscibility is retained above the melting temperature of lipid B.

Another case (Figure 7b) illustrates immiscibility in the fluid phase. Additional separation is observed above the melting temperature of the higher melting lipid B. This type of domain formation is different from the one shown in Figure 7a, because the phase separation is not induced by crystal-like packing in the solid state, but rather by weak attractive forces in the fluid state. Similarly, immiscibility in the solid state can occur in which the molecules are phase-separated below the melting temperature of lipid A. This generates two differently packed arrays of hexagonally ordered lipid grids within the crystalline, solid phase. In summary, domains may consist of solid/fluid, fluid/fluid, or solid/solid incompatibilities.

### *3.2. Binary Mixtures of Structurally Similar Compounds*

Significant phase separation effects can occur despite only a small variation in lipid structure. A classical example of this type is exemplified by phosphatidylcholines with different chain lengths. Nonideal behavior stems purely from an alkyl chain mismatch, since the head groups are kept identical. Knoll et al.[19] and Silvius et al.[20] have studied the phase diagrams by systematically varying the chain length and thereby increasing the chain mismatch between two lipids. Lateral phase segregation was found when the alkyl chains differed in length by four $CH_2$ groups or more. The phase diagram in Figure 8a shows the DLPC ($C_{12}$)/DPPC ($C_{16}$) case. There is distinct immiscibility in the solid phase which leads to solid/solid separation from 60 to 100 mol% DPPC, and both solid phases coexist between 0 and 60 mol% of DPPC. There is full miscibility in the fluid state, with phases coexisting between the phase-transition temperatures $T_{mA}$ and $T_{mB}$ over the whole composition range.

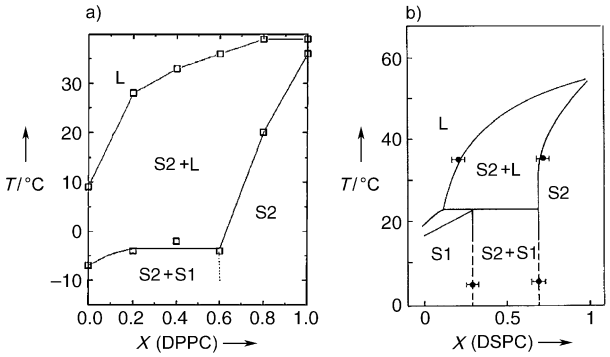



***Figure 8.*** Phase diagram of DMPC/DPPC (a) and DLPC/DSPC (b). There is a difference of four $(CH)_2$ units in the hydrophobic chains of both lipid mixtures and there is a coexistence between liquid (L) and solid phase (S). Reprinted with permission from Elsevier Science[19] and the American Chemical Society.[20a]

A similar picture is indicated in Figure 8b for the higher homologues where the lengths of both lipids are increased by two more $CH_2$ units: DMPC ($C_{14}$) mixed with DSCP ($C_{18}$). The region of coexistence between the fluid and solid phases constitute domains, which, as we have seen, can be detected by a variety of methods. The sizes of these domains may vary between several nanometers and several micrometers. Thus, 100 to more than 100000 lipids can reside within these domains. The size of the domains and their behavior will be explained in Section 4.

Another type of lipid mixture consisting of a symmetric double-chain lipid (such as DSPC) and a lipid consisting of the same head group but with acyl chains of differing length ($C_{18}$-$C_{10}$-PC) was studied by Mason. The mixing behavior of the two lipids was investigated as shown in Figure 9.[21] One lipid chain "disturbs" the lipid bilayer as a result of it having an eight-methylene shorter chain and leads to a very different phase behavior, namely three different immiscibilities in the solid state (S1, S2, and S3). In the solid state S1—low amounts of asymmetrical lipid—a "normal" lipid bilayer is formed with

 © 2003 Wiley-VCH Verlag GmbH & Co. KGaA, Weinheim 

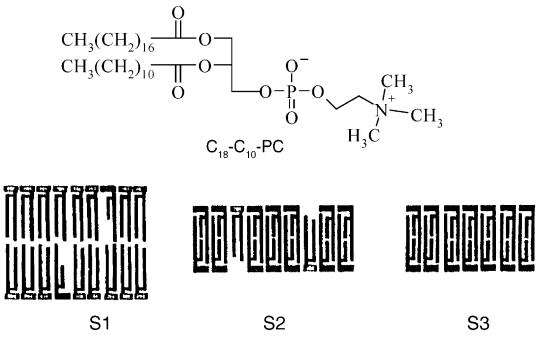



***Figure 9.*** Miscibility of DSPC with a highly unsymmetrical lipid ($C_{18}/C_{10}$-PC). The models of interdigitation of the unsymmetrical lipid chains indicate the different types of solid phases $S_1$, $S_2$, and $S_3$. Reprinted from Ref. [21] with permission from the American Chemical Society.

no apparent compensation for the defect. At concentrations above 50 mol% of $C_{18}$-$C_{10}$-PC, two phases are in coexistence with each other: one phase S2 where the lipid bilayer is partially interdigitated leaving "holes" for the symmetrical DSPC, and phase S3, which consists of purely interdigitated $C_{18}$-$C_{10}$-PC. Phase separation therefore occurs in the solid state as a result of the weak forces among the longer $C_{18}$ chains of the asymmetrical lipid favoring separate crystallization of identical components.

Variation within the lipid backbone (for example, the glycerol moiety) can lead to nonideal effects even if the acyl-chain length and the polar head group of a lipid are the same. The mixing of the ester DPPC and ether 1,2-dihexadecylphosphatidylcholine (DHPC) clearly indicate the presence of different types of phase structures in the solid state. Thus DHPC forms an interdigitated phase,[22] where self-assembly creates a monolayer rather than the usual bilayer.

### 3.3. Binary Mixtures of Structurally Differing Lipids

The most common examples of domain formation involve situations where the two lipid components differ appreciably. This might arise from a) different types of head groups within a similar class of lipids, b) lipids with widely differing phase transition temperatures, and c) mixtures of lipids with cholesterol.

#### 3.3.1. Mixtures of Charged and/or Neutral Lipids

Silvius[23] and other researchers have published a number of phase studies where the miscibilities of lipids with different head groups but identical chain length have been analyzed. In the following ranking, pairs of lipids (charged/neutral or neutral/neutral) are compared with each other (PE = phosphatidylethanolamine, PS = phosphatidylserine, PA = phosphatidic acid, and PC = phosphatidylcholine). In general terms the miscibility of (PE,PS) is equal to that of the (PE,PA) pair, while (PC,PS) and (PC,PA) are less miscible, and (PE,PC) is the least miscible. Most systems exhibited solid/solid immiscibility but full miscibility in the liquid state. Again, there was a broad coexistence region between the liquid and solid phases of the differing lipids, as a result of the strongly differing phase-transition temperatures. Clearly the chemical differences in the head groups are not so significant as to induce strong phase separation phenomena in these lipid mixtures.

#### 3.3.2. Lipids with Strongly Differing Phase-Transition Temperatures $T_m$

Sphingolipids and phospholipids have very different structures with respect to their head groups and hydrophobic tails, thus implying a strong possibility for lateral phase separation effects. Two differing types of investigations were performed: a) traditional thermal (DSC) and fluorescence methods and b) fluorescence microscopy of mixed monolayers consisting of sphingomyelin, DMPC, and a small amount of a fluorescent lipid. Holopainen et al.[24] have studied the phase behavior by fluorescence microscopy, a method initially developed by Ringsdorf and co-workers.[25] The principle of this method is shown in Figure 10. A binary lipid mixture together with a fluorescent lipid (1 mol%) which is known to reside preferentially in one of the two developing phase is applied as a film onto a Langmuir trough and compressed. After compression and phase separation, the resulting domain formed can be visualized directly by fluorescence microscopy. An advantage of this method is the possibility of reaching different phase states without altering the temperature. Compressing the lipid film allows the stepwise appearance of the liquid expanded, liquid condensed, and finally the solid state. These liquid-expanded and solid states correspond to fluid and solid states in the bilayer membrane, respectively.

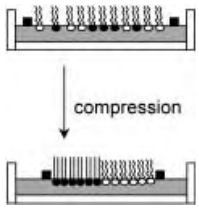



***Figure 10.*** Applying a lipid mixture as a Langmuir film. Phase separation into a solid ordered and a liquid phase takes place upon compression. The process can be followed directly by monitoring a fluorescent lipid which concentrates in one of the two phases.

Sphingolipids and phospholipids (such as DMPC or DPPC) show phase separation in the solid state and a large region of coexisting phases between the two melting points of the lipids.[26] The strong differences are the result of the interactions of the head group within the ceramide backbone.[27] Figure 11 shows fluorescence images of C24:1-galactosylceramide with DMPC obtained from monolayers composed of C24:1-ceramide with DMPC. Phase separation was observed in the liquid as well as in the solid phase when the chain lengths matched, as they do for DMPC and C24:1-ceramide. The phase separation can be visualized by fluorescence microscopy,[24] where domains enriched by C24:1-ceramide appeared as dark spots as a consequence of the enrichment of the fluorescent label in the DMPC-rich fluid phase. The presence of a network of hydrogen bonds interconnecting the ceramide moieties at the surface of the lipid monolayer is likely responsible for this type of domain formation.[28]

 © 2003 Wiley-VCH Verlag GmbH & Co. KGaA, Weinheim 

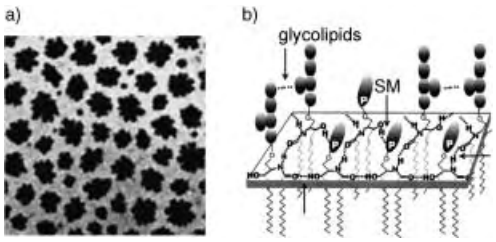



***Figure 11.*** a) Fluorescence microscopy picture of a monolayer composed of DMPC/C24:1-ceramide (30:70) with 1 mol% of a fluorescent probe lipid. b) Schematic representation of the network formed between DMPC and C24:1-ceramide (the arrows show the hydrogen bonds which lead to network formation). Reprinted from Refs. [26, 27] with permission from Elsevier Science.

### 3.3.3. *Cholesterol: Action on Phospholipids*

Cholesterol increases membrane stiffness and imposes a higher lateral mobility. The phenomenological mode of action is shown as a phase diagram in Figure 12.[29] A new phase ($l_o$)

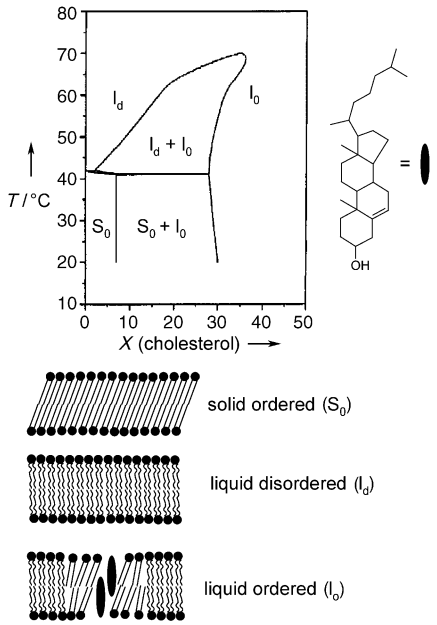



***Figure 12.*** Influence of cholesterol on the lipid bilayer structure. An increasing amount of cholesterol stabilizes the $l_d$ phase above the chain-melting temperature of DPPC. The phase transition disappears at levels above 30 mol% cholesterol, which leads soley to the $l_o$ phase. Reprinted from Ref. [29] with permission from the National Academy of Sciences.

emerges at a low cholesterol content which is in equilibrium with the $l_d$ phase up to about 30 mol% cholesterol. Only the $l_o$ phase persists at higher cholesterol levels, which results in the thermal phase transition of the phospholipid (DPPC) disappearing. DPPC does not exhibit a difference between its fluid state and its crystalline state in a mixture containing more than 30 mol% cholesterol. This observation explains the necessity of cholesterol in biological membranes (to diminish the presence of a phase transition), where it is often present in amounts up to 35 mol%.

The addition of cholesterol to DPPC also leads to a strong condensation effect of the membrane (reducing the membrane area from 61 to 47 Å),[30] which explains the increase in membrane stiffness. van der Waals interaction occurs preferentially between cholesterol and saturated, long acyl chains occurs than in unsaturated chains. An increase in the number of *trans* conformations within the saturated chains is also observed. Lateral mobility, however, is enhanced as a result of the smaller dimensions of cholesterol relative to DPPC, thus increasing the mobility of membrane components within the lipid bilayer.

### 3.3.4. *Cholesterol–Sphingolipid Mixtures*

The interaction between spingolipids and cholesterol is similar to that of the phospholipids.[30] Table 1 shows the reduction in the areas of the head groups of sphingomyelin and phosphatidylcholine monolayers upon addition of equimolar amounts of cholesterol.

***Table 1:*** Percentage reduction of head group areas of sphingomyelin (SM) and phosphatidylcholine monolayers upon addition of an equimolar amount of cholesterol at a defined compression.

| Lipid | Compression [mN m$^{-1}$] and Area reduction [%] | | |
|---|---|---|---|
| | 5 mN m$^{-1}$ | 20 mN m$^{-1}$ | 30 mN m$^{-1}$ |
| N-18-D1-SM | 35% | 28% | 25% |
| SM (egg) | 39% | 28% | 17% |
| SM (bovine) | 39% | 26% | 16% |
| POPC[a] | 34% | 26% | 23% |
| DPPC | 41% | 12% | 11% |
| MPPC[a] | 43% | 29% | 11% |

[a] POPC = palmitoyloleoylphosphatidylcholine, MPPC = myristoylpalmitoylphosphatidylcholine.

The relative reduction in the size of a monolayer is largest when the lipids are in a more expanded state (that is, at low compression values). The more condensed the lipid monolayer (and, by inference, the bilayer), the less effective cholesterol is in promoting membrane condensation. Thus, the initial phase state of the lipid controls the magnitude of the interaction with cholesterol. The measurement of the leakage of cholesterol from membranes composed of different sphingomyelins showed there was a stronger interaction with increasing length of the sphingolipids *N*-acyl chain.[31]

### 3.4. *Mixtures of Three Components*

Membranes with three or more lipids mimic the real, biological membranes more closely than binary mixtures. Common eukaryotic biomembranes are composed of about 50 mol% sphingolipids and phospholipids and up to 40 mol% cholesterol. Studies on mixtures of two phosphatidylcholines with strongly differing phase-transition temperatures (DLPC/DPPC and 12-BrDPPC/DPPC, DOPC/SLPC)[20] admixed with cholesterol indicates there is an increased tendency for phase separation. The corresponding binary mixtures are known to be phase-separated at temperatures between the

 © 2003 Wiley-VCH Verlag GmbH & Co. KGaA, Weinheim 

two respective transition temperatures. The addition of low levels of cholesterol promotes phase separation as a result of favorable interactions with the longer DPPC chains, while a diminishing effect is observed at higher concentrations.[20a]

A more noticeable effect can be visualized in the phosphatidylcholine/cholesterol mixture.[32] Experiments were carried out with supported bilayer membranes (that is, bilayers coating a solid surface) and with giant vesicles by incorporating a fluorescently labeled lipid selectively into the solid phase of the domains in DLPC/DPPC/cholesterol mixtures (Figure 13).[33] As mentioned above, the formation of patches with sizes of 10 μm or larger was observed directly by confocal fluorescence microscopy. Two different types of fluorescent probes were used: 1,1′-dieicosanyl-3,3,3′,3′-tetramethylindocarbocyanine perchlorate (DiI-C20), which is preferentially incorporated into the solid (ordered) phase, and 2-(4,4-difluoro-5,7-dimethyl-4-bora-3a,4a-diaza-*s*-indacene-3-pentanoyl)-1-hexadecanoyl-*sn*-glycero-3-phosphocholine (Bodipy-PC), which is incorporated into the fluid phase. The solid domains are visualized by a red color, whereas the lipid domains appear green.

There is also a strong effect exerted by the nature of the sterol (Figure 14).[34] The efficiency of promoting phase separation is greatest with ergosterol, followed by 7-dehydrocholesterol, stigmasterol, sitosterol, cholesterol, and $C_{10}$-sterol. Thus, the degree of unsaturation within the B ring and the side chain of the sterol moiety have an appreciable effect for reasons that are not completely understood.

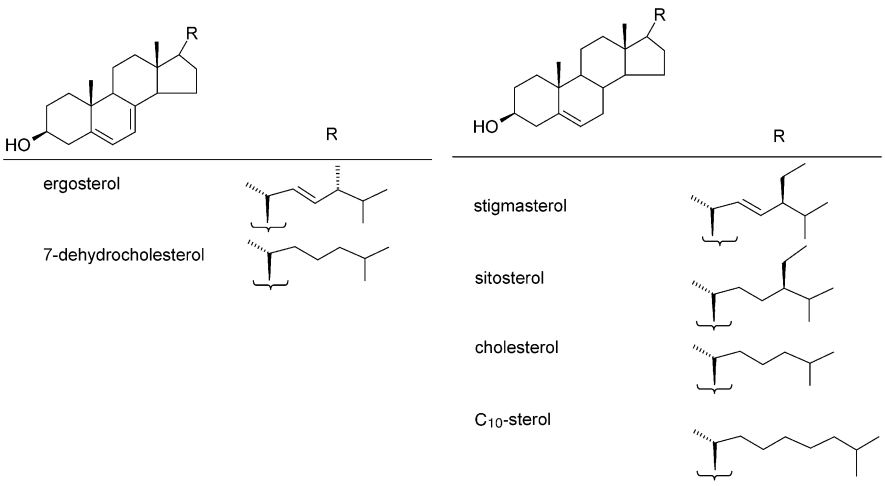



***Figure 14.*** Structures of sterols promoting domain formation in membranes composed of SM/DOPC/sterol mixtures.

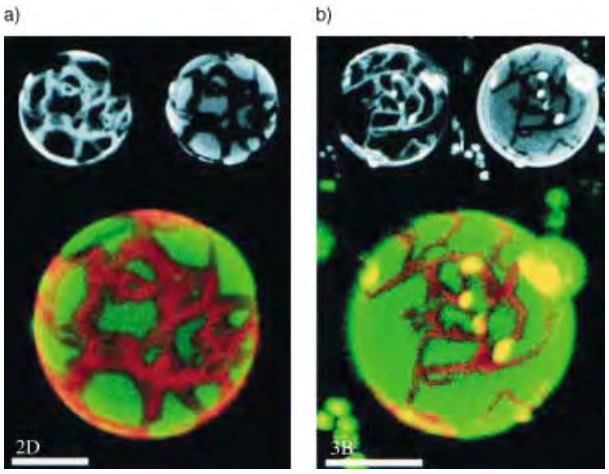



***Figure 13.*** Fluorescence images of giant vesicles with phase separation at 25 °C. a) DLPC/DPPC = 40/60. The red color shows the solid ordered domains (enriched in DPPC), the green color the liquid domains (enriched in DLPC). b) DLPC/DPPC = 50/50 with 5 mol% cholesterol. The scale bar corresponds to 10 μm. Reprinted from Ref. [33] with permission from the National Academy of Sciences.

### *3.5. Induced Phase Separation through Low-Molecular-Weight Compounds*

#### *3.5.1. Influence of $Ca^{2+}$ Ions on Phase Separation*

The action of bivalent ions on mixed phosphatidylserine (PS) bilayers represents one of the most intensively investigated phase-separation processes.[35] Figure 15 shows the dramatic effect of $Ca^{2+}$ ions on the phase behavior on

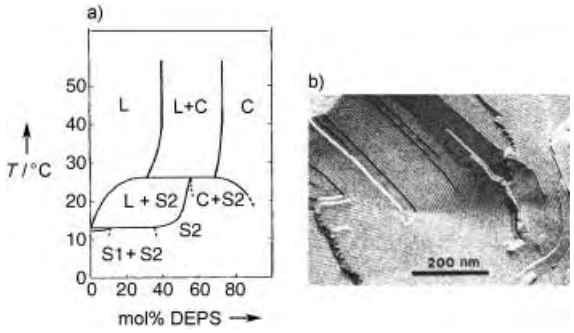



***Figure 15.*** Action of $Ca^{2+}$ ions on a DEPC/DEPS lipid mixture (DE = dielaidoyl). a) DEPC/DEPS lipid bilayers with 30 mM $Ca^{2+}$: A strong demixing effect is observed in both the liquid and solid states (L: liquid-crystalline phase, C: new cochleate-phase, S1: PC-rich phase, S2: PS-rich phase). b) TEM image of a lipid bilayer in a mixture of the cochleate phase/hexagonal phase (DOPE/DOPS = 1/1 plus $Ca^{2+}$). Reprinted from Ref. [35b,c] with permission from the American Chemical Society.

mixtures of DEPC/DEPS. Both lipid pairs are fully miscible in the liquid state (Figure 15a).[35b] A strong demixing is observed both in the solid and liquid state upon addition of 30 mM $Ca^{2+}$ ions (Figure 15b). The most important observation is the occurrence of a new phase, as exemplified by the surface of the vesicles having a different appearance (the so-called "liquid/cochleate phase C") at concentrations between 40 and 80 mol% $Ca^{2+}$ ions. These results are consistent with observations obtained by freeze-fracture electron microscopy on the DOPE/DOPS mixture, which reveal pictorially the

 © 2003 Wiley-VCH Verlag GmbH & Co. KGaA, Weinheim 

details of the phase separation (Figure 15b).[35c] Thus, both the hexagonal phase of DOPE and the cochleate phase of DOPS are visible in a 1:1 mixture of the two lipids in the presence of $Ca^{2+}$ ions. This type of phase separation is also linked to vesicular fusion in biological membranes where, it is assumed, phase transitions in the liquid state promote membrane fusion.

### 3.5.2. Cyclodextrins/Amphotericin B

There is a strong tendency for hydrophobic molecules to insert into the lipid bilayer and form stable complexes with lipids. A highly ordered lipid bilayer is usually disrupted by such an insertion, which leads to its destruction at higher concentrations of the inserted molecule. Molecules able to disturb the lipid bilayer, and also to induce clustering effects, are usually large molecules with molecular weights above 500 g mol$^{-1}$. This insertion effect is important in a variety of pharmacologically active compounds, among which amphotericin B, an antifungal agent, is one of the best known.[36] It is widely accepted that amphotericin B induces enhanced membrane permeability by forming transmembrane ion-pore channels composed of two molecules in opposing parts of the membrane leaflets (Figure 16).

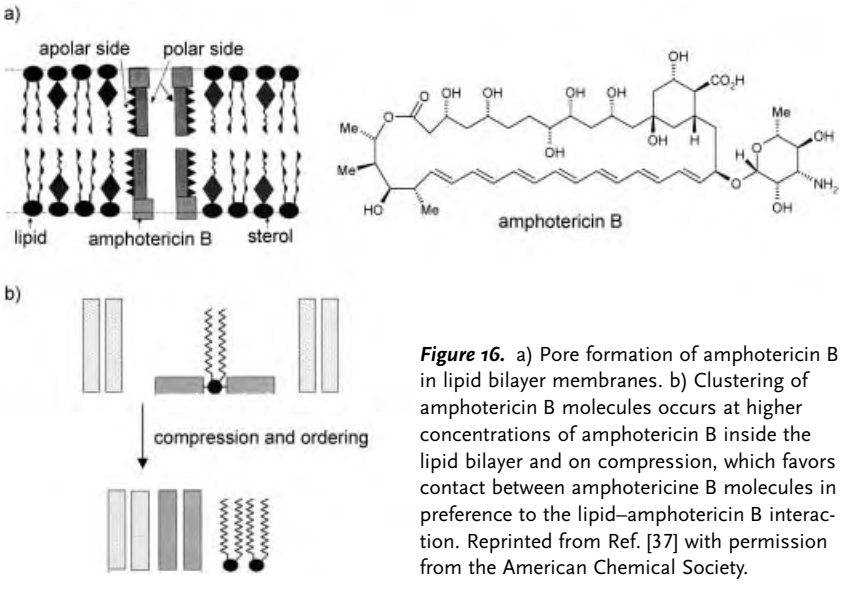



*Figure 16.* a) Pore formation of amphotericin B in lipid bilayer membranes. b) Clustering of amphotericin B molecules occurs at higher concentrations of amphotericin B inside the lipid bilayer and on compression, which favors contact between amphotericine B molecules in preference to the lipid–amphotericin B interaction. Reprinted from Ref. [37] with permission from the American Chemical Society.

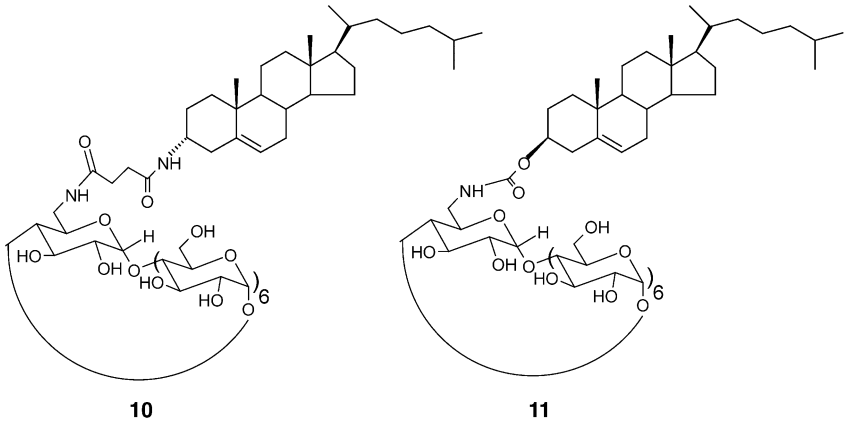



*Figure 17.* β-Cyclodextrin derivatives with (**10**) and without (**11**) a succinimidyl spacer.

According to investigations on model membranes there is a preferential interaction between amphotericin B and cholesterol or phospholipids, which leads to clustering of lipids around the polyene antibiotic. As Miñones et al.[37] have pointed out, the miscibility of amphotericin B with the surrounding lipids is dependent on the phase state of the corresponding monolayer being in the expanded phase (equivalent to the liquid phase in bilayers). In the compressed monolayer (equivalent to the solid bilayer), amphotericin B molecules segregate from the lipids to form their own aggregated phase. In other words, the primary interaction between lipid and amphotericin B is sacrificed for an interaction between two amphotericin B molecules when the phase state changes.

The segregational effect of cholesterol-modified cyclodextrin is another specific example of induced cluster formation in lipid membranes. A cholesterol moiety was linked to a β-cyclodextrin molecule through a succinimidyl spacer and inserted into bilayer membranes composed of DMPC (Figure 17).[38] The formation of two phases was observed: one consisting mainly of pure DMPC, the other being strongly loaded with the cholesterol-substituted cyclodextrin guest. The omission of the succinimidyl spacer (namely, directly linking the cholesterol moiety to the cyclodextrin) led to no segregational effect.

The number of lipid molecules associated with the cholesterol-substituted cyclodextrin guest was found to depend primarily on interactions between the hydrophilic phospholipid head groups and the hydrophilic surface of the cyclodextrin molecule. The attached cholesterol moiety serves mainly as an anchor to fix the cyclodextrin within the membrane.

### 3.5.3. Acylated and Prenylated Peptides and Enzymes

The assembly of peptides into aggregates or domains at the surface of the lipid bilayer membrane is of utmost biological significance. A detailed investigation of peptides with a defined hydrophilicity/hydrophobicity profile has become available through the combination of techniques from molecular biology and membrane technology.

 © 2003 Wiley-VCH Verlag GmbH & Co. KGaA, Weinheim 

The clustering of peptides in an already phase-segregated membrane would seem to require a lipid–peptide interaction. Several authors have recently proven the existence of such a lipid–peptide interaction by fluorescence spectroscopy and microscopy.[39,40] The basic concept is simple and shown in Figure 18.[41] Two types of peptides (A and B) with a defined amino acid sequence are labeled with specific noninteracting fluorescence labels, for example, pyrene, tryptophan, or nondimerizing peptides such as cyan and yellow variants of green fluorescent peptides. These lipids do not show fluorescent radiation energy transfer (FRET) when mixed in a homogenous membrane without domains. Only after clustering together (driven by domain formation) is a FRET transfer possible as a result of the proximity of the two peptides. Vesicle surfaces were composed of lipid mixtures known to phase-separate into domains and also mimic the cell-surface composition. Thus, vesicles composed of PC/SM/cholesterol mixtures phase-separate into liquid-ordered ($l_o$) and liquid-crystalline domains ($l_d$). The effect of the peptides bearing nonpolar chains upon clustering into the $l_o$ phase was investigated with this system. Whereas long-chain fatty acids (myristoyl, palmitoyl) promoted the assembly, the presence of geranylgeraniol chains had no clustering effect.

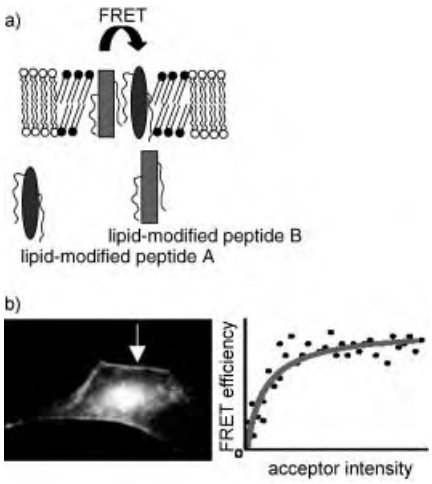



***Figure 18.*** Clustering of lipid-modified peptides in membranes visualized by fluorescent energy transfer. a) Lipid-modified peptides A and B (myristoylated or palmitoylated) and their clustering in the liquid ordered phase ($l_o$) of a membrane. b) Fluorescent image and FRET analysis of the region indicated yield proof of the clustering of the lipid-modified peptides. Reprinted from Ref. [41a] with permission from the AAAS.

The action of enzymes can be influenced significantly by phase-separated domains. Ringsdorf and co-workers[42] have shown that the action of a phospholipase A2 strongly depends on the phase state at the membrane surface. Monolayers consisting of DPPC were prepared exactly at the coexistence point of solid and fluid states. A specific fluorescent label was then incorporated, which led the solid ordered domains having a dark appearance by fluorescence microscopy (Figure 19). When phospholipase A2, an enzyme that cleaves DPPC, was added, the enzyme clearly deformed the round spots through preferential degradation of the DPPC acting preferentially at the solid–liquid phase boundary. The enzyme gravitates preferentially to the solid–liquid phase boundary where it catalyzes the phospholipid hydrolysis.

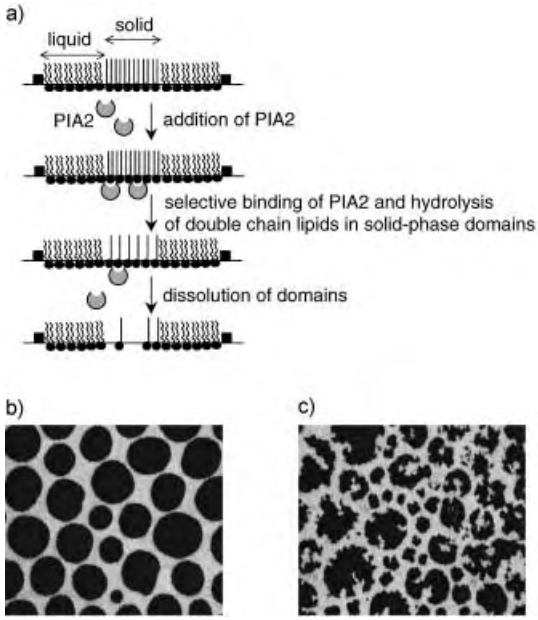



***Figure 19.*** Selective action of enzymes (phopholipase PlA2) on the solid ordered domains of DPPC monolayers. a) Schematic representation of the enzymatic action by selective cleavage of the lipids in the solid ordered domains. b) Round domains before addition of PlA2. c) Destruction of domains by selective hydrolysis and subsequent dissolution. Reprinted from Ref. [42] with permission from Elsevier Science.

## 4. Rafts

### 4.1. Definition

Anyone entering the world of lipid assemblies will encounter three different expressions (Figure 20): caveolae, domains, and rafts. Caveolae[43] are small invaginations (with a size of about 50 nm) within natural membranes and can be observed by electron microscopy. Analysis of the composition of caveolae showed that they are rich in a class of proteins named caveolins as well as in cholesterol and sphingolipids. The term domain[44] is used to describe the formation of lateral assemblies in lipid membranes composed of either of one component lipids (at the solid–liquid equilibrium) or in a mixture with other lipids (see Section 3). The definition of domain is much less specific than that of caveolae, and is used for any type of aggregate within a lipid bilayer/monolayer assembly. The size of domains may vary significantly between several nanometers and many micrometers.

The term raft[45] is more historic in that it is related to membrane fractions isolated in the past by extraction. Natural membranes extracted by cold detergent solutions (4 °C) were

 © 2003 Wiley-VCH Verlag GmbH & Co. KGaA, Weinheim 

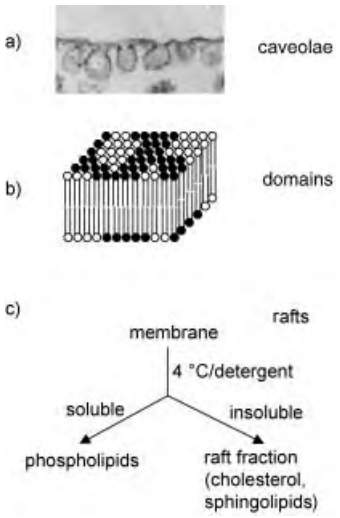



***Figure 20.*** a) Caveolae (TEM image), b) domains (schematic representation), and c) extraction protocol for the isolation of lipid raft fractions.

found to contain a fraction of lipids (so called DRM for detergent-resistant membranes) which were rich in cholesterol and various sphingolipids. This prompted the assumption that aggregates in living cell membranes consist mainly of noncovalent clustering of cholesterol and sphingolipids in the presence of other phospholipids. There is a preferential interaction between sphingomyelin and cholesterol, either through the formation of hydrogen bonds between the cholesterol OH group and the sphingosine NH group or through lipophilic interaction between long-chain sphingolipids and cholesterol. Thus rafts relate to biological membranes as well as to artificial membranes that closely mimick biological membranes.

### *4.2. Properties and Description of Rafts*

In general rafts, domains, and caveolae have three features in common: a) a reduced lateral mobility, b) a chemical composition distinct from the rest of the membrane, and c) variable membrane thickness. A number of analytical techniques has been used to verify all of these features, including AFM and XRD to monitor thickness variations, single-particle tracing (SPT) and fluorescence anisotropy (FRET) to monitor lateral mobility, and ESI-MS and TOF-SIMS to monitor chemical composition. An important development was the visualization of membrane areas by fluorescence microscopy techniques which was made possible by the selective enrichment of fluorescent labels into lipid assemblies, examples of which have already been cited.

The explanation for the occurrence of rafts within the lipid membrane begins with the formation of liquid ordered phases ($l_o$) and fluid phases ($l_d$) because of the action of cholesterol on phospholipids. As mentioned in Section 3, this liquid ordered phase leads to the preferential condensation of the $l_o$ phase over the $l_d$ phase. The addition of sphingolipids then causes the enrichment of sphingomyelin within the ordered phase containing up to 35 mol% cholesterol, an effect that promotes formation of domains. Only the $l_o$ phase exists at a very high cholesterol content (above 50 mol%) which precludes the formation of domains and rafts. Several authors have studied this process in membranes consisting of phospholipid/cholesterol/sphingolipid mixtures.[24,25,32,33]

Dietrich et al.[46] and Korlach et al.[33] have examined giant vesicles (GUVs) by confocal laser microscopy. A specific fluorescence-labeled lipid (laurdan) is selectively incorporated into the lipid bilayer composed of DOPC/cholesterol/sphingomyeline (1/1/1) with 1 mol% of ganglioside (Figure 21). The emission of this lipid depends on the

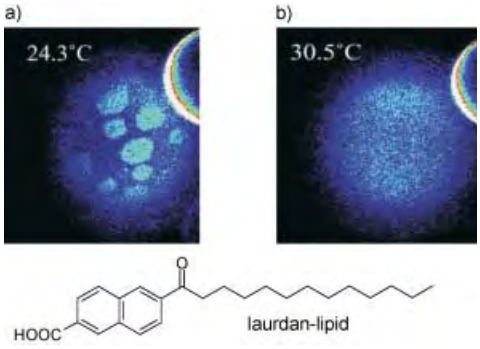



***Figure 21.*** Domain formation in unilamellar giant vesicles (GUVs) composed of DOPC/cholesterol/SM (1/1/1). a) Formation of GUVs at 24.3 °C. b) Destruction of rafts by raising the temperature to 30.5 °C. Reprinted from Ref. [46] with permission from the Biophysical Society.

hydration state of the surrounding media, with a red shift of 50 nm observed in the $l_o$ phase relative to that in the $l_d$ phase. Thus it is possible to discriminate between laurdan–lipid in the two phases by using two-photon absorption processes and an appropriate wave-selective filter. Since GUVs are round structures, the selective photon detection allows the entire surface of the vesicle to be visualized under the microscope rather than merely its cross-section. Dark patches with sizes of around 10 μm were found at the vesicle surface which are indicative of phase separation and the formation of rafts. The patches vanished when the temperature was raised above the phase-transition temperature, thus proving their existence as real phase-separated structures. The measurement of two pictures in a time-resolved mode showed that the patches moved slowly, thus revealing that the rafts were somehow mobile among the more liquid phase.

Studies investigating the changes in the height of phase-separated membranes offer an important way of visualizing the formation of domains/rafts. AFM studies are usually performed to detect these differences in height, which are between 0.5–1 nm.[47] It is necessary to use supported bilayer/monolayer membranes which can be obtained by transfer of Langmuir films onto planar, hydrophobized surfaces (such as mica or silanized glass). It is crucial in these experiments to apply an appropriate compression strength to the monolayer, one that mimics the biological compression. The moving

 © 2003 Wiley-VCH Verlag GmbH & Co. KGaA, Weinheim 

cantilever of the AFM tip can then detect the differences in height caused by changes in the lipid composition. Since phase-segregating lipids often have differing chain lengths, the height differences provide an indirect proof of phase separation and the resulting domain structure (Figure 22).

Milhiet et al.[48] have investigated the influence of increasing amounts of cholesterol on the formation of domains in POPC/SM monolayers (Figure 22a). With no cholesterol present, there are rather large patches (about $10^4$ nm$^2$) which

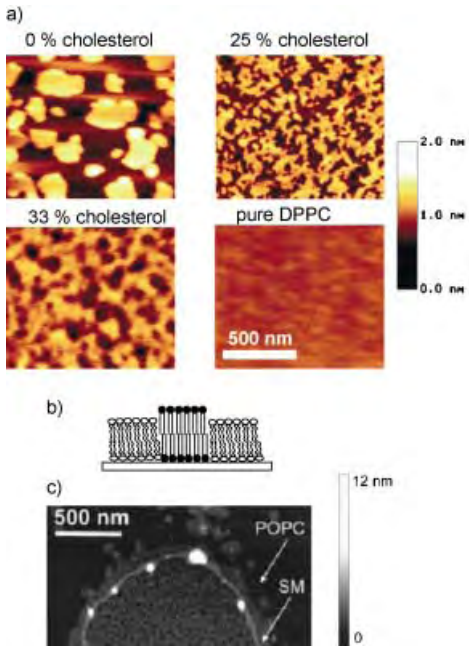



***Figure 22.*** Detection of rafts by AFM. a) Effect of cholesterol on raft formation. b) Schematic representation of raft detection by measuring height differences by AFM. c) Enrichment of ganglioside GM1 (0.2 mol%) at the boundary of a POPC/SM (80/20) monolayer. Reprinted from Ref. [48] with permission from the Biophysical Society.

increase in size with increasing SM concentration. The physical state here is a coexistence of solid and lipid domains. Adding cholesterol induces large changes in the distribution and sizes of the patches. The heights of the domains decrease progressively as the cholesterol content increases from 20 to 55 mol%.

Two additional effects have been demonstrated by AFM spectroscopy: the selective extraction of certain membrane components (similar to DRMs), which proves the selective extraction of specific raft structures,[49] and the clustering of gangliosides (GM1) in the $l_o$ phase.[50,51] The effect of ganglioside clustering is shown by the GM1 appearing as light spots within, or at the border of, the phase-separated domains (Figure 22c), with GM1 clearly concentrated in the $l_o$ phase or the border between the $l_o$ and $l_d$ phases.

Wide-angle X-ray diffraction (WAXRD) can be used to measure the membrane thickness of multilamellar vesicles (MLVs).[52] The bilayers in this type of vesicle are arranged in an onionlike fashion, which enables the distances between the concentric bilayers as well as their thickness to be measured exactly. Membranes composed of sphingomyelin and DOPC were about 0.9–1.1 nm thicker than membranes consisting of DOPC/cholesterol mixtures or pure DOPC bilayer membranes. This observation proves that the membrane composition can modulate the thickness of the membranes.

Rafts have also been investigated by a variety of other methods with the goal of studying their reduced lateral mobility at different chemical compositions. Single-particle tracking (SPT)[53] addresses the different lateral mobility inside rafts. In this method a lipid probe labeled with a gold particle (size 40 nm) is incorporated into a lipid mixture containing rafts. Confocal laser microscopy[54] is then used to detect the domain structure in the lipid monolayer, whereafter the track of the gold-labeled lipid is followed (Figure 23). This method enables the determination of the diffusion coefficients ($D$) in the phase-separated states (inside the dark and bright regions) of the monolayer. It was found that the mobility (that is, $D$) of the lipid probe is reduced by a factor of two in the $l_o$ phase with respect to the $l_d$ phase.

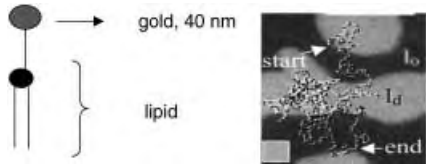



***Figure 23.*** Measurement of the coefficient of diffusion by SPT of a gold-labeled lipid in the $l_d$ (bright) and the $l_o$ phase (dark) of a raft-type lipid monolayer (DOPC/cholesterol/SM = 1/1/1). Particle trajectory of the gold-labeled lipid probe permits the determination of the diffusion coefficient in the $l_d$ ($1.1\times10^{-8}$ cm$^{-2}$ s$^{-1}$) and $l_o$ phase ($0.38\times10^{-8}$ cm$^{-2}$ s$^{-1}$). Reprinted from Ref. [46] with permission from Elsevier Science.

In another study TOF-SIMS[55] was used to check the composition of the rafts compared to the surrounding membrane lipids in DPPC/DOPS lipid monolayers in the presence or absence of $Ca^{2+}$ ions. Clustering into regions enriched in DOPS could be proven in the presence of $Ca^{2+}$ ions together with the formation of domains with sizes of 3–10 μm.

### 4.3. Sizes of Rafts

One of the widely discussed topics is certainly the absolute size of the rafts.[56] Table 2 shows a compilation of values reported in the literature together with their methods of determination. The values center around 10–100 nm by AFM methods and SPT methods and in the range of a few to several micrometers with other methods, such as microscopy, WAXRD, and TOF-SIMS. The number of associated molecules thus varies between several 100 to several 100000.

Three points concerning this problem must be mentioned:

1. Rafts are dynamic features, which means that the components are in dynamic equilibrium between the associated and free forms. It has been demonstrated by fluorescence

 © 2003 Wiley-VCH Verlag GmbH & Co. KGaA, Weinheim 

***Table 2:*** Size and chemical composition of rafts in biomimetic membranes.

| Method | Principle of detection | Membrane type | Composition | Size | Ref. |
|---|---|---|---|---|---|
| AFM | height differences | monolayer | POPC/SM/cholesterol | 15–200 nm | [48] |
| AFM | height differences | monolayer | POPC/SM/cholesterol/GM1 | 30–90 nm | [47b, 48] |
| AFM | height differences | monolayer | DPPC/cholesterol/GM1 | 100 nm | [50] |
| AFM | height differences | monolayer | DOPC/DPPC/GM1 | ca. 1 μm | [51] |
| AFM | height differences | monolayer | DOPC/SM/cholesterol | ca. 0.5 μm | [49] |
| SPT | mobility | murine fibroblasts | | ca. 200 nm | [53a] |
| SPT | mobility | BHK cells | – | 30 nm | [53b] |
| SPT | mobility | monolayer | POPC/SM/cholesterol | – | [46] |
| TOF-SIMS | chemical composition | monolayer | DPPC/DPPS | 3–10 μm | [55] |
| WAXRD | membrane thickness | MLV | – | 9–11 Å thick | [52b] |
| microscopy | fluorescence | monolayer | POPC/SM/cholesterol/GM1 | ca. 1 μm | [46] |
| microscopy | fluorescence | monolayer | DOPC/SM/cholesterol | ca. 0.5 μm | [54b] |
| microscopy | fluorescence | monolayer | DOPE/DPPC/cholesterol | several μm | [54c] |
| microscopy | two-photon absorption | GUV | POPC/SM/cholesterol | ca. 10 mm | [46] |
| microscopy | two-photon absorption | GUV | DLPC/DAPC | $<30$ μm | [54a] |

microscopy and single-particle tracking that the borders between rafts and the surrounding lipids are moving on the time scales of several seconds, therefore making a final determination of the size rather difficult at room temperature.2. The method of detection usually determines the size to which structures can be measured. Thus, it is not astonishing that rafts with sizes below 1 μm cannot be detected by fluorescence microscopy, whereas AFM methods can detect structures down to tens of nanometers.3. Since phase-separation phenomena are the basis for raft formation, the mode of preparation is certainly important as is the physical state of the mono- or bilayer structure. Most experiments have been performed with monolayers transferred from Langmuir–Blodgett films and may be different from unsupported bilayer membranes in GUVs. Additionally, the "growing" of phases has been shown to be time-dependent,[57] which indicates that domains may not always be equilibrium structures. The size of the domains increases significantly with time when a solution of small unilamellar vesicles (DPOC/DPPC) were applied to a surface as a bilayer and monitored by AFM methods (Figure 24). Initial domain sizes centered around 80 nm to 1.1 μm (corresponding to about $10^4$ to $10^6$ molecules) and increased to more than 5 μm over time.

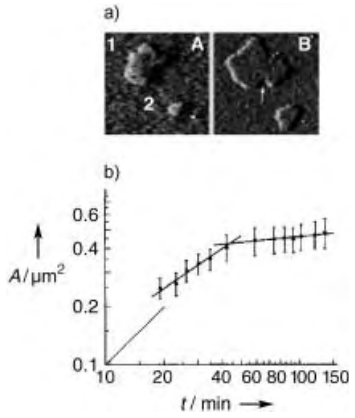



***Figure 24.*** Growth of domains monitored (domains 1 and 2) by AFM spectroscopy. a) The size of the domains of a DPOC/DPPC (3/1) monolayer increases with time (A: after 19 min, B: after 59 min). b) The cross-sectional area grows with time according to a power law. Reprinted from Ref. [57] with permission from the American Chemical Society.

## 5. Polymer-Induced Phase Separation

The previous sections have dealt with spontaneous lateral-phase segregation within a mixed lipid bilayer membrane under the action of temperature, ionic strength, and small-membrane molecules. The following section deals with the phase-separation process induced or exerted by large molecules (polymers), which can lead to clustering effects within lipid membranes. The structure of these membranes might not necessarily be a lipid bilayer membrane but can also be a closed assembly of macromolecular molecules (Figure 25).

The term vesicle can thus be extended to any closed, ball-shaped hollow structure with a diameter from 100 to 500 nm. The shell of these vesicles may consist either of a) polymerized lipids or polymers inserted into a lipid bilayer membrane,[58] b) low-molecular-weight block copolymers, or c) high-molecular-weight block copolymers.[16] The driving force for domain formation usually stems from phase separation of polymer chains and/or solvent molecules, a tendency more common with polymers than low-molecular-weight compounds.[59] Amphiphilic polymers (namely, those consisting of a hydrophilic and a hydrophobic block) in particular show a relatively high selectivity of solubilization in aqueous solvents.[60] This effect ultimately leads to the self-assembly of amphiphilic block copolymers into a variety of highly ordered structures such as micelles, vesicles, gels, and lyotropic phases.[61] The type of structure formed depends mostly on the hydrophilic/hydrophobic balance, the molecular weight, and the solvent.

This aggregation behavior of amphiphilic block copolymers has been covered in a recent review[62] and will not be treated further. However, it should be pointed out that the formation of vesicles and the phase-separation phenomena induced by polymers and block copolymers are just special cases of this very complex phase behavior. Phase separation

 © 2003 Wiley-VCH Verlag GmbH & Co. KGaA, Weinheim 

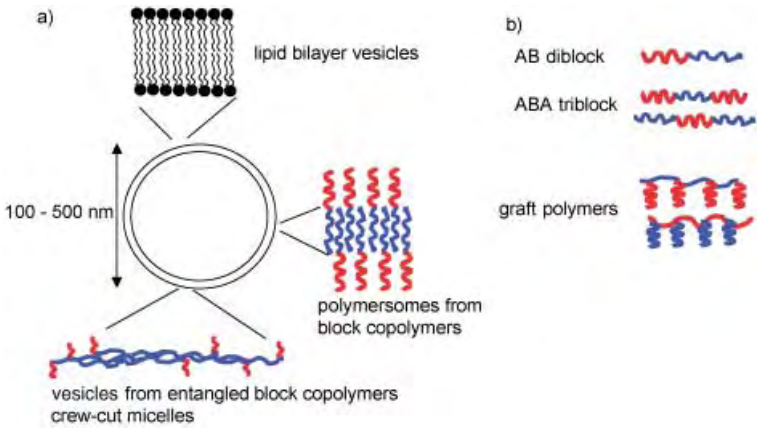



***Figure 25.*** a) The shells of vesicles can be derived from lipid bilayer membranes, diblock copolymers ("polymersomes"), or cross-linked diblock copolymers ("crew-cut vesicles"). b) Different types of block copolymers (red: hydrophilic block, blue: hydrophobic block).

occurs under the influence of polymers and can be either lateral (within the membrane) or vertical (between the outer and inner layers). The following sections give an account of the action of polymers and polymerization reactions on domain formation within membranes.

### *5.1. Action of Polymers on Lipid Bilayer Membranes*

An added amphiphilic/or charged polymer can act in three ways to induce domain formation in a lipid bilayer (Figure 26):

1. by insertion of graft polymers with hydrophobic graft chains, thus inducing a clustering of lipids around the hydrophobic anchoring groups to yield lateral domains; 2. by addition of a charged polymer to a lipid mixture consisting of charged/neutral lipids, thus inducing vertical phase separation by promoting layer-to-layer flip-flop of the charged lipid species in preference over the neutral lipid; and 3. by the insertion of lipid–polymer conjugates, which leads to subsequent clustering of the lipid–polymer conjugates as a result of an enforced increase in the membrane curvature.

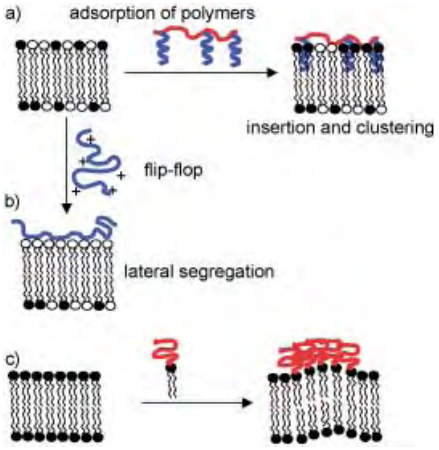



***Figure 26.*** Phase segregation in lipid bilayers induced by polymers. a) Clustering of lipids around a graft polymer with hydrophobic side chains; b) lateral phase segregation by adsorption of a charged polymer (blue) onto the bilayer surface; c) clustering of lipid polymers and induction of membrane curvature.

#### *5.1.1. Insertion of Graft Polymers*

A number of polymers can be adsorbed onto the outer face of a lipid vesicle. Amphiphilic block and graft polymers with hydrophilic backbones and hydrophobic graft chains, respectively, are usually used for this purpose. The hydrophobic polymer chains can insert into the lipid bilayer structure and lead to a fixation of the hydrophilic polymer chains to the outside of the bilayer membrane.

Ladaviere et al.[63] have demonstrated the domain-inducing effect of hydrophilic/hydrophobic graft polymers on the lipid bilayer structure. The formation of domain structures consisting of fluorescent (bright) and nonfluorescent (dark) parts was observed in GUVs with certain polyacrylic acid polymers which exhibited a hydrophilic portion (that is, free acrylic acid fraction) of more than 75 mol% (Figure 27). It was proven that these

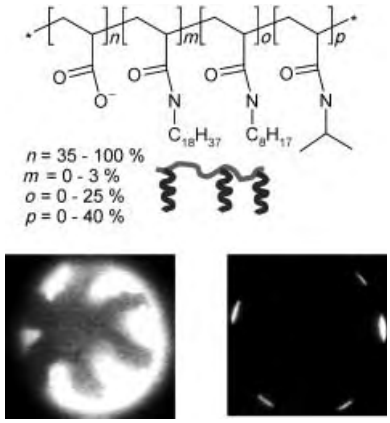



***Figure 27.*** Fluorescence images of GUVs demonstrating the phase segregation after insertion of a graft polymer. Reprinted from Ref. [63] with permission from the American Chemical Society.

polymers were not able to cross the lipid bilayer membrane and that they induced two types of phase separation: a) vertical phase segregation, which corresponds to the external adsorption to the bilayer membrane after inserting the polymers of their hydrophobic graft chains into the membrane and b) lateral segregation as a result of a clustering of the hydrophobic graft chains within the lipid bilayer membrane.

#### *5.1.2. Electrostatic Adsorption of Polymers on Vesicle Surfaces*

Laser microelectrophoresis has been used as an instructive tool in the investigation of polymer/vesicle interac-

 © 2003 Wiley-VCH Verlag GmbH & Co. KGaA, Weinheim 

tions.[64] Ionic vesicles are subjected to an electric field while the sample is illuminated with a laser beam. The addition of a polymer of opposite charge to the system ultimately causes the electrophoretic mobility to reach zero, which signifies that the net charge on the outer surface of the vesicle has been eliminated in the vesicle/polymer complex. By this means it can be determined, for example, whether the polymer senses only ionic lipid in the outer layer (in which case only half the vesicular ions are charge-neutralized) or the entire ionic lipid content of the vesicle (in which case ionic lipid in the inner layer must move in a flip-flop process to the outside under the influence of the polymer).

It was found that a surface-adsorbed cationic polymer (PEVP, Figure 28) can electrostatically drag an anionic surfactant (sodium dodecylsulfate, SDS) from the inner layer to the outer layer of bilayers in the fluid state, as established by the fact that the ratio of the total PEVP charge to the total SDS charge was unity. Bilayers in the solid state do not enable the SDS to undergo a polymer-induced flip-flop process. In this case, the PEVP-to-SDS charge ratio is only 0.5:1 (only the charge of the outer SDS is neutralized). Since the polymer concentrations are much too small to cover the entire vesicle surface, it can be presumed that the polymer gathers either all or half of the SDS (depending upon the phase state of the bilayer) into domains where the charge-neutralization takes place.

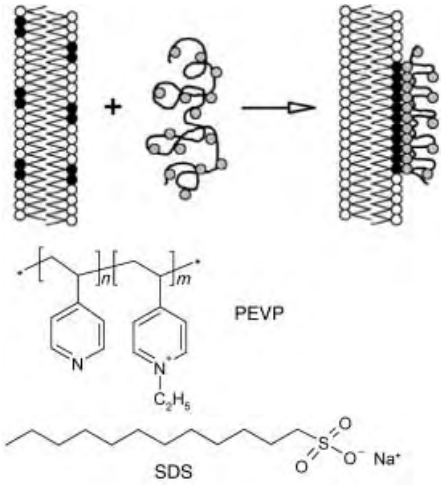



***Figure 28.*** Flip-flop process of an anionic surfactant (SDS) by adsorption of a cationic polymer (PEVP). PEPV = poly(*N*-ethylvinylpyridine-*co*-vinylpyridine). Reprinted from Ref. [64b] with permission from Elsevier Science.

#### *5.1.3.* ***Curvature-Induced Clustering***

Lipid–polymer conjugates constitute a special class of membrane-active polymers. This class of lipids commonly consists of a double-chain lipid molecule onto whose head a polymer of hydrophilic character is bound covalently. If the chain length of the two hydrophobic chains is more than eight $CH_2$ units, such conjugates can be incorporated into lipid bilayers by purely hydrophobic forces. The outer membrane is then covered in part by a hydrophilic polymer shell, which can lead to higher physical and/or biological stability of liposomes—a concept related to the steric stabilization principle of colloids.[65] The polymers used for this purpose are mostly poly(ethyleneglycols), poly(acrylic acids), poly(amino acids), poly(oxazolines), and oligosaccharides. In addition to their stabilizing activities, lipid–polymer conjugates can induce domain formation as well as morphological changes in the membranes.

The induced formation of domains by lipid–polymer conjugates has been proven recently by measurements on bilayer membranes into which a poly(ethyleneglycol)–lipid derivative had been incorporated (Figure 29). Slack et al.[66] determined the spacing of multilamellar membranes with and without a lipid–polymer conjugate. It was found that the lipid–polymer conjugate preferentially enriches the parts of the membrane with higher curvature, and is explained by the hydrophilic polymers and their large head groups having a higher steric demand than conventional lipids with non-polymeric head groups.

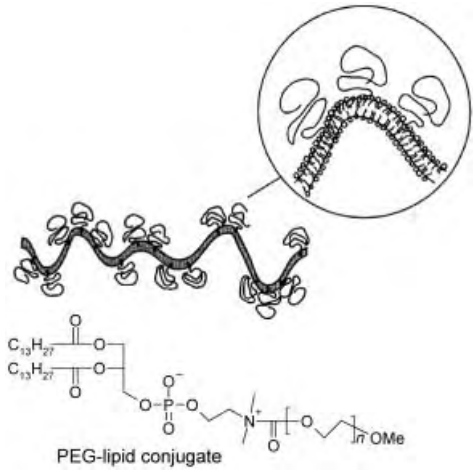



***Figure 29.*** Enrichment of PEG–lipid conjugates in curved parts of the lipid bilayer membrane (PEG = poly(ethyeneglycol). Reprinted from Ref. [66] with permission from the American Institute of Physics.

The concept was developed further by the use of a graft polymer with a thermoresponsive element. Simon et al.[67] used a copolymer of poly(*N*-isopropylacrylamide) (PNIPAM) with a small amount of hydrophobic graft chains (0.5 mol%; Figure 30a), which served as anchoring structures within the lipid bilayer at the outside of preformed vesicles. A fluorescent moiety was also added to enable the lateral diffusion to be monitored and quantified. PNIPAM is known to contract its structure upon heating above a critical temperature of about 42 °C while the curvature of the membrane increases (Figure 30b). As a consequence, the generation of new vesicles is observed as a response to the temperature jump (Figure 30c).[68]

 © 2003 Wiley-VCH Verlag GmbH & Co. KGaA, Weinheim 

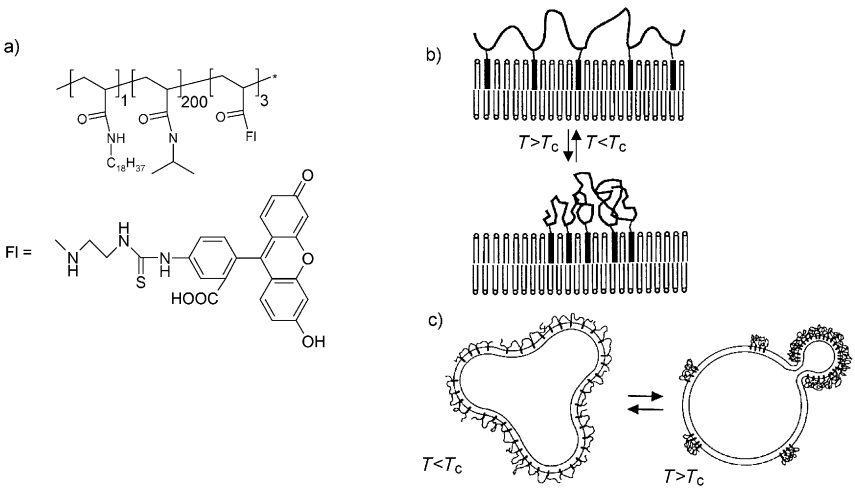



***Figure 30.*** Enrichment of PMPAM–lipid conjugates in curved parts of the a lipid bilayer membrane. a) Structure of the block copolymer; b) temperature-induced contraction ($T > T_c$) of the membrane-inserted polymer; c) effect of temperature-induced contraction on the vesicle shape. The curvature is increased and leads to the "budding" of new vesicles from the surface. Reprinted from Ref. [67] with permission from Elsevier Science.

### *5.2. Polymerization Reactions within the Lipid Bilayer Membrane*

The lipid bilayer membrane permits two different types of polymerization reactions: a) the polymerization of reactive monomers within the hydrophobic shell and b) the polymerization of lipids with polymerizable groups. The latter process has been reviewed thoroughly[58a] and will be mentioned only with respect to vertical phase separation. Both processes can be used to induce either lateral or vertical phase separation within the lipid bilayer membrane.

#### *5.2.1. Lateral Phase Segregation of Growing Polymers within the Lipid Bilayer*

A variety of small hydrophobic monomers, such as styrene, divinylbenzene, and various alkyl acrylates can be incorporated into the hydrophobic part of a lipid bilayer membrane. Two types of structures are generated when the monomers are polymerized thermally or photochemically (Figure 31): a) either a lump of polymer is formed within the lipid bilayer membrane by phase separation during the polymerization reaction[69] or b) the monomer polymerizes homogeneously within the hydrophobic shell.[70]

German and co-workers[71] have studied the phase-segregation process of various monomers within the lipid bilayer occuring by pathway (a) which lead to the formation of a "parachute" architecture.[72] Styrene or alkyl methycrylate monomers were distributed homogeneously between the layers of the membrane (DODAB) by adding the monomer to a preformed vesicle suspension (Figure 31), after which radical polymerization is initiated. The particles formed within the vesicle soon after initiation and without disruption of the lipid bilayer membrane have a uniform size and an ellipsoidal shape.

Critical to this process is the mobility of the monomer within the lipid bilayer membrane. Krafft et al.[73] have forced monomers to polymerize homogeneously within the lipid bilayer structure by reducing the space within the hydrophobic membrane layers. Perfluorinated lipids (FPC) were used as the vesicle-forming lipids. These lipids are known to exhibit a much denser packing (ca. 1 nm) than conventional hydrocarbon lipids (ca. 2.3 nm), thus reducing the lateral diffusion and preventing phase separation during polymerization.

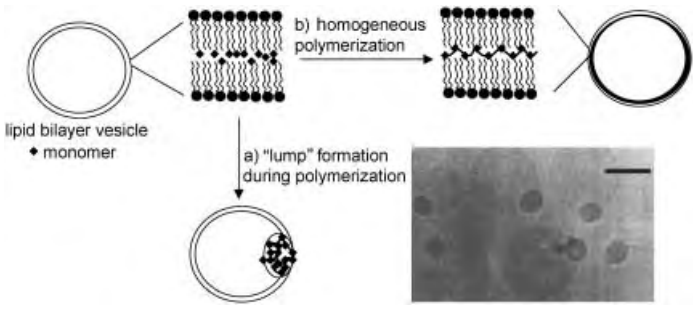



***Figure 31.*** Polymerization of monomers (styrene, methylmethacrylate) inside a bilayer membrane consisting of didodecylammonium bromide (DODAB). The TEM image shows the formation of lumps as a result of the fast diffusion of monomers into the intrabilayer space.[72]

#### *5.2.2. Polymerization in Vertical Phase Segregated Bilayers*

Ravoo et al.[74] used a combination of vertical phase separation and subsequent polymerization to generate stable vesicles with different inner and outer layer structures. A β-nitrostyrene derivative was coupled to the hydrophilic head of a diacylglycerophospholipid and vesicles were formed at neutral pH (Figure 32).

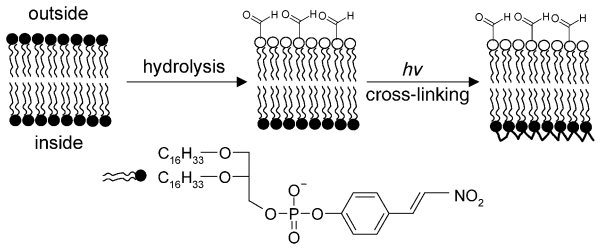



***Figure 32.*** Selective cross-linking of lipids on the inner membrane layer of a vesicle. The hydrolysis leads to a deactivation of the β-nitrostyrene moieties on the outer membrane layer. The remaining β-nitrostyrene moieties on the inside are then cross-linked by irradiation.

The addition of an alkaline solution led to the hydrolysis of the β-nitrostyrene group to form a benzaldehyde derivative. Since the interior of the vesicles remained intact at neutral pH, as a result of hindered diffusion of the hydroxide ion through the vesicle membrane, the hydrolysis occurred on the outside layer only. The remaining β-nitrostyrene groups in

the interior were then cross-linked by photoinduced polymerization, thus stabilizing the vertically phase segregated vesicles against intermixing by flip-flop processes.

### 5.3. Vesicles Formed by Phase Separation of Block Copolymers

In contrast to vesicles formed by small lipid molecules with molecular weights below approximately 1000 g mol$^{-1}$, block copolymers (with molecular weights ranging from 1000 to several 10 000 g mol$^{-1}$) can form vesicles by phase segregation processes. Crucial for this process is an immiscibility of one of the blocks in water as well as an interchain immiscibility between the two blocks. There are two different modes of assembly of the membrane, which lead to two different types of structures.

Block copolymers of intermediate molecular weight (several 1000 g mol$^{-1}$) with a hydrophilic part amounting to 20–40 mol % can be dissolved directly in water where they form vesicles (Figure 33 a)[16] called "polymersomes"[75] as a result of phase-separation processes between the immiscible polymer blocks. The membrane thickness can be adjusted to between 8–20 nm depending on the size of the hydrophobic block, thus enabling membranes to be created with tailored chemical and mechanical properties, such as defined permeability, stiffness, and elasticity. The amphiphilic block copolymers serve as "lipidlike" molecules which assemble as a result of hydrophobic and immiscibility effects between different polymer blocks. The hydrophobic chains are fully extended at low molecular weights, whereas they seem to be entangled at high molecular weights. The mode of assembly has been reviewed recently and will not be discussed further.[76]

Block copolymers with high molecular weights and a hydrophilic portion below 20 mol % fail to from vesicles because of the slow kinetic processes of the longer polymer chains. The polymers are therefore dissolved in a water-miscible solvent which solubilizes both blocks (Figure 33 b).[77] Upon slow addition of water, vesicles are formed with membrane thicknesses between 20 and 40 nm. The membrane of these vesicles is formed by strongly entangled polymer chains, which indicates that the membrane thickness is not solely governed by the length of the hydrophobic block.

Eisenberg and Luo[78] investigated the formation of vesicles from a variety of block copolymers, including PS-*b*-PA, PS-*b*-PEO, and PS-PVP. The important discovery was the that the hydrophobic block was considerably longer (degree of polymerization 200–380) than the hydrophilic block (degree of polymerization 20–80). The vesicles consist of a hydrophobic core of PS and a hydrophilic corona consisting of the hydrophilic PEO, PA, or PVP blocks. The dimensions of the vesicles are determined by a subtle balance between the stretching of the PS block, the repulsive interactions of the hydrophilic blocks in the corona, and the core–corona interface energy.

The interplay of these energies was used to direct polymer chains in a mixture of block copolymers either to the outside or the inside of the vesicle (Figure 34). Thus a mixture of two

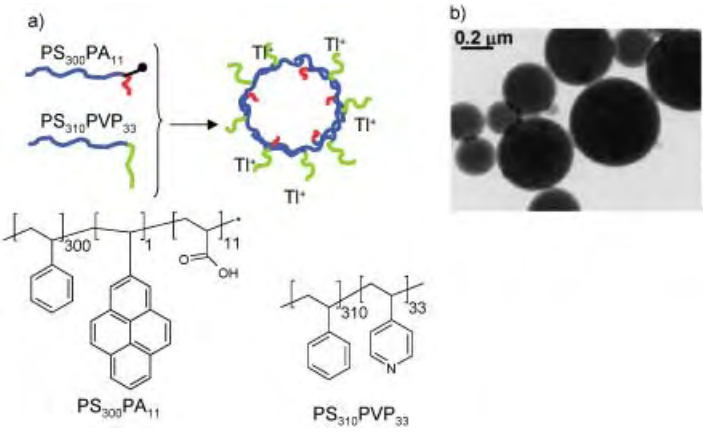



*Figure 34.* Selective phase separation of block copolymers inside/outside of crew-cut micelles. a) A mixture of $PS_{300}PA_{11}$ and $PS_{310}PVP_{33}$ block copolymers forms mixed crew-cut micelles. The longer PVP chains (green) point outwards, while the shorter PAA chains (red) point inwards. The pyrene probe points to the inside of the vesicle and thus remains inaccessible to the $Tl^+$ ions which act as fluorescence quencher molecules. b) TEM image of the formed vesicles.[78]

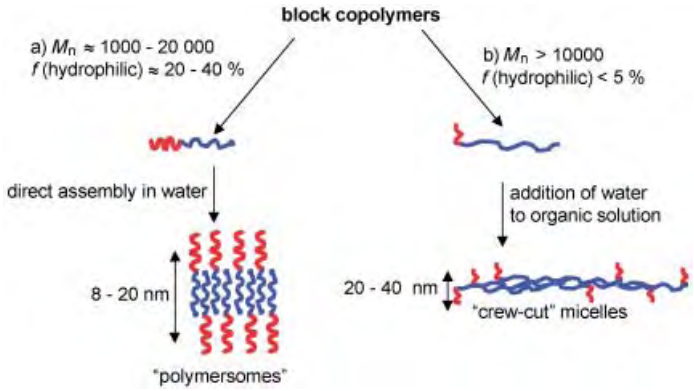



*Figure 33.* Assembly of vesicles from amphiphilic block copolymers in aqueous solution. a) Formation of "polymersomes" by direct assembly of short-length block copolymers with a hydrophilic fraction between 20–40 mol %; b) assembly of hydrophobic, long-chain block copolymers by precipitation from organic solvents to form crew-cut micelles.

block copolymers with equal length PS chains ($m = 300$) and different length hydrophilic chains consisting of either polyacrylic acid (PA, $n = 11$) or poly(4-vinylpyridine) (P-4PV, $n = 33$) was prepared. A pyrene group located directly at the junction between the hydrophilic and hydrophobic blocks served as a label for determining the position of the acrylic acid chains. The two polymers ($PS_{300}PA_{11}$ and $PS_{310}P\text{-}4PV_{33}$) were mixed in solution to form vesicles, after which $Tl^+$ ions were added as a quencher to check for the presence of pyrene molecules on the outside surface of the vesicles. The absence of quenching of the pyrene fluorescence proved that the shorter PA chains were localized exclusively in the interior of the vesicles, while the longer P-4VP chains were located at the exterior of the vesicles. The reason for this arrangement is a purely geometrical constraint: The longer P-4VP chains need more space and prefer the

 © 2003 Wiley-VCH Verlag GmbH & Co. KGaA, Weinheim 

outside with the larger surface area, whereas the shorter PA chains reside at the more highly curved inner surface of the vesicle.

## 6. Biological Impacts of Phase Separation

The primary function of membrane lipids is to form a barrier around the cells and organelles to preserve their integrity. However, the astonishing variety of lipids present in the membrane of living cells suggests that the individual lipids, as well as the physical properties of the membrane bilayer, play important roles in biological events.[79,80] Chemists have studied cholesterol and phospholipid mixtures as well as protein and lipid mixtures in artificial membranes because of their great importance for understanding the function of biological membranes. As pointed out earlier, lipid bilayers can exist in different physical states, depending upon the temperature and the lipid composition: the solid–gel state (Lβ) and the liquid-crystalline state (Lα). A liquid ordered state $l_o$, which has properties intermediate between Lβ and Lα has been identified in model membranes formed from mixtures of cholesterol and sphingolipids. Whether such domains exist in vivo has been a controversial subject for many years.

Evidence that rafts may exist in cell membranes has come from studies of human and hamster fibroblasts in which membrane fractions rich in glycosphingolipids but insoluble in the cold non-ionic detergent Triton X-100 have been detected.[81] Since then, an increasing number of experiments focusing on cell membranes have underlined the importance of rafts in biological activities. Moreover, some proteins have been found to associate within those domains, an association which is likely to be important in many biological events such as signal transduction, protein and lipid sorting, cell adhesion, motility, and various diseases.

### 6.1. Caveolae, Caveolins, and Cholesterol

A special class of lipid domains are caveolae, a subset of rafts, which are rich in cholesterol, glycosphingolipids, sphingomyelin, and lipid-anchored membrane proteins (see Section 4.1).[43,82,83] Caveolae, first reported in the 1950s,[84,85] are dynamic structures that have been characterized by electron microscopy as small cavities with diameters of 50 nm or higher.[86,87] However, the shape of caveolae can change to non-invaginated structures as a consequence of their activity and consequently domains found in cells can be not only invaginations of the plasma membrane but also flat or tubular domains within the membrane (Figure 35).[73,88,89]

Caveolae are present in many cell types and are coated with a cholesterol-binding 22 kDa protein called caveolin-1.[86] The protein is comprised of a central 33 amino acid hydrophobic domain which allows its association with the membrane, while the amino and carboxyl termini of the protein face the cytoplasm. This protein belongs to a family of integral membrane proteins of 21 to 25 kDa which interact with themselves to form homo- and hetero-oligomers, and

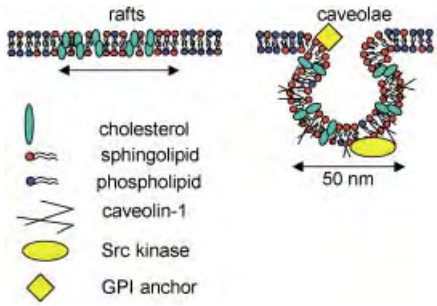



*Figure 35.* Schematic structure of caveolae and the associated proteins caveolin-1, GPI anchors, and Src-kinases.

which are implicated in many cellular functions.[86,90–92] Caveolin-1 is encountered in a large number of cells (for example, endothelial cells, adipocytes, fibroblastic cell types), but the protein is associated with domains in membranes that are rich in cholesterol, whatever the cell type.

It is known that caveolin requires cholesterol to self-associate into oligomers and to bind to biological membranes.[93–97] Caveolin-1 is thought to be necessary for the formation of the invaginated structure of caveolae[43,98] and serves as a marker for caveolae. The invaginated structure of caveolae is a consequence of the hairpin loop of the hydrophobic core of the protein within the membrane and of the binding of the protein with cholesterol and glycosphingolipids.[87,93,99,100] It has to be emphasized that domains have been found in organelles without the presence of the protein being detected. As some cells do not express caveolin but have domains of molecular composition similar to caveolae, those domains are sometimes referred to "noncaveolae rafts" or simply "rafts".[87,1]

When cholesterol levels get too low the coat disassembles[86] and the number of caveolae decreases.[101] As the removal of cholesterol compromises the function of rafts,[102] the relationship between caveolae and cholesterol is most easily summarized as functional.

### 6.2. Caveolae and Cholesterol: Their Roles in Cell Signaling

Caveolin-1 has been detected in caveolae of plasma membranes as well as in intracellular organelles such as the endoplasmic reticulum (ER) and the trans-Golgi network.[92,94,103] The endoplasmic reticulum is a large intracellular compartment made up of tubular and sack-shaped structures and composed of the rough ER and the smooth ER. The former is the site of protein synthesis, which can be, but not necessarily, transported to the Golgi apparatus by transport vesicles. The Golgi apparatus is, like the ER, a network of membrane-enclosed space, and is the site of protein maturation and sorting. The modified proteins are then transported to various sites within the cell, such as the plasma membrane.

Cholesterol (like all the lipids found in raftlike domains) is synthesized in the endoplasmic reticulum (ER) and transported to the plasma membrane where it is distributed to raft and other domains. Cellular lipids are not necessarily trans-

 © 2003 Wiley-VCH Verlag GmbH & Co. KGaA, Weinheim 

ported by vesicles, as is done with most of transmembrane proteins, since carrier proteins can transport lipids through the cytoplasm. The exogenous cholesterol (and sterols in general) can be internalized inside the cells by endocytosis, but cholesterol trafficking also involves caveolin-1 as a shuttle. Caveolin-1 binds cholesterol at the surface of the cell and then transports the lipid intracellularly and also between the intracellular compartments and the plasma membrane.[88]

In summary, the relationship between cholesterol, the protein, and caveolae is really tight and, as pointed out earlier, the formation of caveolae can be suppressed or increased according to the level of caveolin-1 in the cell.[104] Since caveolin-1 is involved in cholesterol regulation, the amount of cholesterol transported to the membranes, and consequently the organization of cholesterol in membrane domains, follows the same rule. The specific interaction between the protein and the lipid is of crucial importance for many surface-signaling pathways, as cholesterol permits the presence of signaling proteins within the domains of the cell membranes. Many biological processes are inhibited if the amount of cholesterol gets too low to keep the proteins assembled.

### 6.3. Protein Targeting to Domains in Membranes

The lipid domains can selectively include or exclude specific classes of proteins which are undoubtedly involved in the function of the rafts in vivo.[99] In general, the fixation of a protein in a membrane is accomplished by a lipophilic anchor. Proteins can become acylated by a palmitic chain, a myristic chain (for example, Src kinases), or prenylated chain (for example, small GTP chains). They can also be covalently linked to glycosylated phosphatidylinositol (GPI) or to cholesterol itself (Figure 35).

Caveolin is not the only lipid-anchored protein implicated in the structure and functions of caveolae. Acylated proteins, GPI-anchored proteins linked to membranes by a carboxy end group, and a few prenylated proteins are among the other proteins present in those domains.[105] These proteins (caveolin, GPI-anchored proteins, etc) come from the ER and are transported into the lipid core of the raft domain (glycosphingolipid/sphingomyelin/cholesterol) in the Golgi complex where they assemble to form caveolae.

The targeting of the selected proteins to rafts depends upon the nature of their saturated lipid anchors (mainly myristoyl–palmitoyl chains, or palmitoyl double chains).[105] The high concentration of acylated proteins in rafts has resulted in it now being widely accepted that acylation is the general targeting signal for the formation of membrane microdomains within a membrane. Multiple hydrophobic modifications of the protein anchor seems to be required as a high concentration of acyl chains is necessary for an efficient targeting of some proteins (for example, *Influenza Hemagglutinin*[106]) to the membrane domains. The relatively low amount of prenylated-anchored proteins found in rafts could be explained by the steric bulk of the prenyl groups. Indeed, prenyl groups are highly hydrophobic but their bulky structure prevents them fitting efficiently into the ordered domains. The mechanism by which proteins associate with rafts requires additional investigation.

Although the existence of rafts in the plasma membrane as well as in the membrane of vacuolar systems of living cells is established, the molecular composition of rafts remains to be further investigated. In spite of the wealth of information available, the nature of the protein components that can insert into rafts is still not well defined. However, normal cell events as well as pathologies are intimately tied to the presence of those components in rafts.

### 6.4. Signal Transduction and Endocytic Functions of Membrane Domains in Cells

Most hydrophilic signal substances that cannot cross the membrane bilayer (for example, hydrophilic hormones) exert their effects by binding to specific receptors present on the outside of the cell surface. The receptors involved in this process are integral membrane proteins of three different types: 1) Type I receptors, which have enzyme activity (usually a tyrosine kinase); 2) Type II receptors, which are ion channels, and 3) Type III receptors, which are transmembrane proteins that transfer their signal via the G-proteins. After binding the signal substance, a modification in the structure of the receptor triggers the release of a signal on the inside of the membrane. This mechanism of action is called signal transduction.

Caveolae and rafts are enriched in molecules involved in intracellular signal transduction, for example, G-protein-coupled receptors, Src family tyrosine kinases, and endothelial nitric oxide synthase (eNOS).[87] The concentration of receptors for interaction with signaling molecules might enable domains to serve as centers of signaling events. Such distinct morphological zones which are assembled within a membrane to carry out signaling processes are named signaling platforms. An example of the role of caveolae as a signaling platform can be taken from the cholera toxin. Signal transduction by this toxin requires the caveolae system to internalize the toxin–receptor complexes through a vesicular transport process. This example demonstrates the tight relation between signal transduction and endocytosis in membrane domains.[107]

Cytosis is an active transport used by the cell to take up macromolecules (endocytosis) or to expel them (exocytosis). Transcytosis refers to the internalization of molecules at one plasma membrane and their transport to the opposite membrane. Both mechanisms involve the formation of membrane-enclosed vesicles, which are constricted off from the plasma membrane or from the membranes of the organelles within the cell. Such endocytic vesicles are coated with special proteins (usually clathrin), however, it seems that caveolae could be involved in endocytosis and transcytosis[108] independently of clathrin vesicles.[109]

The role of the lipids clustering in rafts for the regulation of endocytosis is clear for sterols, but not for sphingolipids. It has been shown that cholesterol is essential for endocytosis, as its depletion prevents internalization by caveolae.[108]

 © 2003 Wiley-VCH Verlag GmbH & Co. KGaA, Weinheim 

If caveolae are vesicles involved in the transport of specific molecules, they should be able to bud off from the membrane. A mechanism for caveolae budding has been proposed in which the invagination of the membrane must be followed by the fission of the neck to generate the transport vesicle. Thus, proteins might be associated with caveolae to allow the formation of independent vesicles. This fission has been shown to be mediated by the GTPase dynamin in endothelial cells and hepatocytes.[87,109,110]

Internalization by caveolae does not seem to be restricted to macromolecules. Anderson et al. have shown that small molecules (folic acid) can be internalized by caveolae. This mechanism for the uptake of molecules and solutes independently from the endocytic pathway has been named potocytosis.[111]

### 6.5. Rafts and Human Diseases

Domains in membranes containing caveolae and caveolin are implicated in the molecular pathology of numerous diseases, such as cancers, atherosclerosis, neurodegenerative diseases, and AIDS. In this section, an overview of the implication of domains in some human diseases is presented.

#### 6.5.1. Transmissible Spongiform Encephalopathies

Prions are a class of proteins of about 35 kDa that cause degenerative, fatal neurologic disorders called transmissible spongiform encephalopathies (TSEs). A PrP gene is a normal component of the host genome. One form of the host PrP has a GPI anchor and localizes in rafts in the extracellular face of the plasma membrane.

The mechanism of transmission and pathogenesis implies the conversion of cellular host prion protein PrP into the scrapie isoform PrPsc. This conversion is inhibited by several factors, for example, lowering the level of cellular cholesterol disperses raft-associated proteins. This is also true in the case of the prion protein, the result of which prevents PrPsc formation. Moreover, the replacement of the GPI anchor of the protein with 62 residues (coded for the transport of "coated pits") inhibited the transport of host PrP to raft domains. These experiments suggest that the conversion of the PrP protein into PrPsc occurs in caveolae.[112,113]

#### 6.5.2. Cancers

Caveolae populations have been shown to decrease in many types of oncogenically transformed cells[114] as a consequence of the loss (or the reduction) of caveolin-1 expression from the transformed cells. Caveolin-1 is expressed in most normal cells, and its expression is essential for normal signal transduction from caveolae, for the mediation of differentiation, and for contact inhibition.[115] Caveolin-1 has been identified as a suppressor of human tumors. Its gene has been mapped to a region of the genome that is often deleted in human cancers, which shows that the region contains a tumor suppressor.[116] The down-regulation of caveolin-1 is related to cell transformation and proliferation in many cancer cell lines.[117] When caveolin-1 is absent, the number of caveolae decreases and cell proliferation becomes uncontrolled.[114] In addition, various proteins involved in the modulation of cell proliferation localize within caveolae or interact with caveolin-1.[118]

Interestingly, it has been shown that multidrug-resistant cancer cells express very high levels of caveolin-1 and caveolae.[119,120] This up-regulation of caveolin-1 may be a consequence of the role of caveolin and caveolae in cholesterol efflux[121] (that is, the transport of cholesterol to the plasma membrane). This pathway has been postulated to play a role in the transport and ultimate expulsion of drugs from intracellular membranes to the plasma membrane, which leads to the acquisition of multidrug resistance.

The articles published up to now lead to the conclusion that the level of caveolin-1 seems to change during differentiation, oncogenic transformation, and multidrug resistance, which shows the complexity of the role of membrane domains in cancers.

#### 6.5.3. Virology

Rafts have been implicated in the infection of many viruses, with the human immunodeficiency virus being the most studied.[122] Strong evidence points to the conclusion that the human immunodeficiency virus-1 (HIV-1) buds through lipid rafts.[123,124] Virus budding is a key step in the infection from all enveloped viruses. The interaction between the virus and the cell surface involves the attachment of a surface protein of the virus to a specific receptor on the targeted cell, which leads to the fusion and entry of the virus. A question arose, as to whether or not this interaction takes place in ordered domains or not.

As pointed out earlier, rafts can include or exclude certain transmembrane molecules selectively. For example, it appears that a 200 kDa transmembrane phosphatase protein CD45 is abundant in all cell membranes except within rafts. Surprisingly, the HIV-1 envelope also excludes this molecule, whereas the virus incorporates other membrane proteins that are present at lower levels than CD45.[125] This result has led researchers to suspect that the virus may bud from rafts, and not from the surrounding membrane.

Virologists have observed that the lipid composition of membranes from many viruses is different from the membrane of host cells from which they are derived.[126–130] Moreover, the HIV-1 lipid bilayer is enriched in cholesterol and sphingolipids,[123] similar to rafts. Thus, it is not surprising that depletion of cholesterol, which disrupts lipid rafts, impairs HIV-1 production.[131] More and more evidence leads to the same conclusion: viral particles may use raft domains of the host cells to start the infection process.

A significant example of viral assembly and cell entry via rafts has been demonstrated by the Ebola virus.[132] The existence of patches of Ebola virus particles in domains rich in lipid rafts has been observed by fluorescence microscopy (Figure 36). This result opens the way for new strategies to fight against virus growth by new antiviral pathways in medicine and biology.

 © 2003 Wiley-VCH Verlag GmbH & Co. KGaA, Weinheim 

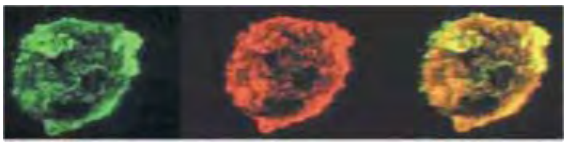


***Figure 36.*** Cluster formation within the membrane of the Ebola viral particles visualized by a fluorescent marker and observed by light microscopy. Green: raft marker, yellow: ganglioside GM1, red: viral glycoprotein. The localization of all the colors at the same spots proves the association of the viral particles in the rafts. Reprinted from Ref. [132] with permission from the Rockefeller University Press.

## 7. Outlook

In this article a new dimension of order in membranes has been reviewed, starting from conventional lipid bilayer model membranes, whose investigations has kept many researchers occupied during the past decades. Historically, there was a "simple" bilayer model, derived from electron microscopy pictures of native cell membranes, which was followed by the first artificial vesicles discovered by Kunitake et al.[133] This has opened the way to the implicit investigations of lipid bilayer membranes by using physicochemical methods to determine the influence of lipid molecules on the structure and dynamics of lipid bilayer membranes. Most such experiments, however, where performed on membranes composed of only one type of lipid.

The complex behavior of lipid mixtures in membranes and the subsequent action of large molecules (polymers and proteins) that leads to the formation of domains has been postulated for a long time. The past decade has brought the definite discovery of these domains, together with explicit proof of their biological significance as rafts in living cell membranes. This definitely has opened a new dimension in membrane research. Today it is known that both the hydrophobic lipid chains as well as their hydrophilic head groups together with membrane proteins are important in inducing clustering effects on membranes. Such clustering effects can also be mimicked by nonlipid molecules derived from synthetic polymers.

Anatole France wrote, "Do not try to satisfy your vanity by teaching a great many things  Put there just a spark. If there is some good flammable stuff, it will catch fire." Writers of reviews always face the problem of following this advice while, simultaneously, providing sufficient fuel to permit the lighting of a bright flame. Thus, reviews are often written after the cream has been skimmed off. This does not seem to be relevant yet to domains and rafts: despite all the information on domains and rafts that has been accumulated, we are just at the beginning of revealing their chemical and biological consequences. Future progress in biology will depend upon scientists of all types, including chemists, continuing to address membrane structure, dynamics, and function where domains and rafts play a key role. Even now it can be assumed that new strategies for fighting viral infections, lipid storage disease, cancer, and other persistent illnesses of mankind will arise through the understanding of rafts.

*W.B. thanks the Austrian Science Foundation (grants FWF 14844 CHE and FWF 13294 CHE) and the Österreichische Nationalbank (OenB 7702) for financial support. Special thanks go to Prof. H. Gruber for proofreading the manuscript. F.M.M. thanks the National Institutes of Health (NIH).*

Received: February 18, 2003 [A586]

[1] R. G. W. Anderson, K. Jacobson, *Science* **2002**, *296*, 1821 – 1825.
[2] R. R. C. New, *Liposomes, A Practical Approach*, IRL Press, Oxford, **1990**.
[3] G. van Meer, *Trends Cell Biol.* **1998**, *8*, 29 – 33.
[4] K. Simons, J. Gruenberg, *Trends Cell Biol.* **2000**, *10*, 459 – 462.
[5] K. Simons, E. Ikonen, *Science* **2000**, *290*, 1721 – 1726.
[6] K. Jacobson, D. Papahadjopoulos, *Biochemistry* **1975**, *14*, 152 – 161.
[7] W. Hartmann, H.-J. Galla, *Biochim. Biophys. Acta* **1978**, *509*, 474 – 490.
[8] E. J. Shimshick, H. M. Connell, *Biochemistry* **1973**, *12*, 2351 – 2360.
[9] D. A. Wilkinson, J. F. Nagle, *Biochemistry* **1979**, *18*, 4244 – 4249.
[10] R. M. Epand, S. Maekawa, C. M. Yip, R. F. Epand, *Biochemistry* **2001**, *40*, 10514 – 10521.
[11] M. Uragami, N. Tokutake, X. Yan, S. L. Regen, *J. Am. Chem. Soc.* **2001**, *123*, 5124 – 5125.
[12] L. J. Pike, X. Han, K.-N. Chung, R. W. Gross, *Biochemistry* **2002**, *41*, 2075 – 2088.
[13] T.-Y. Wang, R. Leventis, J. R. Silvius, *Biophys. J.* **2000**, *79*, 919 – 933.
[14] a) P. Dynarowicz-Latka, A. Dhanabalan, O. N. Oliveira, *Adv. Colloid Interface Sci.* **2001**, *91*, 221 – 293; b) M. Ross, C. Steinem, H.-J. Galla, A. Janshoff, *Langmuir* **2001**, *17*, 2437 – 2445.
[15] a) M. D. Houslay, K. K. Stanley, *Dynamics of Biological Membranes*, Wiley, New York, **1982**, pp. 1 – 92; b) W.-G. Wu, L.-M. Chi, *J. Am. Chem. Soc.* **1991**, *113*, 4683 – 4685.
[16] D. E. Discher, A. Eisenberg, *Science* **2002**, *297*, 967 – 973.
[17] a) X.-M. Li, J. M. Smaby, M. M. Momsen, H. L. Brockman, R. E. Brown, *Biophys. J.* **2000**, 78, 1921 – 1931; b) J. M. Holopainen, J. Y. A. Lehtonen, P. K. J. Kinnunen, *Chem. Phys. Lipids* **1997**, *88*, 1 – 13.
[18] a) D. E. Wolf, *Curr. Top. Membr.* **1994**, 40, 143 – 165; b) R. Welt, M. Glaser, *Chem. Phys. Lipids* **1994**, *73*, 121 – 137.
[19] W. Knoll, G. Schmidt, H. Rötzer, T. Henkel, W. Pfeiffer, E. Sackmann, S. Mittler-Neher, J. Spinke, *Chem. Phys. Lipids* **1991**, *57*, 363 – 374.
[20] a) J. R. Silvius, D. del Giudice, M. Lafleur, *Biochemistry* **1996**, *35*, 15198 – 15208; b) S. N. Ahmed, D. A. Brown, E. London, *Biochemistry* **1997**, *36*, 10944 – 10953.
[21] J. T. Mason, *Biochemistry* **1988**, *27*, 4421 – 4429.
[22] J. T. Kim, J. Mattai, G. G. Shipley, *Biochemistry* **1987**, *26*, 6599 – 6603.
[23] J. R. Silvius, *Biochim. Biophys. Acta* **1986**, *857*, 217 – 228.
[24] J. M. Holopainen, H. L. Brockman, R. E. Brown, P. K. J. Kinnunen, *Biophys. J.* **2001**, *80*, 765 – 775.
[25] D. W. Graninger, A. Reichert, H. Ringsdorf, C. Salesse, *Biochim. Biophys. Acta* **1990**, *1023*, 365 – 379.
[26] M. Gardam, J. R. Silvius, Biochim. *Biophys. Acta*, **1989**, *980*, 319 – 325.
[27] M. Masserini, D. Ravasi, *Biochim. Biophys. Acta* **2001**, *1532*, 149 – 161.
[28] R. E. Brown, *J. Cell Sci.* **1998**, *111*, 1 – 9.
[29] H. B. Sankaram, T. E. Thompson, *Procl. Natl. Acad. Sci.* **1991**, *88*, 8686 – 8690.

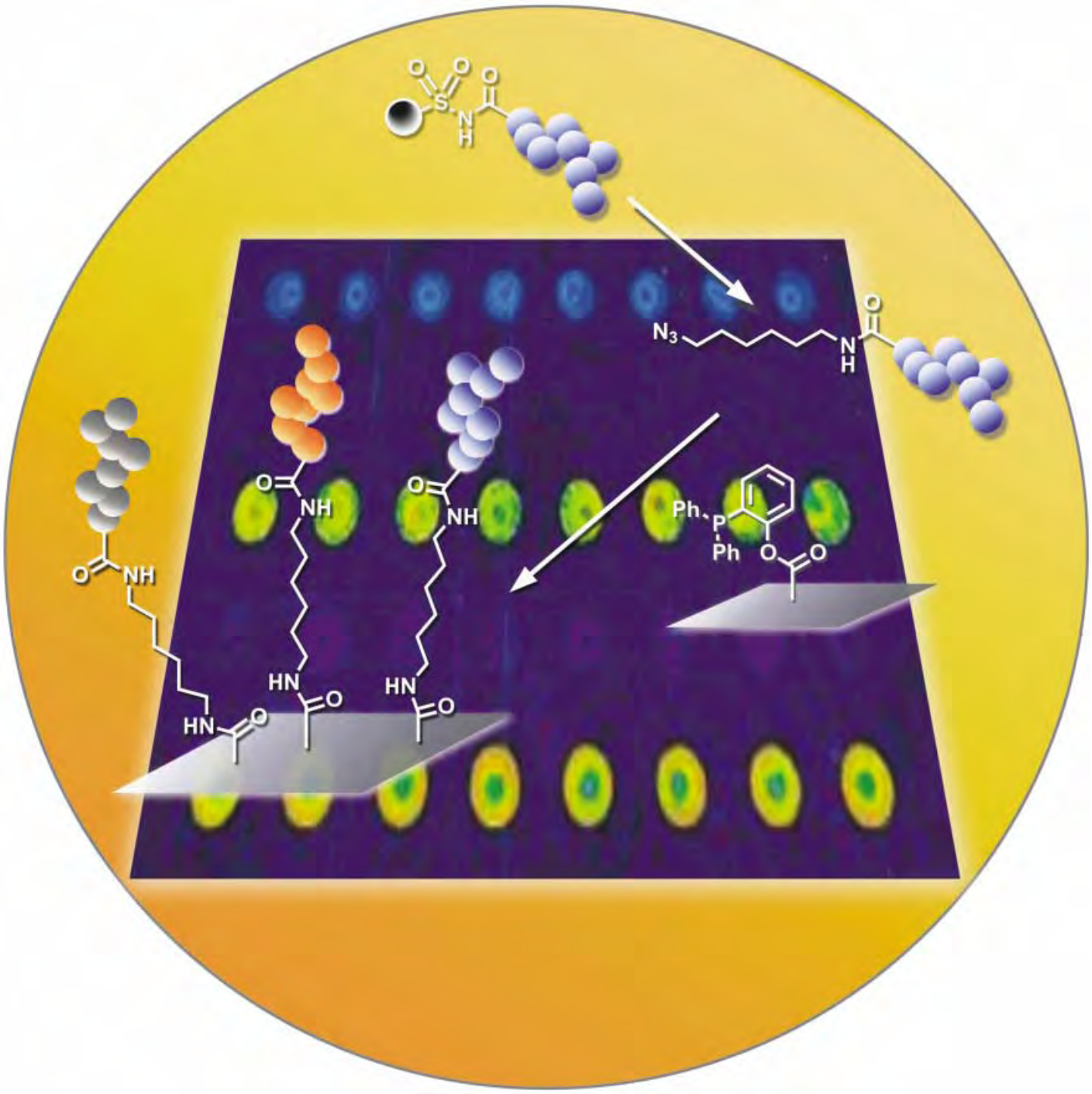
 © 2003 Wiley-VCH Verlag GmbH & Co. KGaA, Weinheim 

[30] J. H. Smaby, H. L. Brockman, R. E. Brown, *Biochemistry* **1994**, *33*, 9135 – 9142.
[31] B. Ramstedt, J. P. Slotte, *Biophys. J.* **1999**, *76*, 908 – 915.
[32] Y.-H. Hao, J.-W. Chen, *J. Membr. Biol.* **2001**, *183*, 85 – 92.
[33] J. Korlach, P. Schwille, W. W. Webb, G. W. Feigenson, *Proc. Natl. Acad. Sci. USA* **1999**, *96*, 8461 – 8466.
[34] X. Xu, R. Bittman, G. Duportail, D. Heissler, C. Vilchez, E. London, *J. Biol. Chem.* **2001**, *276*, 33540 – 33546.
[35] a) W. Knoll, G. Schmidt, H. Rötzer, T. Henkel, W. Pfeiffer, E. Sackmann, S. Mittler-Neher, J. Spinke, *Chem. Phys. Lipids* **1991**, *57*, 363 – 374; b) J. R. Silvius, J. Gagne, *Biochemistry* **1984**, *23*, 3241 – 3247; c) C. P. S. Tilcock, M. B. Bally, S. B. Farren, P. R. Culis, S. M. Gruner, *Biochemistry* **1984**, *23*, 2696 – 2703.
[36] J. Bolard, *Biochim. Biophys. Acta* **1986**, *864*, 257 – 304.
[37] J. Miñones, Jr., J. Minones, O. Conde, J. M. Rodriguez Patino, P. Dynarowicz-Latka, *Langmuir* **2002**, *18*, 2817 – 2827.
[38] M. Roux, R. Auzely-Velty, F. Djedaini-Pilard, B. Perly, *Biophys. J.* **2002**, *82*, 813 – 822.
[39] S. Morein, J. A. Kilian, M. M. Sperotto, *Biophys. J.* **2002**, *82*, 1405 – 1417.
[40] a) T.-Y. Wang, R. Leventis, J. R. Silvius, *Biochemistry* **2001**, *40*, 13031 – 13040; b) J. B. McCabe, L. G. Berthiaume, *Mol. Biol. Cell* **2001**, *12*, 3601 – 3617.
[41] a) D. A. Zacharias, J. D. Violin, A. C. Newton, R. Y. Tsien, *Science* **2002**, *296*, 913 – 916; b) D. Shigematsu, M. Matsutani, T. Furuya, T. Kiyota, S. Lee, G. Sugihara, S. Yamashita, *Biochim. Biophys. Acta* **2002**, *1564*, 271 – 280.
[42] D. W. Grainger, A. Reichert, H. Ringsdorf, C. Salesse, *Biochim. Biophys. Acta* **1990**, *1023*, 365 – 379.
[43] J. Marx, *Science* **2001**, *294*, 1862 – 1865.
[44] M. Edidin, *Trends Cell Biol.* **2001**, *11*, 492 – 496.
[45] a) D. A. Brown, E. London, *J. Biol. Chem.* **2000**, *275*, 17221 – 17224; b) G. van Meer, *Science* **2002**, *296*, 855 – 857.
[46] C. Dietrich, L. A. Bagatolli, Z. N. Vololyk, N. L. Thompson, M. Levi, K. Jacobsen, E. Gratton, *Biophys. J.* **2001**, *80*, 1417 – 1428.
[47] a) P. E. Milhiet, M.-C. Giocondi, C. Le Grimellec, *J. Biol. Chem.* **2002**, *277*, 875 – 878; b) A. S. Muresan, H. Diamant, K. Y. C. Lee, *J. Am. Chem. Soc.* **2001**, *123*, 6951 – 6952; c) C. Yuan, J. Furlong, P. Burgos, L. J. Johnston, *Biophys. J.* **2002**, *82*, 2526 – 2535; d) C. Le Grimellec, M.-C. Giocondi, R. Pujol, E. Lesniewska, *Single Mol.* **2000**, *1*, 105 – 107; e) S. Kumar, J. H. Hoh, *Traffic* **2001**, *2*, 746 – 756; f) E. Sparr, K. Ekelund, J. Engblom, S. Engström, H. Wennerström, *Langmuir* **1999**, *15*, 6950 – 6955.
[48] a) P. E. Milhiet, C. Domec, M.-C. Giocondi, N. V. Mau, F. Heitz, C. Le Grimellec, *Biophys. J.* **2001**, *81*, 547 – 555; b) M.-C. Giocondi, L. Pacheco, P. E. Milhiet, C. Le Grimellec, *Ultramicroscopy* **2001**, *86*, 151 – 157; c) P. E. Milhiet, V. Vie, M.-C. Giocondi, C. Le Grimellec, *Single Mol.* **2001**, *2*, 109 – 112.
[49] H. A. Rinia, M. M. E. Snel, J. P. J. M. van der Eerden, B. de Kruijff, *FEBS Lett.* **2001**, *501*, 92 – 96.
[50] a) M. Menke, S. Künneke, A. Janshoff, *Eur. Biophys. J.* **2002**, *31*, 317 – 322; b) C. Yuan, L. J. Johnston, *Biophys. J.* **2000**, *79*, 2768 – 2781.
[51] V. Vie, N. Van Mau, E. Lesniewska, J. P. Goudonnet, F. Heitz, C. Le Grimellec, *Langmuir* **1998**, *14*, 4574 – 4583.
[52] a) J. Majewski, T. L. Kuhl, G. S. Smith, *Biophys. J.* **2001**, *81*, 2707 – 2715; b) M. Gandhavadi, D. Allende, A. Vidal, S. A. Simon, T. J. McIntosh, *Biophys. J.* **2002**, *82*, 1469 – 1482.
[53] a) C. Dietrich, B. Yang, T. Fujiwara, A. Kusumi, K. Jacobson, *Biophys. J.* **2002**, *82*, 274 – 284; b) A. Pralle, P. Keller, E.-L. Florin, K. Simons, J. K. H. Hörber, *J. Cell Biol.* **2000**, *148*, 997 – 1007.
[54] a) L. A. Bagatolli, E. Gratton, *Biophys. J.* **2000**, *79*, 434 – 447; b) C. Dietrich, Z. N. Volovyk, M. Levi, N. L. Thompson, K. Jacobson, *Proc. Natl. Acad. Sci. USA* **2001**, *98*, 10642 – 10647; c) A. V. Samsonov, I. Mihalyov, F. S. Cohen, *Biophys. J.* **2001**, *81*, 1486 – 1500.
[55] M. Ross, C. Steinem, H.-J. Galla, A. Janshoff, *Langmuir* **2001**, *17*, 2437 – 2445.
[56] R. G. W. Anderson, K. Jacobson, *Science* **2002**, *296*, 1821 – 1825.
[57] M.-C. Giocondi, V. Vie, E. Lesniewska, P.-E. Milhiet, M. Zinke-Allmang, C. Le Grimellec, *Langmuir* **2001**, *17*, 1653 – 1659.
[58] a) B. A. Armitage, D. E. Bennett, H. G. Lamparski, D. F. O'Brien, *Adv. Polym. Sci.* **1996**, *126*, 54 – 84; b) C. G. Clark, K. L. Wooley, *Curr. Opin. Colloid Interface Sci.* **1999**, *4*, 122 – 129; c) H. Ringsdorf, B. Schlarb, J. Venzmer, *Angew. Chem.* **1988**, *100*, 117 – 162; *Angew. Chem. Int. Ed. Engl.* **1988**, *27*, 113 – 158.
[59] S. Förster, M. Zisenis, E. Wenz, M. Antonietti, *J. Chem. Phys.* **1996**, *104*, 9956 – 9970.
[60] Z. Tuzar, P. Kratochvil, *Surface and Colloid Science, vol 15* (Ed.: E. Matijevic), Plenum, New York, **1993**.
[61] P. Alexandridis, R. J. Spontak, *Curr. Opin. Colloid Interface Sci.* **1999**, *4*, 130 – 139.
[62] S. Förster, T. Plantenberg, *Angew. Chem.* **2002**, *114*, 712 – 739; *Angew. Chem. Int. Ed.* **2002**, *41*, 688 – 714.
[63] C. Ladaviere, C. Tribet, S. Cribier, *Langmuir* **2002**, *18*, 7320 – 7326.
[64] a) A. A. Yaroslavov, O. Yu. Udalykh, N. S. Melik-Nubarov, V. A. Kabanov, Yu. A. Ermakov, V. Azov, F. M. Menger, *Chem. Eur. J.* **2001**, *7*, 4835 – 4843; b) V. A. Kabanov, A. A. Yaroslavov, *J. Controlled Release* **2002**, *78*, 267 – 271.
[65] a) D. D. Lasic, D. Needham, *Chem. Rev.* **1995**, *95*, 2601 – 2628; b) H. E. Warriner, S. L. Keller, S. H. J. Idziak, N. L. Slack, P. Davidson, J. A. Zsadzinski, C. R. Safinya, *Biophys. J.* **1998**, *75*, 272 – 293.
[66] N. L. Slack, P. Davidson, M. A. Chibbaro, C. Jeppesen, P. Eiselt, H. E. Warriner, H.-W. Schmidt, P. Pincus, C. R. Safinya, *J. Chem. Phys.* **2001**, *115*, 6252 – 6257.
[67] J. Simon, M. Kühner, H. Ringsdorf, E. Sackmann, *Chem. Phys. Lipids* **1995**, *76*, 241 – 258.
[68] a) I. Tsafrir, S. Sagi, T. Arzi, M.-A. Guedeau-Boudeville, V. Frette, D. Kandel, J. Stavans, *Phys. Rev. Lett.* **2001**, *86*, 1138 – 1141; b) J. Stavans, *Phys. A* **2002**, *306*, 368 – 375.
[69] D. H. W. Hubert, M. Jung, A. L. German, *Adv. Mater.* **2000**, *12*, 1291 – 1294.
[70] a) W. Meier, *Curr. Opin. Colloid Interface Sci.* **1999**, *4*, 6 – 14; b) J. Hotz, W. Meier, *Langmuir* **1998**, *14*, 1031 – 1036; c) J. D. Morga, C. A. Johnson, E. W. Kahler, *Langmuir* **1997**, *13*, 6447 – 6451.
[71] M. Jung, B. H. Robinson, D. C. Steytler, A. L. German, R. K. Heenan, *Langmuir* **2002**, *18*, 2873 – 2879.
[72] a) M. Jung, D. H. W. Hubert, P. H. H. Bomans, P. M. Frederik, J. Meuldijek, A. M. van Herk, H. Fischer, A. L. German, *Langmuir* **1997**, *13*, 6877 – 6880.
[73] M. P. Krafft, L. Schieldknecht, P. Marie, F. Giuleri, M. Schmutz, N. Poulain, E. Nakache, *Langmuir* **2001**, *17*, 2872 – 2877.
[74] B. J. Ravoo, W. D. Weringa, J. B. F. N. Engberts, *Langmuir* **1996**, *12*, 5773 – 5780.
[75] a) B. M. Discher, Y.-Y. Won, D. S. Ege, J. C.-M. Lee, F. S. Bates, D. E. Discher, D. Hammer, *Science* **1999**, *284*, 1143 – 1146; b) C. Nardin, T. Hirt, J. Leukel, W. Meier, *Langmuir* **2000**, *16*, 1035 – 1041; c) B. M. Discher, H. Bermudez, D. A. Hammer, D. E. Discher, Y.-Y. Won, F. S. Bates, *J. Phys. Chem. B* **2002**, *106*, 2848 – 2854.
[76] a) B. M. Discher, D. A. Hammer, F. S. Bates, D. E. Discher, *Curr. Opin. Colloid Interface Sci.* **2000**, *5*, 125 – 131; b) D. A. Hammer, D. E. Discher, *Annu. Rev. Mater. Res.* **2001**, *31*, 387 – 404.
[77] a) A. Eisenberg, H. Shen, *Angew. Chem.* **2000**, *112*, 3448 – 3450; *Angew. Chem. Int. Ed.* **2000**, *39*, 3310 – 3312; b) K. Yu, C.

Bartels, A. Eisenberg, *Macromolecules* **1998**, *31*, 9399 – 9402; c) L. Luo, A. Eisenberg, *Langmuir* **2001**, *17*, 6804 – 6811.
[78] A. Eisenberg, L. Luo, *Angew. Chem.* **2002**, *114*, 1043 – 1046; *Angew. Chem. Int. Ed.* **2002**, *41*, 1001 – 1004.
[79] S. Mukherjee, F. R. Maxfield, *Traffic* **2000**, *1*, 203 – 211.
[80] E. London, D. A. Brown, *Biochim. Biophys. Acta* **2000**, *1508*, 182 – 195.
[81] W. G. Carter, S. Hakomori, *J. Biol. Chem.* **1981**, *256*, 6953 – 6960.
[82] D. A. Brown, E. London, *Annu. Rev. Cell Dev. Biol.* **1998**, *14*, 111 – 136.
[83] R. G. Parton, *Curr. Opin. Cell Biol.* **1996**, *8*, 542 – 548.
[84] G. E. Palade, *J. Appl. Phys.* **1953**, *24*, 1424.
[85] E. Yamada, *J. Biophys. Biochem. Cytol.* **1955**, *1*, 445 – 458.
[86] K. G. Rothberg, J. E. Heuser, W. C. Donzell, Y. S. Ying, J. R. Glenney, R. G. Anderson, *Cell* **1992**, *68*, 673 – 682.
[87] E. J. Smart, G. A. Graf, M. A. McNiven, W. C. Sessa, J. A. Engelman, P. E. Scherer, T. Okamoto, M. P. Lisanti, *Mol. Cell. Biol.* **1999**, *19*, 7289 – 7304.
[88] R. Anderson, *Annu. Rev. Biochem.* **1998**, *67*, 199 – 225.
[89] S. Matveev, X. Li, W. Everson, E. J. Smart, *Adv. Drug Delivery Rev.* **2001**, *49*, 237 – 250.
[90] J. A. Engelman, X. Zhang, F. Galbiati, D. Volontè, F. Sotgia, R. G. Pestell, C. Minetti, P. E. Scherer, T. Okamoto, M. P. Lisanti, *Am. J. Hum. Genet.* **1998**, *63*, 1578 – 1587.
[91] M. Way, R. G. Parton, *FEBS Lett.* **1996**, *378*, 108 – 112.
[92] T. V. Kurzchalia, P. Dupree, R. G. Parton, R. Kellner, H. Virta, M. Lehnert, K. Simons, *J. Cell Biol.* **1992**, *118*, 1003 – 1014.
[93] M. Murata, J. Peranen, R. Schreiner, F. Wieland, T. V. Kurzchalia, K. Simons, *Proc. Natl. Acad. Sci. USA* **1995**, *92*, 10339 – 10343.
[94] S. Monier, R. G. Parton, F. Vogel, J. Behlke, A. Henske, T. V. Kurzchalia, *Mol. Biol. Cell* **1995**, *6*, 911 – 927.
[95] M Sargiacomo, P. E. Scherer, Z. Tang, E. Kubler, K. S. Song, M. C. Sanders, M. P. Lisanti, *Proc. Natl. Acad. Sci. USA* **1995**, *92*, 9407 – 9411.
[96] S. Monier, D. J. Dietzen, W. R. Hastings, D. M. Lublin, T. V. Kurzchalia, *FEBS Lett.* **1996**, *388*, 143 – 149.
[97] S. Li, K. S. Song, M. P. Lisanti, *J. Biol. Chem.* **1996**, *271*, 568 – 573.
[98] S. Li, K. S. Song, S. S. Koh, A. Kikuchi, M. P. Lisanti, *J. Biol. Chem.* **1996**, *271*, 28647 – 28654.
[99] K. Simons, E. Ikonen, *Nature* **1997**, *387*, 569 – 572.
[100] A. M. Fra, M. Masserini, P. Palestini, S. Sonnino, K. Simons, *FEBS Lett.* **1995**, *375*, 11 – 14.
[101] W. J. Chang, K. G. Rothberg, R. G. W. Anderson, *J. Cell Biol.* **1992**, *118*, 63 – 69.
[102] K. G. Rothberg, Y. S. Ying, B. A. Kamen, R. G. W. Anderson, *J. Cell. Biol.* **1990**, *111*, 2931 – 2938.
[103] E. Smart, Y.-S. Ying, P. Conrad, R. G. W. Anderson, *J. Cell Biol.* **1994**, *127*, 1185 – 1198.
[104] A. M. Fra, E. Williamson, K. Simons, R. G. Parton, *J. Biol. Chem.* **1994**, *269*, 30745 – 30748.
[105] K. A. Melkonian, A. G. Ostermeyer, J. Z. Chen, M. G. Roth, D. A. Brown, *J. Biol. Chem.* **1999**, *274*, 3910 – 3917.
[106] P. Scheiffele, M. G. Roth, K. Simons, *EMBO J.* **1997**, *16*, 5501 – 5508.
[107] A. A. Wolf, M. G. Jobling, S. Wimer-Mackin, M. Ferguson-Maltzman, J. L. Madara, R. K. Holmes, W. I. Lencer, *J. Cell Biol.* **1998**, *141*, 917 – 927.
[108] H. A. Anderson, Y. Chen, L. C. Norkin, *Mol. Biol. Cell* **1996**, *11*, 1825 – 1834.
[109] J. E. Schnitzer, *Adv. Drug Delivery Rev.* **2001**, *49*, 265 – 280.
[110] J. R. Henley, E. W. Krueger, B. J. Oswald, M. A. McNiven, *J. Cell Biol.* **1998**, *141*, 85 – 99.
[111] R. G. W. Anderson, B. A. Kamen, K. G. Rothberg, S. W. Lacey, *Science* **1992**, *255*, 410 – 411.
[112] K. Kaneko, M. Vey, M. Scott, S. Pilkuhn, F. E. Cohen, S. B. Prusiner, *Proc. Natl. Acad. Sci. USA* **1997**, *94*, 2333 – 2338.
[113] A. Taraboulos, M. Scott, A. Semenov, D. Avraham, L. Laszlo, S. B. Prusiner, *J. Cell Biol.* **1995**, *129*, 121 – 132.
[114] A. J. Koleske, D. Baltimore, M. P. Lisanti, *Proc. Natl. Acad. Sci. USA* **1995**, *92*, 1381 – 1385.
[115] D. Volonte, F. Gabialti, M. P. Lisanti, *FEBS Lett.* **1999**, *445*, 431 – 439.
[116] R. Sager, S. Sheng, A. Anisowicz, G. Sotiropoulou, Z. Zou, G. Stenmann, K. Swisshelm, Z. Chen, M. J. Hendrix, P. Pemberton, *Cold Spring Harbor Symp. Quant. Biol.* **1994**, *59*, 537 – 546.
[117] L. Campbell, M. Gumbleton, K. Ritchie, *Adv. Drug Deliv. Rev.* **2001**, *49*, 325 – 372.
[118] T. Okamoto, A. Schlegel, P. E. Scherer, M. P. Lisanti, *J. Biol. Chem.* **1998**, *273*, 5419 – 5422.
[119] Y. Lavie, G. Fiucci, M. Liscovitch, *J. Biol. Chem.* **1998**, *273*, 32380 – 32383.
[120] C.-P.H. Yang, F. Galbiati, D. Volonte, S. B. Horwitz, M. P. Lisanti, *FEBS Lett.* **1998**, *439*, 368 – 372.
[121] C. J. Fielding, P. E. Fielding, *J. Lipid Res.* **1997**, 38, 1503 – 1521.
[122] For a recent review, see J. Raulin, *Prog. Lipid Res.* **2002**, *41*, 27 – 65.
[123] R. C. Aloia, H. Tian, F. C. Jensen, *Proc. Natl. Acad. Sci. USA* **1993**, *90*, 5181 – 5185.
[124] D. H. Nguyen, J. E. K. Hildreth, *J. Virol.* **2000**, *74*, 3264 – 3272.
[125] R. J. Orentas, J. E. K. Hildreth, *AIDS Res. Hum. Retroviruses* **1993**, *9*, 1157 – 1165.
[126] J. J. McSharry, R. R. Wagner, *J. Virol.* **1971**, *7*, 59 – 70.
[127] O. Renkonen, L. Kaarainen, K. Simons, C. G. Gahmberg, *Virology* **1971**, *46*, 318 – 326.
[128] J. P. Quigley, D. B. Rifkin, E. Reich, *Virology* **1972**, *50*, 550 – 557.
[129] J. E. Pessin, M. Glaser, *J. Biol. Chem.* **1980**, *255*, 9044 – 9050.
[130] B. N. Slosberg, R. C. Montelaro, *Biochim. Biophys. Acta* **1982**, *689*, 393 – 402.
[131] A. Ono, E. O. Freed, *Proc. Natl. Acad. Sci. USA* **2001**, *98*, 13925 – 13930.
[132] S. Bavari, C. N. Bosio, E. Wiegand, G. Ruthel, W. Gordon, B. Amy, T. W. Geisbert, M. Hevey, C. Schmaljohn, A. Schmaljohn, J. M. Aman, *J. Exp. Med.* **2002**, *195*, 593 – 692.
[133] a) T. Kunitake, *J. Macromol. Sci. Chem.* **1979**, *13*, 587 – 595; b) Y. Okahata, T. Kunitake, J. *Am. Chem. Soc.* **1979**, *101*, 5231 – 5232; c) T. Tunikate, *Angew. Chem.* **1992**, *104*, 692-710; *Angew. Chem. Int. Ed. Engl.* **1992**, *31*, 792 – 726.

 © 2003 Wiley-VCH Verlag GmbH & Co. KGaA, Weinheim 

# Communications




A novel cleavage–activation strategy which links combinatorial solid phase synthesis to the preparation of microarrays via chemoselective Staudinger-ligation is described by R. Breinbauer, C. M. Niemeyer, H. Waldmann et al. on the following pages.


DOI: 10.1002/anie.200352877
© 2003 Wiley-VCH Verlag GmbH & Co. KGaA, Weinheim

Microarrays

# Staudinger Ligation: A New Immobilization Strategy for the Preparation of Small-Molecule Arrays**

*Maja Köhn, Ron Wacker, Carsten Peters, Hendrik Schröder, Laurent Soulère, Rolf Breinbauer,* Christof M. Niemeyer,* and Herbert Waldmann**

*Dedicated to Professor Manfred T. Reetz on the occasion of his 60th birthday*

Over the last few years, small-molecule arrays have been developed as a tool for high-throughput experimentation in biological research.[1,4a] This discipline has been inspired by the now almost routine application of DNA chips[2] and protein microarrays,[3] and shares with these techniques the advantage of spatial addressability of the probe molecules and the requirement of only small amounts of analytes. Crucial to the further development of small-molecule microarrays is the utilization of methods that allow the chemoselective attachment of the compounds under very mild conditions. For this to be possible reaction types are necessary that are compatible with a wide variety of functional groups typically occuring in biologically relevant classes of small molecules. So far only a limited set of reactions has been described for the attachment of small molecules to appropriately functionalized glass slides,[4] with most of them involving functional groups that are crucial for the biological properties of the compounds under investigation, such as -$NH_2$, -OH, -SH, or -COOH.

[*] Dr. R. Breinbauer, Prof. H. Waldmann, Dipl.-Chem. M. Köhn, Dr. C. Peters, Dr. L. Soulère
Department of Chemical Biology
Max-Planck-Institut für molekulare Physiologie
Otto-Hahn-Strasse 11, 44227 Dortmund (Germany)
and
Universität Dortmund
Fachbereich Chemie, Organische Chemie
44227 Dortmund (Germany)
Fax: (+49) 231-133-2499
E-mail: rolf-peter.breinbauer@mpi-dortmund.mpg.de
herbert.waldmann@mpi-dortmund.mpg.de
Prof. C. M. Niemeyer, Dipl.-Biol. R. Wacker
Universität Dortmund
Fachbereich Chemie, Biologisch-Chemische Mikrostrukturtechnik
Otto-Hahn-Strasse 6, 44227 Dortmund (Germany)
Fax: (+49) 231-755-7082
E-mail: cmn@chemie.uni-dortmund.de
Dipl.-Biol. R. Wacker, Dr. H. Schröder
Chimera Biotec GmbH
Emil-Figge-Strasse 76a, 44227 Dortmund (Germany)

[**] This work was supported by the Deutsche Forschungsgemeinschaft, the Max-Planck Society, the Alexander von Humboldt Foundation (Research Fellowship to L.S.), and the Fonds der Chemischen Industrie (Liebig Fellowship to R.B.). We acknowledge the University of Dortmund for financial support through the research program "Molecular Basics of Biosciences".

Our objective was to develop a new coupling strategy that fulfills the following design criteria: employment of a uniquely reactive functional group, which 1) tolerates a diverse array of other functionalities, 2) reacts efficiently under mild reaction conditions in an atmosphere containing oxygen and water, and 3) is compatible to the very efficient strategies of solid-phase combinatorial chemistry. Ideally this functional group would be introduced into the compound library to be immobilized during the process of release from the solid support, namely at the end of the synthesis. In this way additional activating reagents would be rendered unnecessary. We identified the azide moiety as an almost ideal functional group for our purposes, as azides undergo chemoselective ligation with a limited set of reaction partners despite their high intrinsic reactivity. Wong and co-workers have recently reported the fabrication of carbohydrate arrays using Sharpless conditions for the Cu-catalyzed [3+2] cycloaddition of azides and alkynes.[5]

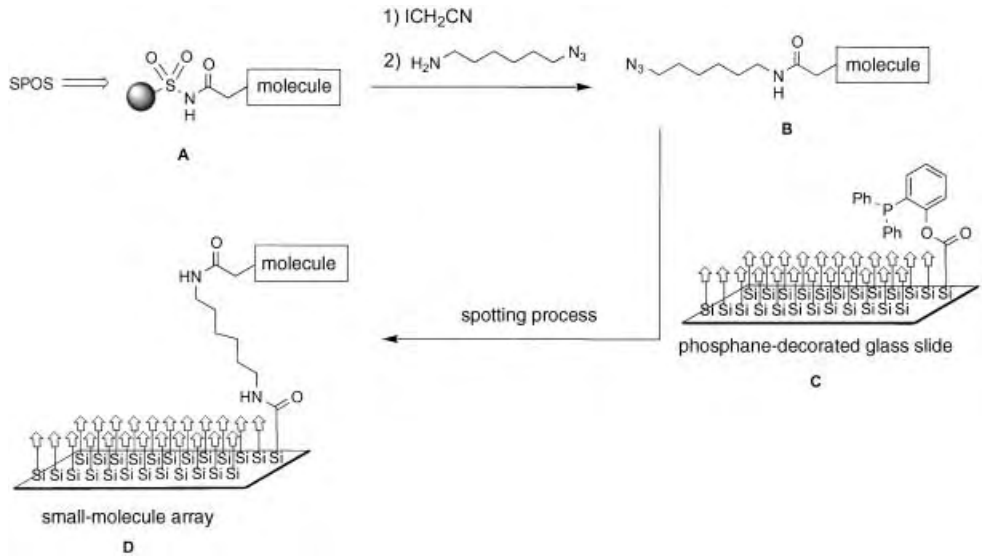
An alternative metal-free coupling strategy is the Staudinger ligation between azides and appropriately substituted phosphanes in which a chemically stable amide bond is formed. The research groups of Bertozzi and Raines have demonstrated the superior chemoselectivity of this approach, for example, in the recently highlighted metabolic engineering of cell surfaces.[6]

We report here that azide-functionalized small molecules can be generated by solid-phase organic synthesis (SPOS) and covalently linked to glass surfaces (Scheme 1). The application of a Kenner-type linker[7] allows the azide moiety to be introduced within the safety-catch cleavage step. The activated library molecules **B**, formed from immobilized sulfonamides **A** after *N*-alkylation and subsequent treatment with an azido-substituted amine, can be selectivley immobilized by Staudinger ligation to glass substrates through covalently linked phosphane groups (**C**). Since the surface-ordered molecules (**D**) are susceptible to ligand-binding reactions using, for example, fluorescently labeled proteins, this approach offers a novel and efficient strategy for the preparation of small-molecule arrays of compounds generated by combinatorial chemistry.[8]

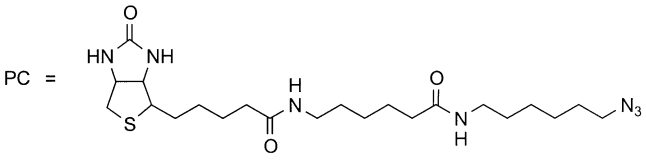
To achieve maximum surface coverage, glass slides were initially modified with an intermediate layer of fourth generation polyamidoamine (PAMAM) dendrimers, as previously described.[9] The primary $NH_2$ groups of the PAMAM were treated with glutaric acid anhydride to introduce free HOOC groups, which were then esterified with 2-(diphenylphosphanyl)phenol[6a] by using a standard esterification protocol.[10] The resulting slides, which contained the azide-reactive phosphane groups (**C**, Scheme 1), were used as the substrate for the deposition of the azide compounds by means of a piezo-driven spotting robot.[11]

As an initial test we spotted various concentrations of solutions of the biotin–aminocaproic–amidohexane azide conjugate **1** (positive control, PC) onto phosphane-modified slides (Figure 1). We used the corresponding azide-free analogue **2** as a negative control (NC). Subsequent to the spotting process the slides were washed with buffer and then treated with Cy5-labeled antibiotin immunoglobulin G (abIgG).[12] The fluorescent signals were recorded and

 © 2003 Wiley-VCH Verlag GmbH & Co. KGaA, Weinheim DOI: 10.1002/anie.200352877 




***Scheme 1.*** Preparation of a library of azide-terminated small molecules using a Kenner-type linker (**A**) and spotting of the azide-compounds onto a phosphane-modified glass slide (**C**) for the preparation of small-molecule arrays (**D**).



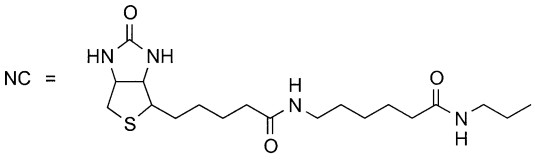




***Figure 1.*** Biotin derivatives used in the solid-phase Staudinger ligation

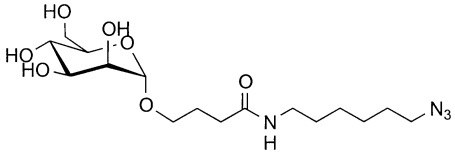
quantified after removal of excess reagent by rinsing with buffer.

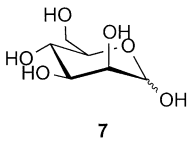
As indicated in Figure 2, the immobilization of biotin compound **1** down to a concentration of 100 μM produced signals with excellent signal-to-noise ratio, whereas no significant signals were obtained at any concentration for the negative control **2** (Figure 2a). Treatment of the slides with a buffer containing 0.1% sodium dodecylsulfate (15 min, 60°C) led to an approximately sixfold reduction in the signal intensity (Figure 2b). Notably and importantly, the continual existence of the small molecules, covalently attached through a peptide bond, was then proven by a renewed incubation with the Cy5-labeled abIgG (Figure 2c). Fluorescent signals of nearly the same intensity were again observed. This observation suggests that the slides manufactured as described above may potentially be amenable to repeated use.

In the next step the biotin-labeled peptide fragment **3** (14% yield over 7 steps) and the biphenyl–antibiotic analogue[13] **4** (6% yield over 7 steps) were prepared by employing our multistep tandem SPOS–activation strategy outlined in Scheme 1 and using the Kenner-type linker **5** (Scheme 2).[7b] The two syntheses involved a variety of different reaction types, such as a Pd-catalyzed cross-coupling, reductive amination, and formation of an amide bond. Compounds **3** and **4** may be regarded as prototypical examples of small molecules accessible by a solid-phase method that are typical for pharmaceutical and chemical biology research.

The fluorescent signals obtained after spotting haptens **3** and **4** onto phosphane-functionalized slides and incubation with Cy5-labeled streptavidin (STV) and also Cy5-abIgG clearly demonstrated the specific attachment as well as the undisturbed functionality of these hapten compounds (Figure 3).[12]

To demonstrate that the approach described above is not limited to biotinylated haptens but can also be applied to other kinds of small molecules, mannose-derivatized azide **6**




was synthesized and immobilized on phosphane-derivatized glass slides. Unsubstituted mannose (**7**) was used as a negative control (Figure 4). Incubation with concanavalin A labeled with AlexaFluor 647 revealed that the attachment of the mannose azide **6** by Staudinger ligation was selective, thus

 © 2003 Wiley-VCH Verlag GmbH & Co. KGaA, Weinheim 

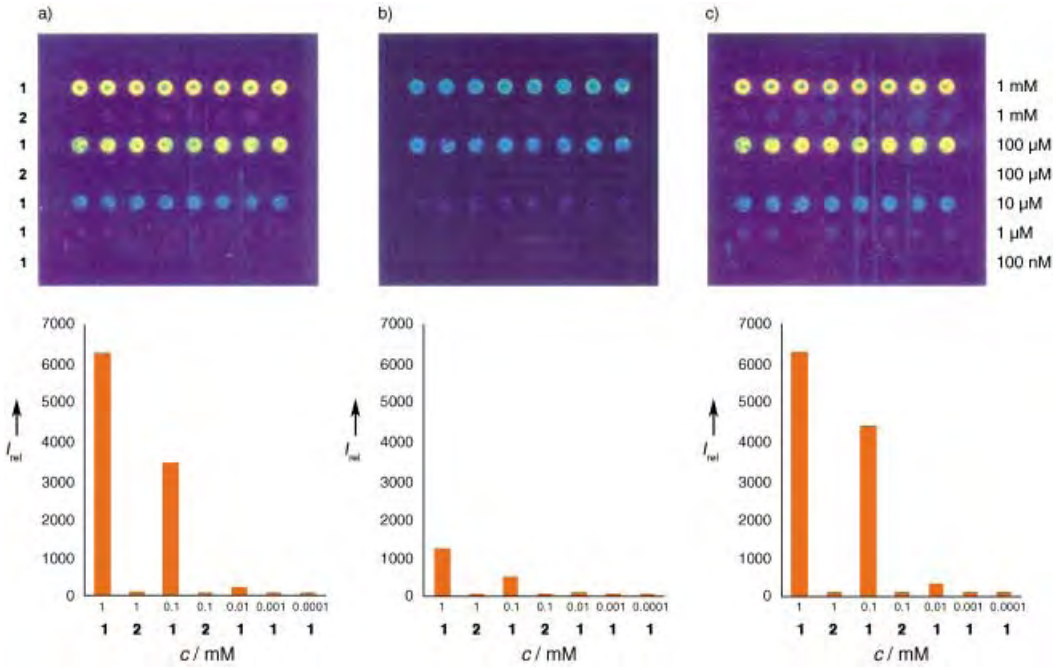
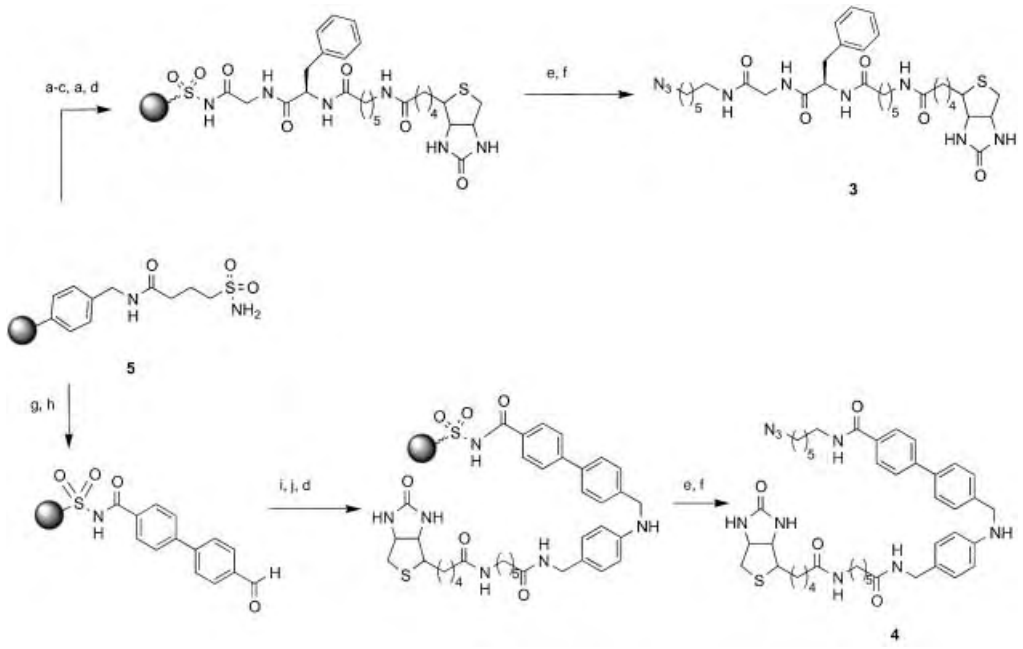



***Figure 2.*** Binding of Cy5-labeled abIgG antibody to compounds **1** and **2** immobilized on a glass slide by Staudinger ligation.[12] The histograms represent signal intensities by quantification of the Cy5 fluorescence. The slide can be regenerated, as demonstrated in (b) and (c).




***Scheme 2.*** Tandem SPOS–activation synthesis of haptens **3** and **4**. a) Fmoc-Gly-OH, PyBOP, DIPEA, DMF, 16 h; b) piperidine/DMF (1:4), 2×10 min; c) Fmoc-Phe-OH, HBTU, HOBt, DIPEA, DMF, 1 h; d) biotin-ACA, HBTU, HOBt, DIPEA, 1 h; e) TMS-$CHN_2$, hexane/$CH_2Cl_2$ (1:1), 3 h, RT; f) 6-azidohexanamine, DMF, 40 °C, DMF; g) 4-iodobenzoic acid, PyBOP, DIPEA, DMF, 16 h; h) 4-formylphenylboronic acid, $Pd(OAc)_2$, $K_2CO_3$, DIPEA, 16 h, 90 °C; i) 4-(*N*-Boc-aminomethyl)aniline, $NaBH(OAc)_3$, $Na_2SO_4$, AcOH, $CH_2Cl_2$, 12 h, ultrasonication; j) TFA/$CH_2Cl_2$ (1:1). Fmoc = 9-fluorenylmethoxycarbonyl, Py = pyridine, BOP = 1-benzotriazolyloxytris(dimethylamino)phosphonium, DIPEA = *N*,*N*-diisopropylethylamine, HBTU = *O*-(benzotriazol-1-yl)-*N*,*N*,*N*′,*N*′-tetramethyluronium hexafluorophosphate, HOBt = 1-hydroxy-1*H*-benzotriazole, TMS = trimethylsilyl, Boc = *tert*-butoxycarbonyl, TFA = trifluoroacetic acid.

enabling its biomolecular recognition by the lectin.[12] In contrast, no signals were obtained for native mannose (Figure 4). These results provide additional indication for the chemoselectivity of the Staudinger ligation, and its applicability to the fabrication of small-molecule arrays.

In conclusion, we have shown that the Staudinger ligation using 2-(diphenylphosphanyl)phenol-modified glass slides can be used as a novel and efficient coupling strategy for the preparation of small-molecule arrays. In comparison with previous approaches, Staudinger ligation offers the advantage

 © 2003 Wiley-VCH Verlag GmbH & Co. KGaA, Weinheim 

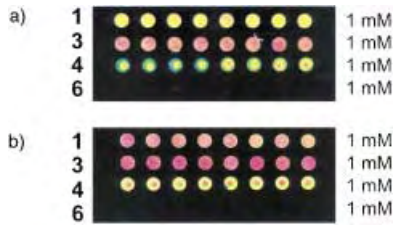



***Figure 3.*** Small-molecule arrays with haptens **3** and **4** (**1** as a positive control, **6** as a negative control). Visualization with a) Cy5–abIgG, and b) Cy5–streptavidin.

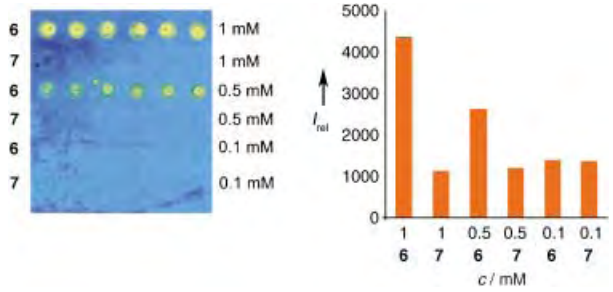



***Figure 4.*** Binding of concanavalin A labeled with AlexaFluor 647 to compounds **6** and **7**.

of chemical compatibility with functional groups, which is often required for interactions in biological systems (for example, hydroxy, carboxy, or sulfanyl groups). Our tandem SPOS–activation strategy links the synthetic efficiency of combinatorial solid-phase synthesis with the analytical advantages of small-molecule arrays, such as the option for rapid high-throughput screening of many different compounds with the requirement of only very small amounts of analytes and probes.

Received: September 16, 2003 [Z52877]
Published Online: October 20, 2003

**Keywords:** bioorganic chemistry · combinatorial chemistry · microarrays · solid-phase synthesis · Staudinger ligation

[1] Reviews: a) K. S. Lam, R. Renil, *Curr. Opin. Chem. Biol.* **2002**, *6*, 353–358; b) C. Ortiz Mellet; J. M. Garcia Fernandez, *ChemBioChem* **2002**, *3*, 819–822; c) R. Breinbauer, M. Köhn, C. Peters in *Bioorganic Chemistry II* (Eds.: C. Schmuck, H. Wennemers), Wiley-VCH, Weinheim, in press.

[2] For a recent review, see M. C. Pirrung, *Angew. Chem.* **2002**, *114*, 1326–1341; *Angew. Chem. Int. Ed.* **2002**, *41*, 1276–1289.

[3] For recent reviews, see a) M. F. Templin, D. Stoll, M. Schrenk, P. C. Traub, C. F. Vohringer, T. O. Joos, *Trends Biotechnol.* **2002**, *20*, 160–166; b) D. S. Wilson, S. Nock, *Angew. Chem.* **2003**, *115*, 510–517; *Angew. Chem. Int. Ed.* **2003**, *42*, 494–500.

[4] Small-molecule immobilization using sulfanyl-modified compounds: a) G. MacBeath, A. N. Koehler, S. L. Schreiber, *J. Am. Chem. Soc.* **1999**, *121*, 7967–7968; with hydroxy groups: b) P. J. Hergenrother, K. M. Depew, S. L. Schreiber, *J. Am. Chem. Soc.* **2000**, *122*, 7849–7850; oxime formation: c) J. R. Falsey, M. Renil, S. Park, S. Li, K. S. Lam, *Bioconjugate Chem.* **2001**, *12*, 346–353; by hybridization of PNA tags: d) N. Winssinger, J. L. Harris, B. J. Backes, P. G. Schultz, *Angew. Chem.* **2001**, *113*, 3254–3258; *Angew. Chem. Int. Ed.* **2001**, *40*, 3152–3155; e) N. Winssinger, S. Ficarro, P. G. Schultz, J. L. Harris, *Proc. Natl. Acad. Sci. USA* **2002**, *99*, 11139–11144; f) F. G. Kuruvilla, A. F. Shamji, S. M. Sternson, P. J. Hergenrother, S. L. Schreiber, *Nature* **2002**, *416*, 653–657; carbohydrate arrays: g) D. Wang, S. Liu, B. J. Trummer, C. Deng, A. Wang, *Nat. Biotechnol.* **2002**, *20*, 275–281; h) S. Fukui, T. Feizi, C. Galustian, A. M. Lawson, W. G. Chai, *Nat. Biotechnol.* **2002**, *20*, 1001–1017; i) B. T Houseman, M. Mrksich, *Chem. Biol.* **2002**, *9*, 275–281; peptide arrays: j) C. M. Salisbury, D. J. Maly, J. A. Ellman, *J. Am. Chem. Soc.* **2002**, *124*, 14868–14870; k) Q. Zhu, M. Uttamchandani, D. Li, M. L. Leasaicherre, S. Q. Yao, *Org. Lett.* **2003**, *5*, 1257–1260; immobilization of small molecules with a moderately acidic proton: l) D. Barnes-Seeman, S. B. Park, A. N. Koehler, S. L. Schreiber, *Angew. Chem.* **2003**, *115*, 2478–2481; *Angew. Chem. Int. Ed.* **2003**, *42*, 2376–2379.

[5] F. Fazio, M. C. Bryan, O. Blixt, J. C. Paulson, C.-H. Wong, *J. Am. Chem. Soc.* **2002**, *124*, 14397–14402.

[6] a) E. Saxon, J. I. Armstrong, C. R. Bertozzi, *Org. Lett.* **2000**, *2*, 2141–2143; b) E. Saxon, C. R. Bertozzi, *Science* **2000**, *287*, 2007–2010; c) H. C Hang, C. R. Bertozzi, *Acc. Chem. Res.* **2001**, *34*, 727–736; d) K. L. Kiick, E. Saxon, D. A. Tirrell, C. R. Bertozzi, *Proc. Natl. Acad. Sci. USA* **2002**, *99*, 19–24; e) E. Saxon, S. J. Luchansky, H. C. Hang, C. Yu, S. C. Lee, C. R. Bertozzi, *J. Am. Chem. Soc.* **2002**, *124*, 14893–14902; f) M. B. Soellner, B. L. Nilsson, R. T. Raines, *J. Org. Chem.* **2002**, *67*, 4993–4996; g) B. L. Nilsson, R. J. Hondal, M. B. Soellner, R. T. Raines, *J. Am. Chem. Soc.* **2003**, *125*, 5268–5269.

[7] a) G. W. Kenner, J. R. McDermott, R. C. Sheppard, *Chem. Commun.* **1971**, 636–637; b) H. S. Overkleeft, P. R. Bos, B. G. Hekking, E. J. Gordon, H. L. Ploegh, *Tetrahedron Lett.* **2000**, *41*, 6005–6009.

[8] During the preparation of this manuscript, Raines and coworkers have applied a Staudinger ligation between (diphenylphosphanylmethyl)thioester-functionalized glass slides and azide-modified peptides to generate arrays containing RNase proteins: M. B. Soellner, K. A. Dickson, B. L. Nilsson, R. T. Raines, *J. Am. Chem. Soc.* **2003**, *125*, 11790–11791.

[9] a) R. Benters, C. M. Niemeyer, D. Wöhrle, *ChemBioChem* **2001**, *2*, 686–694; b) R. Benters, C. M. Niemeyer, D. Drutschmann, D. Blohm, D. Wöhrle, *Nucleic Acids Res.* **2002**, *30*, E10; c) H. Schroeder, R. Wacker, C. M. Niemeyer, *Nachr. Chem.* **2003**, *51*, 28.

[10] Dry $CH_2Cl_2$, 4-dimethylaminopyridine (DMAP, 0.96 mM), 2-(diphenylphosphanyl)phenol (1.2 mM), and diisopropylcarbodiimide (DIC, 1.32 mM) were added to a Schlenk flask containing a COOH-terminated PAMAM glass slide (Chimera Biotec, Dortmund) mounted on a teflon rack. The mixture was stirred under argon overnight. The supernatant solution was removed, and the slide was stirred in dry $CH_2Cl_2$ for 30 min. After thoroughly rinsing the slide with $CH_2Cl_2$, it was dried in vaccuo. The slides were stored under argon, but can be handled on air without any loss of activity.

[11] The spotting process was carried out using a GeSiM Nanoplotter (Gesim, Dresden, Germany) by spotting 0.25 nL droplets of compounds **1**–**4**, **6**, **7** (in water/1,4-dioxane 1:2; spot size 400 μm diameter) followed by incubation overnight.

[12] To reduce nonspecific binding of reagents, all slides were incubated for 30 min with a blocking solution (Chimera Biotec GmbH) after small-molecule immobilization. After drying, hybridization chambers (Schleicher & Schuell) were tied on the slide and abIgG-Cy5 (100 nM) in TETBS buffer (150 mM NaCl, 20 mM Tris, 5 mM EDTA, 0.05% Tween20) was added to each chamber and incubated for 60 min at room temperature. The slide was washed with TETBS and deionized $H_2O$. The slides were dried by centrifugation and the fluorescence intensity

 © 2003 Wiley-VCH Verlag GmbH & Co. KGaA, Weinheim 

was measured using a microarray laser scanning system (Axon; pmt: 500; 100% laser power). Signals were analyzed and quantified using GenePix pro 4.1 software (Axon). For experiments shown in Figure 3, the binding of abIgG-Cy5 (100 nM) or 100 nM Cy5-labeled STV was carried out in a similar way. For the binding of concanavalin A (Figure 4), the slide was blocked with TBSTS buffer (150 mM NaCl, 20 mM Tris, 0.05% Tween20, 1 mM $CaCl_2$, 1 mM $MnCl_2$, 1 mM $MgCl_2$ containing 1% BSA) and concanavalin A (19.2 μM) was also incubated in this buffer for 60 min at room temperature.

[13] M. Artico, A. Mai, G. Sbardella, S. Massa, G. Lampis, D. Deidda, R. Pompei, *Bioorg. Med. Chem. Lett.* **1998**, *8*, 1493–1498.

 © 2003 Wiley-VCH Verlag GmbH & Co. KGaA, Weinheim 

*Electron Transport Mechanism*

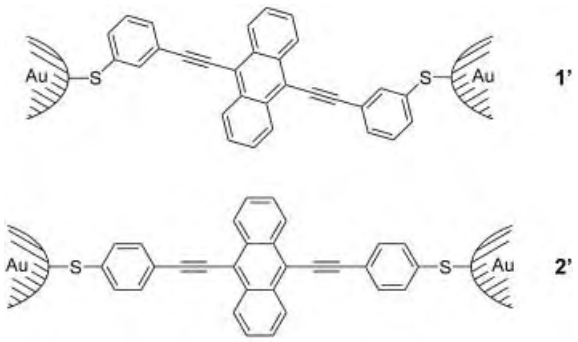
# Electric Current through a Molecular Rod—Relevance of the Position of the Anchor Groups**

*Marcel Mayor,* Heiko B. Weber,* Joachim Reichert, Mark Elbing, Carsten von Hänisch, Detlef Beckmann, and Matthias Fischer*

The understanding of electronic transport through a single molecule is an interesting scientific challenge, which became experimentally addressable only very recently. This interest is further enhanced by the possibility of building electronic devices with molecules, a vision often referred to as "molecular electronics".[1] Tunnel currents through molecular films have been studied on surfaces with STM[2] or with electrode pairs provided by crossed wire junctions[3] and mercury droplets against metallic surfaces.[4] Contacts between single molecules were either made by STM techniques on diluted molecular films[5] or by the mechanically controlled break-junction (MCB) technique.[6–9] The latter has turned out to be particularly powerful to contact single molecules that are covalently linked to both electrodes, as has been demonstrated by the comparison of the electronic characteristics of molecules differing in spatial symmetry.[8] The observed current–voltage (*I*/*U*) characteristics depend not only on the molecular properties but also on the configuration of the microscopic contacts. The rather strong covalent bonding to the atomically disordered metallic electrode causes sample-to-sample fluctuations, which are undesired for both controlled scientific investigation and engineering of electronic properties. Herein we present a strategy to decouple electronically molecular properties from disordered electrodes by varying the relative position (*meta* versus *para*) of the thiol anchor group on the molecular rod. The lack of conjugation in the *meta* position and therefore the reduced electronic communication compared to the *para* position in rodlike π-systems is known and has been shown, for example, in electrochemical investigations[10] and in theoretical studies.[11] Herein we demonstrate the validity of this concept for the anchor groups of single immobilized molecular rods between two electrodes.

A complementary attempt, in which the current was suppressed by internally interrupting the molecular π system with a *trans*-configured $Pt^{II}$ ion increased the junction resistance considerably.[9]

We present the synthesis and characterization of the molecular rods **1** and **2**, both consist of a bis-9,10-phenylethynylanthracene core and acetyl protected thiol anchor groups in *meta* and *para* positions respectively (Scheme 1). Analogously with our previous experiments,[8] deprotection of the acetylsulfanyl groups at the gold surfaces of the electrodes of an MCB yields the immobilized molecular rods (**1′** and **2′**) as single-molecule junctions. By using this set-up the electron transport properties of **1′** and **2′** have been investigated.



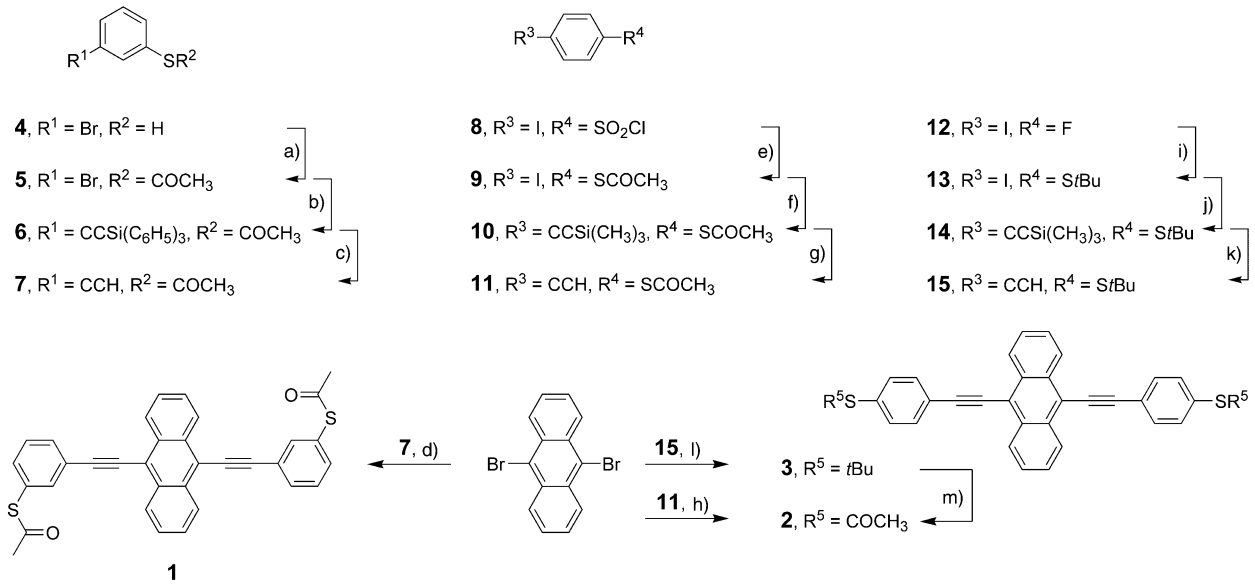

The synthesis of the molecular rods **1** and **2** is shown in Scheme 1. Protection of 3-bromothiophenol **4** with acetic anhydride in acetonitrile with $CoCl_2$ as catalyst gave the acetyl-protected 3-bromothiophenol **5**. The bromine ion of **5** was substituted with triphenylsilyl(TPS)ethynyl by using Sonogashira coupling conditions to yield the TPS-protected **6**. Deprotection of the TPS group of **6** with tetrabutylammonium fluoride (TBAF) in THF and subsequent reprotection of the thiol group with acetic anhydride in acetic acid gave the ethynylbenzene **7**. In a Sonogashira coupling reaction the acetylene **7** substituted both bromine atoms of 9,10-dibromoanthracene with $[Pd(PPh_3)_4]$ and CuI as catalysts. The strongly fluorescent target compound **1** was isolated as an orange solid after column chromatography with a yield of 3%. Compound **1** is soluble in aprotic organic solvents such as THF, toluene, $CH_2Cl_2$, and $CHCl_3$.

The molecular rod **2** with its sulfur anchor groups in the *para* position was synthesized by two different synthetic routes. In analogy to the synthesis of **1**, the corresponding acetylsulfanyl-4-ethynylbenzene (**11**) was synthesized starting

[*] Dr. M. Mayor, Dr. H. B. Weber, Dr. J. Reichert, M. Elbing, Dr. C. von Hänisch, Dr. D. Beckmann, M. Fischer
Institute for Nanotechnology
Forschungszentrum Karlsruhe GmbH
Postfach 3640, 76021 Karlsruhe (Germany)
Fax: (+49) 7247-82-5685
E-mail: marcel.mayor@int.fzk.de
heiko.weber@int.fzk.de

[**] Financial support from the Strategiefond of the Helmholtz Foundation is gratefully acknowledged.

 © 2003 Wiley-VCH Verlag GmbH & Co. KGaA, Weinheim DOI: 10.1002/anie.200352179 




***Scheme 1.*** Synthesis of the acetyl protected molecular rods **1** and **2**. a) $Ac_2O$, $CoCl_2$, $CH_3CN$, RT, 93%; b) $HCCSi(C_6H_5)_3$, $Pd(OAc)_2$, $PPh_3$, CuI, $iPr_2NH$,reflux, 38%; c) TBAF, THF, AcOH, $Ac_2O$, 0°C, 68%; d) $[Pd(PPh_3)_4]$, CuI, $Et_3N$, $C_6H_5CH_3$, 90°C, 3%; e) 1) Zn, $Me_2SiCl_2$, DMA, $(CH_2Cl)_2$, 75°C; 2) AcCl, 50°C, 98%; f) $HCCSi(CH_3)_3$, $[Pd(PPh_3)_2Cl_2]$, CuI, $iPr_2EtN$, 40°C, 98%; g) TBAF, THF, AcOH, $Ac_2O$, 0°C, 69%; h) $[Pd(PPh_3)_4]$, CuI, $Et_3N$, $C_6H_5CH_3$, 90°C, 5%; i) NaS*t*Bu, DMF, 70°C, 44%; j) $HCCSi(CH_3)_3$, $[Pd(PPh_3)_2Cl_2]$, CuI, $iPr_2EtN$, RT, 93%; k) TBAF, THF, 0°C, 100%; l) $[Pd(PPh_3)_2Cl_2]$, CuI, $Et_2NH$, rfl., 71%; *m)* $BBr_3$, AcCl, $CH_2Cl_2$, $C_6H_5CH_3$, RT, 49%.

with 4-iodobenzenesulphonyl chloride (**8**), which was transformed into the acetyl protected 4-iodothiophenol **9** in 98% yield by using reported reaction conditions.[12] As iodide is a better leaving group than bromide, milder conditions could be used for the Sonogashira coupling reaction of **9** than those of **5**. Thus, the introduction of the trimethylsilyl(TMS)-protected acetylene gave the ethynylbenzene **10**. By using similar reaction conditions as those described above for **6**, compound **10** was deprotected to give **11**. Similar conditions to those used for the Sonogashira coupling reactions to obtain **7** were applied to substitute both bromine groups of 9,10-dibromoanthracene with acetylene **11** to yield the molecular rod **2** in 5% yield after column chromatography. Compound **2** is strongly fluorescent with comparable solubility properties to those of **1**. The limited availability of **2**, due to the poor yield of the final synthetic step and the fact that all attempts to crystallize **2** failed, tempted us to investigate an alternative route to **2** with the intermediate **3** as a model compound for X-ray analysis. Substitution of the fluoride of **12** by using sodium *tert*-butylthiolate gave the 1-*tert*-butylsulfanyl-4-iodobenzene (**13**). As with **9**, the TMS-protected acetylene was introduced and deprotected to yield the ethynylbenzene **15**. Both bromides of 9,10-dibromoanthracene were substituted with **15** to yield the *tert*-butyl-protected rod **3**. Finally, the conversion of the *tert*-butylsulfanyl groups into acetylsulfanyl groups with $BBr_3$ in the presence of acetyl chloride,[13] gave the rod **2** in 49% yield.

All compounds were characterized by mass spectroscopy, $^1H$- and $^{13}C$ NMR spectroscopy, and elemental analysis. In addition, the solid-state structures of rods **1** and **3** were analyzed by X-ray analysis (Figure 1).[14] Slow evaporation of a solution of **1** in chloroform and a solution of **3** in diethyl ether gave single crystals suitable for X-ray analysis. The inversion symmetric compound **1** crystallizes in the triclinic space group $P\bar{1}$ and shows an almost coplanar orientation of the phenyl rings and the anthracene motif (torsion angle C(6)-C(7)-C(10)-C(11): 9.1(1)°). The intramolecular sulfur-to-sulfur distance in **1** is 1.78(2) nm. Compound **3** crystallizes in the monoclinic (space group $C2/c$).[14] Surprisingly, the molecular structure has no inversion centre and reveals two different *t*BuS-phenyl groups. While the phenyl ring C(17)–C(22) is 78.2(1)° twisted relative to the anthracene fragment, the phenyl ring C(29)–C(34) departs only by 8.1(1)° from the anthracene plain. These different orientations of the substituents probably result from packing forces, as NMR investigations in solution show no evidence of distinguishable phenyl or *tert*-butyl groups. As both sulfur atoms are on the molecules axis, the intramolecular sulfur-to-sulfur distance (1.99(2) nm) is only slightly affected by these packing forces and slightly shorter than the calculated distance (2.18 nm).[15]

The electronic transport properties have been investigated by using the MCB technique to immobilize in different experiments single molecules **1′** and **2′** between Au-electrodes. Both acetyl-protected rods **1** and **2** have been immobilized from $5\times10^{-4}$ M solutions in THF. Details of the immobilizing protocol and the *I*/*U* characteristics of **2′** have been described elsewhere.[8,9] The rod fixed in the *para* position, **2′**, displayed *I*/*U* curves at room temperature, which are reproducible for a stable junction but are subject to considerable sample-to-sample fluctuations when the experiment is repeated. These fluctuations arise from the single-molecule nature of the experiment. A typical example is shown in Figure 2a. Often, broad steplike increases of the currents were observed, the current ranges from 0.2 μA to

 © 2003 Wiley-VCH Verlag GmbH & Co. KGaA, Weinheim 

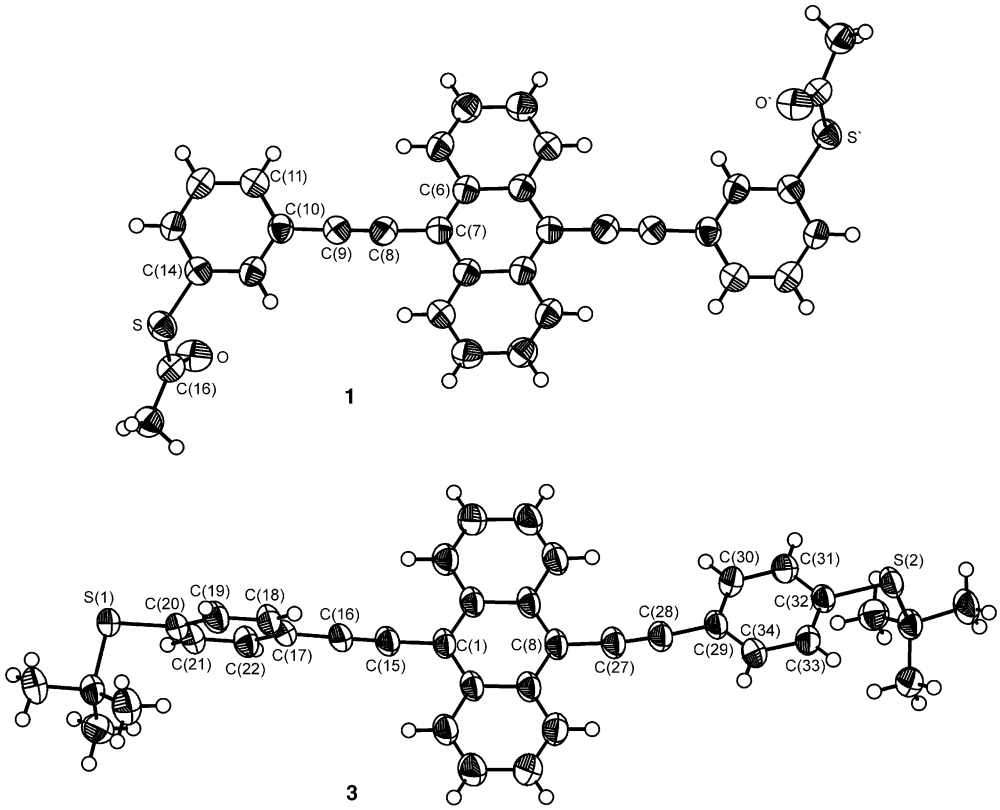



***Figure 1.*** Molecular structures of **1** and **3** (ORTEP, thermal ellipsoids set at the 50% probability level). Selected bond lengths [pm] and bond angles [°]: **1**: S-(14) 176.6(3), S-C(16) 177.6(4), C(16)-O 119.8(4), C(7)-C(8) 141.3(5), C(8)-C(9) 119.7(5), C(9)-C(10) 142.8(5); C(14)-S-C(16) 101.2(2), C(7)-C(8)-C(9) 178.0(4), C(8)-C(9)-C(10) 179.5(4); **3**: C(1)-C(15) 144.4(4), C(15)-C(16) 119.8(4), C(16)-C(17) 144.6(4), C(8)-C(27) 143.9(4), C(17)-C(28) 120.1(4), C(28)-C(29) 144.1(4); C(1)-C(15)-C(16) 175.1(3), C(15)-C(16)-C(17) 177.0(3), C(8)-C(27)-C(28) 173.6(3), C(27)-C(28)-C(29) 175.1(3).

1 μA at $U = 1$ V for different junctions. The immobilization of **1** between the Au electrodes of a bridge contact resulted in a stable configuration **1′** that also allowed us to record reproducible $I/U$ curves at room temperature (Figure 2c). The recorded currents for **1′** were about 10 nA at $U = 1$ V almost two orders of magnitude smaller than the values recorded for **2′** under similar conditions. The $I/U$ curves of **1′** have a barely visible less-resolved steplike feature at $U \approx 0.75$ V, which can better be visualized in the broad maximum of the first derivative (Figure 2d). This can presumably be attributed to resonant tunneling through the HOMO, as has already been calculated theoretically for molecule **2′**.[16] Our recent progress with the MCB technique[17] allowed to record **1′** at low temperatures of $\approx 30$ K (Figure 2e) as well. The low-temperature $I/U$ curves of **1′** display a beautifully resolved steplike feature at $U \approx 0.75$ V. This clear difference indicates that the molecule junction is fluctuating considerably at room temperature and the measurement averages over various microscopic configurations. The observed conductance values are not exponentially suppressed compared to room temperature data, which indicates that not thermally activated hopping, but mainly tunneling governs the electron propagation.[18]

The comparison between the molecules **1′** and **2′** allows the following conclusions to be drawn: a) The conductance does depend on the structure of the molecule and can thus be intentionally altered on a molecular level by varying the position of the anchor group in the synthesis of the molecules. b) The obtained reduction of the current level observed for **1′** with respect to **2′** with anchor groups in the *meta* positions is particularly useful for designing stable molecular junctions as the reduction in the current allows for higher stability. However, the room temperature data are still quite noisy. c) The dominating current path seems to be through the Au–S–C bonds (and not direct injection from the metal to the π system of the rod). d) According to our limited data set, the reproducibility of the $I/U$ curves seems to be improved because the molecule is electronically less coupled to the disordered electrodes.

The data further corroborate that the low-temperature technique[17] gives the expected result: the appearance of highly symmetric $I/U$ curves indicate that both contacts are equivalent.

The results indicate that electronic properties can be tuned by carefully designing molecular structures. Here we have addressed exclusively the aspect of the anchor group position. Many particular electronic functions may be composed by the design of the molecules. To this end, we are currently working on rectifying and switching systems based on molecular structures.

 © 2003 Wiley-VCH Verlag GmbH & Co. KGaA, Weinheim 

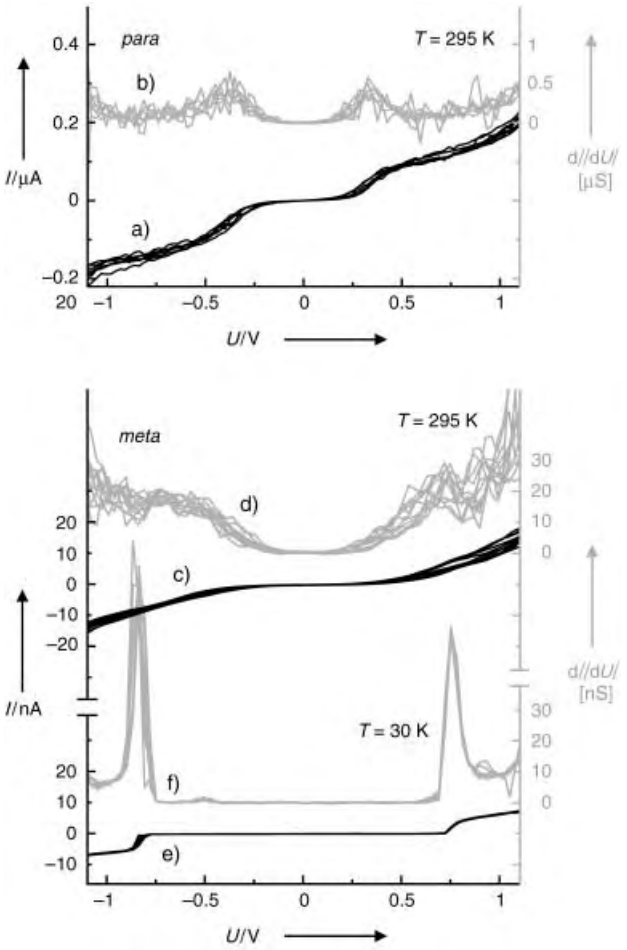



***Figure 2.*** *I*/*U* characteristics reproducibly recorded for a stable junction in a MCB and their numerical derivative d*I*/d*U*. a) *I*/*U* and b) d*I*/d*U* for Au-**2**′-Au at room temperature. c) *I*/*U* and d) d*I*/d*U* for Au-**1**′-Au at room temperature and e) *I*/*U* and f) d*I*/d*U* at $T \approx 30$ K.

## *Experimental Section*

9,10-Bis{[3-(acetylsulfanyl)phenyl]ethynyl}anthracene **1:** 9,10-Dibromoanthracene (0.200 g; 0.595 mmol) was dissolved in argon-saturated triethylamine (1 mL) and toluene (15 mL). Tetrakis(triphenylphosphane)palladium(**0**) (0.0688 g, 0.0595 mmol), copper iodide (0.017 g, 0.0893 mmol) and (3-ethynyl)phenyl thioacetate (0.262 g, 1.488 mmol) were added subsequently. The reaction mixture was heated to 90 °C under an argon atmosphere for 25 h and, cooled, then poured on 2N hydrochloric acid/ice. The aqueous phase was extracted with toluene, the toluene layers dried over $MgSO_4$ and evaporated to dryness. The crude product was purified by column chromatographies (silica gel, cyclohexane, $CH_2Cl_2$) to afford **1** (0.010 g, 0.019 mmol; 3%) as an orange solid. M.p.: 203–205 °C (decomp); $^1$H NMR (300 MHz, $CDCl_3$): $\delta = 8.65$–$8.69$ (m, 4H), 7.80–7.83 (m, 4H), 7.64–7.68 (m, 4H), 7.46–7.52 (m, 4H), 2.49 ppm (s, 6H); $^{13}$C NMR (75 MHz, $CDCl_3$): $\delta = 193.61$ (*C*O), 137.34, 134.77, 132.65, 132.15, 129.42, 128.55, 127.23, 127.05, 124.64, 118.36 (Ar), 101.31, 87.53 (C≡C), 30.34 ppm ($CH_3$); MALDI-TOF-MS: 525.81 [$M^+$], 514.75, 505.75, 451.70 [$M^+$−SAcetyl], 409.70; elemental analysis calcd (%) for $C_{34}H_{22}O_2S_2$: C 77.54, H 4.21; found: C 77.17, H 4.35.

9,10-Bis{[4-(acetylsulfanyl)phenyl]ethynyl}anthracene **2:** 9,10-Bis{[4-(*tert*-butylsulfanyl)phenyl]ethynyl}anthracene **3** (0.0234 g, 0.042 mmol) was dissolved in a mixture of dry argon-saturated $CH_2Cl_2$ (1.5 mL) and dry argon-saturated toluene (1.5 mL). The mixture was cooled to 0 °C, acetyl chloride (0.1256 g, ca. 0.12 mL, 1.6 mmol) was added, then boron tribromide (1.0 M solution in $CH_2Cl_2$; 0.09 ml; 0.09 mmol) was added dropwise. After removal of the ice bath, the reaction was stirred at room temperature for 3 h and poured into ice-water (about 100 mL). The aqueous phase was extracted with diethyl ether, the ethereal layers washed with water until neutral, dried over $MgSO_4$ and evaporated to dryness. Column chromatography (silica gel, $CH_2Cl_2$/hexane 2:1) and subsequent washing with diethyl ether afforded **2** (0.0108 g, 0.021 mmol; 49%) as a yellow-red solid. m.p. 248–249 °C; $^1$H NMR (300 MHz, $CDCl_3$): $\delta = 8.65$–$8.69$ (m, 4H), 7.81 (d, $J = 8$ Hz, 4H), 7.65–7.68 (m, 4H), 7.51 (d, $J = 8$ Hz, 4H), 2.48 ppm (s, 6H); $^{13}$C NMR (75 MHz, $CDCl_3$): $\delta =$ 193.43 (*C*O), 134.47, 132.26, 132.17, 128.63, 127.21, 127.06, 124.57, 118.41 (Ar), 101.74, 88.14 (C≡C), 30.38 ppm ($CH_3$); MALDI-TOF-MS: 525.91 [$M^+$], 452.80 [$M^+$−SAc]; elemental analysis calcd (%) for $C_{34}H_{22}O_2S_2$: C 77.54, H 4.21; found: C 77.38, H 4.32.

Received: June 23, 2003 [Z52179]

**Keywords:** anchor-group position · electron transport · molecular electronics · single-molecule studies · structure–activity relationships

[1] a) C. Joachim, J. K. Gimzewski, A. Aviram, *Nature* **2000**, *408*, 541–548; b) M. A. Reed, J. M. Tour, *Sci. Am.* **2000**, *282*, 86–93; c) R. L. Carroll, C. B. Gorman, *Angew. Chem.* **2002**, *114*, 4556–4579; *Angew. Chem. Int. Ed.* **2002**, *41*, 4378–4400; d) M. Mayor, H. B. Weber, *Chimia* **2002**, *56*, 494–499.

[2] F.-R. F. Fan, J. Yang, S. M. Dirk, D. W. Price, D. Kosynkin, J. M. Tour, A. J. Bard, *J. Am. Chem. Soc.* **2001**, *123*, 2454–2455.

[3] a) J. G. Kushmerick, D. B. Holt, S. K. Pollack, M. A. Ratner, J. C. Yang, T. L. Schull, J. Naciri, M. H. Moore, R. Shashidhar, *J. Am. Chem. Soc.* **2002**, *124*, 10654–10655; b) J. G. Kushmerick, D. B. Holt, J. C. Yang, J. Naciri, M. H. Moore, R. Shashidhar, *Phys. Rev. Lett.* **2002**, *89*, 086802/1–086802/4; c) T. L. Schull, J. G. Kushmerick, C. H. Patterson, C. George, M. H. Moore, S. K. Pollack, R. Shashidhar, *J. Am. Chem. Soc.* **2003**, *125*, 3202–3203.

[4] R. E. Holmlin, R. F. Ismagilov, R. Haag, V. Mujica, M. A. Ratner, M. A. Rampi, G. M. Whitesides, *Angew. Chem.* **2001**, *113*, 2375–2378; *Angew. Chem. Int. Ed.* **2001**, *40*, 2316–2320.

[5] a) L. A. Bumm, J. J. Arnold, M. T. Cygan, T. D. Dunbar, T. P. Burgin, L. Jones II, D. L. Allara, J. M. Tour, P. S. Weiss, *Science* **1996**, *271*, 1705–1707; b) Z. J. Donhauser, B. A. Mantooth, K. F. Kelly, L. A. Bumm, J. D. Monnell, J. J. Stapelton, D. W. Price Jr., A. M. Rawlett, D. L. Allara, J. M. Tour, P. S. Weiss, *Science* **2001**, *292*, 2303–2307; c) L. Patrone, S. Palacin, J. P. Bourgoin, J. Lagoute, T. Zambelli, S. Gauthier, *Chem. Phys.* **2002**, *281*, 325–332.

[6] M. A. Reed, C. Zhou, C. J. Muller, T. P. Burgin, J. M. Tour, *Science* **1997**, *278*, 252–254.

[7] a) C. Kergueris, J. P. Bourgoin, S. Palacin, D. Esteve, C. Urbina, M. Magoga, C. Joachim, *Phys. Rev. B* **1999**, *59*, 12505–12513; b) C. Kergueris, J. P. Bourgoin, S. Palacin, *Nanotechnology* **1999**, *10*, 8–13.

[8] a) J. Reichert, R. Ochs, D. Beckmann, H. B. Weber, M. Mayor, H. von Löhneysen, *Phys. Rev. Lett.* **2002**, *88*, 176804/1–176804/4; b) H. B. Weber, J. Reichert, F. Weigend, R. Ochs, D. Beckmann, M. Mayor, R. Ahlrichs, H. von Löhneysen, *Chem. Phys.* **2002**, *281*, 113–125.

[9] M. Mayor, C. von Hänisch, H. B. Weber, J. Reichert, D. Beckmann, *Angew. Chem. Int. Ed.*. **2002**, *114*, 1228–1231; *Angew. Chem. Int. Ed.* **2002**, *41*, 1183–1186.

[10] M. Mayor, M. Büschel, K. M. Fromm, J.-M. Lehn, J. Daub, *Ann. N. Y. Acad. Sci.* **2002**, *960*, 16–28.

 © 2003 Wiley-VCH Verlag GmbH & Co. KGaA, Weinheim 

[11] S. N. Yaliraki, M. A. Ratner, *Ann. N. Y. Acad. Sci.* **2002**, *960*, 153 – 162.
[12] D. T. Gryko, C. Clausen, K. M. Roth, N. Dontha, D. F. Bocian, W. G. Kuhr, J. S. Lindsey, *J. Org. Chem.* **2000**, *65*, 7345 – 7355.
[13] N. Stuhr-Hansen, J. B. Christensen, N. Harrit, T. Bjørnholm, *J. Org. Chem.* **2003**, *68*, 1275 – 1282.
[14] **1**: $a = 629.7(1)$, $b = 909.0(2)$, $c = 1108.5(2)$ pm, $\alpha = 85.83(3)$, $\beta = 89.55(3)$, $\gamma = 79.36(3)°$, $V = 621.9(2) \times 10^6$ pm$^3$; triclinic $P\bar{1}$, $Z = 1$, $\rho_{calcd} = 1.406$ g cm$^{-1}$, $\mu(Mo_{K\alpha}) = 0.247$ mm$^{-1}$, STOE IPDS2, $Mo_{K\alpha}$ radiation, $\lambda = 0.71073$ Å, $T = 200$ K, $2\theta_{max} = 45°$; 2929 reflections measured, 1542 independent reflections ($R_{int} = 0.0733$), 1321 independent reflections with $F_o > 4\sigma(F_o)$. The structure was solved by direct methods and refined, by full-matrix least-square techniques against $F^2$, 172 parameters (S, O, C refined anisotropically, H atoms were calculated at ideal positions); $R1 = 0.0602$; $wR2 = 0.1806$ (all data); Gof: 1.057; maximum peak 0.305 e Å$^{-3}$. **3**: $a = 2691.8(5)$, $b = 594.7(1)$, $c = 3779.9(8)$ pm, $\beta = 96.88(3)°$, $V = 6007(2) \times 10^6$ pm$^3$; monoclinic $C2/c$, $Z = 8$, $\rho_{calc.} = 1.227$ g cm$^{-1}$, $\mu(Mo_{K\alpha}) = 0{,}203$ mm$^{-1}$, STOE IPDS2, $Mo_{K\alpha}$ radiation, $\lambda = 0.71073$ Å, $T = 200$ K, $2\theta_{max} = 48°$; 9082 reflections measured, 4476 independent reflections ($R_{int} = 0.0661$), 3156 independent reflections with $F_o > 4\sigma(F_o)$. The structure was solved by direct methods and refined, by full-matrix least-square techniques against $F^2$, 361 parameters (S, C refined anisotropically, H atoms were calculated at ideal positions); $R1 = 0.0540$; $wR2 = 0.1438$ (all data); Gof: 0.928; maximum peak 0.262 e Å$^{-3}$. CCDC-210255 (**1**) and CCDC-210256 (**3**) contain the supplementary crystallographic data for this paper. These data can be obtained free of charge via www.ccdc.cam.ac.uk/conts/retrieving.html (or from the Cambridge Crystallographic Data Centre, 12, Union Road, Cambridge CB21EZ, UK; fax: (+44) 1223-336-033; or deposit@ccdc.cam.ac.uk).
[15] MM+ Calculations for **3**.
[16] J. Heurich, J. C. Cuevas, W. Wenzel, G. Schön, *Phys. Rev. Lett.* **2002**, *88*, 256803/1 – 256803/4.
[17] J. Reichert, H. B. Weber, M. Mayor, *Appl. Phys. Lett.* **2003**, *82*, 4137 – 4139.
[18] Data were also recorded at four intermediate temperatures between room temperature and 30 K which are not shown. The improvement of the data quality towards lower T develops continuously.

 © 2003 Wiley-VCH Verlag GmbH & Co. KGaA, Weinheim 

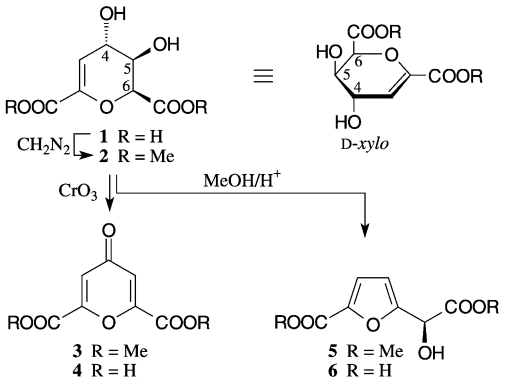
Plant Acids

# (−)-Daucic Acid: Revision of Configuration, Synthesis, and Biosynthetic Implications**

*Frieder W. Lichtenthaler,* Katsumi Nakamura, and Jürgen Klotz*

*In memory of Friedrich Cramer*

(−)-Daucic acid, a $C_7$-sugar dicarboxylic acid found in carrots (*Daucus carota*), sugar beet, wheat, sunflowers, and tobacco, was first isolated from mature carrots in 1971[1] and later assigned the structure of a 2,6-anhydro-3-deoxy-D-hept-2-enaric acid and D-*xylo* configuration with respect to the three chiral centers (Scheme 1, **1**).[2] The assignment of a dihydro-




***Scheme 1.*** Reactions of (−)-daucic acid, isolated from *Daucus carota*, from which the structure of a 2,6-anhydro-2-deoxyhept-2-enaric acid was derived; the D-*xylo* configuration **1** was determined on the basis of $^1$H NMR spectroscopic data (60 MHz).[2]

pyran structure was based on the oxidative conversion of its dimethyl ester into dimethyl chelidonate (**2**→**3**), and its affiliation to the D series of sugars (that is, its configuration at C6) followed convincingly from the high positive optical rotation of the furanoid rearrangement product **5** ($[\alpha]_D$ = +79.3 in $CHCl_3$), which correlated well with the equally high negative $[\alpha]_D$ value of the synthetically prepared L-enantiomer.[2] This assignment was later corroborated by the isolation of osbeckic acid **6** from *Osbeckia chinensis* L., the dimethyl ester of which proved to be fully congruent to **5**.[3]

[*] Prof. Dr. F. W. Lichtenthaler, Dr. K. Nakamura, Dr. J. Klotz
Clemens-Schöpf-Institut für Organische Chemie und Biochemie
Technische Universität Darmstadt
Petersenstrasse 22, 64287 Darmstadt (Germany)
Fax: (+49) 6151-16-6674
E-mail: lichtenthaler@chemie.tu-darmstadt.de

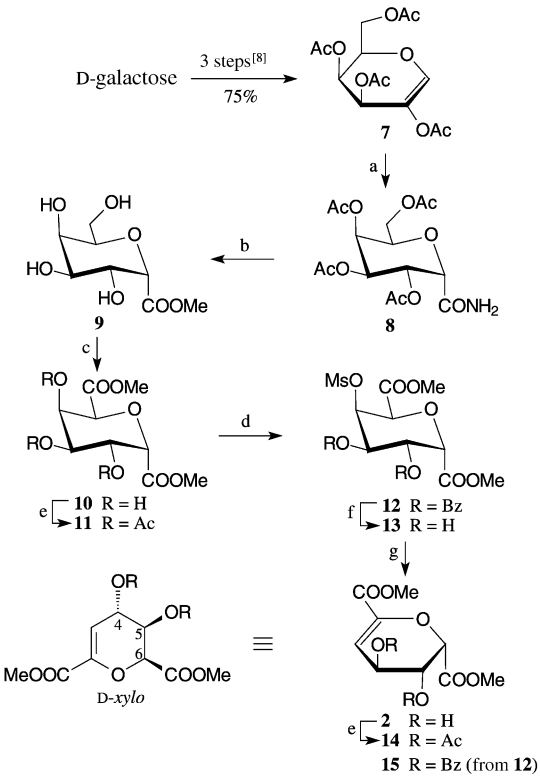
[**] We thank the Deutsche Forschungsgemeinschaft and the Fonds der Chemischen Industrie for support. K.N. thanks the Alexander von Humboldt Foundation for a fellowship.

 © 2003 Wiley-VCH Verlag GmbH & Co. KGaA, Weinheim DOI: 10.1002/anie.200352718 

The assignment of the configuration at C4 and C5 was less conclusive (Scheme 1), as it was inferred from low-resolution (60 MHz) $^1$H NMR spectroscopic data for dimethyl daucate (**2**) and its di-*O*-acetyl derivative, primarily from the coupling constants for 4-H and 5-H and comparison of these with analogous NMR spectroscopic data for certain 4,5-unsaturated hexuronates,[4] which on close inspection prove unreliable.[5] Moreover, the half-chair forms of sugar-derived dihydropyrans usually exist in complex conformational equilibria, which are virtually impossible to predict, thus resulting in coupling patterns that have little bearing on the actual configuration. Therefore, the verification of the stereochemistry at C4 and C5 of (−)-daucic acid was deemed imperative, particularly as reflections on its biosynthetic origin—its formation from 3-deoxy-D-*arabino*-heptulosonate 7-phosphate (DAHP), an early intermediate of the shikimic acid pathway,[6] is a likely possibility—would lead one to expect the D-*arabino* configuration.

These considerations, together with the notion that daucic acid is a possible biosynthetic precursor of chelidonic acid (**4**), a leaf-closing factor in *Cassia mimosoides*,[7] prompted us to devise a stereocontrolled synthesis, which should be practical enough to furnish sufficient amounts for biological studies. Accordingly, herein we report expedient syntheses of the daucic acids with the D-*xylo*, D-*ribo*, L-*arabino*, and D-*lyxo* configuration. Our conceptual approach for developing stereochemically unambiguous access to the D-*xylo*-heptenaric acid **1** and the three alternate configurations of this acid was based upon the anomeric one-carbon-atom homologation of suitable D-hexoses (D-galactose or D-mannose), subsequent oxidation at both termini to the corresponding pyranoid $C_7$ dicarboxylic acids, and controlled β elimination into the pyranoid ring through the judicious choice of leaving groups.

The synthesis of the dimethyl D-*xylo*-dicarboxylate **2** started from tri-*O*-acetyl-2-acetoxy-D-galactal (**7**), readily accessible from D-galactose in a three-step, one-pot procedure[8] involving acetylation, treatment with HBr/HOAc, and dimethylamine-promoted elimination of HBr (Scheme 2). The acetone-initiated photoaddition of formamide to **7**, albeit complex,[9] is α selective to give the heptonamide **8** as the major product (54%), which can be converted into the methyl heptonate **9** by methanolysis under acidic conditions. Oxidation of the primary hydroxy group was effected smoothly with oxygen in the presence of the Adams catalyst to afford, after esterification with methanolic HCl, the dimethyl heptarate **10**. Although the axial orientation of the 5-OH group in **10** would suggest preferential 5,6-elimination from the corresponding tri-*O*-acetyl (**11**) or tri-*O*-benzoyl derivative, their exposure to a variety of suitable conditions (e.g. NaOAc/$Ac_2O$, 70°C or $Al_2O_3$/lutidine, 40°C) led to multicomponent mixtures. Thus, a better leaving group had to be introduced at C5. Low-temperature benzoylation of the equatorial hydroxy groups in **10** and subsequent treatment with methanesulfonyl chloride provided **12**. Now 5,6-elimination could be effected cleanly, either from **12** by briefly heating in NaOAc/$Ac_2O$ to afford the dibenzoate **15** (59%), or from the debenzoylated product **13** through exposure to NaOMe/MeOH to deliver dimethyl D-*xylo*-heptenarate **2** (77%) directly. Gratifyingly, all products in this reaction sequence were obtained in readily




***Scheme 2.*** Conversion of D-galactose into the D-*xylo*-heptenarate **2**: a) $HCONH_2$, $Me_2CO$, *hν*, 3 days, RT, 54%;[9] b) HCl (8%)/MeOH, reflux, 3 h, 86%; c) Pt/$O_2$, water (pH 8), 70°C, 4 h, then saturated methanolic HCl, RT, 1 h, 56%; d) BzCl, pyridine, −40°C, 2 h; then MsCl, −40°C→RT, 2 h, 58%; e) pyridine/$Ac_2O$ (2:1), RT, 12 h, 85%; f) saturated methanolic HCl, reflux, 14 h, 73%; g) NaOMe (0.1 N)/MeOH, RT, 1 h, 77%. Ms = methanesulfonyl.

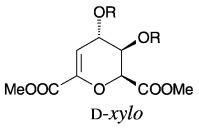
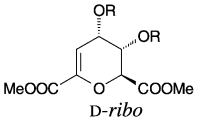
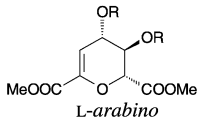
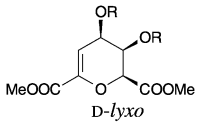
characterizable, crystalline form; only the di-*O*-acetyl and di-*O*-benzoyl derivatives **14** and **15** have so far resisted crystallization.

The melting point for the product **2** of this reaction sequence was close to that of the *Daucus carota* derived compound. However, its optical rotation, although similar in size, was opposite in sign (Table 1). The notion that the natural product might therefore have the enantiomeric (i.e. L-*xylo*) configuration was invalidated by the distinct differences in the $^1$H NMR spectroscopic data of synthetic **2** and **14**, compared to those reported for the respective products of natural origin. The chemical shifts observed for 4-H, 5-H, and 6-H vary by $\delta = 0.3$–$0.6$ ppm in each case, and the coupling constants $J_{3,4}$ and $J_{4,5}$ have significantly different values (Table 1). Thus, a D-*xylo* or L-*xylo* configuration for natural (−)-daucic acid can be excluded unequivocally.

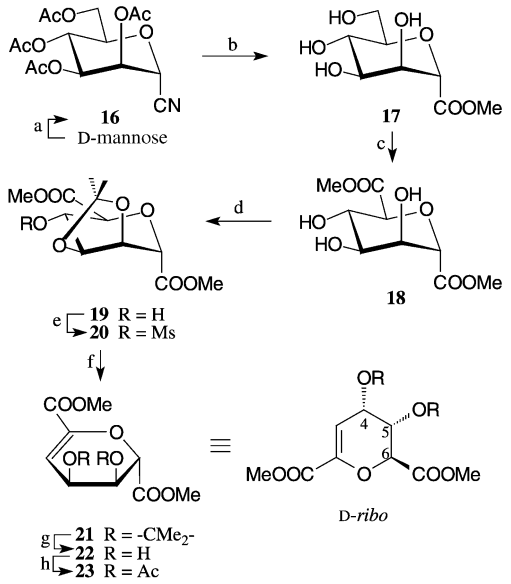
Of the remaining possible configurations—D-*ribo*, D-*lyxo*, and D-*arabino*—the synthesis of the D-*ribo* analogue **22**, the C5 epimer of **2**, was addressed next. We took advantage of the ready accessibility of heptononitrile **16** from D-mannose through a two-step, one-pot reaction comprising acetylation and anomeric cyanation (Scheme 3).[10] Acid hydrolysis followed by esterification with methanol then provided the mannosyl-*C*-carboxylate **17**. The Pt/$O_2$ oxidation of the primary hydroxy group in **17** proved unusually capricious,

 © 2003 Wiley-VCH Verlag GmbH & Co. KGaA, Weinheim 

***Table 1:*** Relevant physicochemical data for dimethyl 2,6-anhydro-3-deoxyhept-2-enarates of D-*xylo*, D-*ribo*, L-*arabino*, and D-*lyxo* configuration and their diacetates, as compared with those reported for the analogous *Daucus carota* derived daucic acid derivatives.[2]

| Compound | | M.p. [°C] | $[\alpha]_D^{20}$[a] | $^1$H NMR [ppm, Hz] | | | | | | | |
|---|---|---|---|---|---|---|---|---|---|---|---|
| | | | | 4-H | 5-H | 6-H | $J_{3,4}$ | $J_{3,5}$ | $J_{4,5}$ | $J_{5,6}$ | solvent |
| (−)-dimethyl daucate[2] | | 130–131 | −102[b] | 4.51 | 4.30 | 4.66 | 3 | 1 | ? | 2 | $CDCl_3$ |
| diacetate[2] | | oil | ? | 5.73 | | 4.82 | 2.3 | ? | ? | 1.8 | $CDCl_3$ |
| | | | | 5.63 | 5.85 | 4.35 | 2.6 | 1.5 | 4.4 | 1.8 | $C_6H_6$ |
|  D-*xylo* | **2** R = H | 133–135 | +106 | 4.19 | | 4.60 | 4.8 | 1.3 | ? | 1.5 | $CDCl_3$ |
| | **14** R = Ac | syrup | +146 | 5.13 | 5.38 | 4.61 | 5.3 | 1.5 | 2.2 | 1.4 | $CDCl_3$ |
| | | | | 5.20 | 5.57 | 4.41 | 5.3 | 1.5 | 2.2 | 1.0 | $C_6H_6$ |
|  D-*ribo* | **22** R = H | syrup | +150.4 | 4.32 | 4.12 | 4.63 | 4.4 | – | 4.3 | 7.6 | $CDCl_3$ |
| | **23** R = Ac | syrup | +171.1 | 5.52 | | 4.84 | 3.7 | – | ? | 6.8 | $CDCl_3$ |
| | | | | 5.62 | 5.71 | 4.74 | 3.8 | 0.7 | 4.2 | 6.3 | $C_6H_6$ |
|  L-*arabino* | **29** R = H | syrup | +30.0 | 4.25 | 4.19 | 4.73 | 4.3 | 0.9 | 2.2 | 5.4 | $CDCl_3$ |
| | **30** R = Ac | 104–106 | +72.1 | 5.14 | 5.44 | 5.06 | 5.4 | 1.5 | 2.1 | 2.2 | $CDCl_3$ |
| | | | | 5.22 | 5.58 | 4.89 | 5.3 | 1.5 | 2.3 | 2.6 | $C_6H_6$ |
|  D-*lyxo* | **35** R = H | 128–129 | −98.3 | 4.50 | 4.30 | 4.67 | 3.3 | 1.1 | 4.3 | 2.3 | $CDCl_3$ |
| | **36** R = Ac | syrup | −54.1 | 5.74 | | 4.84 | 2.2 | 1.7 | ? | 1.4 | $CDCl_3$ |
| | | | | 5.56 | 5.81 | 4.27 | 2.3 | 1.7 | 4.5 | 1.7 | $C_6D_6$ |

[a] Optical-rotation values for the free diols in acetone, for the diacetates in $CHCl_3$. [b] $[\alpha]_D$ value at 24.5 °C.

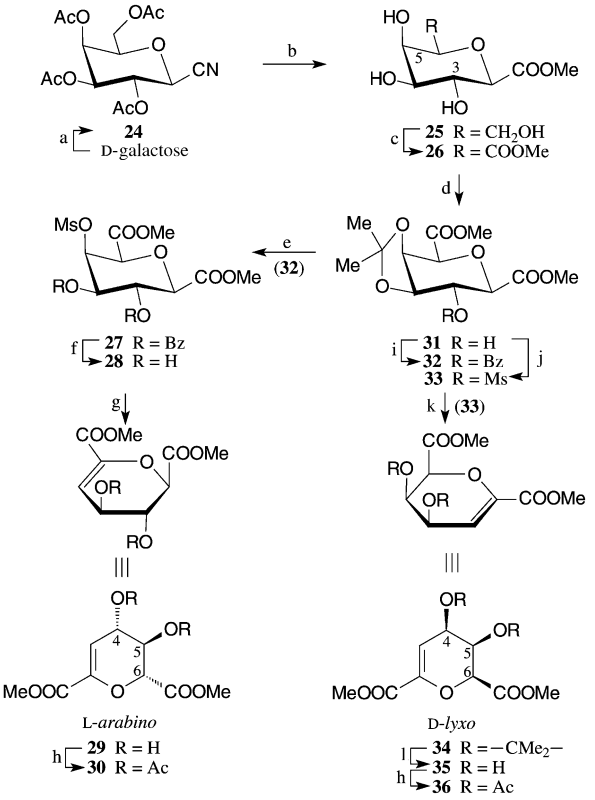



***Scheme 3.*** Synthesis of the D-*ribo*-heptenarate **22** from D-mannose: a) pyridine/$Ac_2O$ (1.3:1), 0 °C, 2 days,[10a] then $Me_3SiCN$, $BF_3{\cdot}Et_2O$, $CH_3NO_2$, 35 °C, 2 h;[10b] b) aqueous HCl (25%), 50 °C, 24 h, then saturated methanolic HCl, RT, 2 h, 85%; c) TEMPO/NaOCl, $H_2O/CH_2Cl_2$, 0 °C, 20 h, then saturated methanolic HCl, RT, 2 h, 83%; d) $Me_2CO/H_2SO_4$, RT, 4 h, 75%; e) MsCl, pyridine, 0 °C, 3 h, 94%; f) basic $Al_2O_3$, lutidine, 40 °C, 30 min, 75%; g) $CHCl_3$/TFA/water (50:10:1), RT, 1 h, 86%; h) pyridine/$Ac_2O$ (2:1), RT, 5 h, 91%. TEMPO = 2,2,6,6-tetramethylpiperidinyl-1-oxyl, TFA = trifluoroacetic acid.

and the conversion of this compound into the desired dicarboxylate was instead effected by a TEMPO-catalyzed oxidation with sodium hypochlorite,[11] to provide, upon esterification with methanolic HCl, the dimethyl heptarate **18** in high yield. Subsequent protection of the hydroxy groups at C3 and C4 through acetonide formation (→**19**), followed by mesylation (→**20**), set the stage for the 5,6-elimination of methanesulfonic acid, which was effected simply by briefly exposing **20** to $Al_2O_3$/lutidine at 40 °C (→**21**). Finally, removal of the isopropylidene group in **21** with aqueous trifluoroacetic acid smoothly delivered the desired dimethyl D-*ribo*-heptenarate **22**, which was acetylated to the di-*O*-acetyl derivative **23**. Both **22** and **23** were isolated as syrups with high positive optical-rotation values. Substantially smaller negative values were observed for the *Daucus carota* derived product. As distinct differences were also observed in the respective $^1$H NMR spectroscopic data (see Table 1), the D-*ribo* and L-*ribo* stereochemistry for natural (−)-daucic acid can also be excluded.

To finally unravel the stereochemistry of the natural product—*arabino* or *lyxo* configurations were still possible—we investigated a convergent synthetic pathway from β-D-galactosyl cyanide **24**,[12] under the premise that $\Delta^{2,3}$ (or $\Delta^{5,6}$) unsaturation could be introduced selectively through an elimination reaction if the 3-OH (or, alternatively, the 5-OH) group in the $C_7$-dicarboxylate **26** was converted into a displaceable leaving group (Scheme 4). Indeed, this key intermediate was prepared in a straightforward manner by

 © 2003 Wiley-VCH Verlag GmbH & Co. KGaA, Weinheim 



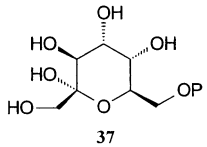

***Scheme 4.*** Conversion of D-galactose into dimethyl heptenarates with the L-*arabino* (**29**) and the D-*lyxo* configuration (**35**); the stereochemistry of **35** corresponds to that of natural (−)-daucic acid: a) NaOAc/$Ac_2O$, 100 °C, 2 h,[12a] then $Me_3SiCN$, $BF_3{\cdot}Et_2O$ in $CH_3NO_2$, 35 °C, 2 h,[12b] 79%; b) 1. NaOMe/MeOH, 2 h, RT; 2. NaOH (6 N), 4 h, reflux; 3. saturated methanolic HCl, RT, 2 h, 85%; c) TEMPO/NaOCl, $H_2O$/$CH_2Cl_2$, 0 °C, 20 h, then saturated methanolic HCl, RT, 2 h, 76%; d) $Me_2CO/H_2SO_4$, RT, 4 h, 83%; e) $CHCl_3$/TFA/water (50:10:1), RT, 30 min, then BzCl (1.2 equiv), pyridine, −40 °C, 2 h, then MsCl, pyridine, RT, 3 h, 53%; f) saturated methanolic HCl, reflux, 24 h, 86%; g) NaOMe (0.1 N)/MeOH, 15 min, RT, 90%; h) pyridine/$Ac_2O$ (2:1), RT, 14 h, 90%; i) MsCl, pyridine, 0 °C, 3 h, 85%; j) basic $Al_2O_3$, lutidine, 40 °C, 30 min, 74%; k) $CHCl_3$/TFA/water (50:10:1), RT, 1 h, 83%.

base hydrolysis of **24**,[12] esterification (→**25**), and TEMPO/NaOCl oxidation in an overall yield of 51%. Attempts to selectively benzoylate the equatorial OH groups in **26**, a protocol successful with its C2 epimer **10** in the synthesis of 5-*O*-mesylate **12**, failed as a result of the distinctly different reactivities of the hydroxy groups in **26** and **10**. As an alternate, albeit less direct route to the desired 3,4-di-*O*-benzoyl-5-*O*-mesylheptarate **27**, the 4,5-*cis*-diol in **26** was protected through isopropylidenation (→**31**, the key intermediate for the generation of the D-*lyxo* compounds; see below), which was followed by benzoylation and acid hydrolysis of the acetonide. The resulting 3-benzoate of **26**, unlike **26** itself, could be monobenzoylated readily at the 4-OH at low temperature, and subsequent in situ mesylation delivered **27** in a tolerable overall yield of 40% for the five steps from **26**. Introduction of the $\Delta^{5,6}$ unsaturation in the L-*arabino* heptenarate **29** was effected by brief exposure of the de-*O*-benzoylated heptarate **28** to NaOMe (0.1N)/MeOH. Whereas **29** was obtained as a syrup, its diacetate **30** crystallized well.

A similar sequence of reactions led from the isopropylidene-protected dimethyl heptarate **31** to the corresponding D-*lyxo* compounds **35** and **36**. Mesylation (→**33**) and $Al_2O_3$/lutidine-induced elimination gave **34**, which was then exposed to aqueous trifluoroacetic acid to remove the isopropylidene group.

Unlike the L-*arabino*-heptenarates **29** and **30**, whose $^1$H NMR spectroscopic data differed markedly from those of the *Daucus carota* derived compounds,[2] the D-*lyxo* analogues **35** and **36** showed almost perfect agreement, not only in the sign and magnitude of their optical-rotation values, but most notably in the chemical shifts and coupling patterns in their $^1$H NMR spectra (Table 1). The slight deviations observed in the coupling constants undoubtedly result from the different field strengths (60[2] versus 300 MHz) and, conceivably, from temperature differences. The temperature affects the equilibrium between the respective half-chair forms ($^5H_6 \rightleftarrows {}^6H_5$) and hence the NMR coupling patterns observed. This evidence is cogent enough to allow the unambiguous assignment of the D-*lyxo*-configuration to carrot-derived (−)-daucic acid.

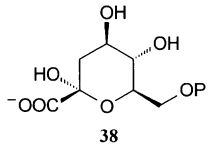
The synthetic (−)-dimethyl daucate (**35**) could be saponified readily by exposure to aqueous trifluoroacetic acid (4:1, 2 days, 25 °C), to provide the free acid in crystalline form (m.p. 87–88 °C, $[\alpha]_D^{20} = -85$ in MeOH, 80%). More vigorous acid conditions led to the pyran→furan rearrangement observed previously for the natural product (Scheme 1):[2] Heating **35** in methanolic HCl afforded dimethyl osbeckate (**5**) (60%), whereas heating **35** in water in the presence of a strongly acidic ion-exchange resin gave the free osbeckic acid (**6**; 81%).




**37**

(sedoheptulose 7-P)

D-*altro*




**38**

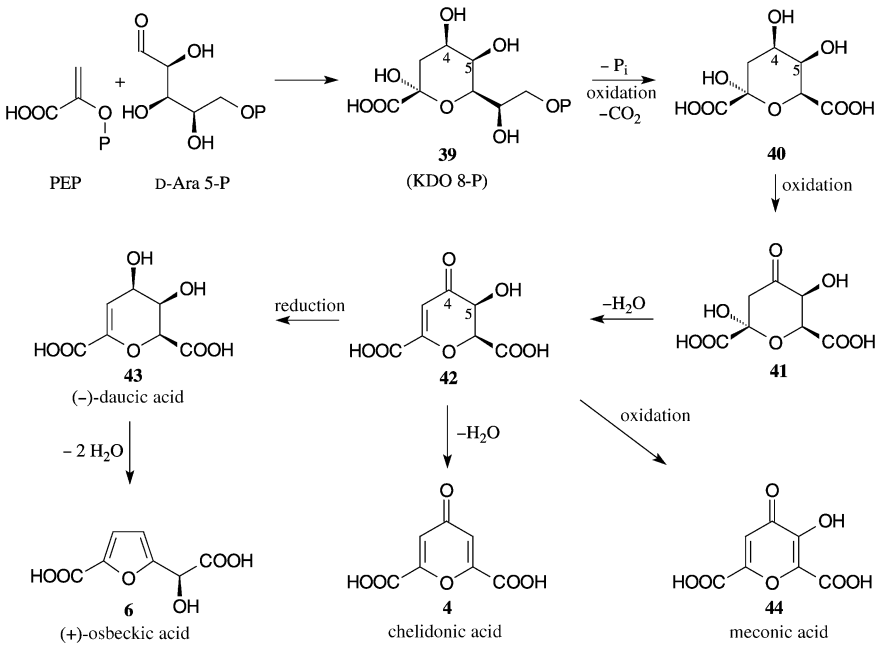
(DAH 7-P)

D-*arabino*

Not only is the biosynthetic origin of (−)-daucic acid intriguing—sedoheptulose 7-phosphate (**37**) and 3-deoxy-D-*arabino*-heptulosonate 7-phosphate (DAHP, **38**), both established intermediates of the pentose phosphate and shikimic acid pathways, respectively, are potential precursors—but also its close structural relationship with chelidonic acid (**4**). The elaboration of the γ-pyrone system would merely require oxidation of daucic acid at C4 and 5,6-elimination of water.

Studies on the biosynthesis of chelidonic acid with $^{14}$C-labeled sugars have uniformly shown that D-glucose, and to an even greater extent D-ribose, are incorporated well,[13,14] whereas **37** is not.[13] Although the assumption that DAHP (**38**) is therefore the likely precursor[14] persisted for 30 years, it was convincingly disproved recently by quantitative carbon-flux analyses of $^{13}$C-labeled sugars, which suggested a biosynthetic assembly of chelidonic acid from one molecule each of pentose phosphate and phosphoenolpyruvate (PEP;

 © 2003 Wiley-VCH Verlag GmbH & Co. KGaA, Weinheim 




***Scheme 5.*** Possible mechanism for the biosynthesis of $C_7$ dicarboxylic acids in plants from common precursors. The suggestion is based on the identical configurations in the pyranoid rings of daucic acid (**43**) and KDO 8-P (**39**), the conjecture that the generation of the structurally similar daucic, chelidonic (**4**), and meconic acid (**44**) may occur via a common intermediate, and on studies[15] on the biosynthesis of **4**.

Scheme 5).[15] Such a biosynthetic process is well-established for Gram-negative bacteria, in which PEP and D-arabinose 5-phosphate (D-Ara 5-P), in turn generated from D-ribulose 5-phosphate by isomerization, undergo an aldol-type condensation to form 3-deoxy-D-*manno*-octulosonate 8-phosphate (KDO 8-P, **39**).[16,17] As the KDO 8-P synthase catalyzed aldol addition proceeds with exclusive *Si* attack by PEP to the *Re* face of the sugar carbonyl group, the 4*R* isomer is formed stereospecifically, so that the product **39** has the D-*manno* configuration.[18] The existence of such a KDO 8-P based mechanism in plants has not yet been proved. However, the fact that DAH 7-P synthase, a key enzyme of the shikimic acid pathway[6] and abundant in higher plants, catalyzes the aldol addition of PEP not only to its natural substrate D-erythrose 4-phosphate, but to D-ribose 5-phosphate (D-Rib 5-P) and D-Ara 5-P as well,[19] may be regarded tentatively as evidence that an octulosonate 8-phosphate based pathway is also operative in plants.

Based on the newly established D-*lyxo* stereochemistry of (−)-daucic acid (**37** and **38** as precursors would lead to the D-*arabino* configuration), on the conjecture that the biosynthetic elaboration of daucic acid is closely related to that of chelidonic (**4**) and meconic acid (**44**), and on available evidence[15] about the biosynthesis of **4**, a biosynthetic pathway readily unfolds as depicted in Scheme 5: D-Ara 5-P and PEP undergo an aldol-type condensation to KDO 8-P (**39**), in which the stereochemistry of the pyranoid ring correlates with the D-*lyxo* configuration of daucic acid. If D-Rib 5-P was involved in the aldol addition step, the $C_8$-sugar phosphate would have the D-*altro* configuration, thus requiring an (unnecessary) epimerization at a later stage.

Unlike in Gram-negative bacteria, in which the $C_8$ chain of KDO 8-P is incorporated into the lipopolysaccharides of cell walls,[16] in this case the terminal carbon is removed by dephosphorylation and oxidative decarboxylation. Although only loss of water is formally required from the resulting intermediate **40** to give daucic acid, a direct 3,2-elimination is unlikely—"cells obey the laws of chemistry"[20]—as the hydrogen atom involved (3-H) is not activated. As activation is usually provided by a vicinal carbonyl group—the conversion of D-glucose into kojic acid by *Aspergillus oryzae* has been rationalized on this basis[21]—the oxidation of **40** at C4 appears plausible as the next step. Dehydration of the resulting ketodicarboxylic acid **41** is thought to proceed spontaneously to give the dihydropyranone **42**, a furcation point towards these $C_7$ dicarboxylic acids. Daucic acid is formed from **42** by reduction (**42**→**43**), chelidonic acid by elimination of water (**42**→**4**), and meconic acid, plentiful in Papaveraceae, by oxidation (**42**→**44**). The furanoid osbeckic acid is likely to be formed from daucic acid through ring contraction and double dehydration (**43**→**6**).

The alluring consistency of this proposed biosynthetic pathway, particularly the configurational identity of KDO 8-P and daucic acid in their pyranoid rings, clearly calls for the systematic investigation of higher plants for the occurrence of a $C_8$-sugar-phosphate pathway with the possible intermediates **40**–**42**, in particular in those species in which these $C_7$ dicarboxylic acids have been detected: daucic acid in carrots, sugar beets, wheat, sunflowers, and tobacco, osbeckic acid in *Osbeckia chinensis* L., meconic acid in Papaveraceae, and chelidonic acid in a plethora of plant families.

Received: August 25, 2003 [Z52718]
Published Online: November 18, 2003

**Keywords:** carbohydrates · chelidonic acid · configuration determination · daucic acid · osbeckic acid

[1] A. J. Keys, C. J. Leaver, D. H. R. Barton, B. D. Brown, D. A. Widdowson, *Nature* **1971**, *232*, 423–424.
[2] D. H. R. Barton, B. D. Brown, D. D. Ridley, D. A. Widdowson, A. J. Keys, C. J. Leaver, *J. Chem. Soc. Perkin Trans. 1* **1975**, 2069–2076.
[3] J.-D. Su, T. Osawa, S. Kawakishi, M. Namiki, *Agric. Biol. Chem.* **1987**, *51*, 2449–3450.
[4] J. Kiss, W. Arnold, *Helv. Chim. Acta* **1975**, *58*, 297–302.
[5] A detailed evaluation of the $^1$H NMR spectroscopic data for 4,5-unsaturated hexopyranuronates in reference [4] revealed a number of serious inconsistencies: The formulae for starting

materials III–V and VII–XI are identical, yet lead to different products, namely, to a β anomer VI and an α anomer X; moreover the coupling constants for the β (VI) and α compound (X) seem to have been interchanged, as only the latter can adopt a half-chair conformation with a $H^2$-C-C-$H^3$ torsion angle of ≈ 130°, and hence result in a coupling constant $J_{2,3} = 7.5$ Hz. Consequently, these data are not useful for comparative purposes.

[6] E. Haslam, *Shikimic Acid: Metabolism and Metabolites*, Wiley, Chichester, **1993**.

[7] E. Miyoshi, Y. Shizuri, S. Yamamura, *Chem. Lett.* **1987**, 511–514; M. Ueda, H. Shigemori, N. Sata, S. Yamamura, *Phytochemistry* **2000**, *53*, 39–44.

[8] a) Acetylation and bromination: R. W. Jeanloz, P. J. Stoffyn, *Methods Carbohydr. Chem.* **1962**, *1*, 224–225; J. Conchie, G. A. Levy, *Methods Carbohydr. Chem.* **1963**, *2*, 336; b) HBr elimination: K. Maurer, A. Müller, *Ber. Dtsch. Chem. Ges. A* **1930**, *63*, 2069–2073. When purification of the two intermediates is avoided, an overall yield of 75% is observed for the three steps.

[9] M. Chmielewski, J. N. BeMiller, D. P. Ceretti, *J. Org. Chem.* **1981**, *46*, 3903–3908.

[10] a) E. Fischer, B. Oetker, *Ber. Dtsch. Chem. Ges.* **1913**, *46*, 4029–4040; R. K. Irani, J. L. Bose, *Indian J. Chem.* **1975**, *13*, 529; b) G. D. Kini, C. R. Petrie, W. J. Hennen, N. K. Dalley, B. E. Wilson, R. K. Robins, *Carbohydr. Res.* **1987**, *159*, 81–94.

[11] N. J. Davis, S. L. Flitsch, *Tetrahedron Lett.* **1993**, *34*, 1181–1184; A. E. J. de Nooy, A. C. Besemer, H. van Bekkum, *Recl. Trav. Chim. Pays-Bas* **1995**, *51*, 8023–8032; Z. Györgydeák, J. Thiem, *Carbohydr. Res.* **1995**, *268*, 85–92.

[12] a) E. Erwig, W. Koenigs, *Ber. Dtsch. Chem. Ges.* **1889**, *22*, 2207–2213; b) F. G. de las Heras, P. Fernández-Resa, *J. Chem. Soc. Perkin Trans. 1*, **1982**, 903–907.

[13] B. A. Bohm, *Arch. Biochem. Biophys.* **1966**, *115*, 181–186.

[14] M. J. Malcolm, J. R. Gear, *Can. J. Biochem.* **1971**, *49*, 412–416.

[15] Z.-W. Shen, U. Fisinger, A. Poulev, W. Eisenreich, I. Werner, E. Pleiner, A. Bacher, M. H. Zenk, *Phytochemistry* **2001**, *57*, 33–42.

[16] F. M. Unger, *Adv. Carbohydr. Chem. Biochem.* **1981**, *38*, 378–388.

[17] M. D. Bednarski, D. C. Crans, R. Dilosimo, E. S. Simon, P. D. Stein, G. M. Whitesides, M. J. Schneider, *Tetrahedron Lett.* **1988**, *29*, 427–430.

[18] G. A. Dotson, P. Nanjappan, M. D. Reily, R. W. Woodard, *Biochemistry* **1993**, *32*, 12392–12397.

[19] G. Y. Sheflyan, D. L. Howe, T. L. Wilson, R. W. Woodard, *J. Am. Chem. Soc.* **1998**, *120*, 11027–11032; H. S. Duewel, R. W. Woodard, *J. Biol. Chem.* **2000**, *275*, 22824–22831.

[20] Dictum attributed to Sir Robert Robinson.

[21] F. W. Lichtenthaler, *Pure Appl. Chem.* **1978**, *50*, 1358.

 © 2003 Wiley-VCH Verlag GmbH & Co. KGaA, Weinheim 

Azide Complexes (1)

# Binary Tellurium(IV) Azides: $Te(N_3)_4$ and $[Te(N_3)_5]^-$**

*Thomas M. Klapötke,* Burkhard Krumm, Peter Mayer, and Ingo Schwab*

*In memory of Marianne Baudler*

Apart from some early reports on the elusive and extremely labile tellurium nitride compounds TeN, $Te_3N_4$, and $Te_4N_4$, and the recently discovered $[Te_6N_8(TeCl_4)_4]$,[1] the only structurally characterized binary Te–N species is the salt $[Te(N_3)_3][SbF_6]$.[2] The triazidotelluronium cation was obtained as an unexpected product during an attempted preparation of $[Te_2N]^+$. The chemistry of tellurium azides was initiated by Wiberg in the 1970s.[3] Various examples of homoleptic azido transition and main-group metalates and nonmetalates are reported,[4] but none of the chalcogen group. The groups of Wiberg and Passmore have indicated the possible existence of a highly explosive $Te(N_3)_4$ and warned of their potential danger. In pursuit of our recent efforts to explore the chemistry of covalent and ionic tellurium azides,[5,6] we describe here the synthesis, isolation, and properties of $Te(N_3)_4$ (**1**),[7] $[Me_4N][Te(N_3)_5]$ (**2a**) and [pyH] $[Te(N_3)_5]$ (**2b**), the latter containing a rare pentacoordinated polyazido anion, the only other example being the $[Fe(N_3)_5]^{2-}$ ion.[8]

As is known from the syntheses of $TeCl_3(N_3)$ and $TeCl_2(N_3)_2$,[3] and confirmed by our own studies, treatment of $TeCl_4$ with excess $Me_3SiN_3$ does not result in the substitution of all chlorine atoms. All successful preparations for $R_2Te(N_3)_2$ and $RTe(N_3)_3$ (R = alkyl, aryl, trifluoromethyl and perfluoroaryl) proceed via the corresponding tellurium di- or trifluorides $R_2TeF_2$ and $RTeF_3$.[5,6a] Thus, for the synthesis of $Te(N_3)_4$ (**1**) and $[Te(N_3)_5]^-$ (**2**), the fluorinated species $TeF_4$ and $[Me_4N][TeF_5]$ were preferred as starting materials. Tellurium tetrafluoride rapidly reacts with $Me_3SiN_3$ in $CFCl_3$ (0 °C) suspension to form a yellowish precipitate of **1** that is soluble in DMSO [Eq. (1)]. On one occasion, the solid

$$TeF_4 + 4\,Me_3SiN_3 \xrightarrow[-4\,Me_3SiF]{CFCl_3/0\,^\circ C} Te(N_3)_4\ (\mathbf{1}) \qquad (1)$$

exploded violently when obtained from a suspension in $CH_2Cl_2$. Solutions of **1** in $[D_6]$DMSO exhibit a very broad

[*] Prof. Dr. T. M. Klapötke, Dr. B. Krumm, Dr. P. Mayer, Dipl.-Chem. I. Schwab
Department of Chemistry
University of Munich (LMU), Butenandtstrasse 5–13 (D)
81377 Munich (Germany)
Fax: (+49) 89-2180-77492
E-mail: tmk@cup.uni-muenchen.de

[**] Financial support from the University of Munich and the Fonds der Chemischen Industrie is gratefully acknowledged. We thank Prof. P. Klüfers for generous allocation of X-ray diffractometer time, and Prof. K. O. Christe and his colleagues for exchange of information about their independent syntheses of $Te(N_3)_4$ and $[Te(N_3)_6]^{2-}$.

 DOI: 10.1002/anie.200352656 © 2003 Wiley-VCH Verlag GmbH & Co. KGaA, Weinheim 

$^{125}$Te NMR resonance at $\delta = 1380$ ppm, deshielded compared to that of $TeF_4$ ($\delta = 1195$ ppm). The resonance for **1** is identical to that detected in a mixture of the dismutation products of $C_6F_5Te(N_3)_3$, $Te(N_3)_4$, and $(C_6F_5)_2Te(N_3)_2$.[6a] Due to our experience with the unpredictable explosiveness of neat **1**, vibrational spectra, mass spectra, and elemental analysis were omitted.[9]

In a similar fashion, $[Me_4N][TeF_5]$ reacts with $Me_3SiN_3$ in $CH_2Cl_2$ to form a yellow solution of $[Me_4N][Te(N_3)_5]$ (**2a**) [Eq. (2)], from which yellow crystals can be grown at below

$$[Me_4N][TeF_5] + 5\,Me_3SiN_3 \xrightarrow[-5\,Me_3SiF]{CH_2Cl_2/0\,^\circ C} [Me_4N][Te(N_3)_5]\ (\mathbf{2a}) \qquad (2)$$

−20 °C. In some cases, an extremely sensitive yellow oil also separates, which in one case exploded when the cold mixture was stirred. For **2a**, a sharp $^{125}$Te NMR resonance was observed at $\delta = 1258$ ppm ($CD_2Cl_2$), again downfield from that of $[TeF_5]^-$. The $^{125}$Te NMR resonance of $[TeF_5]^-$ was observed at 25 °C in $CH_2Cl_2$ solution in the presence of $[Ph_4P]^+$ ions as a doublet of quintets at $\delta = 1161$ ppm ($^1J(^{125}Te\text{-}F_{apical}) = 2918$ Hz; $^1J(^{125}Te\text{-}F_{basal}) = 1386$ Hz). The Raman spectrum of **2a** shows bands at 2105/2055 [$\nu_{as}(N_3)$] and 409/347 [$\nu$(TeN)] cm$^{-1}$, which are detected in the typical regions for tellurium azides.[5,6] A reaction between $[Me_4N]_2[TeCl_6]$ and $Me_3SiN_3$ did not occur, and the $[TeF_6]^{2-}$ ion remains still unknown.[10]

In an attempt to stabilize the tetraazide **1**, and to gain products more easily characterizable, an effort was made to react a pyridine·$TeF_4$ adduct with azide. Such $TeF_4$ adducts are reported, but except for elemental analysis, no analytical information is available.[11] In order to confirm that compounds of the proposed form $[L{\cdot}TeF_3][TeF_5]$ ($L = Me_3N$, pyridine etc.) were prepared,[12] further analytical information was desirable. In the course of the preparation of such a proposed pyridine·$TeF_4$ adduct, the results of the crystal-structure determination unexpectedly revealed a complex mixture of pyridinium pentafluorotellurate(IV) and dimeric units of $TeF_4$ solvated by pyridine.[13]

Since crystals of **2a** grown from the reaction solution tend to deliquesce very rapidly, crystallization was attempted from solutions of the mixture of pyridine with $TeF_4$ and $Me_3SiN_3$. Although the crystals obtained after several weeks were shown to be the pyridinium salt $[pyH][Te(N_3)_5]$ (**2b**), probably formed by reaction of $TeF_4$ with fluoride in the employed glass vessel to give $[TeF_5]^-$ ions, the resulting pentaazidotellurate(IV) anion was unaffected. The pyridinium salt **2b** crystallizes in the triclinic space group $P\bar{1}$, for the anion a distorted $\Psi$-octahedral $TeEN_5$ coordination is found (Figure 1). The $[Te(N_3)_5]^-$ ion represents the first structurally characterized anionic tellurium azide.[7] Similar to neutral organotellurium(IV) azides,[5,6a] secondary Te···N interactions below the sum of the van der Waals radii (3.61 Å)[14] create network structures, which result in the octacoordinated tellurium atoms in **2b** (Figure 2). The Te–N bond lengths vary from 2.075(2) Å (Te-N7) for the apical azide group, to between 2.175(2) and 2.256(2) Å for the basal azide groups. The apical $N_3$ unit has the shortest $N_\alpha$–$N_\beta$/$N_\beta$–$N_\gamma$ bond lengths and the smallest N-N-N angle. The N-Te-N bond angles range between 74.53(7) and 165.99(8)°, and the N-N-N bond angles

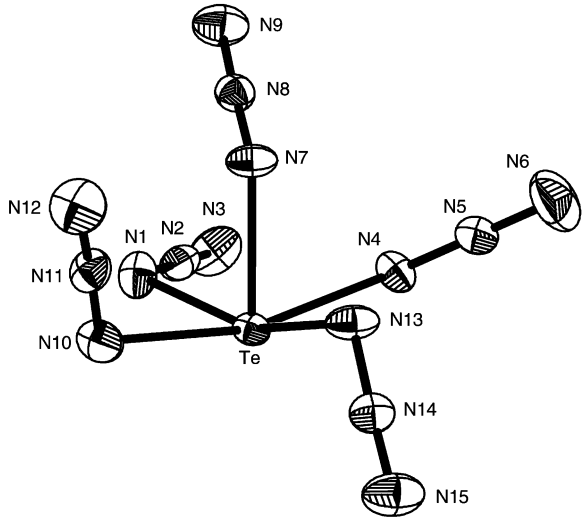



***Figure 1.*** Molecular structure of the anion in **2b** with thermal ellipsoids at 50% probability. Selected bond lengths [Å] and angles [°]: Te-N1 2.185(2), Te-N4 2.256(2), Te-N7 2.075(2), Te-N10 2.175(2), Te-N13 2.242(2); N1-N2-N3 176.9(2), N7-N8-N9 175.8(2), N1-Te-N7 85.34(8), N7-Te-N13 74.53(7).

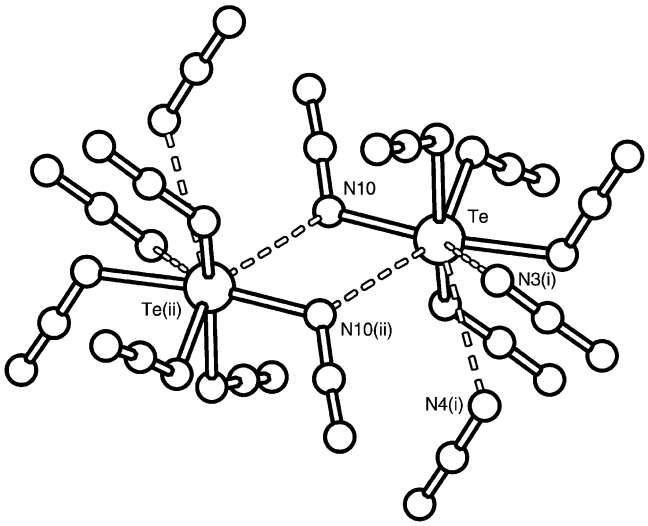



***Figure 2.*** Secondary Te···N interactions between $[Te(N_3)_5]^-$ ions in **2b**. Selected separations [Å]: Te···N3(i) 3.324(2), Te···N4(i) 3.227(2), Te(ii)···N10 3.127(2). Symmetry operations: i = 1−*x*, 1−*y*, −*z*; ii = −*x*, 1−*y*, −*z*.

are 175.8(2)–177.9(3)°. The rather irregular square-pyramidal structure likely results from electrostatic repulsions of the differently polarized $N_\alpha$ and $N_\beta$ atoms of the azide groups, both between each other, and with the lone pair of the $Te^{IV}$ center. Two sets of virtually identical Te–N distances for two geminal basal azide groups are present with four different orientations towards the apical position (Figure 1).

The electronic structure of the $[Te(N_3)_5]^-$ ion was calculated using different ab initio and density functional methods and basis sets (Table 1). All geometries have been fully optimized at the level chosen and led to distorted $C_1$-

 © 2003 Wiley-VCH Verlag GmbH & Co. KGaA, Weinheim 

*Table 1:* Experimental and calculated parameters of $[Te(N_3)_5]^-$.

| Method experiment | *E* [Hartree] | zpe [kcal mol$^{-1}$] | *d*(Te-$N_{apical}$) [Å] | *d*(Te-$N_{basal}$) [Å] | $\tilde{\nu}_{as}(N_3)$ [cm$^{-1}$][a] |
|---|---|---|---|---|---|
| | – | – | 2.075 | 2.175–2.256 | 2112–2037 |
| RHF/SDD | −823.791 | 41.0 | 2.058 | 2.108–2.218 | 2311–2203 |
| MPW1PW91/SDD | −828.642 | 37.9 | 2.124 | 2.159–2.218 | 2133–2097 |
| B3LYP/SDD | −828.877 | 36.7 | 2.140 | 2.179–2.245 | 2067–2030 |
| MP2(FC)/SDD | −825.815 | 36.5 | 2.113 | 2.156–2.238 | 2275–2144 |
| RHF/SDB-cc-pVTZ[20b] | −824.538 | 44.7 | 2.020 | 2.098–2.209 | 2488–2369 |
| B3LYP/SDB-cc-pVTZ[20b] | −829.440 | 39.9 | 2.077 | 2.159–2.229 | 2226–2171 |

[a] Vibrational frequencies are unscaled.

symmetric minimum structures in good agreement with the experimental crystal-structure determination. Best results regarding bond lengths and vibrational frequencies were obtained by using the B3LYP/SDD combination. However, this finding may be due to accidental compensation of pseudopotential and basis deficiencies, which may suggest a higher degree of accuracy for this cheaper method.

After the structural characterization of binary Te azide species of the type $[Te(N_3)_3]^+$[2] and $[Te(N_3)_5]^-$ (**2a** and **b**) and the first direct synthesis and NMR spectroscopic characterization of the neutral tellurium azide molecule, $Te(N_3)_4$ (**1**), the race is now on for the isolation of the first selenium azide species. Studies in this regard are currently in progress.[15]

## *Experimental Section*

All manipulations of air- and moisture-sensitive materials were performed under an inert atmosphere of dry argon using flame-dried glass vessels and Schlenk techniques. Tellurium tetrafluoride and $[Me_4N][TeF_5]$ were prepared according to the literature,[16] trimethylsilyl azide (Aldrich) was used as received. Solvents were dried by standard methods, distilled, and stored over molecular sieves. Raman spectra were recorded on a Perkin Elmer 2000 NIR FT spectrometer fitted with a Nd-YAG laser (1064 nm). NMR spectra were recorded on a JEOL Eclipse 400 instrument, and chemical shifts were referenced to $CH_3NO_2$ ($^{14}$N) and $Me_2Te$ ($^{125}$Te).

**CAUTION**: Binary tellurium azides are extremely hazardous shock-, friction-, and moisture-sensitive materials, which can explode unexpectedly. Appropriate safety precautions, such as Kevlar gloves (Sahlberg, Munich), face shield, leather jacket (Quadratfuss, Berlin), and teflon spatulas (Merck, Darmstadt; customized by LMU) must be employed; the quantities of substances handled in pure form by experienced personnel should not exceed 100 mg.

**1**: A suspension of $TeF_4$ (0.3 mmol, 60 mg) in $CFCl_3$ (10 mL) was treated with $Me_3SiN_3$ (1.2 mmol, 150 mg) at 0 °C. After stirring for 2 h the supernatant was decanted. The residue was dissolved in [D$_6$]DMSO for NMR experiments. $^{14}$N NMR (28.9 MHz, [D$_6$]DMSO, 25 °C; $\Delta\nu_{1/2}$ (Hz)): $\delta = -141$ (80, $N_\beta$), −234 (1000, $N_\gamma$), ≈ −270 ppm (extremely broad, $N_\alpha$); $^{125}$Te NMR (126.1 MHz, [D$_6$]DMSO, 25 °C): $\delta = 1380$ ppm.

**2a**: A solution of $[Me_4N][TeF_5]$ (0.15 mmol, 45 mg) in $CH_2Cl_2$ (5 mL) was reacted with $Me_3SiN_3$ (0.75 mmol, 85 mg) at 0 °C. After a few minutes, a yellow solution formed. After removal of all volatile materials in vacuo, a yellow solid remained. Raman (100 mW, 25 °C): $\tilde{\nu}$ = 3037(20), 2979(20), 2921(20), 2105(40)/2055(15) [$\nu_{as}(N_3)$], 1472(10), 1459(10), 1447(15), 1312(15) [$\nu_s(N_3)$], 1263(10), 948(15), 753(20), 668(10), 639(20), 409(100)/347(85) [ν(TeN)], 255(30), 203(40), 174(50) cm$^{-1}$; $^{14}$N NMR (28.9 MHz, $CD_2Cl_2$, 25 °C, $\Delta\nu_{1/2}$ (Hz)): $\delta = -139$ (20, $N_\beta$), −236 (270, $N_\gamma$), ≈ −250 (extremely broad, $N_\alpha$), −337.8 ppm (3, $Me_4N$); $^{125}$Te NMR (126.1 MHz, $CD_2Cl_2$, 25 °C): $\delta$ = 1258 ppm.

**2b**: A suspension of $TeF_4$ (1 mmol, 205 mg) in dry pyridine (5 mL) was stirred for 12 h. All volatile materials were removed in vacuo and a part of the obtained residue (100 mg) was treated with $Me_3SiN_3$ (1.1 mmol, 125 mg) at 0 °C. After stirring for 1 h, the resulting yellow mixture was decanted. Upon cooling at −25 °C for 30 min, yellow crystals of **2b** can be carefully separated from the supernatant. Raman (100 mW, 25 °C): $\tilde{\nu}$ = 3109(5), 3052(5), 2112(30)/2079(10)/2064(5)/2037(15) [$\nu_{as}(N_3)$], 1640(2), 1618(2), 1490(2), 1323(10) [$\nu_s(N_3)$], 1298(5), 1272(5), 1245(5), 1200(5), 1029(10), 1011(20), 667(5), 651(5), 639(10), 406(100)/342(50) [ν(TeN)], 300(20), 253(15), 193(35), 170(30) cm$^{-1}$. $^{14}$N NMR (28.9 MHz, $CDCl_3$, 25 °C, $\Delta\nu_{1/2}$ (Hz)): $\delta = -115$ (400, py), −141 (25, $N_\beta$), −234 (360, $N_\gamma$), −245 ppm (extremely broad, $N_\alpha$); $^{125}$Te NMR (126.1 MHz, $CDCl_3$, 25 °C): $\delta$ = 1334 ppm.

Crystal data for **2b**: $C_5H_6N_{16}Te$ ($M_r$ = 417.81), yellow block, 0.14 × 0.22 × 0.30 mm, triclinic, space group $P\bar{1}$, $a$ = 7.6459(1), $b$ = 10.3875(1), $c$ = 10.5173(2) Å, $\alpha$ = 117.6238(8), $\beta$ = 91.5610(9), $\gamma$ = 107.847(1)°, $V$ = 690.13(2) Å$^3$, $Z$ = 2, $\rho_{calcd}$ = 2.011 g cm$^{-3}$, $\mu$ = 2.184 mm$^{-1}$, $F(000)$ = 400, Nonius Kappa CCD, $Mo_{K\alpha}$ ($\lambda$ = 0.71073 Å), $T$ = 200 K, $\theta$ range = 3.35 to 27.52°, $-9 \le h \le 9$, $-13 \le k \le 13$, $-13 \le l \le 13$, reflections collected: 10103, independent reflections: 3134 ($R_{int}$ = 0.0376), observed reflections: 2940 [$I > 2\sigma(I)$], structure solution: SIR97,[17] direct methods, data to parameters ratio: 14.0:1 [13.2:1 $I > 2\sigma(I)$], final $R$ indices: $R1$ = 0.0228, $wR2$ = 0.0545 for [$I > 2\sigma(I)$]; $R1$ = 0.0257, $wR2$ = 0.0554 for all data, GOF on $F^2$ = 1.160.

CCDC-215495 (**2b**) contains the supplementary crystallographic data for this paper. These data can be obtained free of charge via www.ccdc.cam.ac.uk/conts/retrieving.html (or from the Cambridge Crystallographic Data Centre, 12, Union Road, Cambridge CB2 1EZ, UK; fax: (+44) 1223-336-033; or deposit@ccdc.cam.ac.uk).

Ab initio calculations: Gaussian03 program package,[18] HF-SCF, DFT, and MP2 methods, basis sets (N: Dunning/Huzinaga valence double-zeta, cc-pVTZ basis sets;[19] Te: double-zeta or triple-zeta basis sets for the valence electrons and energy-consistent large-core ECPs for 46 core electrons[20]) as implemented in Gaussian.

Received: August 15, 2003 [Z52656]

**Keywords:** azides · fluorides · hazardous materials · tellurium

[1] a) R. Metzner, *Ann. Chim. Phys.* **1898**, *15*, 257; b) A. Damiens, *Ann. Chim. Phys.* **1923**, *19*, 74; c) W. Strecker, W. Ebert, *Ber. Dtsch. Chem. Ges.* **1925**, *58*, 2527; d) W. Strecker, C. Mahr, *Z. Anorg. Allg. Chem.* **1934**, *221*, 199; e) O. Schmitz-DuMont, B. Ross, *Angew. Chem.* **1967**, *79*, 1061; *Angew. Chem. Int. Ed. Engl.* **1967**, *6*, 1071; f) H. Garcia-Fernandez, *Bull. Soc. Chim. Fr.* **1973**, 1210; g) W. Massa, C. Lau, M. Möhlen, B. Neumüller, K. Dehnicke, *Angew. Chem.* **1998**, *110*, 3008; *Angew. Chem. Int. Ed.* **1998**, *37*, 2840.

[2] J. P. Johnson, G. K. MacLean, J. Passmore, P. S. White, *Can. J. Chem.* **1989**, *67*, 1687.

[3] N. Wiberg, G. Schwenk, K. H. Schmid, *Chem. Ber.* **1972**, *105*, 1209.

[4] a) H. Sussek, F. Stowasser, H. Pritzkow, R. A. Fischer, *Eur. J. Inorg. Chem.* **2000**, 455; b) A. Kornath, *Angew. Chem.* **2001**, *113*, 3231; *Angew. Chem. Int. Ed.* **2001**, *40*, 3135, and references therein; c) W. Beck, T. M. Klapötke, P. Klüfers, G. Kramer, C. M.

 © 2003 Wiley-VCH Verlag GmbH & Co. KGaA, Weinheim 

Rienäcker, *Z. Anorg. Allg. Chem.* **2001**, *627*, 1669; d) W. Fraenk, T. Habereder, A. Hammerl, T. M. Klapötke, B. Krumm, P. Mayer, H. Nöth, M. Warchhold, *Inorg. Chem.* **2001**, *40*, 1334; e) W. Fraenk, H. Nöth, T. M. Klapötke, M. Suter, *Z. Naturforsch. B* **2002**, *57*, 621; f) A. C. Filippou, P. Portius, G. Schnakenburg, *J. Am. Chem. Soc.* **2002**, *124*, 12396; g) K. Karaghiosoff, T. M. Klapötke, B. Krumm, H. Nöth, T. Schütt, M. Suter, *Inorg. Chem.* **2002**, *41*, 170.

[5] a) T. M. Klapötke, B. Krumm, P. Mayer, O. P. Ruscitti, *Inorg. Chem.* **2000**, *39*, 5426, and references therein; b) T. M. Klapötke, B. Krumm, P. Mayer, H. Piotrowski, O. P. Ruscitti, A. Schiller, *Inorg. Chem.* **2002**, *41*, 1184, and references therein.

[6] a) T. M. Klapötke, B. Krumm, P. Mayer, D. Naumann, I. Schwab, *J. Fluorine Chem.*, in press; b) T. M. Klapötke, B. Krumm, P. Mayer, H. Piotrowski, I. Schwab, M. Vogt, *Eur. J. Inorg. Chem.* **2002**, 2701, and references therein.

[7] a) Presented at the *225th ACS National Meeting* (New Orleans, USA), **2003**, Abstr. INOR-456; b) Independently determined crystal structure of $[Te(N_3)_6]^{2-}$ ion, see: R. Haiges, J. A. Boatz, M. Gerken, S. Schneider, T. Schroer, K. O. Christe, *Angew. Chem.* **2003**, *115*, 6027; *Angew. Chem. Int. Ed.* **2003**, *42*, 5847.

[8] a) W. Beck, W. P. Fehlhammer, P. Pollmann, E. Schuierer, K. Feldl, *Chem. Ber.* **1967**, *100*, 2335; b) J. Drummond, J. S. Wood, *J. Chem. Soc. Chem. Commun.* **1969**, 1373.

[9] On two separate occasions, small amounts of neat, noncrystalline $Te(N_3)_4$ (**1**) exploded within the glassware just before an attempted Raman characterization and caused severe damage, therefore we refrained from handling the compound further. A detailed description of the vibrational data of **1** is presented explicitly in Ref. [7b].

[10] A. R. Mahjoub, D. Leopold, K. Seppelt, *Z. Anorg. Allg. Chem.* **1992**, *618*, 83.

[11] E. E. Aynsley, G. Hetherington, *J. Chem. Soc.* **1953**, 2802.

[12] N. N. Greenwood, A. C. Sarma, B. P. Straughan, *J. Chem. Soc. A* **1968**, 1561.

[13] T. M. Klapötke, B. Krumm, P. Mayer, I. Schwab, unpublished results.

[14] A. Bondi, *J. Phys. Chem.* **1964**, *68*, 441.

[15] T. M. Klapötke, B. Krumm, K. Polborn, unpublished results.

[16] a) K. Seppelt, *Inorg. Synth.* **1980**, *20*, 33; b) N. N. Greenwood, A. C. Sarma, B. P. Straughan, *J. Chem. Soc. A* **1966**, 1446.

[17] A. Altomare, M. C. Burla, M. Camalli, G. L. Cascarano, C. Giacovazzo, A. Guagliardi, A. G. G. Moliterni, G. Polidori, R. Spagna, *J. Appl. Crystallogr.* **1999**, *32*, 115.

[18] Gaussian 2003 (Revision B.0), M. J. Frisch, G. W. Trucks, H. B. Schlegel, G. E. Scuseria, M. A. Robb, J. R. Cheeseman, J. A. Montgomery, Jr., T. Vreven, K. N. Kudin, J. C. Burant, J. M. Millam, S. S. Iyengar, J. Tomasi, V. Barone, B. Mennucci, M. Cossi, G. Scalmani, N. Rega, G. A. Petersson, H. Nakatsuji, M. Hada, M. Ehara, K. Toyota, R. Fukuda, J. Hasegawa, M. Ishida, T. Nakajima, Y. Honda, O. Kitao, H. Nakai, M. Klene, X. Li, J. E. Knox, H. P. Hratchian, J. B. Cross, C. Adamo, J. Jaramillo, R. Gomperts, R. E. Stratmann, O. Yazyev, A. J. Austin, R. Cammi, C. Pomelli, J. W. Ochterski, P. Y. Ayala, K. Morokuma, G. A. Voth, P. Salvador, J. J. Dannenberg, V. G. Zakrzewski, S. Dapprich, A. D. Daniels, M. C. Strain, O. Farkas, D. K. Malick, A. D. Rabuck, K. Raghavachari, J. B. Foresman, J. V. Ortiz, Q. Cui, A. G. Baboul, S. Clifford, J. Cioslowski, B. B. Stefanov, G. Liu, A. Liashenko, P. Piskorz, I. Komaromi, R. L. Martin, D. J. Fox, T. Keith, M. A. Al-Laham, C. Y. Peng, A. Nanayakkara, M. Challacombe, P. M. W. Gill, B. Johnson, W. Chen, M. W. Wong, C. Gonzalez, J. A. Pople, Gaussian, Inc., Pittsburgh, PA, **2003**.

[19] a) T. H. Dunning, Jr., P. J. Hay in *Modern Theoretical Chemistry*, *Vol. 3* (Ed.: H. F. Schaefer III), Plenum, New York, **1976**; b) T. H. Dunning, Jr., *J. Chem. Phys.* **1989**, *90*, 1007.

[20] a) A. Bergner, M. Dolg, W. Küchle, H. Stoll, H. Preuss, *Mol. Phys.* **1993**, *80*, 1431; b) J. M. L. Martin, A. Sundermann, *J. Chem. Phys.* **2001**, *114*, 3408; see also http://theochem.weizmann.ac.il/web/papers/SDB-cc.html.

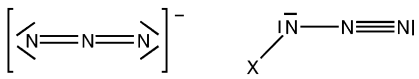
 © 2003 Wiley-VCH Verlag GmbH & Co. KGaA, Weinheim 

*Azide Complexes (2)*

# Polyazide Chemistry: Preparation and Characterization of $Te(N_3)_4$ and $[P(C_6H_5)_4]_2[Te(N_3)_6]$ and Evidence for $[N(CH_3)_4][Te(N_3)_5]$**

*Ralf Haiges, Jerry A. Boatz, Ashwani Vij, Michael Gerken, Stefan Schneider, Thorsten Schroer, and Karl O. Christe**

The azido group is highly energetic and adds about 70 kcal mol$^{-1}$ to the energy content of a molecule. It is, therefore, not surprising that polyazides are highly endothermic compounds, and that their energy content increases with an increasing number of azido ligands. Compared to the relatively stable azide anion, which possesses two double bonds, the bonds in covalent azides are polarized towards a single and a triple bond, which greatly facilitates $N_2$ elimination and enhances their shock sensitivity.



Consequently, the synthesis and characterization of covalent binary azides containing multiple azido ligands can present great experimental challenges, and binary tellurium azides are no exception to this general rule.

Whereas numerous, partially azide-substituted tellurium compounds have been reported,[1–14] only one binary tellurium azide, the $[Te(N_3)_3]^+$ ion, has previously been reported.[5] In this paper, we wish to communicate the synthesis and characterization of three novel binary tellurium azides, $Te(N_3)_4$, $[Te(N_3)_5]^-$, and $[Te(N_3)_6]^{2-}$.

In the presence of catalytic amounts of CsF, the reaction of $TeF_6$ with excess $(CH_3)_3SiN_3$ in acetonitrile solution at room temperature results in the reduction of $Te^{VI}$ to $Te^{IV}$, while the azide ion is oxidized to dinitrogen. Furthermore, complete fluoride–azide exchange takes place, to yield a clear yellow solution of $Te(N_3)_4$ according to Equation (1).

$$TeF_6 + 6\,(CH_3)_3SiN_3 \xrightarrow{CH_3CN} Te(N_3)_4 + 6\,(CH_3)_3SiF + 3\,N_2 \qquad (1)$$

Removal of the volatile products ($CH_3CN$, $(CH_3)_3SiF$, and excess $(CH_3)_3SiN_3$) in vacuo results in the isolation of $Te(N_3)_4$ as a bright-yellow solid. In the absence of CsF, no fluoride–azide exchange reaction was observed even after several days at room temperature. The catalytic function of the fluoride ion in these reactions probably involves the generation of intermediate free azide ions from the reaction of $(CH_3)_3SiN_3$ and $F^-$ ions, and these free azide ions might be the actual reagent. The need for fluoride-ion catalysis, found in our study, is in contrast to the results from a previous $^{19}F$ NMR study[9] in which $TeF_6$ was reported to undergo facile fluoride–azide exchange with $(CH_3)_3SiN_3$ in $CD_3CN$ solution to produce all the members of the $TeF_n(N_3)_{6-n}$ ($n = 1$–5) series. In their study, these authors also observed the azide-ion-mediated reduction of $Te^{VI}$ to $Te^{IV}$ as a side reaction.

As expected for a highly endothermic, binary covalent polyazide, $Te(N_3)_4$ is very sensitive and can explode violently. Its identity was established by the observed material balance, and through vibrational and NMR spectroscopy. The presence of single $\delta(^{125}Te)$ signals at $\delta = 1427$ ppm ($CH_3CN$ solution) and $\delta = 1376$ ppm (DMSO solution), and the absence of any signals that would indicate Te–F spin–spin coupling in $CH_3CN$ solution at 25 °C confirm complete fluoride–azide exchange and a pronounced solvent dependency of these shifts. The observed $^{125}Te$ shifts are in accord with our expectations for a multi-azido-substituted $Te^{IV}$ compound; the shift reported for the closest known analogue, $CH_3Te(N_3)_3$, is $\delta = 1405$ ppm.[12] Furthermore, the presence of covalent azido ligands[11–16] is confirmed by the observed $^{14}N$ NMR shifts of $\delta = -139.8$ ppm ($N_\beta$, $\Delta\nu_{1/2} = 63$ Hz) and $-238$ ppm ($N_\gamma$, $\Delta\nu_{1/2} = 680$ Hz) in DMSO solution at 25 °C. In addition to quadrupolar broadening, rapid ligand exchange on the NMR timescale by the Berry pseudorotation mechanism[17] might contribute to the observation of only one set of azide signals and the relative broadness of the $N_\beta$ resonance.

The observed Raman spectrum of solid $Te(N_3)_4$ is shown in Figure 1, and the observed infrared and Raman frequencies and intensities are listed in the Experimental Section. Assignments of the observed spectra were made by comparison with those calculated at the B3LYPSBKJC + (d) level of theory.[18]

These calculations resulted in two minimum-energy structures of $C_2$ symmetry (Figure 2a and b). Both structures are derived from pseudo trigonal bipyramids, in which one of the equatorial positions is occupied by the sterically active free valence-electron pair of the tellurium center. The two structures differ in energy by only 1.8 kcal mol$^{-1}$. Their main structural difference is the orientation of the axial azido ligands. In structure **2a**, the axial azido ligands point in the same direction and toward the free valence-electron pair of the Te center. This compresses the free pair in the axial direction and exerts additional pressure on the two equatorial

[*] Prof. Dr. K. O. Christe, Dr. R. Haiges, Dr. M. Gerken, Dr. S. Schneider, Dr. T. Schroer
Loker Research Institute
University of Southern California
Los Angeles, CA 90089-1661 (USA)
Fax: (+1) 213-740-6679
E-mail: kchriste@usc.edu
Prof. Dr. K. O. Christe, Dr. J. A. Boatz, Dr. A. Vij
ERC, Inc. and Space and Missile Propulsion Division
Air Force Research Laboratory (AFRL/PRSP)
10 East Saturn Boulevard, Bldg 8451
Edwards Air Force Base, CA 93524 (USA)

[**] This work was funded by the Defense Advanced Research Projects Agency, with additional support from the Air Force Office of Scientific Research and the National Science Foundation. R.H. thanks the Deutsche Forschungsgemeinschaft for a postdoctoral fellowship. We thank Drs. A. Morrish, D. Woodbury, and M. Berman for their steady support, and Drs. R. Wagner, I. Tsyba, and Prof. R. Bau for their help and stimulating discussions. We also thank Prof. T. Klapötke and his colleagues for exchange of information about their independent syntheses of $Te(N_3)_4$ and $Te(N_3)_5^-$.

 DOI: 10.1002/anie.200352680 © 2003 Wiley-VCH Verlag GmbH & Co. KGaA, Weinheim 

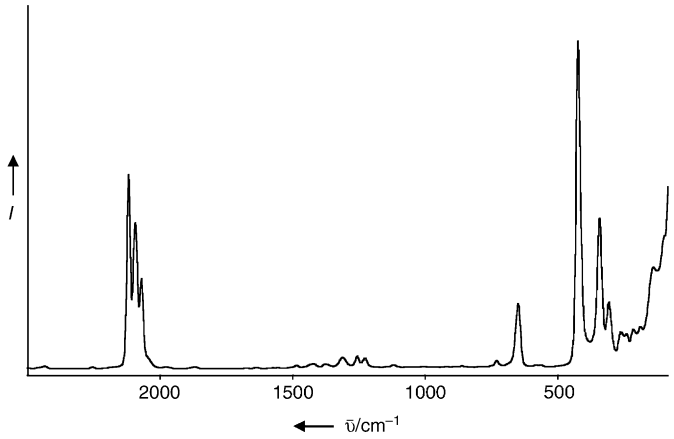



***Figure 1.*** Raman spectrum of solid $Te(N_3)_4$.

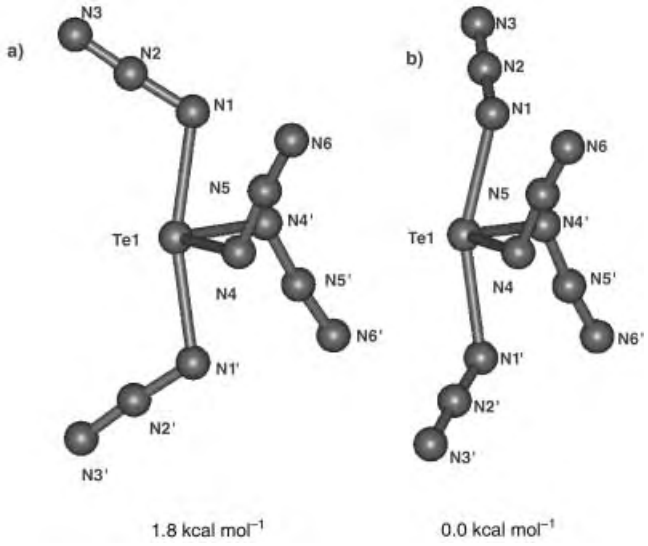



***Figure 2.*** The two minimum energy structures calculated for $Te(N_3)_4$ at the B3LYPSBKJC+(d) level of theory.

ligands, compressing their bond angle by 11° compared to structure **2b**, in which the axial azido ligands point in different directions and away from the free pair.

The vibrational spectra, calculated for **2a** and **2b**,[18] are almost identical and do not permit a distinction between the two models. Nevertheless, they strongly support the presence of highly covalent azido ligands, the absence of Te–F bonds, and the identification of this compound as $Te(N_3)_4$. Because the two isomers have similar Te–N skeletal geometries and differ only in the orientation of the highly fluxional azido ligands, the vibrational spectra should deviate significantly only in the torsional modes. However, these modes are difficult to observe because of their low frequencies and intensities. A further complication might arise from the solid state, where coordinatively unsaturated polyazides might seek higher coordination numbers by the formation of nitrogen bridges. Consequently, crystal-structure data are required for a reliable determination of the precise arrangement of the azido ligands.

The reaction of $Te(N_3)_4$ with ionic azides leads to the formation of the $[Te(N_3)_6]^{2-}$ ion, according to Equation (2).

$$Te(N_3)_4 + 2\,[P(C_6H_5)_4]N_3 \xrightarrow{CH_3CN} [P(C_6H_5)_4]_2[Te(N_3)_6] \qquad (2)$$

The $[P(C_6H_5)_4]_2[Te(N_3)_6]$ salt is a yellow solid which is stable at room temperature and, because of the presence of two large counterions, is much less sensitive to shock than $Te(N_3)_4$. It was characterized from its crystal structure,[19] and by infrared, Raman, and $^{125}Te$ and $^{14}N$ NMR spectroscopy.

$[P(C_6H_5)_4]_2[Te(N_3)_6]$ crystallizes in the triclinic space group $P\bar{1}$ and is the first structurally characterized anionic tellurium(IV) azide.[20] The structure of the dianion shows roughly 50% positional disorder in two azide groups, i.e., N10-N11-N12 and N16-N17-N18. Figure 3 depicts the $TeN_6$ skeleton that is strongly distorted from octahedral symmetry by the sterically active free valence-electron pair of the Te center. If this electron pair were sterically inactive, one would expect perfect $S_6$ symmetry for a $Te(N_3)_6$ species, as predicted by our theoretical studies for $Te(N_3)_6$ and $[Te(N_3)_6]^{2-}$. The possibility of the distortion in $[Te(N_3)_6]^{2-}$ being caused by nitrogen bridging with other anions can be ruled out because, in its $P(C_6H_5)_4^+$ salt, the anions are well separated by twice as many large counterions, and the closest Te···N contacts between neighboring anions are 6.2 Å.

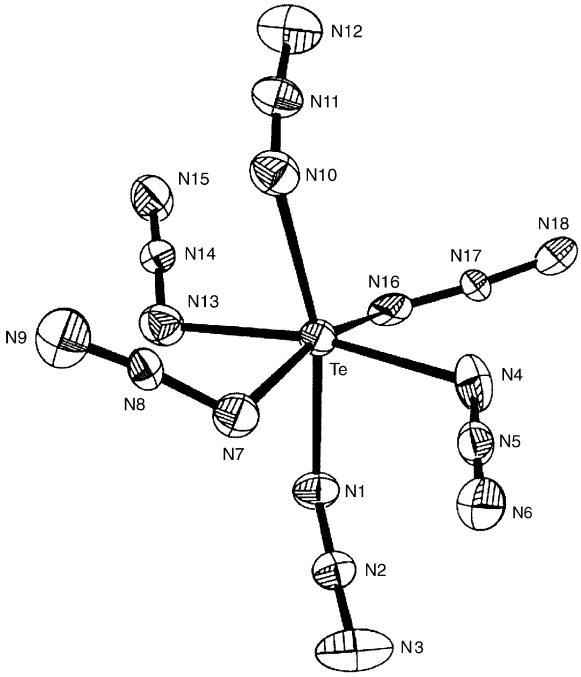



***Figure 3.*** ORTEP drawing of the dianionic part of the crystal structure of $[P(C_6H_5)_4]_2[Te(N_3)_6]$. Thermal ellipsoids are shown at the 50% probability level without any disordered components. Selected bond lengths [Å] and angles [°]: Te-N1 2.136(2), Te-N4 2.240(2), Te-N7 2.094(2), Te-N10 2.416(2), Te-N13 2.197(2), Te-N16 2.542(2), N1-N2 1.228(2), N2-N3 1.115(3), N10-N11 1.223(3), N11-N12 1.143(10), N16-N17 1.206(10), N17-N18 1.159(10); N1-N2-N3 174.4(3), N13-N14-N15 177.6(3), Te-N10-N11 109.3(2), Te-N4-N5 121.2(2), N1-Te-N16 78.0(4), N7-Te-N10 80.63(8), N1-Te-N7 83.59(8), N4-Te-N7 83.79(9), N1-Te-N13 84.32(8), N7-Te-N13 85.33(8), N10-Te-N13 87.89(8), N1-Te-N4 88.87(9), N13-Te-N16 88.5(3), N4-Te-N10 95.87(8), N4-Te-N16 100.1(3), N10-Te-N16 117.1(4).

 © 2003 Wiley-VCH Verlag GmbH & Co. KGaA, Weinheim 

From the bond angles observed for $[Te(N_3)_6]^{2-}$, it appears that the free pair is located primarily between the N10 and N16 atoms (widening of the N10-Te-N16 angle to 120.6(4)° (av)) and displaced somewhat toward N4. Therefore, the $[Te(N_3)_6]^{2-}$ structure is best described as a distorted pseudo pentagonal bipyramid, in which the free valence-electron pair of the Te center is sterically active and occupies one of the equatorial positions. Because of increased ligand crowding in the equatorial plane, the free pair is located somewhat above the N1-N7-N10-N16 plane. This interpretation of the structure is also supported by the observed Te–N bond lengths, which exhibit remarkable differences and can be separated into three sets of pairs: N1 (2.136(2)) and N7 (2.094(2)), N4 (2.240(2)) and N13 (2.197(2)), and N10 (2.416(2)) and N16 (2.535(9) Å (av)). The N1-N2-N3 and N7-N8-N9 ligands are highly covalent, as shown by their very short Te–N bond lengths of about 2.1 Å and the large differences between the $N_\alpha$–$N_\beta$ and $N_\beta$–$N_\gamma$ bonds. In contrast, the $N_3$ ligand, composed of N16-N17-N18, is partially ionic with a Te–N bond length of 2.535(9) Å (av) and with similar $N_\alpha$–$N_\beta$ and $N_\beta$–$N_\gamma$ bond lengths.

In contrast to the observed crystal structure, the global minimum energy structure, predicted for free gaseous $[Te(N_3)_6]^{2-}$ at the B3LYPSBKJC + (d) level of theory,[18] shows ideal $S_6$ symmetry. Local minima of $C_1$ symmetry with asymmetric arrangements of the azido groups were also found which are only slightly higher in energy. The distortions in these $C_1$ structures are relatively minor and are caused by mutual repulsion effects among the azido ligands. These findings indicate that in our calculations the free valence-electron pair of the Te center is sterically inactive. Similar problems with correctly predicting the steric activity of free valence-electron pairs by these methods have been encountered by us for related species, such as $[IF_6]^-$. This ion is known to have a sterically active free valence-electron pair and a strongly distorted octahedral structure,[21,22] but the theoretical studies predict an ideal octahedral structure with a sterically inactive free valence-electron pair.[23]

The NMR spectra provide further support for the presence of the $[Te(N_3)_6]^{2-}$ ion. The observed $^{125}$Te shift of 1250 ppm ($CH_3CN$, 25 °C) is in the range expected for a covalent multi-azido-substituted $Te^{IV}$ compound (see above) and, relative to $Te(N_3)_4$, its shielding is increased by 177 ppm due to the addition of two negatively charged azide ions. By analogy with $Te(N_3)_4$, the $^{14}$N NMR spectra ($CH_2Cl_2$, 25 °C) show resonances characteristic for covalent azido groups at $\delta = -138.6$ ($N_\beta$, $\Delta\nu_{1/2} = 33$ Hz) and $-239$ ppm ($N_\gamma$, $\Delta\nu_{1/2} = 240$ Hz), while $N_\alpha$ is too broad for a reliable assignment. Again, the observation of a single set of signals implies rapid exchange of the different type of ligands on the NMR time scale.

The observed infrared and Raman spectra of $[P(C_6H_5)_4]_2[Te(N_3)_6]$ are shown in Figure 4, and the observed frequencies are listed in the Experimental Section. Again, the agreement between the observed and the calculated spectra is good for the azido vibrations, however, the agreement is poor for the skeletal $TeN_6$ modes because of the failure of the calculations to properly predict the distortion caused by the steric activity of the free valence-electron pair of the Te center.

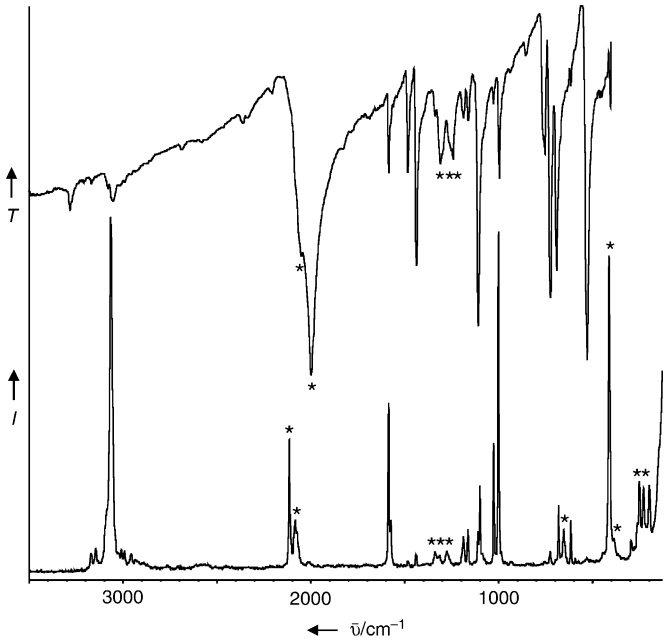



***Figure 4.*** IR and Raman spectra of $[P(C_6H_5)_4]_2[Te(N_3)_6]$. The bands belonging to the $[Te(N_3)_6]^{2-}$ ion are marked with asterisks.

During an attempted synthesis of the $[Te(N_3)_7]^-$ ion from $[TeF_7]^-$ and trimethylsilylazide (either neat or in $CH_3CN$ solution at room temperature), single crystals of $[N(CH_3)_4]^+[Te(N_3)_5]^-$ were obtained and identified by their crystal structure. Again the reduction of $Te^{VI}$ to $Te^{IV}$ by $N_3^-$ ions had occurred [Eq. (3)]:

$$[TeF_7]^- + 7\,(CH_3)_3SiN_3 \rightarrow [Te(N_3)_5]^- + 7\,(CH_3)_3SiF + 3\,N_2 \qquad (3)$$

The structure had a low $R$ factor of 0.016 and clearly showed the expected pseudooctahedral geometry with the free valence-electron pair of the Te center occupying one of the axial positions. However, this structure suffers from a partial occupancy of one equatorial azide position by a chloride ion (which is introduced during recrystallization from a $CH_2Cl_2$ solution), a positional disorder of a second equatorial azide ligand, and a twofold disorder of the $[N(CH_3)_4]^+$ ion along a $C_3$ axis. Consequently, this structure is not discussed in further detail because an ordered structure for this anion has already been obtained by Klapötke and coworkers.[20]

Tellurium azides are remarkable in that the nature of their Te–N bonds can vary in closely related compounds, or even within the same compound, from highly ionic to highly covalent with correspondingly large changes in bond lengths. For example, in $R_3TeN_3$ ($R = CH_3$ or $C_6H_5$),[14] the Te–N bond lengths have average values of about 3.0 Å and the two N–N bonds in the azido groups are almost identical in length, which indicates the presence of highly ionic azides. The other extreme, that is the presence of highly covalent azido ligands, is found in the $[Te(N_3)_3]^+$ ion[5] and $RTe(N_3)_3$ (R = Et, *n*Pr, *i*Pr, or 2,4,6-$Me_3C_6H_2$).[12] In these compounds, the Te–N bond lengths range from 1.99 to 2.25 Å, and the $N_\alpha$–$N_\beta$ and $N_\beta$–$N_\gamma$ lengths differ by about 0.1 Å. As might be expected,

 © 2003 Wiley-VCH Verlag GmbH & Co. KGaA, Weinheim 

compounds with bond lengths that fall between these extremes are also known. For example, the Te–N bond in $[(C_6H_5)_2TeN_3]_2O$ is 2.397(8) Å in length.[10]

Although the bond lengths for $Te(N_3)_4$ could not be measured experimentally, the values of 2.071 and 2.185 Å, predicted for the free gaseous molecule at the B3LYPSBKJC+(d) level of theory,[18] and the observed vibrational and NMR spectra suggest the presence of highly covalent Te–N bonds, similar to those predicted for free $Te(N_3)_6$. In contrast, the Te–N bond lengths observed for $[Te(N_3)_6]^{2-}$ cover a wide range from 2.094(2) to 2.542(9) Å, which indicates the simultaneous presence of highly covalent and partially ionic Te–N bonds within the same ion. The increase of 0.20 Å in the predicted average Te–N bond length on going from $Te(N_3)_6$ to $[Te(N_3)_6]^{2-}$ can be explained by a higher ionicity of the Te–N bonds in $[Te(N_3)_6]^{2-}$, caused by the two formal negative charges.

## Experimental Section

Caution! Covalent azides are potentially hazardous and can decompose explosively under various conditions. They should be handled only on a small scale with appropriate safety precautions (face shields, leather gloves, and protective clothing).

All reactions were carried out in teflon-FEP ampules closed by stainless steel valves. Volatile materials were handled in a stainless steel–teflon-FEP or pyrex glass vacuum line. Nonvolatile materials were handled in the dry argon atmosphere of a glove-box. All reaction vessels and the stainless steel line were passivated with $ClF_3$ prior to use.

Raman spectra were recorded in the range 4000–80 $cm^{-1}$ on a Bruker Equinox 55 FT-RA spectrophotometer using a Nd-YAG laser at 1064 nm. Pyrex melting point tubes were baked out at 300 °C for 48 h at $10^{-2}$ Torr and teflon-FEP tubes with stainless steel valves, passivated with $ClF_3$, were used as sample containers. Infrared spectra were recorded on a Midac M Series FT-IR spectrometer using KBr or AgCl pellets. The pellets were prepared inside the glove-box using an Econo press (Barnes Engineering Co.). NMR spectra were recorded unlocked at 500.13 MHz ($^1$H), 125.76 MHz ($^{13}$C), 202.46 MHz ($^{31}$P), 158.03 MHz ($^{125}$Te) and 36.13 MHz ($^{14}$N) on a Bruker AMX 500 spectrometer using solutions of the compounds in acetonitrile or dichloromethane in sealed standard glass tubes. Neat TMS ($\delta$ = 0.00 ppm) was used as external reference for $^1$H and $^{13}$C, 85% aqueous $H_3PO_4$ ($\delta$ = 0.00 ppm) as external reference for $^{31}$P, saturated aqueous $Te(OH)_6$ ($\delta$ = 710.9 ppm)[24] as external reference for $^{125}$Te and neat $CH_3NO_2$ ($\delta$ = 0.00 ppm) was the external reference for $^{14}$N.

The starting materials $TeF_6$ (Ozark Mahoning) and $[(C_6H_5)_4P]I$ (Aldrich) were used without further purification. $(CH_3)_3SiN_3$ (Aldrich) was purified by fractional condensation prior to use. Solvents were dried by standard methods and freshly distilled prior to use. $[(C_6H_5)_4P]N_3$ was prepared from $[(C_6H_5)_4P]I$ and $AgN_3$.

Preparation of $Te(N_3)_4$: On the stainless steel vacuum line, $TeF_6$ (0.438 mmol) was condensed at −196 °C into a teflon-FEP ampoule containing CsF (0.05 mmol). The ampoule was then attached to a glass vacuum line and after evacuation, $CH_3CN$ (50 mmol) and $(CH_3)_3SiN_3$ (3.21 mmol) was condensed into the ampoule at −196 °C. The mixture was allowed to warm to ambient temperature, resulting in weak gas-evolution and a yellow-colored solution. After 8 h, the temperature was lowered to −20 °C, and all volatile compounds were pumped off over a period of 8 h, leaving behind a yellow liquid. Additional pumping at ambient temperature for 2 h resulted in a bright yellow solid (0.130 g, weight calculated for 0.438 mmol $Te(N_3)_4$ = 0.129 g). Inspection of the volatile material trapped at −196 °C by gas-FTIR spectroscopy showed $CH_3CN$ and $(CH_3)_3SiF$[25,26] as the sole reaction by-product. IR: $\tilde{\nu}$ = 2111(w)/2082(m)/2063(m)/2048(s)/1998 (vs) ($\nu_{as}N_3$), 1294(mw)/1251(m)/1241 $cm^{-1}$ (mw) ($\nu_sN_3$). Raman: $\tilde{\nu}$ = 2116(4.2)/2085(1.7)/2075 (1.3)/2065(0.7)/2057(0.4) ($\nu_{as}N_3$), 1334(0.6)/1313(0.6)/1277(0.7)/1260(0.4) ($\nu_sN_3$), 654(1.4)/647(0.9)/639(0.5) ($\delta N_3$), 412(10.0)/385(1.1) $cm^{-1}$ ($\nu$TeN).

Preparation of $[(C_6H_5)_4P]_2[Te(N_3)_6]$: $[(C_6H_5)_4P]N_3$ (0.6 mmol) was loaded into a teflon-FEP ampoule containing $Te(N_3)_4$ (0.3 mmol), followed by the addition of $CH_3CN$ (30 mmol) in vacuo at −196 °C. The mixture was warmed to room temperature, which resulted in the formation of an orange solution. After 3 h, all volatile material was pumped off, leaving behind an orange solid (0.310 g, weight calculated for 0.3 mmol $[(C_6H_5)_4P]_2[Te(N_3)_6]$ = 0.317 g). Single crystals were grown from a solution in $CH_3CN$. IR: $\tilde{\nu}$ = 2110(vs)/2060(vs) ($\nu_{as}N_3$), 1317(m)/1236 $cm^{-1}$ (m) ($\nu_sN_3$). Raman: $\tilde{\nu}$ = 2119(4.3)/2094(3.3)/2070(2.1) ($\nu_{as}N_3$), 1312(0.3)/1257(0.4)/1227(0.3) ($\nu_sN_3$), 649(1.9) ($\delta N_3$), 424(10.0) ($\nu_{sym}TeN_{2eq}$), 343(4.6) ($\nu_{sym}TeN_{2ax}$) and ($\nu_{as}TeN_{2eq}$), 307(2.1) ($\nu_{as}TeN_{2ax}$), 262(1.2), 241(1.1), 216(1.3), 183(1.4), 138(3.4) $cm^{-1}$.

Preparation of $[N(CH_3)_4][Te(N_3)_5]$: A sample of $[N(CH_3)_4][TeF_7]$ (0.5 mmol) was loaded into a Teflon-FEP ampoule in a glove-box, followed by the addition of $CH_3CN$ (50 mmol) in vacuo at −196 °C. The mixture was warmed to room temperature to form a solution, cooled again to −196 °C, and $(CH_3)_3SiN_3$ (4.0 mmol) was condensed into the mixture. The ampoule was allowed to warm to ambient temperature resulting in a yellow solution. All volatile components were pumped off to leave a yellow solid residue (0.199 g, weight calculated for 0.5 mmol of $[N(CH_3)_4]$ $[Te(N_3)_5$ = 0.206 g). Recrystallization of the crude product from $CH_2Cl_2$ solution by cooling to −30 °C resulted in yellow crystals. Raman (selected values): $\tilde{\nu}$ = 2109(8.4)/2094(1.9)/2074(1.9)/2057(2.6)/2047(2.7)/2036(2.0) ($\nu_{as}N_3$), 1311(1.7)/1266(1.2) ($\nu_sN_3$), 679(0.9)/664(0.8)/656(0.7) ($\delta N_3$), 400(10.0)/337(6.7) $cm^{-1}$ ($\nu$TeN). IR (selected values): $\tilde{\nu}$ = 2086(vs)/2057(vs)/2022(vs) ($\nu_{as}N_3$), 1306(s) ($\nu_sN_3$), 645(w) $cm^{-1}$ ($\delta N_3$). $^{14}$N NMR ($CH_3CN$, 25 °C): $\delta$ = −138 ($N_\beta$, $\Delta\nu_{1/2}$ = 40 Hz), −233 ($N_\gamma$, $\Delta\nu_{1/2}$ = 210 Hz), −337.8 ppm (($CH_3)_4N$, $\Delta\nu_{1/2}$ = 6 Hz); $^{125}$Te NMR ($CH_3CN$, 25 °C) $\delta$ = 1256 ppm.

Received: August 19, 2003 [Z52680]

**Keywords:** azides · density functional calculations · hazardous materials · structure elucidation · tellurium

[1] N. Wiberg, G. Schwenk, K. H. Schmid, *Chem. Ber.* **1972**, *105*, 1209.
[2] R. F. Ziolo, K. Pritchett, *J. Organomet. Chem.* **1976**, *116*, 211.
[3] a) T. N. Srivastava, R. C. Srivastasa, M. Singh, *J. Organomet. Chem.* **1978**, *157*, 405; b) T. N. Srivastava, R. C. Srivastasa, H. B. Singh, *Indian J. Chem. Sect. A* **1979**, *18*, 71; c) T. N. Srivastava, R. C. Srivastasa, H. B. Singh, M. Singh, *Indian J. Chem. Sect. A* **1979**, *18*, 367.
[4] P. Raj, K. Singhal, R. Rastogi, *Polyhedron* **1986**, *5*, 677.
[5] J. P. Johnson, G. K. MacLean, J. Passmore, P. S. White, *Can. J. Chem.* **1989**, *67*, 1687.
[6] P. C. Srivastava, A. Trivedi, *Indian J. Chem. Sect. A* **1989**, *28*, 1110 (It should be noted that the properties given in this reference for $[(CH_3)_2Te(N_3)_2]$ are very different from those given in Ref. [12]).
[7] W. Fimml, F. Sladky, *Chem. Ber.* **1991**, *124*, 1131.
[8] I. D. Sadekov, A. A. Maksimenko, A. G. Maslenkov, V. I. Minkin, *J. Organomet. Chem.* **1990**, *391*, 179.
[9] I. B. Gorrell, C. J. Ludman, R. S. Matthews, *J. Chem. Soc. Dalton Trans.* **1992**, 2899.
[10] P. Magnus, M. B. Roe, V. Lynch, C. Hulme, *J. Chem. Soc. Chem. Commun.* **1995**, 1609.

 © 2003 Wiley-VCH Verlag GmbH & Co. KGaA, Weinheim 

[11] T. M. Klapötke, B. Krumm, P. Mayer, O. P. Ruscitti, *Inorg. Chem.* **2000**, *39*, 5426.
[12] T. M. Klapötke, B. Krumm, P. Mayer, H. Piotrowski, O. P. Ruscitti, A. Schiller, *Inorg. Chem.* **2002**, *41*, 1184.
[13] W. Fraenk, T. M. Klapötke in *Inorganic Chemistry Highlights* (Eds.: G. Meyer, D. Naumann, L. Wesemann), Wiley-VCH, Weinheim, Germany, **2002**.
[14] T. M. Klapötke, B. Krumm, P. Mayer, H. Piotrowski, I. Schwab, M. Vogt, *Eur. J. Inorg. Chem.* **2002**, 2701.
[15] J. Mason in *Multinuclear NMR* (Ed.: J. Mason), Plenum, New York, **1987**.
[16] S. Berger, S. Braun, H. O. Kalinowski, *NMR Spectroscopy of the Non-Metallic Elements*, Wiley, Chichester, England, **1997**.
[17] R. S. Berry, *J. Chem. Phys.* **1960**, *32*, 933.
[18] The molecular structures and vibrational frequencies were calculated at the DFT level using the B3LYP hybrid functional (A. D. Becke, *J. Chem. Phys.* **1993**, *98*, 5648; P. J. Stephens, F. J. Devlin, C. F. Chablowski, M. J. Frisch, *J. Phys. Chem.* **1994**, *98*, 11623; R. H. Hertwig, W. Koch, *Chem. Phys. Lett.* **1997**, *268*, 345), which included the VWN5 correlation functional (S. H. Vosko, L. Wilk, M. Nusair, *Can. J. Phys.* **1980**, *58*, 1200). The SBKJC effective core potential (W. J. Stevens, H. Basch, M. Krauss, *J. Chem. Phys.* **1984**, *81*, 6026; W. J. Stevens, M. Krauss, H. Basch, P. G. Jasien, *Can. J. Chem.* **1992**, *70*, 612) and the corresponding valence-only basis set augmented with d polarization functions (the d function exponents for Te and N are 0.237 and 0.8, respectively; see S. Huzinaga, J. Andzelm, M. Klobukowski, E. Radzio-Andzelm, Y. Sakai, H. Tatewaki, *Gaussian Basis Sets for Molecular Calculations*, Elsevier, Amsterdam, **1984**, and P. C. Hariharan, J. A. Pople, *Theor. Chim. Acta* **1973**, *28*, 213) and a diffuse s + p shell on each atom (the diffuse s + p exponents for Te and N are 0.0306 and 0.0639, respectively; see T. Clark, J. Chandrasekhar, G. W. Spitznagel, P. von R. Schleyer, *J. Comput. Chem.* **1983**, *4*, 294) were used, denoted as B3LYPSBKJC + (d). All calculations were performed using GAMESS (M. W. Schmidt, K. K. Baldridge, J. A. Boatz, S. T. Elbert, M. S. Gordon, J. H. Jensen, S. Koseki, N. Matsunaga, K. A. Nguyen, S. J. Su, T. L. Windus, M. Dupuis, J. A. Montgomery, *J. Comput. Chem.* **1993**, *14*, 1347). Unscaled calculated frequencies, (infrared) and [Raman] intensities for **2a**: 2200 (92.9) [381.6], 2187 (833.1) [103.4], 2165 (901.8) [141.6], 2141 (1380.5) [207.2], 1284 (105.4) [8.7], 1274 (297.7) [0.4], 1227 (137.2) [1.7], 1218 (334.8) [0.9], 632 (30.5) [5.1], 628 (1.0) [15.8], 622 (3.4) [1.7], 611 (7.5) [2.3], 547 (9.0) [0.5], 546 (0.0) [1.8], 526 (3.6) [0.7], 524 (3.8) [0.2], 401 (10.4) [119.1], 381 (67.9) [12.3], 360 (6.1) [21.3], 355 (251.6) [2.6], 242 (7.0) [12.2], 234 (19.0) [9.5], 214 (4.8) [15.7], 170 (3.3) [3.0], 162 (1.4) [11.8], 160 (7.3) [2.0], 130 (0.2) [12.9], 91 (1.4) [2.0], 66 (0.8) [1.7], 59 (1.0) [9.6], 38 (0.5) [16.8], 28 (0.0) [4.6], 21 (1.2) [7.6]. **2b**: 2200 (147.7) [424.1], 2191 (989.2) [91.7], 2180 (80.3) [456.3], 2162 (1941.3) [41.6], 1297 (11.2) [4.0], 1288 (482.0) [0.6], 1230 (405.8) [0.7], 1223 (73.5) [2.3], 629 (0.0) [5.7], 626 (30.3) [3.7], 616 (16.1) [0.5], 611 (0.2) [10.6], 556 (8.7) [0.2], 555 (2.1) [2.5], 524 (4.7) [0.5], 523 (7.3) [1.0], 394 (8.3) [121.2], 381 (72.7) [13.9], 358 (228.1) [0.7], 355 (2.2) [23.2], 245 (17.4) [4.8], 236 (4.5) [18.4], 216 (18.2) [0.4], 196 (15.1) [6.7], 159 (0.1) [15.4], 126 (2.2) [1.5], 116 (0.4) [2.1], 88 (1.5) [1.6], 84 (0.0) [23.3], 82 (2.5) [3.2], 40 (0.0) [6.5], 36 (0.0) [8.7], 25 (0.7) [5.7].
[19] Crystal data for $C_{48}H_{40}N_{18}P_2Te$: $M_r = 1058.52$, triclinic, space group $P\bar{1}$, $a = 10.198(1)$, $b = 15.170(1)$, $c = 15.927(2)$ Å, $\alpha = 78.781(2)$, $\beta = 88.424(2)$, $\gamma = 78.315(2)°$, $V = 2366.6(4)$ Å$^3$, $Z = 2$, $F(000) = 1072$, $\rho_{calcd} = 1.485$ g cm$^{-3}$, $\mu = 0.753$ mm$^{-1}$, approximate crystal dimensions $0.19 \times 0.14 \times 0.04$ mm$^3$, $\theta$ range = 1.30 to 25.33°, $Mo_{K\alpha}$ ($\lambda = 0.71073$ Å), $T = 85$ K, 12464 measured data (Bruker 3-circle, SMART APEX CCD with $\chi$ axis fixed at 54.74°, using the SMART V 5.625 program, Bruker AXS: Madison, WI, 2001), of which 8426 ($R_{int} = 0.0141$) unique. Lorentz and polarization correction (SAINT V 6.45 program, Bruker AXS), absorption correction (SADABS program, Bruker AXS). Structure solution by Patterson methods (SHELXTL 6.14, Bruker AXS), full-matrix least-squares refinement on $F^2$, data-to-parameters ratio: 13.20:1, final $R$ indices [$I > 2\sigma(I)$]: $R1 = 0.0305$, $wR2 = 0.0772$, $R1 = 0.0348$, $wR2 = 0.0796$ (all data), GOF on $F^2 = 1.054$. CCDC-217066 contains the supplementary crystallographic data for this paper. These data can be obtained free of charge via www.ccdc.cam.ac.uk/conts/retrieving.html (or from the Cambridge Crystallographic Data Centre, 12, Union Road, Cambridge CB21EZ, UK; fax: (+44) 1223-336-033; or deposit@ccdc.cam.ac.uk).
[20] An independent study has also obtained a structure of an anionic tellurium(IV) azide, $[Te(N_3)_5^-]$, see: T. M. Klapötke, B. Krumm, P. Mayer, I. Schwab, *Angew. Chem.* **2003**, *115*, 6024; *Angew. Chem. Int. Ed.* **2003**, *42*, 5843.
[21] K. O. Christe, W. W. Wilson, *Inorg. Chem.* **1989**, *28*, 3275.
[22] A. R. Mahjoub, K. Seppelt, *Angew. Chem.* **1991**, *103*, 309; *Angew. Chem. Int. Ed. Engl.* **1991**, *30*, 323.
[23] D. A. Dixon, K. O. Christe, unpublished results.
[24] M. J. Collins, G. J. Schrobilgen, *Inorg. Chem.* **1985**, *24*, 2608–2614.
[25] K. Licht, P. Koehler, H. Kriegsmann, *Z. Anorg. Allg. Chem.* **1975**, *415*, 31.
[26] H. Bürger, *Spectrochim. Acta Part A* **1968**, *24*, 2015.

 © 2003 Wiley-VCH Verlag GmbH & Co. KGaA, Weinheim 

*Surface UV/Vis Spectroscopy*

# The Usefulness of Time-Dependent Density Functional Theory to Describe the Electronic Spectra of Ti-Containing Catalysts**

*Victor. A. de la Peña O'Shea, Maricarmen Capel-Sanchez, Gema Blanco-Brieva, Jose M. Campos-Martin, and Jose L. G. Fierro**

Several Ti-containing catalysts, including TS-1,[1] Ti-β,[2] Ti-containing ordered mesoporous silica,[3] amorphous xerogels,[4] and Ti-supported silica,[5] have exhibited a remarkably high efficiency and molecular selectivity in oxidation reactions with $H_2O_2$ under mild conditions. As a result of their relevance in industrial applications, they have been widely studied in recent years by several techniques, such as diffuse-reflectance spectroscopy coupled with UV/Vis spectroscopy

[*] Prof. Dr. J. L. G. Fierro, V. A. de la Peña O'Shea, M. Capel-Sanchez, G. Blanco-Brieva, Dr. J. M. Campos-Martin
Instituto de Catálisis y Petroleoquímica, CSIC
Marie Curie, s/n; Cantoblanco, 28049 Madrid (Spain)
Fax: (+34) 91-585-4760
E-mail: jlgfierro@icp.csic.es

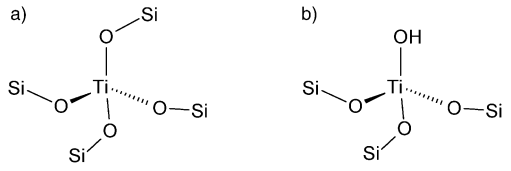
[**] The authors acknowledge financial support from Repsol-YPF (Spain). M.C.-S., G.B.-B., and J.M.C.-M. gratefully acknowledge fellowships granted by Repsol-YPF. Thanks are due to Dr. A. Delgado and Dr. P. de Frutos for helpful discussions.

Supporting information for this article is available on the WWW under http://www.angewandte.org or from the author.

 DOI: 10.1002/anie.200351452 © 2003 Wiley-VCH Verlag GmbH & Co. KGaA, Weinheim 

(DRS-UV/Vis),[6] X-ray absorption spectroscopy,[7] and computer modeling studies.[8]

Although there is currently a general agreement that the active site is a titanium center with tetrahedral coordination, there is still a considerable debate over the type of species present in the catalysts. The two widely accepted models are shown in Scheme 1. The stability of the species has been examined using computer modeling methods, and these suggest that the two species could be interconverted relatively easily by hydrolysis. Both species have been postulated to be present based on UV/Vis and photoluminescence experiments.[6]




***Scheme 1.*** Proposed models of tetrahedral Ti sites in dehydrated titanium catalysts: a) tetrapodal and b) tripodal.

One of the most useful tools to study the titanium environment is UV/Vis spectroscopy. The electronic spectra show an absorption associated with the ligand to metal charge transfer (LMCT) from the oxygen atom to the $Ti^{IV}$ ion, namely $Ti^{4+}O^{2-} \rightarrow Ti^{3+}O^{-}$. The wavelength at which this transition occurs is highly sensitive to the coordination at the titanium sites, and this peculiarity has been proposed as a probe to test the coordination environment around a titanium center.[6]

However, to our knowledge no studies aimed at correlating UV/Vis absorption with the photophysical properties calculated using time-dependent density functional theory (TD-DFT) has been reported. Thus, the two structures depicted in Scheme 1 have been studied. Tetrakis(trimethylsiloxy)titanium and titanosilicalite (TS-1) was selected as examples of the tetrapodal structure (Scheme 1a), whereas a titanium-grafted amorphous silica substrate was taken as a model of the tripodal structure (Scheme 1b). The initial geometry of the cluster selected for DFT calculations was taken from the literature[7,8] and then the geometry fully optimized (see the Supporting Information). As already stated in an earlier study,[9] the silicon atoms are terminated with hydrogen atoms. The geometry corresponds to that determined with experimental X-ray absorption fine structure (XAFS) data.[7] Differences could be observed in the Si-O-Ti bond angles between the two models: the crystalline structure imposes a constrained geometry to the tetrapodal system, while the amorphous model has a more relaxed geometry. A good correlation between the experimental UV/Vis spectra and the electronic transitions derived from the TD-DFT analysis was found (Figures 1, 2, and 3).

The region of the electronic transitions calculated by TD-DFT on the tetrapodal model tetrakis(trimethylsiloxy)titanium (Figure 1) shows a sharp band centered at 214 nm, which is in excellent agreement with the spectrum determined experimentally. Good agreement is also observed between

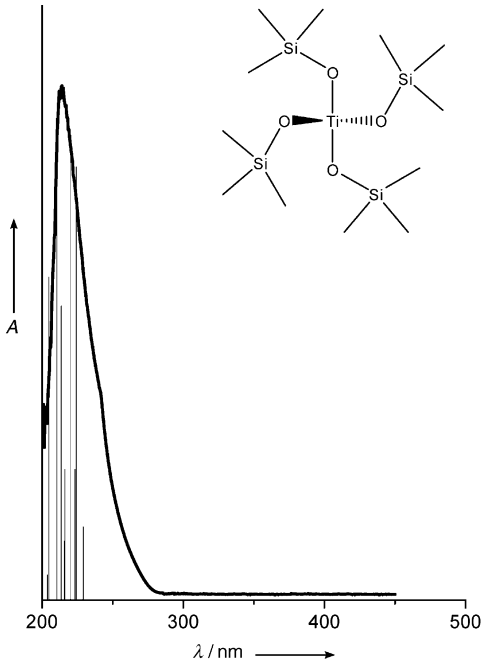



***Figure 1.*** Experimental UV/Vis spectra and calculated transitions (bars) of tetrakis(trimethylsiloxy)tianium diluted in cyclohexane ($10^{-5}$ M).

the calculated and experimental spectra of TS-1 (Figure 2a). This finding indicates clearly that the major species present in TS-1 dried at high temperature (773 K) is the tetrapodal form. The electronic transitions of the tripodal system calculated by TD-DFT give rise to a broader band which is simultaneously shifted towards a greater wavelength (225 nm). These findings are in agreement with experimental observations (Figure 3a) and with other results previously reported by other researchers using titanium-grafted mesoporous MCM-41 systems.[6c]

The introduction of water molecules within the coordination sphere of the titanium cluster leads to a shift of the electronic transition calculated by TD-DFT to a greater wavelength (Figures 2b and 3b). This finding agrees with the experimental observation that an increase in the coordination number of the titanium center causes the wavelength of the LMCT transition to shift. It can be noted that the experimental spectrum of the TS-1 sample exhibits an absorption centered at 215 nm, with a shoulder at 250 nm (Figure 2b), whereas that of the $Ti/SiO_2$ sample shows a shift of the peak to approximately 250 nm (Figure 3b). As previously suggested by other researchers,[6] this difference in the experimental spectra can be explained in terms of the different nature of TS-1 and $Ti/SiO_2$ substrates. The surface of TS-1 is hydrophobic by nature, which strongly hinders the access of molecular water to the titanium center. As a consequence, the number of titanium centers coordinated with water molecules are significantly reduced and a simultaneous decrease in the intensity of the signal at 250 nm occurs. However, since the silica surface is hydrophilic, the coordination of water molecules on surface $Ti^{IV}$ centers is favored. It is emphasized here that the electronic spectrum of TS-1 with adsorbed water calculated by TD-DFT virtually coincided with that of $Ti/SiO_2$. Since the selected cluster for TS-1 does

 © 2003 Wiley-VCH Verlag GmbH & Co. KGaA, Weinheim 

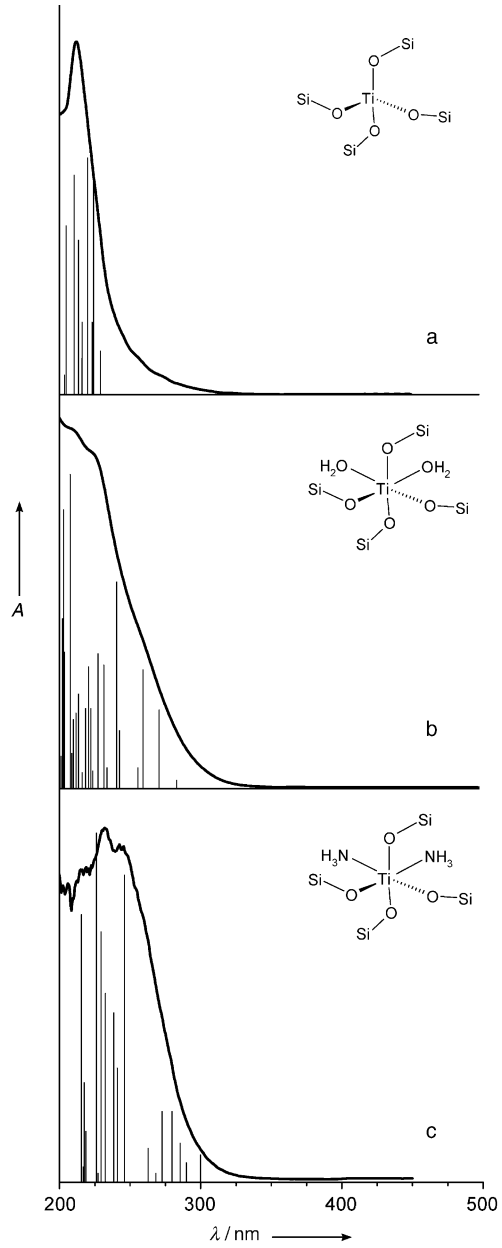



***Figure 2.*** Experimental UV/Vis spectra and calculated transitions (bars) of TS-1: a) dried, b) exposed to water, and c) exposed to ammonia.

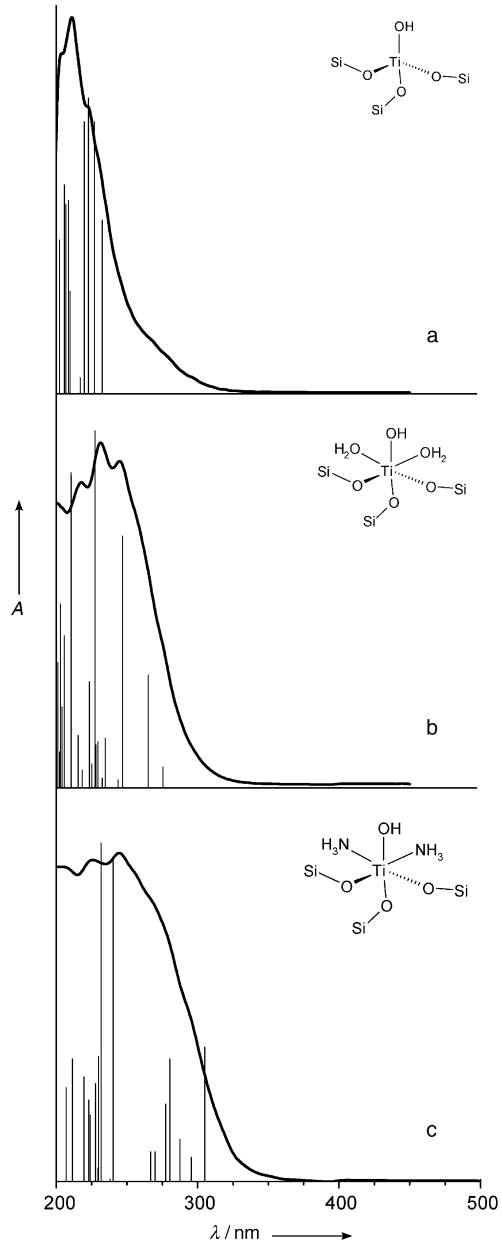



***Figure 3.*** Experimental UV/Vis spectra and calculated transitions (bars) of $Ti/SiO_2$: a) dried, b) exposed to water, and c) exposed to ammonia.

not account for the hydrophobic character of the TS-1 channels, it is concluded that the presence of transitions at lower wavelength arise from LCMT transitions at $Ti^{IV}$ centers with high coordination number as a result of coordinated water.

Similarly to the above, TD-DFT calculations were performed on the titanium cluster with coordinating ammonia molecules. In this case, the ammonia molecules entering the coordination sphere of the titanium cluster leads to a greater shift in the wavelength of the band relative to that observed with adsorbed water (Figure 2c and Figure 3c). Such a larger shift comes from the more basic character of ammonia molecules. This result is consistent with the experimental spectra of both samples, which mirror the shift of the LMCT toward a longer wavelength. In accord with the adsorption of water molecules, no changes in the electronic spectra of the tetrapodal and tripodal structures were observed.

In conclusion, the photophysical properties of the titanium clusters were calculated using time-dependent density functional theory (TD-DFT)[10] with a double zeta basis set (6-31G**). The electronic spectra of titanium-containing tetrapodal (TS-1) and tripodal ($Ti/SiO_2$) structures have been successfully described by time-dependent density functional theory (TD-DFT). The electronic transitions of the tetrapodal model calculated by TD-DFT gives a band centered at 216 nm, which is in excellent agreement with the experimen-

 © 2003 Wiley-VCH Verlag GmbH & Co. KGaA, Weinheim 

tal UV/Vis spectrum of TS-1. Similar TD-DFT calculations on the tripodal structure predicted a broader band which is shifted to a longer wavelength (225 nm). This prediction agrees with the experimental spectrum (Figure 3a) and with results previously reported on titanium-grafted mesoporous MCM-41 systems.[6c] These TD-DFT calculations were also extended to the two titanium clusters into which either water or ammonia adsorbates were incorporated. In both cases a shift of the TD-DFT-calculated LMCT electronic transition to greater wavelength was predicted, thus showing clear differences between tetrahedrally and octahedrally coordinated Ti sites. This shift was larger with ammonia than with water because of the more basic character of ammonia molecules.

## Experimental Section

A sample of TS-1 (1.5 Ti wt%) was synthesized following a literature procedure.[1a] The supported titanium catalyst was prepared as described in the literature.[5c]

UV/Vis transmission spectra were recorded on a solution of tetrakis(trimethylsiloxy)titanium ($10^{-5}$ M) in cyclohexane with a Shimadzu UV-2401PC spectrometer. DRS-UV/Vis spectra were recorded with the same spectrometer to which an integrating sphere was incorporated. Solvent or pure $BaSO_4$ was taken as a reference. DRS-UV/Vis spectra were recorded from samples degassed under high vacuum at 773 K. Degassed samples were exposed to an excess of water or ammonia (25 mbar) and the gas phase was removed by degassing the solution at room temperature for 15 minutes.

Calculations were performed with the Gaussian 98 A.10. version suite of programs.[11] Photophysical properties were calculated using TD-DFT.[10] The validity of this theory for transition-metal ions has been checked by several authors.[12] The gradient-corrected density functional methodology was employed: Becke's exchange functional (B)[13] and Becke's three-parameter adiabatic connection (B3) hybrid[14] exchange functional were used in combination with the Lee–Yang–Parr correlation functional.[15] In all cases, the standard 6–31G** basis set of DZP (double-zeta + polarization) quality was used for orbital expansion to solve the Kohn–Sham equations.

Received: March 20, 2003
Revised: July 17, 2003 [Z51452]

**Keywords:** density functional theory · heterogeneous catalysis · surface chemistry · titanium · UV/Vis spectroscopy

[1] a) M. Taramasso, G. Perego, B. Notari, US Patent 4410501, **1983**; b) B. Notari, *Adv. Catal.* **1996**, *41*, 253; c) M. G. Clerici, G. Bellusi, U. Romano, *J. Catal.* **1991**, *129*, 159; d) M. G. Clerici, P. Ingallina, *J. Catal.* **1993**, *140*, 71; e) M. C. Capel-Sanchez, J. M. Campos-Martin, J. L. G. Fierro, *Appl. Catal. A* **2003**, *246*, 69.

[2] a) R. Hutter, D. C. M. Dutroit, T. Mallat, T. M. Schneider, A. Baiker, *J. Chem. Soc. Chem. Commun.* **1995**, 163; b) P. J. Saxton, W. Chester, J. G. Zajacek, G. L. Crocco, K. S. Wijesekera, US Patent 5621122, **1997**.

[3] a) G. Sankar, F. Rey, J. M. Thomas, G. N. Greaves, A. Corma, B. R. Dobson, A. J. Dent, *J. Chem. Soc. Chem. Commun.* **1994**, 2279; b) P. T. Tanev, M. Chibwe, T. J. Pinnavaia, *Nature* **1994**, *368*, 321; c) T. Maschmeyer, F. Rey, G. Sankar, J. M. Thomas, *Nature* **1995**, *378*, 159.

[4] a) R. Hutter, T. Mallat, A. Baiker, *J. Catal.* **1995**, *153*, 177; b) R. van Grieken, J. L. Sotelo, C. Martos, J. L. G. Fierro, M. López-Granados, R. Mariscal, *Catal. Today* **2000**, *61*, 49.

[5] a) J. M. Fraile, J. I. García, J. A. Mayoral, L. C. de Ménorval, F. Rachdi, *J. Chem. Soc. Chem. Commun.* **1995**, 539; b) E. Jorda, A. Tuel, R. Teissier, J. Kerneval, *J. Chem. Soc. Chem. Commun.* **1995**, 1775; c) M. C. Capel-Sanchez, J. M. Campos-Martin, J. L. G. Fierro, M. P. de Frutos, A. Padilla Polo, *Chem. Commun.* **2000**, 855; d) M. C. Capel-Sanchez, J. M. Campos-Martin, J. L. G. Fierro, *J. Catal.* **2003**, *217*, 195.

[6] a) F. Geobaldo, S. Bordiga, A. Zecchina, E. Giamello, G. Leofanti, G. Petrini, *Catal. Lett.* **1992**, *16*, 109; b) D. Trong On, L. LeNoc, L. Bonneviot, *Chem. Commun.* **1996**, 299; c) L. Marchese, T. Maschmeyer, E. Gianotti, S. Coluccia, J. M. Thomas, *J. Phys. Chem. B* **1997**, *101*, 8836; d) C. Lamberti, S. Bordiga, A. Zecchina, G. Vlaic, G. Tozzola, G. Petrini, A. Carati, *J. Phys. IV* **1997**, *7*, 851.

[7] a) J. M. Thomas, G. N. Greaves, *Science* **1994**, *265*, 1675; b) D. Gleeson, G. Sankar, C. R. A. Catlow, J. M. Thomas, G. Spano, S. Bordiga, A. Zecchina, C. Lamberti, *Phys. Chem. Chem. Phys.* **2000**, *2*, 4812; c) J.-D. Grunwaldt, C. Beck, W. Stark, A. Hagen, A. Baiker, *Phys. Chem. Chem. Phys.* **2002**, *4*, 3514; d) J. M. Fraile, J. Garcýa, J. A. Mayoral, M. G. Proietti, M. C. Sanchez, *J. Phys. Chem.* **1996**, *100*, 19484; e) P. E. Sinclair, G. Sankar, C. R. A. Catlow, J. M. Thomas, T. Maschmeyer, *J. Phys. Chem. B* **1997**, *101*, 4232; f) J. M. Thomas, C. R. A. Catlow, G. Sankar, *Chem. Commun.* **2002**, 2921.

[8] a) H. Munakata, Y. Oumi, A. Miyamoto, *J. Phys. Chem. B* **2001**, *105*, 3493; b) G. Ricchiardi, A. Damin, S. Bordiga, C. Lamberti, G. Spano, F. Rivetti, A. Zecchina, *J. Am. Chem. Soc.* **2001**, *123*, 11409; c) G. Ricchiardi, A. de Man, J. Sauer, *Phys. Chem. Chem. Phys.* **2000**, *2*, 2195; d) A. J. M. de Man, J. Sauer, *J. Phys. Chem.* **1996**, *100*, 5025; e) P. E. Sinclair, C. R. A. Catlow, *Chem. Commun.* **1997**, 1881; f) P. E. Sinclair, C. R. A. Catlow, *J. Phys. Chem. B* **1999**, *103*, 1084.

[9] C. M. Barker, D. Gleeson, N. Kaltsoyannis, C. R. A. Catlow, G. Sankar, J. M. Thomas, *Phys. Chem. Chem. Phys.* **2002**, *4*, 1228.

[10] *Recent advances in density functional methods*, part 1 (Eds.: D. P. Chong, M. E. Casida), World Scientific, Singapore, **1995**.

[11] Gaussian 98 (Revision A.7), M. J. Frisch, G. W. Trucks, H. B. Schlegel, G. E. Scuseria, M. A. Robb, J. R. Cheeseman, V. G. Zakrzewski, J. A. Montgomery, R. E. Stratmann, J. C. Burant, S. Dapprich, J. M. Millam, A. D. Daniels, K. N. Kudin, M. C. Strain, O. Farkas, J. Tomasi, V. Barone, M. Cossi, R. Cammi, B. Mennucci, C. Pomelli, C. Adamo, S. Clifford, J. Ochterski, G. A. Petersson, P. Y. Ayala, Q. Cui, K. Morokuma, D. K. Malick, A. D. Rabuck, K. Raghavachari, J. B. Foresman, J. Cioslowski, J. V. Ortiz, B. B. Stefanov, G. Liu, A. Liashenko, P. Piskorz, I. Komaromi, R. Gomperts, R. L. Martin, D. J. Fox, T. Keith, M. A. Al-Laham, C. Y. Peng, A. Nanayakkara, C. Gonzalez, M. Challacombe, P. M. W. Gill, B. G. Johnson, W. Chen, M. W. Wong, J. L. Andres, M. Head-Gordon, E. S. Replogle, J. A. Pople, Gaussian, Inc., Pittsburgh, PA, **1998**.

[12] a) C. Adamo, V. Barone, *Theor. Chem. Acc.* **2000**, *105*, 169; b) V. Cavillot, B. Champagne, *Chem. Phys. Lett.* **2002**, *354*, 449; c) M. A. Freitag, M. S. Gordon, *J. Phys. Chem. A* **2002**, *106*, 7921.

[13] A. D. Becke, *Phys. Rev. A* **1988**, *38*, 3098.

[14] A. D. Becke, *J. Chem. Phys.* **1993**, *98*, 5648.

[15] C. Lee, W. Yang, R. G. Parr, *Phys. Rev. B* **1988**, *37*, 785.

 © 2003 Wiley-VCH Verlag GmbH & Co. KGaA, Weinheim 

*Natural Product Synthesis*

# Intramolecular Organocatalytic [3+2] Dipolar Cycloaddition: Stereospecific Cycloaddition and the Total Synthesis of (±)-Hirsutene**

*Jian-Cheng Wang and Michael J. Krische**

Nucleophilic catalysis represents an important subset of organocatalytic transformations.[1,5] As part of a program devoted to the design of phosphane-catalyzed C–C bond-forming reactions,[2] we recently reported the first intramolecular phosphane-catalyzed [3+2] cycloaddition of 2-butynoates with electron-deficient alkenes.[2a] A challenge inherent to the intramolecular cycloaddition resides in suppression of competitive internal redox isomerization, that is, phosphane-catalyzed conversion of the 2-alkynoates to the corresponding 2,4-dienoates.[3] Indeed, whereas diquinane formation proceeds smoothly, presumably owing to the enhanced rate of five-membered-ring formation, competitive isomerization circumvents hydrindane formation. Notably, unlike the parent intermolecular cycloaddition discovered in 1995,[4,5] which generally provides cycloadducts as mixtures of regio- and diastereomers, the intramolecular process affords cycloadducts in isomerically pure form.[2a] In this account, the first application of this intramolecular organocatalytic cycloaddition methodology in natural product synthesis is reported, as demonstrated by the synthesis of the linear triquinane hirsutene. These studies highlight the utility of this cycloaddition methodology vis-à-vis diastereoselective construction of quaternary centers and establish the intramolecular cycloaddition as a stereospecific process.

Since the first structural elucidation of a polyquinane natural product in 1966 (hirsutic acid-C, Figure 1),[6] over 250 polyquinane natural products have been isolated.[7] Over 80 of these natural products belong to the structural subset known as linear triquinanes, which are isolated from plants, microbes, and marine organisms.[7b] The discovery of structurally novel linear triquinanes continues unabated. For example, chlorinated linear triquinanes such as chloriolin C have been isolated from fungal cultures taken from a *Jaspis* marine sponge.[8] Efforts toward the synthesis of linear triquinane

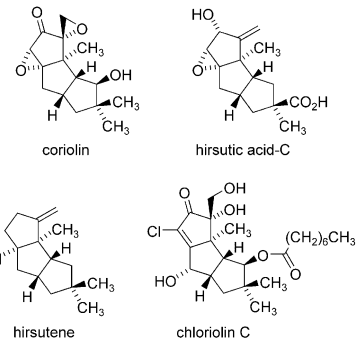



***Figure 1.*** Representative linear triquinanes.

natural products are fueled, in part, by their biological activity. Hirustic acid-C and coriolin exhibit antibiotic and antitumor activity, respectively.[9] Owing to their novel structure, the linear triquinanes have also captured the interest of synthetic chemists as a testing ground for new cyclopentannulation strategies. In this latter capacity, hisutene, a metabolite of the basidiomycete *Coriolus consors* and presumed biogenetic precursor to coriolin and hirsutic acid-C,[10] has been the focus of considerable attention.[7] Here we present a concise and stereocontrolled approach to (±)-hirsutene based on phosphane-catalyzed intramolecular [3+2] cycloaddition methodology developed in our lab.

Retrosynthetically, hirsutene is envisioned to derive from cycloadduct **6** by means of aldol cyclization–methylenation (Scheme 1). The diquinane **6**, which contains three of the four stereogenic centers in hirsutene, will be obtained directly through phosphane-catalyzed [3+2] dipolar cycloaddition of the 1,7-enyne **5**. The cycloaddition of **5** serves as a means of exploring the utility of the intramolecular cycloaddition methodology vis-à-vis stereoselective formation of quaternary carbon centers. Moreover, by examining the cycloaddition of both (*E*)- and (*Z*)-**5**, information regarding the stereospecificity of the intramolecular cycloaddition may be obtained. Finally, cycloaddition substrate **5** will be obtained from dimethylhexenol **1** through sequential introduction of enone and ynoate moieties.

The synthesis of cycloaddition substrate **5** begins with tosylation of 3,3-dimethyl-hex-5-en-1-ol (**1**, Scheme 2).[11] Displacement of the tosylate was attempted with an assortment of acetylides under a range of conditions, but it could only be achieved with lithium acetylide ethylenediamine complex in DMSO. Under these conditions the resulting 1,7-enyne **2** is produced in 68% yield.[12] Treatment of 1,7-enyne **2** with methyllithium followed by methyl chloroformate provides the corresponding ynoate **3** in 81% yield. Selective ozonolytic cleavage of the terminal alkene residue in the presence of the ynoate occurs smoothly to provide aldehyde **4** in 85% yield. Finally, olefination of **4** using 3-diethylphosphono-2-butanone[13] occurs in 60% yield to afford cycloaddition addition substrate **5** as a 5.5:1 ratio of *E*/*Z* isomers.

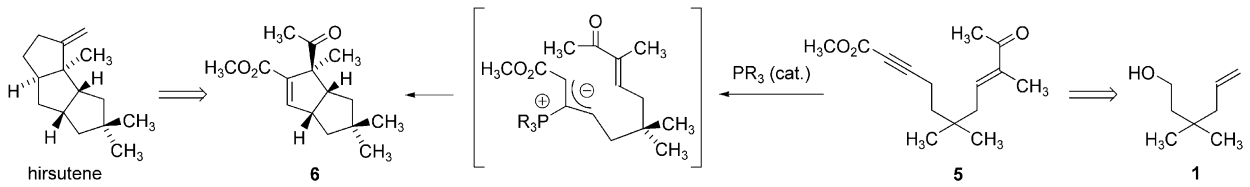
The acquisition of mono(enone)–mono(ynoate) **5** sets the stage for phosphane-catalyzed cycloaddition. Gratifyingly, exposure of (*E*)-**5** to our previously defined conditions[2a] for intramolecular phosphane-catalyzed [3+2] dipolar cycloaddition results in the formation of cycloadduct **6** in 88% yield.

[*] Prof. M. J. Krische, J.-C. Wang
University of Texas at Austin
Department of Chemistry and Biochemistry
1 University Station–A5300
Austin, TX 78712-1167 (USA)
Fax: (+1) 512-471-8696
E-mail: mkrische@mail.utexas.edu

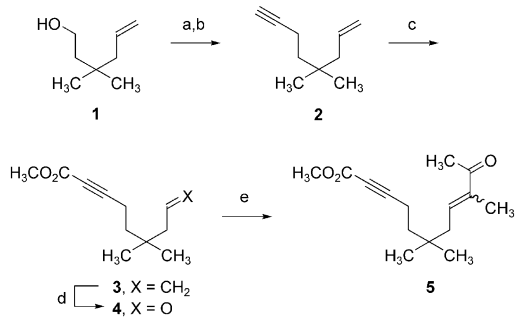
[**] Acknowledgment is made to the Robert A. Welch Foundation (F-1466), the NSF-CAREER program (CHE0090441), the Herman Frasch Foundation (535-HF02), the NIH (RO1 GM65149-01), donors of The Petroleum Research Fund administered by the ACS (34974-G1), the Research Corporation Cottrell Scholar Award (CS0927), the Alfred P. Sloan Foundation, the Camille and Henry Dreyfus Foundation, and Eli Lilly for support of this research.

Supporting information for this article is available on the WWW under http://www.angewandte.org or from the author.

 DOI: 10.1002/anie.200352218 © 2003 Wiley-VCH Verlag GmbH & Co. KGaA, Weinheim 



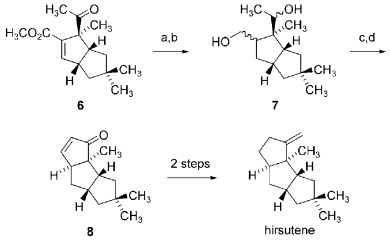

***Scheme 1.*** Retrosynthetic analysis of hirsutene based on a phosphane-catalyzed [3+2] dipolar cycloaddition.




***Scheme 2.*** Preparation of cycloaddition substrate **5**. Conditions: a) TsCl, Pyr, 0 °C, 76 %; b) LiC≡CH, DMSO, 5 °C, 68 %; c) $CH_3Li$, THF, −78 °C, then $ClCO_2CH_3$, −30 °C, 81 %; d) $O_3$, $CH_2Cl_2$, −78 °C, then $PPh_3$, 85 %; e) 3-diethylphosphono-2-butanone, NaH, THF, 35 °C, 60 %, 5.5:1 *E*/*Z* ratio. DMSO = dimethyl sulfoxide, Pyr = pyridine, Ts = toluenesulfonyl.

Moreover, **6** is obtained as a single stereoisomer with placement of the methyl residue on the concave face of the diquinane ring system, that is, formation of the quaternary center occurs readily and with a stereochemistry consistent with the structural features of hirsutene. To probe the stereospecificity of the cycloaddition, (*Z*)-**5** was exposed to identical conditions. Formation of the epimeric diquinane *epi*-**6** is observed, without any detectable formation of the cycloadduct derived from (*Z*)-**5**. These results firmly establish the intramolecular phosphane-catalyzed [3+2] dipolar cycloaddition as a stereospecific process. This result is significant in view of the fact that evidence for both stepwise and concerted mechanisms exists for related intermolecular cycloadditions.[4e,5] A model accounting for the stereospecific cycloaddition of (*E*)- and (*Z*)-**5** is given below (Scheme 3).

Elaboration of cycloadduct **6** to hirsutene is achieved in six manipulations. Hydrogenation of **6** followed by $LiAlH_4$ reduction occurs in yields of 93 % and 92 %, respectively, to provide diol **7** as a mixture of diastereomers. Swern modification of the Moffatt oxidation provides an intermediate keto-aldehyde in 78 % yield, which upon exposure to base affords the aldol cyclodehydration product **8** in 95 % yield as a single stereoisomer. Enone **8** is identical in all respects to the previously reported material, which has been converted to hirsutene in two manipulations.[14] As such, the synthesis of **8** represents a formal total synthesis of (±)-hirsutene. Whereas the previously reported material is prepared in 18 steps from 2,2′-dimethylpentenal, the present route allows access to enone **8** in 12 steps from the very same precursor (Scheme 4).

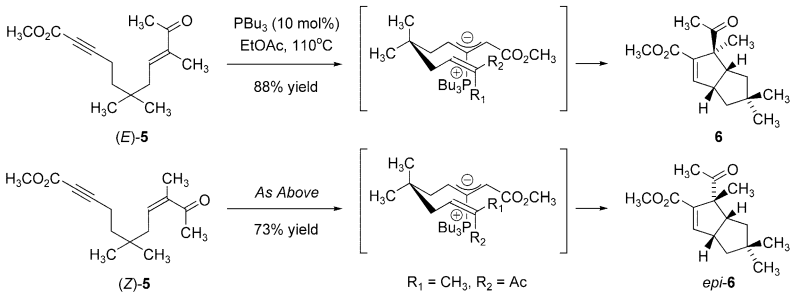



***Scheme 4.*** Conversion of cycloadduct **6** to (±)-hirsutene. Conditions: a) $H_2$, Pd/C, $CH_3OH$, 25 °C, 93 %; b) $LiAlH_4$, $Et_2O$, 25 °C, 92 %; c) $(COCl)_2$, DMSO, $CH_2Cl_2$, −78 °C, then TEA, 78 %; d) KOH, $Bu_4NOH$ (aq), THF/$Et_2O$ (1:1), reflux, 95 %. TEA = triethylamine.

In summation, intramolecular phosphane-catalyzed [3+2] dipolar cycloaddition enables a concise approach to the linear triquinane hirsutene, whereby three contiguous stereogenic centers, including a quaternary center, are created in a single manipulation with control of relative stereochemistry. In addition to demonstrating the applicability of this methodology vis-à-vis triquinane synthesis, these studies also reveal that the intramolecular cycloaddition is stereospecific. Future studies will be devoted to the design of related phosphane-catalyzed transformations including enantioselective variants of the methodology reported herein.

Received: June 24, 2003 [Z52218]

**Keywords:** cycloaddition · natural products · organocatalysis · phosphanes




***Scheme 3.*** Phosphane-catalyzed cycloaddition of **5** is stereospecific.

[1] For selected reviews that include discussions on nucleophilic catalysis, see: a) P. I. Dalko, L. Moisan, *Angew. Chem.* **2001**, *113*, 3840–3864; *Angew. Chem. Int. Ed.* **2001**, *40*, 3726–3748; b) D. Basavaiah, A. J. Rao, T. Satyanarayana, *Chem. Rev.* **2003**, *103*, 811–891.

[2] a) J.-C. Wang, S.-S. Ng, M. J. Krische, *J. Am. Chem. Soc.* **2003**, *125*, 3682–3683; b) B. G. Jellerichs, J. R. Kong, *J.*

 © 2003 Wiley-VCH Verlag GmbH & Co. KGaA, Weinheim 

*Am. Chem. Soc.* **2003**, *125*, 7758 – 7759; c) K. Agapiou, M. J. Krische, *Org. Lett.* **2003**, *5*, 1737 – 1740; d) L.-C. Wang, A.-L. Luiz, K. Agapiou, H.-Y. Jang, M. J. Krische, *J. Am. Chem. Soc.* **2002**, *124*, 2402 – 2403.

[3] a) B. M. Trost, U. Kazmaier, *J. Am. Chem. Soc.* **1992**, *114*, 7933 – 7935; b) C. Guo, X. Lu, *J. Chem. Soc. Perkin Trans. 1* **1993**, 1921 – 1923.

[4] a) C. Zhang, X. Lu, *J. Org. Chem.* **1995**, *60*, 2906 – 2908; b) Z. Xu, X. Lu, *Tetrahedron Lett.* **1997**, *38*, 3461 – 3464; c) Z. Xu, X. Lu, *Tetrahedron Lett.* **1999**, *40*, 549 – 552; d) G. Zhu, Z. Chen, Q. Jiang, D. Xiao, P. Cao, X. Zhang, *J. Am. Chem. Soc.* **1997**, *119*, 3836 – 3837; e) Z. Xu, X. Lu, *J. Org. Chem.* **1998**, *63*, 5031 – 5041; f) Y. Du, X. Lu, Y. Yu, *J. Org. Chem.* **2002**, *67*, 8901 – 8905.

[5] For a review, see: X. Lu, C. Zhang, Z. Xu, *Acc. Chem. Res.* **2001**, *34*, 535 – 544.

[6] F. W. Comer, J. Trotter, *J. Chem. Soc. Phys. Org.* **1966**, *1*, 11 – 18.

[7] Prior syntheses of hirsutene are summarized in the following reviews: a) G. Mehta, A. Srikrishna, *Chem. Rev.* **1997**, *97*, 671 – 719; b) V. Singh, B. Thomas, *Tetrahedron* **1998**, *54*, 3647 – 3692.

[8] X.-C. Cheng, M. Varoglu, L. Abrell, P. Crews, E. Lobkovsky, J. Clardy, *J. Org. Chem.* **1994**, *59*, 6344 – 6348.

[9] L. A. Paquette, *Top. Curr. Chem.* **1979**, *79*, 41 – 165.

[10] K. Tatsuta, K. Akimoto, M. Kinoshita, *J. Am. Chem. Soc.* **1979**, *101*, 6116 – 6118.

[11] G. Pattendon, S. J. Teague, *Tetrahedron* **1987**, *43*, 5637 – 5652.

[12] O. F. Beumel, Jr., R. F. Harris, *J. Org. Chem.* **1963**, *28*, 2775 – 2779.

[13] R. I. Ishchenko, B. G. Kovalev, V. M. Rastegaeva, *Russ. J. Org. Chem.* **1982**, *18*, 2005 – 2007.

[14] D. D. Sternbach, C. L. Ensinger, *J. Org. Chem.* **1990**, *55*, 2725 – 2736.

 © 2003 Wiley-VCH Verlag GmbH & Co. KGaA, Weinheim 

*Carbohydrate Sensors*

# Continuous Glucose Sensing with a Fluorescent Thin-Film Hydrogel**

*Jeff T. Suri, David B. Cordes, Frank E. Cappuccio, Ritchie A. Wessling, and Bakthan Singaram**

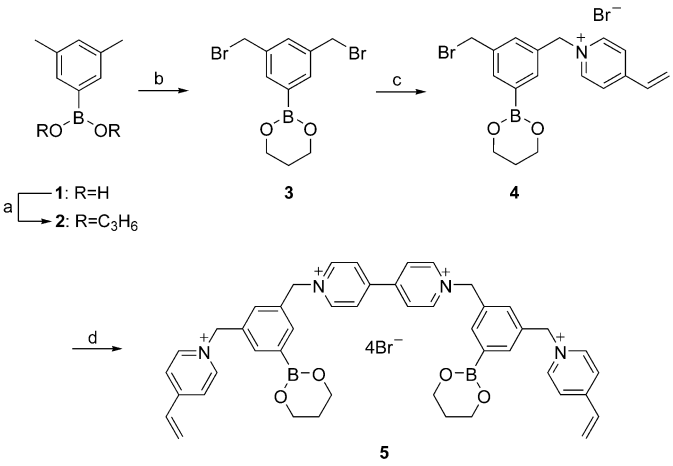
Diabetes mellitus is a chronic disease that impairs the ability of the body to manufacture or use insulin, a hormone necessary to metabolize glucose. Although there is no cure for the disease, tight glucose control substantially reduces morbidity and mortality among diabetes patients.[1] Consequently, there is a consensus that continuous glucose monitoring would be highly beneficial for the diabetic community.[2]

Many different approaches to developing a continuous glucose monitor (CGM) are being pursued.[3] Among them, the enzymatic method, which uses fluorescence-based biosensors, has attracted much attention.[3b,c] In contrast, our approach involves the use of a chemosensor that utilizes the interaction between a negatively charged fluorescent dye and a positively charged boronic-acid-functional quencher.[4]

Boronic acids are known to bind to glucose reversibly under aqueous conditions.[5] When attached to a fluorophore, the acid molecules can modulate the fluorescence as a function of saccharide concentration.[6] In our approach, the boronic acid group is attached to a quencher instead of a dye, and the fluorescence is modulated upon binding of glucose to the boronic-acid-functional quencher. The signal transduction in this two-component system is based on the electrostatic attraction between the fluorophore and the quencher and is a function of the charge on the boron moiety.[4]

For a glucose sensor to be useful in a device, the sensing components must be immobilized to allow real-time monitoring. For in vivo use, the device must operate at physiological temperature, ionic strength, and pH values. In addition, it is preferable to use visible light for optical sensors to avoid complications associated with UV light and autofluorescence. To date, there has been no report of a boronic-acid-based glucose sensor that fulfils all these criteria.[7] We report the development of a two-component sensing system immobilized in a thin film hydrogel. The combination of a cationic boronic-acid-functional quencher **5** and an anionic dye **10** is shown to function as a CGM under physiological conditions.

Viologen **5** was prepared as indicated in Scheme 1. Commercially available 3,5-dimethylphenylboronic acid was first protected as a 1,3-propanediol ester in dichloroethane and then treated with NBS to give, after recrystallization from $CH_3OH$, the dibrominated species **3** in 52% yield. Reaction of **3** with vinylpyridine in a $CH_2Cl_2/CH_3OH$ solution[8] gave




***Scheme 1.*** Synthesis of positively charged quencher monomer **5**. a) 1,3-propanediol, $C_2H_4Cl_2$, $CaH_2$, reflux 3 h; b) *N*-bromosuccinimide (NBS), azobisisobutyronitrile, $C_2H_4Cl_2$, reflux, 3 h, 52%, 2 steps; c) vinylpyridine, $CH_2Cl_2/CH_3OH$ (3:1), 40°C, 22 h, 52%; d) 4,4′-bipyridine, $CH_3OH$/dimethyl formamide (3:1), 40°C, 42 h, 39%.

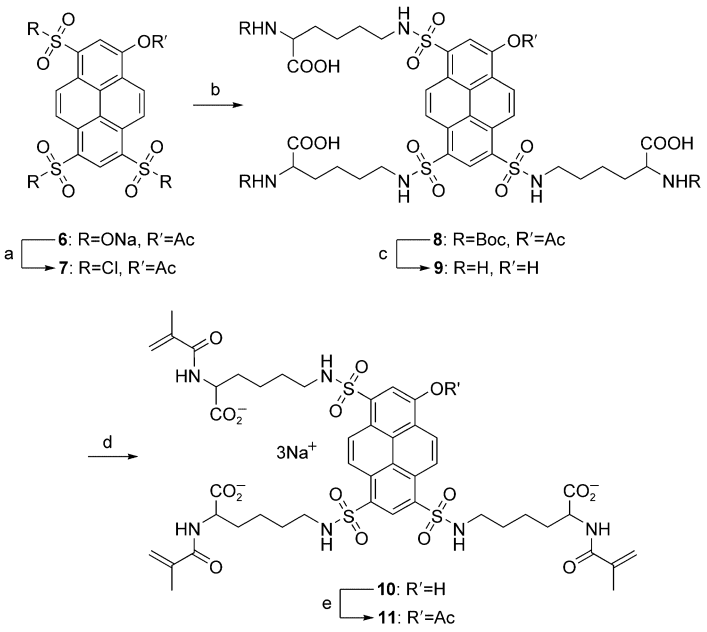
[*] Prof. Dr. B. Singaram, J. T. Suri, D. B. Cordes, F. E. Cappuccio, Dr. R. A. Wessling
Department of Chemistry and Biochemistry
University of California, Santa Cruz
Santa Cruz, CA 95064 (USA)
Fax: (+1) 831-459-2935
E-mail: singaram@chemistry.ucsc.edu

[**] We thank the BioSTAR Project and the Industry–University Cooperative Research Program with Glumetrics for their financial support. Julie Congdon is thanked for her assistance in the synthesis of starting materials.

 DOI: 10.1002/anie.200352405 © 2003 Wiley-VCH Verlag GmbH & Co. KGaA, Weinheim 

the monobromomethylphenylboronate **4**. Further quaternization with 4,4′-dipyridyl and chromatographic purification on C18-silica gel afforded tetracationic viologen **5** in 39%.

Monomeric dye **10** was synthesized in five steps from the commercially available sodium salt **6** (Scheme 2). Chlorination followed by sulfonamide formation gave the Boc-protected derivative **8** in 88%. Deprotection and reaction with methacryol chloride under standard conditions afforded the trifunctionalized derivative **10**, which was converted into the acetoxy-protected monomer **11** for use in polymerization. Pyranine derivatives functionalized with three sulfonamides have shifted excitation and emission peaks in comparison to unfunctionalized pyranine ($\lambda_{ex} = 454$ nm and $\lambda_{em} = 510$ nm)[9] and this shift is observed for **10**, for which $\lambda_{ex} = 491$ nm and $\lambda_{em} = 540$ nm.




***Scheme 2.*** Synthesis of negatively charged dye monomer **11**. a) $SOCl_2$, reflux, 3 h, then $H_2O$, 81%; b) Boc-lysine, NaOH, terahydrofuran/$CH_3CN$/$H_2O$ (2:7:1), RT, 24 h, then HCl, 94%; c) trifluroacetic acid, RT, 2 h, 65%; d) methacroyl chloride, $H_2O$, NaOH, RT, 1 h, 17%; e) acetic anhydride, NaOAc, 24 h, 70%. Boc = *tert*-butoxycarbonyl; Ac = acyl.

To evaluate the ability of **5** to quench the fluorescence of **10** in the absence and presence of different saccharides, fluorescence spectroscopic measurements were carried out in aqueous buffer solutions at pH 7.4. Upon titrating **10** with **5**, significant fluorescence quenching was observed (Figure 1), with an apparent Stern–Volmer quenching constant of $K_{sv} = 1.3 \times 10^4\,\text{M}^{-1}$. Titration of **10** with **5** in the presence of 5 mM glucose decreased the quenching efficiency of **5** ($K_{sv} = 7.2 \times 10^3\,\text{M}^{-1}$).

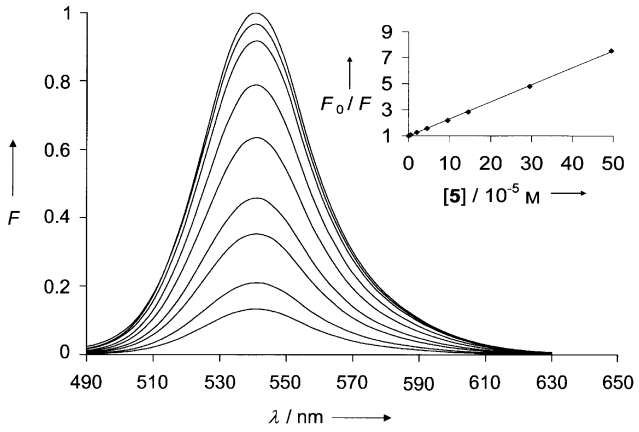
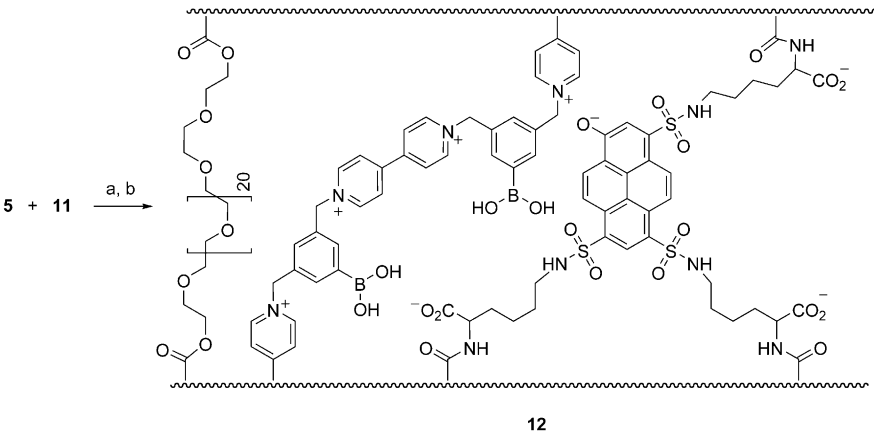



***Figure 1.*** Fluorescence emission spectra of **10** ($4 \times 10^{-6}$ M) with increasing concentrations of **5**. Inset: Stern–Volmer plot, where $F$ is the fluorescence intensity of **10** in the presence of **5** and $F_0$ is the fluorescence intensity of **10** in the absence of **5**. $\lambda_{ex} = 470$ nm.

The relative affinity of **5** towards different saccharides was then determined. Titration of solutions containing **10** ($4 \times 10^{-6}$ M) and **5** ($1.2 \times 10^{-4}$ M) were carried out with fructose, glucose, and galactose. Binding constants for each sugar were calculated from the binding isotherms.[10] The measured affinities are ranked in the order: fructose ($2063\,\text{M}^{-1}$) > glucose ($275\,\text{M}^{-1}$) > galactose ($210\,\text{M}^{-1}$). Phenyl boronic acids normally show a 3:1 greater affinity for galactose over that for glucose[6] but **5** binds glucose more strongly than galactose.

With the quenching and sugar-sensing ability of the dye/quencher combination established, the sensing elements were immobilized in a thin film (Scheme 3). A 50% aqueous solution containing **5, 11**, 2-hydroxyethyl methacrylate, polyethyleneglycol dimethacrylate, and an initiator was injected between two glass plates separated by a 25.4-μm teflon spacer. Free-radical polymerization was carried out at 40 °C for 15 h. The resultant film was leached in pH 9 buffer for one day and equilibrated in pH 7.4 buffer for one day. The swollen




***Scheme 3.*** Synthesis of a glucose-sensing polymer **12** with its sensing elements in proximity to one another. a) 2-Hydroxyethyl methacrylate, polyethylene glycol dimethacrylate ($M_w = 1000$), VA-044 (initiator), 40 °C, 15 h; b) NaOH solution, pH 9, 24 h.

 © 2003 Wiley-VCH Verlag GmbH & Co. KGaA, Weinheim 

hydrogel was found to contain 40% water (by weight). The deprotected film was subsequently tested for its sugar-sensing ability.

The hydrogel was mounted into a flow cell and phosphate buffer of ionic strength 0.1M was circulated through the cell. The film was excited at 470 nm by front-face illumination and the emission at 540 nm was monitored over time. The temperature was kept constant at 37°C. After a stable baseline had been obtained, the buffer solution was replaced with saccharide solution and the change in fluorescence intensity was measured. As indicated in Figure 2, the infusion

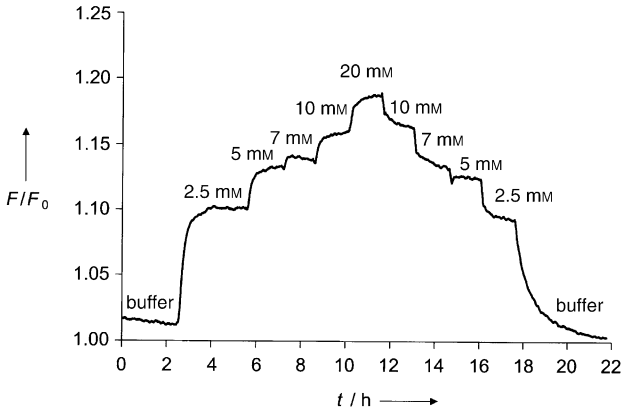



***Figure 2.*** Relative fluorescence intensity change of emmission from **12** over time in the presence of a range of concentrations of glucose. $F$ is the fluorescence intensity of **12** in the presence of glucose and $F_0$ is the fluorescence intensity of **12** in the absence of glucose. $\lambda_{ex} = 470$ nm and $\lambda_{em} = 540$ nm.

of glucose into the hydrogel resulted in a stepwise change in fluorescence intensity that was dependent on sugar concentration. Importantly, the sensor detected glucose in the physiological range of 2.5–20 mM. Moreover, the changes in fluorescence were completely reversible. Similar profiles were obtained for fructose and galactose and the apparent binding constants for each sugar were determined. The selectivity for each saccharide changed once the components were immobilized in a polymer. The immobilized system is more selective for glucose and less selective for fructose and galactose than the free components; the relative affinities are: fructose ($666\,M^{-1}$) > glucose ($333\,M^{-1}$) > galactose ($111\,M^{-1}$).

Hydrogels are known to mimic the behavior of polymer chains in solution in that a high degree of segmental mobility is possible even though long-range diffusion cannot occur. Functional groups attached to the polymer chains are free to move about and interact at least locally. This movement appears to occur in **12**. Since the quenching mechanism appears to be predominately static,[11] the dye and quencher units in the polymer chain must have the freedom to associate and dissociate within the polymer matrix depending on the local saccharide concentration.

The saccharide-sensitive hydrogel reported herein shows promise as the basis for a continuous glucose monitoring system. Through a reversible electrostatic interaction within its polymer matrix, the chemosensor **12** is able to 1) detect glucose in the physiologically important range of 2.5–20 mM and 2) operate under physiological conditions (37°C, 0.1 μM ionic strength, pH 7.4). Moreover, the fluorescence signal obtained is completely reversible, which allows real-time monitoring of glucose levels. Further studies are underway to determine the scope of this approach in continuous glucose monitoring.

Received: July 17, 2003 [Z52405]

**Keywords:** boronic acid · carbohydrates · fluorescence · gels · sensors

[1] The Diabetes Control and Complications Trial Research Group, *N. Engl. J. Med.* **1993**, *329*, 977.
[2] G. Freckmann, B. Kalatz, B. Pfeiffer, U. Hoss, C. Haug, *Exp. Clin. Endocrinol. Diabetes* **2001**, *109*, S347.
[3] a) T. Koschinsky, L. Heinemann, *Diabetes/Metab. Res. Rev.* **2001**, *17*, 113; b) R. J. Russell, M. V. Pishko, C. C. Gefrides, M. J. McShane, G. L. Cote, *Anal. Chem.* **1999**, *71*, 3126; c) R. Ballerstadt, J. S. Schultz, *Anal. Chem.* **2000**, *72*, 4185.
[4] a) J. T. Suri, D. B. Cordes, F. E. Cappuccio, R. A. Wessling, B. Singaram, *Langmuir* **2003**, *19*, 5145; b) J. N. Camara, J. T. Suri, F. E. Cappuccio, R. A. Wessling, B. Singaram, *Tetrahedron Lett.* **2002**, *43*, 1139.
[5] J. P. Lorand, J. O. Edwards, *J. Org. Chem.* **1959**, *24*, 769.
[6] T. D. James, S. Shinkai, *Top. Curr. Chem.* **2002**, *218*, 159.
[7] Boronic acid based sensors have been prepared that use UV light as the excitation source, see A. E. Colvin, U.S. Pat. Appl. Publ. 2002039793, **2002**.
[8] Vinylpyridinium salts are very unstable and are known to spontaneously polymerize, see a) T. Kanbara, M. G. Mikhael, A. B. Padias, H. K. Hall, *J. Polym. Sci. Part A* **1997**, *35*, 2787; b) S. A. Ross, M. Pitie, B. J. Meunier, *J. Chem. Soc. Perkin Trans. 1* **2000**, 571; c) W. K. Fife, P. Ranganathan, M. A. Zeldin, *J. Org. Chem.* **1990**, *55*, 5610. We found that the use of methanol as a cosolvent inhibits polymerization.
[9] a) E. Koller, R. Moser, *Appl. Fluoresc. Technol.* **1989**, *1*, 15; b) G. J. Mohr, T. Werner, O. S. Wolfbeis, *J. Fluoresc.* **1995**, *5*, 135.
[10] K. A. Connors, *Binding Constants—The measurement of Molecular Complex Stability*, Wiley, New York, **1987**.
[11] UV/Vis measurements in solution studies confirmed the formation of a ground-state complex between **5** and **10**.

 © 2003 Wiley-VCH Verlag GmbH & Co. KGaA, Weinheim 

Carbene Complexes

# Three/Four/Five-Component Diastereoselective Cyclization of Fischer Carbene Complexes, Lithium Enolates, and Allylmagnesium Bromide**

*José Barluenga,* Iván Pérez-Sánchez, Eduardo Rubio, and Josefa Flórez*

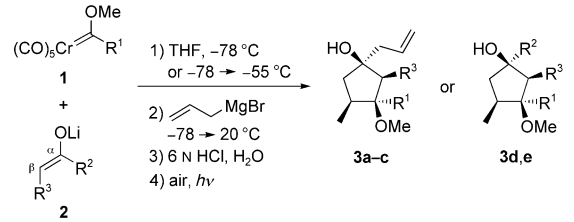
The 1,2-addition reaction of metal enolates to Group 6 Fischer alkoxy carbene complexes produces anionic (1-alkoxy-3-oxoalkyl)pentacarbonylmetalate species, which evolve further to give different organic products, depending on the reaction conditions and the structural features of the reaction partners.[1] Aryl methoxy carbene complexes react with lithium or potassium enolates of ketones[2] and with lithium enolates of α-haloesters[3] to provide open-chain products after hydrolysis with acid. Alkenyl methoxy carbene complexes also undergo nucleophilic attack at the carbene carbon atom when they are treated with methyl ketone lithium enolates, leading to acyclic unsaturated ketones[2] when the reaction mixture is quenched at low temperature and to five-[4] or seven-membered[4a] carbocycles when the reaction is allowed to reach room temperature. These diastereoselective cyclizations involve intramolecular addition of lithium allylmetalate intermediates, generated in situ, to either the carbonyl group or the β carbon atom of an alkenyl ketone. However, to date no examples have been reported of the nucleophilic addition of metal enolates to the carbene carbon atom of either alkynyl or alkyl carbene complexes.

On the other hand, 1-alkoxyalkyl pentacarbonylmetalate species, generated by reduction of alkoxy carbene complexes with *N*-methyl-1,4-dihydropyridine[5] or samarium diiodide/methanol[6], underwent insertion of CO to give α-alkoxyacyl tetracarbonylmetalate intermediates.[7] These acyl chromate or tungstate complexes undergo intermolecular 1,4-addition to electron-deficient olefins,[5,6] intramolecular insertion of an alkene or alkyne,[5] or intramolecular cyclopropanation of a carbon–carbon double bond.[5]

Herein we describe a novel selective synthesis of highly substituted cyclopentanols and 1,4-cyclohexanediols by a three-, four-, or five-component sequential coupling reaction[8] of a Fischer carbene complex, a ketone or ester lithium enolate, and allylmagnesium bromide.

The successive reaction of chromium carbene complexes **1** with β-substituted lithium enolates **2** and then with allylmagnesium bromide under the reaction conditions summarized in Table 1 led, after hydrolysis with acid and decoordination of the metal center, to 1,2,3,3,4-pentasubstituted cyclopentanols **3**, which were obtained in each case as a single diastereoisomer. 1-Allylcyclopentanols **3a-c** were formed when ester lithium enolate **2a**[9] was used in a process that involves four reacting components and the formation of four new C–C bonds (Table 1, entries 1–3). Other 1-substituted cyclopentanols **3d,e** were isolated from the reactions with ketone lithium enolates **2b,c**[10] and represent the coupling of three reacting components with the formation of three new C–C bonds (Table 1, entries 4 and 5). This sequential one-pot synthesis of cyclopentanols proceeded successfully with aryl and heteroaryl carbene complexes **1a,d** and **1b**, respectively, and even with alkyl carbene complex **1c**, which contains an acidic hydrogen atom at the tertiary center α to the carbene carbon atom.

***Table 1:*** 1,2,3,3,4-Pentasubstituted cyclopentanols **3** prepared by one-pot three- or four-component coupling of carbene complexes **1**, lithium enolates **2**, and allylmagnesium bromide.




| Entry | 1 | $R^1$ | 2 | $R^2$ | $R^3$ | Method[a] | 3 | Yield [%][b] |
|---|---|---|---|---|---|---|---|---|
| 1 | **a** | 2-naphthyl | **a** | MeO | Me | A | **a** | 79 |
| 2 | **b** | 2-furyl | **a** | MeO | Me | A | **b** | 73 |
| 3 | **c** | $(CH_2)_4CH$[c] | **a** | MeO | Me | A | **c** | 87 |
| 4 | **d** | Ph | **b** | Et | Me | B | **d** | 80 |
| 5 | **a** | 2-naphthyl | **c** | $(CH_2)_4$ | | B | **e** | 78 |

[a] Reaction conditions: Method A: **2a** (1.2 equiv), −78 °C, 15 min; $CH_2=CHCH_2MgBr$ (2.5 equiv), −78 °C, 30 min; then 20 °C, 20 min. Method B: **2b,c** (1.2 equiv), −78 → −55 °C, 45 min; $CH_2=CHCH_2MgBr$ (1.5 equiv), −78 °C, 30 min; then 20 °C, 20 min. [b] Yield of isolated product based on the corresponding carbene complex **1**. [c] Cyclopentyl.

The analogous consecutive treatment of carbene complexes **1** with β-unsubstituted lithium enolates **4** and allylmagnesium bromide resulted in the diastereoselective formation of 1,3,3,5-tetrasubstituted cyclohexane-1,4-diols **5** (Table 2). The reaction proceeded similarly to that with β-substituted enolates (Table 1): The experiments with ester lithium enolate **4a** afforded 1-allylcyclohexane-1,4-diols **5a-c** in which five reacting components have been joined together with the formation of five new C–C bonds (Table 2, entries 1–3). On the other hand, the reactions with ketone lithium enolates **4b,c** provided 1-substituted cyclohexane-1,4-diols **5d-f** by the assembly of four reacting components with the creation of four new C–C bonds (Table 2, entries 4–6). Aryl

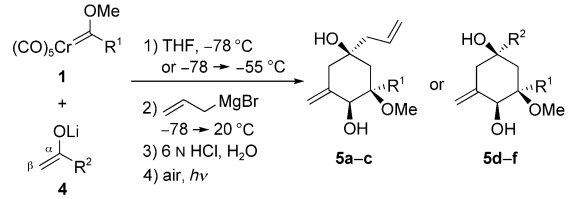
[*] Prof. Dr. J. Barluenga, I. Pérez-Sánchez, Dr. E. Rubio, Dr. J. Flórez
Instituto Universitario de Química Organometálica "Enrique Moles"
Unidad Asociada al CSIC, Universidad de Oviedo
Julián Clavería 8, 33006 Oviedo (Spain)
Fax: (+34) 98-510-3450
E-mail: barluenga@sauron.quimica.uniovi.es

[**] Financial support for this work from the MCYT (BQU2001-3853) and from the FICYT (PR-01-GE-9) is acknowledged. I.P.-S. thanks the Principado de Asturias (FICYT) for a predoctoral fellowship.

Supporting information for this article, including experimental procedures, spectral data, and analytical data for all products, is available on the WWW under http://www.angewandte.org or from the author.

 © 2003 Wiley-VCH Verlag GmbH & Co. KGaA, Weinheim DOI: 10.1002/anie.200352489 

***Table 2:*** 1,3,3,5-Tetrasubstituted cyclohexane-1,4-diols **5** prepared by one-pot four- or five-component coupling of carbene complexes **1**, lithium enolates **4**, and allylmagnesium bromide.

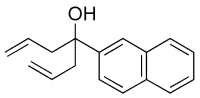



| Entry | 1 | $R^1$ | 4 | $R^2$ | Method[a] | 5 | Yield [%][b] |
|---|---|---|---|---|---|---|---|
| 1 | **a** | 2-naphthyl | **a** | EtO | A | **a** | 79 |
| 2 | **e** | 3-furyl | **a** | EtO | A | **b** | 81 |
| 3 | **f** | *t*BuC≡C | **a** | EtO | A | **c** | 83 |
| 4 | **d** | Ph | **b** | Me | B | **d** | 82 |
| 5 | **c** | $(CH_2)_4CH$[c] | **b** | Me | B | **e** | 87 |
| 6 | **a** | 2-naphthyl | **c** | Ph | B | **f** | 91 |

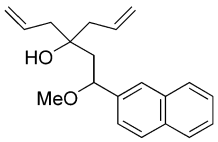
[a] Reaction conditions: Method A: **4a** (1.2 equiv), −78 °C, 15 min; $CH_2=CHCH_2MgBr$ (2.5 equiv), −78 °C, 30 min; then 20 °C, 20 min. Method B: **4b,c** (1.2 equiv), −78 → −55 °C, 45 min; $CH_2=CHCH_2MgBr$ (1.5 equiv), −78 °C, 30 min; then 20 °C, 20 min. [b] Yield of isolated product based on the corresponding carbene complex **1**. [c] Cyclopentyl.

(**1a**,**d**), heteroaryl (**1e**), alkyl (**1c**), and also alkynyl (**1f**) carbene complexes can be used as starting materials for the construction of cyclohexane-1,4-diols **5**.

The addition of ester lithium enolates **2a** and **4a** to the carbene carbon atom of carbene complexes **1** occurred smoothly at −78 °C, but in the case of ketone lithium enolates **2b**,**c** and **4b**,**c** it was necessary to raise the temperature of the reaction to −55 °C to drive the addition reaction to completion. Indeed, a mixture of product **5f** (61 %) and tertiary alcohol **6** (16 %) was isolated in the experiment in which the temperature of the reaction step of **1a** with the lithium enolate of acetophenone, **4c**, was maintained at −78 °C for 45 min (instead of 45 min between −78 and −55 °C; see Table 2, entry 6). Compounds **5** and **6** were easily separated by column chromatography. The formation of alcohol **6**, whose structure does not contain the enolate framework, can be explained by direct addition of allylmagnesium bromide to the carbene carbon of starting carbene complex **1a**, which remains in the reaction mixture as a result of an incomplete addition of ketone enolate **4c** at −78 °C. Furthermore, a shorter reaction time in the second reaction step led also to a mixture of two products, of which the major is a non-annulated derivative. Thus, treatment of the reaction mixture obtained by addition of enolate **4a** to carbene complex **1a** with allylmagnesium bromide at −78 °C for only 5 min (instead of 30 min; see Table 2, entry 1) and then at room temperature for 20 min, furnished cyclohexanediol **5a** (32 %) along with tertiary alcohol **7** (45 %), which does incorporate the enolate framework in its structure. These two compounds **5a** and **7** were, likewise, separable by column chromatography.



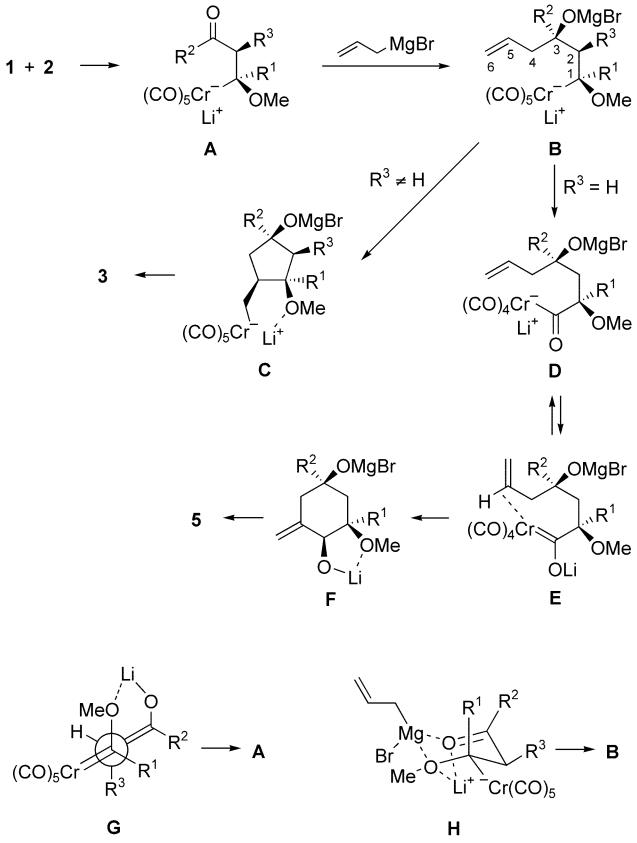

**6** 16%




**7** 45%

The structure and relative stereochemistry of products **3** and **5**–**7** were ascertained by 1D and 2D NMR spectroscopy experiments. The latter were carried out with compounds **3a**,**d**,**e**, **5a**,**b**, and **7**.[11] Furthermore, X-ray single-crystal analysis of **5d** confirmed the structural assignment of cyclohexane-1,4-diols **5**.[12]

The ring skeleton of cyclopentanols **3** combine the carbene ligand, the enolate framework, and one or two allyl units, whereas that of cyclohexanediols **5** also incorporates a carbonyl ligand. Based on this information, a plausible mechanism to explain the formation of **3** and **5** is outlined in Scheme 1 and involves initial 1,2-addition of the appropriate lithium enolate **2** or **4** (= **2**, $R^3=H$) to carbene complex **1**, which generates lithium 1-methoxy-3-oxoalkyl pentacarbonylchromate intermediate **A**. Subsequent addition of the organomagnesium reagent at low temperature to the corresponding ketone or ester functional group produces 5-hexenylchromate intermediate **B**, whose reactivity depends on the degree of substitution at C2. Complexes **B** with an organic group at C2 ($R^3\neq H$) undergo an intramolecular carbometalation reaction to give cyclopentylmethylchromate derivatives **C**, which finally furnish cyclopentanols **3** upon protonation. On the other hand, tetrahedral intermediates **B** that do not have a substituent at C2 ($R^3=H$) undergo migratory insertion of carbon monoxide to provide lithium acyl tetracarbonylchromate species **D**, which lead to 5-

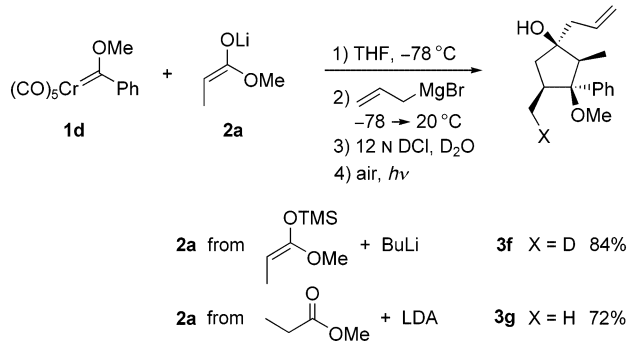



***Scheme 1.*** Proposed mechanism for the formation of compounds **3** and **5**.

 © 2003 Wiley-VCH Verlag GmbH & Co. KGaA, Weinheim 

methylenecyclohexane-1,4-diols **5**, presumably after intramolecular insertion of the carbene carbon atom into the secondary vinylic C–H bond, as indicated in intermediate **E**, and subsequent protonation of **F** (Scheme 1).[13,14,15] The observed diastereoselectivity in the first reaction step can be explained in terms of approach topology **G**, which is favored by coordination of the lithium center to the oxygen atom of the methoxy group. The diastereoisomer formed in the second reaction step can be rationalized by a chelation-controlled transition state in which the nucleophile (organomagnesium) adds to the less-hindered face (back face of model **H**) of the carbonyl group (Scheme 1).[16] Protonation of intermediate **B** before ring closing would account for the isolation of product **7**.

Evidence for the formation of intermediate **C** was provided by quenching the reaction with deuterium oxide and deuterated hydrochloric acid. However, the lithium




***Scheme 2.*** Formation of deuterated compound **3f** in the absence of $i$Pr$_2$NH.

enolate was derived from the corresponding silyl enol ether to avoid the presence of diisopropylamine, which at room temperature promotes protonation of the lithium alkyl chromate moiety. As shown in Scheme 2 the reaction of **1d** with **2a** (prepared from (*E*)-1-methoxy-1-trimethylsilyloxypropene[17] by treatment with BuLi) and allylmagnesium bromide afforded deuterated cyclopentanol **3f**, whereas the same experiment carried out with lithium enolate **2a** (generated from methyl propionate and LDA) produced undeuterated cyclopentanol **3g**.

In conclusion, a new synthetic sequence has been developed for the one-pot diastereoselective preparation from three simple precursors of singular cyclopentanols and cyclohexane-1,4-diols with up to four contiguous stereogenic centers. These formal [2+2+1] and [2+2+1+1] cyclization processes seem to involve intramolecular alkene insertion into an alkyl pentacarbonylchromate[18] and unprecedented lithioxycarbene complex insertion into a vinylic C–H bond, respectively.

Received: July 28, 2003 [Z52489]

**Keywords:** carbenes · chromium · cyclization · enolates · multicomponent reactions

[1] J. Barluenga, J. Flórez, F. J. Fañanás, *J. Organomet. Chem.* **2001**, *624*, 5.
[2] C. P. Casey, W. R. Brunsvold, *Inorg. Chem.* **1977**, *16*, 391.
[3] J. M. Concellón, P. L. Bernad, Jr., *Tetrahedron Lett.* **1998**, *39*, 7967.
[4] a) J. Barluenga, J. Alonso, F. Rodríguez, F. J. Fañanás, *Angew. Chem.* **2000**, *112*, 2555; *Angew. Chem. Int. Ed.* **2000**, *39*, 2460; b) J. Barluenga, J. Alonso, F. J. Fañanás, *J. Am. Chem. Soc.* **2003**, *125*, 2610.
[5] For *N*-methylpyridinium 1-alkoxyalkyl metalates (Cr, W), see: a) H. Rudler, A. Parlier, V. Certal, J. Vaissermann, *Angew. Chem.* **2000**, *112*, 3559; *Angew. Chem. Int. Ed.* **2000**, *39*, 3417; b) H. Rudler, A. Parlier, T. Durand-Réville, B. Martin-Vaca, M. Audouin, E. Garrier, V. Certal, J. Vaissermann, *Tetrahedron* **2000**, *56*, 5001.
[6] For $SmI_2^+$ 1-alkoxyalkyl chromates, see: K. Fuchibe, N. Iwasawa, *Chem. Eur. J.* **2003**, *9*, 905.
[7] Furthermore, alkyl or aryl pentacarbonylchromate complexes, generated by addition of an organometallic compound (Li, Zn) to [Cr(CO)$_5$L] (L = NMe$_3$, THF), have been converted into acyl pentacarbonylchromate complexes in the presence of carbon monoxide (1 atm): a) I. Lee, N. J. Cooper, *J. Am. Chem. Soc.* **1993**, *115*, 4389; b) H. Stadtmüller, P. Knochel, *Organometallics* **1995**, *14*, 3163.
[8] For reviews on multicomponent reactions, see: a) G. H. Posner, *Chem. Rev.* **1986**, *86*, 831; b) L. Weber, K. Illgen, M. Almstetter, *Synlett* **1999**, 366; c) H. Bienaymé, C. Hulme, G. Oddon, P. Schmitt, *Chem. Eur. J.* **2000**, *6*, 3321; d) A. Dömling, I. Ugi, *Angew. Chem.* **2000**, *112*, 3300; *Angew. Chem. Int. Ed.* **2000**, *39*, 3168.
[9] Ester lithium enolate (*E*)-**2a** was prepared by deprotonation of methyl propionate with lithium diisopropylamide (LDA) in THF: a) C. H. Heathcock, C. T. Buse, W. A. Kleschick, M. C. Pirrung, J. E. Sohn, J. Lampe, *J. Org. Chem.* **1980**, *45*, 1066; b) D. A. Oare, C. H. Heathcock, *J. Org. Chem.* **1990**, *55*, 157.
[10] Ketone lithium enolates **2b** (*E*/*Z* ≈ 70:30) and (*E*)-**2c** were prepared by deprotonation of 3-pentanone and cyclohexanone, respectively, with LDA/THF: R. E. Ireland, R. H. Mueller, A. K. Willard, *J. Am. Chem. Soc.* **1976**, *98*, 2868, and reference [9a].
[11] $^1$H, $^{13}$C, DEPT, gHMQC, gHMBC, gCOSY, and NOESY NMR spectra were measured.
[12] Full details of the X-ray crystal-structure study will be described separately.
[13] C–H insertion reactions of Group 6 Fischer carbene complexes are known for nonheteroatom-stabilized (a,b,c), acetoxy- (d), methoxy- (e) or boroxycarbene complexes (f) and alkyl C(sp$^3$)–H bonds in an intramolecular fashion: a) H. Fischer, J. Schmid, R. Märkl, *J. Chem. Soc. Chem. Commun.* **1985**, 572 (intermolecular process); b) S. L. B. Wang, J. Su, W. D. Wulff, *J. Am. Chem. Soc.* **1992**, *114*, 10665; c) N. Iwasawa, M. Shido, H. Kusama, *J. Am. Chem. Soc.* **2001**, *123*, 5814; d) K. Takeda, Y. Okamoto, A. Nakajima, E. Yoshii, T. Koizumi, *Synlett* **1997**, 1181; e) J. Barluenga, F. Aznar, M. Fernández, *Chem. Eur. J.* **1997**, *3*, 1629; f) J. Barluenga, F. Rodríguez, J. Vadecard, M. Bendix, F. J. Fañanás, F. López-Ortiz, M. A. Rodríguez, *J. Am. Chem. Soc.* **1999**, *121*, 8776; and for alkoxy carbene complexes and olefinic C(sp$^2$)–H bonds in an intermolecular process: g) A. Wienand, H.-U. Reissig, *Angew. Chem.* **1990**, *102*, 1156; *Angew. Chem. Int. Ed. Engl.* **1990**, *29*, 1129, and references therein.
[14] An alternative reaction path for the transformation **D** → **F**, which could include intramolecular insertion of the C–C double bond into the C–Cr bond of lithium acyl chromate intermediate **D** followed by a β hydrogen elimination and reduction of the carbonyl group with the hydrido tetracarbonylchromate complex generated in situ, seems to us to be more unlikely.

 © 2003 Wiley-VCH Verlag GmbH & Co. KGaA, Weinheim 

[15] Substitution at C2 ($R^3 \neq H$) presumably favors a conformation of intermediate **B** in which an intramolecular alkene-insertion reaction into the C–Cr bond (**B**→**C**) is favored over a CO-insertion process (**B**→**D**) owing to an effect that facilitates cyclization by increasing alkyl substitution on the open chain of **B**: P. G. Sammes, D. J. Weller, *Synthesis* **1995**, 1205.
[16] a) W. C. Still, J. A. Schneider, *Tetrahedron Lett.* **1980**, *21*, 1035; b) M. T. Reetz, M. Hüllmann, T. Seitz, *Angew. Chem.* **1987**, *99*, 478; *Angew. Chem. Int. Ed. Engl.* **1987**, *26*, 477.
[17] T. V. RajanBabu, *J. Org. Chem.* **1984**, *49*, 2083.
[18] For a proposed intramolecular olefin-insertion reaction into the $C(sp^2)$–Cr bond of a triallyl alkenyl chromate, see: T. Nishikawa, H. Kakiya, H. Shinokubo, K. Oshima, *J. Am. Chem. Soc.* **2001**, *123*, 4629; we thank one of the referees for calling our attention to this reference.

 © 2003 Wiley-VCH Verlag GmbH & Co. KGaA, Weinheim 

*Solid-State Structures*

# Packing Motifs in Porphyrazine Macrocycles Carrying Peripherally Annulated Thiadiazole Rings: Crystal Growths of Metal-Free and Cobalt Tetrakis(1,2,5-thiadiazole)porphyrazines**

*Masato Fujimori, Yosuke Suzuki, Hirofumi Yoshikawa, and Kunio Awaga**

Phthalocyanine compounds have received extensive attention in the last three decades because of their commercial applications as dyes and catalysts, as well as because of their interesting electrooptical and magnetic properties.[1–3] Various chemical modifications have been carried out, mainly on the benzo ring in phthalocyanine, to modify the physical properties.[4–6] Recently Ercolani and co-workers synthesized tetrakis(thiadiazole)porphyrazine ($TTDPzH_2$) and the corresponding metal(II) derivatives (TTDPzM; M = Mg, Cu, Mn, Fe, Co, Ni, and Zn).[7,8] While intermolecular interactions of the thiadiazole ring in symmetrical macrocycles are expected in the solid state, no structural data have been reported so far, although structural studies on the related low-symmetry macrocycles have recently appeared in the literature.[9,10]

Herein we consider the crystal growths of $TTDPzH_2$ and TTDPzCo as well as magnetic measurements on the latter compound. We report polymeric structures of these two compounds, which are completely different from the structures of phthalocyanines.

[*] Prof. K. Awaga, M. Fujimori, Y. Suzuki, Dr. H. Yoshikawa
Department of Chemistry
Graduate School of Science
Nagoya University
Furo-cho, Chikusa-ku, Nagoya 464-8602 (Japan)
Fax: (+81) 52-789-2484
E-mail: awaga@mbox.chem.nagoya-u.ac.jp

[**] K.A. expresses his gratitude to Prof. Tamotsu Inabe for fruitful discussions.

The materials $TTDPzH_2$ and TTDPzCo were prepared by literature methods.[7,8] Single crystals of the compounds were obtained by sublimation under a reduced pressure (a few mbar) with a continuous flow of $N_2$ (30 mL min$^{-1}$). The conditions were optimized so that the sublimation temperatures for $TTDPzH_2$ and TTDPzCo were 500 and 550 °C, respectively. It is notable that crystals, which were suitable for X-ray crystal analyses, were not grown without the gas flow.

$TTDPzH_2$ crystallized in a monoclinic $P2_1/n$ space group with half of the molecule crystallographically asymmetric.[11] The molecules form a layered structure (Figure 1). The layer is formed by a 2D hexagonal close packing of $TTDPzH_2$ with very short S···N contacts of 2.948(2) and 3.245(2) Å. In addition, the layers are stacked along the *c* axis by π–π interactions, with an interlayer distance of 3.45 Å. One molecule interacts with four molecules in adjacent layers.

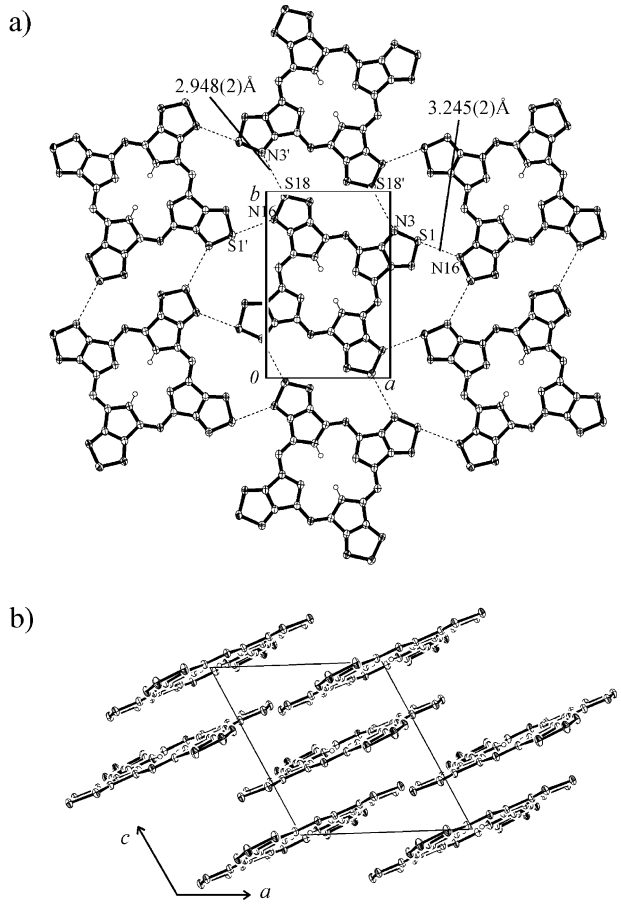



***Figure 1.*** Top (a) and side (b) views of the layered crystal structure in $TTDPzH_2$.

Epitaxial growths of phthalocyanines have been extensively studied on various surfaces, and it was recognized that the surface interactions seriously affected the solid-state structures of phthalocyanines.[12] $TTDPzH_2$ can potentially self-assemble into a planar 2D network in which the molecular planes are all parallel, thus it could have an application in the preparation of oriented thin films.

 DOI: 10.1002/anie.200352571 © 2003 Wiley-VCH Verlag GmbH & Co. KGaA, Weinheim 

TTDPzCo crystallized into a monoclinic $P2_1/c$ space group, in which one molecule was crystallographically independent.[13] The TTDPzCo molecules form a 1D coordination polymer along the *b* axis (Figure 2a). A nitrogen atom on the thiadiazole ring occupies the axial position around the Co ion in the neighboring molecule at a distance of 2.300(2) Å. The two molecules are related by a twofold screw axis parallel to the *b* axis, with a dihedral angle of 82.96(1)°. A similar edge to face interaction was observed for the Zn species containing 3,4-annulated pyridine units.[14] Furthermore, the coordination chains of TTDPzCo are stacked in the *bc* plane, thus forming face-to-face π dimers (Figure 2b). Figure 2c shows a projection of the dimer onto the molecular plane. The axial position around the cobalt ion is occupied by the nitrogen atom of the pyrrole ring in the neighboring molecule at a distance of 3.401(2) Å. The intradimer Co···Co distance is 4.0252(6) Å, which is much shorter than the shortest Co···Co distance in the coordination chain (7.3535(5) Å). A superexchange magnetic interaction is expected in the dimer through the Co-N···Co pathway.

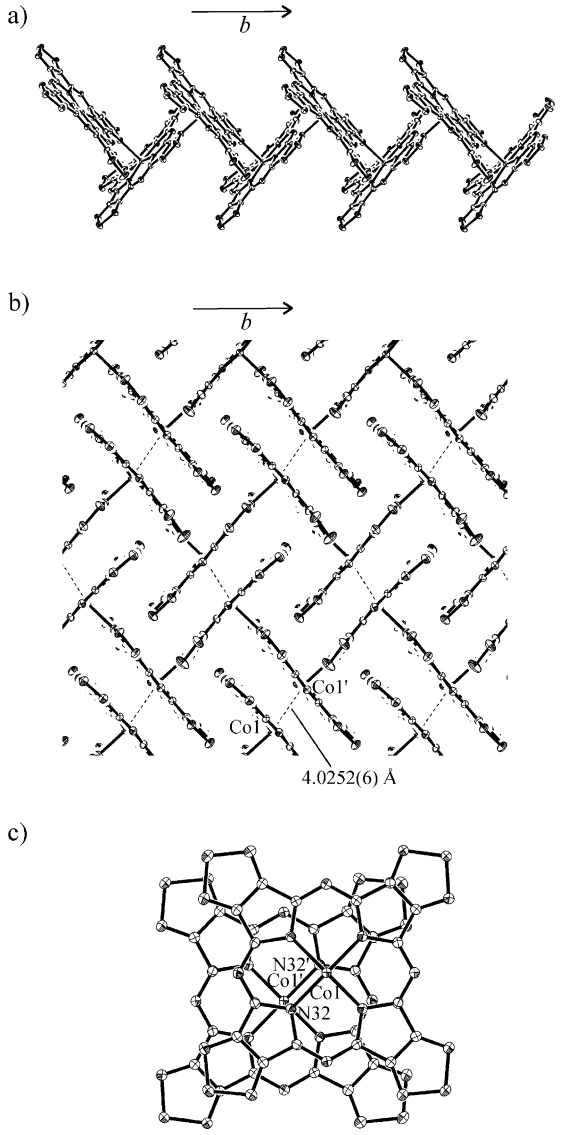



***Figure 2.*** Views of the crystal structure in TTDPzCo; a) coordination polymer along the *b* axis; b) a projection onto the *bc* plane; c) face-to-face π dimer in the interchain arrangement.

It is well known that the structures of metal-containing and metal-free phthalocyanines are nearly identical in either the α or β forms.[15,16] Their structures are governed by the condensation energy associated with the π–π interaction of the planar molecules. In contrast the structures of $TTDPzH_2$ and TTDPzCo are completely different, although they have a common feature; the interactions of the thiadiazole ring play an essential role in their solid-state structure: the electrostatic interaction between the thiadiazole rings is responsible for the 2D close packing in $TTDPzH_2$, while the coordination bond between the ring and the cobalt ion results in the chain structure in TTDPzCo.

Figure 3 depicts the temperature dependence of the paramagnetic susceptibility $\chi_p$ for TTDPzCo.[17] The values of $\chi_p$ show a gradual increase as the temperature decreases down to 12 K, and, after reaching a rather sharp maximum at

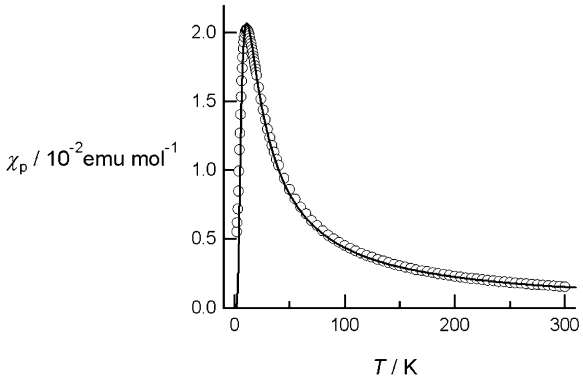



***Figure 3.*** Temperature dependence of the paramagnetic susceptibility $\chi_p$ for TTDPzCo. The solid curve is the theoretical best fit of the dimer model.

12 K, the $\chi_p$ value exhibits a quick decrease down to zero. The data were interpreted in terms of the antiferromagnetic dimer model.[18] The solid curve shows the theoretical best fit of this model obtained with $g = 2.21$ and $2J/k_B = -17.8$ K, where $g$ is the $g$ factor, $J$ is the intradimer coupling constant, and $k_B$ is the Boltzmann constant. The experimental data were in good agreement with the dimer model, but could not be explained in terms of a 1D antiferromagnetic chain. Thus, the result is in agreement with the structure.

In conclusion, single crystals of $TTDPzH_2$ and TTDPzCo were grown by vacuum sublimation under a reduced pressure with a continuous gas flow. While $TTDPzH_2$ adopts a 2D hexagonal close packing, which could have an application in self-assembling films, TTDPzCo crystallizes into a coordination polymer even though the intrachain magnetic exchange interaction is weaker than the interchain interaction. Highly conductive phthalocyanines have recently attracted much interest,[19] and the network structures in the present materials could have application in obtaining 3D molecular conductors.

Received: August 5, 2003 [Z52571]

 © 2003 Wiley-VCH Verlag GmbH & Co. KGaA, Weinheim 

**Keywords:** crystal growth · magnetic properties · porphyrazines · structure elucidation · sulfur heterocycles


[1] a) *Phthalocyanines: Properties and Applications, Vol. 4* (Eds.: C. C. Leznoff, A. B. P. Lever), VCH, New York, **1996**; b) *The Porphyrin Handbook, Vols. 17* and *19* (Eds.: K. M. Kadish, K. M. Smith, R. Guilard), Academic Press, New York, **2003**.

[2] M. J. Cook, *J. Mater. Chem.* **1996**, *6*, 677.

[3] a) S. Mitra, A. Gregson, W. Hatfield, R. Weller, *Inorg. Chem.* **1983**, *22*, 1729; b) K. Awaga, Y. Maruyama, *Phys. Rev. B* **1991**, *44*, 2589; c) M. Evangelisti, J. Bartolomé, L. J. de Jongh, G. Filoti, *Phys. Rev. B* **2002**, *66*, 144410.

[4] R. R. Linstead, E. G. Noble, J. M. Wright, *J. Chem. Soc.* **1937**, 911.

[5] O. E. Sielcken, M. M. van Tilborg, M. F. M. Roks, R. Hendriks, W. Drenth, R. J. M. Nolte, *J. Am. Chem. Soc.* **1987**, *109*, 4261.

[6] P. A. Stuzhin, C. Ercolani in *The Porphyrin Handbook, Vol. 15* (Eds.: K. M. Kadish, K. M. Smith, R. Guilard), Academic Press, New York, **2003**, pp. 263–364.

[7] P. A. Stuzhin, E. M. Bauer, C. Ercolani, *Inorg. Chem.* **1997**, *36*, 1533.

[8] E. M. Bauer, D. Cardarrilli, C. Ercolani, P. A. Stuzhin, U. Russo, *Inorg. Chem.* **1999**, *38*, 6114.

[9] M. P. Donzello, C. Ercolani, A. A. Gaberkorn, E. V. Kudrik, M. Meneghetti, G. Marcolongo, C. Rizzoli, P. A. Stuzhin, *Chem. Eur. J.* **2003**, *9*, 4009.

[10] E. V. Kudrik, E. M. Bauer, C. Ercolani, A. Chiesi-Villa, C. Rizzoli, A. Gaberkorn, P. A. Stuzhin, *Mendeleev Commun.* **2001**, 45.

[11] X-ray diffraction data were collected with graphite-monochromated $MoK_\alpha$ ($\lambda = 0.71073$ Å) radiation on an imaging plate system (Mac Science DIP-3200). The absorption collection was applied by integration using the crystal shape. The structures were solved by a direct method (SHELXS-97). A full-matrix least-squares method on $F^2$ with anisotropic thermal parameters was employed for the structural refinements (SHELXL-97). Hydrogen atoms were found by the difference Fourier syntheses and they were refined. Crystal data for $TTDPzH_2$: $C_{16}H_2N_{16}S_4$ ($M_r = 546.58$), red block, $0.10 \times 0.20 \times 0.2$ mm, monoclinic, space group $P2_1/n$ $a = 8.9250(3)$, $b = 12.0340(5)$, $c = 9.8650(4)$ Å, $\beta = 116.500(2)°$, $V = 948.21(6)$ Å$^3$, $Z = 2$, $\rho_{calcd} = 1.914$ g cm$^{-1}$, $T = 293$ K, $2\theta_{max} = 59.76°$, $F(000) = 548$, reflections collected/unique 10020/2715 ($R_{int} = 0.032$)), parameters 167. Final $R$ indices $R1(I > 2\sigma(I)) = 0.0419$, $wR2 = 0.1019$ (all data), $S = 1.101$ (all data).

[12] a) D. E. Hooks, T. Fritz, M. D. Ward, *Adv. Mater.* **2001**, *13*, 227; b) A. Yamashita, T. Hayashi, *Adv. Mater.* **1996**, *8*, 791 and references therein.

[13] Crystal data for TTDPzCo: $C_{16}N_{16}S_4Co$ ($M_r = 603.49$), purple block, $0.10 \times 0.15 \times 0.20$ mm, monoclinic, space group $P2_1/c$, $a = 13.2660(4)$, $b = 9.1170(3)$, $c = 18.5140(5)$ Å, $\beta = 122.382(2)°$, $V = 1890.99(10)$ Å$^3$, $Z = 4$, $\rho_{calcd} = 2.120$ g cm$^{-1}$, $T = 293$ K, $2\theta_{max} = 59.80°$, $F(000) = 1196$, reflections collected/unique 18880/5194 ($R_{int} = 0.033$), parameters 334. Final $R$ indices $R1(I > 2\sigma(I)) = 0.0392$, $wR2 = 0.1024$ (all data), $S = 1.042$ (all data). CCDC 216083 (for $TTDPzH_2$) and -216084 (for TTDPzCo) contain the supplementary crystallographic data for this paper. These data can be obtained free of charge via www.ccdc.cam.ac.uk/conts/retrieving.html (or from the Cambridge Crystallographic Data Centre, 12 Union Road, Cambridge CB2 1EZ, UK; fax: (+44) 1223-336-033; or deposit@ccdc.cam.ac.uk).

[14] M. J. Cook, A. Jafari-Fini, *J. Mater. Chem.*, **1997**, 7, 2327.

[15] J. M. Robertson, *Organic crystals and molecules*, Cornell University Press, New York, **1953**.

[16] F. H. Moser, A. L. Thomas, *Phthalocyanine compounds*, Reinhold, New York, **1963**.

[17] The magnetic measurements were carried out with a SQUID susceptometer (Quantum Design MPMS-XL). The paramagnetic susceptibility $\chi_p$ was obtained from the susceptibility data, from which the diamagnetic susceptibility was subtracted by assuming that $\chi_p$ follows the Curie–Weiss law at high temperatures.

[18] R. L. Carlin, *Magnetochemistry*, Springer, Heidelberg, **1986**, p. 75.

[19] a) T. J. Marks, *Angew. Chem.* **1990**, *102*, 886; *Angew. Chem. Int. Ed. Engl.* **1990**, *29*, 857. b) T. Inabe, *J. Porphyrins Phthalocyanines* **2001**, *5*, 3 and references therein.


 © 2003 Wiley-VCH Verlag GmbH & Co. KGaA, Weinheim 

*Addition reactions*

# Palladium-Catalyzed Equilibrium Addition of Acidic OH Groups across Dienes**

*Masaru Utsunomiya, Motoi Kawatsura, and John F. Hartwig**

Transition-metal-catalyzed additions of the O–H groups of water and alcohols across substrates with carbon–carbon multiple bonds could provide ethers and alcohols under mild conditions, with the potential for regio and enantiocontrol, and without the by-products of substitution chemistry.[1] However, such metal-catalyzed reactions have been difficult to develop, despite recent advances in the addition of C–H[2–5] and N–H[6–8] groups to olefins.

Palladium-catalyzed telomerization of dienes in the presence of alcohols[9–11] and the 1,4-oxidation of dienes[12] are well-known reactions. Yet, few examples of the formation of allylic ethers by the 1:1 addition of an alcohol across a diene without accompanying oxidation have been reported.[5] A catalyst for the addition of substrates with O–H bonds across dienes that is general enough to encompass additions of mildly acidic O–H groups and that selectively catalyzes 1:1 addition over telomerization is unknown.[13]

In parallel with our efforts to develop catalysis for olefin hydroamination,[7,8,14,15] we have sought transition-metal catalysts for the addition of the O–H groups of alcohols and carboxylic acids across substrates with carbon–carbon multiple bonds. Herein we report the transition-metal-catalyzed formation of allylic ethers and esters by the 1:1 addition of

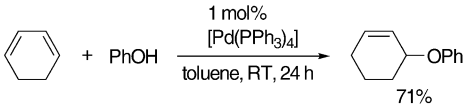
[*] Prof. J. F. Hartwig, M. Utsunomiya, Dr. M. Kawatsura
Department of Chemistry, Yale University
P.O. Box 208107
New Haven, CT 06520-8107 (USA)
Fax: (+1) 203-432-6144
E-mail: john.hartwig@yale.edu

[**] We thank the NIGMS (GM-55382) for support. We thank Mr. Tatsuhiko Kushino for calculation of activity coefficients. M.U. was supported by Mitsubishi Chemical Corporation.

Supporting information for this article is available on the WWW under http://www.angewandte.org or from the author.

 DOI: 10.1002/anie.200352621 © 2003 Wiley-VCH Verlag GmbH & Co. KGaA, Weinheim 

phenols and carboxylic acids across dienes [Eq. (1)]. These addition reactions are reversible, and the measurement of the equilibrium constant for this new type of OH-addition process shows that $\Delta G \approx 0$.




(1)

A series of metal complexes were tested for the addition of phenols across cyclohexadiene. $[Pd(PPh_3)_4]$ displayed good reactivity for the generation of cyclohexenyl phenyl ether under mild conditions (Table 1, entry 1). This simple complex catalyzes the addition of the O–H group of phenols and carboxylic acids across dienes without a co-catalyst. In contrast, this complex required an acid co-catalyst, such as trifluoroacetic or triflic acid, to catalyze the hydroamination of vinyl arenas and dienes.[8,14] The combination of $[\{Pd(allyl)Cl\}_2]$ and $PPh_3$ (4 equiv), which generates $[Pd(PPh_3)_4]$,[16] also catalyzes the addition of phenol to cyclohexadiene.

***Table 1:*** Effect of phosphane ligand on the addition of phenol to cyclohexadiene.[a]

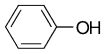
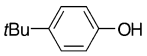
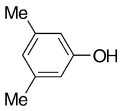
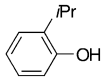
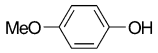
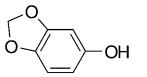
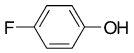
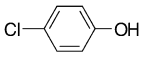
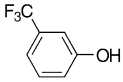
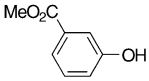
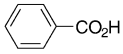
| Entry | Pd precursor | Ligand[b] | Yield [%][c] |
|---|---|---|---|
| 1 | $[Pd(PPh_3)_4]$ | none | 73 |
| 2 | $[\{Pd(allyl)Cl\}_2]$ | $PPh_3$ | 62 |
| 3 | $[\{Pd(allyl)Cl\}_2]$ | $PPh_2Cy$ | 56 |
| 4 | $[\{Pd(allyl)Cl\}_2]$ | $PCy_3$ | 0 |
| 5 | $[\{Pd(allyl)Cl\}_2]$ | $P(p\text{-}MeOC_6H_4)_3$ | 25 |
| 6 | $[\{Pd(allyl)Cl\}_2]$ | $P(p\text{-}ClC_6H_4)_3$ | 25 |
| 7 | $[\{Pd(allyl)Cl\}_2]$ | $P(OPh)_3$ | 0 |
| 8 | $[\{Pd(allyl)Cl\}_2]$ | dppe | 0 |
| 9 | $[\{Pd(allyl)Cl\}_2]$ | dppf | 3 |
| 10 | $[\{Pd(allyl)Cl\}_2]$ | binap | 0 |
| 11 | $[\{Pd(allyl)Cl\}_2]$ | xantphos | 71 |

[a] Reactions were conducted on a 0.4-mmol scale in toluene (0.2 mL) at room temperature for 24 h (phenol/cyclohexadiene/$[Pd(PPh_3)_4]$ or $[\{Pd(allyl)Cl\}_2]$ 100:400:1). [b] P/Pd = 4. [c] Yields determined by GC.

Reactions of phenol with cyclohexadiene catalyzed by $[\{Pd(allyl)Cl\}_2]$ and a variety of phosphanes (Table 1) showed that monodentate ligands, such as $PPh_3$ (Table 1, entry 2) and cyclohexyldiphenylphosphane (Table 1, entry 3), generated catalysts for the addition of phenol across cyclohexadiene. Of the bisphosphanes[17] that we evaluated, only xantphos generated an active catalyst for the addition of the O–H bonds across dienes. Reactions conducted in the absence of catalyst did not form the O–H addition product in amounts detectable by GC. $[Pd(PPh_3)_4]$ was chosen to study the scope of the reaction because it led to faster reaction rates than $[\{Pd(allyl)Cl\}_2]$ and xantphos.

Table 2 summarizes the yields from the addition of various phenols and carboxylic acids across cyclohexadiene. The reactions were typically run at room temperature and at a high concentration (2 M) to favor the addition process. Aryl alcohols with electron-withdrawing groups, such as 4-halophenols (Table 2, entries 7 and 8) and 3-trifluoromethylphenol (Table 2, entry 9), reacted with cyclohexadiene to form the addition product in moderate to good yields. Aryl alcohols with electron-donating groups (Table 2, entries 5 and 6) also formed the addition product in good yields. Phenols with a single *ortho* substituent, including an isopropyl group, reacted in good yields under the same conditions (Table 2, entry 4), but 2,6-disubstituted phenols gave only trace amounts of the addition product at room temperature or 100 °C. The addition reaction also occurred with methyl 3-hydroxybenzoate (Table 2, entry 10), which would react at the ester under classic acid-catalyzed conditions. All reactions in Table 2 gave 2-cyclohexenyl aryl ethers as the sole regioisomer. No 3- or 1-cyclohexenyl aryl ether was detected by GC/MS or NMR spectroscopy. In all cases, the addition processes were clean, and only excess aryl alcohol or ether product were found. Thus, the reaction yields largely paralleled the conversions.

***Table 2:*** Pd-catalyzed addition of acidic OH bonds to cyclohexadiene.[a]

| Entry | ROH | Yield [%][b] | Conversion [%][c] |
|---|---|---|---|
| 1 |  | 71 | 73 |
| 2 |  | 73 | 75 |
| 3 |  | 72 | 73 |
| 4 |  | 61 | 61 |
| 5 |  | 67 | 67 |
| 6[d] |  | 53 | 90 |
| 7[d,e] |  | 62 | 63 |
| 8[d,e] |  | 57 | 60 |
| 9[d–f] |  | 44 | 50 |
| 10[f–h] |  | 47 | 85 |
| 11 |  | 50 | 51[k] |
| 12[i] | $CH_3CO_2H$ | 52 | 52[k] |

[a] Reaction conditions: ROH (1.0 mmol), cyclohexadiene (4.0 mmol), $[Pd(PPh_3)_4]$ (0.01 mmol), toluene (0.5 mL), room temperature, 24 h, unless otherwise noted. [b] Yields of isolated products. [c] Calculated by GC. [d] 50 °C. [e] $[Pd(PPh_3)_4]$: 0.02 mmol. [f] 18 h. [g] Toluene: 1.0 mL [h] $[Pd(PPh_3)_4]$: 0.05 mmol. [i] 2.0-mmol scale, 48 h. [j] Yields determined by GC. [k] Calculated by $^1$H NMR spectroscopy.

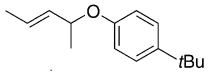
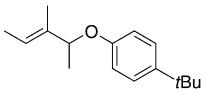
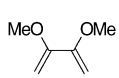
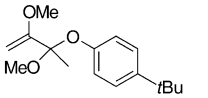
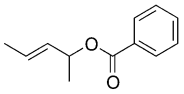
Substrates with O–H groups that are more acidic than those in phenols also underwent additions across dienes. Benzoic acid reacted with 1,3-cyclohexadiene in the presence of the palladium catalyst to form 2-cyclohexenyl benzoate in moderate yield (Table 2, entry 11). Acetic acid added to cyclohexadiene in the presence of the palladium catalyst to form the O–H addition product in 52% yield. Again, no

 © 2003 Wiley-VCH Verlag GmbH & Co. KGaA, Weinheim 

addition product was observed at room temperature or at 70 °C in the absence of catalyst, and the reaction yields were similar to the conversions.

Table 3 summarizes reactions of acyclic dienes with aryl alcohols and carboxylic acids in the presence of $[Pd(PPh_3)_4]$ catalyst. These reactions demonstrate that acyclic allylic ethers can also be prepared by the O–H addition process.

***Table 3:*** Pd-catalyzed addition of acidic OH groups to acyclic dienes.[a]

| Entry | Diene | Product | Yield [%] ($E/Z$)[b] | Conversion [%][c] |
|---|---|---|---|---|
| 1 |  |  | 63 (88:12) | 68 |
| 2 |  |  | 59 (89:11) | 62 |
| 3[d] |  |  | 62 | 64 |
| 4[e] |  |  | 41 (85:15) | 42[f] |

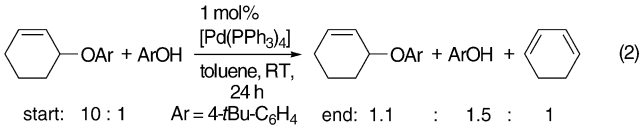
[a] Reaction conditions: 4-tert-butylphenol or benzoic acid (1.0 mmol), dienes (4.0 mmol), $[Pd(PPh_3)_4]$ (0.01 mmol), toluene (0.5 mL), room temperature, 24 h, unless otherwise noted. [b] Yields of isolated products. [c] Calculated by GC. [d] Diene (2.0 mmol), $[Pd(PPh_3)_4]$ (0.05 mmol). [e] Diene (8.0 mmol), $[Pd(PPh_3)_4]$ (0.02 mmol), toluene (1.0 mL), 50 °C. [f] Calculated by $^1$H NMR spectroscopy.

The reactions of 4-*tert*-butylphenol and benzoic acid with *trans*-1,3-pentadiene and (*E*)-3-methyl-1,3-pentadiene gave products with the aryloxy group at the more hindered, internal position by either 1,2- or 1,4-addition (Table 3, entries 1–2, 4). The reaction of 2,3-dimethoxybutadiene with 4-tert-butylphenol also formed the product with the more substituted carbon atom, this time by a clear 1,2-addition (Table 3, entry 3).

The reaction of $[D_1]$4-*tert*-butylphenol with 1,3-pentadiene formed products with the deuterium label at the two methyl groups in a 1:1 ratio, and the reaction of $[D_1]$4-*tert*-butylphenol with cyclohexadiene formed four products in equal amounts from both *syn* and *anti* additions with 1,2- and 1,4-regiochemistry. These labeling experiments suggest the intermediacy of a π-allyl intermediate and reversible C–O bond cleavage in the product. Indeed, catalytic exchange of the phenoxy group of the ether with another aryl alcohol was faster than the catalytic addition of phenol across cyclohexadiene.[18]

The similarities between the yields and conversions of the reactions between dienes and phenols or carboxylic acids suggest that the addition processes are reversible and that thermodynamic factors affect the conversion. This hypothesis was supported by two sets of results: First, reactions at lower temperatures provided higher yields than those conducted at higher temperatures. For example, the reaction of phenol and cyclohexadiene catalyzed by $[Pd(PPh_3)_4]$ at room temperature consumed 73 % of the phenol and formed the addition product in 71 % yield (Table 2, entry 1), whereas the reaction at 60 °C consumed 51 % of the phenol and formed the addition product in 46 % yield. Second, the addition of a second portion of catalyst did not lead to further reaction.

To determine definitively if the reaction was reversible, we subjected 4-*tert*-butylphenyl cyclohexenyl ether to catalytic quantities of $[Pd(PPh_3)_4]$ at room temperature, along with 4-*tert*-butylphenol (0.1 equiv) to activate the catalyst. Consistent with the proposed equilibrium, 55 % of the ether was consumed to give a 1.1:1.5:1 ratio of ether/4-*tert*-butylphenol, and cyclohexadiene after 24 h [Eq. (2)]. The final concentrations from both the forward and reverse reactions at room temperature indicated that the $K_{eq}$ was $1.7 \pm 0.7$; with estimated activity coefficients, the equilibrium constant was $0.62 \pm 0.25$. These values are smaller than those for the addition of methanol to isobutylene.[19]




This thermodynamic analysis of the addition process underscores that the value of $\Delta G$ for O–H addition across olefins is close enough to 0 that small changes in the structures and concentrations of the reactants can influence the conversion. Catalysts active enough to allow the reactions to be conducted under low temperatures conditions with high reactant concentrations are important to obtain high yields of products. Under these conditions, we have shown that the transition-metal-catalyzed addition of phenolic and carboxylic acids across dienes occurs in good yields and with broad scope.

## *Experimental Section*

General procedure (Table 2, entry 1): In a glovebox, 1,3-cyclohexadiene (381 μL, 4.00 mmol) and phenol (94 mg, 1.00 mmol) were added to a suspension of $[Pd(PPh_3)_4]$ (12 mg, 0.01 mmol) in toluene (0.5 mL) in a screw-capped vial. The vial was sealed with a teflon-lined septum, capped, and removed from the glovebox. The reaction mixture was then stirred at room temperature for 24 h. The mixture was absorbed onto silica gel and purified by flash column chromatography to give a colorless oil (124 mg, 71 %).

Received: August 11, 2003
Revised: September 23, 2003 [Z52621]

**Keywords:** addition · alcohols · alkenes · carboxylic acids · dienes · palladium

[1] S. A. Godleski, B. M. Trost, I. Fleming in *Comprehensive Organic Synthesis, Vol. 4* (Eds.: S. A. Godleski, B. M. Trost, I. Fleming), Pergamon, New York, **1991**, p. 585.
[2] L. J. Gooßen, *Angew. Chem.* **2002**, *114*, 3929; *Angew. Chem. Int. Ed.* **2002**, *41*, 3775.
[3] T. Pei, R. A. Widenhoefer, *J. Am. Chem. Soc.* **2001**, *123*, 11290.

 © 2003 Wiley-VCH Verlag GmbH & Co. KGaA, Weinheim 

[4] B. M. Trost, C. Jäkel, B. Plietker, *J. Am. Chem. Soc.* **2003**, *125*, 4438.
[5] P. W. Jolly, N. Kokel, *Synthesis* **1990**, 771.
[6] T. E. Müller, M. Beller, *Chem. Rev.* **1998**, *98*, 675.
[7] M. Utsunomiya, R. Kuwano, M. Kawatsura, J. F. Hartwig, *J. Am. Chem. Soc.* **2003**, *125*, 5608.
[8] M. Kawatsura, J. F. Hartwig, *J. Am. Chem. Soc.* **2000**, *122*, 9546.
[9] W. Keim, A. Behr, M. Roper in *Comprehensive Organometallic Chemistry*, *Vol. 8* (Eds.: G. Wilkinson, F. G. A. Stone), Pergamon, Oxford, **1982**, p. 371.
[10] J. Tsuji, *Acc. Chem. Res.* **1973**, *6*, 8.
[11] R. Jackstell, A. Frisch, M. Beller, D. Rottger, M. Malaun, B. Bildstein, *J. Mol. Catal. A* **2002**, *185*, 105.
[12] J. E. Backvall, *Adv. Met.-Org. Chem.* **1989**, *1*, 135.
[13] For an example of a nickel-catalyzed addition of phenol to for a mixture of telomerization and 1:1 addition products, see: V. J. Beger, C. H. Duschek, G. W. Füllbier, *J. Prakt. Chem.* **1974**, *316*, 26.
[14] O. Löber, M. Kawatsura, J. F. Hartwig, *J. Am. Chem. Soc.* **2001**, *123*, 4366.
[15] J. Pawalas, Y. Nakano, M. Kawatsura, J. F. Hartwig, *J. Am. Chem. Soc.* **2002**, *124*, 3669.
[16] C. F. J. Barnard, M. J. H. Russell in *Comprehensive Organometallic Chemistry*, *Vol. 5* (Eds.: G. Wilkinson, R. D. Gillard, J. A. McCleverty), Pergamon, Oxford, **1987**, p. 1101.
[17] DPPE = 1,2-Bis(diphenylphosphino)ethane, DPPF = 1,1′-Bis(-diphenylphosphino)ferrocene, BINAP = 2,2′-Bis(diphenylphosphino)-1,1′-binaphthyl, Xantphos = 9,9-Dimethyl-4,5-bis(diphenylphosphino)xanthene
[18] See supporting information for data.
[19] J. F. Izquierdo, F. Cunill, M. Vila, M. Iborra, J. Tejero, *Ind. Eng. Chem. Res.* **1994**, *33*, 2830.

 © 2003 Wiley-VCH Verlag GmbH & Co. KGaA, Weinheim 

*Asymmetric Catalysis*

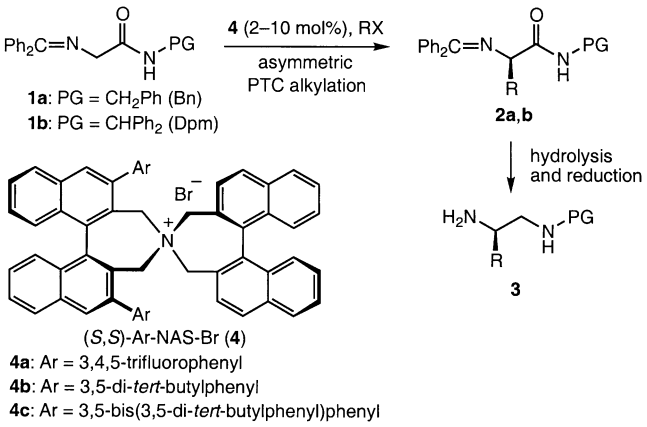
# Practical Asymmetric Synthesis of Vicinal Diamines through the Catalytic Highly Enantioselective Alkylation of Glycine Amide Derivatives**

*Takashi Ooi, Daiki Sakai, Mifune Takeuchi, Eiji Tayama, and Keiji Maruoka**

Optically active vicinal diamines are of great medicinal importance, as they are incorporated in a variety of compounds that display a broad spectrum of biological activity.[1] In organic synthesis, there has also been considerable interest in this class of compounds because of their use as chiral ligands and auxiliaries in asymmetric synthesis.[2] Accordingly, numerous efforts have been made toward their stereoselective preparation, and a number of useful methodologies have been elaborated.[3] Unfortunately, however, only a few practical and general procedures are available even for the asymmetric synthesis of monosubstituted vicinal diamines.[4]

Although the reduction of amides derived from natural α-amino acids is probably one of the most straightforward methods for the synthesis of optically active monosubstituted vicinal diamines,[5] critical structural limitations on the availability of α-amino acids (existing chiral pool) and possible partial racemization encountered in the formation of the amide constitute severe drawbacks. The direct stereoselective introduction of the required side chain onto glycine amides has emerged as a powerful strategy to overcome this intrinsic problem. However, the successful catalytic asymmetric functionalization of prochiral glycine amide derivatives has never been reported, and all previous examples have been diastereoselective transformations involving substrates with chiral auxiliaries.[6] Herein we report the first highly enantioselective phase-transfer catalytic (PTC) alkylation of protected glycine amides **1** with the designer chiral quaternary ammonium salt **4** as the catalyst.[7] The chiral ammonium enolate generated from **1b** and **4c** was found to be very reactive and underwent smooth alkylation even with less reactive *secondary* alkyl halides, thereby facilitating the practical catalytic asymmetric synthesis of a broad range of optically active monosubstituted vicinal diamines (Scheme 1).

First, we examined the feasibility of the stereoselective alkylation of prochiral glycine amide derivatives under phase-transfer catalytic conditions by using the benzophenone Schiff base **1a** of *N*-benzylglycinamide as a representative substrate[8] and the N-spiro chiral quaternary ammonium bromide **4a** as the catalyst. Treatment of **1a** with benzyl bromide (1.2 equiv) and **4a** (2 mol%) in toluene/aqueous KOH (50%) (3:1) at 0°C for 10 h gave only a trace amount of the corresponding alkylation product **2a** (R = $CH_2Ph$). In contrast, the reaction proceeded smoothly under similar con-




***Scheme 1.*** Practical synthesis of a wide range of optically active vicinal diamines through the asymmetric phase-transfer catalytic alkylation of **1** in the presence of the catalyst (*S*,*S*)-**4**. RX = primary, secondary, allylic, or benzylic alkyl halide.

[*] Prof. K. Maruoka, Dr. T. Ooi, D. Sakai, M. Takeuchi, E. Tayama
Department of Chemistry, Graduate School of Science
Kyoto University, Sakyo, Kyoto, 606-8502 (Japan)
Fax: (+81) 75-753-4041
E-mail: maruoka@kuchem.kyoto-u.ac.jp

[**] This work was partially supported by the Uehara Memorial Foundation and a Grant-in-Aid for Scientific Research from the Ministry of Education, Culture, Sports, Science, and Technology, Japan. M.T. thanks the Japan Society for the Promotion of Science for a Research Fellowship for Young Scientists.

Supporting information for this article is available on the WWW under http://www.angewandte.org or from the author.

 © 2003 Wiley-VCH Verlag GmbH & Co. KGaA, Weinheim DOI: 10.1002/anie.200352658 

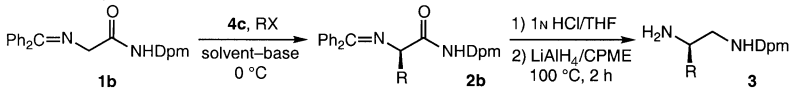
ditions with the catalyst **4b**, which has the substituent 3,5-di-*tert*-butylphenyl, to furnish **2a** (R = $CH_2Ph$) almost quantitatively with 36% *ee*. This result suggested that the steric effect of the 3,3′ aromatic substituent of the catalyst is more important than the electronic effect of this group on the reactivity. Compound **2a** (R = $CH_2Ph$) was obtained with higher enantioselectivity (69% *ee*) when **4c**, which is sterically more hindered, was employed. We then focused on screening the amide substituent, based on these initial results. The diphenylmethyl (Dpm) derivative **1b** was a good substrate, and the phase-transfer catalytic benzylation of **1b** in the presence of **4c** afforded the desired α-amino amide **2b** (R = $CH_2Ph$) in 98% yield with 92% *ee* (Table 1, entry 1).

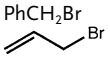
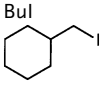
Next, we studied the transformation of **2b** (R = $CH_2Ph$) into the corresponding vicinal diamine. We found that acidic hydrolysis of the imine functionality of **2b** (R = $CH_2Ph$) followed by treatment with $LiAlH_4$ in cyclopentyl methyl ether (CPME)[9] afforded the optically active partially protected vicinal diamine **3** (R = $CH_2Ph$) in 96% yield without loss of enantiomeric excess (Table 1, entry 1).[10] This procedure facilitates the straightforward preparation of a variety of optically active vicinal diamines with primary alkyl side chains. Representative examples are shown in Table 1. A saturated aqueous solution of CsOH was used to ensure consistently high chemical yields in the alkylation with less reactive alkyl halides (Table 1, entries 3 and 4).

This system, which consists of the amide **1b** and the chiral catalyst **4c**, is remarkably reactive, thus enabling the hitherto difficult catalytic asymmetric alkylation of a glycine anion equivalent with simple secondary alkyl halides.[11,12] For instance, the reaction of **1b** with 2-iodopropane (5 equiv) under otherwise similar conditions gave **2b** (R = *i*Pr) in 82% yield with 82% *ee* (Table 1, entry 5). The use of mesitylene in place of toluene enhanced the enantioselectivity to 90% *ee*, and increasing the catalyst loading to 5 mol% led to improvement of the chemical yield (Table 1, entries 6 and 7).[13] Moreover, various cycloalkyl side chains could be introduced in satisfactory chemical yields with excellent enantioselectivities when 2–10 mol% of **4c** was used as the catalyst (Table 1, entries 8–10). Regardless of the steric demand of the newly introduced side chain at the α position, the resulting α-alkyl α-amino amides **2b** can be readily converted into the corresponding optically active partially protected vicinal diamine **3** in excellent chemical yields, as shown in Table 1 and Scheme 2, thus greatly expanding the scope of the present method. Reprotection of the free amine in **3** gave **5**, which could be derivatized further to the partially protected diamine hydrochloride **6** (91%) by simple hydrogenolysis (Scheme 2).

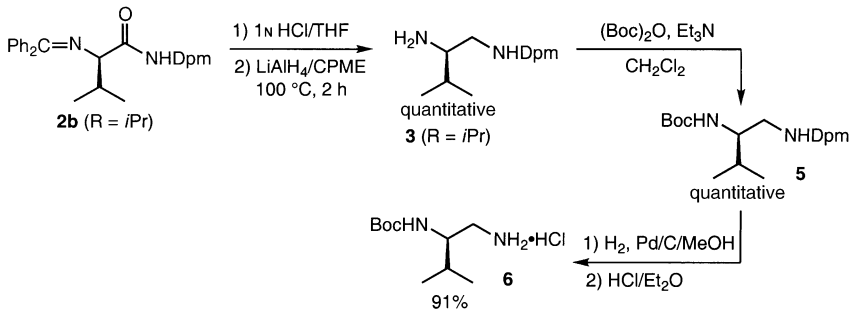
Finally, our approach has been successfully extended to the catalytic asymmetric synthesis of optically active vicinal diamines with sterically congested quaternary stereogenic centers. Thus, vigorous stirring of a mixture of the alanine diphenylmethyl amide derived aldimine Schiff base **7**, iodocyclopentane (5 equiv), $CsOH·H_2O$ (5 equiv), and **4c** (2 mol%) in mesitylene at 0°C for 3 h gave α-amino amide **8** almost quantitatively with 93% *ee*. Subsequent hydrolysis and reduction of **8** cleanly produced the corresponding partially protected diamine **9** (96%),[14] which is not readily accessible by other asymmetric methodologies (Scheme 3).

***Table 1:*** Asymmetric synthesis of optically active vicinal diamines by the catalytic enantioselective phase-transfer alkylation of **1b**.[a]



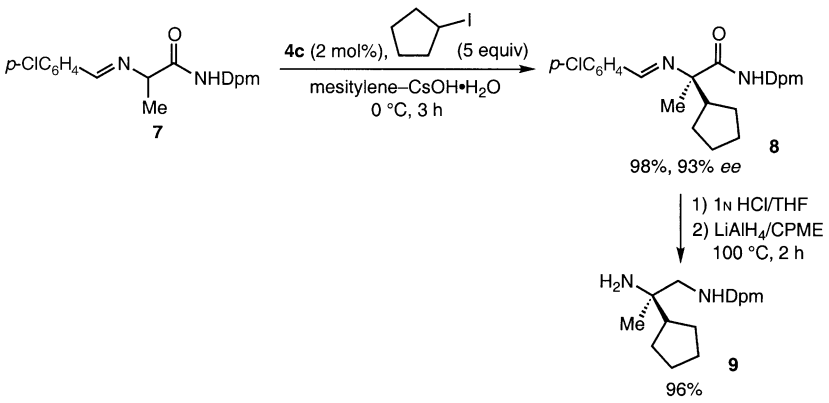

| Entry | RX | **4c** [mol%] | Solvent | Base[b] | *t* [h] | Yield of **2b** [%][c] | *ee* [%][d] | Yield of **3** [%][c] |
|---|---|---|---|---|---|---|---|---|
| 1[e] | $PhCH_2Br$ | 2 | toluene | KOH | 3 | 98 | 92 (*R*) | 96 |
| 2[e] |  | 2 | toluene | KOH | 2 | 99 | 98 (*R*) | 88 |
| 3[e] | BuI | 2 | toluene | CsOH | 3 | 94 | 97 (*R*) | 91 |
| 4[e] |  | 2 | toluene | CsOH | 3 | 82 | 98 (*R*) | 92 |
| 5 |  | 2 | toluene | CsOH | 5 | 82 | 82 (*R*) | |
| 6 | | 2 | mesitylene | CsOH | 5 | 81 | 90 (*R*) | |
| 7 | | 5 | mesitylene | CsOH | 5 | 90 | 90 (*R*) | >99 |
| 8 |  | 2 | mesitylene | CsOH | 3 | 91 | 96 | 97 |
| 9[f] |  | 10 | mesitylene | CsOH | 5 | 71 | 95 | 90 |
| 10 |  | 10 | mesitylene | CsOH | 3 | 80 | 89 | 85 |

[a] Unless otherwise specified, the reaction was carried out with 5 equivalents of RX in the presence of a catalytic amount of **4c** under the reaction conditions given. [b] Aqueous KOH (50%) or saturated, aqueous CsOH. [c] Yield of the isolated product. [d] Enantiopurity was determined by HPLC analysis of the alkylated imine on a chiral phase (Daicel Chiralcel OD (entry 1), Chiralcel OD-H (entry 2), and Chiralpak AD (entries 3–10)) with hexane/2-propanol as the solvent. The absolute configuration of the major enantiomer (given in brackets) was determined by comparison of the HPLC retention time with that of an authentic sample that had been synthesized independently. [e] RX: 1.2 equivalents. [f] Iodocyclohexane: 10 equivalents.




***Scheme 2.*** Facile derivatization of optically active **2b** (R = *i*Pr) to the corresponding differently protected diamines **3** (R = *i*Pr), **5**, and **6**. Boc = *tert*-butoxycarbonyl.

 © 2003 Wiley-VCH Verlag GmbH & Co. KGaA, Weinheim 




***Scheme 3.*** Catalytic asymmetric synthesis of the vicinal diamine **9**, which possesses a sterically congested quaternary stereogenic center.

In conclusion, we have presented a practical procedure for the asymmetric synthesis of vicinal diamines based on the catalytic highly enantioselective alkylation of **1b** under phase-transfer conditions in the presence of the designer chiral quaternary ammonium bromide **4c**. As this substrate–catalyst combination enables the previously difficult catalytic asymmetric construction of α-alkyl α-amino amides that contain a tertiary β carbon center,[15] our approach offers efficient access to structurally diverse optically active vicinal diamines, including those with sterically very congested quaternary α carbon centers.

Received: August 15, 2003 [Z52658]

**Keywords:** alkyl halides · alkylation · asymmetric catalysis · phase-transfer catalysis · vicinal diamines

[1] E. T. Michalson, J. Szmuszkovicz, *Prog. Drug Res.* **1989**, *33*, 135.
[2] See, for example: A. Togni, L. M. Venanzi, *Angew. Chem.* **1994**, *106*, 517; *Angew. Chem. Int. Ed. Engl.* **1994**, *33*, 497.
[3] For an excellent recent review, see: a) D. Lucet, T. Le Gall, C. Mioskowski, *Angew. Chem.* **1998**, *110*, 2724; *Angew. Chem. Int. Ed.* **1998**, *37*, 2581, and references therein; for selected leading references, see also: b) A. Alexakis, I. Aujard, P. Mangeney, *Synlett* **1998**, 873; c) S. Demay, A. Kotschy, P. Knochel, *Synthesis* **2001**, 863; d) P. Saravanan, A. Bisai, S. Baktharaman, M. Chandrasekhar, V. K. Singh, *Tetrahedron* **2002**, *58*, 4693.
[4] For some impressive contributions, see: a) D. Enders, R. Schiffers, *Synthesis* **1996**, 53, and references therein; b) K. Yamada, S. J. Harwood, H. Gröger, M. Shibasaki, *Angew. Chem.* **1999**, *111*, 3713; *Angew. Chem. Int. Ed.* **1999**, *38*, 3504.
[5] a) G. Buono, C. Triantaphylides, G. Peiffer, F. Petit, *Synthesis* **1982**, 1030; b) H. Brunner, M. Schmidt, G. Unger, H. Schönenberger, *Eur. J. Med. Chem.* **1985**, *20*, 509; c) B. E. Rossiter, M. Eguchi, G. Miao, N. M. Swingle, A. E. Hernández, D. Vickers, E. Fluckiger, R. G. Patterson, K. V. Reddy, *Tetrahedron* **1993**, *49*, 965.
[6] For recent examples, see: a) G. Guillena, C. Nájera, *J. Org. Chem.* **2000**, *65*, 7310, and references therein; b) H. J. Kim, S.-k. Lee, Y. S. Park, *Synlett* **2001**, 613.
[7] For the synthetic utility of this type of ammonium salts as chiral phase-transfer catalysts, see: a) T. Ooi, M. Kameda, K. Maruoka, *J. Am. Chem. Soc.* **1999**, *121*, 6519; b) T. Ooi, M. Takeuchi, M. Kameda, K. Maruoka, *J. Am. Chem. Soc.* **2000**, *122*, 5228; c) T. Ooi, M. Kameda, H. Tannai, K. Maruoka, *Tetrahedron Lett.* **2000**, *41*, 8339; d) T. Ooi, M. Takeuchi, K. Maruoka, *Synthesis* **2001**, 1716; e) T. Ooi, Y. Uematsu, M. Kameda, K. Maruoka, *Angew. Chem.* **2002**, *114*, 1621; *Angew. Chem. Int. Ed.* **2002**, *41*, 1551; f) T. Ooi, M. Takahashi, K. Doda, K. Maruoka, *J. Am. Chem. Soc.* **2002**, *124*, 7640; g) T. Ooi, M. Taniguchi, M. Kameda, K. Maruoka, *Angew. Chem.* **2002**, *114*, 4724; *Angew. Chem. Int. Ed.* **2002**, *41*, 4542; h) T. Ooi, E. Tayama, K. Maruoka, *Angew. Chem.* **2003**, *115*, 599; *Angew. Chem. Int. Ed.* **2003**, *42*, 579.
[8] For excellent reviews on the use of Schiff bases of glycine derivatives, see: a) T. Abellán, R. Chinchilla, N. Galindo, G. Guillena, C. Nájera, J. M. Sansano, *Eur. J. Org. Chem.* **2000**, 2689; b) M. J. O'Donnell, *Aldrichimica Acta* **2001**, *34*, 3.
[9] Cyclopentyl methyl ether, kindly supplied by Zeon Corporation, Japan, has a higher boiling point (106 °C) than *tert*-butyl methyl ether. Both ethers are regarded as a potential substitute for diethyl ether.
[10] No loss of enantiomeric excess was observed, as determined by HPLC analysis.
[11] The catalytic enantioselective preparation of α-amino acid derivatives that contain a tertiary β carbon atom from glycine anion equivalents is commonly regarded as extremely difficult. For a diastereoselective approach, see: a) J. M. McIntosh, R. K. Leavitt, P. Mishra, K. C. Cassidy, J. E. Drake, R. Chadha, *J. Org. Chem.* **1988**, *53*, 1947; b) W. Oppolzer, R. Moretti, C. Zhou, *Helv. Chim. Acta* **1994**, *77*, 2363; c) D. Seebach, M. Hoffmann, *Eur. J. Org. Chem.* **1998**, *1337*; d) S. D. Bull, S. G. Davies, A. C. Garner, N. Mujtaba, *Synlett* **2001**, 781. Because of the low reactivity observed in reactions with some alkyl halides, such as iodocycloalkanes,[11a] an extra reaction step is sometimes necessary, for example, alkylation with a reactive secondary allylic halide and subsequent reduction; see: e) J. M. McIntosh, R. K. Leavitt, *Tetrahedron Lett.* **1986**, *27*, 3839.
[12] An alternative solution to this long-standing problem is based on elegant boron alkylation chemistry: M. J. O'Donnell, M. D. Drew, J. T. Cooper, F. Delgado, C. Zhou, *J. Am. Chem. Soc.* **2002**, *124*, 9348; see also: M. J. O'Donnell, J. T. Cooper, M. M. Mader, *J. Am. Chem. Soc.* **2003**, *125*, 2370.
[13] The attempted reaction of **1b** with 2-iodopropane in the presence of *O*-allyl-*N*-(9-anthracenylmethyl)cinchonidinium bromide (10 mol%),[16] one of the most reliable and most commonly used catalysts, under otherwise similar conditions proceeded sluggishly to afford **2b** (R = *i*Pr) in 15% yield with 19% *ee* after 12 h. The use of excess $CsOH·H_2O$ as a solid base and $CH_2Cl_2$ as the solvent at −78 °C to −40 °C did not lead to the formation of the product, and **2b** (R = *i*Pr) was obtained in approximately 23% yield, although with only 7% *ee*, after 5 h at −20 °C.
[14] The absolute configuration of the product **8** was determined to be *R* by X-ray crystallographic analysis after conversion into a dipeptide with *N*-benzyloxycarbonyl-L-alanine; see Supporting Information.
[15] For the importance of optically active α-amino amides, see, for example: a) A. Rockwell, M. Melden, R. A. Copeland, K. Hardman, C. P. Decicco, W. F. DeGrado, *J. Am. Chem. Soc.* **1996**, *118*, 10337; b) K. Kaljuste, J. P. Tam, *Tetrahedron Lett.* **1998**, *39*, 9327; c) G. Liu, N. S. Kozmina, M. Winn, T. W. von Geldern, W. J. Chiou, D. B. Dixon, B. Nguyen, K. C. Marsh, T. J. Opgenorth, *J. Med. Chem.* **1999**, *42*, 3679; d) M. J. Fray, M. F. Burslem, R. P. Dickinson, *Bioorg. Med. Chem. Lett.* **2001**, *11*, 567.
[16] E. J. Corey, F. Xu, M. C. Noe, *J. Am. Chem. Soc.* **1997**, *119*, 12414.

 © 2003 Wiley-VCH Verlag GmbH & Co. KGaA, Weinheim 

*Rh-Catalyzed 1,4-Additions*

# Asymmetric Addition of Aryl Boron Reagents to Enones with Rhodium Dicyclophane Imidazolium Carbene Catalysis**

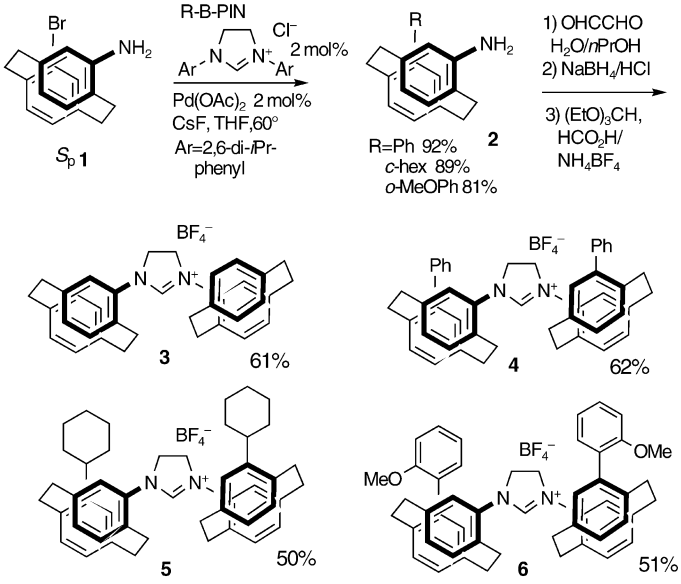
*Yudao Ma, Chun Song, Changqing Ma, Zhijun Sun, Qiang Chai, and Merritt B. Andrus**

Rhodium–binap catalysts have been used with great success for asymmetric conjugate additions of aryl boron compounds to enones and other electron-deficient alkenes.[1] The approach, pioneered by Miyaura, Hayashi, and co-workers offers particular advantages over copper-based methods,[2] including high selectivities, ligand availability, water tolerance, and moderate temperatures. Limitations remain to be addressed, including expanding the scope to alkyl reagents, lowering the amount of borane needed for high reactivity, and identifying new ligands that can be modified readily to accommodate new substrates.[3] As a first step to address these issues and as part of an effort to identify new asymmetric catalysts, we report herein the synthesis and use of a novel class of chiral dicyclophane imidazolium, N-heterocyclic carbene (NHC) ligands. Conditions are reported for the highly selective conjugate addition of aryl borane reagents (1.5 equiv) to cyclic and acyclic enones at moderate temperature. These new $C_2$-symmetric dicyclophane imidazolium ligands can be readily modified to allow substrate–ligand matching with this process and in applications to other asymmetric transformations.

Complexes of N-heterocyclic carbenes (NHC) with transition metals[4] have been developed to catalyze Heck,[5] Suzuki–Miyaura,[6] Stille, and Kumada coupling reactions,[4] hydrogenation reactions,[7] and ruthenium metathesis reactions.[8] We recently reported base-free conditions with NHC–palladium catalysts for Heck and Suzuki coupling reactions and the use of novel, bulky NHC ligands for Sonogashira reactions.[9] Imidazolium carbene ligands provide higher stability and reactivity than phosphanes through strong σ-bond donation to the metal, together with attenuated back-bonding through donation of the nitrogen lone pair of electrons.[10] This combination of electronic effects renders the metal more electron-rich, allowing a more favorable oxidative insertion step. Typical NHC complexes, formed by treatment of an imidazolium salt with base and a metal, are air-stable and can be purified by chromatography in some cases. Alternatively, the NHC–Pd complex can be formed in situ from the imidazolium precursor without added base. Although numerous recent reports of NHC ligands can be found, the area of asymmetric catalysis with chiral imidazolium ligands remains in its infancy.[11]

Planar chiral [2.2]paracyclophane ligands previously have included diphosphanes,[12] oxazoline-phosphanes,[13] oxazoline-imidazolium,[7c] oxazoline-selenides,[14] oxazoline-alcohols,[15] and Schiff base phenols. These have been used for hydrogenation, allylic substitution, and organozinc addition reactions.[16] Dimeric chiral [2.2]paracyclophanes are rare and their use as catalysts has not been reported previously.[17]

The synthesis of the new ligands began with the known compound $S_p$-pseudo-*ortho*-bromoamino[2.2]paracyclophane (**1**; Scheme 1). This material can be readily accessed either from the resolved $S_p$-dibromo[2.2]paracyclophane or from the




***Scheme 1.*** Synthesis of chiral [2.2]paracyclophane imidazolium carbene precursor ligands. R-B-PIN = *B*-aryl pinnacolatoborane

amino[2.2]paracyclophane.[18] The $S_p$-pseudo-*ortho*-dibromide was treated with ammonia under palladium-coupling conditions to give **1**. Alternatively, Boc-protected $S_p$-amino[2.2]paracyclophane[19] can be brominated with NBS (*N*-bromosuccinimide) to give **1**. Suzuki–Miyaura coupling with aryl and cyclohexyl pinacolatoboron compounds under palladium–NHC catalysis gave the amino[2.2]cyclophanes **2** in high yields.[9a,20] A one-pot three-step procedure[21] was then used to generate the $S_p$ $C_2$-symmetric dicyclophane imidazolium ligands **3**–**6**. Ligand **3** was obtained directly from the known $S_p$-amino[2.2]paracyclophane.[19] Treatment with aqueous glyoxal gave the corresponding diimine, which was reduced to the diamine with sodium borohydride. Triethyl orthoformate with catalytic formic acid followed by anion exchange with ammonium tetrafluoroborate gave the dicyclophane imidazolium target **3** in 61% yield. Ligands **4**–**6**

[*] Prof. M. B. Andrus, C. Song
Department of Chemistry and Biochemistry, Brigham Young University
Provo, UT 84602-5700 (USA)
Fax: (+1) 801-422-0153
E-mail: mbandrus@chem.byu.edu
Prof. Y. Ma, C. Ma, Z. Sun, Q. Chai
Chemistry College of Shandong University
Shanda South Road No. 27, Jinan, Shandong, 250100 (P. R. China)

[**] This work was funded by the National Institutes of Health (GM57275, M.B.A.), Brigham Young University, and The Chemistry College of Shandong University (Y.M.).

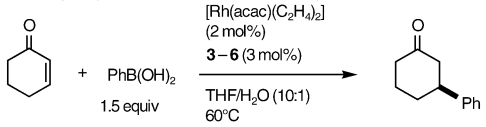
Supporting information for this article is available on the WWW under http://www.angewandte.org or from the author.

 DOI: 10.1002/anie.200352679 © 2003 Wiley-VCH Verlag GmbH & Co. KGaA, Weinheim 

were made by following the same sequence from the $S_p$-amino[2.2]cyclophanes **2** (R = phenyl, cyclohexyl, and *o*-anisyl, respectively).

These new ligands **3–6** were screened in the reaction of phenyl boronic acid (1.5 equiv) and 2-cyclohexenone under standard conditions in THF/water (Table 1). TLC was used to establish when the reaction had gone to completion. The yields shown are for isolated, purified (silica-gel chromatography) (*S*)-3-phenylcyclohexanone product based on 2-cyclohexenone. In the presence of $[Rh(acac)(C_2H_4)_2]$ (2 mol%) and imidazolium ligand (3 mol%), high yields were obtained at 60°C for all ligands investigated. In contrast, when the reaction was carried out with the same rhodium source but with binap ligand, only adequate reactivity was found at 100°C.[1] Only when 0.2 mol% of the rhodium catalyst was used did the yield of the isolated product decrease to 75% in this case. The unsubstituted dicyclophane NHC ligand **3** gave product with only moderate enantioselectivity (61% *ee*). Ligand **4**, the diphenyl variant, reacted at a slower rate, but gave product with improved enantioselectivity (91% *ee*). The dicyclohexyl ligand **5** showed further improvement (97% *ee*). Dianisyl derivative **6** proved to be superior (98% *ee*), and the product was isolated in an excellent yield of 96% after only 3 h.

***Table 1:*** Rh–dicyclophane imidazolium catalysis.

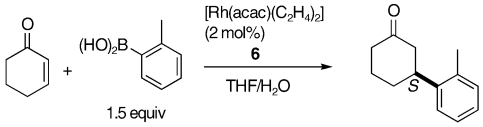



| Entry | Ligand | *t* [h] | Yield [%][a] | *ee* [%][b] |
|---|---|---|---|---|
| 1 | **3** | 4 | 69 | 61 |
| 2 | **4** | 8 | 86 | 91 |
| 3 | **5** | 6.5 | 89 | 97 |
| 4 | **6** | 3 | 96 | 98 |
| 5 | **6** | 3 | 75 | 95[c] |

[a] Yield of product isolated after silica-gel chromatography. [b] Determined by chiral HPLC (OD-H column, heptane/*i*-propyl alcohol 98:2). [c] Catalyst loading changed: Rh (0.2 mol%), ligand (0.3 mol%).

Numerous variations of the reactions conditions were explored for the addition of *o*-tolylboronic acid to cyclohexanone in the presence of the rhodium–**6** complex (Table 2). With the amount of rhodium held constant at 2 mol%, the amount of imidazolium **6** was varied from 0 to 4 mol%. Without added ligand, no product was obtained after 3 h (Table 2, entry 1). The yield was very low, 27% when 1 mol% of **6** was used (Table 2, entry 2), but the selectivity remained high at 89% *ee*. The optimal amount of **6** was found to be 3 mol%, 2:1 ligand/Rh, which resulted in 91% yield, 95% *ee* at 60°C after 3 h (Table 2, entry 4). When the reaction was stopped after 2 h, the product was obtained in 56% yield (96% *ee*) (Table 2, entry 5). At 35°C (Table 2, entry 6) a lower yield was obtained with no improvement in selectivity. At 80°C, the selectivity dropped to 66% *ee* (Table 2, entry 7). When THF alone was used without water, the reaction was much slower and gave a lower yield and selectivity (Table 2, entry 8). The rate was faster when a greater proportion of water was used, however the selectivities were much lower (Table 2, entries 9 and 10). The use of a dioxane/water (10:1) solvent mixture, typical conditions for Rh–binap-catalyzed reactions, gave the product in 89% yield with 95% *ee* after 5 h. Methanol and methanol/water combinations gave good reaction rates, but with lower selectivities. Added bases investigated ($Na_2CO_3$, $NaHCO_3$, $Cs_2CO_3$, CsF, and $K_2CO_3$); all increased the rate of the reaction but gave poor selectivity. When the amount of boronic acid was lowered to 1.2 equivalents, the high selectivity was maintained, but the yield decreased (82%; Table 2, entry 12). A similar effect was noted when the counteranion on the imidazolium salt **6** was changed from tetrafluoroborate to chloride (Table 2, entry 13).

***Table 2:*** Variations on the conditions.




| Entry | **6** [mol%] | $THF/H_2O$ | *T* [°C] | *t* [h] | Yield [%] | *ee* [%] |
|---|---|---|---|---|---|---|
| 1 | 0 | 10:1 | 60 | 3 | 0 | - |
| 2 | 1 | 10:1 | 60 | 3 | 27 | 89 |
| 3 | 2 | 10:1 | 60 | 3 | 82 | 93 |
| 4 | 3 | 10:1 | 60 | 3 | 91 | 95 |
| 5 | 4 | 10:1 | 60 | 3 | 90 | 95 |
| 6 | 3 | 10:1 | 35 | 3 | 83 | 94 |
| 7 | 3 | 10:1 | 80 | 2 | 95 | 66 |
| 8 | 3 | 10:0 | 60 | 6 | 80 | 81 |
| 9 | 3 | 5:1 | 60 | 2 | 85 | 68 |
| 10 | 3 | 3:1 | 60 | 2 | 43 | - |
| 11 | 3 | 10:1 | 60 | 1 | 97 | 36[a] |
| 12 | 3 | 10:1 | 60 | 3 | 82 | 95[b] |
| 13 | 3 | 10:1 | 60 | 5 | 82 | 93[c] |

[a] Reaction performed with added $Na_2CO_3$ (1 equiv). [b] Aryl boronic acid: 1.2 equiv. [c] The chloride salt of ligand **6** was used instead of $BF_4^-$.

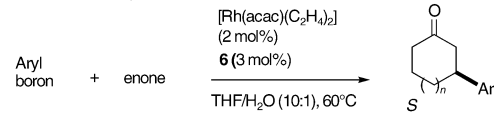
The optimal reaction conditions with ligand **6** were applied in the addition of various aryl boronic acids and potassium trifluoroborates[1f] to several cyclic enones (Table 3). Phenylboronic acid added to all three enones in high yield and with good selectivity. The *p*-methoxyphenyl- and *o*-tolylboron reagents gave similar results. The electron-deficient reagents *p*-acetyl- and trifluoromethylboronic acid also gave excellent yields and selectivities. Under these conditions, the potassium trifluoroborate reagents reacted at a faster rate, but with lower selectivity.

The reactions of acyclic enones with the phenylboron reagents were also explored (Table 4). In general, the yields were again excellent; however, the selectivities were significantly lower. The highest selectivity in this case was found with isopropylvinyl methyl ketone (91% *ee*). The trifluoroborate reagent again reacted at a faster rate, but with lower selectivity.

The origin of the selectivity appears to be related to the binap-catalyzed process proposed by Miyaura, Hayashi, and co-workers.[1] These new $C_2$-symmetric biscyclophane carbene ligands also present four asymmetric quadrants for substrate binding and nucleophile delivery (Scheme 2). In the absence

 © 2003 Wiley-VCH Verlag GmbH & Co. KGaA, Weinheim 

***Table 3:*** Addition to cyclic enone substrates.



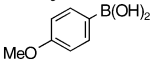
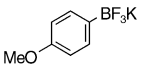
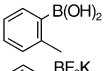
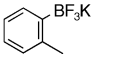
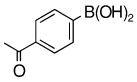
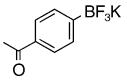
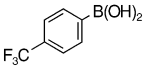
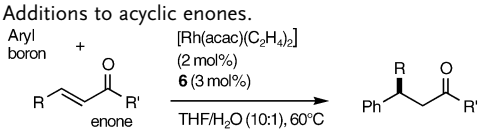
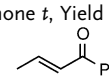
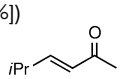

| Aryl boron | Enone *t*, Yield [%] (*ee* [%]) | | |
|---|---|---|---|
| $PhB(OH)_2$ | 3 h,96 (98) | 3.5 h, 94 (93) | 3.5 h, 97 (92) |
| $PhBF_3K$ | 1 h, 96 (91) | 1 h, 93 (85) | 1 h, 95 (90) |
|  | 3 h, 90 (93) | 3.5 h, 90 (85) | |
|  | 1 h, 89 (96) | 1 h, 89 (85) | |
|  | 3 h, 91 (95) | 4 h, 92 (90) | |
|  | 1 h, 95 (90) | 45 min, 94 (87) | |
|  | 4 h, 92 (95) | 4 h, 89 (92) | |
|  | 30 min, 93 (94) | 45 min, 92 (83) | |
|  | 3.5 h, 96 (97) | 4 h, 93 (92) | |

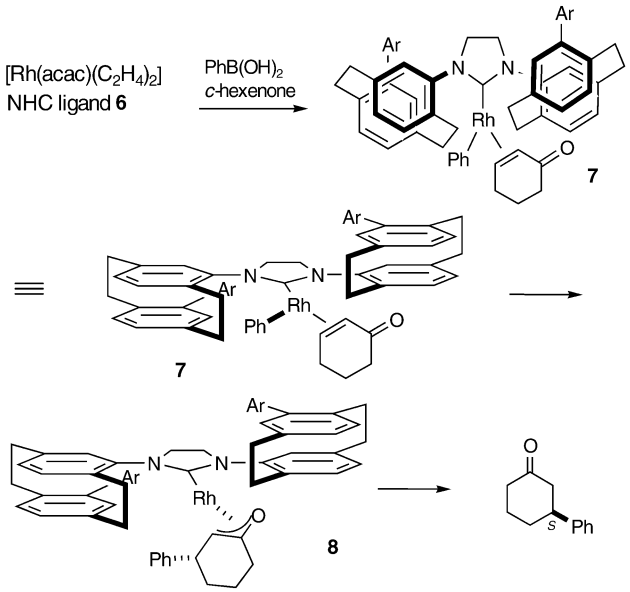
***Table 4:*** Additions to acyclic enones.




| Aryl boron | Enone *t*, Yield [%] (*ee* [%]) | | |
|---|---|---|---|
| |  |  |  |
| $PhB(OH)_2$ | 2.5 h, 95 (81%) | 2.5 h, 92 (78%) | 2.5 h, 83 (91%) |
| $PhBF_3K$ | 45 min, 96 (80%) | 45 min, 95 (73%) | 45 min, 94 (81%) |

of base, the anion of acetylacetone may function as base to produce the rhodium carbene. Palladium–NHC complexes can form in the absence of base. In this case, the aryl boron transmetallates with the NHC–rhodium complex. Complexation with the enone gives **7**. From a 3D view, preferred placement of the enone in an unobstructed quadrant can be assumed. The cyclophane groups, with the aryl substituent rotated back, away from the metal, sterically obstruct the upper right- and lower left-hand quandrants, flanking the central metal carbene. Transfer of the aryl group to the *Si* face of the enone then generates oxallyl–rhodium intermediate **8**. Hydrolysis with water liberates the *S* product and regenerates the catalyst (Scheme 2).

In summary, a new class of asymmetric biscyclophane carbene ligands has been developed. For the first time, very high selectivities are obtained in the presence of a chiral imidazolium ligand for carbon–carbon bond formation in an addition process. The route to these ligands is flexible and




***Scheme 2.*** Origin of asymmetric induction.

allows the synthesis of numerous variations with different electronic and steric properties. This opens up opportunities for other rhodium-based processes and asymmetric, transition-metal-catalyzed reactions with these ligands for which high reactivity at lower temperatures can be found. Efforts to this end are now underway in our laboratories.

Received: August 19, 2003 [Z52679]

**Keywords:** addition · boron · cyclophanes · homogeneous catalysis · rhodium

[1] a) T. Hayashi, M. Takahashi, Y. Takaya, M. Ogasawara, *J. Am. Chem. Soc.* **2002**, *124*, 5052; b) Y. Takaya, M. Ogasawara, T. Hayashi, M. Sakai, N, Miyaura, *J. Am. Chem. Soc.* **1998**, *120*, 5579; c) M. Sakai, H. Hayashi, N. Miyaura, *Organometallics* **1997**, *16*, 4230; for a review, see: d) T. Hayashi, K. Yamasaki, *Chem. Rev.* **2003**, *103*, 2829; for a recent report with aryl siloxanes, see: e) S. Oi, A. Taira, Y. Honma, Y. Inoue, *Org. Lett.* **2003**, *5*, 97; for a recent approach with a Rh phosphoramidite, see: J.-G. Boiteau, R. Imbos, A. J. Minnaard, B. L. Feringa, *Org. Lett.* **2003**, *5*, 681; for the use of potassium trifluoroborates, see: f) M. Pucheault, S. Darses, J.-P. Genêt, *Tetrahedron Lett.* **2002**, *43*, 6157; g) M. Pucheault, S. Darses, J.-P. Genêt, *Eur. J. Org. Chem.* **2002**, 3552.

[2] a) B. L. Feringa, *Acc. Chem. Res.* **2000**, *33*, 346; b) A. Alexakis, J. Burton, J. Vastra, C. Benhaim, X. Fournioux, A. van den Heuvel, J.-M. Levesque, F. Maze, *Eur. J. Org. Chem.* **2000**, 4011; c) L. Liang, T. T. L. Au-Yeung, A. S. C. Chan, *Org. Lett.* **2002**, *4*, 3799; d) H. Mizutani, S. J. Degrado, A. H. Hoveyda, *J. Am. Chem. Soc.* **2002**, *124*, 779.

[3] For a recent report of the use of an achiral cationic palladium catalyst at lower temperatures, see: T. Nishikata, Y. Yamamoto, N. Miyaura, *Angew. Chem.* **2003**, *115*, 2874; *Angew. Chem. Int. Ed.* **2003**, *42*, 2768.

[4] W. A. Herrmann, *Angew. Chem.* **2002**, *114*, 1342; *Angew. Chem. Int. Ed.* **2002**, *41*, 1290.

[5] C. Yang, H. M. Lee, S. P. Nolan, *Org. Lett.* **2001**, *3*, 1511.

 © 2003 Wiley-VCH Verlag GmbH & Co. KGaA, Weinheim 

[6] a) A. Fürstner, A. Leitner, *Syn. Lett.* **2001**, 290; b) G. A. Grasa, A. C. Hillier, S. P. Nolan, *Org. Lett.* **2001**, *3*, 1077.
[7] For asymmetric hydrogenation, see: a) M. C. Perry, X. Cui, M. T. Powell, D. R. Hou, J. H. Reibenspiess, K. Burgess, *J. Am. Chem. Soc.* **2003**, *125*, 113; b) H. Seo, H. J. Park, B. Y. Kim, J. H. Lee, S. U. Son, Y. K. Chung, *Organometallics* **2003**, *22*, 618; c) C. Bolm, T. Focken, G. Raabe, *Tetrahedron: Asymmetry* **2003**, *14*, 1733.
[8] a) T. J. Seiders, D. W. Ward, R. H. Grubbs, *Org. Lett.* **2001**, *3*, 3225; b) J. J. Van Veldhuizen, S. B. Garber, J. S. Kingsbury, A. H. Hoveyda, *J. Am. Chem. Soc.* **2002**, *124*, 4954.
[9] a) M. B. Andrus, C. Song, *Org. Lett.* **2001**, *3*, 3761; b) M. B. Andrus, C. Song, J. Zhang, *Org. Lett.* **2002**, *4*, 2079; c) Y. Ma, C. Song, W. Jiang, Q. Wu, X. Liu, M. B. Andrus, *Org. Lett.* **2003**, *5*, 3317.
[10] W. A. Herrmann, C. Kocher, *Angew. Chem.* **1997**, *109*, 2256; *Angew. Chem. Int. Ed. Engl.* **1997**, *36*, 2162.
[11] For hydrosilylations, see: a) W. A. Herrmann, L. J. Gooßen, C. Köcher, G. R. J. Artus, *Angew. Chem.* **1996**, *108*, 2980; *Angew. Chem. Int. Ed. Engl.* **1996**, *35*, 2805; b) D. Enders, H. Gielen, K. Breuer, *Tetrahedron: Asymmetry* **1997**, *8*, 3571; for the addition of organozinc reagents, see: c) F. Guillen, C. L. Winn, A. Alexakis, *Tetrahedron: Asymmetry* **2001**, *12*, 2083; d) J. Pytkowicz, S. Roland, P. Mangeneney, *Tetrahedron: Asymmetry* **2001**, *12*, 2087; For the Stetter reaction, see: e) D. Enders, U. Kallfass, *Angew. Chem.* **2002**, *114*, 1822; *Angew. Chem. Int. Ed.* **2002**, *41*, 1743; see references [7] and [8] for additional examples.
[12] For use in hydrogenation reactions, see: a) P. J. Pye, K. Rossen, R. A. Reamer, N. N. Tsou, R. P. Volante, P. J. Reider, *J. Am. Chem. Soc.* **1997**, *119*, 6207; b) P. J. Pye, K. Rossen, R. A. Reamer, R. P. Volante, P. J. Reider, *Tetrahedron Lett.* **1998**, *39*, 4441.
[13] For use in allylic substitution reactions, see: X.-W. Wu, X. K. Yuan, W. Sun, M.-J. Zhang, X.-L. Hou, *Tetrahedron: Asymmetry* **2003**, *14*, 107.
[14] X.-L. Hou, X.-W. Wu, L.-X. Dai, B.-X. Cao, J. Sun, *Chem. Commun.* **2000**, 1195.
[15] For use in addition of organizinc reagents, see: X.-W. Wu, X.-L. Hou, L.-X. Dai, J. Tao, B.-X. Cao, B. J. Sun, *Tetrahedron: Asymmetry* **2001**, *12*, 529.
[16] a) T. I. Danilova, V. I. Rozenberg, E. V. Sergeeva, E. Z. A. Starikova, S. Bräse, *Tetrahedron: Asymmetry* **2003**, *14*, 2013; b) S. Dahmen, S. Bräse, *Chem. Commun.* **2002**, 26; c) N. Hermanns, S. Dahmen, C. Bolm, S. Bräse, *Angew. Chem.* **2002**, 114, 3844; *Angew. Chem. Int. Ed.* **2002**, *41*, 3692.
[17] E. Ludger, L. Wittkowski, *Eur. J. Org. Chem.* **1999**, *7*, 1653.
[18] a) K. Rossen, P. J. Pye, A. Maliakal, R. P. Volante, *J. Org. Chem.* **1997**, *62*, 6462; b) P. Pye, K. Rossen, R. P. Volante, U.S. Patent A-5874629.
[19] H. Falk, P. Reich-Rohrwig, K. Schlögl, *Tetrahedron* **1970**, *26*, 511.
[20] Y. Ma, C. Song, M. B. Andrus, unpublished results for aryl halides.
[21] This is a modification of a known procedure: A. J. Arduengo III, *Acc. Chem. Res.* **1999**, *32*, 913.

 © 2003 Wiley-VCH Verlag GmbH & Co. KGaA, Weinheim 

Covalent Catalysis

# Sulfoxide Covalent Catalysis: Application to Glycosidic Bond Formation**

*Timothy A. Boebel and David Y. Gin**

The discovery of novel catalyst systems for hydroxy group functionalization has significant implications in synthesis, both in terms of functional group interconversions as well as fragment-coupling reactions. The development of nonmetallic catalysts for hydroxy group derivatization is an active area of investigation, with the bulk of the work focusing on the discovery of nucleophilic catalysts derived from either nitrogen or phosphorus(III) to enhance acylation or alkylation reactions.[1] On the other hand, the paucity of methods for hydroxy group activation by sulfoxide catalysts is notable despite the diverse reactivity profile of this functional group. Although sulfoxides have been employed as ligands in metal-centered catalysis[2] and as additives to effect coordinative rate acceleration,[3] the use of substoichiometric sulfoxide reagents as stand-alone covalent catalysts has not been exploited.[4] Herein we describe the development of a method for hemiacetal hydroxy sulfonylation that not only establishes the feasibility of sulfoxide turnover in covalent catalysis but also proceeds by a mechanism distinct from the traditional pathway for nucleophilic catalysis. As a demonstration of its practical utility in synthesis, this transformation is applied in conjunction with a subsequent nucleophilic substitution event to effect anomeric bond construction.[5]

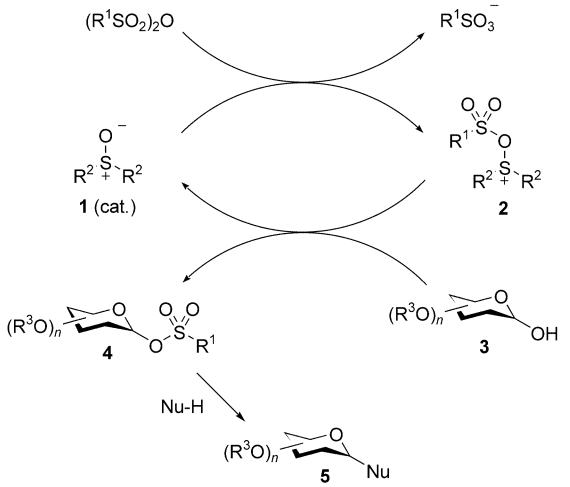
We have previously demonstrated that activated sulfoxide reagents (i.e., $Ph_2SO$ and $Tf_2O$) can effect efficient hemiacetal activation and anomeric bond formation with C1-hydroxy carbohydrates, although the process is only possible when excess sulfoxide reagent is employed in the coupling process.[6] As a result, this glycosylation reaction serves as an ideal setting to establish sulfoxide covalent catalysis, in which the process of hemiacetal sulfonylation is explored. A reasonable pathway for sulfoxide-catalyzed C1-hydroxy sulfonylation (Scheme 1) is envisioned to involve initial *O*-sulfonylation of a sulfoxide catalyst ($R^2_2SO$, **1**) by an appropriate sulfonic anhydride $(R^1SO_2)_2O$ to generate the sulfonyloxysulfonium sulfonate **2**. Ideally, activation of the hemiacetal **3** by **2** leads to the formation of the anomeric sulfonate **4** with concomitant regeneration of the sulfoxide catalyst ($R^2_2SO$, **1**) for subsequent turnovers. The feasibility of sulfoxide turnover is

[*] Prof. Dr. D. Y. Gin, T. A. Boebel
Department of Chemistry, University of Illinois
Urbana, IL 61801 (USA)
Fax: (+1) 217-244-8024
E-mail: gin@scs.uiuc.edu

[**] This research was supported by the National Institutes of Health (GM58833) and the Camille and Henry Dreyfus Foundation. A Pharmacia Graduate Fellowship awarded to TAB is gratefully acknowledged.

Supporting information for this article is available on the WWW under http://www.angewandte.org or from the author.

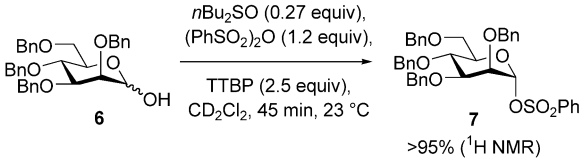
 © 2003 Wiley-VCH Verlag GmbH & Co. KGaA, Weinheim DOI: 10.1002/anie.200352761 




***Scheme 1.*** Proposed pathway for sulfoxide-catalyzed C1-hydroxy sulfonylation (cat. = catalyst).

governed by the requirement that the sulfonate anion derived in the activation process ($R^1SO_3^-$) be of sufficient nucleophilicity so that the glycosyl sulfonate **4** serves as the resting state for the activated hemiacetal.[7] In addition, the anomeric sulfonate **4** must exhibit the desired balance between stability and reactivity if such a process is to be useful for further fragment couplings in glycoconjugate synthesis. For example, unproductive condensation of **4** with unconverted hemiacetal (**4**+**3**) must be avoided in the activation stage,[8] yet substitution at C1 with an external nucleophile (Nu–H, **4**→**5**) must proceed efficiently in the subsequent coupling stage in the absence of additional activating agents.

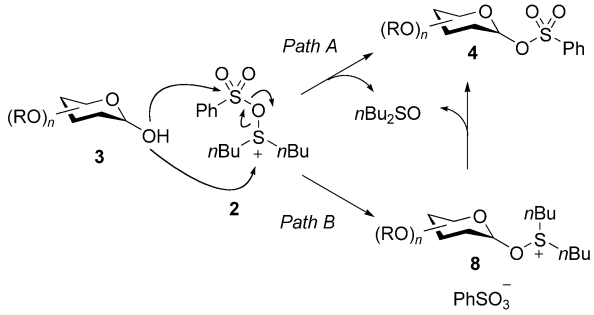
Screening of various sulfonic anhydrides and potential sulfoxide catalysts revealed the combination of $n$Bu$_2$SO and $(PhSO_2)_2O$ to be a suitable system to effect efficient formation of the glycosyl sulfonate **4** by the catalytic turnover of substoichiometric quantities of sulfoxide (Scheme 2).




***Scheme 2.*** Formation of α-mannosyl sulfonate **7** with $n$Bu$_2$SO catalyst and $(PhSO_2)_2O$.

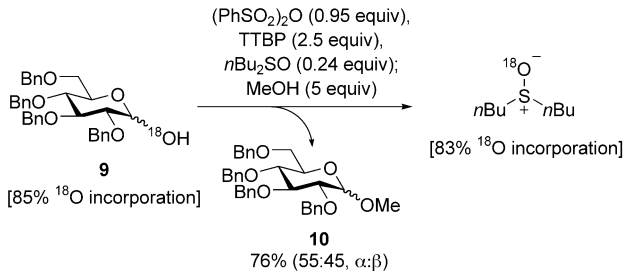
When 2,3,4,6-tetra-*O*-benzyl-D-mannopyranose (**6**) is treated with $(PhSO_2)_2O$ (1.2 equiv) and $n$Bu$_2$SO (0.27 equiv) in the presence of 2,4,6-tri-*tert*-butylpyridine (TTBP; 2.5 equiv) in $CD_2Cl_2$ at 23 °C, near quantitative formation (> 95 %) of the corresponding α-mannosyl sulfonate **7** is observed by $^1$H NMR within 45 min. Importantly, hemiacetal sulfonylation does not proceed in the absence of the sulfoxide when the reaction is performed under otherwise-identical conditions,[9] thereby establishing the critical catalytic role of the sulfoxide species.

Mechanistic consideration of the hemiacetal activation and sulfoxide turnover events suggests two reasonable pathways (Scheme 3), including: (1) Lewis base nucleophilic catalysis[1] to form glycosyl sulfonate **4** (Scheme 3 path A) in




***Scheme 3.*** Two possible pathways for the formation of **4**.

which the sulfoxide species functions sequentially as a transient nucleophile and leaving group; and (2) hemiacetal addition at the sulfonium center of **2** (Scheme 3 path B) to generate the glycosyl oxosulfonium **8**, which then undergoes expulsion/regeneration of the sulfoxide catalyst by nucleophilic substitution by $PhSO_3^-$ to form **4**. A key isotope-labeling experiment (Scheme 4) reveals that addition of

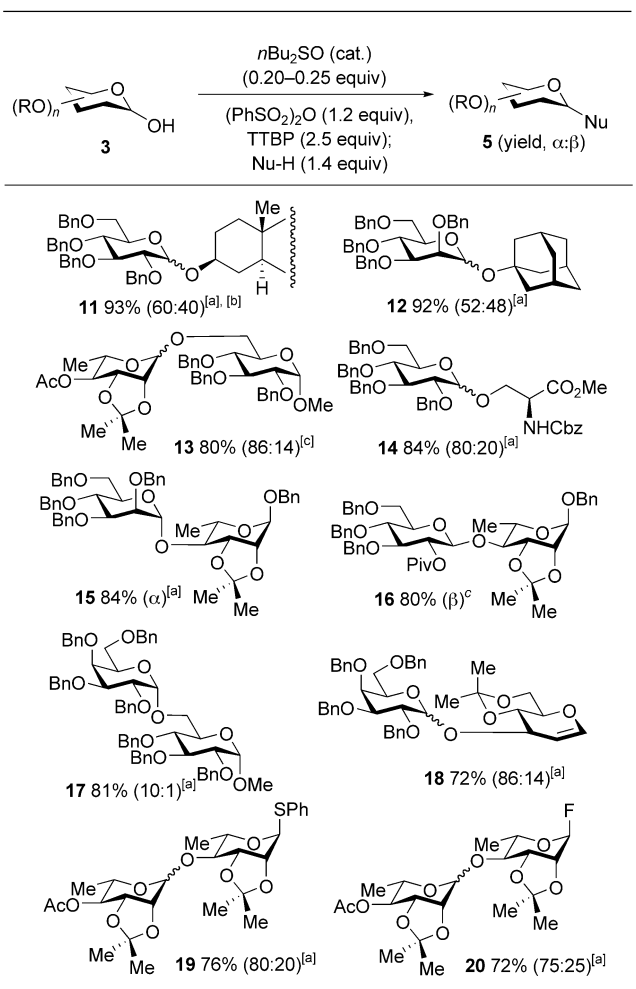



***Scheme 4.*** Isotope-labeling experiment.

methyl alcohol to the glycosyl sulfonate derived from C1–$^{18}$O-labeled 2,3,4,6-tetra-*O*-benzyl-D-glucopyranose (**9**, 85 % $^{18}$O-atom incorporation) by the sulfoxide-catalyzed sulfonylation protocol led to isolation of the recovered sulfoxide catalyst with 83 % $^{18}$O-incorporation, along with methyl 2,3,4,6-tetra-*O*-benzyl-D-glucopyranoside (**10**, 76 %). Factors such as sulfoxide turnover and sulfonate exchange notwithstanding, this level of hemiacetal-to-sulfoxide $^{18}$O-atom transfer indicates that C1–OH activation and sulfoxide turnover proceed at least in part (if not exclusively) through path B of Scheme 3[10,11] in which the sulfur(IV) center serves as a conduit for oxygen-atom transfer, a pathway markedly distinct from both traditional nucleophilic catalysis[1] and simple coordinative rate acceleration.[4]

The production of the methyl glycoside **10** in this experiment also highlights the potential utility of sulfoxide-catalyzed hemiacetal sulfonylation in glycosylation through the introduction of an external nucleophile following hemiacetal activation. Thus, this $n$Bu$_2$SO-catalyzed activation and cou-

 © 2003 Wiley-VCH Verlag GmbH & Co. KGaA, Weinheim 




***Scheme 5.*** Glycoconjugates obtainable by the described reaction; [a] 0.25 equivalents of $n$Bu$_2$SO; [b] Nu–H = dihydrocholesterol; [c] 0.20 equivalents of $n$Bu$_2$SO.

pling is amenable to the construction of a diverse array of glycoconjugates (Scheme 5) in a procedure conveniently conducted entirely at room temperature. In terms of nucleophile variability, primary, secondary, and tertiary alcohols are glycosylated in good yields.[12,13] The range of α:β ratios in the glycoconjugates indicates that the anomeric selectivities vary with the nature of the substrate, although the process does appear to respond to the effects of neighboring group participation (i.e., **16**). Notably, the method tolerates acid-sensitive functionalities such as those present in glycal nucleophiles (**18**). Moreover, the successful couplings with glycals (**18**) as well as nucleophiles bearing latent leaving groups such as sulfide (**19**) and fluoride (**20**) underscore the potential of this reaction to engage in orthogonal glycosylation approaches to oligosaccharide construction.[14]

In summary, the process of sulfoxide turnover in covalent catalysis has been achieved through the development of a versatile glycosylation reaction that employs a simple, commercially available, nonmetallic catalyst for anomeric hydroxy activation and subsequent coupling. The sulfoxide catalyst functions uniquely in three capacities, first as an O nucleophile, then as a $S^+$-electrophile, and finally as a leaving group to fulfill turnover. Investigations are currently underway to further probe the scope and mechanism of this novel mode of sulfoxide catalysis as well as expand it to other oxygen activation/substitution reactions in synthesis.[15]

## *Experimental Section*

General glycosylation procedure with $n$Bu$_2$SO catalyst/(PhSO$_2$)$_2$O: **15**: Benzenesulfonic anhydride (59.9 mg, 0.20 mmol) was added to a solution of 2,3,4,6-tetra-*O*-benzyl-D-mannopyranose (92.1 mg, 0.17 mmol), *n*-butyl sulfoxide (7.0 mg, 0.04 mmol), and 2,4,6-tri-*tert*-butylpyridine (104.6 mg, 0.42 mmol) in dichloromethane (1.3 mL) at 23 °C. After the reaction mixture had stirred for 1 h, a solution of benzyl 2,3-di-*O*-isopropylidene-α-L-rhamnopyranoside (70.3 mg, 0.24 mmol) in dichloromethane (400 μL) was added by syringe and the reaction mixture was then allowed to stir for an additional 19 h. The reaction was then quenched with triethylamine (235 μL, 1.69 mmol), concentrated under high vacuum, and purified by silica gel flash chromatography (5% → 17% ethyl acetate in benzene) to afford the (1→4) α-disaccharide **15** (116.3 mg, 84%) as a single anomer. $R_f = 0.19$ (5% ethyl acetate in benzene); $^1$H NMR (500 MHz, $CDCl_3$): $\delta = 7.18$–$7.42$ (m, 25H), 5.03 (s, 1H), 4.96 (d, 1H, $J = 1.5$ Hz), 4.92 (d, 1H, $J = 10.5$ Hz), 4.80 (d, 1H, $J = 12.6$ Hz), 4.77 (d, 1H, $J = 12.2$ Hz), 4.72 (d, 1H, $J = 12.6$ Hz), 4.69 (d, 1H, $J = 11.7$ Hz), 4.68 (d, 1H, $J = 11.9$ Hz), 4.65 (d, 1H, $J = 11.8$ Hz), 4.57 (d, 1H, $J = 10.6$ Hz), 4.52 (d, 1H, $J = 12.8$ Hz), 4.50 (d, 1H, $J = 12.1$ Hz), 4.24 (t, 1H, $J = 9.7$ Hz), 4.12 (d, 1H, $J = 5.7$ Hz), 4.05 (m, 1H), 4.02 (dd, 1H, $J = 5.8$, 7.3 Hz), 3.92 (dd, 1H, $J = 3.0$, 10.9 Hz), 3.87 (dd, 1H, $J = 3.0$, 9.8 Hz), 3.76 (dd, 1H, $J = 2.0$, 3.0 Hz), 3.70 (dd, 1H, $J = 1.9$, 10.7 Hz), 3.64 (qd, 1H, $J = 6.3$, 10.1 Hz), 3.36 (dd, 1H, $J = 7.4$, 9.9 Hz), 1.49 (s, 3H, $CH_3$), 1.27 (s, 3H), 1.06 ppm (d, 3H, $J = 6.3$ Hz); $^{13}$C NMR (126 MHz, $CDCl_3$): $\delta = 138.7$, 138.7, 138.5, 138.3, 137.0, 128.5, 128.4, 128.3, 128.2, 128.2, 128.1, 128.0, 127.9, 127.7, 127.6, 127.5, 127.4, 109.0, 98.9, 96.1, 80.2, 80.0, 76.0, 75.2, 74.7, 74.0, 73.4, 72.6, 72.3, 71.8, 69.0, 68.6, 65.0, 28.1, 26.3, 17.2 ppm; FTIR (neat film): $\tilde{\nu} = 2932$ (w), 1496 (w), 1454 (w), 1381 (w), 1220 (w), 1093 (s), 1052 (s), 1028 cm$^{-1}$ (m); HRMS (FAB) $m/z$: calcd for $C_{50}H_{56}O_{10}Na$ $[M+Na]^+$ 839.3771; found 839.3770.

Received: September 1, 2003 [Z52761]

**Keywords:** glycosylation · homogeneous catalysis · reaction mechanisms · sulfonylation · synthetic methods

[1] a) E. F. V. Scriven, *Chem. Soc. Rev.* **1983**, *12*, 129–161; b) E. Vedejs, S. T. Diver, *J. Am. Chem. Soc.* **1993**, *115*, 3358–3359; c) E. Vedejs, O. Daugulis, *J. Am. Chem. Soc.* **1999**, *121*, 5813–5814; d) J. C. Ruble, H. A. Latham, G. C. Fu, *J. Am. Chem. Soc.* **1997**, *119*, 1492–1493; e) T. Kawabata, M. Nagato, K. Takasu, K. Fuji, *J. Am. Chem. Soc.* **1997**, *119*, 3169–3170; f) S. J. Miller, G. T. Copeland, N. Papaioannou, T. E. Horstmann, E. M. Ruel, *J. Am. Chem. Soc.* **1998**, *120*, 1629–1630; g) G. C. Fu, *Acc. Chem. Res.* **2000**, *33*, 412–420; h) Y. Chen, S.-K. Tian, L. Deng, *J. Am. Chem. Soc.* **2000**, *122*, 9542–9543; i) D. Basavaiah, A. J. Rao, T. Satyanarayana, *Chem. Rev.* **2003**, *103*, 811–891.

[2] For the use of sulfoxide ligands in metal-centered catalysis, see also: a) B. R. James, R. S. McMillan, *Can. J. Chem.* **1977**, *55*, 3927–3932, b) H. Grennberg, A. Gogoll, J. E. Bäckvall, *J. Org. Chem.* **1991**, *56*, 5808–5811; c) N. Khiar, I. Fernández, F. Alcudia, *Tetrahedron Lett.* **1993**, *34*, 123–126, d) M. C. Carreño, J. L. G. Ruano, M. C. Maestro, L. M. M. Cabrejas, *Tetrahedron: Asymmetry* **1993**, *4*, 727–734; e) M. Ordoñez, V. Guerrero-de la Rosa, V. Labastida, J. M. Llera, *Tetrahedron: Asymmetry*

 © 2003 Wiley-VCH Verlag GmbH & Co. KGaA, Weinheim 

**1996**, *7*, 2675 – 2686; f) G. Chelucci, D. Berta, A. Saba, *Tetrahedron* **1997**, *53*, 3843 – 3848; g) K. Hiroi, Y. Suzuki, *Heterocycles* **1997**, *46*, 77 – 81; h) D. G. I. Petra, P. C. J. Kamer, A. L. Spek, H. E. Schoemaker, P. W. N. M. van Leeuwen, *J. Org. Chem.* **2000**, *65*, 3010 – 3017; i) K. Hiroi, Y. Suzuki, I. Abe, R. Kawagishi, *Tetrahedron* **2000**, *56*, 4701 – 4710; j) K. Hiroi, K. Watanabe, I. Abe, M. Koseki, *Tetrahedron Lett.* **2001**, *42*, 7617 – 7619; k) J. Priego, O. G. Mancheño, S. Cabrera, J. C. Carretero, *J. Org. Chem.* **2002**, *67*, 1346 – 1353; l) K. Watanabe, T. Hirasawa, K. Hiroi, *Chem. Pharm. Bull.* **2002**, *50*, 372 – 379; m) G. J. Rowlands, *Synlett* **2003**, 236 – 240.

[3] Select sulfoxides have been employed as phase-transfer catalysts: a) M. Mikolajczyk, S. Grzejszczak, A. Zatorski, F. Montanari, M. Cinquini, *Tetrahedron Lett.* **1975**, 3757 – 3760; b) N. Furukawa, K. Kishimoto, S. Ogawa, T. Kawai, H. Fujihara, S. Oae, *Tetrahedron Lett.* **1981**, *22*, 4409 – 4412.

[4] The use of excess chiral sulfoxide (3 equiv) for asymmetric allylation of hydrazones through coordinative acceleration has recently appeared: S. Kobayashi, C. Ogawa, H. Konishi, M. Sugiura, *J. Am. Chem. Soc.* **2003**, *125*, 6610 – 6611.

[5] a) K. Toshima, K. Tatsuta, *Chem. Rev.* **1993**, *93*, 1503 – 1531; b) B. G. Davis, *J. Chem. Soc. Perkin Trans. 1* **2000**, 2137 – 2160.

[6] a) B. A. Garcia, J. L. Poole, D. Y. Gin, *J. Am. Chem. Soc.* **1997**, *119*, 7597 – 7598; b) B. A. Garcia, D. Y. Gin, *J. Am. Chem. Soc.* **2000**, *122*, 4269 – 4279.

[7] For examples of glycosyl sulfonate donors, see: a) V. Maroušek, T. J. Lucas, P. E. Wheat, C. Schuerch, *Carbohydr. Res.* **1978**, *60*, 85 – 96; b) V. K. Srivastava, C. Schuerch, *J. Org. Chem.* **1981**, *46*, 1121 – 1126; c) S. Koto, T. Miura, M. Hirooka, A. Tomaru, M. Iida, M. Kanemitsu, K. Takenaka, S. Masuzawa, S. Miyaji, N. Kuroyanagi, M. Yagishita, S. Zen, K. Yago, F. Tomonaga, *Bull. Chem. Soc. Jpn.* **1996**, *69*, 3247 – 3259; d) W. Szeja, *Synthesis* **1988**, 223 – 224; e) S. Koto, N. Morishima, M. Uchino, M. Fukuda, M. Yamazaki, S. Zen, *Bull. Chem. Soc. Jpn.* **1988**, *61*, 3943 – 3950.

[8] Dehydrative glycosylations mediated by $Ph_2SO$ and $Tf_2O$ require the use of excess sulfoxide to minimize self-condensation of the hemiacetal donor since highly reactive glycosyl triflates would necessarily serve as the resting state during the initial activation process with substoichiometric quantities of sulfoxide.

[9] In the absence of sulfoxide catalyst, activation of hemiacetal **6** (1.2 equiv $(PhSO_2)_2O$, 2.5 equiv TTBP) does not occur even after 4 h at 23 °C as evidenced by $^1$H NMR analysis.

[10] Approach of nucleophiles to the sulfonium center of **2** is consistent with the reactivity of oxosulfonium species with nucleophiles: T. T. Tidwell, *Synthesis* **1990**, 857 – 870.

[11] Partial $^{18}$O-atom transfer to the sulfoxide catalyst by way of exclusive reaction through path A of Scheme 3 is possible only if rapid exchange of sulfonate anions with both the sulfonium intermediate **2** and the glycosyl sulfonate **4** occur throughout the activation process. However, participation of the other pseudoequivalent $^{16}$O atoms (present in five-fold excess of the lone hemiacetal $^{18}$O atom) within the sulfonate anions in this exchange process would result in at most a statistical incorporation of $^{18}$O atoms into sulfoxide, even in the limiting case where sulfonate exchange in **2** and **4** might be extremely fast.

[12] Glycosylations to form disaccharide **15** with lower catalyst loadings of $Bu_2SO$ resulted in lower yields of **15** accompanied by some self-condendensation of the hemiacetal donor. With 10 mol% catalyst loading, 75% of **15** and 11% of the corresponding 1,1′-α,α′-symmetrical mannodisaccharide was isolated. At 4 mol% catalyst, 60% of **15** and 20% of the 1,1′-α,α′-symmetrical disaccharide were isolated. Glycosylations to form disaccharide **15** with catalytic 4-dimethylaminopyridine (4-DMAP; 0.25 equiv) instead of $n$Bu$_2$SO under otherwise identical conditions led to 18% yield.

[13] Glycosylation to form disaccharide **15** with catalytic dimethyl sulfoxide (DMSO; 0.25 equiv) instead of $n$Bu$_2$SO under otherwise identical conditions led to 56% yield. An attempted $n$Bu$_2$SO-catalyzed glycosylation to form **15** with $Tf_2O$ (1.2 equiv) instead of $(PhSO_2)_2O$ produced a complex mixture that does not contain **15**.

[14] See, for example: a) S. Raghavan, D. Kahne, *J. Am. Chem. Soc.* **1993**, *115*, 1580 – 1581; b) O. Kanie, Y. Ito, T. Ogawa, *J. Am. Chem. Soc.* **1994**, *116*, 12073 – 12074; c) H. Yamada, T. Harada, T. Takahashi, *J. Am. Chem. Soc.* **1994**, *116*, 7919 – 7920; d) T. Zhu, Boons, G.-J. *Angew. Chem.* **1999**, *111*, 3704 – 3707; *Angew. Chem. Int. Ed.* **1999**, *38*, 3495 – 3497.

[15] See, for example: O. Mitsunobu, *Synthesis* **1981**, 1 – 28.

 © 2003 Wiley-VCH Verlag GmbH & Co. KGaA, Weinheim 

*Hydrogen Shifts*

# Breaking Down Barriers: The Liaison Between Sigmatropic Shifts, Electrocyclic Reactions, and Three-Center Cations**

*Roald Hoffmann* and Dean J. Tantillo**

In a recent computational study we found that the antarafacial [1,8] hydrogen shift in the octatrienyl cation has a very low activation barrier (only 6.3 kcal mol$^{-1}$).[1–2] The transition structure for this rearrangement (Figure 1, two views) is

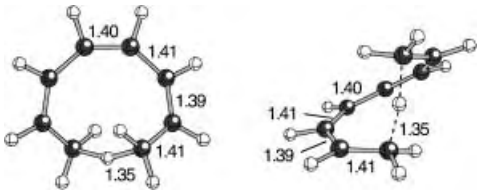



***Figure 1.*** Two views of the transition structure for the antarafacial [1,8] hydrogen shift in the octatrienyl cation. Selected distances are shown in Å.

[*] Prof. Dr. R. Hoffmann
Department of Chemistry & Chemical Biology
Cornell University, Ithaca, NY 14853-1301 (USA)
Fax: (+1) 607-255-5707
E-mail: rh34@cornell.edu

Prof. Dr. D. J. Tantillo
Department of Chemistry, University of California, Davis
One Shields Avenue, Davis, CA 95616 (USA)
Fax: (+1) 530-752-8995
E-mail: tantillo@chem.ucdavis.edu

[**] We gratefully acknowledge support from the National Science Foundation (CHE02–04841) and the National Computational Science Alliance. We also thank Barry Carpenter, Bruce Hietbrink, and Ken Houk for helpful comments.

Supporting information for this article (coordinates and energies (calculated at the B3LYP6-31G(d) level) for all structures shown in Figures 3, 5, and 7) is available on the WWW under http://www.angewandte.org or from the author.

 DOI: 10.1002/anie.200352853 © 2003 Wiley-VCH Verlag GmbH & Co. KGaA, Weinheim 

remarkably delocalized; all bonds (carbon–carbon, and even carbon–hydrogen) are about equal in length. Herein we note an intriguing connection between different types of pericyclic transition structures and carbocations that emerged during our scrutiny of this rearrangement.

## Three-Center Cations

From one perspective, the [1,8] transition structure is simply a cationic extension of a standard sigmatropic reaction (Figure 2, top). But there are other ways to look at this

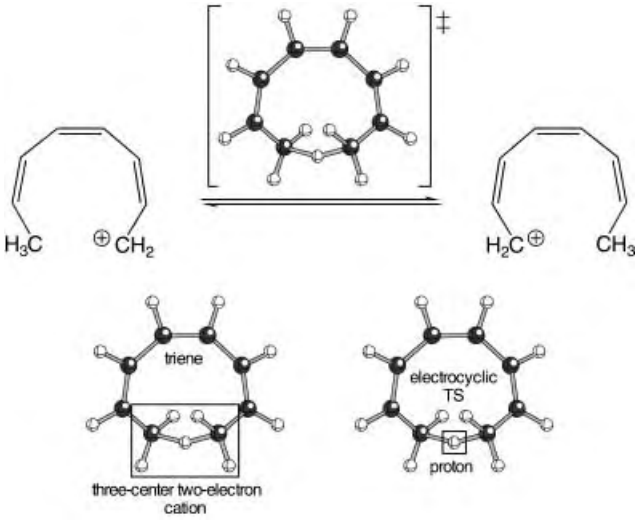
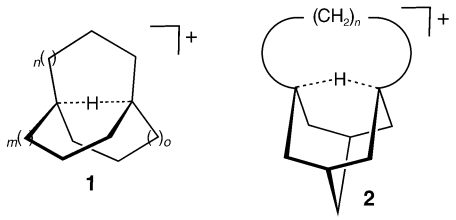



***Figure 2.*** Different ways to view the transition structure for the antarafacial [1,8] hydrogen shift in the octatrienyl cation.

transition structure. For instance, this geometry may be viewed (Figure 2, bottom left) as the transition structure for a hydride transfer from an alkyl group to a carbocation center through a three-center two-electron cationic array, the two reaction partners linked by a triene.[3–4]

Let's examine this perspective a little further. With appropriate geometrical constraints, delocalized $[C\cdots H\cdots C]^+$ arrays can even persist as ground-state molecules, for example, **1** and **2**.[3] Molecules such as **1** and **2** are therefore




sometimes described as "stable transition states"[5] for transannular hydride shifts. The [1,8] transition structure in Figure 1, however, is just that—a transition structure (albeit of low energy), rather than a minimum. Nonetheless, one can play games with that transition structure that lead to species which *are* minima and for which the distinction between [1,8] transition structure and stable $[C\cdots H\cdots C]^+$ cation is effectively lost. Consider, for example, the optimized[6–8] but still theoretical pinwheel cation shown in Figure 3, in which a central $[C\cdots H\cdots C]^+$ array is supported by three hexatriene bridges.

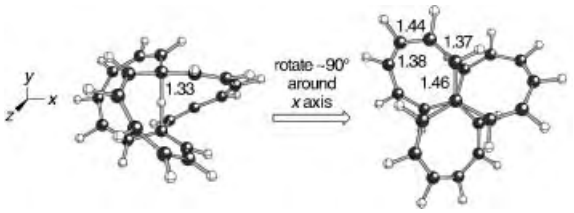



***Figure 3.*** Two views of a pinwheel cation:[8] a "side" view that emphasizes the C···H···C unit and a "top" view that emphasizes the overall threefold symmetry of the structure. Selected distances are shown in Å.

## Protonating Electrocyclic Reactions

There's more. Might one not describe the parent [1,8] transition structure as the product of protonation of another pericyclic transition structure, that for the conrotary electrocyclic closure of an octatetraene to a cyclooctatriene (Figure 2, bottom right)? The calculated[6–7] transition structures for the charged [1,8] sigmatropic hydrogen shift and the neutral 8π electrocyclic reaction are shown side-by-side in Figure 4. Note how similar these are!

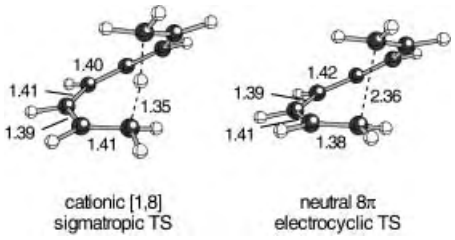



***Figure 4.*** Transition structures for the antarafacial [1,8] hydrogen shift in the octatrienyl cation and the eight-electron electrocyclic ring closure of octatetraene. Selected distances are shown in Å.

This relationship—transition structures for sigmatropic hydrogen shifts resembling protonated electrocyclic transition structures—is quite general.[9] Figure 5 shows the calculated geometries of a series of sigmatropic and electrocyclic transition structures involving different charges, different numbers of electrons, and different topologies (antarafacial/suprafacial; conrotatory/disrotatory).[2,10] In every case, the geometries of the corresponding electrocyclic and sigmatropic transition structures are strikingly similar.[11]

This actually makes quite good sense. Imagine the transition structure for an allowed disrotatory ($C_s$ symmetry) or conrotatory ($C_2$ symmetry) electrocyclic reaction. Such a transition structure, for an allowed reaction, is characterized by a substantial gap between filled and unfilled levels. Now bring in a proton in the mirror plane or along the $C_2$ axis. The empty proton 1s orbital is symmetric and it will interact

 © 2003 Wiley-VCH Verlag GmbH & Co. KGaA, Weinheim 

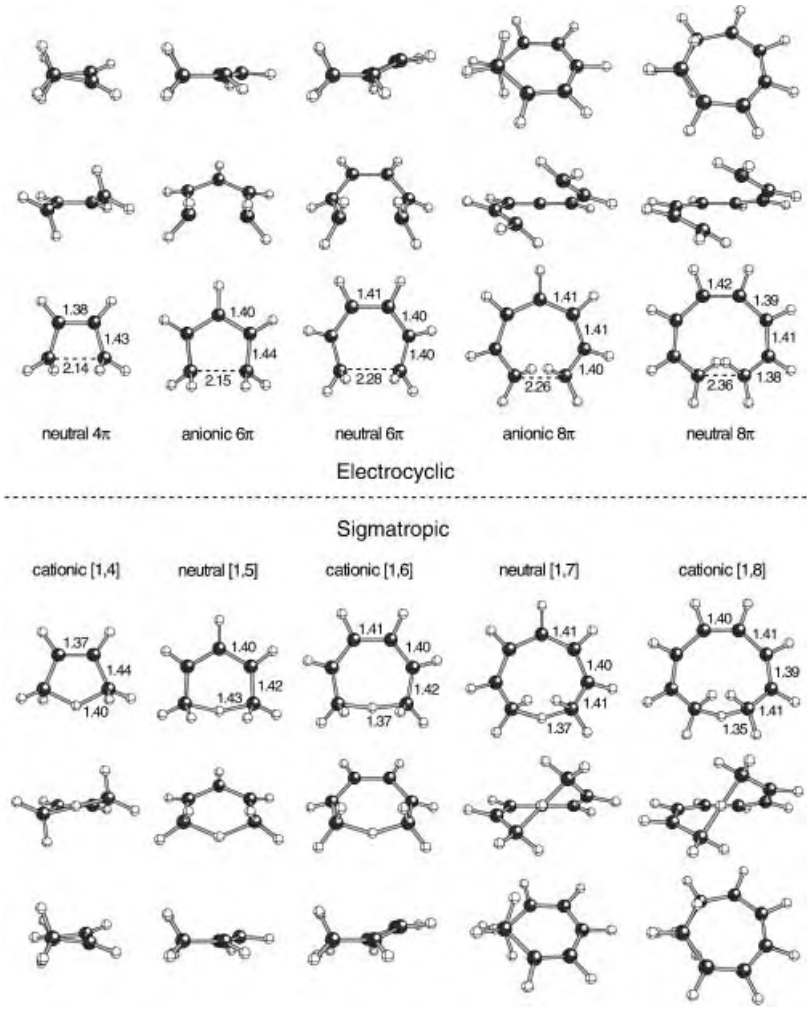



***Figure 5.*** Optimized geometries of electrocyclic and sigmatropic transition structures. Three views of each are shown: a "top" view (closest to dividing line), a "side" view (middle row for each), and a view down the C···(H)···C axis. Selected distances are shown in Å.

(entirely in a one-electron method; mostly, in an all-electron approach) with the filled symmetric levels of the electrocyclic transition structure, stabilizing them (Figure 6a). Perhaps accommodating that proton also "pushes" the ends of the polyene apart slightly, but the primary effect is simply stabilization of the system, without change of electron count or orbital topology. Of course, the proton will also interact with the reactant and product of the rearrangement, making it difficult to predict how the activation barrier will change (see below).

That the "aromaticity" of the transition structures shown in Figure 5, gauged by the delocalization of the bond lengths (and other criteria[12]), is so well-expressed, was not expected. The particularly impressive congruence between the geometries of the electrocyclic and sigmatropic transition structures is likely due, at least in part, to the metrical similarity of a "natural" $[C\cdots H\cdots C]^+$ separation in a hydride shift to a carbonium ion (around 2.5–2.7 Å for the sigmatropic transition structures in Figure 5)[13] to a typical C···C separation in the transition state for an electrocyclic reaction (around 2.1–2.4 Å).[11]

## Transition-State Proton Affinities

If we view the transition structures for sigmatropic hydrogen shifts as protonated electrocyclic transition structures, then we can talk about *transition-state proton affinities*—in other words, the affinities of parti-

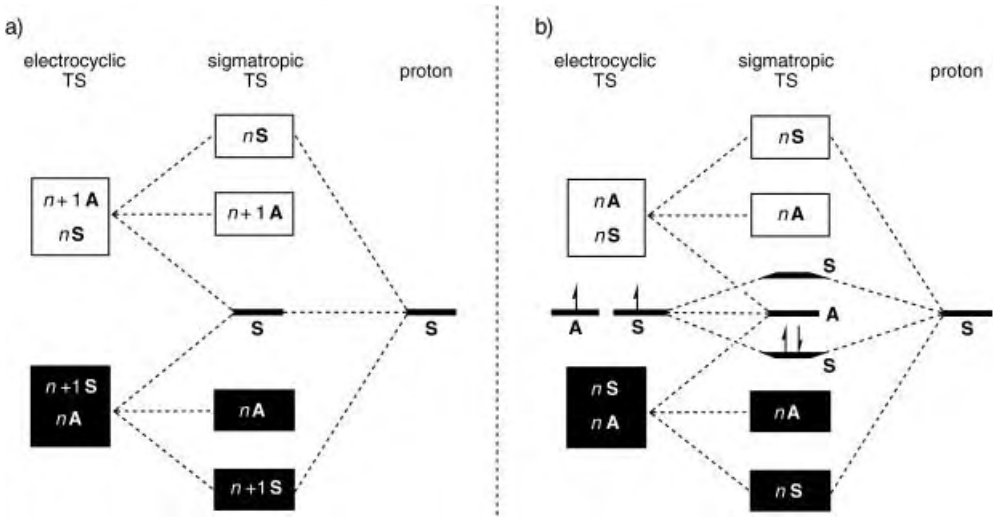



***Figure 6.*** A schematic view of orbital interactions between the symmetric unfilled orbital of a proton with the symmetric filled (black) and unfilled (white) π orbitals of an allowed (a) and forbidden (b) transition structure for a generic electrocyclic reaction involving $4n+2$ orbitals and the same number of electrons. Only the numbers of filled and unfilled orbitals (and the reaction topology) change for $4n$ orbitals, or for different numbers of electrons or orbitals.

 © 2003 Wiley-VCH Verlag GmbH & Co. KGaA, Weinheim 

ally formed or broken carbon–carbon bonds in pericyclic transition structures for protons.[14]

The calculated proton affinities of the anionic electrocyclic transition structures shown in Figure 5 (i.e. the energy differences between the electrocyclic and corresponding sigmatropic transition structures) are 389 kcal mol$^{-1}$ for the anionic 6π ring closure and 366 kcal mol$^{-1}$ for the anionic 8π ring closure. For comparison, proton affinities for benzylic anions are typically ~380–395 kcal mol$^{-1}$ and for alkyl anions are typically ~410–420 kcal mol$^{-1}$.[15a,b] The delocalized anionic electrocyclic transition structures thus appear to be of comparable basicity to other resonance-stabilized anions.

The calculated proton affinities for the neutral electrocyclic transition structures shown in Figure 5 are 203 kcal mol$^{-1}$ for the 4π system and 216 kcal mol$^{-1}$ for both the 6π and 8π systems. For comparison, the proton affinities of typical alkanes are generally ~130–145 kcal mol$^{-1}$,[15a] of simple alkenes are ~165 kcal mol$^{-1}$,[15a] and of conjugated alkenes are ~200–230.[15c] Again, the basicity of the delocalized electrocyclic transition structures appears to be comparable to that of stable delocalized π-systems.

## Different Surfaces, but Similar Transition Structures

The potential energy surfaces for the electrocyclic reactions in Figure 5 are, of course, asymmetric (Figure 7a). Whether the ring-closed or ring-opened form is favored in a given case is determined by many factors (strain, delocalization, charge). On protonation, however, symmetrical sigmatropic shift potential energy surfaces result (Figure 7b). In one case, that of the neutral 6π electrocyclization/cationic suprafacial [1,6] sigmatropic shift pair, the activation barrier for the sigmatropic reaction is lower than that for either electrocyclic ring opening or ring closure.

The surfaces we describe are curious, hundreds of kcal/mol apart on an absolute energy scale, yet gently shaped into unmistakable congruence at their transition states by the stringent demands of orbitals and electrons.

## What Protonation Might Change

In general, it is difficult to locate true transition structures for orbital-symmetry-forbidden processes. Our searches (and those of others) for forbidden transition structures for electrocyclic reactions, for example, have not been fruitful.[16–17] Being unstable and with nothing good going for them, these transition states escape, so to speak. To put it another way, molecules, even quite constrained, find other ways to effect the transformation than by a forbidden process.

However, if protonation stabilizes an allowed transition state without altering its topology, what might it do to a forbidden reaction? A simple orbital argument (analogous to that used for analyzing the effects of protonating the transition structures for allowed reactions) indicates that the "pair of electrons in a degenerate level" problem of a potential forbidden electrocyclic transition structure is partially removed[18] upon protonation (see Figure 6b). So we set out in search of protonated forbidden electrocyclic transition structures, with interesting results.

We were able to locate a $C_2$-symmetric transition structure for formally forbidden antarafacial interconversion of two hexadienyl cations (Figure 8).[19] Much higher in energy (by approximately 16 kcal mol$^{-1}$) than that for the orbital symmetry-allowed rearrangement,[20] the formally forbidden [1,6] transition structure now has lost the high degree of delocalization that characterizes all the allowed structures shown in Figure 5. Instead, it resembles a three-center $[C\cdots H\cdots C]^+$ cation, whose ends are tethered by a simple diene (notice the localized C=C and C–C bonds in the diene linker and the shortened C···H bonds in the $[C\cdots H\cdots C]^+$ array).

We've also looked at the cationic [1,4] case. Our preliminary results suggest that the potential energy surface in the vicinity of the allowed [1,4] transition structure is quite flat and may be populated by both antarafacial and suprafacial structures. More extensive calculations will be required, however, to pin down the nature of this system.

To summarize, the forbidden transition states are certainly stabilized. But they also escape, by localizing into a $[C\cdots H\cdots C]^+$ cation and a polyene. Thus, we have come full circle, returning again to our first analogy, that between sigmatropic shifts and three-center carbocations.

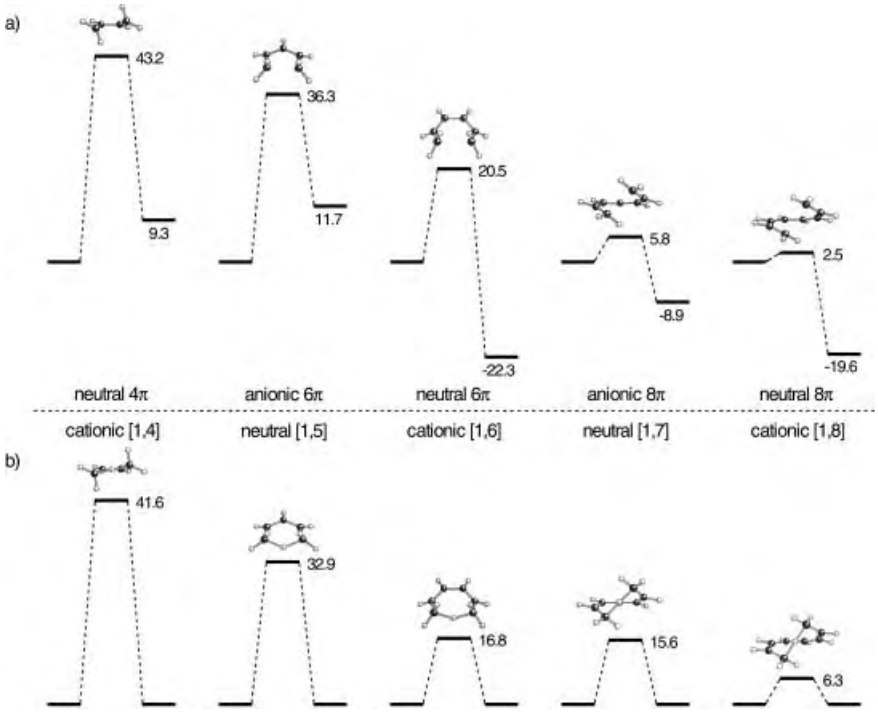



***Figure 7.*** Calculated (B3LYP/6-31G(d)) barriers (in kcal mol$^{-1}$) for electrocyclic (a) and sigmatropic (b) reactions shown in Figure 5. These are from productive conformers, and for electrocyclic reactions, are shown in the ring-closing direction.

 © 2003 Wiley-VCH Verlag GmbH & Co. KGaA, Weinheim 

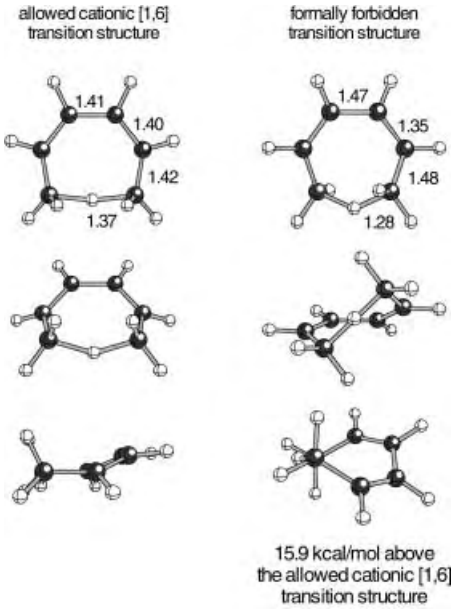



***Figure 8.*** Optimized geometries of allowed and formally forbidden transition structures for cationic [1,6] hydrogen shifts. Three views of each are shown: a "top" view, a "side" view, and a view down the C···(H)···C axis. Selected distances are shown in Å.

## Forward to the Past

The remarkable similarities between electrocyclic and sigmatropic transition states reinforce what was just a plausible argument in early orbital-symmetry days[21]—that there is an underlying electronic unity to all pericyclic reactions. As we can see, now three-center cations are drawn into the game.

Received: September 12, 2003 [Z52853]
Published Online: November 19, 2003

**Keywords:** carbocations · electrocyclic reaction · pericyclic reaction · proton affinity · sigmatropic rearrangement · transition states

[1] From the *all-cisoid* reactant conformer; see: a) D. J. Tantillo, R. Hoffmann, *Helv. Chim. Acta*, in press; b) D. J. Tantillo, C. Ranjan, R. Hoffmann, unpublished results.

[2] For leading references on calculations and experiments on other related sigmatropic shifts, see: a) C. W. Spangler, *Chem. Rev.* **1976**, *76*, 187–217; b) D. J. Tantillo, R. Hoffmann, *J. Am. Chem. Soc.* **2002**, *124*, 6836–6837; c) I. V. Alabugin, M. Manoharan, B. Breiner, F. D. Lewis, *J. Am. Chem. Soc.* **2003**, *125*, 9329–9342; d) O. Dmitrenko, R. D. Bach, R. R. Sicinski, W. Reischl, *Theor. Chem. Acc.* **2003**, *109*, 170–175; e) B. A. Hess, Jr., *J. Org. Chem.* **2001**, *66*, 5897–5900; f) N. J. Saettel, O. Wiest, *J. Org. Chem.* **2000**, *65*, 2331–2336; g) reference [1a].

[3] Cationic three-center two-electron arrays have been studied extensively; for leading references, see: a) J. E. McMurry, T. Lectka, *Acc. Chem. Res.* **1992**, *25*, 47–53; b) M. Saunders, H. A. Jimenez-Vazquez, *Chem. Rev.* **1991**, *91*, 375–397; c) C. A. Grob, *Acc. Chem. Res.* **1983**, *16*, 426–431; d) H. C. Brown, *Acc. Chem. Res.* **1983**, *16*, 432–440.

[4] a) Other researchers have made similar analogies for neutral sigmatropic shifts. See, for example, K. N. Houk, Y. Li, J. D. Evanseck, *Angew. Chem.* **1992**, *104*, 711–739; *Angew. Chem. Int. Ed. Engl.* **1992**, *31*, 682–708; and F. Jensen, *J. Am. Chem. Soc.* **1995**, *117*, 7487–7492; b) it has been proposed that the nature (protonic or hydridic) of the migrating hydrogen in sigmatropic shifts can vary considerably, depending on the nature of the hydrocarbon framework over which it migrates; see: S. D. Kahn, W. J. Hehre, N. G. Rondan, K. N. Houk, *J. Am. Chem. Soc.* **1985**, *107*, 8291–8292; see also: I. V. Alabugin, M. Manoharan, B. Breiner, F. D. Lewis, *J. Am. Chem. Soc.* **2003**, *125*, 9329–9342.

[5] For leading references, see: a) R. V. Williams, *Chem. Rev.* **2001**, *101*, 1185–1204; b) H. Quast, M. Seefelder, C. Becker, M. Heubes, E.-M. Peters, K. Peters, *Eur. J. Org. Chem.* **1999**, 2763–2779; c) R. V. Williams, *Eur. J. Org. Chem.* **2001**, 227–235.

[6] All calculations were performed with GAUSSIAN98 (Gaussian 98 (Revision A.9), M. J. Frisch, G. W. Trucks, H. B. Schlegel, G. E. Scuseria, M. A. Robb, J. R. Cheeseman, V. G. Zakrzewski, J. A. Montgomery, R. E. Stratmann, J. C. Burant, S. Dapprich, J. M. Millam, A. D. Daniels, K. N. Kudin, M. C. Strain, O. Farkas, J. Tomasi, V. Barone, M. Cossi, R. Cammi, B. Mennucci, C. Pomelli, C. Adamo, S. Clifford, J. Ochterski, G. A. Petersson, P. Y. Ayala, Q. Cui, K. Morokuma, D. K. Malick, A. D. Rabuck, K. Raghavachari, J. B. Foresman, J. Cioslowski, J. V. Ortiz, B. B. Stefanov, G. Liu, A. Liashenko, P. Piskorz, I. Komaromi, R. Gomperts, R. L. Martin, D. J. Fox, T. Keith, M. A. Al-Laham, C. Y. Peng, A. Nanayakkara, C. Gonzalez, M. Challacombe, P. M. W. Gill, B. G. Johnson, W. Chen, M. W. Wong, J. L. Andres, M. Head-Gordon, E. S. Replogle, J. A. Pople, Gaussian, Inc., Pittsburgh, PA, **1998**.

[7] Geometries were optimized (without symmetry constraints) at the B3LYP/6-31G(d) level (A. D. Becke, *J. Chem. Phys.* **1993**, *98*, 5648–5652; A. D. Becke, *J. Chem. Phys.* **1993**, *98*, 1372–1377; C. Lee, W. Yang, R. G. Parr, *Phys. Rev. B* **1988**, *37*, 785–789; P. J. Stephens, F. J. Devlin, C. F. Chabalowski, M. J. Frisch, *J. Phys. Chem.* **1994**, *98*, 11623–11627), whose effectiveness in describing structures and energetics for pericyclic reactions is well-documented (see, for example: O. Wiest, D. C. Montiel, K. N. Houk, *J. Phys. Chem. A* **1997**, *101*, 8378–8388; K. N. Houk, B. R. Beno, M. Nendel, K. Black, H. Y. Yoo, S. Wilsey, J. K. Lee, *J. Mol. Struct.* **1997**, *398–399*, 169–179; D. A. Hrovat, B. R. Beno, H. Lange, H.-Y. Yoo, K. N. Houk, W. T. Borden, *J. Am. Chem. Soc.* **2000**, *122*, 7456–7460); all structures were characterized by frequency calculations at the B3LYP/6-31G(d) level, and zero-point energy corrections (scaled by 0.9806 as recommended in A. P. Scott, L. Radom, *J. Phys. Chem.* **1996**, *100*, 16502–16513) from these calculations are included in the reported energies. Ball-and-stick drawings were produced with *Ball & Stick* (N. Müller, A. Falk, Ball & Stick V.3.7.6, molecular graphics application for MacOS computers, Johannes Kepler University Linz, **2000**).

[8] This optimized structure has one imaginary frequency, corresponding to displacement of the bridging H atom along the C···H···C axis; however, the barrier associated with the H shift is less than 1 kcal mol$^{-1}$ in terms of electronic energies, and disappears when zero-point energy corrections are included.

[9] For a discussion of a different sort of connection between the properties of sigmatropic and electrocyclic transition structures (specifically in transition structures for certain rearrangments of α-lactams), see: D. J. Tantillo, K. N. Houk, R. V. Hoffman, J. Tao, *J. Org. Chem.* **1999**, *64*, 3830–3837.

[10] Only anionic and neutral electrocyclic transition structures and neutral and cationic sigmatropic transition structures are shown, since protonation of cationic electrocyclic transition structures would lead to dicationic sigmatropic transition structures and deprotonation of anionic sigmatropic transition structures would lead to dianionic electrocyclic transition structures.

[11] The similarities in forming and breaking bond lengths for different types of pericyclic transition structures have been discussed previously.[4a]

 © 2003 Wiley-VCH Verlag GmbH & Co. KGaA, Weinheim 

[12] Calculated nucleus-independent chemical-shift (NICS) values (GIAO-B3LYP/6-31G(d); for details on the NICS method, see: P. von R. Schleyer, C. Maerker, A. Dransfeld, H. J. Jiao, N. J. R. von E. Hommes, *J. Am. Chem. Soc.* **1996**, *118*, 6317–6318; P. von R. Schleyer, M. Manoharan, Z.-X. Wang, B. Kiran, H. Jiao, R. Puchta, N. J. R. von E. Hommes, *Org. Lett.* **2001**, *3*, 2465–2468) for all of these transition structures are negative (ranging from −13.6 to −7.2). For small systems, there is no clear connection between the NICS calculated for the electrocyclic and sigmatropic transition structures, but for larger systems, nearly identical NICS values were calculated for the electrocyclic and corresponding sigmatropic transition structures (−11.0 for the anionic 8π electrocyclic transition structure and −11.1 for the neutral [1,7] transition structure, and −9.6 for the neutral 8π electrocyclic transition structure and −9.9 for the cationic [1,8] transition structure). This reflects comparable degrees of delocalization in these structures, consistent with the similarities of their geometries. Deviations in the smaller systems may be due to differences in ring size for the electrocyclic and sigmatropic transition structures affecting the proximity of the points at which NICS values were calculated to the carbon–carbon bonds; such problems should be minimized in the larger systems.

[13] For the simple $[H_3C\cdots H\cdots CH_3]^+$ model system, a bent structure with a C···C distance of 2.1 Å is preferred.

[14] "Transition-state acidity" has been discussed previously; for leading references, see: J. L. Kurz, *Acc. Chem. Res.* **1972**, *5*, 1–9 and A. B. Watts, H. Patel, *J. Theor. Biol.* **2001**, *209*, 417–429. This concept does deal with the differences in rate for reactions involving protonated and unprotonated transition states, but is often (although not always) cast in terms of the protonation state of a catalytic molecule, rather than that of a transition structure itself. To our knowledge, this concept has not previously been applied to the analysis of pericyclic reactions.

[15] a) F. A. Carroll, *Perspectives on Structure and Mechanism in Organic Chemistry*, Brooks/Cole, Pacific Grove, **1998**, and references therein; b) http://webbook.nist.gov/chemistry/; c) based on B3LYP6-31G(d) calculations on the reactants for the reactions corresponding to the transition structures in Figure 5.

[16] It was previously reported that the disrotatory "transition state" for the cyclobutene–butadiene interconversion is actually a second-order saddle point; see: J. Breulet, H. F. Schaefer III, *J. Am. Chem. Soc.* **1984**, *106*, 1221–1226.

[17] It was shown previously that formally forbidden electrocyclic transition structures can be stabilized significantly through complexation to certain transition metals; see: D. J. Tantillo, R. Hoffmann, *Helv. Chim. Acta* **2001**, *84*, 1396–1404; D. J. Tantillo, R. Hoffmann, *J. Am. Chem. Soc.* **2001**, *123*, 9855–9859, and references therein.

[18] We say "partially" because the Jahn–Teller-like situation in the forbidden transition structure is replaced upon protonation by a second-order Jahn–Teller system.

[19] High-energy, but real, transition structures for formally forbidden suprafacial [1,7] shifts over cycloheptatriene were previously described; see: T. Okajima, K. Imafuku, *J. Org. Chem.* **2002**, *67*, 625–632.

[20] The effects of substituents on the stereochemical preferences of sigmatropic shifts have been discussed previously; see: M. T. Zoeckler, B. K. Carpenter, *J. Am. Chem. Soc.* **1981**, *103*, 7661–7663 and N. D. Epiotis, *J. Am. Chem. Soc.* **1973**, *95*, 1206–1214.

[21] R. B. Woodward, R. Hoffmann, *The Conservation of Orbital Symmetry*, Verlag Chemie, Weinheim, Germany, **1970**.

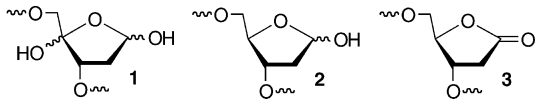
 © 2003 Wiley-VCH Verlag GmbH & Co. KGaA, Weinheim 

Synthesis of Oligonucleotides

# Synthesis and Characterization of Oligonucleotides Containing the C4′-Oxidized Abasic Site Produced by Bleomycin and Other DNA Damaging Agents**

*Jaeseung Kim, Jun Mo Gil, and Marc M. Greenberg**

Exposure of DNA to oxidative stress produces strand scission and a variety of damaged nucleotides, which can be mutagenic and/or cytotoxic. The determination of the effects of specific lesions on nucleic acid structure, stability, and their interaction with polymerase and repair enzymes provide a chemical basis for the biological effects of DNA damage.[1,2] The execution of such investigations is greatly facilitated by the preparation of oligonucleotides containing lesions at defined sites.[3] Oxidized abasic site **1** results from formal abstraction of the C4′-hydrogen atom of a nucleotide in DNA. This alkali-labile lesion accounts for ≈40% of the DNA damage induced by the antitumor antibiotic bleomycin.[4] The C4′-oxidized abasic lesion is also produced following exposure of DNA to the neocarzinostatin chromophore, the enediynes, γ-radiolysis, and a variety of other damaging agents.[5] This oxidized abasic lesion is believed to be mutagenic and cytotoxic, and gives rise to deletions and substitutions in bacteria and mammalian cells.[6] Investigations of **1** have relied upon its sequence nonspecific and nonexclusive generation by the oxidizing agents mentioned above. In contrast, studies concerning related abasic sites (**2**, **3**) are facilitated by the accessibility of oligonucleotides containing them at defined sites.[7–9] Herein we report the first method for chemically synthesizing oligonucleotides that contain **1** at a defined site, and preliminary investigation of the lesion's effects on DNA.




The mechanism by which **1** is produced during DNA oxidation by bleomycin was investigated, and information regarding the source of oxygen at the C4 position was obtained.[4d] To our knowledge there are no reports that describe the ultimate stereochemistry of **1** in DNA, let alone

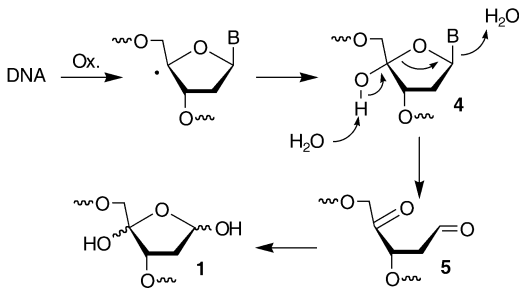
[*] Prof. Dr. M. M. Greenberg, J. Kim, J. M. Gil
Department of Chemistry
Johns Hopkins University
3400 N. Charles St., Baltimore, MD 21218 (USA)
Fax: (+1) 410-516-8420
E-mail: mgreenberg@jhu.edu

[**] We are grateful for support of this research by the National Institutes of General Medical Sciences (GM-63028).

Supporting information for this article is available on the WWW under http://www.angewandte.org or from the author.

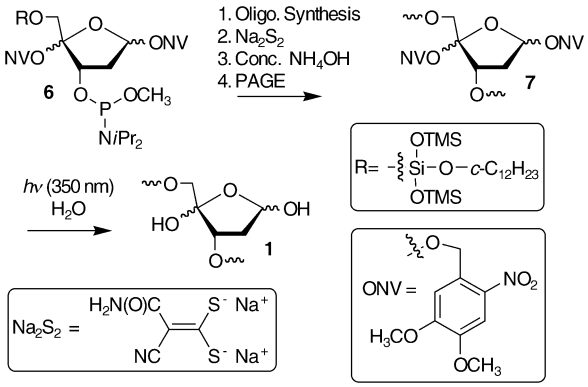
 © 2003 Wiley-VCH Verlag GmbH & Co. KGaA, Weinheim DOI: 10.1002/anie.200352102 

the stepwise mechanism by which it is formed from **4**. A plausible mechanism that was put forth suggests that initial oxidation of the C4′ position activates hydrolysis of the glycosidic bond (Scheme 1).[4c,d] The formation of **1** from the




***Scheme 1.*** Proposed mechanism for the activation of the glycosidic bond.

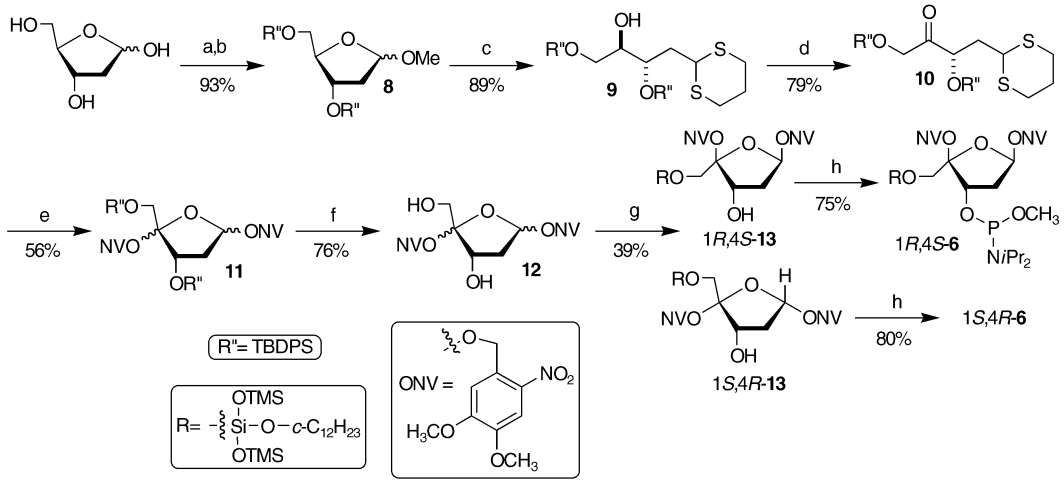
acyclic precursor **5** should result in a mixture of diastereomers.[4c,d] This expectation is consistent with NMR characterization of **2** in DNA, which also leads us to believe that the stereoisomers of **1** should exist in equilibrium with each other and small amounts of **5**.[10] As there was no reason for us to expect that **1** will exist in DNA as a single isomer, we saw no reason to attempt to generate it from individual stereoisomers of a stable precursor. While devising our approach, we also took into account that chemical syntheses of biopolymers that contain **2** and **3** are able to utilize the alkaline deprotection conditions typically employed during oligonucleotide synthesis by unmasking the alkali-labile lesions in a final photochemical step.[7,8] These considerations led us to design **6** as the phosphoramidite used during the automated synthesis to ultimately synthesize **1** in DNA (Scheme 2). Notable features of **6** include the *o*-nitroveratryl moiety (ONV), which serves as the alkali-resistant phototrigger, and the silyloxy protecting group for the primary alcohol. The latter allows us to synthesize protected oligonucleotides




***Scheme 2.*** Synthesis of **1** in DNA.

without exposing the bisacetal (**7**) to acid.[11] The *o*-nitroveratryl group is a member of the class of *o*-nitrobenzyl photolabile protecting groups that are of general use in synthesis, and oligonucleotide synthesis in particular.[12] It was anticipated that oligonucleotides containing **7** would be purified, stored, and used to generate **1** as needed.

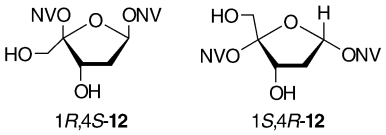
Phosphoramidite **6** was prepared from the 3′,5′-*O*-silyloxy deoxyribose acetal **8** (Scheme 3). Cleavage of the methyl acetal in the presence of 1,3-propane dithiol provided the dithiane **9** with a C4-hydroxy group, which was then oxidized.[13] Subsequent oxidative cleavage of the dithiane ketone, **10**, in the presence of 3,4-dimethoxy-6-nitrobenzyl alcohol provided **11** as a mixture of four stereoisomers.[14] Although separation of the isomers was not practical at this step, the corresponding $^1$H NMR spectrum indicated that two were formed in significantly greater amounts. Analytical samples of the individual diastereomers were obtained upon desilylation (**12**). $^1$H NMR spectroscopy was used to determine that 1*R*,4*S*-**12** and 1*S*,4*R*-**12** accounted for $>80\,\%$ of the mixture of cyclized compounds. In practice, the major diastereomers were separated upon preparation of the cyclododecyloxy bis-trimethylsilyloxy silyl ethers (1*R*,4*S*- 1*S*,4*R*-




***Scheme 3.*** a) $Me_2SiCl_2$, MeOH; b) *tert*-butyldiphenylsilylchloride (TBDPSCl), imadazole; c) propane dithiol, $BF_3{\cdot}Et_2O$, $CH_2Cl_2$, −10 °C; d) oxalyl chloride, dimethyl sulfoxide (DMSO), $Et_3N$, −78 °C; e) *N*-bromosuccinimide, 3,4-dimethoxy-6-nitrobenzyl alcohol (NVOH), $CH_3CN$:$CH_2Cl_2$ (2:1), −10 °C; f) tetrabutylammonium fluoride (TBAF), THF; g)cyclododecyloxy-bis-trimethylsilyloxysilyl chloride (RCl), diisopropylamine, $CH_2Cl_2$ 0–25 °C; h) methyl *N*,*N*-diisopropylchlorophosphoramidite, diisopropylethylamine, $CH_2Cl_2$, 0–25 °C.

 © 2003 Wiley-VCH Verlag GmbH & Co. KGaA, Weinheim 

**13**), which were carried on to their respective phosphoramidites (1*R*,4*S*- 1*S*,4*R*-**6**).




The use of fluoride ions to unmask the primary hydroxy group during synthesis required that oligonucleotides be prepared on polystyrene solid-phase supports by using *O*-methyl phosphoramidites.[11] Solid-phase oligonucleotide synthesis was carried out in the 3′- to 5′-direction on 1 μmol scale by using modified versions of previously reported cycles.[11] With the exception of **6**, all phosphoramidites are commercially available, and were used to prepare oligonucleotides containing as many as 30 nucleotides (**14**–**16**). 5′-*O*-Dimethoxytrityl phosphoramidites containing "fast deprotecting" exocyclic amine protecting groups were used prior to incorporating **6**. This enabled us to monitor the progress of the synthesis by measuring the amount of the dimethoxytrityl cation released. Because of an absence of a similar UV-absorbing chromophore, it was not possible to directly measure the coupling of **6** or subsequent silylated phosphoramidites of the native nucleotides. Consequently, the coupling efficiency of 1*R*,4*S*-**6** was determined indirectly by comparing the isolated yield of **14a** to an otherwise identical oligonucleotide prepared entirely with 5′-*O*-dimethoxytrityl phosphoramidites, which contained thymidine in place of **7**. After the resin loading had been taken into account, the yield of **14a** was 89%, which was as much as the control oligonucleotide, and this yield can be used to estimate the lower limit for the coupling yield of **6**. No differences in coupling yields were observed when a mixture of 1*R*,4*S*- and 1*S*,4*R*-**6** was used, and for simplicity oligonucleotide synthesis with this mixture is currently the method of choice. All oligonucleotides were deprotected in two steps (Scheme 2). Phosphate triester demethylation by using $Na_2S_2$ preceded concentrated aqueous $NH_3$ deprotection/cleavage. After deprotection, photolabile oligonucleotides, **14**–**16**, were isolated by denaturing polyacrylamide gel electrophoresis, and characterized by ESIMS.[15]

5′-d(CGC ATG XGT AGT)
**14a, b**
5′-d(GAA GAC CCX GGC GCC)
**15a, b**
5′-d(GTC ACG TGC TGC AXA CGA CGT GCT GAG CCT)
**16a, b**
**a**: X = **7**; **b**: X = **1**

Photolytic liberation of **1** proved to be extremely efficient. HPLC analysis of photolyzed **14** showed 100% conversion in five minutes of irradiation to a single faster eluting product that did not absorb at 360 nm (Figure 1). In all cases 100% conversion of **7** was achieved during 20 min photolyses. Mass spectral analysis of the photolysates of **14**–**16** verified

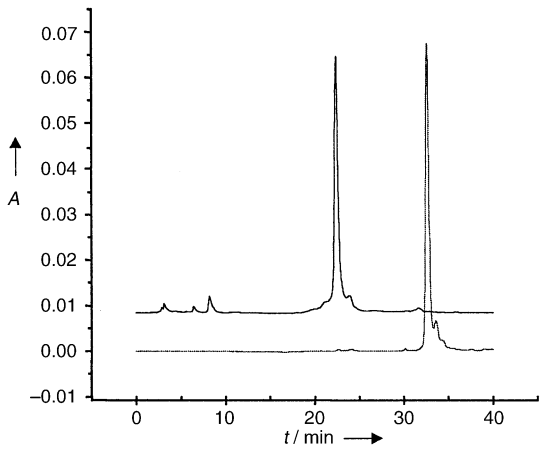



***Figure 1.*** HPLC analysis of (bottom) **14a** (prior to photolysis) and (top) **14b** (after 20 min photolysis at $\lambda_{max} = 350$ nm; intensity: 4.2 mW cm$^{-2}$ @ 360 nm). UV detection at 260 nm.

formation of the desired products, which were observed as a mixture of the cyclic and acyclic (-$H_2O$) forms.[15] The relative amounts of the cyclic and acyclic forms varied from sample to sample.

The stability of **1** in an oligonucleotide (5′-$^{32}$P-**15b**) towards cleavage (phosphate buffer (10 mM), pH 7.5; NaCl (100 mM)) was measured as a function of temperature by using denaturing gel electrophoresis (Figure 2). The C4′-

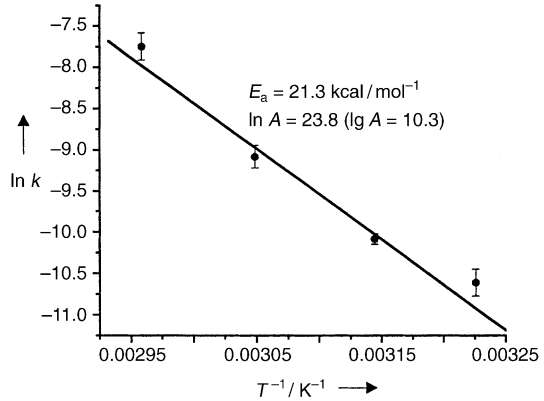
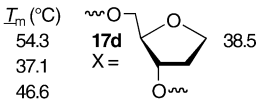



***Figure 2.*** Arrhenius plot describing the cleavage of **1** in **15b**.

oxidized abasic site ($k = 2.46 \times 10^{-5}$ s$^{-1}$, $t_{1/2} = 7.8$ h) was > 10 times as susceptible to cleavage than **3** under comparable conditions (37 °C, pH 7.5), which was found to be 20 times more reactive than a non-oxidized abasic site (**2**).[16] Despite the relative lability of **1**, these studies clearly indicate that **1**

5′-d(CGC ATG XGT AGT)
3′-d(GCG TAC ACA TCA)
**17a-d**

| | X | $T_m$ (°C) |
|---|---|---|
| **17a** | T | 54.3 |
| **17b** | **1** | 37.1 |
| **17c** | **7** | 46.6 |




 © 2003 Wiley-VCH Verlag GmbH & Co. KGaA, Weinheim 

will be sufficiently long-lived to warrant attention by DNA repair enzymes.

A preliminary characterization of the effect of **1** on duplex thermal stability was carried out with the dodecamer **14b**. The lability of **1** at 55 °C led us to investigate the hybridization of **14b** to a complement containing A opposite the lesion at 37 °C to avoid cleaving **1** during hybridization. The suitability of the hybridization conditions was established by using the tetrahydrofuran abasic site analogue, **17d**. Identical $T_m$'s were obtained for **17d** whether the duplex was hybridized at 37 °C (30 min, followed by 2 h at 25 °C) or at 95 °C (5 min, followed by slow cooling to 25 °C). Consequently, the mild conditions (37 °C) were used for the hybridization of **14b**, and the temperature was not allowed to go above 55 °C during the melting process. The $T_m$ for **17b** (37.1 °C, 2.2 μM) did not change over three annealing/melting cycles.[15] Furthermore, no decomposition of **14b** subjected to the identical heating conditions side-by-side with **17b** was detected by HPLC.[15] The $T_m$ for the resulting duplex containing **1** (**17b**) was comparable to that for **17d**, as might be expected for the structurally similar abasic sites. The higher $T_m$ measured for **17c** may reflect the stabilization of the duplex due to π-stacking of the *o*-nitroveratryl groups.

In conclusion, we have developed an efficient method for synthesizing oligonucleotides that contain the C4′-oxidized abasic site, **1**, a common alkali-labile lesion. Despite the lability of **1**, the studies described above clearly indicate that the lesion is amenable to routine handling necessary for carrying out biochemical and biophysical characterization. Specifically, the C4′-oxidized abasic site **1** is sufficiently stable to enable examination of its interactions in a variety of environments such as those that include polymerases and DNA repair enzymes. The ability to store oligonucleotides that contain a stable, convenient photochemical precursor for the C4′-oxidized abasic site **6** in oligonucleotides will facilitate such studies on the lesion.

Experimental procedures for the synthesis of **6**, a description of oligonucleotide synthesis cycles, deprotection, photolysis, melting experiments, and HPLC analysis conditions are available in the Supporting Information. A table of the UV-melting data and sample melt for **17b**, HPLC traces of **14b** before and after 3 annealing/melting cycles, mass spectra of **14**–**16** are also available.

Received: June 10, 2003
Revised: August 25, 2003 [Z52102]

**Keywords:** bioorganic chemistry · DNA damage · oligonucleotides

[1] a) H. Kamiya, *Nucleic Acids Res.* **2003**, *31*, 517; b) D. Wang, D. A. Kreutzer, J. M. Essigmann, *Mutat. Res.* **1998**, *400*, 99.
[2] a) J. Cadet, C. D'Ham, T. Douki, J. P. Pouget, J. L. Ravanat, S. Sauvaigo, *Free Radical Res.* **1999**, *29*, 541; b) M. Dizdaroglu, *Free Radical Res.* **1998**, *29*, 551; c) L. Gros, M. Saparbaev, J. Laval, *Oncogene* **2002**, *21*, 8905.
[3] a) J. Butenandt, L. T. Burgdorf, T. Carell, *Synthesis* **1999**, 1085; b) K. Haraguchi, M. O. Delaney, C. J. Wiederholt, A. Sambandam, Z. Hantosi, M. M. Greenberg, *J. Am. Chem. Soc.* **2002**, *124*, 3263; c) S. Iwai, *Chem. Eur. J.* **2001**, *7*, 4343.
[4] a) J. Stubbe, J. W. Kozarich, *Chem. Rev.* **1987**, *87*, 1107; b) H. Sugiyama, C. Xu, N. Murugesan, S. M. Hecht, *J. Am. Chem. Soc.* **1985**, *107*, 4104; c) L. E. Rabow, J. Stubbe, J. W. Kozarich, *J. Am. Chem. Soc.* **1990**, *112*, 3196; d) L. E. Rabow, G. H. McGall, J. Stubbe, J. W. Kozarich, *J. Am. Chem. Soc.* **1990**, *112*, 3203.
[5] For reviews see: a) C. von Sonntag, *The Chemical Basis of Radiation Biology*, Taylor and Francis, London, **1987**; b) M. M. Greenberg in *Comprehensive Natural Products Chemistry*, *Vol. 7* (Ed. E. T. Kool), Pergamon, Amstedam, **1999**, p. 371; c) Z. Xi, I. H. Goldberg in *Comprehensive Natural Products Chemistry*, *Vol. 7* (Ed. E. T. Kool), Pergamon, Amstedam, **1999**, p. 553.
[6] a) R. A. O. Bennett, P. S. Swerdlow, L. F. Povirk, *Biochemistry* **1993**, *32*, 3188; b) L. F. Povirk, W. Houlgrave, *Environ. Mol. Mutagen.* **1988**, *11*, 461; c) L. F. Povirk, I. H. Goldberg, *Biochimie* **1987**, *69*, 8150.
[7] a) H. J. Lenox, C. P. McCoy, T. L. Sheppard, *Org. Lett.* **2001**, *3*, 2415; b) M. Kotera, A. Bourdat E. Defrancq, J. Lhomme, *J. Am. Chem. Soc.* **1998**, *120*, 11810; c) C. Tronche, B. K. Goodman, M. M. Greenberg, *Chem. Biol.* **1998**, *5*, 263; d) J. T. Hwang, K. A. Tallman, M. M. Greenberg, *Nucleic Acids Res.* **1999**, *27*, 3805; e) B. K. Goodman, M. M. Greenberg, *J. Org. Chem.* **1996**, *61*, 2.
[8] a) J. J. Vasseur, D. Peoc'h, B. Rayner, J. L. Imbach, *Nucleosides Nucleotides* **1991**, *10*, 107; b) T. Horn, K. Downing, Y. Gee, M. S. Urdea, *Nucleosides Nucleotides* **1991**, *10*, 299.
[9] a) G. R. Stuart, R. W. Chambers, *Nucleic Acids Res.* **1987**, *15*, 7451; b) M. Takeshita, C. N. Chang, F. Johnson, S. Will, A. P. Grollman, *J. Biol. Chem.* **1987**, *262*, 10171.
[10] a) J. A. Wilde, P. H. Bolton, A. Mazumder, M. Manoharan, J. A. Gerlt, *J. Am. Chem. Soc.* **1989**, *111*, 1894; b) M. Manoharan, S. C. Ransom, A. Mazumder, J. A. Gerlt, J. A. Wilde, J. A. Withka, P. H. Bolton, *J. Am. Chem. Soc.* **1988**, *110*, 1620.
[11] S. A. Scaringe, F. E. Wincott, M. H. Caruthers, *J. Am. Chem. Soc.* **1998**, *120*, 11820.
[12] a) G. H. McGall, A. D. Barone, M. Diggelmann, S. P. A. Fodor, E. Gentalen, N. Ngo, *J. Am. Chem. Soc.* **1997**, *119*, 5081; b) M. C. Pirrung, *Angew. Chem. Int. Ed.* **2002**, *41*, 1276; c) V. N. R. Pillai, *Synthesis* **1980**, 1.
[13] Y. Honda, A. Ori, G. Tsuchibashi, *Chem. Lett.* **1989**, 1259.
[14] E. J. Corey, B. W. Erickson, *J. Org. Chem.* **1971**, *36*, 3553.
[15] See Supporting Information.
[16] a) Y. Roupioz, J. Lhomme, M. Kotera, *J. Am. Chem. Soc.* **2002**, *124*, 9129; b) S. Shibutani, M. Takeshita, A. P. Grollman, *J. Biol. Chem.* **1997**, *272*, 13916.

 © 2003 Wiley-VCH Verlag GmbH & Co. KGaA, Weinheim 

Molecular Shuttles

# Entropy-Driven Translational Isomerism: A Tristable Molecular Shuttle**

*Giovanni Bottari, Francois Dehez, David A. Leigh,* Phillip J. Nash, Emilio M. Pérez, Jenny K. Y. Wong, and Francesco Zerbetto**

Stimuli-responsive molecular shuttles translocate a macrocycle between different sites ("stations") on a rotaxane thread under the influence of an external trigger.[1] In bistable shuttles the relative macrocycle binding affinities of the stations are reversed by the stimulus, generally through it bringing about a chemical change in the molecule that targets the enthalpy of binding of the macrocycle to one or both stations.[2] Immediately following the chemical transformation the molecule is no longer in the most energetically favored co-conformation and the macrocycle moves along the thread to its newly preferred position through biased Brownian motion as the system relaxes to the global minimum.[3] Although many external stimuli can be used to induce shuttling in this way, for example pH change,[4] light,[5] and electrochemistry[4a,6], a simple temperature change is not generally considered one of them.[7] The Boltzmann distribution of the macrocycle between the different binding sites within a shuttle ensures that heating or cooling changes the degree of discrimination the macrocycle expresses for the various stations, but not the actual station preference of the macrocycle. However, a change of relative-station binding affinity with temperature is possible in principle, since $\Delta G_{binding} = \Delta H_{binding} - T\Delta S_{binding}$. If the entropy terms are sufficiently different then the relative binding affinity of the macrocycle for the two stations can be reversed by increasing or lowering the temperature. Here we describe an example of this phenomenon.[8] The [2]rotaxane **1** is, in fact, a tristable molecular shuttle; the first rotaxane in which a ring can be switched between three different positions on a thread (Figure 1).[9]

Rotaxane *E*-**1** was prepared in 32% yield from thread *E*-**2** (Scheme 1). *E*-**2** has previously[5g] been utilized as the thread for a light- and heat-switchable bistable molecular shuttle **3**, and contains two sites designed to hydrogen bond to a benzylic amide macrocycle, namely a fumaramide group (shown in green) and a succinic amide ester unit (orange), separated by a dodecane chain (purple). Shuttle **1** differs from **3** only in that the macrocycle contains *endo*-pyridine units instead of isophthalamide groups. Photoisomerization of *E*-**1** at 254 nm afforded the *cis*-rotaxane *Z*-**1** in 54% yield. Since the xylylene units of the macrocycle shield the encapsulated regions of the thread, the position of the ring in *E*- and *Z*-**1** could be determined by comparing the chemical shift of the protons in the [2]rotaxanes with those of the corresponding threads (Figure 2).

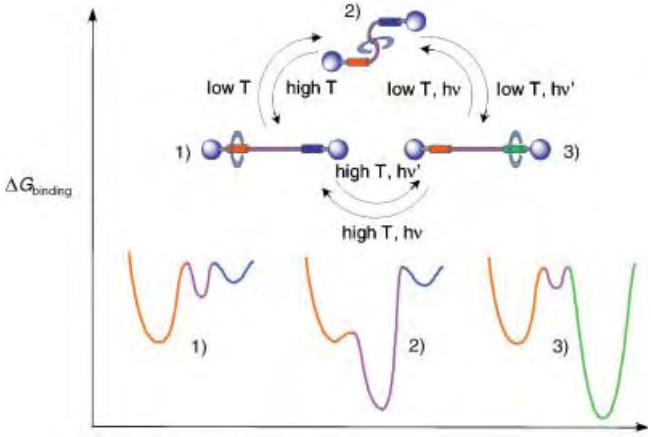



***Figure 1.*** Macrocycle translation in a tristable molecular shuttle. Macrocycle movement between 1) and 2) is an entropy-driven process involving no change to the covalent structure of the molecule.

The $^1$H NMR spectra (400 MHz, 298 K; Figure 2a and b, see page 5888) confirm the position of the macrocycle over the fumaramide station of *E*-**1** in $CDCl_3$. The olefin protons $H_i$ and $H_j$ are shielded by more than 1.5 ppm in the rotaxane relative to the thread, while the chemical shifts of the succinic amide ester protons $H_c$ and $H_d$ are unchanged. Lowering the temperature had no effect on the chemical-shift values, the only significant change in the spectra being that the macrocycle $H_E$ protons sharpen as the ring pirouetting about the thread becomes slow on the NMR timescale.

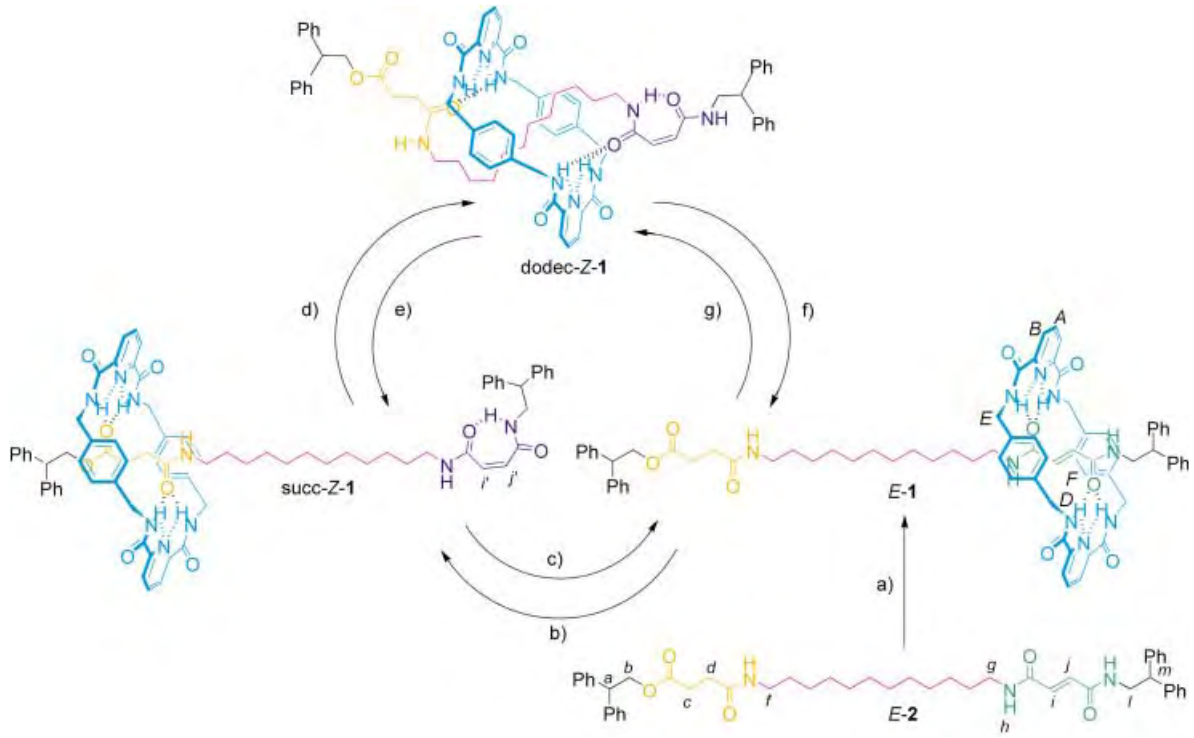
In *Z*-**1**, the strong binding fumaramide station is replaced with a group of much poorer macrocycle-binding affinity (maleamide) and we expected the macrocycle to be displaced to the succinic amide ester site on the thread (that is, co-conformer succ-*Z*-**1**), as occurs with *Z*-**3**.[5g] Whilst the chemical-shift differences (> 1.2 ppm, COSY) of the $H_c$ and $H_d$ protons confirm that this is largely the case[10] at room temperature and above (e.g., at 308 K; Figure 2d), to our surprise the $^1$H NMR spectrum of *Z*-**1** proved highly temperature dependent. Indeed, at 258 K (Figure 2e) the major signals for $H_c$ and $H_d$ of *Z*-**1** appear at the same chemical shifts as they do in the thread (*Z*-**2**). In addition the olefin protons $H_{i'}$ and $H_{j'}$ are also unchanged indicating that the macrocycle is not primarily located over either of the designed stations! In fact, it is the alkyl protons of the $C_{12}$ chain that experience significant upfield shifts (up to 1 ppm at 258 K), which indicates that the pyridine macrocycle is actually positioned

[*] Prof. D. A. Leigh, Dr. G. Bottari, P. J. Nash, E. M. Pérez, Dr. J. K. Y. Wong
School of Chemistry, University of Edinburgh, The King's Buildings, West Mains Road, Edinburgh EH9 3JJ (UK)
Fax: (+44) 131-667-9085
E-mail: David.Leigh@ed.ac.uk
Prof. F. Zerbetto, Dr. F. Dehez
Dipartimento di Chimica "G. Ciamician", Università degli Studi di Bologna, via F. Selmi 2, 40126 Bologna (Italy)
Fax (+39) 051-2099456
E-mail: gatto@ciam.unibo.it

[**] This work was supported by the European Union Future and Emerging Technology Program *MechMol*, the EPSRC, and the MURST project "Dispositivi Supramolecolari". D.A.L. is an EPSRC Advanced Research Fellow (AF/982324).

Supporting information for this article is available on the WWW under http://www.angewandte.org or from the author.

 © 2003 Wiley-VCH Verlag GmbH & Co. KGaA, Weinheim DOI: 10.1002/anie.200352176 




***Scheme 1.*** A tristable molecular shuttle **1**. a) Pyridine 2,6-dicarbonyl chloride, *p*-xylylenediamine, $Et_3N$, $CHCl_3$, 32%; b) *hν* (254 nm), 20 min, $CH_2Cl_2$, 298 K, 54%, or *hν* (350 nm), catalytic benzophenone, 5 min, 65%; c) *hν* (312 nm), 35 min, $CH_2Cl_2$, 298 K, >95%, or *hν* (400–670 nm), catalytic $Br_2$, 2 min, $CH_2Cl_2$, 298 K, ~100%; d) $CDCl_3$, 258 K, 85%; e) $CDCl_3$, 308 K, 90%; f) *hν* (312 nm), 35 min, $CH_2Cl_2$, >95%, or *hν* (400–670 nm), catalytic $Br_2$, 2 min, $CH_2Cl_2$, ~100%; g) *hν* (254 nm), 20 min, $CDCl_3$, 258 K, 54%.

over the $C_{12}$ unit. To satisfy the hydrogen-bonding requirements of the macrocycle, the amide groups of the thread must still act as hydrogen-bond acceptors and so the alkyl chain presumably adopts a folded "S-shape" conformation so that the amides at both ends of the chain can reach the macrocycle binding sites, thus accounting for the shielding seen for the alkyl protons (Scheme 1; co-conformer dodec-*Z*-**1**). Interestingly, two sets of signals are observed for the macrocycle indicating that the two halves of the ring experience magnetically different environments (pirouetting of the macrocycle about the S-shaped thread is slow on the NMR timescale at 258 K).

What is the reason for the unexpected behavior of *Z*-**1**? The reversal of the binding affinity of the macrocycle for the succinic amide ester and the alkyl-chain stations at different temperatures suggests that the $T\Delta S$ term is reversing the relative $\Delta G_{binding}$ of the two stations (Figure 1). In co-conformer succ-*Z*-**1** two hydrogen bonds from the macrocycle occur to an ester carbonyl group, a significantly weaker[11] interaction than an amide–amide hydrogen bond, whereas in the dodec-*Z*-**1** co-conformer four intercomponent amide–amide hydrogen bonds can be formed, providing ~2 kcal mol$^{-1}$ [11] greater enthalpic stabilization. It seems that at low temperatures the energy gain from forming the two extra amide–amide hydrogen bonds overcomes the entropic cost required for the thread to bridge the macrocycle binding sites; a $C_{12}$ chain has >500000 ($3^{12}$) possible C–C rotamers and a significant number of these degrees of freedom must be lost upon forming the dodec-*Z*-**1** structure. Raising the temperature increases the contribution of the $T\Delta S$ term to the $\Delta G_{binding}$ of the dodec-*Z*-**1** co-conformer much more than for succ-*Z*-**1** until, at higher temperatures, the relative stabilities of the two positional isomers are actually reversed and the *Z*-rotaxane predominantly adopts the enthalpically weaker but entropically more favorable succ-*Z*-**1** co-conformation. Indeed, evidence that the stability of dodec-*Z*-**1** is much more temperature dependent than succ-*Z*-**1** is provided by molecular dynamics simulations (see Supporting Information).

The structural requirements for temperature to markedly affect the position of the macrocycle on the thread are quite specific (Figure 3). Similar rotaxanes missing either station (**4** or *Z*,*Z*-**5**) or without the *endo*-pyridyl macrocycle (*Z*-**3**) do not show the same temperature-dependent $^1H$ chemical shifts as *Z*-**1**. However, the "S" shape of the dodec-*Z*-**1** co-conformer binding site is, remarkably, observed in the solid-state structure of an isophthalamide macrocycle-containing [2]rotaxane of a thread consisting of two amide groups separated by a $C_{12}$ chain (**6**, Figure 4). In fact, this type of structure may be a reasonably low-energy co-conformation for many two-amide-station [2]rotaxanes with flexible spacers, which with particular molecular components (poor alternative binding stations) and the right environmental conditions (low temperature), can sometimes become the global minimum arrangement seen for *Z*-**1** at 258 K.

Changing the position of a macrocycle on a thread by varying the temperature is potentially a useful means of controlling translational isomerism in a rotaxane, not least

 © 2003 Wiley-VCH Verlag GmbH & Co. KGaA, Weinheim 

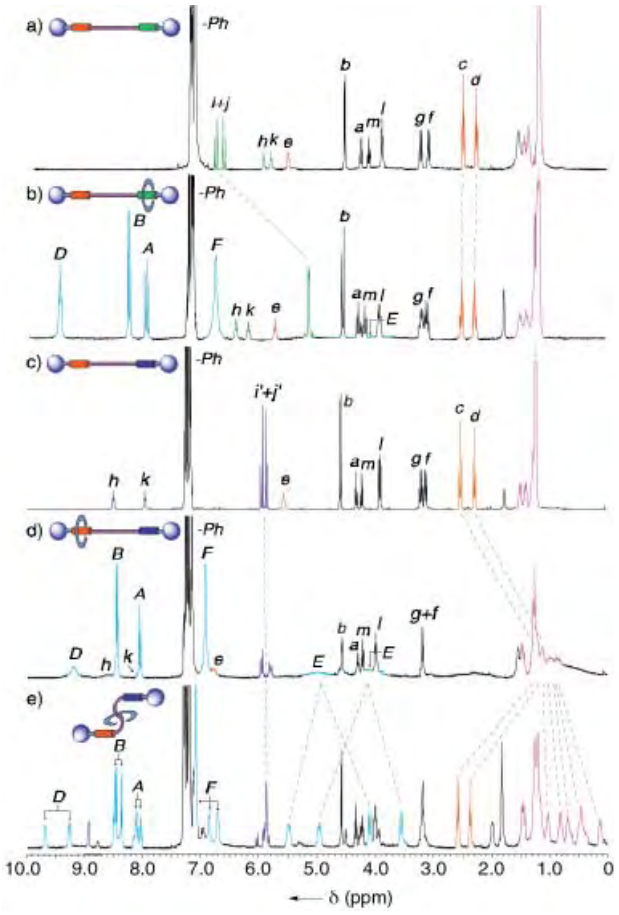



***Figure 2.*** 400 MHz $^1$H NMR spectra ($CDCl_3$) of a) thread *E*-**2** at 298 K, b) rotaxane *E*-**1** at 298 K, c) thread *Z*-**2** at 308 K, d) rotaxane *Z*-**1** at 308 K, and e) rotaxane *Z*-**1** at 258 K. The assignments correspond to the lettering shown in Scheme 1.

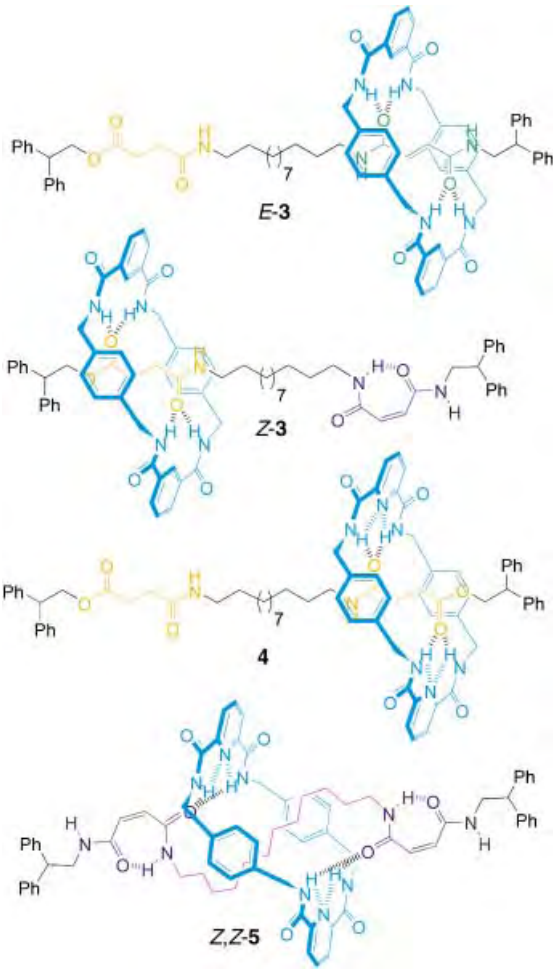



***Figure 3.*** Rotaxane structures related to *Z*-**1**, which do not show temperature-dependent translational isomerism.

because no chemical reaction is involved and no change to the covalent structure of the molecule occurs. The photostationary state of **1** at 312 nm consists of $>95\%$ of the *trans*-isomer (again, dissimilar behavior to shuttle **3** where the steady state at 312 nm is ~55:45 *E*:*Z*). This provides the tristable shuttle with the intriguing property that, starting with the ring on the central station (i.e., dodec-*Z*-**1**), the macrocycle can be moved selectively in one direction along the thread by irradiation with light at 312 nm, or selectively in the other direction by simply raising the temperature.

Received: June 23, 2003
Revised: October 13, 2003 [Z52176]

**Keywords:** entropy · macrocycles · molecular devices · photochemistry · rotaxanes

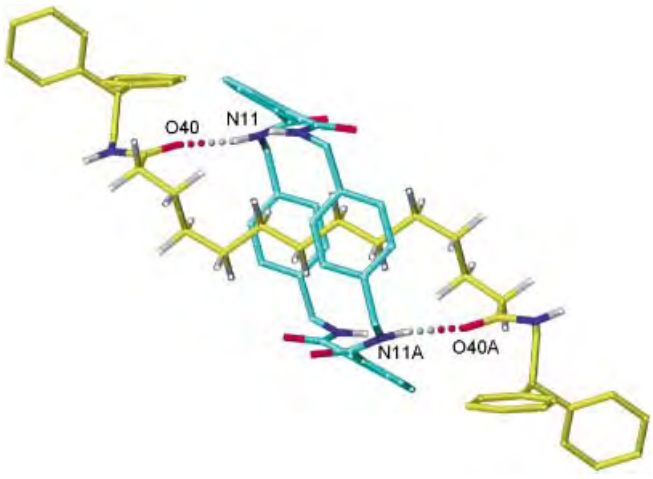



***Figure 4.*** X-ray crystal structure of a benzylic isophthalamide macrocycle-based [2]rotaxane **6** where two amide groups are separated by a $C_{12}$ alkyl chain. Atoms: C (macrocycle) blue, C (thread) yellow, O red, N dark blue. The amide and $C_{12}$ methylene hydrogen atoms are shown in white while all others are removed for clarity. Intramolecular hydrogen-bond distances and angles: O40-HN11/O40A-HN11A 1.92 Å, 156.4°.

[1] a) *Molecular Catenanes, Rotaxanes and Knots* (Eds.: J.-P. Sauvage, C. Dietrich-Buchecker), Wiley-VCH, Weinheim, **1999**; b) V. Balzani, A. Credi, F. M. Raymo, J. F. Stoddart, *Angew. Chem.* **2000**, *112*, 3483–3530; *Angew. Chem. Int. Ed.* **2000**, *39*, 3348–3391; c) Special issue on Molecular Machines: *Acc. Chem. Res.* **2001**, *34*, 409–522; d) M. Venturi, A. Credi, V. Balzani,

 © 2003 Wiley-VCH Verlag GmbH & Co. KGaA, Weinheim 

*Molecular Devices and Machines—A Journey into the Nanoworld*, Wiley-VCH, Weinheim, **2003**.

[2] Exceptions are environment-sensitive shuttles where the preferred position of the macrocycle is determined by the differing solvation of the binding sites in various solvent systems. a) A. S. Lane, D. A. Leigh, A. Murphy, *J. Am. Chem. Soc.* **1997**, *119*, 11092 – 11093; b) C. Gong, H. W. Gibson, *Angew. Chem.* **1997**, *109*, 2426 – 2428; *Angew. Chem. Int. Ed. Engl.* **1997**, *36*, 2331 – 2333; c) T. Da Ross, D. M. Guldi, A. Farran Morales, D. A. Leigh, M. Prato, R. Turco, *Org. Lett.* **2003**, *5*, 689 – 691. Indeed, as an alternative to cooling to 258 K in $CDCl_3$ the macrocycle in *Z*-**1** (but not *E*-**1**) can be positioned over the dodecane chain at room temperature by dissolving it in [$D_6$]DMSO.

[3] The energy potentially available to do useful mechanical work through such a process corresponds to the $\Delta\Delta G_{binding}$ of the macrocycle for the two stations in the chemically transformed shuttle.

[4] a) R. A. Bissell, E. Córdova, A. E. Kaifer, J. F. Stoddart, *Nature* **1994**, *369*, 133 – 137; b) P. R. Ashton, R. Ballardini, V. Balzani, I. Baxter, A. Credi, M. C. T. Fyfe, M. T. Gandolfi, M. Gómez-López, M.-V. Martínez-Díaz, A. Piersanti, N. Spencer, J. F. Stoddart, M. Venturi, A. J. P. White, D. J. Williams, *J. Am. Chem. Soc.* **1998**, *120*, 11932 – 11942; c) J. W. Lee, K. Kim, K. Kim, *Chem. Commun.* **2001**, 1042 – 1043; d) A. M. Elizarov, S.-H. Chiu, J. F. Stoddart, *J. Org. Chem.* **2002**, *67*, 9175 – 9181.

[5] a) H. Murakami, A. Kawabuchi, K. Kotoo, M. Kunitake, N. Nakashima, *J. Am. Chem. Soc.* **1997**, *119*, 7605 – 7606; b) N. Armaroli, V. Balzani, J. P. Collin, P. Gaviña, J. P. Sauvage, B. Ventura, *J. Am. Chem. Soc.* **1999**, *121*, 4397 – 4408; c) P. R. Ashton, R. Ballardini, V. Balzani, A. Credi, K. R. Dress, E. Ishow, C. J. Kleverlaan, O. Kocian, J. A. Preece, N. Spencer, J. F. Stoddart, M. Venturi, S. Wenger, *Chem. Eur. J.* **2000**, *6*, 3558 – 3574; d) A. M. Brouwer, C. Frochot, F. G. Gatti, D. A. Leigh, L. Mottier, F. Paolucci, S. Roffia, G. W. H. Wurpel, *Science* **2001**, *291*, 2124 – 2128; e) G. W. H. Wurpel, A. M. Brouwer, I. H. M. van Stokkum, A. Farran, D. A. Leigh, *J. Am. Chem. Soc.* **2001**, *123*, 11327 – 11328; f) C. A. Stanier, S. J. Alderman, T. D. W. Claridge, H. L. Anderson, *Angew. Chem.* **2002**, *114*, 1847 – 1850; *Angew. Chem. Int. Ed.* **2002**, *41*, 1769 – 1772; g) A. Altieri, G. Bottari, F. Dehez, D. A. Leigh, J. K. Y. Wong, F. Zerbetto, *Angew. Chem.* **2003**, *115*, 2398 – 2402; *Angew. Chem. Int. Ed.* **2003**, *42*, 2296 – 2300.

[6] a) P.-L. Anelli, M. Asakawa, P. R. Ashton, R. A. Bissell, G. Clavier, R. Górski, A. E. Kaifer, S. J. Langford, G. Mattersteig, S. Menzer, D. Philp, A. M. Z. Slawin, N. Spencer, J. F. Stoddart, M. S. Tolley, D. J. Williams, *Chem. Eur. J.* **1997**, *3*, 1113 – 1135; b) J.-P. Collin, P. Gaviña, J.-P. Sauvage, *New J. Chem.* **1997**, *21*, 525 – 528; c) N. Armaroli, V. Balzani, J.-P. Collin, P. Gaviña, J.-P. Sauvage, B. Ventura, *J. Am. Chem. Soc.* **1999**, *121*, 4397 – 4408; d) R. Ballardini, V. Balzani, W. Dehaen, A. E. Dell'Erba, F. M. Raymo, J. F. Stoddart, M. Venturi, *Eur. J. Org. Chem.* **2000**, 591 – 602; e) C. P. Collier, J. O. Jeppesen, Y. Luo, J. Perkins, E. W. Wong, J. R. Heath, J. F. Stoddart, *J. Am. Chem. Soc.* **2001**, *123*, 12632 – 12641.

[7] A temperature change has been used to induce shuttling by bringing about a *cis–trans* isomerization reaction in one of the stations.[5g] For a [2]rotaxane where a temperature increase is used to overcome a significant kinetic barrier to shuttling following a chemical change, see ref [4c]. A bistable [2]rotaxane that appears to undergo translational isomerism as a result of differences in the entropy of solvation of two stations has recently been reported (J. O. Jeppesen, K. A. Nielsen, J. Perkins, S. A. Vignon, A. Di Fabio, R. Ballardini, M. T. Gandolfi, M. Venturi, V. Balzani, J. Becher, J. F. Stoddart, *Chem. Eur. J.* **2003**, *9*, 2982 – 3007).

[8] A series of interesting theoretical designs for entropy-driven mechanical motion in mechanically interlocked molecules have recently been suggested (A. Hanke, R. Metzler, *Chem. Phys. Lett.* **2002**, *359*, 22 – 26).

[9] For other types of tristable switch see a) (supramolecular) P. R. Ashton, V. Balzani, J. Becher, A. Credi, M. C. T. Fyfe, G. Mattersteig, S. Menzer, M. B. Nielsen, F. M. Raymo, J. F. Stoddart, M. Venturi, D. J. Williams, *J. Am. Chem. Soc.* **1999**, *121*, 3951 – 3957; b) (molecular) F. M. Raymo, S. Giordani, A. J. P. White, D. J. Williams, *J. Org. Chem.* **2003**, *68*, 4158 – 4169; c) ([2]- and [3]catenanes) D. A. Leigh, J. K. Y. Wong, F. Dehez, F. Zerbetto, *Nature* **2003**, *424*, 174 – 179.

[10] At 308 K the ratio of succ-*Z*-**1**:dodec-*Z*-**1** is ~90:10; at 258 K it is ~15:85.

[11] F. G. Gatti, D. A. Leigh, S. A. Nepogodiev, A. M. Z. Slawin, S. J. Teat, J. K. Y. Wong, *J. Am. Chem. Soc.* **2001**, *123*, 5983 – 5989.

 © 2003 Wiley-VCH Verlag GmbH & Co. KGaA, Weinheim 

*Coordination Isomers*

# Towards the Rational Design of Magnetic Resonance Imaging Contrast Agents: Isolation of the Two Coordination Isomers of Lanthanide DOTA-Type Complexes**

*Mark Woods, Zoltan Kovacs, Shanrong Zhang, and A. Dean Sherry**

The high spin state and long electronic relaxation time of the gadolinium(III) ion renders it an ideal basis for contrast media for use in magnetic resonance imaging (MRI). The through-space dipole–dipole interactions by which the unpaired f electrons of gadolinium catalyze the relaxation of proximate water-molecule protons are strongly distance dependent. For this reason, the protons of water molecules coordinated to gadolinium are the most effectively relaxed. Exchange of

[*] Prof. A. D. Sherry, Dr. M. Woods, Dr. Z. Kovacs
Department of Chemistry
University of Texas at Dallas
P.O. Box 830668, Richardson, Texas 75080 (USA)
Fax: (+1) 972-8832925
E-mail: sherry@utdallas.edu

Dr. Z. Kovacs
Macrocyclics Inc.
17815 Davenport Road, Suite 120
Dallas, Texas 75252 (USA)

Prof. A. D. Sherry, Dr. S. Zhang
Rogers Magnetic Resonance Center
Department of Radiology
University of Texas Southwestern Medical Center
5801 Forest Road, Dallas, Texas 75235 (USA)

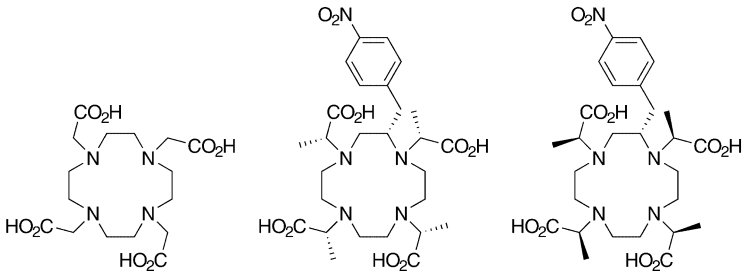
[**] M.W. thanks Craig Sheehan for the translation of an invaluable article (ref. [9]). The authors also gratefully acknowledge financial assistance from the National Institutes of Health (NIH) Biotechnology Research Program (Grant no. RR-02584), NIH Grant no. CA-84697, the Robert A. Welch Foundation (Grant no. AT-584), and the Texas Advanced Technology Program. DOTA = 1,4,7,10-tetraaza-1,4,7,10-tetrakis(carboxymethyl)cyclododecane.

Supporting information for this article is available on the WWW under http://www.angewandte.org or from the author.

 DOI: 10.1002/anie.200352234 © 2003 Wiley-VCH Verlag GmbH & Co. KGaA, Weinheim 

these coordinated water molecules with the bulk solvent is essential for the efficiency or relaxivity of an effective contrast agent.[1] To maximize relaxivity, it is imperative that coordinated water molecules reside on the gadolinium ion just long enough to be relaxed; any longer and they needlessly occupy coordination sites that could be used for relaxing other water molecules. If the residence lifetime is too short, the relaxation process will be less effective. An optimal water residence lifetime ($\tau_M$) of 30 ns has been calculated[1] by using the theory of Solomon, Bloembergen, and Morgan[2–6]

The toxicity of the aqua gadolinium ion necessitates that this paramagnetic agent must be administered in the form of a kinetically and thermodynamically robust chelate. Octadentate polyaminocarboxylate ligands such as DOTA (1,4,7,10-



DOTA *S-RRRR*-**1** *S-SSSS*-**1**

tetraazacyclododecane-1,4,7,10-tetraacetic acid) have proven particularly effective for this purpose.[7] DOTA effectively sandwiches the central gadolinium ion between the four coplanar nitrogen atoms of the macrocycle and four coplanar oxygen atoms of the pendant arms. A water molecule occupying the apical position completes the coordination of the gadolinium ion. The macrocyclic ring in lanthanide–DOTA complexes adopts a [3333] conformation and the torsion angle between the square formed by the nitrogen atoms and a second square made up of coordinating oxygen atoms defines the coordination geometry of the complex. A large torsion angle of around 39° defines a capped square antiprismatic geometry (SAP), whereas a smaller torsion angle of around 25° defines a capped twisted square antiprismatic geometry (TSAP).[8]

These two coordination isomers are in dynamic equilibrium in solution and interconvert either by a flip in the macrocyclic ring conformation or by rotation of the oxygen pendant arms relative to the square defined by the nitrogen atoms.[9] Since the conformation of an ethylene bridge in a macrocycle may be defined as λ or δ (according to the sign of the torsion angle), the conformation of the macrocycle in DOTA may be defined as either (δδδδ) or (λλλλ). In addition, the orientation of the pendant arms (namely, the O-Gd-N torsion angle) may be defined as Δ or Λ. Thus, four stereoisomeric coordination geometries related as two enantiomeric pairs are possible: Δ(λλλλ) and Λ(δδδδ) (square antiprisms), and Δ(δδδδ) and Λ(λλλλ) (twisted square antiprisms). Sequential rotation of the arms and flipping of the ring interconvert the enantiomers.[9] Recent studies have suggested that the rate of water exchange in the two enantiomeric coordination isomers may differ by as much as two orders of magnitude.[10–13] The $\tau_M$ value measured for $[Gd(dota)]^-$ (244 ns) is a weighted average of the values for the coordination isomers present.[14] Although adequate for low-relaxivity agents, such a long average residence lifetime of water molecules is considered undesirable in the design of high-relaxivity contrast media.

Woods et al. recently demonstrated that an α substituent on an acetate arm of DOTA could "sterically lock" the conformation of that pendant arm in complexes.[12,15] The orientation of the arms is determined by the configuration at the α-carbon atom; the Λ orientation is generated by an *R* configuration, while an *S* configuration gives rise to a Δ orientation. We have shown that the conformation of the macrocycle may also be locked by substitution on the ring.[16] Although four methyl groups are necessary to "sterically lock" the macrocycle,[17,18] we found that the same effect can be achieved by using one nitrobenzyl substituent.[16] These observations suggest that a DOTA complex may be "locked" into one or other coordination geometry by suitably substituting both the macrocyclic ring and the pendant arms of the complex. The coordination isomer obtained may be determined by controlling the chirality at each center: if the configuration at the chiral centres in the macrocycle and in the pendant arms is the same, then a twisted square antiprism (TSAP) is obtained, whereas opposite configurations define a square antiprism (SAP).

With this in mind, two stereoisomers of the DOTA-like 2-(*p*-nitrobenzyl)-DOTMA (**1**; DOTMA = (1*R*,4*R*,7*R*,10*R*)-α,α′,α″,α‴-tetramethyl-1,4,7,10-tetraazacyclododecane-1,4,7,10-tetraacetic acid)) were synthesized. The *p*-nitrobenzyl macrocycle was synthesized from L-*p*-nitrophenylalanine by known methods,[19] which led to an *S* configuration at the macrocyclic ring. By altering the configuration at the pendant arms (*RRRR* or *SSSS*), we envisioned that it should be possible to produce two ligands, each of which exclusively adopts one of the coordination geometries. *S*-2-(*p*-nitrobenzyl)-1,4,7,10-tetraazacyclododecane was alkylated by treatment with either D- or L-ethyl *O*-trifluoromethansulfonyl lactate in chloroform in the presence of Hünig's base, to afford the tetraethyl esters of the (*S-SSSS*) and (*S-RRRR*) isomers of 2-(*p*-nitrobenzyl)-DOTMA, respectively. After purification by column chromatography ($SiO_2$, 20% tetrahydrofuran in chloroform), the esters were hydrolyzed by treatment with lithium hydroxide in tetrahydrofuran and water, followed by acidification with hydrochloric acid. Purification of the two ligands at this stage proved impractical so they were used in this crude state to form the corresponding complexes upon addition of the appropriate lanthanide chloride (pH 5.5, 60 °C, 48 h). The complexes so obtained were purified by reverse-phase (C-18) semi-preparative HPLC.

Extended-sweep-width high-resolution $^1H$ NMR analysis of the two europium complexes $[Eu(S\text{-}RRRR\text{-}\mathbf{1})]^-$ and $[Eu(S\text{-}SSSS\text{-}\mathbf{1})]^-$ clearly reveals the presence of only one isomeric coordination geometry in each case (Figure 1). The shifts of the axial proton resonances (34–44 ppm) in the $[Eu(S\text{-}RRRR\text{-}\mathbf{1})]^-$ isomer are consistent with the expected SAP geometry, Δ(λλλλ), while those of the $[Eu(S\text{-}SSSS\text{-}\mathbf{1})]^-$ isomer, at 14–

 © 2003 Wiley-VCH Verlag GmbH & Co. KGaA, Weinheim 

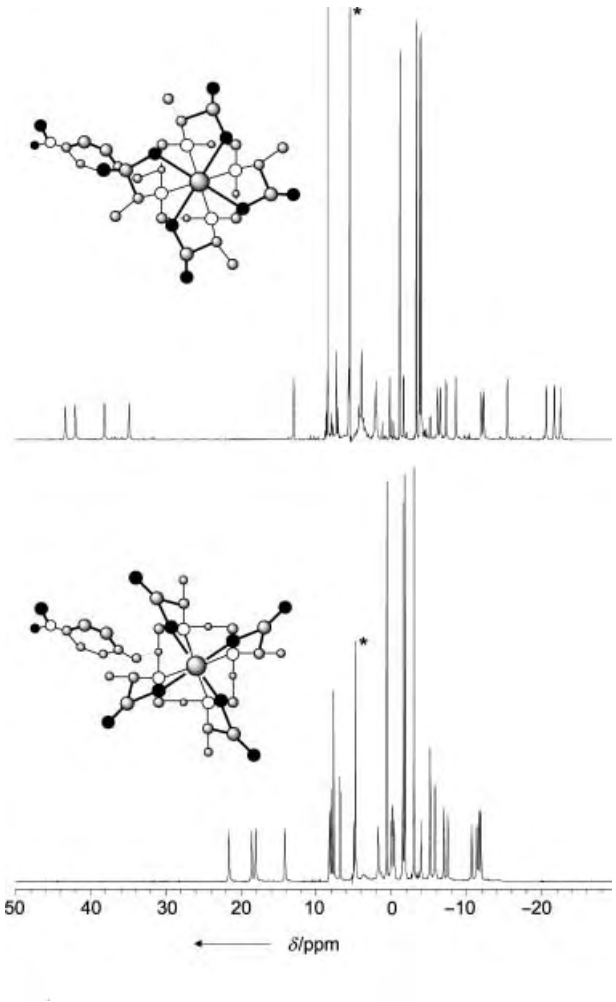



***Figure 1.*** The extended-spectral-width high-resolution $^1$H NMR spectra of the SAP [Eu(*S-RRRR*-**1**)]$^-$ (Δ(λλλλ); top) and TSAP [Eu(*S-SSSS*-**1**)]$^-$ (Δ(δδδδ); bottom) complexes, with schematic representations of the coordination geometries adopted by each isomer. The spectra were recorded at 270 MHz in $D_2O$ at pH 5 and 25 °C (* denotes the HOD peak).

22 ppm, correspond to the more open TSAP geometry, Δ(δδδδ).[12] These results demonstrate that the coordination geometry of DOTA-like complexes may be controlled by the appropriate choice of substituent chirality at the ring and pendant arms. We next took advantage of this unique opportunity to examine some of the physical-chemical differences between the two coordination geometries.

Both isomers were expected to have one inner-sphere water molecule coordinating the central lanthanide ion. The quenching effect of proximate OH oscillators on the luminescence of europium may be used to establish the hydration state $q$ of the europium ion.[20,21] This method is subject to errors arising from other closely diffusing OH or NH oscillators and often gives rise to non-integer hydration states. A revised method has recently been developed to account for the contributions of these diffusing oscillators.[22] The hydration states of [Eu(*S-RRRR*-**1**)]$^-$ and [Eu(*S-SSSS*-**1**)]$^-$ determined by this method show that one coordinated water molecule is present in each complex. The values of $q$ given by the method of Horrocks and Sudnick[20,21] and the revised method of Beeby et al.[22] are given in Table 1. Regardless of the method employed, the hydration state of TSAP [Eu(*S-SSSS*-**1**)]$^-$ is around 0.2 water molecules smaller

***Table 1:*** The hydration states, relaxivity, and water residence lifetimes of the europium/gadolinium complexes.

| | Lanthanide Ion | [Ln(*S-RRRR*-**1**)]$^-$ Δ(λλλλ) | [Ln(*S-SSSS*-**1**)]$^-$ Δ(δδδδ) |
|---|---|---|---|
| $q$[a] | Eu | 1.16 | 0.98 |
| $q'_{corr}$[b] | Eu | 1.00 | 0.81 |
| $r_1^{298}$[c] [mM$^{-1}$s$^{-1}$] | Gd | 4.96 | 5.20 |
| $r_1^{310}$[d] [mM$^{-1}$s$^{-1}$] | Gd | 3.84 | 3.84 |
| $\tau_M^{298}$[e] [ns] | Gd | 120 | 15 |

[a] Hydration state measured by Horrock's method ($q$). [b] Hydration state measured by the revised method of Beeby ($q'_{corr}$) and co-workers. [c] Relaxivity at 25 °C. [d] Relaxivity at 37 °C (20 MHz). [e] Residence lifetimes measured by $^{17}$O NMR spectroscopy at 67.8 MHz.

than that obtained for the SAP [Eu(*S-RRRR*-**1**)]$^-$ isomer. Given the strong distance dependence of the quenching effects of OH oscillators, this observation is consistent with a longer $Eu^{3+}$–water bond distance for [Eu(*S-SSSS*-**1**)]$^-$, with the twisted square antiprismatic geometry, than for the other isomer.[22]

The most important comparison, with respect to the design of high-relaxivity contrast agents, is that of the rate at which these water molecules exchange with the bulk solvent. The rate of water exchange is reflected in the transverse relaxation rate of $^{17}$O nuclei in the bulk solvent. Thus, water exchange rates may be obtained by line-width analysis of the $^{17}$O NMR spectrum of the solvent recorded as a function of temperature.[10] The two complexes [Gd(*S-RRRR*-**1**)]$^-$ and [Gd(*S-SSSS*-**1**)]$^-$ are characterized by extremely different transverse relaxation rate temperature profiles (Figure 2). The profile of [Gd(*S-RRRR*-**1**)]$^-$ (SAP), which rises to a maximum and then falls away with increasing temperature, is indicative of fairly slow exchange. In contrast, the profile of [Gd(*S-SSSS*-**1**)]$^-$ (TSAP) does not reach a maximum within a

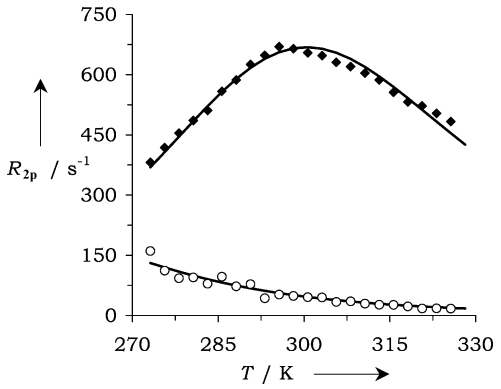



***Figure 2.*** The profiles of the transverse relaxation rates ($R_{2p}$) of the SAP [Gd(*S-RRRR*-**1**)]$^-$ (◆) and the TSAP [Gd(*S-SSSS*-**1**)]$^-$ (○) complexes as a function of temperature, measured by $^{17}$O NMR spectroscopy at 67.8 MHz. The differences in the shapes of the profiles are indicative of differences in water exchange rates.

 © 2003 Wiley-VCH Verlag GmbH & Co. KGaA, Weinheim 

measurable temperature range, which is indicative of much more rapid exchange. The values of $\tau_M$ obtained from fitting these data by using the procedures described by Merbach and co-workers[14,23] are consistent with this observation (Table 1). Indeed, the value obtained for the TSAP isomer [Gd(*S-SSSS*-**1**)]$^-$ is one order of magnitude smaller than that of the SAP isomer [Gd(*S-RRRR*-**1**)]$^-$. This difference is smaller than that observed by Dunand et al.[13] for the more slowly exchanging [Eu(dotam)]$^{3+}$) isomers (dotam = 1,4,7,10-tetrakis(carbamoylmethyl)-1,4,7,10-tetraazacyclododecane). However, the two complexes [Gd(*S-RRRR*-**1**)]$^-$ and [Gd(*S-SSSS*-**1**)]$^-$ are related as individual coordination isomers of two separate diasteroisomeric systems and the relationship between these isomers therefore may not be the same as that between the [Eu(dotam)]$^{3+}$ isomers. Nonetheless, such a large difference in water exchange rates clearly renders the more quickly exchanging isomer preferable for use in the design of high-relaxivity MRI contrast agents.

The effect of these differing water exchange rates upon the relaxivities of the complexes [Gd(*S-RRRR*-**1**)]$^-$ and [Gd(*S-SSSS*-**1**)]$^-$ (20 MHz) is relatively small (Table 1). The water relaxivity of low-molecular-weight chelates at this frequency is strongly influenced by rotational reorientation of the complex ($\tau_R$).[1] Since the two complexes are isomeric and are expected to exhibit identical $\tau_R$ values, the relaxivity will be limited to a similar extent in each case, regardless of water exchange rate. So, even though [Gd(*S-SSSS*-**1**)]$^-$ (TSAP) has a near-optimal water exchange rate, its relaxivity at 25 °C is only about 5 % higher than that of the more slowly exchanging [Gd(*S-RRRR*-**1**)]$^-$ (SAP). At 37 °C even that advantage has disappeared and both complexes exhibit the same relaxivity (Table 1). Indeed, the improvement in relaxivity over that of [Gd(dota)]$^-$ ($r_1 = 4.2\ \mathrm{mM^{-1}s^{-1}}$, 20 MHz, 25 °C)[24] is comparatively small. However, the benefits of an optimally exchanging system may only be evident upon slowing the rotation of the complex (longer $\tau_R$). In practice, this is likely to be achieved by either covalent or noncovalent association of the chelate with a slowly rotating macromolecular structure. That experiment, however, was not within the scope of this paper.

In conclusion, we have demonstrated that the coordination geometry of a DOTA-type lanthanide complex may be controlled by careful consideration of the chirality when substituting both the macrocycle and the pendant arms. The bound water molecule lies further from the lanthanide ion in the twisted square antiprismatic geometry as compared to the square antiprism. This increased bond distance is reflected in more rapid exchange of the bound water molecule with the bulk solvent. The rate of water exchange observed for the twisted square antiprismatic geometry (15 ns) is close to the theoretical optimum value for the design of high-relaxivity contrast agents.

Received: June 26, 2003
Revised: September 16, 2003 [Z52234]

**Keywords:** coordination modes · lanthanides · macrocyclic ligands · MRI contrast agents

[1] S. Aime, M. Fasano, E. Terreno, *Chem. Soc. Rev.* **1998**, *27*, 19.
[2] N. Bloembergen, E. M. Purcell, R. V. Pound, *Phys. Rev.* **1948**, *73*, 679.
[3] I. Solomon, *Phys. Rev.* **1955**, *99*, 559.
[4] I. Solomon, N. Bloembergen, *J. Chem. Phys.* **1956**, *25*, 261.
[5] N. Bloembergen, *J. Chem. Phys.* **1957**, *27*, 572.
[6] N. Bloembergen, L. O. Morgan, *J. Chem. Phys.* **1961**, *34*, 842.
[7] P. Caravan, J. J. Ellison, T. J. McMurry, R. B. Lauffer, *Chem. Rev.* **1999**, *99*, 2293.
[8] M. Meyer, V. Dahaoui-Gindrey, C. Lecomte, R. Guilard, *Coord. Chem. Rev.* **1998**, *178–180*, 1313.
[9] S. Hoeft, K. Roth, *Chem. Ber.* **1993**, *126*, 869.
[10] S. Aime, A. Barge, M. Botta, D. Parker, A. S. De Sousa, *J. Am. Chem. Soc.* **1997**, *119*, 4767.
[11] S. Aime, A. Barge, J. I. Bruce, M. Botta, J. A. K. Howard, J. M. Moloney, D. Parker, A. S. De Sousa, M. Woods, *J. Am. Chem. Soc.* **1999**, *121*, 5762.
[12] M. Woods, S. Aime, M. Botta, J. A. K. Howard, J. M. Moloney, M. Navet, D. Parker, M. Port, O. Rousseaux, *J. Am. Chem. Soc.* **2000**, *122*, 9781.
[13] F. A. Dunand, S. Aime, A. E. Merbach, *J. Am. Chem. Soc.* **2000**, *122*, 1506.
[14] D. H. Powell, O. M. Ni Dhubhghaill, D. Pubanz, L. Helm, Y. S. Lebedev, W. Schlaepfer, A. E. Merbach, *J. Am. Chem. Soc.* **1996**, *118*, 9333.
[15] J. A. K. Howard, A. M. Kenwright, J. M. Moloney, D. Parker, M. Woods, M. Port, M. Navet, O. Rousseau, *Chem. Commun.* **1998**, 1381.
[16] M. Woods, Z. Kovacs, S. Zhang, A. D. Sherry, unpublished results. 2D $^1$H exchange spectrospy (EXSY) was used to establish the mechanism of interconversion of the two diastereoisomeric coordination isomers of [Eu(2-(*p*-$NO_2$Bn)dota)]$^-$. The presence of only two of the four possible diastereoisomeric coordination isomers indicated that one exchange process had been "frozen out." The EXSY spectrum showed that the protons of the macrocycle remained in the same position, that is, axial to axial, equatorial to equatorial, which indicates that exchange occurs by arm rotation alone.
[17] R. S. Ranganathan, R. K. Pillai, N. Raju, H. Fan, H. Nguyen, M. F. Tweedle, J. F. Desreux, V. Jacques, *Inorg. Chem.* **2002**, *41*, 6846.
[18] R. S. Ranganathan, N. Raju, H. Fan, X. Zhang, M. F. Tweedle, J. F. Desreux, V. Jacques, *Inorg. Chem.* **2002**, *41*, 6856.
[19] O. Renn, C. F. Meares, *Bioconjugate Chem.* **1992**, *3*, 563; T. J. McMurry, M. Brechbiel, K. Kumar, O. A. Gansow, *Bioconjugate Chem.* **1992**, *3*, 108.
[20] W. D. Horrocks, Jr., D. R. Sudnick, *J. Am. Chem. Soc.* **1979**, *101*, 334.
[21] W. D. Horrocks, Jr., D. R. Sudnick, *Acc. Chem. Res.* **1981**, *14*, 384.
[22] A. Beeby, I. M. Clarkson, R. S. Dickins, S. Faulkner, D. Parker, L. Royle, A. S. de Sousa, J. A. G. Williams, M. Woods, *J. Chem. Soc. Perkin Trans. 2* **1999**, 2, 493.
[23] G. Gonzàlez, D. H. Powell, V. Tissières, A. E. Merbach, *J. Phys. Chem.* **1994**, *98*, 53.
[24] E. Toth, D. Pubanz, S. Vauthey, L. Helm, A. E. Merbach, *Chem. Eur. J.* **1996**, *2*, 1607.

 © 2003 Wiley-VCH Verlag GmbH & Co. KGaA, Weinheim 

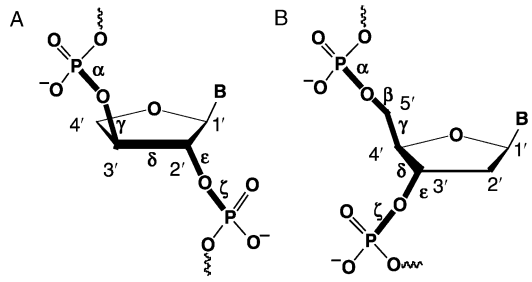
Nucleic Acids

# Why Does TNA Cross-Pair More Strongly with RNA Than with DNA? An Answer From X-ray Analysis**

*Pradeep S. Pallan, Christopher J. Wilds, Zdzislaw Wawrzak, Ramanarayanan Krishnamurthy, Albert Eschenmoser, and Martin Egli**

Research directed toward a chemical etiology of nucleic acid structure has recently established that L-α-threofuranosyl (3′→2′) nucleic acid (TNA) is an efficient Watson–Crick base-pairing system capable of informational cross-pairing with both RNA and DNA.[1–3] TNA is constitutionally the simplest oligonucleotide-type nucleic acid system found so far that possesses this capability. Its cross-pairing with RNA is stronger than with DNA.[1,2] The backbone of TNA is shorter than that of DNA and RNA since the sugar moiety in TNA contains only four carbon atoms and the phosphodiester groups are attached to the 2′- and 3′-positions of the threofuranose ring, as opposed to the 3′- and 5′-positions as in DNA and RNA (Scheme 1).

TNA and RNA, and to a lesser extent DNA sequences can act as templates for the ligation of TNA fragments. Such ligations proceed with high fidelity and are greatly accelerated when adenine is replaced by 2,6-diaminopurine in the TNA ligands.[4] Nitrogenous analogues of TNA in which either O3′ or O2′ is substituted by an NH group are equally efficient Watson–Crick base-pairing systems; they also cross-pair with TNA, RNA, and DNA.[5] It was recently shown that certain DNA polymerases are able to copy a TNA template sequence, albeit of limited length and at a slower rate than with a DNA template.[6] Moreover, a DNA polymerase has been identified that is capable of significant TNA synthesis.[7] The combination of a DNA-dependent TNA polymerase and a TNA-directed DNA polymerase may enable in vitro evolution experiments to be carried out with TNA molecules in the future.[7]




***Scheme 1.*** Configuration, atom numbering, and backbone torsion angle definition in a) TNA and b) DNA.

The remarkable properties of TNA warrant a detailed investigation of its three-dimensional structure and potential conformational plasticity. Specifically, structures of TNA may provide insight into the origins of the more stable pairing between TNA and RNA relative to that between TNA and DNA. We initially analyzed the conformational properties of TNA nucleotides in a B-form DNA dodecamer.[8] The crystal structure of the oligonucleotide with sequence CGCGAAT*TCGCG (T* = TNA T; residues of strands 1 and 2 are numbered 1–12 and 13–24, respectively) was determined at 1.20-Å resolution and revealed a C4′-*exo* conformation of the threose sugar, coupled with a quasi *trans*-diaxial orientation of the 3′ and 2′ substituents (Figure 1 A). The TNA backbone conformation can be characterized by five torsion angles (instead of the six needed for DNA; Scheme 1). The values of these angles in the single TNA thymidine residue present per strand in the B-form DNA duplex fall into the *sc*$^-$, *ap, ap, ac*$^-$, *ac*$^-$ ranges (*α, γ, δ, ε, ζ*; Table 1, Figure 1 A).

The structure of the B-form dodecamer with a single TNA thymidine residue per strand also shows a virtually seamless fit of TNA within a B-DNA context.[8] However, the intra-nucleotide P···P distance in the two TNA residues (5.79 Å in residue T*7; Figure 1 A) is significantly shorter than that between the 5′ and 3′ phosphorus atoms in 2′-deoxyribonucleotides in B-form DNA (for example, 6.77 Å in residue T20; Figure 1 B).[9,10]

To assess the potential of the TNA nucleotide unit to conformationally adapt to different overall helix geometries, we analyzed the crystal structure of an A-form DNA duplex containing a single TNA adenosine residue (A*) per strand. The structure of the decamer with the sequence GCGTAT $^{M}$A*CGC ($T^{M}$, 2′-*O*-methyl-thymidine) was refined to an R factor of 13.3 % at 1.16-Å resolution. The $T^{M}$ residue was

[*] Prof. M. Egli, Dr. P. S. Pallan
Department of Biochemistry
Vanderbilt University
Nashville, TN 37332 (USA)
Fax: (+1) 615-322-7122
E-mail: martin.egli@vanderbilt.edu
Prof. C. J. Wilds
Department of Chemistry and Biochemistry
Concordia University
Montreal, Quebec H4B 1R6 (Canada)
Dr. Z. Wawrzak
DND-CAT Synchrotron Research Center
Sector 5, Advanced Photon Source
Argonne National Laboratory
Argonne, IL 60439 (USA)
Prof. R. Krishnamurthy, Prof. A. Eschenmoser
The Skaggs Institute for Chemical Biology
The Scripps Research Institute
La Jolla, CA 92037 (USA)
Prof. A. Eschenmoser
Laboratorium für Organische Chemie
Eidgenössische Technische Hochschule
8093 Zürich (Switzerland)

[**] Financial support from the National Institutes of Health (Grant GM55237 to M.E.) is gratefully acknowledged. Parts of this work were performed at the DuPont-Northwestern-Dow Collaborative Access Team (DND-CAT) Synchrotron Research Center located at Sector 5 of the Advanced Photon Source, Argonne, IL (USA). DND-CAT is supported by the E. I. DuPont de Nemours & Co., The Dow Chemical Company, the U.S. National Science Foundation through Grant DMR-9304725, and the State of Illinois through the Department of Commerce and the Board of Higher Education Grant IBHE HECA NWU 96.

 DOI: 10.1002/anie.200352553 © 2003 Wiley-VCH Verlag GmbH & Co. KGaA, Weinheim 

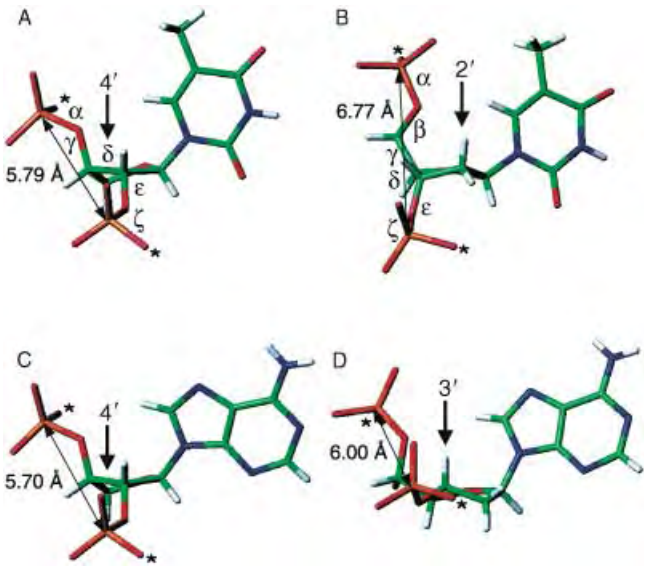



***Figure 1.*** Conformations adopted by TNA and DNA nucleotides in B- and A-form duplexes: a) B-TNA (with residue T*7); b) B-DNA (T20); c) A-TNA (A*7); d) A-DNA (A15). Asterisks in the figure designate the directions of the backbone chain, torsions angles in TNA and DNA are labeled, and carbon atoms of the L-α-threofuranose and D-β-deoxyribose sugars positioned either *exo* (TNA) or *endo* (DNA) to the best plane (defined by the other sugar ring carbon and oxygen atoms) are indicated by arrows.

***Table 1:*** TNA backbone torsion angles in degrees.

| Residue | Helix | $\alpha$ | $\gamma$ | $\delta$ | $\varepsilon$ | $\zeta$ |
|---|---|---|---|---|---|---|
| T*7 | B-form | −84 | −173 | 157 | −100 | −136 |
| T*19 | B-form | −86 | −170 | 160 | −130 | −98 |
| A*7 | A-form | −88 | −172 | 152 | −97 | −132 |
| A*17 | A-form | −87 | −166 | 153 | −108 | −115 |

incorporated to lock the duplex in the A-form geometry. Residues in strands 1 and 2 of the decamer are numbered 1 to 10 and 11 to 20, respectively. A summary of the crystal data, data statistics, and refinement parameters is provided in Table 2.

***Table 2:*** Selected crystal data and refinement parameters.

| | |
|---|---|
| space group | orthorhombic $P2_12_12_1$ |
| unit cell constants [Å] | $a=24.43$, $b=44.52$, $c=47.33$ |
| resolution [Å] | 1.16 |
| no. of unique reflections | 18289 |
| completeness (1.20–1.16 Å) [%] | 98.8 (94.5) |
| R-merge (1.20–1.16 Å) [%] | 6.2 (29.7) |
| R-work (1.20–1.16 Å) [%, no $\sigma$ cutoff] | 13.3 (21.1) |
| R-free [%] | 18.8 |
| no. of refinement parameters | 4921 |
| data-to-parameter ratio | 3.53 |
| no. of restraints | 10197 |
| no. of DNA atoms | 404 |
| no. of water molecules | 125 |
| r.m.s[a] deviation bonds [Å] | 0.017 |
| r.m.s.[a] deviation angles [1···3 dist., Å] | 0.026 |

[a] r.m.s. = root mean square.

The conformations of the two adenine TNA nucleotides in the A-form environment are remarkably similar to those of the two thymidine TNA residues in the B-form duplex (Figure 1C, A). In both environments, the conformation of the two threose sugar units is C4′-*exo* and the intranucleotide P···P distances of the TNA residues in the B- and A-DNA duplexes differ only by 0.1 Å. The five backbone torsion angles in the TNA residues in the A-form duplex also fall into the *sc*$^-$, *ap*, *ap*, *ac*$^-$, *ac*$^-$ ranges ($\alpha$, $\gamma$, $\delta$, $\varepsilon$, $\zeta$; Table 1, Figure 1C). In both the A- and B-form duplexes with incorporated TNA nucleotides, the sugar puckers of residues surrounding the TNA nucleotide are altered minimally relative to those in the respective unmodified duplexes, and local helical parameters (i.e. rise and twist) are only slightly changed (data not shown).[8]

The combined structural data demonstrate that TNA behaves in a conformationally rigid fashion in these duplexes. Minor deviations between the geometries of L-α-threofuranosyl nucleotides in A- and B-form duplexes are limited to the $\varepsilon$ and $\zeta$ backbone torsion angles (Table 1; the glycosidic torsion angles of DNA and TNA nucleotides in the A- and B-form environments differ to a similar extent). The preferred sugar pucker is C4′-*exo*, independent of whether TNA is in an RNA or DNA environment, or indeed exists as an isolated nucleotide (Figure 1).[1] This observation is also in accordance with the conformation of the TNA sugar in the recently determined NMR solution structure of an all-TNA duplex with sequence CGAATTCG.[11] The quasi *trans*-diaxial orientation preferred by the 3′ and 2′ phosphate groups leads to an intranucleotide P···P distance with an upper limit of around 5.8 Å. This distance is similar to that between adjacent phosphate groups in A-form DNA double helices (up to about 6 Å; see Figure 1D).[9,10]

The structural results lead us to conclude that cross-pairing between TNA and DNA is possible because the latter can conformationally adjust to the structural requirements of TNA and not vice versa. To achieve this adjustment, DNA sugars have to assume a conformation in which the inter-phosphate P···P distance is reduced from approximately 7 Å (B-form; Figure 1B) to around 6 Å (A-form; Figure 1D), a conformational adaptation that is similar to that required for DNA when it pairs with RNA. Double-helical RNA cannot assume an extended backbone variant with the sugars in a C2′-*endo* conformation because the quasi-equatorial orientation of the 2′-hydroxy group associated with this pucker would result in a steric clash with the 5′-phosphate oxygen atom of the following ribose unit.[12] Contrary to the apparent conformational uniformity of threoses in TNA–DNA and TNA–RNA hybrid duplexes, the 2′-deoxyribose sugars in DNA–RNA hybrids assume a variety of conformations, including the C3′-*endo* and O4′-*endo* puckers.[13–15] A more important fact with regard to the relative pairing stabilities of TNA with RNA and DNA is that the thermodynamic stability of DNA–RNA hybrids is commonly lower than that of RNA duplexes with identical sequence.[16]

We hypothesize that TNA is a poor substitute for DNA in chemical reactions and molecular recognition events that require a canonical B-form helix geometry. Conversely, TNA appears to be an excellent mimic of A-form DNA and

 © 2003 Wiley-VCH Verlag GmbH & Co. KGaA, Weinheim 

therefore also of A-form RNA as far as geometry and conformation of the nucleotide building blocks are concerned. Thus, our structural observations provide a convincing qualitative rationalization of the experimental observations that 1) TNA hybridizes more strongly with RNA than with DNA,[1,2] and 2) RNA constitutes a better template for ligating TNA fragments than DNA.[4]

The close and specific resemblance between TNA and RNA with respect to the intranucleotide P···P distance, one of the structural parameters that determine the capabilities of oligonucleotide systems for cross-pairing and for serving as cross-templates, is of interest in the context of the notion of a possible etiological relationship between RNA and TNA.

## Experimental Section

Materials: The synthesis of the 3′-*O*-dimethoxytrityl-L-α-*threo*-furanosyladenine-2′-*O*-(2-cyanoethyl)-*N,N*′-diisopropyl phosphoramidite monomer has been described previously.[1,2] 2′-Deoxynucleotide phosphoramidites and 3′-terminal nucleoside controlled-pore glass support were purchased from Glen Research (Sterling, VA). All other chemicals for solid-phase oligonucleotide synthesis were also purchased from Glen Research (Sterling, VA).

Oligonucleotide synthesis: The TNA-modified oligonucleotide was synthesized on an Applied Biosystems 381A DNA synthesizer with slight modifications to published procedures.[17] Monomer coupling times were 90 sec for 3′-CE phosphoramidites and 10 min for the TNA amidite, with the oligomer synthesized with the 5′-terminal trityl group "off". Deprotection and cleavage from the solid support were achieved by treatment with 28–30% $NH_4OH$ at 55 °C for 8 h. The sequence was analyzed and purified by strong anion exchange chromatography on a Pharmacia AKTA Purifier HPLC instrument with a DIONEX DNAPAC PA-100 analytical column (4 × 25 mm) purchased from Dionex Corp (Sunnyvale, CA). For preparative runs, 25 OD units were purified on the analytical column at a time with a gradient of 25 mM tris(hydroxymethyl)aminomethane-HCl (pH 7.8) to 1 M NaCl over 30 min and a flow rate of 1.0 mL $min^{-1}$. The purified oligomer was desalted on a SEP PAK cartridge (Waters Inc., Milford, MA). The cartridge was pre-equilibrated with acetonitrile followed by water. The oligonucleotide solution was applied to the cartridge, washed with water, and a solution of 75% methanol in water was then used to elute the desalted oligomer with a final yield of 56%. Molecular weights of the products were determined by MALDI-TOF mass spectrometry.

Crystallization and data collection: Crystals were grown at 18 °C by the hanging drop vapor diffusion method. Droplets (4 μL) containing oligonucleotide (0.5 mM), sodium cacodylate (20 mM, pH 6.0), sodium chloride (40 mM), barium chloride (10 mM), spermine tetrahydrochloride (6 mM), and 2-methyl-2,4-pentanediol (MPD; 5% (v/v)) were equilibrated against a reservoir of MPD (1 mL, 35%). Hexagonal rods of reasonable size appeared after two weeks. For data collection, a crystal (0.3 × 0.1 × 0.05 mm) was picked up from a droplet with a nylon loop and transferred into a cold $N_2$ stream (120 K). High- and low-resolution data sets were collected on the 5-ID beam line ($\lambda = 1.0$ Å) of the DND-CAT at the Advanced Photon Source (Argonne, IL) by using a MARCCD detector. Data were integrated and merged with the DENZO and SCALEPACK programs, respectively.[18] Selected crystal data and data quality and completeness are summarized in Table 2.

Structure determination and refinement: The structure was determined by the molecular replacement technique by using the program CNS,[19] with an A-form DNA decamer duplex as the search model. Initially, the decamer duplex was refined as an all-DNA molecule. At a later stage, atoms of TNA A*7 and A*17 were renumbered and the former 2′-deoxyribose C5′ atoms in these residues were deleted. Isotropic and anisotropic refinements of the model were carried out with the program SHELX-97,[20] and 5% of the reflections were set aside at random for calculating the R-free value.[21] Hydrogen atoms were added to the SHELX-97 calculations and all DNA and TNA atoms, as well as selected solvent water molecules, were treated anisotropically. Final refinement parameters and r.m.s. deviations from ideal bond lengths and angles are listed in Table 2.

Data deposition: Final coordinates and structure factors have been deposited in the Protein Data Bank[22]: PDB entry code 1PWF.

Received: August 4, 2003 [Z52553]

**Keywords:** conformation analysis · DNA · RNA · structure elucidation · TNA

[1] K. U. Schöning, P. Scholz, S. Guntha, X. Wu, R. Krishnamurthy, A. Eschenmoser, *Science* **2000**, *290*, 1347 – 1351.
[2] K. U. Schöning, P. Scholz, X. Wu, S. Guntha, G. Delgado, R. Krishnamurthy, A. Eschenmoser, *Helv. Chim. Acta* **2002**, *85*, 4111 – 4153.
[3] A. Eschenmoser, *Science* **1999**, *284*, 2118 – 2124.
[4] X. Wu, G. Delgado, R. Krishnamurthy, A. Eschenmoser, *Org. Lett.* **2002**, *4*, 1283 – 1286.
[5] X. Wu, S. Guntha, M. Ferencic, R. Krishnamurthy, A. Eschenmoser, *Org. Lett.* **2002**, *4*, 1279 – 1282.
[6] J. C. Chaput, J. K. Ichida, J. W. Szostak, *J. Am. Chem. Soc.* **2003**, *125*, 856 – 857.
[7] J. C. Chaput, J. W. Szostak, *J. Am. Chem. Soc.* **2003**, *125*, 9274 – 9275.
[8] C. J. Wilds, Z. Wawrzak, R. Krishnamurthy, A. Eschenmoser, M. Egli, *J. Am. Chem. Soc.* **2002**, *124*, 13716 – 13721.
[9] W. Saenger, *Principles of Nucleic Acid Structure*, Springer, New York, **1984**.
[10] A. Rich, *Nat. Struct. Biol.* **2003**, *10*, 247 – 249.
[11] M.-O. Ebert, Ph.D. thesis, ETH-Zürich **2003**; B. Jaun, M.-O. Ebert, personel communication.
[12] A. Eschenmoser, M. Dobler, *Helv. Chim. Acta* **1992**, *75*, 218 – 259.
[13] M. Egli, N. Usman, A. Rich, *Biochemistry* **1993**, *32*, 3221 – 3237.
[14] O. Y. Fedoroff, M. Salazar, B. R. Reid, *J. Mol. Biol.* **1993**, *233*, 509 – 532.
[15] G. Minasov, M. Teplova, P. Nielsen, J. Wengel, M. Egli, *Biochemistry* **2000**, *39*, 3525 – 3532.
[16] E. A. Lesnik, S. M. Freier, *Biochemistry* **1995**, *34*, 10807 – 10815.
[17] C. J. Wilds, M. J. Damha, *Nucleic Acids Res.* **2000**, *28*, 3625 – 3635.
[18] Z. Otwinowski, W. Minor, *Methods Enzymol.* **1997**, *276*, 307 – 326.
[19] A. T. Brünger, P. D. Adams, G. M. Clore, W. L. DeLano, P. Gros, R. W. Grosse-Kunstleve, J.-S. Jiang, J. Kuszewski, M. Niges, N. S. Pannu, R. J. Read, L. M. Rice, T. Simonson, K. L Warren, *Acta Crystallogr. Sect. D* **1998**, *54*, 905 – 921.
[20] G. M. Sheldrick, T. R. Schneider, *Methods Enzymol.* **1997**, *277*, 319 – 343.
[21] A. T. Brünger, *Nature* **1992**, *355*, 472 – 475.
[22] Web address: http://www.rcsb.org.

 © 2003 Wiley-VCH Verlag GmbH & Co. KGaA, Weinheim 

Electron Transfer

# Ultrafast Dynamics in DNA-Mediated Electron Transfer: Base Gating and the Role of Temperature**

*Melanie A. O'Neill, Hans-Christian Becker, Chaozhi Wan, Jacqueline K. Barton,* and Ahmed H. Zewail**

Electron transfer (ET) in double-helical DNA has been the subject of major interest, both experimentally and theoretically.[1,2] The role of dynamic base motions in DNA ET is not fully understood, as it involves a range of timescales and different motions. We previously showed that motions of an intercalated photooxidant on the picosecond timescale can modulate ET in what we termed the gate effect.[3] More recently, incorporation of DNA base dynamics into theoretical treatments of DNA ET[4,5,6] suggests not only that rapid base motions dramatically modulate electronic coupling between DNA bases,[5] but that these motions may facilitate DNA-mediated ET.[6] Herein, to explore the effects of base dynamics, we examine ET between DNA bases directly as a function of temperature through femtosecond spectroscopy.

Our investigations employ photoexcited 2-aminopurine (Ap*) as a dual reporter of DNA base dynamics and DNA-mediated ET. Ap undergoes normal Watson–Crick pairing with T and is well-stacked.[7] ET reactions between Ap* and nucleotides,[8] as well as Ap* and bases in DNA[9–11] have been extensively characterized. In DNA, ET between Ap* and G can be distinguished from other modes of quenching by comparing redox-active G-containing duplexes to otherwise identical duplexes in which the G is replaced by inosine (I), an analogue of G that is essentially inactive towards ET with Ap*.[9a] Femtosecond transient absorption spectroscopy was used to determine the rate constant for ET, $k_{ET}$, which was evaluated as $k_G$–$k_I$ (where $k_G$ and $k_I$ are the rate constants for G- and I-containing duplexes, respectively); other nonradiative processes were examined and they contribute in a relatively minor way, primarily because of the thermodynamically favorable oxidation/reduction in these systems.[8–10,12] On the other hand, steady-state measurements determine the yield of ET according to the fraction of fluorescence quenched, $F_q$, in redox-active relative to redox-inactive DNA assemblies ($F_q = 1 - \Phi_G/\Phi_I$). In this case, to probe the influence of temperature-dependent base dynamics on ET in duplex DNA, 35-mer DNA assemblies (Scheme 1) with melting temperatures of approximately 60 °C were used.[13]

**ApG/ApI**

5'-GATTATAGACATATTI**ApY**ITATTAAGTACATTAC-3'
3'-CTAATATCTGTATAA**CT** **C**CATAATTCATGTAATG-5'

**ApAG/ApAI**

5'-GATTATAGACATATTI**ApAY**ITATTAAGTACATTAC-3'
3'-CTAATATCTGTATAA**CT** **TC**CATAATTCATGTAATG-5'

***Scheme 1.*** Sequences of the 35-mer Ap-oligonucleotides and complementary strands used to investigate the influence of temperature on the rate constants and yields of ET in DNA (Y = I, G). The single strands referred to in the text correspond to the Ap-containing strands.

Figure 1 shows the decay of Ap* following excitation (325 nm, ~100 fs) of Ap in ApG and ApAG 35-mers between 0 and 78 °C. Consistent with all other time-resolved investigations of Ap* in DNA, these decays are characterized by the ultrafast decay due to ET followed by ns-type decays. In both assemblies, but particularly in ApG, a distinct fast decay component can be resolved below the $T_m$. This fast quenching is not found in the reference duplexes, ApI and ApAI, for which ET is not thermodynamically favorable.

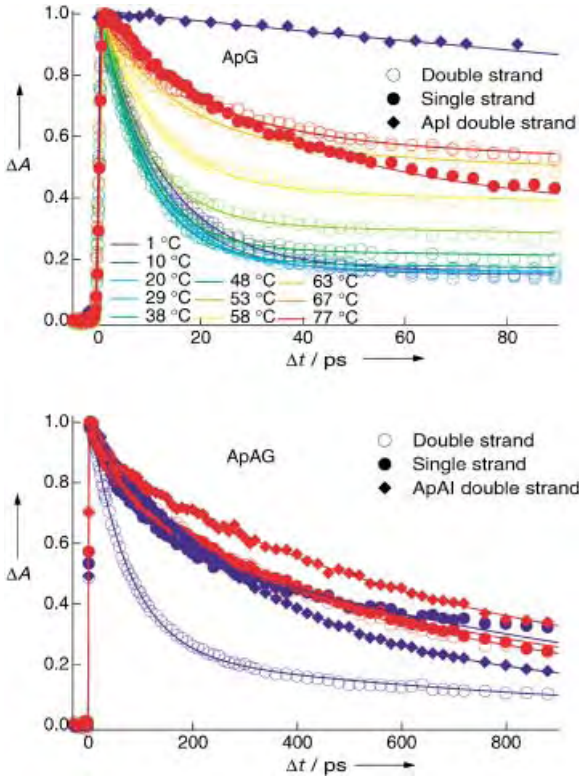



***Figure 1.*** Time-resolved decay of excited Ap in ApG (top) and ApAG (bottom) 35-mers as a function of temperature. Samples were excited with a femotsecond pulse at 325 nm and the decay of Ap* was monitored by transient absorption at 600 nm.

The rate constant for ET, along with the relative amplitudes of the ET component (and slower decay compo-

[*] J. K. Barton, A. H. Zewail, M. A. O'Neill, H.-C. Becker, C. Wan
Laboratory for Molecular Sciences
Arthur Amos Noyes Laboratory of Chemical Physics
California Institute of Technology
Pasadena CA, 91125 (USA)
Fax: (+1) 626-792-8456
E-mail: jkbarton@its.caltech.edu
zewail@caltech.edu

[**] This work was made possible through the support of the Laboratory for Molecular Sciences and the NSF. M.A.O. and H.-C.B. are grateful to NSERC and the Wenner-Gren Foundation, respectively, for postdoctoral fellowships.

 © 2003 Wiley-VCH Verlag GmbH & Co. KGaA, Weinheim DOI: 10.1002/anie.200352831 

nents), exhibits a pronounced temperature dependence (Figure 2). These may be characterized within three temperature regimes. At lower temperatures, in which the assemblies are in the duplex form, $k_{ET}$ exhibits an increase with temperature, more pronounced for ApG than ApAG, whereas the amplitudes of the fast ET and slower decay components show a shallow decrease and shallow rise, respectively. Through the duplex-melting regime, both the rate constant and the amplitude for fast ET decrease dramatically with a correspondingly sharp increase in the amplitude of the slower components. At higher temperatures, significantly less variation is evident. Steady-state measurements of the ET yields (i.e. $F_q$, data not shown) in ApG and ApAG parallel the amplitude ($C_1$) of $k_{ET}$ observed in time-resolved experiments. For both ApG and ApAG, the yield of ET decreases markedly through the melting and displays little variation at higher temperatures.

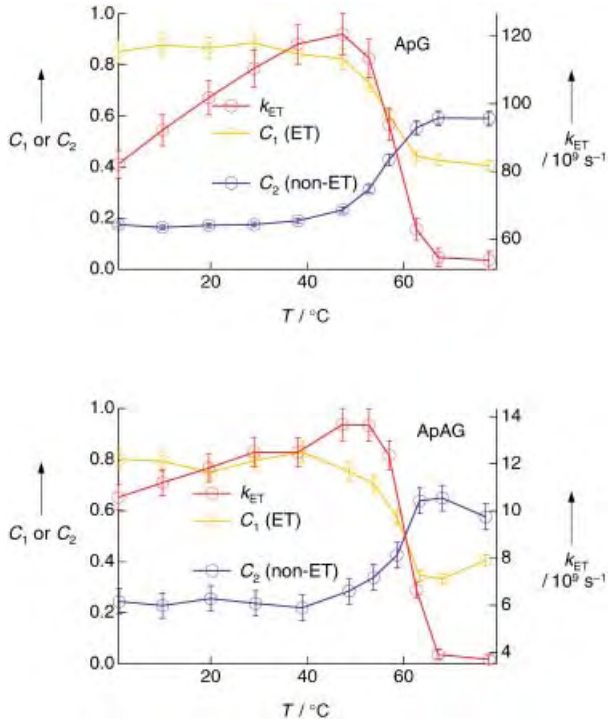



***Figure 2.*** Rate constants for ET, $k_{ET}$, and the amplitudes of the fast ($C_1$) and slower ($C_2$) decay components for ApG (top) and ApAG (bottom) 35-mers as a function of temperature. The decays for both assemblies were analyzed by using a biexponential model. The rate constants and amplitudes are the average of two independent trials.

Given the significant changes in rates and amplitudes associated with melting, a comparison with the single-stranded 35-mer is warranted. In the single-stranded ApG, the rate constant and amplitude of the fast component at ambient temperature decrease by ~50% relative to duplex ApG. Notably, in the single-stranded ApAG there is no significant fast decay component. In fact, the decay times in these single strands (~20 and 420 ps for ApG and ApAG, respectively) are similar to those observed after melting of the DNA duplexes. Thus we conclude that stacking is a prerequisite for efficient ET and that for single-stranded DNA the temperature effect is much-less pronounced than for duplex DNA.

In the premelting regime, we first considered the change in rates with temperature by using the Marcus equation.[14] For a driving force of $-200$ mV,[9a] we obtained electronic couplings and reorganization energies of 92 $cm^{-1}$ and 0.67 eV, respectively for ApG, and 14 $cm^{-1}$ and 0.51 eV, respectively for ApAG. These values, particularly the electronic couplings, are significantly low, especially given other experimental estimates of electronic couplings in DNA,[15] and that the lowest calculated electronic couplings between adjacent bases are about 200 $cm^{-1}$.[16] In Figure 3, we calculate the predicted dependence of rate on temperature using the known driving force of $-200$ mV, and a calculated reorganization energy, assuming that the driving force and the reorganization energy are, to a first approximation, functions only of the donor and acceptor, and thus are relatively independent of temperature in the premelting regime.

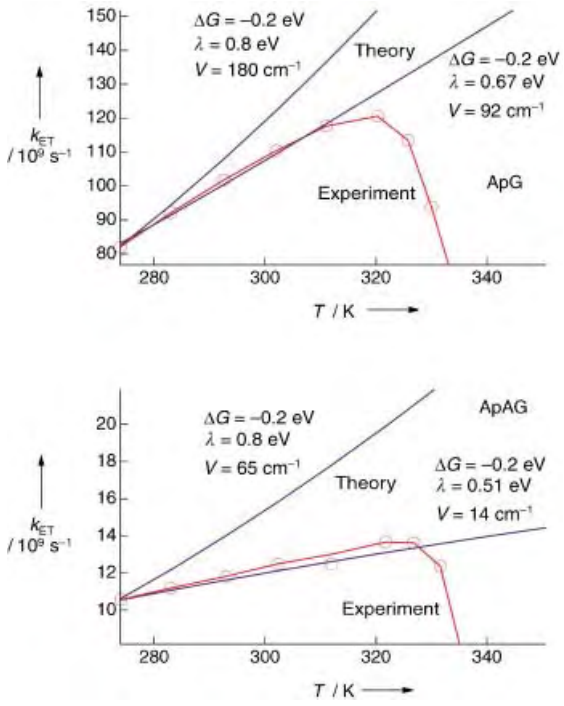



***Figure 3.*** Measured (red lines) and calculated (blue lines) rate constants for ET in ApG and ApAG duplexes are shown for two sets of values (see text).

From the calculated (B3LYP6-311G* level) energy of one-electron-reduced Ap at the geometry of neutral Ap, and the energy of the relaxed (optimized) Ap radical anion, we estimate the reorganization energy[16d] for Ap radical anion formation to be 0.31 eV. This, combined with an experimentally determined reorganization energy for the formation of the G radical cation (0.47 eV),[17] gives a total reorganization energy of 0.8 eV (neglecting solvent effects), which is close to the experimentally determined base-intercalator reorganization energies.[15b] The results are shown in Figure 3, where the experimental temperature dependence of $k_{ET}$ is compared

 © 2003 Wiley-VCH Verlag GmbH & Co. KGaA, Weinheim 

with the calculated change in the ET rate constant. However, this approach neglects the temperature-dependent motion of the DNA bases, which should influence base–base coupling and the change of rates with temperature. The importance of donor, acceptor, and bridge dynamics in bridge-mediated ET reactions of biological assemblies was recently discussed, and modifications of the Marcus theory have been incorporated into the theoretical description of ET in proteins.[18]

From the results presented herein we propose the following model: On the timescale of ET, a DNA solution consists of assemblies with a heterogeneous distribution of base conformations. In some of these assemblies, the donor, the acceptor, and the DNA bridge, if present, are in conformations that upon excitation, facilitate immediate ET. This we assign to direct ET, observed as the fastest decay component in our femtosecond measurements; these conformations can be termed ET-active. Other DNA assemblies do not adopt ET-active conformations at the time of excitation, but can undergo significant base motions, and therefore conformational reorganization, during the lifetime of Ap*. Some of these assemblies may not assume ET-active conformations and, consequently, Ap* decays through non-ET pathways. In DNA assemblies that do adopt ET-active conformations within the lifetime of Ap*, Ap* decays through ET that is gated by initial reorganizational motion. It is this population of assemblies in which DNA dynamics have the most profound impact on ET. This gating concept has been proposed and confirmed by anisotropy measurements on the femtosecond timescale.[3] The model presented herein is reminiscent of the behavior of ethidium-modified DNA duplexes, except that it is the motion of the DNA bases themselves that act as the gate. A recent theoretical study of DNA conformational order has actually reproduced the biphasic temporal behavior and is entirely consistent with the gating model.[6]

In ApG duplexes, in which the donor and acceptor are in direct contact, the probability of being in an ET-active conformation is high and ET occurs in 10 ps, leaving little time for conformational reorganization. In ApAG, however, the ET is mediated by the DNA bridge and requires ~100 ps, during which time some reorganizational motion may occur. Therefore, it is not surprising that for ApAG duplexes, $k_{ET}$ is even less dependent on the temperature and that the deviation from the conventional model is more pronounced (Figure 3). In this case, we are observing ET in those assemblies that assume ET-active conformations at the moment of excitation, as well as assemblies that undergo fast conformational reorganization prior to ET. The temperature dependence of $k_{ET}$ thus reflects both the direct ET and the rate-limiting reorganizational motions.

The variation in yield of ET with temperature is also consistent with this model. In the steady-state experiments, one probes the fraction of assemblies that are not ET active, and the active fraction ($F_q$) is deduced by subtraction. Thus there is a parallel with $C_1$ (Figure 2), the fraction undergoing ET, provided that there are no other significant channels on this timescale. In ApG, a relatively large population of assemblies assumes ET-active conformations at the time of excitation, and thus dynamical motions are not needed for ET. For ApAG, the yield of ET is nearly parallel with $C_1$, but with some subtle differences: It initially decreases (~10%) with increasing temperature, but then rises (~20%). This increase in yield with increasing temperature is consistent with a gating mechanism. For assemblies initially in ET-inactive conformations, enhanced motion results in a higher probability of an ET-active conformation within the lifetime of Ap*. Consequently, increased base dynamics, within a certain regime, can enhance the efficiency of bridge-mediated ET.

According to the model, the fraction of gated ET, relative to direct ET, should increase with the number of bases that separate the donor and acceptor. In fact, our investigations of longer DNA bridges strongly support this interpretation. In DNA duplexes with four adenine residues between Ap and G, the yield of ET, determined through steady-state measurements, exhibits a marked rise with increasing temperature. This increase begins at ~30 °C below the melting and continues almost to the melting, at which point the yield of ET plummets as the duplex is lost (Figure 4). The increase in ET yield indicates that enhanced base dynamics can facilitate DNA-mediated ET. Additional evidence is derived from the temperature dependence of the ET yield through the same length DNA bridge but with an A–A mismatch (Figure 4). Although the mismatch does not change the base sequence of the strand through which ET proceeds, the disruption in stacking induced by the mismatch results in significantly less ET quenching at low temperatures than in the fully matched DNA. In fact, there is no observable ET at low temperatures in the mismatched duplex. Remarkably, however, with increasing temperature the enhanced motion of the DNA bases enables the mismatched duplex to access ET-active conformations and reach an efficiency that is comparable to that of the fully matched duplex. Again, ET is lost as the

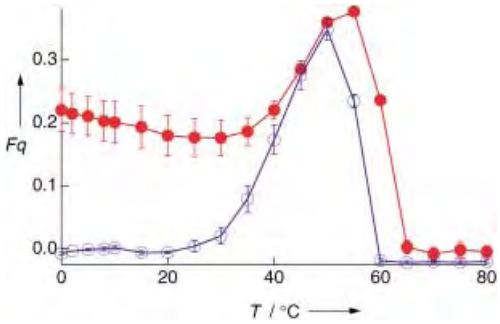



***Figure 4.*** Temperature-dependent yield of ET between Ap* and G through four intervening adenine residues (closed, red circles) and through four intervening adenine residues in which the duplex possesses an A–A mismatch at the third adenine (open, blue circles). The yield of ET is defined by $F_q$, where $F_q = 1 - \Phi_G/\Phi_I$, and $\Phi_G$ and $\Phi_I$ are the relative fluorescence quantum yields in the G- and I-containing duplexes, respectively (relative to free Ap in sodium phosphate (pH 7; 100 mM) at each temperature). The ApAAAAY assemblies (Y = I, G) are 35-mers with the same A–T content and melting temperatures as the ApY and ApAY assemblies. The $F_q$ values are the average of three or four independent trials.

 © 2003 Wiley-VCH Verlag GmbH & Co. KGaA, Weinheim 

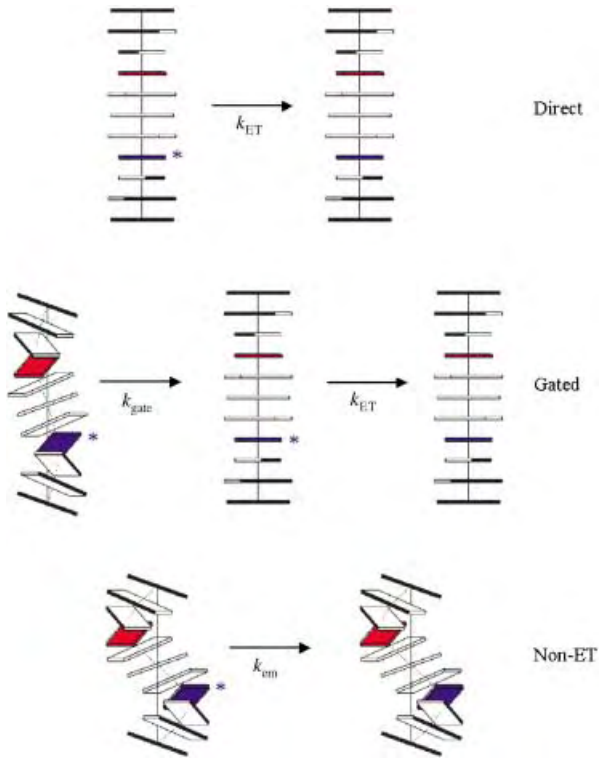



***Figure 5.*** Schematized model depicting the role of DNA base dynamics in DNA-mediated ET. In an ensemble mixture, certain DNA assemblies may adopt conformations that, upon excitation, facilitate direct ET ($k_{ET}$). Other DNA assemblies do not assume such conformations at the time of excitation, but can reorganize during the lifetime of Ap* ($k_{gate}$). Assemblies may not attain ET-active conformations and Ap* decays through non-ET pathways such as emission ($k_{em}$).

duplex melts (~3 °C lower owing to the mismatch) to yield the single strands. Our model is illustrated in Figure 5.

In summary, we used femtosecond spectroscopy to show that ultrafast DNA dynamics play a defining role in DNA-mediated ET. This role originates from the fact that base motions occur on the ET timescale. As ET occurs only through DNA assemblies that have a specific, well-coupled alignment of the DNA bases, motions of the DNA bases that lead to these ET-active conformations can serve as a gate for ET reactions, and thus modulate the rate constants and yields of ET. These data provide compelling experimental evidence that DNA ET cannot be approximated by models designed for more static donor–acceptor assemblies. Fluctuations of DNA bases must be a part of the descriptions of ET dynamics, especially because conformational gating necessarily becomes more important as the DNA bridge is lengthened.

## *Experimental Section*

The femtosecond transient absorption setup has been described previously.[19] Briefly, a pump pulse at 325 nm (< 0.2 μJ per pulse) was used to selectively excite Ap, and then a probe pulse (< 0.01 μJ per pulse) at 600 nm with variable time delay relative to the pump pulse was used to measure the transient absorption initiated by the pump pulse. The polarization of the probe pulse was at the magic angle (54.7°) relative to that of the pump pulse to avoid contributions from the reorientation motion of the molecules. The sample was contained in a stirred 5-mm quartz cell. The temperature was controlled by using a 4-position cell holder under thermostat control, and the temperature was measured with a thermocouple in an identical cuvette. Estimated uncertainties in the determined lifetimes are less than 5% for ApG, and less than 10% for ApAG, and experiment-to-experiment variations in lifetimes are less than 5%. Steady-state fluorescence measurements were conducted on an ISS K2 fluorimeter (pathlength: 5 mm) equipped with a peltier-controlled sample holder (Quantum Northwest) under thermostat control. DNA oligonucleotides were synthesized (trityl on) on an ABI DNA Synthesizer by using standard solid-phase techniques. They were then purified twice on a Hewlett Packard HPLC on a reverse-phase C-18 column with an acetonitrile/ammonium acetate gradient, and subsequently analyzed by mass spectrometry (MALDI). DNA oligonucleotides were quantified through UV/Vis spectroscopy and annealed with regulated cooling from 90–10 °C over a period of 3 h. Duplex melting temperatures were evaluated from the temperature derivative of the absorbance of Ap at 325 nm. Time-resolved and steady-state measurements were carried out on DNA duplexes (50 μM) in sodium phosphate (pH 7; 100 mM).

Received: September 9, 2003 [Z52831]

**Keywords:** DNA dynamics · electron transfer · femtochemistry · intercalations · purines

[1] For recent review, see:a) C. R. Treadway, M. G. Hill, J. K. Barton, *Ann. Rev. Biochem.* **2002**, *71*, 51; b) F. D. Lewis, R. L. Letsinger, M. R. Wasielewski, *Acc. Chem. Res.* **2001**, *34*, 159; c) G. B. Schuster, *Acc. Chem. Res.* **2000**, *33*, 253; d) B. Giese, A. Biland, *Chem. Commun.* **2002**, 667; e) K. Nakatani, C. Dohno, I. Saito, *J. Am. Chem. Soc.* **2000**, *122*, 5893.

[2] For recent reviews, see also:a) M. Bixon, J. Jortner, *Chem. Phys.* **2002**, *281*, 393; b) Y. A. Berlin, A. L. Burin, M. A. Ratner, *Chem. Phys.* **2002**, *275*, 61.

[3] C. Z. Wan, T. Fiebig, S. O. Kelley, C. R. Treadway, J. K. Barton, A. H. Zewail, *Proc. Natl. Acad. Sci. USA* **1999**, *96*, 6014.

[4] F. C. Grozema, L. D. A. Siebbeles, Y. A. Berlin, M. A. Ratner, *ChemPhysChem* **2002**, *3*, 536.

[5] a) A. A. Voityuk, K. Siriwong, N. Rosch, *Phys. Chem. Chem. Phys.* **2001**, *3*, 5421; b) A. Troisi, G. Orlandi, *J. Phys. Chem. B* **2002**, *106*, 2093.

[6] R. Bruinsma, G. Gruner, M. R. D'Orsogna, J. Rudnick, *Phys. Rev. Lett.* **2000**, *85*, 4393.

[7] T. M. Nordlund, S. Andersson, L. Nilsson, R. Rigler, A. Graslund, L. W. McLaughlin, *Biochemistry* **1989**, *28*, 9095.

[8] T. Fiebig, C. Z. Wan, A. H. Zewail, *ChemPhysChem* **2002**, *3*, 781.

[9] a) S. O. Kelley, J. K. Barton, *Science* **1999**, *283*, 375; b) C. Z. Wan, T. Fiebig, O. Schiemann, J. K. Barton, A. H. Zewail, *Proc. Natl. Acad. Sci. USA* **2000**, *97*, 14052; c) M. A. O'Neill, J. K. Barton, *J. Am. Chem. Soc.* **2002**, *124*, 13053; d) M. A. O'Neill, J. K. Barton, *Proc. Natl. Acad. Sci. USA* **2002**, *99*, 16543.

[10] O. F. A. Larsen, I. H. M. van Stokkum, B. Gobets, R. van Grondelle, H. van Amerongen, *Biophys. J.* **2001**, *81*, 1115.

[11] J. M. Jean, K. B. Hall, *Biochemistry* **2002**, *41*, 13152.

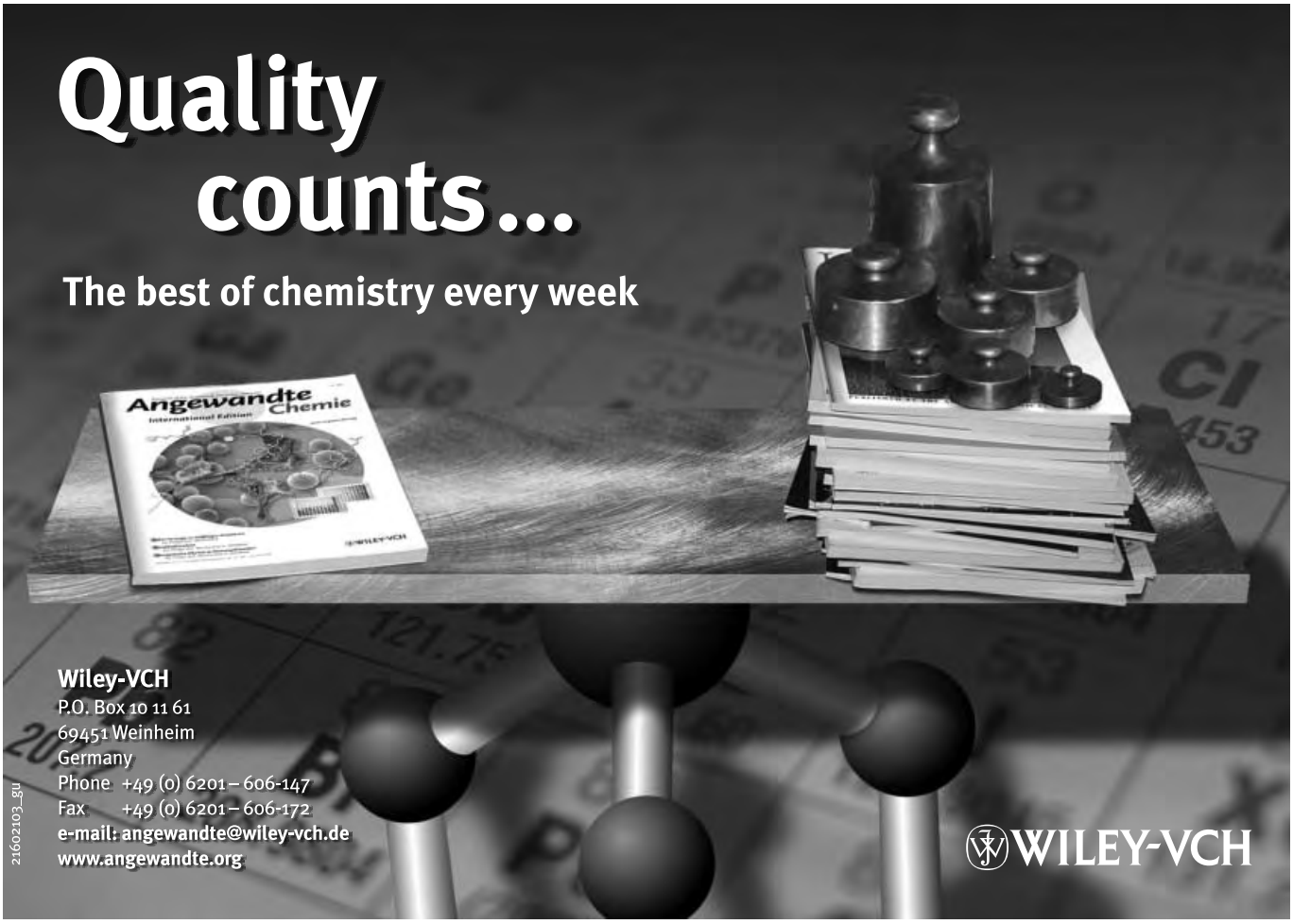
[12] Recent results in our laboratory provide direct chemical evidence for ET between Ap* and G. Irradiation of Ap in DNA that contains $N^2$-cyclopropyldeoxyguanosine ($^{CP}$G) initiates hole transfer from Ap* followed by rapid ring opening of the $^{CP}$G radical cation and subsequent trapping by oxygen and water to yield oxidized products: M. A. O'Neill, C. Dohno, J. K. Barton, unpublished results.

[13] The duplex melting temperatures are 61 and 63 °C for Y = I and G, respectively (50 μM duplexes, 100 mM sodium phosphate, pH 7).

[14] R. A. Marcus, N. Sutin, *Biochim. Biophys. Acta* **1985**, *811*, 265.

 © 2003 Wiley-VCH Verlag GmbH & Co. KGaA, Weinheim 

[15] a) F. D. Lewis, R. S. Kalgutkar, Y. S. Wu, X. Y. Liu, J. Q. Liu, R. T. Hayes, S. E. Miller, M. R. Wasielewski, *J. Am. Chem. Soc.* **2000**, *122*, 12346; b) G. D. Reid, D. J. Whittaker, M. A. Day, D. A. Turton, V. Kayser, J. M. Kelly, G. S. Beddard, *J. Am. Chem. Soc.* **2002**, *124*, 5518.
[16] a) A. A. Voityuk, N. Rosch, M. Bixon, J. Jortner, *J. Phys. Chem. B* **2000**, *104*, 9740; b) A. A. Voityuk, J. Jortner, M. Bixon, N. Rosch, *J. Chem. Phys.* **2001**, *114*, 5614; c) A. Troisi, G. Orlandi, *Chem. Phys. Lett.* **2001**, *344*, 509; d) J. Olofsson, S. Larsson, *J. Phys. Chem. B* **2001**, *105*, 10398; e) G. Brunaud, F. Castet, A. Fritsch, M. Kreissler, L. Ducasse, *J. Phys. Chem. B* **2001**, *105*, 12665.
[17] a) V. M. Orlov, A. N. Smirnov, Y. M. Varshavsky, *Tetrahedron Lett.* **1976**, *17*, 4377; b) N. S. Hush, A. S. Cheung, *Chem. Phys. Lett.* **1975**, *34*, 11.
[18] a) I. Daizadeh, E. S. Medvedev, A. A. Stuchebrukhov, *Proc. Natl. Acad. Sci. USA* **1997**, *94*, 3703; b) E. S. Medvedev, A. A. Stuchebrukhov, *Pure Appl. Chem.* **1998**, *70*, 2201.
[19] T. Fiebig, C. Z. Wan, S. O. Kelley, J. K. Barton, A. H. Zewail, *Proc. Natl. Acad. Sci. USA* **1999**, *96*, 1187.



# Cover Picture




**Stéphane Quideau,* Michael Jourdes, Cédric Saucier, Yves Glories, Patrick Pardon, and Christian Baudry**

**Human DNA topoisomerase II** is inhibited in vitro by acutissimin A, a flavano-ellagitannin, with an activity much higher than that of the clinically used antitumor drug etoposide. Acutissimin A is formed by a non-enzymatic, yet diastereoselective, condensation reaction occurring during the aging of red wine in oak barrels. S. Quideau et al. report its high-yielding semi-synthesis in their Communication on page 6012 ff.

# Contents

## Angewandte EarlyView

***The following articles are available online (in Wiley InterScience). You can find them at www.angewandte.org, under Full Text, Early View.***

*K. Koszinowski, D. Schröder, H. Schwarz*:*
**Coupling of Methane and Ammonia by Dinuclear Bimetallic Platinum–Coinage-Metal Cations PtM$^+$**
DOI: 10.1002/anie.200352817
Published online: December 5, 2003

*C. Lemire, R. Meyer, Sh. Shaikhutdinov, H.-J. Freund*:*
**Do Quantum Size Effects Control CO Adsorption on Gold Nanoparticles?**
DOI: 10.1002/anie.200352538
Published online: December 2, 2003

*L. Zhao, S. K. Pal, T. Xia, A. H. Zewail*:*
**Dynamics of Ordered Water in Interfacial Enzyme Recognition: Bovine Pancreatic Phospholipase $A_2$**
DOI: 10.1002/anie.200352961
Published online: December 8, 2003

Articles judged by the referees or the editor as being either very important or very urgent are immediately edited, proof-read, and electronically published once the manuscript has arrived in the editorial office in final form. As long as there is no page number available these articles should be cited in the following manner:

Author(s) *Angew. Chem. Int. Ed.*, online publication date, DOI.

## News


Materials Science: German Future Award for Merck Team ——— **5922**

Biophysical Chemistry: C. Griesinger Recognized ——— **5922**

Biochemistry: H. Waldmann Receives Bergmann Medal ——— **5922**


## Books


Bioinorganic Chemistry ——— **5924** — Rosette M. Roat-Malone — *reviewed by F. Meyer*

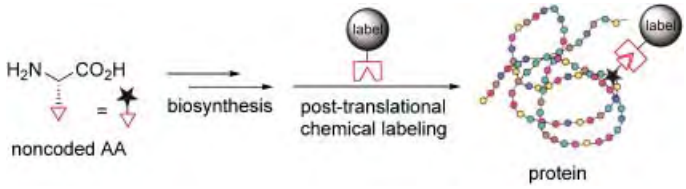
Chemical Discovery and the Logicians' Program ——— **5924** — Jerome A. Berson — *reviewed by S. J. Weininger*


## Highlights

### Protein Design


J. H. van Maarseveen,*
J. W. Back ——— **5926 – 5928**

Re-Engineering the Genetic Code: Combining Molecular Biology and Organic Chemistry

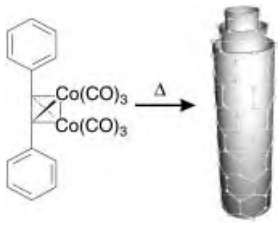

**Imagine...** if the biomachinery of nature accepted every uncoded amino acid site-specifically as desired. Spectacular advances in breaking the genetic code to expand the set of amino acids available for protein biosynthesis are highlighted, and examples of the post-translational chemical modification of proteins containing these nonnatural amino acids are presented (see scheme).

### Nanotechnology

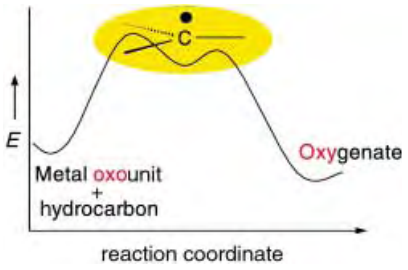

M. Burghard* ——— **5929 – 5930**

Carbon Nanotubes by Quantitative Solid-State Conversion of an Organometallic Precursor


**Optimization of synthesis methods** for carbon nanotubes is an essential requirement for realizing their potential applications in field-emission devices, (bio)sensors, or as electrical interconnections in microchips. Procedures directly yielding clean nanotubes from a single molecular precursor (see picture) are highly desired and are expected to provide important clues to the general mechanism of nanotube formation.



# Reviews



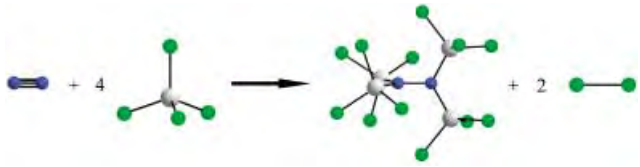

**A radical view of oxygenation**: As revealed by recent research, radical intermediates are almost ubiquitous during metal-assisted oxo-functionalizations of organic substrates (see picture). This review covers examples from the areas as diverse as homogeneous and heterogeneous chemistry, as well as metalloenzyme systems.

## Oxygenation

C. Limberg* _____ 5932 – 5954

The Role of Radicals in Metal-Assisted Oxygenation Reactions

# Communications

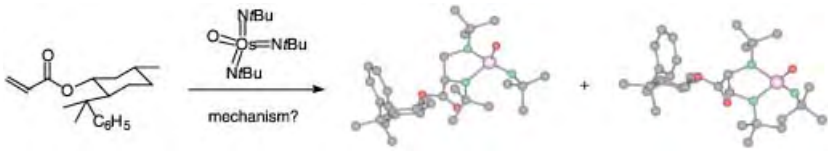



**Microwave magic:** GC–MS analysis and quantum chemical calculations were used to show that $N_2(SiCl_3)_4$ was a product of the reaction of $SiCl_4$ with $N_2$ activated with a gas plasma generated by microwaves. $N_2(SiCl_3)_4$ is the first known perhalogenated silyl hydrazine (see scheme: N blue, Si gray, Cl green).

## Plasma chemistry

N. Schiefenhövel, H.-J. Himmel, M. Binnewies* _____ 5956 – 5957

$N_2(SiCl_3)_4$—A Tetrakissilylhydrazine as an Unexpected Product of the Reaction between $N_2$ and $SiCl_4$

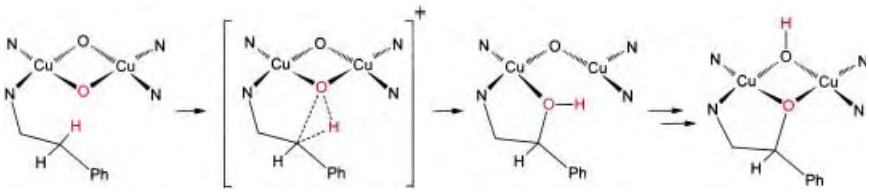



**A mechanistic puzzle** in the field of osmium(VIII)-mediated functionalization of olefins: How do the diaminations of olefins to give osmaimidazolidines with a stereogenic osmium center proceed (see scheme: C: gray, N: green, red: O, Os: pink)?

## Asymmetric Synthesis

K. Muñiz,* M. Nieger, H. Mansikkamäki _____ 5958 – 5961

Stereochemically Defined Osmium Centers from Asymmetric Diamination of Olefins: Mechanistic Implications for Osmium-Mediated Acrylate Functionalization




**The core of the problem**: The selective hydroxylation of benzylic C–H bonds by a $[Cu_2O_2]^{2+}$ core is a nonsynchronous concerted process (see scheme). This is the result of density functional calculations on the mechanistic scenario of the monooxygenase reactivity of a bis(μ-oxo)dicopper(III) complex.

## Modeling Metalloproteins

P. Spuhler, M. C. Holthausen* _____ 5961 – 5965

Mechanism of the Aliphatic Hydroxylation Mediated by a Bis(μ-oxo)dicopper(III) Complex

**For the USA and Canada:**
ANGEWANDTE CHEMIE International Edition (ISSN 1433-7851) is published weekly by Wiley-VCH PO Box 191161, D 69451 Weinheim, Germany. Air freight and mailing in the USA by Publications Expediting Inc. 200 Meacham Ave., Elmont, NY 11003. Periodicals postage paid at Jamaica NY 11431. US POSTMASTER: send address changes to *Angewandte Chemie*, Wiley-VCH, 111 River Street, Hoboken, NJ 07030. Annual institutional subscription price for institutions: Europe € 3430.00/3118.00. Outside Europe US$ 4499.00/4090.00 (valid for print and electronic/print or electronic delivery); for individuals who are personal members of a national chemical society, or whose institution already subscribes, or who are retired or self-employed consultants, print only. Europe € 248.00/Outside Europe US$ 378.00. Postage and handling charges included. All Wiley-VCH prices are exclusive VAT.

 © 2003 Wiley-VCH Verlag GmbH & Co. KGaA, Weinheim 

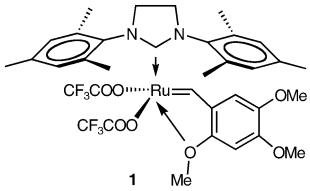
# Contents


## Poly(acetylene)s

J. O. Krause, M. T. Zarka, U. Anders, R. Weberskirch, O. Nuyken,* M. R. Buchmeiser* ——— **5965 – 5969**

Simple Synthesis of Poly(acetylene) Latex Particles in Aqueous Media

**The metathesis catalyst 1** allows the first living cyclopolymerization of 1,6-heptadiynes. With the chiral 4-(ethoxycarbonyl)-4-(1*S*,2*R*,5*S*)-(+)-menthoxycarbonyl-1,6-heptadiyne highly tactic polymers with an alternating *cis–trans* structure and a stereoregularity of greater than 95% are obtained. Fixation of **1** on poly(2-oxazoline) block copolymers provides access to poly(acetylene)s under aqueous conditions by micellar catalysis.

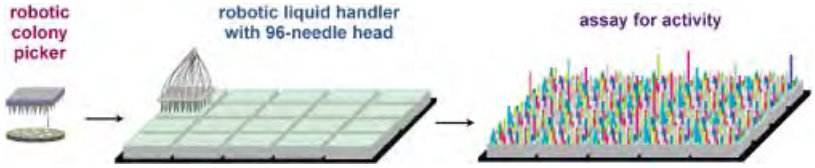



1

## Screening for Protein Catalysts

J. Gildersleeve, A. Varvak, S. Atwell, D. Evans, P. G. Schultz* ——— **5971 – 5973**

Development of a High-Throughput Screen for Protein Catalysts: Application to the Directed Evolution of Antibody Aldolases

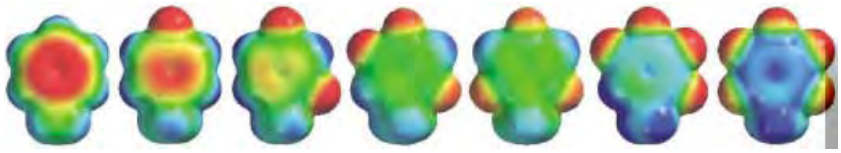



**A semiautomated high-throughput system** has been developed to express and purify proteins and assay their catalytic activity. The screen can be used to evolve activity, selectivity, and expression levels of proteins directly or in combination with selections. To illustrate its potential, the system was applied to the directed evolution of catalytic antibodies with aldolase activity.

## DNA Structures

J. S. Lai, J. Qu, E. T. Kool* ——— **5973 – 5977**

Fluorinated DNA Bases as Probes of Electrostatic Effects in DNA Base Stacking



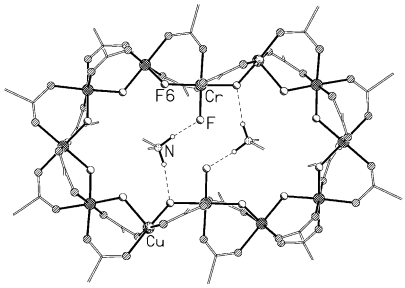
**Stacking the deck**: A series of aromatic fluorinated nucleosides (the electrostatic surface potentials are depicted) was used to probe electrostatic effects in the stacking of DNA bases in water. Although increasing fluorine substitution (from zero through five) generally increases stacking ability, a new tetrafluorinated analogue is, surprisingly, the strongest helix stabilizer, while the pentafluorinated base is the weakest.

## Cage Compounds

F. K. Larsen,* J. Overgaard, S. Parsons, E. Rentschler, A. A. Smith, G. A. Timco,* R. E. P. Winpenny* ——— **5978 – 5981**

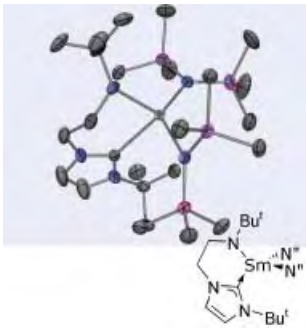
Horseshoes, Rings, and Distorted Rings: Studies of Cyclic Chromium-Fluoride Cages

**Running rings around ammonium**: Use of amine templates leads to a rich structural chemistry for heterometallic cyclic compounds. For example, use of two diethylammonium cations leads to the formation of the $\{Cr_{10}Cu_2\}$ cage, which is stabilized by N–H···F bonds (see picture). The results suggest a new method for making sophisticated polymetallic architectures.





 © 2003 Wiley-VCH Verlag GmbH & Co. KGaA, Weinheim 




**Organolanthanides** with amido-tethered N-heterocyclic carbenes: a new bidentate ligand that tethers an N-heterocyclic carbene group to a trivalent lanthanide complex (samarium, depicted, $N'' = N(SiMe_3)_2$; or yttrium) affords the first organolanthanide amido–carbene complexes and an opportunity to explore the strength and reactivity of the early metal–N-heterocyclic carbene fragment.

## Organolanthanide Complexes

P. L. Arnold,* S. A. Mungur, A. J. Blake, C. Wilson ——— 5981 – 5984

Anionic Amido N-Heterocyclic Carbenes: Synthesis of Covalently Tethered Lanthanide–Carbene Complexes

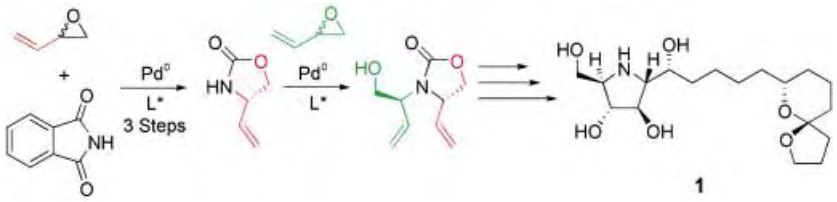



**Blue lights the way!** The rapid evaluation of enantiomeric excess in the high-throughput screening of libraries has been a hurdle to the discovery of effective catalysts. A blue-fluorescent monoclonal antibody (mAb) addresses this problem; mAb 19G2 is used as a fluorescent sensor (see picture) to evaluate a panel of *Cinchona* alkaloid derivatives in the synthesis of asymmetric amino acids by phase-transfer catalysis.

## Sensors

M. Matsushita,* K. Yoshida, N. Yamamoto, P. Wirsching, R. A. Lerner, K. D. Janda* ——— 5984 – 5987

High-Throughput Screening by Using a Blue-Fluorescent Antibody Sensor

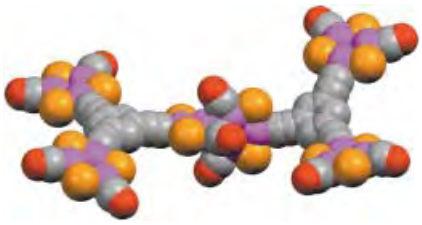



**A potential general approach** to potent N-heterocyclic glycosidase inhibitors is illustrated by the first total synthesis of (+)-broussonetine G (**1**). The key transformation of the synthesis relies on two successive palladium-catalyzed asymmetric allylic alkylations of butadiene monoxide with a nitrogen nucleophile to construct the pyrrolidine core.

## Natural Product Synthesis

B. M. Trost,* D. B. Horne, M. J. Woltering ——— 5987 – 5990

Palladium-Catalyzed DYKAT of Vinyl Epoxides: Enantioselective Total Synthesis and Assignment of the Configuration of (+)-Broussonetine G



**Sterically protected** tri- and hexanuclear platinum clusters were used as building blocks for the high-yield synthesis of a first-generation dendrimer (see picture; *t*Bu groups are omitted for clarity), which is chemically and thermally stable, and in which the cluster units are separated by conjugated 1,3,5-triethynylphenyl groups.

## Pt Dendrimer Synthesis

VIP

A. Albinati, P. Leoni,* L. Marchetti, S. Rizzato ——— 5990 – 5993

Assembling Metal Clusters with Covalent Linkers: Synthesis and Structure of a Quasi-Planar $Pt_{18}$ Dendrimer Containing Five Clusters Connected by σ-Alkynyl Spacers

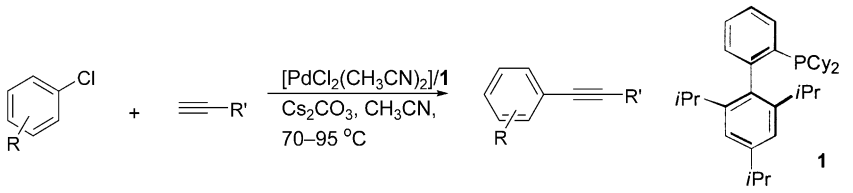
 © 2003 Wiley-VCH Verlag GmbH & Co. KGaA, Weinheim 

# Contents


## Pd-Catalyzed C–C Coupling

D. Gelman, S. L. Buchwald* **5993 – 5996**

Efficient Palladium-Catalyzed Coupling of Aryl Chlorides and Tosylates with Terminal Alkynes: Use of a Copper Cocatalyst Inhibits the Reaction

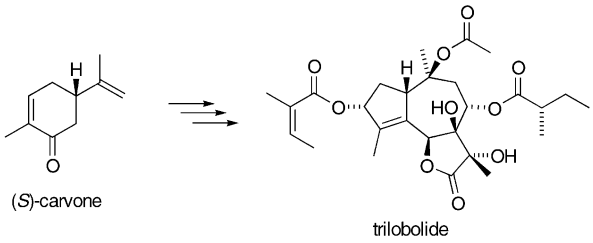



**Less catalyst, lower temperature,** and greater generality are the advantages of the new general protocol over those previously described for the palladium-catalyzed coupling of aryl chlorides and alkynes (see scheme). Better results are obtained without a copper cocatalyst, which has been found to inhibit product formation in the coupling reaction of aryl chlorides with terminal alkynes.

## Natural Products

S. F. Oliver, K. Högenauer, O. Simic, A. Antonello, M. D. Smith, S. V. Ley* **5996 – 6000**

A Route to the Thapsigargins from (*S*)-Carvone Providing a Substrate-Controlled Total Synthesis of Trilobolide, Nortrilobolide, and Thapsivillosin F

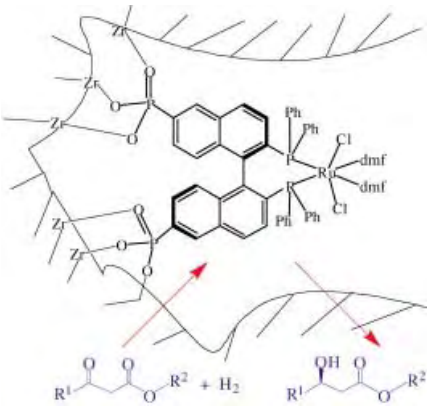



**An entirely substrate-controlled** total synthesis of three members of the thapsigargin family (e.g. trilobolide) is achieved starting from (*S*)-carvone. The synthesis is linear in nature but is achieved in high yield (>90% per step). The route permits late-stage divergence, providing access to a range of natural products and structural analogues.

## Supported Catalysts

A. Hu, H. L. Ngo, W. Lin* **6000 – 6003**

Chiral, Porous, Hybrid Solids for Highly Enantioselective Heterogeneous Asymmetric Hydrogenation of β-Keto Esters

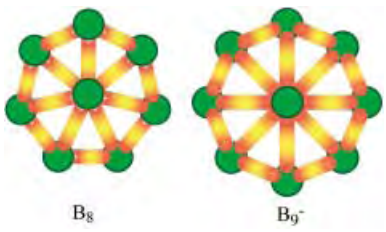



**Catalytic building blocks**: Chiral porous zirconium phosphonates containing Ru-binap moieties are synthesized by a molecular building-block approach, and characterized by a variety of techniques. These hybrid solids are used for enantioselective heterogeneous asymmetric hydrogenation of β-keto esters with *ee* values of up to 95% (see picture). Ready tunability of such a molecular building-block approach promises to lead to useful heterogeneous asymmetric catalysts.

## Molecular Wheels

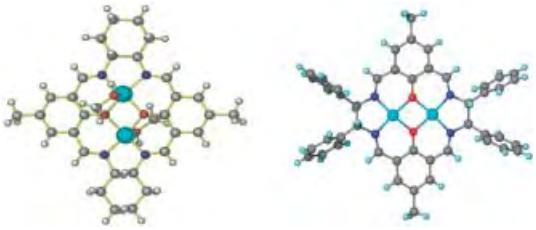
H.-J. Zhai, A. N. Alexandrova, K. A. Birch, A. I. Boldyrev, L.-S. Wang* **6004 – 6008**

Hepta- and Octacoordinate Boron in Molecular Wheels of Eight- and Nine-Atom Boron Clusters: Observation and Confirmation




**Two types of aromaticity**: Experimental and theoretical evidence shows that eight- and nine-atom boron clusters are perfectly planar molecular wheels, with a hepta- or octacoordinated central boron atom, respectively (see picture, B green). The radii of the miniature molecular wheels are found to be 1.8 and 2.0 Å. Analyses of their chemical bonding reveal that they possess double (σ and π) aromaticity, which is responsible for the wheel structures and the extreme coordination environments.


 © 2003 Wiley-VCH Verlag GmbH & Co. KGaA, Weinheim 



**Copper(II)-based complex catalysts** (see crystal structures) were prepared and characterized by X-ray crystallography. They were shown to be active catalysts for asymmetric oxidative coupling of 2-naphthol with high enantioselectivity.

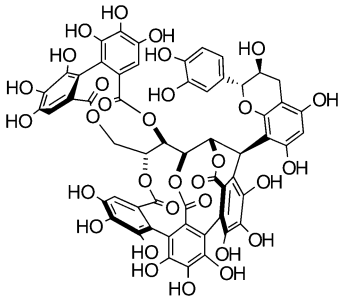

**Asymmetric Oxidative Coupling**

J. Gao,* J. H. Reibenspies, A. E. Martell ——— **6008 – 6012**

Structurally Defined Catalysts for Enantioselective Oxidative Coupling Reactions


---

**Good health!** Although not initially present in red wine, acutissimin A (see picture) and other flavano-ellagitannins are formed during aging in oak barrels by a diastereoselective nonenzymatic condensation reaction between flavan-3-ols present in grapes and ellagitannin vescalagin from oak. Acutissimin A is a DNA topoisomerase inhibitor that is 250-fold more potent in vitro than the clinically used anicancer drug etoposide.



acutissimin A


**Natural Product Synthesis**

S. Quideau,* M. Jourdes, C. Saucier, Y. Glories, P. Pardon, C. Baudry ——— **6012 – 6014**

DNA Topoisomerase Inhibitor Acutissimin A and Other Flavano-Ellagitannins in Red Wine


---



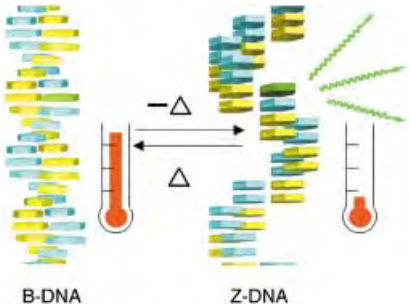
**In a supermolecular system**, the sum of properties is more than that of the individual components. The combination of rod and disc shaped groups (see picture) in the right ratio allows the design of a material with nematic and several layered (smectic) phases. Shape-induced nanophase segregation of rods and discs leads to the formation of distinct sublayers.


**Liquid Crystals**

P. H. J. Kouwer, G. H. Mehl* ——— **6015 – 6018**

Multiple Levels of Order in Linked Disc–Rod Liquid Crystals


---




**Taking the temperature**: The electronic properties of DNA largely depend on the orientation of the π stacking. Based on the discrete clusters of interstrand four-base π stacks in Z-form DNA, a molecular thermometer that exploits the differences in the π stackings of B- and Z-DNA has been designed (see picture).


**Molecular Devices**

R. Tashiro, H. Sugiyama* ——— **6018 – 6020**

A Nanothermometer Based on the Different π Stackings of B- and Z-DNA


 © 2003 Wiley-VCH Verlag GmbH & Co. KGaA, Weinheim 

# Contents


**Helical Polymers**

S. Hecht,* A. Khan ——— **6021 – 6024**

Intramolecular Cross-Linking of Helical Folds: An Approach to Organic Nanotubes





**The tubular secondary structure** of a folded helical polymer—a poly(*m*-phenyleneethynylene) derivative carrying multiple cinnamate moieties—is stabilized by intramolecular cross-linking through topochemically controlled photodimerizations (see schematic representation). This approach should enable the generation of organic nanotubes with controlled dimensions and surface functionality that constitute attractive building blocks for functional nanostructures.

---

Communications labeled with this symbol have been judged by two referees as being "very important papers".

The publication of Communications labeled with this symbol has been accelerated because of their topical or highly competitive nature.


## Looking for outstanding employees?

**Do you need another expert for your excellent team?**
**... Chemists, PhD Students, Managers, Professors, Sales Representatives...**

Place an advert in the printed version and have it made available online for 1 month, free of charge!

***Angewandte Chemie International Edition***
**Advertising Sales Department: Marion Schulz**
**Phone: 0 62 01 - 60 65 65**
**Fax: 0 62 01 - 60 65 50**
**E-Mail: MSchulz@wiley-vch.de**


## Service


***Keywords*** ——— ***6028***

***Authors*** ——— ***6029***

***Angewandte's Sister Journals*** ——— ***6026 – 6027***

***Index*** ——— ***6031***

***Preview*** ——— ***6157***



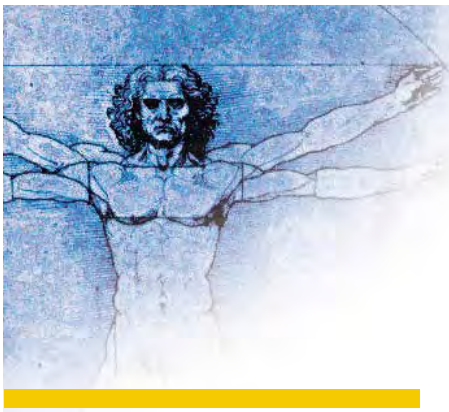

*The editorial staff and the publishers thank all readers, authors, referees, and advertisers for their interest and support over the past year and wish them all a Happy New Year.*

# Corrigenda

In the Communication "Ligand and Metal Effects on the Formation of Main-Group Polyhedral Clusters" by M. P. Coles, A. E. H. Wheatley et al. (*Angew. Chem. Int. Ed.* **2003**, *42*, 5593 – 5596), Figure 2 refers to compound **11** and not to compound **9**.

In the Communication "A Stable Salt of the Tris(ethene)silver Cation: Structure and Characterization of $[Ag(\eta^2\text{-}C_2H_4)_3]^+$-$[Al\{OC(CF_3)_3\}_4]^-$" by I. Krossing and A. Reisinger (*Angew. Chem. Int. Ed.* **2003**, *42*, 5725 – 5728) the last entry in column 2 (correct version: 1610 (vw; $a_1'$)) and the penultimate entry in column 3 of Table 1 (correct version: 1575 (3 km mol$^{-1}$, e′)[a]) were erroneously switched during the editing process.

 © 2003 Wiley-VCH Verlag GmbH & Co. KGaA, Weinheim 



## Future Award to Researchers at Merck

This year the Prize of the German President for Technology and Innovation (Future Award) goes to physicist Kazuaki Tarumi (team leader) and chemists Melanie Klasen-Memmer and Matthias Bremer, a research team at the company Merck in Darmstadt (Germany). They have been distinguished for their project "Lighter, Brighter, Faster: Liquid Crystals for Television Screens". Since the mid-1990s they have systematically synthesized a large number of liquid-crystalline substances, improved them, and tested them in new mixtures, until mixtures were found that were suitable for use with vertical-alignment technology in large LCD (liquid crystal display) television screens. With the materials developed at Merck this technology allows the high contrast, rapid switching times, and large viewing angle required for large screens, so that even fast movements look fluid. In contrast with the more widespread twisted-nematic displays, liquid-crystal molecules are first oriented perpendicular to the glass, and then aligned perpendicular to the field when a parallel voltage is applied.

One tends to assume that everything to do with the manufacturing of display screens happens in the Far East. The majority of displays for wristwatches, laptops, and televisions are indeed manufactured there. However, in the case of liquid crystals that allow changes in contrast, 50 of the 60 tons produced annually come from Darmstadt, including 100% of those used for large television screens. The secret lies not only in the synthesis of new components, but also in the formulation of mixtures, which can be used to tailor-make materials according to each customer's individual requirements in terms of properties (e.g. switching time and contrast). Typically such mixtures contain 20–30 components. Peer Kirsch and Matthias Bremer described the design and synthesis of nematic liquid crystals for active-matrix displays in a Review in issue 23/2000 of *Angewandte Chemie*.[1]

Tarumi studied physics at Waseda University (Japan) and completed his PhD in 1985 in Bremen (Germany). He returned to Japan as associate professor at Gunma University, then joined Merck in Darmstadt in 1990. Bremer completed his PhD in 1989 at the Universität Erlangen-Nürnberg (Germany) under the supervision of P. von R. Schleyer and started at Merck in 1991 after a postdoctoral period in the research group of A. Streitwieser (Berkeley, USA). Klasen-Memmer joined Merck in 1998 after completing her PhD under the guidance of H.-G. Kuball in Kaiserslautern (Germany).



K. Tarumi M. Klasen-Memmer C. M. Bremer

## Otto Bayer Prize to C. Griesinger

The Otto Bayer Foundation has awarded its Prize worth €50000 to Christian Griesinger, director of the Max-Planck-Institut (MPI) für Biophysikalische Chemie (Göttingen, Germany), in recognition of his outstanding achievements in NMR spectroscopy. His research group develops methods for multidimensional NMR spectroscopy in solution and carries out the synthesis and structural elucidation of peptides, proteins, and oligonucleotides. This research has provided important insight into the function of enzymes and into biological events in cells, and has enabled possible starting points for new drugs to be identified. The Communication by Griesinger and coworkers on the binding of epithilone A to tubulin was the cover-picture article in issue 22/2003 of *Angewandte Chemie*.[2]



C. Griesinger

Griesinger completed his PhD in 1986 under the supervision of H. Kessler in Frankfurt am Main (Germany) and carried out postdoctoral research with R. Ernst at the ETH Zürich (Switzerland). In 1990 he accepted a position as Professor of Organic Chemistry at the Universität Frankfurt and has been director at the MPI für Biophysikalische Chemie in Göttingen since 1999.

The Otto Bayer Prize has been awarded since 1984 in memory of Otto Bayer, the pioneer of polyurethane chemistry.

## H. Waldmann Receives the Max Bergmann Medal

Herbert Waldmann, director of the Max-Planck-Institut für Molekulare Physiologie in Dortmund (Germany), has been awarded the Max Bergmann Medal of the Max Bergmann Society this year for his work on the synthesis of lipo- and glycopeptides and proteins.



H. Waldmann

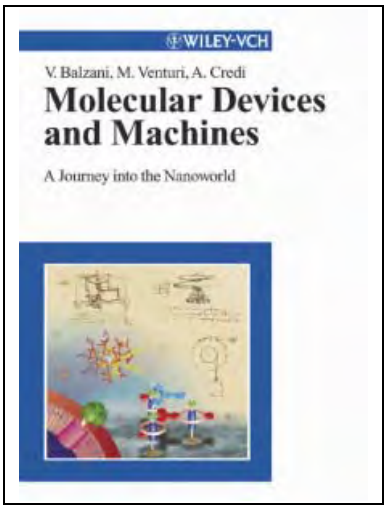
Waldmann completed his PhD in 1985 under the supervision of H. Kunz at the Universität Mainz (Germany), undertook postdoctoral research with G. Whitesides (Harvard University, USA), and completed his habilitation in 1991 in Mainz (Germany). After periods as professor in Bonn and Karlsruhe he was made director of the MPI für Molekulare Physiologie in Dortmund in 1999.

 © 2003 Wiley-VCH Verlag GmbH & Co. KGaA, Weinheim 

He recently reported on the use of natural products as lead compounds for the design and synthesis of compound libraries in a Review in *Angewandte Chemie*.[3]

[1] P. Kirsch, M. Brehmer, *Angew. Chem.* **2000**, *112*, 4384; *Angew. Chem. Int. Ed.* **2000**, *39*, 4216.
[2] T. Carlomagno, M. J. J. Blommers, J. Meiler, W. Jahnke, T. Schupp, F. Petersen, D. Schinzer, K.-H. Altmann, C. Griesinger, *Angew. Chem.* **2003**, *115*, 2615; *Angew. Chem. Int. Ed.* **2003**, *42*, 2511.
[3] R. Breinbauer, I. R. Vetter, H. Waldmann, *Angew. Chem.* **2002**, *114*, 3002; *Angew. Chem. Int. Ed.* **2002**, *41*, 2878.

Key-Technologies of the Future




ISBN 3-527-30506-8
€ 99,-* / sFr 146,-

*The Euro price is only valid for Germany.

*VINCENZO BALZANI, Italy, ALBERTO CREDI, and MARGHERITA VENTURI, all of University of Bologna, Italy*

**Molecular Devices and Machines**
*A Journey into the Nanoworld*
*2003. XVII, 494 pp Hbk*

The miniaturization of bulky devices and machines is a process that confronts us on a daily basis. However, nanoscale machines with varied and novel characteristics may also result from the enlargement of extremely small building blocks, namely individual molecules. This bottom-up approach to nanotechnology is already being pursued in information technology, with many other branches about to follow.
Written by Vincenzo Balzani and his team of co-authors, this book provides a comprehensive overview of this fascinating and multifarious topic, offering newcomers and experts alike a wealth of information.

- Most important new technologies for a broad audience
- Unifying, critical, and stimulating overview of red-hot topics

Wiley-VCH Verlag
Fax: +49 (0)6201 606 184
e-Mail: service@wiley-vch.de
www.wiley-vch.de

Register now for the free
**WILEY-VCH Newsletter!**
***www.wiley-vch.de/home/pas***

WILEY-VCH

50303032_kn

 © 2003 Wiley-VCH Verlag GmbH & Co. KGaA, Weinheim 

Protein Design

# Re-Engineering the Genetic Code: Combining Molecular Biology and Organic Chemistry

*Jan H. van Maarseveen* and Jaap Willem Back*

**Keywords:**
amino acids · biosynthesis · protein engineering · protein modifications · tRNA

Major breakthroughs have been made in the biosynthetic incorporation of noncoded amino acids into proteins.[1] The research groups of Schultz,[2] Yokoyama,[3] and Tirrell[4] in particular have shown that the diversity of proteins may be expanded to include a far wider range of residues than the 20 proteogenic amino acids by using nature's own biosynthetic machinery. Examples are the inclusion in proteins of amino acids bearing functional groups that serve as photoactivatable cross-linkers, spin labels, fluorescence labels, or metal chelators, of glycosylated amino acids, and of a biotinylated amino acid for affinity labeling.[5] Herein we will focus on amino acids labeled with biologically inert but chemically reactive (bioorthogonal) functional groups that allow the selective post-translational covalent modification of proteins (Scheme 1). The incorporation of such reactive amino acids into proteins brings together the worlds of molecular biology and organic chemistry to open up a fertile research area with many applications.

The incorporation of nonproteogenic amino acids into proteins has been successfully carried out in a wide range of systems, both in vitro and in vivo (Figure 1). tRNA can be charged with an amino acid outside or inside the cell, either by stoichiometric chemical ligation or by catalytic means. Because of the different options available and requirements posed, a single method does not yet exist for the incorporation of any given amino acid. However, investigations are being directed toward self-perpetuating living-model systems. Wonderful examples have been set in studies involving the acetylcholine receptor in *Xenopus* oocytes[6] and cultured human neurons.[7]

tRNAs can be chemically charged extracellularly with a noncoded amino acid of choice. The success of this method depends on the ability of the ribosome to handle the resulting AA-tRNA for translation. However, the absolute amounts of protein thus obtained are generally limited because any single tRNA has to be stoichiometrically ligated and delivered to the cells. AA-tRNAs produced catalytically are less limited in supply, but bring about other considerations. When the substrate tolerance of native aminoacyl-tRNA synthases (aaRSs) is exploited, intracellular acylation results in the proteome-wide expression of modified proteins. For example, Met-aaRS allows selenomethione as well as amino acids with less closely related side chains to be loaded.[8]

When the site-specific incorporation of a noncoded amino acid is intended, an aaRS suitable for the acylation of a specific tRNA that can not be loaded with coded amino acids by the target expression system is required. Together with a plasmid specifying the desired protein product, these orthogonal tRNA/aaRS pairs must then be transfected into the host system. Several such pairs have been described that mediate the incorporation of the desired amino acid at the specified position by acylating suppressor tRNAs, thus enabling read-through at amber codons (pathway A, Figure 1),[9] or take advantage of specific Watson–Crick base pairing at the third (wobble) codon residue (pathway B, Figure 1).[4] This latter method does, however, result in the incorporation of the nonnatural amino acid into other cellular proteins in which the redundant codon is used to code for the "expected" natural amino acid by nature itself. Alternatively, the use of four-base codons in *E. coli* has been exploited, whereby nonnatural amino acids are incorporated by the cognate four-base-anticodon AA-tRNAs within the context of a three-base coding frame (pathway C, Figure 1).[10] Another possibility is the use of ribozymes to acylate tRNA.[11] Currently this is done outside the cell, but in the future ribozymes may be found to tolerate even more unusual side chains than altered aaRSs do. The in vivo application of ribozymes will certainly be welcomed.

As expected, the less-complicated and better-documented translational machinery of prokaryotes has allowed more rapid progress to be made in bacteria than has been possible in eukaryotes. It was even shown that the enzymes required for a complete biosynthetic route to *p*-aminophenylalanine (pAF) could be added to *E. coli*, which had also been transfected with a tRNA/aaRS pair specific for this amino acid,[12] to give a truly autonomous system with a repertoire of 21 amino acids to build up proteins.

However, issues of post-translational modification or folding may require

[*] Dr. J. H. van Maarseveen
Institute of Molecular Chemistry
University of Amsterdam
Nieuwe Achtergracht 129
1018 WS Amsterdam (The Netherlands)
Fax: (+31) 20-525-5670
E-mail: jvm@science.uva.nl
Dr. J. W. Back
Swammerdam Institute for Life Sciences
Mass Spectrometry Group
University of Amsterdam
Nieuwe Achtergracht 166
1018 WV Amsterdam (The Netherlands)

 © 2003 Wiley-VCH Verlag GmbH & Co. KGaA, Weinheim DOI: 10.1002/anie.200301698 

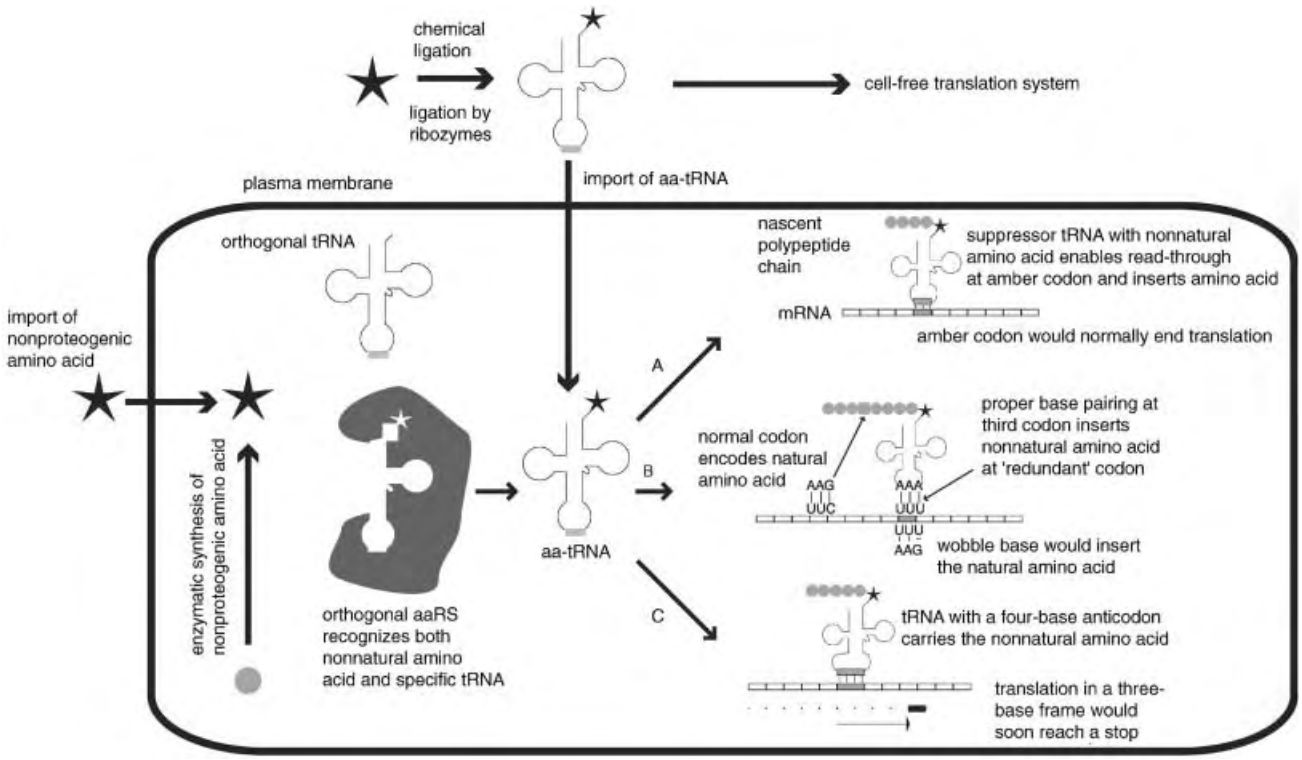


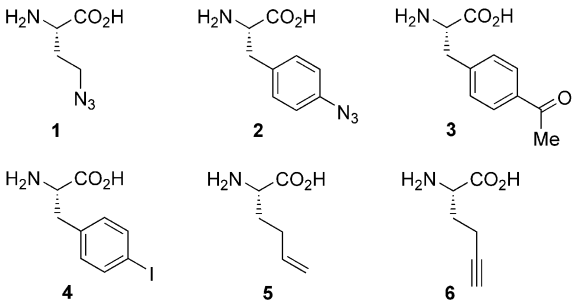

***Figure 1.*** Biochemical strategies for the incorporation of nonproteogenic amino acids into proteins.

eukaryotic expression. To this end, cell lines may be supplemented with a prokaryotic orthogonal tRNA/aaRS pair. This has been demonstrated in cell-free systems[13] and may prove especially useful when the toxicity of the amino acid or the delivery of chemically ligated AA-tRNA could preclude a living-cell approach. Recent progress includes the introduction of orthogonal tRNA/aaRS pairs into living eukaryotic cells, such as yeast[1] and cultured-human-cell lines.[3,14]

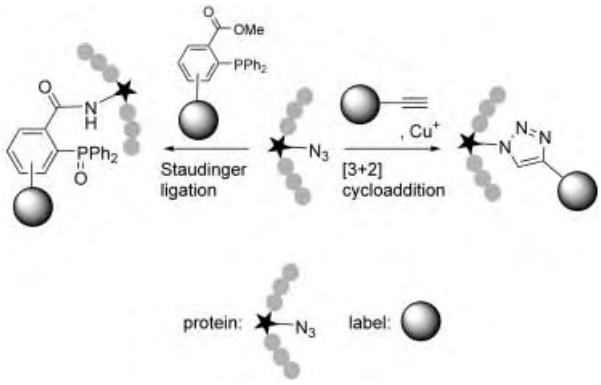
To date over 100 nonproteogenic amino acids have been incorporated into proteins biosynthetically.[5] To emphasize the potential of proteins bearing chemically reactive nonnatural amino acids, the azidohomoalanine (**1**) should be highlighted (Scheme 1). The small, inert, and biocompatible azido group in **1** has shown its versatility in further post-translational bioorthogonal (or abiotic) chemical transformations. The research groups of Bertozzi and Tirrell substituted the eight methionines in the reporter protein murine dihydrofolate reductase (mDHFR) for **1** and selectively labeled this protein with antigenic FLAG peptides[15] or fluorophoric coumarin dyes[16] through a Staudinger ligation reaction in crude cell lysates (Scheme 2).

The copper(I)-catalyzed azide–alkyne [3+2] dipolar cycloaddition (a so-called click reaction[17]) in proteins is also noteworthy (Scheme 2). Link and Tirrell incorporated **1** into the outer-membrane protein C and subsequently allowed the azide groups to react with a biotinylated alkyne reagent, as could be monitored after staining with fluorescent avidin.[18] Although not strictly bioorthogonal owing to the presence of many endogenous keto groups in living cells (e.g. in sugars), *p*-acetyl-L-phenylalanine (**3**) has also been used for in vivo chemical decoration with hydrazide-containing exogenous reagents.[19]

We would like to end this Highlight with some hints for future directions. Expanding the still very limited palette of truly bioorthogonal reactions is an important task for syn-




***Scheme 1.*** Nonnatural amino acids bearing a bioorthogonal chemical handle.




***Scheme 2.*** Covalent functionalization of an azide-labeled protein through bioorthogonal reactions.

 © 2003 Wiley-VCH Verlag GmbH & Co. KGaA, Weinheim 

thetic organic chemists. As an example, the transition-metal-mediated and mild Suzuki cross-coupling reaction between the pseudo proteogenic *p*-iodo-L-phenylalanine (**4**) and an exogenous aryl or alkyl boronic acid can be envisaged.[20] The pseudo proteogenic homoallylglycine (**5**) and homopropargylglycine (**6**) might be used for further post-translational chemical modification by the very mild alkene-, alkyne-, or enyne-metathesis reactions.[21] Intramolecular metathesis reactions within a protein by incorporation of multiple homoallylglycine residues (**5**) would lead to cross-links that could serve as highly stable disulfide-bridge isosteres. Finally, one could envisage such cross-links resulting from a [3+2]-cycloaddition reaction between the azide-containing amino acids **1** or **2** and the alkyne-containing amino acid **6**. A slight preview of the enhanced stability of proteins containing non-natural amino acids has been given by incorporating trifluoroleucine instead of leucine into leucine zipper proteins, which led to higher temperature and denaturant tolerance.[22]

In conclusion, it is clear that exciting developments are taking place at the interface of molecular biology and organic chemistry. The recently discovered biotechnological tools that make it possible to include noncoded amino acids in proteins give access to tailor-made proteins for which numerous applications can be envisaged. The results obtained so far have whetted our appetite for the things to come, and we expect them to have a heavy impact on several fields, such as proteomics, (bio)materials, biomedical research, (combined homogeneous and bio)catalysis, and synthesis.


[1] For a seminal review, see: V. W. Cornish, D. Mendel, P. G. Schultz, *Angew. Chem.* **1995**, *107*, 677–690; *Angew. Chem. Int. Ed. Engl.* **1995**, *34*, 621–633.

[2] J. W. Chin, T. A. Cropp, J. C. Anderson, M. Mukherji, Z. Zhang, P. G. Schultz, *Science* **2003**, *301*, 964–967.

[3] K. Sakamoto, A. Hayashi, A. Sakamoto, D. Kiga, H. Nakayama, A. Soma, T. Kobayashi, M. Kitabatake, K. Takio, K. Saito, M. Shirouzu, I. Hirao, S. Yokoyama, *Nucleic Acids Res.* **2002**, *30*, 4692–4699.

[4] I. Kwon, K. Kirshenbaum, D. A. Tirrell, *J. Am. Chem. Soc.* **2003**, *125*, 7512–7513.

[5] L. Wang, P. G. Schultz, *Chem. Commun.* **2002**, 1–11.

[6] M. W. Nowak, J. P. Gallivan, S. K. Silverman, C. G. Labarca, D. A. Dougherty, H. A. Lester, *Methods Enzymol.* **1998**, *293*, 504–529.

[7] S. L. Monahan, H. A. Lester, D. A. Dougherty, *Chem. Biol.* **2003**, *10*, 573–580.

[8] a) D. B. Cowie, G. N. B. Cohen, *Biochim. Biophys. Acta* **1957**, *26*, 252–261; b) J. C. M. van Hest, K. L. Kiick, D. A. Tirrell, *J. Am. Chem. Soc.* **2000**, *122*, 1282–1288; c) K. L. Kiick, J. C. M. van Hest, D. A. Tirrell, *Angew. Chem.* **2000**, *112*, 2232–2236; *Angew. Chem. Int. Ed.* **2000**, *39*, 2148–2152.

[9] a) D. R. Liu, T. J. Magliery, M. Pastrnak, P. G. Schultz, *Proc. Natl. Acad. Sci. USA* **1997**, *94*, 10092–10097; b) L. Wang, A. Brock, B. Herberich, P. G. Schultz, *Science* **2001**, *292*, 498–500.

[10] T. Hohsaka, Y. Ashizuka, H. Taira, H. Murakami, M. Sisido, *Biochemistry* **2001**, *40*, 11060–11064.

[11] H. Murakami, H. Saito, H. Suga, *Chem. Biol.* **2003**, *10*, 655–662.

[12] R. A. Mehl, J. C. Anderson, S. W. Santoro, L. Wang, A. B. Martin, D. S. King, D. M. Horn, P. G. Schultz, *J. Am. Chem. Soc.* **2003**, *125*, 935–939.

[13] D. Kiga, K. Sakamoto, K. Kodama, T. Kigawa, T. Matsuda, T. Yabuki, M. Shirouzu, Y. Harada, H. Nakayama, K. Takio, Y. Hasegawa, Y. Endo, I. Hirao, S. Yokoyama, *Proc. Natl. Acad. Sci. USA* **2002**, *99*, 9715–9720.

[14] C. Kohrer, L. Xie, S. Kellerer, U. Varshney, U. L. RajBhandary, *Proc. Natl. Acad. Sci. USA* **2001**, *98*, 14310–14315.

[15] K. L. Kiick, E. Saxon, D. A. Tirrell, C. R. Bertozzi, *Proc. Natl. Acad. Sci. USA* **2002**, *99*, 19–24.

[16] G. A. Lemieux, C. L. de Graffenried, C. R. Bertozzi, *J. Am. Chem. Soc.* **2003**, *125*, 4708–4709.

[17] a) H. C. Kolb, M. G. Finn, K. B. Sharpless, *Angew. Chem.* **2001**, *113*, 2056–2075; *Angew. Chem. Int. Ed.* **2001**, *40*, 2004–2021; b) V. V. Rostovtsev, L. G. Green, V. V. Fokin, K. B. Sharpless, *Angew. Chem.* **2002**, *114*, 2708–2711; *Angew. Chem. Int. Ed.* **2002**, *41*, 2596–2599.

[18] A. J. Link, D. A. Tirrell, *J. Am. Chem. Soc.* **2003**, *125*, 11164–11165.

[19] Z. Zhang, B. A. C. Smith, L. Wang, A. Brock, C. Cho, P. G. Schultz, *Biochemistry* **2003**, *42*, 6735–6746.

[20] A. Suzuki, *J. Organomet. Chem.* **1999**, *576*, 147–168.

[21] T. M. Trnka, R. H. Grubbs, *Acc. Chem. Res.* **2001**, *34*, 18–29.

[22] Y. Tang, G. Ghirlanda, W. A. Petka, T. Nakajima, W. F. DeGrado, D. A. Tirrell, *Angew. Chem.* **2001**, *113*, 1542–1544; *Angew. Chem. Int. Ed.* **2001**, *40*, 1494–1496.


 © 2003 Wiley-VCH Verlag GmbH & Co. KGaA, Weinheim 

Nanotechnology

# Carbon Nanotubes by Quantitative Solid-State Conversion of an Organometallic Precursor

*Marko Burghard**

**Keywords:**
carbon · cobalt · heterogeneous catalysis · nanotubes · thermolysis

Carbon nanotubes can be made from a source of carbon at elevated temperatures. Although this "recipe" sounds highly oversimplified, it works sufficiently well to stimulate a vast amount of research devoted to the chemical synthesis of this remarkable allotrope of carbon. Three main synthesis procedures have been established to date: arc discharge,[1] laser ablation,[2] and chemical vapor deposition (CVD).[3] All three methods can produce single-walled (SWCNTs) and multi-walled carbon nanotubes (MWCNTs). While graphite is utilized as the carbon source in the laser ablation and arc-discharge methods, small molecules such as hydrocarbons or carbon monoxide serve as the feedstock in CVD (Figure 1).

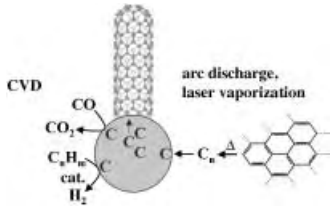



***Figure 1.*** Schematic illustration of the formation of carbon nanotubes, exemplified by the root-growth mechanism leading to single-walled nanotubes. The catalytic decomposition of hydrocarbons, disproportionation of carbon monoxide, and vaporization of graphite are shown as possible sources for carbon atoms. The carbon atoms dissolved in the metal catalyst particle get incorporated into metal–carbon bonds at the growing end of the tube.

The first two processes yield SWCNTs in the presence of an appropriate transition-metal catalyst (for example, iron, cobalt, or nickel), whereas MWCNTs are obtained without catalyst. In CVD, by contrast, amorphous carbon is mainly produced if no metal catalyst is present. Whether MWCNTs or SWCNTs predominate in this process depends on the carbon feedstock, type of metal catalyst, presence of additives, as well as reaction temperature. In general, high temperatures ($\geq 1000\,^{\circ}C$), a low supply of carbon, and the presence of a sulfur source, such as thiophene, favor the formation of SWCNTs.[4] The catalyst required for CVD can be prepared by applying pure metals, metal salts, or complexes onto the substrate by a variety of physical techniques, including vapor deposition or casting from solution. In many cases, further treatments are performed to induce the formation of small metal particles, for example, by gas-phase etching or plasma ion bombardment, or to decompose the metal precursors.

The major difficulties in the synthesis of nanotubes is that the obtained purity and degree of graphitization often lie far behind the needs of the experimentalists. Specifically, the formation of unwanted by-products such as amorphous carbon, fullerenes, and carbon nanospheres is hard to suppress. Moreover, low yields as well as high costs associated with exotic equipment or necessary additives impede the widespread application of some of these procedures. Various attempts have been made to eliminate these complications, and the CVD method in particular has developed into a highly effective synthesis tool.

One central goal in the optimization of the CVD method has been to synthesize SWCNTs directly on patterned surfaces as a basis for fabricating electrical devices or chemical sensors.[5] Application of an electric field has been demonstrated as an effective means to align the SWCNTs during synthesis.[6] The development of a growth process from prefabricated electrodes has opened up the possibility to directly integrate SWCNTs into electronic circuits.[7] Considerable progress has also been made towards controlling the diameter distribution of the SWCNTs by using almost monodispersed, nanosized catalyst particles. A correlation between the SWCNT diameter and the size of the catalyst particles is now well-established.[8] CVD has furthermore enabled the production of extremely long SWCNTs. For example, millimeter-long SWCNTs have been obtained from the catalytic decomposition of carbon monoxide.[9]

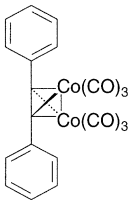
The introduction of the floating catalyst process in 1997 was an important step forward in the synthesis of MWCNTs.[10] In this method, a catalyst is continuously supplied to the gas phase instead of being supported on the substrate, which allows for a high-throughput growth of MWCNTs. For this purpose, metal carbonyl complexes, metallocenes, or metallophthalocyanines have mainly been employed as the catalyst precursors.[11] More recently, plasma-enhanced chemical vapor deposition has been investigated in detail, since this method appears to yield better vertical alignment of the MWCNTs than thermal CVD. Vertically aligned tubes have considerable application potential

[*] Dr. M. Burghard
Max-Planck-Institut fuer
Festkörperforschung
Heisenbergstrasse 1
70569 Stuttgart (Germany)
Fax: (+49) 711-689-1010
E-mail: m.burghard@fkf.mpg.de


DOI: 10.1002/anie.200301705
© 2003 Wiley-VCH Verlag GmbH & Co. KGaA, Weinheim

in field-emitting devices (for example, flat panel displays), as electrodes in biosensors, and as molecular-filtration membranes. Horizontal arrangements of MWCNTs, on the other hand, are of importance for the realization of electric circuits. Such architectures have been fabricated, for example, in the form of mm-scale bridges by capturing as-grown MWCNT bundles between parallel-standing staples.[12]

An alternative, single-component approach to MWCNTs is the pyrolysis of suitable organometallic precursors, which simultaneously function as a carbon source and a catalyst. The first molecules reported to directly yield MWCNTs in a CVD process were metallophthalocyanines containing nickel, iron, or cobalt.[13] It is worth noting that the use of phthalocyanines leads to incorporation of nitrogen atoms close to the periphery and the inner cylinder of the MWCNTs.[14] Direct solid-state generation of nanotubes without CVD was later demonstrated by Vollhardt and co-workers, who found that certain cobalt–oligoalkyne complexes yield MWCNTs upon pyrolysis (ca. 800 °C);[15] however, only modest yields (up to 60 %) and graphitic by-products have so far been obtained. An important milestone in the solid-state synthesis of nanotubes was recently set by the same research group[16] in which the nearly quantitative conversion of the cobalt diphenylethyne complex (**1**) into MWCNTs was observed after thermolysis (650 °C), without formation of other carbon materials.




**1**

The MWCNTs produced under optimized conditions contain well-graphitized inner shells. The open morphology of the resulting networks permits access of dilute acids to dissolve most the contained metal particles, thus allowing the raw material to be purified. This synthesis method has so far produced free-standing MWCNT films and should allow the direct growth of MWCNTs from surface regions containing the metal complex. Although confinement of the complex from solution into small patterns on a substrate will probably be hard to achieve by lithographic techniques, ink-jet printing may be a suitable tool for that task. This method has been employed by Ago et al. to create patterned regions of cobalt nanoparticles useful for the site-selective growth of MWCNTs.[17]

Moreover, in view of the promising results recently obtained in the CVD of iron phthalocyanine,[18] direct control over the diameter of the tubes may be possible. A first step in this direction has already been made by the observation of narrower tubes with only three to five walls after pyrolysis of **1** in the presence of molybdenum hexacarbonyl, [Mo(CO)$_6$]. It will be of special importance in the future to analyze the different stages of the solid-state conversion process, which could also provide important clues to the growth mechanism operative in the alternative production methods.

[1] T. W. Ebbesen, P. M. Ajayan, *Nature* **1992**, *358*, 220 – 222.
[2] T. Guo, P. Nikolaev, D. T. Colbert, R. E. Smalley, *Chem. Phys. Lett.* **1995**, *243*, 49 – 54.
[3] M. Endo, K. Takeuchi, S. Igarashi, K. Kobori, M. Shiraishi, H. W. Kroto, *J. Phys. Chem. Solids* **1993**, *54*, 1841 – 1848.
[4] H. M. Cheng, F. Li, G. Su, H. Y. Pan, L. L. He, X. Sun, M. S. Dresselhaus, *Appl. Phys. Lett.* **1998**, *72*, 3282 – 3284.
[5] H. J. Dai, *Acc. Chem. Res.* **2002**, *35*, 1035 – 1044.
[6] A. Ural, Y. M. Li, H. J. Dai, *Appl. Phys. Lett.* **2002**, *81*, 3464 – 3466.
[7] N. R. Franklin, Q. Wang, T. W. Tombler, A. Javey, M. Shim, H. J. Dai, *Appl. Phys. Lett.* **2002**, *81*, 913 – 915.
[8] a) Y. Li, W. Kim, Y. Zhang, M. Rolandi, D. Wang, H. Dai, *J. Phys. Chem. B* **2001**, *105*, 11 424 – 11 431; b) C. L. Cheung, A. Kurtz, H. Park, C. M. Lieber, *J. Phys. Chem. B* **2002**, *106*, 2429 – 2433.
[9] S. Huang, X. Cai, J. Liu, *J. Am. Chem. Soc.* **2003**, *125*, 5636 – 5637.
[10] L. C. Qin, *J. Mater. Sci. Lett.* **1997**, *16*, 457 – 459.
[11] A. Huczko, *Appl. Phys. A* **2002**, *74*, 617 – 638.
[12] A. Y. Cao, P. M. Ajayan, G. Ramanath, *Appl. Phys. Lett.* **2003**, *83*, 356 – 358.
[13] M. Yudasaka, R. Kikuchi, Y. Ohki, E. Ota, S. Yoshimura, *Carbon* **1997**, *35*, 195 – 201.
[14] K. Suenaga, M. Yudasaka, C. Colliex, S. Ijima, *Chem. Phys. Lett.* **2000**, *316*, 365 – 372.
[15] P. I. Dosa, C. Erben, V. S. Iyer, K. P. C. Vollhardt, I. M. Wasser, *J. Am. Chem. Soc.* **1999**, *121*, 10 430 – 10 431.
[16] V. S. Iyer, K. P. C. Vollhardt, R. Wilhelm, *Angew. Chem.* **2003**, *115*, 4515 – 4519; *Angew. Chem.* **2003**, *42*, 4379 – 4383.
[17] H. Ago, K. Murata, M. Yumura, J. Yotani, S. Uemura, *Appl. Phys. Lett.* **2003**, *82*, 811 – 813.
[18] A. R. Harutyunyan, G. Chen, P. C. Eklund, *Appl. Phys. Lett.* **2003**, *82*, 4794 – 4796.

 © 2003 Wiley-VCH Verlag GmbH & Co. KGaA, Weinheim 

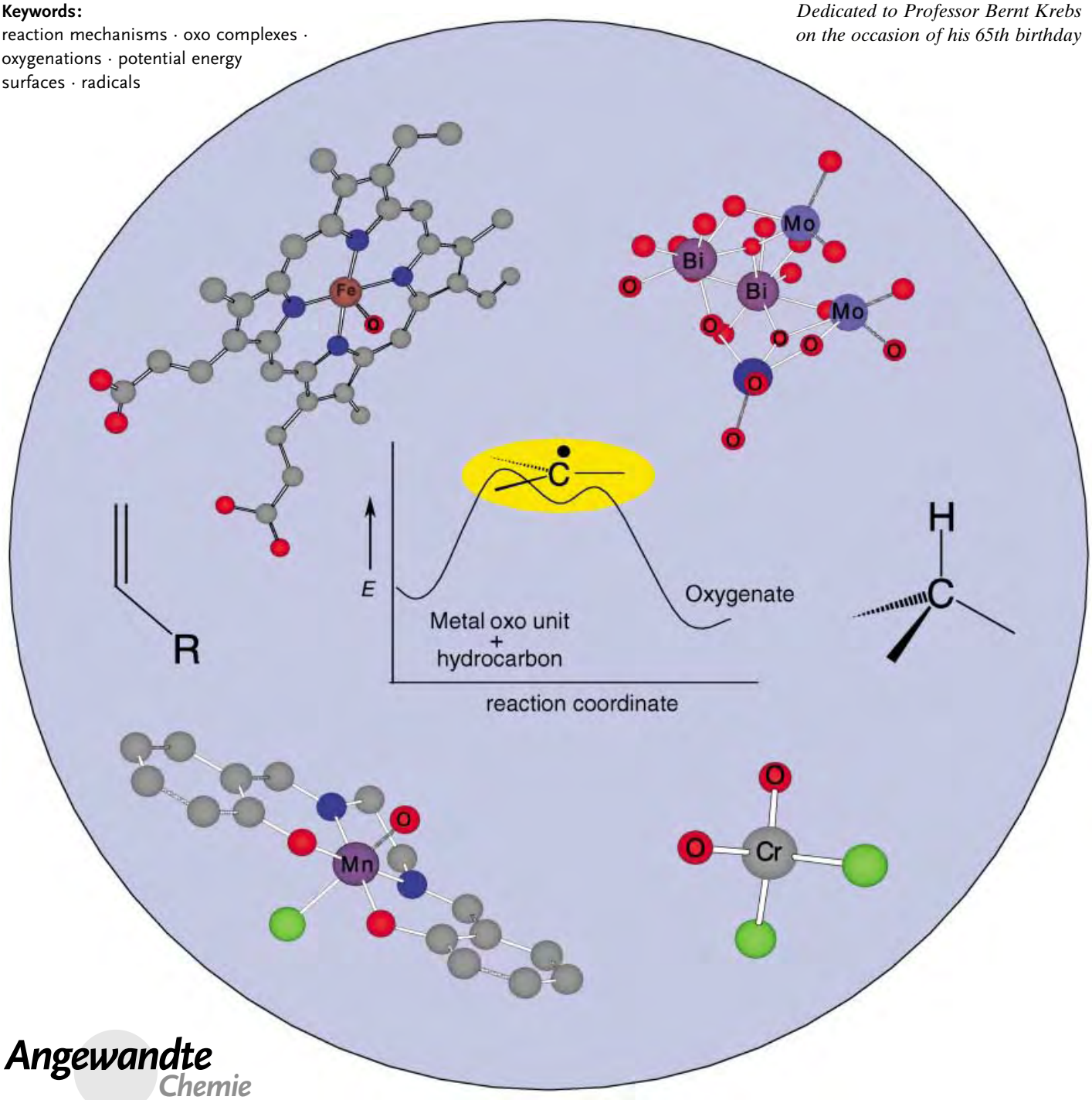
Oxygenation

# The Role of Radicals in Metal-Assisted Oxygenation Reactions

*Christian Limberg**

**Keywords:**
reaction mechanisms · oxo complexes · oxygenations · potential energy surfaces · radicals

*Dedicated to Professor Bernt Krebs on the occasion of his 65th birthday*





© 2003 Wiley-VCH Verlag GmbH & Co. KGaA, Weinheim
DOI: 10.1002/anie.200300578

*The oxo-functionalization of organic substrates with the aid of metal oxo moieties is of fundamental importance not only in nature but also in academic and industrial research. Nevertheless the corresponding reaction mechanisms remain among the most enigmatic in chemistry and few of them are understood in detail. Recent research efforts have resulted in significantly improved information: In the cases of many oxygenation reactions evidence has been provided for the occurrence radical intermediates, even though the high selectivity observed suggests to a different mechanism. Examples stem from various areas of chemistry and include processes involving molecular metal oxo complexes, gas-phase and matrix-isolated species, metalloenzymes, and solid-state oxide surfaces. This Review treats this seemingly wide variety of systems with the aim of providing an overview of common reactivity patterns and principles, as well as open problems.*

**From the Contents**

1. Introduction 5933
2. The Oxygenation of C–H Bonds 5933
3. The Oxidation of C–C Bonds 5946
4. Conclusions 5950

## 1. Introduction

The selective oxidation of hydrocarbons by homogeneous, heterogeneous, and enzymatic processes is of considerable fundamental and industrial interest,[1] because the use of hydrocarbons as feed-stocks, both in nature and in the industrial synthesis of commodity and fine chemicals, typically requires an oxidation step. The oxidation step is, in turn, usually mediated by a transition-metal compound, so that progress with regard to the preparation of valuable products will be directly facilitated by a better mechanistic understanding of how an oxidizing metal site interacts with hydrocarbons. One possible reaction pathway—the generation of radicals—represents the topic of this article.

In basically all areas of chemistry, radical-reactions are mainly thought to occur only when initialized by open-shell species, and they are usually associated with low regio- and stereoselectivities. However, recent advances made in elucidating the mechanisms of metal-mediated oxygenation reactions revealed, that both features are not necessarily concurrent in oxygenation chemistry: There are many examples of long-known reactions, that for many years were assumed to proceed by concerted mechanisms on the basis of the selectivities observed and which are now believed to in fact proceed by radical mechanisms. This review focuses on such classical systems as well as on recent examples which show that radicals are quite frequently involved in metal-mediated oxygenation processes and some of these even proceed with high selectivity. It has to be emphasized that within the space limitations such an article cannot represent a complete overview covering all literature available; it rather concentrates on representative instructive examples to highlight general trends and principles as well as common reactivity patterns and to stress open questions, problems, and possibilities for future developments.

## 2. The Oxygenation of C–H Bonds

The area of selective alkane transformations via radicals and radical cations has been the topic of a recent review;[2] this, however, concentrates mainly on reactions where the step generating the organic radical is metal-free, and it is thus complementary to the theme under discussion here.

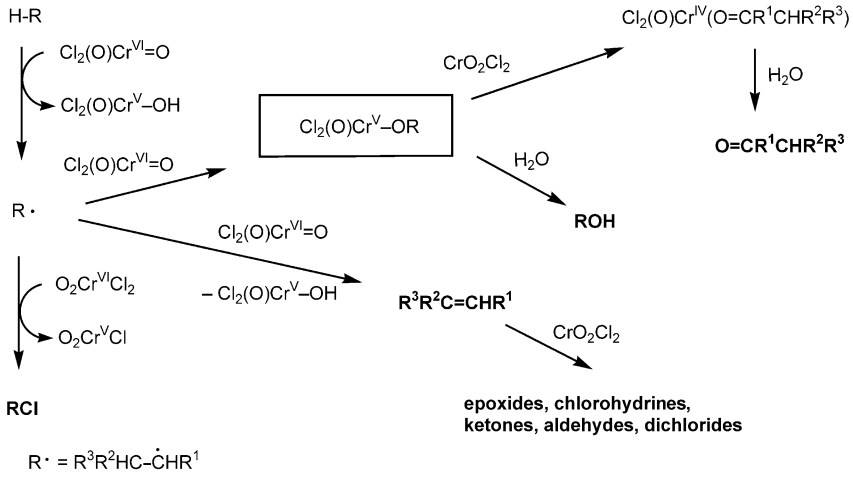
### 2.1. Molecular Oxo Complexes

#### 2.1.1. Molecular Oxo Complexes with Terminal Oxo Ligands

There are various simple metal oxo complexes that have been applied in academic research for many decades to oxofunctionalize organic residues. For instance, the oxidation of hydrocarbons by chromyl chloride, $CrO_2Cl_2$, now known as the Etard reaction,[3] was developed as early as 1877. Despite its fame, the course of this reaction and the nature of its intermediates remained unknown for more than 100 years until Mayer and Cook provided strong evidence—mainly by kinetic studies and trapping experiments—that in reactions of alkanes with chromyl chloride ($CrO_2Cl_2$) the first step consists of a proton-coupled electron transfer (PCET):[4] The addition of an electron to the Cr=O $\pi^*$ orbital significantly increases the basicity of the oxo group and—in contrast—protonation of the oxo ligand makes the complex a much stronger electron acceptor, so that, in combination, the addition of a hydrogen atom results in a strong $Cr^{V}O$–H bond. Consequently, the Cr=O functions of $CrO_2Cl_2$ are capable of abstracting aliphatic hydrogen atoms (as had been suggested by K. B. Wiberg[5]) thereby generating organic radicals, which in subsequent reactions with $CrO_2Cl_2$ (Scheme 1) give rise to the various organic oxidation products[6] (DFT studies involving chromyl chloride and methanol as a model substrates also indicate C–H bond activation by a hydrogen atom abstraction channel[7]). However, the finding of simple alcohols among the products required the assumption of an

[*] Prof. Dr. C. Limberg
Humboldt-Universität zu Berlin
Institut für Chemie
Brook-Taylor-Strasse 2, 12489 Berlin (Germany)
Fax: (+49) 30-2093-6966
E-mail: christian.limberg@chemie.hu-berlin.de

 DOI: 10.1002/anie.200300578 © 2003 Wiley-VCH Verlag GmbH & Co. KGaA, Weinheim 



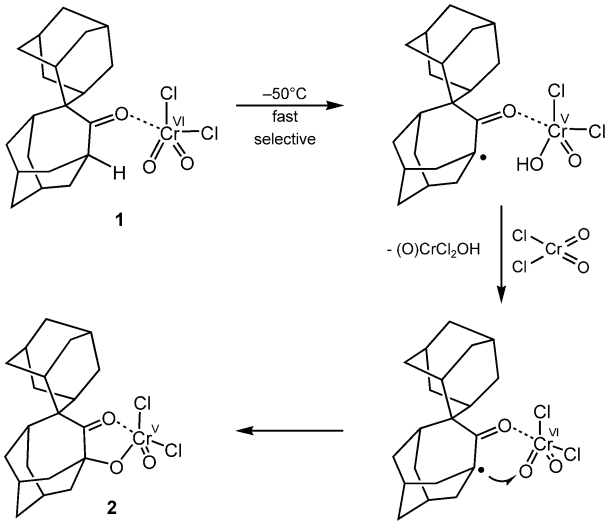

***Scheme 1.*** The oxidation of hydrocarbons with $CrO_2Cl_2$.

additional important step: Radicals resulting from the primary hydrogen-atom abstraction were proposed to add to Cr=O groups of excess $CrO_2Cl_2$ to yield $Cr^V$ alkoxides (framed in Scheme 1), which should then release the alcohols during aqueous work up.[4] Investigating the behavior of $CrO_2Cl_2$ in the presence of epoxides, we succeeded for the first time in isolating and characterizing such a $Cr^V$ alkoxide after radical trapping:[8] In contact with $CrO_2Cl_2$ tetraalkyl- or tetraaryl-substituted epoxides undergo Lewis acid catalyzed isomerizations to give the corresponding ketones. Consequently, bisadamantylidene epoxide rearranges after its complexation to $CrO_2Cl_2$ to give a spiroketone complex **1** (Scheme 2). The subsequent reaction of $CrO_2Cl_2$ with the spiroketone ligand leads to the selective cleavage of only the α-keto C–H bond finally yielding the $Cr^V$ complex **2** under very mild conditions (−50 °C). This is remarkable, since C–H activation by $CrO_2Cl_2$, as discussed above, normally proceeds (with sufficient rates) at temperatures around 70 °C and then not in a selective fashion.[4] To explain this finding, it was concluded that the rigid framework of the ketone forces the complex to adopt an arrangement where a Cr=O group of $CrO_2Cl_2$ comes to lie in close proximity to the α-keto C–H bond.[8,9] The system is thus already positioned quite high on the Hydrogen atom-transfer barrier, and consequently an increase in reactivity and selectivity is reached.



*Christian Limberg was born in 1965 in Essen and studied chemistry in Bochum. He earned his doctorate with Professor A. Haas in 1992 and concluded a postdoctoral work with Professor A. J. Downs at Oxford University with a further Ph.D. thesis in 1995. After his Habilitation with Professor G. Huttner in Heidelberg (1999) and deputizing for Professor Herrmann in the Inorganic Chemistry Chair at the TU Munich (2001) he became full professor at the Humboldt University of Berlin. His main research interest is the synthesis and reactivity of metal oxo complexes, and his awards include the Carl Duisberg prize of the German chemical Society (GDCh).*

The same principle is used in nature by the cytochromes P450: These metalloenzymes are capable of catalytically hydroxylating C–H bonds by using high valent, highly reactive (porphyrin$^{+\cdot}$)$Fe^{IV}$=O units formed in situ during the process of $O_2$ activation[10] (see Section 2.2.1). These oxygenation reactions proceed under physiological conditions with excellent selectivities, as the organic substrates are prearranged in a manner, that allows only one C–H unit to be attacked by the oxo ligand.[11] The hypothesis, that the same is true for **1**, too, was supported by DFT calculations for **1** (which is far too reactive to be studied directly):[8,9] In the thermodynamically stable geometry, the α-keto hydrogen atom is located very closely to a Cr=O unit. This conformation facilitates the intramolecular Hydrogen atom transfer which results in a radical coordi-




***Scheme 2.*** Selective hydrogen-atom abstraction and radical trapping with $CrO_2Cl_2$.

nated to the reduced metal species $HOCr^V(O)Cl_2$. Radical trapping by $HOCr^V(O)Cl_2$ has been shown for related systems not to represent a mayor reaction pathway,[4] and in line with that finding the above-mentioned reaction proceeds with the conversion of the radical/$HOCr^V(O)Cl_2$ intermediate into a radical/$CrO_2Cl_2$ complex. Finally, the addition of the radical to a $Cr^{VI}$=O unit yields a stable $Cr^V$ alkoxide **2**, which could be isolated and investigated by single-crystal X-ray analysis.[8] Its identification, which became possible because of the special advantageous geometric conditions of the substrate, provides forthright evidence on a molecular level for both radical steps discussed above; that is, $d^0$-metaloxo moieties are not only capable of abstracting hydrogen atoms to generate organic radicals, but also of trapping them again. According to Wiberg et al.[5] and Stephenson et al.,[12] who found predominant retention of configuration after oxidation of chiral hydrocarbon units, the rate of radical trapping is very high[4,13] and the process itself solvent-cage supported; Cook and Mayer

 © 2003 Wiley-VCH Verlag GmbH & Co. KGaA, Weinheim 

determined its rate as being close to the diffusion rate—independent of a solvent cage.[4] The findings summarized in Scheme 2 demonstrate that even for a reagent as reactive as $CrO_2Cl_2$ selectivity can be significantly enhanced if the substrate is preorganized in close proximity to the reactive unit, which suggests further research aimed at incorporating high-valent oxo metal centers into a ligand environment that can direct incoming substrates. Such ligand spheres might also help to prevent the aggregation of the reduced metal species after the oxidation step thereby setting a basis for the establishment of catalytic cycles.

Traditionally Hydrogen atom transfer onto oxo metal species had been rationalized based on an analogy with organic radical chemistry, that is, unpaired electron density was thought to be transferred to the oxygen atoms of the metal compounds, which are then ready to enter into radical reactions. The studies mentioned, however, established, that $CrO_2Cl_2$—a $d^0$ system having no unpaired spin density anywhere—is capable of abstracting hydrogen atoms from saturated organic systems, primarily because of the strength of the O–H bond formed in $[Cl_2(O)CrOH]$.[4,14] The reactivity of $CrO_2Cl_2$ is therefore reminiscent of that of oxygen-centered radicals, even though it is not a radical, and its reactions with alkanes can consequently be viewed as examples of "molecule-assisted homolysis", organiclike reactions in which two radicals are formed from two closed-shell molecules.[15,16] As a result of these findings a progression has occurred from thinking about radicals and spin density to an approach based on the thermochemistry of the Hydrogen atom transfer step.[14,6]

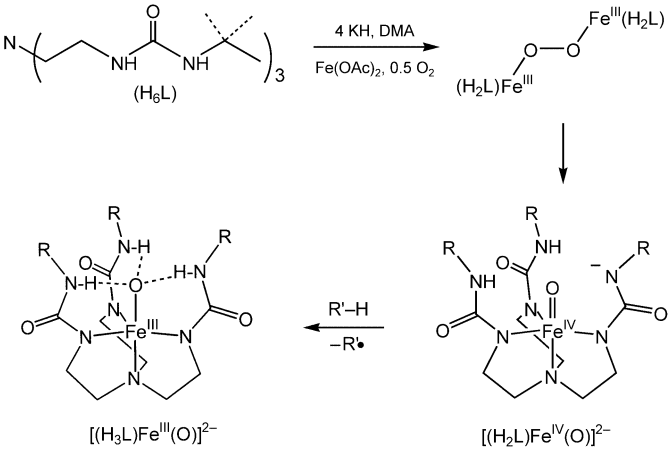
Based on this "bond-strength approach" the reinvestigation of the system $MnO_4^-$/alkyl aromatics considerably improved the understanding of the reactivity principles characteristic for permanganate oxidations: Mayer et al. showed that in aprotic organic media permanganate can abstract hydrogen atoms similarly to $CrO_2Cl_2$.[17] The energetics involved were investigated later on by means of DFT calculations.[18] The results showed, that the transition state of the $MnO_4^-$/methane system has the character of a radical ion pair, that, after its formation, collapses without a further barrier to give the ester product $HOMn^{V}O_2(OCH_3)$ [Eq. (1)].

$$MnO_4^- + CH_4 \longrightarrow [(HO)Mn^{VI}O_3^{\bullet -} / CH_3^{\bullet}]^{\ddagger} \longrightarrow (HO)MnO_2(OCH_3) \qquad (1)$$

In solution the radical pair could be envisaged to partly escape out of the solvent cage, which would explain the observation of only partial retention of configuration during alkane oxidations.[19]

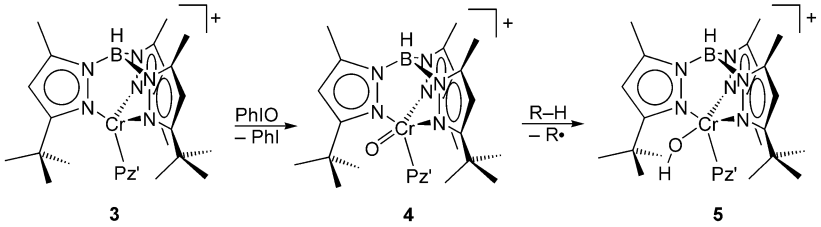
The behavior of $RuO_4$ in contact with alkanes has also been investigated thoroughly,[20] and a comparatively high reactivity has been observed. This reactivity has its origin in a low activation barrier and an early transition state, as found in DFT calculations.[21]

The importance of bond strengths in hydrogen-atom abstraction reactions is not limited to $d^0$-metal oxo complexes. The arguments are transferable to various situations, that is, in principle, any active oxo site with affinity for an electron and a proton should be able to abstract hydrogen atoms,[14] and as research of the last few years showed, this includes metal-oxide active sites in heterogeneous catalysts (see Section 2.2), active sites in metalloenzymes (see Section 2.3) as well as typical coordination complexes with partly occupied d shells that will be discussed below. In doing so attention is kept first on hydrogen-atom-abstracting complexes with terminal oxo ligands that were either formed in situ or isolated. Borovik et al. were able to isolate the iron(III) complex $[(H_3L)Fe^{III}(O)]^{2-}$ proposed to have formed by way of an oxoiron(IV) intermediate $[(H_2L)Fe^{IV}(O)]^{2-}$, that subsequently abstracted a hydrogen atom from solvent or added 9,10-dihydroanthracene. The generation of $[(H_2L)Fe^{IV}(O)]^{2-}$ is plausible, when an $Fe^{II}$ complex of the deprotonated potential ligand $H_6L$ is formed in situ and activates dioxygen to give a dinuclear peroxo bridged species, which then undergoes O–O bond homolysis (Scheme 3).[22] Another example where an




***Scheme 3.*** Proposed mechanism for the formation of $[(H_3L)Fe^{III}(O)]^{2-}$.

oxo complex (in this case well-defined) abstracts hydrogen atoms to yield the corresponding hydroxy complex was published recently: Theopold et al. succeeded in isolating the chromium(IV)oxo complex **4** after the reaction of the cation **3** (Scheme 4) with iodosyl benzene, when external hydrogen atom sources were excluded.[23] However, in the presence of any molecules with weak C–H bonds such as 1,4-hexadiene or 9,10-dihydroanthracene, **4** abstracts a hydrogen atom to give the isolable complex **5** with a $Cr^{III}$-OH unit. Similarly, the chromium(IV) complex $Cr_{aq}O^{2+}$ abstracts hydrogen atoms from $Me_3CCHO$ in aqueous solutions.[24] The observation, that this reaction proceeds 100-times faster than the corresponding one with the superoxochromium complex $Cr_{aq}OO^{2+}$ was rationalized in terms of the respective differ-



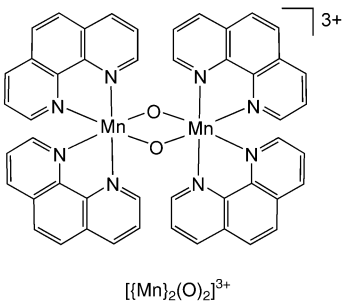

***Scheme 4.*** Synthesis of **4** and its reactivity toward R–H; Pz = 3-*tert*-butyl-5-methylpyrazole.

 © 2003 Wiley-VCH Verlag GmbH & Co. KGaA, Weinheim 

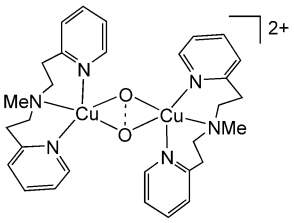
ence between the O–H bonds formed in both cases (see above). Furthermore, in close analogy to $RuO_4$, the $d^2$-complex $[Ru(O)_2(OOCMe)_4]^{2-}$ oxidizes alkanes with a product distribution that suggests hydrogen-atom abstraction by a $Ru^{VI}$=O unit as the initializing step.[25a] Very recently the results of detiled studies concerning hydrogen-atom-abstraction reactions with $[(bipy)_2(py)Ru^{IV}O]^{2+}$ were reported.[25b]

#### 2.1.2. *Molecular Oxo Complexes with other Types of Oxo- or Oxygen-Containing Ligands*

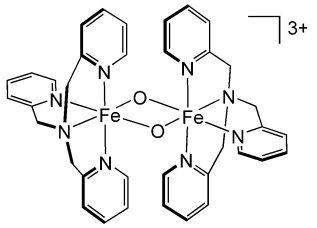
As examples of complexes containing bridging oxo ligands with oxidation capabilities bis(μ-oxo)dimanganese complexes are worth mentioning. These compounds have long been studied, particularly with regard to modeling the manganese active site of the oxygen-evolving center in photosystem II (OEC in PSII, see Section 2.2.3).[26–28] While in PSII the manganese oxo moiety is oxidized by a tyrosyl residue (until it reductively eliminates dioxygen), the reverse type of reactivity is displayed by the complexes $[(phen)_2Mn^{IV}(\mu\text{-}O)_2Mn^{III}(phen)_2](PF_6)_3$ (**$[Mn_2(O)_2]^{3+}$**, Scheme 5; phen = phenanthrolin) and $[(phen)_2Mn^{III}(\mu\text{-}O)(\mu\text{-}OH)Mn^{III}(phen)_2](PF_6)_3$ (**$[Mn_2(O)(OH)]^{3+}$**): both oxidize alkyl aromatics, namely by hydrogen-atom abstractions.[29,30] On the other hand oxidations with the highly oxidized manganese(IV) complex $[(phen)_2Mn^{IV}(\mu\text{-}O)_2Mn^{IV}(phen)_2](ClO_4)_4$ (**$[Mn_2(O)_2]^{4+}$**) proceed by a preequilibrium electron transfer or by an initial hydride transfer.[30] This poses the question, how does the oxidation state of the manganese atoms influence the reaction? The answer is straight forward: Neither **$[Mn_2(O)_2]^{3+}$** nor **$[Mn_2(O)(OH)]^{3+}$** are good outer-sphere oxidants, that is, their tendency to accept an electron is low. However, they can form strong O–H bonds and thus readily accept an electron in combination with a proton (compare the case of chromyl chloride in Section 2.1.1): Consequently, they react by hydrogen-atom abstraction. The highly oxidized **$[Mn_2(O)_2]^{4+}$**, on the other hand, is a powerful one-electron oxidant, however, **$[Mn_2(O)_2]^{3+}$** generated in such a one-electron oxidation has a very low basicity so an accompanying proton is undesired. **$[Mn_2(O)_2]^{4+}$** therefore reacts either by electron transfer or it can accept a hydride ion (a proton and two electrons) to form the stable dimer **$[Mn_2(O)(OH)]^{3+}$**. In reactions with alkyl aromatic compounds there is a large thermodynamic bias for **$[Mn_2(O)_2]^{4+}$** to accept a hydride rather than an electron.[30] Similarly to **$[Mn_2(O)_2]^{3+}$** other complexes containing $M_2(\mu_2\text{-}O)_2$ diamond cores (M = Fe,[31] Cu,[32] Ni[33]), such as, **6**[32a] and **7**[31b] (Scheme 5) have been shown to abstract hydrogen atoms either intramolecularly from their ligands or intermolecularly from added substrates. Displaying this type of reactivity, they potentially model the function of certain metalloenzymes, such as tyrosinases, oxygenases (see Section 2.2), as has very recently been reviewed for iron and copper.[34] Chen and Que obtained evidence, that high-spin iron(III) hydroperoxo species (e.g. **8** ) obtained from $[Fe^{II}(TPA)(MeCN)_2]^{2+}$ complexes (TPA = tris(2-pyridylmethyl)amine, with either two or three α-substituents) and HOOH can selectively cleave C–H bonds




$[\{Mn\}_2(O)_2]^{3+}$

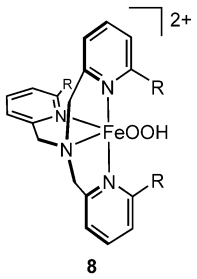



6



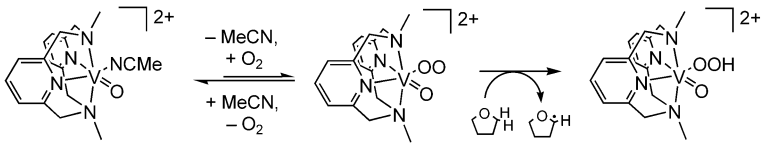

7

***Scheme 5.*** Hydrogen-atom-abstracting complexes with $\{M_2(\mu_2\text{-}O)_2\}$ diamond cores.




8

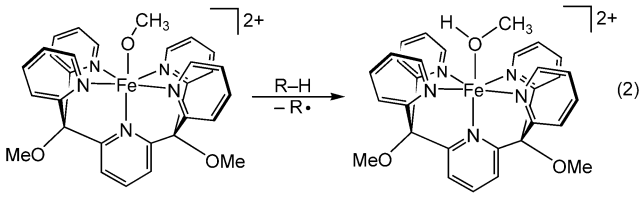
yielding alkyl radicals that epimerize or are trapped by $O_2$.[35] Not surprisingly, also $d^0M(\eta^1\text{-}O_2)$ moieties are capable of abstracting hydrogen atoms: Kelm and Krüger showed that the oxosuperoxovanadium(V) species, **9**, formed in situ from a vanadium(IV) precursor and dioxygen, abstracts hydrogen atoms from THF molecules, to yield an oxohydroperoxovanadium(V) complex **10** that is subsequently deprotonated to finally give an oxoperoxovanadium product (Scheme 6).[36]




9 10

***Scheme 6.*** Hydrogen-atom abstraction by a vanadiumsuperoxo complex.

There are also cases of metal alkoxide moieties displaying hydrogen-atom abstraction capabilities. The ferric-methoxide complex **11** [Eq. (2)], which was designed and synthesized to mimic the Lewis acidic iron site in lipoxygenases, oxidizes

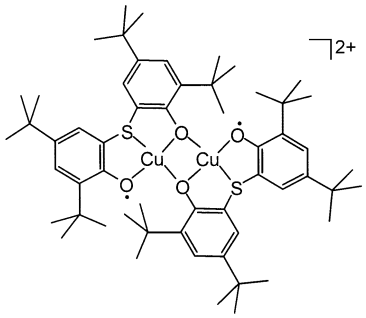



11 12 (2)

 © 2003 Wiley-VCH Verlag GmbH & Co. KGaA, Weinheim 

substrates with weak C–H bonds to yield the ferrous-methanol complex **12** in a process that is consistent with hydrogen-atom abstraction from the substrate.[37] This provided not only the first chemical precedent for the proposed rate-determining step in the mechanism of lipoxygenases but also a thermodynamic rational of why this reaction is favorable.

Another example for hydrogen-atom abstraction from an organic substrate by an alkoxide ligand (which, however, already has unpaired spin density at the oxygen atom) has been reported by Wieghardt and co-workers:[38] In the presence of $O_2$ complex **13** containing two coordinated




**13**

phenoxyl radicals is capable of catalytically oxidizing ethanol to acetaldehyde with $H_2O_2$ as a by-product. Compound **13** can thus be viewed as a functional model for the galactose oxidase. The oxidation is proposed to proceed by addition of the ethanol HO group to one of the Cu(μ-OAr) bonds, so that a copper ethanolate group is generated. The coordinated phenoxyl radical then abstracts a hydrogen atom from the ethanolate methylene group thereby producing acetaldehyde, and $O_2$ reoxidizes the complex, regenerating **13**.

#### 2.1.3. Oxo Complexes in the Gas Phase

Metal oxo cations in the gas phase typically react by non-radical pathways with the exception of species that possess radical character anyway. Radical-type reactions of this kind often have low selectivities:[39] The formally hypervalent $TiO_2^+$ ion, for instance, behaves as a typical oxygen-centered radical, as the three valence electrons of titanium cannot satisfy the needs of two oxo ligands. Thus $TiO_2^+$ is a potent reagent for bond activation and it not only activates alkanes but even abstracts a hydrogen atom from water [Eq. (3)].[40,41]

$$TiO_2^+ + H_2O \longrightarrow Ti(O)OH^+ + OH\cdot \quad (3)$$

Likewise the 4d congener $ZrO_2^+$ oxidizes in a radical-type manner[41]and the reactivity patterns of hafnium oxide cations suggest a similar behavior of $HfO_2^+$.[42] Correspondingly $MoO_3^+$[43,44] and $OsO_4^+$[45] can also be described as hypervalent with high radical character at the oxygen atoms, and therefore it is not surprising that they undergo typical radical reactions analogous to the $TiO_2^+$ ion. The $MoO_3^+$ ion is rather reactive and can even oxidize methane.[43] Most dioxide cations of lanthanide and actinide metals are either of low reactivity or show radical-type behavior.[46]

While the reactivities of the above-mentioned hypervalent species are predictable, the case of $FeO^+$ is more complicated:[47] This species has a high-spin ground state, that naturally can only undergo single-bond reactions, such as, atom abstractions and radical-type processes, as the barriers for two-bond processes (for instance bond insertions) are too high. On the low-spin potential-energy surface (PSE) these barriers are much lower so that, both single- as well as two-bond processes can occur.[39] There is an increasing number of examples (see below) providing evidence, that the reactivity of metal-oxo species is dominated by interaction of various surfaces (spin inversion, intersystem crossing), and this, in turn, means that such species do not only show the reactivity characteristic for the one electronic state, such as the ground state ("single-state reactivity" = SSR), but also the behavior of a second (excited) state differing in spin ("two-state reactivity" = TSR).[48] On this basis there are two different possibilities for a reaction of the system $FeO^+/CH_4$, one of which [Eq. (4)] consists of a hydrogen-atom transfer leading

$$FeO^+ + CH_4 \longrightarrow FeOH^+ + CH_3\cdot \quad (4)$$
$$FeO^+ + CH_4 \longrightarrow Fe^+ + CH_3OH \quad (5)$$

to the release of a methyl radical; considering the high-spin ground state of $FeO^+$ this reaction can occur by TSR or SSR. The second type of reaction [Eq. (5)] leads to $Fe^+$ and the closed-shell hydroxylation product MeOH, and as this is a two-bond process (two new covalent bonds are formed), it requires TSR (reaction on the low spin PES). At high kinetic energies the branching ratio of the two pathways is approximately 50:50, while at lower energies the process in Equation (5) is favored.[47]

Cyclopropane is the only hydrocarbon which also gives rise to the formation of open-shell neutrals upon reaction with $Fe_2O_2^+$, that is, $C_3H_5\cdot$ is formed concomitant with $Fe_2O_2H^+$; the latter ion continues to react with cyclopropane to afford $Fe_2O_2H_2^+$ by means of a second hydrogen-atom abstraction from cyclopropane.[49]

### 2.2. Biological Systems

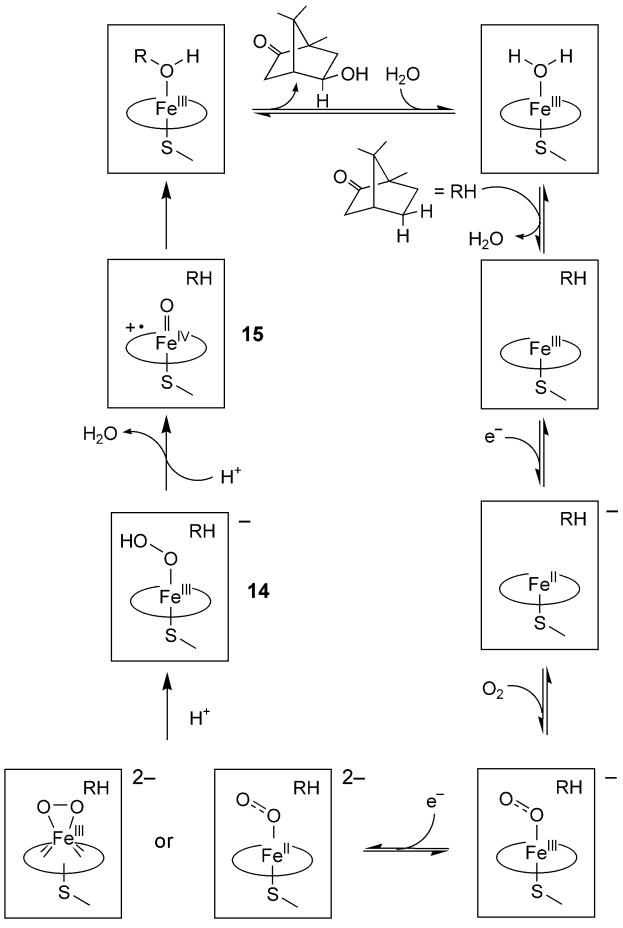
There are also a variety of biochemical processes that appear to involve one or more hydrogen-atom transfer steps, these include metal-free systems, such as the anticancer drug bleomycin and other DNA cleaving reagents,[50] but also systems where metals play decisive roles: Hydrogen-atom transfer has been implicated in the catalytic cycles of a variety of metalloenzymes, including the oxidation of fatty acids by lipoxygenases[51] (see above), the biosynthesis of dopamine,[52] and the processing of various metabolites and xenobiotics by cytochrome P450 enzymes.

#### 2.2.1. Cytochromes P450

The cytochrome P450 enzymes are ubiquitous in nature and effect numerous oxidations of physiologically important

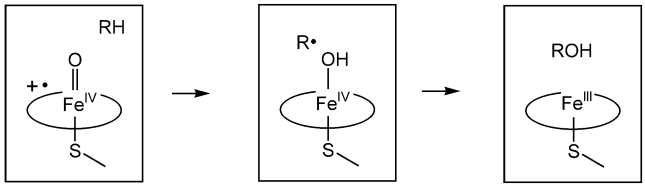
 © 2003 Wiley-VCH Verlag GmbH & Co. KGaA, Weinheim 

natural and foreign substrates. This includes the difficult hydroxylation of unactivated C–H bonds in hydrocarbons and other compounds during processes such as carcinogenesis, drug metabolism as well as the biosyntheses of steroids and lipids.[10] The prosthetic group characteristic to these enzymes is an iron(III) protoporphyrin IX complex (heme) with a thiolate from protein cysteine serving as a fifth ligand to iron. Structurally and biochemically, the best characterized P450 is $P450_{cam}$, which catalyzes the regio- and stereospecific hydroxylation of camphor. Several of the less reactive intermediates in the sequence of hydroxylation have been characterized within the last two decades spectroscopically or even structurally.[53,54] Spectral investigations that focused on the ultimate (short-lived) oxidants in the P450 catalytic cycle[54] as well as in the related nitric oxide synthase[55] have met with partial success, and recent developments in transient-state crystallographic techniques have tentatively identified this oxidant and other elusive intermediates in the reaction cycle of $P450_{cam}$.[11] Taking all the information together, the complete $P450_{cam}$ cycle can be formulated as shown in Scheme 7, and as such it should be exemplary also for other P450 enzymes: First the substrate enters the protein, where it is bound near to the prosthetic group. In the next step an electron transfer occurs reducing the iron center to the oxidation state +II, so that it can bind $O_2$. The rate-determining step is the second electron transfer, followed by a proton transfer, that yields a hydroperoxo complex **14**. Compound **14** then decomposes by heterolytic O–O bond cleavage to give an iron(IV) oxo porphyrin cation radical **15**, which is assumed to be the active electrophilic oxidant in P450, structurally similar to the intermediate "Compound I" that forms in reactions of the heme-containing peroxidase enzymes with hydrogen peroxide.[56] The iron oxo species is capable of formally inserting an oxygen atom into a C–H bond of the substrate, so that the alcohol product is finally obtained.




***Scheme 7.*** Reaction pathway of $P450_{cam}$. The frames indicate the surrounding enzyme.

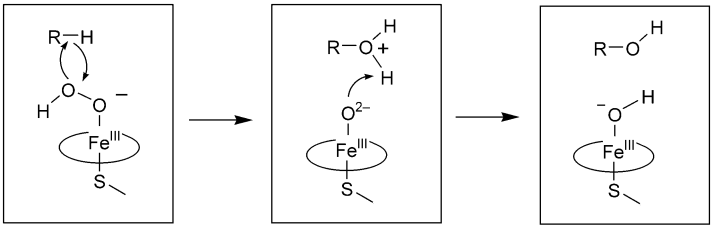
There has, however, been much debate concerning the mechanism of the last step, the hydroxylation, in P450s. A consensus view evolved over the past two decades, primarily based on the results of mechanistic probe studies and kinetic isotope effects.[10,56] This view is, that the iron-oxo species abstracts a hydrogen atom from the substrate to give an iron-hydroxy species and an alkyl radical intermediate; the alkyl radical then displaces the hydroxy ligand from iron in a process termed "oxygen-rebound" (Scheme 8, compare




***Scheme 8.*** The hydrogen-abstraction–oxygen-rebound mechanism.

ref. [10] for the historical development). Results of the past few years indicate, however, that the hydroxylation reaction is more complex than previously thought.[57] For instance, oxidations of two hypersensitive radical clock substrates (*trans*, *trans*-2-methoxy-3-phenylmethylcyclopropane and methylcubane), which undergo characteristic rearrangements allowing a differentiation between radical and cationic intermediates, were performed with wild-type and mutant P450 isozymes.[58] Evidence for cationic rearrangement products (but not for radical rearranged products) was obtained. This result led to a modified mechanistic description of P450-catalyzed hydroxylation reactions that is also consistent with the previous results.[58] The new features of this description are: 1) two electrophilic oxidants, a hydroperoxo-iron complex (**14** in Scheme 7) and an iron-oxo complex (**15**), effect hydroxylation reactions by "insertion processes" and 2) cationic rearrangements occur by insertion of $OH^+$ ions from the hydroperoxo iron species to give protonated alcohol products (Scheme 9) that can rearrange in solvolytic-type reactions. The latter would explain the mechanistic confusion from early work using probes that could not differentiate between radical and cationic intermediates.[58] On the other hand, two groups simultaneously and independently found small amounts of cation- but also putative radical-derived rearrangement products in P450 (and also soluble methane monoxygenase, see Section 2.2.2) enzyme-catalyzed hydroxylations of norcarane.[60,61] The opinions concerning this outcome differ: Newcomb, Lippard and co-workers regard

 © 2003 Wiley-VCH Verlag GmbH & Co. KGaA, Weinheim 



***Scheme 9.*** Hydroxylation withP450 cytochromes by a cationic pathway.

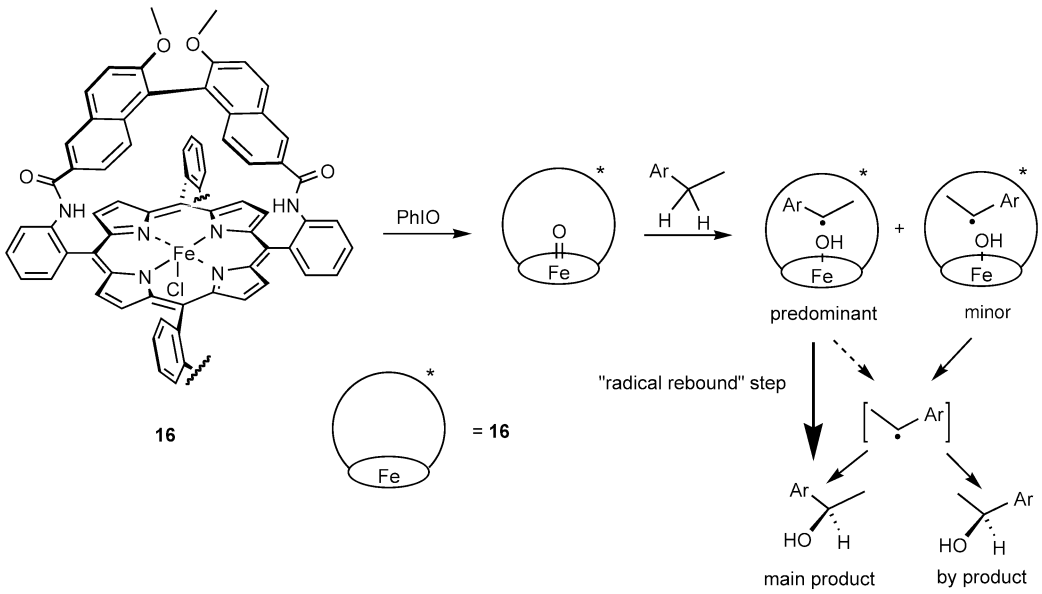
the formation of the cationic rearrangement products as consistent with the aforementioned growing consensus that some type of cation-forming reaction (such as the one depicted in Scheme 9) is possible with these enzymes and note that "formation of small amounts of the radical rearrangement product might indicate the extent of radical formation by minor pathways of the ultimate oxidants in the enzymes and it is not necessarily a measure of the radical life times in a single reaction pathway".[60] They also put forward the possibility, that the production of the radical-derived product is artificial and reflects an unappreciated aspect of norcaranyl cation chemistry.[60] However, Ortiz de Montellano, Groves, and co-workers state that the norcarane results fit well into the data obtained with related substrates and that they are consistent with a radical rebound process (radical life times of 16–52 ps were derived).[61] The cation products observed were attributed to a competing electron-transfer process and the lack of radical-rearranged products (see above) with rapidly rearranging probes was explained by steric and electronic effects.[61] An especially perceptive alternative explanation for the formation of cationic rearrangement products (and thus the lack of uniform experimental results) considers the effects of transitions between different electronic states (state crossing effects) expected in the reaction of a high-spin compound **15** and an organic substrate in analogy to the reactions of $Fe{=}O^{+}$ (Section 2.1.3); state crossing to a low-spin complex would permit insertion, whereas reaction on the high-spin PES would result in a radical pair in which oxidation of the radical to a cation was possible.[48]

The entire debate shows, that a consensus as to whether or not the classical rebound mechanism (Scheme 8) should still be regarded as *the* process responsible for hydroxylation within P450 enzymes has not been reached yet—there is not even agreement that it can serve to describe the reactivity of **15**. There is, however, general agreement that the transition state for C–H bond activation at the iron oxo species **15**, in agreement with Scheme 8, has radical character, and the key question is now whether in fact discrete radical intermediates are occurring. In this context the rebound step was recently analyzed in theoretical investigations on both the high-spin (quartet) and low-spin (doublet) potential energy surfaces, as any barrier would point to discrete radical intermediates. Such a barrier was found on the high-spin PES suggesting a finite radical life-time, while the rebound on the low-spin PES proceeds with virtually no barrier. This finding and the spin-state distribution could be an additional explanation for the confusing experimental results: The percentage of the radical rearrangement depends on the initial concentration of the radicals—as determined by the distribution of the reacting complexes with regard to the high-spin and low-spin processes—as well as the rebound barrier on the high-spin surface. The latter in turn is influenced by the polarity, acidity, and steric effects within the surroundings of the prosthetic group as well as the oxidation potential of the radical (that is, the radical life time is substrate dependent, too).[62]

Although in recent years a giant step forward has been made in understanding the reactivity principles of the P450 enzyme, several questions remain open. Is there a second (or even a third) oxidation-active species within the hydroxylation cycle? Has the hydroperoxide complex **14** oxidative power and could its protonated form (a $H_2O_2$ complex)[59,63] represent a further site where hydroxylation by radicals occurs? Beyond studies of a broader range of P450 enzymes, experimentalists might attempt to design studies to test the multistate scenario for hydroxylation[48,62,64,65] currently being addressed computationally.[57] The preparation and characterization of synthetic analogues of postulated intermediates will also play an important role, and in this context a recent report concerning the first crystal structure obtained for a $Fe^{IV}{=}O$ complex provides a source of optimism and stimulus.[66]

Additional knowledge with respect to the P450 enzymes will also facilitate the design of appropriate model complexes, that analogously realize the catalytic regio- and stereoselective functionalization of non-activated C–H bonds using $O_2$, this type of rection is of great interest in synthetic chemistry.[67] With the aim of mimicking this function of the P450 core with molecular complexes, many optically active iron porphyrin complexes have been synthesized to effect enantioselective oxygen transfer reactions, and only one particularly sophisticated and instructive example is discussed here:[69] In 1990, Groves and Viski reported the first asymmetric benzylic oxidation with iodosyl benzene using the chiral iron porphyrin complex **16** as a catalyst (Scheme 10).[70] The mechanism is envisaged as follows: PhIO transfers its oxygen atom onto complex **16** in the first step to yield the corresponding iron(IV) oxo species, which, in turn, abstracts a benzylic hydrogen atom. Owing to the chiral reaction pocket one of the two possible enantiomeric radical intermediates is enriched and this intermediate undergoes radical-rebound smoothly under retention of configuration to give the enantiomer of benzylic alcohol, that is isolated as the major product. The minor radical intermediate, however, undergoes radical decay (racemization) to a considerable extent, probably owing to the unfavorable interaction with the surrounding chiral binaphthyl bridge moiety; thereby it further enhances the enantioselectivity attained in the hydrogen-abstraction step: when tetralin was used as a substrate it even amounted to 72 % *ee* (Scheme 10).[69] On the other hand Patzelt and Woggon were the first to show, that a synthetic P450 model compound (an iron porphyrin carrying a thiolate ligand) was capable of cleaving molecular oxygen and inducing oxygen-insertion into a non-activated C–H bond (by a proposed radical mechanism).[68]

 © 2003 Wiley-VCH Verlag GmbH & Co. KGaA, Weinheim 



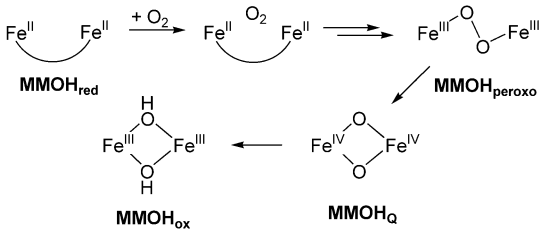

***Scheme 10.*** Asymmetric benzylic oxidation with the iron porphyrin complex **16**.[69,70]

#### 2.2.2. *The Methane Monooxygenase*

Like the P450 cytochromes, the soluble methane monooxygenase (sMMO) also catalyzes the hydroxylation of alkanes. In nature its role is the bacterial conversion of methane into methanol. However, cytochromes P450 and sMMO represent two different solutions to the problem of dioxygen activation for hydrocarbon oxidation:[71] While cytochrome P450 enzymes activate dioxygen at a Fe-porphyrin unit (Section 2.2.1), non-heme diiron centers are employed by sMMO components.[72] Dioxygen activation and methane hydroxylation by sMMO has been recently reviewed.[71] Nevertheless a brief summary of the function is given, to facilitate a subsequent focus on the oxygenation mechanism with special attention to potential radical intermediates and most recent results.[81]

The three protein components that form the soluble MMO enzyme system, MMOH, MMOR, and MMOB, have been characterized by a variety of kinetic, spectroscopic, and structural techniques. Although all of them are necessary for efficient catalysis, the dioxygen activation and substrate hydroxylation takes place at the diiron centers in the $\alpha$ subunits of MMOH (even in the absence of the other components).[71] Scheme 11 shows species in the catalytic cycle that have been detected during the single-turnover reaction of $MMOH_{red}$ with $O_2$ in the absence and presence of substrate.[73–76] Apparently, binding of dioxygen at the reduced iron(II) centers initially yields a species with a peroxo unit ($MMOH_{peroxo}$) which decomposes by either a homolytic or a heterolytic O–O bond cleavage to give $MMOH_Q$. This species has been identified in the course of spectroscopic studies as the intermediate that reacts not only with methane but also with a variety of other alkanes.[71]

How does $MMOH_Q$ hydroxylate substrate molecules? Since no intermediates have been observed for this step by using rapid-mixing spectroscopic methods, indirect methods

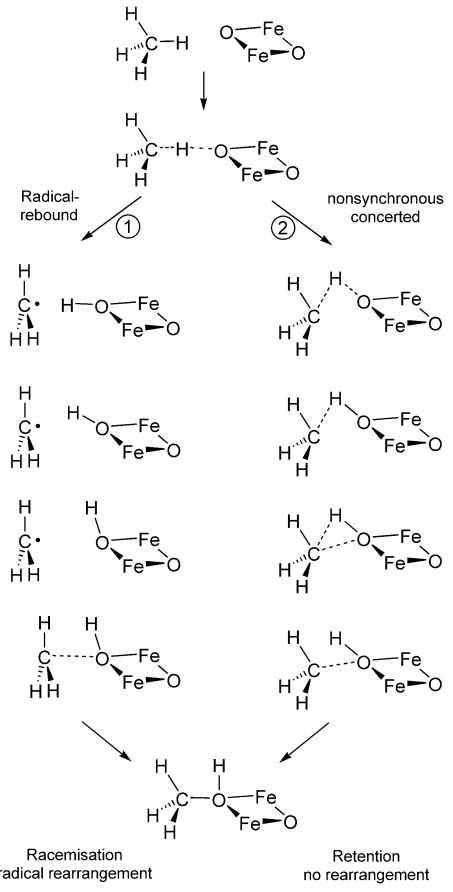



***Scheme 11.*** Overview of the intermediates observed in a single-turnover reaction of $MMOH_{red}$ with $O_2$.

have been applied to find an answer to this question. For instance, substrate probes have helped to delineate the chemical characteristics of the hydroxylation steps, which—as in the case of the P450s—could principally proceed via radical, cationic, or concerted insertion mechanisms.[81] The employment of reporter substances like enantiomerically pure [1-$^2$H, 1-$^3$H]ethane or [2-$^3$H]butane led mainly (though not completely!) to hydroxylation with retention of configuration, thus arguing against radical intermediates and for concerted insertions.[77] The results of experiments with radical clocks seemed to point to the same conclusion.[71] However, after the hydroxylation of a few substrates, which allow radical and cationic mechanisms to be distinguished (including *trans*, *trans*-2-methoxy-3-phenylmethylcyclopropane, see Section 2.2.1), beside cation-derived products also the products of radical-rearrangements were found. Furthermore, in recent studies concerning norcarane oxidation by some soluble MMOs again small amounts of radical-derived products were found[60,78] leading some researchers to conclude that both a cationic species and a discrete radical intermediate were produced (consistent with two different reaction channels for the reaction),[78] while others recommended a very careful interpretation, as mechanistic generalizations based on results with norcarane are unwarranted (see

Section 2.2.1).[60] Hence, on the basis of the experimental results currently available no clear-cut answer is possible yet.

To probe the mechanistic details, many theoretical studies[2,71,81] have been employed, too, offering different results depending on the size of the model, the assumptions made to treat the magnetic coupling between the two iron centers, and the number of ligands coordinated to the iron centers. Of these investigations only a very recent one[79] shall be mentioned here, as it employed a large-scale quantum mechanical model for the active center revealing results that are in line with most of the experimental observations made on employment of reporter substances, spin traps, and isotopically enriched substrates:[71,81] The model of $MMOH_Q$ used in this study has a bis(μ-oxo)diiron(IV) core, and the only energetically reasonable reaction pathway for methane was a straight-on approach to the bridging oxygen atom (Scheme 12). In the corresponding transition state, the hydrogen atom facing the bridging oxide is partially bound to both oxygen and carbon (Scheme 12). From this starting point two different reaction pathways were identified. Pathway 1 involves methyl radical recoil and formation of the O–H bond yielding a (μ-hydroxo)diiron center (Scheme 12, left).[79] The motion the system has to undergo to allow the methyl radical to rebound should provide time enough for racemization, which, however, could be retarded somewhat by steric clash, for instance in the case of ethane.[71,80] Pathway 2 is a nonsynchronous concerted pathway that affords methanol from the same transition state with a negligible energy barrier (Scheme 12, right). The presence of two reaction channels with comparable activation energies can explain the partial loss of configuration observed with chiral [1-$^2$H-$^3$H]ethane:[80] Products derived from the radical rebound channel (pathway 1) undergo partial racemization, while those deriving from the concerted channel (pathway 2) retain their configuration. The partitioning between these two reaction channels should be substrate dependent: Larger radical-clock substrates will favor the concerted mechanism because they have more difficulty reversing their trajectory to form a separate radical once the transition state is reached.[80]




***Scheme 12.*** A model mechanism of hydroxylation with sMMO.[71] Pathways 1 and 2 are explained in the main text.

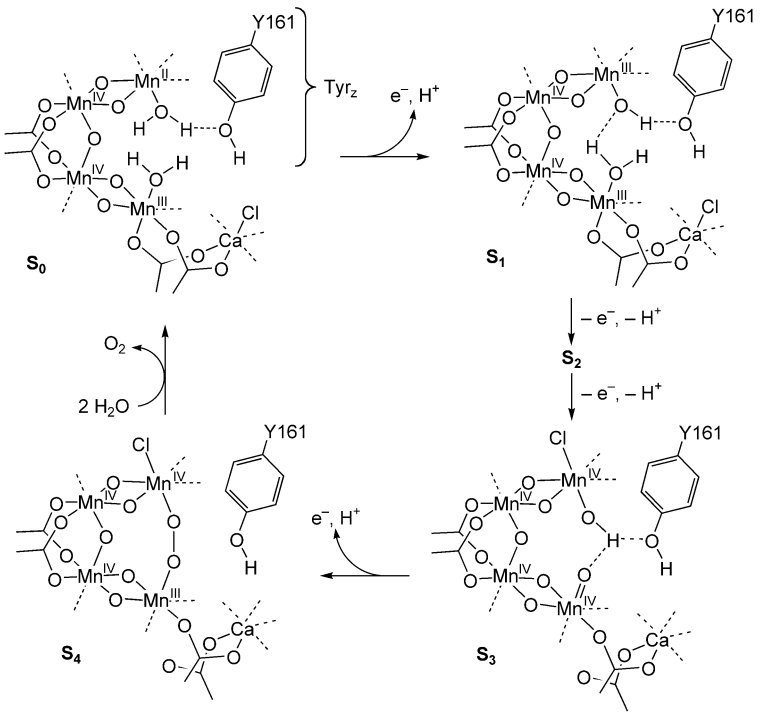
Hence, there are still many questions open also with respect to the hydroxylation mechanism of sMMO, although significant progress has been made in understanding them and instructive, plausible theories have been provided. For instance, it remains unclear, whether the reacting form of $MMOH_Q$ has indeed a bis(μ-oxo)diiron(IV) core or in fact a $Fe^{III}$-O-$Fe^{V}$(=O) structure.[34,71] Furthermore, possible spin-state crossing effects, that are currently under intense discussion for the P450 cytochromes (see Section 2.2.1), are in need of careful scrutiny.[82] An ultimate test for the current understanding of MMO catalysis would be the successful design of a synthetic MMO model that catalyzes the hydroxylation of methane with an efficiency and specificity similar to that of the native enzyme.[71]

### 2.2.3. *Oxidation of a Purely Inorganic Substrate: Hydrogen-Atom Abstraction from Water and Metalloradical Mechanisms in PSII*

The focus of this review is primarily on the radical-like reactivity of metal oxo units with organic substrates. However, it might be instructive to go briefly a little bit beyond this border to illustrate the scope the principles found might have.

Photosynthetic water oxidation to evolve dioxygen occurs at an active site of the photosystem II (the so-called OEC or oxygen evolving center) comprising four oxo-bridged manganese atoms and an oxidizable tyrosine residue ($Tyr_z$). The information available until the mid 1990s led to a mechanistic model, where the OEC was believed to serve as an electron donor to the radical cation of a chlorophyll aggregate P680 (formed in the course of light absorption), the electron transfer being mediated by the $Tyr_z$ residue. Hence the manganese oxo cluster was thought to represent a kind of charge-storage center, from which electrons are extracted by $Tyr_z$ thereby giving rise to five intermediate states from $S_0$ to $S_4$ (the Kok cycle) before reductive elimination of dioxygen occurs.[83] However, experimental and theoretical insights from several areas of chemistry and biochemistry (some of which are discussed in the preceding Sections) led to a reevaluation by Babcock et al. in 1995 and a new theory,[84] that has been modified during the ensuing years:[85,86] $Tyr_z$ (or correctly the tyrosyl radical, $Tyr_z^{\bullet}$) was proposed to oxidize the manganese complex by hydrogen-atom transfer reactions rather than by electron transfer (Scheme 13). This new role for $Tyr_z$ necessitated that the subsequent electron transfer from $Tyr_z$ to $P680^+$ is combined with a rapid loss of a proton (which is transferred ultimately to the aqueous phase), since

 © 2003 Wiley-VCH Verlag GmbH & Co. KGaA, Weinheim 




***Scheme 13.*** Proposed model of S-state cycle in the OEC of PSII[85,86], $Tyr_z^{\bullet}$ is not shown, it reacts immediately by PCET.

only that way is production of more $Tyr_z^{\bullet}$ possible ($Tyr_z^{\bullet}$ is not shown in Scheme 13, as it immediately reacts via PCET). A histidine residue, hydrogen-bonded to $Tyr_z$, was suggested to serve as the first acceptor of protons from $Tyr_z$ in this model.[86] The manganese complex consequently lost its identity as a charge storage center, and its S-state cycle is now envisaged as being essentially electrically neutral (Scheme 13):[86,87] Following Babcocks theory the $Tyr_z^{\bullet}$ abstracts hydrogen atoms from water molecules bound as terminal ligands to two of the four manganese atoms. Each loss of a hydrogen atom thus advances the substrate ligands successively from aquo to hydroxo, and ultimately, to oxo ligands. The first three oxidations of the cycle are characterized as manganese-centered, with the electrons lost being unpaired metal d electrons, while the protons are lost from the ligands. The fourth oxidation is not stabilized at manganese, but instead results directly in $O_2$ formation and release.[87] Accordingly, oxygen–oxygen bond formation occurs only during the transition from $S_3$ to $S_4$ in a radical reaction that requires direct participation of the tyrosyl radical $Tyr_z^{\bullet}$. Especially this last step ($S_3 \rightarrow S_4$) can be rationalized on the grounds of the chemistry displayed by molecular metal oxo complexes (see Section 2.1.1). In detail the Babcock mechanism envisions that a manganese-bound OH group is attacked simultaneously by electrophilic $Tyr_z^{\bullet}$ (which abstracts the hydrogen atom) and by the electron-rich oxygen center of a $O{=}Mn^{IV}$ species, which is suggested to act as an efficient radical trap within the same site, to form the O–O single bond (a crucial function of the manganese complex is thus also to bind the two substrate ligands in a geometry that will promote O–O bond formation). In proposing this idea, reference was made to radical-trapping reactions exhibited by $MnO_4^-$ and $CrO_2Cl_2$,[87] as carbon-centered radicals react with these reagents at diffusion-controlled rates (see Section 2.1.1). Similar radical-trapping reactions are discussed for hydroxylations with cytochromes P450 ("rebound mechanism", see Section 2.2.1), where it is a $Fe^{IV}$-OH group to which the organic radical adds, which demonstrates that a doubly bonded ligand is not essential for radical trapping. Passing from C- to O-centered radicals, there is evidence that analogous reactions exist. For instance, the permanganate ion releases $O_2$ upon illumination.[88] This reaction starts with a ligand-to-metal charge-transfer excitation, which converts an oxo ligand into a radical oxyl ligand. The oxyl radical then can add to a "normal" oxo ligand to make the new O–O single bond. Theoretical considerations also support the plausibility of a radical mechanism of O–O bond-formation in PSII.[89]

The Babcock model (which is supported by other experimental results, not mentioned here)[84–87] is different from previous models in that 1) for the oxidation of water to dioxygen it employs minimal structural changes of the manganese cluster and 2) thermodynamically it is based just on bond enthalpy considerations. However, it invokes large-scale movement of the $Cl^-$ ions and other than assistance in binding the chloride it has no clear essential function for $Ca^{2+}$, particularly in the lower S states.[83] Furthermore, the recent successes of X-ray crystallographic investigations with respect to the structure of PSII revealed that the arrangement of the Mn ions resembles a "Y" (i.e. a 3+1 geometry) and $Tyr_z$ is located 7–8 Å apart from the manganese oxo cluster,[90] so that a further refinement of the model seems appropriate. A water network might be located between the tyrosine and the manganese cluster, and a transfer of several hydrogen nuclei along a hydrogen-bonded chain connecting the tyrosine radical with the manganese cluster (in form of a PCET) could be envisaged.[91] There may, in fact, be a good reason for the two oxidants not to be too close to each other: The oxidized manganese cluster in the $S_3$ state should be a radical trap, but it should not be allowed to trap the tyrosine radical.[92] Irrespective of these open questions, the hydrogen-atom transfer mechanism is an appealing idea supported by the reasonable thermodynamic differences of bond enthalpies as well as functional analogies in molecular chemistry.[83]

### 2.3. Heterogeneous Systems

The general features and reaction steps of oxidation catalysis mechanisms on surfaces can still, in many cases, be regarded as poorly defined,[93] which may in part be due to the difficulties encountered during characterization of reaction intermediates on surfaces.[94] Heterogeneous catalysts for oxidation reactions thus sometimes have to be regarded as "black boxes": Reactants are injected and products are formed in good yields with good selectivities, but a complete understanding of the origin of the catalytic behavior is not yet available. In many instances, however, evidence for radical intermediates has accumulated.

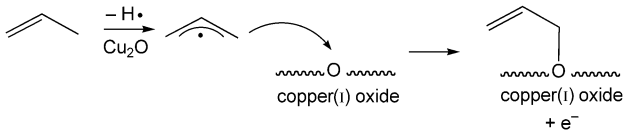
 © 2003 Wiley-VCH Verlag GmbH & Co. KGaA, Weinheim 

### 2.3.1. The Allylic Oxidation of Propylene

Adams and co-workers were the first to discover that copper(I) oxide is a selective catalyst for the oxidation of unsaturated hydrocarbons,[95,96] and one of the more useful reactions is the formation of acrolein from propene[95] at temperatures between 300 and 400 °C with a 10–12% conversion to acrolein and a 60–85% selectivity [Eq. (6)].[97]

$$\mathbf{CH_3}\text{–}CH{=}CH_2 + O_2 \xrightarrow{300\text{–}400\,^\circ C,\ Cu_2O} \mathbf{O{=}CH}\text{–}CH{=}CH_2 + H_2O \qquad (6)$$

This finding marked the beginning of the current process of catalytic olefin oxidation to aldehydes over metal oxide surfaces.[98] In 1959 Shell began producing acrolein by the gas-phase oxidation of propene over a copper(I) oxide catalyst,[100] although the catalysts performance was very poor at that time. Heterogeneous oxidation catalysis on copper oxide surfaces has received significant attention since then, and research on understanding the nature of the copper oxide catalyst has focused on the oxidation state and form of the catalytically active copper oxide as well as on the mechanism for the formation of acrolein from propene including the rates of the various reaction steps. It has become clear that $Cu_2O$ is an efficient catalyst in the partial oxidation of propene to acrolein, while propene oxidation on CuO leads to complete combustion.[93] Recently, the interaction of propene with copper(I) and copper(II) oxide at elevated temperature and elevated pressure has been investigated with core level X-ray photoemission spectroscopy (XPS), resonant photoemission, and temperature-programmed desorption.[93] It was found that the reaction of both oxides at lower temperatures produces a surface intermediate which exhibits XPS peaks for carbon 1s consistent with an allyl alkoxide surface species (Scheme 14). This result indicates a reaction mechanism

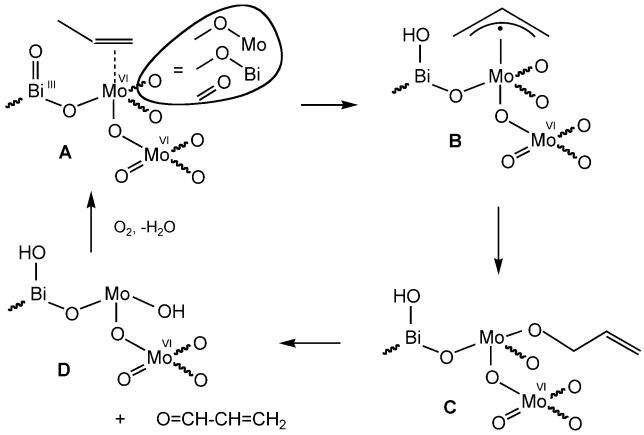



***Scheme 14.*** Model for the formation of allyloxy moieties on copper(I) oxide surfaces.

involving an initial hydrogen-atom abstraction from propene followed by rapid oxide insertion. The initial hydrogen-atom abstraction has been extensively investigated also through isotopic labeling studies, and it was found to be rate-determining step of the oxidation process.[99] The presence of a significant amount of the aforementioned surface alkoxide is consistent with a relatively slow alkoxide decomposition step yielding acrolein.

In 1957 Standard Oil of Ohio (SOHIO) discovered the $MoO_3/Bi_2O_3$ catalyst system, which yielded a fairly good selectivity but still a low propene conversion. In the ensuing decades catalyst performance has been significantly improved (bismuth and molybdenum are still essential components of the modern commercial catalysts, which, however, also contain metal oxide additives), and at present the maximum acrolein yield at high propene conversion (90–95%) using commercial catalysts is approximately 80% in average.[100] Hence, despite the long history of the process an improvement of the selectivity is still desirable, as the production capacities of acrolein are high. However, the exact role of the oxides employed is still not understood in detail making their targeted replacement to give catalysts capable of reaching higher selectivities difficult.

Scheme 15 summarizes some of the mechanistic proposals made in the 1980s on the basis of results from experiments with isotopically labeled substrates and spectroscopic inves-



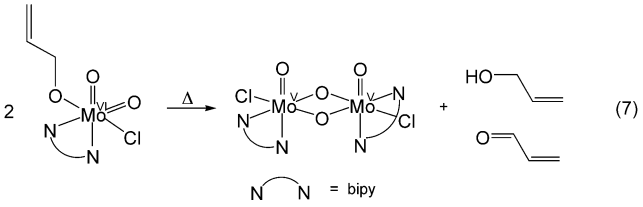

***Scheme 15.*** Mechanistic proposals for the oxidation of propene on bismuth molybdates.

tigations.[101] It is assumed that propene is initially coordinated/chemisorbed at the catalysts surface, followed by a rate-determining step (similar to the copper oxide system (Scheme 14)), in which a hydrogen atom is abstracted—presumably by a bismuth oxo unit. This step leads to an allyl radical, which is symmetrically $\eta^3$ $\pi$ bound at a molybdenum center before it is trapped in a fast subsequent step, thus again organic radicals are trapped by highly oxidized metal oxo moieties, as discussed in Sections 2.1 and 2.2. Early work[101] assigned terminal oxo ligands the role of the trapping site and this theory is still discussed today.[101,102] The results of more recent work,[103] however, also raised the alternative idea, that in heterogeneous oxidation catalysis with $MoO_3/Bi_2O_3$ ($\alpha$-$[Bi_2MoO_6]$) bridging oxo ligands or terminal ligands being in close contact to a second metal might be the ones responsible for oxygenation, that is, the allyl radical would then be trapped by a $\mu$-oxo-type group at the metal. In any case, a subsequent second hydrogen-atom transfer, probably to a Mo=O group, finally yields acrolein, and oxidation of the reduced catalyst with $O_2$ and elimination of water regenerates the starting situation.

As the occurring short-lived intermediates (such as **A**–**D**, Scheme 15) are part of the bismuthmolybdate surface, their

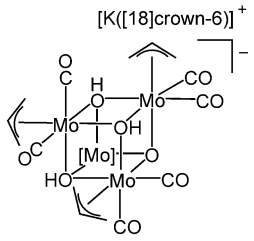
 © 2003 Wiley-VCH Verlag GmbH & Co. KGaA, Weinheim 

direct identification and investigation is difficult. However, attempts have been made to support the mechanistic postulates by studying related molecular complexes. For instance, model complexes for species **C** have been prepared by Osborn and co-workers which on warming indeed decompose to give acrolein [Eq. (7)].[104]




(7)

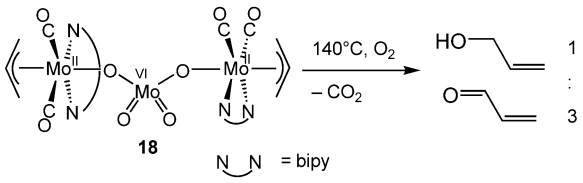
Even the initial formation of a species **A** (Scheme 15) nowadays seems plausible, as several cases have been reported, where coordination of an olefin to a $d^0$ metal center has been demonstrated.[105] In addition, studies in solution have shown that O=$Mo^{IV}$ units can bind olefins,[106] and interactions of olefins with O=$Mo^{V}$ moieties have also been observed.[107] Only recently, it has been reported[108] that bismuth alkoxides, $Bi(OR)_3$, with bulky ligands (R = 2,6-di-*tert*-butylphenyl) decompose by homolytic Bi–O bond cleavage yielding unstable $Bi^{II}$ radicals, as proposed in the hydrogen-atom abstraction from propylene (**A**→**B**; Scheme 15). However, models for surface intermediates such as **B**, which according to the mechanism in Scheme 15 should decompose to give allyloxymolybdenum complexes, are not known to date. This situation does not seem surprising as **B** was often termed "radical-like π-allylmolybdenum complex",[101] which could mean two things (and thus a formal assignment of oxidation states in Scheme 15 has been avoided): it could be formulated as a chemisorbed radical, weakly bound to a $Mo^{VI}$ center. Alternatively, it is discussed, that the electron that is transferred together with a proton onto the Bi=O group, "flows back" to the Mo center thereby lowering the oxidation state of the molybdenum center to +v. This Mo center is proposed to subsequently form an $\eta^3$ complex with the allyl radical, although the electron-deficient metal center is barely able to stabilize such an allylmolybdenum unit through back bonding. However, considering the rapidly developing organometallic chemistry of metals in high oxidation states,[109] the occurrence of an intermediate with a π-allyl ligand bound to a $Mo^{VI}$ center under catalytic conditions seems today not as unrealistic as at the time it was first mentioned. Compounds designed to model these intermediates structurally or functionally should contain a π-allyl molybdenum group covalently bound to an oxo ligand as a minimum requirement, and recently we have prepared the first two precedent cases for complexes, fulfilling this requirement.[110,111] Compound **17** contains—in form of a $\{Mo_4(\mu\text{-}OH)_3(\mu\text{-}O)\}$ moiety—an oxomolybdenum core with allyl ligands bound at the surface. Studies showed that **17** is very fluxional in solution:[110] The allyl molybdenum moieties rotate in the planes formed by the three oxygen donor centers, and this might give an impression, how mobile such units could be on the surfaces of molybdenum oxide solids. While **17** can thus be viewed as a




**17**

structural model for **B** (Scheme 15), its molybdenum atoms are all in the oxidation states +II and thus lower than those discussed for the corresponding centers in **B**. It is probably this detail which makes the isolation of **17** possible, while **B** rapidly decomposes by an allyl shift.

To synthesize model complexes which are somewhat more authentic, the following strategy was followed: allyl molybdenum units were connected to $Mo^{VI}$ centers by oxo ligands, as this could be imagined to result in a weakening of the allyl–molybdenum bonds, which in this form are easily cleaved homolytically, for instance by warming. Hence, this type of construction was anticipated to be capable of artificially providing a situation comparable to the one of **B**, and **18** [Eq. (8)] is an example of a compound containing such a moiety (oxo bridges between allyl molybdenum units and a $Mo^{VI}$ center).[111]




**18**

(8)

The $Mo^{VI}$ center in **18** enhances the model character in comparison to **17** and indeed on warming **18** generates allyl radicals, which, however, are not trapped by the oxo ligands, instead they abstract hydrogen atoms to yield propene. However, it is advisable not to draw immediate conclusions from this finding to the mechanism of the propene oxidation during the SOHIO process, since—although the constitution of the model is acceptable—there remains a topological problem: on the catalysts surface the allyl and oxo groups are in close proximity, in **18** they are a long way apart, so that competing reaction paths gain in importance. However, with **18** it is possible to generate neighboring allyl and oxo groups in situ by warming in the presence of $O_2$. For metal carbonyl compounds these conditions lead to the oxidation of the CO ligands to $CO_2$ and thus replacement of CO by $O^{2-}$ ions.[112] These $O^{2-}$ ions increase the oxidation state of the metal center, whichc in the case of a metal allyl compound is accompanied by production of allyl radicals. Thus allyl molybdenum carbonyl complexes in a dioxygen atmosphere can act, in principle, as sources for both allyl radicals and high-

 © 2003 Wiley-VCH Verlag GmbH & Co. KGaA, Weinheim 

valent molybdenum oxo species. Thermolysis of **18** in the presence of $O_2$ yielded not only allyl alcohol but also acrolein as the volatile products. Thus, not only the generation and trapping of allyl radicals has been achieved, but also a reaction in analogy to the subsequent step **B**→**C** (Scheme 15), a hydrogen-atom abstraction to give acrolein. Hence, a molybdenum compound such as **18** is already capable of mimicking the last two steps of the mechanism in Scheme 15. Naturally, it cannot model the rate-determining first step, of the SOHIO process which undoubtedly proceeds at bismuth oxo units. It would be very informative to gain access to molecular Mo/O/Bi compounds, and first steps in this direction have been taken.[113]

#### 2.3.2. *The Oxidation of Methane*

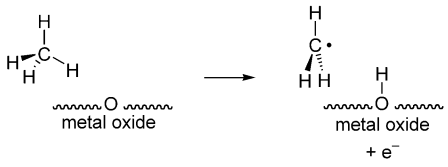
The rate-determining step of the propene oxidation—hydrogen-atom abstraction—plays the decisive role in the heterogeneous oxygenation of methane, too (also compare the case of sMMO, see Section 2.2.2). A wide variety of heterogeneous catalysts for $O_2$ oxidation of $CH_4$ has been described, which are able to formally abstract a hydrogen atom from methane to give gas-phase radicals. These recombine to form ethane[114,115] and after subsequent dehydrogenation, ethene can be obtained [Eq. (9)]. The catalyst is regenerated by oxidation with $O_2$.

The more active catalysts can be divided into five groups:

a) strongly basic, pure oxides, of which the oxides of the lighter lanthanides show the best properties
b) alkaline- and alkaline-earth metal ions supported on basic oxides
c) single-phase oxides
d) some transition-metal oxides containing alkali metal ions
e) any of these materials activated by chloride ions.[114]

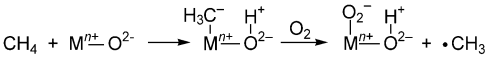
$$CH_4 + O_2 \rightleftharpoons C_2H_4 + 2\,H_2O \quad \Delta H = -67\ \text{kcal mol}^{-1} \tag{9}$$

A question, which is the subject of controversy discussed—also in this area—concerns the mechanism of C–H activation. A reduced surface oxide center having radical character has been invoked to explain the hydrogen-atom abstraction. However, in view of the results described in Section 2.1.1, the presence of an oxo ligand with radical character is not necessary for an efficient hydrogen-atom abstraction, if it proceeds as a PCET:[116] Incipient proton loss from $CH_4$ facilitates electron transfer because the resulting $CH_3^-$ carbanion gives up an electron more readily. The proton acceptor and the electron acceptor could be separate centers within the same oxide, that is, although it causes net hydrogen-atom loss, the oxide does not have to contain radical sites [Eq. (10)].




(10)

As increasing the basicity of the catalysts in some cases increases the rate of $C_2$-product formation[118] it has been proposed alternatively that the C–H-bonds are cleaved heterolytically according to Equation (11), where $CH_4$ functions as a Lewis acid.[117,118]



(11)

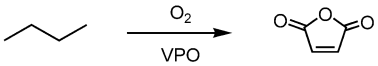
Instructive in this respect are the results of a study by Lunsford and co-workers on a Ba/MgO catalyst.[119] This catalyst apparently contains at least two types of active centers on the surface, the more basic type is indeed capable of heterolytically cleaving the C–H bonds. These, however, are poisoned under the standard conditions of oxidative coupling by $CO_2$. The less basic centers can "only" catalyze the homolysis of the C–H bonds, thereby directly generating methyl radicals that finally form ethane.

On redox-active catalysts (e.g. $MoO_3/SiO_2$), partial methane oxidation yields MeOH and HCHO.[115,120] Reasonable yields can be obtained, but at a very low conversion. Methyl radicals are again proposed as the key intermediates being trapped by surface oxide species to give metal methoxide moieties. These can be converted into methanol by hydrolysis or formaldehyde by hydride transfer to the surface.[120]

While research in the area of oxidative coupling and oxygenation of methane brought about insights in interesting homogenous and heterogeneous radical reactions, to date it has not resulted in a commercial process (a pilot plants exist, though).[121] This situation is not much different for the industrial oxidation of other alkanes: There is only one heterogeneously catalyzed, alkane-selective oxidation reaction in commercial use,[121] which is discussed in the subsequent section.

#### 2.3.3. *The n-Butane Oxidation Catalyzed by Vanadium Phosphates to give Maleic Anhydride*

Maleic anhydride, a precursor to polyester resins, is made industrially by oxidation of *n*-butane over vanadium phosphate catalysts [VPO, Eq. (12)].[123]

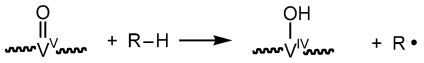



(12)

VPO catalysts are redox-active (as are $MoO_3$ catalysts, see Section 2.3.2), consequently in the course of oxidations on their surfaces, metal centers in varying oxidation states can be found, each playing a different role in the reaction mechanism. To clarify the role of $V^V$ in the butane oxidation on VPO catalysts, time-resolved in situ X-ray absorption spectroscopy has been applied.[122] The results show that when either α-$VOPO_4/SiO_2$ or $(VO)_2P_2O_7/SiO_2$ catalysts are exposed to *n*-butane, the rate of maleic anhydride formation is proportional to the rate of decrease in the concentration of $V^V$ species in the catalyst. Thus $V^V$ species are kinetically


© 2003 Wiley-VCH Verlag GmbH & Co. KGaA, Weinheim

significant for the production of maleic anhydride and not just for the production of by-products. Instead, $V^{IV}$ sites appear to be responsible for by-product formation. The results also suggest that $V^{V}$ species may play a vital role in the initial hydrogen-atom abstraction from *n*-butane. Analogous to the hydrogen-atom abstraction for $d^0$-metaloxo compounds (Section 2.1.1), this rate determining step could be formulated as a PCET to a $O{=}V^{V}$ site [Eq. (13)].



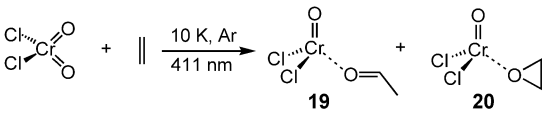

(13)

## 3. The Oxidation of C–C Bonds

In Section 2 it has been shown that metal oxo functions—independently of their d-electron count and environment—are capable of homolytically cleaving C–H bonds by hydrogen-atom abstraction, when this is thermodynamically favorable, that is, when a strong O–H bond is formed. In consequence, it should also be possible that M=O groups homolytically cleave C=C π bonds in olefins, and there is now evidence that many epoxidations proceed this way. The necessary condition is, that the thermochemistry is favorable, which means that the MO–C bond formed in the course of the M=O attack at the carbon center of an unsaturated bond must be sufficiently strong. Addition of an organic radical to a M=O group is indeed likely to be very exothermic in many cases,[4b] and the energy released should be of comparable magnitude as the π-bonding energy lost.

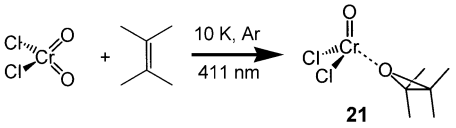
### 3.1. Simple Stoichiometric Reagents

To investigate the early stages of the oxidation of ethene by $CrO_2Cl_2$ at very low temperatures and to obtain direct information about primary and secondary intermediates we have successfully employed matrix isolation techniques: If the activation energy necessary to trigger the reaction in argon at 10 K is provided by means of irradiation, the species **19** and, **20**, are formed [Eq. (14)].[124,125]



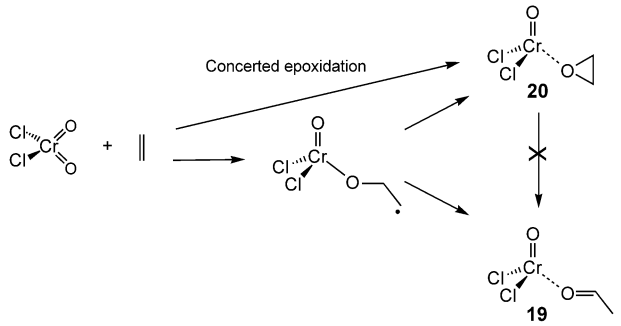

(14)

The extension of this matrix study to substituted olefins[125] yielded additional mechanistic information: the epoxidation proceeds stereoselectively as a *cis* addition and carbonylation occurs regioselectively at the least substituted carbon atom. Furthermore an increase of the degree of methylation at the olefinic bond appeared to decrease the yield of the corresponding carbonyl compound relative to the epoxide. Hence the oxidation of tetramethylethylene leads selectively to the epoxide complex **21** [Eq. (15)].[125]




(15)

The epoxide complexes were found to be photolytically stable which excludes the possibility that the complexes of the carbonyl compounds are generated by rearrangement of them. Thus, both types of species are generated by independent routes. In principle they can be envisaged to form via a common primary product, one possible candidate is a radical intermediate or transition state formed by homolysis of the π bond (Scheme 16). This intermediate could yield either the



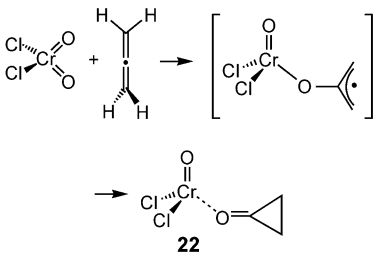

***Scheme 16.*** Product formation in the photolytic oxygenation of ethene by chromyl chloride in an argon matrix at 10 K.

observed carbonyl compounds after a 1,2-H migration (the activation barriers for this process can be easily crossed under the photolytic conditions) or the epoxide complexes after trapping by the alkoxidic oxygen atom. With higher olefins, the most-stable radicals should be formed initially, which accounts for the regioselectivity found for the carbonylations. The limited space and rigidity within the matrix could explain the selective *cis* epoxidation (for a *trans* oxo addition a rotation around the C–C bond would have to occur first). The *cis* selectivity could also hint at a second nonradical oxygenation pathway in which the epoxidation proceeds in a concerted step, but this is difficult to clarify.[6]

The occurrence of intermediate radical species in at least one of the pathways is supported by the results of experiments where alkynes and allene were used as substrates: Photolytically activated, matrix-isolated $CrO_2Cl_2$ reacts with alkynes to yield complexes of the type $[O{=}CrCl_2(\eta^1\text{-}O{=}C{=}CR_2)]$ (R = H, Me) featuring ketene ligands in a $\eta^1$-coordination mode which is unprecedented in structurally characterized compounds,[126] and the oxidation of allene yields the cyclopropanone complex **22** [Eq. (16)].[126]

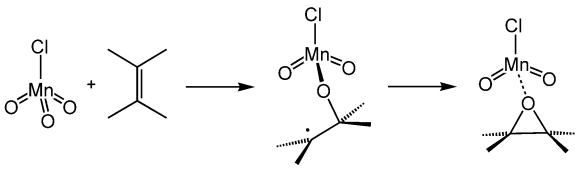
The formation of **22** provides strong evidence for the hypothesis of a π-bond homolysis initiated by the attack of $CrO_2Cl_2$ at the unsaturated bonds leading to radical intermediates in the matrices. These results with $CrO_2Cl_2$ were obtained under photolytic conditions, so that it is not entirely clear, whether or not it is an excited state of $CrO_2Cl_2$ that reacts and shows the behavior observed.[6] The system $MnO_3Cl$/olefin could be investigated in the absence of

 © 2003 Wiley-VCH Verlag GmbH & Co. KGaA, Weinheim 



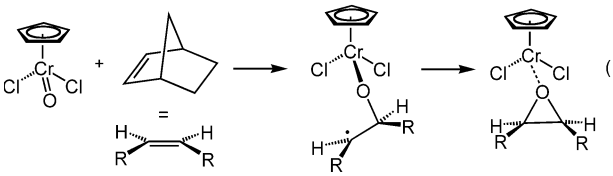
(16)

irradiation, so that it was possible to examine the ground-state reactivity.[127] It was found that in the reaction of tetramethylethylene with $MnO_3Cl$, the transition state undergoes a spin crossover from the singlet potential-energy surface (PES) to the triplet PES, on which a local minimum is reached, which corresponds to a β-alkoxide radical [Eq. (17)]. The carbon-centered radical is then trapped by the alkoxidic oxygen atom to finally yield the corresponding epoxide complex.[127]



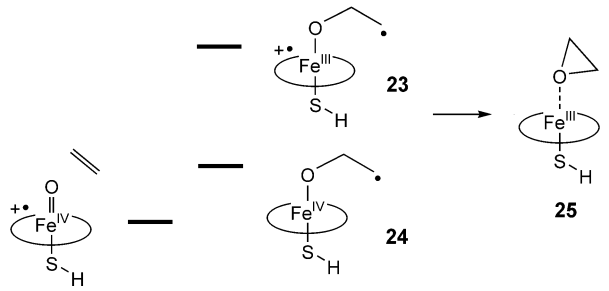
(17)

A behavior very similar to the one displayed by $MnO_3Cl$ is exhibited by $[CpCrOCl_2]$ ($Cp = C_5H_5$) in its reactions with olefins, such as norbornene [Eq. (18)]. The systems reacts starting from the doublet state, reaches a local minimum corresponding to a β-alkoxide radical, which after a spin crossover to the quartet PES, produces the epoxide complex.[128]



(18)

What holds true in the laboratory should proceed similarly in nature and indeed recent investigations in this respect support this hypothesis. Cytochrome P450 enzymes represent efficient catalysts not only for the oxidation of saturated hydrocarbons (as outlined in Section 2.2.1) but also for olefin epoxidation, and DFT calculations concerning the epoxidation of ethene by a representative model for the reactive, oxidizing intermediates in the calalytic cycles of these metalloenzymes, point to radical intermediates, two-state reactivity (TSR), and multiple valence tautomeric species, that is, "multi-state epoxidation":[129] In line with experimental results obtained with molecular models,[130,131,10] that support a stepwise mechanism involving some kind of intermediate, Shaik and co-workers found the reaction to proceed through TSR in stepwise and/or effectively concerted manners. The reactant studied was an (oxo)iron(IV) porphyrin cation radical complex with two closely lying spin states (quartet and doublet), both of which react with ethene to form intermediate complexes with a covalent C–O bond and a carbon-centered radical (radical intermediates).[129] These quartet and doublet radical intermediates additionally exist in two valence tautomeric forms that differ in the oxidation state of iron: $[(porphyrin)^{+\bullet}Fe^{III}OCH_2CH_2^{\bullet}]$ (**23**) and $[(porphyrin)Fe^{IV}OCH_2CH_2^{\bullet}]$ (**24**; Scheme 17). While the doublet spin



***Scheme 17.*** Epoxidation of ethene with a P450 model complex via radical intermediates; the horizontal bars indicate qualitatively the energetic arrangement of the intermediates that lead to **25** on either a doublet or quartet potential-energy surface.

radicals collapse to the corresponding (porphyrin)$Fe^{III}$ epoxide complex **25** with virtually no barriers (equivalent to a concerted mechanism on the doublet surface), the quartet spin intermediates have substantial barriers for this transformation, and consequently, the lifetimes of the radical intermediates are much longer on the quartet than on the doublet spin surface. Any loss of stereochemical information on the way to the epoxides as well as rearrangements to other products should arise therefore mostly, if not only, from the quartet processes, and within these processes mainly from the isomers of the type **23** that have substantially higher barriers for the transformation into the epoxide complexes, than the valence tautomers of type **24**.[129] While this study has to be regarded as a very simplified modeling of a natural epoxidation by P450 cytochromes, its results are in line with findings made in experimental investigations involving molecular iron porphyrin complexes.[132,133] For instance, they can rationalize (on the assumption that the reaction proceeds via the quartet intermediates) the observed pronounced effect of the axial ligand on the lifetimes of the spectroscopically detected radicals: Axial ligands that support the iron(III) form of the intermediate, will give rise to the corresponding valence tautomer **23**, that is associated with longer radical lifetimes as well as side reactions[132,133] such as aldehyde formation. Ligands that support the iron(IV) form will in turn lead to short-lived radicals and a suppression of side products.

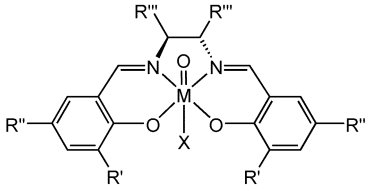
A recent DFT study instructively compares epoxidation and hydroxylation for the substrate propene[134] with a model for the reactive iron(IV) oxo form of the enzyme cytochrome P450. A two-state reactivity (TSR) with quartet and doublet states was located for both processes. The quartet processes were found to be stepwise, whereas the doublet processes were characterized as nonsynchronous but effectively concerted pathways (see above). The computed kinetic

 © 2003 Wiley-VCH Verlag GmbH & Co. KGaA, Weinheim 

isotope effects for C–H hydroxylation with and without tunneling corrections are large ($>7$), and they support the assignment of the corresponding transition states to hydrogen-abstraction processes (compare Section 2.2.1). In the gas phase, epoxidation is energetically favorable by 3.4 kcal mol$^{-1}$ over the hydroxylation.[134]

### 3.2. Epoxidation Catalysts

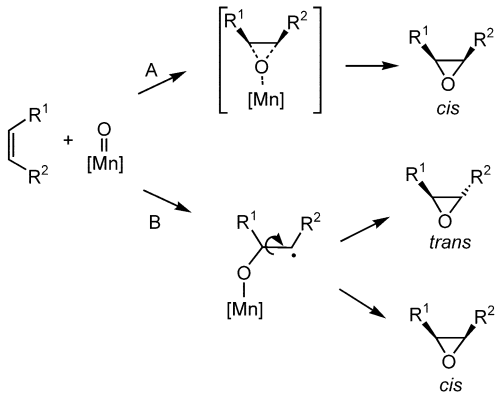
One of the most elegant methods for the selective formation of C–O bonds is the catalytic Jacobsen–Katsuki epoxidation, the enantioselective synthesis of optically active epoxides by oxygen-transfer reactions with chiral, nonracemic manganese[135] and chromium[136] oxo salen complexes such as **26** and **27**. While the chromium oxo complexes are often




M = Cr (**26**), Mn (**27**)

isolable,[137] the manganese oxo complexes are not (at room temperature only stable (L)Mn$^{V}$=O species with other types of ligands L are known).[138,139] Nevertheless compounds such as **27** are now the accepted reactive intermediates in the catalytic Jacobsen–Katsuki epoxidation[135,140] having been identified as such by a series of techniques.[141] The Jacobsen–Katsuki epoxidation, where the catalysts are employed in form of the manganese(III) complexes, that is, **27** without the terminal oxo ligand, leads to high enantiomeric excesses and the best selectivities are achieved with *cis* olefins. As stoichiometric oxidizing agents PhIO, NaOCl or *meta*-chloroperbenzoic acid can be employed.[142,143,135b] The first step of the catalytic cycle seems straight forward: The manganese(III) complex is converted into the corresponding manganese(V) complex bearing a terminal oxo ligand (**27**). To explain the high enantiomeric selectivities with *cis* olefins, it has been proposed that the olefinic double bond approaches the Mn=O group in a side-on fashion, that is, parallel to the salen ligand, bulky groups R′ shield the aryl rings.[143,140,142] There is also consensus about the role of the substituents R″:[144] If they have donor properties, they stabilize the reactive Mn=O intermediate, which lowers the reaction rate of the oxo transfer step resulting in a late transition state. This in turn increases the enantiomeric selectivity, as then the interaction between the olefin and the chiral salen ligand is more intense. Accordingly, the selectivities are also influenced by the addition of potential ligands which coordinate in positions *trans* to the terminal oxo ligand.[145]

On the other hand, the mechanism of the actual oxygenating step is still a focus of intense discussion. In the first examples of the Jacobsen–Katsuki epoxidation it had been found already, that conjugated olefins yield mixtures of *cis* and *trans* epoxides, while alkyl substituted isolated *cis* olefins yield exclusively *cis* epoxides. These results were interpreted in terms of a concerted pathway A (Scheme 18) for the alkyl-substituted olefins and a radical mechanism B for the




***Scheme 18.*** Possible mechanisms for the oxo transfer in the Jacobsen–Katsuki epoxidation.

conjugated olefins.[142] However, it still did not seem plausible, that some olefins, such as *cis*-β-methyl styrene, that are clearly envisaged to react by the radical pathway B, gave *cis*:*trans* product ratios between 95:5 and 5:95 depending on the oxidizing agent used, the catalyst (including the counterion), and the additives.[142] Neither it could be explained, why the employment of radical clocks led to ring-opened products, when PhIO was used as the oxidant, but not when NaOCl was used.[142]

These peculiarities have been addressed in the last 5 years. Within this time, the importance of the spin state of the manganese oxo moiety has been recognized.[140,146–149] Both theoretical and experimental studies agree that the catalytic cycle starts with the Mn$^{III}$ complex in the quintet state.[140,141,146–150] The theoretical studies agree that all spin states (singlet, triplet, quintet) of the actual epoxidizing species, the Mn$^{V}$=O complex **27**, are energetically accessible. Hence, if spin change within these systems is slow, the reaction can proceed completely on the quintet surface, where it starts—in a very asynchronous but concerted fashion, when an axial ligand X is absent (Figure 1, dotted line;[146] compare, however, ref. [148b]). However, if spin change does occur, the addition will proceed on the triplet surface to give a radical intermediate (analogously to the $MnO_3Cl$/olefin system described in Section 3.1) with subsequent formation of product either on the triplet or quintet surface (Figure 1)[140]—according to theoretical considerations the singlet state can be neglected for catalytic processes,[140] although all the spectroscopically characterized LMn$^{V}$=O compounds are uniformly diamagnetic and accordingly possess singlet ground states.[139] The relative stabilities of the radical intermediates as well as the relative activation barriers for product formation and rotation determine the amount of *cis*–*trans* isomerization within this channel[148]. Radical intermediates can also occur without the preceding spin change. Finally, the shape of the quintet PES on which

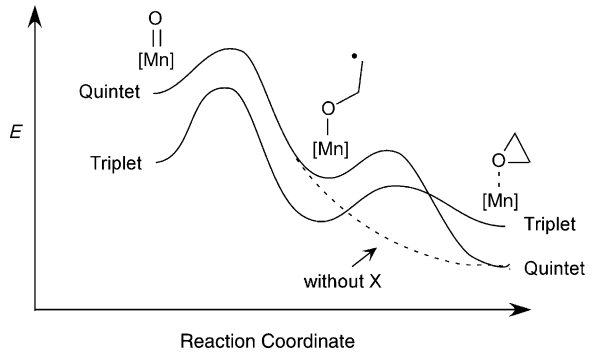
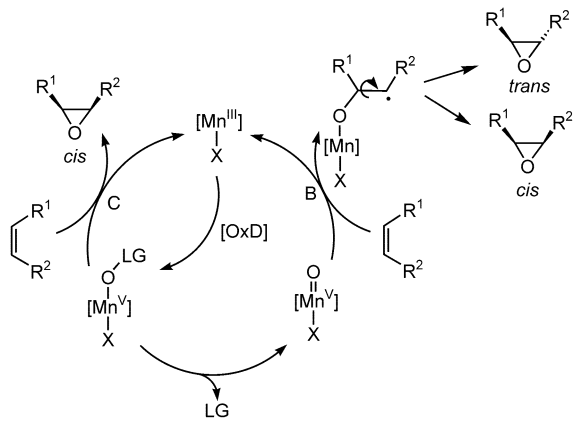



***Figure 1.*** Qualitative potential variations for the reaction of **27** with olefins for various spin states.[140]




***Scheme 19.*** Catalytic cycle for the manganese(III)-catalyzed epoxidation by Lewis acid activation (path C) and via the $Mn^{V}$=O species (path B), see also Scheme 18; OxD = stoichiometric oxygen donor, LG = leaving group.

the reaction starts seems very responsive to the nature of the counterion X. As mentioned, in the absence of a ligand in the axial position, the surface has been found to display no minimum for a radical-intermediate and a concerted, diastereoselective epoxidation would be observed in this case (see, however, ref. [148b]). Counterions with donor properties, such as chloride, will, however, move into the axial position of the manganese complex leading to a quintet PES, which is very similar to the triplet PES and has local minima indicating radical intermediates (Figure 1).[148,149] The experimentally observed counterion effect as well as the effects of additives should thus be attributed to ligand-dependent reaction profiles and stereoselectivities on the individual PESs.[151]

Recently, Linde et al. studied the electronic effects of the substrate on the diastereoselectivity and enantioselectivity of the catalytic epoxidation by employing *para*-substituted *cis* stilbenes in reaction with PhIO and the manganese salen catalyst.[154] They concluded that *cis* and *trans* epoxide formation follow separate pathways, and that the possibility that the reaction mixture contains multiple, rapidly equilibrating oxidizing species, each of which preferentially follows one of the reaction pathways cannot be excluded.

The results could also be interpreted in such a way that starting from a common electrophilic oxidizing species attacking the olefin, a branching of the oxidizing channel to a radical intermediate occurs before the transition state for the concerted *syn* addition is reached—a scenario which could be imagined to occur by spin-surface crossing as outlined above.[155]

The idea of at least two oxidizing species is shared by Adam et al., who suggested a bifurcation step in the catalytic cycle to account for the dependence of the diastereoselectivities on the oxygen source.[152] A concerted Lewis acid activated oxygen transfer (as has been suggested for the case of PhIO by Valentine et al.[153] and recently by Que et al. for iron porphyrin complexes[156]) was proposed to compete with stepwise epoxidation via the Mn=O species[151] (Scheme 19, compare ref. [141c]). Based on this hypothesis and the experimentally observed *cis*:*trans* ratios, the oxygen donors fall into two classes: PhIO, $C_6F_5IO$, $IO_4^-$, and $O_3$ afford the $Mn^{V}$=O species as the dominant oxidant with extensive isomerization (pathway B) through the stepwise radical process; for $HSO_5^-$, NaOCl, and dimethyldioxirane, the concerted process through Lewis acid catalysis (pathway C) is also operative, as reflected by the higher *cis* selectivity.[152] This mechanism might explain, too, why vinylcyclopropane radical clocks survive oxidations with NaOCl but not with PhIO.[154] Adam et al. additionally employed a probe (1α,2β,3α-2-ethenyl-3-methoxycyclopropyl)benzene), with which it is possible to differentiate between radical and cationic intermediates, and were thus able to show, that isomerized epoxide product obtained in PhIO oxidation indeed arises from intermediary radicals and not from cations.[152] With respect to the influence of the oxidant on the stereoselectivity of the reaction a further effect has to be born in mind: oxidants, such as PhIO, containing a heavy atom possibly facilitate spin changes and thus TSR.[140]

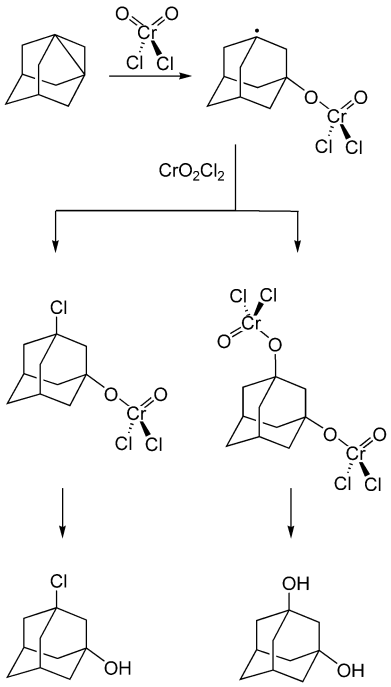
On the basis of all these results and hypotheses described, a possible explanation for the varying *cis*:*trans* product ratios and the contrasting experimental observations would be the following: The catalyst and the oxidant chosen determine the relative importance of the two routes shown in Scheme 19, which influences the observable *cis*–*trans* isomerization ratio even at that stage. Reaction along the $Mn^{V}$=O channel further depends on the outer conditions. If these are such that no spin change occurs, the system remains on the quintet PES where in the absence of a counterion with significant donor properties the epoxidation might proceed in a concerted fashion leading to virtually no isomerization (compare refs. [148b] and [146b]). In the presence of donor ligands, however, the reaction proceeds via radical intermediates as local minima, with the depth of these minima determining the lifetime of the radicals. If on the other hand spin change occurs, epoxidation proceeds on the triplet surface via radical intermediates. The shapes of the surfaces within the $Mn^{V}$=O channel (which are of course also influenced by the substrates themselves) thus influence the frequency of radical formation, their lifetime and isomerization probability. Hence the *cis*:*trans* product ratio observed experimentally is determined by the relative importance of all these pathways and surfaces, which are also influenced by the external conditions.

 © 2003 Wiley-VCH Verlag GmbH & Co. KGaA, Weinheim 

The manganese-based systems, **27** are more useful than the related chromium species **26**; they show a wider range of reactivity and, can be integrated into a catalytic cycle. On the other hand the active species of the stoichiometric chromium systems (the $Cr^{V}$=O complexes) are more easily studied experimentally than the $Mn^{V}$=O species, and thus they were also the subject of a combined experimental–theoretical investigation.[140] The studies show that the Cr and Mn based reactions have many similarities, but also a few critical differences, which could explain the dramatic differences in selectivities (for instance, in the chromium systems high enantioselectivities are obtained in the epoxidation of *trans* alkenes and not for *cis* alkenes). As for the manganese series, both theoretical and experimental results for oxidation with the chromium systems indicate the existence of an intermediate along the reaction path. The DFT calculations identified this intermediate as a β-alkoxy radical bound to chromium (also compare with $CpCrOCl_2$, Section 3.1). The calculations suggest almost complete degeneracy between the low-spin (doublet) and high-spin (quartet) state at this point on the reaction coordinate, and this degeneracy facilitates spin-surface crossing. The fact that the system must change between high- and low-spin during the oxygenation process (the $Cr^{V}$=O reactant has a high-spin, the $Cr^{III}$ product a low-spin ground state) could affect both the diastereoselectivity and the rate of reoxidation of the catalyst, and account for differences to the manganese system. Axial donor ligands significantly lower the barrier of the reaction and dramatically change the conformation of the complexes (as shown earlier for the manganese system[150,132d]). This conformational change brings the salen ligand closer to the substrate in the selectivity-determining transition state and thereby increases enantioselectivity. A difference in conformational preference could also be the origin of differences in substrate selectivity between [Mn(salen)] and [Cr(salen)] reagents.[140]

After the detailed description of the current mechanistic views concerning epoxidations catalyzed by salen-based metal complexes, it should not be forgotten, that metal porphyrin compounds are also capable of acting as catalysts, not only for C–H activation (Section 2.2.1) but also for epoxidations. The mechanism should be very similar to that of the metal salen catalysts.

As epoxidations with metal salen complexes proceed via β-alkoxy radicals it is not surprising that some manganese salen epoxidation catalysts can also carry out hydrogen-atom abstractions. Some complexes are capable of catalyzing benzylic hydroxylation reactions, which correspondingly also proceed through radical intermediates.[157] This link between these two types of reactions (epoxidation and hydrogen-atom abstraction) was mentioned in the first paragraph of Section 3. The discussion can now even be extended: Since the above mentioned results convincingly demonstrate that metal oxo compounds can indeed homolytically cleave C=C π bonds, it might be asked now whether they are capable of cleaving C–C σ bonds as well. Yet again, it can be stated that this possibility exists under the condition that the thermodynamics are acceptable, that is, that the energy lost on breaking the C–C bond (as well as the M=O π bond) is compensated at least mainly by the energy gained on formation of the C–O bond. The oxidation of propellanes (that naturally posses very weak C–C bonds) with $CrO_2X_2$ (X = Cl, OAc; Scheme 20) might be formally regarded as such an oxidative C–C σ-bond cleavage:[16,158] The formation of the isolated products can be explained by attack of a chromium oxo moiety at the quaternary carbon atom, which leads to cleavage of the C–C bond and formation of a radical that is subsequently trapped by reaction with excessive $CrO_2X_2$.




***Scheme 20.*** C–C σ-bond homolysis of propellane with chromyl chloride.

## 4. Conclusions

Oxygenation chemistry in general is still a subject of intense debate which on the one hand is due to the importance the corresponding reactions have for synthetic chemistry, but also due to the difficulty of the questions it raises. The mechanisms of oxygenations by metal oxo species remain among the most enigmatic in chemistry, and they are far from being understood completely. However, "patterns" have emerged that might explain the origin of their complexity as well as confusing experimental observations:

a) Radicals are far more frequently involved in oxygenation reactions than originally assumed, in fact, they appear almost omnipresent. This is stressed in this review, which covers systems as (seemingly) different as $CrO_2Cl_2$, $[(phen)_2Mn^{IV}(\mu\text{-}O)_2Mn^{IV}(phen)_2]^{2+}$, $FeO^{+}$, the P450 cytochromes, the catalyst of the SOHIO process, and metal salen complexes. A common factor, however, in all these systems is that the initial steps in reactions with hydrocarbons involve radicals, which determine the subsequent proceedings.

 © 2003 Wiley-VCH Verlag GmbH & Co. KGaA, Weinheim 

b) The observation of selectivity and retention of configuration is not an argument against radicals, as it can have its origin simply in very short radical lifetimes.
c) In a number of systems there is more than one oxidizing site/oxygenation channel.
d) Last but not least the crossing of different PESs and thus multistate reactivity with all its consequences has to be considered.

On this basis future research will be able to give more detailed information. Contributions will for instance come from the design of instructive model systems containing well-defined sites, in situ studies involving a variety of spectroscopic techniques, appropriate to identify reactive intermediates as well as active sites/phases, and the utilization of computational chemistry to determine structure–function relationships of oxidizing sites, to support mechanistic proposals based on experimental results, as well as to analyze PES crossing scenarios.

*I am grateful to the Deutsche Forschungsgemeinschaft for scholarships as well as funding. I also would like to thank the Fonds der Chemischen Industrie, the BMBF, the Karl-Winnacker-Stiftung and the Dr. Otto-Röhm Gedächtnisstiftung for financial benefits, and Professor Dr. G. Huttner for his continuous interest in and support of our work.*

Received: February 6, 2003 [A578]

[1] a) R. A. Sheldon, J. K. Kochi, *Metal-Catalyzed Oxidation of Organic Compounds*, Academic Press, New York, **1981**; b) G. A. Olah, A. Molnár, *Hydrocarbon Chemistry*, Wiley, New York, **1995**; c) Special issue on bioinorganic enzymology: *Chem. Rev.* **1996**, *96*, 2237; d) K. Weissermel, H.-J. Arpe, *Industrial Organic Chemistry*, VCH, Weinheim, **1997**; *Organic Synthesis by Oxidation with Metal Compounds* (Eds.: W. Mijs, C. R. H. I. de Jonge), Plenum, New York, **1986**.
[2] A. A. Fokin, P. R. Schreiner, *Chem. Rev.* **2002**, *102*, 1551.
[3] M. A. Etard, H. M. Moissan, *C. R. Hebd. Seances Acad. Sci.* **1877**, *84*, 127.
[4] a) G. K. Cook, J. M. Mayer, *J. Am. Chem. Soc.* **1994**, *116*, 1855; b) G. K. Cook, J. M. Mayer, *J. Am. Chem. Soc.* **1995**, *117*, 7139.
[5] G. Cainelli, G. Cardillo, *Chromium Oxidations in Organic Chemistry*, Springer, Berlin, **1984**; K. B. Wiberg in *Oxidation in Organic Chemistry* (Ed.: K. B. Wiberg), Academic Press, New York, **1965**, p. 69.
[6] C. Limberg, *Chem. Eur. J.* **2000**, *6*, 2083.
[7] L. Deng, T. Ziegler, *Organometallics* **1996**, *15*, 3011; T. Ziegler, J. Li, *Organometallics* **1995**, *14*, 214.
[8] T. Wistuba, C. Limberg, P. Kircher, *Angew. Chem.* **1999**, *111*, 3222; *Angew. Chem. Int. Ed.* **1999**, *38*, 3037.
[9] T. Wistuba, C. Limberg, H. Pritzkow, *Z. Anorg. Allg. Chem.* **2002**, *628*, 2340.
[10] a) *Cytochrome P-450: Structure, Mechanism, and Biochemistry*, 1st ed. (Ed.: R. R. Ortiz de Montellano), Plenum, New York, **1986**; b) *Cytochrome P-450: Structure, Mechanism, and Biochemistry*, 2nd ed. (Ed.: R. R. Ortiz de Montellano), Plenum, New York, **1995**.
[11] I. Schlichting, J. Berenzen, K. Chu, A. M. Stock, S. A. Maves, D. E. Benson, R. M. Sweet, D. Ringe, G. A. Petsko, S. G. Sligar, *Science* **2000**, *287*, 1615.
[12] L. M. Stephenson, J. Egnatchik, D. R. Speth, *J. Org. Chem.* **1979**, *44*, 346.
[13] M. Al-Sheikhly, W. L. McLaughlin, *Radiat. Phys. Chem.* **1991**, *38*, 203; S. Steenken, P. Neta, *J. Am. Chem. Soc.* **1982**, *104*, 1244.
[14] J. M. Mayer, *Acc. Chem. Res.* **1998**, *31*, 441.
[15] C. Rüchardt, M. Gerst, J. Ebenhoch, *Angew. Chem.* **1997**, *109*, 1474; *Angew. Chem. Int. Ed. Engl.* **1997**, *36*, 1406.
[16] A. A. Fokin, B. A. Tkachenko, O. I. Korshunov, P. A. Gunchenko, P. Schreiner, *J. Am. Chem. Soc.* **2001**, *123*, 11248.
[17] K. A. Gardner, J. M. Mayer, *Science* **1995**, *269*, 1849; K. A. Gardner, L. L. Kuehnert, J. M. Mayer, *Inorg. Chem.* **1997**, *36*, 2069.
[18] T. Strassner, K. N. Houk, *J. Am. Chem. Soc.* **2000**, *122*, 7821.
[19] J. I. Braumann, A. J. Pandell, *J. Am. Chem. Soc.* **1970**, *92*, 329.
[20] J. M. Bakke, A. E. Froehaug, *J. Phys. Org. Chem.* **1996**, *9*, 310 und 507; J. M. Bakke, A. E. Froehaug, *Acta Chem. Scand.* **1994**, *48*, 160; J. M. Bakke, D. Bethell, *Acta Chem. Scand.* **1992**, *46*, 644; J. M. Bakke, M. Lundquist, *Acta Chem. Scand. Ser. B* **1986**, *40*, 430.
[21] T. Strassner, Habilitation thesis, Technische Universität Munich, **2002**.
[22] C. E. MacBeth, A. P. Golombek, V. G. Young, Jr., C. Yang, K. Kuczera, M. P. Hendrich, A. S. Borovik, *Science* **2000**, *289*, 938.
[23] K. Qin, C. D. Incarvito, A. L. Rheingold, K. H. Theopold, *J. Am. Chem. Soc.* **2002**, *124*, 14008.
[24] A. Bakac, *J. Am. Chem. Soc.* **2000**, *122*, 1092.
[25] a) T.-C. Lau, C.-K. Mak, *J. Chem. Soc. Chem. Commun.* **1993**, 766; b) J. R. Bryant, J. M. Mayer, *J. Am. Chem. Soc.* **2003**, *125*, 10351.
[26] a) K. Wieghardt, *Angew. Chem.* **1989**, *101*, 1179; *Angew. Chem. Int. Ed. Engl.* **1989**, *28*, 1153; b) V. L. Pecoraro, W.-Y. Hsieh in *Metals in Biological Systems*, *Vol. 37* (Eds.: A. Sigel, H. Sigel), Marcel Dekker, Basel, **2000**, pp. 429; c) See ref. [83–92] (Section 2.2.3).
[27] J. Limburg, J. S. Vrettos, H. Chen, J. C. de Paula, R. H. Crabtree, G. W. Brudvig, *J. Am. Chem. Soc.* **2001**, *123*, 423.
[28] M. Baldwin, N. A. Law, T. L. Stemmler, J. W. Kampf, J. E. Penner-Hahn, V. L. Pecoraro, *Inorg. Chem.* **1999**, *38*, 4801.
[29] a) K. Wang, J. M. Mayer, *J. Am. Chem. Soc.* **1997**, *119*, 1470; b) M. A. Lockwood, K. Wang, J. M. Mayer, *J. Am. Chem. Soc.* **1999**, *121*, 11894.
[30] A. S. Larsen, K. Wang, M. A. Lockwood, G. L. Rice, T.-J. Won, S. Lovell, M. Sadílek, F. Tureček, J. M. Mayer, *J. Am. Chem. Soc.* **2002**, *124*, 10112.
[31] a) L. Que, Jr., *J. Chem. Soc. Dalton Trans.* **1997**, 3933, and refs. therein; b) C. Kim, Y. Dong, L. Que, Jr., *J. Am. Chem. Soc.* **1997**, *119*, 3635.
[32] a) H. V. Obias, Y. Lin, N. N. Murthy, E. Pidcock, E. I. Solomon, M. Ralle, N. J. Blackburn, Y.-M. Neuhold, A. D. Zuberbühler, K. D. Karlin, *J. Am. Chem. Soc.* **1998**, *120*, 12960; C. X. Zhang, H.-C. Liang, E. Kim, J. Shearer, M. E. Helton, E. Kim, S. Kaderli, C. D. Incarvito, A. D. Zuberbühler, A. L. Rheingold, K. D. Karlin, *J. Am. Chem. Soc.* **2003**, *125*, 634; b) W. B. Tolman, *Acc. Chem. Res.* **1997**, *30*, 227; S. Itho, M. Taki, H. Nakao, P. L. Holland, W. B. Tolman, L. Que, Jr., S. Fukuzumi, *Angew. Chem.* **2000**, *112*, 409; *Angew. Chem. Int. Ed.* **2000**, *39*, 398; V. Mahadevan, M. J. Henson, E. I. Solomon, T. D. P. Stack, *J. Am. Chem. Soc.* **2000**, *122*, 10249.
[33] a) K. Shiren, S. Ogo, S. Fujinami, H. Hayashi, M. Suzuki, A. Uehara, Y. Watanabe, Y. Moro-oka, *J. Am. Chem. Soc.* **2000**, *122*, 254; b) S. Itoh, H. Bandoh, M. Nakagawa, S. Nagatomo, T. Kitagawa, K. D. Karlin, S. Fukuzumi, *J. Am. Chem. Soc.* **2001**, *123*, 11168.
[34] Review on modeling of metalloenzymes with iron and copper centers: L. Que, Jr., W. B. Tolman, *Angew. Chem.* **2002**, *114*, 1160; *Angew. Chem. Int. Ed.* **2002**, *41*, 1821.
[35] K. Chen, L. Que, Jr., *J. Am. Chem. Soc.* **2001**, *123*, 6327.
[36] H. Kelm, H.-J. Krüger, *Angew. Chem.* **2001**, *113*, 2406; *Angew. Chem. Int. Ed.* **2001**, *40*, 2344.

 © 2003 Wiley-VCH Verlag GmbH & Co. KGaA, Weinheim 

[37] C. R. Goldsmith, R. T. Jonas, T. D. P. Stack, *J. Am. Chem. Soc.* **2002**, *124*, 83.
[38] P. Chaudhuri, M. Hess, U. Flörke, K. Wieghardt, *Angew. Chem.* **1998**, *110*, 2340; *Angew. Chem. Int. Ed.* **1998**, *37*, 2217.
[39] D. Schröder, H. Schwarz, S. Shaik, *Struct. Bonding (Berlin)* **2000**, *97*, 91.
[40] J. Berkowitz, G. B. Ellison, D. Gutman, *J. Phys. Chem.* **1994**, *98*, 2744.
[41] J. N. Harvey, M. Diefenbach, D. Schröder, H. Schwarz, *Int. J. Mass Spectrom.* **1999**, *182*/183, 85.
[42] K. K. Irikura, J. L. Beauchamp, *J. Phys. Chem.* **1991**, *95*, 8344.
[43] I. Kretzschmar, A. Fiedler, J. N. Harvey, D. Schröder, H. Schwarz, *J. Phys. Chem. A* **1997**, *101*, 6252; I. Kretzschmar, D. Schröder, H. Schwarz, *Int. J. Mass Spectrom. Ion Processes* **1997**, *167/168*, 103.
[44] C. J. Cassady, S. W. McElvany, *Organometallics* **1992**, *11*, 2367.
[45] K. K. Irikura, J. L. Beauchamp, *J. Am. Chem. Soc.* **1989**, *111*, 75.
[46] H. H. Cornehl, R. Wesendrup, M. Diefenbach, H. Schwarz, *Chem. Eur. J.* **1997**, *3*, 1083; C. Heinemann, H. H. Cornehl, D. Schröder, M. Dolg, H. Schwarz, *Inorg. Chem.* **1996**, *35*, 2463.
[47] D. Schröder, H. Schwarz, D. E. Clemmer, Y. Chen, P. B. Armentrout, V. I. Baranov, D. K. Bohme, *Int. J. Mass Spectrom. Ion Processes* **1997**, *161*, 175.
[48] S. Shaik, M. Filatov, D. Schröder, H. Schwarz, *Chem. Eur. J.* **1998**, *4*, 193; D. Schröder, S. Shaik, H. Schwarz, *Acc. Chem. Res.* **2000**, *33*, 139; S. Shaik, S. P. de Visser, F. Ogliaro, H. Schwarz, D. Schröder, *Curr. Opin. Chem. Biol.* **2002**, *6*, 556.
[49] P. Jackson, J. N. Harvey, D. Schröder, H. Schwarz, *Int. J. Mass Spectrom.* **2001**, *204*, 233.
[50] R. A. Marusak, C. F. Meares in *Active Oxygen in Biochemistry* (Eds.: J. S. Valentine, C. S. Foote, A. Greenberg, J. F. Liebman), Blackie Academic, New York, **1995**, p. 336.
[51] R. T. Jonas, T. D. P. Stack, *J. Am. Chem. Soc.* **1997**, *119*, 8566, and refs. therein.
[52] J. P. Klinman, *Chem. Rev.* **1996**, *96*, 2541.
[53] T. L. Poulos, B. C. Finzel, I. C. Gunsalus, G. C. Wagner, J. Kraut, *J. Biol. Chem.* **1985**, *260*, 16122; T. L. Poulos, B. C. Finzel, A. J. Howard, *Biochemistry* **1986**, *25*, 5314; T. L. Poulos, R. Raag, *FASEB J.* **1992**, *6*, 674; H. Li, S. Narasimhulu, L. M. Havran, J. D. Winkler, T. L. Poulos, *J. Am. Chem. Soc.* **1995**, *117*, 6297.
[54] R. C. Blake II, M. J. Coon, *J. Biol. Chem.* **1989**, *264*, 3694; T. Egawa, H. Shimada, Y. Ishimura, *Biochem. Biophys. Res. Commun.* **1994**, *201*, 1464; R. Davydov, T. M. Makris, V. Kofman, D. E. Werst, S. G. Sligar, B. M. Hofman, *J. Am. Chem. Soc.* **2001**, *123*, 1403; I. G. Denisov, T. M. Makris, S. G. Sligar, *J. Biol. Chem.* **2001**, *276*, 11648; D. G. Kellner, S.-C. Hung, K. E. Weiss, S. G. Sligar, *J. Biol. Chem.* **2002**, *277*, 9641.
[55] N. Bec, A. C. F. Gorren, C. Voelker, B. Mayer, R. Lange, *J. Biol. Chem.* **1998**, *273*, 13502.
[56] R. E. White, M. J. Coon, *Annu. Rev. Biochem.* **1980**, *49*, 315; J. T. Groves, Y.-Z. Han in *Cytochrome P450 Structure, Mechanism, and Biochemistry*, 2nd ed. (Ed.: P. R. Ortiz de Montellano), Plenum, New York, **1995**, pp. 3–48; F. P. Guengerich, T. L. Macdonald, *FASEB J.* **1990**, *4*, 2453; W. D. Woggon, H. Fretz in *Advances in Detailed Reaction Mechanisms, Vol. 2* (Ed.: J. M. Coxon), JAI, Greenwich, CT, **1992**, p. 111; M. Sono, M. P. Roach, E. D. Coulter, J. H. Dawson, *Chem. Rev.* **1996**, *96*, 2841; J. T. Groves, R. C. Haushalter, M. Nakamura, T. E. Nemo, B. J. Evans, *J. Am. Chem. Soc.* **1981**, *103*, 2884.
[57] M. Newcomb, P. H. Toy, *Acc. Chem. Res.* **2000**, *33*, 449.
[58] M. Newcomb, R. Shen, S.-Y. Choi, P. H. Toy, P. F. Hollenberg, A. D. N. Vaz, M. J. Coon, *J. Am. Chem. Soc.* **2000**, *122*, 2677.
[59] F. Ogliaro, S. P. de Visser, S. Cohen, P. K. Sharma, S. Shaik, *J. Am. Chem. Soc.* **2002**, *124*, 2806; T. Kamachi, Y. Shiota, T. Ohta, K. Yoshizawa, *Bull. Chem. Soc. Jpn.* **2003**, *76*, 721.
[60] M. Newcomb, R. Shen, Y. Lu, M. J. Coon, P. F. Hollenberg, D. A. Kopp, S. J. Lippard, *J. Am. Chem. Soc.* **2002**, *124*, 6879.
[61] K. Auclair, Z. Hu, D. M. Little, P. R. Ortiz de Montellano, J. T. Groves, *J. Am. Chem. Soc.* **2002**, *124*, 6020.
[62] N. Harris, S. Cohen, M. Filatov, F. Ogliaro, S. Shaik, *Angew. Chem.* **2000**, *112*, 2070; *Angew. Chem. Int. Ed.* **2000**, *39*, 2003; F. Ogliaro, M. Filatov, S. Shaik, *Eur. J. Inorg. Chem.* **2000**, 2455; F. Ogliaro, N. Harris, S. Cohen, M. Filatov, S. P. de Visser, S. Shaik, *J. Am. Chem. Soc.* **2000**, *122*, 8977.
[63] J. M. Pratt, T. I. Ridd, L. J. King, *J. Chem. Soc. Chem. Commun.* **1995**, 2297; M. Newcomb, D. Aebisher, R. Shen, R. E. P. Chandrasena, P. F. Hollenberg, M. J. Coon, *J. Am. Chem. Soc.* **2003**, *125*, 6064.
[64] J. C. Schöneboom, H. Lin, N. Reuter, W. Thiel, S. Cohen, F. Ogliaro, S. Shaik, *J. Am. Chem. Soc.* **2002**, *124*, 8142.
[65] K. Yoshizawa, T. Kamachi, Y. Shiota, *J. Am. Chem. Soc.* **2001**, *123*, 9806; T. Kamachi, K. Yoshizawa, *J. Am. Chem. Soc.* **2003**, *125*, 4652.
[66] J.-U. Rohde, J.-H. In, M. H. Lim, W. W. Brennessel, M. R. Bukowski, A. Stubna, E. Münck, W. Nam, L. Que, Jr., *Science* **2003**, *299*, 1037.
[67] B. A. Arndtsen, R. G. Bergmann, T. A. Mobley, T. H. Peterson, *Acc. Chem. Res.* **1995**, *28*, 154.
[68] H. Patzelt, W.-D. Woggon, *Helv. Chim. Acta* **1992**, *75*, 523.
[69] T. Katsuki in *Comprehensive Asymmetric Catalysis I–III* (Eds.: E. N. Jacobsen, A. Pfaltz, H. Yamamoto), Springer, Berlin, **2000**, p. 753.
[70] J. Groves, P. Viski, *J. Org. Chem.* **1990**, *55*, 3628.
[71] M. Merkx, D. A. Kopp, M. H. Sazinsky, J. L. Blazyk, J. Müller, S. J. Lippard, *Angew. Chem.* **2001**, *113*, 2861; *Angew. Chem. Int. Ed.* **2001**, *40*, 2783.
[72] V. Guallar, B. F. Gherman, S. J. Lippard, R. A. Friesner, *Curr. Opin. Chem. Biol.* **2002**, *6*, 236.
[73] K. E. Liu, A. M. Valentine, D. Wang, B. H. Huynh, D. E. Edmondson, A. Salifoglou, S. J. Lippard, *J. Am. Chem. Soc.* **1995**, *117*, 10174.
[74] S.-K. Lee, J. C. Nesheim, J. D. Lipscomb, *J. Biol. Chem.* **1993**, *268*, 21569.
[75] A. M. Valentine, S. S. Stahl, S. J. Lippard, *J. Am. Chem. Soc.* **1999**,*121*, 3876.
[76] J. D. Lipscomb, S.-K. Lee, J. C. Nesheim, Y. Jin, B. J. Wallar, X.-Y. Zhang in *Iron Metabolism: Inorganic Biochemistry and Regulatory Mechanisms* (Eds.: G. C. Ferreira, J. J. G. Moura, R. Franco), Wiley-VCH, Weinheim, **1999**, p. 323.
[77] a) N. D. Priestley, H. G. Floss, W. A. Froland, J. D. Lipscomb, P. G. Williams, H. Morimoto, *J. Am. Chem. Soc.* **1992**, *114*, 7561; b) A. M. Valentine, B. Wilkinson, K. E. Liu, S. Komar-Panicucci, N. D. Priestley, P. G. Williams, H. Morimoto, H. G. Floss, S. J. Lippard, *J. Am. Chem. Soc.* **1997**, *119*, 1818.
[78] B. J. Brazeau, R. N. Austin, C. Tarr, J. T. Groves, J. D. Lipscomb, *J. Am. Chem. Soc.* **2001**, *123*, 11831.
[79] B. D. Dunietz, M. D. Beachy, Y. Cao, D. A. Whittington, S. J. Lippard, R. A. Friesner, *J. Am. Chem. Soc.* **2000**, *122*, 2828; B. F. Gherman, B. D. Dunietz, D. A. Whittington, S. J. Lippard, R. A. Friesner, *J. Am. Chem. Soc.* **2001**, *123*, 3836.
[80] V. Guallar, B. F. Gherman, W. H. Miller, S. J. Lippard, R. A. Friesner, *J. Am. Chem. Soc.* **2002**, *124*, 3377; M.-H. Baik, B. F. Gherman, R. A. Friesner, S. J. Lippard, *J. Am. Chem. Soc.* **2002**, *124*, 14608.
[81] M.-H. Baik, M. Newcomb, R. A. Friesner, S. J. Lippard, *Chem. Rev.* **2003**, *103*, 2385.
[82] R. N. Austin, H.-K. Chang, G. J. Zylstra, J. T. Groves, *J. Am. Chem. Soc.* **2000**, *122*, 11747.
[83] M. Yagi, M. Kaneko, *Chem. Rev.* **2001**, *101*, 21.
[84] G. T. Babcock in *Photosynthesis: From Light to Biosphere, Vol. 2* (Ed.: P. Mathis), Kluwer, Dordrecht, **1995**, p. 209; C. W. Hoganson, N. Lydakis-Simantiris, X.-S. Tang, C. Tommos, K.

Warncke, G. T. Babcock, *Photosynth. Res.* **1995**, *46*, 177; C. Tommos, X.-S. Tang, K. Warncke, C. W. Hoganson, S. Styring, J. McCracken, B. A. Diner, G. T. Babcock, *J. Am. Chem. Soc.* **1995**, *117*, 10325.

[85] C. W. Hoganson, G. T. Babcock, *Science* **1997**, *277*, 1953; C. W. Hoganson, G. T. Babcock in *Manganese and its Role in Biological Systems*, *Vol. 37* (Eds.: A. Sigel, H. Sigel), Marcel Dekker, New York, **2000**, p. 613; C. Tommos, G. T. Babcock, *Biochim. Biophys. Acta* **2000**, *1458*, 199; C. Tommos, C. W. Hoganson, M. Di Valentin, N. Lydakis-Simantiris, P. Dorlet, K. Westphal, H.-A. Chu, J. McCracken, G. T. Babcock, *Curr. Opin. Chem. Biol.* **1998**, *2*, 244.

[86] C. Tommos, G. T. Babcock, *Acc. Chem. Res.* **1998**, *31*, 18; C. Tommos, *Philos. Trans. R. Soc. London Ser. B* **2002**, *257*, 1383.

[87] C. W. Hoganson, 12th *International Congress on Photosynthesis*, CSIRO publishing, Melbourne, **2001**.

[88] W. Rüttinger, G. C. Dismukes, *Chem. Rev.* **1997**, *97*, 1.

[89] P. E. M. Siegbahn, R. H. Crabtree, *J. Am. Chem. Soc.* **1999**, *121*, 117.

[90] A. Zouni, H. T. Witt, J. Kern, P. Fromme, N. Krauss, W. Saenger, P. Orth, *Nature* **2001**, *409*, 739; P. Fromme, J. Kern, B. Loll, J. Biesiadka, W. Saenger, H. T. Witt, N. Krauss, A. Zouni, *Philos. Trans. R. Soc. London Ser. B* **2002**, *257*, 1337.

[91] M. R. A. Blomberg, P. E. M. Siegbahn, G. T. Babcock, *J. Am. Chem. Soc.* **1998**, *120*, 8812; M. R. A. Blomberg, P. E. M. Siegbahn, *Mol. Phys.* **2003**, *101*, 323.

[92] C. W. Hoganson, personal communication.

[93] J. B. Reitz, E. I. Solomon, *J. Am. Chem. Soc.* **1998**, *120*, 11467.

[94] M. Hunger, J. Weitkamp, *Angew. Chem.* **2001**, *113*, 3040; *Angew. Chem. Int. Ed.* **2001**, *40*, 2954.

[95] G. W. Hearne, M. L. Adams (Shell Development Co.), US Patent 2,451,485, **1948**.

[96] H. H. Voge, C. R. Adams, *Adv. Catal.* **1967**, *17*, 151.

[97] C. R. Adams, T. J. Jennings, *J. Catal.* **1964**, *3*, 549.

[98] D. J. Hucknall, *Selective Oxidations of Hydrocarbons*, Academic Press, London, **1974**.

[99] H. H. Voge, C. D. Wagner, D. P. Stevenson, *J. Catal.* **1963**, *2*, 58; C. R. Adams, T. J. Jennings, *J. Catal.* **1963**, *2*, 63.

[100] D. Arntz, M. Höpp, S. Jacobi, J. Sauer, T. Ohara, T. Sato, N. Shimizu, G. Prescher, H. Schwind, O. Weiberg in *Ullmann's Encyclopedia of Industrial Chemistry*, Wiley-VCH, Weinheim, **2002**.

[101] a) J. D. Idol, US Patent 2,904,580, **1959**; J. L. Callahan, R. W. Foreman, F. Veatch, US Patent 3,044,966, **1962**; G. W. Keulks, L. D. Krenzke, T. M. Notermann, *Adv. Catal.* **1978**, *27*, 183; b) R. K. Grasselli, J. D. Burrington, *Adv. Catal.* **1981**, *30*, 133; c) R. K. Grasselli, J. D. Burrington, *Ind. Eng. Chem. Prod. Res. Dev.* **1984**, *23*, 394; d) A. B. Anderson, D. W. Ewing, Y. Kim, R. K. Grasselli, J. D. Burrington, J. F. Brazdil, *J. Catal.* **1985**, *96*, 222; e) J. Belagem, J. A. Osborn, J. Kress, *J. Mol. Catal.* **1994**, *86*, 267; f) R. K. Grasselli in *Handbook of Heterogeneous Catalysis* (Eds.: G. Ertl, H. Knözinger, J. Weitkamp), Wiley-VCH, Weinheim, **1997**, p. 2302.

[102] Y. H. Jang, W. A. Goddard III, *J. Phys. Chem. B* **2002**, *106*, 5997; Y. H. Jang, W. A. Goddard III, *Top. Catal.* **2001**, *15*, 273.

[103] a) $MoO_3/Bi_2O_3$: T. Ono, N. Ogata, Y. Mijaryo, *J. Catal.* **1996**, *161*, 78; T. Ono, H. Numata, N. Ogata, *J. Mol. Catal. A* **1996**, *105*, 31; b) V-O-M: I. E. Wachs, J.-M. Jehng, G. Deo, B. M. Weckhuysen, V. V. Guliants, J. B. Benzinger, S. Sundaresan, *J. Catal.* **1997**, *170*, 75; F. B. Abdelouahab, R. Olier, M. Ziyad, J. C. Volta, *J. Catal.* **1995**, *157*, 687; c) $Bi_2O_3$: M. Kinne, A. Heidenreich, K. Rademann, *Angew. Chem.* **1998**, *110*, 2637; *Angew. Chem. Int. Ed.* **1998**, *37*, 2509.

[104] J. Belgacem, J. Kress, J. A. Osborn, *J. Chem. Soc. Chem. Commun.* **1993**, 1125; J. Belgacem, J. Kress, J. A. Osborn, *J. Am. Chem. Soc.* **1992**, *114*, 1502.

[105] a) J. Kress, J. A. Osborn, *Angew. Chem.* **1992**, *104*, 1660; *Angew. Chem. Int. Ed. Engl.* **1992**, *31*, 1585; C. P. Casey, S. L. Hallenbeck, D. W. Pollock, C. R. Landis, *J. Am. Chem. Soc.* **1995**, *117*, 9770; P. T. Witte, A. Meetsma, B. Hessen, *J. Am. Chem. Soc.* **1997**, *119*, 10561; b) R. F. Nalewajski, A. Michalak, *J. Phys. Chem.* **1996**, *100*, 20076; Z. Wu, R. F. Jordan, J. L. Peterson, *J. Am. Chem. Soc.* **1995**, *117*, 5867.

[106] J. M. Mayer, K. A. Hall, *J. Am. Chem. Soc.* **1992**, *114*, 10402.

[107] C. Limberg, R. Boese, B. Schiemenz, *J. Chem. Soc. Dalton Trans.* **1997**, 1633.

[108] T. A. Hanna, A. L. Rieger, P. H. Rieger, X. Wang, *Inorg. Chem.* **2002**, *41*, 359.

[109] P. Ledgins, S. J. Rettig, L. Sanchez, *Organometallics* **1985**, *4*, 1470; G. N. Schrauzer, N. H. Liu, X. Zang, E. O. Schlemper, *Organometallics* **1988**, *7*, 279, and refs. therein; W. A. Herrmann, *J. Organomet. Chem.* **1990**, *382*, 1; J. W. Faller, R. R. Kucharczyk, Y. Ma, *Inorg. Chem.* **1990**, *29*, 1662; N. Meijboom, C. J. Schaverien, A. G. Orpen, *Organometallics* **1990**, *9*, 774; J. Sundermeyer, U. Radius, C. Burschka, *Chem. Ber.* **1992**, *125*, 2379; J. Sundermeyer, K. Weber, H. Pritzkow, *Angew. Chem.* **1993**, *105*, 751; *Angew. Chem. Int. Ed. Engl.* **1993**, *32*, 731; J. Sundermeyer, *Angew. Chem.* **1993**, *105*, 1195; *Angew. Chem. Int. Ed. Engl.* **1993**, *32*, 1144; P. A. van der Schaaf, J. Boersma, W. J. J. Smeets, A. L. Spek, G. van Knoten, *Inorg. Chem.* **1993**, *32*, 5108; W. Adam, J. Putterlik, R. M. Schuhmann, J. Sundermeyer, *Organometallics* **1996**, *15*, 4586; V. Pfennig, K. Seppelt, *Science* **1996**, *271*, 626, and refs. therein; U. Radius, J. Sundermeyer, *Chem. Ber.* **1992**, *125*, 2183; J. Sundermeyer, J. Putterlik, H. Pritzkow, *Chem. Ber.* **1993**, *126*, 289; R. R. Schrock, *Chem. Rev.* **2002**, *102*, 145.

[110] C. Borgmann, C. Limberg, S. Cunskis, P. Kircher, *Eur. J. Inorg. Chem.* **2001**, 349.

[111] C. Borgmann, C. Limberg, L. Zsolnai, *Chem. Commun.* **1998**, 2729.

[112] M. J. Almond, *Chem. Soc. Rev.* **1994**, *23*, 309.

[113] W. G. Klemperer, R.-S. Lin, *Inorg. Chem.* **1980**, *19*, 3863; M. Hunger, C. Limberg, P. Kircher, *Angew. Chem.* **1999**, *111*, 1171–1174; *Angew. Chem. Int. Ed.* **1999**, *38*, 1105; M. Hunger, C. Limberg, P. Kircher, *Organometallics* **2000**, *19*, 1044; M. Hunger, C. Limberg, E. Kaifer, P. Rutsch, *J. Organomet. Chem.* **2002**, *641*, 9; C. Limberg, M. Hunger, W. Habicht, E. Kaifer, *Inorg. Chem.* **2002**, *41*, 3359.

[114] J. H. Lunsford, *Angew. Chem.* **1995**, *107*, 1059; *Angew. Chem. Int. Ed. Engl.* **1995**, *34*, 970.

[115] J. H. Lunsford, *Catal. Today* **2000**, *63*, 165.

[116] R. H. Crabtree, *Chem. Rev.* **1995**, *95*, 987.

[117] V. R. Choudary, V. H. Rane, *J. Catal.* **1991**, *130*, 411; A. M. Maitra, I. Campbell, R. J. Tyler, *Appl. Catal. A* **1992**, *85*, 27; J. A. Lapszewicz, X.-Z. Jiang, *Catal. Lett.* **1992**, *13*, 103.

[118] V. D. Sokolovskii, S. M. Aliev, O. V. Buyevskaya, A. A. Davydov, *Catal. Today* **1989**, *4*, 293; O. V. Buyevskaya, A. I. Suleimanov, S. M. Aliev, V. D. Sokolovskii, *React. Kinet. Catal. Lett.* **1987**, *33*, 223.

[119] D. Dissanayake, J. H. Lunsford, M. P. Rosynek, *J. Catal.* **1994**, *146*, 613.

[120] H. F. Liu, R.-S. Liu, K. Y. Liew, R. E. Johnson, J. H. Lunsford, *J. Am. Chem. Soc.* **1984**, *106*, 4117.

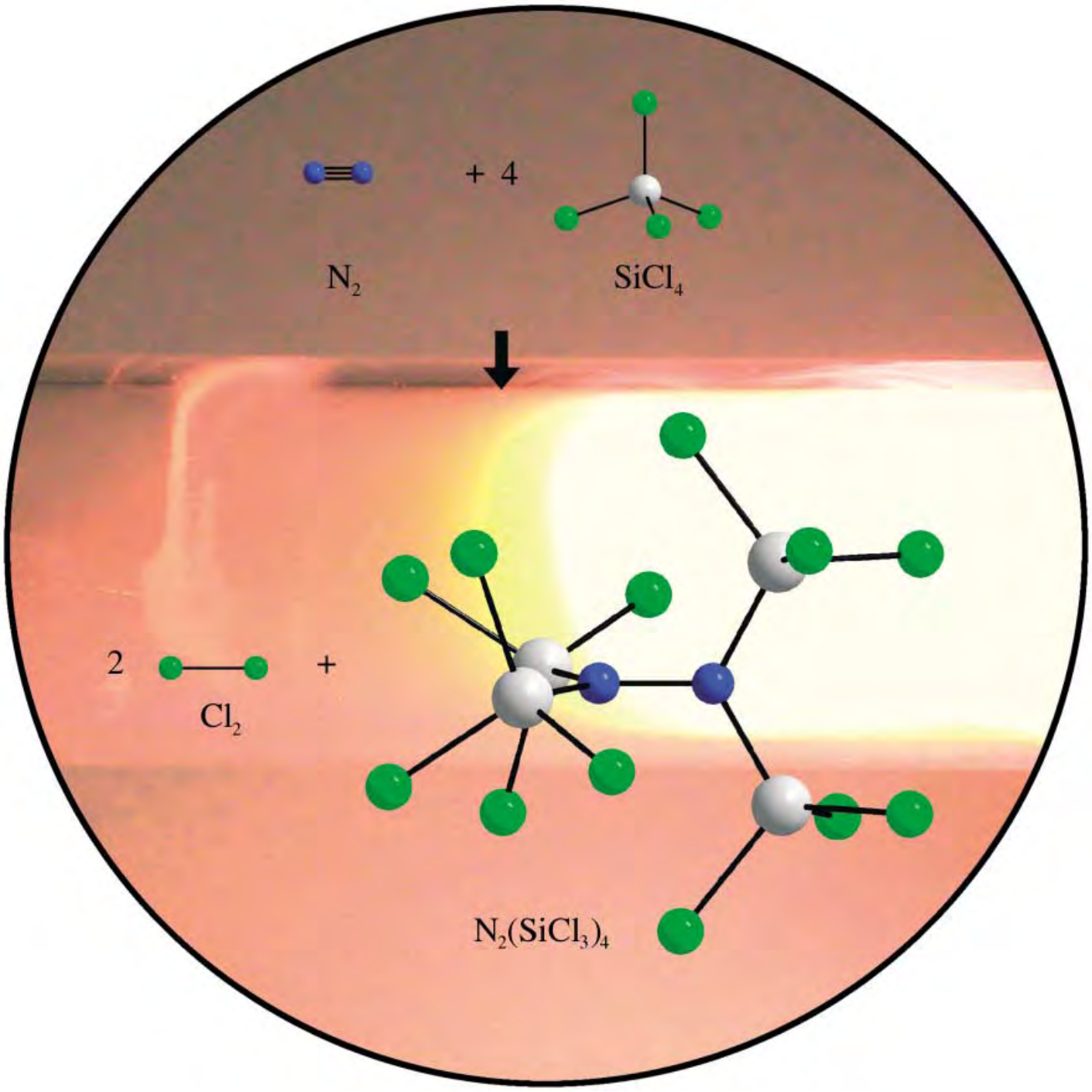
[121] H. Arakawa, M. Aresta, J. N. Armor, M. A. Barteau, E. J. Beckman, A. T. Bell, J. E. Bercaw, C. Creutz, E. Dinjus, D. A. Dixon, K. Domen, D. L. Dubois, J. Eckert, E. Fujita, D. H. Gibson, W. A. Goddard, D. W. Goodman, J. Keller, G. J. Kubas, H. H. Kung, J. E. Lyons, L. E. Manzer, T. J. Marks, K. Morokuma, K. N. Nicholas, R. Periana, L. Que, J. Rostrup-Nielson, W. M. H. Sachtler, L. D. Schmidt, A. Sen, G. A. Somorjai, P. C. Stair, B. R. Stults, W. Tumas, *Chem. Rev.* **2001**, *101*, 953.

 © 2003 Wiley-VCH Verlag GmbH & Co. KGaA, Weinheim 

[122] G. W. Coulston, S. R. Bare, H. Kung, K. Birkeland, G. K. Bethke, R. Harlow, N. Herron, P. L. Lee, *Science* **1997**, *275*, 191.
[123] T. R. Felthouse, J. C. Burnett, S. F. Mitchel, M. J. Mummy, *Kirk-Othmer Encyclopedia of Chemical Technology*, Wiley, New York, **1995**, p. 893.
[124] C. Limberg, R. Köppe, H. Schnöckel, *Angew. Chem.* **1998**, *110*, 512; *Angew. Chem. Int. Ed.* **1998**, *37*, 496.
[125] C. Limberg, R. Köppe, *Inorg. Chem.* **1999**, *38*, 2106.
[126] T. Wistuba, C. Limberg, *Eur. J. Inorg. Chem.* **1999**, 1335.
[127] T. Wistuba, C. Limberg, *Chem. Eur. J.* **2001**, *7*, 4674.
[128] J. S. Hess, S. Leelasubchareoen, A. L. Rheingold, D. J. Doren, K. H. Theopold, *J. Am. Chem. Soc.* **2002**, *124*, 2454.
[129] S. P. de Visser, F. Ogliaro, N. Harris, S. Shaik, *J. Am. Chem. Soc.* **2001**, *123*, 3037.
[130] D. Ostovic, T. C. Bruice, *Acc. Chem. Res.* **1992**, *25*, 314.
[131] B. Meunier, A. Robert, G. Pratviel, J. Bernadou in *The Porphyrin Handbook*, *Vol. 4* (Eds.: K. M. Kadish, K. M. Smith, R. Guilard), Academic Press, San Diego, **2000**, p. 119.
[132] J. T. Groves, Z. Gross, M. K. Stern, *Inorg. Chem.* **1994**, *33*, 5065.
[133] Z. Gross, S. Nimri, C. M. Barzilay, L. Simkhovich, *J. Biol. Inorg. Chem.* **1997**, *2*, 492.
[134] S. P. de Visser, F. Ogliaro, P. K. Sharma, S. Shaik, *J. Am. Chem. Soc.* **2002**, *124*, 11809.
[135] a) E. N. Jacobsen, *Acc. Chem. Res.* **2000**, *33*, 421; b) E. N. Jacobsen, M. H. Wu in *Comprehensive Asymmetric Catalysis* (Eds.: E. N. Jacobsen, A. Pfaltz, H. Yamamoto), Springer, Berlin, **1999**, chap. 18.2, p. 64; c) T. Katsuki in *Catalytic Asymmetric Synthesis*, 2nd ed. (Ed.: I. Ojima), Wiley, New York, **2000**, p. 287; d) T. Katsuki, *J. Mol. Catal. A* **1996** ,*113*, 87.
[136] a) C. Bousquet, D. G. Gilheany, *Tetrahedron Lett.* **1995**, *36*, 7739; b) C. T. Dalton, K. M. Ryan, V. M. Wall, C. Bousquet, D. G. Gilheany, *Top. Catal.* **1998**, *5*, 71; c) K. M. Ryan, C. Bousquet, D. G. Gilheany, *Tetrahedron Lett.* **1999**, *40*, 3613; d) A. M. Daly, C. T. Dalton, M. F. Renehan, D. G. Gilheany, *Tetrahedron Lett.* **1999**, *40*, 3617; e) A. M. Daly, M. F. Renehan, D. G. Gilheany, *Org. Lett.* **2001**, *3*, 663; f) C. P. O'Mahony, E. M. McGarrigle, M. F. Renehan, K. M. Ryan, N. J. Kerrigan, C. Bousquet, D. G. Gilheany, *Org. Lett.* **2001**, *3*, 3435; g) N. J. Kerrigan, I. J. Langan, C. T. Dalton, A. M. Daly, C. Bousquet, D. G. Gilheany, *Tetrahedron Lett.* **2002**, *43*, 2107.
[137] E. G. Samsel, K. Srinivasan, J. K. Kochi, *J. Am. Chem. Soc.* **1985**, *107*, 7606; T. L. Sidall, N. Miyaura, J. C. Huffmann, J. K. Kochi, *J. Chem. Soc. Chem. Commun.* **1983**, 1185; K. Srinivasan, J. K. Kochi, *Inorg. Chem.* **1985**, *24*, 4671.
[138] C. G. Miller, S. W. Gordon-Wylie, C. P. Horwitz, S. A. Strazisar, D. K. Peraino, G. R. Clark, S. T. Weintraib, T. J. Collins, *J. Am. Chem. Soc.* **1998**, *120*, 11540; F. M. MacDonnell, N. L. P. Fackler, C. Stern, T. V. O'Halloran, *J. Am. Chem. Soc.* **1994**, *116*, 7431; J. M. Workman, R. D. Powell, A. D. Procyk, T. J. Collins, D. F. Bocian, *Inorg. Chem.* **1992**, *31*, 1548; T. J. Collins, R. D. Powell, C. Slebodnick, E. S. Uffelman, *J. Am. Chem. Soc.* **1990**, *112*, 899; T. J. Collins, S. W. Gordon-Wylie, *J. Am. Chem. Soc.* **1989**, *111*, 4511.
[139] B. S. Mandimutsira, B. Ramdhanie, R. C. Todd, H. Wang, A. A. Zareba, R. S. Czernuszewicz, D. P. Goldberg, *J. Am. Chem. Soc.* **2002**, *124*, 15170.
[140] P. Brandt, P.-O. Norrby, A. M. Daly, D. G. Gilheany, *Chem. Eur. J.* **2002**, *8*, 4299.
[141] a) D. A. Plattner, D. Feichtinger, *Angew. Chem.* **1997**, *109*, 1796; *Angew. Chem. Int. Ed. Engl.* **1997**, *36*, 1718; b) D. A. Plattner, D. Feichtinger, J. El-Bahraoui, O. Wiest, *Int. J. Mass Spectrom.* **2000**, *195*/196, 351; c) D. Feichtinger, D. A. Plattner, *J. Chem. Soc. Perkin Trans. 2* **2000**, 1023; d) J. El-Bahraoui, O. Wiest, D. A. Plattner, D. Feichtinger, *Angew. Chem.* **2001**, *113*, 2131; *Angew. Chem. Int. Ed.* **2001**, *40*, 2073; e) D. Feichtinger, D. A. Plattner, *Chem. Eur. J.* **2001**, *7*, 591; f) EPR: K. A. Campbell, M. R. Lashley, J. K. Wyatt, M. H. Nantz, R. D. Britt, *J. Am. Chem. Soc.* **2001**, *123*, 5710; g) EPR/NMR: K. P. Bryliakov, D. E. Babushkin, E. P. Talsi, *J. Mol. Catal. A* **2000**, *158*, 19; h) EPR/MS: W. Adam, C. Mock-Knoblauch, C. R. Saha-Moller, M. Herderich, *J. Am. Chem. Soc.* **2000**, *122*, 9685.
[142] T. Linker, *Angew. Chem.* **1997**, *109*, 2150; *Angew. Chem. Int. Ed. Engl.* **1997**, *36*, 2060.
[143] E. N. Jacobsen, *Asymmetric Catalytic Epoxidation of Unfunctionalised Olefins in Catalytic Asymmetric Synthesis* (Ed.: I. Ojima), VCH, Weinheim, **1993**, p. 159.
[144] M. Palucki, N. S. Finney, P. J. Pospisil, M. L. Güler, T. Ishida, E. N. Jacobsen, *J. Am. Chem. Soc.* **1998**, *120*, 948; E. N. Jacobsen, W. Zhang, M. L. Güler, *J. Am. Chem. Soc.* **1991**, *113*, 6703; S. Chang, R. M. Heid, E. N. Jacobsen, *Tetrahedron Lett.* **1994**, *35*, 669; S. L. Vander Velde, E. N. Jacobsen, *J. Org. Chem.* **1995**, *60*, 5380.
[145] R. Irie, Y, Ito, T. Katsuki, *Synlett* **1991**, 265; R. Irie, K. Noda, Y. Ito, N. Matsumoto, T. Katsuki, *Tetrahedron: Asymmetry* **1991**, *2*, 481; M. Palucki, P. J. Pospisil, W. Zhang, E. N. Jacobsen, *J. Am. Chem. Soc.* **1994**, *116*, 9333.
[146] C. Linde, B. Åkermark, P.-O. Norrby, M. Svensson, *J. Am. Chem. Soc.* **1999**, *121*, 5083.
[147] T. Strassner, K. N. Houk, *Org. Lett.* **1999**, *1*, 419.
[148] L. Cavallo, H. Jacobsen, *Angew. Chem.* **2000**, *112*, 602; *Angew. Chem. Int. Ed.* **2000**, *39*, 589; L. Cavallo, H. Jacobsen, *Chem. Eur. J.* **2001**, *7*, 800; b) With another functional basis set combination a minimum was localized that corresponds to a radical intermediate: L. Cavallo, H. Jacobsen, *Eur. J. Inorg. Chem.* **2003**, 892.
[149] Y. G. Abashkin, J. R. Collins, S. K. Burt, *Inorg. Chem.* **2001**, *40*, 4040.
[150] Y. N. Ito, T. Katsuki, *Bull. Chem. Soc. Jpn.* **1999**, *72*, 603.
[151] W. Adam, W. Malisch, K. J. Roschmann, C. R. Saha-Möller, W. A. Schenk, *J. Organomet. Chem.* **2002**, *661*, 3.
[152] W. Adam, K. J. Roschmann, C. R. Saha-Möller, D. Seebach, *J. Am. Chem. Soc.* **2002**, *124*, 5068.
[153] Y. Yang, F. Diederich, J. S. Valentine, *J. Am. Chem. Soc.* **1991**, *113*, 7195; W. Nam, J. S. Valentine, *J. Am. Chem. Soc.* **1990**, *112*, 4977.
[154] a) H. Fu, G. C. Look, W. Zhang, E. N. Jacobsen, C.-H. Wong, *J. Org. Chem.* **1991**, *56*, 6497; b) C. Linde, M. Arnold, P.-O. Norrby, B. Åkermark, *Angew. Chem.* **1997**, *109*, 1802; *Angew. Chem. Int. Ed. Engl.* **1997**, *36*, 1723.
[155] C. Linde, N. Koliaï, P.-O. Norrby, B. Åkermark, *Chem. Eur. J.* **2002**, *8*, 2568.
[156] W. Nam, S. K. Choi, M. H. Lim, J.-U. Rohde, I. Kim, J. Kim, C. Kim, L. Que, Jr., *Angew. Chem.* **2003**, *115*, 113.
[157] T. Katsuki, *J. Mol. Catal. A* **1996**, *113*, 87; T. Katsuki, *Coord. Chem. Rev.* **1995**, *140*, 189; E. N. Jacobsen in *Catalytic Asymmetric Synthesis* (Ed.: I. Ojima), VCH, Weinheim, **1993**, p. 159; J. F. Larrow, E. N. Jacobsen, *J. Am. Chem. Soc.* **1994**, *116*, 12129; K. Hamachi, R. Irie, T. Katsuki, *Tetrahedron Lett.* **1996**, *37*, 497914; T. Hamada, R. Irie, J. Mihara, K. Hamachi, T. Katsuki, *Tetrahedron* **1998**, *54*, 10017.
[158] A. A. Fokin, P. A. Gunchenko, B. A. Tkachenko, E. D. Butova, A. G. Yurchenko, *Tetrahedron Lett.* **1997**, *38*, 639.

 © 2003 Wiley-VCH Verlag GmbH & Co. KGaA, Weinheim 

# Communications




The reactivity of usually inert elemental nitrogen can be increased significantly by microwave-induced plasma activation. An application of this phenomenon is the reaction of $SiCl_4$ with $N_2$ under plasma conditions to give the hydrazine derivative $N_2(SiCl_3)_4$, as shown by M. Binnewies and co-workers on the following pages.


**DOI: 10.1002/anie.200352575**
© 2003 Wiley-VCH Verlag GmbH & Co. KGaA, Weinheim

Plasma chemistry

# $N_2(SiCl_3)_4$—A Tetrakissilylhydrazine as an Unexpected Product of the Reaction between $N_2$ and $SiCl_4$

*Nils Schiefenhövel, Hans-Jörg Himmel, and Michael Binnewies**

*Dedicated to Professor Bernt Krebs on the occasion of his 65th birthday*

The formation of silicon–nitrogen compounds, such as $Si_3N_4$, by the reaction of $N_2$ with $SiCl_4$ is not possible for thermodynamic reasons. The Gibbs free energy $\Delta G^0_{298}$ for Equation (1) is calculated to be 1211.7 kJ mol$^{-1}$.

$$3\,SiCl_4(g) + 2\,N_2(g) \rightarrow Si_3N_4(s) + 6\,Cl_2(g) \quad (1)$$

The equilibrium for this reaction thus lies completely on the side of the reactants. Si–N–Cl compounds, so-called chlorosilazanes, can be considered as formal intermediate products of this reaction. Thus similar states of equilibrium can be expected. However, the reaction can be initiated if a gas plasma is used for activation. The synthesis of $N(SiCl_3)_3$ (**1**) and $Cl_3SiN(SiCl_2)_2NSiCl_3$ (**2**) in a glow discharge and a detailed characterization of these compounds has been reported.[1,2] Presumably the described reaction proceeds because of the formation of nitrogen atoms under plasma conditions. These nitrogen atoms have a relatively long lifetime—up to several minutes under suitable conditions.[3] The Gibbs free energy for Equation (2) is calculated to be −610.2 kJ mol$^{-1}$, and therefore the formation of $Si_3N_4$ should occur readily. Thus the formation of chlorosilazanes should also be thermodynamically allowed.

$$3\,SiCl_4(g) + 4\,N(g) \rightarrow Si_3N_4(s) + 6\,Cl_2(g) \quad (2)$$

We also studied the reaction of $SiCl_4$ with $N_2$. Instead of a glow discharge, we used microwaves to generate a plasma.[4] We also found **1** and **2** as main products of the reaction under these conditions. Furthermore, we observed another chlorosilazane, albeit in small amounts, which was identified by means of GC–MS to be $N_2(SiCl_3)_4$ (**3**; Figure 1).[5,6] The only reasonable structure for **3** is that of a silylhydrazine derivative (Figure 2). As only small quantities of **3** could be obtained from the plasma process, it is currently impossible to isolate the compound and to determine its crystal structure.

[*] Prof. Dr. M. Binnewies, Dr. N. Schiefenhövel
Institut für Anorganische Chemie der Universität Hannover
Callinstrasse 9, 30167 Hannover (Germany)
Fax: (+49) 511-762-19032
E-mail: binn@mbox.aca.uni-hannover.de
Dr. H.-J. Himmel
Institut für Anorganische Chemie der Universität Karlsruhe
Engesserstrasse 15, 76128 Karlsruhe (Germany)

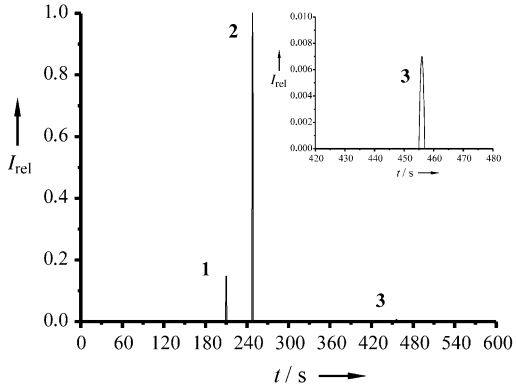



***Figure 1.*** Gas chromatogram of the plasma reaction products of $N_2$ with $SiCl_4$. The expansion (inset) shows the signal for **3**.

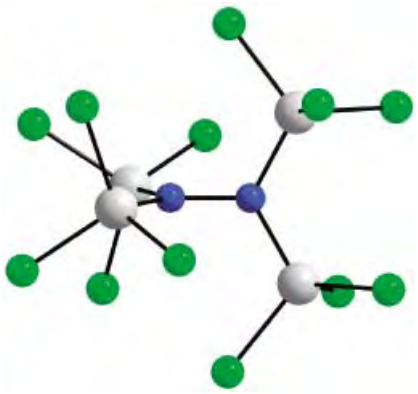


***Figure 2.*** Calculated molecular structure of **3** (N blue; Si gray; Cl green).

The structure given in Figure 2 was obtained by quantum chemical calculations with the TURBOMOLE program.[7] The BP functional was used in combination with the SV(P) and the TZVPP basis sets. For comparison, we also calculated the structure of the hydrogen-substituted analogue $N_2(SiH_3)_4$ (**4**; Figure 3), whose bond lengths and angles are known from electron-diffraction studies.[8] The calculated data agree well with experimental data (Table 1). The calculations support our assumption that **3** can be described as tetrakis(trichlorosilyl)hydrazine (Figure 2). The N–N bond length of **3** is nearly identical to that in hydrazine. In contrast to hydrazine, the two

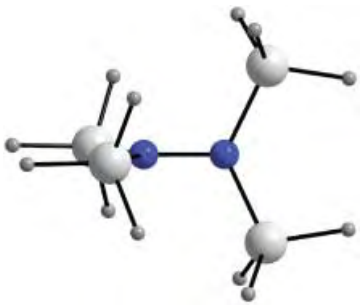


***Figure 3.*** Calculated molecular structure of **4** (N blue; Si light gray; H gray).

 © 2003 Wiley-VCH Verlag GmbH & Co. KGaA, Weinheim DOI: 10.1002/anie.200352575 

nitrogen atoms of the $C_2$-symmetrical compounds **3** and **4** adopt a trigonal planar geometry (Table 1).

Compound **3** is the first known tetrakis(silyl)hydrazine with completely halogenated silyl groups. The classic methods for the preparation of silylhydrazines are based on the elimination of hydrogen chloride from hydrazine and dichlorosilanes or on reactions between lithium hydrazides and halosilanes.[9–11] The tetrakis(silyl)hydrazine **4** was obtained in the gas-phase reaction of hydrazine with excess $SiH_3I$.[8,12] The first crystal structure of a tetrakis(silyl)hydrazine was described by Schmidbauer and co-workers, who obtained $N_2(PhH_2Si)_4$ (**5**) in the reaction of hydrazine with $PhH_2SiCl$.[13]

***Table 1:*** Comparison of the bond lengths [pm] and bond angles [°] of **3**, **4**, and $N_2H_4$.

| | **3**[a] | **4**[a] | **4**[b] | $H_2NNH_2$[a] |
|---|---|---|---|---|
| N–N | 145.0 | 147.2 | 145.7 ± 1.6 | 144.2 |
| N–Si | 177.3 | 176.1 | 173.1 ± 0.4 | – |
| N–H | – | – | – | 102.0/102.4 |
| Si–Cl | 204.9/205.4/ 205.7[c] | – | – | |
| Si–H | – | 149.3/149.6[d] | 148.7 ± 1.4 | |
| Si-N-Si | 123.94 | 129.39 | 129.7 ± 0.7 | |
| H-N-H | – | – | – | 107.10 |
| Si-N-N | 118.03 | 115.30 | 115.15 ± 0.7 | |
| H-N-N | – | – | – | 107.29 |

[a] Calculations carried out with the BP functional and the TZVPP basis set. [b] Data from electron-diffraction studies.[8] [c] The Si–Cl bond lengths in $SiCl_4$ were calculated to be 205.0 pm. [d] The Si–H bond lengths $SiH_4$ were calculated to be 149.3 pm.

According to our quantum chemical calculations, the reaction enthalpy $\Delta H_0^0(0)$ for reaction in Equation (3) amounts to 180.9 kJ mol$^{-1}$ (BP/SV(P)) and 179.7 kJ mol$^{-1}$ (BP/TZVPP). As an almost constant molar heat capacity is expected for the reaction, the reaction enthalpy can be estimated to be about 180 kJ mol$^{-1}$.

$$N_2H_4(g) + 4\,SiCl_4(g) \rightarrow N_2(SiCl_3)_4(g) + 4\,HCl(g) \quad (3)$$

When the known thermochemical data[14] are considered, the standard enthalpy of formation for **3** is calculated as $\Delta H_{298}^0 = -1994$ kJ mol$^{-1}$. As $SiI_4$ and **3** have similar molecular weights, the value of the standard entropies of formation of both gaseous compounds should be almost the same: $S_{298}^0(N_2(SiCl_3)_4) \approx S_{298}^0(SiI_4) = 417$ J mol$^{-1}$ K$^{-1}$.

A matter of particular interest is the reaction pathway that leads to the formation of **3**. According to thermodynamic data, **3** cannot be obtained by the reaction of $N_2$ with $SiCl_4$. However, the reaction of $N_2$ with $SiCl_3$ radicals—whose existence can be anticipated under plasma reaction conditions—may lead to **3**. A formation pathway via $N_2$, $SiCl_2$, and $SiCl_4$ is also possible from a thermodynamic point of view. Both pathways would lead to **3** with preservation of the N–N bond. However, we presume a formation mechanism for **3** that includes the cleavage of the N–N bond of $N_2$. The occurrence of $\cdot N(SiCl_3)_2$ radicals as intermediates seems to be reasonable. The latter pathway would be consistent with the chemical characteristics of $N_2F_4$, which partially dissociates into $NF_2$ radicals at room temperature.

Received: August 6, 2003 [Z52575]
Published Online: November 24, 2003

**Keywords:** hydrazines · nitrogen · plasma chemistry · silazanes

[1] A. Pflugmacher, H. Dahmen, *Z. Anorg. Allg. Chem.* **1957**, *290*, 184–190.
[2] U. Wannagat, R. Flindt, D. J. Brauer, H. Bürger, F. Dörrenbach, *Z. Anorg. Allg. Chem.* **1989**, *572*, 33–46.
[3] N. N. Greenwood, A. Earnshaw, *Chemistry of the Elements*, 1st ed., Pergamon, Oxford, **1989**.
[4] The apparatus contains needle valves to regulate the gas flow of the reactants (a high-precision needle valve for $N_2$ (Linde 4.0), a precision needle valve (Young) for $SiCl_4$ (Riedel 99%, purified by fractional condensation in vacuo)), a quartz tube ($\varnothing$ = 20 mm), and cold traps for condensation of the products. The microwaves were produced in a microwave generator (Electromedical Supplies, Mikrotron 100, Mark 3, 2450 MHz) and applied to the reaction zone through a hollow conductor. The reaction is carried out in a dynamic vacuum, with $p(N_2) = p(SiCl_4) = 100$ Pa.
[5] GC–MS: gas chromatograph Varian Star 3400 CX, mass spectrometer Finnigan MAT SSQ7000; ionization: EI (70 eV), CI (reactant gas: methane 10 mbar). The fragments were identified on the basis of the *m*/*z* values and the isotope pattern. Only the *m*/*z* values of the most intense peak of each group are given (relative intensity in parenthesis: MS (EI): [$M^+$] 566 (15), [$M^+-SiCl_4$] 396 (100), [$M^+-SiCl_5$] 361 (4), [$M^+-NSi_2Cl_8$] 212 (20), [$SiCl_3^+$] 133 (30); MS (CI): [$M^+$+H] 567 (87), [$M^+-Cl+CH_4$] 547 (15), [$M^+-Cl$] 531 (100).
[6] A colorless liquid product (1 mL) was obtained after a reaction period of 20 h. Condensation in vacuo led to the separation of 90% of the more volatile products **1** and **2**. The residue was analyzed by means of GC–MS.
[7] R. Ahlrichs, M. Bär, M. Häser, H. Horn, C. Kölmel, *Chem. Phys. Lett.* **1989**, *162*, 165; K. Eichkorn, O. Treutler, H. Öhm, M. Häser, R. Ahlrichs, *Chem. Phys. Lett.* **1995**, *240*, 283; K. Eichkorn, O. Treutler, H. Öhm, M. Häser, R. Ahlrichs, *Chem. Phys. Lett.* **1995**, *242*, 652; K. Eichkorn, F. Weigend, O. Treutler, R. Ahlrichs, *Theor. Chem. Acc.* **1997**, *97*, 119; F. Weigend, M. Häser, *Theor. Chem. Acc.* **1997**, *97*, 331; F. Weigend, M. Häser, H. Patzelt, R. Ahlrichs, *Chem. Phys. Lett.* **1998**, *294*, 143.
[8] C. Glidewell, D. W. H. Rankin, A. G. Robiette, G. M. Sheldrick, *J. Chem. Soc. A* **1970**, 318.
[9] U. Klingebiel, S. Schmatz, E. Gellermann, C. Drost, M. Noltemeyer, *Monatsh. Chem.* **2001**, *132*, 1105.
[10] E. Gellermann, U. Klingebiel, T. Pape, F. Dall′Antonia, T. R. Schneider, S. Schmatz, *Z. Anorg. Allg. Chem.* **2001**, *627*, 2581.
[11] K. Bode, U. Klingebiel, *Adv. Organomet. Chem.* **1996**, *40*, 1.
[12] B. J. Aylett, *J. Inorg. Nucl. Chem.* **1956**, *2*, 325.
[13] N. W. Mitzel, P. Bissinger, H. Schmidbaur, *Chem. Ber.* **1993**, *126*, 345.
[14] M. Binnewies, E. Milke, *Thermochemical Data of Elements and Compounds*, 2nd ed., Wiley-VCH, Weinheim, New York, **2002**.

 © 2003 Wiley-VCH Verlag GmbH & Co. KGaA, Weinheim 

Asymmetric Synthesis

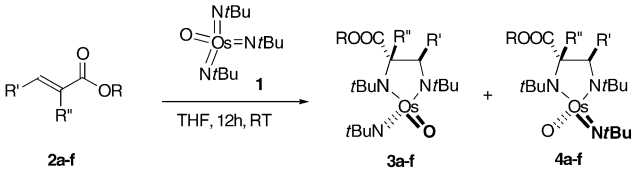
# Stereochemically Defined Osmium Centers from Asymmetric Diamination of Olefins: Mechanistic Implications for Osmium-Mediated Acrylate Functionalization**

*Kilian Muñiz,* Martin Nieger, and Heidi Mansikkamäki*

*Dedicated to Professor Ryoji Noyori*

Investigations on transition-metal complexes with stereogenic metal centers were pioneered by Brunner in 1969, who achieved the resolution of a complex with a pseudo-tetrahedrally coordinated chiral manganese atom.[1] Such complexes, which are also referred to as "chiral-at-metal complexes", [2] have gained important application in organic synthesis,[3] chiral recognition,[4] material sciences,[5] and fundamental basic research.[6] For example, in the area of enantioselective catalysis seminal work by Noyori on transfer hydrogenation of ketones and imines relies on a catalyst with a continuously regenerated stereogenic ruthenium center.[7] All these compounds usually originate either from stereoselective modification of racemic chiral-at-metal complexes with enantiomerically pure auxiliaries or from complexation of prochiral metal centers to chiral, non-racemic ligands.

Herein we report on a conceptually novel approach for the synthesis of stereogenic, tetrahedrally coordinated osmium atoms in an asymmetric diamination. Osmium(VIII) complexes have been most successful in oxidative C–C double-bond transformations. Among these reactions, Sharpless dihydroxylation and aminohydroxylation have been highly acclaimed,[8] whereas related diamination reactions have received only scant attention.[9–11] We have recently reported on the stereoselective diamination of olefins by reaction of bis(*N*-*tert*-butylimido)dioxoosmium(VIII) with fumaric and acrylic ester derivatives[10] to give stable monomeric osmaimidazolidines.[11] When the corresponding trisimidoosmium complex **1** is allowed to react with unsymmetrical esters such as methyl cinnamate **2a**, clean formation of two new compounds is observed (Scheme 1). These were identified as a pair of diastereomeric chiral-at-metal osmaimidazolidines.[12] The two diastereomers, which, according to NMR spectroscopy, were formed in the ratio of 62:38, could be separated by conventional column chromatography. The (2*R*,4*R*,5*S*)/(2*S*,4*S*,5*R*) configuration for the major diastereomer **3a** was determined by X-ray structure analysis.[13]




***Scheme 1.*** Stereogenic osmium centers from diamination of electron-deficient olefins with trisimidoosmium reagent **1**.

Other cinnamates and crotonates gave comparable diastereomeric ratios. In contrast, diastereomeric ratios for osmaimidazolidines obtained from the methyl and *tert*-butyl esters of acrylic and methacrylic acid were significantly higher (Table 1). Apparently, steric bulk in the 3-position has a deteriorating effect on the diastereomeric ratio, whereas it is advantageous when placed in the ester group. A Hammett correlation revealed a $\rho$ value of $+0.28$ for diamination of various 4-aryl substituted ethyl cinnamates.[14] This points to an increase in the rate of the reaction with increasing electrophilicity of the olefin in the presence of the imidoosmium reagent **1** with strongly nucleophilic character.[15] For all reactions of cinnamic esters, diastereomeric ratios were unchanged between 10 and 95% conversion within NMR accuracy and did not show temperature dependence between $-5$ and 30 °C. Moreover, NMR experiments in [$D_8$]toluene confirmed that the isolated products did not epimerize between $-80$ to 90 °C. These results prove the configurational stability of the chiral-at-metal osmaimidazolidines reported.

There has been a pronounced interest in the mechanism of the Sharpless AD reaction over the past years[8,16,17] which was

***Table 1:*** Diastereomeric ratios for syntheses of chiral-at-metal-osmaimidazolidines.

| Entry | Compound | R′ | R″ | R | Products | d.r.[a] | Yield [%][b] |
|---|---|---|---|---|---|---|---|
| 1 | **2a** | $C_6H_5$ | H | $CH_3$ | **3a/4a** | 62:38 | 90 |
| 2 | **2b** | $CH_3$ | H | $CH_3$ | **3b/4b** | 60:40 | 91 |
| 3 | **2c** | H | H | $CH_3$ | **3c/4c** | 90:10 | 97 |
| 4 | **2d** | H | H | $C(CH_3)_3$ | **3d/4d** | 93:7 | 95 |
| 5 | **2e** | H | $CH_3$ | $CH_3$ | **3e/4e** | 96:4 | 97 |
| 6 | **2f** | H | $CH_3$ | $C(CH_3)_3$ | **3f/4f** | $>98:<2$ | 99 |

[a] Diastereomeric ratio (d.r.) as determined from $^1$H NMR spectra of the crude reaction mixture. [b] Yield after isolation of the two diastereoisomers by column chromatography.

[*] Dr. K. Muñiz
Kekulé-Institut für Organische Chemie und Biochemie
Rheinische Friedrich-Wilhelms-Universität
Gerhard-Domagk-Strasse 1, 53121 Bonn (Germany)
Fax: (+49) 228-73-5813
E-mail: kilian.muniz@uni-bonn.de
Dr. M. Nieger, H. Mansikkamäki
Institut für Anorganische Chemie
X-ray Structure Analysis
Rheinische Friedrich-Wilhelms-Universität
Gerhard-Domagk-Strasse 1, 53121 Bonn (Germany)

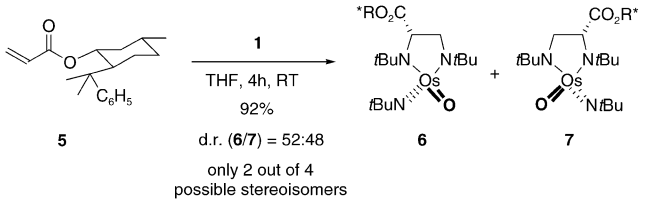
[**] K.M. gratefully acknowledges generous support from Prof. Dr. K. H. Dötz and from the Fonds der Chemischen Industrie (Liebig fellowship 2000–2003). H.M. thanks the Finnish Academy for a grant. The authors thank Mr. A. Schneider for assistance with HPLC measurements.

Supporting information for this article is available on the WWW under http://www.angewandte.org or from the author.

 © 2003 Wiley-VCH Verlag GmbH & Co. KGaA, Weinheim DOI: 10.1002/anie.200352244 

debated to proceed either by a concerted [3+2] mechanism[18] or an alternative stepwise [2+2] mechanism.[19] The present example constitutes a novel reaction in that it concomitantly creates stable and isolable products with both stereogenic carbon and osmium centers. For the mechanism of this oxidative diamination, the resulting chirality of the osmium center may therefore serve as a stereochemical probe.

Since standard Cinchona alkaloid ligands do not complex **1**,[11] synthesis of optically active products was accomplished with the aid of chiral, enantiomerically pure auxiliaries. We have previously employed (−)-8-phenylmenthol as auxiliary in asymmetric diaminations with the related bisimido complex.[10,11] In the present case, diamination of (−)-8-phenylmenthyl cinnamate and crotonate yielded four stereoisomers in different ratios of about 7:3:1:1 and 6:3:1:1, respectively. In contrast, (−)-8-phenylmenthyl acrylate **5a** and the corresponding 8-phenylmenthyl methacrylate reacted faster and produced an almost equal mixture of only two diastereomers (ratio = 1:1:0:0) that could be separated by semipreparative HPLC (Scheme 2).




***Scheme 2.*** Asymmetric diamination to yield enantiomerically pure chiral-at-metal osmaimidazolidines. The diastereomeric ratios were determined by analytical HPLC and $^1$H NMR spectroscopy. R*OH = (−)-8-phenylmenthol.

The structures of the two diastereomers **6** and **7** were characterized by X-ray crystallography (Figure 1). They are the first structural elucidations of osmaimidazolidines with defined absolute configuration at the osmium center.

Formation of up to four stereoisomers is conceivable in the reaction of **1** with enantiopure α,β-unsaturated esters. These are indeed observed for the respective crotonate and cinnamate substrates, although in rather unequal amounts. However, only two products are formed in the reaction of **1** with acrylates and methacrylates. This dependence of stereoselectivity on olefin geometry is noteworthy. Regarding the formation of the two diastereomers from **1** and the chiral acrylate **5** within a [3+2] process, the necessary stereoselection would be assumed to arise from an efficient π interaction between the phenyl group of the terpene and the *Si* face of the olefin, as observed in corresponding diamination reactions with the related bisimido reagent.[10,11] Such a selection step with an approach of the achiral **1** to the free *Re* face of the substrate would result in two diastereomeric products **6** and **8** with opposite absolute configuration at the central Os atom but with the same absolute configuration in the backbone of the osmaimidazolidine (Figure 2).

However, the two products **6** and **7** differ both in absolute configuration at Os and in the osmaimidazolidine backbone, and these absolute configurations are inconsistent with a concerted, *syn*-specific [3+2] mechanism of olefin face differ-

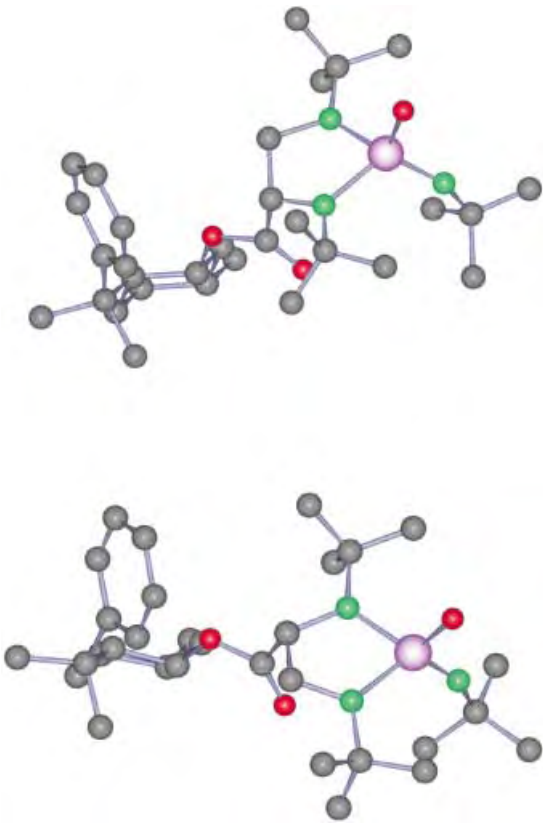


***Figure 1.*** Solid-state structures of the compounds **6** (top) and **7** (bottom);[20] C: gray, N: green, O: red, Os: pink.

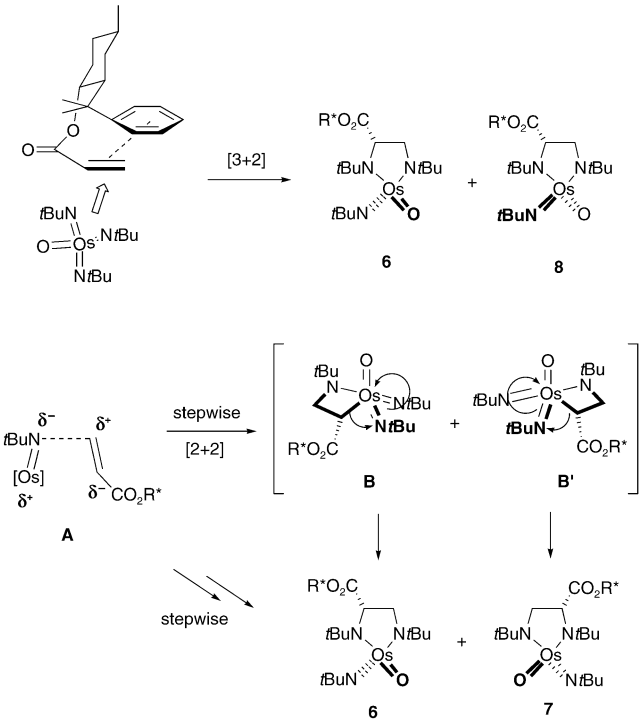



***Figure 2.*** Incompatible π-stacking model for [3+2] transition state and the proposed stepwise sequence for the equimolar formation of the diastereomers **6** and **7**. R*OH = (−)-8-phenylmenthol.

 © 2003 Wiley-VCH Verlag GmbH & Co. KGaA, Weinheim 

entiation. Since there is no apparent alternative stereoselection for a concerted [3+2] reaction, the observed product formation in acrylate diamination must occur by a different pathway.

In view of the high polarity of acrylates and given the strong nucleophilic character of **1**, a stepwise reaction sequence appears reasonable. Such a sequence would be initiated by interaction (**A**) between a nucleophilic imido ligand in **1** and the electrophilic 3-position of the acrylate. This initial regioselective step of 1,4-addition to the acrylate terminus is then followed by either direct C–N bond formation to give **6** or **7**, or occurrence of an intermediary Os–C bond formation to give osmaazetane intermediates **B**/**B**′ and subsequent rearrangement to the osmaimidazolidine products. In such a case the formal product of a [2+2] addition is formed, from which the product arises by stereospecific rearrangement. In both of these cases, there is necessarily no stereoselection regarding the resulting chiral carbon center. Product formation through a stepwise process with reversed regioselectivity can be excluded rigorously for electronic and stereochemical reasons. Apart from the steric involvement, the chiral terpene auxiliary does not exercise any further influence on the course of the reaction but delivers the crucial stereochemical information for differentiation between **6** and **7**. The steric influence of the 8-phenylmenthyl ester group on the reaction course is in agreement with the increase in the diastereomeric ratio for the achiral acrylic and methacrylic substrates **2c**–**f** (Table 1, entries 3–6). Such an overall stepwise reaction pathway explains the occurrence of only two diastereomeric products, the observed diastereomeric ratio, and the absolute configurations of the osmaimidazolidine backbone, much better than any [3+2] mechanism does.

We therefore consider such a stepwise mechanism the most reasonable pathway for osmaimidazolidine formation from the trisimido complex **1** and an acrylic or methacrylic ester. Given the different outcome of the reaction for 3-substituted olefins such as crotonates and cinnamates, alternative mechanisms and/or additional reaction pathways must be involved in these cases. Owing to the reactivity of the osmium complex **1** with its special steric and electronic properties,[11,14] this diamination cannot be directly compared to the catalytic Sharpless AD and AA reactions that involve osmium tetroxide and its monoimido complexes. However, the present example confirms that investigation on the mechanistic pathways of osmium-mediated olefin functionalization may still provide surprises.

In summary, we have described the synthesis of new osmaimidazolidine complexes that contain osmium atoms with defined absolute stereochemistry by an asymmetric diamination of olefins. The analysis of the absolute configuration at the osmium atom suggests the occurrence of a nonconcerted mechanism for the olefin functionalization in the case of the acrylic esters. We are currently investigating other substrates and olefin geometries to determine the general mechanistic pathways involved in osmaimidazolidine formation from diaminations with **1**.

Received: June 27, 2003
Revised: October 29, 2003 [Z52244]

**Keywords:** alkenes · asymmetric synthesis · osmium · oxidation

[1] H. Brunner, *Angew. Chem.* **1969**, *81*, 395 – 396; *Angew. Chem. Int. Ed. Engl.* **1969**, *8*, 382 – 383.
[2] a) H. Brunner, *Angew. Chem.* **1999**, *111*, 1248 – 1263; *Angew. Chem. Int. Ed.* **1999**, *38*, 1194 – 1208; b) C. Ganter, *Chem. Soc. Rev.* **2003**, *32*, 130 – 138; c) H. Brunner, *Eur. J. Inorg. Chem.* **2001**, 905 – 912.
[3] For example: a) S. G. Davies, *Pure Appl. Chem.* **1988**, *60*, 13 – 20; b) S. G. Davies, *Aldrichimica Acta* **1990**, *23*, 31; c) J. W. Faller, M. R. Mazzieri, J. T. Nguyen, J. Parr, M. Tokunaga, *Pure Appl. Chem.* **1994**, *66*, 1463 – 1469.
[4] J. A. Gladysz, B. J. Boone, *Angew. Chem.* **1997**, *109*, 566 – 602; *Angew. Chem. Int. Ed. Engl.* **1997**, *36*, 550 – 583.
[5] R. Dembinski, T. Bartik, M. Jaeger, J. A. Gladysz, *J. Am. Chem. Soc.* **2000**, *122*, 810 – 822.
[6] P. Schwerdtfeger, J. Gierlich, T. Bollwein, *Angew. Chem.* **2003**, *115*, 1331 – 1334; *Angew. Chem. Int. Ed.* **2003**, *42*, 1293 – 1296.
[7] a) K.-J. Haack, S. Hashiguchi, A. Fujii, T. Ikariya, R. Noyori, *Angew. Chem.* **1997**, *109*, 297 – 300; *Angew. Chem. Int. Ed. Engl.* **1997**, *36*, 285 – 288; b) R. Noyori, M. Yamakawa, S. Hashiguchi, *J. Org. Chem.* **2001**, *66*, 7931 – 7944.
[8] a) K. B. Sharpless, *Angew. Chem.* **2002**, *114*, 2126 – 2135; *Angew. Chem. Int. Ed.* **2002**, *41*, 2024 – 2032; b) H. C. Kolb, M. S. VanNieuwenhze, K. B. Sharpless, *Chem. Rev.* **1994**, *94*, 2483 – 2547; c) C. Bolm, J. P. Hildebrand, K. Muñiz in *Catalytic Asymmetric Synthesis* (Ed.: I. Ojima), Wiley-VCH, Weinheim, **2000**, p. 299; d) H. C. Kolb, K. B. Sharpless in *Transition Metals for Organic Synthesis* (Eds.: M. Beller, C. Bolm), Wiley-VCH, Weinheim, **1998**, p. 219.
[9] a) A. O. Chong, K. Oshima, K. B. Sharpless, *J. Am. Chem. Soc.* **1977**, *99*, 3420 – 3426; b) M. H. Schofield, T. P. Kee, J. T. Anhaus, R. R. Schrock, K. H. Johnson, W. M. Davis, *Inorg. Chem.* **1991**, *30*, 3595 – 3604.
[10] K. Muñiz, M. Nieger, *Synlett* **2003**, 211 – 214.
[11] K. Muñiz, A. Iesato, M. Nieger, *Chem. Eur. J.* **2003**, *9*, 5581 – 5596.
[12] Recent synthetic approaches to pseudo-tetrahedral chiral-at-metal osmium complexes: a) H. Brunner, M. Weber, M. Zabel, T. Zwack, *Angew. Chem.* **2003**, *115*, 1903 – 1907; *Angew. Chem. Int. Ed.* **2003**, *42*, 1859 – 1862; b) H. Brunner, T. Zwack, M. Zabel, W. Beck, A. Bohm, *Organometallics* **2003**, *22*, 1741 – 1750; c) J. W. Faller, J. Parr, *Organometallics* **2001**, *20*, 697 – 699; d) J. W. Faller, A. R. Lavoie, *Organometallics* **2002**, *21*, 3493 – 4395; e) see references [1] and [2].
[13] Full data on this X-ray analysis will be published elsewhere.
[14] a) K. Muñiz, unpublished results; b) The observed scenario of a positive $\rho$-value has been discussed by Sharpless as an electronically extreme case in dihydroxylation reactions with $OsO_4$. See ref [8d] and D. W. Nelson, A. Gypser, P. T. Ho, H. C. Kolb, T. Kondo, H.-L. Kwong, D. V. McGrath, A. E. Rubin, P.-O. Norrby, K. P. Gable, K. B. Sharpless, *J. Am. Chem. Soc.* **1997**, *119*, 1840 – 1858.
[15] This nucleophilic character originates from the electronic properties by the three alkylimido ligands with basic lone pairs.[11] Thus, **1** can be regarded as an electron-rich complex with a formal electron count of 18 and an alternating nitrogen–osmium triple bond. For a discussion on osmium complexes with 18 or more electrons, see: E. J. Corey, S. Sarshar, M. D. Azimioara, R. C. Newbold, M. C. Noe, *J. Am. Chem. Soc.* **1996**, *118*, 7851 – 7852.
[16] Selected work: a) T. Göbel, K. B. Sharpless, *Angew. Chem.* **1993**, *105*, 1417 – 1418; *Angew. Chem. Int. Ed. Engl.* **1993**, *32*, 1329 – 1331; b) P.-O. Norrby, H. Becker, K. B. Sharpless, *J. Am. Chem. Soc.* **1996**, *118*, 35 – 42; c) H. C. Kolb, P. G. Andersson, K. B. Sharpless, *J. Am. Chem. Soc.* **1994**, *116*, 1278 – 1291; d) E. J.

 © 2003 Wiley-VCH Verlag GmbH & Co. KGaA, Weinheim 

Corey, M. C. Noe, *J. Am. Chem. Soc.* **1996**, *118*, 319 – 329; e) E. J. Corey, S. Sarshar, M. D. Azimioara, R. C. Newbold, M. C. Noe, *J. Am. Chem. Soc.* **1996**, *118*, 7851 – 7852; f) E. J. Corey, M. C. Noe, *J. Am. Chem. Soc.* **1996**, *118*, 11038 – 11053; g) for a more detailed discussion, see reference [8c].

[17] Selected theoretical investigations: a) A. J. DelMonte, J. Haller, K. N. Houk, K. B. Sharpless, D. A. Singleton, T. Strassner, A. A. Thomas, *J. Am. Chem. Soc.* **1997**, *119*, 9907 – 9908; b) D. V. Deubel, G. Frenking, *Acc. Chem. Res.* **2003**, *36*, 645 – 651; c) N. Moitessier, C. Henry, C. Len, Y. Chapleur, *J. Org. Chem.* **2002**, *67*, 7275 – 7282.

[18] a) J. Böseken, *Recl. Trav. Chim. Pays-Bas* **1922**, *41*, 199 – 207; b) R. Criegee, *Justus Liebigs Ann. Chem.* **1936**, 522, 75 – 96.

[19] K. B. Sharpless, A. Y. Teranishi, J. E. Bäckvall, *J. Am. Chem. Soc.* **1977**, *99*, 3120 – 3128.

[20] X-ray structure analysis for compound **6**: $C_{31}H_{53}N_3O_3Os$: red crystals, crystal dimensions $0.10 \times 0.15 \times 0.20\ mm^3$; $M_r = 705.96$; trigonal, space group $P\bar{3}$ (no. 143), $a = 29.0798(7)$, $c = 10.1329(2)$ Å, $V = 7420.7(3)$ Å$^3$, $Z = 12$, $\mu(Mo_{K\alpha}) = 3.899\ mm^{-1}$, $T = 123(2)$ K, $F(000) = 3240$. A total of 67901 reflections up to $2\theta_{max.} = 50°$ were measured on a Nonius KappaCCD diffractometer with $Mo_{K\alpha}$ radiation, 17327 of which were independent and used for all calculations. The structure was solved by direct methods and refined anisotropically (full-matrix least-squares refinement against $F^2$, 1027 parameters, 1 restraint), the H atoms were refined with a riding model ($wR2(F^2) = 0.0796$, $R1 = 0.0445$ for $I > 2\sigma(I)$). The absolute configuration was determined by refinement of Flack's $x$ parameter, $x = 0.003(6)$). X-ray structure analysis for compound **7**: $C_{31}H_{53}N_3O_3Os$: red crystals, crystal dimensions $0.10 \times 0.20 \times 0.45\ mm^3$; $M_r = 705.96$; monoclinic, space group $P2_1$ (no. 4), $a = 13.2337(1)$, $b = 10.2559(1)$, $c = 25.1757(3)$ Å, $\beta = 103.008(1)°$, $V = 3329.25(6)$ Å$^3$, $Z = 4$, $\mu(Mo_{K\alpha}) = 3.862\ mm^{-1}$, $T = 123(2)$ K, $F(000) = 1440$. A total of 57089 reflections up to $2\theta_{max.} = 50°$ were measured on a Nonius KappaCCD diffractometer with $Mo_{K\alpha}$ radiation, 11733 of which were independent and used for all calculations. The structure was solved by direct methods and refined anisotropically (full-matrix least-squares refinement against $F^2$, 685 parameters, 1 restraint), the H atoms were refined with a riding model ($wR2(F^2) = 0.0539$, $R1 = 0.0340$ for $I > 2\sigma(I)$). The absolute configuration was determined by refinement of Flack's $x$ parameter, $x = -0.029(5)$). CCDC-213515 (**6**) and CCDC-213516 (**7**) contain the supplementary crystallographic data for this paper. These data can be obtained free of charge via www.ccdc.cam.ac.uk/conts/retrieving.html (or from the Cambridge Crystallographic Data Centre, 12, Union Road, Cambridge CB2 1EZ, UK; fax: (+44) 1223-336-033; or deposit@ccdc.cam.ac.uk).

 © 2003 Wiley-VCH Verlag GmbH & Co. KGaA, Weinheim 

Modeling Metalloproteins

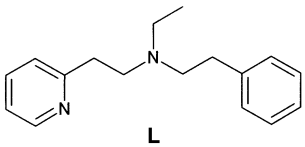
# Mechanism of the Aliphatic Hydroxylation Mediated by a Bis(μ-oxo)dicopper(III) Complex**

*Philipp Spuhler and Max C. Holthausen**

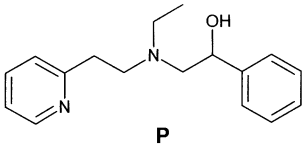
*Dedicated to Professor Helmut Schwarz on the occasion of his 60th birthday*

In the past two decades major research activities have been devoted to the understanding of structure–activity relationships related to binding and activation of dioxygen by copper-based metalloproteins, such as hemocyanin, tyrosinase, catecholoxidase, dopamine β-hydroxylase, or particulate methane monooxygenase.[1] Along these lines of investigation remarkable progress in bioinorganic research has led to a number of studies in which small synthetic $Cu^I$ complexes in solution bind $O_2$, cleave the O–O bond, and/or incorporate $O_2$-derived oxygen atoms into the C–H bonds of organic substrates at low temperatures.[2] By design, these complexes contain a $[Cu_2O_2]$ core as a key structural motif to mimic the biocatalytically active species.[3] Experimental efforts to characterize the active copper species, intermediates, and products have been successful for a variety of model systems that selectively mediate the aromatic hydroxylation,[4] whereas such achievements are less numerous for systems mediating the hydroxylation of aliphatic C–H bonds.[5]

Recently, Itoh et al. published a detailed kinetic study of the intramolecular hydroxylation of benzylic C–H bonds, which occurred after exposure of an acetone solution of $[Cu^I(\mathbf{L})(CH_3CN)]PF_6$ ($\mathbf{L}$ = *N*-ethyl-*N*-[2-(2-pyridyl)ethyl]-2-phenylethylamine) to $O_2$ gas and lead to formation of the product alcohol **P** in 46% yield.[6]




**L**




**P**

An intermediate formed at the start of the reaction and detectable at −90 °C was proposed to be a dinuclear bis(μ-oxo)dicopper(III) species. The suggestion was based on the intermediate's characteristic UV/Vis absorption and reso-

[*] Dr. M. C. Holthausen, Dipl.-Chem. P. Spuhler
Fachbereich Chemie, Philipps-Universität Marburg
Hans-Meerwein-Strasse
35032 Marburg (Germany)
Fax: (+49) 6421-282-5566
E-mail: Max.Holthausen@chemie.uni-marburg.de

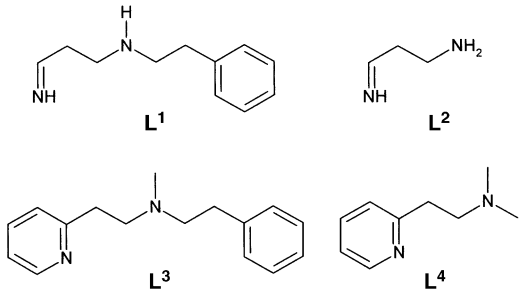
[**] This work has been supported by the Fonds der Chemischen Industrie. We gratefully acknowledge the generous assignment of computer time by the CSC at Frankfurt University and use of the HHLR at the TU Darmstadt.

Supporting information for this article is available on the WWW under http://www.angewandte.org or from the author.

 DOI: 10.1002/anie.200352231 © 2003 Wiley-VCH Verlag GmbH & Co. KGaA, Weinheim 

nance Raman signature, and from its ESR silence. Kinetic measurements revealed a free activation energy of $\Delta G^{\neq} = 12.7\ \text{kcal mol}^{-1}$ and a large deuterium kinetic isotope effect (KIE) of 35.4 for the intramolecular decay of the intermediate at −80 °C. During this decay one of the ligands is nearly quantitatively hydroxylated. Close analogies to related work[5a] led the authors to propose as reaction mechanisms either a H· abstraction followed by an OH· rebound or a concerted O insertion.

Herein we augment the experimental results with a detailed quantum chemical study unveiling the mechanistic scenario. We used a small molecular model with **L**$^{1}$ as the active ligand which has benzylic C–H bonds available to




model the activation, and **L**$^{2}$ as the inactive ligand. Stationary points identified along the reaction path for this computational model were reinvestigated employing **L**$^{3}$ and **L**$^{4}$ as more realistic active and inactive ligands, respectively.[7] We denote stationary points optimized for the small and the large model by superscripts **S** and **L**, respectively.

Starting from the peroxo complex $[Cu_2\mathbf{L}^1\mathbf{L}^2(\mu\text{-}\eta^2\text{:}\eta^2\text{-}O_2)]^{2+}$ (**1**$^{S}$), the first elementary step along the reaction coordinate of the small system is an isomerization of the $[Cu_2O_2]$ core to form the bis(μ-oxo) intermediate **2**$^{S}$ (Figure 1). This step requires a barrier of 6.1 kcal mol$^{-1}$ connected with **TS12**$^{S}$, the transition structure of the O–O bond cleavage to be crossed. Intermediate **2**$^{S}$ is 4.0 kcal mol$^{-1}$ more stable than **1**$^{S}$ supporting the nature of the reactive intermediate postulated by Itoh et al.[6] Subsequent cleavage of the benzylic C–H bond in **2**$^{S}$ via **TS23**$^{S}$ has a barrier of only 4.2 kcal mol$^{-1}$. Quite unexpectedly, **TS23**$^{S}$ does not connect minimum **2**$^{S}$ to a hydroxo(μ-oxo) intermediate, the putative product of this elementary step.[5a,8] Intrinsic reaction coordinate (IRC) calculations following the transition mode in **TS23**$^{S}$ down the product side of the barrier and subsequent geometry optimizations led instead directly to the formation of a C–O bond to yield the alcohol **3**$^{S}$ (Figure 2). We corroborated this finding by repeating the geometry optimizations using the larger basis set BS2, and we confirmed the absence of a hydroxo(μ-oxo) intermediate or alternative lower-energy triplet pathways[9,10] in this region of the potential energy surface by unrestricted calculations (UB3LYP). A subsequent acid–base reaction between the hydroxy group in **3**$^{S}$ and the remaining bridging oxygen atom (formally an $O^{2-}$) takes place via **TS34**$^{S}$, which results in the exothermic formation of **4**$^{S}$. Rotation of the inactive (μ-hydroxo)copper unit via **TS45**$^{S}$ forms the final product, the μ-alkoxo(μ-hydroxo) complex **5**$^{S}$.

Calculations employing the extended model ligands **L**$^{3}$ and **L**$^{4}$ resulted in the same overall reaction path with essentially unaltered structural characteristics of the stationary points (see Supporting Information). Also for the large model we find the bis(μ-oxo) species **2**$^{L}$ to be more stable than **1**$^{L}$ (by 2.3 kcal mol$^{-1}$). **2**$^{L}$ is characterized by a harmonic O–O stretching frequency of 605 cm$^{-1}$, which shifts by −27 cm$^{-1}$ to 578 cm$^{-1}$ upon $^{18}O_2$ isotopic substitution, in excellent agreement with experiment (607 cm$^{-1}$, $\Delta\tilde{\nu}(^{18}O_2) = -29\ \text{cm}^{-1}$). The barrier for the formation of **2**$^{L}$ is 7.4 kcal mol$^{-1}$ and that of the reverse reaction amounts to 9.7 kcal mol$^{-1}$. Both are lower than the barrier of the subsequent hydroxylation via **TS23**$^{L}$ (12.7 kcal mol$^{-1}$), which implies that the isomerization of the copper core between **1**$^{L}$ and **2**$^{L}$ is fast compared to the

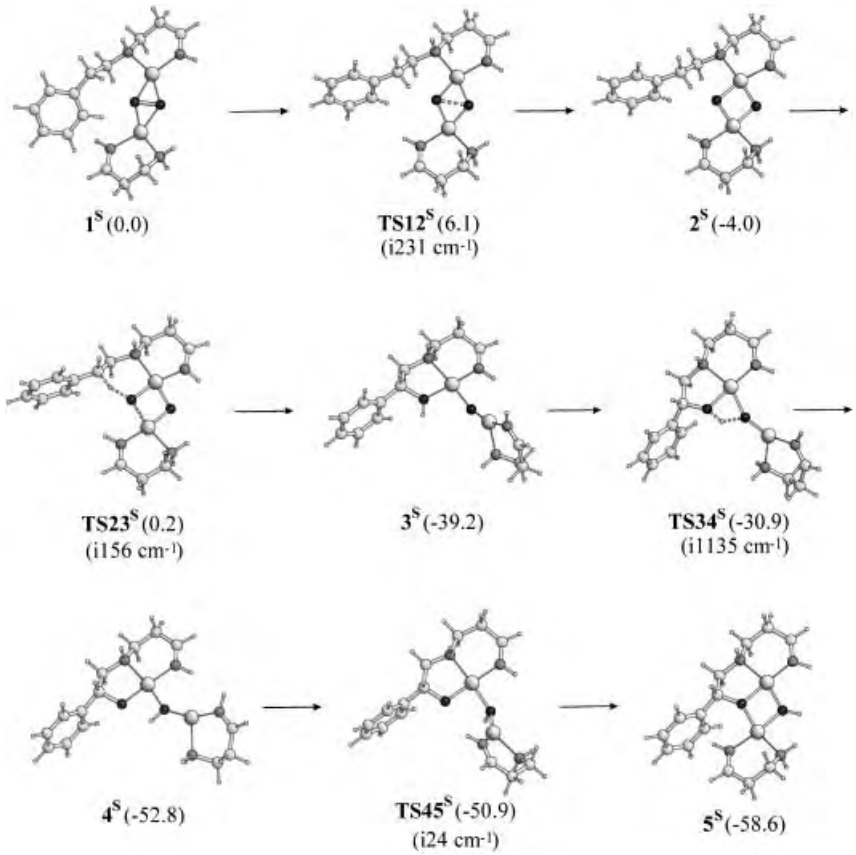



***Figure 1.*** Stationary points (minima and transition structures) identified along the reaction path of the hydroxylation of the benzylic C–H bonds in the small computational model $[Cu_2\mathbf{L}^1\mathbf{L}^2(\mu\text{-}\eta^2\text{:}\eta^2\text{-}O_2)]^{2+}$; relative energies (right, $\Delta G^{-80\,^{\circ}C}$ in kcal mol$^{-1}$, 1 atm, acetone) and calculated imaginary frequencies for transition structures (below) are given in parentheses.

 © 2003 Wiley-VCH Verlag GmbH & Co. KGaA, Weinheim 

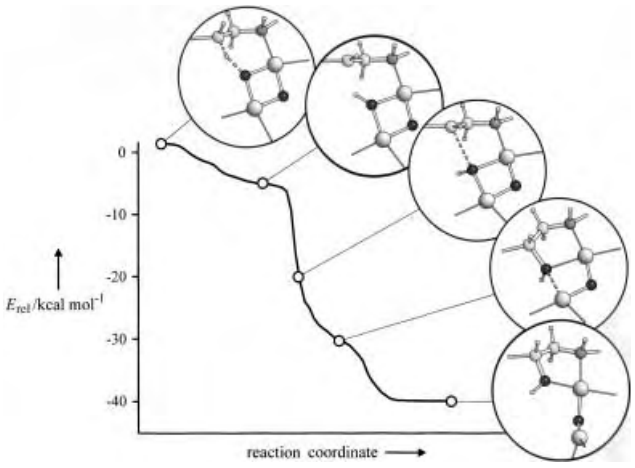
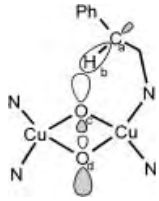



***Figure 2.*** Energy profile for the IRC calculations starting from **TS23$^S$** illustrating the characteristic bond rearrangements involved in the non-synchronous concerted hydroxylation for the small model (Figure 1).

subsequent hydroxylation step via **TS23$^L$**. The corresponding barrier of 12.7 kcal mol$^{-1}$ is in perfect agreement with the experimentally determined rate-limiting barrier (12.7 kcal mol$^{-1}$). The barrier for the reverse reaction from **3$^L$** is prohibitively high (43.0 kcal mol$^{-1}$) making this step irreversible. Thus, once an equilibrium between **1$^L$** and **2$^L$** is established, the rate of hydroxylation via **TS23$^L$** determines the decay of the bis(μ-oxo) species **2$^L$**. After passing **TS23$^L$**, product formation occurs fast in a series of exothermic steps (**TS23$^L$**→**3$^L$**→**TS45$^L$**→**4$^L$**→**TS45$^L$**→**5$^L$**). This mechanistic scenario is fully in line with the large KIE observed experimentally upon deuteration of ligand **L**.[6] For the large model system with a deuterated active ligand **L$^3$** we compute an activation barrier of 13.8 kcal mol$^{-1}$, which corresponds to a classical KIE of 14.7. Taking tunnel effects into account[11] we obtain an improved KIE of 27.9 pleasingly close to the experimental value of 35.4.

A comparison of relative energies in Table 1 reveals that the activation energy for the hydroxylation in the small model is significantly lower than in the large model (4.2 versus 12.7 kcal mol$^{-1}$), whereas we find very similar barriers for the preceding isomerization of the [$Cu_2O_2$] core via **TS12** (6.1 versus 7.4 kcal mol$^{-1}$). Clearly, the results for the small model contradict the experimental findings, which can only be explained with the aid of the larger computational model. These qualitative differences are caused by an orbital interaction between the σ*-antibonding O–O fragment orbital of the bis(μ-oxo)dicopper core and the C–H σ-bonding orbital in **2$^S$** (Scheme 1). This interaction dominates the character of the HOMO of **TS23** for both the small and the large model, but is not present in **2$^L$**. Indeed, a Bader analysis[12] of the electron density of **2$^S$** indicates a bond critical point between $H_b$ and $O_c$ (Figure 3), and a comparison of bond lengths (Table 2) reveals a significantly stretched C–H bond and a very short O–H separation already present in **2$^S$**, whereas no such interaction is present in **2$^L$**. Accordingly, only minor structural and electronic changes are connected with the activation step **2$^S$**→**TS23$^S$** for the small system, which explains the small barrier. Introduction of the pyridyl moiety in **L$^4$** leads to significant steric interactions with the phenylethyl substituent in **L$^3$**, which prevents formation of an




***Scheme 1.***

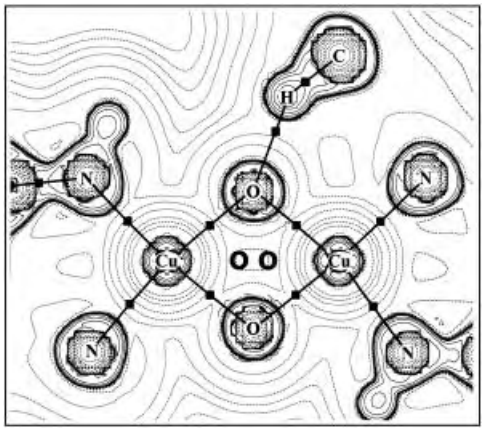



***Figure 3.*** Laplacian and bond paths from a Bader analysis of the electron density of **2$^S$** showing the interaction of the $Cu_2O_2$ moiety with the C–H bond. Solid squares represent bond critical points and bold open circles represent ring critical points.

***Table 1:*** Relative energies including solvation contributions computed employing the COSMO continuum model (Δ*G* in kcal mol$^{-1}$).

| Species | Small Model | | | Large Model | | |
|---|---|---|---|---|---|---|
| | $\Delta G^{[b]}$ | $\Delta G^{\neq[c]}$ (→) | $\Delta G^{\neq[d]}$ (←) | $\Delta G^{[b]}$ | $\Delta G^{\neq[c]}$ (→) | $\Delta G^{\neq[d]}$ (←) |
| **1** | 0.0 | – | – | 0.0 | – | – |
| **TS12** | 6.1 | 6.1 | 10.0 | 7.4 | 7.4 | 9.7 |
| **2** | −4.0 | – | – | −2.3 | – | – |
| **TS23** | 0.2 | 4.2 | 39.3 | 10.5 | 12.7 | 43.0 |
| **3** | −39.2 | – | – | −32.6 | – | – |
| **TS34** | −30.9 | 8.3 | 21.9 | −27.5 | 5.0 | 17.6 |
| **4** | −52.8 | – | – | −45.1 | – | – |
| **TS45** | −50.9 | 1.9 | 7.7 | −42.3 | 2.8 | 3.3 |
| **5** | −58.6 | – | – | −45.6 | – | – |

[a] −80 °C, 1 atm, solvent acetone, $\varepsilon = 20.7$ [b] Energies relative to **1**. [c] Activation energy for the forward reaction relative to the preceding minimum. [d] Activation energy for reverse reaction relative to the preceding minimum.

***Table 2:*** Comparison of relevant bond lengths [Å] for selected stationary points (for atom references see Scheme 1).

| Species | Small Model | | | Large Model | | |
|---|---|---|---|---|---|---|
| | $C_a$–$H_b$ | $H_b$–$O_c$ | $O_c$–$O_d$ | $C_a$–$H_b$ | $H_b$–$O_c$ | $O_c$–$O_d$ |
| **1** | 1.099 | 2.279 | 1.515 | 1.098 | 2.405 | 1.523 |
| **TS12** | 1.122 | 1.783 | 1.863 | 1.098 | 2.307 | 1.857 |
| **2** | 1.136 | 1.679 | 2.296 | 1.096 | 2.554 | 2.271 |
| **TS23** | 1.207 | 1.406 | 2.299 | 1.290 | 1.256 | 2.258 |

 © 2003 Wiley-VCH Verlag GmbH & Co. KGaA, Weinheim 

analogous preactivated C–H bond in complex $\mathbf{2^L}$. Accordingly, much larger structural and electronic changes are connected with the activation step in the large system (Table 2) increasing the C–H activation barrier substantially and making it rate limiting.

The mechanistic scenario established in the preceding discussion features a rate limiting C–H bond cleavage followed directly by an OH rebound step, which leads to the formation of the product alcohol without occurrence of an intermediate. In analogy to mechanistic proposal from Newcomb et al. for Cytochrome P-450[13] we term this elementary step a nonsynchronous concerted process. In the region of the rate-limiting transition structure, however, this process has no radical character. In line with qualitative frontier-orbital arguments discussed elsewhere,[1e,2e,5a] the C–H activation is effectively mediated through an orbital interaction between a C–H σ-bonding orbital and an O–O σ*-antibonding orbital in the bis-(μ-oxo)dicopper unit, which serves as an electrophilic active oxidant. Our finding that a modification of the steric properties of the N-donor ligands can completely change the rate-limiting step is in accord with experimental observations for related bioinorganic model complexes with tridentate ligands, for which the peroxo/bis(μ-oxo) isomerization is found to be rate limiting.[5f,g] While the experimental studies involve a change in denticity of ligands for a change in the character of the rate limiting step, our present study shows that this mechanistic shift can also be controlled for bidentate ligands. We rationalized this shift on the basis of orbital interactions. Further theoretical studies along these lines are in progress and will be published in due course.

Received: June 26, 2003 [Z52231]

**Keywords:** C–H activation · copper · density functional calculations · hydroxylations · reaction mechanisms

[1] a) K. A. Magnus, H. Ton-That, J. E. Carpenter, *Chem. Rev.* **1994**, *94*, 727–735; b) Á. Sánchez-Ferrer, J. N. Ródriguez-López, F. García-Cánovas, F. García-Carmona, *Biochim. Biophys. Acta* **1995**, *1247*, 1–11; c) C. Gerdemann, C. Eicken, B. Krebs, *Acc. Chem. Res.* **2002**, *35*, 183–191; H.-H. Nguyen, S. J. Elliott, J. H.-K. Yip, S. I. Chan, *J. Biol. Chem.* **1998**, *273*, 7957–7966; d) H. Decker, F. Tuczek, *Trends Biochem. Sci.* **2000**, *25*, 392–397; e) H. Decker, R. Dillinger, F. Tuczek, *Angew. Chem.* **2000**, *112*, 1656–1660; *Angew. Chem. Int. Ed.* **2000**, *39*, 1591–1595.

[2] Reviews: a) W. B. Tolman, *Acc. Chem. Res.* **1997**, *30*, 227–237; b) S. Schindler, *Eur. J. Inorg. Chem.* **2000**, 2311–2326; c) "Metal-Oxo and Metal-Peroxo Species in Catalytic Oxidations": A. G. Blackman, W. B. Tolman, *Struct. Bonding (Berlin)* **2000**, *97*; d) K. D. Karlin, A. D. Zuberbühler in *Bioinorganic Catalysis*, 2nd ed. (Eds.: J. Reedijk, E. Bouwman), Marcel Dekker, New York, **1999**, pp. 469–534; e) E. I. Solomon, P. Chen, M. Metz, S.-K. Lee, A. E. Palmer, *Angew. Chem.* **2001**, *113*, 4702–4724; *Angew. Chem. Int. Ed.* **2001**, *40*, 4570–4590 .

[3] a) L. Que, Jr., W. B. Tolman, *Angew. Chem.* **2002**, *114*, 1160–1185; *Angew. Chem. Int. Ed.* **2002**, *41*, 1114–1137; b) P. L. Holland, W. B. Tolman, *Coord. Chem. Rev.* **1999**, *190–192*, 855–869.

[4] a) K. D. Karlin, S. Kaderli, A. D. Zuberbühler, *Acc. Chem. Res.* **1997**, *30*, 139–147; b) L. Santagostini, M. Gullotti, E. Monanzi, L. Casella, R. Dillinger, F. Tuczek, *Chem. Eur. J.* **2000**, *6*, 519–522; c) P. L. Holland, K. R. Rodgers, W. B. Tolman, *Angew. Chem.* **1999**, *111*, 1210–1213; *Angew. Chem. Int. Ed.* **1999**, *38*, 1139–1142; d) M. Becker, S. Schindler, K. D. Karlin, T. A. Kaden, S. Kaderli, T. Palanché, A. D. Zuberbühler, *Inorg. Chem.* **1999**, *38*, 1989–1995; e) H. Ma, M. Allmendinger, U. Thewalt, A. Lentz, M. Klinga, B. Rieger, *Eur. J. Inorg. Chem.* **2002**, 2857–2867.

[5] a) S. Mahapatra, J. A. Halfen, W. B. Tolman, *J. Am. Chem. Soc.* **1996**, *118*, 11575–11586; b) T. Osako, Y. Tachi, M. Taki, S. Fukuzumi, S. Itoh, *Inorg. Chem.* **2001**, *40*, 6604–6609; c) I. Blain, M. Giorgi, I. De Riggi, M. Réglier, *Eur. J. Inorg. Chem.* **2001**, 205–211; d) I. Blain, M. Giorgi, I. De Riggi, M. Réglier, *Eur. J. Inorg. Chem.* **2000**, 393–398; e) I. Blain, P. Bruno, M. Giorgi, E. Lojou, D. Lexa, M. Réglier, *Eur. J. Inorg. Chem.* **1998**, 1297–1304; f) S. Itoh, H. Nakao, L. M. Berreau, T. Kondo, M. Komatsu, S. Fukuzumi, *J. Am. Chem. Soc.* **1998**, *120*, 2890–2899; g) S. Itoh, T. Kondo, M. Komatsu, Y. Ohshiro, C. Li, N. Kanehisa, Y. Kai, S. Fukuzumi, *J. Am. Chem. Soc.* **1995**, *117*, 4714–4715.

[6] S. Itoh, M. Taki, H. Nakao, P. L. Holland, W. B. Tolman, L. Que, Jr., Lawrence, S. Fukuzumi, *Angew. Chem.* **2000**, *112*, 409–411; *Angew. Chem. Int. Ed.* **2000**, *39*, 398–400.

[7] Geometry optimizations and analytical Hessian computations were performed using the program package Gaussian98[14a] at the B3LYP level of theory employing the LANL2DZ standard basis (BS1). All connections of minima and transition states were verified by intrinsic reaction coordinate (IRC) following calculations. Final energies were obtained from single-point energy calculations using the B3LYP functional as implemented in the TURBOMOLE code.[14b] The TZVP standard basis set has been used for H, C, N, and O atoms and the relativistic ECP/basis-set combination of Dolg and co-workers (ecp-10-mdf)[14c] for Cu atoms (BS2). Solvation effects have been included at this level using the COSMO continuum model[14d] (solvent acetone, dielectric constant at room temperature $\varepsilon = 20.7$). The topology analysis of the electron density of $\mathbf{2^S}$ was performed using MORPHY.[14e]

[8] C. J. Cramer, Y. Pak, *Theor. Chem. Acc.* **2001**, *105*, 477–480.

[9] S. Shaik, D. Danovich, A. Fiedler, D. Schröder, H. Schwarz, *Helv. Chim. Acta* **1995**, *78*, 1393–1407.

[10] Based on the optimized geometries of selected singlet species, we computed vertical triplet-excitation energies, all of which are positive: $\mathbf{1^S}$: 1.0, $\mathbf{TS12^S}$: 14.5, $\mathbf{2^S}$: 17.1, $\mathbf{TS23^S}$: 12.7 ($\Delta E_{tot}$ (B3LYP/BS2) in kcal mol$^{-1}$ including solvent contributions). As the B3LYP functional quite generally overestimates the stability of high-spin states relative to low-spin states, the true triplet energies are most likely well above the singlet surface and play no role in the rate-limiting region of the reaction investigated here—see, for example, chapter 9 in W. Koch, M. C. Holthausen, *A Chemist's Guide to Density Functional Theory*, Wiley-VCH, Weinheim, **2000**. The reliability of B3LYP relative energies for closely related molecular systems has been substantiated recently: P. E. M. Siegbahn, *J. Biol. Inorg. Chem.* **2003**, *8*, 577–585.

[11] R. T. Skodje, D. G. Truhlar, *J. Phys. Chem.* **1981**, *85*, 624–628.

[12] R. F. W. Bader, *Atoms in Molecules: A Quantum Theory*, Oxford University Press, Oxford, **1990**.

[13] M. Newcomb, M.-H. Le Tadic-Biadatti, D. L. Chestney, E. S. Roberts, P. F. Hollenberg, *J. Am. Chem. Soc.* **1995**, *117*, 12085–12091.

[14] a) Gaussian 98 (Revision A.7), M. J. Frisch, G. W. Trucks, H. B. Schlegel, G. E. Scuseria, M. A. Robb, J. R. Cheeseman, V. G. Zakrzewski, J. A. Montgomery, R. E. Stratmann, J. C. Burant, S. Dapprich, J. M. Millam, A. D. Daniels, K. N. Kudin, M. C. Strain, O. Farkas, J. Tomasi, V. Barone, M. Cossi, R. Cammi, B. Mennucci, C. Pomelli, C. Adamo, S. Clifford, J. Ochterski, G. A. Petersson, P. Y. Ayala, Q. Cui, K. Morokuma, D. K. Malick,

 © 2003 Wiley-VCH Verlag GmbH & Co. KGaA, Weinheim 

A. D. Rabuck, K. Raghavachari, J. B. Foresman, J. Cioslowski, J. V. Ortiz, B. B. Stefanov, G. Liu, A. Liashenko, P. Piskorz, I. Komaromi, R. Gomperts, R. L. Martin, D. J. Fox, T. Keith, M. A. Al-Laham, C. Y. Peng, A. Nanayakkara, C. Gonzalez, M. Challacombe, P. M. W. Gill, B. G. Johnson, W. Chen, M. W. Wong, J. L. Andres, M. Head-Gordon, E. S. Replogle, J. A. Pople, Gaussian, Inc., Pittsburgh, PA, **1998**; b) Turbomole 5.5, Universität Karlsruhe, **2003**; c) M. Dolg, U. Wedig, H. Stoll, H. Preuss, *J. Chem. Phys.* **1987**, *86*, 866 – 872; d) A. Klamt, G. Schüürmann, *J. Chem. Soc. Perkin Trans. 1* **1993**, *2*, 799; e) P. L. A. Popelier, *Comput. Phys. Commun.* **1996**, *93*, 212 – 240.

 © 2003 Wiley-VCH Verlag GmbH & Co. KGaA, Weinheim 

*Poly(acetylene)s*

# Simple Synthesis of Poly(acetylene) Latex Particles in Aqueous Media**

*Jens O. Krause, M. Tobias Zarka, Udo Anders, Ralf Weberskirch, Oskar Nuyken,* and Michael R. Buchmeiser**

Since the discovery of the conductive properties of poly(acetylene),[1–3] conjugated polymers have been widely used in organic light-emitting diodes (OLEDS), solar cells, photovoltaic devices, field-effect transistors, and lasers.[1–6] Despite significant improvements, materials derived from poly(acetylene)s still suffer from certain drawbacks from a technical point of view. These include insufficient stability and processability, poorly defined composition in terms of connectivity, end groups, and molecular weight, and difficult synthetic accessibility. Any successful application of these systems requires a high degree of definition and variability in monomer structure and depends on the stability and processability of the final polymeric material. Furthermore, straightforward synthetic methods are essential to allow comercialization.

In contrast to 1-alkyne polymerization, the cyclopolymerization of 1,6-heptadiynes offers attractive access to poly(acetylene)s with cyclic recurring units along the backbone, where 1,3-interactions of the substituents, which are responsible for low effective conjugation lengths in poly(1-alkyne)s, are absent.[7,8] Poly(acetylene)s obtained by cyclopolymerization display good solubility in common organic solvents such as benzene, toluene, dichloromethane, and chloroform, good long-term stability towards oxidation, and low energy transitions between the valence and conductivity bands.[7–10] They can be synthesized by using Ziegler catalysts,[11,12] Pd catalysts,[13] anionic polymerization,[14] or binary/ternary Mo or W catalysts.[15] Well-defined molybdenum carbenes in high oxidation states (Schrock catalysts **I**, Figure 1) must be regarded as superior since they cyclopolymerize 1,6-heptadiynes in a living manner[15,16] and can be tuned so that only one single repeat unit, for example, 1,3-(cyclopent-1-enylene)vinylenes[17,18] or 1,3-(cyclohexen-1-enylene)methylidenes,[9,10] is obtained. Despite their unique catalytic properties, the strictly air- and moisture-free conditions that are required for the use of Schrock catalysts are a major limitation to technically relevant applications.

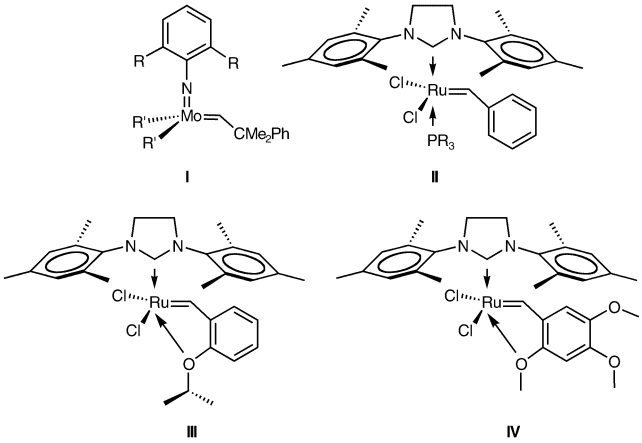



***Figure 1.*** Schrock catalysts **I**, Grubbs–Herrmann catalysts **II**, Grubbs–Hoveyda catalyst **III**, and an asarone-type Grubbs–Hoveyda catalyst **IV**.

Therefore, for any technological use these systems have to be synthesized by more straightforward routes. Grubbs–Herrmann catalysts (e.g. $[RuCl_2(=CHC_6H_5)$(1,3-bis(2,4,6-trimethylphenyl)-4,5-dihydroimidazolin-2-ylidene)$(PCy_3)]$, **II**, Figure 1) and Grubbs–Hoveyda catalysts (e.g. $[RuCl_2(=CH$-(2-(2-PrO)-$C_6H_4)$)(1,3-bis(2,4,6-trimethylphenyl)-4,5-dihydroimidazolin-2-yliden)], **III**, **IV**)[19] are air- and moisture-stable metathesis catalysts with remarkable activity, sometimes rivaling that of highly active Schrock catalysts.[20] Despite their activity in ring-opening metathesis polymerization (ROMP) as well as ring-closing, enyne, and ring-opening cross metathesis reactions, none of the existing systems is capable of polymerizing alkynes or cyclopolymerizing 1,6-heptadiynes. Poly(acetylene)s can, in principle, be prepared

[*] Prof. Dr.-Ing. O. Nuyken, Dipl.-Chem. J. O. Krause, Dipl.-Chem. M. T. Zarka, Dr. U. Anders, Dr. R. Weberskirch
Lehrstuhl für Makromolekulare Stoffe
Technische Universität München
Lichtenbergstrasse 4, 85747 Garching (Germany)
Fax: (+49) 89-289-13562
E-mail: oskar.nuyken@ch.tum.de
A.Univ.-Prof. Dr. M. R. Buchmeiser
Institut für Analytische Chemie und Radiochemie
Universität Innsbruck
Innrain 52a, 6020 Innsbruck (Austria)
Fax: (+43) 512-507-2677
E-mail: michael.r.buchmeiser@uibk.ac.at

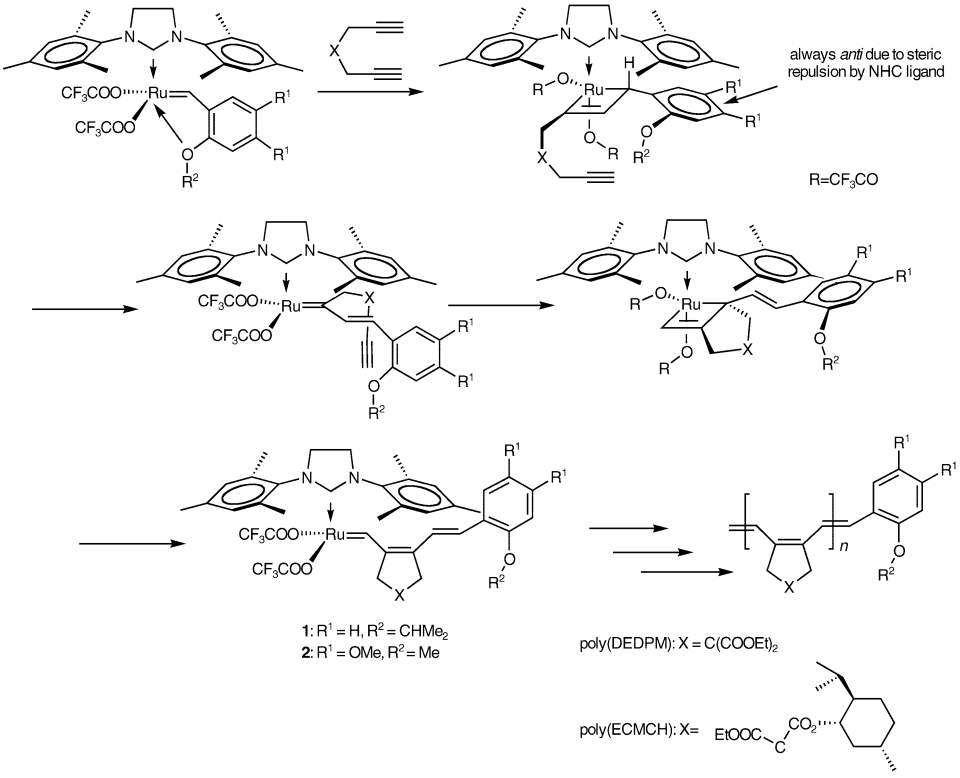
[**] Financial support provided by the Austrian Science Fund, the Freistaat Bayern, the BMBF, and the VCI is gratefully acknowledged.

Supporting information for this article is available on the WWW under http://www.angewandte.org or from the author.

 DOI: 10.1002/anie.200352637 © 2003 Wiley-VCH Verlag GmbH & Co. KGaA, Weinheim 

with these catalysts, but ROMP-based routes are required.[21] The synthesis presented herein of a modified Grubbs–Hoveyda catalyst that can accomplish the cyclopolymerization of 1,6-heptadiynes in both a living and stereoregular way now closes the gap between molybdenum and ruthenium metathesis catalysts.

The reaction of $[RuCl_2(=CH\text{-}(2\text{-}(2\text{-}PrO)\text{-}C_6H_4)(1,3\text{-}dimesityl\text{-}4,5\text{-}dihydroimidazolin\text{-}2\text{-}ylidene)]$ with two equivalents of silver trifluoroacetate provided $[Ru(CF_3COO)_2(=CH\text{-}(2\text{-}(2\text{-}PrO)\text{-}C_6H_4)(1,3\text{-}dimesityl\text{-}4,5\text{-}dihydroimidazlin\text{-}2\text{-}ylidene]$ (**1**, Scheme 1).[22] The enhanced polarization across the Ru–C double bond directly translates into an increased reactivity, thus allowing the cyclopolymerization of diethyl dipropargylmalonate (DEDPM). Interestingly, none of the existing Ru metathesis catalysts, such as $[RuCl_2(=CH\text{-}(2\text{-}(2\text{-}PrO)\text{-}C_6H_4)(NHC)]$, $[RuCl_2(=CHC_6H_5)(PCy_3)(NHC)]$ ($PCy_3$ = tricyclohexylphosphane, NHC = 1,3-dimesitylimidazolin-2-ylidene, 1,3-dimesityl-4,5-dihydroimidazlin-2-ylidene), $[RuCl_2(=CH\text{-}(2\text{-}(2\text{-}PrO)\text{-}C_6H_4)(1,3\text{-}dimesitylimidazolin\text{-}2\text{-}ylidene)]$, or $[RuCl_2(=CH\text{-}(2,4,5\text{-}(MeO)_3\text{-}C_6H_2))(1,3\text{-}dimesityl\text{-}4,5\text{-}dihydroimidazolin\text{-}2\text{-}ylidene)]$, is reactive enough to accomplish this task. Although it is highly active, **1** did not allow a living polymerization of DEDPM.[23]




***Scheme 1.*** The *trans* selectivity and stereoselectivity in the cyclopolymerization of DEDPM.

Irrespective of stoichiometry, polymers with molecular weights of about 12000 g mol$^{-1}$ were obtained (Table 1, entries 1, 2). The ratio of the rate constants for propagation and initiation ($k_p/k_i$)[24] was greater than 1000, which indicated the negative role of the 2-(2-propoxy)benzylidene ligand. Exchange by the 2,4,5-trimethoxybenzylidene ligand[25] led to the formation of $[Ru(CF_3COO)_2(=CH\text{-}(2,4,5\text{-}(MeO)_3\text{-}C_6H_4))(1,3\text{-}dimesityl\text{-}4,5\text{-}dihydroimidazolin\text{-}2\text{-}ylidene)]$ (**2**). This complex turned out to be an excellent catalyst for the cyclopolymerization of DEDPM, as it allowed full control over the molecular weight. Thus, polymerizations of DEDPM initiated with **2** in dichloromethane proceeded in a class VI living manner (Figure 2).[26] Excellent agreement between the theoretical and experimentally determined molecular weights was observed. For all polymers the polydispersity index (PDI) was less than 1.65. The value for $k_p/k_i$ was 3, thus indicating a well-behaved system. In fact, the polymerization system **2**/DEDPM was living

***Table 1:*** Results of the polymerization with catalysts **1**–**4**.[a]

| Poly(acetylene) | Cat. | Solvent | $M_n$ (theor.) | $M_n$ (LS) | $M_w$ (LS) | PDI (LS) | $n$ (LS) | $\lambda_{max}$ [nm] | $E$ [eV] |
|---|---|---|---|---|---|---|---|---|---|
| poly(DEDPM)$_{100}$ | **1** | $CH_2Cl_2$ | 11975 | 10400 | 16800 | 1.62 | 43 | 584 | 2.123 |
| poly(ECMCH)$_{50}$ | **1** | $CH_2Cl_2$ | 17485 | 11100 | 28700 | 2.59 | 32 | 586 | 2.116 |
| poly(DEDPM)$_5$ | **2** | $CH_2Cl_2$ | 1389 | 5600 | 7300 | 1.30 | 23 | 573 | 2.164 |
| poly(DEDPM)$_{10}$ | **2** | $CH_2Cl_2$ | 2571 | 7000 | 11000 | 1.57 | 29 | 576 | 2.153 |
| poly(DEDPM)$_{30}$ | **2** | $CH_2Cl_2$ | 7296 | 13100 | 21400 | 1.63 | 55 | 578 | 2.145 |
| poly(DEDPM)$_{50}$ | **2** | $CH_2Cl_2$ | 12021 | 16200 | 26400 | 1.63 | 68 | 580 | 2.138 |
| poly(DEDPM)$_{70}$ | **2** | $CH_2Cl_2$ | 16747 | 20000 | 22000 | 1.10 | 84 | 583 | 2.127 |
| poly(DEDPM)$_{100}$ | **2** | $CH_2Cl_2$ | 23835 | 27500 | 42400 | 1.54 | 116 | 584 | 2.123 |
| poly(ECMCH)$_{50}$ | **2** | $CH_2Cl_2$ | 17517 | 13000 | 22400 | 1.72 | 37 | 586 | 2.116 |
| poly(DEDPM)$_{50}$ | **3** | $H_2O$ | 11975 | 7700 | 16000 | 2.08 | 32 | 584 | 2.123 |
| poly(ECMCH)$_{50}$ | **3** | $H_2O$ | 17485 | 8100 | 10400 | 1.28 | 23 | 584 | 2.123 |
| poly(DEDPM)$_{50}$ | **4** | $H_2O$ | 12021 | 9500 | 13100 | 1.38 | 40 | 580 | 2.138 |
| poly(DEDPM)$_{100}$ | **4** | $H_2O$ | 23835 | 12700 | 15600 | 1.23 | 53 | 584 | 2.123 |

[a] LS = light scattering, $n$ = degree of polymerization, $\lambda_{max}$ = UV/Vis absorption maximum, E = energy gap between the valence and conductivity bands; molecular weights in g mol$^{-1}$. The polymers were obtained in virtually quantitative yields (> 95 %).

 © 2003 Wiley-VCH Verlag GmbH & Co. KGaA, Weinheim 

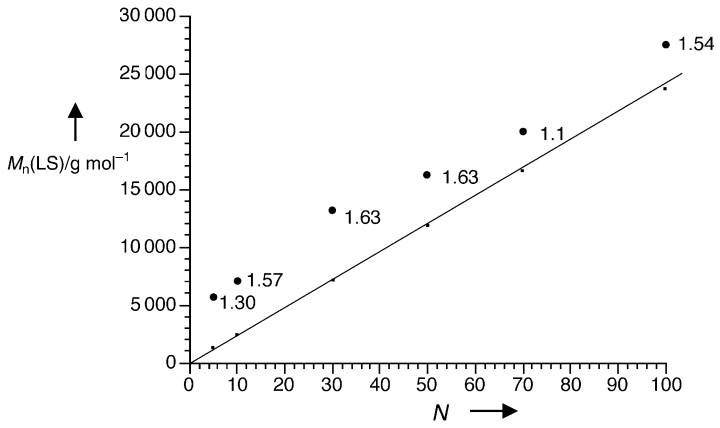



***Figure 2.*** The living character of the polymerization of DEDPM with **2**. $N$ = number of monomer equivalents added; solid line: theoretical values.

even after two days, as shown by the stepwise addition of monomer.

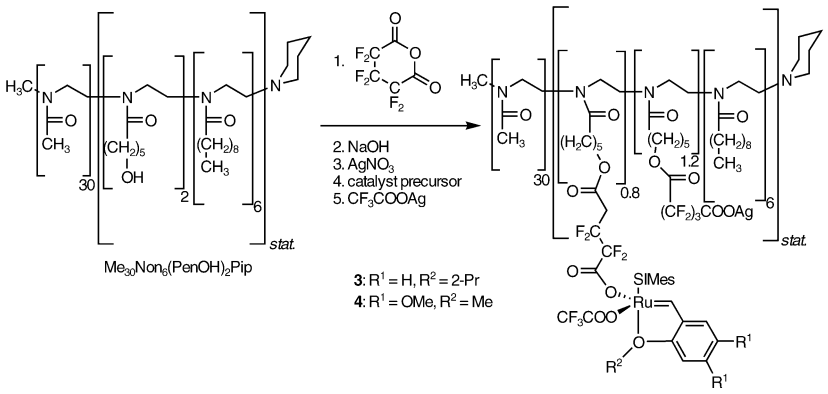
Interestingly, the unsaturated analogue of **1**, [Ru($CF_3$-$COO)_2$(=CH-(2-(2-PrO-$C_6H_4$))(1,3-dimesitylimidazolin-2-ylidene)] was totally inactive. Keeping in mind all the (sometimes incremental) changes that have been made in the original first-generation Grubbs catalyst, [$RuCl_2$-(=$CHC_6H_5$)($PCy_3)_2$], or the Herrmann catalyst, [$RuCl_2$(=$CHC_6H_5$)$(NHC)_2$] (NHC = 1,3-dimesitylimidazolin-2-ylidene), these results illustrate the drastic effects of even small changes in the ligand sphere of a catalyst.

In terms of microstructure, poly(DEDPM) prepared with **1** or **2** consists virtually solely (> 95 %) of 1,3-cyclopent-1-enylenevinylene units, as shown by $^{13}$C NMR spectroscopic measurements.[17,18] Energy band gaps were calculated from the absorption maximum ($\lambda_{max}$)[27] and are summarized in Table 1. The polymerization mechanism certainly follows that of molybdenum-catalyzed cyclopolymerizations and is shown in Scheme 1.[7]

Upon addition of DEDPM to **1**, signals corresponding to the first insertion products at $\delta = 15.63$, 18.67, 19.90, 20.84, and 21.63 ppm were observed in the $^1$H NMR spectrum. The high *trans* selectivity of the vinylene groups probably originates from the steric repulsion of the 2-(2-PrO-$C_6H_4$) groups and the growing poly(acetylene) chain by the NHC ligand. In contrast, the selective insertion is most likely governed by the steric demands of the carboxylate groups. A conformation of the intermediate ruthenacyclobutene with one carboxylate ligand in a *trans* orientation with respect to the NHC ligand was assumed[28] and fits the stereochemical data.

By using MALDI-TOF mass spectrometry, 2-propoxybenzylidene was found to be the end group in polymers prepared with **1**, which indicates the absence of any chain-transfer reactions. In no case was backbiting observed. The polymerization of the chiral 4-(ethoxycarbonyl)-4-(1*S*,2*R*,5*S*)-(+)-menthoxycarbonyl-1,6-heptadiyne (ECMCH, Scheme 1) by **1** proceeded in a stereo- and regioselective manner to provide tactic poly(*trans*-1,3-(cyclopent-1-enylene)vinylene) with greater than 95 % stereoregularity, as shown by $^{13}$C NMR spectroscopy.[17,18] This finding is of particular interest, since polymers prepared by ROMP by using other Ru catalysts revealed a *trans* content of 90 % or less and low stereoregularity.[20,29]

One of the advantages of ruthenium-based catalysts is their tolerance to polar functional groups and water as a reaction medium. Polyenes that are synthesized in the form of stable aqueous dispersions are particularly attractive for many industrial applications, since they can be directly deposited on suitable supports such as clays. We therefore tried to establish a system capable of polymerizing DEDPM under aqueous conditions and providing stable latices in a single step. The use of **1** in combination with micelle-forming compounds such as sodium dodecylsulfate (SDS) resulted only in the formation of oligomeric precipitates. As an alternative, the amphiphilic poly(2-oxazoline)-derived block copolymer $Me_{30}Non_6(PenOH)_2Pip$, which is known to undergo micellization in water,[30] was synthesized by living cationic polymerization (Scheme 2).[31] Again, its use with **1** only resulted in oligomeric precipitates. We therefore focused on fixation of the catalyst on the micelle-forming, amphiphilic block copolymers.




***Scheme 2.*** Immobilization of [$RuCl_2$(=CH-2-(2-PrO-$C_6H_4$))(SIMes)] on poly(2-oxazoline)-based block copolymers. SIMes = 1,3-bis(2,4,6-trimethylphenyl)4,5-dihydroimidazolin-2-ylidene.

The synthesis of a polymer-bound catalyst had to fulfill two requirements: On one hand, perfect mimics of **1** and **2** had to be generated to maintain their reactivity and stereoselectivity. On the other hand, and in contrast to any suspension or emulsion polymerization, the catalyst had to be *permanently* linked to the block copolymer. The catalyst is best located in the hydrophobic micellar core, where, upon micelle formation of the functionalized block copolymer, the monomer will also be dissolved. The functionalized block copolymers were prepared by allowing $Me_{30}Non_6(PenOH)_2$-Pip, which bears two randomly distributed hydroxy groups in the side chain of the hydrophobic block, to react with hexafluoroglutaric anhydride. Subsequent deprotonation with aqueous NaOH and reaction with Ag($NO_3$) yielded the

 © 2003 Wiley-VCH Verlag GmbH & Co. KGaA, Weinheim 

corresponding polymer-bound silver carboxylate. The last steps involved reaction with the catalyst precursors, [$RuCl_2$-(=CH-2-(2-PrO)-$C_6H_4$)(1,3-bis(2,4,6-trimethylphenyl)-4,5-dihydroimidazolin-2-ylidene)] and [$RuCl_2$(=CH-2,4,5-$(OMe)_3$-$C_6H_2$)(1,3-bis(2,4,6-trimethylphenyl)-4,5-dihydroimidazolin-2-ylidene)],[25] respectively, followed by reaction with silver trifluoroacetate to replace the second, unchanged chloride ligand of the catalyst. In the course of this two-step chloride exchange, the corresponding ruthenium compounds were fixed to the support to yield the poly(2-oxazoline)-immobilized catalysts [$Me_{30}Non_6${(PenOCO$(CF_2)_3$COO)($CF_3$-COO)Ru(=CH-2-(2-PrO)-$C_6H_4$)(SIMes)}$_{0.8}$(PenOCO$(CF_2)_3$-COOAg)$_{1.2}$Pip] (**3**) and [$Me_{30}Non_6${(PenOCO$(CF_2)_3$-COO)($CF_3$COO)Ru(=CH-2,4,5-$(OMe)_3$-$C_6H_2$)(SIMES)}$_{0.8}$-(PenOCO$(CF_2)_3$COOAg)$_{1.2}$Pip] (**4**; Scheme 2).

The catalyst immobilization was followed by $^1$H NMR spectroscopy (in $CD_3OD$), which provided exact information on the quality and selectivity of this reaction. The alkylidene protons of the polymer-bound catalyst **3** gave a single signal at $\delta = 17.51$ ppm, which is in excellent agreement with the single signal at $\delta = 17.58$ ppm in the $^1$H NMR spectrum of the free catalyst. On one hand, the similarity of these two chemical shifts indicates a selective immobilization in which no free catalyst or any other catalytic species was observed. On the other hand, it underlines the degree of similarity between **1** and the supported analogue **3**, even more so as the chemical shift for the alkylidene protons in this type of catalyst is very sensitive towards changes in the ligand sphere. It is noteworthy that a successful immobilization requires both straightforward synthetic routes and the careful design of the block sizes in the amphiphilic copolymer. Whereas the use of $Me_{30}Non_4(PenOH)_4Pip$ resulted in insoluble, catalyst-loaded species, $Me_{30}Non_6(PenOH)_2Pip$ could be successfully used for these purposes.

The quantification of the ruthenium content in **3** and **4** by means of ICP-OES measurements indicated that 40 % of the polymeric silver salt had reacted with the catalyst precursors **1** and **2**, which led to ruthenium loadings in the block copolymer of 0.16 mmol $g^{-1}$ upon use of **3** and **4**. For the polymerization of DEDPM with **4**, a value of 11 was found for $k_p/k_i$. Poly(DEDPM) prepared with **4** in water was characterized by lower polydispersity indices ($< 1.40$) compared to poly(DEDPM) prepared with **2**.

Owing to the increased concentration of DEDPM within the micelles, the reaction times required to reach complete conversion were reduced to 30 min with **3** and **4** compared to 2 h with **2**. This illustrates the effect of the micellar "nanoreactors" formed in an aqueous medium. Nevertheless, the polymerization itself cannot be regarded as living.

The TEM analysis of the resulting polymer latices revealed particle sizes between 100 and 200 nm, which is typical for an emulsion-based process (Figure 3). Stabilized by the amphiphilic structure of the block copolymer, the latices could be stored for over two weeks without any change in terms of particle size, molecular weight, or UV/Vis absorption maximum. In addition, immobilization of the catalyst allowed separation of the catalyst from the product to obtain virtually Ru-free poly(acetylene)s with a Ru content of 0.35 ppm or less. Poly(DEDPM) prepared by any of the methods reported herein was stable in the solid state under ambient conditions, including in the presence of air and moisture, which is relevant for technical use.

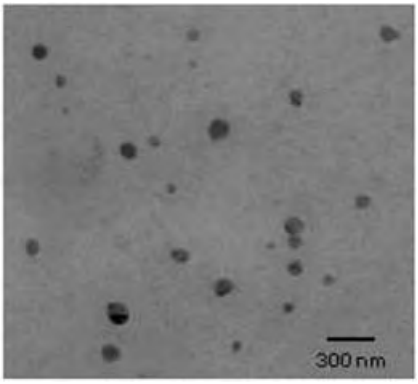



***Figure 3.*** The TEM micrograph of the stable poly(DEDPM) latex particles.

In summary, we have elaborated the first synthetic protocol that allows the preparation of highly conjugated polyenes by cyclopolymerization of 1,6-heptadiynes with a ruthenium metathesis catalyst in a living manner. Furthermore, these polyenes are accessible even under aqueous, micellar conditions. We are convinced that these findings will revitalize poly(acetylene) chemistry and related research areas.

Received: August 13, 2003 [Z52637]

**Keywords:** metathesis · micelles · polyacetylenes · polymerization · ruthenium

[1] A. G. MacDiarmid, *Angew. Chem.* **2001**, *113*, 2649 – 2659; *Angew. Chem. Int. Ed.* **2001**, *40*, 2581 – 2590.
[2] A. J. Heeger, *Angew. Chem.* **2001**, *113*, 2660 – 2682; *Angew. Chem. Int. Ed.* **2001**, *40*, 2591 – 2611.
[3] H. Shirakawa, *Angew. Chem.* **2001**, *113*, 2642 – 2648; *Angew. Chem. Int. Ed.* **2001**, *40*, 2574 – 2580.
[4] T. A. Skotheim, R. L. Elsenbaumer, J. R. Reynolds, *Handbook of Conducting Polymers*, 2nd ed., Dekker, New York, **1997**.
[5] J. L. Brédas, R. J. Silbey, *Conjugated Polymers*, Kluwer, Dordrecht, **1991**.
[6] T. Masuda, S. M. Abdul Karim, R. Nomura, *J. Mol. Catal. A* **2000**, *160*, 125 – 131.
[7] H. H. Fox, R. R. Schrock, *Organometallics* **1992**, *11*, 2763 – 2765.
[8] H. H. Fox, M. O. Wolf, R. O'Dell, B. L. Lin, R. R. Schrock, M. S. Wrighton, *J. Am. Chem. Soc.* **1994**, *116*, 2827 – 2843.
[9] F. J. Schattenmann, R. R. Schrock, W. M. Davis, *J. Am. Chem. Soc.* **1996**, *118*, 3295 – 3296.
[10] F. J. Schattenmann, R. R. Schrock, *Macromolecules* **1996**, *29*, 8990 – 8991.
[11] J. K. Stille, D. A. Frey, *J. Am. Chem. Soc.* **1961**, *83*, 1697 – 1701.
[12] H. W. Gibson, A. J. Epstein, H. Rommelmann, D. B. Tanner, X. Q. Yang, J. M. Pochan, *J. Phys. Colloq.* **1983**, *C3*, 651 – 656.
[13] K. J. S. Harrell, S. T. Nguyen, *Abstr. Pap. Am. Chem. Soc.* **1999**, *217*, 121 – 122.
[14] C. Sivakumar, T. Vasudevan, A. Gopalan, T.-C. Wen, *Polymer* **2002**, *43*, 1781 – 1787.

 © 2003 Wiley-VCH Verlag GmbH & Co. KGaA, Weinheim 

[15] S.-K. Choi, Y.-S. Gal, S.-H. Jin, H.-K. Kim, *Chem. Rev.* **2000**, *100*, 1645 – 1661.
[16] M. R. Buchmeiser, *Chem. Rev.* **2000**, *100*, 1565 – 1604.
[17] U. Anders, O. Nuyken, K. Wurst, M. R. Buchmeiser, *Macromolecules* **2002**, *35*, 9029 – 9038.
[18] U. Anders, O. Nuyken, K. Wurst, M. R. Buchmeiser, *Angew. Chem.* **2002**, *114*, 4226 – 4230; *Angew. Chem. Int. Ed.* **2002**, *41*, 4044 – 4047.
[19] S. B. Garber, J. S. Kingsbury, B. L. Gray, A. H. Hoveyda, *J. Am. Chem. Soc.* **2000**, *122*, 8168 – 8179.
[20] C. W. Bielawski, R. H. Grubbs, *Angew. Chem.* **2000**, *112*, 3025 – 3028; *Angew. Chem. Int. Ed.* **2000**, *39*, 2903 – 2906.
[21] O. A. Scherman, I. M. Rutenberg, R. H. Grubbs, *J. Am. Chem. Soc.* **2003**, *125*, 8515 – 8522.
[22] J. O. Krause, K. Wurst, O. Nuyken, M. R. Buchmeiser, *Chem. Eur. J.* **2003**, *9*, 5031.
[23] T. R. Darling, T. P. Davis, M. Fryd, A. A. Gridnev, D. M. Haddleton, S. D. Ittel, R. R. Matheson, Jr., G. Moad, E. Rizzardo, *J. Polym. Sci. Part A* **2000**, *38*, 1706 – 1708.
[24] G. C. Bazan, E. Khosravi, R. R. Schrock, J. W. Feast, V. C. Gibson, M. B. O'Regan, J. K. Thomas, W. M. Davis, *J. Am. Chem. Soc.* **1990**, *112*, 8378 – 8387.
[25] K. Grela, M. Kim, *Eur. J. Org. Chem.* **2003**, 963 – 966.
[26] K. Matyjaszewski, *Macromolecules* **1993**, *26*, 1787 – 1788.
[27] R. Schlund, R. R. Schrock, W. E. Crowe, *J. Am. Chem. Soc.* **1989**, *111*, 8004 – 8006.
[28] T. J. Seiders, D. W. Ward, R. H. Grubbs, *Org. Lett.* **2001**, *3*, 3225 – 3228.
[29] J. G. Hamilton, U. Frenzel, F. J. Kohl, T. Weskamp, J. J. Rooney, W. A. Herrmann, O. Nuyken, *J. Organomet. Chem.* **2000**, *606*, 8 – 12.
[30] G. Riess, *Prog. Polym. Sci.* **2003**, *28*, 1107 – 1170.
[31] M. T. Zarka, O. Nuyken, R. Weberskirch, *Chem. Eur. J.* **2003**, *9*, 3228 – 3234.

 © 2003 Wiley-VCH Verlag GmbH & Co. KGaA, Weinheim 

*Screening for Protein Catalysts*

# Development of a High-Throughput Screen for Protein Catalysts: Application to the Directed Evolution of Antibody Aldolases**

*Jeff Gildersleeve, Alex Varvak, Shane Atwell, Doug Evans, and Peter G. Schultz**

High-throughput screens can be powerful methods for identifying and evolving biological catalysts.[1–3] To date, nearly all high-throughput screens (e.g. blue/white colony screens, plate lifts, cell sorting, etc.) assay catalytic activity in live cells or crude cell lysates. As a result, there are significant limitations on the substrates, reactions, and conditions that can be used. In addition, detection of products in the presence of many proteins, lipids, nucleic acids, and other cellular components can be problematic. To circumvent these limitations, we have developed a high-throughput system to express, purify, and assay the catalytic activity of proteins. By carrying out assays on purified proteins, a much wider range of substrates and reactions can be explored, including those involving cell-impermeable substrates, endogenous background activities, and nonchromogenic products. To illustrate the potential of this system, we have applied it to the directed evolution of catalytic antibodies with aldolase activity.

The first step involved the development of a general system for expressing and purifying large numbers of antibodies in parallel.[4] The system should be amenable to optimization of expression levels and catalytic activity as both are important properties for antibody development. Our approach was to grow high-density 1-mL cultures of *E. coli* in 96-well plates, lyse the cells, and then capture the His-tagged antibodies with Ni-NTA beads. To maximize the utility of the system, a single set of expression and purification conditions was required that would accommodate many different antibodies. In addition, sufficient quantities of purified antibodies must be produced to obtain good signal-to-noise ratios in catalytic assays. The expression levels and purity of protein must also be reproducible so that mutants with incremental changes in activity and expression levels can be detected with confidence. Finally, protocols should be compatible with automation and high-throughput formats; steps requiring extensive manipulation of plates such as centrifugation and sonication were avoided.

After extensive optimization, we developed a semiautomated system capable of routinely screening 6000 clones/run in a parallel 96-well format. Yields of protein range from 0.5–3 μg/well (1 mL culture/well) and purities are greater than 90%. In addition, a wide range of antibodies have been successfully expressed and purified using the system without modifying the protocol.[5] A typical screen starts by transforming bacteria (Top10) with a library of plasmids encoding mutant antibodies (mouse–human chimeric Fabs) fused to His6 tags.[6] The expression vector is a modified pBAD plasmid with expression controlled by the arabinose promoter. Single colonies are picked into individual wells of shallow, 96-well plates containing 2xYT/amp using a robotic colony picker. These starter cultures are grown overnight and then 10 μL is transferred from each well to a corresponding 1 mL expression culture in a 2-mL, deep, 96-well plate.[7] To expedite the process, the 96 liquid transfers required for each plate are done in parallel using a robotic liquid handler fitted with a 96-needle head. The starter cultures are grown to saturation to ensure that each expression culture is inoculated at about the same density. In addition, the starter cultures serve as a source of plasmid DNA for hits identified during the screen (starter cultures are stored at 4 °C until completion of the screen). The cultures are then grown for 7 h at 37 °C and 250 rpm, and protein production is induced by parallel addition of arabinose (4%, 50 μL/well). Cultures are shaken at 25 °C and 250 rpm for an additional 12 h, and then 100 μL/well of 10x PBS that contains 10units DNase $mL^{-1}$ is added. Cells are lysed by addition of 100 μL/well of deoxycholic acid (10 mg $mL^{-1}$), and His6-tagged proteins are captured by addition of 50 μL/well of Ni-NTA resin. Each of these additions is carried out with the robotic liquid handler. After shaking for an additional 4 h, the plates are allowed to sit for 5 min to allow the Ni-NTA resin to settle to the bottom of the wells. The needles of the liquid handler are inserted into the wells just above the resin, and the lysate is removed. The resin is then washed once with 500 μL/well of PBS that contains 5 mM imidazole and then three times with 500 μL/well of PBS to afford the immobilized, purified antibodies.

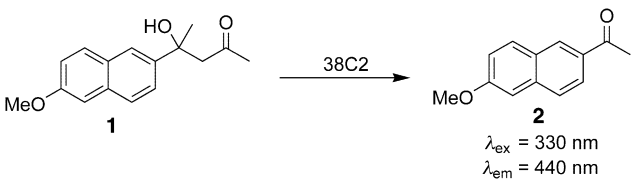
To test the performance of the system, we conducted a series of model studies using catalytic antibody 38C2, an aldolase developed by Wagner, Lerner, and Barbas.[8] This antibody efficiently catalyzes aldol reactions with a broad range of substrates; it has also been extensively characterized both mechanistically and structurally.[9,10] We found that 38C2 retains activity while immobilized on Ni-NTA resin (~50% relative to the antibody in solution) and can be assayed directly without elution. In a representative assay, 38C2 was expressed and purified in 80 wells distributed over 20 plates and then assayed for activity by addition of 200 μL/well of substrate **1** (20 μM in PBS).[11] The product of the retro-aldol reaction, **2** (Scheme 1), can be detected easily using a fluorescent plate reader ($\lambda_{ex} = 330$ nm, $\lambda_{em} = 440$ nm). After incubating the plates for 1 h at 25 °C and 250 rpm, the reaction was transferred to white 96-well plates, and fluorescent signals were measured. The average signal was 1100 with a CV of 30% (signal variation from well to well and plate to plate).

[*] Prof. P. G. Schultz, Dr. J. Gildersleeve, Dr. A. Varvak, Dr. S. Atwell
Department of Chemistry, The Scripps Research Institute
La Jolla, CA 92037 (USA)
Fax: (+1) 858-784-9440
E-mail: schultz@scripps.edu
D. Evans
The Genomics Institute of the Novartis Research Foundation
3115 Merryfield Row, San Diego, CA 92121 (USA)

[**] This research was supported by the NIH (Grant No. GM56528). J.G. gratefully acknowledges a postdoctoral fellowship from the NIH (Grant No. 5 F32 AI10419). This is manuscript number 15847-CH of The Scripps Research Institute.

Supporting information for this article is available on the WWW under http://www.angewandte.org or from the author.

 DOI: 10.1002/anie.200352117 © 2003 Wiley-VCH Verlag GmbH & Co. KGaA, Weinheim 




***Scheme 1.*** 38C2-Catalyzed conversion of substrate **1** into **2**.

With this level of variation, a two- to threefold change in activity is detectable. For comparison, the initial signal for substrate alone was about 220, the background signal after incubation of substrate for 1 h in wells containing a catalytically inactive antibody was about 250, and the fluorescent signal of cell cultures and crude cell lysates lacking substrate was about 3000. The products were also analyzed by mass spectrometry using an LC–TOF instrument equipped with a MUX eight-channel unit, albeit with lower overall throughput ($\sim 500$ samples day$^{-1}$). Moreover, because the assays are performed on resin-bound catalyst, up to three catalytic assays can be conducted on the same sample of protein without significantly affecting the signal-to-noise ratio and variability by simply washing the resin twice with PBS between assays. Furthermore, the antibodies can then be eluted from the resin and analyzed by SDS-PAGE (sodium dodecyl sulfate polyacrylamide gel electrophoresis) or ELISA (enzyme-linked immunosorbent assay) to probe expression levels and hapten binding. By conducting multiple assays, we can simultaneously screen for mutants with improved activity, selectivity, and/or expression levels.

To test the high-throughput screen as a tool for directed evolution, we constructed two antibody aldolase libraries in which key amino acid residues in the active site were randomized to all 20 possible amino acid. One library had residues 96–98 on the heavy chain randomized and the other had residues 27B-D on the light chain randomized. From these libraries, 17 unique mutants were identified that produced signals two- to threefold higher than the 38C2 controls. The four heavy-chain mutants and 13 light-chain mutants were then crossed and rescreened (with 20 μM **1**) in an effort to find combinations of mutations with additive effects. Two clones, 2G7 and 3D6, resulted in yields 15-fold higher than those for 38C2 in the screen. These mutants were expressed in 1-L cultures, purified, and characterized in detail (see Table 1). Both mutants have a 2.4-fold higher $k_{cat}$ value and express at levels five- to sixfold higher levels than those for the wild-type antibody, 38C2, demonstrating that improved antibodies can be reliably identified using the high-throughput screen.

***Table 1:*** Amino acid sequences, catalytic properties, and expression levels for selected antibodies.

| Antibody | Residues | | | | $k_{cat}$[a,b] | $K_M$[a,c] | Expression[d] |
|---|---|---|---|---|---|---|---|
| | L27B-D | H96-98 | L92 | H34 | [min$^{-1}$] | [μM] | [mg L$^{-1}$] |
| 38C2 | L-H-T | F-Y-S | T | M | 0.63 | 15 | 0.25 |
| 2G7 | D-V-L | G-Q-K | T | M | 1.55 | 30 | 1.2 |
| 3D6 | L-V-S | G-Q-K | T | M | 1.51 | 21 | 1.5 |
| 1A4 | L-V-S | G-Q-K | N | V | 2.35 | 9 | 6.0 |

[a] $k_{cat}$ and $K_M$ were measured using racemic substrate **1**. [b] $\pm 0.04$ min$^{-1}$. [c] $\pm 1$ μM. [d] $\pm 0.05$ mg L$^{-1}$.

To further improve the activity and expression levels of the aldolase antibodies, 26 single amino acid positions in close proximity to the active site of 3D6 were randomized. These residues included 31–36 (CDR1) and 89–97 (CDR3) on the light chain and 33–37 (CDR1), and 94, 95, and 99–103 (CDR3) on the heavy chain. The 26 single amino acid libraries were combined and then screened (with 10 μM **1**).[12] Two unique mutants, Thr92 LAsn and Met34HVal, were identified that resulted in yields threefold higher than those for 3D6 in the high-throughput screen. The double mutant (1A4) was generated, expressed, and characterized. Antibody 1A4 was found to have a sixfold improvement in catalytic efficiency ($k_{cat}/K_M$) and a 25-fold improvement in expression level over 38C2, corresponding to an overall 150-fold increase in product yield. As with 38C2, 1A4 was found to be highly selective for the *S* enantiomer of substrate **1**. The generation of antibody 1A4 from high-throughput screens of two iterative focused libraries demonstrates that this is a reliable and effective tool for directed evolution.

In conclusion, we have developed a high-throughput screen capable of rapidly analyzing thousands of protein mutants. The screen can be used to evolve activity, selectivity, and expression levels of proteins directly or in combination with selections. In addition to identifying mutants with improved properties, one can use the screen to rapidly compare protein library design strategies, evaluate the quality of protein libraries, and determine the effectiveness of rounds of selections.

Received: June 11, 2003 [Z52117]

**Keywords:** aldol reaction · antibodies · directed evolution · high-throughput screening · proteins

[1] N. Cohen, S. Abramov, Y. Dror, A. Freeman, *Trends Biotechnol.* **2001**, *19*, 507.
[2] M. T. Reetz, *Angew. Chem.* **2002**, *114*, 1391; *Angew. Chem. Int. Ed.* **2002**, *41*, 1335.
[3] P. Soumillion, J. Fastrez, *Curr. Opin. Biotechnol.* **2001**, *12*, 387.
[4] For other approaches, see: a) S. Yokoyama, *Curr. Opin. Chem. Biol.* **2003**, *7*, 39, and references therein; b) A. Heyhurst, G. Georgiou, *Curr. Opin. Chem. Biol.* **2001**, *5*, 683, and references therein.
[5] In addition to expressing and purifying thousands of mutants of 38C2, the following antibodies have also been successfully expressed: a) 43C9: K. D. Janda, D. Schloeder, S. J. Benkovic, R. A. Lerner, *Science* **1988**, *241*, 1188; b) 136.1: J. R. Jacobsen, J. R. Prudent, L. Kochersperger, S. Yonkovich, P. G. Schultz, *Science* **1992**, *256*, 365; c) 28B4: L. C. Hsieh, J. C. Stephans, P. G. Schultz, *J. Am. Chem. Soc.* **1994**, *116*, 2167; d) 7G12: A. G. Cochran, P. G. Schultz, *Science* **1990**, *249*, 781; e) AZ28: A. C. Braisted, P. G. Schultz, *J. Am. Chem. Soc.* **1994**, *116*, 2211.
[6] Detailed procedures for a typical high-throughput screen, the construction of the expression vector, the construction of the antibody libraries, and characterization of the antibodies can be found in the Supporting Information.
[7] A control antibody (typically 38C2) is expressed in 2–4 wells/plate to serve as an internal control.

 © 2003 Wiley-VCH Verlag GmbH & Co. KGaA, Weinheim 

[8] J. Wagner, R. A. Lerner, C. F. Barbas III, *Science* **1995**, *270*, 1797.
[9] T. Hoffmann, G. Zhong, B. List, D. Shabat, J. Anderson, S. Gramatikova, R. A. Lerner, C. F. Barbas III, *J. Am. Chem. Soc.* **1998**, *120*, 2768.
[10] C. F. Barbas III, A. Heine, G. Zhong, T. Hoffmann, S. Gramatikova, R. Bjornestedt, B. List, J. Anderson, E. A. Stura, I. A. Wilson, R. A. Lerner, *Science* **1997**, *278*, 2085.
[11] B. List, C. F. Barbas III, R. A. Lerner, *Proc. Natl. Acad. Sci. USA* **1998**, *95*, 15351.
[12] The 26 libraries were constructed in four groups, based on the location of the randomized residue: light CDR1, light CDR3, heavy CDR1, and heavy CDR3 (see Supporting Information). The four groups were transformed separately and screened as described in the supporting information with a unique clone in each well. Plasmid DNA from each hit identified in the screen was obtained by isolating the DNA from the corresponding starter culture well.

 © 2003 Wiley-VCH Verlag GmbH & Co. KGaA, Weinheim 

DNA Structures

# Fluorinated DNA Bases as Probes of Electrostatic Effects in DNA Base Stacking**

*Jacob S. Lai, Jin Qu, and Eric T. Kool**

The noncovalent interactions affecting the thermodynamic stability of natural and modified DNA have been topics of broad interest in recent years. The effects of sterics, stacking, hydrogen bonding, and minor-groove solvation have been considered as contributing factors.[1–4] Probably the dominant stabilizing factor in helical DNA is base stacking.[5,6] In order to probe the physical factors that contribute to the stability of this stacking in water, measured melting data of short DNA oligomers, both naturally and nonnaturally substituted, has been studied.[5,7,8] Such experiments have suggested that van der Waals and solvophobic forces can be important contributors to the stabilization of stacking. Beyond this, theoretical work has pointed out the possible importance of electrostatic interactions in the stability and preferred geometry of stacked bases in DNA.[9–14] Understanding these issues could allow for better design of modified DNAs, but relatively little experimental information is available on such electrostatic factors.

[*] Prof. Dr. E. T. Kool, J. S. Lai, Dr. J. Qu
Department of Chemistry, Stanford University
Stanford, CA 94305-5080 (USA)
Fax: (+1) 650-725-0259
E-mail: kool@leland.stanford.edu

[**] This work was supported in part by the U.S. National Institutes of Health (GM52956/EB002059).

Supporting information for this article is available on the WWW under http://www.angewandte.org or from the author.

It is well documented that aromatic rings can exhibit significant dipolar and quadrupolar electrostatic interactions in certain environments. Studies in nonpolar solvents using aromatic compounds containing various electron-donating and -withdrawing substituents have demonstrated significant electrostatic effects in stacking energetics and geometries.[15–17] Although in aqueous systems the electrostatic dipole effects are greatly diminished, localized electrostatic effects are still believed to play a role in governing neighboring base-pair geometries in DNA.[6,12] Studies with small-molecule model systems in water have suggested that electrostatic effects are relatively weak, and that dispersive effects are a major factor governing stacking stability.[18,19] Hydrophobic effects in such model systems appear to play only a small role, although this issue has been debated.[18,20,21]

Quadrupolar interactions have also been documented in specialized cases; for example, benzene is capable of electrostatic interactions with molecules containing a positive charge, as demonstrated by well-documented cation–π interactions, even in aqueous systems.[22] By contrast, perfluorobenzene, with its opposite quadrupolar sign, can stack well (in low polarity environments) with electron-rich aromatic rings.[23] A recent computational study also showed the coordination by water in interactions with benzene and perfluorobenzene.[24] Although benzene-,[25] 2,4-difluorobenzene-,[26] 2,4,5-trifluorobenzene-,[26] and pentafluorobenzene-substituted[27] deoxyribonucleosides and 4-monofluorobenzene ribonucleoside[28] have been previously described, no information on their relative stacking abilities is available, nor is there any data on their interactions with varied neighboring DNA bases.

We now describe a series of fluorinated aromatic nucleoside analogues having a wide range of dipole and quadrupole moments. We have studied the stacking thermodynamics of these compounds in short synthetic DNA duplexes, with all four neighboring nucleobases. The results shed light on the importance and origins of electrostatic interactions in DNA base stacking, and reveal some previously unrecognized structural and electrostatic effects that will be useful in future molecular designs.

The seven deoxynucleosides studied here are shown in Figure 1. In all cases, the deoxyribose moiety is constant, but the "base" groups vary in the extent and orientation of fluorine substitution, from zero substitutions (benzene) to the maximum of five (pentafluorobenzene). These compounds were prepared by treating the appropriate lithiated aromatic species with an O-protected deoxyribonolactone derivative.[29]

Figure 1b depicts calculated electrostatic surface potentials of the aromatic base analogues, in which the effects of the deoxyribose 1′-carbon are approximated with an attached methyl group. The electrostatics vary widely over the series, with the phenyl nucleoside showing a negative potential at the center of the flat aromatic face, and the pentafluorinated case having a strongly positive potential. Thus the quadrupoles are gradually inverted over this series. By comparison, natural DNA bases are not as strongly polarized (in the quadrupolar sense), and the potentials are generally close to neutral (similar to monofluorobenzene, see the Supporting Informa-

 DOI: 10.1002/anie.200352531 © 2003 Wiley-VCH Verlag GmbH & Co. KGaA, Weinheim 

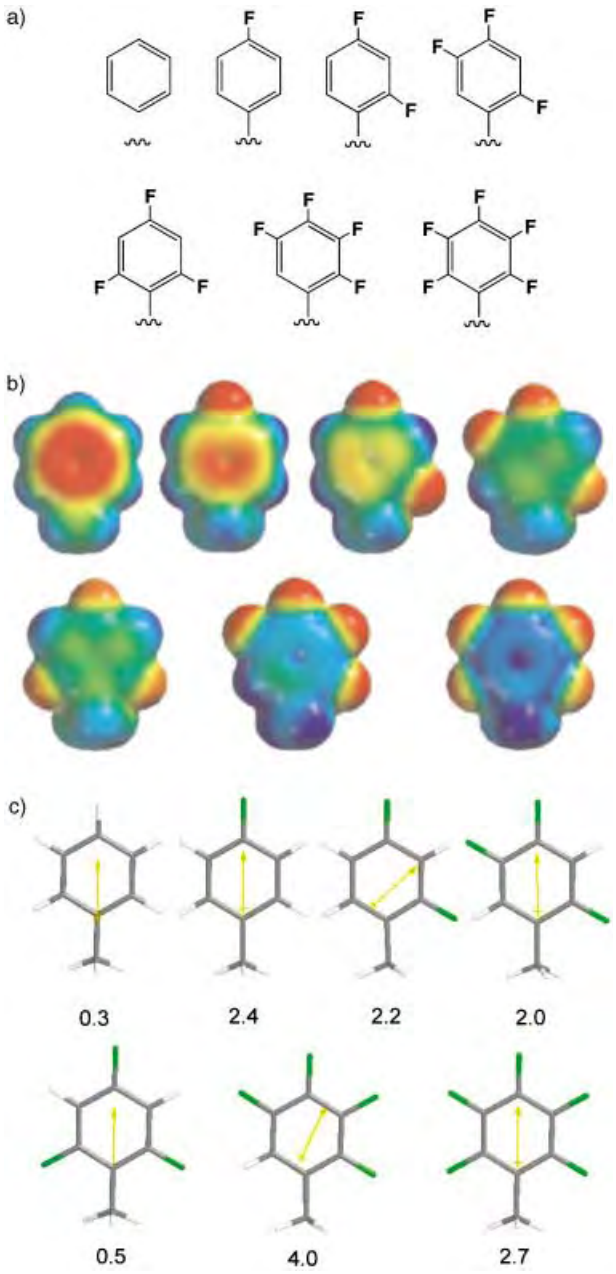



***Figure 1.*** Structures and properties of the seven nucleoside analogues in this study. a) Molecular structures of the nucleobases (all are attached at C1′ of the deoxyribose). b) Calculated electrostatic surface potentials of six progressively fluorinated aromatic base analogues, with an attached methyl group to approximate the effects of the deoxyribose 1′-carbon (red depicts negative potential and blue, positive). c) Calculated dipole moments (debye) of aromatic fluorinated base analogues; dipole orientations are shown with yellow arrows, fluorine atoms are in green. Electrostatics were calculated with Spartan'02 (Wavefunction Inc.) employing the AM1 Hamiltonian.

tion). In addition to differences in quadrupoles, this series has a broad range of dipole moments (Figure 1c), ranging from a calculated 0.4 (for the phenyl case) to 4.5 debye (for the tetrafluorinated compound). Generally, the dipole directional orientations are quite similar over the series (Figure 1c). By comparison, natural DNA bases have dipole moments that are generally large, but with orientations that vary widely (Supporting Information). Finally, to test the effects of location of the fluorine substituents on the base, we studied two different trifluoro-substituted analogues: the 2,4,5-trifluorophenyl and 2,4,6-trifluorophenyl deoxyribonucleosides.

The seven nucleoside analogues were incorporated into synthetic oligonucleotides to study their stacking propensities with natural DNA bases as neighbors. They were incorporated by standard methods on an automated DNA synthesizer, and were characterized in DNA by NMR spectroscopy and by mass spectrometry.

The dangling-end experimental method[30,31] was utilized to evaluate the ability of the fluorinated aromatic base analogues to stabilize DNA duplexes when placed directly adjacent to the helix. The relative stabilizations were measured by comparison of the energetics for helix–coil melting transition of the "core" duplex (lacking any "dangling" nucleotide) to that containing the extra nucleotide. Five short self-complementary sequence contexts were used; the sequences were chosen because they had been shown previously to be well-behaved thermodynamically in the dangling-end configuration.[7,32] Data from two of the contexts are shown in Table 1, and data for the remaining three (showing similar trends) are given in the Supporting Information. By use of these five contexts we were able to compare stacking effects of the base analogues with all four neighboring DNA bases in the helix.

Thermodynamics were obtained both by curve fitting and by the van't Hoff method. All the duplexes appeared to behave in a two-state fashion and had well-shaped melting curves indicative of cooperative interactions of the dangling ends (data not shown). All of the seven unnatural bases displayed significant stabilization of the duplexes relative to the core sequences (Table 1). The least stabilized is the case with a dangling pentafluorophenyl nucleotide on the $(dCGCGCG)_2$ core duplex, which gives an increase in $T_m$ of only 2.9 °C and contributes $-0.5$ kcal mol$^{-1}$ of stability ("$\Delta\Delta G°$ stacking" in Table 1). Almost as poorly stabilizing is the 2,4,6-trifluorinated case, which will be discussed below. The largest stabilizing interaction is observed with the 2,3,4,5-tetrafluorophenyl dangling nucleotide in that same sequence, with a $T_m$ increase of 12.6 °C and a large stabilization of $-2.2$ kcal mol$^{-1}$ compared to the unsubstituted core sequence.

Figure 2 shows the $T_m$ data graphically, illustrating trends over the series with lines connecting data points. The "C adjacent" and "A adjacent" series have the most data available; here we see that mono-, di-, and trifluorinated bases (omitting, for the moment, the 2,4,6-trifluoro isomer) all stabilize the core sequences with similar propensity. For most cases the previously unknown tetrafluoro analogue stacks somewhat more stably than the rest, while in all cases the previously known pentafluoro compound is surprisingly poor at stacking, behaving quite differently than the other compounds across the series.

It is worth noting that simple placement in a 5′-dangling position does not always guarantee a stacked orientation with the neighboring DNA bases. However, we expect that, since these analogues are relatively similar in size and geometry, their propensities for preferred geometries in DNA might

 © 2003 Wiley-VCH Verlag GmbH & Co. KGaA, Weinheim 

***Table 1:*** Stacking of fluoroaromatic nucleotides as measured by thermal denaturation studies in two sequence contexts.[a]

| Dangling residue | $T_m$ [°C][b] | $\Delta T_m$ [°C] | $-\Delta H$ [kcal][c] | $-\Delta S$ [eu][c] | $-\Delta G_{37}$ [kcal][c] | $-\Delta G_{37}$ [kcal][d] | $\Delta\Delta G°$ stacking |
|---|---|---|---|---|---|---|---|
| **XCGCGCG** | | | | | | | |
| none (core duplex) | 41.4 | — | 43.6 | 115 | 8.0±0.1 | 8.1±0.1 | |
| phenyl | 49.1 | 7.8 | 44.7 | 115 | 9.2±0.1 | 9.4±0.1 | 1.2±0.1 |
| 4-fluorophenyl | 51.2 | 9.8 | 64.9 | 175 | 10.3±0.3 | 9.9±0.2 | 2.0±0.2 |
| 2,4-difluorophenyl | 52.5 | 11.2 | 51.7 | 134 | 10.0±0.1 | 10.2±0.1 | |
| 2,4,5-trifluorophenyl | 52.2 | 10.8 | 55.0 | 145 | 10.1±0.3 | 10.0±0.1 | 2.0±0.2 |
| 2,4,6-trifluorophenyl | 45.3 | 4.0 | 37.3 | 104 | 8.4±0.2 | 8.6±0.1 | 0.4±0.1 |
| 2,3,4,5-tetrafluorophenyl | 53.9 | 12.6 | 53.8 | 93 | 10.3±0.2 | 10.2±0.2 | 2.2±0.2 |
| pentafluorophenyl | 44.2 | 2.9 | 39.1 | 99 | 8.5±0.2 | 8.7±0.1 | 0.5±0.2 |
| **XACAGCTGT** | | | | | | | |
| none (core duplex) | 40.0 | — | 44.8 | 119 | 7.9±0.1 | 8.1±0.1 | |
| phenyl | 44.4 | 4.4 | 57.6 | 157 | 8.9±0.2 | 9.0±0.1 | 1.0±0.1 |
| 4-fluorophenyl | 48.7 | 8.7 | 66.6 | 183 | 9.9±0.1 | 9.6±0.1 | 1.8±0.1 |
| 2,4-difluorophenyl | 47.8 | 7.8 | 62.4 | 170 | 9.7±0.2 | 9.6±0.1 | 1.7±0.1 |
| 2,4,5-trifluorophenyl | 48.9 | 9.0 | 67.8 | 186 | 10.1±0.2 | 9.7±0.1 | 1.9±0.2 |
| 2,4,6-trifluorophenyl | 47.8 | 7.9 | 53.6 | 143 | 9.3±0.2 | 9.4±0.2 | 1.3±0.2 |
| 2,3,4,5-tetrafluorophenyl | 50.9 | 10.0 | 76.3 | 212 | 10.7±0.2 | 9.8±0.2 | 2.3±0.2 |
| pentafluorophenyl | 47.3 | 7.0 | 55.2 | 148 | 9.3±0.0 | 9.3±0.2 | 1.3±0.1 |

[a] Free energy of stacking ($\Delta\Delta G°$) is calculated as the difference between the free energies of the duplexes containing dangling residues from the energy of the core duplex. Data from three other sequence contexts is given in the Supporting Information. [b] Conditions: 1 M NaCl, 10 mM sodium phosphate pH 7.0; 5.0 μM DNA-strand concentration for the $T_m$ value shown. [c] Thermodynamic values calculated from van't Hoff plots. [d] Average free energy from fits to individual melting curves.

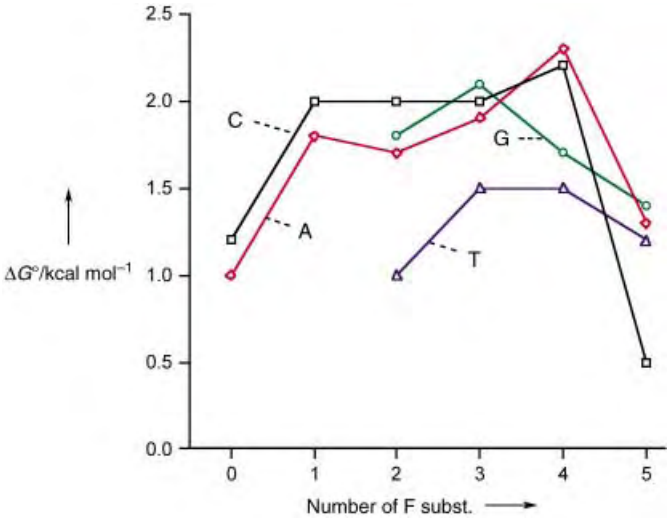



***Figure 2.*** Plot showing trends in stacking free energies as a function of the number of fluorine substitutions on the phenyl deoxyribose adjacent to cytosine (black), adenine (red), guanine (green), and thymine (blue). Primary data are given in Table 1 and in Table S1 in the Supporting Information; the 2,4,6-trifluorinated case is omitted here.

also be similar. It will be important in the future to confirm geometries by structural studies, particularly in a strongly stabilizing case such as the tetrafluorinated analogue, as well as in a poorly stabilized (and potentially distorted) case such as with pentafluorobenzene. Regardless of geometry, however, the present results do indicate which structures are most stabilizing for future molecular designs.

We hypothesized that steric factors might contribute to the poor stabilization by the pentafluorinated species. Although fluorine is a relatively small substituent, it is generally accepted that even small groups can alter the glycosidic orientational preference in nucleosides, presumably by steric interactions with neighboring bonds and substituents.[33,34] To test this further we prepared a second trifluorinated species, this one with 2,4,6 substitution, for direct comparison to the 2,4,5-substituted case. Measurement in the dangling-end contexts revealed that, like the pentafluorinated case, the bis-*ortho*-substituted trifluorobenzene case was very poor at stabilization (Table 1). This is a remarkable difference: a change of 6.8 °C (1.6 kcal) on moving one fluorine atom from the *ortho* to the *meta* position.

Thus the data establish that bis-*ortho* substitution by even small fluorine groups can have a surprisingly large effect on stabilization, causing stacking of both the pentafluoro- and 2,4,6-trifluoronucleosides to be disrupted. We hypothesize that this may be due to a sterically induced twist in the glycosidic bond and/or in the sugar; structural studies will be helpful in evaluating this in the future. This finding explains the previously observed strong destabilizations seen in DNAs containing pentafluorobenzene.[27]

There is a gradual inversion of electrostatic potential at the centers of the flat aromatic surfaces going from the phenyl nucleoside to the pentafluorophenyl nucleoside across this series (see the electrostatic potential maps in Figure 1b). It was anticipated that this difference in electrostatic potential might be a significant factor in the stacking of these compounds in duplex DNA, particularly with differing natural adjacent bases. Electrostatic maps of the four natural DNA bases suggest that adenine is the most electron-rich, while thymine is the least (see the Supporting Information), although the differences are relatively small. However, from the $T_m$ and $\Delta G°$ differences observed here (Table 1 and

 © 2003 Wiley-VCH Verlag GmbH & Co. KGaA, Weinheim 

Figure 2)), there appears to be relatively poor correlation between numbers of fluorine groups and stabilization. For example, in the "C adjacent" and "A adjacent" series, the mono-, di-, and trisubstituted cases show nearly the same stacking propensities (Figure 3a). (Note that we omit the two bis-*ortho* cases from the analysis because of their unusual steric effects.) Since the tetrafluorinated species does stack somewhat more strongly, we cannot entirely rule out a quadrupolar effect, but the data suggest (see below) that simple dipole effects may provide a more consistent explanation for the results. Thus we conclude that, when at least one natural DNA base is involved, quadrupole effects are small or nonexistent, even with one strongly polarized partner. It remains to be seen, however, whether *two* adjacent non-natural stacking partners (which could be more strongly polarized than natural bases are) might exhibit quadrupolar stabilization or destabilization in water.

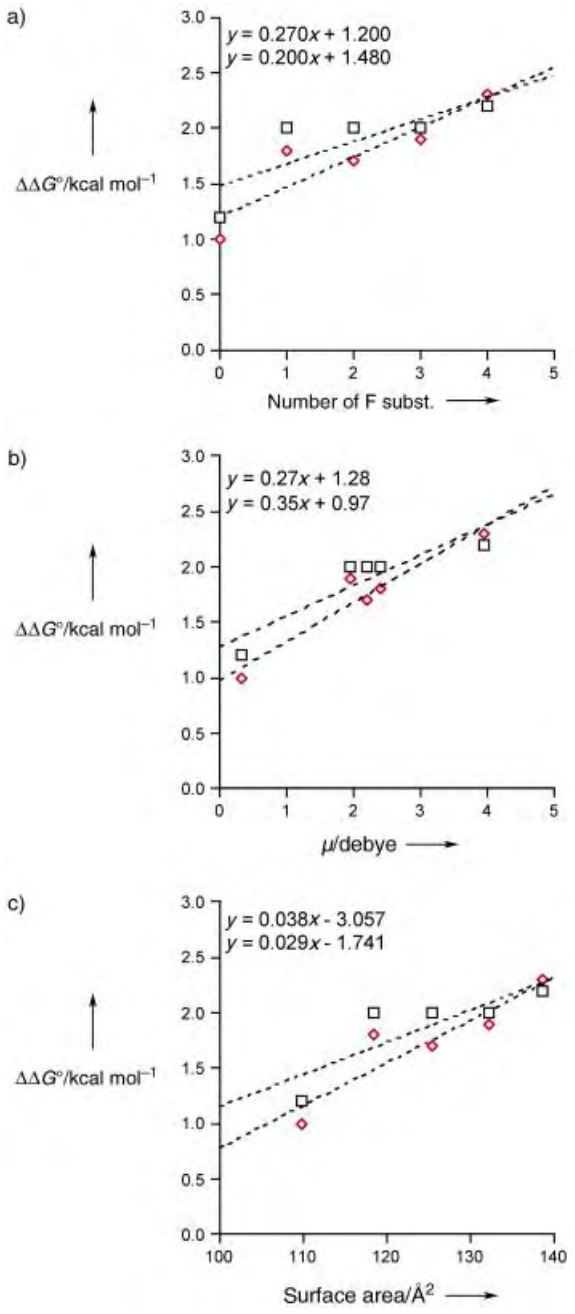



***Figure 3.*** Testing possible linear relationships between stacking free energies and calculated physical properties of aromatic analogues in two comparative sequences with C adjacent (black) and with A adjacent (red) (see Table 1). a) Number of fluorine substitutions (a rough measure of quadrupole strength). b) Dipole moment μ (debye) of the methylated base. c) Estimated surface area of the dangling residue excluded from solvent on stacking. The two compounds with bis-*ortho* effects were omitted.

Dipole moments of the aromatic nucleobase analogues were calculated and plotted against $\Delta T_m$ and $\Delta\Delta G°$ (stacking) for both the "C adjacent" and "A adjacent" series (Figure 3b). Overall, it does appear that there is a linear correlation between dipole moments and stacking stabilization across these series. However, if permanent dipole effects are real, then the orientation of the analogue dipoles relative to the dipole orientations of adjacent bases should play a role in the electrostatic effects. Since the analogue dipole orientations are all similar (Figure 1c), one should compare the dipole orientations of the neighboring bases, which differ more greatly. The dipole directions for adenine and cytosine are oriented roughly 45° relative to one another (see the Supporting Information). If one assumes that a 5′-stacked base takes on the standard B-form conformation, then the dipole orientations of the analogues should be nearly opposed (180°) to that of a cytosine in the neighboring helix, whereas they should be only partially opposed to that of a neighboring adenine. Also possibly significant is the much stronger dipole of C (6.0 debye as the 1-methyl derivative) relative to that of A (2.3 debye). These factors lead to the prediction of stronger dipole effects for a C neighbor than for an A neighbor. However, the plot (Figure 3b) shows very similar slopes for the two series, which is not consistent with these predictions.

A dipole in an end-stacked nucleobase can have two types of electrostatic effects on stacking: as a direct electrostatic interaction with a nearby permanent dipole, and also in the dispersive sense, by inducing an opposing dipole in the neighboring base. One would predict a stronger dispersive effect for a dangling base with a neighboring A than with a neighboring C, because of the greater polarizability of A. However, in the converse sense, C should induce a stronger dipole in the dangling base because of C's strong dipole. These opposing effects might tend to make C and A somewhat similar in stacking abilities, which is consistent with the similar slopes in Figure 3b.

Thus we tentatively conclude that, while dipole effects appear to be significantly stabilizing to DNA base stacking, the origin of the effect may lie in their contribution to van der Waals dispersive forces. Overall, dipole effects can explain only roughly half (and likely less) of the stabilization observed here. Extrapolation to zero dipole still leaves about half of the stacking stabilization intact. Moreover, the compound with largest dipole (the tetrafluorobenzene case) also has greater surface area than the parent benzene compound, a factor that likely also contributes favorably. Plots of surface area vs. stacking (Figure 3c) do show an apparent loose correlation of stabilization with surface area. A correlation of stacking with surface area has been reported

 © 2003 Wiley-VCH Verlag GmbH & Co. KGaA, Weinheim 

previously.[5] It remains to be seen whether the favorable effects of size in this case are due to solvophobic or dispersive effects.

Overall, our data are consistent with the notion that dispersive van der Waals attractions may be among the most important factors in DNA base stacking. The current results suggest that the electrostatic effects of nucleobase dipoles are significant in stabilizing stacking, but may explain only one-third to one-half of the stabilization for bases with strong dipoles. We further suggest that this dipole effect may be a result of dispersive induced-dipole attractions rather than of attractions between permanent dipoles. This leads to the suggestion that aromatic bases with large size and large dipole may be generally well-suited for stacking. Overall the data suggest that quadrupole interactions appear to be small for the natural bases, which have weak quadrupole moments. Finally, a previously unrecognized bis-*ortho* difluoro substitution effect was the largest factor observed in this series. This effect is clearly to be avoided in future designs of base analogues for helix stabilization.

## Experimental Section

All synthetic methods and characterizations of compounds, oligonucleotide synthesis and characterizations, and thermal-denaturation methods and data are reported in the Supporting Information.

Received: July 31, 2003 [Z52531]

**Keywords:** DNA structures · electrostatic interactions · fluorine · pi interactions

[1] S. Smirnov, T. J. Matray, E. T. Kool, C. de los Santos, *Nucleic Acids Res.* **2002**, *30*, 5561 – 5569.
[2] M. L. Waters, *Curr. Opin. Chem. Biol.* **2002**, *6*, 736 – 741.
[3] a) J. Sponer, J. Leszczynski, P. Hobza, *J. Mol. Struct. THEOCHEM* **2001**, *573*, 43 – 53;b) J. Sponer, J. Leszczynski, P. Hobza, *Biopolymers* **2001**, *61*, 3 – 31.
[4] U. Rychlewska, B. Warzajtis, *Acta Crystallogr. Sect. B* **2001**, *57*, 415 – 427.
[5] K. M. Guckian, B. A. Schweitzer, R. X. F. Ren, C. J. Sheils, D. C. Tahmassebi, E. T. Kool, *J. Am. Chem. Soc.* **2000**, *122*, 2213 – 2222.
[6] C. A. Hunter, *J. Mol. Biol.* **1993**, *230*, 1025 – 1054.
[7] a) S. Bommarito, N. Peyret, J. SantaLucia, Jr., *Nucleic Acid Res.* **2000**, *28*, 1929 – 1934; b) J. SantaLucia, Jr., H. T. Allawi, P. A. Seneviratne, *Biochemistry* **1996**, *35*, 3555 – 3562.
[8] S. Nakano, Y. Uotani, S. Nakashima, Y. Anno, M. Fujii, N. Sugimoto, *J. Am. Chem. Soc.* **2003**, *125*, 8086 – 8087.
[9] V. K. Misra, B. Honig, *Biochemistry* **1996**, *35*, 1115 – 1124.
[10] S. C. Harvey, C. L. Wang, S. Teletchea, R. Lavery, *J. Comput. Chem.* **2003**, *24*, 1 – 9.
[11] C. A. Hunter, X. J. Lu, *J. Mol. Biol.* **1997**, *265*, 603 – 619.
[12] P. Hobza, J. Sponer, *J. Am. Chem. Soc.* **2002**, *124*, 11 802 – 11 808.
[13] a) J. Sponer, I. Berger, N. Spackova, J. Leszczynski, P. Hobza, *J. Biomol. Struct. Dyn.* **2000**, *2*, 383 – 407; b) J. Sponer, H. A. Gabb, J. Leszczynski, P. Hobza, *Biophys. J.* **1997**, *73*, 76 – 87.
[14] R. Luo, H. S. R. Gilson, M. J. Potter, M. K. Gilson, *Biophys. J.* **2001**, *80*, 140 – 148.
[15] a) F. Cozzi, F. Ponzini, R. Annunziata, M. Cinquini, J. S. Siegel, *Angew. Chem.* **1995**, *107*, 1092 – 1093; *Angew. Chem. Int. Ed. Engl.* **1995**, *34*, 1019 – 1020; b) F. Cozzi, R. Annuziata, M. Cinquini, J. S. Siegel, *J. Am. Chem. Soc.* **1993**, *115*, 5330 – 5331; c) F. Cozzi, M. Cinquini, R. Annunziata, T. Dwyer, J. S. Siegel, *J. Am. Chem. Soc.* **1992**, *114*, 5729 – 5733.
[16] F. J. Carver, C. A. Hunter, D. J. Livingstone, J. F. McCabe, E. M. Seward, *Chem. Eur. J.* **2002**, *8*, 2848 – 2859.
[17] M. J. Rashkin, M. L. Waters, *J. Am. Chem. Soc.* **2002**, *124*, 1860 – 1861.
[18] T. J. Liu, H. J. Schneider, *Angew. Chem.* **2002**, *114*, 1418 – 1420; *Angew. Chem. Int. Ed.* **2002**, *41*, 1368 – 1370.
[19] B. S. Palm, I. Piantanida, M. Zinic, H. J. Schneider, *J. Chem. Soc. Perkin Trans. 2* **2000**, *2*, 385 – 392.
[20] L. F. Newcomb, S. H. Gellman, *J. Am. Chem. Soc.* **1994**, *116*, 4993 – 4994.
[21] R. A. Friedman, B. Honig, *Biophys. J.* **1996**, *71*, 3525 – 3526.
[22] a) J. C. Ma, D. A. Dougherty, *Chem. Rev.* **1997**, *97*, 1303 – 1324; b) D. A. Dougherty, *Science* **1996**, *271*, 163 – 168.
[23] E. A. Meyer, R. K. Castellano, F. Diederich, *Angew. Chem.* **2003**, *115*, 1244 – 1287; *Angew. Chem. Int. Ed.* **2003**, *42*, 1210 – 1250.
[24] M. Raimondi, G. Calderoni, A. Famulari, L. Raimondi, F. Cozzi, *J. Phys. Chem. A* **2003**, *107*, 772 – 774.
[25] N. C. Chaudhuri, R. X. F. Ren, E. T. Kool, *Synlett* **1997**, 341 – 347.
[26] Z. X. Wang, W. Duan, L. I. Wiebe, J. Balzarini, E. De Clercq, E. E. Knaus, *Nucleosides Nucleotides Nucleic Acids* **2001**, *20*, 11 – 40.
[27] G. Mathis, R. Hunziker, *Angew. Chem.* **2002**, *114*, 3335 – 3338; *Angew. Chem. Int. Ed.* **2002**, *41*, 3203 – 3205.
[28] J. Parsch, J. W. Engels, *Helv. Chim. Acta* **2000**, *83*, 1791.
[29] U. Wichai, S. A. Woski, *Org. Lett.* **1999**, *1*, 1173 – 1175.
[30] M. Petersheim, D. H. Turner, *Biochemistry* **1983**, *22*, 256 – 263.
[31] D. H. Turner, N. Sugimoto, S. M. Freier, *Annu. Rev. Biophys. Biophys. Chem.* **1988**, *17*, 167 – 192.
[32] K. M. Guckian, B. A. Schweitzer, R. X. F. Ren, C. J. Sheils, P. L. Paris, D. C. Tahmassebi, E. T. Kool, *J. Am. Chem. Soc.* **1996**, *118*, 8182 – 8183.
[33] M. S. Cooke, K. E. Herbert, P. C. Butler, J. Lunec, *Free Radical Res.* **1998**, *28*, 456 – 469.
[34] J. Cadet, R. Ducolomb, C. Taieb, *Tetrahedron Lett.* **1975**, 3455 – 3458.

 © 2003 Wiley-VCH Verlag GmbH & Co. KGaA, Weinheim 

Cage Compounds

# Horseshoes, Rings, and Distorted Rings: Studies of Cyclic Chromium-Fluoride Cages**

*Finn K. Larsen,* Jacob Overgaard, Simon Parsons, Eva Rentschler, Andrew A. Smith, Grigore A. Timco,* and Richard E. P. Winpenny**

We recently reported the first heterometallic rings, $[NH_2R_2][Cr_7MF_8(O_2CCMe_3)_{16}]$ (R = a range of alkyl side chains; M = $Ni^{II}$, $Co^{II}$, $Fe^{II}$, $Mn^{II}$, or $Cd^{II}$),[1] based on the neutral homometallic ring, $[Cr_8F_8(O_2CCMe_3)_{16}]$ **1**.[2] These cyclic structures are interesting because they are antiferromagnetically coupled rings, but have a resulting ground state spin. This should allow studies of the dynamics in antiferromagnetic rings, which are often used as models for 1D antiferromagnets.[3] It has also been suggested that such compounds should show macroscopic quantum coherence.[4]

The heterometallic complexes are isolable based on the simple principle that replacement of a single $Cr^{III}$ ion in **1** by a dication generates a ring that is a monoanion.[1] Therefore, in the presence of a suitable counterion—provided by a secondary ammonium ion—it is possible to separate the charged heterometallic species from **1**. The synthesis left several questions unanswered: first, what would happen if the reaction was performed under the usual reaction conditions, but in the absence of the second metal? Second, what might result if the second metal could not occupy the octahedral metal coordination sites found in **1** and in the heterometallic rings? Herein we consider both these questions: the answer is of much wider interest because the resulting structures suggest new methods for controlling the shape of cyclic cage complexes, and perhaps future routes to designed polycyclic metal cages.

[*] Prof. F. K. Larsen, Dr. J. Overgaard
Department of Chemistry, University of Aarhus
8000 Århus C (Denmark)
Fax: (+45) 86-196199
E-mail: kre@chem.au.dk

Dr. G. A. Timco
Institute of Chemistry, Moldovan Academy of Sciences
Kishinev (Moldova)
Fax: (+373) 272-9761
E-mail: Timg@nor.md

Prof. R. E. P. Winpenny, Dr. A. A. Smith
Department of Chemistry, The University of Manchester
Oxford Road, Manchester, M13 9PL (UK)
Fax: (+44) 161-275-4616
E-mail: richard.winpenny@man.ac.uk

Dr. S. Parsons
Department of Chemistry
The University of Edinburgh, Edinburgh (UK)

Dr. E. Rentschler
Max Planck Institut für Strahlenchemie
Mülheim (Germany)

[**] This work was supported by the EPSRC(UK), INTAS (Contract 00-0172) and The Royal Society.

Complex **1** is formed from reaction of hydrated chromium trifluoride with pivalic acid in the presence of dimethylformamide (DMF), followed by crystallization from a range of solvents.[2] To produce the heterometallic rings,[1] a source of a second metal is required and also the addition of a secondary amine, to act as the cation for the ion pair produced. If only the secondary amine is added, dark green crystals can still be grown; however, the X-ray structural analysis[5] of these crystals reveals the formation of a new structural type (Figure 1).

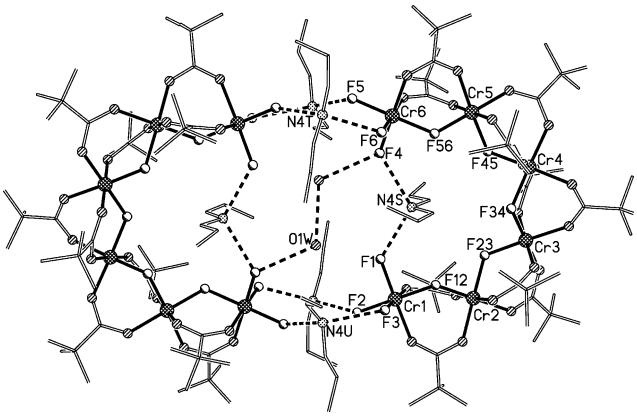



***Figure 1.*** The structure of **2** in the crystal. The hydrogen atoms not involved in hydrogen bonding have been omitted for clarity. Hydrogen bonds are shown as dotted lines. Selected bond-length ranges [Å]: Cr-F(terminal) 1.855–1.883, Cr-F(bridging) 1.899–1.963, Cr(terminal)-O 1.991–2.001, Cr(internal)-O 1.931–1.970; average estimated standard deviation (esd) 0.006 Å. Selected bond angle ranges [°]: *cis* at Cr 86.1–93.3, *trans* at Cr 177.2–179.5; average esd 0.2°.

The general formula for these new cages is $[(R_2NH_2)_3\{Cr_6F_{11}(O_2CCMe_3)_{10}\}sol]_2$ (sol = solvent molecule): here we restrict discussion to R = *n*Pr, sol = $H_2O$ **2** (Figure 1); derivatives have been made with other secondary ammonium ions. The $[Cr_6F_{11}(O_2CCMe_3)_{10}]^{3-}$ horseshoes can be described as derived from **1** by removal of two of the Cr sites. The Cr sites within the horseshoe are bridged by $\mu_2$-F atoms and 1,3-bridging carboxylates in an analogous manner to that found in **1**. The two Cr sites at the tips of the horseshoe have three terminal fluoride ligands, and these terminal fluorides are involved in the hydrogen bonding that links the horseshoes. Two fluoride ions on each chromium hydrogen bond to H atoms of $[R_2NH_2]^+$ ions, which lie between the tips of the horseshoes. These eight F···H–N bonds therefore create a dodecanuclear pseudo-macrocycle. The third fluoride ion on each terminal Cr site is involved in an additional hydrogen-bonding interaction. These four fluoride ions accept hydrogen bonds from two further $[R_2NH_2]^+$ ions that are encapsulated within the pseudo-macrocycle.

Two water molecules are encapsulated within the pseudo-macrocycle (Figure 1). The water molecule hydrogen bonds to two fluoride ligands, with one fluoride ion derived from each of the pair of fluoride ions within the supramolecule. This interaction therefore provides an additional bridge between the two horseshoes. The result is a supramolecule

 © 2003 Wiley-VCH Verlag GmbH & Co. KGaA, Weinheim DOI: 10.1002/anie.200352541 

consisting of two hexametallic trianions, six ammonium ions, and two water molecules.

The bond lengths to chromium in **2** show two clear trends. First, the Cr–F bonds to the terminal fluoride ligands are significantly shorter (about 1.87 Å) than the Cr–F bonds involving the bridging fluoride ligands (about 1.91 Å). Second, bond lengths to the bridging carboxylate oxygen atoms depend on the position of Cr center. For the terminal chromium sites, the bond lengths are close to 1.99(1) Å, while for the inner chromium atoms the Cr–O bonds average 1.95(1) Å. It is noticeable that the hydrogen bonding only involves the terminal F ligands, and not those that bridge between Cr centers. The N···F distances range between 2.64 Å and 2.73 Å.

If a second metal ion that does not favor a regular octahedral geometry is added, further new structural types are formed. If the second metal ion is vanadyl, one site is blocked by the oxide, thus fewer sites are available for bridging. The resulting cage **3**,[5] from the reaction of chromium trifluoride, pivalic acid, and diethylamine in the presence of vanadyl acetate, is shown in Figure 2. Complex **3**

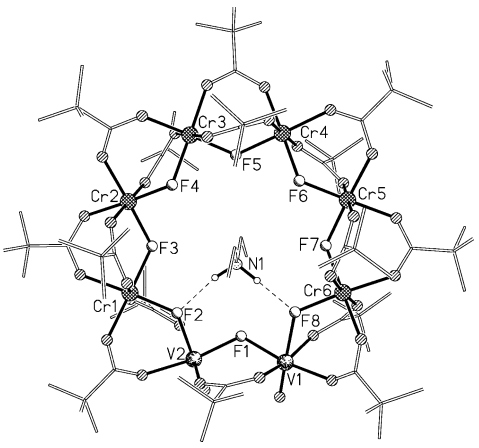



***Figure 2.*** The structure of **3** in the crystal. The hydrogen atoms not involved in hydrogen bonding have been omitted for clarity. Bond-length ranges [Å]: Cr-O($O_2CCMe_3$) 1.932–1.980, Cr-F 1.886–1.945 V-O 1.569–1.578, V-O($O_2CCMe_3$) 2.006–2.036, V-F 1.979–2.210; average esd 0.006.

has the formula $[Et_2NH_2][Cr_6(VO)_2F_8(O_2CCMe_3)_{15}]$ and contains an octanuclear core, bridged by eight fluorides as in **1**. The two vanadyl units are next to one another, and bridged by one pivalate in addition to a μ-fluoride ion, whereas all the Cr···Cr and Cr···V vectors are bridged by two pivalates and a fluoride ion. The ring is a monoanion, and encapsulates a secondary ammonium ion as in the $\{Cr_7M\}$ rings. It is noticeable that the V–F bond *trans* to the oxo group is very long (av 2.20 Å) compared to the V–F bonds *cis* to the oxo (av 1.98 Å). The coordination geometry about the V atom is therefore an extremely distorted octahedron, while the $Cr^{III}$ ions have comparatively regular geometries. The relationship between **3** and the "horseshoes" in **2** appears clear: the horseshoe has been completed by the addition of two $VO^{2+}$ ions. The $\{Cr_6(VO)_2\}$ anion can be isolated with other secondary ammonium counterions.

If we use basic copper carbonate in the same reaction, the resulting cage is less easily rationalized:[5] $[Me_2NH_2]_2[Cr_{10}Cu_2F_{14}(O_2CCMe_3)_{22}]$ (**4**) contains a distorted dodecanuclear ring in which five $Cr^{III}$ centers lie between the two $Cu^{II}$ centers (Figure 3). The copper(II) centers are five-coordinate, bridged to one $Cr^{III}$ through one fluoride ligand and two pivalates, and to a second $Cr^{III}$ through only one fluoride ion and one pivalate. A terminal fluoride ion (F7) is found on the neighboring chromium. The Cr···Cr vectors are all bridged in an analogous manner to **1**–**3**.

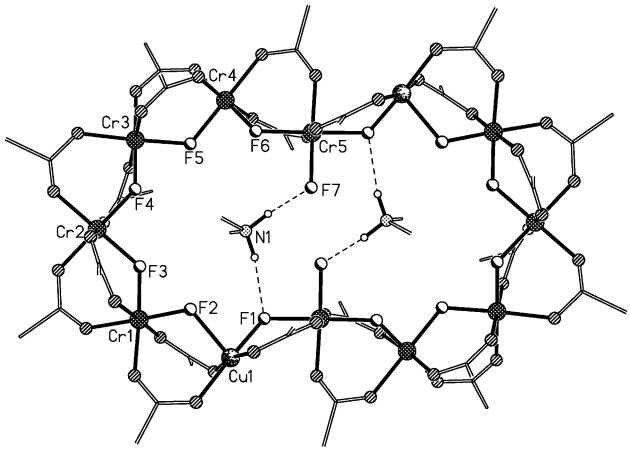



***Figure 3.*** The structure of **4** in the crystal. The hydrogen atoms not involved in hydrogen bonding have been omitted for clarity. Bond-length ranges [Å]: Cr-O($O_2CCMe_3$) 1.853–2.013, Cr-F 1.853–1.931, Cu-O($O_2CCMe_3$) 1.916–1.957, Cu-F 1.878–2.104; average esd 0.013.

The presence of two dicationic metal ions in the ring makes the ring a dianion. Therefore two secondary ammonium ions are found at the center of the structure. They form hydrogen bonds to the terminal fluoride ions (N···F 2.65 Å), and to the fluoride ion that bridges the $Cu^{II}$ and $Cr^{III}$ centers (N···F 3.03 Å). It is possible that this need to form hydrogen bonds leads to a pronounced distortion of the dodecanuclear ring. In previous dodecanuclear rings, the structure is regular, for example, in $\{Ni_{12}\}$[7] and $\{Co_{12}\}$ rings[8] the molecule has $S_6$ crystallographic symmetry, while in a recently reported $\{Fe_{12}\}$ ring[9] the array of metal centers has approximate sixfold symmetry. Complex **4** is the first example of a cyclic 3d-metal complex in which there are regions of negative and positive curvature: Müller et al. have stressed that growth of nanoscale polyoxomolybdates (and other nanoscale molecules) may depend on such symmetry breaking.[10] The distortion also suggests that if the two terminal fluoride bridges could be displaced by a single extended bridge it might be possible to convert **4** into a bicyclic system. This would be a first for coordination chemistry.

The next rational extension was to try a metal ion with a preference for tetrahedral geometry, which led us to try $Zn^{II}$. However, this ion can adopt an octahedral geometry when required and the reaction produced $[NH_2Et_2][Cr_7ZnF_8(O_2CCMe_3)_{16}]$ (**5;** Figure 4), which is the analogue of the heterometallic derivatives of **1**, found with other metal dications.[1] The structure consists of an octametallic ring, with

 © 2003 Wiley-VCH Verlag GmbH & Co. KGaA, Weinheim 

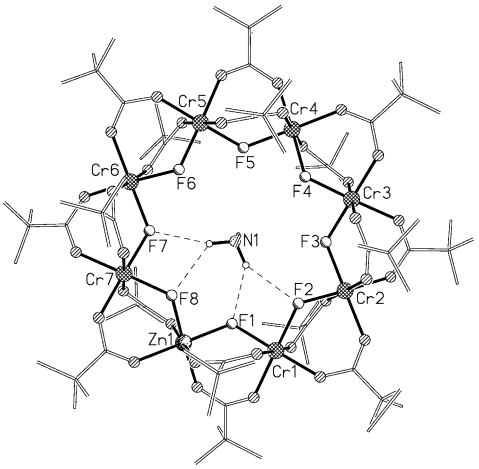



***Figure 4.*** The structure of **5** in the crystal. The hydrogen atoms not involved in hydrogen bonding have been omitted for clarity. Bond length ranges [Å]: Cr-O($O_2CCMe_3$) 1.937–1.989, Cr-F 1.915–1.966, Zn-O($O_2CCMe_3$) 1.946–1.977, Zn-F 1.940–1.957; average esd 0.0026.

each edge bridged by two fluoride ions and a carboxylate ligand. Unlike in the other heterometallic rings,[1] the $Zn^{II}$ ion may be ordered, with one of the eight octahedral metal sites refining well as a Zn site. The unique site is bound to two fluoride ions that both hydrogen bond to the central ammonium ion: it is noticeable in **3** that the fluoride ions involved in hydrogen bonding are bound to vanadyl centers.

Magnetic studies of the complexes show antiferromagnetic exchange between the paramagnetic metal centers. For **2** the room temperature value of $\chi_m T$ per horseshoe, is around 9.4 emu K $mol^{-1}$, lower than predicted for six noninteracting $S = 3/2$ centers ($S$ = spin angular momentum; calcd for $g =$ 1.99, 11.1 emu K $mol^{-1}$; $g$ is the $g$ factor). Complex **2** is diamagnetic at low temperature. For **3** the antiferromagnetic exchange again leads to a diamagnetic ground state; the magnetic behavior has been fitted by using a single exchange parameter, which gives $g = 2.007$ and $J = -14.9$ $cm^{-1}$. The fit is excellent, but clearly the Cr···Cr exchange should be different to the (VO)···(VO) exchange; previously we have found[1,2] that the Cr···Cr exchange is around $-12$ $cm^{-1}$. This suggests the (VO)···(VO) exchange is a little larger to obtain an average exchange of $-14.9$ $cm^{-1}$. For **5** the magnetic data can be modeled with $g = 1.98$, $J = -11.8$ $cm^{-1}$. However at low temperature the model diverges from the measured values, possibly because intermolecular exchange between the $S = 3/2$ spin ground states becomes important.

The magnetic behavior of **4** also suggests a very low spin, probably diamagnetic, ground state. Analysis of the magnetism is complicated because a cyclic $\{Cr_{10}Cu_2\}$ array is too large to be solved by matrix diagonalization. By using an imaginary $\{Cr_8Cu_2\}$ ring as a model allows approximate exchange parameters to be derived; a similar procedure has been used for $\{Fe_{10}\}$ rings previously.[11] By this procedure we derive the Cr···Cr exchange as antiferromagnetic, with a magnitude of $-6.8$ $cm^{-1}$. One of the Cr···Cu exchange paths involves the Cu $d_{x^2-y^2}$ orbital in the exchange path, and this exchange is also considered to be $-6.8$ $cm^{-1}$. The second Cr···Cu exchange involves the Cu $d_{z^2}$ orbital, and this is modeled as $+2$ $cm^{-1}$; the model is not very sensitive to this final parameter, except at very low temperature.

The key result here relates to structural chemistry. Saalfrank et al. have previously shown that use of alkali-metal ions can control the size of metallocrowns.[12] Here we have demonstrated that hydrogen-bonding templates can be used to influence complex topology in cyclic structures. Specifically exciting is the observation of the "templating" of the $\{Cr_{10}Cu_2\}$ cage by incorporation of two ammonium ions. This suggests that use of designed di- and polyamine templates might lead to still greater structural complexity—in a designed manner.

## *Experimental Section*

**2**: $CrF_3 \cdot 4H_2O$ (3.0 g, 17 mmol), $nPr_2NH$ (1.7 g, 16 mmol), and pivalic acid (9.0 g, 88 mmol) were stirred together at 115 °C for 2.0 h. The mixture was cooled to about 80 °C and MeCN (100 mL) added. The solution was heated to reflux for 5 min, and the resulting microcrystalline precipitate was collected by filtration and washed with MeCN prior to recrystallization from acetone. Yield 0.90 g (19 %). Elemental analysis calcd (%) for $C_{136}H_{280}Cr_{12}F_{22}N_6O_{42}$: Cr 16.80, C 43.99, H 7.60, N 2.26, F 11.25; found: Cr 16.48, C 43.73, H 7.52, N 2.22, F 11.10.

**3:** $CrF_3 \cdot 4H_2O$ (5.0 g, 28 mmol), $Et_2NH$ (0.85 g, 12 mmol), and pivalic acid (14.0 g, 140 mmol) were stirred together at 140 C for 1.5 h in a Teflon flask. $[VO(O_2CCMe_3)_2]_n$[13] (1.5 g) was added and the temperature of reaction increased to 160 °C for 2 h. A green crystalline product was formed. The flask was cooled to room temperature and acetone/acetonitrile (50 mL; 1:1) was added with stirring. The product was filtered, washed with a large quantity of acetone/acetonitrile (1:1), dried in air, and recrystallized from hexane. Yield 3.7 g (37 %). Elemental analysis calcd (%) for $C_{79}H_{147}Cr_6F_8N_1O_{32}V_2$: Cr 14.25, V 4.65, C 43.35, H 6.77, N 0.64, F 6.94; found: Cr 13.66, V 5.06, C 42.46, H 6.72, N 0.63. F 6.65. ES-MS (THF): $m/z$: $-2113$ $[Cr_6(VO_2F_8(O_2CCMe_3)_{15}]^-$; $+2188$ $M^+$; $+2211$ $[M+Na]^+$.

**4:** $CrF_3 \cdot 4H_2O$ (3.0 g, 17 mmol), dimethylamine (3.0 mL, 2.0 M solution in THF, 6.0 mmol), and pivalic acid (14.0 g, 140 mmol) were stirred together at 140 °C for 2.0 h in a Teflon flask. Basic copper carbonate (1.0 g, 4.5 mmol) was added and the solution heated for a further 3 h. The flask was cooled to room temperature and acetone (30 mL) was added with stirring. A green crystalline product was formed. The product was filtered, washed with a large quantity of acetone, dried in air and recrystallized from ethyl acetate/acetone (1:1). Yield 3.2 g (60 %). Elemental analysis calcd (%) for $C_{114}H_{214}Cr_{10}Cu_2F_{14}N_2O_{44}$: Cr 16.10, Cu 3.93, C 42.80, H 6.68, N 0.87, F 8.23; found: Cr 14.93, Cu 3.76, C 43.47, H 7.04, N 0.68. F 7.23.

**5:** $CrF_3 \cdot 4H_2O$ (3.0 g, 17 mmol), $Et_2NH$ (0.85 g, 12 mmol), and pivalic acid (14.0 g, 140 mmol) were stirred together at 140 °C for 1.5 h in a Teflon flask. $[Zn(O_2CCMe_3)_2]_n$ (1.0 g) was added and the temperature of reaction increased to 160 °C for 2.5 h. The flask was cooled to room temperature and acetone (50 mL) was added and the solution was stirred for 15 min. A green crystalline product was formed. The product was collected by filtration, washed with a large quantity of acetone and dried in air, then recrystallized from ethyl acetate. Yield: 2.1 g (39 %). Elemental analysis calcd (%) for $C_{84}H_{156}Cr_7F_8N_1O_{32}Zn$: Cr 16.01, Zn 2.88, C 44.38, H 6.92, N 0.62, F 6.69; found: Cr 15.74, Zn 2.99, C 44.41, H 6.99, N 0.60, F 6.57. ES-MS (THF): $m/z$: $-2199$ $[Cr_7ZnF_8(O_2CCMe_3)_{16}]^-$; $+2296$ $[M+Na]^+$.

Measurements: Magnetic susceptibility measurements were performed on polycrystalline samples in the temperature range 2.0 to 298 K in an applied field of 1 T by using a Quantum Design MPMS SQUID magnetometer. Corrections for diamagnetic contributions

 © 2003 Wiley-VCH Verlag GmbH & Co. KGaA, Weinheim 

were applied by using Pascal's Constants. The sample holder diamagnetism was measured and substracted from the raw data.

Received: August 1, 2003 [Z52541]

**Keywords:** cage compounds · chromium · heterometallic complexes · supramolecular chemistry · template synthesis

[1] F. K. Larsen, E. J. L. McInnes, H. El Mkami, J. Overgaard, S. Piligkos, G. Rajaraman, E. Rentschler, A. A. Smith, G. M. Smith, V. Boote, M. Jennings, G. A. Timco, R. E. P. Winpenny, *Angew. Chem.* **2003**, *115*, 105 – 109; *Angew. Chem. Int. Ed.* **2003**, *42*, 101 – 105.

[2] a) N. V. Gerbeleu, Yu. T. Struchkov, G. A. Timco, A. S. Batsanov, K. M. Indrichan, G. A. Popovich, *Dokl. Akad. Nauk SSSR* **1990**, *313*, 1459 – 1462; b) J. van Slageren, R. Sessoli, D. Gatteschi, A. A. Smith, M. Helliwell, R. E. P. Winpenny, A. Cornia, A.-L. Barra, A. G. M. Jansen, G. A. Timco, E. Rentschler, *Chem. Eur. J.* **2002**, *8*, 277 – 285; c) J. Overgaard, B. B. Iversen, S. P. Palii, G. A. Timco, N. V. Gerbeleu, F. K. Larsen, *Chem. Eur. J.* **2002**, *8*, 2775 – 2786.

[3] a) L. J. De Jongh, A. Miedema, *Adv. Phys.* **1974**, *23*, 1; b) K. L. Taft, C. D. Delfs, G. C. Papaefthymiou, S. Foner, D. Gatteschi, S. J. Lippard, *J. Am. Chem. Soc.* **1994**, *116*, 823; c) O. Waldmann, *Phys. Rev. B* **2001**, *65*, 024424 – 024421; d) J. Schnack, M. Luban, *Phys. Rev. B* **2000**, *63*, 0144418; e) A. Chiolero, D. Loss, *Phys. Rev. Lett.* **1998**, *80*, 169.

[4] F. Meier, D. Loss, *Phys. Rev. B* **2001**, *64*, 224411/1 – 224411/14.

[5] Crystal data for **2**. $1.5\,Me_2CO$: $C_{140.5}H_{289}Cr_{12}F_{22}N_6O_{43.5}$; $M_r = 3800.8\ g\,mol^{-1}$): dark green block, monoclinic, space group $P2_1/c$, $a = 19.807(4)$, $b = 25.715(5)$, $c = 21.874(5)$ Å, $\beta = 111.747(3)°$, $V = 10348(4)$ Å$^3$, $Z = 2$ (the supramolecule lies on an inversion center), $T = 150.0(2)$ K, $\rho = 1.220\ g\,cm^{-3}$, $F(000) = 4016$, $\mu(Mo_{K\alpha}) = 0.685\ mm^{-1}$. Crystal data for **3**: ($C_{79}H_{147}Cr_6F_8NO_{32}V_2$; $M_r = 2189.02\ g\,mol^{-1}$): green plate, orthorhombic, space group $Aba2$, $a = 30.173(2)$, $b = 35.201(2)$, $c = 23.449(1)$ Å, $V = 24906(2)$ Å$^3$, $Z = 8$, $T = 120.0(2)$ K, $\rho = 1.167\ g\,cm^{-3}$, $F(000) = 9168$, $\mu(Mo_{K\alpha}) = 0.718\ mm^{-1}$. Crystal data for **4**: ($C_{114}H_{214}Cr_{10}Cu_2F_{14}N_2O_{44}$; $M_r = 3230.08\ g\,mol^{-1}$): dark green plate, tetragonal, space group $I4cd$, $a = 30.950(1)$, $c = 37.950(2)$ Å, $V = 36351(3)$ Å$^3$, $Z = 8$, $T = 120.0(2)$ K, $\rho = 1.180\ g\,cm^{-3}$, $F(000) = 13504$, $\mu(MoK_\alpha) = 0.875\ mm^{-1}$. Crystal data for **5**: ($C_{86}H_{160}Cr_7F_8NO_{33}Zn$; $M_r = 2317.68\ g\,mol^{-1}$): dark green plate, monoclinic, space group $P2_1/c$, $a = 25.000(1)$, $b = 16.6383(9)$, $c = 30.884(2)$ Å, $\beta = 110.037(1)°$, $V = 12069(1)$ Å$^3$, $Z = 4$, $T = 120.0(2)$ K, $\rho = 1.275\ g\,cm^{-3}$, $F(000) = 4868$, $\mu(Mo_{K\alpha}) = 0.879\ mm^{-1}$. Data were collected on Bruker SMART CCD diffractometer ($Mo_{K\alpha}$, $\lambda = 0.71069$ Å). In all cases the selected crystals were mounted on the tip of a glass pin by using Paratone-N oil and placed in the cold flow (120 K) produced with an Oxford Cryocooling device. Complete hemispheres of data were collected by using $\omega$ scans (0.3°, 30 seconds/frame). Integrated intensities were obtained with SAINT+[6] and they were corrected for absorption using SADABS.[6] Structure solution and refinement was performed with the SHELX-package.[6] The structures were solved by direct methods and completed by iterative cycles of $\Delta F$ syntheses and full-matrix least-squares refinement against $F^2$ to give: for **2**: by using 927 parameters and 147 restraints, $wR_2 = 0.2316$ (13519 unique reflections), $R_1 = 0.0713$ (9155 reflections with $I > 2\sigma(I)$); for **3:** using 1152 parameters, $wR_2 = 0.077$ (14988 unique reflections), $R_1 = 0.046$ (11779 reflections with $I > 3\sigma(I)$); for **4:** 673 parameters, $wR_2 = 0.114$ (10560 unique reflections), $R_1 = 0.095$ (5352 reflections with $I > 3\sigma(I)$); for **5:** 1219 parameters, $wR_2 = 0.077$ (27372 unique reflections), $R_1 = 0.057$ (18955 reflections with $I > 3\sigma(I)$). CCDC-216507 (**2**) and CCDC-216509 to CCDC-216511 (**3**–**5**) contain the supplementary crystallographic data for this paper. These data can be obtained free of charge via www.ccdc.cam.ac.uk/conts/retrieving.html (or from the Cambridge Crystallographic Data Centre, 12 Union Road, Cambridge CB21EZ, UK; fax: (+44) 1223-336-033; or deposit@ccdc.cam.ac.uk).

[6] SHELX-PC Package. Bruker Analytical X-ray Systems: Madison, WI, **1998**.

[7] H. Andres, R. Basler, A. J. Blake, E. K. Brechin, C. Cadiou, G. Chaboussant, C. M. Grant, H.-U. Güdel, S. G. Harris, M. Murrie, S. Parsons, C. Paulsen, F. Semadini, V. Villar, W. Wernsdorfer, R. E. P. Winpenny, *Chem. Eur. J.* **2002**, *8*, 4867 – 4876.

[8] E. K. Brechin, O. Cador, A. Caneschi, C. Cadiou, S. G. Harris, S. Parsons, M. Vonci, R. E. P. Winpenny, *Chem. Commun.* **2002**, 1860 – 1861.

[9] C. P. Raptopoulou, V. Tangoulis, E. Devlin, *Angew. Chem.* **2002**, *114*, 2492 – 2495; *Angew. Chem. Int. Ed.* **2002**, *41*, 2386 – 2389.

[10] A. Müller, E. Beckmann, H. Bögge, M. Schmidtmann, A. Dress, *Angew. Chem.* **2002**, *114*, 1210 – 1215; *Angew. Chem. Int. Ed.* **2002**, *41*, 1162 – 1167.

[11] K. L. Taft, C. D. Delfs, G. C. Papaefthymiou, S. Foner, D. Gatteschi, S. J. Lippard, *J. Am. Chem. Soc.* **1994**, *116*, 823 – 832.

[12] R. W. Saalfrank, I. Bernt, E. Uller, F. Hampel, *Angew. Chem.* **1997**, *109*, 2596 – 2599; *Angew. Chem. Int. Ed. Engl.* **1997**, *36*, 2482 – 2485.

[13] R. C. Paul, A. Rumar, *J. Inorg. Nucl. Chem.* **1965**, *27*, 2537 – 2547.

 © 2003 Wiley-VCH Verlag GmbH & Co. KGaA, Weinheim 

*Organolanthanide Complexes*

# Anionic Amido N-Heterocyclic Carbenes: Synthesis of Covalently Tethered Lanthanide–Carbene Complexes**

*Polly L. Arnold,* Shaheed A. Mungur, Alexander J. Blake, and Claire Wilson*

Deprotonation of a bidentate amine-imidazolium bromide affords a new amine-functionalized carbene, and by a protonolysis reaction, the first f-element complex with a covalently bound, potentially hemilabile, N-heterocyclic carbene.

Since the early use of di-*N*-phenyl, -methyl, and -adamantyl functionalized imidazolium salts and electron-rich alkenes as precursors for metal–carbene complexes and stable nucleophilic carbenes,[1] it is now apparent that a wide range of *N*-functional groups are tolerated in nucleophilic

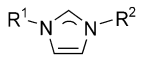
[*] Dr. P. L. Arnold, S. A. Mungur, A. J. Blake, C. Wilson
School of Chemistry
University of Nottingham
University Park, Nottingham, NG7 2RD (UK)
Fax: (+44) 115-9513-563
E-mail: polly.arnold@nottingham.ac.uk

[**] We thank the EPSRC (UK; fellowship for PLA, studentship for SAM, and a diffractometer) and the Royal Society for funding.

Supporting information for this article is available on the WWW under http://www.angewandte.org or from the author.

 DOI: 10.1002/anie.200352710 © 2003 Wiley-VCH Verlag GmbH & Co. KGaA, Weinheim 

imidazol-2-ylidenes (**A**) or N-heterocyclic carbenes (NHCs). These bind as two-electron donors to almost all metals in the



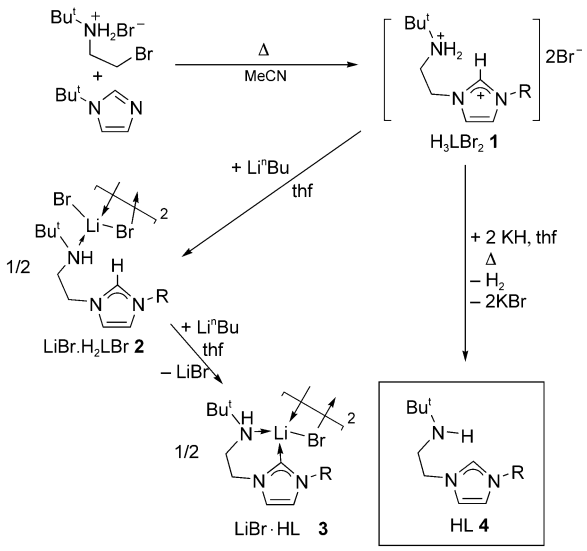

periodic table.[2] NHCs form extremely strong dative bonds to late d-block metals such as ruthenium and palladium, with little or no backbonding,[3] and are easily *N*-functionalized. The overwhelming majority of these ligands are neutral, and incorporate chiral hydrocarbyl groups, or additional donor groups (e.g. pyridyl, ether, NHC), to tune the catalytic activity of the complexes in reactions such as C–Si, C–C, C–N, and now methane C–H activation.[4] To date, the NHC complexes of the most electropositive metals, including Groups 4, 5, and the s- and f-block, have been reported only as "curiosities", in which the NHC binds simply as a solvate.[5] Although interesting electronic properties of the early metal–NHC bond has been suggested,[6] no complexes have been available in which the strength or reactivity of the bound NHC may be studied. Monodentate, unfunctionalized NHCs have already been used to good effect in $Al^{III}$ mediated C–C bond forming reactions,[7] so the development of NHC-functionalized ligands which are asymmetric, and in which the NHC is hemilabile, has potential in areas of homogeneous catalysis.

We have been studying NHC ligands that incorporate a pendant anionic functional group for this purpose.[8] We now report a synthesis of the first amido-functionalized NHC ligand, and syntheses of trivalent samarium(III) and yttrium(III) adducts of this asymmetric bidentate ligand.

The reaction of 2-bromoethyl-*tert*-butyl-ammonium bromide with *N*-*tert*-butyl imidazole proceeds cleanly in acetonitrile to afford the alkylammonium imidazolium bromide *t*BuNH$_2$CH$_2$CH$_2$[HC{*t*BuN(CHCH)N}]Br $H_3LBr_2$, **1** (Scheme 1). A single crystal X-ray diffraction study (see Supporting Information) shows that both cationic groups—amine $NH_2$ and imidazolium CH—form networks of hydrogen bonds through lattice bromide ions.

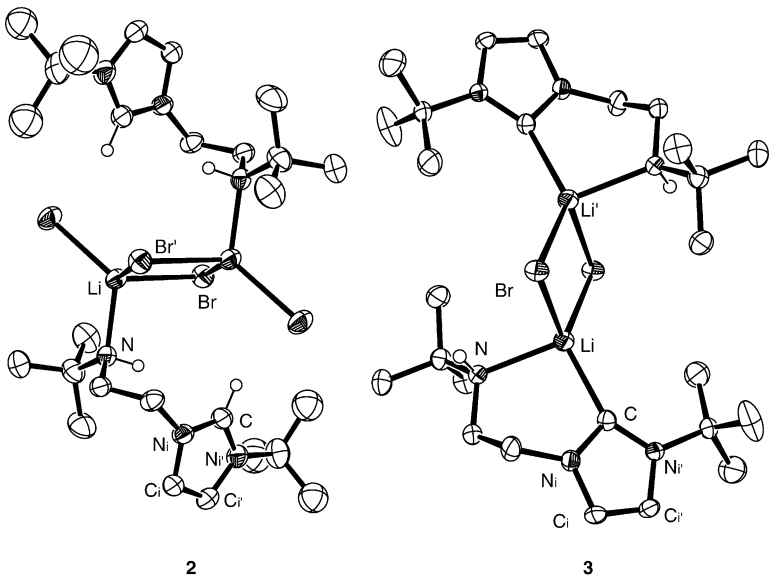
Complex **1** may be deprotonated in sequential steps: The reaction of **1** with an equivalent of lithium *n*-butyl affords the amine-imidazolium bromide $H_2LBr$. Removal of volatiles, and recrystallization from THF affords the LiBr adduct [LiBr($H_2LBr$)] **2**. The reaction of **2** with a further equivalent of lithium *n*-butyl yields the lithium bromide adduct of the target amine–carbene [LiBr(HL)] **3**, Scheme 1. Whilst it is possible to crystallize salt-free $H_2LBr$ from a solution of **2**, (see Supporting Information), the dative bonds from the amine and NHC in **3** bind to the Li cation; we could not displace the bound LiBr from **3** by trituration or other extraction procedures.

Figure 1 shows the structures of **2** and **3**. The molecular structures obtained for all three complexes, and the LiBr-free $H_2LBr$, show the typical change in C–N distance (increase) and ∢ NCN angle (decrease) of the unsaturated NCN fragment upon deprotonation, reflecting the increase in s character in the carbene lone pair.[9]




***Scheme 1.*** Syntheses of complexes **1**–**4**

Lithium carbenes are extremely rare; in **3** the Li–C distance is longer than the 2.155 Å bond length measured in the only other simple lithium NHC adduct, [Li{$C_5H_2$(Si-Me$_3$)$_3$}{C(N*t*BuCH)$_2$}], and longer than the average Li–$C_{NHC}$ distance of 2.162 Å (calculated by including bridging Li–C distances in the other two reported structures).[10] The *tert*-butyl groups of the two molecules of the dimer are geared with a short C–C closest distance of 3.91 Å (H···H separation = 2.41 Å), and although the [$LiCN_iN_{i'}$] fragment is planar, Li···$N_{i'}$ is shorter than Li···$N_{i'}$, which suggests the ligand is too large for the lithium cation. The geometry of the neutral chelate in **3** compares closely with the recently reported [$PdCl_2$(L′)] and [Rh(cod)(L′)][$BF_4$] (L′ = [1-{C(MesN(CHCH)N)-3-{CH=C(*t*Bu)NH*i*Pr]; Mes = 2,4,6-Me$_3$C$_6$H$_2$) complexes of a bidentate neutral imine–NHC [1-




**2** **3**

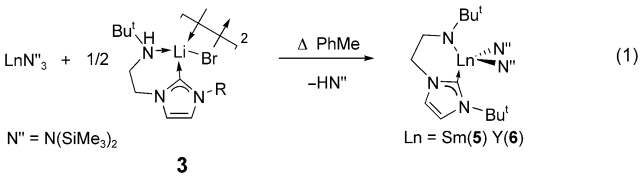
***Figure 1.*** X-ray crystal structures of **2** and **3** (ORTEP, thermal ellipsoids set at the 50% probability level).

 © 2003 Wiley-VCH Verlag GmbH & Co. KGaA, Weinheim 

{C(MesN(CHCH)N)-3-{$CH_2C(t\text{Bu})$=N*i*Pr], which tautomerizes to an enamine upon binding.[11]

To preclude salt incorporation, a mixture of **1** and two equivalents of potassium hydride was heated to reflux in THF for 12 h; filtration and removal of volatiles afforded the carbene–amine HL **4** in 86% yield as a distillable yellow oil.

Transamination of the lithium carbene–amine **3** with $[Sm\{(NSiMe_3)_2\}_3]$ proceeded cleanly in toluene over 48 h to afford **5** [Eq (1)] with complete displacement of lithium




(1)

bromide from the coordination sphere. No samarium bromide-containing complexes were found in the product mixture. After removal of the volatiles, dark yellow, very air-sensitive crystals of $[Sm(L)\{N(SiMe_3)_2\}_2]$ **5** were isolated by recrystallization from diethyl ether, or by sublimation (140 °C, $10^{-3}$ mbar). The paramagnetism of the complex precludes $^{13}C$ NMR spectroscopic identification of the carbenoid carbon, but a carbene–samarium bond in solution is inferred from the absence of the carbene $^{13}C$ NMR spectral resonance, and strongly shifted CH backbone resonances of the heterocycle. Single crystals of **5** suitable for structural analysis were grown by sublimation; the structure is shown in Figure 2.

The geometry at the Sm ion is pseudo-tetrahedral, with one possible close contact with a silicon atom suggested by a Sm–Si distance of 3.3334(5) Å. The amido α-$CH_2$ group is also close to the metal at 2.918 Å. The $Sm-C_{carbene}$ distance of 2.588(2) Å is the shortest yet recorded, compared to the three published monodentate Sm–NHC complexes (av 2.76 Å, range 2.62–2.83 Å).[12] The $Sm-N_{silylamide}$ bonds (av 2.216(2) Å) are short (average for simple samarium amido derivatives = 2.37 Å; range 2.19–2.70 Å). The N-Sm-N angle between the two silylamides of 129° is wider than the tetrahedral angle measured in unconstrained four-coordinate Sm(III) silylamides (av 112.7°).[13]

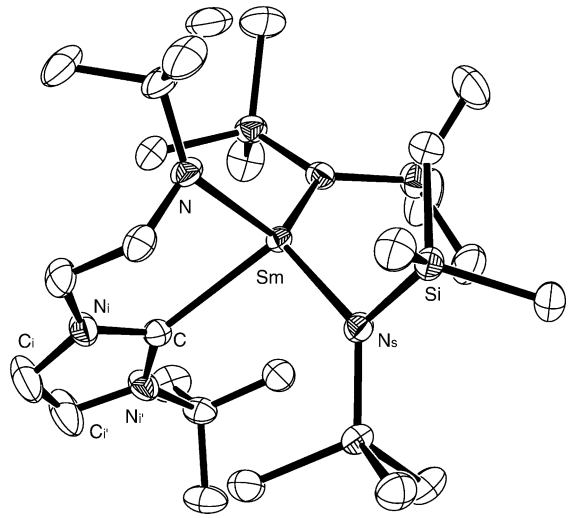



***Figure 2.*** X-ray crystal structures of **5** (ORTEP, thermal ellipsoids set at the 50% probability level).

The long C–N distances and narrow ∢ NCN angle that were observed for **3** are again observed, but in this structure, the Sm-heterocycle fragment is almost completely planar and now symmetrically bifurcates the external $N_i$-C-$N_{i'}$ angle, which suggests the bite angle of this ligand is well-suited to the large cation.

The only isolable complex obtained from the reaction of the divalent compound $[Sm\{(NSiMe_3)_2\}_2]$ with **4** is the trivalent **5**, in a lower yield. We have yet to identify the byproducts arising from the oxidation of the $Sm^{II}$ centre.

Compelling evidence of NHC binding in this system was obtained by the synthesis of the analogous $f^0$ yttrium complex. The complex $[Y(L)\{N(SiMe_3)_2\}_2]$ **6**, made from $[Y\{N(SiMe_3)_2\}_3]$ by the same method as **5**, is isostructural (see Supporting Information) but the $Y-C_{carbene}$ distance is 2.501(5) Å. In NMR spectroscopic solution, the $^{13}C$ $C_{carbene}$ resonates at 186 ppm with a $^1J$ $^{89}Y-C_{carbene}$ coupling of 54.7 Hz, larger than any $^1J_{YC}$ value reported for a σ-bound yttrium alkyl or an yttrium-NHC adduct.[14]

These are the first complexes that combine a metal–amide bond and a metal–NHC bond in a ligand. The strength of the metal–amide bond in **5** and **6** makes a controlled study of the reactivity of the electropositive metal–NHC fragment possible for the first time by precluding ligand redistribution processes that can complicate lanthanide coordination chemistry and allowing us to monitor the fate of both the metal cation and the nucleophilic NHC. It is suggested that the softness of the NHC makes it a poor donor for a lanthanide. A preliminary series of competition reactions of **6** with potential donor ligands was carried out to determine the lability of the NHC bond in this system: THF, diethyl ether, triphenylphosphane, and trimethylamine oxide are unreactive; tetramethylethlenediamine (TMEDA) and triphenylphosphane oxide successfully displace the NHC group and bind to the metal; the $^{13}C$ NMR spectra lose $^1J_{YC}$ coupling, and the latter solution NMR spectrum shows a $^{31}P$ chemical shift of 57 ppm, with $^2J_{PY}$ 6 Hz.

In summary, the first anionic, amido-functionalized *N*-heterocyclic-carbene ligand has been prepared and used to tether covalently the unusual σ-donor NHC group to an electropositive metal atom to afford new organolanthanide complexes. This has allowed the first systematic study of the lability of an early-metal–NHC moiety. The tethered, hemilabile carbene in these complexes may find use in catalysis, for example, as a new Lewis acid–Lewis base catalyst,[15] and a study of the reactivity of the metal-labilized NHC group is now in progress.

## *Experimental Section*

CCDC-218135–218140 contain the supplementary crystallographic data for this paper. These data can be obtained free of charge via www.ccdc.cam.ac.uk/conts/retrieving.html (or from the Cambridge Crystallographic Data Centre, 12 Union Road, Cambridge CB21EZ,

 © 2003 Wiley-VCH Verlag GmbH & Co. KGaA, Weinheim 

UK; fax: (+44) 1223-336-033; or deposit@ccdc.cam.ac.uk). CCDC, codes. Selected characterizing data for **3**: Yield 77%. $^1$H NMR (300 MHz, $C_6D_6$): $\delta = 1.17$ (9H, s, *t*Bu), 1.62 (9H, s, *t*Bu), 2.41 (2H, t, $CH_2$), 4.02 (2H, t, $CH_2$), 6.15 (1H, d, CH), 6.51 ppm (1H, d, CH); $^{13}$C NMR (75 MHz, $C_6D_6$): $\delta = 197$ ppm ($C_{carbene}$). Elemental analysis calcd (%) for $C_{13}H_{25}N_3LiBr$: C 50.33, H 8.12, N 13.54; found C 50.13, H 8.00, N 13.30.

**4**: Yield 86%. $^1$H NMR (300 MHz, $C_6D_6$): $\delta = 0.95$ (9H, s, *t*Bu), 1.47 (9H, s, *t*Bu), 2.81 (2H, q, $CH_2$), 3.96 (2H, t, $CH_2$), 6.59 (1H, s, CH), 6.69 ppm (1H, s, CH); $^{13}$C NMR (75 MHz, $C_6D_6$): $\delta = 211.0$ ppm ($C_{carbene}$). Elemental analysis calcd (%) for $C_{13}H_{25}N_3$: C 69.91, H 11.28, N 18.81; found C 69.94, H 11.49, N 18.75.

**5**: Yield 20% $^1$H NMR (300 MHz, $C_6D_6$): $\delta = -0.97$ (9H, s, *t*Bu), $-0.29$ (9H, s, *t*Bu), 0.13 (36H, s, 2 ($N(SiMe_3)_2$)), 3.97 (1H, s, CH), 5.2 (1H, s, CH), 6.42 (2H, br s, $CH_2$), 11.52 ppm (2H, br s, $CH_2$). Elemental analysis calcd (%) for $C_{25}H_{60}N_5Si_4Sm{\cdot}2\,Et_2O$: C 47.09, H 7.18, N 8.32; found: C 33.59, H 6.79, N 8.08.

**6**: Yield 25%. $^1$H NMR (300 MHz, $C_6D_6$): $\delta = -0.97$ (9H, s, *t*Bu), $-0.29$ (9H, s, *t*Bu), 0.13 (36H, s, ($N(SiMe_3)_2$)), 3.97 (1H, s, CH), 5.2 (1H, s, CH), 6.42 (2H, br s, $CH_2$), 11.52 ppm (2H, br s, $CH_2$); $^{13}$C NMR (75 MHz, $C_6D_6$): $\delta = 186.28$ ppm ($C_{carbene}$, $J_{C\text{-}Y}$ 53 Hz). Elemental analysis calcd (%) for $C_{25}H_{60}N_5Si_4Y.Et_2O$: C 49.32, H 8.56, N 9.92; found: C 43.32, H 8.71, N 9.64.

Received: August 25, 2003 [Z52710]

**Keywords:** carbene ligands · heterocycles · lanthanides · N ligands

[1] H. W. Wanzlick, *Angew. Chem.* **1962**, *74*, 129; *Angew. Chem. Int. Ed.* **1962**, *1*, 75; D. J. Cardin, B. Cetinkaya, E. Cetinkaya, M. F. Lappert, *J. Chem. Soc. Dalton Trans.* **1973**, 514; V. P. W. Bohm, W. A. Herrmann, *Angew. Chem.* **2000**, *112*, 4200; *Angew. Chem. Int. Ed.* **2000**, *39*, 4036.

[2] W. A. Herrmann, *Angew. Chem.* **2002**, *114*, 1342. *Angew. Chem. Int. Ed.* **2002**, *41*, 1290.

[3] J. C. Green, R. G. Scurr, P. L. Arnold, F. G. N. Cloke, *Chem. Commun.* **1997**, 1963.

[4] R. H. Grubbs, *Adv. Synth. Catal.* **2002**, *344*, 569; S. Lee, J. F. Hartwig, *J. Org. Chem.* **2001**, *66*, 3402; I. E. Marko, S. Sterin, O. Buisine, R. Mignani, P. Branlard, B. Tinant, J. P. Declercq, *Science* **2002**, *298*, 204; M. Muehlhofer, T. Strassner, W. A. Herrmann, *Angew. Chem.* **2002**, *114*, 1817; *Angew. Chem. Int. Ed.* **2002**, *41*, 1745.

[5] a) U. Kernbach, M. Ramm, P. Luger, W. P. Fehlhammer, *Angew. Chem.* **1996**, *108*, 333; *Angew. Chem. Int. Ed. Engl.* **1996**, *35*, 310; b) W. A. Herrmann, F. C. Munck, G. R. J. Artus, O. Runte, R. Anwander, *Organometallics* **1997**, *16*, 682; c) W. J. Oldham, Jr., S. M. Oldham, B. L. Scott, K. D. Abney, W. H. Smith, D. A. Costa, *Chem. Commun.* **2001**, 1348.

[6] C. D. Abernethy, G. M. Codd, M. D. Spicer, M. K. Taylor, *J. Am. Chem. Soc.* **2003**, *125*, 1128.

[7] H. Y. Zhou, E. J. Campbell, S. T. Nguyen, *Org. Lett.* **2001**, *3*, 2229; P. K. Fraser, S. Woodward, *Tetrahedron Lett.* **2001**, *42*, 2747.

[8] P. L. Arnold, A. C. Scarisbrick, A. J. Blake, C. Wilson, *Chem. Commun.* **2001**, 2340.

[9] A. J. Arduengo III, *Acc. Chem. Res.* **1999**, *32*, 913.

[10] A. J. Arduengo III, M. Tamm, J. C. Calabrese, F. Davidson, W. J. Marshall, *Chem. Lett.* **1999**, 1021.

[11] K. S. Coleman, H. T. Chamberlayne, S. Turberville, M. L. H. Green, A. R. Cowley, *J. Chem. Soc. Dalton Trans.* **2003**, 2917.

[12] D. Baudry-Barbier, N. Andre, A. Dormond, C. Pardes, P. Richard, M. Visseaux, C. J. Zhu, *Eur. J. Inorg. Chem.* **1998**, 1721; A. J. Arduengo III, M. Tamm, S. J. McLain, J. C. Calabrese, F. Davidson, W. J. Marshall, *J. Am. Chem. Soc.* **1994**, *116*, 7927; M. Glanz, S. Dechert, H. Schumann, D. Wolff, J. Springer, *Z. Anorg. Allg. Chem.* **2000**, *626*, 2467.

[13] M. Karl, G. Seybert, W. Massa, K. Harms, S. Agarwal, R. Maleika, W. Stelter, A. Greiner, W. Heitz, B. Neumüller, K. Dehnicke, *Z. Anorg. Allg. Chem.* **1999**, *625*, 1301; O. Just, W. S. Rees, Jr., *Inorg. Chem.* **2001**, *40*, 1751.

[14] 49.6 Hz for $Y[N(SiHMe_2)_2]_3$(*N*,*N*′-dimethyl-NHC), ref [5b], otherwise commonly 30–48 Hz for s-bound Y-alkyls: S. Arndt, T. P. Spaniol, J. Okuda, *Organometallics* **2003**, *22*, 775; W. E. Piers, D. J. H. Emslie, *Coord. Chem. Rev.* **2002**, *233*, 131.

[15] H. Groger, *Chem. Eur. J.* **2001**, *7*, 5246.

 © 2003 Wiley-VCH Verlag GmbH & Co. KGaA, Weinheim 

Sensors

# High-Throughput Screening by Using a Blue-Fluorescent Antibody Sensor**

*Masayuki Matsushita,* Kazuhiro Yoshida, Noboru Yamamoto, Peter Wirsching, Richard A. Lerner, and Kim D. Janda**

Phase-transfer catalysis (PTC) has received increasing attention in recent years, particularly with regard to asymmetric synthesis, because of its simplicity, mild reaction conditions, and moderate-to-high product yields.[1,2] *Cinchona* alkaloid-derived quaternary ammonium salts have been the most frequently employed chiral catalysts given their efficiency, low cost, ease of preparation, and suitability for introducing structural diversity.[2] Notably, a number of important natural and nonnatural amino-acid derivatives have been synthesized by α-C–C bond formation by quaternary *Cinchona*-based catalysts.[2,3] Yet, despite their successful application to catalytic asymmetric synthesis, dramatic effects of the catalyst structure, solvent, temperature, and metal-ion base on the enantioselectivity have often been problematic with regard to PTC reaction optimization.[2–5]

Combinatorial synthesis can afford large libraries of molecules as a source of new and improved catalysts.[6] However, considerable effort is often entailed in the screen-

[*] Dr. M. Matsushita, Prof. Dr. K. D. Janda, Dr. K. Yoshida, Dr. N. Yamamoto, Dr. P. Wirsching, Prof. Dr. R. A. Lerner
Department of Chemistry and The Skaggs Institute for Chemical Biology
The Scripps Research Institute
10550 N. Torrey Pines Road, La Jolla, CA 92037 (USA)
Fax: (+1) 858-784-2595
E-mail: masayuki@scripps.edu
kdjanda@scripps.edu

[**] This work was supported by funding from the Skaggs Institute for Chemical Biology. We thank Prof. Hyung-geun Park (Seoul National University, Korea) and Prof. Nobuyuki Mase (Shizuoka University, Japan) for helpful discussions.

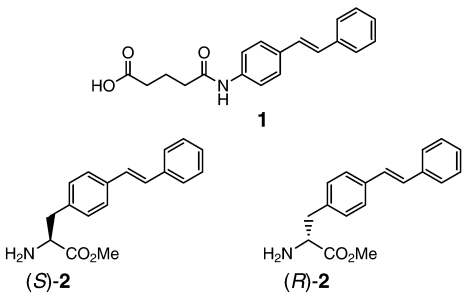
Supporting information for this article is available on the WWW under http://www.angewandte.org or from the author.

 © 2003 Wiley-VCH Verlag GmbH & Co. KGaA, Weinheim DOI: 10.1002/anie.200352793 

ing of these libraries, particularly with regard to enantioselective reactions. In high-throughput screening (HTS) for the evaluation of catalyst libraries, the determination of the enantiomeric excess (*ee*) of the products is generally the rate-limiting procedure.[6c] Hence, the application of HTS to enantioselective transformations has not been straightforward. In 1997, Reetz and coworkers developed the first HTS of reaction *ee* values by using UV/Vis spectroscopy.[7] Following their pioneering work, other methods that use, for example, IR-thermography,[8] circular dichroism,[9] capillary electrophoresis,[10] fluorescence,[11] mass spectrometry,[12] chemosensing,[13] competitive immunoassay,[14] and enzymatic methods[15] have emerged for particular applications. Most of these techniques have been used to screen the *ee* values of asymmetric reduction or hydrolysis reactions, but, to our knowledge, HTS of the *ee* values of products from an asymmetric C–C bond forming reaction has not been reported.

Recently, we described a series of monoclonal antibodies (mAbs), for example, mAb 19G2, prepared against the *trans*-stilbene hapten **1** (Scheme 1), in which the 19G2-**1** complex produced a blue fluorescence in high quantum yield ($\lambda_{ex}$ = 327 nm, $\lambda_{em}$ = 410 nm, $\Phi_f$ = 0.78).[16] During subsequent studies to find alternative ligands for these mAbs, we discovered that each of the chiral *trans*-stilbene amino acid esters (*S*)-**2** and (*R*)-**2** (Scheme 1) could bind to 19G2, but only the 19G2-(*S*)-**2** complex afforded a blue fluorescence. Hence, it occurred to us that 19G2 could act as a sensor in the HTS of chiral catalysts used for the synthesis of (*S*)-**2** and (*R*)-**2**. Herein, the aim was to evaluate a panel of derivatized *Cinchona* alkaloids in the PTC of an asymmetric α-alkylation reaction by using a HTS fluorescence plate-reader format for the rapid estimation of *ee* values of products.

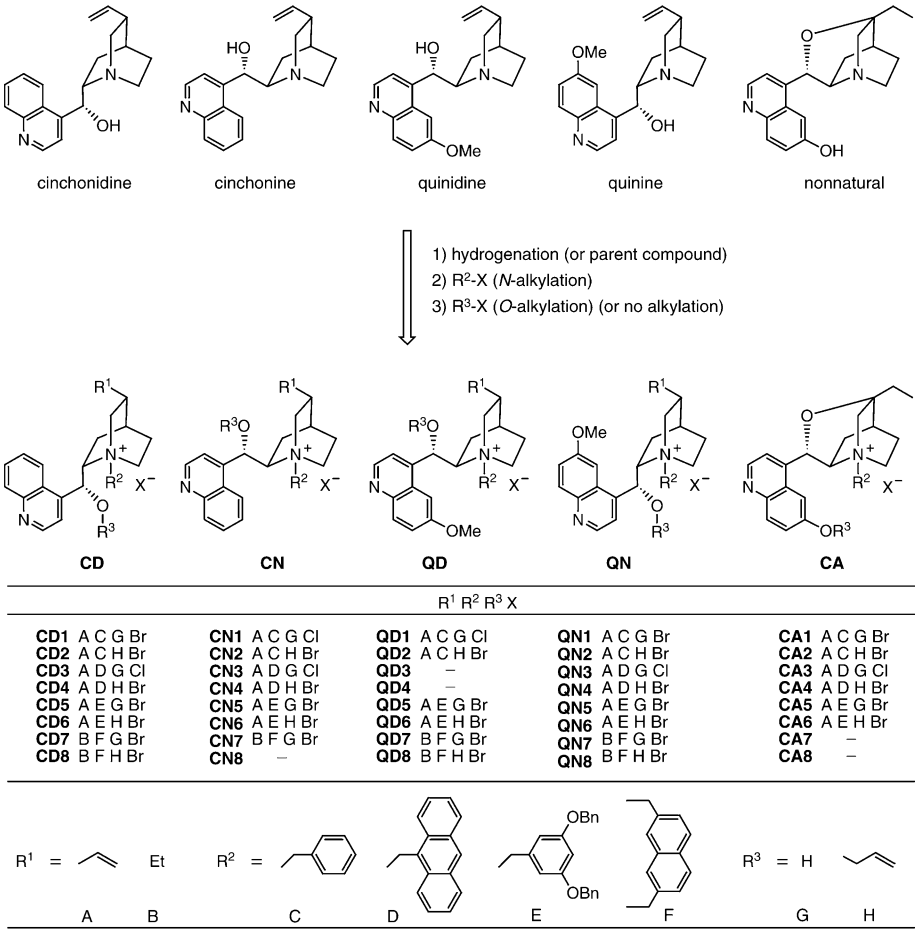
A catalyst library derived from *Cinchona* alkaloids was constructed by individual compound synthesis. Four natural *Cinchona* alkaloids (cinchonidine, cinchonine, quinidine, quinine) and one nonnatural *Cinchona*-type alkaloid[17] were hydrogenated, or left as the parent compound, then derivatized with four different *N*-alkyl substituents, and finally *O*-alkylated, or the hydroxyl was kept unmodified (Scheme 2). Out of a possible 40 *Cinchona* alkaloid ammonium salts, 35 were obtained in high yield and purity. Among these 35 catalysts, 11 had been previously reported[3,4,18] and 24 were new compounds. Each catalyst was then employed in PTC for the




***Scheme 1.*** Blue-fluorescent mAb 19G2 hapten and chiral ligands for sensor applications.

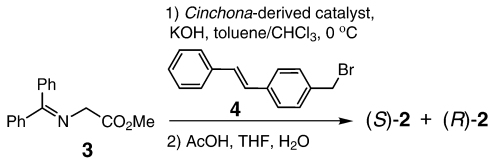
alkylation of *N*-(diphenylmethylene)glycine methyl ester **3** with 4-bromomethyl-*trans*-stilbene **4** (Scheme 3). After the alkylations were complete, the benzophenone Schiff base group was hydrolyzed and the product mixture of (*S*)-**2** and (*R*)-**2** was purified. The simplicity of the sequence allowed us to carry out 35 parallel reactions in two days. Yields of the isolated product mixture ranged from 47% to 83%.

To determine the *ee* values of the 35 product mixtures, we constructed a calibration curve by using independently synthesized (*S*)-**2** and (*R*)-**2**. To this end, (*S*)- and (*R*)-*N*-Boc-iodoalanine methyl ester (Fluka) were each reacted with zinc dust, followed by Pd-catalyzed cross-coupling to 4-




***Scheme 2.*** Preparation of a *Cinchona* alkaloid-derived catalyst library.

 © 2003 Wiley-VCH Verlag GmbH & Co. KGaA, Weinheim 




***Scheme 3.*** Synthesis of chiral ligands for mAb 19G2 by using *Cinchona*-based PTC.

bromo-*trans*-stilbene in analogy with reported procedures.[19] Both (*S*)-**2** and (*R*)-**2** were obtained in $>99\%$ *ee* as analyzed by chiral HPLC. Precise mixtures of these isomers were then prepared (0, 25, 50, 75, 100 % (*S*)-**2**, corresponding to 100 % *ee* (*R*)-**2**, 50 % *ee* (*R*)-**2**, 0 % *ee*, 50 % *ee* (*S*)-**2**, 100 % *ee* (*S*)-**2**) as solutions in DMF. Each calibration standard (50 μM) was mixed with 19G2 (25 μM; 50 μM binding sites) in PBS (10 mM sodium phosphate, 150 mM NaCl, pH 7.4) with 5 % DMF cosolvent, and the fluorescence intensities ($\lambda_{ex} = 327$ nm, $\lambda_{em} = 416$ nm) were measured by using a 96-well plate reader. The data fitted well to a hyperbolic, as required by the specific binding of (*S*)-**2** and (*R*)-**2** by the mAb 19G2. The fluorescence values for each of the 35 product mixtures were then obtained in the same way as above, and the corresponding *ee* values were then calculated (Figure 1). The process of sample preparation, plate reading, and catalyst evaluation took less than one hour.

To confirm the validity of the method, 10 samples were randomly chosen across the range of *ee* values of (*S*)-**2** and (*R*)-**2** and reanalyzed by chiral HPLC. The fluorescence sensor and HPLC measurements varied, on the average, $\approx 10\%$ and afforded an excellent linear correlation (slope = 0.92, $r^2 = 0.99$). We note that the *tert*-butyl ester analogue of **3** generally gave higher enantioselectivities in asymmetric PTC alkylations.[3] However, it was necessary to use **3** as the alkylation substrate, as 19G2 did not show selective fluorescence with the *tert*-butyl ester derivatives corresponding to (*S*)-**2** and (*R*)-**2**.

Significantly, the blue-fluorescent mAb sensor identified high-performance catalysts that were the same as those found by others to give excellent enantioselectivity, as well as one previously unknown catalyst. If we choose $\approx$ 70 % *ee* as a preliminary cut-off point for catalyst efficiency, then, based on our test panel, such a value would give a reasonable $\approx$ 5–10 % member selection from large libraries for further analysis. The catalyst **CD2** (68 % *ee*, fluorescence; 78 % *ee*, HPLC) was reported by O'Donnell et al. in their seminal work on *Cinchona*-based PTC.[18b] **CD8** (75 % *ee*, fluorescence; 85 % *ee*, HPLC) was also observed by Park et al. to exhibit the highest enantioselectivity among this class of catalysts.[18a] Notably, **QN4** (63 % *ee*, fluorescence; 68 % *ee*, HPLC) is a new quinine-based structure for PTC. Lygo et al.[4b] described a catalyst of this type that afforded a $>80\%$ *ee* in reactions by using the *tert*-butyl ester analogue of **3**.

We have presented the foundation for a novel HTS method that uses a blue-fluorescent mAb to assay the enantionselectivity of products from, for example, a catalytic asymmetric alkylation. The method is: 1) sensitive, as expected for fluorescence detection, with only 10 nmol of sample required for each measurement, 2) rapid, hundreds of catalysts could potentially be screened and ranked in less than a day, and 3) accurate, and with a wide dynamic range, as demonstrated by the comparison to HPLC determinations from 100 % *ee* (*S*)-**2** to 100 % *ee* (*R*)-**2**. However, since the method is based on the catalysis of a reference reaction, the intent is to provide a HTS to obtain a subset of catalysts that produce the highest *ee* values. Then, these candidates can be tested and rigorously analyzed, in this case, for efficiency in preparing other amino acids of interest. Importantly, blue-fluorescent HTS has broad applicability. By using the preparation of the same reference compounds, catalysts of other types could be evaluated in both alkylation and nonalkylation strategies for amino acid syntheses. For example, the latter could include Jacobsen-type catalysts for the Strecker reaction.[20] Finally, we are also currently extending the diversity of the *trans*-stilbene moiety, which will allow the application of the blue-fluorescent mAb sensor in screening asymmetric catalysis for other C–C bond-forming reactions, as well as other classes of reactions, such as oxidations, reductions, and hydrolyses.

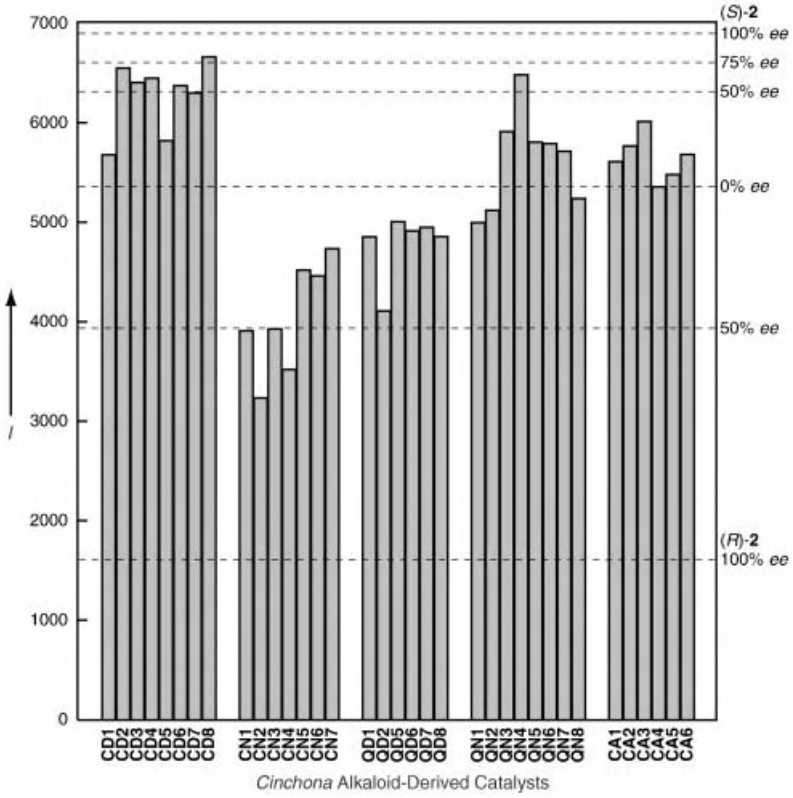



***Figure 1.*** The *ee* values from *Cinchona*-based PTC measured with the mAb 19G2 sensor.

Received: September 4, 2003 [Z52793]

 © 2003 Wiley-VCH Verlag GmbH & Co. KGaA, Weinheim 

**Keywords:** alkaloids · antibodies · enantioselectivity · high-throughput screening · phase-transfer catalysis


[1] For recent reviews of PTC, see: a) K. Maruoka, T. Ooi, *Chem. Rev.* **2003**, *103*, 3013 – 3028; b) P. I. Dalko, L. Moisan, *Angew. Chem.* **2001**, *113*, 3840 – 3864; *Angew. Chem. Int. Ed.* **2001**, *40*, 3726 – 3748; c) M. J. O'Donnell, J. Martin in *Catalytic Asymmetric Synthesis*, 2nd ed. (Ed.: I. Ojima), Wiley-VCH, New York, **2000**, pp. 727 – 755; d) T. Shioiri, S. Arai in *Stimulating Concepts in Chemistry* (Eds.: F. Vogtle, J. F. Stoddart, M. Shibasaki), Wiley-VCH, Weinheim, **2000**, pp. 123 – 143.

[2] M. J. O'Donnell, *Aldrichimica Acta* **2001**, *34*, 3 – 15.

[3] E. J. Corey, F. Xu, M. C. Noe, *J. Am. Chem. Soc.* **1997**, *119*, 12414 – 12415.

[4] a) P. Mazon, R. Chinchilla, C. Najera, G. Guillena, R. Kreiter, R. J. M. K. Gebbink, G. van Koten, *Tetrahedron: Asymmetry* **2002**, *13*, 2181 – 2185; b) B. Lygo, P. G. Wainwright, *Tetrahedron Lett.* **1997**, *38*, 8595 – 8598.

[5] T. Okino, Y. Takemoto, *Org. Lett.* **2001**, *3*, 1515 – 1517.

[6] a) J. P. Stambuli, J. F. Hartwig, *Curr. Opin. Chem. Biol.* **2003**, *7*, 420 – 426; b) A. Berkessel, *Curr. Opin. Chem. Biol.* **2003**, *7*, 409 – 419; c) M. T. Reetz, *Angew. Chem.* **2001**, *113*, 292 – 320; *Angew. Chem. Int. Ed.* **2001**, *40*, 284 – 310; d) K. W. Kuntz, M. L. Snapper, A. H. Hoveyda, *Curr. Opin. Chem. Biol.* **1999**, *3*, 313 – 319; e) A. H. Hoveyda, *Chem. Biol.* **1999**, *6*, R305 – R308.

[7] M. T. Reetz, A. Zonta, K. Schimossek, K. Liebeton, K.-E. Jaeger, *Angew. Chem.* **1997**, *109*, 2961 – 2963; *Angew. Chem. Int. Ed. Engl.* **1997**, *36*, 2830 – 2832.

[8] M. T. Reetz, M. H. Becker, K. M. Kuhling, A. Holzwarth, *Angew. Chem.* **1998**, *110*, 2792 – 2795; *Angew. Chem. Int. Ed.* **1998**, *37*, 2647 – 2650.

[9] K. Ding, A. Ishii, K. Mikami, *Angew. Chem.* **1999**, *111*, 519 – 523; *Angew. Chem. Int. Ed.* **1999**, *38*, 497 – 501.

[10] M. T. Reetz, K. M. Kuhling, A. Deege, H. Hinrichs, D. Belder, *Angew. Chem.* **2000**, *112*, 4049 – 4052; *Angew. Chem. Int. Ed.* **2000**, *39*, 3891 – 3893.

[11] G. Klein, J.-L. Reymond, *Helv. Chim. Acta* **1999**, *82*, 400 – 407.

[12] a) J. Guo, J. Wu, G. Siuzdak, M. G. Finn, *Angew. Chem.* **1999**, *111*, 1868 – 1871; *Angew. Chem. Int. Ed.* **1999**, *38*, 1755 – 1758; b) M. T. Reetz, M. H. Becker, H.-W. Klein, D. Stockigt, *Angew. Chem.* **1999**, *111*, 1872 – 1875; *Angew. Chem. Int. Ed.* **1999**, *38*, 1758 – 1761.

[13] G. T. Copeland, S. J. Miller, *J. Am. Chem. Soc.* **1999**, *121*, 4306 – 4307.

[14] F. Taran, C. Gauchet, B. Mohar, S. Meunier, A. Valleix, P. Y. Renard, C. Creminon, J. Grassi, A. Wagner, C. Mioskowski, *Angew. Chem.* **2002**, *114*, 132 – 135; *Angew. Chem. Int. Ed.* **2002**, *41*, 124 – 127.

[15] P. Abato, C. T. Seto, *J. Am. Chem. Soc.* **2001**, *123*, 9206 – 9207.

[16] A. Simeonov, M. Matsushita, E. A. Juban, E. H. Thompson, T. Z. Hoffman, A. E. Beuscher, M. J. Taylor, P. Wirsching, W. Rettig, J. K. McCusker, R. C. Stevens, D. P. Millar, P. G. Schultz, R. A. Lerner, K. D. Janda, *Science* **2000**, *290*, 307 – 313.

[17] Y. Iwabuchi, M. Nakatani, N. Yokoyama, S. Hatakeyama, *J. Am. Chem. Soc.* **1999**, *121*, 10219 – 10220.

[18] a) H.-g. Park, B.-S. Jeong, M.-S. Yoo, J.-H. Lee, M.-k. Park, Y.-J. Lee, M.-J. Kim, S.-s. Jew, *Angew. Chem.* **2002**, *114*, 3162 – 3164; *Angew. Chem. Int. Ed.* **2002**, *41*, 3036 – 3038; b) M. J. O'Donnell, W. D. Bennett, S. Wu, *J. Am. Chem. Soc.* **1989**, *111*, 2353 – 2355.

[19] a) Y. Tamaru, H. Ochiai, T. Nakamura, Z. Yoshida, *Tetrahedron Lett.* **1986**, *27*, 955 – 958; b) R. F. W. Jackson, K. James, M. J. Wythes, A. Wood, *J. Chem. Soc. Chem. Commun.* **1989**, 644 – 645.

[20] a) P. Vachal, E. N. Jacobsen, *J. Am. Chem. Soc.* **2002**, *124*, 10012 – 10014; b) M. S. Sigman, P. Vachal, E. N. Jacobsen, *Angew. Chem.* **2000**, *112*, 1336 – 1338; *Angew. Chem. Int. Ed.* **2000**, *39*, 1279 – 1281; c) M. S. Sigman, S. Mattew, E. N. Jacobsen, *J. Am. Chem. Soc.* **1998**, *120*, 4901 – 4902.


 © 2003 Wiley-VCH Verlag GmbH & Co. KGaA, Weinheim 

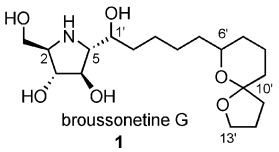
Natural Product Synthesis

# Palladium-Catalyzed DYKAT of Vinyl Epoxides: Enantioselective Total Synthesis and Assignment of the Configuration of (+)-Broussonetine G**

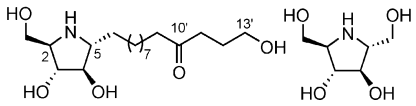
*Barry M. Trost,* Daniel B. Horne, and Michael J. Woltering*

The ability of polyhydroxylated pyrrolidines and pyrrolizidines to inhibit numerous glycosidases continues to draw attention to such structural types.[1] The broussonetines are a class of polyhydroxylated alkaloids that were isolated from the branches of the deciduous tree *Broussontia kazinoki*. Thus far, G. Kusano and co-workers have isolated and characterized 29 unique compounds from this family of natural products.[2] These compounds show striking glycosidase-inhibitory properties, and as such have enormous therapeutic potential as antitumor and anti-HIV agents.[3] The members of the broussonetine family all share a polyhydroxylated pyrrolidine core and a 13-carbon-atom side chain that contains various functional groups.

(+)-Broussonetine G (**1**), one of the most active inhibitors of this class ($IC_{50} = 3$ nM, β-galactosidase; 24 nM, β-glucosidase), contains a structurally interesting 5,6-spiroketal in the side chain.[4] The synthesis of **1** presents an additional




broussonetine G
**1**




broussonetine C
**2**

DMDP
**3**

[*] Prof. B. M. Trost, D. B. Horne, M. J. Woltering
Department of Chemistry, Stanford University
Stanford, CA 94305-5080 (USA)
Fax: (+1) 650-725-0002
E-mail: bmtrost@stanford.edu

[**] DYKAT = dynamic kinetic asymmetric transformation. We thank the National Science Foundation and the National Institutes of Health (GM-13598), the Eli Lilly Corporation (fellowship to DBH), and the Deutsche Forschungsgemeinschaft (fellowship to MJW) for their generous support of our programs. We also thank Dr. Maiko Shibano and Prof. G. Kusano (Osaka University of Pharmaceutical Sciences) for NMR spectra and their donation of a sample of natural broussonetine G. Mass spectra were provided by the Mass Spectrometry Regional Center of the University of California-San Francisco supported by the NIH Division of Research.

Supporting information for this article is available on the WWW under http://www.angewandte.org or from the author.

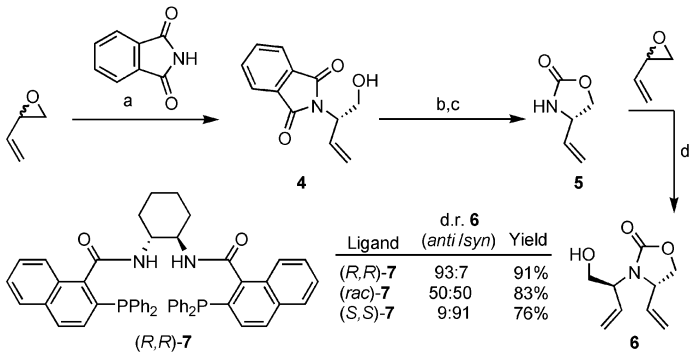
 DOI: 10.1002/anie.200352857 © 2003 Wiley-VCH Verlag GmbH & Co. KGaA, Weinheim 

challenge in that the assignment of the relative stereochemistry of the spiroketal and the 1′-hydroxy group has not been reported.

Despite the interesting structural features and biological activity of these compounds, only one synthesis has been reported: Yoda et al. described the chiral-pool-based synthesis of broussonetine C (**2**).[5] Herein we describe an enantioselective synthesis that involves a palladium-catalyzed dynamic kinetic asymmetric transformation (DYKAT)[6] process, which potentially allows access to all members of the broussonetine family as well as many other pyrrolidine-containing glycosidase inhibitors, including pyrrolizidine and indolizidine types.

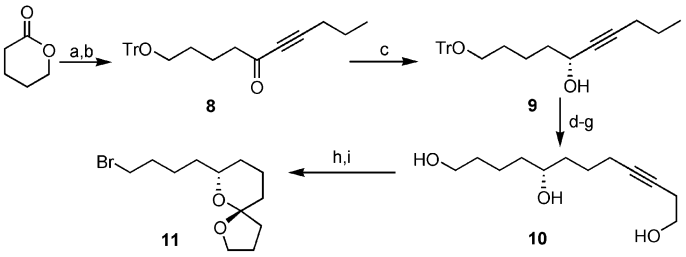
We envisioned that two successive palladium-catalyzed asymmetric allylic alkylations of butadiene monoxide with a suitable nitrogen nucleophile followed by ring-closing metathesis (RCM) could provide a unique access to chiral, substituted pyrrolidines. This strategy could potentially be used to provide all diastereomers of the proposed structure, a key feature for us since the full stereochemistry of our target was not known. Furthermore, we hoped that this strategy could also be used to access many other important polysubstituted pyrrolidine alkaloid natural products, such as (2*R*,3*R*,4*R*,5*R*)-2,5-dihydroxymethyl-3,4-dihydroxypyrrolidine (DMDP; **3**).[7]

The synthesis began with the addition of phthalimide to butadiene monoxide to give **4**[8] in a highly regio- and enantioselective fashion (94% yield, 98% *ee*) (Scheme 1). After deprotection of the diimide to give a vinylglycinol, formation of the cyclic carbamate with triphosgene gave vinyloxazolidinone **5**, the substrate for the second palladium-catalyzed DYKAT reaction. Despite our attempts with various other vinylglycinol surrogates in this reaction, we found the best results were obtained with oxazolidinone **5**, which gave the desired product **6** in 91% yield with excellent diastereoselectivity (d.r. 93:7). We observed that the diastereoselectivity of the product is completely dependent on the choice of ligand (see Table in Scheme 1).




***Scheme 1.*** Synthesis of the chiral core subunit. Reagents and conditions: a) $[\{(C_3H_5)PdCl\}_2]$ (0.4 mol%), (*R*,*R*)-**7** (1.2 mol%), $Na_2CO_3$, $CH_2Cl_2$, room temperature, 94%, 98% *ee*; b) ethylenediamine, EtOH, reflux, 84%; c) triphosgene, $NaHCO_3$, toluene/$H_2O$, 0°C, 85%; d) $[Pd_2(dba)_3]\cdot CHCl_3$ (0.25 mol%), (*R*,*R*)-**7** (0.75 mol%), DBU (1 mol%), $CH_2Cl_2$, room temperature, 91%, 93:7 d.r. dba = *trans*,*trans*-dibenzylideneacetone, DBU = 1,8-diazabicyclo[5.4.0]undec-7-ene.

The synthesis of the side chain began with the addition of 1-pentyne to δ-valerolactone, followed by protection of the primary alcohol with trityl chloride to give alkynone **8** (Scheme 2). Reduction of **8** by using Noyori's enantioselective transfer hydrogenation protocol[9] gave propargyl alcohol



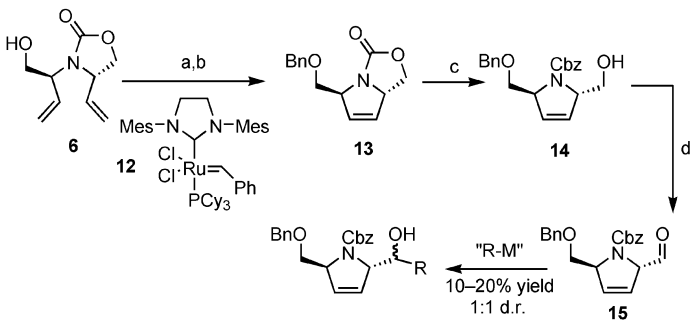

***Scheme 2.*** Synthesis of the spiroketal side chain **11**. Reagents and conditions: a) *n*BuLi, 1-pentyne, THF, −78°C→RT, 94%; b) TrCl, $NEt_3$, DMAP, DMF, room temperature, 77%; c) [($\eta^6$-*p*-cymene)Ru{(1*R*,2*R*)-*p*-TsNCH(Ph)CH(Ph)NH}] (3 mol%), *i*PrOH, room temperature, 95%, 97% *ee*; d) KH (10 equiv), 1,3-diaminopropane, THF, 79%; e) 3,4-dihydro-2*H*-pyran, PPTS, $CH_2Cl_2$, room temperature, 76%; f) *n*BuLi, $AlMe_3$, $BF_3\cdot OEt_2$, $Et_2O$, −78°C; then ethylene oxide, −78°C→RT, 76%; g) HCl/MeOH (1%), 95%; h) $[PdCl_2(PhCN)_2]$ (2 mol%), $CH_3CN$/THF (3:2), 85%, 97:3 d.r.; i) $PPh_3Br_2$, imidazole, THF, 91%. Tr = trityl = triphenylmethyl, DMAP = 4-dimethylaminopyridine, DMF = *N*,*N*-dimethylylformamide, Ts = *p*-toluenesulfonyl, PPTS = pyridinium *p*-toluenesulfonate.

**9** (97% *ee*). The alkyne zipper reaction[10] (KH, 1,3-diaminopropane) was performed to give the desired terminal alkyne. Protection of the secondary alcohol followed by alkylation of the terminal alkyne with ethylene oxide provided the desired homopropargyl alcohol. After acid-catalyzed global deprotection, the resulting triol **10** underwent the requisite regioselective palladium-catalyzed spiroketalization reaction[11] to give the desired 5,6-spiroketal with excellent diastereoselectivity (d.r. 97:3). The high stereoselectivity of this cyclization reaction is attributed to the anomeric affect.[12] Subsequent bromination of the primary alcohol gave bromide **11**.

The synthesis of the pyrrolidine core continued with the protection of the homoallylic alcohol with benzyl bromide, followed by RCM with a Grubbs second-generation catalyst[13] **12** to give 2,5-dihydropyrrole **13** (Scheme 3). The absolute stereochemistry was assigned based on the stereochemical assignment of vinylglycinol performed previously[8] and single-crystal X-ray analysis of oxazolidinone **13**.[14] Unfortunately, oxidation of the primary alcohol derived from **13** after deprotection of the benzyl group led only to decomposition products. We surmised that the oxazolidinone moiety was probably responsible for the lability of the aldehyde intermediate and therefore adopted an alternative pathway. Saponification of the oxazolidinone and protection of the resulting amine with BnOCOCl gave alcohol **14**. Subsequent oxidation with Dess–Martin periodinane delivered the aldehyde **15**. Our attempts to add various alkyl nucleophiles to aldehyde **15** resulted in very poor yields of the desired products and always produced a 1:1 diastereomeric ratio of alcohols.

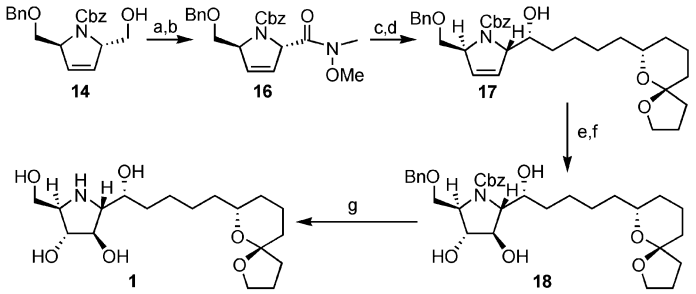
The failure of the coupling reaction led us to consider an alternate strategy. Oxidation of alcohol **14** (TEMPO/bleach/

 © 2003 Wiley-VCH Verlag GmbH & Co. KGaA, Weinheim 




***Scheme 3.*** Synthesis and attempted coupling of aldehyde **15**. Reagents and conditions: a) NaH; BnBr, TBAI, THF, room temperature, 84%; b) **12** (1.2 mol%), $CH_2Cl_2$, reflux, 87%; c) 1) NaOH, EtOH/$H_2O$ (3:1), reflux; 2) BnOCOCl, $NaHCO_3$, $Na_2CO_3$, $H_2O$, 0°C→RT, 99% from **13**; d) Dess–Martin periodinane, $CH_2Cl_2$, 0°C, 95%; TBAI = tetrabutylammonium iodide; Cbz = benzyloxycarbonyl.

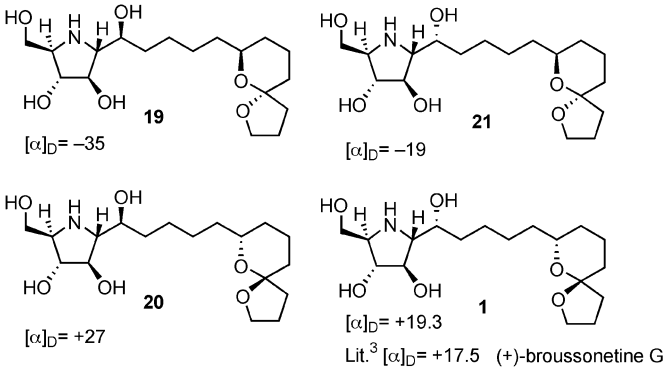
KBr) led to a carboxylic acid, which was converted into Weinreb amide **16** (Scheme 4). Gratifyingly, the subsequent coupling of the two fragments via the alkyl magnesium reagent derived from alkyl bromide **11** led to a ketone.




***Scheme 4.*** Completion of the synthesis of **1**. Reagents and conditions: a) TEMPO, KBr, NaOCl, $NaHCO_3$, acetone/$H_2O$, 0°C, 89%; b) HNMe(OMe)·HCl, pybop, *i*$Pr_2NEt$, $CH_2Cl_2$, 81%; c) 1) **11** (1.2 equiv), Mg, THF, reflux→RT; **16**, room temperature, 65%; d) DIBAL-H, $Et_2O$, 0°C, 76%, 4.3:1 d.r.; e) $F_3CC(O)CH_3$, oxone, $Na_2CO_3$, $CH_3CN/H_2O$, 0°C, 68%; f) TFA, THF/$H_2O$, 65°C, 73%; g) Pd/C, MeOH, HCl, $H_2$ (1 atm), room temperature, 95%; TEMPO = 2,2,6,6-tetramethyl-1-piperidinyloxy, free radical, pybop = (benzotriazol-1-yloxy)tripyrrolidinophosphonium hexafluorophosphate, DIBAL-H = diisobutylaluminum hydride, TFA = trifluoroacetic acid.

Subsequent diastereoselective reduction of the ketone with DIBAL-H gave a 4.3:1 (*R*/*S*) diastereomeric mixture of secondary alcohols. The major diastereomer, alcohol **17**, presumably results from a four-centered transition state.[15] In contrast, reduction of the ketone with $NaBH_4$ led to a diastereomeric mixture of alcohols (*R*/*S* 1:2.6, 83%), the major product of which was the expected Cram product. The stereochemistry of the secondary alcohol was established by $^1$H NMR analysis of the (*R*)- and (*S*)-*O*-methylmandelates.[16] The assignment of the stereochemistry of the C1′ center as *R* also agrees with the assignment of several other broussonetines that contain an hydroxy group at C1′ whose configurations were determined by Kusano et al. by using the Mosher method.[2] Epoxidation of dihydropyrrole **17** led to a mixture of epoxides, both of which gave the same triol **18** as a single diastereomer upon hydrolysis with aqueous TFA. To complete the synthesis, removal of the protecting groups by hydrogenolysis gave **1**, whose spectra and optical rotation matched those of an authentic sample of the natural product in all respects. This constitutes the first synthesis of (+)-broussonetine G.

In addition to the natural product, the remaining three possible diastereomers of broussonetine G were synthesized during the course of our investigations by using the procedures outlined above (Schemes 1–4). Diastereomers **19** and **20** did not correlate with the spectroscopic data of the natural product (Scheme 5). However, the $^1$H and $^{13}$C NMR spectra




***Scheme 5.*** $[\alpha]_D$ Values of diastereomers **1**, **19**, **20**, and **21**.

of **21** were nearly identical to that of **1** and the natural product.[17] Fortunately, the optical rotation was significantly different and led to our assignment of the structure of broussonetine G as shown (Scheme 5).

Received: September 12, 2003 [Z52857]

**Keywords:** asymmetric synthesis · inhibitors · natural products · structure elucidation · total synthesis

[1] For reviews on the importance and use of glycosidase inhibitors, see: a) *Iminosugars as Glycosidase Inhibitors: Nojirimycin and Beyond* (Ed.: A. E. Stutz), Wiley-VCH, Weinheim, **1999**; b) N. Asano, R. J. Nash, R. J. Molyneux, G. W. Fleet, *Tetrahedron: Asymmetry* **2000**, *11*, 1645.

[2] For a recent review of the isolation, biology, and chemistry of broussonetines, see: M. Shibano, D. Tsukamoto, G. Kusano, *Heterocycles* **2002**, *57*, 1539.

[3] a) R. Saul, J. P. Chambers, R. J. Molyneux, A. D. Elbein, *Arch. Biochem. Biophys.* **1983**, *221*, 593; b) R. Saul, J. P. Chambers, R. J. Molyneux, A. D. Elbein, *Arch. Biochem. Biophys.* **1984**, *230*, 668; c) B. Winchester, G. W. Fleet, *J. Carbohydr. Chem.* **2000**, *19*, 471.

[4] M. Shibano, S. Nakamura, N. Akazawa, G. Kusano, *Chem. Pharm. Bull.* **1998**, *46*, 1048.

[5] H. Yoda, T. Shimojo, K. Takabe, *Tetrahedron Lett.* **1999**, *40*, 1335.

[6] a) B. M. Trost, *Chem. Pharm. Bull.* **2002**, *50*, 1; b) B. M. Trost, D. L. Van Vranken, C. Bingel, *J. Am. Chem. Soc.* **1992**, *114*, 9327.

[7] For a review on the synthesis and biology of DMDP, see: T. M. Wrodnigg, *Monatsh. Chem.* **2002**, *133*, 393.

 © 2003 Wiley-VCH Verlag GmbH & Co. KGaA, Weinheim 

[8] B. M. Trost, R. C. Bunt, R. Lemoine, T. L. Calkins, *J. Am. Chem. Soc.* **2000**, *122*, 5968.
[9] K. Matsumura, S. Hashiguchi, T. Ikariya, R. Noyori, *J. Am. Chem. Soc.* **1997**, *119*, 8738.
[10] C. A. Brown, A. Yamashita, *J. Am. Chem. Soc.* **1975**, *97*, 891.
[11] K. Utimoto, *Pure Appl. Chem.* **1983**, *55*, 1845.
[12] P. Deslongchamps, *Stereoelectronic Effects in Organic Synthesis*, Pergamon, Elmsford, NY, **1983**.
[13] M. Scholl, S. Ding, C. W. Lee, R. H. Grubbs, *Org. Lett.* **1999**, *1*, 953.
[14] CCDC-218668 contains the supplementary crystallographic data for this paper. These data can be obtained free of charge via www.ccdc.cam.ac.uk/conts/retrieving.html (or from the Cambridge Crystallographic Data Centre, 12, Union Road, Cambridge CB21EZ, UK; fax: (+44) 1223-336-033; or deposit@ccdc.cam.ac.uk).
[15] a) M. M. Midland, Y. C. Kwon, *J. Am. Chem. Soc.* **1983**, *105*, 3725.b) S. Ono, S. Shuto, A. Matsuda, *Tetrahedron Lett.* **1996**, *37*, 221.
[16] B. M. Trost, J. L. Belletire, S. Godleski, P. G. McDougal, J. M. Balkovec, J. J. Baldwin, M. E. Christy, G. S. Ponticello, S. L. Varga, J. P. Springer, *J. Org. Chem.* **1986**, *51*, 2370.
[17] For an example of diastereoisomeric products with similar NMR spectra, see the synthesis of mosin B: N. Maezaki, N. Kojima, A. Sakamoto, H. Tominaga, C. Iwata, T. Tanaka, M. Monden, B. Damdinsuren, S. Nakamori, *Chem. Eur. J.* **2003**, *9*, 389.

 © 2003 Wiley-VCH Verlag GmbH & Co. KGaA, Weinheim 

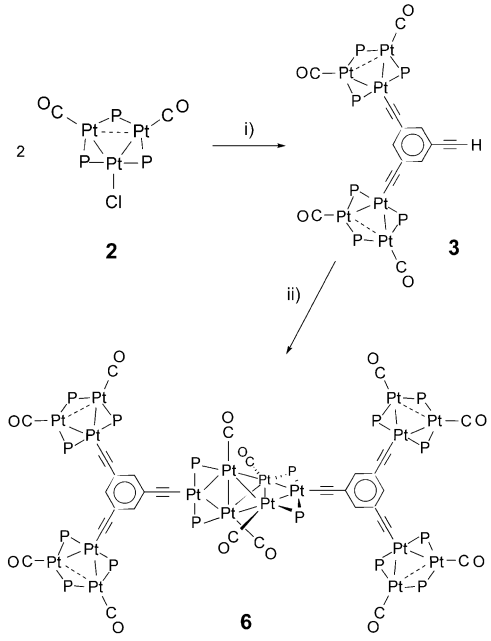
Pt Dendrimer Synthesis

# Assembling Metal Clusters with Covalent Linkers: Synthesis and Structure of a Quasi-Planar $Pt_{18}$ Dendrimer Containing Five Clusters Connected by σ-Alkynyl Spacers**

*Alberto Albinati, Piero Leoni,* Lorella Marchetti, and Silvia Rizzato*

Transition-metal σ-alkynyl derivatives[1] are emerging as potentially useful precursors for advanced materials due to their promising magnetic,[2] liquid-crystalline,[3] nonlinear optical,[4] and luminescence[5] properties. Moreover, there is considerable and increasing interest for their application in the synthesis of metal-containing macrocyclic,[6] dendritic,[7] and rigid-rod molecular frameworks with delocalized π systems. These compounds include derivatives of various dimensions, actively investigated for their potential use in molecular electronics,[8,9] and contain isolated metal centers either located at the extremes[8–11] or regularly intercalated[8,12] into the main chain. Ordered structures with alternated metal clusters (or metal–metal-bonded bimetallic units[13]) and conjugated σ-alkynyl spacers[14–15] are extremely rare,[16] although of great potential interest.[10] This may be due to: 1) the tendency of metal clusters to undergo fragmentation or condensation, 2) their multiple and undistinguishable reactive positions, which facilitate the formation of complex mixtures of products, and 3) the preferred π interaction between the cluster and the alkynyl units[1,17] (the metal–alkynyl σ linkage usually results in increased electronic delocalization[9]).

In this paper we show that tri- and hexanuclear platinum clusters with sizable bridging phosphide groups are suitable precursors to ordered materials. Indeed, the bulky P*t*$Bu_2$ ligands in $[Pt_3(\mu\text{-P}t\text{Bu}_2)_3(L)_2(X)]^{n+}$[18] and $[Pt_6(\mu\text{-P}t\text{Bu}_2)_4(CO)_4(X)_2]^{2n+}$[19] (X = neutral ligand, $n = 1$; X = monoanionic ligand, $n = 0$; L = neutral ligand) impart remarkable thermal and chemical stability to the $\{Pt_x(\mu\text{-P})_y\}$ cores and leave a limited number of reactive sites properly positioned to build ordered structures. Moreover, they force alkynyl ligands to bind the polynuclear system with $\sigma,\eta^1$- rather than $\pi,\eta^2$-interactions.[20] Several structures with predefined molecular shape can therefore be engineered through the combination of these building blocks with well-chosen σ-alkynyl spacers, one of which is shown in Scheme 1. The trinuclear precursor




***Scheme 1.*** Synthesis of complex **6**. i) 1,3,5-$C_6H_3(CCH)_3$, CuI, $NEt_2H$, 25 °C, 24 h (80%); ii) **3** (2 equiv), **5**, CuI, $NEt_2H$, 25 °C, 24 h (85%) (**5** = $[Pt_6(\mu\text{-P}t\text{Bu}_2)_4(CO)_4Cl_2]$).

[*] Prof. P. Leoni, Dr. L. Marchetti
Dipartimento di Chimica e Chimica Industriale
Università di Pisa
Via Risorgimento 35. 56126 Pisa (Italy)
Fax: (+39) 050-2219246
E-mail: leoni@dcci.unipi.it
Prof. A. Albinati, Dr. S. Rizzato
Dipartimento di Chimica Strutturale e Stereochimica Inorganica (DCSSI). Università di Milano
Via Venezian 21, 20133 Milano (Italy)

[**] This work was supported by Ministero dell'Istruzione, dell'Università e della Ricerca (MIUR), Programmi di Interesse Nazionale, 2002–2003.

Supporting information for this article is available on the WWW under http://www.angewandte.org or from the author.

 © 2003 Wiley-VCH Verlag GmbH & Co. KGaA, Weinheim DOI: 10.1002/anie.200352954 

$\{Pt_3\}Cl$ (**2**) [$\{Pt_3\} = Pt_3(\mu\text{-}PtBu_2)_3(CO)_2$] was easily prepared from [$\{Pt_3\}(CO)$]-$(CF_3SO_3)$ (**1**)[18] and a chloride salt. Coupling two equivalents of **2** with 1,3,5-triethynylbenzene,[21] under the classical Sonogashira conditions,[22] gave $C_6H_3$-1,3-(CC-$\{Pt_3\}$)$_2$-5-(CCH) (**3**) as a green solid. This can be further modified either by substituting the carbonyl ligands or by exploiting the reactivity of the residual CCH unit, and may thus be considered an interesting pivot intermediate for the synthesis of dendrimeric structures.

Finally, by coupling (2:1 ratio) complex **3** with the dichloride $\{Pt_6\}Cl_2$ (**5**) [$\{Pt_6\} = Pt_6(\mu\text{-}PtBu_2)_4(CO)_4$], which can straightforwardly be prepared from the known [$\{Pt_6\}(CO)_2](CF_3SO_3)_2$ (**4**),[19] we obtained (in 85% yield) the title compound [($\{Pt_3\}$-CC)$_2$-$C_6H_3$-CC]$_4${$Pt_6$} (**6**), as an orange, microcrystalline solid that was thermally and air stable. All complexes were characterized by microanalytical, IR, and multinuclear NMR data.

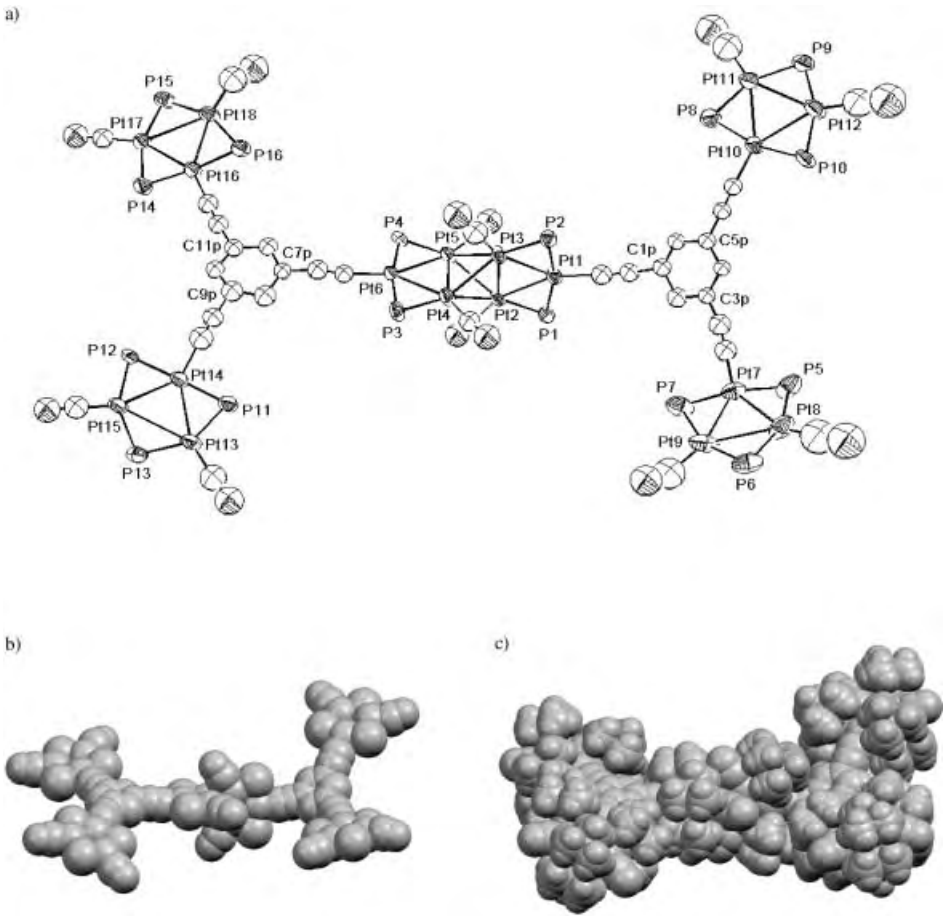



***Figure 1.*** a) ORTEP view of **6** showing the atom numbering scheme; b,c) space-filling models of the molecular structure of **6** (*t*Bu groups omitted for clarity in a) and b)).

Diagnostic signals at $\approx$166 (4P) and 96 ppm (2P) and at $\approx -6100$ (2Pt) and $-5700$ ppm (4Pt) were observed in the $^{31}P\{^1H\}$ and $^{195}Pt\{^1H\}$ NMR spectra of **3**, which suggested the presence of two equivalent triangular cluster units. This was confirmed by the ethynyl CH resonances, found at $\delta = 3.08$ ($\delta_H$) and 75.7 ppm ($\delta_C$), and by the features of the aromatic C–H region (signals in the 2:1 ratio at $\delta = 7.22$ and 7.38 ppm and at $\delta = 131.0$ and 134.3 ppm, respectively, observed in the $^1H$ and $^{13}C\{^1H\}$ NMR spectra). Significant IR absorptions were found at 3300 ($\nu_{CC\text{-}H}$), 2094 ($\nu_{CC}$) and 2024 $cm^{-1}$ ($\nu_{CO}$).

Similar spectral parameters were observed for complex **6**, whose spectra showed additional resonances due to the central hexanuclear cluster ($\delta_P = 335.1$ (4P); $\delta_{Pt} = -4664$ (2Pt), $-2996$ ppm (4Pt)), while the signals of the CCH unit disappeared. Single crystals of **6** suitable for X-ray crystallographic analysis were obtained by slow solvent evaporation from a $CHCl_3$ solution. Figure 1 shows space-filling and ORTEP views of **6**.[23]

The hexanuclear core of the structure may be described as being obtained by the condensation of two "$Pt_3$" units resulting in two edges of the triangles (i.e., Pt4–Pt5 and Pt2–Pt3) at bonding distances in the range of 2.62–2.87 Å. This gives rise to a central tetrahedral unit with two edge-bridging "$PtP_2$" moieties (the "Pt1Pt3" and "Pt4Pt6" triangles are mutually perpendicular, the dihedral angle defined by their mean planes being 89.8°). All the Pt–Pt separations are shorter relative to those found in other triangular clusters such as [$Pt_3(\mu\text{-}PtBu_2)_3(H)(CNR)_2$][18] (2.91–3.03 Å) or [$Pt_3(\mu\text{-}PtBu_2)_3(H)(CO)_2$][24] (2.72–3.61 Å); distances that fall in the lower end of the reported range.

The four chemically identical peripheral triangular units contain one long and two short Pt–Pt bonds[25] and lie approximately in the same mean planes defined by the alkynyl spacers (dihedral angles between planes in the range 16–18°) with the exception of the "Pt7-Pt9" cluster, for which the dihedral angle is $\approx$37°. Moreover, one of the alkynyl groups is roughly coplanar with the nearby triangular portion of the central $Pt_6$ core, while the other is more tilted (dihedral angles between the mean planes C7P–C12P/Pt4–Pt6 and C1P–C6P/Pt1–Pt3 are 13.6 and 51.3°, respectively). Given these distortions, possibly due to steric hindrance, compound **6** can be described as being only approximately planar. It is worth noting that the atoms in this dendrimer show quite large displacement parameters indicating the presence of positional disorder, consistent with the large amount of conformational freedom allowed by the long alkynyl spacers.

 © 2003 Wiley-VCH Verlag GmbH & Co. KGaA, Weinheim 

We are presently pursuing the utilization of compounds **1**–**6** in the synthesis of other ordered structures. The spectroscopic characterization of a linear analogue of complex **6** has also been recently described.[27]

## Experimental Section

$[Pt(\mu\text{-}PtBu_2)(CO)]_3(CF_3SO_3)$ (**1**),[18] $[Pt_6(\mu\text{-}PtBu_2)_4(CO)_6](CF_3SO_3)_2$ (**4**),[19] and 1,3,5-triethynylbenzene[21] were prepared as previously described.

**2:** $nBu_4NCl$ (250 mg, 0.90 mmol) was added to a brown solution of **1** (825 mg, 0.66 mmol) in acetone (20 mL). After stirring for 12 h at room temperature, the mixture was concentrated to ≈5 mL. Addition of $H_2O$ (5 mL) caused the precipitation of **2** as a microcrystalline brown solid (720 mg, 98%). Elemental analysis calcd (%) for $C_{26}H_{54}ClO_2P_3Pt_3$: C 28.1, H 4.89; found: C 28.0 H 4.93. $^{31}P\{^1H\}$ NMR (80.9 MHz, $CDCl_3$, 25°C) (in this spectrum and the following ones # denotes the presence of $^{195}Pt$ satellites): $\delta = 167.8^{\#}$ (d, $^2J_{PP} = 130$ Hz), $46.7^{\#}$ (t, $^2J_{PP} = 130$ Hz); $^1H$ NMR (200 MHz, $C_6D_6$, 25°C): $\delta = 1.47$ (vt, $^3J(H,P) + {}^5J(H,P) = 7.4$ Hz, 36H, $CCH_3$), 1.27 ppm (d, $^3J(H,P) = 15$ Hz, 18H, $CCH_3$); $^{13}C\{^1H\}$ NMR (50.3 MHz, $CDCl_3$, 25°C): $\delta = 172.6^{\#}$ (s, *C*O), $39.8^{\#}$ (m, *C*$CH_3$), $38.8^{\#}$ (m, *C*$CH_3$) 33.4 ppm (br s, C*C*$H_3$); $^{195}Pt\{^1H\}$ NMR (42.8 MHz, $CDCl_3$, 25°C): $\delta = -6389.8$ (1Pt), −5320.0 ppm (2Pt). IR ($CH_2Cl_2$): 2025 $cm^{-1}$ (CO).

**5**: $NH_4Cl$ (9.6 mg, 0.18 mmol) was added to a red solution of complex **4** (120 mg, 0.054 mmol) in acetone (5 mL). Complex **5** precipitated out as a red solid and was filtered and vacuum dried (101 mg, 97%). Elemental analysis calcd (%) for $C_{36}H_{72}Cl_2O_4P_4Pt_6$: C 22.3, H 3.75; found: C 22.1, H 3.70. $^{31}P\{^1H\}$ NMR (80.9 MHz, $CDCl_3$, 25°C): $\delta = 328.9^{\#}$ ppm (s); $^1H$ NMR (200 MHz, $CDCl_3$, 25°C): $\delta =$ 1.51 ppm (vt, $^3J(H,P) + {}^5J(H,P) = 7.2$ Hz); $^{195}Pt\{^1H\}$ NMR (42.8 MHz, $CDCl_3$, 25°C): $\delta = -4152.9$ (2Pt), −3462.7 ppm (4 Pt); $^{13}C\{^1H\}$ NMR (50.3 MHz, $CDCl_3$, 25°C): $\delta = 203.7^{\#}$ (weak br s, 4CO), 44.8 (s, P*C*), 31.5 ppm (s, *C*$H_3$). IR ($CH_2Cl_2$): 2017 $cm^{-1}$ (CO).

**3**: 1,3,5-triethynylbenzene (14.1 mg, 0.094 mmol) and CuI (0.38 mg, 0.002 mmol) were added to a solution of complex **2** (210 mg, 0.189 mmol) in diethylamine (25 mL). After 24 h the solvent was evaporated and the green/brown residue was extracted with $Et_2O$ to give, after chromatography (silica gel, eluent: $CH_2Cl_2$/*n*-hexane 1:5), 172.6 mg of **3** (80%). Elemental analysis calcd (%) for $C_{64}H_{112}O_4P_6Pt_6$: C 33.4, H 4.90; found: C 33.3, H 4.86. $^{31}P\{^1H\}$ NMR (80.9 MHz, $CDCl_3$, 25°C): $\delta = 165.7^{\#}$ (d, $^2J(PP) = 128$ Hz), 95.8# ppm (t, $^2J(PP) = 128$ Hz). $^1H$ NMR (200 MHz, $CD_2Cl_2$, 25°C): $\delta = 7.38$ (s, 1H), 7.22 (s, 2H), 3.08 (s, 1H, ≡C-*H*), 1.41 (vt, $^3J(H,P) + {}^5J(H,P) =$ 7.4 Hz, 36H), 1.32 ppm (d, $^3J(H,P) = 15.4$ Hz, 18H). $^{13}C\{^1H\}$ NMR (50.3 MHz, $CDCl_3$, 25°C): $\delta = 175.2^{\#}$ (s, CO), 134.3, 131.0, 129.3, 121.1 (s, $C_6H_3$), $86.4^{\#}$ (s, Pt-*C*C), 84.7 (s, *C*≡C-H), 75.7 (C≡*C*-H), 39.0, 38.7 (s, *C*-$CH_3$), 33.5 ppm (s, C-*C*$H_3$). $^{195}Pt\{^1H\}$ NMR (42.8 MHz, $CDCl_3$, 25°C): $\delta = -6104.1$ (dt, 2Pt), −5708.3 ppm (dd, 4Pt). IR ($CH_2Cl_2$): 3300 (≡C-H), 2094 (C≡C), 2024 $cm^{-1}$ (CO).

**6:** Complex **3** (93 mg, 0.040 mmol) and CuI (0.08 mg, $0.4 \times 10^{-3}$ mmol) were added to a solution of complex **5** (39.1 mg, 0.02 mmol) in diethylamine (20 mL). After 24 h the solvent was evaporated and the orange residue was extracted with $Et_2O$ to give, after chromatograpy on silica gel (eluent: $CH_2Cl_2$/*n*-hexane 1:3), 110 mg of **6** (85%). Elemental analysis calcd (%) for $C_{164}H_{294}O_{12}P_{16}Pt_{18}$: C 30.5, H 4.58; found: C 30.6, H 4.65. $^{31}P\{^1H\}$ NMR (80.9 MHz, $CDCl_3$, 25°C): $\delta = 335.1^{\#}$ (s), $164.7^{\#}$ (d, $^2J(PP) = 128$ Hz), $96.7^{\#}$ ppm (t, $^2J(PP) = 128$ Hz). $^1H$ NMR (200 MHz, $CD_2Cl_2$, 25°C): $\delta = 7.23$ (s, 2H), 7.16 (s, 4H), 1.55 (vt, $^3J(H,P) + {}^5J(H,P) = 7.0$ Hz, 72H), 1.45 (vt, $^3J(H,P) + {}^5J(H,P) = 7.8$ Hz, 144H), 1.34 ppm (d, $^3J(H,P) = 14.8$ Hz, 72H). $^{13}C\{^1H\}$ NMR (50.3 MHz, $CD_2Cl_2$, 25°C): $\delta = 217.2^{\#}$ (s, 4*C*O), $175.7^{\#}$ (s, 8*C*O), 130.7, 129.3, 129.0 (s, $C_6H_3$), $123.4^{\#}$, $122.0^{\#}$ (s, Pt-*C*C), $99.5^{\#}$, $84.9^{\#}$ (s, Pt-*C*C), 44.3, 39.3, 39.1 (s, *C*-$CH_3$), 33.7, 31.8 ppm (s, C-*C*$H_3$). $^{195}Pt\{^1H\}$ NMR (42.8 MHz, $CDCl_3$, 25°C): $\delta = -6093$ (dt, 4Pt), −5712 (dd, 8Pt), −4664 (m, 2Pt), −2996 ppm (m, 4Pt). IR ($CH_2Cl_2$): 2098 (C≡C), 2019 $cm^{-1}$ (br, CO).

Received: September 25, 2003 [Z52954]
Published Online: November 24, 2003

**Keywords:** alkyne ligands · cluster compounds · dendrimers · metal–metal interactions · platinum

[1] N. J. Long, C. K. Williams, *Angew. Chem.* **2003**, *115*, 2690; *Angew. Chem. Int. Ed.* **2003**, *42*, 2586.
[2] T. Weyland, K. Costuas, A. Mari, J. F. Halet, C. Lapinte, *Organometallics* **1998**, *17*, 5569.
[3] D. W. Bruce in *Inorganic Materials* (Eds.: D. W. Bruce , D. O'Hare), Wiley, Chichester, **1996**, p. 429.
[4] N. J. Long, *Angew. Chem.* **1995**, *107*, 37; *Angew. Chem. Int. Ed. Engl.* **1995**, *34*, 21; S. Barlow, D. O'Hare, *Chem. Rev.* **1997**, *97*, 637; A. M. McDonagh, M. G. Humphrey, M. Samoc, B. Luther-Davies, *Organometallics* **1999**, *18*, 5195.
[5] V. W. W. Yam, *Acc. Chem. Res.* **2002**, *35*, 555; M. Younus, A. Köler, S. Cron, N. Chowdhury, M. R. A. Al-Mandhari, M. S. Khan, J. Lewis, N. J. Long, R. H. Friend, P. R. Raithby, *Angew. Chem.* **1998**, *110*, 3180; *Angew. Chem. Int. Ed.* **1998**, *37*, 3036; M. J. Irwin, J. J. Vittal, R. J. Puddephatt, *Organometallics* **1997**, *16*, 3541; W. Lu, N. Zhu, C. M. Che, *J. Organomet. Chem.* **2003**, *670*, 11; K. M. C. Wong, C. K. Hui, K. L. Yu, V. W. W. Yam, *Coord. Chem. Rev.* **2002**, *229*, 123.
[6] C. Müller, J. A. Whiteford, P. J. Stang, *J. Am. Chem. Soc.* **1998**, *120*, 9827; S. M. Al-Qaisi, K. J. Galat, M. Chai, D. G. Ray III, P. L. Rinaldi, C. A. Tessier, W. J. Youngs, *J. Am. Chem. Soc.* **1998**, *120*, 12149; R. J. Puddephatt, *Coord. Chem. Rev.* **2001**, *216–217*, 313.
[7] S. Leininger, P. J. Stang, S. Huang, *Organometallics* **1998**, *17*, 3981; K. Onitsuka, M. Fujimoto, N. Oshiro, S. Takahashi, *Angew. Chem.* **1999**, *111*, 751; *Angew. Chem. Int. Ed.* **1999**, *38*, 689; V. W. W. Yam, C. H. Tao, L. J. Zhang, K. M. C. Wong, K. K. Cheung, *Organometallics* **2001**, *20*, 453; A. M. McDonagh, C. E. Powell, J. P. Morrall, M. P. Cifuentes, M. G. Humphrey, *Organometallics* **2003**, *22*, 1402.
[8] R. Ziessel, M. Hissler, A. El-ghayouri, A. Harrimen, *Coord. Chem. Rev.* **1998**, *178–180*, 1251.
[9] F. Paul, C. Lapinte, *Coord. Chem. Rev.* **1998**, *178–180*, 431.
[10] S. Le Stang, F. Paul, C. Lapinte, *Organometallics* **2000**, *19*, 1035; W. E. Meyer, A. J. Amoroso, C. R. Horn, M. Jaeger, J. A. Gladysz, *Organometallics* **2001**, *20*, 1115; M. I. Bruce, P. J. Low, K. Costuas, J.-F. Halet, S. P. Best, G. A. Heat, *J. Am. Chem. Soc.* **2000**, *122*, 1949; S. Kheradmandan, K. Heinze, H. W. Schmalle, H. Berke, *Angew. Chem.* **1999**, *111*, 2412; *Angew. Chem. Int. Ed.* **1999**, *38*, 2270.
[11] S. Rigaut, J. Perruchon, L. Le Pichon, D. Touchard, P. H. Dixneuf, *J. Organomet. Chem.* **2003**, *670*, 37; H. Lang, *Angew. Chem.* **1994**, *106*, 569; *Angew. Chem. Int. Ed. Engl.* **1994**, *33*, 547; A. Buttinelli, E. Viola, E. Antonelli, C. Lo Sterzo, *Organometallics* **1998**, *17*, 2574; S. Back, R. A. Gossage, M. Lutz, I. del Rio, A. L. Speck, H. Lang, G. van Koten, *Organometallics* **2000**, *19*, 3296.
[12] J. Lewis, P. R. Raithby, W. Y. Wong, *J. Organomet. Chem.* **1998**, *556*, 219; E. Antonelli, P. Rosi, C. Lo Sterzo, E. Viola, *J. Organomet. Chem.* **1999**, *578*, 210; A. J. Deeming, G. Hogarth, M. Lee, M. Saha, S. P. Redmond, H. Phetmung, A. G. Orpen, *Inorg. Chim. Acta* **2000**, *309*, 109; O. Lavastre, J. Plass, P. Bachmann, S. Guesmi, C. Moinet, P. H. Dixneuf, *Organometallics* **1997**, *16*, 184; W. Weng, T. Bartik, M. Brady, B. Bartik, J. A. Ramsden, A. M. Arif, J. A. Gladysz, *J. Am. Chem. Soc.* **1995**, *117*, 11922; M. A. MacDonald, R. J. Puddephatt, *Organometal-*

 © 2003 Wiley-VCH Verlag GmbH & Co. KGaA, Weinheim 

*lics*, **2000**, *19*, 2194; M. S. Khan, S. J. Davies, A. K. Kakkar, D. Schwartz, B. Lin, B. F. G. Johnson, J. Lewis, *J. Organomet. Chem.* **1992**, *424*, 87; K. Sonogashira, K. Ohga, S. Takahashi, N. Hagihara, *J. Organomet. Chem.* **1980**, *188*, 237; H. B. Fyfe, M. Mlekuz, D. Zargarian, N. J. Taylor, T. B. Marder, *J. Chem. Soc. Chem. Commun.* **1991**, 188.

[13] K. T. Wong, J.-M. Lehn, S. M. Peng, G. H. Lee, *Chem. Commun.* **2000**, 2259; T. Ren, G. Zou, J. C. Alvarez, *Chem. Commun.* **2000**, 1197; M. J. Irwin, G. Jia, J. J. Vittal, R. J. Puddephatt, *Organometallics* **1996**, *15*, 5321.

[14] Structures containing two triangular clusters connected by a π-alkynyl spacer or a $C(C{\equiv}C)_nC$ chain have been described in: M. I. Bruce, M. E. Smith, N. N. Zaitseva, B. V. Skelton, A. H. White, *J. Organomet. Chem.* **2003**, *670*, 170; M. Akita, A. Sakurai, M. C. Chung, Y. Moro-oka, *J. Organomet. Chem.* **2003**, *670*, 2; D. Osella, L. Milone, C. Nervi, M. Ravera, *J. Organomet. Chem.* **1995**, *488*, 1; G. H. Worth, B. H. Robinson, J. Simpson, *Organometallics* **1992**, *11*, 501; G. H. Worth, B. H. Robinson, J. Simpson, *Organometallics* **1992**, *11*, 3863; M. P. Jensen, D. A. Phillips, M. Sabat, D. F. Shriver, *Organometallics* **1992**, *11*, 1859.

[15] Metal clusters connected by conjugate non-alkynyl spacers are reported in: B. K. Roland, C. Carter, Z. Zheng, *J. Am. Chem. Soc.* **2002**, *124*, 6234; Z. Zheng, T. G. Gray, R. H. Holm, *Inorg. Chem.* **1999**, *38*, 4888; A. M. Bradford, E. Kristof, M. Rashidi, D.-S. Yang, N. C. Payne, R. J. Puddephatt, *Inorg. Chem.* **1994**, *33*, 2355.

[16] V. W.-W. Yam, W. K.-M. Fung, K. K. Cheung, *Chem. Commun.* **1997**, 963; M. I. Bruce, B. C. Hall, B. W. Skelton, M. E. Smith, A. H. White, *J. Chem. Soc. Dalton Trans.* **2002**, 995.

[17] S. B. Falloon, A. M. Arif, J. A. Gladysz, *Chem. Commun.* **1997**, 629; M. I. Bruce, *Coord. Chem. Rev.* **1997**, *166*, 91; P. Blenkiron, G. D. Enright, P. J. Low, J. F. Corrigan, N. J. Taylor, Y. Chi, J.-Y. Saillard, A. J. Carty, *Organometallics* **1998**, *17*, 2447.

[18] P. Leoni, F. Marchetti, M. Pasquali, L. Marchetti, A. Albinati, *Organometallics* **2002**, *21*, 2176.

[19] P. Leoni, F. Marchetti, L. Marchetti, M. Pasquali, S. Quaglierini, *Angew. Chem.* **2001**, *113*, 3729; *Angew. Chem. Int. Ed.* **2001**, *40*, 3617.

[20] C. Cavazza, P. Leoni, F. Marchetti, L. Marchetti, M. Pasquali, unpublished results.

[21] E. Weber, M. Hecker, E. Koepp, W. Orlia, M. Czugler, I. Csöregh, *J. Chem. Soc. Perkin Trans. 2* **1988**, 1251.

[22] K. Sonogashira, Y. Tohda, N. Hagihara, *Tetrahedron Lett.* **1975**, 4467.

[23] Crystal data for **6**·($CHCl_3$): $C_{165}H_{295}Cl_3O_{12}P_{16}Pt_{18}$, triclinic, space group $P\bar{1}$ (no. 2), $a = 17.341(1)$, $b = 22.574(1)$, $c = 30.140(2)$ Å, $\alpha = 80.375(2)$, $\beta = 86.231(2)$, $\gamma = 79.132(2)°$, $V = 11\,416.7(1)$ Å$^3$, $Z = 2$, $\rho_{calcd} = 1.915$ g cm$^{-3}$, $\mu$ ($Mo_{K\alpha}$) = 111.67 cm$^{-1}$, dimensions $0.08 \times 0.1 \times 0.25$ mm. 99 337 data were collected, at room temperature, on a Bruker APEX CCD diffractometer, of which 40 489 were unique ($R_{int} = 0.1805$). A multi-scan absorption correction was applied using the program SADABS (transmission factors in the range 1.0000–0.4122). Structure solution was by direct and Fourier methods and refinement by full-matrix least-squares on $F^2$ (SHELX-PC program) using anisotropic displacement parameters for the Pt and P atoms and the CO groups. Final agreement factors were $R_1 = 0.0844$, $R_{w2} = 0.2016$ for 14 218 observed reflections [$I \geq 2\sigma(I)$]; data/restraints/parameters 40489/0/1087; GOF = 0.908. A disordered molecule of solvent ($CHCl_3$) was found in the final Fourier-difference maps and its contribution was taken into account. CCDC-217686 contains the supplementary crystallographic data for this paper. These data can be obtained free of charge via www.ccdc.cam.ac.uk/conts/retrieving.html (or from the Cambridge Crystallographic Data Centre, 12, Union Road, Cambridge CB21EZ, UK; fax: (+44) 1223-336-033; or deposit@ccdc.cam.ac.uk).

[24] P. Leoni, S. Manetti, M. Pasquali, A. Albinati, *Inorg. Chem.* **1996**, *35*, 6045.

[25] The Pt–Pt separations span a rather broad range (3.066–3.380 Å and 2.785–2.914 Å, respectively, with the longer separation increasing as the two shorter ones decrease). A similar soft potential for the deformation of the Pt–Pt bonds has been previously observed in other triangular $[Pt_3(\mu\text{-}PR_2)_3(L)_2(X)]$ derivatives with σ-donor X ligands.[18,26]

[26] R. Bender, P. Braunstein, A. Dedieu, P. D. Ellis, B. Huggins, P. D. Harvey, E. Sappa, A. Tiripicchio, *Inorg. Chem.* **1996**, *35*, 1223.

[27] P. Leoni, F. Marchetti, L. Marchetti, M. Pasquali, *Chem. Commun.* **2003**, 2372.

 © 2003 Wiley-VCH Verlag GmbH & Co. KGaA, Weinheim 

*Pd-Catalyzed C–C Coupling*

# Efficient Palladium-Catalyzed Coupling of Aryl Chlorides and Tosylates with Terminal Alkynes: Use of a Copper Cocatalyst Inhibits the Reaction**

*Dmitri Gelman and Stephen L. Buchwald**

Aryl alkynes are important intermediates in organic synthesis.[1] Currently, palladium and copper cocatalyzed alkyne synthesis, the Sonogashira reaction, is the most straightforward and powerful method for the construction of $C(sp^2)$–C(sp) bonds. The original protocol[2] has been repeatedly modified and improved to overcome several significant limitations: a) the use of various palladacycles led to catalytic systems with higher turnover numbers,[3] b) copper-free[4] or silver cocatalyzed[5] protocols eliminated the undesired dimerization of terminal alkynes,[6] c) Sonogashira coupling of aryl bromides and iodides at room temperature is now possible.[7] However, unlike other cross-coupling reactions, the use of aryl chlorides as coupling partners for alkyne synthesis, until recently, had remained largely unexplored. Significant progress in this field has recently been made.[4c,8] In particular the work of Plenio and co-workers represents the most general procedure for Sonogashira coupling of aryl chlorides described to date. They used a catalyst derived from bis(adamantyl)benzylphosphane and $Na_2PdCl_4$/CuI for the coupling of

[*] Prof. S. L. Buchwald, D. Gelman
Department of Chemistry, Room 18–490
Massachusetts Institute of Technology
Cambridge, MA 02139 (USA)
Fax: (+1) 617-253-3297
E-mail: sbuchwal@mit.edu

[**] We thank the National Institutes of Health (GM46059) for support of this work. We are grateful to Merck, Pfizer, Lundbeck, Rhodia, and Novartis for additional support.

Supporting information for this article is available on the WWW under http://www.angewandte.org or from the author.

 DOI: 10.1002/anie.200353015 © 2003 Wiley-VCH Verlag GmbH & Co. KGaA, Weinheim 

aryl chlorides with terminal acetylenes. Although excellent yields were obtained for activated chloroarenes at 100 °C, the reactions of electron-neutral and electron-rich substrates were less successful, even at 120 °C. In addition, no examples of the coupling of alkyl acetylenes with *ortho*-substituted aryl chlorides were reported. Clearly, the need for improved catalysts remains. Herein we report the most general and efficient method for the coupling of alkynes with aryl chlorides available so far. In addition, we demonstrate for the first time, that a copper cocatalyst, rather than being beneficial, can lead to complete inhibition of the catalytic activity.

Our work began with the intention of discovering a general catalytic system for the Sonogashira coupling of aryl chlorides, based on a family of bulky, electron-rich *ortho*-biphenylphosphane ligands developed in our laboratories.[9] An important observation was made during our initial experiments: for a catalyst derived from **1** and $[PdCl_2(CH_3CN)_2]$, the presence of a copper cocatalyst has a deleterious effect on the desired transformation. In contrast, in the absence of copper the desired transformation proceeds smoothly. As can be seen from Figure 1, 0.5 mol% of CuI, either added prior to the start of the reaction or one hour after its initiation (~35% conversion), causes suppression of the coupling process.

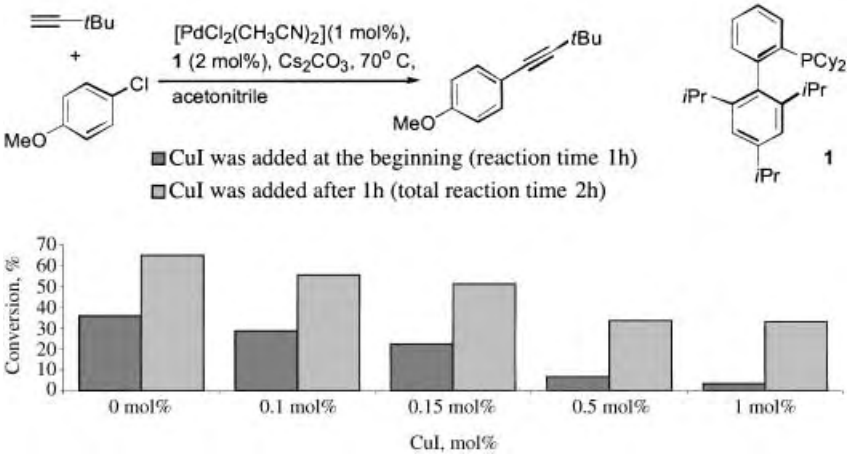


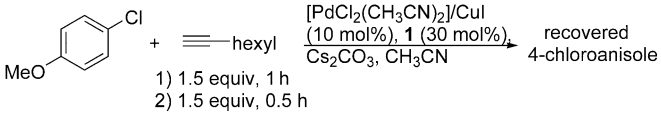




***Figure 1.*** Effect of the copper additive on the efficiency of alkyne coupling of 4-chloroanisole.

Interestingly the inclusion of copper compounds (copper(I) chloride, copper phenylacetylide, copper(II) bis(isobutyrate)), in either the +1 or +2 oxidation state, suppresses the desired transformation. By monitoring the reaction, we discovered that in all reactions that included a copper cocatalyst complete consumption of the starting alkyne takes place by a competitive process, presumably oligomerization. For example, an experiment performed in the presence of 10 mol% of a catalyst derived from **1** and $[PdCl_2(CH_3CN)_2]$ and 10 mol% of CuI showed complete conversion of the 1-octyne after 1 h. An additional injected portion of the alkyne was consumed as well, yet almost no coupling product was observed (Scheme 1).

After further experimentation it was discovered, that if the alkyne is added slowly in a reaction that used CuI/




***Scheme 1.***

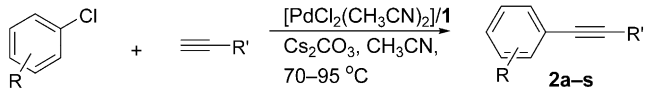
$[PdCl_2(CH_3CN)_2]$/**1**, the side reaction is suppressed and the coupling product cleanly forms. This indicates that no irreversible poisoning of the $[PdCl_2(CH_3CN)_2]$/**1** catalyst with copper takes place and that a lower concentration of the acetylene slows down the rate of oligomerization.

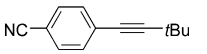
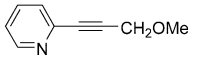
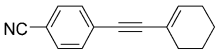
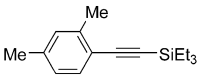
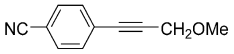
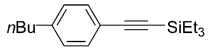
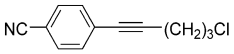
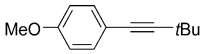
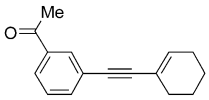
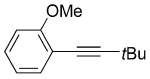
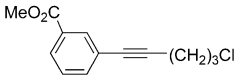
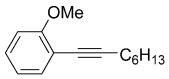
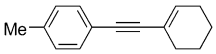
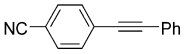
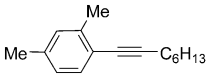
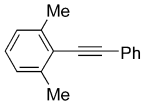
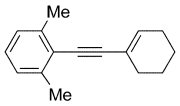
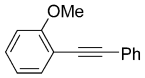
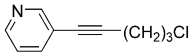
These findings led us to the discovery of a new protocol for the palladium-catalyzed coupling of alkynes with aryl chlorides. The reaction conditions employed (1 mol% of $[PdCl_2(CH_3CN)_2]$, 3 mol% of **1**, 1.3 equivalents of the terminal alkyne, and 2.6 equivalents of $Cs_2CO_3$ in acetonitrile at 70–90 °C) typically provided very fast and selective transformation of aryl chlorides to the desired product (Table 1). The choice of the solvent as well as of the base was important for the success of the reaction described here: only moderately polar aprotic solvents (acetonitrile, dioxane), in combination with inorganic bases ($Cs_2CO_3$, $K_3PO_4$) proved to be useful. In contrast to these observations, no critical role of the precatalyst was detected, although the best results were obtained with $[PdCl_2(CH_3CN)_2]$ or $PdCl_2$ (**2g**, Table 1). The catalyst derived from $[PdCl_2(CH_3CN)_2]$ and **1** was found to promote a high-yielding coupling even when used at 0.1 mol% loading. This corresponds to a turnover number of about 890 (**2a**, Table 1).

As illustrated by Table 1, the reactions of electron-deficient aryl chlorides could be carried out at 70 °C. The transformation with electron-neutral and electron-rich aryl chlorides necessitated a reaction temperature of 90 °C. The coupling of aryl acetylenes required that the alkyne be added over 2 h (**2q–s**, Table 1), otherwise incomplete conversion of the aryl chlorides and nonproductive consumption of the alkynes again takes place. The present method was found to be relatively insensitive to the steric hindrance of the starting aryl chloride. For example, 2-chloro-*m*-xylene was converted to the corresponding acetylene in excellent yield (**2r** Table 1). This is also the first demonstration of the coupling of an *ortho*-substituted aryl chloride with an alkyl acetylene. Good functional group compatibility and wide scope of alkynes highlight the new method. Functionalized as well as unfunctionalized alkynes can be successfully coupled with a variety of aryl and heteroaryl chlorides to yield the corresponding disubstituted acetylenes. While we found that the use of trimethylsilyl-protected acetylenes was inefficient due to the significant desilylation of the product that takes place under our reaction conditions, the use of triethylsilylacetylene was a suitable surrogate (**2l**, **m**, Table 1). Noteworthy is that aryl tosylates, which, to the

 © 2003 Wiley-VCH Verlag GmbH & Co. KGaA, Weinheim 

***Table 1:*** Coupling of aryl chlorides with terminal alkynes catalyzed by $[PdCl_2(CH_3CN)_2]$/**1**.

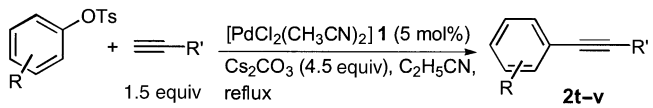


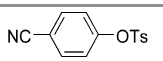
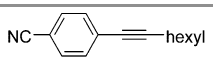
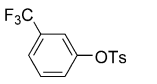
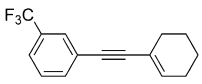
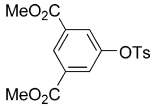
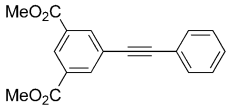

| | Compound | Conditions temp. [°C] | time [h] | Yield[a] [%] | | Compound | Conditions temp. [°C] | time [h] | Yield[a] [%] |
|---|---|---|---|---|---|---|---|---|---|
| **2a**[b] |  | 70 | 9 | 89 | **2k** |  | 90 | 1.5 | 79 |
| **2b** |  | 70 | 1.5 | 93 | **2l** |  | 90 | 2 | 85 |
| **2c** |  | 70 | 1.5 | 94 | **2m** |  | 90 | 2.5 | 77 |
| **2d** |  | 70 | 2 | 84 | **2n** |  | 70 | 3 | 87 |
| **2e** |  | 70 | 1.5 | 94 | **2o** |  | 90 | 1.5 | 93 |
| **2f** |  | 70 | 2 | 92 | **2p** |  | 90 | 2 | 93 |
| **2g** |  | 90 | 4 | 82 | **2q**[c] |  | 82 | 2.5 | 93 |
| **2h** |  | 90 | 2 | 90 | **2r**[c] |  | 97 | 2.5 | 88 |
| **2i** |  | 90 | 2 | 92 | **2s**[c] |  | 97 | 3 | 95 |
| **2j** |  | 90 | 3 | 85 | | | | | |

[a] Yield of isolated product is the average of two runs. [b] The reaction was performed by using 0.1 mol% of the catalyst. [c] The alkyne was added slowly over the course of the reaction.

best of our knowledge[10] have never been reported as coupling partners in Sonogashira processes, react under similar conditions (**2t**–**v**, Table 2). For these substrates slow addition of an alkyne is necessary to obtain a high yield of the desired product.

***Table 2:*** Coupling of aryl tosylates with terminal alkynes catalyzed by $[PdCl_2(CH_3CN)_2]$/**1**.




| Entry | ArOTs | Product | Yield [%][a] |
|---|---|---|---|
| **2t** |  |  | 73 |
| **2u** |  |  | 78 |
| **2v** |  |  | 62 |

[a] Yield of isolated product is the average of two runs.

In summary, we have developed a general protocol for the palladium-catalyzed coupling of aryl chlorides and alkynes. The new protocol requires less catalyst, lower temperature, and has greater generality than those previously reported. We have also demonstrated for the first time that the Sonogashira coupling of aryl tosylates is possible. Moreover, we have uncovered an unexpected phenomenon: the addition of a copper cocatalyst can inhibit product formation in the coupling reaction of aryl chlorides with terminal alkynes. An important ramification of our finding that the presence of a copper cocatalyst can lead to a decrease in yield in a Sonogashira process is that, particularly in the case of highly active catalysts, screening for new catalyst systems needs to be carried out both in the presence and absence of added copper.

## *Experimental Section*

General procedure for preparation of compounds **2a**–**p**: An oven-dried Schlenk tube was evacuated and backfilled with argon (the cycle was performed twice) and then charged under a positive pressure of argon with $[PdCl_2(CH_3CN)_2]$ (1.2 mg, 4.62 μmol, 1 mol%), **1** (6.6 mg, 14 μmol, 3 mol%), $Cs_2CO_3$ (391 mg, 1.20 mmol), followed by anhydrous acetonitrile (924 μL) and the aryl chloride (0.462 mmol). The slightly yellow suspension was stirred for 25 min. Then the alkyne (0.6 mmol) was injected, the Schlenk tube was sealed with a Teflon

 © 2003 Wiley-VCH Verlag GmbH & Co. KGaA, Weinheim 

valve, and the reaction mixture was stirred at the desired temperature for the indicated period of time. The resulting suspension was allowed to reach room temperature, diluted with water (3 mL), and extracted with diethyl ether (4 × 4 mL). The combined organic layers were dried over $MgSO_4$, concentrated, and the residue was purified by flash chromatography on silica gel to provide the desired product.

General procedure for preparation of compounds **2q–s**: An oven-dried two-necked flask, equipped with reflux condenser, gas inlet/outlet, and rubber stopper, was evacuated and backfilled with argon (the cycle was performed twice) and then charged under a positive pressure of argon with $[PdCl_2(CH_3CN)_2]$ (5.9 mg, 22.7 μmol, 1 mol%), **1** (32.5 mg, 68.2 μmol, 3 mol%), $Cs_2CO_3$ (1.63 g, 4.99 mmol), followed by anhydrous acetonitrile (for **2q**) or propionitrile (for **2r**,**s**) (4.5 mL) and the aryl chloride (2.27 mmol). The slightly yellow suspension was stirred for 25 min at room temperature. Then the reaction mixture was heated to reflux and the alkyne (0.6 mmol) was injected slowly over the course of reaction (2 h) by means of a syringe pump. The reaction mixture was stirred for additional 30 min after the addition was complete and the resulting suspension was allowed to reach room temperature, diluted with water (3 mL), and extracted with diethyl ether (4 × 4 mL). The combined organic layers were dried over $MgSO_4$, concentrated, and the residue was purified by flash chromatography on silica gel to provide the desired product.

General procedure for coupling of aryl tosylates with terminal acetylenes (**2t–v**): An oven-dried two-necked flask, equipped with reflux condenser, gas inlet/outlet, and rubber stopper, was evacuated and backfilled with argon (the cycle was performed twice) and then charged under a positive pressure of argon with $[PdCl_2(CH_3CN)_2]$ (7.7 mg, 29.6 μmol, 5 mol%), **1** (42.4 mg, 89 μmol, 15 mol%), $Cs_2CO_3$ (0.87 g, 2.66 mmol), followed by propionitrile (1.8 mL) and the aryl tosylate (0.59 mmol). The slightly yellow suspension was stirred for 25 min at room temperature. (The efficient stirring of the reaction mixture and a high purity of the starting tosylate are important for the transformation to be successful.) Then the reaction mixture was heated to the reflux temperature and the alkyne (0.88 mmol diluted with 1 mL of propionitrile) was injected slowly over the course of reaction (8 h) by means of a syringe pump. The reaction mixture was stirred for additional 2 h after the addition was complete and the resulting suspension was allowed to reach room temperature, diluted with water (3 mL), and extracted with diethyl ether (4 × 4 mL). The combined organic layers were dried over $MgSO_4$, concentrated, and the residue was purified by flash chromatography on silica gel to provide the desired product.

Received: October 3, 2003 [Z53015]

**Keywords:** alkynes · aryl chlorides · C–C coupling · cross-coupling · palladium

[1] a) K. C. Nicolaou, E. J. Sorensen, *Classics in Total Synthesis*, Wiley-VCH, Weinheim, **1996**, pp. 582–586; b) L. Brandsma, S. F. Vasilevsky, H. D. Verkruijsse, *Application of Transition Metal Catalysts in Organic Synthesis*, Springer, Berlin, **1998**, pp. 179–225; c) J. Tour, *Acc. Chem. Res.* **2000**, *33*, 791.

[2] K. Sonogashira, Y. Tohda, N. Hagihara, *Tetrahedron Lett.* **1975**, 4467.

[3] a) W. A. Herrmann, V. P. W. Böhm, C. P. Reisinger, *J. Organomet. Chem.* **1998**, *576*, 23; b) D. A. Alonso, C. Najera, M. C. Pacheco, *Org. Lett.* **2000**, *2*, 1283; c) D. A. Alonso, C. Najera, M. C. Pacheco, *Tetrahedron Lett.* **2002**, *43*, 9365.

[4] a) M. Pal, K. Parasuraman, S. Gupta, K. R. Yeleswarapu, *Synlett* **2002**, *14*, 1976; b) T. Fukuyama, M. Shinmen, S. Nishitani, M. Sato, I. Ryu, *Org. Lett.* **2002**, *4*, 1691; c) D. Méry, K. Heuze, D. Astruc, *Chem. Commun.* **2003**, 1934.

[5] A. Mori, J. Kawashima, T. Shimada, M. Suguro, K. Hirabayshi, Y. Nishihara, *Org. Lett.* **2000**, *2*, 2935.

[6] P. Siemsen, R. C. Livingston, F. Diederich, *Angew. Chem.* **2000**, *112*, 2740; *Angew. Chem. Int. Ed.* **2000**, *39*, 2632.

[7] a) V. P. W. Böhm, W. A. Herrmann, *Eur. J. Org. Chem.* **2000**, 3679; b) T. Hundertmark, A. F. Littke, S. L. Buchwald, G. C. Fu, *Org. Lett.* **2002**, *4*, 1729.

[8] a) M. R. Eberhard, Z. Wang, C. M. Jensen, *Chem. Commun.* **2002**, 818.b) B. M. Choudary, S. Madhi, N. S. Chowdari, M. L. Kantam, B. Sreedhar, *J. Am. Chem. Soc.* **2002**, *124*, 14127; c) A. Kollhofer, T. Pullmann, H. Plenio, *Angew. Chem.* **2003**, *115*, 1086; *Angew. Chem. Int. Ed.* **2003**, *42*, 1056; d) J. W. Faller, R. G. Kultyshev, J. Parr, *Tetrahedron Lett.* **2003**, *44*, 451.

[9] a) H. Tomori, J. M. Fox, S. L. Buchwald, *J. Org. Chem.* **2000**, *65*, 5334; b) S. Kuwabe, K. E. Torraca, S. L. Buchwald, *J. Am. Chem. Soc.* **2001**, *123*, 12202; c) J. Yin, M. P. Rainka, X.-X. Zhang, S. L. Buchwald, *J. Am. Chem. Soc.* **2002**, *124*, 1162; d) T. Hamada, A. Chieffi, J. Ahman, S. L. Buchwald, *J. Am. Chem. Soc.* **2002**, *124*, 1261; e) X. Huang, K. W. Anderson, D. Zim, L. Jiang, A. Klapars, S. L. Buchwald, *J. Am. Chem. Soc.* **2003**, *125*, 6653.

[10] Activated vinyl tosylates have been used previously for Sonogashira reaction: see, for example: X. Fu, S. Zhang, J. Yin, D. P. Schumacher, *Tetrahedron Lett.* **2002**, *43*, 6673.

 © 2003 Wiley-VCH Verlag GmbH & Co. KGaA, Weinheim 

*Natural Products*

# A Route to the Thapsigargins from (*S*)-Carvone Providing a Substrate-Controlled Total Synthesis of Trilobolide, Nortrilobolide, and Thapsivillosin F**

*Steven F. Oliver, Klemens Högenauer, Oliver Simic, Alessandra Antonello, Martin D. Smith, and Steven V. Ley**

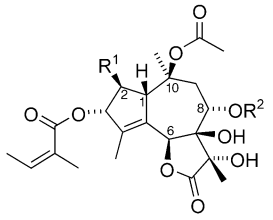
Investigations into the biologically active components of the Mediterranean plant species *Thapsia* led to the isolation of thapsigargin (**1**) and fifteen closely related guaianolides,

[*] Prof. S. V. Ley, Dr. S. F. Oliver, Dr. K. Högenauer, Dr. O. Simic, A. Antonello, Dr. M. D. Smith
University Chemical Laboratory
University of Cambridge
Lensfield Road
Cambridge, CB2 1EW (UK)
Fax: (+44) 1223-336442
E-mail: svl1000@cam.ac.uk

[**] This work was supported by a Wellcome Trust Research Fellowship (to S.F.O.), a Marie Curie Fellowship (to K.H.), the Deutsche Forschungsgemeinschaft (to O.S.), The Royal Society (to M.D.S.), and Novartis Research Fellowships (to S.V.L.). We thank Prof. S. B. Christensen for providing natural product samples for reference purposes and Dr. John Davis for X-ray crystallographic analyses. Early synthesis efforts by Dr. Helen Gold, Dr. Alison Woolford, and Emily Balskus are also gratefully acknowledged.

 © 2003 Wiley-VCH Verlag GmbH & Co. KGaA, Weinheim DOI: 10.1002/anie.200353140 

collectively termed "thapsigargins".[1] The members of this family of sesquiterpene lactones have a highly oxygenated tricyclic framework containing seven or eight stereogenic centers and are functionalized with a range of different acyl groups derived from acetic, butyric, angelic, and octanoic acids. The trilobolide subfamily (**2**–**4**) lack the acyloxy substituent at C2 and it is the first total synthesis of these



**1**: thapsigargin: $R^1$ = octanoyl, $R^2$ = butanoate
**2**: trilobolide: $R^1$ = H, $R^2$ = (*S*)-2-methylbutanoate
**3**: nortrilobolide: $R^1$ = H, $R^2$ = butanoate
**4**: thapsivillosin F: $R^1$ = H, $R^2$ = 3,3-dimethylacrylate

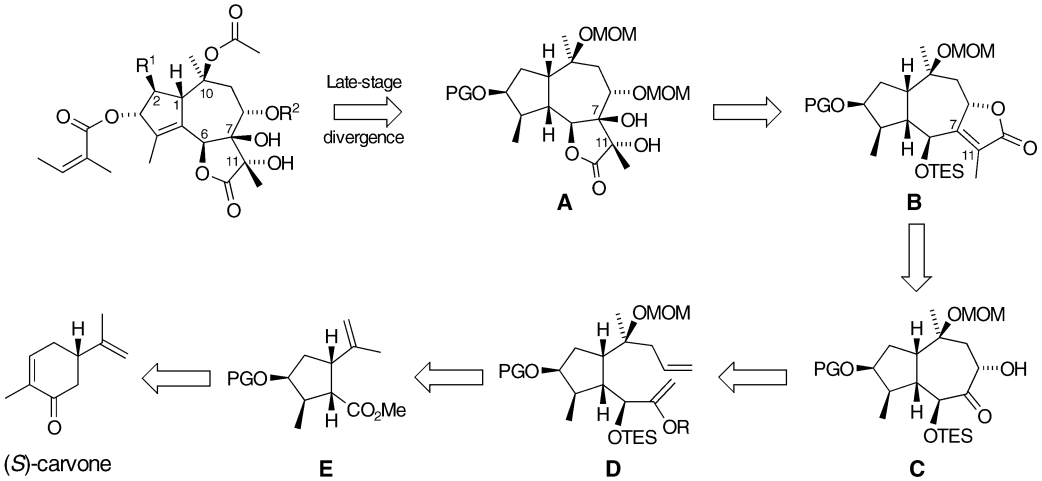
three thapsigargins that we report herein.

Interest in the thapsigargins arose after they were recognized to be potent histamine liberators[2] and selective and irreversible inhibitors of the ubiquitous sarco-endoplasmic reticulum $Ca^{2+}$ ATP dependent pumps (SERCAs) up to subnanomolar concentrations.[3] When applied to intact cells, thapsigargin (**1**) is able to penetrate the cell where it binds to and locks the SERCA into a conformation that has a poor affinity for $Ca^{2+}$ and ATP.[4] Trilobolide (**2**) ($K_D = 1.0$ nM) binds only 2.5 times less tightly to SERCA than **1** ($K_D =$ 0.4 nM).[5] Thapsigargins demonstrate a remarkable specificity for the SERCA isozymes, and have hence become powerful tools to manipulate and study intracellular $Ca^{2+}$-dependent signalling pathways.[6] Thapsigargin (**1**) has also been shown to restore apoptotic function in cancer cell lines.[7] This has recently led to the development of a potential treatment for prostate cancer using a prodrug conjugate of **1** that is cleaved and activated by prostate-specific antigen.[8]

Despite the prevalence of the thapsigargins in the fields of molecular biology and oncology (a scan of the past 10 years' literature reveals almost 5000 hits for the keyword "thapsigargin"), the synthetic community has been slow to reflect its significance. To date, no total or partial synthesis of any member of this family has been reported. Using degradation,[1] Christensen and co-workers have carried out a number of modifications on the periphery of the natural substance to investigate some of the important structure–activity relationships. However, no modification of the core has been possible using this strategy. A flexible synthetic route to the thapsigargins would allow the preparation of simplified analogues and permit the investigation of detailed structure–activity relationships, which would not be otherwise possible.

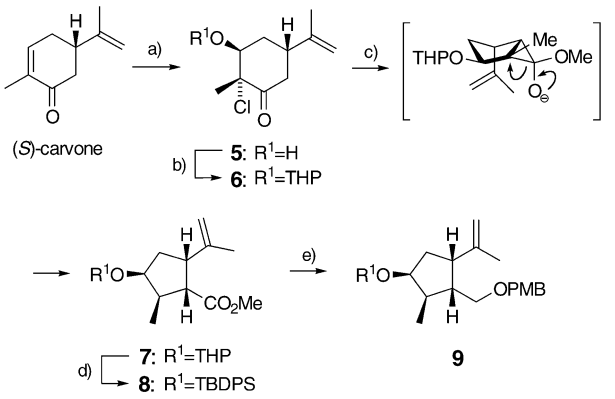
Our general approach to the thapsigargins is outlined in Scheme 1. To allow access to all 16 natural compounds in the series and a number of potential analogues, our plan leads to the common intermediate **A** (PG = *tert*-butyldiphenylsilyl (TBDPS)) as the point of late-stage divergent functionalization of the cyclopentane ring prior to sequential introduction of the various ester functionalities required. We envisaged the installation of the two quarternary centers at C7 and C11 by a stereoselective *cis*-dihydroxylation of butenolide **B**. Assembly of this lactone should be possible from the α-hydroxy ketone **C**, which we planned to generate by an enol ether metathesis/oxidation sequence from diene **D**. Cyclopentane **E** (PG = tetrahydropyranyl (THP)), has already served as an intermediate in a synthesis of two other guaianolides: cladantholide and estafiatin.[9]

The synthesis begins with the stereoselective epoxidation of commercially available (*S*)-(+)-carvone with basic hydrogen peroxide (Scheme 2).[10] Opening of the resulting oxirane with lithium chloride in the presence of trifluoroacetic acid (TFA)[11] led exclusively to chlorohydrin **5**, which was protected to yield a diastereomeric mixture of the THP ethers **6**. Treatment of **6** with sodium methoxide effected a regio- and stereoselective Favorskii rearrangement to give methyl ester **7** as the sole product. At this point, the protecting group was exchanged to the more robust TBDPS group (**7**→**8**). It should be noted that the Favorskii rearrange-




***Scheme 1.*** The synthesis plan. PG = protecting group, MOM = methoxymethyl, TES = triethylsilyl.

 © 2003 Wiley-VCH Verlag GmbH & Co. KGaA, Weinheim 

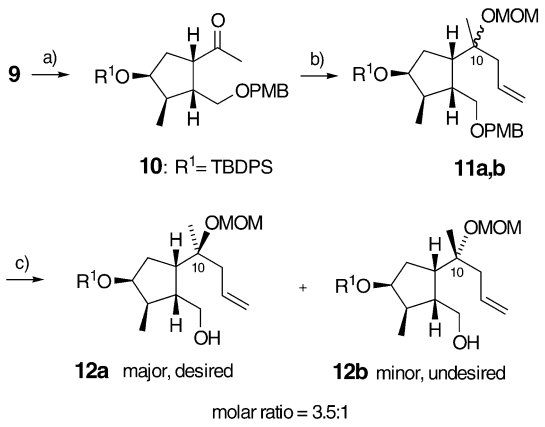



***Scheme 2.*** Synthesis of left-hand fragment **9**. Reagents and conditions: a) 1. $H_2O_2$, NaOH, MeOH, 10°C, 88%, 2. LiCl, TFA, THF, RT, 95%; b) DHP, PPTS cat., $CH_2Cl_2$, RT, 87%; c) NaOMe, MeOH, 0°C, 95%, d.r. > 95:5; d) 1. PPTS cat., MeOH, 40°C, 84%; 2. TBDPSCl, imidazole, DMF, RT, 98%; e) 1. LAH, THF, 0°C; 2. NaH, PMBCl, DMF, RT. TFA = trifluoroacetic acid, DHP = dihydropyran, PPTS = pyridinium *p*-toluenesulfonate, THP = tetrahydropyranyl, TBDPS = *tert*-butyldiphenylsilyl, PMB = *p*-methoxybenzyl.

ment with the TBDPS-protected alcohol was also investigated, but the yields and selectivities were inferior to the THP case. Reduction of ester **8**, followed by protection of the primary alcohol gave 4-methoxybenzyl ether **9**.

As testament to the efficiency of this chemistry, no column chromatography was necessary in this opening eight-step sequence, allowing the preparation of more than 50 g of **9** per batch.

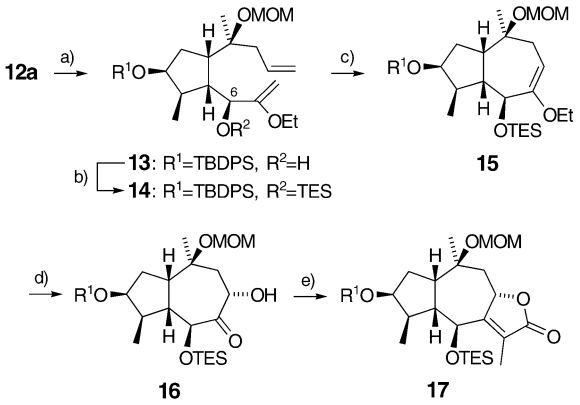
Osmylation and in situ diol cleavage provided the ketone **10** (Scheme 3). Addition of allyl magnesium bromide resulted in the formation of an inseparable diastereomeric mixture of homoallylic alcohols (d.r. = 3.5:1), with preference for the Felkin product.[12] After MOM protection of the tertiary alcohol (→**11a,b**) and removal of the PMB group, this




***Scheme 3.*** Synthesis of the C10 epimeric alcohols **12a** and **12b**. Reagents and conditions: a) 1. $OsO_4$ cat., NMO, acetone, $H_2O$, RT; 2. $NaIO_4$, RT, 74% over four steps; b) 1. AllylMgBr, THF, −78°C, 99%, d.r. = 3.5:1; 2. MOMCl, DIPEA, DMAP cat., $CH_2Cl_2$, RT, 88%; c) DDQ, aq. pH 7 phosphate buffer, $CH_2Cl_2$, RT, 93%. DIPEA = *N*,*N*-diisopropylethylamine, DDQ = 2,3-dichloro-5,6-dicyano-1,4-benzoquinone, DMAP = 4-(*N*,*N*-dimethylamino)pyridine.

mixture could be separated by column chromatography to give the C10 epimeric alcohols **12a** and **12b**.

Continuing the synthesis, alcohol **12a** was oxidized with tetra-*n*-propylammonium perruthenate (TPAP)[13] and *N*-morpholine-*N*-oxide (NMO) (Scheme 4) and the resulting aldehyde was treated with the lithium anion of ethyl vinyl



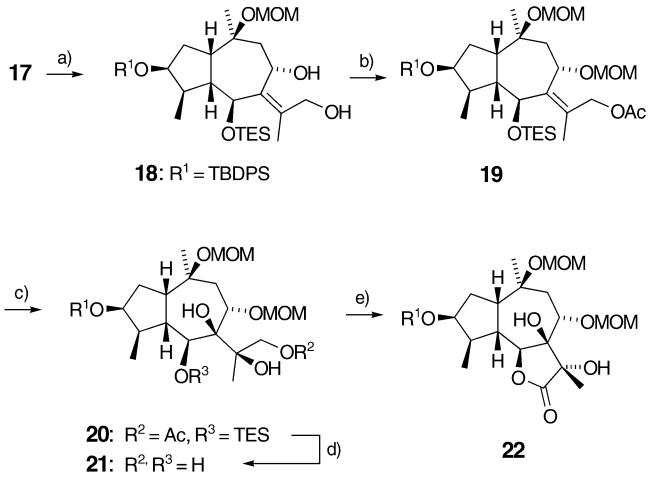

***Scheme 4.*** Synthesis of the α,β-unsaturated lactone **17**. Reagents and conditions: a) 1. TPAP cat., NMO, 4 Å MS, $CH_2Cl_2$, RT, 90%, 2. $CH_2$=CHOEt, *t*BuLi, THF, −78°C, 96%, d.r. > 95:5; b) TESCl, imidazole, DMF, RT, 95%; c) 2.5 mol% Grubbs' dihydroimidazolidine Ru cat., $CH_2Cl_2$, reflux, 92%; d) $K_2OsO_2(OH)_4$ cat., $K_3Fe(CN)_6$, $NaHCO_3$, $MeSO_2NH_2$, $K_2CO_3$, *t*BuOH, $H_2O$, RT, 90%, d.r. = 16:1; e) 1. $HO_2CCH(Me)P(O)(OEt)_2$, EDCI, $CH_2Cl_2$, RT; 2. NaH, THF, reflux, 79% over two steps.

ether to give alcohol **13** as a single diastereoisomer. The stereochemical outcome of this addition is again consistent with the Felkin–Anh model. TES protection gave enol ether **14**, which was subjected to the key ring-closing metathesis reaction using only 2.5 mol% of Grubbs' dihydroimidazoline ruthenium catalyst[14] to form the required cyclic enol ether **15** in remarkable yield.[15]Osmylation in the absence of a chiral ligand led predominantly to the desired α-hydroxy ketone epimer **16** (d.r. = 16:1), resulting from attack on the concave face.[16] The C8 alcohol of **16** was then esterified with 2-(diethoxyphosphoryl)propionic acid, and a subsequent intramolecular Horner–Wadsworth–Emmons reaction resulted in the formation of butenolide **17**.

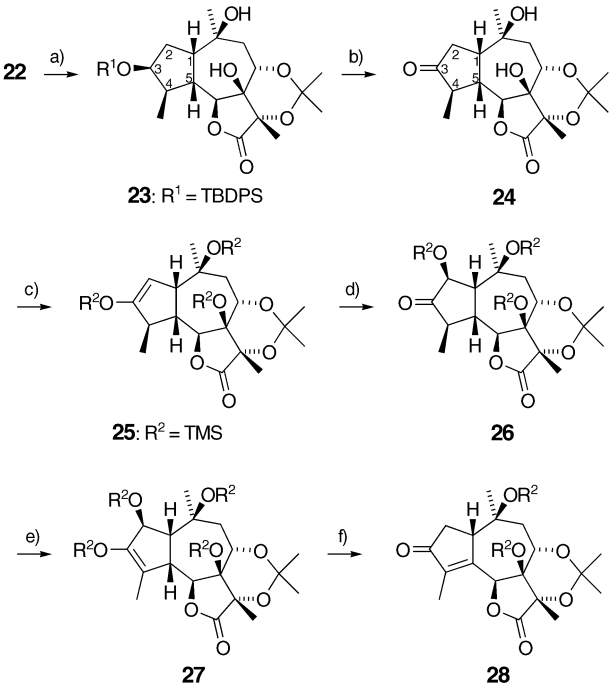
Attempts to effect the intended *syn*-dihydroxylation of lactone **17** proved unsuccessful, most likely due to a combination of unfavorable steric and electronic factors. After some experimentation, we found that carrying out the osmium-mediated dihydroxylation of a reduced derivative was possible (Scheme 5). Thus, formation of diol **18** by lithium borohydride reduction of lactone **17** was followed by orthogonal protection of the primary and secondary alcohol functions to give olefin **19**. At this stage, the dihydroxylation proceeded smoothly to give diol **20** as a single diastereoisomer.[17] Concomitant removal of TES and acetate protecting groups from **20** afforded the tetraol **21**.

The carbon framework was completed by a highly selective TPAP oxidation that first oxidized the primary alcohol of **21**, facilitated intermediate lactol formation, and

 © 2003 Wiley-VCH Verlag GmbH & Co. KGaA, Weinheim 




***Scheme 5.*** Completion of the tricyclic framework. Reagents and conditions: a) $LiBH_4$, THF, reflux, 92%; b) 1. $Ac_2O$, DMAP, 2,6-lutidine, $CH_2Cl_2$, RT, 95%, 2. MOMCl, DIPEA, DMAP, $CH_2Cl_2$, RT, 92%; c) 20 mol% $K_2OsO_2(OH)_4$, quinuclidine, $K_2CO_3$, $MeSO_2NH_2$, $K_3Fe(CN)_6$, *t*BuOH, $H_2O$, RT, d.r. > 95:5; d) $K_2CO_3$, MeOH, RT, 85% over two steps; e) 10 mol% TPAP, 40 equivalents NMO, 4 Å MS, MeCN, RT, 73%.




***Scheme 6.*** Synthesis of ketone **28**. Reagents and conditions: a) Amberlyst-15, acetone, RT, 85%; b) 1. TBAF, THF, RT, 98%, 2. TPAP cat., NMO, 4 Å MS, $CH_2Cl_2$, RT, 93%; c) TMSCl, $Et_3N$, DMF, 120°C, 88%; d) dimethyldioxirane, acetone, $CH_2Cl_2$, 0°C, 99%, d.r. > 95:5; e) TMSCl, $Et_3N$, DMF, 150°C, 90%; f) 10 mol% PhSeBr, $CH_2Cl_2$, 0°C to RT, 94%.

effected a second oxidation to lactone **22** in a single transformation. The 26-step sequence to the core **22** has been carried out on multigram scale (to make > 10 g of **22**) with a minimum of chromatography. It is intended that this intermediate will also serve as a precursor for a number of designed analogues.

Removal of the MOM groups in **22** with simultaneous acetonide formation gave **23** (Scheme 6). Of particular note here is the observation that the acetonide protecting group imparted remarkable chemical stability and crystallinity to all tetracyclic products in the sequence thereafter. Consequently, unmasking of the C3 hydroxy group and TPAP oxidation furnished crystalline ketone **24**, which provided proof for the correct configuration of all stereocenters.

Generation of the C4,C5 α,β-unsaturation from **24** either by a direct (IBX) or indirect (via enol ether) approach was unsuccessful due to an inherent preference for enolization to the less substituted (C2) side. However, a previous model study carried out within our laboratory[18] had shown that enolization in the desired sense could be achieved after installation of the C2 hydroxy group.

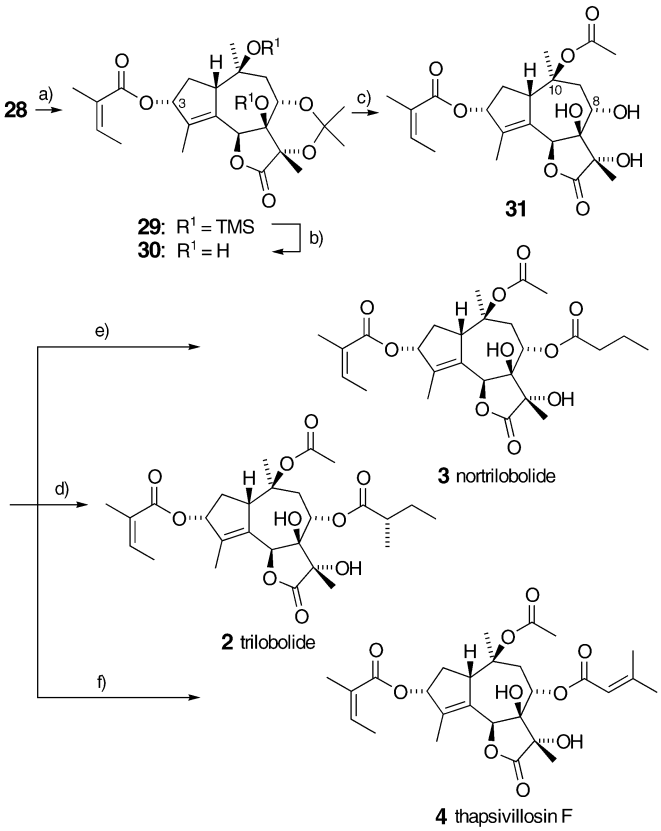
Accordingly, ketone **24** was transformed into silyl enol ether **25** which was oxidized with dimethyldioxirane to afford α-silyloxy ketone **26**. X-ray crystal structure analysis of **26** confirmed that oxygen incorporation occurred exclusively from the convex face. Submitting ketone **26** to TMSCl/$Et_3N$ at 150°C afforded the tetrasubsitituted silyl enol ether **27** in excellent yield.

A range of standard conditions was then tested for the oxidation of enol ether **27** to its corresponding α,β-unsaturated ketone. This screening process led to the discovery of an unprecedented catalytic selenium reaction that provides a direct route to the trilobolide series of the thapsigargins. Treatment of **27** with a catalytic quantity of phenylselenyl bromide gave enone **28** as the sole product, in which the C2 silyloxy group has been lost. The exact mechanism of this formal elimination reaction is still subject to investigation and will be reported later.

Ketone **28** was then stereoselectively reduced with sodium borohydride (d.r. = 4:1) to give alcohol **29** (Scheme 7). To distinguish the five hydroxyl groups in the molecule, the endgame strategy had been designed to minimize protecting group manipulation and take advantage of the inherent order of reactivity of the alcohols in a concise fashion. Accordingly, the C3 hydroxy group was first esterified with angelic acid under Yamaguchi conditions[19] to provide **29** before unmasking the tertiary alcohols with TBAF to yield **30**. Selective acylation of the C10 hydroxy group was then achieved with isopropenyl acetate mediated by polymer-supported tosic acid. Removal of the acetonide led to triol **31**. Finally, esterification with (*S*)-2-methylbutyric anhydride occurred exclusively at the secondary alcohol of C8 to provide trilobolide (**2**). Reaction of **31** with butyric anhydride and senecioic anhydride also furnished nortrilobolide (**3**) and thapsivillosin F (**4**), respectively. All spectral and analytical characteristics of synthetic **2**–**4** are in full accordance with the data obtained from the samples from natural sources.

In summary, the total synthesis of three thapsigargins has been achieved. Stereocontrol during this synthesis relies entirely upon efficient substrate control with all seven stereocentres of the natural product core set from the initial stereochemistry in (+)-carvone. The synthesis is robust (average yield of 90.3% per step), amenable to scale up,

 © 2003 Wiley-VCH Verlag GmbH & Co. KGaA, Weinheim 




***Scheme 7.*** Completion of the synthesis of trilobolide, nortrilobolide, and thapsivillosin F. Reagents and conditions: a) 1. $NaBH_4$, MeOH, 0°C, 86%, d.r. = 4:1, 2. angelic acid, $Et_3N$, 2,4,6-trichlorobenzoyl chloride, toluene, 80°C, 76%; b) TBAF, THF, RT, quant; c) 1. isopropenyl acetate, PS-TsOH, $CH_2Cl_2$, RT, 68%, 2. HCl (aq), MeOH, 40°C; d) (*S*)-2-methylbutyric anhydride, DMAP, $CH_2Cl_2$, RT, 78% over two steps; e) butyric anhydride, DMAP, $CH_2Cl_2$, RT, 72% over two steps; f) senecioic anhydride, DMAP, $CH_2Cl_2$, RT, 73% over two steps. TBAF = tetrabutylammonium fluoride.

and its divergent nature will allow the syntheses of other thapsigargins as well as a number of analogues. After biological assessment of these compounds, further insight into the remarkable biological properties of this substance class should be possible.

Received: October 22, 2003 [Z53140]

**Keywords:** asymmetric synthesis · natural products · terpenoids · total synthesis

[1] S. B. Christensen, A. Andersen, U. W. Smitt, *Fortschr. Chem. Org. Naturst.* **1997**, *71*, 129, and references therein.
[2] S. A. Patkar, U. Rasmussen, B. Diamant, *Agents Actions* **1979**, *9*, 53.
[3] a) J. Lytton, M. Westlin, M. Hanley, *J. Biol. Chem.* **1991**, *266*, 17067–17071; b) C. Caspersen, M. Treiman, *FEBS Lett.* **1995**, *377*, 31–36.
[4] Y. Sagara, J. B. Wade, G. Inesi, *J. Biol. Chem.* **1992**, *267*, 1286–1292.
[5] M. Wictome , Y. M. Khan, J. M. East, A. G. Lee, *Biochem. J.* **1995**, *310*, 859–868.
[6] M, Treiman, C. Caspersen, S. B. Christensen, *Trends Pharmacol. Sci.* **1998**, 19, 131–135, and references therein.
[7] Y. Furuya, P. Lundmo, A. D. Short, D. L. Gill, J. T. Isaacs, *Cancer Res.* **1994**, *54*, 6167–6175.
[8] S. R. Denmeade, C. M. Jakobsen, S. Janssen, S. R. Khan, E. S. Garrett, H. Lilja, S. B. Christensen, J. T. Isaacs, *J. Natl. Cancer Inst.* **2003**, *95*, 990–1000.
[9] E. Lee, J. W. Lim, C. H. Yoon, Y. Sung, Y. K. Kim, *J. Am. Chem. Soc.* **1997**, *119*, 8391–8392.
[10] K. C. Nicolaou, J. Y. Xu, S. Kim, J. Pfefferkorn, T. Ohshima, D. Vourloumis, S. Hosokawa, *J. Am. Chem. Soc.* **1998**, *120*, 8661–8673.
[11] J. S. Bajwa, R. C. Anderson, *Tetrahedron Lett.* **1991**, *32*, 3021–3024.
[12] The configuration of C10 and all subsequently formed stereocenters was unambiguously proven by X-ray analysis of **24** and **26** (vide infra).
[13] S. V. Ley, J. Norman, W. P. Griffith, S. P. Marsden, *Synthesis* **1994**, *7*, 639–666.
[14] M. Scholl, S. Ding, C. W. Lee, R. H. Grubbs, *Org. Lett.* **1999**, *1*, 953–956.
[15] Slow addition of catalyst was required to obtain high yield at low catalyst loading. For examples of enol ether metathesis reactions with Grubbs' Ru catalysts see: J. D. Rainier, J. M. Cox, S. P. Allwein, *Tetrahedron Lett.* **2001**, *42*, 179–181; A. Okada, T. Ohshima, M. Shibasaki, *Tetrahedron Lett.* **2001**, *42*, 8023–8027; V. K. Aggarwal, A. M. Daly, *Chem. Commun.* **2002**, *21*, 2490–2491.
[16] Force field calculations suggest that the OTES group blocks the convex face. Using AD mix α, **16** could be obtained as a single diastereomer (matched case).
[17] An inconsequential side product resulting from protecting group migration under the reaction conditions was also observed. As its deprotection also gave tetraol **21**, the separation from **20** was not necessary.
[18] E. P. Balskus, University of Cambridge, unpublished results.
[19] B. Hartmann, A. M. Kanazawa, J. P. Depres, A. E. Greene, *Tetrahedron Lett.* **1991**, *32*, 5077–5080.

 © 2003 Wiley-VCH Verlag GmbH & Co. KGaA, Weinheim 

*Supported Catalysts*

# Chiral, Porous, Hybrid Solids for Highly Enantioselective Heterogeneous Asymmetric Hydrogenation of β-Keto Esters**

*Aiguo Hu, Helen L. Ngo, and Wenbin Lin**

The chemistry of hybrid solids constructed from organic linkers and metal nodes has received much recent attention, owing to the propensity of incorporating and fine-tuning

[*] Prof. W. Lin, Dr. A. Hu, H. L. Ngo
Department of Chemistry, CB 3290
University of North Carolina
Chapel Hill, NC 27599 (USA)
Fax: (+1) 919-962-2388
E-mail: wlin@unc.edu

[**] We acknowledge financial support from NSF (CHE-0208930). W.L. is an Alfred P. Sloan Fellow, an Arnold and Mabel Beckman Young Investigator, a Cottrell Scholar of Research Corp, and a Camille Dreyfus Teacher-Scholar.

Supporting information for this article is available on the WWW under http://www.angewandte.org or from the author.

 © 2003 Wiley-VCH Verlag GmbH & Co. KGaA, Weinheim DOI: 10.1002/anie.200351264 

desired properties by judicious choice of the building blocks.[1] The use of biphenyl-derived bridging ligands has, for example, led to novel microporous pillared zirconium phosphonates[2] as well as ordered mesoporous organosilica hybrid solids.[3] We believe that the incorporation of axially chiral rigid organic linkers into such hybrid materials can lead to porous solids exploitable for heterogeneous asymmetric catalysis and chiral separations.[4] We have recently synthesized single-crystalline, chiral porous lanthanide bisphosphonates for potential chiral separations.[4a,b] Herein we report novel chiral porous zirconium phosphonates for the highly enantioselective asymmetric hydrogenation of β-keto esters.

Catalytic asymmetric hydrogenation is one of the most efficient strategies for the synthesis of optically active molecules.[5] The ruthenium and rhodium complexes of 2,2′-bis(diphenylphosphanyl)-1,1′-binaphthyl (binap) are particularly useful for the reduction of a wide range of substrates including keto esters, alkenes, and ketones with high enantioselectivity.[5a,6] Both high costs of Ru–binap and Rh–binap precatalysts and the necessity to remove trace amounts of metals from the organic products have, however, hindered their applications in many industrial processes. Heterogenization of these homogeneous asymmetric catalysts presents an interesting solution to both recycling and reusing expensive catalysts and preventing the leaching of metals. To date, several approaches have been used to heterogenize homogeneous asymmetric catalysts including attachment to porous inorganic-oxide and insoluble organic-polymer supports, incorporation into soluble organic macromolecules and membranes, and immobilization through biphasic systems.[7] We envision that metal phosphonates containing pendant chiral chelating bisphosphanes can be designed using rigid bisphosphonic acid ligands, 2,2′-bis-(diphenylphosphanyl)-1,1′-binaphthyl-6,6′-bis(phosphonic acid), $\mathbf{L_1}$-$\mathbf{H_4}$, and 2,2′-bis(diphenylphosphanyl)-1,1′-binaphthyl-4,4′-bis(phosphonic acid), $\mathbf{L_2}$-$\mathbf{H_4}$. Such hybrid materials will combine the robust framework structure of metal phosphonates[8] and enantioselectivity of metal complexes of the pendant chiral bisphosphanes,[5] and may find applications in heterogeneous asymmetric catalysis.

Enantiopure $\mathbf{L_1}$-$H_4$ was synthesized in three steps starting from previously reported 2,2′-dihydroxy-1,1′-binaphthyl-6,6′-bis(diethylphosphonate)[4b] in 47% overall yield (Figure 1). The key step involves nickel-catalyzed phosphonation of 2,2′-bis(triflato)-1,1′-binaphthyl bis(diethylphosphonate). All the intermediates and $\mathbf{L_1}$-$H_4$ were characterized by $^1H$, $^{13}C\{^1H\}$, and $^{31}P\{^1H\}$ NMR spectroscopy and mass spectrometry. $\mathbf{L_2}$-$H_4$ was synthesized according to a literature procedure.[9]

$[Ru(\mathbf{L_1}\text{-}H_4)(dmf)_2Cl_2]$ and $[Ru(\mathbf{L_2}\text{-}H_4)(dmf)_2Cl_2]$ intermediates were synthesized by treating $\mathbf{L_1}$-$H_4$ and $\mathbf{L_2}$-$H_4$ with 0.46 equivalents of $[\{Ru(benzene)Cl_2\}_2]$ in DMF at 100 °C.[10] Chiral porous zirconium phosphonates with approximate formulae $[Zr\{Ru(\mathbf{L_1})(dmf)_2Cl_2\}]\cdot 2\,MeOH$ (Zr-Ru-$\mathbf{L_1}$) and $[Zr\{Ru(\mathbf{L_2})(dmf)_2Cl_2\}]\cdot 2\,MeOH$ (Zr-Ru-$\mathbf{L_2}$) were synthesized

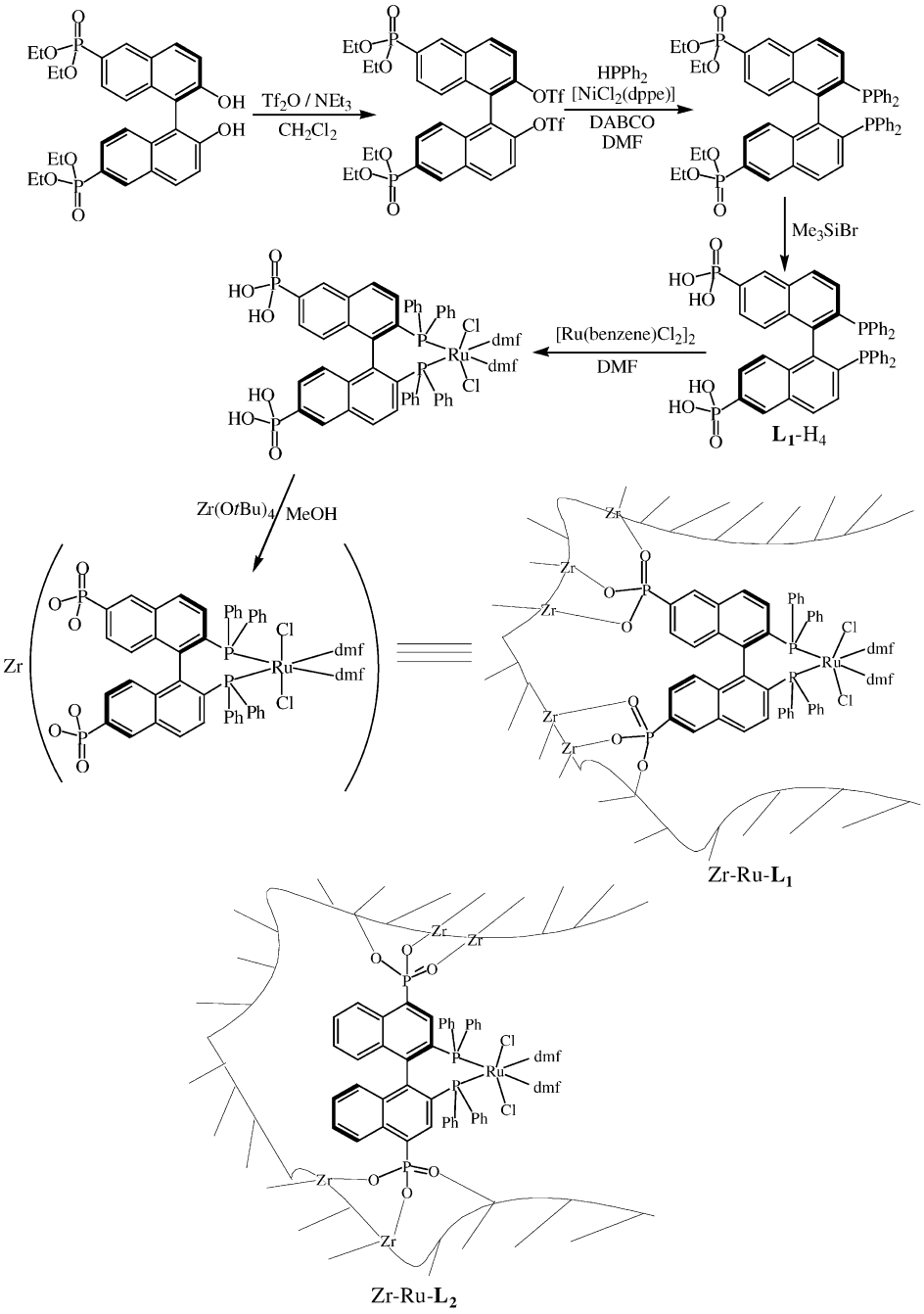



***Figure 1.*** Preparation of $\mathbf{L_1}$-$H_4$, Zr-Ru-$\mathbf{L_1}$, and Zr-Ru-$\mathbf{L_2}$. dppe = 1,2-bis(diphenylphosphanyl)ethene, DABCO = 1,4-diazabicyclo[2.2.2]octane, Tf = Trifluoromethanesulfonyl.

 © 2003 Wiley-VCH Verlag GmbH & Co. KGaA, Weinheim 

by refluxing $Zr(OtBu)_4$ and 1 equivalent of $[Ru(\mathbf{L_1}\text{-}H_4)(dmf)_2Cl_2]$ and $[Ru(\mathbf{L_2}\text{-}H_4)(dmf)_2Cl_2]$ in methanol. These chiral porous zirconium phosphonates have been characterized with a variety of techniques including thermogravimetric analysis (TGA), nitrogen adsorption isotherms, X-ray diffraction (XRD), SEM, IR spectroscopy, and microanalysis.

While the compositions of Zr-Ru-$\mathbf{L_1}$ and Zr-Ru-$\mathbf{L_2}$ were established by TGA and microanalysis results, the IR spectra supported the formation of zirconium phosphonate bonds as the P–O stretches at 950–1150 $cm^{-1}$ are at lower wave numbers than those of $[Ru(\mathbf{L_1}\text{-}H_4)(dmf)_2Cl_2]$ and $[Ru(\mathbf{L_2}\text{-}H_4)(dmf)_2Cl_2]$. The IR spectra also exhibit intense and broad O–H stretching vibrations at around 3400 $cm^{-1}$, consistent with the presence of MeOH solvates.[11] Nitrogen-adsorption measurements indicate that both Zr-Ru-$\mathbf{L_1}$ and Zr-Ru-$\mathbf{L_2}$ are highly porous with rather wide pore size distributions (Figure 2). Zr-Ru-$\mathbf{L_1}$ exhibits a total BET surface area of

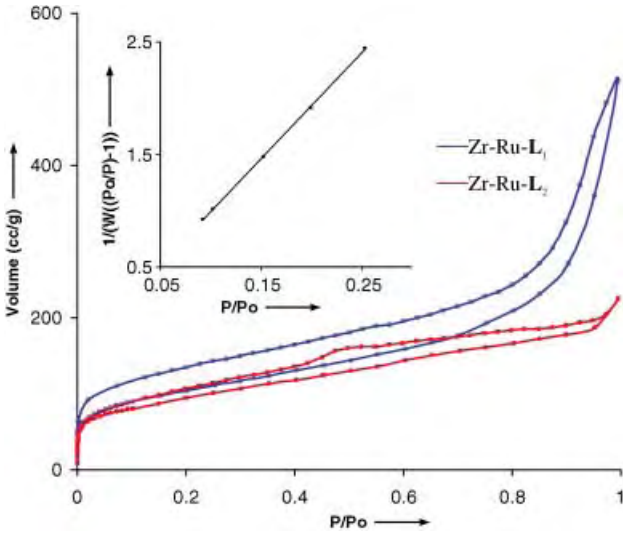



***Figure 2.*** $N_2$ adsorption isotherms for Zr-Ru-$\mathbf{L_1}$ and Zr-Ru-$\mathbf{L_2}$ at 77 K. The inset shows BET plot for Zr-Ru-$\mathbf{L_1}$ in the mesoporous region.

475 $m^2g^{-1}$ with a microporous surface area of 161 $m^2g^{-1}$ and a pore volume of 1.02 $cm^3g^{-1}$ (by BJH method). Zr-Ru-$\mathbf{L_2}$ exhibits a total BET surface area of 387 $m^2g^{-1}$ with a microporous surface area of 154 $m^2g^{-1}$ and a pore volume of 0.53 $cm^3g^{-1}$ (by BJH method). SEM images show that both solids are composed of sub-micrometer particles (Figure 3), while powder X-ray diffraction (PXRD) indicate that both solids are amorphous.

Although the amorphous nature of the present chiral porous zirconium phosphonates has prevented us from elucidating their exact structures, we have successfully utilized the binap-Ru moieties on the surfaces for heterogeneous asymmetric catalysis. As Table 1 shows, both Zr-Ru-$\mathbf{L_1}$ and Zr-Ru-$\mathbf{L_2}$ are highly active catalysts for asymmetric hydrogenation of β-keto esters. Zr-Ru-$\mathbf{L_1}$ catalyzes the hydrogenation of a wide range of β-alkyl-substituted β-keto esters with complete conversions and *ee* values ranging from 91.7 to 95.0% with the same enantio-enrichment as the parent

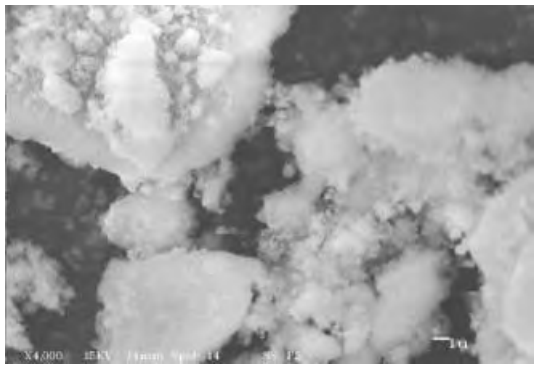
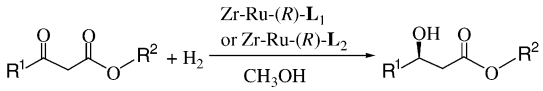


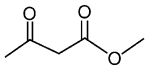
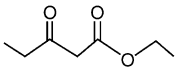
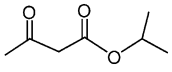
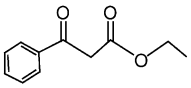
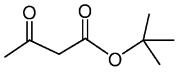
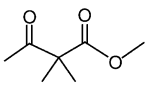
***Figure 3.*** SEM image of the Zr-Ru-$\mathbf{L_1}$ solid precatalyst. The scale bar indicates 1 μm.

homogeneous binap-Ru catalyst. This level of enantioselectivity is only slightly lower than that of their best homogeneous counterparts.[5,6,12] Zr-Ru-$\mathbf{L_1}$ gave a turnover frequency (TOF) of 364 $h^{-1}$ with a 0.1% solid loading, in comparison with a TOF of 810 $h^{-1}$ for the homogeneous binap-Ru catalyst under identical conditions.[13] Similar to the binap-Ru catalyst,[6a] Zr-Ru-$\mathbf{L_1}$ catalyzes the hydrogenation of β-aryl-substituted β-keto esters with modest *ee* value.[14]

In contrast, Zr-Ru-$\mathbf{L_2}$ catalyzes the hydrogenation of β-keto esters with only modest *ee* values. Supernatants of Zr-Ru-$\mathbf{L_1}$ and Zr-Ru-$\mathbf{L_2}$ in MeOH did not catalyze the hydrogenation of β-keto esters, which unambiguously demonstrates

***Table 1:*** Heterogeneous asymmetric hydrogenation of β-keto esters.[a]




| Substrate | Catalyst loading [%] | *T* | $H_2$ pressure [psi][b] | Zr-Ru-$\mathbf{L_1}$ *ee* (yield [%]) | Zr-Ru-$\mathbf{L_2}$ *ee* (yield [%]) |
|---|---|---|---|---|---|
|  | 1 | 60 °C | 700 | 94.0 (100) | |
| | 1 | RT | 1400 | 95.0 (100) | 73.1 (90) |
| | 0.1 | 60 °C | 700 | 93.3 (100) | |
|  | 1 | RT | 1400 | 92.0 (100) | 65.0 (90) |
|  | 1 | RT | 1400 | 91.7 (100) | 68.1 (85) |
|  | 1 | RT | 1400 | 69.6 (100) | 15.7 (50) |
|  | 1 | RT | 1400 | 93.1 (100) | 64.0 (100) |
|  | 1 | RT | 1400 | 93.3 (100) | 78.8 (70) |

[a] All the reactions were carried out in 20 h, and the *ee* values (%) were determined by GC on a Supelco γ-Dex 225 column. The absolute configurations of the products are identical to those obtained by the Ru-(*R*)-binap catalyst. The conversions were determined by the integrations of $^1H$ NMR spectra. [b] 1 psi = 6.89476 kPa.

 © 2003 Wiley-VCH Verlag GmbH & Co. KGaA, Weinheim 

heterogeneous nature of the present asymmetric catalytic systems. We have further confirmed the heterogeneous nature of the present systems using direct current plasma (DCP) spectroscopy. DCP results indicated that less than 0.01% of the ruthenium has leached into the organic solution for each round of hydrogenation.

We have also successfully reused the Zr-Ru-$\mathbf{L_1}$ system for asymmetric hydrogenation of methyl acetoacetate without significant deterioration of enantioselectivity. The Zr-Ru-$\mathbf{L_1}$ system was used for five cycles of hydrogenation with complete conversions and *ee* values of 93.5, 94.2, 94.0, 92.4, and 88.5%, respectively.

In summary, we have synthesized novel chiral porous zirconium phosphonates. These ruthenium-containing chiral porous solids have been used for heterogeneous asymmetric hydrogenation of β-keto esters with *ee* values of up to 95% and can be readily recycled and reused. Ready tunability of such a molecular building-block approach will allow the optimization of the catalytic performance of these hybrid materials and lead to practically useful heterogeneous asymmetric catalysts.

## Experimental Section

Zr-Ru-$\mathbf{L_1}$: $\mathbf{L_1}$-$H_4$ was synthesized in three steps from 2,2′-dihydroxy-1,1′-binaphthyl-6,6′-bis(diethylphosphonate) and treated with [{Ru(benzene)$Cl_2$}$_2$] (0.46 equivalents) in DMF at 100°C under argon for 40 min and then cooled to 40°C. All the volatile components were removed under vacuum, and the dark-red solid was directly used for the synthesis of Zr-Ru-$\mathbf{L_1}$ solid precatalyst. This solid was first dissolved in anhydrous degassed methanol, and heated overnight under reflux with Zr(O*t*Bu)$_4$ (1 equivalent). After centrifugation and rinsing with anhydrous methanol three times, the residue was dried under vacuum to give a dark-brown solid in 96% yield. This dark-brown solid is not soluble in common organic solvents including methanol. Elemental analysis (%) calcd for $C_{52}H_{52}Cl_2N_2O_{10}P_4RuZr$, [Zr{Ru($\mathbf{L_1}$)(dmf)$_2$Cl$_2$}]·2 MeOH: C 49.9, H 4.19, N 2.24, Cl 5.66, P 9.90, Ru 8.07, Zr 7.29; found: C 50.6, H 3.87, N 2.54, Cl 4.98, P 9.32, Ru 7.87, Zr 7.70.

*General procedure for catalysis:* Methyl acetoacetate (55 μL, 0.5 mmol) and anhydrous methanol (1 mL) were added to solid precatalyst (6.0 mg, 5 μmole) in a test tube under argon. The test tube was quickly transferred into a stainless steel autoclave, and sealed. After purging with $H_2$ six times, the final $H_2$ pressure was adjusted to 1400 psi or 700 psi (9652.664 and 4826.332 kPa). $H_2$ pressure was released 20 h later, and methanol was removed in vacuo. The hydrogenated product was extracted with diethyl ether and passed through a mini silica-gel column. The conversions were assessed based on the integration of peaks in the $^1$H NMR spectra of the products and starting materials, while the *ee* values were determined using chiral GC.

Received: February 24, 2003
Revised: June 10, 2003 [Z51264]

**Keywords:** asymmetric catalysis · hybrid materials · hydrogenation · ruthenium · supported catalysts · zirconium

[1] a) J.-M. Lehn, *Supramolecular Chemistry: Concepts and Perspectives*, VCH, New York, **1995**; b) O. R. Evans, W. Lin, *Acc. Chem. Res.* **2002**, *35*, 511; c) M. Eddaoudi, D. B. Moler, H. Li, B. Chen, T. M. Reineke, M. O'Keeffe, O. M. Yaghi, *Acc. Chem. Res.* **2001**, *34*, 319; d) M. J. Zaworotko, B. Moulton, *Chem. Rev.* **2001**, *101*, 1629; e) P. J. Hagrman, D. Hagrman, J. Zubieta, *Angew. Chem.* **1999**, *111*, 2798; *Angew. Chem. Int. Ed.* **1999**, *38*, 2638; f) C. Janiak, *Angew. Chem.* **1997**, *109*, 1499; *Angew. Chem. Int. Ed.* **1997**, *36*, 1431.

[2] a) A. Clearfield, Z. Wang, *J. Chem. Soc. Dalton Trans.* **2002**, 2937; b) G. Alberti, *Comprehensive Supramolecular Chemistry*, *Vol. 7*, Pergamon, New York, **1996**.

[3] a) M. P. Kapoor, Q. Yang, S. Inagaki, *J. Am. Chem. Soc.* **2002**, *124*, 15176; b) S. Inagaki, S. Guan, T. Ohsuna, O. Terasaki, *Nature* **2002**, *416*, 304–307.

[4] a) O. R. Evans, H. L. Ngo, W. Lin, *J. Am. Chem. Soc.* **2001**, *123*, 10395; b) H. L. Ngo, W. Lin, *J. Am. Chem. Soc.* **2002**, *124*, 14298; c) Y. Cui, O. R. Evans, H. L. Ngo, P. S. White, W. Lin, *Angew. Chem.* **2002**, *114*, 1207; *Angew. Chem. Int. Ed.* **2002**, *41*, 1159; d) J. S. Seo, D. Whang, H. Lee, S. I. Jun, J. Oh, Y. J. Jeon, K. Kim, *Nature* **2000**, *404*, 982.

[5] a) R. Noyori, *Angew. Chem.* **2002**, *114*, 2108; *Angew. Chem. Int. Ed.* **2002**, *41*, 2008, and references therein; b) W. S. Knowles, *Adv. Synth. Catal.* **2003**, *345*, 3–13; c) Y.-G. Zhou, W. Tang, W.-B. Wang, W. Li, X. Zhang, *J. Am. Chem. Soc.* **2002**, *124*, 4952.

[6] a) R. Noyori, H. Takaya, *Acc. Chem. Res.* **1990**, *23*, 345; b) M. Kitamura, T. Ohkuma, S. Inoue, N. Sayo, H. Kumobayashi, S. Akutagawa, T. Ohta, H. Takaya, R. Noyori, *J. Am. Chem. Soc.* **1988**, *110*, 629; c) Z. Zhang, H. Qian, J. Longmire, X. Zhang, *J. Org. Chem.* **2000**, *65*, 6223.

[7] Q. H. Fan, Y.-M. Li, A. S. C. Chan, *Chem. Rev.* **2002**, *102*, 3385, and references therein.

[8] a) A. Clearfield, *Prog. Inorg. Chem.* **1998**, *47*, 371; b) G. Alberti, U. Costantino, F. Marmottini, R. Vivani, P. Zappelli, *Angew. Chem.* **1993**, *105*, 1396; *Angew. Chem. Int. Ed. Engl.* **1993**, *32*, 1357; c) T. E. Mallouk, J. A. Gavin, *Acc. Chem. Res.* **1998**, *31*, 209.

[9] M. Kant, S. Bischoff, R. Siefken, E. Gruendemann, A. Koeckritz, *Eur. J. Org. Chem.* **2001**, 477.

[10] A slight excess of ligand is used to ensure that no ligand-free Ru centers are present in the solid catalyst.

[11] There may also be residual protons on the bisphosphonic acids that contribute to the O–H stretching vibrations.

[12] Both [Ru($\mathbf{L_1}$-$H_4$)(dmf)$_2$Cl$_2$] and [Ru($\mathbf{L_2}$-$H_4$)(dmf)$_2$Cl$_2$] gave 98.3% *ee* for homogeneous hydrogenation of methyl acetoacetate in MeOH.

[13] This level of TOF value is comparable to those reported in the literature for the Ru-bisphosphane catalysts. See: H.-U. Blaser, C. Malan, B. Pugin, F. Spindler, H. Steiner, M. Studer, *Adv. Synth. Catal.* **2003**, *345*, 103.

[14] The homogeneous Ru-binap catalyst gave an *ee* value of 80.3% for hydrogenation of ethyl benzoylacetate.

 © 2003 Wiley-VCH Verlag GmbH & Co. KGaA, Weinheim 

Molecular Wheels

# Hepta- and Octacoordinate Boron in Molecular Wheels of Eight- and Nine-Atom Boron Clusters: Observation and Confirmation**

*Hua-Jin Zhai, Anastassia N. Alexandrova, K. Alexander Birch, Alexander I. Boldyrev, and Lai-Sheng Wang**

Clusters of atoms can adopt different atomic arrangements from bulk materials. They often exhibit novel structures and properties, which provide opportunities for new types of chemical bonding and stoichiometry. Herein we report experimental and theoretical evidence that 8- and 9-atom boron clusters are perfectly planar molecular wheels, with a hepta- or octacoordinated central boron atom, respectively, despite the predominance of three-dimensional structures normally found in bulk boron and its compounds.[1–3] Hepta- and octacoordinated planar boron compounds are highly unusual. The radii of the miniature molecular wheels are found to be 1.8 and 2.0 Å for the 8- and 9-atom clusters, respectively. Analyses of their chemical bonding reveal that they possess double (σ and π) aromaticity, which is responsible for the novel molecular structures and the extreme coordination environments.

We produced the $B_8^-$ and $B_9^-$ clusters with a laser vaporization cluster source and probed their electronic structure with photoelectron spectroscopy (PES), analogous to our previous study on the smaller $B_5^-$ and $B_6^-$ clusters.[4,5] Figure 1 shows the PES spectra of $B_8^-$ at three photon energies and those of $B_9^-$ at two photon energies. The 193 nm spectrum of $B_8^-$ revealed four distinct features labeled X, A, B, C (Figure 1b). A fifth band (D) can be tentatively identified, but the signal-to-noise ratios are poor at the high-binding-energy side. At 266 nm (Figure 1a), fine vibrational features were observed for the X band, which were resolved more clearly in the 355 nm spectrum. Two vibrational modes were observed with frequencies of $510 \pm 50$ and $1160 \pm 60\ cm^{-1}$. A sharp peak (B′), which appeared as a shoulder in the 193 nm spectrum, was also resolved in the 266 nm spectrum of $B_8^-$ (Figure 1a). All the vertical detachment energies (VDEs) are given in Table 1 and compared with theoretical calculations (see below). The sharp peak of the X band in the spectrum of $B_8^-$ defines the electron affinity (EA) of neutral $B_8$ to be $3.02 \pm 0.02$ eV.

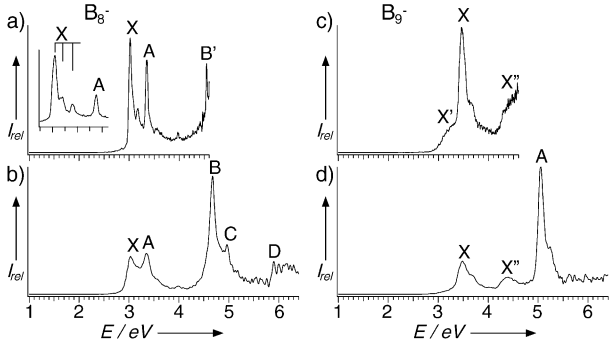



***Figure 1.*** Photoelectron spectra of a) $B_8^-$ at 266 nm (4.661 eV), the inset shows the spectrum taken at 355 nm (3.496 eV), and b) at 193 nm (6.424 eV). c) The photoelectron spectrum of $B_9^-$ at 266 nm and d) at 193 nm.

***Table 1:*** Experimental and theoretical vertical detachment energies in eV for $B_8^-$ and $B_9^-$.

| Observed features | VDE (exp.)[a] | Molecular orbital | Final state | VDE (calcd)[b] | VDE (calcd)[c] |
|---|---|---|---|---|---|
| | | $B_8^-$ ($C_{2v}$, $^2B_1$) | | | |
| X | 3.02(2) | HOMO-1 ($1a_2$) | $^3B_2$ | 2.99[d] | |
| A | 3.35(2) | HOMO ($2b_1$) | $^1A_1$ | 3.45[d] | 3.41 |
| | | HOMO-1 ($1a_2$) | $^1B_2$ | | 3.45 |
| B′ | 4.55(4) | HOMO-2 ($6a_1$) | $^3B_1$ | 4.74[d] | |
| B | 4.68(6) | HOMO-3 ($4b_2$) | $^3A_2$ | 4.78[d] | |
| | | HOMO-3 ($4b_2$) | $^1A_2$ | | 4.79 |
| C | 4.98(6) | HOMO-2 ($6a_1$) | $^1B_1$ | | 5.15 |
| | | HOMO-4 ($1b_1$) | $^3A_1$ | 5.86[d] | |
| | | $B_9^-$ ($D_{8h}$, $^1A_{1g}$) | | | |
| X | 3.46(6) | HOMO ($1e_{1g}$) | $^2E_{1g}$ | 3.47[e] (3.38)[e] | |
| A | 5.04(6) | HOMO-1 ($2e_{1u}$) | $^2E_{1u}$ | 5.07[e] (4.84)[e] | |
| | | HOMO-2 ($1a_{2u}$) | $^2A_{2u}$ | (5.78)[e] | |

[a] Numbers in parentheses indicate the uncertainties of the last digit. [b] CCSD(T)/6-311+G(2df), [c] EOM-RCCSD(T)/6-311+G(2d) [d] Calculations were done at the RCCSD(T) level of theory. [e] Data in parenthesis are at the ROVGF/6-311+G(2df) level of theory and at the UCCSD(T) level of theory otherwise.

The spectral features of $B_9^-$ (Figure 1c, d) seemed to be broader and are dominated by three main bands (X, X″, A). The weak signals at the low-binding-energy side (X′, Figure 1c) depended on source conditions and could be due to either hot band or isomer contributions. The X″ band around

[*] Prof. Dr. L.-S. Wang, Dr. H.-J. Zhai
Department of Physics, Washington State University
2710 University Drive, Richland, WA 99352 (USA)
and
W. R. Wiley Environmental Molecular Sciences Laboratory
Pacific Northwest National Laboratory, MS K8-88
P. O. Box 999, Richland, WA 99352 (USA)
Fax: (+1) 509-376-6066
E-mail: ls.wang@pnl.gov
A. N. Alexandrova, K. A. Birch, Prof. Dr. A. I. Boldyrev
Department of Chemistry and Biochemistry
Utah State University, Logan, UT 84322-0300 (USA)

[**] The theoretical work done at Utah State University was supported by the donors of The Petroleum Research Fund (PRF No. 38242-AC6), administered by the American Chemical Society. The experimental work done at Washington was supported by the US National Science Foundation (DMR-0095828) and performed at the W. R. Wiley Environmental Molecular Sciences Laboratory, a national scientific user facility sponsored by DOE's Office of Biological and Environmental Research and located at Pacific Northwest National Laboratory, operated for DOE by Battelle.

Supporting information for this article (alternative structures and calculated molecular properties) is available on the WWW under http://www.angewandte.org or from the author.

 © 2003 Wiley-VCH Verlag GmbH & Co. KGaA, Weinheim DOI: 10.1002/anie.200351874 

4.4 eV is very broad and not well defined even under the higher resolution condition at 266 nm (Figure 1c). The X and A bands are sharper and more intense, each with a short vibrational progression (vibrational spacing $\approx$1300–1400 $cm^{-1}$). From the threshold of the X band, we estimated an EA of $3.39 \pm 0.06$ eV for $B_9$. The VDEs of the X and A bands are listed in Table 1, and compared with theoretical calculations.

Combining PES and computational chemistry is a powerful means to elucidate the electronic structure and chemical bonding of novel clusters.[6–8] We performed an extensive computational search for the global minimum structures for $B_8$, $B_8^-$, $B_8^{2-}$, $B_9$, $B_9^-$ by using a hybrid (density functional and Hartree–Fock) method. We found that all five species have planar wheel structures (Figure 2): $B_8$ and $B_8^{2-}$ are perfect heptagons and $B_9^-$ is a perfect octagon, whereas $B_8^-$ and $B_9$ have slight in-plane distortions within the heptagonal and octagonal structures, respectively. $B_8$, $B_9$, and $B_9^-$ have been calculated previously,[9–13] but there is no consensus among the different studies. Our heptagon triplet structure for $B_8$ agrees with the theoretical predictions by Bonacic-Koutecky et al.[9] and Boustani.[12] Our octagon structure for $B_9^-$ agrees with a date by Wang and Schleyer.[13]

To confirm our computational results and facilitate comparison with the experimental data, we further calculated the low-lying VDEs for $B_8^-$ and $B_9^-$ using sophisticated ab initio methods (Table 1). To interpret the $B_8^-$ spectra, it is convenient to start from the high symmetry $B_8^{2-}$ structure (Figure 2b). The $B_8^{2-}$ ion is closed-shell and has a degenerate highest occupied molecular orbital (HOMO; $1e_1''$, Figure 3a). Upon one-electron detachment, the resulting doublet $B_8^-$ undergoes a slight Jahn–Teller distortion to $C_{2v}$ symmetry (Figure 2c) with the following valence electron configuration: $1a_1^2 2a_1^2 1b_2^2 2b_2^2 3a_1^2 4a_1^2 3b_2^2 5a_1^2 1b_1^2 4b_2^2 6a_1^2 1a_2^2 2b_1^1$. The doubly degenerate $1e_1''$-HOMO is now split into $2b_1$ (HOMO) and $1a_2$ (HOMO-1) in the $C_{2v}$ structure. When a further electron is removed from $B_8^-$, the final state can be either a singlet (detachment from the singly occupied $2b_1$ MO) or a triplet (detachment from the doubly occupied $1a_2$ MO). The lowest energy peak at 3.02 eV in the $B_8^-$ spectra (Figure 1) corresponds to electron detachment from the $1a_2$ orbital resulting in a triplet state (Table 1), which upon geometry optimization relaxes to the perfect heptagon triplet ground state of $B_8$

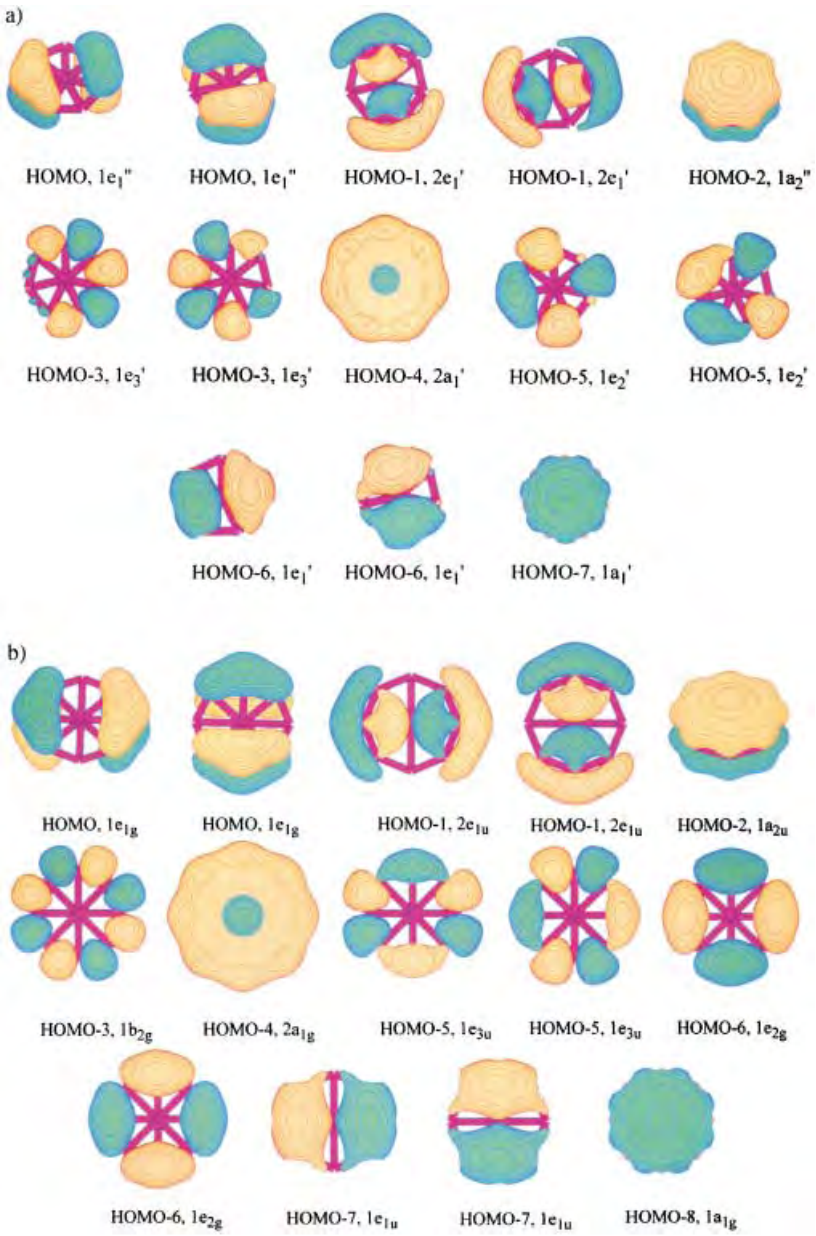



***Figure 3.*** Molecular orbital pictures. a) $D_{7h}$ $B_8^{2-}$, b) $D_{8h}$ $B_9^-$.

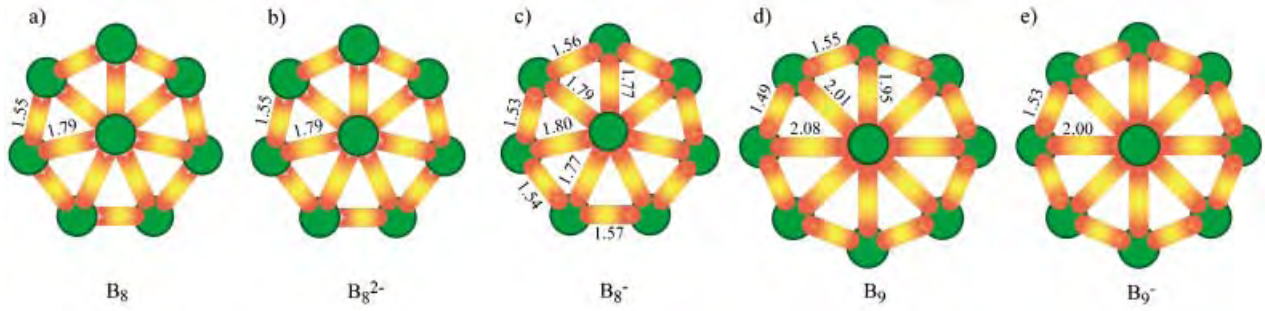



***Figure 2.*** Optimized global minimum structures. a) $D_{7h}$ $B_8$, b) $D_{7h}$ $B_8^{2-}$, c) $C_{2v}$ $B_8^-$, d) $D_{2h}$ $B_9$, e) $D_{8h}$ $B_9^-$. Selected bond lengths given in Å.

 © 2003 Wiley-VCH Verlag GmbH & Co. KGaA, Weinheim 

(Figure 2a). The calculated VDE of 2.99 eV is in excellent agreement with the experimental value of 3.02 eV. According to our calculations two vibrational modes (481 and 1243 $cm^{-1}$) can be responsible for the $C_{2v}$–$D_{7h}$ transformation and these frequencies agree well with the experimentally observed frequencies at $510 \pm 50$ and $1160 \pm 60$ $cm^{-1}$.

The second feature A of the $B_8^-$ spectrum is observed at 3.35 eV (Figure 1a), in excellent agreement with the calculated VDE from the $2b_1$ orbital (Table 1). Our calculated VDE for the singlet final state from detachment from the $1a_2$ orbital is nearly degenerate with that of the $2b_1$ orbital and may also contribute to the A band. The next calculated VDE is at 4.74 eV for the triplet final state from detachment from the $6a_1$ orbital (HOMO-2), which is assigned to the B′ band at 4.55 eV (Table 1). Two other detachment channels, the triplet and singlet final states from the $4b_2$ orbital (HOMO-3), have VDEs very close to each other and are assigned to the intense B band at 4.68 eV. The triplet final state from the $6a_1$ orbital has a calculated VDE of 5.15 eV and is assigned to the C band at 4.98 eV. There are no single-electron detachment channels between 3.4 and 4.7 eV. This calculated spectral pattern is in excellent agreement with the PES spectra of $B_8^-$ (Figure 1a, b). The weak feature around 4 eV in the PES spectra is likely to be due to a two-electron transition. The next calculated VDE is at 5.86 eV from HOMO-4 ($1b_1$). Although the signal-to-noise ratio is poor in the high-binding-energy side of the $B_8^-$ spectrum (Figure 1b), we can tentatively identify a detachment feature (D) around 5.9 eV. The overall agreement between the calculated VDEs and the PES spectra of $B_8^-$ is excellent, confirming unequivocally its heptagonal structure.

The $D_{8h}$ $B_9^-$ has closed shell with a highly degenerate electronic configuration: $1a_{1g}^2 1e_{1u}^4\ 1e_{2g}^4 1e_{3u}^4 2a_{1g}^2 1b_{2g}^2 1a_{2u}^2$-$2e_{1u}^4 1e_{1g}^4$. Detachment from the $1e_{1g}$ HOMO results in a $^2E_{1g}$ state for $B_9$. The calculated VDE for this detachment channel is 3.47 eV, in excellent agreement with the measured VDE of the X band at 3.46 eV (Table 1). However, the $^2E_{1g}$ state is expected to undergo a Jahn–Teller distortion to the $D_{2h}$ ground state of $B_9$ ($^2B_{1g}$). Our calculated adiabatic detachment energy (ADE) or the EA of $B_9$ is 3.43 eV, which is very similar to the calculated VDE and agrees well with the experimental ADE of $3.39 \pm 0.06$ eV. The similarity between the VDE and ADE suggests that the Jahn–Teller effect in $B_9$ is small, consistent with the minor geometry changes between $B_9^-$ and $B_9$ (Figure 2d, e) and the sharp spectral pattern of the X band. The next detachment channel is from the $2e_{1u}$ orbital (HOMO-1) with a calculated VDE at 5.07 eV. The experimental VDE of the A band is in excellent agreement with this detachment channel. This calculated spectral pattern gives a large energy gap between 3.5 and 5 eV, which suggests that there are no single-electron transitions in this energy range. Thus, the broad X″ band may have two origins: either owing to two-electron transitions or arising from a strong Jahn–Teller splitting of the detachment from the degenerate $2e_{1u}$ HOMO-1. We suspect that both of these mechanisms may contribute to the X″ band, but at this point we are not able to definitely resolve this issue because it is challenging to calculate the Jahn–Teller distortions for the excited states. The next detachment is from the $1a_{2u}$ orbital with a calculated VDE of 5.78 eV at the ROVGF level of theory (Table 1). The ROVGF method may have significantly underestimated the VDE because no intense detachment channels were observed between 5.08 and 6.4 eV in the PES spectrum of $B_9^-$ (Figure 1d).

The overall excellent agreement between the predicted detachment energies and the PES spectra of $B_8^-$ and $B_9^-$ lend considerable credibility to the wheel structures found for $B_8$, $B_8^-$, $B_8^{2-}$, $B_9$, and $B_9^-$. Now the question is why these clusters adopt such unusual and beautiful structures? Insight can be gained from a detailed analysis of their valence MOs, as shown in Figure 3 for the closed shell $B_8^{2-}$ (Figure 3a) and $B_9^-$ (Figure 3b). For each molecule, we can identify two sets of MOs, one set responsible for the peripheral B–B bonding and the other set for bonding between the central atom and the peripheral B atoms. The latter set is the same in both molecules: the $1e_1''$, $2e_1'$, $1a_2''$, and $2a_1'$ for $B_8^{2-}$; $1e_{1g}$, $2e_{1u}$, $1a_{2u}$, and $2a_{1g}$ for $B_9^-$. To confirm this classification of the MOs, we performed a model MO calculation of a cyclic $Be_8$, which would have similar peripheral bonding as that in $B_9^-$. Indeed we found that the eight MOs of the cyclic $Be_8$ are very similar to the eight MOs responsible for the peripheral B–B bonding in $B_9^-$.

Among the six MOs responsible for the central B atom and peripheral B atom bonding, three are π orbitals ($1e_1''$ and $1a_2''$ in $B_8^{2-}$; $1e_{1g}$ and $1a_{2u}$ in $B_9^-$). These π-orbital patterns are very similar to those in the prototypical aromatic molecule, benzene. Thus, the $B_8^{2-}$ and $B_9^-$ molecules can be considered to be aromatic, each with six π electrons conforming to the $(4n+2)$ Hückel rule. The π aromaticity in $SiB_8$, which is valence isoelectronic to $B_9^-$, was discussed by Minyaev et al.[14] However, we believe that the $B_8^{2-}$ and $B_9^-$ molecules are not only π aromatic, but also σ aromatic. The three σ orbitals in each molecule ($2e_1'$ and $2a_1'$ in $B_8^{2-}$; $2e_{1u}$ and $2a_{1g}$ in $B_9^-$), which describe bonding between the central atom and the ring, are also highly delocalized and look very similar to the π MOs, thus conferring σ aromaticity on these clusters. We believe that the double aromatic characters in the chemical bonding of $B_8^{2-}$ and $B_9^-$ are responsible for their planarity and their unique coordination environments. When one electron is detached from $B_8^{2-}$ or $B_9^-$, the π aromaticity is reduced and the Jahn–Teller effect leads to a slightly distorted $B_8^-$ or $B_9$, but they are still strongly bonded systems because the σ bonding framework remains the same. When two electrons are removed from $B_8^{2-}$, the degenerate $1e_1''$ HOMO becomes half-filled, which resulting in the triplet $B_8$ ground state with very little structural change (Figure 2a and b). The triplet ground state ($^3A_g$) of $B_8$ is highly π aromatic according to the alteration of the Hückel rule for triplet states.[15,16]

To further confirm aromaticity in the molecular wheels, we calculated nucleus-independent chemical shifts (NICS)[17] for the two doubly aromatic closed-shell boron clusters: $B_8^{2-}$ and $B_9^-$. In Table 2 we presented the NICS values calculated above the center of the cluster and above the $B_3$ triangular ring in $B_8^{2-}$ and $B_9^-$. The very high NICS values (compared to benzene with NICS = −8.0 ppm at B3LYP6-311++G**) clearly show the presence of σ and π aromaticity in the two clusters.

 © 2003 Wiley-VCH Verlag GmbH & Co. KGaA, Weinheim 

*Table 2:* Calculated NICS in ppm at B3LYP6-311+G* for $B_8^{2-}$ and $B_9^-$.

| R [Å] | NICS above the center of the cluster | NICS above the center of the $B_3$ ring |
|---|---|---|
| | $B_8^{2-}$ | |
| 0.5 | −27.0 | −35.7 |
| 1.0 | −24.8 | −20.8 |
| 1.5 | −14.0 | −11.3 |
| 2.0 | −8.5 | −6.9 |
| 2.5 | −5.5 | −4.5 |
| 3.0 | −3.7 | −3.1 |
| | $B_9^-$ | |
| 0.5 | −23.2 | −33.0 |
| 1.0 | −25.6 | −21.0 |
| 1.5 | −15.3 | −12.1 |
| 2.0 | −9.2 | −7.3 |
| 2.5 | −5.8 | −4.7 |
| 3.0 | −3.8 | −3.1 |

The chemical bonding between the central boron and the ring can be viewed as spokes of the molecular wheels. However, the delocalized nature of MOs describing the center-to-ring bonding suggests that individual spokes cannot be identified, much like a bicycle wheel spinning at a high speed. Hence, instead of spokes, the molecular wheels are strengthened by a "disk". Recently, two aromatic planar pentacoordinate iron cations ($[FeSb_5]^+$ and $[FeBi_5]^+$) have been predicted,[18] which exhibit similar delocalized bonding between the central Fe and the $Sb_5$ or $Bi_5$ ring. This is an unprecedented delocalization pattern, which is different from the familiar cyclic delocalization in benzene. It may be appropriate to call this delocalization in the molecular wheels "disk delocalization".

Tetracoordinate planar carbon was proposed 30 years ago by Hoffmann et al.[19] and has been confirmed experimentally.[20,21] More highly coordinated planar carbon and other main-group atoms have been proposed.[13,14] Our work is the first confirmation of hepta- and octacoordinated boron atoms and demonstrates that σ and π aromaticity are responsible for the highly unusual coordination environments. It should be emphasized that detailed understanding of novel molecular structures using concepts of chemistry will be increasingly important in nanotechnology as device features rapidly approach the atomic and molecular scale.

## Methods

*Photoelectron Spectroscopy*: Details of the experimental apparatus have been published elsewhere.[22,23] Briefly, a compressed disk made with pure $^{10}B$ isotope (98% enriched) was used as the laser vaporization target with helium carrier gas. Clusters from the source underwent a supersonic expansion and collimated with a skimmer. Negatively charged clusters were extracted from the cluster beam and were analyzed by a time-of-flight (TOF) mass spectrometer. The $B_8^-$ and $B_9^-$ cluster ions were mass-selected before photodetachment with one of the three photon energies: 355 nm (3.496 eV), 266 nm (4.661 eV), and 193 nm (6.424 eV). The use of a single isotope target greatly simplified the mass spectra and allowed clean mass selections without any contamination. Photoelectron spectra were measured using a magnetic-bottle TOF photoelectron analyzer with an electron kinetic energy resolution of $\Delta E_k/E_k \approx 2.5\%$. The spectrometer was calibrated with the known spectrum of $Rh^-$.

*Theoretical Calculations*: Theoretical methods used in this work were described in more detail elsewhere.[4,5] The initial search for the global minima of $B_8$, $B_8^-$, $B_9$, and $B_9^-$ and vibrational frequency calculations were performed using analytical gradients with polarized split-valence basis sets (6-311+G*) and the hybrid method, known as B3LYP. Some geometries and vibrational frequencies were further refined with the multiconfigurational method CASSCF with various active spaces. The coupled-cluster method [CCSD(T)] with 6-311+G* basis set was used for additional geometry optimizations, and for refinement of energies with the 6-311+G(2df) and 6-311+G(2d) basis sets. Vertical electron detachment energies were calculated using the restricted and unrestricted coupled-cluster methods R(U)CCSD(T)/6-311+G(2df), at the equation-of-motion method based on RCCSD(T) [EOM-RCCSD(T)] with the same 6-311+G(2df) basis set and at the outer-valence Green Function method (ROVGF). Molecular orbitals were calculated at the U(R)HF/6-311+G* levels of theory. U(R)HF, B3LYP, CASSCF, ROVGF, and CCSD(T) calculations were performed using Gaussian 98.[24] RCCSD(T) and EOM-RCCSD(T) calculations—using MOLPRO 1999 program.[25] Molecular orbital pictures were made using MOLDEN3.4 program.[26] All calculations were performed on a 63-nodes Birch-Retford Beowulf cluster computer built at Utah State by K. A. Birch and B. P. Retford.

Received: May 12, 2003
Revised: July 25, 2003 [Z51874]

**Keywords:** ab initio calculations · aromaticity · boron · cluster compounds · photoelectron spectroscopy

[1] W. L. Lipscomb, *Boron Hydrides*, W. A. Benjamin, New York, **1963**.
[2] *Boron Hydride Chemistry* (Ed.: E. L. Meutterties), Academic Press, New York, **1975**.
[3] F. A. Cotton, G. Wilkinson, C. A. Murillo, M. Bochmann, *Advanced Inorganic Chemistry*, 6th ed., Wiley, New York, **1999**.
[4] H. J. Zhai, L. S. Wang, A. N. Alexandrova, A. I. Boldyrev, *J. Chem. Phys.* **2002**, *117*, 7917.
[5] A. N. Alexandrova, A. I. Boldyrev, H. J. Zhai, L. S. Wang, E. Steiner, P. W. Fowler, *J. Phys. Chem. A* **2003**, *107*, 1359.
[6] X. Li, A. E. Kuznetsov, H. F. Zhang, A. I. Boldyrev, L. S. Wang, *Science* **2001**, *291*, 859.
[7] A. I. Boldyrev, L. S. Wang, *J. Phys. Chem. A* **2001**, *105*, 10759.
[8] J. Li, X. Li, H. J. Zhai, L. S. Wang. *Science* **2003**, *299*, 864.
[9] V. Bonacic-Koutecky, P. Fantucci, J. Koutecky, *Chem. Rev.* **1991**, *91*, 1035.
[10] H. Kato, K. Yamashita, K. Morokuma, *Chem. Phys. Lett.* **1992**, *190*, 361.
[11] A. K. Ray, I. A. Howard, K. M. Kanal, *Phys. Rev. B* **1992**, *45*, 14247.
[12] I. Boustani, *Phys. Rev. B* **1997**, *55*, 16426.
[13] Z. X. Wang, P. von R. Schleyer, *Science* **2001**, *292*, 2465.
[14] R. M. Minyaev, T. N. Gribanova, A. G. Starikov, V. I. Minkin, *Mendeleev Commun.* **2001**, 1–2.
[15] N. C. Baird, *J. Am. Chem. Soc.* **1972**, *94*, 4941.
[16] V. I. Minkin, M. N. Glukhovtsev, B. Y. Simkin, *Aromaticity and Antiaromaticity*, Wiley, New York, **1994**.
[17] P. von R. Schleyer, C. Maerker, A. Dransfeld, H. Jiao, N. J. R. v. E. Hommes, *J. Am. Chem. Soc.* **1996**, *118*, 6317.
[18] M. Lein, J. Frunzke, G. Frenking, *Angew. Chem.* **2003**, *115*, 1341; *Angew. Chem. Int. Ed.* **2003**, *42*, 1303.
[19] R. Hoffmann, R. W. Alder, C. F. Wilcox, Jr., *J. Am. Chem. Soc.* **1970**, *92*, 4992.

 © 2003 Wiley-VCH Verlag GmbH & Co. KGaA, Weinheim 

[20] D. Rottger, G. Erker, *Angew. Chem.* **1997**, *109*, 840; *Angew. Chem. Int. Ed.* **1997**, *36*, 812.
[21] L. S. Wang, A. I. Boldyrev, X. Li, J. Simons, *J. Am. Chem. Soc.* **2000**, *122*, 7681.
[22] L. S. Wang, H. Wu in *Advances in Metal and Semiconductor Clusters. IV. Cluster Materials* (Ed.: M. A. Duncan), JAI, Greenwich, CT, **1998**, pp. 299 – 343.
[23] L. S. Wang, X. Li in *Clusters and Nanostructure Interfaces* (Eds.:P. Jena, S. N. Khanna, B. K. Rao), World Scientific, New Jersey, **2000**, pp. 293 – 300.
[24] Gaussian 98 (Revision A.7), M. J. Frisch, G. W. Trucks, H. B. Schlegel, G. E. Scuseria, M. A. Robb, J. R. Cheeseman, V. G. Zakrzewski, J. A. Montgomery, R. E. Stratmann, J. C. Burant, S. Dapprich, J. M. Millam, A. D. Daniels, K. N. Kudin, M. C. Strain, O. Farkas, J. Tomasi, V. Barone, M. Cossi, R. Cammi, B. Mennucci, C. Pomelli, C. Adamo, S. Clifford, J. Ochterski, G. A. Petersson, P. Y. Ayala, Q. Cui, K. Morokuma, D. K. Malick, A. D. Rabuck, K. Raghavachari, J. B. Foresman, J. Cioslowski, J. V. Ortiz, B. B. Stefanov, G. Liu, A. Liashenko, P. Piskorz, I. Komaromi, R. Gomperts, R. L. Martin, D. J. Fox, T. Keith, M. A. Al-Laham, C. Y. Peng, A. Nanayakkara, C. Gonzalez, M. Challacombe, P. M. W. Gill, B. G. Johnson, W. Chen, M. W. Wong, J. L. Andres, M. Head-Gordon, E. S. Replogle, J. A. Pople, Gaussian, Inc., Pittsburgh, PA, **1998**.
[25] MOLPRO 1999 program is by J. H. Werner, P. J. Knowles with contributions from R. D. Amos, A. Bernhardsson, A. Berning, P. Celani, D. L. Cooper, M. J. O. Deegan, A. J. Dobbyn, F. Eckert, C. Hampel, G. Hetzer, T. Korona, R. Lindh, A. W. Llpyd, S. J. McNicholas, F. R. Manby, W. Meyer, M. E. Mura, A. Nicklass, P. Palmieri, R. Pitzer, G. Rauhut, M. Schutz, H. Stoll, A. J. Stone, R. Tarroni, T. Thorsteinsson.
[26] G. Schaftenaar, MOLDEN3.4, CAOS/CAMM Center, The Netherlands, **1998**.

 © 2003 Wiley-VCH Verlag GmbH & Co. KGaA, Weinheim 

*Asymmetric Oxidative Coupling*

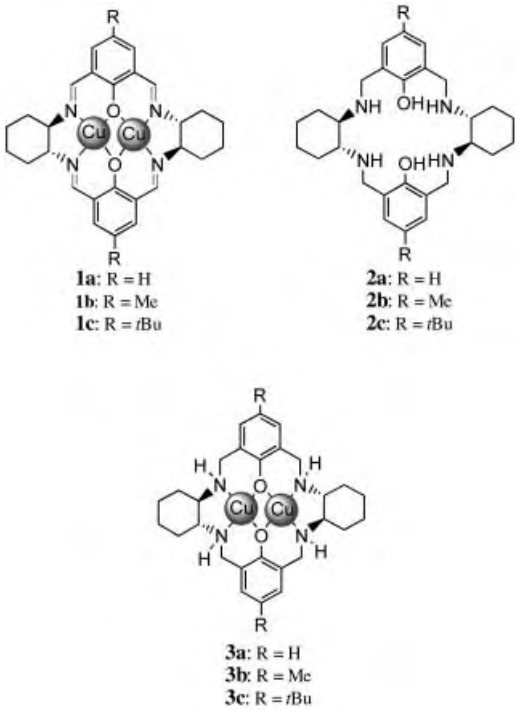
# Structurally Defined Catalysts for Enantioselective Oxidative Coupling Reactions**

*Jian Gao,* Joseph H. Reibenspies, and Arthur E. Martell*[+]

Pure binaphthol enantiomers and their derivatives are important chiral ligands for a wide range of asymmetric syntheses.[1] The facile conversion of binaphthol into 2,2′-(diphenylphosphanyl)-1,1′-binaphthyl (BINAP) is particularly noteworthy because BINAP greatly expanded the synthetic utilities of binaphthol in asymmetric catalysis.[2] In light of the wide-ranging and important applications of these compounds, catalytic asymmetric preparation of chiral binaphthols and improvements in the enantioselectivity of the associated catalysts have continued to attract the attention of many researchers.[3]

Existing catalysts for the asymmetric preparation of chiral binaphthols include copper complexes of chiral amines or their derivatives[4] and chiral $V^{IV}O$ complexes with either one or two stereogenic metal centers.[5] Recently, dimeric copper(II) complexes[4b,e,f] or dinuclear $V^{IV}O$ complexes[5d,e] have been shown to be better catalysts with a high enantioselectivity. In the above reports, the catalytic metal complexes were prepared in situ by reacting a chiral ligand with a desired metal ion ($Cu^{I}$, $Cu^{II}$, or $V^{IV}O$). Generally, this method produces at least three species in solution: metal-free ligand, mononuclear, and dinuclear complexes. However, it is not easy to identify the active species that contribute to the overall reaction rate. Furthermore, the X-ray crystal structures of the above catalysts have never been determined, and this has restricted mechanistic investigations aimed at further improving the catalytic enantioselectivity and robustness. Given the success of Jacobsen's salen catalysts[6] in a broad range of asymmetric catalytic reactions, we decided to investigate whether coupled salen complexes would catalyze reactions that require two catalytic centers. Herein we describe the syntheses and crystal structures of a family of dicopper catalysts for the asymmetric oxidative coupling of 2-naphthol.

The reaction of (1*R*,2*R*)-1,2-diaminocyclohexane (*R*,*R*-DACH) with 2,6-diformylphenol or its derivatives in the presence of $Cu^{II}$ gave yellow-green solids of **1a–c** (Scheme 1),




***Scheme 1.*** Structures of Schiff base dicopper(II) complexes **1a–c**, macrocyclic ligands **2a–c**, and polyamino dicopper(II) complexes **3a–c**.

[*] Dr. J. Gao, Dr. J. H. Reibenspies, Prof. A. E. Martell[+]
Department of Chemistry, Texas A & M University
College Station, Texas 77843-3255 (USA)
Fax: (+1) 979-845-4719
E-mail: gao@mail.chem.tamu.edu

[+] Sadly, Dr. Arthur E. Martell passed away on October 15, 2003. He was a fine chemist, a stimulating advisor, and always full of ideas. It was our privilege to work with him and we shall always be indebted to him for sharing his scientific insight with us. Along with the chemistry community, we mourn his passing.

[**] This research program was supported by a grant from the Welch Foundation A-259. We thank Dr. Li Sun for helping with the revision of the manuscript.

 © 2003 Wiley-VCH Verlag GmbH & Co. KGaA, Weinheim DOI: 10.1002/anie.200351978 

which were recrystallized from DMF/MeOH. X-ray crystal-structure analysis showed that **1b** contains two $Cu^{II}$ centers, each coordinated in a $N_2O_2$-coordination compartment (Figure 1a). Within the macrocycle, the Schiff-base bonds are essentially coplanar with the adjacent phenolic rings, and the $Cu^{II}$ ions reside in this plane. Each $Cu^{II}$ ion adopts a square-pyramidal geometry with a coordinated methanol molecule in the axial direction. The space-filling representation of the dicationic complex (Figure 1b) exhibits $D_2$ symmetry and a substantial orbital overlap of the two Cu centers (Cu1–Cu2 distance, 2.8887 Å).

The preparation of **2a–c** was initially attempted by the Schiff-base condensation of *R*,*R*-DACH with the corresponding dialdehyde at room temperature, but this led to an oligomer. After adopting a metal-template approach, followed by hydrogenation, **2a–c** were successfully prepared in high yields (65–85%). ESI MS spectrum of **2b** (Figure 2) (*m*/*z*, [**2b**+$H^+$] 493.3476; [**2b**+2$H^+$] 247.1748) shows the correct molecular weight, and $^1$H NMR and $^{13}$C NMR spectra are entirely consistent with the proposed structure. Dicopper(II) complexes **3a–c** were readily prepared by reacting the corresponding macrocyclic ligands with 2 equivalents of $Cu^{II}$ in MeOH.

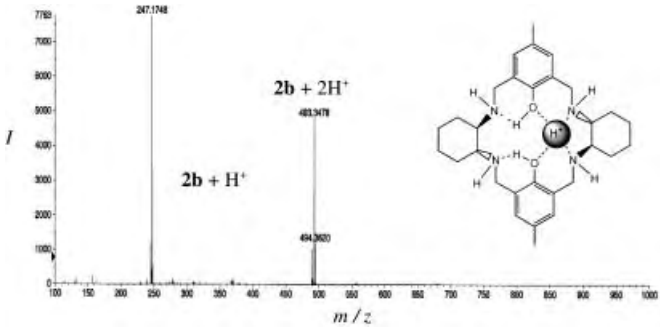
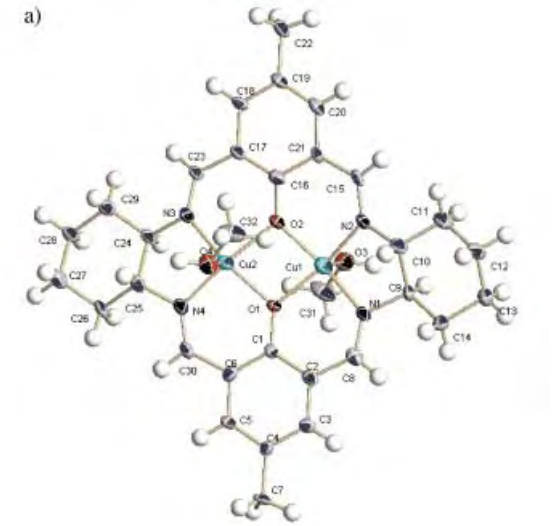



***Figure 2.*** ESI MS spectrum of the macrocyclic ligand **2b**.

By utilizing a similar synthetic approach, Schiff base dicopper(II) complex **1d**, the chiral polyamino macrocycle **2d**, and the corresponding dicopper(II) complex **3d** were successfully prepared (Scheme 2). The X-ray crystal structure of **1d** (Figure 3) shows that the whole molecule adopts a starlike shape with four extended phenyl groups. The C–H bonds from the stereogenic centers in both **1b** and **1d** are essentially perpendicular to the $N_4O_2$-plane (Figure 4), giving an α,β,α,β-



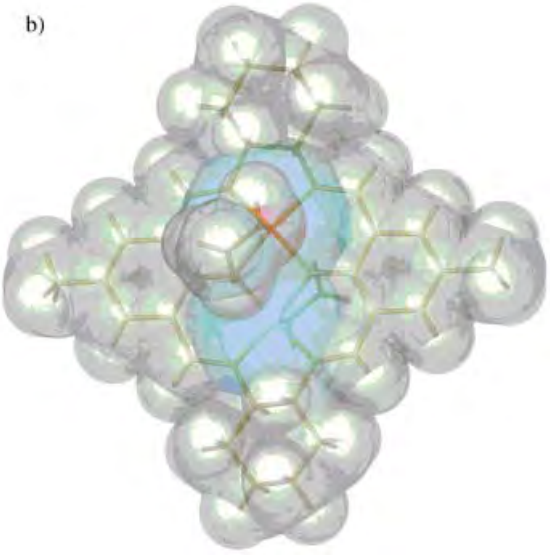
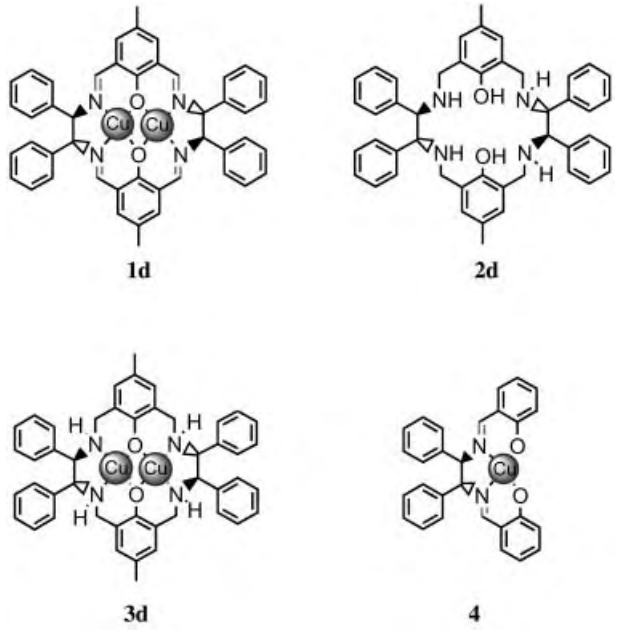




***Figure 1.*** a) ORTEP drawing of **1b**. Selected bond lengths [Å] and angles [°]: Cu(1)-Cu(2) 2.8887(9), Cu(1)-N(1) 1.878(6), Cu(1)-O(1) 1.879(7), Cu(1)-O(2) 1.889(6), Cu(1)-N(2) 1.913(7), Cu(1)-O(3) 2.303(5); N(1)-Cu(1)-O(1) 92.7(3), N(1)-Cu(1)-O(2) 168.1(2), O(1)-Cu(1)-O(2) 81.5(2), N(1)-Cu(1)-N(2) 91.3(3). b) Space-filling representation of **1b**: gray: carbon, red: oxygen, blue: copper.




***Scheme 2.*** Structures of Schiff base dicopper(II) complex **1d**, macrocyclic ligand **2d**, polyamino dicopper(II) complex **3d**, and the control compound **4**.

 © 2003 Wiley-VCH Verlag GmbH & Co. KGaA, Weinheim 

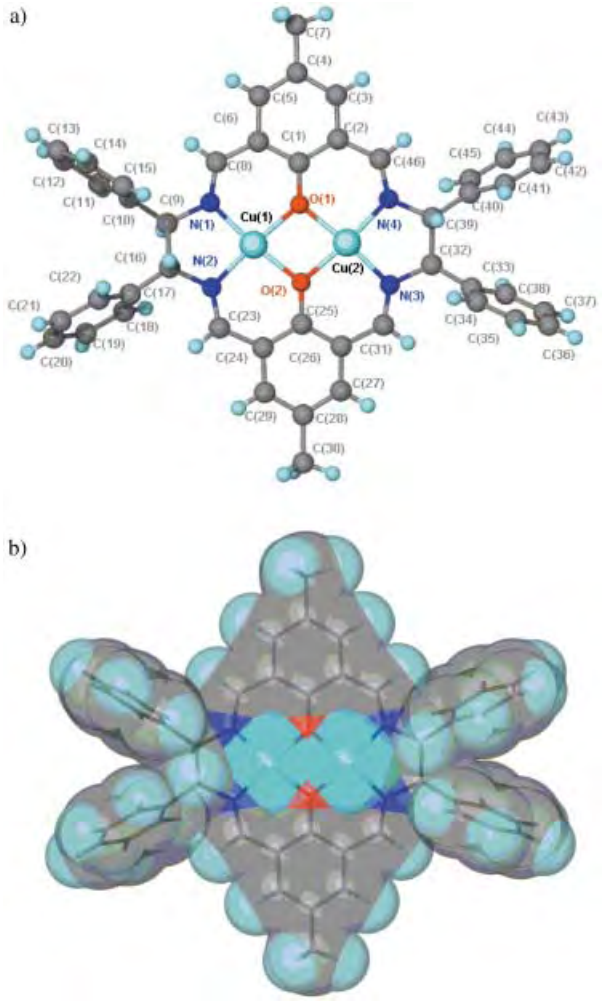
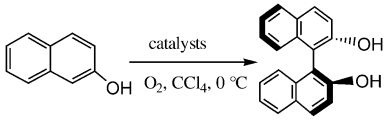



***Figure 3.*** a) ORTEP drawing of **1d**. Selected bond lengths [Å] and angles [°]: Cu(1)-Cu(2) 2.8989(9), Cu(1)-N(1) 1.884(11), Cu(1)-O(1) 1.907(4), Cu(1)-O(2) 1.903(4), Cu(1)-N(2) 1.887(5), Cu(1)-O(1 ме) 2.305(5); N(1)-Cu(1)-O(1) 94.1(2), N(1)-Cu(1)-O(2) 171.9(2), O(1)-Cu(1)-O(2) 80.07(18), N(1)-Cu(1)-N(2) 90.5(3). b) Space-filling representation of **1d**: gray: carbon, red: oxygen, blue: copper.

chiral molecule reminiscent of the chiral porphyrin-amino derivative α,β,α,β-TAPP.[7] Complex **4** was synthesized by condensation of 2 equivalents of salicylaldehyde with 1*R*,2*R*-diphenylethylenediamine (*R*,*R*-DPEN) in the presence of $Cu^{II}$. This complex serves as a control in the following catalytic experiments.

The oxidative coupling of 2-naphthol was employed as a model reaction to compare the catalytic activity and enantioselectivity of the dicopper(II) macrocycle complexes, **1a–d** and **3a–d**. All reactions were carried in the presence of the catalysts (10 mol%) in $CCl_4$ at 0°C with molecular oxygen as oxidant (Table 1). The use of complex **1b** resulted in a yield of

***Table 1:*** Catalytic enantioselective coupling of 2-naphthol in the presence of catalysts (10 mol%).[a]




| Entry | Catalyst | *T* [°C] | *t* [days] | Yield [%][b] | *ee* [%][c] | Config. |
|---|---|---|---|---|---|---|
| 1 | **1a** | 0 | 7 | 75 | 69 | *S* |
| 2 | **1b** | 0 | 7 | 79 | 82 | *S* |
| 3 | **1b** | 10 | 5 | 80 | 61 | *S* |
| 4 | **1b** | 20 | 3 | 89 | 45 | *S* |
| 5 | **1c** | 0 | 7 | 80 | 84 | *S* |
| 6 | **1d** | 0 | 7 | 79 | 80 | *S* |
| 7 | **3a** | 0 | 7 | 92 | 84 | *S* |
| 8 | **3b** | 0 | 7 | 84 | 86 | *S* |
| 9 | **3b** | 10 | 5 | 90 | 74 | *S* |
| 10 | **3b** | 20 | 3 | 93 | 62 | *S* |
| 11 | **3c** | 0 | 7 | 85 | 87 | *S* |
| 12 | **3d** | 0 | 7 | 85 | 88 | *S* |

[a] The reaction was carried out at 0, 10 or 20°C in the presence of 10 mol% of catalyst in $CCl_4$ solution. [b] Yield of isolated product. [c] The enantiomeric excess was determined by HPLC (Chiralpak AD) and the absolute configuration was assigned by comparison to literature.

79% and a moderate enantioselectivity of 82% *ee* (Table 1, entry 2). When polyamino complex **3b** was used (Table 1, entry 8), slightly increases in the *ee* value (86%) and the yield (84%) were observed. In general, polyaza complexes are more robust than their corresponding Schiff base complexes in terms of reproducibility and stability. Catalytic efficiency seems to be insensitive to the bulk of the peripheral groups (compare **1a–c** and **3a–c** series). At higher temperatures, the reaction rate increases, but lower enantioselectivities are observed. For instance, the ee value for **1b** decreased by 37% when the temperature was increased from 0 to 20°C.

Increased bulk of the diamino residues (compare **1b** with **1d** and **3b** with **3d**) does not significantly affect the enantioselectivity. Furthermore, the control compound with one metal center (**4** with $C_2$ symmetry) leads to a low enantioselectivity at 0°C (only 19% *ee*). These results suggest

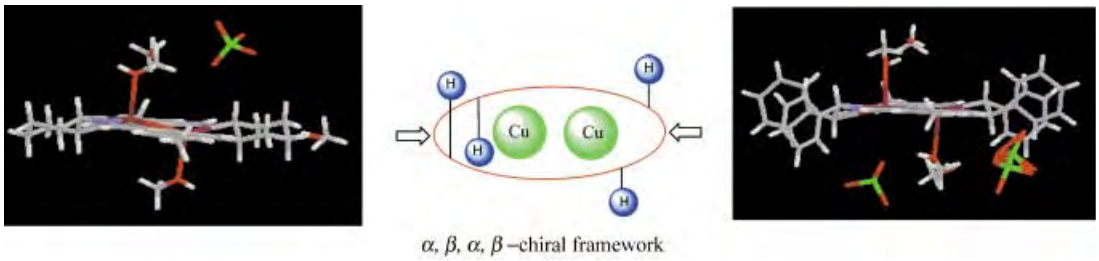



***Figure 4.*** Alternate views of **1b** and **1d**, showing the positions of the chiral C–H bonds.

 © 2003 Wiley-VCH Verlag GmbH & Co. KGaA, Weinheim 

that a rigid dinuclear platform is essential for high enantioselectivity.

The $Cu^{II}$ complex mediated oxidative coupling can proceed through three mechanistic pathways:[4e,g] 1) homolytic coupling of two radical species, 2) radical insertion of one aryl into the C–H bond of another aryl, and 3) reaction of an anion with a carbocation. For the coupling reaction mediated by **1b** (Figure 5), a substrate molecule may undergo ligand exchange with MeOH (on Cu1) to form a $Cu^{II}$–substrate complex **5**, which is followed by the generation of a radical intermediate **6**, which results from one-electron transfer from the substrate to $Cu^{II}$. Simultaneously, the same process may occur on the Cu2 center. Minimization of steric interactions between the radical intermediates and the axial hydrogen atoms of the chiral cyclohexyl rings should favor the orientation shown in Figure 5A. This should produce the *S* product, **8**. The above hypothesis is essentially the same as the pathway 1 mentioned above. This seems to be reasonable given the fact that the two catalytic centers are structurally symmetric. However, more quantitative experiments are required to completely verify our hypothesis or to disprove the remaining two reaction pathways.

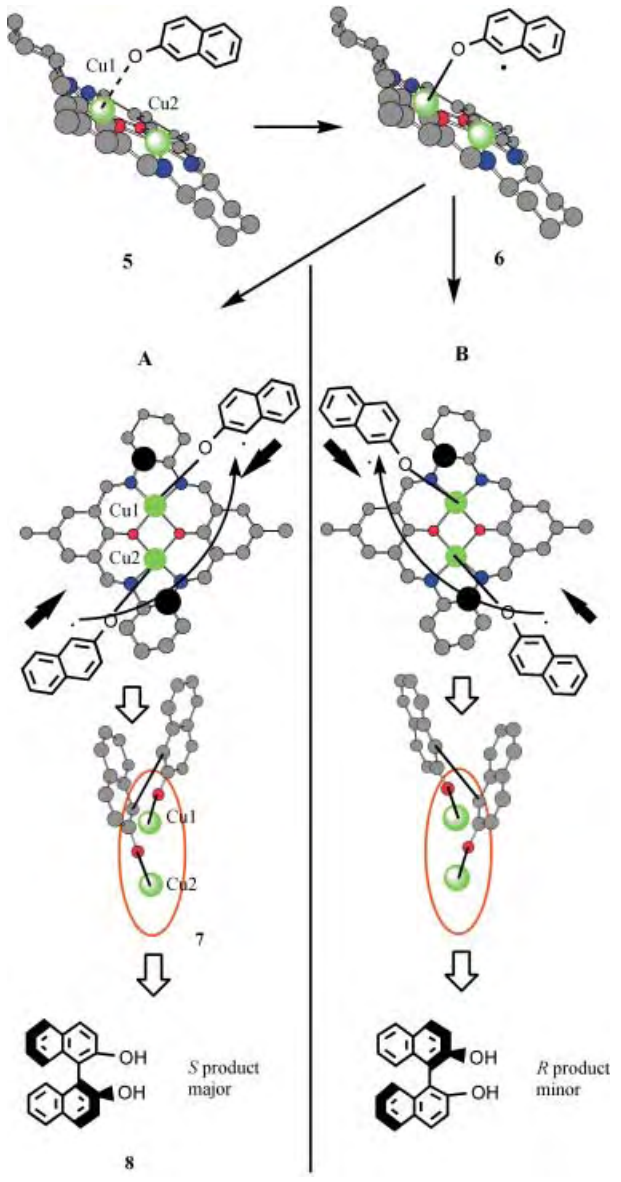



***Figure 5.*** Illustration of enantioselectivity in **1b**-catalyzed oxidative coupling of 2-naphthol. Viewed from above the basal plane of the complex. Hydrogen atoms are omitted for clarity: green: copper, blue: nitrogen, gray: carbon, red: oxygen, black: stereogenic carbon center, which sterically hinders the substrate molecules.

## *Experimental Section*

[**1b**–$Cu_2$]$(ClO_4)_2 \cdot 4CH_3OH$: A solution of 2-hydroxy-5-methyl-1,3-benzenedicarboxaldehyde (0.1 mmol) was added dropwise to a solution of $Cu(ClO_4)_2$ (0.1 mmol) and *R*,*R*-DACH (0.1 mmol) in EtOH (10 mL). After stirring for 4 h, a yellow-green product was obtained in 56% yield. Elemental analysis: calcd (%) for $C_{34}H_{50}Cl_2Cu_2N_4O_{14}$: C 43.6, H 5.4, N 6.0; found: C 43.6, H 5.5, N 6.0. Green crystals were obtained by diffusion of MeOH into a solution of the sample in *N*,*N*-dimethylformamide. Crystal dimensions: $0.3 \times 0.3 \times 0.02$ mm$^3$, $C_{34}H_{50}Cl_2Cu_2N_4O_{14}$, $M = 936.76$, monoclinic, space group $P2(1)$, $a = 11.996(3)$ Å, $b = 13.439$ (3) Å, $c = 12.303(3)$ Å, $\alpha = 90.0°$, $\beta = 102.747(5)°$, $\gamma = 90.0°$, $V = 1934.5(8)$ Å$^3$, $Z = 2$, $\rho_{calcd} = 1.6478$ cm$^{-3}$, $F(000) = 976$, $T = 110(2)$ K, $Mo_{K\alpha}$ radiation, $\lambda = 0.71073$ Å. A total of 7901 independent reflections ($R_{int} = 0.0371$) were obtained. Nonhydrogen atoms were refined with anisotropic thermal parameters. Hydrogen atoms were included in the calculated positions refined with isotropic thermal parameters riding on those of the parent atoms. Full-matrix least-squares refinement on $F^2$ converged to $R_1 = 0.0786$, $wR_2 = 0.2078$ ($I > 2\alpha(I)$) with a goodness of fit $F^2 = 1.060$. CCDC-210825 contains the supplementary crystallographic data for this compound. These data can be obtained free of charge via www.ccdc.cam.ac.uk/conts/retrieving.html (or from the Cambridge Crystallographic Data Centre, 12, Union Road, Cambridge CB21EZ, UK; fax: (+44) 1223-336-033; or deposit@ccdc.cam.ac.uk).

[**1d**–$Cu_2(ClO_4)_2$]$\cdot 4CH_3OH$: The complex was prepared by following a similar procedure to that described above (68% yield). Elemental analysis: calcd (%) for $C_{50}H_{54}Cl_2Cu_2N_4O_{14}$: C 53.0, H 4.8, N 5.0; found: C 53.0, H 4.7, N 5.1. Crystal data: green block $0.05 \times 0.2 \times 0.3$ mm$^3$; $C_{50}H_{54}Cl_2Cu_2N_4O_{14}$, $M = 1132.95$, monoclinic, space group $P2(1)$, $a = 15.8000(2)$ Å, $b = 9.4030$ (12) Å, $c = 16.883(2)$ Å, $\alpha = 90.0°$, $\beta = 98.298(2)°$, $\gamma = 90.0°$, $V = 248.9(6)$ Å$^3$, $Z = 2$, $\rho_{calcd} = 1.516$ cm$^{-3}$, $F(000) = 1172$, $T = 110(2)$ K, $Mo_{K\alpha}$ radiation, $\lambda = 0.71073$ Å. A total of 5485 independent reflections ($R_{int} = 0.0323$) were obtained. Full-matrix least-squares refinement on $F^2$ converged to $R_1 = 0.0419$, $wR_2 = 0.0986$ ($I > 2\alpha(I)$) with a goodness of fit $F^2 = 1.020$. CCDC-210826 contains the supplementary crystallographic data for this compound. These data can be obtained free of charge via www.ccdc.cam.ac.uk/conts/retrieving.html (or from the Cambridge Crystallographic Data Centre, 12, Union Road, Cambridge CB21EZ, UK; fax: (+44) 1223-336-033; or deposit@ccdc.cam.ac.uk).

**2b**: *R*,*R*-DACH (15 mmol) in MeOH (200 mL) was added dropwise to a stirred solution of 2-hydroxy-5-methyl-1,3-benzenedicarboxaldehyde (99%; 2.15 g, 15 mmol) in the presence of $Pb^{II}(OA_C)_2$ in MeOH (300 mL). The yellow solid formed was filtered, washed with MeOH, dried in air, and suspended in MeOH (50 mL). Solid $NaBH_4$ (4.0 g, 100 mmol) was used to reduce the metal complex at 0 °C in an ice bath. The suspension was magnetically stirred for about 2 h at room temperature. Water (5 mL) was added to neutralize excess unreacted $NaBH_4$. The resulting yellow-colored solution was filtered to remove any suspended material. The filtrate was diluted with water (100 mL), acidified (pH 2.0) with $H_2SO_4$ (8 M), and was then filtered. The filtrate was treated with aqueous ammonia (12.5 ml), and was then extracted with chloroform ($3 \times 50$ mL). The combined organic layer was washed with water, dried with $Na_2SO_4$, and the solvent removed on a rotary evaporator nearly to dryness.

 © 2003 Wiley-VCH Verlag GmbH & Co. KGaA, Weinheim 

The crude product was purified by column chromatography (silica gel, $CH_2Cl_2$/MeOH ~ 1:1) and was identified as **2b** (75% yield). ESI MS: $m/z$: 493.3478 $[M+H]^+$; calcd for $C_{30}H_{44}N_4O_2$: 492.3464, m.p. 208 °C; $[\alpha]_D^{25} = -21.7$ ($c = 0.01$, $CH_2Cl_2$); $^1$H NMR ($CDCl_3$): $\delta = 1.17$–$1.80$ (m, 8H; $CH_2$ of cyclohexane), 2.31 (m, 3H; $CH_3$-Ar), 3.79 (s, 2H; CH of cyclohexane), 4.30–4.52 (m, 4H; $CH_2$-Ar), 7.36 ppm (s, 2H; Ar-H); $^{13}$C NMR ($CDCl_3$): $\delta = 20.78$ ($CH_2$ of cyclohexane), 24.75 ($CH_2$ of cyclohexane), 44.74 (CH of cyclohexane), 54.81 ($CH_2$-Ar), 121.86 (Ar-H), 133.75 ($C$(Ar)-$CH_2$), 134.36 ($C$(Ar)-$CH_3$), 152.10 ppm (C(Ar)-OH). Elemental analysis: calcd (%) for $C_{30}H_{44}N_4O_2$: C 73.13, H 9.00, N 11.37; found: C 73.13, H 9.06, N 11.38%.

**2d**: Prepared by a similar reaction procedure from *R*,*R*-DPEN as that for **2b**. Yield: 80%; ESI MS: $m/z$: 689.36 $[M+H]^+$; calcd for $C_{46}H_{48}N_4O_2$: 688.38; m.p. 164 °C; $[\alpha]_D^{25} = +31.3$ ($c = 0.01$, $CH_2Cl_2$); $^1$H NMR,($CDCl_3$): $\delta = 2.18$ (s, 3H; $CH_3$-Ar), 3.80–3.92 (d, 2H; CH-Ar), 4.76 (m, 4H; $CH_2$-Ar), 7.08–7.42 (m, 12H; Ar-H), 7.78 ppm (s, 1H; OH); elemental analysis: calcd (%) for $C_{46}H_{48}N_4O_2$: C 80.20, H 7.02, N 8.13, found: C 80.11, H 7.06, N 8.10%.

Received: May 26, 2003 [Z51978]

**Keywords:** asymmetric catalysis · binaphthols · copper · cross-coupling · enantioselectivity

[1] a) M. Shibasaki, N. Yoshikawa, *Chem. Rev.* **2002**, *102*, 2187–2209; b) M. Shibasaki, H. Sasai, T. Arai, *Angew. Chem.* **1997**, *109*, 1290–1310; *Angew. Chem. Int. Ed. Engl.* **1997**, *36*, 1236–1256; c) R. Noyori, *Asymmetric Catalysis in Organic Synthesis*, Wiley, New York, **1994**; d) K. Ishihara, H. Nakamura, H. Yamamota, *J. Am. Chem. Soc.* **1999**, *121*, 7720; e) *Comprehensive Asymmetric Catalysis* (Eds.: E. N. Jacobsen, A. Pfaltz, H. Yamamoto), Springer, Berlin, **1999**.

[2] a) A. Miyashita, H. Yasuda, H. Takaya, K. Toriumi, T. Ito, T. Souchi, R. Noyori, *J. Am*, *Chem. Soc*, **1980**, *102*, 7932; b) R. Noyori, *Chem. Rev.* **1989**, *89*, 187; c) R. Noyori, H. Takaya, *Acc. Chem. Res.* **1990**, *23*, 345; d) R. Noyori, *Angew. Chem.* **2002**, *114*, 2108–2123; *Angew. Chem. Int. Ed.* **2002**, *41*, 2008.

[3] "Chiral Chemistry": S. C. Stinson, *Chem. Eng. News* **2002**, *80*(20), 45.

[4] a) J. Brusse, A. C. A. Jansen, *Tetrahedron Lett.* **1983**, *24*, 3261; b) M. Hovorka, J. Zavada, *Tetrahedron*, **1992**, *48*, 9517; c) M. Smrcina, M. Lorenc, V. Hanus, P. Sedmera, P. Kocovsky, *J. Org. Chem.* **1992**, *57*, 1993; d) M. Smrcina, J. Polakowa, S. Vyskocil, P. Kocovsky, *J. Org. Chem.* **1993**, *58*, 4534; e) M. Smrcina, S. Vyskocil, B. Maca, M. Polasek, T. A. Claxton, A. P. Abbott, P. Kocovsky, *J. Org. Chem.* **1994**, *59*, 2156; f) M. Nakajima, L. Miyoshi, K. Kanayanma, S. L. Hashimoto, M. Noji, K. Koga, *J. Org. Chem.* **1999**, *64*, 2264; g) X. Li, J. Yand, M. C. Kozlowski, *Org. Lett.* **2001**, *3*, 1137.

[5] a) C. T. Chen, S. W. Hon, S. S. Weng, *Synlett*, **1999**, 816; b) S. W. Hon, C. H. Li, J. H. Kuo, N. B. Barhate, Y. H. Liu, Y. Wang, C. T. Chen, *Org. Lett.* **2001**, *3*, 869; c) N. B. Barhate, C. T. Chen, *Org. Lett.* **2002**, *4*, 2529; d) Z. Liu, Q. Liu, L. Gong, X. Cui, A. Mi, Y. Jiang, *Chem. Commun.* **2002**, 914; e) Z. Luo, Q. Liu, L. Gong, X. Cui, A. Mi, Y. Jiang, *Angew. Chem.* **2002**, *114*, 4714–4717; *Angew. Chem. Int. Ed.* **2002**, *41*, 4532–4535.

[6] T. P. Yoon, E. N. Jacobsen, *Science* **2003**, *299*, 1691.

[7] J. P. Collman, L. Fu, *Acc. Chem. Res.* **1999**, *32*, 455.

 © 2003 Wiley-VCH Verlag GmbH & Co. KGaA, Weinheim 

Natural Product Synthesis

# DNA Topoisomerase Inhibitor Acutissimin A and Other Flavano-Ellagitannins in Red Wine**

*Stéphane Quideau,* Michael Jourdes, Cédric Saucier, Yves Glories, Patrick Pardon, and Christian Baudry*

Polyphenols are ubiquitous in fruits, vegetables, and various plant-derived foods and beverages that have been claimed to be beneficial for human health.[1–3] Among the most evocative examples are red wine, green tea, and chocolate, which all contain polyphenols that are believed to reduce the risk of certain degenerative diseases.[1] The trademark of polyphenols is their antioxidant activity, which puts them center-stage in debates on the prevention of coronary heart disease and atherosclerosis by polyphenol-rich diets. Another widely recognized property of polyphenols is their ability to precipitate proteins through formation of noncovalent complexes. Such complexation of polyphenols with salivary proteins underlies the perception of astringency, a major taste property of red wine and several other beverages.[4] Their potential for application in the food and beverage industry is fueling research ultimately aimed at designing sensors for taste measurement,[4] but the significance of investigations is often limited by lack of access to structurally well-defined polyphenols.

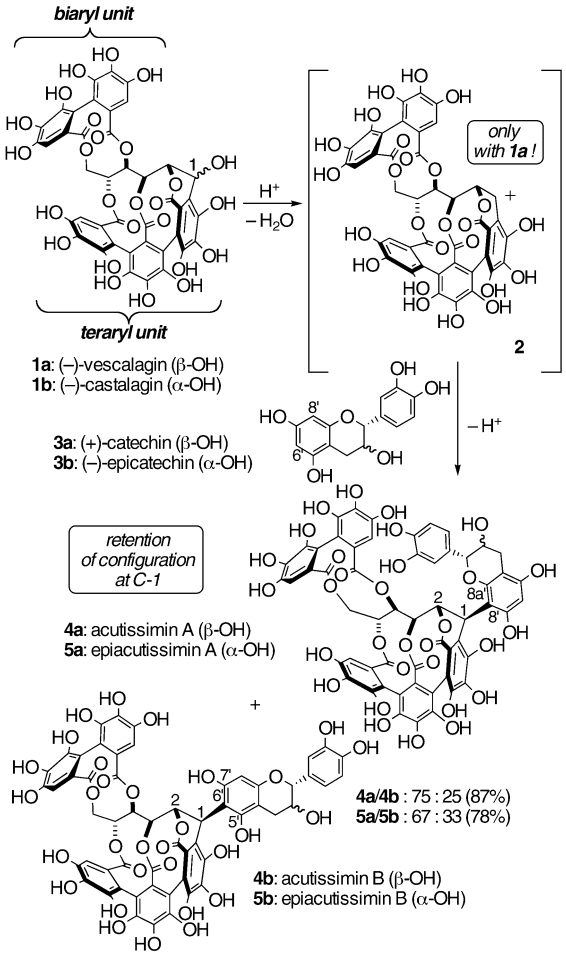
Polyphenols comprise two major classes of natural products: the condensed tannins (proanthocyanidins), which are derived from C–C-linked flavan-3-ols,[1,5,6] and the hydrolyzable tannins (gallo- and ellagitannins), which are derived from galloyl units usually linked by esterification to a sugar core such as glucose.[1,7] Hundreds of purified ellagitannins have been characterized and biologically evaluated as active constituents of plant extracts used in traditional medicine.[7,8] Yet the potential of ellagitannin-based drugs has so far remained untapped, even though pyrogallol-type biaryl and teraryl units (Scheme 1) confer onto this tannin class rigid and stereochemically defined motifs which are well-suited for specific interactions with proteins.[7,9,10]

[*] Dr. S. Quideau
Institut Européen de Chimie et Biologie
2 Rue Robert Escarpit, 33607 Pessac Cedex (France)
Fax: (+33) 540-006439
E-mail: s.quideau@iecb-polytechnique.u-bordeaux.fr
Dr. S. Quideau, M. Jourdes, Dr. P. Pardon, C. Baudry
Laboratoire de Chimie des Substances Végétales
Université Bordeaux 1, 33405 Talence Cedex (France)
Dr. C. Saucier, Dr. Y. Glories
Faculté d'Œnologie
Université Bordeaux 2, 33405 Talence Cedex (France)

[**] We gratefully acknowledge funding from the Conseil Interprofessionnel du Vin de Bordeaux and the Conseil Régional d'Aquitaine.

Supporting information (detailed descriptions of experimental procedures, liquid chromatograms, and NMR and electrospray mass spectra of compounds **4a**, **4b**, **5a**, **5b**, and mixtures thereof) for this article is available on the WWW under http://www.angewandte.org or from the author.

 © 2003 Wiley-VCH Verlag GmbH & Co. KGaA, Weinheim DOI: 10.1002/anie.200352089 




***Scheme 1.*** Formation of acutissimins. Only the *C*-glycosidic ellagitannin (−)-vescalagin (**1a**) reacts under mildly acidic conditions with the flavan-3-ols (+)-catechin (**3a**) and (−)-epicatechin (**3b**) to produce the acutissimins **4a/b** and **5a/b** through a diastereoselective nucleophilic substitution that occurs with retention of configuration at the C-1 center of **1a**.

The work presented herein concerns the formation in red wine of acutissimin A (**4a**) and related flavano-ellagitannins from flavan-3-ols and *C*-glycosidic ellagitannins such as (−)-vescalagin (**1a**) and its C-1 epimer (−)-castalagin (**1b**) that feature an unusual open-chain glucose core C–C-linked to a galloyl-derived teraryl unit (Scheme 1).[11] These *C*-aryl glycosides are characteristic metabolites of durable hardwood species. Acutissimin A (**4a**) was first isolated from the bark of the sawtooth oak (*Quercus acutissima*),[12] a pest- and disease-free oak used as an ornamental tree in air-polluted urban areas in the United States. The compound was later found to be an inhibitor of human DNA topoisomerase II that is 250-fold more potent in vitro (concentration required for 100% inhibition, $IC_{100} = 0.2\ \mu M$) than the clinically used anticancer drug etoposide (VP-16).[13]

The chemistry of the formation of **4a** is simple and involves an acid-catalyzed nucleophilic substitution reaction between either (−)-**1a** or (−)-**1b** at the C-1 center and (+)-catechin (**3a**) at its nucleophilic C-8 center (Scheme 1). Initial attempts by others[12] to use this hemisynthetic approach to produce **4a** from (−)-castalagin (**1b**) resulted in minute amounts (3.7%) of the desired product. The reactions we carried out between purified (−)-**1b** and (+)-**3a** in tetrahydrofuran containing 1% trifluoroacetic acid at 60°C confirmed this failure. However, the use of (−)-**1a** instead of (−)-**1b** led, over a period of 7 h, to the clean formation of acutissimin A (**4a**) as the major product, together with its C-6 regioisomer acutissimin B (**4b**; Scheme 1). Both compounds have the same configuration at C-1 as **1a**. This mixture was then separated by semipreparative HPLC and the individual isomers **4a** and **4b** were obtained in a 75:25 ratio and 87% yield. Interestingly, the isomers have been isolated in a similar ratio (81:19) from *Quercus acutissima*.[12] The identity of the hemisynthetic compounds was confirmed by comparison of $^1H$ and $^{13}C$ NMR data as well as optical rotations with published data.[12]

Initial failures to synthesize the target compound were essentially the result of incorrect selection of the starting *C*-glycoside epimer. (−)-Vescalagin (**1a**) is a much more efficient reaction partner than its α-anomer **1b**. This difference in chemical reactivity can be rationalized in terms of the difference in orientation of the reacting hydroxy group at C-1. In **1b**, this OH group is α-oriented and embedded in the *endo* face of the molecule, whereas in **1a**, it is β-oriented and points outward from the *exo* face of the molecule. The latter OH group is consequently more accessible and its oxygen atom probably has a more basic character than that of the OH group in **1b**, which is also involved in intramolecular hydrogen bonding.[14,15]

The same reaction was performed with the flavan-3-ol (−)-epicatechin (**3b**) and gave two new flavano-ellagitannins that we refer to as "epiacutissimins" A (**5a**) and B (**5b**) in a 67:33 ratio and 78% yield, again with retention of configuration at C-1 (Scheme 1). The position at which the flavanoid unit is connected to the *C*-glucoside C-1 center in these two regioisomers was confirmed by the observation of two- and three-bond couplings of H-1 with C-8′ and C-8′a in the NMR HMBC spectrum of **5a**, and with C-5′ and C-6′ in that of **5b**. The stereochemistry at C-1 was deduced from the small NMR coupling constant between the glucose unit H-1 and H-2 protons; this weak coupling indicates that the dihedral angle between these two protons is close to 90° and such an angle is observed when H-1 is β-oriented.[12] In fact, all known naturally occurring C-1-substituted *C*-glycosidic ellagitannins have their C-1 substituent in this β orientation. It is likely that all these compounds are derived from (−)-**1a** and not from (−)-**1b**. A mechanistic description of the reaction follows a classical $S_N1$-type pathway with protonation of the OH group at C-1 assisting the formation of a benzylic cation **2** (Scheme 1).[1] This stable carbocation intermediate is attacked by the flavan-3-ol units mainly from their C-8 center and, to a lesser extent, from their more encumbered and less nucleophilic C-6 center, with full diastereofacial differentiation (Figure 1).

The hemisynthesis described herein constitutes an in vitro mimicry of the nonenzymatic yet stereoselective formation of acutissimin flavano-ellagitannins. With this sound knowledge of the reactivity of *C*-glycosidic ellagitannins with flavan-3-ols in acidic medium, we turned our attention to the chemistry of red wine because this beverage contains both precursors of

 © 2003 Wiley-VCH Verlag GmbH & Co. KGaA, Weinheim 

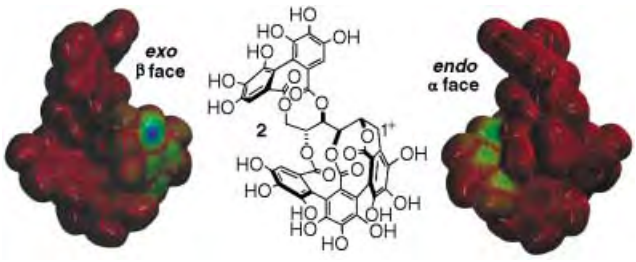



***Figure 1.*** Diastereofacial differentiation of the benzylic carbocation intermediate. These Spartan-generated Hartree–Fock models show the two faces of the lower-energy unoccupied molecular orbital (LUMO) of the benzylic cation **2** mapped onto its 0.002-electron au$^{-3}$ electron density isosurface. The diagrams clearly explain the observed stereochemical preference of the reaction by showing that the carbocation LUMO is indeed more accessible from the exo face (blue spot) than the endo face of the C-1 locus.

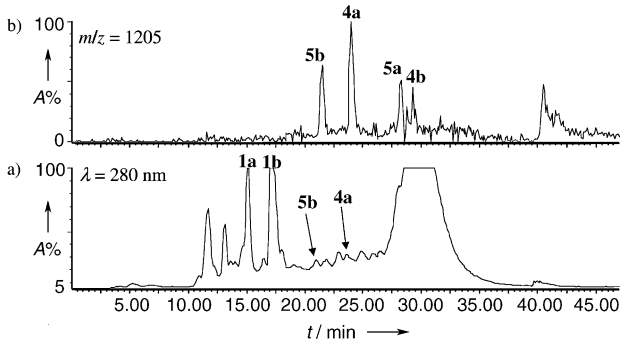



***Figure 2.*** Detection of acutissimins in red wine. HPLC/MS profiles of a partially purified red wine sample. a) UV detection at 280 nm, b) negative-mode electrospray ion trace chromatogram ($m/z = 1205$). **1a**: vescalagin, **1b**: castalagin, **4a**: acutissimin A, **4b**: acutissimin B, **5a**: epiacutissimin A, **5b**: epiacutissimin B.

flavano-ellagitannins. Grape juice brings both catechin (**3a**) and epicatechin (**3b**) to red wine, while vescalagin (**1a**) is extracted from oak by the aqueous alcoholic wine solution during aging in barrels and/or is added by treatment of the wine with enological tannins. We verified that the oak heartwood used to make barrels, from which we isolated **1a** and **1b**,[16] does not contain any detectable amounts of flavano-ellagitannins. Several hundred compounds present in red wine have been characterized so far, so the chances of finding the acutissimins in such a chemically complex medium would have been small without having the compounds already to hand. We first carried out a model reaction by mixing **1a** and **3a** at room temperature in a wine model consisting of a 12% ethanolic aqueous solution containing 5 g L$^{-1}$ tartaric acid at pH 3.2. Formation of both acutissimins **4a/b** was clearly shown by HPLC and electrospray mass spectrometric analysis over a period of 25 days; once again, **4a** was the major product. These results confirmed our hypothesis that acutissimins can be found in red wine and the only remaining challenge was to develop an appropriate extraction protocol (see the Supporting Information). The two acutissimins **4a/b** and the two previously unknown "epiacutissimins" **5a/b** were detected in a sample of red wine that had been aged for 18 months in an oak barrel. Each of the four compounds has a molecular mass of 1206 Da, and their presence was validated by mass spectrometry and comparison of their chromatographic retention times and mass fragmentation patterns with those of the hemisynthetic compounds (Figure 2).

While it would be quite inappropriate to infer from the presence of acutissimin A in red wine that this beverage possesses antitumor properties, our work shows for the first time that wine contains polyphenolic molecules displaying both ellagitannin and flavanoid structural features. These hybrid tannin molecules are accessible through the hemisynthesis reported herein and should be part of molecular-level studies on the effects of polyphenol–protein interactions. Furthermore, the efficacy of the chemistry involved led us to speculate that higher-molecular-mass flavano-ellagitannins similarly constructed from oligomeric *C*-glycosidic ellagitannins and proanthrocyanidins are present in red wine. The amounts of acutissimins in an aging red wine at any given time can appear rather low when measured by any available method, but it should be remembered that wine is a slow but continuously evolving mildly acidic and aerobic reaction mixture. The acutissimins are certainly transformed in wine during aging, but they will form as long as grape-derived flavan-3-ols and oak-derived vescalagin are present in the medium.

Received: June 10, 2003 [Z52089]
Published Online: November 11, 2003

**Keywords:** antitumor agents · diastereoselectivity · natural products · polyphenols · topoisomerase

[1] E. Haslam, *Practical Polyphenolics—From Structure to Molecular Recognition and Physiological Action*, Cambridge University Press, Cambridge, **1998**.
[2] T. Hatano, T. Yoshida, R. W. Hemingway in *Plant Polyphenols 2: Chemistry, Biology, Pharmacology, Ecology* (Eds.: G. G. Gross, R. W. Hemingway, T. Yoshida), Kluwer Academic/Plenum, New York, **1999**, p. 509.
[3] M.-T. Huang, C.-T. Ho, C. Y. Lee, *Phenolic Compounds in Food and their effects on Health*, Vol. II, *ACS Symp. Ser. 507*, American Chemical Society, Wahington, DC, **1992**.
[4] A. Edelmann, B. Lendl, *J. Am. Chem. Soc.* **2002**, *124*, 14741.
[5] D. Ferreira, D. Slade, *Nat. Prod. Rep.* **2002**, *19*, 517.
[6] A. P. Kozikowski, W. Tückmantel, G. Böttcher, L. J. Romanczyk, *J. Org. Chem.* **2003**, *68*, 1641.
[7] S. Quideau, K. S. Feldman, *Chem. Rev.* **1996**, *96*, 475.
[8] T. Okuda, *Curr. Org. Chem.* **1999**, *3*, 609.
[9] D. R. Spring, S. Krishnan, H. E. Blackwell, S. L. Schreiber, *J. Am. Chem. Soc.* **2002**, *124*, 1354.
[10] K. Saeki, S. Hayakawa, M. Isemura, T. Miyase, *Phytochemistry* **2000**, *53*, 391.
[11] G.-I. Nonaka, T. Sakai, T. Tanaka, K. Mihashi, I. Nishioka, *Chem. Pharm. Bull.* **1990**, *38*, 2151.
[12] K. Ishimaru, G.-I. Nonaka, I. Nishioka, *Chem. Pharm. Bull.* **1987**, *35*, 602.
[13] Y. Kashiwada, G.-I. Nonaka, I. Nishioka, K. J.-H. Lee, I. Bori, Y. Fukushima, K. F. Bastow, K.-H. Lee, *J. Pharm. Sci.* **1993**, *82*, 487.
[14] T. Yoshida, H. Ohbayashi, K. Ishihara, W. Ohwashi, K. Haba, Y. Okano, T. Shingu, T. Okuda, *Chem. Pharm. Bull.* **1991**, *39*, 2233.
[15] N. Vivas, M. Laguerre, Y. Glories, G. Bourgeois, C. Vitry, *Phytochemistry* **1995**, *39*, 1193.
[16] A. Scalbert, L. Duval, S. Peng, B. Monties, C. Du Penhoat, *J. Chromatogr.* **1990**, *502*, 107.

 © 2003 Wiley-VCH Verlag GmbH & Co. KGaA, Weinheim 

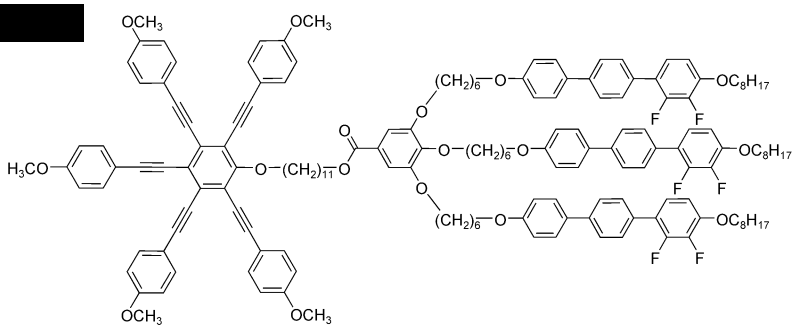
*Liquid Crystals*

# Multiple Levels of Order in Linked Disc–Rod Liquid Crystals**

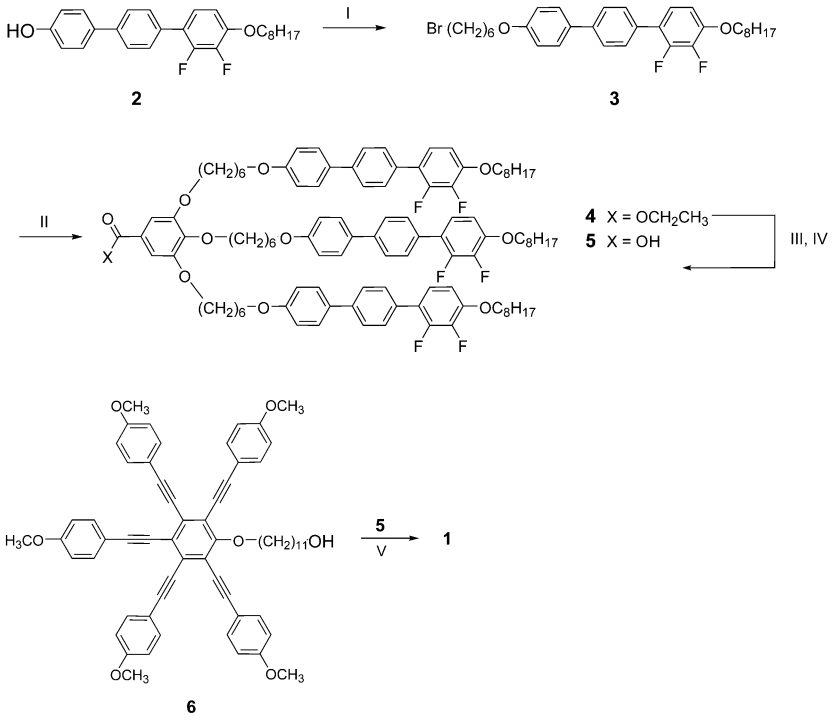
*Paul H. J. Kouwer and Georg H. Mehl**

For thermotropic liquid-crystalline systems, molecular shape and mesophase structure is, in most cases, closely linked. Rod-shaped mesogens form layered (smectic) liquid-crystal phases showing 1D positional order; disc-shaped mesogens order into columnar structures with 2D order. Notable exceptions are various classes of rod-shaped mesogens that self-organize into columnar phases, such as polycatenars,[1a] neat soaps,[1b] mesogens with strongly interacting lateral substituents,[2] and oligomeric/dendritic structures,[3] in which steric factors prevent a layered organization. So far, all reported layered phases of discotic molecules are actually highly ordered columnar lamellar ($Col_L$) phases.[4] Disc-shaped molecules self-organizing into 1D layered phases (smectic A or C) have not been explored systematically.[5] Current developments in nanoscience have caused a resurgence of research on disc-shaped self-assembly systems, particularly in view of applications such as easy-processable and self-healing, organic, photo- and electron-conducting systems. A combination of these properties with the advantages of smectic systems (fast, bistable switching) is of technological relevance as well as fundamental interest, as it extends the basic understanding of structure–property relationships in soft self-organizing systems.

Herein, we present an example of a class of materials that contain a disc-shaped moiety and rod-shaped groups (see Scheme 1), which exhibits a nematic and various smectic mesophases. This work is crucially different from earlier research[6] in that in this system, the (volume-)fractions of the discs and rods are better matching and, importantly, the cross-sections of the disc matches the cross-section of the three rods,[7] thus favoring a layered organization.



***Scheme 1.*** Structure of the investigated disc-rod mesogen.



***Scheme 2.*** Synthesis of the disc–rod mesogen. Key: I) $Br(CH_2)_6Br$ (5 equiv), $K_2CO_3$, KI, butanone, reflux 16 hrs; II) Ethyl gallate, $K_2CO_3$, KI, butanone, reflux 16 hrs; III) aqueous KOH, EtOH/THF (1:1), heat to reflux 2 hrs; IV) aqueous HCl; V) DCC, DMAP, *p*TSA, $CH_2Cl_2$, room temperature 5 days.

The synthesis of target compound **1** is outlined in Scheme 2. Preparation of the discotic mesogen **6** and the rod-shaped terphenyl **2** have been described elsewhere.[8] A spacer was attached to **2** by means of a Williamson alkylation under standard conditions. Alkylation of **3** to ethyl gallate yielded **4**, which was saponified to the free carboxylic acid under basic conditions. A DCC-mediated esterification with the discotic mesogen **6** yielded the target material. Detailed reaction procedures and structure analysis are provided in the Supporting Information. The mesophase behavior of the target material and its precursors was investigated by optical polarizing microscopy (OPM) and differential scanning calorimetry (DSC). The results are summarized in Table 1.

Terphenyl moieties are known to display smectic mesophases.[5a] Also in **4**, in which three mesogens have been linked, smectic phases are observed. Attachment of the discotic nematogen in **1** introduces an additional nematic phase at high temperatures. The nematic phase (Figure 1a),

[*] Dr. G. H. Mehl, Dr. P. H. J. Kouwer
University of Hull
Department of Chemistry
Cottingham Road
Hull, HU6 7RX (UK)
Fax: (+44) 1482-466411
E-mail: g.h.mehl@hull.ac.uk

[**] Financial support was provided by the Ramsay Memorial Fellowship Trust and the EU ("LCDD" contract HPRN-CT2000-00016). We are grateful to Prof. S. J. Picken, Delft University of Technology, for conducting SAXS experiments in his laboratory.

Supporting information for this article is available on the WWW under http://www.angewandte.org or from the author.

 DOI: 10.1002/anie.200352488 © 2003 Wiley-VCH Verlag GmbH & Co. KGaA, Weinheim 

***Table 1:*** Mesopmorphic properties of **1** and its precursors.

| Mesogen | Phase behavior[a,b] | | | | | | | | | | |
|---|---|---|---|---|---|---|---|---|---|---|---|
| **6** | Cr | 132 (37) | | | | | | | N | 246 (0.2) | I |
| **3** | Cr | 107 (50) | | | SmC | 137 (<0.1) | SmA | 172 (5.5) | | | I |
| **4** | $Crx_1$ | 83 (5.5) | $Crx_2$ | 123 (35) | SmC | 165 (0.3) | SmA | 205 (18) | | | I |
| **1** | $Crx_1$ | 83 (10.5) | $Crx_2$ | 115 (31) | SmC | 134 (17) | SmA | 135 (<0.2) | N | 159 (1.5) | I |

[a] Transition temperatures (measured for heating runs) in [°C] and latent heat values (between the brackets) in [kJ mol$^{-1}$]. [b] Phase assignments: Cr = crystalline; Crx = soft crystal; $x_1$, $x_2$ = undetermined phase structure, SmC = smectic C; SmA = smectic A; N = nematic; I = isotropic.

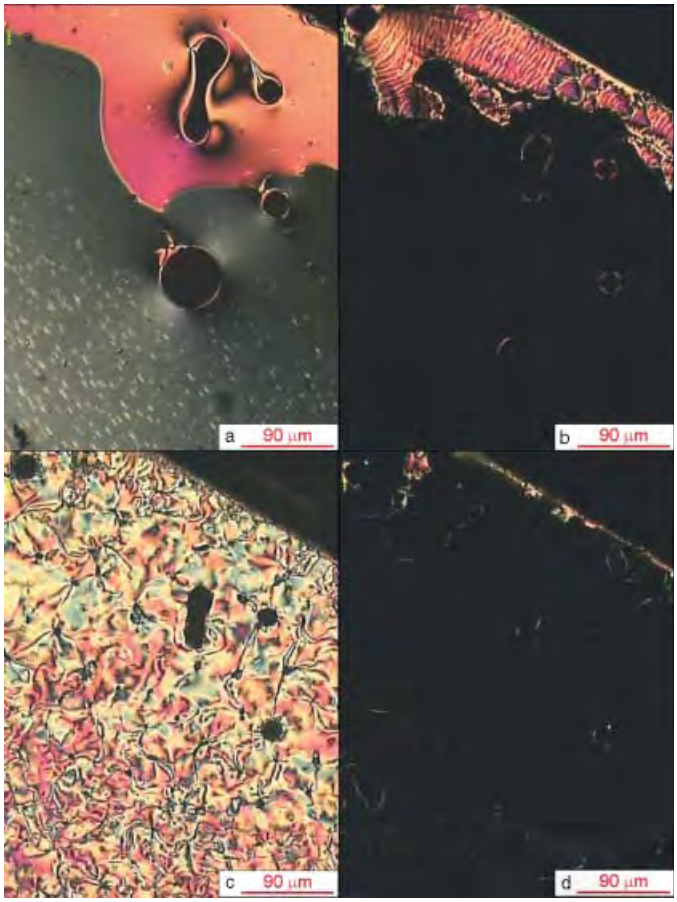



***Figure 1.*** Optical microscopy pictures of **1** at a) $T = 150$ °C (nematic); b) $T = 132$ °C (SmA); c) $T = 130$ °C (SmC); and d) $T = 90$ °C ($Crx_2$). All pictures are taken with crossed polarizers. The scale bar represents 90 µm.

which displays a characteristic Schlieren texture with twofold and fourfold brushes, has a low viscosity and aligns easily between two unprepared glass slides. When the nematic phase is cooled, typical textures of a SmA (fan texture with homeotropic areas, from 135°) and a SmC phase (Schlieren texture, from 132 °C) are observed (Figures 1b and c). At the transition to the soft-crystalline $Crx_2$ phase, a very low birefringent texture appears (Figure 1d). In this phase the viscosity has increased drastically and no further changes in the optical texture are observed on cooling into the crystalline phase. The DSC traces of **1** are shown in the Supporting Information.

The phase structure of **1** in the various mesophases was further investigated by using detailed X-ray diffraction (XRD), see Figure 2. In the nematic phase two diffuse reflections are observed, which indicates a complete absence of positional order. The broad small angle reflection with a *d*-spacing of 29 Å corresponds to the average length of the rods (≈32 Å) and diameter of the discs (≈20 Å), which indicates a molecularly mixed nematic phase and confirms chemical compatibility of the different entities (Figure 3a).[9] Close to the transition to the SmA phase, some pretransitional ordering (small angle reflections with $d = \approx 50$ Å and ≈25 Å) is observed, thus pointing towards phase segregation between the discs and rods and indicating that at lower temperatures in the nematic phase, the entire mesogen is the building block rather than the submolecular units.

In the SmA and the SmC phase, sharp small angle reflections become apparent, attributed to layer formation. The layer spacing of ≈102 Å ($d_{002} = \approx 51$ Å) corresponds to a bilayer lamellar system with the discs and the rods segregated (thus $SmA_2$ and $SmC_2$ phases),[10] schematically shown in Figure 3b. The sharp reflections and the presence of a number of higher-order reflections show that the layered organization is well-defined. The lack of sharp reflections in the wide-angle area indicates the absence of positional order both in the rod layer and in the disc layer. Thus, the discs are essentially organized as calamitic mesogens within a SmA or SmC phase. However, because of free-volume requirements, rotation around the long axis parallel to the layer normal is suppressed and hence, some orientational order of the short axis of the disc perpendicular to the layer normal must be assumed. However, the homeotropic optical texture does not suggest any correlation between adjacent disc layers.

In the SmC phase, characterized by a Schlieren texture and indicative of some correlation of the tilt across the layers, the spacing decreases with decreasing temperature, which is a signature for tilting of the mesogenic units. As the partly fluorinated terphenyls show strong SmC behavior, it was expected that these moieties are responsible for the tilting. Hence, a tilt angle $\theta_t$ was calculated considering that only the rods are tilting [Eq (1)].

$$\theta_t = \cos^{-1}\left(\frac{d_{rod,SmC}}{d'_{rod,SmA}}\right) = \alpha(T_{CA} - T)^{\gamma} \qquad (1)$$

Here $\frac{d_{rod,SmC}}{d'_{rod,SmA}}$ is the ratio between the thickness of the rod layer in the SmC and the extrapolated SmA phase[11a] at temperature $T$, $\alpha$ is a material constant, $T_{CA}$ is the SmC–SmA transition temperature and $\gamma$ is a empirically determined constant: $\gamma = 0.35$.[11b] To check this assumption, the temperature dependence of the tilt was compared to that of precursor **4**. The values obtained after fitting the experimental data with Equation (1) are in close proximity for **1** and **4** ($\alpha(\mathbf{1}) = 5.4 \pm 0.1\,°K^{-0.35}$ and $\alpha(\mathbf{4}) = 5.1 \pm 0.1\,°K^{-0.35}$), and hence there is a strong argument that indeed the rods are tilting and the discs remain essentially oriented perpendicular to the layer normal. However at present, based on these results, we can not exclude fully any tilting of the discs.

 © 2003 Wiley-VCH Verlag GmbH & Co. KGaA, Weinheim 

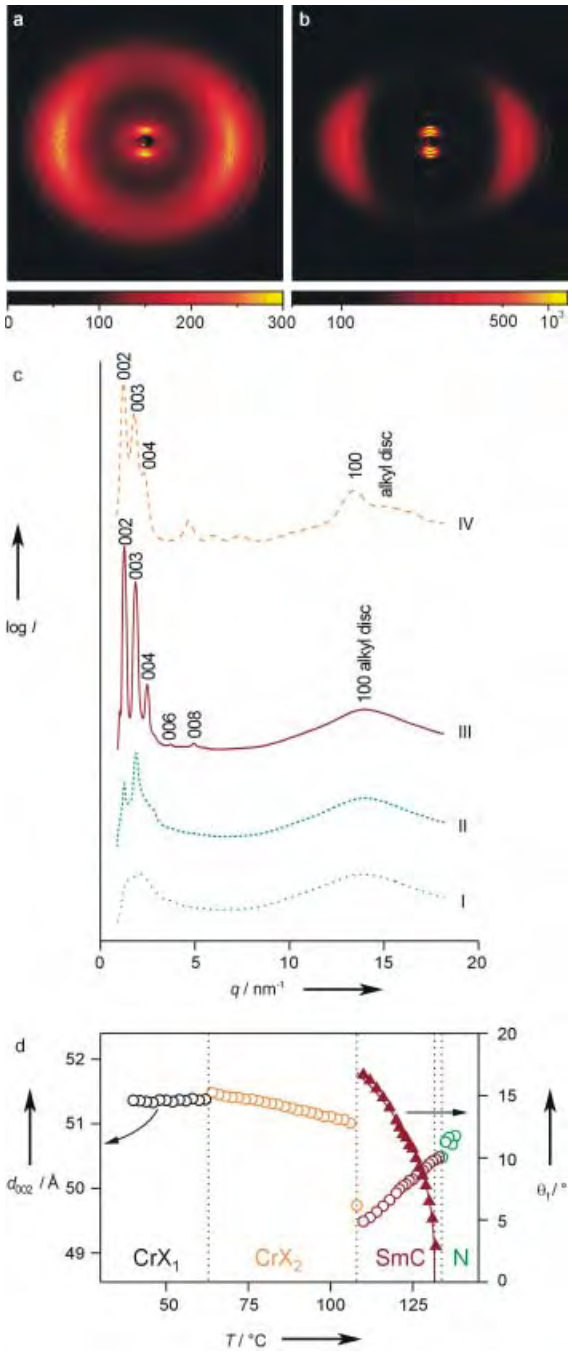



***Figure 2.*** a) Aligned X-ray diffractogram of **1** at 150 °C (nematic, linear *z* scale). b) Aligned X-ray diffractogram of 1 at 132 °C (SmC, logarithmic *z*-scale). c) Integrated X-ray diffraction patterns of **1** at (I) 150 °C (nematic); (II) 136 °C (nematic); (III) 132 °C (SmC); (IV) 90 °C ($Crx_2$). d) Temperature dependence of the layer spacing, *d* (open circles) and the tilt angle, $\theta_t$ (in the SmC phase, triangles), taken from the (002) reflection. Note that $\theta_t$ is calculated based on the assumption that only the rods are tilting. The solid line represents a fit by using Equation (1), in which $\alpha$ is the (only) fitting parameter.[11]

The diffraction pattern in the $Crx_2$ and the $Crx_1$ phase is characterized by a slight widening of the small angle reflections and the presence of a sharp wide angle reflection at 4.7 Å, thus indicating positional order of the mesogens within the layers. The absence of the characteristic reflection

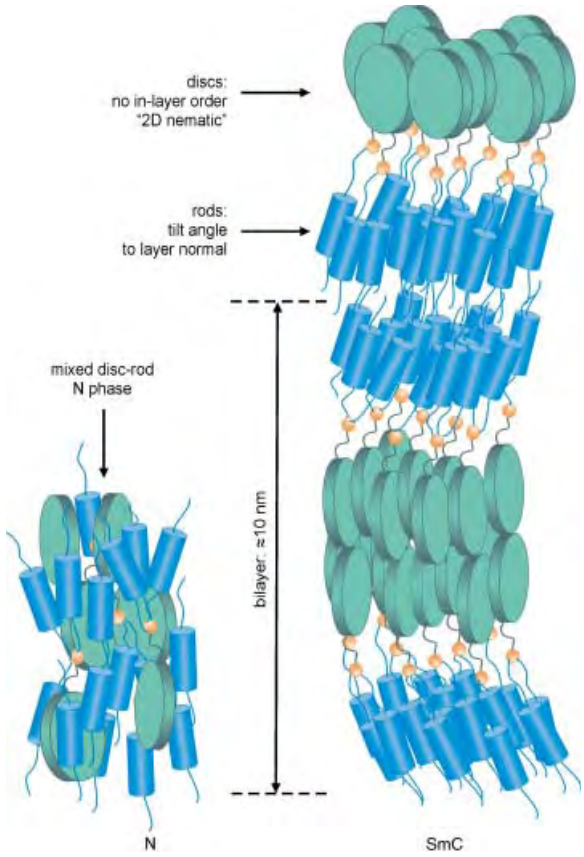



***Figure 3.*** Representation of the order in the N (left) and $SmC_2$ (right) phase of **1**.

at 3.5 Å, assigned to the close (columnar-like) packing of the disc-shaped moieties, indicates that both the SmC–$Crx_2$ and the $Crx_2$–$Crx_1$ transition can be assigned to a further ordering of the rods.[12] These localized phase transitions of the rod-shaped moieties again show the independence of the phase behavior of different layers.

In summary, we have prepared a novel liquid-crystalline material, in which discotic and calamitic mesogens are combined. The material shows a rich phase behavior with a nematic and several smectic phases. To our knowledge this is the first molecular system with discotic mesogens that shows a 1D SmA/C phase. Two levels of order are present in the smectic phases. The first is the well-defined layering, induced by the incompatibility of the discs and rods. Independent of the lamellar order and, indeed, independent of each other, there is another level of organization in the different layers. Phase transitions can occur, which can be solely assigned to a change in organization in one of the two sublayers (e.g. the tilting of the rods at the SmA to SmC phase transition). It is anticipated that also phase transitions may occur in the layer of discs, giving rise to phases in which a layer of columns is formed between layers of rods. The concept of shape-induced phase segregation is a versatile approach to such systems and a wide range of new nanosized phase architectures is anticipated.

Received: July 28, 2003 [Z52488]

 © 2003 Wiley-VCH Verlag GmbH & Co. KGaA, Weinheim 

**Keywords:** liquid crystals · mesophases · nanostructures · self-assembly


[1] a) For a review on polycatenars: H. T. Nguyen, C. Destrade, J. Malthête in *Handbook of Liquid Crystals*, *Vol. 2B* (Eds.: D. Demus, J. W. Goodby, G. W. Gray, H. W. Spiess, V. Vill), Wiley VCH, Weinheim, **1998**, pp. 865–885; b) A. M. Giroud-Godquin, P. M. Maitlis, *Angew. Chem.* **1991**, *103*, 370; *Angew. Chem. Int. Ed. Engl.* **1991**, *30*, 375, and references therein.

[2] For a review on nonconventional mesophases resulting from strong intermolecular interactions: C. Tschierske, *J. Am. Chem. Soc.* **2003**, *125*, 10977, and references therein.

[3] a) R. M. Richardson, S. A. Ponomarenko, N. I. Boiko, V. P. Shibaev, *Liq. Cryst.* **1999**, *26*, 101; b) M. Marcos, R. Giménez, J. L. Serrano, B. Donnio, B. Heinrich, D. Guillon, *Chem. Eur. J.* **2001**, *7*, 1006, and references therein; c) R. Elsäßer, G. H. Mehl, J. W. Goodby, D. J. Photinos, *Chem. Commun.* **2000**, 851.

[4] a) It is noted that the lamellar columnar phases ($Col_L$ or $D_L$ phases) in which mesogens are ordered in layers and in columns that are 2D positionally ordered phases, and are therefore not comparable to SmA or SmC phases, which show 1D order. The first example of $Col_L$ phase is published in: b) K. Ohta, H. Muroki, A. Takagi, K. Hatada, H. Ema, I. Yamamoto, K. Matsuzaki, *Mol. Cryst. Liq. Cryst.* **1986**, *140*, 131.

[5] Highly ordered smectic phases have been reported for a macromolecular samples with strong backbone interactions: D. Janietz, R. Festag, C. Schmidt, J. H. Wendorff, *Liq. Cryst.* **1996**, *20*, 459.

[6] Previously prepared linked disc-rod mesogens: a) W. Kreuder, H. Ringsdorf, O. Herrmann-Schönherr, J. H. Wendorff, *Angew. Chem.* **1987**, *99*, 1300; *Angew. Chem. Int. Ed. Engl.* **1987**, *26*, 1249; b) I. D. Fletcher, G. R. Luckhurst, *Liq. Cryst.* **1995**, *18*, 175; c) J. J. Hunt, R. W. Date, B. A. Timimi, G. R. Luckhurst, D. W. Bruce, *J. Am. Chem. Soc.* **2001**, *123*, 10115; d) P. H. J. Kouwer, G. H. Mehl, *J. Am. Chem. Soc.* **2003**, *125*, 11172.e) P. H. J. Kouwer, G. H. Mehl, *Mol. Cryst. Liq. Cryst.* **2003**, *397*, 301.

[7] The cross section is considered the cross-sectional area of the mesogens perpendicular to the phase normal. For the discs, the cross section is the $\varnothing_D \times d_D$ (diameter × widh) $= 20 \times 4 = \approx$ 80 Å$^2$. Rods have characteristic cross sections of $\approx$25 Å$^2$, and thus three rods in the molecule will have a cross section of $\approx$ 75 Å$^2$. Exact values depend on side groups and the exact organization of the mesogens in the layers.

[8] a) P. H. J. Kouwer, W. F. Jager, W. J. Mijs, S. J. Picken, *Macromolecules* **2002**, *35*, 4322; b) C. C. Dong, M. Hird, J. W. Goodby, P. Styring, K. J. Toyne, *Ferroelectrics* **1996**, *180*, 245.

[9] Also mesogens with incompatible submolecular units (e.g. with siloxane or fluoroalkyl groups) often show microphase segregation. In these systems the phase segregation is already observed in the isotropic phase.

[10] To confirm the presence of the (001) reflection, which is missing in our X-ray diffraction data, additional SAXS measurements were conducted. In these experiments reflections (001) to (004) were observed at $q_{00l} = 0.617$, 1.222, 1.847 and 2.420 nm$^{-1}$, corresponding to layer spacings of $d_{00l} = 101.9$, 51.4, 34.0 and 26.0 Å.

[11] a) Note that the thickness of both the disc and rod layers are estimated after calculating the (sub)molecular dimensions by molecular modeling software. b) P. G. de Gennes, J. Prost in *The Physics of Liquid Crystals*, 2nd ed., Oxford University Press, New York, **1993**, p. 528.

[12] The rod-shaped precursor **4** shows a similar phase transition SmC–$Smx_1$–$Smx_2$ phase transitions and, hence, the transitions are assigned to phase transitions predominantly localized in the rod-layer.


 © 2003 Wiley-VCH Verlag GmbH & Co. KGaA, Weinheim 

Molecular Devices

# A Nanothermometer Based on the Different π Stackings of B- and Z-DNA

*Ryu Tashiro and Hiroshi Sugiyama**

The design and construction of molecular-scale devices are now challenging issues in nanotechnology. Molecular machines, with a two state on–off function, such as catenane,[1,2] rotaxane,[2,3] and ratchet[4] may be candidates for such devices. A nanomechanical device that uses DNA conformational change has recently been developed.[5,6] Double-helical DNA has a unique π-stack structure, and modulation of the π stackings through DNA, controlled by external stimuli coupled with an easily monitored output, is attractive for designing novel DNA-based nanodevices. It has been shown that the electronic properties largely depend on the orientation of the π stacking.[7–9] Because the overall base π stackings of B- and Z-DNA are different, the electronic properties of these two duplexes are also assumed to be different. Based on this hypothesis, a molecular thermometer that uses the different π stackings of B- and Z-DNA was designed. 2-Aminopurine,[10–12] which is a fluorescent probe for charge-transfer processes, was introduced into B- and Z-DNA and the emission monitored. Z-DNA showed a marked increase in fluorescence compared with B-DNA, with the fluorescence intensity correlating reproducibly with temperature.

Inspection of the X-ray structures of Z-form and B-form DNA suggests that there is significant difference in base π-stack orientation in both structures, that is, discrete clusters of interstrand four-base π stacks of G-C-C-G exist in the Z-form,[13] whereas there is a continuous π stack along each strand in B-DNA (Figure 1). We expected that the four-base π stacks would largely contribute to the electronic properties of Z-DNA, and that the different electronic properties between B- and Z-DNA could be monitored by 2-aminopurine (Ap), because the quenching of Ap fluorescence has been used as a probe for charge transfer within DNA duplexes, in which the purine bases (G and A) and pyrimidine bases (C and T) function as donors and acceptors, respectively.[8–11] Thus, the fluorescence intensity of the Ap-containing duplex decamer, 5′-d(CGCApCGCGCG)-3′ (ODN 1)/5′-d(CGCGCGTGCG)-3′ (ODN 2), was monitored under various conditions. The duplex decamer, 5′-d(CGCApC-

[*] Prof. H. Sugiyama, R. Tashiro
Division of Biofunctional Molecules
Institute of Biomaterials and Bioengineering
Tokyo Medical and Dental University
2-3-10 Surugadai, Kanda, Chiyoda, Tokyo 101-0062 (Japan)
E-mail: hs@kuchem.kyoto-u.ac.jp
Prof. H. Sugiyama
Department of Chemistry, Graduate School of Science, Kyoto University, Kitashirakawa-Oiwakecho, Sakyo, Kyoto 606-8502 (Japan)
Fax: (+81) 352-808-127

Supporting information for this article is available on the WWW under http://www.angewandte.org or from the author.

 © 2003 Wiley-VCH Verlag GmbH & Co. KGaA, Weinheim DOI: 10.1002/anie.200352752 

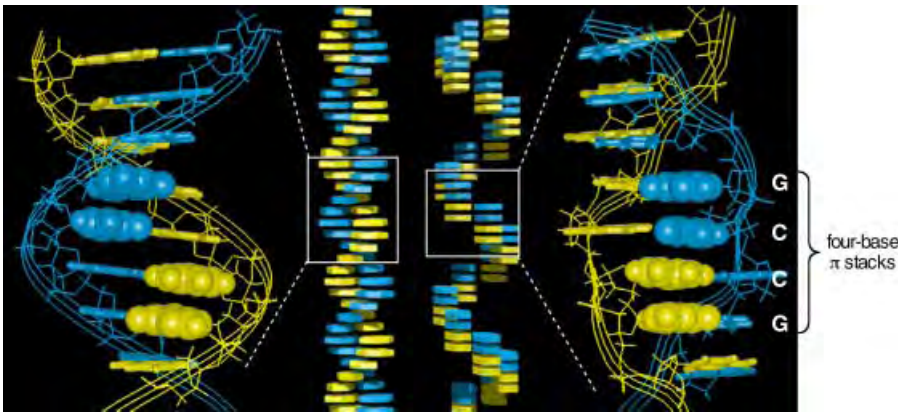



***Figure 1.*** Molecular models of B-form (left) and Z-form DNA (right). The models were constructed by using the Insight II program (Accelrys) with standard B- and Z-form helical parameters. The two strands are in yellow and blue.

G*A*GCG)-3′ (ODN 3)/5′-d(CGC*T*CGTGCG)-3′ (ODN 4), which does not convert to the Z-conformation (even in 5 M NaCl because of the disordering of the preferred altenative purine–pyrimidine sequence of Z-DNA),[13] was used as a control. In 1 M NaCl, ODN 1–2, which mainly exists in the B-conformation (> 95 %), as assessed by using circular dichroism (CD) spectroscopy, showed very weak fluorescence, similar to ODN 3–4. The fluorescence of ODN 1–2 increased proportionally upon increasing the ratio of Z-conformation by increasing the NaCl concentration (1–5 M, Figure 2a), whereas no such evident increase of the fluorescence was observed in the control ODN 3–4. These results indicate that the electronic property of Z-DNA is different from that of B-DNA. The intense fluorescence of Ap in Z-DNA is in accord with the previous finding of almost no charge-transfer between the different four-base π stacks observed in the $^{Br}$U photoreaction of Z-DNA.[14] The intense fluorescence of ODN 1–2 in the Z-conformation can be explained by the following reasons for disruption of charge-transfer. 1) Ap is located at the 5′-end of the four-base π stacks lacking a quenching base at the 5′-side. In fact, fluorescence of 5′-ApCCG-3′ is found to be twice as intense as 5′-CApCG-3′ (see Figure S3 in the Supporting Information). 2) Disruption of continuous π stacking[15] is due to the four-base π stacks in Z-DNA. Analogous slow interstrand charge transfer relative to the intrastrand process in B-DNA has been pointed out.[15,16]

We designed a molecular thermometer based on the change in π stacks upon converting from B- to Z-DNA. It is known that the equilibrium between the Z- and the B-conformation can be controlled by temperature.[17] At low temperature, the proportion of the Z-conformation is high due to its lower entropy. Therefore, an increase in temperature increases the proportion of the B-conformation. Thus, the fluorescence of ODN 1–2 was monitored at different temperatures in 3 M NaCl. Thermal denaturation studies revealed that ODN 1–2 and ODN 3–4 formed a duplex (> 95 %) below 32 °C.[18] As shown in Figure 3, it was found that the intensity of the fluorescence linearly correlated with the temperature. At $T = 32$ °C, at which 23 % of the ODN 1–2 was in the Z-conformation, the fluorescence of the ODN 1–2 was very weak, whereas the fluorescence of the ODN 1–2 dramatically increased at $T = 2$ °C (Figure 3a), when 53 % of the ODN 1–2 was in the Z-conformation. In clear contrast, such a response was not observed in the control ODN 3–4 sample under the same conditions (see Figure 3b). This function is fully reversible. Under repetitive temperature changes, a reproducible fluorescence of ODN 1–2 was observed according to the change in the proportion of B- and Z-conformations (Figure 3c).

These results clearly indicate that the B–Z transition induced by a change in temperature can be readily monitored by using the fluorescence intensity of Ap. Such a molecular thermometer can be applied in the investigation of localized temperature on a microscale. Because we previously reported that the pathway for electron transfer is different between B- and Z-DNA,[14] the B–Z transition could be useful

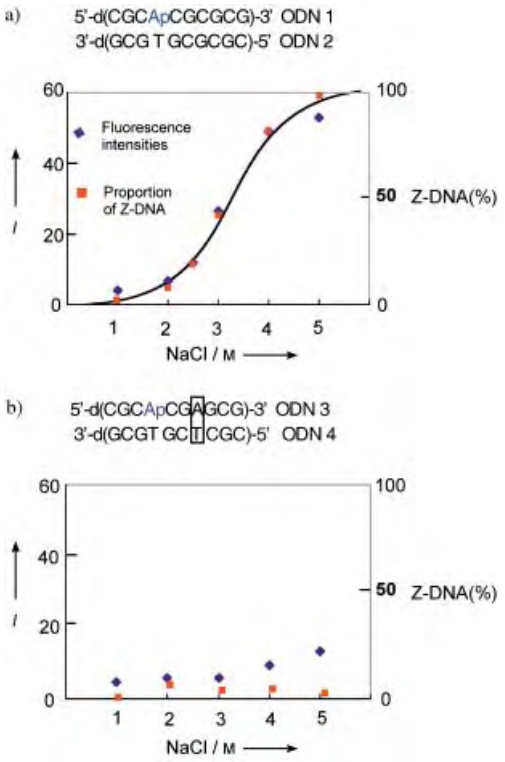



***Figure 2.*** Steady-state fluorescence emission intensities and proportion of the Z-conformation of a) 5′-(CGCApCGCGCG)-3′/5′-(CGCGCGTGCG)-3′ (ODN 1–2), and b) 5′-(CGCApCGAGCG)-3′/5′-(CGCTCGTGCG)-3′ (ODN 3–4), as a function of NaCl concentration (1–5 M). Emission intensities for 30 μM (total base concentration) duplex samples in 20 mM phosphate buffer (pH 7.0) at 10 °C were measured. The samples were excited at 317 nm, and emission intensities were determined by monitoring emission at 360 nm. $I$ = Intensity of fluorescence (arbitrary units).

 © 2003 Wiley-VCH Verlag GmbH & Co. KGaA, Weinheim 

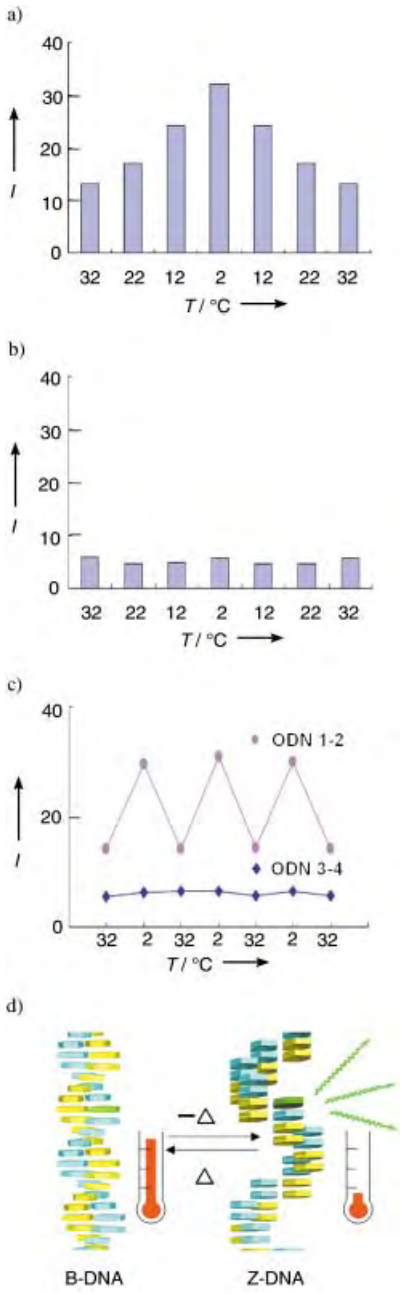



***Figure 3.*** Steady-state fluorescence emission intensities of a) ODN 1–2, and b) ODN 3–4 at different temperatures (32–2 °C). Emission intensities of 30 μM (total base concentration) duplex oligomers in 20 mM phosphate buffer (pH 7.0) and 3 M NaCl were measured. c) Repeating experiments of fluorescence emission of ODN 1–2 and ODN 3–4 at 32 and 2 °C. d) Schematic representation of nanothermometer.

for new types of nanoelectronic devices, such as sensor, wire, memory, and molecular switches.

## *Experimental Section*

CD spectra were measured with an AVIV MODEL 62 DS/202 CD spectrophotometer. Duplexes were hybridized by heating to 90 °C, followed by slow cooling to room temperature. CD spectra of ODN 1–2 and ODN 3–4 (30 μM base concentration in 50 mM sodium phosphate buffer, pH 7.0, at various NaCl concentrations) were recorded by using a 1 cm path-length cell. The proportions of Z, B and SS for these oligmers were estimated as previously reported.[19,20] To obtain the population of B- and Z-DNA ($P_B$ and $P_Z$), we analyzed the CD spectra taking into account the three form (B, Z, SS) present in solution. Hence, at each temperature we made the following assumptions [Eq. (1) and (2)].

$$\Delta\varepsilon^{295} = \Delta\varepsilon_B^{295} P_B + \Delta\varepsilon_Z^{295} P_Z + \Delta\varepsilon_{SS}^{295} P_{SS} \quad (1)$$

$$1 = P_B + P_Z + P_{SS} \quad (2)$$

The $P_B$, $P_Z$, and $P_{SS}$ are the molar fractions of the B, Z, and single strand components, respectively. The $\Delta\varepsilon$ values, relative to the limit forms, have been estimated from the CD signal at 295 nm. They were considered to be independent of the temperature and salt concentration. A UV melting experiment indicated that $P_{SS}$ is negligible under the experimental conditions. Therefore, Equation (1) and (2), relative to each CD spectrum at a given temperature, were solved to provide estimates of $P_B$ and $P_Z$.

Steady-state fluorescence measurements on Ap-containing DNA were conducted by using a JASCO FP-6300 spectrofluorometer. Measurements were performed by using fluorescence cells with a 1 cm path length. The duplex concentration for emission measurements was 30 μM (total base concentration). Steady-state fluorescence emission spectra and CD spectra of ODN 1–2 and 3–4 under different salt conditions are available in the Supporting Information.

Received: September 1, 2003 [Z52752]

**Keywords:** DNA structures · fluorescent probes · molecular devices · nanomaterials · sensors

[1] D. A. Leigh, J. K. Y. Wong, F. Dehez, F. Zerbetto, *Nature* **2003**, *424*, 174.
[2] J.-P. Sauvage, *Acc. Chem. Res.* **1998**, *31*, 611.
[3] A. M. Brouwer, C. Frochot, F. G. Gatti, D. A. Leigh, L. Mottier, F. Paolucci, S. Roffia, G. W. H. Wurpel, *Science* **2001**, *291*, 2124.
[4] T. R. Kelly, H. D. Silva, R. A. Silva, *Nature* **1999**, *401*, 150.
[5] N. C. Seeman, *Nature* **2003**, *421*, 427.
[6] C. Mao, W. Sun, Z. Shen, N. C. Seeman, *Nature* **1999**, *397*, 144.
[7] H. Sugiyama, I. Saito, *J. Am. Chem. Soc.* **1996**, *118*, 7063.
[8] J. M. Jean, K. B. Hall, *Proc. Natl. Acad. Sci. USA* **2001**, *98*, 37.
[9] J. M. Jean, K. B. Hall, *Biochemistry* **2002**, *41*, 13152.
[10] M. A. O'Neill, J. K. Barton, *J. Am. Chem. Soc.* **2002**, *124*, 13053.
[11] C. Wan, T. Fiebig, O. Schiemann, J. K. Barton, A. H. Zewail, *Proc. Natl. Acad. Sci. USA* **2000**, *97*, 14052.
[12] S. O. Kelley, J. K. Barton, *Science* **1999**, *283*, 375.
[13] A. Rich, A. Nordheim, A. H.-J. Wang, *Annu. Rev. Biochem.* **1984**, *53*, 791.
[14] R. Tashiro, H. Sugiyama, *J. Am. Chem. Soc.*, in press.
[15] H.-A. Wagenknecht, S. R. Rajski, M. Pascaly, E. D. A. Stemp, J. K. Barton, *J. Am. Chem. Soc.* **2001**, *123*, 4400.
[16] F. D. Lewis, X. Zuo, J. Liu, R. T. Hayes, M. R. Wasielewski, *J. Am. Chem. Soc.* **2002**, *124*, 4568.
[17] H. Sugiyama, K. Kawai, A. Mastunaga, K. Fujimoto, I. Saito, H. Robinson, A. H.-J. Wang, *Nucleic Acids Res.* **1996**, *24*, 1272 .
[18] Thermal denaturation studies revealed that the melting temperatures of ODN 1–2 and ODN 3–4 are 56 °C and 54 °C, respectively, under the same conditions described in the legend of Figure 3.
[19] L.-E. Xodo, G. Manzini, F. Quadrifoglio, G. A. van der Marel, J. H. van Boom, *Biochemistry* **1988**, *27*, 6327.
[20] E. O. Otokiti, R. D. Sheardy, *Biochemistry* **1997**, *36*, 11419.

 © 2003 Wiley-VCH Verlag GmbH & Co. KGaA, Weinheim 

Helical Polymers

# Intramolecular Cross-Linking of Helical Folds: An Approach to Organic Nanotubes**

*Stefan Hecht* and Anzar Khan*

The design and synthesis of hollow tubular, functional nanostructures of controlled dimensions and defined surface chemistry remains a challenging and attractive target in both bio- and nanosciences.[1,2] Integration of these molecular building blocks into larger, more complex structures by self-assembly or manipulation promises potential applications in several areas, including chemical and charge transport as well as sensing and catalysis.

Here, we report on an approach to organic nanotubes[1] that is based on intramolecular cross-linking[3–5] of helically folded polymer backbones.[6] Our concept (Figure 1) is inspired by the hierarchical structural evolution in nature and involves polymerization of an appropriately functionalized monomer containing folding-promoting features as well as cross-linking units. The formed polymer strand (primary structure) is able to adopt a helical conformation (secondary structure), in which reactive groups are oriented within proximity to allow for subsequent covalent stabilization of the tubular nanoobject.

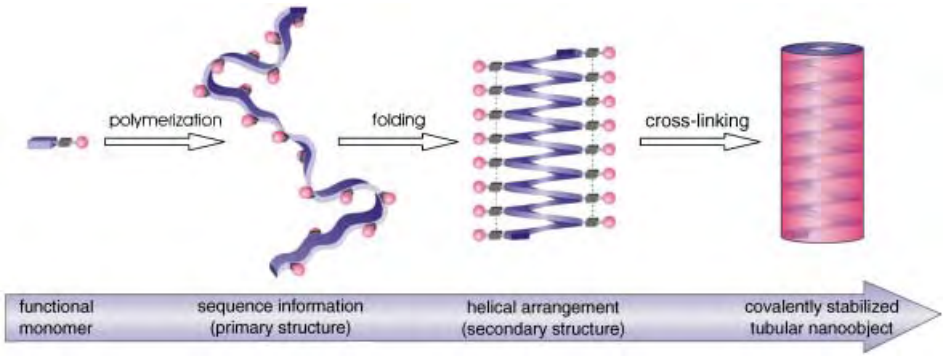



***Figure 1.*** Formation of organic nanotubes by the intramolecular cross-linking of folded helical polymer backbones: Polymerization of a functional monomer carrying both solvophilic (magenta) and cross-linking groups (gray) generates a polymer strand that folds (solvophobically driven) into a helical conformation that is subsequently stabilized by covalent cross-linking using adjacent reactive groups.

Amphiphilic poly(*m*-phenyleneethynylene)s[7] were chosen as the backbone for several reasons: 1) the corresponding (oligomeric) foldamer family pioneered by Moore and co-workers[8] displays well-characterized conformational behavior that can easily be monitored by using a variety of spectroscopic techniques, including UV/Vis absorption and fluorescence spectroscopy; 2) $\pi$–$\pi$ stacking of neighboring units in adjacent turns positions the reactive groups in proximity (ca. 3.4 Å) to ensure efficient cross-linking reactions; 3) the 6-helix[9] enables several cross-links to be introduced per turn, thus potentially increasing the stability of the structure, and contains a large internal void (diameter ca. 0.8 nm). The reactive groups were incorporated as cinnamates to utilize [2+2] photodimerization reactions for intramolecular cross-linking,[10,11] thereby minimizing the structural changes during the cross-linking process.[12]

A newly developed $A_2+BB'$ polycondensation route[13] starting from the diiodocinnamate monomer **1** affords poly(*m*-phenyleneethynylene) **2** (Scheme 1), which has a respectable number-average degree of polymerization (DP ca. 60)[14] and a typical polydispersity index (PDI = 1.3). Most importantly, the polymer does not contain diyne defects as evidenced by $^{13}C$ NMR spectroscopy.[15] Such defects would perturb the folding process and disrupt the tubular helical structure.

Solvent denaturation experiments carried out using UV/Vis spectroscopy (Figure 2a) to monitor the population of random-coiled and helical conformations through differences in transoid and cisoid absorptions,[8a,c] respectively, reveal a typical sigmoidal, that is, cooperative, folding behavior (Figure 3). A similar solvent titration curve with a slightly shifted transition point[8b,c] is obtained independently by monitoring the emission of isolated versus packed "pseudoexcimer"-like repeat units by fluorescence spectroscopy.[15] Denaturation occurs at higher chloroform content than that of shorter oligomers of similar structure,[8] which indicates that a more-stable helix is formed, as predicted by the helix–coil model.[6a,16] Both UV/Vis and fluorescence spectroscopic studies performed in THF at 40 °C (to simulate conditions used in gel-permeation chromatography (GPC)) suggest a major population of the helical conformation and, therefore, the molecular weight determined by GPC most likely represents a lower limit.

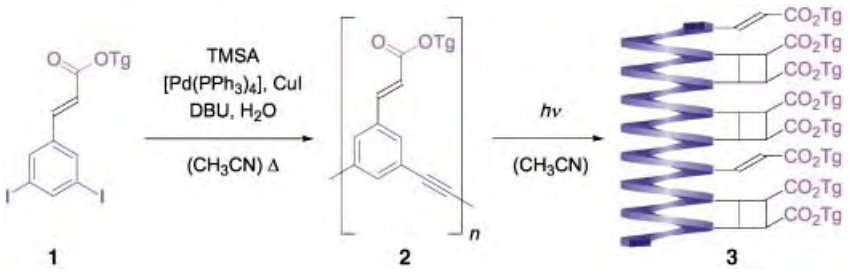
Polymer **2** was irradiated under high-dilution conditions in the folding-promoting solvent acetonitrile.[17] Clean photoconversion of the cinnamate moieties was observed, as evidenced by a smoothly decreasing UV/Vis absorbance and the corresponding extinction difference analysis.[15] After

[*] Dr. S. Hecht, A. Khan
Institut für Chemie/Organische Chemie
Freie Universität Berlin
Takustrasse 3, 14195 Berlin (Germany)
Fax: (+49) 30-838-52551
E-mail: shecht@chemie.fu-berlin.de

[**] The authors thank Melanie Müller for synthesizing some of the starting materials, Dieter Lentz for use of the irradiation equipment, and Andreas Schäfer for his invaluable help with NMR experiments. Generous support by the Sofja Kovalevskaja Award of the Alexander von Humboldt Foundation, endowed by the Federal Ministry of Education and Research (BMBF) within the Program for Investment in the Future (ZIP) of the German Government, is gratefully acknowledged.

Supporting information for this article is available on the WWW under http://www.angewandte.org or from the author.

 DOI: 10.1002/anie.200352983 © 2003 Wiley-VCH Verlag GmbH & Co. KGaA, Weinheim 




***Scheme 1.*** Synthesis and irradiation of amphiphilic poly(*m*-phenyleneethynylene) **2** (Tg = $CH_2CH_2OCH_2CH_2OCH_2CH_2OCH_3$). TMSA = trimethylsilylacetylene, DBU = 1,8-diazabicyclo[5.4.0]undec-7-ene.

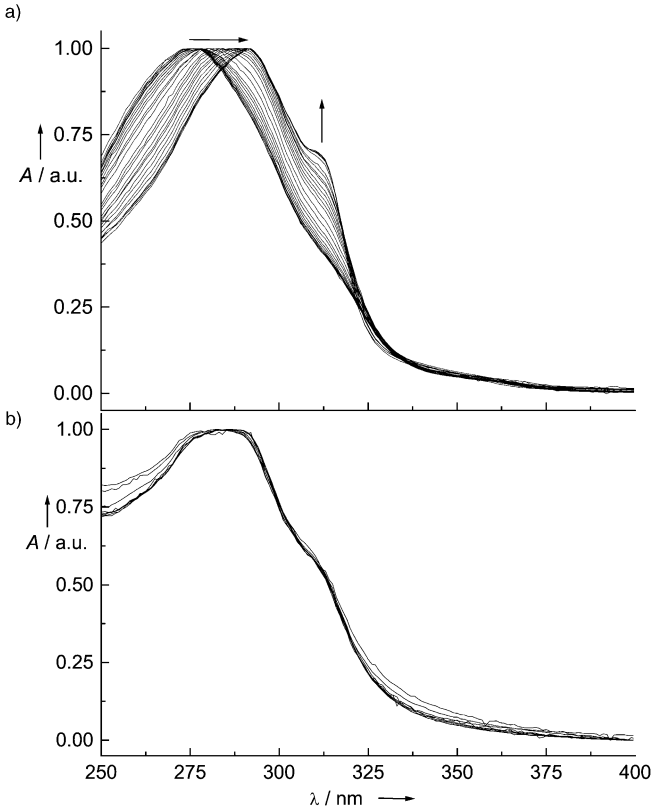



***Figure 2.*** UV/Vis absorption spectra of: a) polymer **2** and b) cross-linked polymer **3** recorded in acetonitrile with increasing chloroform content (100% $CH_3CN \rightarrow 100\%$ $CHCl_3$). The spectra, measured at approximately the same concentration, have been normalized with respect to their maximum intensity.

20 minutes of irradiation, the resulting cross-linked polymer **3** was again subjected to a UV/Vis titration experiment (Figure 2b and 3). No significant spectral changes were observed with increasing amounts of the chloroform denaturant,[17] thus clearly demonstrating the presence of the locked helical conformation. The slightly higher absorbance ratio ($A_{312nm}/A_{292nm}$) relative to that of folded polymer **2** is presumably a result of the structural changes occurring during the photodimerization leading to a slightly twisted cisoid conformation. Further support for the cross-linked helical structure arises from the fluorescence spectrum of **3** recorded in chloroform (Figure 4). The almost negligible emission band (Figure 4, inset) is reminiscent of "pseudoexcimer" **4**. However, the much lower emission intensity can be explained by the diminished π–π overlap in **5** resulting from a considerable tilt angle (ca. 30°) introduced during cross-linking, as evident from molecular mechanics calculations (Figure 5).

Considering the possible geometrical isomers in the cinnamate photodimerization process, the helical structure should exclusively lead to the formation of truxinates, that is, head–head dimers.[18] Following the topochemical principle,[12] the least conformational changes occur during the formation of β-truxinate **5** (*syn* head–head photodimer). Structural evidence for the proposed stereochemistry of **5** arises from NMR spectroscopic analysis (Figure 6), since the doublet at $\delta = 4.0$ ppm is diagnostic for β-truxinates.[19] Furthermore, the signal corresponding to the

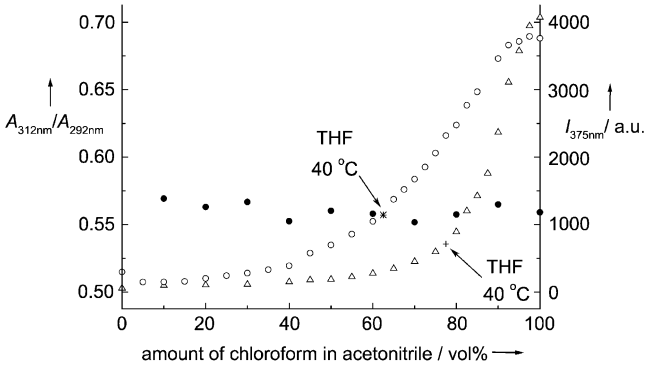



***Figure 3.*** Solvent denaturation curves for amphiphilic poly(*m*-phenyleneethynylene) before (**2**) and after (**3**) irradiation: plot of the UV/Vis absorbance ratio ($A_{312nm}/A_{292nm}$) and corrected normalized fluorescence intensity ($I_{375nm}$), respectively, as a function of the volume percent of chloroform in acetonitrile (25 °C). ○: UV/Vis data of **2**, △: fluorescence data of **2**, ●: UV/Vis data of **3**. The UV/Vis data (*) and fluorescence data (+) of **2** recorded in THF at 40 °C are also shown.

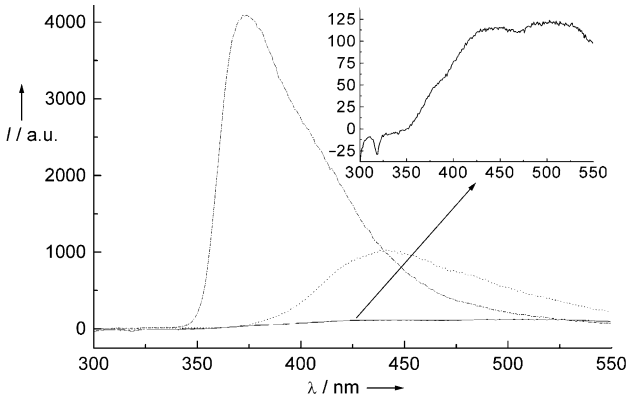



***Figure 4.*** Corrected normalized fluorescence spectra of amphiphilic poly(*m*-phenyleneethynylene) before (**2**) and after (**3**) irradiation (25 °C): –•–•: **2** in $CHCl_3$, •••••: **2** in $CH_3CN$, ——: **3** in $CHCl_3$. The inset shows a magnification of the spectrum of **3** in $CHCl_3$.

 © 2003 Wiley-VCH Verlag GmbH & Co. KGaA, Weinheim 

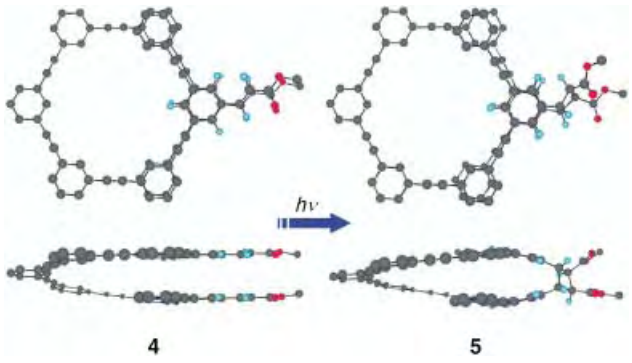



***Figure 5.*** Molecular models of two π–π-stacking cross-linking units in the folded helical conformation of amphiphilic poly(*m*-phenyleneethynylene) **2**. Left: parallel-stacked cinnamate pair **4** (3.4 Å apart) before irradiation,. Right: β-truxinate **5** (*syn* head–head) dimer after irradiation, with a 3.4 Å distance between the centers of the phenyl rings that are tilted by 30.5°. The models were optimized by using molecular mechanics calculations (MM2). For clarity, only the carbon atoms (gray) of the helical backbone as well as the oxygen (red), hydrogen (cyan), and carbon atoms of the cinnamate units are shown.

vinyl protons illustrates that not all the cinnamate moieties have reacted, which is in agreement with the UV/Vis spectra.[15] The pronounced upfield shift of the vinyl protons and the diminished signal of the aryl protons provide additional support for the locked helical structure.[20] As a consequence of the overlapping signals in the $^1$H NMR spectrum, the degree of cross-linking can only roughly be estimated to be about 20–30%. This value is in reasonable agreement with the decrease in the UV/Vis absorption during the course of irradiation.[15]

Short irradiation times favor the formation of mainly intramolecularly cross-linked polymers, as indicated by GPC.[15] However, extensive irradiation leads to additional intermolecular cross-linking of cinnamate moieties in aggregating adjacent tubes, as suggested by the strongly bimodal distribution in the GPC trace after two hours of irradiation. In a control experiment, irradiation in chloroform yielded a polymer with a high degree of intermolecular cross-links and transoid conformations.

In summary, all the experimental methods employed thus far[21] are consistent with a covalent stabilization of the helical conformation and therefore demonstrate the feasibility of our approach to the formation of organic nanotubes (Figure 1). Current work in our laboratories involves in-depth characterization of the generated tubes, increasing their aspect ratio, and improving the cross-linking chemistry to further minimize structural reorganization and include polymeric instead of dimeric cross-links. By utilizing our concept, organic nanotubes of controlled dimensions[22] and specific local surface functionality[23] should ultimately be realized.

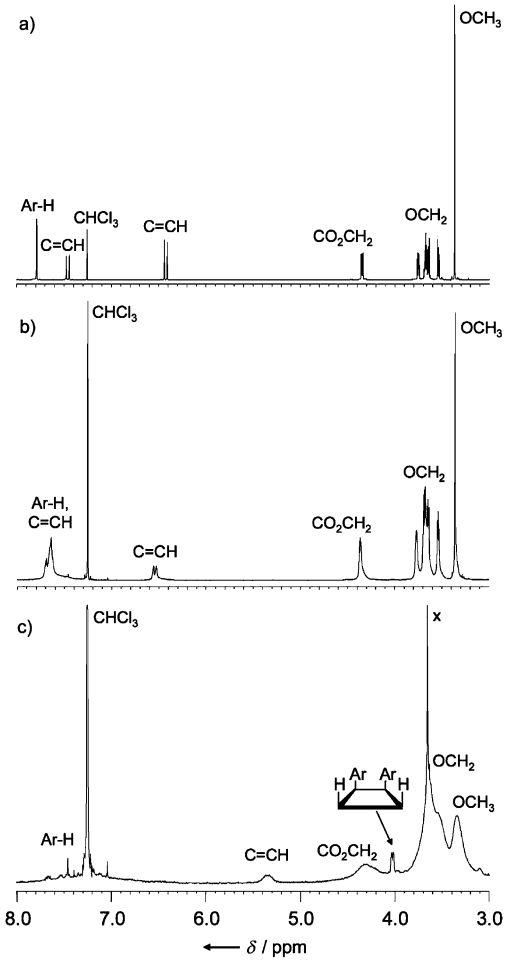



***Figure 6.*** $^1$H NMR spectral comparison ($CDCl_3$, 23 ± 2 °C): a) monomer **1**, b) polymer **2**, and c) polymer **3** (after 20 min irradiation period).

Received: October 1, 2003 [Z52983]

**Keywords:** cross-linking · helical structures · materials science · nanotubes · topochemistry

[1] For a comprehensive review on organic nanotubes, see D. T. Bong, T. D. Clark, J. R. Granja, M. R. Ghadiri, *Angew. Chem.* **2001**, *113*, 1016–1041; *Angew. Chem. Int. Ed.* **2001**, *40*, 988–1011.

[2] For a recent review on inorganic nanostructures, see Y. Xia, P. Yang, Y. Sun, Y. Wu, B. Mayers, B. Gates, Y. Yin, F. Kim, H. Yan, *Adv. Mater.* **2003**, *15*, 353–389.

[3] For a review on regioselectively cross-linked nanostructures, see C. G. Clark, K. L. Wooley in *Dendrimers and other Dendritic Polymers* (Eds.: J. M. J. Fréchet, D. A. Tomalia), Wiley, Chichester, **2001**, pp. 147–170.

[4] Recently, hollow tubes were generated using peripheral cross-linking of dendronized oligomers followed by removal of the inner core: a) Y. Kim, M. F. Mayer, S. C. Zimmerman, *Angew. Chem.* **2003**, *115*, 1153–1158; *Angew. Chem. Int. Ed.* **2003**, *42*, 1121–1126. This approach is related to the concept of cored dendrimers: b) M. S. Wendland, S. C. Zimmerman, *J. Am. Chem. Soc.* **1999**, *121*, 1389–1390.

[5] Short α-helical peptides (without an internal void) have been stabilized by a single covalent cross-link: a) H. E. Blackwell, R. H. Grubbs, *Angew. Chem.* **1998**, *110*, 3469–3472; *Angew. Chem. Int. Ed.* **1998**, *37*, 3281–3284, or their conformation switched using a single azobenzene linker: b) J. R. Kumita, O. S. Smart, G. A. Woolley, *Proc. Natl. Acad. Sci. USA* **2000**, *97*, 3803–3808; c) D. G. Flint, J. R. Kumita, O. S. Smart, G. A. Woolley, *Chem. Biol.* **2002**, *9*, 391–397.

 © 2003 Wiley-VCH Verlag GmbH & Co. KGaA, Weinheim 

[6] For a comprehensive review on foldamers, see a) D. J. Hill, M. J. Mio, R. B. Prince, T. S. Hughes, J. S. Moore, *Chem. Rev.* **2001**, *101*, 3893 – 4011; for a review on synthetic helical polymers, see b) T. Nakano, Y. Okamoto, *Chem. Rev.* **2001**, *101*, 4013 – 4038; for a review on supramolecular helical architectures, see c) J. J. L. M. Cornelissen, A. E. Rowan, R. J. M. Nolte, N. A. J. M. Sommerdijk, *Chem. Rev.* **2001**, *101*, 4039 – 4070.

[7] For a comprehensive review about poly(phenyleneethynylene)s, mostly of the *para*-type, see U. H. F. Bunz, *Chem. Rev.* **2000**, *100*, 1605 – 1644.

[8] a) J. C. Nelson, J. G. Saven, J. S. Moore, P. G. Wolynes, *Science* **1997**, *277*, 1793 – 1796; b) R. B. Prince, J. G. Saven, P. G. Wolynes, J. S. Moore, *J. Am. Chem. Soc.* **1999**, *121*, 3114 – 3121; c) R. B. Prince, PhD thesis thesis, University of Illinois (Urbana-Champaign), **2000**.

[9] The 6-helix is defined as a helix having six repeat units per turn. Experimental evidence for this structure arises from ESR double spin labeling experiments: K. Matsuda, M. T. Stone, J. S. Moore, *J. Am. Chem. Soc.* **2002**, *124*, 11836 – 11837.

[10] For a review on topochemical [2+2] photodimerization of cinnamates, see a) G. M. J. Schmidt, *Pure Appl. Chem.* **1971**, *27*, 647 – 678; for an example in a two-dimensional crystal, that is, on a surface, see b) M. M. S. Abdel-Mottaleb, S. De Feyter, A. Gesquiere, M. Sieffert, M. Klapper, K. Müllen, F. C. De Schryver, *Nano Lett.* **2001**, *1*, 353 – 357; for an example in a liquid-crystalline phase, see c) C. Mertesdorf, H. Ringsdorf, J. Stumpe, *Liq. Cryst.* **1991**, *9*, 337 – 357.

[11] The preparation of polymers from di-olefinic monomers by [2+2] photodimerization has been reviewed in: a) W. L. Dilling, *Chem. Rev.* **1983**, *83*, 1 – 47; b) M. Hasegawa, *Chem. Rev.* **1983**, *83*, 507 – 518.

[12] This is related to the topochemical principle: a) V. Kohlschütter, *Z. Anorg. Allg. Chem.* **1918**, *105*, 1 – 25; for a comprehensive review, see b) V. Ramamurthy, K. Venkatesan, *Chem. Rev.* **1987**, *87*, 433 – 481.

[13] A. Khan, S. Hecht, unpublished results. For related approaches, see a) V. A. Solomin, W. Heitz, *Macromol. Chem. Phys.* **1994**, *195*, 303 – 314; b) H. Haeger, W. Heitz, *Macromol. Chem. Phys.* **1998**, *199*, 1821 – 1826; the in situ deprotection/coupling conditions are inspired by: c) M. J. Mio, L. C. Kopel, J. B. Braun, T. L. Gadzikwa, K. L. Hull, R. G. Brisbois, C. J. Markworth, P. A. Grieco, *Org. Lett.* **2002**, *4*, 3199 – 3202.

[14] According to optical spectroscopy, the molecular weight determined by GPC is most likely underestimated (see Figure 2).

[15] See the Supporting Information.

[16] B. H. Zimm, J. K. Bragg, *J. Chem. Phys.* **1959**, *31*, 526 – 533.

[17] D. J. Hill, J. S. Moore, *Proc. Natl. Acad. Sci. USA* **2002**, *99*, 5053 – 5057.

[18] In bulk cinnamate phases, β- and δ-truxinates (*syn* and *anti* head–head photodimers) constitute the major photodimerization products: P. L. Egerton, E. M. Hyde, J. Trigg, A. Payne, P. Beynon, M. V. Mijovic, A. Reiser, *J. Am. Chem. Soc.* **1981**, *103*, 3859 – 3863.

[19] D. A. Ben-Efraim, B. S. Green, *Tetrahedron* **1974**, *30*, 2357 – 2364; F. D. Lewis, S. L. Quillen, P. D. Hale, J. D. Oxman, *J. Am. Chem. Soc.* **1988**, *110*, 1261 – 1267.

[20] Strong upfield chemical shifts upon transition to the folded helical structure have been reported in reference [8a] and S. Lahiri, J. L. Thompson, J. S. Moore, *J. Am. Chem. Soc.* **2000**, *122*, 11315 – 11319.

[21] Visualization attempts using STM and TEM have so far been unsuccessful because of the significant thickness (low tunneling current) and the low contrast (all carbon material), respectively, of the tubes.

[22] The outer and inner diameters are encoded in the foldamer motif used. Length control—currently not possible by means of self-assembly—could be achieved using a folding polymer of low polydispersity prepared by advanced living polymerization techniques.

[23] In principle the use of heterosequences (alternating as well as block copolymers) enables nonstatistical, location-specific outer/inner functionalization. Currently, such control over surface chemistry cannot be realized in carbon or inorganic nanotubes.

 © 2003 Wiley-VCH Verlag GmbH & Co. KGaA, Weinheim 